



Türkiye 21. Uluslararası  
Petrol ve Doğal Gaz  
Kongre ve Sergisi  
27-29 Eylül 2023

Sheraton Otel ve Kongre Merkezi  
Ankara, Türkiye

*21<sup>th</sup> International  
Petroleum and Natural Gas  
Congress and Exhibition of Turkey  
September 27<sup>th</sup>-29<sup>th</sup> 2023*

*Sheraton Hotel & Convention Center  
Ankara, Türkiye*

**BİLDİRİLER KİTABI**  
**CONGRESS PROCEEDINGS**

## DAVET

Türkiye Uluslararası Petrol ve Doğal Gaz Kongre ve Sergisi (IPETGAS 2023), Türkiye Petrol Jeologları Derneği, TMMOB Petrol Mühendisleri Odası ve TMMOB Jeofizik Mühendisleri Odası tarafından 27-29 Eylül 2023 tarihleri arasında Ankara'da, Türkiye Cumhuriyeti'nin 100. kuruluş yılında "Denizinde, dağında, taşında Cumhuriyetimiz 100 yaşında" sloganı ile düzenlenecektir.

IPETGAS'23'ün amacı, petrol endüstrisinin üç disiplini, yatırımcıları ve servis firmalarını seçkin bir atmosferde buluşturmaktır. Bu bilimsel şölenimizde; Ülkemizin kara ve deniz alanları ile bunların uzantısı komşu ülkelerde petrol ve doğalgaz aramacılığında son dönemdeki bulgular paylaşılacak, altyapı ve stratejiler tartışılacak, yenilenebilir enerji kaynaklarındaki gelişmeler uzmanlarca değerlendirilecektir. Her disiplinden uzmanların özgün sözlü ve poster sunumları yanında seçkin davetli konuşmacılar da geniş perspektiften katılımcıları aydınlatacaklar. Geleceğimiz, her üç disiplinden öğrencilerimiz için sunum fırsatı sağlanacak ve en iyi sunumlar ödüllendirilecektir. Kongremiz sergi alanında endüstrimizin çözüm ortakları, teknoloji ve ürünlerini sergileme fırsatı bulacaklardır. Kongremiz öncesinde tam günlük kurslar ile meslektaşlarımızın yetkinliklerine katkı sunulacaktır. Petrol endüstrisi düzenleyici kuruluşu Maden ve Petrol İşleri Genel Müdürlüğü (MAPEG), sergi alanımızda yatırımcılara ülkemizin arama fırsatları hakkında bilgiler verecektir. Milli Petrol Şirketimiz Türkiye Petrolleri A.O. (TPAO) başta olmak üzere, arama ve üretim şirketleri, Boru Hatları ile Taşımacılık A.Ş. (BOTAS) ve Maden Tetkik Arama (MTA) Genel Müdürlüklerimiz sergi alanımızda servis sağlayıcı firmalarla yeni işbirliklerini tartışabileceklerdir.

Türkiye, zengin hidrokarbon rezervlerine sahip Ortadoğu ve Hazar bölgesi ile tüketimi büyük ölçüde ithalata bağımlı olan Avrupa arasında stratejik bir konumda yer almaktadır. Bu coğrafi konumu ve son yıllarda kara ve deniz alanlarında artan arama faaliyetleri neticesinde Karadeniz'de gerçekleştirdiği doğal gaz keşfi yanı sıra kara alanlarında da bir çok keşfe imza atmıştır. Bu keşifler ülkemizin kara ve deniz alanlarındaki fırsatları ve potansiyeli göstermiş, yeni yatırımcıların ilgi odağında yer almasını da sağlamıştır. Bugün Türkiye, dört ultra derin deniz sondaj ve iki sismik gemi filosu ile Akdeniz ve Karadeniz'de kendi imkanları ile aramacılık yapabilen yegâne ülkedir. Bunun yanında, Karadeniz kuzeyinde Ukrayna-Rusya savaşının oluşturduğu güvenlik sorunu ve istikrarsızlık, Avrupa Birliği ülkelerinin enerji arz güvenliğinde Türkiye'nin konumunu daha da güçlendirmiştir.

Kongremiz Cumhuriyetimizin başkenti ve petrol endüstrisinin karargâhı Ankara'da düzenlenecektir. Ankara ili, Tunç Çağı'ndan beri sürekli yerleşim görmüştür. Kentteki müzeler Hitit, Frigler, Lidyalılar, Persler, Romalılar, Bizanslılar, Selçuklular ve Osmanlılar gibi Anadolu'dan geçmiş ve yaşamış bir çok kültürü yaşatmaktadır. Ankara aynı zamanda bir çok sosyal ve kültürel aktivite, otantik mağazalar ve çok sayıda birinci sınıf restoran ve otel ile öne çıkmaktadır.

Türkiye Uluslararası Petrol ve Doğal Gaz Kongre ve Sergisi'nde (IPETGAS'23) Düzenleme Kurulu adına, sizleri 27-29 Eylül 2023 tarihlerinde Ankara'da yapılacak konferansa bildiri göndermeye ve katılıma davet ediyorum. Katılımınız Kongremizin teknik ve sosyal kalitesini artıracaktır. Cumhuriyetimizin 100.yılında 27 Eylül 2023 tarihinde Türkiye petrol endüstrisi şöleninde, katılımınız bizleri onurlandıracaktır.

Kongre Düzenleme Kurulu Adına  
İsmail Bahtiyar / Başkan

## INVITATION

IPETGAS 2023, International Petroleum and Natural Gas Congress and Exhibition of Türkiye is going to held by the Turkish Association of Petroleum Geologists, the UCTEA Chamber of Petroleum Engineers and the Chamber of Geophysical Engineers of Türkiye between 27-29 September 2023 in Ankara on the 100th anniversary of the establishment of the Republic of Türkiye. The aim of IPETGAS'23 is to bring together the three disciplines, investors and service companies of the petroleum industry in an outstanding atmosphere. In this scientific feast; recent innovations in onshore and offshore petroleum and natural gas exploration of our country and their extension in neighboring countries will be shared, infrastructure and strategies will be discussed, and developments in renewable energy sources will be evaluated by experts. In addition to the oral presentations of experts from all disciplines, distinguished keynote speakers will enlighten the participants in a broad perspective. Our students are our future! Students from three disciplines will be able to deliver oral presentations and best presentations will be rewarded. The shareholders of the market will have a chance to introduce their technologies and products in exhibition. Pre-congress courses will contribute to the competency of our colleagues. The General Directorate of Mining and Petroleum Affairs (MAPEG) as the regulatory body of the petroleum industry will inform the investor of the market about the exploration opportunities of our country.

In the exhibition area, our national petroleum company, Turkish Petroleum Corporation (TPAO), exploration and production companies, Petroleum Pipeline Corporation (BOTAS) and General Directorate of Mineral Research and Exploration (MTA) will be able to discuss new collaborations with service providers.

Türkiye is strategically located between the Middle East and the Caspian region, which has rich hydrocarbon reserves, and Europe, whose consumption is heavily dependent on imports. As a result of this geographical location and the increasing onshore and offshore exploration activities in recent years, many onshore discoveries have been made as well as the natural gas discovery in the Black Sea. These discoveries have shown onshore and offshore opportunities and potential of our country and enabled our country to be become the focus of interest for new investors. Türkiye, with its four fleets of ultra-deep-sea drilling and two seismic vessels, is the only country that can conduct exploration in the Mediterranean and Black Seas with its own means. In addition, the security problem and instability created by the Ukraine-Russia war in the north of the Black Sea have further strengthened Türkiye's position in the energy supply security of the European Union countries.

IPETGAS'23 will be held in Ankara, the capital of our Republic and the headquarters of the oil industry. Ankara Province has been continuously inhabited since the Bronze Age. The museums in the city keep alive many cultures that have passed and lived from Anatolia such as Hittites, Phrygians, Lydians, Persians, Romans, Byzantines, Seljuks and Ottomans. Ankara also stands out for its social and cultural activities, authentic shops and a large number of first class restaurants and hotels.

On behalf of the Organizing Committee of the International Petroleum and Natural Gas Congress and Exhibition of Türkiye (IPETGAS'23), we would like to invite you to present papers and participate in the congress that will be held in Ankara on 27-29 September 2023. Your participation will increase the technical and social quality of our congress.

Your participation in the feast of the Turkish petroleum industry will honor us on the 100th anniversary of our Republic of Türkiye.

On Behalf of the Organizing Committee  
İsmail Bahtiyar / President

**KURULLAR**

Başkanlar Kurulu

**Hasan SARIKAYA**

Başkan (TPJD)

**Şevket DEMİRBAŞ**

Başkan (JFMO)

**İnanç Alptuğ HİDİROĞLU**

Başkan (PMO)

Düzenleme Kurulu

**İsmail BAHTİYAR**

Başkan (TPJD)

**Tayfun BEŞEVLİ**

II.Başkan (JFMO)

**Nurhan TEKAYAK**

II.Başkan (PMO)

**Ş. Gökhan KÖSE**

Genel Sekreter (TPJD)

**Mustafa YILMAZ**

Teknik Sekreter (PMO)

**Ayşegül CANATALI**

Sayman (TPJD)

**Gökhan HACİMEHMETOĞLU**

Üye (JFMO)

**Selda GÜRPINAR**

Üye (JFMO)

**Emel KURU**

Üye (PMO)

**PRESIDENTS**

**Hasan SARIKAYA**

President (TPJD)

**Şevket DEMİRBAŞ**

President (JFMO)

**İnanç Alptuğ HİDİROĞLU**

President (PMO)

Organizing Committee

**İsmail BAHTİYAR**

President (TPJD)

**Tayfun BEŞEVLİ**

II.President (JFMO)

**Nurhan TEKAYAK**

II.President (PMO)

**Ş. Gökhan KÖSE**

General Secretary of the Congress (TPJD)

**Mustafa YILMAZ**

Technical Secretary (PMO)

**Ayşegül CANATALI**

Accountant (TPJD)

**Gökhan HACİMEHMETOĞLU**

Member (JFMO)

**Selda GÜRPINAR**

Member (JFMO)

**Emel KURU**

Member (PMO)

27 Eylül 2023, Çarşamba / 27 September 2023, Wednesday	
08:00-10:30	<b>KAYIT / REGISTRATION</b>
10:30-11:30	<b>AÇILIŞ OTURUMU / OPENING CEREMONY</b>
	<b>İsmail Bahtiyar</b> Düzenleme Kurulu Başkanı <i>Organizing Committee President</i>
	<b>Hasan Sarıkaya</b> TPJD Başkanı-Düzenleyici Kuruluşlar Adına <i>TAPG President on behalf of the Organizers</i>
	<b>Melih Han Bilgin</b> TPAO Genel Müdürü <i>Turkish Petroleum Chairman and CEO</i>
11:30-12:30	Ipetgas'2023 Sergi Açılışı Ve Protokol Turu <i>Ipetgas'2023 Exhibition Opening</i>
12:30-13:30	<b>ÖĞLE YEMEĞİ / LUNCH</b>
13:30-14:00	<b>ÇAĞRILI KONUŞMA:</b> Türkiye Cumhuriyeti'nin 100.yılında, Geçmişten Günümüze Türkiye Petrolleri A. O. <b>KEYNOTE SPEECH:</b> Turkish Petroleum from past to present on the 100th anniversary of the Republic of Türkiye
	<b>Melih Han Bilgin</b> TPAO Yönetim Kurulu Başkanı ve Genel Müdürü <i>Chairman and CEO of Turkish Petroleum</i>
14:00-16:30	<b>PANEL:</b> Türkiye Cumhuriyeti'nin 100. Yılında Geçmişten Günümüze Petrol ve Doğalgaz Sektörü <b>PANEL:</b> Oil and Natural Gas Sector from Past to Present on the 100th Anniversary of the Republic of Turkey
	<b>Prof. Dr. Volkan Ş. Ediger</b> Kadir Has Üniversitesi Enerji Sistemleri Mühendisliği Bölüm Başkanı (Moderatör ve Panelist) <i>Head of Kadir Has University Energy Systems Engineering Department (Moderator and Panelist)</i>
	<b>Prof. Dr. Özdoğan Yılmaz</b> CTO, GeoTomo (Panelist) <i>CTO, GeoTomo (Panelist)</i>
	<b>Sami Sarıyıldız</b> MAPEG Genel Müdür Yardımcısı (Panelist) <i>MAPEG Deputy General Manager (Panelist)</i>
	<b>Enver Çetinkaya</b> TPAO Mühendislik Daire Başkanı (Panelist) <i>TPAO Head of Engineering Department (Panelist)</i>
	<b>Güleşan Demirbaş</b> Shell Türkiye Kamu İlişkileri Direktörü (Panelist) <i>Shell Türkiye Public Relations Director (Panelist)</i>
	<b>Çağatay Beydoğan</b> PETFORM Arama ve Üretim Grubu Başkanı (Panelist) <i>Chairman of PETFORM Exploration and Production Group (Panelist)</i>
20:00-23:00	<b>GALA YEMEĞİ / GALA DINNER</b>
	* Teşrifleri halinde / * To be confirmed

28 Eylül 2023, Perşembe / 28 September 2023, Thursday

	GRAND BALL ROOM-1	GRAND BALL ROOM-2	GRAND BALL ROOM-3	MAGNOLIA	GERBERA	CAMELLIA
09:10 10:30	<b>OTURUM/SESSION 1</b> Cumhuriyetimizin En Büyük Doğal Gaz Keşfi: Sakarya Gaz Sahası <i>The Largest Natural Gas Discovery of the Republic of Türkiye: Sakarya Gas Field</i>  Oturum Yürütücileri Conveners: <b>Derya Kılıç DEMİRCİ,</b> <b>Emir ERSAY</b>	<b>OTURUM/SESSION 2</b> Rezervuar Çalışmaları <i>Reservoir Studies</i>  Oturum Yürütücileri Conveners: <b>Çağlar SINAYUÇ,</b> <b>Sinem Setenay ERDOĞAN</b>	<b>OTURUM/SESSION 3</b> Aşlımadık Hidrokarbon Kaynakları <i>Unconventional Hydrocarbon Resources</i>  Oturum Yürütücileri Conveners: <b>Ahmet MENGİN,</b> <b>Deniz YILDIRIM</b>	<b>OTURUM/SESSION 4</b> Bölgesel Jeoloji ve Tektonik <i>Regional Geology and Tectonics</i>  Oturum Yürütücileri Conveners: <b>Aytaç EREN,</b> <b>Mehmet MUTAFCILAR</b>	<b>OTURUM/SESSION 5</b> Hidrokarbon Aramalarında Elektromanyetik ve Potansiyel Alan Yöntemleri <i>Hydrocarbon Explorations using Electromagnetic and Potential Field Methods (Gravity and Magnetic)</i>  Oturum Yürütücileri Conveners: <b>M. Emin CANDANSAYAR,</b> <b>Sema ARABACI</b>	<b>OTURUM/SESSION 6</b> Yapay Zeka ve Özdevimli Öğrenme <i>Artificial Intelligence and Machine Learning</i>  Oturum Yürütücileri Conveners: <b>Nuri DEMİRDÖVEN,</b> <b>Mehmet Onur DOĞAN</b>
09:10 09:30	<i>Seismic Trace Correlation Approach for Gas Probability Mapping in Sakarya Gas Field Reservoirs, Western Black Sea, Turkey</i> <b>Sait Baytok,</b> <b>Ergin Karaca</b>	<i>Minimization of the Noise in the Calculated Pressure Derivative Data for the Interpretation of Transient Tests</i> <b>Doğuhan Coşar,</b> <b>Çağlar Sinayuç</b>	Aşlımadık Hidrokarbon Kaynak Aramaçlığında Dünya'da Ve Türkiye'de Yapılan Çalışmalar <b>Ahmet Ergin Mengin,</b> <b>Canalp Özkul,</b> <b>Mehmed Ekrem Yazaroğlu, Sezer Sevinc</b>	Foça-Karaburun Açıklan Aktif Tektoniği Ve Stratigrafisinin Deniz Sismliği Verileriyle İncelenmesi: İlkeli Sonuçlar <b>Derman Dondurur,</b> <b>Ashhan Nasif,</b> <b>Özkan Özel,</b> <b>Orhan Atgan,</b> <b>Denizhan Vardar,</b> <b>Muhammet Duman</b>	<i>Experience and Prospects of Magnetotelluric Method Application for Hydrocarbon Prospecting</i> <b>Nikolay Palshin,</b> <b>Elena Aleksanova,</b> <b>Dmitry Epishkin,</b> <b>Denis Yakovlev,</b> <b>Andrey Yakovlev</b>	<i>Machine Learning Assisted Forecasting of Field Performance: A Case Study</i> <b>Emre Artun,</b> <b>Serhat Canbolat,</b> <b>Elif Cihan Yıldırım,</b> <b>Cansu Açıkçöz,</b> <b>Onur Yürükler</b>
09:30 09:50	<i>High-Resolution Visco-Acoustic Fwi Model Building and Lead-Squares Migration in the Black Sea Resolving Imaging And Illumination Challenges For A Deep-Water Dataset</i> <b>Samuel Madden,</b> <b>Kelly Mistry,</b> <b>Zengbao Chen,</b> <b>Cara Smith,</b> <b>Olivia Lewis,</b> <b>Maria Shadrina,</b> <b>Sait Baytok, Can Özsoy,</b> <b>Can Ören,</b> <b>Emir Yusuf Ersay,</b> <b>Kenan Yazan,</b> <b>Ergin Karaca</b>	<i>Integrating Various Sources of Indicators and Water Measurements Data of Different Degree of Uncertainty to Understand Aquifer Encroachment and Resulted Water Breakthrough to Gas Producers</i> <b>Murat Zhiyenkulov,</b> <b>Michael Nashaat,</b> <b>Hassan Kolvand,</b> <b>Oleh Lukin,</b> <b>Abdurrahman Shah,</b> <b>Kassem Ghorayeb,</b> <b>Viacheslav Filatov,</b> <b>Densy Grytsai</b>	<i>Petroleum: How Long More, How Much More</i> <b>Salih Saner</b>	Sapanca Gölü Tabanından Gaz/Sıvı Çıkslarını Sağlayan Poçmarkların Yan-Otomatik Morfolojik Analizi <b>Enes Sönmez,</b> <b>Hülya Kurt</b>	Manyetotellurik Yöntemin Güneydoğu Anadolu'Da Petrol Arama Amaçlı Kullanımın Değerlendirilmesi <i>Evaluation of Magnetotelluric Method for Petroleum Exploration in Southeast Anatolia</i> <b>Ahmet Tuğrul Basokur</b>	<i>Determining Hydrocarbon-Bearing Volcanic Sediments Using Neural Network Method - Based NPHI Cubes: A case Study</i> <b>Nur Gücer Ersay,</b> <b>Musa Çetin</b>
09:50 10:10	<i>An Integrated Petrophysical Technique Leads to Resolve Ultra-Thin Bed Reservoir Properties in Highly Laminated Shale-Sand Sequences Of Black Sea, Turkey</i> <b>Mert Kılıç,</b> <b>Batur İydiken,</b> <b>Tanmoy Dutta,</b> <b>Uğur Yüce</b>		<i>Impact of Numerics on Monte-Carlo Based Type-Well Generation for Unconventional Fields</i> <b>Duruk Alp</b>	İzmir Körfezi'nin Aktif Tektoniğinin ve Stratigrafisinin Deniz Sismliği Verileriyle İncelenmesi: İlkeli Sonuçlar <b>Ashhan Nasif,</b> <b>Derman Dondurur,</b> <b>Özkan Özel,</b> <b>Orhan Atgan,</b> <b>Denizhan Vardar</b>	<i>A Multiphysics Approach to Evaluating Gas Prospectivity with Case Examples</i> <b>Daniel Baltar Pardo,</b> <b>Isag Helland Hansen,</b> <b>Elias Andre Nerland</b>	<i>Leveraging Edge Computing with Artificial Intelligence and Machine Learning for Subsurface Assets</i> <b>Alife Gozde Celik,</b> <b>Ratish Kumar Selvaraj</b>
10:10 10:30	<i>Lithogram: An Innovative Approach for Net-Sand and Lithofacies Estimation in Thin to Laminated Clastic Reservoirs by Using Synthetic Seismogram Method</i> <b>Emir Yusuf Ersay,</b> <b>Batur İydiken,</b> <b>Ergin Karaca,</b> <b>Ömer Akbas, Derya Kılıç Demirci, Tanmoy Dutta,</b> <b>Suat Aktepe</b>	<i>Unlocking New Reservoir Zones at Shallow Depth Based on Integrating Post-Hydraulic Fracture Performance with Reservoir, Petrophysics and Geology Data</i> <b>Murat Zhiyenkulov,</b> <b>Michael Nashaat,</b> <b>Hassan Kolvand,</b> <b>Yerlan Seilov,</b> <b>Abdurrahman Shah,</b> <b>Kassem Ghorayeb,</b> <b>Roman Madatov,</b> <b>Svetlana Grytsai,</b> <b>Viacheslav Filatov</b>	<i>The Fracability Evaluation of Dadas Shale in Southeastern Turkey Based on its Geomechanical Properties</i> <b>Öğüz Cihaner,</b> <b>Betül Yıldırım</b>	<i>Implications for the Neotectonics of the NW Margin of the Arabian Plate: A Case Study of the E-W-trending Altınbaş Basin (Gaziantep, Türkiye)</i> <b>Aydın Çiçek, Ali Koçyığıt</b>	Gravite Tabaka Sıyırma Yöntemi ile Doğu Akdeniz'de Gravite Anomalilerinin Analizi ve Tektonik Yapıların İncelenmesi <b>İlkin Özsöz</b>	<i>Prediction of Flow Rates From Using P1-p-T Measurements in A Horizontal Well By Machine Learning Methods</i> <b>Muharem Hilmi Cevik,</b> <b>Murat Çınar</b>
10:30 10:50	<b>KAHVE ARASI / COFFEE BREAK</b>					

28 Eylül 2023, Perşembe / 28 September 2023, Thursday					
GRAND BALL ROOM-1	GRAND BALL ROOM-2	GRAND BALL ROOM-3	MAGNOLIA	GERBERA	CAMELLIA
<p>10:50 12:30</p> <p><b>OTURUM/SESSION 7</b> Cumhuriyetimizin En Büyük Doğal Gaz Keşfi: Sakarya Gaz Sahası <i>The Largest Natural Gas Discovery of the Republic of Türkiye: Sakarya Gas Field</i> (12:30-12:50)</p> <p>Oturum Yürütücülere Conveners: <b>Murat Fatih TUĞAN,</b> <b>Ergin KARACA</b></p>	<p><b>OTURUM/SESSION 8</b> Rezervuar Çalışmaları <i>Reservoir Studies</i></p> <p>Oturum Yürütücülere Conveners: <b>İsmail DURGUT,</b> <b>İbrahim KOCABAŞ</b></p>	<p><b>OTURUM/SESSION 9</b> Aşılımsız Hidrokarbon Kaynakları <i>Unconventional Hydrocarbon Resources</i></p> <p>Oturum Yürütücülere Conveners: <b>Gökhan Hacımehmetoğlu,</b> <b>Sezer SEVİNÇ</b></p>	<p><b>OTURUM/SESSION 10</b> Kuyu Tamamlama Uygulamaları <i>Well Completion Applications</i></p> <p>Oturum Yürütücülere Conveners: <b>Evren AKBAS,</b> <b>Eren Emre GEÇER</b></p>	<p><b>OTURUM/SESSION 11</b> Dünya'da ve Türkiye'de Enerji Dönüşümü <i>Energy Transition in the World and Türkiye &amp; Petrol ve Doğalgaz Sektöründe</i> <i>Sustainability in the Oil and Gas Industry</i></p> <p>Oturum Yürütücülere Conveners: <b>Metin Talat GÜLERYÜZLÜ,</b> <b>Erdinç ŞENTÜRK</b></p>	<p><b>OTURUM/SESSION 12</b> Yapay Zeka ve Özdevimli Öğrenme <i>Artificial Intelligence and Machine Learning</i></p> <p>Oturum Yürütücülere Conveners: <b>Arzu AKTEPE,</b> <b>Aziz ELİBÜYÜK</b></p>
<p>10:50 11:10</p> <p><i>The Link Between Seismic and Stratigraphic Analysis: How Pre-stack Stochastic Inversion Improves Seismic Resolution in Ultra-Thin Clastic Reservoirs</i> <b>Ergin Karaca,</b> <b>Emir Yusuf Ersay,</b> <b>Burak Salantur</b></p>	<p><i>Analysis of the Effect of Salt Zones on Gas Production From Gas Hydrates in the Mediterranean Sea</i> <b>Sikriü Mercy, Lin Chen</b></p>	<p><i>Hamitabat Formation Tight Sandstone Reservoirs Sweet Spot Identification</i> <b>Sezer Sevinç,</b> <b>Ahmet Ergün Mengen,</b> <b>Kirill Ezhov</b></p>	<p><i>Comparative Analysis of Acid Fracturing in SEHIT ESMA CEVİK - Field Well Using 3 1/2" and 2 7/8" Tubings: A Comprehensive Study</i> <b>Görkem Kaya</b></p>	<p>Türkiye'deki İklim Değişikliği ve Karbon Yakalama-Depolama Uygulamaları ile İlişkili Mevzuatın İncelenmesi <b>Seytaç Bilibil,</b> <b>Çağlar Sınayıcı,</b> <b>Mehmet Onur Doğan</b></p>	<p><i>Quantitative Interpretation Using Rock Physics Driven Convolutional Neural Network</i> <b>Ufuk Durmuş</b></p>
<p>11:30 11:30</p> <p><i>Quantitative Seal Analysis of the Compaction Faults in Western Black Sea Basin, Turkey</i> <b>Bulut Tortopoglu,</b> <b>Nisansu Balci</b></p>	<p><i>Estimation of Missing Well-Log Sections Using Machine Learning Assisted Multivariate Imputation: A Case Study</i> <b>Emre Artun,</b> <b>Serhat Canbolat,</b> <b>Elif Cihan Yıldırım,</b> <b>Canva Açıkşögür,</b> <b>Onur Yürüker</b></p>	<p><i>Evaluation of Dadas Formation Potential: A Case Study From Southeast Türkiye</i> <b>Mehmed Ekrem Yazaroglu,</b> <b>Sinem Artan Ercengiz,</b> <b>Canalp Ozkul,</b> <b>Suzan Mişge Yetim,</b> <b>Ahmet Ergün Mengen,</b> <b>Can Ercan,</b> <b>Yinal Neşes Huvaj</b></p>	<p>Coiled Tubing ile Açık Kuyu Sondaj Operasyonu <b>Seckin Öztel</b></p>	<p><i>A Simulation Study of Underground Hydrogen Storage in the Northern Marmara Field</i> <b>Hasan Gürsel,</b> <b>Murat Fatih Tuğan,</b> <b>Çağlar Sınayıcı</b></p>	<p><i>Implementing Adaptive Neuro-Fuzzy Inference System for Analysis of Heavy Oil Behavior Through Magneto-Rheology</i> <b>Uğur Özveren</b></p>
<p>11:30 11:50</p> <p><i>Critical Strain Approach for Critical Drawdown Analysis with the Advance of Cambridge Clay Model in Sakarya Gas Field, Western Black Sea Basin, Turkey</i> <b>Bulut Tortopoglu,</b> <b>Adil Gürkan Ceyhan,</b> <b>Nisansu Balci</b></p>	<p><i>Coal Bed Methane Characterization for Gas Production Recovery Optimization - Zonguldak, Türkiye</i> <b>Sofiane Belhocine,</b> <b>Ahmet Ergün Mengen,</b> <b>Muhammed Emin Bulguroglu,</b> <b>Rabah Boudissa</b></p>	<p><i>Development Of A Computational Tool for Wellbore Stability Analysis and Mud Weight Optimization</i> <b>Ekrem Alagoz,</b> <b>Ahmet Ergun Mengen,</b> <b>Fethi Benzenouci,</b> <b>Emre Can Dundara</b></p>	<p><i>Radial Drilling</i> <b>Duruk Kırac,</b> <b>Görkem Kaya</b></p>	<p><i>Evaluation of Sustainability Aspects of CO2 Sequestration in Depleted Shale Reservoirs Using Data Analytics</i> <b>Kanan Alınev,</b> <b>Emre Artun,</b> <b>Burak Kulga</b></p>	<p><i>AI Seismic Interpretation: A Deeper Understanding of the Subsurface</i> <b>Luis Gomer Martinez,</b> <b>Abdulqadir Cader,</b> <b>Ryan Williams,</b> <b>Peter Szafian</b></p>
<p>11:50 12:10</p> <p><i>Solutions to Complex Well-Testing Challenges and Proving Production Potential: Successful Well Test operations on the Sakarya Ultra-deep Water Gas Field in the Black Sea, Türkiye</i> <b>Cosan Ayan, Suat Aktepe,</b> <b>Köksal Çiğ,</b> <b>Mehi Gökmen,</b> <b>Adil Gürkan Ceyhan,</b> <b>Murat Fatih Tuğan,</b> <b>Yakov Shumakov,</b> <b>Bertrand Theuveny</b></p>	<p><i>Assessing CO2 Enhanced Geothermal Potential and CO2 Storage in A Red Sea Rift Basin, Al Wajh: A Comprehensive Reservoir Model and Simulation Study</i> <b>Bora Yalcin,</b> <b>Justin Ezekiel,</b> <b>Martin Paul Mai</b></p>	<p><i>Pore Characterization and FESEM Analysis of the Niobrara Formation in Aristocrat Angus PC H11-07 Core, Wattenberg Field, Denver Basin, CO</i> <b>Elvan Aydın</b></p>	<p>Coiled Tubing ile Canlı Kuyuda Slickline Tahliyesi <b>Seckin Öztel</b></p>	<p><i>Sustainability in Energy From Oil &amp; Gas to Geothermal Energy</i> <b>Harun Yaram</b></p>	<p><i>Leveraging AI in Automating Geophysical Feasibility Studies: A Leap Forward in CCS Monitoring</i> <b>Mehdi Paydayesh,</b> <b>Amir Shamsa,</b> <b>Maria Perezhogina</b></p>
<p>12:10 12:30</p> <p><i>Formation Damage Mechanisms and Solutions in Sakarya Field</i> <b>Uğur Paköz</b></p>	<p><i>Calculation of Natural Gas Viscosity of A Gas Reservoir using Correlations and Comparison with Manual Readings Through Well Known Charts</i> <b>Abdullah Gürkan İcşan</b></p>	<p><i>Characterizing an Unconventional Reservoir with Onshore Conventional 3d Seismic Data: Case Study Using Seismic Inversion for The Dadas-1 Member</i> <b>Artem Orlov,</b> <b>Kirill Ezhov,</b> <b>Mehmed Ekrem Yazaroglu,</b> <b>Canalp Ozkul,</b> <b>Ahmet Ergün Mengen</b></p>	<p><i>Resolving Cement Evaluation in the Challenging Environment of Large and Thick Casing</i> <b>Alhadi Zahmwil,</b> <b>Rob Loov, Diana Vargas</b></p>	<p>Modüler Çelik Yapılar, Petrol ve Gaz Sahalarının da İdeal Çözüm <b>Mert Özdemir</b></p>	<p>Yapay Zeka ile Sisimik Hız Modellerinin Doğrudan Kestirimi: Eğitim Veri Seti ve Derin Ağ Eğitimi <b>Mojtaba Najafikhahoumahad,</b> <b>Hacer Yahni Keleş,</b> <b>Selma Kadoğlu</b></p>
<p>(12:30-12:50)</p> <p><i>Utilization of Particle Size Distribution Data for Field Development: Unconsolidated Laminated Sandstone Formation Case</i> <b>Buse Göral, Uğur Paköz</b></p>					
<p>12:30 13:30</p>	<b>ÖĞLE YEMEĞİ / LUNCH</b>				

28 Eylül 2023, Perşembe / 28 September 2023, Thursday							
	GRAND BALL ROOM-1	GRAND BALL ROOM-2	GRAND BALL ROOM-3	MAGNOLIA	GERBERA	CAMELLIA	BEGONIA
13:30 14:50	<b>OTURUM/SESSION 13</b> Derin Deniz Operasyonları <i>Deep Water Operations</i>  Oturum Yürütücülere Conveners: <b>Fatih KARAKAYA,</b> <b>Süleyman ABRAVCI</b>	<b>OTURUM/SESSION 14</b> Kuyu Tamamlama Uygulamaları <i>Well Completion Applications</i>  Oturum Yürütücülere Conveners: <b>Hüseyin Kerem GÜNER,</b> <b>Mehmet GÖÇ</b>	<b>OTURUM/SESSION 15</b> Petrol Sistemleri Analizi, Harıza Modellemesi ve Jeokimya <i>Petroleum Systems Analysis, Basin Modeling, Geochemistry</i>  Oturum Yürütücülere Conveners: <b>Cengiz SOYLU,</b> <b>Zeynep Özlem ÇIHAN</b>	<b>OTURUM/SESSION 16</b> Rezervuar Çalışmaları <i>Reservoir Studies</i>  Oturum Yürütücülere Conveners: <b>Hüseyin ÖZDEMİR,</b> <b>Zafer ÖZER</b>	<b>OTURUM/SESSION 17</b> Petrol, Doğal Gaz, LPG ve LNG Pazarı <i>Oil, Gas, LPG and LNG Market &amp; Geothermal Energy</i>  Oturum Yürütücülere Conveners: <b>Okan YARDIMCI,</b> <b>Ahmet ÜÇER</b>	<b>OTURUM/SESSION 18</b> Aşılımadık Hidrokarbon Kaynakları <i>Unconventional Hydrocarbon Resources</i>  Oturum Yürütücülere Conveners: <b>Mahmut PARLAKTUNA,</b> <b>Günay ÇİFÇİ</b>	<b>Öğrenci Bildiri Yarışması Student Paper Contest</b> (14:00-16:20)  Oturum Yürütücülere Conveners: <b>Hakkı AYDIN,</b> <b>Damla ALTINTAŞ</b>
13:30 13:50	Karadeniz Derin Deniz Sahalarında Operasyonel Oncesi Dizayn Hususları <i>Top Hole Design Considerations in Black Sea Deepwater Fields</i> <b>Burak Büyükkıncı,</b> <b>Fatih Karakaya,</b> <b>Amit Sankhe</b>	<i>Advanced Tractor Techniques in Extended Reach Wells Allow Confirmation of Well Integrity and Execution of Perforation Services in Key Turkish Offshore Gas Fields</i> <b>Daniel Steen Haase</b> Sorensen, Uğur Ezer, Mohammed Ameen Al Ganad, Fadil Duman	<i>A Case Study of The Regional 3-D Basin Modeling in Anu Darya and Afghanistan Basins</i> <b>Yücel Deniz Erdal,</b> Zeynep Adıgüzel, Şükür Gökhan Köse, Hasan Güney, Helby Ellen, Awdeji Temitope Ajayi, Mustafa Demirci, Emrah Dölek	<i>An Integrated Approach to Carbonate Reservoir Characterization: A Case Study From Se of Turkey</i> <b>Mustafa Kamil Yüksek,</b> Aslıhan Deliktas, Atilla Aydemir	LPG'nin Günümüzde Konvansiyonel ve Alternatif Kullanımı <b>Can Toydemir,</b> Lpg Dairesi, Yasin Ersöz	Tuna Deltası (Romanya ve Bulgaristan Açık Deniz) Kitassal Yamacı'nın Gaz Hidrat Potansiyeli ve Sismik Stratigrafisi <b>Orhan Atgan,</b> Günay Çifci	<i>Predicting Bottomhole Temperature of Offshore Production Wells In the North Sea</i> <b>Tuğberk Berat Günel</b>  <i>Application of CT in Reservoir Characterization</i> <b>Efe Erkek</b>  <i>Energy Transition</i> <b>Yaren Esra Kahya</b>
13:50 14:10	Derin Deniz Operasyonlarında İkili Kulenin Avantajları <i>The Advantage of Dual Derrick in Ultra-Deepwater Operations</i> <b>Evren Bektaş,</b> <b>Fatih Karakaya,</b> <b>Hüseyin Kasapoğlu,</b> <b>Amit Sankhe,</b> <b>Okan Kirgiz</b>	<i>Overview of Acid Fracturing Operations in Carbonate Reservoirs of Turkey</i> <b>Ufuk Kılıçaslan,</b> Ahmet Ergin Mengen, Özlem Özcan, Mutlu Daşdemir, Yasin Ünal, Bekir Onay, Bülent Şahinbaş, Vasily Semenovich Mironov, Aleksei Vasilevich Khlopkov	<i>Exploring Hydrocarbons in 1.75 Billion-Year-Old Precambrian Deposits of South Africa Using Environment Friendly SDDT Technology</i> <b>Öngün Yoldemir,</b> Joerg Enge	<i>Physics-Informed Neural Networks for Solving Partial Differential Equations: Applications and Challenges</i> <b>Amir Shamsa,</b> Mehdi Paydayesh, Maria Perezhogina	Kahramanmaraş Depremi'nin Türk Akaryakıt Piyasasına Etkisi <b>Sinem Okumus,</b> Aysin Korucan	<i>A Study Of An Experimental Possible Production Mechanisms Of Hydrate Formation</i> <b>Hasan Hüseyin Engitci</b>	Türkiye'de Buhar ve Karbondioksit Enjeksiyonu, Faydaları ve Zorlukları <b>Mehmet Merican Doğan</b>  <i>Steamflooding Interval Horizontal Wells</i> <b>Öğuzhan Ucar</b>
14:10 14:30	Derin Deniz Jetleme Operasyonlarında Etkinliğin ve Stabilitenin Artırılması & Matkap Pozisyonlanmasının Etkisi <i>Enhancing Efficiency and Stability in D/W Jetting Operations &amp; Role of Bit Stick-Out Length</i> <b>Öğuzhan Kaylan,</b> <b>Fatih Karakaya</b>	<i>Importance of Cement Slurry Density &amp; GEO-LITE</i> <b>Yigit Altunal,</b> <b>Burak Ekiçi</b>	<i>Pitfalls in Basin Modeling - A Case Study From the Eastern Black Sea</i> <b>Turan İçsimer</b>	<i>Integrated Reservoir Characterization of Fractured Carbonates: Garzan Limestone Case</i> <b>Ufuk Durmus</b>	Jeotermal Sahalarda Mikrosismik İzleme Yöntemi ile Rezervuar Takibi <b>Burcu Turhan,</b> Tuğçe Bilgiç, Ünal Selçik, Kadir Balci, Ali Yıldırım, Bülent Kaypak	Bati Karadeniz Kitassal Kenarının Gaz Hidrat Potansiyeli <b>Özkan Özel,</b> Aslıhan Nasif Dondurur, Derman Dondurur	<i>Stimulation of a Tight Sandstone Reservoir Through Hydraulic Fracturing: Taylor Sandstone Case, Texas</i> <b>Muhoh Gariba, Sheron</b>  <i>Forecasting the Performance of Shale Gas Wells Using Machine Learning</i> <b>Mohammed Shedaiva</b>
14:30 14:50	Derin Deniz Emniyet Vanaları Kontrol Sistemleri Güvenilirliği <i>Subsea BOP Control System Reliability</i> <b>Fatih Karakaya,</b> <b>Yasin Demiralp,</b> <b>Necip Bektaş</b>	<i>Tight Gas Field Development in Thrace Basin by Hydraulic Fracturing</i> <b>Ufuk Kılıçaslan,</b> Ahmet Ergin Mengen, Özlem Özcan, Sofiane Belhocine, Rabah Boudissa, Vasily Semenovich Mironov, Aleksei Vasilevich Khlopkov	Rock Eval Piroiz Analizi ile Kinetik Parametrelerin Karakterizasyonu ve Silüryen Yaşlı Dadaş Formasyonu'nun Kinetik Parametrelerinin Belirlenmesi Projesi <b>Cihan Çan,</b> Zeynep Özlem Çihan, Şükür Gökhan Köse, Yücel Deniz Erdal	<i>Unlocking New Discovery in Thrace Basin, Turkey: Probabilistic Neural Network Application to Estimate Nphi and Acoustic Impedance Cross Plotting for Hydrocarbon Mapping</i> <b>Sait Baytok,</b> Ergin Karaca	Sismik Hız ile Boşluk Basıncı İlişkisi Örnek Çalışma: Denizli Havzası <b>Orhan Güreli</b>	<i>A Deep Dive Into the Black Box of Artificial Intelligence</i> <b>Orhan Kurt</b>	<i>Approximating Hydraulic Fracture Permeability Enhancement</i> <b>Onuralp Mete Yağmur</b>
14:50 15:10	<b>KAHVE ARASI / COFFEE BREAK</b>						

28 Eylül 2023, Perşembe / 28 September 2023, Thursday						
	GRAND BALL ROOM-1	GRAND BALL ROOM-2	GRAND BALL ROOM-3	MAGNOLIA	GERBERA	CAMELLIA
15:10 16:30	<b>OTURUM/SESSION 19</b> Akdeniz Baseni Petrol Potansiyeli ve Yeni Gelişmeler <i>Petroleum Potential and New Developments of the Mediterranean Basin</i>  Oturum Yürütücileri Convener: <b>Ali DEMİRER,</b> <b>Fatih ÖZDAMAR</b>	<b>OTURUM/SESSION 20</b> Petrol ve Doğal Gaz Politikaları, Hükuki ve Ekonomik Gelişmeler <i>Oil and Gas Policies, Legal and Economic Developments</i>  Oturum Yürütücileri Convener: <b>Uğur GÖNÜLALAN,</b> <b>Emre ÖZGÜR</b>	<b>OTURUM/SESSION 21</b> Petrol Sistemleri Analizi, Havza Modellemesi ve Jeokimya <i>Petroleum Systems Analysis, Basin Modeling, Geochemistry</i>  Oturum Yürütücileri Convener: <b>Şükrü Gökhan KÖSE,</b> <b>Ayşegül CANATALI</b>	<b>OTURUM/SESSION 22</b> Rezervuar Çalışmaları <i>Reservoir Studies</i>  Oturum Yürütücileri Convener: <b>Hüseyin ÖZDEMİR,</b> <b>Korhan AKIN</b>	<b>OTURUM/SESSION 23</b> Jeotermal Enerji <i>Geothermal Energy</i>  Oturum Yürütücileri Convener: <b>Serhat AKIN,</b> <b>Harun YARIM</b>	<b>OTURUM/SESSION 24</b> Aşılılmadık Hidrokarbon Kaynakları <i>Unconventional Hydrocarbon Resources</i>  Oturum Yürütücileri Convener: <b>Turhan AYYILDIZ,</b> <b>Sergin AYTUNA</b>
15:10 15:30	<i>Geochemical Characteristics and Palaeoenvironmental Conditions of the Organic-Rich Triassic Facies in the Western Taurides.</i> <b>Zeynep Dincer Kırmızı,</b> <b>İsmail Ömer Yılmaz,</b> <b>Hasan Çağlar Üsdün</b>	Türkiye'deki Petrol ve Doğal Gaz Arama ve Üretim Faaliyetlerinin Teknik ve Ekonomik Analizi <i>Technical and Economic Analysis of Oil and Natural Gas Exploration and Production Activities in Turkey</i> <b>A. Uğur Gönülalan</b>	Doğu Trakya Havzası Basen ve Petrol Sistemi Modellemesi <i>Basin and Petroleum System Modeling in the Eastern Thrace Basin</i> <b>Esra Yalçın Yılmaz,</b> <b>Şükrü Gökhan Köse</b>	<i>Utilizing Seismic Amplitude Information and Extending the Value of The Seismic Beyond Structural Imaging</i> <b>Omar Ab. Aya Ibrahim,</b> <b>Tarek Nafe,</b> <b>Ahmed Hassan,</b> <b>Mohamed Fekry,</b> <b>Amin Al Maktari,</b> <b>Aref Al Shadi,</b> <b>Mohammed Ali Al Rawqi</b>	<i>A Numerical Toolkit for Optimization of Model Parameters for Tracer Tests</i> <b>Doğanhan Barlas,</b> <b>Sevindik,</b> <b>Ali Berkay Tokel,</b> <b>Selçuk Erol,</b> <b>Serhat Akın</b>	<i>Coalbed Methane Exploration, West Black Sea Region, Turkey</i> <b>Muhammed Emin Bulutazgın,</b> <b>Ahmet Ergün Mengen,</b> <b>Fatma Sanal,</b> <b>Onurhan Taç,</b> <b>Tuba Evren Sökmenşier,</b> <b>Ali Sarı</b>
15:30 15:50	Doğu Akdeniz'deki En Büyük İki Delta'nın (Nil ve Seyhan-Ceyhan) Gelişiminde Tektonizmanın Karşılaştırmalı Analizi <i>Comparative Analyses Tectonism on the Development of two Largest Deltas (Nile and Seyhan-Ceyhan) in the Eastern Mediterranean</i> <b>Yasemin Geze,</b> <b>Kalanuvva,</b> <b>Nizamettin Kazancı</b>	<i>Current Status of Türkiye About Carbon Capture and Sequestration: A Case Study Related to Carbon Capture and Sequestration in The Bati Raman Heavy Oilfield Of Türkiye</i> <b>Emre Özgür,</b> <b>Şükrü Meray</b>	Dolomitleşme Sıcaklığının ve Zamanlamasının Rezervuar Kalitesine Etkisi Nedir? Örnek Çalışma: GDA Bölgesindeki Mardin Grubu Dolomitlerinin Kümelennmiş İzotop Sıcaklıkları <i>Deniz Atasoy,</i> <b>Aynur Geçer Büyüktoku,</b> <b>Arzu Aktosun</b>	<i>Seismic Reservoir Characterization of Hydrocarbon-Bearing Sandstones, in A Producing Field, Thrace Basin</i> <b>Taner Arpacı</b>	<i>Carbon Utilization Potential in Geothermal Fields</i> <b>Erdinc Sentürk,</b> <b>Gültekin Tarcan</b>	Doğu Karadeniz'de Gaz Hidratlar ve 2 Camur Volkanının Keseli ve Gwangyang Körfezi'nde Siğ Gaz Birikimleri <i>Sevinç Özel Füzün,</i> <b>Günay Cici,</b> <b>Seda Okay Günaydan,</b> <b>Sermet Gündüz,</b> <b>Dae Choul Kim</b>
15:50 16:10	Levant ve Herodot Basenleri Stratigrafik Birimlerin Benzerliği, Sismik Kesit Örnekleri <b>Fatih Özdamar</b>	<i>Comparison of Host Government Petroleum Contracts And Applicability for Türkiye Deepwater Offshore Licences</i> <b>Fatih Vural</b>	<i>Conceptual Risk Modeling for Biogenic Gas Fields</i> <b>Yücel Deniz Erdal</b>	<i>Multiple Approaches to Reservoir Characterization of Gas-Bearing Sandstone: a Case Study from the Thrace Basin, Turkey</i> <b>Mustafa Kamil Yükek</b>	<i>Top Cementing Job A Lesson Learnt from Geothermal Well Drilling in Alasehir Geothermal Field</i> <b>Enrah Gürel,</b> <b>Ömer Yukseke,</b> <b>Emir Dimici,</b> <b>Cemil Seckin</b>	Bozcahiyuk (Seyitomer/ Kitahya) Yoresindeki Bitümlü Maırları Organik Jeokimyasal Verilerin Değerlendirilmesi ile Senteik Petrol Potansiyelinin Ortaya Konulması <b>Ali Sarı,</b> <b>Fatih Biyükl</b>
16:10 16:30			<i>Investigation the impact of Messinian Event in the Eastern Black Sea according to Biogenic Gas System Perspective</i> <b>Mehmet Hazar,</b> <b>Yücel Deniz Erdal,</b> <b>Şükrü Gökhan Köse</b>	<i>The Critical Role of Velocity in Pore Pressure Estimations and the Impact of the Centroid Effect</i> <b>Ersin Karaca</b>	Kapadokya Bölgesinde Gömülü Kalderanın Manyetotellürik Yöntem ile Görüntülenmesi ve Jeotermal Potansiyelinin Değerlendirilmesi <b>Ahmet Tuğrul Basokur,</b> <b>Özlem Hacıoğlu,</b> <b>Naser Meqbel,</b> <b>Halil İbrahim Arslan,</b> <b>Tevfik Efeçınar</b>	<i>New Generation Approaches for the Manufacturability of Gas Hydrate, One of Turkey's Alternative Energies</i> <b>Güzide Kalyoncu Ergüler</b>



29 Eylül 2023, Cuma / 29 September 2023, Friday						
	GRAND BALL ROOM-1	GRAND BALL ROOM-2	GRAND BALL ROOM-3	MAGNOLIA	GERBERA	CAMELLIA
09:10 10:30	<b>OTURUM/SESSION 25</b> Derin Deniz Operasyonları <i>Deep Water Operations</i>  Oturum Yürütücülere Conveners: <b>Erdal ASKU,</b> <b>Alpaslan SAHİN</b>	<b>OTURUM/SESSION 26</b> Sedimentoloji, Stratigrafi ve Çökülme Ortamları <i>Sedimentology, Stratigraphy and Depositional Systems</i>  Oturum Yürütücülere Conveners: <b>Alaaddin SAYILI,</b> <b>Ash ELMACI</b>	<b>OTURUM/SESSION 27</b> Sismik Veri Toplama ve Sismik Veri İşlem <i>Seismic Data Acquisition and Seismic Data Processing</i>  Oturum Yürütücülere Conveners: <b>Derman DONDURUR,</b> <b>Hakan KARSLI</b>	<b>OTURUM/SESSION 28</b> Rezervuar Çalışmaları <i>Reservoir Studies</i>  Oturum Yürütücülere Conveners: <b>Ceyda ÇETİNKAYA KAYRIN,</b> <b>Yâsemîn GEZE KALANYUVA</b>	<b>OTURUM/SESSION 29</b> Petrol Endüstrisinde Dijitalleşme ve Teknolojik Gelişmeler <i>Digitalization and Technological Developments in Petroleum Industry</i>  Oturum Yürütücülere Conveners: <b>Önder SARAÇOĞLU,</b> <b>Ali BAŞER</b>	<b>OTURUM/SESSION 30</b> Cumhuriyetin 100. Yılında Yerlîmleri'nde Kadın Olmak  Oturum Yürütücülere Conveners: <b>Umur BEŞPINAR</b>
09:10 09:30	Derin Deniz Emniyet Vanası Kuyudan Kuyuya Alınma <i>BOP Hoopings Operation</i> <b>Ahmet Başar Dimez,</b> <b>Fatih Karakaya,</b> <b>Albert Higgins,</b> <b>Firat Dođu Kaya,</b> <b>Yasin Demiralp,</b> <b>Andrew Timms,</b> <b>Uğur Cengiz</b>	<i>Palaeoenvironmental Significance of Pithonellid Calcitrarchs in Se Anatolia: A Discussion on the Use of the Term 'Calcspheres'</i> <b>Öğüz Mülâvîm,</b> <b>İsmail Ömer Yılmaz,</b> <b>Bruno Ferré</b>	<i>Seismic Reprocessing for Carbon Storage</i> <b>Arindam Kanrar,</b> <b>Joseph Sutcliffe,</b> <b>David Barlass,</b> <b>Shona Joyce,</b> <b>James Bailey,</b> <b>Khaled Abdel Aleem Abdel Aleem,</b> <b>Rachel Little,</b> <b>Priyabrata Pradhan</b>	Güneydođu Anadolu Bölgesi Diyarbakır Yöresi Teklonik Süreçlerinin Bir Üretim Sahasına Etkisi <i>Çanberk Güzelcan,</i> <b>Ashhan Deliktaş,</b> <b>Berat Niran Taşdemir,</b> <b>Cansu Güner Çiçek,</b> <b>Ceyda Çetinkaya Kayrın</b>	<i>Development of a Pore-to-Grid Digital Twin and Software Ecosystem: A Case Study for Sakarya Gas Field Development Project</i> <b>Mehmet Çiçek,</b> <b>Nuri Demirdoven</b>	<b>Fatma Umur Beşpinar (ODTÜ)</b>
09:30 09:50	Casing İçinde Gravel Pack Operasyonu <i>Cased Hole Gravel Pack Uğur Cengiz,</i> <b>Eren Emre Geçer,</b> <b>Carlos Anderson Domingos,</b> <b>Atilla Mazman,</b> <b>Bekir Ođulcan Bulut,</b> <b>Yasin Demiralp,</b> <b>Firat Dođu Kaya,</b> <b>Fatih Karakaya</b>	<i>Carbonate Sedimentology, Micropaleontological Analysis and Stable Isotope Geochemistry of the Gercus Formation at the Core of Gercus Anticline and Subsurface Extent, Batman, Se Turkey</i> <b>Damla Altıntaş,</b> <b>İsmail Ömer Yılmaz,</b> <b>Sevinç Özkan Altner</b>	<i>Multi-Year Evolution of Processing Improvements to A 10 Day Delivery: The Edward Grieg Pp and Ps Time-Lapse Obe Story</i> <b>Richard Ford,</b> <b>Francesca Twynam,</b> <b>Alice Ramsden</b> <b>Taylor Leitch,</b> <b>Michael Hooke,</b> <b>Per Eivind Dhelie,</b> <b>Vidar Danielsen,</b> <b>Arnstein Kvilhaug,</b> <b>Knut Richard Straith</b>	<i>Three Dimensional Reservoir Characterization of Dodaan Field as a Candidate Underground Gas Storage (UGS)</i> <b>Nilsu Kızılk,</b> <b>Diether Kratzer,</b> <b>Robert Rieger,</b> <b>Claudia Steimer-Lackbauer,</b> <b>Ceyda Çetinkaya Kayrın,</b> <b>Fevzi Mert Ürsün,</b> <b>Hasan Çađlar Ürsün</b>	<i>Architecting a Big Data Platform for the Oil and Gas Industry: The Dijital TPMO Project</i> <b>Muhsin Gürel,</b> <b>Adil Cem Abayrak,</b> <b>Resul Kayım</b>	<b>Sema Tekin (PMO)</b>
09:50 10:10	Karadeniz Derin Deniz Operasyonlarında Kullanılan İlk Dört Zonlu MSGP <i>First 4 Zone MSGP for Black Sea Deepwater Case Study</i> <b>Eren Emre Geçer,</b> <b>Carlos Anderson Domingos,</b> <b>Fatih Karakaya,</b> <b>Evren Akbaş,</b> <b>Firat Dođu Kaya</b>	<i>Gondwana Burulları ve GD Anadolu Paleozoyik Petrol Sistemlerine Olan Etkileri</i> <b>Nihat Bozdoğan,</b> <b>Bayram Kara</b>	<i>Full Waveform Inversion and Modern Signal Processing Brings Imaging Uplift for Presalt Reservoirs in the Kwanza Basin</i> <b>Samuel Madden,</b> <b>Mina Matter, Alex Cooke,</b> <b>Amr Ghanem,</b> <b>Carina Lansky,</b> <b>Mahmoud Mahfouz,</b> <b>Deepak Rathee</b>	<i>Bypass Pay Identification and Hydrocarbon Quantification with Advanced Pulsed Neutron Behind Casing As a Result of Logging Optimization and Data Analysis</i> <b>Yernur Akashesy,</b> <b>Samira Ahmad,</b> <b>Chiara Cavalleri,</b> <b>Sviatoslav Yuras</b>	<i>An Integrated GIS-based Asset Information Management System: ZEKI GX &amp; ZEKI EX</i> <b>Yavuz Gültekin,</b> <b>Mehmet Çiçek</b>	<b>Güzde Venedik (JFMO)</b>
10:10 10:30	Tanımlama Operasyonlarında Sıvı Kaybı ile Mücadele için Tasarım Optimizasyonu <i>Completion Design Optimization to Tackle Fluid Loss</i> <b>Carlos Anderson Domingos,</b> <b>Eren Emre Geçer,</b> <b>Nuno Carvalho,</b> <b>Evren Akbaş,</b> <b>Atilla Mazman,</b> <b>Fatih Karakaya</b>	<i>Sequence Sequence Analysis and Depositional Models of the Maestrichtian to Early Eocene Succession at the Gercus Anticline, Batman, Southeast of Turkey</i> <b>Mehmet Özen Gürbüz</b>	<i>Dual-Source and Hexa-Source Time-Lapse OBC Acquisition and Imaging for the Edward Grieg Field</i> <b>Richard Ford,</b> <b>Francesca Twynam,</b> <b>Alice Ramsden,</b> <b>Taylor Leitch,</b> <b>Michael Hooke,</b> <b>Per Eivind Dhelie,</b> <b>Vidar Danielsen,</b> <b>Arnstein Kvilhaug</b>	<i>Sub-Seismic Fault and Fracture Analysis Using Conventional and Image Logs: A Case Study In Bozhüyük Field, Southeast Turkey</i> <b>Cansu Güner Çiçek,</b> <b>Onur Yürüker,</b> <b>Osman Merçey,</b> <b>Ceyda Çetinkaya Kayrın</b>	<i>Autonomous Corrosion and Scale Management for ESP Wells</i> <b>Radhish Kumar Sehvaraj,</b> <b>Dana Kayshibaeva,</b> <b>Michael Van Spankeren</b>	<b>Hafize Akılın (Wing)</b>
10:30 10:50	<b>KAHVE ARASI / COFFEE BREAK</b>					

29 Eylül 2023, Cuma / 29 September 2023, Friday						
	GRAND BALL ROOM-1	GRAND BALL ROOM-2	GRAND BALL ROOM-3	MAGNOLIA	GERBERA	CAMELLIA
10:50 12:30	<b>OTURUM/SESSION 31</b> Derin Deniz Operasyonları <i>Deep Water Operations</i> Oturum Yürütücülere Conveners: <b>Erdal ASKU,</b> <b>Selin EDA TEKİROĞLU</b>	<b>OTURUM/SESSION 32</b> Geliştirilmiş Petrol Kurtarımı <i>Enhanced Oil Recovery &amp; Üretim Mühendisliği Production Engineering</i> Oturum Yürütücülere Conveners: <b>Murat ÇINAR,</b> <b>Veli Volkan ÜSTÜN</b>	<b>OTURUM/SESSION 33</b> Sismik Veri Toplama ve Sismik Veri İşlem <i>Seismic Data Acquisition &amp; Seismic Data Processing</i> Oturum Yürütücülere Conveners: <b>Orhan GÜRELİ,</b> <b>Yılmaz SAKALIOĞLU</b>	<b>OTURUM/SESSION 34</b> Rezervuar Çalışmaları <i>Reservoir Studies</i> Oturum Yürütücülere Conveners: <b>Ferit BİNZET,</b> <b>Tugba ÖZDOĞAN</b>	<b>OTURUM/SESSION 35</b> Petrol Endüstrisinde Dijitalleşme ve Teknolojik Gelişmeler <i>Digitalization and Technological Developments in Petroleum Industry</i> Oturum Yürütücülere Conveners: <b>Zübeyir KÜÇÜK,</b> <b>İhsan Burak KULGA</b>	<b>OTURUM/SESSION 36</b> Sedimentoloji, Stratigrafi ve Çökeltim Otakları <i>Sedimentology, Stratigraphy and Depositional Systems</i> Oturum Yürütücüsü Conveners: <b>İsmail Ömer YILMAZ,</b> <b>Fevzi Mert TÜRESİN</b>
10:50 11:10	Sakarya Sahasından Sonadajın Tamamlama Operasyonlarına Entegre Kıyılı İnşası <i>Integrated Well Construction from Drilling To Completion for Sakarya Field</i> <b>Atilla Mazman,</b> <b>Eren Emre Geçer,</b> <b>Carlos Anderson Domingos,</b> <b>Nuno Carvalho,</b> <b>Fatih Karakaya</b>	<i>Recent Activities in Heavy-Oil Batı Raman Field</i> <b>Ufuk Kılıçbaşan,</b> <b>Turgay İnceci,</b> <b>Yusuf Demirel,</b> <b>Ahsen Özesen</b>	Sismik Yansıma Veri İşlemi İçin Geliştirilen Yeni Bir Yazılımın (Ata-Sis) Tanıtımı <b>Alihan Pekivi,</b> <b>Hulya Kurt</b>	<i>Reservoir Saturation Monitoring Over Time: Case Studies From Karacalı Gas Field and Batı Raman Heavy Oil Field</i> <b>Uğur Yüce</b>	Mobil/Web Tabanlı Jeolojik Numune Toplama ve Saha Planlama Sistemi <b>Tünay Öztürk</b>	<i>Preliminary Results of Mineralogical, Organic Petrographical and Rock-Eval Pyrolysis Analyses of the Oligocene Formation in the Şilivri (NE Thrace Basin)</i> <b>Cüneyt Bircan,</b> <b>Rıza Görkem Oskay,</b> <b>Ali İhsan Karayigit</b>
11:10 11:30	Derin Deniz Kuyularında Çok Zonlu Akıllı Tamamlama Dizisi Tasarımı ve Operasyonu <i>Designing and Running Multi-Zone Smart Completions in Deepwater Wells</i> <b>Nuno Carvalho,</b> <b>Bekir Oğulcan Bulut,</b> <b>İlker Kemal Öztürk</b>	A Numerical Study on the Effect of Flue Gas Composition on Oil Recovery in Low-Permeability Formations <b>Yashar Tavakkoli Oskay,</b> <b>Mehmet Onur Dogan,</b> <b>Cağlar Sinayuc</b>	An Acoustic Wave Equation with the Effects of Reflectivity <b>Jiayong Bai,</b> <b>Orhan Yılmaz</b>	Raman Sahası Garzarz Formasyonu Hedefli Rezervuar Karakterizasyonu ve Saha Geliştirme Çalışması <i>Raman Field Garzarz Formation Targeted Reservoir Characterization and Field Development Study</i> <b>Merve Benzek,</b> <b>Ceyda Çetinkaya Kayrın,</b> <b>Safıgül Tuha Kamanlı,</b> <b>Melahat Aslı Akdere</b>	<i>Some Useful Applications of Whole-Core CT Scanning</i> <b>İbrahim Olgun Uğurlu</b>	Güneydoğu Anadolu Bölgesi Üst Kretase Karbonat İstifi (Adıyaman Grubu) Stratigrafisi, Foraminifer Biyostratigrafisi ve Mikroklastik Özellikleri <b>Recep Özkan</b>
11:30 11:50	Sakarya Sahası Faz-1 Üst Tamamlama Operasyonlarında Ana Tasarım Değişimleri ve İyileştirmeleri <i>Major Design Changes &amp; Improvements During Sakarya Phase-1 UC Operations</i> <b>Alparslan Kömür,</b> <b>Eren Emre Geçer,</b> <b>Fatih Karakaya,</b> <b>Nuno Carvalho,</b> <b>İlker Kemal Öztürk</b>	<i>Combustion Tube Experimental Setup Design for Underground Coal Gasification</i> <b>İsmail Hakkı Sarıcam,</b> <b>Murat Çınar</b>	Vibratör Harmonikleri - Sinyal mi Güdültü mü ? <b>Orhan Gürel</b>	3D Jeolojik Modeling Study of the Garzarz Formation in Çakılı Field <b>Safıgül Tuha Kamanlı,</b> <b>Elvan Aydın</b>	<i>Repurposing Pipelines for Hydrogen and Hydrogen Blend Service</i> <b>Nicholas Waple,</b> <b>Robert Preston</b> <b>Callum Peace,</b> <b>Harry Cotton,</b> <b>Hooman Haghighi</b>	<i>Palynological and Paleobiogeographical Findings from the Upper Ordovician Successions in the Central and Eastern Taurides</i> <b>Sinem Tanrikulu,</b> <b>Sevinç Özkan Altner,</b> <b>Demir Altner</b>
11:50 12:10	Sakarya Gaz Sahası Geliştirme Projesinde Hizmet Kalite Yönetimi <i>Service Quality Management in Sakarya Gas Field Development Project (SQFDP), Black Sea, Turkey</i> <b>Esen Nasıroğlu,</b> <b>Hüseyin Savaşçı,</b> <b>Fırat Üstün,Erdal Asku</b>	<i>Overcoming Complex Flow Assurance Issues with Respect to Gas Hydrate Formation in Deep-Water Well Testing Operations</i> <b>Yakov Shumakov,</b> <b>Ozgur Karacali</b>	<i>Innovative Distributed Acoustic Sensing Technology and Applications in Borehole Seismic</i> <b>Rafael Guercra</b>	Elastic Response of Porous Rock to Accumulated Slip on Strike Slip Fault Networks in Geo-Reservoirs <b>Bora Yalçın, Olaf Zieck,</b> <b>Martin Paul Mai</b>	<i>Magnetotelluric System NÖRD</i> <b>Dimitri Epishkin,</b> <b>Denis Yakovlev,</b> <b>Andrey Yakovlev,</b> <b>Nikolay Palshin,</b> <b>Nikita Zorin</b>	<i>Late Paleocene-Early Eocene Stratigraphy and Hydrocarbon Potential, Southeast of Turkey</i> <b>Mehmet Özen Gürbüç,</b> <b>Halil Şeker,</b> <b>İsmail Bahiyyar,</b> <b>Hasan Altunbay,</b> <b>Ali Can Diyarbakırlı,</b> <b>Mehmet Şahin,</b> <b>Deniz Atasoy,</b> <b>Mahir Kaya,</b> <b>Hasan Çağlar Üsdün,</b> <b>Fırat Göçmenoğlu,</b> <b>Sinem Artan Ercengiz,</b> <b>Yinal Neşes Huvaj</b>
12:10 12:30	<i>Evolution of Lower and Upper Completions in Ultra-Deep-Water Gas Wells, Offshore Black Sea: Learnings, Improvements and Potential Innovations</i> <b>Yves Mbiquis</b>	<i>Single Configuration Enables Seamless Workflow From Cleanup to Extended Well Test and to Production in a Harsh Environment</i> <b>Symon Thomas Shiels</b>	<i>Low Frequency Single Geophone Versus Standard Geophone Array: A Field Test Study in the Se Turkey</i> <b>Yılmaz Sakallioğlu,</b> <b>Zhao Mingqiu, Chen Xin</b>	<i>Navigating Complex Carbonate Reservoirs: Use Cases From A Novel Integrated Well-Placement Workflow</i> <b>Kemal Çağrı Hekimoğlu,</b> <b>Melike Özkaya Türkmen,</b> <b>Onur Yürüker,</b> <b>Batur Alp Aydın,</b> <b>Osman Mery,</b> <b>Ceyda Çetinkaya Kayrın</b>	<i>Integrated End-To-End Carbonate Acidizing Workflow</i> <b>Jakub Wittek,</b> <b>Edmund Eswein</b>	<i>Hydrocarbon Exploration and Potential of Mannar Basin of Sri Lanka, Using Environmental Free Sdt Technology</i> <b>Ongun Yoldemir</b>
12:30 13:30	<b>ÖĞLE YEMEĞİ / LUNCH</b>					

29 Eylül 2023, Cuma / 29 September 2023, Friday						
	GRAND BALL ROOM-1	GRAND BALL ROOM-2	GRAND BALL ROOM-3	MAGNOLIA	GERBERA	CAMELLIA
13:30 14:50	<p><b>OTURUM/SESSION 37</b> Rezervuar Çalışmaları <i>Reservoir Studies</i></p> <p>Oturum Yürütücülere Conveners: <b>A.Çoşkun NAMOĞLU,</b> <b>Arzu AKTOSUN</b></p>	<p><b>OTURUM/SESSION 38</b> Üretim Mühendisliği <i>Production Engineering</i></p> <p>Oturum Yürütücülere Conveners: <b>Murat DEMİR,</b> <b>Serhat GÜLE</b></p>	<p><b>OTURUM/SESSION 39</b> Sismik Yorum <i>Seismic Data Interpretation &amp; Hydrocarbon Aramalarında Elektromanyetik ve Potansiyel Alan Yöntemler (Gravite ve Manyetik)</i></p> <p><i>Hydrocarbon Explorations Using Electromagnetic and Potential Field Methods (Gravity and Magnetic)</i></p> <p>Oturum Yürütücülere Conveners: <b>Kadir Baris BAKIOĞLU,</b> <b>Ercan ARABACI</b></p>	<p><b>OTURUM/SESSION 40</b> GDA Kenet Kuvakları ve İlişkili Basenlerin Petrol Potansiyeli <i>Petroleum Potential of Southeastern Anatolia and Surrounding Areas</i></p> <p>Oturum Yürütücülere Conveners: <b>Sule YILMAZ,</b> <b>Atilla AYDEMİR</b></p>	<p><b>OTURUM/SESSION 41</b> Petrol ve Doğal Gaz Endüstrisinde İş Sağlığı, Güvenliği ve Çevre Health, Safety and Environment in the Oil and Gas Industry</p> <p>Oturum Yürütücülere Conveners: <b>Meliha Beyza KOZAK,</b> <b>Yaprak Damla YAGMUR</b></p>	<p><b>OTURUM/SESSION 42</b> Aşılınımdaki Hidrokarbon Kaynakları <i>Unconventional Hydrocarbon Resources</i></p> <p>Oturum Yürütücüsü Conveners: <b>Salih SANER,</b> <b>Süleyman ÇOŞKUN</b></p>
13:30 13:50	<p>Güneydoğu Anadolu Bölgesinde Petrol Üretiminin Rezervuar Birimleri <b>Ercan Yılmaz,</b> <b>Fevzi Mert Türşin</b></p>	<p>ESP Malzeme Kullanım Önemlerinin (Runlife) Adıyaman, Diyarbakır ve Batman Bölgelerinde İncelenmesi <i>Investigation of ESP Equipments Runlife in Adıyaman, Diyarbakir and Batman Regions</i> <b>Ayhan Budak</b></p>	<p><i>Seismic Facies Analysis: From Basin to Prospect, From Visualisation to Value</i> <b>Simon Mann,</b> <b>James Ostrickoff,</b> <b>Stefane Gesbert</b></p>	<p>Paleo-fayların 2023 Depremlerindeki Rolü ve Petrol Havza ile Yapılarına Etkisi <i>The Role of Paleo Faults in The 2023 Earthquakes and Their Effects on the Oil Basin and Its Structure</i> <b>Doğan Perincek</b></p>	<p>Batı Karadeniz'deki Petrol Platformlarının Gemi Trafığına Olan Etkisi ve Oluşabilecek Kazaların Petrol Dağılımı <b>Ersan Başar,</b> <b>Mehmet Kerem Kemeri</b></p>	<p><i>Methane Adsorption Kinetics Of Core Samples From Tight Oil Field in Southeastern Türkiye</i> <b>Artur Türkmenoğlu,</b> <b>S. Esra Safran,</b> <b>Candan Kızıllırmak,</b> <b>Can Ercan</b></p>
13:50 14:10	<p>Rezervuar kompartmanlarının belirlenmesinde jeokimyasal yaklaşım: Cakilli Sahası <i>Geochemical Approaches for Determination of Reservoir Compartments: Cakilli Field</i> <b>Hüsnü Corbacioğlu,</b> <b>Serdar Doğan,</b> <b>Yagmur Sümer</b> <b>Görenekli,</b> <b>Samet Öksüz</b></p>	<p><i>Wireless Monitoring of Artificial Lift Wells</i> <b>GEOM Wireless Well Monitoring</b> <b>Aasitk Saluja,</b> <b>Nick Nazarov</b></p>	<p>Gravite Gradyent Tensörlerinden Doğu Akdeniz Havzalarının Hidrokarbon Potansiyelinin Kestirimi <b>İlkin Özsöz,</b> <b>Bülent Oruç</b></p>	<p>Hoya Formasyonu'nun Petrol Sistemi <b>Deniz Atasoy,</b> <b>Aynur Geçer Büyüktoku,</b> <b>Arzu Aktosun,</b> <b>Fevzi Mert Türşin,</b> <b>Hüsnü Corbacioğlu</b></p>	<p><i>Analysis of Spreading of Oil Spill on the Sea Surface During Gravity-Viscous and Surface Tension-Viscous Regimes</i> <b>Metehan Erdoğan,</b> <b>İsmail Durgut</b></p>	<p><i>Natural Fracture modeling in Unconventional Dadaş-1 Member for 3d Seismic Survey: Case Study, Turkey</i> <b>Artem Orlov,</b> <b>Canalp Özkut,</b> <b>Fethi Benesenouci,</b> <b>Mehmed Ekrem Yazaroğlu,</b> <b>Ahmet Ergün Mengen,</b> <b>İsmail Ömer Yılmaz</b></p>
14:10 14:30	<p><i>Improved Permeability Prediction of a Heterogeneous Carbonate Reservoir Using Pore-Space and Pore Type Characterization</i> <b>İbrahim Olgun Uğurlu</b></p>	<p><i>Integrated Artificial Lift Optimization Workflow and New Technologies Implementation Helps Improving Reciprocating Rod Pumping Performance on Heavy Oil Fields, Onshore Romania</i> <b>George Ditoiu,</b> <b>Vasile Mogos</b></p>	<p><i>Gravity and Magnetic Based Solutions for Integrated Regional-To-Basin Exploration</i> <b>Andrea Sirtori,</b> <b>Luciana De Luca,</b> <b>Giuseppe Bancaia,</b> <b>Samuele Ratti,</b> <b>Massimo Clementi</b></p>	<p><i>Imprints of Late Paleozoic-Early Mesozoic Tethyan Evolution in the Northern Arabian Plate (Se Turkey) and Its Role in the Paleozoic Petroleum System</i> <b>Gökay Yıldız</b></p>	<p>Petrol Döküntülerinde Risk Değerlendirmesi ve Acil Müdahale Planlarının Önemi <b>Pelin Doğruyol,</b> <b>Müge Büyükoğlu,</b> <b>Ayşe Tuna İşsever</b></p>	<p><i>Evaluation of XRD, CEC, and LSM Methods for Fracturing Fluid Optimization: Experimental Findings</i> <b>Ekrem Alagoz,</b> <b>Ahmet Ergun Mengen,</b> <b>Yalcın Yaradilims</b></p>
14:30 14:50	<p><i>Use of Reservoir Geochemistry in High Water Cut Production: A Case Study in the Karakus Field</i> <b>Placido Franco,</b> <b>Roberto Galimberti,</b> <b>Alara Dispeneç,</b> <b>Onur Acilar,</b> <b>Esra Eren Tokoğlu,</b> <b>Sinem Artan Ercengiz,</b> <b>Onur Yürüker,</b> <b>Ceyda Çetinkaya Kayrın,</b> <b>Tufan Tığlı</b></p>	<p>Açık Deniz Gaz Kuyularında Kum ve Su Kontrolü için Uygulanabilen Bazı Kimyasal Yöntemler <b>Nazan N. Topgüder</b></p>	<p>Güney Karolayna Kıyı Kenarındaki Clubhouse Crossroads Mafiklerinin(CAMP) 3 Boyutlu Gravite ve Manyetik Ters Dönüşümü <b>Kübra Sibel Albayrak</b></p>			
14:50 15:10	<b>KAHVE ARASI / COFFEE BREAK</b>					

## 29 Eylül 2023, Cuma / 29 September 2023, Friday

	GRAND BALL ROOM-1	GRAND BALL ROOM-2	GRAND BALL ROOM-3	MAGNOLIA	GERBERA	CAMELLIA
15:10 16:30	<b>OTURUM/SESSION 43</b> Rezervuar Çalışmaları <i>Reservoir Studies</i>  Oturum Yürütücülere Conveners: <b>Hakki ŞİMŞEK,</b> <b>Adnan EROĞLU</b>	<b>OTURUM/SESSION 44</b> Sondaj Mühendisliği <i>Drilling Engineering</i>  Oturum Yürütücülere Conveners: <b>Gürsat ALTUN,</b> <b>Ahmet AY</b>	<b>OTURUM/SESSION 45</b> Jeodezi, Geomatik ve Uzaktan Algılama Çalışmaları <i>Geodesy, Geomatics and Remote Sensing Studies</i>  Oturum Yürütücülere Conveners: <b>Bilent ORUÇ,</b> <b>Ayça KARAÇAY</b>	<b>OTURUM/SESSION 46</b> Jeotermal Enerji <i>Geothermal Energy</i>  Oturum Yürütücülere Conveners: <b>Muzaffer ŞİYAKO,</b> <b>Deniz ATASOY</b>	<b>OTURUM/SESSION 47</b> Petrol ve Doğal Gaz Endüstrisinde İş Sağlığı, Güvenliği ve Çevre <i>Health, Safety and Environment in the Oil and Gas Industry</i>  Oturum Yürütücülere Conveners: <b>Şebnem Doğa ATAY BALLI,</b> <b>BeYZade KAYGISIZ</b>	<b>OTURUM/SESSION 48</b> Aşılınmadık Hidrokarbon Kaynakları <i>Unconventional Hydrocarbon Resources</i>  Oturum Yürütücüsü Conveners: <b>Can S. BAKİLER,</b> <b>Betül YILDIRIM</b>
15:10 15:30	Genetik Ters Çözüm ve Sismik Nitelik Kombinasyonu ile F3 Blok Kuzey Denizi Potansiyel Hidrokarbon Alanlarının Belirlenmesi <i>A Combination of Genetic Inversion and Seismic Attributes for Prospect Identification in F3 Block, North Sea</i> <b>Silvan Alemdar,</b> <b>Ertan Pekşen</b>	<i>Planning and Execution of a Horizontal Well in Southeast Anatolian Field: Advanced Processes and Technologies for Drilling and Logging</i> <b>İhsan Kaya,</b> <b>Davide Di Tommaso,</b> <b>Inan Sare,</b> <b>Shahbazi Kaveh</b>	Doğal Tehlikelerin Değerlendirilmesinde Konumsal Bilgi Teknolojilerinin Kullanımı <b>Sultan KOCAMAN</b>	<i>Geothermal Energy Potential of Radioactive Heat Production and Magnetic Susceptibility Characteristics in Kütahya Sınov Basin</i> <b>Elif Meric İlkimen,</b> <b>Cihan Çolak,</b> <b>Ali Aydın</b>	Büyük Gemi Kazaların Önlenmesi ve Çıkarılma Dersler <b>Mehmet Kerem Kemerli</b>	<i>Reservoir Characterization of Unconventional Dadaş Formation in Southeastern Turkey</i> <b>Canalp Özkul,</b> <b>İsmail Ömer Yılmaz,</b> <b>Ahmet Ergün Mengen,</b> <b>Fethi Bensenouci,</b> <b>Kirill Ezhov,</b> <b>Mehmed Ekrem Yazaroğlu</b>
15:30 15:50		Experimental Investigation Of The Effect Of Type And Concentration Of Polymers On The Rheological Properties Of Drilling Fluids <b>Mehmet Soylu</b>	<i>Bathymetry Effect on Complete Bouguer Anomalies Along the Turkish Shoreline of the Black Sea</i> <b>Sevda Olgun,</b> <b>Aydın Üstün</b>	Jeotermal Kaynakların Yönetiminde Reenjeksiyonun Önemi <b>Nilgün Doğdu,</b> <b>Oktay Çelmen</b>	Petrol ve Doğal Gaz Üretim Faaliyetleri Sonucu Oluşan Atık suların Membran Teknolojileri ile Yönetimi <b>Börte Köse Mutlu,</b> <b>İsmail Koyuncu,</b> <b>Recep Kaya, Hale Özgün,</b> <b>M. Evren Ersahin,</b> <b>Mahmut Altınbaş,</b> <b>Sema Sayılı,</b> <b>Şebnem Doğa Atay Bali,</b> <b>Pelin Hoşhan, Esra Eren</b>	Geomechanics Aided Solution to Support Drilling and Completion of Dadaş Unconventional Reservoirs, Se-Türkiye <b>Fethi Bensenouci,</b> <b>Ahmet Ergun Mengen,</b> <b>Canalp Özkul,</b> <b>Artem Orlov,</b> <b>Kirill Ezhov,</b> <b>Mehmed Ekrem Yazaroğlu,</b> <b>İsmail Ömer Yılmaz</b>
15:50 16:10	Yeraltı Doğalgaz Depolama Rezervuarları: Antropojen Sismisite, Deprem Tehlikesi ve Sürdürülebilirlik <b>Hüseyin Saifi Kuleli,</b> <b>Ekrem Zor,</b> <b>Mehmet Ergin,</b> <b>Haluk Kunter,</b> <b>Taner Teoman,</b> <b>Haldun Bingöl</b>	<i>A Synopsis on Pressure-While-Drilling Applications</i> <b>Korhan Kor</b>	Deniz Alanlarında Radar Uzaktan Algılama Yöntemiyle Hidrokarbon Sızıntıları Tespiti <b>Ayça Karacay</b>	<i>Implications for the Geothermal Potential of the Area Between the Dead Sea Transform Fault System and the East Anatolian Transform Fault System (Karasu Rift)</i> Based on Geochemical, Geological and Deep Well data: S Türkiye <b>Aydın Cicek, Galip Yüce</b>	Petrol ve Doğalgaz Sektörünün İklim Değişikliğine Etkileri <b>Murat Çilingiroğlu</b>	<i>An analytical Study of Hydraulic Fracturing Optimization for Tight Shale Formation</i> <b>Emre Can Dündar,</b> <b>Ahmet Ergun Mengen,</b> <b>Vasily Mironov,</b> <b>Aleksei Khlopkov,</b> <b>Ekrem Alagoz</b>
16:10 16:30	<i>Mature Field Development By Means of Rotary Steerable System and Reservoir Navigation Services, Turkey</i> <b>Paolo Sudiro,</b> <b>Melike Özkaya Türkmen,</b> <b>Elif Cihan Yıldırım,</b> <b>Batur Alp Aydın</b>		Kara Alanlarında Uzaktan Algılama Yöntemleriyle Hidrokarbon Aramacılığı <b>Ayça Karacay</b>		Türkiye Petroleri Anonim Ortaklığı (TPAO)'nda Sera Gazi Emisyon Hesaplama Çalışmaları <b>Eatma Salcı,</b> <b>Erkan Burçnar,</b> <b>Hatice Selcen Köse,</b> <b>Pınar Aydoğdu,</b> <b>Elif Gökçek Küllük,</b> <b>Şebnem Doğa Atay Bali,</b> <b>Muhammet Mustafa Çelebi,</b> <b>Galip Yılmaz,</b> <b>Ali Sercan Malgaz</b>	



## **İÇİNDEKİLER**

*CONTENTS*

---



<b>Alışılmadık Hidrokarbon Kaynak Aramacılığında Dünya'da ve Türkiye'de Yapılan Çalışmalar</b>	<b>29</b>
<u>Ahmet Ergün Mengen, Canalp Özkul, Mehmed Ekrem Yazaroğlu, Sezer Sevinç</u>	
<b>Petroleum: How Long More, How Much More</b>	<b>35</b>
<u>Salih Saner</u>	
<b>Impact of Numerics on Monte-Carlo Based Type-Well Generation for Unconventional Fields</b>	<b>40</b>
<u>Doruk Alp</u>	
<b>The Fracability Evaluation of Dadas Shale in Southeastern Turkey Based on its Geomechanical Properties</b>	<b>50</b>
<u>Oğuz Cihaner, Betül Yıldırım</u>	
<b>Hamitabat Formation Tight Sandstone Reservoirs Sweet Spot Identification</b>	<b>64</b>
<u>Sezer Sevinç, Ahmet Ergün Mengen, Kirill Ezhov</u>	
<b>Evaluation of Dadas Formation Potential: A Case Study from Southeast Türkiye</b>	<b>68</b>
<u>Mehmed Ekrem Yazaroğlu<sup>1</sup>, Sinem Artan Ercengiz<sup>2</sup>, Suzan Müge Yetim<sup>1</sup>, Canalp Özkul<sup>1</sup>, Ahmet Ergün Mengen<sup>1</sup>, Can Ercan<sup>2</sup>, Yinal Neşes Huvaj<sup>2</sup></u>	
<b>Development of a Computational Tool for Wellbore Stability Analysis and Mud Weight Optimization</b>	<b>73</b>
<u>Ekrem Alagoz, Ahmet Ergün Mengen, Fethi Bensenouci, Emre Can Dündar</u>	
<b>Pore Characterization and FESEM Analysis of the Niobrara Formation in Aristocrat Angus PC H11-07 Core, Wattenberg Field, Denver Basin, CO</b>	<b>79</b>
<u>Elvan Aydın</u>	
<b>Characterizing an Unconventional Reservoir with Onshore Conventional 3d Seismic Data: Case Study Using Seismic Inversion for The Dadas-1 Member</b>	<b>83</b>
<u>Artem Orlov, Kirill Ezhov, Mehmed Yazaroğlu, Canalp Özkul, Ahmet Mengen</u>	
<b>Tuna Deltası (Romanya ve Bulgaristan Açık Denizi) Kitasal Yamaç'ının Gaz Hidrat Potansiyeli ve Sismik Stratigrafisi</b>	<b>85</b>
<u>Orhan Atgın<sup>1</sup>, Günay Çifci<sup>2</sup></u>	
<b>A Study Of An Experimental Possible Production Mechanisms Of Hydrate Formation</b>	<b>93</b>
<u>Hasan Hüseyin Engüçlü</u>	
<b>Batı Karadeniz Kitasal Kenarının Gaz Hidrat Potansiyeli</b>	<b>98</b>
<u>Özkan Özel, Aslıhan Nasif Dondurur, Derman Dondurur</u>	
<b>Doğu Karadeniz'de Gaz Hidratlar ve 2 Çamur Volkanının Keşfi ve Gwangyang Körfezi'nde Sığ Gaz Birikimleri</b>	<b>103</b>
<u>Sevinç Özel Füzün<sup>1</sup>, Günay Çifci<sup>2</sup>, Seda Okay Günaydın<sup>3</sup>, Sermet Gündüz<sup>4</sup>, Dae Choul Kim<sup>5</sup></u>	
<b>Bozcahüyük (Seyitömer/Kütahya) Yöresindeki Bitümlü Marlarnın Organik Jeokimyasal Verilerinin Değerlendirilmesi ile Sentetik Petrol Potansiyelinin Ortaya Konulması</b>	<b>111</b>
<u>Ali Sari<sup>1</sup>, Fatih Büyük<sup>2</sup></u>	
<b>New Generation Approaches for The Manufacturability of Gas Hydrate, One of Turkey's Alternative Energies</b>	<b>121</b>
<u>Güzide Kalyoncu Ergüler</u>	
<b>Methane Adsorption Kinetics Of Core Samples From Tight Oil Field in Southeastern Türkiye</b>	<b>125</b>
<u>Artuğ Türkmenoğlu, S. Esra Safran, Candan Kızılırmak, Can Ercan</u>	
<b>Natural Fracture Modeling in Unconventional Dadaş-1 Member for 3d Seismic Survey: Case Study, Turkey</b>	<b>131</b>
<u>Artem Orlov<sup>1</sup>, Canalp Özkul<sup>1</sup>, Fethi Bensenouci<sup>1</sup>, Mehmed Yazaroğlu<sup>1</sup>, Ahmet Mengen<sup>1</sup>, İsmail Yılmaz<sup>2</sup></u>	
<b>Evaluation of XRD, CEC, and LSM Methods for Fracturing Fluid Optimization: Experimental Findings</b>	<b>133</b>
<u>Ekrem Alagoz, Ahmet Ergun Mengen, Yalcin Yaradilmis</u>	
<b>Reservoir Characterization of Unconventional Dadaş Formation in Southeastern Turkey</b>	<b>143</b>
<u>Canalp Özkul<sup>1</sup>, Ahmet Ergün Mengen<sup>1</sup>, İsmail Omer Yılmaz<sup>2</sup>, Fethi Bensenouci<sup>1</sup>, Kirill Ezhov<sup>1</sup>, Mehmed Ekrem Yazaroglu<sup>1</sup></u>	

<b>Geomechanics Aided Solution to Support Drilling and Completion of Dadaş Unconventional Reservoirs, SE-Türkiye</b>	<b>145</b>
<i>Fethi Bensenouci<sup>1</sup>, Ahmet Ergun Mengen<sup>1</sup>, Canalp Ozkul<sup>1</sup>, Artem Orlov<sup>1</sup>, Kirill Ezhov<sup>1</sup>, Mehmed Ekrem Yazarođlu<sup>1</sup>, Ismail Omer Yilmaz<sup>2</sup></i>	
<b>An Analytical Study of Hydraulic Fracturing Optimization for Tight Shale Formation</b>	<b>148</b>
<i>Emre Can Dündar<sup>1</sup>, Ahmet Ergun Mengen<sup>1</sup>, Vasily Mironov<sup>2</sup>, Aleksei Khlopkov<sup>2</sup>, Ekrem Alagoz<sup>1</sup></i>	
<b>Foça-Karaburun Açıkları Aktif Tektoniđi Ve Stratigrafisinin Deniz Sismiđi Verileriyle İncelenmesi: İlkeli Sonuçlar</b>	<b>159</b>
<i>Derman Dondurur<sup>1</sup>, Aslıhan Nasıf<sup>1</sup>, Özkan Özel<sup>1</sup>, Orhan Atgın<sup>1</sup>, Denizhan Vardar<sup>2</sup>, Muhammet Duman<sup>1</sup></i>	
<b>The Semi-Automatic Morphological Analysis of The Pockmarks Enable Gas/Liquid Emissions From The Bottom Of Sapanca Lake</b>	<b>165</b>
<i>Enes Sönmez, Hülya Kurt</i>	
<b>İzmir Körfezi'nin Aktif Tektoniđinin ve Stratigrafisinin Deniz Sismiđi Verileriyle İncelenmesi: İlkeli Sonuçlar</b>	<b>168</b>
<i>Aslıhan Nasıf<sup>1</sup>, Derman Dondurur<sup>1</sup>, Özkan Özel<sup>1</sup>, Orhan Atgın<sup>1</sup>, Denizhan Vardar<sup>2</sup></i>	
<b>Implications for the Neotectonics of the NW margin of the Arabian Plate: A case study of the E-W-trending Altıntaş Basin (Gaziantep, Türkiye)</b>	<b>175</b>
<i>Aydın Çiçek<sup>1</sup>, Ali Koçyiđit<sup>2</sup></i>	
<b>Seismic Trace Correlation Approach for Gas Probability Mapping in Sakarya Gas Field Reservoirs, Western Black Sea, Turkey</b>	<b>181</b>
<i>Sait Baytok, Ergin Karaca</i>	
<b>High-Resolution Visco-Acoustic Fwı Model Building and Least-Squares Migration in The Black Sea – Resolving Imaging and Illumination Challenges for a Deep-Water Dataset</b>	<b>182</b>
<i>Samuel Madden<sup>1</sup>, Kelly Mistry<sup>1</sup>, Zengbao Chen<sup>1</sup>, Cara Smith<sup>1</sup>, Olivia Lewis<sup>1</sup>, Maria Shadrina<sup>1</sup>, Sait Baytok<sup>3</sup>, Can Özsoy<sup>2</sup>, Can Ören<sup>2</sup>, Emir Yusuf Ersay<sup>3</sup>, Kenan Yazan<sup>3</sup>, Ergin Karaca<sup>3</sup></i>	
<b>An Integrated Petrophysical Technique Leads To Resolve Ultra-Thin Bed Reservoir Properties in Highly Laminated Shaly-Sand Sequences of Black Sea, Turkey</b>	<b>184</b>
<i>Mert Kılıç<sup>1</sup>, Batur İşdiken<sup>1</sup>, Tanmoy Dutta<sup>1</sup>, Uđur Yüce<sup>2</sup></i>	
<b>Lithogram: An Innovative Approach for Net-Sand and Lithofacies Estimation in Thin to Laminated Clastic Reservoirs by Using Synthetic Seismogram Method</b>	<b>185</b>
<i>Emir Yusuf Ersay, Batur İşdiken, Ergin Karaca, Ömer Akbaş, Derya Kılıç Demirci, Tanmoy Dutta, Suat Aktepe</i>	
<b>The Link Between Seismic and Stratigraphic Analysis: How Pre-stack Stochastic Inversion Improves Seismic Resolution in Ultra-Thin Clastic Reservoirs</b>	<b>186</b>
<i>Ergin Karaca<sup>1</sup>, Emir Yusuf Ersay<sup>1</sup>, Burak Salantur<sup>2</sup></i>	
<b>Quantitative Seal Analysis of the Compaction Faults in Western Black Sea Basin, Turkey</b>	<b>187</b>
<i>Bulut Tortopoglu, Nisansu Balcı</i>	
<b>Critical Strain Approach for Critical Drawdown Analysis with the Advance of Cambridge Clay Model in Sakarya Gas Field, Western Black Sea Basin, Turkey</b>	<b>188</b>
<i>Bulut Tortopoglu<sup>1</sup>, Adil Gürkan Ceyhan<sup>2</sup>, Nisansu Balcı<sup>1</sup></i>	
<b>Solutions to Complex Well-Testing Challenges and Proving Production Potential: Successful Well Test Operations on the Sakarya Ultra-deep Water Gas Field in the Black Sea, Türkiye</b>	<b>189</b>
<i>Coşan Ayan<sup>1</sup>, Suat Aktepe<sup>1</sup>, Köksal Çiđi<sup>1</sup>, Melih Gökmen<sup>1</sup>, Adil Gürkan Ceyhan<sup>1</sup>, Murat Fatih Tuđan<sup>1</sup>, Yakov Shumakov<sup>2</sup>, Bertrand Theuveny<sup>2</sup></i>	
<b>Formation Damage Mechanisms and Solutions in Sakarya Field</b>	<b>195</b>
<i>Uđur Paköz</i>	
<b>Utilization of Particle Size Distribution Data for Field Development: Unconsolidated Laminated Sandstone Formation Case</b>	<b>196</b>
<i>Buse Göral, Uđur Paköz</i>	
<b>Top Hole Design Considerations in Black Sea Deepwater Fields</b>	<b>199</b>
<i>Burak Büyükkadıncı, Fatih Karakaya, Amit Sankhe</i>	



<b>The Advantage of Dual Derrick Activity in Ultra-Deepwater Operations</b> <u>Evren Bektaş, Fatih Karakaya, Hüseyin Kasapoğlu, Amit Sankhe, Okan Kırıl</u>	206
<b>Enhancing Efficiency and Stability in Deepwater Jetting Operations: The Role of Bit Stick-Out Length</b> <u>Oğuzhan Kaylan, Fatih Karakaya</u>	212
<b>Subsea BOP Control System Reliability</b> <u>Yasin Demiralp, Fatih Karakaya, Necip Bektaş</u>	217
<b>BOP Hopping Operation</b> Ahmet Başar Dimez, Fatih Karakaya, Albert Higgins, Fırat Doğu Kaya, <u>Yasin Demiralp</u> , Andrew Timms, Uğur Cengiz	228
<b>Cased Hole Gravel Pack</b> Uğur Cengiz, Eren Emre Geçer, Carlos Anderson Domingos, Atilla Mazman, <u>Bekir Oğulcan Bulut</u> , Yasin Demiralp, Fırat Doğu Kaya, Fatih Karakaya	237
<b>The First 4 Zone Modular Screen Gravel Pack for Black Sea Deepwater – Case Study</b> <u>Eren Emre Geçer</u> , Carlos Anderson Domingos, Fatih Karakaya, Evren Akbaş, Fırat Doğu Kaya	249
<b>Completion Design Optimization to Tackle Fluid Loss</b> <u>Carlos Anderson Domingos</u> , Eren Emre Geçer, Nuno Carvalho, Evren Akbaş, Atilla Mazman, Fatih Karakaya	255
<b>Integrated Well Construction from Drilling to Completion for Sakarya Field</b> <u>Atilla Mazman</u> , Eren Emre Geçer, Carlos Anderson Domingos, Nuno Carvalho, Fatih Karakaya	260
<b>Designing and Running Multi-Zone Smart Completions in Deepwater Wells</b> <u>Nuno Carvalho</u> , Bekir Oğulcan Bulut, İlker Kemal Öztürk	267
<b>Major Design Changes &amp; Improvements During Sakarya Phase-1 UC Operations</b> <u>Alparslan Konbul</u> , Eren Emre Geçer, Fatih Karakaya, Nuno Carvalho, İlker Kemal Öztürk	273
<b>Service Quality Management in Sakarya Gas Field Development Project (Sgfdp), Black Sea, Türkiye</b> Esen Nasıroğlu, Hüseyin Savaşçı, <u>Fırat Üstün</u> , Erdal Asku	281
<b>Evolution of Lower and Upper Completions in Ultra-Deep-Water Gas Wells, Offshore Black Sea: Learnings, Improvements and Potential Innovations</b> <u>Yves Mbiguis</u>	293
<b>Türkiye'deki İklim Değişikliği ve Karbon Yakalama-Depolama Uygulamaları ile İlişkili Mevzuatın İncelenmesi</b> <u>Sevtaç Bülbül<sup>1</sup>, Çağlar Sınayuç<sup>2</sup>, Mehmet Onur Doğan<sup>3</sup></u>	305
<b>A Simulation Study of Underground Hydrogen Storage in the Northern Marmara Field</b> <u>Hasan Gürsel</u> , Murat Fatih Tuğan, Çağlar Sınayuç	312
<b>Recent Activities in Heavy-Oil Batı Raman Field</b> Ufuk Kılıçaslan, <u>Turgay İnceşiçi</u> , Yusuf Demirel, Ahsen Özesen	319
<b>A Numerical Study on the Effect of Flue Gas Composition on Oil Recovery in Low-Permeability Formations</b> <u>Yashar Tavakkoli Osgouei</u> , Mehmet Onur Dogan, Çağlar Sınayuc	325
<b>Combustion Tube Experimental Setup Design for Underground Coal Gasification</b> <u>İsmail Hakkı Sarıçam</u> , Murat Çınar	329
<b>Predicting Bottomhole Temperature of Offshore Production Wells in the North Sea</b> <u>Tuğberk Berat Günel</u>	339
<b>Application of CT in Reservoir Characterization</b> <u>Efe Ereğ</u>	349
<b>Energy Transition</b> <u>Yaren Esra Kahya</u>	352
<b>Türkiye'de Buhar ve Karbondioksit Enjeksiyonu. Faydaları ve Zorlukları</b> <u>Mehmet Mertcan Doğan</u>	353

<b>Steamflooding Interval Horizontal Wells</b>	354
<a href="#">Oğuzhan Uçar</a>	
<b>Stimulation of a Tight Sandstone Reservoir Through Hydraulic Fracturing: Taylor Sandstone Case, Texas</b>	355
<a href="#">Muloh Gariba Sheron</a>	
<b>Approximating Hydraulic Fracture Permeability Enhancement</b>	363
<a href="#">Onuralp Mete Yağmur</a>	
<b>Forecasting the Performance of Shale Gas Wells Using Machine Learning</b>	365
<a href="#">Mohammed Shedaiva</a>	
<b>Experience and Prospects of Magnetotelluric Method Application for Hydrocarbon Prospecting</b>	371
<a href="#">Nikolay Palshin<sup>1</sup>, Elena Aleksanova<sup>2</sup>, Dmitry Epishkin<sup>3</sup>, Denis Yakovlev<sup>2</sup>, Andrey Yakovlev<sup>4</sup></a>	
<b>Manyetotellürük Yöntemin Güneydoğu Anadolu'da Petrol Arama Amaçlı Kullanımının Değerlendirilmesi Evaluation of Magnetotelluric Method for Petroleum Exploration in Southeast Anatolia</b>	380
<a href="#">Ahmet Tuğrul Başokur</a>	
<b>A Multiphysics Approach To Evaluating Gas Prospectivity With Case Examples</b>	387
<a href="#">Daniel Baltar Pardo, Dag Helland Hansen, Elias Andre Nerland</a>	
<b>Gravite Tabaka Sıyırma Yöntemi ile Doğu Akdeniz'de Gravite Anomalilerinin Analizi ve Tektonik Yapıların İncelenmesi</b>	390
<a href="#">İlkin Özsöz</a>	
<b>Gravite Gradyent Tensörlerinden Doğu Akdeniz Havzalarının Hidrokarbon Potansiyelinin Kestirimi Estimation of the Hydrocarbon potentials of the Eastern Mediterranean basins from the Gravity Gradient Tensors</b>	399
<a href="#">İlkin Özsöz<sup>1</sup>, Bülent Oruç<sup>2</sup></a>	
<b>Gravity and Magnetic Based Solutions aor Integrated Regional-To-Basin Exploration</b>	404
<a href="#">Andrea Sirtori, Luciana De Luca, Giuseppe Bancalà, Samuele Ratti, Massimo Clementi</a>	
<b>Güney Karolayna Kıyı Kenarındaki Clubhouse Crossroads Mafiklerinin(CAMP) 3 Boyutlu Gravite ve Manyetik Ters Dönüşümü</b>	407
<a href="#">Kübra Sibel Albayrak</a>	
<b>Bathymetry effect on complete Bouguer Anomalies along the Turkish shoreline of the Black Sea</b>	417
<a href="#">Sevda Olgun, Aydın Üstün</a>	
<b>Deniz Alanlarında Radar Uzaktan Algılama Yöntemiyle Hidrokarbon Sızıntıları Tespiti</b>	420
<a href="#">Ayça Karaçay</a>	
<b>Kara Alanlarında Uzaktan Algılama Yöntemleriyle Hidrokarbon Aramacılığı</b>	427
<a href="#">Ayça Karaçay</a>	
<b>Jeotermal Sahalarda Mikrosismik İzleme Yöntemi ile Rezervuar Takibi</b>	439
<a href="#">Bürçü Turhan<sup>1</sup>, Tuğçe Bilgiç<sup>2</sup>, Ünal Selek<sup>2</sup>, Kadir Balcı<sup>3</sup>, Ali Yıldırım<sup>3</sup>, Bülent Kaypak</a>	
<b>Sismik Hız İle Boşluk Basıncı İlişkisi Örnek Çalışma: Denizli Havzası</b>	445
<a href="#">Orhan Güreli</a>	
<b>A Numerical Toolkit for Optimization of Model Parameters for Tracer Tests</b>	455
<a href="#">Doğuhan Barlas Sevindik<sup>1</sup>, Ali Berkay Tokel<sup>1</sup>, Selçuk Erol<sup>2</sup>, Serhat Akın<sup>1</sup></a>	
<b>Carbon Utilization Potential in Geothermal Fields</b>	461
<a href="#">Erdiçe Şentürk, Gültekin Tarcan</a>	
<b>Top Cementing Job A Lesson Learnt from Geothermal Well Drilling in Alasehir Geothermal Field</b>	470
<a href="#">Emrah Gürel, Omer Yukselec, Emir Dimici, Cemil Seckin</a>	
<b>Kapadokya Bölgesinde Gömülü Kalderranın Manyetotellürük Yöntem ile Görüntülenmesi ve Jeotermal Potansiyelinin Değerlendirilmesi</b>	475
<a href="#">Ahmet Tuğrul Başokur<sup>1</sup>, Özlem Hacıoğlu<sup>2</sup>, Naser Meqbel<sup>3</sup>, Halil İbrahim Arslan<sup>1</sup>, Tevfik Efeçinar<sup>4</sup></a>	

<b>Geothermal Energy Potential of Radioactive Heat Production and Magnetic Susceptibility Characteristics in Kütahya Simav Basin</b> <u>Elif Meriç İlkimen, Cihan Çolak, Ali Aydın</u>	482
<b>Jeotermal Kaynakların Yönetiminde Reenjeksiyonun Önemi</b> <u>Nilgün Dođdu, Oktay Çelmen</u>	486
<b>Implications for the Geothermal Potential of the Area between the Dead Sea Transform Fault System and the East Anatolian Transform Fault System (Karasu Rift) Based on Geochemical, Biological and Deep well Data: S Türkiye</b> <u>Aydın Çiçek<sup>1</sup>, Galip Yüce<sup>2</sup></u>	495
<b>Comparative Analysis of Acid Fracturing in ŞEHİT ESMA ÇEVİK Field Using 3 1/2" and 2 7/8" Tubings: A Comprehensive Study</b> <u>Görkem Kaya</u>	503
<b>Coiled Tubing ile Açık Kuyu Sondaj Operasyonu</b> <u>Seçkin Öztel</u>	505
<b>Radial Drilling</b> <u>Doruk Kırac, Görkem Kaya</u>	513
<b>Coiled Tubing ile Canlı Kuyuda Slickline Tahliyesi</b> <u>Seçkin Öztel</u>	517
<b>Resolving Cement Evaluation in the Challenging Environment of Large and Thick Casing</b> <u>Alhadi Zahmuw, Rob Loov, Diana Vargas</u>	522
<b>Advanced Tractor Techniques in Extended Reach Wells Allow Confirmation of Well Integrity and Execution of Perforation Services in Key Turkish Offshore Gas Fields</b> <u>Daniel Steen Haase Soerensen<sup>1</sup>, Ugur Ezer<sup>1</sup>, Mohammed Ameen Al Ganad<sup>1</sup>, Fadi Duman<sup>2</sup></u>	530
<b>Overview of Acid Fracturing Operations in Carbonate Reservoirs of Turkey</b> <u>Ufuk Kılıçaslan, Ahmet Ergün Mengen, Özlem Özcan, Mutlu Daşdemir, Yasin Ünal, Bekir Onay, Bülent Şahinbaş, Vasily Semenovich Mironov, Aleksei Vasilevich Khlopkov</u>	535
<b>Importance of Cement Slurry Density &amp; GEO-LITE</b> <u>Yigit Altunal, Burak Ekici</u>	539
<b>Tight Gas Field Development in Thrace Basin by Hydraulic Fracturing</b> <u>Ufuk Kılıçaslan, Ahmet Ergün Mengen, Özlem Özcan, Sofiane Belhocine, Rabah Boudissa, Vasily Semenovich Mironov, Aleksei Vasilevich Khlopkov</u>	546
<b>Geochemical Characteristics and Depositional Conditions of the Organic-Rich Triassic Facies in the Western Taurides, Turkey</b> <u>Zeynep Dincer Kırman<sup>1</sup>, İsmail Ömer Yılmaz<sup>2</sup>, Hasan Çağlar Üsdün<sup>3</sup></u>	555
<b>Dođu Akdeniz'deki En Büyük İki Deltanın (Nil ve Seyhan-Ceyhan) Gelişiminde Tektonizmanın Karşılaştırmalı Analizi</b> <b>Comparative Analyses Tectonism on the Development of two Largest Deltas (Nile and Seyhan-Ceyhan) in the Eastern Mediterranean</b> <u>Yasemin Geze Kalanyuva<sup>1</sup>, Nizamettin Kazancı<sup>2</sup></u>	556
<b>Levant ve Herodot Basenleri Stratigrafik Birimlerin Benzerliği, Sismik Kesit Örnekleri</b> <u>Fatih Özdamar</u>	561
<b>Development of a Pore-to-Grid Digital Twin and Software Ecosystem: A Case Study for Sakarya Gas Field Development Project</b> <u>Mehmet Cicek, Nuri Demirdoven</u>	565
<b>Architecting a Big Data Platform for the Oil and Gas Industry: The Dijital TPAO Project</b> <u>Muhsin Gürel, Adil Cem Albayrak, Resul Kayım</u>	567
<b>An Integrated GIS-based Asset Information Management System: ZEKI GX &amp; ZEKI EX</b> <u>Yavuz Gültekin, Mehmet Cicek</u>	568
<b>Autonomous Corrosion and Scale Management for ESP Wells</b> <u>Dana Kayshibaeva, Michael Van Spankeren</u>	570

<b>Mobil&amp;Web Tabanlı Jeolojik Numune Toplama ve Saha Planlama Sistemi</b> <u>Tünay Öztürk</u>	571
<b>Some Useful Applications of Whole-Core CT Scanning</b> <u>İbrahim Olgun Uğurlu</u>	573
<b>Repurposing Pipelines for Hydrogen and Hydrogen Blend Service</b> <u>Nicholas Waple<sup>1</sup>, Callum Peace<sup>2</sup>, Harry Cotton<sup>1</sup>, Hooman Haghghi<sup>3</sup></u>	578
<b>Magnetotelluric System NORD</b> <u>Dmitrii Epishkin<sup>1</sup>, Denis Yakovlev<sup>2</sup>, Andrey Yakovlev<sup>3</sup>, Nikolay Palshin<sup>4</sup>, Nikita Zorin</u>	584
<b>Integrated end-to-end Carbonate Acidizing Workflow</b> <u>Jakub Witek, Edmund Eswein</u>	591
<b>A Case Study of the Regional 3-D Basin Modeling in Amu Darya and Afghan-Tajik Basins</b> <u>Yücel Deniz Erdal<sup>1</sup>, Zeynep Adıgüzel<sup>1</sup>, Şükrü Gökhan Köse<sup>1</sup>, Hasan Güney<sup>2</sup>, Helby Ellen<sup>2</sup>, Ayodeji Temitope Ajayi<sup>2</sup>, Mustafa Demirci<sup>1</sup>, Emrah Dölek<sup>1</sup></u>	597
<b>Exploring Hydrocarbons in 1.75 Billion-Year-Old Pre-Cambrian Deposits of South Africa Using Environment Friendly SDDT Technology</b> <u>Ongun Yoldemir, Joerg Enge</u>	600
<b>Pitfalls in Basin Modeling - A Case Study From the Eastern Black Sea</b> <u>Turan İşçimen</u>	602
<b>Rock Eval Piroiliz Analizi ile Kinetik Parametrelerin Karakterizasyonu ve Silüriyen Yaşlı Dadaş Formasyonu'nun Kinetik Parametrelerinin Belirlenmesi Projesi</b> <u>Cihan Can<sup>1</sup>, Zeynep Özlem Cihan<sup>1</sup>, Şükrü Gökhan Köse<sup>2</sup>, Yücel Deniz Erdal<sup>2</sup></u>	605
<b>Doğu Trakya Havzası Basen ve Petrol Sistemi Modellemesi (Basin and Petroleum System Modeling in the Eastern Thrace Basin)</b> <u>Esra Yalcın Yılmaz, Şükrü Gökhan Köse</u>	607
<b>Dolomitleşme Sıcaklığının ve Zamanlamasının Rezervuar Kalitesine Etkisi Nedir? Örnek Çalışma: GDA Bölgesindeki Mardin Grubu Dolomitlerinin Kümelmiş İzotop Sıcaklıkları</b> <u>Deniz Atasoy<sup>1</sup>, Aynur Geçer Büyüktutku<sup>2</sup>, Arzu Aktosun<sup>3</sup></u>	611
<b>Conceptual Risk Modeling for Biogenic Gas Fields</b> <u>Yücel Deniz Erdal</u>	616
<b>Investigation the impact of Messinian Event in the Eastern Black Sea from a Biogenic Gas System Perspective</b> <u>Mehmet Hazar, Yücel Deniz Erdal, Şükrü Gökhan Köse</u>	619
<b>Batı Karadeniz'deki Petrol Platformlarının Gemi Trafikğine Olan Etkisi ve Oluşabilecek Kaza Sonrası Petrol Yayılımı</b> <u>Ersan Başar<sup>1</sup>, Mehmet Kerem Kemerli<sup>2</sup></u>	623
<b>Analysis of Spreading of Oil Spill on The Sea Surface During Gravity-Viscous and Surface Tension-Viscous Regimes</b> <u>Metehan Erdoğan<sup>1</sup>, İsmail Durgut<sup>2</sup></u>	625
<b>Petrol Döküntülerinde Risk Değerlendirmesi ve Acil Müdahale Planlarının Önemi</b> <u>Pelin Doğruyol, Müge Bıyıklıoğlu, Ayşe Tuna İşsever</u>	629
<b>Büyük Gemi Kazaların Önlenmesi ve Çıkarılan Dersler</b> <u>Mehmet Kerem Kemerli</u>	631
<b>Petrol ve Doğal Gaz Üretim Faaliyetleri Sonucu Oluşan Atıksuların Membran Teknolojileri İle Yönetimi</b> <u>İsmail Koyuncu<sup>1</sup>, Recep Kaya<sup>2</sup>, Börte Köse Mutlu<sup>1</sup>, Hale Özgün<sup>1</sup>, M.Evren Erşahin<sup>2</sup>, Mahmut Altınbaş<sup>2</sup>, Sema Sayılı<sup>3</sup>, Şebnem, Doğa Atay Bali<sup>3</sup>, Pelin Hoşhan<sup>3</sup>, Esra Eren<sup>3</sup></u>	633
<b>Petrol ve Doğalgaz Sektörünün İklim Değişikliğine Etkileri</b> <u>Murat Çilingiroğlu</u>	635

<b>Türkiye Petrolleri Anonim Ortaklığı (TPAO)'nda Sera Gazı Emisyon Hesaplama Çalışmaları</b> <u>Fatma Salçın</u> , Erkan Buzpınar, Hatice Selcen Köse, Pınar Aydoğdu, Elif Gökçek Küllük, Şebnem Doğa Atay Bali, Muhammet Mustafa Çelebi, Galip Yılmaz, Ali Sercan Malgaz	637
<b>Türkiye'deki Petrol ve Doğal Gaz Arama ve Üretim Faaliyetlerinin Teknik ve Ekonomik Analizi</b> <b>Technical and Economic Analysis of Oil and Natural Gas Exploration and Production Activities in Turkey</b> <u>A.Uğur Gönülalan</u>	643
<b>Current Status of Türkiye about Carbon Capture and Sequestration: A Case Study Related to Carbon Capture and Sequestration in the Bati Raman Heavy Oilfield of Türkiye</b> <u>Emre Özgür<sup>1</sup></u> , Şükrü Merye <sup>2</sup>	652
<b>Comparison Of Host Government Petroleum Contracts And Applicability For Türkiye Deepwater Offshore Licences</b> <u>Fatih Vural</u>	657
<b>Evaluation of Sustainability Aspects of CO<sub>2</sub> Sequestration in Depleted Shale Reservoirs Using Data Analytics</b> Kanan Aliyev <sup>1</sup> , Emre Artun <sup>2</sup> , <u>Burak Kulga<sup>2</sup></u>	663
<b>Sustainability in Energy From Oil &amp; Gas to Geothermal Energy</b> <u>Harun Yarım</u>	669
<b>Modüler Çelik Yapılar, Petrol ve Gaz Sahalarınında İdeal Çözüm</b> <u>Mert Özdemir</u>	678
<b>LPG'nin Günümüzde Konvansiyonel ve Alternatif Kullanım Alanları</b> <u>Can Toydemir<sup>1</sup></u> , Lpg Dairesi <sup>2</sup> , Yasin Ersöz <sup>3</sup>	683
<b>Kahramanmaraş Depremlerinin Türk Akaryakıt Piyasasına Etkisi</b> <u>Sinem Okumuş</u> , Aysun Korucan	688
<b>Minimization Of The Noise In The Calculated Pressure Derivative Data For The Interpretation Of Transient Tests</b> <u>Doğuhan Coşar</u> , Çağlar Sınayuç	699
<b>Integrating Various Sources Of Indicators And Water Measurements Data Of Different Degree Of Uncertainty To Understand Aquifer Encroachment And Resulted Water Breakthrough To Gas Producers</b> <u>Murat Zhiyenkulov<sup>1</sup></u> , Michael Nashaat <sup>2</sup> , Hassan Kolivand <sup>2</sup> , Oleh Lukin <sup>1</sup> , Abdurrahman Shah <sup>2</sup> , Kassem Ghorayeb <sup>2</sup> , Viacheslav Filatov <sup>3</sup> , Denys Grytsai <sup>3</sup>	702
<b>Unlocking New Reservoir Zones at Shallow Depth Based on Integrating Post-Hydraulic Fracture Performance with Reservoir, Petrophysics and Geology Data</b> <u>Murat Zhiyenkulov<sup>1</sup></u> , Michael Nashaat <sup>2</sup> , Hassan Kolivand <sup>2</sup> , Yerlan Seilov <sup>1</sup> , Abdurrahman Shah <sup>2</sup> , Kassem Ghorayeb <sup>2</sup> , Roman Madatov <sup>1</sup> , Svetlana Grytsai <sup>3</sup> , Viacheslav Filatov <sup>3</sup>	706
<b>Analysis of the Effect of Salt Zones on Gas Production from Gas Hydrates in the Mediterranean Sea</b> <u>Şükrü Merye<sup>1</sup></u> , Lin Chen <sup>2</sup>	710
<b>Estimation of Missing Well-Log Sections Using Machine Learning Assisted Multivariate Imputation: A Case Study</b> Emre Artun <sup>1</sup> , <u>Serhat Canbolat<sup>2</sup></u> , Elif Cihan Yıldırım <sup>2</sup> , Cansu Açıköz <sup>2</sup> , Onur Yürüker <sup>2</sup>	717
<b>Coal Bed Methane Characterization for Gas Production Recovery Optimization-Zonguldak, Turkey</b> <u>Sofiane Belhocine</u> , Ahmet Ergün Mengen, Muhammed Emin Bulguroğlu, Rabah Boudissa	726
<b>Assessing CO<sub>2</sub> Enhanced Geothermal Potential and CO<sub>2</sub> Storage in a Red Sea Rift Basin, Al Wajh: A Comprehensive Reservoir Model and Simulation Study</b> <u>Bora Yalcın</u> , Justin Ezekiel, Martin Paul Mai	735
<b>Calculation of Natural Gas Viscosity of a Gas Reservoir Using Correlations and Comparison with Manual Readings Through Well Known Charts</b> <u>Abdullah Gürkan Işcan</u>	741
<b>An Integrated Approach to Carbonate Reservoir Characterization: A Case Study from Se of Turkey</b> <u>Mustafa Kamil Yüksek<sup>1</sup></u> , Ashlan Deliktaş <sup>1</sup> , Attıla Aydemir <sup>2</sup>	749

<b>Physics-Informed Neural Networks for Solving Partial Differential Equations: Applications and Challenges</b>	754
<u>Amir Shamsa, Mehdi Paydayesh, Maria Perezhogina</u>	
<b>Integrated Reservoir Characterization of Fractured Carbonates: Garzan Limestone Case</b>	758
<u>Ufuk Durmus</u>	
<b>Unlocking New Discovery in Thrace Basin, Turkey: Probabilistic Neural Network Application to Estimate NPHI and Acoustic Impedance Cross Plotting for Hydrocarbon Mapping</b>	763
<u>Sait Baytok, Ergin Karaca</u>	
<b>Utilizing Seismic Amplitude Information and Extending The Value of The Seismic Beyond Structural Imaging</b>	766
<u>Omar Aly<sup>1</sup>, Aya Ibrahim<sup>1</sup>, Tarek Nafie<sup>1</sup>, Ahmed Hassan<sup>1</sup>, Mohamed Fekry<sup>1</sup>, Amin Al Maktari<sup>2</sup>, Aref Al Shadadi<sup>2</sup>, Mohammed Ali Al Rawqi<sup>2</sup></u>	
<b>Seismic Reservoir Characterization of Hydrocarbon-Bearing Sandstones, In A Producing Field, Thrace Basin</b>	772
<u>Taner Arpacı</u>	
<b>Multiple Approaches to Reservoir Characterization of Gas-Bearing Sandstone: a Case Study from the Thrace Basin, Turkey</b>	776
<u>Mustafa Kamil Yüksek</u>	
<b>The Critical Role of Velocity in Pore Pressure Estimations and the Impact of the Centroid Effect</b>	780
<u>Ergin Karaca</u>	
<b>Güneydoğu Anadolu Bölgesi Diyarbakır Yöresi Tektonik Süreçlerinin Bir Üretim Sahasına Etkisi</b>	782
<u>Canberk Güzelcan, Aslıhan Deliktaş, Berat Niran Taşdemir, Cansu Güner Çiçek, Ceyda Çetinkaya Kayrın</u>	
<b>Three Dimensional Reservoir Characterization of Dodan Field as a Candidate Underground Gas Storage (UGS)</b>	784
<u>Nilsu Kıştaç<sup>1</sup>, Diethard Kratzer<sup>2</sup>, Robert Rieger<sup>2</sup>, Claudia Steiner – Luckbauer<sup>2</sup>, Ceyda Çetinkaya Kayrın<sup>1</sup>, Fevzi Mert TÜresin<sup>3</sup>, Hasan Çağlar Üsdün<sup>3</sup></u>	
<b>Bypass Pay Identification and Hydrocarbon Quantification with Advanced Pulsed Neutron Behind Casing as a Result of Logging Optimization and Data Analysis</b>	791
<u>Yemur Akashev<sup>1</sup>, Samira Ahmad<sup>1</sup>, Chiara Cavalleri<sup>1</sup>, Sviatoslav Yuras<sup>2</sup></u>	
<b>Sub-Seismic Fault and Fracture Analysis Using Conventional and Image Logs: A Case Study In Bozhüyük Field, Southeast Turkey</b>	800
<u>Cansu Güner Çiçek<sup>1</sup>, Onur Yürüker<sup>1</sup>, Osman Meroy<sup>2</sup>, Ceyda Çetinkaya Kayrın<sup>1</sup></u>	
<b>Reservoir Saturation Monitoring over time: Case Studies from Karacali Gas Field and Batı Raman Heavy Oil Field</b>	804
<u>Uğur Yüce</u>	
<b>Raman Sahası Garzan Formasyonu Hedefli Rezervuar Karakterizasyonu ve Saha Geliştirme Çalışması Raman Field Garzan Formation Targeted Reservoir Characterization and Field Development Study</b>	808
<u>Merve Benzek, Ceyda Çetinkaya Kayrın, Safiğül Tuba Kamanlı, Melahat Aslı Akdere</u>	
<b>3D Geological Modeling Study of the Garzan Formation in Cakilli Field</b>	811
<u>Safiğül Tuba Kamanlı, Elvan Aydın</u>	
<b>Elastic Response of Porous Rock to Accumulated Slip on Strike Slip Fault Networks in Geo-Reservoirs</b>	815
<u>Bora Yalcin, Olaf Zielke, Martin Paul Mai</u>	
<b>Navigating Complex Carbonate Reservoirs: Use Cases from a Novel Integrated Well-Placement Workflow</b>	820
<u>Kemal Çağrı Hekimoğlu<sup>1</sup>, Melike Özkaya Türkmen<sup>2</sup>, Onur Yürüker<sup>2</sup>, Batur Alp Aydın<sup>2</sup>, Osman Meroy<sup>2</sup>, Ceyda Çetinkaya Kayrın<sup>2</sup></u>	
<b>Güneydoğu Anadolu Bölgesi'nde Petrol Üretilen Rezervuar Birimler</b>	829
<u>Erhan Yılmaz<sup>1</sup>, Fevzi Mert TÜresin<sup>2</sup></u>	
<b>Rezervuar kompartmanlarının belirlenmesinde jeokimyasal yaklaşım: Çakıllı Sahası Geochemical Approaches for Determinaiton of Reservoir Compartments: Çakıllı Field</b>	846
<u>Hüsnü Corbacioğlu, Serdar Doğan, Yağmur Sümer Görenekli, Samet Öksüz</u>	

<b>Improved Permeability Prediction of a Heterogeneous Carbonate Reservoir Using Pore-Space and Pore Type Characterization</b>	<b>848</b>
<u>İbrahim Olgun Uğurlu</u>	
<b>Use of Reservoir Geochemistry in High Water Cut Production: A Case Study in The Karakuş Field</b>	<b>855</b>
Placido Franco <sup>1</sup> , Roberto Galimberti <sup>1</sup> , Alara Dispençe <sup>2</sup> , Onur Acilar <sup>2</sup> , Esra Eren Tokoğlu <sup>3</sup> , Sinem Artan Ercengiz <sup>3</sup> , Onur Yürüker <sup>4</sup> , Ceyda Çetinkaya Kayrın <sup>4</sup> , Tufan Tıgh <sup>4</sup>	
<b>Genetik Ters Çözüm ve Sismik Nitelik Kombinasyonu ile F3 Blok Kuzey Denizi Potansiyel Hidrokarbon Alanlarının Belirlenmesi</b>	<b>862</b>
<b>A Combination of Genetic Inversion and Seismic Attributes for Prospect Identification in F3 Block, North Sea</b>	
<u>Süleyman Alemdar<sup>1</sup>, Ertan Pekşen<sup>2</sup></u>	
<b>Yeraltı Doğalgaz Depolama Rezervuarları: Antropojen Sismisite, Deprem Tehlikesi ve Sürdürülebilirlik</b>	<b>872</b>
<u>Hüseyin Sadi Kuleli<sup>1</sup>, Ekrem Zor<sup>2</sup>, Mehmet Ergin<sup>2</sup>, Haluk Kunter<sup>3</sup>, Taner Teoman<sup>3</sup>, Haldun Bingöl<sup>3</sup></u>	
<b>Palaeoenvironmental Significance of Pithonellid Calcitarchs in Se Anatolia: A Discussion on the Use of the Term ‘Calcispheres’</b>	<b>883</b>
<u>Oğuz Mülayim<sup>1</sup>, İsmail Ömer Yılmaz<sup>2</sup>, Bruno Ferré<sup>3</sup></u>	
<b>Carbonate Sedimentology, Micropaleontological Analysis and Stable Isotope Geochemistry of the Garzan Formation at the Core of Gercus Anticline and Subsurface Extent, Batman, SE Turkey</b>	<b>889</b>
<u>Damla Altuntaş<sup>1</sup>, İsmail Ömer Yılmaz<sup>2</sup>, Sevinç Özkan Altuner<sup>2</sup></u>	
<b>Gondwana Paleozoyik Buzulları ve GD Anadolu Paleozoyik Petrol Sistemlerine Olan Etkileri</b>	<b>893</b>
<u>Nihat Bozdoğan<sup>1</sup>, Bayram Kara<sup>2</sup></u>	
<b>Sequence Sequence Analysis and Depositional Models of the Maastrichtian to Early Eocene Succession at the Gercus Anticline, Batman, Southeast of Turkey</b>	<b>903</b>
<u>Mehmet Özen Gürbüz</u>	
<b>Preliminary Results of Mineralogical, Organic Petrographical and Rock-Eval Pyrolysis Analyses of the Oligocene Formation in the Silivri (NE Thrace Basin)</b>	<b>907</b>
<u>Cüneyt Bircan<sup>1</sup>, Rıza Görkem Oskay<sup>2</sup>, Ali İhsan Karayığit<sup>3</sup></u>	
<b>Güneydoğu Anadolu Bölgesi Üst Kretase Karbonat İstifinin (Adıyaman Grubu) Stratigrafisi, Foraminifer Biyostratigrafisi Ve Mikrofasiyes Özellikleri</b>	<b>912</b>
<u>Recep Özkan</u>	
<b>Palynological and Paleobiogeographical Findings from the Upper Ordovician Successions in the Central and Eastern Taurides</b>	<b>915</b>
<u>Sinem Tanrikulu<sup>1</sup>, Sevinç Özkan Altuner<sup>2</sup>, Demir Altuner<sup>2</sup></u>	
<b>Late Paleocene-Early Eocene Stratigraphy and Hydrocarbon Potential, Southeast of Turkey</b>	<b>916</b>
<u>Mehmet Özen Gürbüz, Halil Şeker, İsmail Bahtiyar, Hasan Altınbay, Ali Can Diyarbakırlı, Mehmet Şahin, Deniz Atasoy, Mahir Kaya, Hasan Çağlar Üsdün, Fırat Göçmenoğlu, Sinem Artan Ercengiz, Yinal Neşes Huvaj</u>	
<b>Hydrocarbon Exploration And Potential Of Mannar Basin Of Srilanka, Using Environmental Free Sddt Technology</b>	<b>919</b>
<u>Ongun Yoldemir</u>	
<b>Seismic Reprocessing for Carbon Storage</b>	<b>923</b>
<u>Arindam Kanrar, Joseph Sutcliffe, David Barlass, Shona Joyce, James Bailey, Khaled Abdel Aleem Abdel Aleem, Rachel Little, Priyabrata Pradhan</u>	
<b>Multi-Year Evolution of Processing Improvements to A 10 Day Delivery. The Edvard Grieg Pp And Ps Time-Lapse OBC Story</b>	<b>927</b>
<u>Richard Ford<sup>1</sup>, Francesca Twynam<sup>1</sup>, Alice Ramsden<sup>1</sup>, Taylor Leitch<sup>1</sup>, Michael Hooke<sup>1</sup>, Per Eivind Dhelie<sup>2</sup>, Vidar Danielsen<sup>2</sup>, Arnstein Kvilhaug<sup>2</sup>, Knut Richard Straith<sup>2</sup></u>	
<b>Full Waveform Inversion And Modern Signal Processing Brings Imaging Uplift for Presalt Reservoirs in The Kwanza Basin</b>	<b>932</b>
<u>Samuel Madden, Mina Matter, Alex Cooke, Amr Ghanem, Carina Lansky, Mahmoud Mahfouz, Deepak Rathee</u>	
<b>Dual-Source and Hexa-Source Time-Lapse Obc Acquisition And Imaging for the Edvard Grieg Field</b>	<b>937</b>
<u>Richard Ford<sup>1</sup>, Francesca Twynam<sup>1</sup>, Alice Ramsden<sup>1</sup>, Taylor Leitch<sup>1</sup>, Michael Hooke<sup>1</sup>, Per Eivind Dhelie<sup>2</sup>, Vidar Danielsen<sup>2</sup>, Arnstein Kvilhaug<sup>2</sup></u>	

<b>Sismik Yansımaya Veri İşlemi İçin Geliştirilen Yeni Bir Yazılımın (ATA-SIS) Tanıtımı</b> <u>Alican Pekiyi<sup>1</sup>, Hulya Kurt<sup>2</sup></u>	941
<b>An Acoustic Wave Equation with the Effects of Reflectivity</b> <u>Jianyong Bai, Orhan Yilmaz</u>	951
<b>Vibratör Harmonikleri - Sinyal mi Gürültü mü ?</b> <b>Vibrator Harmonics - Signal or Noise ?</b> <u>Orhan Güreli</u>	957
<b>Innovative Distributed Acoustic Sensing Technology and Applications in Borehole Seismic</b> <u>Rafael Guerra</u>	966
<b>Low Frequency Single Geophone Versus Standard Geophone Array; A Field Test Study in the SE Turkey</b> <u>Yılmaz Sakallıoğlu, Zhao Mingqiu, Chen Xin</u>	972
<b>Seismic Facies Analysis: From Basin to Prospect, From Visualisation to Value</b> <u>Simon Mann<sup>1</sup>, James Ostrikoff<sup>2</sup>, Stefane Gesbert<sup>3</sup></u>	979
<b>Planning and Execution of A Horizontal Well in Southeast Anatolian Field: Advanced Processes and Technologies for Drilling and Logging</b> <u>Ishan Kaya<sup>1</sup>, Davide Di Tommaso<sup>2</sup>, Inan Sare<sup>2</sup>, Shahbazi Kaveh<sup>2</sup></u>	985
<b>Experimental Investigation of the Effect of Type And Concentration of Polymers On The Rheological Properties Of Drilling Fluids</b> <u>Mehmet Soylu</u>	992
<b>A Synopsis on Pressure-While-Drilling Applications</b> <u>Korhan Kor</u>	998
<b>Mature Field Development by Means of Rotary Steerable System and Reservoir Navigation Services. Turkey</b> <u>Paolo Sudiro<sup>1</sup>, Melike Özkaya Türkmen<sup>2</sup>, Elif Cihan Yıldırım<sup>2</sup>, Batur Alp Aydın<sup>2</sup></u>	1007
<b>Paleo-Fayların 2023 Depremlerindeki Rolü ve Petrol Havza ile Yapılarına Etkisi</b> <b>The Role of Paleo-Faults in the 2023 Earthquakes and Their Effects on the Oil Basin and its Sturcture</b> <u>Doğan Perinçek</u>	1015
<b>Hoya Formasyonu'nun Petrol Sistemi</b> <b>Petroleum System of Hoya Formation</b> <u>Deniz Atasoy<sup>1</sup>, Aynur Geçer Büyüktutku<sup>2</sup>, Arzu Aktosun<sup>3</sup>, Fevzi Mert Türesin<sup>3</sup>, Hüsnü Çorbacıoğlu<sup>3</sup></u>	1028
<b>Imprints of Late Paleozoic-Early Mesozoic Tethyan Evolution in The Northern Arabian Plate (SE Turkey) and Its Role in The Paleozoic Petroleum System</b> <u>Gökay Yıldız</u>	1039
<b>Overcoming Complex Flow Assurance Issues with Respect to Gas Hydrate Formation in Deep-Water Well Testing Operations</b> <u>Yakov Shumakov, Ozgur Karacali</u>	1047
<b>Single Configuration Enables Seamless Workflow From Cleanup to Extended Well Test and to Production in a Harsh Environment</b> <u>Symon Thomas Shields</u>	1054
<b>ESP Malzeme Kullanım Ömürlerinin (Runlife) Adıyaman, Diyarbakır ve Batman Bölgelerinde İncelenmesi</b> <b>Investigation of ESP Equipments Runlife in Adıyaman, Diyarbakir and Batman Regions</b> <u>Ayhan Budak</u>	1056
<b>Wireless Monitoring of Artificial Lift Wells – Techno-Commercial Feasibility of GEOEM Wireless Well Monitoring</b> <u>Aastik Saluja, Nick Nazarovs</u>	1063
<b>Integrated Artificial Lift Optimization Workflow And New Technologies Implementation Helps Improving Reciprocating Rod Pumping Performance on Heavy Oil Fields, Onshore Romania</b> <u>Gheorghe Ditoiu, Vasile Mogos</u>	1068



---

<b>Açık Deniz Gaz Kuyularında Kum ve Su Kontrolü için Uygulanabilen Bazı Kimyasal Yöntemler</b> <u>Nazan N Topgüder</u>	1079
<b>Machine Learning Assisted Forecasting of Field Performance: A Case Study</b> Emre Artun <sup>1</sup> , Serhat Canbolat <sup>2</sup> , Elif Cihan Yıldırım <sup>2</sup> , Cansu Açıkgoz <sup>2</sup> , Onur Yürüker <sup>2</sup>	1087
<b>Determining Hydrocarbon-Bearing Volcanic Sediments using Neural Network Method Based NPHI Cubes: A case Study</b> <u>Nur Göçer Ersay</u> , Musa Çetin	1095
<b>Leveraging Edge Computing with Artificial Intelligence and Machine Learning for Subsurface Assets</b> <u>Afife Gozde Celik</u> , Ratish Kumar Selvaraj	1099
<b>Prediction of Flow Rates from Using Plt p-T Measurements in a Horizontal Well By Machine Learning Methods</b> <u>Muharrem Hilmi Çevik</u> , Murat Çınar	1104
<b>Quantitative Interpretation Using Rock Physics Driven Convolutional Neural Network</b> <u>Ufuk Durmuş</u>	1114
<b>Implementing Adaptive Neuro-Fuzzy Inference System for Analysis of Heavy Oil Behavior Through Magneto-Rheology</b> <u>Uğur Özveren</u>	1118
<b>AI Seismic Interpretation: A Deeper Understanding of the Subsurface</b> <u>Luis Gomez Martinez</u> , Abdulqadir Cader, Ryan Williams, Peter Szafian	1121
<b>Leveraging AI in Automating Geophysical Feasibility Studies: A Leap Forward in CCS Monitoring</b> <u>Mehdi Paydayesh</u> , Amir Shamsa, Maria Perezhogina	1125
<b>Yapay Zeka ile Sismik Hız Modellerinin Doğrudan Kestirimi: Eğitim Veri Seti ve Derin Ağ Eğitimi</b> <u>Mojtaba Najafikhatounabad<sup>1</sup></u> , Hacer Yalım Keleş <sup>2</sup> , Selma Kadioğlu <sup>1</sup>	1129
<b>A Deep Dive Into The Black Box of Artificial Intelligence</b> <u>Orhan Kurt</u>	1134

- Babadağ ( Denizli ) Metabazik Birimlerinin Petrojenetik Karakteristikleri** 1145  
Cihan Çolak, Ali Kaya
- Complex Characterization Through Logging Data of a Heterogenous Faulted Zone** 1152  
Constantin Laurian Ciuperca, Vladimir Andrei Hanumolo
- The Magnetotelluric Method in Geothermal Exploration: Case Studies** 1159  
Nikita Zorin<sup>1</sup>, Dmitrii Epishkin<sup>1</sup>, Denis Yakovlev<sup>2</sup>, Andrey Yakovlev<sup>3</sup>, Nikolay Palshin<sup>4</sup>
- Organofacies and Paleo-depositional Environment of the Northeast Java Basin, Indonesia: Hydrocarbon Generation and Expulsion Potentials Based on Hydrocarbon Geochemical Analysis** 1167  
Syahronidavi Al Ghifari
- Distribution Of Terpane and Sterane Biomarkers as Indicators of Organic Matter Input and Depositional Environments in Eocene Sediments Around Zara and Bozbel (Sivas-Türkiye)** 1171  
Nazan Yalçın Erik
- COVID-19 Pandemisinin Türkiye'deki Enerji Tüketimine Etkisi** 1179  
Kıvanç Peker
- Küresel Enerji Talebinin Arktik Deniz'indeki LNG Gemi Trafikine Etkisi** 1189  
Arzu Bal, Ersan Başar
- Optimizing Oil Production in Naturally Fractured Carbonate Reservoirs with Gas Coning under Gas Production Constraint** 1195  
Abdulmalik Ibragimov<sup>1</sup>, Kamshat Ussenova<sup>2</sup>, Murat Zhiyenkulov<sup>2</sup>
- Evaluation of Paleo-depositional Environment Properties of Miocene coals of Divriği-Selimoğlu Region (Sivas-Türkiye) Using Organic Geochemical and Organic Petrographic Properties** 1199  
Harun Çakır, Nazan Yalçın Erik
- A New Depositional and Stratigraphic Framework for Jurassic Marrat Formation: Implications in Reservoir Management in Greater Burgan Field, Kuwait** 1203  
Bashar Alenezi<sup>1</sup>, Kalyan Datta<sup>1</sup>, D. Saucier<sup>2</sup>, L. Faisal<sup>2</sup>, R. Former<sup>2</sup>
- An Example of Seismic Interpretations on Listric Faults; Gulf of Gökova, Dağca Fault** 1211  
Yeliz Mert, Damla Doğan, Hülya Kurt
- Hesaplanmış Yansıma Katsayısı Değerleri Kullanılarak 2-B Sentetik Sismik Kesitin MATLAB Yazılımı ile Oluşturulması** 1215  
Mehmet Mert Doğu<sup>1</sup>, Altay İsa Tok<sup>1</sup>, Göktürk Mehmet Dilci<sup>2</sup>, Rahmi Mert Bolat<sup>2</sup>, Fatih Özdamar<sup>2</sup>
- Predicting Shear Stress in Heavy Crude Oil Using Random Forest Analysis of Magneto Rheological Behavior** 1221  
Uğur Özveren



**Alışılmadık Hidrokarbon Kaynakları**  
*Unconventional Hydrocarbon Resources*

---



# Alışılmadık Hidrokarbon Kaynak Aramacılığında Dünya’da ve Türkiye’de Yapılan Çalışmalar

**Ahmet Ergün Mengen, Canalp Özkul, Mehmed Ekrem Yazaroğlu, Sezer Sevinç**  
Türkiye Petrolleri Anonim Ortaklığı



Sanayi devrimiyle buharlı makinelerin icad edilmesi, gelişen ülkeleri sürekli bir enerji kaynağı arayışına sürüklemiş ve enerji hammaddesi olarak kömür; endüstriyel üretim makineleri ve ulaşımda lokomotif ağırlarına güç vermek için yüzyılı aşkın bir süre kullanılmıştır. 19. asrın ikinci yarısından itibaren petrol ve doğal gaz üretimi ticari olarak artan bir hacimde devam etmekte olup sosyal hayatın her alanında hem enerji kaynağı ve hem de mamül üretim süreçlerinde kullanılmaktadır. Dünyada artan nüfus ve yükselen hayat standartları, petrol ve doğal gaza olan bağımlılığımızı arttırmakta olup, sınırlı rezervler ve yeni rezervlerin keşfedilmesindeki zorluklar belli dönemlerde arz sıkıntılarının yaşanmasına yol açmıştır. Sınırlı geleneksel rezervuarların tükenmesi sonucunda yerlerine yeni rezervler eklenebilmesi için petrol endüstrisi geleneksel olmayan hidrokarbon kaynaklara (şeyl petrolü, şeyl gazı, bitümlü şistler, kömür bantlarındaki metan gazı, kesif kumtaşları ve gaz hidratlar gibi) yönelmiş, maliyet etkin üretim metotlarını geliştirerek hidrokarbon kaynaklarımıza yeni kaynaklar ilave edilmektedir. Geleneksel hidrokarbon rezervuarlarından üretim, rezervuar kayaçlarının akışkana olan geçirgenlikleri makul düzeyde iyi olduğundan dikey kuyu tamamlama şeklinde gerçekleştirilebilirken alışılmadık hidrokarbon kaynak kayaçlarından üretim, genellikle hidrolik olarak çatlatılmış yatay kuyular içinden yapılabilir.

Yukarıdaki üçgende gösterildiği gibi devasa hacimde yerinde rezerve sahip alışılmadık hidrokarbon kaynak kayaçlarından üretim yapabilmek için çok daha pahalı yüksek teknolojiler kullanılarak yatay açılımlı kuyuların kazılıp tamamlanması gerekmektedir. 1980’li yıllarda kesif kumtaşları ve kömür bantlarından metan üretmek için geleneksel kazılan dikey kuyulardan hidrolik çatlatma ile ticari hacimde üretim alınarak alışılmadık kaynaklara ilgi artmış ve çalışmalar o istikamette artarak günümüze kadar gelmiştir. Şekil-1’de yer alan üçgenin sağ ve sol alt köşelere doğru yaklaştıkça üretim maliyetleri artmakta ve kullanılan teknolojiler daha karmaşık hale gelmektedir. Örneğin şeyl petrol kaynaklarından üretim yapabilmek için çok uzun yatay açılımlı kuyular kazmakla kalınmıyor, yatay kuyu boyunca kaynak kayaç içinde her yüz metrede bir çok-basamaklı hidrolik çatlatma operasyonları yapılarak kaynak kayacının iletkenliği geliştirilip gözenekli ortamda hapsolmuş hidrokarbon kuyuya atkılıp kuyu içinde kurulu pompalar yardımıyla yüzeye taşınmaktadır.

Alışılmadık (ankonvansiyonel) hidrokarbon kaynak kayaçlardan artan hacimde petrol ve gaz üretimi yapılarak özellikle Kuzey Amerika’da Şeyl Devrimi’nin kıvılcımı ateşlenmiş ve alışılmadık kaynaklardan elde edilen üretimler, geleneksel kaynaklardan yapılan günlük üretim hacimlerini de aşarak petrol ve doğal gaz üretim arz güvenliğinde çok sağlam adımlar atılmıştır.

## DÜNYA’DA ANKONVANSİYONEL HİDROKARBON ÜRETİM ÇALIŞMALARI

Üretimi nispeten kolay olan konvansiyonel petrolün azalan arzı göz önüne alındığında hızla artan enerji talepleri, petrol fiyatlarının 100 \$/varil’e dayanması ve teknolojik gelişmeler, konvansiyonel ve ankonvansiyonel arama ve üretim alanlarında petrol endüstrisini, teknik olarak geliştirilmesi ve üretimi çok daha zor olan ankonvansiyonel kaynaklara doğru yönlendirmiştir. Ankonvansiyonel rezervler aşağıdaki kaynakların tamamını kapsamaktadır:

1. Kömür yataklarındaki metan gazı (CBM),
2. Çok düşük permeabiliteli formasyonlarda kesif kumtaşı gaz kaynakları,
3. Çok düşük permeabiliteli şeyl kayaçlarında bulunana şeyl gazı ve petrolü,
4. Petrollü şeyl (ya da Bitümlü şist)
5. Katranlı kumlar (tar sands)
6. Metan hidratlar

Dünyanın ispat edilmiş 6600 + trilyon fit küp (TCF) konvansiyonel doğal gaz rezervleriyle kıyaslandığında, yukarıda sıralanan tüm ankonvansiyonel kaynaklarda bulunan gaz rezervlerinin 730000 TCF (20674 trilyon metre küp) olduğu tahmin edilmektedir.1-3 Benzer bir şekilde yeryüzünde bulunan 9 ile 13 trilyon varil arasında değiştiği tahmin edilen petrol rezervinin sadece %30’u konvansiyonel petrole karşılık gelirken geri kalan %70’i ağır petrol, oldukça ağır petrol, katranlı kum ve bitümlü şistlerden müteşekkil kaynaklardan oluşmaktadır.4 İlaveten şeyl kökenli petrol kaynaklarının dünya çapında rezerv hacminin de 6 ile 8 trilyon varil arasında değiştiği tahmin edilmektedir.5

Amerikan Enerji Bilgi Ajansı’nın (EIA) 2013’de yayımladığı rapora göre dünyada teknik olarak kurtarılabılır 7299 trilyon fit küp (TCF) (yaklaşık 207 trilyon metreküp) şeyl gazı ve 345 milyar şeyl petrol kaynağı bulunduğu ifade edilmektedir.

## Amerika Birleşik Devletleri’nde Şeyl Petrol ve Gaz Potansiyeli

Sondaj Bilgi Veritabanına göre ABD’de 180 000 şeyl kuyusundan üretim yapılıyor olup her yıl ilave 18000 kuyu kazılarak ankonvansiyonel kaynaklar ekonomiye kazandırılmaktadır. Şu anda ABD’de teknik olarak kurtarılabılır 665 TCF (18.83 trilyon metreküp) şeyl gazı ve 58 milyar varil şeyl petrol kaynağı bulunmaktadır. ABD’de 11 farklı şeyl baseninde kuyular kazılmaya devam edilip ankonvansiyonel üretim yapılmaktadır. Üretim yapılan basenler; başlıca Barnett, Marcellus, Fayetteville, Woodford, Haynesville, Bakken, Eagle

Ford, Niobrara, Utica, Wolfcamp ve Monterey olarak sıralanabilir.

ABD’de ankonvansiyonel aramacılığın geçmişi 1970’li yıllara kadar uzanmakta 1980’lerde saha geliştirme çalışmaları yoğunlaştırıldıktan sonra meyveler 2000’li yıllardan sonra alınmaya başlanmıştır.

Şekil 2’de gösterilen ankonvansiyonel petrol üretim eğrisine gene ankonvansiyonel kaynaklardan üretilen kondensat debisi de ilave edilmiştir. Şeyl basenlerinden 2022 yılında günde ortalama 8.5 milyon varil petrol ve 2 milyar metreküpü aşkın gaz üretim debilerine ulaşılmıştır. Şekil 3’te ise konvansiyonel ve ankonvansiyonel basenlerden üretilen petrol debileri kıyaslanmaktadır. Her iki eğride üretilen ham petrole, gene aynı kaynaklardan üretilen kondensat ve gazın petrol eşdeğerleri de ilave edilmiştir. 2011 yılından sonra ankonvansiyonel petrol ve gaz üretimi konvansiyonel üretimi geçmiş ve konvansiyonel kaynaklardan elde edilen üretim zamanla azalırken ankonvansiyonel kaynaklardan üretim sürekli bir artış eğilimi göstermeye devam etmektedir.

### Çin’de Şeyl Petrol ve Gaz Potansiyeli

Çin’de müstakbel yedi basende mebzul miktarda şeyl petrolü ve gazı bulunmaktadır. Bunlar; Sichuan, Tarim, Junggar, Songliao, the Yangtze Platform, Jianghan ve Subei basenlerinden oluşmaktadır. Çin’de teknik olarak kurtarılabilir 1115 TCF (31.6 trilyon metreküp) şeyl gazı olduğu tahmin edilmektedir ki bu rezerv denizel ve göl birikintileri oluşmuş şeyl kaynak kayaçlarında bulunmaktadır. Bu rezervin 626 TCF’lik (17.73 trilyon metreküp) kısmı Sichuan baseninde, 216 TCF’lik (6.12 trilyon metreküp) kısmı Tarim baseninde, 36 TCF’lik (1.02 trilyon metreküp) kısmı Junggar, ve 16 TCF’lik (453 milyar metreküp) kısmı da Songliao baseninde bulunmaktadır. İlave olarak teknik kurtarılabilir 222 TCF’lik (6.29 trilyon metreküp) şeyl gaz kaynağı da daha küçük ama yapısal olarak karmaşık Yangtze Platform, Jianghan ve Subei basenlerinde bulunmaktadır.

Çin’de jeolojik olarak iyi tanımlanamayan oldukça fazla şeyl petrol potansiyeli olduğu düşünülmektedir. Junggar, Tarim ve Songliao basenlerinde yerinde şeyl petrol kaynağı 643 milyar varil olup bunun sadece 32.2 milyar varillik kısmı teknik olarak kurtarılabilir bir rezervdir. Çin’deki şeyl petrol kaynakları daha çok parafinik petrol barındırmakta olup çoğunlukla göl çökelti alanlarındaki yüksek kil mineralli şeyller olduğundan hidrolik çatlatma açısından çok tercih edilmeyen kaynaklardır.

Şekil 4’te görüldüğü gibi ankonvansiyonel basenlerden elde edilen petrol ve gaz üretimi son yirmi yılda istikrarlı bir şekilde artmaktadır. 2022 yılında şeyl basenlerden günlük ortalama 660 bin varil petrol ve 205 milyar metreküp doğal gaz üretilmiştir. Şekil 5’te de konvansiyonel formasyonlardan yapılan üretimle şeyl basenlerinden elde edilen üretimler kıyaslanmaktadır. Her iki eğride üretilen gazın petrol eşdeğeri de petrol üretim debilerine dahil edilmiştir.

### Arjantin’de Şeyl Petrol ve Gaz Potansiyeli

Arjantin, başlıca Neuquen baseni içinde olmak üzere Kuzey Amerika dışında birinci kalite muhtemelen en verimli şeyl gaz ve petrol potansiyeli bulunduran ülkedir. Ek olarak test edilmemiş diğer sedimanter havzalarda şeyl kaynak potansiyeli vardır. Neuquen baseni içinde bulunan Los Molles ve Vaca Muerta formasyonlarında kalın, organik maddece zengin denizel ortamda çökelmiş siyah şeyller bulunmaktadır. Bu formasyonlardan üretim yapılmaktadır. Arjantin, 3244 TCF (91.87 trilyon metreküp) hacimde yerinde şeyl gaz potansiyeline sahip olup bu rezervin 802 TCF’lik (22.71 trilyon metreküp) kısmı teknik olarak kurtarılabilir kaynak olduğu tahmin edilmektedir. Yerinde şeyl petrol potansiyeli 480 milyar varil olup bu kaynağın 27 milyar varillik kısmı teknik olarak kurtarılabilir görülmektedir.

Son 20 yılda yapılan saha geliştirme ve rezerv ekleme çalışmaları neticesinde 2010 yılından itibaren ankonvansiyonel kaynaklarda elde edilen petrol ve gaz üretimi hissedilir bir şekilde artmış, konvansiyonel kaynaklarda yaşanan üretim kaybı dengelenmiştir. Şekil 6’da gösterildiği gibi 2022 yılında şeyl basenlerinden günlük ortalama 250 bin varil petrol ve 70 milyon metreküp gaz üretilmiş ve üretim artışı yeni kazılan ve tamamlanan kuyularla beraber artış eğilimini sürdürdüğü izlenmektedir. Şekil 7’de görüldüğü gibi konvansiyonel rezervuarlardan yapılan üretimler günlük ama yıllara sari olarak şeyl kaynaklardan elde edilen hidrokarbon üretim debileriyle kıyaslanmaktadır. 2004’ten itibaren konvansiyonel rezervlerden üretim sürekli bir azalış eğilimi gösterirken 2012 yılından itibaren şeyl kaynaklardan elde edilen üretimin zamanla istikrarlı bir artış göstermesi, günlük toplam üretim kaybını minimize ederek ülkenin hidrokarbon üretim kapasitesini olumlu yönde dengelemiştir.

Türkiye’de Şeyl Petrol ve Gaz Potansiyeli: Türkiye Güneydoğu Anadolu bölgesinde Dadaş formasyonuna yönelik olarak gerçekleştirilen arama faaliyetleri 2010 yılında başlamıştır. 2011 yılında Shell firması ile imzalanan Ortaklık Anlaşması gereğince Diyarbakır ili civarında K-1 ve A-1 kuyuları açılmıştır. K-1 kuyusunda 500 metrelik yatay sondaj yapıp 5 kademe hidrolik çatlatma operasyonu gerçekleştirilmiştir ve akabinde yapılan üretim testlerinde yüksek graviteli (42 API) petrol elde edilmiştir.

Türkiye Petrolleri olarak Dadaş Formasyonuna yönelik G-1 arama kuyusu 3001 m’de dikey kuyu olarak bitirilmiştir. Pilot kuyudan gelen veriler neticesinde yatay kuyunun açılacağı derinlik belirlendikten sonra yatay kuyu sondajına 5 Haziran 2019 da başlanıp 20 Temmuz 2019 tarihinde bitmiştir. Toplamda 1031 m uzunlukta yatay kuyu (Türkiye’de kazılan en uzun yatay kuyu) olacak şekilde son derinliği 4017 m’de bitirilmiştir. Tamamlanan sondaj faaliyetlerinden sonra G-1 yatay kuyusunda 10 kademeli hidrolik çatlatma operasyonu yapılmıştır. Bunu takiben geri akış testlerinde 35 API graviteli petrol alınmıştır.

Ayrıca 2014 yılında sondajı tamamlanan ve Petrol Emareli Sulu Kuyu olarak terk edilen B-1 kuyusunda

yapılan 373 m derinleştirme sondajı ile kuyunun son derinliği 3255 m olarak bitirilmiştir. Bu kuyuda Dadaş Formasyonu ve Bedinan Formasyonlarında olmak üzere 2 kademeli çatlatma operasyonu yapılmıştır.

Dadaş Formasyonuna yönelik alışılmadık hidrokarbon potansiyelin belirlenmesine yönelik olarak Dadaş yayılım baseni içerisinde yer alan daha önce açılmış kuyularda petrol üretim potansiyelini keşfetme amaçlı dik kuyuda yapılacak hidrolik-çatlatma operasyonu için Dadaş Formasyonunda 10 adet hidrolik çatlatma operasyonuna karar verilmiştir. Basenin çeşitli yerlerinde bulunan bu kuyuların çatlatma operasyonları tamamlanmış ve geri akışlara başlanmıştır. Mevcut veriler ışığında basende dik kuyu ve yatay kuyu prospektleri verilmesi planlanmaktadır.

Trakya Baseni'nde, havzanın şeyl gaz ve kesif kumtaşı gazlarına yönelik potansiyel belirleme faaliyetleri 2015 yılından beri devam etmektedir. 2015 ve 2018 yıllarında yapılan Hamitabat Formasyonu kaynak kaya seviyesine yönelik yapılan sondajlar jeolojik olarak olumlu sonuç vermiş fakat akabinde yapılan hidrolik çatlatmalar yüksek çevresel stresler nedeni ile tam olarak başarıya ulaşamamıştır. Bunun üzerine çalışmalar kesif kumtaşları (tight sand) üzerine yoğunlaşmıştır.

2019 yılında açılan Orta Eosen yaşlı Hamitabat Formasyonu hedefli kuyular ile kesif kumtaşı (tight sand) sahası keşfi yapılmıştır. 2019 yılından bu yana Soğucak Formasyonu Değirmenköy üyesi ve Osmancık Formasyonlarında çeşitli kuyularda hidrolik çatlatmalar yapılmış ve üretime alınmıştır. Bugüne kadar kümülatif gaz üretimi 71 milyon m<sup>3</sup> olmuştur. 2023 yılında ise Mezardere Formasyonu Teslimköy üyesi kumtaşları çatlatılarak ilk defa kesif kumtaşı petrolü üretimine başlanmıştır.

Bu kapsamda Güneydoğu Anadolu'da Dadaş Formasyonu ve Trakya Bölgesinde Hamitabat, Soğucak, Mezardere ve Osmancık Formasyonlarının kesif kumtaşı seviyelerinde jeolojik, jeofiziksel, petrofiziksel ve jeomekanik olarak analizler devam etmekte olup eş zamanlı olarak hidrolik çatlatma operasyonları da devam etmektedir.

### **Türkiyede Alışılmadık Hidrokarbon Arama Projeleri**

Dadaş formasyonunun potansiyelinin belirlenmesi amacıyla formasyonun yayılım alanı içerisinde rezervuar özellikleri 3 boyutlu olarak sismik rezervuar karakterizasyon yöntemiyle çalışılmıştır. Dadaş Projesinde kullanılan sismik veriler farklı yıllarda elde edilen ve işlenen çeşitli 3B ve 2B sismik hattı içermektedir (Şekil9).

Rezervuar karakterizasyonu çalışmasında 3 boyutlu sismik veriler çeşitli analizler için kullanılmıştır:

1. Yapısal yorumlama ve rezervuar haritalama
2. Doğal çatlak dağılımını gösteren atribütelerin çıkartılması
3. Elastik parametreler, mineral bileşimi, organik madde içeriği, gözeneklilik gibi rezervuar kalitesini

ve üretkenliğini kontrol eden bazı temel özellikler arasındaki ilişkiyi anlamak. Kuyular arası rezervuar özelliklerinin belirsizliğini tahmin etmek için

4. Ayrık doğal çatlak ağı modellemesi (DFN) için sismik verileri ve logları kullanmak

5. Gözeneklilik basıncı analizi ve dağılımı için 3D sismik kapsama ve sismik inversiyonun gücünü kullanmak

Dadaş yayılım alanı içerisinde planlanan yeni kuyu prospektlerini oluşturmak, mevcut rezervi değerlendirmek ve hidrolik çatlatma operasyonlarını başarılı şekilde yapmak için bölgenin tamamını kapsayacak bir statik jeolojik modelin yapılmasına başlanmıştır. Dadas-1 formasyonunun jeolojik modellemesi, toplam havza yüzeyinin %75'ini kaplayan 7 sismik alanda yorumlanan faylar, Dadas-1 ve Bedinan Formasyonu sismik yorumlarına dayanılarak yapılmıştır. Yapısal model oluşturulurken bölgede mevcut olan 66 kuyudan edinilen datalar kullanılmıştır (Şekil 10).

Dadas-1 formasyonunun dinamik simülasyon modellemesi için kullanılacak 3 boyutlu statik modeli detaylandırmak için kullanılan statik modelleme iş akışı.

Yapısal modellerin oluşturulmasında Dadas-1 ve Bedinan Formasyonu girişlerinin sismik yorumları ve faylar kullanılmıştır. Tamamlanan 7 statik modelde toplam 204 fay yorumlanmıştır.

Çalışma alanında tamamlanan yapısal modeller üzerinde petrofiziksel modellerden elde edilen toplam gözeneklilik, efektif gözeneklilik ve su doymuşluğu gibi rezervuar parametreleri Dadaş-1 için 3B olarak modellenmiştir (Şekil 11).

Ayrıca hacim hesaplaması 3 boyutlu modeller üzerinde yapılmıştır. Hacim hesaplamasının bir parçası olarak model için bir petrol su dokanağı oluşturulması gerekmektedir. Dadas-1 bir şeyl rezervuarı olduğundan serbest su dokanağı mevcut değildir. Dadas-1 formasyonunda hacim hesaplaması yapmak için Bedinan Formasyonu yüzeyi kullanılarak bir dokanak oluşturulmuştur. Rezerv hesaplamasında PHIT, Sw, Bo=1,6 ve geri kazanım faktörü 0.007 olarak kullanılmıştır (Tablo 1).

### **SONUÇ**

Alışılmadık (ankonvansiyonel) kaynaklar, girişte grafiklerle gösterildiği gibi Amerika Birleşik Devletleri ve Arjantin'de geleneksel hidrokarbon kaynaklarından elde edilen üretimi aşmış ve gerçekleşen şeyl devrimi, dünya üzerinde benzer kaynaklara sahip diğer ülkeler nezdinde dikkatlice takip edilmekte olup ilham verici bir başarı olarak addedilmektedir. Örnek olarak ABD'deki şeyl devrimini mercek altına alırsak bu alanda yapılan ilk deneme çalışmaların 1970'li yıllarda başladığını ve 80'li yıllardan sonra yoğunluk kazanıp alışılmadık kaynak kayaçların üretim mekanizmaları çözülüp iyice anlaşılmasıyla yoğun sondaj kampanyası ve ardından 2000'li yıllardan itibaren göz alıcı ticari üretimlerin arttığını ve devam ettiğini müşahade etmekteyiz. Buradan alınan ilhamla 2011 yılında TPAO tarafından

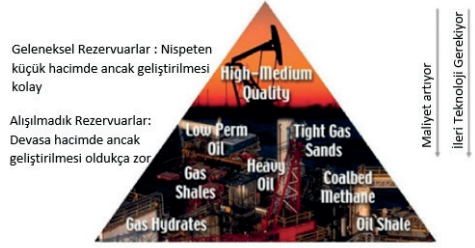
Türkiye’de ankonvansiyonel projeler başlatılmış olup Shell ile ortaklaşa ilk şeyl petrolü hedefli kuyular kazılmıştır. Türkiye’de başlıca ankonvansiyonel hidrokarbon kaynak kayaçlarımız olarak biri güneydoğu anadolu bölgesinde Dadaş baseni ve diğeri de Trakya’da Hamitabat basenini gösterebiliriz. Literatüre göre Güney Doğu Anadolu Bölgesi Dadaş baseni ile Trakya bölgesi Hamitabat basenlerinde toplam 163 TCF (4.62 trilyon metreküp) yerinde şeyl gazı olup bunun 24 TCF’i (680 milyar metreküp) teknik olarak kurtarılabilir rezerv olduğu düşünülmektedir. Gene aynı iki basende 94 milyar varil yerinde şeyl petrolü olup bunun 4.7 milyar varilinin teknik olarak üretilebilir olduğu tahmin edilmektedir. TPAO kendi rezervuar modellerini inşa etmeye devam etmekte olup anılan rezerv hacimlerini kendi veri tabanına dayanarak güncelleme çalışmalarını yürütmektedir.

## KAYNAKÇA

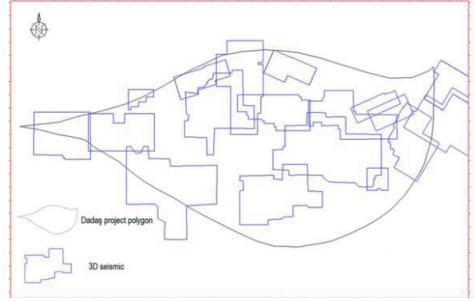
1. <http://www.eia.gov/analysis/studies/worldshalegas/>
2. Kawata, Y. and Fujita, K., Some Predictions of Possible Unconventional Hydrocarbons Availability until 2100, Society of Petroleum Engineers (SPE) paper number 68755.
3. <http://www.netl.doe.gov/kmd/cds/disk10/collett.pdf>
4. [https://www.slb.com/~media/Files/resources/oilfield\\_review/ors06/sum06/heavy\\_oil.ashx](https://www.slb.com/~media/Files/resources/oilfield_review/ors06/sum06/heavy_oil.ashx)
5. Biglarbigi, K., Crawford, P., Carolus, M. and Dean, C., Rethinking World Oil-Shale Resource Estimates, Society of Petroleum Engineers (SPE) paper number 135453.
6. Bayram Kara, Veysel Isik.,2021. “Reservoir characteristics and unconventional oil potential of Silurian aged Dadas shale in southeast Turkey.” Journal of Petroleum Science and Engineering.
7. Dilci, Gokturk Mehmet.,2019. “Investigations on influences of faults and related stress fields on naturally fractured reservoirs in Adiyaman area, Estern Turkey.” A thesis submitted to the graduate school of natural and applied sciences of Middle East Technical University. 50.
8. Nelson, Ronald A.,2001. “Geological analysis of natural fractured reservoir.”
9. Luthi, S. M. 2000. Geological Well Logs, Springer, Berlin, p373.
10. Stephen E. Laubach, Jon E. Olson, Julia F.W. Gale. 2004. “Are open fractures necessarily aligned with maximum horizontal stress?” Earth and Planetary Science Letters 222.
11. US Energy Information Administration (EIA) Report, September 2015. “Technically Recoverable Shale Oil and Gas Resources: Turkey”.

Anahtar Kelimeler: Şeyl petrolü, Şeyl gazı

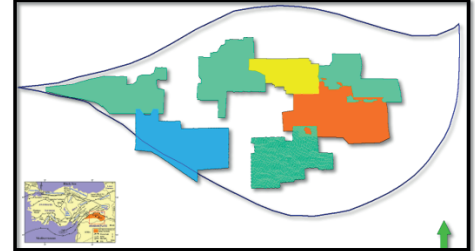
Şekil 1. Hidrokarbon Kaynak Çeşitliliği Üçgeni



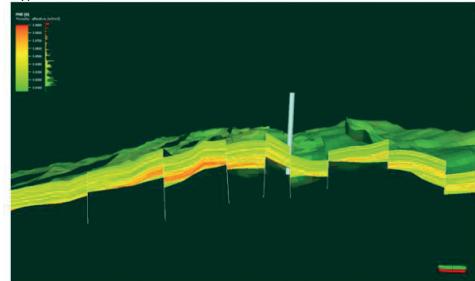
Şekil 10. Dadaş Formasyonu yayılım alanı içerisinde mevcut olan 3D sismik alanlar.



Şekil 13. Dadaş yayılım alanı içerisinde modellemesi biten 3B sismik veri alanları

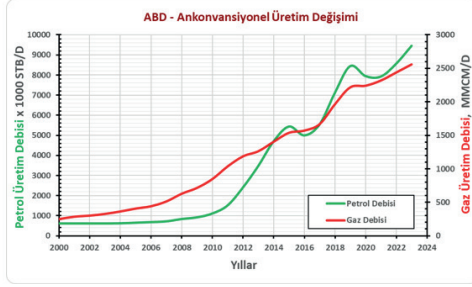


Şekil 16. Dadas Formasyonu 3B Modelinde Toplam Gözeneklilik Dağılımı Kesiti

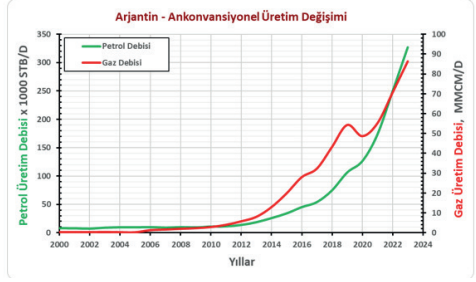




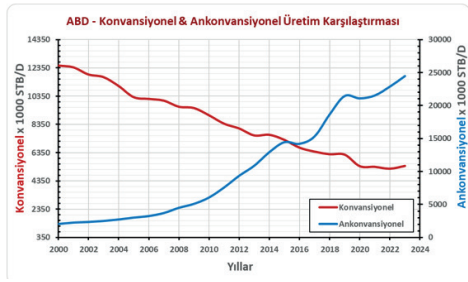
Şekil 2. ABD'de son yirmi yılda ankonvansiyonel üretim grafiği.



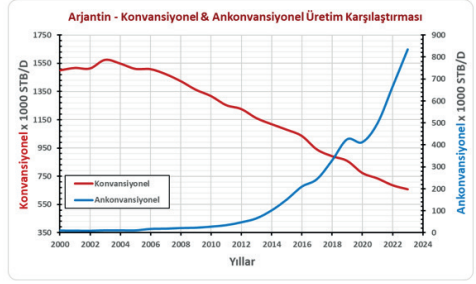
Şekil 6. Arjantin'de son yirmi yılda ankonvansiyonel üretim grafiği.



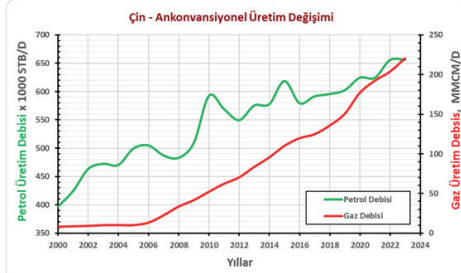
Şekil 3. ABD'de son yirmi yılda konvansiyonel ve ankonvansiyonel üretim grafiği.



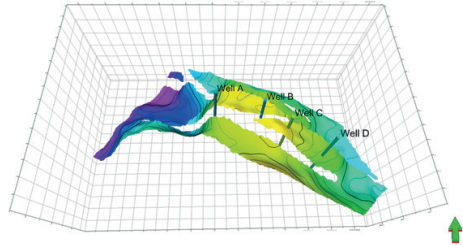
Şekil 7. Arjantin'de son yirmi yılda konvansiyonel ve ankonvansiyonel üretim grafiği.



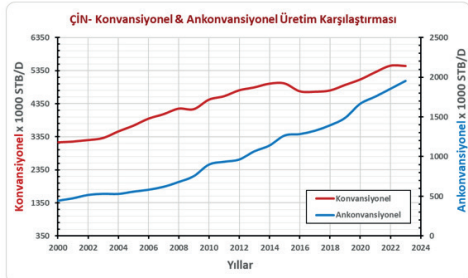
Şekil 4. Çin'de son yirmi yılda ankonvansiyonel üretim grafiği.



Şekil 9. Trakya Baseni 3B jeolojik model ve kuyu lokasyonları



Şekil 5. Çin'de son yirmi yılda konvansiyonel ve ankonvansiyonel üretim grafiği.



Tablo 1: Dadaş-1 rezerv hesaplamaları

	Bulk volume MM m3	STOHP MM sm3	STOHP MM bbl	Recoverable oil MM	Recoverable oil MM bbl
BLOK A	66 086	649	4 082	45	283
BLOK B	7 742	67	421	5	31
BLOK C	82 520	2,416	15 194	169	1 063
BLOK D	14 892	32	201	2	13
BLOK E	54 577	253	1 591	18	113
BLOK F	42 062	873	5 490	61	384
BLOK G	42 150	574	3 610	40	252
7 Blocks	310 029	4 864	30 590	340	2 138

# Petroleum: How Long More, How Much More

**Salih Saner**

Near East University, Engineering Faculty, Nicosia / North Cyprus



## ABSTRACT

As conventional hydrocarbon reserves decrease in time, exploring and exploiting unconventional hydrocarbons using new technologies extends the life of fossil fuel utilization. Besides being most important primary energy source today the world industry and economy are dependable on petrochemical products. Simply escalation of the strategic importance of hydrocarbons will propagate further in the future.

Massive unconventional resources will become the reserves for tomorrow with evolving technology. Mature oil fields, heavy oil reservoirs, tar sands, tight oil, tight gas, shale oil, shale gas, coalbed methane, and gas hydrates each involve a particular technology for bringing them to human consumption. Assessment of recent re-coverable conventional and unconventional resources indicated 7 712 Ttbb crude oil and 15 488 Tcf natural gas. If 89.877 MMbbl/day present consumption remains at the same level, crude oil will last 235 years, and natural gas with a consumption rate of 140 Tcf/yr will last 110 years. Gas hydrates, which are not producible yet, will become a primary energy source if technological improvements are accomplished to recover methane from hydrates. At that time, the natural gas volume is expected to reach 458331.22 Tcf and natural gas's life will be prolonged 3274 years more.

## 1 INTRODUCTION

It is a fact that fossil fuels, which are said to be depleted, will be replaced by alternative sources. Fossil fuels consist of crude oil, natural gas, and coal. Oil and natural gas consumption will be faster in the next fifty years. The main reasons for this upsurge are the increasing world population, a growing share of underdeveloped countries, and the need for more energy for growing technologies and industry.

The usage rates of alternative energy sources are low compared to fossil fuels, but some renewable energy has increased rapidly in recent years. Fig. 1 shows the percentage share of each energy source in the total according to BP (2021) statistics. Currently, the energy obtained from fossil fuels is four times higher than from alternative sources. It is seen that the highest consumed crude oil decreased from 40 percent to 32 percent between 1995 and 2020. However, the use of natural gas increased from 20 percent to 24 percent. Although the advantages of using gas increase its share, it will enter a swift consumption phase after 2050.

## 2. UNCONVENTIONAL HYDROCARBON RESOURCES

Conventional petroleum exploration, drilling, and production operations are conducted with an understanding of the petroleum systems concept that includes generation, migration, entrapment, and gravity segregation. The evolving technologies promoted obtaining hydrocarbon production from unconventional accumulations.

Conventional hydrocarbons are trapped structurally or stratigraphically in a porous and permeable reservoir rock. A trap commonly spreads under an impermeable cover rock. The gravitational segregation principle is essential in conventional hydrocarbon accumulations. However, economic deposits in non-conventional reservoirs may occur in very low porosity and low permeable rocks, without structural and stratigraphic traps, and without cover rock. Most of the time, source rocks, rich in organic matter are also reservoir rocks. Production techniques are different. New developed chemical injection techniques are conducted in conjunction with horizontal drilling and hydraulic fracturing. As stated by Ma and Holditch, (2016) the production price of conventional oil was around \$28/bbl, where the cost in non-conventional reservoirs was \$40-80/bbl in 2016.

## 3. BASIC UNCONVENTIONAL RESERVOIR TYPES

Nine main unconventional reservoirs exist, 1. Mature fields, 2. Heavy oil reservoirs, 3. Tar sands, 4. Tight oil, 5. Tight gas, 6. Shale oil, 7. Shale gas, 8. Coal bed methane (CBM), and 9. Gas hydrate. Two of the first, mature fields and heavy oil reservoirs, are conventional-type accumulations, but their production requires superior Enhanced Oil Recovery (EOR) techniques. Others are intrinsic types.

### 3.1 Mature Fields

Each reservoir has an economic life. The daily production of a well increases for a while and reaches a maximum. Then the yield decreases over the years. From the time it starts to decline, it is called a mature reservoir (Fig. 2). At this stage, primary and secondary production methods are insufficient; hence advanced Enhanced Oil Recovery (EOR) methods are necessary.

### 3.2 Heavy Oil Reservoirs

Heavy oil reservoirs, like mature reservoirs, contain high residual oil that cannot produce conventionally. Heavy oils do not flow even at reservoir temperature due to their high viscosities (Fig. 3a). Their weights

range from 10 to 22.3 °API. A good example is the Batu Raman field in Southeastern Türkiye which contains 11°API oil in a carbonate reservoir.

### 3.3 Tar Sands

Tar sands are deposits containing heavy and viscous bitumen in their pores. These are formations cropping out on the surface or at very shallow depths. In association with the atmosphere, for a long geological time, light hydrocarbon molecules evaporated, but heavy molecules remained within the formation. Pore liquids contain asphalt and water. The rock matrix consists of sand and clay. A tar sand sample is displayed in Fig. 3b.

Production from outcropping tar sands can be performed by the open mining method. Shoveled sands are transported to special facilities, and oil is separated from the sand by heating and chemical treatments. Fig. 3c shows an open tar-sand mining pit in Alberta. Deep tar sands are exploited by in situ mining methods, of which the most common one is hot steam injection.

It is reported that the total geologic resource in the world is 3.509 Tbbbl, and the amount of oil that can be extracted is 0.449 Tbbbl. The recovery factor today is about 13 percent, but this may increase with new techniques in the coming years.

### 3.4 Tight Oil

They are compact sandstone or limestone reservoirs with very low porosity and permeability (Fig. 3d) and without a trap or cover rock. The oil they contain is a light oil with a conventional character. Production is accomplished with horizontal drilling techniques and some chemical injections following hydraulic fracturing.

The estimated geological amount of tight oil in the world is 7.853 Tbbbl. It is the unconventional hydrocarbon type with the lowest recovery factor at 3.6 percent. Accordingly, the total crude oil that can be produced is estimated to be 0.290 Tbbbl.

### 3.5 Shale Oil

Shale is a laminated sedimentary rock composed of fine-grained silt (quartz) and clay (Fig. 3e). Oil production from shale is of two types. One is shale containing abundant oil prone organic matter but did not reach enough temperature. This is oil shale which oil could be generated by heating (pyrolysis) in special plants. The other type is shale oil, produced from a source rock. Terminologically two terms are not distinct in the literature. Shale oil is produced in the Catagenesis zone, above 50°C, where temperature increases with burial. The generated oil is expelled from the shale by overburden pressure and migrates to the porous and permeable reservoir rock. A portion of the oil is confined in the shale pores and forms shale oil

Shale oil is also exploited by open mining or in situ methods. For in situ methods, horizontal drilling and

hydraulic fracturing are basic operations followed by fluid injections. Since shale is a plastic matter, brittle carbonate intercalations are chosen for hydraulic fracturing.

The average 25 percent recovery factor for shale oil is the highest among all unconventional crude oil reservoirs. The world's geological resources are 5.842 Tbbbl, and the producible reserves are 1.469 Tbbbl.

### 3.6 Shale Gas

Like shale oil, organic-rich shale forms the source rock for gas. Generation occurs in the zone of biogenesis, at a shallower depth and lower temperature (<50°C) than oil generation. There is no structural or stratigraphic entrapment for shale gas. A portion of generated gas could not be expelled during overburden and was confined within the micro matrix pores of shale and in porous kerogen. Shale gas production is also through horizontal drilling and hydraulic fracturing techniques. Open mining for gas is out of the question because the gas escapes from the outcropping formations. Geological resources of unconventional shale gas reservoirs of the world are 22 954 Tcf. Production is expected to be 5 686 Tcf with a production factor of 25 percent.

### 3.7 Tight Gas Reservoirs

As in tight oil reservoirs, these are gas-containing sandstone and limestone formations with very low porosity and exceptionally low permeability. Unlike Shale gas, it does not contain organic matter and has no source rock characteristics. Gas was formed in a source rock formation and moved into the reservoir before deep overburden and tightening took place. They are usually found in the basin depths, for this reason, they are also known as mid-basin gases.

In the production of tight gas reservoirs, horizontal drilling, hydraulic cracking, and injection methods are applied in situ. Geologically 3 355 Tcf of tight-gas is available in the world and it is assumed that 18 percent, that is 600 Tcf, is producible.

### 3.8 Coalbed Methane

In coalbed methane reservoirs, gas generation and accumulation processes are in the coal seam. Coal is both source rock and reservoir rock. Microbiologically and thermally formed gas exists in three forms. 1. In the free pores and cracks of the coal called cleats, 2. Adsorbed by the coal matrix, and 3. Dissolved in the water of the coal layer. Coal bed methane may contain small amounts of ethane, propane, and butane. There is no H<sub>2</sub>S in Coalbed methane. Coalbed methane causes firedamp explosions in coal mines. Its geological potential is 2 860 Tcf, and the recoverable amount is 1 730 Tcf. It is the unconventional gas with the highest recovery factor of 60 percent.

### 3.9 Gas Hydrates

Gas hydrate is known as burning ice (Fig. 3f). Methane gas molecules are trapped in the centers of ice crystal cages. The hydrate crystal structure is formed by high pressure and low temperature. For the occurrence of gas hydrate, temperature, and pressure must be in equilibrium. Hydrate occurrences in deep sea floors, where pressure is high, can occur at higher temperatures than in shallower depths.

Commercial gas production from oceanic hydrates has not started yet. Research seeking a feasible production procedure examines three essential Methods: 1. Reducing the pressure, 2. Increasing the temperature, and 3. Chemical injection. Promising production methods in Japan, China and USA were announced in 2013, 2017, and 2023; respectively.

When the trapped methane molecules are freed from the ice, their volumes expand under atmospheric conditions. In reservoir conditions, 1 m<sup>3</sup> gas hydrate consists of 0.8 m<sup>3</sup> water and 0.2 m<sup>3</sup> methane. When brought to the atmospheric conditions, methane expands 820 times, giving 164 m<sup>3</sup> of methane gas (Fig. 4).

The natural gas amount expected from hydrate resources of the world has been estimated using the Kvenvolden (1988) organic carbon distribution shown in Fig 5. Recoverable and nonrecoverable fossil fuels are 27 percent. If natural gas is used as organic carbon indicator, gas equivalences of crude oil and coal will allow estimation of total fossil fuel equivalence (27 percent) gas. Equivalence of 1 bbl average crude oil is 6040 Cft natural gas. Global 1074108-million-ton coal produces 2205560575 million kWh of power which is equivalent to 16217.35 Tcf of gas. 27 percent of fossil fuel totally corresponds to 233489.49 TCft gas. As a result, 53 percent gas hydrate is calculated to be 458331.22 Tcf. As such, it is 69 times the conventional gas reserves.

## 4. TOTAL CONVENTIONAL AND UNCONVENTIONAL HYDROCARBON RESOURCES OF THE WORLD

### 4.1 Amount of Crude Oil Available

The total world hydrocarbon potential has been assessed by adding up conventional reserves and anticipated producible portions of unconventional resources. Some assumptions have been applied as needed after consideration of world statistics.

The total oil reserve of the world, which designates the producible portion, is calculated as 1.732 Ttbl (BP Statistics, 2021). This amount is presumed to be 30 percent of the Original Oil In Place (OOIP). The remaining 70 percent (4.041 Ttbl) portion is residual oil (Sor) and is targeted as mature unconventional potential. Considering the consent that up to an average of 50 to 80 percent recovery could be accessed, with an appropriate EOR application. Recovery from Sor will be around 2.885 Ttbl. Eventually, conventional, and

unconventional production summation will be 4.616 Ttbl. The inaccessible 20 percent, 1.154 Ttbl, will remain underground forever (Fig. 6).

Table 1 presents geologic resources and the estimated reserves that can be produced from each (Ma and Holditch, 2016). The total geologic and producible potentials are summarized in Table 2.

### 4.2 Available Natural Gas Amount

Table 3. shows the geographical quantities of unconventional natural gas resources in the world for each reservoir type. Estimated producible reserves after Ma and Holditch (2016) are also shown in the table. The bottom rows include the gas volumes in Tcf and recovery factors. (RF) Table 4 is the assessment of future world gas potential.

## 5. CONCLUSIONS

With the new hydrocarbon discoveries, the oil will maintain its prominence in the future. In parallel with renewable energy, the exploitation of unconventional resources will continue for a longer period than earlier estimates. The life span of oil, which has become a strategic product, will depend on its wise use, the making of discoveries, and the innovation of exploitation and production technologies.

This study aimed to contribute to energy planning by interpreting the inventory of hydrocarbons of today. The existence of 29.863 Ttbl geological liquid petroleum re-sources in the world is estimated. About 7.712 Ttbl of the total is recoverable. Assuming that the current consumption rate of 89.877 MMbbl/day does not change, it is calculated that oil will last for 235 years.

Today, the world's conventional and unconventional total gas resources are about 37 472 Tcf. Estimations showed that 15 488 Tcf of this total can be produced. If the production is kept constant at 140 Tcf/yr, it can be concluded that natural gas has a life span of 110 years. Since natural gas is easier to produce and transport than liquid oil, it is more economical and more environmentally friendly, and its consumption is much faster than oil.

Gas hydrate-based methane, which is still not economically producible, has not been included in the preliminary calculations. In a previous study world estimates of natural gas in gas hydrate deposits were estimated as 706 293 Tcf (Collett, 2004). With the recent research herein another 458331.22 Tcf of natural gas from hydrate will extend gas life 3274 years more,

## REFERENCES

- BP, (2021). Statistical Review of World Energy, 70th edition.
- Collett, T. S., (2004). Gas Hydrates: Energy resource potential of Gas Hydrates, in Encyclopedic of Energy, ed. Cleveland, C.J., ISBN 978-0-12-176480-7.

Çiftci, G. (2020). Gaz Hidratlar: Yakın geleceğin enerji kaynağı. BRIQ Journal, p61-75.

Jarvie, D. M., (2012). Shale resource systems for oil and gas: Part 2— Shale-oil resource systems, in J. A. Breyer, ed., Shale reservoirs—Giant resources for the 21st century: AAPG Memoir 97, p. 89 – 119.

Kvenvolden, K.A., (1988). Methane Hydrate – A Major Reservoir of Carbon in the Shallow Geosphere. Chemical Geology, 71, 1-3, 41-51.

Ma, Y. Z. and Holditch, S. A. (2016). Unconventional Oil and Gas Resources Handbook. Evaluation and Development, 535p. Elsevier, Gulf Professional Publishing.

Merey, Ş. and Longinos, S. N. (2021) The gas hydrate potential of the Eastern Mediterranean basin, Bulletin of the Mineral Research and Exploration, Bull. Min. Res. Exp. (2019) 160: 117-13.

Tuğan, M. F. ve Yardımcı, O. (2020). 21. Yüzyılda Petrol ve Doğal Gaz Mühendisliği. Gazi Kitabevi, Ankara, Turkey.

Yaycı, C. (2012). Doğu Akdeniz’de Yetki Alanlarının Paylaşılması Sorunu Ve Türkiye. Bilge Strateji, 4 (6), 1-70. Retrieved from <https://dergipark.org.tr/tr/pub/bs/issue/3804/51021>.

Keywords: World reserves, unconventional resources

Fig. 2. Extending life of a mature well and increasing production with the application of EOR.

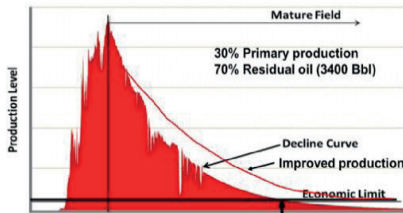


Fig. 3. Unconventional hydrocarbons: (a) Heavy oil not flowing easily due to its high viscosity; (b) A tar sand sample in which bitumen and asphalt fill the pores; (c) An open tar sand mining pit in Alberta; (d) A laminated oil shale sample and lab-



Fig. 4. 1 m<sup>3</sup> of gas hydrate produces 164 m<sup>3</sup> of methane under atmospheric conditions.

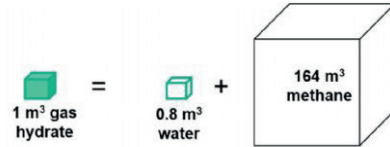


Fig. 5. Distribution of organic carbon in nature (Kvenvolden, 1988).

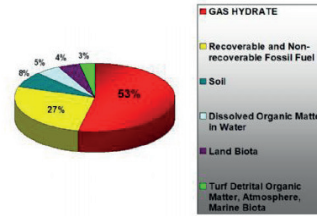


Fig. 6. The expected total production amounts from conventional, mature, and heavy oil reservoirs.

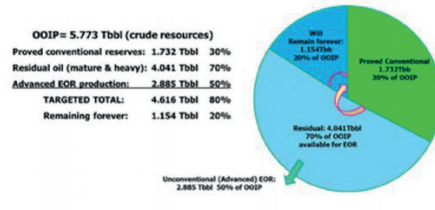


Fig. 1. Percent share of the primary world energy resources in total (BP, 2021).

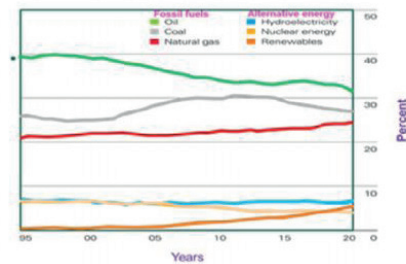


Table 1. Geologic and recoverable global resources of unconventional oil.

Unconventional Type	Geological (Tbbl)	Recoverable (Tbbl)	Recovery (%)
Heavy residual	6.888	0.887	13
Tar sand	3.509	0.449	13
Tight oil	7.853	0.290	3.6
Shale oil	5.842	1.469	25
<b>TOTAL</b>	<b>24.090</b>	<b>3.095</b>	<b>13</b>

Table 2. Geological and producible petroleum potentials of conventional and unconventional crude oil sources.

Oil Type	Amount Tbbl
<b>Total geological conventional oil resources (OoIP):</b>	<b>5.773 #</b>
Residual conventional oil (mature and heavy) 70%:	4.041
Proved (moveable) conventional reserves 30%:	1.732 *
Targeted conventionals after EOR applications) 80%:	4.616
Remaining forever 20%:	1.154
<b>Global geological unconventional oil:</b>	<b>24.090 #</b>
Total recoverable (13%) unconventional oil:	3.095 *
Advanced EOR in conventional mature reservoirs:	2.885 *
World producible unconventional oil potential:	5.980
<b>Total geological world oil resources (#):</b>	<b>29.863 #</b>
<b>Total expected producible world oil potential (*):</b>	<b>7.712 *</b>

Table 3. Geologic and recoverable global resources of unconventional gas.

Unconventional Type	Geological (Tcf)	Recoverable (Tcf)	Recovery (%)
Shale gas	22954	5686	25
Tight gas	3355	600	18
Coalbed methane	2860	1730	60
Gas hydrate	Not included		0
<b>TOTAL</b>	<b>29170</b>	<b>8016</b>	<b>28</b>

Table 4. Geological and producible potentials of conventional and unconventional natural gas re-sources.

Gas Type	Amount Tcf
Geological conventional gas reserves and resources (OGIP):	8 302 #
Residual conventional gas (20%):	1 660
Producible proved conventional gas reserves (80%):	6 642
Production (10%) from residual conventional gas:	830 *
Global geological unconventional gas:	29 170 #
Global recoverable (28%) unconventional gas:	8 016 *
Gas hydrates: Not included	458331,22
Total world gas resources:	37 472 #
The total world expected producible gas potential:	15 488 *

# Impact of Numerics on Monte-Carlo Based Type-Well Generation for Unconventional Fields



**Doruk Alp**

Petrol ve Doğalgaz Mühendisliği, ODTÜ Kuzey Kıbrıs Kampusu, Güzelyurt / KKTC

## EXTENDED ABSTRACT

For decision making purposes and to evaluate reserves, we would like to forecast production from producing, newly drilled and future wells in a field (Haskett & Brown 2005). A type-well is a representation of probabilistic production forecast for a newly drilled or future well. This representation involves multiple probable rate forecasts over time. One can use type-wells to mitigate risk of drilling a low performance well, guide required well count and drilling schedule (Minin 2011), and investment decisions. Type-wells could be generated with any method, numerical (reservoir simulation), analytical or empirical models. An overview of forecasting for oil & gas fields, and the place of type-well methodology in the overall scheme is presented as a chart in Fig. 1-1.

Underground hydrocarbon (HC) accumulations are broadly classified as conventional and unconventional. Unconventional fields are also called unconventional resources as the HC is typically produced from the source rock where it is generated, to distinguish conventional case of migration to a reservoir rock (Russel 2012). Unconventional fields in this context are tight and ultra-low permeability (0.1 – 0.001 mD) subsurface HC deposits, such as shale oil, shale gas, tight gas and coal bed methane fields (Haskett & Brown 2005).

Unconventional fields often require horizontal wells and stimulation with multiple man-made “hydraulic” fractures to produce at commercial rates (Russell et al. 2012, Ma & Holditch 2016, p3). On the other hand, in unconventional fields there is practically no interference between wells due to ultra-low permeability. This renders type-well generation based on empirical decline curve analysis (DCA) a viable tool for forecasting (Russel 2012), as well as a sense-check on more sophisticated physics-based models (Miller et al. 2017).

## MOTIVATION

Miller et al. (2020) confirms that generating type-wells is among the most important exercises for decision making in unconventional fields. While there is commercial software (e.g. IHS Harmony, or Kappa Citrine) available, because source code is not accessible, it would not be possible to implement changes to the workflow at will (there are various methodologies for type-well generation). Depending on the methodology, and to repeat the workflow numerous times with consistency, it is necessary to establish the type-well workflow in a procedural programming environment (i.e. computer code) instead of a spreadsheet environment. In this study, we develop a portable computer code for generating type-wells based on the fundamental Monte-Carlo (MC) methodology using multi-segment Arps

(MS-Arps. Fig. 3-1. Pratikno et al. 2014, Stright 1983, Arps 1945) decline curve model for unconventional field forecasting.

## RESEARCH QUESTIONS

We utilize the MS-Arps based MC simulation code developed in this study to answer following research questions:

- 1) Is there an appropriately small hyperbolic exponent  $b$  value for which Arps (1945) hyperbolic equation can practically substitute for the exponential equation.
- 2) Is there an appropriately small  $\Delta t$  value for which trapezoidal rule can substitute for analytical cumulative production (estimated ultimate recovery - EUR) equation(s).

Overall MS-Arps based type-well algorithm can be significantly simplified using only hyperbolic rate equation with an appropriate  $b$ , and the trapezoidal rule for EUR calculations. Such implementations avoid the extra-care needed for computational traps due to original equations becoming undefined at particular values of  $b = 0$  (exponential), and  $b = 1$  (harmonic). Thus, instead of having to switch analytical equations, entire algorithm can use only the hyperbolic equation but change  $b$  value for segments.

- 3) What is the impact of number of MC simulations (experiments) on generated type-wells.
- 4) What is the impact of number of samples on the uncertainty band developed in the plot of aggregation of mean type-wells from repeated MC simulations.

Taji and Alp (2021) previously observed that type-wells showed sensitivity to repeating MC experiments. However, because their implementation was spreadsheet based, high number of manual repetitions of MC simulation was not possible.

## BACKGROUND

In fact, a type-well is a set of percentile (P10-P50-P90) rate forecasts for a single newly drilled or future well in a field. It is based on data from multiple wells grouped by similar characteristics. For instance, the P10 curve implies that, there is 10% probability the production decline profile of the newly drilled/future well will look like the P10 decline curve generated by the method. Similarly, there is 10% probability the EUR will be the EUR of the P10 decline curve. Here, 10 % probability implies the expected behavior of 1 out of 10 newly drilled wells.

Neither typical type-well methodology nor the model developed herein is aimed at forecasting a single well based on its own production data (i.e. forecasting a



currently producing well). Forecasting individual well production is the subject of other methods such as numerical simulations (Fakcharoenphol et al. 2013, Alharthy et al. 2012), analytical models (Torcuk et al. 2013, Stalgorova & Mattar 2012), or probabilistic decline curve analysis (pDCA, Yehia et al. 2023, Gong et al. 2014). For general overview of pDCA, reader is encouraged to see the literature review by Yehia et al. (2023).

Numerical and analytical models can also be utilized for the probabilistic forecasting of a single well. This would require history-matching (HM) single well models with same historical production data but different subsurface characteristics to generate percentile forecasts. This is the typical probabilistic forecasting workflow.

## METHODOLOGY

The MC based EUR targeted type-well methodology is the recommended methodology in the literature, as we cited earlier in the Motivation and Background sections. This methodology can be outlined as:

- 1) Scaling & normalizing historical production data of wells that belong to a subset in the field.
- 2) Fit individual well data with Arps hyperbolic equation, extract  $D_i$  &  $b$  parameters (super-hyperbolic  $b$  for the linear transient flow regime).
- 2b) IF boundary dominated flow is observed, also extract the value of  $D$  where  $b = 0$  (exponential decline) begins.
- 3) Seek correlation between extracted DC parameters, as well as between parameters & well characteristics.
- 4) Obtain statistical distributions of  $D_i$  &  $b$ , and  $D_{exp}$  (or  $D_{lim}$  when exponential decline begins).
- 5) Randomly sample from  $D_i$  &  $b$
- 6) Co-sample if a correlation was established in step 3.
- 7) Based on sampled values, calculate EURs, and obtain the cumulative distribution curve (CDF) of EURs.
- 8) Use the  $D_i$  &  $b$  pairs resulted in the percentile EURs to construct the type-wells (i.e. percentile/P10-P50-P90 decline profiles).

Our implementation follows the same procedure beginning with step 4 above. Hence, we do not attempt to further validate the workflow itself within the frame of this study. The reason for random sampling of  $D_i$  &  $b$  parameters is to realize a probabilistic approach (which is where our workflow begins in the absence of real field data); i.e. based on the observed  $D_i$  &  $b$  parameters from actual wells in the field, what would be the  $D_i$  &  $b$  of a newly drilled well, even without actually producing this well.

Similarly, we did not utilize real field data as our purpose is to test impact of numerics which, we believe, is best observed through MMS. MMS involves using a controlled data set such as synthetic well data generated by us (i.e. the normal distributions we defined for the  $D_i$  &  $b$  parameters of the DCA). However, we used range of values from the literature:

- 1) In the absence of actual field data, we generate normal probability distributions for hyperbolic equation parameters  $D_i$  and  $b$  based on unconventional field data from the literature.
- 2) We do not generate a distribution for  $q_i$  as we assume rates are normalized by the initial rate (per discussion in the pertinent section earlier), hence  $q_i = 1$  for all wells.
- 3) We do not assume any correlation between parameters.
- 4) We assume a constant  $D_{min}$  (effective decline value) to switch from super-hyperbolic to exponential.
- 5) Randomly sample (the MC process) the distributions of  $D_i$  &  $b$  to generate pairs representing synthetic wells.
- 6) Generate DC for synthetic wells using the pairs from MC simulation.
- 7) Assume a well life of 30 years = 360 months for all wells.
- 8) Opt to use analytical equations to reduce run time For the MC process.
- 9) Calculate EURs and rates as a function of time unit (months).
- 10) Generate CDF for EURs and find P10-50-90 values, as well as the mean value.
- 11) To generate and display type-wells, plot DCs using  $D_i$  &  $b$  pairs corresponding to the percentile and mean EUR values.

To assess the impact of repetition of MC simulations following steps are added:

- 1) Repeat the MC experiment starting with a new random sampling each time.
- 2) Save data for percentile & mean EURs for each MC run.
- 3) Once total number of MC experiments are completed, plot:
  - 3a) experiment count vs mean EUR values, and
  - 3b) DCs corresponding to each mean EUR to observe spread in results.

As our goal is to evaluate impact of numerics on developing DCA based type-wells, we choose a coding environment to run the algorithm(s). Among plethora of options, we settled on python for a number of reasons, one being its availability to run online.

Although we did not utilize real field data, instead utilized a normal distribution based on parameter ranges from literature, we do not anticipate the variations in parameter ranges and distribution types to significantly change our observations on numerics. Nevertheless, such variations can easily be included in the code for a new analysis.

Within the frame of this study, we do not attempt to compare our results to commercial software, or other workflows from the literature. Different workflows were compared in an earlier study by Taji & Alp (2021). Nevertheless, according to literature, the type-well methodology used in commercial software has been the time-slice (TS) method (unless changed since then),

which is not recommended based on the issues identified (Freeborn et al. 2012 and Russel et al. 2012). For instance, using the method of manufactured solutions (MMS), Russell et al. (2012) show that percentile decline curves obtained with the TS method does not correspond to percentile estimated ultimate recovery values (EURs). Further, a type-well methodology should establish uncertain parameter(s) and probability of achieving certain values of the parameter(s). With the TS method, uncertain parameter is not clear, and uncertainty in IP or EUR is not estimated (Freeborn 2016, 2015). Besides, as actual rates from wells are utilized, it is not clear how survivor bias (skewing of results due to some wells reaching abandonment rate much earlier) can be mitigated (Freeborn 2016, 2015). Consequently, MC based EUR targeted methodology, which we implemented herein, is pioneered and recommended by the practitioners in the industry.

The type-well algorithm we implemented does not currently include a probabilistic decline curve analysis (pDCA) module, as we focus on the overall type-well workflow itself. However, a regression algorithm from ready-to-use python packages can be utilized to curve-fit DCA parameters ( $b$  &  $Di$  or  $a$ ) to single well historical data. Slight deviations from the best fit can be adopted to generate percentile curves for the single well, to complete the pDCA. Incorporating a pDCA module would alter results of the type-well methodology as the number of EUR data points would increase (we would now have 3 additional EURs for each well), and the EUR distribution itself would expand (due to added uncertainty band in calculated EURs for each well). Finding the synthetic well that corresponds to a percentile EUR (the inverse problem) will also require finding the parameter governing the deviation in DC profile as well as the  $Di$  &  $b$  pair.

## RESULTS & DISCUSSION

### Hyperbolic Exponent $b$ for Exponential Decline

By definition, decline is exponential when  $b = 0$ . Customarily, the exponential equation is utilized for the case of  $b = 0$  because hyperbolic equation is undefined for this substitution. Herein, we show that error introduced due to use of hyperbolic equation with a small  $b$  value in lieu of exponential decline is admissible for practical purposes. Per our observations during this exercise, the rate ( $q$ ) error grows with initial decline ( $Di$  or corresponding  $ai$ ) as well as time. Hence, we check the error at various  $Di$  (or  $ai$ ) values to find the  $b$  value applicable for a wider range of cases. We decide the range of  $ai$  values based on effective decline  $Di$  because  $ai$  is not bounded whereas  $Di$  is limited to range  $[0 - 1]$ . Table 6-1 suggest that a reasonable  $ai$  range to scan is  $[0.01 - 11.5]$ . In Fig. 6-1, we plot the error between dimensionless rates and dimensionless EUR values predicted by exponential and hyperbolic equations for small  $b$  values. In the pertinent calculations we assume a time unit of 1 month. Hence, 360 time units corresponds to 30 years, approximate mechanical life expectancy for

a well. Per Fig. 6-1, at the end of 30 years, dimensionless rate error grows beyond 8 % for  $ai = 11.5$  &  $b = 1.0e-8$ , which is not admissible. For  $b = 1.0e-16$ , rate error is in the range of 1.0e-6 %. For a well with  $q = 1$  MM bpd (1 million barrels per day) at the end of 30 years, 1.0e-6 % error corresponds to a mere 0.01 bpd. The error could be further reduced using an even smaller  $b$ , as long as one can increase arithmetic precision in the computing environment accordingly.

Also in Fig. 6-1, we see the plot of dimensionless EUR values calculated using exponential equation at 360 time units, for the range of  $ai$  values. In Fig. 6-1, dimensionless EUR error shows an asymptotic behavior, converging at a maximum of 1e-14 % for  $b = 1e-16$ . Considering that maximum EUR is 97 [-] for an  $ai \sim 0.01$  (Fig. 6-3), 1e-14 % error corresponds to a mere 9.70e-09 stb for a well with  $qi = 1$  MM bpd. These results confirm that hyperbolic equation can safely substitute for exponential equation with  $b \leq 1e-16$ .

### Trapezoidal Rule in lieu of Analytical EUR Equation

To determine a proper  $\Delta t$  for the trapezoidal rule, we compare calculated EURs to the analytical integral of hyperbolic equation. The range of expected  $ai$  values are established in Table 6-2 for  $b$  parameters typical for unconventional fields. Fig. 6-4a (left hand side) shows the error % in 30 year (360 time unit) EUR due to using trapezoidal equation in lieu of the integral of hyperbolic equation. We see that error can be as large 0.5 % for  $b \sim 0$  with  $dt = 1e-2$  for trapezoidal equation. When we set  $dt = 1e-3$ , we see that error % decreases 2 orders of magnitude in Fig. 6-4b (right hand side).

Also according to Fig. 6-4, EUR error grows with increasing  $ai$ , and decreasing  $b$ . Dimensionless EUR for the largest 0.005 % error is 0.04 volume units. For a well with  $qi = 1$  MM bpd,  $ai = 25$  and  $b \sim 0$  this EUR corresponds to 40 Mstb. Thus, 0.005 % error corresponds to a mere 0.4 stb. Consequently, it is safe to conclude that calculating EURs with trapezoidal equation is admissible for  $dt = 1e-3$  &  $b = [0-4]$ .

### Impact of Number of Experiments

The foundation of MC based type-well methodology is random sampling of parameters governing decline curve. In theory, if we were to sample primary probability distributions sufficiently large number of times, we should replicate the same distribution in the (secondary) distributions observed after sampling. In that case, if entire experiment was to be repeated, no variation in resultant type-wells is expected, as long as primary distributions remain the same. To assess if repeating the MC experiments has an impact on the resultant type-wells, and how number of samples impact such variation in type-wells, we carry out numerous MC repetitions using the code developed in this study.

We use normal (Gaussian) distributions for parameters  $Di$  and  $b$  as presented in Table 6-3. Fig. 6-5 shows the secondary distributions in cumulative density plots

(CDFs) after truncated (reject negatives) sampling in abundance and keeping 999 & 9999 of the samples, respectively. Fig. 6-6 is the representation of both data sets in a normal quantile (Q-Q) plot. Here, we see that the case of 9999 samples provides a distribution closer to the normal distribution (covering more of the diagonal line), per our expectations.

In the second stage of this exercise, we repeat the M-C experiments 100 times for 999 & 9999 samples. EUR distribution and type-wells generated for the first M-C experiment with 999 samples is provided in Fig 6-7. Fig. 6-8 (top row) shows plot of experiment number vs mean EUR value. We see that with increased number of samples, mean EUR spread is in fact reduced. When we look at Fig. 6-8 (lower row) which is aggregation of mean type-wells from all the MC experiments, we see a band of uncertainty develops for earlier rates and gradually diminishes with time (only due to wells declining). Yet, we do not observe any significant reduction in the uncertainty band based on number of samples.

## CONCLUSIONS

In this study, we developed a portable computer code for generating type-wells based on the fundamental Monte-Carlo methodology using multi-segment Arps (Stright 1983, Arps 1945) decline curve model for unconventional fields. Using this code we established following answers to the research questions we set out to explore:

- 1) Our results confirm that hyperbolic equation can safely substitute for exponential equation with  $b \leq 1e-16$ , if computational precision is adjusted beyond default double precision.
- 2) We only recommend substituting hyperbolic equation for exponential equation when evaluator can control the operational precision of computational platform. Contemporary spreadsheet applications are typically limited to double precision and do not allow arbitrary precision by default, and thus should not be preferred for such substitution as sporadic results ensue.
- 3) Calculating EURs with trapezoidal equation is admissible for  $dt = 1e-3$  [time unit used in calculations], and  $b = [0-4]$ .
- 4) 100 repetitions of overall M-C experiments shows slight variations in mean EURs. Mean EUR uncertainty decreased with increased number of samples. However, the uncertainty band observed in the aggregate plot of mean type-wells for early times, did not show significant difference with number of samples.
- 5) Increasing number of M-C samples 10 fold from 999 to 9999 rendered truncated distributions closer to a normal distribution. This reduced the uncertainty band for mean EUR values from M-C experiments.

Keywords: Unconventional, Type-well

Figure 1-1: An overview of forecasting for oil & gas fields

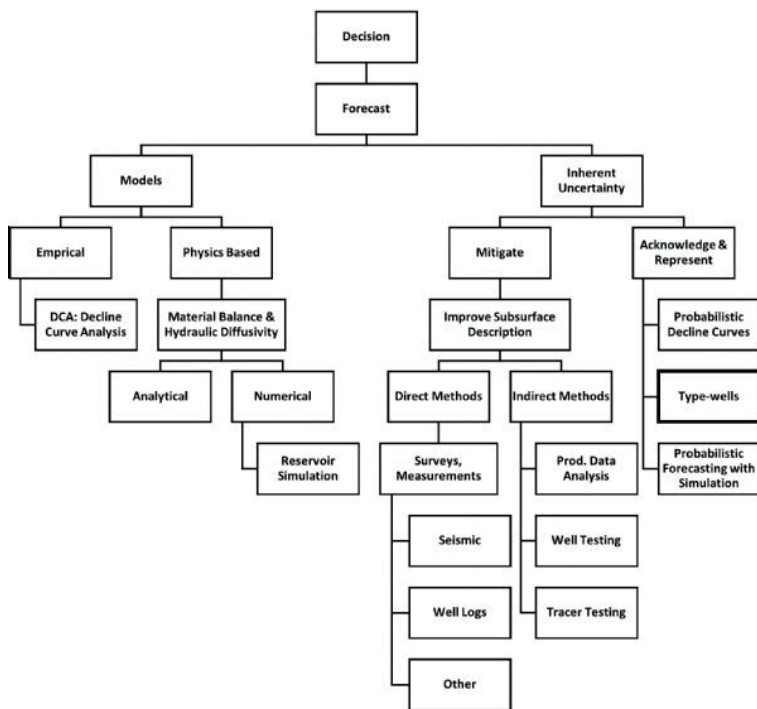


Figure 3-1: Typical Flow regimes identified on a decline curve.

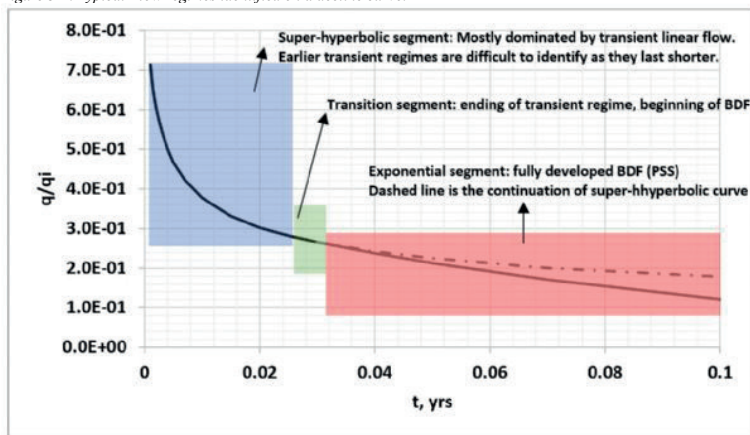


Figure 6-1: Error % using parameter b to replicate exponential decline, Di range [0.01 – 0.99999]

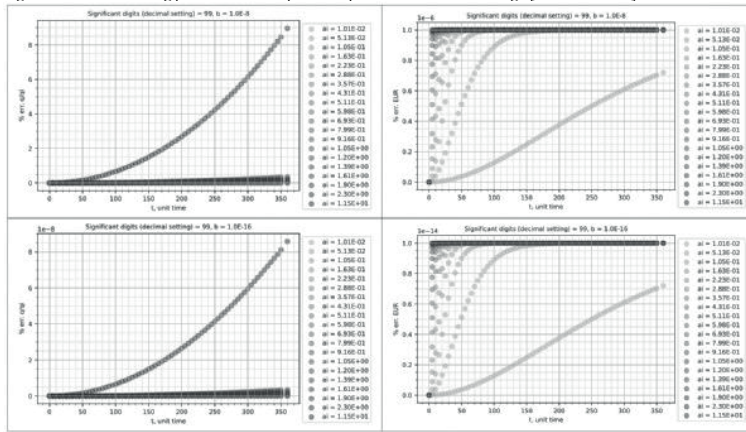


Figure 6-3: Dimensionless EURs at 360 time units, based on exponential equation, Di range [0.01 – 0.99999]

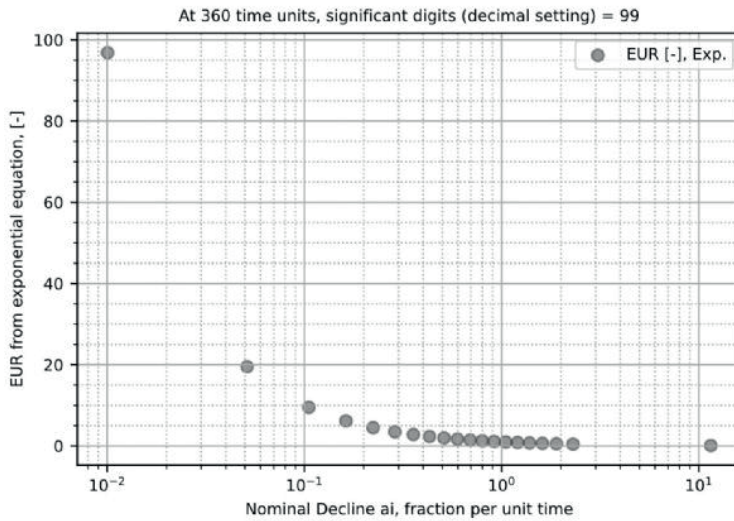


Figure 6-4: EUR error % using trapezoidal equation

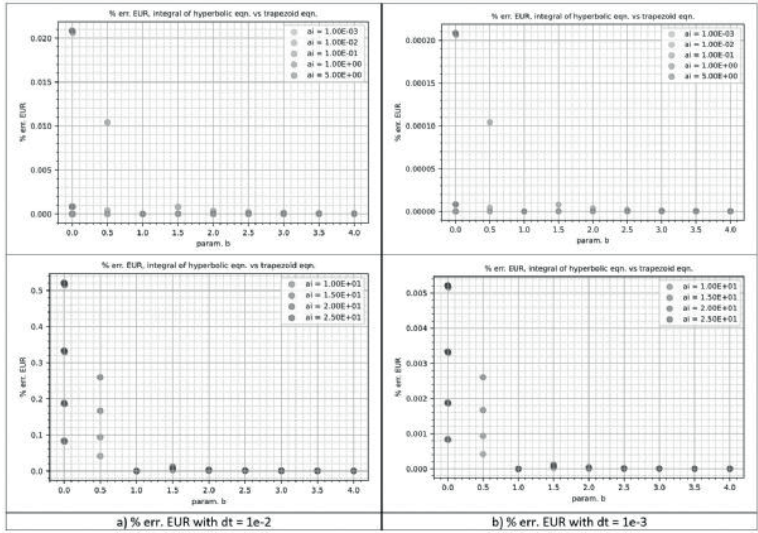


Figure 6-5: CDFs for sampled parameters  $D_i$  &  $b$  (secondary distributions).

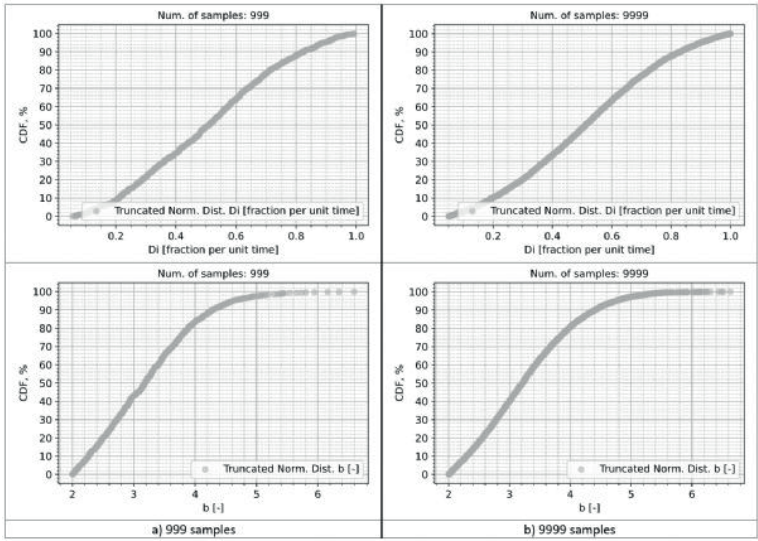


Figure 6-6: Normal Quantile (Q-Q) plots for sampled parameters  $D_i$  &  $b$  (secondary distributions).

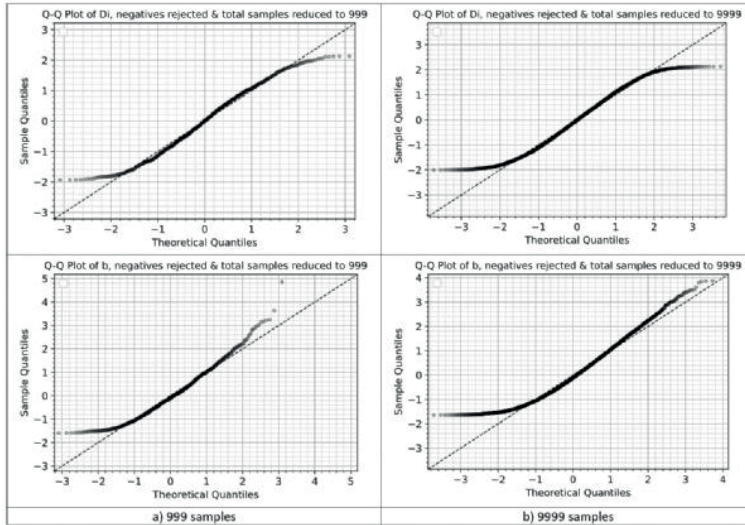


Figure 6-7: EUR distribution and type-wells generated by a single MC experiment with 999 samples

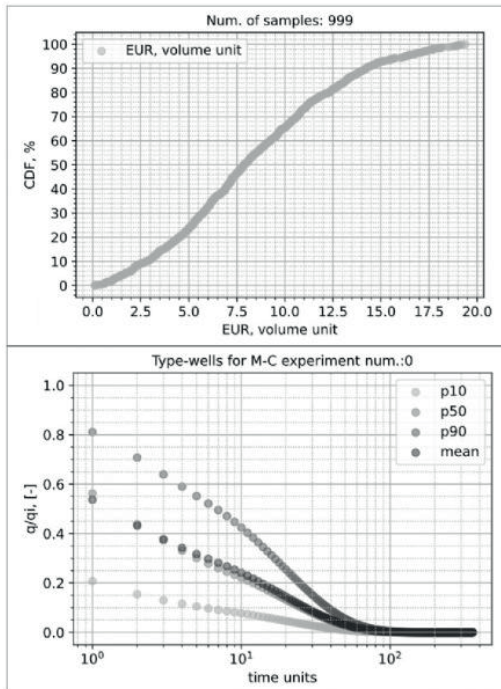


Figure 6-8: Mean EURs and mean type-wells from 100 MC experiments for 999 & 9999 samples.

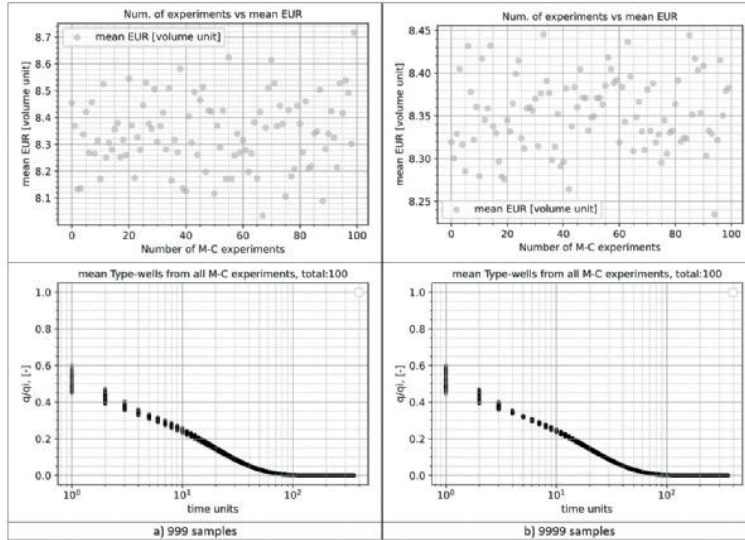


Table 6-1: Nominal decline (ai) values corresponding to Effective Decline (Di) for small values of parameter b.

b values =	1.00E-01	1.00E-02	1.00E-04	1.00E-08	1.00E-12	0.00E+00
	<b>Hyperbolic: <math>a_i = \frac{(1-D_i)^{-b}-1}{b}</math></b>					<b>Exponential: <math>a_i = -\ln(1 - D_i)</math></b>
Di values	ai values					ai values
1.00E-02	1.01E-02	1.01E-02	1.01E-02	1.01E-02	1.02E-02	1.01E-02
5.00E-02	5.14E-02	5.13E-02	5.13E-02	5.13E-02	5.13E-02	5.13E-02
1.00E-01	1.06E-01	1.05E-01	1.05E-01	1.05E-01	1.05E-01	1.05E-01
2.00E-01	2.26E-01	2.23E-01	2.23E-01	2.23E-01	2.23E-01	2.23E-01
3.00E-01	3.63E-01	3.57E-01	3.57E-01	3.57E-01	3.57E-01	3.57E-01
4.00E-01	5.24E-01	5.12E-01	5.11E-01	5.11E-01	5.11E-01	5.11E-01
5.00E-01	7.18E-01	6.96E-01	6.93E-01	6.93E-01	6.93E-01	6.93E-01
6.00E-01	9.60E-01	9.21E-01	9.16E-01	9.16E-01	9.16E-01	9.16E-01
7.00E-01	1.28E+00	1.21E+00	1.20E+00	1.20E+00	1.20E+00	1.20E+00
8.00E-01	1.75E+00	1.62E+00	1.61E+00	1.61E+00	1.61E+00	1.61E+00
9.00E-01	2.59E+00	2.33E+00	2.30E+00	2.30E+00	2.30E+00	2.30E+00
9.9999E-01	2.16E+01	1.22E+01	1.15E+01	1.15E+01	1.15E+01	1.15E+01



Table 6-2: Range of nominal decline (ai) values for typical values of parameter b observed in unconventional fields

b values =	4.00E+00	3.00E+00	2.00E+00	1.00E+00	1.00E-01	0.00E+00
	<b>Hyperbolic: <math>\alpha_i = \frac{(1-D_i)^{-b}-1}{b}</math></b>					<b>Exponential: <math>\alpha_i = -\ln(1 - D_i)</math></b>
Di values	ai values					ai values
1.00E-02	1.03E-02	1.02E-02	1.02E-02	1.01E-02	1.01E-02	1.01E-02
5.00E-02	5.69E-02	5.55E-02	5.40E-02	5.26E-02	5.14E-02	5.13E-02
1.00E-01	1.31E-01	1.24E-01	1.17E-01	1.11E-01	1.06E-01	1.05E-01
2.00E-01	3.60E-01	3.18E-01	2.81E-01	2.50E-01	2.26E-01	2.23E-01
3.00E-01	7.91E-01	6.38E-01	5.20E-01	4.29E-01	3.63E-01	3.57E-01
4.00E-01	1.68E+00	1.21E+00	8.89E-01	6.67E-01	5.24E-01	5.11E-01
5.00E-01	3.75E+00	2.33E+00	1.50E+00	1.00E+00	7.18E-01	6.93E-01
6.00E-01	9.52E+00	4.88E+00	2.63E+00	1.50E+00	9.60E-01	9.16E-01
7.00E-01	3.06E+01	1.20E+01	5.06E+00	2.33E+00	1.28E+00	1.20E+00
8.00E-01	1.56E+02	4.13E+01	1.20E+01	4.00E+00	1.75E+00	1.61E+00
9.00E-01	2.50E+03	3.33E+02	4.95E+01	9.00E+00	2.59E+00	2.30E+00
9.9999E-01	2.50E+19	3.33E+14	5.00E+09	1.00E+05	2.16E+01	1.15E+01

Table 6-3: Variables controlling secondary (sampled) distributions of effective decline (Di) & parameter b.

	Effective Decline Di	Hyperbolic Exponent b
Primary distribution	Normal (Gaussian)	Normal (Gaussian)
Mean value	0.5	3.0
Standard deviation	0.3	1.0
Desired range	[Dmin – 1]	[2 – 4]
Truncation Lower Bound	Dmin = 0.05 (=5%)	2.0
Truncation Upper Bound	1.0	+ infinity

# The Fracability Evaluation of Dadas Shale in Southeastern Turkey Based on its Geomechanical Properties

**Oğuz Cihaner, Betül Yıldırım**

Petroleum and Natural Gas Engineering, Middle East Technical University, Ankara / Türkiye



## 1. INTRODUCTION

Although a significant part of oil and gas is still produced from conventional reservoirs, the production potential of unconventional reservoirs has become a groundbreaking agenda in petroleum industry since the beginning of 21st century. Unconventional reservoirs, especially shale oil/gas reservoirs, have been regarded as alternative oil and natural gas resources not only in the United States but also in many parts of the world. The development of shale oil/gas reservoirs is even more vital for energy-dependent countries such as Turkey. On the other hand, the development of shale reservoirs requires the application of improved technology in technical processes, such as horizontal drilling and hydraulic fracturing (HF). Accordingly, hydraulic fracturing (HF) of horizontal wells has been applied for the past twenty-five years to produce oil and gas commercially from ultra-low permeable shale reservoirs.

While geochemical and petrophysical properties assess the production potential of an unconventional shale reservoir, its primary and sustained productivity is strongly dependent on geomechanical parameters. The fracability may be the most critical geomechanical parameter in HF operations, which aims to increase the stimulated reservoir volume (SRV) so the productivity. The fracability can be defined as the ability of unconventional rocks to be effectively fractured and create complex fracture-network systems. Accordingly, the fracability index (FI) term has evolved as a theoretical benchmark in geomechanics literature, which defines the easiness of rocks to be fractured mathematically. FI is a guiding factor in identifying ideal reservoir intervals, i.e., the sweet spots. Hence, the reservoir zones with a higher FI are classified to be sweet spots, whereas the zones with a lower FI may be considered as a fracture barrier. Consequently, it should be avoided to perforate the fracture barrier zones while performing HF in shales (Jin et al., 2015).

One of the most critical parameters used to assess the fracability of rock is brittleness. Generally, brittleness refers to the property of a material that either fails with no plastic deformation or low plastic deformation under the action of external forces (Huang et al., 2021). From the geomechanical perspective, brittleness is the point at which the elastic strain controlling the deformation of rock exceeds the strength of the rock, which leads the rock to rupture (Salah et al., 2019). As shown in Figure 1, ductile rocks can hold permanent deformation (plastic strain) for long period of time without losing the ability to resist load. On the contrary, brittle rocks have much shorter plastic deformation, and their ability to resist load decreases with plastic strain. Therefore, brittle shales are more likely to be naturally fractured, tending to response to HF positively. Accordingly, a brittleness

index (BI) can be used to differentiate brittle shales from ductile shales in unconventional reservoirs (Bai, 2016; Salah et al., 2019).

BI is mainly derived either from rock mineralogy (proportion of brittle minerals in shale) or from rock mechanics parameters, particularly the Young's modulus (E) and Poisson's ratio ( $\nu$ ). From mineralogical aspect, as the amount of non-brittle mineral (clay) increases and the amount of brittle minerals (quartz minerals and carbonates) decreases in a rock, the rock tends to show ductile behavior. From mechanical aspect, generally shales with low Young's modulus and high Poisson ratio tend to be ductile, whereas rocks with high Young's modulus (E) and low Poisson's ratio ( $\nu$ ) tend to be brittle.

BI has been widely used in the past years as a single parameter to represent sweet spots in HF operations of unconventional shale reservoirs (Jin et al., 2015). However, it is not certain that brittle rocks can be easily fractured compared to ductile rocks, since brittle rocks may have greater strength than ductile rocks (Bai, 2016; Salah et al., 2019). This fact has been demonstrated by the recent research activities and field experiences, which have shown that BI alone is inadequate to detect easily-fracable spots of unconventional shale formations precisely (Huang et al., 2021; Jin et al., 2015). From this fact, besides the BI, researchers have integrated the effects of fracture toughness ( $K_{Ic}$  &  $K_{IIc}$ ), minimum horizontal stress ( $\text{MinHS}$ ,  $\sigma_h$ ), and differential horizontal stress (DHS,  $\Delta\sigma$ ) into fracability evaluation. As a matter of fact, the formation with higher FI is a good fracturing candidate which has higher brittleness (does not continue absorbing energy after applied stress reaching rock strength) and lower fracture toughness (fracture propagation consumes less internal work). Besides, such formation is surrounded by relatively lower minimum horizontal stress (less external energy by closure stress) and resides in horizontal stresses with relatively lower anisotropy (better interaction between hydraulic fractures and natural fractures).

This study aims to calculate the fracability index (FI) of Dadaş shale based on BI,  $K_{Ic}$  &  $K_{IIc}$ ,  $\text{MinHS}_{grad}$  ( $\sigma_h \cdot G$ ) and DHS ( $\Delta\sigma$ ), all of which are crucial in mechanical characterization. For this, three mathematical fracability models were used through both deterministic and probabilistic approaches. Accordingly, the degree of influence of mechanical properties on FI are discussed within the context of probabilistic research.

## 2. STATEMENT OF PROBLEM

The assessment of shale reservoirs cannot be specified by one unique geological factor, but two quality categories may be useful for assessing the main characteristics of shale reservoirs. The first category

is reservoir quality, symbolizing hydrocarbon (HC) potential, HC amount in place, and HC deliverability. The critical variables in reservoir quality are kerogen, total organic carbon (TOC), thermal maturity, lithology, porosity, permeability, pore pressure, and fluid saturations (Zee Ma, 2016). The second category is completion quality, which shows the HF potential or the ability to create and maintain fracture surface area and complex fracture systems. Completion quality is mainly affected by geomechanical parameters and it is closely linked to fracability. Geomechanical parameters include mineralogy, in-situ stress regime, Young's modulus (E), Poisson's ratio ( $\nu$ ), brittleness, fracture toughness ( $K_{Ic}$ ,  $K_{IIc}$ ), the presence and characteristics of natural fractures (NFs), unconfined compressive strength (UCS), tensile strength ( $T_o$ ), internal friction angle ( $\phi$ ), and cohesion (C). Production in shale reservoirs is mostly positively correlated with reservoir quality and completion quality, yet the reservoir quality has to reach a certain level for the completion to be efficient. For rocks with a very low reservoir quality, production is low regardless of the completion quality, whereas, for moderate to high reservoir-quality rocks, completion quality is the decisive element in production (Zee Ma, 2016). In the light of all the facts mentioned above, parameters of reservoir quality and completion quality listed in Table 1 should be considered when evaluating shale reservoirs.

The main problem regarding Turkey's promising shale formations (e.g., Dadaş shale) is stated to be the higher clay percentage (>40%) as obtained by X-ray diffraction (XRD) mineralogical analysis (Table 2), so the lower BI. However, when the mineralogical contents of some of the most productive shale formations in North America are analyzed comparatively by using the ternary diagram (Figure 2), the results propose similar ranges of BIs with Dadaş shale, whereas the well-proven HF performance in North American shales is observed to be high. Similarly, Dadaş shale is found to show unattractive elastic properties (relatively lower Young's modulus and higher Poisson's ratio) in terms of mechanical BI (Table 3). However, it can be observed from the Figure 3, some of the most productive shale formations in North America (having high HF performance) present a close mechanical tendency with Dadaş shale. All these findings, indeed, imply that using a single parameter (brittleness index, BI) to define the overall fracability of formation would be misleading; thus, a more complex and multivariable fracability parameter is required. To this end, a field-scale study that considers the selection of ideal reservoir zones in HF operations from a different angle was applied for the better development of Turkey's domestic shale oil and gas resources.

### 3. METHODOLOGY

The Silurian-aged, black, organic-rich Dadaş Shale (Figure 4) resides in the north-central portion of Southeast Anatolia Basin, which contains the most productive hydrocarbon reservoirs of Turkey. As represented in Figure 5, the Dadaş Formation consists

of three units from bottom to top: Dadaş-I, Dadaş-II, and Dadaş-III. Among these units, the Dadaş-I unit, the lowest part in Dadaş shale, attracted attention due to its favorable properties. Considering petrophysical and geochemical differences, the Dadaş-I unit is divided into four stratigraphic subunits by Kara & Isik (2021) as L1, L2, L3, and L4 from bottom to top (Figure 5).

In this study, the fracability of Dadaş shale is discussed within the scope of composite well-log data (gamma-ray log, density log, and compressional sonic log) obtained from Çalıktepe-2 well (Kara & Isik, 2021) (Figure 5). For this, first the well-log data of Çalıktepe-2 well was digitized by Neuralog software, then critical geomechanical parameters were estimated using the fundamental empirical correlations provided in Figure 6. Finally, three fracability models listed in Figure 7 were implemented deterministically and stochastically to quantify FIs (as a function of BI,  $K_{Ic}$  &  $K_{IIc}$ ,  $\text{MinHSgrad}(\sigma_h/\sigma_v)$ , and DHS ( $\Delta\sigma$ )) of aforementioned zones.

Yuan et al.'s model (2017) proposes a fracability equation including  $BI_{\text{mech}}$ ,  $K_{Ic}$  &  $K_{IIc}$ , and  $\sigma_h/\sigma_v$  but neglecting  $\Delta\sigma$ . On the other hand, Dou et al.'s model (2022) suggests an improved method by integrating the DHS into fracability model but the technique lacks the mode-II fracture toughness ( $K_{IIc}$ ). It is an undeniable fact that DHS affects the structure of complex fracture networks and the size of SRV (Dou et al., 2022; Lihong et al., 2019), whereas the  $K_{IIc}$  is pertinent to shear fracture growth and fracture conductivity (He et al., 2019; Yuan et al., 2017). Moreover, strike-slip and reverse faulting regimes are dominantly observed around Diyarbakir region according to the world stress map (WSM) data (Merey et al., 2021) and the study of Inan & Kavak (2019). In the light of all the facts mentioned above, a new fracability model that integrates both  $K_{IIc}$  and DHS into the same fracability equation has been proposed mainly taking the study of Dou et al. (2022) as a reference. In this new model, mode-I and mode-II fracture toughnesses ( $K_{Ic}$  &  $K_{IIc}$ ) are assumed to equally impact fracability index as in Yuan et al.'s study.

For the fracability evaluation, Yuan et al.'s model presents only a relative comparison among candidate zones instead of using specific ranges describing fracable and non-fracable spots. Conversely, in Dou et al.'s model, candidate reservoir zones have been classified based on three distinct fracability index (FI) ranges as follows:

(1) Type-I:  $FI \geq 0.3 \left[ \frac{\text{MPa}}{\text{m}} \right]^{-1}$ . For this type, there is a high probability of obtaining a complex fracture network, a greater SRV, and high fracture conductivity. The fracability is ranked as high. Zones correspond to this range are regarded as ideal spots for HF.

(2) Type-II:  $0.22 \left[ \frac{\text{MPa}}{\text{m}} \right]^{-1} \leq FI < 0.3 \left[ \frac{\text{MPa}}{\text{m}} \right]^{-1}$ . For this type, there is an intermediate probability of obtaining a complex fracture network and a greater SRV. The fracability is ranked as intermediate. The HF may be recommended for this type of zones, but not strongly supported.

(3) Type-III:  $FI < 0.22 [(MPa)]^{(-1).m}$ . For this type, it is difficult to obtain a complex fracture network and a greater SRV. To this end, the fracability is ranked as low. This type of reservoir zones tends to behave as fracture barrier and the HF is not advised in these zones.

As for the newly Proposed model, the aforementioned FI ranges in Dou et al.'s model were taken as a basis for fracability evaluation.

## 4. RESULTS & DISCUSSION

### 4.1 Deterministic Method

The calculated geomechanical parameters were averaged over the zones to express the fracability in terms of a discrete, constant value of constituents. Table 4 shows the representative values of geomechanical properties used to evaluate the FI deterministically.

Inserting input parameters in Table 4 into equations in Figure 6 provided constant-valued FIs as listed in Table 5. For each reservoir zone, FI results were obtained in descending order as the Proposed model, Dou et al.'s model, and Yuan et al.'s model. According to the Yuan et al.'s model, L3 (in first place) and L4 (in second place) zones are found to be much better targets for HF operation compared to L2 zone. However, Dou et al.'s model and the Proposed model suggest that all studied zones are observed highly-fracable. Additionally, the FI values obtained from Yuan et al.'s correlation is apparently smaller from Dou et al.'s and newly Proposed model's values. Accordingly, this may reflect that the DHS ( $\Delta\sigma$ ) has a strong effect on the fracability of Dadaş shale. Besides, it is observed that the results of Dou et al. and newly Proposed model are considerably close to each other, which suggests that the mode-II fracture toughness ( $K_{Ic}$ ) plays a small role in fracability evaluation for Dadaş shale.

### 4.2 Probabilistic Method

Considering Kara & Isik's findings (Table 6), and the list of critical or desired values in shale rock characterization (Table 1), it can be easily observed that the L2 subunit is by far the most favorable zone among all subunits (L1, L2, L3, and L4) of Dadaş-I member in terms of reservoir quality and completion quality. From this fact, the probabilistic risk analysis has been performed only over the L2 facies.

The uncertainties that each mechanical parameter has necessitate the utilization of probabilistic approach for a more reliable evaluation process. To this end, after optimally fitting the input data to specific distributions with @RISK software, probabilistic risk analysis have been performed by Monte Carlo simulation.

Best-fitted distribution type for each parameter (Figure 8) was selected among the distribution options automatically recommended by @RISK software. Normalized Young's modulus (EN) and normalized Poisson's ratio ( $\nu_N$ ) data in L2 are exponentially distributed. Fracture toughness parameter in itself

showed different distribution tendencies ( $K_{Ic}$ : PERT distribution, and  $K_{Ic}$ : Triangular distribution). On the other hand, the normalized versions of fracture toughness ( $K_{Ic\_N}$  &  $K_{IIc\_N}$ ) optimally matched with the PERT distribution in L2 zone. In addition, the data range for MinHS ( $\sigma_h$ ) and DHS ( $\Delta\sigma$ ) best fit in with triangular distribution. As an interval of any normalized parameter are inherently bounded by 0 and 1, it is not a coincidence that profiles of fracability components are dominated by triangular distribution and PERT distribution, which are highly suitable for bounded-interval inputs.

Subsequent to distribution specification procedure, a Monte Carlo simulation with 10000 iterations has been applied to evaluate the fracability index (FI) stochastically. In this context, the graphs of probability density functions (PDFs) and cumulative distribution functions (CDFs) were obtained for the each fracability model (Figure 9).

The behavior of output data in response to changing input data can be examined by performing a sensitivity analysis. By ranking inputs quantitatively, the sensitivity analysis facilitates evaluating the relative effect of different factors and identifying the most critical factor in fracability evaluation. Accordingly, an input with a greater impact score on a sensitivity assessment tool includes more uncertainty, requiring risk mitigation and developed investigation and modeling studies (Lumivero, 2023c). Tornado charts and spider graphs can represent the analysis visually to make more informed and sound judgments. A spider chart presents more information than a tornado diagram since a tornado diagram reflects only the overall change in output value. However, a spider chart informs about the change rate in output value as the input data changes within its range (Lumivero, 2023a, 2023b).

Tornado and spider graphs for three fracability models were generated to analyze how the model inputs affect the behavior of the FI.

For Yuan et al.'s model (Figure 10), normalized Poisson's ratio (PR) and normalized Young's modulus (YM) have the by far the largest impact score on FI. This result matches up with the fact that the PDF of the fracability index resembles the exponential distribution, which is best fitted for normalized YM and PR.

In Dou et al.'s model, FI is found to be mostly sensitive to (at an almost equal rate) the DHS index and normalized mode-I fracture toughness (Figure 11). Thus, it is an expected result that the FI profile seems as the projection of the combination of Triangular and PERT distributions. Then, the effect size on the output gradually decreases from minimum horizontal stress to normalized PR and YM, respectively.

As for proposed model, since the DHS index has the largest bar on the tornado graph and has the steepest line on the spider graph (Figure 12), it may be easily inferred that FI distribution is predominantly affected by the uncertainty of DHS index. MinHS ranks number two at the effect ranking on the FI after the DHS index. The rest of the input parameters almost shares the same portion at

the scale. In addition, the shape of the PDF distribution of FI in this model nearly corresponds to triangular distribution, which accords with the distribution of the most-dominant input parameter (DHS index).

## 5. CONCLUSIONS

The FI results of Dadaş-I member were calculated by implementing three different FI models deterministically and stochastically (Table 7). The deterministic and probabilistic FI results for L2 zone were listed in descending order as the Proposed model, Dou et al.'s model and Yuan et al.'s model. Deterministic and probabilistic FI results for each model generally showed no significant difference. To clarify, only a slight but noticeable difference in Yuan et al.'s model was observed; the deterministic FI value (0.241) corresponds to the P65 percentile in stochastic distribution. As for Dou et al.'s model and Proposed model, the deterministic FI values correspond to the P53 and P54 percentiles in stochastic approach, respectively. Both for Dou et al.'s model and for Proposed model, the stochastic approach suggested that P50 values are almost equal to statistical mean values. On the other hand, a considerable difference is observed between the mean value and P50 value for Yuan et al.'s model.

Model comparison analysis indicated that all deterministic and probabilistic FI values obtained from Dou et al.'s model and Proposed model are much bigger than those of the two other models. This, indeed, implies that the fracability of Dadaş shale is highly affected by differential horizontal stress (DHS,  $\Delta\sigma$ ). Besides, it was observed that the results of Proposed model are highly close to results of Dou et al.'s model. This suggests that the mode-II fracture toughness (KIIC), which is mainly correlated with the shear failure, plays a small role in FI evaluation for Dadaş shale. Moreover, the results of the Proposed model for Dadaş-I shale are found to be consistent with those of Dou et al.'s model. The proposed model emphasizes the importance of differential horizontal stress and the type-II fracture toughness parameter in fracability evaluation of shale reservoirs, which especially reside in strike-slip faulting environments (e.g., Dadaş shale).

All in all, according to the Yuan et al.'s model, the L2 zone has low-fracable structure, and it is difficult to obtain an effective HF performance from this zone. However, the model inspires not much confidence due to the absence of differential horizontal stress in fracability equation. On the other hand, for L2 zone, Dou et al.'s model and the Proposed model (the most comprehensive fracability model in this research) suggested a highly promising picture regarding obtaining a complex fracture network, a greater SRV, and a higher conductivity. Besides, as opposed to all other zones, L2 zone has a favorable petrophysical and geochemical properties in addition to its geomechanical properties. From this viewpoint, it was concluded that L2 zone is the most likely ideal option in the matter of the effective stimulation of Dadaş shale by HF. In the near future, the results obtained from this research,

along with the modified fracability model (Proposed model), may be extended and used to evaluate the fracability of unconventional shale reservoirs in Turkey.

## REFERENCES

- Akkoca, D. B., & Işık, Ü. (2018). Geochemistry of paleozoic dadaş shales from the foreland of southeastern Turkey, Bismil, Diyarbakır. *Periodico Di Mineralogia*, 87(3), 207–225. <https://doi.org/https://doi.org/10.2451/2018PM683>
- Bai, M. (2016). Why are brittleness and fracability not equivalent in designing hydraulic fracturing in tight shale gas reservoirs. *Petroleum*, 2(1), 1–19. <https://doi.org/10.1016/j.petlm.2016.01.001>
- Belyadi, H., Fathi, E., & Belyadi, F. (2017). Chapter Thirteen - Rock Mechanical Properties and In Situ Stresses. In *HYDRAULIC FRACTURING IN UNCONVENTIONAL RESERVOIRS Theories, Operations, and Economic Analysis* (pp. 207–224). Gulf Professional Publishing. <https://doi.org/https://doi.org/10.1016/B978-0-12-849871-2.00013-7>
- Dobson, P., & Houseworth, J. (2014). Inventory of Shale Formations in the US, Including Geologic, Geochemical, Hydrological, Mechanical, and Thermal Characteristics. Lawrence Berkeley National Laboratory. LBNL Report #: LBNL-6749E. <https://escholarship.org/uc/item/1vb4c0vh#author>
- Dou, L., Zuo, X., Qu, L., Xiao, Y., Bi, G., Wang, R., & Zhang, M. (2022). A New Method of Quantitatively Evaluating Fracability of Tight Sandstone Reservoirs Using Geomechanics Characteristics and In Situ Stress Field. *Processes*, 10(5), 1040. <https://doi.org/10.3390/pr10051040>
- Eaton, B. A. (1975). The Equation for Geopressure Prediction from Well Logs. <https://doi.org/10.2118/5544-ms>
- EIA. (2015). Technically Recoverable Shale Oil and Shale Gas Resources: Turkey. [https://www.eia.gov/analysis/studies/worldshalegas/pdf/Turkey\\_2013.pdf](https://www.eia.gov/analysis/studies/worldshalegas/pdf/Turkey_2013.pdf)
- Ercengiz, S. A., Alper, M. Z., Sancay, R. H., Blair, G. J., & Ekinci, M. K. (2014). Characteristics of Lower Silurian Rocks as an Unconventional Resource in Diyarbakir Basin, SE Turkey. *International Conference & Exhibition*. <https://www.searchanddiscovery.com/abstracts/html/2014/90194ice/abstracts/1948896.html>
- Fjær, E., Holt, R. M., Horsrud, P., Raen, A. M., & Risnes, R. (2008). Chapter 5 Elastic wave propagation in rocks. In *Petroleum Related Rock Mechanics 2nd Edition* (Vol. 53, pp. 175–218). Elsevier. [https://doi.org/https://doi.org/10.1016/S0376-7361\(07\)53005-0](https://doi.org/https://doi.org/10.1016/S0376-7361(07)53005-0)
- He, R., Yang, Z., Li, X., Li, Z., Liu, Z., & Chen, F. (2019). A comprehensive approach for fracability evaluation in naturally fractured sandstone reservoirs based on analytical hierarchy process method. *Energy Science and Engineering*, 7(2), 529–545. <https://doi.org/10.1002/ese3.303>

- Higgins-Borchardt, S., Sitchler, J., & Bratton, T. (2016). Chapter 7 - Geomechanics for Unconventional Reservoirs. In Y. Zee Ma & S. A. Holditch (Eds.), *Unconventional Oil and Gas Resources Handbook* (pp. 199–213). Elsevier. <https://doi.org/10.1016/B978-0-12-802238-2.00007-9>
- Horsrud, P. (2001). Estimating mechanical properties of shale from empirical correlations. *SPE Drilling and Completion*, 16(2), 68–73. <https://doi.org/10.2118/56017-PA>
- Huang, Z. X., Yang, K., Peng, C. Y., Ai, C. Z., Jiang, M., Deng, J. T., & Liu, W. J. (2021). How to identify the best candidate fracturing zone: A review of current fracability evaluation method. *IOP Conference Series: Earth and Environmental Science*, 861(6). <https://doi.org/10.1088/1755-1315/861/6/062071>
- Inan, M. A., & Kavak, O. (2019). Shale resource potential of the Silurian Dadas Formation in Diyarbakır (SE Anatolia of Turkey) and its surroundings. *Arabian Journal of Geosciences*, 12(22). <https://doi.org/10.1007/s12517-019-4837-7>
- Jin, X., Shah, S. N., Roegiers, J. C., & Zhang, B. (2015). An integrated petrophysics and geomechanics approach for fracability evaluation in shale reservoirs. *SPE Journal*, 20(3), 518–526. <https://doi.org/10.2118/168589-PA>
- Kara, B., & Isik, V. (2021). Reservoir characteristics and unconventional oil potential of Silurian aged Dadaş shale in southeast Turkey. *Journal of Petroleum Science and Engineering*, 200(December 2020), 108365. <https://doi.org/10.1016/j.petrol.2021.108365>
- Lihong, Z., Xuwei, L., Daqi, F., Dongping, L., Xingsong, L., Shengchuan, Z., Gongquan, C., Min, Z., Fuchun, T., Yudong, Z., Xiugang, P., Jianfeng, L., & Shunli, Y. (2019). Evaluation and application of influencing factors on the fracturability of continental shale oil reservoir : a case study of Kong 2 Member in Cangdong sag. 24(5).
- Lumivero. (2023a). Spider Graphs. <https://help.palisade.com/v8/en/@RISK/Graphing/Spider-Graphs.htm?Highlight=spider>
- Lumivero. (2023b). Tornado Graphs. <https://help.palisade.com/v8/en/@RISK/Graphing/Tornado-Graphs.htm?Highlight=tornado>
- Lumivero. (2023c). What is Sensitivity Analysis and How Does it Work. <https://lumivero.com/software-features/sensitivity-analysis/>
- Merey, S., Polat, C., & Eren, T. (2021). Design of horizontal wellbore in Dadas shales of Turkey by considering wellbore stability and reservoir geomechanics. *Proceedings of the SPE/IADC Middle East Drilling Technology Conference and Exhibition, 2021-May*. <https://doi.org/10.2118/202183-MS>
- Ozturk, S. S., Demirel, I. H., & Günay, Y. (2016). Petroleum source rock potential of the Silurian Dadaş shales in the Hazro and Korudağ regions of Southeast Anatolia, Turkey. *Marine and Petroleum Geology*, 75, 53–67. <https://doi.org/10.1016/j.marpetgeo.2016.04.007>
- Rickman, R., Mullen, M., Petre, E., Grieser, B., & Kundert, D. (2008). A practical use of shale petrophysics for stimulation design optimization: All shale plays are not clones of the Barnett Shale. *Proceedings - SPE Annual Technical Conference and Exhibition, 2(Wang)*, 840–850. <https://doi.org/10.2118/115258-ms>
- Salah, M., Ibrahim Mohamed, M., Ibrahim, M., & Pieprzica, C. (2019). A Newly Developed Approach to Evaluate Rock Brittleness and Fracability for Hydraulic Fracturing Optimization in Shale Gas. *SPE Western Regional Meeting*, 23–26. <https://doi.org/10.2118/195196-MS>
- Şen, Ş., Aysal, N., & Kaygısız, E. (2021). Mineralogical Composition of the Silurian (Llandovery) Dadaş Hot Shales: Implication to Hydraulic Fracture Propagation. In O. Parlak, K. Sayit, B. L. Mesci, H. Akilli, & M. Akyıldız (Eds.), *73rd Geological Congress of Turkey with International Participation*. [https://www.researchgate.net/publication/351971786\\_Mineralogical\\_Composition\\_of\\_the\\_Silurian\\_Llandovery\\_Dadas\\_Hot\\_Shales\\_Implication\\_to\\_Hydraulic\\_Fracture\\_Propagation](https://www.researchgate.net/publication/351971786_Mineralogical_Composition_of_the_Silurian_Llandovery_Dadas_Hot_Shales_Implication_to_Hydraulic_Fracture_Propagation)
- Yildirim, B. (2019). An Experimental and Numerical Investigation Into Hydraulic Fracture Propagation in Naturally Fractured Shale Gas Reservoirs [Doctoral Dissertation, Imperial College London]. <https://spiral.imperial.ac.uk/handle/10044/1/80287>
- Yuan, J., Zhou, J., Liu, S., Feng, Y., Deng, J., Xie, Q., & Lu, Z. (2017). An improved fracability-evaluation method for shale reservoirs based on new fracture toughness-prediction models. *SPE Journal*, 22(5), 1704–1713. <https://doi.org/10.2118/185963-pa>
- Zee Ma, Y. (2016). Chapter 1 - Unconventional Resources from Exploration to Production. In Y. Zee Ma & S. A. Holditch (Eds.), *Unconventional Oil and Gas Resources Handbook Evaluation and Development* (pp. 3–52). Gulf Professional Publishing. <https://doi.org/https://doi.org/10.1016/B978-0-12-802238-2.00001-8>
- Zoback, M. (2007). Chapter 1 - The tectonic stress field. In *Reservoir Geomechanics* (pp. 3–26). Cambridge University Press. <https://doi.org/10.1017/CBO9780511586477.002>

Keywords: Fracability Index, Shale Reservoir Geomechanics

Figure 1. The brittle and ductile behavior of material from stress vs. strain plot (Salah et al., 2019)

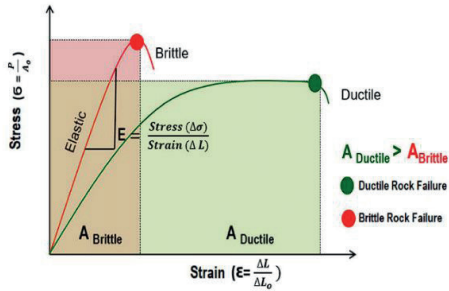


Table 1. Some Important Parameters in Evaluation of Shale Reservoirs (Zee Ma, 2016)

Parameter	Critical or Desired Values
TOC	> 2% (weight)
Thermal Maturity	Oil window: $0.5 < Ro < 1.3$ , Gas window: $1.3 < Ro < 2.6$
Mineralogy	Clay < 40%, Quartz or Carbonate > 40%
Average Porosity	> 4%
Average Water Saturation	< 45%
Average Permeability	> 100 nanoDarcy
Pressure	Overpressure is preferable
Reservoir Temperature	> 230 °F
Stress	< 13.80 MPa (2000 psia) net lateral stress
Young's Modulus	> 20.68 GPa (3 MM psia)
Poisson's Ratio	< 0.25

Figure 2. A ternary diagram showing the comparison of Dadaş shale (indicated by triangles) with some major North American shales (indicated by circles) and one European-origin Derbyshire shale (indicated by red stars) (Modified after Yildirim, 2019)

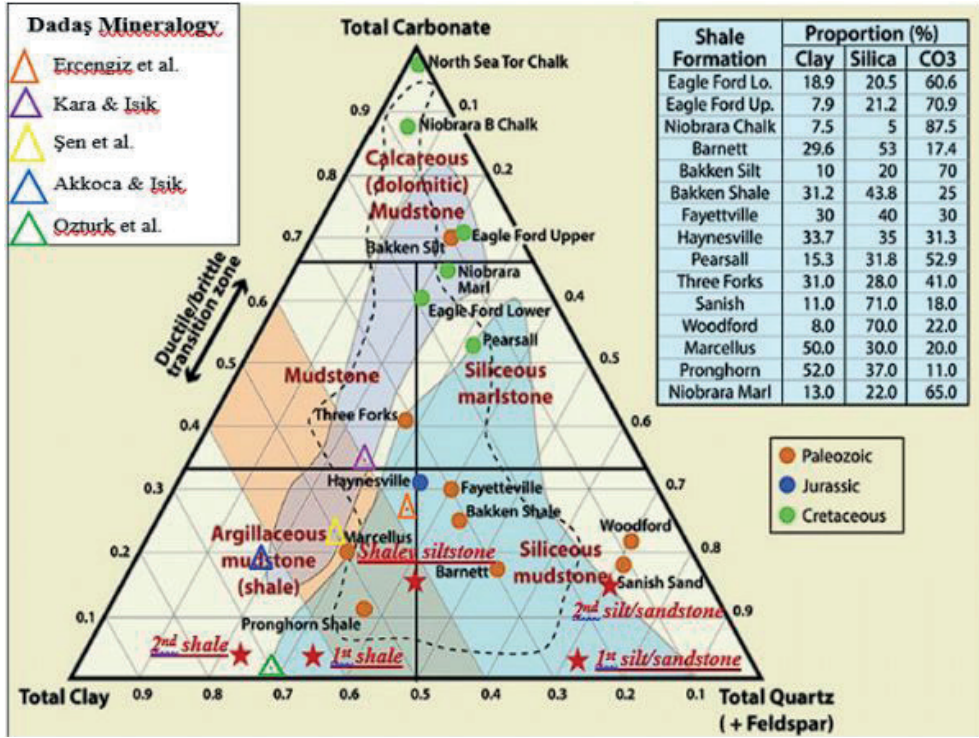


Table 2. Total clay, quartz, and carbonate percentages of Dadaş Shale from various sources.

Data Source	Total Clay	Total Quartz	Total Carbonate
(Ercengiz et al., 2014)	38	35	27
(Kara & Isik, 2021)	40	24	33
(Şen et al., 2021)	50	27	23
(Akkoca & Işık, 2018)	63	18	19
(Ozturk et al., 2016)	70	28	2



Figure 3. A graph showing the mechanical elasticity comparison between Dadaş shale and some major North American shales.

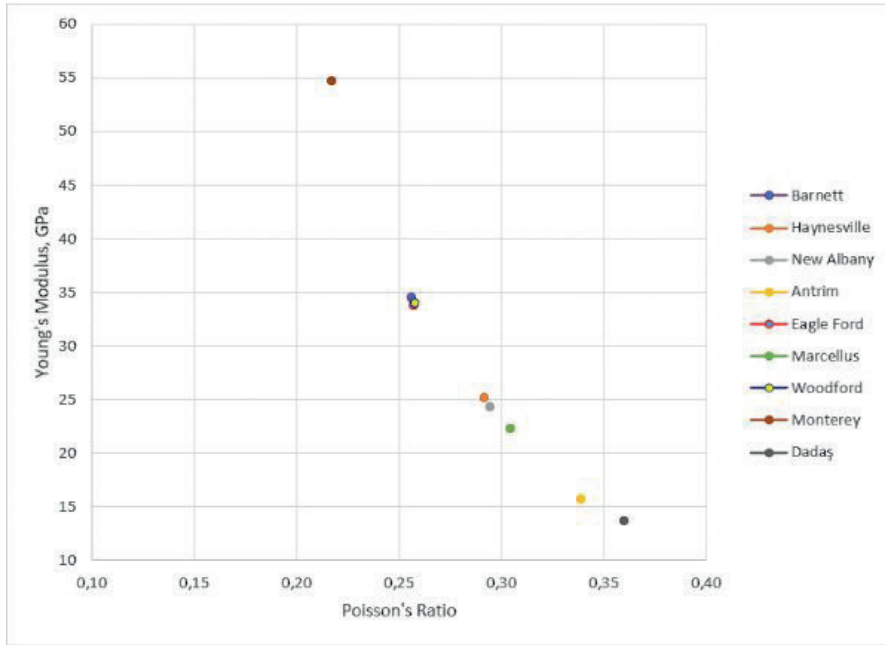


Table 3. Poisson's ratio and Young's modulus values of some of the most productive North American shales and Dadaş shale (Modified after Dobson & Houseworth, 2014).

Shale Formations	Poisson's Ratio	Young's Modulus (GPa)
Barnett	0.26	34.51
Haynesville	0.29	25.09
New Albany	0.29	24.33
Antrim	0.34	15.71
Eagle Ford	0.26	33.78
Marcellus	0.30	22.28
Woodford	0.26	34.00
Monterey	0.22	54.66
Dadaş	0.36	13.70

Figure 4. Dadaş Shale Prospective Area, SE Anatolian Basin, Turkey (EIA, 2015).

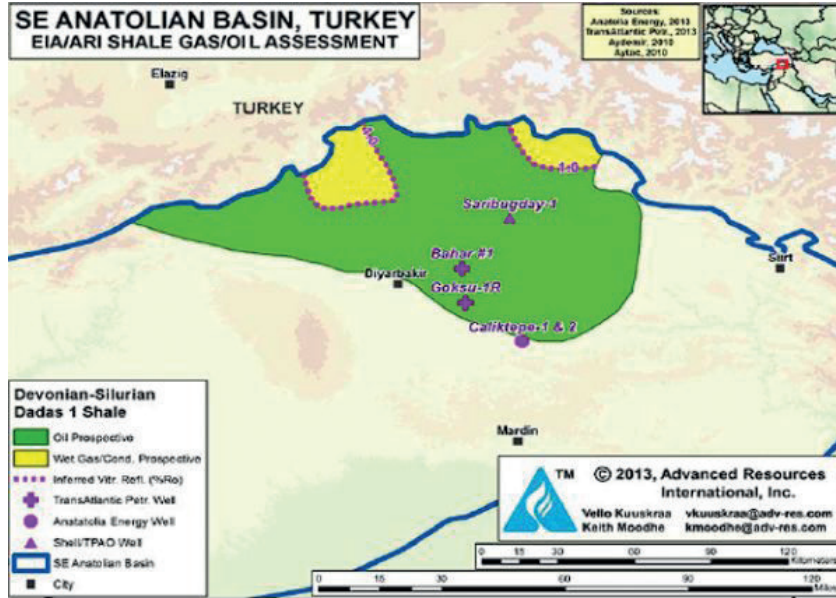


Table 4. The averaged value of input data for deterministic fracability evaluation.

Input Parameters	L4 Zone	L3 Zone	L2 Zone
Poisson's Ratio, $\nu$	0.35	0.34	0.38
Young's Modulus, E (GPa)	14.55	16.37	11.17
Static Young's Modulus, E <sub>S</sub> (GPa)	2.80	3.10	2.19
Biot's Constant, $\alpha$	0.69	0.70	0.70
Pore Pressure Gradient, P <sub>(P,grad)</sub> (psi/ft)	0.871	0.871	0.871
Vertical Stress, $\sigma_V$ (MPa)	59.14	60.36	60.76
Maximum Horizontal Stress, $\sigma_H$ (MPa)	71.09	70.98	77.28
Minimum Horizontal Stress, $\sigma_h$ (MPa)	67.38	66.63	75.04
Differential Horizontal Stress Index, $[(\Delta\sigma)]_{\text{Index}}$	0.49	0.40	0.68
Mechanical Brittleness Index, BI <sub>mech</sub>	0.38	0.44	0.24
Mode-I Fracture Toughness (MPa.m <sup>0.5</sup> )	1.00	1.01	0.95
Mode-II Fracture Toughness (MPa.m <sup>0.5</sup> )	2.02	2.05	2.04

Figure 5. Lithofacies of Dadaş-I Member (from Çalkıtepe-2 well) (Kara & Isik, 2021).

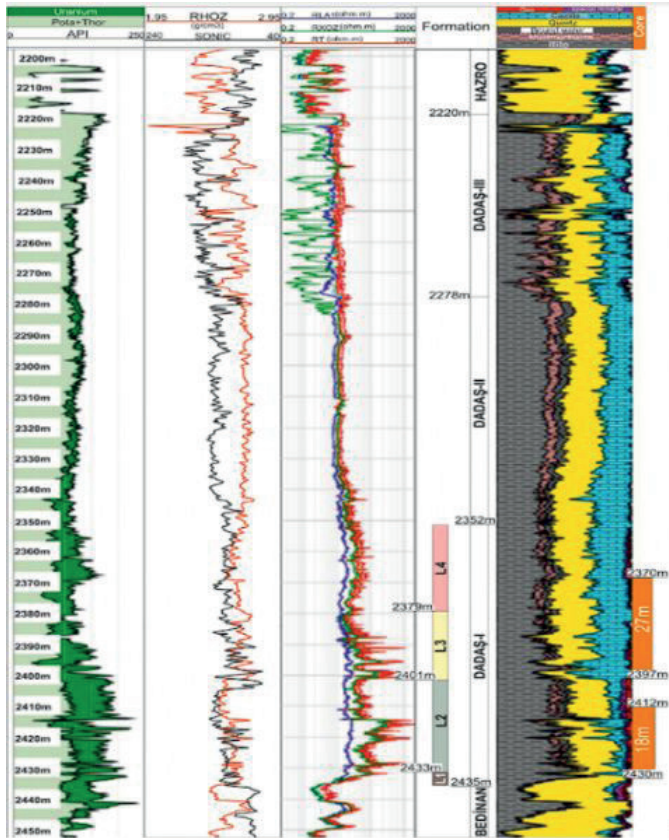


Table 5. Deterministic fracability index results for selected models.

Zones	FI by Yuan et al.	FI by Dou et al.	FI by Proposed Model
L4	0.404	0.611	0.683
L3	0.468	0.586	0.663
L2	0.241	0.629	0.660

Figure 6. The list of geomechanical properties used in fracability evaluation.

Estimated Parameter	Equation/Correlation	Reference
Poisson's Ratio	$\nu = \frac{(V_P^2 - 2V_S^2)}{2(V_P^2 - V_S^2)}$	(Fjær et al., 2008)
Young's Modulus	$E = \frac{\rho V_S^2 (3V_P^2 - 4V_S^2)}{(V_P^2 - V_S^2)}$	
Static Young's Modulus	$E_S = 0,076 * V_P^{3,23}$	(Horsrud, 2001)
Biot's Constant	$\alpha = 0.64 + 0.854 * \phi$	(Belyadi et al., 2017)
Pore Pressure Gradient	$P_{p,grad} = \sigma_{v,grad} - (\sigma_{v,grad} - P_{hyd,grad}) \left( \frac{\Delta t_n}{\Delta t} \right)^3$	(Eaton, 1975)
Vertical Stress	$\sigma_v = \frac{\bar{\rho} H}{144}$	(Zoback, 2007)
Maximum Horizontal Stress	$\sigma_H = \frac{\nu}{1-\nu} (\sigma_v - \alpha P_p) + \alpha P_p + \frac{E_S}{1-\nu^2} (\epsilon_H + \nu \epsilon_h)$	(Higgins-Borchardt et al., 2016)
Minimum Horizontal Stress	$\sigma_h = \frac{\nu}{1-\nu} (\sigma_v - \alpha P_p) + \alpha P_p + \frac{E_S}{1-\nu^2} (\epsilon_h + \nu \epsilon_H)$	
Differential Horizontal Stress Index	$\Delta\sigma_{Index} = 1 - \frac{\Delta\sigma}{\Delta\sigma_{max}}$	(Dou et al., 2022)
Mechanical Brittleness Index	$BI_{mech} = 0.5E_N + 0.5\nu_N$	(Rickman et al., 2008)
Mode-I Fracture Toughness	$K_{IC} = 0.450\rho - 0.151e^{Vsh} + 0.201 \ln(DT) - 0.877$	(Yuan et al., 2017)
Mode-II Fracture Toughness	$K_{IIC} = 2.119\rho - 0.245e^{Vsh} + 1.152 \ln(DT) - 8.378$	

Table 6. Reservoir Parameters of Dadaş Units and Dadaş-I Subunits Obtained from Log Analyses in Çalkıtepe-2 well (Kara & Isik, 2021). Note: (f: Faulty contact), \* Rounded to a nearest whole number.

Unit	Depth (m)	Gross pay (m)	Net pay* (m)	Por. (avg) (%)	Sw (avg) (%)	Perm. (avg) (nD)	TOC (avg) (%)	Cum. OIP (MMbbls/km <sup>2</sup> )
Dadaş-III	2220f	58	0	3.12	100	0	1.06	0
Dadaş-II	2278	74	0	4.00	98	0.2	1.03	0.20
Dadaş-I (L4)	2352	27	26	6.00	50	130	1.69	4.21
Dadaş-I (L3)	2379	22	14	3.60	73	50	1.79	1.67
Dadaş-I (L2)	2401	32	31	7.60	28	423	2.69	8.76
Dadaş-I (L1)	2433	3	1	1.80	96	0	2.70	0

Figure 7. Selected fracability models for this study.

Fracability Model	Fracability Equation	FI Unit
Yuan et al.	$FI = \frac{BI_{mech}}{0.5 \times K_{IC} + 0.5 \times K_{IIC}} \times \frac{1}{\sigma_h^G}$	$MPa^{-2} \cdot m^{0.5}$
Dou et al.	$FI = (0.33BI_{mech} + 0.33K_{IC,N} + 0.34S_N) / \sigma_h^G$	$MPa^{-1} \cdot m$
Proposed Model	$FI = (0.33BI_{mech} + 0.33[0.5K_{IC,N} + 0.5K_{IIC,N}] + 0.34S_N) / \sigma_h^G$	$MPa^{-1} \cdot m$

Table 7. Collective fracability index results of L2 zone for three different models.

Value Type	Yuan et al.	Dou et al.	Proposed Model
Mean Value	0.213	0.618	0.646
P50 Value	0.177	0.612	0.644
Deterministic Value	0.241	0.629	0.660
Probabilistic Corresponding Value of Deterministic Value	P65	P53	P54

Figure 8. Fitting results of input data for L2 zone

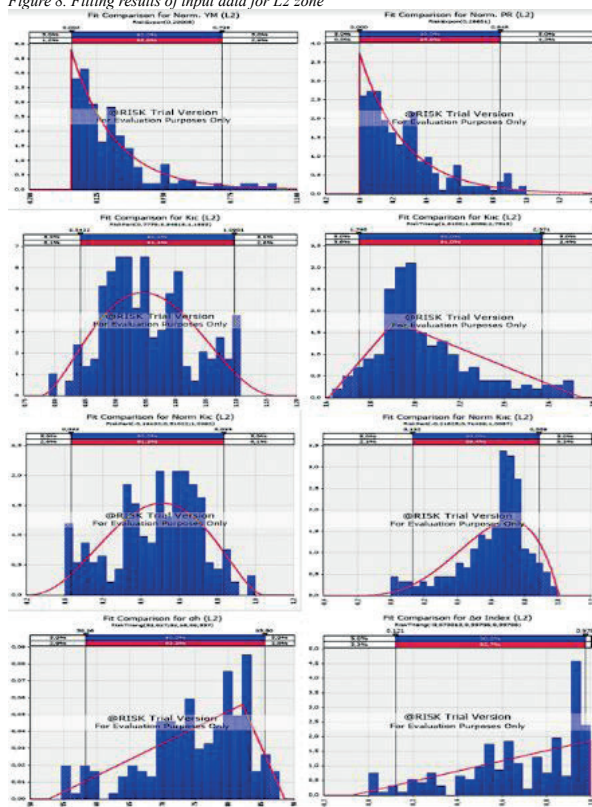


Figure 9. Distribution graphs of the probability density function (PDF) and cumulative probability function (CDF) a-) for Yuan et al.'s model b-) for Dou et al.'s model c-) for Proposed model.

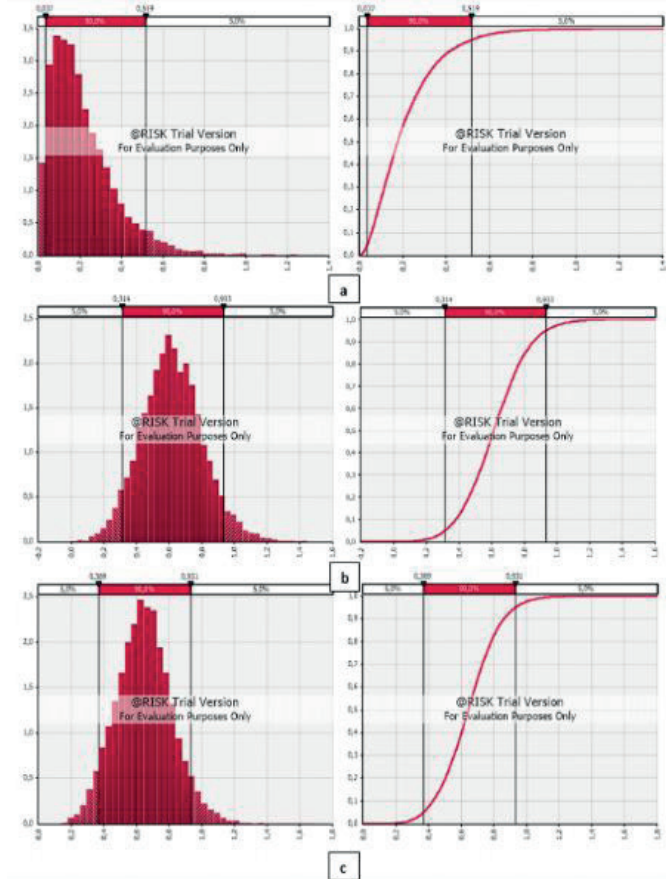


Figure 10. a-) Tornado chart and b-) spider chart of L2 zone for Yuan et al.'s model.

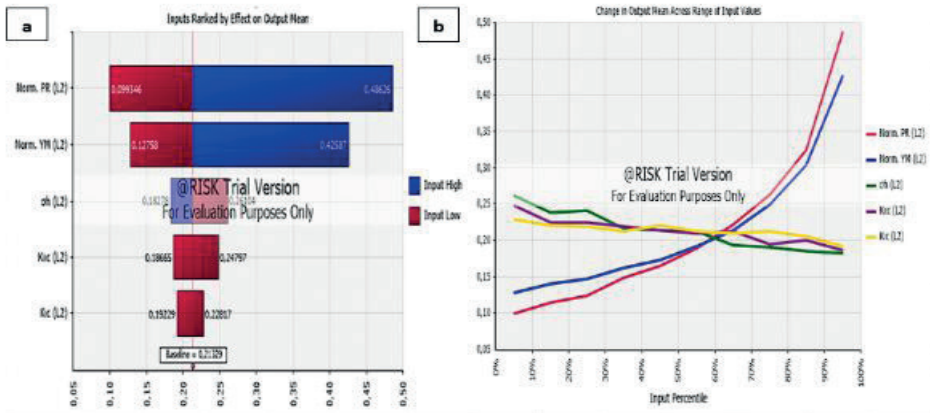


Figure 11. a-) Tornado chart and b-) spider chart of L2 zone for Dou et al.'s model.

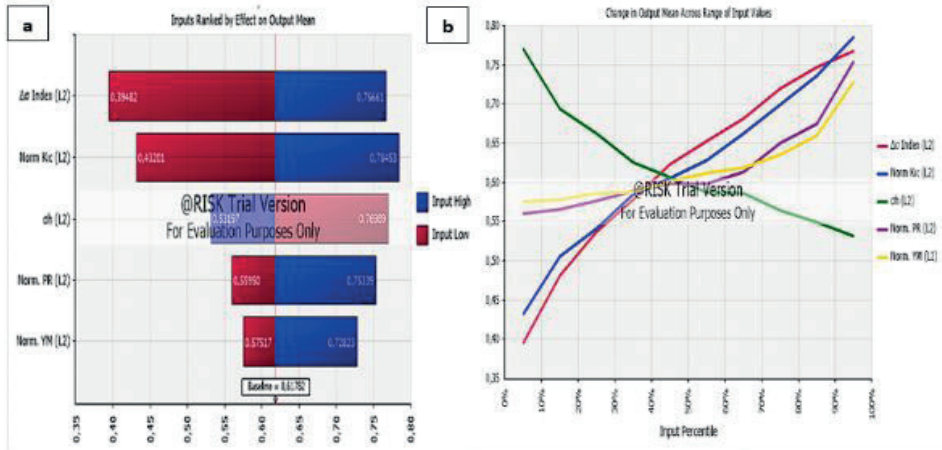
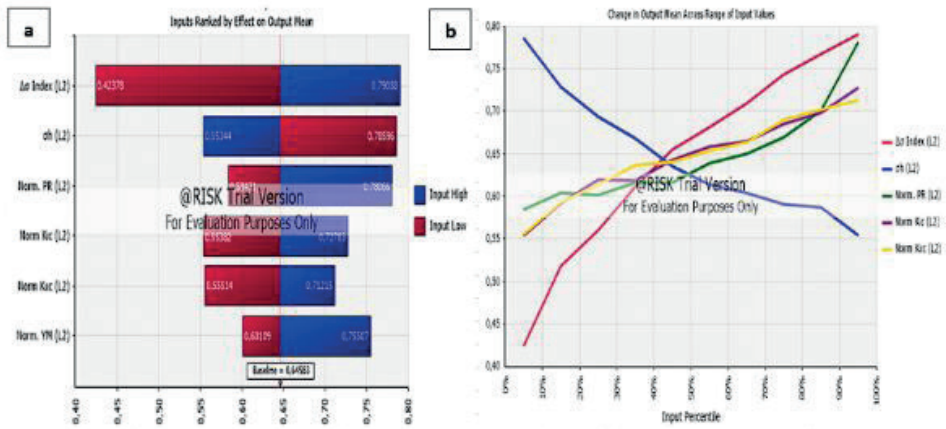


Figure 12. a-) Tornado chart and b-) spider chart of the L2 zone for Proposed model.



# Hamitabat Formation Tight Sandstone Reservoirs Sweet Spot Identification



**Sezer Sevinc, Ahmet Ergün Mengen, Kirill Ezhov**  
Türkiye Petrolleri Anonim Ortaklığı

## 1. INTRODUCTION

Considering the production performances of the wells targeted Hamitabat Formation some factors emerge as sweet spots such as thickness and lithology, tectonics and timing, reservoir pressures, porosity and water saturations.

Thrace Basin is the main gas producing basin located in NW Turkey. Natural gas is produced from many reservoirs including both carbonates and clastics. Petroleum systems are divided into two as Eocene and Oligocene petroleum systems, including source rock and reservoir rock. The Eocene oil system differs from the Oligocene in terms of cumulative production and reserve amounts. In the Eocene petroleum system, Hamitabat Formation emerges. Although the Hamitabat Formation is the Formation containing the largest reserves of the Thrace Basin, the high feldspar ratio is transformed into clay minerals through diagenetic processes within the tectonic development of the basin. Clay minerals, on the other hand, reduce the porosity and permeability and transform the Hamitabat Formation into a high potential tight sand play.

All along the Eocene, volcanism accompanied the sedimentary sequence and affected the mineralogical composition. Middle-Upper Eocene aged andesitic-rhyolitic volcanism was formed both in the Istranca massif and in the east-west line passing through Keşan and Silivri districts. In the Hamitabat Formation, which developed simultaneously with volcanism, volcanic effects appear in the mineralogical composition with high feldspar ratio.

The Turbiditic Hamitabat Formation was deposited with the rifting formed by the back arc spreading in the Middle Eocene. The Hamitabat Formation is defined by the cores taken from the gas wells in the Hamitabat gas field and does not outcrop. The turbiditic character of the formation was confirmed in sedimentological descriptions made with cores, well cuttings and wireline logs. The upper parts of the formation, which also includes reservoir levels, are mainly composed of grayish beige colored arcotic turbiditic sandstones. A heterolithic structure with intermittent sand-shale intercalation and volcanic tuff is also observed. These levels, which usually contain the uppermost section of 100 m, show the reservoir characteristics. The middle parts of the formation contain thick massive sandstone levels. The lower parts are generally of distal turbiditic character and consist mostly of shale and silt stones.

## 2. METHODS AND DISCUSSION

Eight wells targeted Hamitabat Formation were studied for their sweet spots properties and best criterias were determined regarding production performances. Only

well C and D have economic production. Others only have gas flared. Sweet spot properties; thickness and lithology, tectonics and timing, reservoir pressures, porosity and water saturations were studied in Hamitabat Formation depositional area and relationships between productivity and sweet spots criterias are explained.

In general, the sand ratio in the formation is higher in areas where Hamitabat Formation is thick, and it is expected to be high in reservoir quality at the same time. Hamitabat Formation is typical example of deep marine turbidite system. Therefore, formation shows a variety of architectural elements including incised valleys, levees and sheet sands. Having the thickest sandstone sequences, sheet sand parts in the reservoirs of the Hamitabat Formation are known as the parts with the best reservoir properties with high flow rates and high recovery rates since having relatively simple reservoir geometries, horizontal continuity, high sandstone ratios, and relatively good porosity and permeability. Tubiditic currents flow in a NW to SE direction. Incised valleys are in the NW part (figure 1) of the basin and the deep sea fans/sheet sands are in the central part of the basin through the SE. Deep sea fans creates the thickest sections (figure 2). Wells from inner fans to outer parts display higher gross thickness and higher net to gross (NTG) ratio (figure 3).

Tectonics and timing of the petroleum system is an essential part when evaluating the sweet spot for the tight sand play of the Hamitabat Formation. The Thrace Basin developed mainly in three tectonic phases. First and second phases are strictly related to Hamitabat Tight gas sweet spot prediction. The first phase is the Middle-Upper Eocene rifting, which also represents the formation of the basin, and continues until the Late Oligocene. This rifting phase is confirmed by angular unconformity clearly observed in the seismic data between Lower and Middle Eocene in the center of the basin. In the southern margin of the basin outcrops shows a series starting with the blocks up to 15-20 meters at the base showing the first stages of a rifting phase and continues with deep sea sediments. The second phase is the compression regime, which starts at Middle Oligocene and continues until the end of the Oligocene and is represented by an uplift in the basin. At this stage, inversion structures are formed on Eocene normal faults by compression regime. Trap mechanisms of the fields producing from Hamitabat Formation are formed by both Eocene normal faults and Oligocene inverted and strike slip faults. The third and also the recent tectonic period is an extensional tectonic regime that creates angular unconformity between Upper Oligocene and Early Miocene. Maximum expulsion rate from source rock is at Upper Eocene to Middle Oligocene. Therefore, considering the petroleum system timing Eocene structures displays enough trap



properties while Oligocene structures are not much successful as Eocene structures to hold hydrocarbons in place. Production performances of the wells penetrated Eocene and Oligocene structures shows the differences of the trap and expulsion timing criteria for sweet spot identification.

Reservoir pressures are the main driving mechanism affects the production performances. Pore pressure profiles were built to evaluate how it changes across the wells North to South and West to East. Well X on the West side of the study area has a reservoir pressure of 0.45 psi/ft. The wells (Y and Z), penetrating the thickest part of the Hamitabat Formation, reservoir pressures are up to 0.76 psi/ft. Wells on the North and Eastern sides, have a pore pressure around 0.49-0.64 psi/ft. Pore pressure profiles are built with Eaton Method (1975) and calibrated with well events and well tests.

Totally 8 wells penetrated the Hamitabat bottom were analyzed. According to well logs interpretation, cuttings and core data analysis, the Gross thickness varies between 300 m and 1600 m with the average value of 675 m. One of the observations that the top of Hamitabat formation can be recognized by the significant increasing of Gamma Ray and especially Thorium concentration. Identification of the bottom is more complex and depends on the underlying formation: Lower Eocene ophiolites, source rock etc.

Due to the lack of grain size analysis data, sand intervals were estimated based on conventional well log data with the support of NMR logs, assuming that the inversion of the larger pore volumes should represent larger grain sizes e.g. sand and gravel. This assumption was also confirmed with the mineralogical composition based on pulsed neutron spectroscopy logs. Resulted net sand ratio and the total gross thickness are presented on the Figure 5a. We can see, that the fraction of sand intervals is increasing together with the gross thickness increasing.

Not all Sand intervals are Reservoirs, but all potential Reservoirs are associated with Sands. Using indications from conventional well logs (mud invasion on resistivity and caliper logs, neutron-density crossover) and, again, support information from NMR (Free Fluid Volume) Net Reservoirs were identified. Petrophysical properties are the following: average Porosity is 8.6%, average matrix Permeability is 0.14 mD. Relationship between Net Reservoirs fraction and Hamitabat Gross Thickness presented on the Figure 5b. As you may notice the correlation becomes more scattered and many wells have almost zero NTG values. Also, it is observed that NTG starts to increase if Gross Thickness is greater than 400 m., what could be one of the possible criteria for efficient well placement. Figure 6 and 7 shows the relationships between gross thickness, net sand, net reservoir and porosity.

**3. CONCLUSION**

Productive wells and sweet spot criteria such as thickness and lithology, tectonic and timing, reservoir pressures, porosity and water saturation show high correlations.

These criterias give the most suitable prospect points for exploration and development purposes.

Keywords: Tight sandstone, sweet spot

Figure 1 Eocene Stratigraphic Chart of Thrace Basin

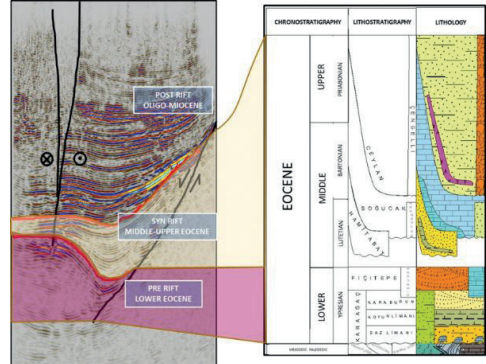


Figure 2 Relation of Architectural Elements and Thickness of Hamitabat Formation

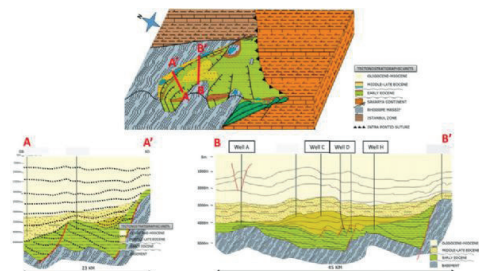


Figure 3 Location Map of Wells

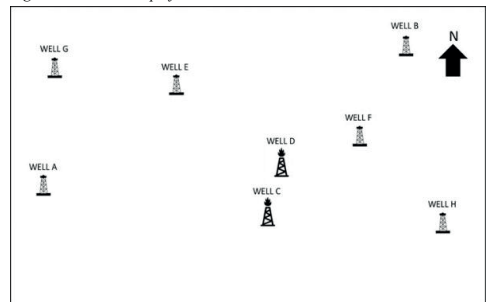


Figure 4 Pore Pressure Profiles

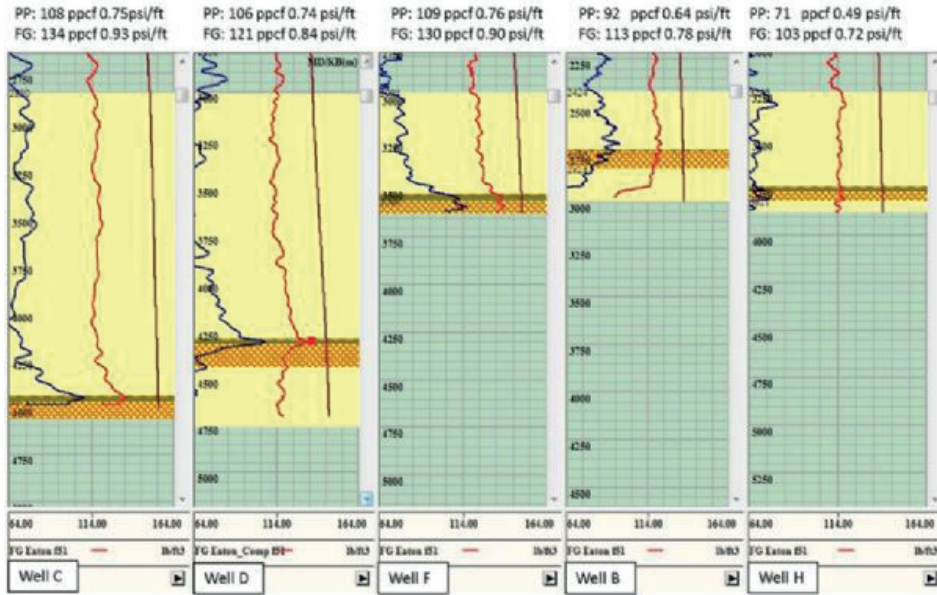


Figure 5 NTG and Gross Thickness Relationship

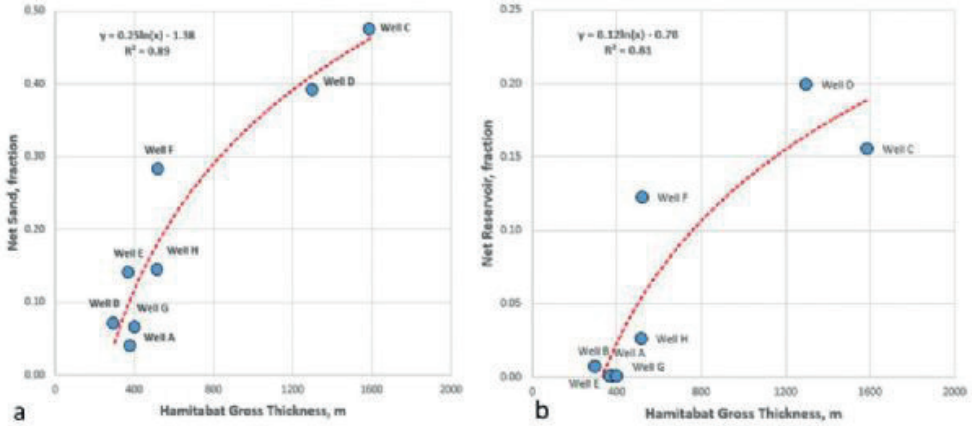


Figure 6 Net Sand, Clay Volume, Net Reservoir and Porosity Variations East to West

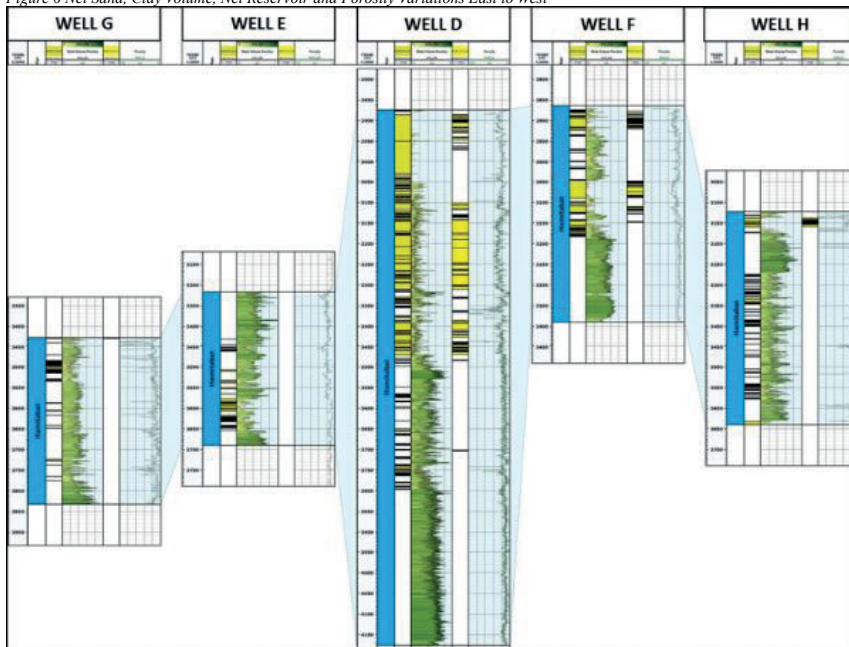
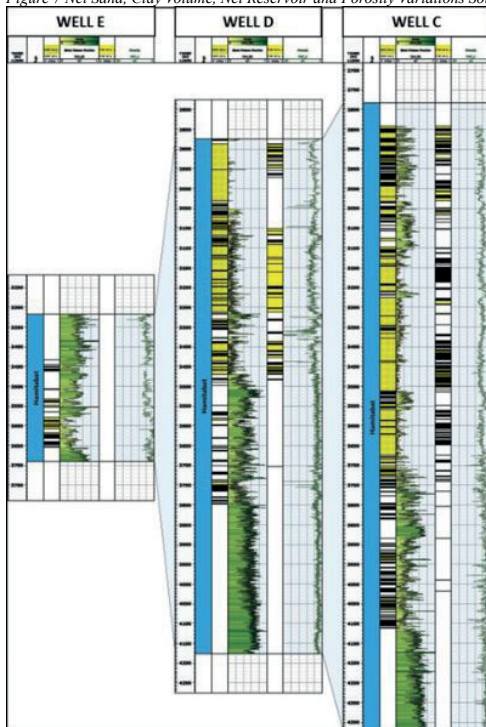


Figure 7 Net Sand, Clay Volume, Net Reservoir and Porosity Variations South to North



# Evaluation of Dadas Formation Potential: A Case Study from Southeast Türkiye



**Mehmed Ekrem Yazaroğlu<sup>1</sup>, Sinem Artan Ercengiz<sup>2</sup>, Suzan Müge Yetim<sup>2</sup>, Canalp Özkul<sup>1</sup>, Ahmet Ergün Mengen<sup>1</sup>, Can Ercan<sup>2</sup>, Yinal Neşes Huvaj<sup>2</sup>**

<sup>1</sup>Turkish Petroleum, Exploration Department, 06530 Ankara / Türkiye

<sup>2</sup>Turkish Petroleum, R&D Center Department, 06530, Ankara / Türkiye

## INTRODUCTION

Unconventional plays are identified in all hydrocarbon basins around the world. The exploration and production strategies are an increasingly important for the oil and gas industry. However, the complexity of unconventional formations associated with limited data sets and comprehensive analysis and high production costs leads to significant uncertainties and risks when it comes to the development of these reservoirs. Unconventional formations show generally high heterogeneity in a wide range of scales such as their mechanical, chemical and petrophysical properties. Therefore, comprehensive sedimentological and geochemical studies based on abundant core and cutting samples are particular crucial in the analysis of hydrocarbon generation and maturation processes in unconventional reservoirs. Horizontal wells are drilled in unconventional reservoirs to not only increase production rates but also provide larger area of contact with the formations which can provide more information.

The early Silurian to the earliest Devonian age Dadaş Formation in the Diyarbakır basin, SE Anatolian Basin is characterized as the most prospective unconventional reservoir in Turkey. However, the potential of this unconventional formation has not been studied in adequate amount of wells. UNC-1 well was drilled with vertical part and 1000m horizontal section within Dadas-I member of Dadas formation. Geochemical and sedimentological analyses on large data sets consists of cores and cuttings, petrographic analysis on thin sections and SEM images, well log data interpretation and cores from UNC-1 well are carried out to understand the potential of Dadaş unconventional reservoir. The results showed that the Dadaş-I member of the Dadaş formation has potential of source rock for the Paleozoic oil system.

Performing a single well model study around UNC-1 well using the available above data and with the integration of hydraulic fracture and production data for that well would help to understand the range of natural fracture permeability we are dealing with for Dadas formation especially for that area and may be used as reference for other data. A full single well simulation model has been carried out for UNC-1 well and results are shared in the coming sections.

## SAMPLING AND METHODS

A series of 131 core samples were collected from Dadas-I Member of Dadas Formation in UNC-1 well located in the Diyarbakır Basin, SE Anatolia. These samples were analyzed by using Rock Eval-6 Turbo to identify the source rock potential of the lower part

of Dadas Formation known as Dadas-I. The results of pyrolysis analyses are shown in Figure 1 through the UNC-1 well. Based on the geochemical analyses, the basal “hot shale member” of the formation, Dadas-I shows the best source rock potential. Mean total organic carbon (TOC) values obtained from core samples have a wide range up to 13 wt% as oil-prone Type II kerogene.

The core analyses have been performed by using GRI method to measure petrophysical properties of the cores in UNC-1 well. Porosity and permeability graphs (Figure 3) are plotted in order to observe the relationship between porosity and permeability values based on dry helium porosity and dry permeability measurements in core analysis (CSP). Porosity values are up to 10%, on the other hand permeability values are too low.

In order to reveal the brittle and ductile mineral content in Dadas-I Member of Dadas Formation in UNC-1 Well, X-ray Diffraction Method (XRD) is used. 69 core samples were selected to define the type and percentage of minerals in whole rock sample and type and percentage of clay minerals. By differentiating brittle and ductile mineral content in the rock sample, cross-plots are obtained to show whether formation is suitable for fracturing or not.

The sample which is delivered to the XRD laboratory grind with brass mortar by hand gently. If the sample contains minerals which have higher hardness levels, than Retsch's RS 200 vibratory disc mill is preferred to have smooth powder. After the sample is powdered, XRD sample holder is filled by the powder and bulk XRD analysis is performed. As preparing the sample for the bulk XRD analysis, any kind of pretreatment process is not preferred in order to protect the original conditions of the sample. By performing this analysis, the general mineralogical content is determined as analyzing the bulk XRD diffractogram by using the “MDI's Jade 7.0” software. Such mineralogical content consists of non-clay minerals such as rock forming minerals, accessory minerals, total clay and mica minerals, excluding clay types. After the completion of bulk XRD analysis, the sample is prepared for clay mineral analyses by following the “Smear Mount Method” described in Moore and Reynolds (1997) in order to determine the clay mineral types. Chemical pretreatments, such as removal of iron oxides or removal of organic materials, are not followed unless it is mandatory as suggested also in Moore and Reynolds (1997) in order to prevent altering the clay minerals.

The bulk powder diffractogram is interpreted based on the Inorganic Crystal Structure Database (ICSD) of International Centre for Diffraction Data (ICDD) by using MDI's “Jade 7.0” software, and semi-quantitative analysis is performed according to the profile-based

matching of the software and reference intensity ratios (RIR) of minerals by using “Easy Quant” patch of the software. The clay fraction XRD diffractograms are interpreted based on the rules described in Moore and Reynolds (1997) and Brown and Brindley (1980), and semi-quantitative clay mineral analysis is performed by following the procedures in Underwood and Pickering (1996).

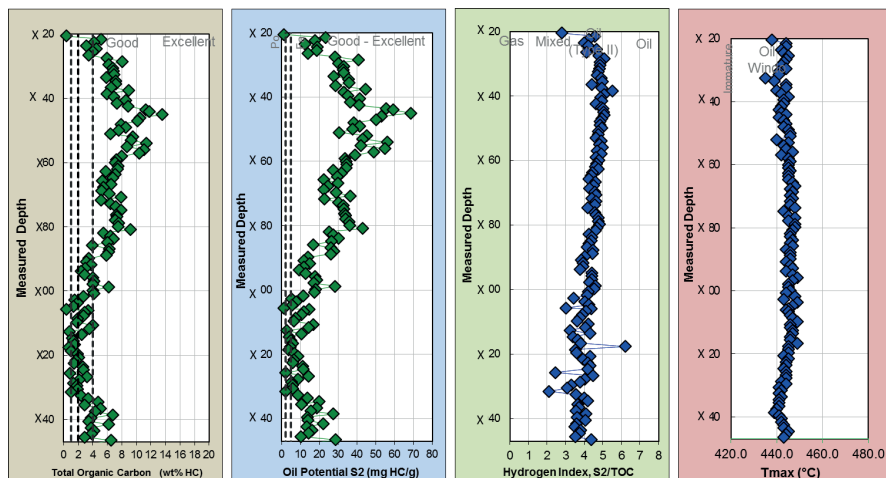


Fig.1: Geochemical analysis in Dadaş-1 member.

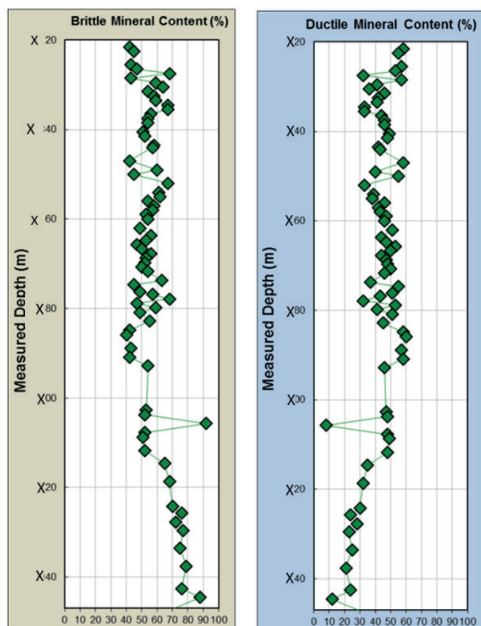


Fig.2: XRD mineralogical analysis in Dadaş-1 member.

### UNC-1 well multi-stage hydraulic fracture and production

The geomechanic model as well as reservoir properties derived from the pilot well UNC-1 serve as a basis for 3D single well model for the horizontal well. These provide information about the reservoir properties as well as adjacent areas because it is important to understand the fracture geometry modeling and the SRV (simulated reservoir volume). A DFN was created based on the natural fracture appearance and orientation observed in lower section of Dadas 1 formation. DFN was generated using a statistical approach with some assumptions:

Fracture set	Properties	Length (s)	Orientation (deg)	Spacing (m)
1	Average	15	165	24
	Std.dev	5	20	5

Fig.3: DFN inputs for frac model UNC-1 well

Preliminary staging and perforation design was mainly based on the completion quality, primarily focusing on minimum horizontal stress magnitude and its difference to the overburden. The Reservoir quality appears to be consistent through out the lateral section.

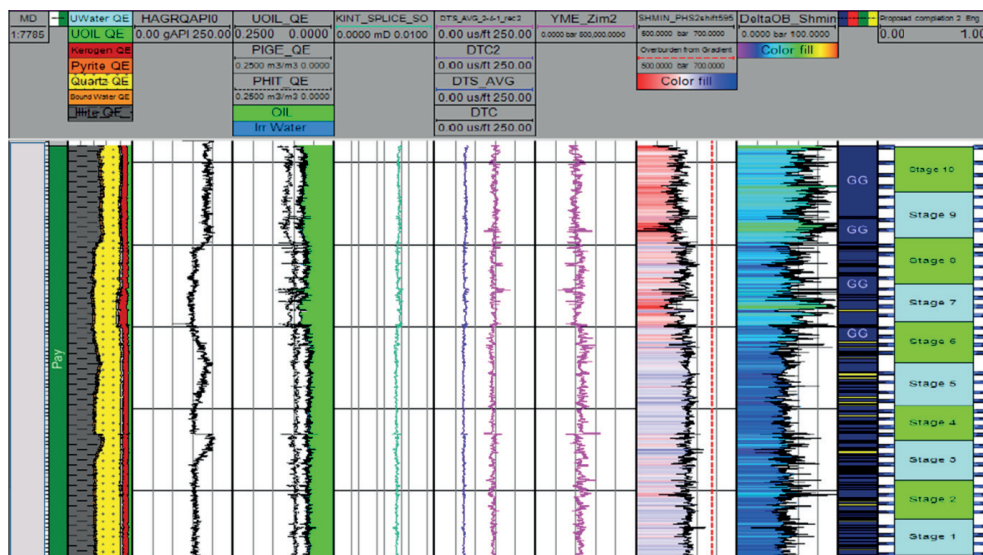


Fig.4: Completion design for UNC-1 well

The simulated multi stage hydraulic fracture (10 stages: 4 clusters each) results are shown in the figure bellow:

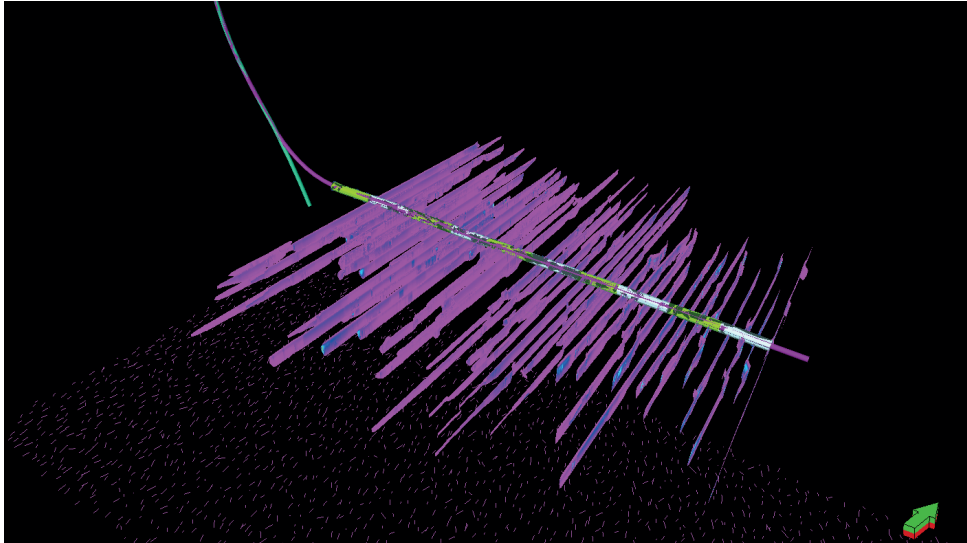


Fig 5: Hydraulic fracture simulation results

In the aim of understanding the production profiles for UNC-1 well and the reservoir parameters especially the natural fracture properties, a single well model has been carried out for UNC-1 well. The preliminary characteristics of UNC-1 area are shown in the bellow table (based on available core data):

Propriety	Value	Source
Matrix Permeability (NanoD)	136	Core data
Average Matrix Porosity (%)	4	Core data
Fracture porosity (%)	0.2	Fracture Analysis
Average Swi (%) (irreducible water saturation)	40	Core / Log data
Fracture permeability (md)	Matching parameter	
Sigma (m-2)	Matching parameter	

Fig 6. UNC-1 well single well model data

Assuming an area of 1700m\*600m\*80m, a reservoir model has been constructed to simulate the behavior of UNC-1 w

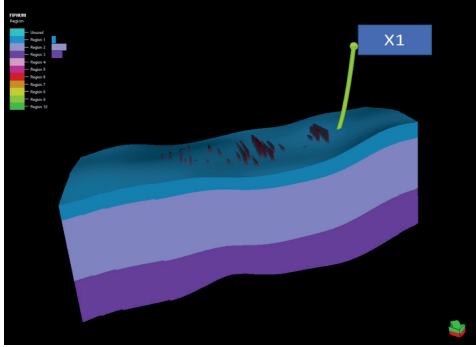


Fig 7. UNC-1 well single well model grid

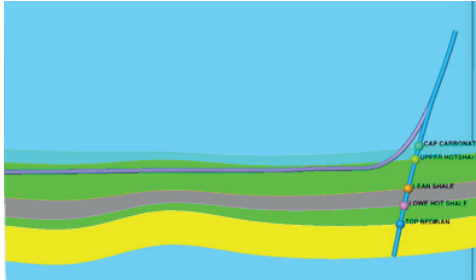


Fig 8. 3D Geological model Cross Section

In the absence of pressure survey from any source, we have analysed the drilling data where the well UNC-1 has been with 1.4 to 1.46 sg mud weight, a partial loss at top Dadas formation and no evidence of underbalancing, a pressure gradient of 0.58 psi/ft has been used to estimate the initial reservoir pressure.

To confirm the presence and the contribution of natural fractures in UNC-1 well production, first the well has been run only with single porosity system, which mean only matrix, will contribute to production, even though the well has been fractured with 10 stages and 4 clusters each, matrix only cannot produce the reality:

We then switch to double porosity system, which means the integration of natural fracture data, based on the available core data for UNC-1 well, we populate natural fracture porosity, natural fracture permeability and sigma factor.

After some history matching iterations, we found that a permeability value of 0.02 md for the natural fracture system can honor the oil production rate for UNC-1 well. This has given insight on the order of natural fracture permeabilities we are expecting out of Dadas formation.

## RESULTS

As a result of the analyses, the core samples of the UNC-1 well has the general decreasing trend of "total clay and mica" content and the increasing trend of quartz content with the increasing depth. As considering the clay mineral content, illite and kaolinite are the most dominant types of clays in almost each samples and illite is always in higher amounts than kaolinite. On the other hand, the amount of smectite which has the highest plasticity than other types of clays is barely found in all samples. Based on these mineralogical trends, the fracturing operations was considered as suitable for the UNC-1. The detailed rock parameters and petrophysical evaluation, carried on the core samples of UNC-1 well, indicates that the lower part of Dadaş Formation (Dadaş-I) has a very rich organic matter content (up to 13 wt% TOC) which is convenient for an unconventional resource. The porosity values, up to 10 %, and the low permeability, having the similar trend with the well logs, supports to find the best the pay zone for the UNC-1 well. XRD results show that, brittle mineral percentage is increasing whereas ductile mineral percentage is decreasing with depth just below the X05 meters in UNC-1 well. This change in mineral content of Dadaş-I Member of Dadas Formation shows that fracturing operations can be applied to this interval with abundant brittle mineral content in this well.

The single well model of UNC-1 well has validated the presence of natural fractures around that well which has contribute to the total oil production, an estimated average natural permeability of 0.02 md has been found. These value may be used as reference for other formation and alsoas a guide for the performed DFN's in other reservoir areas.

## CONCLUSION

In conclusion, for the first time in the Diyarbakır Basin in Southeast Turkey, horizontal well was successfully drilled. Using core and cutting samples obtained from the vertical and the horizontal well of UNC-1 an integrated workflow analysis is created. This workflow is focused on the identification of the unconventional potential of Dadas-I member of Dadas Formation. The results revealed that the Early Silurian aged Dadas-I member of the Dadaş Formation has a very good potential of source rock as an unconventional reservoir in the Paleozoic oil system in Diyarbakır Basin, SE Anatolia.

The single well model study performed on UNC-1 well confirm that natural fractures are the main contributor to shale well production in Dadas formation, eventhough we perform multi stage fractures, we need to look on highly natural fracture areas to increase our chance of better production performances of our shale well.

A better natural fracture characterization is a must to understand fracture distribution and look for hot spots for the new prospects.



# Development of a Computational Tool for Wellbore Stability Analysis and Mud Weight Optimization

**Ekrem Alagöz, Ahmet Ergün Mengen, Fethi Bensenouci, Emre Can Dündar**  
Turkish Petroleum Corporation



## ABSTRACT

This paper presents the development of a computational tool for wellbore stability analysis and mud weight optimization, written in Python language. The tool utilizes well log data as input parameters and correlations to calculate stresses, and performs wellbore stability analysis to create a mud weight window. The computational tool's performance is evaluated and compared to traditional methods, and a case study is presented. The results demonstrate that the computational tool provides an efficient and accurate solution for wellbore stability analysis and mud weight optimization. Future research directions are also discussed.

Keywords: Wellbore stability analysis, Mud weight optimization.

## 1. INTRODUCTION

Wellbore stability analysis is a critical aspect of drilling operations in the oil and gas industry. It involves assessing the mechanical integrity of the wellbore and ensuring its stability to prevent issues such as wellbore collapse, formation damage, and lost circulation. Mud weight optimization, on the other hand, refers to the process of determining the optimal density of drilling mud to maintain wellbore stability while minimizing the risk of formation damage and ultimately reduce NPTs (Cole et al., 2017). Traditionally, wellbore stability analysis and mud weight optimization have relied on manual calculations and empirical models, which can be time-consuming and may not always yield accurate results. With the advancement of computational tools and programming languages, there is a growing opportunity to develop more efficient and reliable solutions. The development of a computational tool for wellbore stability analysis and mud weight optimization addresses the need for a more streamlined and accurate approach in the industry. By automating the calculation process and utilizing well-log data and correlations, the tool can provide a faster and more precise evaluation of wellbore stability conditions (Zhang et al., 2006). The significance of this computational tool lies in its potential to improve drilling efficiency, reduce operational risks, and optimize drilling mud costs. By enabling engineers and drilling professionals to make well-informed decisions based on comprehensive analysis, the tool can contribute to safer and more cost-effective drilling operations.

The primary objectives of this paper are as follows:

- To present the development of a computational tool for wellbore stability analysis and mud weight optimization.
- To describe the methodology employed in the tool, including the utilization of well log data, correlations, and stress calculations.

- To evaluate the performance of the computational tool and compare it with traditional methods commonly used in the industry.
- To present a case study demonstrating the application of the computational tool and its outcomes.
- To provide the Python code implementation of the tool.
- To discuss the accuracy, efficiency, and potential future research directions for the computational tool.

## 2. METHODOLOGY

The development of the computational tool involved a systematic approach to address wellbore stability analysis and mud weight optimization. The tool was designed and implemented using the Python programming language to ensure flexibility, ease of use, and compatibility with existing industry practices. The computational tool utilizes various input parameters derived from well log data which are tabulated in Table 1. Additionally, the tool incorporates empirical correlations established through previous research and field data to estimate the relevant geomechanical properties of the formation. One of the key components of the computational tool is the calculation of stresses within the wellbore. By analyzing well log data, the tool employs relevant equations and correlations to determine the magnitudes and orientations of the stresses. This information is crucial for assessing wellbore stability conditions and potential failure mechanisms.

Table 1. Well Log input parameters used in the calculations

Input Parameters	Units
Depth	m, meter
Bit size	in, inches
caliper	in, inches
DT_compression	$\mu\text{s}/\text{ft}$
DT_shear	$\mu\text{s}/\text{ft}$
Gamma Ray	API
Rhob	(density) g/cc
V_clay	(clay volume) percent

Calculations have been performed in three domains. The first one is the calculation of rock properties. Then, using the calculated rock properties, stresses have been calculated using densities and poroelastic model. Subsequently, wellbore stability analysis based on Mohr-Coulomb criteria has been conducted. Finally, a mud weight window graph has been generated. These steps will be discussed sequentially.

**2.1. Rock Properties Calculations**

Drilling case is primarily based on the interpretation of rock properties, determination of stresses around the wellbore, in-situ stress characterization, and rock failure criteria (Alpkiray et al., 2022). The equations used in the calculation of rock properties are listed below as Equations 1-13. Dynamic elastic properties are converted to static using Equations 5-6 (Fjaer et al., 1992), whereas Equation 8 is used to calculate UCS calculation (Plumb, 1994). Tensile strength or TSTR is assumed equivalent to 10 % of UCS (Fjaer et al., 1992)

$$G_{dyn} = (13474.45) * (\rho_b / (\Delta t_{shear})^2) \dots\dots\dots(1)$$

$$K_{dyn} = (13474.45) * (\rho_b) [(\Delta t_{comp})^2 - (4/3) * G_{dyn}] \dots\dots\dots(2)$$

$$E_{dyn} = (9 * G_{dyn} * K_{dyn}) / (G_{dyn} + 3 * K_{dyn}) \dots\dots\dots(3)$$

$$PR_{dyn} = [0.5 * (\Delta t_{shear} / \Delta t_{comp})^2 - 1] / [(\Delta t_{shear} / \Delta t_{comp})^2] \dots\dots\dots(4)$$

With  $G_{dyn}$  is dynamic shear modulus in Mpsi,  $K_{dyn}$  is dynamic bulk modulus in Mpsi,  $\rho$  is bulk density in g/cc,  $E_{dyn}$  is dynamic Young’s modulus in Mpsi and  $\nu_{dyn}$  is dynamic Poisson’s ratio;  $\Delta t_{shear}$  and  $\Delta t_{comp}$  are shear slowness and compressional slowness (both in  $\mu s/ft$ ), respectively.

$$YME_{stat} = 0.6 * YME_{dyn} \text{ (for shales)} \dots\dots\dots(5)$$

$$YME_{stat} = 0.8 * YME_{dyn} \text{ (for sandstones)} \dots\dots\dots(6)$$

$$PR_{stat} = PR_{dyn} \text{ (assumed)} \dots\dots\dots(7)$$

$$UCS = 2.280 + 4.1089 * E_{stat} \text{ (Plumb, 1994)} \dots\dots\dots(8)$$

$$TSTR = 0.1 * UCS \text{ (assumed)} \dots\dots\dots(9)$$

$$V_{clay} > 0.45 \text{ (for shales)} \dots\dots\dots(10)$$

$$V_{clay} < 0.45 \text{ (for sandstone)} \dots\dots\dots(11)$$

$$FANG = 30 \text{deg (in shales)} \dots\dots\dots(12)$$

$$FANG = 40 \text{deg (in sandstone)} \dots\dots\dots(13)$$

**2.2. Stress Calculations**

Understanding of stress conditions is an essential part of drilling and instability analysis. Before drilling operation, stresses are considered in cartesian coordinate system. Once drilling begins, a cylindrical shape is presented and the analysis is considered in cylindrical coordinate system (Jaeger et al., 2009). In this section, minimum and maximum horizontal stresses have been calculated using the rock properties obtained in the previous section. The equations used in these calculations are listed below as Equation 14-22 (Fjaer et al., 1992).

$$\sigma_h = [v / (1 - v)] * (\sigma_v - \alpha * P_p) + \alpha * P_p + [E / (1 - v^2)] * \epsilon_h + [(v * E) / (1 - v^2)] * \epsilon_H \dots\dots\dots(14)$$

$$\sigma_H = [v / (1 - v)] * (\sigma_v - \alpha * P_p) + \alpha * P_p + [(v * E) / (1 - v^2)] * \epsilon_h + [E / (1 - v^2)] * \epsilon_H \dots\dots\dots(15)$$

$$S_v = \text{depth(m)} * 3.281 * \sigma_v \dots\dots\dots(16)$$

$$P_p = \text{depth(m)} * 3.281 * (\text{Pore pressure gradient}) \dots\dots\dots(17)$$

The overburden and pore pressure gradients are considered here as 1 psi/ft and 0.55 psi/ft respectively. A Closure gradient of 0.79 psi/ft is used to calibrate minimum horizontal stress

For wellbore stability analysis effective stresses are used:

$$\sigma_{h-min} \text{ (effective)} = \sigma_{h-min} \text{ (calculated)} - \text{Pore Pressure} \dots\dots\dots(18)$$

$$\sigma_{h-max} \text{ (effective)} = \sigma_{h-max} \text{ (calculated)} - \text{Pore Pressure} \dots\dots\dots(19)$$

**2.3. Failure Criteria**

Analysis for the determination of the rock requires to apply failure criteria. One of the most common and applied failure criteria is Mohr-Coulomb. It uses the unconfined compressive strength (UCS) and the Friction Angle (FANG) to construct the yield envelope (Alpkiray, 2021).

Figure 1 – Mohr-Coulomb representation under triaxial test (Alpkiray, 2021)

**2.4. Wellbore Stability Analysis And Mud Weight Optimization Process**

The computational tool performs wellbore stability analysis by evaluating the mechanical integrity of the wellbore under various operational conditions. It considers factors such as formation strength, pore pressure, mud weight, and wellbore geometry. Based on the calculated stresses and other relevant parameters, the tool determines the stability of the wellbore and identifies potential issues that may arise during drilling operations such as drill-pipe sticking, lost circulation, wellbore collapse, and non-productive time (Aadnoy et al., 2010). Furthermore, the tool facilitates mud weight optimization required to limit drilling problems by generating a mud weight window i.e MWW (Zoback et al., 1985). MWW is defined by four boundaries (Figure 2):

- 1 From the left, the first is the pore pressure limit, which should be exceeded to maintain an overbalance in the well and avoid kicks.
- 2 The second lowest boundary, is the shear failure limit. If the mud weight drops below this limit shear failure at the wellbore wall occurs. This can lead to diametrically opposing pairs of breakouts.
- 3 The third limit from the left is fracture gradient assumed overall as mud loss limit. It is defined by the least principal stress in equivalent mud weight. When the mud weight exceeds this limit mud losses can start to occur as a result of pre-existing fractures being opened.
- 4 The fourth limit represents the tensile failure of the rock (i.e Breakdown), is caused when the mud weight is too high. Severe mud losses can occur when this pressure is exceeded in intact formations.

Figure 2 – Mud Weight Window Explanation

The principal stress tensor around the borehole is computed as a function of the far field principal stresses, mud weight, the borehole orientation and azimuth with respect to the principal stress axes (Fjaer et al.). The Mohr-Coulomb criterion can thus be used to predict the minimum mud weight needed to prevent shear failure of the wellbore. The equations used in these calculations are listed below as Equations 23-30.

$$N = [1 + \sin(\text{FANG})] / [1 - \sin(\text{FANG})] \dots\dots\dots(23)$$

$$P_w = (\text{Mud Weight}/2.31) * \text{Normal Gradient} * \text{Depth(m)} * 3.281 \dots\dots\dots(24)$$

$$\sigma_R = P_w - P_p \dots\dots\dots(25)$$

$$\sigma_{\theta \min} = 3 * [\sigma_{\text{h-min}}(\text{effective})] - [\sigma_{\text{h-max}}(\text{effective})] - \sigma_R \dots\dots\dots(26)$$

$$\sigma_{\theta \max} = 3 * [\sigma_{\text{h-max}}(\text{effective})] - [\sigma_{\text{h-min}}(\text{effective})] - \sigma_R \dots\dots\dots(27)$$

$$\text{Kick Limit (Pore pressure)} = 8.34 * 2.31 * P_p / (\text{Depth} * 3.281) \dots\dots\dots(28)$$

$$\text{BreakoutPoint (Shear Failure)} = (3 * [\sigma_{\text{h-max}}(\text{effective})] - [\sigma_{\text{h-min}}(\text{effective})] + P_p - \text{UCS} * 1000 + N * P_p) / ([1 + N] * [3.281 * \text{depth(m)} * 0.052]) \dots\dots\dots(29)$$

$$\text{Fracture Gradient (Sh-min)} = (8.34 * 2.31 * \sigma_{\text{h-min}}) / (\text{Depth} * 3.281) \dots\dots\dots(30)$$

$$\text{Breakdown limit (Tensile)} = (3 * [\sigma_{\text{h-min}}(\text{effective})] - [\sigma_{\text{h-max}}(\text{effective})] + P_p + 145.037 * \text{TSTR}) / ([3.281 * \text{depth(m)} * 0.052]) \dots\dots\dots(31)$$

**3. CASE STUDY AND IMPLEMENTATION OF CODES**

To demonstrate the practical application of the developed computational tool for wellbore stability analysis and mud weight optimization, real data is used. The wellbore stability analysis and mud weight optimization results obtained from the computational tool are summarized in Figure 3. The analysis includes the assessment of wellbore stability conditions, identification of potential failure mechanisms, and the determination of an optimal mud weight range for maintaining wellbore stability while minimizing formation damage. The results are presented in a clear and concise manner. For instance, it is easy to notice from Figure 3 that a mud weight of 16 ppg would be able to stabilise the boreholes walls, avoid formations kicks, mud losses and formation breakdown.

Figure 3 – Example of wellbore stability analysis using our Program.

**4. CONCLUSION**

- The equations used in Equation 5-13 can be modified based on the laboratory studies of the fields for which the data will be used. Additional correlation will be added to enrich the program library.
- Biot constant can be modified and instead of assuming 1.
- The code successfully calculated rock properties, in-situ stresses using real data which allows to perform wellbore stability analysis and define the optimum mud weight for one well section

- This code will be converted into a program with interface to be much more user friendly.
- More applications like Pore Pressure Prediction and impact of wellbore trajectory are planned to be developed.

**REFERENCES**

Aadnoy, B. S., Fazaelizadeh, M., and Hareland, G. (2010). A 3d analytical model for wellbore friction. *Journal of Canadian Petroleum Technology*, 49(10):25–36

Alpkiray, M., Nguyen, T., Saasen A. (2022) Thermal Effects on Wellbore Stability and Fluid Loss in High-Temperature Geothermal Drilling. AAE Conference, Houston.

Alpkiray, M. (2021). Implementation of Geomechanical Approach in Geothermal Drilling During Lost Circulation Phenomena (Doctoral dissertation, New Mexico Institute of Mining and Technology).

Cole, P., Young, K., Doke, C., Duncan, N., and Eustes, B. (2017). Geothermal drilling: a baseline study of nonproductive time related to lost circulation. In *Proceedings of the 42nd Workshop on Geothermal Reservoir Engineering*, Stanford, CA, USA, pages 13–15.

Fjaer, E., Holt, R. M., Horsrud, P., Raaen, A. M., and Risnes, R., 1992. *Petroleum Related Rock Mechanics*, Elsevier, Amsterdam.

Jaeger, J. C., Cook, N. G., and Zimmerman, R. (2009). *Fundamentals of rock mechanics*. John Wiley & Sons.

Plumb, R.A. “Influence of composition and texture on the failure properties of clastic rocks.” Paper presented at the *Rock Mechanics in Petroleum Engineering*, Delft, Netherlands, August 1994. doi: <https://doi.org/10.2118/28022-MS>

Zhang, J., Keane, G., and Standifird, W. (2006). Wellbore stability with consideration of pore pressure and drilling fluid interactions. In *Golden Rocks 2006, The 41st US Symposium on Rock Mechanics (USRMS)*. OnePetro

Zoback, Mark D., Daniel Moos, Larry Mastin, and Roger N. Anderson. “Well bore breakouts and in situ stress.” *Journal of Geophysical Research: Solid Earth* 90, no. B7 (1985): 5523-5530.

Zoback, M., 2010, *Reservoir Geomechanics*: New York, Cambridge University Press.

**APPENDIX**

The appendix section provides a description of the Python codes that have been included as supplementary material to the paper. Each code is briefly explained, highlighting its purpose and functionalities within the context of wellbore stability analysis and mud weight optimization.

“””

Created on Wed Apr 12 12:26:09 2023

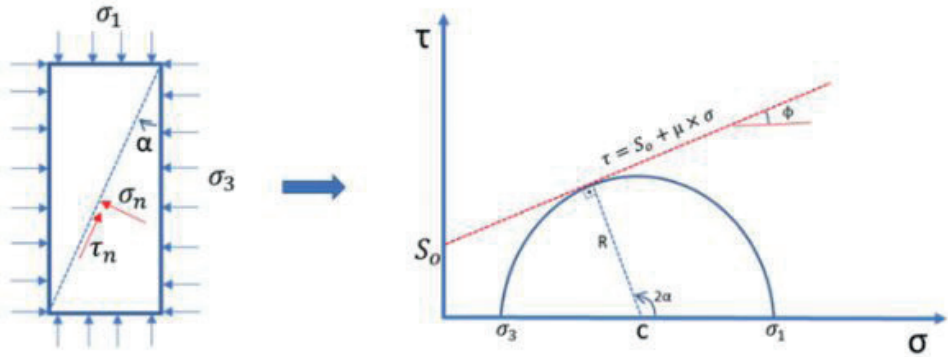
@author: calagoz

“””

```
import pandas as pd
import numpy as np
import matplotlib.pyplot as plt
# Load log data from Excel file
df = pd.read_excel('04-Well_A_data.xlsx')
# Calculate rock properties
Rhub = df['Rhub']
DT_shear = df['DT_shear']
DT_comp = df['DT_comp']
V_clay = df['V_clay']
Bit_size = df['bit size']
depth = df['depth']
caliper = df['caliper']
G = (13474.45 * Rhub) / (DT_shear**2)
K = (13474.45 * Rhub / (DT_comp**2)) - (4/3) * G
YME_dyn = (9*G*K) / (3*K+G)
PR_dyn = (0.5*(DT_shear/DT_comp)**2-1) / ((DT_shear/DT_comp)**2-1)
df['Rock Type'] = np.where(V_clay > 0.45, 'Shale', 'Sandstone')
df['FANG'] = np.where(df['Rock Type'] == 'Shale', 30, 40)
df['YME_stat'] = np.where(df['Rock Type'] == 'Shale', 0.6 * YME_dyn, 0.8 * YME_dyn)
YME_stat_GPa = 6.895 * YME_dyn
UCS_MPa = (4.1089 * YME_stat_GPa + 2.28) / 2
UCS_Mpsi = UCS_MPa / 6.895
TSTR_MPa = 0.1 * UCS_MPa
# User inputs
normal_gradient = float(input("Enter normal gradient in psi/ft: "))
pore_pressure_gradient = float(input("Enter pore pressure gradient in psi/ft: "))
closure_gradient = float(input("Enter closure gradient in psi/ft: "))
alpha = float(input("Enter biot constant, alpha: "))
MW_SG = float(input("Enter mud weight in SG: "))
# Calculate stresses
df['Sv'] = df['depth'] * 3.281 * normal_gradient
df['Pp'] = df['depth'] * 3.281 * pore_pressure_gradient
df['Sh_min'] = df['depth'] * 3.281 * closure_gradient
# Calculate PR_stat
PR_stat = PR_dyn
# Calculate teta_hmin and teta_hmax
epsilon_h = 0.0005
epsilon_H = 0.00108
```

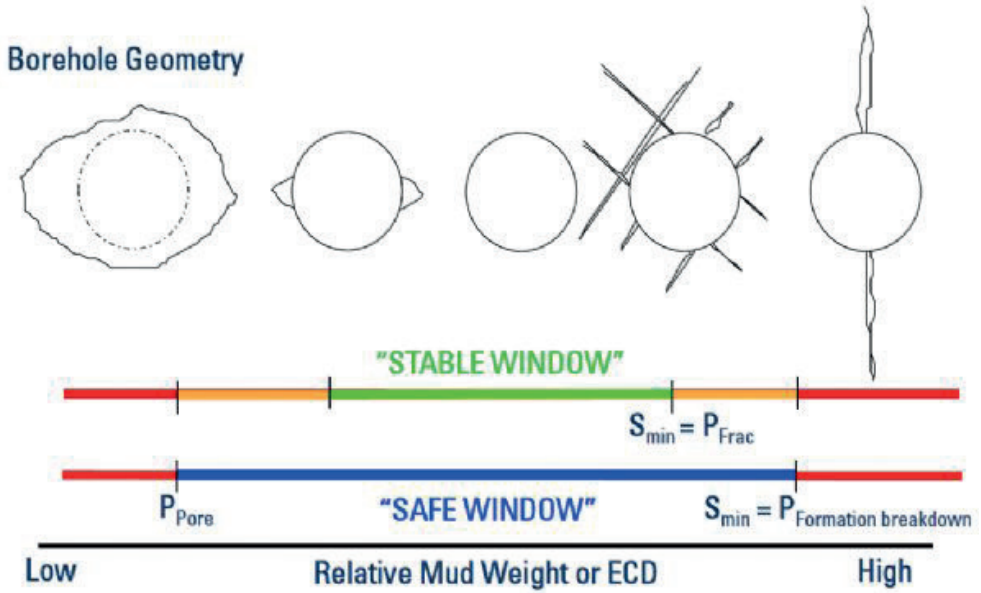
```
teta_hmin = (PR_stat/(1-PR_stat)) * (df['Sv']-alpha*df['Pp']) + alpha*df['Pp'] + (df['YME_stat']/(1-PR_stat**2))*epsilon_h + ((PR_stat*df['YME_stat']/(1-PR_stat**2))*epsilon_H)
teta_hmax = (PR_stat/(1-PR_stat)) * (df['Sv']-alpha*df['Pp']) + alpha*df['Pp'] + ((PR_stat*df['YME_stat']/(1-PR_stat**2))*epsilon_h + (df['YME_stat']/(1-PR_stat**2))*epsilon_H)
teta_hmin_eff = teta_hmin - df['Pp']
teta_hmax_eff = teta_hmax - df['Pp']
FANG_rad = np.radians(df['FANG'])
# Calculate N
N = (1 + np.sin(FANG_rad)) / (1 - np.sin(FANG_rad))
# Calculate pore pressure, tensile, and shear failure
Pw = (MW_SG/2.31)*normal_gradient*df['depth']*3.281
sigma_teta_R = Pw - df['Pp']
sigma_teta_min = (3*teta_hmin_eff) - teta_hmax_eff - sigma_teta_R
sigma_teta_max = (3*teta_hmax_eff) - teta_hmin_eff - sigma_teta_R
Pore_Pressure = (8.34 * 2.31 * df['Pp']) / (df['depth'] * 3.281)
Shear Failure = ((3*teta_hmax_eff) - teta_hmin_eff + df['Pp']) - UCS_Mpsi*1000 + N * df['Pp'] / ((1+N)*(3.281*df['depth']*0.052))
Tensile Failure = ((3*teta_hmin_eff) - teta_hmax_eff + df['Pp']) - TSTR_MPa*145.037 / ((3.281*df['depth']*0.052))
Fracture Gradient = (8.34 * 2.31 * teta_hmin) / (df['depth'] * 3.281)
# plot Depth vs Pore Pressure, Shear Failure, Tensile Failure and Fracture Gradient
plt.plot(Pore_Pressure, df['depth'], label='Pore Pressure(Kick Limit)')
plt.plot(Shear_Failure, df['depth'], label='Shear Failure(Breakout)')
plt.plot(Tensile_Failure, df['depth'], label='Tensile Failure(Breakdown)')
plt.plot(Fracture_Gradient, df['depth'], label='Fracture Gradient(Sh_min)')
plt.gca().invert_yaxis()
#plt.xlim(4, 24) # Set x-axis limits
#plt.ylim(3520, 3660) # Set y-axis limits
plt.xlabel('PPG')
plt.ylabel('Depth (m)')
plt.legend()
plt.savefig('figure2.jpg', dpi=1000)
plt.show()
Keywords: Wellbore stability analysis, Mud weight optimization
```

Figure 1 – Mohr-Coulomb representation under triaxial test (Alpkiray, 2021)



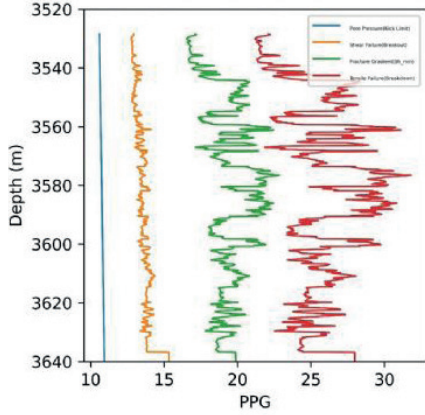
2.3. Failure Criteria bölümüne ait figure

Figure 2 – Mud Weight Window Explanation



2.4. Wellbore stability analysis and mud weight optimization process bölümü içerisinde

Figure 3 – Example of wellbore stability analysis using our Program.



3. Case Study and Implementation of codes bölümü içerisinde

Table 1. Well Log input parameters used in the calculations

Input Parameters	Units
Depth	m, meter
Bit size	in, inches
Caliper	in, inches
DT_compression	µs/ft
DT_shear	µs/ft
Gamma Ray	API
Rhob (density)	g/cc
V_clay (clay volume)	percent

2.Methodology ilk paragraph tan sonra

- AbstractTshales).....(5)
- YMEstat = 0.8 \* YMEdyn (for sandstones).....(6)
- PRstat = PRdyn (assumed).....(7)
- UCS = 2.280 + 4.1089\*Estat (Plumb, 1994).....(8)
- TSTR = 0.1 \* UCS(assumed).....(9)
- Vclay > 0.45 (for shales).....(10)
- Vclay < 0.45 (for sandstone).....(11)
- FANG = 30deg (in shales).....(12)
- FANG = 40deg (in sandstone).....(13)

# Pore Characterization and FESEM Analysis of the Niobrara Formation in Aristocrat Angus PC H11-07 Core, Wattenberg Field, Denver Basin, CO



**Elyan Aydin**

Turkish Petroleum, Production Department, Sogutozu Mah. Sht. Ogretmen Senay Aybuke Yalcin Cd., No:10, 06530, Cankaya / Ankara / Türkiye

## INTRODUCTION

The Niobrara Formation in the Denver Basin is a prolific unconventional, self-sourced oil and gas play in Wattenberg Field, Colorado (Figure 1). It is divided into two members: The Fort Hays Limestone at the base and the overlying Smoky Hill Member (Figure 3). The Smoky Hill Member is further divided into seven chalk-rich and marl-rich intervals. The organic-rich marls within the Niobrara Formation are source rocks while the chalks are reservoirs. The Wattenberg Field in the Denver Basin has been productive for 50 years. Due to the little research that has been performed last 50 years, this project aims to give a comprehensive account of the pore system and storage capacity in the Niobrara Formation. Qualitative data was collected by field emission scanning electron microscope (FE-SEM) analysis, while quantitative data was collected by quantitative image, nitrogen gas adsorption, mercury injection capillary pressure (MICP) analyses, and liquid saturation and immersion experiments from the samples of the Aristocrat Angus PC H11-07 core.

## METHODOLOGY AND RESULTS

FE-SEM analysis was performed on sixteen representative samples of the Niobrara Formation in the studied core. After a detailed FE-SEM analysis of the samples from the chalk and marl intervals, matrix-related interparticle (interP) and intraparticle (intraP) pores, and organic matter (OM) pores were the most common pore types observed in this research. Fracture-related pores were only identified in the B and C Chalks of the studied core. Additionally, the FE-SEM analysis results show that the transition from euhedral to anhedral micrite moving deeper in the Smoky Hill Member implies the porosity decrease from shallow to deep within the Smoky Hill Member. The quantitative image analysis data indicates that the pore sizes ranged from 0.085  $\mu\text{m}$  - 368.600  $\mu\text{m}$  in the chalks and 0.166  $\mu\text{m}$  - 221.600  $\mu\text{m}$  in the marls.

Porosity values reported from MICP analysis agree with those determined by liquid saturation and immersion experiments (Figure 4). This indicates that using kerosene as the immersion liquid is more suitable than DI water on the Niobrara Formation samples (Figure 5). Furthermore, permeability values obtained from MICP analysis show a high correlation with porosity values obtained by the same analysis.

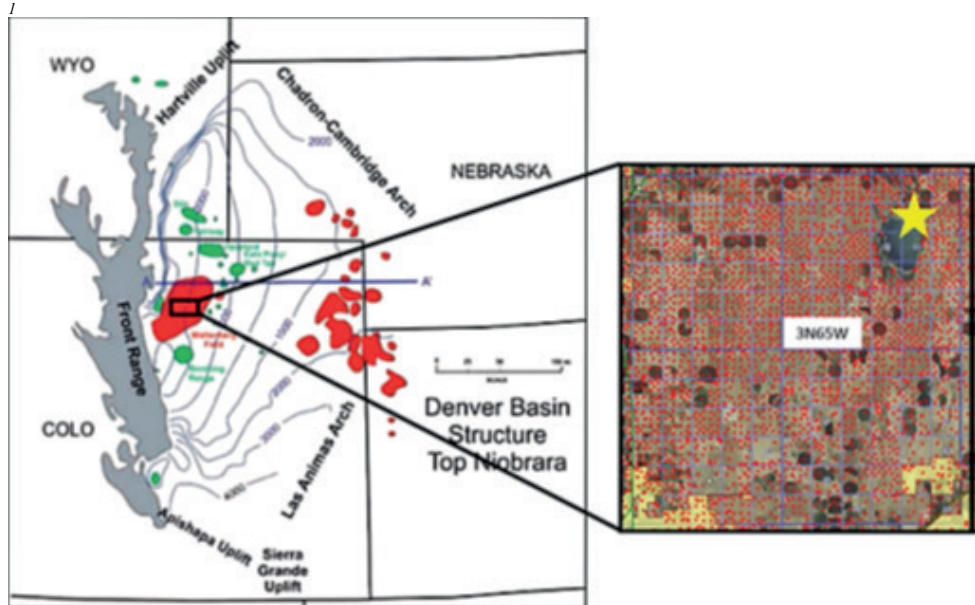
Pore size distributions were determined by MICP, and nitrogen gas adsorption analyses in order to capture micro- and nano-pore distributions (Figure 6). According to the nitrogen gas adsorption results, a trimodal pore size distribution is present within the chalks

and marls of the Niobrara Formation with a major peak at 10-20 nm, a small peak around 6 nm, and a big peak at 30-40 nm. In addition, the most abundant pore type observed by the MICP analysis is nanopores (1 nm-1  $\mu\text{m}$ ). This suggests that the nanometer size pores are the main contributors to the porosity of the Niobrara Formation in the studied core. Summing up the results, it can be concluded that the A Chalk is the best reservoir, while the A and C Marls are the best source rocks in the Niobrara Formation of the studied core.

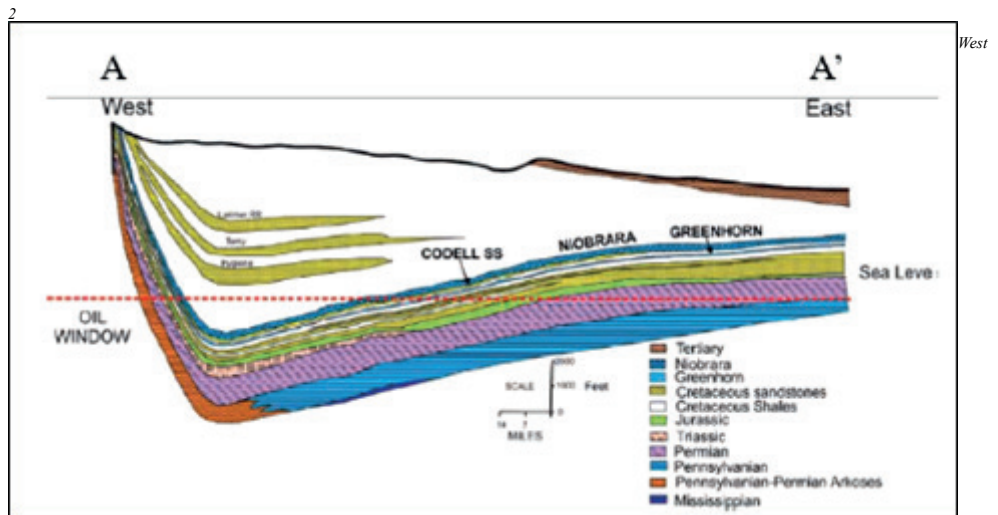
## REFERENCES

- Barlow, L.K., 1985, Event stratigraphy, paleoenvironments, and petroleum source rock potential of the Niobrara Formation (Cretaceous), Northern Front Range, Colorado: Master's thesis, University of Colorado, Boulder, Colorado, 288 p.
- Kauffman, E.G., 1985, Cretaceous evolution in the Western Interior Basin of the United States, in Pratt, L.M., Kauffman, E.G., and Zelt, F.B., eds., Fine-grained deposits and biofacies of the Cretaceous Western Interior Seaway: Evidence of cyclic sedimentary processes: Society for Sedimentary Geology Second Annual Midyear Meeting, Golden, Colorado, Field Trip No. 9, p. 90-99.
- Longman, M.W., Luneau, B.A., and Landon, S.M., 1998, Nature and distribution of Niobrara lithologies in the Cretaceous Western Interior Seaway of the Rocky Mountain Region: The Mountain Geologist, v. 35, p. 137-170.
- Sonnenberg, S.A., 2011, The Niobrara Petroleum System: A new resource play in the Rocky Mountain Region: Search and Discovery Article, v. 10355, p. 1-32.
- Sonnenberg, S.A., 2015, New reserves in an old field, the Niobrara/Codell resource plays in the Wattenberg Field, Denver Basin, Colorado: First Break, v. 33, no. 12, p. 55-62.

Keywords: mudrocks, pore characterization



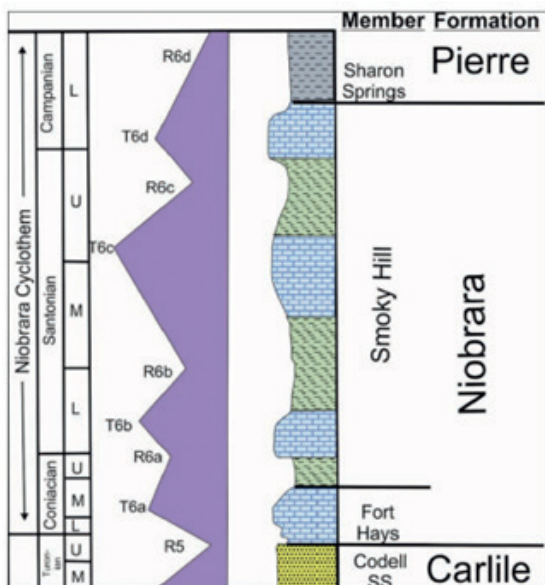
Structure contour map of the Denver Basin showing the location of Niobrara gas fields shown by red color; oil fields by green color. Cross section A-A' shown in Figure 2 Wattenberg Field is located along the synclinal axis of the Denver Basin (modified from Sonnenberg, 2015). The studied well location is highlighted by the star.



to east schematic cross section through the central part of the Denver Basin. The Niobrara Formation is in a thermally mature area in the deep part of the basin. Biogenic gas accumulations occur in the Niobrara along the shallow east flank of the basin. Location of cross section is shown on Figure 1 (Sonnenberg, 2015).

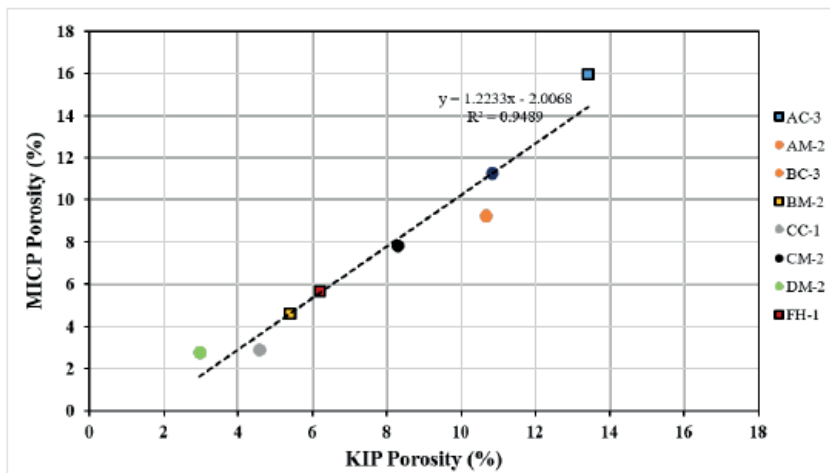


3

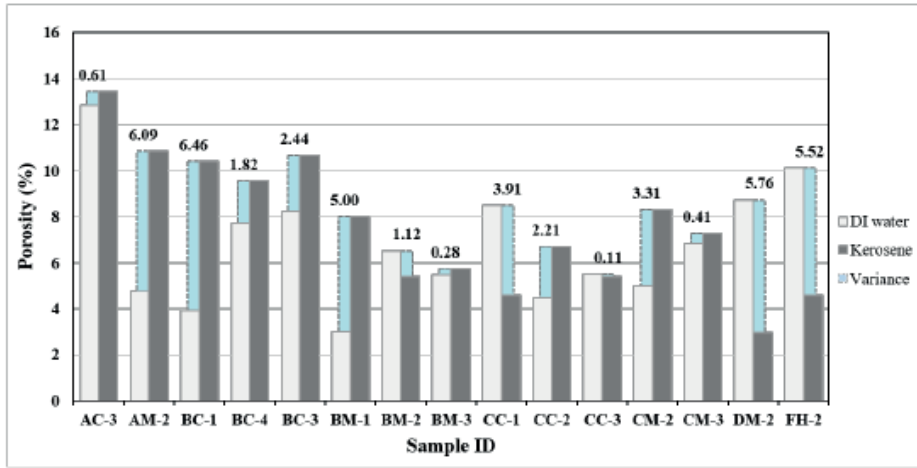


Generalized stratigraphic column for the Niobrara in the northern Denver Basin. The Niobrara ranges in age from Coniacian to lower Campanian. Several transgressive and regressive cycles are noted for the Niobrara interval. Four chalk-rich intervals were deposited during transgressive events and marls during regressive events (modified from Kaufman, 1985; Barlow, 1985; Longman et al., 1998; Sonnenberg, 2011).

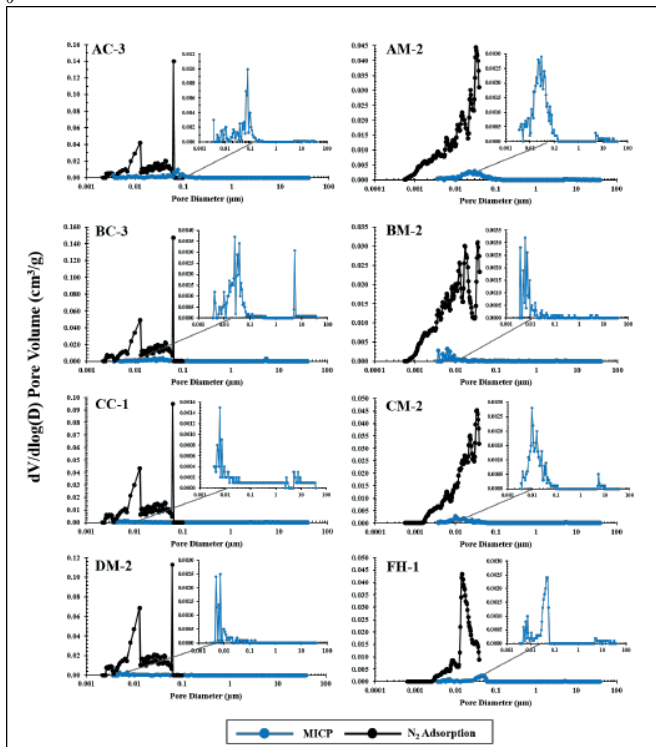
4



Comparison of measured porosity using kerosene saturation and immersion experiment (KIP) and MICP analysis performed on samples from the same depth.



Comparison of measured porosity using kerosene and DI water for the liquid saturation and immersion experiments from the same samples.



Comparison of pore size distributions obtained from nitrogen gas adsorption analysis (DFT model) and MICP analysis from the eight studied samples.

# Characterizing an Unconventional Reservoir with Onshore Conventional 3d Seismic Data: Case Study Using Seismic Inversion for the Dadas-1 Member



**Artem Orlov, Kirill Ezhov, Mehmed Ekrem Yazaroğlu, Canalp Özkul, Ahmet Ergün Mengen**  
Turkish Petroleum

## OBJECTIVE AND SCOPE

The seismic reservoir characterization of unconventional reservoir normally requires wide-azimuth long offset 3D seismic data. These type of data are normally hardly available in exploration stage of the project. Presented case study aims at using a narrow-azimuth 3D seismic volume to utilize for Amplitude Variation with Offset (AVO) inversion analysis methods to characterize Late Silurian – Lower Devonian age Dadas-1 organic rich shale member that acts as one of the main source rocks in SE Turkey and represents a self-sourced unconventional play. The seismic reservoir characterization by application of AVO methods where both well and seismic data are closely integrated is able to provide a new insight into distribution of porosity, TOC and more brittle versus ductile rocks to maximize reservoir recovery since the economic hydrocarbon production in unconventional plays requires hydraulic fracture stimulation. In addition, inverted elastic properties offers an opportunity to improve a reservoir modeling (static and dynamic), to provide the basic for design of an optimum well placement and could serve as a guide on how to improve the seismic acquisition/ resolution to highlight valuable “sweet spots”.

## METHODS, PROCEDURES, PROCESS

The first stage is well data analysis to determine petrophysical, rock-physics and geomechanical information. The 30 wells spread across Dadas project polygon were studied (Figure 1) to establish a crucial link between seismic inversion and reservoir parameters needed to create a rock-physics templates for interpreting crossplots of inversion attributes. To understand, quantify and formalize key factors for successful and efficient exploration, well completion and production a petrophysicist identified four rock types using various reservoir cut-off values: Rock-Type-1 if  $PHIE \geq 0.03\%$  and mineralogical brittleness (MBI)  $\geq 0.55$ , Rock-Type-2 if  $PHIE < 0.03$  and  $MBI \geq 0.55$ , Rock-Type-3 if a kerogen volume  $> 0.05$  and Rock-Type-4 is all the rest. The rock typing allowed to analyze the data on quantitative (PHIT, PHIE, WCLAY, TOC) and qualitative levels and looked at characterization of unconventional reservoir from different prospective. Afterwards a simultaneous AVO seismic inversion was performed to determine the desired elastic properties in 3D space using the seismic data. The study uses three 3D seismic volumes acquired in the period of 2009-2021 that were combined in one survey 3D for a processing in the year 2021. The inverted an acoustic impedance and the Lamé parameters ( $\lambda$  and  $\mu$ ) allowed to compute the LMR logs and the elastic properties of Poisson's ratio and Young's Modulus. The optimum

Silurian unconventional Dadas-1 shale reservoir in Diyarbakir basin were successfully characterized using LMR crossplot method. Lambda parameter is the measure of incompressibility of the rock and Mu is the measure of rigidity. The potentially hydrocarbon bearing zones can be separated from shales due to their high quartz content giving them a high  $\mu/\rho$  value and low  $\lambda/\rho$ . Besides, to support the derived intervals for the optimum brittleness values a plot proposed by the Rickman (2008) between Young's modulus and Poisson's ration were utilized for cross-validation. Rock with low Poisson's ratio and high Young's modulus describes a relatively hard and rigid formation that makes it less ductile and potentially brittle (Figure 2). In addition, to contribute to the static geological modeling a multilinear regression analysis was utilized to predict a porosity from the pre-stack seismic inversion attributes (acoustic impedance, AI and  $V_p/V_s$  ratio,  $V_p/V_s$ ). Since no single property was sensitive enough, both the (AI and  $V_p/V_s$ ) were simultaneously used as inputs to train multi-attribute regression that established a maximum correlation with the least mean square error.

## RESULTS, OBSERVATIONS, CONCLUSIONS

The interpretation of AVO inversion data has certainly become an important tool for reservoir identification and description, nevertheless, it is important to be aware of some limitations and assumptions behind conventional seismic data approach: 1). similar elastic properties of AI and  $V_p/V_s$  for sandstone and shale coupled with limited useful seismic frequency of 30-40Hz in the target interval caused inability of a Bayesian lithoclassification to distinguish all lithoclasses describing shale properties in details, 2). the limited offset data up to 28-30 degree resulted AVO effect from density not fully observed introducing uncertainty to inversion result, 3). LMR crossplot assumes isotropy which is suitable for the identification of reservoir at the well. Since the elastic properties of the rock are anisotropic the number of well as control points is directly proportional to ambiguity of seismic inversion, 4). the effect of the band-passed seismic wavelet used to calculate the low-frequency model introduce a bias to the seismic inversion result from log data. However, the analysis confirmed that the Dadas-1 member is prospective unconventional reservoir due to its relatively high quartz content and therefore is likely to respond positively to hydraulic fracturing. The conventional 3D seismic data together with petrophysical interpretation and rock-physics analysis enabled to understand the relationship between the elastic parameters derived from AVO inversion and some of the key properties that control productivity in shale plays, such as TOC, porosity and brittleness.

Crossplot study indicated that elastic log information, derivable from seismic data, could be used to indicate the spatial distribution of sweet spots away from the wells and enhanced the value of seismic data beyond conventional structural interpretation and attribute analysis.

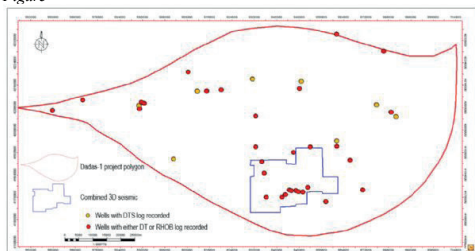
Elastic moduli, TOC and brittleness are all related to each other. Rock with high Young's modulus and low Poisson's ratio is more brittle that caused a low TOC and vice versa. The trade-off value between these critical parameters of brittleness and TOC must be estimated. The 3D output volumes of elastic moduli from the seismic reservoir characterizations can be further used for in-situ stress calculations and 3D mechanical earth model building. Analysis presented in this work could be bolstered through the generation of an Amplitude Variation with offset and Azimuth (AVAZ) inversion volume that could be further used to investigate fracture orientation, fracture closer stress distribution and derivation of a principal axes of the elastic stiffness tensor for understanding of fault activity.

**NOVEL/ADDITIVE INFORMATION**

The novel aspect of this project is the multi-scale approach rooted in 3D pre-stack seismic inversion, petro physical evaluation, rock-physics analysis and the Bayesian estimation theory to determine the location of the most promising brittle zones for optimum hydraulic fracturing well placement.

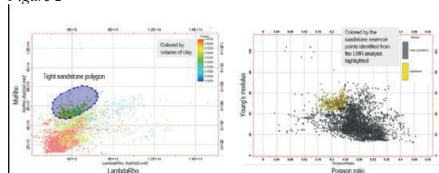
Keywords: Unconventional resources, seismic inversion

Figure



The Dadas project polygon and wells with petrophysical interpretation that were used for a rock-physics crossplot analysis

Figure 2



Lithology and brittleness analysis using LambdaRho/MuRho crossplot versus Young's modulus/Poisson ration. The tight sandstone intervals that are separated using LMR plot are highlighted on the Young's modulus and Poisson ratio plot in the most brittle area

# Tuna Deltası (Romanya ve Bulgaristan Açık Denizi) Kıtasal Yamacı'nın Gaz Hidrat Potansiyeli ve Sismik Stratigrafisi



**Orhan Atgun<sup>1</sup>, Günay Çiçik<sup>2</sup>**

<sup>1</sup>Dokuz Eylül Üniversitesi, Deniz Bilimleri ve Teknolojisi Enstitüsü

<sup>2</sup>Dokuz Eylül Üniversitesi, Jeofizik Mühendisliği Bölümü ve Deniz Bilimleri ve Teknolojisi Enstitüsü

## ÖZET

Avrupa'nın en büyük ikinci nehir havzasının oluşmasına neden olan Tuna Nehri, bu tortul girişimi nedeni ile Karadeniz'de birçok jeolojik unsurlara sebep neden olmuştur. Günümüzde Vitez olarak adlandırılan güncel kanal dışında gömülü halde bulunan birçok kanal yapısı bulunmaktadır. Hem güncel kanal hem de gömülü kanallar nedeni ile yamaçta ve abisal düzlükte oldukça büyük bir alana yayılmış deltalar oluşmuştur. Yamaçta gömülü halde bulunan kanal geometrileri sismik yansıma kesitlerinde açıkça görülmektedir. Bu kanalların geometrilerini ortaya koymak hidrokarbon rezervleri açısından oldukça önemlidir. Alışlagelik hidrokarbon kaynaklarının yanı sıra alışlagelmedik kaynaklardan biri olan gaz hidratlar açısından da alandaki kanal geometrileri ve bunların taşınış olduğu tortulları araştırmak gereklidir. Karadeniz'in birçok bölgesinde BSR (bottom simulating reflector) yansıması denilen gaz hidratın varlığını kesin olarak ifade eden yansıma türlerini görmek mümkündür. Yapılan çalışmada, GEOMAR'ın yürüttüğü SUGAR (Submarine Gas Hydrate Reservoirs) projesinin ortak işbirliğinin bir parçası olarak Dokuz Eylül Üniversitesi DBTE-SeisLab bünyesinde bulunan sismik ekipmanlar ile R/V Maria S. Merian gemisiyle 2013 yılında yaklaşık 2300 km çok kanallı yüksek ayrımlı çok kanallı sismik yansıma verisi toplanmıştır. SUGAR projesinin amacı bölgedeki gaz hidrat rezervlerinden doğal gaz üretimini sağlamak olsa da bölgede toplanan sismik veriler sayesinde gaz hidratın yanı sıra kanal geometrilerine yönelik çalışmalar da gerçekleştirilmiştir. Tüm denizaltı yelpazelerinin dağılımını haritalamak çalışma alanı içerisinde mümkün olmasa da sismik kesitlerde bu tortulların tabanına kadar nüfuz edildiğinden bu deltaları oluşturan paleokanalların haritalanması mümkün olmuştur. Ayrıca alanın en dikkat çekici özelliklerinden biri de hala tam olarak nedeni ispatlanmamış olan çoklu BSR yansımalarının alanda oldukça fazla gözlemlenmesidir. Gaz hidrat araştırmalarında cevaplanması gereken önemli sorulardan biri olan çoklu BSR yansımalarının nedenleri ve sonuçları da bu çalışmanın hedefleri arasında yer almaktadır.

## ABSTRACT

The formation of the second largest river basin in Europe, the Danube River, has resulted in numerous geological features in the Black Sea due to its sedimentary input. Today, there are many channel structures buried apart from the current channel called Vitez. Both the active and buried channels have contributed to the formation of extensive deltas on the slope and abyssal plain. The geometries of the buried channels on the slope are clearly visible in seismic reflection profiles.

Revealing the geometries of these channels is crucial for hydrocarbon reserves. In addition to conventional hydrocarbon sources, it is also necessary to investigate the channel geometries in the area and the sediments they carry in terms of unconventional resources, such as gas hydrates. In many regions of the Black Sea, it is possible to observe reflection types known as BSR (bottom simulating reflector), which indicate the presence of gas hydrates definitively. In the conducted study, approximately 2300 km of high-resolution multi-channel seismic reflection data was collected in 2013 using seismic equipment at Dokuz Eylül University's DBTE-SeisLab, as part of the collaborative efforts of the SUGAR (Submarine Gas Hydrate Reservoirs) project led by GEOMAR, and aboard the R/V Maria S. Merian. Although the primary objective of the SUGAR project is to exploit gas hydrate reservoirs in the region for natural gas production, the seismic data collected in the area have also facilitated studies on channel geometries. While mapping the distribution of all submarine fans within the study area might not be entirely feasible, the seismic sections have penetrated down to the base of these sediments, enabling the mapping of paleochannels that constitute these deltas. Furthermore, one of the most striking features of the area is the abundant presence of multiple BSR reflections, the exact causes of which have not been fully proven yet. Investigating the reasons and implications of these multiple BSR reflections is one of the significant questions that need to be addressed in gas hydrate research and is also among the objectives of this study.

## AMAÇ

Tuna Fanı kıyı şerifinden geniş bir şelf ile ayrılan (yaklaşık 120 km) ince taneli bir türbidit sistemidir (Popescu et al., 2001). Tuna derin deniz yelpazesi, şelf kırığında 100 m su derinliğinden abisal düzlükte 2200 m su derinliğine kadar eğimli bölgede gelişmiştir (Wong et al., 1997). Tuna yelpazesinin en son aktif kanalı şelf kırığında Vitez Kanyonu ile birlikte Tuna Nehri'ne bağlanan Tuna Kanalı'dır (Popescu et al., 2001). Aşındırıcı olan Vitez Kanyonu yaklaşık 800 m su derinliğinde bir kanal-levee sisteminde sona ermektedir (Le Ricolais et al., 2013). Tuna kanalı, yaklaşık 25 ka önce son buzul dönemde deniz seviyesinin bugünkünden 150 m daha düşük olduğu dönemde gelişmiştir (Winguth et al., 2000). Tuna yelpazesindeki gaz hidrat oluşumu, sığ denizaltı tortullarında ilk hidrat keşiflerinden beri bilinmektedir (Ginsburg and Soloviev, 1998). Daha yakın zamanlarda, derin tortullarda gaz hidratın varlığı yelpazenin güneyindeki BSR gözlemlerinden çıkarılmıştır (Ion et al., 2002). Bölgedeki gaz çıkışları, esas olarak %99,1–99,9 konsantrasyonları ile biyojenik kaynaklı metandan oluşmaktadır (Poort et al., 2005;

Römer et al., 2012; Bialas, 2014). Dünyadaki en çarpıcı örneklerden biri olup çalışma alanını da içerisinde bulunduran Tuna Fan Deltası'nda (Popescu et al., 2006) gözlemlenmiştir. Bu çalışmada Tuna deniz yelpazesini oluşturan kanal-levece sistemindeki BSR yansımalarının karakterleri ve dağılımını araştırmak amacıyla yüksek çözünürlüklü 2 boyutlu çok kanallı sismik yansıma verileri kullanılmıştır. Çoklu BSR'ların farklı gaz bileşenlerine sahip olabileceği hipotezinden yola çıkılarak çalışma alanında üst üste sıralanmış 5 adet BSR yansımalarının faz diyagramı ile araştırılması çalışmanın amaçlarından biridir. Gaz hidratların potansiyel bir doğalgaz rezervi olduğu hesaba katıldığında ve BSR olan bölgelerin gaz hidrat rezervi olduğu düşünüldüğünde, bu bölgelerdeki yansımalara dayanarak tüm çalışma alanı boyunca rezerv hesaplamalarının yapılması çalışmanın bir diğer amacını oluşturmaktadır.

Ayrıca çalışma alanı kıtasal yamaçta bulunduğundan, abisal düzlüğe kadar ilerleyen gömülü kanalları da haritalamak mümkün olmuştur. Bölgedeki paleokanallar hidrokarbon rezervleri açısından oldukça önem teşkil ettiğinden bu bölgeyi stratigrafik olarak incelemek de çalışmanın bir başka amacını yansıtmaktadır.

## GEREÇ VE YÖNTEM

Çalışmada kapsamında, GEOMAR'ın yürüttüğü SUGAR (Submarine Gas Hydrate Reservoirs) projesinin ortak işbirliğinin bir parçası olarak Dokuz Eylül Üniversitesi Deniz Bilimleri ve Teknolojisi Enstitüsü'ne ait olan sismik ekipmanlar ile R/V Maria S. Merian gemisiyle Aralık 2013 yılında yaklaşık 2300 km çok kanallı yüksek ayrımlı çok kanallı sismik yansıma verisi toplanmıştır. Çok kanallı sismik verilere ait hatlar Şekil 1'de gösterilmiştir. 6.25 kanal aralığı ile toplamda 196 kanala sahip 1050 metre uzunluğundaki sismik alıcı kablo 4 metre derinlikten çekilmiştir. Sismik kaynak olarak 3 metre derinlikten çekilen ve 45+45 inç3 hacme sahip olan GI-gun ile 12,5 m ve 18,75 m atış aralıkları ile 2000 psi basınçlı atışlar gerçekleştirilmiştir. Sismik kayıt ise 1 ms örnekleme aralığı ile 4000 ms kayıt uzunluğuna sahiptir. Çok kanallı sismik veriler geleneksel veri işlem adımlarına tabi tutulmuştur ve bunları sırası ile; veri yükleme, geometri tanımlama, bant geçişli filtre (8-220 Hz), iz ayıklama, f-k eğim filtresi, CDP gruplarını oluşturma, hız analizi, tekrarlı yansımaların bastırılması (SRME), yığılma öncesi zaman migrasyonu ve genlik düzeltmeleridir. Stratigrafik yorumlamalar için otomatik kazanç kontrolü (AGC) kullanılırken BSR yorumlamaları için gerçek genlik düzeltmesi (TAR) uygulanmıştır. BSR seviyeleri üzerinde yapılan denge eğrilerinin hesaplandığı sismik kesitler yığılma öncesi derinlik migrasyonuna tabi tutulmuştur. Karmaşık sismik nitelik analizleri için final kesitlerden görünür polarite, anlık frekans ve zarf kesitleri elde edilmiştir.

Çok ışınlı batimetri verisi için gemi gövdesine monte edilmiş olan EM122 ekosandır (Kongsberg) cihazı tüm sismik hatlar toplanırken veri toplamıştır ve bu verilerden 25m x25m çözünürlükte harita elde edilmiştir.

Tüm yorumlamalar ve haritalama işlemleri IHS Kingdom yorumlama programında gerçekleştirilmiştir.

## BULGULAR

Çoklu BSR'ların varlığı Popescu et al. (2006) 'da tanımlandığı üzere 10 yıldan fazla süredir 3 farklı kayıt sistemi ile görüntülenmiştir. Bu gözlemler ile beraber bölgedeki 5 adet BSR yansımalarının artefakt ya da sistemden kaynaklanan gerçek olmayan görüntüler olmadığı kanıtlanmıştır. Çalışma kapsamında kullanılan veri setinde gözlemlenen BSR yansımaları, önceki çalışmalarda gözlemlenen çoklu BSR yansımalarına uygundur.

Tuna Kanalı'nın yanı sıra çalışma alanında birçok kanal sistemi bulunmaktadır. Bunlardan hiçbirisi Tuna Kanalı ölçeğinde olmamakla birlikte kanalların 3 tanesi Tuna Kanalı'nın batısında 3 tanesi de doğusunda yer almaktadır. Tuna Kanalı'nın batısında şelf kırığından bir kanyon sistemi ile başlayıp kıtasal yamaçın içerisinde son bulan yan yana 3 adet kanal bulunmaktadır ve bu kanallar Zander et al; 2016'da "Sugar Kanalları" olarak isimlendirilmiştir. Tuna Kanalı'nın doğusunda ise yine şelf kırığından bir kanyon sistemi ile başlayıp kıtasal yamaç içerisinde son bulan Hillman et al 2018 'de "S1, S2 ve S3" olarak adlandırılan 3 adet kanal sistemi bulunmaktadır.

Tüm Karadeniz'i kapsayan çalışmalardan biri olan Nikishin et al., 2015'teki sismik hatlarda, Tuna denizaltı fanlarının olduğu bölgedeki fan sistemlerinin maksimum derinliği geliş-gidiş zamanı cinsinden 4 saniye olarak görülmektedir. Çalışmada kullanılan sismik yansıma kesitlerinin kayıt uzunluğunun geliş-gidiş zamanı cinsinden 5 saniye olması, alan içerisinde kalan kanal-levece sistemlerinin oluşturduğu tüm seviyeleri gözlemlenmeyi mümkün kılmıştır. Kanal-levece sistemlerinin oluşturduğu seviyeler içerisinde farklı 3 farklı alanda BSR'lar gözlemlenmiştir ve bu BSR alanlarından bazılarındaki yansımalar çoklu BSR'lar olarak gözlemlenmektedir.

Çalışma alanı içerisinde farklı alanlarda BSR'lar gözlemlenmiştir ve bunlar "X, Y ve Z" olmak üzere üçe ayrılmıştır (Şekil 2). Alanın batısında bulunan "X" BSR alanı yüz ölçümü olarak en büyük alandır. Daha sonra alansal olarak bunu "Z" alanı izler ve "Y" alanı ise BSR alanları arasında yüz ölçümü olarak en küçük alandır. BSR alanları, çalışma alanının kuzeyinde gaz hidrat stabilite zonu (GHSZ) olarak 720 metre hesaplanan kontur ile sınırlanmaktadır. BSR alanlarından en dikkat çekici olan alan "X" alanıdır ve bunun nedeni bu bölgedeki çoklu BSR'ların 5 katmandan oluşmasıdır (Şekil 3).

Tuna Kanalı'nı dikine kesen hatlardan biri olan MSM34 8 hattında, kanal-levece sistemlerinin neden olduğu jeolojik unsurların tamamını görmek mümkündür. Bu sistemlerin oluşturduğu birimler akustik verilerde 1'den 10'a kadar sıralanmıştır ve Tuna Kanalı'nın oluşturduğu birim 10 numara ile ifade edilmiştir. Ayrıca akustik verilerde içerisinde düzenli yansımaların bulunmadığı kaotik yansımalar şeklinde görülen MTD'ler de bulunmaktadır.

Önceki çalışmalardan biri olan Winguth et al., 2000 tarafından bu alandaki kanal-levee sistemlerinin yaşları tanımlanmıştır. Bu birimlerden Tuna kanal-levee sistemi (TKS), son büyük buzul döneme karşılık gelen 0-75 ka'dır. 7 numaralı gömülü kanal-levee sisteminin (GKS) üzerinde ve paleokanalın batısında bulunan 9 numaralı seviye olarak tanımlanan birim 73-320 ka'dır. Tuna Kanalı'nın batısında yer alan GKS'ye karşılık gelen yaş ise 320 ka'dır (Şekil 4).

Çalışma alanı içerisinde farklı ölçeklerde birçok MTD bulunmaktadır. Bunlardan bazıları lokal MTD'ler bazıları ise yüzlerce kilometre karelik alana yayılmış MTD'lerdir. BSR'ların 2000 ms ve 2700 ms aralığındaki derinliklerde gözlemlendiği göz önüne alındığında özellikle bu derinliklerdeki MTD yapılarının yorumlanması önemlidir.

“X” BSR alanında çoklu BSR'ların gözlemlendiği bölgede yapılan “heat flow” ölçümleri MSM34\_07 sismik hattı ve grafik üzerinde aynı ölçekte sıralanmıştır. Batıdan doğuya doğru sıralanmış 8 adet heat flow ölçümünden elde edilen ısı akışı ve sıcaklık gradyanı değerleri her bir nokta için BSR üzerinde de gösterilmiştir ve bu noktalardeki BSR derinlikleri de hesaplanmıştır (Şekil 5). HF\_1'den HF\_9'a doğru ölçüm noktalarına bakıldığında bu noktalardeki BSR kalınlıkları MTD yapısının olduğu bölüme kadar 350 metre olarak gözlemlenmiştir. MTD yapısının batı sınırı ile birlikte diğer ölçüm noktalarındaki BSR kalınlık değerleri doğuya gittikçe artmıştır. En batıdaki ölçüm noktası ile en doğudaki ölçüm noktası arasında 30 metrelik bir kalınlık farkı olduğu görülmüştür. Daha önce denge eğrisinden hesaplanan 24,5 0C'lik jeotermal gradyan sarı kesikli çizgi ile gösterilmiştir ve tam olarak MTD'nin batı sınırının olduğu yerde gerçek BSR yansımaları (mor çizgi) hesaplanan sarı çizgili gradyandan daha derine gitmiştir ve bu fark giderek artmıştır. Deniz tabanını tam olarak paralel oluşmayan MSM34\_07 hattındaki BSR'ın yansımaları özellikleri aynı şekilde MSM34\_08 hattında görülmektedir ve bu hat için de paralelliğin bozulduğu yer MTD'nin batı sınırı ile başlamaktadır. Ayrıca ikincil BSR da MTD yapısının görülmesi ile birlikte birincil BSR yansımaları ile olan paralelliğini kaybetmiştir ve doğuya doğru aradaki kalınlık farkı artmıştır. Birincil ve ikincil BSR arasındaki kalınlık farkı batıda 90 metre iken en batıda 140 metreye kadar çıkmıştır. Sıcaklık gradyan değerlerine bakıldığında, dt/dz (K/m) değerlerini MTD yapısı dışında kalanlar ve içinde kalanlar şeklinde değerlendirmek gereklidir. MTD yapısının olduğu bölümdeki sıcaklık gradyan değerleri dışında kalanlara göre daha yüksek hesaplanmıştır (Şekil 5a). Celsius cinsinden (0C) hesaplandığında grafikten de görüldüğü üzere MTD yapısının bulunduğu bölgedeki sıcaklık değerleri 33 0C ve 370C arasında gözlemlenmektedir. MSM34\_08 hattında seçilen nokta için, daha önce denge eğrisinden 24 0C olarak hesaplanan gradyan kullanıldığında, bu noktadaki gradyan 30 0C olarak hesaplanmaktadır. Fakat grafikteki gradyan değerlerine göre, saf metana göre hesaplanmış bu 30 0C'lik gradyanın sıcaklığı MTD bölgesinde kalan gradyanlara kıyasla daha düşüktür. Kısacası gerçek gradyan değerleri

%100 metan eğrisine göre hesaplandığında, denge eğrisinde tam olarak BSR seviyesinde keşimlenmektedir. Isı akışı değerleri ise (Kossel et al., 2013)'de aynı çalışma alanı için hesaplanan termal kondaktivite değeri olan 1,3 W/m/K değerine göre hesaplanmıştır ve sonuçlar Şekil\_5a'daki grafikte gösterilmiştir.

Gaz hidratların yanı sıra çalışma alanı stratigrafik olarak ele alındığında birçok kanal-levee yapısı ortaya çıkmaktadır. Bu kanallardan en güncel olan Tuna Kanalı dışında kalan kanallar gömülü halde bulunmaktadır ve kanalların geometrisi yamaç boyunca haritalanmıştır. Tuna Fan Deltasında diğer kanal-levee sistemlerinde olduğu gibi yüksek genlikli yansımalar gözlemlenmiştir. Genel olarak bu yansımalar tipleri iki jeolojik unsura kendini göstermektedir. Bunlardan ilki kanal eksenlerinin içerisindeki yüksek genlikli yansımalar (HAR) ve bu yansımalar kanalın gözlemlendiği tüm sismik hatlarda kanal boyunca görülmektedir. Bu yüksek genlikli yansımalar paketleri kanal içerisindeki dolgularda görülmektedir ve bu dolguların, kanaldaki kayma yapılarına bağlı olarak kanalın ilk oluştuğu andaki seviyeden günümüzdeki seviyeye kadar geçen sürede batıdan doğuya doğru biriktiği gözlemlenmiştir (ŞEKİL 6a). Kanal-levee sistemlerinde sıkça görülen diğer bir yansımalar türü ise yüksek genlikli yansımalar paketleri denilen HARPlardır (high amplitude reflection packets). HARPlar kanal-levee paketlerinin altında paralel şekilde birikmişlerdir levee sistemini oluşturan birikimlerden göreceli olarak çok daha yüksek genliklere sahiptir. Sismik hatlarda gözlemlenen HARPlar, kanal içerisindeki HARlara oranla çok daha ince bir tabaka olarak birikmişlerdir ve geniş alanlara yayılmışlardır. Göreceli genlik değerleri tüm sismik hatlarda açıkça fark yaratmadığı ve ince bir tabaka olarak biriktiği için bazı hatlarda HARPları yorumlamak ve haritalamak HARlara oranla daha zordur. HARPlar çalışma alanındaki eğimin azaldığı ve klasik kanal-levee yapısının görüldüğü sismik hatlarda ortaya çıkarken HARlar kanalın ilk oluştuğu yerden itibaren çalışma alanındaki son sismik hatta kadar tüm hatlarda gözlemlenmiştir.

Batimetri haritası en güncel kanyon olan Viteaz Kanyonu'nu ve Tuna Kanalı'nı açıkça ortaya koymaktadır. Kanalın thalweg doğrultusu, genişliği ve kanal boyunca değişim gösteren eğimi gibi birçok morfolojik bilgi batimetri sayesinde elde edilmektedir. Nikishin'in yapmış olduğu çalışmada yaklaşık 4. Saniyede biten Tuna Fanına ait birimlerde çalışma alanı içerisinde kalan bölümde Şekil 4'te de gösterilen sismik yansımalar kesitinde güncel Tuna Kanalı'nın yanı sıra gömülü halde bulunan 3 adet paleokanal gözlemlenmiştir. Bu paleokanallar 3,4 ve 7 numaralı seviyelere ait kanallardır ve neredeyse kuzeybatı- güneydoğu doğrultulu olan tüm sismik kesitlerde görülmektedir. Kuzeybatı-güneydoğu sismik kesitlerde gözlemlenen paleokanallara ait seviyeler yorumlandığında paleokanallar ortaya çıkmaktadır. Bu seviyelerde görülen kanal duvarlarının en yüksek olduğu bölümler çizildiğinde Şekil\_7'deki paleokanalların haritası oluşmaktadır. Bu paleokanalların tamamı güncel Tuna Kanalı'nın batısında yer almaktadır ve thalwegleri Tuna Kanalı ile aynı doğrultudadır.

## SONUÇLAR

Çalışma alanı içerisinde kalan tüm gömülü kanalları haritalamak mümkün olmuştur ve bu kanallar içerisinde yüksek genlikli yansımalar (HAR) keşfedilmiştir. Bu yansımaların kum kanalları olduğu düşünülmektedir ve hidrokarbon rezervleri açısından oldukça önem teşkil etmektedir. Ayrıca alandaki MTD yapısı diğer çalışmalarda gözlemlenen MTDler ile birleştirilmiştir ve Karadeniz'deki alansal olarak en büyük MTDlerden birini haritalamak mümkün olmuştur. Gaz hidratlar açısından bakıldığında da, kıtasal yamaç boyunca 3 alandan oluşan gaz hidrat rezervleri haritalanmıştır. Bu haritalar daha önce yapılan çalışmalar ile kıyaslandığında bu alan için en ayrıntılı BSR dağılım haritalarıdır. Bunlardan X gaz hidrat alanındaki çoklu BSR yansımaları üzerinde denge eğrileri hesaplanmıştır ve aynı jeotermal gradyan ile yapılan hesaplamalarda kalınlığın artmasının sebebinin basınca bağlı olduğu ortaya çıkmıştır. Ayrıca farklı denge eğrileri ile BSR seviyelerinde farklı gaz bileşenleri üzerine farklı gaz kompozisyonları ile yeni eğriler oluşturulmuştur.

## REFERANSLAR

- Bialas, J., Klaucke, I., and Haeckel, M. (Eds.), 2014. FS MARIA S. MERIAN Fahrtbericht / Cruise Report MSM-34/1 & 2 - SUGAR Site, 06.12.13-16.01.14, Varna – Varna. GEOMAR Report, N. Ser. 015. GEOMAR Helmholtz-Zentrum für Ozeanforschung Kiel, Germany, 111 pp., doi:10.3289/GEOMAR\_REP\_NS\_15\_2014
- Ginsburg, G. D., & Soloviev, V. A. (1995). Submarine Gas Hydrate Estimation: Theoretical and empirical approaches. All Days. <https://doi.org/10.4043/7693-ms>
- Hillman, J. I. T., Klaucke, I., Bialas, J., Feldman, H., Drexler, T., Awwiller, D., Atgin, O., Çiğci, G., & Badhani, S. (2018). Gas migration pathways and slope failures in the Danube fan, Black Sea. *Marine and Petroleum Geology*, 92, 1069–1084. <https://doi.org/10.1016/j.marpetgeo.2018.03.025>
- Ion G, Lericolais G, Nouzé H, Panin N, Ion E (2002) Seismo-acoustic evidence of gases in sedimentary edifices of the paleo-Danube realm. CIESM Workshop Series 17: 91-95
- Kossel, E., Bigalke, N., Pinero, E., Haeckel, M., 2013. The SUGAR Toolbox – A Library of Numerical Algorithms and Data for Modelling of Gas Hydrate Systems and Marine Environments. GEOMAR Report Nr. 8. 160 pp.
- Lericolais, G., Bourget, J., Popescu, I., Jermannaud, P., Mulder, T., Jorry, S., & Panin, N. (2013). Late quaternary deep-sea sedimentation in the western Black Sea: New insights from recent coring and seismic data in the Deep Basin. *Global and Planetary Change*, 103, 232–247. <https://doi.org/10.1016/j.gloplacha.2012.05.002>
- Nikishin, A. M., Okay, A. I., Tüysüz, O., Demirel, A., Amelin, N., & Petrov, E. (2015). The Black Sea basins structure and history: New model based on new deep penetration regional seismic data. part 1: Basins structure and fill. *Marine and Petroleum Geology*, 59, 638–655. <https://doi.org/10.1016/j.marpetgeo.2014.08.017>

Poort, J., Vassilev, A., & Dimitrov, L. (2005). Did postglacial catastrophic flooding trigger massive changes in the Black Sea Gas Hydrate Reservoir? *Terra Nova*, 17(2), 135–140. <https://doi.org/10.1111/j.1365-3121.2005.00599.x>

Popescu, I., De Batist, M., Lericolais, G., Nouzé, H., Poort, J., Panin, N., Versteeg, W., & Gillet, H. (2006). Multiple bottom-simulating reflections in the Black Sea: Potential proxies of past climate conditions. *Marine Geology*, 227(3–4), 163–176. <https://doi.org/10.1016/j.margeo.2005.12.006>

Popescu, I., De Batist, M., Lericolais, G., Nouzé, H., Poort, J., Panin, N., Versteeg, W., & Gillet, H. (2006a). Multiple bottom-simulating reflections in the Black Sea: Potential proxies of past climate conditions. *Marine Geology*, 227(3–4), 163–176. <https://doi.org/10.1016/j.margeo.2005.12.006>

Römer, M., Sahling, H., Pape, T., Bahr, A., Feseker, T., Wintersteller, P., & Bohrmann, G. (2012). Geological control and magnitude of methane ebullition from a high-flux seep area in the Black Sea—the Kerch Seep Area. *Marine Geology*, 319–322, 57–74. <https://doi.org/10.1016/j.margeo.2012.07.005>

Winguth, C., Wong, H. K., Panin, N., Dinu, C., Georgescu, P., Ungureanu, G., Krugliakov, V. V., & Podshuveit, V. (2000). Upper quaternary water level history and sedimentation in the northwestern Black Sea. *Marine Geology*, 167(1–2), 127–146. [https://doi.org/10.1016/s0025-3227\(00\)00024-4](https://doi.org/10.1016/s0025-3227(00)00024-4)

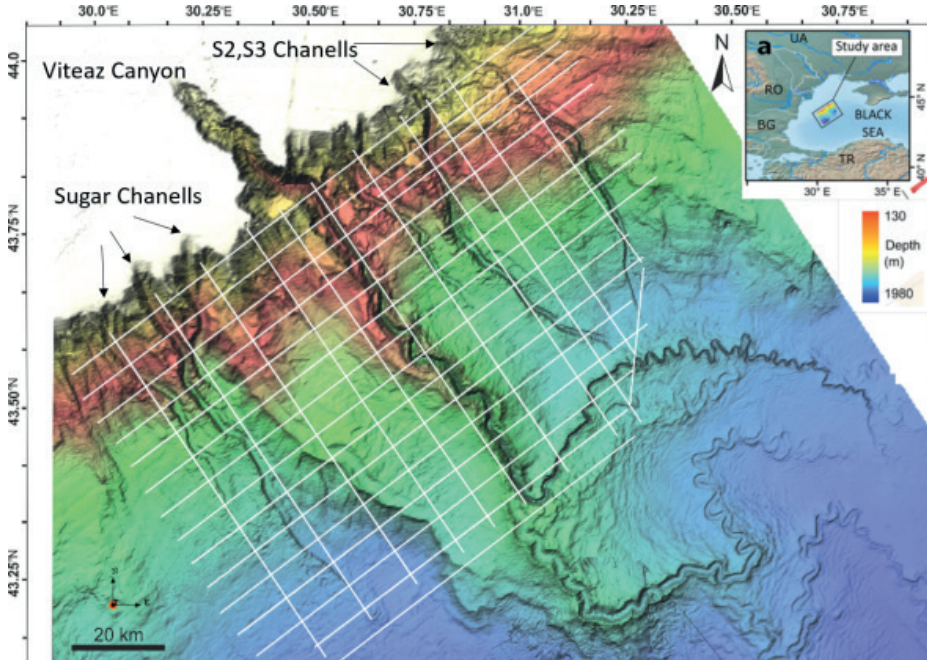
Wong, H.K., Winguth, C., Panin, N., Dinu, C., Wollschläger, M., Georgescu, P., Ungureanu, G., Krugliakov, V.V., Podshuveit, V., 1997. The Danube and Dniepr fans, morphostructure and evolution. *GeoEcoMarina* 2, 77–102

Zander, T., Haeckel, M., Berndt, C., Chi, W.-C., Klaucke, I., Bialas, J., Klaeschen, D., Koch, S., & Atgin, O. (2017). On the origin of multiple bsrs in the Danube deep-sea fan, Black Sea. *Earth and Planetary Science Letters*, 462, 15–25. <https://doi.org/10.1016/j.epsl.2017.01.006>

Anahtar Kelimeler: Gaz Hidrat, Tuna Paleokanalları

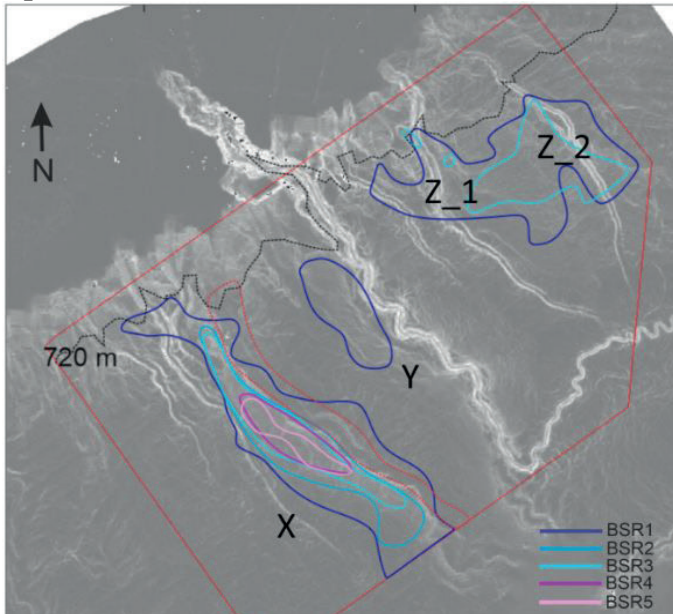


Şekil 1



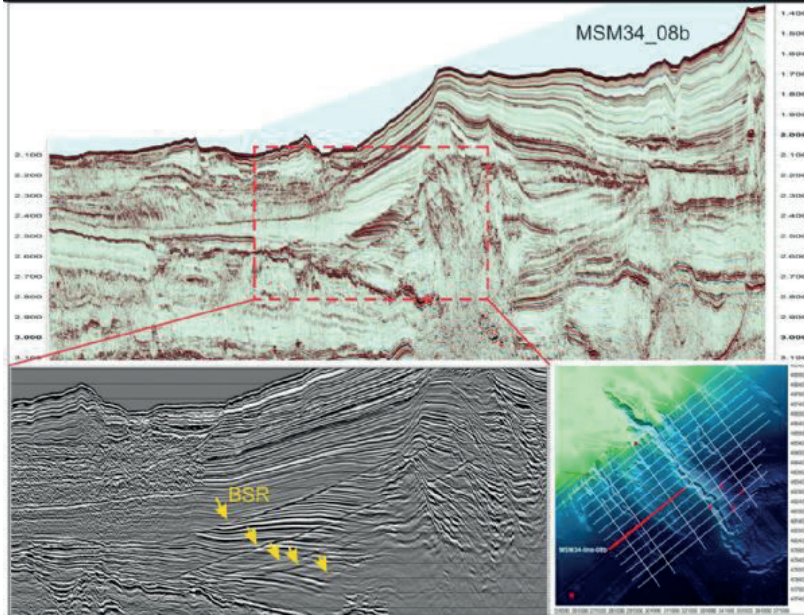
Çalışma alanı, alan içerisindeki kanallar ve sismik yansımalar

Şekil 2



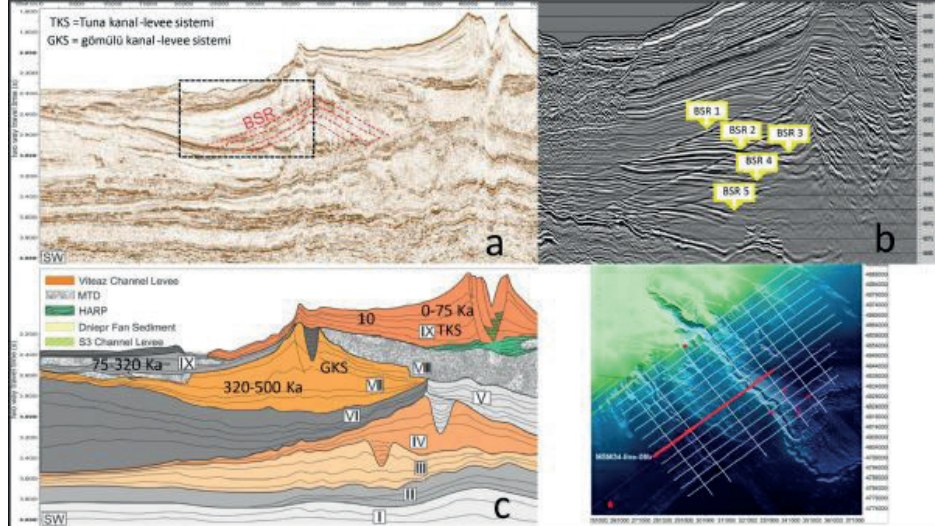
Gaz hidrat dağılım haritası

Şekil\_3



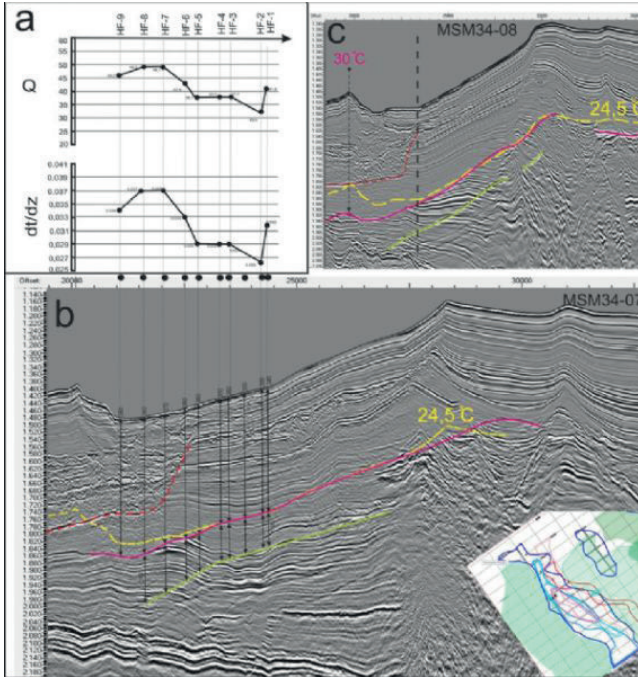
MSM34\_8b hattına ait sismik kesit ve 5 katlı BSR yansımaları

Şekil 4



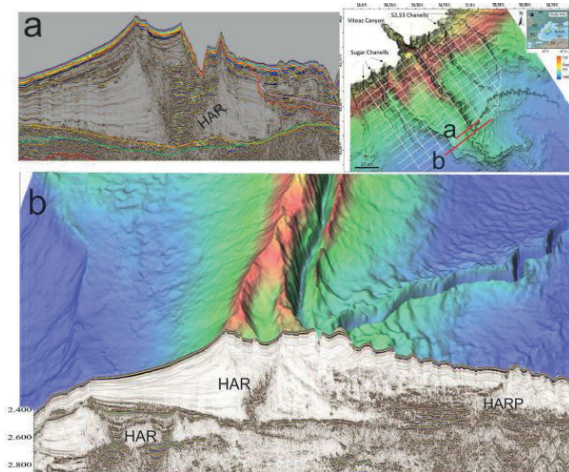
Alandaki sismik birimler, paleokanallar ve birimler içerisindeki çoklu BSR yansımaları

Şekil\_5



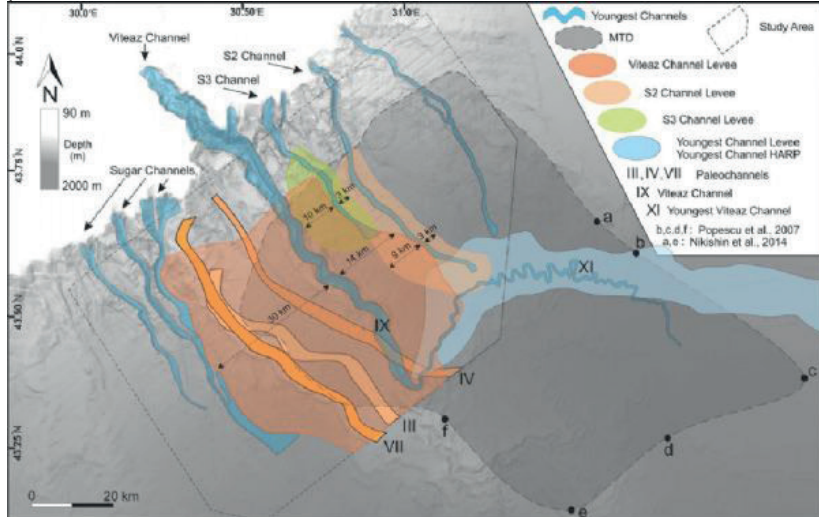
Çoklu BSR alanı üzerinde alınan ısı akısı ölçümlerinin profil boyunca değişimi ve MTD ile ilişkisi

Şekil\_6



Kanallar boyunca taşınan yüksek genlikli yansıma paketleri (HAR, HARP)

Şekil 7



Çalışma alanı içerisinde gözlemlenen paleokanalların geometrileri ve sismik kesitlerde gözlemlenen en büyük MTD yapısının dağılımına ait harita.

# A Study of an Experimental Possible Production Mechanisms of Hydrate Formation

**Hasan Hüseyin Engüclü**

Department of Petroleum and Natural Gas Engineering, Middle East Technical University, Ankara / Türkiye



## ABSTRACT

In this study, the temperature and pressure values of the formation and dissociation of methane hydrate are determined using various production techniques under laboratory conditions. A cylindrical high pressure hydrate cell in constant temperature room is used in the experiment to provide the actual field conditions for the hydrate reservoirs. Methane gas is injected into the cell at high pressure into which sand and water are filled at low temperatures. The hydrate reservoir is formed in the 21.2 liter hydrate formation cell according to the thermodynamic conditions. The ¼ inch production lines are used to produce methane and water. In the experiment, two different production stages are presented. The first stage uses a combination of depressurization method and thermal recovery method to provide constant temperature water circulation inside the spiral pipe. The effect of the thermal recovery method decreases and disappears in the second stage, it leaves its place only to the depressurization method.

Due to endothermic dissociation during the production phase, the heat removed from the environment causes pores to become blocked due to hydrate reformation. As a result, the production slows down and sometimes stops. By combining depressurization with thermal recovery, the gas hydrate production becomes more efficient and the rate at which hydrate dissociates increases. The depressurization method itself becomes less efficient and the dissociation rate decreases.

## PURPOSE

As our civilization progressed, energy became the primary source of its following growth. With the industrial revolution, fossil fuels became one of the primary energy sources for a variety of functions ranging from heating to transportation. Following the negative repercussions of increased greenhouse effect, demand for hazardous to the environment fossil fuels is falling. To meet the Paris Agreement's goals, emissions must decline to 9.7 Gt in 2050 for an emissions pathway compatible with the 2°C objective (Gielen et al., 2019). However, natural gas consumption in the category of fossil fuels is anticipated to be higher because it is less damaging to the environment and pollutes the air less. As a result, natural gas has remained popular in comparison to other fossil fuels. It can also serve to support the policies of the 197 member countries of the United Nations Framework Convention on Climate Change. Furthermore, according to the IEA's 2020 policy scenario, natural gas demand is expected to rise until 2040. The rising trend in natural gas demand may need the development of new yet unconventional gas resources to meet the demand. Natural gas hydrate reserves are predicted to have the most gas of any

unconventional source. Although there is no commercial realization yet, some of the practical production trials carried out in the world can be listed as; Mallik Field/McKenzie Delta-Canada, Nankai Trench-Japan, Shenhu Field-South China Sea. With an experimental study, this study intends to explore the effectiveness of two possible gas hydrate production mechanisms, namely depressurization and thermal stimulation. Methane hydrates will form in a porous medium composed of crushed-unconsolidated sand particles. Then, to produce gas from hydrate reservoirs, two alternative production methods (depressurization + thermal stimulation and depressurization alone) will be used.

## MATERIALS AND METHODS

In order to produce a gas hydrate in a laboratory environment, it must first be formed. Hydrate can occur only when both pressure and temperature are in the hydrate area, which is highlighted in yellow in Figure 1. The equilibrium line (red line in Figure 1) is the boundary between the hydrate and non-hydrate regions. Figure 1 displays the hydrate equilibrium line calculated using the CSMHYD software (Sloan, 1990).

Figure 1 demonstrates potential gas production methods (thermal stimulation, depressurization, and inhibitor injection) from hydrate reservoirs. Thermal stimulation procedures include any form of releasing gas that involves raising the temperature of the hydrate reservoir. The temperature can be raised by circulating hot water/steam pumped into a reservoir well or by lowering a heater into the well. Depending on the method used, the temperature increase may be limited to the neighborhood of the well. Larger regions can also be heated by flooding water from the injection well to the production well in the reservoir. Whatever method is utilized, the goal is to raise the reservoir temperature above the hydrate equilibrium temperature and let the gas to flow towards the production well. For this there might be different well patterns to inject the warm water such as injection production well pair (Nearby) or horizontal well pair (SAGD-like). The "Injection-Production Well Pair (Nearby)" offers direct heating and simplicity, but it may have problems with pressure building and uneven heat distribution. The "Horizontal Well Pair (SAGD-like)" on the other hand, while potentially encountering drilling challenges and potential well interference, offers improved heat distribution and controlled pressure.

In the Figure 2, a high-pressure hydrate cell is saturated with water and high-pressure methane gas for hydrate generation. The materials utilized during the study's hydrate formation and gas production periods are illustrated in Figure 3.

A high pressure hydrate cell filled with unconsolidated sand and water has been injected with methane gas.

After 90 days of hydrate growth, gas hydrate production began. The graphic displays gas production with a green arrow. The dissociation of hydrates generated in a high-pressure hydrate cell is required for gas production from hydrate reservoirs. This is accomplished through the reduction of pressure (depressurization) and/or the circulation of warm water around the artificial well (thermal stimulation).

## RESULTS AND DISCUSSIONS

When the cell pressure reached 51.44 bar-g at the end of the hydrate formation period, it was decided to begin the gas production stage. Warm water circulation was begun through a spiral channel to ease circulation around the artificial well in the cell in order to achieve hydrate dissociation. The circulation temperature is set at a constant temperature of 20 degrees Celsius. In one day, a slow circulation rate of warm water raised the temperature around the artificial well by about 10 degrees Celsius. A modest rise in cell temperature caused a pressure increase to the average value of 51.82 bar-g immediately before production began (Figure 4).

Figure 5 displays data acquired during the experiment's gas production stage: This data consists of average temperature, average pressure, wellhead pressure (or back-pressure regulator set pressure), gas flow rate, and cumulative water output over time. This data leads to the following

## CONCLUSIONS

1. There is no gas flow at initially, but there is some water production due to the expansion of compressed water that enters the artificial well. During this time, no gas could enter the wellbore because the free gas water interface was higher than the perforation depth.
2. Furthermore, the average cell pressure was higher than the wellhead pressure, which was caused by compressed free gas at the top of the cell.
3. Later, with no or very little gas flow, an increase in water output was noted. This is linked to the gas locking effect caused by extremely high water saturation in porous media, which blocks gas passage due to relative permeability.
4. A distinct indicate of temperature reduction is detected at around 1000 sec of the production stage, which is an indication of hydrate dissociation due to the endothermic nature of dissociation.
5. Later intermittent character of gas production is encountered with greater rate of water generation till water production is eliminated.
6. The greatest gas flow occurred when the water flow got extremely low.

Figure 6 presents temperature distributions at various depths in the cell based on average temperature values of thermocouples of various lengths such as 60 mm, 120 mm, 180 mm and 240 mm from the top cover to inside of the reservoir. The deeper the layer in the cell from the top cover, the less the temperature changes during

dissociation / gas production, as seen. The uppermost layer (60 mm from the top cover) showed the greatest cooling due to hydrate dissociation. After 1000 seconds, when dissociation begins, the temperature drops by around 2 degrees Celsius. This can be interpreted as indicating that the majority of hydrates formed around the top cover or near the water-gas contact.

## CONCLUSION

The interpretation of this study's gas hydrate production data reveals the following results.

1. Thermal stimulation when combined with depressurization is a more effective production strategy than depressurization alone since dissociation is an endothermic process that might result in subsequent hydrate formation or ice.
2. Initially, high water flow rates block gas flow. It is due to higher water saturation in porous media, which has a larger relative permeability of water. Furthermore, increased water flow rates could hinder gas movement in the wellbore. This raises the challenge of how to regulate water production following dissociation.
3. Since heat transfer is not good in hydrates, well pattern to inject warm water may require wells to be as close as possible. However, the decision is based on the reservoir characteristics, efficiency objectives, technical potential, and economics.

Keywords: Gas Hydrate Dissociation, Gas Hydrate Production Mechanisms

Figure 1. Hydrate equilibrium curve of pure methane

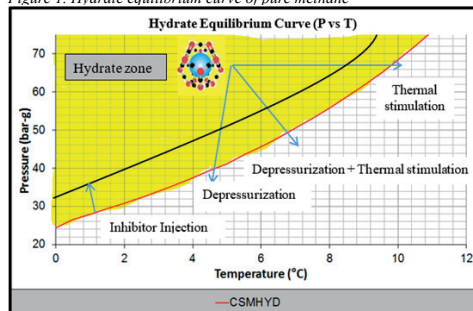


Figure 2. Cylindrical high pressure cell used for hydrate formation experiments



Figure 3. Experimental Set-up and Procedure

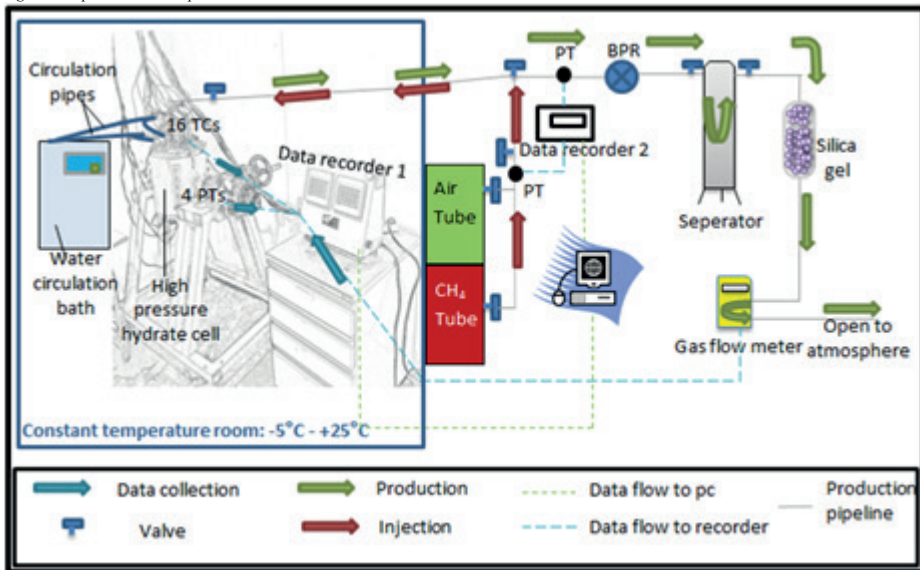


Figure 4. Pressure – temperature traverse during hydrate formation and gas production stages

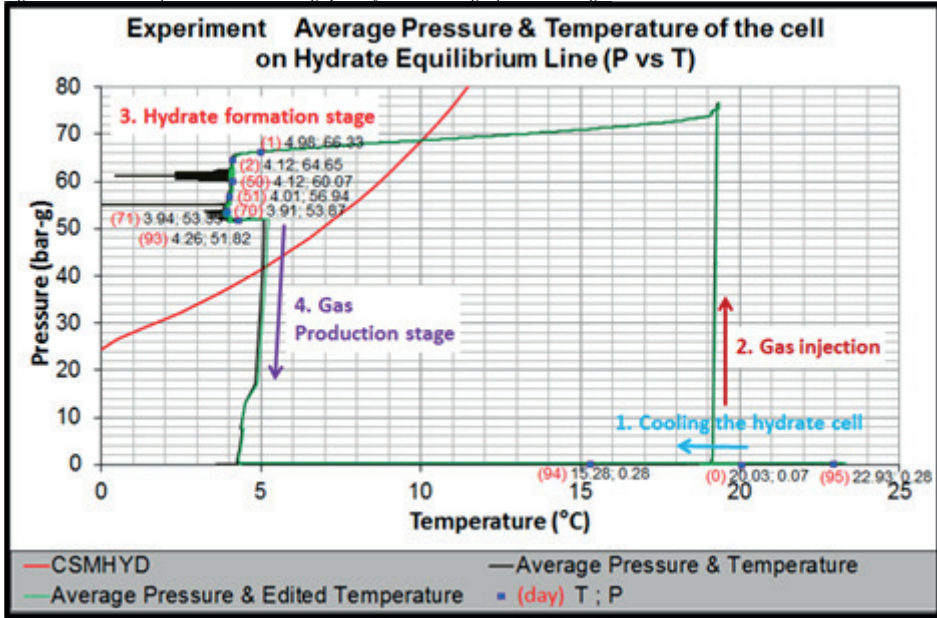


Figure 5. Production stage (Pressure, Temperature, Gas Flow Rate, Cumulative water production vs time)

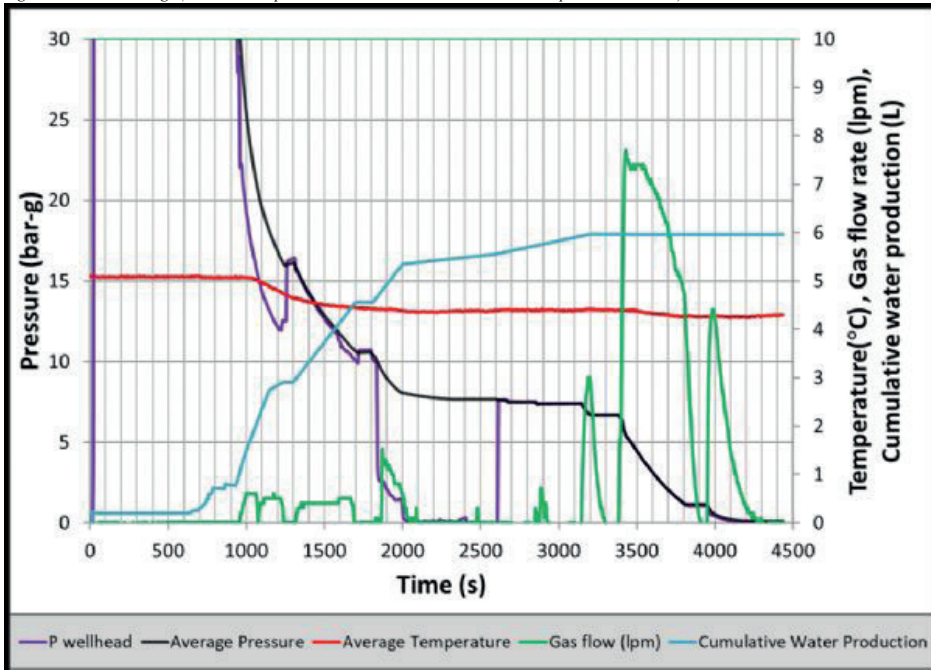
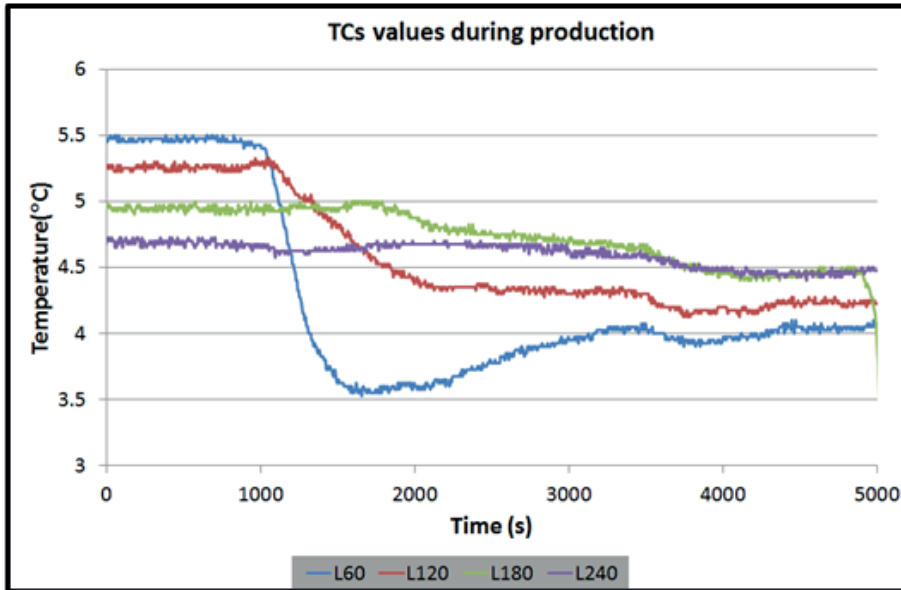




Figure 6. Thermocouple values in different depths during production



## ÖZ

Çalışma alanı, Batı Karadeniz kıta sahasında şelf, kıtasal yamaç ve yükselimini kapsamaktadır. Akustik veri setleri 2010 ve 2012 yıllarındaki deniz araştırmaları kapsamında toplanmıştır. Toplanan veriler değerlendirilerek, çalışma alanı, morfolojik, sıg gaz ve gaz hidrat birikimleri açısından incelenmiştir. Dokuz Eylül Üniversitesi R/V K. Piri Reis Araştırma gemisi ile 2 farklı sefer kapsamında yaklaşık 3000 km uzunluğunda, çok kanallı sismik yansıma, CHIRP sıg mühendislik sismigi ve çok ışınlı batimetri verileri toplanmıştır. Çalışma kapsamında ortaya çıkarılması hedeflenen gaz hidrat birikimlerinin varlığı açısından önemli bulgular akustik verilerin yorumlanması sonucunda haritalanmıştır. Çok kanallı sismik verilerin tamamının değerlendirilmesi sonucunda gaz hidrat birikimlerine karşılık gelen alanlar belirlenmiştir. BSR seviyesinden deniz tabanına kadar olan bölümden gaz hidratın depolanacağı düşünüldükçe gaz hidrat rezerv kestirimi hesaplamaları gerçekleştirilmiştir. Buna göre Batı Karadeniz bölgesindeki denizel sediment içerisindeki iki farklı oranda gaz hidrat satürasyonu için (%10 ve %40 gaz hidrat satürasyonu) ve %20 porozite değerine göre 110 - 440 tcf'lik doğal gaz rezervi hesaplanmıştır. Bu da iyi ve kötü senaryoya göre gaz hidratın üretilmesi durumunda Türkiye'nin yıllık 2.1 Tcf'lik gaz tüketimi ile oranlanırsa yaklaşık 54 - 216 yıllık doğal gaz ihtiyacını karşılayacağı hesaplanmıştır.

The study area covers the shelf, continental slope and rise on the offshore Western Black Sea. Acoustic datasets were collected as part of two research expeditions in 2010 and 2012. The study area was examined in terms of morphological, shallow gas and gas hydrate deposits. Approximately 3000 km long, multi-channel seismic reflection, CHIRP sub-bottom profiler seismic and multi-beam bathymetry data were collected with the Dokuz Eylül University R/V K. Piri Reis. Finally, presence of hydrocarbons in the form of gas hydrate was mapped as a result of the interpretation of the acoustic data. It has been observed that BSR reflections are distributed under ridge-type sedimentary structures in the continental slope and continental rise regions

After evaluating all the multi-channel seismic data, areas corresponding to gas hydrate accumulations have been identified. Gas hydrate reserve estimations were conducted, assuming gas hydrates would be stored from the BSR level down to the seafloor. Accordingly, natural gas reserves ranging from 110 to 440 trillion cubic feet (tcf) were calculated for two different gas hydrate saturations within the marine sediments of the Western Black Sea region (%10 and %40 gas hydrate saturation) and with a porosity value of %20. Considering Turkey's annual gas consumption of 2.1 tcf, this would fulfill approximately 54 to 216 years of natural gas demand under favorable and unfavorable scenarios if gas hydrates were extracted.

## 1. GİRİŞ

Gaz hidrat araştırmaları günümüzde konvansiyonel olmayan kaynaklar açısından değerlendirilmektedir. Standart basınç ve sıcaklık koşullarında, 1 m<sup>3</sup> gaz hidrat, 164 m<sup>3</sup> metan gazı ve 0,8 m<sup>3</sup> su içermektedir. Bu denli yüksek oranda metan içeren gaz hidratlardaki organik karbon miktarı, dünyadaki tüm fosil kaynaklarda bulunan organik karbonun 2 katıdır ve Kvenvolden, (1988)'e göre doğadaki organik karbonun %50'sini aşkın miktarı gaz hidratların bünyesinde bulunmaktadır. 19. yüzyılın ortalarında yakın geleceğin enerji kaynağı olarak görülen gaz hidratlar (Kelland, 1994), denizel sedimentler içerisinde uygun termobarik koşullar altında bulunmakta olup günümüzde üretim testleri aşamasına geçilmiştir (Hancock vd., 2005; Zhou vd., 2014; Li, Moridis, Zhang ve Li, X.S., 2010). Gaz hidratların sunduğu diğer bir ekonomik önem ise bu tipteki yapıların oluştukları tortul ortamları çimentolaması sebebiyle örtü kayaç özelliği sunmasıdır. Bu sebeple gaz hidrat içeren tortul ortamların altı, serbest gaz birikimi için oldukça uygun bir ortamdır. Gaz hidratlar genellikle metan gazı içeriyor olsa da gaz bileşiminde bazı ağır hidrokarbon gazları da yer alabilmektedir. Böyle bir durum tespit edilebilmesi ise derinlerdeki termojenik kökenli hidrokarbonun varlığını gösterir nitelikte bir bulgudur. Bu bağlamda sıra dışı (unconventional) enerji kaynakları arasında yer alan gaz hidratlar, geleneksel hidrokarbon aramaçılığında dolaylı belirteç olarak sayılmaktadır. Kanyonların tortul erozyonuyla tanımlanan kıtasal yamaç yapıları olarak tanımlanmakta ve sıg sulardan derin sulara tortul taşınımını sağlayan en önemli sistemler olduğu bilinmektedir (Laursen ve Normark, 2002; Antrobreh ve Krastel, 2006). Son yıllardaki çalışmalar deniz altı kanyonlarının karmaşık bir kökene sahip olduğunu ortaya koymuş olup, oluşumları nehir kazılmaları, karadaki yüzey erozyonu, türbidite akıntıları erozyonu, faylanma, su seviyesi değişimleri ve denizel bentik faunanın aktivitesiyle ilişkilendirilmiştir (Shepard ve Dill, 1966; Shepard 1981; Belderson ve Kenyon, 1976; Twichell ve Roberts, 1982). Deniz altı kanyonlarının oluşumunda kıta kenarlarında kayma, tortul erozyonu, heyelan, moloz akıntıları ve türbidite akıntıları olmak üzere kütle hareketlerinin etkili olduğu vurgulanmıştır (Laursen ve Normark, 2002; Casas, Ercilla, Baraza, Alonso ve Maldonado, 2003).

Bu çalışmanın amacı Batı Karadeniz kıtasal yamacındaki olası gaz hidrat birikimlerinin haritalandırılması ve bölgenin morfolojik olarak tanımlanmasını kapsamaktadır.

## 2. YÖNTEM

Çalışma alanında çok kanallı sismik yansıma, çok ışınlı batimetri ve CHIRP sıg mühendislik sismigi çalışmaları

gerçekleştirilmiştir. Çok kanallı yansıma verileri 96-168 kanallı, 6,25 grup aralığına sahip alıcı kablo ve 2000 psi basınca sahip GI hava tabancası ile toplanmıştır. Veri yüklemesi, geometri tanımlama, top-mute, bandpass filtre, f-k eğim filtresi, CDP sıralama, hız analizi, nmo düzeltmesi, pre-stack kirrhoff zaman migrasyonu, genlik düzenleme işlemleri uygulanmıştır. Çok ışınlı batimetri verisi 126 adet ışına sahip olarak toplanmış olup, spike temizleme, enterpolasyon ve 100 m grid aralığı ile 3 boyutlu batimetri haritası oluşturulmuştur. CHIRP sığ mühendislik sismiği verileri için herhangi bir veri işlem uygulanmamış olup sadece koordinat düzenlemesi gerçekleştirilmiştir.

### 3. BULGULAR

Gaz hidratlar içerdiği oldukça yüksek miktardaki doğal gaz miktarı ile hem bilimsel hem de enerji üretimi anlamında birçok çalışmanın konusudur. Bu anlamda gaz hidratların varlığının ortaya konması amacıyla, Batı Karadeniz Kıtasa yamacında 2010 ve 2012 yılları arasında Tübitak 108Y110 kodlu proje kapsamında Dokuz Eylül Üniversitesi Deniz Bilimleri ve Teknolojisi Enstitüsü araştırma gemisi R/V K. Piri Reis ile Kefken ve Kuruçay ile arasında gerçekleştirilen araştırma seferi kapsamında yaklaşık 3000 km<sup>2</sup>'lik hat üzerinde çok kanallı sismik yansıma, CHIRP mühendislik sismiği, çok ışınlı batimetri verileri toplanmıştır (Şekil 1a). Verilerin değerlendirilmesi sonucu 5510 km<sup>2</sup>'lik oldukça geniş bir alanda gaz hidrat varlığına işaret eden BSR (Bottom Simulating Reflector) yansımaları haritalandırılmıştır (Şekil 1b).

Toplanan batimetri verilerinden 3 boyutlu batimetri haritası elde edilmiş olup, çok sayıda kanyon ve kanal yapısının varlığı da ilk kez ortaya konmuştur (Şekil 2). Çalışma alanında gözlenen kanyon yapılarının oluşumu incelendiğinde, özellikle alanın en batısında yer alan Sakarya Kanyonu'nun oluşumunda karadaki nehir bağlantıları ve kütle hareketlerinin etkin rol üstlendiği önerilmiştir. Ayrıca Sakarya Kanyonu'nun tabanını dik kesen şekil 3 üzerinde gömülü moloz birikimi (MTD) kanyon oluşumunda gravitasyonel kütle hareketlerinin de oldukça etkin olduğu anlaşılmaktadır.

Çalışma alanının en batısında Sakarya kanyon tabanında gözlenen BSR yansıması Şekil 3'te gösterilmiştir. Normal stratigrafik seviyeleri kesen bu yansımalar deniz tabanından yaklaşık 200-230 ms derinliklerde deniz tabanına paralel olarak uzanmaktadır. Şekil 4'te Akçakoca açıklarında sedimanter sırt yapılarının altında gözlenen BSR yansımaları ve sığ gaz birikimlerine karşılık gelen akustik türbidite birikimleri görülmektedir.

Zonguldak açıklarında gözlenen BSR yansımaları da yaklaşık olarak deniz tabanından itibaren 250-300 ms altında yer almaktadır. BSR yansımalarının altında gözlenen sığ gaz birikimleri olduğu düşünülen akustik boşluk alanları gaz hidrat birikimlerinin iyi bir örtü kaya (cap-rock) özelliğine sahip olduklarını göstermektedir (Şekil 5).

### 4. SONUÇLAR

Çok kanallı sismik verilerin tamamının değerlendirilmesi sonucunda gaz hidrat birikimlerine karşılık gelen alanlar belirlenmiştir. BSR seviyesinden deniz tabanına kadar olan bölümde gaz hidratın depolanacağı düşünülmektedir. Buna göre Batı Karadeniz bölgesindeki denizel sediment içerisindeki iki farklı oranda gaz hidrat saturasyonu için (%10 ve %40 gaz hidrat saturasyonu) ve %20 porozite değerine göre 110 - 440 tcf'lik doğal gaz rezervi hesaplanmıştır. Bu da iyi ve kötü senaryoya göre gaz hidratın üretilmesi durumunda Türkiye'nin yıllık 2.1 Tcf'lik gaz tüketimi ile oranlanırsa yaklaşık 54 - 216 yıllık doğal gaz ihtiyacını karşılayacağı söylenebilir.

### REFERANSLAR

- Antobreh, A. ve Krastel, S. (2006). Morphology, seismic characteristics and development of Cap Timiris Canyon, offshore Mauritania: A newly discovered canyon preserved off a major arid climatic region. *Marine and Petroleum Geology* 23, 37-59.
- Belderson, R.H. ve Kenyon, N.H. (1976). Long-range sonar views of submarine canyons. *Marine Geology*, 22(3), 1769-74.
- Casas, D., Ercilla, G., Baraza, J., Alonso, B. ve Maldonado, A. (2003). Recent mass-movement processes on the Ebro continental slope (NW Mediterranean). *Marine and Petroleum Geology*, 20, 445-457.
- Dondurur, D., Çifçi, G. ve Ergün, M. (2012). Karadeniz Sedimentasyonu ve Akdeniz Su Değişimi Arasındaki Karşılıklı Etkileşimi (Boğaz ve Sakarya Nehri Çıkışları Laboratuvarı), Tuna Deltası Abisal Düzlüğü ve Boğaz Cıvarı Sedimentasyonu Arasındaki Bağlantı, Sediman Duyarlılığı ve Hareket Yolları, Karadeniz Pliyosen Kuvaterner Masif Taban Kaymaları ve Kıyusal İnsan Aktiviteleri Arasındaki Bağlantı, TUBITAK Projesi sonuç raporu, Proje Kodu: 108Y110.
- Hancock, S.H., Dallimore, S.R., Collett, T.S., Carle, D., Weatherill, B., Satoh, T. ve Inoue, T. (2005). In Scientific Results from the Mallik 2002 Gas Hydrate Production Research Well Program, Mackenzie Delta, Northwest Territories, Canada. *Geological Survey of Canada Bulletin* 585,134.
- Kelland, M. (1994). Natural gas hydrates: Energy for the future. *Marine Pollution Bulletin*, 29(6-12), 307-311. [https://doi.org/10.1016/0025-326x\(94\)90645-9](https://doi.org/10.1016/0025-326x(94)90645-9)
- Küçük H.M. (2016). Batı Karadeniz Zonguldak-Amasra açıklarında gaz ve gaz hidratların jeolojik ve jeofizik yöntemlerle araştırılması [Doktora Tezi]. Dokuz Eylül Üniversitesi.
- Kvenvolden, K.A. (1988). Methane hydrate a major reservoir of carbon in the shallow geosphere. *Chemical Geology*, 71, 41-51.
- Laursen, J. ve Normark, W. R. (2002). Late Quaternary evolution of the San Antonio Submarine Canyon in the central Chile forearc (~33°S). *Marine Geology*, 188,

365-390.

Li, G., Moridis, G., Zhang, K. ve Li, X.S. (2010). Evaluation of the gas production potential of marine hydrate deposits in the shenhu area of the South China Sea. Proceedings of Offshore Technology Conference. <https://doi.org/10.2523/20548-ms>.

Nasif Dondurur, A. (2021). Sakarya Kanyonu'nun morfo-akustik yapısı [Doktora Tezi]. Dokuz Eylül Üniversitesi, Fen Bilimleri Enstitüsü.

Shepard, F.P. ve Dill, R.F. (1966). Submarine Canyons and other Sea Valleys. Rand McNally, 3, 381.

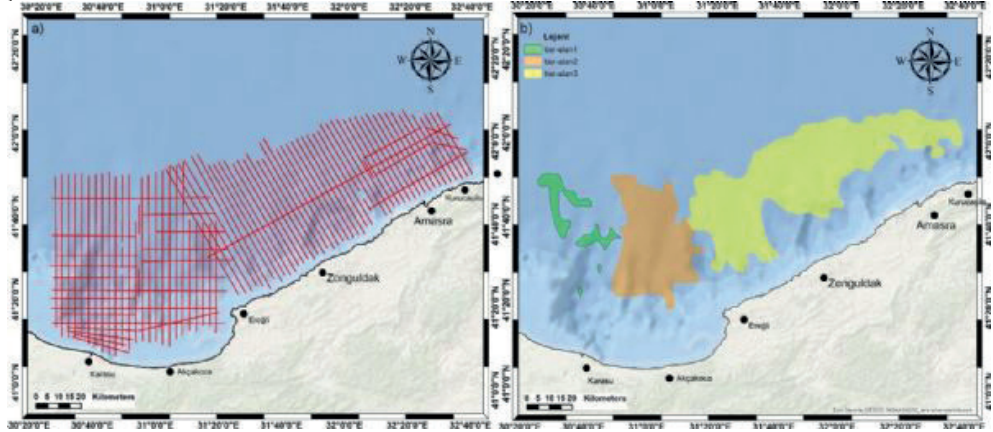
Shepard, R. (1981). The eucharistic presence and reconciliation of opposing realities. The Heythrop Journal, 22(2), 123-134. <https://doi.org/10.1111/j.1468-2265.1981.tb00463.x>

Twichell, D.C. ve Roberts, D.G. (1982). Morphology, distribution, and development of submarine canyons on the United States Atlantic continental slope between Hudson and Baltimore Canyons. Geology, 10, 408-412

Zhou, M., Soga, K., Xu, E., Uchida, S. ve Yamamoto, K. (5 - 8 Mayıs 2014). Numerical Study on eastern nankai trough gas hydrate production test. 4. Offshore Technology Conference Houston Texas United States of America. <https://doi.org/10.4043/25169-ms>.

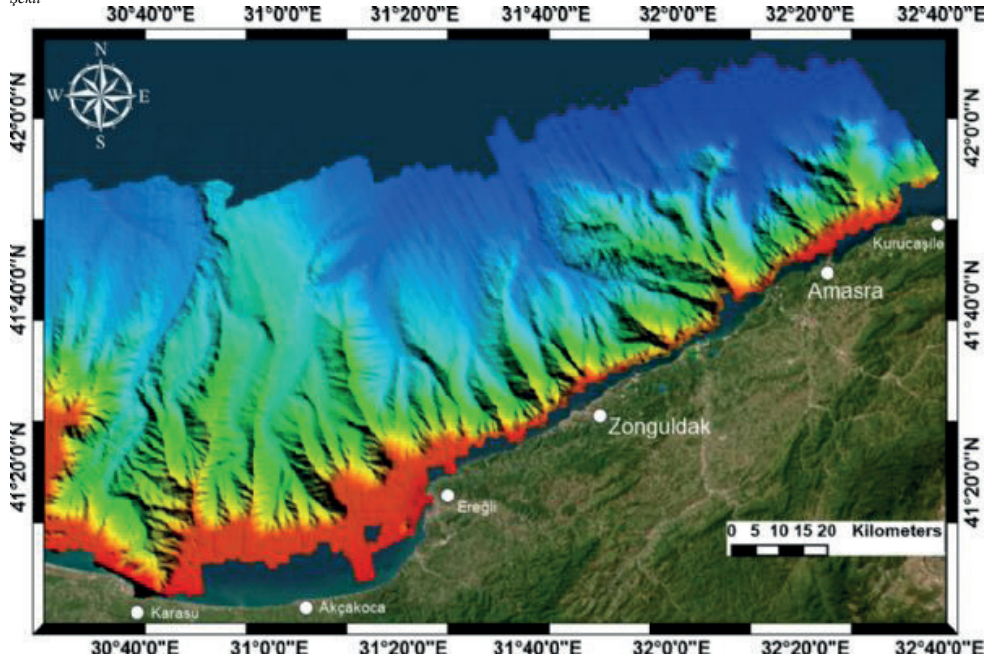
Anahtar Kelimeler: Batı Karadeniz, BSR

Şekil 1



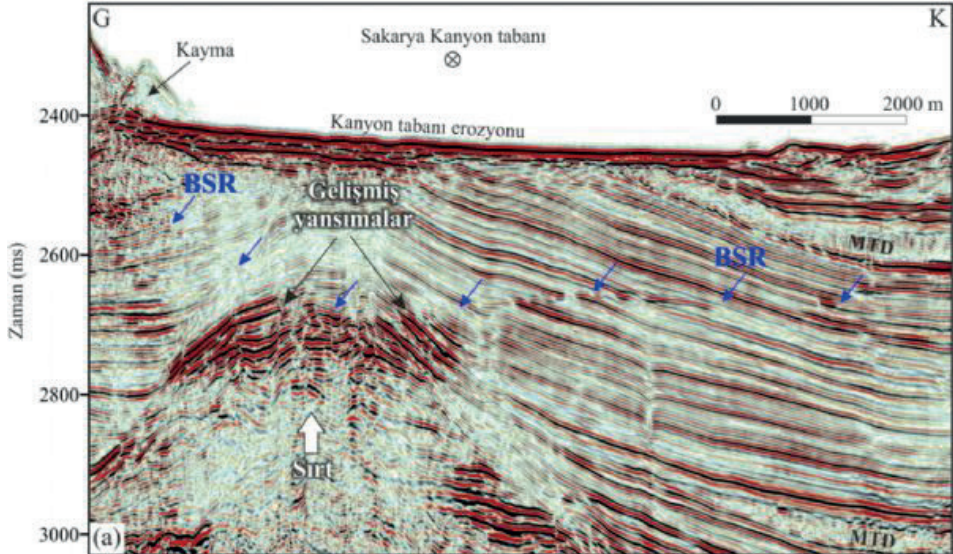
(a) çok kanallı sismik, çok ışınlı batimetri ve CHIRP mühendislik sismikliği hat haritası, (b) çalışma alanında gözlenen gaz hidrat belirteçleri olarak bilinen BSR yansıma alanları (Dondurur ve diğer., 2012; Nasif 2021; Özel 2023 ve Küçük 2016)

Şekil



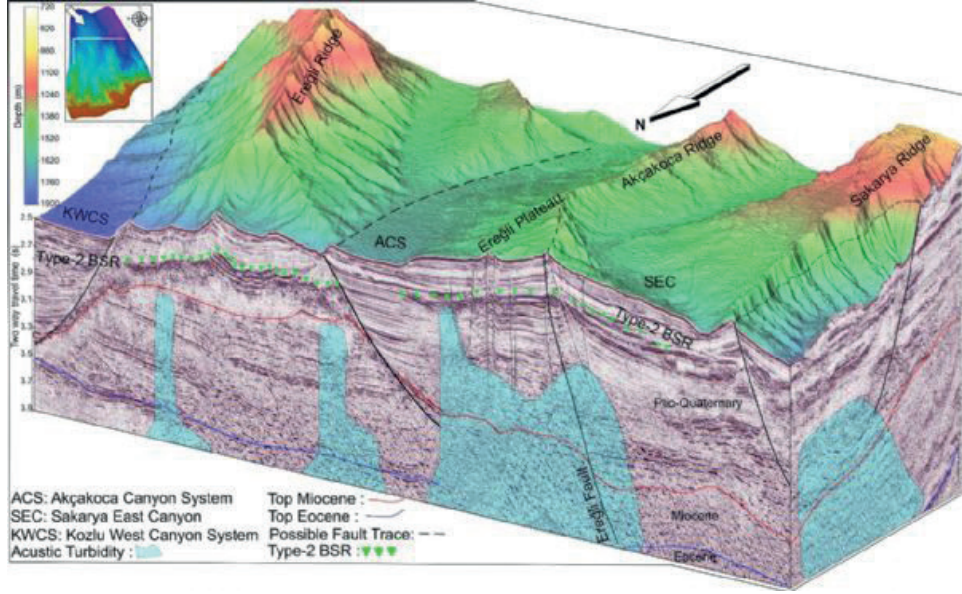
Çalışma alanının 3 boyutlu batimetri haritası (Dondurur ve diğer., 2012; Nasif 2021; Ozel 2023 ve Küçük 2016).

Şekil 3



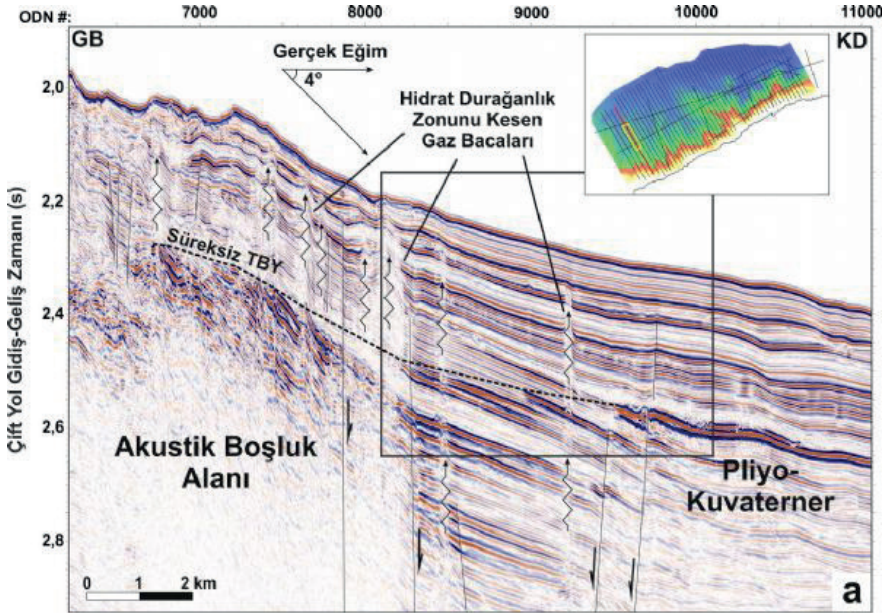
Sakarya kanyon tabanında gözlenen BSR yansımaları (Nasif 2021)..

Şekil 4



Akçakoca açıklarında gözlenen BSR yansımaları ve sıg gaz yapıları (Ozel 2023).

Şekil 5



Zonguldak açıklarında gözlenen BSR yansımaları ve sıg gaz yapıları (Küçük 2016).

# Doğu Karadeniz'de Gaz Hidratlar ve 2 Çamur Volkanının Keşfi ve Gwangyang Körfezi'nde Sığ Gaz Birikimleri



Sevinc Özel Füzün<sup>1</sup>, Günay Çifci<sup>2</sup>, Seda Okay Günaydın<sup>3</sup>, Sermet Gündüz<sup>4</sup>, Dae Choul Kim<sup>5</sup>

<sup>1</sup>Dokuz Eylül Üniversitesi, İzmir Meslek Yüksekokulu, İzmir / Türkiye

<sup>2</sup>Dokuz Eylül Üniversitesi, Mühendislik Fakültesi, Jeofizik Mühendisliği Bölümü, İzmir / Türkiye

<sup>3</sup>Dokuz Eylül Üniversitesi, Deniz Bilimleri ve Teknoloji Enstitüsü, İzmir / Türkiye

<sup>4</sup>Maden Tetkik ve Arama Genel Müdürlüğü, İzmir / Türkiye

<sup>5</sup>Pukyong National University, Busan / Güney Kore

Ülkemiz kıyılarında şelf, açık denizde ve uluslararası sularda yapılan aramalarda gaz hidrat ve altındaki sığ gaz rezervleriyle ilişkili olarak; BSR yapıları, çamur volkanları, çamur diyapirleri, gaz sızıntıları vb. yapılar gözlemlenmiş ve bazı lokasyonlarda alınan örnekler ile gaz hidratın varlığı ispatlanmıştır. Karadeniz son yıllarda özellikle barındırdığı hidrokarbon potansiyeli ile gündeme gelmiştir.

2010 yılında Deniz Bilimleri ve Teknoloji Enstitüsü ve Pukyong Ulusal Üniversitesi araştırmacıları Türk-Güney Kore ikili işbirliği projesi 108Y244 no'lu TÜBİTAK projesi kapsamında Doğu Karadeniz'de çok kanallı sismik yansıma verisi ile 2009 yılında Güney Kore'de Gwangyang Körfezi'nde CHIRP mühendislik sismiği verisi toplanarak piston karot örnekleri alınmıştır. Bu bağlamda, sığ gaz ve gaz hidrat oluşumlarının, çeşitli hidrokarbon sızıntılarının (pockmarklar, çamur volkanları, neden olan faylar) haritalanması için Doğu Karadeniz'de çok kanallı sismik yansıma ve tortulların fiziksel ve akustik özelliklerini ortaya koymak açısından da Kore'nin güneyindeki Gwangyang Körfezi'nde CHIRP sismik yansıma yöntemi ile veri toplanarak, piston karot yöntemiyle de numuneler alınmıştır.

Gwangyang Körfezinde elde edilen veri seti ile tortulların akustik ve fiziksel özelliklerinin belirlenmesi yoluyla varlığı bilinen akustik yapıların incelenmesi ve sığ gaz birikimlerinin kökenini araştırmak için kullanılmıştır.

Doğu Karadeniz'de çalışma alanı kıta yamacı, apron ve abisal düzlüğü kapsamaktadır. Alanının en doğusuna ait kesitlerde bottom simulating reflector (tabana benzeyen yansıtıcı), parlak noktalar ve gaz kolonları gözlenmiştir. Ayrıca bölgede iki çamur volkanı bulunmuş ve bunlar sırasıyla İzmir ve Pusan olarak adlandırılmıştır. Kıtasal yamaçta kayma çökelleri gözlenmiştir. Sismik nitelik analizlerinde bu alanlar, zarf ve görünür polarite bölümlerinde güçlü yansımalar gösterirken, anlık frekans bölümünde aynı alanda düşük frekans içeriği ile kendini göstermektedir. Bu durum, bu ortamda sığ gazın varlığı olasılığını desteklemektedir.

Gas hydrates and shallow gas accumulation relates structures; BSR's, mud volcanoes, mud diapirs, gas seeps, etc. are observed on the coastlines of our Turkey under the shelf, in the open sea and in international waters. The presence of gas hydrates are proved with the samples taken at some locations. Due to its potential for hydrocarbons, the Black Sea has gained attention recently.

In 2010, researchers from the Institute of Marine Sciences and Technology and Pukyong National

University collected multi-channel seismic reflection data in the Eastern Black Sea Region within the scope of the Turkish-South Korean bilateral cooperation project TUBITAK project number 108Y244. And in 2009 CHIRP seismic data collected and piston core samples were collected in South Korea, Gwangyang Bay.

In this context, multi-channel seismic reflection data were collected in the Eastern Black Sea region for mapping shallow gas and gas hydrate formations, various hydrocarbon seeps (pockmarks, mud volcanoes, causative faults) and to reveal the physical and acoustic properties of sediments in Gwangyang Bay in the south of Korea, CHIRP seismic reflection data were collected and piston core samples were taken. By identifying the acoustic and physical characteristics of the sediments, the data set collected in Gwangyang Bay are used to study the known acoustic structures and to investigate the origin of shallow gas deposits.

In the Eastern Black Sea, the study area covers the continental slope, the apron and the abyssal plain. Bottom simulating reflector, bright spots and gas columns are observed in the easternmost sections of the area. In addition, two mud volcanoes are discovered in the region and they are named as İzmir and Pusan, respectively. Slump deposits are observed on the continental slope. In seismic attribute analysis, these areas show strong reflections in the envelope and apparent polarity sections, while they show low frequency content in the same area in the instantaneous frequency sections. This supports the possibility of the presence of shallow gas in the area.

Keywords: eastern Black Sea, gas hydrate

## AMAÇ

Karadeniz bölgesi daha önce gerek tektonik açıdan, gerekse barındırdığı enerji kaynakları açısından birçok bilim adamı tarafından araştırılmıştır. 2005 yılında Gürcistan açıklarında R/V Prof. Logachev araştırma gemisi ile yapılan Araştırma ile Eğitim-TTR seferinden elde edilen sismik yansıma kesitlerinde kanyon sırtlarında gözlenen çamur diyapiri yapılarından alınan gravite karot örneklerinde büyük gaz hidrat kütleleri ile birlikte petrol örneklenmiştir (Şekil 1). Ayrıca alanda deniz yüzeyinde petrol sızıntıları gözlenmiştir. Ancak bu çalışmalar Doğu Karadeniz bölgesinde, özellikle de bölgenin tektonik açıdan incelenmesi konusunda yetersiz kalmıştır. Bu doğrultuda çalışmanın bir bölümünün amacı, bölgede daha önce

yapılan çalışmalar ışığında, Doğu Karadeniz' in yüksek ayrımlı çok kanallı sismik yansıma yöntemiyle detaylı incelemesi ve elde edilen sonuçlar ile tektonik yapısının yorumlanması ve sıgı gaz birikimleri ve gaz hidratların varlığının araştırılması hedeflenmiştir. Ayrıca Çalışmanın bir diğer amacı da yüksek ayrımlı akustik ve sismik yöntemler kullanılarak iki farklı bölgede (Doğu Karadeniz'de Türkiye kıta sınırı ve Kore'nin güneyinde yer alan Gwangyang Körfezi'nde), farklı jeolojik tarih ve bileşime sahip tortulların akustik ve fiziksel özelliklerini ortaya konarak varlığı saptanan serbest gaz ve gaz hidrat alanları haritalanmasıdır.

Gaz hidratların belirteci olan tabana benzeyen yansıtıcı olarak adlandırılan BSR yapılarının araştırılması çalışmanın hedeflerinden biridir. Katı gaz hidrat fazında büyük miktarlarda gaz depolanabilmesi nedeniyle, gaz hidratlara geleceğin enerji kaynağı gözüyle bakıldığından araştırılması önem taşımaktadır.

Güney Kore'de Gwangyang körfezinde yüksek ayrımlı CHIRP sismik çalışmalar ve karot örnekleme çalışma alanındaki tortulların fiziksel ve akustik özelliklerini incelemek için yapılmıştır. Tortulların çoğunluğu Seomjin nehrinden taşınmıştır. Tortullar Yesou Boğazı ve Gwangyang Körfezi aracılığıyla taşınmaktadır. Karot örnekleri tortulların içeriklerini (tane boyu, kum, silt ve kil oranları), fiziksel özelliklerini (porosite, su içeriği, bulk yoğunluğu, tane yoğunluğu ve kesme kuvveti) ve akustik özelliklerini (sıkışma dalga hızları ve atenuasyon) analiz etmek için toplanması amaçlanmıştır.

Şekil 1. Gürcistan açıklarında kanyon sırtlarında gözlenen çamur diyapiri yapılarından alınan karotlarda petrol ile birlikte örneklenen büyük gaz hidrat kütlelerinin yanması.

## YÖNTEM

Çalışmadaki veriler 108Y244 numaralı TÜBİTAK Türkiye-Güney Kore ikili işbirliği projesi kapsamında Doğu Karadeniz ve Gwangyang körfezi olmak üzere iki farklı alanda toplanmıştır. 2009 yılında Gwangyang körfezinde, 2010 yılında ise Doğu Karadeniz'de seferler gerçekleştirilmiştir.

Doğu Karadeniz'de Trabzon-Rize açıklarında yüksek ayrımlı çok kanallı sismik yansıma verileri Dokuz Eylül Üniversitesi Deniz Bilimleri ve Teknolojisi Enstitüsü jeofizik ekibi ve lisansüstü öğrencileri ve tarafından R/V Koca Piri Reis gemisi ile toplanmıştır. Alanda Şekil'de konumları verilen çok kanallı sismik yansıma verileri toplanmıştır. Veriler 216 kanallı ve 1350 m uzunluğunda sayısal streamer ve enerji kaynağı olarak da GI hava tabancası 2x(45+45) kullanılarak toplanmıştır. Toplamda 1700 km sismik yansıma verisi toplanmıştır.

Gwangyang Körfezinde very seti Chirp II, Datasonics cihazı kullanılarak üniversiteye ait R/V Tamyang araştırma gemisi ile toplanmıştır. Sismik hatlar boyunca 36 piston karot örnekleme de aynı gemi ile toplanmıştır. Fiziksel özellikler (gözeneklilik, su içeriği ve yoğunluğu) ağırlıklı-hacim yöntemi kullanılarak belirlenmiştir. Fiziksel ve akustik özelliklerin ölçümünde

aynı karot derinliğinden elde edilen numuneler için dane boyu dağılımı belirlenmiştir. Şekil 3'te Gwangyang Körfezi'nde toplanan CHIRP mühendislik sismiği hatları ile piston karot numunelerinin konumları verilmiştir.

Şekil 2. Doğu Karadeniz bölgesinde toplanan çok kanallı sismik hatlara ait lokasyon haritası,

Şekil 3. Güney Kore, Gwangyang körfezinde alına piston karot noktaları ve CHIRP sismik hatlarının lokasyonları.

## BULGULAR

Doğu Karadeniz'de Rize ve Trabzon açıklarında toplanan çok kanallı yüksek ayrımlı sismik hatlar şelfin bir kısmını, kıtasal yamacı ve apronun bir kısmını kapsamaktadır. Çalışma alanında da birden fazla fay sistemi ile kıvrım kuşakları gözlenmiş ve gözlenen bu yapıların, fay zonu içerisinde birbirleriyle bağlantılı olarak geliştiği düşünülmektedir. Çalışma alanında gözlenen Trabzon fayının, kuzey-güney yönlü bindirme kuvvetlerinin oluşturduğu, kuzeydoğu-güneybatı uzanımlı, sol yönlü doğrultu atımlı bir fay olduğu yorumu getirilmiştir. Şekil 4'te verilen sismik hat deniz kıyısına dik olup, uzunluğu yaklaşık olarak 55 km'dir. Sismik kesit üzerinde Trabzon-1 ve Trabzon-2 fayları kırmızı ve yeşil renkte çizilmiş ve bölgede hakim olduğu düşünülen ana normal fay da mavi renkte gösterilmiştir. Karadeniz bölgesinin genelinde meydana gelen erozyonel olaylar ve kütle hareketleri de aynı sismik kesitte gözlenmiştir. Kıtasal yamaçlarda deniz tabanı eğiminin yüksek olması; kütle kayması, heyelan, tortul dalgaları gibi oluşumlara sebep olmaktadır.

Şekil 4. DK 10-29 No'lu K-G sismik hattında gözlenen Trabzon fayı ve kıtasal yamaçta kayma yapıları.

Çalışma alanının doğusunda gaz hidratın varlığını işaret eden BSR yansımaları sismik hatlarda gözlenmiştir. Bu hatlara örnek Şekil 5'te verilmiştir. Sismik hattın en kuzeyinde, yüksek genlikli seviyenin taban topografyasını takip etmesi, yüksek genlik değerlerine sahip olması ve deniz tabanına göre ters polariteli olmasından dolayı tabana benzeyen yansıtıcı (Bottom Simulating Reflector-BSR) olduğu yorumu yapılmıştır.

Dk10-11 ve dk10-12 (Şekil 5a) numaralı sismik hatlardaki BSR yansımalarının altında gazın varlığına rastlanmazken, BSR içeren diğer sismik hatlarda serbest gaz içeren alanlara rastlanmıştır.

Alanda genellikle BSR yansımaları deniz tabanından itibaren yaklaşık olarak 1800-2700 ms derinlikte gözlenmiş ve ortalama genişliği 2000-4000 m arasında hesaplanmıştır

Şekil 5a. K-G yönlü DK 10-12 no'lu sismik kesitte gözlenen BSR yapısı

Şekil 5b. DK 10-12 no'lu sismik kesitte gözlenen BSR yapısını büyütülmüş görüntüsü

Şekil 6'da kesitin ortasına yakın bölgede gözlenen akustik türbidite zonu gazın varlığı olarak yorumlanmıştır. Güneybatıda deniz tabanında gözlenen kaotik içsel yansıma sahip yükselti çamur volkanı



olarak yorumlanmıştır. Alanda ilk kez saptanan bu çamur volkanına İzmir Çamur Volkanı adı verilmiştir. Çamur volkanının beslenme kanalı akustik maskelenme olarak gözlenmekte ve kenarlarında hız düşmesi nedeniyle tabakalar aşağıya doğru dalmaktadır. Tepe noktasında yüksek genlikli yansımalar şeklinde BSR yapıları mevcuttur.

Şekil 6: Yorumlanmış DK10- X04 nolu sismik yansıma kesiti.

Şekil 7. Yorumlanmış DK10-13 nolu sismik yansıma kesiti

Şekil 8. DK 10-13 hattına ait zarf, görünür polarite ve frekans kesiti

Şekil 7’de gözlenen çamur volkanına ise Busan çamur volkanı adı verilmiştir. BSR yapısının altında gözlenen akustik maskelenmeler gazın varlığını işaret etmektedir. BSR’in varlığı literatür de birçok çamur volkanında örneklenen gaz hidratların çamur volkanları ile birlikte yer almasına bir örnek daha teşkil etmektedir. Ayrıca bu yapıları içerisinde yer alan hız düşmeleri de gazın varlığını ortaya koymaktadır

Sismik kesitin KD’ sunda ise kayma düzlemi gibi gözlenen yansımalar olası kanal varlığını işaret etmektedir. Bu paralel yansımalar içerisinde gözlenen kaotik yansımalar Gürcistan tarafından gelen nehrin Lowstand (düşük susevyesi) zamanında taşıdığı tortullar olarak yorumlanabilir.

Şekil 8’de Nitelik analizinde, anlık frekans, zarf ve görünür polarite kesitlerinde yüksek genlikli ters polariteli seviyeler, anlık frekans kesitlerinde ise düşük frekanslı seviyeler gözlenmiştir. Şekilde zarf kesitinde deniz tabanının hemen altında güçlü yansımalar elips ile belirtilmiştir. Aynı şekilde görünür polarite kesitinde negatif polarite içeren yansımalar ve anlık frekans kesitinde de düşük frekans içerikleri siyah elipsler ile gösterilmiştir. Bu analizler tortullarda gaz birikimlerinin varlığını doğrular niteliktedir. Bu yansımaların BSR olup olmadığını anlamak için AVO analizi uygulanmıştır. AVO analizi ve enine kesit çizimi ve Gradyan analizi, Sınıf 1 AVO anomalisini ve tortulardaki gazın varlığını işaret etmektedir.

Gwangyang körfezinde elde edilen CHIRP verilerine örnek Şekil 9’da verilmiştir. Bu kesitte çalışma alanında çamur diyapiri yapısı gözlenmektedir. Çamur diyapirleri sıg gaz birikimleri ile ilişkili yapılara olarak yorumlanmaktadır.

Şekil 9. Gwangyang Körfezi’nde yüksek ayrımlı CHIRP sismik sistemi ile elde edilen kesitte gözlenen çamur diyapiri.

## SONUÇLAR

Çalışma alanında, sırt yapılarında diyapirik yapılarla gelişen ve bu çalışma kapsamında saptanan 2 çamur volkanı gözlenmiş olup, Busan (Pusan) ve İzmir çamur volkanları isimleri verilmiştir. Çalışma alanının doğusunda kuzey-güney yönlü bindirme kuşaklarının sebep olduğu doğu-batı uzanımlı kıvrım kuşağı bölgedeki ters faylarla ilişkilendirilmiştir. Bölgede

büyük bir olasılıkla sıkışma tektonik rejimi altında çok miktarda sıvı içeren tortulların yüzeye doğru yükselmesi ile çamur volkanları meydana gelmiştir. Sonuç haritasında çalışma alanındaki olası gaz birikimleri, BSR’lar ve çamur volkanları yaklaşık batimetri haritası üzerinde gösterilmiştir (Şekil 10).

Şekil 10. Çalışma alanında yorumlanan yapıları gösteren sonuç haritası.

Bölgenin doğusunda gaz hidratın varlığını işaret eden BSR yansımaları gözlenmiştir. BSR yansımaları deniz tabanından itibaren yaklaşık olarak 1800-2700 ms derinlikte gözlenmiş ve ortalama genişliği 2000-4000 m arasında hesaplanmıştır. Gaz ve BSR alanı olarak haritalanan sismik kesite uygulanan nitelik analizleri ortamda olası gaz varlığına işaret etmektedir.

Gwangyang Körfezi’nde sıg gazla ilişkili gözlenen akustik anomaliler körfezde yaygın olarak dağılım göstermektedir. Bu anomaliler sıg gazın varlığını işaret eden, deniz tabanına yakın gözlenen akustik maskelenme ve akustik tuurbidite alanları olarak gözlenmiştir. gaz içeren tortullardan alınan örneklerde gaz kabarcıkları gözlenmiştir.

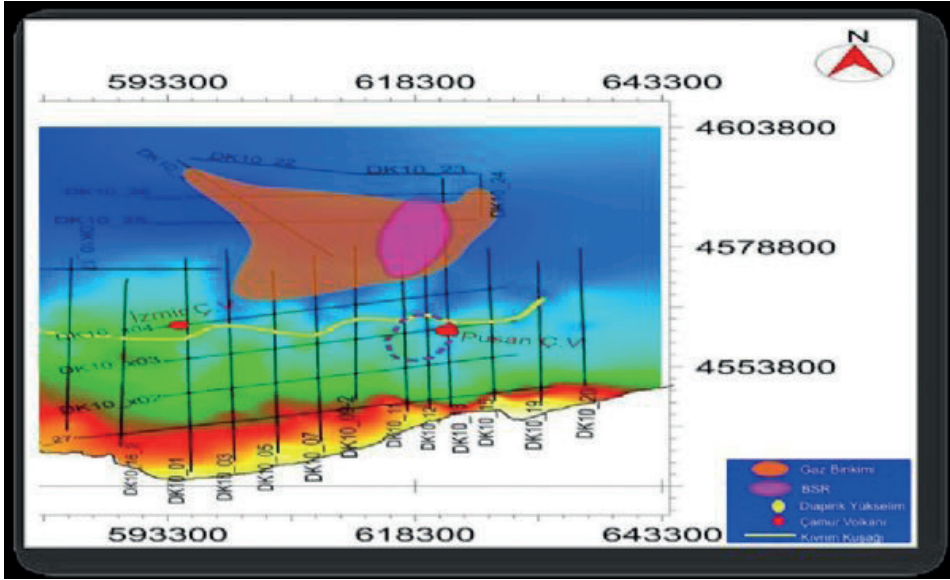
Bu çalışma ile dünyanın iki farklı alandaki çalışmalar yaparak sıg alandaki her yapının derinlerle bağlantılı olduğu ve yüzeyde deniz tabanındaki tortullarda derinlerin imzasını taşıdığı görülmüştür.

Anahtar Kelimeler: Doğu Karadeniz, gaz hidrat

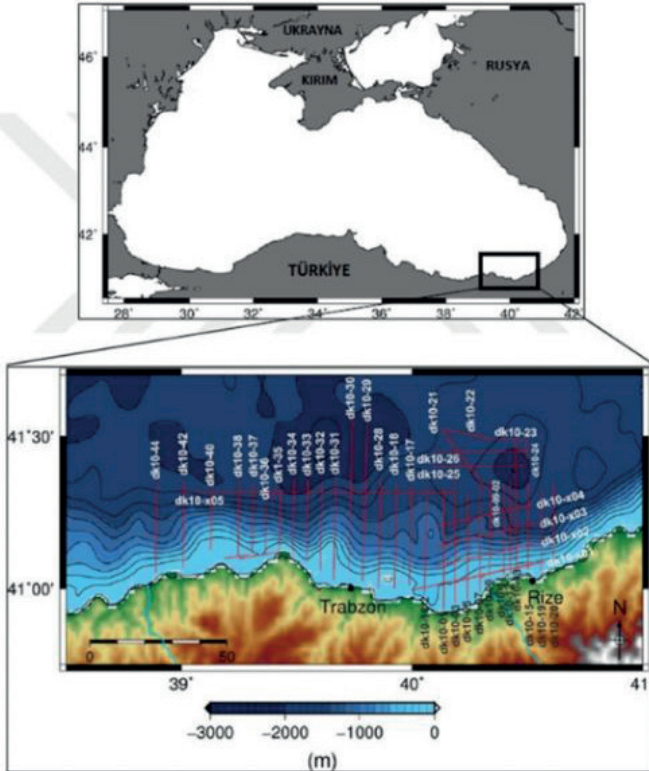
Şekil 1



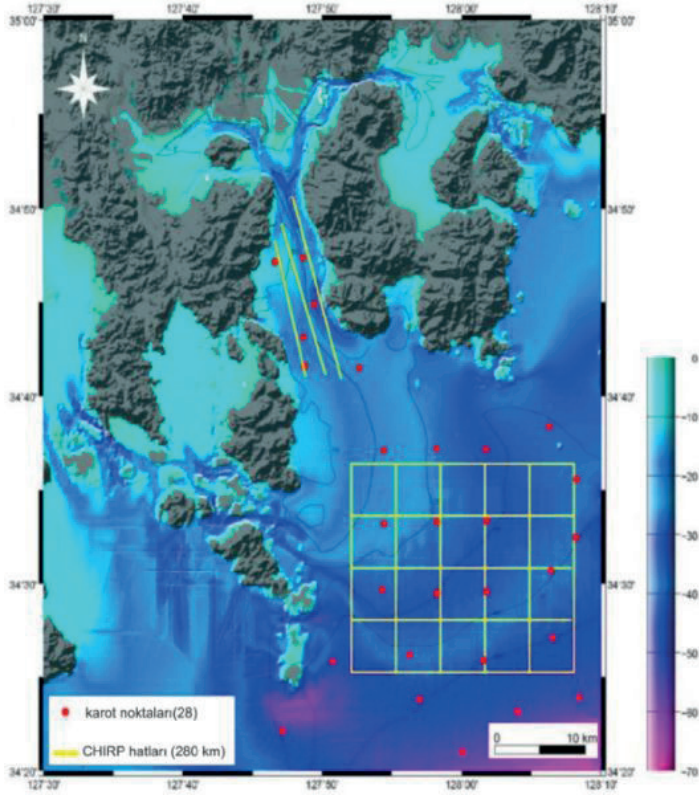
Şekil 10



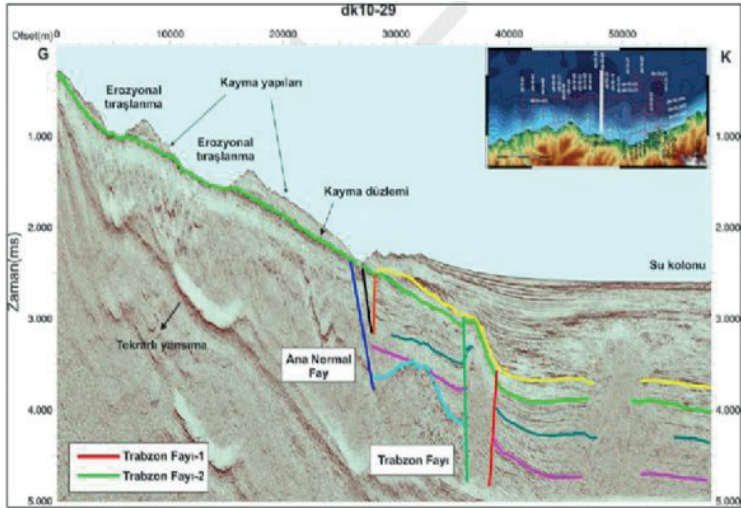
Şekil 2



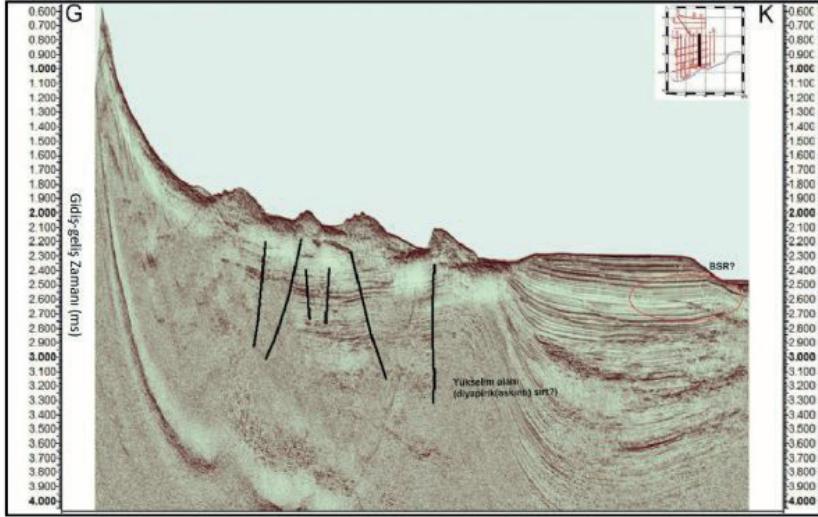
Şekil 3



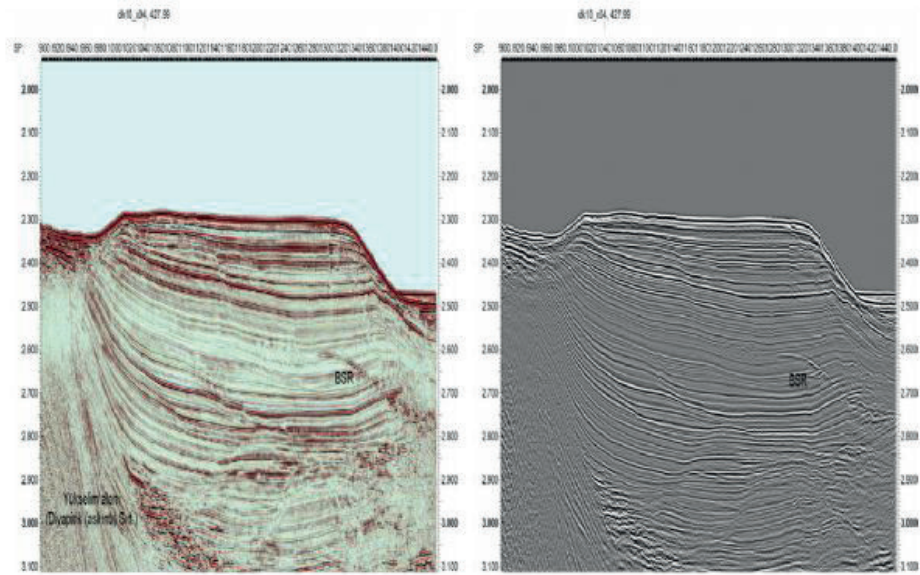
Şekil 4



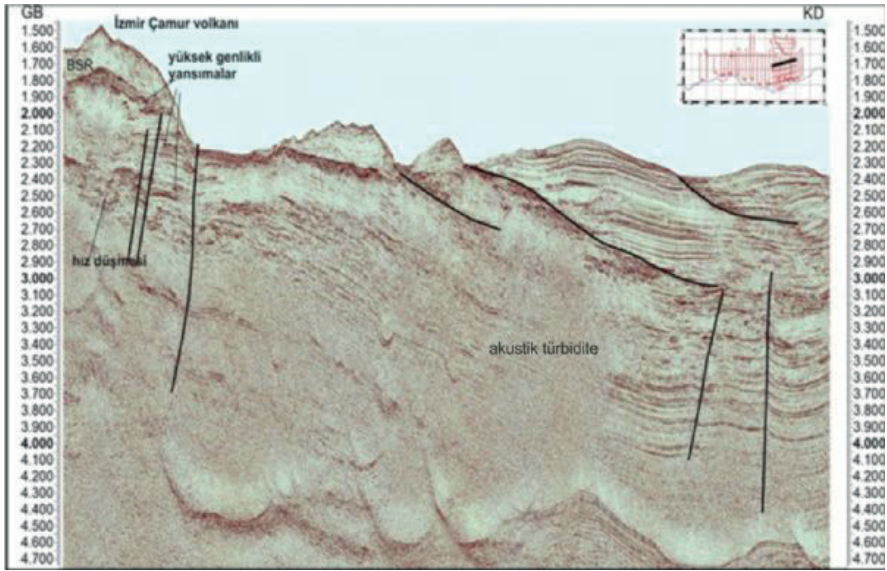
Şekil 5a



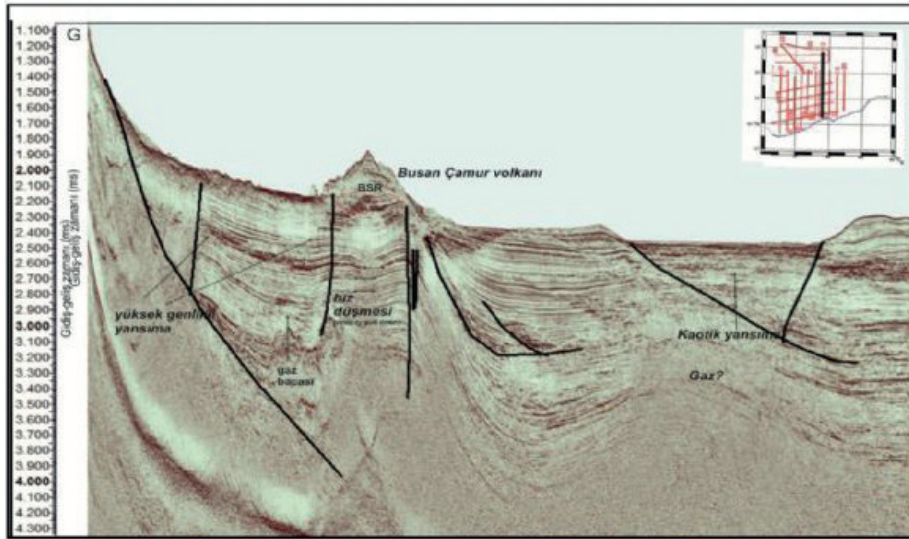
Şekil 5b



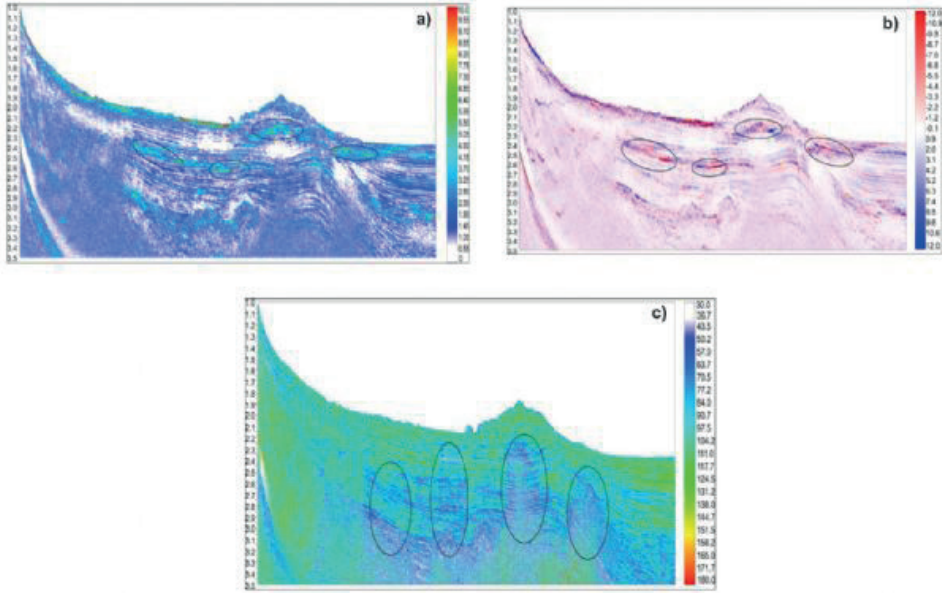
Şekil 6



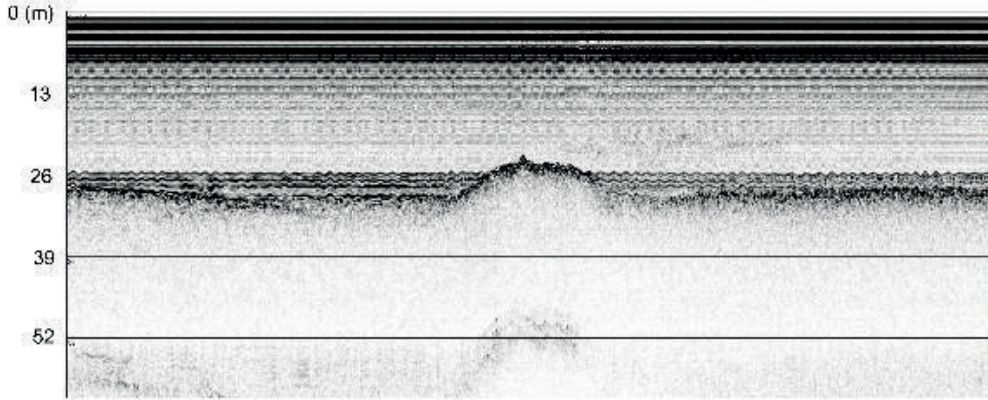
Şekil 7



Şekil 8



Şekil 9



YEOSU 2009 - LINE 10 A

# Bozcahüyük (Seyitömer/Kütahya) Yöresindeki Bitümlü Marlarnın Organik Jeokimyasal Verilerinin Değerlendirilmesi ile Sentetik Petrol Potansiyelinin Ortaya Konulması



Ali Sarı<sup>1</sup>, Fatih Büyüç<sup>2</sup>

<sup>1</sup>Ankara Üniversitesi, Mühendislik Fakültesi, Jeoloji Mühendisliği Bölümü, 50. Yıl Yerleşkesi, 06830, Gölbaşı, Ankara / Türkiye.

<sup>2</sup>Enerji ve Tabii Kaynaklar Bakanlığı, Tabii Kaynaklar Dairesi Başkanlığı, Nasuh Akar Mahallesi, Türkocağı Caddesi, No:2, 06520, Çankaya, Ankara / Türkiye.

## ÖZ

Bozcahüyük (Seyitömer/Kütahya) yöresinde yüzeylenen gri-yeşil renkli, baskın olarak marn, marn-kiltaşı ardalanmasından oluşan organik karbon yönünden oldukça zengin bitümlü marnların organik jeokimyasal özelliklerinin incelenmesi ile çökeltme ortamı koşulları ve hidrokarbon potansiyeli değerlendirilmiştir. Bu kapsamda, çalışma sahasından alınan örneklerin Rock-Eval piroliz, Gaz Kromatografisi (GC), Gaz Kromatografisi-Kütle Spektrometresi (GC-MS) ve Modified Fischer Assay (MFA) analizleri yapılmıştır. Gastropoda, lamellibranshiata ve ostrakoda fosillerinin yanı sıra kömürleşmiş yaprak ve dal kalıntılarını içeren Seyitömer Formasyonu'nun linyit işletmesi içindeki Höyük panosunda bitümlü marnlardan alınan örneklerin ince kesitlerinde karasal fitoklast ve palinomorfların yanı sıra Botryococcus Braunii gibi Tip-I kerogeni işaret eden tatlı su alglerine rastlanmıştır. Dolayısıyla bölgedeki marnların bir siğ/durgun göl ve bataklık ortamında çökeldiği değerlendirilmektedir. Çalışma sahasında, organik maddece zengin bitümlü marn istifinden alınan örnekler (23 adet) ortalama TOC %9,27 değerine sahip olup mükemmel kaynak kaya özelliği taşımaktadır. HI-OI, HI-Tmax ve S2-TOC, HI diyagramları, (S2/S3) hidrokarbon tip indeksi ile (S1+S2) potansiyel ürün değerleri, ortamın baskın Tip I (gösel) ve nadir Tip II kerogen içerebileceğine işaret eder. İncelenen örneklerin Tmax ortalaması 432 °C olması ve GC-MS verilerinin değerlendirilmesi ile bölgedeki bitümlü marnların henüz olgunlaşmamış olması nedeniyle konvansiyonel petrol türetemediği belirlenmiştir. MFA yöntemi ile analiz edilen bitümlü marn örneklerinin petrol içeriği ortalaması %12,6 olup, 133 L/ton sentetik petrole karşılık gelmektedir. MFA verimi ile TOC, HI ve S2 ilişkileri birlikte değerlendirildiğinde, mükemmel kaynak kaya özelliğine sahip olan bu kayaçlardan, retortlama ve/veya ekstraksiyon yöntemleri ile sentetik petrol üretilebileceği değerlendirilmektedir.

Anahtar Kelimeler: Bitümlü Marn, Sentetik Petrol.

## REVEALING OF SYNTHETIC PETROLEUM POTENTIAL BY EVALUATION OF ORGANIC GEOCHEMICAL DATA OF BITUMINOUS MARLS IN BOZCAHÜYÜK (SEYİTÖMER/KÜTAHYA) REGION

By examining the organic geochemical properties, sedimentation conditions and hydrocarbon potential of the bituminous marls, having quite rich organic carbon content, composed of gray-green colored, dominant

marl, marl-claystone intercalation in the Bozcahüyük (Seyitömer/Kütahya) Basin has been evaluated. In this context, Rock-Eval pyrolysis, Gas Chromatography (GC), Gas Chromatography-Mass Spectrometry (GC-MS) and Modified Fischer Assay (MFA) analyses of the samples taken from the study area were performed. The Seyitömer Formation contains fossils of gastropoda, lamellibranshiata and ostracoda, as well as coalized leaf and branch remains and in the thin sections of samples taken from bituminous marls of the Formation on the "Höyük Panosu" in the lignite mine, terrestrial phytoclasts and palynomorphs as well as freshwater algae such as Botryococcus Braunii indicating Type-I kerogen were encountered. Therefore, it is considered that the marls in the region were deposited in a shallow/stagnant lake and swamp environment. Samples (23 pieces) taken from the organic matter-rich bituminous marl sequence in the study area have an average TOC ratio of 9.27% and have excellent source rock characteristics. HI-OI, HI-Tmax and S2-TOC, HI diagrams, (S2/S3) hydrocarbon type index and (S1+S2) potential product values may indicate that the environment may contain dominant Type I (lacustrine) and rare Type II kerogen. The average of the Tmax values of analysed samples is 432 °C and according to evaluation of the GC-MS data it was determined that the bituminous marls in the region could not produce conventional petroleum due to their immaturity. The average oil content of the bituminous marl samples analysed by the MFA method is 12.6%, corresponding to 133 L/ton of synthetic oil. When the MFA yield and TOC, HI and S2 relations are evaluated together, it is possible to say that synthetic oil with economic potential can be produced from these excellent source rocks by retorting and/or extraction methods.

Keywords: Bituminous Marl, Synthetic Oil.

## 1. GİRİŞ

Çalışma sahası, Kütahya Seyitömer Beldesine bağlı Bozcahüyük mevkinde 1/25.000 ölçekli İ23-c3 ve c4 paftalarında yer alır (Şekil 1).

Bitümlü şeyl, petrollü şeyl (oil shale), bitümlü şist, bitümlü kiltası ve bitümlü marn şeklinde adlandırılabilen organik maddece zengin kayaçlar; genellikle siyah, koyu gri, gri, koyu kahve renkli ve çoğunlukla laminalı olup içermiş olduğu maddenin bir kısmı organik çözücülerde çözünen bitümden, diğer kısmı ise organik çözücülerde çözünmeyen kerojenden oluşmaktadır (Dyini, 2003). Bitümlü kayaçlar, retortlama ve ekstraksiyon prosesleri ile petrol ve gaz üretilebilen ve geriye proses sonrası farklı sektörlerde kullanılabilen

kül bırakırlar. Bitümlü kayaçlar; kalorifik değeri nedeniyle termik santrallerde düşük kaliteli linyitlerle birlikte katı yakıt olarak kullanıldığı, ana, iz ve nadir toprak elementleri ile aktif karbon üretiminde, kağıt, plastik, boya, seramik, gübre ve çimento sanayisinde kullanıldığı bilinmektedir.

Ülkemizde MTA ve diğer araştırmacılar tarafından geçmiş yıllarda yapılan çalışmalarda, mümkün ve muhtemel rezerv kategorisinde yaklaşık 10 milyar ton bitümlü kayac kaynağı tespit edilmiş olup enerji kaynakları içerisinde yaklaşık 20 milyar ton olan linyit kaynağından sonra ikinci sırada yer almaktadır (Büyük ve Sarı, 2021).

Enerji talebi ve fosil yakıtlarda dışa olan bağımlılığın artması, petrol fiyatlarındaki dalgalanmalar ve artan enerji faturaları, enerji arz güvenliği kapsamında kaynak çeşitliliğinin artırılması ve alternatif yerli kaynakların değerlendirilmesi ihtiyacı nedeniyle bitümlü kayaçlardan üretilebilecek sentetik petrole ihtiyaç duyulmaktadır.

## 2. MATERYAL VE YÖNTEM

Çalışma sahasından alınan toplam 23 adet örneğin organik jeokimya analizleri, Türkiye Petrolleri'nin (TP) AR-GE Merkezi laboratuvarlarında yapılmıştır. Bu örneklerin tamamı Rock Eval piroliz analizine tabii tutulmuş ve yüksek TOC, S2 ve HI değerlerine göre seçilen 6 adet örnek ise Modified Fischer Assay (MFA) analizinde, MFA analiz sonuçları ile korelasyonunun yapılabilmesi için değişken TOC, S2 ve HI değerlerine göre çoğunlukla MFA numunelerinden seçilen 3 adet örnek de gaz kromatografisi (GC) ve gaz kromatografisi-kütle spektrometresi (GC-MS) analizlerinde ve değişken TOC, HI ile OI değerlerine ve organik petrografi (kerojen tip tayini) analizlerine göre seçilen 5 adet örnek ise organik fasiyes analizinde kullanılmıştır.

## 3. GENEL JEOLojİ

Seyitömer Neojen Havzası, Brinkmann (1971) tarafından tanımlanan "İzmir-Ankara Okyanus Zonu" üzerinde bulunmaktadır. Erken Miyosen'de, bölgedeki D-B yönünde etkili olan gerilme rejimi altında Seyitömer Havzası gibi K-G yönlü havzalar oluşmaya başlamıştır. Miyosen-Pliyosen yaşlı havza dolgusu, bu havzanın temelini oluşturan metamorfikler, ofiyolitik kayaçlar ve granitoidleri uyumsuz olarak üzerlemektedir (Çelik, 2003). Havzadaki bu dolgu malzemelerini, Sarıyıldız (1987) genel olarak eski akarsu, göl ve yeni akarsu çökeltileri olarak ayırmıştır.

Erken-Orta Miyosen yaşlı zengin linyit yataklarını içeren Seyitömer Formasyonu'nun tabanında yer alan yeşil plastik kili üzerinde sırasıyla alt linyit (ana damar) seviyesi, bitümlü marnlar ve üst linyit damarı yer alır. En üst seviyelerde ise açık sarı, gri, yeşilimsi gri renkli mam ve yer yer silisifiye kireçtaşı mercekli tuf ve diyatomeli marn ardalannmasından oluşan sarı kil üyesi bulunur (Şengüler, 1999) (Şekil 2-4).

## 4. ORGANİK JEOKİMYASAL BULGULAR VE DEĞERLENDİRMELER

### 4.1. Kaynak Kaya Potansiyeli

%1,06 ile %29,87 arasında değişen TOC değerlerinin ortalaması %9,27'dir. İncelenen örnekler; Tissot ve Welte (1984)'e göre zengin (TOC>2), Jarvie (1991)'e göre yeterli (TOC>1) ve Peters ve Cassa (1994)'e göre mükemmel (TOC>4) kaynak kaya potansiyeline sahiptir. Ortalama 2,11 mg HC/g kaya S1 ve ortalama 66,40 mg HC/g kaya S2 hidrokarbon değerleri; Peters ve Cassa (1994)'e göre örneklerin S1 için genellikle iyi (1<S1<2) ve mükemmel (4<S1) arasında ve S2 için ise mükemmel (20<S2) petrol potansiyeline sahip kaynak kaya olduğunu ve tüm örneklerde S2>S1 olmasının da kaynak kayada herhangi bir organik kirlenmenin olmadığını gösterir.

### 4.2. Organik Madde Tipi

290 ile 769 mg HC/g TOC arasında değişen HI değerlerinin ortalaması 654,59 mg HC/g TOC'dir. Şekil 5 ve Şeki 6'da HI-OI ve HI-Tmax diyagramlarından da görüleceği üzere ve 3,01-31,26 arasında değişen (S2/S3) hidrokarbon tip indeksi (Peters ve Cassa, 1994) dikkate alınarak yapılan kerojen tipi değerlendirmesinde, baskın Tip I kerojen (15<S2/S3) ve nadir Tip II kerojen (10<S2/S3<15) türleri ve Şekil 7'de HI ile ilişkilendirilmiş S2-TOC diyagramında incelenen örneklerin Tip I-Tip II kerojen olduğu görülmektedir.

### 4.3. Organik Maddenin Isısal Olgunluğu

İncelenen örneklerin Tmax ortalaması 432 °C olup 426°C ile 441°C arasında değişmekte olup olgunlaşma parametresi; Espitalie vd. (1984)'e göre olgunlaşmamış-petrol penceresinde (430<Tmax(°C)<435), Peters ve Cassa (1994)'e göre ise olgunlaşmamış (Tmax (°C)<435) evrededir. Şekil 6'da yer alan HI-Tmax diyagramında örnekler, genellikle Tmax<435°C olması sebebiyle olgunlaşmamış olup hidrokarbon türetmeyeceği görülmektedir. Şekil 8'de PI değerlerinin 0,1'den daha düşük olması nedeniyle olgunlaşmamış zonda olduğundan hidrokarbon türümünün gerçekleşemeyeceğine işaret eder.

### 4.4. Hidrokarbon Türetme Potansiyeli

Kaynak kayanın petrolü dışarı atmaya başladığı derinliğin tespit edilmesinde kullanılan "Bitümen indeksi" (S1/TOC) değerlendirmesinde; incelenen örneklerden 10'nunun atım başlangıcında (0,1<S1/TOC<0,2), diğer 10'unda ise atımın çok fazla olduğu (0,2<S1/TOC) ve geriye kalan 3'ünde ise atımın hiç olmadığı (S1/TOC<0,1) görülmüştür (Smith, 1994; Hunt, 1995).

Hidrokarbon Tip İndeksi (S2/S3) ortalama değeri 18,95 olup örneklerin Clementz (1979)'a ve Peters (1986)'ya göre petrol türetme (5,0<S2/S3) potansiyeline sahip olduğu görülmüştür. Yine bu örneklerin Potansiyel Ürün



PY (ppm/mg HC/g kaya) (S1+S2) ortalamasının 68.508 ppm olması, Tissot ve Welte (1978)'e göre iyi kaynak kaya potansiyeline (6.000 ppm<S1+S2) işaret eder.

#### 4.4.1. Modified Fischer Assay (MFA) Analizi ile Sentetik Petrol Üretimi

İncelenen örneklerin MFA verimi ile TOC, S1 ve S2 ilişkileri şekil 9-11'de incelendiğinde, çok iyi ekonomik potansiyelde petrol üretilebileceği değerlendirilmektedir. MFA petrol içeriğinin %TOC ( $r=0,848$ ,  $p=0,033$ ) ve S2 ile ( $r=0,875$ ,  $p=0,022$ ) pozitif yönde güçlü korelasyon ilişkisi vardır. %TOC ve S2 değerlerinin artmasıyla birlikte MFA verimi de arttığından Tip I kerojen özelliğindeki bu örneklerden çok iyi ekonomik seviyede petrol türetilebileceği anlaşılmaktadır.

#### 4.5. Biyomarker İncelemeleri

##### 4.5.1. Gaz Kromatografisi Analizi (GC)

n-Alkan Dağılımları: GC analizleri ile çökeltme ortamı, biyolojik bozunma, ısısal olgunluk ve organik madde tipi hakkında değerlendirme yapılmıştır. İncelenen örnekler için gaz kromatogramlarında; nC23-nC30 dizisine doğru çarpık bir n-alkan dağılımı yani uzun zincirli C23, C25, C27 ve C29 piklerinin diğerlerine göre yüksek olmasından dolayı çökeltme ortamı karasal yüksek bitki ve denizel olmayan fitoplankton alg içeren göl ortamını işaret eder (Tissot ve Welte, 1984; Peters ve Moldowan, 1993).

Pristan/Fitan Oranı (Pr/Ph): Pr/Ph oranlarının 1'den küçük olmasından dolayı ortamın redoks koşullarının indirgen/anoksik olduğunu gösterir (Tissot ve Welte, 1984).

Karbon Tercih İndeksi (CPI): İncelenen örneklerin CPI değerleri Bray ve Evans (1961)'e göre HB-7'de 1,18, HB-12'de 5,88 ve HB-18'de 3,06 değerleri bulunmuştur. HB-7 denizel planktonları içerdiğini, HB-12 ve HB-18 ise yüksek karasal bitkilerle beslenen denizle bağlantısı olan bir karasal/gösel ortamı göstermektedir. Ayrıca CPI>1 ise tek sayılı karbonların baskın olması ve HB-12 ve 18 no.lu örneklerin CPI verilerinin yüksek olması, örneklerin olgunlaşmamış safhada olduğunu göstermektedir (Tran ve Philippe, 1993).

İzoprenoid/n-Alkan Oranları: HB-12 örneğinde Pr/nC17: 0,15 ve Ph/nC18: 1,00 ve HB-7 numunesinde ise Pr/nC17:0,70 ve Ph/nC18: 1,82 değerleri incelendiğinde, Petersen vd. (2001)'e göre ortamın anoksik, Chaula vd. (1987)'ye göre de kerojenin algal kökenli (Tip I kerojen) olduğuna işaret etmektedir.

##### 4.5.2. Gaz Kromatografisi-Kütle Spektrometresi Analizi (GC-MS)

m/z 191 kütle kromatogramlarında, HB-12 ve HB-18 numaralı örneklerde tuzluluk göstergesi olan Gameseranın (sırasıyla 0,25 ve 0,13) varlığı bölgenin denizel etki altında kaldığına ve ortamın indirgen

olduğuna işaret eder (Peters ve Moldowan, 1993).

İncelenen örneklerin m/z 191 kromatogramlarında C31 22R/C30 hopan oranının 0,25'den yüksek çıkmasının, marn kaynak kayası olduğunu (Koralay, 2009), [C29 Ts/(C29Ts+C29 Norhopan)] oranının 1'den küçük olmasının ise kil içeriği yüksek gösel çökeltme ortamını yansıttığı görülmüştür (Philip and Gilbert, 1986).

Diasteran/steran oranlarının (HB-7: 13,4; HB-12: 4,7; HB-18: 21,2) yüksek çıkması, çökeltme ortamının alg kökenli organik madde içeren kil oranı yüksek klastik sediman içerdiğini gösterir (Mello vd., 1988; Peters ve Moldowan, 1993).

m/z 191 ve m/z 217 GC-MS kromatogramlarında incelenen örneklerde, steran/hopan oranının  $\geq 1$  olması, örneklerin algal organik madde içerdiğine işaret eder (Peters ve Moldowan, 1993).

#### 5. TARTIŞMA VE SONUÇLAR

Bu çalışmada, Bozcahöyük (Seyitömer/Kütahya) yöresinde yayılım gösteren Seyitömer Formasyonuna ait bitümlü marnların ortalama %9,27 TOC içermesi nedeniyle mükemmel kaynak kaya özelliğine sahip, kerojen tipinin baskın Tip I ve nadiren Tip II ve çökeltim redoks koşullarının ise indirgen anoksik ortam olduğu, karasal fitoklast ve palinomorfaların yanı sıra Botryococcus Braunii gibi tatlı su algleri içermesi nedeniyle çökeltim ortamının göl olduğu anlaşılmıştır. Ancak incelenen organik jeokimya verilerine göre; CPI verilerinin yanı sıra C27, C28 ve C29 steran bolluk dağılımının ve tuzluluk ortam göstergesi olan Gameseranın varlığının tespit edilmesi, zaman zaman göl ortamının lagüner denizel etki altında kalmış olabileceğine işaret eder. Bölgedeki bitümlü marnların, Tmax ortalamasının 432°C olması ve GC ile GC-MS verilerinin değerlendirilmesi neticesinde henüz olgunlaşmamış olması sebebiyle konvansiyonel petrol türetmediği değerlendirilmiştir.

Seyitömer Havzası'ndaki bitümlü marnların geçmiş yıllarda petrol içeriğine (%2,4-%5,9) ve bu marnlardan sentetik petrol üretimine yönelik yapılan çalışmalara kıyasla, çalışma sahasından alınan örneklerin MFA analizlerinde, petrol içeriği ortalama %12,6 (%3,22-%21,57) yani ortalama 133 L/ton (30 L/ton -230 L/ton) gibi yüksek değerler elde edilmiştir. Bu kapsamda bölgede, Hufnagel (1989)'a göre bitümlü kayaçların ekonomik ve teknolojik olarak kazanılabileceği uluslararası minimum petrol içeriği sınırının %4 olması kriterinin sağlanmasının yanı sıra, baskın Tip-I kerojen, yüksek TOC, S2 ve HI piroliz verileri değerlendirildiğinde, çalışma sahasındaki bitümlü marnlardan sentetik petrol üretme potansiyeli olduğu ortaya konulmuştur.

#### DEĞİNİLEN BELGELER

Bray, E.E., Evans, E.D. 1961. Distribution of n-paraffins as a clue to recognition of source beds. *Geochimica et Cosmochimica Acta* 22, 2-15.

- Brinkmann, R. 1971. The geology of western Anatolia. Geology and history of Turkey. The Petroleum exploration society of Libya.
- Büyük, F. 2019. Bozcahüyük (Seyitömer/Kütahya) Havzası bitümlü şeyllerinin organik jeokimyasal değerlendirmesi ve hidrokarbon potansiyeli. Yüksek Lisans Tezi, Ankara Üniversitesi, Fen. Bil. Ens., Jeoloji Mühendisliği Anabilim Dalı, Ankara.
- Büyük, F. ve Sarı, A. 2021. Bozcahüyük (Seyitömer/Kütahya) Havzası'ndaki bitümlü marnların organik jeokimyasal özellikleri, çökeltme ortamı ve hidrokarbon potansiyeli. MTA Dergisi, 164:55-75, Ankara.
- Chaula, B.R., Chopra, A.K., Shukla, R.K. 1987. Geochemistry of sedimentary organics of Jurassic of India. In Petroleum Geochemistry Exploration in the Afro-Asian Region, Balkema, Rotterdam.
- Clementz, D.M. 1979. Effect of oil and bitumen saturation on source-rock pyrolysis. AAPG Bulletin 63, 2227-2232.
- Çelik, Y. 2003. Seyitömer (Kütahya) Neojen Havzası linyitlerinin petrografisi, jeokimyası ve depolanma ortamı. İ.Ü. Mühendislik Fakültesi, Mühendislik Bilimleri Genç Araştırmacılar I. Kongresi, İstanbul, 691-700.
- Dikmen, D. 2005. Seyitömer (Kütahya) yöresindeki kömür-bitümlü marn geçişinin organik fasiyesi özellikleri. Yüksek Lisans Tezi, İstanbul Üniversitesi, Fen. Bil. Ens., Jeoloji Mühendisliği Anabilim Dalı, İstanbul.
- Dyni, J. R. 2003. Geology and resources of some world oil-shale deposits. Oil Shale 20, 193-252.
- Espitalie, J., Marquis, F., Barsony, I. 1984. Geochemical logging. In: Analytical pyrolysis: techniques and applications, Voorhees, London. Butterworth & Guildford 276-304.
- Hufnagel, H. 1989. Investigation of oil shale deposits in Western Turkey. Bundesanstalt für Geowissenschaften und Rohstoffe, Project no.84.2127.3, Hannover, Germany (unpublished).
- Hunt, J.M. 1995. Petroleum geochemistry and geology. W. H. Freeman and Company, New York, 743 p.
- Jarvie, D.M. 1991. Factors affecting rock-eval derived kinetic parameters. Chemical Geology 93, 79-99.
- Koralay, D.B. 2009. Bolu Havzası bitümlü şeyllerinin hidrokarbon potansiyeli ve iz element dağılımlarının belirlenmesi. Doktora Tezi, Ankara Üniversitesi, Fen. Bil. Ens., Jeoloji Mühendisliği Anabilim Dalı, Ankara.
- Langford, F.F., Blanc-Valleron, M.M. 1990. Interpreting rock-eval pyrolysis data using graphs of hydrocarbons vs. total organic carbon. AAPG Bulletin 74, 799-804.
- Mello, M.R., Telnaes, N., Gaglianone, P.C., Chicarelli, M.I., Brassell, S.C., Maxwell, J.R. 1988. Organic geochemical characterisation of depositional paleoenvironments of source rock and oils in Brazilian Marginal Basins. In, Advances in Organic Geochemistry 1987 (L. Mattavelli and L. Novelli, eds.), Oxford, Pergamon Press, 31-45.
- Mukhopadhyay, P.K., Wade, J.A., Kruge, M.A. 1995. Organic facies and maturation of Jurassic/Cretaceous rocks, and possible oil-source rock correlation based on pyrolysis of asphaltenes, Scotian Basin, Canada. Organic Geochemistry 22(1), 85-104.
- Peters, K.E. 1986. Guidelines for evaluating petroleum source rock using programmed pyrolysis. The American Association of Petroleum Geologists Bulletin 70(3), 318-329.
- Peters, K.E., Cassa, M.R. 1994. Applied source rock geochemistry, in L.B. Magoon and W.G. Dow, eds., The petroleum system from source to trap. AAPG Memoir 60, 93-120.
- Peters, K.E., Moldowan, J.M. 1993. The biomarker guide: Interpreting molecular fossils in petroleum and ancient sediments. Englewood Cliffs, N.J.: Prentice-Hall.
- Peters, K.E., Walters, C.C., Moldowan, J.M. 2005. The biomarker guide. Cambridge University Press, V. 1, 471, UK.
- Petersen, H.I., Andersen, C., Anh, P.H., Bojesen-Koefoed, J.A., Nielsen, L.H., Nytoft, H.P., Rosenberg, P., Thanh, L. 2001. Petroleum potential of Oligocene lacustrine mudstones and coals at Dong Ho, Vietnam an outcrop analogue to terrestrial source rocks in the greater Song Hong Basin. Journal of Asian Earth Sciences 19, 135-154.
- Philip R.P., Gilbert T.D. 1986. Biomarker distributions in oil predominantly derived from terrigenous source material. Advances in Organic Geochemistry, Oxford, United Kingdom, Pergamon Press, 73-84.
- Sarıyıldız, M. 1987. Seyitömer (Kütahya) kuzeybatısındaki kömürlü Neojen kayalarının jeolojisi. Yüksek Lisans Tezi, Dokuz Eylül Üniversitesi, Fen. Bil. Ens., Jeoloji Mühendisliği Anabilim Dalı, İzmir (yayınlanmamış).
- Seifert, W.T., Moldowan, J.M. 1986. Use of biological markers in petroleum exploration. In, Methods in Geochemistry and Geophysics (P. B. Johns, ed.) 24, 261-290.
- Smith, J.T. 1994. Petroleum system logic as an exploration tool in frontier setting, in L. P. Magoon, and W. G. Dow (eds.), The petroleum system from source to trap. AAPG Memoir 60, 25-49.
- Şengüler, İ. 1999. Seyitömer (Kütahya) Petrollü şeyllerin ekonomik kullanım olanaklarının araştırılması. Doktora Tezi, Ankara Üniversitesi, Fen. Bil. Ens., Jeoloji Mühendisliği Anabilim Dalı, Ankara.
- Tissot, B.P., Welte, D.H. 1978. Petroleum formation and occurrence, Springer -Verlag, Berlin.
- Tissot, B.P., Welte, D.H. 1984. Petroleum formation and occurrence. Springer-Verlag, Berlin, 699 p.
- Tran, K.L., Philippe, B. 1993. Oil and rock extract analysis, in: Applied petroleum geochemistry (M.L., Bordenave, eds.), Paris.
- Van Krevelen, D.W. 1993. Coal. 3rd Edition, Elsevier Science Publishers, Amsterdam.

Sekil 1. Çalışma alanının Google Earth uydur görüntüsü ve yer bulduru haritası (Büyü ve Sari, 2021).



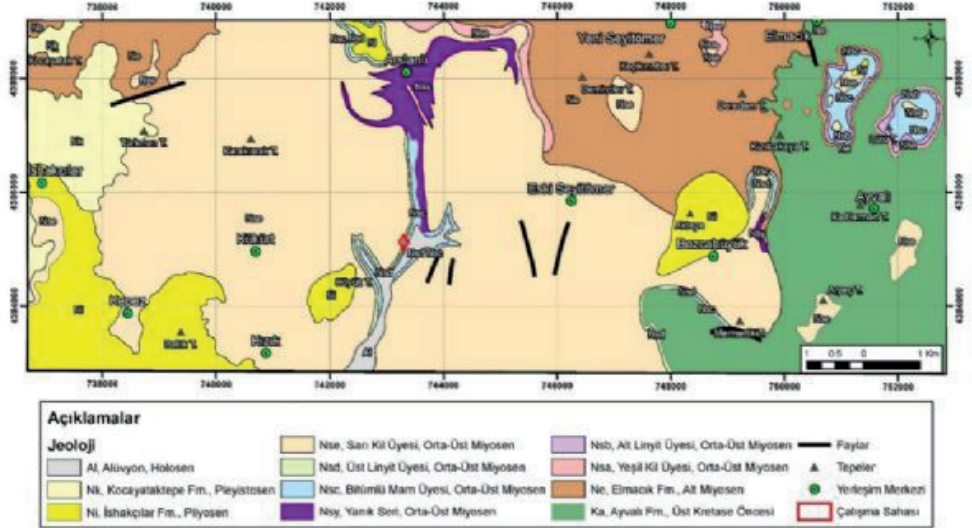
Tablo 1. m/z 191 ve m/z 217 GC-MS kromatogramlarına göre örneklerin içerdiği organik maddenin olgunlaşmasına ilişkin hesaplanan biyomarker parametreleri (Büyü ve Sari, 2021).

OLGUNLUK PARAMETRELERİ	HB-7	HB-12	HB-18
20S/(20S+20R) Steran Oranı (C29)=[18/(18+21)] piklerinin yüksekliği (m/z 217 GC-MS) Bu oran<0,5 ise olgunlaşmamıştır (Hunt, 1995).	0,04 Olgunlaşmamış	0,12 Olgunlaşmamış	0,06 Olgunlaşmamış
$\beta\beta/(\beta\beta+aa)$ Steran Oranı (C29)=[(19+20)/(18+19+20+21)] piklerinin yüksekliği (m/z 217 GC-MS) Bu oranda, ısasal olgunlaşma dengesi, petrol oluşum zonunda 0.72'dir (Peters vd., 2005).	0,23 Olgunlaşmamış	Tayin edilemedi.	0,26 Olgunlaşmamış
22S/(22S+22R) Homohopan İndeksi (C31)=[25/(25+26)] piklerinin yüksekliği (m/z 191GC-MS) Bu oranda ısasal denge değeri, petrol oluşum zonunda 0.5'e ulaşır (Peters vd., 2005).	0,02 Olgunlaşmamış	0,10 Olgunlaşmamış	0,05 Olgunlaşmamış
$Ts/(Ts+Tm) = [13/(13+14)]$ piklerinin yüksekliği(m/z 191 GC-MS) Bu oran, geç olgun petrol oluşum safhasında 1.0'e ulaşır (Peters vd., 2005).	Tayin edilemedi.	0,11 Olgunlaşmamış	Tayin edilemedi.
Moretan/Hopan Oranı (C30) = (24/23) piklerinin yüksekliği (m/z 191 GC-MS) Bu oran, ısasal olgunluğun artmasıyla 0,8'den 0,15-0,05'lere kadar düşebilir (Seifert ve Moldowan, 1986).	0,95 Olgunlaşmamış	5,52 Olgunlaşmamış	0,87 Olgunlaşmamış

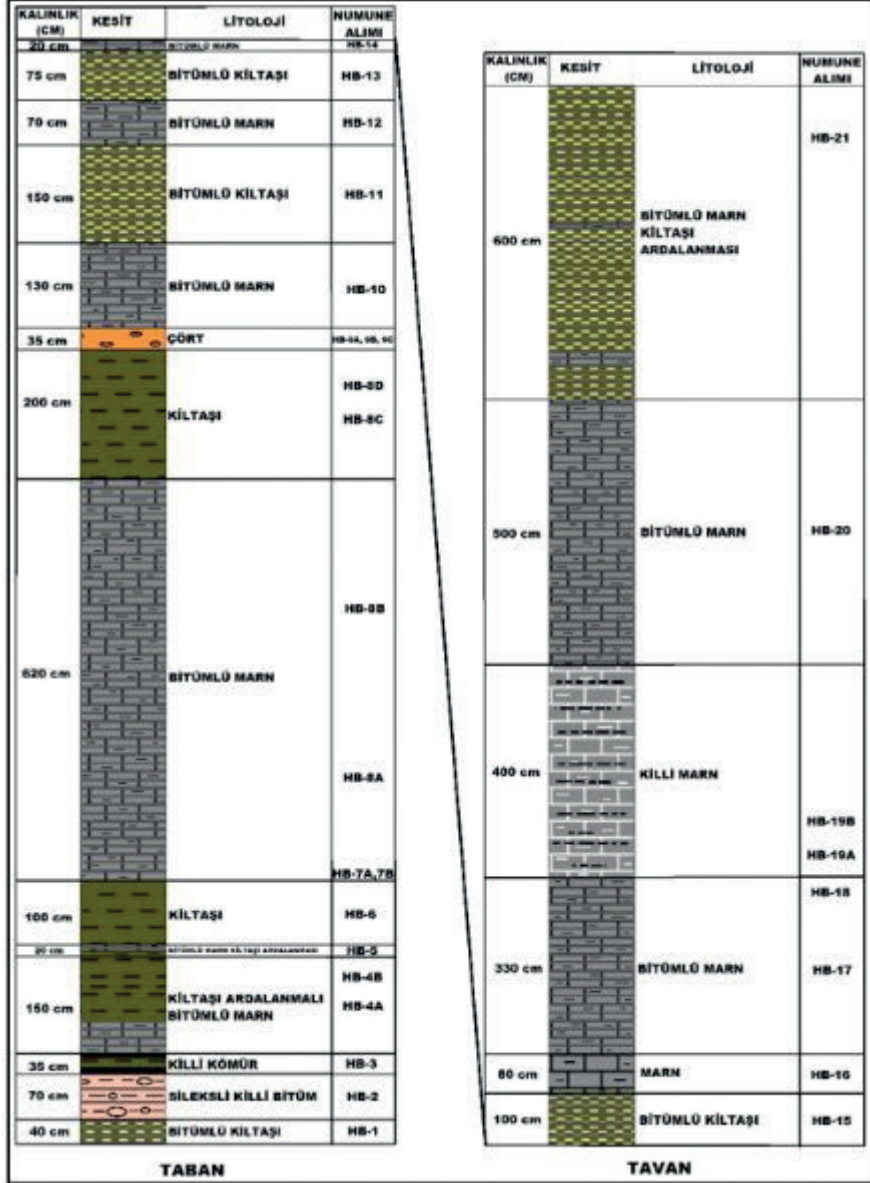
Şekil 2. Seyitömer (Kütahya) genelleştirilmiş stratigrafik kesiti (Şengül, 1999; Dikmen, 2005; Büyük, 2019).

SİSTEM	SERİ	FORMASYON	ÜYE	SİMGE	KALINLIK (m)	LİTOLOJİ	AÇIKLAMA					
KUVATERNER	HOLOSEN PLEYİSTOSEN	KOCAYATAKTEPE	Nk	Qh	20		Tutturulmamış çakıl, kum, mil ve kil					
					50		Kırmızımsı ve krem renkli, az tutturulmuş konglomera, kumtaşı ve yer yer tuf ve kil					
NEOJEN	PLİYOSEN	İSHAĞÇILAR	Ni		150		Üst seviyelerinde kireçtaşı, Orta seviyelerinde marn, Alt seviyelerinde tuf					
					SEYİTÖMER	Sarı Kil	Nse	25	Sarı lül, sarı, gri, yeşilimsi gri, krem marn, ve silisli kireçtaşı, mercelik tuf, diatomeli marn ardalanması			
						Üst Linyit	Nsd	10	Üst linyit gri ve açık gri renkli marn ardalanması			
					BİTİMLİ MARN	Nsc	30	Gri, yeşilimsi gri kireçtaşı, silisli kireçtaşı, marn yer yer çört ardalanması				
						Alt Linyit	Nsb	20 - 40	Alt linyit: linyit, kılı linyit, kumtaşı, silttaşı, kilitaşı ve marn ardalanması			
					YEŞİL PLASTİK KİL	Nsa	50	Yeşil plastik kil Üst seviyelerinde gri kilitaşı Alt seviyelerinde kumlu kilitaşı				
						Yeşil kil						
					ELMACIK	Ne	75 - 150					Çakıltası, kumtaşı ve kilitaşı ardalanması köfli boylanma, iri taneli, çapraz katmanlaşma, üst seviyelere doğru incelen tane boyu düğümlü akarsu ortamı
					ÜST KRETASE ÖNCESİ	ATVALI	Ka	>300				Ofiyolitik Melanj Serpantin, radyolarit, kireçtaşı blokları

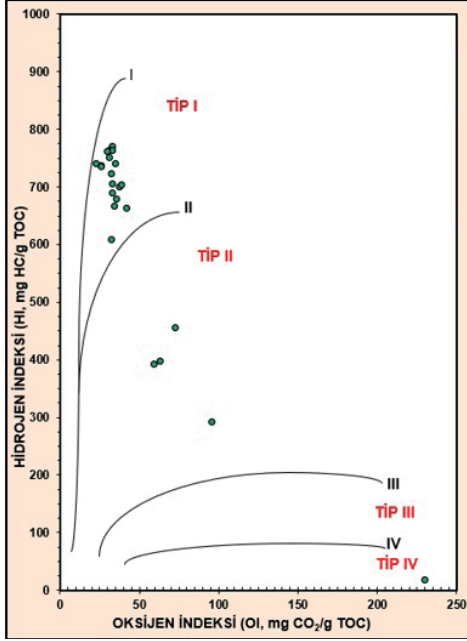
Şekil 3. Seyitömer (Kütahya) civarının jeoloji haritası (Şengül, 1999; Dikmen, 2005; Büyük, 2019).



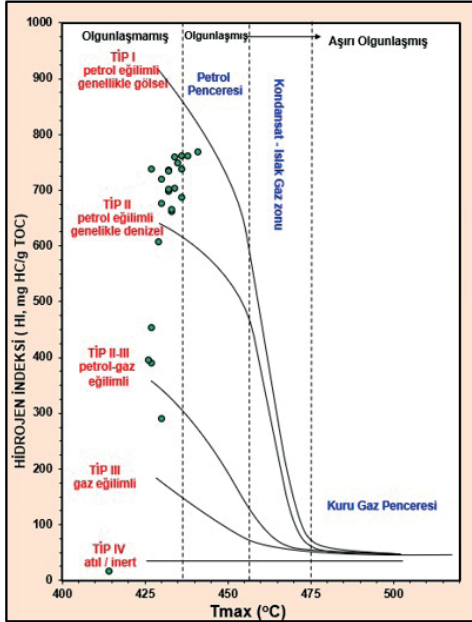
Şekil 4. Bozcahöyük (Seyitömer/Kütahya) Havzası Höyük Panosu'ndaki bitümlü marnların ölçülü stratigrafi kesiti (Büyük ve Sarı, 2021).



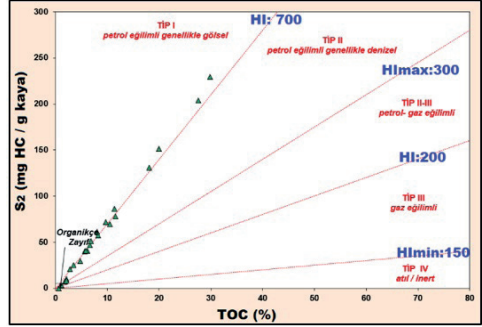
Şekil 5. HI-OI diyagramı (Van Krevelen, 1993; Büyük ve Sarı, 2021).



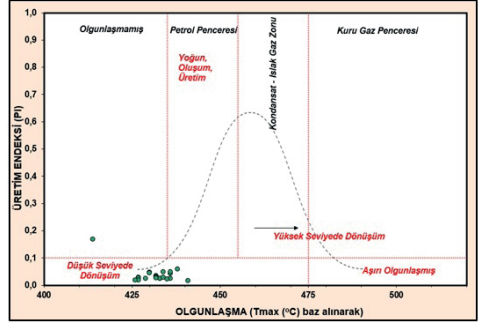
Şekil 6. HI-Tmax diyagramı (Hunt, 1995; Mukhopadhyay vd., 1995; Büyük ve Sarı, 2021).



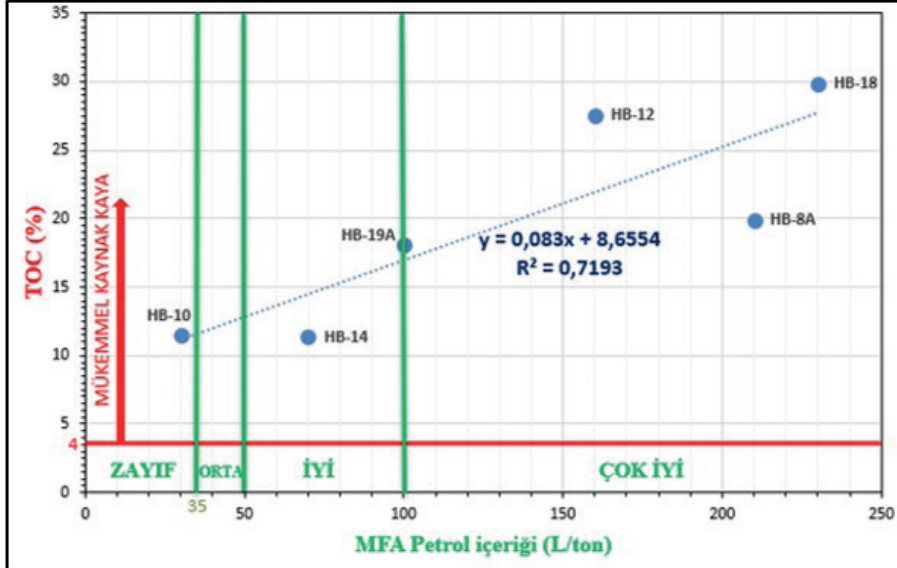
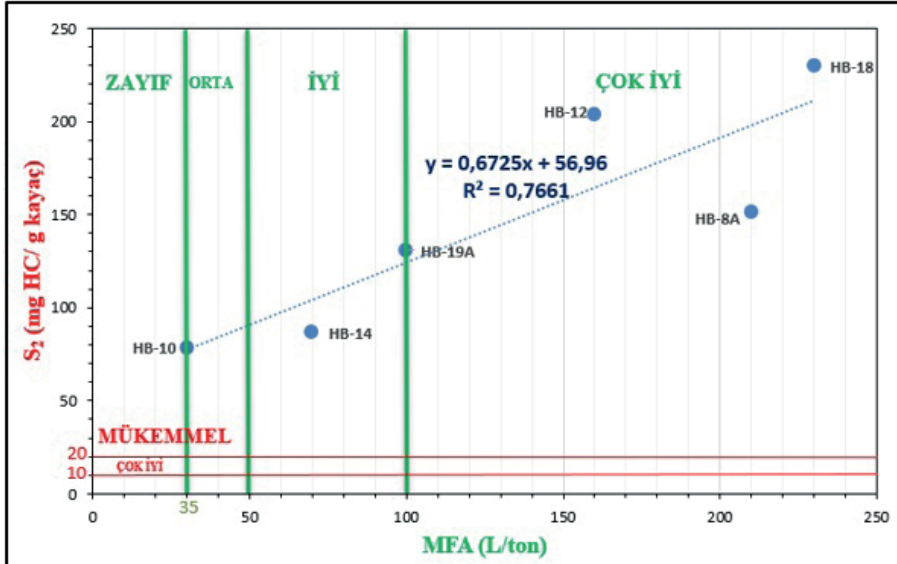
Şekil 7. S2-TOC, HI diyagramı (Langford ve Blanc- Valleron, 1990; Büyük ve Sarı, 2021).



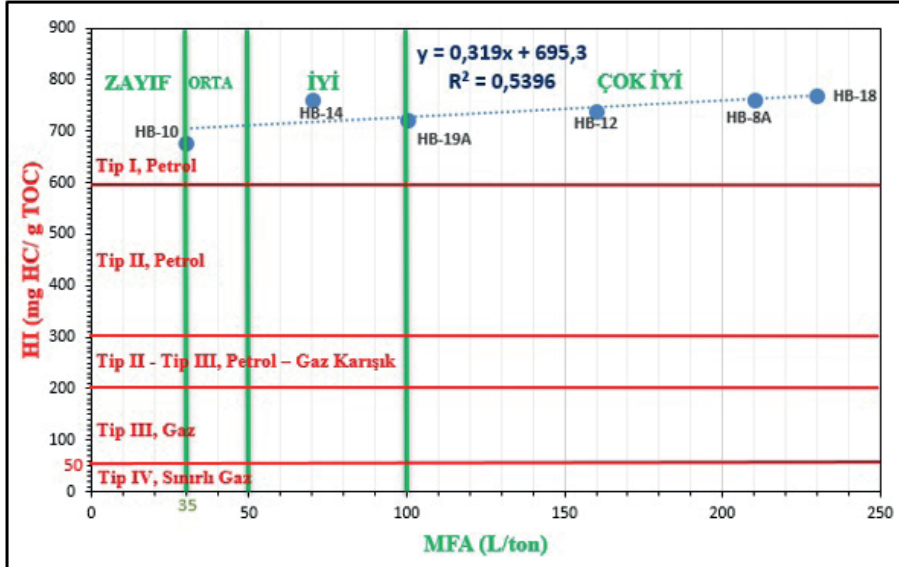
Şekil 8. PI-Tmax olgunlaşma ile kerojen dönüşüm diyagramı (Peters, 1986; Büyük ve Sarı, 2021).



Şekil 9. MFA petrol içeriği (L/ton)-TOC (%) diyagramı (Büyük ve Sarı, 2021).

Şekil 10. MFA petrol içeriği (L/ton)-S<sub>2</sub>(mg HC/ g kaya) diyagramı (Büyük ve Sarı, 2021).

Şekil 11. MFA petrol içeriği (L/ton)-HI (mg HC/ g TOC) diyagramı (Büyük ve Sarı, 2021).





# New Generation Approaches for the Manufacturability of Gas Hydrate, one of Turkey's Alternative Energies



## Güzide Kalyoncu Ergüler

Dumlupınar University, Department of Geological Engineering, Kütahya / Türkiye

### ABSTRACT

The need for project proposals that can come out of the vicious circle of climate change, which will be created as a result of the rapidly changing energy needs of developing countries and the energy sources of the future, which are within their own potential, and the carbon emission of traditional fuels, is increasing. Establishing systems that include the production of sustainable energy resources and new generation method applications for future generations is one of the most important issues that researchers have recently focused on. Based on the energy realities of Turkey, the general framework of the project titled "Carbon Capture, Storage and Utilization for Production of Natural Gas from Gas Hydrate Deposits in the Eastern Black Sea" will be mentioned within the scope of European Union IPA 3. In this context, it has been tried to present predictions about the studies carried out in the world and the studies that our country can do due to its potential.

Keywords: Eastern Black Sea, Gas hydrate.

### INTRODUCTION

Although not a conventional energy source, natural gas hydrate, which has achieved important steps in its commercialization, is a polyhedral lattice crystal, formed under high pressure and low temperature between methane and small amounts of non-hydrocarbon gases and water molecules by hydrogen bonding (Sloan and Koh, 2007). Natural gas hydrates are commonly located in the earth's crust as widely found in deep water areas and much lesser quantities permafrost.

The production methods of natural gas hydrate mining can be listed as depressurization, heating, inhibitor, CO<sub>2</sub> exchange methods and solid absorption. Recently, mixed production methods have been found in experimental studies. It is seen that the most common heating method and pressure reduction method also finds its place in the production of natural gas hydrates.

The main principle in production is possible by changing the structure of the hydrate, in which the hydrate is located. It is the formation of new ambient conditions by deteriorating the hydrate equilibrium state by changing the conditions of presence; temperature and pressure.

Thus, it is to ensure that the hydrate is decomposed into natural gas and water. Due to its great resource potential, natural gas hydrate is in the focus of attention of both oil producing countries, developing countries and industry. Determining the hydrate phase equilibrium under experimental conditions and determining the theoretical Gibbs free energy offer a promising option for storing CO<sub>2</sub> as solid hydrates in sediments and simultaneously recovering methane from gas hydrate reservoirs (Ohgaki

et al., 1996; Uchida et al., 2005). Theoretically, under favorable heat and mass transfer conditions, the CO<sub>2</sub> displacement process can be fast and efficient (Jung and Santamarina, 2011; Miyazaki et al., 2016; Ersland et al., 2010; Graue et al., 2008; Ota et al., 2005; Yuan et al., 2013; Ota et al., 2007).

Hassanpouryouzband and other researchers (2020) evaluated the current situation in gas hydrate in their literature review. In these evaluations, attention was drawn to the importance of heat and mass transfer due to CO<sub>2</sub> exchange in sediments, fine pores and secondary hydrate formation. Yang et al. (2008) the study in was concluded that the presence of excess clay and water in the hydrate crystals causes CO<sub>2</sub>-CH<sub>4</sub> exchange in a time-consuming process and the formation of the CO<sub>2</sub> hydrate shells surrounding the methane hydrate crystals acts as a shield to prevent the diffusion of the CO<sub>2</sub> molecule to the methane. In this process, thermal stimulation can destabilize methane hydrates. Therefore, the CO<sub>2</sub> exchange reaction process is highly affected by heat transfer (Bertolazzo et al., 2018; Ree and Kelland, 2018; Zhang, et al., 2018).

When Xiao and Adidharma (2009) and Khan et al. (2019) studies are examined, it is seen that CO<sub>2</sub>-N<sub>2</sub> mixtures can increase methane recovery from methane hydrate well by injection of compressed air or flue gas, while N<sub>2</sub> molecules can allow some of the methane molecules to be removed. In small lattice hydrate structures, CO<sub>2</sub> molecules replace methane molecules. This has been confirmed by thermodynamic modeling (McMullan et al., 1966; Cha et al. (2015). The beginning application of the CO<sub>2</sub> replacement method was carried out on the North Slope of Alaska with very significant results. Chen et al., (2008) CO<sub>2</sub>' 54% of methane was stored underground. In addition, just over 50% of the recovered methane remained in the hydrate reservoir until the well pressure dropped the methane hydrate decomposition pressure. It can also be used as a part in chemical methods to obtain gas hydrate in CO<sub>2</sub> storage processes. In chemical methods, thermodynamic hydrate inhibitors are used. The problem of clogging of amino acids can be overcome, thus protecting the marine environment in pipelines (Longinos and Parlaktuna, 2021).

As a result of the process evaluations, direct injection of unwanted flue gas into methane hydrate-containing sediments was first investigated experimentally in order to reduce the cost of CO<sub>2</sub> capture, increase the applicability, in other words, to ensure its availability/commercialization. Nitrogen in the injected flue gas changed the hydrate structure (equilibrium) conditions and caused most of the methane hydrate to decompose (Hassanpouryouzband et al., 2019; Yang et al., 2017). CO<sub>2</sub> has different structures from dissociated methane hydrate; It can form CO<sub>2</sub>-CH<sub>4</sub> +N<sub>2</sub>/non or

CO<sub>2</sub> hydrates. However (Sun et al. 2016; Schicks et al., 2018) it is possible to observe CO<sub>2</sub> exchange in sediments containing methane hydrate. It has been stated that about 82% CO<sub>2</sub> in the injected flue gas can be captured and stored in frozen sediments containing methane hydrate at an average of 261 K.

Although there are better approaches to how CO<sub>2</sub> molecules replace methane molecules trapped in methane hydrate, no obvious active process has been modeled. (Qi et al., 2011 and Bai et al., 2012) While initial dynamic models and three-dimensional simulations show that methane hydrate first decomposes after contact with CO<sub>2</sub> and then regenerates CO<sub>2</sub> hydrate or CO<sub>2</sub> mixed hydrates, while subsequent simulation studies show that direct displacement of methane and It can be formed by the displacement or temporary occupation of CO<sub>2</sub> molecules or a hydrate lattice. Molecular dynamics simulation by Wu et al. (2019) is that the adsorption of CO<sub>2</sub> molecules to on methane hydrate contact surfaces and penetrating into the content can directly help stabilize methane hydrate displacement and co-existence of hydrates in contact with CO<sub>2</sub>. Methane hydrate decomposition has been observed in different studies (Wu et al., 2019) using several different methods such as magnetic resonance imaging, Lee et al., (2013) electrical resistance, Erslund et al., (2010) and Graue et al. (2008) differential scanning calorimetry. In Raman spectroscopy, it has been determined that the free water phase emerges during the CO<sub>2</sub> exchange (Jung and Santamarina, 2010) and Yoon et al., in 2004, adopting the idea of the transition process from solid methane hydrate to solid carbon dioxide hydrate, physical models of the CO<sub>2</sub>-CH<sub>4</sub> molecular exchange were created (Salamatin et al., 2017; Yasunami et al., 2010).

In today's technology, it is understood that the required production value for a well in optimum conditions for the commercialization of natural gas hydrate is at least 160,000 m<sup>3</sup>/day (Chen et al., 2022). About 35 countries are actively involved in technology development studies for hydrate exploration and production (Yushan, 2012). Especially China and Japan have successfully carried out gas hydrate test production with short and long term trials (Le and She, 2021). However, sustainable production; Due to pre-development technology, environmental concerns and high cost, commercial (household and industrial) natural gas hydrate continues to be the fuel of the near future (Makogon et al., 2007).

### The Aim and Scope

In this study, it is aimed to give general information about the project and to evaluate the possible production models of the Eastern Black Sea gas hydrates located in the exclusive area of Turkey. In this context, it is aimed to create an application ecosystem by giving general information about the project titled "Carbon Capture, Storage and Utilization for Production of Natural Gas from Gas Hydrate Deposits in the Eastern Black Sea". In addition, gas hydrate production methods and the devices used are included in this paper.

## MATERIALS AND METHODS

Methane hydrate, which is the energy of the near future, also known as gas hydrate reserves, is located on almost three sides of Turkey. R&D studies are continuing to operate the gas hydrate reserve, which has the potential to be the most important key to our country's energy independence. There is some methane release inherent in the possible operating models of gas hydrate. "The Usability of CO<sub>2</sub> Gas Emitted 41,000,000 Euros within the scope of clean energy technologies such as carbon capture and offshore energy sources, which is under the title of Increase and promote utilisation of clean, sustainable and efficient technologies across the energy" The project titled "Tea Factories In The Production Of Gas Hydrates In The Eastern Black Sea" was proposed to our Ministry of Energy and Natural Resources in 2021. A production model is planned with the displacement of CO<sub>2</sub> to CH<sub>4</sub>. It is a pilot project planned for five years.

Environmental sensitivity (CO<sub>2</sub> emissions, analysis of its impact on global warming, consideration of fish migration when determining the drilling application time, etc.) in application projects is very important in terms of reserve acquisition and environmental vision. The inclusion of these issues in the works will give both a perspective in terms of sustainability and a privileged meaning in the national and international dimension of the project. Based on the fact that the settlement in the Eastern Black Sea Region is on the coast, stability studies for drilling and tests include both permitted seafloor movements and possible tsunami impact studies. It is planned to obtain methane from the Eastern Black Sea Gashydrate deposit by capturing the CO<sub>2</sub> from the Tea Factories. For this purpose, the flue gas content was investigated. It includes the establishment of a laboratory capable of advanced field modelling, the grading of the relevant parameters in this laboratory, and numerical, empirical and field modeling studies. With the developed method, the process of capturing CO<sub>2</sub> and transporting it to the gas hydrate area and replacing it with CH<sub>4</sub> will be evaluated. The production of tea factories is directly related to the tea season. This study is the first advanced technology R&D study in the world in terms of CO<sub>2</sub> production.

## RESULTS AND CONCLUSIONS

A more environmentally friendly, safe and efficient natural gas hydrate production process that prevents climate change is being developed for the future. In this development process, new technologies in physical and numerical simulation technology, new processes and new equipment and methods for deep sea studies are rapidly needed.

Each simulation study creates new boundaries with new unknowns. Comprehensive monitoring system equipment and high-efficiency technological equipment will ignite long-term production. The interest in natural gas hydrate sustains new generation production techniques conformity assessment and optimization studies through experimental and numerical simulations or field application for widespread trading development

in the after now.

In order to achieve sustainable CH<sub>4</sub>-hydrate production by CO<sub>2</sub> injection, it is necessary to consider the geomechanical properties of CO<sub>2</sub>-hydrate sediments. In laboratory experiments, process control modeling should be done by applying experimental methods including triaxial compression tests drained on artificial CO<sub>2</sub>-hydrated sand samples.

## REFERENCES

- Bai, D. Zhang, X. Chen G. Wang, W. 2012. Replacement mechanism of methane hydrate with carbon dioxide from microsecond molecular dynamics simulations. *Energy & Environmental Science* 5, 7033–7041.
- Bertolazzo, A. A. Naullage, P. M. Peters B. Molinero, V. 2018. The clathrate–water interface is oleophilic. *J. Phys. Chem. Lett.* 9, 3224–3231
- Cha, M. Shin, K. Lee, H. Moudrakovski, I. L. Ripmeester J. A. Seo, Y. 2015. Kinetics of methane hydrate replacement with carbon dioxide and nitrogen gas mixture using in situ NMR spectroscopy. *Environ. Sci. Technol.* 49, 1964–1971.
- Chen, Q. Yu, Y. Zeng, P. Yang, W. Liang, Q. Peng, X. Liu Y. Hu, Y. 2008. Effect of 1-butyl-3-methylimidazolium tetrafluoroborate on the formation rate of CO. *Journal of Natural Gas Chemistry* 17, 264–267.
- Chen, X., Lu, H., Gu, L., Shang, S., Zhang, Y., Huang, X., et al. 2022. Preliminary Evaluation of the Economic Potential of the Technologies for Gas Hydrate Exploitation. *Energy* 243, 123007. doi:10.1016/j.energy.2021.123007
- Chun L K. Jaafar, A. 2013. Ionic liquids as low dosage hydrate inhibitor for low assurance in pipeline. *Asian J Sci Res* 6(2):374–380.
- Ersland, G. Husebo, J. Graue, A. Baldwin, B. A. Howard J. Stevens J. 2010. Measuring gas hydrate formation and exchange with CO<sub>2</sub> in Bentheim sandstone using MRI tomography. *Chemical Engineering Journal* 158, 25–31.
- Graue, A. Kvamme, B. Baldwin, B. Stevens, J. Howard, J. J. Aspenes, E. Ersland, G. Husebo J. and Zornes, D. 2008. MRI Visualization of Spontaneous Methane Production From Hydrates in Sandstone Core Plugs When Exposed to CO<sub>2</sub>. *SPE J.* 13, 146–152.
- Hassanpouryouzband, A., Joonaki, E. et. al, 2020. Gas Hydrates In Sustainable Chemistry. *Chem. Soc. Rev.* 49, 5225–5309. <https://pubs.rsc.org/en/content/articlehtml/2020/cs/c8cs00989a>.
- Jung J. W. Santamarina J. C. 2010. CH<sub>4</sub>-CO<sub>2</sub> replacement in hydrate-bearing sediments: A pore-scale study. *Geochemistry, Geophysics, Geosystems* 11, 1–8.
- Jung J. W. Santamarina, J. C. 2011. Hydrate adhesive and tensile strengths. *Geochemistry, Geophysics, Geosystems* 12, 1–9.
- Khan, M. S. Lal, B. Shariff A. M. Mukhtar H. 2019. Ammonium hydroxide ILs as dual-functional gas hydrate inhibitors for binary mixed gas (carbon dioxide

and methane) hydrates. *Journal of Molecular Liquids* 274, 33–44.

Kim K. Kang, S.-P. 2011. Investigation of pyrrolidinium- and morpholinium-based ionic liquids into kinetic hydrate inhibitors on structure i methane hydrate. *Proceedings of the 7th International Conference on Gas Hydrates (ICGH 2011)*, 17–21.

Le, Z., He, J. 2021. Research Progress of Numerical Simulation Technology of Natural Gas Hydrates Production. *Sci. Technology Eng.* 21 (28), 11891–11899. doi:10.3969/j.issn.1671-1815.2021.28.001.

Lee, S. Lee, Y. Lee, J. Lee H. Seo, Y. 2013. Experimental Verification of Methane–Carbon Dioxide Replacement in Natural Gas Hydrates Using a Differential Scanning Calorimeter. *Environ. Sci. Technol.* 47, 13184–13190.

Longinos, S.N. Parlaktuna, M. 2021. Kinetic study of the effect of amino acids on methane (95%)—propane (5%) hydrate formation. *Reaction Kinetics, Mechanisms and Catalysis* 133:753–763.

Makogon, Y. F., Holditch, S. A., Makogon, T. Y. (2007). Natural Gas-Hydrates - A Potential Energy Source for the 21st Century. *J. Pet. Sci. Eng.* 56 (1-3), 14–31. doi:10.1016/j.petrol.2005.10.009.

McMullan, R. K. Mak T. C. Jeffrey, G. A. 1966. Polyhedral Clathrate Hydrates. XI. Structure of Tetramethylammonium Hydroxide Pentahydrate. *The Journal of Chemical Physics* 44, 2338–2345.

Miyazaki, K. Oikawa, Y. Haneda H. Yamaguchi, T. 2016. Triaxial Compressive Property of Artificial CO<sub>2</sub>-Hydrate Sand. *Int. J. Offshore Polar Eng.* 26, 315–320.

Ohgaki, K. Takano, K. Sangawa, H. Matsubara T. Nakano, S. 1996. Methane Exploitation by Carbon Dioxide from Gas Hydrates—Phase Equilibria for CO<sub>2</sub>-CH<sub>4</sub> Mixed Hydrate System. *Journal of Chemical Engineering Of Japan* 29, 478–483.

Ota, M. Abe, Y. Watanabe, M. Smith R. L. Inomata, H. 2005. Methane recovery from methane hydrate using pressurized CO<sub>2</sub>. *Fluid Phase Equilibria* 228–229, 553–559.

Ota, M. Saito, T. Aida, T. Watanabe, M. Sato, Y. Smith R. L. Inomata, H. 2007. Macro and microscopic CH<sub>4</sub>-CO<sub>2</sub> replacement in CH<sub>4</sub> hydrate under pressurized CO<sub>2</sub>. *AIChE J.* 53, 2715–2721.

Qi, Y. Ota M. Zhang, H. 2011. Molecular dynamics simulation of replacement of CH<sub>4</sub> in hydrate with CO<sub>2</sub>. *Energy Conversion and Management* 52, 2682–2687.

Ree L. H. S. Kelland, M. A. 2018. Polymers of N-(Pyrrolidin-1-yl) Methacrylamide as High Cloud Point Kinetic Hydrate Inhibitors. *Energy Fuels* 32, 10639–10648.

Salamatin, A. N. Falenty A. and Kuhs, W. F. 2017. Diffusion Model for Gas Replacement in an Isostructural CH<sub>4</sub>-CO<sub>2</sub> Hydrate System. *J. Phys. Chem. C* 121, 17603–17616.

Schicks, J. M. Strauch, B. Heeschen, K. U. Spangenberg E. and Luzi-Helbing, M. 2018. From Microscale (400 μl) to Macroscale (425 L): Experimental Investigations of the CO<sub>2</sub>/N<sub>2</sub>-CH<sub>4</sub> Exchange in Gas Hydrates

Simulating the İgnik Sikumi Field Trial. *JGR Solid Earth* 123, 3608–3620.

Sloan, E. D., Koh, C. A. 2007. *Clathrate Hydrates of Natural Gases*. Boca Raton, FL 33487-2742. CRC Press

Sun, D. Ripmeester, J. Englezos, P. 2016. Phase Equilibria for the CO<sub>2</sub>/CH<sub>4</sub>/N<sub>2</sub>/H<sub>2</sub>O System in the Hydrate Region under Conditions Relevant to Storage of CO<sub>2</sub> in Depleted Natural Gas Reservoirs. *J. Chem. Eng. Data* 61, 4061–4067.

Uchida, T. Ikeda, I. Y. Takeya, S. Kamata, Y. Ohmura, R. Nagao, J. Zatsepina, O. Y. Buffett, B. A. 2005. Kinetics and Stability of CH<sub>4</sub>–CO<sub>2</sub> Mixed Gas Hydrates during Formation and Long-Term Storage. *Chem. Phys. Chem.* 6, 646–654.

Wu, G. Tian, L. Chen, D. Niu M. Ji, H. 2019. CO<sub>2</sub> and CH<sub>4</sub> Hydrates: Replacement or Cogrowth?. *J. Phys. Chem. C* 123, 13401–13409.

Xiao, C. Adidharma, H. 2009. Dual function inhibitors for methane hydrate. *Chemical Engineering Science* 64, 1522–1527.

Yang, J. Chapoy, A. Tohidi, B. Jadhawar, P. S. Lee, J. 2008. Thermodynamic Conditions and Kinetics of Integrated Methane Recovery and Carbon Dioxide Sequestration. *Offshore Technology Conference*. USA.

Yang, J. Okwananke, A. Tohidi, B. Chuvilin, E. Maerle, K. Istomin, V. Bukhanov B. Cheremisin, A. 2017. Flue gas injection into gas hydrate reservoirs for methane recovery and carbon dioxide sequestration *Energy Convers. Manage* 136, 431–438.

Yasunami, T. Sasaki, K. Sugai, Y. 2010. CO<sub>2</sub> Temperature Prediction in Injection Tubing Considering Supercritical Condition at Yubari ECBM Pilot-Test. *J. Can. Pet. Technol.* 49, 44–50.

Yoon, J. H. Kawamura, T. Yamamoto Y. and Komai, T. 2004. Transformation of Methane Hydrate to Carbon Dioxide Hydrate: In Situ Raman Spectroscopic Observations. *J. Phys. Chem. A* 108, 5057–5059.

Yuan, Q. Sun, C. Y. Liu, B. Wang, X. Ma, Z. W. Ma, Q. L. Yang, L. Y. Chen, G. J. Li, Q. P. Li, S. Zhang, K. 2013. Methane recovery from natural gas hydrate in porous sediment using pressurized liquid CO<sub>2</sub>, *Energy Conversion and Management* 67, 257–264.

Yushan, L. (2012). New Trend of Exploration and Exploitation of Marine natural Gas Hydrate (II). *Mineral. Deposits.* 31 (1), 176–177. doi:10.16111/j.0258-7106.2012.01.014.

Zhang, Q. Heyns, I. M. Pflukwa, R. Klumperman B. and Kelland, M. A. 2018. Improving the Kinetic Hydrate Inhibition Performance of 3-Methylene-2-pyrrolidone Polymers by N-Alkylation, Ring Expansion, and Copolymerization. *Energy Fuels* 32, 12337–12344.

# Methane Adsorption Kinetics Of Core Samples From Tight Oil Field in Southeastern Türkiye

**Artuğ Türkmenoğlu, S. Esra Safran, Candan Kızılırmak, Can Ercan**  
Türkiye Petrolleri A.O. Research & Development Center, Ankara / Türkiye



Unconventional reservoirs, characterized by low permeability and high organic content, are important hydrocarbon sources. In this research, tight oil samples from SE Anatolia, Türkiye, were used to investigate the methane adsorption kinetics through adsorption tests at different temperatures (40 – 60 – 80 – 100 °C) and thermodynamic calculations. Same sample was sieved in two different sizes to understand the effect of particle size on gas diffusion/adsorption mechanism and gas adsorption capacity. Gas diffusion is modeled by applying intra-particle diffusion model. Langmuir adsorption isotherm model was applied to calculate gas adsorption capacity of the sample and it was varied between 62 and 137 scf/ton for coarse samples and between 41 and 97 scf/ton for finer samples. Kinetic calculations showed that methane adsorption onto rock is an exothermic process and spontaneously occurring. It was observed that physical adsorption mechanism took place rather than chemical reaction during the methane adsorption onto the sample.

## INTRODUCTION

Adsorption is the tendency of liquid or gas phase molecules' to adhere to solid surface. In industrial applications, this separation technique is widely utilized for wastewater treatment, pharmaceutical applications, virus removal, gas purification and the removal of contaminants like aromatic sulfur [1]. However, in nature, adsorption is the main mechanism in gas bearing organic-rich rocks like coal bed methane, shale gas and tight sand reserves. In 2000, percentages of natural gas production from CBM, tight sand and shale gas reserves in United States are 7%, 20% and 2%, respectively. In 2013, more than the quarter of natural gas comes from the shales and by 2035, it is predicted that half of natural gas will be produced from shales [2]. Türkiye has also, prospective basins in Southeastern Anatolia and Thrace Region as shown in Figure 1. According to EIA, Dadas Shale in SE Anatolia and Hamitabat Shale in Thrace Region contain 163 Tcf shale gas in place. Dadas Shale with 130 Tcf of shale gas in place, has relatively favorable properties for gas development whereas heavy faulting and moderate clay content could cause development risks [3].

Natural gas in unconventional rocks is deposited in three ways: (1) as free gas in pores, (2) as adsorbed phase on rock/organic matter surface and (3) as dissolved phase in formation water. Latter has the minimum percentage both in conventional and unconventional so, it is usually ignored in reserve estimations. Shales are characterized by low permeability and relatively low porosity. Hence, it can be clearly seen that most of the natural gas in tight rocks is in the form of adsorbed state. Changes in pressure and temperature conditions

disturb the interaction between rock and gas molecule. Consequently, desorption of gas molecule proceeds and then, production develops.

Recently, numerous researchers investigated the thermodynamics of gas adsorption onto shale rocks. These parameters gives insights about the reaction pathway, occurrence and progress. Dang et. al. measured supercritical methane adsorption on shale samples from Ordos Basin, China. Applying different adsorption and kinetic models, they calculated thermodynamic variables such as enthalpy ( $\Delta H$ ), entropy ( $\Delta S$ ) and Gibbs free energy ( $\Delta G$ ) changes. They concluded that methane adsorption onto shale rock is an exothermic, spontaneous and physical adsorption process [4]. In another study, effect of water presence in gas adsorption process is studied. 77% decrease in gas adsorption capacity and 70% decrease in  $\Delta H$  coupled with 97% decrease in  $\Delta S$  were reported. In addition, diffusion rate is diminished [5]. A recent Molecular Dynamics (MD) study revealed that the average sorption energy varied from -30 to -120 kcal/mol with a pressure increase from 500 to 2500 psi. van der Waals forces are the main interactions between gas-shale surface and gas-gas molecules. Also, it was observed that CH<sub>4</sub> molecule has a tendency to adsorb onto carbon contents and feldspar [6].

In our study, Dadas Shale sample is sieved into two different sizes, namely coarse and fine samples. Methane gas adsorption experiments are conducted at 4 different temperature values (40 – 60 – 80 – 100 °C). Using Langmuir and Toth adsorption models, gas adsorption capacities are calculated. Through intra-particle diffusion (IPD) model, rate constants are determined. Thermodynamic properties and activation energy of methane adsorption onto Dadas Shale are also, presented.

## MATERIALS AND METHODS

High pressure methane gas is provided from a local supplier at purity level of 99.95%. Numerous studies are conducted to characterize Dadas Shale and average properties are as follows: Kerogen type: Type II and III, TOC: 5.5%, Ro: 0.7-0.8%, clay content: 40%, porosity: 6.8%, permeability: 0.1 mD and medium occurrence of natural fracture [7]. Roughly, 100 g of samples are prepared and specific gravity of sample is measured as 2.12 g/cc by using He picnometer.

### Volumetric gas adsorption measurement

Gas adsorption amount can be done experimentally by using three different Methods: (1) Gravimetric method, in which mass of the sample is continuously monitored, (2) Volumetric method, in which pressures of the cell and reference cell are monitored [8].

In this study, GAI100 Gas Adsorption Test System (Corelab, USA) is used. Schematic of the system is presented in Figure 2. Approximately 100 psi air is required to operate the valves and gas booster.

Prior to the experiments, samples are categorized into two different sizes. Coarse sample contain particles less than 20 mesh whereas fine one contain particles greater than 40 mesh. Then, samples are heated in an oven up to 80 °C to remove the moisture. During the experiments, samples are placed into the cell and whole system is vacuumed. Oil bath temperature is set to the test temperature. After that, valves before the tanks (A1, A2, A3) are opened and methane is allowed to flow into the system. Then, those valves are closed and gas pressure is monitored. When the pressure is stabilized, gas is allowed to flow into the cell and consequently the samples by opening A2, B2 and C3 valves. Again, system pressures are monitored and after equilibrium is achieved, the experiment continues with the next pressure step. At the end of the experiment, pressure is released through A3, B3 and C3 valves and cells are emptied.

### ADSORPTION ISOTHERM MODELS

In unconventional gas systems, gas content of the rock is of great importance for reserve calculations and further operations. To evaluate the experimental data, various adsorption isotherms with different assumptions are developed. Langmuir adsorption isotherm is the most commonly used model and it simply assumes the following criteria: (1) adsorption occurs only at energetically equivalent sites, (2) only one adsorbate can be loaded into one site and (3) the interaction between the adsorbent and the adsorbate should be as strong as enough to prevent movement or escaping [9]. Langmuir adsorption isotherm is in the following form [10]:

$P$  is the relevant pressure step (MPa),  $n_e$  is the adsorbed gas amount (mmol/g),  $KL$  is Langmuir constant (1/MPa) and  $n_{max}$  is the maximum adsorption capacity (mmol/g).

Toth adsorption model is accounted for the adsorption onto heterogeneous surface unlike Langmuir model. The model is given below:

$KT$  is the maximum adsorption capacity (mmol/g),  $\alpha T$  is Toth model constant (1/MPa),  $1/t$  is the isotherm exponent. Here,  $1/t$  is related to surface heterogeneity or (a measure of the deviation from Langmuir model) and if  $t=1$ , the model reduces to Langmuir adsorption isotherm [11]. Detailed information about the adsorption isotherms and other models can be found in the literature [12].

### RESULTS

Toth and Langmuir adsorption isotherm model parameters are calculated and presented in Table 1. Langmuir model constants ( $KL$  and  $n_{max}$ ) are inversely proportional with temperature. However, Toth model does not show a significant trend. Toth isotherm exponent ( $t$ ) is very close to unity so, it can

be claimed that shale surface is not heterogeneous or in other words, Toth adsorption isotherm can be reduced to Langmuir adsorption isotherm model. Hence, further calculations are done by using Langmuir model constants. Adsorbed gas amounts for both samples are calculated by using Langmuir model and presented in Figure 3. More gas is adsorbed onto coarse shale sample at all temperature values. Maximum adsorption amounts are varied between 0.186 and 0.082 mmol/g (147 – 65 scf/ton rock) for coarse sample and between 0.128 and 0.052 mmol/g (101 – 41 scf/ton rock) for finer samples. Maximum adsorption capacity for Longmaxi, Barnett, Eagle Ford, Marcellus shales and San Juan coals are 0.056, 0.0716, 0.0110, 0.0261 and 0.678 mmol/g, respectively [13]. The difference between coarse and finer samples can be attributed to the blockage of free gas molecules by previously adsorbed gas molecules. Consequently, gas molecules could not reach the active sites and the adsorption is interrupted.

In thermodynamics, free energy concept is used to define if a process occurs spontaneously or not at constant temperature. One of those, Gibbs free energy, is chosen at a reference point and its change determines if the reaction will continue by itself. Hence, in equilibrium conditions at constant  $T$  and  $P$ ,  $\Delta G=0$ .

In an adsorption process, Gibbs free energy change is calculated using Eq. 5:

$$\Delta G = -RT \ln(K_L) \quad (5)$$

Here,  $\Delta G$  is Gibbs free energy change (J/mol),  $T$  is temperature (K),  $R$  is universal gas constant (8.314 J/mol/K) and  $KL$  is Langmuir adsorption equilibrium constant (1/MPa).

Other important parameters in a thermodynamic process are enthalpy and entropy variations. Enthalpy change ( $\Delta H$ ) defines the interaction strength between the adsorbate and the adsorbent whereas entropy change ( $\Delta S$ ) is a measure of the gas molecule's degree of freedom. The changes in enthalpy and entropy are calculated through the well-known Van't Hoff equation. This equation relates the temperature and the adsorption equilibrium constant and the linear form is given in Eq. 6:

Table 2 summarizes the thermodynamic parameters and negative  $\Delta G$  values show that the adsorption of supercritical methane onto the samples is a spontaneous process. Lower absolute values of Gibbs energy for the finer samples indicate that energy required to maintain the adsorption onto the sample is easier [4]. Higher surface area of finer sample creates more places for sc-CH<sub>4</sub> to accommodate and consequently, adsorption onto finer samples is more favorable.

For coarse sample, enthalpy change is very close to the half of that for finer sample. Negative value of  $\Delta H$  demonstrates that sc-CH<sub>4</sub> adsorption onto rock sample has an exothermic nature. Adsorption is divided into three categories with respect to change in enthalpy. When  $\Delta H < 20$  kJ/mol, physisorption, dominated by weak van der Waals interaction, occurs in the system. Between 20 – 80 kJ/mol, electrostatic interaction takes place. When there is a chemical interaction between the

adsorbate and the adsorbent, chemisorption develops and bond strengths vary between 80 – 450 kJ/mol [13]. Low enthalpy change for sc-CH<sub>4</sub> and rock sample refers to physisorption is the main mechanism. Chen et. al. reported that same mechanism is valid for methane adsorption onto Chinese shale sample and average of our findings ( $\Delta H_{\text{ave}} \approx 8.2$  kJ/mol) is in the range of shale's enthalpy change during methane adsorption [14].

For coarse and fine samples, values of  $\Delta S$  are -7.35 J/mol/K and -28.63 J/mol/K, respectively. Negative entropy values suggest that methane molecules proceed into more ordered phase after the adsorption. As seen on Fig. 5, free gas molecules move onto the rock sample and then their vibration and movement capacity is significantly decreased. This reduction is due to the adsorbate-adsorbent binding effect. Adsorbed phase is no longer in gaseous state. Although it is not covered in that study, adsorbed methane density on shale sample will be in the range of 0.30 – 0.40 g/cc [15], whereas density of sc-CH<sub>4</sub> is in the vicinity of 0.02 – 0.20 g/cc. Increase in density may be the result of volume decrease due to the interactions at the solid interface

For coarse sample, lower absolute values of  $\Delta H$  and  $\Delta S$  are calculated. Since adsorption is a surface phenomenon and coarse sample has less surface area, energy of molecules is concentrated in a narrower area and less scattered [11].

Intra-particle diffusion model and activation energy Prior to adsorption, free gas molecules occupy the void in the adsorption cell. Then, bulk diffusion and film diffusion phases occur. In this phase, concentration difference is the driving force for gas molecule to diffuse. Finally, intra-particle diffusion and then, adsorption onto the rock take place. Flow process is given in Fig. 6.

The case of C constant being close to zero states that pore diffusion is the rate limiting factor for the methane adsorption onto Dadas Shale. As seen on Table 3,  $k_i$  values decrease with increasing temperature. This clearly demonstrates that gas diffusion-adsorption process is inversely proportional to temperature. Significant difference and trend for the particle size and diffusion rate constant are not observed in our study.

In chemical engineering, activation energy should be supplied into the system to initiate the reaction. That energy is the minimum energy level to achieve a chemical process. Activation energy and specific rate constant (or diffusion rate constant in our case) are expressed by Arrhenius equation, given in Eq. 8:

Calculated activation energy values are presented in Table 3. Lower adsorption energy for finer particles is due to higher surface area. Since gas adsorption occurs on the surface, higher surface area of finer sample promotes the diffusion. Consequently, the abundance of active sites for adsorption catalyzes the reaction and it requires less energy to happen.

## CONCLUSION

This study aims to investigate the effect of particle size of Dadas Shale on adsorption capacity, kinetics and thermodynamics. Using two different sample sizes, volumetric methane adsorption experiments are conducted at 4 different temperature values. The following conclusions are obtained throughout this study:

1. Total adsorption isotherm model for methane – Dadas Shale pair can be reduced to Langmuir adsorption isotherm due to the almost homogenous surface. Hence, Langmuir model is recommended to calculate and model the experimental data.
2. At each temperature, coarse sample exhibits more adsorption capacity than finer particles. Adsorption capacity varies between 147 – 65 scf/ton for coarse sample and between 101 – 41 scf/ton for fine particles. Temperature has an adverse effect on adsorption capacity.
3. Maximum methane adsorption capacity of Dadas Shale is close or higher than Longmaxi, Barnett and Marcellus Shale formations and hence, potential of the field should be evaluated in other aspects and production options should be considered. Considering the remark above, shallower points of the formation can be a better hot spot for production, since more gas is adsorbed at lower temperature values.
4. Negative values of  $\Delta S$ ,  $\Delta H$  and  $\Delta G$  show that methane adsorption onto Dadas Shale is an exothermic, spontaneous process. Also, physical adsorption occurs between methane molecule and Dadas Shale.
5. Intra-particle diffusion model is used to determine diffusion rate constants.  $k_i$  constants change from 0.0014 to 0.0072 min<sup>-1</sup>. Significant trend and difference with respect to particle could not be observed. Pore diffusion is the rate limiting factor instead of film diffusion.
6. More activation energy is required for methane to be adsorbed onto coarse sample.

Keywords: Gas adsorption, Shale gas

Figure 1. Shale gas/oil assessments in Turkiye [3]



Figure 2. Gas adsorption test system.

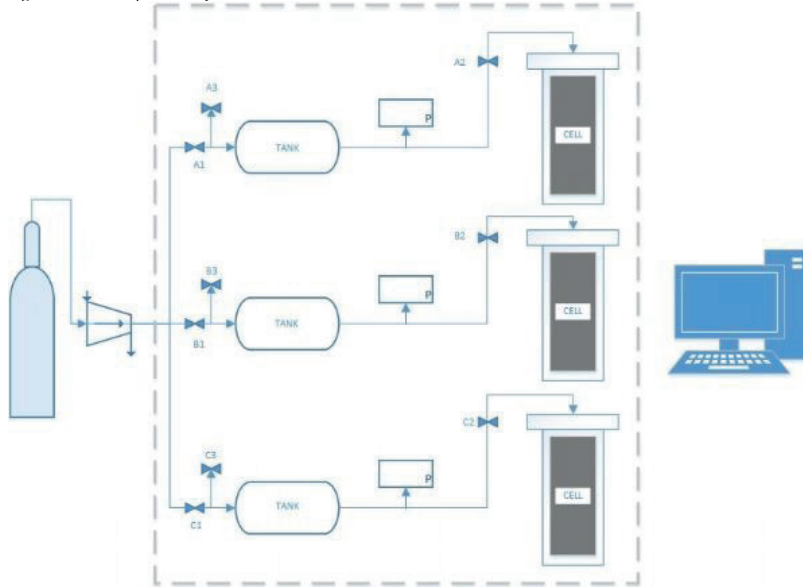


Figure 3. Adsorbed gas amount at different temperature values and particle sizes.

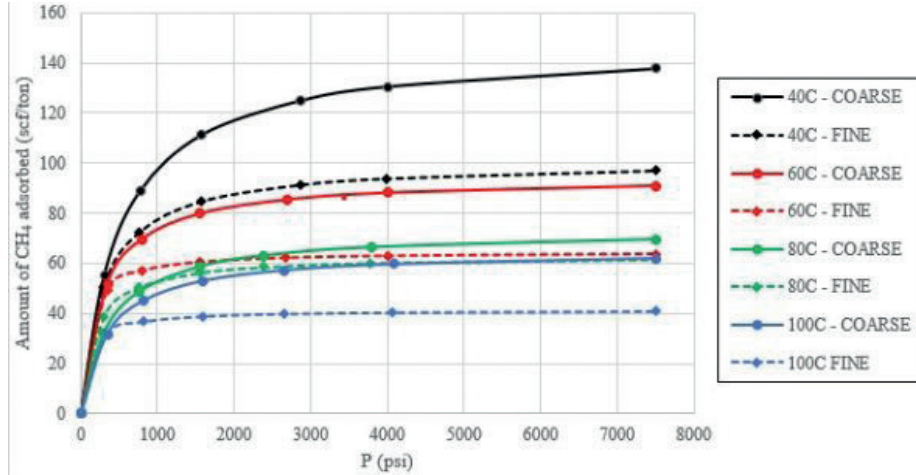




Figure 4. Van't Hoff plots for coarse and fine samples.

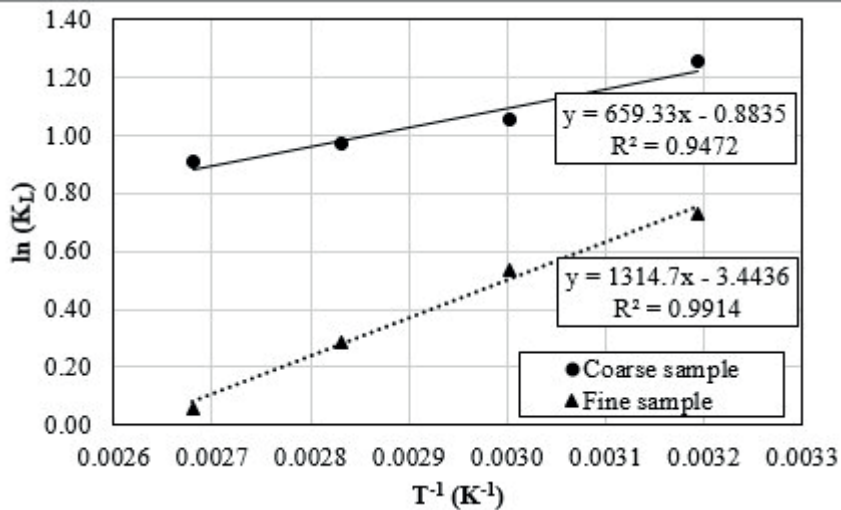


Figure 5. Movement capacity of gas molecules before (left) and after (right) adsorption.

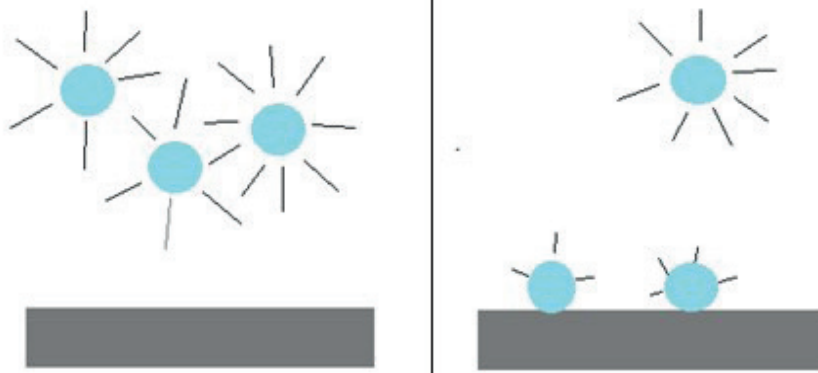


Figure 6. Mass transfer steps [15].

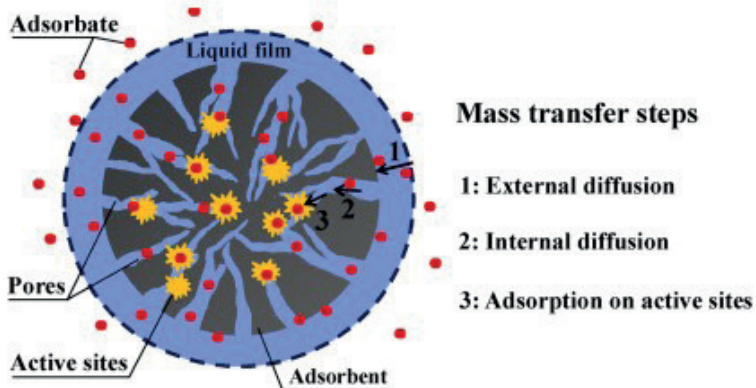


Figure 7. Arrhenius plots for methane adsorption onto Dadas Shale.

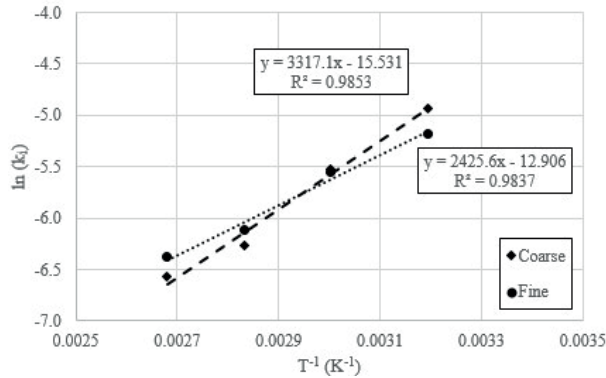


Table 1. Langmuir and Toth adsorption isotherm parameters.

T (°C)	Coarse samples					Fine samples				
	Toth			Langmuir		Toth			Langmuir	
	K <sub>T</sub> (mmol/g)	σ <sub>T</sub> (1/MPa)	t	K <sub>L</sub> (1/MPa)	q <sub>max</sub> (mmol/g)	K <sub>T</sub> (mmol/g)	σ <sub>T</sub> (1/MPa)	t	K <sub>L</sub> (1/MPa)	q <sub>max</sub> (mmol/g)
40	0.14	1.77	1.07	3.50	0.186	0.16	1.24	0.94	2.08	0.128
60	0.10	1.87	1.05	2.86	0.119	0.13	3.05	0.96	1.71	0.082
80	0.14	4.28	0.91	2.65	0.092	0.13	3.23	0.92	1.34	0.080
100	0.11	3.41	0.94	2.48	0.082	0.13	3.81	0.81	1.06	0.052

Table 2. Thermodynamic variables of sc-CH4 onto coarse and fine parricles.

Sample	Parameter	T (K)			
		313	333	353	373
Coarse	ΔG (kJ/mol)	-3.26	-2.91	-2.86	-2.81
	ΔH (kJ/mol)			-5.48	
	ΔS (J/mol/K)			-7.35	
Fine	ΔG (kJ/mol)	-1.90	-1.49	-0.85	-0.19
	ΔH (kJ/mol)			-10.93	
	ΔS (J/mol/K)			-28.63	

Table 3. IPD model results.

	Coarse sample				Fine Sample			
	40 °C	60 °C	80 °C	100 °C	40 °C	60 °C	80 °C	100 °C
k <sub>T</sub> (min <sup>-1</sup> )	0.0072	0.0040	0.0019	0.0014	0.0056	0.0039	0.0022	0.0017
C	0.0786	0.0943	0.0741	0.0875	0.0970	0.0840	0.0681	0.0754

Table 4. Activation energies for coarse and fine samples.

	Coarse	Fine
E <sub>A</sub> (kJ/mol)	-27.58	-20.17

# Natural Fracture Modeling in Unconventional Dadaş-1 Member for 3D Seismic Survey: Case Study, Turkey



Artem Orlov<sup>1</sup>, Canalp Özkul<sup>1</sup>, Fethi Bensenouci<sup>1</sup>, Mehmed Yazaroğlu<sup>1</sup>, Ahmet Ergün Mengen<sup>1</sup>, İsmail Ömer Yılmaz<sup>2</sup>

<sup>1</sup>Turkish Petroleum

<sup>2</sup>Middle East Technical University Research Information System

## OBJECTIVE AND SCOPE

Traditional description of unconventional reservoir like any natural fracture reservoirs relies heavily on quality and analysis of image logs and core data at discrete well locations. These data provide high vertical resolution information but soon becomes challenging to use and propagate away from the borehole. The presented modeling process is generally based on pure stochastic workflow that tries to achieve realistic 3D model of fractured reservoir by matching the well information, in-situ stress and capture inter-well heterogeneity using 3D seismic data. This workflow has been tested on unconventional natural fracture reservoir in Diyarbakir basin where late Silurian – lower Devonian age Dadaş-1 organic rich shale member exhibits both low porosity and extremely low matrix permeability. Acting as one of the main source rocks in SE Turkey, it represents a self-sourced unconventional play. The interpretation of image logs and core samples reveals clusters of fractures suggesting a naturally fracture reservoir type I. This study aims at using an integrated approach spanning from seismic interpretation to image log data analysis and 3D geomechanics to develop a discrete fracture network model (DFN) and to provide new insights into distribution of hydrocarbons since fractures is solely responsible for making this reservoir producible (Figure 1). In addition, a derived DFN model offers an opportunity to improve a reservoir modeling (static and dynamic), to provide the basis for design of an optimum well placement, stimulation, completion, production and could serve as a guide on how to improve the seismic acquisition/resolution to highlight valuable fracture zones.

## METHODS, PROCEDURES, PROCESS

This integrated study uses borehole image log data acquired in the Dadaş-1 member interval of 3 exploration wells: A, B and C, 3D seismic volume and 3D geomechanical model. Fracture modeling was performed using a fracture modeling software that calculates fracture permeability, porosity and matrix block size on 3D reservoir grids by constructing the DFN model. The main steps of the workflow were: 1) to use previously interpreted image log data and classify the natural fractures by fracture sets using dip azimuth distribution. The wellbore fracture data is dominantly striking in E-W and N-S directions with a large number having a high (> 60 degree) dip angle. Important to note is that the statistical likelihood of intersecting high (>50 degree) angled fractures is reduced by drilling vertical wells, suggesting that the vertical wells used in this study may be underestimating the true fracture density; 2) evaluate possible fracture drivers, defined

as any 3D properties that can be sensitive to or capture directly fracture intensity information in the inter-well space. The fracture drivers used in our workflow are various post-stack seismic attributes: Variance, Curvature, Chaos, Ant-Tracking, Sweetness and etc. All tested seismic attributes are used as input to a multi-scale statistical correlation analysis where previously derived 1D intensity logs using image logs were matched. Because seismic domain comes with inherent resolution limitations compared to borehole data the fracture intensity logs were generated with different window filter size to evaluate the best scaling factor for optimizing correlation with the seismic domain. The best fracture drivers for the total intensity log before splitting on sets appear to be 3D Curvature ( $\approx 0.66$  correlation factor), Chaos ( $\approx 0.43$  correlation factor) and flatness ( $\approx 0.55$ ). These 3 seismic cubes supervised by interpreted intensity values at well locations were used to derive 3D fracture intensity cube (or 3D fracture driver). The QC crossplot between interpreted and predicted intensity logs shows correlation value 0.88; 3) to review this analysis in the context of the seismic structural interpretation and regional tectonic framework. Since the fracture distribution and density relate to the tectonic features (faults), Ant-tracking 3D seismic attribute was used to derive seismically resolved faults/fractures. All captured by Ant-tracking discontinuities were split into two tectonic sets based in the strike direction and relationship to tectonic events: Set-1 fault polygons in black that have West-East orientation and formed during 1st tectonic event and Set-2 fault polygons in red that striking in North-South and formed during 2nd tectonic period (Figure 2); 4) to employ 3D geomechanical model to determine the likelihood of natural fractures undergoing tensile reactivation. This model does not consider variables such as fracture plane roughness, cementation, pressure variation, or the possibility of crystal bridging, which has been shown to enable fractures to remain open and permeable albeit not preferentially aligned with  $\sigma_1$ . Importantly, all fracture types (conductive, partially conductive and resistive) were used for the modeling. Natural fractures in shale, as weak planes of mechanical heterogeneity, can reactive and widen the treatment zone, affect propagation and intensity of artificial fractures. Even the cemented fractures, i.e. mineral veins, can considerably contribute to efficient hydraulic fracture treatment, because of the weak chemical bond between the fracture-filling minerals and their wall rocks that can be easily broken apart.

**RESULTS, OBSERVATIONS, CONCLUSIONS**

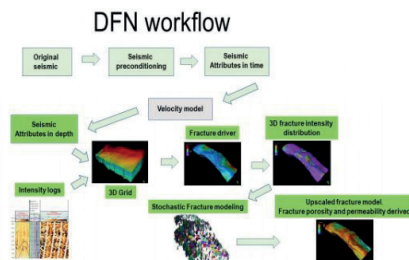
The analysis of natural fracture orientation, dip, aperture together with petrophysical data, seismic interpretation, paleo- and current stress regimes enable to build a 3D discrete fracture model, predict their occurrence in the Dadas-1 interval and used this output for dynamic reservoir modeling (Figure 3). Adopting the reasonable assumption that lateral heterogeneity of the fracture network is related to the major tectonic events, the seismic attribute analysis together with regional geology reveals two major sets of fractures: strike in ESE-WNW that relate to the first extensional tectonic event and the second with a strike NNE-SSW after paleo-stress rotation from E-W to N-S. Application of 3D geomechanical model reveals that not all fractures should be considered as point of weakness for the future fracking campaign. Only natural discontinuities that are favorably oriented to in-situ stress more likely to be critically stressed and hydraulically conductive. The result of this interpretation were used to predict hydrocarbon flowing zones (in the absence of PLT data). Accordingly, the selection of testing intervals on the basis of the highest density of fractures only is not a valid approach to determine prospective zones. From the structural point of view, in the current strike-slip/compressional regime, the fracture direction is the main control to hydrocarbon flow with the best contribution coming from natural fractures oriented close to the present day maximum horizontal stress.

**NOVEL/ADDITIVE INFORMATION**

The novel aspect of this project is the multi-scale approach rooted in seismic interpretation, detailed fault imaging and interpretation combined with attribute analysis, image log analysis combined together with 3D geomechanical model to determine the orientation of flow contributing fractures for optimizing well testing and design.

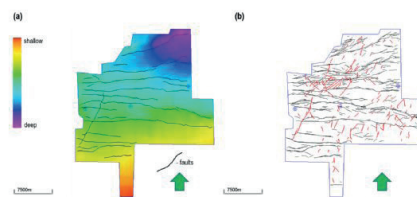
Keywords: Unconventional resources, fracture modeling

Figure 1



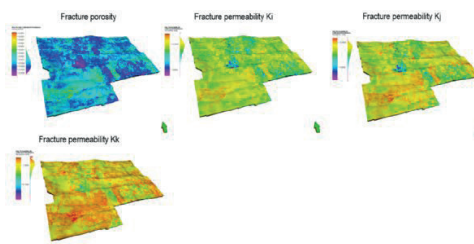
Discrete Natural fracture model (DFN) workflow

Figure 2



(a) The Top Dadas-1 structural map in depth and seismically interpreted fault polygons; (b) Fault polygons extracted from the Ant-Tracking seismic attribute. The polygons in black color are associated with the 1st tectonic event and the polygons in red color with the 2nd tectonic event

Figure 3



Derived from DFN model the fracture porosity and fracture permeability maps for unconventional reservoir of Dadas-1 member

# Evaluation of XRD, CEC, and LSM Methods for Fracturing Fluid Optimization: Experimental Findings

**Ekrem Alagöz, Ahmet Ergün Mengen, Yalçın Yaradılmış**  
Turkish Petroleum Corporation



This article explores the optimization of fracturing fluids for shale rock properties. X-ray diffraction, cation exchange capacity, and linear swell meter tests were used to evaluate the effectiveness of various fracturing fluid additives. The study found that clay stabilizers and potassium chloride work well together to reduce the rate of fluid imbibition into the porous rock formation, while biocides, surfactants, and friction reducers were also effective in enhancing the hydraulic fracturing process. The results provide valuable insights into how shale-fluid interactions can be influenced by different materials, and can be used to optimize the extraction of resources from shale formations.

**Key words:** Shale Rock Properties, Frac Fluid Optimization

## 1. INTRODUCTION

Fracturing fluids, also known as fracking fluids, are liquids used in the process of hydraulic fracturing. They are injected into rock formations at high pressure to create fractures, which allow for the extraction of natural gas and oil. Fracturing fluids typically consist of water, sand, and chemicals. The water helps to create and propagate the fractures, while the sand acts as a proppant to keep the fractures open. The chemicals are added for various purposes, such as to reduce friction, prevent bacterial growth, and control the pH of the fluid. The composition of the fracturing fluid can vary depending on the specific characteristics of the rock formation and the type of hydrocarbon being extracted. Rock-fluid and fluid-fluid interactions have been studied by many researchers before [1-4]. The fracturing fluid additives used in this study are biocide, surfactant, friction reducer, and clay stabilizer. The abbreviations of the chemicals used are given in Table 1. The general properties of these additives are given below, respectively.

Table 1. Frac fluids chemicals

Abbreviations Fluid Concentration

DI DI Water 98-99%

TAP Tap Water 98-99%

S2 Surfactant 0.1-0.5%

FR3 Friction Reducer 0.1-1%

CSTAB2 Clay Stabilizer 0.1-1%

CIDE Biocide 0.01-0.1%

Biocides are added to hydraulic fracturing fluids to kill or inhibit the growth of microorganisms that can be present in the rock formations. These microorganisms can consume the nutrients in the hydraulic fracturing fluid, which can cause the fluid to become less effective.

They can also produce gases that can increase the pressure in the fractures, which can cause them to close. Additionally, they can cause corrosion in the pipelines and other equipment used in the hydraulic fracturing process. Biocides are added to the fluid to kill or inhibit the growth of these microorganisms, which helps to maintain the effectiveness of the fluid and prevent damage to equipment.

Surfactants are used in hydraulic fracturing fluids as they reduce the surface tension between the fluid and the rock, allowing the fluid to more easily flow into the fractures in the rock. They also help to prevent the fractures from closing after the fluid is injected, which helps to keep the fractures open and increases the effectiveness of the hydraulic fracturing process.

Friction reducers, also known as viscosity reducers, are added to hydraulic fracturing fluids to decrease the fluid's resistance to flow, allowing it to move more easily through the fractures in the rock. This in turn allows the fluid to be pumped into fractures at a higher rate, increasing the efficiency and effectiveness of the hydraulic fracturing process. Additionally, friction reducers can also help to reduce the amount of energy required to pump the fluid into the fractures, which can lower costs and reduce the environmental impact of the process.

Clay stabilizers, also known as clay inhibitors, are added to hydraulic fracturing fluids to prevent the clays in the rock from swelling and closing fractures created during the hydraulic fracturing process. These clays can absorb water and increase in volume, which can cause fractures to close, reducing the effectiveness of fracturing process. Clay stabilizers work by altering properties of clay minerals, inhibiting their ability to absorb water, and maintaining fractures open. By preventing clays from swelling, clay stabilizers help to keep fractures open and increase the effectiveness of fracturing treatment.

## 2. EXPERIMENTAL METHODS

XRD, CEC and LSM tests were carried out, respectively. Each step was carried out in the procedure described below and the experiments were completed.

### 2.1. X-Ray Diffraction (XRD)

XRD is a technique used to determine the crystal structure of a material. It is based on the interaction of X-rays with the atoms in a crystal, which causes X-rays to be scattered in many directions. Pattern of these scattered X-rays can be used to determine the arrangement of atoms in the crystal. XRD is used in a variety of fields, including materials science, chemistry, and mineralogy, to identify and study the crystal structures of materials, such as minerals, metals, and polymers. It is also used to determine the purity, crystallinity, and defects of a material.

Cutting samples taken from the wells, which are in the hydraulic fracturing program for XRD bulk powder mineral, and clay mineral analyses. The samples ground with Retsch RS-200 vibratory disc mill to have bulk powder and then representatively selected and plated for the XRD bulk powder analyses. After the bulk XRD analyses, two glass slides were prepared from each powdered samples for clay fraction analysis by using the “smear mount method” described in Moore and Reynolds [5]. After the completion of analyses of air-dried slides, same slides left in the 60°C ethylene glycol vapor bath for 2.5 hours and then analyzed. The other slides heated up to 540°C for 2.5 hours and then analyzed. The semi-quantitative XRD bulk powder and clay mineral analyses performed under conditions given below:

- Generator: Rigaku D/Max-2200 Ultima
- X-ray Tube: Cu
- Voltage: 40 kV
- Current: 20 mA
- Wavelength: (CuK $\alpha$ 1) 1.54059 Angstrom
- Scan Speed: 1°/min.
- Software: MDI Jade 7.0

The X-ray diffractograms interpreted based on the Inorganic Crystal Structure Database (ICSD) of International Center for Diffraction Data (ICDD) by using MDI’s “Jade 7.0” software. The outputs of the XRD analysis evaluated according to profile-based matching of software and reference intensity ratios (RIR) by using “Easy Quant” patch of the software. The relative abundances of bulk and clay minerals in samples were determined as weight percentages are given on Table 2.

Table 2. XRD Analysis Results of Cutting Samples

Based on the XRD results of the samples, quartz and clay minerals are dominant mineral types in all samples. Calcite, dolomite and feldspar are common and close to the original abundances of the XRD results of cutting samples of these wells that have presented in previous studies. In terms of clay mineral content, Illite and smectite, which has the highest swelling potential, are the most abundant clay types with minor amounts of kaolin, chlorite and mixed-layer Illite-smectite minerals.

## 2.2. Cation Exchange Capacity (CEC)

CEC is the total capacity of a rock to hold exchangeable cations. The higher CEC value, the more the shale sample tends to exchange cations, which increases shale swelling. CEC is measured in milli-equivalents (meq) of methylene blue dye adsorbed per 100 g dry clay. According to API RP 13B-1 [6] standard, methylene blue capacity of a water-based fluid is an indication of the amount of reactive clays present as determined by methylene blue test. The methylene blue capacity provides an estimate of the total cation exchange capacity of the drilling cuttings. The test for Methylene blue capacity of cuttings performed according to API RP 131 [7] procedure, which shows the methodology

below. Organic materials, if present in the sample, destroyed by oxidation with hydrogen peroxide. The sample is titrated with standard methylene blue solution until adsorptive capacity is satisfied.

## METHODOLOGY

1. Drill cuttings are grinded.
2. Grinded cuttings dried for CEC tests.
3. 25 cc %2 Tetra Sodium Pyrophosphate solution added to erlenmeyer.
4. 1 gram of cutting sample added to erlenmeyer.
5. Erlenmeyer is magnetically stirred and boiled.
6. After 10 minutes boiling, 15 cc %3 Hydrogen Peroxide and 1 cc 5N Sulfuric Acid added to solution and boiled 10 minutes more.
7. Erlenmeyer kept cool.
8. Methylene Blue (MB) solution started adding to erlenmeyer.
9. Clay mineral with absorbed MB dropped to Whatman No.1 filtrate paper with a pipette.
10. MB solution continued adding up to observing the full-saturated blue circle and turquoise ring near the blue circle.
11. Test repeated again in ten minutes later. If turquoise ring occurs again, test is completed.

CEC results for all samples illustrated in Table 2. CEC values of the samples vary from 1.5 meq/100 gr to 8 meq/100 gr. Based on these results, reactivity of cutting samples are about 1/9 or 1/10 less than Sodium Montmorillonite Bentonite clay which has CEC with 70-130 meq/100 gr according to literature [8] in Table 3.

Table 3. CEC Values of Clay Minerals [8]

Clay Mineral	CEC, (meq/100 gr)
Montmorillonite	70-130
Vermiculite	100-200
Illite	10-40
Chlorite	10-40
Attapulgite-Sepiolite	10-35
Kaolinite	3-15

## 2.3 Linear Swell Meter (LSM)

LSM device used for determining shale hydration or swelling by measuring the expansion just in vertical axis of radially confined sample plugs, which exposed to HVFR fracturing fluids. Testing procedure of LSM test is not exist in API Specifications or Recommended Practice documents as a standard procedure. Therefore, performed experimental test results used for comparisons between candidate fluids. Due to the nature of the experimental application and multiple components availability, measurement inconsistencies may occur in LSM tests. Maximum effort and consideration has made to minimize the measurement inconsistencies and to provide high accuracy, high

precision and standardization in all LSM tests.

Grace Instrument M4600 HPHT LSM equipment used to perform the tests, which is an automated, dual core, high pressure and high temperature linear swell meter as seen in Figure 1. Dual compactor was also used to create cylindrical plugs from ground samples by applying 6,000-psi pressure for 3-hours shown in Figure 2. M4600 includes a windows based software for data acquisition. Real-time data displayed along with customized charts during a test. Test data exported to Microsoft Excel for reporting after a test is completed.

Figure 1. M4600 LSM Equipment

Figure 2. Dual Core Plug Compactor and Pump

All LSM tests conducted at ambient temperature. Results recorded as plots of swelling percent versus time in minutes. These tests provide a graphical comparison of multiple inhibitive fluids simultaneously. The M4600 is composed of two independent pressure cells: Cell A and Cell B (Figure 3). Each cell has its own controls, and one can get them worked either individually or simultaneously.

Figure 3. Pressure Cell Components [9]

Each pressure cell assembly is comprised of the following components.

- A. Sample Cup A B. Sample Cup B
- C. Wafer Holder A D. Wafer Holder B
- E. LVDT sensor tip A F. LVDT sensor tip B
- G. Bottom Plate A H. Bottom Plate B
- I. Steel Rod with Top Plate A J. Steel Rod with Top Plate B

M4600 apparatus uses a LVDT (Linear Variable Differential Transformer) sensor, which detects mechanical linear movement as displacement occurs and converts it to electrical signals. Contact displacement sensors based on this method read changes in the shape of the target by converting it into electrical signals. These requests and guidance include which reservoir sample to test and which brine composition to use. Testing procedure of LSM Test is below.

## METHODOLOGY

1. Drill cuttings are grinded.
2. Grinded cuttings dried for Linear Swell Meter tests.
3. 10.5-gr sample poured into the steel cylinder to create the plug. The steel cell is hit manually on a hard surface, allowing air between the particles to escape and the first compaction.
4. Top and bottom acrylic spacers used to compress the cutting particles.
5. Plugs created by applying 6,000-psi for 3-hours with compactor pistons.
6. Prior to every test, Grace Instrument M4600 HPHT LSM equipment calibration is done by using steel spacers which have exact length of 0.40-in, 0.65-in and 0.90-in for both Cell A and Cell B.

7. The height of the plugs measured with a caliper manually.

8. Plugs placed in the LVDT sensors and bottom plate tightened.

9. LVDT sensor tightened to LSM device.

10. The length of the plug, the tested solution information for Cell A and Cell B, and the material information for the plug defined to the LSM device.

11. 80 ml of solutions poured to pressure Cell A and Cell B. Test started before introducing liquid sample with the plug.

12. As soon as test started, pressure cell screwed into the LSM device. Pressure Cell already covers the LVDT sensor in this position.

13. Swelling and hydration between solution and plug starts immediately. Swelling percentage vs time displayed in real time graph on computer.

This method always followed based on the advices of manufacturer manual and our experiences for R&D research studies. Total 65 LSM tests carried out by using mentioned methodology. Test results of LSM demonstrated in Figures 4-8.

## 3. RESULTS AND DISCUSSION

### 3.1. CEC vs LSM

#### 3.1.1. Effect of Fracturing Fluids on Swelling

Use of frac fluid in fracturing can have a significant impact on the swelling of shale rock. When the fluid is injected into the rock formation at high pressure, it can cause an increase in the volume of the shale rock, known as "swelling." This swelling occurs because the fluid can interact with the minerals in the rock and cause a chemical reaction that leads to an expansion of the rock. The swelling of shale rock can have a negative impact on the hydraulic fracturing process. When the rock swells, it can cause the fractures created by the high-pressure injection to close, which reduces the flow of gas or oil from the well. This can make it difficult to extract the desired resources, and it can also lead to damage to the well. The pressure created by the swelling can cause the well bore to become -severely damaged, which can make it difficult to repair.

Figure 4. Clay stabilizer with KCL worked better together

Figure 5. Clay stabilizer with KCL worked better together

The studies [1-4] on shale-fluid interaction have investigated the impact of different factors on the rate of imbibition, which is the process by which fluids are absorbed into a porous material. One of the key findings from these studies is that the use of clay stabilizers in conjunction with KCL can effectively decrease the rate of imbibition. This means that by using these materials together, the fluid is absorbed at

a slower rate into the porous material. These findings were determined through the use of two specific test Methods: proppant embedment and NMR. Proppant embedment is a technique that measures the amount of fluid that is absorbed into a porous material, while NMR is a non-destructive testing method that is used to study the properties of fluids. Both of these methods provided detailed information on the rate of imbibition and how it was affected by the presence of clay stabilizers and KCL. The test setup used in this study also revealed that clay stabilizer and KCL work well together. This means that when these materials are used in combination, they have a synergistic effect, resulting in an even greater decrease in the rate of imbibition than when used individually. Overall, these research studies provide valuable insights into how shale-fluid interactions can be influenced by different materials, and can be used to optimize the extraction of resources from shale formations.

Figure 6. When CEC= 8, the Fracturing fluid effect is not seen much

Figure 7. Optimization of Clay stabilizer with different CEC values

Figure 8. Optimization of Clay stabilizer with different CEC values

## 5. CONCLUSIONS

1. By looking at the XRD results, the effect of clays on swelling observed independently of the fracturing fluids.
2. An increase in CEC values observed according to the amount of active clays and the degree of activity.
3. Clay stabilizers inhibit more effectively with KCL.
4. Presented methods can be used to optimize fracturing fluids before the treatments.
5. The most active mineral is Smectite. The reason for its high activity is due to its weak bonding and high repulsive potentials on its surface. This unique characteristic allows water to enter between the layers, which in turn causes an increase in the c-spacing. This expanding lattice greatly increases the colloidal activity of Smectite by making all the layer surfaces available for hydration and cation exchange. This results in a significant increase in specific surface, as observed in reference 8.

## REFERENCES

1. Alagoz, E., Wang, H., Russell, R.T. and Sharma, M.M. (2020). New Experimental Methods to Study Proppant Embedment in Shales. Paper ARMA 2020-1933, 54th US Rock Mechanics/Geomechanics Symposium held in Golden, Colorado, USA, 28 June-1 July. <https://onepetro.org/ARMAUSRMS/proceedings-abstract/ARMA20/All-ARMA20/ARMA-2020-1933/447713>
2. Alagoz, E. and Sharma, M.M. (2021). Investigating Shale-Fluid Interactions and Its Effect on Proppant Embedment Using NMR techniques. Paper ARMA 2021-1129, 55th US Rock Mechanics/Geomechanics

Symposium held in Houston, Texas, USA, 20-23 June. <https://onepetro.org/ARMAUSRMS/proceedings-abstract/ARMA21/All-ARMA21/ARMA-2021-1129/467923>

3. Alagoz, E., Wang, H., Russell, R.T. et al. New Experimental Methods to Study Proppant Embedment in Shales. *Rock Mech Rock Eng* 55, 2571-2580 (2022). <https://doi.org/10.1007/s00603-021-02646-1>
4. Alagoz, E. Interaction of Fracturing Fluids with Shales: Proppant Embedment Mechanisms. MS Thesis, The University of Texas at Austin, Austin/Texas, December 2020. <https://repositories.lib.utexas.edu/handle/2152/89282>
5. Moore, D. M. and Reynolds, R. C. Jr.: "X-Ray Diffraction and the Identification and Analysis of Clay Minerals, Oxford University Press", New York, pp.215-225, 1997
6. API Recommended Practice 13B-1, Third Edition, December 2003
7. ANSI/API Recommended Practice 13I, Eighth Edition, March 2009
8. From Grim, R.E., 1953. *Clay Mineralogy*. McGraw Hill Book Co., New York and Weaver, C.E. and Pollard, L.D., 1973. *The Chemistry of Clay Minerals*. Elsevier Scientific Publ. Co., New York. <http://dx.doi.org/10.1016/B978-0-12-804751-4.00004-3>
9. M4600 HPHT Liner Swell Meter, Grace Instrument Operational Manual, 2012

Keywords: Frac Fluid Optimization, Shale Rock Properties



Figure 1. M4600 LSM Equipment

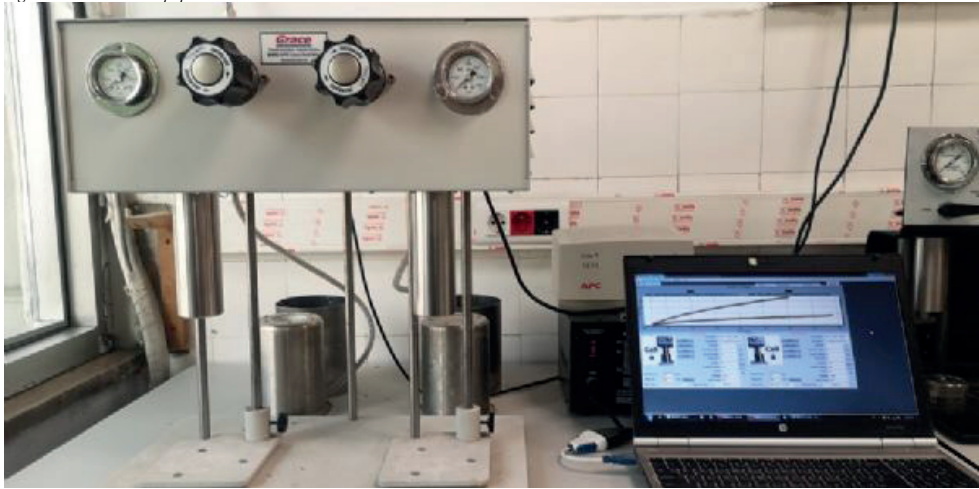


Figure 2. Dual Core Plug Compactor and Pump



Figure 3. Pressure Cell Components [9]



Figure 4. Clay stabilizer with KCl worked better together

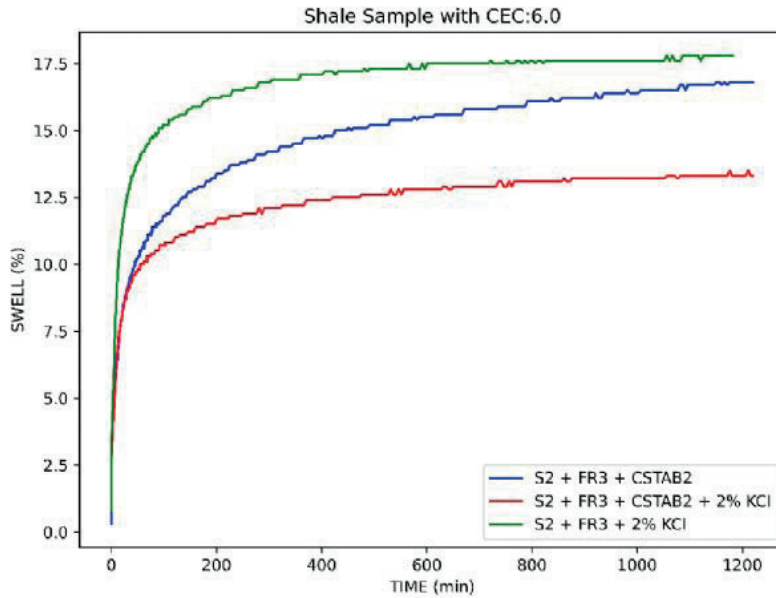


Figure 5. Clay stabilizer with KCl worked better together

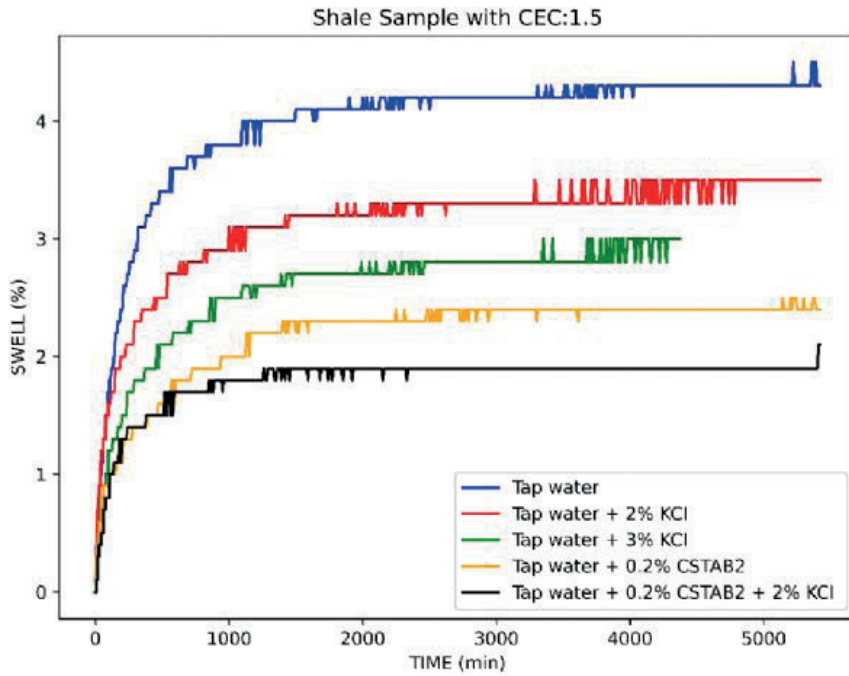


Figure 6. When CEC= 8, the Fracturing fluid effect is not seen much

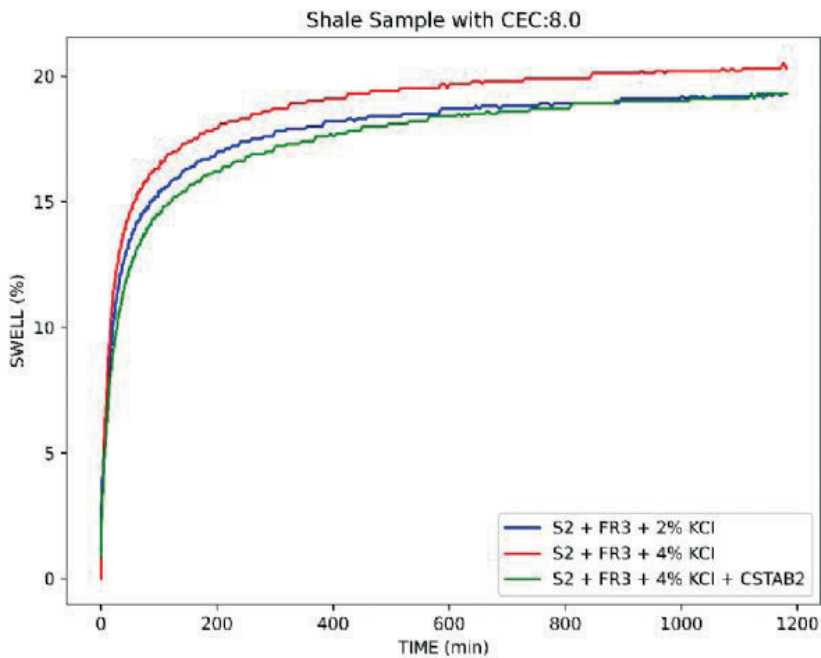


Figure 7. Optimization of Clay stabilizer with different CEC values

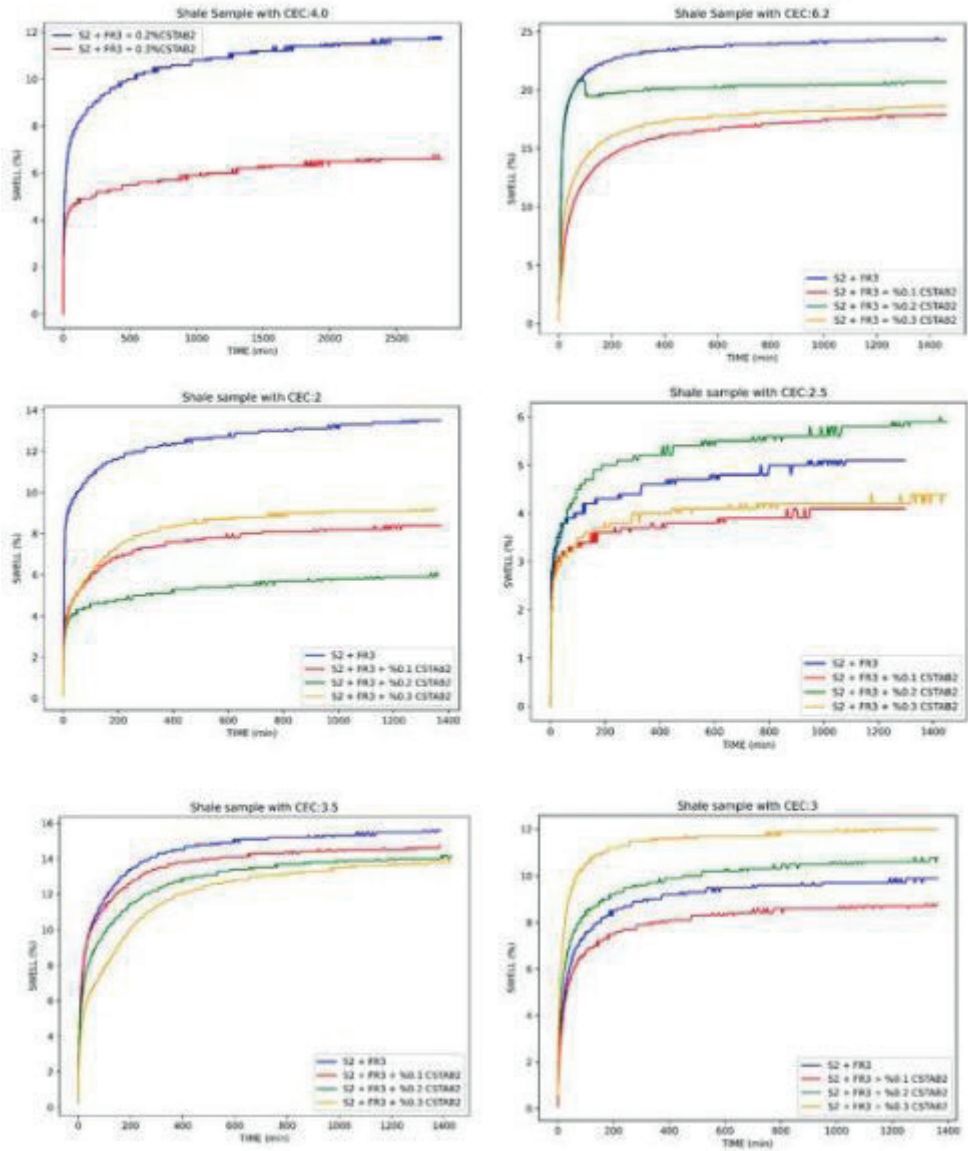


Figure 8. Optimization of Clay stabilizer with different CEC values

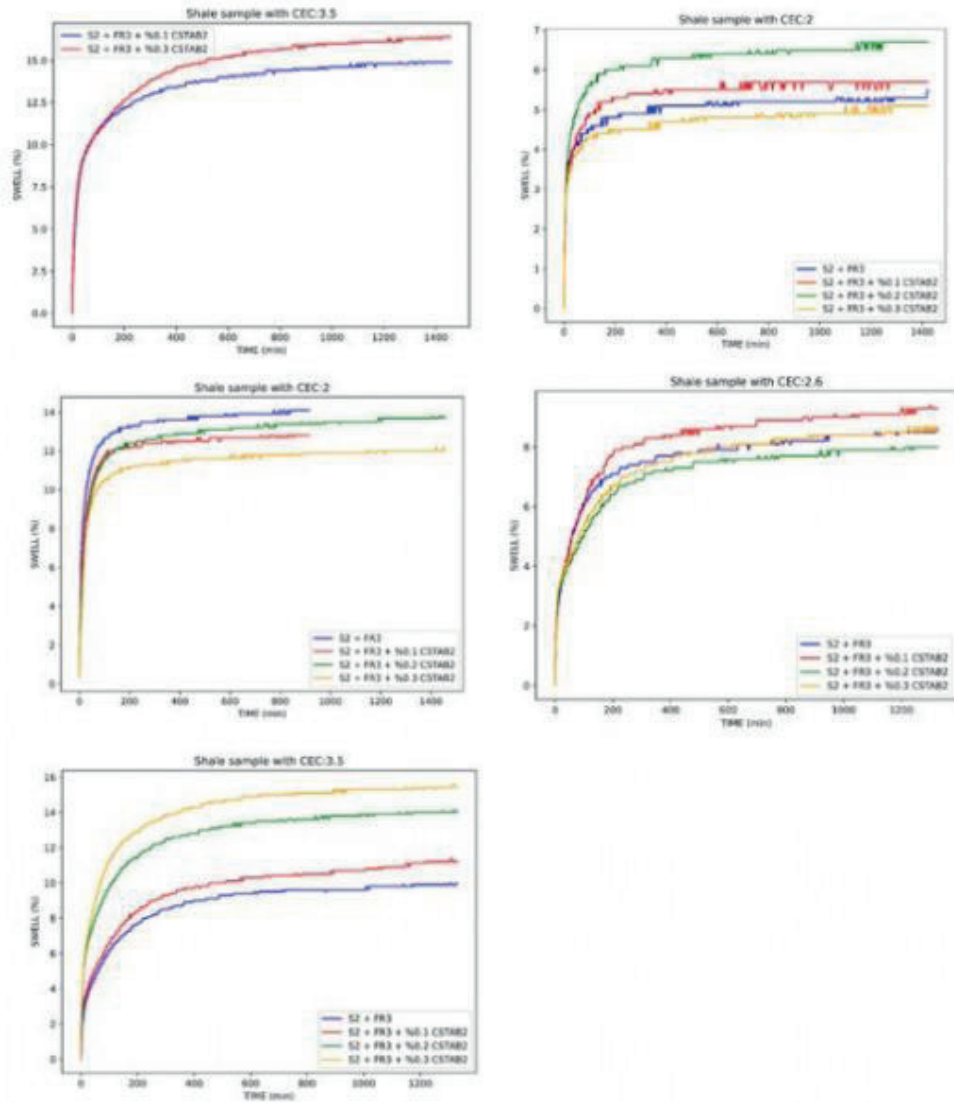


Table 2. XRD Analysis Results of Cutting Samples

	XRD Bulk Powder Mineralogy (wt%)							XRD Clay Mineralogy (wt%)					Total % CEC, (meq/100g)		
	Quartz	Feldspar	Calcite	Dolomite	Pyrite	Barite	Siderite	Gypsum	Total Clay+Mica	Illite-Mica	Smectite	Kaolin		Chlorite	Mixed-Layer Illite-Smectite
19	2	0	8	2	6	0	0	63	28	1	20	10	4	100	8
23	2	1	2	2	0	4	0	66	16	1	37	12	0	100	6
33	7	6	6	3	2	0	0	43	19	1	16	6	1	100	5
26	4	9	3	4	4	0	0	50	30	2	10	5	3	100	4
39	5	8	7	4	0	0	0	37	29	1	3	1	3	100	3
46	4	11	0	3	6	0	0	30	18	1	6	4	1	100	1,5
34	4	10	2	0	0	0	3	47	15	0	19	4	10	100	6,2
40	5	8	2	0	0	1	4	40	25	0	8	7	2	100	2,5
33	5	0	21	0	0	1	5	35	21	0	8	4	2	100	2
36	0	23	3	7	0	0	0	31	12	0	12	6	1	100	3,5
21	0	35	14	4	0	1	0	25	7	0	9	6	2	100	3
22	0	33	6	6	0	0	0	33	19	1	10	2	1	100	3,5
16	0	48	10	4	0	4	0	18	3	0	7	3	5	100	5
34	0	13	6	6	0	1	0	40	25	0	9	4	2	100	3
21	0	2	41	3	0	0	0	33	17	1	9	2	5	100	3
31	13	12	4	4	0	1	0	35	25	0	7	2	1	100	2
25	0	15	16	5	0	3	0	36	17	0	8	8	3	100	4
23	4	17	34	1	0	0	0	21	12	0	4	3	2	100	2,6
35	41	1	4	3	0	0	0	16	8	0	4	4	0	100	3,5
30	8	3	7	10	0	2	0	40	22	1	10	7	1	100	3

Tablo içeriği, sistemdeki "tablo oluşturma" kısmıyla yapılmadığından, resim olarak eklenmiştir. Edit için lütfen benimle iletişime geçiniz.

Table 1. Frac fluids chemicals

Abbreviations	Fluid	Concentration
DI	DI Water	98-99%
TAP	Tap Water	98-99%
S2	Surfactant	0.1-0.5%
FR3	Friction Reducer	0.1-1%
CSTAB2	Clay Stabilizer	0.1-1%
CIDE	Biocide	0.01-0.1%

# Reservoir Characterization of Unconventional Dadaş Formation in Southeastern Turkey



**Canalp Özkul<sup>1</sup>, İsmail Ömer Yılmaz<sup>2</sup>, Ahmet Ergün Mengen<sup>1</sup>, Fethi Bensenouci<sup>1</sup>, Kirill Ezhov<sup>1</sup>, Mehmed Ekrem Yazaroğlu<sup>1</sup>**

<sup>1</sup>Turkish Petroleum, Exploration Department, 06530 Ankara / Türkiye

<sup>2</sup>Department of Geological Engineering, Middle East Technical University, 06800, Ankara / Türkiye

## INTRODUCTION

Unconventional resources are increasingly important in the future of oil and gas industry as they potentially hold substantial amount of hydrocarbon. Economical production from shale reservoirs is still strongly dependent on reservoir characterization of the formations that are generally conducted by using mineralogical content of the rocks and geochemical properties including total organic carbon content (TOC) and maturation of the source rocks. However, the integrated approach by describing, from microscopic to reservoir scales, the sedimentological, petrophysics, geomechanical parameters and structural aspects are also required. The Silurian age Dadaş Shale in the Diyarbakır basin, SE Anatolian Basin are the most prospective unconventional reservoir in Turkey. However, the potential of this unconventional formation still remained ambiguous. Thus, sedimentological analysis on cores and cuttings, petrographic analysis on thin sections and SEM images, well log data interpretation, natural fracture characterization using Borehole Imagers (BHI) and cores are conducted to unlock the potential of Dadaş unconventional reservoir and results revealed that the Dadaş-I member of the Dadaş formation has potential of source rock for the Paleozoic oil system.

## METHODS

First, all available wellbore data is collected, checked and harmonized. All required preparation steps like depth shifting, data corrections etc. are done according to the standards. Petrophysical properties, such as TOC, Total and Effective Porosity

(PHIT, PHIE), Water Saturation (SW), Mineralogical Composition, Matrix Permeability, and also Brittleness Index (BI) are estimated based on the custom designed workflow: on the first step TOC estimated based on Delta Log R method, and calibrated on pyrolysis results, after that based on multiminerall inversion algorithm reservoir properties are estimated, and on the last step different Rock Types are estimated: "1" - Reservoir + Completion Quality intervals (higher PHIE and BI values), "2" - Completion Quality intervals (higher BI values only), "3" - EOR Quality intervals (higher kerogen content) and "4" - non-productive shales.

Intervals "1" or RCQ are the best candidates for hydraulic fracture operations as they can store and produce hydrocarbons. Intervals "2" or CQ are also meaningful for hydraulic fracturing if they are connecting some RCQ zones as a so called "technical conductors". Intervals "3" or EORQ could be used on later stages, as a focus for tertiary treatment techniques. Intervals

"4" have no potential and should be avoided. Natural fracture characterization analysis was done based on the BHI and core data. All Images were processed, interpreted, and compared with the corresponding core intervals. Fully conductive, partially conductive and resistive fractures were identified, as well faults, beddings, unconformities etc. Critically stressed fractures are identified by integrating 1D in-situ stresses and geomechanical properties of natural fractures. The integration of all the results helps to identify the best perforation intervals for hydraulic fracturing operations and define landing points for planned horizontal wells.

## RESULTS

The studied Dadaş-I interval is characterized and divided into four lithofacies (L1, L2, L3, and L4) by using lithological data from logs of the offset wells supported by the core data (porosity, permeability, saturation, pyrolysis, SEM and XRD data). Petrophysical properties of the highlighted lithofacies reveal that L1 (Lower Hotshale) and L3 (Upper Hotshale) have the highest amount of RCQ intervals and hence the highest potential. L4 (Cap Carbonate) has also reasonable properties, but the fraction of CQ intervals is a bit higher. However, hydrocarbon potential of the L2 (Lean Shale) is poor and not considered to be a good candidate for unconventional reservoir. In addition, petrographic analysis indicate Dadaş-I includes kerogen porosity and low amount of fracture porosity. Natural fracture characterization analysis show that fracture orientations are unique in facies L4, striking parallel to an E-W major faults group whereas the rest of fractures are striking NE-SW, parallel to the second group of fault in the area. As the E-W faults are known to be created first, L4 facies seems to be naturally fractured before the rest of facies. The geomechanics parameters calculated for each facies shows that L4 present higher elastic parameter, higher brittleness but also higher strength properties. Since Dadaş Formation has experienced high deformation during the tectonic history of the region, L4 formation could have concentrate more stress due to their higher elastic properties and hence fractured before of the rest of facies. The process of fracturing is also promoted by a higher brittleness. However, further analysis of major controlling parameters of fracture intensity reveal that there is no distinctive correlation with lithological variation such as total clay content, brittle index, total organic carbon, and reservoir properties such as porosity. Moreover, detailed core analysis revealed that some of the fractures characterized as open fractures may be misinterpreted due to limitation in WBI analysis. Geomechanical approach indicates the critically stress fractures that are more prone to impact on production

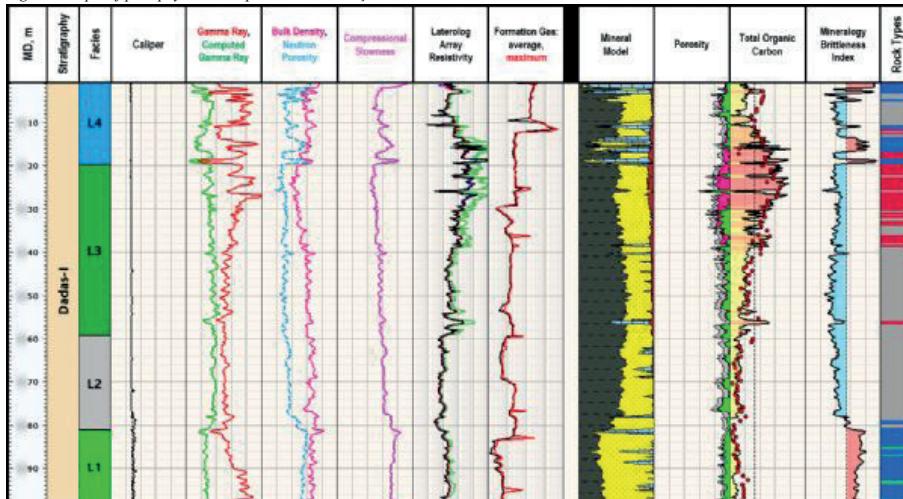
have higher intensity in L3 and L4 reservoir properties which are also favorable as reservoirs.

**CONCLUSION**

For the first time in Dadaş field an integrated workflow for the wellbore data analysis is created. This workflow is focused on the identification of the most producible intervals before fracking operations. It combines variety of data from core analysis to petrophysical interpretation together with natural fractures characterization and geomechanics modeling. It is worth to mention, that this approach has proven to work better in Dadaş formations based on the recent production results.

Keywords:Reservoir evaluation, Natural Fractures

Fig.1: Example of petrophysical interpretation in Dadaş-1 member.





# Geomechanics Aided Solution to Support Drilling and Completion of Dadaş Unconventional Reservoirs, SE -Türkiye



**Fethi Bensenouci<sup>1</sup>, Ahmet Ergün Mengen<sup>1</sup>, Canalp Özkul<sup>1</sup>, Artem Orlov<sup>1</sup>, Kirill Ezhov<sup>1</sup>, Mehmed Ekrem Yazaroglu<sup>1</sup>, İsmail Ömer Yılmaz<sup>2</sup>**

<sup>1</sup>Exploration Department, Türkiye Petrolleri Anonim Ortaklığı (TPAO), Ankara / Türkiye

<sup>2</sup>Department of Geological Engineering, Middle East Technical University, Ankara / Türkiye

## INTRODUCTION

Exploring unconventional reservoirs is known to be technically and economically challenging from drilling to reservoir evaluation and stimulation. In order to develop unconventional reservoirs, oil companies have to drill and stimulate high number of wells which makes geomechanics studies crucial to provide necessary insights for successful operations. Dadaş Silurian shale, located in SE- Türkiye, are being explored as unconventional reservoir by the TPAO for decades. Numerous problems related to formations instability and or pore pressure have been reported while drilling these formations. Hydraulic fracturing completed in some wells turned out to be also very challenging in various intervals. Considering these different problems, a geomechanics study is completed at different scales in Dadaş field to help improving, in the short term, hydraulic fracturing operations and provide solutions for drilling optimization to limit drilling-related non-productive time and bad hole conditions.

## METHODS

The study starts by collecting all relevant and available data that can be used as input in geomechanical parameters calculations or help to calibrate the obtained results. Then, the collected data is reviewed, classified and corrected when required. The lack of data like shear slowness logs is tackled using rock physics. Rock properties are calculated using wireline logs and calibrated with mechanical core tests. Pore pressure calculation is predicted using Eaton and Bowers methods, calibrated by drilling events and hydraulic fracturing results. Vertical stresses are calculated based on bulk density, whereas horizontal stresses calculation is done using a poro-elastic model. Considering the 1D modeling limitations e.g. effects of geological attributes such as: non-horizontal horizons, faults, fractures and evolution of stresses away from the wellbore wall, it was decided to complete the study with an advanced 3D geomechanical modelling. The 3D model offer a solution that provides stresses in magnitudes and directions computed over the whole field or reservoir. The 3D modeling integrates 1D data and 3D seismic inversion results available in one block of Dadaş field. The main tools used for this study are Techlog™ for 1D modelling and Petrel™ with VISAGE™ for 3D modeling.

## RESULTS

After a data audit including core analysis, daily drilling reports (DDR) review and wireline logs QC, 12 post-drill 1D Geomechanics models known also as 1D

MEMs (for Mechanical Earth Models) are completed to provide, in a low Turnaround Time, necessary data for hydraulic fracturing design. Elastic properties and rock strength parameters are found to vary with depth and rock mineralogy. Rock properties calculated along the studied sections show some similarities with Vacca Muerta shale in Argentina. However, more mechanical lab tests are still needed to complete better the characterization of the mechanical properties of Dadaş shale. Pore pressure in the different wells show some lateral variability in Dadaş-I member even within one block. Overall, we see that pore pressure gradients tend to increase toward the center of basin. This parameter will be subject to further investigation after receiving additional data from the current operations. Horizontal stresses calculations show vertical and lateral heterogeneities over the field. The minimum horizontal stress gradient ranges from 0.75 psi/ft to 1.1 psi/ft, with a stress regime varying from normal to strike/slip and, locally, reverse (Figure 1). The maximum horizontal stress calculation is validated with wellbore stability analysis. Sensitivity analysis of wellbore stability with respect to hole deviation and azimuth is completed at selected depths in Dadaş-I member. This analysis aims at defining the most stable azimuth for planned horizontal sections; however the results do not show high sensitivity on borehole direction for deviation angles close to 90°. In that case drilling toward the minimum horizontal stress direction is recommended. The 1D geomechanics results are integrated with petrophysics outputs to select and rank the wells candidate for fracking operations and also to define the best perforation intervals for each well. The 1D results are also used as inputs in the 3D modelling phase.

A 3D geomechanical model is completed based on the most complete structural model available for the reservoir, including geological attributes, seismic, pore pressure field and spatial grid. It aims at calculating rock properties and in-situ stresses at 3D scale over a field or a block. In this study, rock properties are populated within a structural model in Dadaş by integrating 1D MEMs, acoustic impedance and Vp/Vs ratio from seismic inversion in depth domain. In-situ stresses are calculated in the pre-production condition using the finite element simulator VISAGE, calibrated with 1D stress profiles and closure pressures from hydraulic fracturing. The final 3D stress results capture well enough the heterogeneity noticed at well scales. Limited variation of stresses magnitudes and orientations is noticed near the major faults acting as discontinuities within the field. Also, the impact of the faults in the field is different between the ones striking E-W and those striking NNE-SSW. The combination of 3D in-situ stresses and 3D rock properties allows the calculation

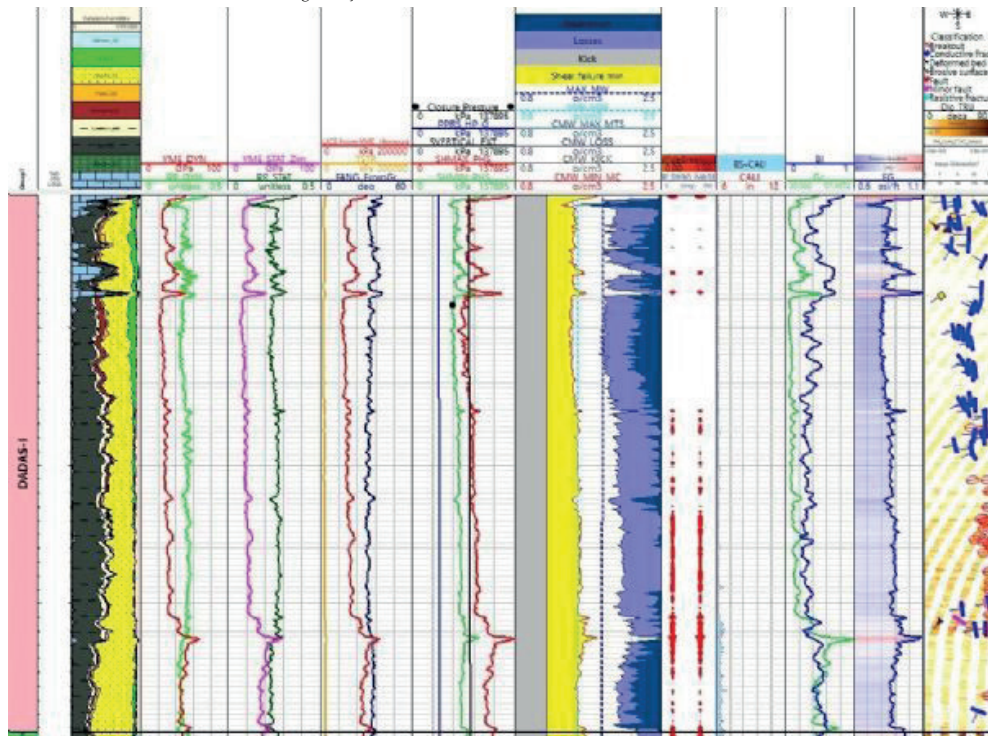
of 3D wellbore stability parameters, an important tool in drilling designs. The 3D analysis provides also additional attributes to investigate the best future wells locations in the field (Figure 2) and to support the natural fracture modeling (DFN). Finally in-situ stresses are used as input in a discontinuity stability analysis to define the most critically stressed natural fractures and faults. The combinations of all these attributes will help to define the best locations of the future wells.

## CONCLUSION

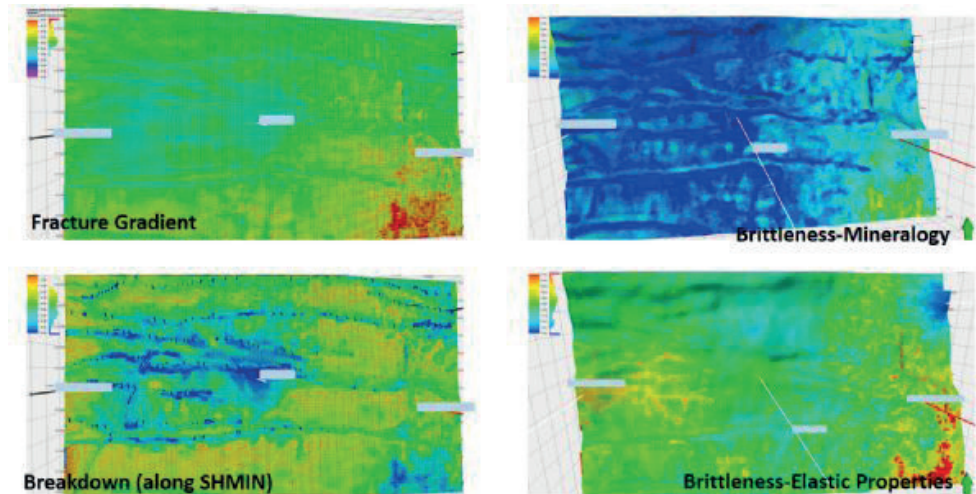
For the first time in Dadaş field, a multi-scale Geomechanics study is completed to support decision making during the exploration phase. The post-drill 1D Geomechanics integrated with Petrophysics allows to select the well candidates for the hydraulic fracturing campaign and also to define the perforation intervals. Rock properties calculated at well scale show vertical variability related to mineralogy but low lateral heterogeneity in the same facies. Regarding pore pressure and horizontal stresses slightly higher lateral variability is noticed. By combining 1D rock properties and seismic inversion results, rock properties are populated within a structural model obtained from 3D seismic and stresses are calculated using finite element code. Stress magnitudes are calibrated with 1D profiles at well scale and closure pressures. The 3D model is able to capture the stress heterogeneity seen between the wells. The 3D results are used to provide more attributes like Fracture Gradient, Breakdown gradients, Stress Anisotropy, Brittleness... to support new prospect locations identification. The 3D results are also used to model natural fractures network within the studied block. As way forward, the integration of stresses, natural fractures network and reservoir properties will be integrated in a Two-way Coupling Geomechanical model to estimate the impact of reservoir depletion on fracture porosity and permeability and on production forecast.

Keywords: Dadaş shale, Multi-scale Geomechanics

1D Geomechanical results in one well crossing Dadaş-1 member



Examples of 3D Geomechanical results used as completion quality attributes



# An Analytical Study of Hydraulic Fracturing Optimization for Tight Shale Formation

Emre Can Dündar<sup>1</sup>, Ahmet Ergün Mengen<sup>1</sup>, Vasily Mironov<sup>2</sup>,  
Aleksi Khlopkov<sup>2</sup>, Ekrem Alagöz<sup>1</sup>

<sup>1</sup>Turkish Petroleum Corporation

<sup>2</sup>Turkish Petroleum Offshore Technology Center



Hydraulic fracturing optimization is a critical aspect of improving the recovery of unconventional shale formation. This paper discusses the use of different types of proppants, rate optimization, and proppant amount optimization to improve hydraulic fracturing techniques.

The paper begins with a discussion of proppant selection, which is a critical aspect of hydraulic fracturing. The authors highlight the importance of proppant endurance in holding the fracture opening and provide a range of proppants suitable for different confining pressures. Tables and charts are included to illustrate the permeability values of various proppants under different closure stress values. This section also emphasizes the significance of proppant shape in creating a more conductive path in the fracture.

The next section of the paper discusses the methodology used in the study, including the Fracpro software simulation parameters. The authors then delve into the optimization of proppant specific gravity and the results of their experiments with five different types of proppants. The paper highlights the impact of proppant specific gravity on fracture width and dimensionless conductivity (FCD).

The authors also focus on the optimization of pumping rate, which is an essential parameter of hydraulic fracturing operations. The paper includes simulation studies conducted to determine the effects of pumping rate on fracture parameters such as propped length and propped height. The authors highlight the relationship between rate and FCD and how it is affected by permeability values of the proppant.

Finally, the paper discusses proppant amount optimization, which is a critical point of hydraulic fracturing optimization. The authors provide an overview of the results of the experiments conducted to determine the optimal amount of proppant required for different hydraulic fracturing operations.

Overall, this paper provides valuable insights for researchers and engineers working to improve hydraulic fracturing techniques for tight shales formation. The authors use a combination of theory, experiments, and charts to provide a comprehensive overview of the various aspects of hydraulic fracturing optimization.

**Key Words:** Hydraulic Fracturing Optimization, Proppant Optimization, FracPro Software

## 1. INTRODUCTION

This article discusses various aspects of hydraulic fracturing optimization for unconventional shale formation. The authors provide an overview of the

different types of proppants, rate optimization, and proppant amount optimization used in hydraulic fracturing operations. The article also delves into the methodology used in the study, including the Fracpro Simulation Parameters. The authors use a combination of theory, experiments, and charts to provide valuable insights for researchers and engineers working to improve hydraulic fracturing techniques for tight shale formation.

## 2. A LOOK INTO THE PROPPANT SELECTION

Proppant is used for creating a conductive path through the induced hydraulic fracture from wellbore towards the formation. Typical proppant was sand historically, at the beginning of the hydraulic fracturing operations. Now, coated sand and ceramic materials are in different size and strength in use.

Figure 1: A typical view of the embedded proppant in the fracture (Suponik et al., 2023).

Proppant selection is based on many critical parameters, namely, transport and durability performances of it in the fractures. Since the endurance of the proppant is one of the most important factor in holding the fracture opening, a range of the proppant for different confining pressures are listed in table 1.

Proppant Type Density (g/cm<sup>3</sup>) Resistance (psi)

Pure Sand 2,65 <6000 (≈41 Mpa) Resin-Coated sand (RCS) 2,55 <8000 (≈55 Mpa)

Intermediate Resistance Ceramic (IRC) 2,7-3,3 5000-10000 (34-69 Mpa)

High Resistance Ceramic (HRC) 3,40 >10000 (69 Mpa)

Bauxite 2,00 >7000 (48 Mpa)

Table 1: Proppant resistance pressure and approximate density values (Economides & Nolte, 2000).

After proppants placed in the fracture aperture, a conductive path is created. This created media in the fracture is based on many factors like proppant resistance and proppant shape. Figure 2 shows the permeability values of different type of proppants under different closure stress values.

Figure 2: Permeability change of the proppant types under closure stress (Economides & Nolte, 2000).

Proppant shape is one of the other important variable that has a great impact on the fracture permeability, conductivity and the proppant pack stability. The expected shape of the proppant is spherical shape with uniform distribution. The sphericity is defined by The International Organization for Standardization (ISO) as "a measure of how close a proppant partical look like the shape of a sphere". Moreover, it describes the roundnes

as “a measure of the relative sharpness of corners or of curvature”. Figure 3 shows how more rounded and spherical proppants create a more conductive path in the fracture than not spherical and not rounded proppant pack.

Figure 3: Rounded and spherical proppants create a more conductive fracture (Nash, 2018)

### 3.METHODOLOGY

There are three different optimization steps are determined to simulate the hydraulic fracture operation on frackpro software. The first step is deciding the optimum proppant specific gravity, and five different proppant are used in this optimization part. Since the rate is very critical for fracture geometry as second step rate optimization is simulated with the already decided specific gravity from the first step. As the last part of the operation, proppant amount is optimized with the decided specific gravity and rate values from the former steps.

#### 3.1 Optimization of Proppant Specific Gravity

There are five different proppant types are taken as example for hydraulic fracturing design. The first type of the proppant is CR4000 20/40 resin coated sand which is a low strength proppant with a specific gravity of 2.53. Second type of the proppant is THS EconoProp 20/40 with a specific gravity of 2.61. Third type of proppant is Carbo Bond 20/40RCP with a specific gravity of 2.72. Forth type proppant is CarboProp 20/40 which is a medium strength ceramic proppant with a specific gravity of 3.28. The fifth type of proppant is CarboHSP 20/40 with a specific gravity of 3.56. For both cases, 100 mesh sand and 40/70 mesh proppants are used. In total, 60 tonnes of proppant is used in each case. A summary table is given below.

Table 2: Created Hydraulic Fracture Properties of 4000CR 20/40 and CarboProp 20/40.

Table 2 depicts that using THS EconoProp 20/40 results in increase in the fracture width, and it has the value of dimensionless conductivity (FcD) which is so close to optimum value. FcD value increases with the use of higher specific gravity proppant. The increase can be described well with the equation (1) which shows the formula of FcD. According to the formula, fracture width is directly proportional with FcD. Additionally, permeability and the fracture length are inversely proportional. Moreover, such critical increase in FcD, brings it close to the optimum value of it. Figure 4 shows optimum FcD value is around 10 and lower or higher than around 10 is actually not desired in terms of hydraulic fracturing design. If you go above 30, you are adding too much effort which is not add more conductivity in return. Figure 5 shows for each proppants, the effective stress on proppant for permeability values which also shows that low specific gravity proppant also has a lower strength value.

$$C_{fd} = (k_f w) / (k X_f) \quad (1)$$

Figure 4: Equivalent wellbore radius as a function of dimensionless fracture conductivity and fracture length (Economides & Nolte, 2000).

Figure 5: Effective Stress on Proppant vs. Proppant Permeability.

#### 3.2 Optimization of Rate

Pumping rate is an essential parameter of hydraulic fracturing treatments, because it directly affects the hydraulic horsepower that is used in the hydraulic fracturing operation. Therefore, pumping slick water, proppant and any other chemicals are under direct impact of the rate parameter.

There is a simulation is conducted to see the effect of pumping rate on the fracture parameters. Figure 6 and figure 7 show the changes in both propped length and propped height. Therefore, with the increase of rate causes the geometry of fracture increase in both cases. In these two figures the optimum values for 60 bpm rate look sufficient, and they are circled with red.

Figure 6: Rate vs. Propped Length for two different specific gravity of proppants

Figure 7: Rate vs. Propped Height for two different specific gravity of proppants.

On the other hand, on the fracture width and FcD values there are respectively proportional increase and decrease are detected. In figure 8, rate 60 bpm looks very promising in the light of the length and height graphs. Moreover, figure 9 shows that FcD gives an optimum value which is close to 10, at 60 bpm.

Figure 8: Rate vs. Width Relationship for Each Proppants

Figure 9: Rate vs. FcD Relationship for Each Proppants

#### 3.3 Optimization of Proppant Amount

Proppant amount optimization is a vital point of optimization of hydraulic fracturing because the operation price can be very high or low according the success of it. To decide the proppant amount in this simulation study; 40, 60, 80, 100, 120 ton of proppant amounts are used for comparing the results. Figure 10 shows that propped length generally increases with the increasing proppant amount, but it is not directly proportional with the proppant amount, and when proppant amount increases from 80 to 100 the length slightly increases or stays stable. Figure 11 shows propped height behaviour for given proppant amounts. When proppant amount increases to 100, propped height slightly increases.

Figure 10: Proppant Amount vs. Propped Length

Figure 11: Proppant Amount vs. Propped Height

Figure 12 shows fracture width response to increase of proppant amount. Generally, with the increase of the proppant amount the fracture width increases. Specifically, the increase in the proppant amount from 80 to 100 results an increase in the fracture width.

Figure 13 shows FcD responses for different amount of proppants, and it generally shows a steady increasing line as a response of the proppant amount change. When the proppant amount reaches a certain point, in this case its 100 tons, FcD gets the highest value. If you use more proppant above 100 tons, this will not help the increase in FcD, so production.

Figure 12: Proppant Amount vs. Fracture Width

Figure 13: Proppant Amount vs. FcD

In the light of the fracture length, fracture height, fracture width and FcD graphs 100 tonnes of proppant use looks reasonable for the sake of optimization.

### 3.4 Pad Volume Optimization

By attending different pad volume values for each of the treatment, a more suitable value tried to obtain. In this study from 500 bbls to 2100 bbls pads are pumped, and around 500 bbls pad volume the optimum point is detected. While 500 bbls giving the highest FcD, in terms of the price it will costs the minimum when we also consider other expenses like sweep fluid in the treatment.

## 4. RESULT

Hydraulic fracturing optimization should be done with consideration of many factors. The ones taken account in this optimization study are specific gravity, rate, proppant amount and pad volume optimization. To obtain these most important features for a hydraulic fracturing operation, the parameters and Fracpro software runs were conducted.

The specific gravity simulations show higher the specific gravity higher a proppant has the strength and FcD. Therefore, in Fracpro runs, the FcD value was in a trend of increase with the increase of the specific gravity. The reason FcD increases is because the strength of the proppant increases with the specific gravity. Thus, proppant cruhses less than the weak ones. For this step, THS EconoProp 20/40 proppant with a specific gravity of 2.61 was decided to be utilized.

The rate study gives results as the increase in the rate results with the increase in the fracture geometries. Therefore, propped length and height values increase. Specifically at 60bpm level the fracture length and height look the optimum.

Proppant amount is one of the vital step of the hydraulic fracturing optimization, and in this study different proppant amounts are taken into consideration, namely, 40, 60, 80, 100, 120 tonnes proppant were pumped. The results depicted that 100 tonnes of proppant use gives the optimum proppant amount to pump.

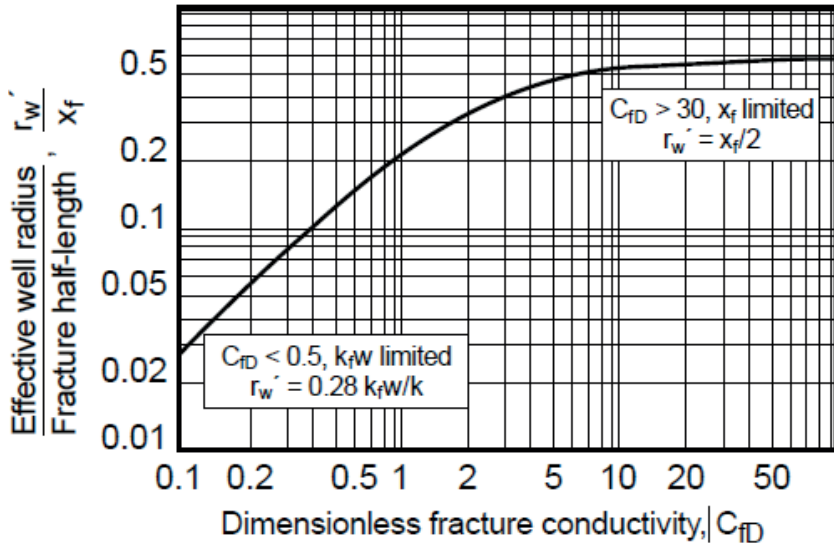
Pad volume was decided to be taken as 500 bbls considering the operation efficiency at optimum. Eventhough with low amount of pad volume the fracture width increases, with low permeability formation, it will not impact our production directly positively.

## REFERENCES

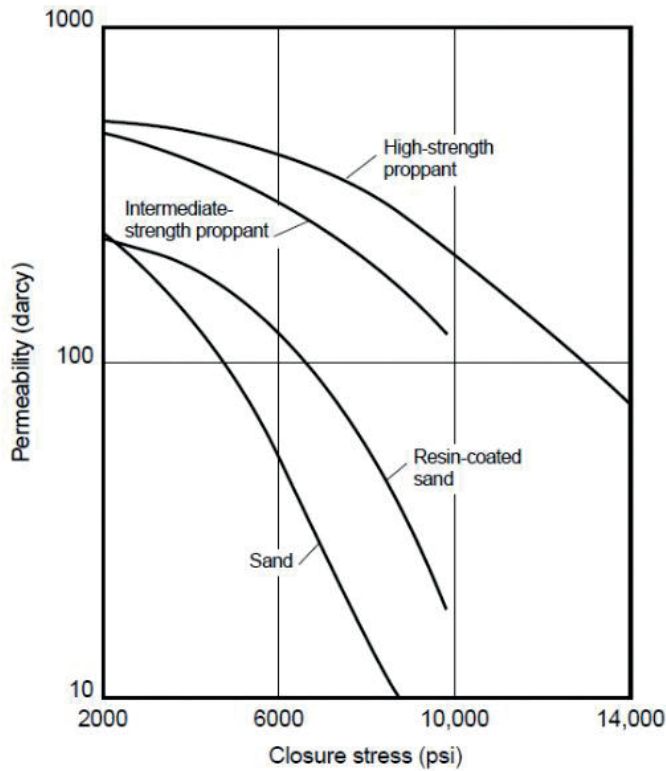
- 1- Suponik, T., Labus, K., & Morga, R. (2023). Assessment of the suitability of coke material for Proppants in the hydraulic fracturing of Coals. *Materials*, 16(11), 4083. <https://doi.org/10.3390/ma16114083>
- 2- Economides, M. J., & Nolte, K. G. (2000). *Reservoir stimulation*. Wiley.
- 3- Nash, Susan. (2018). *Proppant Technology Advances and Reservoir Performance*.

Keywords: Hydraulic Fracturing Optimization, FracPro Software

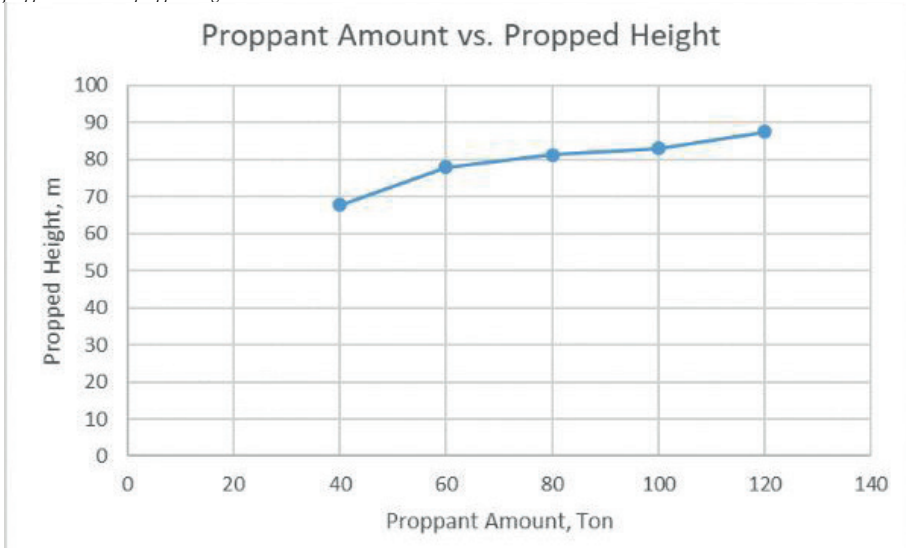
FcD



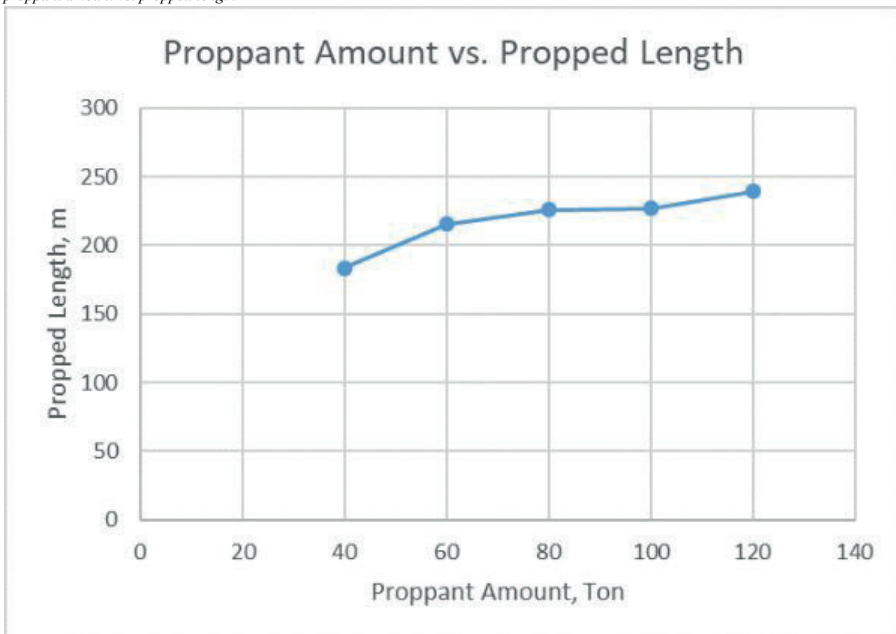
Permeability vs. Closure Stress



*proppant amount vs. propped height*

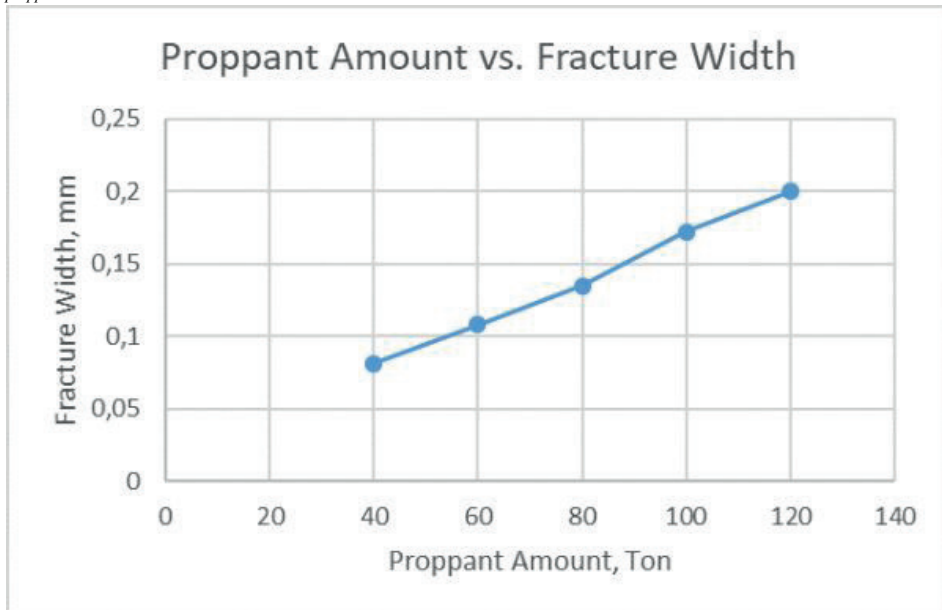


*proppant amount vs. propped length*

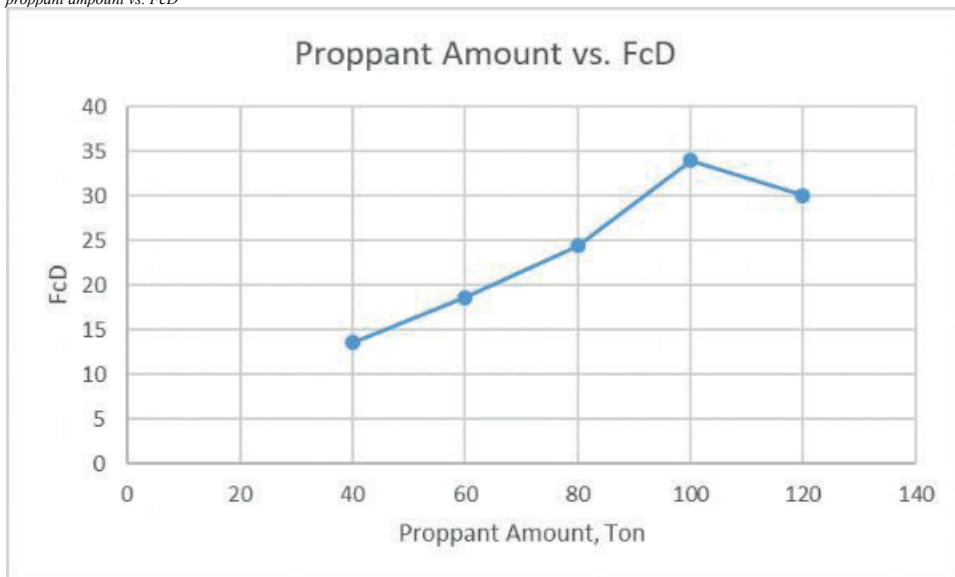


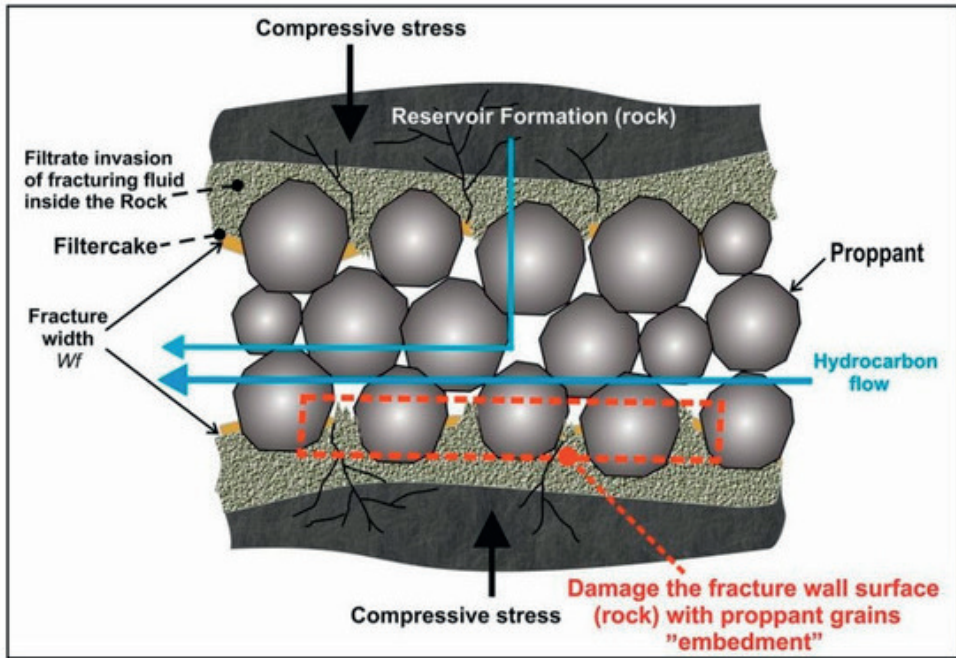


*proppant amount vs. width*

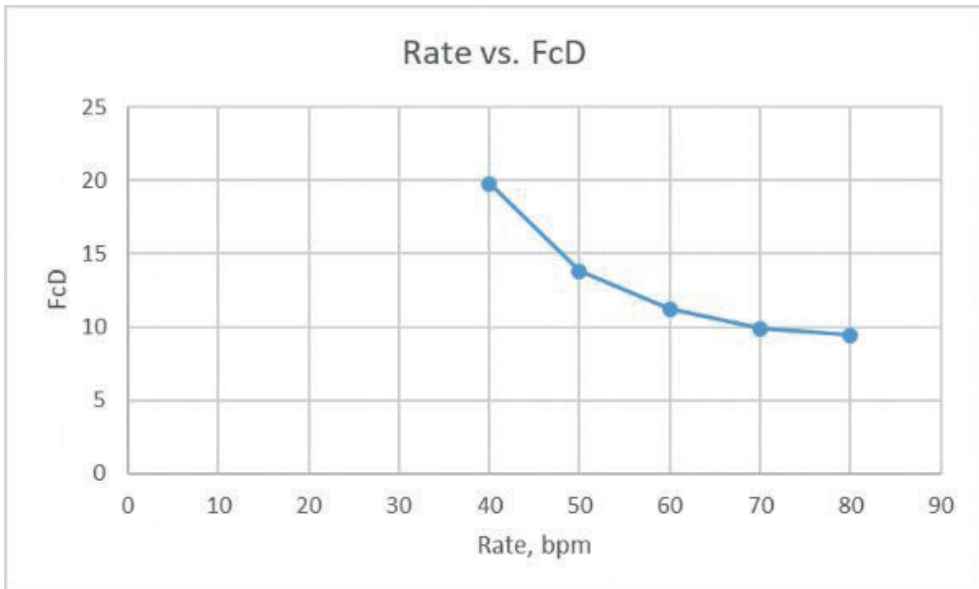


*proppant amount vs. FcD*

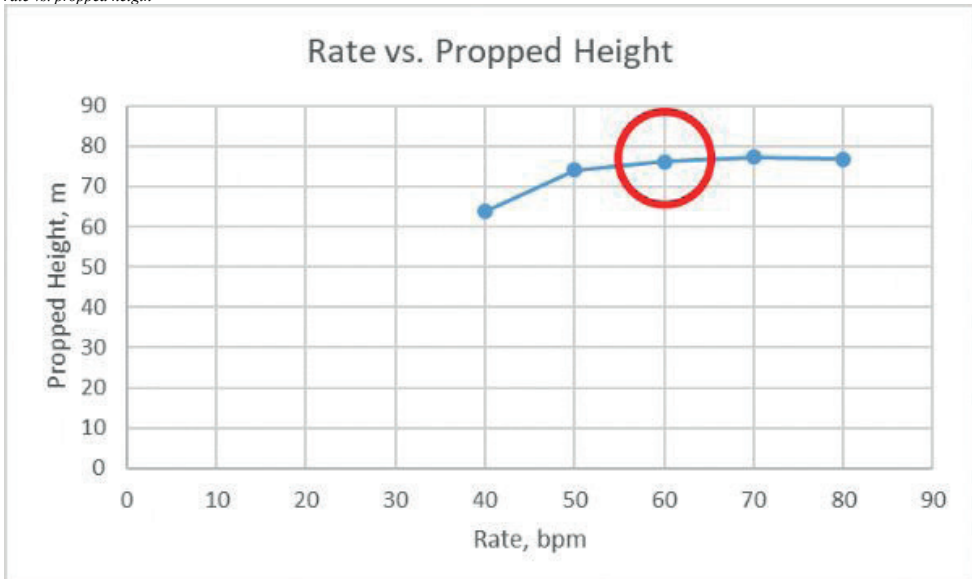




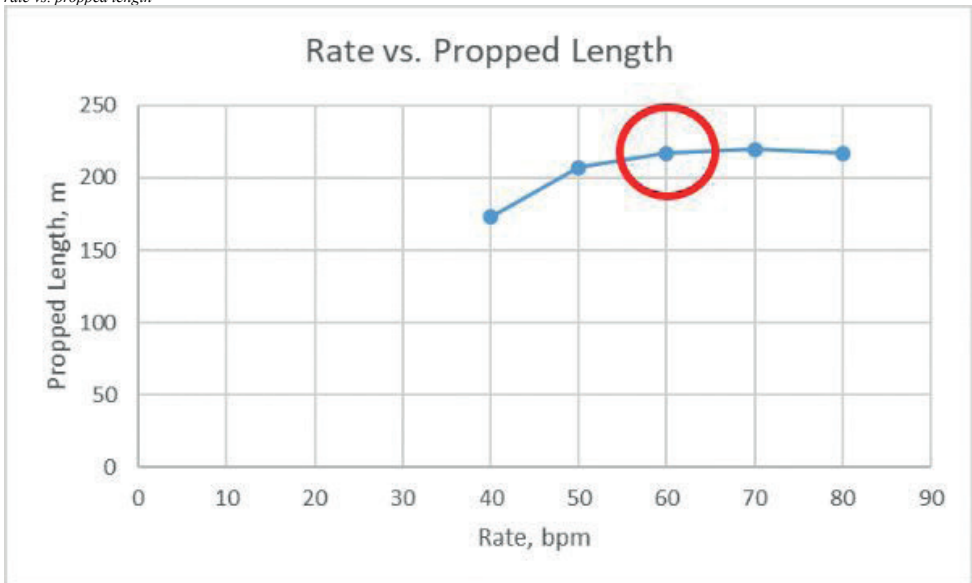
rate vs.  $F_{cD}$



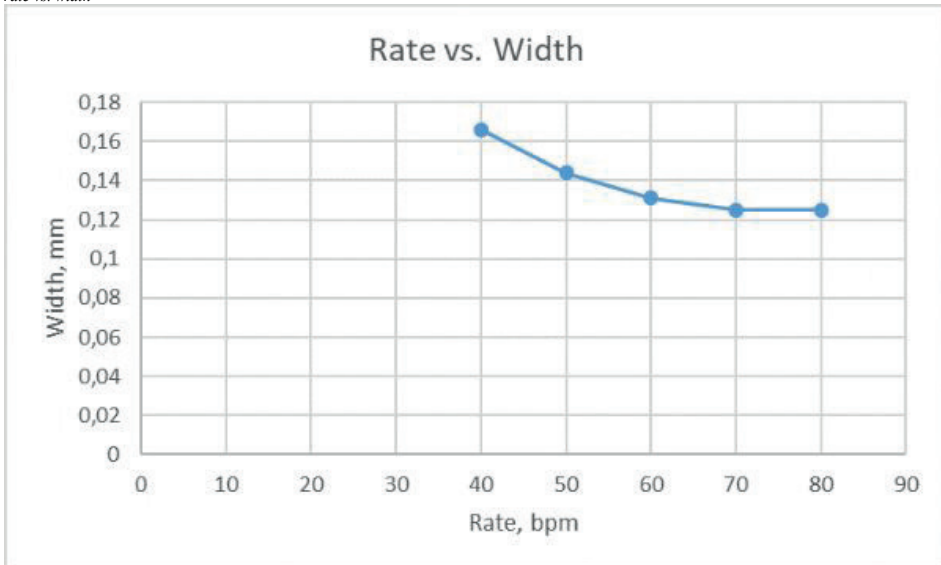
rate vs. propped height



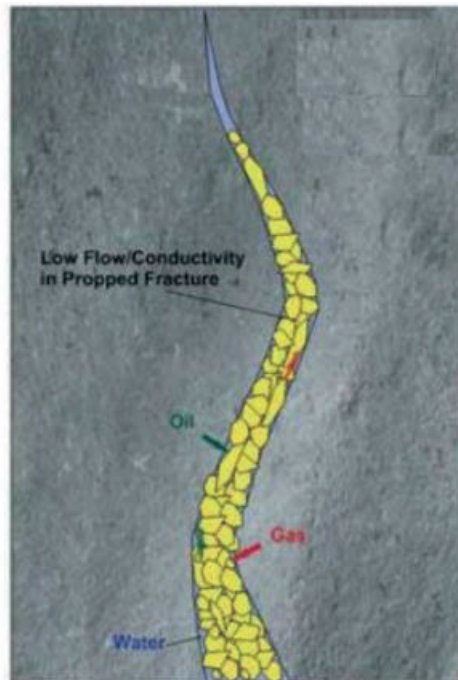
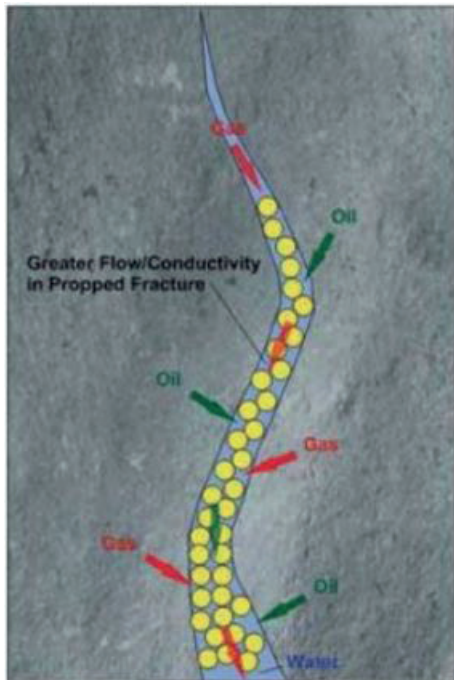
rate vs. propped length



rate vs. width



roundness





**Bölgesel Jeoloji ve Tektonik**  
*Regional Geology and Tectonics*

---



# Foça-Karaburun Açıkları Aktif Tektoniği ve Stratigrafisinin Deniz Sismiği Verileriyle İncelenmesi: İlk Sonuçlar



Derman Dondurur<sup>1</sup>, Ashlhan Nasıf<sup>1</sup>, Özkan Özel<sup>1</sup>, Orhan Atgın<sup>1</sup>, Denizhan Vardar<sup>2</sup>, Muhammet Duman<sup>1</sup>

<sup>1</sup>Dokuz Eylül Üniversitesi, Deniz Bilimleri ve Teknolojisi Enstitüsü, İzmir / Türkiye

<sup>2</sup>İstanbul Üniversitesi, Deniz Bilimleri ve İşletmeciliği Enstitüsü, İstanbul / Türkiye

İzmir Dış Körfezi, Karaburun-Foça ve Çandarlı Körfezi açıklarını içerisine alan bir alanda, Şubat 2023 döneminde çok kanallı sismik ve Chirp mühendislik sismik verileri toplanmıştır. Çalışma alanının çok ışıklı batimetri verisi ise Seyir Hidrografi ve Oşinografi Dairesi (SHOD)'dan temin edilmiştir. Çalışma alanında toplanan yaklaşık 1000 km uzunluğundaki sismik veri işlenerek yorumlamaya hazır hale getirilmiştir.

İşlenen sismik ve batimetrik veriden elde edilen ilksel sonuçlara göre, çalışma alanı morfolojik olarak 5 farklı alana ayrılabilir. Bunlar güneyden kuzeye İzmir Körfezi'nin çıkışına karşılık gelen İzmir Dış Körfezi alanı, Karaburun ve Çandarlı Basenleri, bu basenlerin arasında kalan Foça Sırtı bölgesi ve Çandarlı İç Körfez alanıdır.

İzmir Dış Körfezi'nde su derinliği kuzeye doğru tekdüze şekilde artmaktadır. Bu bölgede metamorfik temel 1.2 s civarında çok az ondülasyon göstererek uzanır. Sismik veri, bölgede KB-GD yönlü uzanan aktif fayların varlığını işaret etmektedir. Karaburun ve Çandarlı Basen'lerinin her ikisi de faylarla kontrol edilmekte, faylar basenlerin hem marjinalini ve hem de basen dolgusunu etkilemektedir. Çandarlı Baseni'nin, güneyde, olasılıkla KB-GD yönlü uzanan oldukça belirgin iki ana doğrultu atımlı fayla sınırlandırıldığı görülmüştür. Bu fayların basenin güney kısmında Foça'nın kuzeyinde karaya çıktıkları düşünülmektedir. Chirp kesitleri her iki fayın da deniz tabanını kestiğini ve dolayısıyla aktif olduğu göstermektedir.

Multi-channel seismic and Chirp subbottom profiler data were collected in February 2023 in an area that covers the İzmir Outer Bay, Karaburun-Foça and Çandarlı Bay. The multi-beam bathymetry data of the study area was obtained from the Office of Navigation, Hydrography and Oceanography (SHOD). Approximately 1000 km of seismic data collected in the study area were processed and interpreted.

According to the preliminary results obtained from the processed seismic and bathymetric data, the study area can be morphologically divided into 5 different areas. These are the İzmir Outer Bay area, which corresponds to the exit of İzmir Bay from south to north, Karaburun and Çandarlı Basins, Foça Ridge region between these basins and Çandarlı Inner Bay area.

The water depth in İzmir Outer Bay increases uniformly towards the north. In this region, the metamorphic basement extends around 1.2 s with almost no relief. Seismic data indicate the presence of active faults extending in NW-SE direction in this region. Both the Karaburun and Çandarlı Basins are fault-controlled, affecting both the margins and the basin fills. It has been observed that the Çandarlı Basin is bounded in the south by two very prominent main strike-slip faults, possibly

extending in a NW-SE direction. It is suggested that these faults can also be traced onshore in the south of the basin, in the north of Foça. Chirp sections show that both faults deform the sea floor and are therefore active.

## GİRİŞ

Batı Anadolu'nun neotektoniği, Ege levhasının K-G açılmasıyla ilişkili olan bir dizi D-B yönlü graben ile karakterize edilir (Dewey and Sengor, 1979; Angelier vd., 1981; Bozkurt, 2001). Bu graben sisteminde normal faylarla ilişkili büyük depremlerin meydana geldiği bilinmektedir (Eyidoğan ve Jackson, 1985; Aktar vd., 2007). Ancak yüzey morfolojisi ve deniz sismik verilerine (Ocakoğlu vd., 2005) dayanarak yapılan son gözlemler, bölgede geniş çaplı aktif doğrultu atımlı fayların varlığını da işaret etmektedir. Aksu vd. (1987), günümüz kıyı çizgisine paralel K-KB yönelimli bir dizi fayın, İzmir Dış Körfezi ve Çandarlı Baseni'ni sınırladığını öne sürmektedir. Ege Bölgesi'nin GPS ve depremsellik verilerine dayanan anlık deformasyonu ve topoğrafik ve batimetrik özellikleri, kuzeyden güneye yapıların karmaşıklığını işaret etmekte ve tüm bölgenin K-G yönlü açılma rejimine maruz kalıp kalmadığı ile ilişkili sorular oluşturmaktadır (Ocakoğlu vd., 2005). Batı Anadolu neotektoniğini şekillendiren bu graben ve horst sistemi, genellikle batıya doğru akan bir drenaj sistemi de meydana getirmiştir. Ege marjinalindeki kıtasal şelf alanları, bu drenaj sistemlerini oluşturan nehirlerin delta yapılarını içermektedir (Aksu vd., 1987).

Ege Denizi, Yunanistan'la olan sınır anlaşmazlığı, çok sayıdaki adanın varlığı ve Ege kıyılarının aşırı derece girintili-çukurluğu olması nedeniyle, sismik çalışmalar anlamında Karadeniz ve Akdeniz'e oranla daha az çalışılabilmiştir. Aksu vd. (1987), İzmir orta-dış körfezi ve Çandarlı Körfezi'ni de içerisine alan geniş bir alanda, tek kanallı düşük ayrımlı ve sınırlı penetrasyona sahip rejyonel sismik veriler ve 3.5 kHz mühendislik sismik verileri toplamı ve bölgenin ilk rejyonel fay haritası ile düşük ayrımlı batimetri konturlarını vermişlerdir. Ocakoğlu vd. (2005) ise, İzmir dış körfezi, Seferihisar Körfezi ve Çandarlı Dış Körfezi'ni içerisine alan bir alanda, geniş aralıklı rejyonel sismik verilerin yorumundan, bölgenin tektonik çatısını ortaya koymaya çalışmıştır.

Çalışma alanı Gediz (İzmir Dış Körfezi) ve Bakırçay (Çandarlı Körfezi) grabenlerinin batıya doğru uzanan denizel alanlarını kapsamakta olup, alan Şekil 1'de verilmiştir. Çalışmanın temel amacı, Foça-Karaburun arasındaki alan ile İzmir Dış Körfezi'ni ve Çandarlı Körfezi'ni de içeren denizel alanın deniz jeofiziği verileri kullanılarak, yapısal, stratigrafik, morfolojik ve olası hidrokarbon birikimleri açısından incelenmesidir.

## ÇALIŞMANIN TEMEL AMAÇ VE HEDEFLERİ AŞAĞIDAKİ ŞEKİLDE ÖZETLENEBİLİR

### i. Morfolojik unsurlar

Yorumlamadan elde edilmesi beklenen çıktı, kanallar, sırtlar, basenler ve denizel taraçalar gibi morfolojik unsurların varlığı, dağılımı, içsel yapısı ve oluşum mekanizmasıdır. Ayrıca deniz tabanında aktif faylanmayı işaret edebilecek çizgiselliklerin incelenmesi de amaçlanmıştır.

### ii. Alanın sığ ve derin stratigrafisi

Derin stratigrafinin, Foça-1 kuyusunu kesen çok kanallı sismik kesitler üzerinden tüm alana yayılması amaçlanmıştır. Elde edilmesi beklenen çıktı, (olasılıkla) Neojen ve sonrası derin stratigrafisi ve izopak haritaları, Holosen sonrası detay stratigrafisi ile ana birikim alanları ve izopak haritası, şelf üzerindeki olası delta klinoformları, düşük deniz seviyesi terasları ile Ege'deki deniz seviyesi değişimleri hakkında yeni bilgilerdir.

### iii. Yapısal jeoloji

Olası aktif fayların varlığının Chirp verisinden, yönelimleri ise çok ışınlı batimetri verisinden elde edilmesi hedeflenmiştir. Kör (blind) faylar ise sismik yansıma verileri kullanılarak yorumlanmıştır.

### iv. Olası hidrokarbon belirtileri

Çalışma alanındaki olası çopurlar (pockmarks), çamur volkanları ve diyapirleri, su kolonuna gaz çıkışları (plumes) ve sığ gaz birikimleri gibi oluşumların varlığı ve dağılımının Chirp verilerinden elde edilmesi amaçlanmıştır. Ayrıca çok kanallı sismik veriden olası yapısal, stratigrafik kapanlar ve doğrudan hidrokarbon belirteçleri (DHI) ile ilgili bilgiler elde edilmeye çalışılmıştır.

## YÖNTEM

Çalışmada, çok kanallı sismik yansıma, Chirp mühendislik sismiği ve çok ışınlı batimetri verileri kullanılmıştır. Çok kanallı sismik yansıma ve Chirp mühendislik sismiği verileri, Şubat 2023 döneminde DEÜ-Deniz Bilimleri ve Teknolojisi Enstitüsü (DBTE) araştırma gemisi R/V K. Piri Reis ile eş zamanlı olarak toplanmıştır. Çok ışınlı batimetri verileri ise Seyir Hidrografi ve Oşinografi Dairesi (SHOD)'dan temin edilmiştir. Veri toplama çalışması sırasında toplam 1012 km sismik ve Chirp verisi toplanmıştır. Çalışmada toplam 58 adet hat üzerinde çok kanallı sismik yansıma verisi ve 64 adet hat üzerinde de Chirp sismik verisi toplanmıştır. Sismik hatların konumu Şekil 1'de verilmiştir.

Çalışma sırasında gemi hızı 4.0-4.5 knot arasında tutulmuş olup, günlük veri üretimi ortalama 145 km civarında olmuştur. Çok kanallı sismik yansıma verileri 96 kanallı bir kayıtçı kullanılarak toplam 600

m uzunluğunda dijital alıcı kablo ile toplanmıştır. Kayıt uzunluğu 3 s, Örnekleme aralığı 1 ms, Minimum ofset mesafesi 50 m alınmıştır. Alıcı kablo ve sismik kaynak derinliği sırasıyla 4 ve 3 m'de sabit tutulmuştur. Sismik kaynak olarak 45+45 inç3 kapasiteli GI gun kullanılmış ve 2000 psi basınçta her 18.75 m'de patlatılmıştır. Toplanan verinin optimum katlama sayısı 16'dır. Chirp mühendislik sismiği verileri 9 transducerli Batho2010 sistemi ile toplanmıştır. Sweep frekansı 2.75-6.75 kHz arasında olup, kayıt uzunluğu 40 ms, örnekleme aralığı ise 0.05 ms alınmıştır. Çok ışınlı batimetri verileri ise SHOD tarafından 50 kHz frekansında çalışan SeaBeam 1050D batimetri sistemi ile toplanmıştır. Sistemin ayrımlılığı 1.5° olup, toplam 126 ışın kullanılmaktadır.

Çok kanallı sismik yansıma verileri, SeisSpace/ProMAX kullanılarak aşağıdaki standart işlemler uygulanarak işlenmiştir: Veri yükleme, geometri tanımlama, bantgeçişli süzgeç (~6-200 Hz), iz ayıklama ve silme (mute) işlemi, f-k süzgeci, tekrarlı yansımaların atılması (SRME yöntemi), CDP sıralama, hız analizi (max. 500 CDP'de bir), NMO düzeltmesi ve yığma, yığma sonrası içgencikleştirme dekonvolüsyonu, Kirchhoff zaman göçü, Kazanç uygulama (AGC ve t<sup>2</sup>), SegY çıktı.

Chirp mühendislik sismiği verilerinin işlenmesi için veri toplama çalışmalarında kullanılan Batho2010 Chirp sistemi, veri toplama sırasında Chirp verilerine gerekli standart veri işlem adımlarını uygulamakta ve veriyi işlenmiş şekilde kaydetmektedir. Bu nedenle Chirp verilerine, veri toplama sonrası ek bir veri işlem uygulanması gerekmemektedir. Bu standart veri işlem adımları Chirp kaynak imzası ile ilişkilendirme (de-chirping), zarf (envelope) hesaplama, kazanç uygulamadır. Buna ek olarak verinin yorumlama sistemine yüklenerek yorumlanabilmesi amacıyla, Chirp sistemi ham veri formatı olan ODEC formatından 16 bit standart SegY formatına dönüştürülmüş, su kolonundaki sinyal yayılımı nedeniyle oluşan gecikme zamanları (delay times) giderilmiş ve verinin başlık kısmındaki koordinatlar coğrafik koordinatlardan UTM35 formatına dönüştürülmüştür.

Çok ışınlı batimetri verileri SHOD tarafından işlenmiş olarak teslim edilmiştir. Verilere veri yükleme, navigasyon düzeltme, navigasyon ve batimetrik verinin birleştirilmesi, gürültü ayıklama (spike edit), gridleme, enterpolasyon işlemleri uygulanmıştır.

## BULGULAR

Çalışma alanının morfolojisi, çok ışınlı batimetri verisi kullanılarak incelenmiştir. Batimetri ve sismik veri birlikte yorumlanarak, çalışma alanı morfolojik olarak 5 farklı alana ayrılabilir. Bunlar güneyden kuzeye İzmir Körfezi'nin çıkışına karşılık gelen İzmir Dış Körfezi alanı, Karaburun ve Çandarlı Basenleri, bu basenlerin arasında kalan Foça Sırtı bölgesi ve Çandarlı İç Körfez alanıdır (Şekil 2).

İzmir Dış Körfezi alanı, Uzunada'nın kuzeyi ile İzmir Körfezi'nin Ege Denizi'ne bağlandığı alan arasındaki kısım olup, su derinliği 50-80 m arasında değişmektedir. Batimetri verisi, bu bölgede deniz tabanında belirgin bir morfolojik yapının varlığını işaret etmektedir. Deniz



tabanı kuzeye doğru tekdüze şekilde derinleşir (Şekil 2). Foça-1 kuyusunun stratigrafisi İzmir Dış Körfezi'ne yayılmaya çalışılmıştır. Buna göre, metamorfik temel 1.2 s civarında çok az ondülasyon göstererek uzanmaktadır. İzmir Dış Körfezi'nde neredeyse yatay uzanan Miyosen ve Pliyosen üst yüzeyleri kuzeye Karaburun Baseni'ne yaklaştıkça derinleşmektedir (Şekil 3). Körfezi bu bölgesinin metamorfik temeli de etkileyen küçük atma sahip normal faylarla deforme olduğu görülmektedir. Foça-1 kuyusunun kuzeyinde fayların atımının da arttığı gözlenmektedir (Şekil 3). BGB-DGD yönlü uzanan sismik kesitlerde fay atımlarının daha büyük olduğu gözlenmiştir. Bu kesitlerde fayların deniz tabanını da etkilediği görülmektedir (Şekil 3). Henüz çalışma alanının bütüncül bir fay haritası çıkarılmamış olmakla birlikte, fayların bu özellikleri, körfezin bu kısmındaki faylarının yönelimlerinin kabaca KB-GD yönlü olduğunu işaret etmektedir.

Şekil 4, Karaburun Baseni, Foça Sırtı ve Çandarlı Baseni'ni kesen bir sismik kesiti göstermektedir. Kesitte her iki basenin tabanı sismik kesitte belirgin şekilde haritalanamamıştır ve basenlerin faylarla kontrol edildiği görülmektedir. Faylar basenlerin hem marjinalini ve hem de basen dolugusunu etkilemektedir. Özellikle Karaburun Baseni son derece deforme olmuş durumda olup, baseni etkileyen fayların bazılarının deniz tabanına kadar uzandığı görülmektedir. Basenleri ayıran Foça sırtının doğu kısmında doğuya ilerleyen bir deltanın klinoformlarını gözlemek mümkündür. Çalışma kapsamında, özellikle Karaburun ve Çandarlı Basen'lerinin kuzey sınırında hem deniz tabanında uzanan ve hem de gömülü şekilde bu delta yapılarının varlığı görülmüştür. Çalışmanın ilerleyen aşamalarında söz konusu deltalar haritalanacak ve Ege Denizi deniz seviyesi değişimleri ile ilişkilendirilecektir.

Çandarlı Baseni Çandarlı Körfezi'nin batı çıkışında yaklaşık K-G yönlü uzanır ve çalışma alanındaki derinli 75-135 m arasında değişir. Çandarlı baseni'ni kesen sismik kesitler, basenin faylarla kontrol edildiğini ve özellikle güney kısmında, olasılıkla KB-GD yönlü uzanan oldukça belirgin iki ana doğrultu atımlı fayla sınırlandığını göstermektedir (Şekil 5). Bu faylar henüz haritalanamamış olup, basenin güney kısmında Foça'nın kuzeyinde karaya çıktıkları düşünülmektedir. Fayların atımları Chirp kesitlerinde de oldukça belirgin olup, her iki fayın da deniz tabanını kestiği ve dolayısıyla aktif olduğu görülmektedir (Şekil 5).

## SONUÇLAR

Sismik ve batimetrik veriden yola çıkılarak çalışma alanı morfolojik olarak 5 farklı alana ayrılmıştır. Bunlar güneyden kuzeye İzmir Körfezi'nin çıkışına karşılık gelen İzmir Dış Körfezi alanı, Karaburun ve Çandarlı Basenleri, bu basenlerin arasında kalan Foça Sırtı bölgesi ve Çandarlı İç Körfez alanıdır.

İzmir Dış Körfezi'nde su derinliği 50-80 m arasında değişmektedir ve belirgin bir morfolojik yapıya ev sahipliği yapmamaktadır. Bu bölgede metamorfik temel 1.2 s civarında çok az ondülasyon göstererek uzanır. Bölgede özellikle BGB-DGD yönlü uzanan sismik

kesitlerde belirgin olan fay fayların deniz tabanını da etkilediği görülmekte, körfezin bu kısmındaki faylarının yönelimlerinin kabaca KB-GD yönlü olduğu düşünülmektedir.

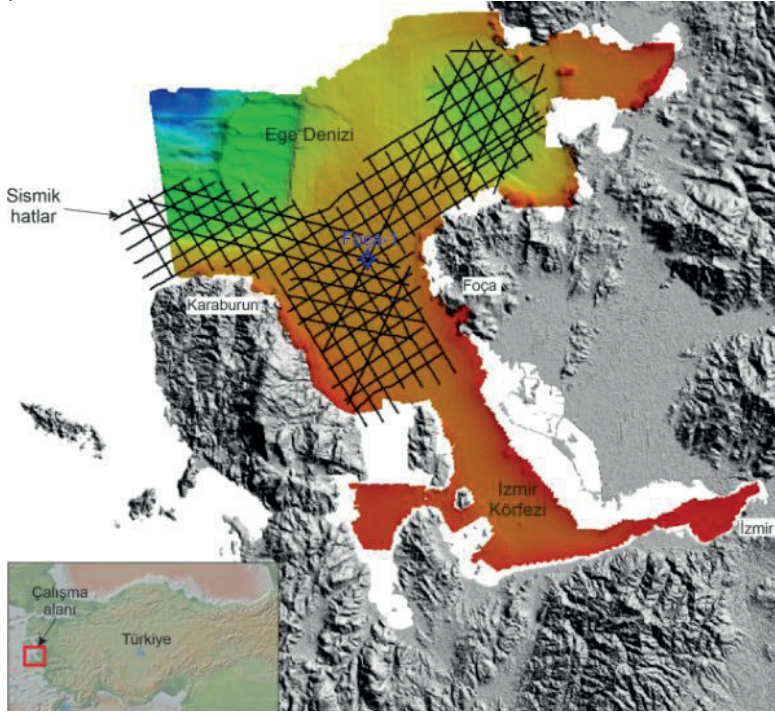
Karaburun ve Çandarlı Basen'lerinin her ikisi de faylarla kontrol edilmektedir. Faylar basenlerin hem marjinalini ve hem de basen dolugusunu etkilemektedir. Özellikle Karaburun Baseni son derece deforme olmuş durumda olup, baseni etkileyen fayların bazılarının deniz tabanına kadar uzandığı görülmektedir. Çandarlı Baseni'ni kesen sismik kesitler, basenin güney kısmında, olasılıkla KB-GD yönlü uzanan oldukça belirgin iki ana doğrultu atımlı fayla sınırlandığını göstermektedir. Bu fayların basenin güney kısmında Foça'nın kuzeyinde karaya çıktıkları düşünülmektedir. Chirp kesitleri her iki fayın da deniz tabanını kestiğini ve dolayısıyla aktif olduğu göstermektedir.

## KAYNAKLAR

- Aksu, A.E., Piper, D.J.W., and Konuk, T., 1987. Late Quaternary tectonic and sedimentary history of outer İzmir and Çandarlı Bays, western Turkey, *Marine Geology*, 76, 89-104.
- Aktar, M., Karabulut, H., Özalaybey, S., and Childs, D., 2007. A conjugate strike-slip fault system within the extensional tectonics of western Turkey, *Geophys. J. Int.*, 171, 1363-1375.
- Angelier, J., Dumont, J.K., Karamandereci, H., Poisson, P., Şimşek, S., and Uysal, S., 1981. Analysis of fault mechanisms and expansion of southwestern Anatolia since the Late Miocene, *Tectonophysics*, 75, T1-T9.
- Bozkurt, E., 2001. Neotectonics of Turkey, a Synthesis, *Geodinamica Acta*, 14, 3-30.
- Dewey, F.J., and Şengör, A.M.C., 1979. Aegean and surrounding regions: complex multiplate and continuum tectonics in a convergent zone, *Geol. Soc. Am. Bull.*, 90, 84-92.
- Eyidoğan, H., and Jackson, J.A., 1985. A seismological study of normal faulting in the Demirci, Alasehir, and Gediz earthquakes of 1969-1970 in the western Turkey: implications for the nature geometry and deformation in the continental crust, *Geophys. J. R. Astr. Soc.*, 81, 569-607.
- Ocakoğlu, N., Demirbağ, E., and Kuşçu, İ., 2005. Neotectonic structures in İzmir Gulf and surrounding regions (western Turkey): evidences of strikeslip faulting with compression in the Aegean extensional regime, *Marine Geology*, 219, 155-171.

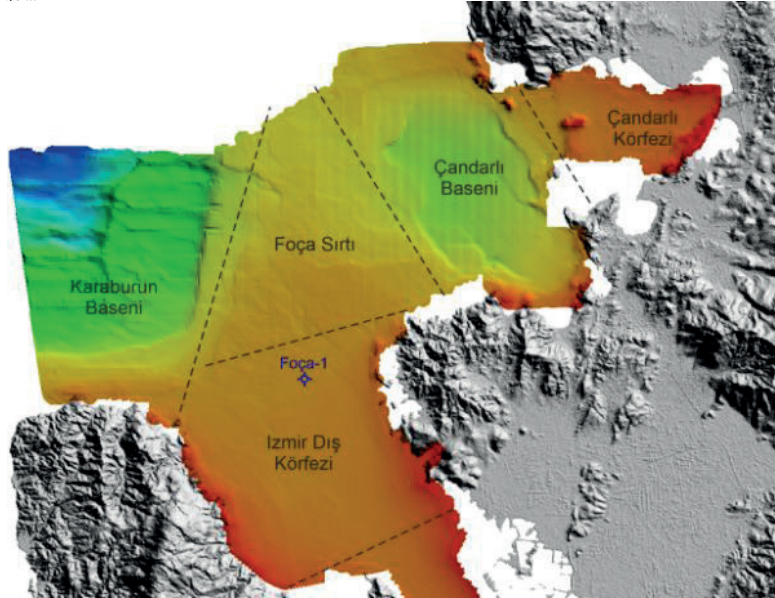
Anahtar Kelimeler: Deniz sismliği

Şekil 1



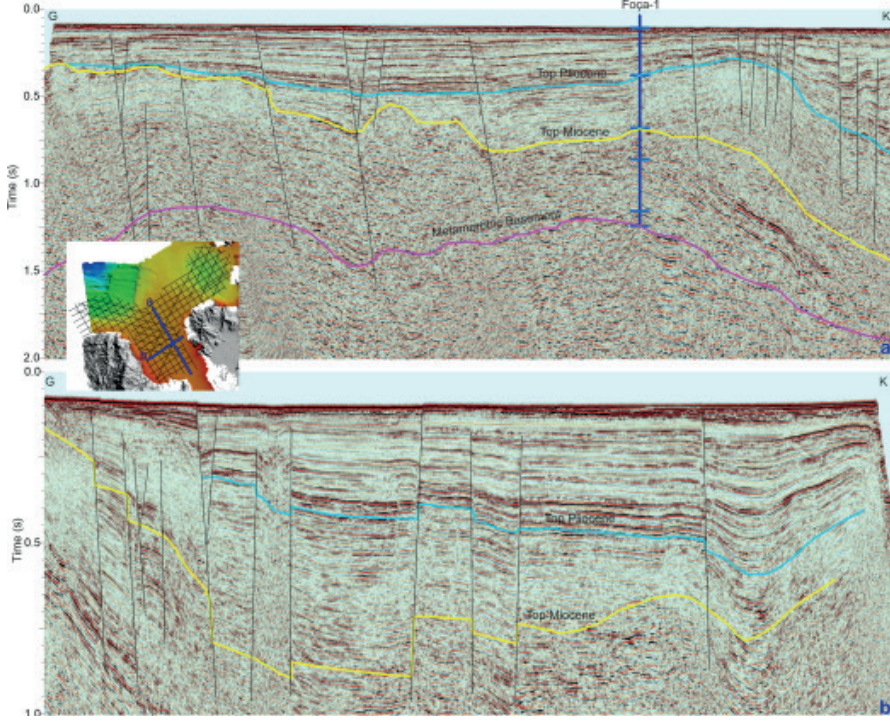
Şekil 1. Çalışma alanı ve toplanan çok kanallı ve Chirp sismik hatları.

Şekil 2



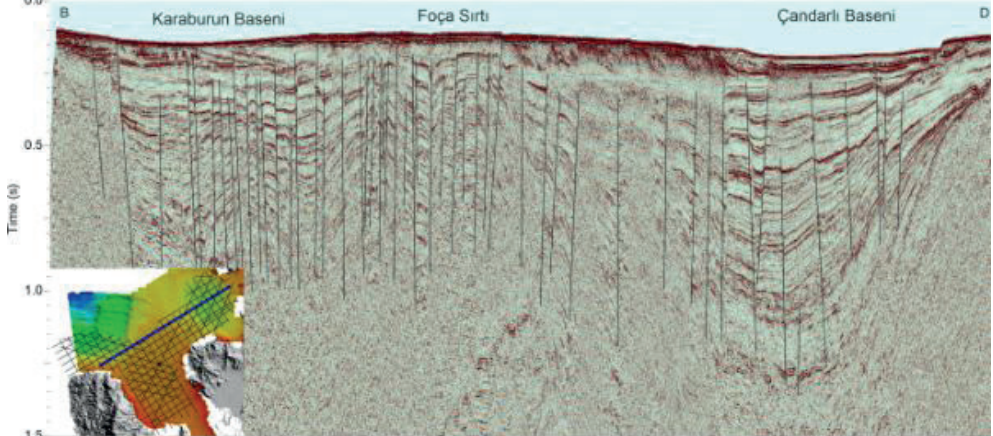
Şekil 2. Çalışma alanının morfolojik bölümleri.

Şekil 3



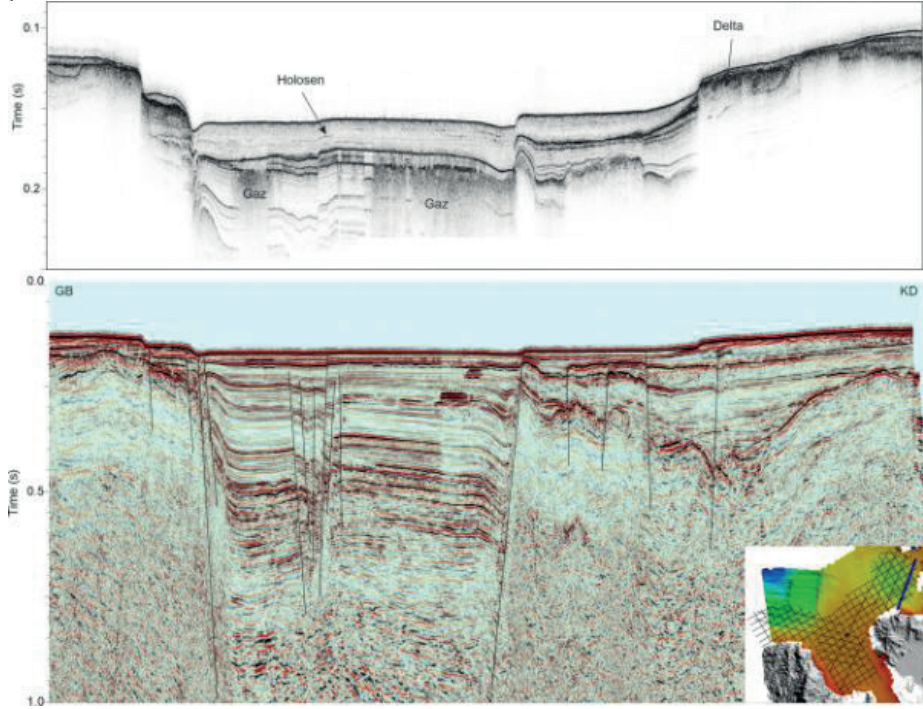
Şekil 3. İzmir Dış Körfezi'nden kuzeye uzanan ve Foça-1 kuyusunu kesen çok kanallı bir sismik hat (üstte) ve BGD-DGD yönlü uzanan bir başka örnek sismik kesit (altta).

Şekil 4



Şekil 4. Karaburun Baseni, Foça Sırtı ve Çandarlı Baseni'ni kesen ve BGD-DGD yönlü uzanan örnek bir sismik kesit.

Şekil 5



Şekil 5. Çandarlı Baseni'ni kesen bir Chirp (üstte) ve çok kanallı sismik kesit (altta).

# The Semi-Automatic Morphological Analysis of The Pockmarks Enable Gas/Liquid Emissions From The Bottom Of Sapanca Lake



**Enes Sönmez, Hülya Kurt**

Department of Geophysical Engineering, Istanbul Technical University, Istanbul / Türkiye  
İstanbul Üniversitesi, Deniz Bilimleri ve İşletmeciliği Enstitüsü, İstanbul / Türkiye

## ABSTRACT

In this study, the geometric characteristics and distribution of pockmark structures developed in relation to active faults in Sapanca Lake, located on the northern branch of the North Anatolian Fault (NAF), were investigated using multi-beam bathymetric data. The multi-beam bathymetric data was collected in an area of approximately 18 km<sup>2</sup> as part of the TUBITAK-1001 Project titled «Investigation of the Active Tectonics of Sapanca Lake and its Surroundings using Geophysical Methods» (Project No: 117Y130) (Kurt et al., 2020). Contour and relief maps were created using GIS-based software, and the traces of active faults and pockmark areas in the lake were investigated. A semi-automatic system was employed to detect and classify pockmarks using attributes such as area, perimeter, diameter, and depth of the pockmark structures. Based on the evaluations, a total of 439 pockmarks were identified in the lake, with diameters ranging from 1 to 50 meters and depths ranging from 0.1 to 3.91 meters. Among these, 49 were identified as normal pockmarks as in Hovland et al. (2002). Pockmarks are predominantly concentrated in the northeast of the lake but also exist in the southeast. It is believed that these pockmarks, which have a shape close to circular, are formed by strong and sudden fluid escapes associated with seismic activity along the fault on the lake floor.

## ÖZET

Bu çalışmada, Kuzey Anadolu Fayı'nın (KAF) kuzey kolu üzerinde bulunan Sapanca Gölü'nde toplanan çok ışımlı batimetrik veriler kullanılarak buradaki aktif faylara bağlı olarak gelişen pockmark yapılarının geometrik özellikleri ve göldeki dağılımları araştırılmıştır. Çok ışımlı batimetrik veriler "Sapanca Gölü ve Civarının Aktif Tektoniğinin Jeofizik Yöntemlerle Araştırılması" başlıklı TÜBİTAK-1001 Projesi (Proje No: 117Y130) (Kurt ve diğ., 2020) çerçevesinde yaklaşık 18 km<sup>2</sup>'lik bir alanda toplanmıştır. GIS tabanlı yazılımlar kullanılarak kontur ve kabartı haritaları oluşturulmuş ve gölde aktif fayların izleri ve pockmark alanları araştırılmıştır. Pockmarkların belirlenmesi ve sınıflandırması bu yapıların alan, çevre, çap ve derinlik gibi öznitelikleri kullanarak yarı-otomatik bir sistemle gerçekleştirilmiştir. Yapılan değerlendirmelerde gölde çapları 1-50 m, derinlikleri ise 0.1-3.91 m arasında değişen toplam 439 adet pockmark belirlenmiş, bunlardan 49 tanesinin normal pockmark (Hovland ve diğ., 2002) olduğu anlaşılmıştır. Pockmarklar yaygın olarak gölün kuzeydoğusunda yoğunlaşmakla beraber güneydoğusunda da varlığını göstermektedir. Hemen hemen dairesel yakın şekle sahip pockmarkların, göl tabanındaki fayın deprem aktivitesi ile güçlü ve ani bir

akışkan çıkışı tarafından oluştukları düşünülmektedir.

## INTRODUCTION

In marine areas, multi-beam bathymetric methods are mainly used to determine the active tectonics and the topographic characteristics of the seabed. Pockmarks are hollow areas on the seabed formed by the eruption of fluids such as gases and liquids accumulated in the sediments on the ocean, sea and lake floors due to tectonic activities, sediment movements and decomposition of organic materials. In this study, the development of the pockmarks around the traces of the NAF, which can be traced on the floor of Sapanca Lake, due to this fault activity and the relationship of some geometric features of the pockmarks with the earthquakes that have occurred in the region were investigated (Figure 1). The study area is an active tectonic structure connected to the NAF and has the capacity to produce earthquakes of magnitude up to Mw > 7. It has been proven by some studies that pockmarks become active before, during and after earthquakes (Field and Jennings, 1987; Hovland and Judd 1988). This feature may enable pockmarks to be used as an earthquake warning system before earthquakes. Pockmarks can also be used as earthquake recording systems thanks to the information they provide about previous earthquakes. For this reason, determining the number of pockmarks in the region, pockmark type and shape will prepare a research ground for a wider interpretation. Within the scope of this study, the pockmarks in Sapanca Lake, located in the Eastern Marmara region, were identified with a semi-automatic system in order to minimize the errors that may be caused by manual mapping. Manual mapping and characterization of pockmarks is subjective and requires long computation times. In this sense, the semi-automatic filtering method offers a faster and more reliable system. In the study area, detailed geometric and distributional characteristics of the pockmark structures, which are thought to be formed by fluid outflows such as gas and liquid surrounding active faults in the water table where sedimentation is high, were determined and classified.

(Figure 1)

## MATERIALS AND METHODS

In the multi-beam bathymetry method applied in Sapanca Lake, data were collected over an area of approximately 17.85 km<sup>2</sup> of the lake with the "Norbit iWBMS Multi-beam Echosounder" device installed on the 10 m long "Curt Kosswig" research boat of Istanbul University, Faculty of Aquatic Sciences (Figure 2). The operating frequency range of the device is between 360

- 440 kHz and the resolution of the data is in the order of centimeters on the lake bottom.

(Figure 2)

### MULTI-BEAM BATHYMETRIC DATA PROCESSING

After the data processing stages applied to the raw data, bathymetric data in (x,y,z) format were gridded in GMT software. QGIS and ARCGIS programs were mainly used in the following stages of the study since they provide practical ease of use in bathymetric mapping and sectioning. The bathymetric data set with a grid spacing of 0.5 m was transferred to QGIS software and lake bottom contour and relief maps were created. For the morphological analysis of the pockmarks, the use of ARCGIS program, which has a rich variety of modules, was preferred more. Figure 3 shows the flow chart for determining the geometric characteristics of the pockmarks. In the diagram, just below the module names used in the ARCGIS program, the purpose for which they are used is briefly stated.

(Figure 3)

At the beginning of the study, the hollow areas thought to be pockmarks on the lake bottom were visually identified on the relief map prepared using the QGIS program. Then, the area covered by the pockmarks on the lake bottom was manually analyzed and marked from the contour geometry in the contour maps prepared. In addition, cross-sections were taken in different directions in these parts identified as pockmarks and information on the depth and flank slopes of the pockmarks were derived. However, such manual assessments of the morphology of pockmarks are limited to the evaluation criteria that the interpreter can see at the time and may present relative changes. In addition, the manual evaluation of such pockmarks, which can number in the hundreds, is time-consuming and increases the likelihood of error. For these reasons, there is a need for systematic and automated assessments to determine the geometric characteristics of pockmark structures observed on the lake bottom. Over the last 20 years, there have been many studies on pockmark assessments on marine and lake bottoms using GIS-based software with fully or semi-automated approaches (Gaferia et al., 2012; Gaferia et al., 2018; Audsley et al., 2019). GIS-based programs have a rich variety of modules that can be used for these purposes, and the identification of pockmarks in this way requires a multi-stage process. In the data processing phase, the minimum threshold parameter must be selected correctly in order to distinguish pockmarks from depressions due to topographic changes on the lake bottom. This parameter is determined by trial and error. Thus, polygons representing the water bottom areas shaped by the pockmarks are created. As a result of the semi-automatic approach, a total of 439 pockmarks with diameters ranging from 1-50 meters and depths ranging from 0.1-3.91 meters were identified in Sapanca Lake

(Figure 4)

### RESULTS

Morphological Interpretations of Bottom of Sapanca Lake High resolution multi-beam bathymetry data indicate that the deepest point of the lake is -52.78 m in the central part of the lake. Although pockmarks are mostly seen in the northeast of the lake, these structures are also encountered in the southeast of the lake. Figure 5 shows the distribution of the pockmarks identified in this study on the map of the bottom of Sapanca Lake showing the lake bottom sediment types prepared by Ertürk (1994). According to the map, it is observed that pockmarks are generally concentrated in muddy sand sediments in the lake.

(Figure 5)

Eccentricity, used in morphological assessments, is a measure of the distance of a shape from roundness or symmetry. The eccentricity of a circle-like shape can be calculated by taking the ratio of the longest axis passing through the center of the shape and the axis perpendicular to it. Pockmarks in Sapanca Lake have an eccentricity dominance of approximately 0.3. In this sense, it can be interpreted that normal pockmarks in the lake generally have a shape close to circular. It can be interpreted that the pockmarks in Sapanca Lake were formed as a result of the earthquake activity of the fault at the base of the lake and instantaneous fluid eruptions. In addition, the eccentricity orientation map, which generally presents a NE-SW distribution, is given in Figure 6.

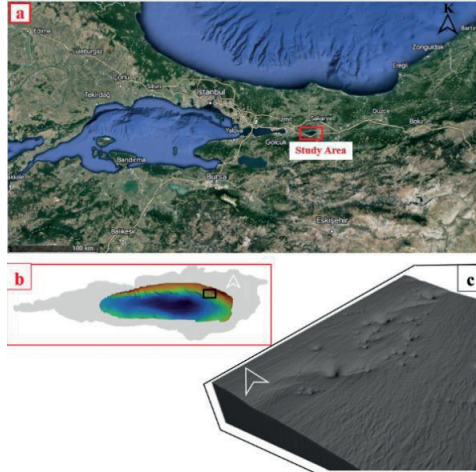
(Figure 6)

### CONCLUSIONS

In the morphological evaluation of the multi-beam bathymetric data of Sapanca Lake using GIS-based programs, it was observed that the pockmarks distributed on the lake bottom are mainly located around the active faults of the NAF and in the northeast of the lake. A total of 439 pockmarks were detected and morphometrically characterized by semi-automated approach and 49 of them were determined to be normal pockmarks. The pockmarks, which were generally concentrated in the muddy sand sediments of the lake, ranged from 1-50 meters in diameter and 0.1-3.91 meters in depth. It was observed that normal pockmarks generally have a circular shape and eccentricity measurements are concentrated at 0.3. Therefore, it is thought that the pockmarks in Sapanca Lake were formed by instantaneous and powerful fluid eruptions due to the earthquake activity of the fault at the lake bottom. Approximately 50% of the normal pockmarks in Sapanca Lake were found to extend along the lake floor in the NE-SW direction. The consistent orientation of the pockmarks may indicate that all pockmarks were formed in a short period of time or that the bottom current regime in the lake has been effective for a long time. Semi-automated morphological approaches to the high-resolution bathymetric data used in this study provide information on the distribution, size, orientation and formation mechanisms of pockmarks in addition to active fault traces in Sapanca Lake.

Keywords: Pockmark, Sapanca Lake

Figure 1



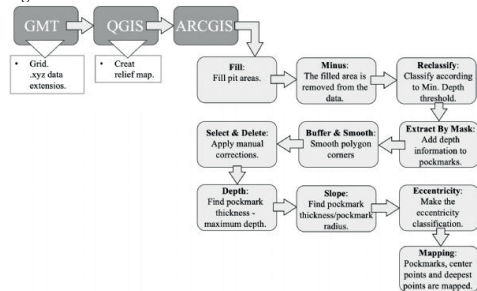
a) Map showing the location of the study area b) Location of multi-beam bathymetric data in Sapanca Lake c) 3D view of pockmarks in Sapanca Lake

Figure 2



a) Research boat (Curt Koswig) used in the collection of geophysical data in Sapanca Lake b) Equipment used in the collection of multi-beam bathymetry data

Figure 3



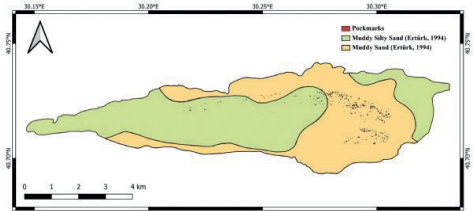
Flowchart for processing multi-beam bathymetric data

Figure 4



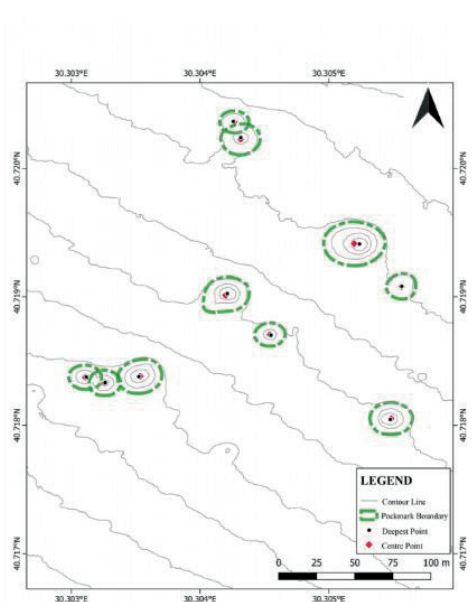
Map showing the location of all pockmarks in the study area

Figure 5



Distribution of pockmarks on the map showing the lake bottom sediment types of Sapanca Lake

Figure 6



Map showing the deepest points, center points and boundary lines of normal pockmarks

# İzmir Körfezi'nin Aktif Tektoniğinin ve Stratigrafisinin Deniz Sismiği Verileriyle İncelenmesi: İlk Sonuçlar



**Aslıhan Nasıf<sup>1</sup>, Derman Dondurur<sup>1</sup>, Özkan Özel<sup>1</sup>, Orhan Atgın<sup>1</sup>, Denizhan Vardar<sup>2</sup>**

<sup>1</sup>Dokuz Eylül Üniversitesi, Deniz Bilimleri ve Teknolojisi Enstitüsü, İzmir / Türkiye

<sup>2</sup>İstanbul Üniversitesi, Deniz Bilimleri Ve İşletmeciliği Enstitüsü, İstanbul / Türkiye

İzmir metropol alanı ve çevresi, geçmiş dönemde yoğun sismolojik etkinliğin gözlemlendiği, tarihsel dönemde 6.5 ve üzerinde depremlerin ciddi şekilde hasar verdiği 1. derece deprem bölgesidir. Bu anlamda, bölgeyi etkileyebilecek aktif fayların varlığı, uzanımı, aktif olup olmadıkları, olası hareket mekanizmaları ve karadaki aktif faylarla olan olası ilişkisinin araştırılması ve ortaya konulması önem taşımaktadır. İzmir ve çevresinin karasal alanındaki aktif faylar nispeten iyi derece araştırılmış olmakla birlikte, İzmir Körfezi faylarının uzanımı ve aktivitesi ile ilişkili bilgimiz yetersizdir.

Çalışmanın temel amacı, İzmir İç ve Dış Körfez alanının deniz jeofiziği verileri kullanılarak, (i) stratigrafik (delta, deniz seviyesi değişimleri ve Miyosen sonrası derin stratigrafi), (ii) yapısal jeoloji (fay haritası, aktif fayların varlığı ve uzanımı, mevcut tektonik yapı) ve (iii) sığ gaz birikimleri açısından incelenmesidir. Çalışılan alan yaklaşık 370 km<sup>2</sup> olup, su derinliği 10-70 m arasında değişmektedir. Çalışma sırasında İzmir İç ve Dış Körfez alanında farklı penetrasyon ve ayrımlılığa sahip sismik veriler toplanmıştır. Veri toplama DEÜ-Deniz Bilimleri ve Teknolojisi Enstitüsü' ne ait R/V K. Piri Reis ve Dokuz Eylül 4 gemileriyle gerçekleştirilmiştir.

Sismik veriler ile sismolojik veriler karşılaştırılarak yorumlanacak ve halen oldukça tartışmalı olan İzmir İç Körfezi'nin aktif tektoniği ve fayların mekanizmaları ile uzanımları ortaya konulmaya çalışılmıştır. Bu sunum, İzmir için yapılacak deprem modellemeleri, İzmir ili deprem senaryosu ve deprem master planı çalışmalarını için oldukça önemli ve gerçekçi bilgiler temin edecek ilksel sonuçları içermektedir. Bu çalışma Dokuz Eylül Üniversitesi tarafından, Bilimsel Araştırma Projeleri kapsamında desteklenmiştir. (Proje Kodu: FBG-2023-3159)

**Anahtar Kelimeler:** İzmir Körfezi Aktif Tektoniği, Deniz Sismiği

The Izmir metropolitan area and its surroundings are a first-degree earthquake zone where intense seismic activity has been observed in the past. Historical records indicate that earthquakes with a magnitude of 6.5 and above have caused significant damage in the region. Therefore, it is crucial to investigate and determine the presence, extent, activity, possible movement mechanisms, and potential relationship with on-land active faults that could affect the area. While the active faults in the terrestrial (land-based) areas of Izmir and its surroundings have been relatively well studied, our knowledge about the extent and activity of faults in Izmir Bay (Izmir Körfezi) is insufficient.

The main objective of the study is to investigate the Izmir Inner and Outer Gulf area using marine geophysical data. The study focuses on three main aspects: (i) stratigraphy, which includes the study of

delta formations, sea-level changes, and post-Miocene deep stratigraphy, (ii) structural geology, involving fault mapping, presence and extent of active faults, and existing tectonic structures, and (iii) shallow gas accumulations. The study area covers approximately 370 km<sup>2</sup> with water depths ranging from 10 to 70 meters.

During the research, seismic data with different penetration and resolution capabilities were collected in the Izmir Inner and Outer Gulf area. The data collection was carried out using the R/V K. Piri Reis and Dokuz Eylül 4 research vessels, both belonging to the Institute of Marine Sciences and Technology.

The seismic data compared and interpreted in conjunction with seismological data to shed light on the active tectonics and fault mechanisms in Izmir Inner Gulf, which is currently a subject of significant debate. The aim is to determine the orientations of faults in the region. This presentation will provide essential and realistic information for earthquake modeling, earthquake scenarios, and earthquake master planning studies in Izmir. The primary results obtained from this study will be crucial in providing valuable insights.

This research has been supported by Dokuz Eylül University under the scope of Scientific Research Projects (Project Code: FBG-2023-3159).

## GİRİŞ-AMAC

İzmir Körfezi, halen gelişmekte olan sığ bir deniz havzasıdır. Körfez morfolojik olarak iki ana bölüme ayrılabilir (Aksu ve Piper, 1983; Aksu ve diğ., 1987, 1990). Körfezin iç bölümü ("L" şeklinin yatay kısmı) doğuda Kavak Nehri deltasından Güzelbahçe'ye kadar uzanır. Dış kısım ("L" şeklindeki dikey kısım) KKB-GGD'ye doğru uzanır ve körfez kuzeyde Ege Denizi'ne açılır. Seferihisar Fayı, körfezin iç ve dış kesimleri arasındaki kara, güney sınırı olarak Sığacık Körfezi'nden Güzelbahçe'ye kadar uzanır ve Holosen'den beri aktiftir. Sağ yanal doğrultu-atım özelliği ile Bornova Fliş Zonu ile Neojen sedimanları arasında sınır görevi görür (Emre ve diğ., 2005). Gediz Grabeni'nin devamı olarak körfezin iç kısmı kuzey ve güneyden iki fayla çevrilidir. Körfezin güney kıyı şeridinde İzmir Fay Zonu gözlenir. İzmir'in yakın doğusundan başlar ve Balçova'nın doğusuna kadar devam eder (Emre ve Barka, 2000). Balçova jeotermal sahası bu fay sistemi üzerinde yer almaktadır. Ancak Balçova Narlıdere'den batıya doğru açık denizde devam ettiğine dair herhangi bir araştırma yoktur. İzmir Fayı geçmişte aktif bir normal fay zonu olarak kabul edilmiştir (Sözbilir ve diğ., 2004; Emre ve diğ., 2005). Sözbilir ve diğ. (2008), İzmir Fayı'nın en güneydeki segmentinin yaklaşık 500



m genişliğinde olan fay zonundaki ana fay segmenti olduğunu belirtmişlerdir.

Aksu ve diğ. (1987), İzmir Orta-Dış Körfezi ve Çandarlı Körfezi'ni de içerisine alan geniş bir alanda, tek kanallı düşük ayrımlı ve sınırlı penetrasyona sahip rejyonel sismik veriler ve 3.5 kHz mühendislik sismiği verileri toplamış ve bölgenin ilk rejyonel fay haritası ile düşük ayrımlı batimetri konturlarını vermişlerdir. Ocakoğlu ve diğ. (2005) ise, İzmir Dış Körfezi, Seferihisar Körfezi ve Çandarlı Dış Körfezi'ni içerisine alan bir alanda, geniş aralıklı rejyonel sismik verilerin yorumundan, bölgenin tektonik çatısını ortaya koymaya çalışmıştır. Çalışma alanının derin stratigrafik yapısı hakkında literatürde sadece Ocakoğlu ve diğ. (2005) tarafından yayınlanan ve 1990'lı yıllarda MTA tarafından toplanan sismik hatlardan haritalanan düşük ayrımlı Miyosen temel derinliği haritası mevcuttur. Buna göre Miyosen yaşlı temel çalışma alanının kuzey kısımları ve Çandarlı Körfezi açıklarında 1800 ms derinliklere ulaşırken, Karaburun-Foça açıkları, İzmir Dış Körfezi'nde ortalama 500 ms derinliklerdedir. Aynı çalışma alanının Holosen'den Miyosen girişine detay derin stratigrafik bilgisi ise literatürde bulunmamaktadır.

Çalışmanın temel amacı, İzmir İç ve Dış Körfezi'ni içeren denizel alanın deniz jeofiziği verileri kullanılarak, yapısal ve stratigrafik açıdan incelenmesidir. Çalışma alanı Gediz (İzmir Dış Körfezi) grabeninin batıya doğru uzanan denizel alanını kapsamakta olup, alan Şekil 1'de verilmiştir. İncelenen alan yaklaşık 370 km<sup>2</sup> boyutlarında olup, su derinliği 10-70 m arasında değişmektedir.

Şekil 1. Çalışma alanı.

#### Projenin temel amaç ve hedefleri aşağıdaki şekilde özetlenebilir:

- Alanın sığ ve derin stratigrafisi: Derin stratigrafik bilgi sismik yansıma verisinden, Holosen sonrası stratigrafisi ise Chirp ve sparker verisinden elde edilmiştir. Derin stratigrafisi, Foça yakınlarında bulunan Foça-1 kuyusunu kesen çok kanallı sismik kesitler üzerinden tüm alana yayılmıştır. Elde edilmesi beklenen çıktı, (olasılıkla) Neojen ve sonrası derin stratigrafisi ve izopak haritaları, Holosen sonrası detay stratigrafisi ile ana birikim alanları ve izopak haritası, dış körfezdeki Gediz delta klinoformları, olası düşük deniz seviyesi terasları ile Ege'deki deniz seviyesi değişimleri hakkında yeni bilgilerdir. Ayrıca, denizel alanın derin stratigrafisinin, karada gözlenen stratigrafik birimler ile arasındaki bağlantı kurulması hedeflenmektedir.

- Olası hidrokarbon belirtileri: Çalışma alanındaki olası çopurlar (pockmarks), su kolonuna gaz çıkışları (plumes) ve sığ gaz birikimleri gibi oluşumların varlığı ve dağılımı Chirp ve sparker verilerinden elde edilmiştir. Çalışma, elde edilen sismik verinin olası sığ gaz birikimleri bunlarla ilişkili yapıların anlaşılması bakımından da ekonomik öneme sahiptir. Uzunada'nın hemen doğusunda gözlenen çok sayıda deniz tabanına gaz çıkışlarının derinlerdeki rezervuarın varlığı ile ilişkilendirilmesi, derin HC birikimleri açısından önem taşıyabilir.

- Yapısal jeoloji: Çalışmadaki en önemli hedef, alanın yapısal durumudur. Olası aktif fayların varlığı Chirp ve Sparker verisinden elde edilmiştir. Kör (blind) faylar ise sismik yansıma verileri kullanılarak yorumlanmıştır. Yorumlamadan elde edilen çıktı, Neojen ve sonrası fay haritası ve körfezdeki etkin tektonik mekanizmadır.

- Çalışma, İzmir İç ve Dış Körfezi alanlarını kapsayan bölgedeki yapısal jeolojik unsurları haritalamayı da amaçlayan en kapsamlı deniz jeofiziği çalışmasıdır. Sismolojik veriler, çalışma alanının deprenselliğinin yüksek olduğunu işaret etmektedir. Elde edilen yeni sismik verilerle, halen tartışmalı olan bölgenin aktif tektoniği ve fayların mekanizmaları ile uzanımları ortaya konulmuştur. Bu veri, İzmir için yapılacak deprem modelleri, İzmir deprem senaryosu ve deprem master planı çalışmaları için oldukça önemli ve gerçekçi bilgiler temin etmiştir. Ekim 2020 döneminde yaşadığımız ve İzmir ve çevresini son derece olumsuz etkileyen Samos depreminde anlaşıldığı üzere, bu bilgi çevre şehirlerimizin deprem güvenliği açısından büyük önem taşımaktadır.

Bölgedeki fayların aktivitesinin risk hesaplamasının yapılabilmesi için, tüm alanın ve çevresinin sistematik şekilde sismik verilerle taranması gerekmektedir. Buna göre,

a. Özellikle İzmir Fayı, karada yapılan çalışmalarda Balçova bölgesinde DB yönlü haritalanmış ancak denizdeki uzanımı ve iç körfezdeki (olası) devamı bilinmemektedir. Bu aktif fayın İzmir metropol alanına uzandığı düşünülmektedir. Toplanan sismik veriler bu konuda ilk kez bilgi sahibi olmamızı sağlamıştır.

b. Gülbahçe Fayı'nın körfez içerisindeki uzanımı net olarak bilinmemekte, fayın karayla olan olası bağlantısı ilk kez ortaya konulmuştur.

c. Uzunada'nın doğusunda uzanan Uzunada Fayı'nın tüm körfez boyunca özellikle kuzeye uzanımı bu çalışmadan elde edilen verilerle ilk kez ortaya konulmuştur.

d. Çalışmada toplanan yüksek ayrımlı sismik veriler, İzmir Dış Körfezi'nde daha derinlerdeki gömülü fayların uzanımının ilk kez ortaya konulmasını sağlamıştır.

Bahsi geçen tüm bu fayların aktivite ve uzanımlarının ortaya konulması, deprem risk hesapları için bir gerekliliktir. Herhangi bir fayın üzerindeki risk hesabının yapılabilmesi için fayın başlangıcının ve bitişinin, yani fayın toplam uzunluğunun bilinmesi bir zorunluluktur. Bu anlamda, İzmir Körfez alanının faylarının uzanımı ve aktivitesi hakkında ilk kez bütüncül bir bilgi ortaya konulmuştur.

#### GEREÇ VE YÖNTEM

Çalışmada, 2023 Yılı'nın Mayıs Ayı'nda çok kanallı sismik yansıma ve Chirp mühendislik sismiği verileri eş zamanlı olarak toplanmıştır. Veri toplama, Dokuz Eylül Üniversitesi, Deniz Bilimleri ve Teknolojisi Enstitüsü (DBTE) araştırma gemisi R/V K. Piri Reis ile gerçekleştirilmiştir. Aynı zamanda Temmuz 2023 tarihi itibarıyla iç ve dış körfezde gerçekleştirilen sparker araştırma seferinde yine Deniz Bilimleri Enstitüsü'

ne ait Dokuz Eylül 4 gemisi kullanılmıştır. Ulusal sularımızda deniz sismliği ve diğer akustik çalışmaların yapılabilmesi, bu tür akustik verilerin toplanması, işlenmesi ve yorumlanması amacıyla, 2003 yılından bu yana yapılan yatırımlarla DEÜ-DBTE bünyesinde, SeisLab adı altında bir akustik laboratuvarı kurulmuştur (<http://web.deu.edu.tr/seislab>). Bu laboratuvarın etkin şekilde çalıştırılması halen proje ekibi tarafından sürdürülmekte olup, veri toplama sırasında kullanılacak akustik sistemler, DEÜ-DBTE Jeofizik Laboratuvarı (SeisLab) tarafından 2005 yılından beri başarılı şekilde kullanılmaktadır.

**Çok kanallı sismik yansıma yöntemi:** Tamamlanan araştırma seferleri süresince, İzmir Dış Körfezi'nde 2B çok-kanallı sismik yansıma verisi toplanmıştır. Sismik veri, projenin ana araştırma veri setini temin ettiğinden, veri toplama sırasındaki veri kalitesine azami önem gösterilmiştir. Toplanmış olan her hattın hemen ardından, SeisLab-ISO belgelerimizde tanımlanmış olan standart kalite kontrol (QC) analizleri veriye uygulanarak, toplanan verinin kalitesi güvence altına alınmıştır. Çalışma süresince kullanılan sismik veri toplama parametreleri Tablo 1'deki gibidir:

Tablo 1. Çalışmada kullanılan çok kanallı sismik veri toplama parametreleri.

Kanal sayısı 24

Streamer uzunluğu 150 m

Kayıt uzunluğu 3000 ms

Gecikme (Delay) 0 ms

Örnekleme aralığı 1 ms

Streamer derinliği 4 m

Atış aralığı 18.75 m

Grup aralığı 6.25 m

Kaynak GI gun (45+105 inç3)

Kaynak derinliği 3 m

Kaynak basıncı 2000 psi (140 bar)

Minimum ofset mesafesi 50 m

Kullanılan bird sayısı 3 adet 5010/5011 I/O DigiBird

Veri formatı IEEE 32 bit SegY

**Chirp mühendislik sismliği yöntemi:** Çok kanallı yüksek ayrımlı sismik yansıma verileri ile birlikte, Chirp mühendislik sismliği (subbottom profiler) verileri de toplanmıştır. Sistem 2.75-6.75 kHz frekans bandında 3.5 kHz'de merkezlenmiş süpürme (sweep) sinyali üretmektedir. Çalışma süresince kullanılan Chirp sismik veri toplama parametreleri Tablo 2'deki gibidir.

Tablo 2. Chirp mühendislik sismliği veri toplama parametreleri.

Transduser sayısı 9

Sweep frekansı 2.75-6.75 kHz

Kayıt uzunluğu 40 ms

Gecikme (Delay) Su derinliği bağımlı

Örnekleme aralığı 0.05 ms

Bant genişliği 4 kHz

Veri formatı 16 bit integer

Sample/trace 800

**Sparker sismik yansıma yöntemi:** Özellikle İzmir İç Körfezi gibi gemi trafiğinin yoğun olduğu kısımlarda, sparker tek kanallı sismik yansıma verisi toplanmıştır. Sparker verisi 17 m uzunluğunda tek kanallı bir alıcı kablo (streamer) kullanılarak 2000 Joule sismik kaynak ile toplanmış ve Triton SBlogger yazılımı ile kaydedilmiştir. Sparker sistemi, sparker sismik kaynağı olarak bilinen ve her atış noktasında sparker elektrodlarına gönderilen 4000 Volt elektrik akımının suda oluşturduğu patlama ile ses sinyali üretir. Sismik hat boyunca patlatmalar, 2000 Joule kaynak için her 2s'de bir yapılmıştır. Üretilen sinyalin frekans bandı yaklaşık 60- 450 Hz aralığındadır. Çalışma süresince kullanılan sparker sismik veri toplama parametreleri Tablo 3'deki gibidir:

Tablo 3. Çalışmada kullanılan sparker

sismik veri toplama parametreleri.

Kanal sayısı 1

Streamer uzunluğu 17 m

Kayıt uzunluğu 1000 ms

Gecikme (Delay) 0 ms

Örnekleme aralığı 0.5 ms

Streamer derinliği 0.5 m

Atış aralığı 2 s

Kaynak gücü 2000 Joule

Kaynak derinliği 0.5 m

Yanal ofset mesafesi 5 m

Veri formatı IBM 32 bit SegY

Veri toplama çalışmalarında kullanılan Bathy2010 Chirp sistemi, veri toplama sırasında Chirp verilerine gerekli standart veri işlem adımlarını uygulamakta ve veriyi işlenmiş şekilde kaydetmektedir. Bu nedenle Chirp verilerine, veri toplama sonrası ek bir veri işlem uygulanması gerekmemiştir. Bu standart veri işlem adımları aşağıdaki gibidir:

- Chirp kaynak imzası ile ilişkilendirme (de-chirping)

- Zarf (envelope) hesaplama

- Kazanç uygulama

Şekil 2' de alandan toplanan hatların haritası görülmektedir.

Şekil 2. Çalışma alanı ve toplanan çok kanallı sismik, Chirp ve Sparker hatlarının tamamı.

## BULGULAR

Çalışma alanı morfolojik olarak genellikle düz ve ondülasyon göstermeyen batimetriye sahiptir (Şekil 3). Alan toplanan hatların türüne ve aranan fayların yönelim ve doğrultularına göre 3 farklı bölgede incelenmiştir. Bunlardan en doğuda bulunan İç Körfez bölümü oldukça sığ (20m) derinliğe sahipken Dış Körfez ve Gülbahçe Körfezi Uzunada' nın hemen kuzeyinde 70 metre derinliğe ulaşmaktadır (Şekil 3). Dış Körfezi İç

Körfezden ayrılan sınır ise güneyde Yenikale, Kuzeyde ise Gediz Nehrinin oluşturduğu Gediz Deltası' nın GB kısmıdır.

Şekil 3. Çalışma alanının batimetri ve DEM haritası ve çalışılan alanlar.

Dış Körfez' in yapısal durumu çok kanallı sismik yansıma verileriyle incelenmiştir. Dış Körfez' deki en belirgin yapısal unsur Uzunada' nın doğusu boyunca KB-GD yönlü uzanan Uzunada Fayı' dır (Şekil 4). Uzunada fayı Urla-Güzelbahçe ile Uzunada' nın kuzeyine kadar batimetri verisinden izlenecek şekilde devam etmektedir. Fayın sismik kesitlerdeki görünümü düşey bileşenin yanı sıra doğrultu atım özelliği göstermektedir. Fayın yanıl atımı henüz hesaplanmamıştır. Düşey bileşeni ise Uzunada' nın doğusunda Holosen seviyesinin hemen altında 60 ms civarında iken, güneye Çiçek Adaları' na doğru daha da artar. Atım KD yönünde Dış Körfez basenine doğrudur. Bu bölgede sismik veri fayın aynı zamanda sentetik ve antitetik bileşenlere de sahip olduğunu göstermektedir. Bu bileşenler de deniz tabanını etkilemekte olup, bunların düşey atımı da batimetri verisinde görülebilir (Şekil 3). Uzunada Fayı, denizel alanda en güneyde, sismik kesitlerde tamamen karakter değiştirmekte olup düşey bileşenini yitirdiği gözlenmekte ve Zeytinalanı mevkiinden karaya çıkmaktadır. Bu bölgede karadaki devamı bilinmemektedir. Dış Körfezin KD sınırı boyunca, Uzunada fayının karşısında Foça-Süzbeyli Fayı uzanır (Şekil 4). Bu fayın atım yönü ise GB olup, Uzunada Fayı ile birlikte bir graben sistemi oluşturduğu ve dış körfezin dış kısmını sınırladıkları görülmektedir.

Şekil 4.Uzunada Fayı ve Foça-Süzbeyli Fayı' nı gösteren çok kanallı deniz sismiği yansıma kesiti.

İzmir Dış Körfezi'nde uzanan ikinci önemli yapısal unsur İzmir Fayı'dır. Fay, karada Balçova bölgesinde haritalanmış ancak denizel devamlılığı hakkında çok az bilgi edinilebilmiştir. Mevcut sismik veride, İzmir fayının D-B yönünde Balçova kıyı çizgisine paralel uzandığı görülmektedir (Şekil 5). Fay, atımı kuzeye doğru olan bir normal fay görünümündedir. Fay batıya doğru Zeytinalanı mevkiî açıklarına kadar takip edilebilir. Doğuda ise Yenikale bölgesinde karaya çıkmakta, Üçkuyular civarında İç Körfez' de tekrar denizel alanda D-B yönünde takip edilebilmektedir.

Şekil 5. İzmir Fayı' nı gösteren çok kanallı deniz sismiği yansıma kesiti.

Gülbağçe Körfezi yapısal olarak oldukça karmaşık bir görünüme sahiptir. Körfezin güney kısımları, akustik temelin 1 s civarında derinliklerde uzandığı asimetrik bir basen yapısındadır. Bu basenin hem sınırları hem de merkez kısmı, kabaca K-G yönlü uzanan belirgin doğru atımlı faylarla deforme olmaktadır (Şekil 6). Fayların her iki yanında sıkışma yapıları belirgin olup, transpresyon özelliği gösteren doğrultu atımlı faylardan oluştuğu düşünülmektedir. Gerçekten de, körfezin güney kısmında belirgin olan bu bükülmeler, kuzeye doğru ilerledikçe son derece belirgin hale gelmektedir. Uzunada' nın batısında ise artık bu sıkışma yapıları son derece dik yansımalar şeklinde kesitlerde kendisini gösterir. Tabakaların eğim yönü daima batıya Karaburun

Yarımadası' na doğrudur.

Şekil 6. Gülbağçe Fayı' nı gösteren çok kanallı deniz sismiği yansıma kesiti.

İzmir İç Körfez alanı oldukça sığ ve dar olduğundan, ayrıca mevcut denizcilik faaliyetleri nedeniyle çok kanallı sismik çalışmaların yapılmasına elverişli değildir. Bu nedenle bu bölgede sadece tek kanallı sparker sismik verisi toplanabilmiştir. Verinin penetrasyonu en çok 300 m civarındadır. İç Körfezi' in kuzey kısımları Gediz Deltası' nın etkisi altında olup, bu kısımdaki biyojenik gaz birikimleri nedeniyle kuzey kısımdaki fayların haritalanması mümkün olmamıştır. Bununla birlikte, İzmir Fayı' nın iç körfezdeki devamı sparker verilerinde gözlenmektedir. Bu kısımdaki fayın atımı genellikle Holosen birikimi altında olup dış körfezdekine oranla daha küçüktür. Ayrıca, sismik verinin ilksel analizleri, iç körfezin orta kısmında kabaca BKB-DGD yönlü uzanan olası bir doğrultu atımlı fayın varlığını da işaret etmektedir. Fayın doğu tarafında olası transpresyon izleri mevcuttur. Holosen sedimentlerinde deformasyon oluşturan bu fayın karayla bağlantısı henüz yapılmamıştır.

## SONUÇLAR

Çalışma alanında deniz tabanı düz bir morfolojiyle izlenmektedir. Su derinliği iç körfezde 20 metreye kadar, dış körfezde ise 70 metreye kadar ulaşmaktadır. Çalışma alanında toplanan yüksek ayrımlı ve çok kanallı deniz sismiği verisi ve Sparker verileri, literatürde, karadaki varlıkları bilinen ama denizel devamlılıkları hakkında bilgimizin olmadığı Gülbağçe Fayı, İzmir Fayı ve Foça-Süzbeyli denizdeki uzanımlarını göstermektedirler. Uzunada fayının ise karasal devamlılığının olmadığı yine veri setlerinden ortaya konmuştur. İzmir fayının İç Körfez' deki devamlılığı D-B uzanımlı olarak görülmüş, kıyı şeridinde paralel şekilde devam ederek Bornova Ovası' na doğru ilerleyen normal atımlı fay olduğu belirlenmiştir.

## REFERANSLAR

- Aksu, A.E., Piper, D.J.W., 1983. Progradation of the late Quaternary Gediz delta, Turkey, *Marine Geology*, 54, 1-25.
- Aksu, A.E., Konuk, T., Uluğ, A., Duman, D., Piper, D.J.W., 1990. Quaternary tectonic and sedimentary history of Eastern Aegean Sea shelf area. *Jeofizik* 4, 3-35.
- Aksu, A.E., Piper, D.J.W., Konuk, T., 1987. Late Quaternary tectonic and sedimentary history of outer İzmir and Çandarlı Bays, western Turkey, *Marine Geology*, 76, 89-104.
- Emre, O., Barka, A., 2000. Active faults between Gediz graben and Aegean Sea (İzmir region). *Batı Anadolu' nun depremselliği sempozyumu*, DEÜ yayınları. Bildiri kitabı, 131132
- Emre, Ö., Özalp, S., Doğan, A., Özaksoy, V., Yıldırım, C., Göktaş, F., 2005. İzmir yakın çevresinin diri fayları ve deprem potansiyelleri, *Maden Tetkik ve Arama*

Genel Müdürlüğü, Jeoloji Etütleri Dairesi, MTA Rapor No: 10754

Ocakoğlu, N., Demirbağ, E., Kuşçu, İ., 2005. Neotectonic structures in İzmir Gulf and surrounding regions (western Turkey): evidences of strikeslip faulting with compression in the Aegean extensional regime, Marine Geology, 219, 155-171.

Sözbilir, H., Sümer, O., Uzel, B., Saygılı, A., Ramazanoğlu, I., Uysal, E., 2004. İzmir Fayı'nın jeolojik ve jeomorfolojik parametreleri. ATAG 8. Toplantısı Bildiri Kitabı, 22.

Sözbilir, H., Uzel, B., Sümer, O., İnci, U., Ersoy, E.Y., Koçer, T., Demirtas, R., Özkaymak, Ç., 2008. D-B Uzunlmlı İzmir Fayı ile KD-uzunlmlı Seferihisar Fayı'nın birlikte çalıştığına dair veriler: İzmir Körfezi'ni oluşturan aktif faylarda kinematik ve paleosismolojik çalışmalar. Batı Anadolu. TJK Bull. 51, 91e114.

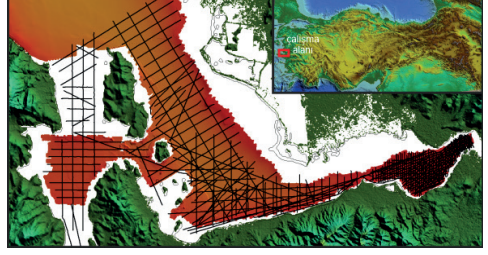
Anahtar Kelimeler: İzmir Körfezi Aktif Tektoniği, Deniz Sismiği

Şekil 1



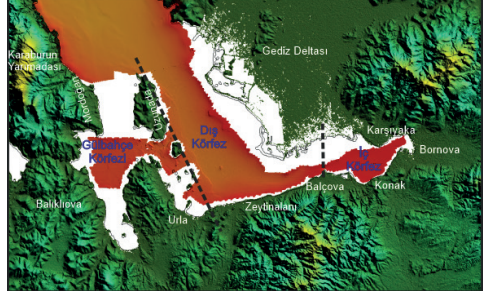
Çalışma alanı

Şekil 2



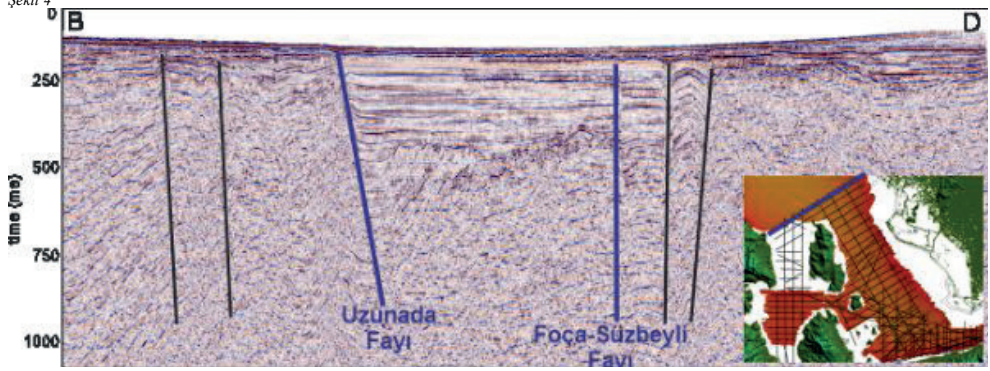
Çalışma alanı ve toplanan çok kanallı sismik, Chirp ve Sparker hatlarının tamamı

Şekil 3



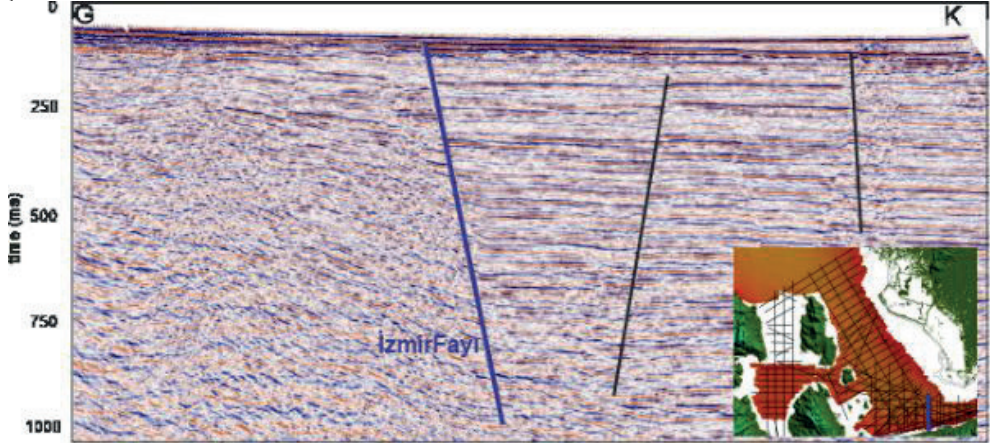
Çalışma alanının batimetri haritası ve çalışılan alanlar

Şekil 4



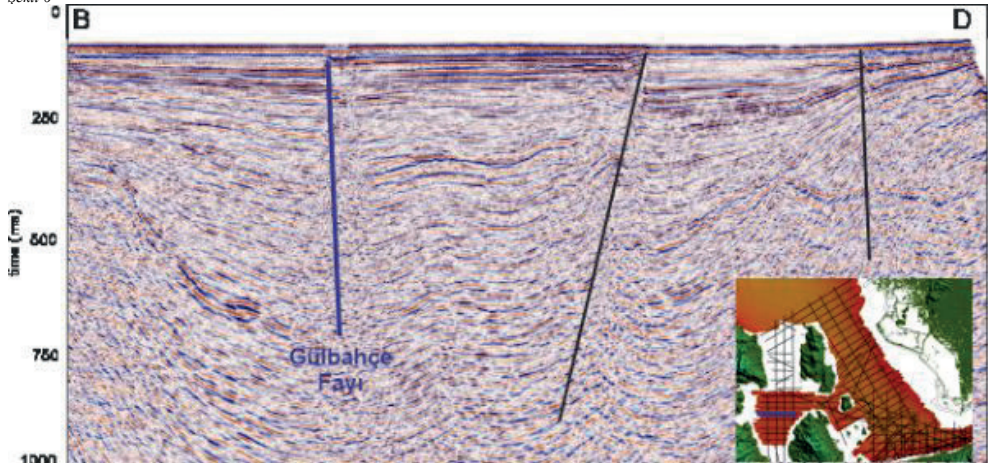
Uzunada Fayı ve Foça-Süzbeyli Fayı' nı gösteren çok kanallı deniz sismiği yansıma kesiti.

Şekil 5



İzmir Fayı' nı gösteren çok kanallı deniz sismiği yansıma kesiti

Şekil 6



Gülbahçe Fayı' nı gösteren çok kanallı deniz sismiği yansıma kesiti.

*Tablo 1.*

Kanal sayısı	24
Streamer uzunluğu	150 m
Kayıt uzunluğu	3000 ms
Gecikme (Delay)	0 ms
Örnekleme aralığı	1 ms
Streamer derinliği	4 m
Atış aralığı	18.75 m
Grup aralığı	6.25 m
Kaynak	GI gun (45+105 inç3)
Kaynak derinliği	3 m
Kaynak basıncı	2000 psi(140 bar)
Minimum ofset mesafesi	50 m
Kullanılan bird sayısı	3 adet 5010/5011 I/O DigiBird
Veri formatı	IEEE 32 bit SegY

*Çalışmada kullanılan çok kanallı sismik veri toplama parametreleri.*

*Tablo 2*

Transduser sayısı	9
Sweep frekansı	2.75-6.75 kHz
Kayıt uzunluğu	40 ms
Gecikme (Delay)	Su derinliği bağımlı
Örnekleme aralığı	0.05 ms
Bant genişliği	4 kHz
Veri formatı	16 bit integer
Sample/trace	800

*Chirp mühendislik sismik veri toplama parametreleri*

*Tablo 3*

Kanal sayısı	1
Streamer uzunluğu	17 m
Kayıt uzunluğu	1000 ms
Gecikme (Delay)	0 ms
Örnekleme aralığı	0.5 ms
Streamer derinliği	0.5 m
Atış aralığı	2 s
Kaynak gücü	2000 Joule
Kaynak derinliği	0.5 m
Yanal ofset mesafesi	5 m
Veri formatı	IBM 32 bit SegY

*Çalışmada kullanılan sparker sismik veri toplama parametreleri.*

# Implications for the Neotectonics of the NW margin of the Arabian Plate: A case study of the E-W-trending Altıntaş Basin (Gaziantep, Türkiye)



**Aydın Cicek<sup>1</sup>, Ali Koçyiğit<sup>2</sup>**

<sup>1</sup>General Directorate of Mineral Research and Exploration (MTA), Department of Energy Raw Materials and Survey, 06530 Ankara / Türkiye

<sup>2</sup>Middle East Technical University, Geological Engineering Department, Active Tectonics and Earthquake Research Unit, 06531 Ankara / Türkiye

## ABSTRACT

Altıntaş Basin is an approximately 6-9 km wide, 50 km long and nearly E-W-trending basin located close to the NW margin of the Arabian Plate. Study area is controlled by the Güllüce Fault Zone in the north, the Bağlıca, Akdurak, Erenbağ and Fistiklidağ Fault Sets in the northeast, the Kemerli Fault Set in the east, the Karasu Fold Set in the south, and the Kırkpınar Fault Zone in the west.

The Altıntaş basin has two basin fills separated by an intervening regional angular unconformity. These are: (a) Middle Eocene-Pliocene Late Early Miocene deformed basin fill and, (b) Quaternary undeformed neotectonic fill. These two different packages of basin fills reveal obviously an episodic development history for the Altıntaş Basin. They also indicate a Latest Pliocene (?) to Quaternary onset age for the strike-slip neotectonic regime along the NW margin of the Arabian Plate.

Key words: Altıntaş Basin, strike-slip neotectonic regime, Arabian Plate.

## INTRODUCTION

Even though the neotectonics of Türkiye has been a quite hot topic among the earth scientists due to complex deformation history and structure patterns, SE Türkiye has not attracted numerous researchers. Therefore, the area has a significant potential to shed light on the neotectonics of the region.

The main scope of this study is to present new field geological data about the Altıntaş (Araban) Basin. Because it is located in a triangular area bounded by both the dextral Bozova strike-slip Fault Zone and the East Aantolian sinistral strike-slip Fault System (Figure 1). In addition, it is very close to the NW margin of the Arabian plate, and has some diagnostic field geological data related to onset age of the strike-slip neotectonic regime affecting whole of SE Türkiye

### Altıntaş Basin (AB)

Altıntaş Basin is an approximately 6-9 km wide, 50 km long, nearly E-W-trending complex tectonic structure (Figures 1 and 2). It is bounded by the Güllüce Fault Zone to the north, Akdurak, Bağlıca, Erenbağ and Fistiklidağ Fault Sets in the NE, Kemerli Fault Set in the east, Karasu Fold Set in the south and the Kırkpınar Fault Zone in the west. The AB is characterized by two

basin fills separated by an intervening regional angular unconformity, which is the most significant key structure for the variation in the tectonic regime at the end of the Pliocene (?) or beginning of the Quaternary period.

### Stratigraphic Outline of the Altıntaş Basin

The rocks exposing in the study area are classified into two main categories: (1) Paleotectonic units, and (2) neotectonic units. The paleotectonic units are also subdivided into two packages as the relatively younger allochthonous rocks and older autochthonous units. Allochthonous units are made up of the Latest Cretaceous Karadut Complex (Kka) and the Latest Cretaceous Koçali Ophiolitic Melange (Kko). However, only the Germav formation of the older autochthonous units exposes in the study area. Their detailed discussion is the behind of the study.

### Pre-Modern Basin Fill

Pre- neotectonic (modern) basin fill is explained under six rock packages. They are:(1) the middle Eocene Hoya formation, (2) the middle Eocene-middle Oligocene Gaziantep formation, (3) the middle Oligocene-Early Miocene Fırat formation, (4) the Late Oligocene (?) -Early Miocene Cingife formation, (5) The Early Miocene-middle Miocene Yavuzeli volcanics, and (6) the middle Miocene-Early Pliocene Şelmo formation. Although Cingife formation is regarded as a member of the Şelmo formation, it was renamed as a new formation here. Because there are clear differences in their ages (K/Ar ages) (Tatar et al., 2004), stratigraphic relationships and lithostratigraphic content between them (Figure 3).

Hoya formation is made up cream to light gray colored massive, thick-bedded fossiliferous porous limestone, dolomitic limestones and dolomites. The Hoya formation was dated as the middle Eocene by Terlemez et al. (1992).

The Gaziantep formation includes gray, cream to light red, pinkish red clayey to chalky limestone and partly marls. Based on rich fossil content and stratigraphic relationships, it was dated as the middle Eocene - the middle Oligocene in age by previous researchers (Ulu et al., 1991; Terlemez et al., 1992).

The Fırat formation exposes almost every part of the Altıntaş Basin, and consists of light dirty yellow, cream colored, massive- thick bedded and porous fossil-rich limestone. Ulu et al. (1991) assigned the late Oligocene to Early Miocene age to the Fırat Formation.

The Cingife formation is composed of conglomerates,

loose sandstone, claystone and mudstone in various colors in the western half of the study area. It also contains dark tile-red to cream colored massive limestone and beige colored marls in the nature of intercalations in places. Based on both the stratigraphic relationships and some new K/Ar radiometric ages (Tatar et al., 2004) reveal that the Cingife formation is the Late Oligocene (?)–Early Miocene in age.

Yavuzeli volcanics are regarded as the continuation of the Syrian volcanics due to geologic distribution, geochemical characteristics and radiometric ages (Trifonov et al. 2011; Tatar et al. 2004). Tatar et al. (2004) dated some samples and obtained K/Ar ages ranging from  $21.24 \pm 0.04$  to  $16.53 \pm 0.35$  Ma for the stage-1 volcanic rocks in the study area. In addition, Çemen (1987) dated stage-2 volcanics exposed near north of the study area as  $15.1 \pm 0.4$  Ma at the bottom and  $12.01 \pm 0.4$  Ma at the top. Based on these data, the Yavuzeli volcanics in the study area are the Early Miocene to middle Miocene in age.

The Şelmo formation consists mostly of light red, orange to grey colored claystone, grey to dirty white, beige colored marls and tuffite alternation. Based on both the K/Ar age of the stage-2 volcanics and the pollen ages coming from the upper levels of the Şelmo formation, a middle Miocene–Early Pliocene age was also assigned to the Şelmo formation (Çemen, 1987; Çemen et al., 1990).

### Modern (neotectonic) Basin Fill

In the study area, the modern basin fill is represented by only the Lahti group's rocks and sedimentary deposits. This unit was previously dated to be the Plio-Quaternary (Tolun, 1956; Ulu et al., 1991). However, this age needs revision, i.e., it seems as Quaternary in age owing to the revision of the lower boundary of the Quaternary (from 1.8 Ma to 2.588 Ma) carried out by the International Stratigraphy Commission (ICS) in 2009. Hereafter, previous Late Pliocene ages are replaced by the Early Quaternary.

In general, the modern basin fill consists of two common facies assemblages based on both the depositional settings and grain size. These are: (1) coarse-grained marginal facies, and (2) finer-grained depocentral facies.

### Coarse-grained marginal facies assemblage

It is made up of terrace deposits, slope scree deposits, renewed alluvial fan deposits and fan-apron deposits. At some localities, caliche occurrences are common and bound clasts. The sediments comprising the coarse-grained marginal facies assemblage were transported and accumulated at suitable places by both the debris flows and running waters such as the Karasu River.

### Finer-grained depocentral facies assemblage

This facies assemblage consists of brown to red colored soil and other alluvial sediments. The axial plain deposits include beige, gray, yellow, brown and

light red colored muds/mudstone, clays/claystone and organic material-rich swamp deposit alternations with the intercalations of lenticular sand, pebble and calichy.

## STRUCTURES IN THE STUDY AREA

The Altıntaş basin is controlled, shaped and characterized by two major groups of tectonic structures. These are: (1) the paleotectonic structures of pre-Quaternary age, and (2) the neotectonic structures of the Quaternary age.

They structures have been observed, mapped and analyzed in terms of newly collected field geological data obtained in the frame of the present this work. The common structures in and adjacent to the study area are folds, faults, beds, unconformities and mesoscopic structures such as shear fractures, tension gashes and stylolites. Here fold, faults and some mesoscopic structures will be explained briefly for the sake of brevity.

### Folds

They are classified into three groups based on their trends: (a) E-W-trending folds, (b) NNE to NW-trending folds, and (c) NE-trending folds. This situation implies that these structures may have originated from the N-S, NW-SE and E-W-directed compression/contraction except for the fault-bounded folds (Figure 2). Folds seem to have formed before the latest Pliocene (?) / Early Quaternary time (i.e., during the paleotectonic period). This is evidenced by both the deformed pre-modern basin fill of middle Eocene–Early Pliocene age and the relatively non-deformed neotectonic units (Figure 3).

### Faults

Indeed, the study area is located inside the East Anatolian Fault System (Figure 1). It is an about 700 km long, 80 km wide and NE-trending left-lateral strike-slip shear zone, which separates the Anatolian platelet to the north from the Arabian plate to the south. A number of faults were identified, mapped and named in the study area during the field geological mapping studies. They are: (1) Çatboğazı Thrust Fault Zone, (2) Güllüce Fault Zone, (3) Bağlıca Fault Set, (4) Akdurak Fault Set, (5) Erenbağı Fault Set, (6) Fıstıklıdağ Fault Set, (7) Kemerli Fault Set, (8) Taşdeğirmen Fault Set, (9) Karadağ Fault Zone, (10) Yavuzeli Fault Set, (11) Dağdağancık Fault Zone, (12) Çatlaklar Fault Set, (13) Yakuplu Fault Set, and (14) Kırkpınar Fault Zone. They are explained briefly below.

The Çatboğazı Fault Zone is a low-angle thrust fault zone exposing in a limited area in northern section of the study area. Two nappe packages (Karadut and Koçali complexes) crop out in a tectonic window (Çatboğazı tectonic window) there. This structure is a paleotectonic structure.

The Güllüce Fault Zone is a 50 km-long, 1 to 1.5 km wide and approximately ENE-trending deformation zone characterized by the combination of northward steeply dipping reverse faults and the strike-slip faults



with significant dip-slip component.

The Bağlıca Fault Set is a 35 km-long, nearly 0.1-1.5 km-wide and NW-SE-trending shear zone.

The Akdurak Fault Set is an 11.2 km long, approximately 1-2.5 km-wide and NW-trending dip-slip fault with considerable amount of dextral-strike slip component.

The Erenbağ Fault Set is an approximately 8.2 km-long, 0.4 km-wide and NW-trending shear zone.

The Fıstıklıdağ Fault Set is a 10 km-long, 0.4-1.1 km-wide and NW-trending shear zone observed at the NE corner of the study area.

The Kemerli Fault Set is 1.2 km-wide, 40 km-long and NE-trending deformation zone in the nature of active sinistral strike-slip fault. It cut and offset the ancient Roman-Byzantine water storage tank. Therefore, it is active.

The Taşdeğirmen fault set is an approximately 13 km-long, 9 km-wide and NE-trending deformation zone in the nature of sinistral strike-slip faulting. The Karadağ Fault Zone is an 1-1.5 km-wide, 30 km-long and E-W-trending oblique-slip normal fault with a significant dextral slip-slip component.

The Yavuzeli fault is 33 km long and E-W-trending blind thrust.

The Dağdağancık Fault Zone is an approximately 30 km-long, 0.2-4 km-wide and NW-SE-trending zone of deformation characterized by a dextral strike-slip faulting.

The Çatlaklar fault set is nearly 15 km-long, 5 km-wide and NE-trending deformation zone composed of a set of sinistral strike-slip fault segments.

The Yakuplu fault set is about 3-6 km-wide, 37 km-long and NW-trending shear zone. It is observed near both the Yeni yurt and Ballık sections of the study area (Figure 2).

The Kırkpınar fault zone is a 14.4 km-long, 5 km-wide and NE-trending deformation belt characterized by the left-lateral strike-slip faulting. This fault zone is an active fault zone.

## MESOSCOPIC STRUCTURES

During the field studies many mesoscopic structures were observed. They are briefly: (1) tension gashes, (2) stylolites and (3) conjugate shear fractures.

The tension gashes occur in various forms such as single gashes, en-echelon type gashes, single sigmoidal veins, en-echelon type sigmoidal veins, hybrid shear veins (Pinnate or feather joints) and the stepped veins. They were used in stress analysis.

The conjugate shear fractures developed as a result of compressive stresses (Dunne and Hancock, 1994). They were measured and used in the kinematic analysis to determine the operation directions of the stress state in the study area.

The stylolites are serrated sub-planar surfaces where mineral material is dissolved and then removed

away by pressure dissolution processes at the time of deformation (Railsback, 2003). Orientations of stylolite surfaces and the associated features (spikes and teeth) mark the operation direction of the local maximum principal stress axis ( $\sigma_1$ ) (e.g. Suppe, 1985). Whole of these outcrop-scale features were measured and used in the kinematic analysis in the present study.

## DISCUSSION AND CONCLUSION

The Altıntaş Basin has two basin fills: (1) Pre-Quaternary (paleotectonic) basin fill, and (2) Quaternary modern (neotectonic) basin fill. The paleotectonic basin fill is made up of deformed units ranging from the middle Eocene to the Early Pliocene in age. In contrast, the modern basin fill consists of both the coarse-grained marginal and finer-grained axial plain facies assemblages. It is nearly flat-lying (nondeformed) except for the areas adjacent to the faulted contacts, and Quaternary in age.

Various facies of the paleotectonic basin fill display both vertical and lateral transitional boundary relationships with each other. Following the sedimentation (post-early Pliocene) the pre-modern basin fill was deformed into a series of anticlines and synclines as a natural response to the prominent NW to N-S directed compressive stress (first phase of deformation). This is evidenced by a series of fold axes and some strike-slip faulting-related slip-plane data. Later on, these structures were re-deformed by the E-W to NW-SE-directed compressional stress (phase two deformation). This is revealed by the E-W trending strike-slip faults, N-S trending fold axes, and mesoscopic features such as tension gashes, stylolites and conjugate shear fractures.

The Quaternary basin fill, which rests on the erosional surface of older basin fill with regional angular unconformity, consists mostly of coarse-grained marginal facies such as slope-scar deposits, fan-apron deposits and alluvial fans transported and accumulated by the debris flows under the control of active faulting. The modern basin fill is nearly flat-lying. The sedimentation seems to continue under the control of NNE to N-S directional strike-slip regime (third phase of deformation or neotectonics regime) since the beginning of Early Quaternary. Consequently, the onset age of the strike-slip neotectonic regime in the study area is Quaternary in age. Here, the basic evidence is more than one deformation phases and the regional unconformity between the paleotectonic and neotectonic basin fills. For this reason, the development history of the Altıntaş basin is episodic, not continuous.

## REFERENCES

- Çemen, İ. 1987. Structural geology of the western part of the Araban block: Implications concerning Petroleum potential of the region. TPAO Exploration Group, Report No: 2239.
- Çemen, İ., Perinçek, D., Ediger, V.Ş. and Akça, L. 1990. Güneydoğu Anadolu'daki Bozova Doğrultu Atımlı Fayı: Üzerindeki ilk hareket ters faylanma olan faylara

ait bir örnek. Proceedings in 8th Petroleum Congress of Turkey, 169-179. [in Turkish with English abstract].

Dunne, W. M. and Hancock, P. L. 1994. Paleostress analysis of small-scale brittle structures. 101-120 [in P. L. Hancock, (ed.) 1994. Continental Deformation. Pergamon Press, Oxford, 421 p.].

Railsback, L. B. 2003. Stylolites. 690-692. [in Encyclopedia of Sediments and Sedimentary Rocks edited by Middleton, J. C., Coniglio, M., Hardie, L. A., Longstaffe, F. J. 2003] Kluwer Academic Publishers, Dordrecht, 821 p.

Suppe, J., 1985. Principles of Structural Geology. Prentice-Hall, New Jersey, 537 p.

Tatar, O., Gürsoy, H. Piper, J.D.A, Heinmann, A., Parlak, O., Yurtmen, S., Koçbulut, F. and Mesci, B.L. 2004. Ölüdeniz ve Doğu Anadolu Fay Zonlarının Kesişim bölgesinde kabuksal deformasyonun Paleomanyetik ve jeokronolojik açıdan incelenmesi. TÜBİTAK, Report No: YDABAG-101Y023, 129p. [in Turkish with English abstract]

Terlemez, H.Ç.İ., Şentürk, L., Ateş, Ş., Sümengen, M. and Oral, A.1992. Gaziantep dolayının ve Pazarcık-Sakçagöz-Kilis-Elbeyli-Oğuzeli arası jeolojisi. MTA, Report No: 9526, 112p. [Unpublished]. [in Turkish].

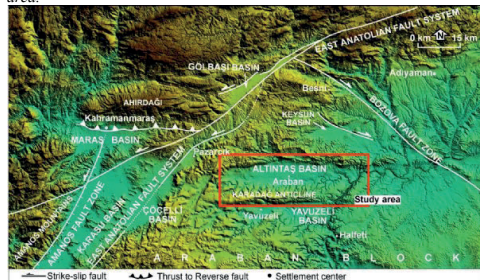
Tolun, N., 1956. Pazarcık (Maraş) Birecik ve Gaziantep dolaylarının jeolojik incelemesi. MTA Report No: 2389, 79p. [Unpublished]. [in Turkish]

Trifonov, V.G., Dodono, A.E., Sharkov, E.V., Golovin, D.I., Chernyshev, I.V., Lebedev, V.A., Ivanova, T.P., Bachmanov, D.M., Rukieh, M., Ammar, O. Minini, H., Al-Kafri, A.-M. and Ali, O. 2011. New data on the Late Cenozoic basaltic volcanism in Syria, applied to its origin. Journal of Volcanology and Geothermal Research, 199, 177-192.

Ulu, Ü., Genç, Ş., Giray, S., Metin, Y., Çörekçiöğlu, E., Orçen, S, Ercan, T., Yaşar, T. and Karabiyiçoğlu, M. 1991. Belveren-Araban-Yavuzeli-Nizip-Birecik alanının jeolojisi, Senozoyik yaşlı volkanik kayaların petrolojisi ve bölgesel yayılımı. MTA, Report No: 9226, 225p. [Unpublished]. [in Turkish].

Keywords: Altıntaş, neotectonic

Figure 1. Shuttle Radar Topography Mission (SRTM) image of the study area.



Shuttle Radar Topography Mission (SRTM) image of the study area.

Figure 2. Map showing the mapped structures and neotectonic units of the study area.

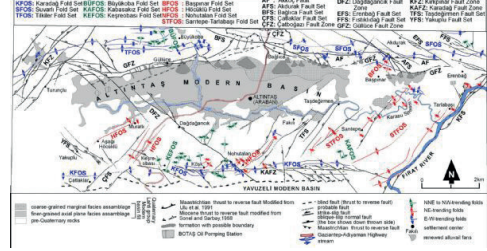
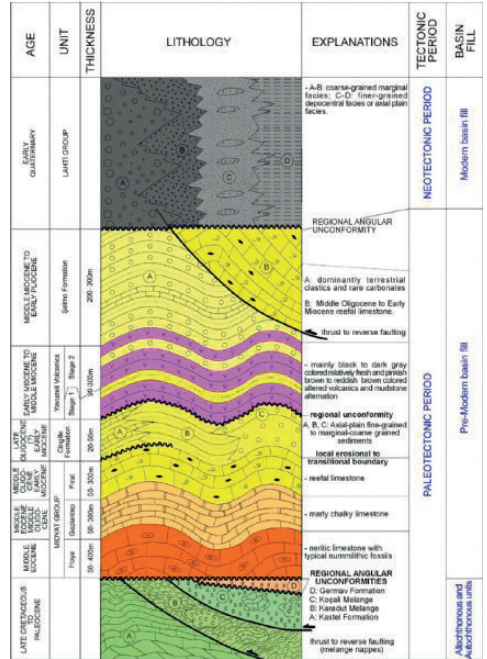


Figure 3. Generalized tectonostratigraphic column section of the Altıntaş basin and its environs.





**Cumhuriyetimizin En Byk Keşfi:  
Sakarya Gaz Sahası**

*The Largest Natural Gas Discovery of the  
Republic of Trkiye: Sakarya Gas Field*

---



# Seismic Trace Correlation Approach for Gas Probability Mapping in Sakarya Gas Field Reservoirs, Western Black Sea, Turkey



**Sait Baytok, Ergin Karaca**

Turkish Petroleum Offshore Technology Center (TP-OTC)

The Sakarya Gas Field produces gas from multiple reservoir intervals within a deep submarine fan system of Pliocene-Pleistocene-Upper Miocene age. Seismic time and depth volumes are the main data used to map extent of these reservoirs since amplitude anomalies correspond well to saturation. However, in some cases, relying solely on amplitude anomaly maps is insufficient to accurately map the distribution of gas-bearing reservoir intervals. Additionally, classifying gas-bearing intervals based on thickness changes can be useful in identifying sweet spots.

To address this challenge, a cross-correlation approach is employed to search for similarities between synthetic traces generated for specific cases and the seismic field data. This approach allows for the generation of correlation coefficient maps that indicate gaseous areas with specific thicknesses. The correlation attribute used in this method measures the similarity between different digital waveforms by computing the correlation coefficient. It is commonly used in Time Lapse Analysis to analyze the correlation between two seismic traces  $f$  and  $g$ , quantifying the sample reflective correlation.

$$R_{fg} = \frac{\sum f_i g_i}{\sqrt{(\sum f_i^2)(\sum g_i^2)}}$$

The approach requires a workflow that involves several steps to generate a correlation coefficient volume. Firstly, a wedge model is created for the desired case with variable thickness. Zero-offset synthetic traces are generated using measured well logs for different scenarios such as water, gas, or water-gas mixtures with varying thicknesses. Alternatively, trace extraction from an existing well with the desired case can be used instead of synthetic traces. Secondly, the target seismic cube is flattened to align all traces horizontally. This is achieved by picking the top of the reservoir interval to ensure that all traces are aligned at the same level. This step is crucial for the accuracy of the correlation process. Finally, a correlation volume is generated by comparing the similarity between each synthetic case and the seismic field data.

The results of the correlation analysis are promising, as the generated correlation maps align well with well observations. Correlation can be performed between seismic field data and any given case, with cases being synthetic scenarios generated through AVO forward modeling using Fluid Replacement Modeling (FRM) or extracted traces from known wells. This method has been tested at different levels in the field and the results have proven to be reliable.

Keywords: Cross-Correlation, Seismic

# High-Resolution Visco-Acoustic FWI Model Building and Least-Squares Migration in The Black Sea – Resolving Imaging And Illumination Challenges for A Deep-Water Dataset



**Samuel Madden<sup>1</sup>, Kelly Mistry<sup>1</sup>, Zengbao Chen<sup>1</sup>, Cara Smith<sup>1</sup>, Olivia Lewis<sup>1</sup>, Maria Shadrina<sup>1</sup>, Sait Baytok<sup>3</sup>, Can Özsoy<sup>2</sup>, Can Ören<sup>2</sup>, Emir Yusuf Ersay<sup>3</sup>, Kenan Yazan<sup>3</sup>, Ergin Karaca<sup>3</sup>**

<sup>1</sup>SLB, London, United Kingdom

<sup>2</sup>Turkish Petroleum (TPAO), Ankara / Türkiye

<sup>3</sup>Turkish Petroleum Offshore Technology Center (TP-OTC), Ankara / Türkiye

## INTRODUCTION

The Western Black Sea (WBS) is an active area of hydrocarbon exploration with the recent discoveries of the Domino and Lira gas fields in the Romanian sector, and the Sakarya gas field in the Turkish sector of the basin. The shallow structure is complex, with rapid lateral and vertical velocity variations arising from shallow-channel systems, mass-transport complexes, shallow gas, and faulting leading to seismic imaging challenges. These include short-scale undulations in the overburden, amplitude dimming, and fault shadow effects, all of which were seen in the legacy imaging, which used an earth model derived by reflection tomography. The small-scale nature of the velocity complexity requires a velocity model building technique capable of deriving a correspondingly high-resolution model and to this end, full-waveform inversion (FWI) (Vigh et al., 2011) was employed as the primary model building tool to resolve these challenges. In addition to the model building, pre-stack image-domain Least-Squares Kirchhoff Depth Migration (LSQKDMi) (Leone et al., 2018) was employed to gain as much resolution as possible while taking advantage of the high-resolution FWI model to accurately capture, and correct for, illumination effects of the complex overburden. This study presents the results of the high-resolution model building and imaging performed at the Sakarya field.

Vigh, D., Kapoor, J. and Li, H., Full-waveform inversion application in different geological settings. SEG Technical Program Expanded Abstracts 2011

Leone, C., Osen, A., Cavalca, M., Fletcher, R.P. and Ferriday, M. [2018]. Improving Quantitative Interpretation beneath Sand Injectites: A North Sea Case Study. 80th EAGE Conference & Exhibition, Extended Abstracts.

## METHODS

A legacy Q-VTI model built by reflection tomography was taken as the starting point for this study. Conditioning included anisotropy calibration and mild smoothing for FWI, as initial testing indicated that overall a good fit was achieved between the observed and modelled shot data. A combination of input towed streamer seismic data with excellent signal to noise ratio at the lowest available frequencies, and a robust tomography model to act as a starting point meant that minimal conditioning of the legacy velocities was required.

## FWI Model Building

With water depths up to 2.1 km and a maximum 8-km offset recorded by the acquisition geometry, no diving-wave energy was recorded. Consequently, the FWI workflow was driven only by reflected energy. A high number of least-squares FWI iterations were performed in gradually increasing frequency bands to derive the resulting velocity model, with more than half of the total iterations performed at the lowest useable frequencies (below 8 Hz peak frequency). This was of particular importance without the presence of diving wave energy to constrain the low-wavenumber model.

Absorption anomalies related to shallow gas accumulations were considered as a potential cause of amplitude dimming seen in the project area. From the outset, visco-acoustic FWI (Cheng et al., 2015) was performed, initially with a smooth background interval Q model. Simultaneous inversion for  $V_p$  and Q was performed at 5-Hz peak frequency. This was found to update the Q model with clear anomalies related to the shallow gas accumulations in the overburden channel systems. The updated Q model was included in all visco-acoustic propagation within the FWI from this point onwards. FWI continued through five further frequencies bands, completing at 20 Hz peak frequency, and giving us a model reflecting the final inversion bandwidth of ~2 to 35 Hz. This limit was sufficient to resolve the imaging challenges, however the behaviour of the data and the updates suggested that higher frequencies would be achievable for future studies and would bring further resolution to the model and the resulting FWI reflectivity image (e.g. Vigh et al., 2021). The resulting model is well resolved, even at this bandwidth, due to the iterative nature of FWI.

Cheng, X., Jiao, K., Sun, D. and Vigh, D., 2015. A new approach of visco-acoustic waveform inversion in the time domain. In SEG Technical Program Expanded Abstracts 2015 (pp. 1183-1187). Society of Exploration Geophysicists.

Vigh, D., Cheng, X., Jiao, K., Kang, W. and Brand, N., 2021. The impact of acquisition geometry on full-waveform inversion updates. The Leading Edge, 40(5), pp.335-341.

Intermediate quality control images demonstrated the uplift in the structure after the FWI workflow, with the imaging challenges of fault shadows and structural undulations being clearly resolved after the high-resolution FWI. The FWI reflectivity image was shown

to have naturally compensated for the illumination and resolution losses (Vigh et al., 2021) caused by the acquisition and imaging system in a similar fashion to a data domain Least Squares RTM (LSRTM), with two added benefits in terms of image quality. Firstly, that the FWI reflectivity image is the result of a non-linear process and so is not dependent on a fixed initial velocity model, and secondly that it uses the full wavefield and is therefore not subject to the signal processing compromises involved in removing all non-primary reflection energy from the dataset prior to final migration.

Pre-stack least-squares migration in the image domain

Least-squares Q-Kirchhoff migration in the image domain (LSQKDMi) was performed on pre-stack angle gathers after pre-stack Q-Kirchhoff depth migration using the final high-resolution model. In the framework of pre-stack LSQKDMi applied to angle gathers in the image domain, each angle gather is regarded as the result of a non-stationary convolution of the subsurface reflectivity with a blurring operator. This operator is approximated through a grid of point spread functions (PSFs). PSFs capture space-, depth- and dip-variant illumination effects due to complexity in the overburden, limitations of the acquisition system and restricted bandwidth on the diffractor point in the subsurface (Fletcher et al., 2012). PSFs are explicitly modelled for each angle gather, based on the velocity field and the source and receiver locations. PSFs generation is data independent and the ability of PSFs to capture the illumination pattern in the subsurface depends on how accurate and detailed the velocity model representation of the earth is.

Fletcher, R. P., S. Archer, D. Nichols, and W. Mao, 2012, Inversion after depth imaging: 72nd Annual International Meeting, SEG, Expanded Abstracts, 1–5

The pre-stack LSQKDMi workflow was applied to partial angle stacks for the full-depth interval of 12 km. Computed PSF angle gathers are deconvolved from the respective seismic volumes to remove the 'blurring operator' present in the seismic data and deliver angle gather volumes corrected for the illumination footprint. The reflectivity volumes resulting from the LSQKDMi workflow were more representative of the subsurface response and provided enhanced amplitude fidelity for quantitative interpretation. Decoupling of the wave propagation and reflectivity effects in the image domain LSM facilitates preservation of complex seismic signatures, allowing further advanced reservoir characterization analysis. Application of pre-stack least squares QKDM demonstrated effective mitigation of the illumination footprint. More balanced amplitudes were observed throughout the volume as well as enhanced resolution and sharper imaging of the geological structures. Extension of the LSQKDMi workflow into the pre-stack domain delivered not only improved imaging but additionally allowed for the removal of the angle-dependent illumination variation from the seismic amplitudes leading to more accurate amplitude signature with offset and bringing it closer to the true subsurface reflectivity response.

## FINDINGS

The high-resolution model building and LSQKDMi workflow has resulted in a significant uplift in the imaging. The high-frequency FWI model building has captured the velocity complexity at high resolution which is clearly visible in the resultant image via simplification of the overburden stratigraphy and the much-improved imaging of fault segments and their associated fault shadows. The overall resolution and structure of the seismic image has been improved with Q-KDM and the final FWI derived Q and Vp models, and further resolution and image uplift has been gained through the pre-stack LSQKDMi workflow. In addition, the FWI reflectivity image as a standalone deliverable has added significant value as an early out product at the end of the model building and prior to the LSQKDMi.

## CONCLUSIONS

The LSQKDMi process has taken advantage of the accurate velocity model produced by the FWI and compensated for the illumination effects of the stacked channel sequences which it would not have been able to do otherwise.

## ACKNOWLEDGEMENTS

We thank TP for permission to present the results, and Azza Salem and Aashna Kumar for their contributions during this project.

Keywords: FWI, Least-Squares Migration

# An Integrated Petrophysical Technique Leads to Resolve Ultra-Thin Bed Reservoir Properties In Highly Laminated Shaly-Sand Sequences of Black Sea, Turkey



**Mert Kılıç<sup>1</sup>, Batur İşdiken<sup>1</sup>, Tanmoy Dutta<sup>1</sup>, Uğur Yüce<sup>2</sup>**

<sup>1</sup>Turkish Petroleum Offshore Technology Center (TP-OTC)

<sup>2</sup>Turkish Petroleum (TPAO)

The Western Black Sea's deep water gas reservoirs are made up of complex and heterogeneous sand/shale sequences with thin to ultra-thin sand layers.. High-resolution wireline image tools with a vertical resolution of over 0.5 cm can capture bed thicknesses and boundaries of these sand layers, enabling the determination of the net to gross sand ratio. However, accurate porosity and water saturation cannot be derived from image tools alone. Consequently, a petrophysical model was developed to better evaluate low-resistivity pay zones in highly laminated shaly sand sequences by integrating the Thomas-Stieber (1975) sand-shale volumetric model with triaxial induction resistivity data, including vertical-horizontal resistivity measurements.

A more reliable assessment of the hydrocarbon pore volume in such reservoirs is made possible by core data and an integrated petrophysical model that has been properly calibrated. Furthermore, the inclusion of both conventional and advanced wireline measurements, such as multi-component induction resistivity logs and high-resolution image logs, enables the quantification of hydrocarbon pore volume with reduced uncertainty.

To improve calculations of other petrophysical properties, like porosity and water saturation, which are linearly or non-linearly derived from the sand/shale fraction of the rock volume, it is essential to accurately estimate the laminar shale volume in shaly sand sequences. Laminar shale volume, calibrated by image tools and validated by LamCount core data, has been considered the ground truth in the petrophysical analysis. Lamcount data is an external visual measurement of shale and sand laminae. To achieve the accurate petrophysical evaluation both net reservoir and net sand results are required to be calibrated throughout the complete spectrum of shaliness.

In difficult, highly laminated clastic reservoirs, using the methods presented in this work significantly reduces uncertainty for volumetric petrophysical estimates. The findings indicate that low resistive laminated clastic reservoirs with substantial amounts of shale fractions can be highly productive, exhibiting reservoir quality equivalent to that of productive thick sands.

Keywords: laminated reservoirs, petrophysics



# Lithogram: An Innovative Approach for Net-Sand and Lithofacies Estimation in Thin to Laminated Clastic Reservoirs by Using Synthetic Seismogram Method



**Emir Yusuf Ersay, Batur İřdiken, Ergin Karaca, Ömer Akbař, Derya Kılıç Demirci, Tanmoy Dutta, Suat Aktepe**

Turkish Petroleum Offshore Technology Center, Ankara / Türkiye

Identifying thin-to-laminated beds and their fluid content in clastic sediments from seismic data and conventional well logs is a challenge for geoscientists in oil and gas industry. High resolution resistivity based image logs with vertical resolution ranging from 0.5-3.0 cm have been used as an industry standard to determine thin-to-laminated bed boundaries and estimate Net-Sand in calibration of core data. However, the image logs tend to get affected from salinity changes and invasion of oil-based mud in some extend by its nature. In this paper, a new approach has been introduced to predict a salinity independent lithofacies and Net-Sand estimation by using synthetic seismogram method. A conventional synthetic seismogram in oil and gas industry is mainly generated by using density and sonic logs. The purpose of generating a synthetic seismogram is to correlate the information that were acquired from borehole with seismic reflection data along the well. A seismic reflection data, whether it is a 2D or 3D, include information kilometers away from the well location in horizontal direction but lacks of resolution in vertical direction with comparison to well logs which include information only a few decimeters in horizontal level but with much higher vertical resolution than the seismic data. Synthetic seismogram is generated with the convolution of a predetermined wavelet with a frequency of the seismic reflection data and a reflection coefficient which is calculated by density and sonic logs with a specified sampling rate. In order to establish a high correlation between well and seismic data, the sampling rate of the reflection coefficient and the frequency of the wavelet are chosen to fit with the seismic reflection data. In this study, a reflection coefficient with very small sampling rate was created by conventional density and sonic logs and a phase shifted ultra-high frequency wavelet was determined to match with the bed thickness instead of seismic data. The final output trace, called Lithogram, now has a resolution comparable with high resolution image logs. A seismic-to-well tie analysis is not required for Lithogram since it does not depend on seismic reflection data. This approach could be an efficient tool to identify bed boundaries that cannot be captured due to the resolution of the conventional well logs. Besides, Lithogram can be used to estimate Net-Sand in clastic reservoirs with thin-to-laminated beds. In addition to this, it can help operators to estimate Net-Sand in a cost effective way without running expensive image tools.

Keywords: synthetic seismogram, Net-Sand

# The Link Between Seismic and Stratigraphic Analysis: How Pre-stack Stochastic Inversion Improves Seismic Resolution in Ultra-Thin Clastic Reservoirs



**Ergin Karaca<sup>1</sup>, Emir Yusuf Ersay<sup>1</sup>, Burak Salantur<sup>2</sup>**

<sup>1</sup>Turkish Petroleum Offshore Technology Center, Ankara / Türkiye

<sup>2</sup>TPAO, Ankara / Türkiye

The primary focus of this study is to enhance the seismic resolution for thin-to-laminated sand intervals. These layers in the Sakarya Gas Field often fall not just beneath the seismic resolution, but also notably extend beyond the typical constraints of wireline resolution limits. Traditional Amplitude Versus Offset (AVO) inversion methods are ineffective in resolving thinly laminated successions unless the overall thickness of the multiple layers is compatible with tuning thickness and has a high Net-to-Gross (NTG) ratio. The challenge amplifies more when the outputs of the AVO inversion which is approximately close to the seismic frequency are incorporated into the geomodel that is designed as to be ultra-high resolution to investigate the lateral and vertical distribution of the ultra-thin reservoir properties. The application of geostatistical inversion using multiple wells significantly enhances the resolution, providing vertical resolutions of approximately 0.6 meters, demonstrating a notable improvement compared to the outputs generated by AVO inversion methods. This approach not only improves the resolution in the frequency through variogram, but also provides valuable insights into the distribution of thin-bedded sequences across the field.

The successful implementation of this geostatistical inversion method within the Sakarya Gas Field indicates a promising opportunity for similar complex reservoirs around the world. Furthermore, this research implies a direct correlation between the enhanced seismic frequency bandwidth and improved predictability of thin-to-laminated sand intervals. By integrating multiple well data into the inversion process, there is a significant reduction in the ambiguity that typically accompanies traditional AVO inversion methods. Moreover, a considerable increase in the accuracy of geomodels is observed, particularly in capturing the spatial distribution of the ultra-thin reservoir properties. This advancement facilitates a more refined stratigraphic interpretation, contributing to the optimization of extraction techniques and overall reservoir management strategies. The future scope of this study aims at expanding the application of this method to other production fields, and evolving it further to tackle even more challenging geological settings.

Keywords: Ultra-thin beds, Stochastic inversion

# Quantitative Seal Analysis of the Compaction Faults in Western Black Sea Basin, Turkey

**Bulut Tortopoğlu, Nisansu Balci**

Turkish Petroleum - Offshore Technology Center (TP-OTC), Ankara / Türkiye



The Sakarya Gas Field in the western portion of the Black Sea Basin is observed to be a deep submarine fan system deposited in the Upper Miocene-Pleistocene-Pliocene time. It is far from the tectonically active region along the North Anatolian Fault System in the south. While there were several gravity driven Mass Transport Complexes in the past forming small scale deformation zones having distinctive fold geometry on ramp-flat-ramp basement, the entire region is currently under compaction-controlled stress conditions. Performing structural geology studies result in structural features such as compaction faults, stress arches, deformation axis and subsidence shaped seabed being interpreted in seismic data. Therefore, the geomechanical response of them remains to be thoroughly observable against the stress field analysis in the region professionally regarded in this study. A quantitative approach reveals that stress tendency anomalies refer to conductive and sealing zones of structural features.

The ongoing naturally formed compaction process is of prime importance to model the sealing potential of structural features in the region. It provides an opportunity to detect the stress tendencies in 3D space very well due to be critically stressed in terms of magnitude  $\sigma_1$  ( $S_v$ )  $>$   $\sigma_2$  ( $S_{Hmax}$ )  $>$   $\sigma_3$  ( $S_{Hmin}$ ). The proportion of shear stresses to normal stresses, Slip Tendency, plays a key role to understand the sealing potential in any case of slip generated. However, observing an amount of slip on the modelled structures is not obvious because some parts of the planes are not in the failure mode, but the yield mode because of high confining stress conditions. Additionally, having a cap failure on the yield surface motivates to run dilation tendency analysis to determine zones dominated by plastic strain induced pore collapse and pore shrinkage. Populated dilation tendency and slip tendency properties are assigned to map structural planes dividing as conductive and sealing portions. This analysis is also verified by a series of well tests performed in the Sakarya Gas Field.

Keywords Compaction Faults, Seal Potential

# Critical Strain Approach for Critical Drawdown Analysis with the Advance of Cambridge Clay Model in Sakarya Gas Field, Western Black Sea Basin, Turkey



**Bulut Tortopoglu<sup>1</sup>, Adil Gürkan Ceyhan<sup>2</sup>, Nisansu Balcı<sup>1</sup>**

<sup>1</sup>Turkish Petroleum - Offshore Technology Center (TP-OTC), Ankara / Türkiye

<sup>2</sup>Turkish Petroleum - Offshore Technology Center (TP-OTC), Istanbul / Türkiye

Sakarya Gas Field is deposited as the distal part of a deep submarine fan system in the Upper-Miocene-Pleistocene-Pliocene time. The dominant force is the gravity-controlled overburden in the region because the region is far from tectonically active right lateral strike slip faults system in the south, North Anatolian Fault System. This results in the overburden stress being the preconsolidation stress in the field. Several Mass Transport Complexes (MTC) observed to demonstrate distinctive fold geometries on ramp-flat-ramp basement, which have only effect on the variation in the strain field currently. MTCs explicitly have a limited amount of boundary effect due to strain history, which has an impact on the stress path evolution. Therefore, naturally formed compaction-controlled stress conditions ( $\sigma_1(Sv) > \sigma_2(SHmax) > \sigma_3(SHmin)$ ) shrinks the porous media in consistent with the Dickinson Compaction Model in response to progressive burial diagenesis.

The geomechanical response of the Sakarya Gas Field to production is deductively noticeable against the naturally formed compaction induced structural features observed in seismic, log and core dataset such as deformation axis, stress arches, compaction faults, compaction & shear bands etc. It is of prime importance on selecting the right material model to calculate volumetric plastic strain regarding the Cambridge Clay Model because a significant amount of slip is missing on the structural features assigning to dilation although burial diagenesis causes an amount of porosity loss. Quantitative analysis of plastic strains is evaluated to be on the cap of the compaction domain rather than on the dilation domain since cohesive failure is very less observed in unconsolidated and low cemented material in the field. Production increases deviatoric stress and effective mean stress resulting the radius of ellipse being larger as a result of plastic strain generated because the region is critically stressed. Additionally, it is reasonable to express the loading path ranges close through the isotropic compression line because there is a limited amount of differential stress in the field. It runs through an comparatively stable path curved very slightly to the critical state line. That's is also because the material behavior is strain hardening due to ductile behavior, so it is really rare to have a localized deformation on a plane, but micro-fracturing in grain scale. So, reservoir material has a potential to sustain higher load in response to production because the strain hardening response manages a relatively stable process.

Quantitative analysis of the material behavior in response to production is performed to calculate both elastic and plastic components of both deviatoric stress and effective mean stress and to evaluate stress path in p-q space. Volumetric plastic strain values are calculated in the advance of strain decomposition principle. Grain

compressibility values are also used to update porosity near wellbore in response to production because grain crush generates an amount of deformation in addition to pore shrinkage. The amount of deformation is diffused in the porous media, so shear and compaction bands are mostly formed rather than shear enhanced faults.

Keywords: Critical Drawdown and Strain Hardening

# Solutions to Complex Well-Testing Challenges and Proving Production Potential: Successful Well Test Operations on the Sakarya Ultra-deep Water Gas Field in the Black Sea, Türkiye



**Cosan Ayan<sup>1</sup>, Suat Aktepe<sup>1</sup>, Köksal Çığ<sup>1</sup>, Melih Gökmen<sup>1</sup>, Adil Gürkan Ceyhan<sup>1</sup>, Murat Fatih Tuğan<sup>1</sup>, Yakov Shumakov<sup>2</sup>, Bertrand Theuveny<sup>2</sup>**

<sup>1</sup>Turkish Petroleum

<sup>2</sup>Slb

## INTRODUCTION

Exploration activities in deep water environments are taking more attention with the increasing demand for reliable energy resources. Türkiye, have a strong commitment to energy independency and thus show great appetite to deep water exploration activities. Country's efforts finally yield its fruits with the giant Sakarya gas discovery, which is developed with a fast-track approach.

In Sakarya field, a live field development planning approach was applied in which the development plans were updated rapidly, in parallel with the dynamic reservoir characterization process. Therefore, a strong link between static modeling, advanced logging, and dynamic well behavior analysis had to be established. In addition, proof of concept for the well completion design had to be validated.

Conventional drill stem tests (DST) have always been a primary source of information for reservoir characterization and field development planning at exploratory and appraisal phases of the field. Along with multiple formation testing techniques, conventional well test operations are still relevant today and provide unique, dynamic reservoir information to determine reservoir pressures, distance to boundaries, areal extent, fluid properties, permeability and formation heterogeneities, vertical layering, production capacity, formation damage, productivity index, completion efficiency, and more to de-risk the field development plan. This is especially valid concerning complex reservoirs with high vertical heterogeneity, laminated structures, or high-permeability gas reservoirs.

Following an unprecedented, detailed formation evaluation and fine-scale reservoir and transient wellbore simulations, five well tests (DSTs) were designed and executed. The design considerations and execution challenges of DSTs in Sakarya Field included the completion type, fluid losses and high risk of hydrate formation in the deepwater environment. The well tests successfully performed in Sakarya Field led to the initiation of the first ultra deepwater natural gas field development in Türkiye. The detailed formation testing campaign played a key role in selecting production intervals and optimizing well completion. In light of the high-resolution vertical formation evaluation, well tests were designed to prove reservoir extent, connectivity and long-term production potential of the field. Completion design and the results observed while placing the completion were compiled and simulated using fine-scale reservoir modeling and transient wellbore simulations to assess all potential risks during

the well tests. The tests were executed successfully, revealing critical well deliverability and reservoir characterization information, including production logging tool (PLT) surveys. Completion brine losses into the formation, hydrate formation risks at low subsea and surface temperatures, completion and formation differential pressure considerations were evaluated with real-time data analysis. The well test execution plan was updated in real time to achieve critical reservoir information. This closely integrated characterization and field development planning approach led to keeping the tested wells as production wells, thus improving efficiency, minimizing cost and environmental impact, thus accelerating time to first production.

Many technical challenges and time limitations were overcome during this project. Application of detailed formation testing practices, cased hole gravel pack completion in an offshore environment with hydrate risks and close integration of the observations with the well test design by a multiskilled team led to accurate well test simulations, correct test design and successful execution with excellent quality information.

## SAKARYA FIELD

The Sakarya field is a large gas discovery located approximately 170 km north of the Turkish coast in the Black Sea at 2117 m water depth, within the block AR/TPO/KD/C26-C27-D26-D27. The gas-bearing reservoirs are in the clastic rocks of the Miocene-Pliocene age and shale-dominated intervals within the same deposits have also been considered as the biogenic source rock of the system (Fig. 1). Wells in the field produce via a subsea natural gas production system and an onshore natural gas processing facility within the Filyos Industrial Zone.

Fig. 1—Sakarya gas field location in the Black Sea.

To accelerate the time to first gas production and fast-track field development, it was deemed necessary to conduct flow tests of the reservoirs to acquire critical reservoir information and assess the production potential and completion efficiency while reducing the number of wells. This was achieved by drilling and testing several appraisal wells with multiple target intervals that will be later used as producers.

A preliminary review of project challenges led to a set of system goals that would allow alternative development options to be compared. Ranking of development alternatives against these design criteria resulted in the selection of multizone cased hole gravel pack completions with intelligent-well flow control valves

across the target intervals. To acquire critical reservoir information, reduce the number of wells and minimize the geological and completion efficiency uncertainties, it was decided to test target intervals individually in two appraisal wells later to be used as producers.

### Well-Test Design and Operations Planning

The deep water well test operations performed on gas reservoirs introduce a unique challenge related to flow assurance aspects, such as hydrate formation that needs to be assessed at the design stage of the test and develop mitigation actions. To accelerate the first production from the field and fast-track the field development, it was decided to keep the appraisal wells and later use them as producers. This approach allows reducing the number of wells, leading to improved efficiency, minimized cost and environmental impact, and accelerated time to first production. However, it raises the complexity of DST operations with the requirement of seamless integration of the DST string with the lower vertical completion. The lower completion was installed in the well prior to the well test operations and comprised of cased-hole gravel packs that increased the fluid losses into the reservoir, making well clean-up operations more challenging (Fig. A-1).

Well testing in all well categories is a relatively nonstandard operation addressed to put the well on temporary production through the provisional completion string and surface well test package installed on the rig to acquire critical well and reservoir information. At the design stage of the well test on Sakarya field, the following key factors that increase the complexity of well test operations were considered:

- There is high fluid loss into the formation during the TCP and the gravel pack installation process which uses a water-based completion fluid system that makes the well clean-up operations more complicated.
- Destabilization of the formation around wellbore in combination with the liquid loss into formation increases the risk of solids and fines migration and gravel pack destabilization due to the high-pressure drawdown or the drag force applied by the liquid and gas production during the well test. To prevent this, monitoring of drawdown pressure throughout the test is essential.
- There is high risk of hydrate formation in the landing string and at the surface due to the nature of offshore deep-water environment with high fluid cooling effect across the 2150 m water column in combination with low reservoir temperature. The fluid losses of water-based completion brine and gravel pack fluid and vapor water in combination with any potential formation water production can introduce severe risks of hydrate formation during the tests. With awareness of the safeguard requirements and hazards associated with methanol handling on the drillship, methanol was selected as the hydrate inhibitor during the tests. The injection capacity was optimized, and methanol was injected at the seabed during flow tests.
- Long perforation intervals introduce uncertainties

in the net contributing interval to be used in well-test interpretation and the risk of potential crossflows during pressure buildups. This uncertainty can lead to incorrect determination of key reservoir properties such as skin, reservoir permeability, radius of investigation and distances to flow boundaries. Therefore, to reduce the uncertainties in well test interpretation and determine producing intervals during the, it was decided to perform production logging surveys through the DST string.

To evaluate the transient well and reservoir flow behavior and assess the time required to clean-up the well during well test, the transient multiphase flow wellbore simulator coupled with the near wellbore hydrodynamic model was used (Fig.2). For an accurate prediction of flow behavior and liquid recovery process during the clean-up flow, additional attention was paid to the description of the reservoir model and especially the description of the vertical heterogeneity of the thin-layered reservoir structure. This was achieved by splitting the perforation section into 25 to 45 layers, depending on the length and vertical heterogeneity of tested interval, respecting the permeability contrast and net-to-gross ratio.

To ensure operations will be performed safely with no health, safety, and environment (HSE) incidents and within the operational envelope of the equipment, the following operational constraints were set:

- Maximum pressure drawdown that can be applied during the operations to preserve wellbore stability and prevent sand and/or proppant production
- Choke bean-up rate to prevent fast and extensive drawdown change that should not exceed 4/64-in. at once
- Maximum water production rate constraint by the water filtration system and chemical injection to prevent hydrate formation
- The maximum flow rate of oil and gas within the constraints of the temporary surface well-test package installed on the rig
- Minimum gas flow rate required to lift the water and completion brine to prevent water accumulation in the wellbore
- Minimal flowing temperature limited by the temperature rating of the pipework at the surface and the chemical injection capabilities to mitigate hydrate formation

Fig. 2—The simulation results of well clean-up process using a transient wellbore simulator for one of the DST well tests performed on the Sakarya field.

Surface Well-Test Package. The surface well test package was designed to handle anticipated flow rate up to 60 MMscf/D and to provide fluid handling capabilities at surface, safe and environmentally friendly disposal of the well effluent and perform accurate and reliable flow rate measurements during the test. The surface well test package was equipped with two choke manifolds and two indirect heat exchangers to heat up the produced fluids (Fig. 3). In case of any solids production at the surface and to prevent the potential risk of erosion and

plugging the choke, a cyclonic de-sander was used.

Fig. 3—The schematics of the surface well test package used during DST operations.

Accurate and reliable flow rate measurements of water, oil and gas are among the most critical information acquired during the test. Flow rate measurements were performed by using Coriolis flow meters installed in a new generation high-rate well test separator with enhanced fluid-handling and separation efficiency.

DST String. The designed DST string comprised of a seal assembly with the shifting tool, several sets of downhole memory gauges, downhole dual valve providing downhole shut-in and reverse circulation functionalities and a PVT sample carrier to collect representative uncontaminated downhole PVT samples (Fig. A-2). The DST string also included an acoustic telemetry system that provided real-time surface readout of the downhole pressure gauges and control of all downhole DST tools during the tests; the annulus pressure commands remained for redundancy. The application of the acoustic telemetry system to control the downhole tools increased the efficiency of the operations and reduced the annulus pressure while providing all required functions, including a collection of multiple sets of downhole PVT samples. Multiple pressure and temperature gauges were placed at different depths along the bottomhole assembly to record pressure in the annulus as well as the tubing pressure below and above the downhole shut-in valve including the gauges installed below the packer.

To prevent hydrate formation during the test, the landing string was equipped with two ½-in. umbilical lines and one dedicated 3/7-in. chemical injection line with a total pumping capacity up to 14 L/min of methanol. For hydrate monitoring and prevention during the test, a high-tensile-rating gauge carrier below the fluted hanger was installed. The gauge carrier accommodated two sets of gauges measuring pressure and temperature at the seabed and transmitting the data to the surface wirelessly.

## JOB EXECUTION

During the operations large quantities of data, both surface and downhole, with more than 250 channels were acquired and transmitted in real time to a fully secured remote web-based server. Using dedicated software with enhanced data visualization, remote experts could access large amounts of real-time information. This enabled fast processing and live well test interpretation. With specially designed software, the operational support center could remotely access wellsite acquisition units, validate data and assist with any troubleshooting on a 24/7 basis. In addition, together with the chat functionalities, data exchange, screen sharing and conference call facilities at the core of the real-time operations, all team members could communicate, share ideas and provide recommendations. Thus, the entire work force could work together, even if the team members were in different locations. Such a fast information turnaround across all involved parties

also improved the decision-making process and makes conventional well-testing operations more interactive and allows optimization of the well-test program toward the achievement of test objectives within the optimum time frame.

Real-time data delivery of bottomhole pressures, recorded by memory pressure and temperature gauges was essential for hydrate monitoring and prevention, optimizing the chemical injection process, monitoring of pressure drawdown and for a real-time quick-look well-test interpretation that assisted in optimizing the duration of pressure build-up. An example of a diagnostic log-log plot is shown in Fig. 4, comparing two buildup tests, with the final test showing lesser skin factor.

Fig. 4—The log-log plot with the plotted bottomhole pressure data transmitted to the surface by the acoustic telemetry system during the initial and final pressure buildups. The plot also shows the improvement of skin with the formation clean-up during the test.

Figs. 5 and 6 present a comparison of actual field data acquired during cleanup flow on one of the DSTs with the results of the modeling work performed using a transient wellbore simulator at the design stage. During the operation, the choke sequences were adjusted in real-time according to actual well production behavior, but for the sake of comparison, the data were recomputed using actual flow and choke sequences.

Fig. 5—Comparison of actual surface data and flow rates acquired during cleanup flow on one of the DSTs performed on Sakarya field with modeled results using actual choke sequences.

Fig. 6—Comparison of actual flowing conditions at the seabed and calculated using a transient wellbore simulator.

During the entire well clean-up operation, as was expected, there was a severe risk of hydrate formation, which was mitigated by methanol injection at the seabed at 30% to 40% of the total volume of produced water. The risk subsequently declined as the flowing temperature increased (Fig. 7).

Fig. 7—Hydrate curves with the different methanol concentration and actual operating conditions during the clean-up operations at the wellhead and seabed

The flow profile surveys using a production logging tool (PLT) with several flow rates and shut-in conditions provided essential information on contributing intervals and crossflow when the well was shut-in at the surface (Table 1). Figs. A-3 and A-4 show examples of shut-in and flowing flow profiles from one well.

## CONCLUSIONS

This case study shows how successful well-testing operations can be performed in complex, deepwater gas reservoirs with careful planning, including contingency scenarios and integration of all disciplines. The deepwater nature of the operations requires special attention on the risk of hydrate formation and ensuring

that mitigation actions are in place.

The well test operations, especially the clean-up flow can be enhanced by proper forward modeling using a transient wellbore simulator coupled with a hydrodynamic reservoir model. This is especially important in the case of high fluid losses into the formation, such as cased hole or open hole gravel pack completions or hydraulic fracturing operations. This modeling is very different from the completion optimization workflow or flow assurance analysis typically done with a good understanding of well and reservoir performance. When the expected well and reservoir behavior was understood, the DST string and surface well test spread were optimized to handle well effluent in a deepwater offshore environment.

The use of umbilical lines and a dedicated chemical injection line in combination with two indirect steam exchangers as part of the surface well test setup were instrumental to preventing hydrate formation during well test operations. The well test separator equipped with Coriolis meters simplified operations, reducing environmental risk and allowing acquisition of accurate flow rate measurements throughout the entire test duration.

The application of an acoustic telemetry system was instrumental for monitoring the pressure drawdown, hydrate monitoring and prevention and observing well operating conditions at the seabed. The implemented real-time data transmission process of acquiring bottomhole and surface well-test data has significantly improved collaboration between the experts at the wellsite and facilitated a seamless operation. Real-time data transmission with real-time collaboration of experts at multiple sites was instrumental in acquiring high-quality data, providing concurrent feedback, and optimizing the well test program. The ability to ensure data interpretability while the test was ongoing ensured that the test met the objectives and added significantly to de-risking future field development.

Although this case study involved five DSTs from two wells, at the time of writing this paper, more than 30 well tests/clean-up periods have been completed in the field all with transient interpretations. All well test objectives have been successfully achieved safely and efficiently. The acquired dynamic data during these tests enabled assessing each individual well and reconfiguring completions technologies thereby expediting a fast field development program.

**APPENDIX**

Fig. A-1—The lower completion schematic for one of the production/appraisal wells with three main flow intervals. The completion contains the cased hole gravel packs, sump packers, and mechanical fluid loss control valves to prevent extensive fluid loss into formation.

Fig. A-2—DST string used during the well test operations.

Fig. A-3—PLT production profile: shut-in survey.

Fig. A-4—PLT production profile: flow survey.

Keywords: Sakarya Welltest

Fig. 1—Sakarya gas field location in the Black Sea.



Fig. 2—The simulation results of well clean-up process using a transient wellbore simulator for one of the DST well tests performed on the Sakarya field.

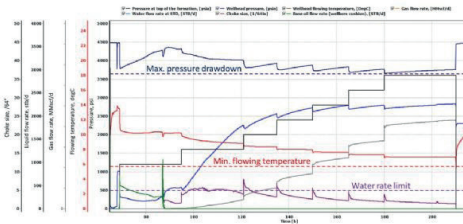


Fig. 3—The schematics of the surface well test package used during DST operations.

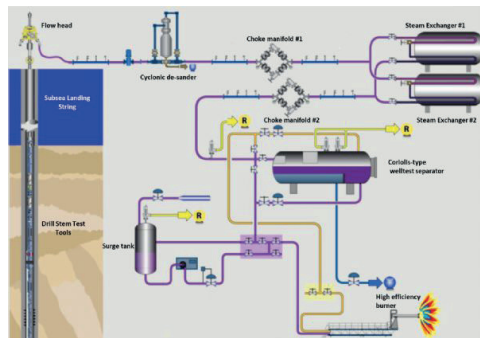




Fig. 4—The log-log plot with the plotted bottomhole pressure data transmitted to the surface by the acoustic telemetry system during the initial and final pressure buildups. The plot also shows the improvement of skin with the formation clean-up duri

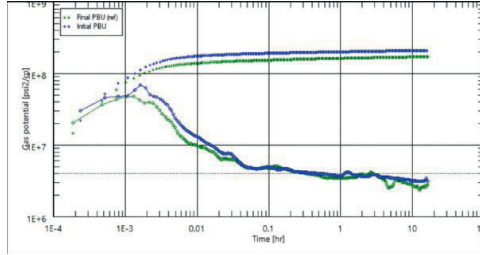


Fig. 5—Comparison of actual surface data and flow rates acquired during cleanup flow on one of the DSTs performed on Sakarya field with modeled results using actual choke sequences.

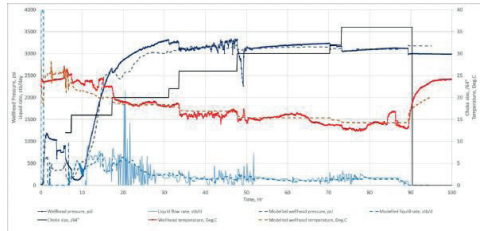


Fig. 6—Comparison of actual flowing conditions at the seabed and calculated using a transient wellbore simulator.

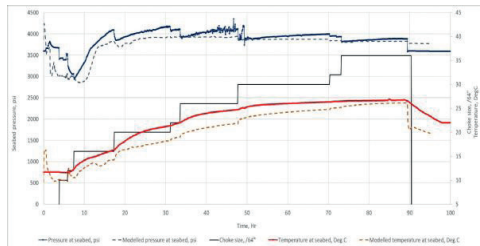


Fig. 7—Hydrate curves with the different methanol concentration and actual operating conditions during the clean-up operations at the wellhead and seabed.

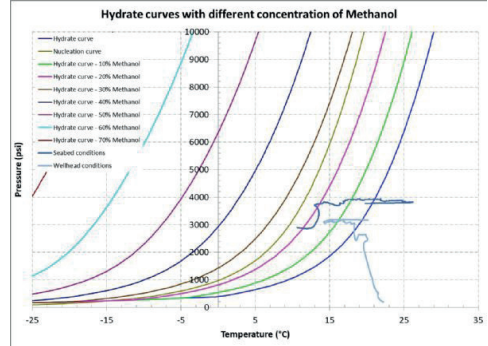
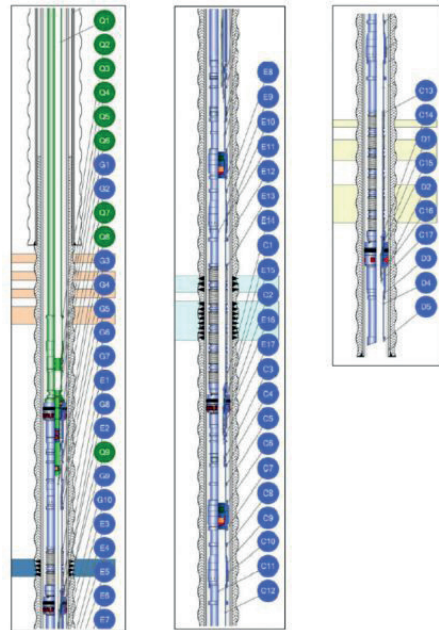
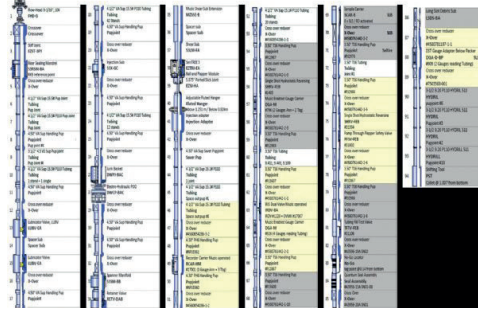


Fig. A-1—The lower completion schematic for one of the production/appraisal wells with three main flow intervals. The completion contains the cased hole gravel packs, sump packers, and mechanical fluid loss control valves to prevent extensive fluid l



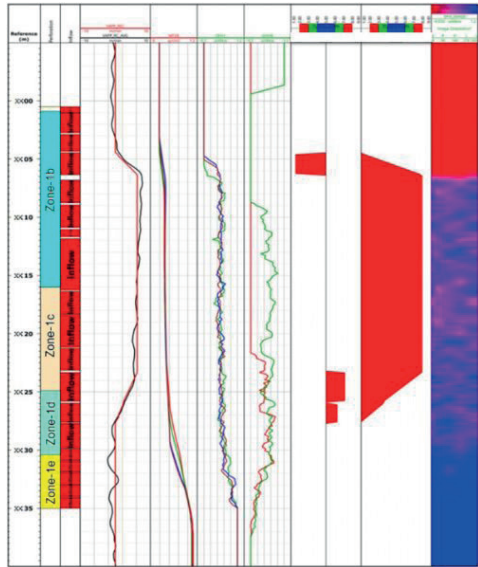
Appendix A1

Fig. A-2—DST string used during the well test operations.



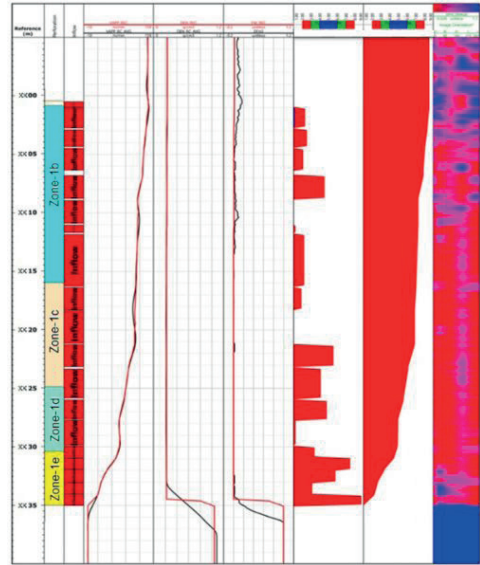
Appendix A2

Fig. A-3—PLT production profile: shut-in survey.



Appendix A3

Fig. A-4—PLT production profile: flow survey.



Appendix A4

# Formation Damage Mechanisms and Solutions in Sakarya Field

**Uğur Paköz**

Turkish Petroleum Offshore Technology Center (TP-OTC)



Sakarya field contains gas in thinly laminated and unconsolidated shaly silty sandstone reservoirs with sensitive clays and cementing carbonates. Complex lithology and unconsolidated nature of these reservoirs necessitates detailed engineering during well operation sequences. Presence of sensitive clays requires using oil-based mud to prevent swelling and presence of gas at multiple zones and possible sanding issues requires multi-zone cased hole gravel pack completion.

Predicting possible production impairment mechanisms and acting to tackle detected issues may only be possible through detailed formation damage testing. Formation rock and fluid data acquisition and interpretation is the first and the most important stages since rock and fluid properties are the base parameters that cannot be changed. Clay swelling tests, fluid-fluid and rock-fluid compatibility studies are the next follow-up work in the context of formation damage. For Sakarya field, a carefully designed and executed formation damage studies were conducted at laboratory and field phases.

Fluid-fluid compatibility studies are the first and preliminary step in formation damage testing. At this stage, drilling fluid, completion fluid, remedial and operational fluids were mixed with representative formation water at different ratios and temperature values in accordance with operational sequences in Sakarya field. Static bottle tests were supported by additional analysis such as total suspended solids, particle size distribution, dry scanning electron microscopy and pH measurements. Once fluid-fluid compatibility stage was finalized, problematic fluids were eliminated and most compatible fluids were identified, rock-fluid compatibility (core flood) testing was conducted. A completely representative and novel experimental setup was used to replicate operational sequences during drilling, cased hole gravel pack completions, early and late cleanup periods and long-term production by using representative encapsulated core plug samples. Outputs were application pressure and permeability, SEM images, micro-CT interpretations and core plug and experimental setup photographs at before and after test conditions.

Defined formation damage mechanisms with the most compatible drilling fluid and completion brine formulations were hysteresis due to fluid retention, cementing material dissolution by HCl acid injected to enhance injectivity for gravel packing, compaction, sanding and proppant embedment. Solutions were determined and applied in the field to minimize these damaging mechanisms. Solutions implemented were minimizing fluid loss into the formation and overbalance pressure in wellbore at any stage, flowing fluid invaded well in the shortest time possible to minimize non-native fluid exposure in the reservoirs, minimizing acid exposure and finding a more compatible acid and

implementing optimum gravel pack design with the most accurate data. In the next stage, short and medium term gas production will be monitored to evaluate and enhance formation damage assessment in Sakarya Field.

Keywords: formation damage, compatibility

# Utilization of Particle Size Distribution Data for Field Development: Unconsolidated Laminated Sandstone Formation Case



**Buse Göral, Uğur Paköz**

Turkish Petroleum - Offshore Technology Center (TP-OTC)

Particle size determination allows for quantification of particle shape anisotropy and assessment of surface area regularity. Particle size distribution (PSD) is a crucial descriptive method for classification of solid particles into each size ranges as a proportion of total solids of all sizes present. Representative PSD of unconsolidated reservoirs is one of the key inputs for field development. PSD data is key to drilling fluid formulation, gravel pack completion design, identification and prevention of formation damage issues, sand production assessment and scaling and corrosion prediction. PSD data is also used to estimate permeability in the absence of core data.

In this study, PSD data was utilized in many different aspects of field development of an unconsolidated gas bearing laminated sandstone formation in Sakarya Field. In addition to conventionally known PSD acquisition methods such as sieve and laser particle size analysis, PSD data was obtained by thin section imaging, microscopic view and SEM images. Depending on how the data was used, different source of material was analyzed for PSD measurements. These materials included cores and plugs whenever available as the first choice, well cuttings, debris, solids and scaling/precipitation products collected during clean-up, flowback and DST of wells, scaling/precipitation products collected from core flow tests and proppants used for gravel pack well completion. Due to heterogeneous nature of Sakarya field in terms of lithology and mineralogy, PSD data was observed to vary significantly. Detailed engineering approaches were utilized to filter, compile and use PSD data for cased hole gravel pack completion design, formation damage evaluations, drilling fluid optimization and permeability estimation.

It was found that properly sized CaCO<sub>3</sub> could be used as an effective bridging agent for the formation of interest since formation rock with given PSD could aid in a good filter cake development. Based on formation PSD, a quite small wire wrap of 150 micron size screen and the smallest proppant size of 40/70 mesh was used for the cased hole gravel pack. No significant sand production was observed in the field, proving gravel pack assembly's success in preventing sanding. Good correlation between air permeability measured on cleaned and humidity dried plugs at confining stress and air permeability derived from different equations was established. It was noticed that although permeability trends matched, there were significant differences between the plug measured data and PSD estimated data. This difference could easily be explained by the lack of confining stress in permeability estimated from PSD data, which ultimately resulted in overestimation in permeability. PSD of precipitates created and collected

during formation damage tests and actual flowback and well tests was also effectively used to understand source and mechanisms of such precipitates.

Keywords: particle size distribution (PSD), unconsolidated formation



## **Derin Deniz Operasyonları**

*Deep Water Operations*

---



# Top Hole Design Considerations in Black Sea Deepwater Fields

**Burak Büyükkaçmıcı, Fatih Karakaya, Amit Sankhe**  
Turkish Petroleum Off-Shore Technology Center A.Ş.



1. The uppermost part of the well, known as the top-hole section, plays a crucial role in supporting the rest of the well. This section is drilled and sealed with cement, typically without the use of a riser, which makes it difficult to effectively monitor and control any losses or influxes. The top-hole section frequently encounters challenges due to unstable formations, leading to issues such as packing off, subsidence, the presence of sticky clay-like material called gumbo, and the loss of drilling fluid.

Deepwater top hole design is crucial in establishing the structure of the wellbore, which is determined by different pressures, loads, and conditions that determine the well's arrangement. The conventional design of tubulars used in the wellbore and the loads they experience, such as burst, collapse, axial, and combined operational and service loads, remain unchanged.

This paper examines top-hole design considerations for Black Sea wells. Particularly, as we delve further into the design considerations for the top hole, certain recommendations will be made to optimize the specific requirements of the wells in the Black Sea, based on priceless experiences gained since the beginning of the Sakarya Gas Field Development Project.

## 2. INTRODUCTION

When designing structures for deepwater wells, it is necessary to consider all the loads imposed during the drilling, completion, and production life cycle, both in static and cyclic modes; which defines the fatigue life. The casing design for drilling operations is influenced by operational loads, including lateral (shear) force, axial load, and bending moments. The analysis conducted by various companies focused on evaluating the maximum bending moment effects on the wellhead (conductor). The results indicated that these effects were relatively minor or not a significant concern when considering a standalone XT left on the wellhead. However, it was observed that during the drilling phase, when the BOP was latched, the wellhead was exposed to the highest bending forces. These forces increased significantly with greater water depths. Another important factor that contributes to bending forces and significantly reduces the well's lifespan is the wellhead stick-up.

To assess fatigue life and various aspects of the well's operating systems, such as wear and tear, annular pressure-volume, and temperature effects, it is necessary to determine the production well and field life cycle loads. These loads are used to calculate stress concentration factors and spectral loads that are applied.

When designing the structural strings, several factors must be considered, including the depth of penetration below the mud line, the characteristics of the soil,

the pipe's wall thickness, diameter, length, material strength, and the method of installation. The analysis conducted should consider the nonlinear behavior of soil loads, their strengths, and the resulting deflection of the structural pipe.

In that manner, ensuring a vertical conductor is quite significant. Although having cement between the conductor and the surface casing is not necessary for fatigue life, to have good cement to drill ahead is important. While going deeper into design considerations regarding the top hole, recommendations will be made to optimize Black Sea field specifics, throughout this abstract.

## 3. NOMENCLATURE

Bending Moment, the response that occurs in a structural element when an external force or moment is applied, resulting in the element undergoing deformation and curving.

Conductor, the casing string, and the initial component are inserted into a well to protect against the collapse of the wellbore. Referred to as the drive pipe, is often a short length and may be driven/jetted into the ground. Conductors are used as the uppermost section of many wells drilled through loose or unconsolidated sediments, as opposed to the more solid formations encountered at greater depths.

Fatigue Life refers to the number of cycles or duration that a material or structure can endure before failure under repeated or fluctuating loads. It represents the lifespan under cyclic loading conditions.

Jetting, A method that uses high-pressure water or fluid jets to create holes in soft seabed sediments, facilitating the installation of conductor pipes.

Mud Mat, is a large, flat, and heavy structure placed on the seabed. It assists in preventing the formation of gas hydrates.

Pack Off, to plug the wellbore surrounding a drill string, this action can occur due to various factors, with the primary ones being inadequate removal of drill cuttings and debris by the drilling fluid or sections of the wellbore collapsing around the drill string.

Riser, the riser is a significant pipe with a wide diameter that links the subsea blowout preventer (BOP) stack to a floating surface rig, allowing for the upward flow of mud returns to the surface. Its purpose is to prevent the mud from spilling out of the top of the stack and onto the seafloor. In a way, the riser can be viewed as a temporary extension of the wellbore, reaching the surface.

Riser Tensioner, a marine riser tensioner (MRT) is a device employed on offshore drilling vessels to exert a

consistent upward force on the drilling riser, regardless of the movement of the floating drill vessel. This ensures the stability and proper positioning of the riser during drilling operations.

Structural Strings, 36" surface conductor and 22" surface casing strings.

Subsidence refers to the sinking or downward movement of the wellhead structure. It can occur due to various factors and can impact well integrity and drilling safety. Monitoring and management of wellhead subsidence are significant for the long-term success of deepwater drilling operations.

#### 4. PRESUMPTIONS

This article considers and makes recommendations for only the wells drilled in the Sakarya Gas Field of the Black Sea since the beginning of the project.

#### 5. METHODOLOGY

##### 5.1 Riser Analysis

After designing the top hole, the next critical step is to make a riser analysis. Riser analysis aims to evaluate if the riser system is fit for purpose, including evaluation of functional requirements and structural integrity. In general, the primary objectives of riser analysis are:

- Determine minimum riser tension requirements,
- Determine operating envelopes and drift off limits,
- Determine riser, conductor, and casing installation envelopes,
- Determine the fatigue life of the wellhead, conductor, casing, and riser system.

The evaluation part of the riser analysis can be conducted against API standards. API RP 16Q, titled "Design, Selection, Operation, and Maintenance of Marine Drilling Riser Systems" offers guidelines for assessing the structural integrity of drilling riser systems. These guidelines provide acceptance criteria for various global responses of the riser, such as allowable flexible joint angle, permissible stresses, and top tension requirements.

##### 5.2 Deepwater Top Hole Installation Systems

The installation method chosen has a significant impact on the axial capacity of all structural strings. In deepwater applications, the most used method is jetting, which involves driving a conductor string into the soft clay sediments beneath the seafloor until the desired shallow depth is reached. Throughout the jetting process, it is essential to follow best practices to ensure that the skin friction between the soil and the outer wall of the conductor develops sufficient axial load resistance, exceeding the buoyant weight of the conductor.

However, if the subsurface conditions consist of hard ground, glacial till, debris, gravel beds, or nonclay particle grain sizes, the installation of structural

strings follows a standard procedure. This involves drilling a wellbore, running the string into position, and cementing it from a predetermined depth to the seafloor. This method is typically employed when the soil composition is not suitable for jetting and requires a more traditional installation approach.

Among all the methods used, jetting is known to cause the most significant degradation in axial capacity. If the structural pipe is not properly designed or installed, there is a high risk of the structure slumping and failing under axial and bending loads. Numerous documented cases serve as evidence of such failures.

The axial capacity of the structural pipe is heavily influenced by factors such as soil strength, soil type, interval length, nature of soil constituents, and the disturbance caused during the jetting process. It is crucial to adhere to best practices during the jetting operation for each string to reach the required depth.

There are significant hazards associated with jetting installations. Setting a conductor too short and unable to support the necessary axial load or running a conductor length that is too long is a big issue. When the conductor length for jetting is too much, being unable to jet further down is a major problem and will leave the wellhead sticking up above. Difficulties in achieving the required setting depth during jetting, which may necessitate excessive reciprocation, can lead to severe and permanent damage to the soil strength and holding capacity, with potentially unknown consequences.

Excessive jetting practices in specific soil types and conditions can result in broaching, where the structural casing breaches outside the intended area. This can cause soil liquefaction, slump failure, and the need to respud wells in some cases.

The level of soil disturbance during jetting operations depends on various factors, including the pumping rate, the difference in outer diameter (OD) between the connector and the casing, the number of reciprocations conducted, and the time allowed for the soil to recover after jetting. The use of flush connectors can significantly improve the development of skin friction by reducing the geometric disturbance since the pipe diameter is flush with no protrusions to disrupt the soil. However, these connectors typically have to handle pad eyes that need to be cut off and removed before running, which adds time and cost to the rig operations.

In Türkali wells, where jetting is relatively easier and takes approximately 3 hours, it may be worth considering the use of flush connectors. Although there might be some loss in pick-up time due to the removal of pad eyes, overall time savings may be achieved by reducing soaking time.

Once the jetted pipe reaches the desired depth, the design criteria must ensure that it can initially support its own buoyant weight and, to some extent, the weight of the inner drill string bottom hole assembly until it is considered operationally safe to be released.

Mud mats also referred to as hydrate deflectors, are large and flat structures placed on the seabed. However,



the exact benefit of using mud mats in many cases should be questioned. Although some operators do not prefer to use it, it will be good practice to continue using it at the Black Sea since the current at the seabed is almost none to monitor the exact placement of the 36" conductor to the right depth at 2200 m water depth. Therefore, watching the mud mat rod indicator via ROV is quite useful. Please see Figure 1, taken during jetting, in which the conductor string is hardly seen.

### 5.3 Conductor Depths

The design lengths for installations are primarily determined based on available data. In cases where limited data is available, particularly for the first wells drilled in a new area, a penetration test of the bottom hole drilling assembly, possibly in conjunction with a pilot hole, can be conducted. Also, coring might be an option to assess soil strength. These tests help assess and gather information on the soil type and characteristics of the first approximately 100 meters below the seafloor. The obtained data is then used to determine the optimal foundation and/or conductor lengths.

The setting lengths, diameters, means, and methods of installation are highly dependent on the shallow soil conditions and the depositional environment in the area. In deepwater applications, installations can vary in length and diameter. Self-penetrating foundation pipes can be as short as a few meters with varying diameters ranging from 2 to 5 meters. Conductor Anchor Node (CAN) type units typically have lengths of 8 to 15 meters and diameters ranging from 3 to 6 meters. These units are self-penetrating and then pumped (suctioned) to the desired depth. For more extensive foundation pipes, lengths can range from 36 to 42 inches or even more in diameter, and they can be up to 20 to 50 meters long. These pipes are installed using various methods depending on the specific requirements.

Figure 2 and Figure 3 depict an illustration of a suction-installed foundation unit called the Conductor Anchor Node (CAN). The CAN consists of a cylindrical structure that is open at its base and closed at the top, with a vent in the roof and internal ring or longitudinal stiffeners. When the CAN is lowered to the seabed, it utilizes its own weight to self-penetrate the soil until it reaches an equilibrium with the soil resistance conditions.

To further embed the CAN into the seabed, water is pumped out from the interior of the cylinder using an ROV-installed or carried pump. This creates a differential pressure between the unit's roof and the soil surface, generating a suction force that pulls the unit deeper into the seabed. The pressure applied must be sufficient to overcome the soil resistance but not excessive enough to cause fluidization of the soil inside the CAN.

The suction-installed foundation unit technology, CAN-ductor, is a proven method and is typically performed by Neodrill in Norway. This technique is conducted offline by Platform Supply Vessels (PSVs) and is particularly suitable for relatively harder formations. The use of

this technology can be considered a viable option for fields where jetting is not suitable in the Black Sea and Mediterranean Sea.

In deepwater applications, the most used method for installing conductor pipe is either jetted or drilled and cemented. The typical range for conductor pipe lengths in these methods is around +/- 40-50 meters when used in conjunction with a foundation, CAN unit, or similar structures. In specific ultra-deepwater environments, the conductor pipe lengths can extend up to approximately +/- 80-100 meters.

Increasing the conductor pipe depth, i.e., 110-120m, instead of ~90m, can reduce the likelihood of cement shortfall for the 22" surface casing. By extending the conductor setting depth, there is a better chance that sufficient cement will be available for the surface casing, mitigating any potential issues that could arise from cement shortfall. Although this adjustment can be considered for future Black Sea or Mediterranean Sea wells, for Türkali wells it seems not suitable since the loss zone is deeper. Please note that increasing conductor depth comes with the challenge of being able to jet depth required and not getting stuck before section TD.

### 5.4 Penetration Tests

In regions where seismic data is poor or non-existent, there have been instances of conductor failure events, which cost millions of dollars. To address this issue and make informed decisions, conducting penetration tests can be justified. These tests aim to assess the suitability of soil conditions and gather data on formation characteristics throughout the depth interval necessary for jetting the conductor pipe below the seafloor. By analyzing the test data, it becomes possible to distinguish between clay and non-clay formations using a non-rotational drilling assembly penetration jetting test.

The obtained data from the penetration tests is then utilized to evaluate the optimal conductor lengths required and determine the best practices to employ for each specific well. These tests help in making data-driven decisions and optimizing conductor length and depth to ensure efficient operations.

In cases where the penetration test is deemed insufficient or inconclusive, the operator may choose to invest further and drill pilot holes to gather more definitive and evident data. This additional information allows for a more accurate assessment of the soil conditions and aids in making well-informed decisions regarding conductor length and depth optimization.

Note that a slick or stabilized drilling BHA can behave very differently with regards to a jetting conductor much larger diameter string. However, penetration test data and trends obtained have proved worthy if no subsurface data is available.

### 5.5 Pilot Holes

Pilot holes are drilled to detect, identify, evaluate, plan, prevent, and mitigate unknown hazards and operational risks that may exist in the target area. By drilling pilot holes, operators can obtain valuable data about the subsurface conditions, such as geological formations, rock properties & geomechanical data, and potential drilling challenges such as shallow hazards, and water flow zones. The data collected from pilot holes assists in determining casing and cementing programs, well trajectory planning, drilling fluid properties, and equipment selection.

Pilot holes are also used to obtain pore and fracture pressure data. This information is crucial for understanding the subsurface pressure regime and assessing the risks associated with drilling operations. Accurate pressure data allows for more informed decisions regarding well design, drilling fluid selection, and wellbore stability.

In the Türkali field, where cement shortfall issues have been experienced, three pilot holes were drilled recently. And, valuable data was obtained about subsurface conditions, such as geological formations, rock properties & geomechanical data, and potential drilling challenges such as shallow hazards, and gas/water flow zones primarily from LWD. They are also used to predict PPFG profiles.

### 5.6 Surface Casing Depths and Cementing

The main objective of designing the primary structural surface casing is to establish a fracture gradient that allows for safe drilling, casing, and cementing of the first intermediate casing at the desired depth. It is crucial to ensure that the wellbore formation can withstand the pressure exerted by the hydrostatic weighted mud, circulating fluids, cuttings, and all other static and dynamic pressure effects within the subsea BOP and marine riser. Additionally, the wellbore formation must be able to handle full returns to the rig, considering the presence of the marine riser. This ensures operational safety and enables the efficient functioning of the drilling operation.

When primary well control situations or operating conditions approach the predetermined safe limits, it is necessary to run casing strings as part of the well design.

Since formation is softer in general at the Black Sea, by current cement design and +/-450 m for Türkali wells (+/-2000 m WD), we observed by 22" USIT logs that there is a cement shortfall behind the surface casing. However, +/-650 m for Amasra wells (+/-2000 m WD), observed no cement shortfall since having better PPFG profile.

Successful surface casing cementing requires improved drilling fluids management, reduced slurry transition times, and compatibility between drilling fluids and cement slurry weights with formation gradients. Challenges include placing cement in weak formations prone to fracturing. Design parameters include pump time, fluid loss, rheology, density, and compressive

strength.

The surface casing shoe must have competent cement surrounding the casing and the wellbore. This shoe serves as the first barrier in case of a well control event, where it is exposed to shut-in kick pressures before drilling into the next section. Ensuring a secure cement bond in the surface casing shoe is vital for maintaining well integrity during potential well control situations.

In cases where fracture gradients in the area do not allow for the circulation of a heavy slurry back to the seafloor, a combination of a lightweight slurry for the upper section and a heavier tail slurry is utilized. Despite this design approach, there have been instances of cement shortfall observed in Türkali wells. To improve this situation:

- Prior to cement operation, during circulation, bridging materials can also be pumped. Or, they can be added to the cement slurry itself. Fiber was added to our slurry to cure potential loss intervals in one of the drilled & cemented Black Sea wells recently.
- Special spacer systems can be employed. One used for a well in the Black Sea, claiming an increase of up to 0.1 ppg to fracture gradient by sealing off micro-fractures in the formation.
- Gasblock additive can be utilized to prevent gas migration. However, one should be careful while using it since if pumps are stopped for any reason during the operation, Gasblock makes the slurry hard to pump in a short time. For our wells, Gasblock was in use only for the tail slurry. Then, it is used both for tail and lead slurries to improve the chance of good cement.
- Cement slurry weights should be kept as low as possible.
- Before considering more expensive options like LiteCrete lightweight cement slurry, we may even think of not bringing cement slurry till seabed intentionally, since having cement between the conductor and surface casing is not so critical for the fatigue life of the wellhead.
- Two stage cementing can be considered.
- As for centralizer design, cement baskets can be used to prevent losses due to the weight of the cement column.

## 6. CONCLUSIONS

General design criteria for the top hole section are examined throughout this article, with the help of drilled ultra-deepwater wells in Black Sea Fields. The following are the significant conclusions achieved:

- Jetting practices are so critical that they can affect all life cycles of a well.
- PPFG and shallow hazard data are very important for surface casing cement design.
- Usage of Gasblock additive in cement slurry is notable to prevent gas migration. Additionally, it provides better rheology.
- Special spacer systems used ahead of cement slurry may increase the fracture gradient of formation up to 0.1

ppg by sealing off micro fractures.

- Fiber use can prevent losses during cement jobs.

#### 7. Acknowledgements

I would like to thank the Management of Turkish Petroleum Off-Shore Technology Center Incorporation for their support in publishing this paper.

I wish to state my sincere regards and thanks to my manager Fatih Karakaya for his motivation, guidance, and valuable feedback. I appreciate Senior Drilling Supervisors (SDSV) Albert Higgins and Wallace Smith for their motivation, and sharing experiences gained by working offshore for years.

Lastly, I would like to express my profound gratitude to my wife Aybüke, and priceless family members.

#### 8. References

Aird, P. (2019). Deepwater Drilling. Elsevier Ltd.

Neodrill. Retrieved June 19, 2023, from <http://www.neodrill.com>

Enhanced Drilling. Retrieved June 19, 2023, from <https://www.enhanced-drilling.com/>

ABS. (July 2023). Drilling Riser Analysis. American Bureau of Shipping Incorporated by Act of Legislature of the State of New York.

2H Offshore. (April 2020). TPAO Drilling Riser and WH Analysis.

SDSV Albert Higgins and Wallace Smith. (June 1, 2023).

## 9. APPENDIX

### 9.1 Abbreviations and Acronyms

BOP Blow Out Preventer

CAN Conductor Anchor Node

HPWHH High-Pressure Wellhead Housing

LPWHH Low Pressure Wellhead Housing

MRT Marine Riser Tensioner

WD Water Depth

WH Wellhead

XT Christmas Tree

### 9.2 List of Figures

Figure 1

Indicator Rod During Jetting

Figure 2

Conventional vs CAN-ductor System

Keywords: Top Hole Design, deep-water surface casing cementing

Figure 2 Conventional vs CAN-ductor System

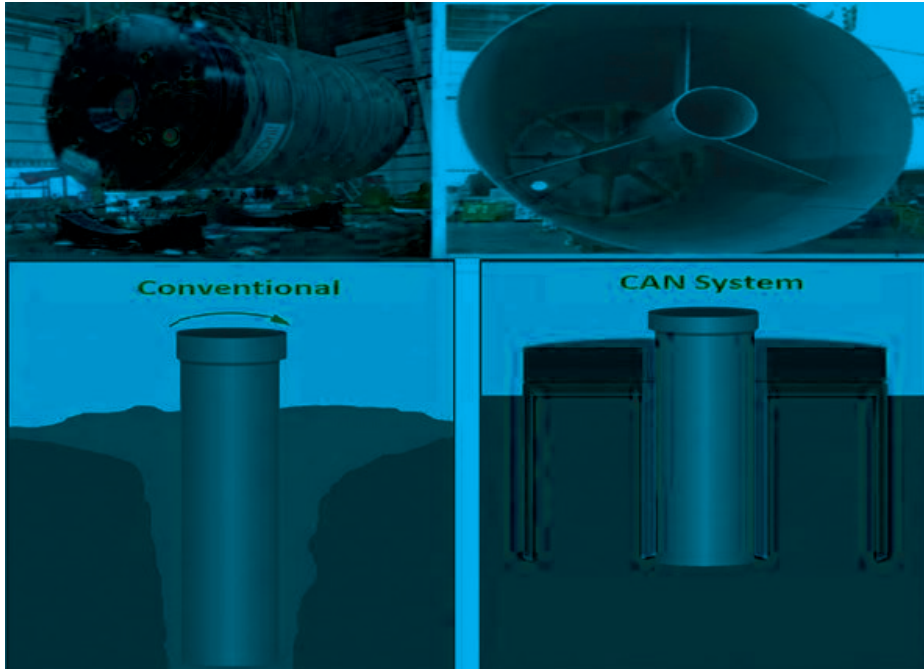
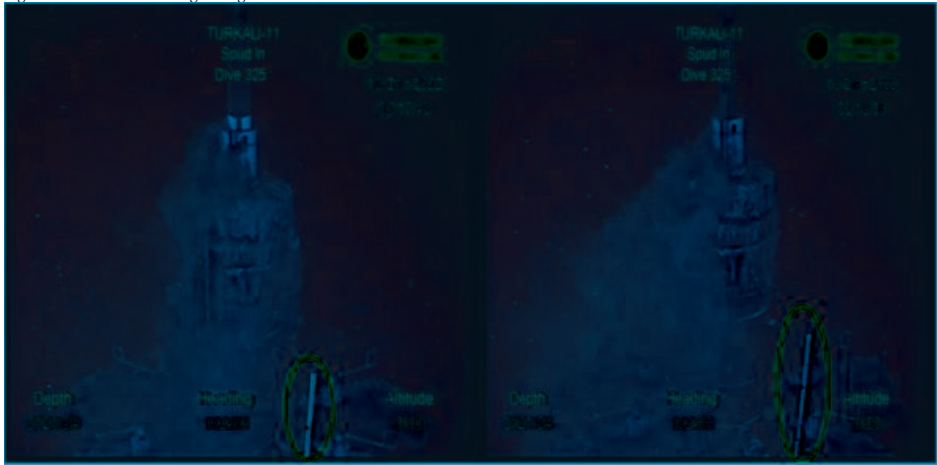


Figure 3 Running CAN-ductor Offline by Boats



Figure 1 Indicator Rod During Jetting



# The Advantage of Dual Derrick Activity in Ultra-Deepwater Operations

**Evren Bektas, Fatih Karakaya, Hüseyin Kasapoğlu, Amit Sankhe, Okan Kurgul**  
Turkish Petroleum Off-Shore Technology Center A.Ş.



This paper presents the advantages of Dual Derrick Activities, how to reduce the drilling costs and to reduce operational time. In detail, the paper focuses on how to design the well and plan operational steps for Dual Derrick floating vessel, how to deal with logistics for Dual Derrick Activities, challenges of Dual Derrick Activities, equipment design, and properties, and a case study to show the advantages of Dual Derrick to reduce drilling costs and to save time for the operations.

The experiences in the Mediterranean Sea with eight (8) exploration wells and in Black Sea with seven (7) exploration wells and fourteen (14) Appraisal wells show that there is a significant time reduction on the drilling operation using the advantage of having Dual Derrick Activity floating vessel. This study also shows the importance of logistic plan, coordination and good communication while executing the operations.

## 2 INTRODUCTION

Many of the rigs contracted during the late nineties building boom are equipped with some sort of efficiency boost tools. The simplest is an onboard make-and-break assembly that builds or breaks out bottom-hole assemblies, drill pipe stands and casing stands. The more advanced in this respect is the full capability twin derrick systems. There is a huge potential in removing activities from the critical path and having parallel activities done, thus reducing overall time to perform the operations. Dual derrick can greatly improve the efficiency of drilling operations in deep-water area.

The idea is to build two completely independent rotaries, traveling blocks, and everything else necessary for drilling operations, all under the same derrick. Thus, it will be possible to perform many operations concurrently, instead of sequentially, providing significant advantages for both exploratory and development operations.

It is possible to run casing with one derrick set and drill with the other, thus reducing total rig time to complete the operation. Of course, the latter operation is accomplished before running the BOP stack.

The forward and aft rotary tables will support each other in an orchestrated manner that maximizes progress along the critical path. For example, in an exploratory or single-well scenario, the forward rotary can be used to run conductor and perform jetting operation and prepare to run the BOP stack and riser at the same time that the aft rotary run and cement surface casing and pull out of hole with the inner string that we perform cement operation.

Once the surface casing string is cemented, the critical path moves from the aft rotary to the forward rotary in order to run the riser and BOP stack. This type of dual

activity is facilitated by dynamically repositioning the drill ship.

From this point, the aft rotary table converts to a full support role for the forward rotary table, eliminating operations from the critical path and reducing the time required for performing sequential operations

After running BOP on the riser and landing in on the wellhead, there are also advantages of having a dual derrick such as making up BHAs for the next sections, picking up casing joints and making up casing stands, and racking them back in the derrick, laying out drill pipe and BHAs, prepare any wear bushings or MPD tools, etc. These off-line activities serve to reduce the time needed to run casing once total depth is reached, continuing onward as the hole progresses to smaller casing strings.

There should be good planning not only operational but also logistically to use the advantage of Dual Derrick activities. Support vessels transfer the top hole equipment consisting bulks, 36" Conductors, 22" Surface Casing joints to load to the rig and one of the support vessels keep the backup top hole equipment by waiting alongside and 2 ROVs are also operational especially for the riserless section. Apart from the advantages of having dual derrick, it might also bring challenges. Coordination and good communication are extremely important for safe Dual Activity operations. Detailed work plan and instruction for each well activity center, more personnel are required to run dual activity operations. There should be good deck management plan and good coordination in terms of the logistics on the rig site.

## 3 NOMENCLATURE

**Exploration Well**, a well drilled in order to establish the existence of a possible petroleum deposit or to acquire information in order to delimit an established deposit. Exploration well is a generic term for wildcat and appraisal wells.

**Appraisal Well**, exploration well drilled to establish the extent and size of a petroleum deposit that has already been discovered by a wildcat well.

**Non-Productive Time (NPT)**, is the time when the well operations in the program are interrupted or delayed for any reason.

**Drawworks**, it reels in the cable (drilling line) on the drum to lift the pipe. It allows the cable to be spooled out as the pipe is lowered into the well.

**Top Drives**, mechanical device on a drilling rig that provides clockwise torque to the drill string.

**Rotary Table**, a mechanical device on a drilling rig that provides clockwise rotational force to the drill string to

facilitate the process of drilling a borehole.

Pipe Racking System, a computer-assisted, dual-arm, vertical pipe handling system. It provides remote handling of drill pipe, drill collar, and casing stands between the pipe setback area and well centre.

Hydra Tong, hydraulic machinery used to makeup and breakout drill pipe, drill collars.

Travelling Block, the set of the sheaves that move up and down in the derrick.

#### 4 PRESUMPTIONS

This study considers eight (8) exploration wells drilled in the Mediterranean Sea between the years of 2018 and 2020, and seven (7) exploration wells drilled in the Black Sea and fourteen (14) Appraisal Wells drilled in the Sakarya Gas Field of the Black Sea between the years of 2020 and 2023. The statistical studies are based on actual well time data starting from the first operational step and ends at the last operational step.

#### 5 METHODOLOGY

The wells with the lowest Non-Productive Time (NPT) are taken into account for this study to have more clear information about the advantage of Dual Derrick Activities. It starts with the operational steps that we perform on both Main Rig Floor and Aux Rig Floor simultaneously. Then, the offline activities performed at both the Main and Aux Rig Floor are explained. The study continues with the comparison of Dual Derrick Activity and Single Derrick Activity.

### 6 DUAL DERRICK ACTIVITY

#### 6.1 Dual Derrick Equipment

Dual Derrick Activity Rigs are designed to safely perform activities simultaneously; it is equipped with two independent drilling systems as:

- Drawworks
- Top Drives
- Rotary Tables • Pipe Racking Systems
- Hydra Tongs
- Travelling Blocks

Dual Activity Rigs have a single derrick, riser, and one (1) or two (2) BOP Stacks. DA Rigs are able to provide enough power, pumping capacity, storage volumes, and crane for both Aux and Main Rig Floors. There should be efficient deck and derrick use in order to perform DA operations safely and efficiently. Derrick raking (size, length, and setback) must account for activities performed on both Main and Aux RFs. For the Rig limitations, Riser and Wireline operations can only be performed from the Main RF in most cases unless a rotary sock is installed.

#### 6.2 Dual Derrick Operations

Activities performed for the riserless section at both Main RF and Aux RF are summarized below.

List of Activities that is performed on the Main RF

- Rig up 36" Conductor Running Tools
- Pick up and Run 36" Conductor joints
- Pick up and Make up 36" LPWHH
- Make up and Run 26" Jetting BHA into 36" conductor
- Run 36" Conductors and 26" Jetting BHA to sea bed on drill pipe
- Jet 36" Conductor, Release 36" DAT and drill 26" Hole Section.
- POOH and rack back 26" Jetting BHA.

• Rig Up Riser Running Equipment

• Skid BOP below Main RF

• Run Subsea BOP on Riser & Land onto 18 3/4" HPWHH

List of Activities that is performed on the Aux RF

- Rig up 22" Surface Casing Running Tools
- Run 22" Surface Casing
- Run 5 7/8" Cement Stinger into 22" Surface Casing
- Pick up and Make up 18 3/4" CART
- Run 22" Surface Casing on Landing String
- Stab 22" Guide Shoe into 36" LPWHH.
- Run 22" Surface Casing and Land out 18 3/4" HPWHH into 36" LPWHH
- Perform 22" Surface Casing Cement Operation
- Release 18 3/4" CART and POOH with 5 7/8" Cement Stinger and Landing String

Activities performed after landing BOP (riser section) at Aux RF, outside of critical path.

- Drill Pipe Stands building
- Special stands building – Side Entry Stand, Double Dutch Stand, Cement Stand etc.
- Casing Stands building
- BHA stands building
- BHA tools testing (MWD/LWD) and downloading
- Break down BHA once out of the hole from Main RF
- Casing Hanger Stand, Wear Bushing Stand building

Case1 Türkali-11 Appraisal Well

Türkali-11 has the following well data

Water Depth (RKB): 2144.3 m

Well TD: 3801 m

Well Program: four (4) casing strings

The Well AFE including 10 % NPT contingency is 43.1 days. The well finished in 38.02 days with 0.2%

NPT which is 5.08 days ahead of the planned days.

The main phases and the durations of the sections are:

36" Conductor Jetting: 1.14 days  
Drill 26" Hole Section: 0.7 days  
Run and Cement 22" Casing: 0.39 days  
Run BOP on Riser: 2.01 days  
Drill 17 ½" Hole Section: 2.47 days  
Run and Cement 13 5/8" Casing: 1.91 days  
Drill 12 ¼" Hole Section: 2.74 days  
Log and Evaluation: 21.01 days  
Run and Cement 9 5/8" Casing: 3.63 days  
P & A: 2.02 days

The main phase activities are simulated with single rig assuming all offline activities performed as online activity. Tripping time, running time and handling time are take into account identical with the dual rig activity.

36" Conductor Jetting: 1.14 days  
Drill 26" Hole Section: 1.14 days  
Run and Cement 22" Casing: 0.9 days  
Run BOP on Riser: 2.21 days  
Drill 17 ½" Hole Section: 2.85 days  
Run and Cement 13 5/8" Casing: 2.52 days  
Drill 12 ¼" Hole Section: 3.11 days  
Log and Evaluation: 21.01 days  
Run and Cement 9 5/8" Casing: 4.87 days  
P & A: 2.27 days

Based on the simulated single rig activity durations, Türkali-11 Appraisal Well would have terminated in 42.02 days.

## 7 CONCLUSIONS

Total time of the Türkali-11 Well is 38.02 days. 4.24 days are related to the riserless sections (Conductor jetting to land BOP) and 33.78 days are related to the remaining sections. In the riserless section, time-saving is 1.15 days, which is 27.1 %, time-saving after landing BOP (riser section) is 2.85 days, which is %8.4 compared to single rig activity. It can be concluded that the total time reduction on Türkali-11 is 10.5% compared to a single activity rig. These results exclude time spent prior and post execution i.e. move in/out the rig well location, sea bed survey, deploy/recover beacons etc.

## 8 ACKNOWLEDGEMENTS

I would like to thank the Offshore Operations Department of Turkish Petroleum Off-Shore Technology Center Incorporation for their support to publish this paper. I also would like to thank all of my managers, colloquies and service company personnel who have contributed to the execution of the successful Ultra-Deepwater operations.

## 9 REFERENCES

Soegaard, L.M., Nergaard, A. (2001). Offshore Drilling Experience with Dual Derrick Operations. SPE/IADC 67706.  
Avignon, B., Simondin, A. (2002). Deepwater Drilling Performance. SPE 77356.  
TP-OTC. (2023). Türkali-11 Drilling Program. Ankara: Turkish Petroleum Off-Shore Technology Center Inc.  
TP-OTC. (2023). Türkali-11 Weekly Performance Report Report. Ankara: Turkish Petroleum Off-Shore Technology Center Inc.

## 10 APPENDIX

### 10.1 Abbreviations and Acronyms

AFE Authorizations for Expenditure  
BOP Blow out Preventer  
BHA Bottom Hole Assembly  
ROV Remotely Operated Vehicle  
MPD Managed Pressure Drilling  
NPT Non-Productive Time  
RF Rig Floor  
DA Dual Activity  
LPWHH Low Pressure Wellhead Housing  
HPWHH High-Pressure Wellhead Housing  
DAT Drill Ahead Tool  
POOH Pull Out of Hole  
CART Cam Actuated Running Tool  
MWD Measurement While Drilling  
LWD Logging While Drilling  
RKB Rotary Kelly Bushing  
P & A Plug and Abandonment  
TDS Top Drive System

### 10.2. List of Figures

Figure 1  
Dual Derrick Activity Rig Layout  
Figure 2  
Main & AUX TDS and Pipe Racking System  
Figure 3  
Main & Aux Rotary Table and Driller's Cabin

### 10.3. List of Tables

Table 1  
Example of Drilling Systems in Dual Derrick Activity Rigs  
Table 2  
Derrick Management in Dual Derrick Activity Rigs  
Table 3  
General Dual Derrick Activity Operation Sequence



Keywords: Dual Derrick Activity, Ultra-Deepwater Drilling

Figure 1 — Dual Derrick Activity Rig Layout

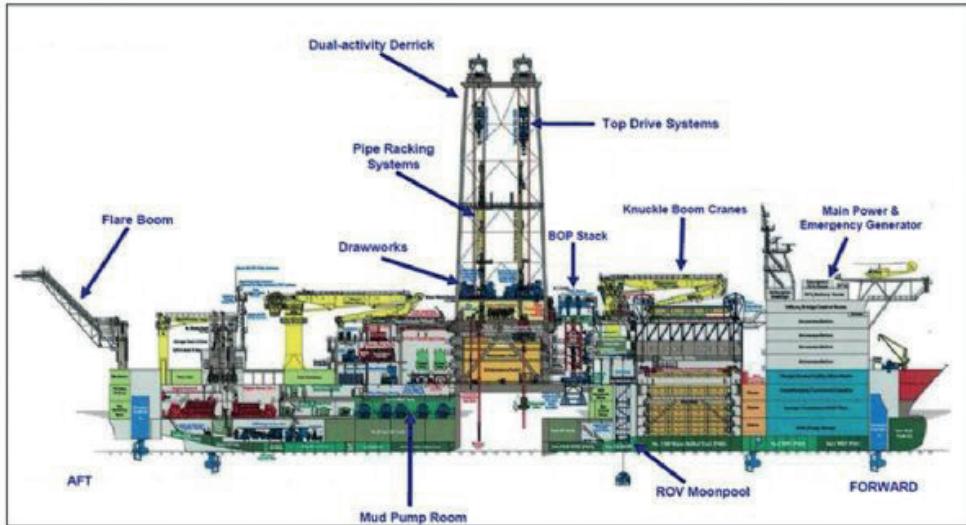


Figure 2 — Main & AUX TDS and Pipe Racking System



Figure 3 — Main & Aux Rotary Table and Driller's Cabin



Table 1 — Example of Drilling systems in Dual Derrick Activity Rigs

	<b>Main WC</b>	<b>Aux WC</b>
Travelling Block	2500 klbs	1500 klbs
Drawworks w/Active Heave Compensation	Hoisting Capacity of 2000 klbs	Hoisting Capacity of 1500klbs
Top Drive	2000 klbs, 65.5 kft-lbs, 270rpm	1500 klbs, 65.5 kft-lbs, 270rpm
Rotary Table	75 1/2", 45 kft-lbs	60 1/2", 45 kft-lbs
Pipe Racking System	Yes	Yes
Hydra Tong	3 1/2" to 9 3/4", 103.2 kft-lbs MUT- 147.5 kft-lbs BOT, 100 rpm	3 1/2" to 9 3/4" 103.2 kft-lbs MUT- 147.5 kft-lbs BOT, 100 rpm

Table 2 — Derrick Management in Dual Derrick Activity Rigs

Drill Pipe and BHA racking capacities				
Tubular Type	Stands	Joints	Feet (ft)	Metres (m)
6 5/8" or 5 7/8" Drill Pipe	450	1800	55800	17000
6 5/8" HWDP	20	80	2500	760
6 3/4" Drill Collars	14	56	1700	520
8 1/4" Drill Collars	24	96	3000	915
9 1/2" Drill Collars	8	32	1000	305

Racking Information		
	Height (ft)	Height (m)
Minimum Stand Height	105	32
Maximum Stand Height	138	42.06
Fingerboard Height	101	30.79
Bellyboard Height	50	15.24

Casing racking capacities				
Tubular Type	Stands	Joints	Feet (ft)	Metres (m)
20" & 18" Casing	24	72	2950	900
16" Casing	32	96	3930	1200
13 5/8" Casing	70	210	8610	2620
11 3/4" Casing	77	231	9470	2890
10 5/8" Casing	84	252	10330	3150
9 5/8" Casing	91	273	11190	3410
7" Casing	112	336	13780	4200

Table 3 — General Dual Derrick Activity Operation Sequence

Main Rotary	Online	Offline	Auxiliary Rotary
	Online	Offline	
-Pick up and rack back jetting BHA -Pick up and rack back 36" DAT -Rig up 36" conductor running tools -Pickup and run 36" conductors			-Pick up 5-7/8" cement stand -Pick up 18-3/4" CART tool -Rig up 22" casing running tools
-Run 36" conductors & jetting BHA to seabed on drill pipe			-After starting to run 36" conductor & jetting BHA on drill pipe, P/U and RH with 22" casing joints
-Jet 36" conductor -Release DAT and drill 26" hole section			-Finish running any remaining 22" casing -Run 5-7/8" inner string and install 18-3/4" CART tool -Run 22" casing to 100m above seabed
-POOH and rack back 26" drilling assembly -Install riser handling tools -Skid BOP below main rotary			-Skid aux. rotary with 22" casing over 36" LPWH#1 -Run 22" casing in hole -Perform cement job on 22" casing -Release 18-3/4" CART, pull 5-7/8" inner string if HPWHH
-Begin running BOP subsea -Testing C&K Lines every 500meters			
-Continue running BOP subsea -Testing C&K Lines every 500meters			-Pull 5-7/8" inner string out of hole -Pick up and rack back the 17-1/2" BHA
-Continue running BOP subsea -Testing C&K Lines every 500meters -Land BOP on HPWH#1, install diverter -Perform required BOP testing			
-P/U 17-1/2" BHA; run in hole below BOP -Perform BOP pressure and function tests with test rams			-Pick up and M/U 13-5/8" casing stand and rack back in derrick -Pick up and M/U 13-5/8" Casing Hanger and rack back in Derrick. -Pick up and M/U 13-5/8" Cement head and rack back in Derrick.
-Drill 17-1/2" hole section			-Pick up and rack back the 12-1/4" BHA -Pick up, M/U and rack back 13-5/8" WBRRT in Derrick
-Run and cement 13-5/8" casing string			
-Drill 12-1/4" hole section -Perform Wireline Operation			-Break out 13-5/8" PADPRT tool -R/B 9-5/8" cement head in derrick -Pick up and M/U 9-5/8" casing stand and rack back in derrick -Pick up, M/U and rack back 9-5/8" WBRRT in Derrick
-Run and cement 9-5/8" casing string			-Pick up, M/U Scraper BHA

1.

# Enhancing Efficiency and Stability in Deepwater Jetting Operations: The Role of Bit Stick-Out Length

**Oğuzhan Kaylan, Fatih Karakaya**

Turkish Petroleum Off-Shore Technology Center A.Ş..



This research paper examines the importance of bit stick-out in surface conductor jetting drilling for deepwater operations. Surface conductor jetting drilling is an innovative deepwater drilling technique specifically designed for time savings on the rig and the elimination of conductor cementing operations. Eliminating cementing work reduces the complexity and time required to construct a well. In addition to these benefits, the surface jetting drilling method offers other notable advantages, such as overcoming the challenges of the loose deep seabed and avoiding geological disasters at shallow depths.

In jetting drilling, the length of the drill bit at the bottom of the conductor shoe is referred to as bit stick-out and is kept constant, i.e. the drill bit and conductor are combined into one whole in the vertical direction run into the formation concurrently. This ensures that the formation around the bit bottom is fully flushed, and broken formation cuttings can flow back from the inner annulus of conductors, thus enhancing the conductor's running speed.

TP-OTC, operating in the challenging Sakarya fields of the Black Sea, employs a specific equipment configuration comprising a 36-inch conductor casing and a 26-inch Milled Tooth Smith Bit. Through careful analysis, it is determined that a stick-out length of approximately 5.5 inches is optimal for their jetting operations at the Sakarya fields. This selection ensures efficient hole, friction, and jetting of the formation, providing correct drilling fluid circulation and enhancing overall drilling efficiency.

In conclusion, the research demonstrates the significance of bit stick-out in surface conductor jetting drilling. The established calculation model and field tests validate the theoretical assumption and emphasize the importance of selecting an appropriate bit stick-out length. The analysis demonstrates a significant time reduction of 46.56 hours per well when comparing jetting operations to non-jetting operations. This substantial time savings underscores the enhanced operational efficiency and adherence to safety requirements achieved through the implementation of the jetting method with the appropriate bit stick-out selection.

## 2. NOMENCLATURE

$\Delta h$ —reasonable bit stick-out, mm;

$H$ —the distance between the plane of the bit nozzle tip center and that of the bit top, mm;

$D$ —outer diameter of conductor, mm;

$r$ —wall thickness of conductor, mm;

$L$ —vertical distance between bit nozzle tip center and bit axis, mm;

$\theta$ —included angle between bit nozzle axis and bit axis (°);

$R_o$ —nozzle tip radius, mm;

$\alpha$ —jet flow divergence angle, (°), generally 25°-30°

## 3. INTRODUCTION

Surface conductor jetting drilling is an innovative technique that has gained prominence in Deepwater operations. This drilling method offers several advantages, making it a preferred choice for reducing rig time and eliminating the need for cementing operations associated with conductor casing. In surface conductor jetting drilling, the 26" BHA and conductor casing are run together and connected by the DAT Tool.

After the jetting operation is completed, a soak time is required to provide soil stress recovery around the conductor to allow the formation to hold the conductor casing securely. This waiting period ensures the stability and integrity of the wellbore, contributing to the overall success of the drilling operation. Then, the BHA in the running assembly will be unlocked by operating the DAT tool. The DAT tool will be removed from the running assembly, and then the drilling process will continue. Finally, the DAT tool is tripped out at the end of the drilling process and the installation of the conductor pipe is completed.

In jetting operations, the selection of an appropriate bit stick-out length holds paramount importance. An optimal bit stick-out length ensures efficient penetration, enhances the removal of cuttings, and promotes the desired flow path of drilling fluid.

This research paper focuses on the significance of bit stick-out selection in surface conductor jetting drilling. The study aims to examine the impact of bit stick-out length on operational efficiency and drilling performance. In the following sections, the research investigates the distinction between reasonable and unreasonable bit stick-out lengths, shedding light on the factors that contribute to successful jetting operations.

## 4. METHODOLOGY

### Research Design

This study employs an analytical research design to investigate the impact of bit stick-out length on jetting operations in deepwater drilling. Analyzing data from previous jetting operations, we aim to identify correlations and trends that shed light on the optimal bit stick-out length.

## DATA COLLECTION

Data for this study were collected from a comprehensive review of existing literature on jetting operations, as well as through the analysis of field operational data and field experiences. The literature review provided valuable insights into established best practices, while operational data and case studies allowed for a real-world assessment of bit stick-out length's influence.

### 4.3. Variables

The primary independent variable in this study is the bit stick-out length, measured as the distance from the endpoint of the drill bit to the conductor endpoint of the cut joint. Dependent variables include drilling efficiency, conductor installation velocity and soak time.

### 4.4. Controlled Variables

To isolate the impact of bit stick-out length, we controlled variables such as flow rate, bit type, flow rate, slack-off weight, and conductor size, which are known to influence jetting operations. These controls ensured that any observed effects could be attributed to variations in bit stick-out length.

The methodology employed in this study provides a robust framework for investigating the role of bit stick-out length in deepwater jetting operations. It allows for a comprehensive assessment of its impact on drilling efficiency, conductor installation velocity, and soak time.

## 5. DIFFERENT SCENARIOS FOR BIT STICK-OUT

A critical factor in deepwater jetting operations is the establishment of a reasonable bit stick-out, which plays a crucial role in ensuring effective penetration in the formation at the bottom of the bit. The selection of a reasonable bit stick-out length allows for efficient penetration of the formation, promotes the desired jetting rate, and correct flow line, and ultimately contributes to the successful execution of deepwater jetting operations.

During the jetting process, various hydraulic parameters such as drilling pressure, flow rate, and WOB can be modified to optimize the operation. It is vital to note that once the conductor casing is run in water, the bit stick-out length cannot be adjusted. Recognizing this limitation, TP-OTC has focused on modifying the hydraulic parameters, WOB, frictions, reciprocations, and pumping Hi-Vis during the jetting operation.

### 5.1. Reasonable Bit Stick-Out

A reasonable bit stick-out [Figure 1] is crucial in surface conductor jetting drilling to ensure sufficient penetration in the formation at the bottom of the bit. It enables the drilling fluid jet to effectively break down the formation and promotes the removal of cuttings. By optimizing the bit stick-out, drilling operations can achieve improved

jetting rates and enhanced drilling performance.

In deepwater jetting drilling, the selection of the optimum bit stick-out length is influenced by various factors, including the angle of the nozzle, the size of the bit, the diameter of the conductor, and other relevant parameters. Industrial practices indicate that a range of 4 to 7 inches (approximately 101 to 203 millimeters) is commonly considered reasonable for the bit stick-out length. This range allows for effective engagement with the formation and facilitates the desired penetration through the rocks. Additionally, it promotes proper weight distribution onto the drill bit, ensuring optimal functionality and improved drilling efficiency. Therefore, when determining the ideal bit stick-out length, it is essential to consider the specific characteristics of the bit size, conductor size, and Drill Bit features.

Figure 1

Reasonable Bit Stick Out Length Diagram (Liu et al.,2022)

### 5.2. Unreasonable Bit Stick-Out

#### 5.2.1. Small Stick-Out

When the bit stick-out is too small [Figure 2], several issues arise that result in low drilling efficiency. Firstly, the limited contact area between the drill bit and the formation prevents effective engagement and proper penetration through the rocks. This insufficient contact hinders the bit's ability to break through the formation effectively. Additionally, due to the small bit stick-out, the weight distribution shifts predominantly to the cut joint of the conductor casing instead of being evenly distributed onto the drill bit. Consequently, the drill bit cannot bear the desired load and may not function optimally. Furthermore, the positioning of the bit nozzles at the upper part of the conductor shoe causes the jet beam to be partially or wholly directed toward the internal wall of the conductor. As a result, the jet beam fails to effectively break the formation and adequately clean the bottom hole. These factors collectively contribute to reduced drilling efficiency, emphasizing the importance of selecting an appropriate bit stick-out length to optimize drilling operations.

Figure 2

Unreasonable (Too Small) Bit Stick Out Length Diagram (Liu et al.,2022)

#### 5.2.2. Excessive Bit Stick-Out

When the bit stick-out is excessive [Figure 3], one of the consequences is the formation of cuttings along a return flow path located both behind and inside the conductor casing. That may also result in hole enlargement, which can further impact the overall casing stability and jeopardize the success of the well construction. In addition, a maximum bit stick-out length of 8 inches is typically considered to be the upper

limit based on industry practices. Beyond this limit, the flow line behind the conductor casing decreases friction between the conductor casing and formation. The lack of sufficient friction can also affect the stability and support provided by the formation, potentially compromising the overall integrity of the wellbore. Furthermore, this lack of friction can contribute to an increase in the soak time, which prolongs the operation duration. Increased operation duration, in turn, leads to higher costs for the well construction due to extended rig time and associated expenses.

Figure 3

Unreasonable (Excessive) Bit Stick Out Length Diagram (Liu et al.,2022)

### 6. CALCULATION OF BIT STICK-OUT

According to the analysis presented above, it is postulated that the optimal bit stick-out occurs when the upper edge of the jet beam aligns internally with the lower edge of the conductor. This alignment is achieved when the upper edge QG of the jet beam is tangent to the inner wall AG of the conductor at point G (refer to Figure 4 below). This configuration ensures not only the desired jetting running speed of the conductor but also meets the safety requirements for operations. Based on this theoretical assumption, a model is developed to calculate the appropriate and reasonable bit stick-out.

Figure 4

Bit Stick Out Formula Diagram (Yang et al., 2013)

$$\Delta h = H - \left\{ \left( \frac{D}{2} - r - L \right) \cdot \cot(\theta) \right\} + \left\{ \left( R_o + \left( \frac{D}{2} - r \right) \cdot \tan\left(\frac{\alpha}{2}\right) / \sin(\theta) \right) / \left( \cos(\theta) \cdot \tan\left(\frac{\alpha}{2}\right) + \sin(\theta) \right) \right\}$$

### 7. EXPERIMENTAL STUDY

According to the South China Sea case study [Figure 5] of the relationship between the bit stick-out amount and conductor casing installation velocity (ROP of the conductor), it is found that the installation velocity increases with increasing bit stick-out within a reasonable range. However, if the bit stick-out becomes excessively long, the conductor casing installation velocity decreases. This may occur because when the bottom of the bit is far away from the shoe of the conductor casing, the debris washed by the bit-emitted jetting drilling fluid cannot be returned from the casing annulus in a timely manner. In addition, soak time increases. Thus, conductor installation velocity decreases.

Figure 5

Case Study in South China (Different Bit Stick Out Length vs ROP) (Liu et al., 2022)

### 8. DISCUSSION

TP-OTC is running operations and carries out its activities at the Sakarya Fields located in the Black Sea. To optimize jetting operations, TP-OTC employs a specific equipment configuration consisting of a 36-

inch conductor casing and a 26-inch Milled Tooth Smith Bit. A carefully chosen bit stick-out of approximately 5.5 inches (139.7mm) is utilized by TP-OTC for jetting operations at the Sakarya Fields (Figure 1). Theoretical estimations based on the 26-inch Milled Tooth Smith Bit suggest that a stick-out length of approximately 5.5 inches is also optimal for jetting operations. This carefully chosen bit stick-out ensures efficient penetration, enabling effective removal of cuttings and promoting the correct circulation flow path of drilling fluid. By adhering to these parameters, TP-OTC aims to achieve exceptional drilling efficiency and successful outcomes in their jetting operations within the Black Sea's challenging Sakarya fields.

### 9. CONCLUSION

The bit stick-out parameter plays a crucial role in the surface conductor running technique for deepwater jetting drilling, as it significantly impacts drilling operation efficiency and subsea wellhead stability. This research paper focuses on establishing a reasonable bit stick-out based on theoretical analysis and experimental studies. The model assumes that the optimal bit stick-out occurs when the upper edge of the drilling fluid jet sprayed from the bit's nozzle is internally tangent to the lower edge of the surface conductor. Field tests were conducted to validate the theoretical assumption and the accuracy of the calculation model. The analysis shows a significant average time reduction of 46.56 hours per well between jetting operations and non-jetting operations, highlighting the improved efficiency achieved through optimized bit stick-out selection in the surface conductor running technique.

### 10. ACKNOWLEDGEMENTS

I would like to express sincere gratitude to the Turkish Petroleum Offshore Technology Company for providing the opportunity to observe and gain a comprehensive understanding of surface conductor jetting drilling operations. The valuable insights and firsthand experience gained through collaboration with TP-OTC have significantly contributed to the knowledge and findings presented in this research paper.

### 11. REFERENCES

- Akers, T.J., 2006. Jetting of structural casing in deepwater environments: job design and operational practices. SPE Drill.
- Jeanjean, P., 2002. Innovative Design Method for Deepwater Surface Casings.
- Liu, J., Lin, Y., Yang, J. & Yin, Q. (2022). A robust and efficient method to geometrically calculate the minimum bit stick-out in a deepwater conductor jetting Project. Journal of Petroleum Science and Engineering, 208(2022), 1-9.
- Liu, S., Yang, J., Zhou, J., 2011. Relationship between Weight-on-bit and Drilling Rate during Jetting

Drilling in Sub-bottom deepwater. Oil Drilling & Production Technology.

Quirs, G., Little, R., 2003. Deepwater Soil Properties and Their Impact on the Geotechnical Program.

TP-OTC.(2020). Well Drilling Programs Ankara, Turkish Petroleum Off-Shore Technology Center Inc.

TP-OTC.(2020-2023). End of Well Phase Reports, Ankara: Turkish Petroleum Off-Shore Technology Center Inc.

TP-OTC.(2023). Non-Conformance Report Procedure. Ankara: Turkish Petroleum Off-Shore Technology Center Inc.

Yang, J., Yan, D., Tian, R., Zhou, B., Liu, S., Zhou, J. & Tang, H. (2013). Bit stick-out calculation for he deepwater conductor jetting technique. Petroleum Exploration and Development, 40(3), 394-337.

Zhou, B., et al., 2014. Design of conductor soaking time in deepwater drilling. Pet. Explor. Dev. 41 (2), 257–261.

12. APPENDIX

12.1 Abbreviations and Acronyms

BHA Bottom Hole Assembly

DAT Tool Drill Ahead Tool

ROP Rate of Penetration

WOB Weight on Bit

12.2 List of Figures

Figure 1

Reasonable Bit Stick Out Length Diagram (Liu et al.,2022)

Figure 2

Unreasonable (Too Small) Bit Stick Out Length Diagram (Liu et al.,2022)

Figure 3

Unreasonable (Excessive) Bit Stick Out Length Diagram (Liu et al.,2022)

Figure 4

Bit Stick Out Formula Diagram (Yang et al., 2013)

Figure 5

Case Study in South China (Different Bit Stick Out Length vs ROP) (Liu et al., 2022)

Keywords: Deep Water Jetting, Bit Stick Out

Figure 1 Reasonable Bit Stick Out Length Diagram (Liu et al., 2022)

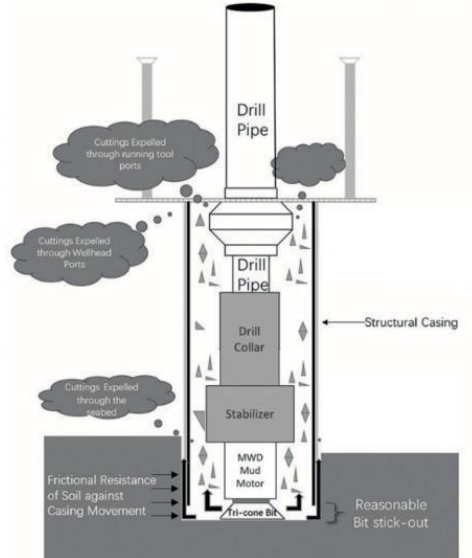


Figure 2 Unreasonable (Too small) Bit Stick Out Length Diagram (Liu et al., 2022)

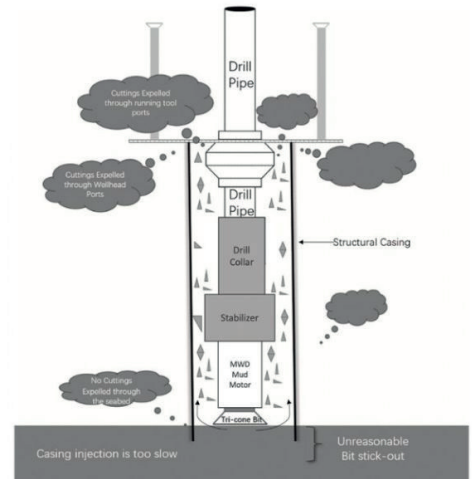


Figure 3 Unreasonable (Excessive) Bit Stick Out Length Diagram (Liu et al., 2022)

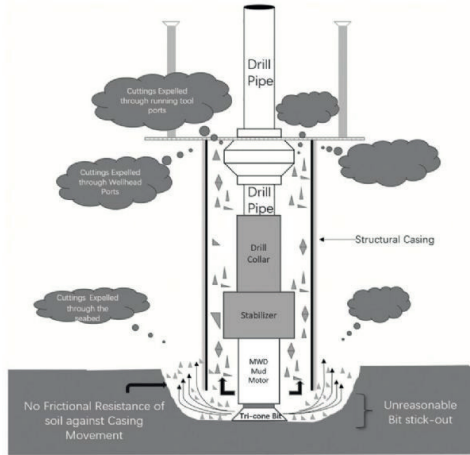


Figure 5 Case Study in South China (Different Bit Stick Out Length vs ROP) (Liu et al., 2022)

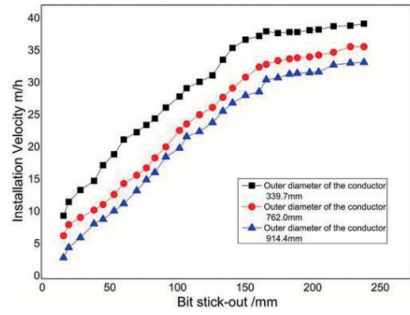
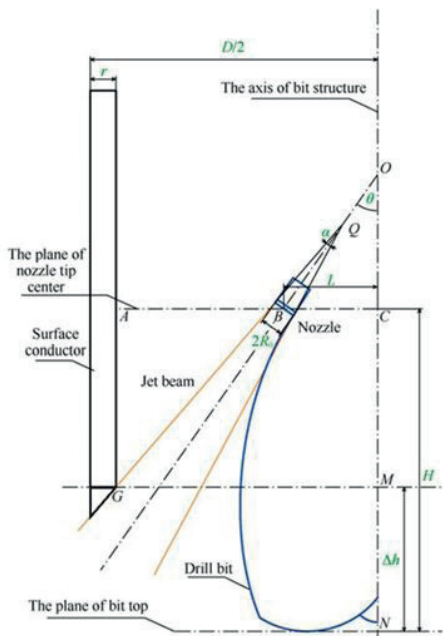


Figure 4 Bit Stick Out Formula Diagram (Yang et al., 2013)





# Subsea BOP Control System Reliability

**Yasin Demiralp, Fatih Karakaya, Necip Bektaş**  
Turkish Petroleum Off-Shore Technology Center A.Ş.



1. Offshore subsea BOP control systems play a critical role in ensuring the safety and integrity of deepwater drilling operations. The reliability and effectiveness of these control systems are of utmost importance, as any failure or malfunction could result in severe consequences such as blowouts and oil spills. This paper investigates the reliability of subsea BOP control systems in offshore drilling and completion operations. Data from 47 wells drilled and completed in Türkiye were analyzed to assess the occurrence of NPT events related to BOP failures. The study identified the main control system, particularly the MUX BOP control system, as the primary contributor to NPT events, accounting for 53.72% of BOP-related NPTs. However, the paper emphasizes that BOP control systems are designed with redundancies, providing backup measures to address failures and enhance reliability. By implementing rigorous maintenance practices and ensuring competent personnel, potential BOP control system failures can be mitigated and prevented. The study underscores the importance of a reliable BOP control system to minimize NPT events and maintain safe and efficient operations. Proactive measures and redundancy within the control system are essential for preventing operational disruptions and improving overall well-control reliability

## 2. INTRODUCTION

Ensuring safe oil and gas drilling operations is paramount, especially when it comes to preventing 'loss of well control.' This scenario, also known as a 'blowout,' can lead to uncontrolled hydrocarbon releases, endangering lives, the environment, and a company's reputation. Offshore drilling rigs are equipped with a BOP system. These systems provide a secondary means of well control, particularly crucial in unbalanced wellbore situations. It's noteworthy that some less-experienced drill crew members might mistake the BOP for the primary well control method. Therefore, rigorous competency training on-site is essential to clarify the distinction between primary and secondary well control mechanisms.

BOP is installed at the wellhead to contain wellbore pressure either in the annular space between the casing and the tubular or in an open hole during drilling, completion, testing, or workover operations (API, 2014). It serves as a secondary barrier, connected to the drilling rig and wellhead via marine risers for drilling fluid conveyance. The system must perform the following operations:

- Close off the top of the wellbore by means of sealing around planned tubular sizing,
- Close off the top of the well without tubulars in the hole,

- Permit monitoring of wellbore pressures to assess bottom hole/formation pressure,
- Allow controlled circulation of hydrocarbons to the surface,
- Be suitably designed/constructed to permit low/high-pressure bull heading,
- Designed to allow various operational requirements to include LOT/FIT, well clean-up flow operations, wireline, and slickline operations,
- Control the release of drilling or completion fluid and other fluids within the column,
- Circulate across the BOP stack to a choke manifold,
- Allow the drill string to strip.

Mainly, the subsea BOP consists of a LMRP and a Lower BOP Stack illustrated in Fig. 1 and Fig. 2, respectively. The BOP stack is mechanically latched to the top of the subsea wellhead by means of a hydraulically operated connector. The lower BOP stack houses the lower Annular (depending on the manufacturer), the ram-type BOPs used to close the well with drill pipe in the hole or on open bore, and kill&choke outlets and valves. The lower BOP stack also houses accumulator bottle racks for the control system which store hydraulic power required by functioning components and emergency conditions such as EDS, EHBS, and ROV intervention panel.

LMRP is an assembly installed on top of the lower BOP stack. It contains a riser adapter with a flex/ball joint; one or two annular preventers (depending on the manufacturer); two independent subsea MUX control pods (Yellow and Blue) which contain the primary system controls for the BOP and LMRP functions, and a hydraulic connector mating the riser system to the lower BOP stack. LMRP is designed to provide a releasable interface between the drilling riser and the BOP stack. Fig. 3 shows the main components of a Subsea BOP system (Kozel, 2015). LMRP is independently retrievable from the BOP and it can be connected/disconnected to BOP by means of a hydraulically operation collet type connector similar to that of the wellhead connector design. This allows the safe disconnection of the LMRP / Marine riser in the event of a POD failure and subsequent recovery to the surface for repair or, a weather event that dictates a disconnect for safety thus allowing the BOP to remain on the wellhead and closed against wellbore pressures.

The continuance and safety of drilling and completion operations severely depend on the reliability of the BOP; because of the importance of this equipment, there are stringent API guidelines that all drilling contractor and operators alike must adhere to. These include but are not limited to, regular BOP function testing (every 7 days) and regular BOP element pressure testing (every

21 days). The only exemption or delay permitted to this is the weekly function test that can be delayed due to current operations at the time of the planned function test. Catastrophic accidents may result from inadequate reliability of the BOP if it's to be used as a consequence of failed 'primary' well control.

### 3. NOMENCLATURE

Actual Well Duration is the reported time required to complete operations.

BOP stands for Blowout Preventer. It is a critical piece of equipment used in drilling operations to prevent the uncontrolled release of oil or gas from a well in the event of a blowout.

BOP failure can result from either a single component failure or a failure of the control system. However, BOP failure does not necessarily require the entire system to be retrieved, as there is redundancy built into the system.

BOP wet days represent the total duration from the time the BOP is splashed in the water and pulled through the splash zone upon completion of the operations or any stack pulls after a failure.

BOP in operation refers to the state of the BOP when it is actively deployed and functioning as a critical well control barrier during drilling or completion operations.

Safety critical failures can occur after the completion of the subsea BOP installation test. Since the BOP serves as a critical barrier in well control, failures in the system are considered critical. The significance of a failure depends on the specific part of the BOP system that experiences the failure.

Non-Productive Time (NPT) refers to the number of hours suspended due to equipment failures. These failures disrupt drilling and completion operations and require corrective actions to restore functionality.

SEM, "Subsea Electronic Module," is a key part of the subsea BOP control system. It decodes surface control panel commands and sends electric signals to control solenoid valves in the subsea control pods, enabling specific BOP stack functions.

A Solenoid valve is an electromechanical device that controls hydraulic fluid in the BOP control system. When an electrical signal activates it, a magnetic field moves a plunger or piston to regulate hydraulic fluid flow, managing various BOP stack functions.

SPM valve stands for "Subplate-mounted valve" and is a crucial hydraulic component in the BOP control system. Mounted on a subplate, it allows remote operation from the surface, ensuring effective well control during drilling and completion operations.

### 4. METHODOLOGY

This study investigates the reliability of subsea BOP systems concerning well control, focusing on main, emergency, and secondary control systems. Redundancies within the BOP control system, aimed at reducing failures, will be explored, highlighting specific

examples. Data will be gathered from Türkiye's well case reports to identify BOP-related NPT, particularly in the MUX control system. The study underscores the importance of maintenance, skilled personnel, and comprehensive training to prevent NPT. This research offers insights into subsea BOP system reliability, potentially guiding system enhancements and operational practices.

## 5. MAIN CONTROL SYSTEMS

### 5.1. Direct Hydraulic Control

Direct hydraulic control is a system used in BOP operations, primarily in onshore drilling rigs. It connects hydraulic lines directly to each BOP stack actuator, enabling control through hydraulic fluid flow regulation. Hydraulic power is sourced from a remote unit at a safe distance from the wellhead.

This system offers cost-effective simplicity in design. However, it becomes less efficient and more expensive for longer hydraulic lines, impacting operational speed. As a result, it's typically used at depths less than 500 feet (GE Oil and Gas, 2010).

### 5.2. Indirect Hydraulic Control

With the growth in complex subsea BOP systems, direct control methods become impractical due to long hydraulic lines required for remote seabed operations. These extended lines lead to slow response times. To address this, two types of indirect control systems have emerged: piloted hydraulic and MUX hydraulic systems.

#### 5.2.1. Piloted Hydraulic Control

These systems use a hydraulic pod positioned on the BOP stack, lowered to the seabed wellhead. The pod contains piloted hydraulic valves to control high-pressure stack valves, activated by small hydraulic lines from the surface. Panels on the rig control these functions. This reduces costs and the size of the umbilical connecting the rig to the BOP stack. However, the hydraulic pod increases complexity and equipment costs. It works effectively up to around 4,000 feet in depth (GE Oil and Gas, 2010). Still, signal transmission through the hydraulic umbilical leads to increased response times, especially with hose type and water depth. Despite these limitations, it's suitable for shallow-water drilling.

#### 5.2.2. MUX Hydraulic Control

The MUX system was developed to overcome the limitations of piloted hydraulic BOP systems, which are ineffective beyond 4,000 feet. In a MUX control system, electrical signals from the surface activate solenoid valves in control pods, which then transmit hydraulic signals to pilot valves for BOP functions (Okohue, 2015). Pilot signals go to both blue and yellow pods simultaneously, while power fluid is directed only to the

active pod, reducing the need for large supply lines and decreasing umbilical size and cost.

MUX systems excel in ultra-deepwater applications due to their rapid response time through electric signals, crucial for emergency LMRP disconnection and quick shut-in of BOP components during well control events. Although they have a more complex design and higher initial costs, the built-in redundancy makes them highly reliable. MUX systems operate effectively up to 10,000 feet in depth, limited by nitrogen pre-charge reactions in accumulator banks under subsea pressures. The MUX BOP control system comprised five major subsystems (GE Oil and Gas, 2010):

### ELECTRICAL

The electrical subsystem consists of two UPSs, two PDPs, and two subsea transformers. Each UPS supplies electrical power to its dedicated battery cabinet and both PDPs. The PDPs are responsible for distributing power to the MUX control system cabinets. Additionally, the PDPs transmit power to the MUX control pods through the subsea transformers.

### COMMUNICATIONS

The communication system includes blue and yellow CCUs, remote processor cabinets, driller's and toolpusher's master control panels, HPTU remote display, HPU, and diverter interface panels. These components monitor the BOP stack status and send hydraulic function commands.

### SURFACE HYDRAULICS

The hydraulic subsystem comprises the HPU, the FRU, the surface accumulator racks, and the diverter skid. These components are responsible for directing and regulating the flow of hydraulic fluid throughout the control system.

### SUBSEA EQUIPMENT

The subsea subsystem includes the annular BOPs, the ram-type BOPs, the subsea control pods (blue and yellow), and the subsea accumulator bottles.

### ANCILLARY EQUIPMENT

Ancillary equipment includes MUX cable and reels, hotline hose and reel, ERA system for real-time riser angle monitoring, HPHT probe, RTU for data collection and transmission, MUX pod test system, solenoid test system, and HPTU.

The subsea MUX control system (Fig. 6) comprises a CCU, driller's panel, toolpusher's panel, MUX cable reel, HPU, accumulators, and two control pods. Control panels initiate commands in the subsea system, which are multiplexed down the umbilical to the subsea pods. Two functionally identical control pods operate on the "blue" and "yellow" sides of the MUX Control System.

While one pod is active, the other remains on standby, mounted on the LMRP, and is integral to the BOP main control system (NOV Shaffer Volume-2). The pod decodes and executes the signal; for example, to close a BOP ram, the command is decoded, activating a solenoid that sends a hydraulic pilot signal to the appropriate valve. This signal shifts the hydraulic valve, directing pressurized fluid to close the BOP ram (Liu et al., 2017).

## 6. EMERGENCY CONTROL SYSTEMS

Emergency control systems provide an alternative means to operate BOP elements when the main control systems are compromised or lost, aiding in equipment failures and well control incidents. They can operate independently or interface with the main BOP control system to activate its components. Understanding their applications is vital to prevent environmental incidents, reduce injuries, and save lives. The main emergency control systems include (Hauser, 2003):

### 6.1. Emergency Disconnect System

In the Oil and Gas Industry, particularly in deep-water exploration, DP systems have become crucial for operating rigs in challenging offshore environments. However, the persistent risk of position loss due to equipment failures or human errors necessitates swift reactions.

The EDS plays a vital role as part of the main control system, triggered when the rig deviates significantly from its designated location, often linked to DP system issues. It initiates a predefined sequence of actions, including BOP stack functions and LMRP disconnection, to secure well integrity. As emergencies can be sudden, well-prepared procedures are essential to minimize damage and blowout risks.

The industry relies on tools like WSOG, categorizing DP statuses and performance limits, and Emergency Disconnection Guidelines, offering clear instructions for managing well control events safely and efficiently (DNV, 2011).

### 6.2. Deadman & AMF

The Deadman system is a safety control mechanism that ensures the BOP stack's activation in the event of a loss of control from the drilling station. It functions as an emergency stop, shutting down all drilling operations and closing the BOPs automatically if there is a sudden loss of hydraulic pressure or a failure in the communication link between the surface control panels and the subsea BOP stack. It is designed to prevent uncontrolled flow or a blowout in the event of a critical failure or human error.

AMF is a feature that automatically activates certain critical BOP functions or control actions in specific conditions or scenarios. It can be programmed to respond to specific emergency situations, such as loss of power, loss of communication, or other predefined

criteria. AMF helps to maintain the safety and integrity of the well in case of unforeseen events or challenges that may compromise regular control functions.

### 6.3. Autoshear

Autoshear, according to IADC, is a standalone system that automatically closes shear rams on the BOP stack if the LMRP disconnects unexpectedly. It has two modes: disarmed and armed. When armed, it activates upon LMRP separation, closing shear rams and/or casing. In uncontrolled well flow events like kicks or blowouts, Autoshear triggers shear ram closure. These specialized components cut and seal off the drill pipe or casing swiftly, preventing potential blowouts and maintaining well control.

### 6.4. Emergency Hydraulic Backup System

The EHBS is a redundant hydraulic system that independently powers the BOP stack if the primary hydraulic system fails. It acts as a backup, ensuring BOP operation and critical functions even during a hydraulic pressure loss. In emergencies or primary system failures, the EHBS activates, supplying hydraulic power to close BOP preventers and regain well control. This enhances BOP system reliability and redundancy, adding an essential layer of protection for drilling operations and personnel safety.

## 7. SECONDARY CONTROL SYSTEMS

### 7.1. ROV Intervention

The ROV plays a crucial role as part of the secondary control system in offshore drilling operations, particularly in relation to well control where the ROV serves as an essential tool for secondary intervention. If a failure or an emergency situation occurs with the main control system or the BOP stack, the ROV can be deployed to perform critical tasks and interventions remotely on the seabed (See Fig. 7). The ROV's functions as part of the secondary control system include:

**Inspection and Monitoring:** The ROV examines and monitors subsea equipment for damage or issues, relaying real-time data and live video to the surface. It can perform tasks like replacing connector gaskets, cleaning wellhead profiles, and installing/removing caps.

**Manual Control:** In the event of a failure in the main control system, the ROV can be used to manually operate specific functions on the BOP stack. For example, it can actuate the BOP rams, shear the pipe, or close the annular preventer using specialized robotic arms.

**Emergency Response:** The ROV can be quickly deployed in emergency situations to initiate the secondary control system and take appropriate actions to regain well control and prevent potential blowouts or

uncontrolled well flows.

**Intervention and Repairs:** If any equipment or components need repair or maintenance, the ROV can be used to carry out minor interventions and perform necessary tasks to restore functionality.

### 7.2. Acoustic System

The acoustic system's primary role is to facilitate remote communication and control between the surface station and subsea equipment, including the BOP stack. It uses underwater acoustic signals to establish a reliable link. These signals are received by transducers, decoded by subsea electronic modules, and activate solenoid valves in the acoustic control pod. These valves provide hydraulic pilot pressure for acoustic SPM valves, enabling hydraulic supply for specific BOP functions (Fig. 8, Kozel, 2015). The acoustic system also handles emergency functions like riser connector unlocking, blind shear ram activation, and upper and middle ram closure. While serving as a secondary control system, it's not mandatory as an emergency backup system per API requirements (API, 2018).

## 8. RELIABILITY OF THE SUBSEA BOP SYSTEMS IN RELATION TO WELL CONTROL

The BOP stack and MUX control system are vital for well control and safety in deepwater operations. MUX control system components are chosen for a 20-year service life based on 25 years of proven experience. Stainless steel piping is extensively used, with some electro-polished to reduce corrosion (GE Oil and Gas, 2010). This design aims to cut maintenance costs, boost system reliability, and simplify troubleshooting, contributing to safer and more efficient drilling.

In deepwater drilling, downtime and revenue loss from LMRP removal due to BOP or control system issues are highly undesirable. This process incurs significant time and costs, impacting the well's AFE. Unscheduled maintenance due to low system reliability can lead to equipment unavailability and NPT. To counter this, redundancies have been added to enhance system reliability and minimize disruptions during drilling and completion operations.

Some of the redundancies that the system employs are listed below (GE Oil and Gas, 2010):

- Two independent uninterruptible power supplies provide electrical power to the system, ensuring continuous operation.
- Two MUX cables establish communication with the subsea components, ensuring data transmission integrity.
- Two separate subsea control pods, one serving as the primary and the other as a "hot backup," both perform the same BOP control functions. Hydraulic flow is directed to the active pod, and a seamless transition can occur if a failure necessitates a MUX control changeover.
- Each subsea control pod contains two separate

SEMs, each with its own power supply, providing dual communication paths to the pod in case of electronic failure.

- Two remote panels, the toolpusher's cabinet, and the driller's panel, are utilized for monitoring and controlling the BOP system.
- Each remote panel features two video monitors, offering alternative control options for the BOP control system.
- Two identical electronic controllers manage communications between the remote panels, CCU, and the subsea pods. Both controllers operate simultaneously, ensuring system continuity in the event of a primary controller malfunction.

In certain well operation stages like pre-deployment testing or initial testing, BOP failures aren't considered significant issues leading to well control incidents. The BOP doesn't act as a well barrier at this point. Official activities start after successful installation, pressure tests, and approval when the BOP is connected to the wellhead. From this stage, the BOP becomes a critical well barrier. Failures occurring afterward are safety-critical, with the degree of criticality depending on the specific BOP component. Maintaining BOP integrity and reliability during active operations is vital for well control and incident prevention.

## 9. BOP-RELATED PROBLEMS ENCOUNTERED IN VARIOUS DRILLSHIPS IN TÜRKİYE

In this study, a total of 47 wells have been investigated since 2018, focusing on drilling and completion activities in Türkiye. The Turkish Petroleum Corporation (TPAO), the National Oil Company of Türkiye, owns four drillships, with three of them currently operating in the Black Sea, specifically engaged in the Sakarya Gas Development Field. The remaining drillship is deployed in the Mediterranean Sea.

During the drilling phase of 30 wells and the completion phase of 17 wells, a range of Subsea BOP Stack equipment from different manufacturers is being employed. Specifically, the equipment utilized includes Cameron (SLB Cameron), Hydril (GE Hydril), and Shaffer (National Oilwell Varco) systems. While specific annular and ram preventers may vary, the BOP control systems on these drillships share functional similarities. This standardization ensures consistent and efficient operations, regardless of the BOP stack's manufacturer or model, all relying on a MUX control system as the primary control system. A subsea well control equipment system encompasses various components and equipment that are crucial for maintaining well control in subsea drilling operations. This study categorizes these components into the following groups: BOP control systems, Subsea BOP stack, riser system, diverter system, and auxiliary equipment.

Fig. 9 illustrates the failure distribution of various BOP studies, highlighting the subsea BOP control system as the primary contributor to equipment failures across all

studies. Notably, approximately 53.72% of all BOP-related NPT is attributed to failures in the primary control systems. Following closely behind is the BOP stack consisting of ram and annular preventers, choke & kill lines, and valves accounting for 23.28% of the failures. Based on the graph, it is evident that the contribution of emergency and secondary control systems to NPT is relatively low. This suggests that failures or issues specifically related to these control systems have a minimal impact on operational disruptions or downtime. This observation underscores the effectiveness and reliability of emergency and secondary control systems, as they demonstrate a lower incidence of failures or issues compared to primary control systems.

Within the control system failures, a significant portion (40.25%) is attributed to issues with components in the BOP Control PODs. Examples include solenoid valve leaks and leakage in the SPM valves. Electrical problems (15.83%) and communication/signal loss (12.51%) are additional types of failures that can occur in BOP control PODs. Furthermore, failures or leaks in the choke and kill valves contribute to 21.88% of the BOP-related NPT, while leaks of control fluid in the conduit manifold account for 12.96%. Leakages often occur due to worn or damaged elastomeric seals rather than steel components.

These findings emphasize the dominance of control system failures in the study. Despite the presence of redundancy designed to enhance reliability, the control systems exhibit vulnerabilities and are susceptible to failures. The complexity and multitude of components within the control system contribute to this risk.

When analyzing the BOP-related failures, it was found that the portion of NPT attributed to BOP issues accounted for only 3.82% of the overall NPT. In contrast, the total NPT across all factors amounted to 17.72%. This relatively low percentage indicates that BOP-related failures constituted a small proportion of the overall NPT events. The majority of NPT events are attributed to operational failures rather than issues specifically related to the BOP systems.

Among the BOP-related NPT experienced, a significant portion, specifically 69.37%, occurred while the BOP was in operation which refers to the state of the BOP when it is actively deployed and functioning as a critical well control barrier during drilling or completion operations. This high percentage indicates that operational issues or malfunctions necessitated the unlatching and removal of the BOP/LMRP from the wellhead on 9 occasions out of a total of 2,351 BOP days. Stack pulls are considered in-operation events and occur when equipment cannot be repaired on-site or if redundant equipment fails to meet operational requirements. None of the stack pulls mentioned are associated with emergency situations. Instead, they primarily occurred due to specific reasons such as leaks, electrical ground faults in the PODs, and failures to function upon command. Indeed, any delays or interruptions caused by these actions can result in increased operational expenses, as the rig may incur additional charges for extended drilling contracts, personnel wages, and equipment rentals. While any

instance of NPT is undesirable and can impact project timelines and costs, the comparatively low contribution of BOP-related NPT signifies a higher level of reliability and performance in the BOP systems. It indicates that the BOP equipment and associated control systems were effective in maintaining well control and minimizing disruptions. Fig. 10 demonstrates a comparison between BOP-related NPTs and non-BOP-related NPTs in drilling and completion operations across various drillships and locations. This comparison provides valuable insights into the impact of BOP failures on operational efficiency.

Fig. 11 serves as an additional example to showcase the reliability of BOP control systems. The graph not only compares BOP-related NPTs with the actual and BOP wet days in drilling operations but also includes upper and lower completion operations. The data clearly demonstrates that BOP-related NPTs represent only a small portion of the total operational days. This comparison strongly indicates that the BOP control systems perform admirably, leading to minimal interruptions and downtime across various operation types. Consequently, this data reinforces the perception that BOP control systems exhibit a high level of reliability, effectively supporting the seamless execution of operations.

## 10. CONCLUSIONS

Based on the findings of this study, it is evident that the reliability of subsea BOP systems plays a crucial role in ensuring well control. Through an examination of various redundancies developed over time to mitigate the possibility of BOP control system failures, it was identified that the main cause of NPT in relation to BOPs is attributed to the MUX control system. Nevertheless, the overall percentage of BOP-related NPT remained relatively low compared to the total NPT events, demonstrating the robustness and effectiveness of the BOP control systems.

However, potential improvements in system design and operational practices to eliminate BOP-related NPTs involve several key strategies. Firstly, continuous research and development can enhance the reliability of BOP control systems, introducing advanced technologies, and materials to withstand harsh operating conditions. Secondly, implementing rigorous preventive maintenance programs and regular equipment inspections will detect and rectify potential issues before they escalate into failures. Thirdly, providing comprehensive training and competency programs for personnel involved in BOP operations will ensure proper handling and response to emergency situations. Additionally, establishing robust communication and coordination protocols between rig crew and onshore support teams can expedite troubleshooting and minimize downtime. Lastly, fostering a culture of safety and adherence to best practices will foster a proactive approach to prevent BOP-related NPTs and enhance overall well control integrity.

## 11. ACKNOWLEDGEMENTS

I would like to express my sincere gratitude to the Management of Turkish Petroleum Off-Shore Technology Center Incorporation for their invaluable support and guidance in the successful completion of this study.

I am indebted to all individuals who have directly or indirectly contributed to this research. Their contributions, whether through discussions, data sharing, or technical support, have played a significant role in shaping the outcomes presented in this paper.

## 12. REFERENCES

- American Petroleum Institute. (2004). Specification for Drill-through Equipment: ANSI/API Specification 16A (3rd ed.).
- DNV. (2011). Recommended Practice DNV-RP-E307, Dynamic Positioning Systems - Operation Guidance (p. 38).
- GE Oil and Gas. (2010). Multiplex (MUX) Blowout Preventer Control System: Basic Training Manual (pp. 2-13).
- Hauser, B. (2003). Evaluation of Secondary Intervention Methods in Well Control for U.S. Minerals Management Service. West Engineering Services Inc (pp. 13-15).
- Holand, P. & Awan, H. (2012). Reliability of Deepwater Subsea BOP Systems and Well Kicks. Exprosoft Final Report (p. 75).
- National Oilwell Varco RS Technical College. (n.d.). Shaffer Subsea Generic (Vol. 1, pp. 25-30).
- National Oilwell Varco RS Technical College. (n.d.). Shaffer Subsea Generic (Vol. 2, p. 51).
- Kozel, K. (2015). Emergency Operation of a Subsea Drilling Blowout Preventer. Offshore / Marine and Subsea Technology.
- Liu, et al. (2017). Reliability Analysis of MUX Control System of Subsea BOP Based on Stochastic Petri Net (p. 2).
- Okohue, L.O. (2015). Deepwater Subsea MUX BOP Control System & Marine Riser System (pp. 8-11).
- TP-OTC. (2018-2023). Daily Drilling and Completions Reports. Ankara: Turkish Petroleum Off-Shore Technology Center Inc.
- TP-OTC. (2018-2023). End of Well Phase Reports. Ankara: Turkish Petroleum Off-Shore Technology Center Inc.

## 13. APPENDIX

### 13.1. Abbreviations and Acronyms

- AFE Authorization for Expenditure  
 AMF Automatic Mode Function  
 API American Petroleum Institute  
 BOP Blowout Preventer

- CCU Central Control Unit
- DCP Driller’s Control Panel
- DP Dynamic Positioning
- EDS Emergency Disconnect System
- EHBS Emergency Hydraulic Backup System
- ERA Electronic Riser Angle
- FRU Fluid Reservoir Unit
- HPTU High Pressure Test Unit
- HPU Hydraulic Power Unit
- LMRP Lower Marine Riser Package
- MUX Multiplex
- NPT Non-Productive Time
- PDP Power Distribution Panel
- PLC Programmable Logical Controller
- ROV Remotely Operated Vehicle
- RTU Remote Terminal Unit
- SEM Subsea Electronic Module
- SPM Subplate Mounted Valve
- SV Solenoid Valve
- TCP Toolpusher’s Control Panel
- UPS Uninterruptible Power Supply
- WSOG Well Specific Operating Guideline

**13.2. List of Figures**

Figure 1

LMRP (Lower Marine Riser Package) - The National Oilwell Varco (NOV) 18-3/4", 15,000 psi Shaffer

Figure 2

Lower BOP Stack - The National Oilwell Varco (NOV) 18-3/4", 15,000 psi Shaffer

Figure 3

Main Components of a Subsea BOP System (Kozel, 2015)

Figure 4

Schematic of MUX Section Used to Transmit Power Fluid and Pilot Fluid (Okohue, 2015)

Figure 5

Blue and Yellow Pods – The National Oilwell Varco (NOV) 18-3/4", 15 000 psi Shaffer

Figure 6

General overview of Subsea BOP MUX control system (Liu et al., 2017)

Figure 7

ROV Applications: BOP Latching on a Wellhead, Cleaning of Wellhead Profile

Figure 8

Acoustic Control System (Konsberg Maritime, Kozel, 2015)

Figure 9

BOP Related NPTs in 47 Drilling and Completion Wells

Figure 10

BOP Related NPTs versus Non-BOP Related NPTs

Figure 11

BOP Related NPTs versus Actual and BOP Wet Days

Keywords: Subsea BOP Systems, Reliability

Figure 01 LMRP (Lower Marine Riser Package) - The National Oilwell Varco (NOV) 18 3-4in, 15,000 psi Shaffer

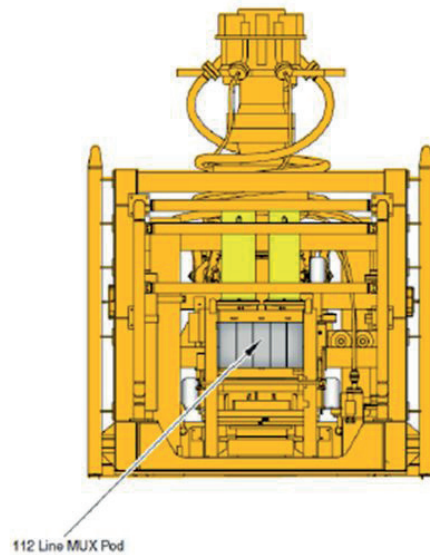


Figure 02 Lower BOP Stack - The National Oilwell Varco (NOV) 18 3-4 in, 15,000 psi Shaffer

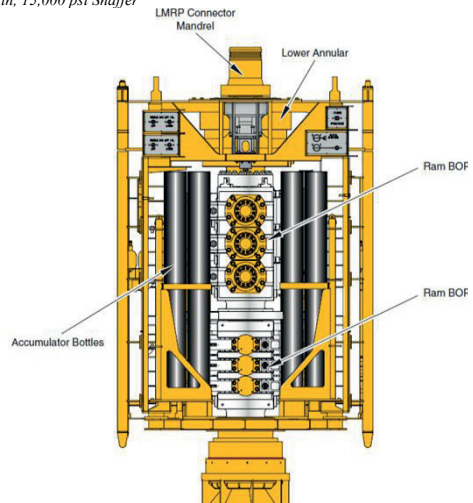


Figure 03 Main components of a Subsea BOP System (Kozel, 2015)

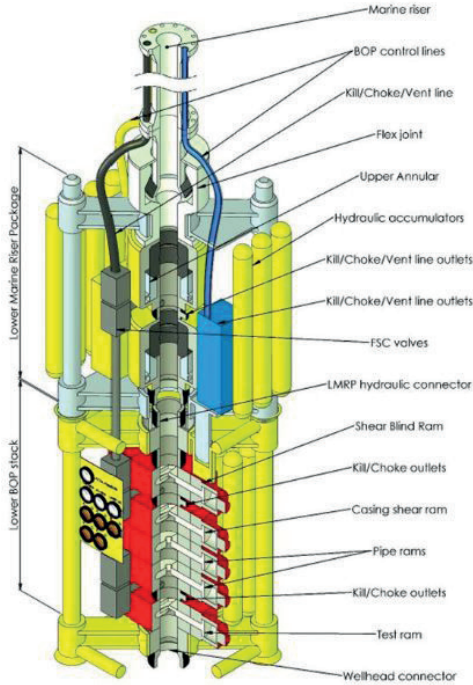


Figure 04 Schematic of MUX section used to transmit power fluid and pilot fluid (Okohue, 2015)

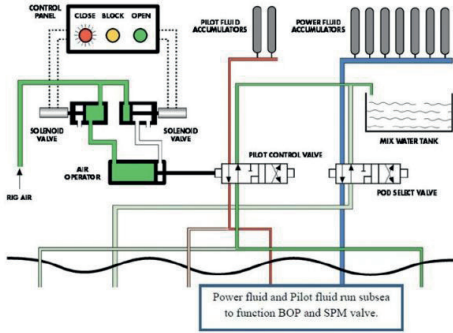


Figure 05 Blue and Yellow Pods - The National Oilwell Varco (NOV) 18 3-4in, 15,000 psi Shaffer



Figure 06 General overview of Subsea BOP MUX control system (Liu et al., 2017)

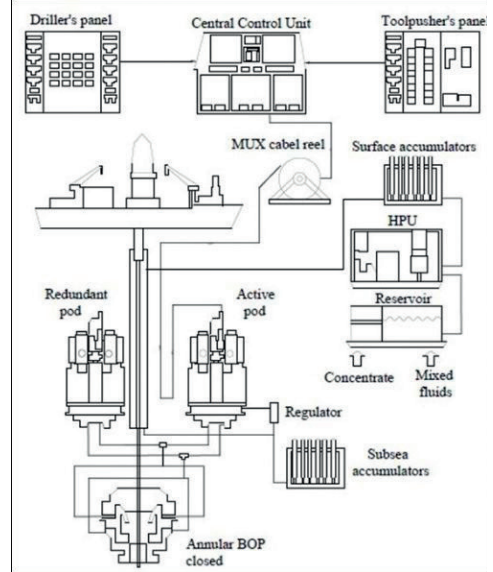




Figure 07 ROV Applications BOP latching on a wellhead, cleaning of wellhead profile

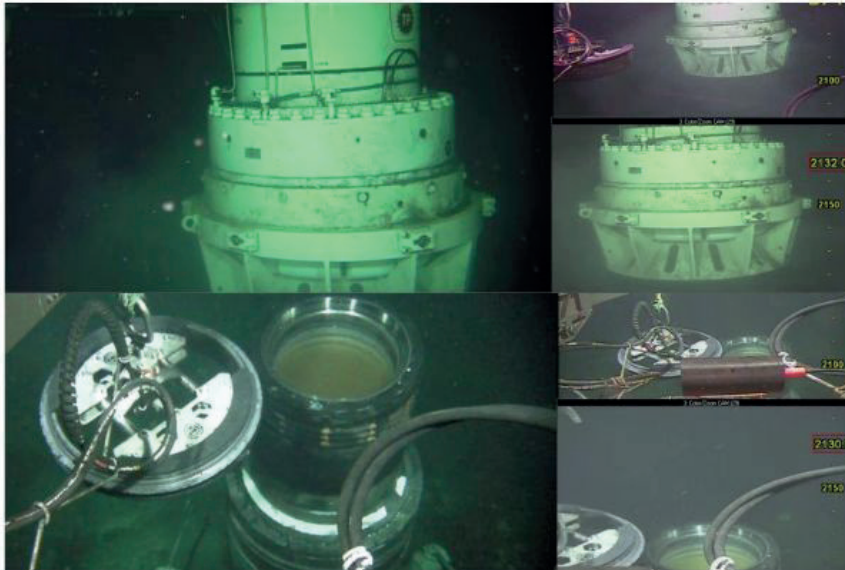


Figure 08 Acoustic Control System (Konsberg Maritime, Kozel, 2015)

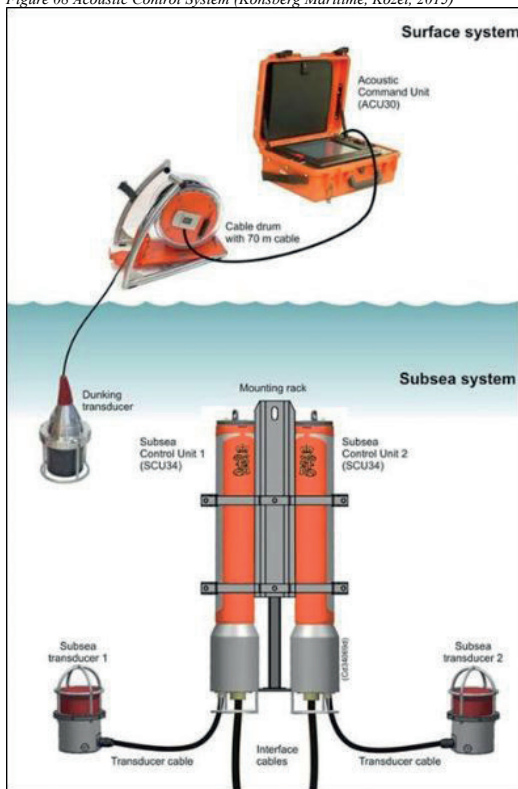


Figure 09 BOP Related NPTs in 47 drilling and completion wells

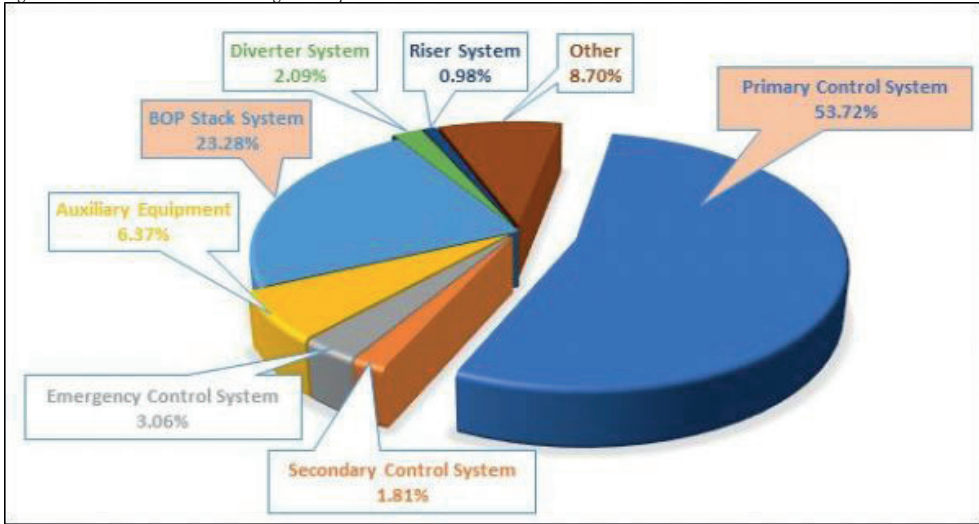


Figure 10 BOP Related NPTs versus Non BOP Related NPTs

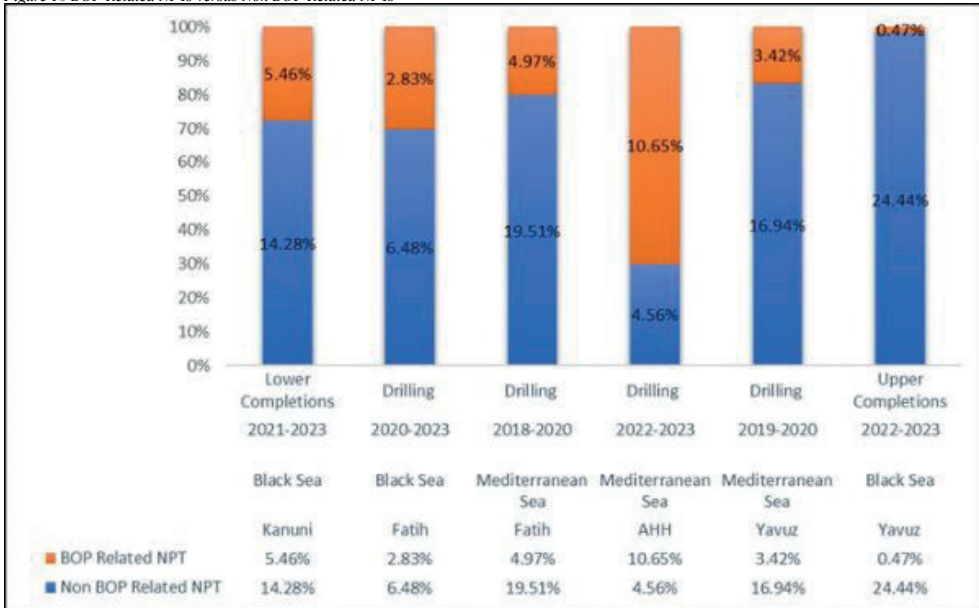
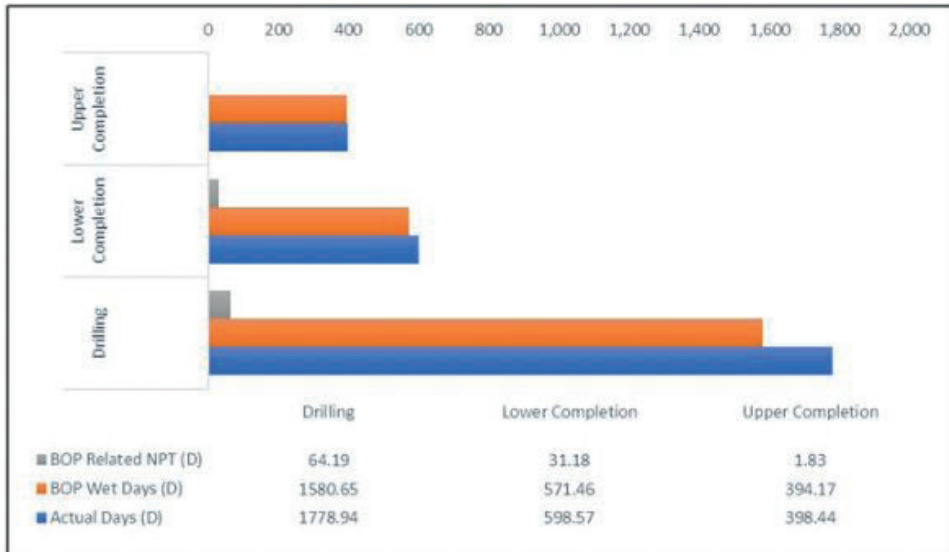


Figure 11 BOP Related NPTs versus Actual and BOP Wet Days



# BOP Hopping Operation

Ahmet Başar Dimez, Fatih Karakaya, Albert Higgins, Fırat Doğu Kaya,  
Yasin Demiralp, Andrew Timms, Uğur Cengiz  
Turkish Petroleum Off-Shore Technology Center A.Ş.



1. Deepwater drilling and completion operations often rely on floating rigs such as semisubmersibles and drillships which are equipped with subsea blowout preventer (BOP) systems (see Figure 1). The traditional process of subsea BOP operations has been time-consuming and occupational risk-involved activities. To address these challenges, the BOP hopping procedure has emerged as a valuable technique to expedite rig mobilization, saving time and mitigating operational risks, especially on rig personnel.

This study presents a comprehensive overview of the BOP hopping procedure, its advantages, and limitations in offshore drilling and completion operations. The process is described step-by-step, along with safety and limitation considerations. Additionally, a comparative analysis considering time and cost implications between conventional BOP running/recovering operations and the BOP hopping procedure is conducted.

The findings indicate that the BOP hopping procedure offers substantial benefits, including reduced rig time, decreased risk exposure for personnel, increased deck space, and eventually considerable cost savings. However, the applicability of the procedure must be evaluated for each specific task, considering limitations. Further research is recommended to explore additional factors and optimize the implementation of the BOP hopping procedure in offshore drilling operations. This study contributes to the understanding of the efficient technique of BOP hopping for deepwater drilling.

## 2. INTRODUCTION

Floating rigs, including semisubmersibles and drillships, are among the costliest assets to operate in the drilling industry. As such, maximizing efficiency during operations with these units is of paramount importance. Practices that effectively reduce rig time are highly valued in the offshore drilling industry, provided they do not compromise personnel safety or increase the risks associated with equipment. Striking a balance between operational efficiency and risk management is crucial to ensuring successful and cost-effective drilling and completion operations while prioritizing the safety and well-being of the workforce and equipment.

Traditionally, BOP (see Figure 2) running and recovering operations have been time-consuming and high-risk activities, especially for the water depths of 1800+ classified as ultra-deepwater operations. To address these challenges, BOP hopping emerged in the 2000s as an innovative technique to expedite the mobilization of rigs between well locations, saving time, and cost and reducing personnel occupational risks. BOP hopping is recognized by API STD 53 as a standard industry practice.

This study presents a detailed overview of the BOP hopping procedure. We describe the process in detail, evaluate safety and environmental considerations, and limitations, and provide a time-cost comparison between conventional BOP running/recovering operations and the BOP hopping procedure by analyzing a case study referencing the operations conducted in the Black Sea.

## 3. NOMENCLATURE

**Rig:** A drilling rig, also known as a drill rig or drilling platform, is a complex mechanical system used for drilling wells in various applications, including oil and gas exploration, mineral exploration, geothermal energy extraction, water well drilling, and construction projects. It is a crucial piece of equipment in the drilling industry.

### Floating Rig

A floating drilling rig, also known as a floating drilling rig or offshore drilling rig, is a type of drilling rig designed to operate in deep water environments, typically in water depths greater than approximately 150 meters (500 feet). These rigs are used for drilling oil and gas wells in offshore locations where the seabed is too deep for fixed-platform drilling operations.

### BOP

A BOP system, which stands for Blowout Preventer system, is a critical safety device used in drilling operations to control the flow of fluids (such as oil, gas, or drilling mud) from a wellbore. It is designed to prevent blowouts, which are uncontrolled releases of pressure and fluids from the well that can lead to catastrophic incidents.

### Semisubmersibles

Semi-submersible rigs, also known as semi-submersible drilling rigs or simply semisubmersibles, are specialized offshore drilling units used for drilling operations in deep water or harsh sea conditions. These rigs are designed to float on the water's surface while partially submerged, using pontoons or columns to provide stability and buoyancy.

### Drill Ships

A drill ship, also known as a drilling vessel or offshore drilling ship, is a specialized maritime vessel designed and equipped for offshore drilling operations. It combines the functions of a drilling rig and a ship, allowing for mobile drilling operations in deep water or remote locations.

### **Rig Mobilization**

Transfer of drilling unit from one location to another upon completion of the operations to be conducted.

### **Rig Time**

The time consumed for a specific operation, since most of the rigs are rented by the operators on a daily basis rig time is one of the most important performance indicators for the evaluation of operational efficiency.

### **Heavy Lifts**

Movement of the equipment which is heavier and bigger than usual can cause harm to equipment or personnel. These operations require dedicated risk assessment prior to proceeding.

### **Manual Handling**

Equipment transfers that involve rig personnel physical interference to the load being carried.

### **Riser**

A marine riser, also referred to as a drilling riser or offshore riser, is a vital component of offshore drilling systems. It is a large-diameter pipe or conduit that connects the subsea wellhead or blowout preventer (BOP) to the surface drilling vessel or platform.

### **Wellhead**

Very top component of an oil or gas well that sticks out from the surface or seabed.

### **Batch Drilling**

Batch drilling, also known as batch drilling operations or batch drilling technique, refers to a drilling practice where multiple wells are drilled consecutively at the same drilling location or within close proximity before moving the drilling rig to a new location. It involves drilling and completing multiple wells in a sequential manner, often without the need to move or mobilize the rig between each well.

### **Diverter Tool**

A drilling diverter tool, also known as a diverter system or diverter valve, is an essential piece of equipment used in drilling operations to divert or redirect the flow of drilling fluids or gases away from the rig in the event of an uncontrolled wellbore situation. It is designed to provide an emergency pressure control mechanism to prevent blowouts and ensure the safety of personnel and equipment on the drilling rig.

### **Slip Joint**

One of the top components of a riser string, the main purpose of the slip joint is to compensate vertical motion of the drilling unit.

### **Moon Pool**

Floating rigs have an opening just below the rotary table which is called a moon pool.

### **Dynamic Positioning System**

It is an advanced system used in ships, offshore vessels, and other maritime platforms to maintain their position and heading automatically without the need for traditional anchoring.

### **Remotely Operated Vehicle**

A type of underwater robot or submersible that is operated from the surface by remote control. ROVs are commonly used in various underwater operations and industries, such as offshore oil and gas exploration, marine research, underwater inspections, and deep-sea exploration.

### **Transponder**

A device that is placed on the sea bed to provide location signal to vessels so that the DP system remains in position over the wellhead precisely.

## **4. CONVENTIONAL BOP/RISER OPERATIONS**

Mobilizing a floating rig from one location to the next one, conventionally subsea BOP stack needs to be recovered on the deck by pulling all the riser joints above it, secured in the setback area. After the end of well maintenance for the BOP stack, it is ready to be run back into depths to be latched on the new wellhead. After the end of well maintenance for BOP, the stack is ready to be run back into depths to be latched on the new wellhead.

The operation sequence of Conventional BOP /Riser Operations consists of 3 main phases which are; recovering BOP/riser, end of well maintenance, and running BOP/riser.

Operation breakdowns for recovering BOP/riser:

1. Rig up for BOP/Riser handling tools.
2. Remove Diverter
3. Pick up and make up the landing joint
4. Collapse slip joint.
5. Unlatch the BOP stack from the wellhead.
6. Rig down moonpool connections.
7. Lay down landing joint and slip joint
8. Recover riser joints one by one and store them in the dedicated area.
9. Recover BOP on the deck and secure on setback area.
10. Rig down riser handling equipment.

End-of-well maintenance is a very detailed and particular task to be conducted by qualified personnel. End-of-well maintenance typically takes 7-14 days (depending on the work scope). High-level breakdowns

of BOP maintenance tasks are as follows:

- Cleaning and flushing the BOP Stack.
- Testing all of the functions.
- Splitting LMRP and lower BOP stack.
- Replacement of all the necessary items as per podrotation.
- Detailed inspection for faults and damages.
- Replacement of necessary filters.
- Full BOP function and pressure test including auxiliary lines and emergency sequences.
- Pre-deployment checks.
- Drift BOP.

### OPERATION BREAKDOWNS FOR RUNNING BOP/RISER

1. As conventional practices, upon the installation of a subsea wellhead on the seabed, BOP/riser handling tools are rigged up.
2. The BOP stack is skidded below the rotary table and connected to the first joint of the riser string.
3. Splash BOP and run until seabed on marine riser string picking up riser joints one by one and pressure testing auxiliary lines periodically.
4. Pick up and make up slip joint.
5. Rig up the moonpool connections.
6. Land on the wellhead and lock connector.
7. Stroke out the slip joint and lay down the landing joint.
8. Install and test the diverter.
9. Rig down riser handling equipment.

#### 4.1. Operational Risks

Conventional BOP/riser operations require for crew to keep focus and good communication during the task to conduct operations safely. The main occupational risk factors during BOP/riser operations are:

- Handling big-sized and heavy lifts, BOP and riser joint sizes and weights are different and mostly specific for the rig, for example; BOP weights: 750klbs (air), 680klbs (water), each marine riser, joint: 50klbs (air), BOP + Marine riser string: 1200klbs
- Manual handling of equipment, there are lots of tasks to be manually handled or assisted during operations.
- Working at height and on water, personnel need to work at height especially in the moonpool area for a long time on the platforms or lifting baskets.
- Stored energy, suspended heavy loads, and lines in tension and pressure are also a source of high potential stored energy bearing a high risk of injuries if they are released in an uncontrolled way.
- Collaborative work of all the departments of rig crew, marine crew, drilling crew, subsea crew, and department supervisors work all together during the task. Good

communication between the departments is the key to success.

- Repetitive task, especially running the riser joint is a long task basically repeating itself over and over again. Considering environmental difficulties offshore such as wind, cold or heavy sun, etc. keeping focus on the task and dealing with complacency can get very difficult for personnel to cope with.

### 5. BOP HOPPING PROCEDURE

BOP running and recovery operations for floating rigs are time-consuming and pose significant risks to personnel. To address the downsides of conventional BOP/Riser operations, BOP hopping emerged in the 2000s as an innovative technique to expedite the mobilization of rigs, and later on, it was recognized as an industry practice by API STD 53.

The BOP hopping procedure (Figure 3) can be basically defined as moving the rig from one location to the next one with the subsea BOP stack remaining suspended below, without the need for full recovery to the surface before rig mobilization. BOP hopping can minimize the time consumed for the mobilization of the rig by minimizing time consumption for operation, and occupational risk exposure of the personnel and the equipment is also minimized. However, it is only applicable in scenarios where the next wellhead has been pre-installed, such as in batch drilling, batch completion operations, or when multiple rigs are involved in different sections of the well construction process.

General operational sequence of the hopping process of a subsea BOP stack includes the following steps:

1. Rig up the riser handling equipment.
2. Recover the diverter.
3. Pick up the landing joint and connect it to the slip joint.
4. Collapse and lock the telescopic slip joint.
5. Unlatch the subsea BOP from the wellhead connector and lift it above the wellhead.
6. Remove subsea connections and control lines.
7. Start pulling riser joints lay down the landing joint and slip the joint back on the deck.
8. Pull the required number of riser joints to a safe space out above the seafloor.
9. Move the rig to the next location with limited cruise speed while observing the subsea BOP stack with a remote-operated vehicle (ROV).
10. Run a sufficient number of riser joints for the new location.
11. Pick up and make up the slip joint and landing joint.
12. Rig up subsea connections and control lines in the moon pool.
13. Move the rig over the wellhead.
14. Land on the wellhead with the subsea BOP and engage the wellhead connector.

15. Perform checks and tests as per procedures.
16. Stroke out the slip joint and lay down the landing joint.
17. Install and test the diverter.
18. Rig down the riser handling equipment.

### 5.1. Equipment Requirements

During BOP hopping operations, the presence of an ROV (Remotely Operated Vehicle) is essential for providing visual data, replacing ring gasket, scanning surroundings with sonar, and ensuring the safety and efficiency of the process. Figure 4 illustrates a visual representation of BOP hopping operations in progress during a voyage. The ROV's duty begins with the unlatching of the BOP stack from the existing wellhead and continues throughout the entire voyage until the BOP stack is landed and latched onto the next wellhead. ROV unit has to be equipped with a sonar system to be able to scan obstacles in the front even with bad sea water visibility, and a ring gasket running tool so that I can place the new ring gasket on the wellhead profile before landing with BOP. Overall, ROV is essential for BOP hopping operations, to provide visual data and conduct dedicated tasks, its continuous presence and real-time visual data transmission enable operators to make informed decisions, ensuring a smooth and successful transition between well locations while minimizing risks and potential challenges.

During the voyage for the BOP hopping operation, it is important to move the vessel in DP (Dynamic Positioning) transit mode. This strategic approach ensures a smooth transition of the vessel and minimizes its motion, thereby maximizing the safety of the hopping operation. DP system relies on a GPS system and the signal from the transponders located on the sea bed. Since there are no transponders during the voyage, reliable and continuous GPS data is essential for the vessel as it is the only source of navigation data.

### 5.2. Advantages of BOP Hopping

BOP hopping brings outstanding advantages such as reduced risk exposure of personnel increased deck space, reduced rig time, and reduced well cost.

For vessels designed with open riser decks, the riser storage area offers essential deck space for the storage of equipment necessary for various operations, which is particularly vital for completion operations due to the diverse range of tools and equipment required. The practice of BOP hopping further optimizes this space as marine riser joints are not recovered on the deck, allowing the riser storage area to remain available and enhancing logistics flexibility.

BOP hopping significantly reduces occupational risks for rig personnel by reducing exposure time and eliminating many high-risk tasks, resulting in a notable decrease in both the frequency and impact of incidents.

By eliminating the most time-consuming phases of conventional BOP/riser operations, BOP hopping offers

a significant reduction in rig time during mobilization. Considering the daily high costs of drilling units, this reduction in rig time translates into substantial cost savings for the project.

## 6. TIME-COST COMPARISON

The primary objective of implementing the BOP hopping procedure is to achieve substantial time and cost savings. When analyzing the sequence of operations, it becomes evident that a significant portion of time is consumed during the handling of the BOP stack on the deck, running and recovering riser joints, moon pool work for BOP/riser system connections, and particularly during the BOP maintenance period. Moon pool work for connections remains a necessary step, regardless of the procedure employed. However, the time-consuming aspects related to BOP stack handling, riser joint running/recovery, and maintenance can be eliminated through the BOP hopping procedure.

To estimate the benefits of BOP hopping, we calculate the total time required for conventional BOP/riser running operations and then deduct the equivalent time saved by omitting specific steps. This analysis allows us to assess the potential time reduction and overall efficiency gains. Referencing operations in the Black Sea with a dynamically positioned drillship, conventional subsea BOP running operations take approximately 83 hours for water depths of around 2100m, as indicated in Table 1. With BOP hopping, steps such as 'Rig up for BOP/ Riser operation,' 'splash BOP,' and 'Run approximately 76 joints of marine riser and periodic pressure tests' are eliminated, resulting in a total of 56.5 hours saved, as shown in Table 2. Similarly, Table 3 illustrates that recovering the BOP on the deck requires approximately 46 hours, through BOP hopping, steps such as 'Recover approximately 76 joints of the marine riser,' 'Recover BOP Stack on the deck and secure on setback area,' and 'Rig down riser handling equipment' are avoided, saving 30.5 hours, as noted in Table 4.

As presented in Table 5, out of the total 129 hours required for a single mobilization of a drillship, a significant 87 hours are recoverable by eliminating certain operational steps. It's essential to acknowledge that during the BOP hopping process, the BOP stack is not fully recovered, leading to the exclusion of the standard 7-day maintenance period for the BOP stack.

It's equally crucial to consider the impact of limited cruise speed for an accurate calculation. In conventional operations, vessel transit is typically an offline activity carried out during maintenance periods. However, when practicing BOP hopping, it becomes an online activity. The effect of this transition is directly linked to the distance of the route. In our case, the distance is 6 nautical miles (NM), and with a limited cruise speed of 0.5 knots, a negative 12 hours should be accounted for in the calculations. This adjustment ensures that the calculations accurately reflect the extended duration caused by the limited cruise speed during BOP hopping operations.

When considering the cumulative benefits of BOP

hopping, which includes the recovered 87 hours from recovering and running BOP/riser, 168 hours from the postponed maintenance period, and the negative 12 hours for online transit of the rig, the total benefit amounts to 243 hours or approximately 10.1 days. This represents roughly 82% of the total rig time required for conventional BOP running and recovery operations, which typically take 297 hours, as indicated in Table 6.

As a summary of the calculations so far, the total operational time for conventional BOP/riser operations in our case was 297 hours. This time could have been reduced to 54 hours if the BOP hopping procedure had been implemented instead.

To provide an alternative perspective on the advantages of BOP hopping, let's consider the daily cost of a floating rig as US\$800,000 for cost calculation purposes. The recoverable 10.1 days translates to approximately US\$8 million for a single mobilization. When projecting this cost reduction to a deep-water campaign consisting of 30 wells, assuming BOP hopping is practiced for every second well, the potential earnings reach US\$120 million for one rig over the entire project. This figure can be multiplied by the number of rigs involved in the project that can employ BOP hopping to determine the total profit derived from this practice.

In conclusion, the BOP hopping procedure offers significant time and cost savings compared to conventional BOP running and recovery operations. Recovering 82% of operational time is an undeniable benefit, particularly for operations with high daily costs, such as offshore drilling and completion operations.

## 7. LIMITATIONS

It is crucial to note that moving a rig with a suspended BOP requires careful planning, equipment handling, and adherence to safety protocols. The rig crew must follow industry best practices and regulations to ensure the safety of personnel and equipment throughout the entire rig move process.

When planning for a BOP hopping operation, several environmental considerations should be considered, including water depth, shallow and mid and deep ocean currents, sea and wind conditions, weather forecasts, and the bathymetry of the sea bed. These factors can impact the safety and feasibility of the operation, proper planning and precautions must be taken accordingly.

Water depth is one of the important considerations while hopping a BOP stack, when there is a significant depth difference between well locations, control system pre-charge values should be calculated and set such that it is suitable for all of the intended depths prior to running BOP into water in the first location.

Ocean currents have to be evaluated by met-ocean data along the route, strong currents can jeopardize operational safety.

Sea and wind conditions should be favorable for the BOP hopping operation as well as the weather forecast. Weather condition limitation more depends on the vessel motion than it does on the weather itself. Figures

being accepted for safe operations in the Black Sea are defined as 1deg for max pitch, 1deg for max roll, and 2 meters for max heave. If weather conditions cause or are likely to cause (according to the weather forecast) the vessel to move above accepted limits, detailed risk assessments need to be conducted before proceeding with the BOP hopping operation.

Even under the best weather conditions, vessel cruise speed is limited by 0.3-0.5 knots (depending on the vessel). This limitation is the consideration of BOP stack stand-off and hydrodynamic damage risk of delicate parts or fittings on the BOP stack. Cruise speed is another measure to take into account when planning for BOP hopping. Any unintended motion of the vessel reaching above accepted limits can cause failure on the integrity of the riser/BOP system or other equipment involved due to substantial weight suspended below the rig which is approximately 1200 klbs for ~2100 meters of water depth.

While evaluating the bathymetry, there might be artificial obstructions as well as natural ones. BOP hopping operations are mostly preferred for batch completion operations in the Black Sea. Simultaneous operations are being conducted in the area for drilling, completion, and the construction of subsea pipelines and structures.

Another major limitation of BOP hopping is the impact on BOP maintenance. Delaying BOP maintenance while conducting BOP hopping can significantly increase the frequency of BOP failures and may outweigh any advantages BOP hopping offers for the project if not carefully planned. It is crucial to assess potential BOP failures before initiating any hopping operation. If there are persisting issues or indications of possible failure, or if the maintenance period has already been delayed too long based on industry best practices, proceeding with BOP hopping instead of prioritizing recovery and maintenance could lead to BOP failures during critical operation stages. Such occurrences pose a serious risk to personnel safety, result in substantial downtime, and profoundly disrupt the well construction process. Proper planning and consideration of maintenance requirements are essential to minimize risks and ensure success and safety.

## 8. CHALLENGES

Limiting factors can be challenged through the application of scientific methods and causality calculations, as long as viable and safe solutions can be derived within the bounds of these approaches.

For instance, in the Sakarya field, there are subsea structures located on the BOP hopping route. Any failure causing to drop BOP on subsea structures can end up a dramatic damage to the structures and lead to significant delays on the project timeline. To mitigate this risk and ensure the safety of the equipment and the subsea structures, the route for BOP hopping needs to be carefully designed to allow smooth navigation for the vessel so that it is achievable with the BOP stack remaining suspended below and also effectively avoid



any intersection with the subsea structures. Planning for cruise speed, route, maneuvers and distances from the subsea structures requires considerable attention and precision.

In another case, vessels were experiencing frequent GPS signal disruptions, raising significant concerns for the safety of the hopping operation during risk assessment. In response, a proactive measure was taken to ensure redundancy in positioning systems. A transponder was attached to the hand of the ROV deployed to accompany the BOP stack during the hopping operation, offering an alternative means to locate the vessel in the event of GPS signal loss. The plan was to drop the transponder to the sea bed and provide location information to the DP system if any GPS data disruption was experienced. Even though GSP data reception was continuous, this redundant system successfully mitigated to risk of losing GPS data during the voyage.

## 9. CONCLUSION

The BOP hopping procedure has demonstrated significant advantages in offshore drilling & completion operations. By employing this procedure, significant time and cost savings can be achieved while reducing the risk exposure of the rig personnel.

The time-cost comparison analysis conducted in the Black Sea case study highlighted the potential benefits of the BOP hopping procedure. By recovering a significant portion of the time consumed by conventional BOP running and recovery operations, the procedure offers the opportunity to optimize rig time and minimize operational costs.

The benefits of the BOP hopping procedure are particularly prominent in cases where greater water depths would require more time to recover the subsea BOP stack to the surface and then re-run into depths. By implementing the hopping procedure, this time can be significantly reduced. Additionally, when mobilizing the rig between closely located well locations, the limited cruise speed and time with the BOP suspended below the rig becomes less of a concern, making the hopping operation more advantageous.

However, it is crucial to evaluate the applicability and effectiveness of the BOP hopping procedure before application. Factors such as water depth, distance between well locations, and environmental conditions and obstructions need to be carefully evaluated. Especially, delaying the BOP maintenance period for too long can cause an increase in the failures of the BOP system and consequently times. Adherence to industry best practices and safety regulations is essential to ensure the well-being of personnel and the protection of the environment and equipment during the rig move process.

In summary, the BOP hopping procedure offers the benefits of, reduced risk exposure for personnel, along with considerable time and cost savings. However, it is important to assess the feasibility of the procedure for each specific case and consider relevant limitations.

Further research and optimization are needed to maximize the benefits and efficiency of the BOP hopping procedure in offshore drilling and completion operations.

## 10. ACKNOWLEDGMENTS

I would like to express my gratitude to Mr. Fatih Karakaya for his valuable mentoring, generous time, and suggestions during the preparation of this study. I wish to extend my gratitude to Mr. Albert Higgins and Mr. Andrew Timms for their suggestions and contributions. Furthermore, I am also thankful to TP-OTC for encouraging me to construct this study.

## 11. REFERENCES

- API Standard 53 Fifth Edition December 2018
- TP-OTC Operation Procedures, "Rig Move Operations", PRO-CORP-OPS-027
- TP-OTC Operation Procedures, "Risk Assessment Form", FORM-CORP-HSE-034
- TP-OTC Daily Drilling/Operation Reports
- Aroona Drilling Operation Plans "Move Rig Between Wells With BOP Suspended"
- Transocean Drilling Practices, Drilling Practices, "Field Moves With BOP Suspended in the Water"

## 12. APPENDIX

### 12.1. Abbreviations and Acronyms

- BOP: Blowout Preventer
- DP: Dynamic Positioning
- ROV: Remotely Operated Vehicle

### 12.2. List of Figures

- Figure 1  
Subsea BOP and Marine Riser System
- Figure 2  
Subsea BOP Stack
- Figure 3  
BOP Hopping
- Figure 4  
ROV Visual During BOP Hopping

### 12.3. List of Tables

- Table 1  
BOP Running Operation Time Breakdown for ~2100m Water Depth
- Table 2

Recoverable Time Breakdown for BOP Running Operation

Table 3

BOP Recovering Operation Time Breakdown for ~2100m Water Depth

Table 4

Recoverable Time Breakdown for BOP Recovery Operation

Table 5

Operational Time Summary for BOP Running and Recovery

Table 6

Recoverable Time by BOP Hopping Operation

Keywords: Move BOP Suspended, BOP Hopping

Figure 1 - Subsea BOP and Marine Riser System

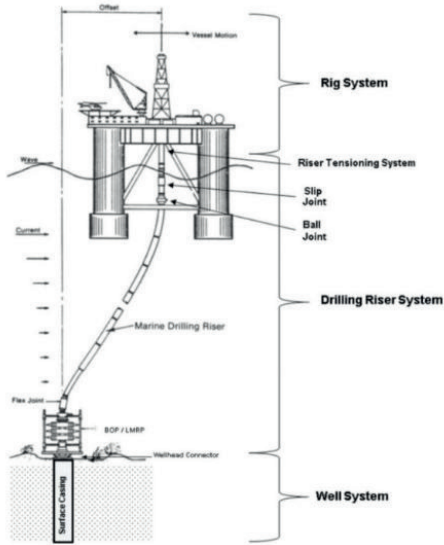


Figure 2 - Subsea BOP and Marine Riser System

Figure 2 – Subsea BOP Stack

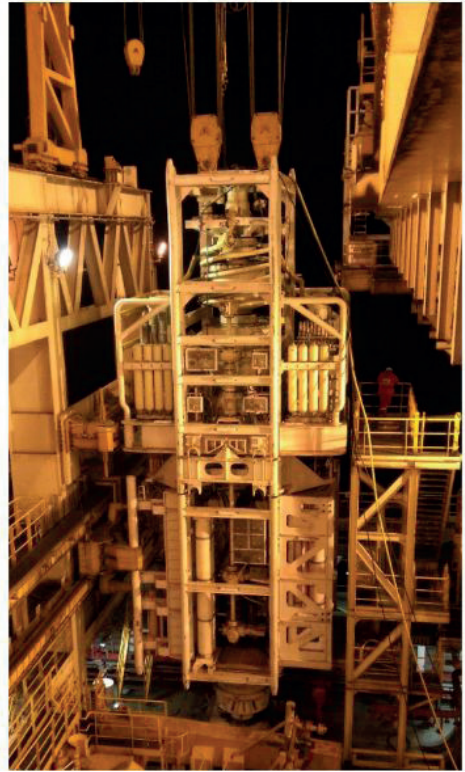


Figure 3 - BOP Hopping

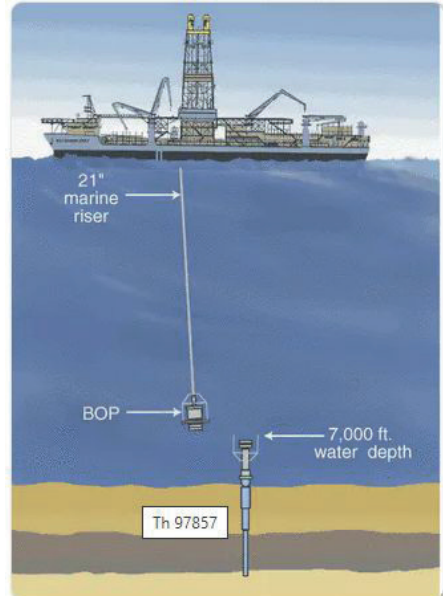


Figure 4 - ROV Visual during BOP hopping

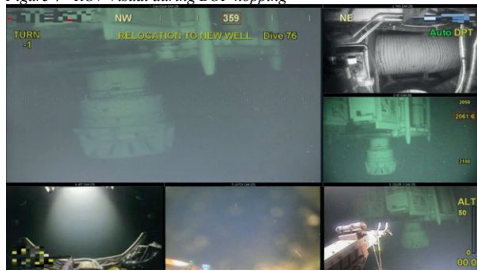


Table 1 - BOP Running Operation Time Breakdown for ~2100m Water Depth

	Time (hours)
BOP/Riser Running Operation	5
Rig up for BOP/Riser operation	2.5
Splash BOP	49
Run ~76 joints of marine riser and periodic pressure tests	5.5
Pick up and make up slip joint	8
Moon pool work for BOP/Riser system connections	3
Land and latch on WH with subsea BOP and final tests	1
Stroke out slip joint and lay down landing riser joint	6
Install diverter	3
Rig down riser handling equipment	83
Total	

Table 2 - Recoverable time breakdown for BOP running operation

	Time (hours)
BOP/Riser Running Operation	5
Rig up for BOP/Riser operation	2.5
Splash BOP	49
Run ~76 joints of marine riser and periodic pressure tests	56.5
Total	

Table 3 - BOP Recovering Operation Time Breakdown for ~2100m Water Depth

	Time (hours)
BOP/Riser Recovery Operation	5
Rig up for BOP/Riser operation and rig down diverter	3
Rig down diverter	1.5
Collapse slip joint	1
Unlatch subsea BOP from wellhead	3.5
Moon pool work to remove BOP/Riser connections	1.5
Lay down slip joint	23.5
Recover ~76 joints of marine riser	4
Recover BOP Stack on the deck and secure on setback area	3
Rig down riser handling equipment	46
Total	

Table 4 - Recoverable time breakdown for BOP recovery operation

Recover ~76 joints of marine riser	23.5
Recover BOP Stack on the deck and secure on setback area	4
Rig down riser handling equipment	3
Total	30.5

*Table 5 - Operational time summary for BOP running and recovery*

Time Recovery by BOP Hopping	Total Time (hours)	Recoverable Time (hours)
Running BOP/Riser	83	56.5
Recovering BOP/Riser	46	30.5
Total	129	87

*Table 6 - Recoverable Time by BOP Hopping Operation*

Time Recovery by BOP Hopping	Total (hours)	Time Recoverable (hours)	Time	Total Time (Days)	Recoverable Time (Days)
Running BOP/Riser	83	56.5		~3.5	~2.4
Recovering BOP/Riser	46	30.5		~1.9	~1.3
Maintenance period	168	168		7	7
Transit time with reduced cruise speed	N/A	-12		N/A	-0.5
Total	297	243		~12.4	~10.1

# Cased Hole Gravel Pack

Uğur Cengiz, Eren Emre Geçer, Carlos Anderson Domingos, Atilla Mazman, Bekir Oğulcan Bulut, Yasin Demiralp, Fırat Doğu Kaya, Fatih Karakaya  
Turkish Petroleum Off-Shore Technology Center A.Ş.



1. The cased hole gravel pack operation is a technique employed in well completion to achieve effective sand control in reservoirs with poor consolidation or non-uniform particle size distribution. This methodology aims to fulfill two primary Objectives: packing the annulus between screens and the cased hole with the appropriate size of gravel sand and filling each perforation tunnel adequately. By achieving these objectives, the operation prevents sand production, enhances long-term productivity, and prevents potential issues such as collapsing perforation tunnels resulting in a decline in production.

The methodology involves meticulous consideration of critical factors such as gravel size and type, fluid selection for gravel transport, screen type, and formation characteristics. Conducting a sand sieve analysis enables the determination of the ideal gravel sand size, facilitating proper sand control while allowing the flow of fines. The selection of a clean and compatible carrier fluid ensures effective gravel transport. Screen selection involves choosing a mesh size smaller than the smallest size of gravel sand to optimize sand filtration and control.

By implementing proper methodology and utilizing the appropriate equipment, cased-hole gravel pack operations can be executed efficiently, controlling solids production to an acceptable range while maintaining high flow capacity, and maximizing production at minimum draw-down pressure.

## 2. INTRODUCTION

Unconsolidated sandstone formations pose a significant challenge in the extraction of oil and gas reserves, as they often lead to sand production in wells. Sand production can occur during the initial production phase and has detrimental effects on the longevity of the well and operational expenses. To mitigate this issue, the gravel pack method has become the preferred technique in the oil and gas industry. By effectively designing and executing gravel pack operations, sand production can be reduced to acceptable levels, extending the well's lifespan. This paper examines the cased hole gravel pack methodology, its objectives, critical design factors, and the essential equipment involved. Understanding and implementing this methodology can ensure optimal sand control and enhance well performance.

## 3. NOMENCLATURE

Unconsolidated formations: loose geological layers lacking strong binding material between the grains or particles. These formations are prone to sand production, where loose particles can dislodge and cause operational issues during oil and gas extraction.

**Cased Hole:** Wellbore section that is lined with a steel casing for stability and protection. It involves operations conducted within this protected section, such as logging and interventions.

**Annulus:** The space or gap between concentric objects, such as the wellbore and casing.

**Perforation:** The process of creating holes or channels in the casing and surrounding rock formation during well completion.

**Gravel:** Small, granular particles, typically made of sand or other durable materials.

NTU (Nephelometric Turbidity Unit): measurement unit used to quantify the turbidity of a liquid sample. Turbidity refers to the cloudiness or haziness of the liquid caused by suspended particles.

**Casing Scraper:** is a mechanical tool used in well operations to clean the inner surface of the well casing.

**Casing Brush:** This is a tool used in oil and gas operations to clean the inner surface of a casing pipe.

**Sand Sieve Analysis:** the method used to determine the particle size distribution of sand. It involves passing a sample of sand through a series of sieves with progressively smaller openings. This analysis provides valuable information about the grain size distribution and helps characterize the properties of the sand.

**Snap latch:** Refers to a mechanical device used for quick and secure fastening or locking of components.

## 4. CASED HOLE GRAVEL PACK OPERATION AND EQUIPMENT

### 4.1. Principle and Objective of Gravel Pack Operation

Cased Hole gravel pack operations involve the installation of screens to effectively manage the flow of sand from the formation while allowing the production of gas or oil. This operation is considered one of the most intricate tasks during the completion phase due to its multifaceted nature, requiring a combination of specialized practices.

The cased-hole gravel pack operation aims to achieve two primary objectives:

1. Packing the annulus between screens and the cased hole with the appropriate size of gravel sand. Properly filling and packing the annulus plays a critical role in preventing sand production from unconsolidated sand formations. By effectively controlling the sand, the operation helps to maintain the long-term productivity and integrity of the well.

2. Packing each perforation tunnel with gravel sand is vital for optimal well production. Failing to fill and pack the perforations properly can result in the collapse of unconsolidated formation sands or their intrusion into the perforations. This can result in pressure drop issues, which can ultimately lead to reduced well production or a complete halt in production.

These objectives highlight the significance of meticulous gravel pack execution, as it directly impacts sand control and the overall performance of the well.

#### 4.2. Design Considerations

The successful execution of gravel pack operations requires thorough design considerations. Preparing the wellbore and selecting the appropriate tools, materials, and techniques are crucial for achieving effective sand control and optimizing well performance. By understanding the unique challenges and characteristics of the formation, operators can develop customized strategies to mitigate sand production and ensure the long-term productivity and integrity of the well.

##### 4.2.1. Size and Type of Gravel

The size and type of gravel play an essential role in the quality and longevity of a well-completion operation. To determine the ideal gravel sand size for a specific well and formation, a sand sieve analysis is conducted using samples obtained from the formation, often through conventional or sidewall core methods.

Accurately determining the size and type of gravel sand is vital to prevent the formation of sand from migrating into the wellbore. Simultaneously, allowing fines, which naturally flow with the formation fluid, into the wellbore is necessary. If fines are allowed to bridge off, they can reduce the flow area and have a negative impact on production.

By conducting a thorough analysis and understanding the size and type of gravel needed, the well's integrity can be maintained, ensuring that sand is controlled while fines are properly managed, ultimately enhancing the overall productivity of the well.

##### 4.2.2. Fluid Selection (to Carry Gravel Sands)

It is of utmost importance that the fluid used in the gravel pack job is thoroughly cleaned and filtered. Additionally, the carrier fluid must be compatible with the formation, similar to other completion fluids. Using incompatible fluids can cause clay swelling or changes in permeability, which in turn can lead to a reduction in well productivity.

Gravel packs conducted using brine as the carrier fluid are commonly known as water/brine packs or conventional packs. On the other hand, gravel packs performed with HEC gel transport fluids are often referred to as slurry packs, gel packs, or viscous packs. Generally, a fluid that does not require a breaker is preferred for gravel pack operations. In cases where

viscosifiers are necessary for the gravel pack fluid, a breaker should also be employed to reduce the carrier fluid's viscosity to a level comparable to that of water after a specific period.

Based on both laboratory experiments and field applications, brine has demonstrated better performance in achieving comprehensive packing within the perforations and annulus across a diverse range of well conditions. As such, it is widely regarded as the preferred, versatile choice for gravel-pack operations in most scenarios. On the other hand, the application of gel transport fluids is best suited for wells with inclinations of less than 45°.

When HEC gel is used as the transport fluid, the gravel particles are suspended within the gel, leading to slow settling due to the high viscosity of the fluid. In contrast, when brine is utilized as the transport fluid, the gravel settles more quickly due to its lower viscosity. As a result, higher pump rates may be necessary when using brines to accommodate the settling of the particles.

##### 4.2.3. Screen Selection

Screen selection is a critical aspect of gravel pack operations as it involves the placement of screens within the wellbore, featuring a mesh of the appropriate size. The primary function of the screen is to allow fluid to flow into the wellbore while effectively preventing the passage of gravel sands. To ensure optimal gravel sand control, it is essential to select screen mesh sizes that are smaller than the smallest size of gravel sand used in the gravel pack operation. This ensures maximum filtration and minimizes the risk of sand production. Proper screen selection plays a vital role in maintaining the integrity and productivity of the well by effectively managing the flow of fluids while preventing the migration of unwanted solids.

##### 4.2.4. Packer Selection

When selecting a packer for cased hole gravel pack operations, it is crucial to choose one that can provide effective zonal isolation and prevent gravel pack fluid from bypassing the target zone. Factors to consider include the pressure and temperature ratings of the packer, its sealing capabilities, and compatibility with the wellbore and gravel pack fluids. Additionally, metallurgy and elastomer considerations should be taken into account based on well conditions, including the presence of H<sub>2</sub>S, CO<sub>2</sub>, etc. The selection process should also consider the specific reservoir and differential pressure requirements. Hydraulic or mechanical packers are commonly used in cased-hole gravel pack operations due to their reliability and performance.

##### 4.2.5. Pumping Equipment and Rates

Proper evaluation and selection of pumping equipment are necessary to achieve efficient gravel pack placement. Pumping rates should be optimized to ensure adequate gravel transport and distribution throughout the annulus.

Monitoring pressure and flow rates during pumping is essential for accurate placement while ensuring that the pressure remains below the fracture pressure of the formation. Exceeding the fracture pressure can result in formation damage which can negatively impact well productivity.

### 4.3. Cased Hole Gravel Pack Equipment

Cased Hole Gravel Pack Equipment is a critical component of gravel pack operations in unconsolidated formations. This equipment includes the gravel pack base (sump packer), seal assembly, screens, gravel pack packer, service tool, wash pipe, and mechanical fluid loss devices such as FIV, MFIC, and MST sleeves. Each component serves a specific purpose in ensuring the success of the gravel pack operation, which involves controlling sand production and optimizing well productivity. The careful selection and utilization of these equipment elements are essential for achieving effective sand control and maintaining the long-term integrity of the well.

#### 4.3.1. Gravel Pack Base (Sump Packer)

The gravel pack base, commonly known as the sump packer, establishes the foundation of cased hole lower completion assemblies including screens, blank pipes, and the gravel pack packer. The sump packer can be deployed using an e-line or drill pipe, positioned below the deepest perforating depth prior to the perforation operation. In the Black Sea completion operation wireline is employed to set the Sump Packer to achieve precise placement as it is critical for the forthcoming zones. Once the sump packer is set and the casing is perforated, the lower completion assemblies can be installed. The seal assembly, located at the lowermost part of the lower completion assembly, securely connects with the sump packer, providing a stable base for the gravel pack operation.

#### 4.3.2. Seal Assembly

The seal assembly creates a secure seal between the sump packer and the lower completion annulus in cased-hole gravel pack applications. Typically, a snap latch-type seal assembly is used. The seal assembly serves two main purposes within the sump packer bore:

1. Preventing gravel pack sand from filling the bottom of the well during gravel pack operations. This ensures that the desired gravel pack placement is achieved without compromising the well's integrity.
2. Providing zonal isolation for each production section, particularly when multiple zones are targeted for gravel pack completion. This allows for effective control and management of production from different reservoir zones.

Additionally, the snap latch locator on the seal assembly provides a surface indication that the lower completion assemblies are accurately positioned, confirming the proper alignment and placement of the components.

#### 4.3.3. Screens

Screens play a pivotal role in gravel pack operations as they form the cornerstone of the sand control process. The primary objective of gravel pack operations is to effectively manage and control sand production. To achieve this, it is crucial to fill and pack the annulus between the casing and production string, as well as the perforation tunnels, with gravel.

Gravel pack screens serve as the essential tools that create an annular space between the production string and casing. This annular space acts as a barrier, retaining the gravel pack during the production phase and preventing the production of sand from the formation. By strategically designing and selecting gravel pack screens, the risk of sand production can be significantly reduced, ensuring a more efficient and reliable production process. Screens are therefore instrumental in maintaining sand control and optimizing the overall performance of the well.

#### 4.3.4. Blank Pipe

Blank pipe acts as a sand reservoir positioned above the screen, important for maintaining the integrity of the screen packing. A general guideline recommends ensuring a minimum of 30 feet of gravel packing above the screen when using brine as the completion fluid. However, in viscous fluids or shorter completion intervals, the length of the blank pipe can be extended to up to twice the length of the screen. This adjustment ensures that the screen remains effectively packed with gravel.

Moreover, blank pipe serves a dual purpose by functioning as an extension to access and connect with the upper zones for subsequent completion operations. This capability allows for efficient completion construction of multiple reservoirs within a single well.

#### 4.3.5. Gravel Pack Packer

Gravel pack packers are integral components positioned above the gravel pack assemblies in the lower completion section. These packers can be classified as either permanent or retrievable, with the retrievable option often being recommended. In the event of any failure during the gravel pack operation or during the packer setting process, retrievable packers can be easily retrieved using a specific tool.

By employing sealbore packer gravel pack systems, the implementation of multiple-zone gravel pack completions can be effectively achieved. The gravel pack packer can also serve as a "sump packer" for the subsequent lower completion zone, provided the spacing between each zone is appropriately arranged. This enables efficient zonal isolation and facilitates the proper execution of the gravel pack operation across multiple zones.

Overall, the selection of the appropriate packer type and the strategic utilization of gravel pack packers enhance the reliability and flexibility of the gravel

pack completion process, ultimately contributing to the overall success of the well.

#### 4.3.6. Gravel Pack Extension

Gravel pack extensions provide a flow path from the tubing above the packer to the screen or casing annulus below the packer. These extensions facilitate the efficient transport of gravel pack fluids during the gravel pack job. This structure comprises two components: the upper extension, which contains flow ports for gravel pack fluids, and a sealbore. The lower extension, on the other hand, is responsible for housing the gravel-pack service tool across its entire operational range. The precise length of the gravel-pack extension is designed to ensure compatibility with a specific gravel-pack packer and its service tool.

#### 4.3.7. Service tool

The service tool is widely utilized in gravel pack operations, gaining global acceptance for its effectiveness. The fundamental principle of gravel pack operations in cased holes involves pumping gravel into the screen and casing annulus through the service tool.

Service tools facilitate the circulation of gravel down the work string, above the packer, and into the screen and casing annulus below the packer. During this process, the return flow, consisting solely of carrier fluid (as the gravel is retained by screens), travels up the washpipe and back through the service tool, directing the flow to the casing and work string annulus above the packer.

To achieve optimal results, the return flow is restricted using a choke, which forces fluid out of the perforations, allowing for some degree of leak-off and enabling the packing of gravel sands into the perforation tunnels. Once the desired or calculated amount of gravel sands has been placed and screen-out (indicating complete packing of the screen, casing annulus, and perforation tunnels) has been achieved, the work string is further raised to manipulate the service tool into the reverse circulation position.

In the reverse circulation position, any excess slurry remaining in the work string above the service tool can be reversed out to the surface for disposal. Once the gravel pack operation is completed, the service tool is removed from the lower completion string by simply pulling the string.

#### 4.3.8. Washpipe

The washpipe is located beneath the service tool and packer. It is installed inside the screens and blank pipes to facilitate the return flow of the gravel pack carrier fluid from the bottom of the screens. The positioning of the washpipe is important, with its bottom placed in close proximity to the bottom of the screens.

This strategic placement allows for the gradual buildup of gravel sands from the bottom of the screens, ensuring a systematic packing sequence from bottom to top.

#### 4.3.9. Mechanical Fluid Loss Devices

Mechanical fluid loss devices minimize fluid loss to the formation. In completion operations in the Türkiye Black Sea, the MST screen system has been used for the sand control. This system consists of sleeves located within the screen, which are utilized as fluid loss control as well as producing the well. These sleeves can be manipulated using a running shifting tool.

Once the gravel pack job is completed and the reverse circulation is finished, the service tool is pulled out, causing the monitoring sleeves to close. These sleeves serve as the flow path into the washpipe to the annulus throughout the gravel pack operation. By closing these sleeves, the loss to the formation is stopped until they are opened again for production or well testing.

### 4.4. Well Preparation Prior to Cased Hole Gravel Pack Operation

Effective preparation of the well is essential before performing a gravel pack operation. The following steps are pivotal in ensuring the efficient execution of the gravel pack job:

#### 4.4.1. Casing Cleaning

Prior to displacing the well with a clean brine, it is important to clean the casing walls using mechanical cleaning tools such as casing scrapers, casing brushes, riser brushes, and well scavengers. This step removes any potential cement or scale debris that could hinder the sealing of packers.

#### 4.4.2. Displacing Well to Clean Completion Fluid

The completion fluid used must be clean, free from solids, and have a low TSS (total suspended solids) and NTU (nephelometric turbidity unit) value. Surface filtration systems should be employed to achieve the required level of cleanliness for the completion fluids. This helps prevent any plugging or reduction in formation permeability and gravel pack sand performance.

#### 4.4.3. Clean Out Run After Perforation

Shape-charged perforations generate debris and may leave metal fragments from the housing in the well. Prior to running the lower completion and performing the gravel pack operations, it is crucial to remove these debris and metals from the well using mechanical cleaning tools such as VACs, well scavengers, and magnets. This step ensures a clean well environment for the subsequent operations.

#### 4.4.4. Pickling:

During the makeup of drill pipe connections, pipe dope is used. However, excessive accumulation of pipe dope inside the drill pipe can pose a problem. When gravel pack fluid is pumped, the excessive pipe dope can be



swept along and deposited in the formation, potentially causing damage and screen plug.

To mitigate this issue, it is important to thoroughly clean and remove any excess pipe dope from the drill pipe prior to the gravel pack operation. This can be achieved through a pickling process, which involves the use of specialized cleaning fluids or solvents to dissolve and remove the accumulated pipe dope. Pickle fluid is pumped down with a specified volume through the string, ensuring it doesn't reach the formation but thoroughly cleans the entire string. Afterward, it is then reversed out.

#### 4.4.5. Acidizing

Additionally, the debris created from the perforations can accumulate around the perforation, leading to reduced well productivity. To maximize well productivity, it is necessary to remove the debris deposits around the perforation. Acidizing is commonly employed as a method to remove such debris buildup in the perforations, restoring their performance.

An injectivity test is conducted to determine the formation's injectivity rates, helping make a decision about whether acidizing is needed.

#### 4.5. Steps of Gravel Pack Operation in Well Site

1. Mobilization: The first step is to mobilize the necessary equipment and personnel to the wellsite. This includes bringing in the gravel pack pumping unit, mixing equipment, screens, packers, service tools, and other required tools and materials.
2. Rigging up: Once at the wellsite, the equipment is rigged up and positioned in the appropriate locations for the gravel pack operation. This includes setting up the pumping unit and silos for gravel sands, connecting the necessary hoses and lines.
3. Pre-job preparation: Before initiating the gravel pack operation, pre-job preparations are conducted. This involves checking and verifying all equipment, ensuring that the screens, packers, and other tools are in good condition, performing pressure tests of pipes and equipment above expected treating pressure, and calibration of flow meters.

Additionally, prior to the gravel pack job conducting a "Screen Out Drill" with the drill crew is essential to ensure they are prepared for immediate gravel reverse-out in the event of a screen out, as failing to do so may necessitate costly and time-consuming coil tubing cleanup procedures.

4. Gravel pack fluid preparation: The gravel pack fluid, which carries the gravel sand, is carefully prepared beforehand. This involves selecting the appropriate fluid composition, cleaning and filtering the fluid to remove any impurities, and ensuring compatibility with the formation and other completion fluids.
5. Wellbore preparation: The wellbore is prepared for the gravel pack operation by cleaning out any debris,

scale, or obstructions that could hinder the proper placement of gravel sand. This may involve using tools such as scrapers or brushes to clean the casing and wellbore surfaces. (section 4.4)

6. Screen and packer installation: The screens and packers are run and installed in the wellbore. The screens are placed at the desired intervals, ensuring they are securely positioned to create an annular space between the production string and casing. The packer is then set above the screens to provide zonal isolation and prevent gravel pack fluid from bypassing the target zone

7. Pickling and Acidizing: (see sections 4.4.4 and 4.4.5)

8. Gravel Pumping: Gravel pack fluid, mixed with the gravels, is pumped down the work string to initiate the gravel pack operation. The fluid flows through the service tool, which acts as a crucial junction point, effectively distributing the gravel into the annulus below the packer. This process requires close monitoring of pressure and flow rates during pumping to ensure the precise placement of the gravel pack material throughout the targeted zones.

Monitoring the pressure and flow rates during pumping is essential for several reasons. Firstly, it helps detect any potential issues or irregularities in the gravel placement, such as voids or areas with insufficient gravel. Adjustments can then be made in real-time to address these concerns and optimize the gravel pack's effectiveness. Secondly, by carefully controlling the pressure and flow, the risk of formation damage can be minimized, ensuring that the reservoir is not negatively impacted by the operation.

During the pumping process, the gravel pack gradually forms, with the gravel sand settling around the screens and inside the perforation tunnels. The goal is to create a robust and permeable barrier that prevents sand production while allowing hydrocarbons to flow freely into the wellbore.

9. Achieve Screen-Out: Close monitoring of the operation enables the determination of when screens reach their full packing capacity, a condition known as "screen-out." Screen-out signifies the optimal filling of the annulus between the casing and screens, as well as the proper packing of gravel into the perforation tunnels, ensuring effective sand control and preventing sand production.

10. Reverse Circulation: Once the desired level of gravel packing has been achieved, typically indicated by a screen-out condition, the next step is to initiate reverse circulation. This involves raising the work string to manipulate the service tool into the reverse circulation position. (see Figure 3)

In the reverse circulation configuration, the fluid flow is reversed, with the carrier fluid and any remaining slurry in the work string above the service tool now flowing upward toward the surface.

As the slurry flows upward, it travels through the work string and is ultimately brought to the surface for disposal. This process effectively removes excess gravel sands remaining in the pipe, mitigating the risk of

potential issues such as stuck pipe or parted washpipe. Failure to reverse out the excess gravel could indeed lead to significant problems and potentially result in losing the well.

11. Surface disposal: The excess slurry is typically directed to appropriate disposal systems or containment units at the surface. This ensures that any environmental or regulatory requirements for waste management are properly met.

#### 4.6. Operational and Risks Associated with Gravel Pack Operation

1. Incomplete Gravel Packing: Achieving uniform and complete gravel packing throughout the well annulus can be challenging due to factors such as uneven fluid flow distribution, screen plugging, and bridging of gravel particles. Inadequate gravel packing can result in the migration of formation sand and reduced sand control effectiveness.

If larger particle sands are able to flow freely through the screens, they can create "hot spots" causing excessive wear and damage to the screen, ultimately leading to the unwanted sands being brought to the surface. This can result in severe damage to the surface production equipment and have a negative impact on overall production operations.

2. Screen Plugging: Unconsolidated sand formations can lead to screen plugging, where sand particles infiltrate the screen openings and restrict fluid flow. This can hinder the effectiveness of gravel pack operations and reduce well productivity. Factors such as screen mesh size, and screen type play a crucial role in mitigating screen plugging risks.

3. Fluid Loss: Fluid loss into the formation during gravel pack operations can result in formation damage, reduced productivity, and ineffective sand control. Controlling fluid loss and selecting appropriate gravel packing fluids that minimize fluid loss are essential considerations.

4. Formation Damage: The process of gravel packing can inadvertently cause formation damage if during the pumping stage fracture pressure is exceeded. These issues can negatively impact well productivity and sand control effectiveness.

Also, the placement of gravel packs may cause formation damage, such as screenouts or plugging of pore throats, which can reduce reservoir permeability and well productivity if not properly managed.

5. Pumping Challenges: Pumping gravel pack fluids into unconsolidated sand formations can be challenging due to high frictional pressure losses, proppant settling, and the need for precise control of fluid rheology. Optimizing pumping rates, pressures, and fluid additives can help overcome these challenges and ensure efficient gravel placement.

In the event of a pump failure during a gravel pack operation, the inability to reverse out can lead to significant consequences such as a stuck pipe and

potential loss of the well. To mitigate such risks, it is important to have a backup pump available as a contingency plan. The backup pump can be used promptly in case of a primary pump failure, ensuring continuous fluid circulation and preventing operational delays or complications.

6. Operational Safety: Gravel pack operations involve handling and pumping abrasive materials, which can pose risks to personnel and equipment integrity. Implementing proper safety protocols, equipment maintenance, and personal protective measures are crucial to mitigate operational safety risks.

7. Cost Considerations: Gravel pack operations can be expensive, especially in offshore operations. Managing costs while maintaining sand control effectiveness is a challenge that requires careful planning and optimization.

## 5. CONCLUSION

Cased-hole gravel pack operations are crucial for managing sand production in unconsolidated sandstone formations and extending the lifespan of oil and gas wells. By effectively controlling the flow of sand, these operations contribute to the long-term productivity and integrity of the well. The key factors outlined above that require thorough consideration in the design process.

The proper placement and use of gravel pack equipment are essential for achieving optimal results in gravel pack operations. Through meticulous well preparation, including casing cleaning, displacement with clean completion fluids, and cleanout run after perforation, the efficiency of the gravel pack operation can be enhanced.

Overall, cased-hole gravel pack operations require careful planning, specialized equipment, and adherence to best practices. When executed successfully, these operations significantly reduce sand production, ensuring the long-term productivity and integrity of oil and gas wells in unconsolidated sandstone formations.

## 6. ACKNOWLEDGEMENTS

We would like to thank the Management of Turkish Petroleum Off-Shore Technology Center A.Ş. for their support in publishing this paper.

## 7. REFERENCES

- Hatcher, W.B., Chilingarian, G.V., Solum, J.R. Surface Operations in Petroleum Production II. [Book]
- Mader, D. Hydraulic Proppant Fracturing and Gravel Packing. [Book]
- Saucier, R.J. (1974). Considerations in Gravel Pack Design. Journal of Petroleum Technology, 26(2), 205-212. doi: SPE-4030-PA.
- Penberthy Jr., W.L. and Echols, E.E. 1993. Gravel Placement in Wells. J Pet Technol 45 (7): 612-613, 670-674. SPE-22793-PA
- SPE PetroWiki. Gravel Pack Equipment and Tools:

[https://petrowiki.spe.org/Gravel\\_pack\\_equipment\\_and\\_tools](https://petrowiki.spe.org/Gravel_pack_equipment_and_tools)

6. TP-OTC. (2021-2023). Well Completion Programs. Ankara: Turkish Petroleum Off-Shore Technology Center Inc.

## 8. APPENDIX

### 8.1 List of Figures

Figure 1

Commercial Gravel Size

Figure 2

Sump Packer (courtesy of Baker Oil Tools)

Figure 3

MST Screen System (courtesy of Baker Oil Tools)

Figure 4

Gravel-Pack Service tool Positions (Courtesy of Baker Oil Tools)

Figure 5

Packing Sequence With Brine Carrier Fluids

Figure 6

Typical Gravel-Pack Completion Equipment in Cased Hole (Courtesy of Baker Oil Tools).

Figure 7

MST Sleeves and Shifting Tool (Courtesy of Baker Oil Tools)

Figure 8

Flow paths during gravel pack operation (courtesy of Baker Oil Tools).

Figure 9

Example Gravel Pack Operation Graph

Keywords: Gravel Pack Operation, Sand Control

Figure 1 Commercial Gravel Size

<u>Gravel Size, U.S. Mesh</u>	<u>Size Range, in.</u>
8/12	.094–.066
12/20	.066–.033
20/40	.033–.017
40/60	.017–.0098
50/70	.012–.0083

Figure 2 Sump Packer (courtesy of Baker Oil Tools)

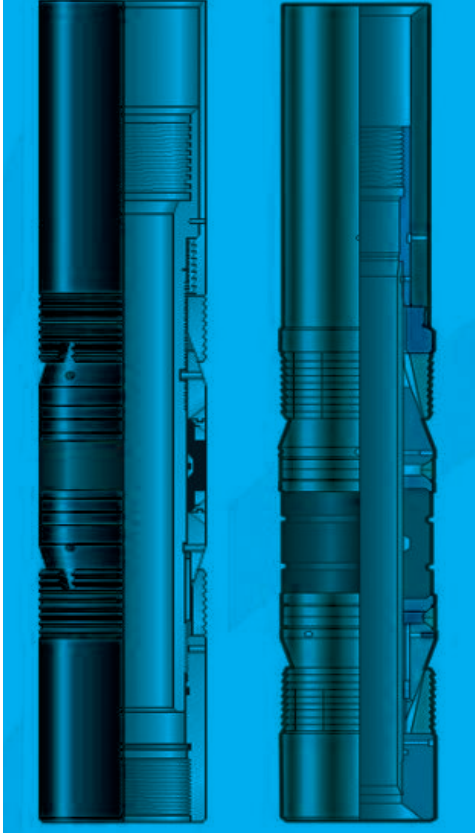


Figure 3 MST Screen System (courtesy of Baker Oil Tools)

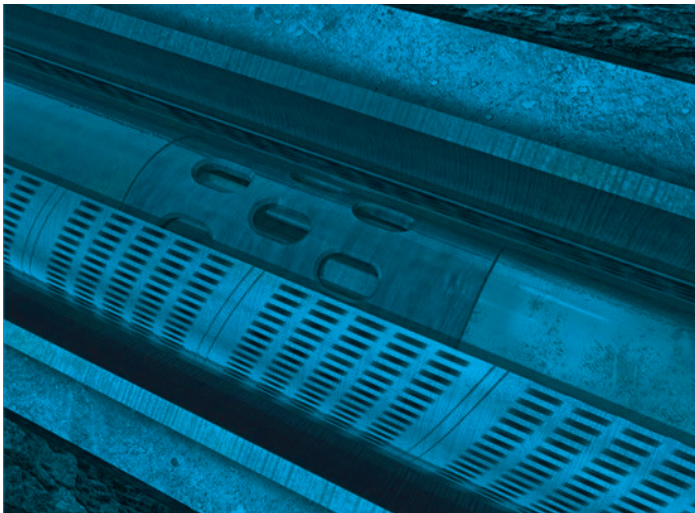


Figure 4 Gravel-pack crossover tool positions (courtesy of Baker Oil Tools)

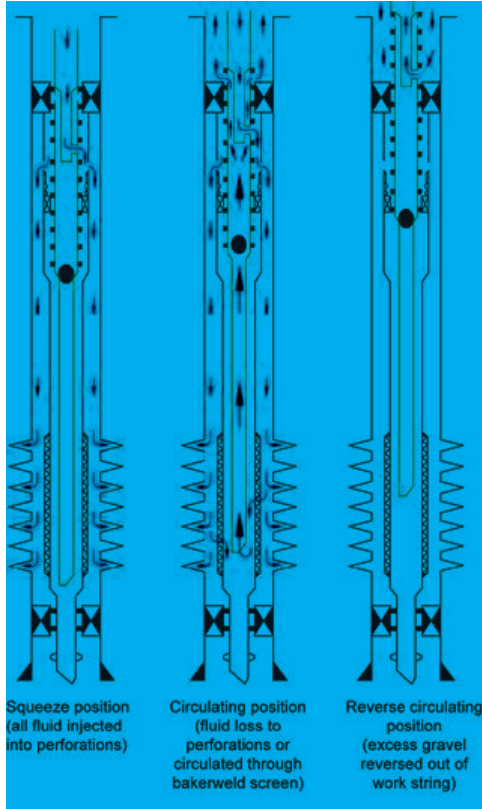


Figure 5 Packing sequence with brine carrier fluids

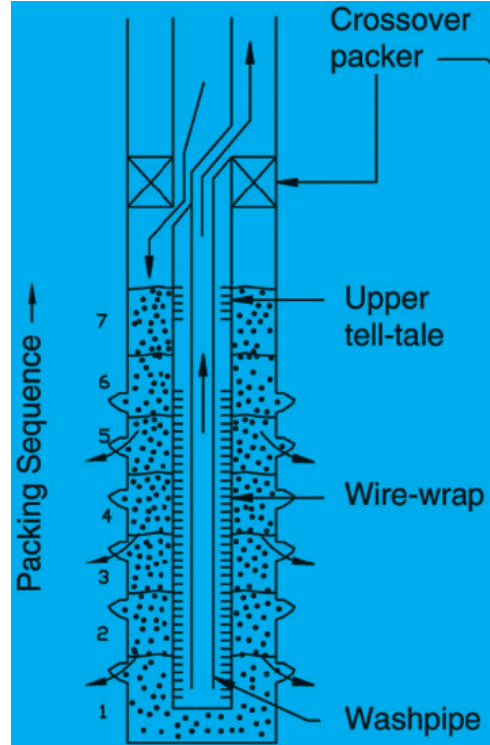


Figure 6 Typical gravel-pack completion equipment in cased hole (courtesy of Baker Oil Tools)

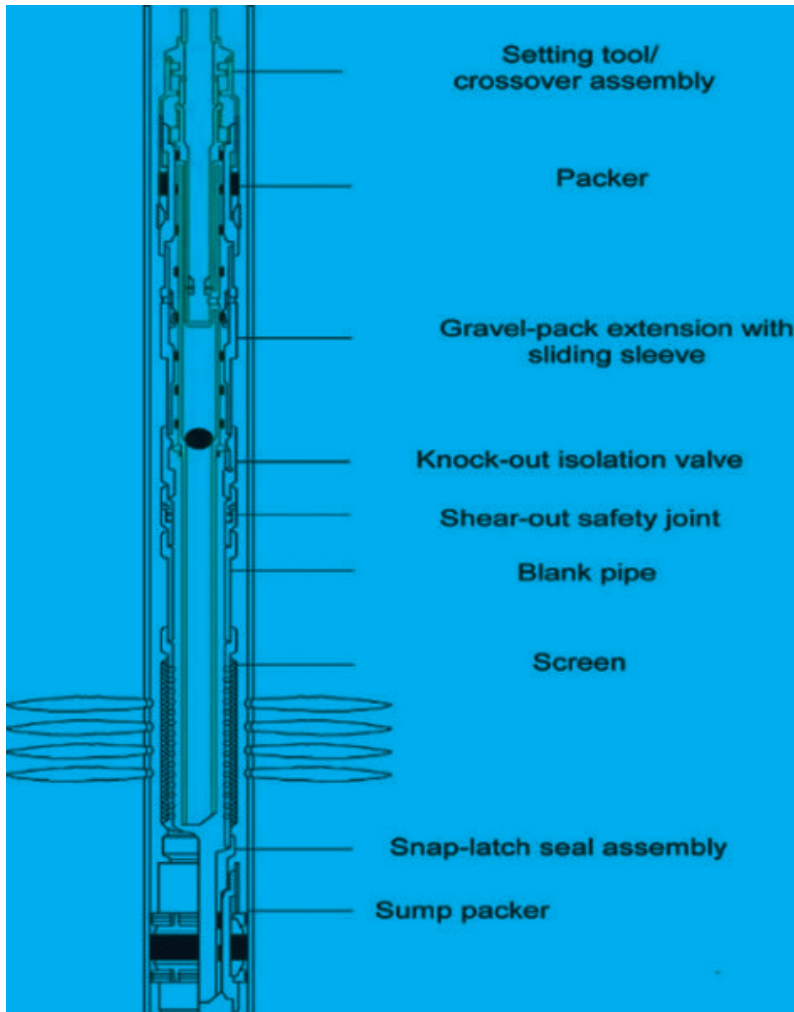


Figure 7 MST sleeves and shifting tool (courtesy of Baker Oil Tools)

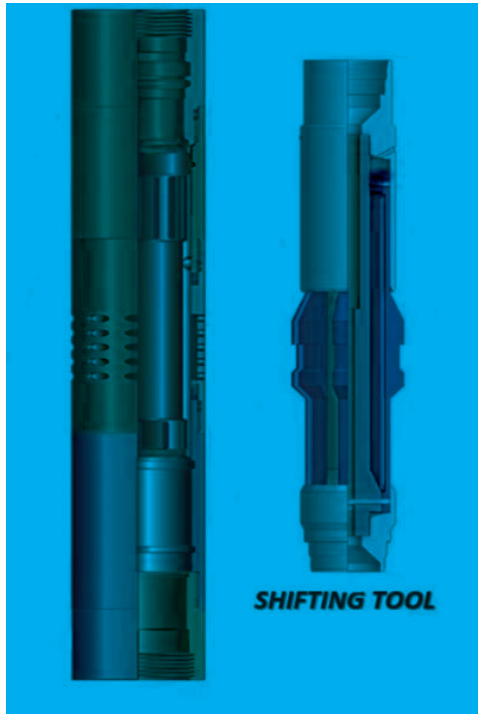


Figure 8 Flow paths during gravel pack operation (courtesy of Baker Oil Tools)

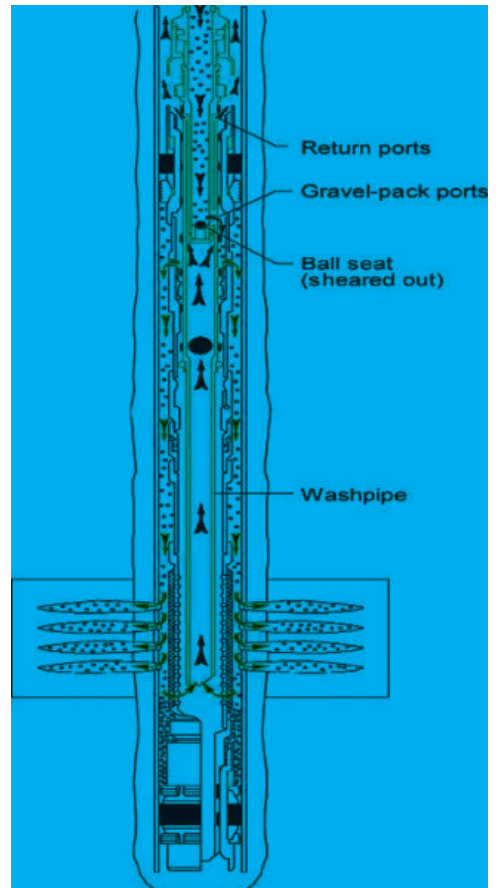
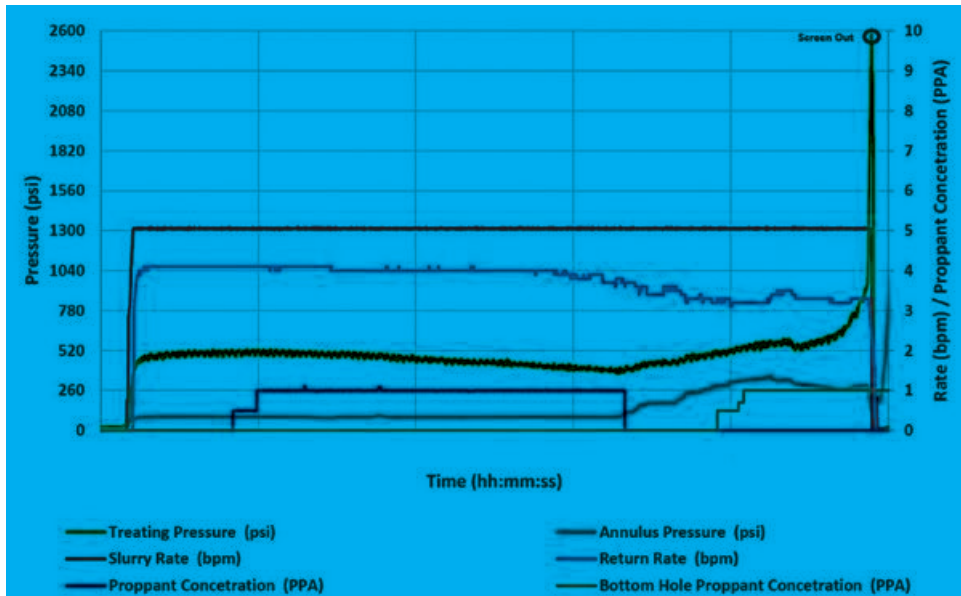


Figure 9 Example Gravel Pack Operation Graph





# The First 4 Zone Modular Screen Gravel Pack for Black Sea Deepwater – Case Study

**Eren Emre Gecer, Carlos Anderson Domingos, Fatih Karakaya, Evren Akbaş, Fırat Doğu Kaya**

Turkish Petroleum Off-Shore Technology Center A.Ş.



1. Deepwater wells are known for their challenge to drill and complete. Since most of the deep-water wells have low compaction because of water above it, the formations are unconsolidated. Unconsolidated sandstone reservoirs always have a challenge of sand and fine production during the production phase of oil and gas wells

Deepwater operations are being carried out usually in West Africa, the Gulf of Mexico, and some parts of SE Asia. These fields all over the world are sandstone reservoirs. To prevent sand production, different sand control methods are applied to reservoirs. The widest one is the gravel pack. The common practice is to run 2 or 3 zones in the other parts of the world.

TPAO & TP-OTC is currently developing the Sakarya Gas Field located in the middle of the Black Sea with more than 2100m water depth. The field has 3 unconsolidated sandstone reservoirs with many sub-layers. To produce without sand production, the Multi Zone Cased Hole Gravel Pack system is selected. Based on well data, 3 to 5 zone Stacked Pack Cased Hole Gravel Pack completions run till now.

To conclude, this paper presents the world's first 4 zone Modular Screen Gravel Pack system application which is successfully deployed in the Deepwater Black Sea exceeding 2000m water depth by TPAO & TP-OTC. The design of 4 zones Lower Completion, Execution Process, and Lessons Learnt Items are given.

## 2. INTRODUCTION

Sand control techniques are widely used in the oil and gas industry to prevent sand migration from the reservoir to the inside of production tubing.

There are 4 types of sand control methods available in the industry. They are;

Stand-alone Screens,

Expandable Sand Screens,

Gravel Pack & Frack Pack,

Chemical Composition.

The stand-alone screen is a system that only consists of screens for sand control runs across the reservoir section. Once production starts, sand particles and fines migrate to the wellbore between the screen and formation and start accumulating across the screens. At the end of the process, it creates a filter cake that covers the whole screen. Following that, this filter media works to separate formation sands and only allows hydrocarbon to be produced through the screens. The most basic type of sand control screen is a Wire-wrapped screen. This includes a base pipe with a mesh that covers the base pipe. For cases where there is more than one

mesh, the type of screen is called Premium Screens. The second type of Sand Control is called Expandable Sand Screens. This system is run with an expansion insert that is located at the end of the screen. Once the Expandable Sand Screens (ESS) string reaches the reservoir section, the packer set and the screen is expanded by means of pulling the expansion insert out of screens. As a result of that, the screen OD gets bigger once the insert is out of the screen. (Figure-1)

Figure 1 Expandable Sand Screens

The third method of sand control is by pumping gravel into a well. This method is based on creating a sand filter between screens and casing as well as inside the perforations. Gravel, also known as proppant, is selected based on the particle size of the formation sands. After cores are taken, Particle Size Distribution and Sleeve Analysis are applied to core sands to understand the size of formation sands. Following that, the Saucier Method is used to find Proppant and Screen Size. In this method, the Gravel is designed so it can hold the formation sands, whereas the screen is designed to hold the gravel in place. To pump the gravel into the wellbore, a carrier fluid is required. The type of carrier fluid depends on the type of treatment, so it can be brine or viscous fluid. When this method is applied while pumping the gravel below fracture pressure, this is called a Gravel Pack. If pumping pressure is above fracture pressure, this method is called Frack Pack. An intermediate method between these two is the High Rate Water Pack. In this method, fluid is pumped slightly over the frack pressure, once the screen out closes, pressure is decreased to close frack channels. Frack Pack allows clients to create long, and high-permeable channels. This is the reason why Frack Pack wells usually have lower skin values than Gravel Pack and High Rater Water Pack completions. The type of screens for these methods can be of any type as per reservoir requirement, where wrapped Screen (WWS) wire is the most common one. Figure 2 shows an example of Gravel Pack and Frack Pack.

Figure 2 Gravel/Frack Pack

The last available method in industry is Chemical Consolidation of the formation. This method aims to strengthen the formation of sand by injecting some chemicals into the reservoir. This method is quite complex compared to other methods as it relies on chemical means rather than mechanical means. Furthermore, this method may require many injections with different chemicals, and chemical compatibility is critical in order to keep retained permeability as high as possible.

The table below summarizes the advantages and disadvantages of the methods given above.

Table 1 Advantages & Disadvantages of Sand Control Methods

As stated above, sand control methods vary from stand-alone screens (SAS) to gravel packing. Sand control design starts with the selection of the right gravel and screen size some methods such as Saucier. Design continues with a selection of sand control methods. Once the sand control method has been selected, it's important to decide how the gravel is going to be placed into the wellbore. For example, gravel packing can be pumped into the wellbore between casing and screen in different ways such as Stacked Pack, Multi-zone Single Trip, and Alternative Path (Shunt).

Figure 3 Typical Gravel Pack

While the Stacked pack system packs the zones individually in multiple trips, the Multi-Zone Single Trip (MZST) system allows the gravel packing to be performed in one trip. For example, Figure 3 shows a typical gravel-packed well, which includes 2 zones. If these zones are gravel packed with 2 different strings, this becomes a Stacked Pack completion. However, if the zones are completed with one string (single trip), the system is called Multi-Zone Single Trip (MZST). On that note, all zones are perforated at once, and gravel pumping is done with the same string. MZST system requires a good pressure profile trend. Also, in terms of well control point of view, a stacked pack has an advantage.

The cased Hole Gravel Pack system includes one special type of hardware. It is called a Modular Screen. The selective Modular Screen system is different from than usual industry screens. Usual screens include base pipe with screen covers on it. Selective Modular Screens have one extra pipe inside screens that provides a conduit for hydrocarbons to flow through called us communication mandrel. The established flow path allows the hydrocarbon to reach the screen's internal Sliding Sleeves to be able to enter the wellbore. These Sleeves are closed after gravel pack operation till the deployment of the Upper Completion. Figure 4 shows the fluid path difference between ordinary screens and modular screens.

Figure 4 Difference between Ordinary & Modular Screen Design

Modular Screen design has a lot of advantages, they are;  
Minimizing well control issue if Upper completion has control lines,

Minimizing loss during upper completion run,

Dropping extra isolation valves between zones,

Internal SSDs can work as fluid loss devices.

As it states SSDs are the way that Modular Screens isolate the zone. If there is more than 1 zone, the profile of SSDs should be different. If all 3-4 zones include the same profile SSD, while running the production string, the most top zone SSD will open and fluid will be lost till the tubing hanger lands. This is the reason why SSD profiles should be different from one another. The only right Shifter (SSD key) should open the specific SSD.

This system is called Selective Modular Screens

### 3. NOMENCLATURE

Tubing Hanger is a completion device connected to the top of the completion string that creates integrity between the wellhead and the completion string as a part of the well barrier envelope.

Gravel Pack is a sand control process that helps companies fulfill the annulus of screen and perforation with proppant.

Multi Zone String Trip Gravel Pack is a sand control system that allows the operator to pack the whole reservoir sections in one run.

Screen out Pressure, a pressure value that is seen during Gravel Pack operations once the whole screen string is covered with proppant.

Shifter is a device that works as a key to open or close the SSD.

Sliding Sleeve, a completion device that can be operated to supply a fluid path between inside and outside of the tool.

System Integrity Test, a test that is done before operations to be able to sure equipment shows the expected performance.

### 4. METHODOLOGY

This case study investigates to show the advantages of Modular Screen Design over standard screens. At the same time, it accounts for the world's First 4 Zone Modular Screen Cased Hole Gravel Pack design and execution which was achieved in Sakarya Phase I operations. Furthermore, it expresses the challenges and Lessons Learned. This methodology aims to contribute not only to upcoming projects but also Oil & Gas industry.

### 5. OPERATION DESIGN

Turkish Petroleum Corporation, TPAO, the national oil company of Turkey, made the biggest gas discovery in the Sakarya Block, located in the ultra-deep waters of the Black Sea. The reservoir consisted of unconsolidated sand layers. Cased Hole Gravel Pack (CHGP) application is used for the Sakarya Gas Field. Although a 2-zone CHGP system is common in the deepwater industry, Sakarya Wells is a pioneer with 3 to 4-zone CHGP completion. In addition to this, the First 4 Zone Selective Modular Screen Design System was applied to wells to prevent sand production. Designing a well with a Selective Modular Screen includes a few processes.

First of all, the OD and ID of the Modular Screen is significant. Since Mesh is already selected as per formation sand particle, OD & ID are down to completion engineering team selection. OD selection plays a key factor in packing efficiency. If Casing ID-Screen OD clearance is small, friction will be high so that perforations won't be filled with proppant. This

creates high skin. Thus, service company SOP and company SOP should be checked. As for ID selection, it is easier than OD. The only decision point for ID is to be able to be big enough to run Intelligent Completion.

Secondly, the material selection of the screen & base pipe should be compatible with reservoir conditions & fluid. If there is a sweet gas, the investor is lucky to use the standard pipe. However, reservoirs usually include Carbon Dioxide or Sour gases. Black Sea reservoirs include some kind of Carbon Dioxide. Sour gas limit is really low. 13CR is more than enough together with pH and reservoir fluid properties evaluation.

Additionally, the monitoring sleeve which serves as a GP return port, is placed as below the perforation as possible as deeper. Nonetheless, if there is a production sleeve that serves as a hydrocarbon production port in the system, production sleeve positions should be located as per the reservoir engineer team's requirement.

There are some other considerations for screens as well. There are Shifter/SSD sequences, screen overlap, SSD flow area, and gauge replacement. Wrong Shifter/SSD sequence may result in losing of zone directly. Screen overlap increases the softness of Screen Out Pressure. SSD Flow Area shall be big enough to flow reservoir capacity. Required pipe modeling should be done. Post Job Analysis gauges can be put at one bottom and one at the top as a backup.

As for Lower Completion Accessories, they have the same metallurgy with screens to prevent any type of corrosion. Selected packer complies with ISO V0 Standards. These parts are compatible with reservoir fluids. Gravel Pack Port should be sealed through the upper zone.

## 6. EXECUTION

Execution of Operations started way before rig operations. All Driller Instructions have been written in the office by the completion engineering team. After that, DIs are reviewed by the offshore team to revise if any. At the same time, the interface works between Lower Completion – Rig has been carried out. Since the draft tally is created by completion engineers, the packing simulations job is started. Many different cases have been run and the best case selected. As per this base case, the pumping schedule is built up.

After Draft Drilling Instructions were completed, hardware started to arrive on Service Company bases. All hardware SIT and QA-QC checks have been done together with completion engineering team representatives. Sub-assembly sheets have been prepared and approved by all parties. All Documentation like proved Subassembly sheets and inspection documents have been shared with the rig.

Risk Register meetings have been held to come up with possible risks. Mitigations are being written and required actions have been taken to prevent associated risks. Key risks added to Driller Instructions to increase rig team attention.

Prepared sub-assemblies shipped to Drillship to start Lower Completion Operations. Tallies are being checked as per the TP-OTC Tally Generation Process given in Appendix 1. Before operations, DIs were reviewed by the office and offshore team together through online calls for fine-tuning. As per the final tally, the pumping schedule is updated.

Completion run performed as per DI, RR, and agreed Tally. Gravel Pack Packer set, located positions, and tested successfully. Planned fluids & proppant have been pumped as per the pumping schedule. 4 Different zone has been completed and packed as per given sequence above.

## 7. LESSONS LEARNED

Lessons Learned items are one of the codes of success through project management, especially for large-scale works like the development of deepwater fields. Throughout the project, each Lessons Learned item is registered by anyone as per office team request & regulations. Every improving item is followed by completion engineers and implemented in the next zone. Project has a lot of Lessons Learned. Two key AAR items are stated below;

It is always better to run gravel packing software by using Lower Completion Draft Schematic. If packing efficiency is low, packing efficiency can be increased by adding a screen joint if applicable.

During the displacement of completion brine, NTU & TSS are decreased by filtration. However, perforation may increase the NTU & TSS. Additional circulation cycles may be required after each perforation based on charge type.

## 8. CONCLUSION

In summary, Sakarya Field is located in the Black Sea with a 2100m water depth. Field consists of gas-bearing sands of unconsolidated reservoirs. Cased Hole Gravel Pack system with a Modular Screen is utilized to prevent sand production.

Since the reservoir includes many zones, it is more feasible to run a multi zone type. That is to say, the 4-zone Modular Screen Gravel Pack with Selective Screens is run for the first time in the Deepwater which is achieved in Sakarya Gas Field by TPAO, TP-OTC, and Baker Hughes. This study demonstrated all phases from the design process to the execution of operations for 4 zone Selective Modular Screen CHGP. In addition to this, lessons learned, recommendations and cost-effective practices for the Ultra-Deepwater Black Sea environment are presented.

## 9. ACKNOWLEDGEMENTS

We would like to thank the Management of Turkish Petroleum Off-Shore Technology Center Incorporation for their support in publishing this paper.

## 10. REFERENCES

IADC. ESS Technology Improves Productivity, Cut Cost. Drilling Contractor Magazine, March/April 2011 pg46.

Retrieved from <http://www.ingenieriadepetroleo.com/fracturing-sand-control-oil-well/> on June 5, 2023.

Retrieved from <https://ppt-online.org/622345> ppt 16 on June 6, 2023.

Figure 1 Expandable Sand Screens



## 11. APPENDIX

### 11.1 Abbreviations and Acronyms

AAR After Actions Review

CGHP Cased Hole Gravel Pack

ESS Expandable Sand Screens

ISO International Organization for Standardization

MZST Multi Zone Single Trip

LC Lower Completion

SSD Side Sleeve Door

QAQC Quality Control – Quality Control

WWS Wire Wrapped Screens

### 11.2. List of Figures

Figure 1

Expandable Sand Screens

Figure 2

Gravel/Frac Pack

Figure 3

Typical Gravel Pack

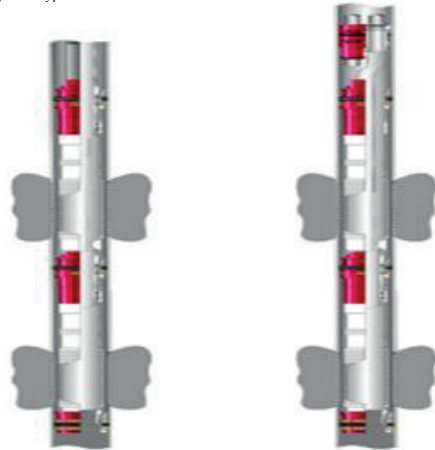
Figure 4

Difference between Ordinary & Modular Screen Design

Figure 5

TP-OTC Tally Generation Process

Figure 3 Typical Gravel Pack



### 11.3. List of Tables

Table 1

Advantages & Disadvantages of Sand Control Methods

Keywords: Gravel Pack Operations, Modular Screen Design

Figure 4 Difference between Ordinary & Modular Screen Design

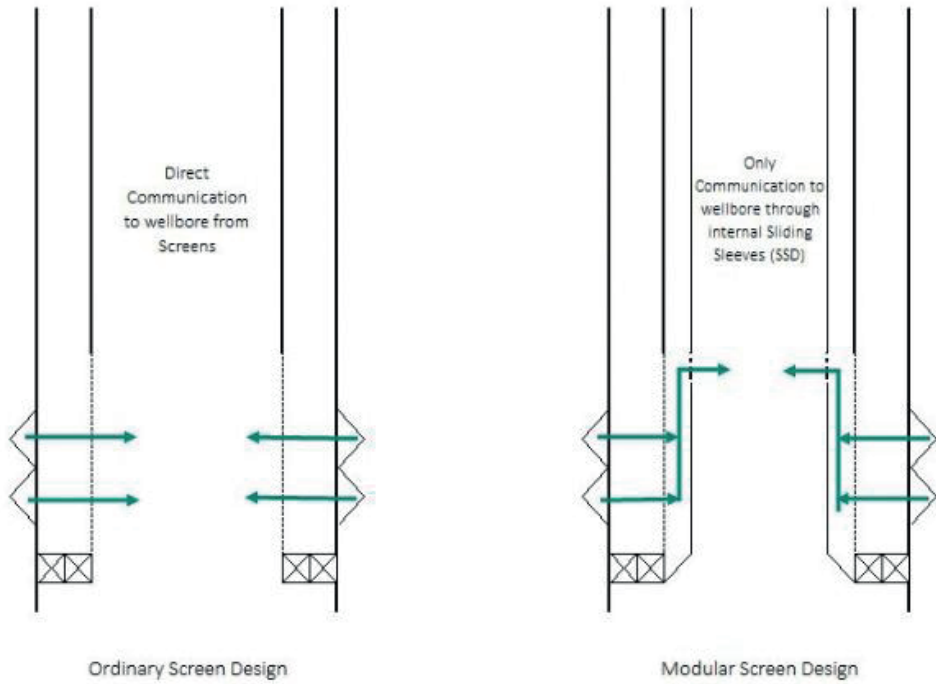


Figure-5 TP-OTC Tally Generation Process

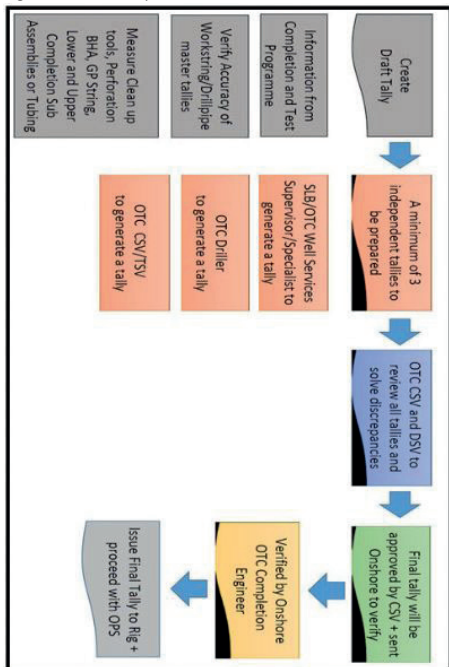


Table 1 Advantages &amp; Disadvantages of Sand Control Methods

Stand Alone Screens	Expandable Screens	G.Pack / F. Pack	Chemical Consolidation
<p>Advantages</p> <ul style="list-style-type: none"> <li>• Low Cost,</li> <li>• Low Operational Complexity.</li> </ul> <p>Disadvantages</p> <ul style="list-style-type: none"> <li>• ID Reduction,</li> <li>• Screen erosional problem.</li> </ul>	<p>Advantages</p> <ul style="list-style-type: none"> <li>• No ID Reduction,</li> <li>• High Flow area.</li> </ul> <p>Disadvantages</p> <ul style="list-style-type: none"> <li>• Screen erosional problem</li> <li>• Intervention issue</li> </ul>	<p>Advantages</p> <ul style="list-style-type: none"> <li>• Low skin,</li> <li>• Wellbore integrity,</li> <li>• Support Screens.</li> </ul> <p>Disadvantages</p> <ul style="list-style-type: none"> <li>• Complex operational job,</li> <li>• High Cost,</li> <li>• Needs more engineering</li> </ul>	<p>Advantages</p> <ul style="list-style-type: none"> <li>• Low kh damage,</li> <li>• Track Record.</li> </ul> <p>Disadvantages</p> <ul style="list-style-type: none"> <li>• Requires a lot of compatibility work,</li> <li>• Lots of injectivity,</li> <li>• Wellbore stability,</li> </ul>

# Completion Design Optimization to Tackle Fluid Loss

**Carlos Anderson Domingos, Eren Emre Geçer, Nuno Carvalho, Evren Akbaş, Atilla Mazman, Fatih Karakaya**

Turkish Petroleum Off-Shore Technology Center A.Ş.



1. Achieving operational excellence is essential for developing offshore deepwater oil and gas assets since drilling and completion activities can present significant risks. Some of these difficulties are linked to risk exposure, water depth, proximity to shore, and unfavorable weather. These can have a significant impact on the day-to-day operation of a drillship (DS) in the form of health and safety issues, logistical delays to deliver essential equipment, NPT from waiting-on-weather, poor performance, and excessive expenses [1]. Therefore, while implementing oil and gas growth strategies, the ability to foresee these difficulties is crucial.

With this vision in mind, several optimizations were implemented in the Sakarya Field completion designs since the beginning of field development to deliver safe, compliant, and reliable well operations. Design optimizations started at the initial FEED stage, and focused on looking at ways to minimize risk exposure and formation damage while completing multiple zones in a single well. The ultimate goal was to implement a completion design that could be safely installed and operated. In this context, safe installation must take into account risks including well control, heavy lifts, chemical exposure, and concurrent operations [9]. Whereas, safe operations need to ensure that well integrity is maintained and sufficient barriers are in place for the life of the well. This was the forefront of the design review as the initial design proposed in the FEED posed some well control concerns, apart from reservoir damage due to excessive losses into the formation.

This paper presents the lessons learned and completion design optimizations that were put in place to minimize the impact of completion brine lost into the reservoir.

## 2. INTRODUCTION

The pace of deepwater developments experienced a moderate decline in 2016, with several major companies around the world reducing their rig fleets and suspending investment decisions, motivated by the low oil price and resource potential uncertainties. Economics was the main driver, as such projects involve substantial capital expenditures, including rig time and equipment, subsea infrastructure, and production facilities. All these need to be accounted for in a strategic approach through sound decision-making to establish a long-term vision and executive commitment with comprehensive data analysis and economic evaluations [3].

Driven by the oil price recovery at the beginning of 2021, the situation has changed more recently, with deepwater projects on the rise again and new regions targeted for oil and gas exploration. Some of the latest discoveries and development start-ups include

Namibia's Block 2913B by Total, Angola's Platina Block 18 by BP, Angola's Block 32 by Total, Mauritania and Senegal's Greater Tortue Ahmeyim by BP, and the Black Sea (Sakarya) Gas Project by Turkish Petroleum (TPAO).

The Sakarya Gas Project case is particularly interesting as it is the first time TPAO has discovered oil or gas in deepwater environments. The first discovery was made in the deepwater Black Sea after drilling the Well-1 well to intercept the natural gas-bearing sandstone reservoir zones in the Pliocene and Miocene formations. Well-1 well data and geophysical analyses indicate a potential of 320 billion cubic meters of lean gas, the greatest discovery in the Black Sea.

## 3. SAKARYA FIELD COMPLETION DESIGN

The deepwater and ultra-deepwater environments in the Black Sea region are probably considered some of the most challenging ones for oil and gas developments due to the limited number of projects until recently. Sakarya Field consists of three main reservoirs, R1, R2, and R3, characterized by thin shale layers interbedding the laminated sandstone and siltstone formations. Hence, the well construction requirement called for a completion design that could address multiple intervals that could be produced individually to maximize recovery.

As part of the well delivery process for the Sakarya field, the wells are presently being completed as stacked pack CHGP across 3 to 5 zones, depending on reservoir management requirements. The current sand-face completion design employs modular wire-wrapped screens with a patented screen communication system and sliding sleeves to isolate the formation and prevent fluid loss after the gravel pack operation. The design also includes sliding sleeves that are shifted open for production when the tubing hanger is landed.

The in-line intelligent completion, as part of the upper completion (UC), is equipped with electro-hydraulically operated downhole flow control valves set within the stacked pack lower completion (LC), allowing production from each of the 3 to 5 zones individually.

Due to the complexity of the Sakarya field reservoir, one of the most challenging tasks was to select the most suitable completion design to achieve sand control, water production management, and production management from multiple zones individually.

The initial design proposed for the LC to achieve these requirements included two designs:

Option A: Multiple-zone Single treatment completed with the MZ-All Frac Packer;

Option B: Two-zone Single treatment completed with the MZ-All Frac Packer.

The single-trip system enables the completion to be run and the gravel pack in multiple zones to be performed in one trip. The system offers the benefit of reducing the number of trips, thus minimizing risk exposure compared to multiple trips, and lowering the overall completion costs [5]. The single-trip system has been used through the years to address the requirement to complete very long intervals where up to five intervals need to be isolated. The system has a track record of being time-efficient, with a clear example coming from the wells completed in the Mahakham Delta oilfield in Indonesia. Typical wells in this field were completed with the stacked pack design across five zones and an average of 30 days of operational time. However, with the single-trip system, the average operational time dropped to an average of 22.2 days per well, that is, 1 to 2 rig days saved per gravel pack zone [6].

Despite the benefits of the single-trip system, during the planning phase of Well-3, it was identified that it could pose numerous challenges during execution, mainly during the TCP operation. Some of the potential challenges are related to:

The possibility of having a long TCP column stuck in the wellbore due to sanding or casing burrs after perforation;

The requirement to manage losses effectively across a wellbore with 3 or 5 zones at different reservoir pressures;

Formation damage due to excessive LCM in an attempt to control losses across 3 to 5 zones at different reservoir pressures.

Furthermore, the team believed that commencing with a single trip early in the project would be overly ambitious. As the first completion to be deployed, it was preferred to take a more careful approach, addressing the planned intervals one by one while gaining experience working as a team and becoming acquainted with the reservoir itself.

In light of this, and after careful discussions, the decision was made to employ the stacked pack design instead. The main difference from the single trip is that with the stacked pack, the well is perforated, and gravel is packed one interval at a time. This design offers a more controllable way to address each zone individually, with the benefit of minimizing possible technical risks.

This choice was then conveyed and debated with the completion supplier to update the initial FEED proposal, and therefore the stacked pack design was suggested in the second FEED submission.

To address each of the proposed LC designs, the UC design included:

Option A: single-trip design that positions Proteus FCV stations, electric monitoring, and isolation packers in each zone of interest.

Option B: TRFC-HD two-zone fully hydraulic intelligent well completion. This design incorporates an intermediate completion that is run after the LC design from option 2 to divide the reservoir into two zones that can be produced separately via distinct flow paths.

These proposed UC designs are independent of the type of LC design selected, and therefore they apply to both the single-trip and stacked-pack systems

#### 4. COMPLETION DESIGN OPTIMIZATIONS

Once the basis of the LC design was set, several other design modifications were implemented before the start of LC operations. Perhaps a very controversial one was the use of the FLCD in each zone to prevent fluid loss after the gravel pack operation. This is in contrast to what was proposed in the FEED, where only one FLCD was proposed to be set in the topmost zone. Such an option posed the following risks:

- Well control due to long-term exposure to completion brine being lost into the formation during the LC operation.
- Well control due to long-term exposure to completion brine being lost into the formation while running the UC.
- Significant losses until the topmost FLCD was closed.
- Well control while opening the FLCDs during the wellbore cleanout operation in the UC phase.
- Significant losses while running the UC string.
- Crossflow between adjacent reservoir zones.
- Formation damage with a consequent high skin factor due to long-term exposure to completion brine in the reservoir

After careful discussions to tackle these possible issues, the decision was made to:

- Add more FLCDs to the design and place the valves according to the pressure differential between adjacent zones.
- Establish an acceptable loss decision tree for after TCP and gravel pack jobs to effectively manage losses throughout operations.
- Establish a Loss Control Material (LCM) strategy.
- Perform a dedicated trip to open all the FLCDs and leave the well in a stable condition before running the UC.
- Establish a well control strategy for running the UC.

A further improvement to the above design modification was to adjust the setting depth of the FLCD in relation to the top of the screens. This arose as a lesson learned from the Well-3 LC and DST, where the bottom zone had approximately 300 m of blank pipe between the top of the screens and the FLCD. This setup allowed gas to be accumulated below the FLCD, thus creating an underbalanced condition when opening the FLCD for DST or in preparation to run the UC string. Therefore, with this setup, as part of the well control strategy, the mitigation was to bullhead brine from the surface to reinject the trapped gas into the formation. However, by changing this setup by lowering the FLCD to 33 m above the top of the screens, the new setup was able to achieve the following for the UC phase:

- Significant reduction of gas accumulated below the



## FLCDs;

- Overbalance condition whenever the FLCD is opened;
- Elimination or reduction of the requirement for bullheading brine after opening the FLCDs;
- Reduction in the number of trips required to open the different FLCDs from 2 to 1 only, to achieve an overall reduction in the amount of fluid lost into the formation.

The advantages and disadvantages of both FLCD configurations are listed in Figure 1 below. Completion brine is depicted in pink, whereas formation gas is shown in yellow.

Figure 1

### FLCD Placement Pros and Cons

Additional design measures were implemented to improve operational efficiency and lessen the reservoir's long-term exposure to completion saline. The latter is of particular interest due to the long suspension period that can be incurred from the LC to the UC phase. LC and UC operations are conducted with two different rigs in the Sakarya Field, with DS Kanuni executing the LC operation and DS Yavuz conducting the horizontal tree installation and executing the UC operation. Depending on the operational efficiency of each drillship, this results in an approximately two-month interval between the end of the LC and the start of the UC. This is the same amount of time that the reservoir is exposed to a considerable volume of completion brine. Notable and recent design measures were taken to address this. Firstly, the implementation of the modular screen gravel pack design by Baker Hughes gives the following benefits:

- Eliminating losses while running the UC;
- Significant well control risk reduction during UC due to the presence of selective shifters and seal assemblies properly spaced out;
- Eliminating gas accumulation on top of the screens due to the presence of sliding sleeves instead of a ball-type Fluid Loss Control Device (FLCD). Second, the flowback of the two bottom zones after the gravel pack job with DS Kanuni to:
- Minimize the amount of fluid that remains in the wellbore during suspension;
- Reduce the rig time of DS Yavuz during flowback operations;
- Test the zones to obtain initial productivity data.

As a result, significant improvements in operational efficiency and skin factor were observed. The flowback operation time in DS Yavuz was reduced by five days, and the skin factors were reduced by half compared to the initial FEED design.

The table below presents a summary of improvements and major impacts on the completion design of Sakarya Gas Field.

Table 1

### Summary of Design Optimizations

## 5. CONCLUSION

This paper described the lessons learned and optimizations made to the Sakarya Field Completion design to mitigate the impact of completion brine lost into the reservoir. During the initial FEED phase, design optimizations focused on minimizing risk exposure reservoir damage while completing multiple zones in a single well.

As of June 2023, a total of seven wells have been completed with the initial FEED design proposed in Phase 1A of Sakarya Field Development, whereas the modular screen design has been deployed in three wells as part of Phase 1B thus far. From these three wells, two have completed the LC phase, and one has completed the UC phase with satisfactory skin factors in all zones.

## 6. ACKNOWLEDGEMENTS

We would like to thank the Management of Turkish Petroleum Off-Shore Technology Center A.Ş. for their support in publishing this paper.

## 7. REFERENCES

- Onugbolu, O., Rodrigues, C., Maueler, R., Lewis, D. W., & Loyola, C. (2012, August 6). Deepwater Drilling Operations Challenges of Exploration Well in Alpha Block, Gulf of Guinea: Lessons Learned. All Days. <https://doi.org/10.2118/162959-ms>
- The challenge of maintaining deepwater wells | Control Engineering. (2016, March 29). Control Engineering. <https://www.controleng.com/articles/the-challenge-of-maintaining-deepwater-wells/>
- Opportunities and challenges for Global Deepwater Players | Arthur D. Little. (n.d.). Opportunities and Challenges for Global Deepwater Players | Arthur D. Little. <https://www.adlittle.com/us-en/insights/prism/opportunities-and-challenges-global-deepwater-players>
- Sakarya Gas Field Development, Black Sea, Turkey. (2023, February 1). Offshore Technology. <https://www.offshore-technology.com/projects/sakarya-gas-field-development-black-sea-turkey/>
- Single-Trip Multizone Completion Systems. (n.d.). Single-Trip Multizone Completion Systems. <https://www.halliburton.com/en/completions/well-completions/sand-control/single-trip-multizone-completion-systems>
- Banman, Mark, Sofyan, Muhammad, Suryadana, Siswara, and Eric Delattre. "Single Trip Multi Zone Gravel Packing - Field case study within Total E&P Indonesia on Handil Bekapai and Sisi Nubi fields." Paper presented at the International Petroleum Technology Conference, Kuala Lumpur, Malaysia, December 2008. doi: <https://doi.org/10.2523/IPTC-12388-MS>
- Sakarya Gas Field Development Completion Design Report Phase – FEED
- Bellarby, J. (2009, February 20). Well Completion Design: Vol. Volume 56.

8. APPENDIX

8.1 Abbreviations and Acronyms

- CHGP Cased Hole Gravel Pack
- DST Drill Stem Testing
- FCV Flow Control Valve
- FLCD Fluid Loss Control Device
- FEED Front-End Engineering Design
- GP Gravel Pack
- LC Lower Completion
- NPT Non-Productive Time
- TCP Tubing Conveyed Perforation
- TR-FC HD Tubing-retrievable Flow Control Hydraulic
- UC Upper Completion

8.2 List of Figures

Figure 1  
FLCD Placement Pros and Cons

8.3 List of Tables

Table 1  
Summary of Design Optimizations

Keywords: Fluid Loss, Completion Design

Figure 1-FLCD Placement pros and cons

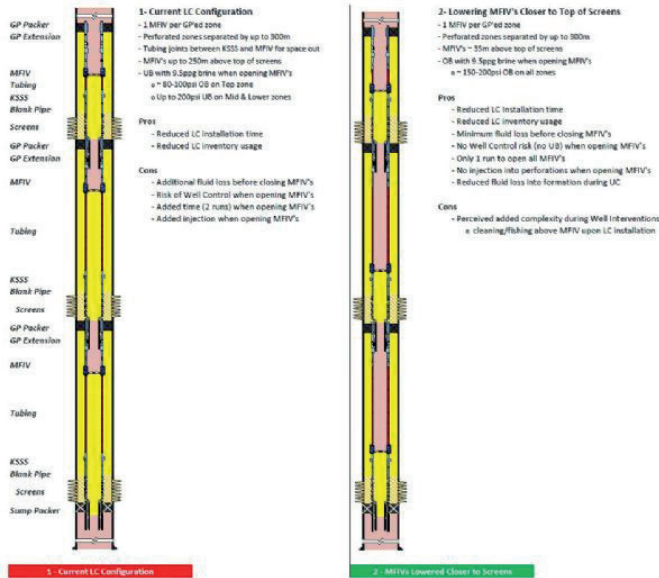


*Table 1-Summary of design optimizations*

Improvement	Major Impacts
Change from single-trip to stacked pack design	Reduce well control concerns after perforation.
Use of multiple FLCDs in the design	Prevent cross-flow between zones.
FLCD relocation closer to the top of screens.	Reduce well control concerns from a possible long column of gas below the FLCD when breaking containment.
Establish a decision tree for Acceptable losses after TCP and after GP	Clear plan on how to handle losses and the use of loss control materials.
Introduction of the modular screen design	Run UC without losses. Minimize the amount and the long term impact of brine lost into the reservoir.
Flowback operation after the gravel pack	Minimize the long term impact of brine lost into the reservoir.

# Integrated Well Construction from Drilling to Completion for Sakarya Field



**Atilla Mazman, Eren Emre Geçer, Carlos Anderson Domingos, Nuno Carvalho, Fatih Karakaya**

Turkish Petroleum Off-Shore Technology Center A.Ş. Turkish Petroleum Off-Shore Technology Center A.Ş.

1. This abstract summarizes the pre-engineering working process for the well construction aspect of the Sakarya Field Phase-1 development, before further detailing the construction strategy through the study cases and preliminary design, to decide the most appreciated and applicable solution for construction in the Sakarya field. This paper discusses the below areas of interest:

## 2. INTRODUCTION

Oil and gas reserve evaluation and development in a deep-water environment is a highly complex process that involves the collaboration of many different disciplines. The construction of a well plays a crucial role in this process as it is responsible for the construction of conduits from the reservoir to the offshore facility. The well construction process can be broken down into five sequential phases of work, as follows:

Preliminary well design

Detailed well design

Prepare drilling program

Execute well program

Analyze and improve performance

Drilling and Completion stages are the major parts of the well construction. For the Sakarya Gas Field below the tree (Fig.1) which is similar to the above steps has been followed and completed in a short time due to the lack of time.

Based on seismic data, geophysical prospects, water depth, and access to supporting resources, 3 different drilling ships have been selected for different purposes. Fatih DS was appointed to drill. Kanuni DS charged on lower completion operations and Yavuz DS selected for upper completion with the horizontal Christmas tree installation.

The process of converting a drilled well into a safe and efficient production well known as Completion. This terminology in offshore wells is used in two distinct contexts. A well completion involves a set of actions taken to convert an individual borehole into an operational system for controlled recovery of underground hydrocarbon resources. Those actions include the installation of the final well casings that isolate fluid migrations along the borehole length while also establishing perforated sections where needed to capture the hydrocarbons from the geologic reservoir into the production casing. A subsea completion refers to a system of pipes, connections, and valves that reside on the ocean bottom and serve to gather hydrocarbons produced from individually completed wells and direct those hydrocarbons to a storage and offloading facility that might be either offshore or onshore. (Subgroup, 2011)

As a general approach all over the world, reservoir parameters and limitations have been decisive during the designing of completion and drilling equipment, work string, etc. In the Sakarya Gas Field, the same approach was used and the reservoir was the major criterion for the lower completion equipment selection. After that bearing in mind the lower completion materials, the upper completion design has been worked. At the final stage taking into consideration these three phases, the construction team decided to hole section, casing size, cementing strategy, and log jobs for the drilling phase.

Specific target of well design in this project is for minimum life cycle cost that allows the realization of forecasted well productivity whilst ensuring optimal sand control and fulfilling well and reservoir management requirements. Following basis of design was used for the Sakarya Gas Field Development.

Field offtake policy is to maximize inflow performance whilst ensuring sand control.

Optimal well integrity without excessive well costs and allowing for remedial repair and usage.

Single Trip Multi Zone Cased Hole Gravel Pack (STMZCHGP) completion (Lower Completion) for effective sand control and zonal isolation.

Intelligent Well Completion (IWC) technology installation (Upper Completion) for effective drawdown and undesired fluid flow control (Flow Control Valves, FCV).

Dynamic surveillance (dynamic pressure and temperature surveys by using downhole dual-type gauges) for well and reservoir management requirements.

To examine in more detail, Sakarya wells can be subdivided into different topic titles. This paper covers 4 different main topic and their sub-topics about integrated well construction.

## 3. NOMENCLATURE

Appraisal Well, exploration well drilled to establish the extent and size of a petroleum deposit that has already been discovered by a wildcard well.

Well Construction, beforehand planned design engineered to cope with well geology and purpose. It is responsible for building conduits from the reservoir to the onshore facility.

Casing is a series of steel pipes that run into a drilled oil well to stabilize the well.

Completion is an operation on an oil and gas well to open up the reservoir to production.

Lower Completion refers to the portion of the well

across the production. Perforation, sand control, and wellbore clean-out operations are performed during these stages.

Upper Completion refers to all components from the bottom of the production tubing upwards.

Packer, a downhole device that can be run into a wellbore with a smaller initial outside diameter that then expands externally to seal the wellbore.

Perforation is a process used to establish a flow path between the near reservoir and the wellbore.

Gravel Pack is a sand-control method used to prevent the production of formation sand.

#### 4. METHODOLOGY

Sakarya Gas Project construction and designing process is considered for this study to summarize 3 major topics. Study starts with the methodology of equipment selection and continues with the pre-engineering and designing process for drilling, lower completion, and upper completion.

#### 5. MATERIAL SELECTION

As a beginning, material selection has been studied based on several criteria. Choosing the right materials was not the only challenge in the project in addition procurement of these materials was another difficulty due to the time limitation of the first phase. The samples taken from the Tuna-1 well were examined and the below information was obtained.

- Gas analyses and molecule percentages
- Expected reservoir pressures
- Expected reservoir temperatures
- H<sub>2</sub>S / CO<sub>2</sub> percentages
- Formation Water / Salinity

In the light of these analyses, additional criteria which have been used are:

- Target production rate
- Expected well life
- Loads
- Working pressures

Well, casings must be designed for worst load cases. Casings load cases are broadly classified into two types based on operation:

Drilling Load Cases - Where loading during drilling operations is considered.

Production Load Cases - Where loading during production operations is considered.

Construction team classified load cases into below categories:

- Burst load Drilling load
- Burst load Production load
- Collapse load Drilling load

- Collapse load Production load
- Axial load Drilling & Production combined

Casings, work strings, production tubing, and packers have been selected based on the above (Table 1) analyses. The below tree (Fig. 2) shows how the decision was made and why current materials were bought.

#### 6. DRILLING

Offshore drilling costs significantly more than land drilling, depending on sea bed depth and well complexity. In this respect, the Sakarya gas field is one of the most challenging fields for drilling operations. As a common approach, start with large diameter holes and casing first then progressively smaller hole sizes as downhole pressures increase. General practice in Sakarya is after drilling the first casing interval, a drilling riser is connected to the wellhead and used to pump drilling fluid to remove cuttings. BOP and riser are placed at the seabed onto a wellhead system. During the wellbore construction process, each depth interval of the well is analyzed and designed. Although some parts vary for each well, the statements mentioned below were determined while the construction process was ongoing.

Drilling fluid composition density, and type.

Drilling BHA's and casing to be run.

The class and amount of cement to be used.

The above statements and many other parts are determined by subsurface pressures, equipment limitations, and other parameters. Casing depth and drilling fluid density are subject to change for every well. This decision is controlled by rock stress, pore pressure, fracture pressure, and casing specifications.

When an offshore deep-water well is spudded, and prior to the installation of the riser, seawater, and sweeps are used to jet or drill the structural and conductor casings. Effective deep-water well designs require that the first casing string is positioned deep enough that the formation has sufficient mechanical strength to withstand the formation pressures anticipated in the next deeper interval. (Subgroup, 2011) (Figure-3)

#### 7. LOWER COMPLETION

Completion planning was one of the major challenges due to the complexity of the Sakarya gas reservoir. Sand control, controlling various productive zones, and managing water production were the difficulties that completion design had to deal with to be able to control sand, water production, and numerous reservoir zones separately, two alternative intelligent well completion technologies have been determined as completion design. If we evaluate the lower completion operations in 2 different sub-topics. Perforation design was one of the critical parts since it creates a flow path for the gas from the reservoir to the wellbore. UCS is very low as it is a deep-water well. Also, the formation is made up of weakly cemented sandstone zones. The main goal of perforating is to ensure maximum area

to flow to reduce fluid velocity. Reduced fluid velocity in the perforations lowers the pressure drop in the perforations, which increases long-term completion integrity and lowers skin. It also reduces the danger of gravel pack destabilization and screen erosion. The selected system is 7" charges. While perforating the guns, there will be some metallic gun debris. The main aim of all lower completion operations is damaging the formation as possible therefore static overbalance with dynamic underbalance perforating has been selected for the TCP design. Volume of the gun BHA and detonation pressures are controlled to create a transient dynamic underbalance just after the perforation is created. This is the primary approach for Sakarya when the interval length facilities to do so. The dynamic response is driven by the interval length and gun loading configuration, this also directly impacts shock generation on the BHA. Dynamic underbalance is a more efficient cleanup mode than conventional static underbalance in particular in more consolidated sands.

Sakarya field reservoirs that have been targeted are laminated sandstone/siltstone formations with interbedded thin shale layers. Analyses on reservoir show that cementation is weak and formation unconsolidated. Therefore, one of the sand control techniques must be applied to protect production string, HXT, and surface pipelines from erosion. Another reason for sand control is water-bearing zones. Targeted gas reservoirs are very thin and covered by water-bearing zones from below and above. These zones separate from each other thin shale barriers. As a result of all this information, the most fit-for-purpose sand control method which is cased hole gravel pack has been selected. Aims of this design are to prevent early water breakthrough and allow solids-free gas.

Designing of cased-hole gravel pack needs some additional tests and an understanding of the reservoir. As an example, to decide the mesh size of the screen and proppant. Formation sand size has to be known. Gravel pack pumping strategy needs to be decided according to formation parameters. As a result of 2 different sand analyses which are Laser Particle Analysis and Dry Sieve Analysis. It has been concluded with 40/60 US mesh gravel with 175-micron screen openings. As a general draft, the below-listed equipment can be considered as a lower completion feature.

Gravel Pack Packer

Gravel Pack Packer Quick Connect / Extension

Safety Shear Sub (optional)

Loss Control Valve

Blank Pipes

Washpipe (inner string)

Service Tool (inner String)

Screen

Snap Latch Assembly

A major target of a cased hole gravel pack treatment is to ensure the perforations, perforation/casing annulus, and casing/screen annulus are packed to minimize

skin. During gravel pack pumping parameters will be managed to stay below the fracture pressure since there is a high possibility of initiating water-bearing zones. Brine is used as a carrier fluid during the circulating gravel pack. Pumping order is listed below.

DP Pickle in reverse position

Injektivty Test

Acid Pumping

Gravel Pack Pumping

## 8. UPPER COMPLETION

Because of the complexity of the reservoir, intelligent well control technology must for Sakarya wells. Production tubing and other IWC equipment will be run to the hole while upper completion operations. Surface-controlled flow control valves (FCV) and downhole gauges (DHG) will allow for the identification and testing of each zone separately. These features will also provide a control on drawdown on the reservoir. Real-time data will help the operator during the production phase to analyze water or sand production for each well and zone. Some devices were explained below with their usage reasons.

Upper completion design has the feature of a subsurface safety valve, which is an emergency flow control mechanism. It will prevent uncontrolled hydrocarbon leaks and protect the environment in the event of a catastrophic accident on the sea floor. It has a nitrogen-charged flapper valve. Another feature of the upper completion design is the safety valve control line and chemical injection lines. Downhole equipment will be operated by these lines. Downhole gauges will be used for monitoring reservoir temperature and pressure. Moreover, data will help in optimizing production and improving reservoir and recovery. Selected production packer will be tubing mounted and hydraulic set by pressure applied through the tubing. It isolates the annulus from production fluids. Another specialty of the packer is cut to release. This specialty provides more robust and high tensile strength (SLB, 2021).

## 9. CONCLUSION

Considering the difficulties created by the ultra-deep-water environment, the studies resulting above have been performed in light of these information. (Figure-4) shows the general completion design as an example.

## 10. ACKNOWLEDGMENTS

I would like to thank the following persons and companies for their support in publishing this paper.

TPAO management

TP-OTC management

SLB – supplier of Sakarya Gas Field

Development Completion Design Report.

## 11. REFERENCES

- SLB. (2021). Sakarya Gas Field Development Completion Design Report.
- Subgroup, O. O. (2011). Subsea Drilling, Well Operations, and Completions.

## 12. APPENDIX

### 12.1. Abbreviations and Acronyms

- BOP Blow Out Preventer
- POOH Pull Out of Hole
- STMZCHGP Single Trip Multi Zone Cased Hole Gravel Pack
- IWC Intelligent Well Completion
- FCV Flow Control Valve
- BHA Bottom Hole Assembly
- UCS Unconfined Compressive Strength
- TCP Tubing Conveyed Perforating
- HXT Horizontal Xmas Tree
- DP Drill Pipe
- DHG Downhole Gauges

### 12.2. List of Figures

- Figure 1  
Sakarya Field Tree Chart of Construction
- Figure 2  
Material Selection Guide
- Figure 3  
Deepwater Well Appearance
- Figure 4  
Completion Design Schematic

### 12.3. List of Tables

- Table 1  
Design Factor

Keywords: Well Construction, Metallurgy

Figure 1. Sakarya Field Tree Chart of Construction



Figure 2. Material Selection Guide

**MATERIAL SELECTION**

For standard applications and the most severe environments.

CO <sub>2</sub> ≤ 2 psi or No-flow-wet pipes			API	J-K-N-R-P-Q types	
H <sub>2</sub> S ≤ 0.05 psi	Carbon Steel	High Collapse High Strength	VM HC - VM CY	VM CYC	
		eXtreme Collapse High Strength	VM CYXC		
H <sub>2</sub> S ≥ 0.05 psi	Sour Service Carbon Steel	Sour Service	VM S - VM SS - VM10MS		* High Collapse eXtreme Collapse
		Enhanced Sour Service	VM RRP - VM RSS VM SS-D - VM ESS VM X3 - VM130MS		
CO <sub>2</sub> ≥ 2 psi and Flow-wet pipes	H <sub>2</sub> S ≥ 6 psi	With S*	Ni based Alloy	VM G3 - VM D30	
		Limited S*	Austenitic	VM 26 - VM 625	
	H <sub>2</sub> S ≤ 6 psi	T ≤ 232°C	Super Duplex	VM 25S	
		T ≤ 232°C	Duplex & Super Duplex	VM 22 - VM25S	
	H <sub>2</sub> S ≤ 1.5 psi	T ≤ 180°C	Enhanced Super 13Cr	VM 13CRSS	
		T ≤ 180°C	Super 13Cr	VM 13CRM VM 13CRSS	
T ≤ 150°C		13Cr	VM 13CR		

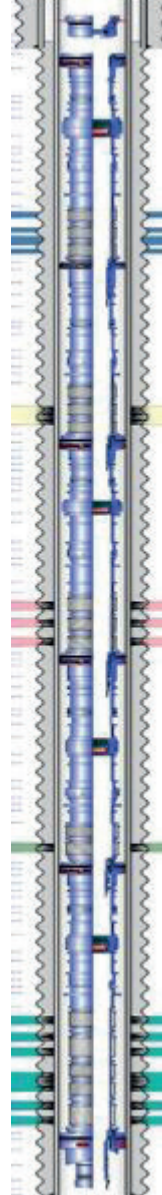
Vallourec grades for Special Applications				
Unconventional Enhanced API	Arctic Low temperature	Riser	Expandable	Corrosion mitigation
EC-HCE-RY T95E-P110MS	VM LT	VM R-RSS	VM ET-13ET	VM 1CR-1CRHC-3CR GRE liner



Figure 3. Deepwater Well Appearance



Figure 4. Completion Design Schematic



*Table 1. Design Factor*

	Pipe Body	Connection
Burst	1.1	1.1
Collapse	1	1
Tension	1.3	1.3
Compression	1.3	1.3
Triaxial	1.25	

# Designing and Running Multi-Zone Smart Completions in Deepwater Wells

**Nuno Carvalho, Bekir Oğulcan Bulut, İlker Kemal Öztürk**  
Turkish Petroleum Off-Shore Technology Center A.Ş.



1. Downhole Flow Control (DHFC) is a technology to improve the management of reservoirs with layered intervals. DHFC can remotely adjust the flow of layers in either production or injection wells. Prior to the advent of DHFC, multi-zone reservoirs required wells dedicated to each zone or costly intervention operations to change the flow or injection profile.

## 2. INTRODUCTION

Prior to the advent of DHFC, multi-zone reservoirs required wells dedicated to each zone or costly intervention operations to change the flow or injection/production profile. With the implementation of DHFC technology, additional value has been realized through the acceleration of production. Drilling fewer wells has allowed wells to be brought forward in the drilling schedule. It is critical that lessons learned in any area are documented and shared with other areas so companies (Operators and Service Providers) do not repeat the same mistakes. The objective of this document is to highlight key areas the operators should look into when considering to implement DHFC technology. This document addresses more detailed technical issues associated with the design, installation, and operation of DHFC wells. The recommendations in this document are intended to relay to all personnel planning, executing, and operating DHFC wells.

## 3. METHODOLOGY

Aspects to consider while designing a project using DHFC wells: planning and organization, reservoir specifications, aspects to consider while drilling and completing the wells and surface facilities.

Shrouded vs in-line configuration: brief description of the main difference between these two types of DHFC designs.

Dual-zone open hole or cased hole completion (either producers or injectors) using the shrouded design: aspects to consider during the design, the benefit of using this design, and the challenges while running this type of completion.

Multi zones cased hole gravel pack (either producers or injectors) using in-line design: aspects to consider during the design, the benefit of using this design, and the challenges while running this type of completion.

## 4. FUNDAMENTALS OF DHFC TECHNOLOGY

Two types of DHFC have been developed: On-Off and Choking. Please refer to Figures 1 and 2 in the Appendix. On-Off DHFC, as the name implies, is either open or closed. It can be used for sequential depletion

of multiple zones, un-modulated commingled flow, alternating production/injection into two zones, etc. Choking DHFC allows modulation of flow from or injection into multiple zones. Choking DHFC's most valuable application is in modulating injection into two or more zones simultaneously above fracture pressure. It is also valuable for independently controlling drawdown on multiple production intervals, and water and gas coning control.

Some cautions that have to be taken into consideration when designing and planning DHFC in producers is the extreme difference in reservoir pressures that can develop over time due to depletion, especially in gas wells. Another difficult case for DHFC is the very high rate of gas applications. To date, the highest gas rate produced through a DHFC completion is around 100 MMSCFD. This is not to say that higher rates are not possible, but modeling and testing are required to verify any design for extremely high rates.

## 5. ASPECTS TO BE CONSIDERED WHILE DESIGNING A DHFC COMPLETION

### 5.1. Planning and Organization

Assets that are considering the application of DHFC should emulate the approach taken by the successful assets.

Competent and experienced personnel dedicated to the evaluation and implementation of DHFC are required.

Establish an integrated relationship between the D&C organization and the Subsurface organization to jointly develop a comprehensive statement of requirements.

Top-side facilities with adequate features to manipulate the DHFC wells.

Evaluations of DHFC should assume failures in the economic analysis while recognizing that the consequence of failure is seldom the complete loss of a well.

### 5.2. Reservoir

- It is critical to understand the injection pressure response of the reservoir before embarking on a DHFC completion program.

### 5.3. Well Construction

- Apply best practices from prior installation programs.
- Mechanical fluid loss devices continue to be problematic and their removal from well plans, where feasible, is encouraged.

- Accommodate DHFC in the base case subsea architecture.
- Rigorous Manufacturing Quality Assurance and Design Reliability programs are essential.

#### 5.4. Operations

- Choking DHFC provides adequate precision of injection distribution.
- Downhole pressure gauges are essential to the effective utilization of DHFC technology.

#### 5.5. Fundamentals of DHFC Technology

The key features of DHFC technology are illustrated in the schematic below (Figure 3 – DHFC with Stand Alone Screen in Open Hole or Cased Hole Application). DHFC technology consists of valves placed in the completion that are connected to the surface through hydraulic or electrohydraulic control lines. At the surface, hydraulic fluid or electric signal is sent downhole. This causes the valves to change position, allowing flow or injection into discrete layers to be remotely controlled without intervention in the well.

### 6. SHROUDED VS IN-LINE CONFIGURATION

#### 6.1. Shrouded

Shrouded DHFC is normally associated with sand control completions. The valves are stacked above the completion because of the restricted bore of the sandface completion. Shrouded DHFC is limited to two zones. It accommodates mechanical fluid loss devices either in the Lower Completion or in a dedicated Intermediate Completion. The shrouded configuration may be less erosion-tolerant because of the tortuous flow paths. Shrouded configuration makes the deployment of sensors across the sandface much more difficult.

#### 6.2. In-Line

In-line DHFC facilitates control of more than 2 zones. Standard size valves used in the shrouded design will not fit inside most sand control sandface completions. Chemical or a mechanical fluid loss control device is required while running the DHFC completion string to reduce or eliminate possible losses from the TCP operations. The In-line flow path is much simpler than the shrouded flow path. Some suppliers have developed technology that allows the deployment of up to 12 zonal monitoring and control systems with only three control lines. Produced fluids exiting perforations might impinge on control lines and erode them. In-line DHFC is well suited for cased & perforated or ESS completions.

### 7. SEVERAL TYPES OF DEEP-WATER MULTI-ZONES SMART COMPLETIONS

#### 7.1. Dual Zone Open hole/Cased hole – Producers / Injectors

Design Concepts: This design, also known as n+1, requires a single open c-line per each DHFC valve and a common close line that gives the ability to close all the DHFC valves in the system at the same time. Please refer to Figure 3 in the Appendix.

By adopting a Shroud design (discussed above), and in particular, for water injector wells, the flow path through a DHFC valve is from inside to outside. Any solids carried out in the injected water could impinge on the casing, causing erosion. Consideration must be given to protecting the casing by installing a shroud around the OD of the valve and a hard material such as tungsten carbide is adopted in some designs.

Optimization of choke settings for modulated water injection is not a trivial exercise. Current designs in choking DHFC valves offer seven to ten discrete choke positions. A range of fairly small choke settings is required to provide sufficient differential pressure to drive injection to a lower injectivity zone. Modeling of injection scenarios with several ranges of choke settings is recommended.

Extreme loads due to temperature changes should also be considered especially in deepwater wells. These thermal swings can produce very high tensile and compressive loads on downhole equipment, even at moderate depth.

Zonal Isolation Packers either for cased or open-hole application are available in the market to guarantee isolation between the upper and lower zones. In particular, for open-hole applications, the use of two open-hole mechanical packer could be considered for redundancy and to ensure no communication between zones is achieved throughout the life of the well. However, may not be possible to test the full integrity of the Open Hole Isolation Packer at high pressures, once it is set, due to the risk of fracturing the formations. That assurance can only be performed once the upper completion is in place and the gauges are connected.

Benefits: The financial benefit can be measured in direct capital savings. A successful well saves drilling and completing a second well. A single DHFC well can deliver the functionality of two single wells. There is also a potential for production acceleration and reserves increase. The value is stated in simple terms of capital expenditure savings. One DHFC well cost is less than two single wells.

Challenges of running this design: a) Fluid cleanliness specs prior to running the completion may have an impact on the tool's functionality.

b) Depending on the supplier, and where the equipment may be positioned on the well, the DHFC valves may present a limitation in terms of max allowable DLS.

c) Failure of one of the DHFC requires a new well to be

drilled or as a second option, an intervention operation to commingle the reservoirs and operate the well as a single zone.

d) In rigs with limited deck space and reduced capability to perform activities offline, making up the c-lines of the DHFC could have to be considered to be performed in the critical path, increasing considerably the completion time.

e) Depending on the DHFC supplier, some companies propose the subassemblies to be pre-made in the workshop. That ends up having long subassemblies (18 to 22m long) which include both upper and lower DHFC valves in the same assembly. Long subassemblies may be a challenge to handle in some rigs. A correct lifting procedure must be in place to handle the assemblies to avoid damaging it or cut the control-lines already pre-made up.

### Failure Mode

a) High diff pressure across internal packing elements led to leaks; b) Stuck in position due to not functioning periodically; c) Tubing pressure caused the closed valve to open.

### 7.2. Multi Zones Cased Hole Gravel Pack – Producers / Injectors

Design Concepts: This design, as mentioned above, is also known as “In-line”. It allows to running of several DHFC valves with a limited number of control lines. As mentioned above, In-line DHFC is well suited for cased & perforated or ESS completions. Please refer to Figure 4 in the Appendix. Based on that, the following aspects are considered:

Upper and Lower Completion Interface: Special consideration must be given to the upper and lower completion interface to ensure the upper completion string with DHFC valves is accommodated inside of the lower completion (either Cased & Perf, Cased Hole Frack/Gravel Pack or Expandable Screens) without issues and at the same time to address additional requirements:

a) Ability to keep formation for all zones isolated until upper completion is deployed.

b) Ability to shift open the sleeves or mechanical isolation valves incorporated in the lower completion during deployment of upper completion in a single trip.

c) Ability to keep formation isolation in place during rig up of surface test tree prior to landing the tubing hanger.

Safety Valve Considerations: A Safety Valve is a key component in a DHFC well design. In deepwater applications, several designs could be considered such as; a) Nitrogen charged spring or b) a Safety Valve with a balance line feature apart from the control line to open the valve. Those two designs will eliminate the internal tubing pressure dependence to open the valve and will allow the valve to be set at depths exceeding 2500m (including water depth), away from the hydrate zone.

DHFC Valves Metallurgy: The metallurgy of the DHFC valves could be different from the completion string tubulars. Some factors that would determine the material selection of the DHFC are differential pressure requirements, hydraulic chamber pressure requirements, production fluids, injection fluids, flowing differential requirements, etc. The material selection is important to ensure functionality for the lifetime of the valves. Would be important to emphasize that, the DHFC valves differ from any other accessory which does not have any moving parts or even has it, but it is mechanical, and no pressure build up is required. It is more sophisticated than just any accessory and requires attention. One of the main DHFC advantages is to cycle remotely from the surface without any well intervention and be able to do it for 20-25 years.

DHFC Valve positioning: flow from the screens to the DHFC valve occurs through the annulus of the production tubing and the screen base pipe and once the fluid enters inside the tubing, then the flow occurs inside the tubing till the wellhead. Depending on the location of the DHFC valves, the length of the annular flow can be decided as well as the tubing flow. Therefore, the frictional pressure differential for the same reference depth flowing through annulus vs. tubing and the location of the DHFC is also decided. Note that this annular space also may include flatpicks in which control cables pass through as well as clamps to protect the completion. Therefore, pressure drop at these sections must also be taken into consideration when choosing the correct DHFC valves positioning.

Feedthrough assemblies: as per the schematic below, all the subassemblies above the lower most DHFC 1, must have a feedthrough feature to accommodate the control lines and tubing encapsulated conductor (TEC). Feedthrough Production Packers, seals, DHFC Valves, and Shifting tools must be qualified to operate under the wells flowing conditions for the life of the well without integrity issues. This equipment must be supplied with different feedthrough options to suit all customer operating requirements.

Downhole Gauges: it will allow monitoring of downhole reservoir pressure and temperatures. By incorporating downhole gauges in the completion design this reduced the costs of well surveillance intervention, well testing and surface facilities. Moreover, this downhole data will assist in optimizing production, improving reservoir drainage and recovery, refining field development plans, and updating/history-matching reservoir models. Dual tubing/annulus gauges should be considered to be run in each production zone to measure pressure and temperature across the DHFC valves.

Thread Connection: considerations must be given to the type of connection that will maximize the reliability of the tubing and reduce any potential tubing leaks during the life of the well, particularly for deep-water subsea gas wells.

Zonal Isolation between Production Zones: Several designs are in the market to guarantee zonal isolation

in between production zones. Isolation packers are used and set in between zones to create a barrier and mechanically isolate production zones. That will prevent communication between zones and commingle production. The use of Polished Bore Receptacles (PBRs) and bonded seals is also an option to provide isolation between zones.

**Bonded Seal Units:** In this type of design, seal units will be utilized to isolate between commingled production zones. A full compatibility test must be carried out to ensure the correct elastomers are selected. Aspects such as fluids, CO<sub>2</sub> and H<sub>2</sub>S content, temperature, flow regimes, etc., are considered when selecting the correct type of elastomers. Benefits: Similar to the shrouded configuration (Dual Zone Open hole/Cased hole – Producers / Injectors) described above, the benefits of this design can be measured as well in direct capital savings with the advantages of completing up to 12 zones in a single well.

Challenges of running this design: a) Similar to the previous design, ensuring fluid cleanliness prior to running the completion is a major request as debris may have a negative impact on the tool's functionality and zonal isolation when using seals and PBRs.

b) In this type of design, it is recommended to feed through the control lines into the assemblies and check their integrity (pressure tests). That preparation is normally done in the workshop. The assemblies are then mobilized offshore with long tails and extra care must be given during basket preparation/transportation, lifting procedures (onshore and offshore), running procedures, removing the encapsulation, terminating the control lines, and clamps installation as required.

c) If multiple seal units are run to engage into the PBRs and isolate the production zones, care must be taken to ensure the seals do not engage into the PBRs at the same time to avoid excessive drags which could buckle the completion string and risk of losing clamps, compromise the integrity of the tubing or even not been able to run the completion to TD.

d) Due to the type of design, multiple control line terminations are required to be done. Based on that, experienced personal are required to ensure the job is done in an efficient way.

Failure Mode: a) Valve gets stuck in position.

## 8. CONCLUSIONS

Although DHFC technology has several benefits, as mentioned above, the application of this type of design requires a detailed study by different disciplines to ensure that not only the preparation and deployment are conducted in an efficient way but also the facilities are set up to take the most advantage of this technology. A robust intervention plan must also be in place in case a failure or malfunction is detected while installing the completion or during the life of the well. Another point that requires deep analysis is the type of design to use (shrouded vs. in-line). The main question to be asked is: Should an operator adopt the n+1 design

or push the boundary and complete up to 12 zones in one completion? Several points must be considered such as personal experience, type of reservoirs, production facilities compatibility with this type of design, expected life of the project, costs of a possible failure, capability to intervene, etc.

## 9. ACKNOWLEDGEMENTS

The authors would like to deeply thank the Management of the Turkish Petroleum Offshore Technology Center Incorporation for their support in publishing this paper.

We also would like to thank our colleagues from Schlumberger and Baker for providing literature about this topic and sharing their experiences in this subject.

Finally, we would like to thank ex-colleagues for sharing their knowledge on these topics.

## 10. REFERENCES

1. Schlumberger Completions: Sakarya Deepwater Completions Design Report
2. Recommended Practices for Downhole Flow Control Design Installation and Operations – Mark Barrilleaux, issued on 18 November 2010.
3. Downhole Flow Control Application Philosophy by Mark Barrilleaux Williams, 3rd December 2009.
4. Completion Design – Section 6 - Material Selection, John Martin, Steve Groves and Paul Adair
5. Sand Control Screen Erosion – Prediction and Avoidance, SPE-174837-MS, Alex Procyk, Xinjun Gou, Srinagesh K. Marti and Robert C Burton.

## 11. APPENDIX

### 11.1. Abbreviations and Acronyms

CHFP Cased Hole Frack Pack  
 CHGP Cased Hole Gravel Pack  
 D&C Drilling and Completions  
 DHFC Downhole Flow Control  
 DLS Dog Leg Severity  
 ESS Expandable Screens  
 ICV Internal Control Valve  
 MMSCFD Million Standard Cubic Feet per Day  
 OHGP Open Hole Gravel Pack  
 PBR Polished Bore Receptacle  
 QAQC Quality Assurance – Quality Control  
 SAS Stand Alone Screen  
 TD Total Depth  
 TEC Tubing Encapsulated Conductor  
 TH Tubing Hanger  
 TP-OTC Turkish Petroleum Offshore Technology Center

11.2.List of Figures

Figure 1

On-Off DHFC

Figure 2

Choking DHFC

Figure 3

DHFC with Stand Alone Screen in

Open Hole or Cased Hole Application

Figure 4

Application Multi Zones Cased hole Gravel Pack – Producers / Injectors

Keywords: Reservoir with different layers, Production enhancement

Figure 1 – On-Off DHFC



Figure 2 – Choking DHFC

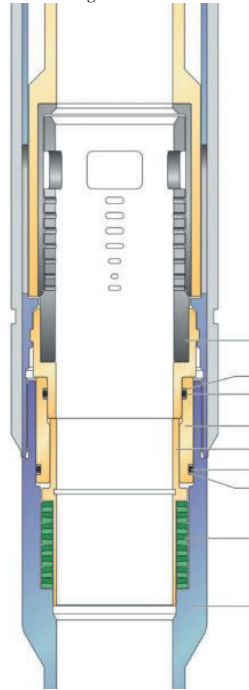


Figure 3 – DHFC with Stand Alone Screen in Open Hole or Cased Hole Application

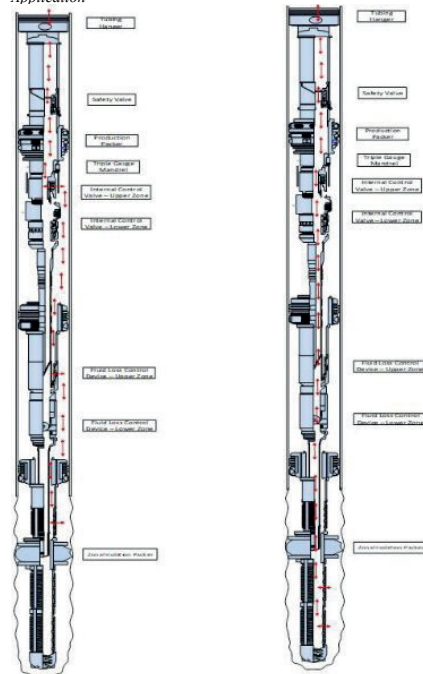
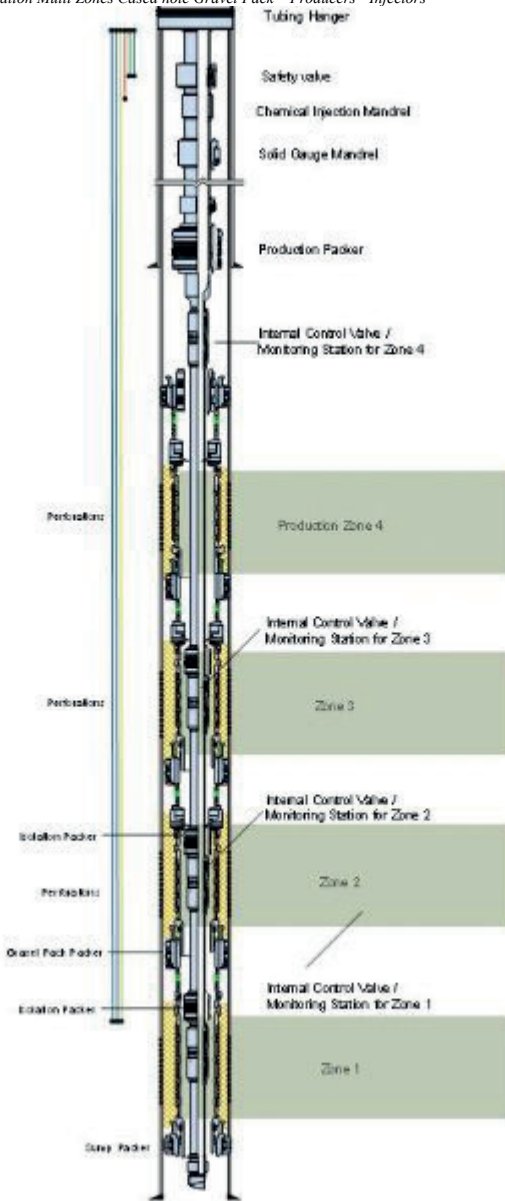


Figure 4 –Application Multi Zones Cased hole Gravel Pack – Producers - Injectors





# Major Design Changes & Improvements During Sakarya Phase-1 UC Operations



**Alparslan Konbul, Eren Emre Geçer, Fatih Karakaya, Nuno Carvalho, İlker Kemal Öztürk**

Turkish Petroleum Off-Shore Technology Center A.Ş.

1. The Upper Completion operations commence by latching BOP to HXT and testing it against the RBP that was set in a 9 5/8" casing. That is followed by the retrieval of the RBPs, clean-up of the wellbore, and jetting and testing of the BOP. After this, displacement of the existing corrosion-inhibited brine to inhibited filtered brine will be done, maintaining a stable fluid column in the well. In-line intelligent completion, with electro-hydraulically operated downhole flow control valves, is going to be run to meet the production requirement. With the integrity of the completion confirmed, part of the completion string is going to be displaced to a light base oil column, in preparation for the well flow back. The objective of the flow back/clean-up operation is to get the well zones ready for production after placing the upper completion. After flowback, well suspension steps are going to be followed. This paper will provide the design changes and improvements made since the beginning of Phase-1 for UC operations conducted with Yavuz DS.

## 2. INTRODUCTION

Turkey is among the world's major energy consumers with its developing economy. Turkey is heavily dependent on imports of natural gas. The rate of foreign dependency on natural gas consumption is higher than oil, and approximately 98.9% of Turkey's natural gas consumption is met by imports. While approximately 44.8 billion m3 of natural gas was consumed in Turkey in 2020, only 1.1% of this amount (441 million m3) was met by domestic production.

Turkish Petroleum Corporation (TPAO or Project Owner) was established to perform hydrocarbon exploration, drilling, production, refinery, and marketing activities on behalf of the Turkish Republic in 1954.

On 12th March 2019, the Turkish Petroleum Offshore Technology Centre (TP-OTC) was founded to conduct and support petroleum and natural gas exploration and production activities on the seas of Turkey.

The name TP-OTC was registered on 2 April 2019 following this resolution, and the company was structured specifically for the conducting of maritime operations.

TP-OTC, 100% owned by TPAO will be conducting Project Management and Engineering, Procurement, Construction, and Installation (EPCI) for the Sakarya Gas Field Development Project.

Offshore exploration activities, which were accelerated in order to increase the rate of meeting Turkey's increasing oil and natural gas demand with domestic production, gave its first results with the natural gas reserve detected in the Sakarya Gas Field in 2020.

The SGFD Project is the first deep-water gas field discovery and the biggest natural gas reserve in the country. Within the scope of the Project, an annual production of 3.5 billion m3 will be achieved in Phase 1, followed by an annual production of 14 billion m3 in Phase 2, and 30% of Turkey's total consumption will be met.

Sakarya Gas Field is located within the Sakarya Gas Field Block C26 in the western Black Sea, 165 km offshore from Filyos, Zonguldak, at a depth of approximately 2,200 m, within Turkey's exclusive economic zone. The natural gas discovery was initiated with the Tuna-1 deep-water exploration well, set at a depth of 2,115 m to reach a depth of 4,525 m.

The Project is going to be completed in two phases, Phase 1 and Phase 2:

- Under Phase 1, natural gas to be produced with the subsea production system from 12 wells in Sakarya Gas Field will be transported onshore through a 16-inch (40.64 cm) diameter carbon steel pipeline, processed at the onshore production facility.
- Under Phase 2, the natural gas whose production will continue in the Sakarya Gas Field will be connected to the subsea production system with up to 30 additional wells reaching a total of up to 40 wells under Phase 2. A 24-inch pipeline (60.96 cm) or above will be needed to transport the additional gas produced in Phase 2.

This paper will focus on the improvements made during the upper completion operations with DS Yavuz at Phase 1.

## 3. NOMENCLATURE

After Action Review (AAR), is a tool used to debrief a project or event to understand what took place, why it happened the way it did, and how to improve on it. When used correctly, it can highlight areas of strength or concern in a project. An AAR occurs at the end of a project, and its purpose is to improve future projects with similar workflows or features.

Subsea Test Tree (SSTT), The Sub Sea Test Tree is the well testing safety device that replicates the BOP functionality in the subsea part of the landing string. The SSTT is a dual 'fail-safe' valve system designed as a primary well control barrier rated 10,000 psi. When activated close the ball valve and the upper flapper valve to ensure sealing from wellbore fluids.

Blowout Preventer (BOP), shuts off the valve leading underneath the machinery to stop any liquid from surfacing in a dangerous explosion, or a kick

K240, inhibitor is a shale inhibitor which are materials or chemicals added to water-based drilling fluids to prevent hydration, swelling, and degradation of the clay

minerals.

#### 4. METHODOLOGY

Case study includes: Removal of K-240 from the Brine and Increasing KCL Percentage from 7% to 9%.

Well test area improvements.

Removal of adjustable chokes on the steam exchangers and flush them with citric acid during PBU's.

The Use of Modular Screens Equipped with Sliding Sleeves Instead of MFIVs.

Changing the Number of Seals of Tubing Seal Nipple and 4.75" Feed Through Seal Assembly.

Addition of 2.5" Pump Bailer Run.

Bleed of pressure limit during flowback has been increased from 4000psi to 5000psi.

Keeping 4100psi in A-annulus for Suspension.

Transfer of SSTT from AWC to MWC with rig equipment instead of PRT.

#### 5. DESIGN CHANGES AND IMPROVEMENTS

##### 5.1. Removal of K-240 from the Brine and Increasing

KCL Percentage from 7% to 9%

K240 (Shale inhibitor) and K302 (Sand control additive) inhibitors have been integrated to the upper-completion fluid program. After performing upper-completion on Well-3 & 5, analysis and observation have been confirmed that using of K240 shale inhibitor increased the PH of the mud and affected to skin factor of formation in a negative way, contributing to the scale deposition on WT surface lines and increased the flow back durations. K240 inhibitor is a shale inhibitor which are materials or chemicals added to water-based drilling fluids to prevent hydration, swelling, and degradation of the clay minerals. This inhibitor has been used only on two wells - Well-3 & 5. Then the decision was made to increase the percentage of KCl in brine from 7% to 9% and not use a K240 inhibitor. Starting from Well-7 only K302 has been used as an inhibitor in our upper-completion fluid system.

##### 5.2. Well Test Area Improvements

Well test equipment was arranged for a compact footprint and required a safe way to get around and inspect or service equipment. Walkways have been constructed to improve safety and reduce tripping hazards. This makes access around easy and improves escape routes in case of an emergency situation. Photos of the walkways installation have been presented in the Appendix section as Figure 1.

##### 5.3. Removal of Adjustable Chokes on the Steam Exchangers and Flush Them with Citric Acid during PBU's

Observed time-to-time scale deposition on STX adjustable chokes and choke bean adaptor stuck on CM during the inspection period between flowing each zone. Cleaning of this scale was extending the PBU period and causing Non-Productive time. Decision was made to prepare citric acid composition and flush the lines with it. Pictures that show the scale deposition on STX and CM, and a video that shows the scale dissolution in citric acid have been presented in the Appendix section (Figure 2-5).

##### 5.4. The Use of Modular Screens Equipped with Sliding Sleeves Instead of MFIVs.

Mechanical isolation valves were used with the old design which allows a mechanical opening or closure with a dedicated shifting tool. To operate it, a shifting tool is run at the end of a wash pipe, slick line, perforated string, or coil tubing. When the shifting tool is passing through the valve, it either opens or closes.

Disadvantages of this old design were:

- Valves were opening separately.
- Fluid losses were increasing between valve opening sequences and the operations until the flowback period.
- Due to the fluid losses into the formation, we were having inconsistent formation performance during flowback periods.

Decision made to use of the modular screens equipped with sliding sleeves instead of MFIV's. By this way, UC and LC runs will be done with minimum losses and less formation damage. Moreover, flowback periods have been shortening and we started getting more consistent formation performance during flowback periods. Fluid losses to the formation have been summarized in Figure 6 for the previous wells completed with the old design.

##### 5.5. Changing the Number of Seals of Tubing Seal Nipple and 4.75" Feed Through Seal Assembly

Tubing Seal Nipple is used as the lower seal assembly or assemblies in multiple packer installations. With sufficient seal units, mis-measurement or tubing movement can be accommodated.

Due to the high drag forces experienced during the Drift Run in one of the wells, also considering the 2 7/8" tubing buckle (especially the section of tubing in casing), it became important to reduce seal friction considerably for the next seal drift run but maintain seal ability. It is decided to remove the seals of the tubing seal nipple from 14 to 7. Seal unit is modified by removing elastomer from the top bonded seal by a knife. After the modification, no major drag has been observed during the drift runs for the following wells. Also, Spacers have been ordered to replace the bonded seals and avoid removing the elastomers with knife. FTSA is also modified due to the high drag forces experienced.

Proposed 4.75" FTSA consisted of 3 bonded seals per seal unit. However, due to high drag forces decision was made to modify FTSA with 2 bonded seals per seal unit by removing elastomer from the top bonded seal.

As a result, zones are isolated by removing 17 out of 51 bonded seals and keeping 34 out of 51 seals on feed-through seal assemblies for Drift Runs and UC runs for the upcoming wells. After the change, no major drag has been observed during the drift runs for the following wells.

Also; A risk assessment was issued, and there is no risk of running fewer seals as initially planned and the space out is done such that at least one seal is inside the PBR at all times even during production with possible tubing movement.

Figure 7 shows the illustration of seal units and bonded seals.

### 5.6. Addition of 2.5" Pump Bailer Run

A 2.5" pump bailer run has been added before retrieving the 3.437" DB plug to clean debris since a huge amount of debris was found on the top of the plug at Well-9. Step-by-step operational details are given below to explain the decision made for the addition of a 2.5" pump bailer run into the UC program.

2.5" GS + Equalizing Prong has been made up to the SL tool string to retrieve the 3.437" DB plug. RIH with SL string to 2806 m. Recorded Neutral weight: 520 klb, PU weight: 550 klb, Running weight: 510 klb. Continued RIH and slowly sit down 2.5"GS+ Eql Prong at 2811m. Laid off weight and monitored pressure, no change. P/U the string and repeated the same many times until equalizing plug shears and pressure equalizes, observed no pressure change across the plug. During the first 2 attempts, observed a 200lb overpull, and then the string weight dropped down to 560lb. Continued working on a string from 200lb to 560lb to be able to engage the plug, with no success. Bled off tubing pressure at WT CM from 1350psi to 1292psi. Checked downhole gauges, and observed no change. Decision made to POOH and check the condition of the 2.5" GS tool. POOH with 2.5" GS + Equalizing Prong to surface. B/O PCE on QTS. B/O 2.5" GS + Equalizing Prong and inspected. GS was unsheared. Collected a small amount of debris inside of the equalizing prong. Very fine sandstone or siltstone 35-40%, Claystone:55-60%. Very few metals. Therefore, the decision was made to RIH with a 2.5" Pump Bailer to clear possible debris/scale from the 3.437" Oilenco plug. Summary of the bailer runs has been mentioned in the Appendix section (Table 1-2).

### 5.7. Increment of Bleed of Annulus Pressure Limit during Flowback from 4000psi to 5000psi

This change has been made to increase the operation window and reduce the frequency of bleeding of A-Annulus pressure. Production packer has been set at 6000psi and the annulus has been tested the same. 5000psi has been also picked up to be on the safe side.

Bleed off procedure: Pump via cement unit to equalize across AAV.

Open AAV, bleed off pressure to a certain point via rig choke to monitoring tank lined up to MGS.

Close rig choke. Close AAV.

Open rig choke and bleed off pressure to MGS.

Record bleed-off volume return to monitoring tank.

Close rig choke and continue monitoring annulus pressure via APTT gauge.

### 5.8. Keeping 4100psi in A-annulus for Suspension It is decided to pressurize A-annulus for suspension since Well-9.

Pressurization procedure of A-Annulus to 4,100 psi for suspension:

Close XT valves, XOY, PMV, AVV, and AWW.

Open AMV and record APTT reading.

Calculate the hydrostatic pressure of the fluid column down to HXT.

Open AAV and pressurize A-annulus via cement unit to 4,100psi on APTT P gauge by keeping the required pressure on the unit.

Once the desired pressure is reached, close the AMV and bleed off the choke line to zero.

Close AAV. Monitor APTT for any pressure build-up for 10 mins.

### 5.9. Transfer of SSTT from AWC to MWC with rig equipment instead of PRT

The Sub Sea Test Tree is the well testing safety device that replicates the BOP functionality in the subsea part of the landing string. The SSTT is a dual 'fail-safe' valve system designed as a primary well control barrier rated 10,000 psi. When activated to close the ball valve and the upper flapper valve to ensure sealing from wellbore fluids.

PRT system has been used for transferring SSTT from AWC to MWC while running upper completion at Wells 3,5,6&7. Decision made to not use PRT winch and continue transferring SSTT with rig equipment to save money and time.

Transfer procedure with rig equipment: SSTT has been lowered into the rotary sock with the AWC TDS and set in slips. 15m soft sling arrangement connected to lift cap. The 7 5/8" elevators are then closed around the pup joint and sit on the dog collar. 50' bails have been installed on MWC TDS. Bails are to be positioned to connect the side door elevators on the SSTT pup joint. Men in the work basket install the bails. MWC driller, with the assistance of the winches, hoists the elevators until they take the weight under the pup joint coupling. Then the man in the work basket removes the dog collar. Black winch on the bails to be kept to assist as the AWC and MWC hoist the SSTT.

Hoist the AWC TD until SSTT is 1m off the floor, before

starting the transfer. Control swinging with tag lines.

Toolpusher co-ordinates the transfer of SSTT from AWC to MWC by picking up on the MWC and slowly slacking off on the AWC while keeping the SSTT vertical and 1m above the rig floor. Use the black winch to assist with the weight of the long bails.

The SSTT should continue to be slowly and carefully transferred until it is vertical in the MWC with two men positioned at fingerboard level with Radios.

Please refer to the pictures that demonstrate the transfer procedure and show the SSTT in the Appendix section (Figure 8-11).

## 6. CONCLUSION

An after-action review (AAR) is a tool used to debrief a project or event to understand what took place, why it happened the way it did, and how to improve on it. When used correctly, it can highlight areas of strength or concern in a project. An AAR occurs at the end of a project, and its purpose is to improve future projects with similar workflows or features. UC programs have always been updated with the latest improvements captured from past UC AAR's from the beginning of the project. All UC teams onshore and offshore have contributed to this system and had weekly meetings to improve the operations. As a result, a lot of improvements have been made as it is reported in this paper.

## 7. ACKNOWLEDGEMENTS

Authors would like to thank the Management of Turkish Petroleum Off-Shore Technology Center Incorporation for their support in publishing this paper.

## 8. REFERENCES

Kadıoğlu, G. (2022). Sakarya Gas Field Development Project - ESIA, Non-Technical Summary. Ankara: TPAO.

TP-OTC. Well Completion Programs. Ankara: Turkish Petroleum Off-Shore Technology Center Inc.

TP-OTC. (2020-2023). End of Well Phase Reports. Ankara: Turkish Petroleum Off-Shore Technology Center Inc.

## 9. APPENDIX

### 9.1. Abbreviations and Acronyms

CM: Choke manifold

SGFD: Sakarya Gas Field Development

UC: Upper Completion

PBU: Pressure Build Up

STX: Steam Exchangers

ADJ: Adjustable

BOP: Blowout Preventer

HXT: Horizontal Christmas Tree

RBP: Retrievable Bridge Plug

KCL: Potassium Chloride

AAR: After Action Review

POOH: Pulling out of the hole

RIH: Run in a hole

WT: Well Test

PCE: Pressure Control Equipment

QTS: Quick Test Sub

AWC: Aux Well Center

MWC: Main Well Center

SSTT: Subsea Test Tree

### 9.2. List of Figures

Figure 1

Walkways constructed in the Well Test Area

Figure 2

Scale in WT Kit after Well-5- ADJ Box - STX1 - Inlet line condition

Figure 3

Scale in WT Kit after Well-5- ADJ Box - STX1 condition

Figure 4

Scale in WT Kit after Well-5- ADJ Box - STX1 Scale Thickness

Figure 5

Scale in WT Kit after Well-5- RHS Choke Box

Figure 6

Fluid Losses with Old Design

Figure 7

Seal Units- Remove Elastomer from top bonded seal from each seal unit- In Total: 17 Seal Units

Figure 8

Transfer procedure of SSTT with rig equipment- The 7 5/8" elevators are closed around the pup joint and sit on the dog collar

Figure 9

Transfer procedure of SSTT with rig equipment- 50' bails have been installed on MWC TDS

Figure 10

Transfer procedure of SSTT with rig equipment- Transfer of SSTT with using soft slings

Figure 11

SSTT

### 9.3. List of Tables

Table 1

Summary of 2,5" Bailer Runs at Well-9

Table 2

Summary of 2,5" Bailer Runs at Well-12

Keywords: Upper Completion Improvements, Completion Optimization

Figure 01-Walkways constructed in Well Test Area



Figure 02-Scale in WT Kit after Well-5- ADJ Box - STX1 - Inlet line condition



Figure 03-Scale in WT Kit after Well-5- ADJ Box - STX1 condition



Figure 04-Scale in WT Kit after Well-5- ADJ Box - STX1 Scale Thickness

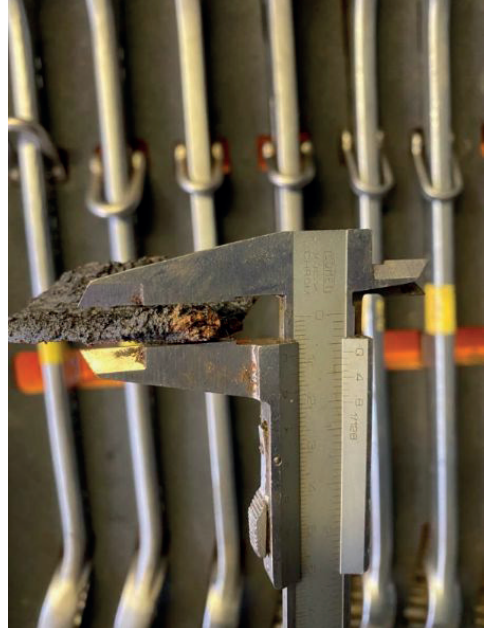


Figure 05-Scale in WT Kit after Well-5- RHS Choke Box



Figure 06-Fluid Losses with Old Design

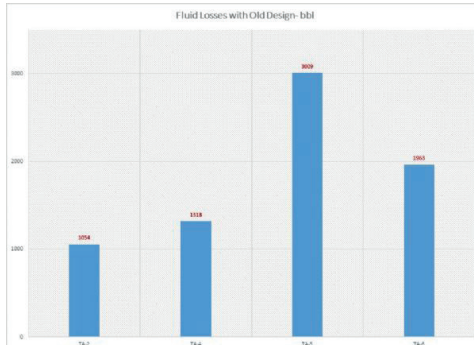


Figure 07 Seal Units- Remove Elastomer from top bonded seal from each seal unit- In Total: 17 Seal Units



Figure 08-Transfer procedure of SSTT with rig equipment- The 7 5-8 elevators are closed around the pup joint and sit on the dog collar



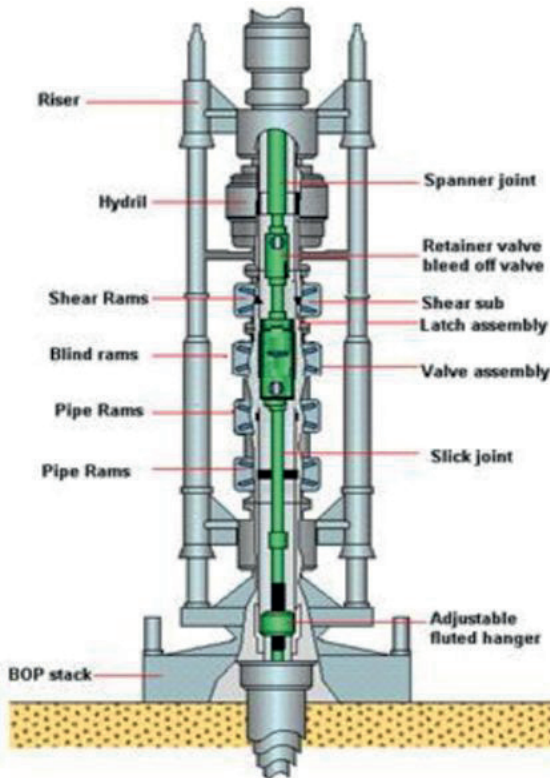
Figure 09-Transfer procedure of SSTT with rig equipment- 50' bails have been installed on MWC TDS



Figure 10-Transfer procedure of SSTT with rig equipment- Transfer of SSTT with using soft slings



Figure 11-SSTT



**IPETGAS 2023**

*Table 1 Summary of 2,5" Bailer Runs at Well-9*

	1st Run	2nd Run	3rd Run	4th Run	5th Run	6th Run	
Wet Debris, gr	610	1+10	363	382	142	180	
Dry Debris, gr	473	1456	252	276	100	121	
Description of Debris	Very fine Sandstone/Siltstone: 10% Metal:90%	Very fine Sandstone/Siltstone: 20% Metal:80%	Very Sandstone: Metal:95%	fine 5%	Metal: 100% Trace of dolomite with presence of two amorphous pieces of cement	M e t a l : 100%	Metal: 100%
Fluid Volume, lt	1.216	4.4	4	4.1	1.8	2	

*Table 2 Summary of 2,5" Bailer Runs at Well-12*

	1st Run	2nd Run	3.437" Plug Retrieval Run	Total Weight
Wet Debris, gr	830	160	218	1208
Dry Debris, gr	586	123	180	889
Description of Debris	Oily Dirt: 20% Metal: 80%	Oily Dirt: 10% Metal: 90%	Metal: 100%	



# Service Quality Management in Sakarya Gas Field Development Project (SGFDP), Black Sea, Türkiye



Esen Nasıroğlu, Hüseyin Savaşçı, Firat Üstün, Erdal Asku  
Turkish Petroleum Off-Shore Technology Center A.Ş.

This paper presents an analysis of operational efficiency in constructing the deepwater wells in Sakarya Gas Field of Black Sea. In greater detail, the paper focuses on how the Service Quality (SQ) has been improved and ensure a cost driven drilling methodology.

The experiences from discovery to world class megaproject holds a number of key lessons, particularly in the challenging conditions of deep water. An effective monitoring and evaluation of key lessons is essential to achieving sustainable Service Quality Management System.

Turkish Petroleum Off-Shore Technology Center (TP-OTC), Integrated Project Management Company (IPM) in the Sakarya Gas Field Development Project (SGFDP), has organized a dedicated Service Quality team of Senior Engineers in early 2021. TP-OTC SQ team has been entrusted to ensure all drilling activities are conducted in the most efficient, safe and cost-effective manner.

In order to manage a more integrated and centralized information of well operations, an up-to-date and well-structured database was implemented. Standard industrial data classification methods were applied to categorize and store information gathered from Daily Drilling Reports over a span of two years covering fourteen wells.

Service Quality Engineering ensured that the operator company and service suppliers work together as a system for accomplishing optimum outcomes by measuring deviations in approved well budgets (AFE) and existing Key Performance Indicator (KPI) metrics. Furthermore, it played an active role in the development of new KPI metrics and controlling Non-Productive Times (NPTs).

## 1 INTRODUCTION

Türkiye, with its growing economy, stands as a prominent global energy consumer with an increasing reliance on natural gas imports to satisfy its escalating energy demand. According to the Energy Market Regulatory Authority Reports, Türkiye's national natural gas production increased by 6% between 2017 and 2021 (Energy Market Regulatory Authority, 2017,2021) yet it is far from meeting the demand.

To access national resources, Turkish Petroleum Corporation (TPAO) has drilled numerous shallow, deep and ultradeepwater wells in offshore Black Sea since 1971. In the last decade, during deepwater drilling campaign in Black Sea, numerous risks were encountered like the presence of shallow gas zones, sections with low fracture pressure gradients, loss circulation zones due to the presence of fractured limestone, long abnormally pressurized intervals, a

high potential for false kicks (breathing formation and ballooning), and the potential for gas migration to the riser (Luiz A. S. Rocha, 2011). Even with increasing amount of geological data, the geoscience studies point that the Black Sea is still characterized by controversy and uncertainty (M. D. Simmons, 2018).

With the objective of supporting petroleum and natural gas exploration and production activities on waters of Türkiye, Turkish Petroleum Off-Shore Technology Center (TP-OTC) was founded in 2019. Shortly after, activities successfully resulted in the discovery of a natural gas reserve in Sakarya Gas Field of Black Sea (Kadıoğlu, 2022). Based on reservoir studies, a multiphase drilling, completions and production campaign was put together that will large number of years and utilize a great number of resources including three of Ultra Deepwater Dual Activity Drillships and twelve of Platform Supply Vessels.

In the early stage of the project, TP-OTC has established a Service Quality Management (SQM) in order to complete the project in the most economical and safe way and to minimize operational downtime.

TP-OTC Service Quality Management System promotes continuous improvement, focuses non-conformity prevention, and seeks to reduce variation and impact of non-productive time in service supply organizations by setting Key Performance Indicators (KPI), analysing and reporting Non-Productive Time (NPT) and High Potential (HiPo) events, managing Non-Conformance Reports (NCR) and performing Root Cause Analysis (RCA) studies. Within these responsibilities, Service Quality Management observes to international standards and industrial practices as its operational guidelines, namely API Specification Q2 (Quality Management System Requirements for Service Supply Organizations) and Rushmore Reviews.

## 2 PRESUMPTIONS

This article considers 14 wells drilled in Sakarya Gas Field of Black Sea by Fatih Drillship between the years of 2020 and 2023. It should be noted that Well-14 well has been excluded in the study due to early well abandonment.

Furthermore, the statistical studies are based on Actual Well Duration (AWD) data starting from the first operational step and ending at the last operational step in AFE program. The wells are non-dry wells normalized for each 1,000 meters drilled and considered all well operations including formation evaluations.

### 3 METHODOLOGY

As presented in Figure-1 Service Quality Management System starts with defining KPIs for the well operations using information from Well Drilling program and service contracts. Since, monitoring KPIs is essential to improve operational efficiency by detecting events of Invisible Lost Time (ILT), TP-OTC took Real-Time Monitoring Center into service, managed by senior engineers shifting for 24/7 work schedule. The actual time and offset information are compared on daily basis and reported for attention of operations team. The reports intend to demonstrate how operations evolve over time and helps to identify improvement areas to reach technical limits of operation over the course of the project.

Similarly, tracking NPT and HiPo cases helps to identify challenging parts of the operation by monitoring severity and frequency of incidents. Therefore, SQM constructed a database of NPT and HiPo records on the basis of industrial norms and practices. The database consists of three main and detailed sub-groups; Event Environment, NPT/ HiPo Category, NCR/RCA Status. Maintaining the database enables to track the NPT/HiPo closure and also to help analyse the NPT statistics over time, well, operation or any other variable. Alerting and taking precautions against HiPo events is also an important part of the process as these might have resulted in NPT events under slightly different circumstances.

For all type of NPT events, the owner of the NPT generates NCR and submits to the Service Quality Management. The initial NCR report contains basic information regarding the NPT incident, aims to inform all related parties about the event and should be sent in earliest time operationally feasible. On the other hand, the Final NCR report contains detailed information regarding the incident. Root causes of the incident, corrective and preventative actions with responsible parties, due dates and supportive documents should be part of the final report and is expected to be finalized within two weeks of the incident date. For NPTs over certain hours of duration, a Root Cause Analysis (RCA) study will be performed by an appointed team to analyze the incident in depth to define ways to prevent future occurrences. Following Subject Matter Expert (SME) approval, final NCR/RCA report recorded and archived with corrective and preventative actions (CAPA). Depending on the nature of the NPT, team meeting may be requested along with publishing Service Quality Alert (SQA). For HiPo events, NCR reports are prepared by directive of managerial decision and follows same rules as NPT caused NCRs. The Figure-2 presents a detailed Root Cause Analysis Process Flow with all elements.

#### 4 SERVICE QUALITY MANAGEMENT

##### 4.1 Key Performance Indicator (KPI)

TP-OTC SQ team monitors and analyzes Performance Trends during drilling of wells by applying records on Table-1. SGFDP Wells consists of four hole sections.

Table-1 presents a set of KPI metrics dedicated for well operations in each well section.

The detailed AFE study delivers operations steps with required time schedule based on offset wells. These are called target or base plan for the operational KPI metrics and KPI analysis is compared against the base plan.

The Last Performance (LT) on the other hand refers to the latest recorded performance of the Rig. Furthermore, calculated Trend presents correlation between the last and previous performances. While a negative (-) Trend indicates poor performance a positive (+) Trend points an improvement in performance.

Year-to-Date Performance (YTDP) gives an arithmetic average of performance metric that recorded through the year. It is a more sensitive indicator when comparing rig performances in a fleet.

The Best of Best (BOB) is also recorded as the benchmark performance in the project. It is expected to change by time, improving or worsening. The BOB is monitored by measuring change between base plan and BOB (Delta) where positive delta shows performance improvement.

The Best in Class (BIC) is another performance qualifier that correlates the company performance with industrial benchmark. It is usually used for operational efficiency in international area.

##### 4.2 Drilling Performance

Drilling wells is a major expense for the upstream oil industry. The economic application of well operations relies on understanding of well costs and the risks involved. Drilling performance can be discussed based on Actual Well Duration (AWD) as presented in Figure-3.

In upstream projects, well time contributes significantly to reduce well costs which governed by efficient well operations. The Figure-4 demonstrates a logarithmic relationship of actual well time in SGFDP wells. The actual well duration decreases through project phase indicating that experience from wells applied to upcoming ones decreasing well and NPT times and increasing efficiency and economics of the project.

Nature of the SQ database construction enables analyzing the operational data in multiple ways. When well duration analyzed based on wellbore section, in Section 1, impact of different operations can be seen. On Figure-5, two distinct deviation from average times can be observed: During EOWM period after Well-5, preparations for next well (simops) could not be performed due to operational issues and negatively affected Section-1 timing on Well-6. Similarly, BOP hopping operations were utilized in Well-10 well which positively affected the timings and AFE. Lessons learned from these operations enables to plan more effectively for the upcoming wells.

A similar analysis that was performed for Section-2 (Figure-6) shows rapid learning curve over the initial wells. Through capturing lessons learned for the section

and implication on upcoming wells, section was drilled more efficiently and on predicted timeline for the remaining wells. A detailed operational analysis of the section and Invisible Loss Time (ILT) study may bring the section times to BIC levels as next step of the study. Looking at Section-3 (Figure-7) we have seen a similar learning curve as Section-2. A rapid decrease in actual well duration over the course of campaign indicates application of lessons learned.

On the reservoir section of the well, there is a sharp spike on the initial stages of the campaign (Figure-8). Upon detailed look at the operations, the first two wells have extensive wireline and coring operations performed at the wells thus effecting the actual well duration. Excluding these operations, it can be observed that the well times in the last section (Section-4) has a flat trend showing that an in depth ILT analysis can be performed to improve section times further.

### 4.3 Non-Productive Time

The operations that are not in the well program or excess time spent for a certain operation that is in the program result in Non-Productive Time. Data from daily reports of 14 wells recorded on a daily basis and statistical analyses of the NPTs observed during the operation have been carried out. NPT details are recorded in accordance with the IADC definitions (such as Event Owner, Owner Function, Month to Date, Event Category, Event Type) and analyses can be performed according to different categories

Following the analysis, results shared with related departments, the causes of the NPT are investigated and the necessary meetings are held to minimize the probability of experiencing same situations in the future. With the preventative measures taken, the total cost of the operation can be significantly reduced as these situations that cause the operation to be stopped or delayed incur significant expenses for the company.

Analyzing total NPT durations of the 14 wells (Figure-9), a clear decline in the NPT hours can be seen over the course of the operation. The decrease in overall NPT hours enables drilling operations become more efficient and economical over time. The two spikes that goes over the curve, namely Well-4 and Well-6, are because of issues that requires long-lead items and excluding these NPT's, the clear improvement trend is obvious.

When further detailing the NPT's over types of failures (Figure-10), it is observed that two main failure points are rig (REF) and well equipment (WEF) related issues (total of 81%). To analyze further, when the NPTs plotted by category and over the years (Figure-11), the effect of REF and WEF related NPT's on the total NPT times can be seen clearly. On the same figure, a distinct decrease in event durations on all types of NPT's can be observed over the years (as seen on previous figures). The sharp decrease in WEF and REF NPT's makes the biggest impact in overall NPT times which coincides with the establishment of Service Quality Management services. Reporting and analyzing the NPT's according

to industry standards, sharing results and recording for future enable all parties to learn from these events and take precautions to prevent future occurrences thus improve overall efficiency of the operations.

### 4.4 Non-Conformance Report Recovery

Analyzing historical data for the given 14 wells drilled during the campaign (Figure-12), data shows that in the first year of the SQM department became active, only a third of the recorded NPT events can be closed with final reports. In 2022, although same number of wells drilled as in 2021 (six wells each), the close out rate increased to 80%. Same trend extends to 2023 and NPT close out numbers stay close to the number of NPT events. As each closed report recorded and archived, a valuable repository of information is created over time. The converging lines on the graph shows the improvement over time for capturing events, onset of NCR culture in the company as well as the emphasis given by the management on the matter.

When comparing the duration between the date of the event and the closure date of the report, a similar improvement recognized over time (Figure-13) since the beginning of the service quality process. Within one-year time, report closeout times drop to less than 20 days on average and stays close with-in the company defined standards in terms of event closure.

In order to analyze the impact of Service Quality Management, an NPT duration versus project timeline plot has been studied (Figure-14). The plot can be analyzed in three sections: For NPT events below 5 hours, there is a clear decrease in the number of events recorded during operations. As majority of these events are related to Rig and Surface Equipment (approximately 69%), it is clearly shown that the process managed to emphasize issues and led to improvements. Similarly, for events between 5 to 10 hours of duration, similar decreasing trend can be observed over time. For events over 10 hours, NPT mostly happened due to BOP or Seal Assembly issues which are either long-lead items or waiting ship to enter SPS period to maintain these issues. Looking at overall frequency of events, it is clearly shown that the Service Quality Management system has beneficial effect on operational efficiency and decreasing number of NPT events.

## 5 CONCLUSIONS

### SQ

Service Quality Management has increased operational efficiency by preventing rework, reducing waiting time, eliminating unexpected situations and reducing NPT.

### KPI

Tracking Key Performance Indicators (KPIs) over time and at various levels revealed areas where operational performance needs to be improved in order to beat benchmarks. It also contributes to optimize the overall cost of drilling oil and gas wells.

## NPT

The NPTs occurred in the operations are indicated in the Daily Drilling Reports and the records are kept by the performance team, statistically analyzed and shared with the relevant units. As a result, the necessary meetings are organized with the event owners who caused the NPT, and these meetings help in the identification of root causes and lessons learned for the future in order to avoid repeating the same situations in operations. This results in a decrease in non-productive time, allowing the company to operate more efficiently and reduce costs overall.

## HIPO

High Potential Events that occur on the field are recorded for future reference. The final reports that explain the situation and the actions that were taken as a result have been examined. As a result, we have solutions for how to proceed in the event of such a situation in the future.

## NCR

Analyzing NPT/NCR data over time, three distinct results can be observed. As project evolves, most of the NPT events are now properly tracked and closed through NCR reports. The time between the event and close-out date is moving below the company standards, and the number of NPT events are decreasing in number. As reporting process of the NPT events are clearly demonstrating the benefits, tracking High Potential Events in similar manner has also been started at the beginning of the year as the next step of the service.

## 6 FUTURE PLANS

To enlarge SQ unit to focus more efficiently ILT and NPT events

To set well delivery process to standardize and simplify engineering and administrate operations in each well phase.

## 7 ACKNOWLEDGEMENTS

We would like to thank the Management of Turkish Petroleum Off-Shore Technology Center A.Ş. for their support to publish this paper.

## 8 REFERENCES

- API. (2021). API Specification Q2 Quality Management System Requirements for Service Supply Organizations for the Petroleum and Natural Gas Industries. API.
- D.F. Bond, P. S. (1996). Step Change Improvement and High Rate Learning are Delivered by Targeting Technical Limits on Sub-Sea Wells. Louisiana: Society of Petroleum Engineers, Inc.
- Energy Market Regulatory Authority. (2017,2021). Turkish Natural Gas Market Report. Ankara: Energy Market Regulatory Authority.
- Gantsho, Y., & Sukdeo, N. (2018). Impact of Organizational Culture on Service Quality. Paris, France: Proceedings of the International Conference on

Industrial Engineering and Operations Management.

IHS Markit. (2023). Sakarya Gas Field Well Location Map. IHS Markit.

Kadioğlu, G. (2022). Sakarya Gas Field Development Project - ESIA, Non-Technical Summary. Ankara: TPAO.

Luiz A. S. Rocha, E. G. (2011). Overcoming Black Sea Ultra Deepwater Drilling Challenges. OTC 21676. Houston, Texas: Offshore Technology Conference.

M. D. Simmons, G. T. (2018). Petroleum Geology of the Black Sea.

Rushmore, P. (2011). Anatomy of the “Best In Class Well”: How Operators Have Organised the Benchmarking of their Well Construction and Abandonment Performance. SPE/IADC 140172.

TP-OTC. (2020). Well Drilling Programs. Ankara: Turkish Petroleum Off-Shore Technology Center Inc.

TP-OTC. (2020-2023). End of Well Phase Reports. Ankara: Turkish Petroleum Off-Shore Technology Center Inc.

TP-OTC. (2023). Non-Conformance Report Procedure. Ankara: Turkish Petroleum Off-Shore Technology Center Inc.

Wardt, J. P. (2016). Measuring Drilling and Completion Efficiency. IADC/SPE-178850-MS.

## 9 APPENDIX

### 9.1 Abbreviations and Acronyms

- AFE Authorization for Expenditure  
 AWD Actual Well Duration  
 BIC Best in Class  
 BOB Best of Best  
 BOP Blowout Preventer  
 CAPA Corrective Action, Preventive Action  
 CH Cased Hole  
 CSG Casing  
 DRL Drilling  
 DS Drillship  
 EOW End of Well  
 h Hour  
 HiPo High Potential  
 ILT Invisible Lost Time  
 ILTA Invisible Lost Time Analysis  
 LCO Lower Completion  
 LS Landing String  
 min Minute  
 MTP Maximum Theoretical Performance  
 NCR Non-Conformance Report  
 NPT Non-Productive Time  
 OH Open Hole

PT Productive Time	No Well and Rig Problem (NWRP), problems other than well and rig problems.
RCA Root Cause Analysis	Post Connection, time interval from the moment the drill string is pulled out of the slips to resume drilling.
ROP Rate of Penetration	Pre-Connection, time interval from the stand or single drilled to drill string is set into the slips.
SME Subject Matter Expert	Rig Equipment Failure (REF), failure of equipment in the rig inventory and operated by rig management.
SQ Service Quality	Surface Equipment Failure (SEF), failure of equipment that is not in the rig inventory and provided and operated by service providers during well operations.
SQM Service Quality Management	Technical Limit (TL), performance against theoretical times for sections and activities based on perfection assumptions.
Std Stand	Theoretical Well Time, the time can be calculated under the assumption of flawless operation based upon current knowledge and design technology (D.F. Bond, 1996).
TD Total Depth	Well Equipment Failure (WEF), failure of equipment which is temporarily or permanently run into hole.
TCP Tubing Conveyed Perforation	Well Problem None Blowout (WPNB), well problems without blowout.
TL Technical Limit	
TPAO Türkiye Petrolleri Anonim Ortaklığı	
TP-OTC Turkish Petroleum Off-Shore Technology Center A.Ş.	
SGFDP Sakarya Gas Field Development Project	
UCO Upper Completion	
UOM Unit of Measure	
WPBO Well Problem Blowout	
WPNB Well Problem None Blowout	
YTDP Year-to-Date Performance	

## 9.2 Nomenclature

Authorization of Expenditure (AFE), A budgetary document prepared to list estimated expenses of drilling a well to a specified depth, casing point or geological objective, and then either completing or abandoning the well.

Actual Well Duration, the reported time required to complete operations required to drill a well.

Best in Class (BIC), comparing overall, sectional, and phase performance with that of other operators on similar wells.

Best of The Best (BOB), internal comparison of an Operator's performance to the best results achieved on past wells.

Connection, time interval from the full string weight set in slips to drill string is pulled out of the slips. Conventional Lost or Down Time, the reported time spent on unplanned and redundant operations while drilling the same well; includes lost time from problems and down time due to equipment failure.

Invisible Lost Time (ILT), time lost due to inefficiency while drilling a well, which is typically reported as Productive Time and thus remains invisible in the record.

Key Performance Indicator (KPI), a set of quantifiable metrics used to evaluate overall long-term performance.

Maximum Theoretical Performance, estimated performance based on the physics of rock drilling from its characteristics and faultless operations using appropriate tools and equipment.

Non-Productive Time (NPT), is the time when the well operations in the program are interrupted or delayed for any reason.

Keywords: Service Quality Management, NPT

Figure 01 — Service Quality Process

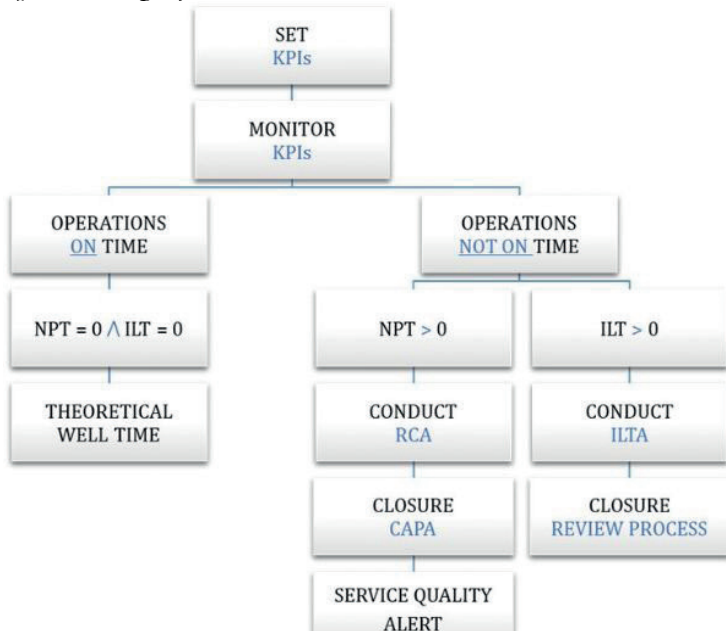


Figure 02 — Root Cause Analysis Process Flow

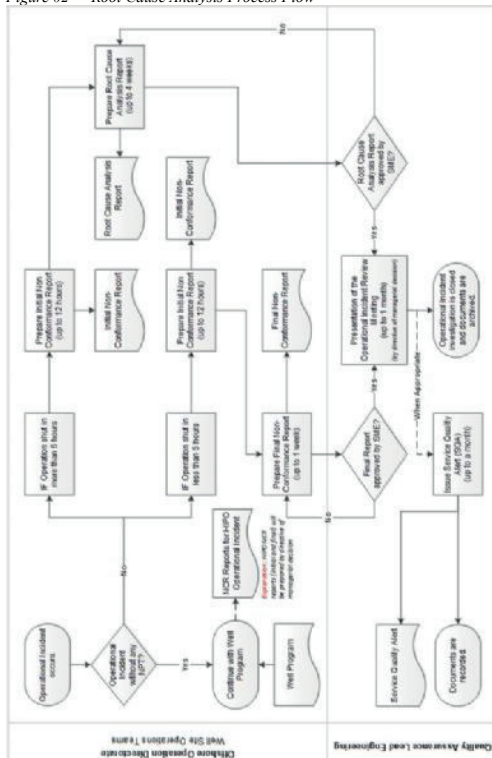


Figure 04 — Drilling Learning Curve

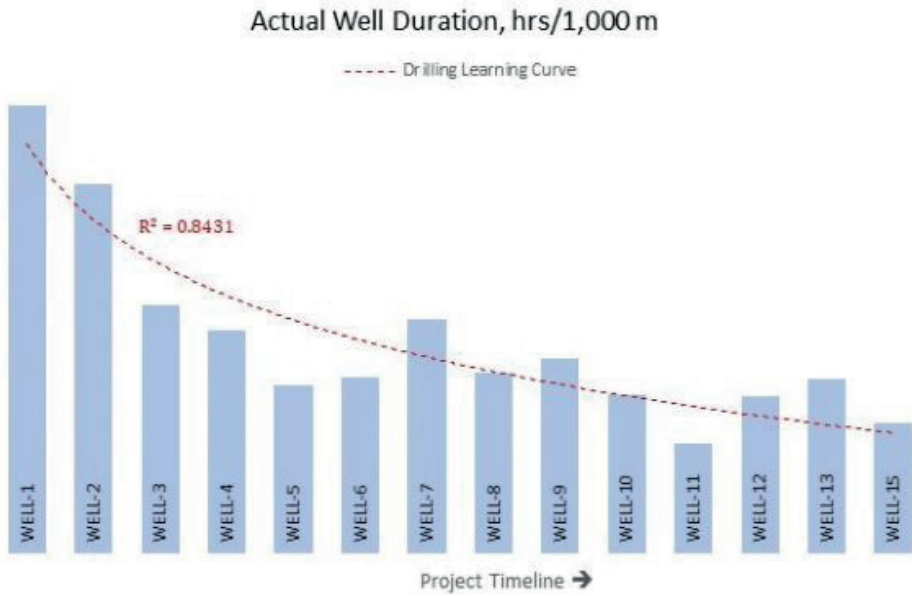


Figure 05 — Section-1 AWD

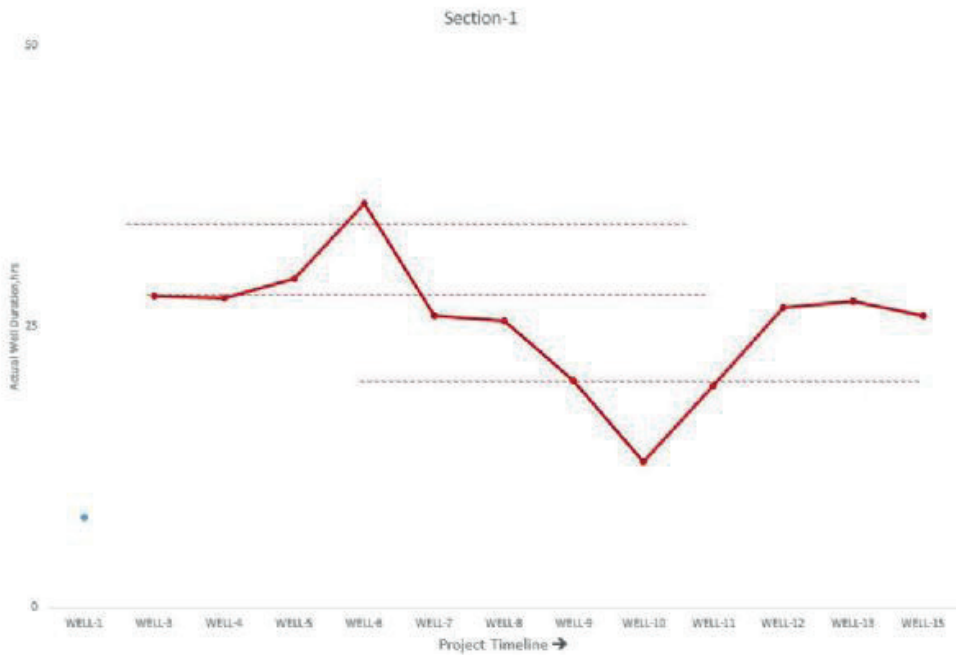


Figure 06 — Section-2 AWD

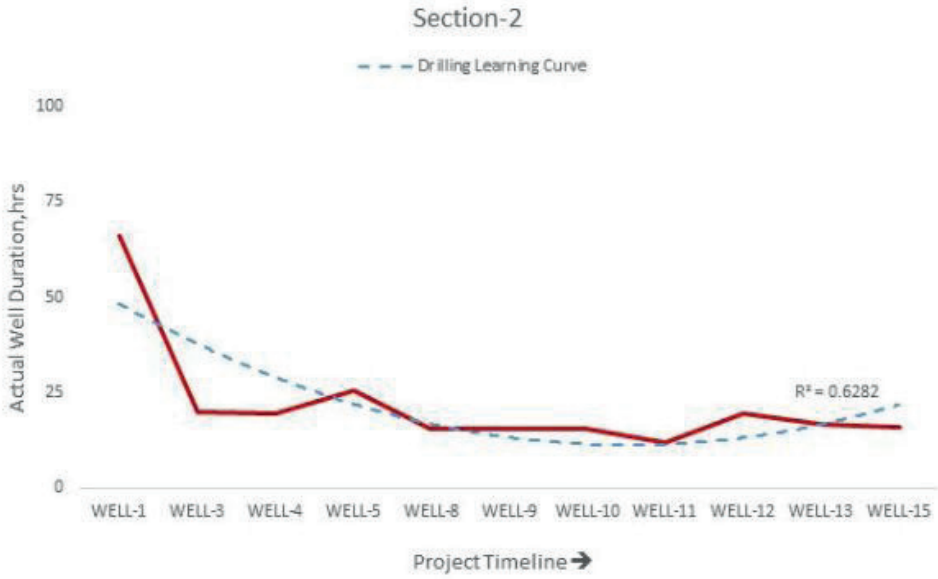


Figure 07 — Section-3 AWD





Figure 08 — Section-4 AWD



Figure 09 — Total NPT Breakdown by Wells

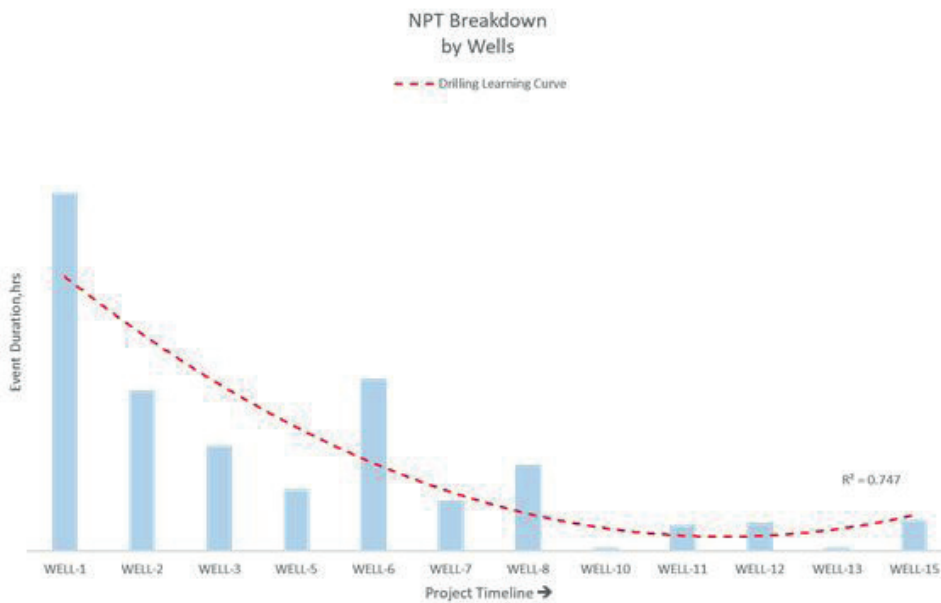


Figure 11 — Total NPT Breakdown by NPT Category and Years

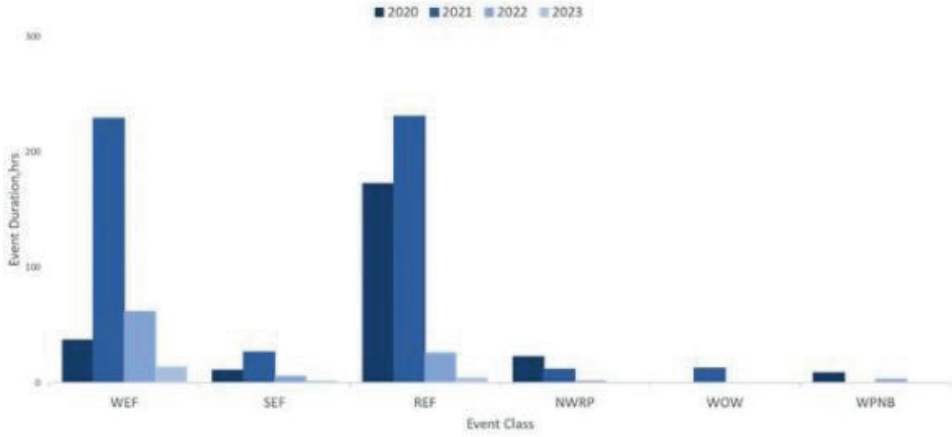


Figure 12 — Non-Conformance Report Recovery

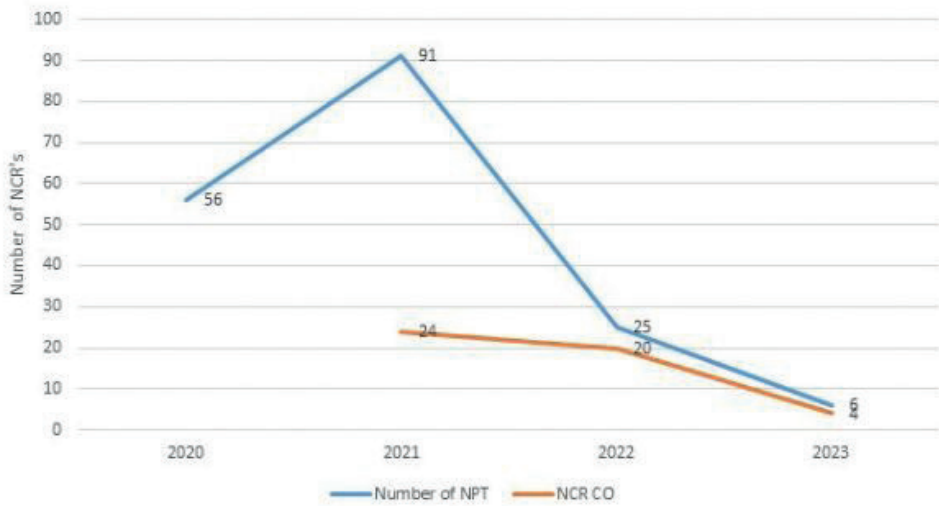


Figure 13 — Non-Conformance Report Recovery Rate (Completion Time)

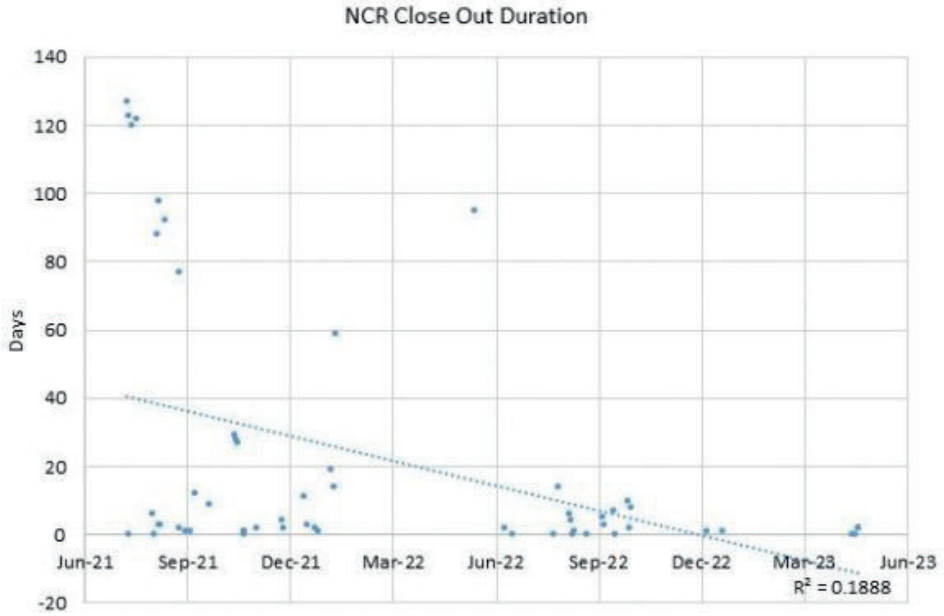


Figure 14 — Non-Productive Time Duration

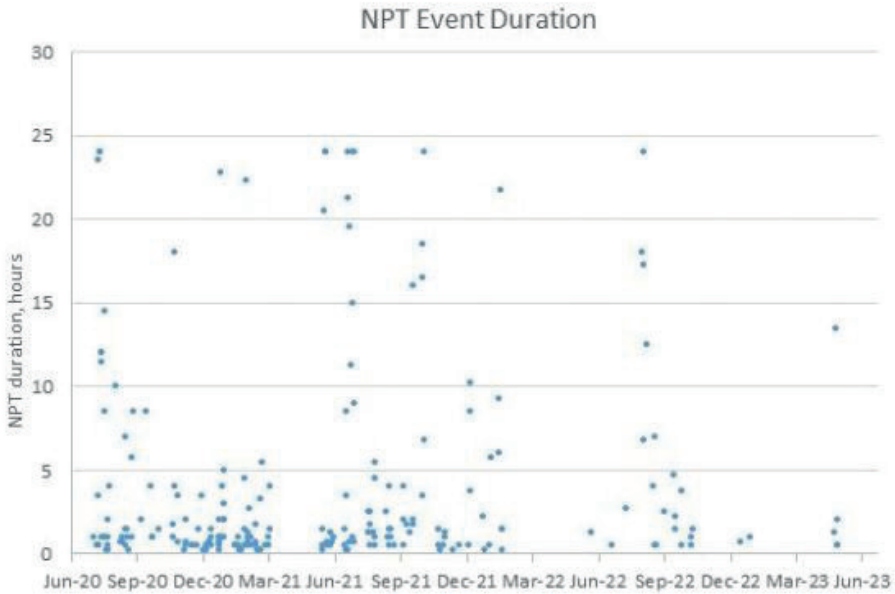


Table 1 — Performance Trend Report

Well Phase	KPI Metric	UOM	AFE Base Plan	LP Rig	LP Trend %	YTDP Rig	BOB Rig	BOB Delta	BIC
Section-1 Hole Drilling	Weight to Weight Time	min							
Section-1 Hole Drilling	Average Net ROP	m/h							
Section-2 Hole Drilling	Weight to Weight Time	min							
Section-2 Hole Drilling	On-Slips Time during Tripping	min							
Section-2 Hole Drilling	Speed Time/Stand during Tripping	min/std							
Section-2 Hole Drilling	Average Net ROP	m/h							
Casing Running	On-Slips Time during Tripping	min							
Casing Running	Speed Time/Stand during Tripping	min/std							
Casing Running	Average Net Tripping Speed	m/h							
BOP/Riser Running	On-Slips Time during Tripping	min							
BOP/Riser Running	Speed Time/Stand during Tripping	min/std							
BOP/Riser Running	Average Net Tripping Speed	m/h							
Clean Out	On-Slips Time during Tripping	min							
Clean Out	Speed Time/Stand during Tripping	min/std							
Section-3 Hole Drilling	Weight to Weight Time during Drilling	min							
Section-3 Hole Drilling	On-Slips Time during Drilling	min							
Section-3 Hole Drilling	On-Slips Time during Tripping	min							
Section-3 Hole Drilling	Speed Time/Stand during Tripping	min/std							
Section-3 Hole Drilling	Average Net ROP	m/h							
Casing Running	On-Slips Time during Tripping	min							
Casing Running	Speed Time/Stand during Tripping	min/std							
Casing Running	On-Slips Time during Tripping	min							
Casing Running	Speed Time/Stand during Tripping	min/std							
Casing Running	On-Slips Time during Tripping	min/std							
Casing Running	Speed Time/Stand during Tripping	min/std							
Casing Running	Average Net Tripping Speed	min							
Casing Running	Casing Stands	min							
Casing Running	Average Net Tripping Speed	m/h							
Section-4 Hole Drilling	Weight to Weight Time during Drilling	min							
Section-4 Hole Drilling	On-Slips Time during Drilling	min							
Section-4 Hole Drilling	On-Slips Time during Tripping	min							
Section-4 Hole Drilling	Speed Time/Stand during Tripping	min/std							
Section-4 Hole Drilling	Average Net ROP	m/h							
Formation Evaluation	On-Slips Time during Tripping OH	min							
Formation Evaluation	On-Slips Time during Tripping CH	min							
Formation Evaluation	Speed Time/Stand during Tripping OH	min/std							
Formation Evaluation	Speed Time/Stand during Tripping CH	min/std							
Formation Evaluation	Average Net Tripping Speed OH	m/h							
Formation Evaluation	Average Net Tripping Speed CH	m/h							
Casing Running	On-Slips Time during Tripping 9" CSG	min							
Casing Running	Speed Time/Stand during Tripping CSG	min/std							
Casing Running	On-Slips Time during Tripping CSG	min							
Casing Running	Speed Time/Stand during Tripping CSG	min/std							
Casing Running	On-Slips Time During Tripping	min							
Casing Running	Speed Time/Stand during Tripping	min/std							
Casing Running	Average Net Tripping Speed	m/h							
Casing Running	Casing Stands	m/h							
Casing Running	Average Net Tripping Speed	m/h							
Plug and Abandonment	On-Slips Time during Tripping	min							
Plug and Abandonment	BOP on Riser	min							
Plug and Abandonment	Speed Time/Stand during Tripping	min/std							
Plug and Abandonment	BOP on Riser	min/std							
Plug and Abandonment	On-Slips Time During Tripping	min							

# Evolution of Lower and Upper Completions in Ultra-Deep-Water Gas Wells, Offshore Black Sea: Learnings, Improvements and Potential Innovations



**Yves Mbiguis**

Turkish Petroleum

With the recovery of the oil price and the increasing demand on reliable energy resources observed in 2021, the world has noticed an increased exploration activity for untapped hydrocarbon resources in deep-water. One of those latest discoveries includes the Black Sea (Sakarya) Gas project by Turkish Petroleum (TPAO).

The recently discovered, but fast-tracked Turkey's Sakarya offshore natural gas field development is also a result of the country's commitment to energy independence.

The current paper focuses on the Lower and Upper Completion designs, preparations and installation activities in the Sakarya Gas Project. Its aims are:

- Describe the key considerations for the design stage of the Lower Completions (LC) and Upper Completions (UC) of the Sakarya Gas Project wells;
- Discuss the currently used Completions designs, their key features, risks and potential improvements.
- Presenting some identified innovations to further de-risk the Completions operations in the Sakarya Gas Project

## SAKARYA FIELD AND PROJECT OVERVIEW

The Sakarya Gas project is the first TPAO oil or gas discovery in deep water environment. The Sakarya natural gas field was discovered in August 2020 by drilling Tuna-1 exploration well using Turkey's sixth generation ultra-deep-water drillship Fatih. Tuna-1 was drilled at a water depth of 2,115m and reached 3,500m in the Black Sea. The well successfully intercepted more than 100m of the natural gas-bearing reservoir in Early Pliocene to Pleistocene sandstone formations. The field was estimated to have a potential natural gas reserves of 320 billion cubic meters (bcm) of lean gas, which is the largest gas reserve discovered in the Turkish Exclusive Economic Zone as well as in the Black Sea.

In October 2020 a second discovery announcement was made in the lower sections of Tuna-1, which increased the potential recoverable reserve estimate to 405 bcm of lean gas. The discovery was found at the deeper part of the well, where an additional 30m of gas pay was encountered in the sandstone reservoir of the Late Miocene. Further, the drilling of the exploratory well Amasra-1, 40 km away from north of Sakarya gas field by Fatih drillship lead to discovery of 135 bcm gas within the similar reservoir concept in June 2021, and increased the potential recoverable cumulative natural gas reserves to 540 bcm

The Sakarya field is located 170 km north of the Turkish coast in the Black Sea at 2117m of water depth. The gas-bearing reservoirs are in the clastic rocks of the Mio-Pliocene age and shale dominated intervals within

the same deposits have also been considered as the biogenic source rock of the system (Fig. 1). The first gas production from the Sakarya gas field has started in 2023 into the Turkish grid from the completed wells of the first phase of the project.

The field consists of three main reservoirs, R1, R2, R3, characterized by thin shale layers interbedding the laminated sandstone and siltstone formations. With well architectures needing optimisation to drain up to 19 layers of poorly consolidated interbedded sand shale delineated across R1, R2 and R3 horizons, the ultra-deep-water environments in the Black Sea region makes this project to be one of the most challenging for oil and gas developments. Key requirements of the Lower and

## Upper Completion systems include:

- Completion life of 25-years
- Utilize key enabling technologies to maximise gas recovery across the pay by incorporating zonal control and monitoring.
- Robustness and reliability are essential to assure successful installation, uptime and operational longevity.
- Well designs eliminate interventions due to deep-water subsea complexities and cost.

Front End Engineering Design (FEED) – LC and UC architectures

In order to overcome the challenges posed by the complex nature of the Sakarya field reservoir, one of the most critical tasks was to select the most suitable completion design for sand control and gas production management from multiple zones.

## LC architectures:

During the FEED and concept framing stage, the initially proposed LC designs included the following designs:

- Design #1: Multiple-zone Single Treatment with MZ-All Frac Packer
- Design #2: Two-zone Single Treatment with MZ-All Frac Packer

For both Design #1 and 2, The lower completion design was a single trip cased hole gravel pack with alternate path screens and a formation isolation valve.

In those designs, a sump packer is at the bottom of the completion this is used to land the lower completion into, OptiPac screens and isolation packers to isolate between distinct reservoir intervals. This is repeated dependent on the number of zones required per well. At the top of the lower completion the Fortress-M Isolation

Valve is used to mitigate fluid losses whilst running the upper completion.

The lower completion is run in a single trip using a standard work string. The gravel is pumped through the shunt tubes, in a single treatment, packing the top zone first and continuing down the shunt tubes to pack the lower zones.

For the Design #2, the Fortress-M Isolation Valve is not required in the Lower completion as the AFIV/FIV is to be run on the intermediate string.

One of the main benefits of the single trip system is the reduction of number of runs, hence a lesser exposure to execution risks and considerable reduction of completion time and costs. However, the benefits here-above mentioned did not outweigh the challenges and operational risks of the single trip system, which were revealed while preparing the execution of the 1st Well

#### **Completion in Türkali-2 (TA-2). These challenges included:**

- Excessive losses into the formation, due to up to 5 sands perforated, could create risk of well control or damage to formation.
- Potential for stuck perforating string, due to excessing sand production from long perforated gross section.
- Challenges in effectively managing cross flow during simultaneous perforation or up to 5 zones with different reservoir pressures.

For the reasons listed above, the LC Design#1 was revisited and FEED was updated with the LC Stacked Gravel Pack design, where the zones are perforated and gravel packed sequentially. This Design #3 allows a more controllable way of working on each each zone individually, with the benefit of minimizing the possible design and installation risks. This was perceived as more cautious approach, as it permitted to complete the intervals one by one, while also increasing team experience in terms of technical and operational capabilities, including reservoir familiarization.

Figures 2, 3 and 4 show the components of Design #1, #2 and #3.

#### **UC architectures:**

During the FEED and concept framing stage, the initially proposed UC designs included the following designs:

- For Design #1 – for LC Design#1 and #3: single trip design that positions Proteus Flow Control Valve (FCV) stations, electric monitoring, and isolation packers in each zone of interest. There is a shifting tool at the bottom of the upper completion, which is to open the Fortress-M Isolation Valve when stinging into the lower completion. The seal will provide a fluid conduit to surface whilst stinging through the FIV. Proteus stations with zonal isolation allow selective production from commingled zones and monitoring of those zones. Above the reservoir there is a production packer that

acts as the primary well barrier during production. A sliding side door (SSD) is to be used to unload kill weight brine from the wellbore. A chemical injection mandrel is to be installed below the SSSV to mitigate any scale concerns. A deep-set safety tubing pressure insensitive valve will be installed, which is a fail-safe device with fully redundant hydraulics.

- Option 2: TRFC-HD two-zone conventional hydraulic intelligent well completion. This design aims at reducing total well cost, complexity and improved lead time. It includes an intermediate completion run immediately after the LC, to allow the 2 zones to produce separately through different flow paths.

These proposed UC designs showing both the design with Proteus FCV's and with the TRFC-HD Hydraulic system are presented below:

#### **Subsequence Learnings and Improvements during Completion Jobs Executions**

After the FEED, the LC and UC designs were further improved, as discussed in this section.

#### **Standardizing MFIV as Fluid Loss Device for each zone:**

As per the agreed FEED, the original plan was to install

only MFIV on the topmost zone, to serve and FLCD before temporary suspension of the well before UC. The other zones below would have viscous pills to help against fluid loss.

During further risk assessments before start of LC activities, it was observed that this design brings several operational risks:

- Potential for well control situation, due to excessive losses during LC and inability to maintain a brine hydrostatic column.
- Possible formation damage due to large volume of brine saturating the reservoir, or due to poor management of the Fluid Loss Pills used to stop the losses.
- Loss of capital, due to excessive brine lost into the formation or too much time needed to clean up the wells before production
- Potential for crossflow between adjacent reservoir zones with no competent fluid barriers between them during LC operations.

To minimize or eliminate the risks above, the improvements below were adopted and included in the revised designs:

- Usage of more MFIV's in the LC designs, whenever reservoir pressures between zones are within a certain range. As per service company standards, the MFIV's were positioned right below the Gravel Pack packer extension, on top of the blank pipes, but far away from the top of screens.
- Establish a clear criterion for acceptable losses after perforating and gravel pack, to define whether a fluid loss pill is required or not to control losses.

• Establish a Well control strategy for running UC, including criteria for pumping in-screen fluid loss pills.

Opening the MFIV's and running UC in 2 separate trips:

As per revised FEED study, the plan was to install MFIV – fluid loss control devices in each zone and close them after each gravel packing operation. The plan was to run the UC with the MFIV in place; a shifting tool at the bottom of the UC string would permit opening the MFIV ball valve during UC installation.

During the detailed design phase of the UC, though kill weight brine was present in the well while running the UC string with control lines, the position of the MFIV in the LC created underbalance conditions, which would have generated a well control situation when opening the MFIV's with the UC string; the gas below each MFIV would migrate up the annulus and activating the shear rams would have been the only option in order to prevent having gas into the riser and at surface.

**The figures 5 below shows an example of under/overbalance assessment done for each zone:**

As a Well Control mitigation, the UC Program was updated with a dedicated trip to open all the MFIVs in a separate run, keep the well in a stable condition with continually monitored kill weight brine and with an accepted amount of fluid losses, while running the UC.

**The bull nose replaced by Bull plug:**

With the UC design no longer needing an MFIV shifting tool at the bottom of the string, a mule shoe was seen as sufficient to be placed at the bottom of the UC string. The risk of potential hang ups during RIH with UC was perceived minimum in these vertical wells, and this risk was mitigated by picking up and applying minimum rotation on the string and running in again.

However, during the UC on the well TA-2, the several hang ups were observed and rotating the string was not effective. The vessel was manipulated to achieve rotation. As a learning from this situation, it was agreed to:

- Replace the mule shoe by a bullet-shaped bull plug.
- RIH the UC with at least one FCV open to allow the string to be self filling.
- RIH with FCV in open-position #4, which allowed enough flow area thru the valve and allowed a short amount of time to close the valve in case of emergency.

**Relocating the MFIV's closer to top of screens:**

The Underbalance situation generated by the locations of the MFIV's in the LC strings was further assessed after the TA-2 LC and UC. To re-establish well control while opening each MFIV, the large volume of gas accumulated below the ball valve had to be bull-headed into the formation. However, by relocating the MFIV's closer to the top of screens, the following could be achieved:

- Regaining overbalance condition across the MFIV's.
- Significant reduction of volume of gas accumulated below MFIVs.
- No need for bull-heading brine after opening MFIVs.
- Reduction in number of trips required to open the different MFIV from 2 to 1 only, to achieve an overall reduction in the amount of fluids lost into the formation.

The figure 6 below shows a summary of the pros and cons of the old and the new configurations. The brown colour represents completion brine, and the yellow colour represents the formation gas.

**Use of Modular screens and Feedthrough Seals for “zero” losses:**

Alternative design were considered in order to reduce the long-term impact of the completion brine over the reservoir. Indeed, up to 9 months could be spent between the time LC is run until the UC is installed, which equates to the time the reservoir is exposed to considerable volume of completion brine.

**In order to mitigate against this, following were implemented:**

- LC design with conventional wire wrapped screens and MFIV fluid loss device to be replaced by screens incorporating sliding sleeves- also known as Modular Screens
- UC design with feedthrough hydraulic, straight-pull-to-release packers to be replaced by feedthrough seals.
- The dedicated trip to open the MFIV before UC deployment to be replaced by incorporating selective SSD shifting tools into the UC string.

**The changes mentioned above offer many benefits:**

- “Zero” fluid losses while running UC.
- Rig time saver and Well Control Risk reduction: No gas accumulation inside the LC, hence possibility of opening the Sliding Sleeves on the screens with UC string.

The completion configuration with this new design is shown in the figures 7 (Lower Completion), 8 (Upper Completion) and 9 (New LC and UC Configuration with Modular Screens) below

Further improvements and innovations

At the time of writing this paper, further improvements are being assessed and planned for upcoming implementations. This include existing as well as innovative technologies.

**Placing the Sliding Sleeve or SSD (Sliding Side Door) below the production packer:**

With the production packer currently used in Phase 1 of the Sakarya project, a V0 rated SSD is run above the production packer, to allow pumping the packer fluid

and spotting the base oil, after the production packer is set. This creates however a potential leak point, thus a well integrity risk. The SSD could not be positioned below the production packer, due to service company limitations with available tools to cut and release the packer in those conditions, if required.

A new type of production packer is planned for Phase 2 of the project, which allows placing the SSD below the packer, hence eliminating the well integrity risk mentioned above.

#### **Increasing the length of feedthrough seals:**

The current UC design features an Expansion Joint, that helps in ensuring a proper landing of the UC seals into their respective and, at the same time, ensures the Tubing Hanger reaches its landing position, with a larger margin of tolerance to space out errors. However, inherent risks due to usage of the expansion joint exist, these are:

- Risk of not being able to shear the ring of the expansion joint, leading to being unable to land the tubing hanger, thus need to pull the UC out of hole.
- Risk of damaging the tubing hanger or landing string, due to sling effect while shearing the expansion joint.

In order to mitigate the risks above, and innovation is being considered to engineers longer feedthrough seals in order to achieve a confidence level that would allow landing the seals and tubing hanger at the same time, without the need for the expansion joint, with still enough margins of tolerance to space out measurement errors. The design of these extended feedthrough seals is still being finalized, at the time of writing this paper.

#### **Other potential improvements and innovations:**

Since the detailed design of Phase-2 of the Sakarya Gas Project is still underway, other improvements and innovations are still pending reviews and full assessments; these are:

- Use of hydrostatic set production packer: to minimize the number of plugs run on slick line before setting the packer.
- Use of slick joint below the tubing hanger: this innovating tool is still under feasibility review by service supplier. If implemented, it would provide a way of circulating gas out of the well, in case the UC needs to be pulled. Shearing the UC string would no longer be the only well control measure.

Capturing lessons learnt and implementing improvements measures and innovative solutions are essentials in the long term success of projects. The details provided in this report are only a snapshot of how the Completion design and operations of the Sakarya project has evolved thus far.

Keywords: Completion, Intelligent



Fig. 1 – Sakarya gas field location in the Black Sea.



Fig. 2 – Design #1: Multiple-zone Single Treatment with MZ-All Frac Packer and Proteus FCV system

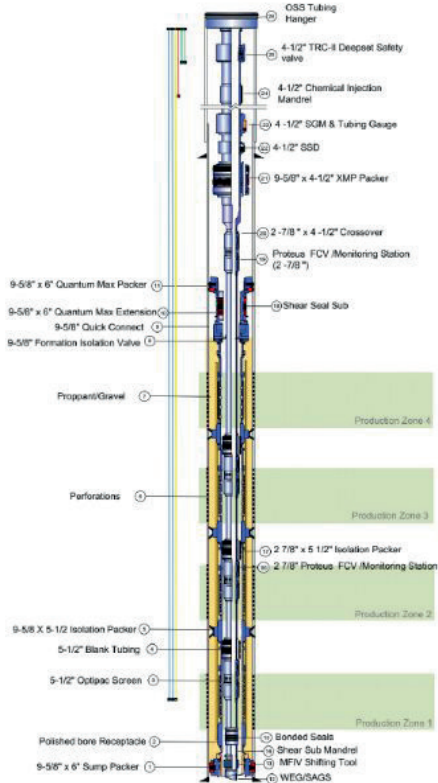


Fig. 3 – Design #2: Two-zone Single Treatment with MZ-All Frac Packer and TRFC-HD system

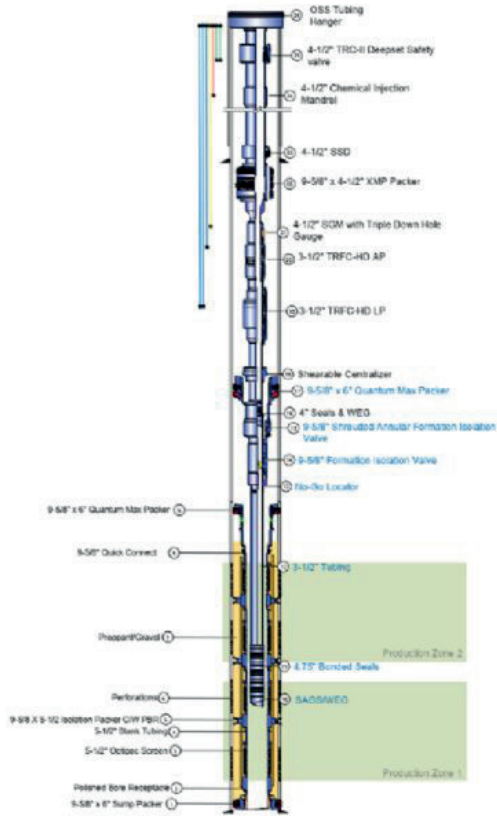


Fig. 4 – Design #3: Multiple-zone Stacked Gravel Packs and Proteus FCV system

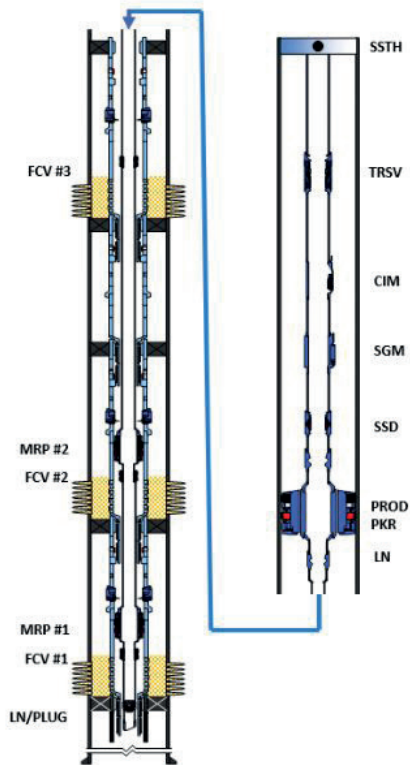


Fig. 5 – Example of MFIV opening assessment

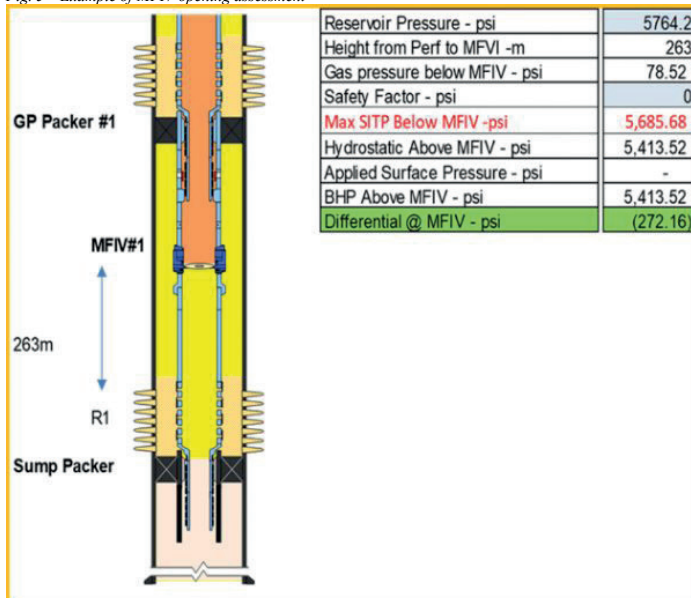


Fig. 6 – LC with Old vs New MFIV positions

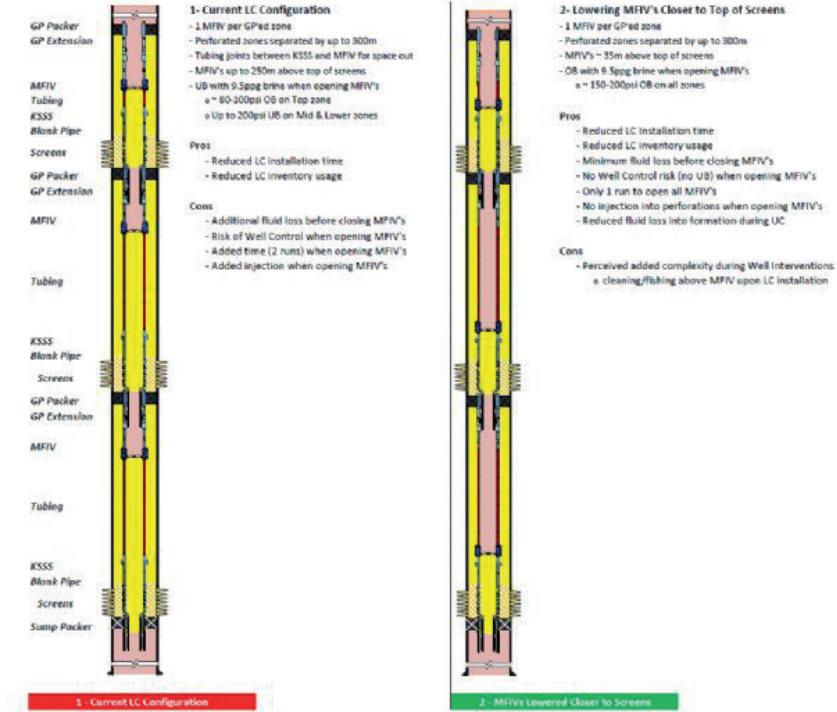


Fig. 7 - Lower Completion

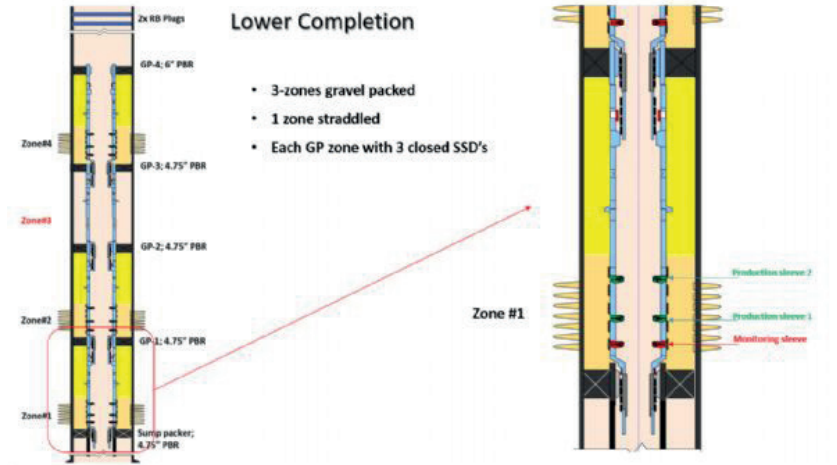


Fig. 8 - Upper Completion

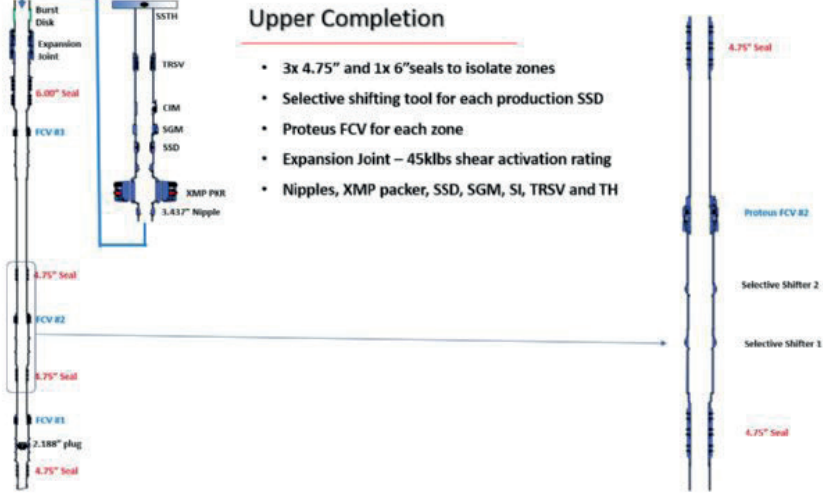
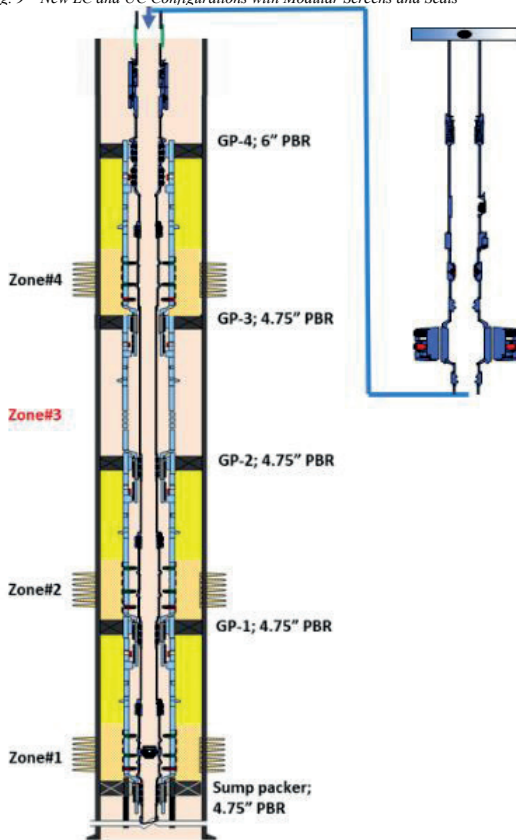


Fig. 9 – New LC and UC Configurations with Modular Screens and Seals







## **Dünya'da ve Türkiye'de Enerji Dönüşümü**

*Energy Transition in the World and Türkiye*

---





# Türkiye’deki İklim Değişikliği ve Karbon Yakalama-Depolama Uygulamaları ile İlişkili Mevzuatın İncelenmesi



**Sevtac Bülbül<sup>1</sup>, Çağlar Sımauç<sup>2</sup>, Mehmet Onur Doğan<sup>3</sup>**

<sup>1</sup>Orta Doğu Teknik Üniversitesi Petrol Araştırma Merkezi, Ankara / Türkiye

<sup>2</sup>Orta Doğu Teknik Üniversitesi Petrol Araştırma Merkezi, Ankara, Orta Doğu Teknik

Üniversitesi Petrol ve Doğal Gaz Mühendisliği Bölümü, Ankara / Türkiye

<sup>3</sup>Orta Doğu Teknik Üniversitesi Petrol ve Doğal Gaz Mühendisliği Bölümü, Ankara / Türkiye

## ÖZ

İklim değişikliğinin etkilerinin azaltılabilmesi için gerekli teknik yeterliliğin sağlanmasının yanı sıra ilgili faaliyetlerin uygulanmasına imkân veren yasal düzenlemelerin geliştirilmesi de büyük önem taşımaktadır. Karbon yakalama ve depolama uygulamaları gibi emisyon azaltma faaliyetlerinin gerçekleştirilebilmesi için, uygun stratejilerin belirlenmesi, uluslararası koşullara uyum sağlanması ve destekleyici mevzuat çalışmalarının yapılması gerekmektedir.

Bu çalışmada, Türkiye’de ilerleyen süreçte endüstriyel tesislerden açığa çıkan baca gazı ve karbondioksitin yakalanma ve depolanma çalışmalarının düzenlenmesi için ihtiyaç duyulan yasal alt yapının geliştirilmesi amacıyla, konu ile ilişkili mevcut mevzuat incelenmiş, iklim değişikliği ile mücadele kapsamında yürütülen çalışmaların tarihsel gelişimi sunulmuştur. Türkiye’nin iklim değişikliği ile ilgili ulusal hedef ve bildirimlerine yer verilmiş ve uluslararası müzakerelerdeki rolü incelenmiştir. Türkiye’de yakıtların yakılması, petrol rafinasyonu, çimento ve demir-çelik üretimi gibi faaliyetlerde belli kapasite üzerindeki tesislerin yürütmesi gereken sera gazı emisyonu izleme, raporlama ve doğrulama süreçleri özetlenmiş ve Avrupa Birliği Karbon Yakalama ve Depolama Direktifi’ne uyum süreci kapsamında yürütülen çalışmalara yer verilmiştir.

As well as the need of the technical competence to mitigate the effects of climate change, it is also of great importance to develop regulations that allow the application of related activities. In order to continue activities for emission reduction such as carbon capture and storage, appropriate strategies must be determined, international conditions must be adapted and supportive legislation must be developed. In this study, the current legislation is investigated in order to develop a legal infrastructure needed in the future to regulate the capture and storage of flue gas and carbon dioxide emitted from industrial facilities in Türkiye. Moreover, historical development of activities carried out against the climate change is presented. Türkiye’s national targets and communication on climate change are included and Türkiye’s role in international negotiations is examined. Regulations related to the greenhouse gas emission monitoring, reporting and verification processes in Türkiye, which are obligatory for the facilities with a specified capacity that carry out activities such as fuel combustion, oil refining, cement and iron and steel production, are summarized. The studies carried out within the scope of the harmonization process with the European Union Carbon Capture and Storage Directive are included.

## AMAÇ

Atmosferdeki karbondioksit miktarının azaltılması ve iklim değişikliği ile mücadele için gerekli süreçlerin düzenlenmesini sağlayan bir yasal alt yapının geliştirilmesi gerekmektedir. Yürütülen çalışma kapsamında, karbon yakalama ve depolama uygulamalarını da içeren iklim değişikliğinin etkilerinin azaltılması çalışmaları ile ilişkili ulusal mevzuat incelenerek sürece ait yasal çerçevenin belirlenmesi amaçlanmıştır. Bu amaçla, Türkiye’nin iklim değişikliği konusunda belirlemiş olduğu hedefler ve yürütülen çalışmaların tarihsel gelişimi incelenmiştir.

## GEREÇ VE YÖNTEM

Çalışmada, iklim değişikliği ve karbondioksitin yakalanması ve depolanması ile ilgili mevcut yasal mevzuat araştırılmıştır. Türkiye’de uygulanmakta olan karbon yakalama ve depolama projeleri ve Avrupa Birliği Karbon Yakalama ve Depolama Direktifi kapsamında çalışmalar incelenmiştir.

## BULGULAR

### Türkiye’nin Uluslararası İklim Değişikliği Müzakerelerindeki Rolü

Birleşmiş Milletler İklim Değişikliği Çerçeve Sözleşmesi (BMİDÇS), 3-14 Haziran 1992’de gerçekleştirilen Birleşmiş Milletler Çevre ve Kalkınma Konferansı (Rio Dünya Zirvesi)’nde imzaya açılmıştır (BM, 2023a, T.C. ÇŞİDB, 2023a). Sözleşme, “ortak fakat farklılaşmış sorumluluklar ve göreceli kabiliyetler” ilkesine dayanmakta ve sera gazı emisyonlarının azaltılması için, ülkelerin kalkınma öncelikleri ve özel koşulları göz önüne alınmaktadır. Ek-I’de yer alan gelişmiş ülkelerin sözleşmenin amacına ulaşılmasında diğer taraflara yardımcı olabileceği belirtilmiştir. Ek-II listesinde yer alan gelişmiş ülkeler ve diğer taraflar ise, gelişmekte olan tarafların Madde 12- Paragraf 1’de üstlendikleri yükümlülükleri yerine getirirken ortaya çıkan, üzerinde mutabık kalınmış tüm masrafların karşılanması için yeni ve ek mali kaynakları sağlayacaklarını taahhüt etmektedir. 1992 yılı itibarıyla BMİDÇS Ek-I’de, OECD üyesi olan ülkeler ve AB ile pazar ekonomisine geçiş sürecindeki ülkeler yer almaktadır. Bir OECD ülkesi olan Türkiye’nin adı, BMİDÇS 1992 yılında kabul edildiğinde Ek-I ve Ek-II listelerinde yer almıştır. 2001’de Marakeş’te gerçekleştirilen 7. Taraflar Konferansı’nda (COP7) alınan 26/CP7 numaralı karar uyarınca, Türkiye, Ek-II listesinden çıkarılmış ve özel şartları tanımlanmış bir Ek-I ülkesi olarak taraf olmuştur.

Türkiye, 21.10.2003 tarihli ve 25266 sayılı Resmî Gazete'de yayımlanan 16.10.2003 tarihli, 4990 sayılı Kanun ile 24 Mayıs 2004'de BMİDÇS'ne katılan 189. taraf olmuştur (T.C. Dışişleri Bakanlığı, 2023a).

BMİDÇS'ni güçlendirmek ve giderek artan iklim değişikliğinin etkilerini azaltabilmek amacıyla hazırlanan Kyoto Protokolü, 1997 yılında 3. Taraflar Konferansı'nda kabul edilmiş ve 16 Mart 1998'de New York'ta imzaya açılmıştır. 16 Şubat 2005'te yürürlüğe giren Kyoto Protokolü'ne 191 ülke ve Avrupa Birliği taraf. BMİDÇS'nde Ek-I'de yer alan ülkeler, Kyoto Protokolü'nün Ek-B listesini oluşturmaktadır. 2008-2012 yılları arasındaki birinci taahhüt döneminde, Ek-I'deki tarafların karbondioksit eş değeri sera gazlarının salımlarının toplamını 1990 yılı seviyelerinin en az %5 aşağısına indirmek için Ek-B'de kayıtlı azaltım taahhütlerine uymaları hedeflenmiştir. 2012 yılında Doha'da düzenlenen 18. Taraflar Konferansı'nda ikinci taahhüt dönemi 2013-2020 yılları olarak belirlenmiş ve Ek-B'deki tarafların salımlarını 2020 yılında 1990 yılına göre en az %18 azaltması kararlaştırılmıştır. Doha Değişikliği'nin yürürlüğe girmesi için 144 ülke tarafından kabul edilmesi şartı, 147 ülkenin kabulü ile Ekim 2020'de sağlanmıştır. Türkiye, 5386 Sayılı Kanun'un 5 Şubat 2009'da kabulü ile 26 Ağustos 2009'da Kyoto Protokolü'ne taraf olmuştur. Türkiye, Kyoto Protokolü kabul edildiğinde BMİDÇS'nin tarafı olmadığından, Ek-I ülkesi olmasına rağmen Ek-B'de yer almamıştır. Türkiye'nin Kyoto Protokolü kapsamında, 1. ve 2. taahhüt dönemlerinde taahhüdü bulunmamaktadır (T.C. ÇŞİDB, 2023a, T.C. Dışişleri Bakanlığı, 2023b).

Paris Anlaşması, 12 Aralık 2015'te, BMİDÇS kapsamında 21. Taraflar Konferansı'nda kabul edilmiş ve 4 Kasım 2016'da yürürlüğe girmiştir. 2020 yılında biten Kyoto Protokolü sonrası dönemin düzenlenmesi ve sanayileşme öncesine oranla küresel sıcaklık artışının 2°C'nin altında tutulması hedeflenmektedir. Anlaşma, gelişmiş ve gelişmekte olan taraf ülkelerin belirledikleri bağlayıcı olmayan hedefleri kapsamında sorumluluk üstlenmeleri esasına dayanmaktadır. Paris Anlaşmasının Onaylanmasının Uygun Bulduğuna Dair Kanun, 7 Ekim 2021 tarihli ve 31621 sayılı Resmî Gazetede yayımlanmıştır. Türkiye'nin Paris Anlaşması'na ilişkin Onay Belgesi ve Ulusal Beyanı, 11 Ekim 2021'de Birleşmiş Milletler Sekretaryası'na bildirilmiştir. 10 Kasım 2021'de Türkiye anlaşmaya taraf olan 192'inci ülke olmuştur. Türkiye'nin 2053 yılı için net sıfır emisyon hedefi ilan edilmiştir (T.C. ÇŞİDB, 2023c).

Türkiye'nin Ulusal İklim Değişikliği Stratejisi ve Eylem Planı, Ulusal Bildirimler

3 Mayıs 2010'da, iklim değişikliğinin önlenmesi faaliyetlerini içeren 2010-2023 Türkiye İklim Değişikliği Stratejisi, Yüksek Planlama Kurulu tarafından onaylanmıştır. Enerji sektöründe 2020 yılına kadar referans senaryoya göre %7 karbondioksit emisyon sınırlaması potansiyeli hedeflenmiştir (T.C. ÇŞİDB, 2023d). Ulusal İklim Değişikliği Stratejisi'nin uygulanması için Ulusal İklim Değişikliği Eylem Planı 2011-2023 hazırlanmıştır. Orman alanlarında karbon tutulumunun 2007 değerinin %15'i oranında artırılması,

temiz kömür teknolojilerinin kullanılması, enerji verimliliğinin artırılması ve yenilenebilir enerjinin payının artırılması azaltım planları arasında yer almaktadır (T.C. ÇŞİDB, 2023e).

Türkiye, müzakereleri devam eden Paris Anlaşması kapsamında, Eylül 2015'te Niyet Edilen Ulusal Katkı Beyanı'nı (Intended Nationally Determined Contribution-INDC), 13 Nisan 2023'te ise Güncellenmiş Birinci Ulusal Katkı Beyanı'nı BMİDÇS Sekretaryası'na sunmuştur. Güncellenmiş Birinci Ulusal Katkı Beyanı'nda, Türkiye'nin 2015 yılında %21 olarak açıklanan niyet beyanının 2030 yılı için % 41 oranında azaltılacağı (2030 yılında 695 Mt CO2 eşdeğeri) ve 2038 yılında emisyonların tepe noktasına ulaştırılması niyetinin olduğu belirtilmiştir. İkincil ETS Mevzuatı ve Türkiye için Karbondioksit Yakalama ve Kullanım Teknolojileri Yol Haritası ve Uygulama Planı'nın en kısa sürede hazırlanması hedeflenmektedir (T.C. ÇŞİDB, 2023f). Türkiye, BMİDÇS kararı 9/CP.16 ve 2/CP.17 ile teyit edildiği üzere, 2019-2022 yıllarını kapsayan 8. Ulusal Bildirim ve 5. İki Yıllık Raporu'nu 23 Mayıs 2023'te, BMİDÇS'a sunmuştur (BM, 2023d).

Avrupa Birliği, 11 Aralık 2019'da açıkladığı Avrupa Yeşil Mutabakatı ile 2050 yılında sıfır sera gazı emisyonunu ve kaynak kullanımından bağımsız bir ekonomik büyümeyi hedeflenmektedir (AB (a), 2023). Türkiye'nin Avrupa Yeşil Mutabakatı'na uyumunun sağlanması amaçlanarak Yeşil Mutabakat Eylem Planı 2021, 16 Temmuz 2021'de 2021/15 sayılı Cumhurbaşkanlığı Genelgesi ile yayımlanmıştır (T.C. Ticaret Bakanlığı, 2023).

İklim değişikliği ile ilgili ulusal koordinasyon, T.C. Çevre, Şehircilik ve İklim Değişikliği Bakanlığı tarafından yürütülmektedir. İklim değişikliği ile ilgili stratejileri belirlemek amacıyla faaliyet gösteren İklim Değişikliği ve Uyum Koordinasyon Kurulu, bakanlıklar, kamu kurumları ve sivil toplum kuruluşlarının aralarında bulunduğu üyelerden oluşmaktadır. (T.C. ÇŞİDB Bakanlığı, 2023g).

T.C. Enerji ve Tabii Kaynaklar Bakanlığı tarafından 31 Aralık 2022'de 2035 yılına kadar olan süreci kapsayan Türkiye Ulusal Enerji Planı yayımlanmıştır (T.C. ETKB, 2023). Net-sıfır emisyon hedefine ulaşabilmek amacıyla enerji sektörü ile elektrik ve ısı sektörü kaynaklı emisyonlar için üst sınır belirlendiği, yatırım maliyetleri incelendiğinde karbon yakalama teknolojilerine sahip kömür ve doğal gaz santral yatırım kararı alınmadığı, ileride bu teknolojilerin değerlendirilebileceği belirtilmiştir.

21-25 Şubat 2022'de düzenlenen İklim Şurası Komisyon Tavsiye Kararları'nda, yeşil hidrojen ve türevleri, karbon yakalama, kullanım ve depolama gibi emisyon azaltımına yönelik çalışmalar yapılmasının gerektiği ve ETS ile ilgili çalışmaların 2024 yılında tamamlanmasının gerekliliği belirtilmiştir (İklim Şurası, 2023).

### **Türkiye’de Sera Gazı Emisyonlarının Raporlanması ve İzlenmesi**

Türkiye’de, belirli kapasitenin üzerinde olan, yakıtların yakılması, petrol rafinasyonu, çimento, kok, demir-çelik üretimi gibi faaliyetlerde bulunan tesisler, sera gazı emisyonları için yıllık izleme, raporlama ve doğrulama süreçlerine tabidir. Sera gazı emisyonlarının izlenmesine, raporlanmasına ve doğrulanmasına dair usul ve esasları içeren Sera Gazı Emisyonlarının Takibi Hakkında Yönetmelik, 25 Nisan 2012 tarihli ve 28274 sayılı Resmi Gazete’de yayımlanarak yürürlüğe girmiştir. Yapılan değişiklikler ile Yönetmelik revize edilerek 17.05.2014 tarihli ve 29003 sayılı Resmi Gazete’de yayımlanmıştır (Mevzuat Bilgi Sistemi, 2023a). Yönetmelik kapsamında sera gazı emisyonlarının ve ilgili faaliyet verilerinin izlenmesi ve raporlanmasına ilişkin yükümlülükler, Sera Gazı Emisyonlarının İzlenmesi ve Raporlanması Hakkında Tebliğ’de (Resmi Gazete Sayı: 29068, Tarih: 22 Temmuz 2014) belirtilmektedir (Mevzuat Bilgi Sistemi, 2023b). Tesisler tarafından hazırlanan emisyon raporları, bağımsız akredite kuruluşlar tarafından doğrulanmaktadır. Sera gazı emisyon raporlarının doğrulanması ve doğrulayıcı kuruluşların niteliklerine ve akreditasyon işlemlerine ilişkin esasları içeren Sera Gazı Emisyon Raporlarının Doğrulanması ve Doğrulayıcı Kuruluşların Akreditasyonu Tebliği, 02.12.2017’de yürürlüğe girmiştir (Resmi Gazete No: 30258) (Mevzuat Bilgi Sistemi, 2023c).

### **AB Karbon Yakalama ve Depolama Direktifi**

Avrupa Birliği’nin 23 Nisan 2009 tarihli 2009/31/EC1 sayılı direktifi, iklim değişikliğine karşı karbondioksitin jeolojik depolanması için yasal bir çerçeve oluşturmaktadır (AB (b), 2023). Direktif, Avrupa Birliği üye ülkelerinde ve bu ülkelerin ekonomik bölgelerinde ve Birleşmiş Milletler Deniz Hukuku Sözleşmesi (UNCLOS) kapsamında ülke kıta sahanlıklarında CO<sub>2</sub>’nin jeolojik olarak depolanmasını kapsamaktadır.

T.C. Çevre, Şehircilik ve İklim Değişikliği Bakanlığı’nın faydalanıcı kuruluş olduğu, “Düşük Karbonlu Kalkınma için Çözümsel Tabanlı Strateji ve Eylem Geliştirilmesi Teknik Yardım Projesi” kapsamında, AB direktifinin ulusal mevzuata uyumlaştırılması çalışmaları yürütülmüştür. AB Karbon Yakalama ve Depolama Direktifi Düzenleyici Etki Analizi (DEA) çalışması gerçekleştirilmiştir. Kamu ve sektör temsilcileri ile yapılan toplantıların sonuçları AB Karbon Yakalama ve Depolama Direktifi Düzenleyici Etki Analizi Raporu’nda sunulmuştur (Düşük Karbonlu Kalkınma Projesi, 2017).

### **Türkiye’de Baca Gazının/ Karbondioksitin Yakalanması ve Depolanması ile İlişkili Yasal Mevzuat**

1986 yılından beri Dodan Gaz Sahası’ndan üretilen karbondioksit kullanılarak Türkiye’nin en büyük sahalarından olan Batı Raman sahasındaki petrolün üretimi sağlanmaktadır ancak sanayi tesislerinden

yakalanan baca gazının/ karbondioksitin petrol sahalarına enjeksiyonu işlemi, Türkiye’de uygulaması henüz olmayan bir işlemdir. Türkiye’de karbon yakalama ve depolama konusunda tamamlanmış ve halen yürütülmekte olan araştırma projeleri ve pilot ölçekli projeler bulunmaktadır (TÜBİTAK KAMAG 2009, CGS Europe 2014, ENOS 2020, ECOBASE 2020, GECO 2022, SUCCEED 2022, TÜBİTAK 1005 2023, CCUS ZEN 2023).

Doğrudan karbon yakalama ve jeolojik depolamayı düzenleyen bir yasa bulunmamakta, 30 Mayıs 2013’de kabul edilen 6491 sayılı Türk Petrol Kanunu, petrol kaynaklarının aranması, geliştirilmesi ve üretimini düzenlemektedir. Türk Petrol Kanunu, Madde 9 (3)’te “Petrol sahalarında üretilen karbondioksit gazı, üretim artırma yönteminde kullanılabilir.” ifadesi yer almaktadır ancak sanayi tesislerinden yakalanan karbondioksitin kullanımı ile ilgili bir bilgi yer verilmemektedir (Mevzuat Bilgi Sistemi, 2023d).

Türk Petrol Kanunu Madde 9 (4)’te, “Yer altı deposu olarak kullanılacak petrol rezervuarları, fiilen veya hesaba boşaltılmadan ve Genel Müdürlüğün uygun görüşü alınmadan yer altı deposu olarak kullanılamaz.” açıklaması yer almaktadır. Madde 9 (5)’te ise, “Depolama ve diğer enerji faaliyetleri ile petrol üretim faaliyetlerinin teknik olarak bir arada yapılmasının mümkün olduğu sahalar hem petrol üretim faaliyetine hem de depolama ve diğer enerji faaliyetlerine konu olabilir.” denmektedir (Mevzuat Bilgi Sistemi, 2023d).

22/1/2014 tarihli ve 28890 sayılı Resmî Gazete’de yayımlanan Türk Petrol Kanunu Uygulama Yönetmeliği’de, yer altı doğal gaz depolama ile ilgili bazı esaslara yer verilmiştir (Mevzuat Bilgi Sistemi, 2023e). Türk Petrol Kanunu Uygulama Yönetmeliği Madde 3- (ggg)’de, yeraltı doğal gaz depolama tesisi, “İşletmecinin ürettiği gazı ya da dışarıdan temin ettiği gazı kendi petrol rezervuarlarında depolamaya mahsus tesis” olarak tanımlanmıştır. Türk Petrol Kanunu Uygulama Yönetmeliği Madde 29 (12)’de, “Yeraltı doğal gaz depolama faaliyeti kapsamında; a) İşletmecinin ürettiği gazı ya da dışarıdan temin ettiği gazı kendi petrol rezervuarlarında depolama faaliyetleri ile ilgili Genel Müdürlükten izin alır.” ifadesi yer almaktadır.

2872 sayılı Çevre Kanunu’nda, karbondioksitin tesislerden yakalanması ile ilgili açıklama bulunmamaktadır. Çevre Kanunu Madde 3(h)’de, “...sera gazı emisyonlarının takibine yönelik karbon ticareti gibi piyasaya dayalı mekanizmalar ile ekonomik araçlar ve teşvikler kullanılır. (Değişik cümle:24/12/2020-7261/12 md.)” denmektedir (Mevzuat Bilgi Sistemi, 2023f). 29.07.2022 tarih ve 31907 sayılı Resmi Gazete’de yayımlanan Çevresel Etki Değerlendirmesi Yönetmeliği Ek-1 bölümünde bulunan Çevresel Etki Değerlendirmesi Uygulanacak Projeler Listesi 45. Madde’de “Yıllık olarak 1.5 milyon ton ve üzerinde karbon yakalama ve jeolojik depolama projeleri” yer almaktadır. Ek-2’de bulunan Çevresel Etkileri Ön İnceleme ve Değerlendirmeye Tabi Projeler arasında ise “Madencilik projeleri- Karbondioksit, metan gazı ve diğer gazların çıkartılması (Madde 45(c))

ve “Karbon yakalama ve depolama amacıyla CO<sub>2</sub>'in boru hatları ile taşınması (Madde 54)” bulunmaktadır (Mevzuat Bilgi Sistemi, 2023g).

Türkiye’de 2005 yılından beri, Gönüllü Karbon Piyasası’na yönelik projeler uygulanmaktadır. 7/8/2010 tarihli ve 27665 sayılı Resmî Gazete’de yayımlanarak yürürlüğe giren Sera Gazı Emisyon Azaltımı Sağlayan Projelere İlişkin Sicil İşlemleri Tebliği ile sera gazı emisyonlarının azaltılması, sınırlandırılması ve yutak alanların artırılması için yürütülen projelerin kayıt altına alınması amaçlanmıştır. 09.10.2013 tarih ve 28790 sayılı Resmî Gazete’de yayımlanan Gönüllü Karbon Piyasası Proje Kayıt Tebliği ile Sera Gazı Emisyon Azaltımı Sağlayan Projelere İlişkin Sicil İşlemleri Tebliği yürürlükten kaldırılmıştır. Türkiye Cumhuriyeti sınırları içerisinde karbon sertifikası elde etmek amacıyla geliştirilen projelerin kayıt altına alınmasına dair esaslar, Gönüllü Karbon Piyasası Proje Kayıt Tebliği’nde yer almaktadır (Mevzuat Bilgi Sistemi, 2023i). Proje sahiplerinin projelerini Bakanlığa kayıt ettirme yükümlülükleri, bağımsız denetleyici kuruluşların onayladıkları ve/veya doğruladıkları proje bilgilerini Bakanlığa iletme yükümlülükleri bulunmaktadır. 6446 sayılı Elektrik Piyasası Kanunu’nun Madde 11 (8)’inde emisyon ticaretine ilişkin hususların T.C. Enerji ve Tabii Kaynaklar Bakanlığının ve Sermaye Piyasası Kurulu’nun görüşü alınarak Enerji Piyasası Düzenleme Kurumu tarafından belirleneceği belirtilmektedir (Mevzuat Bilgi Sistemi, 2023i).

Karbon Piyasalarına Hazırlık Ortaklığı (Partnership for Market Readiness- PMR) Teknik Destek Programı, Dünya Bankası tarafından 2011 yılında başlatılmış ve Türkiye, 2013 yılında programa katılmıştır. Türkiye’deki PMR Projeleri, T.C. Çevre ve Şehircilik Bakanlığı tarafından yürütülmektedir. PMR Türkiye 1. ve 2. Faz çalışmalarında, Türkiye’de emisyon ticareti sisteminin kurulması, piyasa temelli emisyon azaltım politika seçenekleri, karbon fiyatlandırma politikaları ve pilot ETS altyapısı konularında raporlar hazırlanmıştır. Program kapsamında, Taslak Emisyon Ticareti Sistemi Yönetmeliği ve Taslak İklim Değişikliği Kanunu hazırlanmıştır (Karbon Piyasalarına Hazırlık Ortaklığı, 2023a, 2023b). Taslak İklim Değişikliği Kanunu Madde 6 (1)’de, “Azaltım politikaları, iklim değişikliği ile mücadelede sera gazı emisyonlarının kaynağında azaltılması, yakalanması, depolanması ve denkleştirilmesi ile bu yönde kapasitenin artırılması amacı taşıyan strateji, hedef ve eylemlerin belirlenmesini kapsar.” ifadesi yer almaktadır.

Türkiye’de iklim değişikliği, karbondioksit yakalama ve depolama uygulamalarına yönelik gelişmeler, Tablo 1’de verilmektedir.

## SONUÇ

Çalışma kapsamında, baca gazının/ karbondioksitin sanayi tesislerinden yakalanması ve depolanması ile ilişkili yasal mevzuat araştırılmış, uluslararası müzakereler, ulusal hedef ve bildirimler, sera gazı emisyonlarının izlenmesi ve doğrulanması süreçleri, AB Karbon Yakalama ve Depolama Direktifi kapsamında

yürütülen çalışmalar, iklim değişikliği çalışmalarının tarihsel gelişimi incelenmiştir. Türkiye’de doğal bir sahadan üretilen karbondioksitin bir petrol sahasına enjeksiyonu işlemi uzun yıllardır sürdürülmektedir ancak sanayi tesislerinden yakalanan baca gazının/ karbondioksitin yer altına enjeksiyonu işlemi henüz uygulanmamaktadır. Yasal mevzuatta, doğrudan baca gazı/ karbondioksit yakalama ve depolama faaliyetlerini düzenleyen bir yasa bulunmamakta olup bu uygulamaların gerçekleştirilmesi için, sürecin her aşaması ile ilgili düzenlemeleri içeren yasal mevzuatın geliştirilmesi önem kazanmaktadır.

## NOT

Bu çalışma, TÜBİTAK 1005-Ulusal Yeni Fikirler ve Ürünler Araştırma Destek Programı, “Batman Petrol Rafinerisinden Yakalanacak Baca Gazı/ Karbondioksitin Batı Raman Sahasına Enjeksiyonu için En Uygun İş Modelinin Teknik ve Ekonomik Açısından Araştırılması” başlıklı proje (Proje no:221M582) kapsamında yürütülmüştür.

## KAYNAKLAR

Avrupa Birliği(a).“A European Green Deal” [https://ec.europa.eu/info/strategy/priorities-2019-2024/european-green-deal\\_en#Highlights](https://ec.europa.eu/info/strategy/priorities-2019-2024/european-green-deal_en#Highlights)

Son erişim:25.07.2023

Avrupa Birliği(b).“Directive 2009/31/EC of the European Parliament and of the Council of 23 April 2009 on the geological storage of carbon dioxide and amending Council Directive 85/337/EEC, European Parliament and Council Directives 2000/60/EC, 2001/80/EC, 2004/35/EC, 2006/12/EC, 2008/1/EC and Regulation(EC) No 1013/2006 (Text with EEA relevance)” <https://eur-lex.europa.eu/legal-content/EN/TXT/PDF/?uri=CELEX:32009L0031>

Son erişim:25.07.2023

Batman Petrol Rafinerisi’nden Yakalanan Karbondioksitin Batı Raman Sahası’na Enjeksiyonu Yapılabilirlik Çalışması, TÜBİTAK 1005 Projesi, 2020-2023.

Birleşmiş Milletler(a).“Birleşmiş Milletler İklim Değişikliği Çerçeve Sözleşmesi”. [https://unfccc.int/sites/default/files/convention\\_text\\_with\\_annexes\\_english\\_for\\_posting.pdf](https://unfccc.int/sites/default/files/convention_text_with_annexes_english_for_posting.pdf) Son erişim:25.07.2023

Birleşmiş Milletler(b).“Kyoto Protokolü”.<https://unfccc.int/resource/docs/convkp/kpeng.pdf>

Son erişim:25.07.2023

Birleşmiş Milletler(c).“Paris Antlaşması”. <https://unfccc.int/resource/docs/2015/cop21/eng/109r01.pdf>

Son erişim: 25.07.2023

Birleşmiş Milletler(d). “National Communication(NC). NC 8. Biennial Reports(BR). BR 5”.<https://unfccc.int/documents/628372>

Son erişim:26.07.2023

CCUS ZEN-Zero Emission Network,AB Horizon

Europe Projesi, 2022-2025. <https://www.ccusnetwork.eu/>

Düşük Karbonlu Kalkınma için Çözümsel Tabanlı Strateji ve Eylem Geliştirilmesi Teknik Destek Projesi, Faaliyet 2.1 AB Karbon Yakalama ve Depolama Direktifi Düzenleyici Etki Analizi(2009/31/EC) Raporu, Proje No: EuropeAid/136032/IH/SER/TR, Katılım Öncesi Mali Yardım Aracı, 2013 Türkiye Ulusal Programı,2017-2019.

Establishing CO2 Enhanced Oil Recovery Business Advantages in South Eastern Europe(ECOBASE),AB EraNet ACT Projesi, 2017-2020. <https://ecobase-project.eu/>

ENabling Onshore CO2 Storage in Europe(ENOS),AB Horizon 2020 Projesi, 2016-2020. <http://www.enos-project.eu/>

Geothermal Emission Control Project(GECO),AB Horizon 2020 Projesi, 2018-2022. <https://geco-h2020.eu/>

İklim Şurası Kararları. <https://iklimsurasi.gov.tr/sayfa/sonuc-bildirgesi>

Son erişim: 28.07.2023

Karbon Piyasalarına Hazırlık Ortaklığı(Partnership for Market Readiness-PMR) (a). "Taslak Emisyon Ticareti Sistemi Yönetmeliği". <https://pmrturkiye.csb.gov.tr/wp-content/uploads/2020/12/Taslak-ETS-Yonetmeliği-1.pdf>

Son erişim:25.07.2023

Karbon Piyasalarına Hazırlık Ortaklığı(Partnership for Market Readiness-PMR) (b). "Taslak İklim Kanunu". <https://pmrturkiye.csb.gov.tr/wp-content/uploads/2020/12/Taslak-Iklim-Kanunu-1.pdf>

Son erişim:25.07.2023

Pan-European coordination action on CO2 Geological Storage(CGS Europe),AB 7. Çerçeve Projesi, 2010-2014. <http://www.cgseurope.net/>

Synergetic Utilisation of CO2storage Coupled with Geothermal Energy Deployment(SUCCEED),AB Horizon 2020 Projesi, 2019-2022. <https://www.imperial.ac.uk/energy-futures-lab/succeed>

T.C. Cumhurbaşkanlığı Mevzuat Bilgi Sistemi(a).“Sera Gazı Emisyonlarının Takibi Hakkında Yönetmelik” <https://www.mevzuat.gov.tr/File/GeneratePdf?mevzuatNo=19678&mevzuatTur=KurumVeKurulusYonetmeliği&mevzuatTertip=5>

Son erişim:25.07.2023

T.C. Cumhurbaşkanlığı Mevzuat Bilgi Sistemi(b).“Sera Gazı Emisyonlarının İzlenmesi ve Raporlanması Hakkında Tebliğ” <https://www.mevzuat.gov.tr/mevzuat?MevzuatNo=19920&MevzuatTur=9&MevzuatTertip=5>

Son erişim:25.07.2023

T.C. Cumhurbaşkanlığı Mevzuat Bilgi Sistemi(c).“Sera Gazı Emisyon Raporlarının Doğrulanması ve Doğrulanıcı Kuruluşların Akreditasyonu Tebliği” <https://www.mevzuat.gov.tr/MevzuatMetin/yonetmelik/9.5.24128.pdf>

pdf

Son erişim:25.07.2023

T.C. Cumhurbaşkanlığı Mevzuat Bilgi Sistemi(d).“Türk Petrol Kanunu”<https://www.mevzuat.gov.tr/Mevzuat-Metin/1.5.6491.pdf>

Son erişim:25.07.2023

T.C. Cumhurbaşkanlığı Mevzuat Bilgi Sistemi(e).“Türk Petrol Kanunu Uygulama Yönetmeliği” <https://www.mevzuat.gov.tr/File/GeneratePdf?mevzuatNo=19319&mevzuatTur=KurumVeKurulusYonetmeliği&mevzuatTertip=5>

T.C. Cumhurbaşkanlığı Mevzuat Bilgi Sistemi(f).“Çevre Kanunu” <https://www.mevzuat.gov.tr/MevzuatMetin/1.5.2872.pdf>

T.C. Cumhurbaşkanlığı Mevzuat Bilgi Sistemi(g).“Çevresel Etki Değerlendirmesi Yönetmeliği” <https://www.mevzuat.gov.tr/MevzuatMetin/yonetmelik/7.5.39647.pdf>

T.C. Cumhurbaşkanlığı Mevzuat Bilgi Sistemi(i).“Gönlüllü Karbon Piyasası Proje Kayıt Tebliği”<https://www.mevzuat.gov.tr/File/GeneratePdf?mevzuatNo=18934&mevzuatTur=Tebliğ&mevzuatTertip=5>

T.C. Cumhurbaşkanlığı Mevzuat Bilgi Sistemi(i).“Elektrik Piyasası Kanunu” <https://www.mevzuat.gov.tr/MevzuatMetin/1.5.6446.pdf>

T.C. Çevre, Şehircilik ve İklim Değişikliği Bakanlığı(a).“Birleşmiş Milletler İklim Değişikliği Çerçeve Sözleşmesi”. [https://webdosya.csb.gov.tr/db/iklim/webmenu/webmenu12421\\_1.pdf](https://webdosya.csb.gov.tr/db/iklim/webmenu/webmenu12421_1.pdf)

Son erişim:25.07.2023

T.C. Çevre, Şehircilik ve İklim Değişikliği Bakanlığı(b).“Kyoto Protokolü”. [https://webdosya.csb.gov.tr/db/iklim/editordosya/kyoto\\_protokol.pdf](https://webdosya.csb.gov.tr/db/iklim/editordosya/kyoto_protokol.pdf)

Son erişim:25.07.2023

T.C. Çevre, Şehircilik ve İklim Değişikliği Bakanlığı(c).“Paris Anlaşması”. <https://iklim.gov.tr/paris-anlasmasi-i-34>

Son erişim:25.07.2023

T.C. Çevre, Şehircilik ve İklim Değişikliği Bakanlığı(d).“Türkiye İklim Değişikliği Stratejisi 2010-2023”. [https://webdosya.csb.gov.tr/db/iklim/editordosya/file/strateji%20belgesi/Turkiye%20Iklim%20Degisikligi%20Strateji%20Belgesi\\_TR.pdf](https://webdosya.csb.gov.tr/db/iklim/editordosya/file/strateji%20belgesi/Turkiye%20Iklim%20Degisikligi%20Strateji%20Belgesi_TR.pdf)

Son erişim:25.07.2023

T.C. Çevre, Şehircilik ve İklim Değişikliği Bakanlığı(e).“Türkiye İklim Değişikliği Eylem Planı 2011-2023”. [https://webdosya.csb.gov.tr/db/iklim/editordosya/file/eylem%20planlari/Iklim%20Degisikligi%20Eylem%20Plani\\_TR.pdf](https://webdosya.csb.gov.tr/db/iklim/editordosya/file/eylem%20planlari/Iklim%20Degisikligi%20Eylem%20Plani_TR.pdf)

Son erişim:25.07.2023

T.C. Çevre, Şehircilik ve İklim Değişikliği Bakanlığı(f).“İklim Değişikliği Koordinasyon Kurulu”. <https://www.iklim.gov.tr/guncellenmis-birinci-ulusal-katki-beyani-sunuldu-haber-1139>

Son erişim:26.07.2023

T.C. Çevre, Şehircilik ve İklim Değişikliği Bakanlığı(-g).“İklim Değişikliği Koordinasyon Kurulu”.<https://iklim.gov.tr/idukk-i-13>

Son erişim:25.07.2023

T.C. Dışişleri Bakanlığı(a).“BM İklim Değişikliği Çerçeve Sözleşmesi”. <https://www.mfa.gov.tr/bm-iklim-degisikligi-cerceve-sozlesmesi.tr.mfa>

Son erişim:25.07.2023

T.C. Dışişleri Bakanlığı(b).“Kyoto Protokolü”. <https://www.mfa.gov.tr/kyoto-protokolu.tr.mfa>

Son erişim:25.07.2023

T.C. Enerji ve Tabii Kaynaklar Bakanlığı.“Türkiye Ulusal Enerji Planı”. [https://enerji.gov.tr/Media/Dizin/EIGM/tr/Raporlar/TUEP/T%C3%BCrkiye\\_Ulusal\\_Enerji\\_Plan%C4%B1.pdf](https://enerji.gov.tr/Media/Dizin/EIGM/tr/Raporlar/TUEP/T%C3%BCrkiye_Ulusal_Enerji_Plan%C4%B1.pdf)

Son erişim:28.07.2023

Türkiye’de Termik Santraller ve Sanayi Tesislerinden Gelen Karbondioksit Emisyonu Envanterinin Çıkarılması ve Karbondioksitin Yeraltı Jeolojik Ortamlarda Depolanma Potansiyelinin Belirlenmesi, TÜBİTAK KAMAG Projesi-106G110, 2007-2009. <https://www.sciencedirect.com/science/article/pii/S1876610211007314>

T.C. Ticaret Bakanlığı.“Yeşil Mutabakat Eylem Planı 2021”

<https://ticaret.gov.tr/data/60f1200013b876eb28421b23/MUTABAKAT%20YE%C5%9E%C4%B0L.pdf>

Son erişim:25.07.2023

Anahtar Kelimeler: Karbon yakalama ve depolama, mevzuat

Tarih	Gelişme
9 Ağustos 1983	2872 sayılı Çevre Kanunu (Değişik cümle:24/12/2020-7261/12 md. ve (Ek:24/12/2020-7261/17 md.)
3-14 Haziran 1992	Birleşmiş Milletler İklim Değişikliği Çerçeve Sözleşmesi (BMİDÇS)'nin imzaya açılması
11 Aralık 1997	Kyoto Protokolü'nün 3. Taraflar Konferansı'nda kabul edilmesi
16 Mart 1998	Kyoto Protokolü'nün New York'ta imzaya açılması
2001	İklim Değişikliği Koordinasyon Kurulu (İDKK)'nin kurulması
29 Ekim - 6 Kasım 2001	Türkiye'nin, EK-II listesinden çıkarılması ve özel şartları tanımlanmış bir EK-I ülkesi olarak BMİDÇS'ne taraf olma isteğinin kabulü
24 Mayıs 2004	Türkiye'nin 189. taraf olarak BMİDÇS'ne katılması
2008-2012	Kyoto Protokolü Birinci Taahhüt Dönemi
23 Nisan 2009	Avrupa Birliği'nin 2009/31/EC1 sayılı Direktifinin ilanı
26 Ağustos 2009	Türkiye'nin Kyoto Protokolü'ne taraf olması
3 Mayıs 2010	2010-2020 Türkiye İklim Değişikliği Stratejisi'nin onaylanması
2011	Dünya Bankası tarafından Karbon Piyasalarına Hazırlık Ortaklığı (Partnership for Market Readiness-PMR) Teknik Destek Programı'nın başlatılması
25 Nisan 2012	Sera Gazı Emisyonlarının Takibi Hakkında Yönetmelik'in yürürlüğe girmesi
2013	İklim Değişikliği Koordinasyon Kurulu'nun İklim Değişikliği ve Hava Yönetimi Koordinasyon Kurulu (İDHYKK) adını alması
2013	Türkiye'nin Karbon Piyasalarına Hazırlık Ortaklığı (Partnership for Market Readiness- PMR) Teknik Destek Programı'na katılması
30 Mart 2013	6446 sayılı Elektrik Piyasası Kanunu
30 Mayıs 2013	6491 sayılı Türk Petrol Kanunu'nun kabulü
9 Ekim 2013	Gönlüllü Karbon Piyasası Proje Kayıt Tebliği'nin yayımlanması
2013-2020	Kyoto Protokolü İkinci Taahhüt Dönemi
22 Ocak 2014	Türk Petrol Kanunu Uygulama Yönetmeliği'nin yayımlanması
22 Temmuz 2014	Sera Gazı Emisyonlarının İzlenmesi ve Raporlanması Hakkında Tebliğ'in yürürlüğe girmesi
Eylül 2015	Türkiye'nin Niyet Edilen Ulusal Katkı Beyanı'nı (Intended Nationally Determined Contribution-IN-DC) Birleşmiş Milletler İklim Değişikliği Çerçeve Sözleşmesi Sekreteryası'na sunması
12 Aralık 2015	Paris Anlaşması'nın kabulü
2 Aralık 2017	Sera Gazı Emisyon Raporlarının Doğrulanması ve Doğrulayıcı Kuruluşların Akreditasyonu Tebliği'nin yürürlüğe girmesi
26 Aralık 2018	Türkiye'nin İklim Değişikliği Ulusal Bildirimi'ni BMİDÇS Sekreteryasına sunması
1 Ocak 2018	Türkiye'nin Üçüncü İki Yıllık Raporu, BMİDÇS Sekreteryası'na sunması
9 Temmuz 2018	Petrol İşleri Genel Müdürlüğü ve Maden İşleri Genel Müdürlüğü'nün kaldırılarak Maden ve Petrol İşleri Genel Müdürlüğü (MAPEG) kurulması
Mayıs 2019	AB Karbon Yakalama ve Depolama Direktifi Düzenleyici Etki Analizi Raporu'nun sunulması
11 Aralık 2019	Avrupa Birliği'nin Avrupa Yeşil Mutabakatı açıklaması
27 Aralık 2019	Türkiye'nin Dördüncü İki Yıllık Raporu BMİDÇS Sekreteryası'na sunması
2020	Taslak Emisyon Ticareti Sistemi Yönetmeliği ve Taslak İklim Değişikliği Kanunu hazırlanması
16 Temmuz 2021	Türkiye'nin Yeşil Mutabakat Eylem Planı 2021'i yayımlaması
13 Ağustos 2021	Boru Hatları İle Petrol Taşıma A.Ş. Genel Müdürlüğü (Botaş) Ham Petrol ve Doğal Gaz Boru Hattı Tesislerinin Yapımı Ve İşletilmesine Dair Teknik Emniyet ve Çevre Yönetmeliği'nin yayımlanması
29 Ekim 2021	Çevre ve Şehircilik Bakanlığı'nın adının Çevre, Şehircilik ve İklim Değişikliği Bakanlığı olarak değiştirilmesi
29 Ekim 2021	İklim Değişikliği ve Hava Yönetimi Koordinasyon Kurulu (İDHYKK'nın yerini İklim Değişikliği ve Uyum Koordinasyon Kurulu (İDUKK)'nin alması
10 Kasım 2021	Türkiye'nin Paris Anlaşması'na taraf olan 192'inci ülke olması
11 Ocak 2022	İklim Değişikliği ve Uyum Koordinasyon Kurulu'(İDUKK)'nin ilk toplantısı
21-25 Şubat 2022	İklim Şurası
29 Temmuz 2022	Çevresel Etki Değerlendirmesi Yönetmeliği'nin yayımlanması
31 Aralık 2022	Türkiye Ulusal Enerji Planı'nın yayımlanması
13 Nisan 2023	Türkiye'nin Güncellenmiş Birinci Ulusal Katkı Beyanı'nı BMİDÇS Sekreteryası'na sunması
23 Mayıs 2023	Türkiye'nin 8. Ulusal Bildirim ve 5. İki Yıllık Raporu'nu BMİDÇS Sekreteryası'na sunması

# A Simulation Study of Underground Hydrogen Storage in the Northern Marmara Field

**Hasan Gürsel, Murat Fatih Tuğan, Çağlar Sınayuç**

Petroleum and Natural Gas Engineering Department, Middle East Technical University, Ankara / Türkiye



## ABSTRACT

Considering its significant working gas capacity of 2.25 billion cubic meters and its strategic proximity to industrial hubs and ports, an inquiry was conducted to determine the potential viability of repurposing the Northern Marmara depleted gas field for underground hydrogen storage (UHS).

Field-specific evaluation of the potential issues found in the literature was conducted, and microbial consumption of hydrogen and impurities in the withdrawn stream were determined to be the prominent risk factors.

The field was modelled, and simulated using a commercial software suite, previously published field data and previously presented storage schedule and constraints. The simulation spanned an initial depletion period between 1997-2002, 25 years of methane storage between 2007-2032, hydrogen storage between 2032-2057, and finally an extended withdrawal period before the abandonment.

A comparison with the field's current use as a natural gas storage was done by juxtaposition of the energy content of the produced gas streams. Stream composition during the UHS period showed high variability due to methane being withdrawn alongside hydrogen. Overall, 3.12 times less energy was withdrawn during the UHS period compared to methane storage period.

## INTRODUCTION

The Sixth Assessment Report on Climate Change Mitigation of the Intergovernmental Panel on Climate Change (IPCC) states that hydrogen could play a unique role as an energy carrier to enable grid flexibility. Subsequently, Underground Hydrogen Storage (UHS) emerges as a crucial part of the hydrogen value chain to enable large scale seasonal energy storage, and supply security.

Although most UHS demonstrations have been with salt caverns as the storage media, depleted gas field pilot projects of hydrogen storage mixed with methane in Austria by RAG (Underground Sun Project) and in Argentina by HyChico (Patagonia Wind) have resulted with encouraging results for future trials.

A recent study conducted by the Energie Beheer Nederland (EBN) and the Netherlands Organization for Applied Scientific Research (TNO) has concluded that offshore UHS options are technologically feasible to be considered, but storage of pure hydrogen in depleted gas fields still requires field trials to be proven as a concept.

As the first commercial offshore discovery of Turkish Petroleum, the Northern Marmara Gas Field has a unique location with its proximity to many heavy industries, ports and the İzmit Refinery. The trap

consists of a shale cap rock of Ceylan Formation, and a limestone reservoir that belongs to Soğucak Formation at a depth of 1150 meters. Initial reservoir pressure is 14300 kPa while the reservoir temperature is 68.8 °C. The Original Gas in Place (OGIP) and Working Gas Capacity (WGC) for the field are reported by Şahin, Abravcı and Tirek (2012) as 5.5 bcm and 2.25 bcm, respectively. After the termination of the production at the end of 2001, some host gas was left as cushion for future storage endeavors. The field has been serving as the largest natural gas storage media of Türkiye as part of the Silivri Storage Facility since 2007. Currently, it is under further development with new wells being drilled with the aim to increase the WGC up to 4.6 bcm. Moreover, "European potential for hydrogen storage in depleted gas fields and aquifers" by the Hydrogen Underground Storage in Porous Reservoirs (HyUSPRE) Consortium has considered the Northern Marmara Field to be the only known candidate for UHS in Türkiye.

Since UHS is a practice at its infancy, research is being conducted to investigate the potential effect of cyclic storage on the rock and fluid properties, wellbore and near-wellbore elements, transport properties, and overall operational feasibility. While the existing literature indicates that geochemical reactions with brine or rock are not major concerns due to their slow reaction rates, research in this area is still in progress. A particular concern that gained significant attention is the microbial consumption of H<sub>2</sub> and the subsequent formation of biofilms. Estimating the extent of microbial effects on hydrogen loss and transport is a novel scientific challenge.

In this study, Northern Marmara Field's viability is assessed for UHS by comparison of the energy content of the withdrawn gases, and possible technical issues are pointed out. A simulation was conducted involving 25 years of cyclic methane storage followed by 25 years of cyclic hydrogen storage. It is important to note that the model used in this study does not address various challenges that may arise during operation, such as microbial consumption, biofilm formation, leakage, and well integrity problems. Furthermore, potential improvements resulting from production optimization and additional field development have not been taken into account in this investigation.

## METHODS

First, an evaluation of the field in the context of UHS is carried out based on an extensive literature research. Next, the contour map from Kaptanoğlu (1998) was digitized using the Surfer software. A commercial software suite (CMG) was used for the modelling and the compositional simulator (GEM) was used for the simulation. To construct a reservoir model, historical



wellhead pressure and production data from Öztürk (2004) were matched and the model was further validated by the comparison of analytical solution of the dry gas reservoir ( $P/z$  vs  $G_p$  plot) with data extracted from Şahin, Abravcı and Tirek (2012) using the Matlab plugin Grabit. PR-1978 was used as the equation of state. Forward simulations were carried out to assess the purity of the streams, and to compare the energy content of the withdrawn gases between methane and hydrogen storage periods of 25 years each. For the cycling constraints, the field practice presented by Abravcı (2017) is used as 215 days of injection with 9 million m<sup>3</sup>/day and 120 days of withdrawal with 16 million m<sup>3</sup>/day flow rates between 14300 kPa and 8400 kPa pressure limits. Lastly, an extended withdrawal period is simulated to retrieve the hydrogen that has been left behind in the reservoir due to dispersion.

## FINDINGS

### Evaluation of Site-specific Factors

The primary concern associated with any UHS site is the potential microbial impact. Hydrogen, being a universal electron donor, can be utilized by various microbial organisms for their metabolic processes. This could potentially result in the production of methane, acetone, or in severe cases, sulfate as a consequence of hydrogen consumption. Considering that each subsurface structure may inhabit a distinct microbial community, accurately modeling and assessing the extent of these microbial effects pose a scientific challenge that necessitates site-specific laboratory investigations as a starting point.

Currently, there is no data regarding the subsurface biota, nor is there a valid methodology to estimate the extent of biological reactions' effect. However, based on the assumption of a salinity level of 30,000 ppm (Çalışgan, 2005), a preliminary evaluation can be made, referencing the paper by Thaysen et al. (2021) titled "Estimating microbial growth and hydrogen consumption in hydrogen storage in porous media". It can be said that Northern Marmara Field is susceptible to all known kinds of microbial hydrogen reactions.

Although rapid geochemical reactions are unlikely to occur under field temperature conditions, it is highly recommended to perform lithology-specific laboratory experiments and modeling studies. It is worth noting that despite hydrogen's low solubility in water, the composition of the formation brine can still exert a subtle yet significant influence. Various other risk factors have been identified in the final report for the Underground Sun Project, and the HyUSPRE reports. While risks associated with components and environmental factors are not considered major concerns, the Northern Marmara, being an aged field located in a seismically active zone, demands meticulous attention to equipment and hazard protection.

### MODEL VALIDATION

History match for the initial production period of the

field (1997-2002) was conducted based on the field data obtained from Öztürk's MSc. thesis (2004). For the production well locations, Kaptanoğlu, Atalay, Yörük (1998) was used, and later for the storage period, wells from Gümrah et al. (2005) were added. An error margin less than 5% for each well was attained, and the resulting model's performance was validated by the analytical solution of dry gas reservoir compared with the extracted field data from Şahin, Abravcı and Tirek (2012). The resulting model had 51x61x4 blocks with 65x65x8.5 meters lengths with constant porosities of 20% and constant permeabilities of 50 mD. As suggested by Terstappen (2021) numerical dispersion was controlled by the total variation limiting flux limiter (TVD) available in the software and assumed to be a substitute for the physical dispersion.

## SIMULATION OUTCOMES

25 years of CH<sub>4</sub> storage followed by 25 years of H<sub>2</sub> storage were simulated. As visualized in Figure-1, during H<sub>2</sub> injection, the CH<sub>4</sub> present in the reservoir is pushed to the periphery. During the withdrawal periods of H<sub>2</sub>, at some point, the CH<sub>4</sub> that was pushed to the periphery comes back and gets produced alongside with H<sub>2</sub>. The fraction of CH<sub>4</sub> in the withdrawn stream decreases with time, but still remains around 8% after the field reaches equilibrium. The composition of the gas stream, and therefore the energy content, has shown great variations even for the same well within the same cycle. This situation calls for different field constraints and well-specific withdrawal plan to be utilized for H<sub>2</sub> storage.

As a result of dispersion which is also visible in Figure-1, 2:61% of the injected H<sub>2</sub> gets left behind in the reservoir after the last storage cycle. However, further depletion of the field below the threshold pressure of 8400 kPa could enable this remaining hydrogen to be reproduced. In fact, under the model assumptions, depletion down to 6000 kPa is already enough to reproduce 99.5% of the injected hydrogen.

Table-1 presents a concise summary table outlining the results obtained for the CH<sub>4</sub> and H<sub>2</sub> storage periods. In the end, as a result of hydrogen storage, 3.12 times less energy was withdrawn compared to the same duration of methane storage. Furthermore, 10% of the withdrawn energy during H<sub>2</sub> storage came from CH<sub>4</sub> that was withdrawn alongside with H<sub>2</sub>.

## CONCLUSION

When locally produced from renewable sources, hydrogen can offer significant advantages in terms of energy security and addressing climate change. The Northern Marmara Field possesses a strategic location for UHS, being in close proximity to potential end-users and export routes. However, its current utilization as a natural gas storage enables the supply of a larger amount of energy in a more stable manner. The challenge of compositional variations in the produced stream could potentially be overcome through surface purification

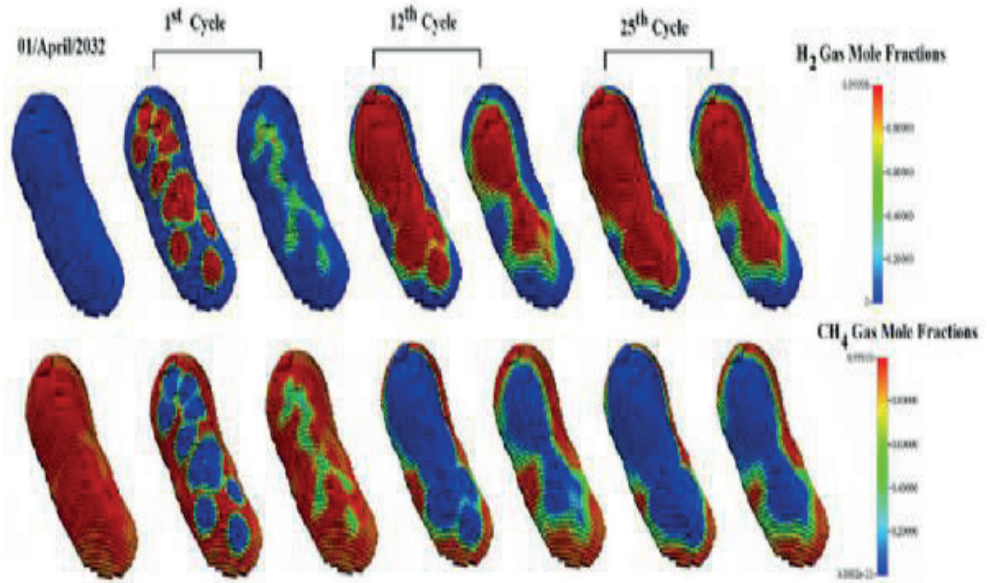
techniques, and real-time monitoring and optimization of the production.

Nevertheless, the issue of microbial hydrogen loss poses a significant threat to the feasibility of UHS in the field, and as of now, no effective method has been proposed to prevent this phenomenon. This study represents the first exploration of the possibility of storing hydrogen in the Northern Marmara Field. However, there are numerous factors that must be carefully considered before making the complex decision of utilizing the field for hydrogen storage. Further research and evaluation are crucial to fully assess the viability and address the challenges associated with hydrogen storage in this location.

## REFERENCES

- [1] Süleyman Abravcı. Silivri doğalgaz depolama tesisi ve güncel durum. World Petroleum Congress, 2017.
- [2] Anne-Catherine Ahn, Adrian Hidalgo-Ulloa, Yehor Pererva, Bart Lomans, and Diana Sousa. Review of the window of viability of the different microbial metabolisms relevant for subsurface h<sub>2</sub> storage application, h2020 hyspre project report., 2022.
- [3] Andrew Cavanagh, Hamid Yousefi, Mark Wilkinson, and Remco Groenenberg. Hydrogen storage potential of existing european gas storage sites in depleted gas fields and aquifers, h2020 hyspre project report., 2022.
- [4] Jacopo de Maigret, and Diego Viesi. Report on equipment requirements and capital as well as operating costs for the hydrogen scenarios, h2020 hyspre project report, 2023.
- [5] F. Gümrah, O Izgec, U. Gokcesu, and S. Bagci. Modeling of underground gas storage in a depleted gas field. Energy Sources, 27:913–920, 7 2005.
- [6] Neda Hassannayebi, Siroos Azizmohammadi, Marco De Lucia, and Holger Ott. Underground hydrogen storage: application of geochemical modelling in a case study in the molasse basin, upper austria. Environmental Earth Sciences, 78, 3 2019.
- [7] Aliakbar Hassanpouryouzband, Remco Groenenberg, Katriona Edlmann, Rama Kotni, Eric Craenmehr, and Jonathan van den Ham. Database of mineral reaction rates with hydrogen and their dependence on temperature and pressure, h2020 hyspre project report. 2022.
- [8] A.A. Kaptanoğlu, Recep Atalay, and Yoruk R. Development of a north marmara field offshore turkiye: A case study. The International Society of Offshore and Polar Engineers, 5 1998.
- [9] Kolin. Kuzey marmara doğalgaz depolama tesisi (faz-iii) projesi. 2022.
- [10] V. Masson-Delmotte, A. P. Zhai, S.L. Pirani, C. Connors, S. P'ean, N. Berger, Y. Caud, L. Chen, M.I. Goldfarb, M. Gomis, K. Huang, E. Leitzell, J.B.R. Lonnoy, T.K. Matthews, T. Maycock, O. T. Waterfield, R. Yelek,ci, R. Yu, B. Zhou, and (eds.). Ipcc, 2021: Summary for policymakers. in: Climate change 2021: The physical science basis. contribution of working group i to the sixth assessment report of the intergovernmental panel on climate change, 2021.
- [11] Julia Michelsen, Eike Marie Thaysen, Sebastian Hogeweg, Birger Hagemann, Aliakbar Hassanpouryouzband, Nils Langanke, Katriona Edlmann, and Leonhard Ganzer. Hydrogen reservoir flow behaviour: measurements of molecular diffusion, mechanical dispersion and relative permeability, h2020 hyspre project report, 2023.
- [12] Ariel Perez, E Perez, Sebastian Dupraz, J Bolcich, A Perez, and S Dupraz. Patagonia wind-hydrogen project: Underground storage and methanation, 2016.
- [13] Austria AG. RAG, angewandte Prozesstechnik GesmbH AXIOM, AG Verbund, MONTANUNIVERSITAT LEOBEN, UNIVERSITAT fur Bondenkultur Wien, and ENERGIEINSTITUT an der Johannes Kepler Universit at Linz. Underground sun storage publishable final report, 2017.
- [14] Secaeddin Sahin, Suleyman Abravci, and Ali Tirek. Design and status of the only underground gas storage project in turkey after three years of operation. pages 16–18. SPE, 9 2012.
- [15] John W. Sheffield. Energy security through hydrogen. pages 1–8. Springer, 2007.
- [16] P.R. Shukla, J. Skea, R. Slade, A. Al Khourdajie, R. van Diemen, D. McCollum, M. Pathak, S. Some, P. Vyas, R. Fradera, M. Belkacemi, A. Hasija, G. Lisboa, S. Luz, J. Malley, and (eds.). IPCC, 2022: Summary for policymakers. in: Climate change 2022: Mitigation of climate change. contribution of working group iii to the sixth assessment report of the intergovernmental panel on climate change, 2022.
- [17] Robin Johannes Terstappen. Analysis of mixing during hydrogen storage in gas reservoirs, 2021.
- [18] Eike M. Thaysen, Sean McMahon, Gion J. Strobel, Ian B. Butler, Bryne T. Ngwenya, Niklas Heinemann, Mark Wilkinson, Aliakbar Hassanpouryouzband, Christopher I. McDermott, and Katriona Edlmann. Estimating microbial growth and hydrogen consumption in hydrogen storage in porous media. Renewable and Sustainable Energy Reviews, 151, 11 2021.
- [19] Serge van Gessel, Bastiaan Jaarsma, Remco Gronenberg, Dennie Kleijweg, Joaquim Judge-Larre, Silke van Klaveren, Walter Eikelenboom, Gijs Rummelts, Renske van Slooten, Esmee Butter, Thijs Huijskes, and Maartje Koning. Haalbaarheidsstudie: Offshore ondergrondse waterstofopslag, 2022.
- [20] Hüseyin Çalışgan. Comprehensive modelling of gas condensate relative permeability and its influence on field performance, 2005.
- [21] Öke İsmet Özkılıç. Simulating co<sub>2</sub> sequestration in a depleted gas reservoir, 2005.
- [22] Bülent Öztürk. Simulation of depleted gas reservoir for underground gas storage, 2004.

Figure-1



Comparison of gas compositions after the end of gas injection and withdrawal phases.

Table-1

Years (25 Cycle)	2007-2032	2032-2057	
Cycled Gas	CH4	H2	CH4
Production (gmol)	$1.66392 \times 10^{12}$	$1.57457 \times 10^{12}$	54980640700
Production (million tons)	26.69	3.17	0.88
Produced Energy (TWh)	371.05	106.65	12.25

Summary of the Results





## **Geliştirilmiş Petrol Kurtarımı**

*Enhanced Oil Recovery*

---



# Recent Activities in Heavy-Oil Batı Raman Field

Ufuk Kılıçaslan, Turgay İnceisci, Yusuf Demirel, Ahsen Özesen

Turkish Petroleum Corporation (TPAO), Ankara / Türkiye



Batı Raman field is known as the highest oil accumulation in Turkey, containing roughly 1.85 billion barrels of initial oil in place. Since its discovery in 1961, the field has produced more than 133 million stock-tank-barrel (stb) of oil and its daily production is still around 5,000 stb. Major contribution of this production has been coming from immiscible CO<sub>2</sub>-EOR project, which started in 1986 as a response to low primary recovery due to its heavy-oil.

In this paper, operational aspects and production contribution of recent practices in the development of Batı Raman field were presented. In addition to on-going CO<sub>2</sub> flooding, polymer gel injection, propriety monomer gel application in production and injection wells were discussed. During last four years, acid fracturing technology was implemented in eastern part of the field, where fissure system is not well developed as in the case of western and central part. Fractured wells yielded more than 185,000 stb of additional oil compared to do-nothing scenario.

## INTRODUCTION

In Batı Raman field, oil gravity ranges from 9° API to 15° API and the viscosity ranges from 450 cp to 1000 cp at reservoir conditions by having 18-20 ft<sup>3</sup>/bbl of dissolved gas. The productive formation is the Garzan limestone having average net thickness of 161 ft. The geological formation, reef limestone, is a long, east-west direction-oriented anticlinal type. The field has 17 km. length and 4 km. width. The reservoir is limited by an oil/water contact at 600 m. in the west and north, by a permeability barrier in the south and southeast, and by a fault system in the southwest and southern part of the field. The reservoir rock is fractured vuggy limestone in the western and central parts, but it is tighter to the east due to the chalky reservoir character. Core analyses demonstrated that the matrix porosity ranges between 15% and 20%, the matrix permeability is around 50 md, and the water saturation is 21%. Additionally, the effective reservoir permeabilities observed between 400 md and 2000 md in the well test results of some wells confirmed natural fractures and vugs (Sahin et al. 2012).

The average reservoir pressure started from 1700 psi and dwindled to below 400 psi in the western and central areas and dropped to 800-1000 psi in the eastern part of the reservoir. Rock and fluid expansion is the primary reservoir production mechanism. Due to its unfavorable reservoir and fluid properties and lack of enough water drive significantly, the Batı Raman field has exhibited a fast production decline since 1961 and resulted a low recovery factor of 1.7% of the OOIP corresponding to 32 MMSTB. The existence of a huge amount of heavy oil has led TPAO to focus and experiment with various methods based on the lithology, reservoir depth,

pressure, temperature, liquid properties, economic parameters and so on.

Pilot tests with steam injection, air injection and water injection conducted as either huff & puff or inverted five-spot pattern scheme didn't yield desired production enhancement (Sahin et al. 2014). The presence of a large CO<sub>2</sub> reservoir in the nearby Dodan field has initiated a feasible project in the Batı Raman field after comprehensive engineering, simulation, and laboratory studies in order to recover the heavy oil by immiscible CO<sub>2</sub> injection. The design and construction of surface facilities in Dodan and Batı Raman were completed between 1980 and 1986. Since 1986, this successful EOR Project, immiscible CO<sub>2</sub> injection, has been operated by the Turkish Petroleum Corporation (TPAO) to produce the heavy oil of Batı Raman. Aside from immiscible CO<sub>2</sub> flooding, development of the field is continuing by in-fill drilling. Polymer and monomer gel applications has been tested to shut-off water influx in production wells and to divert injected gas into untouched matrix from injectors. Recently, acid fracturing has been introduced and applied successfully. Many wells showed two to five fold increase in first month oil production.

## On-going CO<sub>2</sub> Flooding Operations

In 1986, CO<sub>2</sub> flooding started with a cyclic injection and production regime in the pilot area, which has an area of 1200 acres and 33 adjacent wells. The cyclic regime aimed to increase reservoir pressure to 10% higher than the original reservoir pressure with adequate gas injection to saturate oil at this pressure and then put these wells on production by solution-gas drive mechanism with improved oil properties. Due to the dual porosity behavior with fractures and the fissures of the pilot area except for the Northwestern part, the escape of gas observed towards the outside of the pilot area and the required bottomhole pressures for cyclic regime were never reached at that part. Thus, the application was turned into a continuous gas drive process (CO<sub>2</sub> flood) after two years of injection. Recycle systems were constructed in 3TP2 and AP2 stations in 1991 and 2011, respectively.

From that day to today, more than 100 MMstb of incremental oil has been produced, and the recycled gas has been 230 Bscf since 1991. It is crucial to point out that the daily production rate reached 13,830 stb in 1991 after this application. Today, oil production in the field is around 5,000 stb per day, and the gas utilization ratio is 6 Mscf/stb. While 502 Bscf of CO<sub>2</sub> is injected cumulatively, 371 Bscf of gas has been produced back.

### In-fill Drilling

Starting in 2002, an infill drilling campaign was started to slow the downward trend of production rate caused by the reduction in the amount of CO<sub>2</sub> injected. Thanks to this campaign, the production rate was kept at an average of 7,000 stb/day. However, the decrease in the amount of CO<sub>2</sub> injected volume by the depletion of Dodan CO<sub>2</sub> reserves has again led to a falling trend in the production rate since 2017. The production history and the number of wells drilled during this period can be seen in Fig-1.

Figure-1: The production and injection history of Batı Raman

### POLYMER GEL INJECTION

Due to the naturally fractured structure of the Batı Raman reservoir and the low density and viscosity of the compressed gas compared to oil, problems such as unfavorable mobility rate, fingering, and breakthrough adversely affect the CO<sub>2</sub> injection applications (Karaoguz et al. 2007). Besides these problems, a sudden decrease in oil production due to quick increase in water cuts in production wells that have connections to the fractures fed by water has been observed recently. One of the main methods of eliminating these adverse issues, which significantly reduce the spatial and volumetric sweep efficiency of the reservoir and adversely affect production, is conformance improvement applications in the reservoir. It is aimed to increase oil recovery by limiting the permeability of high permeability matrices and natural fractures in the reservoir, directing the fluid injected in the injection wells to the unswept sections of the reservoir, and isolating the water-producing fractures in the production wells.

The main method used to improve the reservoir conformance is the injection of the crosslinked gel-formed liquid into the reservoir (Borling 1994). Polyacrylamide gels, also known as polymer gels, linked with chromium acetate crosslinkers, have been successfully implemented in the Batı Raman field since 2002.

In injection wells, the main concerns are to increase in wellhead injection pressures and in oil production rates of the surrounding production wells. On the other hand, the reduction in water production and the increase in oil production are the primary targets of polymer gel operations in production wells,

The criteria for the well selection of a CO<sub>2</sub> injection well can be summarised as follows:

- Low cumulative production of the offset production wells around the candidate well,
- A quick breakthrough of injected CO<sub>2</sub> gas to the production wells,
- High gas/liquid ratios in the fluid produced from the wells,
- The excess injection capacity of the well, as a result of the decrease in injection pressures,

- No sufficient injection to support the reservoir pressure

For production wells, sudden increases in the water cuts of the well and increases in the fluid level in the annulus are taken into account in the selection of candidate wells.

In polymer gel applications, the gel should be injected gradually to be able to inject the entire planned injection volume (if possible) without exceeding the fracture pressure of the reservoir, to widen the gel's impact area by pushing it as far as possible in the formation, and provide a more durable gel in the vicinity of the well towards the end of the projected injection volume. It is aimed to inject the gel in different densities, such as (35%) low polymer concentration gel, 50% more concentrated and stronger gel for the main application, and 15% the highest concentration for areas close to the well.

It is very important to continuously monitor and record the injection flow rates and injection pressures in gel operations. Flow measurements are made precisely in parallel from the tanks and the flowmeter connected to the wellhead. The injection rate is adjusted according to the injection pressures. The pressure data gives information about the progress of the gel in formation, the decrease in permeability it provides, its adhesion and gelation, and when it begins to occlude a particular fracture or high permeability matrix. The increase in injection pressure during the operation gives clues that the gel operation will be technically successful.

The production wells where polymer gel operation was performed between 2013-2022 in the Batı Raman field are given in Fig.-2. Information on the gel operations carried out in the production wells in the Batı Raman field between 2013 and 2022 is given in Table-1.

Figure-2: Production wells in which polymer gels were applied

Table-1: Production wells in which polymer gels applied by years

As can be seen in Table-1, in the polymer gel operations performed in the production wells over the years, 21 wells were selected from the wells that were temporarily shut-in due to the high water cuts, and 17 wells were selected from the production wells which had a tendency of rapid increase in water cut in recent years. In 14 shut-in wells, the water cut was reduced after the gel operations, and these wells could be put into production. However, no decrease in the water cuts was observed in 7 wells. The effect of the gel application varies from well to well, and the effect of the gel in successful production wells varied between 3 months and 15 months. A total of 70,000 barrels of additional oil was produced from the polymer gel applied wells.

The CO<sub>2</sub> injection wells in which polymer gel operation was performed between 2002-2021 in the Batı Raman field are given in Fig.-3. A summary of gel operations performed in CO<sub>2</sub> injection wells in the Batı Raman field between 2002-2021 can be seen in Table-2.

Figure-3: CO<sub>2</sub> injection wells in which polymer gels were applied



Table-2: CO<sub>2</sub> Injection wells in which polymer gels applied by years

As summarized in Table-2, an increase in injection pressures was achieved in all 20 wells in which gel injection was applied. The increase in injection pressures indicates that the existing flow channels of CO<sub>2</sub> gas are partially closed, and the gas is directed to different channels. When we look at the post-gel performance of the offset production wells, approximately 40,000 barrels of extra oil production were obtained from 55 of the total 109 offset production wells in the one year after the gel operation.

### MONOMER GEL INJECTION

Polymer gel, due to its high molecular weight and long chain structure, cannot be injected in the eastern part of the Batu Raman field, where there are fissures and relatively weak fracture development. As a solution to this problem, the in-situ gel was developed by our R&D (ARGEM) Department. This in-situ gel is prepared by adding monomer, crosslinker, initiator, and retarder to the water taken into the tanks at the wellhead and is activated by temperature after being injected into the reservoir in the form of water. The mixture gets its gel form when it reaches a temperature above 50°C in the fractures it enters.

Upon the positive results of the monomer gel in the core tests performed in the laboratory studies, it is decided to initiate a pilot application in the Batu Raman field. The volumes required to close the fractures in the area 20 m away from the vicinity of the candidate well were roughly calculated, taking into account the fracture densities and fracture spacing obtained from the cores. During the operations, it is aimed to constantly revise the amount of initiator and retarder in order to adjust the timing of gelation according to the pressure increase of the wells. In addition, it is planned to continue the operations until the wells are pressurized and, if necessary, to continue the operations stepwise. In other words, if the well is not pressurized after the injection of 500 barrels of gel volume, the operations will be paused for the gelation in the reservoir and then be resumed in the next day.

Monomer gel pilot applications were carried out in Inj-1 (CO<sub>2</sub> injection well) and Prod-1 & Prod-2. Technically, it was succeeded that the gel was sent to the reservoir in the form of water in all wells, and it was observed that the gelation occurred in the samples taken from the tanks at the wellhead at 65°C.

Monomer gel was injected into Inj-1 CO<sub>2</sub> injection well for three days, but the operation was terminated because no pressure increase could be achieved in the well. After 510 barrels of gel injection to the production well Prod-1, the operation was stopped for one night because the well could not be pressurized. In Prod-2, a pressure increase was achieved in the well on the same day.

The amount of gel injected into the wells during the operations and the highest recorded pressure values are given in Table-3.

Table-3: Monomer gel operation parameters

An increase in wellhead injection pressure was achieved in the CO<sub>2</sub> injection well Inj-1 (Fig.-4). The wellhead pressure, which was 530 psi before the operation, increased to 680 psi after the operation, and the current value is 620 psi. Although the water cuts decreased to 45% after the gel application in well Prod-1 (Fig.-5), the WC went up to 100% within one month, and the well was again shut-in. Post-operation water cut values in well Prod-2 varied between 12-100% (Fig.-6).

Figure-4: Injection Pressure of Inj-1

Figure-5: WC values of well Prod-1

Figure-6: WC values of well Prod-2

The results of the pilot applications of the monomer gel in production wells in the Batu Raman field were not as positive as expected. In the CO<sub>2</sub> injection well, the increase in the wellhead pressure showed that the existing flow channels of the gas could be changed. In the coming period, it will be useful to revise the gel recipe for production wells and to review the procedure for the selection of the candidate wells.

### ACID FRACTURING

Over four years, 20 wells were stimulated by acid fracturing. Before starting acid fracturing operations, wells were completed properly to deliver desired rate at high treating pressure. In this respect, 10K rating RTTS packer was preferred, as expected maximum pressure is less than 10000 psi. Considering the ID and the pressure rating, 3 1/2" EUE N80 tubing was selected to reduce treating pressure. Lastly, the 10K 2 9/16" X-Tree is used to establish the integrity.

28% HCl gelled acid was used as a main treatment fluid. The average acid concentration per perforation length was generally close 400 gal/ft. In some wells, higher and lower concentrations were tried as well. Treating pressures during operations were less than 5,200 psi. Similarly, injection rate varied from 30 bbl/minute to 50 bbl/minute but mostly it was kept above 40 bbl/minute to carry acid into deeper section of the formation as fast as possible. During operation, acid was injected in different stages to divert it into unstimulated zones. Bio-balls were the main mechanical diverter while crosslinked gel helped to divert acid in both wellbore vicinity and far deep reservoir sections. Once bioballs reached to perforations, treating pressure increased, which is a clear indication of diverter effect (Fig.-7). Also, pre and post-job temperature logs were direct tools to evaluate vertical entry profile of acid distribution (Fig.-8).

Figure-7: Bioball Effect on Treating Pressure

Figure-8: Temperature Log for Zonal Contribution (Black is before frac, others are after fracturing)

To understand effect of any well stimulation technique, change in productivity index (PI) is the first thing to be checked. In this respect, PI was calculated for each well based on first month production metrics, either before or after the fracturing operation. As seen in Fig.-9, all acid fracturing operations led to significant enhancement

in PI of the wells. Similarly, oil production increased in almost all the wells. As shown in Fig.-10, average additional oil per month is around 400 stb after acid fracturing. Throughout four years, 185,000 stb of extra oil was produced by this technology compared to do-nothing scenario.

Figure-9: Before-After Productivity Index (PI) Comparison

Figure-10: Production Enhancement After Fracturing Operation

**CONCLUSION**

In this paper, field development activities in Bati Raman field were summarized. Current CO2 flooding operations aims to maximize efficiency of low amount of available CO2 resources. In-fill drilling will continue in relatively undeveloped areas to reduce well spacing. Different gel systems have been successfully implemented in the field to reduce adverse effects of fracture system on CO2 flooding. In addition to those, acid fracturing campaign showed that well stimulation is possible even in low pressure heavy-oil reservoirs. Campaign will continue with upcoming in-fill wells and existing poor performed wells.

**ACKNOWLEDGEMENT**

The authors want to thank the Turkish Petroleum Corporation (TPAO) for allowing the publication of this work and material.

**REFERENCES**

Borling, D. C. "Injection Conformance Control Case Histories Using Gels at the Wertz Field CO2 Tertiary Flood in Wyoming." Paper presented at the SPE/DOE Improved Oil Recovery Symposium, Tulsa, Oklahoma, April 1994. doi: <https://doi.org/10.2118/27825-MS>

Karaoguz, Osman K., Topguder, Nazan N., Lane, Robert H., Kalfa, Ulker, and Demet Celebioglu. "Improved Sweep in Bati Raman Heavy-Oil CO2 Flood: Bullhead Flowing Gel Treatments Plug Natural Fractures." SPE Res Eval & Eng 10 (2007): 164–175. doi: <https://doi.org/10.2118/89400-PA>

Sahin, Secaeddin, Kalfa, Ulker, Celebioglu, Demet, Duygu, Ersan, and Hakki Lahna. "A Quarter Century of Progress in the Application of CO2 Immiscible EOR Project in Bati Raman Heavy Oil Field in Turkey." Paper presented at the SPE Heavy Oil Conference Canada, Calgary, Alberta, Canada, June 2012. doi: <https://doi.org/10.2118/157865-MS>

Sahin, Secaeddin, Kalfa, Ulker, Uysal, Serkan, Kilic, Harun, and Hakki Lahna. "Design, Implementation and Early Operating Results of Steam Injection Pilot in already CO2 Flooded Deep-Heavy Oil Fractured Carbonate Reservoir of Bati Raman Field, Turkey." Paper presented at the SPE Improved Oil Recovery Symposium, Tulsa, Oklahoma, USA, April 2014. doi: <https://doi.org/10.2118/169035-MS>

Keywords: Bati Raman, CO<sub>2</sub>-EOR

Figure-1: The production and injection history of Bati Raman

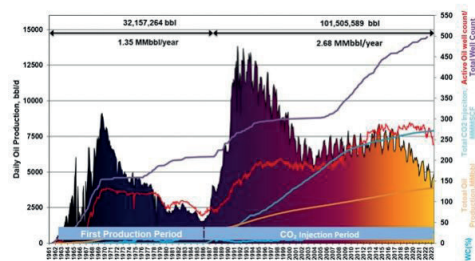


Figure-10: Production Enhancement After Fracturing Operation

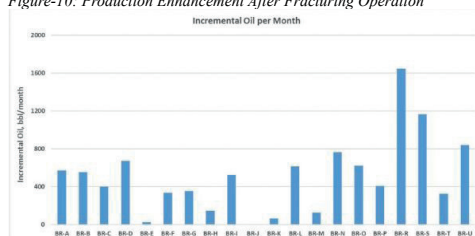


Figure-2: Production wells in which polymer gels were applied

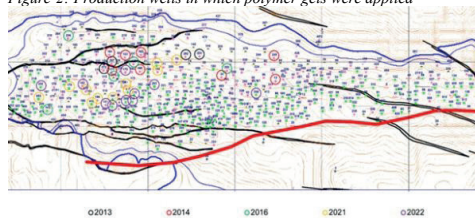


Figure-3: CO<sub>2</sub> injection wells in which polymer gels were applied

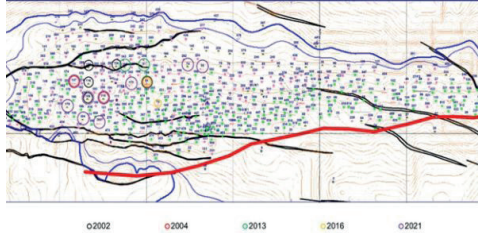


Figure-4: Injection Pressure of Inj-1

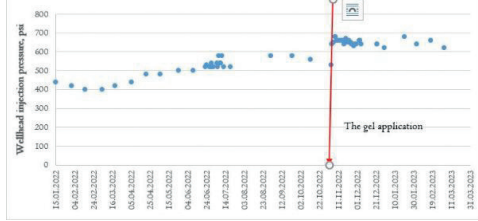


Figure-5: WC values of well Prod-1

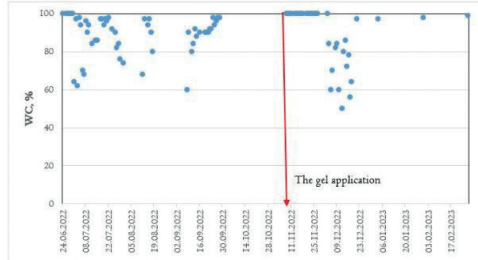


Figure-6: WC values of well Prod-2

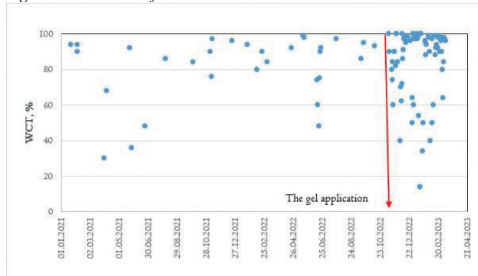


Figure-7: Bioball Effect on Treating Pressure

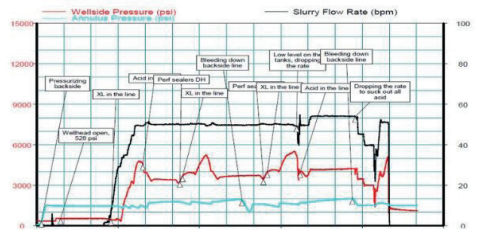


Figure-8: Temperature Log for Zonal Contribution (Black is before frac, others are after fracturing)

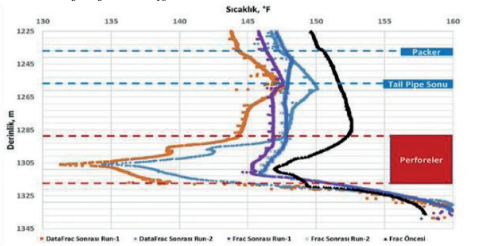


Figure-9: Before-After Productivity Index (PI) Comparison

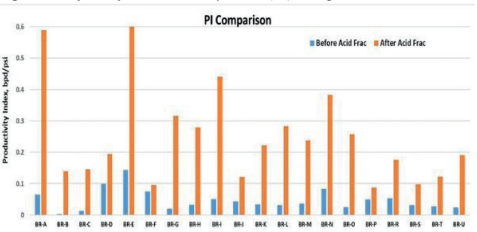


Table-1: Production wells in which polymer gels applied by years

Year	Production wells	Temporary Shut-in wells	Total	Successful operation	Success rate
2013	2	2	4	4	100%
2014	5	3	8	8	100%
2016	0	5	5	3	60%
2021	7	4	11	9	82%
2022	3	7	10	7	70%
<b>Total</b>	<b>17</b>	<b>21</b>	<b>38</b>	<b>31</b>	<b>82%</b>

Table-2: CO2 Injection wells in which polymer gels applied by years

Year	CO2 Injection Well	Injection Pressure before gel app.	First Injection Pressure after gel app.	Injection pressure after one year	Offset well count	Number of wells with production increase
2002	INJ-1	340	590	520	3	3
	INJ-2	240	450	400	5	4
	INJ-3	240	570	540	8	6
2004	INJ-4	350	600	480	6	3
	INJ-5	300	950	800	5	4
	INJ-6	520	850	600	6	3
	INJ-7	340	720	520	4	4
2013	INJ-8	425	650	540	7	2
	INJ-4	400	550	420	7	2
	INJ-9	380	520	450	3	1
2016	INJ-4	560	740	460	5	1
	INJ-10	320	540	370	8	3
2021	INJ-11	680	840	840	3	0
	INJ-12	560	720	460	4	2
	INJ-1	460	600	520	5	1
	INJ-5	400	560	450	5	2
	INJ-13	340	500	400	5	3
	INJ-6	200	650	650	5	3
	INJ-14	360	750	650	5	1
	INJ-15	320	500	480	5	2
	INJ-16	360	440	420	5	3

Table-3: Monomer gel operation parameters

Well	Type	Injected gel volume, bbl	Maximum injection pressure, psi
Inj-1	CO2 injection	1862	0
Prod-1	Production	960	1040
Prod-2	Production	340	550

# A Numerical Study on the Effect of Flue Gas Composition on Oil Recovery in Low-Permeability Formations

**Yashar Tavakkoli Osgouei, Mehmet Onur Doğan, Çağlar Sınayuç**

Department of Petroleum and Natural Gas Engineering, Middle East Technical University,  
Ankara / Türkiye



The production of heavy oil is challenging because of its higher viscosity and lower mobility. Although thermal-based methods are useful to cope with these problems through heat injection, the application of thermal recovery method are expensive and not always effective methods. Therefore, different alternatives were considered with respect to conditions of heavy oil reservoirs. Non-condensate gases like flue gas injection are widely used in heavy oil recovery. The flue gas includes approximately 80% N<sub>2</sub> and 20% CO<sub>2</sub>. The flue gas injection is an effective method for improving not only heavy oil recovery, but also environmental issues. The flue gas injection was simulated as a dual porosity-single permeability model with Eclipse compositional (e300) software. Numerical study was carried out to investigate the effect of flue gas compositions on oil production performance. The numerical results showed that high percentage of N<sub>2</sub> in gas stream improves oil production cumulative, maintaining reservoir pressure. These can be attributed to foam oil formation by N<sub>2</sub> because of good expansibility of N<sub>2</sub> compared to CO<sub>2</sub> in low-permeability oil reservoirs at the same conditions. The flue gas injection into oil reservoirs not only enhances oil production performance, but also reduces CO<sub>2</sub> emission by different industries

## INTRODUCTION

Heavy oil reservoirs are significant energy sources, accounting for 70 % of reserves worldwide. The most challenging problem about heavy oil is its higher viscosity characteristics that impact its mobility in reservoir and surface conditions over production. Steam injection technology is the most widely used method to enhance heavy oil recovery [1]. However, it is not an effective method for recovery of heavy oil in deep reservoirs due to pressure and heat losses. In these cases, the cold recovery technologies can alternatively be applied to improve productivity index. One of these techniques is non-condensate gas injection. In fact, the light gases act as solvents in decreasing the immobile oil fraction by minimizing interfacial tension. In addition, they increase the oil mobility by swelling effect on oil fraction, pushing the oil toward the production wells. The most commonly used non-condensate gases in oil recovery are CO<sub>2</sub>, N<sub>2</sub>, and flue gas [2].

As revealed by the non-condensate gas injection in heavy oil reservoirs, oil recovery increases due to the main mechanism including, the foam oil formation, crude oil viscosity reduction, crude oil volume expansion, interfacial tension reduction, water phases wettability increase, and influence of three-phase relative permeability [3]. In oil reservoirs, the injected CO<sub>2</sub> to be miscible with crude oil, reservoir pressure must be higher than the minimum miscible pressure. In

heavy oil reservoirs API gravity is low and minimum miscible pressure is high. For API gravities less than 22, CO<sub>2</sub> with oil becomes immiscible [4]. In addition, lack of considerable decrease in interfacial tension between gas and oil provides an immiscible process in heavy oil recovery. The non-condensate gas injection improves heavy oil recovery by the following main mechanisms such as crude oil volume expansion, crude oil viscosity reduction, component extraction, and formation energy replenishment [5].

A large amount of flue gas is usually produced by different industrial sectors, especially, oil refinery and petrochemical industry. The flue gas is used to oil field production, which not only improves oil recovery, but also decreases the emission of detrimental gases like CO<sub>2</sub>. The capture of CO<sub>2</sub> from flue gas was mainly carried out to enhance oil recovery rather than reduce greenhouse emission to the atmosphere in the few years ago. However, it attracts many attentions to stabilize the atmospheric concentration of greenhouse gases over the last two decades [6]. In general, the flue gases are a mixture of 20 % CO<sub>2</sub> and 80 % N<sub>2</sub>. Flue gas has some advantages for oil recovery due to its lower cost and higher availability by different industries. The flue gas injection into low-permeability oil reservoirs plays an important role in not only oil recovery, but also CO<sub>2</sub> storage [7].

In the current study, the effect of flue gas compositions on heavy oil recovery in the naturally fractured reservoir was investigated with Eclipse 300 as the compositional numerical simulator using the dual porosity option. A series of simulation were performed to study the effect of nitrogen contamination in the flue gas stream on heavy oil recovery and field pressure in the fractured reservoir with dual porosity models.

## METHODOLOGY

A reservoir pattern of the Bati Raman heavy oil field in Southeast Turkey was chosen with potential flue gas injection to explore the effect of flue gas compositions on heavy oil recovery. In order to conduct this study, the reservoir pattern was defined as a square-shaped box model (Fig. 1). The selected reservoir pattern is 3410×3410 ft<sup>2</sup> in areal extend and 4265 ft in thickness. The gridding system of 31×31×60 blocks in x, y, and z directions respectively provides a proper simulation model to study heavy oil recovery under flue gas injection with different compositions. The model includes four injection wells in the four corner and one production well in the middle of the square-shaped box model. As Bati Raman heavy oil reservoir is highly fractured, it was simulated by using the dual porosity option within Eclipse 300. The dual porosity model assumes that the matrix does not allow the flow

between matrix blocks due to very low permeability of matrix. The dual porosity model consists of two parts like matrix and fracture in formation with different porosities and permeabilities. While the matrix acts as a source for fluid storage, the fracture system provides the path for fluid flow from the formation to the well.

The model was considered with an initial reservoir pressure of 1750 psi in water-oil contact at depth of 1968 ft. Also, the aquifer was defined in the bottom of entire reservoir and water influx moves vertically upward into the oil zone. All of the necessary reservoir rock properties, and fluid specifications together with reservoir fluid compositions have been determined considering the data available in the literature. The reservoir model details are summarized in the Table 1;

## RESULT & DISCUSSION

### Field Pressure

The presence of N<sub>2</sub> in flue gas stream affects reservoir pressure compared to pure CO<sub>2</sub> gas stream injection. Figure 2 indicates that the injection of flue gas with composition of 20%CO<sub>2</sub> and 80%N<sub>2</sub> energizes the reservoir pressure compared to that of pure CO<sub>2</sub> gas injection. According to several studies, the large amount of N<sub>2</sub> migrates to top section of reservoir under the gravity effect during flue gas injection with the composition of 20%CO<sub>2</sub> and 80%N<sub>2</sub>, creating a secondary gas cap. In fact, it simultaneously contributes to the recovery of formation energy [8].

### OIL PRODUCTION CUMULATIVE

The performance of gas injection operation depends on many factors, such as injection time, injected gas volume, and injected gas composition. The effect of N<sub>2</sub> content in flue gas on the oil production cumulative was numerically studied (Fig. 3). It can clearly be seen that the amount of oil production cumulative increases in all kinds of gas streams injection with different compositions. The response of the gas stream with large percentage of N<sub>2</sub> (20% CO<sub>2</sub> and 80% N<sub>2</sub>) to enhance oil production is higher compared to that of pure CO<sub>2</sub> gas stream (100% CO<sub>2</sub>). This is solely due to the presence of N<sub>2</sub> in the gas mixture stream. There is direct relationship between oil production cumulative and the percentage of N<sub>2</sub> in the gas mixture. In fact, the flue gas with the composition of 20% CO<sub>2</sub> and 80% N<sub>2</sub> provides higher oil production in comparison with pure CO<sub>2</sub> gas stream. The presence of N<sub>2</sub> in the gas stream results in the obstruction of large pore throat by foam oil formation, consequently, this leads to increase in reservoir pressure and oil production cumulative [5].

### GAS-OIL RATIO

The amount of foam oil formation can be quantified by the parameter of gas-oil ratio. The higher gas-oil ratio in the flue gas with the composition of 20% CO<sub>2</sub> and 80% N<sub>2</sub> in the Figure 4 represents the role of N<sub>2</sub> in the

formation of foam oil that increases oil mobility and displacement. However, the gas-oil ratio is less for the pure CO<sub>2</sub> gas stream, fluctuating around low constant values [9].

### GAS DISTRIBUTION

Gas distribution profile in the simulation model can be considered as an index to evaluate the amount of free gas in reservoir. In fact, the more gas phase, the higher reservoir pressure. Figure 5 shows the distribution of CO<sub>2</sub> and N<sub>2</sub> in the model for flue gas injection. It can clearly be seen that the diffusivity of N<sub>2</sub> is greater than that of CO<sub>2</sub> in the selected low-permeability formation over flue gas (20% CO<sub>2</sub> and 80% N<sub>2</sub>) injection. It can come from good displacement property, gas lift, and drainage function of N<sub>2</sub> because of its good expansibility compared to CO<sub>2</sub> given the same temperature and pressure [10].

### CONCLUSION

The heavy oil reservoir was simulated by the dual porosity option within Eclipse compositional simulator (e300) to investigate the effect of flue gas component on the performance of heavy oil production. On the basis of the simulation results it is evident that the presence of N<sub>2</sub> in gas stream improves cumulative oil production by foam oil formation because of developing an effective bank, resulting in rising reservoir pressure. In fact, higher displacement efficiency by the flue gas with the composition of 20% CO<sub>2</sub> and 80% N<sub>2</sub> can come from good expansibility of N<sub>2</sub>. In addition, flue gas injection with higher percentage of N<sub>2</sub> contributes to not only improving heavy oil recovery, but also decreasing the CO<sub>2</sub> emission to atmosphere.

### ACKNOWLEDGEMENT

This study was carried out within the scope of TÜBİTAK 1005 - National New Ideas and Products Research Support Program, project titled "Technical and Economical Investigation of the Most Appropriate Business Model for Injection of Flue Gas / Carbon Dioxide Captured from the Batman Oil Refinery into the Bati Raman Field", (Project No: 221M582).

### REFERENCES

- [1] J. Qin, J. Zhang, S. Zhu, Y. Wang, and T. Wan, "Multi-Component Thermal Fluid Injection Performance in Recovery of Heavy Oil Reservoirs," *Front. Energy Res.*, vol. 9, 2021, Accessed: Jan. 03, 2023. [Online]. Available: <https://www.frontiersin.org/articles/10.3389/fenrg.2021.803540>
- [2] Liu, Q. Research on Nitrogen-Foam Flooding Technology in LuKeQin Deep Heavy oil Exploitation; Northeast Petroleum University: Daqing, China, 2017.
- [3] X. He et al., "A Critical Review Using CO<sub>2</sub> and N<sub>2</sub> of Enhanced Heavy-Oil-Recovery Technologies in China," *Appl. Sci.*, vol. 12, no. 24, p. 12585, Dec. 2022,

doi: 10.3390/app122412585.

[4] Taber, J. J., Martin, F. D., and Seright, R. S. (1997). EOR Screening Criteria

Revisited—Part 2: Applications and Impact of Oil Prices. SPE Reservoir Engineering 12, 199-205.

[5] Zhou, X.; Yuan, Q.; Zeng, F.; Zhang, L.; Jiang, S. Experimental study on foamy oil behavior using a heavy oil—methane system in the bulk phase. J. Pet. Sci. Eng. 2017, 158, 309–321.

[6] N. Bueno Zapata, J. M. Mejía Cárdenas, and J. J. Martínez Paternina, “Flue gas and nitrogen co-injection during cyclic steam stimulation in heavy oil reservoirs: a numerical evaluation,” DYNA, vol. 88, no. 218, pp. 127–135, Aug. 2021, doi: 10.15446/dyna.v88n218.90341.

[7] Bender, S; Akin, S; “Flue Gas Injection for EOR and Sequestration: Case Study”, Journal of Petroleum Science and Engineering, 2017, 157, 1033-1045

[8] Guo, X.; Zhao, H.; Guoliang, H.U.; Wang, L.; Zeng, W.; Yang, Y. Ultra-deep wells in fractured-vuggy reservoir nitrogen injection EOR technology. Oil Drill. Prod. Technol. 2013, 35, 98–101

[9] Yue, P.; Xie, Z.; Huang, S.; Liu, H.; Liang, S.B.; Chen, X. The application of N2 huff and puff for IOR in fracture-vuggy carbonate reservoir. Fuel 2018, 234, 1507–1517

[10] Li, Y.B.; Pu, W.F.; Wei, B.; Chen, Y.F.; Bai, B.J. “The feasibility of CO2 and N2 injection for the Tahe fracture-cavity carbonate extra-heavy oil reservoir: An experimental study”, Fuel, 2018, 226, 598–606.

Keywords: Compositional simulation model, Flue gas injection

Fig. 1. The dual porosity modeling of the selected reservoir pattern

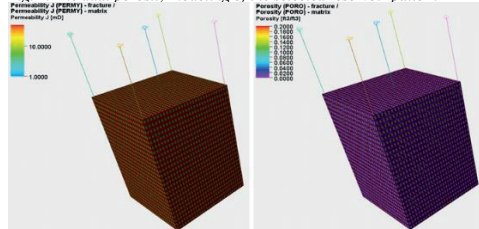


Fig. 2. Reservoir pressure for gas stream injection with different compositions

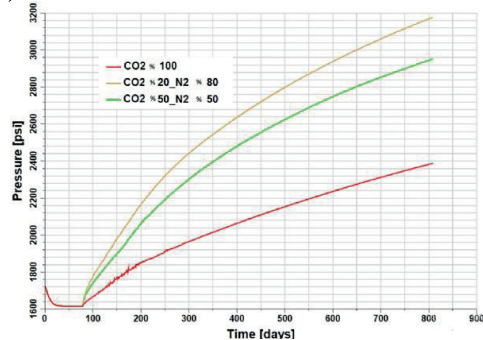


Fig. 3. Oil production cumulative for gas stream injection with different compositions

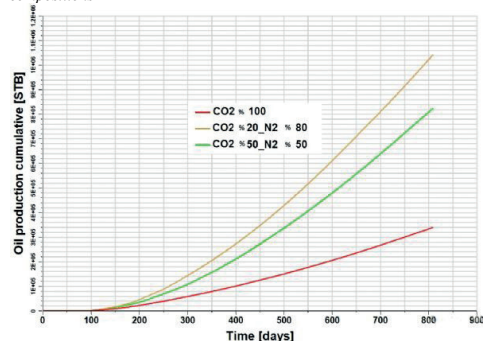


Fig. 4. The gas-oil ratio at the production well for different injection compositions

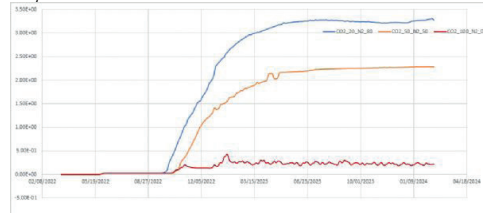


Fig. 5. Gas distribution in the selected reservoir pattern

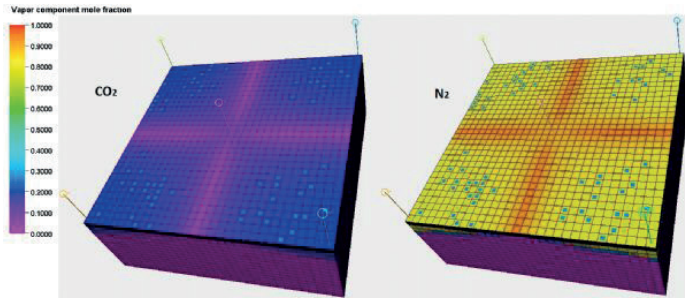


Table. 1. Properties used for simulation

Parameters	Values	Units
Total grid cells	57660	
Matrix porosity	0.18	
Matrix permeability (x,y)	10	md
Matrix permeability (z)	5	md
Fracture porosity	0.018	
Fracture permeability (x,y)	60	md
Fracture permeability (z)	20	md
Sigma	0.1	
Reservoir pressure	1750	psi
Reservoir depth	4265	ft
Reservoir temperature	129	°F
Initial Water saturation	0.21	
Gas oil ratio	18	scf/STB
Bubble point pressure	155	psi
Number of injection wells	4	
Number of production well	1	
Components	CO2, N2, C1, C3, C6, C10, C15, C20	



# Combustion Tube Experimental Setup Design for Underground Coal Gasification

**İsmail Hakkı Sarıcam, Murat Çınar**

Department of Petroleum and Natural Gas Engineering, Faculty of Mines, Istanbul Technical University, Istanbul / Türkiye



## 1. INTRODUCTION

Surface or underground mining of coal takes place in a dangerous working environment. In addition, using coal in conventional ways, such as extracting and exploiting it, adversely affects the environment. On the other hand, coal is needed for our energy demand. That is why unconventional coal usage is required to satisfy global energy demand and cope with environmental issues. Underground coal gasification (UCG) and coal bed methane (CBM) are unconventional coal technologies.

UCG provides utilization of coal seams that are not technologically or economically extracted in conventional techniques. The process of UCG can take place as follows. After determining the target coal seam, production and injection well pairs are drilled. If the desired flow rate is not achieved, different methods, such as hydraulic fracturing and reverse and forward combustion, can be used to generate a link between these well pairs. Later, an oxidant is injected through injection wells, and gasification is initiated. Finally, generated gas is produced through production wells. These gases are named syngas (synthesis gas), mainly consisting of  $\text{CO}_2$ ,  $\text{CO}$ ,  $\text{CH}_4$ , and  $\text{H}_2$ . Produced syngas could be directed through surface pipelines to a power plant. In addition to electricity generation, these gases can be used for hydrogen, methanol, synthetic fuel production, and industrial heating. The general schematic of the process is described in Figure 1.1.

The process of UCG is affected by several factors, such as coal properties, type of injectant, operational parameters, seam depth, seam thickness, and the surrounding medium (Bhutto et al., 2013). When a suitable and optimal operation of UCG is accomplished, it chiefly exploits a coal seam without transferring ash to the surface and releasing any greenhouse gases into the atmosphere. In conventional coal technologies, large amounts of ash come out in power plants which need to be removed and mitigated. UCG also enables the vanishing of hard/hazardous working environments at the coal mines.

Although various/several attempts have been made, only one UCG power plant exists on an industrial scale (Klimenko, 2009). Numerous pilot-scale field trials took place but were terminated due to different operational or environmental problems. If laboratory studies and successful field tests enable us to find optimal ways to accomplish UCG, these unconventional coal technologies can fulfill some energy demands.

In previous combustion tube experiments for the UCG, the experimental designs have some drawbacks. To illustrate, the usage of an adiabatic reactor does not represent the UCG in terms of temperature behavior underground. Moreover, previous designs did not include any  $\text{H}_2\text{S}$  filter (Bell & Gunn, 1980; Sutardi et al.,

2020). In this work, we aimed to develop combustion tube experiments for UCG. Heat losses are taken into account in our design as well as an  $\text{H}_2\text{S}$  removal unit. Proper laboratory studies enable us to understand what mechanism occurs underground and what factors affect the process.

## 2. SCOPE OF THE STUDY

This study aims to update the combustion tube experimental setup built for oil experiments for coal gasification to provide a better model of UCG on a laboratory scale. During the gasification of coal, three main processes occur. First, coal drying takes place and moisture inside the coal evaporates at this stage. Then, dry coal decomposes in the absence of oxygen, called the pyrolysis process. Char, a residue after pyrolysis, spall into the cavity and forms a bed at the bottom of the cavity. Then, char gasification takes place inside the cavity. Thus, a packed bed model is selected to design combustion tube experiments.

Target coal seams for UCG are generally located in deeper or low-ranked coals. Obtaining large coal samples from such fields is not feasible due to their depth. Hence, an experimental system based on available core samples must be used. Core drilling is costly, and a limited amount of coal can be acquired. Dimensions of the experiments are designed such that the gasification's stable behavior can be observed using a small amount of coal sample.

Combustion tube experiments are already used in the petroleum industry to obtain parameters for the in situ combustion process design, an enhanced oil recovery technique to improve oil production. In these experiments, the tube is filled with coal sample and a combustion front is propagated through the tube with continuous air injection. After some time, the combustion front self-propagates, the front velocity becomes nearly constant called the stable period. The necessary data is obtained in this stable period. The length of the tube and the injection rate are important parameters for the success of an experiment and need to be chosen accordingly.

In this study combustion tube experimental setup for in situ combustion of petroleum is adapted for coal gasification. Therefore, the combustion tube is designed such that a stable period can be observed using a low amount of coal. The stable period is when the composition of syngas does not change considerably. The slope of the temperature profile behind and front of the combustion zone are constant during the stable period. Necessary equipment, such as filters and a scrubber, is added to update the experimental system.

The length of the combustion tube and injection rate

are the main components that affect the stable period (Penberthy & Ramey, 1966). The experiments were conducted to determine whether the reactor's length was enough for observing a stable period during the gasification of low-ranked coal. Although it is not the main goal of this study, the effects of different coal samples and oxidants were investigated. Since it is not a sensitivity study, a couple of experiments were executed for this purpose. In addition, an  $H_2S$  filter was needed during the study; thus, an  $H_2S$  filter was also designed.

### 3. MATERIALS AND METHODS

#### Experimental Apparatus

In these experiment series, coal is gasified in a combustion tube called the reactor. An oxidant is injected with a certain pressure and flow rate into the reactor. The composition and flow rate of the produced syngas is measured. The temperature inside the reactor is measured as well with the thermocouples. Produced gas flows through the liquid collector, sand filter,  $H_2S$  filter, and condenser before reaching the flowmeter and gas analyzer.

#### Reactor

The reactor is a cylindrical tube with 1 m in length, 7 cm in diameter, and 1.5 mm in wall thickness. The length of the tube should be long enough to obtain stabilization. A thin wall is needed to minimize heat absorbed by the wall of the combustion tube. There are fluid inlet and outlet, and thermocouple inlets on the upper and lower flanges of the reactor. The reactor and flanges are made up of 316L stainless steel. Schematic of the reactor, flanges, and thermocouples can be seen in Figure 3.1. A copper gasket with thermal paste applied on top and bottom is placed between the flanges and the reactor to prevent gas leaks.

#### $H_2S$ Filter

Since  $H_2S$  in considerable concentration is hazardous for the environment and equipment used in experiments, it is necessary to remove or decrease the concentration of the  $H_2S$  from the syngas. In these experiments, caustic scrubbing is used for  $H_2S$  removal. A scrubber colon is designed in which gas enters the colon from the bottom, and the caustic solution is provided to the colon from above. The "clean" gas flows from the top of the scrubber, and the used caustic solution is collected from the bottom. Sodium hydroxide (NaOH) solution is pumped to the top of the scrubber. NaOH is pumped through a nozzle which enables the pulverization of the caustic to increase the contact area of gas and liquid. Increasing the contact area increases the efficiency of the caustic scrubbing operation. The schematic of the designed caustic scrubber can be seen in Figure 3.2.

#### Coal Samples

Kınık and Çerkezköy lignite samples were used in the experiments. Their properties vary from each other, which can be seen in Table 4.2. In the literature, the particle-sized spalled into the cavity is estimated to be around 1 cm in diameter (Perkins, 2018b). Thus, the samples were crushed and screened by 1 cm grain size before packing them into the reactor. The heating values of the Kınık and Çerkezköy coals were measured as 11.88 MJ/kg and 8.6 MJ/kg, respectively.

#### Execution of the Experiments

Experiments were conducted by following a procedure of several steps. First, the bottom flange of the reactor is connected. Then a mesh is placed inside the bottom of the reactor to prevent the intrusion of solid particles into the flow line. After that, the bottom thermal probe is placed, and fittings and reducers are connected to the bottom flange. Later, almost 400 ml of sand particles are packed into the reactor's bottom to filter the solid particles. In the following step, coal samples that are crushed into particles are packed into the reactor before closing the reactor with the top flange. The upper thermal probe is placed into the reactor after connecting fittings and reducers to the top flange. Then, the reactor is covered with insulation material (pyrogel) to minimize heat losses. The heater is connected at the top of the reactor before vertically placing the reactor into the reactor casing. Later, the top and bottom parts of the reactor are connected to the flow line.

Thermal probes are connected to the ports then the recording system is checked to see whether it works properly. After that, the gas analyzer is calibrated before the heater is powered. When the temperature reaches reasonable values (almost 550 °C) for the ignition of coal, the heater is closed and the injection of oxidant starts. The oxidant enters the reactor from the top, supporting the gasification. Syngas is produced as a result of the gasification, and it flows through the bottom of the reactor. Produced gas first enters the liquid collector and then flows through the sand filter. After that, it flows to the  $H_2S$  filter before reaching the condenser. Then, it flows through the drierite to make sure that the syngas water content is minimized. Syngas enters the gas analyzer after passing through the 15 and 7-micron filters. Finally, the effluent gas flows through the vent. Figure 3.3 shows the flowline of the gasification experiments. After the termination of the gasification of coal, the reactor and equipment in the flow line are demounted.

### 4. RESULTS AND CONCLUSIONS

The scope of this study is to develop a combustion tube experimental setup for UCG. Within this scope, the packed bed model is used. A reactor with a 1 m length, 7 cm diameter, and 1.5 mm wall thickness is designed for coal gasification. The stable behavior can be observed with these dimensions and operating conditions if the composition and temperature profiles in the previous

sections are analyzed. While decreasing the reactor length might cause difficulty in forming a stable period, an increase in the reactor length requires more coal samples. The wall thickness of the reactor can be smaller if it resists the high temperature, high pressure, and corrosive environment.

Seven experiments were executed in this study. Operation parameters of these experiments is shown in Table 4.1. Mainly, coal is packed in the reactor and then gasified. The temperature in the reactor and the composition of the syngas were measured. As seen in the Figure 4.1, the temperatures reached up to 1200 °C and combustion front velocity at stable period is calculated as 0.17 m/hr for gasification with air injection. Different coal samples were used, and the effect of oxygen on the gasification performance was investigated. Furthermore, a caustic scrubber column was designed for removing H<sub>2</sub>S from the syngas.

The composition of the syngas varies with the different coal samples. Since the compositions are different, gas heating values (GHV) can be different. Thus, coal type affects the process as expected. Table 4.2 shows the two different coals' proximate analysis, syngas compositions, and GHV.

GHV increases as the oxygen concentration in the injected gas increases. The heating value of the syngas for 21%, 30%, and 40% oxygen concentrations are 2.98, 4.62, and 4.87 MJ/Nm<sup>3</sup>, respectively. Table 4.3 shows the comparison of these results. The amount of methane, hydrogen, carbon monoxide and carbon dioxide in the syngas is directly proportional to the oxygen concentration of the injected gas. This behavior matches the literature (Mastellone et al., 2012; Park et al., 2018). This study does not involve a sensitivity analysis for the effect of O<sub>2</sub> concentration on UCG performance. Therefore, more experiments must be conducted to determine the relationship between injected O<sub>2</sub> concentration and syngas. The primary aim of using different oxygen concentrations is to test and observe the deficiencies of the experimental system. When the O<sub>2</sub> content inside the reactor increases, the coal consumption rate also increases. It can be seen from the experiments that the duration of the experiment is inversely proportional to the O<sub>2</sub> content of the injected fluid (Figure 4.2). The stable behavior can also be detected in the reactor with a 1 m length when the O<sub>2</sub> concentration of the injected fluid increased up to 40%. Since more coal is gasified in a unit of time when O<sub>2</sub> content increases, an increase in the composition of methane, hydrogen, and carbon monoxide would be expected.

Several experiments are disrupted due to the sand filter and condenser clogging. Liquid moved with syngas trapped at the sand filter and condenser, limiting the gas flow. Thus, a better liquid trap is needed. A liquid trap with a higher length (>30 cm) and higher volume can trap more liquid, decreasing the amount of liquid transported to the sand filter. The sand filter should be designed such that gas flow should not be limited if a liquid intrusion occurs. In these experiments, sand particles between 80 and 100 mesh sizes were used in

the sand filter. Using more coarse sand grains, such as 60 mesh size, can resist clogging. Moreover, the reactor and thermal probes were adversely affected due to high temperatures and corrosive gases. The used reactor and thermal probes are made up of 316L stainless steel. Materials having more resistance to high temperature and corrosion than 316L steel should be selected for future experiments. A pressure jacket can also be added to the design if high operational pressures are desired. The pressure inside the pressure jacket can supply external pressure to the reactor; therefore, a pressure balance can be maintained to operate at high pressures without bursting. Finally, the grain size distribution of the coal particles should be as homogenous as possible and packed well to eliminate the forming of a second combustion front.

#### ACKNOWLEDGEMENTS

I would like to express my gratitude to Istanbul Technical University (ITU) for supporting this study. The study was conducted under the ITU BAP program with the project code MYL-2020-42750. I would like to thank Polyak Eyzec Enerji Üretim Madencilik San. ve Tic A.Ş. as well for providing coal samples to be used in the experiments.

#### REFERENCES

- Bell, G. J., & Gunn, R. D. (1980). Adiabatic Coal Gasification Tube Experiments - Forward Gasification. Sixth Underground Coal Conversion Symposium, 53(9), 1689–1699.
- Bhutto, A. W., Bazmi, A. A., & Zahedi, G. (2013). Underground coal gasification: From fundamentals to applications. *Progress in Energy and Combustion Science*, 39(1), 189–214. <https://doi.org/10.1016/j.pecc.2012.09.004>
- Klimenko, A. Y. (2009). Early ideas in underground coal gasification and their evolution. *Energies*, 2(2), 456–476. <https://doi.org/10.3390/en20200456>
- Mamrosh, D. L., Beitler, C. A. M., Benn, B., McIntush, K. E., & Hileman, O. E. (2009). Use of Caustic in a Short Contact Time Approach to Selectively Scrub H<sub>2</sub>S from CO<sub>2</sub>-Contaminated Gas Streams. Proceedings of the 59th Laurance Reid Gas Conditioning Conference, 94572(510), 445–459.
- Mastellone, M. L., Zaccariello, L., Santoro, D., & Arena, U. (2012). The O<sub>2</sub>-enriched air gasification of coal, plastics and wood in a fluidized bed reactor. *Waste Management*, 32(4), 733–742. <https://doi.org/10.1016/j.wasman.2011.09.005>
- Park, S. W., Lee, S. Y., Jeong, Y. O., Han, G. H., & Seo, Y. C. (2018). Effects of Oxygen Enrichment in Air Oxidants on Biomass Gasification Efficiency and the Reduction of Tar Emissions. *Energies*, 11(10). <https://doi.org/10.3390/en11102664>
- Penberthy, W. L., & Ramey, H. J. (1966). Design and Operation of Laboratory Combustion Tubes. *Society of Petroleum Engineers Journal*, 6(02), 183–198. <https://doi.org/10.1016/j.spe.1966.02.002>

doi.org/10.2118/1290-pa

Perkins, G. (2018b). Underground coal gasification – Part II: Fundamental phenomena and modeling. *Progress in Energy and Combustion Science*, 67, 234–274. <https://doi.org/10.1016/j.pecs.2018.03.002>

Sutardi, T., Wang, L., Karimi, N., & Paul, M. C. (2020). Investigation of thermochemical process of coal particle packed bed reactions for the development of UCG. *International Journal of Coal Science and Technology*, 7(3), 476–492. <https://doi.org/10.1007/s40789-020-00360-x>

V. Bontozoglou, A. J. K. (1989). Simultaneous Absorption of H<sub>2</sub>S and CO<sub>2</sub> in NaOH Solutions: Experimental and Numerical Study of the Performance of a Short-Time Contactor. *Industrial & Engineering Chemistry Research*, 34.

**Keywords:** combustion tube, underground coal gasification

Figure 1.1: Schematic of a UCG process.

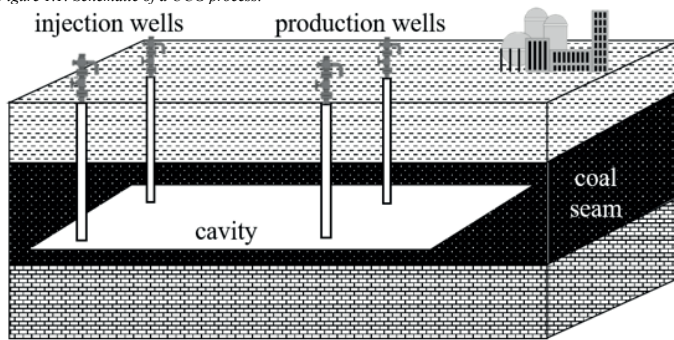


Figure 3.1: Schematic of the reactor and its components.

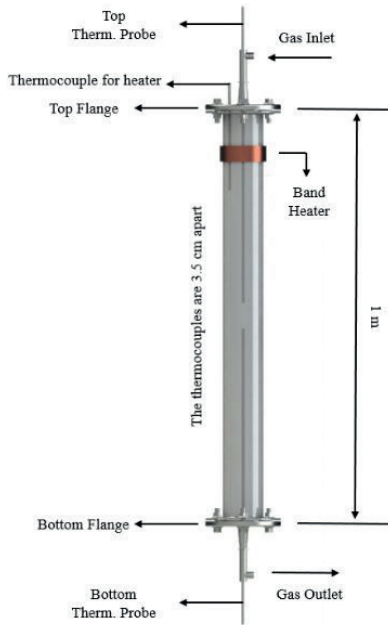


Figure 3.2: Schematic of the designed caustic scrubber.

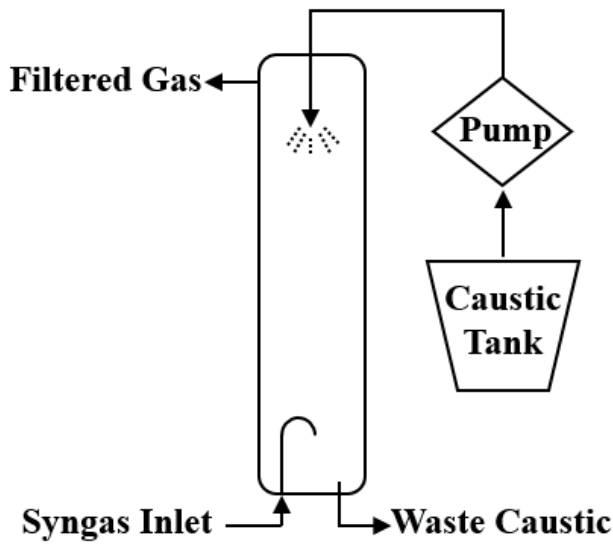


Figure 3.3: Flowline of the gasification experiments

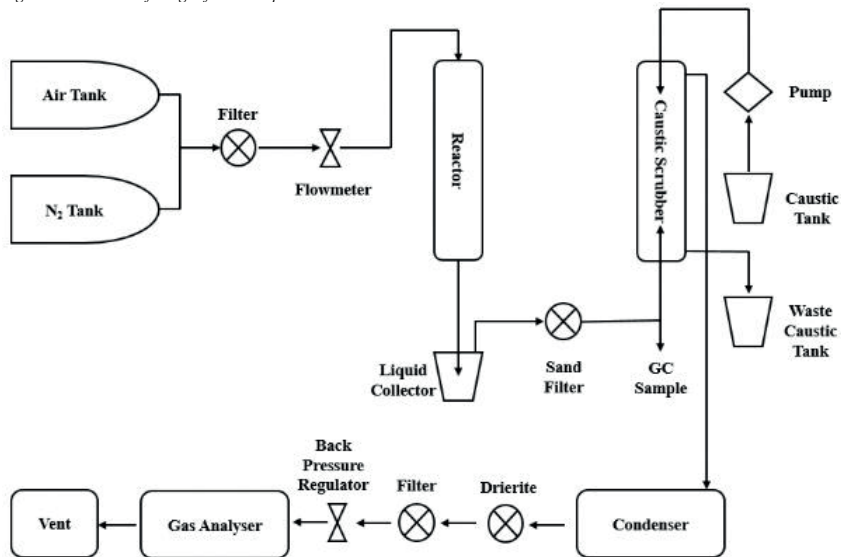


Figure 4.1: Temperature profile in the reactor.

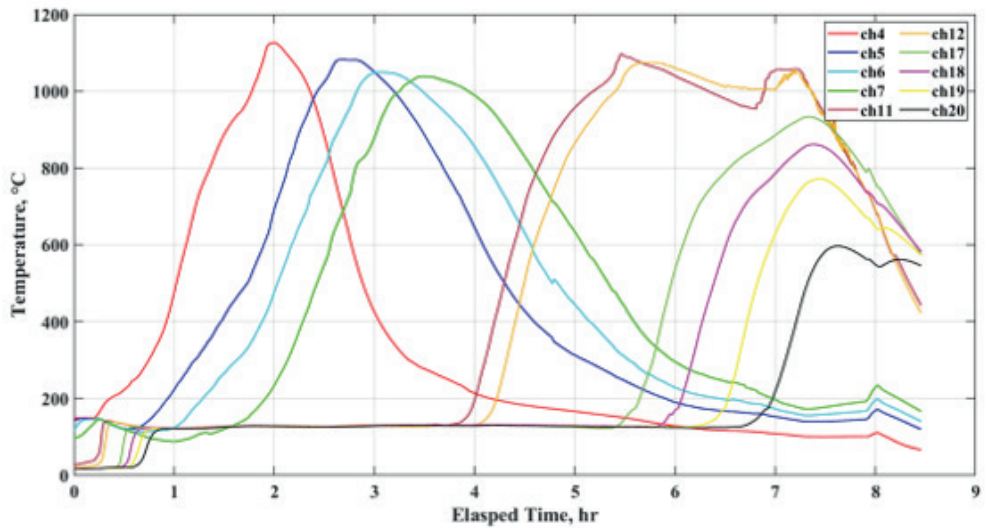


Figure 4.2: Comparison of syngas compositions of experiments with varying oxygen content of the injected fluid (GA: Gas Analyser, GC: Gas Chromatography).

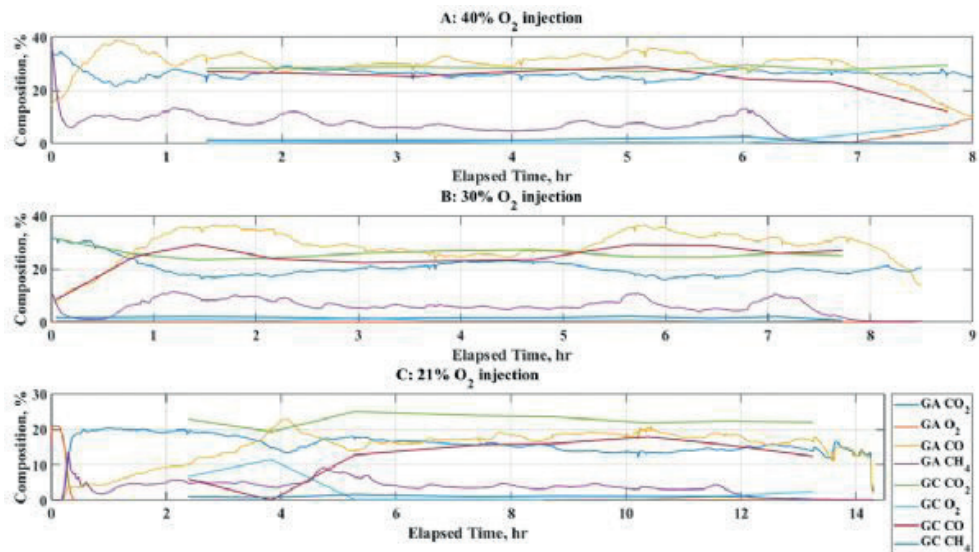


Table 4.1: Operation parameters of the experiments.

Experiment	Location of coal sample	Oxidant	Injection Rate (lt/min)	Pressure (psig)
1	Çerkezköy	Air	6	100
2	Çerkezköy	Air	6	70
3	Kınık	Air	6	70
4	Kınık	Air	6	70
5	Kınık	Air	6	70
6	Kınık	40 % O <sub>2</sub>	6	70
7	Kınık	30 % O <sub>2</sub>	6	70

Table 4.2: Comparison of Çerkezköy and Kınık coals.

Coal	Fixed Carbon (%)	Ash (%)	Moisture (%)	Volatile Matter (%)	GHV (MJ/Nm <sup>3</sup> )
Çerkezköy	24.2	16.8	34.63	24.37	2.33
Kınık	17.91	36.42	8.48	37.19	3.08

Table 4.3: Comparison of syngas compositions and heating values for varying oxygen content of the injected fluid.

O <sub>2</sub> (%)	CH <sub>4</sub> (%)	H <sub>2</sub> (%)	CO <sub>2</sub> (%)	CO (%)	HHV (MJ/Nm <sup>3</sup> )	LHV (MJ/Nm <sup>3</sup> )
21	1.250	3.566	23.843	15.933	3.079	2.987
30	1.720	4.985	26.792	25.826	4.757	4.629
40	1.913	5.324	29.132	26.803	5.016	4.875







## **Öğrenci Bildiri Yarışması**

*Student Paper Contest*

---



# Predicting Bottomhole Temperature of Offshore Production Wells in the North Sea

**Tuğberk Berat Günel**

Istanbul Technical University



## 1. AİM

The importance of data science in the petroleum industry has grown significantly with the rise of digitalization. Estimating crucial properties like temperature and pressure is beneficial for economic and safety purposes. While surface measurements are relatively easy to obtain, downhole measurements require equipment installation, which is time-consuming, costly, and requires maintenance. To address these challenges, historical production data can be used to estimate temperature and pressure in recently drilled production wells within the same formations. In this project, the production data from the Volve Field is utilized to build a model that predicts bottomhole temperatures using known and controllable parameters.

## 2. METHODOLOGY

Achieving a meaningful result requires an extensive work methodology. In this project, the following list represents the stepwise methodology for this work.

- Data Manipulations
- Data Visualizations
- Data Imputations
- Feature Selection
- Building a Machine Learning Model

In the following subsections, each methodology that is mentioned in the above list is going to be examined.

### 2.1. Data Manipulations

In this part, the work of filtering the data to only production wells, and aggregating new columns are done. New columns are aggregated to be cumulative summation of each three phase fluids, oil, gas, and water. Furthermore, the daily production observations are sorted into ascending manner.

### 2.2. Data Visualization

#### 2.2.1. Production Data Visualizations

In order to gain knowledge about the reservoir, and its behavior, the fluid production graphs are plotted as a function of time. Figure 1 represents oil-water production as a function of time, and gas-water production as a function of time. Furthermore, Figure 2 demonstrates the oil production decline curve against time.

#### 2.2.2. Distribution Visualizations of Features

Before getting started with data manipulations, and building a machine learning model, it is found to be necessary to maintain the distributions of the curial features as their statistical behaviours can affect the processing and model building progresses. To achieve this, distribution plots, and statistical properties are used.

### 2.3. Data Imputation

The implementation of a successful data imputation plays a tremendous affect in the data science world, as the wrong imputations may result in huge deviations from the real data. As a results of that, the complete analysis, and the corresponding model will be useless.

In the existing body of literature, numerous imputation methods are available for addressing missing values. Nonetheless, all of these methods necessitate the prior identification of the missingness type and its corresponding statistical distribution before implementation. To determine the specific missingness type for each feature, various beneficial tests or plots can be utilized.

#### 2.3.1. Identifying Missingness Type

Each methodology offers distinct advantages. For instance, the independent t-test detects missing completely random behaviour. On the other hand, the correlation test suits the missing at not random behaviour. Similarly, the KNNImputer proves robust for missing at random behaviour. Furthermore, the incorporation of an msno matrix plot provides a visual representation of missing value distribution per feature. This plot facilitates assessing missingness patterns and identifying trends or clusters within the data structure.

##### 2.3.1.1. Independent T-Test

The independent t-test assesses if there's a significant mean difference between two groups. It calculates a t-statistic by dividing the difference in sample means by the standard error. This t-statistic is compared to a critical value from the t-distribution to gauge significance. The null hypothesis assumes no mean difference, while the alternative suggests a significant one. In this analysis, the null hypothesis is about feature independence in missingness patterns. A lower p-value indicates stronger evidence against the null, supporting group differences. In this context, the null hypothesis pertains to independence of missingness types, positing no systematic relationship between them.

### 2.3.1.2. Correlation Test

The purpose of this analysis is to investigate correlations among missing values. Correlation coefficients, ranging from -1 to 1, are computed to measure the strength and direction of relationships. A coefficient of 1 indicates a strong positive correlation, -1 denotes a strong negative correlation, and values close to 0 represent weak or no correlation. By examining the correlation coefficients, insights into the strength and direction of relationships among the features can be gained. Correlation coefficients close to 1 or -1 indicate strong positive or negative correlations, respectively, suggesting the presence of systematic dependencies in the missingness of features, rather than random characteristics.

### 2.3.1.3. KNNImputer

KNNImputer can be used to handle missing values. This method imputes missing values by leveraging information from nearest neighbors. The imputation process calculates correlations between original and imputed values to evaluate their similarity. KNN imputation estimates missing values based on the assumption that nearby data points exhibit similar values. It involves computing distances between observations and determining the k-nearest neighbors for imputation. The resulting correlation coefficient indicates the success of imputation, with a value close to one indicating a strong positive correlation. This suggests that imputed values closely resemble the true values and implies missingness at random.

### 2.3.2. Imputing Identified Data

In order to handle missing values in datasets, various imputation methods are employed. Each method has its own approach and assumptions based on the type of missingness and the relationships between variables. Two commonly used imputation methods are the KNNImputer for the Missing Not at Random (MNAR) mechanism and the IterativeImputer for the Missing Completely at Random (MCAR) mechanism. These methods aim to estimate missing values by leveraging information from observed variables or through iterative regression modelling, respectively.

#### 2.3.2.1. KNNImputer

The KNNImputer is a technique used to address missing values under the MNAR mechanism. It relies on the assumption that similar observations exhibit similar values. The code employs the concept of nearest neighbours to impute missing values. By calculating the distances between observations using measures like Euclidean distance or cosine similarity, the k-nearest neighbours are determined. The values of these neighbours are then utilized to impute the missing values.

The KNNImputer method allows for the imputation of missing values by incorporating information from other observed variables. It leverages the relationships

between variables to estimate the missing values. This approach is particularly useful when the missingness of variables is related to unobserved data and can assist in addressing the MNAR mechanism.

#### 2.3.2.2. IterativeImputer

The IterativeImputer method imputes missing values assuming MCAR mechanism. It uses an iterative regression-based approach. Missing values start with an initial guess (mean, median, random). Each variable is iteratively treated as target with others as predictors. A regression model trained on observed values predicts missing ones. This process refines imputations iteratively. Considering variable dependencies and regression, IterativeImputer improves accuracy over simple methods. It assumes MCAR where missingness is not related to unobserved data. This incorporates relationships for reliable imputations under MCAR.

### 2.4. Feature Selection

Feature selection is a vital aspect of machine learning, involving the identification and extraction of the most informative features from a dataset. It improves prediction accuracy, reduces overfitting, and enhances model interpretability. By selecting relevant features and discarding irrelevant ones, feature selection techniques help in reducing dimensionality and improving computational efficiency. They contribute to the generalizability of machine learning models by focusing on the most influential factors. In addition to improving model performance, feature selection saves computational resources and aids in model interpretability, making it a crucial step in the machine learning pipeline. To accomplish a solid model, three different approaches are going to be used; these are the correlation matrix plot, the lasso regression test, and the analysis of variance (ANOVA) test.

#### 2.4.1. Correlation Matrix Plot

The correlation matrix and heatmap provide insights into variable relationships within a dataset. Values close to 1 indicate positive correlations, while values near -1 suggest negative correlations. Values around 0 indicate weak or no linear relationship. Analyzing these visualizations helps identify patterns, dependencies, and potential multicollinearity, enhancing dataset understanding. While strong positive or negative correlations may not always indicate meaningful relationships, careful examination of the data ensures validity and significance of these correlations.

#### 2.4.2. Lasso Regression Test

The Lasso regression is a linear regression technique that incorporates regularization by introducing a penalty term to the loss function. This penalty, implemented through L1 regularization, encourages sparsity in the coefficient estimates. By driving the coefficients of irrelevant or less important features towards zero, the

Lasso regression aids in identifying and selecting the most relevant features. The resulting feature importance derived from the Lasso model provide insight into the relative importance of each feature in predicting the target variable. Higher absolute values indicate greater importance, enabling researchers to prioritize the most influential features in their analysis.

#### 2.4.3. ANOVA Test

The ANOVA test is a statistical method that measures the relationship between a categorical target variable and continuous features. It calculates the F-statistic and p-value for each feature, determining if there is a significant difference in means across target variable levels. Features with higher F-statistic scores and lower p-values are considered more relevant. The code selects the top K features based on ANOVA scores to predict the average downhole temperature.

### 2.5. Machine Learning Model

In machine learning, various techniques and algorithms play a significant role in model development and optimization. This introduction highlights some key methodologies that contribute to model evaluation, performance enhancement, and predictive accuracy. These techniques include cross-validation, hyperparameter tuning, pipeline construction, and specific algorithms like linear regression, random forest regressor, gradient boosting, support vector regressor (SVR), and extreme gradient boosting (XGBoost). Each of these approaches has its unique logic and application, enabling researchers and practitioners to build robust and accurate machine learning models.

#### 2.5.1. Cross Validation

Cross-validation is a technique to evaluate a model's performance and estimate its generalization ability. It divides the data into subsets (folds) to simulate performance on new data. The model is trained on one subset and evaluated on the other, repeating this process multiple times. Averaging the results provides a reliable assessment of the model's performance, helps detect issues like overfitting, and enables model tuning. Cross-validation reduces reliance on a single train-test split, providing a more robust estimate of performance.

#### 2.5.2. Hyperparameter Tuning

Hyperparameters are adjustable parameters set before training a model that are not learned from the data. Hyperparameter tuning aims to find the best combination of values to optimize model performance. It systematically explores different hyperparameter values and selects those that yield the best evaluation metric. Tuning hyperparameters improves model performance, enhances predictions, and increases generalization ability. It ensures the model is optimized for the specific problem by accounting for the significant impact of different hyperparameters on the model's behavior and

predictive power.

#### 2.5.3. Pipeline

A pipeline in machine learning is a sequence of data processing steps combined into a single workflow. It allows you to conveniently chain together multiple data preprocessing and modeling steps. The logic behind a pipeline is to ensure that the data transformations applied during preprocessing are consistently applied to both the training and testing data. This prevents information leakage and ensures that the model is trained and evaluated on the same types of data transformations.

#### 2.5.4. Linear Regression

Linear regression is a linear approach to modeling the relationship between a dependent variable and one or more independent variables. The logic behind linear regression is to find the best-fitting line that minimizes the difference between the observed data points and the predicted values on a continuous scale. It assumes a linear relationship between the independent variables and the dependent variable. The general idea behind the linear regression is to coefficients of the correlations. This is done by ordinary least squares (OLS) or gradient descent techniques.

#### 2.5.5. Random Forest Regressor

Random Forest Regressor is an ensemble learning method that combines multiple decision trees to make predictions. The logic behind random forest regression is to create an ensemble of decision trees, where each tree is trained on a random subset of the features and data samples. The predictions from individual trees are then averaged to obtain the final prediction.

#### 2.5.6. Gradient Boosting

Gradient Boosting is another ensemble learning method that combines multiple weak learners (typically decision trees) to make predictions. The logic behind gradient boosting is to sequentially train new models that focus on reducing the errors made by the previous models. Each new model is trained to predict the residuals (the difference between the observed and predicted values) of the previous models.

#### 2.5.7. Support Vector Regressor (SVR)

SVR transforms the data into a higher-dimensional feature space using a kernel function. It then finds the hyperplane that maximizes the margin around the support vectors while allowing for errors within the specified tolerance. The objective function of SVR involves minimizing the empirical risk (error) and maximizing the margin.

### 2.5.8. Extreme Gradient Boosting

XGBoost (eXtreme Gradient Boosting) is an optimized implementation of the gradient boosting algorithm. The logic behind XGBoost is similar to gradient boosting, where weak learners are sequentially combined to form a strong learner. However, XGBoost incorporates several enhancements, such as regularization techniques and parallel processing, to improve performance and accuracy.

### 3. OBSERVATIONS

Upon careful data analysis and statistical examinations, several important observations emerge. Figure 1 shows that gas production surpasses oil and water production, indicating gas as the predominant phase in the reservoir. Additionally, Figure 2 suggests a slight increase in oil production after 2013, potentially indicating the implementation of enhanced oil recovery operations.

The examination of variable distributions reveals distinct patterns. Figure 3 illustrates that Average Downhole Pressure closely resembles a normal distribution with slight left-skewness. Similarly, Figure 4 displays the distribution of Average Annulus Pressure, which also exhibits a normal distribution with a slight left-skewness. Figure 5 demonstrates the lognormal distribution of Average Wellhead Pressure, indicating right-skewness. Furthermore, Figure 6 shows that Average Wellhead Temperature follows a lognormal distribution with left-skewness.

The imputation process successfully filled missing values while preserving data patterns. The imputation process for Average Differential Pressure Tubing revealed some challenges when comparing the statistics before and after imputation in Table 1 and Table 2. However, the density plot in Figure 7 showed a slight increase in kurtosis and similar skewness. Additionally, the boxplot in Figure 8 indicated the absence of outliers and unchanged whisker lengths, further confirming the success of the imputation process.

Regarding feature selection for the machine learning model, the correlation matrix indicates the significant effects of Average Downhole Pressure, Average Wellhead Temperature, and Differential Pressure of Tubing on Average Downhole Temperature. Similarly, the Lasso Regression highlights the importance of Average Downhole Pressure, Gas Production Volume, Average Annular Pressure, and Average Wellhead Temperature in predicting Average Downhole Temperature. Furthermore, the ANOVA test identifies Average Downhole Pressure, Differential Pressure of Tubing, Differential Pressure on Choke, Oil Production Volume, and Gas Production Volume as influential features for predicting Average Downhole Temperature.

The Random Forest Regressor with  $n\_estimators=300$  emerges as the best model for predicting average downhole temperature. The model metrics, including RMSE, cross-validation RMSE, MAE, and r-square, indicate successful performance, demonstrating the model's ability to accurately predict the target variable.

In conclusion, the observations reveal the dominance of gas production, potential enhanced oil recovery operations, and the influence of various parameters on average downhole temperature. The imputation process successfully handled missing data, while the selected features and the Random Forest Regressor exhibited excellent performance in predicting average downhole temperature.

### 4. RESULTS

The Results section provides a concise summary of the main findings obtained from the analysis and experiments conducted. The findings are presented in a logical and organized manner, using appropriate tables, graphs, or figures to support the results. The machine learning model developed in this study, the Random Forest Regressor with 300 estimators, demonstrated excellent performance in predicting average downhole temperature. The model metrics, including an RMSE of 1.619, cross-validation RMSE of 1.446, MAE of 0.309, and an R-squared value of 0.99871, indicate its accuracy and predictive capability. The Random Forest Regressor model's fit is illustrated in Figure 9.

The developed model's prediction is applicable to the following scenarios:

- Offshore fields: The model can be utilized for temperature estimation in offshore petroleum fields, taking into account the specific characteristics and challenges associated with offshore operations.
- Production wells: The model is suitable for predicting bottomhole temperatures in production wells, providing valuable insights for optimizing production and ensuring safety.
- Known parameters: The model requires known parameters such as Average Downhole Pressure, Average Differential Tubing Pressure, Differential Pressure on Choke, Oil Production Volume, Gas Production Volume, and Average Wellhead Temperature. Incorporating these parameters enhances the accuracy and reliability of the temperature predictions.
- Wells with three-phase production: The model is designed to estimate temperatures in wells that produce three phases: oil, gas, and water. This consideration enables the model to account for the complexities and interactions among these phases.
- Saturated reservoirs: The model's prediction is specifically applicable to reservoirs in which saturation occurs, allowing for more accurate temperature estimation in these types of reservoirs.

These findings provide valuable insights into the applicability and scope of the developed machine learning model. By considering offshore fields, production wells, known parameters, three-phase production, and saturated reservoirs, the model can contribute to optimizing production processes and ensuring operational safety in the petroleum industry.

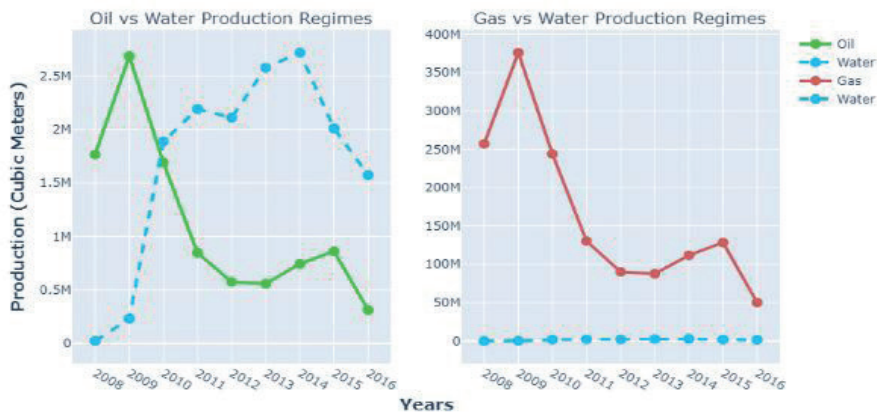
It is important to acknowledge that while the developed model demonstrates promising performance, there

are certain limitations and potential areas for future research. Further validation and testing in diverse offshore fields and production settings are necessary to ensure the model’s generalizability. Additionally, exploring additional features and incorporating advanced modeling techniques may enhance the model’s accuracy and expand its applicability.

In conclusion, the Results section presents the main findings of this study, highlighting the successful performance of the Random Forest Regressor model in predicting average downhole temperature. The model’s applicability to offshore fields, production wells, known parameters, three-phase production, and saturated reservoirs offers valuable insights for the petroleum industry. Further research and validation are recommended to refine and enhance the model’s capabilities.

Keywords: Machine Learning, Predictive Model

Figure 1



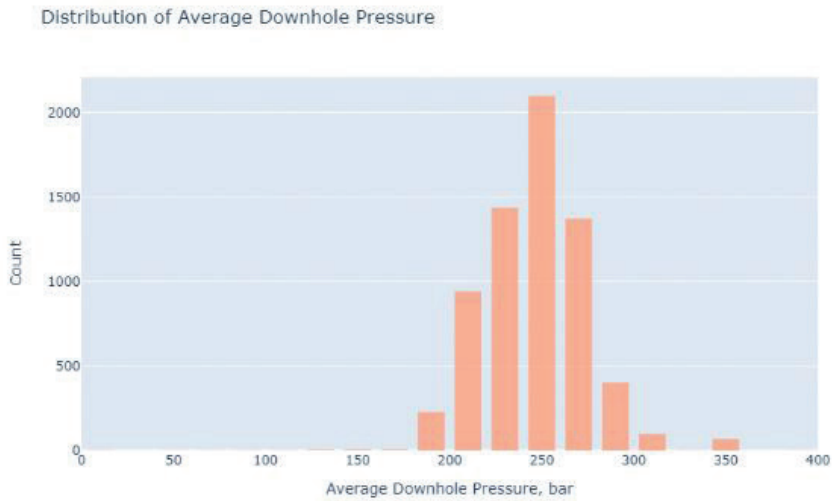
Oil vs water production, and gas vs water production as a function of time.

Figure 2



Oil production peaks and its decline curve as a function of time.

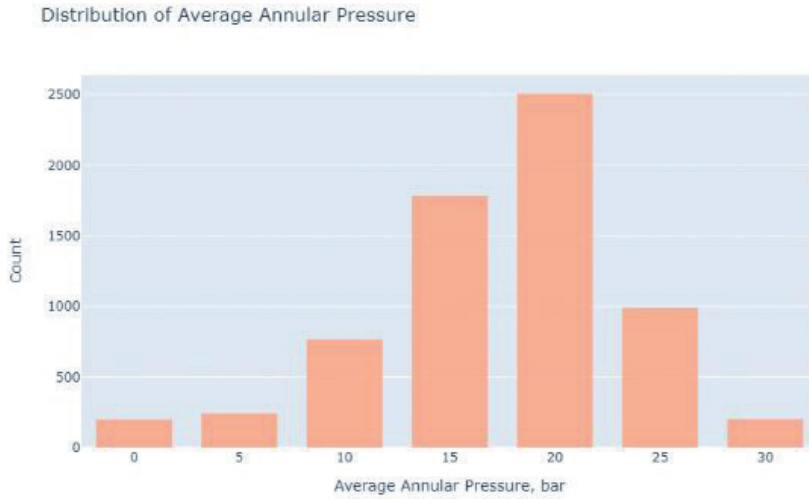
Figure 3



Distribution plot of average downhole pressure.

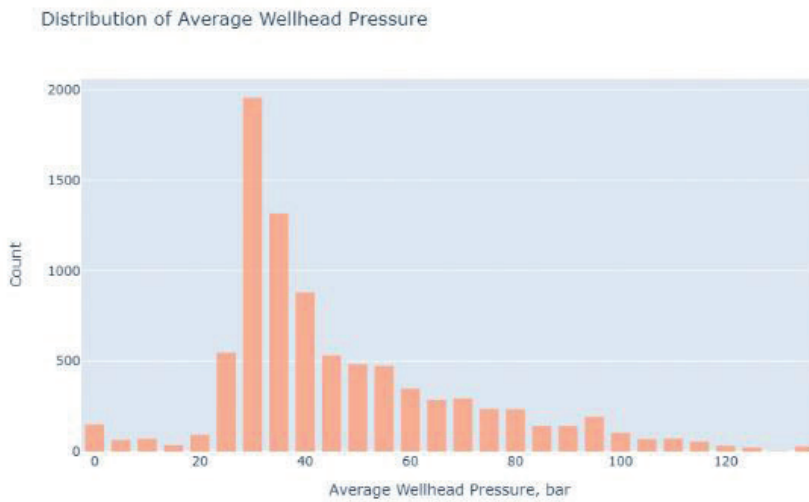


Figure 4



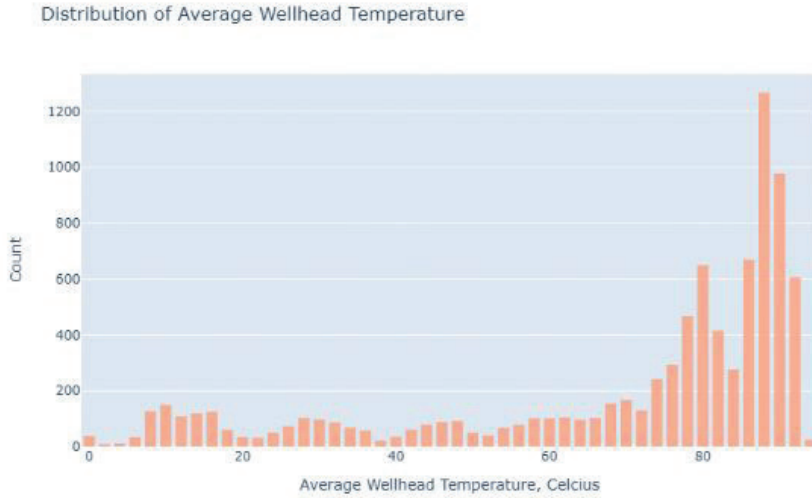
Distribution plot of average annular pressure.

Figure 5



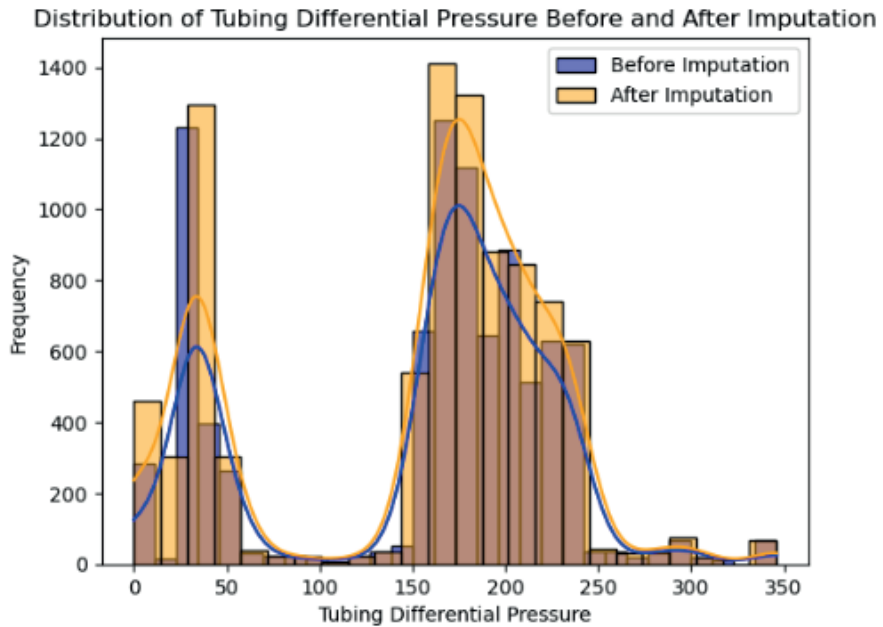
Distribution plot of average wellhead pressure.

Figure 6



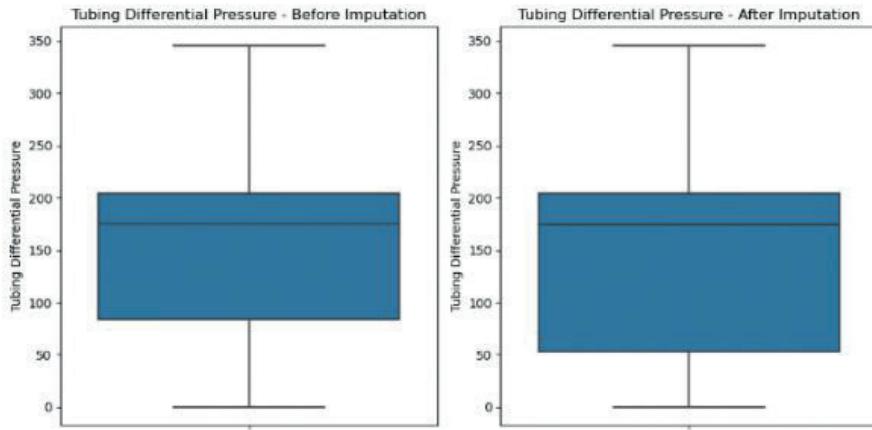
Distribution plot of average wellhead temperature.

Figure 7



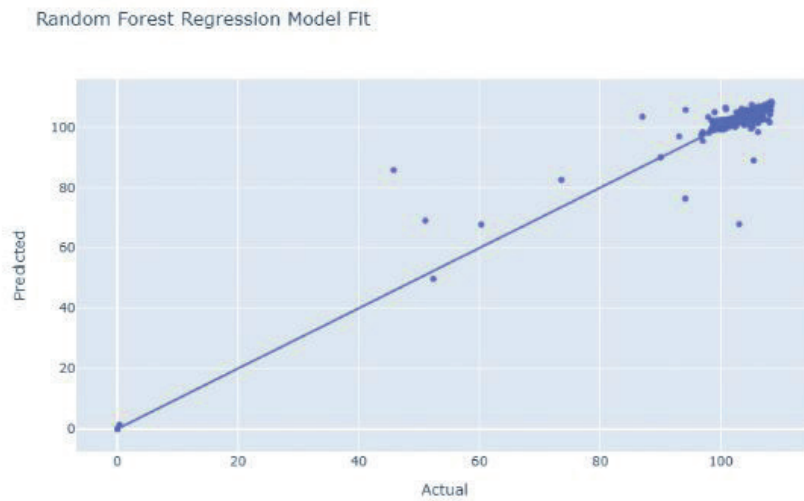
Distribution and density plot of tubing differential pressure before and after data imputation.

Figure 8



Statistical plot of tubing differential pressure before and after data imputation.

Figure 9



Plot of best machine learning model fit.

Table 1

	AVG_DOWNHOLE_ PRESSURE	AVG_DOWNHOLE_ TEMPERATURE	AVG_DP_ TUBING	AVG_ WHP_P	AVG_ WHT_P	DP_CHOKE_ SIZE	AVG_ANNULUS_ PRESS
Count	6668	6668	8792	8876	8844	8692	6686
Mean	244.84	103.91	157.32	46.8	70.04	56.61	17.53
Standard Deviation	27.83	5.18	74.15	23.77	25.15	36.05	6.04
Minimum	0.86	0.35	0.06	0.00007	0.00002	0.000143	0.00002
25%	223.83	101.25	150.11	31.63	61.2	22.9	13.98
50%	245.01	105.7	176.53	38.7	80.44	53.3	18.9
75%	262.45	106.46	204.83	58.3	88.15	99.99	21.81
Maximum	397.58	108.5	345.91	137.31	93.51	100	30.02

Statistical property summaries before the data imputation.

Table 2

	AVG_DOWNHOLE_ PRESSURE	AVG_DOWNHOLE_ TEMPERATURE	AVG_DP_ TUBING	AVG_ANNULUS_ PRESS	AVG_CHOKE_ SIZE_P	AVG_ WHP_P	AVG_ WHT_P	DP_CHOKE_ SIZE
Count	5415	5415	5415	5415	5415	5415	5415	5415
Mean	242.31	104.32	192.67	17.04	49.26	49.65	67.77	21.70
Standard Deviation	25.36	4.26	29.59	5.4	34.85	23.1	23.17	21.58
Minimum	1.93	0.35	7.22	0.00002	0.000143	0.00009	0.99	0.0038
25%	220.81	101.14	168.89	13.95	12.44	31.45	57.36	3.34
50%	244.79	105.91	183.71	15.75	45.88	42.19	77.74	14.11
75%	261.73	106.52	218.88	21.53	84.95	65.32	86.2	33.81
Maximum	317.67	108.5	314.133	30.02	100	125.5	92.07	111.52

Statistical property summaries after the data imputation.

# Application of CT in Reservoir Characterization

**Efe Ereğ**

Geological Engineering, Middle East Technical University, Ankara / Türkiye



## INTRODUCTION, PROBLEM DEFINITION

The scope and purpose of this report is to introduce Core Tomography (CT) and its applications in reservoir rock characterization. CT scan provides high resolution images of core sample, which are constructed by measuring bulk density and effective atomic number of specific minerals without direct contact with the core. CT scan uses two energy level while measuring these two parameters, which are 140 KeV to measure bulk density and 80 KeV to measure effective atomic number.

One of the most important issues in reservoir rocks, deterioration of the core while taking core plug and losing of energy and money. Moreover, knowing the porosity and permeability characters of the reservoir rock from bottom to top is hard to predict from the investigation of thin section samples because of the scaling problem. However, approximately for 500 slices of images per 1 foot are provided by the help of CT scan. Thus, it significantly contributes prediction on porosity and permeability by visualization of internal structure of the rock sample.

Previous studies and algorithm of the application

CT scan uses specific part of the electromagnetic spectrum, which is X-Ray to construct cross sectional image. Multiple projections of the object reconstruct the internal structure of the object. Generally 500 X-Ray slices per foot is utilized in medical CT scans. For each direction of the X-Ray beam, the scanner effectively records the X-Ray adsorption by the core sample.

Then, software is used to compute the brightness of each pixel from the all recordings.

The parts of the CT scan is subdivided into gantry, data acquisition system and operating console. Gantry includes X-Ray tube, slip ring, detector array and collimator. Data acquisition system consist of interaction of the X-ray photons with the detectors and detection of the intensity in the form of current, current is converted to voltage, analog integrator removes spikes, conversion of analog data to digital data, lastly, data can be processed and reconstructed in the computer. Operating console includes set scan parameters, computers and monitors, and the console is protected by lead-shielded walls due to the exposure of threaten levels of radiation energy. Gantry includes two important tool, collimator and detectors.

Collimator is fan shaped exposure reducer, also remove the scattered photons as well as control slice thickness. Detectors capture the energy that is not attenuated by the sample.

The spatial resolution of the object is determined by the size and number of detector elements, the size of X-Ray focal spot, the source of object-detector distance and the

size of the pixel array used to reconstruct the image.

Theory of the CT scan can be introduced by the slice element, which is determined by the width of the X-ray beam and represents the smallest part of the constructed object as a 3D element. Then, matrix follows, which is grid like pattern of the surface of candidate image.

Pixel is the square element of the matrix, and voxel is the 3D element of the matrix where the thickness of the slice is taken into account. Another important term is the CT number determined for each pixel and gives a unique color depending on the windowing property (which also depends on the bit size of the data). Windowing is the CT number range of interest cover the full grey scale in display systems, and by windowing width, contrast of the image is represented; by the window level, brightness of the image is represented. Reproduction of an image from raw data. Image production is provided by filtered back projection (Scan data/matrix form to digital image, then digital to analog conversion to display). Single transmission measurement through the rock sample in a given unit of time by detector is called Ray. Series of ray that passes through the same orientation is called a projection. CT scanner hardware purpose on acquire large number transmission measurements through different orientations.

Representation of transmission measurements (X-ray attenuation) is provided by grid like pattern, matrix. Display matrix is generally 512x512 or 1024x1024 pixel. Lambert's law of absorption, attenuation coefficients can be found. Attenuation coefficient for each voxel is calculated by reconstruction process, then CT number is calculated by following formula.

$$CT\ Number = 1000(\mu_t - \mu_x) / \mu_x.$$

There are some artifact of the CT scan images, which are beam hardening, partial volume and metal streak artifacts. Beam hardening can be expressed by greater attenuation in low energy ray. Partial volume is a result of wrong calculation of the average density for a specific thickness and apply it for another material which has a different thickness. Lastly, metal streak artifact is huge problem for image quality, because of the high density of the metallic minerals, the presence of them cause huge brightness in the image.

## DISCUSSION AND CONCLUSION

To sum up, by the help of CT scan principles which is highly related to provide information about some important geological parameters such as core characterization, fracture characterization, quick preview of the core tubes for sample selection, comparison of FMI/5cm resolution resistivity based log and CT/3mm resolution can be done. Bedding, mineralogical and lithological differences, invasion of

high density mud solids, fractures can be identified by CT before the core is removed from the liner. Aids core orientation when taking plug sample and rapidly and easily evaluates core damage and core heterogeneity.

Porosity Measurement Using Dual-Energy Data can be provided theoretically. Comparison with log data, such as RHOB and photoelectric log can be correlated with dual energy data.

Fluid flow visualization can be characterized before mercury injection or saturation experiments.

**REFERENCES**

- Effective atomic number and density determination of rocks by X-ray microtomography, Eduardo Inocente Jussiani, Carlos Roberto Appoloni, 9 June 2014
- Computed tomography in petroleum engineering research, S. AKIN & A. R. KOVSCEK, September 17, 2016
- Developments in Petroleum Science, Colin McPhee, Jules Reed, Izaskun Zubizarreta, Vol. 64. 2015
- Dual-Energy CT –Scanning Applications in Rock Characterization, Shamem Siddiqui, SPE, and Aon A. Khamees, Saudi Aramco R&D Center, Dhahra, KSA, 2004

Keywords: Reservoir Characterization, Core Tomography

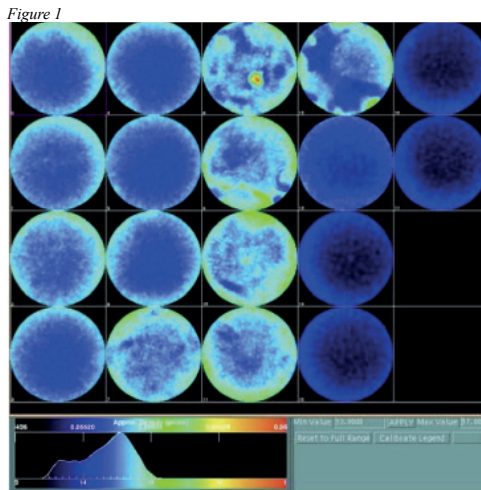


Figure 1  
Cross sectional image of the core is constructed by computation of effective atomic number of materials

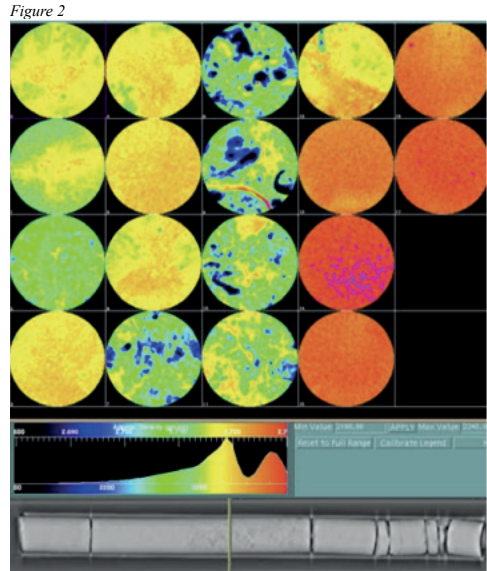


Figure 2  
Cross sectional image of the core is constructed by computation of bulk density of materials

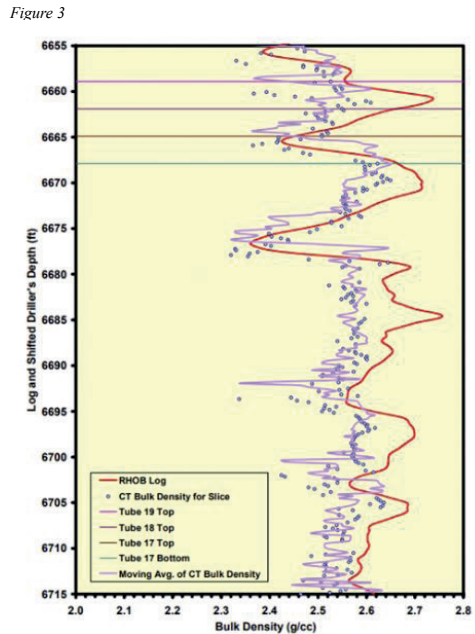
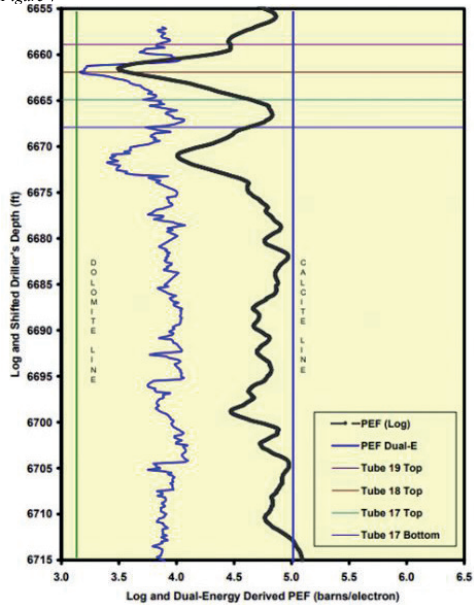


Figure 3  
Comparison of RHOB log and the data is gathered from the CT that is depend on the bulk density

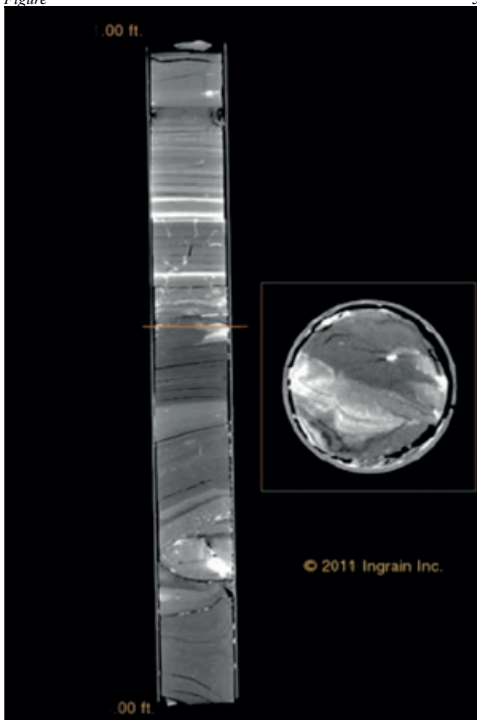
Figure 4



Comparison of PEF log and the data is gathered from the CT that is depend on the effective atomic number

Figure

5



3D cross sectional slice viewer

# Energy Transition

**Yaren Esra Kahya**

Petroleum and Gas Engineering, Istanbul Technical University, Istanbul / Türkiye



The energy transition is the process of transitioning from fossil fuels to renewable energy sources that are cleaner and more sustainable. This transition is important for reducing greenhouse gas emissions, reducing costs and improving environmental quality. The transition process has become mandatory due to factors such as global warming and depletion of fossil fuels in an environment of innovations day by day. Otherwise, humanity will have to face the climate catastrophe. Energy transformation is examined under two headings, in the world and in Turkey.

While the pace and extent of global energy change may differ between continents and nations, it is happening. Countries are researching to produce energy from renewable sources such as solar, wind, geothermal. The studies provide information about the roadmap to be followed. In addition, as a result of these researches, they are working for investments that will give up the fossil fuels that dominate the energy sector in the world. Renewable energy sources, unlike fossil fuels, are less harmful to nature as they are environmentally friendly. This is one of the most important reasons for the transition. Another reason why countries can keep up with this energy transition in the world is the climate change that people have to face today. Energy transition has become a necessity due to the fact that greenhouse gases that cause global warming are released to nature more in fossil fuels than in renewable energy sources. In this way, the future time of the expected climate crisis is postponed. By 2035, 8% of the world's energy needs are expected to be met by renewable energy consumption, which currently accounts for 3% of all energy consumption. According to the 2016 BP Energy Statistics Report, the amount of renewable energy used to generate electricity increased by 15.2%, and renewable energy sources now account for 6.7% of all energy produced globally. It is claimed that traditional energy production methods will change globally in the coming years with these data. In addition, the energy transition has economic benefits. Some of these are the decrease in costs, the decrease in dependence on imported energy with the decrease in costs, more energy efficiency, decrease in residential energy expenditures with increasing efficiency. In short, the energy transition for the environment and society has gained importance all over the world.

Today, Turkey meets most of the energy it needs today from fossil fuels such as coal and oil. Since Turkey is in a geopolitically important position, it acts globally within the framework of some agreements. This situation has to face some problems in supply and production in Turkey's export and import processes in the energy sector. In order to turn these difficulties into an advantage, it first gave importance to energy security. In addition, due to the geographical location of Turkey, some parts of the

country have more sunshine and wind speed in some parts. Owing to these, Turkey is a country that has the potential to produce energy sustainably through renewable energy sources such as solar, wind and geothermal. Although Turkey seems to be advantageous in the production of sustainable energy from renewable energy sources, certain stations are required for the realization of energy production. The infrastructure of the country must be sound for the smooth operation of these stations. In the establishment of the infrastructure, countries should also allocate a special budget for this issue. Although Turkey started its studies a little late, it tries to keep up with the innovations brought by this development in the world where the needs change. Turkey accepted the Paris Agreement and set a goal of having zero carbon emissions by the end of 2053. As it can be understood from here, Turkey is in an energy transformation in order to reach zero emissions. While Turkey is getting used to renewable energy, it should take necessary precautions for energy efficiency in order to use the consumed energy effectively and to reduce waste. Encouraging the public to save energy helps to change the traditional perception of energy production. Through the incentives, the energy transition for Turkey becomes easy. Supportive policies affect Turkey's global attitude.

People live in a time when the effects of climate change are increasing day by day. In order to minimize these effects, the transition to sustainable energy sources has become mandatory both in Turkey and in the world. The change in energy is visibly evident in every region of the world, especially in the countries that dominate the world energy sector. International cooperation facilitates the transition to sustainable resources. On the other hand, Turkey, has more opportunities for transformation due to reasons such as its strategic location and diversity of resources. Being aware of this, the Turkish state uses this advantage in its own favor. Taking advantage of renewable energy sources and producing them sustainably will ensure that the energy transition in the world and in Turkey will be cleaner and social activity.

Keywords: Energy, transition



# Türkiye’de Buhar ve Karbondioksit Enjeksiyonu. Faydaları ve Zorlukları



**Mehmet Mertcan Doğan**

İzmir Katip Çelebi Üniversitesi, Petrol ve Doğalgaz Mühendisliği, İzmir / Türkiye

## **Buhar ve Karbondioksit Enjeksiyonu: Faydaları Zorlukları**

Buhar ve karbondioksit enjeksiyonu, petrol ve gaz sektöründe önemli bir rol oynayan yenilikçi tekniklerdir. Bu teknikler, enerji kaynaklarının geri kazanımını artırmak, petrol ve gaz üretimini artırmak için kullanılmaktadır. Türkiye’de de buhar ve karbondioksit enjeksiyonu, önemli bir potansiyele sahiptir. Bu makalede, buhar ve karbondioksit enjeksiyonunun tanımı ve açıklaması, Türkiye’deki faydaları ve kullanım alanları ile olası zorlukları ele alınacaktır.

Steam and carbon dioxide injection are innovative techniques that play a significant role in the oil and gas industry. These techniques are used to enhance energy resource recovery and increase oil and gas production. In turkey, steam and carbon dioxide injection also hold substantial potential. This article will discuss the definition and description of steam and carbon dioxide injection, their benefits and applications in turkey, as well as potential challenges.

## **Türkiye’de Buhar ve Karbondioksit Enjeksiyonunun Avantajları ve Uygulamaları: Tanımlayıcı Bir Bakış**

Zengin enerji kaynakları ve büyüyen sanayi sektörü ile Türkiye, enerji üretimi ve endüstriyel süreçler için alternatif yöntemler araştırmaktadır. Önemli ölçüde dikkat çeken bu iki yöntem, buhar enjeksiyonu ve karbondioksit enjeksiyonudur.

Buhar enjeksiyonu, petrol geri kazanımını artırmak için rezervuarlara buhar enjeksiyonunu içerirken, karbondioksit enjeksiyonu, çeşitli amaçlar için yer altı oluşumlarına karbondioksit enjekte etmeyi içerir. Bu tekniklerin faydaları oldukça geniştir.

İlk olarak, buhar enjeksiyonu, daha önce erişilemeyen rezervlerin çıkarılmasına izin vererek, petrol geri kazanım oranlarını önemli ölçüde artırabilir. Ayrıca, hidrolik kırma gibi çevreye zarar veren tekniklere olan ihtiyacı en aza indirerek petrol çıkarmanın çevresel etkisini azaltabilir. Türkiye’de, buhar enjeksiyonu Ege bölgesindeki jeotermal enerji santrallerinde başarılı bir şekilde uygulanarak ülkenin yenilenebilir enerji hedeflerine katkıda bulunmaktadır.

Karbondioksit enjeksiyonu ise, sera gazı emisyonlarının azaltılmasına ve iklim değişikliğiyle mücadeleye yardımcı olurken aynı zamanda gelişmiş yağ geri kazanımı için de kullanılabilir. Türkiye’de karbondioksit enjeksiyonu, enerji üretimi, çimento üretimi ve çelik üretimi gibi önemli sektörlerde karbondioksit emisyonlarının azaltılması açısından büyük potansiyel taşımaktadır.

## **Zorluklar ve Gelecek İçin Bakış**

Türkiye’de buhar ve karbondioksit enjeksiyonunun potansiyel uygulamalarını değerlendirirken, bazı zorlukların da dikkate alınması gerekmektedir. Öncelikle, ülkenin jeolojik yapısı bu tekniklerin uygunluğunu etkilemektedir. Bazı bölgeler daha uygunken, diğerleri için farklı bir yöntem daha etkili olabilir.

Ayrıca, buhar ve karbondioksit enjeksiyonu için özel ekipman ve altyapı gerekmektedir. Bu nedenle, Türkiye’nin bu alanda yatırım yapması ve teknolojik altyapısını geliştirmesi önemlidir.

Ancak, bu tekniklerin potansiyel faydaları göz önünde bulundurulduğunda, Türkiye’nin sürdürülebilir enerji politikaları izlemesi ve buhar ve karbondioksit enjeksiyonunu teşvik etmesi önemlidir. Bu sayede enerji üretimi daha verimli hale gelebilir, çevre kirliliği azalır ve enerji bağımlılığı düşer.

Sonuç olarak, buhar ve karbondioksit enjeksiyonu, Türkiye’nin enerji sektöründeki dönüşümünü destekleyecek ve çevresel sürdürülebilirliğe katkı sağlayacak önemli tekniklerdir. Yüksek potansiyele sahip olan bu yöntemlerin, uygun stratejiler ve yatırımlarla ülkemizde yaygınlaştırılması ve kullanım alanlarının genişletilmesi gerekmektedir.

**Anahtar Kelimeler:** Buhar Enjeksiyonu, Karbondioksit Enjeksiyonu

# Steamflooding Interval Horizontal Wells

**Oğuzhan Ucar**

İzmir Katip Celebi University, İzmir / Türkiye



Horizontal wells are being employed because of the physical challenges of the reservoir or to access formations such as very viscous oils and bitumen. In steam injection operations for heavy oil recovery, horizontal wells may be needed to inject into the targeted interval. This paper, the effect of horizontal wells on steamflooding operations is discussed.

The cost of horizontal wells is higher than vertical wells in steam injection operations, but horizontal wells have been found to be more successful in terms of efficiency. Many research and papers have been published on steam injection using various horizontal-vertical well combinations. For example, Chang, Farouq Ali and George (Chang, H.L., Ali, S.M.F., and George, A.E. 1992. Performance Of Horizontal-Vertical Combinations For Steamflooding Bottom Water Formations.) used the five-point injection pattern to study steamflooding and found that a horizontal steam injector and a horizontal producer yielded the highest recovery.

Figure 1 shows that the horizontal producer-vertical injector (HPVI) combination yielded the lowest ultimate recovery of 48.5% while the horizontal producer-horizontal injector (HPHI) combination produced the highest recovery of 60.9%.

Horizontal producer-horizontal injection combination will be very costly. To be economic, the radial spread of heat and the Steam Assisted Gravity Drainage (SAGD) mechanism can be exploited. For example, in a recovery area using the five-point injection pattern, one injection well can be placed in the center of the four producer well intervals instead of four injection and one producer wells. The heat of the steam injected from the center will spread radially and reach the reservoir. At the same time, horizontal producer wells will be placed several feet below the reservoir. As the heavy oil or bitumen in the reservoir heats up, its mobility increases and is forced to move downwards by gravity. In this way, oil is collected in producer wells. Reducing the number of injection wells from four to one will improve the economy. A similar study was attempted in the Duri field in 1999. A seven-point injection pattern was used and the injection well was placed in the center, thereby improving the economy. (Sigit, R., Satriana, D., Peifer, J.P. et al. 1999. Seismically Guided Bypassed Oil Identification in A Mature Steamflood Area, Duri Field, Sumatra, Indonesia. Presented at the SPE Asia Pacific Improved Oil Recovery Conference, Kuala Lumpur, Malaysia, 25-26 October 1999.)

In summary, enhanced oil recovery techniques are applied to produce formations such as heavy oil or bitumen. Steamfloods is one of the most effective methods of these techniques and steamfloods give more successful results with the use of horizontal wells that have become common recently. As mentioned

in detail above, the highest recovery is yielded with the horizontal injector-horizontal producer. The cost increase of horizontal wells can be improved with a suitable model design.

Keywords: Steamflooding, horizontal wells

Figure 1. Comparison of the various injection-production strategies on ultimate oil recovery, for the different bottomwater cases investigated (after Chang, George, and Farouq Ali)

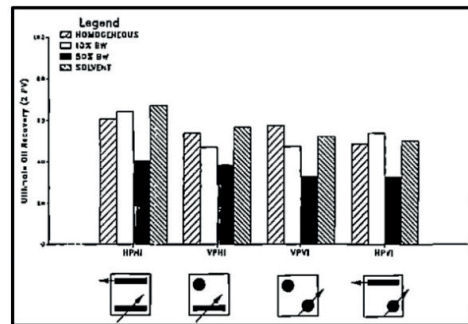
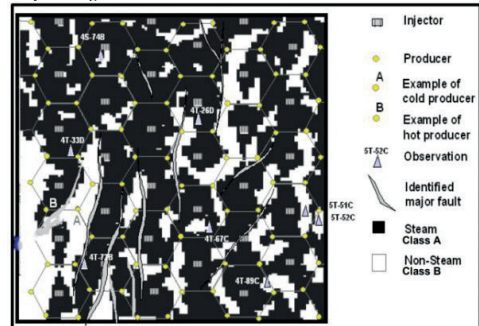


Figure 2. Steam map of the Pertama interval as a result of discriminant analysis using multi seismic attributes.



# Stimulation of a Tight Sandstone Reservoir Through Hydraulic Fracturing: Taylor Sandstone Case, Texas



**Muloh Gariba Sheron**

Near East University, Engineering Faculty, Nicosia, North Cyprus

## ABSTRACT

This research evaluates post-fracture vertical gas well performance in the Cotton Valley Sandstone Formation of Eastern Texas, USA. Fracpro fracture simulator was used to model a hydraulic fracture and a series of scenarios were run with different perforation lengths, fracturing fluids, and proppant types. Sixteen scenarios were used, and numerical results showed that Scenario 16 produced the best propped fracture geometry and dimensionless conductivity. After ten years of forecasting, scenario 16 with the highest recovery increased gas recovery from 13.56% to 63.68% with a flow rate of 110.6 Mscf/day.

## INTRODUCTION

There has been a drastic increase in the development and exploitation of unconventional resources during the last two decades. We have also seen a resurgence in oil and gas production in North America, because of technological breakthroughs in hydraulic fracturing, which allows natural gas and oil to be economically produced from unconventional shale plays, tight oil, and tight gas sandstones (Gharavi et al., 2022).

Hydraulic fracturing, first used in 1947, evolved into “slick water multistage horizontal stimulation” in 1998. This technique enabled low permeability reservoir production, leading to exploration of shale plays and tight sandstone formations worldwide. The industry now shifts from traditional high-permeability resources to unconventional resources like shale, which are easier to find but more challenging to generate their hydrocarbons (Belyadi et al., 2019).

One of the most important aspects of well completion is hydraulic fracturing. Hydraulic fracturing (HF) is the process of breaking up rock by applying high pressure rates and pumping sand, water, and specific chemicals in order to release the hydrocarbon. It reduces skin damage from drilling and increases the permeability of unconventional reservoirs. Tight sandstone reservoirs are known for having low permeability, to raise these reservoirs’ production levels, hydraulic fracturing is used (Belyadi et al., 2019).

Robinson et al. (1992) evaluated hydraulic fracture performance in Gas Research Institute (GRI) well 3 (Taylor Sandstone), using a single-layer model. Shaoul et al. (2016) applied a multilayer model to predict long-term gas production, confirming Robinson et al.’s conclusion that better fracture treatment designs and numerical simulation can increase gas production. This study aims to assess post-fracture vertical gas well performance (GRI Well 3) in Eastern Texas, USA using Taylor Sandstone reservoir data and Fracpro fracture simulator. The study compares the effects of different

fracturing fluid types, proppants, and perforation lengths on production.

Geology of Cotton Valley, Taylor Sandstone Reservoir (Stage Field Experiment Well 3)

Stage Field Experiment (SFE) Well 3 is one of the experimental wells drilled by the GRI. As shown in Figure 1, Well 3 is located in Harrison County, Texas in the Waskom field. In this area, the Taylor Formation is the dominant tight gas reservoir, which is mainly produced from petroleum traps associated with the Sabine arc and many other salt structures (Robinson et al., 1992).

Dutton et al. (1992) described the Taylor Sandstone as a thick upward coarsening sequence from the Upper Jurassic to the Lower Cretaceous period composed of shale at the base, bioturbated, fine-grained sandstones interbedded with siltstones and mudstones in the middle, and clean well-sorted sandstones at the top. This thick upward coarsening sequence was deposited as follows: shoreface, microtidal barrier island, lagoon and washover deposits, a second microtidal barrier island, tidal inlet, and marsh lagoon depositional environments in ascending order (Figure2).

## METHODOLOGY

Fracpro was used to model a vertical hydraulic fracture followed by production analysis. In Fracpro, the 3D user-defined model was used to simulate fracture growth behavior run from job design data. Taylor Sandstone is a multilayered reservoir as seen in Figure 3.

## RESERVOIR DESCRIPTION

Taylor Sandstone consists of shale, siltstone, and sandstone. The permeability of this reservoir is 0.0059 mD and has a subsurface depth of 9200 feet. The reservoir and PVT properties of this study are presented in Table 1.

## Scenarios Used for Simulator Input

Table 2 depicts the 16 Scenarios that were used in this study. Also, different injection rates were utilized for the two types of fracturing fluid (acid was used as a secondary fluid for slick water frac). Slickwater and HCL were injected at a rate of 80 barrels per minute (bpm) while hybrid gel (slickwater and 20% linear GW-32) was injected at a rate of 50 bpm, and the proppants used were 30/50 Ottawa sand and 30/50 Diamond light weight ceramic (LWC). Both primary and secondary fluid types have different viscosities; Slickwater-1.33cp, HCL-0.254cp, and 20% linear GW-32- 4.17cp.

## RESULTS AND DISCUSSIONS

In this study, perforation interval was defined by their lengths (perforation length) as follows; 9315-9335 ft (20 ft), 9225- 9265 ft (40 ft), 9270-9350 ft (80 ft), and 9215-9315 ft (100ft).

### Fracture Geometry Scenarios 1 to 4

Scenarios 1 to 4 utilized slickwater fracturing fluid and Ottawa sand. All four scenarios had different fracture geometries and dimensionless conductivities ( $C_{fd}$ ). Scenario 4 has the longest fracture half-length ( $x_f$ ) of 1604.6 ft, while Scenario 1 recorded the least  $x_f$  of 1220 ft.

### Fracture Geometry Scenarios 5 to 8

Slickwater and Diamond LWC were used for Scenarios 5 to 8. Scenario 8 has the highest  $x_f$  of 1573.3 ft. The shortest fracture half-length (1227.2 ft) was reported in Scenario 5.

### Fracture Geometry Scenarios 9 to 12

Scenarios 9 to 12 utilized hybrid fracturing fluid and Ottawa sand. Scenario 12 measured the longest  $x_f$  of 2680.5 ft. while Scenario 9 recorded the shortest frac half length of 1925.3 ft.

### Fracture Geometry Scenarios 13 to 16

Hybrid fracturing fluid and Diamond LWC were tested for Scenarios 13 to 16. Scenario 16 with a maximum  $x_f$  of 2718.4 ft, and the lowest  $x_f$  of 1933 ft was observed in Scenario 13.

Effect of Perforation Length, Fracturing Fluid, and Proppant on Fracture Geometry

Figure 6 (a) shows the plot of perforation length and fracture half-length for slickwater and hybrid frac treatments.  $x_f$  increases with an increase in perforation length. Scenario 16 produced the longest fracture half-length at a perforation of 100 ft. According to the simulation results, hybrid treatments resulted in longer fractures than slickwater treatments. The assumptions of Stokes' law can be used to explain this. Since the hybrid treatment comprises a linear gel, the viscosity of the fluid increases, limiting the proppant carrying capacity and assisting in moving the proppant further into the formation. Scenarios that employed Ottawa sand exhibited slightly longer fracture half-lengths than Diamond LWC for slickwater frac given that sand had a lower settling velocity than LWC. The reverse was true for hybrid frac, except for Scenario 11 which showed a longer half-length.

Figure 6 (b) displays simulation results for perforation length and fracture height using slickwater (sand/ceramic) and hybrid (sand/ceramic) fracturing fluids. Shorter perforation lengths increased formation friction, thereby pushing the hydraulic fracture upward reducing the pay zone and extending its height into the cap rock

regardless of frac fluid or proppant type. At longer perforations, the fracture is confined inside the reservoir interface. This impact is more severe in slickwater frac than in hybrid. Scenario 1 resulted in the tallest frac. In addition, Diamond LWC displayed taller fractures than Ottawa sand; due to the fact that sand has a somewhat lower density than LWC, it was expected that it would create a slightly larger frac owing to its low settling velocity.

Figure 7 (a) shows fracture widths for Scenarios 1 to 16 using different perforation lengths. However, hybrid treatments resulted in smaller fractures as perforation length increased. Because the formation could not accept higher injection rates for hybrid frac, it was impossible to calculate fracture width only on fluid viscosity. We may deduce that larger injection rates resulted in broader fractures since slickwater frac was injected at a higher pump rate. Perkins et al. (1961) discovered that fracture half-length can also impact fracture width; in this study, there is a relationship between fracture width and half-length (Figure 7 b). Fracture width was decreased in hybrid frac because longer fractures were formed; however, slickwater produced shorter fracs, which increased frac width.

### Effect of Proppant Types on Dimensionless Conductivity

According to Figure 8, Diamond LWC showed higher  $C_{fd}$ s than Ottawa sand, this demonstrates that ceramic proppants have controlled particle sizes and are spherical, resulting in higher conductivity than sand proppants, which have lower conductivity due to a wide range of shapes and sizes, leading to tight packing arrangements, limiting conductivity.  $C_{fd}$  was defined by Belyadi et al. (2019) "as the ability of fractures to transport reservoir fluid to the wellbore divided by the formation's ability to transmit fluid to the fractures" (Eq.1).

$$C_{fd} = k_f * w_f / k * x_f \text{ (Eq.1)}$$

Where  $k_f$ = fracture conductivity (mD. ft),  $w_f$ = fracture width (ft),  $k$ = formation permeability (mD),  $x_f$ = fracture half- length (ft).

## PRODUCTION FORECAST

Results from fracture analysis of each Scenario were simulated using production analysis mode in Fracpro in order to determine the Scenario with the highest cumulative production. The simulator utilized the propped fracture geometries and proppant concentrations to estimate a ten-year production period. The original gas in place (OGIP) is 2.13 BCF.

### Production Forecast Scenario 1 to 4

Scenario 4 resulted in a greater cumulative gas output of 1.218 BCF compared to other cases. This shows that a perforation length of 100 ft produced the best propped fracture geometry and  $C_{fd}$  of 9.306. When Scenarios 4, 3, 2, and 1 were compared gas production increased by

57.28%, 56.70%, 54.71%, and 54.15% respectively.

### Production Forecast Scenarios 5 to 8

According to the findings, Scenario 8 resulted in greater cumulative gas output and flow rate of 1.283 BCF and 129.9 Mscf/day, respectively. A perforation length of 100 ft resulted in better gas production. Comparing Scenarios 8, 7, 6, and 5 showed an increase in gas production by 60.32 %, 59.96%, 58.76%, and 56.75% respectively.

### Production Forecast Scenarios 9 to 12

Scenario 12 showed a higher cumulative gas production of 1.316 BCF and a flow rate of 124.3 Mscf/day. We can deduce that longer perforations yield a better increase in gas production. Scenarios 12, 11, 9, and 10 increased gas production by 61.86%, 60.4%, 59.71%, and 58.58% respectively.

### Production Forecast Scenario 13 to 16

Per the findings, Scenario 16 resulted in greater cumulative gas production of 1.354 BCF and a flow rate of 110.6 Mscf/day. Here perforation length of 100 ft produced the best fracture propped geometry with a  $C_{fd}$  of 18.906. When Scenarios 16,13,14, and 15 were compared, gas production increased by 63.687%, 63.58%, 62.84, and 61.58%, respectively. The propped fracture geometry and their corresponding cumulative gas production for all Scenarios is illustrated in Table 3.

The Taylor sandstone SFE Well 3 was also modeled in Fracpro with no hydraulic fracture, and it produced 288.3 MMscf of gas at a flow rate of 75.58 Mscf/day over ten years with a recovery factor of 13.56%.

## CONCLUSION

Hydraulic fracturing is an efficient technique for increasing productivity. The Cotton Valley Taylor sandstone reservoir is a low porosity, low permeability reservoir that requires specialized technology such as hydraulic fracturing to help generate its hydrocarbons. In this study, the parameters that influenced the attained cumulative production from the hydraulic fracturing process were explored and an optimized fracturing Scenario was proposed. The following conclusions were reached based on the research discussion.

The findings revealed that although production analysis depends on the propped fracture geometry and fracture conductivity, fracture geometry is dependent on the rock mechanical parameters, perforation interval (length), frac fluid type, and proppant type.

As perforation length increases, so does fracture half-length. In comparison to slickwater frac, hybrid fracturing fluid produces substantially longer fractures because it employed a more viscous fluid to help transport proppant. While hybrid treatment provided longer fractures when Diamond LWC was tested, the

usage of slickwater frac with Ottawa sand exhibited somewhat longer frac half lengths. At a perforation length of 100 feet, Scenario 16 yielded the longest frac half-length.

Shorter perforations increased formation friction, causing the hydraulic fracture to spread beyond the reservoir zone. This may reduce stimulation efficiency, resulting in proppant and frac fluid waste, and generate other environmental issues. As a result of the fracture's modest offset away from the pay zone, less gas was produced. The hydraulic fracture was contained at the longer perforations. Scenario 1 created the highest fracture with a perforation length of 20 ft.

In hybrid fracturing, increasing the perforation length resulted in smaller fractures whereas doing so in slickwater fracturing caused broader fractures. The widest fractures were generated by Scenario 6 with a perforation length of 40 feet.

Regardless of the type of frac fluid used, ceramic proppant showed a higher conductivity than sand proppant.

Higher injection rates (80 bpm) are required for slickwater treatment, whereas lower injection rates (50 bpm) are needed for hybrid frac.

Longer perforations improved gas output greatly because they provided a better propped fracture half-length.

With a longer propped fracture half-length and a narrower fracture, cumulative gas output increased.

Although the hybrid frac generated about twice as much as the propped frac half-length of slickwater, the gas output was not as spectacular as expected, most likely due to gel degradation. Gel residue tends to build at extremely small pore throats, reducing fluid flow capacity.

The estimated ultimate recovery (EUR) increased in all scenarios. Better propped fracture geometry and consequently increased productivity came from hybrid fracturing. Scenario 16 demonstrated that the design conditions for best production include an injection rate of 50 bpm, hybrid fracturing fluid, Diamond LWC, and a perforation length of 100 ft, resulting in the maximum increase in EUR. As a consequence, the ideal propped fracture geometry is: propped half-length = 2109.1 ft, propped height = 272 ft, fracture width = 0.339 in, and  $C_{fd}$  = 18.906. After ten years, Scenario 16 generated 1.354 BCF of cumulative gas output at a flow rate of 110.6 Mscf/day.

A thorough economic analysis should be conducted in order to determine the net present value of each scenario.

## REFERENCES

- Abaa, K. N. (2011). New stimulation technologies for ultra-tight gas sandstones. <https://etda.libraries.psu.edu/catalog/11769>
- Belyadi H., Fathi. E & Belyadi R. (2019). Hydraulic fracturing fluid systems. In H. Belyadi, E. Fathi & F. Belyadi (Eds.), *Hydraulic Fracturing in Unconventional*

Reservoirs (47-69). Gulf Professional Publishing. ISBN 9780128176658

Dutton, S. P., Laubach, S. E., Tye, R. S., Baumgartner, R. W., & Herrington, K. L. (1990). Geology of the Lower Cretaceous, Travis Peak formation, East Texas—depositional history, diagenesis, structure, and reservoir engineering implications. Contract, 5082-211.

Gharavi, A., Hassan, M., Zarehparvar Ghoochaninejad, H., Kenomore, M., Fianu, J., Shah, A., & Buick, J. (2022). Rejuvenation of a Mature Tight Sandstone Oil Reservoir through Multistage Hydraulic Fracturing: A Case Study of a North African Basin. *Oil Geomechanic*, 4(3), 59-89.

Perkins, T. K., & Kern, L. R. (1961). Widths of hydraulic fractures. *Journal of petroleum technology*, 13(09), 937-949.

Robinson, B. M., Holditch, S. A., Whitehead, W. S., & Peterson, R. E. (1992). Hydraulic fracturing research in East Texas: third GRI staged field experiment. *Journal of Petroleum Technology*, 44(01), 78-87.

Shaoul, J. R., Park, J., Berentsen, C., & Caballero, J. (2016, September). A new look at a famous well-analysis of Staged Field Experiment# 3 including stress sensitive permeability in a multi-layer reservoir simulation model. In SPE Annual Technical Conference and Exhibition? (p. D021S024R004). SPE.

Smith, D., Rogers, H., Ambrose, W. A., & Shuster, M. (2018). Oil and gas production in Texas. Bureau of Economic Geology. <https://www.beg.utexas.edu/files/content/beg/research/starr/Oil%20and%20Gas%20Map%20of%20Texas%202018.pdf>

Keywords: Hydraulic fracture productivity, treatment parameters

Figure 1. Location of GRI well 3 in east Texas (Robinson et al.,1992; Smith et al.,2018).

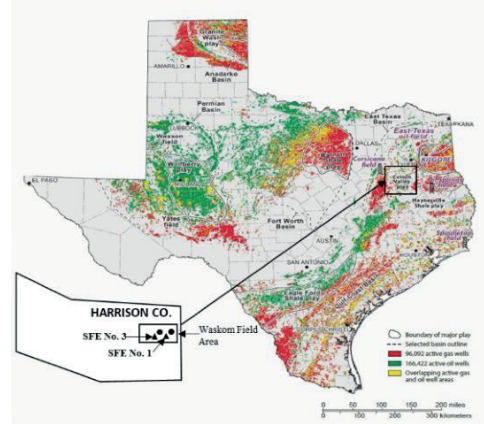


Figure 2. Log representation of Taylor Sandstone (Dutton et al., 1990).

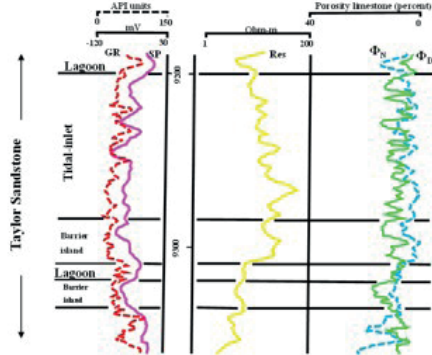


Figure 3. Lithology and log representation of layer properties of the Taylor Sandstone modelled by Fracpro.

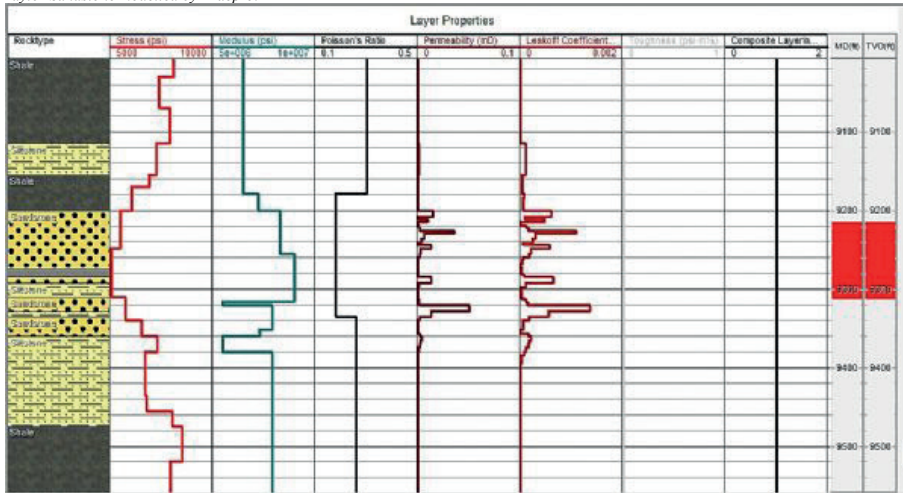


Figure 4. Concentration of proppant in fracture, Scenarios 4 (a) and 12 (b).

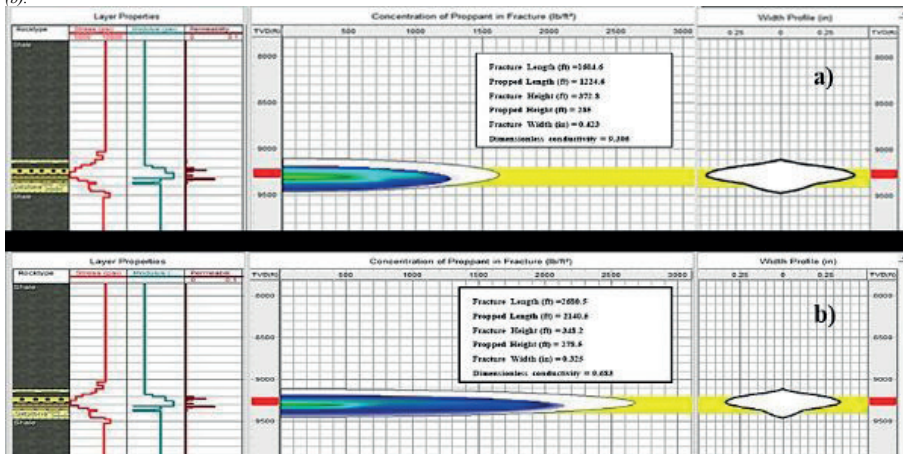


Figure 5. Concentration of proppant in fracture, Scenarios 8 (a) and 16(b).

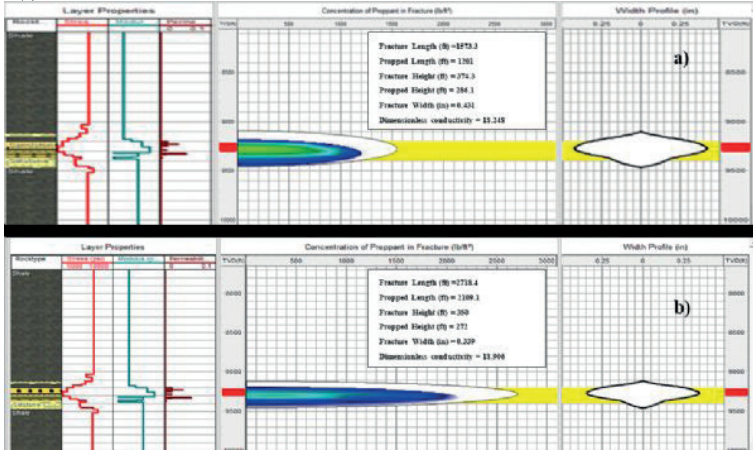


Figure 6. Perforation length vs. fracture half-length for 16 (a), perforation length vs. fracture height for different frac fluids and proppants (b).

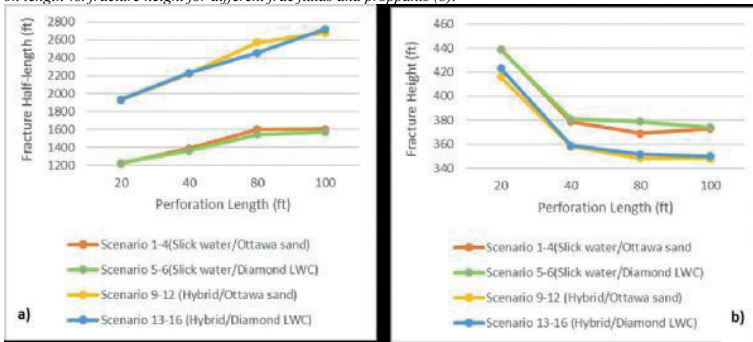


Figure 7. Perforation interval versus fracture width for different fracturing fluids and proppants (a), (b) cross plot of fracture width versus fracture half-length.

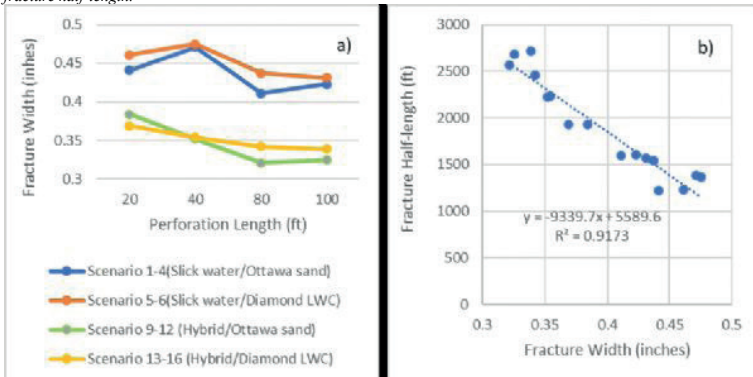




Figure 8. Proppant type vs. dimensionless conductivity for 16 Scenarios.

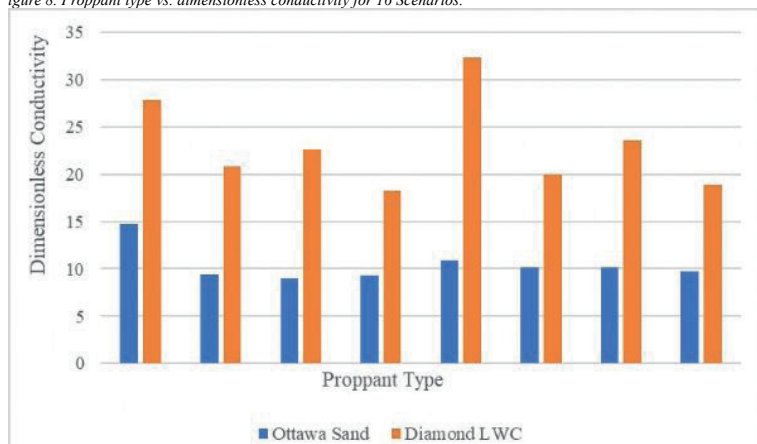


Figure 9. (a) cumulative production versus propped fracture half-length cross plot, (b) cross plot for cumulative production versus fracture width.

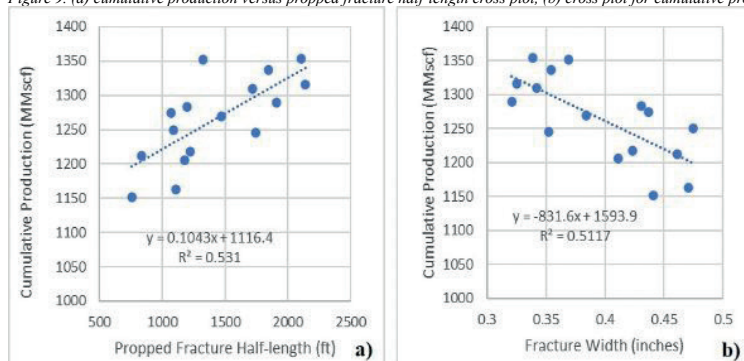


Table 2. 16 different scenarios used in this study.

Scenarios	Perforation interval (ft)	Slickwater	Hybrid	Sand	Ceramic
1	9315-9335	x		x	
2	9225-9265	x		x	
3	9270-9350	x		x	
4	9215-9315	x		x	
5	9315-9335	x			x
6	9225-9265	x			x
7	9270-9350	x			x
8	9215-9315	x			x
9	9315-9335		x	x	
10	9225-9265		x	x	
11	9270-9350		x	x	
12	9215-9315		x	x	
13	9315-9335		x		x
14	9225-9265		x		x
15	9270-9350		x		x
16	9215-9315		x		x

Table 3. Propped fracture geometries and cumulative gas production for 16 Scenarios.

Scenarios	Propped half-length (ft)	Propped height (ft)	Width (inches)	Cumulative production (MMscf)
1	758.9	273.5	0.441	1152
2	1109.1	303.2	0.471	1163
3	1178.9	272.8	0.411	1206
4	1224.6	285	0.423	1218
5	836.6	299.7	0.461	1212
6	1091.7	304	0.475	1250
7	1073	263.6	0.437	1275
8	1201	286.1	0.431	1283
9	1472.6	318.4	0.384	1270
10	1741.7	280.8	0.352	1246
11	1906.2	258	0.321	1290
12	2140.3	278.5	0.325	1316
13	1326	290.5	0.369	1352
14	1843.9	296.6	0.354	1337
15	1717.2	246	0.342	1310
16	2109.1	272	0.339	1354
No fac	-	-	-	255

Table 1. Reservoir/ PVT properties of Taylor Sandstone (Shaoul et al., 2016).

Parameters	Units	Values
Average permeability	mD	0.0059
Average porosity	%	3.5
Drainage area	Acres	177.5
Bottom hole temperature	°F	240
Reservoir pressure	Psi	3600
Surface temperature	°F	70
Water saturation	%	80
Gas viscosity	cp	0.03
Total compressibility	1/Psi	2.48 x10 <sup>-4</sup>
Reservoir thickness	ft	195

# Approximating Hydraulic Fracture Permeability Enhancement

**Onuralp Mete Yağmur**

GEOS Energy Inc.



An important parameter of assessing the success level of a hydraulic fracturing operation is to evaluate the increase of the permeability (Ge & Ghassemi, 2011). This paper introduces a straightforward approach to measure permeability enhancement through hydraulic fracture stimulation data.

## THEORY

Ge & Ghassemi (2011) introduced a method to measure enhanced permeability by matching the failed reservoir volume (FRV) with the stimulated reservoir volume (SRV) which is estimated from microseismic clouds.

With adequate modeling and stochastic approaches the FRV model can be used to determine permeability with higher accuracies. However, FRV model requires the fracture geometry to be known.

The model introduced by (Patel, Sondergeld, & Rai, 2018) eliminates the need to know the fracture geometry by hypothesizing that; the pressure data recorded during hydraulic fracturing might be used to estimate the permeability.

This research is based on the theory that the drop in the injection pressure just after the breakdown during hydraulic fracturing occurs due to the flow of injected fracturing fluid inside the induced hydraulic fracture.

In theory the pressure drop (part which is highlighted in red) is due to the injection fluid flowing inside the hydraulic fracture.

## GOVERNING EQUATIONS

As a simplifying assumption the source of diffusion is an infinite line source located at the center of the sample.

In this case, the pressure will obey the 1D diffusion equation.

## TEST RUN

A MATLAB script was written using the governing equations of pressure drop model.

A sensitivity analysis was made based on frack fluid viscosity and dynamic diffusivity, and it was observed that enhanced permeability has linear relationship with hydraulic diffusivity and injected fluid viscosity.

## COMMENTS AND CONCLUSIONS

- Pressure drop model provides much more reliable and concrete results compared to FRV model since it does not deal with uncertainties related to fracture geometry.
- Pressure drop model is easier to use and model.

According to pressure drop model:

- Higher hydraulic diffusivity yields higher permeability.
- Fracking fluid viscosity has major effect on the created permeability, and higher viscosity yields higher permeability.

The minimum horizontal stress will determine the fluid diffusion inside the fracture. A higher stress value will result in less diffusion, which will reduce the estimated value of fracture permeability (Patel, Sondergeld, & Rai, 2018).

## ACKNOWLEDGEMENTS

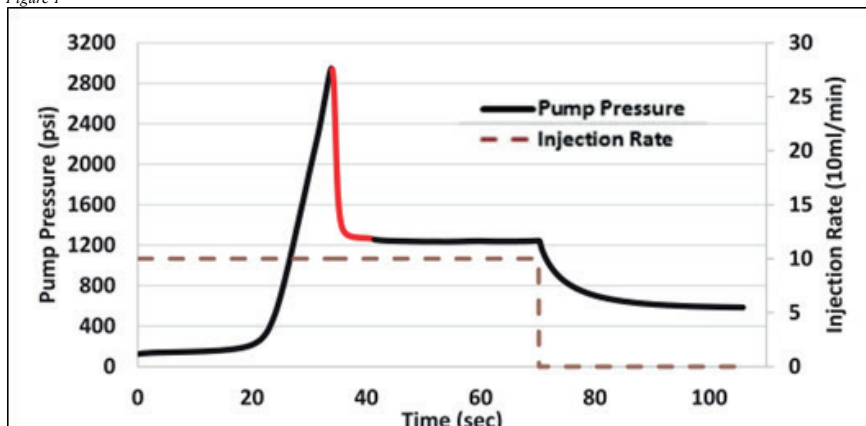
The author is deeply thankful to Asst. Prof. Betül Yıldırım for her support and providing the idea for this research through her course on unconventional oil and gas resources.

## REFERENCES

- Ge, J., & Ghassemi, A. (2011). Permeability Enhancement in Shale Gas Reservoirs after Stimulation by Hydraulic Fracturing. 45th US Rock Mechanics/ Geomechanics Symposium. San Francisco, CA.: American Rock Mechanics Association.
- Patel, S. M., Sondergeld, C. H., & Rai, C. S. (2018). Hydraulic fracture permeability estimation using stimulation pressure data. International Journal of Rock Mechanics and Mining Sciences, 50-53.

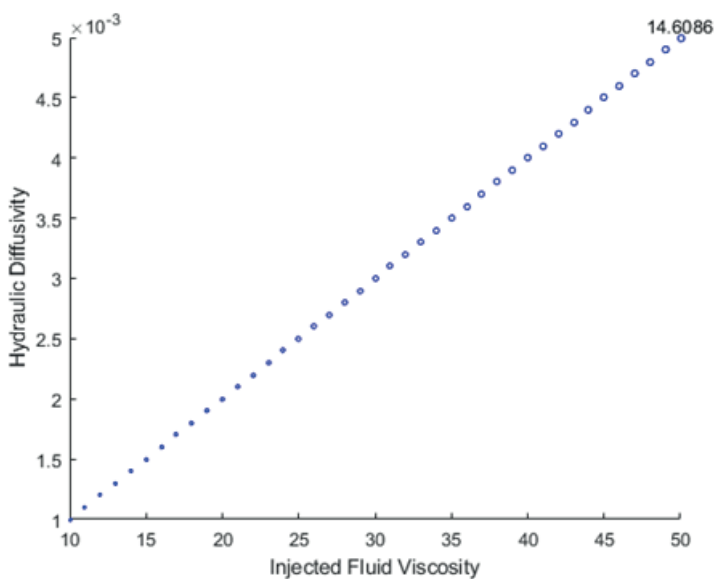
Keywords: Permeability, Pressure

Figure 1



Pump pressure recorded against time during experiment.

Figure 2



Calculated permeability using a range of hydraulic diffusivity and frack fluid viscosity.

Table 1

Variable	Value
Average porosity (%)	6.8
Bulk moduli of fluid (GPa)	1.4
Bulk moduli of dry frame (GPa)	24
Bulk moduli of grain material (GPa)	36.6
Frame shear modulus (GPa)	20.4
Fluid dynamic viscosity (cp)	10-50
Hydraulic diffusivity (m <sup>2</sup> /s)	0.001-0.005

# Forecasting the Performance of Shale Gas Wells Using Machine Learning

**Mohammed Shedaiva**

Istanbul Technical University, Faculty of Mines, Department of Petroleum and Natural Gas Engineering, Istanbul / Türkiye



Utilization of real data to develop data-driven models in the petroleum industry has gained momentum in the past decade. The challenges related to modeling unconventional reservoirs has been recognized as the driving force behind this change in approach. Data-driven models help to enhance operations, increase efficiency, and save time. In the meantime, several numerical reservoir simulators are used to model and forecast the performance of shale gas wells. However, these methods are computationally expensive and the simulators could indirectly face with difficulties in forecasting performance for the unconventional shale reservoirs comparing to conventional ones. In this study, a data analytics approach is utilized to investigate and gain understanding into the key parameters that influence the gas production performance in unconventional reservoirs (i.e. cumulative gas production after 1 year). The dataset utilized in this study is acquired from SPE Data Repository and consist of 53 wells (SPE, 2021). The study essentially utilized two main techniques, namely exploratory data analysis (EDA) and predictive data analytics modeling. Through the utilization of exploratory data analysis (EDA), the correlation between each reservoir and operational parameter with the cumulative gas production (Gp) is clearly identified. A number of reservoir and operational parameters display a strictly monotonic relationship with the gas production. Out of all variables, gas saturation was the variable, which demonstrated the strongest correlation. Furthermore, predictive data-analytics models based on statistical and machine learning algorithms were developed to predict the cumulative gas production after 1 year. Among the five conducted models, extreme gradient boosting machine (XGBoost) proved to be the optimal technique for forecasting gas production, as it yielded the lowest Root Mean Square Error (RMSE) and the highest Coefficient of Determination (R<sup>2</sup>). Finally, an analysis of variable importance was conducted to determine the key variables, which have the highest predictive power in forecasting gas production performance in unconventional shale reservoirs. The operational parameters such as the number of stages, lateral length, and bottom perforation along with reservoir parameter such as gas saturation, porosity, and thickness are more dominant than the other reservoir and operational parameters and gas saturation is the most critical parameter, which is considered as the key driver of forecasting the gas production. The findings of this study will contribute in the development of sustainable designs for similar forecasting modelling projects.

## INTRODUCTION

The increase of energy demand has been the driving force behind the production from unconventional shale reservoirs during the past two decades. This came with the developing horizontal drilling technology and multi-stage hydraulic fracturing techniques (Kulga et al., 2017). These reservoirs are characterized as ultra-low permeability rocks - measured in nanodarcies, not millidarcies. Therefore, the conventional reservoir engineering approaches such as numerical reservoir simulators in such complex systems like unconventional shale have experienced challenges in many different aspects of reservoir analysis. As it become slow and even making it difficult to move forward. Furthermore, it could be computationally ineffective and even more expensive making it difficult to rely in numerical models (Ertekin & Sun, 2019). These challenges have been recognized as the driving force behind the change in approach to the utilization of real data to develop data-driven models in the petroleum industry which has gained momentum in the past decade. Data-driven based machine learning algorithms models help to avoid the difficulties faced with reservoir simulators as well as their ability to reduce the computational load, increase the efficiency, save time and their fast response speed (Schuetter et al., 2018). This would help engineers to achieve the modeling goals and make decisions in a rapid way (Kulga et al., 2017).

## METHODOLOGY

This study utilized recently published dataset (SPE, 2021). The dataset is consisting of 53 shale wells from Eagle Ford, Marcellus and Haynesville shale formations, with 20 parameters distributed among reservoir and operational properties. In the initial stages, the process of parameters selection entailed identifying all features that could logically influence the gas production. Following this, features exhibiting a substantial number of missing values, predominantly comprising nil values, were intentionally omitted from the imputation consideration due to the severity of their missing data. During the data pre-processing stage, missing values were filled using the mean value, which reflects the central tendency of the particular parameter. Notably, only the Spacing parameter underwent this pre-processing, as the other parameters were complete. The dataset was also subjected to feature scaling, aiming to normalize the data on a similar scale. This step holds the potential to enhance the performance of machine learning algorithms. The data analytics approach then is utilized to investigate and gain understanding into the key parameters that influence the gas production performance in unconventional reservoirs (i.e. cumulative gas production after 1 year). The study

essentially utilized two main techniques, namely exploratory data analysis (EDA) and predictive data analytics modeling. EDA including univariate, bivariate, and multivariate analysis is used to examine the structure of the dataset and gain a better understanding into the data. Univariate analysis is the initial step of EDA used to represent graphically each parameter in the dataset including the response (cumulative gas production) in one dimension using boxplots. This will help to outline the characteristics of variables individually including the spread and distributional symmetry as well as detecting outlier values in the dataset. Bivariate analysis used to examine the relationship between each input parameter and the cumulative gas production using scatterplots as well as Pearson and Spearman correlation coefficients is employed to determine the linear relationship strength between the input and response variables. Multivariate analysis as well is employed as an extension of bivariate analysis which help to determine the correlation among all reservoir and operational parameters and between parameters and cumulative gas production at once using the correlation matrix. The EDA used in this study was the primary step to verify the parameters that have a relationship with the cumulative gas production along with understanding patterns, trend, and relationship among variables and between each parameter and cumulative gas production in order to perform predictive modeling. Two primary methods were utilized for model development: multiple linear regression (MLR) and tree-based methods. The tree-based methods included regression tree, bagging, random forest (RF), and extreme gradient boosting machine (XGBoost). The multiple linear regression is a proxy model that make prediction of the target variable based on the slope coefficient of all the predictor variables. The resulted proxy equation then can be used to estimate the cumulative gas production for the unseen data. The regression tree is a straightforward and highly interpretable method. It divides the dataset by initially using the most influential predictor as the primary split (root node). Subsequently, the data branches out to form more decision nodes on both sides of the tree. The decision nodes have less influence on the target variable than the root node. This branching continues as long as further splits are possible; otherwise, the process reaches a terminal node. These terminal nodes ultimately represent the average prediction values of the response variable, in this context, the cumulative gas production after one year. XGBoost is a scalable machine learning method due to the availability of algorithms optimizations. Therefore, the XGBoost model can be tuned to be suitable to the used specific dataset and this help avoid overfitting. Cross-validation technique can be used to estimate the best tune parameters. Differing from RF, where regression trees are built in parallel, XGBoost is a sequential model which mean each subsequent tree is dependent on the output of the last predicted tree. The final predictions of this model is computed by summing up the predictions of all individual trees. Precisely, five statistical and machine learning method including MLR, regression tree, bagging, RF and XGBoost were utilized

to develop a model that is capable to accurately predict the performance of shale gas wells. For each model the dataset is splitted into 80% and 20% for training and test respectively. The training data is used to train our model and the test data is used to validate the model. In this study three common metrics is used to evaluate the performance of each model. These metrics are average absolute error (AAE), root mean square error (RMSE), and coefficient of determination (R<sup>2</sup>). The model with the lowest prediction error and highest R<sup>2</sup> error will be selected with regard to avoiding the overfitting. The final method employed in this study is the variable importance approach which is used to determine the key parameters that have the highest influential impact on the performance of our shale gas wells as well as that have the most predictive power in the developed model.

## FINDINGS

The results of this study illustrate a number of reservoir and operational parameters that display a symmetric distribution and a strictly monotonic relationship with cumulative gas production such as gas saturation, water saturation, porosity, reservoir thickness, lateral length, hydraulic fracturing related number of stages and bottom perforation. Out of all variables, gas saturation was the variable, which demonstrated the strongest correlation. Furthermore, among the five conducted models to predict the cumulative gas production after 1 year, extreme gradient boosting machine (XGBoost) demonstrate the best results proving to be the optimal technique for forecasting gas production, as it yielded the lowest Root Mean Square Error (RMSE) and the highest Coefficient of Determination (R<sup>2</sup>). The XGBoost model used the best tuning parameters, derived through cross-validation, which suggests the use of all observations in the dataset along with only 80% of the available predictors to build the regression trees. Furthermore, it suggests building the regression trees with a maximum size of three levels, which means the number of nodes between the root node and the terminal node of the tree are equal to a maximum of three splits. It also suggests using only 150 boosting rounds (iteration) before stopping the model from a further training process that may cause overfitting. Finally, the key variables which have the highest predictive power in forecasting gas production performance in unconventional shale reservoirs is identified. XGBoost and random forest methods have a good agreement on the top 6 influential parameters that influence the performance of shale wells in unconventional reservoirs. These parameters is distributed between the reservoir and operational parameters. The operational parameters such as the number of stages, lateral length, and bottom perforation along with reservoir parameter such as gas saturation, porosity, and thickness are more dominant than the other reservoir and operational parameters. The overall variable importance approach by XGBoost and RF tend to rank the operational parameters in the top as well as the regression tree used lateral length and the number of clusters per stage as main parameters to partition the tree. These results was consistent with the findings of

similar studies (Schuetter et al., 2018) The gas saturation is the most critical parameter that serve as the key driver of forecasting the cumulative gas production. The findings of this study will contribute in the development of sustainable designs for similar forecasting modelling projects.

## CONCLUSION

Predicting cumulative gas production through data-driven methods is feasible in unconventional shale reservoirs. This approach has proven to be efficient in accurately predicting gas production fast and cost-effective manner.

Five statistical and machine-learning methods, including MLR, regression tree, bagging, RF, and XGBoost regression models, have been used to predict the cumulative gas production after 1 year from unconventional shale reservoirs. Among five models evaluated, XGBoost demonstrated the best prediction performance, with the highest R-squared score of 91% and the lowest RMSE of 1218.54 MMscf. This result agrees with many academia literature that assume XGBoost model as one of the most powerful machine-learning algorithms.

XGBoost and RF agrees on the top 6 influential parameters that influence the production performance from shale gas wells except for the ranking of the third parameter, where lateral length is prioritized for XGBoost and the number of clusters per stage for RF. These 6 main influential parameters are:

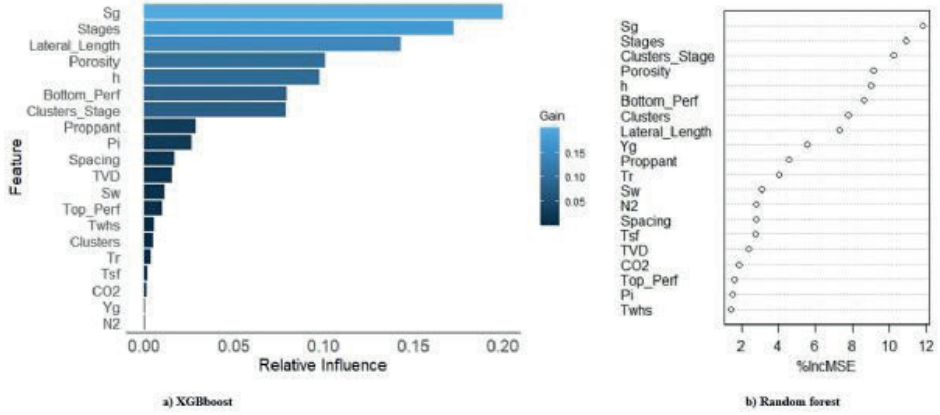
1. Gas saturation (Sg)
2. Number of stages
3. Lateral length (XGboost),  
Number of clusters per stage (RF)
4. Porosity
5. Thickness
6. Bottom perforation

Gas saturation is the most critical parameter in forecasting the cumulative gas production in unconventional shale reservoirs since it ranked first in XGBoost, RF and Regression tree main split (root node).

The multiple linear regression method performed best after reducing the number of contributing parameters to the model from 20 to 13. The number of parameters was determined using k-fold cross-validation and extracted using the best subset selection algorithm.

Keywords: Gas production prediction, Predictive modeling

XGBoost and Random forest models variable importance







**Hidrokarbon Aramalarında Elektromanyetik ve  
Potansiyel Alan Yöntemler (Gravite ve Manyetik)**

*Hydrocarbon Explorations Using Electromagnetic and  
Potential Field Methods (Gravity and Magnetic)*

---



# Experience and Prospects of Magnetotelluric Method Application for Hydrocarbon Prospecting



**Nikolay Palshin<sup>1</sup>, Elena Aleksanova<sup>2</sup>, Dmitry Epishkin<sup>3</sup>, Denis Yakovlev<sup>2</sup>,  
Andrey Yakovlev<sup>4</sup>**

<sup>1</sup>Nord-West Ltd, Moscow / Russia; Shirshov Institute of Oceanology, RAS, Moscow / Russia

<sup>2</sup>Nord-West Ltd, Moscow / Russia

<sup>3</sup>Nord-West Ltd, Moscow / Russia; Schmidt Institute of Physics of the Earth, RAS / Moscow, Russia

<sup>4</sup>Nord-West Ltd, Moscow / Russia; Lomonosov Moscow State University / Russia

## INTRODUCTION

Magnetotelluric (MT) sounding method began its development in 1960s, mainly in application to sedimentary basin imaging. Since 2000 at more than 100 000 stations throughout the globe has been carried out magnetotelluric acquisition by Russian geophysical service companies and most of them have been obtained for hydrocarbon prospecting purposes.

Seismic methods are traditionally considered to be the main instrument in hydrocarbon prospecting and exploration. In most cases modern advanced technologies make it possible to solve tasks of defining prospective geological structures and/or formations. However, there are several geological settings, where seismic methods face serious difficulties, while application of magnetotellurics can substantially increase credibility of geological interpretation of geophysical data. Recently magnetotellurics has been widely used in hydrocarbon prospecting and exploration.

Favorable for magnetotellurics geological settings are sedimentary basins covered with thick flood basalt cover or permafrost. The Siberian traps in Russia, Parana Basin in Brazil, as well as sedimentary basins covered by Deccan basalts in India may serve as examples.

Besides, magnetotellurics proves to be an efficient complementary method of hydrocarbon prospecting in sedimentary basins with a well-developed salt tectonics, for instance, in Pre-Caspian Basin or intracratonic sedimentary basins of the Northern Sea.

Magnetotellurics has certain advantages when applied to map the structure in fold and thrust belts (FTB), such as Zagros in Iran, Subandean fold belt in Peru and Bolivia or Yenisei-Khatanga Depression in Siberia. In FTB the geological boundaries are characterized by large dip angles and disharmonic folding, which also makes interpretation of seismic data challenging. MT studies were carried out in Yenisei-Khatanga Depression in Siberia, Zagros FTB in Iran, Subandean FTB in Bolivia and Colombia.

## METHODS

### Electrical Resistivity of the Rocks

The main result of the MT studies is a subsurface resistivity image – a two- or three-dimensional model describing the distribution of electrical resistivity inside the structure (medium). The ultimate stage of the research is the geological interpretation of the resistivity model obtained. When electromagnetic (EM) methods are

applied for hydrocarbon exploration its interpretation is based on the understanding of mechanisms controlling electrical resistivity (or conductivity) of sedimentary rocks.

The electrical conductivity of sedimentary rocks depends on the clay content, pore space geometry, porosity, fluid saturation, and, finally, the electrical conductivity of the pore fluid. The first four factors characterize the petrophysical and hydrophysical properties of the rock. The latter one is the most important since it's the main factor controlling the electrical conductivity of most non-clay sedimentary rocks. The resistivity of sedimentary rocks depends on several factors and, as a rule, an unambiguous interpretation of the observed anomalies in terms of geological structure is hardly possible without additional petrophysical and hydrophysical information. In many cases, when data or at least some estimates on lithology, petrophysical and hydrophysical properties of sediments (clay content, pore space geometry, fluid saturation, typical salinity of fluids) are available, it becomes possible to estimate the effective porosity as reservoir quality index (or clay content as cap rock quality).

## MT BASICS

MT method is intended to probe electrical conductivity structure of the Earth. It involves measuring variations of orthogonal components of electromagnetic (EM) fields at the surface of the Earth in a broad spectrum of natural geomagnetic variations. Time series of electric and magnetic field are used for estimating two fundamental MT quantities (transfer functions) impedance tensor  $Z$  and magnetic tipper vector  $W$ .

$$E_x = Z_{xx} H_x + Z_{xy} H_y \quad (1)$$

$$E_y = Z_{yx} H_x + Z_{yy} H_y$$

$$H_z = W_{zx} H_x + W_{zy} H_y \quad (2)$$

where  $E$  are a horizontal component of the electric field and  $H$  is horizontal and vertical components of the magnetic fields at a given frequency, respectively, and  $(x,y)$  denotes the orthogonal components of horizontal direction and  $(z)$  - of vertical direction.

EM field behavior and MT transfer functions greatly depend on dimensionality of the Earth. Most real geological situations are 3D, although 2D dimensional approximation is quite often used. In a 2D dimensional case the EM field can be described by two independent modes: TM (horizontal magnetic field is oriented along the strike) and TE (horizontal electric field is oriented along the strike). The 2D inversion technology is

well developed and widely used in magnetotellurics. Nevertheless, the general 3D approach is developing fast and often it finds its application in applied magnetotellurics.

### MT Survey Technology

Over the past decade the amount of MT data collected has increased manifold, which has prompted the development of MT data acquisition technology, data processing and analysis methods and consequently the efficiency of the method achieved a new level. MT survey consists of several sequential steps (see Fig. 1).

Data acquisition is the most important part of MT survey. Only advanced modern MT technology, which includes proper survey planning, use of novel ultrawide band MT instruments including low-noise sensitive induction coils (magnetic field sensors) and electrodes (electric field sensors), which enable EM field measurements in the frequency band from 0.001 Hz to 10 kHz to.

To get reliable data acquisition should last for at least 14-20 hours (an overnight recording) and the use of remote reference site or several remote reference sites is strongly required. The distance from the remote site to regular ones should be  $> 20-30$  km to provide non-coherency of EM noises. The modern efficient and powerful data processing software (robust remote reference RRR) with a user-friendly interface allows to obtain an MT set of transfer function: impedance, tipper and horizontal magnetic tensor. Additional time-domain EM measurements are a reliable technique for adjusting static shift correction procedure.

The data analysis consists of a dimensionality analysis and a static shift correction, which are essential steps before data inversion. While most of MT studies aimed at hydrocarbon prospecting are carried out along seismic profiles a 2D approach is still widely spread in commercial magnetotellurics, but its application should be confirmed by the dimensionality analysis and transfer function transformations if needed. The 2D approach usually uses 2D nonlinear conjugate gradient (NLCG) multi-stage bimodal inversion technology.

## CASE

### Regional-scale geophysical transects in Russia

The main goal of the regional-scale MT surveys is imaging of the structure of the upper part of the Earth crust. For 2D regional-scale surveys, the depth of investigation reaches over 25 km, allowing one to map the structure of the sedimentary basins as well as a crystalline basement.

Along with seismic, magnetotellurics is one of the leading methods utilized in regional-scale geophysical surveys. For MT acquisition, the typical station spacing along the line varies within 1-3 km, while the maximum period for transfer functions' estimation is about 3000 s. In many cases magnetotellurics have been accompanied

by time-domain electromagnetics to achieve a better resolution of the upper part of the section and for static shift correction in MT data.

Regional scale geophysical studies, which include MT data acquisition, in Russia are being conducted as a part of governmental project initiated by the Russian Ministry of Natural Resources. More than 14 000 MT sites have been acquired along 14000 km of profiles. More regional profiles are planned for the near future (Fig. 2).

An example of resistivity image and geological interpretation of a portion of 3-SB transect is shown at Fig. 3. The main goal of the studies was to construct a resistivity model of the sedimentary cover of the northern part of the Baikitskaya antecline and the southern part of the Kureiskaya syncline as a result of joint interpretation of magnetotelluric data, seismic CDP data, well logging and potential fields' data. The model was then analyzed to identify the electrical conductivity anomalies associated with good reservoir rock properties in the Lower Paleozoic, Vendian (Neo-proterozoic) and Riphean (Mezo-proterozoic) formations.

Three major resistivity layers are identified within the sedimentary cover: suprasalt, halogen-carbonate (salt) and subsalt. The resistivity images, graphs and maps of the resistivity distributions in specific layers, derived from the resistivity model, revealed the following features of the resistivity structure.

1. A sequence of layers with varying resistivity can be distinguished within the suprasalt formation. Highly resistive layers and regions are in good correlation with the intrusive bodies (traps), revealed by the borehole data. These high-resistivity features, spread across the survey area, have variable thickness and location depth.
2. Sediments of the halogen-carbonate formation generally have high resistivities (hundreds of Ohm-m), but often include conductive regions that may be associated with the zones of rock alteration caused by magmatic intrusions.
3. The subsalt formation is represented by the Vendian and Riphean (Mesoproterozoic) sediments. Resistivity variations are prominent in the Vendean rocks. A correlation between the increase in thickness and the decrease in resistivity is observed for the terrigenous formation containing high-porosity sandstones (the Vanavara formation). In some parts of the area the Vendean sediments have low resistivity, which can be explained by the increased fracturing of carbonate rocks. Relatively conductive the Riphaean formation has resistivity ranging from tens to a few hundreds of Ohm-m and is found within two large troughs of near North-South strike.

### MT Studies in Parana Basin, Brazil

The similar study was completed in Parana Basin in Brazil in 2014 (see Fig. 4). The studies in the sedimentary Paraná Basin, located in southern Brazil (the states of Mato Grosso do Sul, São Paulo and Paraná) were conducted in 2014 under a contract with

the Brazil's National Agency of Petroleum, Natural Gas and Biofuels. The survey's main goal was to assess prospects of oil and gas potential in the region and delineate licensed areas.

The terms of reference included mapping diabase intrusions, estimating the thickness and depth to bottom surface of the traps, imaging of the lateral inhomogeneity of the traps, identifying fault zones, studying the sedimentary formations beneath the traps, discriminating the layers according to their resistivity, estimating the lateral inhomogeneity of the entire resistivity structure, mapping the surface of the crystalline basement, identifying the low resistivity regions in the Earth's crust.

Resistivity image obtained for Line 3 (see Fig. 4) is shown at Fig. 5.

The data clearly reveal an inhomogeneous high-resistive formation interpreted as Serra Geral traps overlaid by the Bauru sands; vertical and horizontal heterogeneities of the basaltic formation are imaged. The thickening of the high-resistivity layer with two supplying vertical channels, traced in the central part of the line, corresponds to the well-known Ponto Grossa Arch, which is distinctly identified based on magnetic prospecting data and, according to geologists, represents fan-shaped dyke complexes. The depth to the crystalline basement in the survey area was found varying from 3 km in the southeast to 5.5 km in its central part. The obtained results are in good agreement with the available borehole lithological and logging data.

### Taymyr Fold Belt

Since 2005 a large amount of MT data were acquired in the framework of multi-method geophysical studies on the territory of Taymyr Peninsula (North of Siberia, Russia). The total length of the completed survey lines is nearly 20 thousand linear kilometers.

The main components of the geophysical technology applied for the studies of both the Mountain Taymyr and the Yenisei-Khatanga Trough, are the 2D CDP seismic survey and the magnetotellurics.

MT acquisition was conducted along the seismic lines and a joint interpretation of resistivity and seismic images with the involvement of gravity and magnetic prospecting data made it possible to clarify the understanding of the geological structure of the region to identify a series of large previously unknown geological objects that aren't exposed on the earth's surface and identify hydrocarbon-prospective areas as well.

Fig. 6 shows the geophysical studies results along one of the survey lines. In the middle part of the line, a large Gydan-Taymyr Trough has been mapped, with the thickness of the sedimentary formation reaching 20 km (filled with about 10 km of Paleozoic sediments and the Upper Riphean sequence of comparable thickness).

A joint analysis of the seismic and resistivity models has shown that the largest anomalies of the seismic wave field coincide with the resistivity anomalies; taking the available paleo reconstructions into account, it can

be assumed that these anomalies correspond to reef structures and manifestations of salt-dome tectonics (Fig. 7).

It was concluded that the distinct-boundary high-resistivity zones correspond to the regions of loss of correlation between the seismic reflectors and resistivity boundaries. In one case, those anomalies are accompanied by low gravity field, which suggests that they might be associated with low-density anhydrite bodies (salt domes), while other certain resistive regions fall within the elevated gravity field zones, which is the evidence for their carbonate (reef) origin.

MT studies made it possible to predict a generalized lithology pattern of the Phanerozoic formations in the area, to clarify the location of the bottom of the traps and the Jurassic-Cretaceous sediments, to identify the non-outcropped intrusive bodies in the upper part of the section, to make important conclusions about the oil and gas potential of the area, and to outline the strategy for further studies. The application of magnetotellurics confirmed the existence of the previously unknown sufficiently large structures, assessed as prospective in terms of oil and gas potential.

### Subandean Fold Belt

In 2017 two large MT-TDEM projects were carried out in Bolivia under a contract with the Bolivian national oil and gas company YPFB. The main goal was to understand better the geological structure of the sedimentary basin and petroleum system in two study areas: Subandino Sur and Subandino Norte (see 1 and 2 in Fig. 8).

The Subandean fold belt is a thin-skinned in-sequence system with several detachment levels. The geological structure of the Subandean fold belt is typical for many fold belts. Most fold belts are characterized by a quasi-2D structure with wide relatively low resistivity synclines with horizontal layering and narrow complicated anticlines often fragmented by many fault zones and subvertical layering forming mountain ridges with steep slopes. Disharmonic folding also is typical for the Subandean fold belt: folding in upper structural levels does not coincide with those in the lower levels.

The Subandean fold belt is characterized by very complex structures with steep (even vertical) dips in the anticline nuclei. The available seismic data does not provide enough information in the axis of the structures, which might lead to a false interpretation when planning exploration wells. Detailed MT studies were carried out in addition to the seismic acquisition to understand the structural behavior of the study area.

The field work was carried out simultaneously at two survey areas and 3628 MT and 1130 TDEM stations were acquired. Impedance tensor and tipper were obtained in a wide interval of periods from  $10^{-4}$  to  $10^3$  s (7 decades).

Below the results obtained at Subandino Norte (see 1 in Fig. 8) survey are discussed. Broadband MT data

were acquired along 15 profiles following old seismic profiles with lengths from 30 to 50 km oriented across the geological strike. Due to quasi-2D structure of the Subandean fold belt the main tool was a 2D inversion. A TM mode in our case is more informative, but a bimodal inversion with a down weighted TE mode at a limited period band clearly gave the best result. Theoretically TM mode has a better resolution of high resistive targets, while TE is responsible for imaging a low resistive (conductive) object, but practically for real geological settings even for quasi-2D fold belts where targets are geological structures, which could be both resistive (anticlines) and conductive (synclines) a bimodal inversion is preferable. There is also another reason for applying bimodal inversion: a regularized 2D inversion of TM mode only in some cases can result in “overfitting”, when a number of artefacts appear in resistivity images. These artefacts are caused by deviation of a real structure from 2D one. Application of a bimodal inversion even with a down weighted TE mode helps to avoid such situations and obtain reliable resistivity images for both resistive anticlines and conductive synclines.

A case study showed that a 2D bimodal inversion with a reference background resistivity model as a starting one (soft constraint) is the most efficient approach. The procedure consists of three main stages: (1) unconstrained 2D and 3D MT data inversion, (2) construction of 2D reference background resistivity models using all available data: unconstrained MT data inversion, seismic and logging data and (3) constrained inversion – in our case MT data inversion with a reference background model as starting one. An example of resistivity image is shown in Fig. 9.

## CONCLUSION

The MT method is increasingly used in hydrocarbon prospecting. It provides important information about the structure of buried folds, complex salt bodies and fault zones. The results of magnetotelluric studies make it possible to solve both structural and petrophysical problems in the search and exploration of hydrocarbons and deep aquifers.

The experience of studying areas of complex geological structure shows the feasibility of combining various geophysical methods to reduce the uncertainties of geological models. The use of MT data in combination with seismic survey and logging data besides other geological and geophysical studies can significantly increase the reliability of mapping prospective structures and determining the targets of exploratory drilling.

Keywords: magnetotelluric sounding, hydrocarbon prospecting

Fig.1.

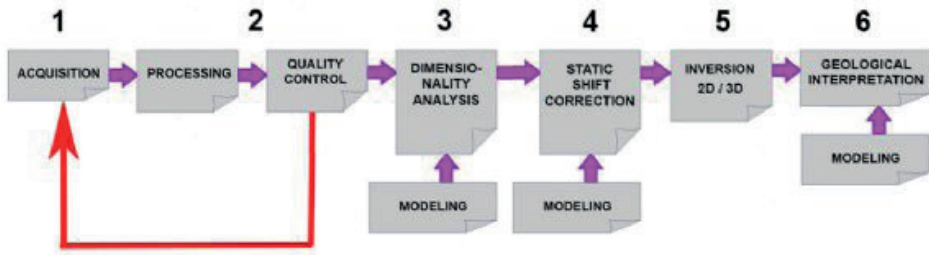


Fig.1. MT flowchart: 1- data acquisition, 2 - data processing, post-processing and quality control 3 - dimensionality analysis, 4 - static shift correction, 5 - MT transfer functions inversion and 6 - geological interpretation (or constructing of geologically meaningful models).

Fig. 2.

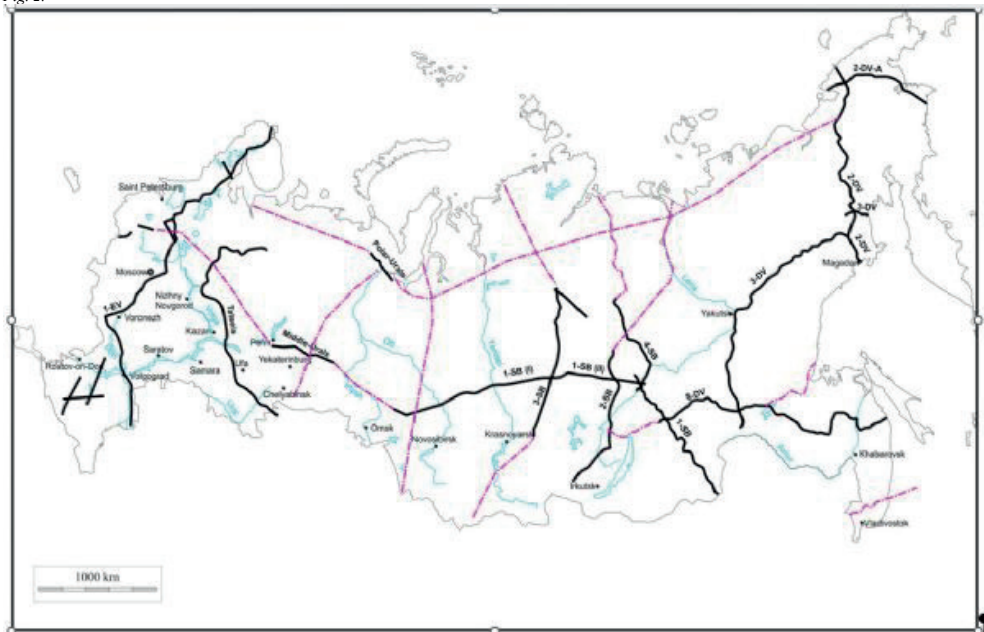


Fig. 2. Regional scale magnetotelluric studies in Russia. Solid black lines represent profile where acquisition of MT data was completed, while dash-dotted magenta lines show planned profiles.

Fig. 3.

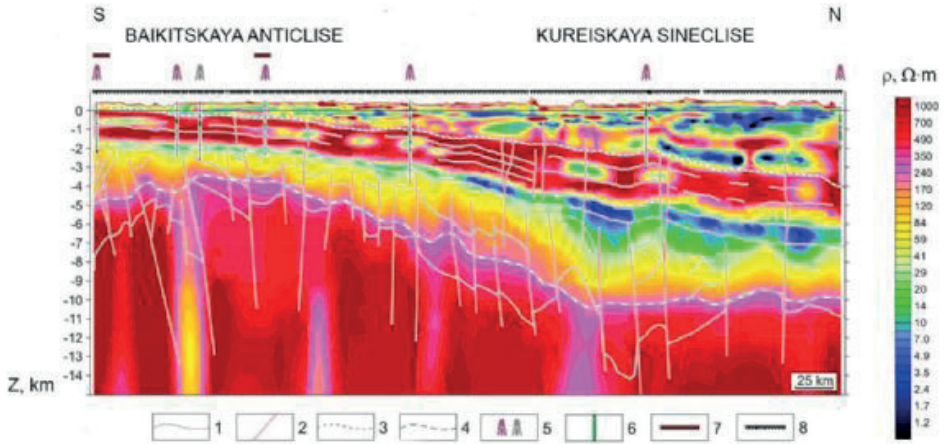


Fig. 3. Resistivity image with geological interpretation for a portion of 3-SB regional transect in the Eastern Siberia: 1 – seismic reflectors as imaged by CDP data; 2 – tectonic fault zones revealed by seismic; 3 - the top of the halogen-carbonate formation determined from CDP and borehole data; 4 - high-resistivity basement according to MT data; 5 - well position; 6 - intrusive rocks according to borehole data; 7 – hydrocarbon fields' locations; 8 – MT stations.

Fig. 4.

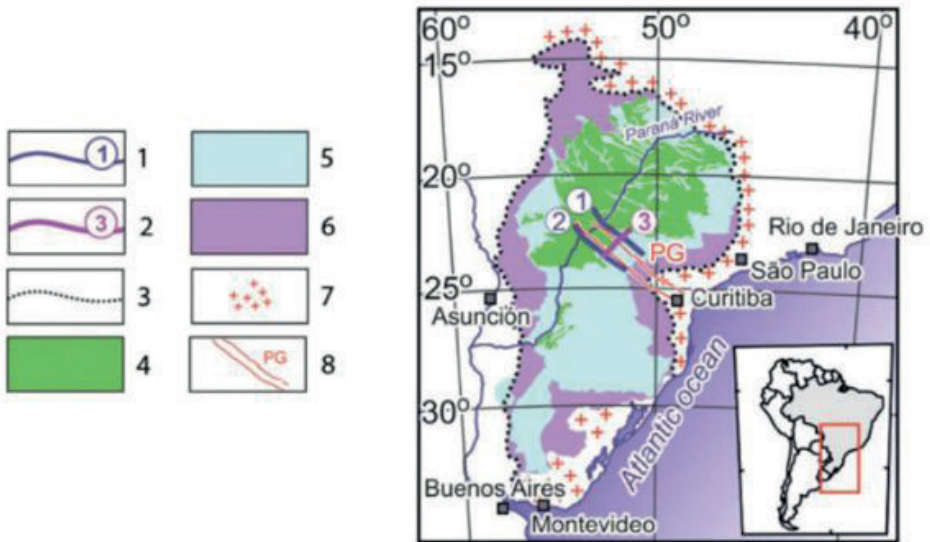


Fig. 4. Survey area map. 1 – location of the lines 1, 2, 3; 2 – location of the line 3; 3 - boundaries of the sedimentary basin; 4 - sandstones of the Bauru formation; 5 – basalts of the Serra Geral formation; 6 – Mesozoic-Paleozoic sedimentary rocks; 7 - crystalline basement rocks; 8 - the position of the Ponta Grossa Rise. The red rectangle on the smaller-scale map of South America approximately indicates the survey region.



Fig. 5.

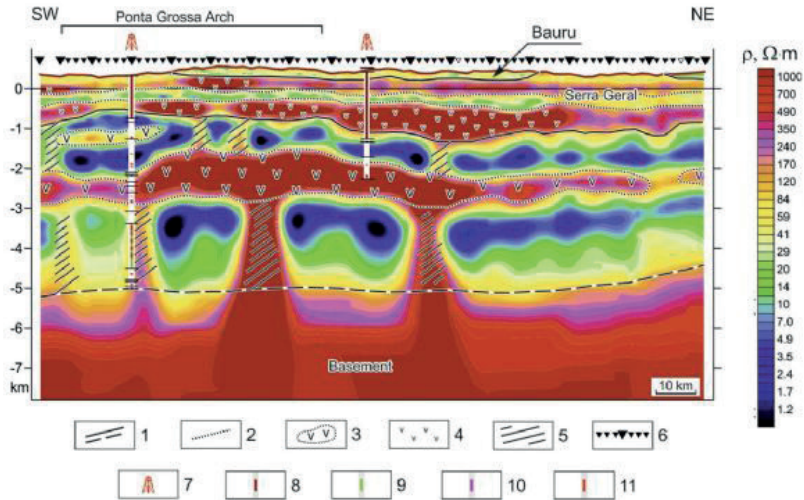


Fig. 5. Resistivity image and geological interpretation for Line 3 at Parana Basin: 1 - the boundaries of the main resistivity layers; 2 - extra boundaries within them; 3 - regions with a significant content of intrusive rocks; 4 - regions with predominance of magmatic rocks in the Serra Geral formation; 5 - zones of altered rocks; 6 - MT stations; 7 - borehole positions and charts; 8 - Serra Geral formation; 9 - rocks of the Ponta Grossa formation (Paleozoic sedimentary rocks); 10 - rocks of Precambrian crystalline basement; 11 - intrusive rocks.

Fig. 6.

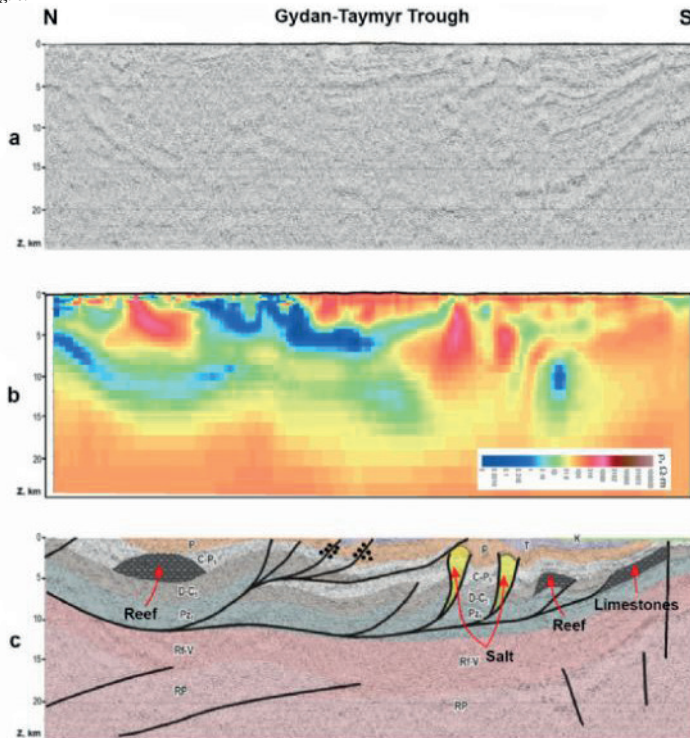


Fig. 6. Seismic image (a), resistivity image (b) and final model interpreted in terms of geological structure (c). The black lines indicate the major faults.

Fig. 7.

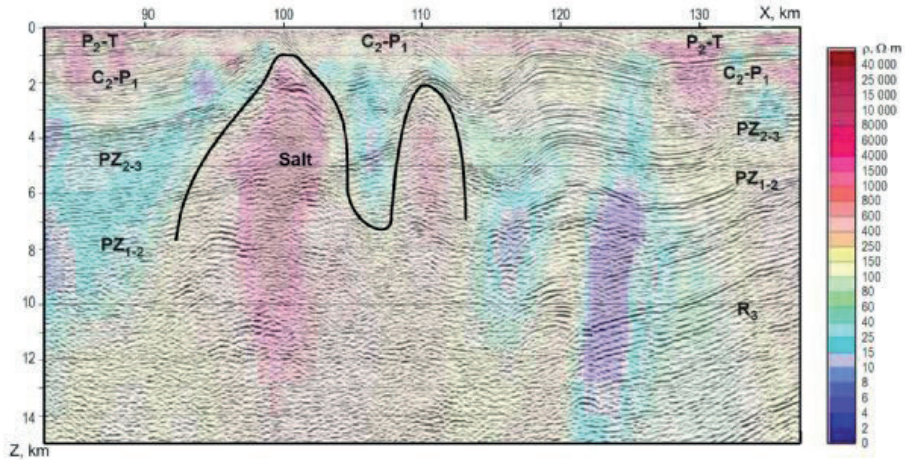


Fig. 7. An example of the identification of salt domes based on the joint analysis of resistivity and seismic images. The top surface of the salt domes is shown with a black line.

Fig. 8.

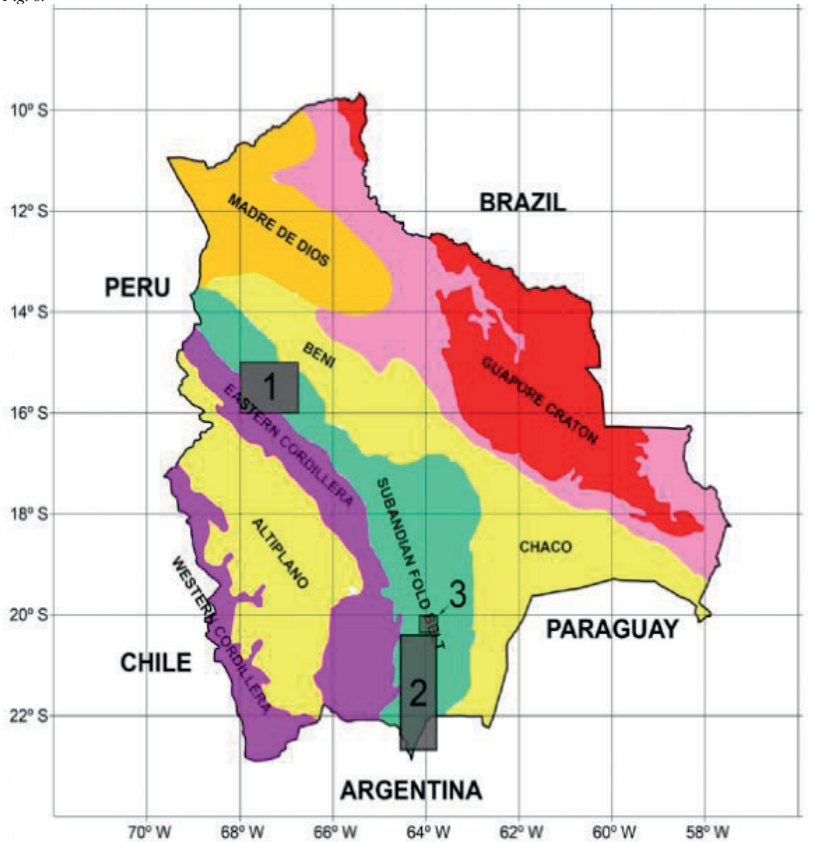


Fig. 8. Three MT projects in Subandean Fold Belt in Bolivia: 1 – Subandino Norte, 2 – Subandino Sur; 3 – Itacaray.

Fig. 9

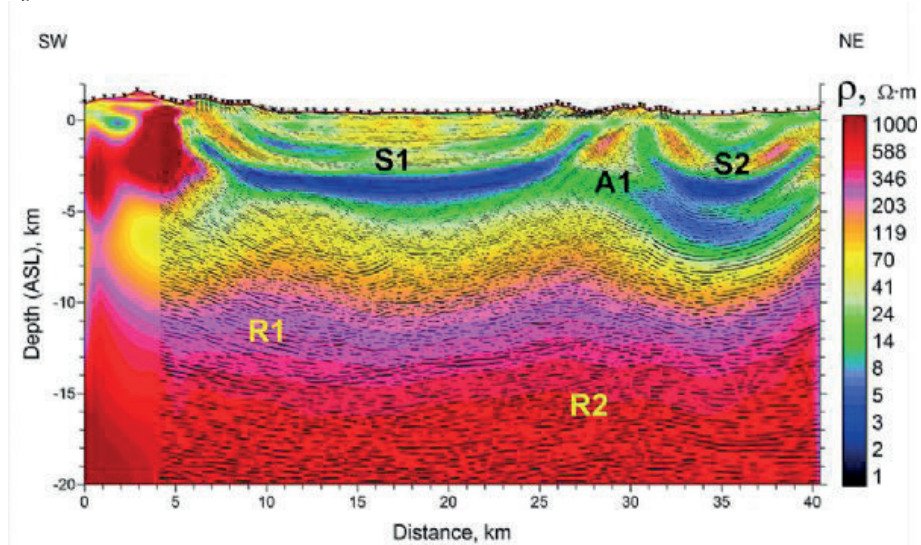


Fig. 9. Resistivity model obtained by 2D bimodal inversion for exemplary profile at Subandino Norte with seismic data overlapped. Positions of acquisition sites are shown by brown triangles. Main structures outlined: A1 – Lliquimuni anticline, A2 – Tacuaral anticline, S1 – Mayaya syncline, S2 – Inicua syncline, R1 – resistive Paleozic sediments, R2 – crystalline basement.

# Manyetotellürük Yöntemin Güneydoğu Anadolu'da Petrol Arama Amaçlı Kullanımının Değerlendirilmesi

## Evaluation of Magnetotelluric Method for Petroleum Exploration in Southeast Anatolia



**Ahmet Tuğrul Basokur**

Lemnis Yerbilimleri

### ÖZ

Sismik yansıma, tortul katmanların araştırılmasında sağladığı yüksek ayrımlılık nedeni ile petrol aramalarının birincil yöntemidir. Yüzeyle yüksek hızlı bir katman olduğunda veya volkanik sahalarda, özellikle bazalt örtüsünün bulunması durumunda yeterli sinyal oluşturulması güçleşir. Bu tür durumlarda, başlıca seçenек manyetotellürük (MT) yöntemidir. Ayrıca, üstteki katmanların daha yüksek sismik hızda olduğu bindirme kuşakları ve benzeri ortamlarda, yorumlamadaki belirsizlikleri azaltmak amacı ile sismik yansıma ile MT yöntemi birlikte kullanılmaktadır. MT yöntemi, sismik yansıma göre daha az maliyetli olduğundan, geniş tortul havzalarda sismik aramadan önce MT çalışmaları ile tortul kalınlıklarının saptanması, daha etkin sismik planlama yapılmasına yardım eder.

Bu çalışmada, MT verisinden hesaplanan üç-boyutlu öz direnç modeli kullanılarak, Güneydoğu Anadolu'da jeolojik formasyonların birbirinden ayırt edilebilme olanakları araştırılmıştır. Sondaj kuyularında ölçülen öz direnç logu bilgilerinden, Midyat formasyonunun yüksek öz direnç (100-300 ohm-m) ve Germav'dan Kastel'e kadarki bütün formasyonların düşük öz direnç değerleri (3-20 ohm) gösterdiği anlaşılmaktadır. Sayındere formasyonu ise yüksek öz direnç değerleri (100-300 ohm-m) ile temsil edilmektedir. Bu bilgiler MT arazi verisinden kestirilen üç-boyutlu öz direnç modelinin yorumlanmasını kolaylaştırmaktadır. Midyat-Germav ve Kastel-Sayındere arayüzeyleri üç-boyutlu öz direnç modelinden türetilen öz direnç kesitlerinde kolaylıkla ayırt edilebilmektedir. Ancak, Germav ile Koçali-Karadut ve Kastel formasyonlarının ayırt edilmesi tümünün düşük öz dirençli olması nedeni olanaklı görülmemektedir. Öz direnç modellerinde bu üç formasyon tek bir katman gibi çözülmektedir.

**Anahtar Kelimeler:** Manyetotellürük Yöntem, Güneydoğu Anadolu'da Petrol Aramacılığı.

The seismic reflection method is the primary method for petroleum exploration because of its high resolution in investigating sedimentary basins. However, obtaining sufficient signals in high-velocity surficial layer cases, especially volcanic cover, is problematic. In such conditions, the main alternative is the magnetotelluric (MT) method. Seismic reflection and MT methods can also be used jointly to decrease the uncertainties in interpreting overthrust zones and similar environments where surficial layers have higher velocity values than the underlying layers. In addition, the MT method can investigate the sedimentary basins at a lower cost before the seismic method's application, leading to efficient seismic survey planning.

This presentation examines the possibility of identification of formation boundaries in Southeast

Anatolia from the three-dimensional resistivity model estimated from the MT data. The well-logging data shows that the Midyat formation has high resistivity values of 100-300 ohm-m, and all formations from the Germav to Kastel have relatively lower resistivity values between 3-20 ohm-m. Sayındere formation is represented by relatively higher resistivity values between 100-300 ohm-m. The information obtained from the well-logging data helps to interpret three-dimensional resistivity models estimated from the MT field data. Identifying the interfaces between Midyat-Germav and Kastel-Sayındere in resistivity sections derived from the three-dimensional resistivity model becomes straightforward. However, identifying the interfaces between the Germav, Koçali-Karadut and Kastel formations is difficult. These formations are resolved as a single layer in the resistivity models.

**Keywords:** Magnetotelluric Method, Petroleum Exploration in Southeast Anatolia.

### GİRİŞ

Petrol aramalarında sismik yansıma ana yöntemi oluşturmakla birlikte, özellikle tuz domları ve yüzeyle bazalt gibi volkanik kayaçlar bulunması (Beamish and Travassos, 1992) veya başka nedenler ile sismik yöntemlerin sorun yaşadığı sahalarda manyetotellürük (MT) yönteme başvurulmaktadır. Şeyl rezervuarlarda MT yöntemi uygulamaları başarılı sonuçlar vermektedir (Kumar and Hoversten, 2012). Bölgesel çalışmalarda MT yöntemi ön bilgilerin elde edilmesinde oldukça başarılıdır. Örneğin Yakovlev ve diğ.(2018), Sibirya platformu üzerindeki permafrost bölgelerdeki toplam 20 bin km uzunluğundaki profiller üzerinde 30 binden fazla MT istasyonunu gaz hidrat arama amacı ile ölçmüşlerdir. İran'da da MT yöntemi petrol arama amaçlı olarak Zagros zonunda kullanılmıştır (Mansoori et al., 2015; (Mansoori et al., 2016). Hindistan'da bazalt altı bölgenin görüntülenmesi amacı ile yaygın bir kullanım alanı bulmuştur (Sarma et al., 1992; Sarma et al., 1998a,b,c; Harinarayana et al., 2000; Harinarayana et al., 2003; Harinarayana et al., 2009; Azeez et al., 2011; Pandey et al., 2008, 2009; Satpal et al., 2006; Strack and Pandey, 2007; Patro et al., 2015). Japonya'da bazalt ve volkanik örtü altındaki karbonat kayaçların incelenmesi için MT uygulanmıştır (Mitsuata et al., 1999). Benzer örnekler Suudi Arabistan (Colombo D, Keho T, McNeice G, 2012), İtalya (De Stefano ve diğ., 2011), Amerika Birleşik Devletleri (Morrison ve diğ., 1991) ve Rusya'da (Spies, 1983) görmek mümkündür. Çalışmaların büyük bölümü ise şirket raporları olarak saklı tutulmuştur. Ülkemizde ise İlkışık ve Jones(1984), Güneydoğu Anadolu'da bazalt ile kaplı bölgelerde MT ile hangi katman sınırlarının çözülebileceği hakkında

kuramsal bir çalışma gerçekleştirmiştir. Bu çalışmada ise Güneydoğu Anadolu'da ölçülen MT verisinden üç-boyutlu ters-çözüm ile hesaplanan öz direnç modeli kullanılarak jeolojik formasyonların ayırt edilebilme olanakları gösterilmiştir.

## MANYETOTELLÜRİK ALAN VE YÖNTEM

Yerküresinin doğal elektromanyetik alanı, manyetotellürik (MT) alan olarak adlandırılır. MT alanın kaynağı değişik olaylara bağlı olarak atmosferde, iyonosferde veya manyetosferde bulunur. 1 hertz (Hz) altındaki elektromanyetik dalgalar güneşten gelen yükler ile manyetosfer sınırındaki girişimlerden oluşur. 1 Hz'in üzerindeki değişimler yere ulaşmadan iyonosfer içinde soğurulduğundan, bu sinyallerin kaynağı atmosferde oluşan yıldırım ve şimşeklerdir. Serbest uzayda 'yerdeğiştirme akımı' ile yayılan elektromanyetik dalga çok az soğurularak çok büyük uzaklıklara erişebilirken, yer içine doğru ilerleyen bir elektromanyetik dalga iletken içerisine girdiğinde 'iletkenlik akımı' baskındır. Bu ise dalganın soğurulması, yani uzaklık ile dalga genliğinin azalmasına neden olur. Soğurulma dalganın frekansına ve ortamın öz direncine bağlı olduğundan, MT alanın incelenmesi ile yeraltı öz direnç dağılımı elde edilebilir. Araştırma derinliği, ölçülerin frekans aralığına bağlı olduğundan inceleme amaçlarına göre denetlenebilir. 'Duyulabilir manyetotellürik' (audio-magnetotellurics, AMT), manyetotellurik (MT) ve jeomanyetik derinlik sondajı (geomagnetic depth sounding, GDS) adları ile sınıflandırılan yöntemlerin ilkeleri aynı olup, kullanılan frekans aralıklarına göre adlandırılmaktadırlar.

## MT ÖLÇÜ DÜZENİ VE VERİ SUNUMU

MT yönteminde doğal elektrik alanının iki bileşeni ve manyetik alanın üç bileşeni zamanın fonksiyonu olarak ölçülürler. Elektrik alan iki ucunda elektrotlar bulunan bir kablo yardımı ile ve manyetik alan ise indüksiyon bobinleri ile ölçülür. Veri kalitesi, MT verisinin önbilmezlik (causality) koşulunu sağlayıp, sağlamadığının denetlenmesi ile gerçekleştirilmelidir. Bu denetimi sağlamak için, eşit aralıklı olmayan verinin Hilbert dönüşümüne dayanan bir yöntem Başokur(2023) tarafından geliştirilmiştir. Ölçülen gerilim farkı ile manyetik alan, geleneksel olarak görünür öz direnç ve faz değerlerine dönüştürülür (Başokur, 1994). Verilerin sunumu ise görünür öz direnç eğrileri, yapma-kesitleri ve haritaları ile gerçekleştirilir. Görünür öz direnç eğrileri, yapma-kesitleri ve seviye haritalarının gözden geçirilmesi ile hedef kütlelerin yeri ve uzanımı hakkında da nitel bir yorum yapılabilir. Ancak, nitel yorum ile hedef kütlelerin derinlik, uzanım ve kalınlıkları hakkında sayısal bilgiler elde edilemez. Bu görselleştirme teknikleri sayısal modelleme yöntemlerinin uygulanmasından önce önsel-bilgi sağlarlar.

## MT VERİLERİNİN EVİRTİMİ

Jeofizik yöntemlerin amacı belirli bir fiziksel parametrenin yeraltındaki dağılımını saptamaktır. Bu işlem doğrudan fiziksel parametrenin ölçülmesi ile gerçekleştirilmez. Bunun yerine, bu fiziksel parametrenin yeraltındaki dağılımı nedeni ile oluşan alan değişimi yer yüzeyinde ölçülür. Bu alan değerleri kullanılarak, evirtim (ters-çözüm-inversion) yöntemleri ile fiziksel parametrenin yeraltındaki dağılımı kestirilmeye çalışılır. Bu amaçla, elektrik ve elektromanyetik yöntemlerde üç tür kavramsal model kullanılmaktadır. Bu modellerden en yalını, tekdüze ve yön-bağımsız katmanlardan oluşan bir-boyutlu (1B) modeldir. Bu modelde, geometrik parametreler katman kalınlıkları iken fiziksel parametreler ise her katmanın kendine özgü öz direncidir. İki-boyutlu (2B) model fiziksel parametrelerin ölçü hattı doğrultusunda ve düşey yönde değiştiği, ancak kesit düzlemine dik yönde değişmediği varsayımı ile elde edilir. Prizmaların kesit düzlemindeki görüntüleri hücre olarak adlandırılır. Üç-boyutlu (3B) modellemeye ise yer altı küp şekilli bloklar ile temsil edilir. Her küpün kendine özgü bir fiziksel parametre değeri vardır. Şekil 1'de, 3B model ağı için bir örnek verilmiştir. Ölçü alanı daha küçük hücrelere bölünmekte, model kenarlarının oluşturacağı etkiyi ortadan kaldırmak için model alanı çok büyük tutulmaktadır. Üç-boyutlu model yeraltının betimlenmesinde gerçeğe daha yakın sonuçlar üretir. Bir-boyutlu modelleme oldukça hatalı sonuçlar üretmesi açısından hesaplama olanaklarının geliştiği günümüzde artık kullanılmamaktadır. İki-boyutlu model kullanımının da birçok sakıncası bulunmaktadır. Sadece aynı doğrusal bir hat üzerinde bulunan belirli sayıda istasyon ters-çözüm amacı ile kullanılabilir. Jeoloji yaklaşık iki-boyutlu olmalı ve ölçü hatları jeolojik doğrultuya dik yönde seçilmelidir. Jeolojik doğrultuya dik olmayan yönlerde modelleme yapılamaz. Kuzey-güney ve doğu-batı yönlerinde ölçülen elektrik ve manyetik alan değerleri jeolojik doğrultuya hesapla dönüştürmek zorundadır. Bu işlem verideki gürültülerin ve dolayısı ile belirsizliklerin artmasına neden olur. Yorumlama, yan yana dizilen iki-boyutlu görüntülerden yapıldığından, iki kesit arasındaki belirsizlikler giderilemez. Yapma üç-boyutlu görüntü elde edilebilir ise de hatlar arasındaki öz direnç değerleri ara değer bulma yöntemleri ile hesaplandığından gerçek model değerleri değildir. Üç-boyutlu modellemeye bu tür kısıtlar bulunmamaktadır. Ancak, model ağı geometrik olarak büyüdüğünden çözülmesi gereken parametre sayısı çok büyük değerlere ulaşır ve çok-çekirdekli hızlı sunucuların ve daha karmaşık yazılımların kullanılmasını zorunlu hale getirir.

Ters-çözüm işleminde fiziksel modelin hesaplanması dolaylı bir yol ile gerçekleştirilir. Türev-tabanlı ters-çözüm yöntemlerinin birinci adımında, model parametreleri için bir ön-kestirim yorumcu tarafından sağlanır ve ön-kestirime karşılık gelen kuramsal veri hesaplanarak, ölçülen veri ile karşılaştırılır. Daha sonra, ölçülen ve kuramsal verinin çakışma derecesini arttırmak amacı ile parametreler yenilenir. Bu işlem, iki veri kümesi arasında yeterli bir çakışma elde edilinceye

kadar yinelenir. Ölçülen veri ile çıkarılan kuramsal veri üretken birden fazla model bulunabileceğinden, çözüm tekil değildir. Model yanıtı ile ölçülen veri arasındaki farkları en aza indirmek için yapılan yineleme işleminin sayısı, ön-kestirim değerlerinin gerçeğe yakınlığı ve verinin gürültü içeriği ile ilişkilidir. Gürültü bazı durumlarda yineleme işleminin yakınsamasını engelleyebilir.

Evirtim işlemi ile hesaplanan üç-boyutlu yeraltı öz direnç modelinin, diğer yerbilim bilgileri de kullanılarak jeolojik açıdan anlamlandırılması yorum sürecini oluşturur. Aynı jeolojik birim içerisindeki küpler, birbirine oldukça yakın öz direnç değerleri gösterir. Küplerden oluşan bu tür öz direnç modellerinin yorumlanmasındaki en büyük güçlük jeolojik birimlerin sınırlarının saptanmasıdır. Çünkü güncel evirtim yöntemleri yeraltının bulanık (blurred) bir görüntüsünü üretir. Bu nedenle, öz direnç modelini oluşturan komşu hücreler birbirleri ile ilişkilendirilerek, jeolojik birimlerin sınırları yorumcu tarafından görsel yol ile belirlenmek zorundadır.

Manyetotellürik yöntemin ana ilkeleri, veri-sunum ve veri-işlem teknikleri ile yer altı öz direnç dağılımının elde edilmesinde kullanılan algoritmalara ait ayrıntılı bilgiler için "Jeotermal, Maden ve Petrol Aramalarında Manyetotellürik Yöntem" adlı kitaba bakılabilir. (Başokur, 2015).

Şekil 1. Üç-boyutlu ters-çözümde kullanılan model ağı. İnceleme alanı sırası ile x, y ve z yönlerinde 80, 103 ve 74 olmak üzere toplam 609.760 hücreye bölünmüştür.

## GÜNEYDOĞU ANADOLU'DA PETROL ARAMA AMAÇLI MT ÇALIŞMA ÖRNEKLERİ

Uygulamalı MT çalışmaları TPAO tarafından çeşitli servis firmalarına yaptırılmakla birlikte, bu çalışmaların içerikleri yayımlanmamıştır. Bu çalışmalar üç-boyutlu modellemelerin bilgisayar kapasiteleri nedeni ile gerçekleştirilemediği dönemlerde yapılmıştır.

Güneydoğu Anadolu'da MT yönteminin uygulanabilirliğini ele alan ilk açık kaynak, İlkışık ve Jones(1984) yayımlanan makaledir ve kuramsal bir çalışma olup, sahada MT ölçmeleri yapılmamıştır. Makalede üstten alta doğru, Bazalt, Midyat kireçtaşı, Gerçüş kumtaşı, Üst ve Alt Germav şeyli, Garzan kireçtaşı, Trias-Permian kireçtaşı, Ordovisiyen kumtaşı ve Kambrien temelden oluşan bir kesit ele alınmıştır (Şekil 2). Kuyu ölçülerinden elde edilen öz direnç değerleri ve bir-boyutlu model kullanılarak MT görünür öz direnç verisi hesaplanmıştır (Şekil 3). Bu veriden parametre kestirim yöntemlerinin uygulanması ile hangi katmanların derinlik ve öz direnç değerlerinin çözülebileceği hakkında yorum yapılmıştır. Germav şeylinin kalınlığının en iyi çözülen parametre olduğu, Germav şeyli üstünde kalan istifin kalınlığının ve temel öz direncinin iyi derecede çözülebildiği gösterilmiştir.

Şekil 2. Öz direnç kuyu loglarından elde edilen kalınlık ve ortalama öz direnç değerlerine göre hazırlanan ve katman çözümlüklerini incelemede kullanılan kesit.

Şekil 3. Bir önceki şekilde verilen kesitteki öz dirençleri kullanarak hesaplanan görünür öz direnç eğrisi (İlkışık ve Jones, 1984).

İkinci örnek, Adıyaman civarında gerçekleştirdiğimiz MT çalışmalarından derlenmiştir. Adıyaman kuzeyinde açılan bir kuyunun öz direnç kuyu ölçülerinden, Çizelge 1'de verilen öz direnç değerleri elde edilmiştir. Çizelgenin incelenmesi ile Midyat formasyonu ile Germav formasyonu arasında öz direnç kontrastı olduğu ve bu sınırın MT yöntemi ile ayırt edilebileceği anlaşılmaktadır. Ancak, Germav, Koçali-Karadut ve Kastel formasyon ara yüzeylerinin ayırt edilmesi tümünün düşük öz dirençli olması nedeni olanaklı görülmemektedir. Öz direnç modelinde bu üç formasyonun tek bir katman gibi yanıt vermesi beklenir. Sayındere formasyonu ise kireçtaşı biriminden oluştuğundan yüksek öz direnç değeri göstermekte ve üstteki formasyon ile olan sınırlarını ayırt edilmesi olanaklıdır. Şekil 4'de ise TPAO'na ait bir sondaj kuyusundaki öz direnç değişimi görüntülenmiştir. Öz direnç değişimi başlıca üç öz direnç katmanına işaret etmektedir. En üstteki 100 ohm-m öz dirençli katmanın Midyat formasyonunu, düşük öz dirençli katmanın Germav, Koçali-Karadut, Kastel formasyonları ve yüksek öz dirençli son katmanın Sayındere ve onun üzerindeki katmanları temsil ettiği gözlenmektedir. Böylece Midyat-Germav ve Kastel-Sayındere arayüzeylerinin öz direnç kesitlerinde kolaylıkla ayırt edilmeleri beklenebilir.

Şekil 5'de MT ölçülerinin üç-boyutlu modellemesi ile üretilen 25 km uzunluğundaki bir hat boyunca hesaplanan öz direnç kesiti görülmektedir. Yukarıda değinildiği gibi düşük öz dirençli zonun derinlik ile değişiminin, ayrıca alt ve üst katmanlar ile arayüzeyinin yüksek ayrımlılık ile çözümlendiği gözlenmektedir.

Çizelge 1. Adıyaman kuzeyinde kuyu bilgilerinden derlenen öz direnç değerleri.

Formasyon Litoloji Öz direnç (ohm-m)

Midyat Kireçtaşı-Dolomit 100

Germav Marn, Şeyl, Kumtaşı 20

Koçali-Karadut Serpantin, Şeyl, Marn, Kireçtaşı 10

Kastel Marn-Kumtaşı 5

Sayındere Killi Kireçtaşı 100

Şekil 4. Öz direnç kuyu ölçülerine göre formasyon öz dirençleri.

Şekil 5. MT ölçülerinin üç-boyutlu modellemesi ile üretilen 25 km uzunluğundaki bir hat boyunca hesaplanan öz direnç kesiti. Hoya-Germav ve Kastel-Sayındere arayüzeyleri yüksek öz direnç kontrastı göstermektedir.

## 5. SONUÇLAR

Güneydoğu Anadolu'da gerçekleştirdiğimiz MT incelemeleri ve üç-boyutlu modellemeler sonucunda, Midyat-Germav ve Kastel-Sayındere geçişlerinin saptanabileceğini, Germav, Koçali-Karadut ve Kastel formasyonlarının tek bir katman gibi çözülebileceği

gösterilmiştir. Ayrıca, sismik yöntemin iyi sonuç vermediği yüksek hızlı yüzey katmanı koşullarında (bazalt gibi volkanik kayalar ve bindirme kuşakları), MT yönteminin sismik yöntem ile birlikte veya tek başına kullanılabilirliği gösterilmiştir.

#### KAYNAKLAR

Abdul Azeez, K. K., T. Satish Kumar, S. Basava, T. Harinarayana and A. M. Dayal (2011). Hydrocarbon prospects across Narmada-Tapti rift in Deccan trap, central India: Inferences from integrated interpretation of Magnetotelluric and geochemical prospecting studies. *Marine and Petroleum Geology*, 28, 1073-1082 doi:10.1016/j.marpetgeo.2011.01.003.

Başokur, A. T., 1994, Definitions of apparent resistivity for the presentation of magnetotelluric sounding data, *Geophysical Prospecting*, 42, 141-149.

Başokur, A. T., 2015, Jeotermal, Maden ve Petrol Aramalarında Manyetotellürik Yöntem, Lemnis Yerbilimleri Ltd. Şti. Yayınları (<http://www.lemnis.com.tr>). 28 sayfa.

Başokur, A. T., 2023, Hilbert transform of unequally sampled data: Application to dispersion relations in magnetotellurics. *Geophysics* 88, 2, E29-E38.

Beamish, D. and Travassos, J.M., 1992, Magnetotelluric of basalt-covered sediments. *First Break*, 10, 345-357.

Christopherson KR (1991) Applications of magnetotellurics to petroleum exploration in Papua New Guinea: a model for frontier areas. *Lead Edge* 10:21-27.

Colombo, Keho and McNeice G., 2012, Integrated seismic-electromagnetic workflow for sub-basalt exploration in northwest Saudi Arabia. *Lead Edge* 31:42-53.

De Stefano M, Andreasi FG, Virgilio M, Snyder F (2011) Multiple-domain, simultaneous joint inversion of geophysical data with application to subsalt imaging. *Geophysics* 76:R69-R80.

Harinarayana, T., D. N. Murthy, R. S. Sastry, S. G. Virupakshi, M. Someswara Rao, K. Veeraswamy, S. P. E. Rao, C. Manoj, B. P. K. Patro, K. K. Abdul Azeez, K. Naganjaneyulu, M. V. C. Sarma, T. Srinivasulu, S. Basava, G. D. Naidu, A. K. Gupta, V. T. C. Kumara Swamy, S. R. K. Kishore, T. V. Phanikiran, K. Ravishankar, S. V. Sreedhar and N. Nageshwara Rao (2009). Integrated Geophysical studies for hydrocarbon exploration in eastern part of the Deccan Syncline, Central, India. NGRI Technical Report No: NGRI-2009-EXP-679-Volume II.

Harinarayana, T., M. Someswara Rao, K. Veeraswamy, D. N. Murthy, M. V. C. Sarma, R. S. Sastry, G. Virupakshi, S. P. E. Rao, B. P. K. Patro, C. Manoj, M. Rao, T. Sreenivasulu, K. K. Abdul Azeez, K. Naganjaneyulu, S. K. Begum, B. F. Kumar, K. Sudha Rani, M. Sreenivas, V. Prasanth and P. Aruna (2003). Exploration Sub-Trappean Mesozoic basins in the western part of Narmada-Tapti region of Deccan syncline. NGRI-2003-EXP-404.

Harinarayana, T., R. S. Sastry, N. Nagarajan, S. P. E. Rao, C. Manoj, K. Naganjaneyulu, G. Virupakshi, D.N. Murthy and S. V. S. Sarma (2000). Integrated Geophysical studies for Hydrocarbon exploration, Kutch, India. NGRI-2000-EXP-296.

Kumar D, Hoversten GM (2012) Geophysical model response in shale gas. *Geohorizons* 17:32-37

Mansoori, I., B. Oskooi and L. Pederson (2015). Magnetotelluric signature of anticlines in Iran's Sehqanat oil field. *Tectonophysics*, 654, 101-112.

Mansoori, I., B. Oskooi, L. Pederson and R. Javaheri (2016). Three - dimensional modelling of magnetotelluric data to image Sehqanat hydrocarbon reservoir in southwestern Iran. *Geophysical Prospecting*, 64, 753-766.

Mitsuhashi, Y., K. Matsuo and M. Minegishi (1999). Magnetotelluric survey for exploration of a volcanic-rock reservoir in the Yurihara oil and gas field, Japan. *Geophysical Prospecting* 47, 195-218.

Morrison HF, Shoham Y, Hoversten GM, Torres-Verdin C (1996) Electromagnetic mapping of electrical conductivity beneath the Columbia basalt. *Geophys Prospect* 44:935-961

Pandey, D., S. Singh, M. Sinha, L. MacGregor (2009). Structural imaging of Mesozoic sediments of Kachchh, India and their hydrocarbon prospects. *Marine and Petroleum Geology*, 26, 1043-1050.

Patro, P. K., K. K. Abdul Azeez, K. Veeraswamy, S. V. S. Sarma, M. K. Sen (2015). Sub-basalt sediment imaging - the efficacy of magnetotellurics. *Journal of Applied Geophysics*, 121, 106-115, DOI: <http://dx.doi.org/10.1016/j.jappgeo.2015.07.010>.

Sarma, S.V. S., G. Virupakshi, D. N. Murthy, T. Harinarayana, T. S. Sastry, M. S. Rao, N. Nagarajan, K. Veeraswamy, M. S. Sarma, S. P. E. Rao, K. R. B. Gupta (1992). Magnetotelluric studies for Oil Exploration over Deccan Traps, Saurashtra, Gujarat, India. NGRI-92-LITHOS-125.

Sarma, S. V. S., G. Virupakshi, T. Harinarayana, D. N. Murthy, M. Someswara Rao, R. S. Sastry, N. Nagarajan, T. S. Sastry, M. V. C. Sarma, M. Rao, K. Veeraswamy, S. P. E. Rao, K. R. B. Gupta, A. Lingaiah, T. Sreenivasulu, A. V. S. N. Raju, B. P. K. Patro, C. Manoj, A. Bansal, V. T. C. Kumaraswamy, S. R. Sannasi, C. Stephen and K. Naganjaneyulu (1998a). Integrated Geophysical studies for Hydrocarbon exploration Saurashtra, India. NGRI-98-EXP-237.

Satpal, O. P. Singh, D. Sar, S. M. Chatterjee and S. Sawa (2006). Integrated interpretation for sub-basalt imaging in Saurashtra Basin, India. *Leading Edge*, July issue, 882-885.

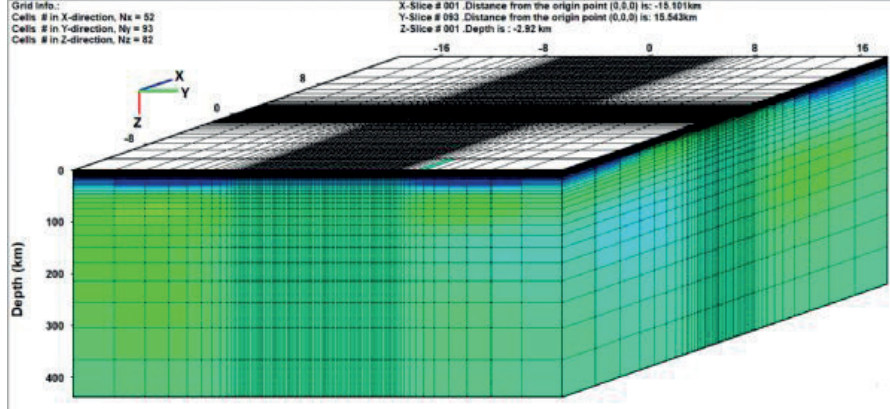
Spies BR (1983) Recent developments in the use of surface electrical methods for oil and gas exploration in the Soviet Union. *Geophysics* 48:1102-1112.

Strack, K. M., P. B. Pandey (2007). Exploration with controlled-source electromagnetic under basalt cover in India. *Leading Edge*, March issue, 360-363.

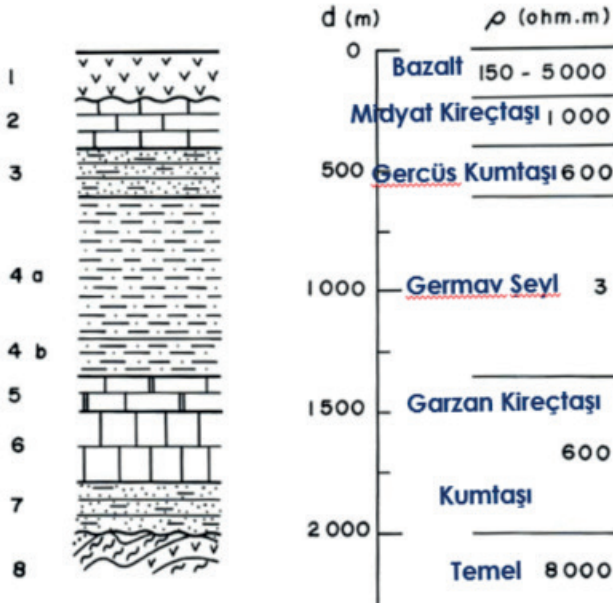
Yakovlev, D. V., Yakovlev, A.G. and Valyasina O.A., 2018, Study in the northern margin of the Siberian platform based on regional geoelectric survey data (in Russian).

Anahtar Kelimeler: Manyetotellürik Yöntem, Güneydoğu Anadolu'da Petrol Aramacılığ

Şekil 1

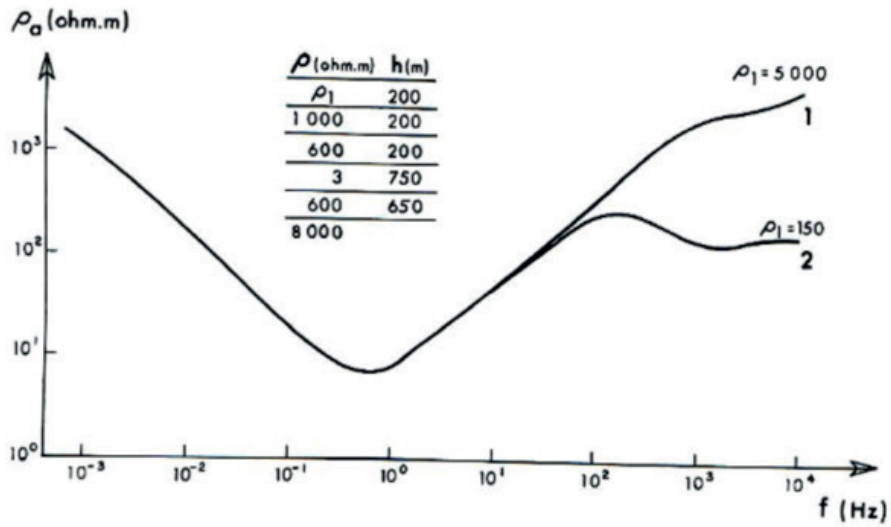


Şekil 2

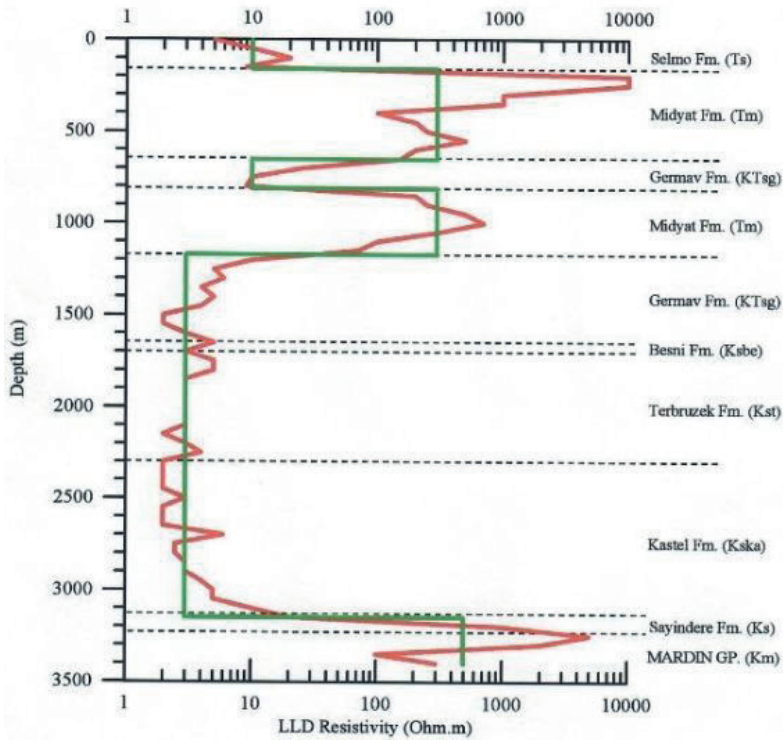




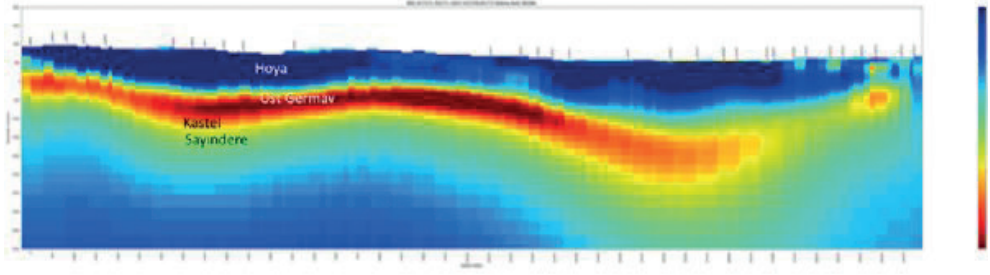
Şekil 3



Şekil 4



Şekil 5



Çizelge 1

Formasyon	Litoloji	Özdirenç (ohm-m)
Midyat	Kireçtaşı-Dolomit	100
Germav	Marn, Şeyl, Kumtaşı	20
Koçali-Karadut	Serpantin, Şeyl, Marn, Kireçtaşı	10
Kastel	Marn-Kumtaşı	5
Sayındere	Killi Kireçtaşı	100

Adıyaman kuzeyinde kuyu bilgilerinden derlenen özdirenç değerleri

# A Multiphysics Approach To Evaluating Gas Prospectivity With Case Examples

**Daniel Baltar Pardo, Dag Helland Hansen, Elias Andre Nerland**  
EMGS



## INTRODUCTION

In a time when the world is in trying to reduce its carbon emissions and the war in Ukraine has created an energy crisis, the demand for gas is increasing beyond supply capacity. The demand surge and price hike has led many companies to re-initiate global exploration for gas. The issue then becomes how to make gas exploration more efficient to improve exploration profitability and reduce the time to first production. Exploration efficiency can be improved, particularly in cases where seismic direct hydrocarbon indicators and CSEM resistivity can be combined in a multiphysics approach.

In this paper we discuss how a multiphysics approach impacts prospect assessment, particularly in gas cases where seismic direct hydrocarbon indicators are present. We illustrate this through a few case examples from several basins in the world where this approach has been proven.

When interpreting 2D and 3D seismic it is often easy to spot bright seismic amplitudes and AVO responses indicating presence of highly-porous shallow gas-filled reservoirs. These seismic bright events often happen in uncompacted young sediments at relatively low pressures, which can mean excellent reservoir properties but also an ambiguous seismic response and interpretation with regards to the presence and extent of full hydrocarbon saturation.

This sort of features often occurs in clusters, with several similar prospects belonging to the same play happening over a region, making the upside potential very attractive, but making it hard to choose an optimal drilling sequence that will allow to encounter the largest accumulations first. This slows down and reduces the success rate of the exploration efforts, reducing its profitability.

## CASES

The challenge with using seismic amplitudes in these plays is that the effect of gas presence in this poorly-consolidated high-porosity sediments is very strong, this means the mere presence of gas will induce a seismic amplitude anomaly, independently of the saturation. At the same the presence of a seal in such unconsolidated sediments is usually uncertain or its capacity limited. Hence, these conspicuous seismic amplitude anomalies can represent paleo gas accumulations that only contain a residual quantity of gas that can't be produced (or just high porosity lithology) but that is extremely difficult to distinguish from a high gas saturation as it may display very similar properties such as amplitude conformance to structure, AVO response, flat spots and low seismic velocity.

This is where CSEM-derived resistivity can make a

large difference, since the main driver of resistivity is the amount of brine in the sediment, it provides the perfect indicator to separate those amplitude anomalies with high hydrocarbon saturation from those with high brine saturation. There are several reasons why CSEM can provide a very significant change in the understanding of gas related features. First, the sensitivity of CSEM is heavily dependent on the target's depth below mudline, this type of targets are often at a depth where CSEM sensitivity is high, making it easy to detect even relatively small lateral changes in reservoir resistivity. Second, given the uncompacted nature of these sediments their porosity/water content is very high with very unlikely occurrence of diagenesis and compaction having reduced the porosity and increased the resistivity. This leads to very homogeneous and low resistivity backgrounds with hardly any occurrences of high resistivity not associated with presence of hydrocarbon in the sediment. Third, there is the reservoir resistivity in this type of sediments, their poorly consolidated nature makes very low residual water saturations common, leading to a great contrast between the high brine content background and the low brine content fully saturated pay.

Therefore, CSEM resistivity --derived independently from any seismic interpretation or models-- provides an independent assessment of the geological model and a large reduction in the pre-drill uncertainty of both the presence and extent of a hydrocarbon accumulation. Which are two of the main pre-drill uncertainties of prospects with good seismic direct hydrocarbon indicators.

We will show several case studies from different parts of the world, where gas prospects with a variety of seismic direct hydrocarbon indicators were supplemented with CSEM derived resistivity. We will analyse the CSEM data, processing and interpretation requirements and the impact of the multiphysics approach in the prospect evaluation. These cases are in relatively young and poorly consolidated clastic sediments, they showed good direct hydrocarbon indications on seismic.

One of the cases is from the Gulf of Mexico, where a Miocene reservoir shows two contacts in the seismic data. The structure is a four-way dip closure much larger than the seismic DHI response. The application of 3D CSEM indicates the presence of a highly resistive body around just one of the contacts. The resistivity indicates a high likelihood of gas presence but a limited areal extent of the hydrocarbon accumulation, which allowed to increase the accuracy of the prospect evaluation.

The second example from the North Sea contains several salt related structures with the same Late Tertiary reservoir and very similar seismic DHI responses: clear amplitude anomalies and structural conformance,

Figure 1 and Figure 4. From a seismic-only evaluation perspective, the largest risk is the presence of seal in the structures. A regional CSEM survey allows us to re-evaluate several of these prospects considering the new physical measurement (Figure 2 and Figure 5) and provide an updated risk and volume. There is extremely high sensitivity to any significant hydrocarbon charged volumes, in terms of the area, net thickness and resistivity of the accumulation, as shown in Figure 3. This will reduce the uncertainty in the presence and extent of the potential hydrocarbon accumulations and allow to confidently set a drilling sequence that will maximize the amount of hydrocarbon found in the first few wells.

## FINDINGS

In cases where the presence of direct hydrocarbon indicators on seismic, which are typically considered as some of the lowest uncertainty cases possible in exploration, the adoption of a multiphysics approach can significantly reduce the uncertainty in the prospect evaluation beyond what would be possible using a conventional approach.

In order to achieve this very low uncertainty evaluations it is paramount to have good seismic information with direct hydrocarbon indicators and independently-processed CSEM data. If this is done in gas cases with young loosely compacted reservoirs, then a geophysical sweet spot is reached, where seismic provides very clear direct seismic hydrocarbon indicators, and CSEM has high sensitivity with excellent contrast between the high porosity-permeability reservoirs and the low-resistivity lithologies in the background.

## CONCLUSIONS

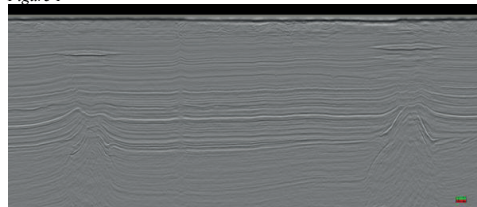
Even in cases with extremely similar seismic direct hydrocarbon indicators, where making a decision on drilling priority would be challenging, using a multiphysics approach will deliver a very large improvement in the prospect evaluation, both in terms of risking and volume assessment, since CSEM derived resistivity will allow to identify the presence of hydrocarbon saturated sediments and the lateral extent of the hydrocarbon accumulation, significantly improving the understanding of the hydrocarbon accumulation size.

We will also look at the impact of the CSEM response on the assessment of the play and how it creates play segments with very different properties and provides the potential for a very significant improvement on the play creaming, exploration efficiency, and its economic attractiveness.

In order to achieve effective improvements in exploration performance it is key to have the information at the right time to impact decision making. This implies having a work program that includes multiphysics at the right scale well ahead of the drilling/drop decision or the decision to prioritize certain prospects, plays, or play segments.

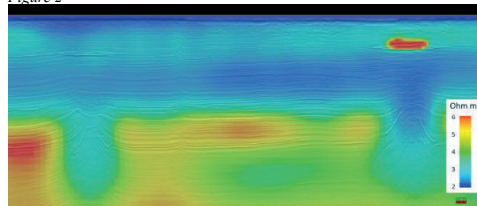
Keywords: Gas Exploration, multiphysics

Figure 1



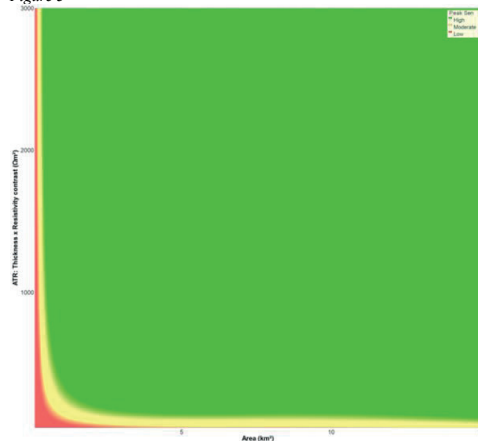
Seismic response of two prospects with clear seismic amplitude anomalies and flat spots. The size and seismic characteristics are extremely similar.

Figure 2



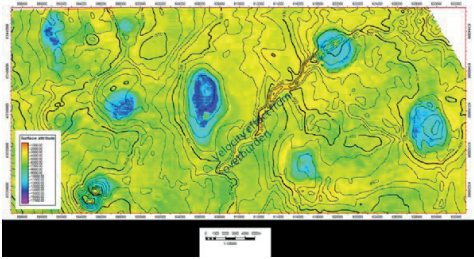
Same seismic line as in Figure 1 with CSEM-derived resistivity. Very different responses can be seen in both prospects, implying an extremely different risk and volume profile for each prospect.

Figure 3



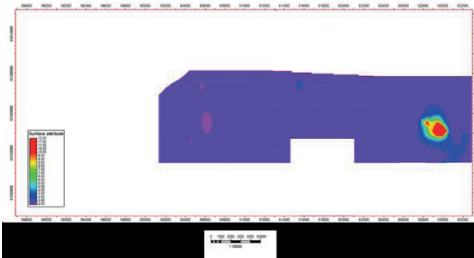
Sensitivity of CSEM to the prospects in Figure 1 and 2. Extremely high sensitivity (green area) to most geological models that include hydrocarbon filled sands with a few square kilometre targets.

Figure 4



Seismic amplitude map of the top reservoir horizon with structural contours every 10 m. There are several seismic amplitudes with good match to structure and others with less obvious structural conformance.

Figure 5



Average normal resistivity from CSEM averaged around the top reservoir horizon. A clear CSEM anomaly is observed in one of the prospects but not the other.

# Gravite Tabaka Sıyırma Yöntemi ile Doğu Akdeniz'de Gravite Anomalilerinin Analizi ve Tektonik Yapıların İncelenmesi



## İlkin Özsöz

Maden Tetkik ve Arama Genel Müdürlüğü

### ÖZET

Bu çalışma, Doğu Akdeniz sahası için gravite tabaka sıyırma yönteminin uygulanmasını ele almaktadır. Yöntemin amacı, sabit yoğunluk kontrastına sahip ve ondülasyonu bilinen bir yüzeyin gravite anomalisinin hesaplanarak, ölçülen gravite anomalisinden elimine edilmesi olarak tanımlanabilir. Çalışmada, Doğu Akdeniz sahasının serbest hava anomalisi ve batimetri verileri kullanılmıştır. Moho arayüzeyi ise Airy-Heiskanen İzostazi Teorisi ile hesaplanmıştır. Daha sonra, su kolonu ve Moho ondülasyonlarının gravite etkileri Parker-Oldenburg yöntemi ile hesaplanmıştır. Hesaplama yapılırken su kolonun yoğunluk kontrastı  $-1670 \text{ kg/m}^3$  ve Moho arayüzeyinin yoğunluk kontrastı  $-200 \text{ kg/m}^3$  olarak varsayılmıştır. Deniz tabanı ve Moho ondülasyonları altında kalan sırasıyla  $-4750 \text{ m}$  ve  $-30000 \text{ m}$  deki düz yüzeyleri gravite etkileri de rejyonel etkiyi gidermek için kullanılmıştır. Su kolonuna ait gravite etkisinin, serbest hava anomalisinden elimine edilmesi ile rezidüel anomali elde edilmiş olup, Moho ondülasyonlarına ait gravite etkisinin, rezidüel anomaliden elimine edilmesi ile izostatik rezidüel anomali elde edilmiştir. Sonraki aşamada, Doğu Akdeniz çalışma alanı için Bouguer, rezidüel ve izostatik rezidüel anomalilerin uzay ve dalga-sayı ortamındaki korelasyonu irdelenmiştir. Ayrıca bu anomalilerin çalışma alanında bulunan Doğu Akdeniz Sırtı'nı ve Ege Yayı'nı temsil etme kabiliyeti yorumlanmıştır. Elde edilen bulgulara göre Bouguer ve rezidüel anomalileri uzay ortamı korelasyonunda  $R^2=0.99$  ile pozitif mükemmel korelasyonu işaret etmesine rağmen, dalga-sayı ortamında kısmi farklılıklar gözlemlenmiştir. Çalışma alanındaki tektonik yapılar rezidüel ve izostatik rezidüel anomalilerde belirgin kontrastlar oluştururken, Bouguer anomalisinde bu yapılar yorumlanabilir olsa bile rezidüel ve izostatik rezidüel anomalilerde olduğu gibi belirgin kontrastlar gözlemlenmemiştir. 3B modelleme ile elde edilen bulgular yüksek dalga sayısı bileşenlerinde daha az genlik kaybı ve tektonik yapıların yorumlanabilirliği açısından Bouguer anomalisine göre daha iyi ve güvenilir sonuçlar sunmuştur.

### ABSTRACT

This study focuses on the application of the gravity layer stripping method for the Eastern Mediterranean region. The method aims to calculate the gravity anomaly of an undulating surface with constant density contrast and eliminate it from the measured gravity anomaly. The study utilizes the free-air anomaly and bathymetry data of the Eastern Mediterranean region, while the Moho interface is calculated using the Airy-Heiskanen Isostasy Theory. Subsequently, the gravity effects of the water column and Moho undulations are calculated using the Parker-Oldenburg method, assuming a constant density

contrast of  $-1670 \text{ kg/m}^3$  for the water column and  $-200 \text{ kg/m}^3$  for the Moho undulations. The gravity effects of flat surfaces located at depths of  $-4750 \text{ m}$  and  $-30000 \text{ m}$  below the sea floor and Moho undulations, respectively, are utilized to remove the regional effects. By eliminating the gravity effect of the water column from the free-air anomaly, the residual anomaly is obtained, while eliminating the gravity effect of the Moho undulations from the residual anomaly yields the isostatic residual anomaly. In the subsequent stage, the correlation of Bouguer, residual, and isostatic residual anomalies in the spatial and wavenumber domains is examined for the Eastern Mediterranean study area. Furthermore, the ability of these anomalies to represent the Eastern Mediterranean Ridge and Aegean Arc is interpreted. The results indicate a positive perfect correlation ( $R^2=0.99$ ) between Bouguer and residual anomalies in the spatial domain, albeit with some moderate differences in the wavenumber domain. While the tectonic structures in the study area exhibit notable contrasts in the residual and isostatic residual anomalies, the Bouguer anomaly shows interpretable but less notable contrasts. The findings obtained through 3D modelling present better and more reliable results in terms of less amplitude loss in high-wavenumber components and interpretability of the tectonic structures compared to the Bouguer anomaly.

### 1. GİRİŞ

Bir statik kütle dağılımının gravitasyonel alanını elde etmek için düz çözüm yöntemleri kullanılabilir. Topoğrafya ve deniz tabanı ondülasyonlarının gravite etkileri (Sandwell ve diğ. 2006), gravite tabaka sıyırma yöntemi (Miroslav ve diğ. 2013), Bouguer ve izostatik anomali hesabı (Vaníček ve diğ. 1999), sediman tabanı morfolojisi (Granser, 1987) ve Moho arayüzeyinin gravite anomalisi (Gómez-Ortiz ve Agarwal, 2005) düz çözüm teknikleri ile çözülebilen problemler ve hesaplamalar arasındadır. Düz çözüm teknikleri ile bu hesapların yapılabilmesi için gravite anomalisine neden olan cismin veya yüzeyin kütleli dağılımının tanımı, geometrik özellikleri ve sabit veya değişken yoğunluk farkı bilgileri gerekmektedir (Hirt ve diğ. 2016).

Düz çözüm teknikleri spektral ortamda veya uzay ortamında gerçekleştirilebilir. Uzay ortamında, çalışma alanı genellikle dikdörtgen prizmalar veya mikro birimler gibi poligonol cisimlere bölünür ve her prizmatik cismin hacim integrali, köşelerdeki fonksiyonların toplamı yoluyla hesaplanabilir (Cordell ve Henderson, 1968; Li ve Oldenburg, 2010). Ancak uzay ortamı düz çözüm yöntemlerinin hesaplama süresi oldukça zaman almaktadır. Spektral ortamda yapılan düz çözüm teknikleri integrasyona gerek duymadığı için daha hızlı sonuç üretebilmektedir

(Parker, 1973; Oldenburg, 1974). Spektral ortamda yapılan düz çözüm tekniklerinin dezavantajları, çalışma alanının kenarlarında veri kaybına neden olması ve spektral ortamda düz çözüm için kullanılan Parker-Oldenburg yönteminin Dünya'nın küreselliğini hesaba katmadığı için kıtasal ölçekli çalışmalarda hatalı çözümler üretmesidir (Chen ve Tenzer, 2020). Bu çalışma kapsamında hızlı çözüm üretmesi ve Dünya'nın küreselliğinden kaynaklı hatanın ihmal edilebilir olması nedeniyle spektral ortam düz çözüm tekniği olan Parker-Oldenburg yöntemi kullanılmıştır.

Spektral alanda uygulanan gravite tabaka sıyırma tekniği, her bir katmanın veya yüzeyin gravite etkisinin toplamının ölçülen toplam gravite anomalisini yarattığını varsaymaktadır. Bu durum süperpozisyon prensibi tanımlanmaktadır (Blakely, 1996). Süperpozisyon prensibi, yüzey ondülasyonu ve yoğunluk kontrastı bilinen tabakanın gravite anomalisinin, toplam ölçülen gravite anomalisinden elimine edilmesine olanak sağlamaktadır. Bu işlem gravite tabaka sıyırma yöntemi olarak adlandırılmaktadır.

Düz çözüm ile modellenen ve gravite anomalisi hesaplanan katmanın dalga-sayısı içeriği yoğunluk farkı, yanal çözünürlük ve derinlik tarafından kontrol edilir. Bu durumda ölçülen gravite anomalisi ve modellenen katmanın gravite anomalisinin yüksek dalga-sayısı bileşenlerinde farklılıklar gözlenecektir. Bu dalga-sayısı bileşenlerindeki farklılıklar, gravite tabaka sıyırma işleminde model bütünlüğünü bozan etkilere sebep olmaktadır. Model bütünlüğünü bozmamak ve yapay etkilerden kaçınmak için, ölçülen ve modellenen gravite anomalisi arasındaki dalga-sayısı bileşenlerinin eşitlenmesi gerekmektedir (Özsöz, 2019; Özsöz ve diğ., 2022).

Çalışmanın amacı, Doğu Akdeniz sahasının serbest hava anomalisinden, aynı sahanın batimetri ve Airy-Heiskanen teorisi (Airy, 1855; Heiskanen, 1931) ile hesaplanan Moho ondülasyonlarının gravite etkilerinin elimine edilmesi için uygulanan gravite tabaka sıyırma yönteminin anlatılması ve elde edilen Bouguer, rezidüel ve izostatik rezidüel anomalilerin yapısal unsurları tanımlama kabiliyetinin ve dalga-sayısı içeriklerinin irdelenmesidir. Çalışma kapsamında 3B modelleme işlemi bu çalışma kapsamında yazılan MATLAB tabanlı "fwgparke3D" programı ile yapılmıştır. Doğu Akdeniz sahasının serbest hava anomalisi International Gravimetric Bureau (BGI) (Bonvalot ve diğ., 2012) tarafından sağlanmış olup, batimetri verileri ise ETOPO1 (Amante and Eakins, 2009) modelinden elde edilmiştir.

## 2. YÖNTEM

### 2.1. Parker-Oldenburg Yöntemi

Ondülasyona sahip sabit yoğunluk kontrastlı bir yüzey ile bu yüzeye ait gravite anomalisinin spektral ortamda düz çözüm ile hesaplanması Parker (1973) ve Oldenburg (1974) tarafından tanımlanmıştır.

$$F[\Delta g(x,y)] = -2\pi G \Delta \rho e^{-(kz_0)} \sum_{n=1}^{\infty} \frac{k^n}{n!} F[\Delta h]^n(x^*, y^*) \quad (1)$$

Eşitlik (1)'de G, gravitasyonel sabiti ( $6.67 \times 10^{-11} \text{ m}^3/(\text{kg} \cdot \text{s}^2)$ );  $F[\Delta g]$ , modellenen gravite anomalisinin 2 boyutlu Fourier Dönüşümü'nü;  $\Delta \rho$ , sabit yoğunluk kontrastını;  $k = \sqrt{k_x^2 + k_y^2}$ , dalga-sayısını;  $z_0$ , arayüzeyin ortalama derinliğini,  $F[\Delta h]^n$ , ondülasyonlu yüzeyin 2 boyutlu Fourier Dönüşümü'nü ve n, Parker-Oldenburg denklemine uygulanacak açılımın derecesini göstermektedir. Teorik olarak Eşitlik (1), Parker-Oldenburg denklemine toplama işleminin sonsuza kadar gitmesi gerektiğini göstermesine rağmen, bu durum pratikte uygulanabilir değildir. Bu çalışmada uygulanan Parker-Oldenburg algoritması,  $z = 0$  yüksekliğinde tanımlanan, yatay bir düzlemle sınırlanan ve yüzey dalgalanması  $h(x,y,z)$  olan sabit yoğunluk kontrastına sahip bir modeli tanımlar.

### 2.2. İki Zaman Serisi Arasındaki Spektral Uyumunun Büyüklüğü (MSCS)

Daha önce bahsedildiği gibi modellenen ve ölçülen gravite anomalisinin dalga-sayısı içeriği birbirleri ile aynı olmayacak ve gravite tabaka sıyırma işlemi esnasında bu farklılıklar model bütünlüğünü bozacaktır. Bu durumdan kaçınmak için uyumsuzluk gösteren dalga-sayısı bileşenleri filtrelenmelidir. Bu işlem MSCS yöntemi ile yapılabilmektedir. MSCS yöntemi, iki zaman serisi arasındaki dalga-sayısına bağlı lineer ilişkiyi ölçmekte kullanılan bir araçtır. Eğer  $x_1(n)$  ve  $x_2(n)$ 'in, iki farklı zaman serisini temsil ettiği düşünülür ise MSCS yöntemi aşağıdaki gibi tanımlanabilir:

$$C_{(x_1, x_2)}(k) = \frac{S_{(x_1, x_2)}(k)}{\sqrt{S_{(x_1, x_1)}(k) \times S_{(x_2, x_2)}(k)}} \quad (2)$$

Bağıntı (2)'de  $S_{(x_1, x_2)}(k)$ ,  $x_1$  ve  $x_2$  zaman serilerine ait çapraz spektrumu;  $S_{(x_1, x_1)}(k)$  ve  $S_{(x_2, x_2)}(k)$ ,  $x_1$  ve  $x_2$  zaman serilerine ait güç yoğunluğu spektrumunu göstermektedir.

## 3. BULGULAR ve TARTIŞMA

Doğu Akdeniz'de, deniz tabanının ve Moho arayüzeyinin gravite etkilerinin ortadan kaldırılması, gravite tabaka sıyırma tekniği ve MSCS yoluyla sağlanmıştır. Çalışma alanı, serbest hava anomalisi ve şematik katman sıyırma diyagramı Şekil 1'de gösterilmektedir; burada gri kısımlar, bu katmanlar için katman sıyırma işleminin yapılmadığını gösterirken renkli kısım, gravite tabaka sıyırma yönteminin uygulandığı yerleri göstermektedir.

Doğu Akdeniz Sırtı (EMR) ve Ege Yayı (AA) ile karakterize edilen çalışma alanında serbest hava anomalisi -100 mgal ile 148 mgal arasında değişmektedir. EMR, yüksek ve düşük gravite anomalileri arasında belirgin bir sınır oluşturmaktadır. Benzer şekilde AA, gravite anomalisindeki düşük dalga boyu bileşeni (güneydoğu kesiminde) ile daha yüksek dalga boyu bileşeni (kuzeybatı kesiminde) arasındaki sınırı göstermektedir.

Moho arayüzeyini belirlemek için, batimetri verileri 1 ark-dakika çözünürlüğünde ETOPO 1 modelinden elde edilmiştir ve 30000 m denge kolunu varsayımı ile Airy-Heiskanen izostazi teorisi kullanılmıştır. Moho arayüzeyi haritası batimetri verilerinden tahmin edildiğinden, iki harita arasında dalga sayısı açısından herhangi bir farklılık bulunmamaktadır. Şekil 2'de, deniz yatağının ve Moho arayüzeyinin 3B yüzey haritası gösterilmiştir. Bu harita Moho arayüzeyinin, deniz tabanındaki ondülasyonları izostatik olarak nasıl kompanse ettiğini göstermektedir.

Deniz tabanının değerleri -4740 m ile -869.33 m arasında değişirken, Moho ondülasyonları -25327.49 m ile -15355.32 m arasında değişmektedir (Şekil 2). Airy-Heiskanen izostazi teorisine göre deniz tabanı, Moho'da anti-köklere ile dengelenmektedir. Bu çalışmada kullanılan "fvg\_parker3d" kodu, her katman için sabit yoğunluk kontrastı varsayımıyla, deniz suyu yoğunluğunun 1030 kg/m<sup>3</sup> ve arka plan yoğunluğunun 2700 kg/m<sup>3</sup> olduğu varsayımı ile çalıştırılmıştır. Bu nedenle su kolonunun yoğunluk farkı -1670 kg/m<sup>3</sup> (1030-2700=-1670 kg/m<sup>3</sup>) olarak elde edilmiştir. Su kolonunun gravite etkisinin, serbest hava anomalisinden gravite tabaka sıyırma yöntemi ile eliminasyonu Şekil 3'de verilmiştir.

Batimetrisinin gravite etkisi ve onun filtrelenmiş halinin gravite etkisi sırasıyla -264 mgal ile -90 mgal ve -251 mgal ile -80 mgal arasında değişmektedir. Rezidüel anomalide ise değişim 80 mgal ile 296 mgal arasındadır. Rezidüel anomalideki değişimler, batimetrisinin gravite anomalisindeki kütle fazlalığı ve eksikliğine bağlı olarak karakterize edilmektedir. Bu kütle fazlalığı veya eksikliği, rezidüel anomalie pozitif veya negatif katkı sunabilmektedir. Bu çalışma özelinde negatif yoğunluk kontrastı ve negatif derinlik değerleri kullanıldığı için batimetrisinin gravite etkisi, deniz seviyesinin altında olduğu için pozitif katkı sunmaktadır ve bu pozitif katkı deniz tabanının derin olduğu yerlerde artmaktadır. Pozitif katkının kompanse edilebilmesi için filtrelenmiş batimetrisinin gravite anomalisinin, serbest hava anomalisinden çıkarılması gerekmektedir.

Şekil 3e'de her ne kadar batimetrisinin gravite etkisi giderilmiş olsa bile, batimetrisinin reyonel gravite etkisi giderilememiştir. Bu etkinin giderilebilmesi için deniz tabanının hemen altından geçen düz bir yüzeyin, rezidüel anomaliden elimine edilmesi gerekmektedir. Bu çalışma için seçilen düz yüzey -4750 m olarak belirlenmiştir. Düz yüzey, deniz tabanı ondülasyonları ile -4750 m arasında olan bir katman olarak seçildiği için yoğunluk farkının su kolonundan farklı olması beklenmektedir. İnce düz yüzey için yoğunluk 2000 kg/m<sup>3</sup> ve yoğunluk farkı 2000-2700=-700 kg/m<sup>3</sup> olarak seçilmiştir. Düz yüzeyin gravite anomalisi, deniz tabanının gravite anomalisine göre pozitif katkı sunmaktadır. Bu nedenle, düz yüzeyin gravite anomalisinin, deniz tabanının gravite anomalisinden çıkartılması gerekmektedir. Daha sonra, aradaki fark, rezidüel anomalie göre yine pozitif katkı sunduğu için farkın, rezidüel anomaliden çıkartılması gerekmektedir. Bu işlem sonuçları Şekil 4'de gösterilmiştir.

Bulgulara göre, -4750 m derinlikte deniz tabanı ile düz tabaka arasındaki gravite etkisi 34 mgal ile 121 mgal arasında değişmektedir. Ayrıca, -4750 m'ye indirgenen rezidüel anomalinin değeri 40 mgal ile 241 mgal arasında değişmektedir. Şekil 4f'deki anomalî, batimetri ile -4750 m'deki düz yüzeyin arasındaki gravite etkisinin, rezidüel anomaliden çıkartılması ile elde edilmiştir.

İzostatik rezidüel anomalinin hesabı yapılırken herhangi bir doğrudan ölçüm ve ek veri olmadığı izostatik düzeltme için kullanılan yoğunluk kontrastı -200 kg/m<sup>3</sup> olarak varsayılmıştır. Şekil 5'de izostatik rezidüel hesabının sonucu, kullanılan yüzeyler ve onların gravite anomalileri gösterilmiştir.

İzostatik etkiler ölçülen anomalie pozitif katkı sunduğu için Moho ondülasyonları ile -30000 m'deki düz yüzey arasındaki gravite anomalisinin, -4750 m'ye indirgenen rezidüel anomaliden çıkartılması gerekmektedir. Elde edilen izostatik rezidüel anomalî üzerinde çok küçük veya çok büyük ölçekli ondülasyon etkileri giderilmiş ve bu anomalî deniz tabanından Moho arayüzeyine kadar uzanan bölgenin gravite etkisini temsil etmektedir.

Son olarak çalışma alanı için elde edilen rezidüel anomalî (Şekil 3e), Bouguer anomalisi ve İzostatik rezidüel anomalî (Şekil 5g) karşılaştırılmış ve her bir anomalinin geniş ölçekli tektonik yapıları (Doğu Akdeniz Sırtı ve Ege Yayı) temsil etme kabiliyeti irdelenmiştir. Ayrıca, Bouguer anomalisi ve rezidüel anomalî yalnızca su kolonunun gravite etkisinin giderilmesi ile hesaplandığı için bu iki anomalinin benzer sonuçlar göstermesi beklenmektedir. Bu iki anomalie ait benzer sonuçlar arasındaki farklılıklar MSCS ve korelasyon grafikleri ile irdelenmiştir. Son olarak Bouguer anomalisi ve izostatik rezidüel anomalî radyal ortalama güç spektrumu (RAPS) ile karşılaştırılmıştır. Sonuçlar Şekil 6'da gösterilmiştir.

Şekil 6'da görüldüğü üzere Bouguer, rezidüel ve izostatik rezidüel anomaliler EMR'nin güneyinde Afrika Levhası ile EMR'nin kuzeyindeki Avrasya Levhası arasında belirgin bir sınır oluşturduğunu göstermektedir. Tüm haritalardaki gravite anomalileri, Avrasya Levhası'na kıyasla Afrika Levhası'nda daha yüksektir. EMR'nin kuzeyindeki kontur çizgileri, EMR'nin güneyine kıyasla daha sık görülmektedir. EMR baz alınarak gravite anomalilerinde en belirgin kontrast izostatik rezidüel anomalide elde edilirken, Bouguer anomalisi bu alanda en düşük kontrastı sunmuştur.

AA etrafında da sık kontur çizgileri gözlenmektedir. Lort ve diğ. (1971) bu bölgeyi "zone of compression" veya sıkışma bölgesi olarak tanımlamıştır. İzostatik rezidüel anomalide, AA civarında veya sıkışma bölgesinde gravite anomalisinde net bir kontrast gözlenirken, Bouguer anomalisinde bu kadar sert geçişler gözlenmemiş olmasına rağmen Bouguer anomalisi de AA'daki çizgisellik sınırlarını belirlemede oldukça başarılı sonuçlar sunmuştur.

MSCS sonuçlarına göre rezidüel anomalî ile Bouguer anomalî dalga-sayısı ortamında orta derecede bir korelasyon sağlamış ve ara ara dalga-sayısı içeriği nedeniyle farklılıklar gözlenmiştir. Buna karşın,



F-F' profilinden alınan veri ile yapılan uzay-zaman ortamındaki korelasyon sonucu iki verinin neredeyse aynı olduğu gözlemlenmiştir ( $R^2=0.99$ ). Bu durumda, uzay-zaman ortamında Bouguer anomalisi ile rezidüel anomalinin benzer olduğu ancak dalga-sayısı içeriği bakımından birbirinden farklı oldukları ortaya çıkarılmıştır.

Şekil 6f'de Bouguer anomalisi ile izostatik rezidüel anomali arasındaki dalga-sayısı bileşenlerindeki farklılıklar irdelenmiştir. Bu bağlamda, düşük dalga-sayısı bileşenlerinde izostatik rezidüel anomali ile Bouguer anomalisi benzer sonuçlar sunarken, dalga-sayısı içeriği yükseldikçe Bouguer anomalisinin genliğinde önemli bir düşüş gözlemlenmiştir. İzostatik rezidüel anomalinin, Bouguer anomalisine göre dalga-sayısı içeriği bakımından daha ayrıntılı sonuçlar verdiği gösterilmiştir.

3B modelleme ve gravite tabaka eliminasyon yöntemi ile elde edilen rezidüel ve izostatik rezidüel anomaliler, Bouguer düzeltmesi ile elde edilen Bouguer anomalisine göre tektonik yapıların gravite anomalilerinde oluşturduğu kontrastlar ve dalga-sayısı içeriği bakımından daha iyi sonuçlar vermiştir. Bu sonuçlar yalnızca deniz tabanı ve Moho ondülasyonlarının gravite etkilerinin giderilmesi ile elde edilmiştir.

Gravite tabaka sıyırma yöntemi ile sismik yorumlama ile elde edilen ara yüzeylerin gravite anomalisi de rezidüel veya izostatik rezidüel anomaliden elimine edilebilir. Özellikle hidrokarbon aramacılığında gravite verilerinden azami verimin alınabilmesi için istenmeyen yüzeylerin gravite anomalileri, ölçülen veriden elimine edilebilir.

## SONUÇLAR

Gravite tabaka sıyırma yöntemi elde edilen bulgular ışığında verinin dalga-sayısı içeriğini değiştirmeden, istenmeyen katmanların gravite etkisinin giderilmesi olarak tanımlanabilir. Diğer bir ifadeyle jeolojik filtreleme olarak adlandırılabilir. Çalışma kapsamında elde edilen sonuçlar aşağıdaki gibi sıralanabilir:

- Deniz tabanının ve onun altında kalan -4750m'deki düz yüzeyin gravite etkileri, serbest hava anomalisine göre pozitif katkı sunmaktadır. Bu pozitif katkı serbest hava anomalisinden çıkarılır ise rezidüel anomali elde edilebilir.
- Moho ondülasyonları ve onun altında kalan -30000m'deki düz yüzeyin arasındaki gravite etkisi serbest hava anomalisine göre aynı şekilde pozitif katkı sunmaktadır. Bu pozitif katkı rezidüel anomaliden elimine edilir ise izostatik rezidüel anomali elde edilebilir.
- Uzay-zaman ortamında yapılan korelasyon ile Bouguer ve rezidüel anomaliler  $R^2=0.99$  değeri ile mükemmel pozitif korelasyon sağlasa bile, MSCS grafiği göstermektedir ki dalga-sayısı içeriği bakımından orta ölçekli farklılıklar mevcuttur.
- Bouguer anomalisi, rezidüel ve izostatik rezidüel anomalilere göre sınırlarda daha düşük kontrast sunmakta ve dalga-sayısı içeriği bakımından, yüksek

dalga-sayısı bileşenlerinde genliğini önemli ölçüde kaybetmektedir. Buna karşın rezidüel ve izostatik rezidüel anomaliler çalışma alanındaki tektonik yapıları Bouguer anomalisine göre daha başarılı bir şekilde tanımlamakta ve yüksek dalga-sayısı bileşenlerinde daha yüksek genliklere sahiptir.

- Sonuç olarak, 3B modelleme ile elde edilen bulgular, 1B Bouguer levha düzeltmesi ile elde edilen Bouguer anomalisine göre sınırlarda daha yüksek kontrast ve dalga-sayısı bileşenlerinin dağılımı açısından daha zengin sonuçlar sunmaktadır.

## KAYNAKLAR

- Airy, B., 1855. III. On the computation of the effect of the attraction of mountain-masses, as disturbing the apparent astronomical latitude of stations in geodetic surveys. *Philos. Trans. R. Soc. London* 145, 101–104. <https://doi.org/10.1098/rstl.1855.0003>
- Amante, C., Eakins, B.W., 2009. ETOPO1 1 Arc-Minute Global Relief Model: Procedures, Data Sources and Analysis. NOAA Tech. Memo. NESDIS NGDC-24 19. <https://doi.org/10.1594/PANGAEA.769615>
- Blakely, R., 1996. Potential theory in gravity and magnetic applications.
- Bonvalot, S., Balmino, G., Briais, A., Kuhn, M., Peyrefitte, A., Vales, N., Biancale, R., 2012. World Gravity Map: a set of global complete spherical Bouguer and isostatic anomaly maps and grids. *EGUGA* 14, 11091.
- Chen, W., Tenzer, R., 2020. Reformulation of Parker-Oldenburg's method for Earth's spherical approximation. *Geophys. J. Int.* 222, 1046–1073. <https://doi.org/10.1093/gji/ggaa200>
- Cordell, L., Henderson, R.G., 1968. Iterative three-dimensional solution of gravity anomaly data using a digital computer. *Geophysics* 33, 596–601. <https://doi.org/10.1190/1.1439955>
- Gómez-Ortiz, D., Agarwal, B.N.P., 2005. 3DINVER.M: A MATLAB program to invert the gravity anomaly over a 3D horizontal density interface by Parker-Oldenburg's algorithm. *Comput. Geosci.* 31, 513–520. <https://doi.org/10.1016/j.cageo.2004.11.004>
- Granser, H., 1987. Three-dimensional interpretation of gravity data from sedimentary basins using an exponential density-depth function. *Geophys. Prospect.* 35, 1030–1041. <https://doi.org/10.1111/j.1365-2478.1987.tb00858.x>
- Heiskanen, W., 1931. Isostatic tables for the reduction of gravimetric observations calculated on the basis of Airy's hypothesis. *Bull. Géodésique* 30, 110–153. <https://doi.org/10.1007/BF03029991>
- Hirt, C., Reubner, E., Rexer, M., Kuhn, M., 2016. Topographic gravity modeling for global Bouguer maps to degree 2160: Validation of spectral and spatial domain forward modeling techniques at the 10 microGal level. *J. Geophys. Res. Solid Earth* 121, 6846–6862. <https://doi.org/10.1002/2016JB013249>

Li, Y., Oldenburg, D.W., 2010. Rapid construction of equivalent sources using wavelets. *Geophysics* 75. <https://doi.org/10.1190/1.3378764>

Lort, J.M., 1971. The tectonics of the eastern Mediterranean: A geophysical review. *Rev. Geophys.* <https://doi.org/10.1029/RG009i002p00189>

Miroslav, B., Michael, R., Michael, L., 2013. Tutorial: The gravity-stripping process as applied to gravity interpretation in the eastern Mediterranean. *Lead. Edge* 32, 410–416. <https://doi.org/10.1190/le32040410.1>

Oldenburg, D.W., 1974. Inversion and interpretation of gravity anomalies. *Geophysics* 39, 526–536. <https://doi.org/10.1190/1.1440444>

Özsöz, İ., 2019. Gravity Layer Stripping for Analysis of Jurassic, Triassic and Pre-Zechstein North Sea Units. University of Leeds.

Özsöz, İ., Chris, G., Fairhead, J.D., Marsden, D., 2022. Gravity Layer Stripping Application in the North Sea, in: *Deu International Symposium Series On Graduate Researches-2022. İzmir, TURKEY.*

Parker, R.L., 1973. The Rapid Calculation of Potential Anomalies. *Geophys. J. R. Astron. Soc.* 31, 447–455. <https://doi.org/10.1111/j.1365-246X.1973.tb06513.x>

Sandwell, D.T., Smith, W.H.F., Gille, S., Kappel, E., Jayne, S., Soofi, K., Coakley, B., Géli, L., 2006. Bathymetry from space: Rationale and requirements for a new, high-resolution altimetric mission. *Comptes Rendus - Geosci.* 338, 1049–1062. <https://doi.org/10.1016/j.crte.2006.05.014>

Vaniček, P., Huang, J., Novák, P., Pagiatakis, S., Véronneau, M., Martinec, Z., Featherstone, W.E., 1999. Determination of the boundary values for the Stokes-Helmert problem. *J. Geod.* 73, 180–192. <https://doi.org/10.1007/s001900050235>

Anahtar Kelimeler: Gravite tabaka sıyırma, Parker-Oldenburg yöntemi

Bağntı 1

⊞

$$\mathcal{F}[\Delta g(x, y)] = -2\pi G \Delta \rho e^{-kz_0} \sum_{n=1}^{\infty} \frac{k^{n-1}}{n!} \mathcal{F}[\Delta h^n(x', y')] \quad (1)$$

Bağntı 2

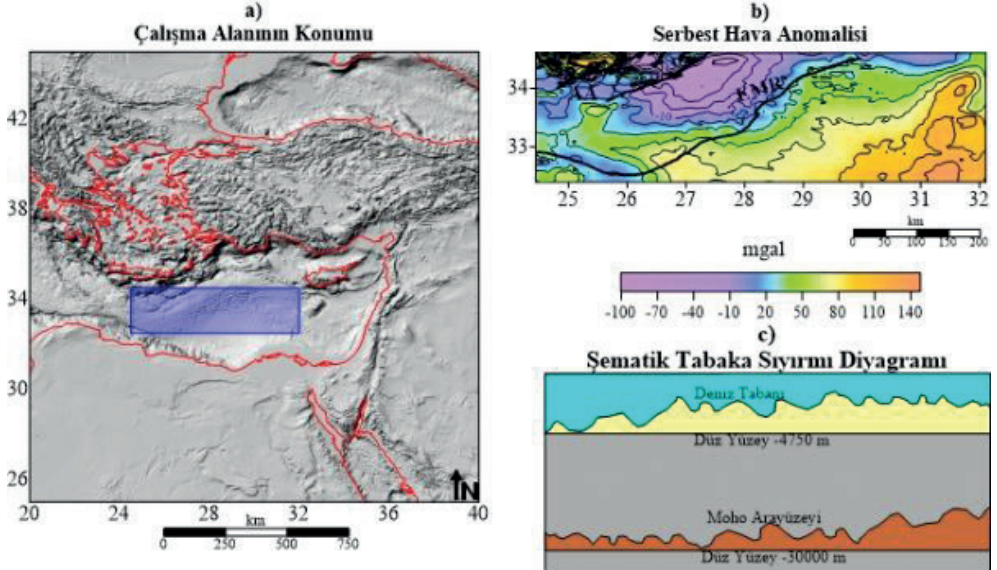
⌋

$$C_{x_1 x_2}(k) = \frac{S_{x_1 x_2}(k)}{\sqrt{S_{x_1 x_1}(k) \times S_{x_2 x_2}(k)}} \quad (2)$$

Bağntı 3

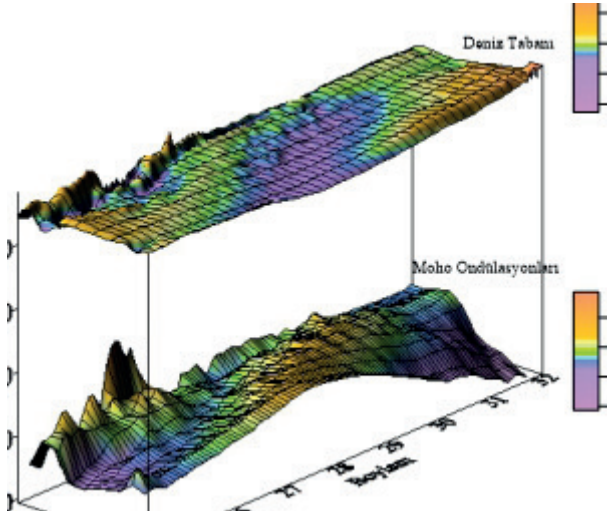
$$z_{moho\_und} = \frac{z_{bath} \Delta \rho_{cw}}{\Delta \rho_{mc}} + T \quad (3)$$

Şekil 1



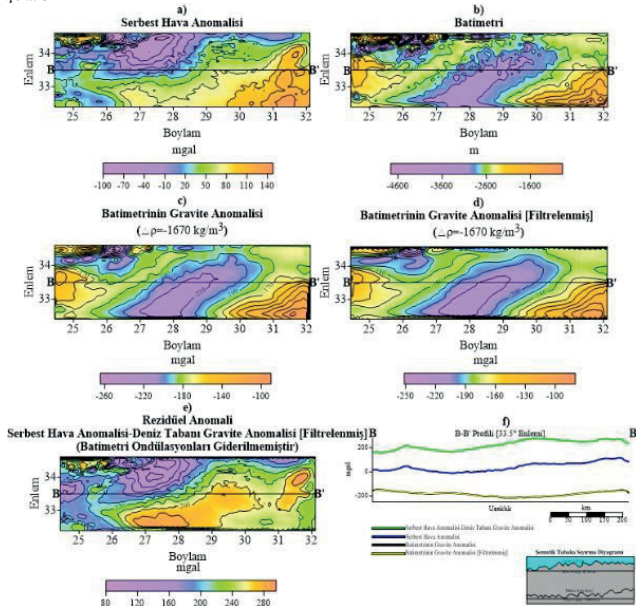
Şekil 1. Gravite tabaka sıyırma yönteminin uygulandığı bölgenin konum haritası ve girdi parametreleri: (a) Çalışma alanının konumu (mavi dikdörtgen), (b) Serbest hava anomalisi (EMR: Doğu Akdeniz Sırtı, AA=Ege Yayı), (c) şematik katman sıyırma diyagramı (tabaka sıyırma işleminin yapıldığı katmanlar mavi, sarı ve kahverengi renklerde gösterilmiştir).

Şekil 2



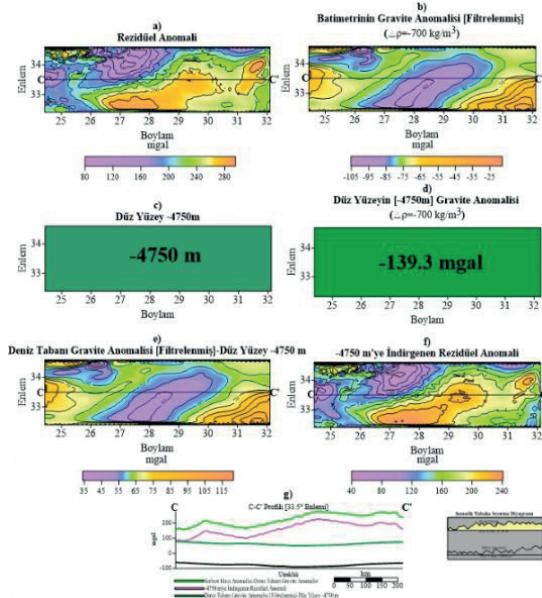
Şekil 2. Deniz tabanının ve Moho ondülasyonlarının 3B yüzey haritası.

Şekil 3



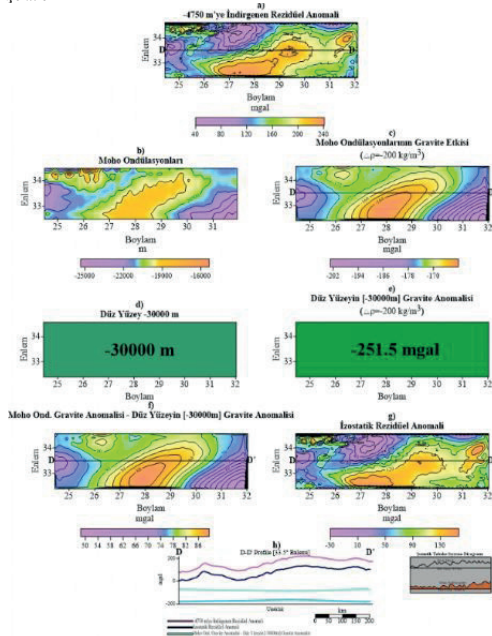
Şekil 3. Su kolonunun gravite etkisinin, serbest hava anomalisinden eliminasyonu: (a) serbest hava anomalisi, (b) batimetri, (c) batimetrisinin gravite anomalisi, (d) alçak geçişli filtre uygulanmış batimetrisinin gravite anomalisi, (e) rezidüel anomali ve (f) serbest hava anomalisi, rezidüel anomali ve filtrelenmiş/filtrelenmemiş batimetrisinin gravite anomalisinin karşılaştırmasını içeren B-B' profili.

Şekil 4



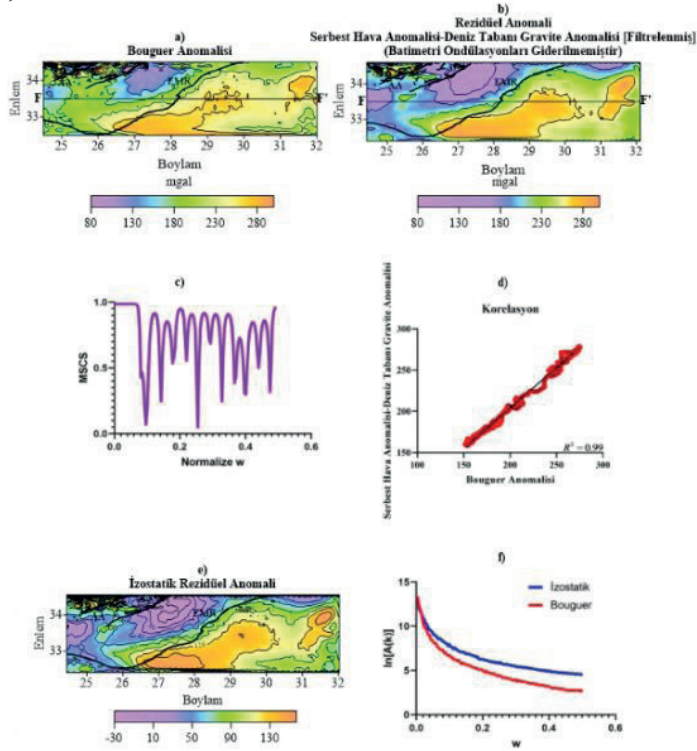
Şekil 4. Su kolonunu ile düz yüzey -4750 m arasındaki gravite etkisinin, rezidüel anomaliden eliminasyonu: (a) rezidüel anomali, (b) batimetrisinin gravite anomalisi, (c) -4750 m'deki düz yüzey (d) -4750 m'deki düz yüzeyin gravite anomalisi, (e) deniz tabanı ile -4750 m'deki düz yüzey arasındaki gravite anomalisi ve (f) -4750 m'ye indirgenen rezidüel anomali ve (g) bahsi geçen gravite anomalilerinin karşılaştırmasını içeren C-C' profili.

Şekil 5



Şekil 5. İzostatik rezidüel anomali hesabı: (a) -4750 m'ye indirgenen rezidüel anomali, (b) Moho ondülasyonları, (c) Moho ondülasyonlarının hesaplanan gravite anomalisi (d) 30000 m'deki düz, (e) 30000 m'deki düz yüzeyin gravite anomalisi, (f) Moho ondülasyonları ile -30000 m'deki düz yüzey arasındaki gravite anomalisi (g) izostatik rezidüel anomali ve (h) bahsi geçen gravite anomalilerinin karşılaştırmasını içeren D-D' profili.

Şekil 6



Şekil 6. Elde edilen anomalilerin karşılaştırılması ve çalışma alanındaki geniş ölçekli tektonik yapıları temsil etme kabiliyetleri: (a) Bouguer anomalisi, (b) rezidüel anomali, (c) Bouguer anomalisi ile rezidüel anomali kullanarak elde edilen MSCS sonucu, (d) Bouguer anomalisi ile rezidüel anomali arasındaki korelasyon ve (e) izostatik rezidüel anomali ve (f) izostatik rezidüel anomali ile Bouguer anomalisinin RAPS ile karşılaştırılması. EMR: Doğu Akdeniz Sırtı, AA: Ege Yayı.

# Gravite Gradyent Tensörlerinden Doğu Akdeniz Havzalarının Hidrokarbon Potansiyelinin Kestirimi

## Estimation of the Hydrocarbon potentials of the Eastern Mediterranean basins from the Gravity Gradient Tensors



**İlkin Özsöz<sup>1</sup>, Bülent Oruç<sup>2</sup>**

<sup>1</sup>Maden Tetkik ve Arama Genel Müdürlüğü; Kocaeli Üniversitesi, Mühendislik Fakültesi, Jeofizik Mühendisliği Bölümü, Kocaeli / Türkiye

<sup>2</sup>Kocaeli Üniversitesi, Mühendislik Fakültesi, Jeofizik Mühendisliği Bölümü, Kocaeli / Türkiye

### ÖZET

Bu çalışmada gravite anomalilerinin gradyent tensörleri kullanılarak doğrultu açıları, kabuk deformasyon analizleri ve invaryant oranlarından hidrokarbon rezervuar potansiyellerinin kestirimine yönelik bölgesel ölçekte yeni yaklaşımlar sunulmaktadır. Bu bağlamda Doğu Akdeniz havzasının küresel gravite anomalileri derlenerek gradyent tensörleri hesaplanmıştır. Daha sonra gradyent tensörlerinden bulunan doğrultu açıları, kabuk deformasyonu ve invaryant oranları gözlemsel olarak yorumlanmıştır. Doğrultu açılarının en önemli özelliği yatay katmanlı sedimanter istif bulunan bölgelerde birbirine paralel açı vektörleri sunmasıdır. Bu nedenle doğrultu açıları aynı zamanda bir tür "taratılmış" özellikleriyle yorumu kolaylaştırmaktadır. Bundan başka deformasyon haritaları tektonik olarak genişleme (açılma) ve sıkışma rejimlerinin etkin olduğu bölgelere yönelik veri setleri sunar. Doğrultu açılarının paralel dizilimlerinin kümelendiği kesimler kayaç dayanımlarının zayıf olduğu ve ağırlıkla genişleme rejimlerinin geliştiği kesimlerde ortaya çıkmaktadır. Bu durumda doğrultu açıları ile kabuk deformasyon süreçleri birbirleriyle iyi korele edilebilmektedir. Doğu Akdeniz havzasında invaryant oranlarının düşük değerlerinin ve doğrultu açılarının yüksek paralellik oranlarına karşılık gelen kesimlerde hidrokarbon rezervuarlarına yönelik kestirim bulgular ortaya çıkarmıştır. Ayrıca bu kesimlerin ağırlıkla genişleme rejiminin etkisi altında olmasrezervuar kestiriminde deformasyon süreçlerinin de değerlendirilmesi gerektiğini göstermiştir.

### ABSTRACT

In this study, new regional-scale approaches are presented for the estimation of hydrocarbon reservoir potentials based on directional angles, crustal deformation analyses, and invariant ratios using gradient tensors of gravity anomalies. In this context, the global gravity anomalies of the Eastern Mediterranean basin were compiled, and gradient tensors were calculated. Subsequently, the strike angles, crustal deformation, and invariant ratios derived from the gradient tensors were interpreted observationally. The most significant characteristic of the strike angles is their presentation of parallel angle vectors in regions with horizontally layered sedimentary sequences. Hence, the strike angles also facilitate interpretation with a kind of "combed" property. Furthermore, the deformation maps provide datasets for regions where tectonic extension (opening) and compression regimes are active. Sections where the strike angles cluster in parallel arrangements appear in

regions with weak rock strengths and predominantly exhibit extensional regimes. In such cases, the directional angles and crustal deformation processes correlate well with each other. In the Eastern Mediterranean basin, regions with low values of invariant ratios and high parallelism rates of directional angles have revealed indicative findings related to hydrocarbon reservoirs. Additionally, the prevalence of extensional regimes in these regions underscores the need to consider deformation processes in reservoir estimation.

### 1. GİRİŞ

Günümüzde gelişen uydu teknolojileriyle birlikte altimetrik ve gravimetrik ölçümler almabilmektedir. Bu ölçümlerle yer kürrenin statik gravite alanı harmonik jeopotansiyel katsayılarla yüksek çözünürlükte elde edilebilmektedir. Bu amaçla Pavlis ve diğ. (2008) tarafından geliştirilen EGM2008 ve Förste ve diğ. (2014) tarafından geliştirilen EIGEN-6C gibi statik gravite alanı modelleri yerbilimlerine önemli katkılar sağlamıştır. Klokočnik ve diğ. (2017) Sahara'da bulunan paleoöller ve Klokočnik ve diğ. (2017a) Doğu Antartika'da, Vostok Gölü yakınlarında potansiyel iki buzulaltı volkanı tespit etmiştir. Aynı çalışma alanında Klokočnik ve diğ., (2018), Gamburtsev Buzulaltı Dağları ile Vostok Gölü arasında potansiyel üç adet buzulaltı göl ve bir göl havzası tespit etmiştir. Ayrıca Wilkes Land buz örtüsünün altındaki büyük darbe yapısının (Klokočnik ve diğ., 2018a), Saginaw darbe yapısının ve Grönland'da buzulların altında bulunan kraterin (Klokočnik et al., 2019) varlığını iddia eden hipotezleri bu çalışmada kullanılacak olan yöntem ve veriler ışığında doğrulanmıştır. Yöntemin petrol ve doğal gaz aramalarında kullanılabilirliği Klokočnik ve diğ., (2021)'de tartışılmış ve Ghawar (Suudi Arabistan), Basra Körfezi, Texas-Oklohama-Meksika Körfezi kapsayan alan ve Alaska Körfezi ile Kodiak (Alaska) arasında kalan alandan elde edilen bulgulara göre yöntemin başarılı sonuçlar verdiği belirlenmiştir.

Bilindiği gibi tek başına gravite anomalileri hedef rezervuarların tanımlanmasında yeterli olmayabilmektedir. Bu çalışmada hidrokarbon arama amacıyla yeni yöntemler olarak gradyent tensörlerinin doğrultu açıları ve deformasyon haritalarının ön etüt çalışmaları kapsamında uygulanabilirliği tartışılmıştır. Bu bağlamda Doğu Akdeniz Bölgesi için doğrultu açıları ve deformasyon haritaları elde edilerek bilinen rezervuarlar üzerinde ve bilinmeyen olası hidrokarbon potansiyellerine yönelik çözümleri analiz edilmiştir. Bu amaçla gravite gradyent

tenörlerinden türetilen doğrultu açıları, invaryant oranları ve kabul deformasyon süreçleri korele edilerek olası hidrokarbon rezervasyonlarına yönelik ön kestirimler yapılmıştır.

## 2. YÖNTEM

### 2.1. Gravite Gradyent Tensör Bileşenlerinin Doğrultu Açısı

MarussıTensör matrisi olarak da tanımlanan (Klokočnik vediğ. 2019)gravite gradyentensör matrisinin bileşenleri

(1)

olarak verilir.Gradyentensör matrisinin en önemli özelliği simetrik olması ve bileşenlerinin koordinat dönmelerinden bağımsız olarak invaryant (değişmez) özelliği göstermesidir. Ana köşegen dışındaki bileşenleri simetrik eşit olduğundan ( $T_{xy} = T_{yx}$  ;  $T_{yz} = T_{zy}$  ;  $T_{zx} = T_{xz}$  ) ve kaynak dışında Laplace denklemini

$$T = \begin{bmatrix} T_{xx} & T_{xy} & T_{xz} \\ T_{yx} & T_{yy} & T_{yz} \\ T_{zx} & T_{zy} & T_{zz} \end{bmatrix} = \begin{bmatrix} \frac{\partial^2 V}{\partial x^2} & \frac{\partial^2 V}{\partial x \partial y} & \frac{\partial^2 V}{\partial x \partial z} \\ \frac{\partial^2 V}{\partial y \partial x} & \frac{\partial^2 V}{\partial y^2} & \frac{\partial^2 V}{\partial y \partial z} \\ \frac{\partial^2 V}{\partial z \partial x} & \frac{\partial^2 V}{\partial z \partial y} & \frac{\partial^2 V}{\partial z^2} \end{bmatrix}$$

sağladığından ( $T_{zz} = -(T_{xx} + T_{yy})$  ) yalnızca beş adet bağımsız bileşeni ( $T_{xx}$ ,  $T_{xy}$ ,  $T_{xz}$ ,  $T_{yy}$ ,  $T_{yz}$ ) bulunmaktadır. Tensörbileşenlerinden yeni veri setleri türetilir. Bu amaçlaKalvoda vediğ. (2013)tarafından doğrultu açısı,tensörlerin doğrultularına bağlı olarak

(2)

eşitliğinden hesaplanabilir.  $\theta_s$  değerleri  $-90^\circ$  ile  $90^\circ$  arasında değişir. Bu durumda her bir koordinat değerine karşılık gelen doğrultu açısı değerlerinden ortalama bir değer

eşitliğinden bulunabilir (Kalvoda ve diğ. 2013). Burada

$$\tan 2\theta_s = 2 \frac{T_{xy}(T_{xx} + T_{yy}) + T_{xz}T_{yz}}{T_{xx}^2 - T_{yy}^2 + T_{xz}^2 - T_{yz}^2}$$

n veri sayısıdır. Karşıt yönleredeki açıların tek bir yöne indirgenmesi için

koşulları değerlendirilir (Kalvoda ve diğ. 2013). Bu durumda  $\theta_i$  açıları yünden bağımsız olarak yalnızca

$$\theta_{ortalama} = \frac{\sum_{i=1}^n \theta_i}{n}$$

doğrultu teriminden elde dilmiş olacaktır. Doğrultu açıların paralel olma özellikleri veya dereceleri ortalama değerden olan sapmalarına göre

eğer  $|\theta_i - \theta_{comb}| > 90^\circ$ ,

$$\theta_i = 180^\circ - |\theta_i - \theta_{comb}|$$

eşitliğinden bulunabilir (Kalvoda ve diğ. 2013).. Paralellik parametresi 1'e yakınsa  $\theta_i$  açıları paralel olma eğiliminde ve 0'a yakınsa rastgele dağılım göstermektedir. Paralellik değerleri ise  $\theta_s$  açıları arasındaki paralelliğin arttığını bölgelerde 1'e

$$r_{msv} = \frac{\sum_{i=1}^n (\theta_i - \theta_{comb})^2}{n} \quad (5)$$

ve

$$Paralellik = 1 - \frac{r_{msv}}{90^\circ} \quad (6)$$

yaklaşırken, farklı doğrultulara sahip  $\theta_s$  açıların olduğu bölgelerde 0'a yaklaşmaktadır. Klokočnik ve diğ., (2021), Paralellik  $< 0.55$  ise çalışma alanında  $\theta_s$  açıların paralel bir dizilim göstermediğini ancak Paralellik  $> 0.65$  ise çalışma alanında  $\theta_s$  açıların paralele yakın olduğunu göstermiştir. Ancak bu değerler ideal koşullar için saptanmıştır. Paralelliğin gözlemsel yorumunda  $\theta$ 'nın ortalama değere göre değişimi de irdelenmelidir. Bu değişim basitçe eşitliği ile verilir (Kalvoda ve diğ. 2013).

### 2.2. Gravite Gradyent Tensör Matrisinin İnvaryantları

$$\theta_i^{göreceli} = 1 - \frac{|\theta_i - \theta_{comb}|}{90^\circ} \quad (7)$$

Gravite Gradyent Tensörleri (GGT) bağımsız bir referans düzlemi üzerinde tanımlanırlar. Başka bir deyişle bu tensörlerin referans koordinat sisteminde dönmelerden bağımsız veya invaryant (değişmez) özelliğinde olan büyüklükleri bulunmaktadır. (2) bağıntısı ile verilen tan gradyentensör matrisinden üç adet invaryant hesaplanabilir. Bu invaryantlar

eşitlikleri ile verilir. Pedersen ve Rasmussen (1990)(10) ve (9) eşitliklerinin oranından bir değişmezlik oranı tanımlamıştır:

(9)

I oranının en önemli özelliği anomali kaynaklarının

$$I_0 = T_{xx} + T_{yy} + T_{zz} \quad (8)$$

$$I_1 = (T_{xx}T_{yy} + T_{yy}T_{zz} + T_{zz}T_{xx}) - (T_{xy}^2 + T_{yz}^2 + T_{xz}^2) \quad (9)$$

$$I_2 = (T_{xx}(T_{yy}T_{zz} - T_{yz}^2) + T_{xy}(T_{yz}T_{zz} - T_{xy}T_{zz}) + T_{xz}(T_{xy}T_{zz} - T_{xz}T_{yy}) \quad (10)$$

boyutlarının kestirimine yönelik bilgiler vermesidir. Bu durumda oranın sıfır ve sıfıra yakın değerleriiki boyutlu yapılarla, 1 ve 1'e yakın değerleri ise üç



$$I = 0 \leq \frac{-(I_2/2)^2}{(I_1/3)^3} \leq 1$$

boyutlu yapılara karşılık gelmektedir (Pedersen ve Rasmussen, 1990). I oranı 0-1 aralığında değişir. Bu bağlamda I oran değeri gradyentensörlerinin işaretinden bağımsız olarak anomali kaynaklarının iki veya üç boyutlu olup olmadıklarına yönelik bilgi taşır (Pedersen ve Rasmussen, 1990). İki boyutlu yapılarda I oranı sıfıra yakınken, üç boyutlu yapılarda I değerine yakın olmaktadır. Hidrokarbon sahalarında jeolojik kapanların iki boyutlu yapılar olduğu bilinmektedir. Bu nedenle I oranının 0'a yaklaştığı bölgeler dikkate alınmalıdır. Bununla birlikte yalnızca I oranından elde edilen çözümler kestirimsel olarak ön-etüd kapsamında değerlendirilerek bu çalışmada ele alınan diğer yaklaşımların sonuçlarıyla birlikte yorumlanmalıdır.

### 2.3. Yatay Gradyent Tensörlerinden Kabuk

#### Deformasyonu

Deformasyon tensörleri, jeodinamik süreçleri açıklamak için kullanılabilir. Yatay yönlü kabuk deformasyonlarına duyarlı veriler olan yatay gravite gradyent tensörleri deformasyon analizlerinde kullanılabilir. Gravite alanı ile kabuk deformasyonu arasındaki ilişkiler çeşitli araştırmacılarla ele alınmıştır. Fung (1965) deformasyonun, gravite alanının koordinat bileşenlerine göre türevleriyle tanımlanabileceğini ileri sürmüştür. Heck ve Mälzer (1983) ve Sanso ve Dermanis (1982) deformasyonun yatay gravite gradient tensörlerine bağlı olarak kuramsal ilkelerini geliştirmiştir. Bu konuda kapsamlı çalışma Dermanis ve Livieratos (1983), tarafından yürütülmüştür.

Klokočnik ve diğ. (2014) tarafından yatay gradyent tensörleri ile yatay deformasyonlar arasındaki ilişki

(10) olarak verilen deformasyon matrisi ile tanımlanmıştır. Bu durumda kabuk dilatasyonu, sıkışmaları ve rotasyonu gibi jeodinamik süreçler yatay gravite gradyent tensör bileşenleri olarak tanımlanan yamulma-deformasyon

$$e = \begin{pmatrix} e_{xx} & e_{xy} \\ e_{yx} & e_{yy} \end{pmatrix} = \begin{pmatrix} \epsilon_{xx} & (\epsilon_{xy} + \epsilon_{yx})/2 \\ (\epsilon_{xy} + \epsilon_{yx})/2 & \epsilon_{yy} \end{pmatrix} \quad (12)$$

matrisinin elemanlarından kestirilebilir. Buradan yedi adet kabuk deformasyon parametresi tanımlanabilir (Klokočnik ve diğ. 2014). Bu parametreler

olarak verilir. Burada toplam dilatasyonu;  $\gamma_1$  ve  $\gamma_2$ , tam makaslama bileşenlerini;  $\gamma$ , toplam makaslama;  $a$ , deformasyon elipsinin ana yarı eksenini;  $b$ , deformasyon elipsinin küçük yarı eksenini ve  $\alpha$ , ana deformasyon ekseninin yönünü temsil eder.

$$\Delta = \epsilon_{xx} + \epsilon_{yy} \quad (13)$$

$$\gamma_1 = \epsilon_{xx} - \epsilon_{yy} \quad (14)$$

$$\gamma_2 = 2\epsilon_{xy} \quad (15)$$

$$\gamma = \sqrt{\gamma_1^2 + \gamma_2^2} \quad (16)$$

$$a = \frac{\Delta + \gamma}{2} \quad (17)$$

$$b = \frac{\Delta - \gamma}{2} \quad (18)$$

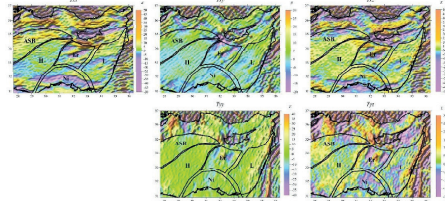
$$\alpha = \frac{\tan^{-1}(\gamma_2/\gamma_1)}{2} \quad (19)$$

### 3. BULGULAR VE TARTIŞMA

Bu bölümde uydu gravite gradyentensör verilerinden türetilen doğrultu açıların, kabuk deformasyonlarının ve invaryantların Doğu Akdeniz havzasının bilinen hidrokarbon alanlarındaki çözüm karakteristikleri araştırılmıştır. Bunun yanı sıra havzaların daha önce bilinmeyen hidrokarbon potansiyellerine yönelik kestirimsel yaklaşımlar tartışılmıştır.

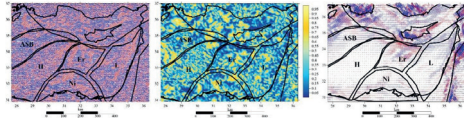
#### 3.1. Doğu Akdeniz Havzasının Doğrultu Açıları, İnvaryant Oranları ve Deformasyon Çözümleri

Bu bölümde Doğu Akdeniz havzasının bilinen ve potansiyel taşıyan hidrokarbon rezervuarları ile ilişkili olarak doğrultu açıların, invaryant oranlarının ve kabuk deformasyonlarının modellenerek haritalanması amaçlanmıştır. Bu amaçla Bucha ve Janák (2013) tarafından geliştirilen, yüksek derecelere (on binlerce ve ötesi) kadar jeopotansiyel fonksiyonlara dayalı MATLAB tabanlı GrafLab (GRAVITYFIELDLABORATORY) yazılımı kullanılarak her iki havzanın GGT bileşenleri haritalanmıştır. Şekil 1'de Doğu Akdeniz havzasının GGT bileşenlerinin değişimleri görülmektedir. Havzanın hidrokarbon rezervuarları olabilecek sahaları için sınıflandırma yapılmıştır. Bu sınıflandırmada Eratostenes Platformu, Levantin Baseni, Nil Deltası Baseni, Herodot Baseni ve Akdeniz Sırtı olmak üzere beş bölge belirlenmiştir.  $T_x$  ve  $T_y$  tensör alanlarının gradyentleri ( $T_{xx}$ ,  $T_{xy}$ ,  $T_{xz}$ ,  $T_{yy}$ ,  $T_{yz}$ ) havzanın kabuk içi deformasyonlarına bağlı olarak farklı doğrultularda vanal



Şekil 1. Doğu Akdeniz havzası GGT bileşenleri. ASB: Akdeniz Sırt baseni. H: Herodot baseni. ER: Eratostenes platformu. L: Levantin baseni. Ni: Nil Deltası baseni. Gradyent tensörleri yoğunluk farklarının yanal ve düşey yönlü değişimlerine duyarlıdır. Bu değişimlerin beş sektörün her birinde gözlenmesine karşılık özellikle Eratostenes platformunda, Levantin baseninde ve Nil deltasında daha etkindir. Sektörler, Schenk ve diğ., (2020) ye ait rapordan temin edilmiştir.

GGT bileşenlerine bağlı olarak hesaplanan doğrultu açıları, invaryant oranları ve sıkışma ve açılma rejimlerine bağlı olarak ortaya çıkan kabuk deformasyonları sırasıyla Şekil 1a, Şekil 1b ve Şekil 1c'de gösterilmiştir. Söz konusu sektörlerin doğrultu açılarının paralellikleri, invaryant oranları ve kabuk deformasyonları birbiriyle korele edilmiştir. Şekil 2'de, Akdeniz sırtının güneyinde paralel  $\theta_s$  açıları gözlemlenirken, *I oranı* Kıbrıs'ın Güneybatısı ve Kuzeydoğusu'nda sıfıra yaklaşmaktadır. Kabuk deformasyonu haritasında, Kıbrıs'ın Doğusu'ndaki Levant Havzası bölgesinde dilatasyona bağlı yamulmalar gözlenirken, Kıbrıs'ın Güneybatısı'ndaki sırt bölgesinde ise sıkışma gerilmesine bağlı yamulmalar ortaya çıkmaktadır. Herodot, Levantin ve Nil sektörleri göreceli olarak daha az deformasyon gözlenen bölgeler olarak öne çıkmaktadır. Bu sektörlerin hidrokarbon açısından zengin olması bu bağlamda dikkate alınması gereken bir özelliktir. Levant Havzası, en düşük *I oranı*'na sahip bölge olarak tespit edilmiştir ( $I=0.30$ ), en yüksek *I oranı* ise Akdeniz Sırt Baseni'nde gözlenmiştir ( $I=0.37$ ). Herodotus Havzası, en fazla paralellüğün gözlemlendiği bölgedir (*Paralellik* =0.56). En düşük paralellik değeri ise Akdeniz Sırt Baseni'nde tespit edilmiştir (*Paralellik* =0.48). Eratosthenes Platformu ( $I=0.37$  ve *Paralellik* =0.55) için elde edilen sonuçlar da Levant Havzası sonuçlarına oldukça yakındır. Buna karşın, yüksek *I oranı* ve düşük *Paralellik* değeri ile Akdeniz Sırt Baseni, ideal rezervuar olma potansiyeli en düşük bölge olarak nitelendirilebilir. Ön bulgulara göre, Herodotus Havzası *Paralellik* değeri açısından ideal sonuçlar sunarken, göreceli olarak yüksek *I oranı* nedeniyle ideal rezervuar olmaktan uzaklaşmaktadır. Nil Deltası Havzası'nda ise  $I=0.33$  ve *Paralellik* =0.54 değerleri, ideal rezervuar modeline yakın sonuçlar elde edilmiştir.



Şekil 2. Doğu Akdeniz havzasının GGT bileşenlerinden hesaplanan doğrultu açıları ( $\theta_s$ ), invaryant oranları (*I*) ve kabuk deformasyon (*KD*) haritaları.  $\theta_s$  haritasında paralelliklerin yoğun olduğu bölgeler kırmızı ve mavi renkler ile izlenmektedir. *I oranı* haritasında 2B yapıların dağılımı küçük *I* değerleri ile yaklaşık 3B yapıların dağılımı ise büyük *I* değerleri ile gözlemlenmektedir. *KD* haritasında kırmızı bölgeler sıkışma ve mavi bölgeler açılma gerilmesi altında deforme olan bölgeleri temsil eder.

#### 4. SONUÇLAR

Jeofizik açıdan değerlendirildiğinde  $\theta_s$ , kayacın dayanımındaki zayıflığıyla ilişkili olarak jeolojik ortamın yatay istiflenmesi gibi paralel olarak dizilimlere duyarlı sonuçlar üretir. Bununla birlikte yerel paralellikler keskin olarak istif içinde petrol ve doğal gaz bulgusunu göstermeyebilir. Yeraltı suyu, paleogöl veya krater tipi yapılarla yönelik çözümlere de işaret edebilir. Bu bağlamda iki boyutlu veya üç boyutlu yapılarla yönelik ayırımı yapan invaryant oranlarının da dikkate alınması gereklidir. Hidrokarbon rezervuarları için jeolojik kapanlar iki boyutlu olduğundan oran

değerine göre bu bilgi de değerlendirilmelidir. Çalışma kapsamında değerlendirilen hidrokarbon potansiyeli alan bölgelerde düşük *I oranı* ve yüksek *Paralellik* gözlemlenmesi durumunda ideal koşullar sağlanmış olacaktır. Bunlardan başka Akdeniz havzasının dalma batma, faylanma ve yamulma süreçleri dikkate alındığında kabuk deformasyonlarının da rezervuar kestiriminde önemli olduğu açıktır. Bununla birlikte bu çalışmada modelleme teknikleri tektonik olarak tam dilatasyon ve tam sıkışma rejimleri ile

sınırlıdır. Daha karmaşık tektonik süreçlerin etkinliği ayrı bir çalışma konusu olarak durmaktadır. Doğu Akdeniz bölgesinde  $\theta_s$  açılarının paralellik ölçüleri veya yoğun tarama alanları kayacın mukavemetindeki zayıflığa bağlı olarak paralel dizilim eğiliminde stratigrafik tabakalanmaya işaret eder. Hidrokarbon potansiyeli olan bölgelerde, düşük *I oranı* ve yüksek *Paralellik* gözlemlendiğinde ideal koşulların sağlandığına yönelik yaklaşık bilgiler elde edilmektedir. Özellikle Levant baseninde  $I=0.30$  ve *Paralellik*=0.55 değerleriyle birlikte, diğer dört sektör içinde en ideal sonuçlar veren bölge olarak belirlenmiştir. Gradyenttenörlerinin kısa dalga boyulu ve ayrıntılı çözüm özelliklerinden hareketle yukarıda tanımlanan yeni veri setleri, arama projelerinde ön-ütüt çalışmaları ve buna bağlı olarak bölge sınırlaması gibi konularda değerlendirilebilir. Doğrultu açıları misten en ölçüde gelişen paralellikleri hidrokarbon birikimlerini içeren sediment istiflerinden başka yer altı suyu, paleogöl ve krater gibi anomalikaynaklarının üzerinde de meydana gelebileceğinden yorumlama için bölgesel jeolojik bulguların da derlenmesi önem kazanmaktadır.

#### KAYNAKLAR

- Bucha, B., Janák, J., 2013. A MATLAB-based graphical user interface program for computing functionals of the geopotential up to ultra-high degrees and orders. *Computers & Geosciences* 56, 186-196.
- Dermanis, A., Livieratos, E., 1983. Applications of deformation analysis in geodesy and geodynamics. *Rev. Geophys.* <https://doi.org/10.1029/RG021i001p00041>
- Förste, C., Bruinsma, S., Abrikosov, O., Flechtner, F., Marty, J.-C., Lemoine, J.-M., Dahle, C., Neumayer, H., Barthelmes, F., König, R., Biancale, R., Förste, C., Bruinsma, S., Abrikosov, O., Flechtner, F., Marty, J., 2014. EIGEN-6C4 - The latest combined global gravity field model including GOCE data up to degree and order 1949 of GFZ Potsdam and GRGS Toulouse. *EGU Gen. Assem.* 16, 3707.
- Fung, Y.C., 1965. Foundations of solid mechanics Prentice-Hall. Inc, New Jersey.
- Heck, B., Mälzer, H., 1983. Determination of vertical recent crustal movements by levelling and gravity data, in: *Developments in Geotectonics*. Elsevier, pp. 251-264. <https://doi.org/10.1016/B978-0-444-42243-9.50039-4>
- Kalvoda, J., Klokočník, J., Kostecký, J., Bezděk, A., 2013. Mass distribution of earth landforms

determined by aspects of the geopotential as computed from the global gravity field model EGM 2008. *Acta Univ. Carolinae, Geogr.* 48, 17–25. <https://doi.org/10.14712/23361980.2015.1>

Klokočník, J., Kostecký, J., Bezděk, A., 2019. The putative Saginaw impact structure, Michigan, Lake Huron, in the light of gravity aspects derived from recent EIGEN 6C4 gravity field model. *J. Great Lakes Res.* 45, 12–20. <https://doi.org/10.1016/j.jglr.2018.11.013>

Klokočník, J., Kostecký, J., Bezděk, A., 2018a. On the detection of the Wilkes Land impact crater. *Earth, Planets Sp.* 70, 1–12. <https://doi.org/10.1186/s40623-018-0904-7>

Klokočník, J., Kostecký, J., Bezděk, A., Čílek, V., 2021. The spatial distribution of the strike angles derived from EIGEN 6C4 gravity model – A new possibility for oil and gas exploration? *Int. J. Oil, Gas Coal Technol.* 28, 306–332. <https://doi.org/10.1504/IJOGCT.2021.118651>

Klokočník, J., Kostecký, J., Bezděk, A., Pešek, I., 2017a. Candidates for volcanoes under the ice of Antarctica detected by their gravito-topographic signal. *Ann. Geophys.* 60, 662. <https://doi.org/10.4401/ag-7427>

Klokočník, J., Kostecký, J., Čílek, V., Bezděk, A., Pešek, I., 2018b. Gravito-topographic signal of the Lake Vostok area, Antarctica, with the most recent data. *Polar Sci.* 17, 59–74. <https://doi.org/10.1016/j.polar.2018.05.002>

Klokočník, J., Kostecký, J., Čílek, V., Bezděk, A., Pešek, I., 2017b. A support for the existence of paleolakes and paleorivers buried under Saharan sand by means of “gravitational signal” from EIGEN 6C4. *Arab. J. Geosci.* 10. <https://doi.org/10.1007/s12517-017-2962-8>

Pavlis, N.K., Holmes, S.A., Kenyon, S.C., Factor, J.K., 2008. The EGM2008 global gravitational model, in: *AGU Fall Meeting Abstracts*. pp. G22A-01.

Pedersen, L.B., Rasmussen, T.M., 1990. The gradient tensor of potential field anomalies: some implications on data collection and data processing of maps. *Geophysics* 55, 1558–1566. <https://doi.org/10.1190/1.1442807>

Sanso, F. and Dermanis, A., 1982. A geodynamic boundary value problem. *Boll. Geod. Sci. Aff.*, 41(1), pp.65-87.

Schenk, J.C., Mercier, J.T., Finn, M.T., Woodall, A.C., Marra, R.K., Müller-Leathers, M.H., Le, A.P., Drake, M.R., 2020. Assessment of Undiscovered Conventional Oil and Gas Resources in the Eastern Mediterranean Area, 2020 (ver.1.1). *U.S. Geol. Surv. Fact Sheet* 2021-3032.

Anahtar Kelimeler: Doğrultu açısı, kabuk deformasyonu

# Gravity and Magnetic Based Solutions or Integrated Regional-To-Basin Exploration

**Andrea Sirtori, Luciana De Luca, Giuseppe Bancalà, Samuele Ratti, Massimo Clementi**

Slb, D&I Geosolutions, Milan / Italy



## INTRODUCTION

Through the years, Potential Fields (PF) methods have proven to be a valuable source of complementary information for different type of studies, with the integration of Potential Fields aided solutions within traditional workflows progressively becoming a standard in the energy industry. Applications are various and heterogeneous, spanning from frontier exploration & basin potentiality assessment, to regional studies and structural framework reconstruction, to basin integrated interpretations and major discontinuities mapping, to seismic-integrated Earth Model Building (EMB), up to Energy Transition applications (e.g. Geothermal) and more. Moreover, PF offer wide degrees of flexibility, since prone to be integrated via both qualitative and quantitative approaches, hence allowing integrated solutions to be case-by-case tailored to scale and objective of the study.

Three different workflows using Potential Fields data to enhance Regional-to-Basin exploration are described: 1) regional study via Gravity and Magnetic interpretation and modelling; 2) Gravity assisted seismic Earth Model building; 3) Gravity & seismic Simultaneous Joint Inversion (SJI) for near-surface modelling. These cases demonstrate how the exploitation of PF data at different stages of the exploration workflow can be of crucial importance both for regional screening, as well as to complement seismic data for exploration purposes by improving seismic imaging through appropriate integration of different geophysical domains and seamless interaction of geoscience disciplines.

## METHODS & FINDINGS

### Regional study via Gravity and Magnetic interpretation and modelling

The first PF integrated workflow has the objective to improve the regional-scale understanding from deep crustal and lithospheric structures to shallower depositional evolution. Gravity and magnetic data are, in fact, very powerful tools to detect variations due to lithological and structural changes, helping the mapping of fault trends and the identification of geologic features strike direction, thus aiding exploration strategies. The workflow applied consists in: the interpretation of key regional structural elements on adequately filtered and enhanced gravity & magnetic maps; the estimation of top-basement relief using prism-based inversion of gravity and magnetic data; the 2.5D and 3D regional modelling via forward modelling techniques.

Initially all the available legacy and public domain data are carefully screened, exploited, and properly

merged with available proprietary data, so to widen the analysis area and to minimize boundary-effects. Then, after the application of spectral analysis, filtering, and anomaly enhancement techniques, lineaments are interpreted and analyzed on bathymetry and PF data. In the presented case, interpreted lineaments, and associated rose diagrams, indicated an overall consistent geodynamical evolution, with one predominant direction related to the evolution of the continental shelf and secondary directions related either to salt-sediment interactions through geological time or to the strong interaction between tectonics and sedimentation close to the coast.

After the lineaments are interpreted, the regional crustal structures are defined using an iterative 2.5D-3D forward-modelling approach: following an initial 2D model-building stage, where main boundaries (basement from prism-based inversion of pseudo-gravity data [Golfrè Andreasi F. and Scandroglio S., 2021, "Basement relief estimation through a two-parameters gravity inversion", 82nd EAGE Annual International Conference and Exhibition], Curie depth, Moho, etc.) and density distribution are defined, the models are interactively perturbed and refined (geometries and lithologies) via gravity and magnetic data-fit minimization (Figure 1). Then, boundaries and densities from the 2.5D modelling are extrapolated into a 3D grid to undergo a full 3D validation via 3D Forward Modelling. Based on the outcome of the last step, further 2.5D-3D loops are executed until reaching an acceptable level of residual misfit. In the presented case, the resulting model provided a refined definition of the deeper regional structures and related sedimentary packages, identifying potential sub-basins and areas with high-density rocks. Also, the resulting basement interface constituted a valuable guidance for acoustic basement interpretation on the seismic data, whose signature was not always evident.

Gravity assisted seismic Earth Model building  
The second PF integrated workflow describes the strategy applied to address an imaging challenge due to a carbonate platform in the Campeche Bay. The area is located approximately 55 km off the coast of Mexico, with a carbonate platform (with ambiguous thickness varying from 1 km to 5 km) overlying a Jurassic section that is attractive for exploration purposes. In this context, PF data were employed to overcome seismic Narrow Azimuth (NAZ) limitations in terms of depth penetration and spatial long-wavelength content.

A dedicated workflow was designed to reduce seismic interpretation uncertainty via gravity data integration: milestone velocity models are converted into density via well-based rock physics law, and then assessed via gravity forward modeling. Through gravity residual

analysis, timely feedback are provided to interpreters to guide the milestone interpretation refinement process: a density deficit (positive residual) suggests the need for an overall denser lithological composition, while density excess (negative residual) suggests the need for lighter lithologies. In the presented case, the deficit might translate into the need for a denser (faster) sediment package, a shallower top of carbonate or a deeper base of carbonate; the excess might instead translate into the need for a lighter (slower) sedimentary package, a deeper top of carbonate or a shallower base of carbonate.

Figure 2 shows the gravity residual evolution from an early-stage model to the final model, highlighting a significant misfit improvement, and thus increasing the confidence in the Final model. Indeed, the statistical distributions of the gravity residual maps confirmed the uplift by a more zero-centric mean value; also, the standard deviation decreased, thus corroborating a better match with observed data. Finally, looking at the final Reverse Time Migration (RTM), improvements of the stratification within the carbonate body can be clearly denoted; at Jurassic pre-carbonate section, series of sands are imaged from the Oxfordian, Kimmeridgian, and Tithonian sequences.

Gravity & seismic Simultaneous Joint Inversion (SJI) for near-surface modelling The third PF integrated workflow describes a solution designed to provide least-square full-waveform inversion (FWI) with a robust near-surface starting model capable of mitigating the risk of cycle skipping in a context of very shallow water (~ 10m), hence where seismic low frequencies are strongly attenuated by the ghost effect. To achieve the objective, Full-Tensor Gradiometry (FTG) data are numerically integrated with seismic refraction First-Break picks (FB) by means of Simultaneous Joint Inversion (SJI) [De Stefano M., Golfré Andreasi F., Re S., Virgilio M., and Snyder F., 2011, "Multiple-domain, simultaneous joint inversion of geophysical data with application to subsalt imaging", *Geophysics*, 76, 69-80], aiming to improve the Starting Model detailing and thus enabling FWI to start at higher frequencies, in presence of higher signal-to-noise (S/N) ratio.

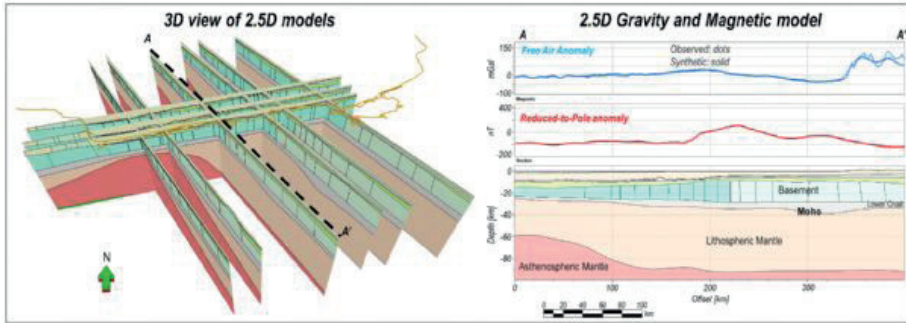
The key differentiator of SJI for seismic model building is the active (or "joint") contribution of an independent dataset that brings into play information coming from a different domain, a different perspective. In this case FTG is helping to laterally constrain the anomalies, thus returning a more detailed model than the refraction-only solution, while also improving the process robustness by honoring multiple data coming from different domains. In the presented case, resulting velocity and density models after SJI revealed many common similarities in terms of both shape and distribution of the main anomalies. Finally, SJI resulting velocity model was compared to 3 Hz FWI model, showing how the first is further reducing the seismic misfit and therefore, in this case, providing a better starting model for the higher frequency FWI at 4 Hz (Figure 3).

## CONCLUSION

The presented examples about exploitation of PF data at different stages of the exploration workflow prove how Potential Fields can be of crucial importance both for regional screening, as well as to complement seismic data for exploration purposes by improving seismic imaging through appropriate integration of different geophysical domains and seamless interaction of geoscience disciplines.

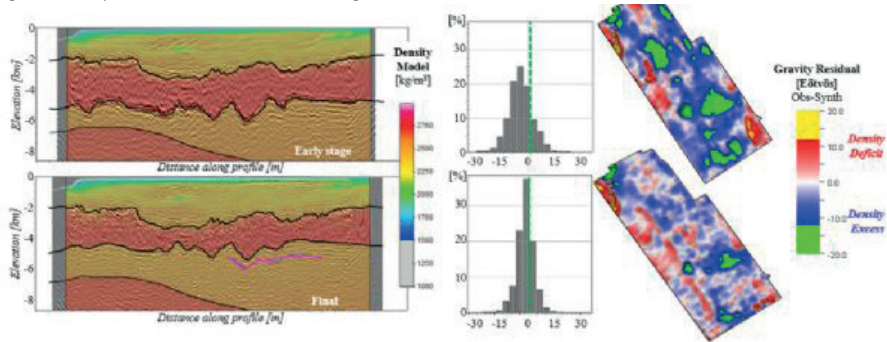
Keywords: Multiphysics, Integration

Figure 1 - Regional study via Gravity and Magnetic interpretation and modelling



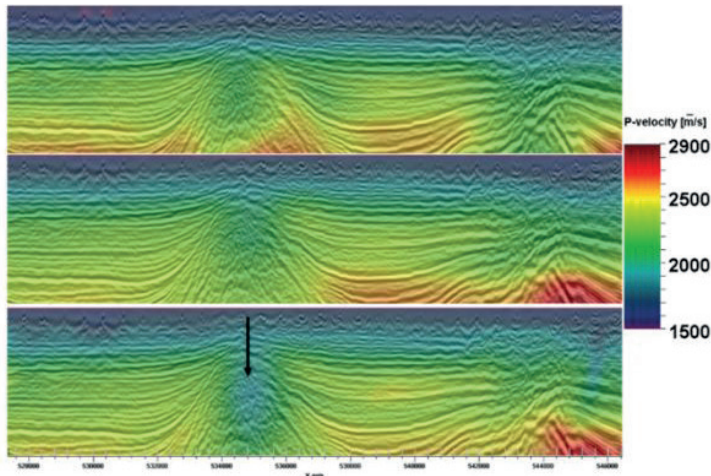
3D view of the 2.5D regional models along the 2D profiles [left]; example of gravity and magnetic interactive 2.5D modelling along a 2D profile [right]

Figure 2 - Gravity assisted seismic Earth Model building



Seismic image with corresponding density model and key interpretations (carbonate, black; salt, pink; and basement, deep black) overlaid [left]; statistical distribution of the gravity residual [center]; gravity residuals [right]. Early-stage model [top], final model [bottom]

Figure 3 - Gravity & seismic Simultaneous Joint Inversion (SJI) for near-surface modelling



3 Hz FWI [top], FB-FTG SJI [center], 4 Hz FWI from FB-FTG SJI [bottom]

# Güney Karolayna Kıyı Kenarındaki Clubhouse Crossroads Mafiklerinin(CAMP) 3 Boyutlu Gravite ve Manyetik Ters Dönüşümü



**Kübra Sibel Albayrak**

Türkiye Petrolleri Anonim Ortaklığı-Gravite Manyetik

## AMAC

Triyasik-Jurasik yaşlı The Central Atlantic Magmatic Province CAMP dünya da bilinen büyük magmatik jeolojik alandır. Fakat bu alanın hem geometrisi hemde hacmi konusunda yeterli bilgi ve çalışma tam olarak bulunmamaktadır. Özellikle Georgia ve Güney Karolayna eyaletlerindeki sismik kesitlerde tariflenmiş J seviyesine CAMP in lav akışının sebep olduğu düşünülmektedir. Triyasın sonunda, ~ 1 m.y. 200 My, The Central Atlantic Mahmatic (CAMP), Pangea dağılımasından hemen önce dünyanın en büyük kıtasal magmatığı olarak kabul edilmektedir. CAMP dört kıtaya yayılmıştır ve tahmini 7-10 ×10<sup>6</sup> km<sup>2</sup>'lik bir alanı kapsamaktadır (Marzoli ve diğerleri, 1999; McHone, 2000). Masif CAMP toleyitik bazalt akıntıları, Trias-Jura kitlesel oranda yok oluşlarıyla ilişkilendirilmiştir. Kıta kenarlarından 2000 km'ye kadar yaygın magmatizma söz konusudur. CAMP'nin jeokimyasal yapısı, yitim süreçleriyle modifiye edilmiş bir üst manto kaynağına işaret eder ve kuzeye karşı güney CAMP lavlarının manto kaynağında yitimle ilgili farklı gözlemlerle tanınır (Whalen ve diğerleri, 2015). Magmatizma, Triyas-Jura sınırındaki büyük bir kitlesel yok oluşla aynı zamana denk gelmektedir. Jeokronolojik ve paleomanyetik veriler, CAMP yaş aralığını ~ 191 ila 205 My arasında sınırlar ve bu yaygın magmatizmanın çoğu 200 My e kadar çıktığı görülür. CAMP yaşları 204 Ma ile 190 Ma arasında değişmektedir (Nomade ve diğerleri, 2005). Ancak Diyabaz ve gabro için herhangi bir yaş yoktur. Güney Georgia havzası, Kuzey Amerika'nın doğu sınırındaki en güneydeki ve en büyük erken Mesozoyik rift havzasıdır. Kuzey Amerika'nın doğu kenarı boyunca erken Mesozoik rift-havzası oluşumu tipik olarak sedimanter gruplarda diyabaz daykları, eşikler ve bazalt akıntıları olarak yerleştirilmiş magmatik aktiviteyi içermiştir (Olsen, 1997). Whalen et al. (2015), eş zamanlı CAMP akışlarının güney yarık havzalarında bulunmadığını, ancak havza dolgusu için yaş kısıtlamalarının biyostratigrafiye, paleomanyetik verilere ve Milankovitch döngüselliğine dayandığını ve zayıf bir şekilde kısıtlandığını öne sürmüştür. (Olsen, 1997). CAMP akışlarının en büyüğünün, Atlantik kıyı düzlüğünün tabanında öne çıkan "J" yansıtıcısı olarak Güney Georgia Rift'te korunduğu uzun süredir varsayılmıştır. "J" reflektörü/ufku, Schilt ve diğerleri (1983) tarafından adlandırılmıştır ve Clubhouse Crossroad bölgesinde yer alan sondajlarda karşılaşılan bir dizi toleyitik bazalt akıntısı ile ilişkilendirilmiştir (Gottfried ve diğerleri, 1983). Heffner ve diğerleri tarafından yapılan son çalışmada (2012), ancak reflektöre giren kuyuların çoğunun bazaltla değil, Kıyı Ovası sedimanlarının tabanında bir empedans kontrastıyla karşılaştığını göstermiştir. Bununla birlikte, çok sayıda kuyu diyabazla karşılaştırılmıştır. Gravite ve manyetik verine göre CAMP'in ana bileşenleri

temsil eden Güney Georgia Rift Havzasında (Chowns ve Williams, 1983) gömülü yaygın eşikler, bentler ve derin kanallar veya plütonları ortaya koymaktadır.1886 Charleston depreminin merkez üssü yakınında yer alan, sismisite ve fayları araştırmak için tasarlanmış birçok sismik hatlar ve sınırlar iyi kalitede veriler çalışma alanında mevcuttur. 1975 yılında, USGS tarafından Charleston-Güney Karolayna'nın 40 km batı-kuzeybatısında üç adet Clubhouse Crossroad (CC) kuyusu açılmıştır. CC kuyuları, Triyas kırmızı yataklarına ve toleyitik bazaltlara girmeden önce kıyı ovası tortullarına girmektedir. CC- 3 numaralı kuyu en büyük pozitif manyetik anomali üzerine açılmıştır. Clubhouse Crossroad mafikleri üzerindeki sismik veriler SEISDATA4 profilini içerir. Güney Karolina için 1958'den 1978'e kadar elde edilen USGS aeromanyetik ve kara gravite verileri kullanılmıştır. Güney Karolayna'da havadan manyetik verileri için uçuş aralığı 1.6 km'dir; arazi gravite verileri yaklaşık 5 km'lik bir çözünürlüğe sahiptir. Havadan manyetik veriler cell size 1 km olacak şekilde gridlenmiştir.Kara gravite verileri ise 2 km'lik bir cell size ile gridlenmiştir.

## YÖNTEM

Gravite yöntemi Newton Yasasına dayanan yerçekimi ivmesindeki değişimden yararlanarak yer altındaki farklı yoğunluk yapılarını araştırır. Güvenilir modelleme için derinlik bilgisi de gereklidir. Bu çalışmada kısıtlı kuyu bilgilerinden yararlanılarak derinlik bilgisi çekilmiş ve modellemede kullanılmıştır. Manyetik yöntemin amacı, Dünya'nın manyetik alanındaki değişiklikleri analiz etmektir. Manyetik alan daha karmaşıktır ve yerçekimi alanından daha fazla değişkenliğe sahiptir.

Manyetik duyarlılık, indüklenen manyetik alanı üreten önemli bir varyanttır, çünkü kaya yoğunlukları yerçekimi alanını üretir.

Potansiyel alan verileri arazide ki faylar, dayklar ve kontaklar gibi yeraltı yapılarını haritalandırmak için yorumlanır. Bu çalışma da yorumlama, Geosoft Oasis Montaj (sürüm 9.2) yazılımında Tilt Derivative, Reduced to Pole, Analytical Signal ve 2-D modelleme gibi teknikleri uygulanarak yapılmıştır.

Eğim türevi (Tilt Türevi) yöntemi, geniş alanlar için manyetik tabana olan derinliği tahmin etmenin ve sığ özellikleri iyileştirmenin basit ve hızlı bir yolu sağlar. Eğim türevi, kutba indirgenmiş (RTP) birinci mertebedir (Fairhead ve diğerleri 2010).

Analitik sinyal (AS), toplam gradyan tekniği olarak da bilinen potansiyel alan verilerini yorumlamak için yaygın yöntemlerden biridir. Teknik, anomali adı verilen herhangi bir bozukluğa neden olan yapının derinliğini ve kenarını tahmin etmek için kullanılır. AS'nin önemli bir

avantajı, kaynağı miktatsızlanma yönünden bağımsız olmasıdır. Kıyı ovası sedimanlarının tabanı, Triyas havzası dolgunun tabanı ve Moho'nun derinliği dahil olmak üzere, kıyı ovası sedimanlarının tabanına açılan üç sondaj deliği, Seisdata-4 sismik yansıma verileri ve bir sismik kırılma hızı modeli ile sınırlandırılmıştır. (Leutgart ve diğerleri, 1994). Bu sınırların geometrisi önemlidir çünkü model profili boyunca en güçlü yoğunluk kontrastlarını temsil ederler. Bu çalışmada ön geometriler ayarlanarak temsili yoğunluk ve manyetik duyarlılık değerleri girilmiştir. Daha sonra, Clubhouse Crossroad mafik plütön anomalisinin kaynağı olan büyük çaptaki gövdeyi çözümlmek için poligon geometrisi ve atanan yoğunluk ve manyetik duyarlılık değerleri, hesaplanan anomalinin gözlenen anomaliye en iyi uyum tutarlı bir model çözümü üretmek için değiştirilmiştir. GM-SYS 3D modelin toplam yanıtını hesaplamak için Hızlı Fourier Dönüşümü (FFT) ve uzay-etki alanı algoritmalarının bir kombinasyonunu kullanır. Bu çalışma da da toplam model yanıtını hesaplamak için Hızlı Fourier Dönüşümü (FFT) kullanıldı. 3 boyutlu ters dönüşüm toplam model yanıtını hesaplamak için Hızlı Fourier Dönüşümü (FFT) ve uzay-etki alanı algoritmalarına dayanır. İleriye dönük hesaplamalar, Parker (1972) ve Blakely (1983) tarafından yapılan frekans alanı tekniğine dayanmaktadır.

## BULGULAR

Geosoft Oasis Montaj'daki VOXI yer modelleme aracı kullanılarak gravite verilerinin 3 boyutlu ters çözümü de gerçekleştirilmiştir. VOXI yer modellemesi, Li ve Oldenburg'un (1998) 2 boyutlu modelleme sonuçlarından elde edilen yoğunluk değerleri ile algoritmasına dayanmaktadır. Kullanılan yöntem, veri uyumsuzluğunu en aza indirir ve model ters dönüşüm tekniğiyle güncellenir. Ters çözüm, ters yoğunluk modelinin yerçekimi ortalaması ile tahmin edilen model arasındaki fark yeterince azaltılıncaya kadar devam eden birkaç yineleme kullanır (Kanthiya ve diğerleri, 2008). Bu durumda ortaya çıkan ters çözüm modelinin sonucu, yer altı katmanlarının geometrik bir modeli olarak kabul edilerek yorumlanır.

Çalışma alanında toplam manyetik yoğunluk anomalisi 414,4 ile -159,1 nT arasında değişmektedir. Manyetik haritada ki maksimum değerler açık pembe renkli CAMP intrüzif plütönlarını göstermektedir. Mavi ve yeşil renkler, düşük anomali değerleri ile ilişkilidir.

Kutuba indirgenmiş (RTP) filtre, gözlemlenen alanı taşımak için kullanılır. RTP filtresi, anomaliyi doğrudan kaynağın üzerine yerleştirir. Yöntem, eğim ve sapma açısının kaldırılmasına dayanır. TMI ve RTP arasında küçük farklar vardır. ~268-~480 nT aralığındaki CAMP mafikleri üzerindeki yüksek değerleri vurgulamaktadır.

Çalışmada önce 2 boyutlu düz (forward) çözüm ile başlanmıştır çünkü profil geometrisi kuyu, sismik, gravite ve manyetik verilerle sınırlandırılabilir. Potansiyel alan verilerinin forward modellemesi, Geosoft GM-SYS yazılımı kullanılarak, Talwani ve diğerleri (1959) ve Talwani ve Heirtzler'in (1964) belirli bir yatay prizmadan yerçekimi ve manyetik

tepkiyi hesaplama metodolojisine dayanan etkileşimli bir yöntemle gerçekleştirildi (Duff ve Kellogg, 2019). CAMP Clubhouse Crossroad mafik plütönü üzerinde kuyu, sismik, gravite ve manyetik verilere dayalı olarak oluşturulmuş 4 model profili bulunmaktadır. Profil 1, kısmen SEISDATA 4 sismik yansıma profiline dayalı olarak Duff (2015) tarafından oluşturulmuş ve diğerleri için referans profili olarak kullanılmıştır.

İlk profil, SEISDATA 4 sismik yansıma hattının bir bölümünü takip eder. Model için hesaplanan yerçekimi ve manyetik alanlar, gözlemlenen alanlara uygundur. Anomali gövdesi ortalama ~1.5 km kalınlığındadır ve 1-3 km derinlikte yer almaktadır.

İkinci profil, birinci profil SEISDATA 4'e diktir. Model hesaplanan gravite ve manyetik anomaliler gözlenen anomalilere uygundur. Modellenen mafik gövde 2 km kalınlığa kadar ve 1-3 km derinlikte yer almaktadır.

Üçüncü profil için hesaplanan gravite anomalileri (Şekil 4.11) gözlenene çok iyi uymaktadır. Mafik gövde 2 km kalınlığa kadar ve 1-3 km derinlikte yer almaktadır.

Model, dördüncü profil için hesaplanan gravite değerleri (Şekil 4.12) gözlenen gravite değerleri ile uymaktadır. Model mafik gövdesi 2 km kalınlığa kadar ve 1-3 km derinlikte yer almaktadır.

## SONUÇLAR

GM-SYS 3B ters dönüşüm modeli için, ilk olarak iyi bilinen kıyı ovası sediman tabakasını modellenmiştir. Varsayılan bir Triyas sediman yoğunluğu kontrastı ile, mafik Triyas sediman kantağının tepesinin derinliğini haritalamak için gravite ters dönüşümü uygulanmıştır. Son olarak, mafik Alt Triyas kantağının tabanına olan derinliği hesaplamak için gravite ters çözümü uygulanmıştır.

Sonuçlanan 3B modelde CAMP mafik yapıların iki kanaldan beslenen diyabaz/gabro CAMP yaşlı lakoliti olduğu görülmüştür. Söz konusu lakolit en fazla 2 km kalınlığında, 1-3 km derinliğinde değişen ve 1900 km<sup>2</sup> lik bir alanı kaplamaktadır. Lakolitin hacmi ise 1300 km<sup>3</sup> bu da Newark Baseninde yer alan Palizat Siltlerin yaklaşık 8 katına karşılık gelmektedir. Yalnızca sondaj ve sismik yansımaya dayanan CC bazalt hacimlerinin önceki tahminleri, Kıyı Ovası altında korunan toplam CAMP hacminden fazladır. Clubhouse Crossroad lakoliti ayrıca CO2 tutulması için büyük bir potansiyel rezervuar sağlayabilir. Clubhouse Kavşağı bazaltlarının ve Summerville petrol kuyusundaki ve kıyı ovasının altındaki başka yerlerdeki diyabazın yaşlarını doğrulamak için daha fazla yaş tarihlemesi gerekmektedir. Bu, ya 200 Ma'daki büyük CAMP Büyük Igneous Province olayı ya da ~ 180 Ma'daki ilk Kuzey Atlantik riftleşmesi ile ilgili olarak meydana gelen mafik aktivitenin yaşlarını parantez içine almak için önemlidir.

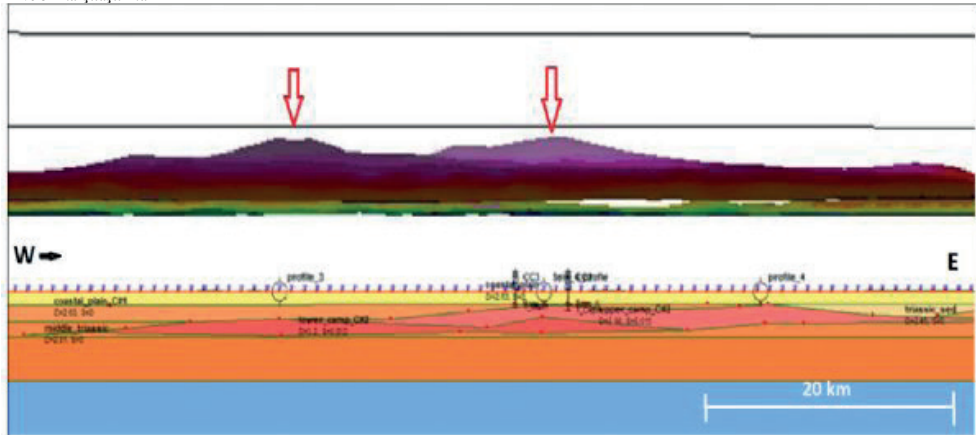
The Central Atlantic Magmatic Province (CAMP) at the Triassic-Jurassic boundary, is the largest known igneous province in the world. However, the geometry and volume of CAMP intrusives under the Coastal Plain of the southeastern United States are poorly known.

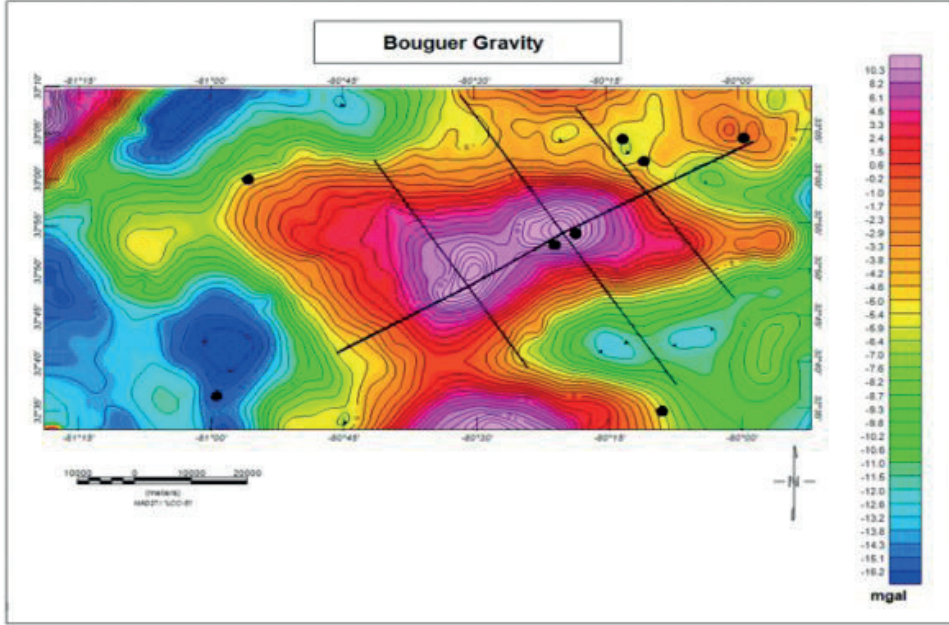


Under the Coastal Plain sediments of Georgia and South Carolina, the “J” seismic reflector was predicted to be produced by a CAMP lava flow. Recent studies of seismic and well data have shown that the “J” reflector is an unconformity and only locally a CAMP lava flow. In the Clubhouse Crossroads area of South Carolina, seismic reflection, seismic refraction, and well data are available to constrain the shallow structure under the Coastal Plain sediments but have not succeeded in imaging the underlying pluton. We take advantage of a rich potential field dataset to predict the deeper structure of the CAMP mafic intrusive pluton at Clubhouse Crossroads for the first time. The CAMP plutons have both very high densities as well as high magnetic susceptibilities, which makes them ideal for 3-D inversion techniques. We forward modeled the shallow structure with seismic and well control and then inverted for the shape of the deeper structures assuming realistic densities and magnetic properties. The inversion methods used include Fast-Fourier Transform inversion with GMSYS 3D, gravity Fourier Matlab depth inversion, and Oasis Montaj-Voxi earth modeling inversion. The resulting 3-D models show that the Clubhouse Crossroads mafic intrusive is a diabase/gabbro CAMP age laccolith fed by two deep conduits. The laccolith is up to 2 km thick and extends from 1 to 3 km depth over an area of 1900 km<sup>2</sup>. The volume of the Clubhouse Crossroads laccolith is 1300 km<sup>3</sup> or over eight times larger than the Palisades Sill in the Newark Basin.

Anahtar Kelimeler: 3Boyutlu Modelleme

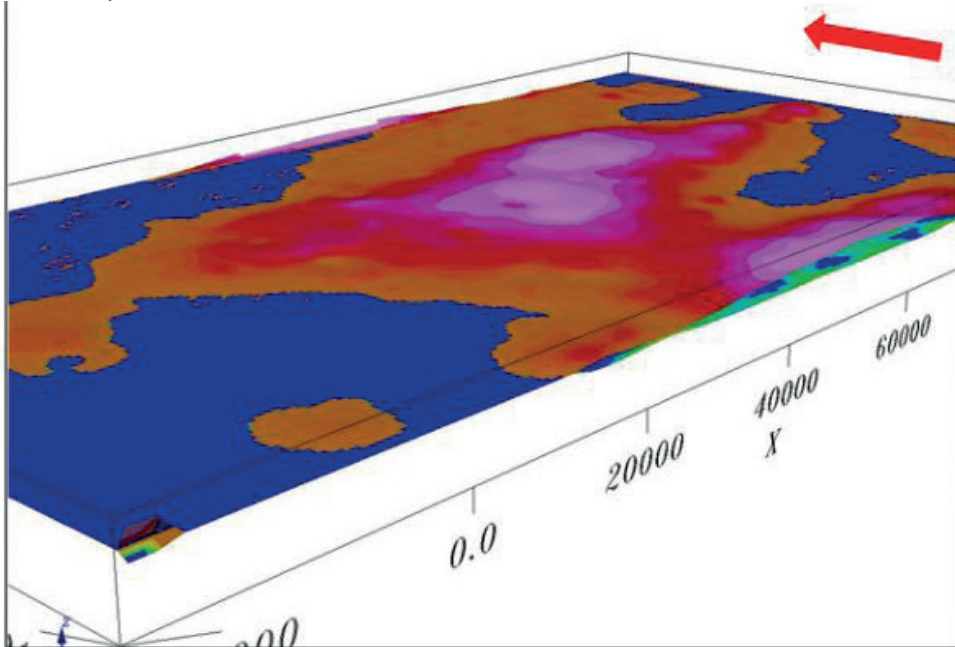
2B ve 3B karşılaştırma

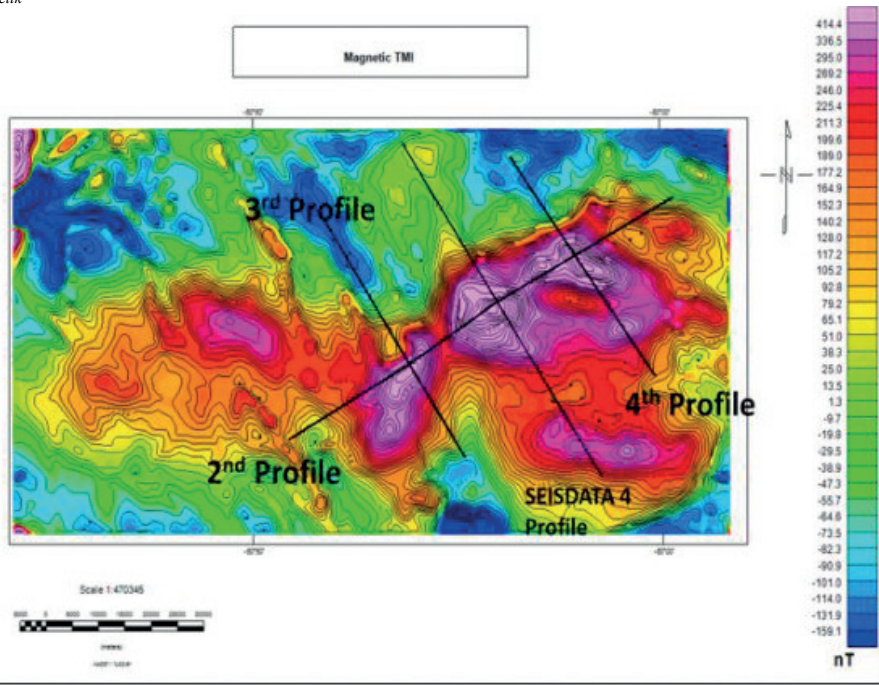




Gravite Grid Datası

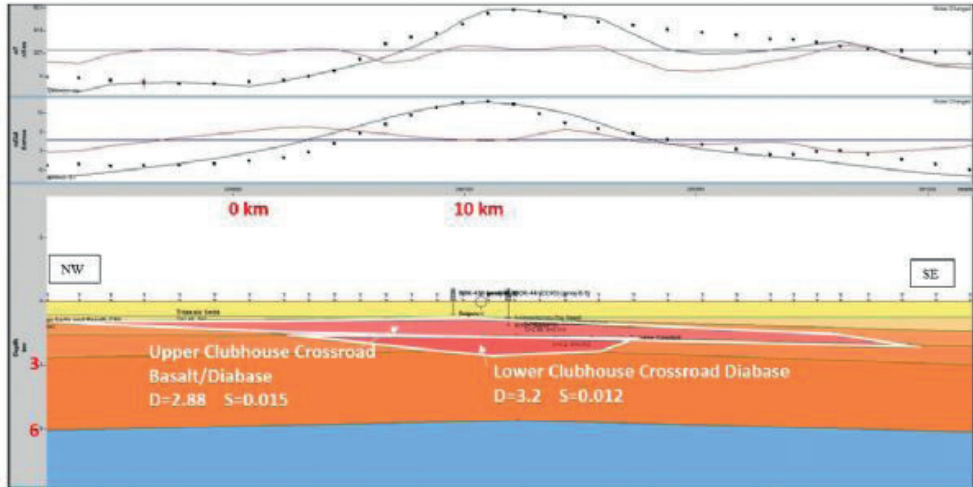
Gravite ters dönüşümü





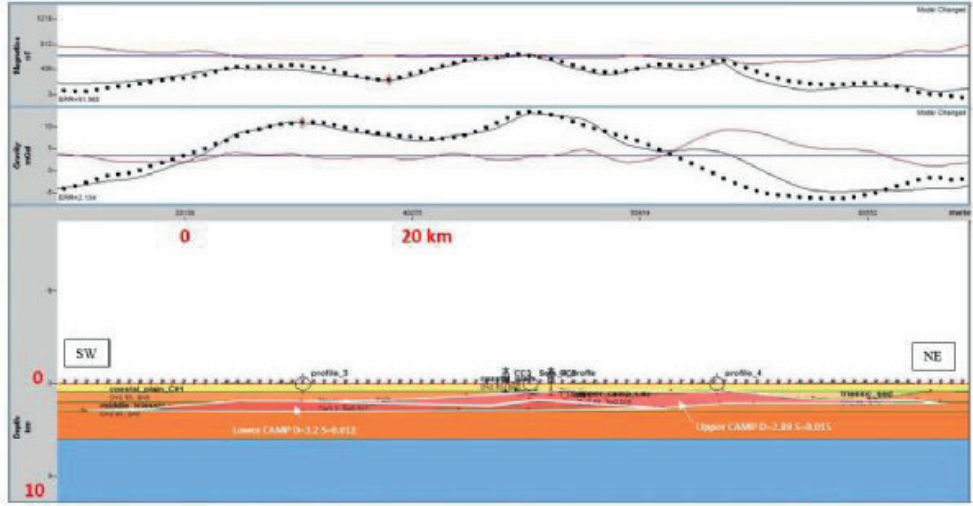
Manyetik Grid datası

Profil 1



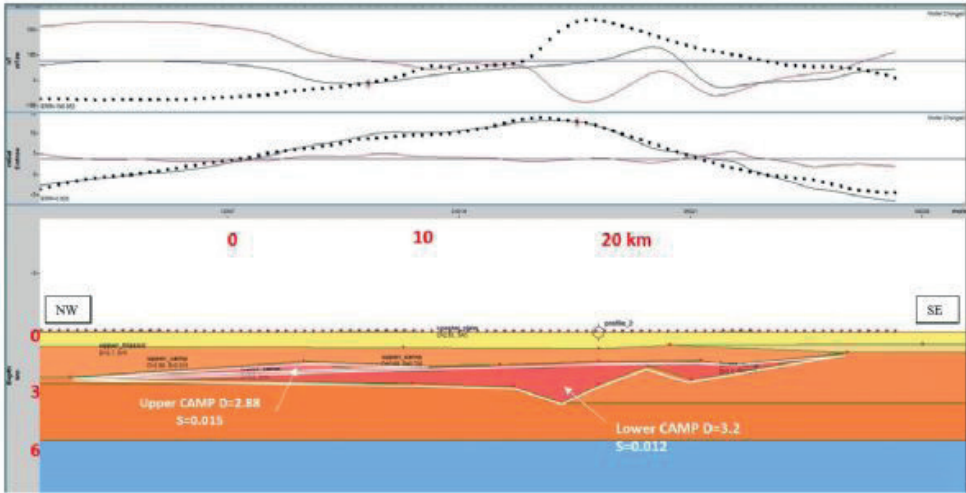
Profil 1 2 Boyutlu modeli

Profil2



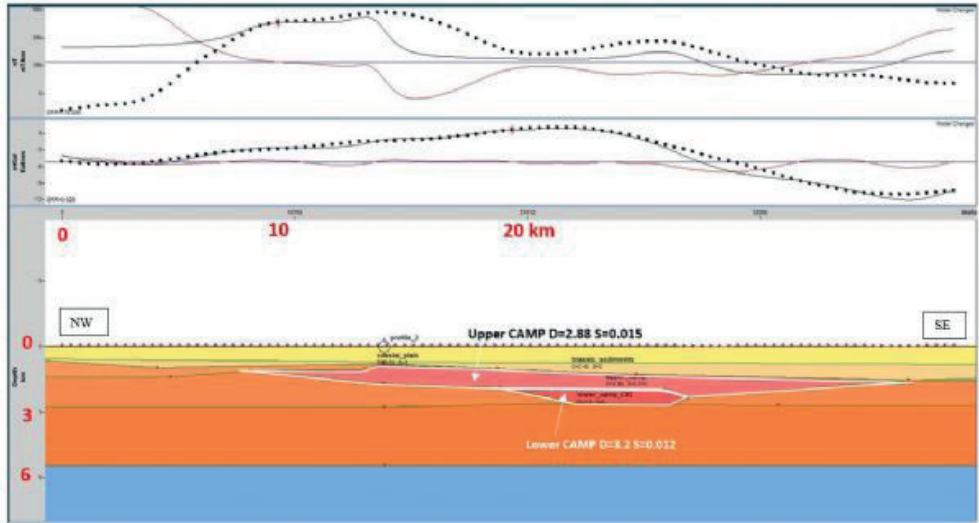
Profil2 2 Boyutlu Modeli

Profil3



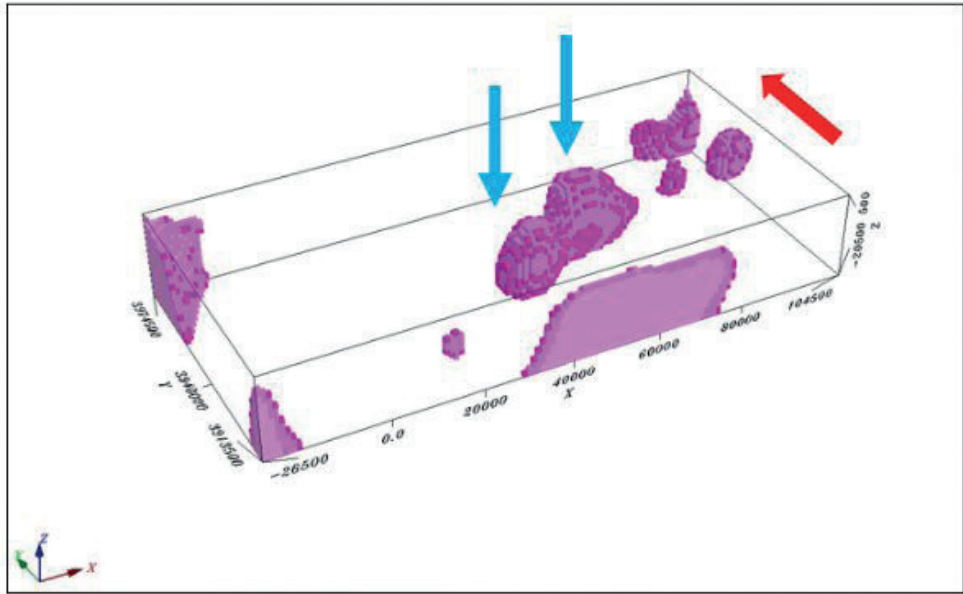
Profil3 2 Boyutlu Modeli

Profil4



Profil4 2 Boyutlu Modeli

Voxi 3 Boyutlu Model







## **Jeodezi, Geomatik ve Uzaktan Algılama Çalışmaları**

*Geodesy, Geomatics and Remote Sensing Studies*

---





# Bathymetry effect on complete Bouguer Anomalies along the Turkish shoreline of the Black Sea



**Sevda Olgun, Aydın Üstün**  
Kocaeli University, Kocaeli / Türkiye

## AIM

Reducing topographic effects on gravity data is required in geodesy, mineral and oil exploration in geophysics, and other gravity field associated studies (see, Hofmann-Wellenhof and Moritz, 2006; Hinze et al., 2013). The local signals of the topographic masses that constitute high frequency spectrum in gravity space must be taken into account for the full modeling of the gravitational field. If a special concern is not taken, gravity anomaly observations reduced to the geoid become topography dependent in particular over severe conditions. This scenario leads to incorrect interpretations of gravity (potential) fields. Therefore, terrain correction (TC) errors must be considered to have best practice. TC values have been found to reach tens of mGal, particularly in high mountain regions (Olgun et al., 2023). Because of these substantial values, complete Bouguer anomalies should be calculated rather than simple Bouguer anomalies (Amos and Featherstone, 2003; Janak and Vanicek, 2005). Calculating terrain corrections for complex terrain and bathymetry, land and ocean stations requires taking into account both the contributions from the land and water bodies (Hwang et al., 2013). This study aims to analyze the magnitude of terrain corrections and the bathymetry effect in the Black Sea line and, consequently, their significance in gravity reduction practices.

## MATERIALS AND METHODS

'tc-cylinder' (Olgun et al., 2023) program is used for TC calculations. In all physical circumstances, the proposed algorithm for segmenting cylinder bodies produces more accurate and effective results for terrain correction. 1 arc-second resolution Digital Elevation Model (DEM) and detailed mass elements utilized for the TC computation. A numerical test is carried out at 100800 grid points in Karadeniz, North Turkey.

A high-resolution DEM is necessary for the reduction and interpolation of gravity measurements. If high accuracy terrain corrections (TC) are required for gravity observations, the DEM resolution in the immediate vicinity of the point of interest should be 30 m or less. However, in terms of computations to be performed on the computer, very high resolution DEMs encounter speed and storage issues. Fast Fourier Transform (FFT) (Parker, 1973; Sideris, 1985; Forsberg, 1985; Kirby and Featherstone, 1999; Tsoulis, 2001a; McCubbine et al., 2017; Goyal et al., 2020), binary linear functions, and Gaussian quadrature techniques (Tsoulis et al., 2003; Hwang 2003; D'Urso and Trotta, 2015). These numerical techniques improve processing efficiency, but the binomial series converge if the topographic slope is less than 45° (Tziavos, 1992; Sideris and Sanso, 2013; Sampietro 2016). The series, on the other hand, must

have higher order terms in order to improve the accuracy of the TC values (see Goyal et al., 2020). As a result, spectral approximations must strike a balance between accuracy and convergence. Tsoulis (2001b) highlights that the balance can be reached using analytical methods applied in the near neighborhood. Analytical methods aim to define topography as geometric shapes such as rectangular prisms (Nagy et al., 2000; 2002), polyhedral masses (Pohanka, 1998; Tsoulis, 2001b; D'Urso, 2014), or cylindrical segmentations (Olgun et al., 2023).

Reduction for topographic masses is generally practiced in three terms (Bullard A, B, C) in the context of Bouguer anomalies. The first term (Bullard A; BA) is to compute the Bouguer slab effect, which is the gravitational effect of a constant density slab with a thickness equal to the gravity observation elevation. Bullard A ignores the earth's sphericity and Simple Bouguer reduction is the correction that takes the plane plate into account. The sphericity correction, represented by Bullard B (BB), changes the plane-plate gravitational action into the spherical gravitational effect of the 166.7 km radius (cover) shell centered at P (Bullard, 1936). However, the actual geometry of the topography around the calculation point differs significantly from these simplified models. Terrain corrections (Bullard C; TC) is determined by accounting for topographic deviations from the spherical Bouguer shell (Figure 1).

Transitions from one form of anomaly to another also use smooth gravity anomalies, like Bouguer, which reveal the internal structure of the Earth. Bouguer anomalies yield gridded high-resolution gravity information or interpolated spatial gravity field information. This can be accomplished by reducing all of the topographic masses, or by using the completed Bouguer approach. Bouguer gravity anomalies are generated by applying Bouguer corrections to free-air gravity anomalies ( $\Delta g_{FA}$ ). The Bouguer reduction seeks to determine the sea level equivalent of earth gravity measurement. Complete Bouguer anomalies have been identified if terrain corrections are used as follows,

$$\Delta g_{CB} = \Delta g_{FA} - (BA + BB) + TC \quad (1)$$

otherwise, simple Bouguer anomalies,

$$\Delta g_{SB} = \Delta g_{FA} - (BA + BB) \quad (2)$$

are determined.

The gravitational effect of this plate ( $BA = 2\pi G\rho H$ ) is obtained for an infinite-radius cylinder of the Newton integral at a point P on the Earth. G denotes the universal gravitational constant, and  $\rho$  is the average topographical density. The Bouguer plate effect is calculated by,

$$BA = 0.1119H \quad (3)$$

for the value of 2.67 gr cm<sup>-3</sup> for  $\rho$ . Using the coefficients of the polynomial equation for the standard density and the Earth radius of 6371 km, Cogbill (1979) calculated

Bullard B correction for the Earth sphericity by,

$$BB=1464.139 \times 10^{-3} H - 3533.047 \times 10^{-7} H^2 + 1002.709 \times 10^{-13} H^3 + 3002.407 \times 10^{-18} H^4. \quad (4)$$

The topography is split into rings using this method, and each ring is divided into compartments based on the sectoral length. The inner radius  $r_i$  and the outer radius  $r_{i+1}$  define the zones. The compartment gravity effect can be calculated by integrating the differential equation provided in:

$$TC = G\rho\Delta\alpha[r_{i+1} - r_i - \sqrt{(r_{i+1})^2 + [\Delta H]^2} + \sqrt{(r_i)^2 + [\Delta H]^2}] \quad (5)$$

(bkz. Heiskanen ve Mortiz, 1967; Vanicek ve Krakivsky, 1986; Olgun ve Üstün, 2021).

The resolution and precision of the DEM have an impact on the correctness of the terrain correction value. The height data closest to the calculation point contributes the most (Long and Kaufmann, 2013), yet the processing time increases as the resolution improves. In order to avoid this negative effect, analytical software use DEMs with high resolution for the immediate environment and reduced resolution for the surrounding region. The estimation of the outer zone effect up to 166.7 km is acceptable (Bullard, 1936; LaFehr 1991; Hinze et al. 2005).

Each of the cylinder segments representing the grid node attributes around the calculation point has average height, density, and coordinates with 'tc-cylinder'. Furthermore, in order to measure the gravity effect with great accuracy, the Newton integral requires smaller cylinder segments. If the height of the model's resolution is insufficient, the integration fills in the empty compartments and prevents the accuracy from deteriorating dramatically.

Since the effect of mass elements close to the point on the result is important, the highest resolution global elevation models were utilized. The SRTM1 model was used to obtain high-resolution terrestrial elevation data, while the SRTM15 model was used to obtain bathymetric data.

## RESULTS

Gravity reduction magnitudes have been calculated at 1' x 1' resolution grid nodes (100800 points) at 27.5° - 41.4° East longitudes and 40.5° - 42.5° North latitudes, including Turkey's Black Sea coastline. The calculation points range in height from -2500 to 3500 m. The study area has been expanded to include this radial distance in order to account for the outer zone effect up to 166.7 km (Figure 2).

The gravitational effect of spherical Bouguer plate (BA) has been calculated with maksimum 389.09 mGal, and mean 40.52 mGal. Bouguer sphericity effect (BB) reached a maximum of 1.52 mGal and was computed as an average of 0.32 mGal. Terrain correction values for constant density of topography (2.67 g cm<sup>-3</sup>) have been calculated with 'tc-cylinder' software using DEMs with 1" interior and 15" exterior resolution. Terrain corrections range between -8.08 and 45.06 mGal, with an

average of 2.88 mGal and 4.03 mGal standard deviation (Figure 3). The complete Bouguer correction is derived by subtracting the gravitational effect of the spherical Bouguer shell from terrain corrections (Table 1). When the TCs are computed without taking into account the bathymetric contribution, there are variations of up to 5.85 mGal over Turkey's northern area.

## CONCLUSIONS

Bouguer reduction calculations were performed in 1' grid intervals along the Black Sea coastline, where the steep and mountainous terrain, as well as the sea, are located. At 100800 points, terrain correction values up to 45 mGal have been obtained. Therefore, disregarding topographic corrections for Bouguer anomalies will lead to substantial errors. Because Turkish territory along the Black Sea has highly irregular topography, relatively large correction values are expected in studies to be performed in different places in Turkey.

The effect of bathymetry is shown to exceed 5.85 mGal in the terrain corrections determined on land. The bathymetry effect can be a significant source of error when taking into account the requirements of sub-mGal accuracy of gravity measurements, according to current studies on the gravity field.

## KAYNAKLAR

- Amos, M., Featherstone, W. (2003). Comparisons of Recent Global Geopotential Models with Terrestrial Gravity Field Observations over New Zealand and Australia. *Geomatics Research Australasia*, 79, 1-20.
- Cogbill, J.R. (1979). The Relationship Between Seismicity and Crustal Structure In The Western Great Basin, Doktora Tezi, Northwestern Üniversitesi, Illinois, 8007361.
- D'Urso, M.G. (2014). Analytical Computation of Gravity Effects for Polyhedral Bodies. *Journal of Geodesy*, 88(1), 13-29.
- Forsberg, R., (1985). Gravity Field Terrain Effect Computations by FFT. *Bull. Géodésique*, 59(4), 342-360.
- Goyal, R., Featherstone, W., Tsoulis, D., Dikshit, O. (2020). Efficient Spatial-spectral Computation of Local Planar Gravimetric Terrain Corrections from High-resolution Digital Elevation Models. *Geophysical Journal International*, 221(3), 1820-1831.
- Janak, J., Vanicek, P. (2005). Mean Free-air Gravity Anomalies In The Mountains. *Studia Geophysica et Geodaetica*, 49(1), 31-42.
- Hinze, W.J., Von Frese, R.R., Von Frese, R., Saad, A.H., 2013. *Gravity and Magnetic Exploration: Principles, Practices, and Applications*. Cambridge University Press, pp. 3-5.
- Hofmann-Wellenhof, B., Moritz, H., 2006. *Physical Geodesy*. Springer Science & Business Media, p. 129.
- Hwang, C., Hsu, H. J., Chang, E. T., Featherstone, W. E., Tenzer, R., Lien, T., & Jai, P. H. (2014). New free-

air and Bouguer gravity fields of Taiwan from multiple platforms and sensors. *Tectonophysics*, 611, 83-93.

Hwang, C., Wang, C.G., Hsiao, Y.S. (2003). Terrain Correction Computation Using Gaussian Quadrature. *Computers & Geosciences*, 29(10), 1259–1268.

Kirby, J.F., Featherstone, W. (1999). Terrain Correcting Australian Gravity Observations Using The National Digital Elevation Model and The Fast Fourier Transform. *Australian Journal of Earth Sciences*, 46(4), 555–562.

Pohanka, V. (1988). Optimum Expression for Computation of The Gravity Field of a Homogeneous Polyhedral Body. *Geophysical Prospecting*, 36(7), 733–751.

Parker, R.L. (1973). The Rapid Calculation of Potential Anomalies. *Geophysical Journal International*, 31(4), 447-455.

Nagy, D., Papp, G., Benedek, J. (2000). The Gravitational Potential and Its Derivatives for The Prism. *Journal of Geodesy*, 74(7), 552–560.

Nagy, D., Papp, G., Benedek, J. (2002). Corrections to “The Gravitational Potential and Its Derivatives for the Prism”. *Journal of Geodesy*, 76(8), 475.

Olgun, S., Üstün, A., Akyılmaz, O. (2023). tc-cylinder: An Optimized Algorithm for Accurate Topography Effect from High-resolution Digital Elevation Models. *Computers & Geosciences*, 170, 105264.

Sampietro, D., Capponi, M., Triglione, D., Mansi, A., Marchetti, P., Sanso, F. (2016). GTE: A New Software for Gravitational Terrain Effect Computation: Theory and Performances. *Pure Appl. Geophys.* 173(7), 2435–2453.

Sanso, F., Sideris, M.G. (2013). *Geoid Determination: Theory and Methods* (1st ed.). London: Springer-Verlag Berlin Heidelberg.

Sideris, M.G. (1985). A Fast Fourier Transform Method for Computing Terrain Corrections. *Manuscripta Geodaetica*, 10(1), 66-73.

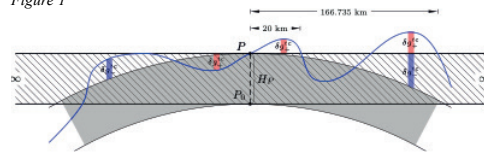
Tsoulis, D. (2001). Terrain Correction Computations for A Densely Sampled DTM In The Bavarian Alps. *Journal of Geodesy*, 75(5), 291–307.

Tsoulis, D., Petrovic, S. (2001). On the Singularities of The Gravity Field of A Homogeneous Polyhedral Body. *Geophysics*, 66(2), 535-539.

Tziavos, I., Sideris, M., Schwarz, K. (1992). A Study of The Contributions of Various Gravimetric Data Types on The Estimation of Gravity Field Parameters In The Mountains. *Journal of Geophys. Res.: Solid Earth*, 97(B6), 8843–8852.

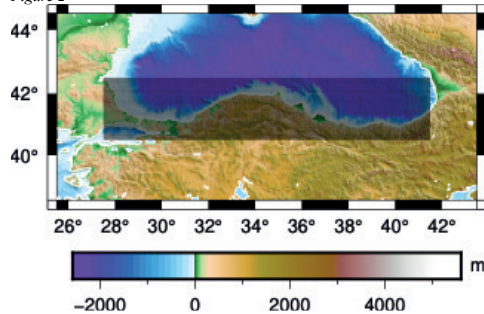
Keywords: Digital Elevation Models, Terrain Corrections

Figure 1



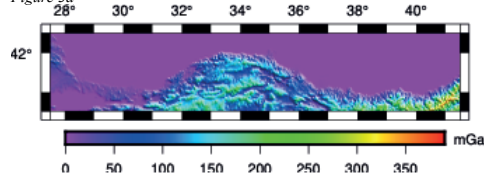
Bouguer plate, spherical Bouguer shell and mass elements of terrain corrections ( $\delta g^{tc}$ ) for onshore areas. The cylinder masses are red or blue indicates whether the gravity total correction amount is positive or negative at the P point. The topography, Bouguer plate and spherical Bouguer shell are shown by a blue curve, an inner hatching plate, and gray region, respectively (Olgun ve Üstün, 2023).

Figure 2



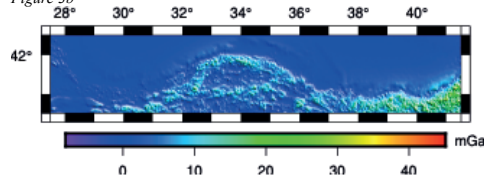
Study area and calculation points distribution

Figure 3a



Gravitational effect of the spherical Bouguer shell

Figure 3b



terrain correction values

Table 1

	Min	Max	Mean	RMS	STD
BA	0	389.09	40.52	76.90	65.36
BB	0	1.52	0.36	0.63	0.52
TC	-8.08	45.06	2.88	4.95	4.03
-(BA+BB)+TC	-15.37	362.61	38.00	73.69	63.14
Bathymetry Effect	0	5.85	0.25	0.56	0.51

Statistics of Bouguer plate, sphericity correction, terrain correction, completed Bouguer correction, and bathymetry effect values

# Deniz Alanlarında Radar Uzaktan Algılama Yöntemiyle Hidrokarbon Sızıntıları Tespiti

**Avca Karacay**

Türkiye Petrolleri Anonim Ortaklığı, AR-GE D. Başkanlığı, Sedimentoloji, Ankara / Türkiye



## ÖZ

Günümüzde gelişen teknoloji ile Petrol sektöründe de çeşitli teknolojik yöntemler kullanılarak hidrokarbon aramacılığı yapmak günden güne önem arz etmektedir. Bu yöntemlerin en başında hem daha hızlı hem de daha düşük maliyetli olması açısından uzaktan algılama yöntemleri gelmektedir. Türkiye üç tarafı denizlerle çevrili bir ülke olarak jeopolitik ve jeolojik açıdan birçok değersahip nadir ülkeler biridir. Bununla birlikte, son 10 yıldır kara alanlarında aramacılık yapılmasının yanı sıra deniz alanlarında da aramacılık yapılmasına önem verilmiş ve bu sayede yeni ve önemli keşifler de yapılmıştır. Deniz alanlarında aramacılığın artması ile yeni sahalar bulmak amacıyla uzaktan algılama yöntemlerine de başvurulmaya başlanmıştır. Deniz alanlarında en iyi sonuç veren uzaktan algılama yöntemlerinden biri olan Radar sistemleri ile projelere destek verilmekte ve yeni keşifler yapılmaya çalışılmaktadır. Bu projede, uzaktan algılama radar yöntemiyle deniz alanlarında hidrokarbon aramacılığının nasıl yapıldığı belirtilmesi amaçlanmıştır. Bu amaçla kullanılmakta olan Avrupa Uzay Ajansı'na (ESA) ait Radar verilerinin temin edilmesi, işlenmesi ve son ürünün elde edilmesine kadar izlenen basamaklar izah edilmiştir. Temin edilen veriler, NEST, ENVI ve ArcGIS programları kullanılarak işlenmiş ve analiz edilmiştir.

Nowadays, with the developing technology, it is important to reconnoiter new hydrocarbons explorations by using various technological methods in the Petroleum sector. Among these technologies, remote sensing takes the first place in terms of being both more time saving and more cost-efficient method. Türkiye, as a country surrounded by seas on three sides, is one of the rare countries with many geopolitical and geological values. For this reason, besides exploration in land areas, importance has been given to exploration in sea areas in last ten years, and new and important discoveries have been made in this way. With the increase in exploration in offshore areas, remote sensing methods have started to be used in order to find new hydrocarbon fields. Radar, one of the best the remote sensing technics which detects hydrocarbon seeps, has been used to support project in order to make new discoveries in offshore areas. In this project, it is aimed to indicate how hydrocarbon exploration is carried out in offshore areas with the remote sensing radar method. For this purpose, the steps followed until the acquisition, processing and final product acquisition of Radar data belonging to the European Space Agency (ESA), are explained in this paper. The provided data has been processed and analyzed using NEST, ENVI and ArcGIS programs.

## 1. GİRİŞ

Birçok alanda (maden, jeotermal, vb.) aramacılık açısından kullanılan uzaktan algılama yöntemlerinin petrol aramacılığı içinde avantajlı bir yöntem olduğu pek çok araştırma sonucunda ortaya konulmuştur. Yapılan araştırmalara göre, radyo dalga boyunda sinyallerin kullanan, aktif uydu sistemi olan Sentetik Aralıklı Radar (SAR) uydularından temin edilen görüntülerin analizi sonucunda petrol sızıntılarına ulaşılmaktadır. Aktif uydu sistemleri pasif uydu sistemlerinden farklı olarak enerji kaynaklarını kendi ürettikleri enerji sinyallerinden sağlamaktadır. Bu ürettikleri enerjinin çarptığı nesneden saçılması veya yansması sonucunda alınan geri sinyaller (back-scattering) sayesinde araştırma yapılan nesne ya da bölge hakkında bilgi elde edilmektedir.

Doğal petrol sızıntılarında deniz tabanından deniz yüzeyine ulaşan petrol sızıntısı, yüzeyde ince bir tabaka hâlinde yayılım göstermektedir. Petrollü bölgeye gelen Radar sinyalleri sakin veya az pürüzlü deniz ortamlarında tam yansımaya uğrayarak verilerin toplandığı uydudan uzaklaşarak bu alana ait bilgi elde edilememesine neden olmaktadır. Bu tam yansımaya sonucunda, istenilen çalışma alanına dair alınan uydu görüntülerinde hidrokarbon sızıntısı olan alanlar koyu bölgeler şeklinde görülmektedir. SAR görüntülerinde tespit edilen koyu alanlar büyüklüğüne, şekline ve kontrastına bakılarak doğal petrol sızıntıları veya benzerleri olarak sınıflandırılmaya çalışılmaktadır.

Bu amaçla, veri temini sırasında Avrupa Uzay Ajansı'ndan (ESA) ücretsiz elde edilen SAR uydu görüntüleri kullanılarak deniz alanlarında petrol sızıntıları belirlenmeye çalışılmıştır.

## 2. UYGULAMA

Bu çalışmada ESA'dan ücretsiz elde edilmiş çeşitli SAR uydularına ait verilere, görüntü oluşturması için toplanan radar sinyallerinin maruz kaldığı atmosferik ya da topoğrafik etkileri minimuma indirmek amacıyla bazı işlemler uygulanmıştır. Bu amaçla sırasıyla NEST (Next ESA SAR Toolbox), ENVI (Environment for Visualizing Images) ve ArcGIS programları kullanılmıştır. (Şekil 1)

ESA'dan alınan veriler SAR IMP 1P (SAR Image Mode Precision Image-SAR Görüntü Modunda Duyarlı Görüntü) ürün tipinde elde edilmiştir. IMP modundaki radar görüntüleri iki farklı banttan oluşmaktadır. Bunlar, yoğunluk (intensity) ve genlik (amplitude) bantlarıdır. NEST programına bu veriler çağırıldıktan sonra bir görüntü toplama sırasındaki hataları düzeltme amaçlı Görüntü Ayarlama-Kalibrasyon işlemi uygulanmıştır.

## 2.1 Kalibrasyon

Kalibrasyon aşaması, alınan ham verinin bileşenlerinin belirli bir hesaplama sonrasında belirli bir standartta düzeltmelerinin yapıp görüntü hâline getirilme işlemidir. Bu projede kullanılan veri tipinden ötürü (IMP verisi) verilerinde ölçümleme işlemini kendi arşivindeki imkanlarını kullanarak yapmaktadır.

Level 1 seviyesinde olan SAR verileri, radyometrik polarlaması bulunmayan ve düzeltmesi yapılmamış verilerdir. Radyometrik düzeltmelerin yapılması yansıma verilerinin piksel verilerinin doğru değerlendirilmesinin yapılması açısından önemlidir. Bir radar sinyali, sinyal vericisinden çıkmaya başladığı andan sinyal alıcısına yeniden ulaşana kadar çeşitli etkilere maruz kalmaktadır. Bu etkileri azaltmak amacıyla daha önceki SAR görüntüleriyle karşılaştırma yapılması önemlidir. SAR verilerinden iyileştirmeye gidilen bu aşama Görüntü Ayarlama-Kalibrasyon adı verilen işlemle gerçekleştirilmektedir.

Kalibrasyon aşamasında üç adet düzeltme uygulanmaktadır; bunlar geliş açısı (incidence angle) düzeltmesi, görüntü ayarlama sabiti (calibration constant) ve analogdan dijital çevirici doğrusalsızlığı (analogue to digital converter non-linearity) düzeltmesidir.

IMP görüntülerinde ölçümleme işlemi yapılırken NEST programı tarafından kullanılan hesaplama formülü aşağıdaki gibidir.

$$\sigma^{\wedge}\theta_{i,j} = \left( \frac{DN(i,j)^2}{K \sin^2(\alpha(i,j))} \right) \gamma(i,j) = (\sigma^{\wedge}\theta_{i,j}) / \cos^2(\alpha(i,j))$$

for  $i=1...L$  ve  $j=1...M$

- $DN_{i,j}$  piksel  $i, j$  için piksel yoğunluğu
- $\theta_{i,j}$  bakış açısı
- $K$  mutlak ayarlama sabiti
- $\alpha_{i,j}$  geliş açısı

## 2.2 Çoklu Bakış (Multilooking)

SAR IMP verisi elde edilirken bazı düzeltmeleri yapıp kullanıcıya sunulmasına rağmen kendi içinde benek gürültüsünü (speckle noise) barındırmaktadır. Bu gürültünün azaltılması için daha önce aynı alan için çeşitli açılardan çekilmiş Radar görüntüleri birleştirilir. Bu işlem çoklu bakış (multilooking) işlemi aşamasında gerçekleştirilmektedir. Çoklu bakış (multilooked) haline getirilen verinin yorumlanabilirliği artmaktadır.

Çoklu bakış (Multilooking) işlemi iki farklı şekilde uygulanabilmektedir;

- 2 boyutlu Kernel sarımı kullanarak ya da kullanmaksızın tek bakışlı görüntünün uzay-tabanlı ortalamasından üretmek
- Ya da frekans-tabanlı metot kullanılarak üretilebilmektedir. NEST programı uzay-tabanlı çoklu bakış metodunu kullanmaktadır.

Bu işlemde SAR görüntülerinin klavuz verilerindeki Number of Range Looks ve Number of Azimuth Looks değerleri sistemin otomatik olarak atadığı

verilerle karşılaştırılmış ve aynı oldukları görülmüştür. Bu nedenle sonraki görüntülerde otomatik olarak algılamasına izin verilmiştir.

## 2.3 Görüntü Projeksiyonlama (Reprojection)

Çoklu Bakış işlemi sonrasında Görüntü Projeksiyonlama (Reprojection) işlemi uygulanmıştır. Görüntü projeksiyonlama (Reprojection) işlemi, alınan SAR verisinin dünya düzleminde konumlandırılmasının yapıldığı aşamadır. Bu konumlama işlemi sırasında Koordinat Referans Sistemi (Coordinate Reference System-CRS) kullanılmaktadır. Projeksiyonlama ve jeodetik başlangıç noktası seçilerek verinin hangi bölgeye ait olduğu bu şekilde programa tanıtılmış olur.

## 2.4 Filtreleme (Filtering)

Projeksiyonlama işleminden sonra Filtreleme (Filtering) işlemine geçilmiştir. Radar verilerindeki gürültülerin yok edilmesi Filtreleme işlemi sayesinde olmaktadır. Radar görüntüleri yapısal olarak tuz ve karabiber (Salt and pepper) görüntüsü veren bir yapıdadır. Bu görünüm verinin kalitesini düşürmekte ve analiz edilmek istenen görüntünün yorumlamasını zorlaştırmaktadır. Benek gürültüsünün azaltılması Çoklu Bakış işlemi ile başlamaktadır fakat asıl uygulama Filtreleme işlemindedir. Bu işlemi bütün görüntüye uygulamadan önce, yapılan araştırmalar sonucunda, uygulanacak en iyi filtreleme yöntemine çeşitli hesaplamalar sonucunda karar verildiği görülmüştür. Bu yüzden öncelikle seçilen bir görüntü üzerinde bütün filtreleme işlemleri uygulanmış, bu işlemler sonucunda her bir işlem için görüntünün istatistiği çıkarılmış ve bu istatistikteki bazı veriler kullanılarak hesaplama yapılmıştır.

Programda 6 farklı filtreleme çeşidi bulunmaktadır. Bunlar;

- Mean • Median
- Frost • Lee
- Refined Lee • Gamma-MAP'tir.

Geçmişte yapılmış çalışmalarına göre filtreleme işlemindeki önemli parametreler;

ENL (Equivalent Number of Looks-Bakının Eşdeğer Sayısı), SSI (Speckle Suppression Index- Benek Yok Etme Katsayısı), ve SMPI (Speckle Suppression and Mean Preservation Index- Benek Yok Etme ve Ortalama Koruma Katsayısı)'dir.

$$ENL = (Mean \div StandardDeviation)^2 (2)$$

Yüksek ENL değeri homojen alanlar için daha uygun bir filtreleme yöntemini işaret eder.

$$SSI = ((\sqrt{var(I_f)}) \div mean(I_f)) \times (mean(I_o) \div (\sqrt{var(I_o)})) (3)$$

$I_f$  = Filtrelenmiş görüntü

$I_o$  = Gürültülü görüntü

Bu hesaplama sonucunda çıkan değer  $1$ 'den daha az olması gerekmektedir. Çıkan sonuç ne kadar küçük olursa kullanılan filtreleme işlemi o görüntü için en

uygun olandır.

$$SMPI = Q \times (\sqrt{\text{var}(If)} \div \sqrt{\text{var}(Io)}) \quad (4a)$$

$$Q = 1 + |\text{mean}(Io) - \text{mean}(If)| \quad (4b)$$

Bu hesaplama sonucunda çıkan sonuç ne kadar küçük olursa o kadar iyi ortalamayı koruyan ve gürültü azaltan bir filtreleme kullanıldığı belirtilmektedir. Bu hesaplamalar sonucunda çıkan tablo aşağıda verilmektedir. (Şekil 2)

Yapılan hesaplamalar sonucunda Median 7\*7'in en iyi ENL ve en düşük SSI ve SMPI değerlerine sahip olduğu görülmüştür. (Şekil 3)

## 2.5 Petrol Sızıntısı Tespiti Aşamaları

Petrol sızıntısı tespiti kısmında NEST programı ile otomatik olarak deniz alanlarının üzerindeki petrol sızıntısı veya benzerlerinin oluşturduğu koyu alanlar tespit edilmektedir. Belirlenen alanlar ENVI programının yardımıyla hücresele veriden vektörel veri hâline getirilip oradan da ArcGIS programına aktarılmaktadır. ArcGIS programında da bu veriler kategorize edilmektedir. Bu sayede petrol benzeri kısımlar ve doğal petrol sızıntılarının birbirinden ayrıştırılmış olur.

### 2.5.1 NEST Programında Otomatik Koyu Alanların Tespiti (Oil Spill Detection)

NEST programında Oil Spill Detection modülü otomatik olarak SAR görüntüsünün deniz alanları üzerindeki koyu alanları yakalamaktadır. Bu işlem sırasında filtrelenmiş her bir SAR görüntüsünün Threshold Shift ve Minimum Cluster boyutu değiştirilip doğru sonuçlara ulaşılmaya çalışılmıştır.

Threshold Shift değeri, sisteme girilen değerler altında ortalama geri-yansıma değeri veren bölgeleri yakalamaktadır.

Minimum Cluster boyutu, sisteme girilen alan boyutunun üzerinde kaplanan koyu alanları yakalamaktadır.

NEST programında otomatik olarak belirlenen sızıntı alanlarının hücresele veriden vektörel veriye çevirimi için ENVI programına aktarılması gerekmektedir. Fakat yukarıdaki şekilde de görüldüğü üzere gereksiz alanların da sızıntıya gibi algılanmasından kaynaklı veriler NEST-OST işlemi yapılmadan direk ArcGIS programına aktarılmıştır. Bu program aracılığıyla sızıntı ve sızıntı benzeri öğeler tespitinin kullanıcı tarafından belirlenmesine karar verilmiştir.

### 2.5.2 ArcGIS Programında Sızıntı Verilerinin Sınıflandırılması

ArcGIS programına aktarılan SAR görüntülerinin sızıntı ve sızıntı benzeri görüntü veren kısımları belirlenerek, kirlilik, olası sızıntı ve sızıntı olarak üç kategoride sınıflandırılmaya çalışılmıştır. Bu amaçla, SAR görüntüleri tek tek incelenmiştir. Analiz edilen her bir görüntüdeki sınıflandırılmış sızıntı ve sızıntı benzeri görüntüler gruplarına göre renklendirilip zamanla olan tekrarlamaları dikkate alınmıştır.

Sınıflandırma yapılırken kullanılan kriterler Görüntü Sınıflandırılması ve Olası Sızıntıların Belirlenmesi kısmında ayrıntılı olarak anlatılmaktadır.

## 2.6 Görüntülerin Sınıflandırılması ve Olası Sızıntıların Belirlenmesi

Yapılan literatür çalışmalarına göre doğal sızıntıların ve sızıntı benzeri yapıların ayırımının nasıl yapıldığına dair bilgiler edinilmiştir. Araştırmalar doğrultusunda biyojenik tabakalara, yağmur hücrelerinin, deniz içi oluşan dalgaların, atmosferik etkilerin ve gemi izlerinin hidrokarbon sızıntısı benzeri görüntüler verildiği görülmüştür. Bu rastlanan tabakaların kirlilik olarak adlandırılmasında karar verilmiştir. (Şekil 4)

Yukarıdaki şekillerde belirtilen görüntüler dışında hidrokarbon sızıntısı görüntüsü veren alanlar belirlendiğinde, bu alanlarda sızıntı görüntülerinin tekrarı görülmüyorsa, bu görüntüler olası sızıntı kategorisi altında sınıflandırılmaya karar verilmiştir.

Eğer doğal sızıntı olarak tespit edilen görüntüler, farklı zamanlardaki SAR verilerinde aynı bölgede ya da yakınında tekrar ediyorsa bunlar kesin sızıntı olarak kategorize edilmiştir.

Sınıflandırma kısmında her bir kategori için kullanılan renkler daha önceki çalışma alanlarında yapılan petrol sızıntısı tayini raporlarına bakılarak renklerinin bozulmaması adına aynı şekilde kullanılmıştır. (Şekil 5)

SAR görüntülerinde tespit edilen sızıntı ve sızıntı benzeri yapıların görüntü olarak nasıl farklılık gösterdiğinin daha açık belirtilmesi için bazı örnekler aşağıda bulunan görüntülerde görülebilmektedir. (Şekil 6)

Yapılan araştırmalar sonucunda hidrokarbon sızıntılarına en yakın görüntü veren gemi izlerinin büyük önem taşıdığı belirlenmiştir. Kirlilik olarak adlandırdığımız bu yapıların doğal sızıntılardan ayrıştırılması için çalışma alanına ait gemi trafiğinin incelenmesi gerektiği anlaşılmış ve bu tarz verilerin elde edildiği Marrine Traffic internet sitesinin interaktif bilgi haritası kaynağına başvurulmuştur. Bunun yanı sıra, doğal sızıntı gibi görünen bazı büyük yapıların gerçek petrol sızıntısı mi yoksa tanker kazası sonrası deniz üzerine yayılan petrol kirliliği mi olduğunun belirlenmesi amaçlı geçmiş dönem gazete ve haberleri de araştırılmıştır. Bu veriler sayesinde doğal sızıntıları, sızıntı benzeri veren yapıardan ayrıştırılmış ve kirlilik olarak adlandırdığımız kısımların da doğruluğunu kanıtlar nitelikte olmuştur. (Şekil 7)

ArcGIS programında analiz edilen görüntülerden elde edilen sonuçlar bir görüntü üzerine yerleştirilip yeniden gözden geçirilmiştir. Bu sonucuna göre yeniden sızıntı ve sızıntı benzeri adı altında kategorize edilen her tabaka yeniden isimlendirilmiştir.

## 2.7 Batimetri Verisi Oluşturma ve Sızıntıların Sınıflandırılması

Deniz yüzeyindeki doğal sızıntılar daha önce de "Deniz Yüzyinde Petrolün Yayılımı" kısmında anlatıldığı gibi hidrokarbonun rezervuardan deniz tabanına bulduğu

çatlak ve açıklıklardan ulaşır, buradan da su kolonunu geçerek yüzeye varmasıyla oluşmaktadır. Bu nedenle, deniz tabanındaki bu çatlak ya da açıklıkların tespiti doğal sızıntıları bulmak açısından önem arz etmektedir. Deniz tabanının yapısını anlamak amacıyla üç boyutlu (3-B) batimetri modeli oluşturulmuş ve modele bazı analizler uygulanmıştır. Çalışma alanına ait 3-B batimetri verisi oluşturmak için Geosoft firmasının Oasis Montaj programından sağlanan 900 metre aralığa sahip noktasal batimetri verisi XYZ formatında elde edilmiştir. Daha sonra bu veriler Excel programına aktararak X ve Y koordinatları ve derinlik verilerinden oluşan bir tablo oluşturulmuştur. Bu Excel tablosu ArcGIS programında önce tablo halinde açılmış, daha sonra bu tablonun verileri kullanılarak noktasal veri bulutu kümesi oluşturulmuştur. Noktasal veri bulutu kümesinden 3-B model oluşturmak için öncelikle Düzensiz Üçgen Ağı-Triangulated Irregular Network (TIN) yüzeyi oluşturulmuştur.

TIN yüzeyi, belirli bir coğrafi bilgi sisteminde üç boyutlu koordinatlara sahip (X,Y,Z) veri yapısında düzensiz dağıtılan noktalardan 3-B model oluşturulması amacıyla bu veriler arasında sanal yüzeyler oluşturulması sonucu ortaya çıkar. Delanuay üçgenleşirmesine dayanan sistem, bir noktanın kendine komşu olan diğer noktasal verilerle olan ilişkisi sonucunda enterpolasyon ile yüzey oluşturmaktır. Oluşturulan TIN yüzeyi hücresel veriye dönüştürülerek 3-B Batimetri modeli oluşturulmuştur. Bu modele çeşitli filtreleme yöntemleri uygulanarak, bu model üzerindeki yapılar daha belirgin hale getirilmiştir. Model üzerinde uygulanan filtrelemeler sonucunda deniz tabanında bulunan yapısal unsurlar belirlenmiştir. Bu unsurlar; faylar ve yeraltındaki çatlaklarından deniz tabanına ulaşan hidrokarbon kil ve mil ile karışarak oluşturduğu çamur volkanlarıdır. Yapılan bu tespitlerin sonucu, bulunan doğal sızıntı ve sızıntı benzerleriyle karşılaştırılarak doğruluk analizi yapılmaya çalışılmıştır. (Şekil 8)

### 3 SONUÇ

Bu çalışmada, elde edilmiş SAR verileri sırasıyla NEST, ArcGIS programlarında işlenmiştir. İzlene metotlar ve yapılan işlemler sonucunda bulunan petrol ve petrol benzeri tabakalar 3 kategoride incelenmiş ve sınıflandırılmıştır. Sınıflandırmaya göre petrol benzerlerinin hepsi (anafolar, rüzgâr gölgeleri, yağmur hücreleri, biyojenik tabakalar, gemi izleri ya da atıkları, nehirlerle taşınan kirlilikler, vb.) 'Kirlilik' olarak kategorize edilmiştir. Diğer yandan tam olarak sızıntı olduğuna karar verilemeyenler 'Olası Sızıntı' olarak adlandırılmıştır. Kesin sızıntı olduğuna kanaat getirilen kısımlar 'Sızıntı' olarak kategorize edilmiştir. Yapılan incelemeler sonucunda kesin sızıntı olarak sınıflandırılan ve zaman içinde bu sızıntıların sürekliliğini gösteren 3 bölge tespit edilmiştir. (Şekil 9)

### KAYNAKLAR

Alpers W., & H. Espedal, 2004a, Oils and surfactants. In "Synthetic Aperture Radar Marine User's Manual", US Department of Commerce: Washington, DC, pp.

263-275

Alpers, W., and W. Huang, 2011, On the discrimination of radar signatures of at- mospheric gravity waves and oceanic internal waves on synthetic aperture radar images of the sea surface, IEEE Trans. Geosci. Rem. Sens., vol. 49, no. 3,

pp. 1114-1126.

Akkartal, A., Sunar, F., 2008, The usage of Radar images in oil spill detection, The International Archives of the Photogrammetry, Remote Sensing and Spatial Informaiton Sciences. Vol XXXVII. Part B8, 271-276

Bilgin, C., 2003, Gemi Kökenli Petrol Kirliliği Biyolojik Yöntemlerle Giderilmesi, Yüksek Lisans Tezi, İstanbul Teknik Üniversitesi

Durna, S., 2014, Denizlerdeki Yağ Tabakasının Tespitinde Radar Görüntülerinin Kullanımı, denizcilik Uzmanlık Tezi, T.C: Ulaştırma, Denizcilik ve Haberleşme Bakanlığı.

Zhang, Y., Li, Y., and Lin, H., 2014, Oil-Spill Pollution-Remote Sensing by Synthetic Aperture Radar, Advanced Geoscience Remote Sensing, Chapter 2, 27-50, <http://dx.doi.org/10.5772/57477>

Anahtar Kelimeler: Hidrokarbon sızıntı, Radar

Şekil 1.

### Ham haldeki SAR verisi temini



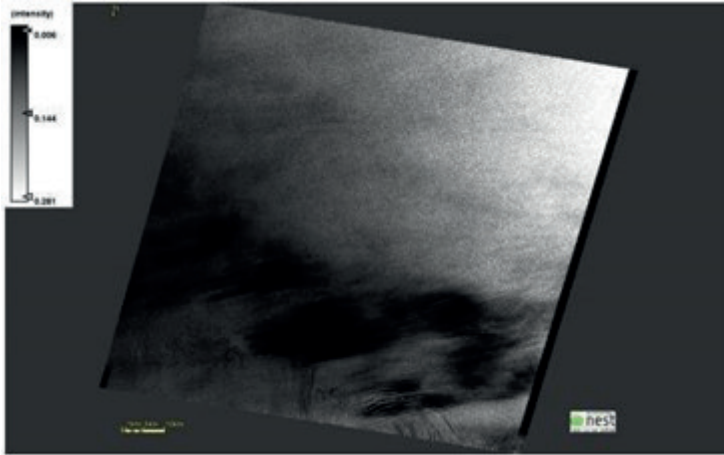
SAR verilerinin işlem aşamaları şeması

Şekil 2.

Filtering	Mean P3	Mean P5	Mean P7	Median P3	Median P5	Median P7	Std P3	Std P5	Std P7	Gamma P3	Gamma P5	Gamma P7	Lee P3	Lee P5	Lee P7	Refined Lee 5000	Refined Lee 6000	Refined Lee 7000	Real Data
Mean total	0.195262	0.190626	0.186488	0.189497	0.189207	0.1895012	0.071672	0.0706276	0.0684888	0.0748943	0.0746963	0.0748495	0.0753162	0.0708136	0.07064988	0.0887921	0.0887921	0.0887921	20921164
Std total	0.028	0.028	0.028	0.028	0.028	0.028	0.028	0.028	0.028	0.028	0.028	0.028	0.028	0.028	0.028	0.028	0.028	0.028	0.028
Median total	1.944	1.127	0.968	2.154	1.87	1.87	2.021	2.402	2.922	2.228	2.228	2.057	1.944	1.638	1.978	1.744	1.744	1.744	702529
Mean	0.108	0.107	0.107	0.101	0.09	0.098	0.106	0.107	0.107	0.107	0.107	0.107	0.104	0.104	0.104	0.104	0.104	0.104	0.104
Std	0.086	0.082	0.081	0.072	0.07	0.075	0.075	0.086	0.086	0.074	0.073	0.073	0.076	0.075	0.081	0.076	0.076	0.076	0.076
BF	0.096	0.096	0.096	0.094	0.09	0.092	0.096	0.092	0.095	0.096	0.092	0.092	0.094	0.094	0.094	0.094	0.094	0.094	0.094
Conf	0.885	0.837	0.816	0.904	0.855	0.872	0.892	0.840	0.827	0.896	0.844	0.822	0.892	0.845	0.821	0.868	0.868	0.868	2.114
SNR	1.268	1.428	1.502	1.196	1.26	1.477	1.254	1.398	1.464	1.244	1.403	1.479	1.254	1.409	1.482	1.322	1.322	1.322	1.322
PS	0.144	0.147	0.148	0.139	0.133	0.136	0.145	0.145	0.143	0.140	0.144	0.145	0.144	0.145	0.147	0.147	0.147	0.147	0.000
PR	0.167	0.170	0.171	0.160	0.159	0.154	0.165	0.164	0.166	0.162	0.164	0.163	0.163	0.168	0.164	0.167	0.167	0.167	0.000
PER	0.194	0.190	0.197	0.185	0.189	0.179	0.193	0.192	0.193	0.192	0.191	0.194	0.194	0.193	0.193	0.194	0.194	0.194	0.000
PR	0.232	0.233	0.233	0.223	0.22	0.212	0.232	0.230	0.229	0.232	0.227	0.233	0.232	0.233	0.232	0.232	0.232	0.232	0.000
PR	0.288	0.291	0.287	0.290	0.27	0.266	0.299	0.292	0.290	0.297	0.288	0.294	0.288	0.290	0.284	0.291	0.291	0.291	0.000
Q	1.052	1.051	1.051	1.089	1.05	1.094	1.052	1.052	1.051	1.051	1.051	1.051	1.054	1.052	1.052	1.054	1.054	1.054	1.000
SMP	0.708	0.688	0.675	0.725	0.69	0.676	0.716	0.692	0.682	0.716	0.699	0.688	0.712	0.694	0.681	0.702	0.702	0.702	1.000
SR	0.081	0.081	0.079	0.089	0.08	0.081	0.086	0.082	0.081	0.083	0.083	0.084	0.084	0.084	0.084	0.082	0.082	0.082	1.000

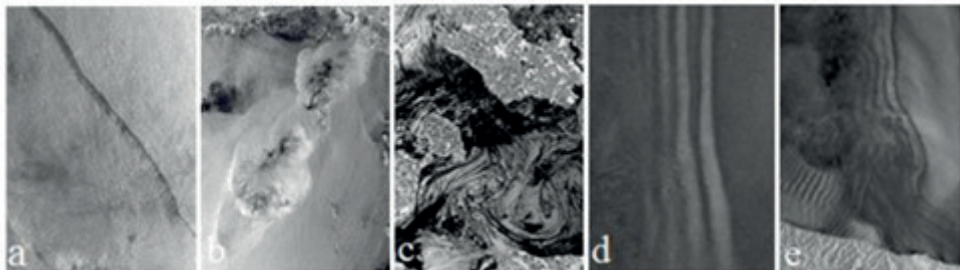
Çeşitli filtreleme yöntemlerinin istatistiksel hesaplamalarının tablosu.

Şekil 3.



Median 7\*7 filtresi uygulanmış SAR görüntüsü.

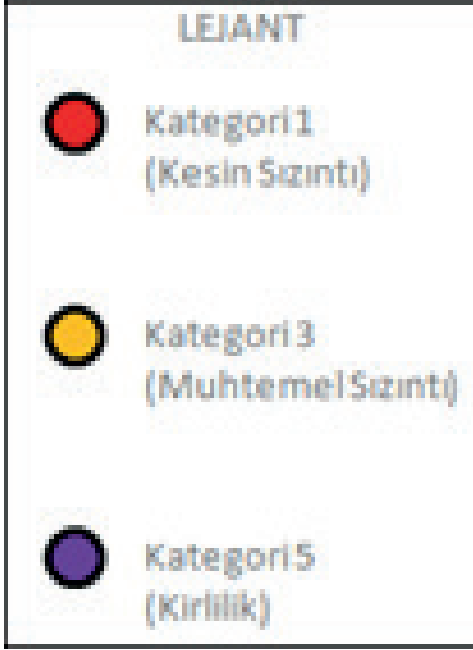
Şekil 4.



SAR görüntüsünde sızıntı vesizinti benzeriyansım gösteren yapılar; a) Tipiksızntı (Foto: Alpers et al. 2004); b) yağmür hücreleri (Foto: ESA); c) biyojenik tabakalar (Foto: Alpers et al. 2004a); d) deniz içi oluşan dalgalar (Foto: Alper et al. 2011); e) atmosferik etkilerle oluşan dalgalar (Alpers et al. 2011), (Zhang et al. 2014)

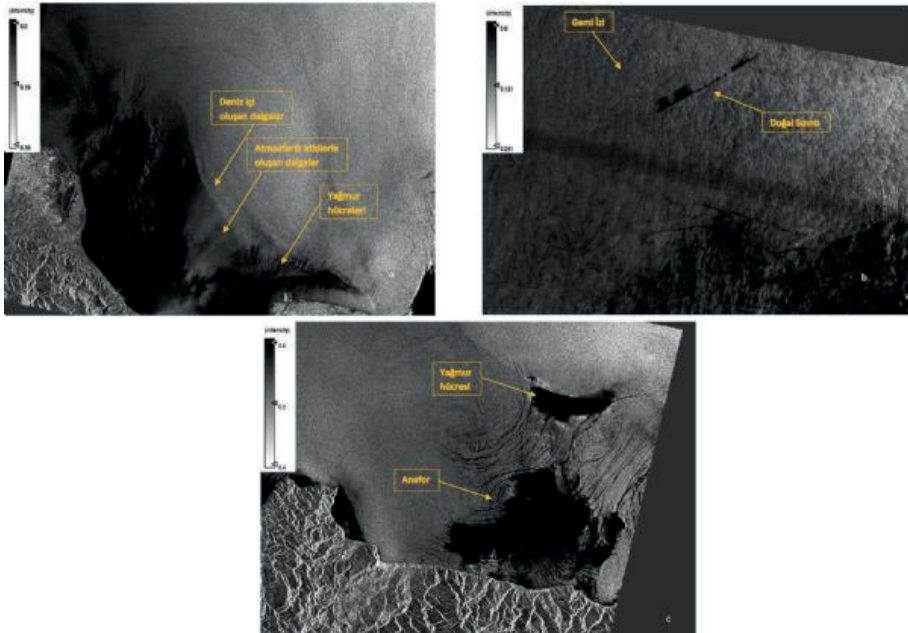


Şekil 5.

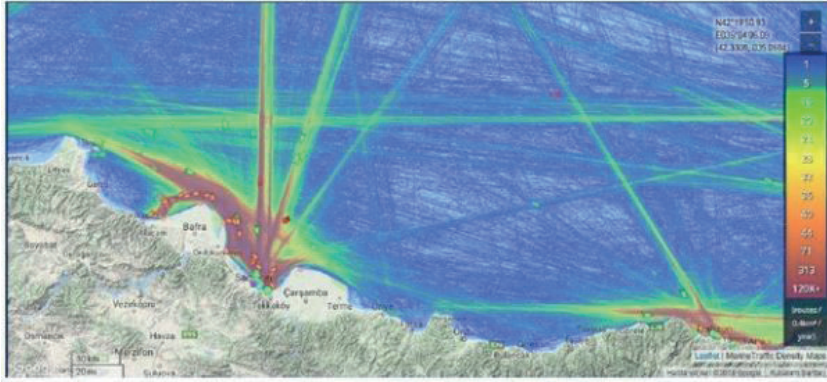


Çalışmada kullanılan renk tanımlaması.

Şekil 6.

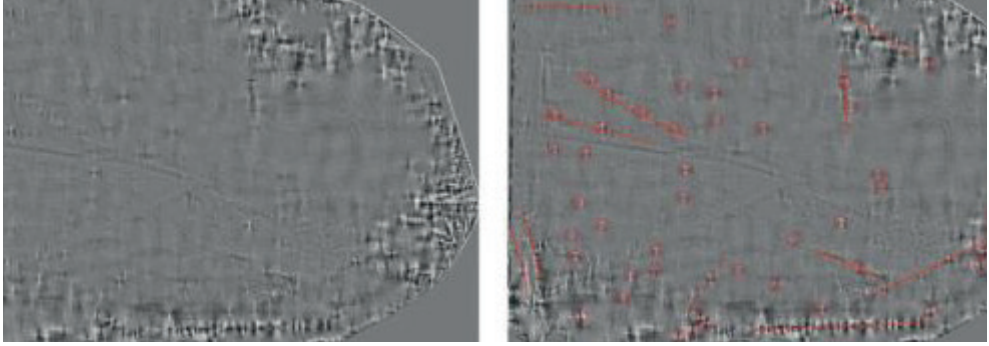


Şekil



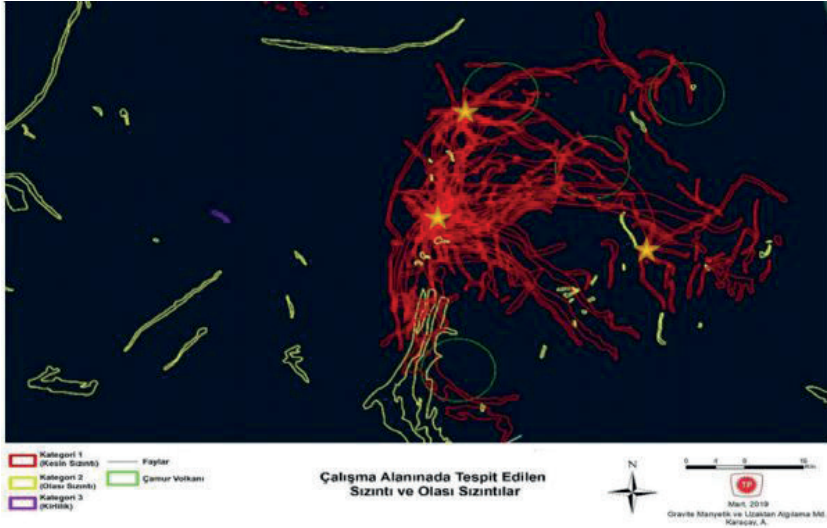
Çalışma alanındaki deniz trafiği yoğunluğunu gösteren harita (Kaynak: MarineTraffic.com).

Şekil 8.



a) Oluşturulan batimetri verisi b) yapısal unsurları belirlenmiş batimetri verisi

Şekil 9.



Kategorize edilmiş sızıntı ve olası sızıntıların haritası

# Kara Alanlarında Uzaktan Algılama Yöntemleriyle Hidrokarbon Aramacılığı

**Avca Karacay**

Türkiye Petrolleri Anonim Ortaklığı, AR-GE D. Başkanlığı, Sedimentoloji, Ankara / Türkiye



## ÖZ

Geçmişten günümüze gelişen teknoloji ile birlikte hem daha hızlı bilgi sağlamak hem de maliyeti azaltmak amacıyla gerek tarım, gerek madencilik, gerek çevre, gerekse petrolcülük vb alanlarda Uzaktan Algılama sistemlerinin kullanılması yaygın hale gelmiştir. Hem kara hem deniz alanlarında kullanılmaya başlanan bu sistemle daha düşük maliyetle makro ya da mikro ölçekli hidrokarbon sızıntıları ve neden oldukları alterasyon alanları tespit edilmeye çalışılmaktadır. Uzaktan Algılama ile araziye çıkmaya gerek kalmadan potansiyel hidrokarbon sızıntısı olan alanların tespiti yapılarak öncelikli prospekt olabilecek alanların belirlenmesinde gerekli başarılar elde edilmektedir. Uzaktan algılama çalışmalarının amacı çok yönlü olup, çalışma alanındaki çizgiselliklerin (fay, mikro ve makro yüzey kırıkları vb.) tespitinin yapılması, daha sonra bu bölgelerde oluşan petrol basenleri ile ilişkili muhtemel hidrokarbon sızıntılarının yüzeyde oluşturduğu mineralojik alterasyonun belirlenmesi ve haritalanmasıdır. Bunlara ek olarak, uzaktan algılama yöntemleri kullanarak inceleme alanına ilişkin topoğrafya ve bitki örtüsü üzerindeki stresin bir arada değerlendirilmesi ile bölgedeki tarım alanları altında kalmış olası kapanların da belirlenmesi sağlanmaktadır. Bu çalışmada, çalışma alanı koşulları göz önüne alınıp bahsi geçen bütün metodlar kullanılarak olası sızıntıların tespiti yapılmaya çalışılmıştır. Bu amaçla, Landsat, ASTER ve Sentinel-2 gibi multispektral veriler üzerinde çalışılmış ve ENVI, ArcGIS ve SNAP programları kullanılmıştır.

With the developing technology from the past to the present, the use of Remote Sensing systems has become widespread in agriculture, mining, environment, petroleum, etc. in order to provide faster information and reduce costs. With this system, which has started to be used in both land and sea areas, macro or micro-scale hydrocarbon leaks and the alteration areas they cause are tried to be detected at lower cost. With Remote Sensing, the areas with potential hydrocarbon leakage can be identified without the need to go to the field and the necessary successes are achieved in determining the areas that can be prioritized prospects. The purpose of remote sensing studies is multifaceted and includes the detection of lineaments (faults, micro and macro surface fractures, etc.) in the study area, and then determining and mapping the mineralogical alteration on the surface caused by possible hydrocarbon seeps associated with the oil basins formed in these regions. In addition, remote sensing methods are used to evaluate the topography and vegetation stresses in the study area and to identify possible traps under agricultural areas in the region. In this study, taking into account the conditions of the study area, all the methods mentioned above were used to detect possible leakages. For this

purpose, multispectral data such as Landsat, ASTER and Sentinel-2 were studied and ENVI, ArcGIS and SNAP are used.

## 1. GİRİŞ

Bir cismin ya da maddenin yapı, şekil veya özelliğindeki tüm kimyasal ve/veya fiziksel değişiklikler alterasyon olarak tariflenmektedir. Jeolojik açıdan alterasyonu ise kayalarla oluşturan minerallerin, fiziksel ve kimyasal etkilerle kompozisyonlarının değişmesi şeklinde ifade edilebilir. (Koyuncu, H., 2012)

Bir bölgedeki hidrokarbon sızıntısı, depolandığı ortam üzerindeki kayaların içindeki fay, kırık, çatlak ve fisürlerle jeolojik tabakaların arasından yüzeye ulaşması olarak tariflenmektedir. Mikro ve makro sızıntı olmak üzere iki çeşit olup, gözle görülebilecek ölçekte olanlar makro sızıntı; gözle görülemeyecek boyutta olmasına rağmen yüzeye ulaştığı ortamda yarattığı kimsayal ya da fiziksel etkiler nedeniyle çeşitli yöntemlerle tespit edilebilen sızıntılar ise mikro sızıntı olarak ifade edilmektedir. (Koyuncu, H., 2012)

Hidrokarbon sızıntıları nedeniyle oluşan mineral alterasyonları petrol aramacılığında son dönemde büyük önem kazanması nedeniyle birçok kişi tarafından araştırılmıştır (Abrams et al., 1984, Donovan, 1974, Petrovic et al. 2008). Rezervuardan mikro ya da makro ölçütlü çatlaklar vasıtasıyla yüzeye ulaşan hidrokarbonlar, yüzeydeki minerallerle tepkimeye girerek minerallerde oksitlenme-indirgeme ya da yüzey sularında pH değişimlerine neden olurlar. Bunlar aynı zamanda sedimanlarda ve toprakta jeokimyasal, biyolojik, jeofiziksel ve mineral olarak anomalilerin oluşmasına sebep olmaktadır (Donovan et al., 1979, Segal and Merin, 1989, Schumacher and Abrams, 1996). Bu anomaliler arasından, kırmızı renkli formasyonlarda oluşan beyazlaşmalar (bozlaşma), +2 değerli demir minerali oluşumları, kil (illit, kaolinit, simektit) ve ikincil karbonat mineralleri oluşumları, ve botanik anomaliler gibi yüzeyde belirgin spektral imzalar uzaktan algılama tekniği ile tespit edilebilmektedir. (Sabins, 1999, Almeida et al., 2002, van der Meer et al., 2002, Fu et al., 2007).

Limonit içerikli kayalarda göç eden hidrokarbonun oluşturduğu indirgen ortam koşulları sonucu kayaçta bulunan ferrik demir sistemden hızla uzaklaştırılır ve/veya pirit olarak yeniden çöker. Bu olay sonucunda kayaç üzerinde açık renkli alanlar gelişir. Buna bozlaşma denir.

Hidrokarbonun ulaştığı ortamda organik maddenin diyajenezini sırasında bakterilerin biyolojik bozunmaya sebep olmasıyla hidrojen sülfid oluşabilmektedir. Bu tepkime ile bikarbonat iyonları ortamda oluşmaya başlar. Bunun sonucunda bu alanlarda

karbonat konsantrasyonunun artmasına paralel olarak ikinci karbonat gelişimi olabilmektedir. Kayacın içinde kararlı olan feldispar ve mikalar, hidrokarbonla girdikleri tepkime sonrasında kaolinit ve illit/simekte dönüşebilmektedir. Bu olay da killeşme olarak adlandırılmaktadır. (Şekil-1)

## 2. UYGULAMA

Bu çalışmada çeşitli kaynaklardan ücretsiz elde edilmiş multispektral verileri çeşitli metotlar ile işlemlere tabi tutulmuştur. Bu amaçla sırasıyla SNAP, ENVI ve ArcGIS programları kullanılmıştır.

### 2.1 Mineralojik Alterasyon Alanlarını Belirleme

Aster ve Landsat gibi optik uzaktan algılama uydularında güneşin dünyaya gönderdiği elektromanyetik enerjinin yerden yansması ile oluşan ışınım berrisi üzerinde dijital rakamlar (DN) ile belirtilmektedir. Uydunun belirli bantlarına kaydolun bu dijital rakamlar dalga boyu aralıklarına göre farklı bilgiler sağlamakta ve bu sayede amaca yönelik çeşitli mineral indeks haritaları oluşturulmaktadır (Hunt,1977). Daha önce minerallerin spektral özelliklerinin belirlenmesi için yapılan laboratuvar çalışmaları sonucunda elektromanyetik spektrumda 0.4 ve 2.5 mikrometre aralığı kayaçlardaki altere olmuş minerallerin tespitinde kullanılabilceği tespit edilmiştir. (Hunt ve diğ.,1971; Hunt,1977; Hunt ve Ashley, 1979; Lee ve Raines, 1984) (Şekil-2).

Elektromanyetik spektrumunun görünür (visible), yakın kızılötesi (NIR) ve kısa dalga boylu kızılötesi (SWIR) dalga boyunda minerallerin spektral soğurma özelliklerinin bazı sebebi vardır (Hunt, 1977). İlk olarak, 1.2 mikrometreden daha kısa dalga boylarındaki spektral soğurma özelliklerinin demir ile bağlantılı elektron geçişinden kaynakladığı bilinmektedir. Fe<sup>3+</sup> ve O<sup>2-</sup> iyonlarının birbiri ile yaptıkları elektron değişimleri, 0.8 mikrometreden daha kısa dalga boylarında ve orta ultraviyole bölgede geniş ve yoğun soğurma özellikleri gösterebilmektedir. Bu yük değişimi Fe<sup>3+</sup> minerallerinin kristal alanları üzerinde alan geçişlerine sebep olabilmekte ve elektron seviyelerindeki değişikliklere bağlı küçük spektral soğurma özellikleri ortaya koyabilmektedir (Lee ve Raines,1984). İkinci olarak ise, Hidroksil (OH, Al-OH) içeren minerallerdeki titreşim mekanizması nedeniyle, 1.2 mikrometreden daha uzun dalga boyunda oluşan soğurma özellikleri görülebilmektedir. Hidroksil (OH, Al-OH) gruplarının en iyi belirleyicisi 2.2 mikrometre dalga boyundaki spektral bölgedir. Karbonat minerallerinin tespit edebilmek için 2.35 mikrometre dalga boyundaki bantlar kullanılmaktadır, çünkü bu bantlar CO<sub>3</sub><sup>2-</sup> titreşimlerini yakalayabilmektedir (Koyuncu, H., vd, 2011). Bu belirteçlerden yola çıkarak hidrokarbon kaynaklı alterasyon alanları tespitinde her bir uydu verisinin yukarıda belirtilen dalga boylarına denk gelen spektral bantlarına göre bant matematikleri oluşturulmuştur. USGS'den indirilen 26 adet ASTER ve 16 adet Landsat verisi üzerinde ön işlemler yapılmasından sonra her bir uyduya göre belirtilmiş bant matematikleri kullanılarak alterasyon alanı belirteci olan Demir-Oksit, Kil ve

Karbonat minerallerinin mineral indeks haritaları ve RGB bant kombinasyonları hazırlanmıştır (Şekil.2). Bu haritaların oluşturulması sonucunda alterasyon alanları çizgisellikler de kullanılarak tespit edilmiştir. (Şema-1) (Şekil 3.)

### 2 Temel Birleşenler Analizi (Principle Component Analysis- PCA)

Temel Birleşen Analizi (PCA) birbiriyle korelasyonu olan spektral bantların temel birleşenlerine dönüştürülme işlemidir. Büyük boyutlu veri kümelerinden anlamlı veriler elde edilirken, bu veriler arasındaki benzerlikler ve farklılıklar ortaya koyulabilmektedir. Bu yöntem, görüntü zenginleştirme ve birleştirme, boyutsal indirgeme ve imge sıkıştırma işlemleri için de kullanılmaktadır. Bu çalışmada Çukurca bölgesine ait ASTER verisi üzerindeki spektral bilgi üzerinde PCA ile istatistiksel analiz yapılarak, hidrokarbonun formasyon içindeki minerallerle girdiği tepkime sonucunda oluşan altere alanlarındaki mineraller tespit edilmeye çalışılmıştır. Bu amaçla DemirOksit (Fe<sub>2</sub>, Fe<sub>3</sub>), Kil (Kaolinit, Alunit vb.) ve Karbonat (Kalsit) mineralleri en hassas oldukları spektral bantlara PCA uygulanmıştır. DemirOksit için ASTER 1-2-3-4 bantları, kil için ASTER 1-3-4-6 bantları ve karbonat için 1-3-6-8 bantları kullanılmıştır (Okyay ve Khan, 2016). ENVI programının ileri temel birleşen analiz aracı kullanılarak istatistiksel hesaplamaları ve çevrimleri yapılmıştır. PCA sonucunda elden edilen istatistiklere göre en düşük eigen değerini veren PC bandının o mineral için en uygun bant olduğu daha önceki çalışmalardan bilinmektedir (Okyay ve Khan, 2016). Her bir mineral için yapılan analiz sonucunda PC4 bandının en uygun bant olduğu tespit edilmiştir. Kırmızı renge DemirOksit, yeşil renge kil ve mavi renge karbonat mineralleri için seçilmiş PC bantları atanmış ve ASTER verisindeki mineral indeks haritalarının birleştirilmesi sonucu bulunan olası alterasyon alanlarının karşılaştırması yapılmıştır. (Şekil 4) rulması sonucunda alterasyon alanları çizgisellikler de kullanılarak tespit edilmiştir.

### 2.3 Çizgisellik Analizi (Fay ve Kırıkların Tespiti)

Uydu verileri kullanılarak yapılmakta olan çizgisellik analizi, çalışma alanındaki jeolojik kökenli çizgisel unsurların (faylar, litoloji veya formasyon sınırları, kırıklar, kıvrımlar, nehir yatakları) belirlenmesi ve olası altere alanlar ile karşılaştırmak için yapılmaktadır. Yapılan işlemler sonucunda kimi zaman jeolojik açıdan ifade etmeyip çizgisellikte görünüm sağlayabilen tarım alanları sınırları, demiryolları, karayolları ve sulama kanalları gibi yapay unsurlar da analiz sonucu çizgisel unsuruşmuş gibi kendini gösterebilmektedir. Bu nedenle, kontrollü bir şekilde çizgisellik analizi yapılmalı, otomatik oluşturulsa dahi kullanıcı tarafından kontrol edilere dikkatli bir şekilde oluşturulmalıdır. Bu çalışmada atmosferik etkilerden neredeyse hiç etkilenmemesi nedeniyle bir Radar sistemi olan STRM verisi kullanılmıştır. USGS'in veri indirme platformundan indirilen toplam 6 adet SRTM verisi

önce tek bir veri haline getirilmiş, daha sonra çalışma alanına göre kesilip üzerinde çeşitli filtreleme teknikleri kullanılarak çizgisel unsurlar daha belirgin hale getirilip yapay çizgisel unsurlardan kaçınmak adına manuel olarak çizilmiştir. Çizgisellik verileri manuel olarak çizilirken filtrelenmiş SRTM verisi ile kabartı verisi eş zamanlı olarak kontrol edilip bulunan çizgiselliklerin uygunluğuna karar verildikten sonra çizgisellik haritası oluşturulmuştur. Uygulanan işlemler Şekil.5'te gösterilmektedir. Çizgisellik haritasında kesin olarak belirtilenler yüzeylenmiş faylar, kırıklar, formasyon ve litoloji sınırları iken, olası olarak belirtilen çizgisellikler ise nehir ya da dere yataklarının ani yön değiştirmelerine neden olan ama kesinliğinden emin olunamayan çizgisellikler için kullanılmıştır

#### 2.4 Bitki Örtüsü İndeks Haritası ve Bitki Stresi Analizi

Hidrokarbonların yer altı rezervuarından mikrosızıntı şeklinde yüzeye sürekli göçü, üstteki toprakta ve/veya sedimanda indirgeyici (anoksik) bir ortam yaratmaktadır. Bitki örtüsünün büyümesi, böyle beslemeye dirençli bir ortamda kısıtlanır ve sonuç olarak, mikro sızıntı alanında bir bitki anomalisi veya stresi gelişir. Bu nedenle, bitki örtüsü stresi, hidrokarbon mikrosızıntısının bir göstergesi olarak gösterilebilmektedir. Bitki indeksleri, bitkilerin farklı dalga boylarındaki yansımaları kullanılarak oluşturulan, bant oranlama tekniğine dayalı matematiksel bir işlemdir. Bitki indekslerinin kullanıldığı mecralar bitkinin büyümesi sırasında maruz kaldığı ortam nedeniyle verimli büyümemesi (bitki stresi), toprağın özelliği ile ürün verimi ilişkisinin saptanması, bitki örtüsü haritalaması, evapotranspirasyon belirlenmesi, tarım politikalarının saptanması ve yerleşim bölgelerindeki yeşil alanların belirlenmesi olarak sıralanabilirler. (Gündeş, 2007). a ~90 m b 16 Çalışma sahasının güney kısmında yer alan Harran ovası ve Suriye sınırı boyunca uydu görüntülerinde tespit edilen tarım alanlarının formasyonları örtmektedir. Bu nedenle, bu bölgede bulunabilecek kapanların tespiti amacıyla bitki stresi analizi çalışması yapılmış ve olası mikro sızıntı alanları tespit edilmeye çalışılmıştır. Yapılan araştırmalar sonucunda, Sentinel-2 verisinin on iki bandından sekizinin görünür ve yakın kızılötesi spektral aralığına yerleştirilmesi nedeniyle bitki örtüsü indeksi ve bitki stresi analizinde en iyi sonucu vermekte olduğu görülmüştür (Verrelst vd., 2015; Clevers vd.,2017). Bu çalışmada, bitki durumunu ve bitki örtüsünü tespit etmek için kullanılan en yaygın bitki indeksi NDVI (Normalized Difference Vegetation Index-Normalize Edilmiş Fark Bitki Örtüsü İndeksi) yerine, bitkinin içindeki sağlık klorofil içeriğini göstermesi ve bitki stresini ve yaşlanması daha doğru bir oranda ortaya koyması nedeniyle IRECI (Inverted Red-Edge Chlorophyll Index-Tersine Çevrilmiş Kırmızı-Sınırı Klorofil İndeksi) kullanılmıştır (Frampton vd., 2013; Majasalmi ve Rautiainen, 2016; Castillo vd., 2017). (Şekil 6)

Çalışma alanı için indirilmiş Sentinel-2 verilerine uygulanan IRECI bitki örtüsü analizi sonuçları Şekil

7'de gösterilmektedir.

Oluşturulan indeks haritaları sonrasında bütün çalışma sahasındaki tarım alanları daha yakından incelenmiş, indirilen verilen kronolojik olarak takip edilerek bitki stresinin olduğu alanlar tespit edilmeye çalışılmıştır (Şekil 8). Bulunan bazı alanların olası hidrokarbon sızıntısı alanları olduğu düşünülmüş ve mineral indeks haritalarında işaretlenen olası sızıntı alanları ile birleştirilmiştir.

### 3 SONUÇ ve DEĞERLENDİRMELER

Bu çalışmada, çeşitli amaçlarla kullanılmış olan ASTER, Landsat, Sentinel-2 ve SRTM verilerine uygulanan işlemler sonucunda olası hidrokarbon mikro sızıntı alanları için gerek mineral indeks haritaları üretilmiş ve buralardan alterasyon alanları bulunmuştur. Çalışma alanına dair fay ve kırıklar hem ani topoğrafya farklılıklarından hem de ani nehir ve dere yataklarının yön değiştirmesinden tespit edilmeye çalışılmış, bunun yanı sıra tarım alanlarındaki bitki stresi analizlerinden de mikro sızıntılar bulunmaya çalışılmıştır. Karşılaştırılarak olası alterasyon alanlarının doğrulukları tespit edilmeye çalışılmış ve bu sayede hata payının minimuma indirilmesi amaçlanmıştır.

ASTER ve Landsat görüntüleri alterasyon alanları tespiti için kullanılmıştır. Veriler üzerinde uygulanan ön işlemler (veri düzenlemesi ve bitki örtüsü, su ve gölge alanların maskelenmesi) sonrası daha önceki çalışmalarda kullanılan bant matematiği yöntemi ile alterasyon sonucu oluşan mineraller haritalanmıştır. Bu haritalar birleştirilerek mikrosızıntı olabilecek alanlar tespit edilmeye çalışılmıştır. Aynı zamanda ASTER verisi üzerinde Temel Birleşen Analizi (PCA-Principle Component Analysis) uygulanarak tespit edilen alterasyon alanları klasik yöntemle bulunan alterasyon alanları ile doğruluğu artırmak amacıyla karşılaştırma yapılmıştır.

Temin edilen SRTM verisinden Sayısal Yükseklik Modeli (Digital Elevation Modal- DEM) verisi oluşturulup bu veri üzerinde yapılan filtreleme işlemleri sonrası yüzey çizgisellikleri (faylar, kırıklar, litolojik sınırlar vb) tespit edilmiştir. Aynı zamanda oluşturulan Kabartı Haritası ile eş zamanlı olarak bulunan çizgisel unsurların doğruluğu karşılaştırılmıştır. Alanın çok geniş olması nedeniyle üretilen drenaj verilerinin sağlıklı sonuçlar verdiği görülmüş ve proje için akış yönü tespiti, baki haritaları oluşturulmuş olsa dahi kullanılmamaya karar verilmiştir. Onun yerine drenaj sisteminin çok net belli olması nedeniyle filtreler uygulanan SRTM verisi üzerinde nehir ve dere yatakları takip edilerek ani yön değiştirdikleri yerlerde olası çizgisellikler manuel olarak çizilmiştir.(Şekil 9)

Çalışma alanının güney kısımlarının büyük bir yüzdesi tarım alanları ile örtülü olması nedeniyle bu bölgelerin ASTER ve Landsat verilerinde maskelenmesi nedeniyle veri kaybı yaşanmıştır. Bu durumun telafisi için, tarım alanlarında olası sızıntı noktalarının tespiti amacıyla bu bölgelerdeki bitkilerin stres analizleri yapılmıştır. Bölgedeki tarım alanlarındaki bir yıllık değişim tek tek incelendikten sonra mikro sızıntı nedeniyle olduğu

düşünülen olası bitki stresi alanları tespit edilmiştir. (Şekil 11)

Bu verilerin birleştirilmesi sonucu çalışma alanındaki hidrokarbon sızıntısı alanları tespit edilmiş ve potansiyel kapanların bulunduğu alanlar için daha spesifik bölgeler üzerinde çalışma yapılması sağlanmıştır.

#### KAYNAKLAR

Abrams, M.A., Eds. (1984); AAPG: Houston, TX, USA, pp. 71–89

Almeida-Filho, R., Miranda, F., Yamakawa, T., Bueno, G., Moreira, F., Celso, E., Bentz, C. (2002). Data integration for a geologic model of hydrocarbon microseepage areas in the Tonã Plateau region, North Tucano basin, Brazil. *Canadian Journal of Remote Sensing*, 28, 96-107. 10.5589/m02-006.

Castillo, J.A.A. Apan, A.A., Maraseni, T.N. ve Salmo, S.G. (2017). Estimation and mapping of above-ground biomass of mangrove forests and their replacement land uses in the Philippines using Sentinel imagery. *ISPRS Journal of Photogrammetry and Remote Sensing*, 134, 70-85

Clevers, J.G.P.W., Kooistra, L. ve Van Den Brande, M.M.M. (2017). Using Sentinel-2 data for retrieving lai and leaf and canopy chlorophyll content of a potato crop. *Remote Sensing*, 405 (9), 1-15.

Donovan TJ, (1974) Petroleum microseeps at Cement Oklahoma: Evidence and mechanism: AAPG Bull, 58(3), pp 429–446.

Donovan, T., Forgey, R.L., Roberts, A.A.. (1979). Aeromagnetic detection of diagenetic magnetite over oil fields. *Am. Assoc. Pet. Geol. Bull.*; (United States). 63:2.

Frampton, W.C., Dash, J., Watmough, G. ve Milton, E.W. (2013). Evaluating the capabilities of Sentinel-2 for quantitative estimation of biophysical variables in vegetation. *ISPRS Journal of Photogrammetry and Remote Sensing*, 82, 83-92.

Fu, Bihong & Zheng, Guodong & Ninomiya, Yoshiki & Wang, Chuanyuan & Sun, Guoqiang. (2007). Mapping hydrocarbon-induced mineralogical alteration in the northern Tian Shan using ASTER multispectral data. *Terra Nova*. 19. 225 - 231. 10.1111/j.1365-3121.2007.00739.x.

Gündeş, S. (2007). Türkiye'nin bitki örtüsü değişiminin NOAA uydu verileri ile belirlenmesi.

Çukurova Üniversitesi Fen Bilimleri Enstitüsü, (Yüksek Lisans Tezi), 83s, Adana.

Hunt. G. R., Salisbury, J. W., and Lenhoff, C. J. (1971). Visible and near infrared spectra of minerals and rocks: III. oxides and hydroxides, *Modern Geology*, 2, s. 195205.

Hunt, G. R. (1977). Spectral signatures of particulate minerals in the visible and near infrared, *Geophysics*, 42, s. 501-503.

Koyuncu, H., Tokatlı, K., Çınar Dağ, R., Yılmaz, U., Cengiz, C. (2011). Hidrokarbon alterasyonunun belirlenmesi ve haritalanması uzaktan algılama projesi, TPAO Rapor No: 5250

Lee, Keenan, and Raines, G. L. (1984). Reflectance spectra of some alteration minerals, a chart compiled from published data, 0.4-2.5 micrometer: U.S. Geological survey Open Report, pp.6, 84-96, chart 1.

Majasalmi, T. ve Rautiainen, M. (2016). The potential of Sentinel-2 data for estimating biophysical variables in a boreal forest: a simulation study. *Remote Sensing Letters*, 7 (5), 427-436.

Okyay, Ü., Khan, S.D. (2016). Remote detection of fluid-related diagenetic mineralogical variations in the Wingate Sandstone at different spatial and spectral resolution.

*International Journal of Applied Earth Observation and Geoinformation*

Petrovic A, Khan SD, Thurmond AK (2012) Integrated hyperspectral remote sensing, geochemical and isotopic studies for understanding hydrocarbon-induced rock alterations. *Mar Pet Geol* 35:292–308

Petrovic, A. & Khan, Shuhab & Chafetz, Henry. (2008). Remote detection and geochemical studies for finding hydrocarbon-induced alterations in Lisbon Valley, Utah. *Marine and Petroleum Geology*. 25. 696–705. 10.1016/j.marpetgeo.2008.03.008.

Sabins, F.F., 1999. Remote sensing for mineral exploration. *Ore Geol. Rev.* 14, 157– 183. [https://doi.org/10.1016/S0169-1368\(99\)00007-4](https://doi.org/10.1016/S0169-1368(99)00007-4).

Saunders, D.F. & Burson, K.R. & Thompson, C.K.. (1999). Model for hydrocarbon microseepage and related near-surface alterations. *AAPG Bulletin*. 83. 170-185.

Schumacher, D., 1996, *Hydrocarbon-Induced Alteration of Soils and Sediments*, ind

Segal, D.B. & Merin, I.S.. (1989). Successful use of Landsat Thematic Mapper data for mapping hydrocarbon microseepage-induced mineralogical alteration, Lisbon Valley, Utah. *Photogrammetric Engineering & Remote Sensing*. 55. 1137-1145.

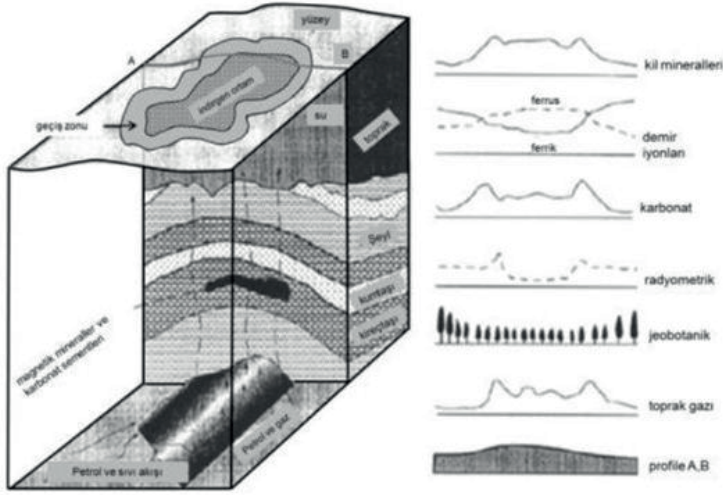
Van der Meer, Freek & Dijk, Paul M. & van der Werff, Harald & Yang, Hong. (2002). Remote sensing and petroleum seepage: A review and case study. *Terra Nova*. 14. 1 - 17. 10.1046/j.1365-3121.2002.00390.x.

Verrelst, J., Rivera, J.P., Veroustraete, F., Mari, J.M., Clevers, J.G.P.W., Vals, G.C. ve Moreno,

J. (2015). Experimental Sentinel-2 LAI estimation using parametric, non-parametric and physical retrieval methods – A comparison. *ISPRS Journal of Photogrammetry and Remote Sensing*, 108, 260-272

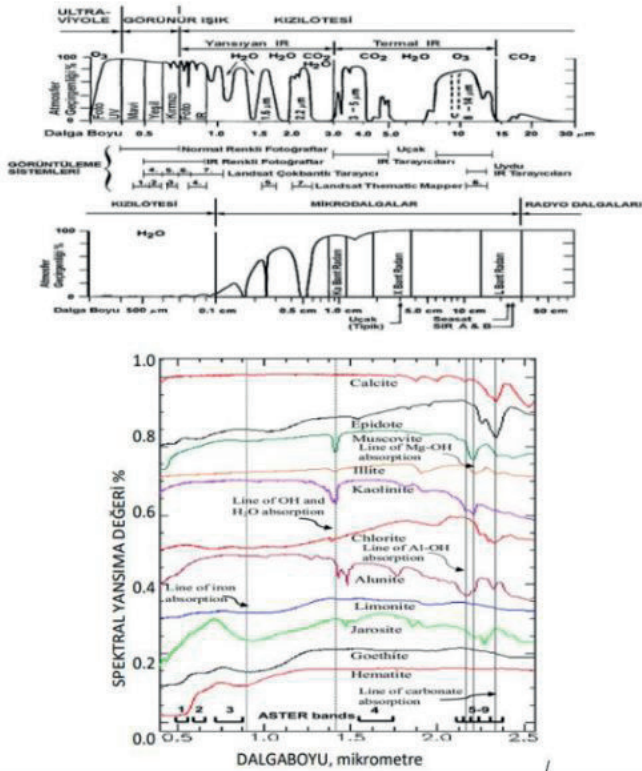
Anahtar Kelimeler: kara alanlar, sızıntı tespiti

Şekil 1.



Hidrokarbon alterasyon etkilerinin şematik gösterimi (Schumacher, D., 1996)

Şekil 2.



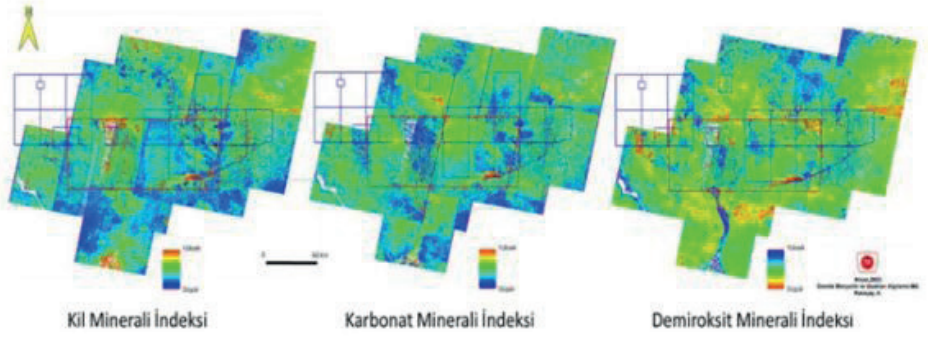
a) Elektromanyetik spektrum, yaygın algılama dalga boyları ve atmosferik soğurma bantları (Sabins, 1986) b) Alterasyon minerallerinin laboratuvar spektrumları.(USGS)

Şema 1.



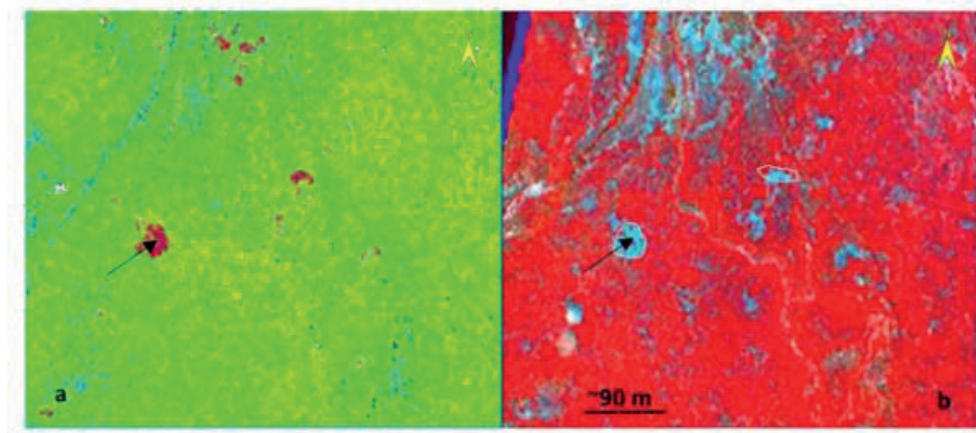
Mineral İndeks Haritaları oluşturma ve alterasyon alanlarının tespiti sırası ile uygulanan yöntemler

Şekil 3.



ENVI programında ASTER görüntüleri ile elde edilen kil, karbonat ve demiroksit mineral indeksi haritaları

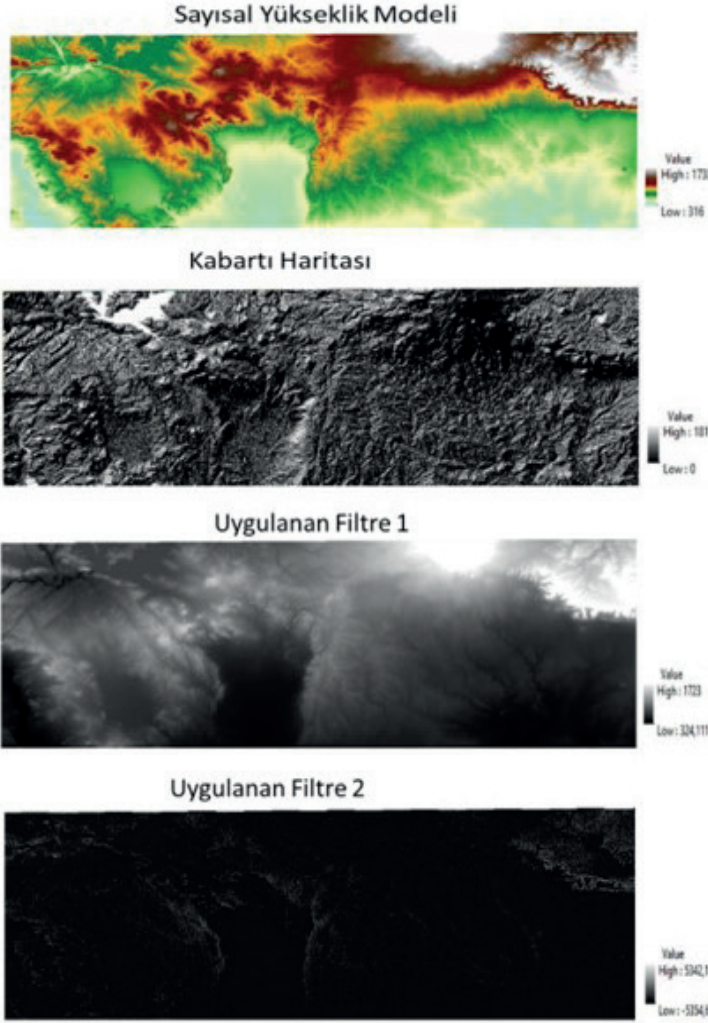
Şekil 4.



ENVI Programında birleştirilmiş kil, karbonat ve demiroksit indeks görüntüleri (a) ile aynı alanda dair yapılan PCA sonucunun(b) karşılaştırılması



Şekil 5.



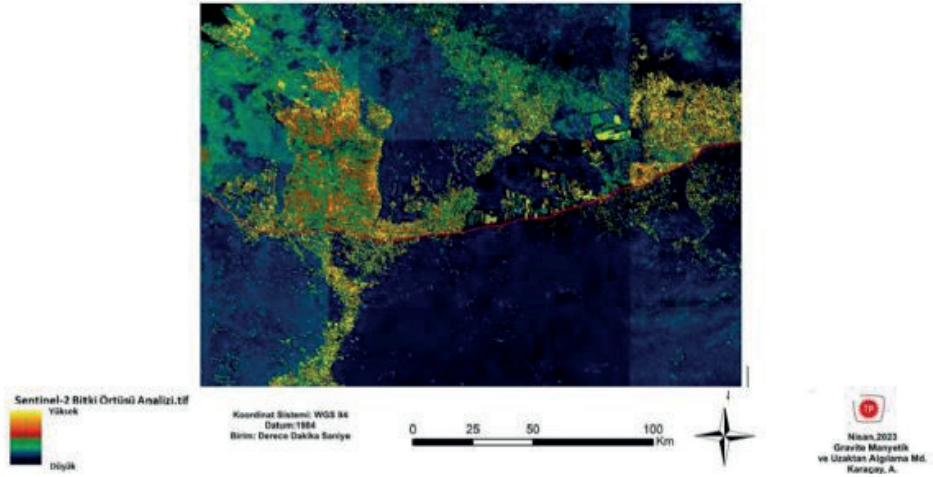
a) SRTM verisinden üretilen Sayısal Yükseklik Modeli (SYM), b) SYM'den üretilen kabartı haritası, c) SYM üzerinde uygulanan 1. Filtre, d) SYM üzerinde uygulanan 2. Filtre

Şekil 6.

$$IRECI = \frac{(IR\_factor * near\_IR - red1\_factor * red1)}{(red2\_factor * red2 / red3\_factor * red3)}$$

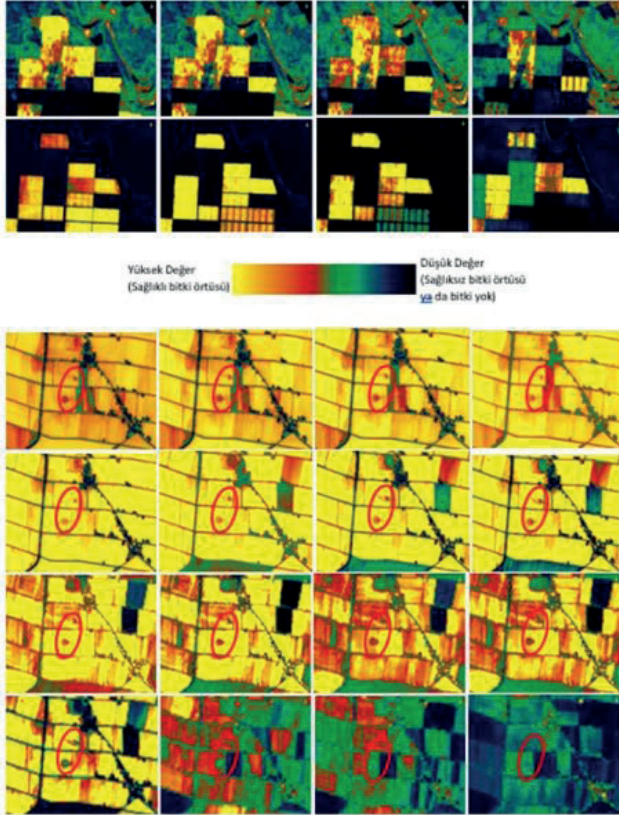
IRECI (Inverted Red-Edge Chlorophyll Index-Tersine Çevrilmiş Kırmızı-Sınırı Klorofil İndeksi)

Şekil 7.



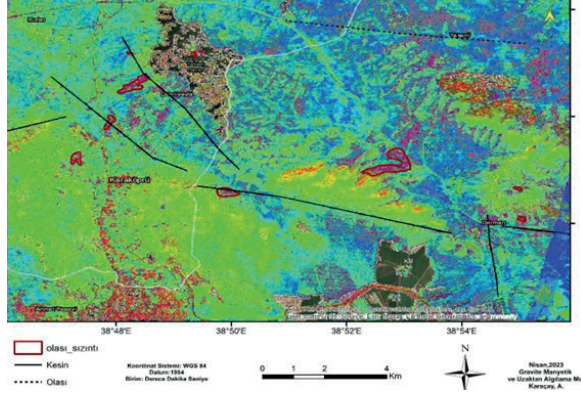
IRECI algoritması ile oluşturulmuş bitki örtüsü analizi haritası

Şekil 8.



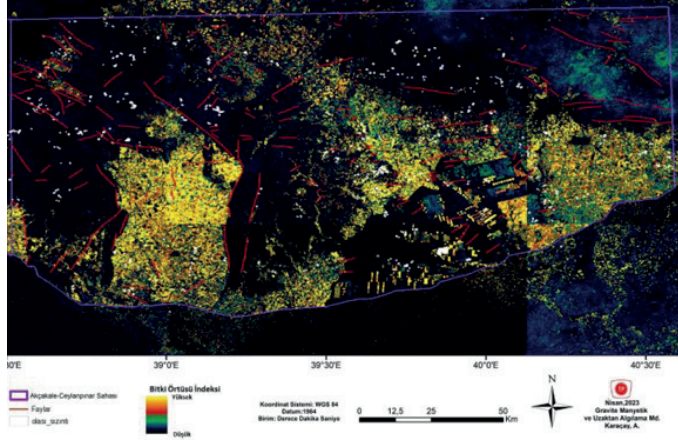
IRECI algoritması ile oluşturulmuş bitki örtüsü indekslerinin zamansal değişimi

Sekil 9.



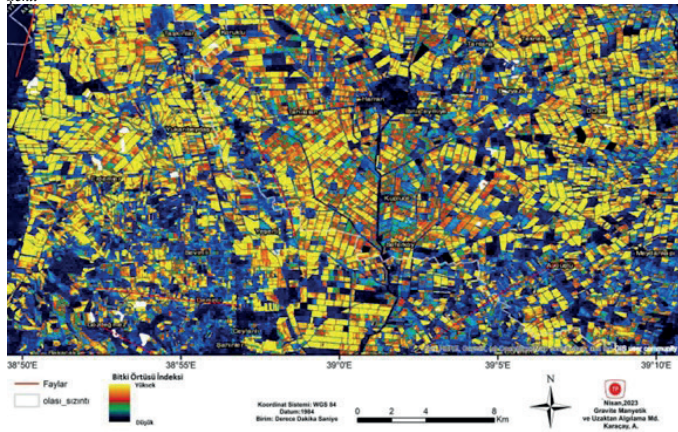
Birleştirilmiş Aster mineral indeks haritaları üzerinde fay-kırıklar ve olası sızıntılar haritası

Sekil 10.



Sentinel-2 verisinden üretilen bitki indeksi görüntüsü üzerinde fay-kırıklar ve olası sızıntılar haritası

Sekil



Harran ovası bitki indeksi görüntüsü üzerinde fay-kırıklar ve olası sızıntılar haritası

11.





**Jeotermal Enerji**

*Geothermal Energy*

---



# Jeotermal Sahalarda Mikrosismik İzleme Yöntemi ile Rezervuar Takibi



**Burcu Turhan<sup>1</sup>, Tuğçe Bilgiç<sup>2</sup>, Ünal Selek<sup>2</sup>, Kadir Balcı<sup>3</sup>, Ali Yıldırım<sup>3</sup>, Bülent Kaypak**

<sup>1</sup>Türkiye Petrolleri Genel Müdürlüğü

<sup>2</sup>Mikrosismik Mühendislik Danışmanlık Ltd. Sti.

<sup>3</sup>Maspo Holding

<sup>4</sup>Ankara Üniversitesi

Yenilenebilir enerji kaynaklarından biri olan jeotermal enerji özellikle ülkemizde önemli bir potansiyele sahiptir. Bu enerji kaynağının belirlenmesine yönelik arama faaliyetleri sonrası, işletilen jeotermal santrallere ait sahalarda işletmenin sürdürülebilirliği için rezervuar takibine ilişkin geleneksel çalışmalar dışında başka bir çalışma yapılmamaktadır. Jeotermal işletme faaliyetleri ile re-enjeksiyon ve üretim kuyularının faaliyetleri esnasında yeraltında kılcal boyutlarda kırılma olayları meydana gelmektedir. Mikrosismik olarak isimlendirilen bu olayların takibi, sahaya kurulacak yüksek frekanslı sensörler ile alınan sürekli kayıtların analizi ile mümkün olmaktadır. Jeotermal sahaların güvenliği ve sürdürülebilirliğini sağlamak mikrosismik izleme yöntemi ile yapılabilmektedir. Bu kapsamda söz konusu yöntemin uygulanmasına dair dünyada birçok örnek olmasına karşın yöntemin endüstriyel anlamda kapsamlı ilk uygulaması TÜBİTAK destekli (3200756 numaralı 1501-TEYDEB Projesi) bir proje ile bu çalışmada yapılmıştır. Çalışmada, mikrosismik izleme ağı ile toplanan kayıtlardan mikrosismik olaylar saptanmış, bunların konumları hesaplanmış ve seçili mikrosismik olayların büyüklükleri hesaplanarak, odak mekanizması çözümleri yapılmıştır. Böylece, rezervuarın güncel durumu hakkında teknik ve bilimsel bilgi elde edilmiş, suyun yer içindeki hareketine dair saptamalar yapılmış ve çatlak yönelimi ile gerilme analizine ait değişimler belirlenmiştir.

Geothermal energy, one of the renewable energy sources, has an important potential especially in our country. After the exploration activities aimed at determining this energy source, no other studies are conducted for reservoir monitoring in the fields of operated geothermal power plants, other than traditional works for the sustainability of the operation. The fractured events have occurred in underground during the activities of re-injection and production wells and geothermal operations activities. The monitoring of these events, called microseismic, is done using continuous recordings taken with high frequency sensors to be installed in the field. Ensuring the safety and sustainability of geothermal fields can be done with microseismic monitoring method. In this context, although there are many studies of the application of the method in the world, the first comprehensive application of the method in the industrial sense was carried out in this study with a project supported by TÜBİTAK (1501 TÜBİTAK-TEYDEB Project No: 3200756). Microseismic events were determined from the continuous records collected by the microseismic monitoring network, the location of events and the magnitudes of selected events were calculated, and their

focal mechanism solutions were done. So, the technical and scientific information are get about the current situation of the reservoir, the results of the movement of water in the ground were obtained and the changes of the fracture orientation and the stress analysis were found.

## GİRİŞ

Dünya genelinde, fosil yakıtların tükenmesi ve artan enerji ihtiyacı ile birlikte yenilenebilir enerji kaynakları önem kazanmıştır. Ülkemizde potansiyeli en yüksek enerji kaynaklarından biri de jeotermal enerjidir. Jeotermal enerji, yer kabuğunun derinliklerindeki doğal ısı kaynaklarından elde edilen, yenilenebilir ve çevre dostu bir enerji türüdür. Jeotermal enerji üretimi, yüksek sıcaklık ve basınç altında bulunan yer altı sularının veya buharının, enerji üretimi için yüzeye çıkarılmasıyla gerçekleşir. Bu kaynakların çıkarılması sırasında, yer içerisinde meydana gelen değişimler nedeniyle enerjileri düşük, yüksek frekanslı, küçük genlikli ve çok hızlı sönmülenen mikrosismik olaylar meydana gelmektedir.

Mikrosismik izleme yöntemi, jeotermal sahalarda meydana gelen değişimleri ve etkileşimleri takip etmek için kullanılan bir yöntemdir. Yöntem, sismik dalgaların hızı, frekansı ve şekli gibi özelliklerinin hassas ölçümünü kapsamaktadır. Yöntemin standart bir şekilde uygulanması, jeotermal rezervuarların etkin bir şekilde izlenmesi ve yönetilmesi jeotermal saha operasyonlarının güvenliği ve verimliliği açısından önemlidir. Çalışma, MASPO Jeotermal Üretim sahasına yerleştirilen yedi adet kuyu tipi sensör ile kaydedilen kayıtların analizi ile yapılmıştır. Mevcut sensörler ile 2021-Temmuz ile 2023-Mayıs aralığında toplanan verilerin sonuçlarından yararlanılmıştır. Söz konusu zaman aralığında toplam 1538 mikrosismik olay belirlenmiştir. Kaydedilen olayların derinliği -0.3 ile 10.9 km arasında değişmektedir. Büyüklük değerleri ise 0.00 ile 1.3 arasında değişmektedir.

## ÇALIŞMA SAHASI JEOLJİSİ

Çalışma sahası Manisa ilinin Alaşehir ilçesi sınırlarında yer almaktadır. Bölge Neojen öncesi temel kayalar, Neojen ve Kuvaterner yaşlı sedimanter birimlerden oluşur. Çalışma alanının jeolojisine ve stratigrafisine ilişkin bilgiler Karamandereci (1994), Karahan (2007), Yolal ve Karahan (2010) 'dan derlenmiştir. Menderes Masifi ile İzmir-Ankara Zonunun kapanması sırasında oluşan eski faylar ve Graben tektoniği bölgenin önemli yapıları arasındadır. Genel yapıya bağlı olarak çalışma sahasında iki farklı stratigrafik istif gözlenmektedir.

En altta Menderes Metafak ünitesini oluşturan yüksek basınç ve yüksek sıcaklık metamorfizması ürünlerinin görüldüğü temel birimler ve bunların üzerinde ise Tersiyer çökel kayaları yer alır. Çalışma bölgesindeki en genç birimler sıcak ve soğuk su kaynakları boşalım noktalarında oluşan travertenler, eski ve yeni alüvyonlardır.

Rezervuar özellikteki çalışma alanı, Gediz Grabeni olarak bilinen stratigrafik yapıda konumlanmaktadır. Graben, kıta içi açılma tektoniğine bağlı olarak şekillenen bir rift havzasıdır (Koçyiğit, 2000). Havzanın Miyosen boyunca sadece güney kenarı aktif olduğu yarı graben olarak gelişmiş, Pliyo-Kuvaterner'de ise kuzey kenar fay sisteminin faaliyete geçmesiyle bugünkü asimetric görünümünü kazanmıştır. Buna bağlı olarak oluşan normal faylar önünde çökelen tortullar Gediz Grabeni'nin en yaşlı tortul dolgusunu meydana getirmiştir (Yılmaz vd., 2000). Kuvaterner çökelleri; alüvyon yelpazesi çökelleri, akarsu çökelleri, gösel çökel arakatlı yelpaze deltası ve delta çökelleri, gösel çökeller olarak sınıflandırılmaktadır. Gediz Grabeni tektonik yapısı bölgenin jeotermal potansiyelini oluşturmaktadır.

### MİKROSİSMİK İZLEME YÖNTEMİ

Yöntemin ilk basamağında, çalışma sahasındaki sismik hareketliliği izlemek üzere kurulacak istasyon noktalarının arka alan gürültü seviyesinin (rüzgar, deniz dalgası, gel-gitler, trafik, endüstriyel hareketler, yapay patlamalar) önceden belirlenmesi için gürültü analizi yapılmaktadır. Böylece uygun bir ağ tasarımı oluşturularak daha temiz kayıtların elde edilmesi sağlanmaktadır. Gürültü analizi çalışması sonuçlarından yararlanılarak, belirlenen lokasyonun gürültü içeriğinin düşük olması için kuyu içi sensörler tercih edilmiş ve böylece yüzey gürültüsünün elemine edilmesi sağlanmıştır. Çalışma sahasında yöntemin sağlıklı bir şekilde uygulanması için S/G (Sinyal/Gürültü) oranı yüksek kayıtlar elde edilmesi sağlanmıştır (Tunç v.d. diğ., 2023).

Yedi sensör tarafından kaydedilen bir mikrosismik olayın kaydına ait görüntü Şekil-1'de verilmiştir. Toplam 22 aylık süreçte kaydedilen 1538 olayın konum, büyüklük değişimi ve derinlik bilgisine ait bilgiler Şekil-2'de görülmektedir. Mikrosismik olayların konumlarının belirlenmesinde çalışma sahasında toplanan sismik yansıma verilerinden elde edilen hız bilgisi başlangıç hız bilgisi olarak kullanılmıştır. Sonrasında verilerin belli bir sayıya ulaşması ile altı aylık süre zarfında kaydedilen mikrosismik olayların kullanılmasıyla sismik tomografi uygulanmış yer altı hız modeli güncellenmiştir. Konumlandırma için ise literatürde genel olarak tercih edilen Geiger (Geiger, 1910) algoritması içeren HYP2000 yazılımı kullanılmıştır.

Olay konumlarının dağılımı incelendiğinde, sahanın güney kesiminde kazıya göre daha fazla yoğunlaşma olduğu görülmektedir. Bu durum, güney kesimde suyun hareketi esnasında daha fazla çatlak kırık dağılımının oluştuğunun bir göstergesidir. Bu sonuç, sahanın güney

kesiminin jeolojik olarak çatlama daha uygun litolojik formasyonlardan oluştuğunun bir göstergesi olup, daha az basınç hareketi ile rezervardaki suyun daha kolay hareket ettiği ve daha derinlere doğru dolaşabildiğini göstermektedir. Diğer taraftan sahanın batısına doğrudan olaylarda çizgisel bir artış olduğu dikkat çekmektedir. Fakat, istasyonların yerleşimi nedeniyle batıda istasyon olmaması nedeniyle kaydedilen bazı olayların konumlandırılması yapılamamıştır. Mikrosismik olayların genellikle 1-5 km arasında yoğunlaştığı görülmüştür. Bu derinlik jeotermal aktivitenin faaliyete gösterdiği derinliklerdir. Diğer taraftan mikrosismik olayların büyüklük dağılımı incelendiğinde, beklenildiği üzere kuyular çevresinde meydana gelen olayların daha çok küçük magnitudüli olaylar olduğu, daha derin tektonik kökenli olabilecek deprem karakterindeki olayların ise kısmen daha büyük magnitudüli olduğu görülmüştür. Mikrosismik olayların büyüklük hesabı olayın süre bilgisinden hesaplanan  $M_d$  (duration magnitude) değeri ile bulunmuştur. Büyüklük değerleri çatlak boyutu hakkında fikir edinmemizi sağlamaktadır. Şekil-3'de mikrosismik olayların konumları 3-boyutlu olarak verilmiştir. Olayların konumları, suyun güneyde daha derinden hareket ederek batıya doğru yönlendiği göstermektedir. Seçili mikrosismik olayların her biri için odak mekanizması çözümü yapılamamaktadır. Odak mekanizması çözümü yapılabilmesi için tüm sensörler tarafından kaydedilmiş olan ve S/G oranı yüksek kayıtlara sahip olaylar seçilmiştir. Bu sebeple toplam 109 olay için odak mekanizma çözümü yapılabilmektedir. Yöntem olarak moment tensör ters çözümü kullanılmıştır. Sensör sayısı az olduğu için ilk hareket yönlerinin kullanıldığı fay düzlemi çözümü yönteminin uygulanması tercih edilmemiştir. Şekil-4'de odak mekanizma çözümleri çalışma sahası haritası üzerinde konumları ile birlikte verilmiştir. Odak mekanizma çözümleri kullanılarak; faylanma türü ve gerilme bileşenleri belirlenebilmektedir. Faylanma türü olarak daha çok doğrultu atımlı faylanmaya uygun çözümler elde edilmiştir. Mikrosismik olaylar; tektonik olaylardan farklı olarak yapay kuvvetlerle neticesinde oluşan zorlanmış olaylardır. Şekil-5'te odak mekanizma çözümleri sonrası fay düzlemlerinin doğrultuları ile elde edilen çatlak-kırık yönelimleri görülmektedir. Genel olarak, çatlak yöneliminin sahanın jeolojik yapısına uygun olacak şekilde KB-GD doğrultulu olduğu görülmüştür. Şekil-6'da 22 aylık dönemde konumları hesaplanmış mikrosismik verilerin aylara göre dağılımı verilmiştir. Sahadaki kuyular genel olarak sabit debi ve sabit basınçla çalışmaktadır. Sadece santrallerdeki operasyonel faaliyetler durduğunda ve kuyulardaki basınç değişimleri değiştiğinde sahadaki debi ve basınç değerleri değişmektedir. Söz konusu değişiklikler olduğunda indüklenmiş olaylarda da genel olarak bağlantılı değişiklikler olduğu gözlenmiştir.

### SONUÇLAR

Çalışma sahasında yedi kuyu tipi sensör ile 22 aylık dönemde toplanan veriler değerlendirilmiştir. Sensörlerdeki sürekli verinin uygun filtrelene işleme tabi tutulması ile yüksek frekans içeriğindeki

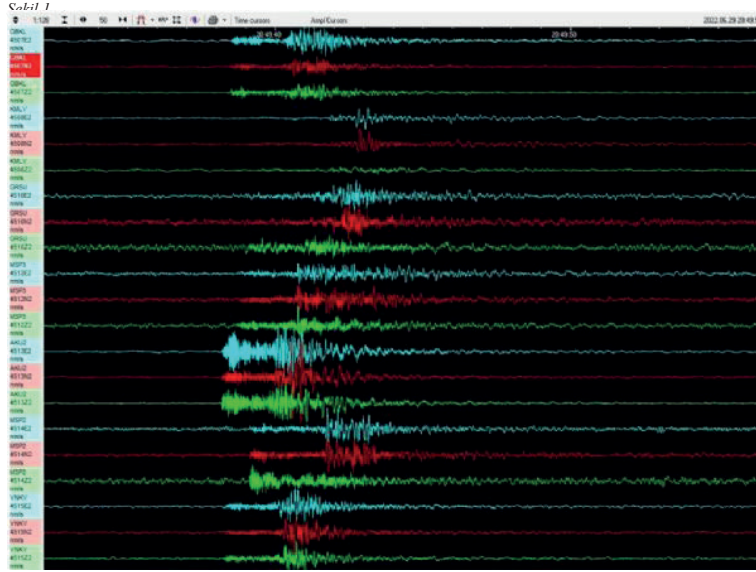


mikrosismik olaylar seçilebilmiştir. Seçilen toplam 1538 mikrosismik olayın konumunun belirlenmesi ile özellikle sahanın güney kesiminde olayların yoğunlaştığı görülmüştür. Bu durum, rezervuar suyunun güneydeki hareketi esnasında daha fazla kırık-çatlak meydana getirdiğini göstermektedir. Diğer taraftan mikrosismik olayların günlük sayılarının sahadaki kuyulardaki enjeksiyon, üretim faaliyetleri ve basınç değişimleri ile genel olarak ilişkili olduğunu göstermiştir. Sahada meydana gelen mikrosismik olayların büyüklük değerleri beklenildiği gibi oldukça küçük değerlerdir. Ortalama büyüklük değeri 0.3'tür. Olayların büyüklükleri çatlak-kırık boyutu hakkında bilgi vermektedir. Diğer taraftan çalışma sahasında tektonik yapıları tetikleyecek herhangi bir faaliyet gerçekleşmediğini ve risk unsuru oluşturmadığı söylenebilir. Genel bir değerlendirme yapıldığında, sahadaki üretim ve re-enjeksiyon faaliyetlerindeki basınç değişiminin mikrosismik olaylardaki etkinliği arttırdığı söylenebilir.

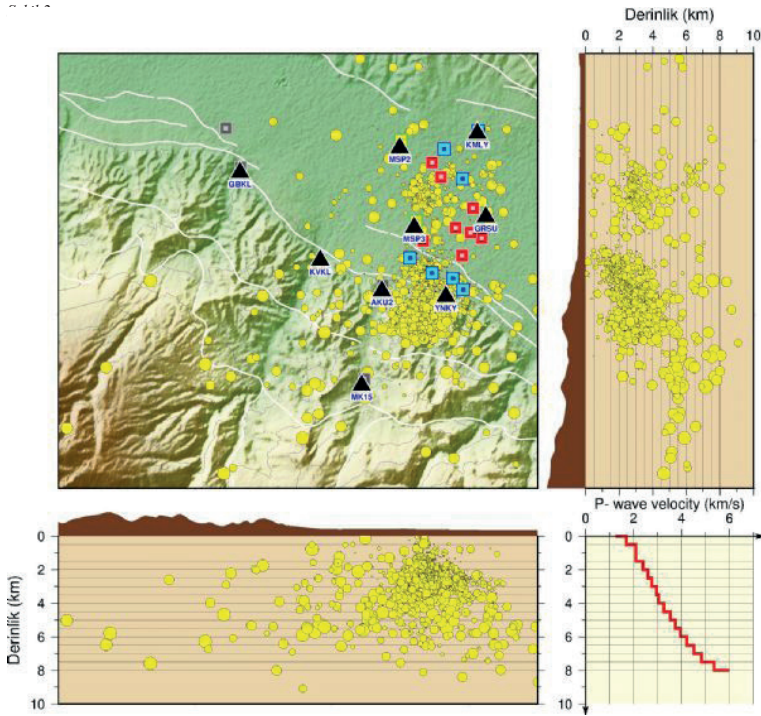
#### KAYNAKLAR

- Geiger, L. (1910). Herdbestimmung bei Erdbeben aus den Ankunftszeiten. Nachrichten von der Königlich Gesellschaft der Wissenschaften zu Göttingen, MathematischPhysikalische Klasse, 331-349.
- Karahan C, S. Bakrac, H. Dünya,2003. Alasehir-Kavaklıdere-Gobekli jeotermal enerji araştırma sondajının (KG-1) değerlendirilmesi. Sondaj Sempozyumu MTA Ege Bölge Müdürlüğü ve TMMOB Maden Müh. Hamdi Deliormanlı A., Seçkin C, İzmir Subesi, 10-11 Nisan 2002. Bildiriler, pp 39-43
- Karamanderesi İ. H., 1997. Salihli-Caferbeyli (Manisa İli) jeotermal sahası potansiyeli ve geleceği.,Dünya Enerji Konseyi Türk Milli Komitesi, Türkiye 7. Enerji Kongresi teknik oturum bildiri metinleri, pp 247-261
- Koçyiğit, A., H. Yusufoglu, E. Bozkurt, 1999. Evidence from the Gediz graben for episodic two-stage extension in Western Turkey. Journal of the Geological Society, London, 156, 605- 616.
- Tunç S., B. Selek, B. Koca, Ü.S. Selek, K. Balcı, A. Yıldırım, B. Kaypak, 2023. Installation of microseismic monitoring networks in geothermal fields. Journal of the Faculty of Engineering and Architecture of Gazi University 38:3, 1307-1319.
- Yılmaz, Y., S.C. Genç, O.F. Gürer, M. Bozcu, K. Yılmaz, Z. Karacık, I. Altunkaynak, and A. Elmas, 2000. When did the western Anatolian grabens begin to develop. in Bozkurt, E., Winchester, J.A., and Piper, J.D.A., eds., Tectonics and magmatism in Turkey and the surrounding area: Geological Society of London Special Publication, 173, 353-384.
- Yolal, A. and Ç. Karahan, 2010, Aydın Pamukören AP-3 Jeotermal Sondajı Kuyu Bitirme Raporu. MTA report, No. 11280.

Anahtar Kelimeler: Jeotermal enerji, mikrosismik izleme

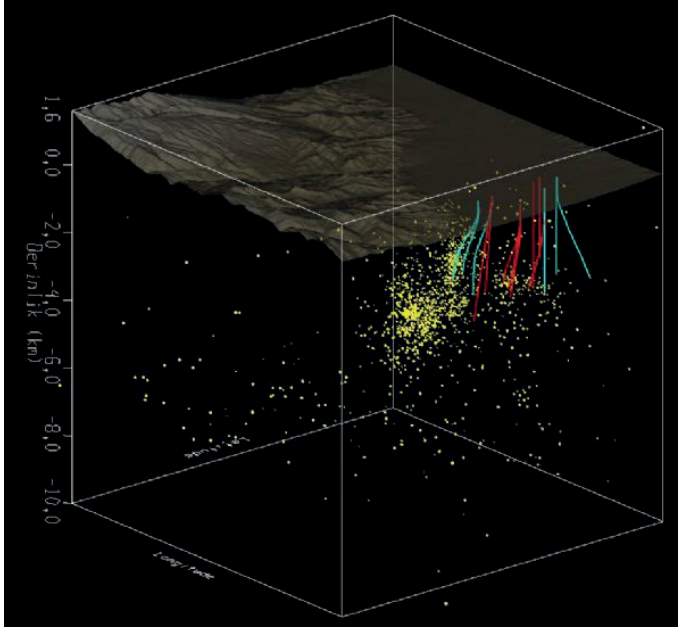


29.06.2022 20:49:35 tarih ve saatinde meydana gelen mikrosismik olay kaydı

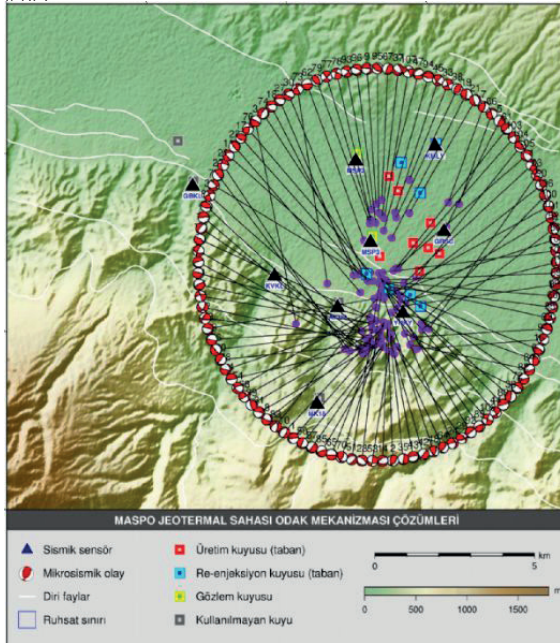


22 aylık dönemde sahada meydana gelen mikrosismik konumlarının (sarı renkli daireler) büyüklük ve derinlik ilişkisi ile birlikte sensör ( mavi üçgen semboller) dağılım ile birlikte gösterimi. Konumların belirlenmesinde kullanılan 1-B sismik hız modeli ise sağ alt köşede verilmiştir.

Sekil 3.

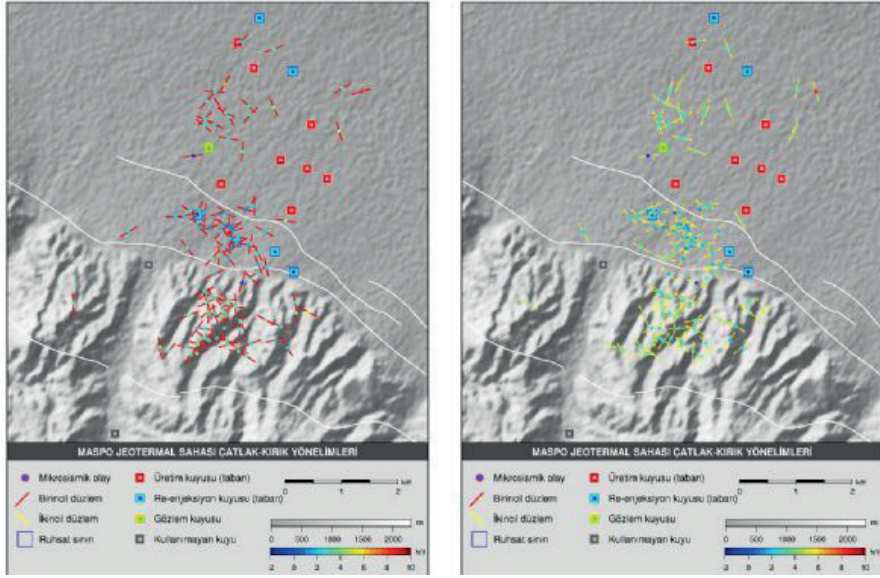


22 aylık dönemde meydana gelen mikrosismik olayların 3-B gösterimi



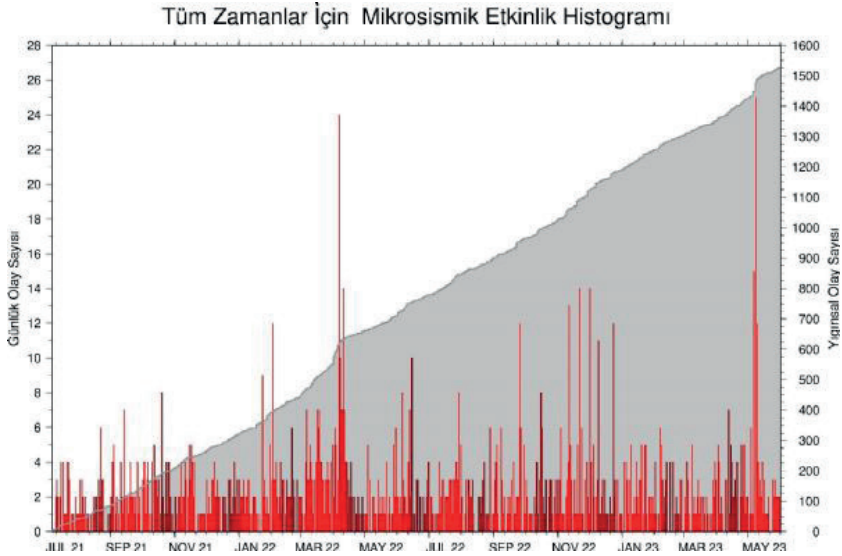
22 aylık dönemde meydana gelen çözümü yapılabilen mikrosismik olayların odak mekanizma çözümleri ve lokasyonlar

Şekil 5.



Sahada meydana gelen seçili mikrosismik olayların odak mekanizma çözümleri ile belirlenen kırık yapılarının düzlem doğrultuları.

Şekil 6.



22 aylık dönem için oluşturulmuş mikrosismik etkinlik histogramı (kırmızı çubuklar) ve sahada meydana gelen olayların yığılma grafiği (gri alan)

# Sismik Hız İle Boşluk Basıncı İlişkisi Örnek Çalışma: Denizli Havzası



## Orhan Güreli

RR Sismik Mühendislik A.Ş., Ankara / Türkiye

Ege bölgesi ve Denizli havzası yüksek sismik aktiviteye ve zengin jeotermal alanlara sahiptir. 2000 yılında Denizli havzası çevresinde artan bir sismik aktivite gözlenmiştir. Bazı araştırmacılar, bölgedeki 635 kayıtlı deprem verisinin seyahat sürelerini kullanarak Denizli havzasının bir boyutlu (1-B) ve üç boyutlu (3-B) Vp ve Vp/Vs yapısını araştırmışlar ve Denizli havzasının 3 boyutlu sismik hız modellerini elde etmişlerdir. Bu modeller, jeolojik ve tektonik birimlerden elde edilen sonuçlarla karşılaştırılmışlardır.

Bu çalışma da, aynı bölgede daha önce elde edilmiş sismik hız bilgisi kullanılarak, aynı bölgenin boşluk basıncı hesabı yapılmıştır. Elde edilen sonuçlar, daha sonra bölgede açılmış kuyular ve doğal sıcak su kaynakları ile karşılaştırılmıştır.

Anahtar Kelimeler: 3-B sismik hız tomografisi, Boşluk basıncı, Sismik hızlar.

## RELATIONSHIP BETWEEN SEISMIC VELOCITY AND PORE PRESSURE

### Case Study: Denizli Basin

The Aegean region and Denizli basin have high seismic activity and rich geothermal fields. In 2000, an increasing seismic activity was observed around the Denizli basin. Some researchers have investigated the one- and three-dimensional Vp and Vp/Vs structure of the Denizli basin by using the travel times of the 635 recorded earthquake data. They were obtain the 3D seismic velocity models of the Denizli basin. They concluded 3D Vp and Vp/Vs seismic velocity models for the upper 20 km of the crust beneath the Denizli basin, then, evaluated with the obtained results from geologic and tectonic units.

In this study, the pore pressure calculation of the region was made using the same seismic velocity information, which is obtained, in the same region. The obtained results were then compared with the drilled wells and hot water spring in the Denizli basin.

Key words: 3D seismic velocity tomography, Pore pressure, Seismic velocities.

## 1. GİRİŞ

Denizli havzası, Anadolu'nun batısında olup Büyük Menderes Grabeni ile Alaşehir Grabeni'nin bulunduğu bir noktadadır. Havzanın kuzey-güney yönündeki genişleme rejimi nedeniyle, doğu-batı yönlü büyük küçük boyutlarda bir çok graben oluşmuştur. Bölgedeki en önemli iki graben, D-B yönlü Büyük Menderes ve KB-GD yönlü Alaşehir grabenidir. Bu grabenler doğuda Denizli havzasında birleşirler. Denizli havzası

ve yakın çevresi, hem jeotermal açıdan önemli bir potansiyele sahip hemde yüksek deprem etkinliği gözlenen bir bölgedir (Şekil 1a). Bölgede geçmişte yıkıcı depremlerin olduğu bilinmektedir. Özellikle son yıllarda görülen depremlerin oluşum sıklığı bölge ile ilgili bilimsel araştırmaların yapılmasına neden olmuştur. Deprem etkinliği bakımından hayli aktif bir bölgede yer alan Denizli havzası ve çevresinin 1-B ve 3-B sismik hız yapısı yerel deprem tomografisi yöntemi ile belirlenmiştir. Bu yöntem ile elde edilen sonuçların bölgenin tektonik, jeolojik, hidrotermal ve depremsellik gibi unsurları ile yorumlanması gibi konularda bir çok araştırmacı çalışmaları yapmışlardır.

Denizli Baseninin tomografik yöntemlerle ortaya çıkarılmış 3B veri kullanarak boşluk basıncının ortaya çıkarılması bu çalışmanın temel amacını oluşturur. Deprem dalgalarının (P ve S dalgaları) seyahat zamanları kullanılarak tomografi yöntemiyle hız yapısı çıkartılır. Bu sahanında aynı şekilde hız yapısı Kaypak ve Gökkaya (2012) tarafından çıkarılmıştır. TÜBİTAK-MAM YDBAE tarafından 3-29.09.2000 tarihleri arasında bölgeye yerleştirilmiş istasyonlar ve kaydedilen mikro depremlere ait lokasyonlar Şekil 1a'da verilmiştir. Bu seçilen deprem kayıtları kullanılarak Denizli Baseninin 3-B sismik tomografik hız yapısı Kaypak ve Gökkaya (2012) tarafından çıkarılmıştır.

Bu çalışmada, Kaypak ve Venedik (2011) tarafından elde edilen Denizli baseninin 3-B Vp hızı kullanılarak boşluk basıncı hesaplanmış ve sonuçları yorumlanmıştır.

## 2. JEOLJİK VE TEKTONİK ORTAMLAR

Batı Anadolu'daki tektonik genişleme hareketleri sonucunda çok fazla graben oluşmuştur. En büyük graben; Büyük Menderes Grabeni (BMG), Küçük Menderes Grabeni (KMG) ve Gediz Grabenidir (GG). Bölgedeki grabenler, K-G yönlü genişleme hareketine bağlı olarak çoğunlukla D-B doğrultulu (sadece Gediz Grabeninin Salihli-Sarıgöl arası KB-GD yönlüdür) ve farklı boyutlardadır. Denizli havzası BMG ile GG'nin kesiştiği yerde oluşmuştur. Bu bölgenin önemli havzalarından biri olan Denizli havzası, yaklaşık 50 km uzunluğunda ve 25 km genişliğinde, BKB-DGD doğrultulu asimetric bir grabendir (Şekil 1b). Havza güneyde Babadağ ve Honaz dağları, kuzeyde ise Çökelez Dağı ile sınırlıdır. Denizli havzası ve çevresi iki ana grup litolojiden oluşur. ilk grup temel kayalar ve ikinci grup ise bunları üzerini örten genç havza çökelleridir.

Menderes masifinin oluşturduğu gerilmeler sonucunda, tektoniğe bağlı olarak D-B ve KB-GD yönlü normal faylar ve gerilme çatlakları ile horst ve grabenler oluşmuştur. Bunların çoğu eğim atımlı normal faylardır. Güncel tektonik olarak, Denizli bölgesi Batı Anadolu genişleme rejimi ile oluşan graben sistemleri içinde yer

alır (Şengör ve diğ. 1987). “Güneyden kuzeye doğru sıralanan Babadağ horstu, Honazdağ horstu, Çürüksu grabeni, Büyükmenderes grabeni, Buldan horstu, Gediz grabeni, Yenice horstu ve Çökelezdağ horstu bölgedeki başlıca yapılarıdır” Kaypak ve Venedik (2011).

### 3. YÖNTEM

Formasyon hızları, formasyon yoğunluğuna, sıcaklığına, üzerindeki ağırlığa ve boşluk içindeki basınca bağlı olarak değişir. Bu konuda, konunun uzmanları uzun süredir çalışmaktalar. Bu çalışmalar daha çok doğal gaz sahalarında uygulanmakta olup “Doğrudan Hidrokarbon Keşfi-Direct HC indicator (DHI)” yöntemlerinden biridir. Aynı zamanda bu yöntem, gazlı sahalarda kuyu dizaynında ve kuyu Casing programında kullanılmaktadır.

Bulk Modülü (K): Hidrostatik basınç altında kalan bir kayadaki gerilme-deformasyon ölçüsüdür. Yani materyalin hacim değişikliğine karşı mukavemetinin ölçüsüdür.

$$K = \text{Hacim Gerilmesi/Hacim Deformasyonu} = P / (dv/V) \quad (1)$$

burada K: Bulk modülü, P: basınç, V: hacim ve dv ise hacim değişimidir.

Dışardan uygulanan üç yönlü basınç artarsa hacimde bir miktar azalma olmaktadır. Hacimin azalması Bulk modülünü (K) artırmaktadır. K modülü arttıkça formasyon sertleşmektedir. Bu sertleşmeye bağlı olarak sismik hızlar artmaktadır.

$$v_p = \sqrt{((K+4/3\mu)/\rho)} \quad (2)$$

$$v_s = \sqrt{(\mu/\rho)} \quad (3)$$

burada  $v_p$ : P dalgasının hızı,  $v_s$ : S dalgasının hızı,  $\mu$ : Rijitide (sıkıştırılabilirlik) ve  $\rho$  ise yoğunluktur.

Sismik hızlar; kayaçların, kimyasal bileşimlerine, sıcaklığına ve basıncına bağlı olarak değişirler. Düşük sıcaklık, yüksek basınç ve katı hal durumu/sertliği sismik hızları artıran faktörlerdir. Yüksek sıcaklık, düşük basınç ve sıvı hal ise sismik hızı azaltan faktörlerdir. Kayaçların içindeki akışkan arttıkça  $V_s$  hızı düşer,  $V_p$  hızı ise akışkanın hızına bağlı olarak, kayaç hızından akışkan hızına doğru değişir.

#### 3.1 Sıcaklık İle Sismik Hız İlişkisi:

Yüksek basınç altındaki kayaçların  $V_p$  hızlarının sıcaklığa bağlı değişimi üzerine Kern (1978, 1979 ve 1982), Lebedev ve diğ. (2021) ve Popp and Kern (1993) çeşitli çalışmalar yapmışlardır. Lebedev ve diğ. (2021)'in yaptığı çalışmaya göre; Kuru koşullarda, incelenen mafik-ultramafik kayaçlardaki sıkışma dalga hızları ( $V_p$ ), 20 ila 700 °C arasındaki tüm sıcaklık (T) aralığında çok az da olsa değişir. Kayacın mineral yapısının etkisi daha önemlidir. Bazaltlarda, daha yüksek gözeneklilik, heterojen yapı, kristal mineral fazlarına bağlı olarak ve ikincil minerallerin varlığı nedeniyle  $V_p$  hız değerlerinde biraz artış vardır. (Şekil 2).

#### 3.2 Boşluk Basıncı İle Sismik Hız İlişkisi

Şeyl, kil, silt, kum, kum taşları gibi sediman çökellerin yüksek poroziteli olmaları nedeniyle sıkıştırma ve boşluk basıncına duyarlıdır. Boşluk basıncının artması ile sismik hızlar düşmektedir. Sediman olmayan diğer kayaçlarda da genleşme katsayısına ve porozitesine bağlı olarak hızlar düşecektir (Şekil 3).

#### 3.3 Sismik Hızlardan Boşluk Basıncının Elde Edilmesi

Sismik hızlardan boşluk basıncının elde edilmesi konusunda çok fazla araştırmacı çalışmıştır ve çalışmaya devam etmektedir. Sismik hızlar kullanılarak boşluk basıncı hesabında en yaygın ve en çok kullanılan yaklaşımlar Eaton (1972) ve Bowers (1995) yaklaşımlarıdır. Bu çalışma için yapılan hesaplamalarda Eaton (1972) denklemleri kullanılmıştır.

Örtü gerilmesi (S) boşluk basıncı (Pp) ile efektif gerilmenin ( $\sigma$ ) toplamına eşittir (Şekil 4).

$$S = \sigma + P_p \quad (4)$$

$$\sigma_n = S - p_n \quad (5)$$

$$S = g \cdot \rho \cdot m \cdot z \quad (6)$$

$$p_n = g \cdot \rho_w \cdot z \quad (7)$$

$$\sigma = g \cdot \rho \cdot m \cdot z - P_p \quad (8)$$

$$\sigma = \sigma_n (v/v_n)^n \quad (9)$$

$$v_n(z) = v_o + k \cdot z \quad (10)$$

$$P_p = S - (S - p_n) \cdot (v/v_n)^n \quad (11)$$

Burada;

$\sigma_n$ : Normal efektif gerilme,

$\sigma$ : h derinliğindeki efektif gerilme,

$p_n$ : Normal boşluk basıncı,

g: yer çekimi ivmesi,

$\rho_m$ : Kütleli yoğunluğu,

$\rho_w$ : Formasyon içindeki akışkanın yoğunluğu,

h: Derinlik,

v: h derinliğindeki sismik ara hız,

z: derinlik,

$v_n$ : h veya z derinliğindeki normal hız değeri,

$v_o$ : Yüzeyleki tabakanın sismik ara hızı,

k: birim hız değişimi,

n: sabit katsayıdır.

Boşluk basıncı hesabında (11) nolu denklem kullanılmıştır.

## 4. VERİ

### 4.1) Verinin Toplanması

Bölgede meydana gelen depremleri takip etmek, gözlemlemek ve diri fayların sismotektonik özelliklerini belirlemek amacı ile TÜBİTAK-MAM YDBAE tarafından bölgeye 24 adet tek bileşen kısa periyodlu (Mark L-28/1D, 4.5 Hz doğal frekanslı) ve 4 adet üç bileşen geniş bantlı (Güralp CMG-40T with 0.033 Hz doğal frekanslı) olmak üzere toplam 28 istasyondan oluşan bir sismik ağ kurularak (Şekil 1a) 3-29.09.2000 tarihleri arasında yaklaşık bir ay süre ile veri toplanmıştır.

### 4.2) Verinin İşlenmesi

Denizli havzası ve dolayına ait sismik hız yapısının belirlenebilmesi için toplanan verilere iki aşamalı yöntem ardışık olarak uygulanmıştır. İlk aşamada ters çözüm yöntemi ile Denizli havzasının 1-B hız yapısı hesaplanmıştır, ikinci aşamada ise elde edilen 1-B hız modeli giriş verisi olarak kullanıldı ve aynı ters çözüm yöntemi ile havzanın 3-B sismik hız yapısı elde edilmiştir.

Denizli havzası ve dolayına ait 1-B ters çözüm işlemi sonucunda önce 1-B  $V_p$ ,  $V_s$  ve  $V_p/V_s$  oranları elde edilmiştir. 1-B ters çözüm sonuçları değerlendirildiğinde, yüzey jeolojisinin çok etkili olduğu, 2.0 km derinliğe kadar olan sık katmanların hızlarının düşük olduğu gözlenmiştir. Veri işlemin bir sonraki aşamasında ise Denizli havzasının 3-B sismik hız yapısının belirleme çalışmalarıdır. Yapılan ardışık ters çözüm işlemleri sonucu, bölgenin 20 km derinliğe kadar olan sismik hız yapısı ( $V_p$  ve  $V_p/V_s$ ) ve önemli yapısal unsurları ortaya çıkarılmıştır. Yeraltındaki kayaların yapısal özellikleri, sıvı içerikleri ve süreksizlikler  $V_p$  ve  $V_s$ 'i önemli ölçüde etkilemektedir.  $V_p$ 'nin uzamsal değişimi kayaç özellikleri ve litolojinin dağılımını yansıtırken,  $V_p/V_s$  değişimleri ise kayaç porozitesi, çatlak yoğunluğu ve sıvı içeriği ile ilişkili olmaktadır (Berge ve Bonner 2002).

Eaton (1972)'in ve diğer araştırmacıların geliştirdiği, sismik hızlardan boşluk basıncı hesabı yöntemi uzun yıllardır kullanılmaktadır. Bu yöntemler daha çok sediman kayaçlar için uygulanmaktadır. Özellikle sondajların uyguladığı bu yöntem "casing" ve sondaj hızı planlanmasında yaygın olarak kullanılmaktadır.

Bu çalışmada, Kaypak ve Venedik (2011)'in hesapladığı hız verileri kullanılarak boşluk basıncı hesabı yapılmıştır.

Şekil 5'de Denizli havzası içindeki depremler, kayıt eden deprem istasyonları, aktif ve pasif faylar görülmektedir. Değerlendirmeler sonucunda, şekilde belirlenen profiller boyunca  $V_p$  hızları,  $V_p/V_s$  oranı değişimi çıkarıldı ve değerlendirilmede bu profiller boyunca hesaplamalar yapıldı. Bu profiller boyunca elde edilen  $V_p$  hızları ve  $V_p/V_s$  oranları Şekil 6a ve Şekil 6b'de verilmiştir.

Elde edilen sonuçlar, doğal sıcak su çıkışları olan Pamukkale, Karahayit ve Gölemezli bölgesindeki sıcaklık bilgileri ile Akça Enerji AŞ'ye ait Ak-3 ve Ak-6 kuyularının sıcaklık ve basınç bilgileri ile karşılaştırılmıştır.

## 5. BULGULAR

Denizli havzasındaki depremlerden elde edilen sismik hızların tamamı derinliğin fonksiyonu olarak Şekil 7a'da verilmiştir. Bu hızlar, 11 nolu denklemde kullanılarak boşluk basıncı hesabı yapılmıştır (Şekil 8b).

Yukardaki formüller ile bulunan değerler 11 nolu denklemde kullanılmıştır. Ayrıca analizler sonucunda en uygun değer  $n=3$  olduğuna karar verilmiş ve çalışmada bu değer kullanılmıştır. Bu değerlere göre 11 nolu denklem aşağıdaki gibi kullanılmıştır.

$$P_p = S - (S - p_n) \cdot (v/v_n)^n \quad (12)$$

Böylece boşluk basıncının derinliğe bağlı olarak değişimi hesaplanmıştır. Boşluk basıncı ve "İlave basınç" olarak Boşluk basıncı iki aşamada değerlendirilmiştir. Burada "İlave basınç" tabiri; boşluk basıncı ile normal şartlardaki basınç (Hidrostatik gerilme) arasındaki fark için kullanılmıştır. Yani formasyon içine sıcaklık ve/veya ilave akışkanın artması ile boşluktaki basıncın ilave artması demektir.

$$\text{İlave basınç} = P_p - P_n \quad (13)$$

Şekil 8'de, Şekil 5'deki profiller boyunca ve Şekil 6'daki aynı kat haritaları için hesaplanan boşluk basıncı ve ilave basınç değişimleri için hazırlanmış kat haritaları verilmiştir. Haritalarda da derinlikle boşluk basıncı ve ilave basınç değerlerinin artırmakta olduğu görülmektedir.

Ak-3 ve Ak-6 kuyularına ait litoloji bilgileri, sıcaklık ve basınç verileri, bu çalışmadaki  $V_p$  hızlarından elde edilen boşluk basıncı değerleri ile karşılaştırılmıştır. Grafikler incelendiğinde, derinliğe bağlı olarak sıcaklık ve basınç değerleri de artmaktadır. Yani kuyular devam etseydi sıcaklık ve basınç değerleri de artmaya devam edecekti. Bu bilgiler, kuyulara en yakın hatların ve hat üzerindeki noktaların hesaplanmış boşluk basıncı değerleri ile karşılaştırılmıştır (Şekil 9).

Şekil 10'da bölgenin  $V_p$ ,  $V_p/V_s$ ,  $P_p$  ve  $P_p - P_n$ 'in kat haritaları (-1500m) görülmektedir. Ayrıca harita üzerinde Ak-3 ve Ak-6 kuyu (1) yerleri, Gölemezli (2), Karahayit (3) ve Pamukkale (4) sıcak su çıkışları gösterilmektedir. Bu dört noktanın ortasında Profil-8 ile Profil-16'nın kesiştiği bölgede  $V_p$  hızları ve  $V_p/V_s$  oranının çok düşük olduğu bölge olup, yine bu bölge boşluk basıncı ( $P_p$ ) ve ilave basıncın ( $P_p - P_n$ ) çok yüksek olduğu bölgedir. Bu bölgenin kuzeyindeki Gölemezli ve doğusundaki Karahayit ve Pamukkale sıcak su çıkışlarının kaynağı burası olabilir. Bu bölgedeki basıncın etkisi ile fay zonu üzerinde olan bu noktalardan sıcak sular doğal olarak çıkıyor olabilir. Bu bölgede fay sisteminin olmaması nedeniyle de basınç artmış ve çevresini sıkıştırıyor.

## 6. SONUÇLAR

Güntümüzde bu tür konularda araştırma yapan araştırmacılar, jeotermal sistem ile depremler arasında bir ilişki olduğunu söylemektedir. Denizli havzası ve dolayındaki aktif jeotermal sistemi de bölgenin sismik etkinliğini artırmada önemli rol oynayan nedenlerden biri olarak sayabilir. Kayaçların yüksek sıcaklık ve basınç altında sismik hızlarının değiştiği bilinmektedir. Yüksek sıcaklık ve basınç altında, ne tür kayaç olursa olsun Vp ve Vs hızlarında az veya çok bir değişim olmaktadır. Sedimanlarda bu değişim çok fazla olurken, mafik ve ultramafik kayaçlarda daha az olmaktadır. Sismik hızlardan boşluk basıncı hesaplama işi, doğalgaz ve petrol arama amacıyla yaygın olarak kullanılmaktadır.

Yapılan hız tomografi sonuçlarına göre de değerlendirilmeler ve yorumlar Kaypak ve Venedik (2011) ve Kaypak ve Gökkaya (2012) tarafından yapılmıştır. Bu yazarların çalışmaları sonucunda elde edilen P dalga hızı (Vp) ve P-S dalga hızı (Vp/Vs) oranı değişimi sonuçları ile bu çalışmada elde edilen boşluk basıncı (Pp) ve ilave basınç (Pp-Pn) sonuçları karşılaştırılmış ve birlikte yorumlanmıştır.

Litolojik değişimler P dalga hızını etkilerken, kayaçların fiziksel özellikleri de Vp/Vs oranını etkilemektedir. Jeotermal sahalarda Vp/Vs anomalileri; genellikle kayacın dokusuna, poroziteye, gözenek içindeki akışkana, boşluk basıncına, sıcaklığa ve gözenek şekline bağlıdır (Takei, 2002). 3-B Vp/Vs anomalilerinin olduğu bölgeler, havza içerisindeki çatlak ve kırıklı bölgelerin yoğun olduğu kısımlardır. Yani bu bölgeler fayların çok olduğu ve fiziksel özelliklerinin değiştiği bölgelerdir. Bu bölgeleri ezilme zonu olarak düşünebiliriz. Vp anomalileri ise kayacın litolojik değişimlerine bağlıdır.

Boşluk basıncı hesabı Vp hızına bağlı olarak hesaplanması nedeniyle, hızın düştüğü yerlerde boşluk basıncı artmaktadır. Tabi bu artış için normal hız trendine göre daha düşük olmalıdır. Bu tür bölgelerde boşluk basıncı yüksek olacaktır. Bununla birlikte Vp/Vs oranında düşerse bu bölgelere basınçlı bölgeler diyebiliriz. Basınçla Vp hızı, Vs hızına göre daha hızlı azaldığından Vp/Vs oranı da düşmektedir. Dolayısıyla hem Vp hızının hem de Vp/Vs oranının düşük olduğu bölgelerde basınç değeri çok yüksektir. Bu tür yerler CO2 bakımından doygun veya yüksek basınçlı akışkanın olduğu yerleri gösterir (Zandomeneghi ve diğ., 2008; Moretti ve diğ., 2009; Husen ve diğ., 2004; Vanorio ve diğ., 2005). Vp hızı düşerken Vp/Vs oranı artarsa bu tür yerlerde çatlakların yani boşlukların fazla olduğu yerler ve bu yerlerin akışkan ile dolu olduğu anlamına gelebilir. Su/gaz gibi akışkanların S hızı olmadığı için Vp/Vs oranı böyle yerlerde artmaktadır. Bu akışkanın Vp hızında bir miktar düşmesine, böyle bölgelerde de boşluk basıncının artmasına neden olur.

Öncelikle Ak-3 ve Ak-6 kuyularındaki kuyu içi basınç değerleri ile en yakın profillerin ve en yakın noktalarındaki basınç değerleri ile kıyaslanmıştır. Ak-3 ve Ak-6 kuyu basınç değerleri ile profillerdeki hesaplanmış basınç değerlerinin birbirleriyle oldukça uyumlu olduğu görülmüştür. Aynı zamanda, elde edilen basınç sonuçları Pamukkale, Karahayıt ve Gölemezli sıcak su çıkışları ile

de kıyaslanmıştır. Kat haritası (Şekil 10) incelendiğinde, Profil-8 ile ile Profil-16'nın keşiştiği bölge yüksek basınçlı bir bölge olarak görülmektedir. Bu bölge ilginç olarak Ak-3, Ak-6 kuyuları ile Pamukkale, Karahayıt ve Gölemezli sıcak su çıkışlarının tam ortasında yer almaktadır. Bu bölgede fay olmaması (Şekil 10) basınç değerinin artmasına neden olmaktadır. Bu bölgedeki yüksek basınç, çevreye baskı yapmaktadır. Bu basınç ile çevrenin Vp hızı artmakta, dolayısıyla Vp/Vs oranını da artırmaktadır. Pamukkale, Karahayıt ve Gölemezli sıcak suyun olduğu bölgeye baskı yapmaktadır. Bu basıncın etkisiyle ve aynı zamanda faylı bir bölge olması nedeniyle sıcak sular yüzeye çıkmaktadır. Yine aynı haritalar incelendiğinde, bölgede pekçok yüksek basınçlı bölgeler görülmektedir.

Sonuç olarak, Jeotermal sahalarda önceden sahaya yerleştirilmiş sismometreler ile depremler belirli bir süre kayıt edilebilir. Sonuçların daha doğru hesaplanabilmesi için çok fazla sismometre kullanılmalı çok fazla deprem kayıt edilmelidir. Sismometreler ile elde edilen kayıtlar çeşitli tomografi programları aracılığıyla ile yerin içinin sismik hız değerleri elde edilir ve bu hızlar kullanılarak bölgenin boşluk basıncı hesabı yapılır. Bu bilgiler ile diğer jeofizik verilerin birlikte yorumlanmasıyla bölgenin jeotermal potansiyeli ortaya çıkarılır. Ayrıca tüm sonuçlar birlikte değerlendirilip, arama amaçlı bir kaç kuyu açılabilir. Daha sonra sahada mutlaka sismik yansıma yöntemi ile veri toplanmalı ve birlikte yeniden yorumlanmalıdır. Ayrıca sismik yansıma verisinden elde edilecek sismik hızlar ile deprem kayıtlarının değerlendirilmesinden elde edilen hızlarla ve basınçlarla karşılaştırılmalıdır. Sahada daha fazla yeni kuyu açmadan, bölgenin fayları, fay atımları, tabaka dalım açıları vs. sismik yansıma verisi ile ortaya çıkarılmalı ve yeni kuyu yerleri sismik veriden belirlenmelidir.

## KAYNAKLAR

- Berge, P. A., and Bonner, B. P., 2002. Seismic velocities contain information about depth, lithology, fluid content and microstructure. In: Symposium on the Application of Geophysics to Engineering and Environmental Problems, pp. UCRL-JC-144792.
- Blangy, J. P., 1992. Integrated seismic lithologic interpretation: The petrophysical basis, Ph.D. thesis, Stanford University.
- Bowers, G. L., 1995. Pore pressure estimation from velocity data: accounting for overpressure mechanisms besides under compaction. In: IADC/SPE drilling conference proceedings. p 515-530.
- Eaton B. A., 1972. Graphical method predicts geopressure worldwide. World Oil 182:51-56.
- Husen, S., Smith, R.B., Waite, G.P., 2004. Evidence for gas and magmatic sources beneath the Yellowstone volcanic field from seismic tomography imaging. J. Volcan. Geotherm. Res. 131, 397-410.
- Kaypak, B., and Gökkaya, G., 2012. 3-D imaging of the upper crust beneath the Denizli geothermal region by local earthquake tomography, western Turkey. Journal of Volcanology and Geothermal Research 211-212, 47-60.



Kaypak, B. ve Venedik, G., 2011. Denizli Havzası 3-B Sismik Hız Yapısının Jeolojik, Tektonik, Hidrotermal ve Depremsellikle İlişkisi, 1. Türkiye Deprem Mühendisliği ve Sismoloji Konferansı, Ankara, 11-14 Ekim.

Kern, H., 1982. P-and S-wave velocities in crustal and mantle rocks under the simultaneous action of high confining pressure and high temperature and the effect of the rock microstructure. In *High-Pressure Researches in Geoscience* (ed. Schreyer, W.) 15–45 (Schweizerbart'sche Verlagsbuchhandlung).

Kern, H., 1979. Effect of high-low quartz transition on compressional and shear wave velocities in rocks under high pressure. *Phys. Chem. Minerals* 4, 161–167.

Kern, H., 1978. The effect of high temperature and high confining pressure on compressional wave velocities in quartz-bearing and quartz-free igneous and metamorphic rocks. *Tectonophysics* 44, 185–203.

Lebedev, E. B., Kern, H., Pavlenkova, N. I., Lukanin, O. A., Lobanov, K. V., Zharikov, A. V., and Popp, T., 2021, Compressional wave velocity measurements on mafic–ultramafic rocks under high aqueous fluid pressure and temperature help to explain low velocity zones in the lithosphere, *Scientific Reports*, 11:13424 <https://doi.org/10.1038/s41598-021-92248-2>

Moretti, M., De Gori, P., Chiarabba, C., 2009. Earthquake relocation and three-dimensional  $V_p$  and  $V_p/V_s$  models along the low angle Alto Tiberina Fault (Central Italy): evidence for fluid overpressure, *Geophys. J. Int.*, 176, 3, 833-846.

Popp, T. and Kern, H., 1993. Thermal dehydration reactions characterised by combined measurements of electrical conductivity and elastic wave velocities. *Earth Planet. Sci. Lett.* 120, 43–57.

Şengör, A.M.C., 1987. Cross-faults and differential stretching of hanging walls in regions of lowangle normal faulting; Examples from western Turkey. In: *Continental Extensional Tectonics*. (Eds. M. P. Coward, J. F. Dewey and P. L. Hancock), *Geol. Soc. Pub.*, 28, 575-589.

Takei, Y., 2002. Effect of pore geometry on  $V_p/V_s$ : from equilibrium geometry to crack, *J. Geophys. Res.* 107, doi:10.1029/2001JB00522.

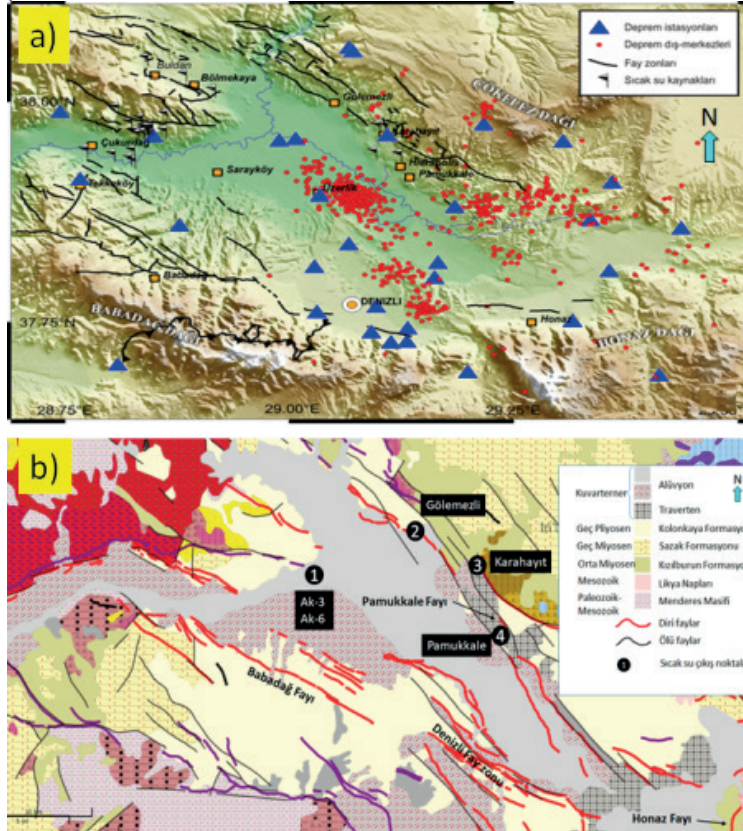
Vanorio, T., Virieux, J., Capuano, P., and Russo, G., 2005. Three-dimensional seismic tomography from P wave and S wave microearthquake travel times and rock physics characterization of the Campi Flegrei Caldera, *J. Geophys. Res.*, 110, B03201, doi:10.1029/2004JB003102

Zandomenighi, D., Almendros, J., Ibanez, J., Saccorotti, G., 2008. Seismic tomography of Central Sao Miguel, Azores, *Phys. Earth Plan. Int.*, 167, 8-18.

<http://yerbilimleri.mta.gov.tr/anasayfa.aspx>

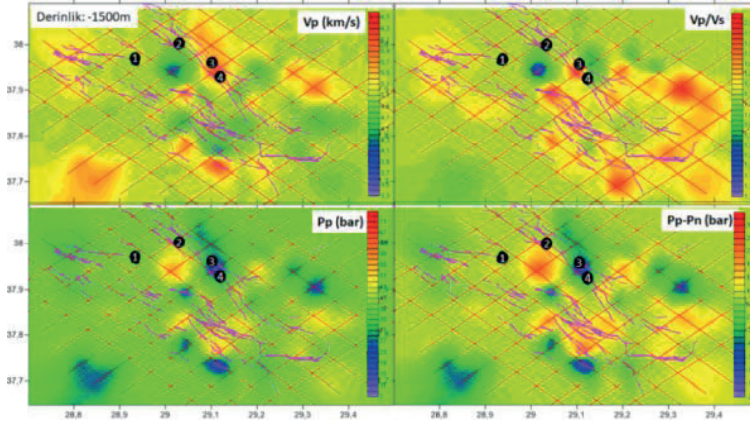
**Anahtar Kelimeler:** 3-B sismik hız tomografisi, Boşluk basıncı

Şekil-1



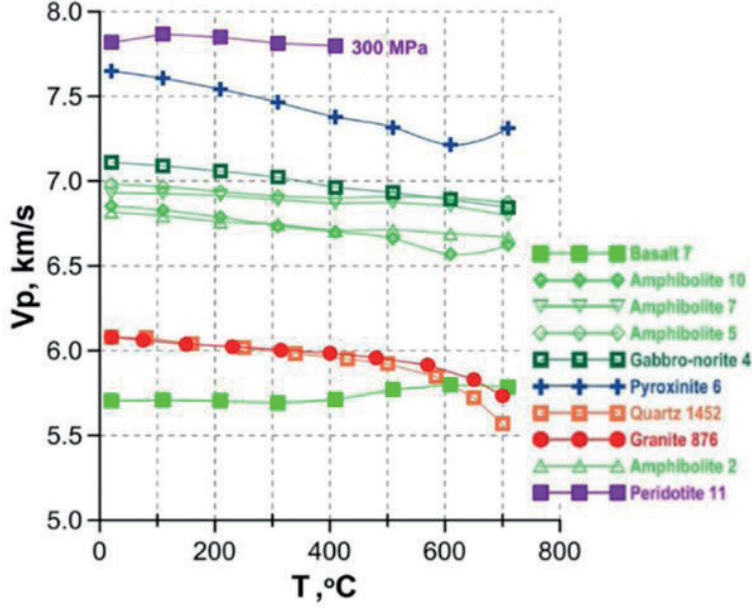
Şekil 1: a) TÜBİTAK-MAM YDBAE tarafından 3-29.09.2000 tarihleri arasında bölgeye yerleştirilmiş istasyonlar (üçgenler) ve kaydedilen mikro depremlere ait lokasyonlar (daireler). Kalın çizgiler ana fay zonlarını, siyah-beyaz bayraklar ise mevcut sıcak su noktalarını göstermektedir (Kaypak ve Gökçaya, 2012'den alınmıştır), b) Denizli havzasının jeoloji haritası (Kaynak: <http://yerbilimleri.mta.gov.tr/anasayfa.aspx> den değiştirilerek alınmıştır)

Şekil-10



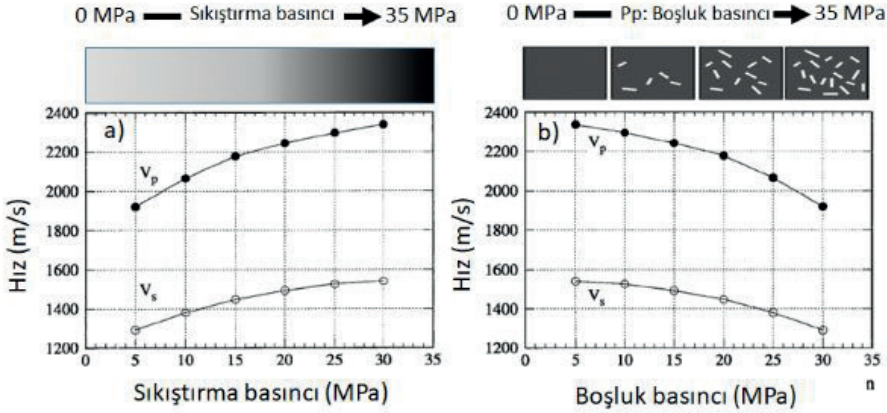
Şekil 10: -1500m kotundaki seviyemin  $V_p$ ,  $V_p/V_s$ ,  $P_p$  ve  $P_p - P_n$  kat haritasının karşılaştırılması

Şekil-2



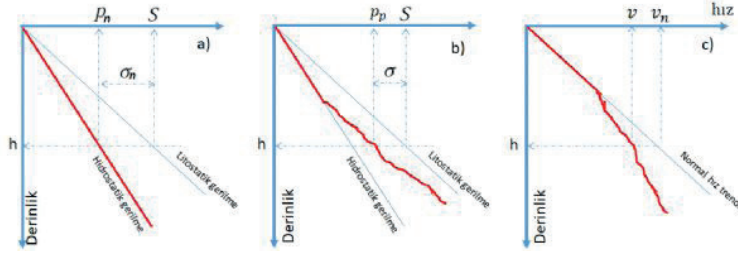
Şekil 2: Kuru koşullarda ve 600 MPa basınç altında kayaçların  $V_p$  hızlarının sıcaklığa bağlı değişimi (Kern 1978, Kern 1979, Lebedev ve diğ. 2021, Popp and Kern 1993)

Şekil-3



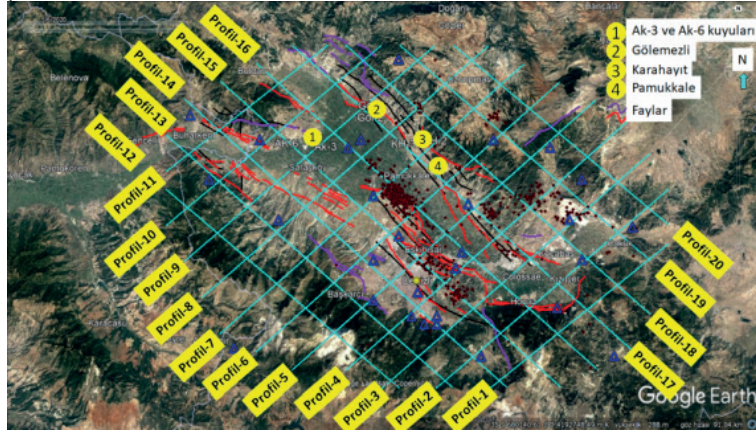
Şekil 3: (a)  $V_p$  ve  $V_s$  hızlarının sıkıştırma basıncına göre değişimi, (b)  $V_p$  ve  $V_s$  hızlarının boşluk basıncına göre değişimi (Blangy 1992'den düzenlenmiştir)

Şekil-4



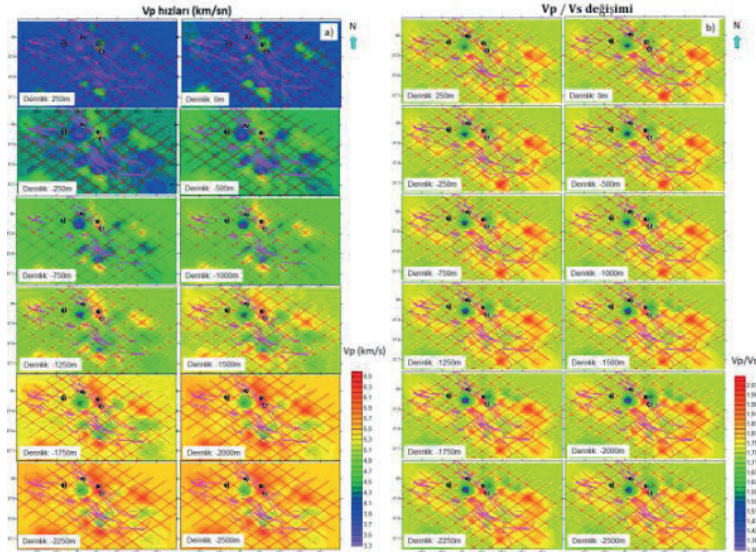
Şekil 4: (a) Normal gerilme ve (b) boşluk basıncı durumuna göre gerilmeler; (c) sismik hızla ilişkisi

Şekil-5



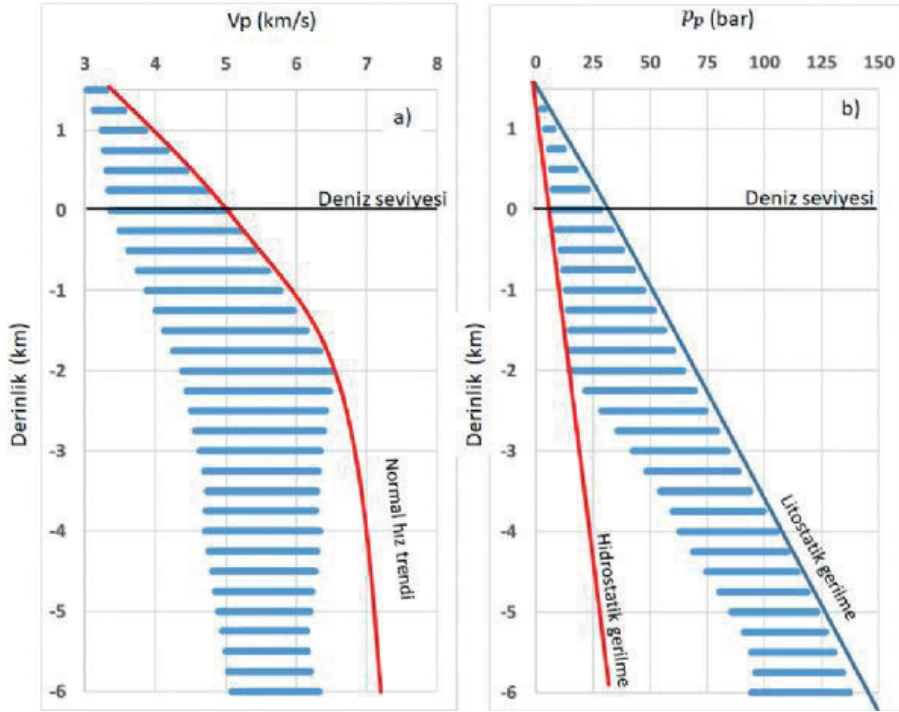
Şekil 5: Denizli havzasında elde edilen hız verisinin sunumu için profiller (Google Earth programı)

Şekil-6

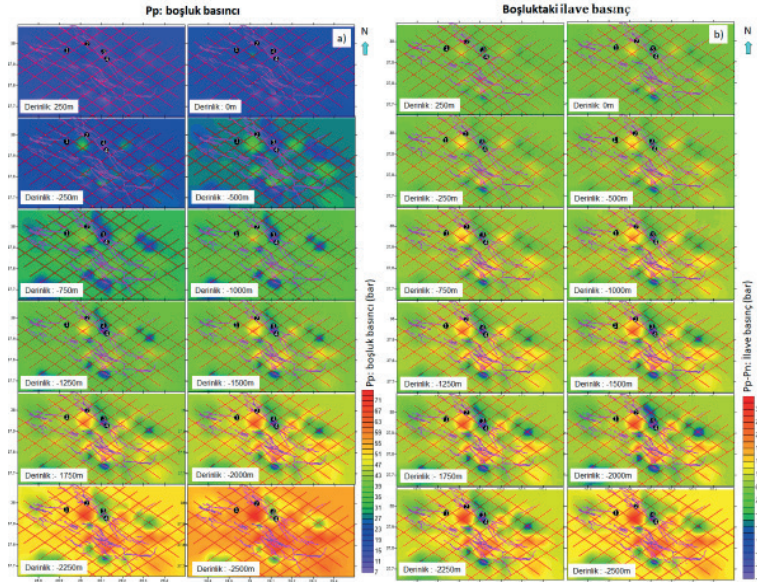


Şekil 6: (a) Sismik hız kat haritası ve (b)  $V_p/V_s$  oranı değişim

Şekil-7

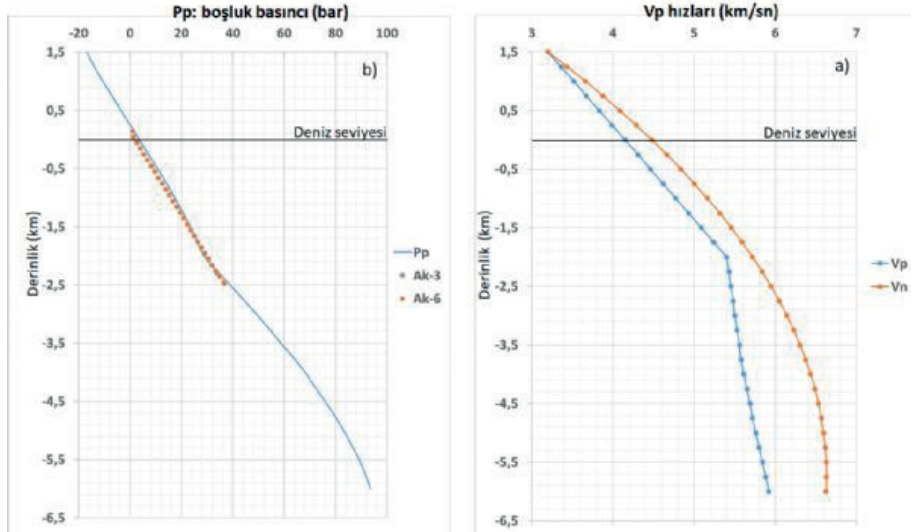
Şekil 7: Denizli havzasında deprem kayıtlarından elde edilmiş (a)  $V_p$  hızları ve (b) hızlardan elde edilmiş boşluk basıncı değerleri

Şekil-8



Şekil 8: Şekil 7'deki hızları kullanarak aynı kat haritalarından elde edilmiş (a) boşluk basıncı ve (b) ilave basınç haritası

Şekil-9



Şekil 9: (a) Profil-9 üzerindeki Ak-3 ve Ak-6 kuyularına en yakın noktadaki Vp ve Vn hızları, (b) Bu hızlardan elde edilen boşluk basıncı ve kuyulardaki basınç değerlerinin karşılaştırılması

# A Numerical Toolkit for Optimization of Model Parameters for Tracer Tests



**Doğuhan Barlas Sevindik<sup>1</sup>, Ali Berkay Tokel<sup>1</sup>, Selçuk Erol<sup>2</sup>, Serhat Akın<sup>1</sup>**

<sup>1</sup>Middle East Technical University, Ankara / Türkiye

<sup>2</sup>Izmir Institute of Technology, Izmir / Türkiye

Interpretation of tracer tests based on the analytical solutions is an essential step for the characterization of subsurface reservoirs. In that manner, initial screening tools are needed to be incorporated for automated calibration of the model parameters rather than intuitive calibration approaches. In this study, a Python-based non-linear optimization package is presented, which implements different analytical models and non-linear optimization methods. The developed numerical package has been tested for two different case studies. It has been observed that the performance of the package agrees well with the observations; hence, the developed tool can be readily used for tracer test interpretations.

## 1. INTRODUCTION

Analytical models based on the convection-dispersion-diffusion equation play a crucial role in the characterization of subsurface mass transport in porous media, complementing numerical simulation models by offering valuable insights into parameters such as the Peclet number and dispersivity, which are essential for understanding subsurface processes. These parameters, which describe the transport behavior, cannot be readily obtained from numerical simulators. By incorporating analytical models alongside numerical simulations, a more comprehensive understanding of subsurface mass transport can be achieved, aiding in improved characterization and analysis. The convection-dispersion-diffusion equation displayed in Figure 1 where  $c$  denotes the solute/tracer concentration,  $t$  is time,  $R$  is the retardation factor,  $D_{x,y,z}$  are hydrodynamic dispersion coefficients,  $u_{x,y,z}$  are the Darcy velocities along the respective direction and  $s$  is the production term respectively.

Although, based on the convection-dispersion-diffusion equation, numerous analytical solutions have been presented (Van Genuchten, 1982, Bullivant and O'Sullivan, 1989, Erol et al. 2022), which differ in analyzed geometry, dimensionality, medium properties, and boundary conditions, those analytical solutions still require accurate parameter estimation methods for adequately describing the hydraulic properties of the subsurface reservoirs.

The parameter estimation procedure can either be accomplished by a trial-and-error procedure, which could be a tedious implementation. On the other hand, the usage of linear or non-linear optimization methods is handy for automating the calibration process. Several studies have been carried out for the parameter estimation based on the analytical solutions of the convection-dispersion-diffusion equation including the Levenberg-Marquardt algorithm (Bullivant and O'Sullivan, 1989) and non-linear least-squares approximation (Akin, 2001). In this study, a Python toolkit for non-linear

parameter estimation is presented by using different non-linear optimization methods including the Nelder-Mead algorithm (Nelder and Mead, 1965), Powell's method (Powell, 1964), and Levenberg-Marquardt algorithm (Levenberg, 1944, Marquardt, 1963). Furthermore, four distinct analytical models are used to determine the transport parameters for parameter estimation including the single-fracture and multi-fracture model (Fossum and Horne, 1982), the fracture-matrix model (Bullivant and O'Sullivan, 1989), and the uniform porous model (Sauty, 1980). A modified Cauchy loss function has been used as the loss function to deal with the outlier values and hyperparameter tuning has been performed. Lastly, the developed package has been tested for two different tracer breakthrough curves (BTC) of a conducted slug tracer injection test, and the results are analyzed accordingly.

## 2. METHODOLOGY

### 2.1. Analytical Models

#### 2.1.1. Multi-Fracture Model

The multi-fracture model presented by Fossum and Horne, (1982) describes the solute transport between the injection and production well along  $n$  number of fractures which can be used for describing transport along a single-fracture or more. The one-dimensional dispersion occurs due to both the high velocity and the presence of molecular diffusion along the fracture. The multi-fracture analytical model has been presented in Figure 2 for which  $C_i$  denotes the transfer function,  $C_r$  is the tracer concentration,  $R_i$  is the apparent fracture length,  $u_i$  is the velocity,  $t_{mi}$  is the mean arrival time and  $Pe_i$  is the Peclet number of the  $i^{\text{th}}$  flow channel respectively.

#### 2.1.2. Fracture-Matrix Model

The fracture-matrix model developed by Bullivant and O'Sullivan, 1989, describes the tracer transport along a single fracture including the fracture-matrix interaction (Figure 3). The tracer transfer can occur between the fracture and the matrix in both ways, however, longitudinal transport only occurs along the fracture and not through the matrix. Furthermore, the model ignores the longitudinal dispersion along the fracture channel. In the fracture-matrix model indicated in Figure 3,  $U$  denotes the Heaviside step distribution,  $w$  is the ratio of transport along the fracture to transport out of the fracture, and  $t_b$  is the response start time.

### 2.1.3. Uniform Porous Model

The uniform porous model, proposed by Saaty in 1980, addresses the hydro-dispersive transport of tracers in one-dimensional and two-dimensional systems, considering both continuous and instantaneous injection schemes. This model describes the mass transport between an injection well and an observation well, with the kinematic dispersion serving as the dominant component. Notably, the models developed for continuous and instantaneous injection schemes exhibit noteworthy differentiation when the Péclet numbers are below 10. The solution for the 1D instantaneous tracer injection is given in Figure 4.

## 2.2. Optimization Package

The parameter estimation procedure of the analytical models with the described optimization methods was implemented in Python. Although different sets of optimized parameters and derived parameters can be chosen for each analytical model, the developed toolkit follows the parameter sets described by Akin, 2001. Table 1 presents the optimized parameters during function minimization as well as the derived parameters for each analytical model respectively.

In Table 1, in terms of optimized parameters,  $Pe$  is the Peclet number,  $t$  is the mean arrival time in days,  $e$  is the flow contribution coefficient of individual fractures,  $w$  is the ratio of transport along the fracture to transport out of the fracture,  $T$  is the response start time in days and  $J$  is a model parameter for each analytical model respectively. On the other hand, in terms of derived parameters,  $m$  is the mass entering the stream tube,  $D$  is the longitudinal dispersion coefficient in  $m^2/day$ ,  $u$  is the flow velocity in  $m/day$ , and  $\alpha$  is the mechanical dispersivity in  $m^2$ .

Furthermore, the loss function used in the optimization methods is chosen to be a modified version of the Cauchy loss function (CLF) indicated in Figure 5 since the actual values observed in the real systems can bear occurrences of both noise and outliers (Mlotshwa et al., 2022). In Figure 5,  $L$  denotes the Cauchy loss function,  $y$  is the model value,  $Y$  is the predicted value,  $c$  is the hyperparameter of the Cauchy loss function that controls the sensitivity to outliers.

The optimization package requires nine inputs from the user regardless of the analytical model desired to be used. In terms of output control, four different outputs are generated by the optimization package for each analytical model respectively. The workflow for the optimization package is indicated in Figure 6.

Firstly, the optimization package requires the user for the selection of the described analytical models followed by a general set of inputs. Those inputs include the initial guess matrix with distinct parameters indicated in Table 1, the observation file directory containing the time-dependent tracer concentrations either in an Excel file or a text file, and the desired optimization method. Furthermore, case-specific inputs are required, which include the distance between the injector and producer,

the mass production rate of the producer, and the observed maximum tracer concentration. An important consideration is that the maximum tracer concentration is only needed to be defined during the execution of 1D or 2D Homogenous analytical models. Furthermore, a matrix for the parameter search range can be defined not only for avoiding unrealistic parameter estimates, for instance,  $Pe=0$ , but also to enable the user to pre-define a desired parameter search space. Furthermore, a search range for the hyperparameter,  $c$ , in the Cauchy loss function is needed to be defined for tuning the hyperparameter for accurately capturing the noise present in the data. Finally, a time duration can be inputted into the package for how long the BTCs are desired to be calculated based on the optimized model, unless, the time-dependent concentrations are calculated until the last observation time.

Secondly, in terms of model outputs, the optimized parameter and derived parameter matrixes are stored in a text file as well as the best SSE value for the optimized model. Furthermore, the resulting BTC for the inputted time duration is displayed and saved to the same file directory.

During the non-linear optimization, the analytical models besides the multi-fracture model are subjected to an unconstrained optimization for the minimization of the loss function; however, according to the multi-fracture model, the flow contribution coefficients must be summed up to 1 hence, it cannot be treated as an unconstrained optimization. The aforementioned optimization methods, the Nelder-Mead method, and Powell's method can only be implemented in unconstrained problems without using a penalty term which increases the computational cost of the optimization, the only method which is available for the minimization of the loss function for the multi-fracture model is the Levenberg-Marquardt algorithm. Thus, the selection of the initial guesses is needed to be more meticulous since the convergence of the Levenberg-Marquardt algorithm is more sensitive to the initial parameter guesses compared to the remaining two algorithms.

## 3. RESULTS AND DISCUSSION

For the implementation of the optimization package, a slug 2-6-naphthalene-disulphonate tracer injection test with 200 kilograms of tracer injection conducted in a geothermal reservoir located in Western Anatolia has been used as the field data for 176 days of sampling. The demonstration of the package is going to be presented in the upcoming sections for the collected tracer concentration history of two different production wells as two distinct case studies respectively. For each demonstration, during the non-linear optimization, each aforementioned optimization method has been incorporated alongside the multi-fracture model, single-fracture model, fracture-matrix model, and the 1D homogenous model respectively.



### 3.1. Case Study 1

For the first case study, a production well located roughly 485 meters away from the injection well has been selected with a total 2-6-naphthalene-disulphonate recovery of approximately 14.85 kilograms alongside a peak tracer concentration of 49.85 ppb. The resulting optimized parameters, derived parameters, and the SSE values for each analytical model are displayed in Table 2 as well as the tracer BTCs in Figure 7 for a time duration of 200 days.

Firstly, the multi-fracture solution can fit the data by using two fractures with a first arrival time of the tracer in 16 days. The characteristics of those fractures differ from one another one being a dominant factor while fitting the advective front of the tracer arrives to the well with a high Peclet number of 27.1 and the secondary fracture displaying a later breakthrough time with lower velocity and a Peclet number of 3.13 indicating a low permeable and more storativity along this fracture as the mass entering the stream tube in this fracture is significantly larger. The single-fracture model displays an earlier first arrival time of the tracer compound with 12 days for which the flow velocity and the Peclet number are smaller than the overall multi-fracture model to match the tailing of the breakthrough curve better. Although the fracture-matrix model displays the latest first arrival time of the tracer with 24 days due to the fracture-matrix model being more sensitive to the observations for the first arrival time of the tracer, the early breakthrough time of the tracer is caught by the model indicating a fast advective front velocity of the tracer along the fracture as a high value of the  $w$  parameter is obtained meaning the transport along the fracture is significant between the wells. Note that as the first arrival time is not certain with observations, the parameter  $w$  can be even larger with an earlier response start time. Lastly, the 1D Homogenous model yielded similar results to the single fracture model with a little bit more advection dominating the transport between the wells.

### 3.2. Case Study 2

For another demonstration of the optimization package, a production well with 720 meters of distance between the injection well alongside a total tracer recovery of approximately 2.19 kilograms and a peak tracer concentration of 7.56 ppb has been selected. The resulting optimized parameters, derived parameters, and the SSE values for each analytical model are displayed in Table 3 as well as the tracer BTCs in Figure 8 for a time duration of 200 days.

Furthermore, like in the case of the previous production well, 2 fractures are suitable during the multi-fracture solution for the well where the first tracer arrives at the well in 18 days according to the model. Although the overall Peclet number is obtained as 19.71, the majority of the tracer that enters the stream tube is transported to the fracture where the fluid velocity is considerably lower than the other which corresponds to a fast advective front and a long tailing section in

the breakthrough curve. In the single-fracture model, a slower fluid velocity has been observed along the fracture compared to the multi-fracture model. A more dominant dispersive transport with similar storativities compared to the multi-fracture model resulted since the fast advective front of the tracer with a long tailing section restricts the single-fracture model in terms of capturing both. The fracture-matrix model yielded similar results with previous production well where it captures the fast advection and long tailing of the breakthrough curve where the  $w$  parameter yielded a value of 0.57 meaning that there exists some degree of flow out of the fracture alongside the flow along the fracture. Lastly, the 1D Homogenous model resulted in a Peclet number of 4.78 indicating that dispersive transport is a dominant mechanism along the flow paths between the injector and the producer.

## CONCLUSION

A user-friendly numerical optimization package for the interpretation of tracer tests has been developed by using different optimization methods and analytical models. The developed package has been verified by testing the models for the tracer concentration histories of two observation wells for a slug tracer test conducted in a geothermal reservoir. It has been observed that the developed numerical package successfully matches the observation data for both cases. Thus, it has been concluded that the proposed numerical package can be used as an interpretation tool for the estimation of the parameters which govern the mass transport in a geothermal reservoir.

## ACKNOWLEDGMENTS

This paper has received funding from the European Union's Horizon 2020 research and innovation program Grant Agreement No.818169-GECO. This publication reflects the views only of the authors, and the Commission cannot be held responsible for any use which may be made of the information contained therein. The authors would like to thank the Zorlu Energy staff for providing the tracer test data.

## REFERENCES

- Akin, S. (2001). Analysis of tracer tests with simple spreadsheet models. *Computers & Geosciences*, 27(2), 171–178. [https://doi.org/10.1016/s0098-3004\(00\)00084-4](https://doi.org/10.1016/s0098-3004(00)00084-4)
- Bullivant, D.P., O'Sullivan, M.J., 1989. Matching a field tracer test with some simple models. *Water Resources Research* 25 (8), 1879–1891.
- Erol, S., Bayer, P., Akin, T., & Akin, S. (2022). Advanced workflow for multi-well Tracer test analysis in a Geothermal Reservoir. *Geothermics*, 101, 102375. <https://doi.org/10.1016/j.geothermics.2022.102375>
- Fossum, M.P., Horne, R.N., 1982. Interpretation of tracer return profiles at Wairakei geothermal field using fracture analysis. *Geothermal Resources Council*,

Transactions 6, 261–264.

Levenberg, Kenneth (1944). “A Method for the Solution of Certain Non-Linear Problems in Least Squares”. Quarterly of Applied Mathematics. 2 (2): 164–168. doi:10.1090/qam/10666

Marquardt, Donald (1963). “An Algorithm for Least-Squares Estimation of Nonlinear Parameters”. SIAM Journal on Applied Mathematics. 11 (2): 431–441. doi:10.1137/0111030.

Mlotshwa, T., van Deventer, H., & Bosman, A. S. (2022). Cauchy Loss Function: Robustness Under Gaussian and Cauchy Noise. In Southern African Conference for Artificial Intelligence Research (pp. 123-138). Cham: Springer Nature Switzerland.

Nelder, J. A., & Mead, R. (1965). A simplex method for function minimization. The Computer Journal, 7(4), 308–313. https://doi.org/10.1093/comjnl/7.4.308

Powell, M. J. D. (1964). “An efficient method for finding the minimum of a function of several variables without calculating derivatives”. Computer Journal. 7 (2): 155–162. doi:10.1093/comjnl/7.2.155. hdl:10338.dmlcz/103029

Sauty, J.P., 1980. An analysis of hydrodispersive transfer in aquifers. Water Resources Research 16 (1), 145–158.

Van Genuchten, M. T. (1982). Analytical solutions of the one-dimensional convective-dispersive solute transport equation (No. 1661). US Department of Agriculture, Agricultural Research Service.

Keywords: numerical optimization, tracers

Figure 1 Convection-dispersion-diffusion equation.

$$R \frac{\partial c}{\partial t} = (D_x \frac{\partial^2 c}{\partial x^2} + D_y \frac{\partial^2 c}{\partial y^2} + D_z \frac{\partial^2 c}{\partial z^2}) - u_x \frac{\partial c}{\partial x} - u_y \frac{\partial c}{\partial y} - u_z \frac{\partial c}{\partial z} + s$$

Table 1 Optimized and derived parameters for each analytical model.

Model	Optimized Parameters	Derived Parameters
Single-fracture	Pe, J, t	m, D, u
Multi-fracture	Pe, J, t, e	m, D, u
Fracture-matrix	w, T, J	m
1D Homogenous	Pe, t	alpha, D, u

Figure 2 Multi-fracture model (Fossum and Horne, 1982)

$$C_t = \sum_{i=1}^n e_i C_r \left( \frac{R_i}{u_i}, Pe_i \right)$$

$$C_r = J \frac{1}{\sqrt{t}} \frac{2tm}{t} \exp \left( \frac{-Pe \cdot (t - t_m)^2}{4t_m t} \right)$$

Table 2 Results of each analytical model for the first production well.

Model	Pe	J	t	D	u	SSE
Multi-fracture	14.26	210.43	85.11	283.52	6.91	167
Single-fracture	4.41	132.35	96.48	550.57	5.02	428
Fracture-matrix	w	J	T			
	0.44	29067.1	17.52			185
1D Homogenous	Pe	t	alpha	D	u	
	6.35	61.62	76.20	598.36	7.85	652

Figure 3 Fracture-matrix model (Bullivant and O'Sullivan, 1989)

$$C_r = JU(t - t_b)^{-\frac{1}{2}} \exp\left(\frac{-t_b}{w(t - t_b)}\right)$$

Table 3 Results of each analytical model for the second production well.

Model	Pe	J	t	D	u	SSE
Multi-fracture	19.72	37.79	56.35	283.22	10.47	4.10
Single-fracture	3.16	19.84	95.61	781.70	5.08	13.24
Fracture-matrix	w	J	T			
	0.57	3786.62	17.01			3.86
1D Homogenous	Pe	t	alpha	D	u	
	4.78	51.17	101.57	964.80	9.50	22.43

Figure 4 1D Homogenous model (Sauty, 1980).

$$C_r = \frac{K}{\sqrt{t_r}} \exp\left(\frac{-P_{e_{up}}}{4t_r} (1 - t_r)^2\right)$$

Figure 5 Cauchy loss function.

$$L(y, \hat{y}) = \log\left(1 + \left(\frac{y - \hat{y}}{c}\right)^2\right)$$

Figure 6 Workflow for the optimization package.

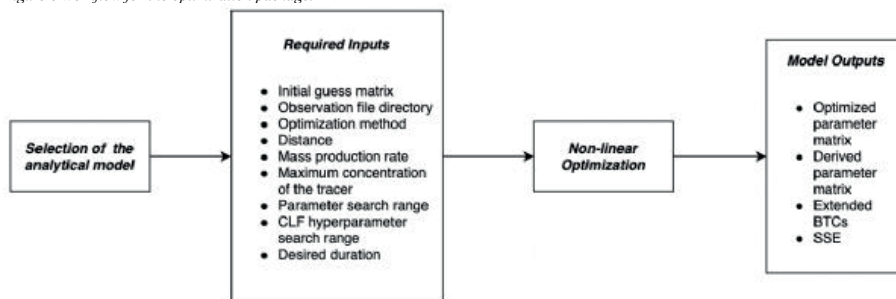


Figure 7 Tracer BTCs for the first production well.

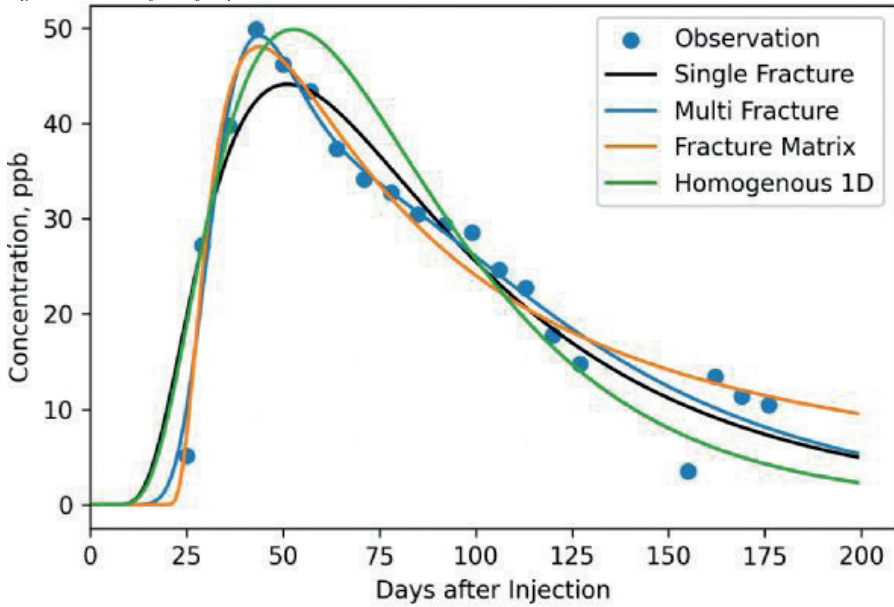
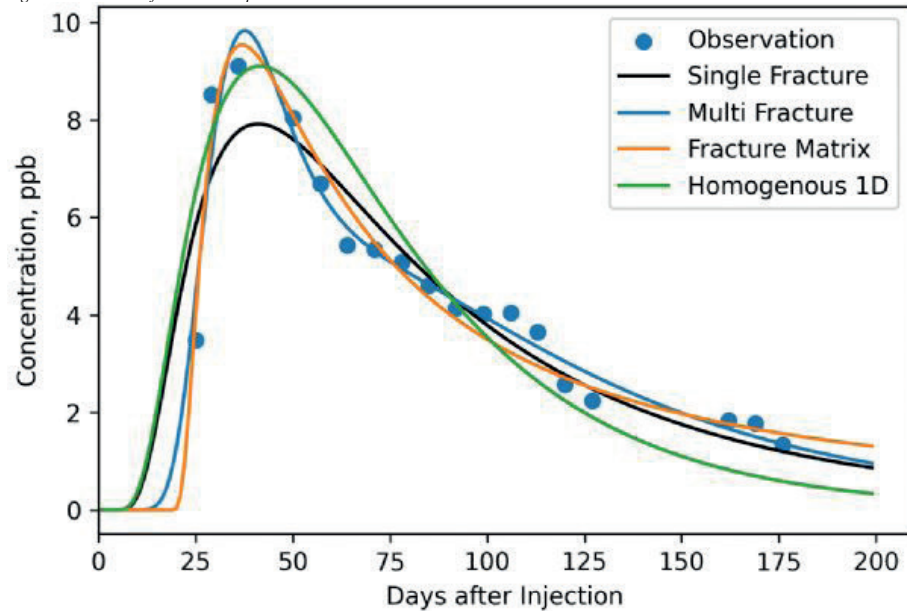


Figure 8 Tracer BTCs for the second production well.



# Carbon Utilization Potential in Geothermal Fields

**Erdinc Sentürk, Gültekin Tarcan**  
Dokuz Eylül University, İzmir / Türkiye



As the world's industries have developed and grown, the consumption of resources such as energy has increased. Along with this consumption, activities that affect the material and thermal balance of natural cycles in various fields for various purposes have become possible. Carbon, which is a substance that has its natural cycle disrupted as a result of these processes, is one such example. In particular, carbon dioxide produced from processes such as energy, agriculture, and land use disrupts this balance. In addition to carbon dioxide, this group of gases, which are known as greenhouse gases, including methane, nitrogen monoxide, and other gases, have the potential to harm the current world order. In particular, when these gases are released into the atmosphere as a result of various processes, the gas capsule created by these gases causes heat to be trapped around the Earth, causing the temperature on the Earth to rise. This increase is not the result of natural processes and has a risk-impact range that extends from major natural disasters to the extinction of living species. For this reason, large agreements and action plans have been created to reduce emissions. One aspect of these plans, which are shaped primarily around reducing emission-increasing activities, is the conversion of emissions into storage or use inputs in different areas. The first studies in this context began with natural gas production plants, and today they are mostly carried out with petroleum and gas production projects. However, with the development of technology and production diversity, there are also potential application areas in the geothermal energy field, which offers options for energy production, for the use and storage of carbon. In this study, a general overview and evaluation of carbon capture, utilization and storage applications will be made from the perspective of geothermal energy.

**Keywords** geothermal, carbon, capture, utilization, storage, ccus

Gelişen ve büyüyen endüstrilerin oluşması ile birlikte Dünya' da enerji başta olmak üzere öz kaynakların tüketimi artmıştır. Bu tüketimle birlikte farklı amaçlar dahilinde farklı alanlarda doğal döngülerin materyal ve ısıl dengesini etkileyen faaliyetler yapılması söz konusu olmuştur. Bu süreçler sonrası doğal döngüsü bozulmakta olan bir madde de karbondur. Özellikle enerji, tarım ve toprak kullanımı gibi süreçler sonrası mevcut proseslerden ortaya çıkan karbondioksit bu dengeyi bozmaktadır. Karbondioksitin yanı sıra sera gazları olarak genel ismiyle anılan metan, diazot monoksit gibi diğer gazları da içeren bu grup gazlar mevcut Dünya düzenine zarar verebilecek niteliktedir.

Özellikle bu gazların çeşitli prosesler sonunda atmosfere salınması durumunda, bu gazların oluşturduğu gaz kapsülü Dünya üzerinden etrafına yayılacak ısının hapsolmesine ve dolayısıyla yeryüzündeki sıcaklığın artmasına sebep olmaktadır. Bu artış doğal süreçlerin

sonucu olmadığı üzere; büyük doğa felaketlerinden, canlı türlerinin yok olmasına kadar uzanan bir risk-etki alanına sahiptir. Bu sebepten emisyonların azaltılması noktasında büyük ölçekli anlaşma ve aksiyon planları oluşturulmuştur. Temelde emisyon artırıcı faaliyetlerin azaltılması ekseninde şekillenen bu planların bir ayağı da emisyonların depolama ya da farklı alanlarda kullanım girdilerine çevrilmesidir. Bu kapsamda yapılan ilk çalışmalar doğal gaz üretim tesisleriyle başlamış günümüzde de ağırlıklı petrol ve gaz üretim projeleriyle birlikte yürütülmüştür. Bununla birlikte gelişen teknoloji ve üretim çeşitliliği ile enerji üretimi noktasında opsiyon sağlayan jeotermal enerji alanında da karbon kullanma ve depolama konusunda potansiyel uygulama alanları mevcuttur. Bu çalışmada karbon yakalama kullanma ve depolama uygulamalarına jeotermal enerji perspektifinden genel bakış ve değerlendirme yapılacaktır.

**Anahtar kelimeler:** jeotermal, karbon, yakalama, kullanım, depolama

## INTRODUCTION

Arising industrial revolutions through the last century has started to show several complications. These complications are associated with the industrial processes that are musts for the daily life we knew of. One and maybe the most severe complication that of those is climate change. Climate change is a process that the ongoing human-made activities affect and distort the rhythm of the natural activities of Earth. As we describe in this context, climate change is a result of human-made activities. On the other hand, it will be a cause for a great variety of events that could hinder the life on Earth irreversibly if it is not taken care of. Extinction of species, devastating natural hazards are major examples of the end results due to climate change. To solve this issue, we need to know the reasons of climate change. Fortunately, it has a simple and clear explanation. There are some gases in Earth's atmosphere forming a layer or a capsulation. These gas are called greenhouse gases(GHG) and are trapped in atmosphere and absorbs some of the heat radiating from Earth surface to space. Although it is a naturally occurring phenomenon, during production or processing of different materials or resources additional amount of these gases come out as the product of the reactions took place in that process and are emitted to atmosphere. This additional gas cause additional warming up at Earth's surface and this temperature increase holds severe risks for life on Earth.

Amongst different GHGs, the most dangerous one, in terms of global warming potential and volumetric contribution to the composition is CO<sub>2</sub>(Figure 1).

CO<sub>2</sub> and other GHGs are emitted by different industrial sectors and processes. Major sectors that emit GHGs are energy, agriculture, forestry and land-use, waste management, chemical production (H. Ritchie, M. Roser and P. Rosado, 2020)

As mentioned, CO<sub>2</sub> is the largest contributor to global warming. Annual CO<sub>2</sub> emissions from fossil fuels and industrial production reach to all time high level at over 35 billion tonnes, which was below 5 billion tonnes at the beginning 19th century (Figure 2).

With this sharp increase global temperature average increased parallelly compared to baseline of pre-industrial baseline reaching a total of 1.1°C in nearly 110 years (Figure 4). All of these developments seem to be a disastrous scenario, but it could be even worse if the actions needed would not be applied immediately which is obviously reducing emissions to lower levels to preserve the warming up as it is.

## METHODOLOGY

### 1. Conventional CCUS

In conventional applications of CCUS, CO<sub>2</sub> is captured from any production process with several methods. After it is captured at production facility, it is transferred to facilities that could process CO<sub>2</sub> for any other use in different manufacturing processes or transferred to oilfields for utilizing in enhanced recovery orientation, or transferred to onshore and offshore storage sites for removal purposes (Figure 3).

The first industrial CCUS application which is still ongoing between Val Verde Natural Gas Production Site to Sharon Ridge Oilfield in US commissioned in 1972. In this project captured CO<sub>2</sub> from Val Verde Natural Gas Production Facilities is transferred to Sharon Ridge Oilfield and used in enhanced oil recovery operations (H. Carr, 2021).

From first case to today, there are 137 CCUS projects which could be categorized as conventional applications, and expected to be more in near future with climate change action plans (CCUS projects footprint, Map of Global CCS Projects, 2022).

#### 1.1. Capture

First process of a CCUS application, capturing CO<sub>2</sub> from the operating system. As in conventional CCUS applications the interested facilities are fossil fuel based energy production facilities, it will involve a combustion procedure. In this process, there are two options to capture CO<sub>2</sub>, which are capturing it before the combustion and capturing it after the combustion. Compared to these alternatives there is another option which involves another set of reactions for capturing CO<sub>2</sub> is oxyfuel combustion. All of these methods are valid and effective in terms of capturing mechanism, but captured CO<sub>2</sub> concentrations vary amongst them (Figure 4).

### 1.2. Utilization and Storage

Once CO<sub>2</sub> is captured, it is transferred to facilities at which CO<sub>2</sub> could be used in different processes or injected to underground formations. Utilization of CO<sub>2</sub> in this aspect, has a great variety of applications in different categories such as biological conversion, chemical, refrigerant, inerting agent, food products. In all of those different applications, captured CO<sub>2</sub> needs to be processed in terms of purification to be able to produce desired product. On the other hand, captured CO<sub>2</sub> could be used directly in storage purposes in which purification is only needed to adjust gas properties to desired injection conditions. In addition to underground storage option, also utilizing CO<sub>2</sub> in enhanced oil recovery as flooding serves to decrease CO<sub>2</sub> emissions as well while creating additional value to current operations.

## 2. Geothermal CCUS

A geothermal system, in classical definition consists of common and basic features as; a heat source to heat the geothermal fluid, a recharge to create and sustain a reservoir, a cap rock that insulates the heat in the geothermal reservoirs. Geothermal fluid in that definition contains some amount of non-condensable gases (NCG) including CO<sub>2</sub>. These gases are originated from three different sources. Firstly, it could have a meteoric origin from the recharge of the geothermal system. Secondly, it could be related to heat source, a magmatic origin. And lastly, it could be originated from the host rocks mostly carbonates (F. Thráinn et al., 2017).

Although the amount of CO<sub>2</sub> emission in geothermal energy production is much less compared to fossil fuel energy production (Carbon emissions of power plants, What are the greenhouse gas emissions of a mini-grid project and how are they calculated?, 2022), geothermal fields could host different CCUS applications for reducing emissions for itself and other industries.

As summarized in Figure 5, geothermal CCUS pathway has options and adaptations that could help solve the climate change problem to some extent. In geothermal fields, CO<sub>2</sub> that is processed in the geothermal power plants, atmospheric CO<sub>2</sub> and captured transferred CO<sub>2</sub> could be used in different utilization and storage applications. Mostly up-to-date applications of utilization of CO<sub>2</sub> in geothermal fields is limited to injection and storage purposes. Some of those applications could be listed as;

GECO (Geothermal Emission Control) project in which at 4 different fields CO<sub>2</sub> injection was tested within different geological structures and thermodynamic processes (GECO Demo-Sites, 2021).

Ngatamariki geothermal field CO<sub>2</sub> capture and injection trial in which Mercury, operator company has accomplished nearly %100 of injection of CO<sub>2</sub> back into reservoir within 7 months of trial period (A. Richter, 2022).

## 2.1. Capture

In geothermal power plants, there are several technologies to produce electricity; dry steam, flash steam, binary and combined systems. For flash power plants especially, non condensable gas handling is a process that could affect efficiency of the system. For this reason, specific NCG removal systems are used. In many applications, injectors and vacuum pumps are used to collect NCG from the different stages of the process (Figure 6).

## 2.2. Utilization and Storage

Once NCG is captured, it could be utilized and stored underground for different purposes. Sequestration of CO<sub>2</sub> in geologically favored fields could be applied for removal purposes. In those fields it is also possible to collect/capture atmospheric CO<sub>2</sub> or use fossil based transferred CO<sub>2</sub> for sequestration. Carbfix and Climeworks (Figure 7) projects in Iceland are two examples of sequestration applications could be took place at geothermal fields.

Addition to storage applications, utilization of CO<sub>2</sub> to create additional value to current operations is promising area that likely to be growing more in near future. There could be several options to utilize CO<sub>2</sub> in geothermal applications. First CO<sub>2</sub> and other NCGs play a crucial role for wellbore performance. As these gases expand in wellbore, they carry geothermal fluid to surface with this expansion by decreasing the weight of fluid column that reservoir pressure needs to overcome. In this regard, there are other parameters as temperature, productivity, index and flowrate in addition to reservoir pressure and gas content of geothermal fluid. Another utilization method for wellbore performance could be brine conditioning application in injection wells. As geothermal liquid has high contents of minerals and processed at different pressure and temperatures, from production to injection there is a risk of precipitation. In this regard, CO<sub>2</sub> charged brines could be used to regulate conditions that affect mineral precipitation by controlling the pH of the brine.

As we produce geothermal fluid and remove NCGs at the power plant process emission to atmosphere, mass balance of gas content in reservoir becomes uneven. Since after removal of gases, injected fluid does not contain any amount NCG or negligible amount of NCG, with dilution effect in reservoir geothermal fluid gas content tends to decrease with production. This decrease cause a decline on well performance. Therefore utilizing CO<sub>2</sub> in injection applications to make it breakthrough to production could prevent this performance decline. A similar approach for this could be using CO<sub>2</sub> as motive fluid in a gas lifting orientation. In gas lifting, basic idea is injecting gas into flowing wellbore and creating an expansion drive of gas to producing fluid (Figure 8).

Besides of wellbore performance applications, direct electricity generation from CO<sub>2</sub> is also another application for utilizing it in geothermal systems. In a basic system, with different thermodynamics processes as compressing and heating of supercritical CO<sub>2</sub> and

generating electricity from this gas in a supercritical CO<sub>2</sub> gas turbine could be an utilizing method as such (Figure 9).

Finally, CO<sub>2</sub> could be used as working fluid for heat transfer in geothermal applications. Wellbore heat exchanger and enhanced geothermal systems are examples of this. For wellbore heat exchangers, main purpose creating a heat transfer loop inside a well while for enhanced geothermal systems it is intended to be in whole reservoir (Figure 10).

## RESULTS

In this study, an overview of carbon capture utilization and storage is given through answering questions of why it matters, what are the conventional ccus applications and how geothermal energy fits in all of these. As climate change is a significant problem for sustaining life on Earth in the form that we knew of today, it should be threatened with sufficient amount of intellectual and economical interest. In that regard, one of the important point needs to be investigated deeper and mitigated the risks and impact of possible occurrences is CO<sub>2</sub> emissions from different industries. Conventionally, CCUS involves a CO<sub>2</sub> emission source; a production facility or atmosphere, a capture mechanism; pre or post combustion and oxyfuel and utilizing in different industries as raw form or stored underground. In geothermal fields, these three could be easily connected as power plant technology involves capturing units and field and current operations serves several utilizing options such as sequestration, breakthrough to production wells via injection, using as motive fluid in a gas lifting system and in a supercritical CO<sub>2</sub> gas turbine, or working fluid in a wellbore heat exchanger and in a enhanced geothermal system doublet orientation.

## REFERENCES

- Greenhouse Gases Factsheet, (2021). 06.01.2023. <https://css.umich.edu/publications/factsheets/climate-change/greenhouse-gases-factsheet>.
- H. Ritchie, M. Roser and P. Rosado (2020). "CO<sub>2</sub> and Greenhouse Gas Emissions". 06.01.2023. <https://ourworldindata.org/co2-and-other-greenhouse-gas-emissions>.
- CO<sub>2</sub> Levels, (2019). 06.01.2023. <https://www.climatecentral.org/graphic/co2-and-the-climate-curve?graphicSet=CO2+Levels&location=Carbon+Dioxide+and+Temperatures&lang=en>.
- Carbon Capture Utilization and Storage (CCUS) (2022). 06.01.2023. <https://www.energy.gov/our-business/carbon-capture-utilization-and-storage-ccus/2/>.
- H. Carr (2021). "The Air That I Breathe, Part 3 - The U.S.'s Existing and Planned CO<sub>2</sub> Pipeline Networks". 06.01.2023. <https://rbnenergy.com/the-air-that-i-breathe-part-3-the-uss-existing-and-planned-co2-pipeline-networks>.

- Map of Global CCS Projects (2022). 06.01.2023. <https://www.iogp.org/bookstore/product/map-of-global-ccs-projects/>.
- Llamas, B., Navarrete, B., Vega, F., Elías Rodríguez, E., Mazadiego, L. F., Cámara, A., & Otero, P. (2016). Greenhouse Gas Emissions – Carbon Capture, Storage and Utilisation. In B. L. Moya, & J. Pous (Eds.), Greenhouse Gases. IntechOpen.
- F. Thráinn et al. (2017). “Greenhouse gas emissions from geothermal power production”, Proceedings 42nd Workshop on Geothermal Reservoir Engineering, Stanford University.
- What are the greenhouse gas emissions of a mini-grid project and how are they calculated?(2022). 06.01.2023. <https://www.usaid.gov/energy/mini-grids/environment-health-safety/emissions>.
- GECO Demo-Sites(2021). 19.08.2023. <https://geco-h2020.eu/demo-sites/>
- Successful tests of capturing and reinjecting geothermal CO<sub>2</sub>, NZ (2022). 19.08.2023. <https://www.thinkgeoenergy.com/successful-tests-of-capturing-and-reinjecting-geothermal-co2-nz/>
- How Iceland’s Carbfix Project is turning carbon dioxide into rock (2019). 06.01.2023. <https://www.weforum.org/agenda/2019/05/carbfix-scientists-in-iceland-are-turning-carbon-dioxide-into-rock/>.
- Direct Air Capture (2022). 06.01.2023. <https://www.carbfix.com/direct-air-capture>.
- K. Andrews (2022). “Gas Lift: How It Works, Why You Should Use It, and Equipment Required”. 06.01.2023. <https://kimray.com/training/gas-lift-how-it-works-why-you-should-use-it-and-equipment-required>.
- Sandia team puts power into local grid with supercritical CO<sub>2</sub> closed-loop Brayton-cycle turbine (2022). 06.01.2023. <https://www.greencarcongress.com/2022/08/20220822-sandia.html>.
- How Does Geothermal Energy Work? (2022). 06.01.2023. <https://www.greenfireenergy.com/how-does-geothermal-energy-work/>.

Keywords: ccus, geothermal



Figure 1 Greenhouse gases summary. Greenhouse Gases Factsheet, (2021).

Compound	Pre-industrial concentration (ppmv <sup>1</sup> )	Concentration in 2020 (ppmv)	Atmospheric lifetime (years)	Main human activity source	GWP <sup>2</sup>
Carbon dioxide (CO <sub>2</sub> )	278	413	variable	Fossil fuels, cement production, land use change	1
Methane (CH <sub>4</sub> )	0.722	1.889	12	Fossil fuels, rice paddies, waste dumps, livestock	28
Nitrous oxide (N <sub>2</sub> O)	0.27	0.333	121	Fertilizers, combustion industrial processes	265
HFC 23 (CHF <sub>3</sub> )	0	0.000024 <sup>3</sup>	222	Electronics, refrigerants	12,400
HFC 134a (CF <sub>3</sub> CH <sub>2</sub> F)	0	0.000062 <sup>3</sup>	13	Refrigerants	1,300
HFC 152a (CH <sub>2</sub> CHF <sub>2</sub> )	0	0.0000064 <sup>3</sup>	1.5	Industrial processes	138
Perfluoromethane (CF <sub>4</sub> )	0.00004	0.000079 <sup>3</sup>	50,000	Aluminum production	6,630
Perfluoroethane (C <sub>2</sub> F <sub>6</sub> )	0	0.0000041 <sup>3</sup>	10,000	Aluminum production	11,100
Sulphur hexafluoride (SF <sub>6</sub> )	0	0.0000073 <sup>3</sup>	3,200	Electrical insulation	23,500

<sup>1</sup>ppmv = parts per million by volume, <sup>2</sup>GWP = 100-year global warming potential, <sup>3</sup>Concentration in 2011  
 Water vapor not included in table, see bullet.

Figure 10 Wellbore heat exchanger & Enhanced Geothermal Systems diagram, How Does Geothermal Energy Work? (2022)

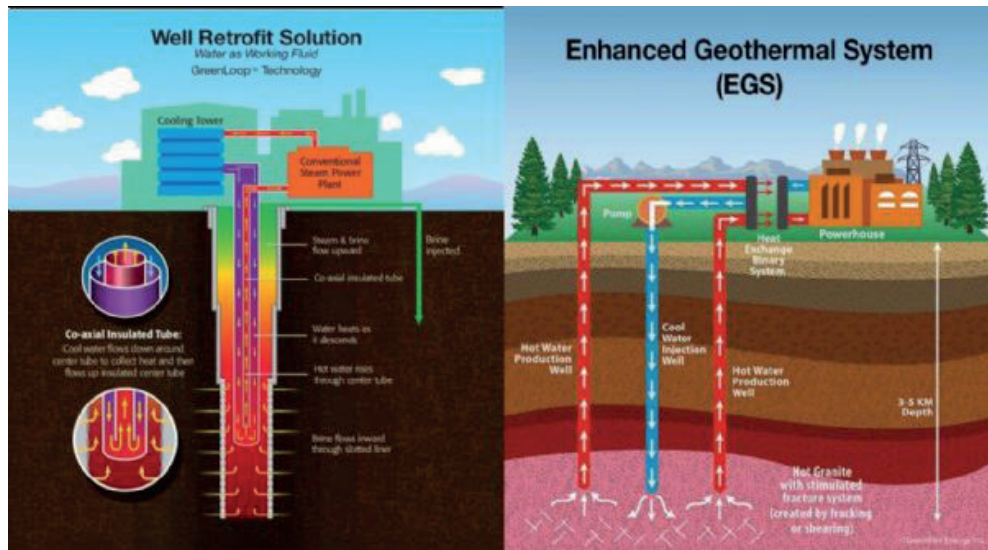


Figure 2 CO2 emissions and temperature change, CO2 Levels, (2019)

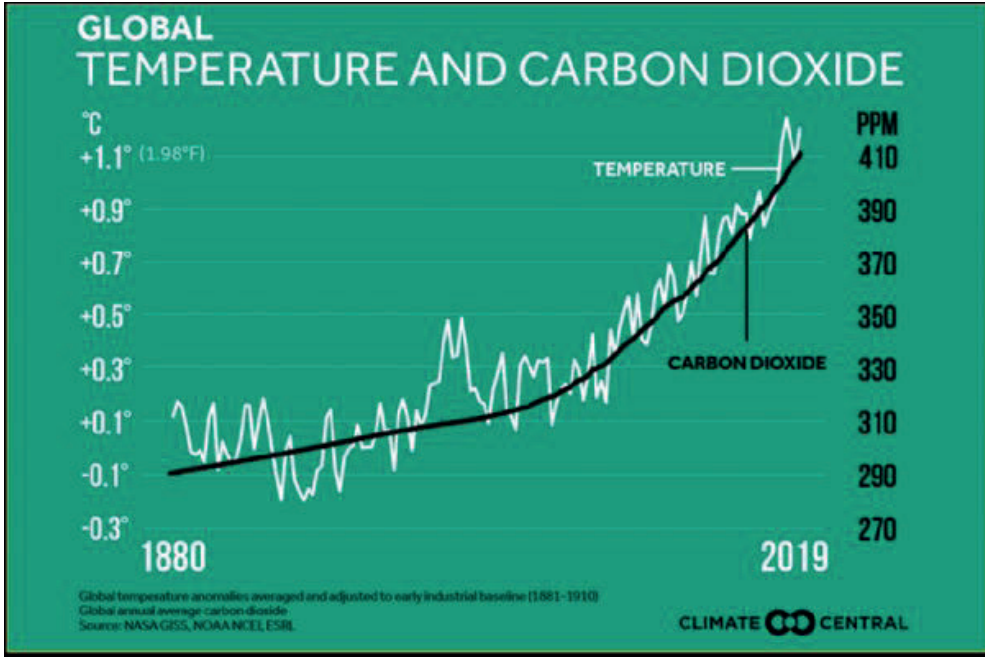


Figure 3 Conventional CCUS summary; Carbon Capture Utilization and Storage(CCUS) (2022)

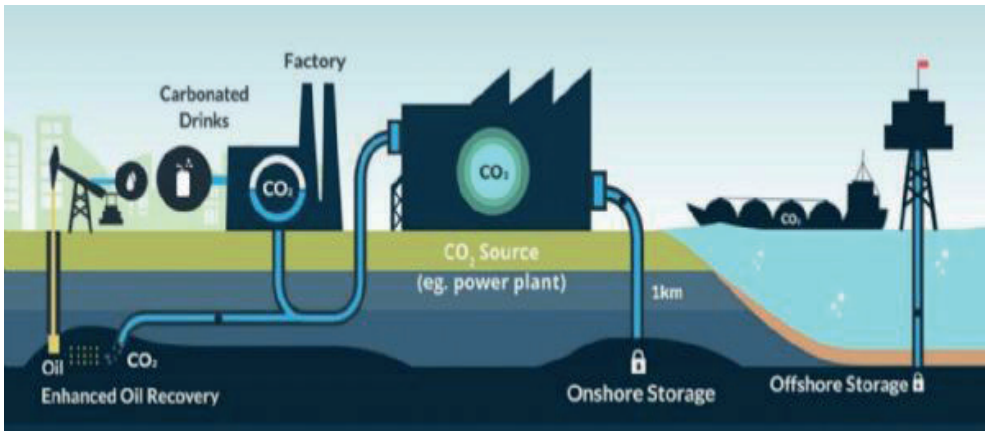


Figure 4 Carbon capture methods, Llamas, B. Et al. (2016)

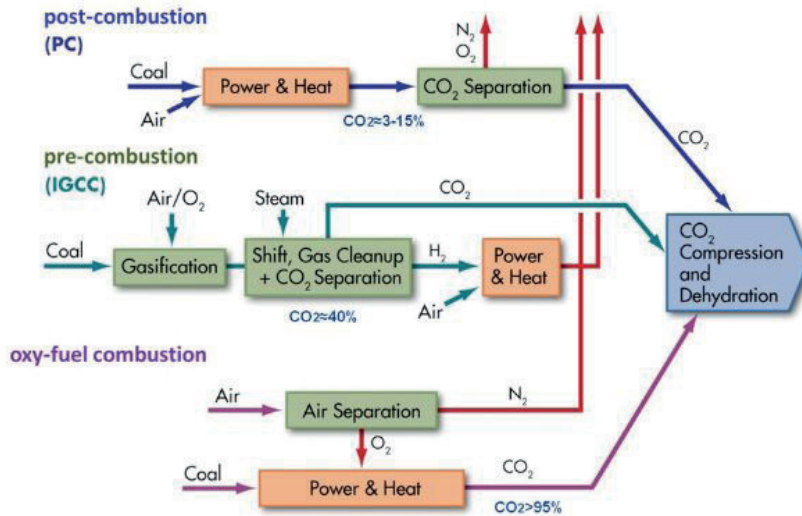


Figure 5 Geothermal CCUS pathways

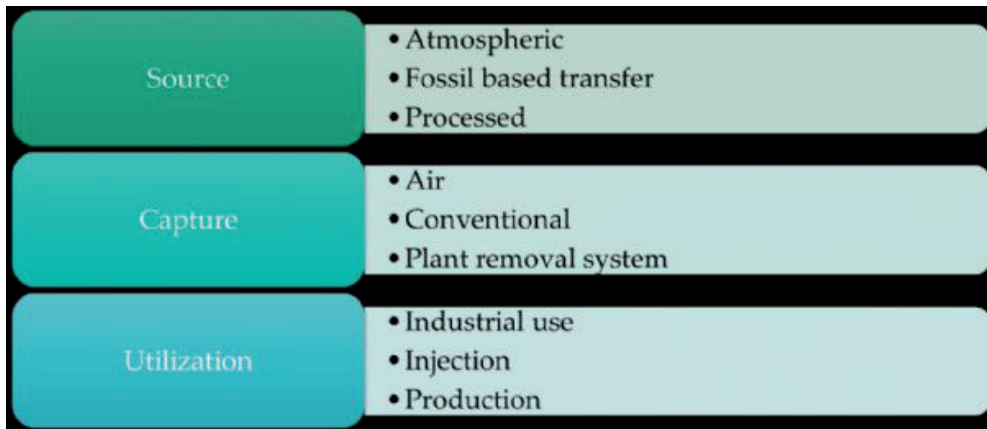


Figure 6 Basic geothermal power plant schematic(Flash)

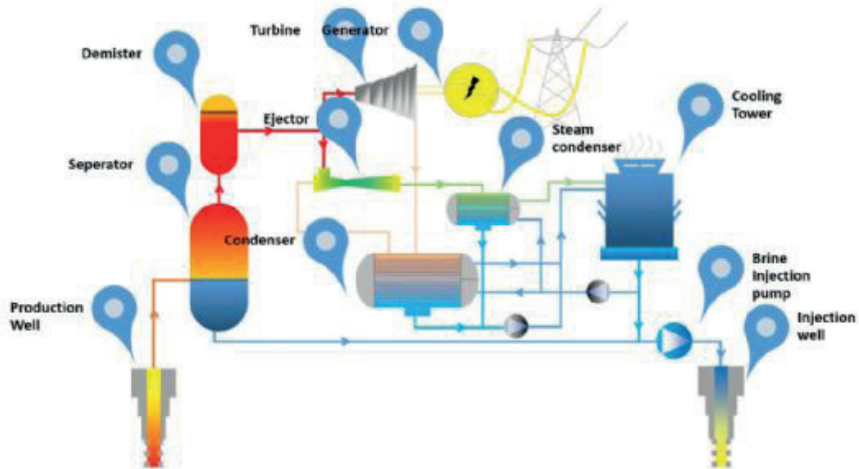


Figure 7 Carbfix: carbon sequestration in a geothermal field, How Iceland

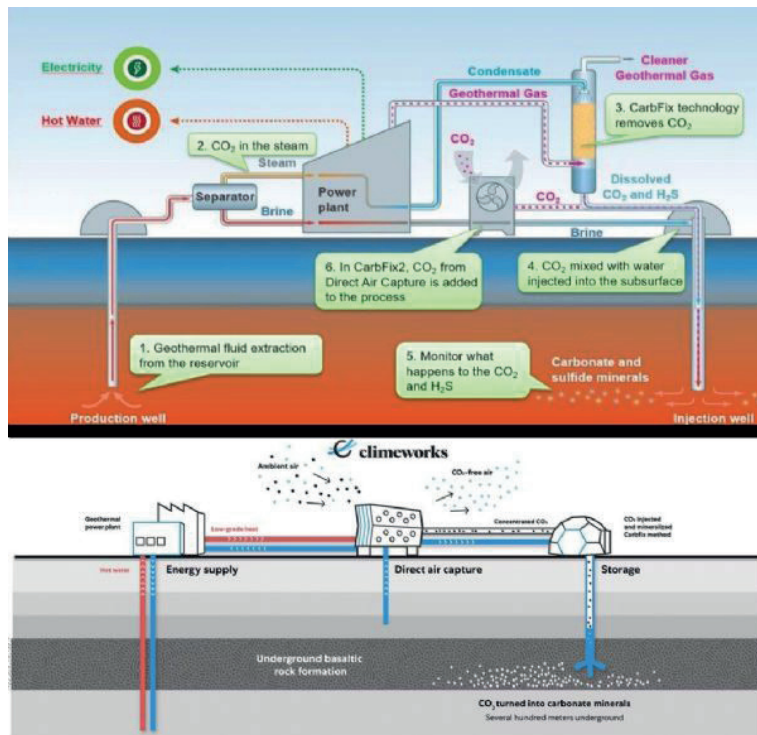


Figure 8 Gas lift diagram, K. Andrews (2022)

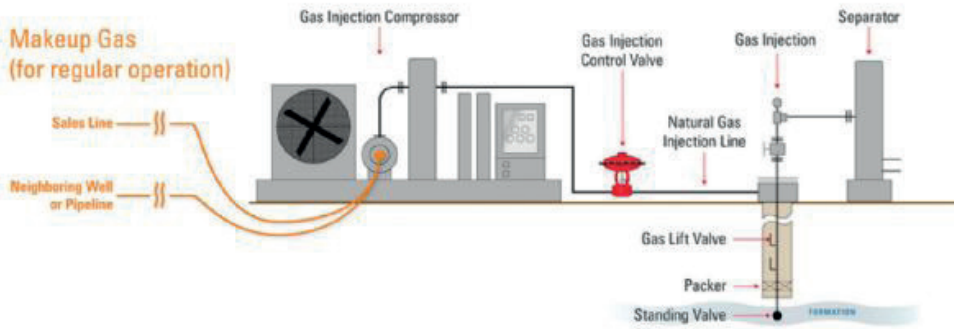
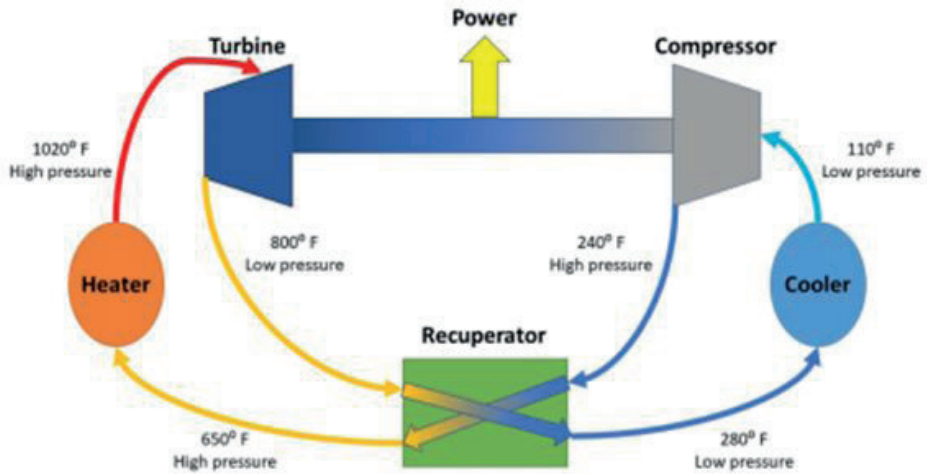


Figure 9 Gas turbine diagram, Sandia team puts power into local grid with supercritical CO<sub>2</sub> closed-loop Brayton-cycle turbine (2022)



# Top Cementing Job A Lesson Learnt from Geothermal Well Drilling in Alasehir Geothermal Field



**Emrah Gürel, Omer Yukselce, Emir Dimici, Cemil Seckin**

Turkerler Geothermal Energy Exploration and Production Co. Inc

## ABSTRACT

Geothermal energy is becoming an important source of energy and geothermal sector is improving in last 15 year in Turkey. Drilling geothermal well is almost the same as drilling an oil or gas wells apart from cementing operations. Although oil and gas wells cemented only above cap rock, geothermal well must be cemented up to surface. Formations to be cemented in geothermal wells are especially weak or unconsolidated causing that cement is not received on surface. Protection of casing and mechanical integrity of well bore gain importance when geothermal well is let to flow. When the temperature increases, there is a risk that the well fails unless surface, intermediate and especially production casings are successfully cemented. Therefore, cementing is curial operation in geothermal well due to protection of the casing and mechanical integrity of well bore.

In this paper, cementing operation challenges, solutions using decision tree and job procedures experienced from drilled wells are presented.

## 1. INTRODUCTION

Formations to be cemented in geothermal wells are especially weak or unconsolidated causing that cement is not received on surface. Protection of mechanical integrity of well bore gain importance when geothermal well starts to flow. When the temperature increases, there is a risk that the well fails unless surface, intermediate and especially production casings are successfully cemented. This paper present cementing operation procedure step by step according to gained experiences in Alaşehir geothermal field for last 10 years.

## 2. ALASEHIR GEOTHERMAL FIELD

The Alasehir Geothermal field is located about 140 km east of Izmir in the Western Anatolian extensional province (Dewey and Sengor, 1979). Nonmarine sediments are dominated formations in the southern and northern margins of the Alasehir graben. Also, it shows lateral and vertical facies variation (Purvis and Robertson, 2005). The Alaşehir Graben are consist of four sedimentary units, which is developed under an extensional tectonic regime. It is also a superimposed graben, which contains possible traps in addition to a high potential for hydrocarbon generation. Furthermore, Alasehir geothermal field has been mapped in five sections according to lithological characteristics, structure, and color. It consists of four main parts according to Yazman at all. (1990). They are Alluvium, Gediz group, Alasehir and Basement. The graben fill contains of four sedimentary units, which can be seen in the figure of Generalized stratigraphic column of the Alasehir area by After Yilmaz and Gelişli, 2003.

## 3. GEOTHERMAL WELLS CEMENTING OPERATION

Figure-2 shows classic design of geothermal wells. All size of casings must be cemented up to surface properly. Especially, cementing of production casing, which is 9 5/8" diameter, has more importance than other size of casing. It is run at the bottom of sandstone, mudstone, or shale, where metamorphic rocks start. In metamorphic rock formation, 7" slotted liner is run from final true depth to 9 5/8" casing shoe. 9 5/8" casing allows production of geothermal brine to surface. Since 9 5/8" casing is cemented up to surface, hydrostatic head of cement is going to be in high value when casing set depth is deeper. Generally, cemented formations, which are Alluvium, Gediz group, Alasehir, are highly fractured and unconsolidated. When cementing operation is performed, cement is generally not able to be received on surface. So that, top job operation is performed lowering 1/2" or 1" pipes from annulus, which is not a good operation that annulus is not cemented as desired because some mud or water stays in annulus. Then, it causes collapse of casing when well starts heat up (Figure-3). Therefore, cementing is critical issue in geothermal wells. In chart 1 and chart 2, cementing procedures are listed according to a lesson learnt from drilling geothermal wells in Alaşehir Geothermal field, which is located at Gediz Graben.

William M. R. at all 2012 mentioned that there are three types of cementing procedures when cement is not observed on surface or cement level dropped while WOC.

1. Top Job Cementing,
2. Top Fill,

## 3. TOP SQUEEZE CEMENTING

### 3.1. Top Job Cementing

When cement cannot receive on surface for 20" and 13 8/8" casings' cementing operation, PH and viscosity of last mud return on shakers will be in high value. Top job operation performed with 1" or 1/2" pipes, which is called macaroni pipes. High PH and viscosity value of mud indicates cement is about to come surface. After let cement become stronger, Wait On Cement, macaroni pipes are lower down from annulus. Firstly, top of cement is tried to be determined. After first macaroni pipes tag and it is assumed as top of cement, one or two more series of macaroni pipes are lowered down and all series are connected to manifold, which is valve system used for connection cementing lines. Then, water pumped to clean and displace the annulus with small flow rate. Later, cement slurry is pump with small flow

rate until cement is observed on surface.

There is a risk that macaroni pipes can be tagged at coupling of casings, where casing cannot be centered properly. Therefore, the depth of the top cement was not clearly identified.

Briefly, top job operation is not proper for geothermal wells, because; mud is contaminated with cement and viscosity is high, which does not allow mud lift out and small annulus can occur. In other words, cementing job cannot be performed as the conduit of small diameter macaroni pipes are not enough wide to flow cement slurry.

### 3.2. Top Fill

When cement is observed at the surface, but the cement subsequently recedes back down the casing-by-casing annulus, immediately or while waiting on cement, which is termed as fallback. When fallback occurs, a specific remedial procedure, termed as 'top fill', will be applied. After fallback, the space in the annulus, initially filled by cement, will be air-filled. It is important to immediately close the annular preventer during WOC.

The top fill technique is only effective when fallback occurs after primary cementing. The appropriate cement slurry is mixed and pumped through the cementing lines before connecting to the side valve. This ensures that the lines are flushed clean and only good cement is pumped into the annular space. water-free cement is pumped into one side of the annulus while the other side remains open. As the cement is pumped, any air in the annular space is displaced and evacuated through the open side outlet valve. Subsequently, pumping continues until there are only good cement returns flowing through the open side outlet valve

### 3.3. Top Squeeze

Partial or total loss of circulation may occur during cementing. This is caused by existing lost circulation zones, induced losses due to the excessive hydrostatic head of the cement column exceeding the formation pressure, or the presence of washouts (hole enlargement) that require more cement than initially calculated. If good cement does not return to surface during the primary cement job, a 'top squeeze' remedial cementing method may be applied. The top of the cement column in the annulus may be above or below the shoe of the previous casing string. In any case, it is imperative to immediately flush the casing-by-casing annulus with at least one annular volume of water to force any cement above the casing shoe out of the annular space and into the formation. Squeezing is the application of differential pressure to force cement into the formation. A minimum of at least one casing-by-casing annular volume of cement is pumped to fill the annulus, and pumping continues until a squeeze is achieved or cement is depleted

## 4. FIELD CASE STUDY for TOP SQUEEZE CEMENT

In XY-2 well, depth for 12 ¼" size is decided as 2275 by checking geological samples and correlation with other wells. Then, 9 5/8" casing is successfully run to 2272 m with two stage cementing tool, which is DV Tool. It is designed to set 1186 m depth.

After cementing head and its cementing lines and circulation lines installed, circulation tried with mud but no mud on surface since there is total loss. Totally, 600 bbl mud and 480 bbl water are pumped at stand pipe pressure of 200-300 psi. Total loss amount is 1080 bbl.

Mud prepared with Lost Circulation Material (LCM) pumped but it did not help to have circulation. It was seen that it was not possible to block this leakage, and it was decided not to risk the cement of the second stage without wasting time. It was decided to perform first stage cementing to avoid any case of the collapse between casing and annulus and bridge of formations.

A total of 390 bbl of cement was pump, of which 250bbl was 15-15.2 ppg and 140bbl 14.7-14.9 ppg, cement. The first stage displacement plug was dropped from the cementing head with 10 bbl of water and displaced with 527 bbl mud (Total displacement volume 530 bbl). Bottom plug set at 2500 psi. Any return from annulus was also not observed during cement and displacement.

Since the DV tool is just 100 meters below the 13 3/8" casing, it was thought that circulation could be observed after the ports were opened. To open the DV Tool ports, the opening bomb was thrown and the free fall to 1186 m was expected. Pressure was applied over 800psi and DV Tool ports were opened. Circulation was tried to be provided through the ports in DV and 358bbl drilling mud was pumped. The annulus volume from DV Tool is 238 bbl. Circulation still was not observed. The total loss amount is 1699 bbl.

For the cement of the second stage to be successful, 9 5/8" casing- 13 3/8" casing annulus must be circulated to the surface through the DV ports. Otherwise, in the cement operation to be carried out as in the first stage, it will not be able to be cemented up to the surface and even all of them will go to loss zone. For this reason, high viscosity sludge (YP>25 lb/ft<sup>2</sup>) was prepared with the prediction that it could provide circulation by blocking the loss zones. After pumping it, again circulation could not be obtained.

It was desired to use mud prepared with Lost Circulation Material (LCM). However, since LCM material in Coarse size should be used for this amount of loss, such LCM usage could also block the DV tool ports by causing DV mechanical properties failure.

A top squeeze cementing operation was decided to perform. Research has been carried out in the literature for this operation, which has not been done before as an application in geothermal wells in Turkey. Operations were planned by using the article "TOP SQUEEZE OR TOP FILL: IMPROVED SECONDARY CEMENTING FOR GEOTHERMAL WELLS" by William M. Rickard, Jonathan Hernandez and Alan Bailey. The

main purpose of this operation is to pump the cement slurry by closing the Annular BOP under pressure.

According to this plan, firstly, DV tool ports should be closed. The closing plug is lowered and displaced with a total of 250 bbl mud and the plug is set. When 1300 psi pressure is applied, the ports were closed, where casing axial movement observed.

After making sure that the first stage cement was set, the top squeeze operation was started. The Annular BOP was closed, and the cementing lines were connected to the kill line. The first stage for the squeeze cementing operation is pumping water. 150 bbl water is pumped through kill line to 600 psi with 3 bpm.

After pumping water was completed, the cementing operation was started. A cement mixture of 260 bbl 14.7-14.9 ppg was printed using the Hooper system starting with 3 bpm to 800 psi pressure, and during the last 80-100 bbl printing the press was observed as 200 psi. After pumping 260 bbl of cement (230 bbl of theoretical annulus volume) was completed, the WOC stage was started with the kill line and the Annular BOP under closed position. The reason for the closure of the Annular BOP is to disconnect the annulus from the atmosphere and prevent it from vacuuming.

After approximately 12 hours of WOC, the Annular BOP was opened and top of cement is measured as 33 meters.

With the Annular BOP and choke valve open, cement was pumped from kill line. After 23 bbl 14.7-14.9 ppg mixture was pumped, cement was observed coming from the choke outlet and the pumping process was stopped. After waiting for 15 minutes, the choke valve and the Annular BOP were closed, 0.4 bbl of 14.8 ppg cement was pumped from the kill line, and the pressure suddenly increased to 300 psi and it was remained constant at 300 psi for 5 minutes.

During the top-filling process, the cement comes from the choke outlet and the 300 psi pressure remains constant, indicating that the operation has been completed successfully. It was ensured that the annulus between 13 3/8" casing and 9 5/8" casing was completely cemented.

## 5. CONCLUSION

Having a proper cement for both 13 3/8" and 9 5/8" is very crucial to avoid any casing integrity problems. There are some steps to follow before cementing and after cementing operation in Geothermal Well. First off all, drilling mud should be treated well before casing running operations and circulation after casings are run since long waiting hours can be observed and high bottom hole temperature will cause to break mud properties. Also, caliper and other formation identification logging can be performed to have healthier data about wellbore. Lastly, cement slurry will be prepared by considering high temperature, high head pressure causing by high cement weight, logging analysis if there is any. In this paper, experiences for cementing operations learnt from Alasehir Geothermal Field in 10 years are shared and

decision tree table is structured to follow to have proper cementing operations. Top Job Cementing, Top Fill, Top Squeeze Cementing are the way of to have proper cementing operation. Top squeeze cementing operation is exemplified with one of the well in Alasehir Geothermal Field.

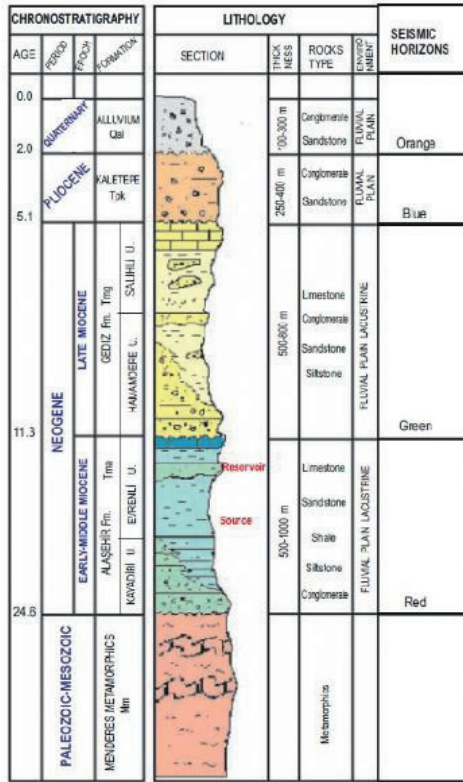
## 6. REFERENCES

- Çiftçi, B. N. (2007). Geological Evolution of the Gediz Graben, SW Turkey: Temporal and Spatial Variation of the Graben. PhD dissertation, The Middle East Technical University, Ankara.
- Dewey, J.F. and Şengör, A.M.C., 1979, Aegean and surrounding regions complex multiplate and continuum tectonics in a convergent zone: Geol. Soc. Am. Bui., 90, 84-92.
- Gürel, E., 2016. Uncertainty Quantification by Using Stochastic Approach In Pore Volume Calculation For Geothermal Reservoir. Msc thesis, Middle East Technical University, Ankara, Turkey.
- Muffler, L. J. P., and Cataldi, R., 1977. Methods for Regional Assessment of Geothermal Resources. Paper presented at Larderello Workshop on Geothermal Resource Assessment and Reservoir Engineering, Larderello.
- Sorey, M.L., Reed, J.M., Mariner, R.H., Nathenson, M.: Assessment of Low Temperature Resources in the United States. GRC Transactions. 6, (1982) 479-487.
- Yazman, M., Yılmaz, M. and İztan, H. 1998. Evaluation report of the Alaşehir Graben and Alaşehir-1 Prospect, Turkish Petroleum Corporation (TPAO) research group progress report no. 3864, Ankara, Turkey, unpublished report [in Turkish].
- Yılmaz, M. and Gelişli, K., 2003. Stratigraphic-structural interpretation and hydrocarbon potential of the Alaşehir Graben, western Turkey. Petroleum Geoscience, Vol. 9, pp. 277-282.
- William M. R., Jonathan H. and Alan B., 2012. Top Squeeze or Top Fill: Improved Secondary Cementing for Geothermal Wells Proceedings of the 4th African Rift Geothermal Conference, Nairobi, Kenya, 21-23 November 2012

Keywords: Top squeeze cementing, Alasehir Geothermal Field



Generalized stratigraphic column of the Alasehir area After Yilmaz and Gelişli, 2003

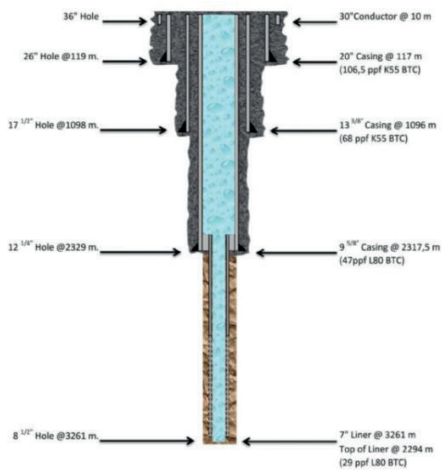


Not to scale

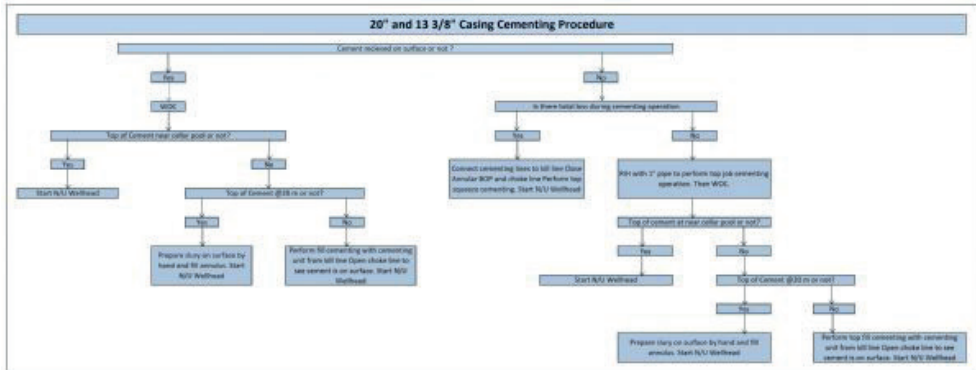
Collapse



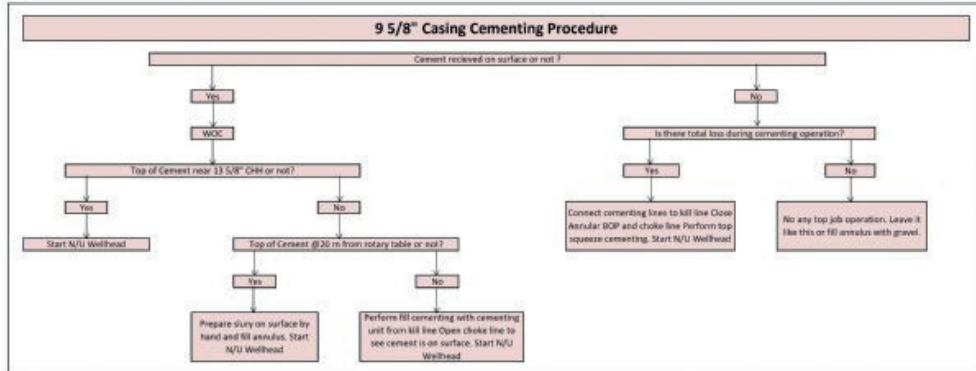
Well Schematic



Decision Tree-1



Decision Tree-2



# Kapadokya Bölgesinde Gömülü Kalderanın Manyetotellürük Yöntem ile Görüntülenmesi ve Jeotermal Potansiyelinin Değerlendirilmesi



**Ahmet Tuğrul Basokur<sup>1</sup>, Özlem Hacıoğlu<sup>2</sup>, Naser Meqbel<sup>3</sup>, Halil İbrahim Arslan<sup>1</sup>, Tevfik Efeçmar<sup>4</sup>**

<sup>1</sup>Lemnis Yerbilimleri, Ankara

<sup>2</sup>Karadeniz Teknik Üniversitesi, Trabzon

<sup>3</sup>National Observatory, Rio de Janeiro

<sup>4</sup>Era Enerji Ltd., Ankara

A hidden caldera imaged by magnetotellurics in the Cappadocia region and evaluation of its geothermal potential

üç-boyutlu olarak görüntülemek ve öz direnç modelini jeotermal arama açısından yorumlamaktır.

## ÖZ

Kapadokya Bölgesinde jeotermal kaynak arama amaçlı manyetotellürük inceleme gerçekleştirilmiştir. Çalışma alanında, öncel jeoloji ve jeokimya verileri ışığında gömülü bir kalderanın olduğu öne sürülmüştür. Manyetotellürük verinin üç-boyutlu modellenmesi ile yeraltı öz direnç dağılımı kestirilmiştir. Hesaplanan öz direnç modeli gömülü kalderanın biçimini başarılı bir şekilde görüntülemiştir. Düşük öz direnç belirtileri ise hidrotermal etkinlik sonucu oluşan alterasyon zonları olarak yorumlanmıştır.

**Anahtar Sözcük:** Üç-boyutlu manyetotellürük Modelleme, Kapadokya Bölgesinde Gömülü Kaldera.

A magnetotelluric survey has been conducted in the Cappadocia region of central Turkey to find new geothermal resources. The survey area has formerly been postulated as the location of a buried caldera that was one of the main eruptive centres of Cappadocian Volcanic Province. Three-dimensional non-linear conjugate gradient inversion of magnetotelluric data by using the full impedance tensor helps to delineate the subsurface resistivity distribution. The derived resistivity model reveals the possibility of a buried caldera. The low resistivity anomalies are interpreted as the clay alteration zones caused by hydrothermal activities.

**Keywords:** Three-dimensional magnetotelluric modelling, Buried Caldera in Cappadocian Volcanic Province.

## GİRİŞ

Kapadokya bölgesi Erciyes, Hasandağ ve Melendiz volkanlarının Neojen-Kuvaterner püskürmeleri ile oluşan tüfler ile örtülmüştür. Volkanik etkinlikler meteorik suların dolaşım nedeni ile ısınmasına ve faylar boyunca yükselerek termal kaynaklar olarak boşalmalarına yardımcı olurlar. Hem termal su dolaşımı hem de dolaşım nedeni ile oluşan alterasyon zonları elektriksel öz direnç değerlerinde önemli düşmelere neden olurlar. Elektromanyetik yöntemler yeraltı düşük öz direnç zonlarına duyarlı olduklarından, jeotermal kaynak aramalarında birincil yöntem olarak kullanılırlar. Bu çalışmanın amacı manyetotellürük (MT) yöntem kullanılarak, yeraltı öz direnç dağılımını

## JEOLOJİ

Kapadokya'da, Neojenden bu yana yoğun volkanik etkinlik sürmektedir (Froger et al., 1998). Volkan bacalarının dağılımı bölgesel tektonik ile bağlantılıdır (Toprak, 1998). Kapadokya bölgesinde sıcak su kaynakları Tuzlusu (25.5–25.9 °C), Yaprakhisar (30.8–33.5 °C), Ziga (44.7–45.4 °C) ve Acıgöl (Narköy; 40–61 °C) kaynaklarıdır (Afşin ve diğ.,2014). Bu kaynaklar Tuz Gölü Fayı veya ona paralel faylar üzerinde bulunmaktadır. Temel kayaları metamorfikler oluşturmaktadır. Bunların üstünde volkanik materyal ve Kuvaterner tortulları bulunmaktadır. Toprak(1998), bölgede volkanik baca dağılımını ve tektonizma ile ilişkisini incelemiştir. Afşin ve diğ. (2014), Kapadokya bölgesindeki hidrotermal kaynak sularını kimyasal yöntemlerle inceleyerek, meteorik su karışımı sürecini ele almışlardır. Yeraltı suyu dolaşımı için kavramsal model önermişlerdir. Şener ve diğ.(2017), Kapadokya bölgesinin jeokimyasal ve jeokronolojik evrimini ele almışlardır. Jeotermal suların fay zonları boyunca yükseldiğini, geçmişteki mineral alterasyonlarının güncel jeotermal sular ile benzer karakterde olduğunu belirtmişlerdir. Önerdikleri kavramsal jeotermal modelde, volkanik olarak ısıtılan rezervuar ve örtü kayaçları yer almaktadır. Yapısal olarak jeotermal bir sistem için koşulların var olduğu belirtilmiştir.

Kapadokya bölgesinde üç püskürme bölgesi önerilmiştir. Nevşehir ve Acıgöl gömülü kalderaları gravite, manyetik ve yerelektrik çalışması ile saptanmıştır (Kaya ve diğ., 1989; Bilginer ve Tokgöz, 1982). Pasquare et al. (1988), üçüncü gömülü kaldera yeri olarak 15 km çapındaki Çiftlik çöküntüsünü önermişlerdir. Gömülü kalderanın ilksel biçimini koruması, daha sonraki aşınma, tektonik ve volkanik etkinliğe bağlıdır. Bu etkinlikler, kalderanın yüzey jeolojisi ile belirlenmesini güçleştirmektedir. Çiftlik çöküntüsü Kuvaterner yaşlı gölsel tortullar ile örtülüdür. MT çalışmasının yapıldığı alan Çiftlik çöküntüsü de kapsadığından, gömülü kaldera önermesinin denetlenmesi ve olası kalderanın biçimini üç-boyutlu öz direnç modeli ile ortaya çıkarılması MT incelemesinin amacı oluşturmaktadır (Şekil 1). MT yöntemi volkanların araştırılmasında etkin bir şekilde kullanılmaktadır (Başokur et al., 2022)

Şekil 1. Sarı çizgiler Kapadokya bölgesindeki Neojen yaşlı çöküntü alanını ve kırmızı çizgiler MT ölçü alanını göstermektedir. Güncel faylar siyah çizgiler ile gömülü faylar kesikli çizgiler ile gösterilmiştir (Hacıoğlu et al., 2023).

### MT VERİ-TOPLAMA VE VERİ-İŞLEM

MT çalışması yaklaşık 1000x1000 aralıklı bir ölçü ağı üzerinde 60 adet istasyonun ölçülmesi ile gerçekleştirilmiştir. Her bir istasyonda üç manyetik (doğu-batı, kuzey-güney ve düşey) ve iki elektrik alan bileşeni (doğu-batı ve kuzey-güney) ölçülmüştür. Beş bileşen kapsayan zaman serisi 'hızlı Fourier dönüşümü' (FFT) ile frekans ortamına aktarılmıştır. Frekans dengelenmiş direntinin gerçel ve sanal bölümleri arasında var olan Hilbert dönüşümü ilişkisi kullanılarak, Lemnis Ltd. şirketine ait yazılım (Başokur 1994, Başokur 1999, Başokur 2023, Zorin ve diğ., 2020) ile empedans değerlerine tutarlılık analizi uygulanmıştır. Empedans değerleri bu teknik ile elektromanyetik alan ile ilgili fiziksel kısıtlar sağlanarak hesaplanmaktadır. Bu tekniğin kullanılması ile doğal elektromanyetik alanın zayıf olduğu 100-10.000 Hz frekans aralığında da güvenilir empedans değerlerinin hesaplanması olanaklı olmuştur. Sonuç çıktısı olarak her istasyon için, 10.000-0.001 Hz frekans aralığında, her dönemde 10 veri olmak üzere toplam 71 adet frekansta empedansın dört bileşeni hesaplanmıştır.

### ÜÇ-BOYUTLU MODELLEME

Jeofizik yöntemlerin amacı belirli bir fiziksel parametrenin yeraltındaki dağılımını saptamaktır. Bu işlem doğrudan fiziksel parametrenin ölçülmesi ile gerçekleştirilmez. Bunun yerine, bu fiziksel parametrenin yeraltındaki dağılımı nedeni ile oluşan alan değişimi yer yüzeyinde ölçülür. Bu alan değerleri kullanılarak, ters-çözüm yöntemleri ile fiziksel parametrenin yeraltındaki dağılımı kestirilmeye çalışılır. Bu amaçla çeşitli kavramsal modeller kullanılmaktadır. Elektrik ve elektromanyetik yöntemlerde üç tür kavramsal model kullanılmaktadır. Bu modellerden en yalını, tekdüze ve yön-bağımsız katmanlardan oluşan bir-boyutlu (1B) modeldir. Bu modelde, geometrik parametreler katman kalınlıkları iken, fiziksel parametreler ise her katmanın kendine özgü öz direncidir. İki-boyutlu (2B) model fiziksel parametrelerin ölçü hattı doğrultusunda ve düşey yönde değiştiği, ancak kesit düzlemine dik yönde değişmediği varsayımı ile elde edilir. Prizmaların kesit düzlemindeki görüntüleri hücre olarak adlandırılır. Üç-boyutlu (3B) modellemede ise yer altı küp şekilli bloklar ile temsil edilir. Her küpten kendine özgü bir fiziksel parametre değeri vardır. Üç-boyutlu model yeraltının gerçeğe en yakın bir modelinin kurulmasında daha başarılıdır. Bir-boyutlu modelleme oldukça hatalı sonuçlar üretmesi açısından hesaplama olanaklarının geliştiği günümüzde artık kullanılmamaktadır. İki-boyutlu model kullanımı halen sürdürülmekte ise de birçok sakıncası bulunmaktadır. Sadece aynı doğrusal bir hat üzerinde bulunan belirli sayıdaki istasyon ters-çözüm amacı ile kullanılabilir. Jeoloji yaklaşık iki-

boyutlu olmalı ve ölçü hatları jeolojik doğrultuya dik yönde seçilmelidir. Jeolojik doğrultuya dik olmayan yönlerde modelleme yapılamaz. Kuzey-güney ve doğu-batı yönlerinde ölçülen elektrik ve manyetik alan değerleri jeolojik doğrultuya hesapla döndürülmek zorundadır. Bu işlem verideki gürültü ve belirsizliklerin artmasına neden olur. Yan yana dizilen iki-boyutlu görüntülerden yorumlama yapılmak zorundadır. Yapma üç-boyutlu görüntü elde edilebilir ise de hatlar arasındaki öz direnç değerleri ara değer bulma yöntemleri ile hesaplandığından gerçek değerler değildir. Üç-boyutlu modellemede bu tür kısıtlar bulunmamaktadır. Ancak, model ağı geometrik olarak büyüdüğünden çözülmesi gereken parametre sayısı çok büyük değerlere ulaşır ve çok-çekirdekli hızlı sunucuların ve daha karmaşık yazılımların kullanılmasını zorunlu hale getirir. Üç-boyutlu modelleme için hesaplama süresi parametre ve yineleme sayılarına bağlı olarak 50-100 saat sürebilir.

Bu çalışmada öz direnç modelleri üç-boyutlu (3B) ters-çözüm yazılımı (Egbert and Kelbert, 2012; Kelbert et. al., 2014) kullanılarak hesaplanmıştır. Modelleme için oluşturulan ağı, x, y ve z yönlerinde sırası ile 52, 93 ve 82 olmak üzere toplam 396552 parametreden oluşmaktadır (Şekil 2). Topoğrafya için SRTM90 verisinden elde edilen her hücre içerisindeki ortalama yükseklik kullanılmıştır. Üç-boyutlu evirtim (ters-çözüm yazılımı çok-çekirdekli iş istasyonu üzerinde çalıştırılmıştır. 10.000-0.001 Hz frekans aralığında her logaritmik onluğa beş veri düşecek şekilde 36 frekans kullanılarak üç-boyutlu evirtim gerçekleştirilmiştir.

Üç-boyutlu öz direnç modeli, öz dirençleri farklı küplerin bileşiminden oluşur. Evirtim işlemi ile bu hücrelerin öz direnci hesaplanır ve elde edilen yer altı öz direnç dağılımının mevcut bilgiler kullanılarak jeolojik açıdan anlamlandırılması yorum sürecini oluşturur. Aynı jeolojik birimi temsil eden küplerin, birbirine oldukça yakın öz direnç değerleri ile temsil edilmesi beklenir.

Şekil 2. Üç-boyutlu ters-çözümde kullanılan model ağı. İnceleme alanı sırası ile x, y ve z yönlerinde 52, 93 ve 82 olmak üzere toplam 396552 hücreden oluşmaktadır.

### SONUÇLAR

Isı kaynağı, rezervuar (kırk ve boşluklardaki doğal akışkan) ve düşük geçirgenlikli örtü kayacı olmak üzere hidrotermal sistemler üç ögeden oluşmaktadır. Örtü kayacı, derinliklerdeki sıcak akışkanın yüzey suları ile karışarak soğumasını engeller. Hidrotermal sistemlerde, su-kayaç etkileşimi yoğundur. Hem tortul kayalar da hem de çatlak ve kırık sistemlerinde, düşük öz direnç değerleri geçirgenlik ve gözenekliliğin artması ile doğrudan ilişkilidir. Suya doygun katmanlar, hidrotermal zonlar ve hidrotermal alterasyona uğramış kayaların varlığı, düşük öz direnç değerleri ile ilişkilendirilir. Bu etkilere bileşimi de düşük öz direnç değerlerinin nedeni olabilir.

Şekil 3'de görüntülenen ve 342 ve 238 metre yükseklik aralığına karşılık gelen öz direnç haritası iki farklı jeolojik doğrultu bulunduğu işaret etmektedir. Bunlardan ruhsat sahasının doğusunda bulunan, yaklaşık 45 derece güneydoğu-kuzeybatı doğrultulu süreksizlik literatürde

Çiftlik Fayı veya Tepeköy Fayı olarak adlandırılan aktif fay ile ilişkili olmalıdır. Diğerleri ise özdirenç haritalarında daha sığ derinliklerde gözlenen ve güneybatı-kuzeydoğu doğrultulu süreksizliklerdir. Şekil 4’de ise yükseklik değeri -504 ve -651 metre aralığına karşılık gelen özdirenç haritasında düşük özdirenç zonu GB-KD doğrultusu boyunca gözlenmektedir. Şekil 5’de ise yükseklik değeri -1435 ve -1682 aralığına karşılık gelen özdirenç haritası, özdirenç değerlerinin görece azalmasına, ancak daha geniş dairesel bir bölgenin varlığına işaret etmektedir. Şekil 6’da görüntülenen batı-doğu yönlü özdirenç kesitinde, doğu ve batıda elektrik temelini yitirdiği orta bölümde ise muhtemel bir alterasyon zonu varlığı dikkat çekmektedir. Bu durum Şekil 5’de görselleştirilen özdirenç haritasından da anlaşılmaktadır. Çalışma sonucunda kaldera biçimsel olarak tanımlanmış ve özdirenç modelinden fay lokasyonları yorumlanmıştır (Şekil 7). Olası jeotermal kaynaklar bu fay zonları ile ilişkili olmalıdır. Çalışma alanına birkaç kilometre uzaklıktaki sondajda, 3957 metre derinliğinde kuyu taban sıcaklığı 341°C olarak ölçülmüştür ve çalışma alanında yüksek sıcaklık beklentisinin diğer bir kanıtıdır.

Şekil 3. Yükseklik değeri 342 ve 238 metre aralığına karşılık gelen özdirenç haritası (üstte) ve Google Earth üzerinde görünümü (altta).

Şekil 4. Yükseklik değeri -504 ve -651 aralığına karşılık gelen özdirenç haritası (üstte) ve Google Earth üzerinde görünümü (altta).

Şekil 5. Yükseklik değeri -1435 ve -1682 aralığına karşılık gelen özdirenç haritası (üstte) ve Google Earth üzerinde görünümü (altta).

Şekil 6. Batı-doğu doğrultulu özdirenç kesiti. Yukarıdaki şekilde mor üçgen kesitin başlangıcını ve kırmızı çizgi kesitin doğrultusunu göstermektedir. Altta özdirenç kesitinde düşey gri çizgi ruhsat sınırına işaret etmektedir.

Şekil 7. Batı-doğu doğrultulu bir kesit boyunca özdirenç değişimi. Yüzeyledeki üçgenler MT istasyonlarını, kırmızı ok çalışma alanındaki bir fayın yüzey izini ve kesik beyaz çizgiler yorumlanan fayları göstermektedir (Hacıoğlu ve diğ., 2023).

### Katkı Belirtme

Era Enerji Ltd Şirketi’ne MT inceleme sonuçlarını yayımlama izni verdiği için teşekkür ederiz. Veri, 21 Kasım ile 10 Aralık 2018 aralığında, Lemnis Yerbilimleri tarafından ölçülmüştür.

### KAYNAKLAR

Afsin, M., Allen, D. M., Kirste, D., Durukan, U. G., Gurel, A. and Oruc, Ö. [2014] Mixing processes in hydrothermal spring systems and implications for interpreting geochemical data: a case study in the Cappadocia region of Turkey. *Hydrogeology Journal*, 22, 7–23.

Başokur, A. T. [1994] Definitions of apparent resistivity for the presentation of magnetotelluric sounding data. *Geophysical Prospecting*, 42, 141-149.

Başokur, A. T. [1999] Properties of the magnetotelluric frequency-normalised impedance function over a layered medium. *Journal of the Balkan Geophysical Society*, 2, 63-74. (available at <http://www.balkangeophysoc.gr/>).

Başokur, A. T., Koçyiğit, A., Hacıoğlu, Ö., Arslan, H. İ. and Meqbel, N., 2022, Magnetotelluric imaging of the shallow-seated magma reservoir beneath the Karadağ stratovolcano, Central Anatolia, Turkey. *Journal of Volcanology and Geothermal Research* 427, 107567. doi.org/10.1016/j.jvolgeores.2022.107567.

Başokur, A. T. [2023] Hilbert transform of unequally sampled data: Application to dispersion relations in magnetotellurics. *Geophysics* 88, 2, E29-E38.

Bilginer, Ö. ve Tokgöz, T., [1982], Nevşehir-Acıgöl kaldera ve çevresi rezistivite etüdü. MTA Rapo No: 7154.

Egbert, G.D., Kelbert, A., [2012] Computational recipes for electromagnetic inverse problems. *Geophys. J. Int.*, 189, 167–251.

Froger, J.L., Lenat, J.F., Chorowicz, J., Le Pennec, J.L., Bourdier, J.L., Köse, O., Zimitoğlu, O., Gündoğdu, N.M. and Gourgaud, A., [1998], Hidden calderas evidenced by multisource geophysical data; example of Cappadocian Calderas, Central Anatolia. *Journal of Volcanology and Geothermal Research*, 185, 99–128.

Hacıoğlu, Ö., Başokur, A.T., Meqbel, N., Arslan, H.I. and Efeçinar, T. [2023] Magnetotellurics unveils a hidden caldera complex beneath the Cappadocia Volcanic Province, central Anatolia, Türkiye. *Journal of Volcanology and Geothermal Research* (in print).

Kaya, C., Aktaş, K. ve Tokgöz, T., [1989], Aksaray Sofular-Acıgöl ve Ziga sahaları jeotermal enerji aramaları jeofizik yapay kaynaklı manyetotellurik (CSAMT) etüdü. MTA Rapor No: 8560.

Kelbert, A., Meqbel, N., Egbert, G. D. and Tandon, K., [2014] ModEM: A modular system for inversion of electromagnetic geophysical data, *Computers & Geosciences*, 66, 40–53.

Pasquare, G., Poli, S., Vezzoli, L., Zanchi, A. [1988] Continental arc volcanism and tectonic setting in central Anatolia, Turkey. *Tectonophysics*, 146, 217–230.

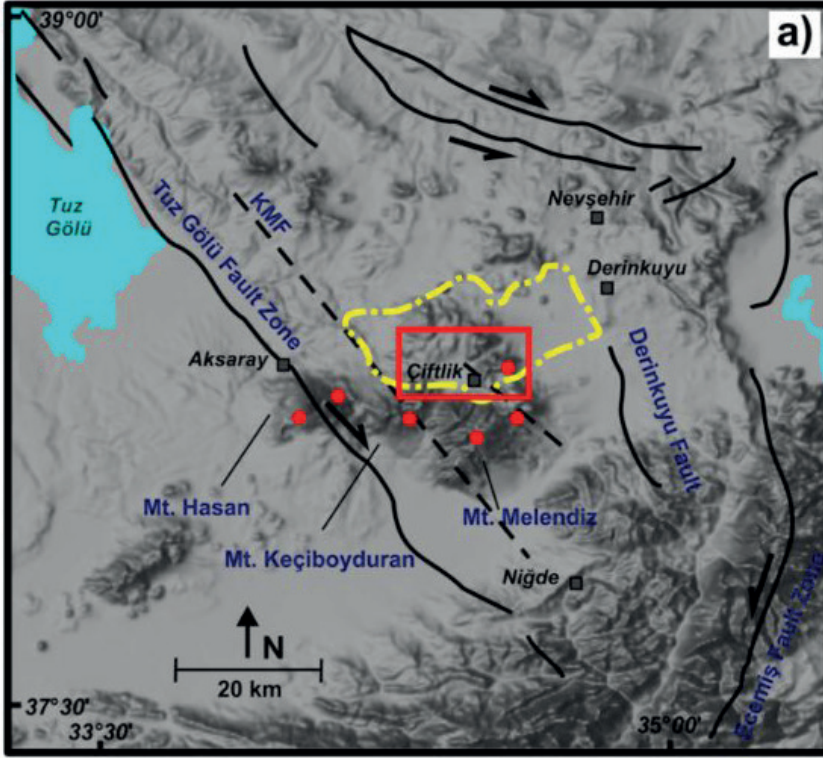
Şener, M. F., Şener, M. and Uysal I. T. [2017] The evolution of the Cappadocia Geothermal Province, Anatolia (Turkey): geochemical and geochronological evidence, *Hidrogeological Journal* 25, 2323-2345.

Toprak, V. [1998] Vent distribution and its relation to regional tectonics, Cappadocian Volcanics, Turkey. *Journal of Volcanology and Geothermal Research*, 85, 55–67.

Zorin, N.L., E. Aleksanova, H. Shimizu, and D. Yakovlev, D. [2020] Validity of the dispersion relations in magnetotellurics: Part I-theory: Earth, Planets and Space, 72, 1-18.

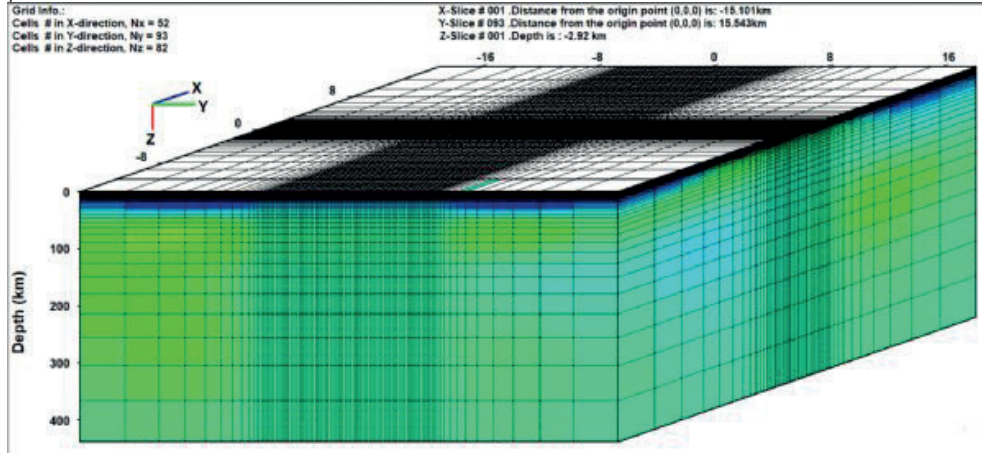
Anahtar Kelimeler: Üç-boyutlu manyetotellurik Modelleme, Kapadokya Bölgesinde Gömülü Kaldera

Şekil 1



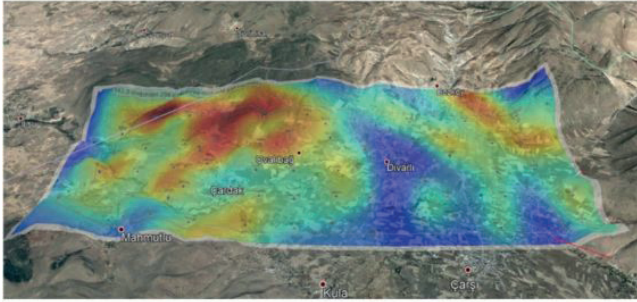
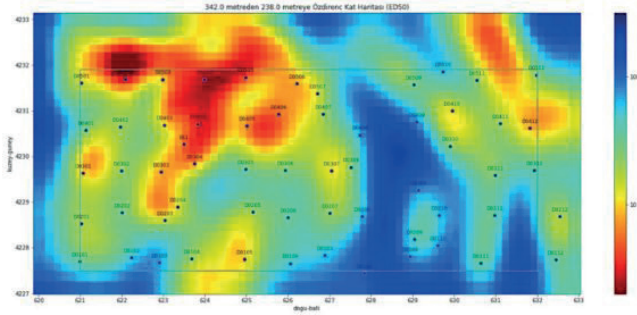
Şekil 1. Sarı çizgiler Kapadokya bölgesindeki Neojen yaşlı çöküntü alanını ve kırmızı çizgiler MT ölçü alanını göstermektedir. Güncel faylar siyah çizgiler ile gömülü faylar kesikli çizgiler ile gösterilmiştir (Hacıoğlu et al., 2023).

Şekil 2



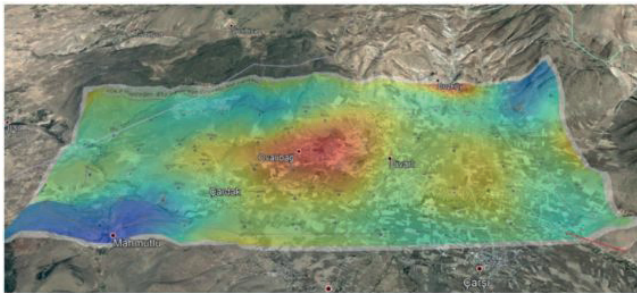
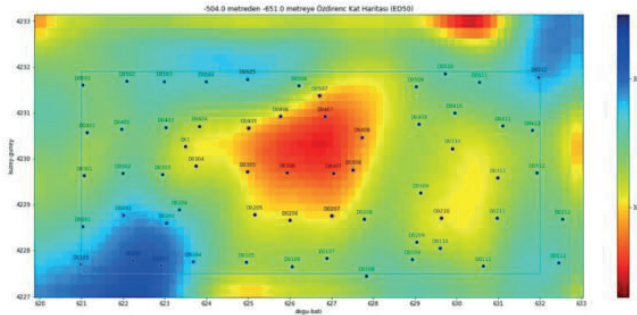
Şekil 2. Üç-boyutlu ters-çözümde kullanılan model ağı. İnceleme alanı sırası ile x, y ve z yönlerinde 52, 93 ve 82 olmak üzere toplam 396552 hücreden oluşmaktadır.

Şekil 3



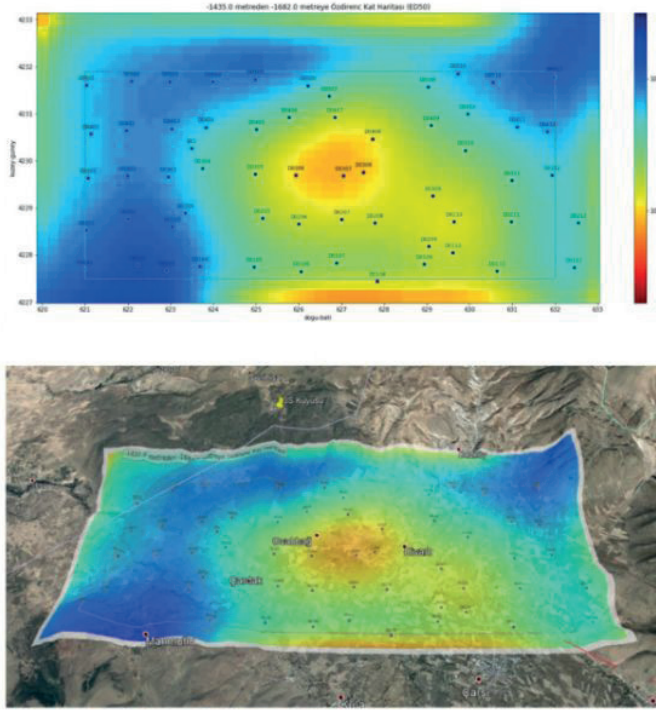
Şekil 3. Yükseklik değeri 342 ve 238 metre aralığına karşılık gelen öz direnç haritası (üstte) ve Google Earth üzerinde görünümü (altta).

Şekil 4



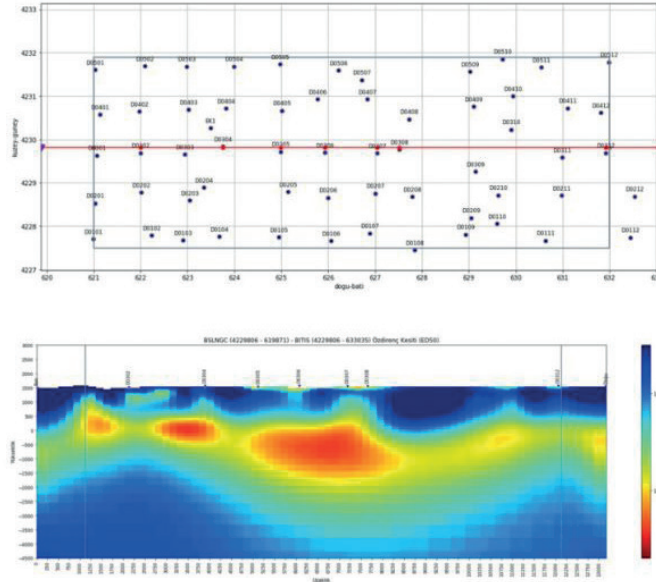
Şekil 4. Yükseklik değeri -504 ve -651 aralığına karşılık gelen öz direnç haritası (üstte) ve Google Earth üzerinde görünümü (altta).

Şekil 5



Şekil 5. Yükseklik değeri -1435 ve -1682 aralığına karşılık gelen öz direnç haritası (üste) ve Google Earth üzerinde görünümü (altta).

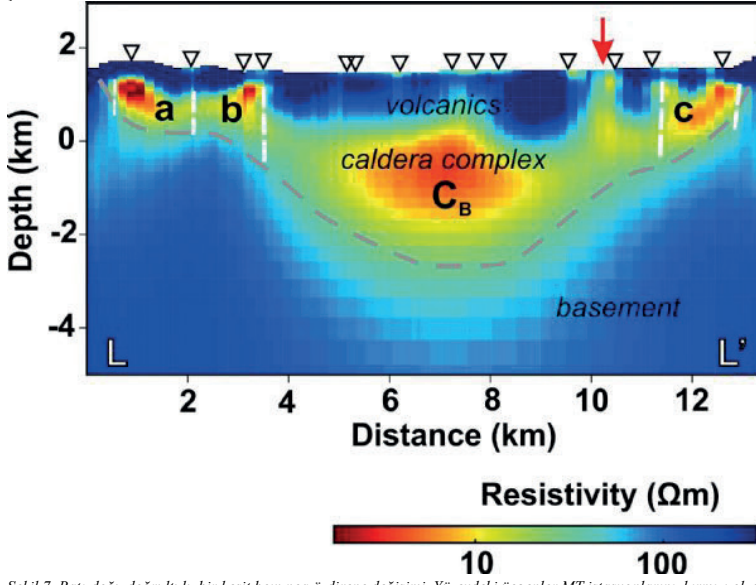
Şekil 6



Şekil 6. Batı-doğu doğrultulu öz direnç kesiti. Yukarıdaki şekilde mor üçgen kesitin başlangıcını ve kırmızı çizgi kesitin doğrultusunu göstermektedir. Altta öz direnç kesitinde dikey gri çizgi ruhsat sınırına işaret etmektedir.



Şekil 7



Şekil 7. Batı-doğu doğrultulu bir kesit boyunca öz direnç değişimi. Yüzeyledeki üçgenler MT istasyonlarını, kırmızı ok çalışma alanındaki bir fayın yüzey izini ve kesik beyaz çizgiler yorumlanan fayları göstermektedir (Hacıoğlu ve diğ., 2023).

# Geothermal Energy Potential of Radioactive Heat Production and Magnetic Susceptibility Characteristics in Kütahya Simav Basin



Elif Meric İlkimen, Cihan Çolak, Ali Aydın

Department of Geological Engineering, Faculty of Engineering, Pamukkale University, 20160 Pamukkale Denizli / Türkiye

## ABSTRACT

Geothermal energy is a renewable and sustainable energy source that holds substantial promise. Radiogenic heat production (RHP) from migmatites is a noteworthy option for geothermal energy production. Migmatites are metamorphic rocks formed through partial melting and exhibit high radiogenic heat due to uranium and thorium decay. This study investigates the magnetic susceptibility and petrophysical properties of migmatites within the Precambrian-age Kalkan formation in the Simav Basin, Turkey. The study establishes a link between migmatites and geothermal energy potential by analyzing magnetic susceptibility, uranium (U), thorium (Th), and potassium (K) concentrations using in-situ XRF measurements, as well as U/Th, Th/U, Th/K, and U/K ratios. Results highlight distinct boundaries separating areas of high and low radiogenic heat production values, indicative of heat-generating rock formations. Overlaying these findings with geothermal drilling locations reveals a correlation between radiogenic heat production and magnetic susceptibility in specific regions. By shedding light on the geological and petrophysical attributes of migmatites, this study provides a solid foundation for future exploration and harnessing of geothermal resources in the Simav Basin. In conclusion, this study underscores the potential of migmatites in the Simav Basin as a viable and promising source of RHP-based geothermal energy.

## INTRODUCTION

Geothermal energy is a significant form of renewable energy with the potential to contribute substantially to the sustainable development of countries worldwide. Among the various sources of geothermal energy, radiogenic heat production (RHP) from migmatites stands out as a promising option, particularly in the context of Turkey's sustainable energy mix. Migmatites are metamorphic rocks that have undergone partial melting, often exhibiting high levels of RHP. The decay of uranium and thorium isotopes within these rocks generates heat that can be harnessed for geothermal energy production. Several regions worldwide are known for their substantial concentrations of uranium and thorium in migmatites, making them attractive sites for RHP-based geothermal energy production. In the specific case of Turkey, the Simav Basin is recognized for its abundant uranium and thorium concentrations within the granitic migmatites present in the region. Consequently, the Simav Basin holds great promise as a location for RHP-based geothermal energy production. RHP-based geothermal energy production offers various advantages compared to other

forms of renewable energy. Its high efficiency, low environmental impact, and reduced reliance on fossil fuels make it a desirable option for meeting Turkey's energy demands. Additionally, the relatively lower exploration and production costs associated with RHP-based geothermal energy further enhance its appeal as a viable investment for Turkey's energy sector. In this study, we aim to investigate the magnetic susceptibility and petrophysical properties of migmatites exposed in the basement rocks of the Simav Basin. By examining these properties, we seek to establish the relationship between migmatites and geothermal energy. The studied Kalkan formation is of Precambrian age, comprising migmatites at the base, wherein aplitic and pegmatitic rocks resulting from partial melting are observed (Figure 1). These migmatites transition into banded migmatites in the upper layers. To calculate the radiogenic heat production values, magnetic susceptibility measurements from migmatite samples in the study area were utilized, alongside U, Th, and K concentration values measured using an in-situ XRF device. Additionally, the ratios of U/Th, Th/U, Th/K, and U/K were examined. The mapping of all obtained values revealed distinct boundaries between regions of high and low values, signifying the presence of heat-generating rock formations in the area. Furthermore, by overlaying the geothermal drilling locations on the obtained maps, we observed a correlation between radiogenic heat production values and magnetic susceptibility values in specific regions. In conclusion, the RHP-based geothermal energy potential of migmatites in the Simav Basin, Turkey, presents a promising source of sustainable energy for the nation. The exploration and utilization of geothermal energy from migmatites hold significant prospects for enhancing Turkey's energy security and supporting its transition to a more sustainable and eco-friendly energy mix. A study focused on investigating the geothermal energy potential of Simav Basin in relation to radioactive heat production and magnetic susceptibility characteristics. Geothermal energy is gaining increasing importance as a sustainable and eco-friendly energy source. Therefore, the primary aim of this research is to assess the potential of geothermal resources in the region, with the objective of contributing to energy production and utilization in Kütahya Simav Basin (Figure 1).

## METHODOLOGY

The research methodology employed in this study entails the systematic collection of geothermal samples from diverse locations within the Kütahya Simav Basin. These samples are subsequently subjected to meticulous laboratory analyses to ascertain their radioactive heat

production potential. In parallel, appropriate techniques are deployed to measure the magnetic susceptibility characteristics of the geothermal samples. The collected data is then subjected to comprehensive analysis and interpretation, yielding invaluable insights into the geothermal resources prevalent in the region. Magnetic susceptibility measurements serve a multitude of geophysical applications, ranging from identifying distinct rock types in geological surveys to determining the depth and thickness of sediment layers in subsurface exploration projects. Additionally, they find utility in environmental studies by enabling the detection and quantification of pollution or contamination in soils and sediments. In essence, the magnetic susceptibility method serves as an indispensable geophysical technique for elucidating the magnetic properties of rocks and sediments. By assessing the magnetic susceptibility of diverse materials, geophysicists can glean valuable information pertaining to their composition and properties. The measurement of magnetic susceptibility in geophysics is typically conducted using either SI (International System of Units) or cgs (centimeter-gram-second) units, contingent upon the application. In SI units, magnetic susceptibility is expressed in  $\text{m}^3/\text{kg}$ , whereas in cgs units, it is rendered dimensionless. To measure magnetic susceptibility in the laboratory using the Bartington MS2B device, a series of standard steps are typically followed, involving the preparation of the sample, its placement into measurement slots, and the actual measurement process. The magnetic susceptibility of minerals is intricately linked to the properties of the minerals and elements present within the substance. In the course of this study, measurements were conducted using the MS2B sensor of the Bartington device. Powdered samples, duly prepared and placed into 10 cc pots, were positioned into the measurement slot of the device at both low (0.47 kHz) and high (4.7 kHz) frequencies, with a sensitivity of 0.1 SI unit. The measured magnetic susceptibility values ( $\chi$ ) were subsequently divided by the densities ( $\rho$ ) of the samples to compute the mass-specific magnetic susceptibility. In the context of calculating the Radiogenic Heat Production (RHP), the concentrations of certain elements, such as uranium (U), thorium (Th), and potassium (K), assume paramount significance. These element concentrations play a pivotal role in estimating the activity concentrations of radioactive isotopes present in the sample, subsequently facilitating the calculation of the RHP of the said sample. The variations in the values of K (%), Th (ppm), U (ppm), and  $\rho$  ( $\text{g}/\text{cm}^3$ ) measured from the rock samples taken from the study area are depicted in figure maps, wherein elevated values are discernible in the regions exhibiting high-value distributions (Figure 2). The Radiogenic Heat Generation Potential (RHP) of a rock or mineral can be calculated through equations developed by many researchers such as Raybach (1976,1988), Birch (1954), Hamza and Beck (1972) and Uyanik et. all (2020). Overall, this study adopts a rigorous and comprehensive approach in investigating the geothermal energy potential of the Simav Basin, particularly with regard to radioactive heat production and magnetic susceptibility

characteristics. Through advanced laboratory analyses and geophysical techniques, the study aims to shed light on the geothermal resources in the region, contributing valuable insights towards harnessing this abundant and sustainable energy source.

## DISCUSSION AND RESULTS

The present study has yielded significant insights into the geothermal energy potential within the Simav Basin, unveiling valuable information through an assessment of the radioactive heat production of geothermal samples. This assessment sheds light on the thermal energy that can be harnessed from these resources, holding promise for sustainable energy generation. Moreover, the identification of magnetic susceptibility characteristics in the geothermal areas offers crucial knowledge regarding the properties of subsurface formations, providing further support for the assessment of geothermal resources.

By evaluating the heat production maps, it was observed that values exceeding  $2 \mu\text{Wm}^{-3}$  could be considered as indicative of geothermal potential areas. Additionally, geothermal drillings within the region are strategically positioned in alignment with these high-value regions. The calculation of radioactive heat production values from migmatite samples, considered as potential heating rocks within the area, involved substituting their K, U, and Th values into the RHP formula. Upon examination of the results, it became evident that the geothermal potential areas in the region exhibit values surpassing 2, and a compelling correlation between the calculated values from magnetic susceptibility measurements and the heat production maps was discerned. Regions lacking geothermal drilling activities may still possess hot dry rock characteristics (Figure 2).

The comprehensive evaluation of the geothermal energy potential in the Simav Basin, based on radioactive heat production and magnetic susceptibility characteristics, is of paramount importance. These findings have significant implications for the energy sector, as they underscore the promising prospects of harnessing geothermal energy as a sustainable and eco-friendly energy source in the region. Furthermore, the sustainable utilization of geothermal resources holds the potential to foster energy security and minimize environmental impacts, aligning with broader sustainable development goals.

In light of the study's outcomes, several key implications arise. Firstly, the identification of geothermal potential areas with heat production values exceeding  $2 \mu\text{Wm}^{-3}$  offers valuable guidance for future geothermal energy development initiatives. These areas present attractive prospects for further exploration and investment in geothermal power generation projects. Additionally, the compatibility between magnetic susceptibility values and geothermal potential areas highlights the role of geophysical measurements in understanding the subsurface properties and enhancing geothermal resource assessment accuracy.

Considering the discussion on future research and

exploration activities, further investigations are warranted to delve into the untapped geothermal potential in the Kütahya Simav district. Geothermal resource mapping efforts, coupled with advanced geophysical surveys and geological studies, can provide a more comprehensive understanding of the subsurface characteristics and geothermal reservoirs in the region. Moreover, in-depth analyses of the thermal properties of migmatites and their spatial distribution could lead to enhanced resource estimations and optimal well-placement strategies.

In conclusion, this study has contributed valuable insights into the geothermal energy potential of the Simav Basin, highlighting its significance as a sustainable energy resource. The assessment of radioactive heat production and magnetic susceptibility characteristics has unveiled promising geothermal potential areas and facilitated a comprehensive evaluation of the region's geothermal resources. The implications of these findings for the energy sector underscore the importance of embracing geothermal energy as a viable and eco-friendly alternative to conventional energy sources. Recommendations for future research and exploration activities will pave the way for further advancements in geothermal energy utilization and contribute to the sustainable energy perspective of the region and beyond.

#### ACKNOWLEDGMENTS

The authors would like to acknowledge The Council of Higher Education (YOK) 100/2000, The SEG Scholarships, The Pamukkale University BAP unit for supporting this study (Projects 2021FEBE042), Zorlu Energy Company who always support academic studies on geothermal energy in Turkey, Kütahya Special Provincial Administration and Governorship of Kütahya, MTA General Directorate - Energy Raw Material Investigation and Exploration Department-Geothermal Reservoir Research and Protected Areas Unit - Phd. Nilgün Dođdu.

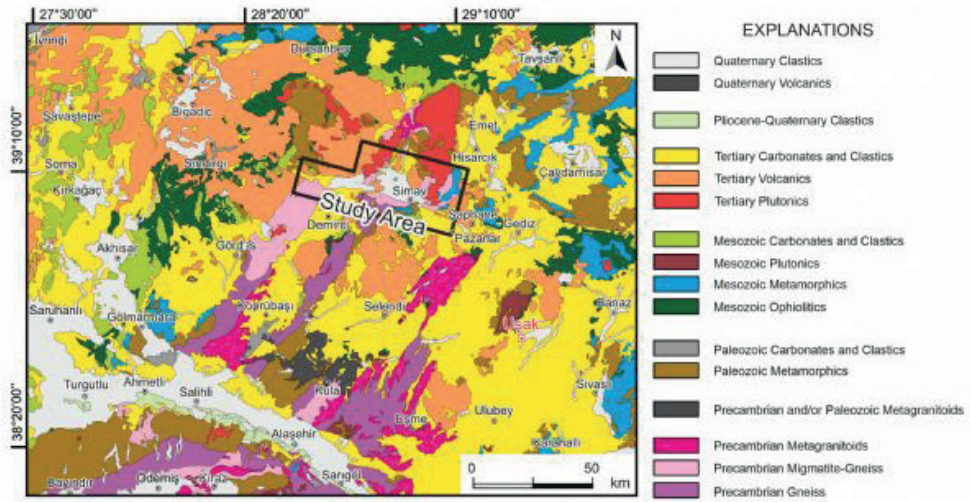
#### REFERENCES

- Birch F., "Heat from Radioactivity", in Nuclear Geology. 1st ed. New York, USA, Wiley, 1954.
- Hazma V.M, Beck A.E., "Terrestrial heat flow, the neutrino problem, and a possible energy source in the core". *Nature*, 240(5380), 343-344, 1972.
- Raybach L. "Radioactive heat production in rocks and its Relation to other petrophysical parameters". *Pure and Applied Geophysics*, 114(2), 309-317, 1976.
- Rybach, L., "Determination of heat production rate". In: Haenel, R., Rybach, L., Stegena, L. (Eds), *Handbook of Terrestrial Heat-Flow Density Determination*. Kluwer, Dordrecht, 125-141, 1988.
- MTA. 2002. 1/500.000 scaled Geological Map of Türkiye, Kütahya Map. Mineral Research and Exploration General Directorate, Ankara.
- Uyanık, N. A., Kurt, B., & Uyanık, O., "Determination of the hot dry rock from radiogenic heat production

for potential geothermal sources and example of Isparta-Yakaören", *Pamukkale University Journal of Engineering Sciences*, 26(6), 1170-1177, 2020.

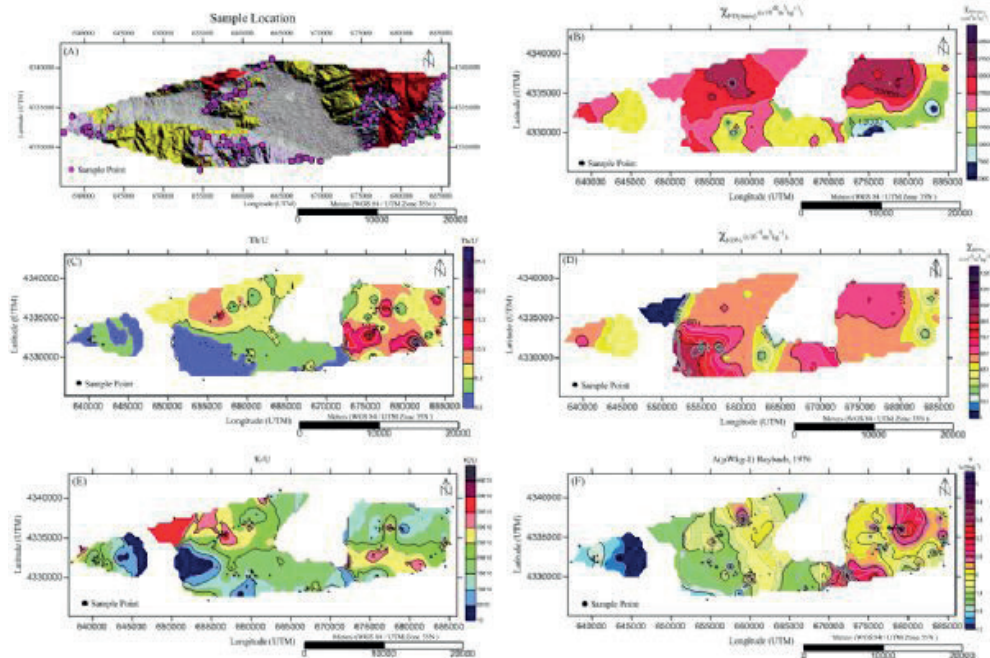
Keywords: Simav Basin, Radioactive Heat Production (RHP)

Figure 1



Study Area (Simav/Kütahya). MTA, 2002, 1:500.000 Scale Geological Map of Turkey, İzmir Quadrangle.

Figure 2



(A) Sample points, (B) Mass-dependent magnetic susceptibility, (C) Th/U ratio, (D) Frequency-dependent magnetic susceptibility, (E) K/U ratio, (F) Radioactive heat generation potential value maps of study area

# Jeotermal Kaynakların Yönetiminde Reenjeksiyonun Önemi

**Nilgün Doğdu, Oktay Çelmen**

Mta Genel Müdürlüğü, Enerji Hammadde Etüt ve Arama Dairesi



## ÖZ

Jeotermal kaynakların yönetimi, jeotermal kaynakların türü (doğal kaynaklar, kuyu), kullanım durumları (termal kullanım, konut-sera ısıtma, elektrik enerjisi vb.), kullanım miktarı (optimum debi, uygun basınç-sıcaklık değişimleri, kimyasal kompozisyon), rezervuar bütünlüğü, çeşitli etkilere dayanarak sürdürülebilirliğinin sağlanması, denetlenmesi, çevreye etkileri, üretim-reenjeksiyon dengesi stratejilerinin planlanması ve uygulamasını kapsamaktadır. Bu kapsamda jeotermal kaynağın reenjeksiyonu ise, sürdürülebilirlik kavramında en önemli hususlardan biridir. Jeotermal sahalarda kullanımdan dönen akışkanın rezervuara geri basımı için, rezervuardaki sıcaklık ve basınç koşullarındaki olumsuz değişimleri önleyici tedbirlerin alınması önemlidir.

Reenjeksiyon, jeotermal enerji üretimi için kullanılan suyun, kullanım sonrası tekrar yer altına geri basılmasını ifade eder. Bu işlemin, doğru lokasyon ve doğru teknik şartlarda yapılması ise jeotermal sahanın sürdürülebilirliğini sağlamak, hidrolojik dengesini ve verimini korumak için en önemli kriterlerden biridir.

Jeotermal kaynakların işletilmesinde reenjeksiyon/deşarj şartları ve yükümlülükleri 5686 Sayılı Kanun ve Yönetmelik hükümlerinde de belirtilmiştir. Jeotermal sahalarda enerji üreten sahalarda ısıtma yapılan sahalarda reenjeksiyon işlemi hem Kanuni hem de teknik bir zorunluluktur.

Bu nedenlerle, jeotermal enerji işletmelerinde reenjeksiyon süreci, sürdürülebilirlik ve çevresel koruma açısından büyük öneme sahiptir. Ayrıca jeotermal enerjinin entegre kullanımı ve bu kullanımın sürdürülebilir bir rezervuar yöntemi ile reenjeksiyon işlemi ile birlikte yapılması jeotermal enerjinin daha geniş çapta, daha etkili ve daha fazla yatırım ile kullanılmasına olanak tanıyacaktır.

Anahtar kelimeler: jeotermal enerji, reenjeksiyon

Reinjection in Geothermal Resources Management and Its Importance

## ABSTRACT

Management of geothermal resources, type of geothermal resources (natural resources, wells), use cases (thermal use, residential-greenhouse heating, electrical energy, etc.), amount of use (optimal flow, appropriate pressure-temperature changes, chemical composition), reservoir integrity, It covers the planning and implementation of production-reinjection balance strategies, ensuring its sustainability by protecting it from various effects, inspection, environmental effects. In this context, the reinjection of the geothermal resource

is one of the most important issues in the concept of sustainability. It is important to take measures to prevent adverse changes in temperature and pressure conditions in the reservoir for the return of the fluid returned from use in geothermal fields to the reservoir.

Reinjection means that the water used for geothermal energy production is pumped back underground after use. Performing this process in the right location and in the right technical conditions is one of the most important criteria to ensure the sustainability of the geothermal field and to maintain its hydrological balance and efficiency.

Reinjection/discharge conditions and obligations in the operation of geothermal resources are also specified in the provisions of Law No. 5686 and Regulation. In geothermal fields, the reinjection process is both a legal and a technical requirement in energy producing fields and heating fields.

For these reasons, the reinjection process in geothermal energy enterprises is of great importance in terms of sustainability and environmental protection. In addition, the integrated use of geothermal energy and the use of this use with a sustainable reservoir method and reinjection process will allow geothermal energy to be used on a larger scale, more effectively and with more investment.

Keywords: geothermal resources, reinjection

## GİRİŞ

5686 sayılı Kanuna göre jeotermal kaynak, jeolojik yapıya bağlı olarak yer kabuğu ısısının etkisiyle sıcaklığı sürekli olarak bölgesel atmosferik yıllık ortalama sıcaklığın üzerinde olan, çevresindeki sulara göre daha fazla miktarda erimiş madde ve gaz içerebilen, doğal olarak çıkan veya çıkarılan su, buhar ve gazlar ile yeraltına insan düzenlemeleri vasıtasıyla gönderilerek yer kabuğu veya kızgın kuru kayaların ısısı ile ısıtılarak su, buhar ve gazların elde edildiği yerler olarak sıcak su ve buharın taşıdığı enerji olarak tanımlanabilir.

İdeal bir jeotermal sistemde (Şekil 1), ekonomik derinlikte jeotermal kaynak oluşturabilecek boyut ve yaşta ısı kaynağı, sıcak su kaynaklarına hidrolik oluk vazifesi yapacak fay ve kırıklar, ısınan rezervuarın ısı kaybını önleyecek bir örtü kaya ile jeotermal sistemi sürekli besleyen uygun bir beslenme alanına sahip olması gerekir.

Ülkemizde jeotermal enerji, yerli, çevre dostu ve sürdürülebilir bir enerji kaynağı olarak önemli bir potansiyele sahiptir.

Türkiye, Alp-Himalaya aktif tektonik kuşak üzerinde yer almakta olup jeolojik olarak genç-diri faylar ile volkanik/mağmatik oluşumlar içermektedir. Bu yapılar

Türkiye’de zengin jeotermal potansiyelin oluşumuna neden olmaktadır. Türkiye’nin ana neotektonik hatları,sıcak ve mineralli su kaynakları ile jeotermal alanların dağılımı Şekil 2’de yer almaktadır.

Ülkemizde jeotermal potansiyelin ortaya çıkarılması çalışmaları 1926 yılında sıcak su kaynakları çalışmaları, 1935 yılında Maden Tetkik ve Arama Enstitüsü’nün kurulması ve özellikle 1960’lı yıllarda MTA projeleri ile yoğunlaşan sıcak ve mineralli sular kaynak arama çalışmaları, 1970’li yıllarda ilk jeotermal santral, 1980’li yıllarda ilk konut ve sera ısıtma projeleri, 1990’lı yıllarda reenjeksiyon çalışmaları, MTA Genel Müdürlüğü’nün 1962 yılında başlattığı jeotermal kaynak arama çalışmaları 2005 yılında Yenilenebilir Enerji Kanunu, 2006 ve 2007 yıllarında da 5686 sayılı Jeotermal Kaynaklar ve Doğal Mineralli Sular Kanunu ve Uygulama Yönetmeliği’nin yürürlüğe girmesi ve özel sektörün de arama ve araştırma faaliyetlerine katılması ile hızla artmış, MTA Genel Müdürlüğü’nün kaynak varlığını ortaya çıkardığı jeotermal sahaları ihale etmesi, yatırımcıların da bu sahaları geliştirerek yatırıma kazanması ile hızla artmıştır.

Jeotermal sistemlerin sürdürülebilirliği, jeotermal rezervardan elde edilen akışkanların sıcaklık, basınç ve hidrokimyasal yapısının olumsuz etkilenmeden korunarak uzun süreli ve çevre dostu bir şekilde kullanılması anlamına gelir. Bunun sağlanması, jeotermal akışkanların uygun üretim koşullarında ve uygun yöntemlerle çıkarılarak işletilmesi ile başlar ve mutlaka uygun lokasyon ve teknik şartlarda reenjeksiyonu ile devam etmelidir. Bu sayede, rezervuarın hidrolik dengesi korunur, jeotermal kaynağın daha uzun süreli ve verimli bir şekilde kullanılması sağlanır ve aynı zamanda çevresel etkilere karşı da koruma sağlanır.

## AMAÇ VE KAPSAM

Çalışmanın amacı, jeotermal kaynakların kullanımında ve işletilmesinde yerli ve sürdürülebilir enerji kaynaklarımızdan olan jeotermal enerji sistemlerinde reenjeksiyonun önemini irdelemek, sıcaklık, basınç, kimyasal kompozisyonunun değişmeden jeotermal kaynakların korunması için kullanımdan dönen jeotermal atık suyun (termal kullanımlar hariç) reenjeksiyonunun yapılması, üretim-reenjeksiyon dengesinin sağlanması, reenjeksiyon lokasyon seçimlerinde dikkat edilmesi gerekli hususlar, ülkemizdeki uygulamalarının sürdürülebilirlik üzerindeki etkilerini araştırmak ve jeotermal kaynak yönetimi koşullarının irdelenmesidir. Jeotermal akışkanın kullanıldığı işletmelerde kullanımdan dönen suyun reenjeksiyonu jeotermal sistemin beslenmesi açısından gerekli olduğu gibi yasal açıdan da bir zorunluluk getirmektedir. 5686 sayılı Jeotermal Kaynaklar ve Doğal Mineralli Sular Kanununa göre, jeotermal enerji ile elektrik üreten sahalar ile ısıtma yapılan sahalarda ve entegre kullanımın söz konusu olduğu sahalarda reenjeksiyon şartı getirilmiştir. Bu tür sahalarda, özellikle entegre kullanımın söz konusu olduğu durumlarda, jeotermal sistemin basınç ve sıcaklık koşullarındaki denge

gözetilerek, kabuklaşma ve korozyon problemleri ile rezervuardaki çatlaklı zonların kısmen veya tamamen tıkanmasına yol açmayacak şekilde gerekli tedbirler alınarak reenjeksiyon yapılmalıdır (5686 sayılı Jeotermal Kaynaklar ve Doğal Mineralli Sular Kanunu 14. Maddesi ve Uygulama Yönetmeliği- 23., 24., 25, ve 26. Maddeleri). Dolayısıyla jeotermal alanlarda, işletme faaliyetine geçmeden önce ruhsat alanı içerisinde yapılacak etütler neticesinde reenjeksiyon bölgesi belirlenmeli, bu bölgede uygun sayıda kuyu açılarak bu kuyularda enjektivite testleri yapılarak, reenjeksiyon uygulamaları yapılmalıdır.

## MATERYAL VE METOD

Çalışma kapsamında, MTA Genel Müdürlüğü’nün özellikle 2007 yılından sonra kamu ve özel sektöre yapmış olduğu Teknik Danışmanlık, Kurumsal Danışmanlık, Kaynak Koruma Alanı Etüt Çalışmaları ile gerek Ücretli İşler gerekse Yatırım programı kapsamında yapılan jeotermal etüt ve sondaj çalışmalarından elde edilen bilgi, birikim ve gözlemler değerlendirilmiştir. Ayrıca jeotermal sistemlerde reenjeksiyona yönelik literatür taraması ve bilimsel makalelerin incelenmesi yoluyla bilgi toplama yöntemi kullanılarak bazı çalışmalar gerçekleştirilmiştir.

MTA Genel Müdürlüğü tarafından yapılan çalışmalar, gözlem ve değerlendirmeler ile literatür taraması sonucunda elde edilen bilgiler, niteliksel analiz yöntemiyle değerlendirilmiştir. Toplanan veriler, tematik analiz ve içerik analizi gibi yöntemlerle analiz edilerek, jeotermal enerji sistemlerinin sürdürülebilirlik açısından reenjeksiyonun önemi, ne kadar etkili olduğu belirlenmeye çalışılmıştır. Ayrıca, reenjeksiyon lokasyon seçimi, dikkat edilmesi gerekli hususlar ve reenjeksiyonun yürürlükteki kanun ve uygulamalardaki yeri de belirtilmeye çalışılmıştır.

## JEOTERMAL KAYNAKLARDA REENJEKSİYON

Dünya’da yapılan çalışmalara bakıldığında ilk reenjeksiyon uygulamaları, The Geysers, ABD (1969), Otake, Japonya (1972), Larderello, İtalya (1974), Hatchobaru, Japonya (1977), Kakkonda, Japonya (1980) ve Onuma, Japonya (1981) gibi yüksek sıcaklıkta elektrik üreten alanlarda başlamıştır. Reenjeksiyon kavramı öncelikle, jeotermal kaynaklardan elde edilen kullanılmış akışkanların doğru bir şekilde bertaraf edilmesi için kullanılmıştır. Ancak günümüzde jeotermal akışkanın reenjeksiyonu, enerjisi azalmış sıcak akışkanların düzenli bir şekilde bertaraf edilmesini sağlarken aynı zamanda rezervuarın etkin bir şekilde beslenmesini de sağlar (Axelsson, 2013). Ayrıca, jeotermal suyun ısıtma ve enerji üretiminde kullanılması sırasında, kullanılmış suyun reenjeksiyonu, yüksek sıcaklık ve basınç koşullarının dengede tutulmasına ve akışkanın debisindeki düşüşün engellenmesine yardımcı olur

MTA Genel Müdürlüğü tarafından kamu ve özel sektöre yapılmış olan Teknik Danışmanlık, Kurumsal

Danışmanlık, Kaynak Koruma Alanı Etüt Çalışmaları sonucunda elde edilen veilere göre; Türkiye’de halen işletmede olan jeotermal enerji santrallerinde, kullanılan jeotermal akışkanın %90-100 oranında reenjeksiyonu, vazgeçilmez rezervuar yönetimi faaliyetlerinden biridir. Alan ısıtmada (konut veya sera), kullanılan jeotermal akışkanın ise yaklaşık %70’i reenjekte edilmekte olup, bazı durumlarda doğrudan ısıtma için kullanılan jeotermal akışkan, termal tesisler ve diğer entegre amaçlar için de kullanılabilir (Doğdu ve Çelmen, 2023).

Ülkemizde jeotermal enerji yatırımı yapan pek çok kamu iştiraki ile özel sektör yatırımcısı bulunmaktadır. MTA Genel Müdürlüğü tarafından yapılan etüt, sondaj, teknik danışmanlık, kurumsal danışmanlık ve Kaynak Koruma Alanı Etüt çalışmaları sonucu elde edilen ve jeotermal sistemin sürdürülebilirliği açısından oldukça önemli pek çok veri bulunmaktadır. Bu verilerin detayları, gizlilik ilkesi ve tüm teknik denetimlerin ilgili İl Özel İdareleri/Valilik koordinasyonunda yürütülmesinden dolayı verilememiştir. Çalışmanın kapsamı, ülkemizdeki jeotermal enerji yatırımlarının sürdürülebilirliğini saha bazlı detaylandırmak değil, elde edilen tüm veri ve gözlemlere dayanarak reenjeksiyonun önemi ve lokasyon seçim kriterlerinden bahsetmek olarak belirlenmiştir. Bu nedenle bilgiler MTA Genel Müdürlüğü tarafından belirlenen jeotermal alanlar bazında verilmiştir.

### REENJEKSİYON KUYU LOKASYONLARININ BELİRLENMESİ

Jeotermal sahanın sürdürülebilirliği, uygun şartlarda reenjeksiyon işlemlerinin tüm teknik özelliklerinin titizlikle göz önünde bulundurulmasıyla sağlanır. Bu bağlamda, jeolojik veriler (stratigrafi, tektonizma, hidrojeoloji), sondaj verileri (litostratigrafi, sıcaklıkta değişim), jeofizik veriler, kuyu logları, akış hızları, hidrojeokimyasal veriler (kaynak ve kuyu sıcaklıkları, kimyasal bileşimler) gibi faktörler, reenjeksiyon kuyusu yerlerinin doğru bir şekilde belirlenmesinde kritik rol oynar. Reenjeksiyon kuyusu yerlerinin seçimini etkileyen diğer önemli etmenlerden biri, jeotermal akışkanın üretim bölgesinden reenjeksiyon bölgesine olan derin sirkülasyonu sırasında, rezervuara ulaşana kadar sıcaklık değişiminin önceden tahmin edilmesidir. Reenjeksiyon kuyu lokasyonu seçiminde en etkili olduğu değerlendirilen 3 (üç) yöntem değerlendirilmiş ve Doğdu ve Çelmen, 2023’te detaylandırılmıştır.

### YERALTISUYU AKIM HARİTALARININ KULLANIMI

Jeolojik etüt ile yapılan detaylı çalışmalar, stratigrafik birimlerin tespiti, tektonik yapıların incelenmesi (fay, graben gibi), kuyu verilerinin analizi ve hidrojeolojik özelliklerin değerlendirilmesiyle birlikte, rezervuar, örtü kaya ve tektonik parametrelerin yorumlanması sayesinde, akım koşulları ve potansiyel reenjeksiyon alanları tespit edilir. Bu çalışmaların sonucunda, bölgedeki beslenme ve boşalım bölgeleri arasındaki akış

yolları, kırık hatları ve hidrokimyasal parametrelerin belirlenmesi, reenjeksiyon alanlarının doğru bir şekilde saptanmasında kritik bir rol oynar.

### İZLEYİCİ TESTLERİNİN KULLANIMI

İzleyici testleri, hidrolojik ve hidrojeolojik çalışmalarda yaygın olarak kullanılmakta olup, yeraltı suyu akış yönü, hızı ve yer altı sularındaki kirleticilerin kaynağını tespit etme gibi amaçlar taşımaktadır. Ayrıca, jeotermal sahada üretim-reenjeksiyon sisteminin dengesi ve sirkülasyonunun belirlenmesi için de izleyici testlerinin yapılması en etkili yöntemlerden biridir.

### DURAYLI İZOTOPLARIN REENJEKSİYON LOKASYON SEÇİMİNDE KULLANILMASI

Jeotermal sahalarda, beslenme bölgesini belirlemek için kullanılan önemli bir yöntem beslenme yüksekliğinin tespittir. Bu yöntem, bölgenin jeolojisi ve suyun hidrokimyasal özellikleri ile birlikte değerlendirilerek jeotermal rezervuarın beslenme alanının tahmin edilmesine yardımcı olur. Jeotermal sahalardaki sıcak su kaynaklarının beslenme alanlarını belirlemek için oksijen-18 ve döteryum izotoplarına dayalı yöntemler kullanılabilir (Mazor, 1991). Ayrıca, atmosferdeki su buharının izotopik oranları deniz seviyesinden yüksek bölgelere doğru azalır ve yükseklikle birlikte de izotop içeriğinde azalma meydana gelir. Bu nedenle, bir jeotermal rezervuarın beslenme yüksekliğini tespit etmek için bölgedeki yağışın oksijen-18 ve/veya döteryum içeriğini bilmek önemlidir. Ancak bu veriler her zaman mevcut olmayabilir, bu durumda yağıştan kısa sürede yeraltına süzülen soğuk su kaynaklarının oksijen-18 değeri de kullanılabilir. Bu soğuk su kaynaklarının yükseklik ve kararlı izotop değeri, sıcak su kaynaklarının yükseklik ve kararlı izotop değeriyle karşılaştırılarak beslenme yüksekliği tespit edilebilir.

### ÜLKEMİZDEKİ JEOTERMAL SAHALARDA REENJEKSİYON DURUMU VE MTA GENEL MÜDÜRLÜĞÜ ÇALIŞMALARI

5686 sayılı Jeotermal Kaynaklar ve Doğal Mineralli Sular Kanunu ve Uygulama Yönetmeliği hükümleri, jeotermal kaynağın sürdürülebilirliği ve etkin rezervuar / jeotermal kaynak yönetimi için, jeotermal enerjinin elektrik üretimi, konut ısıtma ve sera ısıtma amaçlı (Tablo 1,2,3) kullanıldığı jeotermal sahalarda reenjeksiyon uygulaması zorunludur. Bu nedenle gerek özel sektör gerekse kamu iştiraklerinin imtiyaz sahibi olduğu ruhsat sahalarda, jeotermal kaynakların işletilmesinde reenjeksiyon uygulamaları da dahil olmak üzere; yapılan faaliyetlerin sorumluluğu ruhsat sahibine, faaliyetlerin yasa- yönetmeliğe uygunluğu ve denetlenmesi ilgili sorumluluk ise ilgili İl Özel İdare/ Valilik koordinasyonunda yapılması gerekmektedir.

Jeotermal enerjinin elektrik üretimi, sera ısıtma ve konut ısıtma amaçlı kullanıldığı birçok jeotermal sahada jeotermal enerjinin sürdürülebilir kullanımı ve reenjeksiyon kuyusu lokasyonları belirleme çalışmaları



yapılmış ve işletmeye alınmış olup rezervuar yönetimine yönelik araştırmalar devam etmektedir (Tablo 4). Bunlara örnek olarak Kütahya-Simav-Eynal-Çitgöl-Naşa, Nevşehir-Kozaklı alanlarından kısaca aşağıda bahsedilmiş olup bu ve diğer alanlara yönelik detaylı bilgiler Dođdu ve Çelmen, 2023'te verilmiştir.

Simav-Eynal-Çitgöl-Naşa jeotermal sahasında 1985 yılından bu yana MTA Genel Müdürlüğü ve Belediye Başkanlığı tarafından sondaj çalışmaları yapılmakta ve sondajlardan elde edilen jeotermal akışkan konut ısıtma, sera ısıtma ve termal amaçlı kullanılmaktadır. Bölgede 40 adet üretim ve 2 adet reenjeksiyon kuyusu bulunmaktadır. Simav-Eynal jeotermal sahasında Y-1 kuyusu reenjeksiyon amacıyla kullanılmaktadır. Kış aylarında kullanımdan dönen jeotermal akışkanın mevcut Y-1 kuyusuna reenjekte edildiği ancak bunun jeotermal rezervuarın sürdürülebilirliği için yeterli olmadığı görülmüştür. Bu kapsamda, MTA'nın jeolojik, jeofiziksel ve diğer verilerinin multidisipliner değerlendirmesi sonucu reenjeksiyon alanı belirlenmiş, daha sonra Simav ve Eynal'dan dönen suların konut ve sera ısıtma kullanımlarından dönen akışkanın enjeksiyonu amacıyla, EJ-1 reenjeksiyon kuyusu MTA tarafından 2022 yılında açılmıştır (Şekil 3).

Nevşehir-Kozaklı jeotermal sahasında, 1965 yılından itibaren MTA Genel Müdürlüğü, İdare ve Belediye tarafından sondaj çalışmaları yapılmaktadır. Sondajlardan elde edilen jeotermal akışkan Nevşehir-Kozaklı jeotermal sahasında konut ısıtma, sera ısıtma ve termal amaçlı kullanılmaktadır. Sahada 25 adet üretim ve 1 adet reenjeksiyon kuyusu bulunmaktadır. Jeotermal akışkan NEVJET A.Ş. tarafından 1.500 ton kapasiteli toplama/dağıtım tankından konut ısıtma ve termal amaçlı abonelere, kullanımdan dönen akışkan ise 500 ton kapasiteli reenjeksiyon tankından reenjeksiyon kuyusuna geri gönderilmektedir. MTA tarafından yapılan etütlerle Nevşehir-Kozaklı jeotermal sahasında 2 adet reenjeksiyon kuyusu yer belirlenmiştir. Bu çalışmalar sonucunda belirlenen 1 adet reenjeksiyon kuyusu yetkililer tarafından açılmış olup halen reenjeksiyon amacıyla kullanılmaktadır (Şekil 4).

Ruhsatlarda yapılan faaliyetler ile ilgili ihtiyaç duyulursa İl Özel İdare ve YİKOB tarafından MTA Genel Müdürlüğü'nden teknik görüş alınabilir. Bu nedenle işletme ruhsatlarındaki faaliyetlerde yasal olarak reenjeksiyon zorunluluğu, uygunluğu ya da reenjeksiyonun jeotermal kaynaklara etkisi durumları MTA Genel Müdürlüğü'nden teknik görüş istenebilir.

Reenjeksiyonda en önemli parametreler, atık akışkanın kimyasal konsantrasyonu ile sıcaklığıdır. Jeotermal akışkanın çevreye vereceği olumsuzlukları önlemek, üretim kuyusunun rezervini artırmak, jeotermal rezervuarı beslemek ve rezervuar basıncının sabit tutulmasını sağlaması açısından için en etkili yöntem uygun bir lokasyona yapılacak reenjeksiyon olacaktır. Olası bir reenjeksiyon işlemi sırasında alandaki akışkanın hem sıcaklığının düşme ihtimali hem de jeotermal sularda bulunan ağır metal ve Bor içerikleri, bunların insani-tarımsal amaçlı kullanılan sulara karışması gibi durumlarda kimyasal kompozisyonunun değişmesi olasılıkları da göz önüne alınmalıdır.

Ayrıca, termal akışkanlar üretim kuyusundan çekildikten, enerjisi alındıktan sonra atık niteliğindeki soğuk akışkanın çevreye zarar vermeden bertaraf edilmesi amacıyla üretim kuyusunun bulunduğu bölgenin dışında yeniden yeraltına enjekte edilmesi de reenjeksiyon işlemi olarak uygulanabilir.

Belirlenecek lokasyonlarda açılacak reenjeksiyon kuyularının, reenjeksiyona uygun olup olmadığına ilişkin ise gerekli testlerin (enjektivite testi vb.) yapılması; üretim-reenjeksiyon miktarının net olarak bilinmesi, kuyunun reenjeksiyona uygun olması halinde ise, rezervuarda herhangi bir sıcaklık ve basınç düşümüne yol açmayacak uygun sıcaklık/basınçtaki akışkanın reenjeksiyonunun yapılarak rezervuarın olası sıcaklık ve basınç düşümlerine karşı düzenli olarak belirli aralıklarla gözlemlenmesi gerekmekte olup, yapılan reenjeksiyonun rezervuarda sürdürülebilir üretimi etkileyecek sıcaklık ve/veya basınç düşümüne yol açtığı belirlenmesi halinde ise, reenjeksiyona izin verilmemesi önem arz etmektedir.

5686 sayılı Jeotermal Kaynaklar ve Doğal Mineralli Sular Kanunu 14. Madde 4. Fıkrasına göre; "Ruhsat sahibi, kullanım sona erene çıkacak akışkanın çevre limitlerini dikkate alarak deşarj edebilir. Akışkan içeriği çevre limitlerine göre deşarja izin vermiyorsa reenjekte etmekle yükümlüdür. Ancak formasyonun fiziksel ve kimyasal özellikleri nedeniyle reenjeksiyonun gerçekleşmediğinin MTA tarafından onaylanması halinde, çevre kirlenmesini önleyecek tedbirler alınarak deşarj yapılır".

Jeotermal sahalarda reenjeksiyon işlemi düzgün yapılmadığı takdirde rezervuar basıncı düşebilir ve su seviyesinin düşmesi nedeniyle sahada çökmeler meydana gelebilir (Dođdu ve Çelmen, 2023). Öte yandan, yenilenebilir enerji kaynakları olarak sınıflandırılan jeotermal kaynaklar, reenjeksiyonun yapılamaması nedeniyle yenilenemeyip kısa sürede tükenebilir. Ayrıca, reenjeksiyon uygun koşullarda yapılmadığı takdirde, rezervuar veya sistemde soğuma ile kabuklaşma ve korozyon oluşabileceği gibi, uygun şartlarda yapılmayan reenjeksiyon işlemi yüzey sularını da olumsuz etkileyebilir.

## SONUÇLAR VE DEĞERLENDİRME

Jeotermal kaynakların sürdürülebilirliğinin sağlanması ve üretim-reenjeksiyon dengesi politikasının sürdürülebilmesi kaynakların korunmasını sağlar. Doğru koşullarda ve lokasyonlarda reenjekte edilen akışkanlar sayesinde jeotermal rezervuarların mevcut basınçları süreklilik ve güvenilir enerji üretimi sağlanabilir. Aksi durumda akışkan üretiminin fazla olduğu, reenjeksiyonun uygun koşullarda yapılmadığı durumlarda zamanla basınçlar düşebilir ve kaynak olumsuz etkilebilir.

Jeotermal akışkanların içerdiği değerli mineraller ve çözünmüş maddeler, günümüzde ekonomik olmayabilecek ancak çeşitli endüstriyel ve tarımsal amaçlar için kullanılacak miktarlarda olabileceğinden, kullanımdan dönen jeotermal akışkan reenjekte edildiğinde bunlar korunabilir ve teknoloji

ilerledikçe bu potansiyel değerlendirilebilir.

5686 sayılı Jeotermal Kaynaklar ve Doğal Mineralli Sular Kanunu ve Uygulama Yönetmeliği' ne göre jeotermal kaynağın sürdürülebilirliği ve etkin rezervuar / jeotermal kaynak yönetimi için, elektrik üretimi, konut ısıtma ve sera ısıtma amaçlı kullanımlarda reenjeksiyon uygulaması zorunludur. Bu nedenle gerek özel sektör gerekse kamu iştiraklerinin imtiyaz sahibi olduğu ruhsat sahalalarında, jeotermal kaynakların işletilmesinde reenjeksiyon uygulamaları da dahil olmak üzere; yapılan faaliyetlerin sorumluluğu ruhsat sahibine, faaliyetlerin yasa- yönetmeliğe uygunluğu ve denetlenmesi ilgili sorumluluk ise ilgili İl Özel İdare/ Valilik koordinasyonunda yapılması gerekmektedir.

Reenjeksiyon kuyusunun belirlenmesi ve açılması aslında rezervuar yönetiminde sürdürülebilirliğin sağlanması için sadece başlangıçtır. Bundan sonraki adımda, sürekli izlemeler, rezervuar parametrelerinin düzenli gözlemlenmesi ve gerekli tedbirleri almak gerekir. Bu şekilde, uzun vadeli enerji sürdürülebilirliği sağlanabilir, jeotermal enerji kaynakları daha verimli ve güvenilir bir şekilde kullanılabilir.

## TEŞEKKÜR

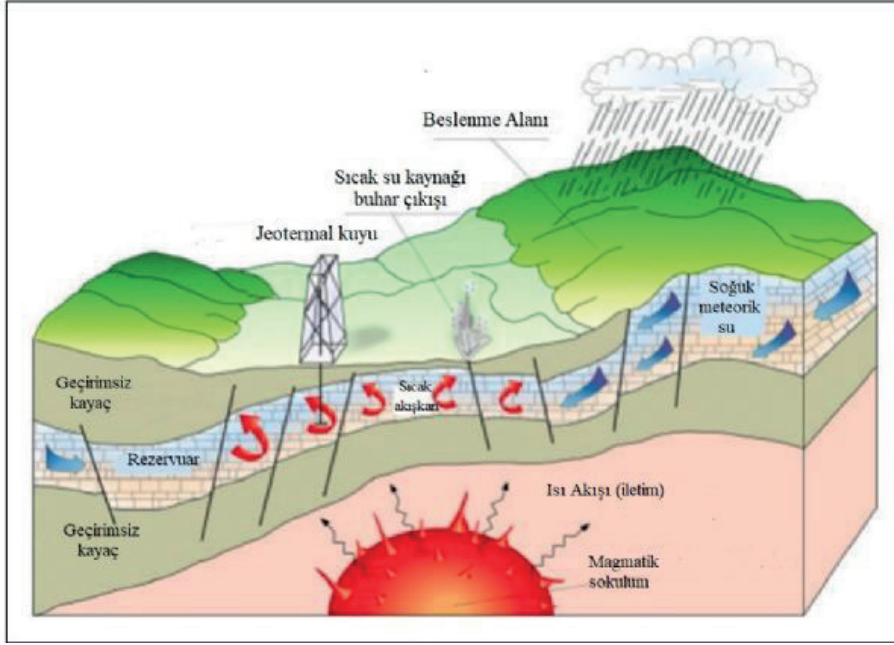
Bu çalışmada, Maden Tetkik ve Arama (MTA) Genel Müdürlüğü Enerji Hammadde Tetkik ve Arama Dairesi Başkanlığı tarafından yürütülen jeotermal enerji etüt ve sondaj çalışmaları ile jeotermal kaynak koruma alanı etütleri kapsamındaki çalışmalardan yararlanılmıştır. Yazarlar bu projelerde görev yapanlara katkılarından dolayı teşekkür ederler.

## KAYNAKLAR

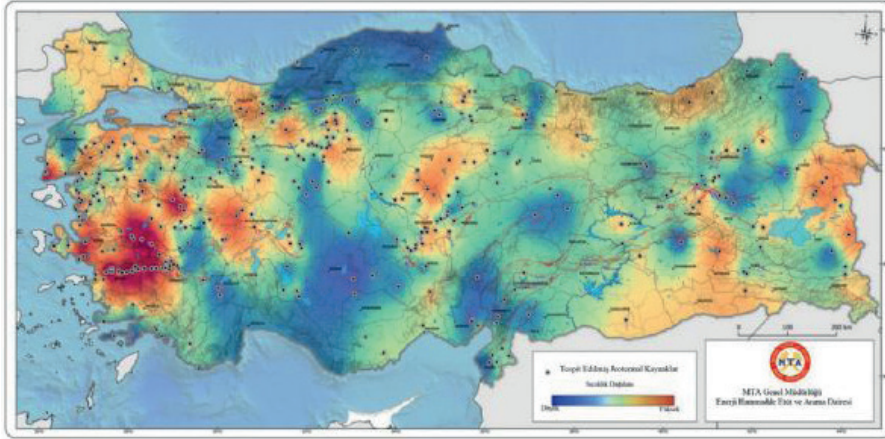
- A Axelsson, G. 2013b. Tracer tests in geothermal resource management. In EPJ Web of Conferences (Vol. 50).
- Doğdu, N. ve Çelmen, O. 2023. Importance of reinjection in sustainability of geothermal resources and reinjection well locations in Türkiye (kabul edildi/basım aşamasında), Bulletin of the Mineral Research and Exploration, Ankara, DOI: 10.19111/bulletinofmre.1316785
- Mazor, E. 1991. Applied Chemical and Isotopic Groundwater Hydrology. Open University Press, Suffolk, 274.

Anahtar Kelimeler: jeotermal enerji, reenjeksiyon

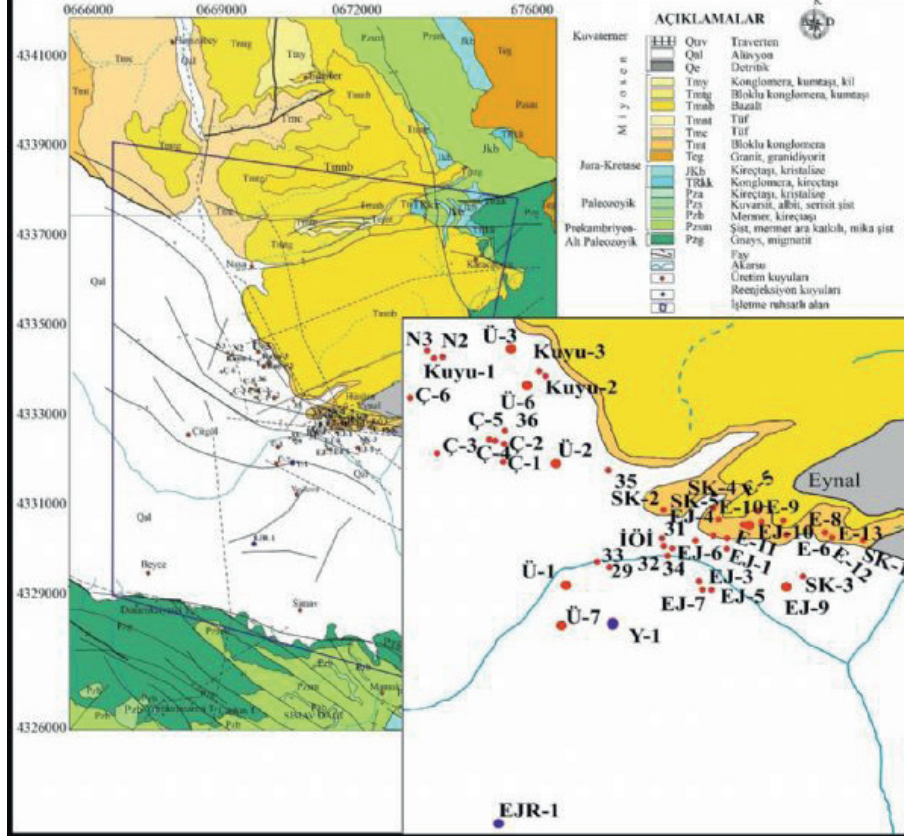
Şekil-1 Bir jeotermal sistemin şematik gösterimi (Barbier, 2002)



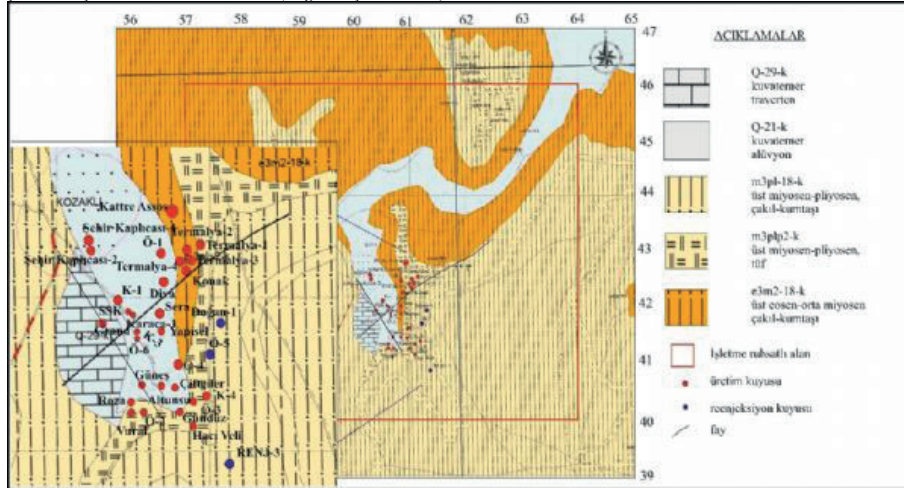
Şekil 2- Türkiye'deki Jeotermal Alanların Dağılımı



Şekil 3- Kütahya-Simav-Eynal-Çitğöl-Naşa Jeotermal Alanı (Doğdu ve Çelmen, 2023)



Şekil 4- Nevşehir-Kozaklı Jeotermal Alanı (Doğdu ve Çelmen, 2023)



Tablo 1. MTA Genel Müdürlüğü kayıtlarına göre ülkemizde jeotermal kaynaktan fiili olarak elektrik üretimi yapan sahalar

Jeotermal saha	İşletmedeki kurulu kapasite (MWe)
Denizli-Kızıldere	280,55
Denizli-Tekkehamam	79,25
Aydın-Germencik	283,9
Aydın - Gümüşköy	13,2
Aydın - Umurlu	24
Aydın - Yılmazköy	24
Aydın - Efeler	24,8
Aydın - Nazilli	10
Aydın - Salavatlı	68,45
Aydın - Bozköy-Çamur	169,8
Aydın - Pamukören	176,55
Aydın - Sultanhisar	36,31
Aydın - Kuyucak	18
Aydın - Buharkent	13,77
Aydın-Merkez	17
Çanakkale – Tuzla	7,5
Çanakkale-Babadere	8
Çanakkale-Ayvacık	30,75
Manisa-Alaşehir	309,74
Manisa-Salihli	69,5
Afyonkarahisar-Ömer-Gecek	2,76
İzmir-Seferihisar	12

Tablo 2. MTA Genel Müdürlüğü kayıtlarına göre ülkemizde jeotermal kaynaktan konut ısıtma yapılan sahalar

Jeotermal saha	Konut (Ke)	Isıtma
Afyon-Ömer Gecek	24.600	
Afyon-Gazlıgöl	500	
Afyon-Heybeli	374	
Afyon-Sandıklı	11.500	
Ağrı-Diyadin	690	
Ankara-Kızılcahamam	2.500	
Balıkesir-Bigadiç	1.950	
Balıkesir-Edremit	4.881	
Balıkesir-Gönen	2.500	
Balıkesir-Güre	1.200	
Denizli-Sarayköy-Bereket En.	2.500	
İzmir- Balçova	36.000	
İzmir-Bergama	450	
İzmir-Dikili	2.500	
Kırşehir	1.800	
Kütahya-Simav-Eynal	13.400	
Manisa-Salihli	7.292	
Nevşehir-Kozaklı	3.000	
Yozgat-Sorgun	1.500	

Tablo 3. MTA Genel Müdürlüğü kayıtlarına göre ülkemizde jeotermal kaynaktan sera ısıtması yapılan sahalara

Jeotermal saha	Sera Alanı (m <sup>2</sup> )
Afyon-Ömer Gecek	300.000
Afyon-Gazlıgöl	10.000
Afyon-Heybeli	100.000
Afyon-Sandıklı	475.000
Ağrı-Diyadin	22.000
Ankara-Kızılcahamam	500
Aksaray-Sarıyahşi	40.000
Aydın-Gümüşküy-Söke-Germencik-Sultanhisar	174.000
Balıkesir-Hisaralan	4.500
Denizli-Gölemezli	184.168
Denizli-Yenicekent	53.566
Denizli-Sarayköy-Bereket En.	276.189
İzmir-Seferihisar	1.000
İzmir- Balçova	6.000
İzmir-Dikili	850.000
Kırşehir	100.000
Kütahya-Simav-Eynal	265.000
Manisa-Urganlı	170.000
Manisa-Salihli	422.000
Nevşehir-Kozaklı	67.000
Şanlıurfa-Karaali	450.000
Yozgat-Sorgun	25.000
Yozgat-Boğazlıyan	56.916

Tablo 4. MTA Genel Müdürlüğü tarafından verilen/yapılan reenjeksiyon kuyu lokasyonlarının bulunduğu jeotermal sahalara

Jeotermal saha	İşletme	İşletme Durumu
Denizli-Kızıldere	Elektrik üretimi	Aktif olarak üretim ve reenjeksiyon yapılıyor
Kütahya-Simav-Eynal-Çitgöl	Konut ve sera ısıtması Termal kullanım Yün kurutma	Aktif olarak üretim ve reenjeksiyon yapılıyor
Nevşehir-Kozaklı	Konut ve sera ısıtması Termal kullanım	Aktif olarak üretim ve reenjeksiyon yapılıyor
Afyonkarahisar-Sandıklı	Konut ve sera ısıtması Termal kullanım	Aktif olarak üretim ve reenjeksiyon yapılıyor
Afyonkarahisar-Ömer Gecek	Elektrik üretimi Konut/sera ısıtması Termal kullanım	Aktif olarak üretim ve reenjeksiyon yapılıyor
Afyonkarahisar-Çobanlar	Sera ısıtma Termal kullanım	Reenjeksiyon kuyusu lokasyonu önerildi
Elazığ-Cıpköy	Sera ısıtma	Proje inşaa aşamasında

# Implications for the Geothermal Potential of the Area between the Dead Sea Transform Fault System and the East Anatolian Transform Fault System (Karasu Rift) Based on Geochemical, Biological and Deep well Data: S Türkiye



**Aydm Cicek<sup>1</sup>, Galip Yüce<sup>2</sup>**

<sup>1</sup>General Directorate of MTA, Department of Energy Raw Materials Survey and Exploration, 06800, Ankara / Türkiye

<sup>2</sup>Hacettepe University, Department of Geological Engineering, 06810, Beytepe, Ankara / Türkiye

## ABSTRACT

The geothermal potential of the region between the East Anatolian Transform Fault System and the Dead Sea Transform Fault System is relatively unknown due to limited studies. Only some detailed geological, geochemical and deep geothermal drilling studies were carried out along the Karasu Rift Valley between 2010 and 2015 by MTA and Hacettepe University. Based on these data, a series of hot and cold groundwaters were sampled, analyzed and evaluated from springs and shallow wells. Based on the obtained new data, Karasu Valley seems to have limited geothermal potential and can be considered as low enthalpy geothermal system. Geothermal gradients along the Karasu Rift range between 20.3 to 42.4 oC/km (average is 30,6 oC/km) based on deep wells reaching up to 4443 m depths. In addition, relatively higher geothermal gradients are observed at shallower depths (i.e. < 1000 m) and the geothermal gradient decreases with increasing depth. Although the Karasu Rift has extensive Quaternary volcanism, some geothermal studies in the region show that young basaltic volcanics have very low geothermal heat source potential. This is most likely due to low viscosity, higher density related rise of mantle sourced melts with respect to surrounding formations and limited residence times at shallow crustal levels in the study area. According to the interpretation of gamma ray well log data obtained from deep wells, radiogenic heat production appears to be low. However, this hypothesis needs more evidence such as calculations based on U, Th, K elements to be measured from rock samples. Low-temperature serpentinization processes may be a possible explanation for anomalous geothermal gradients at least in some limited locations in the study area. However, this hypothesis needs more evidence.

Key words: Karasu Rift, geothermal potential.

## INTRODUCTION

The neotectonics of Türkiye is mainly controlled by four major structure. They are: South Aegean-Cyprus Arc (SACA), North Anatolian Transform Fault System (NATFS), East Anatolian Transform Fault System (EATFS) and Dead Sea Transform Faults System (DSTFS) (Figure 1) (Bozkurt, 2001). The neotectonics is also the major governing reason behind the geothermal potential of Türkiye. Geothermal energy potential of Türkiye is ranked as the fourth in the world and the first in Europe based on the installed power capacity.

The main scope of this study is to present new field

geological, hydrogeochemical and deep well data (between 552 - 4443 m) distributed throughout so called Karasu Rift (Hatay-Gaziantep-Kahramanmaraş) located between EATFS and DSTFS (Figure 1). Karasu Rift is a nearly 185 km long, 10-40 km wide, NNE-trending transtentional megastructure bounded by the DSTFS to the east, Mediterranean Sea to the SSW, the EATFS to the west and Andırın mountain to the north (Boulton and Robertson 2007; Boulton and Robertson 2008; Boulton 2009) (Figure 1). In addition, three tectonic plates meet along this structure, namely, African, Arabian and Anatolian Plates. The structure constitutes also NW margin of the Arabian plate.

## GEOLOGICAL OUTLINE OF THE STUDY AREA

The rocks exposing in the study area are classified into thirty formations or members by Selçuk (1985); Yolal et al. (2015). They are: (1) Precambrian Sadan Formation, (2) lower Cambrian Zabuk Formation, (3) lower-middle Cambrian Koruk Formation, (4) middle to Upper Cambrian Sosink Formation, (5) upper Cambrian-lower Ordovician Kardere Formation (6) middle Ordovician Kızlaç Formation, (7) Middle-Upper Cambrian Bedinan Formation, (8) Lower Silurien Akçadağ Formation, (9) Middle to Upper Silurien Dedeler Formation, (10) Upper Silurien Bahçe Formation, (11) Lower Devonian Quartzite Member, (12) Lower to Upper Devonian Hasanbeyli Formation, (13) Lower Triassic Arılık Formation, (14) Middle to Upper Triassic Çanaklı Formation, (15) Upper Jurassic Keldağ Formation, Kretase aged (16) Tekneçik, (17) Yaylıkdamlar, (18) Kızıldağ ophiolite, (19) Yalaz and (20) Kaleboğaz Formations, (21) Paleosen aged Uluyol Formation, (22) Lower Eocene Okçular Formation, (23) Upper Eocene Kışlak Formation, Miocene aged (24) Balyatağı, (25) Sofular, (26) Tepehan, (27) Nurzeytin and (28) Vakıflı Formations, (29) Samandağ Formation and (30) Quaternary Units such as alluvium and basalts (Figure 2). The readers who are interested in detailed stratigraphy of the study area are referred to Yolal et al. (2016).

The study area includes many structures such as faults and folds. Here, we only discuss faults.

The faults observed in the study area are sub-divided into two based on their trends. They are (1) N to NE-trending faults and (2) mainly WNW-trending faults.

N to NE-trending faults: They are usually included inside the EATFS and DSTFS (Figure 1). They are parallel to sub-parallel, closely-spaced, sinistral strike-

slip faults in character with some dip slip components. It is very well-known that majority of these faults are active as evidenced by some ancient and recent devastating earthquakes such as February 6, 2023 Pazarcık (Kahramanmaraş) (Mw= 7.7) and February 20, 2023 Defne (Hatay) Mw= 6.4 earthquakes. Perinçek (2023) points out that these faults display close relationship with WNW-trending faults. Geological, hydrogeochemical and drilling data supports that these faults play a significant role in the development of the geothermal system as conduits inside the study area.

WNW-trending faults: They are strike-slip faults with some dip-slip components. These faults usually are perpendicular to DSTFS and EATFS and also cut and displace them (Figure 1). Perinçek (2023) stated that some of these faults extend beyond the study area up to Saudi Arabia and might have occurred during Precambrian. It seems that these faults also occur as a barrier during the rapture of N-S to NE-trending faults following the February 6, 2023 Pazarcık (K.Maraş) (Mw= 7.7) and February 20, 2023 Defne (Hatay) Mw= 6.4 earthquakes (Perinçek, 2023). Those earthquakes play a significant role in the development of geothermal system as conduits in the study area.

Geological, hydrogeochemical and deep well data suggest that the geothermal springs take place along the intersection of N to NE-trending and WNW-trending faults (Figure 1).

### **HYDROGEOCHEMISTRY OF THE WATERS IN THE STUDY AREA**

The study was carried out during Eastern Mediterranean Geothermal Project of MTA of Türkiye between 2010-2013 and during 111Y090 COST (1001) TÜBİTAK project during 2012-2014 field campaign. During the fieldwork, electrical conductivity (EC), temperature (T), pH and some Eh values are carefully measured from many cold/hot springs/wells observed in the study area. However, only 39 of them exceeding 25 °C are presented here. Based on the data, T values reach up to 42,8 °C, EC values are between 503-45,300 µS/cm, and pH values range from 6,61 to 11,85.

Based on the Schoeller (1967) diagram, the geothermal waters discussed here display two major water types, namely, Na+K-Ca-Cl-HCO<sub>3</sub> waters and the waters are of almost the same major anions and cations (Figure 3). According to the Piper (1944) diagram, the geothermal waters display a wide range of distribution (Figure 4).

Some pH measurements show hyperalkaline water characteristics as aforementioned above. Although, a comprehensive study has not been performed yet. Some geothermal waters at least partly seem to emerge as a result of low temperature serpentinization as evidenced by anomalous abiogenic CH<sub>4</sub>, H<sub>2</sub> gas occurrences and mild temperatures up to 33,6 °C inside the Kızıldağ ophiolites (Yüce et al. 2015). Similar findings were also reported from many similar rock types such as Oman, Cyprus and Antalya ophiolite complexes (Neal and Shand, 2002; Chavagnac et al. 2013; Hoşgörmez et al. 2008). The CH<sub>4</sub> occurrences in the serpentinites

are commonly observed in geothermal wells during and following the drillings up to 8 bars (115 psi) wellhead pressures observed within one days in the study area. Based on this observation, some low temperature geothermal waters observed in thick serpentinitized rocks seem to be at least partially related to active serpentinization processes in the Karasu Rift.

### **GEOHERMAL POTENTIAL OF THE STUDY AREA**

Although some different processes are attributed to heat source in a geothermal system such as volcanic activities, buried magmas (magma patches), chemical processes (e.g. serpentinization), radiogenic heat production and the friction-induced heating along major faults (Beardmore and Cull, 2001 and some references therein). In fact, it is widely speculated that young basaltic volcanics (0.05±0.03 to 2.0±0.20 Ma) are the heat source for the geothermal waters observed in the Karasu Rift. However, there are some evidences implying that the basaltic volcanics are rare source of high heat potential for the geothermal fields in Türkiye. This is most probably due to low viscosity, high buoyancy relative to surrounding rocks and low extension rates related fast eruptions of basalts without sufficient residence time needed for enough heating in shallow crustal levels. This is supported by deep wells drilled inside the Kula (Manisa), Karacadağ (Diyarbakır) and the Karasu volcanites where relatively average geothermal gradients are observed up to 4443 m (Bülbül et al. 2022; Çiçek et al. 2020; Çiçek et al. 2022, Çiçek et al. 2023). Similar observations exist in many geothermal systems in the world in continental geothermal systems with some exceptions such as Iceland and Hawaii (Wohletz, and Heiken, 1992). Some geochemical data having either almost no or less crustal contamination imply that the volcanics are of the deep origin and had no sufficient residence time to be a heat source during their ascend inside the Karasu Rift System (Çapan et al. 1987; Alıcı et al. 2001). This is further supported by relatively lower geothermal gradients (i.e. 20.3 to 42.4 oC/km with averaged 3,06 oC/km) obtained from the deep wells in the study area (e.g. Yüce et al. 2015). Moreover, relatively high geothermal gradients are limited to shallow levels (<1000 m) and generally decrease with increasing depths.

A number of gamma-ray well logging studies were carried out in deep geothermal and oil wells in the Karasu Rift. The well log data show that the radiogenic heat source seems less likely due to lower gamma-Ray readings (i.e. typically less than 10 API). This particularly occur inside the ophiolites where the highest geothermal gradients are observed in the study area. A quite higher values (typically below 40 API) are observed inside the other rocks such Midyat, Mardin and Cudi groups. This data also implies that radiogenic heat production is relatively low along the Karasu Rift at least upper crustal levels. But this requires further supporting evidence such as detailed chemical analysis and the calculations using radiogenic elements (i.e. U, Th, K). As discussed above, CH<sub>4</sub> and H<sub>2</sub> gas emanations along



with hyperalkaline geothermal waters, isotopic gas studies (Yüce, 2015) and dense serpentinite formations around hot waters within the ophiolitic complex partly imply that serpentinization may be a partial heat source inside the Karasu Rift in some limited localities.

## CONCLUSIONS

The Karasu Rift is located between the East Anatolian Transform Fault System and the Dead Sea Transform Fault System. The study area has some low temperature (20-42,8) geothermal springs. In order to reveal the geothermal potential of the study area, some geothermal research studies were carried out by the MTA of Türkiye and Hacettepe University. Following these studies, deep geothermal potential was tested by some deep geothermal wells and the results were also supported by the data obtained from the deep oil wells in the study area. Based on all this information, following outcomes are obtained:

- (1) The Karasu Rift is a low enthalpy geothermal system with a relatively low geothermal gradient varying between 20.3 and 42.4 °C/km an average of 30.6 °C/km. In addition, the relatively higher geothermal gradients are observed in shallower depths (i.e. < 1000 m) and geothermal gradient values decrease with increasing depth.
- (2) Extensive young basaltic volcanics have a quite lower geothermal heat potential in the study area.
- (3) Basically, temperatures of the thermal waters in the study area are between 20 to 42,8 °C and classified with two major water facies which are Na+K-Ca-Cl-HCO<sub>3</sub>. Na and Cl are the dominant major ions that imply groundwaters in the area having deep circulation.
- (4) Radiogenic heat production seems to be quite less based on the low gamma-ray readings in the boreholes. But this hypothesis needs to be supported by the calculations using radioactive parameters such as U, Th, K within the rock samples from the area. This research is planned in the near future.

## ACKNOWLEDGMENTS

Alper YOLAL, Adnan GÜVEN, Sebhattin ŞAHAN, Orhan KILINÇ, Ünsal TURALI, Güvenç DEMİRKIRAN, Afsin EKMEKYAPAR, Süleyman YILDIZ, Rifat C. SEVİM, Ahmet UTAR, Ömer KESGİN and some others who supported these studies during the fieldwork and drilling are appreciated.

## REFERENCES

Alıcı, P., Temel, A., Gourgaud, A., 2002. Pb-Nd-Sr isotope and trace element geochemistry of Quaternary extension-related alkaline volcanism: a case study of Kula region (western Anatolia, Turkey). *Journal of Volcanology and Geothermal Research* 115, 487-510.

Alıcı, P., Temel, A., Gourgaud, A., Vidal, P., Gündoğdu, M. N., 2001. Quaternary Tholeiitic to Alkaline Volcanism in the Karasu Valley, Dead Sea

Rift Zone, Southeast Turkey: Sr-Nd-Pb-O Isotopic and Trace-Element Approaches to Crust-Mantle Interaction. *International Geology Review*, 43, 120-138.

Beardsmore, G.R., Cull, J.P. 2001. *Crustal Heat Flow. A Guide to Measurement and Modelling*. Cambridge University Press, 324 p., ISBN 0-521-79289-4.

Boulton, S.J. and Robertson, A.H.F., 2007. The Miocene of the Hatay area, S Turkey: Transition from the Arabian passive margin to an underfilled foreland basin related to closure of the Southern Neotethys Ocean. *Sedimentary Geology* 198 (1), 93-124.

Boulton, S.J., 2009. Record of Cenozoic sedimentation from the Amanos Mountains, Southern Turkey: Implications for the inception and evolution of the Arabia-Eurasia continental collision. *Sedimentary Geology* 216 (1-2), 29-47.

Boulton, S.J. and Robertson, A.H.F., 2008. The Neogene–Recent Hatay Graben, South Central Turkey: graben formation in a setting of oblique extension (transtension) related to post-collisional tectonic escape. *Geological Magazine* 145 (6), 800-821.

Bozkurt, E., 2001. Neotectonics of Turkey—a synthesis. *Geodinamica Acta* 14, 3-30.

Chavagnac, V., Monnin, C., Ceuleneer, G., Boulart, C., Hoareau, G. 2008. Characterization of hyperalkaline fluids produced by low-temperature serpentinization of mantle peridotites in the Oman and Ligurian ophiolites. *Geochemistry Geophysics Geosystems*, 7, 14, 2496-2522.

Çapan, U.Z., Vidal, P., Cantagrel, J.M., 1987. K-Ar, Nd, and Pb isotopic study of Quaternary volcanism in Karasu valley (Hatay), N-end of Dead Sea rift zone in SE-Turkey. *Yerbilimleri*, 14, 165-178.

Çiçek, A., Kılınç, O., Öztürk, S., Kılıç, A. R. 2020. Doğu Akdeniz Jeotermal Enerji Aramaları Projesi (2011.33.13.06-1; 2012.33.13.06-1; 2013.33.13.18; 2014.33.13.17-1) AR: 2009210002, 3, 4, 5; AR: 2011210002, 3, 4, 5 ve AR: 2013210002 no.lu jeotermal kaynak arama ruhsat sahaları jeotermal etüt (jeoloji ve jeofizik) ve DMC-2012/14 jeotermal araştırma sondajı kuyu bitirme raporu. MTA Genel Müdürlüğü, Rapor No.: 13918, 78 p., Ankara (unpublished).

Çiçek, A., Öztürk, S., Kılınç, O., Ataman, O., 2022. Diyarbakır Büyükşehir Belediyesi adına kayıtlı Diyarbakır-Sur-Çarıklı AR: 2021210001 no.lu Jeotermal Kaynak Arama Ruhsat Sahası Jeotermal Etüt Raporu. MTA Genel Müdürlüğü, Rapor No.: 14045, 53 p., Ankara (unpublished).

Çiçek, A., Arğün, Z., Kılınç, O., 2023. Diyarbakır Büyükşehir Belediyesi adına Diyarbakır-Sur-Çarıklı AR: 2021210001 no.lu Jeotermal Kaynak Arama Ruhsat Sahasında Tamamlanan DSÇ-1 Jeotermal Araştırma Sondajına Ait Kuyu Bitirme Raporu. MTA Genel Müdürlüğü, Rapor No.: 14222, 57 p., Ankara (unpublished).

Emre, Ö., Duman, T. Y., Özalp, S., Elmacı, H., Olgun, Ş., Şaroğlu, F. 2013. 1/250.000 ölçekli Türkiye diri fay haritası. The General Directorate of Mineral Research

and Exploration of Türkiye, Special Publications Series, 30, Ankara, Türkiye.

Hoşgörmez, H., Etiope, G., and Yalçın, M. N. 2008. New evidence for a mixed inorganic and organic origin of the Olympic Chimaera fire (Turkey): a large onshore seepage of abiogenic gas. *Geofluids* 8, 263-273.

Neal, C. and Shand, P., 2002. Spring and surface water quality of the Cyprus ophiolites. *Hydrology and Earth System Sciences*, 6(5), 797–817.

Perinçek, D. 2023. Paleo-fayların 2023 Depremlerindeki Rolü: Artçı Depremlerin İlerlemesini Durduran Engeller. 75th Geological Congress of Türkiye with International Participation, April 10-14, 2023, Ankara, Türkiye.

Piper, A. M. 1944. A Graphic Procedure in Geochemical Interpretation of Water Analyses. *American Geophysical Union Transactions*, 25, 914–923.

Schoeller, H. 1967. Geochemistry of groundwater. An international guide for research and practice. UNESCO, 15, 1-18.

Selçuk H. 1985. Kızıldağ-Keldağ-Hatay dolayının jeolojisi ve jeodinamik evrimi. MTA. Genel Müdürlüğü Rapor No:7787, 129 s., Ankara (unpublished).

Wohletz, K. and Heiken, G., 1992. Volcanology and geothermal energy. Berkeley, California: 878 University of California Press, 432 p.

Yolal, A., Kahraman, S., Çiçek, A., Arslan, G., Hacısalihoglu, Ö., Bostan, S., Bekar, T., 2016. Doğu Akdeniz Jeotermal Enerji Aramaları Projesi Hatay ili AR:31/2009-1, 2, 3, 4, 5, 6, 7, 9, 10, 11, 12, 13 ve 14 no.lu Jeotermal Kaynak Arama Ruhsat Sahaları Jeotermal Etüt (Jeoloji-Jeofizik) Raporu. MTA Genel Müdürlüğü, Rapor No.: 11883, Ankara (unpublished).

Yüce, G., 2015. Toprak İçi ve Yeraltısularındaki Gaz Çıkışları ile Fay Aktivitesi ve Jeotermal Kökenin Belirlenmesi: Ölü Deniz Fay Zonu (ÖDFZ)'nun Amik Uzantısı-Karasu Fayı İlişkisi ve Amik Ovası Sıcak Sularının Kökeni. TÜBİTAK (COST) Project Report, No: 111Y090, 217 p.

Keywords: Karasu Rift, geothermal potential

Figure 1. Shuttle Radar Topography Mission (SRTM) image of the study area and some major structures.



Figure 2. Generalized stratigraphic columnar section of the study area and its vicinity (Selçuk, 1985; Yolal et al. 2015).

Epoch	System	Series	Formation	Lithology	Explanation
CENOZOIC	Quaternary	Holocene			Quaternary alluvium UNCONFORMITY
		Pleistocene			Quaternary basalts UNCONFORMITY
	NEOGENE	Pliocene	SAMANDAG		Sandstone, clayey limestone and siltstone UNCONFORMITY
			VAKIFLI		gypsum and gypsum interbedded limestone
			NURZEYFİN		sandstone interbedded clayey limestone, claystone, marl — CONFORMABLE CONTACT
		MIOCENE	TEPEHAN		clayey limestone, claystone and marl with marlstone interbeds — CONFORMABLE CONTACT
			SOFULAR		marl limestone
			BALYATAĞI		pebblistone, sandstone and sandy mudstone — UNCONFORMITY
	PALEOGENE	Eocene	KISLAK		limestone, marl, limestone with siliceous nodules
			ÇİNKÖLÜR		limestone, cherty limestone, clayey limestone with detritic siliceous nodules
PALEOCENE		ULUYOL		sandstone, limestone, clayey limestone, claystone	
		KALE BOĞAZI		limestone, clayey limestone, marl — CONFORMABLE CONTACT	
MESOZOIC	CRETACEOUS	YALÇI		pebblistone, pebbly sandstone and sandstone UNCONFORMITY	
		HIZLIÖZGÜN		vectorites, cumulate, diabase dike complex — TECTONIC CONTACT	
		YAYKIMLAR		sandy limestone, cherty limestone and clayey limestone	
		YERZİDE		sandstone, sandy limestone, limestone and cherty limestone	
		KARAKÖLÜ		dolomitic limestone, oolitic limestone and sandy limestone — UNCONFORMITY	
	JURASSIC	UPPER	KELDAG		dolomite, dolomitic, micritic limestone and sandy limestone
	TRIASSIC	MIDDLE	GARAKLI		dolomite, dolomitic, micritic limestone and sandy limestone
		LOWER	AFILIK		pebblistone, metasandstone-slate succession — UNCONFORMITY
		DEVONIAN	UPPER	YIĞIRIBETLİ	
	MIDDLE		YIĞIRIBETLİ		siliceous pebbly sandstone and quartzite
LOWER	YIĞIRIBETLİ			sandstone, shale and slate succession	
UPPER	BAHÇE			shale interbedded metapebblistone-quartzite succession	
MIDDLE	AKÇADIRG			pebblistone, litharenite and shale	
PALEOZOIC	ORDOVICIAN	UPPER	BEDİNHAN		siliceous interbedded sandstone-quartzite intercalation — CONFORMABLE CONTACT
		MIDDLE	KÖKLAC		pyrite, micaceous sandstone-sandstone with quartzite interbeds and clayey carbonaceous shale
		LOWER	KURDERE		quartzite with mudstone interbeds-quartz sandstone
	CAMBRIAN	UPPER	SÖRENK		fine sandstone, siltstone interbeds, mudstone-shale and calcshale succession
		MIDDLE	KÖRÜK		micritic limestone, sandy dolomite and dolomite
		LOWER	ZARLIK		sandy mudstone-shale interbedded metasandstone-quartzite
		PRECAMBRIAN	SADAN		shale-shale interbeds metapebblistone-metasandstone-quartzite succession

Figure 3. Schoeller diagram of the water samples collected from the study area.

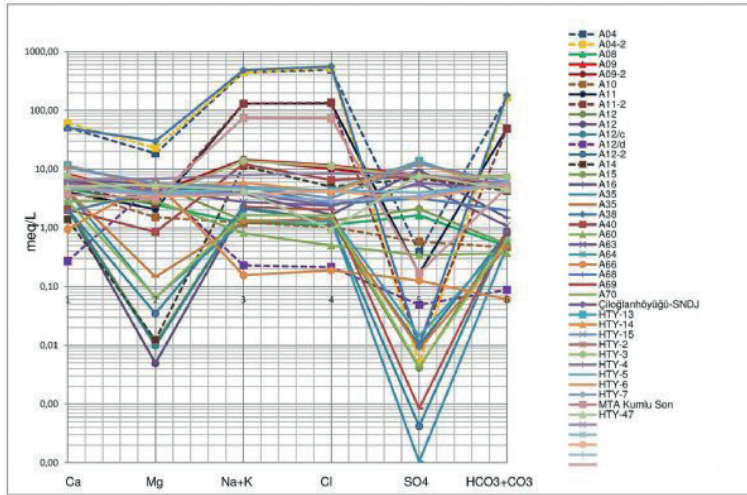
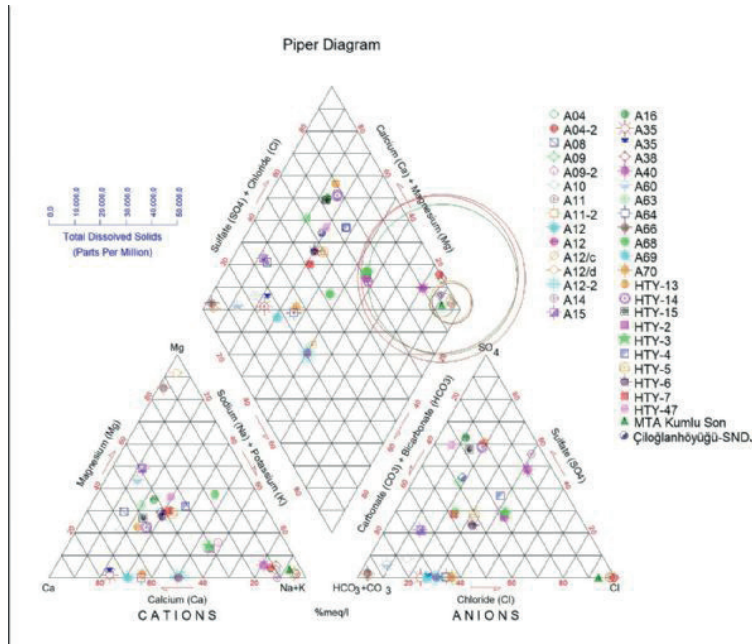


Figure 4. Piper diagram of the water samples collected from the study area.





## **Kuyu Tamamlama Uygulamaları**

*Well Completion Applications*

---



# Comparative Analysis of Acid Fracturing in ŞEHİT ESMA ÇEVİK Field Using 3 1/2" and 2 7/8" Tubings: A Comprehensive Study



**Görkem Kaya**

Türkiye Petrolleri Anonim Ortaklığı

Acid fracturing is a well stimulation technique that plays a crucial role in enhancing the productivity of oil and gas reservoirs. It involves the injection of acid into the formation to create or extend fractures, which allows for improved hydrocarbon flow towards the wellbore. However, the success of acid fracturing operations heavily relies on various factors, including the selection of an appropriate tubing size. In recent years, the oil and gas industry has witnessed a growing emphasis on maximizing hydrocarbon recovery from existing reservoirs. Acid fracturing has emerged as an effective method to achieve this objective, particularly in mature and low-permeability reservoirs. The technique has evolved over time, and advancements in technology have provided more options for operators to tailor the stimulation process to specific reservoir characteristics. Tubing size selection is a critical aspect of acid fracturing design. Different tubing diameters offer distinct advantages and limitations, influencing factors such as injection rates, production efficiency, wellbore integrity, and ultimately, the economic viability of the operation. This comprehensive comparative analysis focuses on acid fracturing in Şehit Esma Çevik-21 (SEÇ-21) using 3 1/2" and 2 7/8" tubings. The study aims to provide valuable insights for decision-makers in the industry to optimize well performance and maximize hydrocarbon recovery.

First of all, the literature review delves into the historical development of acid fracturing techniques, tubing selection criteria, and relevant case studies that have explored the impact of tubing size on well stimulation operations. The origins of acid fracturing can be traced back to the 1930s when it was first introduced as a method to improve well productivity. Over the years, the technique has evolved significantly, with various modifications and enhancements to increase its effectiveness in different reservoir conditions. A critical aspect of acid fracturing design is the selection of tubing size. The review explores the factors that influence this decision, such as reservoir characteristics, fluid properties, and equipment limitations. It also delves into the theoretical considerations and mathematical models used to analyze the flow dynamics and pressure differentials within the wellbore during the acid fracturing process. Case studies from different oil and gas fields provide valuable insights into the practical implications of tubing size selection. These studies demonstrate the correlation between tubing size and production efficiency, highlighting the importance of optimizing this parameter to achieve desirable results. Additionally, the literature review examines the various challenges faced by operators in acid fracturing operations and how the choice of tubing size can impact the overall success of the stimulation process.

Moreover, the field data analysis involves an in-depth examination of historical records from SEÇ-21, where acid fracturing was conducted using both 3 1/2" and 2 7/8" tubings. The data collected includes production rates, pressure differentials, wellbore integrity records, and other relevant parameters. By analyzing the production rates achieved with each tubing size, the study highlights the impact of tubing diameter on the effectiveness of acid fracturing in the specific reservoir. It identifies trends in hydrocarbon recovery and reservoir contact, demonstrating how the larger 3 1/2" tubing facilitates higher injection rates, leading to enhanced fracture initiation and propagation. Moreover, the study explores the pressure differentials experienced during acid fracturing with different tubing sizes. The analysis reveals that the larger diameter of 3 1/2" tubing minimizes pressure drops along the wellbore, reducing the risk of formation damage and casing failures. In contrast, the smaller 2 7/8" tubing experiences higher pressure differentials, potentially leading to undesirable consequences like tubing deformation or fracturing fluid leakage. The examination of wellbore integrity records sheds light on the mechanical performance of the wellbore after acid fracturing. The study compares the structural integrity of wells stimulated with different tubing sizes, highlighting any variations in wellbore stability and potential damage. The field data analysis is a critical aspect of the study, as it provides real-world insights into the performance of acid fracturing operations using different tubing sizes. By examining historical records from SEÇ-21, the analysis can draw meaningful conclusions about the impact of tubing size on production efficiency and wellbore integrity. The production rates achieved during acid fracturing using 3 1/2" and 2 7/8" tubings play a vital role in determining the effectiveness of each stimulation method. The analysis should not only compare the absolute production rates but also investigate the duration and sustainability of the increased productivity. In SEÇ-21, the data might reveal that wells stimulated with 3 1/2" tubing exhibited higher initial production rates compared to those stimulated with 2 7/8" tubing. However, it is essential to explore how production rates change over time and whether one tubing size sustains its enhanced productivity for a more extended period. Factors like reservoir depletion rate, fluid flow dynamics, and pressure behavior should be considered to provide a comprehensive analysis. Additionally, the study should delve into the reservoir contact achieved with each tubing size. The larger 3 1/2" tubing allows for higher injection rates, leading to more extensive and effective fracture initiation and propagation. The analysis should discuss how this increased reservoir contact translates into higher hydrocarbon recovery and how it impacts the long-term performance of the wells.

Pressure differentials experienced during acid fracturing can significantly impact the wellbore integrity and overall success of the operation. The field data analysis should explore the variations in pressure differentials between the two tubing sizes and their implications. The larger diameter of 3 1/2" tubing is expected to result in lower pressure drops along the wellbore, reducing the risk of formation damage and casing failures. The analysis should investigate specific instances where high pressure differentials were observed with 2 7/8" tubing and how it affected the wellbore, such as casing deformation or fluid leakage.

Furthermore, the analysis should consider the wellbore stability records and any indications of mechanical issues after acid fracturing. Comparing the structural integrity of wells stimulated with each tubing size would provide valuable insights into the long-term impacts on wellbore health and the risk of future interventions.

The economic analysis investigates the cost implications associated with acid fracturing using 3 1/2" and 2 7/8" tubings. It takes into account not only the initial investment but also the long-term benefits and returns from each tubing size. The study analyzes the initial costs of acquiring and installing 3 1/2" and 2 7/8" tubings, comparing their respective prices and installation expenses. Additionally, it factors in the operational costs associated with each tubing size, such as acid volumes required, well maintenance, and production monitoring. The economic analysis should encompass a detailed breakdown of operational costs associated with each tubing size. This includes the costs of acquiring and installing 3 1/2" and 2 7/8" tubings, as well as the expenses related to acid volumes, equipment, and manpower during the fracturing process. A comprehensive lifecycle analysis is necessary to understand the long-term economic implications. It should consider factors like maintenance costs, well surveillance, and any potential workover requirements. The analysis should explore how the operational costs differ between the two tubing sizes and their overall impact on the profitability of the project. The economic analysis should include calculations of the Net Present Value (NPV) and Return on Investment (ROI) for each tubing size. These financial metrics help decision-makers evaluate the profitability of the acid fracturing project over its economic life. By discounting cash flows and considering factors like production rates, hydrocarbon prices, and operational costs, the analysis can quantify the long-term benefits and returns associated with 3 1/2" and 2 7/8" tubings. This would provide a clear comparison of the economic performance of each tubing size and inform investment decisions.

Furthermore, the economic analysis considers the long-term benefits of each tubing size in terms of production rates and extended well life. By projecting production profiles and estimating reservoir depletion rates, the study assesses the overall economic viability of using each tubing size in acid fracturing operations.

The comprehensive comparative analysis of acid fracturing using 3 1/2" and 2 7/8" tubings concludes that the selection of tubing size significantly impacts

the success of well stimulation operations. The larger 3 1/2" tubing proves superior in terms of production efficiency, wellbore integrity, and economic viability. An in-depth economic analysis should also include sensitivity analysis and risk assessment. Sensitivity analysis examines how changes in key parameters (e.g., oil prices, production rates, operating costs) affect the project's financial outcome. This helps in understanding the project's robustness under different scenarios and uncertainties. The risk assessment should identify potential risks and uncertainties associated with acid fracturing using each tubing size. Factors like geological uncertainties, reservoir performance, and commodity price fluctuations should be considered. The analysis should discuss risk mitigation strategies and their impact on the overall economic viability of the project. By expanding on these aspects, the field data analysis and economic analysis sections will provide a more comprehensive understanding of the significance of tubing size selection in acid fracturing operations. The additional details will offer valuable insights to oil and gas operators, researchers, and decision-makers in the industry, aiding in the optimization of well performance and maximizing hydrocarbon recovery from reservoirs.

In conclusion, based on the findings, the study recommends using 3 1/2" tubing for acid fracturing operations, particularly in reservoirs with specific characteristics similar to SEÇ-21. Decision-makers and operators in the oil and gas industry can use these insights to optimize well performance, enhance hydrocarbon recovery, and ensure economic sustainability in their acid fracturing projects. Overall, the research contributes valuable knowledge to the field of acid fracturing and emphasizes the importance of tubing size selection as a critical parameter for successful well stimulation in the oil and gas industry. It highlights the need for further studies and applications of tubing size optimization in different geological settings to continue improving well productivity and maximizing reservoir potential.

Keywords: ACID FRAC, TUBING SIZE



# Coiled Tubing ile Açık Kuyu Sondaj Operasyonu

**Seckin Öztel**  
Pars Drilling



Coiled Tubing Drilling uzun yıllardır uygulanan bir sondaj yöntemidir. Gelişen teknoloji ile yapılabilen coiled tubing sondaj derinliği artmak ile birlikte hem hızlanmış hem de E-Coil, E-MWD gibi teknolojilerin uygulamaya eklenmesi ile konvansiyonel sondajın yapılamadığı yerlerde bir çözüm olarak öne çıkmıştır. Bu bildiri Türkiye’de yapılan bir Coiled Tubing Drilling operasyonunun özeti, avantajlarını, karşılaşılan problemleri ve sonucunu anlatmaktadır.

## ABSTRACT

Coiled Tubing Drilling is a drilling method that has been applied for many years. Coiled tubing, which can be done with developing technology, has both accelerated with increasing drilling depth and stood out as a solution in places where conventional drilling cannot be done with the addition of technologies such as E-Coil and E-MWD added to the application. This paper describes the summary, advantages, problems encountered and the result of a Coiled Tubing Drilling operation conducted in Turkey.

## A. AMAÇ

Trakya bölgesinde kazılan shallow gaz kuyuları genel olarak slim hole 4 ½” casing ile tamamlanmakta ve casing içinden gaz üretilmektedir. Yıllar içinde üretimi düşen kuyularda derinleştirme yapılarak alt rezervuarlardan üretim yapmak istenmektedir. Kuyuların şehir içinde kalması lokasyon yapımını zorlaştırmakta ve maliyetini arttırmakta ayrıyeten 4 ½” casing içinde slim hole dizi ile sondaj yapmak operasyonu daha komplike hale getirmektedir. Bu problemleri çözmek için küçük ayak izi, hızlı operasyon kabiliyeti olan ve slim hole BHA’e uygun olarak Coiled Tubing ile sondaj tekniği uygulanmış ve operasyon başarı ile sonuçlanmıştır.

## B. GEREÇ ve YÖNTEM

Coiled Tubing Uygulamaları günümüzden yaklaşık 45 yıl öncesine dayanmaktadır. Günümüzde Coil Tubing Uygulamaları, Kuyu Temizliği, Asitleme Operasyonları, Log operasyonlarına hatta Sondaj ve Tahlisiye uygulamalarına kadar geniş bir yelpazede çalışmalara olanak sağlamaktadır.

En önemli avantajı artezyen kuyularda kuyuyu öldürmeden (basınç altında) müdahale, kuyuya hızlı giriş - çıkış ve manevra esnasında kesintisiz pompalama, hatta underbalanced drilling sayesinde kuyu kirlenmesi olmadan sondaj gibi eşsiz imkanlar sağlamaktadır.

Coiled Tubing Drilling 1991’de uygulanmaya başlamıştır. Yılda ortalama 1000 adet kuyu CTD ile kazılmış yada derinleştirilmektedir. Gelişen Teknoloji ile CTD ile MWD de kullanılabilir. Gelişen Teknoloji ile CTD ile MWD de kullanılabilir.

Coiled Tubing Operasyonları dört ana başlıkta toplanabilir;

### 1. Pumping Operasyonları

Canlı kuyuda Kuyu temizliği Scale, wax, parafin, propan vb.

Milling

Nitrojen ile kuyu canlandırma

Asitleme

Tubing kesimi

Kick Out Dizisi ile Multi Lateral Kuyu Operasyonu

### 2. Mekanik Operasyonlar

Tahlisiye

Perforasyon

Logging

Mekanik kuyu kirliliği temizliği

Velocity String

### 3. Sondaj Operasyonları

Underbalance ve Overbalance Sondaj

4. E-Coil ile Log Alımı

Açık kuyuda full set log alımı

PLT log alımı

Down hole Kamera Logu

Bu bildiri 3. Kısım olan Coiled Tubing ile sondaj operasyonu uygulanarak derinleştirilen DT8 nolu gaz kuyusundaki işlemler ele alınacaktır.

### B.1. KUYU BİLGİLERİ

DT-8 Kuyusu 2007 yılında gaz üretim kuyusu olarak kazılmıştır. 647 metreye kadar 6” matkap ile kazılmış ve 458 metreye 4 ½” casing inilip yüzeye kadar çimentolanmıştır. 458 – 647 metre arası 6” açık kuyu olarak kalmıştır. Açılan çeşitli perforelerden gaz üretimi yapılmış fakat üretim azalınca 950 – 1200 metre arasındaki gaz rezervuarına ulaşıp üst taraf kapatılarak bu rezervuardan üretim yapılması ihtiyacı doğmuştur.

Bu sebep ile derinleştirme operasyonu planlanmıştır. Coiled Tubing operasyonu öncesi workover kulesi alınarak taban kontrolü yapılmış, açık olan perforeler çimento ile kapatılmış ve test edilmiştir. Bunun yapılmasının amacı coiled tubing öncesi kuyunun durumundan emin olmak ve sondaj operasyonu öncesi kuyuyu hazırlamaktır.

## B.2. EKİPMAN

Coiled Tubing sondajı dizayn aşamasında operatörün istekleri göz önüne alınarak bir ön maliyet ve teknik çalışma yapılmıştır. Bu çalışma sonucunda istenen derinliğe uygun ekipman seçilmiştir. Bunlar özet olarak aşağıda belirtilmiştir.

### Yüzey Ekipmanları

Coiled Tubing: CT 2 7/8". Wall Thickness 0,175", min: 81.300 – max 129.300 psi yield strength

Injector Head: 100.000 lbf pull capacity, 50.000 lbf snubbing capacity. 100" Radius Gooseneck

12.000 psi 1000 HP iki adet pumping unit

Well Control Equipment: 4 1/16" 10K Quad BOP, 4 1/16" 10K Stuffing Box

5K Choke Manifold

Elek tankı (Bu operasyona özel dizayn edilmiştir)

Poor Boy Degasser

Çamur Tankları, minimum 600 bbl kapasiteli

BHA Ekipmanları

3 3/4" PDC Matkap

Motor: 2 7/8", Stall Torque 508 ft.lb,

Speed range 240 – 320 RPM 5/6 stage

Motor Head Assy: Connector + Check

Valve + Release Joint + Circulation Sub

Flow Thru Sub

Weight Bar

## B.3. DİZAYN

### i. BHA Dizaynı;

BHA dizaynı 4 1/2" casing içinde çalışacak ve maksimum hidrolik gücü kaldıracak şekilde seçilmiştir. Burada bizi zorlayan kısım kesintilerin yüzeye getirilebilmesi ve PDM için gerekli horse power ile debiyi yakalayabilmek oldu. Bunun için diziyeye flow thru sub eklendi. Flow thru sub'ın amacı kesintileri yüzeye getirmede bir sıkıntı yaşanır ise veya yüksek debide sirkülasyon yapmak gerekir ise PDM'e zarar vemedi matkap üstünden sirkülasyon yapmaktır.

### ii. Hidrolik Dizaynı;

Hidrolik dizaynı coiled tubing ve yüzey ekipmanlarının maksimum çalışma basıncı gözetilerek mümkün olan en optimum basınç, maksimum verim ve süre ile çalışılacak şekilde dizayn edilmiştir.

### iii. Çamur Dizaynı;

Kuyu şartları ve offset dotalar incelenerek KCl – Polymer çamuru kullanılmasına karar verildi. Buradaki amacımız kuyu stabilitesini sağlar iken rezervuarı kirlenmemektir.

## iv. Coiled Tubing Forces;

Coiled Tubing bir iniş çıkış operasyonunda 6 sefer düzleştirilip bükülür. Bu sebep ile limitli bir iniş çıkış kabiliyeti vardır. Bu değer coiled tubing fatigue olarak adlandırılır ve her coiled tubing operasyonundan sonra hesaplanarak kayıt edilir. Dizayn kriterinde ilk hesaplanan bölüm coiled tubing'in bu sondajı tamamlayacak kadar fatigue dayanımına sahip olup olmadığıdır.

Ayrıca Coiled tubing'in hedeflenen derinliğe sorunsuz inebileceğini kontrol amacı ile Tubing Forces simülasyonu yapıldı. Bu simülasyonda sondaj sırasında görülecek yüzey ağırlıkları, Axial Kuvvetler, Von-Miss Stresleri, Maksimum çekme kuvveti, Maksimum verilebilecek matkap ağırlığı ve Coil Tubing collapse limitleri simüle edilerek hesaplandı.

Şekil -1 Tubing bükülme döngüsü

## B.4. OPERASYON

Lokasyon alanı şehir merkezi sınırları içinde kaldığı için operasyon öncesi en büyük zorluklardan biri kısıtlı kuyu lokasyon alanı idi. Bunu aşmak için detaylı bir yerleşim ve dizilim planı hazırlandı. Bazı ekipmanların dizaynı değiştirilerek daha kompakt hale getirildi. Lokasyon hazır edildikten sonra nakliyata başlandı.

Lokasyona ulaşıp kurulum tamamlandıktan sonra yüzey hatları testleri ve çamur hazırlanma işlemlerine başlandı. Yüzey mud log ekipmanları kuruldu. Ardından 3 3/4" PDC matkap ile iniş yapılarak 647 metrede sondaja başlandı. 647 metre ile 1154 metre arası sondajı ortalama 12 metre/saat ROP ile 2 günde tamamlandı. Burada ROP kuyunun sapmasını önlemek ve kuyu temizliğini sağlıklı bir şekilde sağlamak için yavaş tutuldu. Tüm metrajlardan kırıntı numunesi alındı ve belli metrelerde gaz okumaları görüldü.

Sondaj sonrası kuyunun 5 1/2" çapına genişletilebilmesi için underreamer dizisi ile inişe geçildi. Fakat underreamer dizisi ile 458 – 647 metre arasındaki 6" geniş çaplı kuyudan dolayı kazılan kuyuya inilemediği için bu operasyonda vazgeçildi.

Underreamer çıkışı sonrası full set log alımı denendi fakat log dizisi yine aynı sebepten ötürü 3 3/4" kuyuya giremediği için log alınmadı.

Ardından coiled tubing dizisi ile 1144 metreye tekrar inilerek çimento operasyonu için hazırlık yapıldı. Bu metrajda coiled tubing çimentolanarak kuyu başına asıldı.

Sondaj operasyonu sonrası kuyu belirlenen metrajlardan perfore edilerek üretime alındı.

## B.5. LESSON LEARNED

Operasyonun en büyük katkısı yakaladığı başarının yanında bunun ülkemizde milli imkanlarla yapılan ilk Coiled Tubing sondajı olması ve bu operasyondan çıkardığımız dersler ve öğrendiğimiz now-how bölümleridir. Bunlardan başlıcaları;

No. Problem Çözüm Önerisi

1 Flare Hattı çalışma alanına çok yakın. Flare hattı bir sonraki projede daha detaylı planlanarak çalışma alanından daha uzağa konularak flare bacası uzaklaştırılacak.

2 Gece lokasyonun bazı kısımları karanlıkta kalıyor. Daha fazla ışıldak ve seygar projector getirilerek her yerin iyice aydınlatılması sağlanacak. Ayrıca ışık ve ses ölçümleri yapılarak kritik yerler belirlenecek.

3 Coiled Tubing Ünitesi yazılımının güncellemesi gerekiyor. Bir sonraki operasyonda yazılımın güncellenerek ünitenin kullanılması gerekiyor.

4 Hopper olmadığı için çamuru düzgün bir şekilde karıştırmak zor olmaktadır. Buna ek olarak, doğrudan aktif dolaşım sistemine çamur eklenmesi, çamurun homojenliğini olumsuz yönde etkileyebilir. Yeni çamuru hopper sistemi ile aktarmak için başka bir hat olmalıdır. Blender tanklarına hopper sistemi akuple edilmez. Ayrıca bir tabanca hattı ile karışması sağlanmalıdır.

5 Ünitelerin motorlarından olası yağ sızıntısı için pompa ve CT ünitelerinin altında branda veya dökülme kiti bulunmalıdır. Ünitelerin altına serilmesi için branda tedarik edilmesi gerekiyor.

6 Operasyon sırasında formasyondan ve sondaj hızından ötürü eleklerde taşma gözlenmiştir. Elek dizaynı olası sondaj parametrelerine göre güncellenmelidir ve yeterli size da elek yedeği sahada bulunmalıdır.

7 Coiled Tubing Drilling kuyu başının bağlandığı ilk flanş test edilmemiştir. Workover operasyonunda kuyubaşı bırakılmadan önce test edilmelidir.

8 Sondaj sırasında çamur servis firması olmadığına çamur değerlerinin alınması konusunda sıkıntı yaşanmıştır. Çamur servis firması ile anlaşılıp sondaj sırasında çamur servis firması tarafından hazırlanmalıdır.

9 Yedek elek tankı bulunmadığı için operasyon sırasında yaşanabilecek bir aksaklıkta sondajın durma riski vardır. Yedek elek tankı lokasyonda hazır bir şekilde bulunmalıdır.

10 Çimentolama kafası yedeği sahada yoktur. Çimentolama kafası veya bunun gibi yardımcı malzemeler operasyondan önce sahada bulunmalı ve kontrolü sağlanmalıdır.

11 Sondaj sırasında ara ara görülen torq problemleri. Motor seçiminde 7/8 satege - yüksek torq dayanımlı bir motor seçilmelidir.

Tablo -3 Lesson Learned

C. BULGULAR VE SONUÇ

Sonuç olarak Coiled Tubing ile açık kuyuda sondaj operasyonu Türkiye’de ilk defa yapılmış ve başarı ile bitirilmiştir. Mobilite, kolay kurulum, Küçük yerleşim planı, hızlı operasyon kabiliyeti, underbalance sondaj imkanı, minimum kuyu kontrolü riski, düşük görsel ve ses kirliliği gibi avantajları göz önüne alındığında derinleştirme veya yatay kuyu sondajı operasyonlarını başarı ile yapabilecek bir ekipmandır.

D. ŞEKİL VE TABLOLAR

Şekil 6- Yerleşim Planı

Anahtar Kelimeler: Coiled Tubing

BHA

Drilling BHA Schematic						Area	Tool & Assembly	Serial	Tool Submitter
<p>0000                      010 Meter - 60 Meter Power (01000)                      020 Meter - 60 Meter Power (02000)                      030 Meter - 1" Strip Bar                      040 Meter - 1" Strip Bar                      050 Meter - 1" Strip Bar                      060 Meter - 1" Strip Bar                      070 Meter - 1" Strip Bar                      080 Meter - 1" Strip Bar                      090 Meter - 1" Strip Bar                      100 Meter - 1" Strip Bar                      110 Meter - 1" Strip Bar                      120 Meter - 1" Strip Bar                      130 Meter - 1" Strip Bar                      140 Meter - 1" Strip Bar                      150 Meter - 1" Strip Bar                      160 Meter - 1" Strip Bar                      170 Meter - 1" Strip Bar                      180 Meter - 1" Strip Bar                      190 Meter - 1" Strip Bar                      200 Meter - 1" Strip Bar                      210 Meter - 1" Strip Bar                      220 Meter - 1" Strip Bar                      230 Meter - 1" Strip Bar                      240 Meter - 1" Strip Bar                      250 Meter - 1" Strip Bar                      260 Meter - 1" Strip Bar                      270 Meter - 1" Strip Bar                      280 Meter - 1" Strip Bar                      290 Meter - 1" Strip Bar                      300 Meter - 1" Strip Bar                      310 Meter - 1" Strip Bar                      320 Meter - 1" Strip Bar                      330 Meter - 1" Strip Bar                      340 Meter - 1" Strip Bar                      350 Meter - 1" Strip Bar                      360 Meter - 1" Strip Bar                      370 Meter - 1" Strip Bar                      380 Meter - 1" Strip Bar                      390 Meter - 1" Strip Bar                      400 Meter - 1" Strip Bar                      410 Meter - 1" Strip Bar                      420 Meter - 1" Strip Bar                      430 Meter - 1" Strip Bar                      440 Meter - 1" Strip Bar                      450 Meter - 1" Strip Bar                      460 Meter - 1" Strip Bar                      470 Meter - 1" Strip Bar                      480 Meter - 1" Strip Bar                      490 Meter - 1" Strip Bar                      500 Meter - 1" Strip Bar                      510 Meter - 1" Strip Bar                      520 Meter - 1" Strip Bar                      530 Meter - 1" Strip Bar                      540 Meter - 1" Strip Bar                      550 Meter - 1" Strip Bar                      560 Meter - 1" Strip Bar                      570 Meter - 1" Strip Bar                      580 Meter - 1" Strip Bar                      590 Meter - 1" Strip Bar                      600 Meter - 1" Strip Bar                      610 Meter - 1" Strip Bar                      620 Meter - 1" Strip Bar                      630 Meter - 1" Strip Bar                      640 Meter - 1" Strip Bar                      650 Meter - 1" Strip Bar                      660 Meter - 1" Strip Bar                      670 Meter - 1" Strip Bar                      680 Meter - 1" Strip Bar                      690 Meter - 1" Strip Bar                      700 Meter - 1" Strip Bar                      710 Meter - 1" Strip Bar                      720 Meter - 1" Strip Bar                      730 Meter - 1" Strip Bar                      740 Meter - 1" Strip Bar                      750 Meter - 1" Strip Bar                      760 Meter - 1" Strip Bar                      770 Meter - 1" Strip Bar                      780 Meter - 1" Strip Bar                      790 Meter - 1" Strip Bar                      800 Meter - 1" Strip Bar                      810 Meter - 1" Strip Bar                      820 Meter - 1" Strip Bar                      830 Meter - 1" Strip Bar                      840 Meter - 1" Strip Bar                      850 Meter - 1" Strip Bar                      860 Meter - 1" Strip Bar                      870 Meter - 1" Strip Bar                      880 Meter - 1" Strip Bar                      890 Meter - 1" Strip Bar                      900 Meter - 1" Strip Bar                      910 Meter - 1" Strip Bar                      920 Meter - 1" Strip Bar                      930 Meter - 1" Strip Bar                      940 Meter - 1" Strip Bar                      950 Meter - 1" Strip Bar                      960 Meter - 1" Strip Bar                      970 Meter - 1" Strip Bar                      980 Meter - 1" Strip Bar                      990 Meter - 1" Strip Bar                      1000 Meter - 1" Strip Bar                      1010 Meter - 1" Strip Bar                      1020 Meter - 1" Strip Bar                      1030 Meter - 1" Strip Bar                      1040 Meter - 1" Strip Bar                      1050 Meter - 1" Strip Bar                      1060 Meter - 1" Strip Bar                      1070 Meter - 1" Strip Bar                      1080 Meter - 1" Strip Bar                      1090 Meter - 1" Strip Bar                      1100 Meter - 1" Strip Bar                      1110 Meter - 1" Strip Bar                      1120 Meter - 1" Strip Bar                      1130 Meter - 1" Strip Bar                      1140 Meter - 1" Strip Bar                      1150 Meter - 1" Strip Bar                      1160 Meter - 1" Strip Bar                      1170 Meter - 1" Strip Bar                      1180 Meter - 1" Strip Bar                      1190 Meter - 1" Strip Bar                      1200 Meter - 1" Strip Bar                      1210 Meter - 1" Strip Bar                      1220 Meter - 1" Strip Bar                      1230 Meter - 1" Strip Bar                      1240 Meter - 1" Strip Bar                      1250 Meter - 1" Strip Bar                      1260 Meter - 1" Strip Bar                      1270 Meter - 1" Strip Bar                      1280 Meter - 1" Strip Bar                      1290 Meter - 1" Strip Bar                      1300 Meter - 1" Strip Bar                      1310 Meter - 1" Strip Bar                      1320 Meter - 1" Strip Bar                      1330 Meter - 1" Strip Bar                      1340 Meter - 1" Strip Bar                      1350 Meter - 1" Strip Bar                      1360 Meter - 1" Strip Bar                      1370 Meter - 1" Strip Bar                      1380 Meter - 1" Strip Bar                      1390 Meter - 1" Strip Bar                      1400 Meter - 1" Strip Bar                      1410 Meter - 1" Strip Bar                      1420 Meter - 1" Strip Bar                      1430 Meter - 1" Strip Bar                      1440 Meter - 1" Strip Bar                      1450 Meter - 1" Strip Bar                      1460 Meter - 1" Strip Bar                      1470 Meter - 1" Strip Bar                      1480 Meter - 1" Strip Bar                      1490 Meter - 1" Strip Bar                      1500 Meter - 1" Strip Bar                      1510 Meter - 1" Strip Bar                      1520 Meter - 1" Strip Bar                      1530 Meter - 1" Strip Bar                      1540 Meter - 1" Strip Bar                      1550 Meter - 1" Strip Bar                      1560 Meter - 1" Strip Bar                      1570 Meter - 1" Strip Bar                      1580 Meter - 1" Strip Bar                      1590 Meter - 1" Strip Bar                      1600 Meter - 1" Strip Bar                      1610 Meter - 1" Strip Bar                      1620 Meter - 1" Strip Bar                      1630 Meter - 1" Strip Bar                      1640 Meter - 1" Strip Bar                      1650 Meter - 1" Strip Bar                      1660 Meter - 1" Strip Bar                      1670 Meter - 1" Strip Bar                      1680 Meter - 1" Strip Bar                      1690 Meter - 1" Strip Bar                      1700 Meter - 1" Strip Bar                      1710 Meter - 1" Strip Bar                      1720 Meter - 1" Strip Bar                      1730 Meter - 1" Strip Bar                      1740 Meter - 1" Strip Bar                      1750 Meter - 1" Strip Bar                      1760 Meter - 1" Strip Bar                      1770 Meter - 1" Strip Bar                      1780 Meter - 1" Strip Bar                      1790 Meter - 1" Strip Bar                      1800 Meter - 1" Strip Bar                      1810 Meter - 1" Strip Bar                      1820 Meter - 1" Strip Bar                      1830 Meter - 1" Strip Bar                      1840 Meter - 1" Strip Bar                      1850 Meter - 1" Strip Bar                      1860 Meter - 1" Strip Bar                      1870 Meter - 1" Strip Bar                      1880 Meter - 1" Strip Bar                      1890 Meter - 1" Strip Bar                      1900 Meter - 1" Strip Bar                      1910 Meter - 1" Strip Bar                      1920 Meter - 1" Strip Bar                      1930 Meter - 1" Strip Bar                      1940 Meter - 1" Strip Bar                      1950 Meter - 1" Strip Bar                      1960 Meter - 1" Strip Bar                      1970 Meter - 1" Strip Bar                      1980 Meter - 1" Strip Bar                      1990 Meter - 1" Strip Bar                      2000 Meter - 1" Strip Bar                      2010 Meter - 1" Strip Bar                      2020 Meter - 1" Strip Bar                      2030 Meter - 1" Strip Bar                      2040 Meter - 1" Strip Bar                      2050 Meter - 1" Strip Bar                      2060 Meter - 1" Strip Bar                      2070 Meter - 1" Strip Bar                      2080 Meter - 1" Strip Bar                      2090 Meter - 1" Strip Bar                      2100 Meter - 1" Strip Bar                      2110 Meter - 1" Strip Bar                      2120 Meter - 1" Strip Bar                      2130 Meter - 1" Strip Bar                      2140 Meter - 1" Strip Bar                      2150 Meter - 1" Strip Bar                      2160 Meter - 1" Strip Bar                      2170 Meter - 1" Strip Bar                      2180 Meter - 1" Strip Bar                      2190 Meter - 1" Strip Bar                      2200 Meter - 1" Strip Bar                      2210 Meter - 1" Strip Bar                      2220 Meter - 1" Strip Bar                      2230 Meter - 1" Strip Bar                      2240 Meter - 1" Strip Bar                      2250 Meter - 1" Strip Bar                      2260 Meter - 1" Strip Bar                      2270 Meter - 1" Strip Bar                      2280 Meter - 1" Strip Bar                      2290 Meter - 1" Strip Bar                      2300 Meter - 1" Strip Bar                      2310 Meter - 1" Strip Bar                      2320 Meter - 1" Strip Bar                      2330 Meter - 1" Strip Bar                      2340 Meter - 1" Strip Bar                      2350 Meter - 1" Strip Bar                      2360 Meter - 1" Strip Bar                      2370 Meter - 1" Strip Bar                      2380 Meter - 1" Strip Bar                      2390 Meter - 1" Strip Bar                      2400 Meter - 1" Strip Bar                      2410 Meter - 1" Strip Bar                      2420 Meter - 1" Strip Bar                      2430 Meter - 1" Strip Bar                      2440 Meter - 1" Strip Bar                      2450 Meter - 1" Strip Bar                      2460 Meter - 1" Strip Bar                      2470 Meter - 1" Strip Bar                      2480 Meter - 1" Strip Bar                      2490 Meter - 1" Strip Bar                      2500 Meter - 1" Strip Bar                      2510 Meter - 1" Strip Bar                      2520 Meter - 1" Strip Bar                      2530 Meter - 1" Strip Bar                      2540 Meter - 1" Strip Bar                      2550 Meter - 1" Strip Bar                      2560 Meter - 1" Strip Bar                      2570 Meter - 1" Strip Bar                      2580 Meter - 1" Strip Bar                      2590 Meter - 1" Strip Bar                      2600 Meter - 1" Strip Bar                      2610 Meter - 1" Strip Bar                      2620 Meter - 1" Strip Bar                      2630 Meter - 1" Strip Bar                      2640 Meter - 1" Strip Bar                      2650 Meter - 1" Strip Bar                      2660 Meter - 1" Strip Bar                      2670 Meter - 1" Strip Bar                      2680 Meter - 1" Strip Bar                      2690 Meter - 1" Strip Bar                      2700 Meter - 1" Strip Bar                      2710 Meter - 1" Strip Bar                      2720 Meter - 1" Strip Bar                      2730 Meter - 1" Strip Bar                      2740 Meter - 1" Strip Bar                      2750 Meter - 1" Strip Bar                      2760 Meter - 1" Strip Bar                      2770 Meter - 1" Strip Bar                      2780 Meter - 1" Strip Bar                      2790 Meter - 1" Strip Bar                      2800 Meter - 1" Strip Bar                      2810 Meter - 1" Strip Bar                      2820 Meter - 1" Strip Bar                      2830 Meter - 1" Strip Bar                      2840 Meter - 1" Strip Bar                      2850 Meter - 1" Strip Bar                      2860 Meter - 1" Strip Bar                      2870 Meter - 1" Strip Bar                      2880 Meter - 1" Strip Bar                      2890 Meter - 1" Strip Bar                      2900 Meter - 1" Strip Bar                      2910 Meter - 1" Strip Bar                      2920 Meter - 1" Strip Bar                      2930 Meter - 1" Strip Bar                      2940 Meter - 1" Strip Bar                      2950 Meter - 1" Strip Bar                      2960 Meter - 1" Strip Bar                      2970 Meter - 1" Strip Bar                      2980 Meter - 1" Strip Bar                      2990 Meter - 1" Strip Bar                      3000 Meter - 1" Strip Bar                      3010 Meter - 1" Strip Bar                      3020 Meter - 1" Strip Bar                      3030 Meter - 1" Strip Bar                      3040 Meter - 1" Strip Bar                      3050 Meter - 1" Strip Bar                      3060 Meter - 1" Strip Bar                      3070 Meter - 1" Strip Bar                      3080 Meter - 1" Strip Bar                      3090 Meter - 1" Strip Bar                      3100 Meter - 1" Strip Bar                      3110 Meter - 1" Strip Bar                      3120 Meter - 1" Strip Bar                      3130 Meter - 1" Strip Bar                      3140 Meter - 1" Strip Bar                      3150 Meter - 1" Strip Bar                      3160 Meter - 1" Strip Bar                      3170 Meter - 1" Strip Bar                      3180 Meter - 1" Strip Bar                      3190 Meter - 1" Strip Bar                      3200 Meter - 1" Strip Bar                      3210 Meter - 1" Strip Bar                      3220 Meter - 1" Strip Bar                      3230 Meter - 1" Strip Bar                      3240 Meter - 1" Strip Bar                      3250 Meter - 1" Strip Bar                      3260 Meter - 1" Strip Bar                      3270 Meter - 1" Strip Bar                      3280 Meter - 1" Strip Bar                      3290 Meter - 1" Strip Bar                      3300 Meter - 1" Strip Bar                      3310 Meter - 1" Strip Bar                      3320 Meter - 1" Strip Bar                      3330 Meter - 1" Strip Bar                      3340 Meter - 1" Strip Bar                      3350 Meter - 1" Strip Bar                      3360 Meter - 1" Strip Bar                      3370 Meter - 1" Strip Bar                      3380 Meter - 1" Strip Bar                      3390 Meter - 1" Strip Bar                      3400 Meter - 1" Strip Bar                      3410 Meter - 1" Strip Bar                      3420 Meter - 1" Strip Bar                      3430 Meter - 1" Strip Bar                      3440 Meter - 1" Strip Bar                      3450 Meter - 1" Strip Bar                      3460 Meter - 1" Strip Bar                      3470 Meter - 1" Strip Bar                      3480 Meter - 1" Strip Bar                      3490 Meter - 1" Strip Bar                      3500 Meter - 1" Strip Bar                      3510 Meter - 1" Strip Bar                      3520 Meter - 1" Strip Bar                      3530 Meter - 1" Strip Bar                      3540 Meter - 1" Strip Bar                      3550 Meter - 1" Strip Bar                      3560 Meter - 1" Strip Bar                      3570 Meter - 1" Strip Bar                      3580 Meter - 1" Strip Bar                      3590 Meter - 1" Strip Bar                      3600 Meter - 1" Strip Bar                      3610 Meter - 1" Strip Bar                      3620 Meter - 1" Strip Bar                      3630 Meter - 1" Strip Bar                      3640 Meter - 1" Strip Bar                      3650 Meter - 1" Strip Bar                      3660 Meter - 1" Strip Bar                      3670 Meter - 1" Strip Bar                      3680 Meter - 1" Strip Bar                      3690 Meter - 1" Strip Bar                      3700 Meter - 1" Strip Bar                      3710 Meter - 1" Strip Bar                      3720 Meter - 1" Strip Bar                      3730 Meter - 1" Strip Bar                      3740 Meter - 1" Strip Bar                      3750 Meter - 1" Strip Bar                      3760 Meter - 1" Strip Bar                      3770 Meter - 1" Strip Bar                      3780 Meter - 1" Strip Bar                      3790 Meter - 1" Strip Bar                      3800 Meter - 1" Strip Bar                      3810 Meter - 1" Strip Bar                      3820 Meter - 1" Strip Bar                      3830 Meter - 1" Strip Bar                      3840 Meter - 1" Strip Bar                      3850 Meter - 1" Strip Bar                      3860 Meter - 1" Strip Bar                      3870 Meter - 1" Strip Bar                      3880 Meter - 1" Strip Bar                      3890 Meter - 1" Strip Bar                      3900 Meter - 1" Strip Bar                      3910 Meter - 1" Strip Bar                      3920 Meter - 1" Strip Bar                      3930 Meter - 1" Strip Bar                      3940 Meter - 1" Strip Bar                      3950 Meter - 1" Strip Bar                      3960 Meter - 1" Strip Bar                      3970 Meter - 1" Strip Bar                      3980 Meter - 1" Strip Bar                      3990 Meter - 1" Strip Bar                      4000 Meter - 1" Strip Bar                      4010 Meter - 1" Strip Bar                      4020 Meter - 1" Strip Bar                      4030 Meter - 1" Strip Bar                      4040 Meter - 1" Strip Bar                      4050 Meter - 1" Strip Bar                      4060 Meter - 1" Strip Bar                      4070 Meter - 1" Strip Bar                      4080 Meter - 1" Strip Bar                      4090 Meter - 1" Strip Bar                      4100 Meter - 1" Strip Bar                      4110 Meter - 1" Strip Bar                      4120 Meter - 1" Strip Bar                      4130 Meter - 1" Strip Bar                      4140 Meter - 1" Strip Bar                      4150 Meter - 1" Strip Bar                      4160 Meter - 1" Strip Bar                      4170 Meter - 1" Strip Bar                      4180 Meter - 1" Strip Bar                      4190 Meter - 1" Strip Bar                      4200 Meter - 1" Strip Bar                      4210 Meter - 1" Strip Bar                      4220 Meter - 1" Strip Bar                      4230 Meter - 1" Strip Bar                      4240 Meter - 1" Strip Bar                      4250 Meter - 1" Strip Bar                      4260 Meter - 1" Strip Bar                      4270 Meter - 1" Strip Bar                      4280 Meter - 1" Strip Bar                      4290 Meter - 1" Strip Bar                      4300 Meter - 1" Strip Bar                      4310 Meter - 1" Strip Bar                      4320 Meter - 1" Strip Bar                      4330 Meter - 1" Strip Bar                      4340 Meter - 1" Strip Bar                      4350 Meter - 1" Strip Bar                      4360 Meter - 1" Strip Bar                      4370 Meter - 1" Strip Bar                      4380 Meter - 1" Strip Bar                      4390 Meter - 1" Strip Bar                      4400 Meter - 1" Strip Bar                      4410 Meter - 1" Strip Bar                      4420 Meter - 1" Strip Bar                      4430 Meter - 1" Strip Bar                      4440 Meter - 1" Strip Bar                      4450 Meter - 1" Strip Bar                      4460 Meter - 1" Strip Bar                      4470 Meter - 1" Strip Bar                      4480 Meter - 1" Strip Bar                      4490 Meter - 1" Strip Bar                      4500 Meter - 1" Strip Bar                      4510 Meter - 1" Strip Bar                      4520 Meter - 1" Strip Bar                      4530 Meter - 1" Strip Bar                      4540 Meter - 1" Strip Bar                      4550 Meter - 1" Strip Bar                      4560 Meter - 1" Strip Bar                      4570 Meter - 1" Strip Bar                      4580 Meter - 1" Strip Bar                      4590 Meter - 1" Strip Bar                      4600 Meter - 1" Strip Bar                      4610 Meter - 1" Strip Bar                      4620 Meter - 1" Strip Bar                      4630 Meter - 1" Strip Bar                      4640 Meter - 1" Strip Bar                      4650 Meter - 1" Strip Bar                      4660 Meter - 1" Strip Bar                      4670 Meter - 1" Strip Bar                      4680 Meter - 1" Strip Bar                      4690 Meter - 1" Strip Bar                      4700 Meter - 1" Strip Bar                      4710 Meter - 1" Strip Bar                      4720 Meter - 1" Strip Bar                      4730 Meter - 1" Strip Bar                      4740 Meter - 1" Strip Bar                      4750 Meter - 1" Strip Bar                      4760 Meter - 1" Strip Bar                      4770 Meter - 1" Strip Bar                      4780 Meter - 1" Strip Bar                      4790 Meter - 1" Strip Bar                      4800 Meter - 1" Strip Bar                      4810 Meter - 1" Strip Bar                      4820 Meter - 1" Strip Bar                      4830 Meter - 1" Strip Bar                      4840 Meter - 1" Strip Bar                      4850 Meter - 1" Strip Bar                      4860 Meter - 1" Strip Bar                      4870 Meter - 1" Strip Bar                      4880 Meter - 1" Strip Bar                      4890 Meter - 1" Strip Bar                      4900 Meter - 1" Strip Bar                      4910 Meter - 1" Strip Bar                      4920 Meter - 1" Strip Bar                      4930 Meter - 1" Strip Bar                      4940 Meter - 1" Strip Bar                      4950 Meter - 1" Strip Bar                      4960 Meter - 1" Strip Bar                      4970 Meter - 1" Strip Bar                      4980 Meter - 1" Strip Bar                      4990 Meter - 1" Strip Bar                      5000 Meter - 1" Strip Bar                      5010 Meter - 1" Strip Bar                      5020 Meter - 1" Strip Bar                      5030 Meter - 1" Strip Bar                      5040 Meter - 1" Strip Bar                      5050 Meter - 1" Strip Bar                      5060 Meter - 1" Strip Bar                      5070 Meter - 1" Strip Bar                      5080 Meter - 1" Strip Bar                      5090 Meter - 1" Strip Bar                      5100 Meter - 1" Strip Bar                      5110 Meter - 1" Strip Bar                      5120 Meter - 1" Strip Bar                      5130 Meter - 1" Strip Bar                      5140 Meter - 1" Strip Bar                      5150 Meter - 1" Strip Bar                      5160 Meter - 1" Strip Bar                      5170 Meter - 1" Strip Bar                      5180 Meter - 1" Strip Bar                      5190 Meter - 1" Strip Bar                      5200 Meter - 1" Strip Bar                      5210 Meter - 1" Strip Bar                      5220 Meter - 1" Strip Bar                      5230 Meter - 1" Strip Bar                      5240 Meter - 1" Strip Bar                      5250 Meter - 1" Strip Bar                      5260 Meter - 1" Strip Bar                      5270 Meter - 1" Strip Bar                      5280 Meter - 1" Strip Bar                      5290 Meter - 1" Strip Bar                      5300 Meter - 1" Strip Bar                      5310 Meter - 1" Strip Bar                      5320 Meter - 1" Strip Bar                      5330 Meter - 1" Strip Bar                      5340 Meter - 1" Strip Bar                      5350 Meter - 1" Strip Bar                      5360 Meter - 1" Strip Bar                      5370 Meter - 1" Strip Bar                      5380 Meter - 1" Strip Bar                      5390 Meter - 1" Strip Bar                      5400 Meter - 1" Strip Bar                      5410 Meter - 1" Strip Bar                      5420 Meter - 1" Strip Bar                      5430 Meter - 1" Strip Bar                      5440 Meter - 1" Strip Bar                      5450 Meter - 1" Strip Bar                      5460 Meter - 1" Strip Bar                      5470 Meter - 1" Strip Bar                      5480 Meter - 1" Strip Bar                      5490 Meter - 1" Strip Bar                      5500 Meter - 1" Strip Bar                      5510 Meter - 1" Strip Bar                      5520 Meter - 1" Strip Bar                      5530 Meter - 1" Strip Bar                      5540 Meter - 1" Strip Bar                      5550 Meter - 1" Strip Bar                      5560 Meter - 1" Strip Bar                      5570 Meter - 1" Strip Bar                      5580 Meter - 1" Strip Bar                      5590 Meter - 1" Strip Bar                      5600 Meter - 1" Strip Bar                      5610 Meter - 1" Strip Bar                      5620 Meter - 1" Strip Bar                      5630 Meter - 1" Strip Bar                      5640 Meter - 1" Strip Bar                      5650 Meter - 1" Strip Bar                      5660 Meter - 1" Strip Bar                      5670 Meter - 1" Strip Bar                      5680 Meter - 1" Strip Bar                      5690 Meter - 1" Strip Bar                      5700 Meter - 1" Strip Bar                      5710 Meter - 1" Strip Bar                      5720 Meter - 1" Strip Bar                      5730 Meter - 1" Strip Bar                      5740 Meter - 1" Strip Bar                      5750 Meter - 1" Strip Bar                      5760 Meter - 1" Strip Bar                      5770 Meter - 1" Strip Bar                      5780 Meter - 1" Strip Bar                      5790 Meter - 1" Strip Bar                      5800 Meter - 1" Strip Bar                      5810 Meter - 1" Strip Bar                      5820 Meter - 1" Strip Bar                      5830 Meter - 1" Strip Bar                      5840 Meter - 1" Strip Bar                      5850 Meter - 1" Strip Bar                      5860 Meter - 1" Strip Bar                      5870 Meter - 1" Strip Bar                      5880 Meter - 1" Strip Bar                      5890 Meter - 1" Strip Bar                      5900 Meter - 1" Strip Bar                      5910 Meter - 1" Strip Bar                      5920 Meter - 1" Strip Bar                      5930 Meter - 1" Strip Bar                      5940 Meter - 1" Strip Bar                      5950 Meter - 1" Strip Bar                      5960 Meter - 1" Strip Bar                      5970 Meter - 1" Strip Bar                      5980 Meter - 1" Strip Bar                      5990 Meter - 1" Strip Bar                      6000 Meter - 1" Strip Bar                      6010 Meter - 1" Strip Bar                      6020 Meter - 1" Strip Bar                      6030 Meter - 1" Strip Bar                      6040 Meter - 1" Strip Bar                      6050 Meter - 1" Strip Bar                      6060 Meter - 1" Strip Bar                      6070 Meter - 1" Strip Bar                      6080 Meter - 1" Strip Bar                      6090 Meter - 1" Strip Bar                      6100 Meter - 1" Strip Bar                      6110 Meter - 1" Strip Bar                      6120 Meter - 1" Strip Bar                      6130 Meter - 1" Strip Bar                      6140 Meter - 1" Strip Bar                      6150 Meter - 1" Strip Bar                      6160 Meter - 1" Strip Bar                      6170 Meter - 1" Strip Bar                      6180 Meter - 1" Strip Bar                      6190 Meter - 1" Strip Bar                      6200 Meter - 1" Strip Bar                      6210 Meter - 1" Strip Bar                      6220 Meter - 1" Strip Bar                      6230 Meter - 1" Strip Bar                      6240 Meter - 1" Strip Bar                      6250 Meter - 1" Strip Bar                      6260 Meter - 1" Strip Bar                      6270 Meter - 1" Strip Bar                      6280 Meter - 1" Strip Bar                      6290 Meter - 1" Strip Bar                      6300 Meter - 1" Strip Bar                      6310 Meter - 1" Strip Bar                      6320 Meter - 1" Strip Bar                      6330 Meter - 1" Strip Bar                      6340 Meter - 1" Strip Bar                      6350 Meter - 1" Strip Bar                      6360 Meter - 1" Strip Bar                      6370 Meter - 1" Strip Bar                      6380 Meter - 1" Strip Bar                      6390 Meter - 1" Strip Bar                      6400 Meter - 1" Strip Bar                      6410 Meter - 1" Strip Bar                      6420 Meter - 1" Strip Bar                      6430 Meter - 1" Strip Bar                      6440 Meter - 1" Strip Bar                      6450 Meter - 1" Strip Bar                      6460 Meter - 1" Strip Bar                      6470 Meter - 1" Strip Bar                      6480 Meter - 1" Strip Bar                      6490 Meter - 1" Strip Bar                      6500 Meter - 1" Strip Bar                      6510 Meter - 1" Strip Bar                      6520 Meter - 1" Strip Bar                      6530 Meter - 1" Strip Bar                      6540 Meter - 1" Strip Bar                      6550 Meter - 1" Strip Bar                      6560 Meter - 1" Strip Bar                      6570 Meter - 1" Strip Bar                      6580 Meter - 1" Strip Bar                      6590 Meter - 1" Strip Bar                      6600 Meter - 1" Strip Bar                      6610 Meter - 1" Strip Bar                      6620 Meter - 1" Strip Bar                      6630 Meter - 1" Strip Bar                      6640 Meter - 1" Strip Bar                      6650 Meter - 1" Strip Bar                      6660 Meter - 1" Strip Bar                      6670 Meter - 1" Strip Bar                      6680 Meter - 1" Strip Bar                      6690 Meter - 1" Strip Bar                      6700 Meter - 1" Strip Bar                      6710 Meter - 1" Strip Bar                      6720 Meter - 1" Strip Bar                      6730 Meter - 1" Strip Bar                      6740 Meter - 1" Strip Bar                      6750 Meter - 1" Strip Bar                      6760 Meter - 1" Strip Bar                      6770 Meter - 1" Strip Bar                      6780 Meter - 1" Strip Bar                      6790 Meter - 1" Strip Bar                      6</p>									

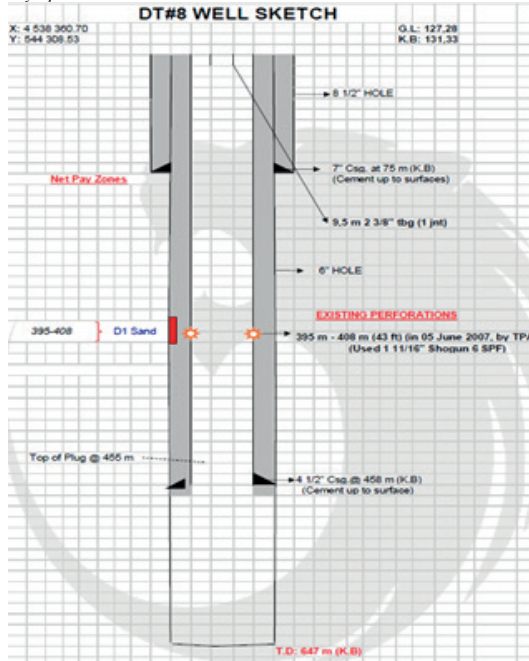
Çamur Dizayn

COMPOSITION	1		2		3		4	
Amount of XCD, ppb	1.0		1.5		2.0		2.5	
Test Temperature, F <sup>1</sup>	77	145	77	145	77	145	77	145
O <sub>300</sub>	21.6	16.9	38.2	26.0	43.9	34.4	54.4	44.8
O <sub>200</sub>	16.2	12.9	28.0	21.7	34.8	27.7	43.1	37.7
O <sub>100</sub>	13.6	12.0	24.8	18.6	30.1	24.7	36.8	34.3
O <sub>500</sub>	10.8	8.9	20.2	15.6	24.9	20.8	32.5	29.6
O <sub>6</sub>	5.1	3.7	11.3	8.0	14.1	11.9	19.7	18.0
O <sub>3</sub>	4.5	3.4	10.1	7.1	13.0	10.6	18.3	16.6
PV	5.4	4.0	10.2	4.3	9.1	6.7	11.3	7.1
YP	10.8	8.9	17.8	17.4	25.7	21.0	31.8	30.6
GeI, 10 sec	5.9	3.7	10.6	8.2	15.2	12.5	19.9	18.5
GeI, 10 min	7.3	3.9	13.7	10.0	20.1	16.7	26.8	24.2
pH	6.85	6.35	6.98	6.45	6.92	6.34	6.85	6.25

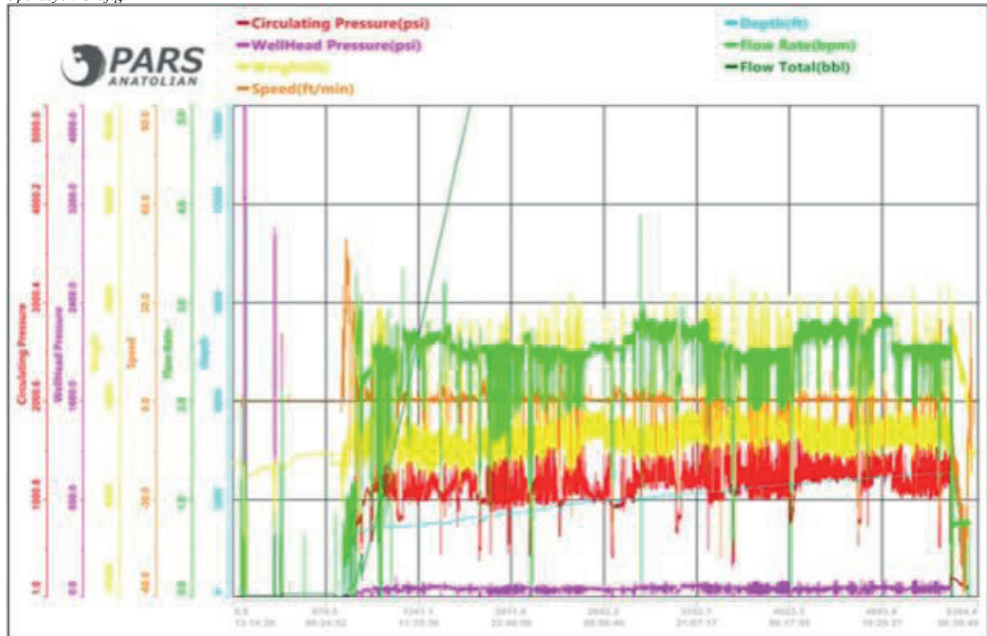
Hidrolik Dizayn

	RIH		POOH	
Calculation Depth (m)	1200		1200	
Pump Pressure (psi)	2421.9		2421.9	
Wellhead Pressure (psi)	50.0		50.0	
Gooseneck Pressure (psi)	2301.9		2301.9	
Downhole Pressure (psi)	2561.5		2561.5	
Downhole Flow Rate (bpm)	3.50		3.50	
Tool Pressure (psi)	2561.5		2561.5	
Pressure Loss across BHA (psi)	1220.0		1220.0	
	Inside CT	Annulus	Inside CT	Annulus
Volume (bbl)	33.7	39.8	33.7	39.8
Fluid Travel Time (min)	9.6	10.5	9.6	10.5
Friction Pressure Loss (psi)	440.1	711.4	440.1	711.4
Hydrostatic Pressure (psi)	1799.8	1799.8	1799.8	1799.8
Flow Regime	Turbulent	Turbulent	Turbulent	Turbulent

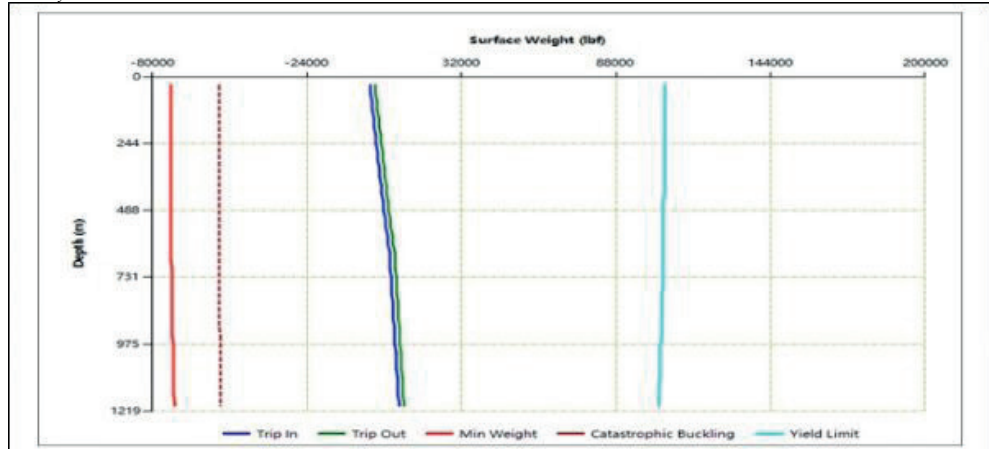
Kuyu Şemasi



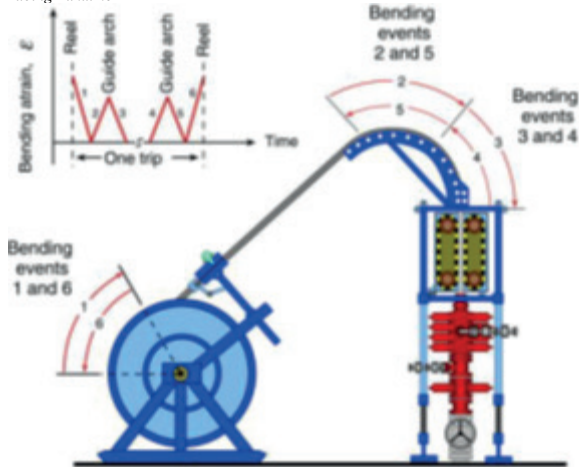
Operasyon Grafiği



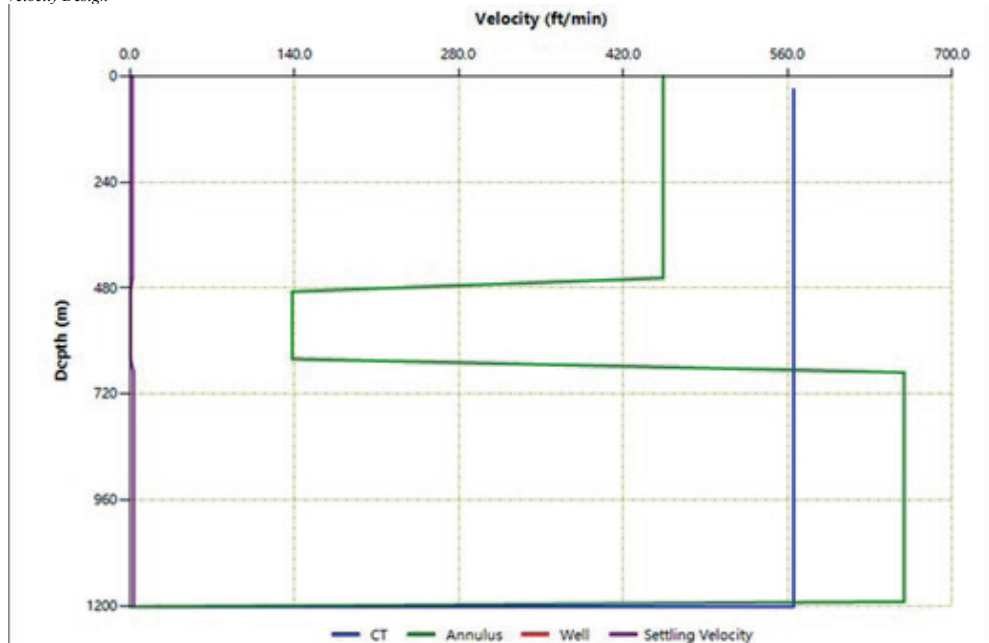
Similasyon 1



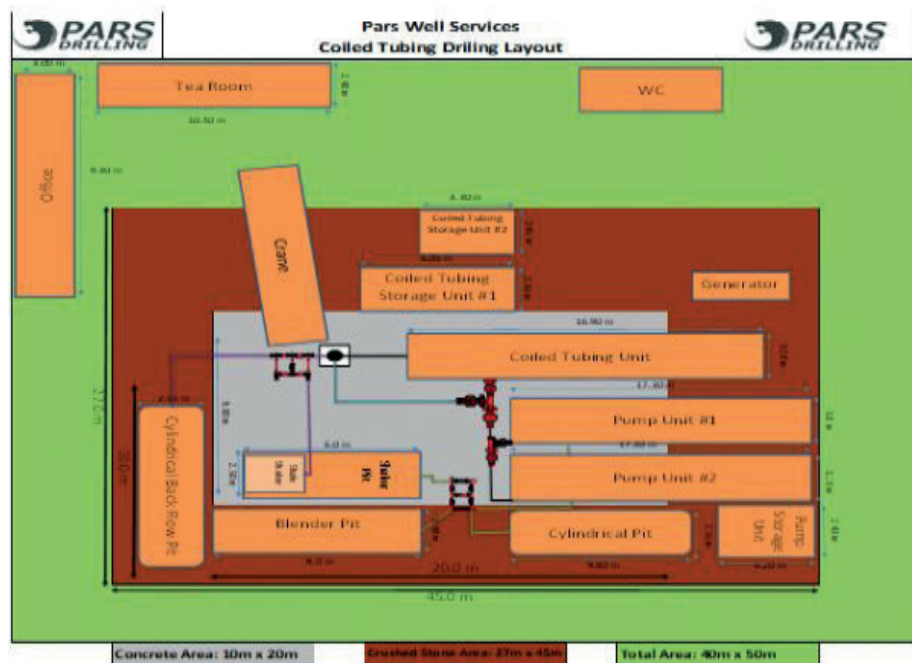
Tubing Bükülme



Velocity Design



Yerleşim



Yerleşim Foto



Yerleşim Foto 2



Yerleşim Foto 3





## Radial Drilling

**Doruk Kırac, Görkem Kaya**  
Türkiye Petrolleri Anonim Ortaklığı



Radial Drilling is an innovative technique used in the oil and gas industry to enhance well productivity and reservoir drainage with its ability to access multiple pay zones and increase hydrocarbon recovery. It involves the creation of radial, high-pressure jetting channels from the wellbore into the surrounding formation. These channels extend horizontally, intersecting and connecting with natural fractures or creating new pathways to increase reservoir contact.

The primary principle behind radial jet drilling is the utilization of high-pressure fluids, typically water or specialized fluids, to create jetting channels. A specially designed downhole tool, known as a jetting tool, is deployed into the wellbore. The tool incorporates nozzles or orifices that direct the high-pressure fluid into the surrounding rock formation, creating radial fractures or pathways.

The primary principle behind radial drilling is the utilization of high-pressure fluids, typically water or specialized fluids, to create jetting channels. The process begins with a workover rig installing a 2 7/8" tubing, along with a 2 3/8" tailpipe that extends 100-150 m. A deflector tool or shoe attached to the desired depth, which can be oriented to the targeted azimuth with the help of the gyro services within the main well. A coil tubing is then inserted through the tubing to the target depth. Utilizing the installed deflector shoe, milling bit connected to a flexible shaft and a positive displacement motor is employed to create the initial exit point. This is accomplished by milling a hole into the existing casing. Following this step, the coil tubing is retrieved from the wellbore. In the subsequent stage, a 100 m long flexible high-pressure hose is run into the wellbore using a coiled tubing. This hose exits the well through the previously created hole. High-pressure water is then pumped into the hose, and it exits through specially designed nozzles with very small diameters. As the fluid exits the jetting nozzles at high velocities, it generates powerful hydraulic jets that penetrate the rock, creating fractures or enlarging existing ones. Finally, suitable acid composition is pumped through to jet nozzles while jetting out of the newly created lateral hole in order to stimulate the formation.

### COMPARISON WITH TRADITIONAL DRILLING METHODS

Radial drilling offers several advantages over traditional drilling methods such as vertical and horizontal drilling. Traditional drilling techniques are limited in their ability to access and stimulate specific zones of a reservoir. In contrast, RJD allows for precise targeting of specific regions within the reservoir, including bypassed pay zones and low-permeability formations.

Unlike conventional drilling methods that rely on mechanical borehole penetration, radial jet drilling creates fractures without the need for extensive rock removal. This non-invasive technique reduces formation damage, minimizing the risk of decreased productivity. Additionally, RJD can be applied in both vertical and deviated wells up to 30°, making it a versatile option for various reservoir configurations.

### BENEFITS OF RADIAL DRILLIN

**Enhanced Production Rates:** Radial drilling has proven to increase production rates by improving wellbore connectivity and drainage efficiency if the targeted reservoir will be suited for creating a extra fractures. The creation of radial jetting channels increases the contact area between the well and the reservoir, allowing for better fluid flow and increased production of hydrocarbons.

**Enhanced Reservoir Access:** RD allows for precise targeting of specific regions within the reservoir, including bypassed pay zones and low-permeability formations. It provides access to previously untapped or difficult-to-reach areas, maximizing the recovery of hydrocarbons.

**Reduced Environmental Impact:** Compared to traditional drilling methods, radial drilling presents a reduced environmental footprint. The non-invasive nature of the technique minimizes formation damage, preserving the integrity of the reservoir.

**Minimized Formation Damage:** Radial drilling minimizes formation damage, which is a common concern in traditional drilling methods. By creating fractures without excessive rock removal, Radial Drilling prevents damage to the reservoir's permeability and preserves the natural fracture network. This preservation enhances long-term productivity and reduces the need for costly remedial treatments.

**Precise Stimulation Control:** RD enables operators to have precise control over the stimulation process. They can target specific zones, adjust flow rates, and optimize the treatment to achieve the desired results. This control helps maximize hydrocarbon recovery and improves overall well performance.

### CHALLENGES AND LIMITATIONS OF RADIAL DRILLING

**Formation Heterogeneity:** The success of radial jet drilling is dependent on the presence and connectivity of natural fractures within the reservoir. In formations with low fracture density or significant heterogeneity, achieving optimal results can be challenging. Proper reservoir characterization and understanding of the

geological properties are essential for identifying suitable target zones for RD.

**Equipment Reliability and Durability:** The tools and equipment used in radial drilling must withstand high-pressure and high-velocity fluid flows. The reliability and durability of these tools are crucial for the successful execution of RD operations. Continuous improvements in tool design, materials, and manufacturing processes are necessary to ensure efficient and reliable operations.

**Fluid and Erosion Management:** The selection and management of fluids used in radial drilling are critical to avoid erosion and maintain the integrity of the wellbore and the created jetting channels. The erosive nature of the high-velocity fluid jets can cause damage to the equipment and wellbore surfaces. Proper fluid selection, flow rate control, and erosion monitoring techniques are essential for mitigating these challenges.

**Limited Reach:** The radial extent of the stimulated zone in radial drilling is typically limited compared to other techniques such as hydraulic fracturing. While it allows for the creation of multiple radial channels, the overall reach of the stimulated zone may be smaller, which can affect the production rates and ultimate recovery from the reservoir.

**Overlapping Casing:** Radial Drilling systems can only penetrate single layer casing. Liners that have an overlap in the hang-off section cannot be milled with the present configuration of the cutting system.

### **Cement Quality**

When the bond between the casing and the cement is weak or compromised, it can hinder the effectiveness of the jetting operation. The jetting fluid may not be able to penetrate the desired zones or create the desired fractures, leading to reduced efficiency and suboptimal results. In such cases, additional measures may be required to improve the bonding or alternative techniques may need to be considered. Therefore, it is important to assess the bond quality before initiating the radial drilling process to ensure that the cement bond is strong and capable of withstanding the forces and pressures associated with the jetting operation. This assessment helps in determining the feasibility and effectiveness of the radial drilling technique in the specific wellbore.

### **Wellbore Inclination**

The angle of inclination affects the gravitational force acting on the system, and as the angle increases, the force pulling the system downward diminishes. This reduction in force can impede the proper seating and stability of the system within the deflector shoe. To ensure successful deployment and operation of the radial drilling system, it is important to consider the wellbore inclination and make sure it remains within the acceptable range (below 30°). If the wellbore inclination exceeds the recommended limit, alternative drilling methods or techniques may need to be employed to achieve the desired objectives

**Bottomhole Temperature:** Excessive temperatures can negatively impact the performance and integrity of the radial drilling tools and components. High temperatures may cause degradation of elastomers, seals, and other sensitive materials, leading to reduced functionality or failure of the equipment. Additionally, extreme temperatures can affect the effectiveness of the drilling fluids, such as acid compositions, used in the process.

## **SURFACE AND DOWNHOLE EQUIPMENTS**

### **Coil Tubing**

Coil tubing is a continuous, flexible pipe that is deployed into the wellbore to perform operations, including milling, jetting, and fluid circulation inside the tubing. It is typically inserted through the tubing and extends to the target depth with the downhole tools.

**Wellhead Equipments:** After running in hole the Radial Drilling Bottom Hole Assembly with the tubing string, several wellhead equipment components should be nipple up to the wellhead. These components include the Downhole Pressure Control Valve (DPSV), Coil Tubing Blowout Preventer (CT BOP), Coil Straightener, and for deeper wells, the Injector Head and Gooseneck. The purpose of these components is to ensure proper control, safety, and functionality during the radial drilling operation.

### **High Pressure Pump**

It is responsible for generating the required flow rate and pressure essential for the downhole jetting and milling operations.

### **Tanks & Filtration**

A 2.5m tall stand for acid tank will be required to gravity feed acid to high pressure pump. In addition to the acid tank stand, it is essential to incorporate a filtration system to maintain the cleanliness of the fluids. A 10-micron filtration system is recommended to remove particles and impurities from the fluids before they enter the high-pressure pump and the coil tubing. This filtration level helps prevent damage to the pump components and minimizes the risk of blockages in the coil tubing, ensuring smooth operation and efficient fluid flow.

### **Deflector Shoe**

A deflector shoe is a key component used in radial drilling operations. Its purpose is to divert the flow of fluid or tools from the main wellbore into a lateral or sidetrack direction. The deflector shoe is typically attached to the bottom of the tubing string or drill pipe, and it helps guide the tools or fluids into the desired trajectory. The deflector shoe is designed with a specific angle or shape that allows for the redirection of the fluid or tools. When the fluid or tools pass through the deflector shoe, the

angled conduit causes them to exit the shoe at an angle, creating a lateral hole or sidetrack away from the main wellbore. The conduit has a j-shaped run which allows for the milling bit to the exit of the deflector shoe at a 90° angle to the vertical and mill the casing. The shape of the conduit is of great importance for both the jetting and the milling process. If the conduit is too narrow or is not of the correct shape it is impossible for the jetting hose to jet through it. If the conduit is too wide it is impossible to direct the flexible shaft and the milling bit through out deflector shoe exit.

#### **Decentralizers:**

The decentralizer used in the radial drilling process is a welded construction composed of five parts: a ring, two interlocking half-shells, and two flat springs. These components are securely joined together to form the centralizer. The primary function of the decentralizer is to position the deflector shoe, which has a smaller diameter, away from the central position and press the conduit exit against the casing to prevent the milling bit from rotating freely. The decentralizer is installed just above the deflector shoe and is fixed to the tubing and the coupling using grub screws. To install the centralizer, it needs to be pulled over the coupling with a ring, and the two half-shells are screwed together before fastening the grub screws. It needs to be adjusted according to the internal diameter (ID) of the casing to achieve the required eccentricity. During assembly, it is crucial to ensure that the flat springs are placed on the opposing side of the conduit exit. This arrangement allows the decentralizer to exert pressure on the conduit exit, ensuring that it remains in contact with the casing wall. By using this decentralizer design, the radial drilling process can effectively position the deflector shoe and secure the milling bit in place. The decentralizer's welded construction and adjustable eccentricity play a vital role in maintaining the desired position and stability during the milling operation.

**UBHO & Gyro:** UBHO (Universal Bottom Hole Oriented) is a specialized tool used in radial drilling operations to provide accurate orientation and measurement of the wellbore trajectory. It combines the capabilities of a gyroscopic tool and a UBHO Assembly to enhance the accuracy and control of the radial drilling process to find the exact direction. The gyro logging tool is typically lowered into the wellbore via wireline inside through the tubing string until it hits the wedge placed into the UBHO. It is crucial to ensure that the wedge inside the UBHO is placed on the same side of the conduit exit. It can provide real-time information on the azimuth (horizontal direction) and inclination (vertical angle) of the wellbore, allowing operators to accurately steer the radial drilling tubing string to the desired direction.

#### **PDM**

A positive displacement motor (PDM) is a type of downhole drilling tool used in radial drilling operations. It is designed to provide rotational power to the drill

bit or milling bit used for creating lateral holes in the wellbore. The PDM operates on the principle of positive displacement, where fluid pressure is used to generate mechanical power. As fluid flows through the motor, it drives the rotation of the lobes or gears, which in turn transmit the torque to the drill bit. In radial drilling, the PDM is typically used in combination with a flexible shaft that connects it to the milling bit. The PDM's rotation powers the cutting or milling action, allowing the bit to penetrate the casing and create the lateral hole.

#### **Torque Arrester Sleeve**

Torque arrester sleeve is a specialized tool used to mitigate and control rotational forces or torque generated by the positive displacement motor during the drilling process. The torque arrester sleeve helps to stabilize the drillstring and minimize the transfer of torque to the flexible shaft and milling bit, improving the efficiency and effectiveness of the radial drilling operation. By reducing torque fluctuations and vibrations, the torque arrester sleeve helps improve drilling efficiency and prolong the life of the drilling motor and other downhole tools. It helps prevent excessive wear and damage that may occur due to high torque loads, enhancing the overall performance and longevity of the drilling system.

#### **Milling Bit**

In radial drilling operations, a milling bit is a specialized tool used to create openings or windows in the existing casing or formation. It is designed to remove material and create pathways for fluid flow in order to access reservoir zones or stimulate well production. The milling bit used in radial drilling is typically a small-diameter cutting tool with sharp, durable teeth or inserts. It is attached to a flexible shaft, which is powered by a PDM. During radial drilling operations, the milling bit is typically operated with a relatively low WOB and rotation speed. The purpose of this approach is to facilitate a grinding or rubbing process rather than a traditional cutting process at the cutting edges of the bit. These low values of WOB and rotation speed are chosen to prevent excessive stress on the milling bit and the downhole motor, particularly to avoid exceeding the motor torque limit.

#### **Flexible Shaft**

In radial drilling, a flexible shaft is an essential component used to transmit torque and rotational force from the surface to downhole tools. It provides the necessary flexibility to navigate through the wellbore and perform various drilling operations. The flexible shaft is designed to withstand the harsh downhole conditions while maintaining its structural integrity.

#### **Jet Nozzle**

The jet nozzle is a critical component in radial drilling that plays a key role in creating the desired hydraulic

jetting effect. It is responsible for delivering high-pressure fluid into the formation through the lateral hole, contributing to the stimulation and reservoir drainage process. The jet nozzle is designed to produce a focused and powerful jet of fluid that effectively erodes the formation, creating fractures and improving well productivity. The jet nozzle typically consists of a small-diameter orifice or series of orifices strategically positioned to direct the fluid flow in a specific pattern or direction. The size and configuration of the nozzle orifices can vary depending on the desired jetting effect and the characteristics of the formation being targeted. The jet nozzle used in radial drilling can have either a static or rotational movement.

### **Jet Hose**

The jetting hose is meant to supply the nozzle with fluid (pressure and flow rate) and whilst doing so create as little pressure loss as possible. The jetting hose used in radial drilling should possess specific characteristics to ensure optimal performance in the field. One crucial aspect is its chemical resistance to substances like water-glycol, diesel, and acids. This resistance is important to ensure the hose remains unaffected by the fluids it comes into contact with during the drilling operation. Another essential feature is the minimum bending radius. Under high pressure, the hose tends to stiffen, making it challenging to navigate through the conduit of the deflector shoe. By having a smaller bending radius, the hose maintains flexibility. Jetting hose should not be excessively heavy. This allows the nozzle to pull the hose into the formation without encountering significant resistance or affecting the drilling process. Additionally, the outer layer of the hose is designed to be abrasion-resistant. This protective layer helps prevent damage to the hose when it comes into contact with rough surfaces, such as the rugged terrain of a side track. By mitigating abrasion, the outer layer ensures the longevity and reliability of the jetting hose during radial drilling operations.

While radial drilling has proven to be a highly effective technique, it is important to note that its success depends on proper planning and execution. Accurate reservoir characterization and fracture mapping are critical to identifying the optimal locations for the laterals. Additionally, advanced drilling and measurement technologies play a crucial role in ensuring precise lateral placement and control.

In conclusion, radial drilling has emerged as a groundbreaking technique in the oilfield industry. Its ability to access multiple pay zones, enhance hydrocarbon recovery, and bypass damaged formations has made it a preferred method for improving well performance and productivity. As the industry continues to seek innovative solutions, radial drilling stands out as a game-changer that will shape the future of oilfield operations, maximizing reservoir potential while reducing costs and environmental impact.

Keywords: Radial Drilling

# Coiled Tubing ile Canlı Kuyuda Slickline Tahliyesi

**Seckin Öztel**  
Pars Drilling



Anahtar Kelime: Coiled Tubing, Tahliyesi

Coiled Tubing küçük çaplı, manşonsuz oluşu, basınç altında iniş çıkış ve iniş çıkış yaparken sirkülasyon yapabildiği için çok önemli bir tahliye ekipmanıdır. Kuyuda kalan malzeme tahliyesi, milling operasyonları, halat yalakama gibi birçok farklı tahliye operasyonu coiled tubing ile yapılabilmektedir. Varınca Hazro 1 kuyusunda yapılan tahliye bunun çok iyi bir örneğidir. Canlı bir kuyuda kablo tahliyesi başarı ile yapılmıştır. Bu bildiride bu operasyonun nasıl yapıldığı anlatılmaktadır.

Coiled Tubing is a very effective equipment because it has a small diameter, no joints, it can circulate when RIH under pressure. Many different fishing operations such as junk fishing, milling operations, wire rope fishing can be performed with coiled tubing. The fishing performed at the Hazro 1 well is a very good example of this. Cable fishing has been performed successfully in a live well. This statement describes how this operation was carried out.

## A. AMAÇ

Varınca Hazro 1 kuyusu 2021 yılında kazılmıştır. 3260 m'ye 7" Casing indirilmiş, ardından 3801 m'ye kadar son section dikey olacak şekilde 6" matkap ile kazılmış ve 7" e genişletilmiştir. Ardından 5 1/2" liner inişine geçilmiş, liner 3733 m'de oturmuş. Bu metrajda çimentosu yapılmıştır. Çimento sırasında kaçak görülmemiş yüzeye 10 bbl kontamine çimento gelişi görülmüştür. 4 3/4" PDC bit + 2 7/8" PDM ile inilerek LC+FC+FS sondajı yapılmış 3767 m'ye kadar açık kuyuda ilerlenmiştir. Daha sonra PLS packer ile inilerek kuyu üretime alınmıştır. Üretim testleri sırasında 3700 m 0.107" slickline ve PT tool'u kuyuya düşerek kuyuda kalmıştır. Kuyu başında basınç olduğu için müdahalenin coiled tubing ile yapılmasına karar verilmiştir.

## B. GEREÇ VE YÖNTEM

Öncelikle operasyon planını kuyu emniyete alıp susturmak amacı ile oluşturduk. Bu sebep ile 1 1/2" Coiled tubing ile 1 11/16" BHA kullanılması kararlaştırıldı.

### B.1. Dizayn

Öncelikle kuyuda 2 7/8" tubing olduğundan dolayı tool fit analysis yapıldı ve 1 11/16" BHA'ın kuyuya en uygun çapda dizi olduğu anlaşıldı. BHA çapı belirlendikten sonra coil çapı olarak 1 1/2" kullanılmasına karar verildi.

BHA ve coil çapı belirlendikten sonra kuyu başındaki basınç ve derinliğinden kaynaklı Coil Tubing Limitleri simülasyonda hesaplanarak coiled tubing'in kuyu dibine sorun yaşamadan inebileceği görüldü

Limit analizine müteakip Real Axial Force, Von Mises Stress, Surface Weight, Max Set down and Pull Force simülasyonları yapılarak kontrol edildi. Tüm hesaplar sonucu operasyonun sorunsuz yapılabileceği anlaşılınca naliyata başlandı.

Sahaya coiled tubing ekipmanları nakliyatı yapılarak kuruluma geçildi. Kuyuyu öldürmek için KCl Brine'ı hazırlandı. Kuyubaşı ve inflow testleri yapıldıktan sonra kuyubaşı açılarak inişe geçildi. İlk iniş de oturma görülmeyen 2000 metreye başarılı bir şekilde inildi ve kuyu brine basılarak susturuldu.

2. runda TPAO ile ortak bir dizayn ile geliştirilen Tahliye Tool'u inildi. Bu tool tamamen yerli malzeme ve işçilik ile Pars Firması tarafından TPAO ile danışılarak bu kuyu şartına özel olarak üretildi.

Tahliye inişinde kuyuda kalan halada 400 metrede rastlandı. Kuyudaki tahliye başarılı bir şekilde yakalandı. Çıkış yapılmak istendiğinde coiled tubing'in sıkışık olduğu görüldü.

Verilen karar doğrultusunda dizi MHA üstünden ayrılarak kuyuda bırakıldı ve kuyu emniyetli bir şekilde workover kulesine teslim edildi.

Workover kulesi gerekli kuyubaşı emniyetini sağladıktan sonra geliş olmayan kuyuda tubing çıkışı yaparak tubing içinde kalan slick line halatını kuyudan çıkardı. Tekrar tubing inişi yapılarak kuyu üretime verildi.

## A. OLGU VE SONUÇ

Varınca Hazro 1 de yapılan operasyon bir petrol firmasının envanterinde farklı çözümler olması gerekliliğinin açık bir örneğidir. Coiled tubing ile kısa sürede yapılan bu başarılı tahliye Türkiye'deki petrol sektörünün gelişmişliğini göstermektedir.

Ayrıca TPAO – Servis firması iş birliğinin hızlı ve olumlu sonuçlandığı operasyonlardan biridir.

Tahliye malzemesi tasarlanarak TPAO Kuyu Tamamlama Birimi ile istişare edilmiş, gerekli malzemenin çizimi bilgisayar ortamında yapılmış, bu çizime kuyu nezdinde özel tırnaklar eklemiş ve bu kuyuya özel bir tahliye ekipmanı dizayn edilmiştir.

Varınca Hazro 1 kuyusu 22.08.2023 tarihi itibarı ile 724 bbl petrol üretmektedir. Su oranı %27 ile 195 bbl'dir. Net petrol üretimi 529 bbl olmuştur.

Bu operasyonun başarıya ulaşmasında hızlı alınan aksiyonun yanında, TPAO Mühendislik Daire Başkanlığı, Kuyu Tamamlama Müdürlüğü ile operasyon dizaynı konusunda verimli işbirliğinin, tahliye ekipmanı üretim sürecinde Pars CNC atölyesinin ve dizayn ekibinin titiz ve hızlı çalışması, ekipmanın 5 gün gibi kısa bir sürede yedeği ile birlikte üretilmesi ile coiled tubing ekibinin hızlı bir şekilde mobilize olması

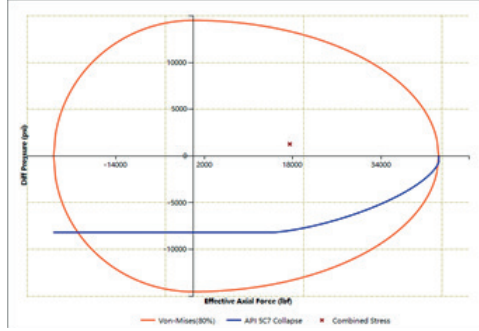
ve operasyona başlaması neden olmuştur.

Bu bağlamda yurtdışından malzeme veya coiled tubing ekipmanı tedarikine gidilse minimum 45 gün sürecek ekipman ve malzeme tedariki 10 gün gibi kısa bir sürede yapılmıştır. Buda operatör firmaya 30 günlük toplam 1.269.000 USD bir petrol üretim kazanımı sağlamıştır.

Tahlisiye operasyonunun başarıya ulaşmasının ardından aynı lokasyonun 700 metre yanına yeni bir kuyu açılmış ve şu anda tamamlaması yapılmaktadır. İlk tamamlama operasyon verileri umut vericidir ve Varınca Hazro 1 kuyusuna yakın bir üretim beklenmektedir.

Anahtar Kelimeler: Coiled Tubing, Tahlisiye

Ct Limits



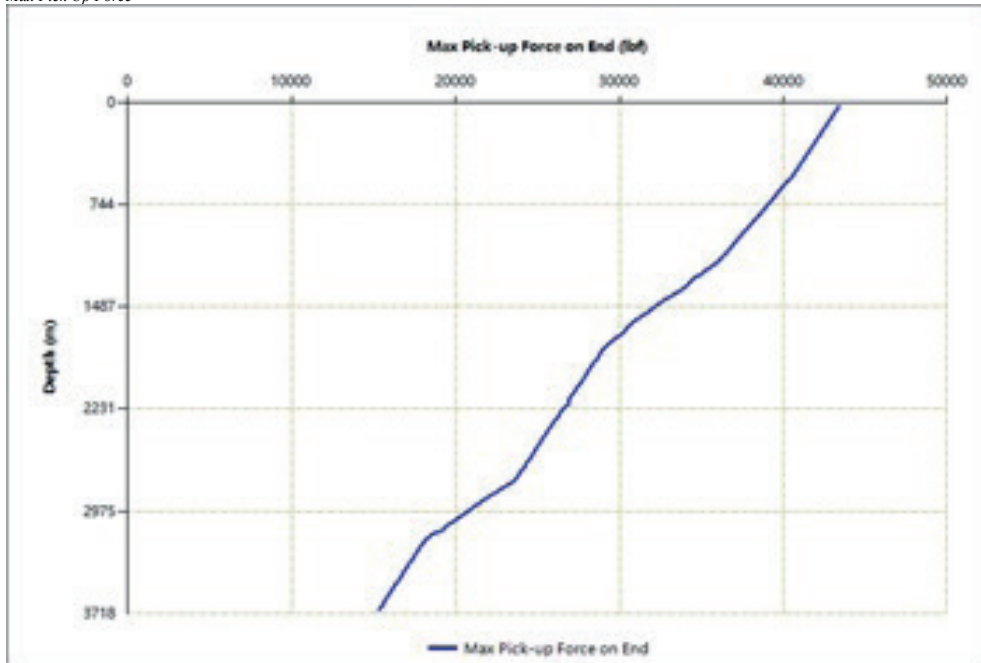
Fishing Tool



Hidrolik Dizayn

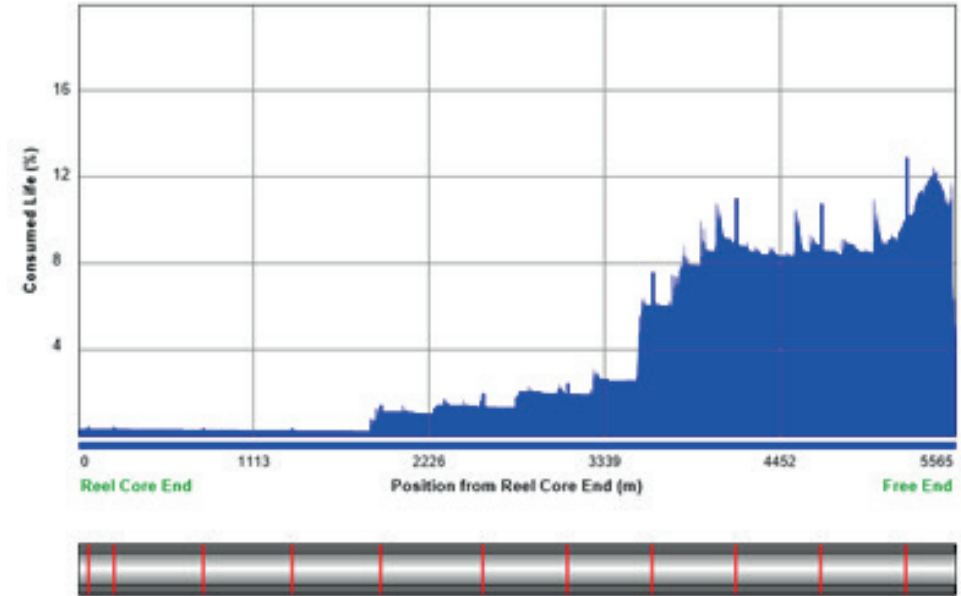
	RIH		POOH	
Calculation Depth (m)	1200		1200	
Pump Pressure (psi)	2421.9		2421.9	
Wellhead Pressure (psi)	50.0		50.0	
Gooseneck Pressure (psi)	2301.9		2301.9	
Downhole Pressure (psi)	2561.5		2561.5	
Downhole Flow Rate (bpm)	3.50		3.50	
Tool Pressure (psi)	2561.5		2561.5	
Pressure Loss across BHA (psi)	1220.0		1220.0	
	Inside CT	Annulus	Inside CT	Annulus
Volume (bbl)	33.7	39.8	33.7	39.8
Fluid Travel Time (min)	9.6	10.5	9.6	10.5
Friction Pressure Loss (psi)	440.1	711.4	440.1	711.4
Hydrostatic Pressure (psi)	1799.8	1799.8	1799.8	1799.8
Flow Regime	Turbulent	Turbulent	Turbulent	Turbulent

Max Pick Up Force





Pipe Fatigue

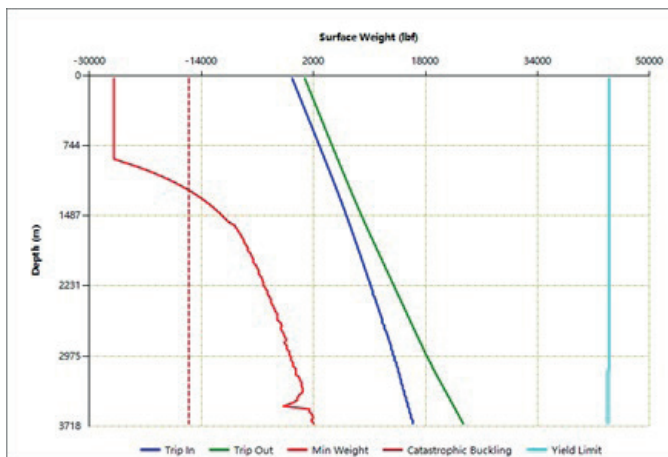




Tahsisive



Tripping forces



# Resolving Cement Evaluation in the Challenging Environment of Large and Thick Casing

**Alhadi Zahmuwl, Rob Loov, Diana Vargas**  
Schlumberger



## INTRODUCTION

Well integrity assurance and zonal isolation have high importance for both new and old wells. Moreover, the stakes are much higher when the well is located offshore and any compromise on cement evaluation could result in very high liability for operators with a critical impact on the environment and carbon footprint.

Recent advances in deepwater exploration technology and operational strategies have allowed oil and gas operators to reach more complex and challenging fields which required large installing large diameter and thicker casings. Hence the need for developing a solution to evaluate cement in these conditions became a necessity.

The conventional ultrasonic technology has been used for many years for well integrity assurance, but it has been challenging in large casings greater than 13 3/8in, heavyweight casing with thick walls above 0.59in, and when the borehole is filled with heavy-weight mud. The solution was to design a powerful and low-noise low-frequency transducer to resonate the casing at low frequency and overcome highly attenuative borehole fluid while properly centralizing the tool in the very large diameter casing.

Using uniquely designed Powerful transducers, new processing algorithms, and a specially designed centralizer kit, the operating range of ultrasonic cement and casing measurement range was extended beyond where conventional ultrasonic tools can function to Extreme conditions. With PowerEcho and PowerFlex technology high-quality pulse-echo and flexural wave signals were achieved in large casings up to 26in and a thickness of 1.25 in Performance has been proven in mud weights from ultralight to those exceeding 19 ppg.

## CEMENT EVALUATION METHODS AND TOOL

Cement bond logging tools have been used successfully for many years to evaluate casing and cement conditions in both production and injection wells. These tools utilize either sonic or ultrasonic measurement techniques designed for the conventional steel casing and cement environment.

The Cement Bond Log (CBL-VDL) type tools, which include all tools that measure amplitude or attenuation, have a common theory of measurement, interpretation principles, strengths, and weaknesses. The principle of measurement of these tools is to measure the amplitude of a sonic signal, produced by a transmitter emitting a 20 kHz acoustic wave, after it has traveled through a section of the casing. This amplitude is then converted into attenuation by either using a ratio of multiple transmitter and receiver amplitudes, or using chart book

conversions. The percent of the circumference of the casing bonded is then computed by calculating a Bond Index.

At this point the interpreter has to select a value for the attenuation of a 100% bonded interval. This can be done based on the CBL data collected in the well or it can come from the cement properties provided by the cementing company. The value for the attenuation in a 100% bonded interval is the key to the interpretation of this type of log and the cement properties are critical to the interpretation. It is important to make accurate estimates of the properties if they are not known from the cementing company. These tools also provide a qualitative indication of bond to the formation through the use of a variable density log (VDL) waveform.

Figure 1 shows the basic tool configuration and measurement principle.

The ultrasonic type tools, such as the UltraSonic Imager (USIT), are designed to measure the acoustic impedance of the material on the outer surface of the casing. This is accomplished by using a transducer to project a short pulse of acoustic energy with a bandwidth of 200 kHz to 700 kHz toward the casing. The transducer then becomes a receiver and measures the returning echo from the casing. The analysis of the returning wave can be performed in several different ways with the outputs being acoustic impedance of the material on the outside surface of the casing and thickness of the casing.

Current versions of the ultrasonic tools have a rotating transducer that provides full radial coverage of the casing circumference. These tools have far better vertical and radial resolution than the CBL/RCBL type tools. The returning waveform is the summation of the echo waveform from the original burst, and an exponentially decaying waveform from the resonant energy trapped between the inner and outer casing walls. The initial acoustic response consists of a large reflection from the internal surface of the casing. The time of arrival of the initial reflection depends on the standoff distance from the transducer to casing and the mud acoustic velocity.

The interpretation of the cement bond for the ultrasonic tools is determined by the selection of a liquid/cement threshold for acoustic impedance. Where the acoustic impedance is greater than the liquid/cement threshold, the casing is interpreted as cemented. Where the acoustic impedance is less than the liquid/cement threshold, the casing annulus material is interpreted to be fluid. An image map of the acoustic impedance measurements and the interpreted data is created to provide a visualization of the cement in place.

Figure 2 shows the basics of the USIT measurement principle and Threshold method.

Comparing the different type cement evaluation logging tools, the main advantage the CBL-VDL type tools have over the ultrasonic tools is the small affect of the borehole fluids. These tools can be run in the very heaviest drilling mud. The CBL tools provide qualitative information about the bond to the formation through the use of the VDL waveform, where the ultrasonic logs provide no information about the cement to formation bond. However, the CBL type tools do not have the ability to determine if the casing is laying against the formation. This condition will result in a lower signal attenuation that would decrease the bond index.

The ultrasonic tools have two main advantages. First, the ultrasonic logging tools are capable of much better vertical and radial resolution. This provides the interpreter with an improved "picture" of what the cement sheath looks like. Second, the interpretation of the cement is not dependent on the acoustic properties of the cement. The ultrasonic interpretation is sensitive to the acoustic properties of the fluids. The accuracy of the acoustic impedance measurement is 0.5 MRayls, which means there must be at least 1 MRayls difference between fluids and cement impedances to distinguish one from the other.

The requirement is that there must be at least a 1 MRayl difference between the acoustic impedance of the fluid and the acoustic impedance of the cement is considered a limitation in evaluating light cement or contaminated cement where the acoustic impedance of the slurry could be low and close to the acoustic impedance of the annulus fluid.

These limitations prompted the development of a new ultrasonic cement evaluation tool ( Isolation Scanner), which is based on the combination of two casing modes that operate at a sufficiently high frequency to keep the required azimuthal and vertical resolutions. The first mode is the thickness resonance mode ( pulse-echo technique), with a normal incidence single transducer. The second mode is the flexural mode where the emitter is firing at a certain angle, The combination of the two modes enables a better evaluation of low-impedance cements, and the flexural mode has the potential to probe the full annulus between the casing and formation without the need of the use of threshold method.

Figure 3 shows the Isolation Scanner sub combining pulse-echo, flexural measurement.

In summary, Ultrasonic measurements have long been the preferred technology for well integrity data acquisition due to their dual ability to perform cement evaluation and casing inspection in a single descent, with a single tool. Various ultrasonic modes inside the casing allow azimuthal and radial assessment of cement quality. The two best-known techniques are based on pulse echo and flexural mode technologies, which in combination, allow evaluation of the cement as well as casing centralization.

## HEAVY WALL, LARGE OD CASING ISSUES

In deep offshore environments, deepwater drilling activities have lead to deep wells designed with large casings ranging from 22 to 28 inches that are thicker than generally used in the past. These casing joints are greater than 0.6" thick and can be up to 2in. In fact, casings with wall thicknesses exceeding 1" are becoming more frequently employed for shallow intermediate and surface casings strings.

The theoretical thickness limits of the standard industry ultrasonic tools are set by the fundamental operating frequency at about 0.591". Casings with wall thickness over 0.6" present challenges resulting from the inability of the transducer to produce acoustic impulse with energy in lower frequency part of the spectrum for pulse-echo measurements. The plot below relates the casing size and thickness showing the improved measurement range of New Generation slb transducers.

Figure 4 Range of casing dimensions for former and new generation transducer

These large and thick casings were a challenge for cement evaluation technologies, it was not possible in the past to evaluate large casing above 13 3/8 inch with thickness above 1 inch due to the following factor:

- 1) The attenuative nature of the ultrasonic signal due to the large standoff when running the in large casing resulted in no return signal or very weak and thus data that was not useable to evaluate the cement bond.
- 2) Most of the transducers in the oilfield have peak energy and sensitivity at a frequency of approximately 250-500 kHz. This bandwidth is required to reliably perform pulse-echo measurements for casings up to 0.6" thick.
- 3) Heavier mud systems, which are utilized to withhold increasing reservoir pressures create problems of their own. Heavy muds tend to have higher acoustic signal attenuation which amplifies the difficulties for cement evaluation and casing inspection measurements and interpretation.
- 4) Current hardware limitations make centralizing the tool in such large casings difficult. The available large hole kit centralizer has a maximum effective operating range 20 inch.

For CBL -VDL measurement in Large Casing, the main challenge obtaining good centralization and the Low contracts between Free pipe CBL amplitude and fully bonded CBL amplitude. For example, 20-inch OD 169 ppf casing, cemented with 12.5 ppg cement slurry which has 3.8 Mrayl acoustic impedance

- Free Pipe CBL amplitude for the 20in casing 169 ppf expected 35mv.
- 80% bond equivalent CBL amplitude expected 27mv.

For the above illustrated example there is only 8mv difference between the CBL amplitude for bond cement and free pipe. In large Casing ID, CBL centralization may be challenging and slight Eccentralization will lead to wrong interpretation with only 8 mv contrast. For a standard pipe with a diameter of 5.5 in (139.7 mm) and

a thickness of 7.72 mm, an eccentricity of 1/4 in could cause the CBL amplitude to be reduced by about 20% (Song, Ruo-Long et al 2013).

The quality of ultrasonic cement evaluation measurements in large and thick wall casing is challenged by higher attenuation caused by heavy muds, large casing and thick casings that reduced sensitivity to the cement. This issue has been addressed with new generation transducer technology that results in thirtyfold increase in signal-to-noise ratio. This improvement was accomplished through a complete redesign and optimization of hardware, software, and data processing/interpretation workflows which know as PowerFlex and PowerEcho services.

### EXTENDING THE RANGE OF CEMENT EVALUATION SOLUTION

Extensive analysis of the challenges for the cement evaluation in large and thick wall casing and how they could be overcome, drove the development of the next generation of transducer including its upgraded hardware, firmware and software. These developments are described in detail in the paper (Thierry et al, 2016).

There are several differentiating features of the new transducers. Two of the most significant improvements are its increased signal strength and wider frequency spectrum. The laboratory test results which were published (Thierry et al, 2016) are shown in figure 6.

Figure 5 Comparison of echoes obtained with legacy and new transducers, and transfer function of the ultrasonic transducer

It has been shown that higher signal strength and wider frequency spectrum allow us to perform logs in heavier muds. It also enables a wider range of distances between transducer and casings, meaning that larger casing strings can be evaluated with smaller sub-sizes provided that we maintain good tool centralization.

The next distinguishing factor: higher energy in the lower frequency range for the transducer impulses, allows us to perform the same measurements but in much thicker casings. This inadvertently also contributes to the ability to log multiple casing strings, as casings usually get thicker as they get larger.

As tool centralization play a major role in data quality for both CBL and Ultrasonic tool, having good centralizers will help to have better confidence in log result. The standard large hole centralizer for the ultrasonic tool has a maximum effective operating range 20-inch; hence it is not effective to be used for casing large 20 inches. The only possible option to centralize the tool effectively is to use a specially manufacture centralizer to suit the casing ID. These centralizers are made for the larger casing OD > 20inch.

It was not possible in the past to evaluate such large OD > 13 3/8in and thick wall casing > 1in; however, with the new generation of powerful ultrasonic transducers, developing a unique data processing solution and hardware modification for the centralization in such large casings became possible and enables to extend the

cement evaluation measurement in large casing up to 26inch OD and thick wall casing up to 1.25inch.

Figure 6 shows the extended measurement range of cement evaluation

### CASE HISTORIES / FIELD EXAMPLES

The operational benefits and financial allowances emerging from the new transducer technology are best illustrated by showing some examples and log responses in a large and thick casing;

#### Example 1

Well 1 is cased with two different casing weights of the 24-inch casing, 171.29 ppf with ID of 22.62 inch and wall thickness of 0.69 inch and 186.2 ppf heavier weight with ID of 22.49 inch and wall thickness of 0.75inch and cemented with 15.8 ppg tail, 12.5 ppg cement leads, logs are performed through 8.9ppg WBM ( Sarah AlArfaj et al 2023).

Figure 7 show Well 1 the cemented section with tail cement of 15.8 ppg slurry weight

Figure 7 shows the cemented section with tail cement of 15.8 ppg slurry weight, as can be seen, all measurements respond correctly in this large casing, with correct casing thickness detected averaging ~0.761 inch, and casing radius averaging ~11.23 inch, cement across this interval appears to be good and acoustic impedance average varies between 5 to 8 Mrayl, the CBL qualitatively appears to detect the cement in many intervals. However, it is used qualitatively.

Figure 8 Well1 the cemented section with 12.5 ppg lead slurry

Figure 8 shows the cemented section with 12.5 ppg lead slurry, as can be seen, all measurements respond correctly, and the transition between the two different casing weights is clearly detected on both the thickness and the radius measurements as casing thickness reduces from ~0.76 inch to ~0.7 inch and casing radius increases from ~11.23 inch to ~11.31 inch, the bottom section appears to have a relatively higher acoustic impedance of ~4 Mrayl while the top section is averaging around 3 Mrayl with some channeling detected, the CBL appears to qualitatively correlate to the acoustic impedance in this section ( Sarah AlArfaj et al 2023).

#### Example 2

Well 2 is cased with two different casing weights of the 24-inch casing, 171.29 ppf with ID of 22.62 inch and wall thickness of 0.69 inch and 186.2 ppf heavier weight with ID of 22.49 inch and wall thickness of 0.75inch and cemented with 15.8 ppg tail, 12.5 ppg cement leads, logs are performed through 8.9 ppg WBM ( Sarah AlArfaj et al 2023).

Figure 9 Well 2 cemented section with 15.8 ppg tail and 12.5 ppg lead

Figure 9 shows the cemented section with the 15.8 ppg tail up to ~3600ft, and 12.5 ppg lead above that.

All measurements are validated, thickness average of ~0.751 inch, and a casing radius averaging ~11.25 inch. Cement across this interval appears to be good, the acoustic impedance average for the tail varies between 6 to 8 Mrayl, the 12.5 ppg lead cement appears, and the transition between the lead and tail cement can be seen very clearly in the log.

### Example 3

Well 3 is cased with 23-inch casing, 450 ppf with wall thickness of 2 inch and logs are performed through 15.6 ppg SOBML, Logging objective is casing inspection.

This example involves the casing inspection of the thick surface casing.

Figure 10 shows the corrosion log, the log shows a clear casing groove and data of good quality in very thick casing.

Figure 10 Casing inspection data for 23" OD 2" thick casing from example

### CONCLUSIONS

The new developments in annular barrier evaluation service PowerFlex and PowerEcho can be used successfully to determine the casing and cement parameters under downhole conditions more extreme than the original tool specifications suggested.

Quantitative evaluation of the casing and cement sheath conditions can be made in most heavy wall casing materials using PowerFlex and PowerEcho service which allows in mud weights exceeding 19ppg (Thierry et al, 2016), and in casings up to 26", through thicknesses of 1" or greater.

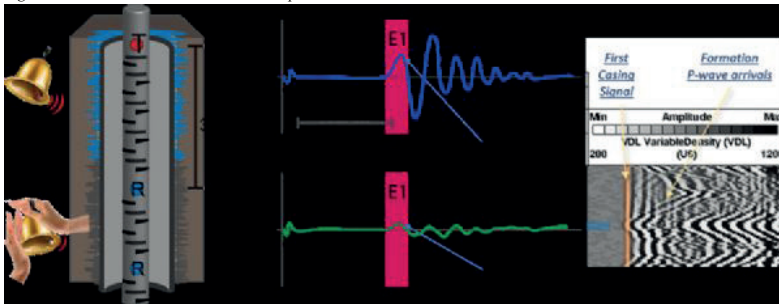
Even in such difficult environments, the high-quality data shows all phases and aspects of the cement. Well set tail cement, the lighter lead cement, transition zone between cement density.

The first 22in OD 224.8 ppf with 1in wall thickness casing cement evaluation in Turkey was performed Mar 2023, since then, evaluating these large casing sizes became a practice and implemented by TPAO/OTC for all deep drilling wells. Since then, more than 3 wells of the 22-inch casing 1in wall thick casing have been evaluated. However, the log example from these jobs could not be used for this paper due to data release.

The cement evaluation logs using PowerEcho have helped TPAO/OTC to understand the cement status behind these large & thick casings and allowed TPAO/OTC to proceed to the next phase in Well completion without delay. The efficiency gains of the new technology resulted in logging the interval more than twice as fast, and saving of direct rig time—the improved log quality made for an easier and more precise cement evaluation.

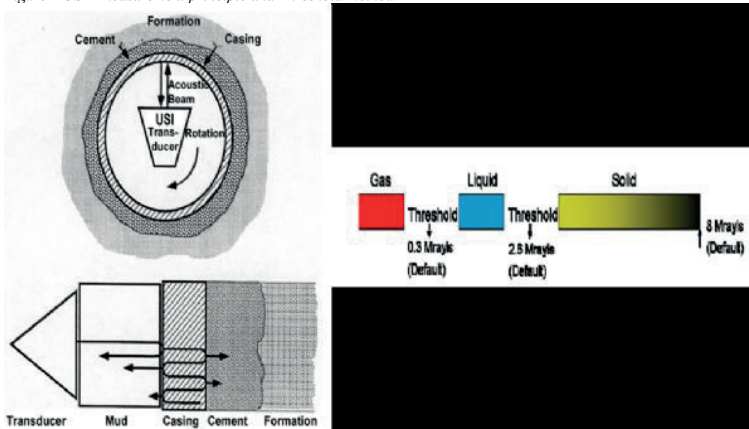
Keywords: Cement Evaluation through Large & Thick Casing

Figure 1 CBL-VDL tool measurement Principle



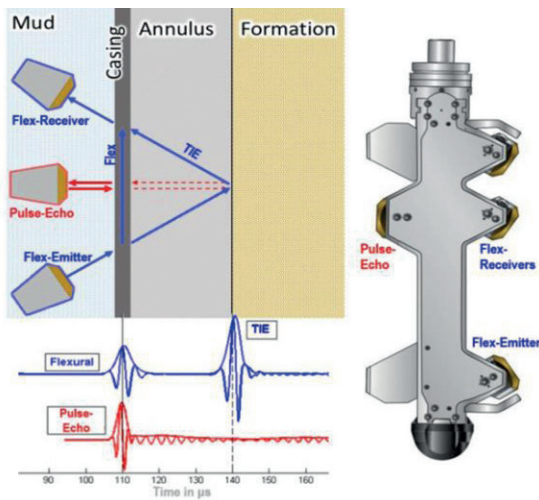
CBL-VDL tool measurement Principle

Figure 2 USIT measurement principle and Threshold method



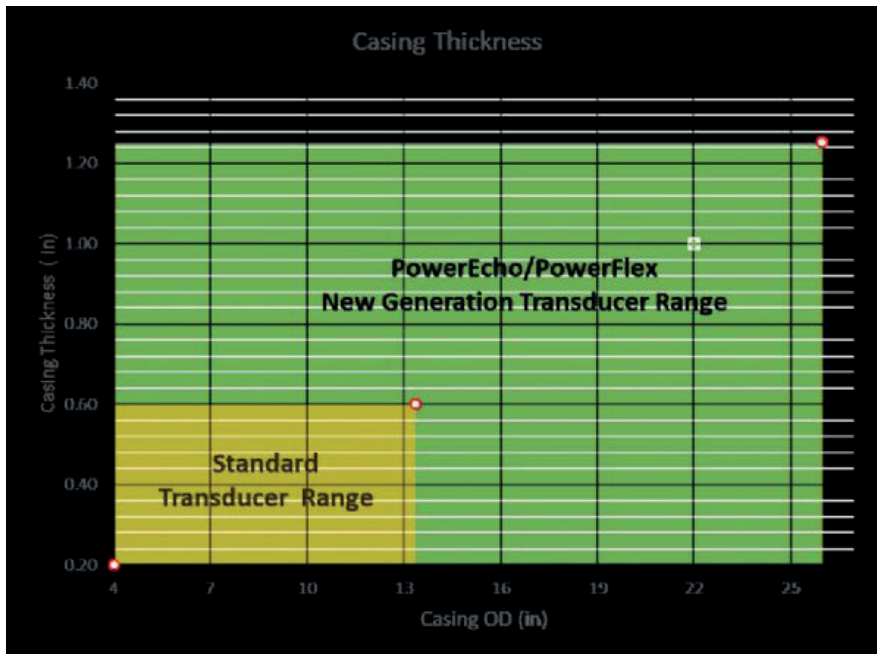
USIT measurement principle and Threshold method

Figure 3 Isolation Scanner sub combining pulse-echo, flexural measurement.



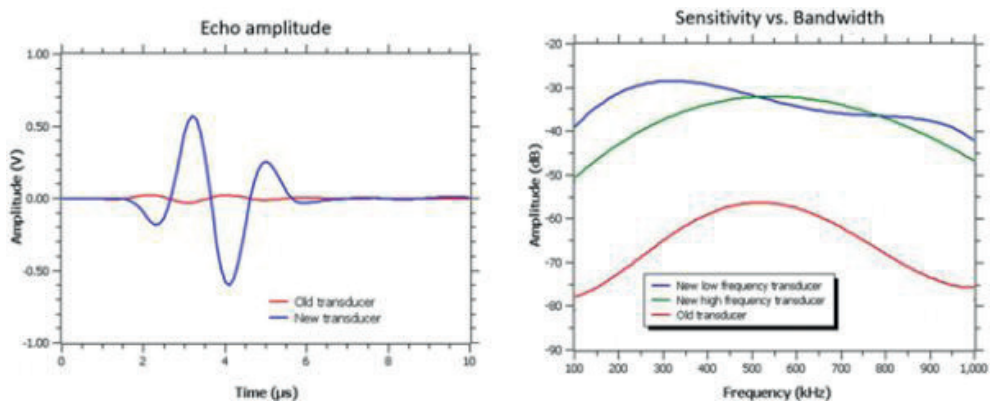
Isolation Scanner sub combining pulse-echo, flexural measurement.

Figure 4 Range of casing dimensions for former and new generation transducer



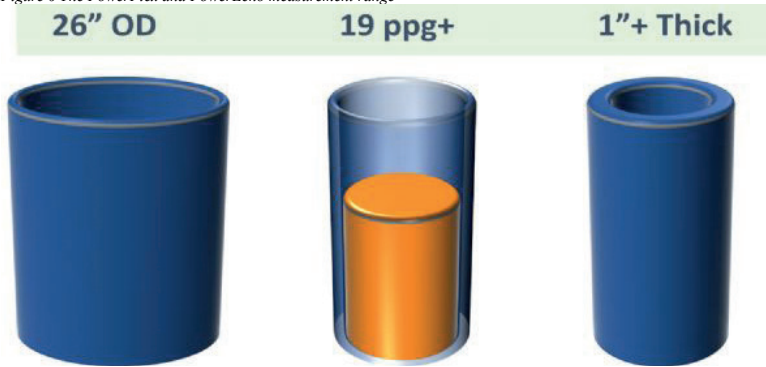
Range of casing dimensions for former and new generation transducer

Figure 5 Comparison of echoes obtained with legacy and new transducers, and transfer function of the ultrasonic transducer



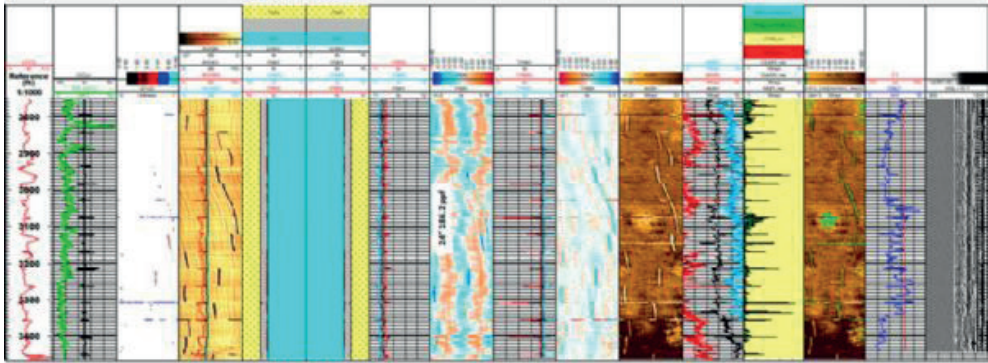
Comparison of echoes obtained with legacy and new transducers, and transfer function of the ultrasonic transducer

Figure 6 The PowerFlex and PowerEcho measurement range



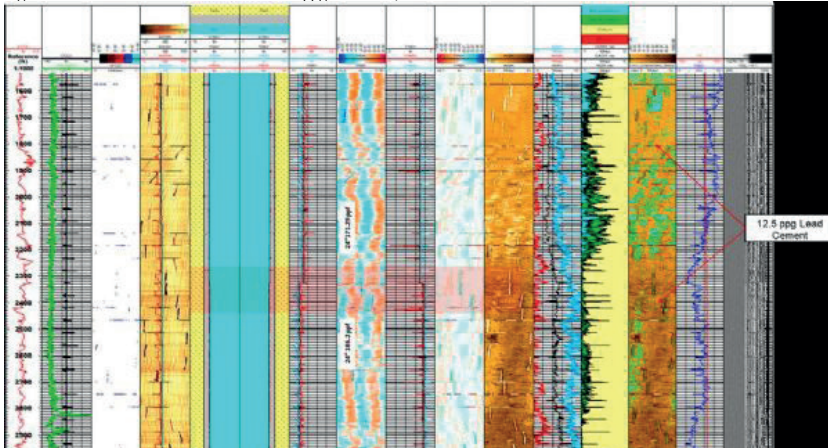
The PowerFlex and PowerEcho measurement range

Figure 7 Well 1 the cemented section with tail cement of 15.8 ppg slurry weight



Well 1 the cemented section with tail cement of 15.8 ppg slurry weight

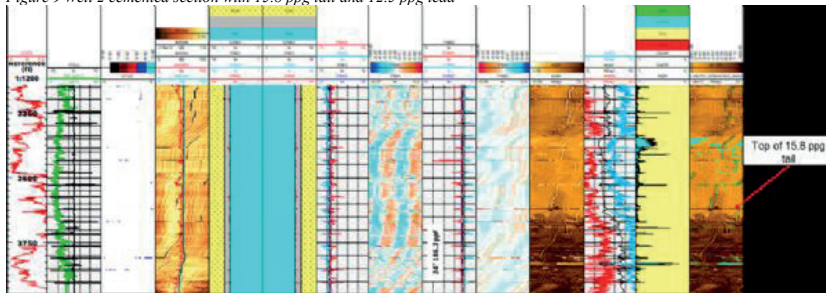
Figure 8 Well1 the cemented section with 12.5 ppg lead slurry



Well1 the cemented section with 12.5 ppg lead slurry

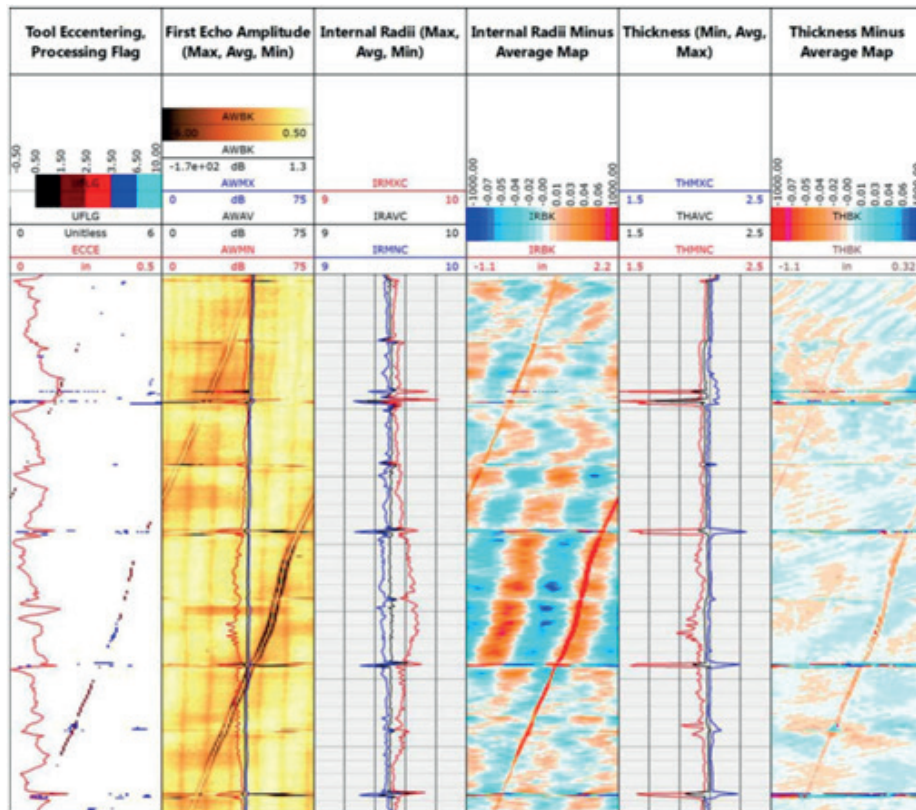


Figure 9 Well 2 cemented section with 15.8 ppg tail and 12.5 ppg lead



Well 2 cemented section with 15.8 ppg tail and 12.5 ppg lead

Figure 10 Casing inspection data for 23" OD 2" thick casing from example



Casing inspection data for 23" OD 2" thick casing from example

# Advanced Tractor Techniques in Extended Reach Wells Allow Confirmation of Well Integrity and Execution of Perforation Services in Key Turkish Offshore Gas Fields



**Daniel Steen Haase Soerensen<sup>1</sup>, Ugur Ezer<sup>1</sup>, Mohammed Ameen Al Ganad<sup>1</sup>, Fadil Duman<sup>2</sup>**

<sup>1</sup>SLB

<sup>2</sup>Park Place Energy

## INTRODUCTION

The South Akcakoca Sub-Basin (SASB) is a key part of Turkish offshore field development, and one of the biggest natural gas projects in the Black Sea. The SASB project consists of four offshore production platforms, linked to shore by 18 km of subsea pipeline. These platforms have a mixture of low deviation wells and extended reach drilled (ERD) wells, as there are at least nine gas fields in the area, spread over a large area (Figure 1).

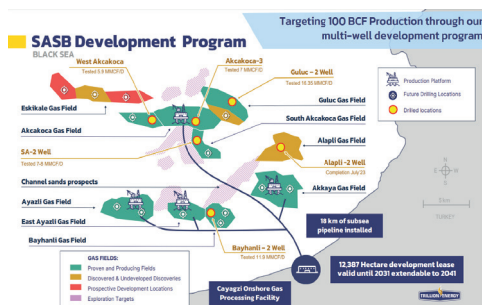


Figure 1: The South Akcakoca Sub-Basin (SASB) and associated gas fields (Trillion Energy Investor Presentation June 2023).

Once the wells are drilled, well integrity logs are required to confirm the cement coverage and identify any potential channelling before running the upper completion. After the upper completion has been run, perforation guns are then run to perforate the reservoir section and bring the wells online. The low deviation wells are relatively accessible on e-line with conventional gravity conveyance. However, the ERD wells cannot be accessed on gravity alone, as e-line gravity conveyance becomes increasingly challenging at deviations above 65 to 70°. Accessing these wells requires either e-line tractor conveyance or an entirely different method of conveyance such as coiled tubing or pipe.

This paper presents two case studies in different fields within the SASB, where tractor conveyance was used to convey well integrity and perforation services to the target depth and fulfil the required objectives to put the wells online. These combined to represent the most tractoring ever performed in Turkey. Due to the specific challenges in these wells, two special tractor capabilities had to be utilized: tandem tractoring and reverse tractoring. These are not commonly utilized capabilities but were critical on both case study wells.

The aim of this paper is to share why they are important capabilities to be aware of and why they should be included in planning and risk mitigation when designing e-line operations in ERD wells such as on the Akcakoca platform (Figure 2).

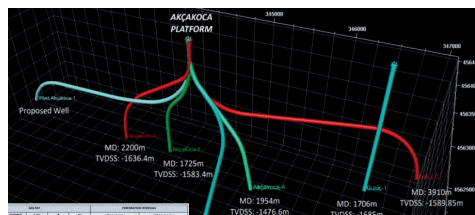


Figure 2: The Akcakoca platform, showing a mixture of low deviation wells and ERD wells (Trillion Energy Investor Presentation June 2023).

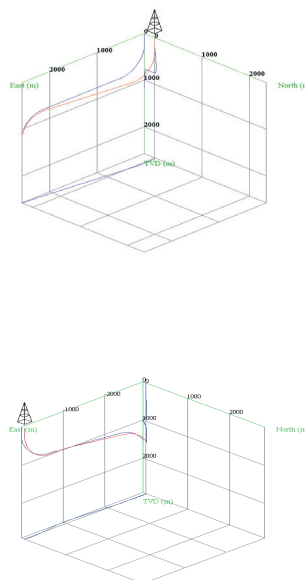


Figure 3: The two case study wells. Top, Well A trajectory with a 3:1 MD to TVD ratio. Bottom, Well B trajectory 2.5:1 MD to TVD ratio.

Case Study Well A: Designing high-force tractoring string to push well integrity service with booster centraliser to TD in ERD well and negotiate downhole restrictions using tandem function.

Well A (Figure 3) is located in the Bayhanli gas field and has an MD to TVD ratio of almost 3:1, with the horizontal section stretching almost 2000 m. Traditionally, these types of wells were only accessible with drillpipe or coiled tubing, but advances in e-line tractors over the last decades have enabled the much lower footprint option of wireline conveyance. However, two further factors complicated the planned scope on Well A.

First, the well has a significant ID change around 600 m from TD and where the well was still highly deviated (72°) as a liner covered the reservoir section. This creates a challenge for the wheeled e-line tractors because they must climb the sudden inside diameter (ID) change while exerting radial force create traction to move the tools forward. Tractors can typically manage instantaneous ID changes of up to 0.5 in, or gradual changes of 2 in/ft, but a 7-in liner hanger generally has an almost instantaneous ID change of at least 1 in and up to 2.5 in, which will cause the tractor to stall.

Second, advanced cement evaluation logging was required to confirm the integrity of the zonal isolation behind the liner and casing, and the absence of channelling. Cement evaluation services rely on acoustic signals and are highly affected by any eccentricalisation of the tools so require extremely stiff and rigid centralisers as well as booster springs to provide centralising force. These can be extremely challenging to squeeze through the ID change at liner hangers, and require around 300lbf of force, adding to the force required to push a heavy >800-kg toolstring along a horizontal well and pull thousands of meters of cable.

To address these two factors, a full tandem configuration was selected for the tractor, consisting of two sets of three drives, independently controllable.

Case Study B: Using reverse tracting capability to reduce cable load in ERD well and to re-enter upper completion safely.

Well B (Figure 3) is located in the western part of the Akcakoca gas field and has an MD to TVD ratio of 2.5:1. The objective of the e-line intervention in this scope was, as in Well A, to perform well integrity logging and then perforate the reservoir section to open the well for production.

Originally, the e-line scope on Well B seemed slightly simpler than that on Well A, as the well trajectory indicated lower tracting forces required and lower tensions. Therefore, the well integrity tool chosen was a simpler design that did not require aggressive booster centralisers. However, two unexpected factors led to quite significant challenges on the well that were only overcome by reverse tracting.

First, on one of the perforation runs, the tension recorded when the toolstring was in the liner was found to be far higher than expected or observed on previous runs. Where previous runs had seen tensions around 2,400 to 3,000 lbf, the tension on this run was up to 5,600 lbf, very close to the cable safe working load of 5,810 lbf. This increased tension was seen during the regular pickups prior to reaching the target perforation interval. Without tractors available, the decision would likely

have been to cancel the run before reaching a depth where the tools could not be safely retrieved without exceeding the cable safe working load.

Second, the e-line operations were all performed after running of the upper completion, and difficulties were encountered with re-entering the upper completion from the liner. This is sometimes a risk with e-line operations in horizontal wells, as there is typically no centralisation at the top of the toolstring when pulling out of hole and the tools will tend to lie on the low side. The large ID change from the 7-in liner to the 4.5-in upper completion coupled with the large outside diameter change from 0.32-in cable to 3.125" cable head can result in the top of the head catching on the tubing shoe and not being possible to pull into the upper completion.

Introduction to e-line tractors:

Wheeled e-line tractors

E-line tractors were first introduced to the oilfield about 25 years ago. While e-line tracting was originally a relatively niche service, improvements in reliability and design combined with the increasing number of highly deviated and horizontal wells have led to a significant growth in the use of e-line tractors worldwide. E-line tractors can be grouped into two types, continuous drive and reciprocating drive (Figure 4). Both have the same two functions: to push a payload (in most cases a toolstring) to the target depth and to pull the cable powering the tools and tractors behind them. Continuous drive tractors have moving parts interacting with the internal surface of the casing or formation to provide continuous forward force, while reciprocating drive tractors anchor on the internal surface and use a linear actuator to push the toolstring forward, with typically at least two sections performing this in tandem to provide relatively steady forward motion.(ref 1)

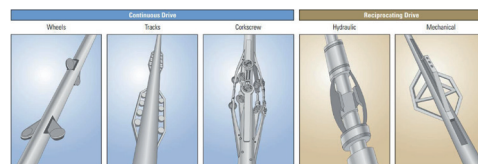


Figure 4: Continuous drive and reciprocating drive tractors (ref 2).

The majority of tractors currently used worldwide are of the wheeled continuous drive design (Figure 5), although both types have advantages and disadvantages. Reciprocating tractors tend to have advantages in open hole tracting while continuous drive have advantages in length, speed, and modularity (ref3).



Figure 5: Wheeled drive tractor with three drives seen inside tubing.

### Tractor Planning

Most tractors are powered from the surface through an e-line cable and are available in monocable and heptacable configurations both requiring significant power to operate effectively, especially for ERD wells. In fact, unlike many other e-line services, power planning is a critical element of tractor planning and means that only certain high-power cables can be considered for tractor operations. The power requirement of an e-line tractor will typically depend on several different factors including the configuration of the tractor, the amount of force it is required to provide, and the tractor speed that is desired.

The amount of force required is a product of the force required to pull the cable behind the tractor, and the amount of force to push the toolstring and tractor itself forward. These factors are in turn dependent on a myriad of factors such as the well trajectory, cable type, well friction coefficients, well fluids or gas, and so on. Due to the number of interrelated factors, tractor planning software is typically used to estimate the amount of force required to reach the target depth, an example of the results of which is shown in Figure 6.

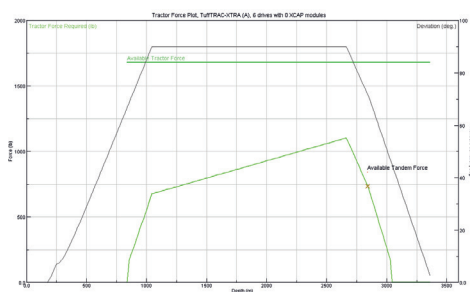


Figure 6: Example of tractor force planning software.

The tractor configuration is selected depending on the amount of force calculated to be required, whether hepta or monocable is being used, and the well completion design. To increase the force capability of the tractors, additional drive sections can be added. These are modules of tractor containing the force-exerting section such as wheels, and each one has an expected force contribution usually ranging from 250 to 350 lbf per

section. Heptacable and monocable will usually dictate the selection of a telemetry and power cartridge, but most tractor drives are capable of running with either cable type. Finally, the well completion design should be reviewed carefully for any abrupt ID changes or complicated well jewellery where the wheeled tractors may hang up or not be able to tractor. A tractor navigation planner can then be used to design the tractor configuration to straddle across this section, or tandem mode can be used to negotiate the restriction.

### Tandem Mode

Some, but not all, tractors have a capability called tandem mode. This is the operation of some drive sections within the tractor toolstring separately from others. Typically, this will be with two sets of drives, one above the other, consisting of between two and four drives each, depending on the force required (Figure 7). These sets of drives can be operated independently of one another, so one can be stopped or closed while the other is open and driving the toolstring forward.



Figure 7: Example of single and tandem drive configurations for the TuffTRAC™ wireline tractor.

An example of tandem operation would be when meeting a restriction that the tractor wheels cannot pass. The lower section of wheels would meet it first and start to stall or skid. The operator would then close this lower set of tractors and continue using only the upper set of tractors. This would continue until the upper set of tractors encountered the restriction and stopped making forward progress. At this point, the operator would close the upper set of tractors, open the lower set of tractors again, and continue past the restriction. Once all the wheels passed, both sets could then be opened, or progress could be continued with just one set on the force and power requirements.

### Reverse Tractoring

Another capability of some but not all wheeled tractors is reverse tractoring (Figure 8). This is simpler with mechanical transmissions using electric motors for wheel rotation where the direction of the electric motor can be reversed (ref 3). Reverse tractoring can help

significantly in stuck tool situations or where the well trajectory reduces the effectiveness of surface pull on downhole tools. In ERD wells, a lot of surface pull is lost to friction along the well, and available overpull on the tools is therefore often very low. Reverse tracting can reduce this risk by applying force directly on the downhole tools mitigating the loss of pull capacity at depth.

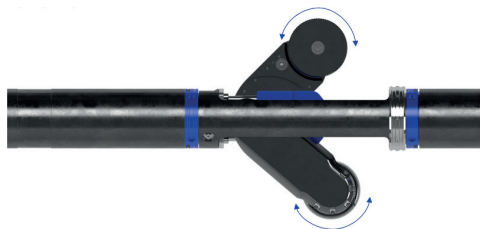


Figure 8: Reverse tracting enabled by reversing direction of wheel rotation.

Reversing the tractor does carry some risk, as cable tension on the head must be maintained above the normal tension to avoid opening of cable armours, or potential birdcaging. This is considerably helped by having a calibrated head tension at the top of the toolstring, which enables the winch operator to appropriately judge the amount of cable pull to apply and winch speed to use.

**RESULTS**

Tandem function for force and restriction negotiation:

**Case Study Well A**

The tractor planning for Well A had shown that it would be a challenging but feasible tractor operation (Figure 9). Relatively high force was seen as required (consistently 600 to 800 lbf) and as logging of the liner was required, the liner hanger would have to be passed. Therefore, tandem tracting was expected to be required. In addition, the well integrity services had full booster kits installed, so high force was expected to be required at the liner hanger depth to force them through the restriction.

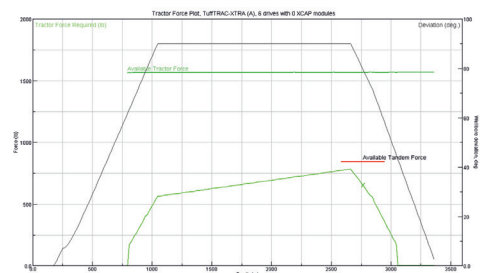


Figure 9: Well A tractor force planning software.

On the operation, the tractor force modelling proved to be very accurate. The force was consistently ~600 to 700 lbf down to the liner hanger, and tractor with a single set of three drives had no difficulty conveying the tools (Figure 10). However, at the liner hanger it was found that the force required suddenly increased, and one set of the drives could not push the spring-boosted centraliser through the ID change. Both tandem drives were therefore engaged and used in unison to provide up to 1,800 lbf of push, easily enough to force it through. Once the booster was in, the lower tractor set then met the liner hanger ID change. It was closed, and the upper section was used to push the lower section fully into the liner. Once the upper section met the liner hanger ID, it was in turn closed, and the lower tractors were used to pull the rest of the toolstring inside.

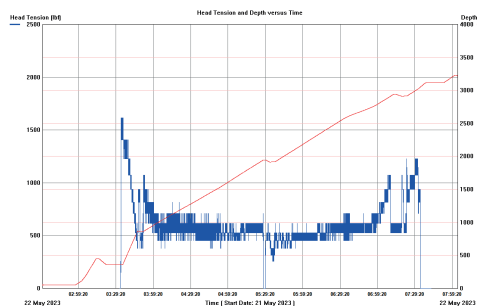


Figure 10: Well A head tension (blue) vs. depth (red) while tracting down, showing ~500lbf of tractor force required to pull the cable behind the tools from 1000 m to 2780 m.

Once in the liner, the force was found to be higher than expected, presumably due to friction caused by the compressed centralisers. Tracting with a combination of both tandem sections was used to provide sufficient force to reach the vertical drop at the end of the well and perform all required well integrity logging. Without the tandem function, it would not have been possible to enter the liner hanger, and without capability to use both sets together, the lower interval would not have been reachable.

Reverse tracting for reducing cable load and re-entering upper completion: Case study Well B

While tracting in hole on Well B through the upper completion, it seemed that the conveyance would be relatively simple. Tractor force requirements were low and pickup tensions were normal. However, after reaching the target depth of 3,600 m and performing correlation passes, tensions suddenly increased with each pickup from the initial 3,000 lbf up to a maximum of 5,600 lbf.

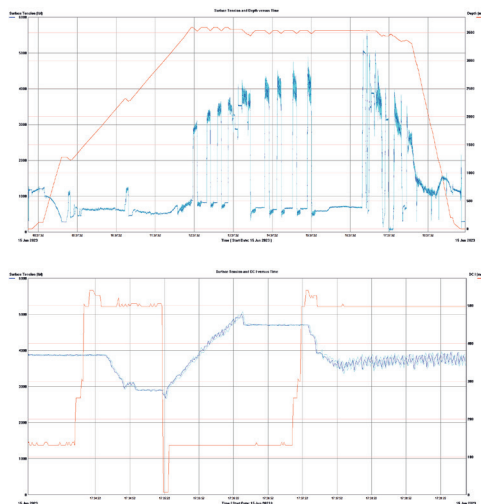


Figure 11: Well A surface tension (blue) vs. depth (red). Top, the high and increasing pickup tensions (spikes in blue) when trying to pull tools upwards (red is depth). Bottom, the tractor current applied to reverse tractor (red) vs. the surface tension (blue), clearly decreasing the surface tension by -1,000 lbf.

It was decided to utilise the reverse capability of the tractor to provide downhole force on the toolstring and reduce the cable load. This was successful in extricating the toolstring from the zone of highest tension and safely retrieving it to surface without risk of damaging the cable by exceeding the safe working load. It was found that reverse tracting reduced the cable tension required by approximately 1,000 lbf (Figure 11).

Once the cable load was safely below the safe working load, the reverse tracting was stopped, and the toolstring was pulled out to the shoe of the upper completion where a sudden tension increase was observed. Correlation indicated the top of the toolstring was catching on bottom of the upper completion (Figure 12).



Figure 12: Illustration of how the cable head of the logging toolstring (in gold) can catch on the entry guide of the upper completion (in red).

Repeated attempts to pull out with cable force were unsuccessful, so the reverse tractor was again engaged. This time, it was not only to provide downhole force,

but also, and mainly, to centralise the top of the toolstring, as the tractor wheels push on all sides to put the toolstring in the middle of the casing. By so doing, it was easily possible to retrieve the toolstring through the shoe and complete the operation successfully.

## CONCLUSIONS

The success of the tractor conveyance in the SASB has proven the feasibility of well integrity and perforation operations based solely on e-line in ERD wells in Turkish offshore projects. Risks associated with e-line tractor conveyance such as restriction navigation, higher-than-expected force requirements, stuck tools, and lost-in-hole risks have been mitigated through the application of the advanced tractor techniques detailed in this paper: tandem tracting and reverse tracting.

The 2023 SASB tractor conveyance has constituted the most extensive tracting ever performed in Turkey, with almost 35,000 m of tracting year to date, and has established Turkey as one of the ERD tracting leaders. It is expected that the future will hold more such operations as Turkey continues to develop its offshore fields, and it is critical that the learnings are recorded and shared for all.

## REFERENCES

- 1) Wireline Tractor for Through-Tubing Intervention in Wells with Barefoot Openhole Completions  
Greg Giem; Todor Sheiretov; Yoann Couble  
Paper Number: SPE-189923-MS
- 2) Advancing Downhole Conveyance.  
Alden, M., Arif, F., Billingham, M. et al. . 2004.  
Oilfield Review 16 (3): 30–43.
- 3) Wireline Tractors and Mechanical Services Tools: Comparative Study of Technical Solutions  
Todor Sheiretov  
Paper Number: SPE-179044-MS

# Overview of Acid Fracturing Operations in Carbonate Reservoirs of Turkey



**Ufuk Kılıçaslan, Ahmet Ergün Mengen, Özlem Özcan, Mutlu Daşdemir, Yasin Unal, Bekir Onay, Bülent Şahinbaş, Vasily Semenovich Mironov, Aleksei Vasilevich Khlopkov**

Turkish Petroleum Corporation (TPAO), Ankara / Türkiye

Over four years, Turkish Petroleum Corporation (TPAO), state owned oil company of Turkish Republic, has put significant efforts to increase production rates from its carbonate reservoirs by acid fracturing. Operational and production aspects of acid fracturing in 44 wells has been discussed in this paper.

Many wells exhibited two to five folds increase in the first month production. Compared to do-nothing scenario, more than 315,000 barrel of additional oil was produced during this period. However, no improvement was observed in deeper wells having high temperature, low porosity and relatively low permeability. Emulsified acid could function better in those kind of subsurface conditions. Diverters are necessary and helpful in displacing acid into undepleted zones.

## INTRODUCTION

Carbonate reservoirs are the main source for oil production in Turkey. Acid fracturing is applied to improve or maintain production from tight carbonate reservoirs. It helps to increase in permeability and reduce in skin factor, thereby it increases the reservoir productivity. By dissolving rock deep within the fracture face, acid fracturing can increase productivity by forming long, conductive channels that are narrow near the wellbore to lessen pressure gradients and wider into the reservoir to better sustain closure stress. In order to accomplish this, the acid formulation must have a slow reaction rate while still having a high capacity for dissolving, decrease leak-off into the matrix by additives and have low friction to support high-rate pumping (Chang, 2022).

The first and main part of the acid fracturing is to select the candidate wells to operate. Because success of a treatment depends on the selection of the correct wells to stimulate. Acid fracturing is usually applied in shallow and low-temperature carbonate reservoirs. The best candidate wells are shallow wells with a reservoir temperature less than 200 °F and that have the maximum effective stress less than 5,000 psi. (Tiab, 2016).

Another important part of the acid fracturing is the treatment design. The goal of the design is to create the best pumping schedule with respect to productivity target, operational limits, available resources and mainly economics. The key variables to be selected for a design are the type and quality of fracturing pad and acid, injection rate and the volume of each stage.

## FRACTURING OPERATIONS

Before starting acid fracturing operations, wells should be completed properly to deliver desired rate at high

treating pressure. In this respect, first thing to do is to decide the correct frac string; packer system, tubing string and wellhead. 10K rating RTTS packer was preferred in our cases, as expected maximum pressure is less than 10000 psi. Generally, wider ID tubing string allows to reduce treating pressure. Considering the ID and the pressure rating, 3 1/2" EUE N80 tubing was selected. Lastly, the 10K 2 9/16" X-Tree is used to establish the integrity. The packs was set around 20 meters above the perforations and a small sub is used under the packer for creating a spacing to protect the packer against the harmful effect of the acid to the packer. During the operation annulus is pressurized at 1500 psi to prevent unsettling the packer and a possible leakage around it because of the differential pressure.

Depth of target zones were in the range of 1,200-3,000 meters while temperature of reservoirs varies from 120 °F to 250 °F. 28% HCl gelled acid was used as a main treatment fluid. The average acid concentration per perforation length was generally close 400 gal/ft. In some wells, higher and lower concentrations were tried as well. Treating pressures during operations were in the range of 1,200 psi to 8,200 psi. Similarly, injection rate varied from 20 bbl/minute to 50 bbl/minute but mostly it was kept above 40 bbl/minute to carry acid into deeper section of the formation as fast as possible. During operation, acid was injected in different stages to divert it into unstimulated zones. Bio-balls were the main mechanical diverter while crosslinked gel helped to divert acid in both wellbore vicinity and far deep reservoir sections. Once bioballs reached to perforations, treating pressure increased, which is a clear indication of diverter effect (Fig.-1). Also, pre and post-job temperature logs were direct tools to evaluate vertical entry profile of acid distribution (Fig.-2).

Figure-1: Bioball Effect on Treating Pressure

Figure-2: Temperature Log for Zonal Contribution

## PRODUCTION TRENDS

To understand effect of any well stimulation technique, change in productivity index (PI) is the first thing to be checked. In this respect, PI was calculated for each well based on first month production metrics, either before or after the fracturing operation. As seen in Fig.-3, almost all acid fracturing operations led to significant enhancement in PI of the wells, except two wells. The first one was an exploration well, where target interval may not have favourable reservoir properties. In second case, decrease in well production rate could be attributed to fines migration, which could plug some of the existing fluid pathways.

Figure-3: Before-After Productivity Index Comparison

Even though acid fracturing operations increased well PI, not the all wells delivered with higher oil production. Especially, wells locating in Adiyaman region didn't show considerable production enhancement after acid fracturing, except latest one which was fractured recently. Some wells started with higher oil production but then they couldn't produce their historical trend. On the other hand, rapid increase in water cut resulted in lower oil rate in some other wells. The wells in Adiyaman region are deeper and hotter than wells drilled in other regions. In addition to relatively poor reservoir characteristics, higher temperature and higher stresses could be underlying reasons for underperformance.

Apart from Adiyaman region, acid fracturing worked well in many heavy-oil fields. Pay-out time was generally less than 8 months. Especially in Batı Raman field, almost all wells responded positively, whether newly drilled or not. As an example, before-after comparison can be seen in Fig.-4, where six months production and associated decline curve are plotted with post performance to understand stimulation effect. These wells were mainly located in eastern part of the field, where fissure system is not well developed as in the case of western and central part. After these promising results, fracturing infill wells to be drilled in eastern part has been common practice, recently. Similar positive results were observed in heavy-oil Çamurlu field and Batı Kozluca field. One exception of them was ÇAM-A well, where frac hit a nearby fault and well started to produce 100% of water. Furthermore, both positive and negative results were experienced for different wells in same field during this campaign. Summary of incremental oil per month throughout production period can be seen in Fig.-5 for each well.

Figure-4: Before-After Comparison for Batı Raman Wells

Figure-5: Production Enhancement After Fracturing Operation

## CONCLUSION

Based on decline curve analysis, acid fracturing operations in 44 wells have added more than 315,000 barrel of additional oil production. Substantial increases were observed in productivity indexes of wells after acid fracturing, even for many heavy-oil wells having relatively low reservoir pressures. On the other hand, this treatment couldn't provide production enhancement in deeper wells having high temperature, low porosity and relatively low permeability, where emulsified acid could work better. Diverters are necessary and helpful in displacing acid into undepleted zones.

## ACKNOWLEDGEMENT

The authors want to thank the Turkish Petroleum Corporation (TPAO) for allowing the publication of this work and material.

## REFERENCES

- Frank F. Chang, Fluid Chemistry, Drilling and Completion Book, 2022, Chapter 10 - Acid fracturing stimulation, pp. 387-419
- D. Tiab, Advanced Well Test Analysis Course Notes, 2016, Ch. 4 –Hydraulically Fractured Wells

Keywords: Acid Fracturing, Gelled Acid



Figure-1: Bioball Effect on Treating Pressure

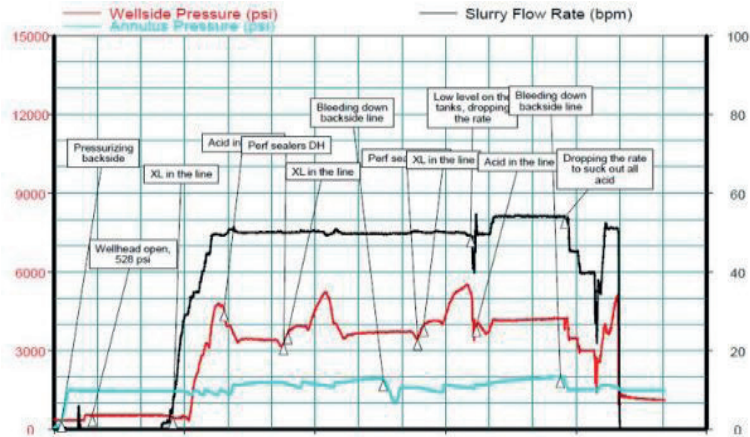


Figure-2: Temperature Log for Zonal Contribution

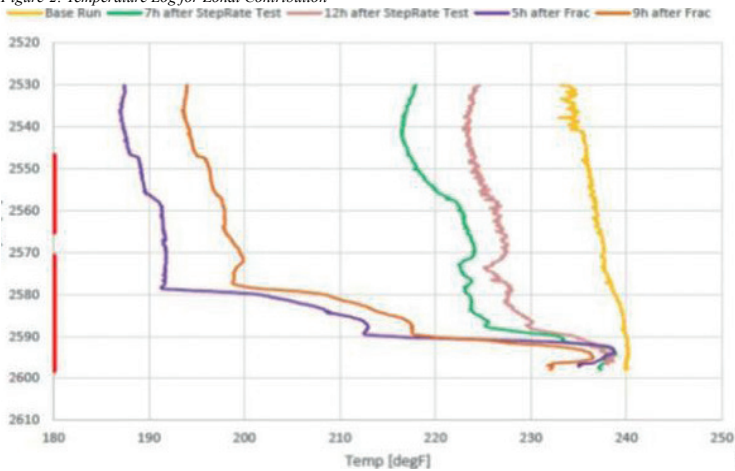


Figure-3: Before-After Productivity Index Comparison

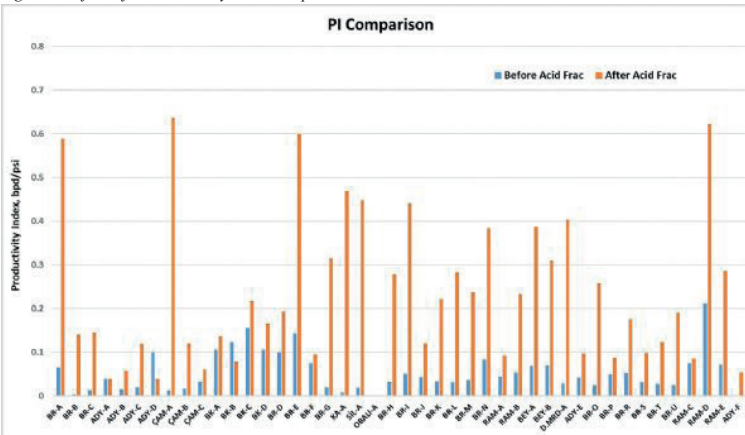


Figure-4: Before-After Comparison for Batu Raman Wells

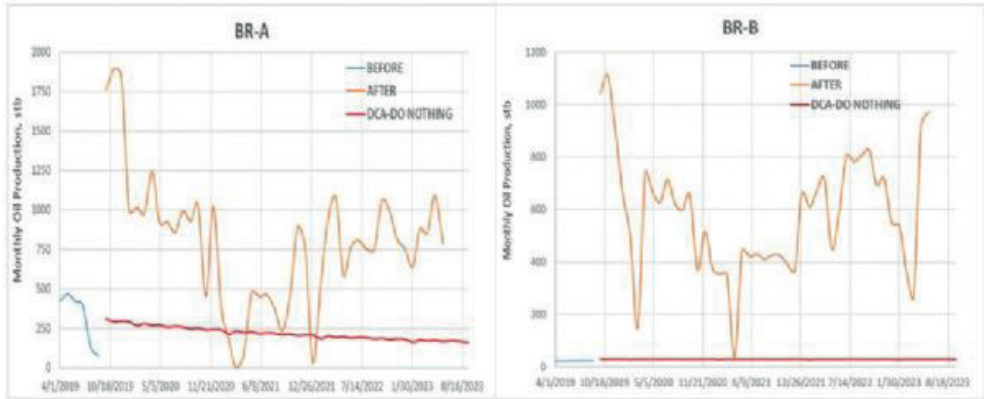
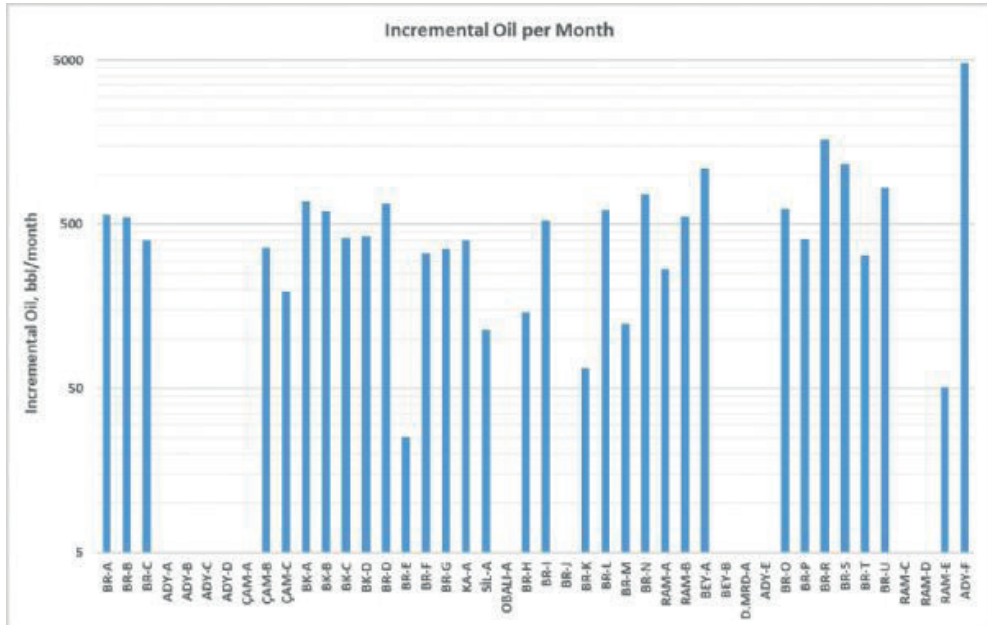


Figure-5: Production Enhancement After Fracturing Operation



# Importance of Cement Slurry Density & GEO-LITE

**Yigit Altunal, Burak Ekici**

GeoChemm Kimya A.Ş., Aydin / Türkiye



The use of lightweight cement (LWC) in oilfield has gained significant attention in recent years, owing to its potential to solve various challenges associated with cementing operations. This study presents a comprehensive analysis of the properties, applications, and advantages of lightweight cement in the oil and gas industry. This study focuses on the development and characterization of lightweight cement formulations, their rheological behavior, and their performance under different temperature and pressure conditions encountered in oilfield operations.

It has been reviewed the key factors influencing the design and composition of lightweight cement, including the selection of lightweight additives, particle-size distribution, and chemical admixtures. It discusses the effect of these factors on important properties, such as density, compressive strength, and setting time. Moreover, it is examined the potential benefits of lightweight cement in enhancing well integrity, reducing the risk of lost circulation, and improving zonal isolation.

Furthermore, it also has been investigated the challenges associated with lightweight cement, including not only gas migration, fluid loss, and long-term durability but also strategies employed to mitigate these challenges using additives and optimized cementing procedures.

The results prove that lightweight cement offers promising opportunities to optimize cementing operations, enhance well performance, and ensure long-term integrity in challenging oilfield environments.

## 1. INTRODUCTION

Cementing operations involve the creation of a strong and impermeable cement sheath between the casing and wellbore, to ensure well integrity and zonal isolation. The process begins with well preparation, which includes drilling and installing a casing to provide structural support and isolating different zones. The cement slurry is then carefully designed considering the well conditions and operational requirements. After mixing the slurry, it is pumped down the wellbore using specialized equipment, displacing drilling fluids, and ensuring complete coverage along the annular space. Once in place, cement undergoes hydration, resulting in hardening and strength development over time. The quality of the cement job is evaluated, and remedial measures may be taken if necessary to address any issues and ensure proper zonal isolation. Effective cementing operations are critical for maintaining well integrity, achieving zonal isolation, and optimizing the overall well performance in the oilfield industry.

## 2. GEO-LITE

In the oil and gas industry, the demand for advanced cementing solutions that can address the unique challenges encountered in well construction and completion processes has never been greater. One solution that has gained significant attention is lightweight cement. As drilling operations are introduced in increasingly complex and demanding environments, the need for lightweight cements has become evident. This introduction explores the reasons why lightweight cement is essential, highlighting its role in pressure control, zonal isolation, lost circulation prevention, and overall wellbore stability.

Pressure control is a critical consideration in oilfield operations, particularly in high-pressure or deep wells. Lightweight cement offers a feasible solution to achieve the desired pressure balance while mitigating risks associated with excessive differentials. By utilizing lightweight cement, operators can effectively manage hydrostatic pressure, thereby reducing the potential for formation damage, wellbore instability, and other related issues. The ability to precisely control pressure is key to successful drilling and production operations.

Zonal isolation is another fundamental requirement in well construction, which aims to prevent fluid migration between different reservoir zones. Lightweight cement plays a crucial role in achieving reliable and effective zonal isolation. Its lower density allows for improved placement and coverage along the annulus between the casing and the wellbore. This characteristic reduces the risk of incomplete cementing and provides a strong cement sheath, minimizing the threat of fluid communication and maintaining a good overall integrity.

The prevention of lost circulation, which is a common challenge in well construction, is significantly enhanced by employing lightweight cement. In formations with fracturing or permeable zones, the lower density of lightweight cement helps mitigate the loss of cement slurry into the permeable formations. This ensures efficient placement, maximizes the threat of achieving a complete cement sheath, and optimizes well performance by minimizing costly circulation losses.

Wellbore stability is a major consideration in drilling and completion. Lightweight cement contributes to maintaining wellbore stability, particularly in weak formations. The reduced density of lightweight cement reduces the stress or strain on surrounding formations, mitigating the risk of wellbore collapse, differential sticking, and other stability-related problems. By developing wellbore integrity, lightweight cement enhances the safety and efficiency of drilling operations.

### Case History

A.S. Al Yami et al. (2008) conducted research on lightweight cements and obtained the following results from field Results:

The lightweight cement was successfully applied to 40 wells, resulting in reduced hydrostatic column and cement placement on the surface. Lightweight cement was placed on the surface, and no losses were reported. (A.S. Al Yami et al., 2008).

Table 1 – Well Properties (A.S. Al Yami et al., 2008)

Table 2 - Result of Field Samples (A.S. Al Yami et al., 2008)

Table 3 – Brine permeability of lightweight cement samples used in the field. (A.S. Al Yami et al., 2008)

Fig. 1 – Low density cement samples collected from field application (A.S. Al Yami et al., 2008)

In conclusion, lightweight cement is essential in cementing operations owing to its significant benefits in terms of pressure control, zonal isolation, lost circulation prevention, and wellbore stability. These advantages are the critical challenges encountered during well construction and completion processes, ensuring operational success, and maintaining the integrity of oil, gas, and geothermal wells. As the industry continues to push boundaries in search of new reserves, lightweight cement has proven to be an indispensable solution for optimizing well performance and enhancing the overall operational efficiency. GeoChem; we applied these processes to create our lightweight product GEO-LITE.

### 3. DESIGNING THE COMPOSITION OF GEO-LITE

The design of the composition of lightweight cement for oilfield applications requires careful consideration of several key factors to ensure an optimal performance. One of the most important factors is the correct selection of aggregates according to the characteristics of the wells. To achieve the desired properties of GEO-LITE, these aggregates should possess characteristics such as controlled particle size distribution, low density, and compatibility with wellbore fluids.

In addition, the selection of cementing materials plays a crucial role in optimizing the performance of GEO-LITE. Specific additives, extenders, or supplementary cementing materials may be employed to enhance properties, such as thickening time, compressive strength development, and rheological behavior. Chemical components also play a crucial role in improving the workability, fluidity, and pumpability of GEO-LITE slurry. Furthermore, achieving an appropriate water-cement ratio is essential to balance the fluid properties, slurry stability, and long-term durability in a challenging well. By carefully designing the composition of GEO-LITE, oilfield applications can benefit from improved rheological properties, better zonal isolation, enhanced wellbore stability, and efficient cementing operations, ultimately leading to enhanced well integrity and successful drilling.

Several important factors should be considered when considering the use of GEO-LITE. These considerations help to ensure successful application and optimal performance. The key considerations are as follows:

**Density and Strength:** The density and compressive strength of GEO-LITE are critical factors that should be considered. To achieve the intended objectives such as pressure control, lost circulation prevention, and zonal isolation, the desired density should be lower than that of conventional cement. However, it is essential to maintain a sufficient strength to provide a durable and reliable cement sheath. The balance between density and strength should be carefully optimized based on the well conditions and operational requirements.

**Lightweight Additives:** The selection and incorporation of lightweight additives are crucial. Patents review revealed that there are several ways other than just mixing hollow microspheres with cement. For example, mixing coarse and fine cement particles, fly ash, fumed silica, hollow microspheres, and water (Dao,2003). Another example is to mix hollow microspheres with plasticizer, cement and aluminum metal powder and sodium sulfate (Dillenbeck,2004). These additives contribute to reducing the density of the cement slurry, while maintaining adequate mechanical properties. The choice of lightweight additives should consider factors such as stability, compatibility, and the desired density reduction.

**Particle Size Distribution:** Controlling the particle size distribution of the lightweight additives is crucial. Particle size influences the rheological properties, pumpability, and settling behavior of the slurry. An optimized particle size distribution helps ensure uniform dispersion, minimizes settling, and enhances the overall stability and performance of GEO-LITE slurries. The particle size distribution should be tailored based on the specific well conditions and desired properties of the cement slurry.

**Chemical Components:** Chemical components can be used to modify the properties of GEO-LITE. These components include fluid-loss control additives, set retarders, accelerators, and strength enhancers. The selection and dosage of chemical components should be carefully evaluated to optimize the rheology, setting time, fluid loss control, and strength development of GEO-LITE slurries.

**Wellbore Conditions:** Wellbore conditions such as temperature, pressure, and formation characteristics should be considered when designing GEO-LITE formulations. High-temperature and high-pressure environments may require specific cement compositions or additives to withstand downhole conditions and maintain desired properties. Understanding wellbore conditions and their potential impact on GEO-LITE is crucial for successful cementing.

**Compatibility and Performance Evaluation:** It is important to assess the compatibility of GEO-LITE with other well fluids and materials. Compatibility testing can help identify any potential issues or interactions that may affect the performance of the GEO-LITE.

Additionally, performance evaluation methods, such as laboratory testing and simulation studies, can provide valuable insights into the behavior and performance of lightweight cement under simulated downhole conditions.

**Operational Considerations:** Practical aspects such as mixing, handling, and pumping of GEO-LITE should be considered. GEO-LITE slurries may exhibit different flow properties compared to conventional cement slurries, requiring adjustments in pumping rates, pressures, and equipment. Proper training and operational guidelines should be provided to ensure successful implementation of GEO-LITE operations.

Considering these important considerations, the design and application of lightweight cement in cementing are optimized for specific well conditions, operational requirements, and performance objectives. Comprehensive and detailed evaluations contribute to successful lightweight cementing operations.

#### 4. LABORATORY STUDIES AND GEO-LITE

In this study, low-weight cement slurries were formulated using class-G cement and GEO-LITE. To create an appropriate LWC for our purposes, the concentration of each additive was adjusted and GEO-LITE was employed at a specific concentration.

#### EXPERIMENTAL STUDIES

i. **Slurry Preparation Procedure:** LWC was prepared in the laboratory using a standard API blender. The slurry was mixed for 15 s at 4,000 rpm and for 35 s at 12,000 rpm.

ii. **Slurry Thickening Time:** The cement slurry was poured into an API standard HPHT consistometer slurry cup for thickening time to evaluate pumpability.

iii. **Slurry Rheology:** The slurry rheology was conditioned in an atmospheric consistometer before obtaining rheological readings. A viscometer was used to measure slurry rheology (Nelson, 1990).

iv. **Free Water and Slurry Sedimentation:** The free water test was designed to measure water separation using a 250 ml graduated cylinder. The duration of the test is 2 h, according to the API 10 B-2 procedure. Having zero free water and no significant settling or sedimentation are good indications of good slurry and good potential of zonal isolation, (Nelson, 1990).

v. **Slurry Fluid Loss:** The HPHT filter press and stirred filter press tester were used to measure the amount of fluid loss. If not carefully controlled, fluid loss can cause the slurry volume to decrease and the pressure to drop, which could allow the formation fluids to enter the slurry, (Stiles, 1997).

vi. **Compressive Strength:** The SGSA was used to measure compressive strength. Tests were completed by following API 10 B-2 procedures. Compressive strength is essential in cementing operations because it ensures structural integrity, supports zonal isolation, promotes wellbore stability, facilitates load distribution, enhances

durability, and aids in cement evaluation. Monitoring and achieving the appropriate compressive strength are crucial for maintaining the integrity and long-term performance of the cement.

Fig 2 - GEO LITE + 35% Silica (only for 250°F)

Figure 2 shows the compressive strengths of the 12.5 ppg cement slurries at different temperatures. The compositions without GEOLITE additives had compressive strengths between 400 and 500 psi.

Table 4 shows that the GEO-LITE can aid in reducing the settling of cement slurries during the waiting-on-cement (WOC) period. The low density of the GEO LITE minimizes sedimentation, helping to maintain the stability of the slurry. Additionally, GEO LITE can contribute to fluid loss control by forming a filter cake and reducing fluid loss in the formation.

The incorporation of GEO-LITE can affect the rheological properties of the cement slurry. The presence of the GEO-LITE can influence the viscosity, yield stress, and fluidity of the slurry. The specific effect depends on the size, concentration, and distribution of GEO-LITE. The addition of GEO-LITE can modify the slurry's flow behavior, potentially improving its pumpability and flow characteristics during the cementing operation.

The use of GEO-LITE affected the mechanical properties of the cement sheath. GEO-LITE contributes to the compressive strength compared to conventional cement slurries without additives. In addition, the impact on the mechanical properties can be mitigated by adjusting the concentration of GEO-LITE and optimizing the cement formulation. It is important to strike a balance between the density reduction and maintaining adequate strength to ensure the durability and integrity of the cement sheath.

Table 4- GEO-LITE, 12.5 ppg @ 120 °F, 3000 psi

Table 5- GEO-LITE, 12.0 ppg, @3000 psi

Table 6- GEO LITE, 11.5 ppg, @3000 psi

Table 7- GEO LITE, 11.0 ppg, @3000 psi

#### REFERENCES

- A.S. Al Yami, H.A. Nasr-El-Din, M.K. Al-Arfaj, S.H. Al-Saleh, A.S. Al-Humaidi., and N.A. Al-Shuker 2008. "Evaluation and Optimization of Low-Density Cement: Laboratory Studies and Field Applications", Presented at the Indian Oil and Gas Technical Conference and Exhibition held in Mumbai, India, 4-6 March, SPE-113090
- Dao, B., Ravi, K. M., Vijn, J. P., Noik, C., and Rivereau, A. 2003. "Lightweight Well Cement Compositions and Methods," U.S. Patent No. 6, 562, 122.
- Dillenbeck, R. L., Heinold, T., Rogers, M. J. And Bray, W. S. 2004 "Ultra Low Density Cementitious Slurries for Use in Cementing of Oil and Gas Wells," U.S. Patent No. 6, 832-652.
- Kutlu, B. 2013. "Rheological Properties of Drilling Fluids Mixed with Lightweight Solid Additives".

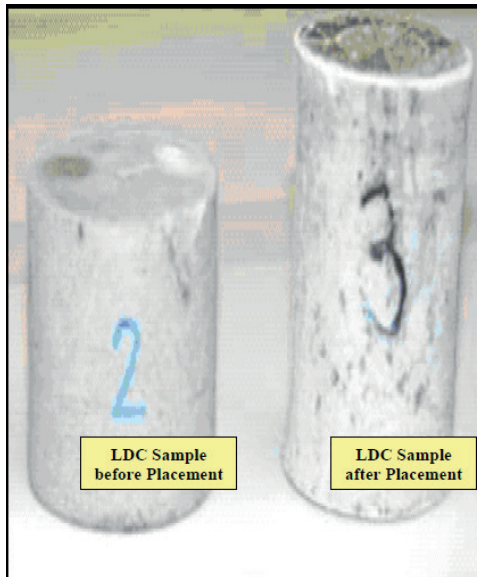
Presented at the SPE Annual Technical Conference and Exhibition, New Orleans, Louisiana, 30 September-2 October, SPE-167619-STU

Nelson, E. B.: "Well Cementing," TSL-4135/ICN-01557200, Schlumberger Educational Services, 1990. P 8-10 and B -1 to B -9

Stiles, D. A.: "Succesfull Cementing in Areas Prone to Shallow Saltwater Flows in Deep-Water Guld of Mexico," paper SPE OTC 8305 presented at the 1997 OTC in Houston, TX, 5-8 May.

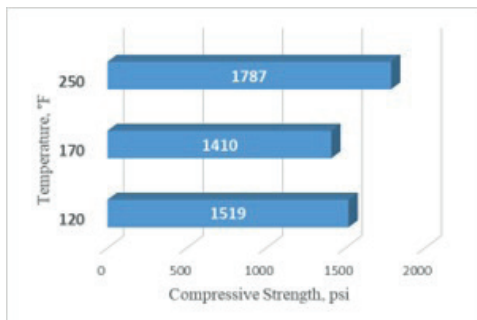
Keywords: Cementing, Geo-LITE

Figure 1



Low density cement samples collected from field application (A.S. Al Yami et al., 2008)

Figure 2



GEO LITE + 35% Silica (only for 250°F)

Table 1

<b>9 5/8" Intermediate Casing @9,110 ft</b>	
Temperature Gradient, °F/100ft	1.5
Estimated Fracture Equivalent Circulating Density, ppcf	82
9 5/8" casing was pressure tested at 3,700 psi after the operation	No Leak
Formation Type	Carbonate

Well Properties (A.S. Al Yami et al., 2008)

Table 2

<b>Parameter</b>	<b>Units</b>	<b>Value</b>
Slurry density before pressurizing at 5,000 psi	lb/gal	9.35
Slurry density after crushing pressurizing at 5,000 psi	lb/gal	10.6
Plastic Viscosity (PV)	cP	93
Yield Point (YP)	lbf/100ft <sup>2</sup>	8.5
Free Water	%	0
Thickening Time	hr:mn	7:42

Result of Field Samples (A.S. Al Yami et al., 2008)

Table 3

Sample Information	Confining Pressure, psi	Injection Pressure, psi	Duration of Injection, days	Permeability, md
Prior Placement	1,800	50	1	0
		100	1	0
		150	1	0
		250	1	0
		500	1	0
	3,500	500	1	0
		1,000	1	0
		1,500	1	0
		2,000	1	0
		2,500	1	0
After Placement	1,800	50	1	0
		100	1	0
		150	1	0
		250	1	0
		500	1	0
	3,500	500	1	0
		1,000	1	0
		1,500	1	0
		2,000	1	0
		2,500	1	0

Brine permeability of lightweight cement samples used in the field. (A.S. Al Yami et al., 2008)

Table 4

Properties	GEO LITE Concentration (%)		
	0%	8%	20%
Fluid Loss, ml/30 min	366	85	40
PV	15	50	216
YP	2	18	28
Free Water, 2 hrs	1%	0%	0%
Settling	Yes	No	No
Compressive Strength 48 hrs, psi	644	1889	3731

GEO-LITE, 12.5 ppg @ 120 °F, 3000 psi



Table 5

Properties	GEO LITE Concentration (%)		
	15%	20%	
Temperature, °F	120	120	170
Fluid Loss, ml/30 min	40	37	44
PV	59	113	78
YP	4	10	7
Free Water, 2 hrs	0%	0%	0%
Settling	No	No	No
Compressive Strength 48 hrs, psi	1690	3300	3086

GEO-LITE, 12.0 ppg, @3000 psi

Table 6

Properties	GEO LITE Concentration (%)	
	25%	
Temperature, °F	120	170
Fluid Loss, ml/30 min	34	46
PV	174	152
YP	19	15
Free Water, 2 hrs	0%	0%
Settling	No	No
Compressive Strength 48 hrs, psi	2826	2535

GEO LITE, 11.5 ppg, @3000 psi

Table 7

Properties	GEO LITE Concentration (%)		
	25%	30%	
Temperature, °F	120	120	170
Fluid Loss, ml/30 min	62	41	44
PV	85	128	109
YP	21	19	17
Free Water, 2 hrs	0%	0%	0%
Settling	No	No	No
Compressive Strength 48 hrs, psi	1834	2982	2598

GEO LITE, 11.0 ppg, @3000 psi

# Tight Gas Field Development in Thrace Basin by Hydraulic Fracturing



**Ufuk Kılıcaslan, Ahmet Ergün Mengen, Özlem Özcan, Sofiane Belhocine, Rabah Boudissa, Vasily Semenovich Mironov, Aleksei Vasilevich Khlopkov**  
Turkish Petroleum Corporation (TPAO), Ankara / Türkiye

In order to reduce the reliance on and costs of imported energy, Turkish Petroleum Corporation (TPAO), the state-owned oil company of the Turkish Republic, has put significant effort into exploration and production activities. In addition to ongoing operations in their conventional reservoir formations, hydraulic fracturing technology has been considered, studied and implemented in tight gas reservoir during last three years. The main challenge of the project was fracturing an over-pressured tight gas reservoir deeper than 3,000 meters (true vertical depth), in a tectonically active area. Performing fracturing operations in a safe, proper, environmentally friendly way was initial priority.

This paper presents not only specific operational experiences, but also the modelling aspects from a tight gas reservoir development using hydraulic fracturing as a real field case study. Different responses were observed both in the fracturing and production characteristics, even within short distances between wells/treatments. These behaviours challenge not only modelling existing experiences but also in designing future operations and their corresponding production profiles.

## INTRODUCTION

Tight gas reservoirs have an intrinsically low permeability value, which is typically less than 0.1 mD. Hydraulic fracturing is the most efficient stimulation method to achieve economical rates in such tight formations. Increases in the effective fracture half-length and effective conductivity generally result in higher initial rates and an increased cumulative gas production behaviour (Holditch and Tschirhart, 2005).

An accurate estimation of the original gas in place and EUR, are key aspects for understanding the commerciality of any project and particularly in the case of tight-gas. A number of techniques can be implemented beginning with simple decline curve analysis, where only production data will be enough for the required assessment. Boundary dominated flow should be seen to determine correct decline exponent- the b value (Alem et al., 2019). Since tight gas reservoirs have relatively low permeability, it is difficult to conduct and analyse a successful pressure transient test. Rate Transient Analysis (RTA) provides a viable alternative to the use of conventional Pressure Transient Analysis (PTA) by using rate and bottomhole flowing pressure data without having to shut the well in. Instead of just a simplified reservoir model and a single-averaged value for a distinct reservoir property, changes in reservoir and fluid properties can be modelled dynamically in a fully 3D environment. However, this requires additional high-quality data and the run-time and analysis period can be much longer than when compared to other techniques. In this case study, all three methods were implemented

for producing wells and comparison was made based on estimated ultimate recovery (EUR).

## HYDRAULIC FRACTURING OPERATIONS

Fracturing over-pressured tight gas reservoir deeper than 3,000 meters (true vertical depth) in tectonically affected areas was the main challenge of the project. Eight hydraulic fracturing operations were performed in four vertical wells, including two wells with multistage fracturing. One of these operations was conducted to test the potential of a shale gas interval that exists within the field.

The Hamitabat Formation is a tight sandstone reservoir, which requires significant propped fracture length to achieve good dimensionless fracture conductivity (FCD). Due to formation depth, the friction pressures are important to stay within the safety region for 15k psi of equipment capacity. To address these issues, high injection rate with low viscosity fluid was preferred. Another consideration was formation damage in case of guar based fracturing fluid. In this respect, High Viscosity Friction Reducer (HVFR) fluid was used in the operations as a fracturing fluid. 40/70 Intermediate Density Ceramic proppant (IDC) was injected during the mini frac to check connection between the formation and the wellbore, to clean perforations and the near wellbore, and to decrease perforation and near wellbore friction. On the other hand, 40/70 IDC and tail in with 20/40 High Strength ceramic Proppant (HSP) were pumped in the main fracture. Also, micro-proppant particles were added during the pad stage to improve the production contribution from deeper reservoir sections; the size of these particles is between 150-325 mesh, and the average is around 200 mesh.

In modelling of the fracture design within the pseudo 3D simulator, a model was created based upon available logs and other data. The formation permeability was assigned in the range of 0.001-0.1 mD, depending upon the tightness of each individual layer. The presence of natural fractures observed in the logs was considered by using a multiplier function, such that their effect on the net pressure match and leak-off rate could be simulated.

As a diagnostic injection, mini-frac was preferred. Standard procedure for mini-frac execution includes injection of mini-frac with proppant slug, shut-in, recording pressure fall-off until fracture closure. Then analysis is done for mini-frac response, model calibration and redesign of the main treatment. Initial target for mini-frac was to test treating pressure level under maximum injection rate. As seen in Fig. 1., treating pressures were too high in shale interval. Also, mini-frac injection includes proppant slug stage to ensure good connection between the wellbore and the formation. It can be observed from Fig. 2., proppant slug hit the

perforations and dropped treating pressure such that fracture entry frictions were diminished. However, there was no such effect observed in some cases meaning that fracture entry frictions are negligible. Formation breakdown pressure was observed clearly in some of the operations (Fig.-3). During the mini-frac, one ton of 40/70 IDC at 0.5 ppg concentration was pumped with HVFR fluid. Injection rates were varied from 40 to 60 bpm.

Figure-1. Mini-frac plot for the Shale Interval.

Figure-2. Cleared Near Wellbore Friction in Mini-frac.

Figure-3. Clear Breakdown Signature.

Mini-frac analysis includes estimation of ISIP, total friction, fluid leak-off, net pressure, and closure pressure using standard methods like G-function Plot, SQRT Plot and Log-Log Plot. From ISIP, we can understand quality of connection between wellbore and nearby formation. G-function derivative analysis showed, for some wells, almost normal leak-off behaviour (Fig. 4.), which is described by constant hydraulic fracture area during shut-in and leak-off through a homogeneous rock matrix. At the same time, several cases were observed with fracture tip extension behaviour, where fracture growth after injection is stopped. Also, tip extension combined with pressure dependent leak-off due to natural fractures were seen in some wells, as illustrated in Fig. 5.

Figure-4. Normal Leak-off Regime.

Figure-5. Effect of natural fractures on G-function

As summarized in Table 1., Diagnostic Fracture Injection Tests (DFIT) showed high closure stress values (up to 1 psi/ft gradient), which resulted in high treating pressures. Net pressures were high for almost all mini-frac treatments except two cases. These high treating pressures can be attributed to either having strong stress barriers above and below the target zone or the initiation of multiple fractures due to formation geo-mechanical properties and the presence of natural fractures. In the field in question, both options are considered to be valid potential outcomes.

Table 1. Minifrac Analysis Summary.

Mini-frac analysis showed significant variety in model parameters proving that relatively homogeneous geological conditions in conjunction with tectonic events results in a wide range of variation in treating pressures, fluid and proppant volumes, maximum proppant concentrations, and finally created fracture geometry and conductivity.

A typical pumping schedule for the main fracture treatment consisted of pad, proppant-laden staged and final flush. In the first fracturing operation, high treating pressure was observed in the shale gas interval. Even reducing pump-rates did not substantially reduce the treating pressure sufficiently, it was decided to reduce the rate and then switch to flush (see Fig. 6).

Figure-6. Main-frac Plot for Shale Gas Interval.

As experience was gained, one or several sweeps were used to separate different proppant mesh sizes, which

allowed the completion of the treatments with the designed proppant volumes (Fig. 7.). Actual numbers and volume of sweeps were dictated by actual treating pressure behaviour. If the pressure started to build with the slope 100 psi/min or more, then pumping was switched to a sweep stage, the sweep was then pumped until pressure dropped or flattened, and then started pumping proppant again. To prevent screen-out, proppant concentration was increased by 0.25 ppg at each step. As can be seen in Fig. 8., freezing concentration even at low values could not keep the pressure stable. It was necessary to cut proppant in order to eliminate screen-out.

Figure-7. Sweep Effect on Treating Pressure.

Figure-8. Proppant Bridging in Main-frac Operation.

As seen in Table 2., even though the injection rates were similar, huge differences were observed in the maximum proppant concentration and ISIP gradients within the same field. This behaviour suggests how difficult it is to design, operate and analyse fracturing operations within this geological system.

Table-2: Summary of Main-frac Operations and Mainfrac Analysis.

## RESERVOIR MODELLING AND FUTURE PREDICTION

None of these wells and associated intervals could provide economic gas rates, some would not initiate flow before fracturing. After hydraulic fracturing operations, we saw commercial gas production during almost all flowback operations, except the initial two stages of Well A. The first stage was conducted on the shale interval, while deeper Hamitabat section was fractured in second stage. To eliminate possible obstacle in gas flow due to water head in the tubing, nitrogen lifting via coiled tubing was utilized. Even though 5-10% of additional fracturing fluid was recovered, these operations did not change well productivity. On the other hand, remaining wells performed very well both in flowback period and production period. Details of flowback & production period for each stage were summarized in Table-3.

Table-3: Summary of Well Productions.

After general understanding of production behaviour in wells, traditional methods of performance prediction were implemented starting with simplistic decline curve analysis up to more sophisticated numerical reservoir simulation. EUR predictions at the end of 20 years with 5,000 m<sup>3</sup>/day economic cut-off were also compared between the various methods.

Instead of classical hyperbolic decline, two newer methods addressing transient flow behaviour at early time of tight gas production were used. The first method was power law method (Ilk et al., 2008) while second was stretched exponential decline method (SEPD), introduced by Valko and Lee (2010). On the other hand, three different RTA methods readily available in conventional industry software were used to find fracture half-length and drainage area as well as predict

future performances under constraints mentioned above. The final method was numerical reservoir simulation, where whole flow physics and geological features were included in calculations. The fine grid size was set to 25 meters by 25 meters for areal discretization while two main zones were created with a layering of 5 meters in vertical direction, which ended up with a geomodel having 360K grid cells. After validating the gas in place, the base case was run under gas rate control. The main mismatch was observed for Well A, due to a low matrix permeability compared to historical gas production rate. Also, a sudden increase in water production observed for this well. As explained previously, this well is located close to a fault where a significant occurrence of natural fractures takes place and a deeper part of the fault is potentially connected to water. In addition to these changes, PI multipliers were used to mimic the hydraulic fracture behaviour with time. As can be seen in Fig. 9., reservoir pressure, water production and oil production were matched at field level.

Figure-9: Field History Match. Dots are Observed Values While Lines are Simulated.

Summary of EUR values from different production forecasts are given in Table-4. Since we have long production history in Well A, all methods yielded similar EUR value. Conversely, significant differences exist in other two wells, which have less than one year production period. Both RTA and reservoir simulation overestimated production. Main reason seems to be permeability used in those models, which matched historical production in numerical simulation. Permeability was assigned based on core porosity-permeability relationship. Considering Well A production, EUR predictions from DCA methods were more dependable than others. Therefore, some refinements in porosity-permeability relationship could converge recovery estimates while providing history match, which has non-unique solutions.

Table-4: Comparison of Prediction Methods in EUR (MMsm<sup>3</sup>).

## CONCLUSIONS

In this study, the lessons learned from eight fracturing operations and modelling of associated production behaviours were discussed. Although wells and target intervals are quite close, almost all the fracturing operations have different characteristics. Regional stress regime associated to basin tectonics, local rock properties and the presence of natural fractures are thought to be major factors in these differences. Similar behaviours were observed in gas production. In order to reduce uncertainty in EUR prediction, decline curve analysis, RTA and reservoir simulation methods were implemented and results were compared. Based on the remaining gas volume and reservoir pressure from simulation study, at least one well could be drilled as an infill well, which is close to one of the major faults. However, its location needs further optimization by placing it at safe proximity to a fault to eliminate early screen-out while getting production benefit of denser

natural fractures as observed in Well A.

## Acknowledgement

The authors want to thank the Turkish Petroleum Corporation (TPAO) for allowing the publication of this work and material.

## Nomenclature

DFIT = Diagnostic Fracture Injection Test  
 EUR = Expected Ultimate  
 Recovery (MMsm<sup>3</sup>) or (mmbbls)  
 FCD = Dimensionless Fracture Conductivity  
 HVFR = High Viscosity Friction reducer  
 IDC = Intermediate Density Ceramic  
 ISIP = Instantaneous Shut-In Pressure (psi) or (kPa)  
 MBT = Material Balance Time  
 PTA = Pressure Transient Analysis  
 RTA = Rate Transient Analysis  
 SEPD = Stretched Exponential Decline Method  
 TPDA = Transient Production Decline Analysis

## REFERENCES

- Alem, M., Baig, T., Ann, M., and Jones, A., 2019, Predicting the Performance of Tight Gas Reservoirs, SPE 195503-MS, Presented at the SPE Europec featured at 81st EAGE Conference and Exhibition, London, England, UK, June.
- Holditch, S.A. and Tschirhart, N.R., 2005, Optimal Stimulation Treatments in Tight Gas Sands, SPE 96104, Presented at the SPE Annual Technical Conference and Exhibition, Dallas, Texas, USA, October 9-12.
- Ilk, D., Rushing, J. A., Perego, A. D., and T. A. Blasingame., 2008, Exponential vs. Hyperbolic Decline in Tight Gas Sands — Understanding the Origin and Implications for Reserve Estimates Using Arps' Decline Curves, SPE 116173-MS, Paper presented at the SPE Annual Technical Conference and Exhibition, Denver, Colorado, USA
- Valkó, P.P., and Lee, W.J., 2010, A Better Way to Forecast Production from Unconventional Gas Wells, SPE 134231-MS, Paper presented at the SPE Annual Technical Conference and Exhibition, Florence, Italy

Keywords: Hydraulic Fracturing, Tight Gas Reservoirs

Figure-1: Mini-frac plot for the Shale Interval.

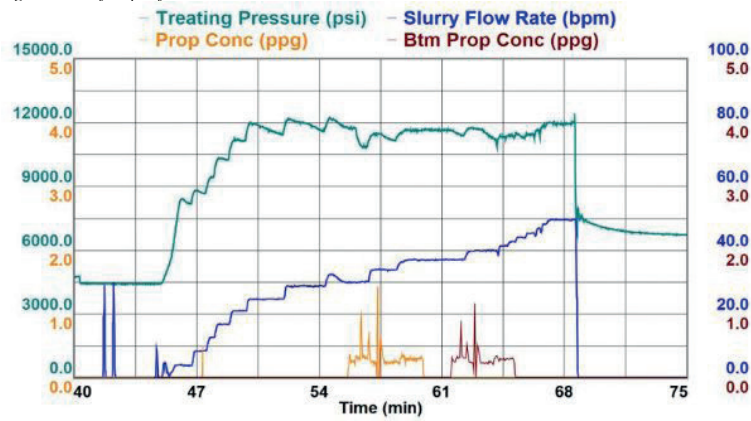


Figure-2: Cleared Near Wellbore Friction in Mini-frac.

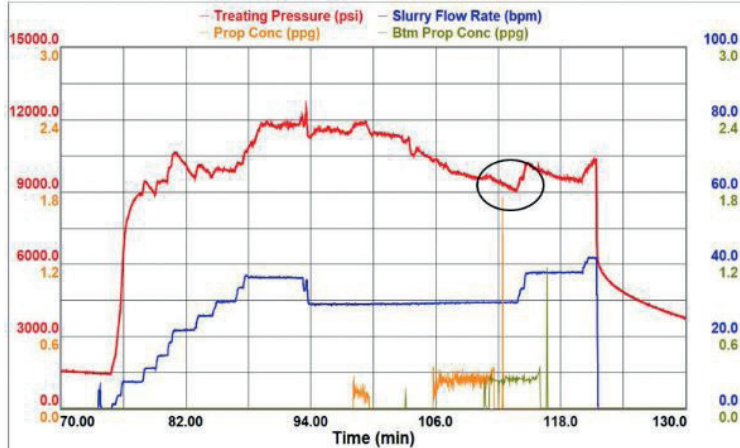


Figure-3: Clear Breakdown Signature.

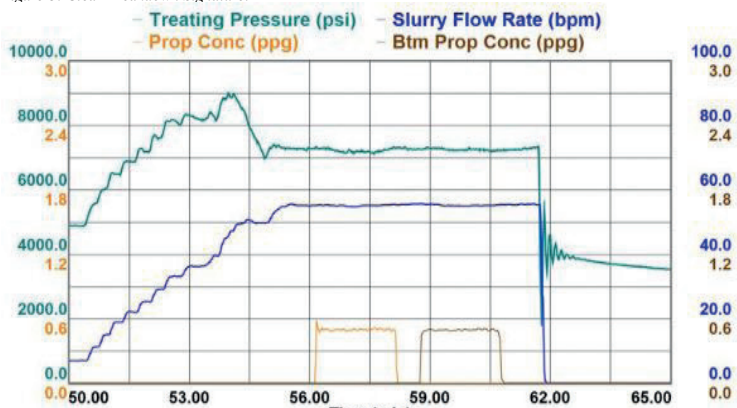


Figure-4: Normal Leak-off Regime.

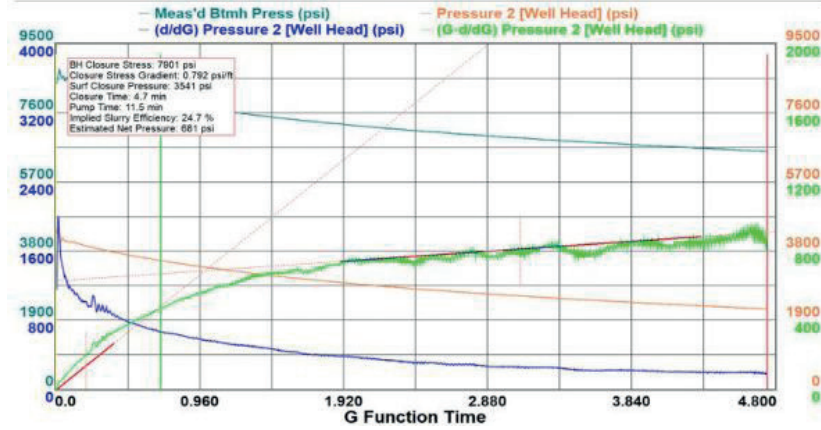


Figure-5: Effect of natural fractures on G-function

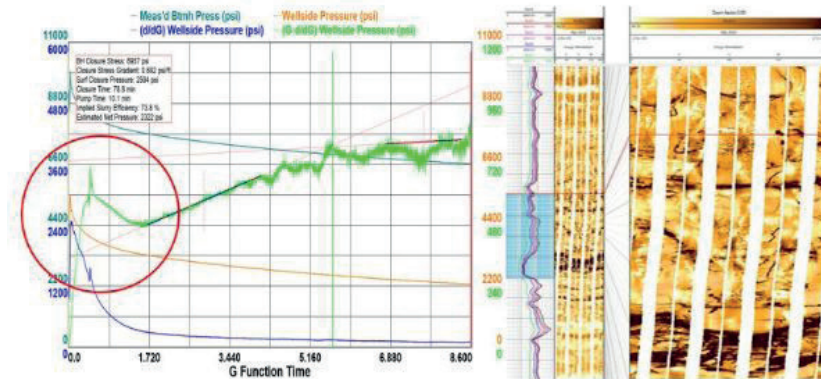


Figure-6: Main-frac Plot for Shale Gas Interval.

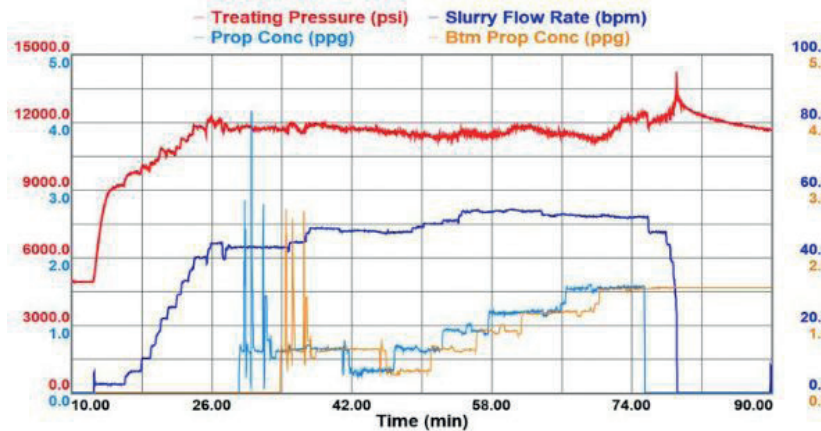


Figure-7: Sweep Effect on Treating Pressure.

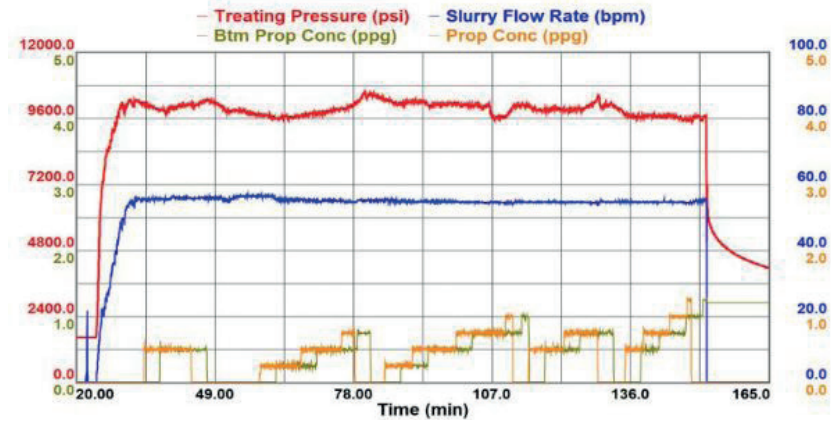


Figure-8: Proppant Bridging in Main-frac Operation

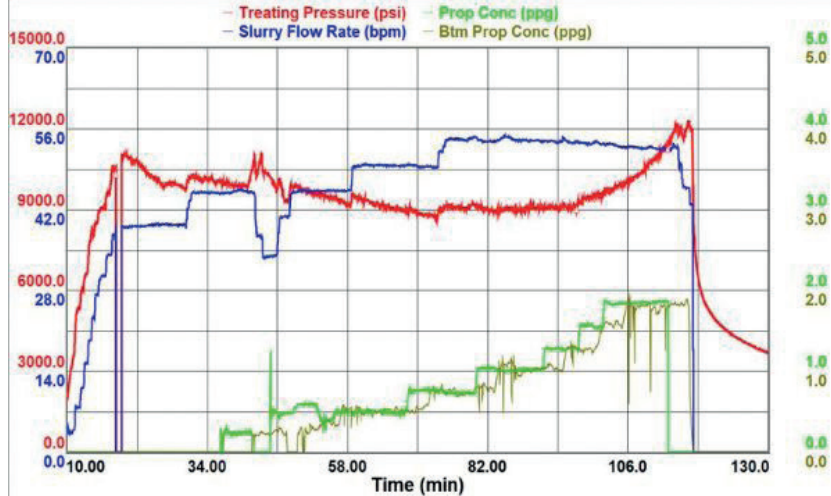


Figure-9: Field History Match. Dots are Observed Values While Lines are Simulated.

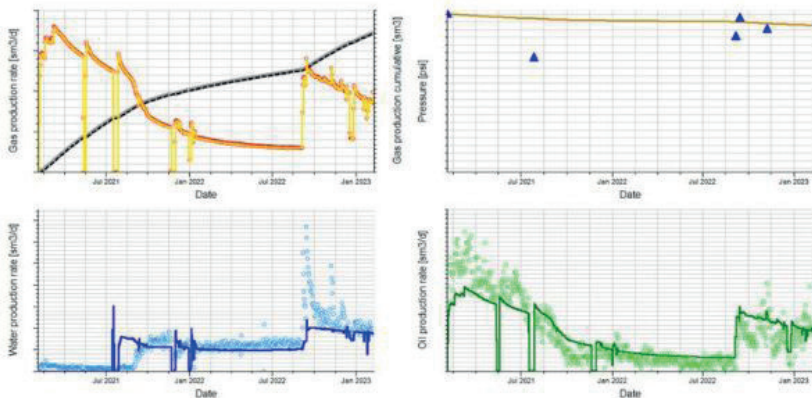


Table 1: Minifrac Analysis Summary.

Well Name	BH ISIP (psi)	ISIP Gradient (psi/ft)	BH Closure (psi)	Total Friction (psi)	Closure Gradient (psi/ft)	SI Time min	Closure Time (min)	Implied Slurry Efficiency (%)	Est. Net Pressure (psi)
Well A_1 <sup>st</sup>	13,868	0.983	13,295	4,342	0.942	68.9	1.20	4.70	573
Well A_2 <sup>nd</sup>	8,753	0.792	7,621	2,778	0.69	145	38.7	50.8	1,167
Well A_3 <sup>rd</sup>	10,326	1.048	7,689	4,369	0.781	84.0	11.7	17.5	2,636
Well B_1 <sup>st</sup>	10,705	1.093	9,314	3,053	0.951	88.0	4.10	19.5	1,391
Well B_2 <sup>nd</sup>	8,583	0.86	7,901	2,953	0.792	68.0	4.70	24.6	681
Well B_3 <sup>rd</sup>	8,392	0.862	7,278	3,184	0.748	59.0	11.4	24.3	1,113
Well C	8,845	0.905	6,274	3,709	0.642	103	15.9	44.9	2,570
Well D	9,279	0.923	6,957	3,668	0.692	159	78.8	73.8	2,322

Table-2: Summary of Main-frac Operations and Mainfrac Analysis.

Well Name	Fluid Volume (bbls)	Rate (bpm)	Proppant Volume (MT)	Max Proppant Conc. (ppg)	BH ISIP (psi)	ISIP Gradient (psi/ft)	Total Friction (psi)	Propped Length (m)	FCD
Well A_1 <sup>st</sup>	2.790	52	39	1.70	-	-	-	301	10.9
Well A_2 <sup>nd</sup>	4.539	54	100	3.00	8,883	0.804	2,419	213	140
Well A_3 <sup>rd</sup>	4.680	53	59.4	1.86	12,918	1.312	3,678	192	3.34
Well B_1 <sup>st</sup>	6.630	55	49	1.25	10,405	1.062	3,623	65	1.03
Well B_2 <sup>nd</sup>	6.224	55	99.3	2.40	9,598	0.962	3,239	112	33.2
Well B_3 <sup>rd</sup>	5.196	56	77.8	1.75	8,691	0.893	3,515	163	2.90
Well C	4.691	62	84	3.50	8,587	0.878	4,040	121	9.00
Well D	4.941	58	86.5	3.00	10,579	1.052	3,446	132	42.1

Table-3: Summary of Well Productions.

Well Name	Flowback Liquid Recovery (%)	Flowback Max Gas Rate (Mm3/d)	Initial Gas Rate, (Mm3/d)	Initial WHP (psi)	Current Gas Rate (Mm3/d)	Current WHP (psi)	Cum Gas (MMm3)
Well A_1 <sup>st</sup>	23.6	1.4	-	-	-	-	-
Well A_2 <sup>nd</sup>	59.8	0.8	-	-	-	-	-
Well A_3 <sup>rd</sup>	39.3	211	180	3000	19.5	491	51.3
Well B_1 <sup>st</sup>	47.3	28.8	33.8	1006	11.1	362	4.1
Well B_2 <sup>nd</sup>	59.5	39.6					
Well B_3 <sup>rd</sup>	40.2	31.5					
Well C	49.7	99.2	87.9	1460	28.7	297	13.8
Well D	51.3	36	19.7	466	-	-	0.3

Table-4: Comparison of Prediction Methods in EUR (MMm3).





## **Akdeniz Baseni Petrol Potansiyeli ve Yeni Gelişmeler**

*Petroleum Potential and New Developments  
of the Mediterranean Basins*

---



# Geochemical Characteristics and Depositional Conditions of the Organic-Rich Triassic Facies in the Western Taurides, Turkey



Zeynep Dincer Kirman<sup>1</sup>, İsmail Ömer Yılmaz<sup>2</sup>, Hasan Çağlar Üsdün<sup>3</sup>

<sup>1</sup>Geochemistry Department, Research&Development Center, TPAO, Ankara / Türkiye

<sup>2</sup>Geological Engineering Department, METU, Ankara / Türkiye

<sup>3</sup>Sedimentology Department, Research&Development Center, TPAO, Ankara / Türkiye

## SUMMARY

Eastern Mediterranean Basin poses importance with respect to not only the drilled and scheduled offshore wells but also the source rock discoveries made in the near past. On the contrary, available limited data and knowledge regarding these source rocks and their spatial distribution throughout the region bring challenges for a solid understanding of the petroleum system of the subject area. To gain an understanding of the petroleum system in the region, it is crucial to undertake a thorough assessment of the source rock units and discern their depositional processes. Utilizing this information as a foundation, conducting field studies on Nappes becomes crucial due to the uncertainty surrounding the number of depocenters in the region. Notably, the presence of Triassic-aged source rock examples in Northern Italy adds to the region's allure for exploration.

## METHODOLOGY

This study focuses on the comprehensive analysis of 98 samples collected from Early Triassic-aged 2 different sections in Western Taurides, Turkey. Systematic sampling was conducted every 25 cm, considering changes in lithology and sedimentological texture. Geochemical assessments including Pyrolysis, Sulphur, GC (Gas Chromatography), and GC-MS (Gas Chromatography – Mass Spectrometry), as well as inorganic and organic carbon isotope analysis and elemental analysis, contribute to the understanding of these units. The integration of geochemical analysis with sedimentological data help build the paleoenvironmental setting of the region.

## RESULTS

Sahin et al., (in press) in their micropaleontological examination of both Yerindere and Pınargözü sections samples have identified the stratigraphic age of Triassic-Olenekian for the first time, and this finding complies with the geochronology of Sr isotope values in this study. The investigations conducted on the Yerindere section reveal a transition in lithology and source rock potential along the samples (Sahin et al., in press). Prior samples consisted of limestone with high clay and sand content and minimal source rock potential. However, after a point, there is a notable decrease in clay and sand content and presence of significant source rock potential. The samples with source rock potentials show a range from poor to excellent, with the majority falling in the excellent category (Sahin et al., in press). Tmax values indicate that the samples are generally immature. Based on the HI and Tmax values, the potential source rock

samples predominantly contain Type II kerogens derived from lacustrine and marine organic matter, indicating the capability of generating liquid hydrocarbons with the highest HI values samples grouped in Type-IIS part. GC and GC-MS analyses on extracted samples indicate a shallow, anoxic depositional environment with a predominantly marine input for all samples. There is a notable increase in the levels of normalized V and P, exhibiting a direct correlation with Total Organic Carbon (TOC). In parallel, the concentrations of Zn, Mo, Cu, and Ni also ascend.

Similar patterns are observed in the Pınargözü section, where normalized V and P samples exhibit a comparable trend to those in the Yerindere section, along with increased concentrations of normalized Zn, Cu, and Mn. The distribution of potential source rock samples in the Pınargözü section appears to be more uniform throughout the sequence. The deposition environment in this section also exhibits sulfidic characteristics, leading to the formation of Type-IIS kerogen, similar to the deposition mechanism observed in the Yerindere section. Hence, a possible interpretation of this deposition scenario is that intrusion of seawater into asymmetrical restricted depocenters promotes bio productivity and converting the environment into relatively deeper anoxic/sulfidic state. In cases where the input of iron is limited (or lower than the Sulfur concentration in the deposition environment), free S binds to the kerogen, promoting the development of Type-IIS kerogen which is capable of generating hydrocarbon at earlier maturation stages.

## REFERENCE

Sahin, N., Altner, D., Dincer-Kirman, Z., 2023. Discovery of Lower Triassic Hydrocarbon Source Rock in a Rift Controlled Tectonic Setting, Antalya Nappes, Southwestern Turkey (in press).

Keywords: Triassic, geochemistry

# Doğu Akdeniz'deki En Büyük İki Deltanın (Nil ve Seyhan-Ceyhan) Gelişiminde Tektonizmanın Karşılaştırmalı Analizi Comparative Analyses Tectonism on the Development of two Largest Deltas (Nile and Seyhan-Ceyhan) in the Eastern Mediterranean



**Yasemin Geze Kalanyuva<sup>1</sup>, Nizamettin Kazancı<sup>2</sup>**

<sup>1</sup>Türkiye Petrolleri A.O (TPAO), Ankara / Türkiye

<sup>2</sup>Ankara Üniversitesi Jeoloji Mühendisliği Bölümü, Ankara

## ÖZ

Doğu Akdeniz'in en büyük aktif iki deltası güneyde Nil, kuzeyde Seyhan-Ceyhan deltalarıdır. Bu iki delta, Tortoniyen'den bu yana, izostatik ve tektonik etkileri kendi istiflerinde taşımakla birlikte sürekli gelişim içinde olmuşlardır. Bu çalışmada sismik kayıtlar ve sondaj verileri kullanılarak incelenen Seyhan-Ceyhan deltası istifleri ile literatürden yararlanılarak elde edilen Nil Deltası istifleri karşılaştırılmıştır. İstiflerin karşılaştırılmaları boyut itibarıyla değil, stratigrafik ve mimari açıdan ele alınmıştır. Amaç aynı denizdeki aynı global seviye değişimlere bağlı iki delta üzerinde tektonizmanın nasıl etki ettiğini belirlemektir.

## GİRİŞ

Teorik olarak, Seyhan-Ceyhan ve Nil deltalarının global deniz seviyesi değişimlerinden birlikte etkilenmeleri ve benzer istifleri oluşturmaları beklenir. Buna karşın deltayik istif stratigrafilerinde farklılıklar göze çarpar. SCD bir kompleks olarak altta Tortoniyen üstte Pliyosen-Pleyistosen yaşlı deltayik istifler ile temsil edilir ve her iki seviye birbirinden Messiniyen evaporitleri ve devamındaki Zankliyen transgresyonu ile ayrılmaktadır. Nil Deltası'nın Geç Oligosen-Erken Miyosen'de başlayan oluşumu, Messiniyen Krizi sırasındaki çökelmezlik dışında sürekli olarak devam etmiştir.

Doğu Akdeniz'in kuzeyinde tektonizma etkin, güneyinde ise göreceli zayıftır. Dolayısıyla deltaların istif mimarilerini kontrol eden birincil etken tektonizmadır. Tortoniyen, Seyhan-Ceyhan Deltası'nın bulunduğu Anadolu levhasının tektoniğinde önemli bir zaman dilimidir. Paleotektonik sona ermiş ve Neotektonik dönem başlamıştır. Bir başka deyişle Anadolu levhası yükselmiş, Akdeniz bugünkü sınırlarına gerilemiştir. Daha da önemlisi, Adana Havzası Misis Yükselimi ile İskenderun Havzası'ndan ayrılmış ve tektonizma kontrollü depolanma başlamıştır. Yükselen Anadolu ve Toroslar, Seyhan-Ceyhan Deltası için aşım ve kaynak alanı haline gelmiştir. Kuzeyde bu tektonik kontrollü deltayik depolanmaya karşın, güneyde Nil deltasının istifleri göreceli daha serbest depolanma alanı içinde akarsu kontrollü olarak gelişime devam etmiştir. Nil Deltası'nın gelişiminde önemli olan Süveyş Körfezi'nin açılımı Anadolu'daki paleotektonik döneme rastlar ve değerlendirme dışında tutulmuştur.

## METOT

Çalışmada Seyhan-Ceyhan Deltası'nın (SCD) sedimantolojisi ve evrimi bölgede yer alan sismik kayıtlar ve sondaj verileri kullanılarak incelenmiştir. SCD'nin stratigrafisi ve fasiyes çalışmalarında çeşitli yıllarda açılmış olan 4 adet kara sondajı (Adana) ve 2 adet deniz sondajının (Mersin Körfezi) kırıntı verilerinden yararlanılmıştır. Karada açılan kuyular çalışmada kuzeyden itibaren "K" sembolüyle 1'den 4'e kadar numaralandırılarak adlandırılmış, deniz kuyuları için ise "D-1" ve "D-2" sembolleri kullanılmıştır. Kuyu kırıntı örneklerinden yapılan tane boyu dağılım analizleri (K-1), bileşen analizleri (K-1, K-2, K-3) ve log verileri yardımıyla deltanın istif mimarisi kurulmuştur. Ayrıca çalışmada kullanılan tüm kara ve deniz kuyularına ait kırıntı örneklerinden seçilen mollusk kavkıklarıyla (Şekil 1) Pliyo-Kuvaterner istifinde paleo-ortamsal yorum ve biyostratigrafik çalışmalar gerçekleştirilmiştir. Havzanın kara alanında çeşitli yıllarda atılan 2B ve 3B sismik veriler söz konusu istifin havza genelinde kalınlık, yayılım ve tektonizmanın çökel sistemindeki etkilerinin yorumlanmasında kullanılmış, körfezde atılan sismik veriler yardımıyla da yorumlanan bu istifin deltayik seviyeleri belirlenmiştir.

Şekil 1. Sondaj kesitlerinden makro fosillerin seçilerek sınıflandırılması ve tanımlanan türlerle yapılan levha çalışmaları (tanımlama için mollusk kavkıkları seçilmiştir)

## BULGULAR

Adana Havzası'nın tortul dolgusu (Oligosen-Kuvaterner) tüm Akdeniz için anahtar olan Messiniyen evaporitleri ile (Gökkuşu Üyesi) iki büyük kısma ayrılabilir. Havzada ilk deltayik istif stratigrafisi Tortoniyen ile başlar. Buradan, Seyhan-Ceyhan Nehirleri'nin doğuşunu da Tortoniyen olarak düşünmek mümkündür. Akdeniz'in kuruma evresi aynı zamanda yeni bir transgresyonun başlangıcı olup (Zanliyen), aynı zamanda SCD kompleksinin de Tortoniyen yaşlı alt deltayik istifini ve Pliyosen-Pleyistosen yaşlı üst deltayik istifini birbirinden ayırır. Transgresyonun devamında önce Avdan Formasyonu oluşmuş (denizel marnlar) daha sonra dört ayrı delta istifli Pliyo-Kuvaterner'de depolanmıştır (Şekil-2). Bu deltayik istifler dört ayrı 3. derece sekanslar (Şekil 3) olarak görülür ve dört ayrı delta istifinin (=SCDK) toplam kalınlığı 2000 m'yi bulmaktadır. Kuraşa Formasyonu olarak ayrılan tortullar Orta Pliyosen-Pleyistosen yaşlıdır.

Şekil 2. Seyhan-Ceyhan Deltası'nda kara alanında açılan kuyuların G-K yönlü korelasyonunda izlenen

Zankliyen transgresyonu ve paleontoloji verileri yardımıyla belirlenen Pliyo-Kuvaterner istifi, Geze Kalanyuva 2021

Nil Deltası sedimanları üzerinde yapılan incelemeler, Nil Nehri'nin Geç Oligosen (Şattaniyen)'de tortul taşımaya başladığı (nehirin doğusu), deltanın da bu sırada oluşmaya başladığını göstermiştir (Fielding vd. 2018).

Delta prizmasından sekans stratigrafisi kurallarına göre ayrılmış 7 adet 3.derece, 11 adet 4. ve 5. Derece istif ayrılabilmıştır (El Fawal 2016). Bunların 1-6'sı Pliyosen, 7.si Pleyistosen yaşlıdır.

Şekil 3. SCD'nin diyagramatik stratigrafik kesiti, Geze Kalanyuva 2021

SCD ve Nil deltalarının karşılaştırılmasında nehir uzunlukları ve drenaj alanı genişliklerinden ileri gelen farklılık dikkate alınmıştır. Ortaya çıkan sonuç, her iki deltanın gelişiminde Tortoniyen sonunda ve Messiniyen başında uzun süreli kesilmelerin söz konusu olmasıdır (Şekil 4). Tortoniyen sonu kesilmesi erozyon olarak görünürken Messiniyen'deki kesilme (Messiniyen krizi) tüm Akdeniz boyunca yörelere göre farklılık gösteren evaporit çökelişi şeklinde olmuştur (tip lokalitesinde 40 m, Mersin Körfezi'nde tuz domu oluşturduğu alanda 2500 m ölçülmüştür).

Çalışma alanına yer alan sismik kesitlerde evaporit kalınlığı tuz tektoniğinin yörelere göre farklılaşması olarak görünür ve kalın evaporitler deltayık istifte daha belirgin deformasyona yol açmıştır. Öte yandan yüzey çalışmaları ve sismik yorumlarla yapılan çalışmalarda; Misis yükselimi'nin tektonik birim olması yanında bölgeyi etkileyen diğer Ecemiş Fay Zonu, Kozan Fay Zonu, Ölü Deniz Fay Zonu ve daha güneydeki Kıbrıs Yayılı'nın varlığı Anadolu'nun bu bölümünün Akdeniz'in güney kenarına göre daha aktif olduğunu, depolanmanın tektonizmadan çokça etkilendiğini ortaya koymaktadır.

Şekil 4. Nile Delta'sının stratigrafik istifi, Mahmoudi ve Gabr 2009 (original referance; Said 1962, Salem 1976, Rizzini vd. 1978).

## SONUÇLAR

Tektonizmanın depolanmadaki görünür etkisi istiflerin yanal yönde önemli kalınlık değişimi göstermesidir. İkinci dikkat çeken husus, Seyhan-Ceyhan deltası Nil'e kıyasla daha küçük iken, denizel delta istiflerinin kalınlığı yer yer Nil deltasına yakındır. Örneğin, Seyhan-Ceyhan deltasında Geç Miyosen delta istifi (Handere Fm) 600 m, Pliyo-Kuvaterner istifinin toplam kalınlığı ise (deltayık ve deltayık olmayanlar birlikte) (Avdan-Kuraşa Fm) ise 2200 m iken, aynı zaman aralığındaki sediman kalınlıkları Nil'de de yaklaşık aynıdır. Bu durum, tektonizmanın yerel olarak daha fazla tortul getirilmesine yol açtığının göstergesidir. Deniz seviyesi değişimlerinin depolanmaya etkileri bu çalışmada tam olarak ortaya konulamamıştır.

## REFERANSLAR

Geze Kalanyuva, Y. 2021. Tarsus –Seyhan-Ceyhan Delta Kompleksinin Kuvaterner Jeolojisi, Adana GD Türkiye, Doktora Tezi, Ankara Üniversitesi Fen Bilimleri Enstitüsü, 252 s., Ankara.

Ilgar, A., Nemec, W., Hakyemez, A. and Karakuş, E. 2013. Messinian forced regressions in the Adana Basin: a near-coincidence of tectonic and eustatic forcing. Turkish Journal of Earth Sciences, doi:10.3906/yer-1208-3.

Kazancı, N. ve Gürbüz, A. 2012. Kuvaterner Bilimi. Ankara Üniversitesi Yayınları. 570s, Ankara.

Karakuş, E. 2011. Tarsus (Mersin) yöresi Messiniyen (Üst Miyosen) evaporitlerinin sedimentolojisi. Yüksek Lisans Tezi, Ankara Üniversitesi Fen Bilimleri Enstitüsü, 143 s., Ankara.

Kozlu, H. 1987. Structural development and stratigraphy of the Misis–Andirin region. In: Proceedings of the 7th Petroleum Congress of Turkey

Kozlu, H. 1997. Doğu Akdeniz bölgesinde yer alan Neojen basenlerinin (İskenderun, Misis-Andirin) tektono-stratigrafik birimleri ve bunların tektonik gelişimi. PhD, Çukurova University, Adana, Turkey (in Turkish).

Mahmoudi, A.E. and Gabr, A. 2009. Geophysical surveys to investigate the relation between the Quaternary Nile channels and Messiniyen Nile Canyon at East Nile Delta, Egypt. Arab J Geosci 2:53–67, DOI 10.1007/s12517-008-0018-9.

Öğrünç, G. 2001. Messiniyen Tuzluluk Krizi Sırasındaki ve Sonrasındaki Çökellerin Stratigrafisi ve Paleokoşoloji, Bir örnek: Adana Baseni Doktora Tezi. Çukurova Üniversitesi, Fen Bilimleri Enstitüsü, Adana, 218 s

Özgül, N. 1976. Toroslara bazı temel jeoloji özellikleri. Türkiye Jeoloji Kurumu Bülteni 19, 65–78.

Özgül, N. ve Kozlu, H. 1993. Kozan-Feke-Mansurlu arasının jeolojisi: TPAO Rapor No: 3380, Ankara.

Poppe, G. T. and Goto, Y. 1991. European Seashells (Polyplacophora, Caudofoveata, Solenogastrea, Gastropoda). Vol: 1, Wiesbaden/Verlag Christa Hemmen. Pp: 352.

Poppe, G.T. and Goto, Y. 1993. European Seashells (Scaphopoda, Bivalvia, Cephalopoda), Vol: 2, Wiesbaden/Verlag Christa Hemen. Pp: 221

Ryan, B. F. W. and Pitman, C. Walter. 1998. Noah's Flood/ The New Scientific Discoveries About The Event That Changed History. Simon&Schuster. New York NY. (Türkçe tercüme 284 s).

Schmidt G. C. 1961. Stratigraphic Nomenclature For The Adana Region Petroleum District VII. Petroleum Administration Bull., v. 6, pp. 47-63.

Tucker, M. E. 1992. Sedimentary Petrology. Black-Well, Oxford, 260p.

Yıldız Çiftçi, S., Hacıköylü, P., Kalanyuva Geze, Y., Kansu, E and Aktepe, A. 2012. Exploration Plays in the Mersin Basin, Turkish Mediterranean Sea. Leading

Edge, Mediterranean Section, 832-845.

Jaffey, N., Robertson, A.H.F. 2005. Non-marine sedimentation associated with Oligocene–Recent exhumation and uplift of Central Taurus Mountains, S Turkey. *Sedimentary Geology* 173, 53–89.

Erol, O. 2003. Ceyhan Deltasının Jeomorfolojik Evrimi. *Ege Coğrafya Dergisi*. 12(2), 59-81.

Fawal, M.F., Sarhan, A., Collier, E.R., Basal, A. and Abdel, H.M. 2016. Sequence Stratigraphic Evolution on The Post Rift Megasequence in The Northern Parth of the Nile Delta Basin, Egypt. *Arab J Geosci* (2016) 9: 585. DOI 10.1007/s12517-016-2602-8

Comparative Analyses Tectonism on the Development of two Largest Deltas (Nile and Seyhan-Ceyhan) in the Eastern Mediterranean

Nile Delta in the south and Seyhan-Ceyhan Delta in the north are two main active sediment prism of the Eastern Mediterranean Sea. They have been developed continuously since Tortonian under controls of isostatic end tectonic effects. As a matter of fact, Tortonian is a critical time on tectonism of Anatolian plate which also carries the Seyhan-Ceyhan Delta. Paleotectonic stage of Anatolia ended and the Neotectonic stage has begun at that time, the Anatolian plate has started to uplift, and thus the Mediterranean Sea gained more or less its present position. The most important event dealing with northern Mediterranean Sea, the Adana Basin was separated from the İskenderun Basin due to emerging of Misis uplift and the deposition has been developed under control of these events. Following the Anatolian uplift, the Taurus Mountains become sediment sources for the Seyhan-Ceyhan Delta. While such a deltaic deposition continues in the north under the control of tectonics, facies of the Nile Delta in the south have been in occurred by effects of river mechanism relatively in an open depositional area. Rifting of the Gulf of Suez was during the Paleotectonic time Anatolia, therefore it hasn't been considered in this study.

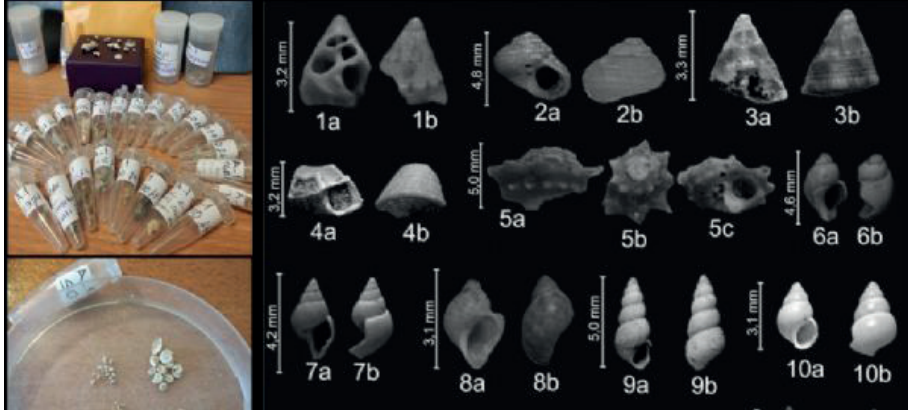
Here, Seyhan-Ceyhan deltaic sequences studied by seismic sections and drilling well data compared with the Nile Delta based on data collected from the literature. The purpose is to define the results of the tectonic effect on delta sequences as the global water level would change parallel at both margins of the same sea. In the delta formation, length of rivers and width of drainage areas are essential which effects on the sediment thickness. Hence, the main comparison was on thicknesses of deltaic sequences. It should be noted that there were discontinuities in development of both deltas at the end of Tortonian and Messinian. While the Late Tortonian discontinuity seems to be done by erosion, Messinian unconformity must be depend on evaporate sedimentation (salinity crisis), resulting different sediment thickness. In some layers evaporates is ca. 40 m, but at domes of Mersin Bay they can reach 2500 m by diapiric deformations.

The apparent effect of tectonism on deposition is the sediment thickness, thus successions can display significant thickness variation in the lateral direction where the tectonism is active. The second point taken

attention is unbalancy between dimension and sediment thickness of two deltas. While Seyhan-Ceyhan delta is highly smaller than the Nile delta, the thickness of its marine sequences are closed to those of the Nile delta in places. For instance while Late Miocene deltaic sequences (Handere Formation) is 600 m and Plio-Quaternary sequence (Kuraşa Fm) is 2200 m in the Seyhan-Ceyhan Delta, the sediment thickness in the same period are approximately the same in the Nile. This may be an indicator for extreme sediment supply provided by the tectonic activity. The effects of sea level changes on deposition couldn't be completely revealed.

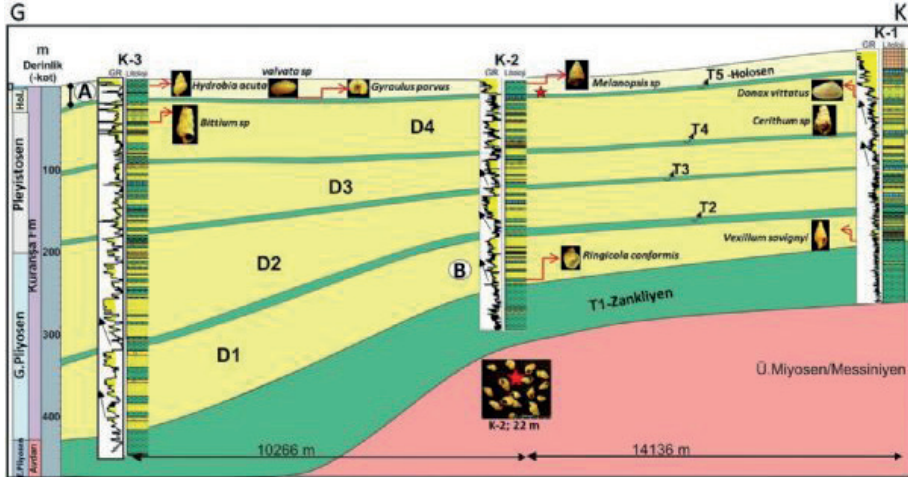
Anahtar Kelimeler: Seyhan-Ceyhan Deltası, Nil Deltası

Şekil 1.



Sondaj kesintilerinden makro fosillerin seçilerek sınıflandırılması ve tanımlanan türlerle yapılan levha çalışmaları (tanımlama için mollusk kavkaları seçilmiştir)

Şekil 2.



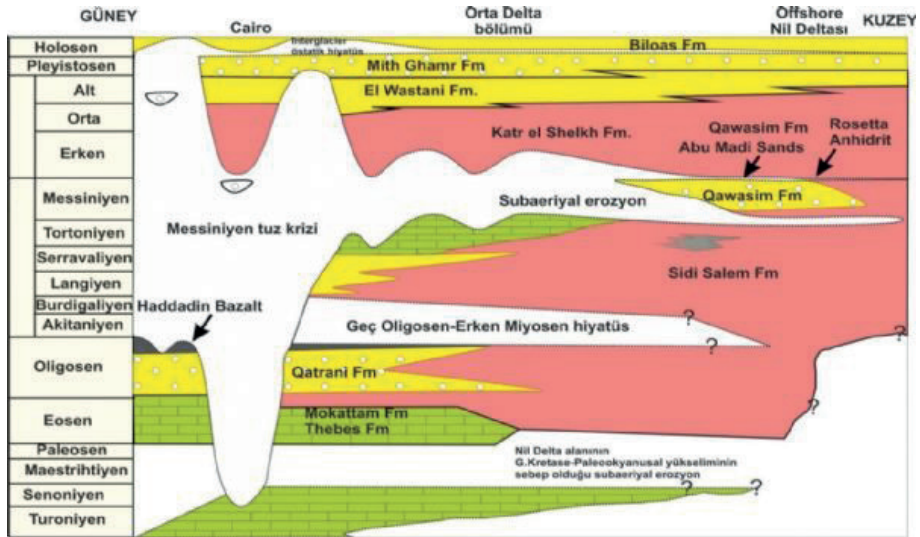
Seyhan-Ceyhan Deltası'nda Zankliyen sonrası istifinin sondaj verileri ve paleontoloji verileriyle korelasyonu; (A: Akarsu ağzı kıyı ortamında yaşayan kavka türleri tanımlanmıştır; B: K-2 ve K-3 sondajlarında Pliyosen kavka türleri tanımlanmıştır), Geze Kalanyuva 2021

Sekil 3.

	Age	3rd order succession	4th order succession	Delta	Formation
Pleistocene	Holocene	karasal			SCD
	Late	5	g	D4	KURANŞA
	Chibanian		f		
	Calabrian	4	e	D3	
	Gelasian	d			
Pliocene	Piacenzian	3	c	D2	
		2	b	D1	
	Zanclean	1	a	1	AVDAN

SCD'nin diyagramatik stratigrafik kesiti, Geze Kalanyuva 2021

Sekil 4.



Nile Delta sının stratigrafik istifi, Mahmoudi ve Gabr 2009 (original reference; Said 1962, Salem 1976, Rizzini vd. 1978).



# Levant ve Herodot Basenleri Stratigrafik Birimlerin Benzerliđi, Sismik Kesit Örnekleri



## Fatih Özdamar

Türkiye Petrolleri Anonim Ortaklığı, Arama Daire Başkanlığı, Ankara / Türkiye

Dođu Akdeniz'in dođu-güneydoğusunda yer alan Levant baseni son yıllarda büyük keşifler ile dikkat çekmektedir. Bu basende kaynak kaya olabilecek seviyelere kadar penetre etmiş çok sayıda sondaj gerçekleştirilmiştir. Basenin paleocoğrafyası, sondaj ve sismik veri setleri modellenerek jeolojik tarihçe birçok yerbilimci tarafından ortaya konmaya çalışılmıştır.

Levant baseninin batısında Herodot baseni yer almaktadır. Bu iki basen Akdeniz denizaltı dađı (Eratosthenes Sea Mount) ile birbirinden ayrılır. Herodot baseni henüz sondaj faaliyetleri ile aranmış durumda değildir. Yalnızca baseninin güney kısmında Kiwi-1 kuyusu açılmıştır. Herodot baseni, 2B sismik verileri değerlendirilmesi sonucunda Levant baseni ile benzer sismik özellikler sergilediđi görülmüştür. Bu benzerlik, iki basenin jeolojik geçmişinin ve hidrokarbon potansiyelinin benzer olabileceđini düşündürmektedir.

Bu çalışmada; Levant, Herodot basenlerini ve Akdeniz denizaltı dađını (Eratosthenes Sea Mount) kapsayan TPAO 2B sismik verileri çalışılarak Levant ve Herodot basenlerinin benzer jeolojik geçmişe sahip olduđu sismik benzeşimleri ile ortaya konmaya çalışılmıştır. Bu sismik veri setleri kullanılarak aynı litolojik formasyonların aynı sismik yansıma karakteri gösterebileceđi değerlendirilmiştir. Sismik veri toplama parametrelerinin farklılıđı, faylar, tuz tektoniđi ve formasyonların içindeki akışkan çeşidi gibi etmenler sismik sinyalde çeşitli sođrulmalar ve genlik artışı-azalışı gibi durumlar ortaya çıkarmaktadır. Yorumlar yapılırken bu bozucu ya da yapıcı etkiler de göz önünde bulundurulmuştur.

The Levant Basin has attracted attention in recent years with major discoveries. Drilling has been carried out in this basin, starting from the seabed and including reservoir rocks and potential source rock levels of the basin. The geological history of the basin has been attempted to be revealed by many geologists by modeling the paleogeography of the basin, drilling and seismic data sets. The Herodotus Basin is located east of the Levant Basin. The Mediterranean submarine mountain (Eratosthenes Sea Mount) is located between the two basins. The Herodot Basin has not yet been explored by drilling activities. There is no well in the basin except the Kiwi-1 well in the southern part of the basin. TPAO seismic data sets cover the Levant and Herodotus basins.

In general, the same lithological formations exhibit the same seismic reflection character. This is because each lithological formation has its own unique acoustic impedance properties. Acoustic impedance is the ability of a material to transmit sound waves. Materials with high acoustic impedance transmit sound waves more effectively and produce stronger reflections.

The Levant Basin, where major hydrocarbon discoveries are made in the Eastern Mediterranean, also extends into the borders of the TRNC-TPAO partnership licenses. The seismic data sets of the Herodotus Basin sedimentary successions, which are included in the licenses of the Republic of Türkiye, and the Levant Basin analogy are mentioned in the present study.

Anahtar Kelimeler: Sismik Yansıma, Stratigrafi





**Petrol Endüstrisi'nde Dijitalleşme ve Teknolojik  
Gelişmeler**

*Digitalization and Technological Developments in  
Petroleum Industry*

---



# Development of a Pore-to-Grid Digital Twin and Software Ecosystem: A Case Study for Sakarya Gas Field Development Project



**Mehmet Cicek, Nuri Demirdoven**

Turkish Petroleum Offshore Technology Center

## 1. INTRODUCTION

The Sakarya Gas Field is a gas reservoir in the Turkish Exclusive Economical Zone of the Black Sea at a water depth of around 2100 m. It is developed via subsea tie-back to an onshore processing facility located more than 170 km away, where it will connect to the national gas grid. This design creates some challenges in engineering, offshore operations and asset operations.

This paper focuses on an integrated Digital Twin and software ecosystem, “ZEKI”, developed by TP-OTC Digital & Analytics Department. With its integrated software and workflow stack, ZEKI aims 1 – to act as a Decision Support System, 2 – to manage risks; and 3 – to be the single source of truth.

## 2. ZEKI ECOSYSTEM

### 2.1. Challenges and Answers to those Challenges

Sakarya Gas Field Development (GFD) project is developed with 170 km subsea tie-back with depth of around 2100 m. This ultra-deep tie-back creates flow assurance challenges such as slugging, water-breakthrough, hydrate formation. These challenges are addressed by Process Twin (ProductionX, PX) software. With this, what-if scenarios and high-level optimizations in production parameters are also made possible.

After exploration of Sakarya Gas Field, engineering studies have started. During this phase a large team is involved and engineering data was started to be produced from different resources. To ensure engineering consistency, a central and robust engineering data management software is used. This software, ZEKI EngineeringX (EX) does not only hold the data and documents (1D/2D/3D, P&IDs, datasheets, CAD models, etc.), but also helped different parties to communicate and mature the documents in a central way. This tool also covers an Asset Information Management System (AIMS) need of the company. This software also holds data based on Capital Facilities Information Handover Specification (CFIHOS) for each tagged item.

Due to large geospatial coverage, no conventional AIMS solution would be applicable to Sakarya GFD project, thus a Geographical Information System (GIS) - based software, called ZEKI GISX (GX) was developed. In addition to many other data types, this software also holds data based on Pipeline Open Data Standard (PODS) for each section of the pipelines.

In such a project many vessels work simultaneously in the project area for many different operation types such as drilling, completion, pipe-lay, subsea construction, and logistics. A proprietary antenna system built in

Filyos Onshore Processing Facility (OPF) collects real-time vessel position and status data and feed this data to ZEKI GX software for monitoring. Remote Operating Vessel (ROV) operation recordings are also available within ZEKI GX.

Operation and maintenance (O&M) phase of the project holds many chances for optimization. Due to the fact that, Sakarya Enterprise Resource Planning (ERP) system is integrated and built in tandem with ZEKI.

Managing the data and business workflow also helped to have a central performance management software (ZEKI DashboardX, DX) and many dashboards in different levels.

### 2.2. Components of ZEKI

ZEKI is composed of 14+ software components currently. All these separate components are integrated with each other. The entire ZEKI ecosystem is also integrated with many other major (like ERP) and minor systems.

ZEKI is highly

- Scalable: can be used for new geographical areas, new engineering disciplines, new user groups, etc.
- Extendable: new use cases can be developed; and
- Agnostic: agnostic to data, agnostic to workflows, agnostic to technologies, etc.

### 2.3. Software Technologies

Web technologies are used whenever (mostly) applicable. API technologies are used extensively. User Interface and User Experience (UI/UX) and performance domains are the top most priority, thus applicable tools and methodologies are selected.

### 2.4. Project and Product Management

Suitably to the pace and ambition in overall Sakarya GFD project, Agile and Scrum methodologies are put in use in software development. Current state of ZEKI and overall Digital maturity are reached in 2.5 years.

## 3. LOOKING FUTURE

### 3.1. Innovation

There will be new technologies and new software products within ZEKI ecosystem. Some examples might be:

- a. Integrated Operator Training Simulator (OTS): This will be a full-field integrity solution as well; where

result of any action would be simulated and monitored.

b. AI-Hybrid Reservoir Simulation: This is an accelerator for conventional reservoir simulators using Machine Learning (ML) methodologies.

c. Robotic Inspection: Repetitive tasks can be automated with robotic solutions. Also, this increases the occupational safety in some duties.

d. Central ML/ Center of ML: This is a central repository to host and run ML models; and an environment for users to reach and play with their own data.

e. Predictive Maintenance: Based on the real-time sensor data and historical failure records, assets will be monitored and a failure will be detected even before it happens.

f. Maintenance Planning & Inventory Optimization: Having the integration with ERP system and predictive maintenance capabilities, maintenance planning and inventory optimization will be possible.

g. Short/Mid-term Production Parameter Optimization: Based on real-time sensor data, physical model and integrated data-flow and workflows, gas production will be able to optimized for short- and mid-term within ZEKI ecosystem.

### 3.2. Diffusion

Software products and use cases will be spread to a larger body of users. With this, users would be able to leverage inter- and intra-connectivity of ZEKI and analytic capabilities to build by themselves.

a. Citizen Developers: A Low-code Application Platform (LCAP) for variety of users to develop their own applications with drag-and-drop capabilities.

b. Citizen Data Scientists: A low-code data analysis environment for ML models to be trained, hosted and run for variety of users to develop their own ML models with drag-and-drop capabilities.

### 3.3. Expansion

New content will be added to software in ZEKI, so that ZEKI will have more use cases. For example, ZEKI Virtual Sakarya (VX) can be used for orientation or for some trainings with appropriate content in it.

## 4. CONCLUSION

The development of the Pore-to-Grid Digital Twin and Software Ecosystem, known as “ZEKI,” has been a crucial endeavor for addressing the engineering, offshore, and asset operations challenges faced in the development of the Sakarya Gas Field Development Project.

Due to design principles and architectural decisions, ZEKI will be applicable to new project phases and uses cases as the commitment in development continues. With this, ZEKI will serve for faster and robust decisions, lower overall risks and optimum parameters for variety of activities.

# Architecting a Big Data Platform for the Oil and Gas Industry: The Dijital TPAO Project



**Muhsin Gürel, Adil Cem Albayrak, Resul Kayım**  
Türkiye Petrolleri Anonim Ortaklığı, Ankara / Türkiye

## PROBLEM STATEMENT

The Oil and Gas industry, where large companies such as TPAO, produces vast and varied data from sources like seismic surveys, drilling logs, production data, maintenance records, and field surveys. However, managing, processing, and analyzing this data is a significant challenge due to its complexity and heterogeneity. The problem addressed in the context of the “Dijital TPAO” project is: How can we effectively utilize a comprehensive big data platform to manage, process, and draw insightful conclusions from the data generated in the Oil and Gas industry, specifically at TPAO?

## MOTIVATION / RELEVANCE

The motivation behind the “Dijital TPAO” project is the potential for vast improvements in cost savings, efficiency, safety, and decision-making if the data can be efficiently harnessed for actionable insights. Currently, the industry faces considerable challenges in managing and processing the immense volume of data. The development and implementation of a big data platform could revolutionize exploration, production, and decision-making processes, potentially fast-tracking TPAO’s digital transformation.

## THEORETICAL FRAMEWORK

The theoretical foundation of the “Dijital TPAO” project is rooted in principles from software frameworks, big data, and analytics. The comprehensive architecture for the big data platform also incorporates elements like large storage systems, parallel processing, sophisticated analytics, and machine learning models. The theoretical framework also acknowledges the need for sound data governance and security practices and the applications of machine learning and AI in predictive analytics, anomaly detection, and decision support.

## METHOD

Within the context of the “Dijital TPAO” project, we propose and implement a comprehensive big data platform architecture specifically tailored for TPAO and, more broadly, the Oil and Gas industry. This architecture integrates cutting-edge technologies and facilitates efficient data ingestion from various sources, data processing and transformation, data storage, and complex analytics tasks. It caters to both structured and unstructured data types and uses machine learning and artificial intelligence algorithms for complex tasks.

## RESULTS

The “Dijital TPAO” project’s big data platform effectively addresses TPAO’s unique data management needs, offering a robust, scalable, and flexible solution that can accommodate future growth and technological advancements. The implementation of this platform could be transformative for TPAO, enabling more efficient and effective exploration, production, and decision-making processes. In addition, the platform’s security measures and data governance protocols assure safe and effective data management practices.

## CONCLUSION

Through the implementation of the “Dijital TPAO” project, this study demonstrates that a big data platform can effectively address the inherent challenges of data management in the Oil and Gas industry, as exemplified by TPAO. The proposed architecture provides a model for a platform that efficiently manages and processes extensive data and facilitates data-driven decision-making. This platform significantly contributes to TPAO’s digital transformation.

Keywords: Big Data Platform, Artificial Intelligence

# An Integrated GIS-based Asset Information Management System: ZEKI GX & ZEKI EX

**Yavuz Gultekin, Mehmet Cicek**

Turkish Petroleum Offshore Technology Center



## 1. INTRODUCTION

The Sakarya Gas field is located in the Turkish sector of the Black Sea at a water depth of around 2100 m. It is planned to be developed via subsea development tied back to an onshore processing facility located more than 170 km away, where it will connect to the national gas grid. The main challenges facing the project include water breakthrough from intermediate reservoir layers, hydrate formation, slugging, and a wide operating envelope through the life of the field.

This study presents two software products from “ZEKI” digital twin and software ecosystem developed by TP-OTC Digital & Analytics Department. The first software to focus on is ZEKI EX (EngineeringX) and the second one is ZEKI GX (GISX) as given below. Both software, as all other software in ZEKI ecosystem, are integrated with each other. ZEKI EX and ZEKI GX complete each other creating a Geographical Information Systems (GIS)-based Asset Information Management System (AIMS) for Sakarya Gas Field Development Project.

## 2. ZEKI EX

ZEKI EX is a web-based information management software that is integrated with other software of ZEKI, where engineering documents and data are managed, updated and their relations with assets are displayed. It shows 1D engineering data, 2D engineering drawings and 3D models in relationship with each other, manages the engineering workflows, and acts as the “single source of truth” with easy and fast access to most up-to-date information for engineering and operational activities.

Its unique strength lies in its ability to showcase complex relationships between assets and associated documents through intuitive visualizations. This feature empowers users to understand the connections between equipment, processes, and documentation, facilitating efficient decision-making and problem-solving. Alongside engineering activities, it provides field operators an improved way of working.

Based on CFIHOS (Capital Facilities Information Handover Standard), ZEKI EX contributes to the creation of 1D, 2D and 3D documents produced in engineering studies, strengthens integrity with data capture feature, helps increasing the quality of engineering documents, measures project performance and reveals true status of data handover processes. Compliant with the CFIHOS international standard, ZEKI EX uses data within the digital twin to provide value-added business processes spanning the entire plant lifecycle, increasing project and operational efficiency while reducing risk.

In addition to all these features, ZEKI EX ensures that communications are immediate, everyone is working

on the same “single source of truth,” and all actions are recorded, traceable, reportable and it is designed to make finding information easy and intuitive.

## 3. ZEKI GX

ZEKI GX is a digital twin platform that enables the meaningful and seamless integration of various data types from different data sources, making use of the Geographical Information Systems infrastructure. The software uses state-of-the-art data processing algorithms to collate, validate and organize asset information, ensuring company-wide data integrity and accuracy.

Wide areal coverage of Sakarya Gas Field Development project creates need for a GIS-based software with advanced search function to use the area from the subsea production facility to the onshore gas processing facility and a large number of data sources covering this region.

ZEKI GX hosts and serve a wide range of data types for a large area. Some data types include bathymetry, geohazard and orthophoto data from surveying studies to include the current project site and future phases, 3D models of all assets from subsea production facility to onshore processing facility, data according to Pipeline Open Data Standard (PODS), real-time data received from proprietary antenna system, real-time sensor readings, among many others.

Some of the other features ZEKI GX have can be mentioned as simultaneous operations for offshore (SIMOPS), valve status management, people and vehicle tracking, heatmap for reports and planned activity mapping throughout the entire project area, etc.

## 4. INTER- AND INTRA-INTEGRATION OF ZEKI SOFTWARE COMPONENTS

ZEKI ecosystem is integrated with Sakarya Enterprise Resource Planning (ERP) systems, other data warehouses and engineering tools. It can display variety of data sources which belong to the project spreading over a large area in one screen, and it provides convenience to planning and workflows.

It shortens the time of accessing information and helps to increase work efficiency. The software’s advanced capabilities provide real-time monitoring of asset data, enabling users to detect anomalies, track changes, and set up alerts for critical events. This proactive approach ensures timely responses to potential issues, minimizing downtime and maximizing asset performance.



## 5. CONCLUSION

ZEKI digital twin and software ecosystem consists of many components and two of those components are used together to create a robust and innovation solution for “GIS-based AIMS” need Sakarya GFD project has.

With these tools, asset data, all communications related to engineering studies and documents, and engineering management of change are all managed, orchestrated and recorded centrally. All data is presented to its users from one environment making it very easy to reach data and give better decisions for operators and engineers.

Keywords: Asset Information Management System, GIS

# Autonomous Corrosion and Scale Management for ESP Wells

**Dana Kayshibaeva, Michael Van Spankeren**  
SLB, Houston



## OBJECTIVES

Producers spend considerable OPEX managing risks associated with corrosion and scale. Monitoring and chemical intervention workflows are typically manual, and performed at low frequencies, leading to delays in event detection, and increasing potential for well failures. This project's scope integrates chemistry domain experience with edge analytics, modeling, and intelligent equipment, to transform manual processes into an autonomous solution. The goal is to optimize operations, reduce well failures and workover costs, and maximize production.

## METHODS, PROCEDURES, PROCESS

This solution is currently deployed in an oilfield, that has been historically challenged with high numbers of ESP failures due to corrosion and scale, resulting in significant production losses and unforeseen workover costs. The digital architecture supports autonomous management of scale and corrosion through remote monitoring and automated chemical injection. Real-time data is acquired from connected equipment, processed in an edge device running artificial intelligence, and autonomously sent to chemical pumps. Data from sensors, connected devices, and models are visualized in cloud applications, or integrated into existing client systems for end user analysis and full visibility of the entire process.

## RESULTS

Improving chemical injection precision through real-time monitoring and control is the driver for this solution. After 3 months, actual injection rate vs target injection rate compliance increased from 60 to 99%, ensuring continuously optimized treatment.

Typically, manual workflows performed monthly, now run in real-time, enabling quick detection of system changes, and resulting in a 99% reduction of elapsed time between risk detection and chemical intervention.

Real-time predictive models for virtual flow metering and scale prediction, when validated against manual methods, produced results within 3% and required no manual intervention. This optimizes chemical injection and will ultimately lead to a reduced number of failures. The new system has been in place for 18 months, and ESPs that were previously failing every 6 months on average continue operating flawlessly.

System uptime achieved 97%, providing full visibility into performance, maintaining continuous protection of the system, and maximizing production uptime.

This solution also resulted in a 75% reduction in carbon footprint and limited exposure to safety risks, due to a

minimization of required trips to the field.

Early economic feasibility analysis shows that by investing in this real-time system and reducing corrosion and scale related failures by just 10% per year, this customer would recover 100% of their investment in the first year, and more than 1000% in less than 5 years.

## CONCLUSION

Although chemical inventory and rate management have been automated in the past, this fully autonomous corrosion and scale control system is a first in the industry. Results support the theory that traditional infrequent and manual monitoring methods may seem less expensive upfront, in fact investing in a digitally enabled real-time corrosion and scale control system may well prove to be a more effective approach, when looking at achieving sustainability targets, and reducing total cost of operations.

Keywords: autonomous chemical injection, corrosion

# Mobil&Web Tabanlı Jeolojik Numune Toplama ve Saha Planlama Sistemi



**Tünay Öztürk**

TPAO, CBS Müdürlüğü, Ankara / Türkiye

## ÖZ

Mobil ve web tabanlı jeolojik numune toplama ve saha planlama sistemi, Coğrafi Bilgi Sistemi (CBS) prensipleriyle entegre bir şekilde tasarlanmıştır. Bu sistem sayesinde saha ekipleri sahadada daha verimli çalışabilir, verileri hızlı ve doğru bir şekilde toplayabilir, analiz edebilir ve paylaşabilir. Sistem, mobil saha uygulaması, web uygulaması ve bir saha planlama dashboard uygulamasını içermektedir.

Mobil saha uygulaması, saha ekiplerinin jeolojik numuneleri toplamasını ve kritik bilgileri kaydetmelerini sağlar. Ayrıca, coğrafi haritalarla etkileşime geçerek konum bilgilerini elde edebilme imkanı sunar. GPS entegrasyonu ile numune noktalarının coğrafi koordinatları otomatik olarak kaydedilir ve özelleştirilmiş domain sub-type özellikleri kullanılarak detaylı bilgiler girilebilir. Web uygulaması sayesinde toplanan veriler merkezi olarak yönetilebilir ve düzenlenebilir. Numunelerin detayları ve saha ekibinin bilgileri bir veritabanında tutulur, bu da takip, analiz ve raporlama süreçlerini kolaylaştırır. Saha planlama dashboard uygulaması ile saha çalışmaları izlenebilir, coğrafi konumlar harita üzerinde gösterilebilir ve ilerleme analizleri yapılabilir.

Bu entegre CBS sistemi sayesinde saha ekipleri, saha çalışmalarını daha verimli ve etkili bir şekilde yönetebilir. Verilerin güvenliği ve kimlik doğrulama Active Directory entegrasyonu ile sağlanırken, kullanıcı dostu arayüzler ve analitik araçlar sayesinde veri analizi ve raporlama kolaylaşır. Sonuç olarak, bu sistemin kullanımı jeolojik saha çalışmalarını daha verimli hale getirirken, veri güvenliğini ve işbirliğini de destekler.

The Mobile and Web-Based Geological Sample Collection and Field Planning System has been designed in integration with Geographic Information System (GIS) principles. This system enables field teams to work more efficiently in the field, collecting, analyzing, and sharing data quickly and accurately. The system comprises a mobile field application, a web application, and a field planning dashboard application.

The mobile field application facilitates the collection of geological samples and the recording of critical information by field teams. Moreover, it allows interaction with geographical maps to obtain location information. GPS integration automatically records the geographical coordinates of sample points, and detailed information can be entered using customized domain sub-type features. Through the web application, collected data can be centrally managed and edited. Details of samples and field team information are stored in a database, facilitating tracking, analysis, and reporting processes. The field planning dashboard application enables the tracking of fieldwork, display of

geographical locations on maps, and progress analysis.

Thanks to this integrated GIS system, field teams can manage fieldwork more efficiently and effectively. Data security and authentication are ensured through Active Directory integration, while user-friendly interfaces and analytical tools facilitate data analysis and reporting. In conclusion, the utilization of this system enhances the efficiency of geological fieldwork and supports data security and collaboration.

## GİRİŞ

Jeolojik çalışmalar ve numune toplama süreçleri, genellikle saha ekiplerinin çeşitli alanlarda veri toplamasını ve analiz etmesini içerir. Bu süreçlerde, verilerin etkin bir şekilde toplanması, doğru şekilde kaydedilmesi ve sonrasında analiz için kullanılabilir hale getirilmesi kritik öneme sahiptir. Bu nedenle, sahadaki ekiplerin verileri hızlı ve güvenilir bir şekilde toplamasını, yönetmesini ve paylaşmasını sağlayacak bir jeolojik numune toplama ve saha planlama sistemi geliştirilmiştir.

Mobil ve web tabanlı jeolojik numune toplama ve saha planlama sistemi, jeologların saha çalışmalarını daha etkili ve verimli bir şekilde yürütmelerine yardımcı olmak amacıyla tasarlanmış bir entegre bir Coğrafi Bilgi Sistemini ifade eder. Bu tür bir sistem, sahadada çalışan jeologların saha çalışmalarını daha iyi organize etmelerine, verileri daha hızlı ve doğru bir şekilde toplamalarına, analiz etmelerine ve paylaşımlarına imkan tanımaktadır.

Söz konusu web tabanlı jeolojik numune toplama ve saha planlama sistemi aşağıdaki temel özelliklere sahip olacak şekilde ESRI altyapısı kullanılarak planlanmıştır.

## MOBİL VE WEB TABANLI JEOLJİK NUMUNE TOPLAMA VE SAHA PLANLAMA SİSTEMİ

Mobil Saha Uygulaması: Bu çalışmada, ESRI tabanlı mobil saha uygulaması geliştirilmiştir. Uygulama, saha ekibinin jeolojik numuneleri toplamasını ve bu numunelere ilişkin kritik bilgileri kaydetmesini kolaylaştırır. Mobil uygulama, kullanıcıların kuyu, sismik, jeoloji ve topografik haritaları istedikleri gibi düzenleyerek saha uygulamasına eklemelerine izin verir. Kullanıcılar, saha çalışmalarını daha iyi planlamak için altlık haritalarıyla etkileşimde bulunabilir ve coğrafi konum bilgilerini kolayca alabilir.

Mobil uygulama aynı zamanda, numune noktalarını doğrudan yerinde işaretlemek ve bu noktaların coğrafi koordinatlarını otomatik olarak eklemek için GPS entegrasyonu kullanır. Kullanıcılar, numuneye ilişkin detaylı bilgileri görmek için özelleştirilmiş domain

sub-type özelliklerini kullanabilirler. Numunenin türü, toplama tarihi, numuneleyen kişi ve diğer ilgili bilgiler, saha ekibi tarafından kolayca kaydedilebilir. Ayrıca, uygulama numune noktalarıyla ilişkilendirilen fotoğrafların çekilmesini ve bu fotoğrafların direkt olarak numune kaydına eklenmesini de sağlar.

Web Uygulaması: Numune toplama ve saha planlama süreçleri sadece mobil uygulama ile sınırlı değildir. Bu nedenle, geliştirilen sistem, verilerin merkezi olarak yönetilebilmesi ve düzenlenebilmesi için bir web uygulaması içerir. Web uygulaması, saha ekibinin topladığı verilere erişim sağlar ve gerektiğinde düzenlemeler yapmalarına olanak tanır. Numunelerin kim tarafından toplandığını, toplandığı tarihi, koordinatlarını ve diğer bilgileri içeren bir veritabanı oluşturulur. Bu veritabanı, saha ekibinin çalışmalarını takip etmesine, verileri analiz etmesine ve raporlamasına yardımcı olur.

### DASHBOARD UYGULAMASI

Son olarak, geliştirilen sistemde bir saha planlama dashboard uygulaması da bulunmaktadır. Bu uygulama, saha ekibinin çalışmalarını izlemek ve analiz etmek için kullanıcı dostu bir arayüz sunar. Dashboard, numunelerin toplandığı coğrafi konumları harita üzerinde gösterir, saha çalışmalarını zaman çizelgeleri ve grafiklerle görselleştirir ve ilerlemeyi takip etmek için faydalı analitik araçlar sağlar.

### Tasarlanan entegre CBS sayesinde elde edilecek avantajlar aşağıda sıralanmıştır:

1. Saha Planlama ve Organizasyon: Jeologlar, saha çalışmalarını sahaya çıkmadan önce ofiste planlayabilir, çalışma bölgelerini haritalarda işaretleyebilir ve saha ekiplerini koordine edebilir.

1. Numune Toplama ve Veri Kaydı: Jeolojik numunelerin türlerine göre veri girişi yapılabilir, numune toplama noktaları koordinatları kaydedilebilir ve numunelere ilişkin saha çalışması öncesinde saha ekiplerince tutulması planlanan fiziksel özellikleri kaydedilebilir.

2. Fotoğraf ve Not Ekleme: Saha çalışması sırasında çekilen fotoğraflar, raporlar ve açıklayıcı notlar sistem içerisine yüklenebilir. Tüm bu veriler numunelerle ilişkilendirilebilir.

3. Veri Analizi ve Çıkarımlar: Toplanan veriler otomatik olarak analiz edilebilir, jeolojik özellikler çıkarılabilir ve elde edilen sonuçlar grafikler veya raporlar şeklinde sunulabilir.

4. Veri Paylaşımı ve İşbirliği İmkânı: Sistem, farklı kullanıcıların verilere erişim sağlamasına olanak tanımaktadır. Daha sonra yapılacak saha çalışmalarında önceki çalışmalarda toplanan numune noktaları referans olarak da kullanılabilir.

5. Coğrafi Haritalama ve CBS Entegrasyonu: Saha çalışmaları haritalar üzerinde gösterilirken, çalışma alanındaki coğrafi veriler sisteme entegre edilerek Coğrafi Bilgi Teknolojilerinin özelliklerinden faydalanılabilir.

6. Mobil Kullanım Kolaylığı: Saha jeolojisi çalışmaları sırasında mobil cihazlar üzerinden erişim sağlanan kullanıcı dostu bir arayüz sunulur.

7. Veri Güvenliği ve Kimlik Doğrulama: Toplanan verilerin güvenliği ve gizliliği sağlanabilir, bunun yanı sıra yetkilendirme ve kimlik doğrulama mekanizmaları da sisteme entegre edilebilir. Kullanıcıların uygulamaya erişimi, Active Directory üzerindeki kimlik bilgileri ve yetkilendirme mekanizmalarının kullanılması yoluyla gerçekleştirilmektedir. Active Directory, kullanıcı kimlik doğrulama süreçlerini merkezi olarak yöneterek, yetkilendirme kontrollerini etkin bir şekilde uygular ve ayrıcalıklı erişim haklarını düzenler. Bu, organizasyonların bilgi güvenliğini artırmalarına, kullanıcı yönetimini kolaylaştırmalarına ve erişim denetimini sağlamalarına yardımcı olur. Kullanıcı girişlerinin Active Directory üzerinden yönetimi, veri bütünlüğünü koruma, izlenebilirliği artırma ve sistem erişimini merkezi bir yaklaşımla yönetme gibi birçok katkı sağlar.

8. Raporlama ve Sunum Hazırlama Kolaylığı: Sistem, saha çalışmalarının sonuçlarını içeren raporları veya sunumları hazırlamayı kolaylaştırabilir, böylece elde edilen verilerin anlamlı bir şekilde sunumu kolaylaşabilir.

### SONUÇ

Bu çalışmada, jeolojik numune toplama ve saha planlama süreçlerini kolaylaştıran entegre bir sistem tanıtılmıştır. Mobil uygulama, verilerin sahadan hızlı bir şekilde toplanmasını sağlar. Web uygulaması, verilerin merkezi olarak yönetilmesini ve saha çalışanlarının toplanan verileri ofiste düzenleyebilmesini kolaylaştırır. Dashboard uygulaması ise yöneticilere saha çalışmasını ve toplanan verileri analiz etme ve raporlama imkânı sunar. Bu entegre sistem, jeolojik saha çalışmalarını daha verimli ve etkili hale getirecek, saha çalışmalarının daha iyi yönetilmesine katkı sağlar.

Anahtar Kelimeler: CBS, Dijitalleştirme

# Some Useful Applications of Whole-Core CT Scanning

**İbrahim Olgun Uğurlu**

Turkish Petroleum Corporation, Ankara, TP R&D Center/Sedimentology&Reservoir Geology Department



X-ray CT (computed tomography) imaging is a powerful nondestructive technique used in the oil industry to evaluate internal structures of cores (Al-Owihan et. al, 2014). The produced images help preview core tubes for core plug selection, determine bulk density, percent (%) of vuggy pores in vuggy carbonate reservoirs, identify lithology variation along the core tube (detection of formation boundary), sedimentary structures, stylolites and fractures; and they help generate mean CT numbers and heterogeneity logs (Figures 1, 2, 3, 4, and 5) The CT scanning system used in this study is a fourth generation medical CT scanner (Figure 6) that can produce continuous whole-core scans at 0.5 mm (500 micron) spacing and derive bulk density and effective atomic number (Zeff) logs along the core interval (Figure 7). Pre-processing, segmentation and digital rock physics calculations are performed using whole-core CT scan to generate quantitative CT data. The high resolution 3D CT images improved the sedimentological descriptions and the quantitative data derived from the X-Ray CT improved the detection of density and mineralogical changes along the scanned core intervals. Single-mineralogy (carbonate cores) and multiple mineralogy (clastic cores) reservoirs are used in order to determine the effect of facies&lithology changes on the CT numbers. The results indicates that visual examination of cores leads to random core sampling and it is insufficient for detailed core characterization. CT imaging provides significant data for selection of core plug samples for highly heterogeneous reservoirs and its ability to scan cores in preserved conditions (aluminium sleeved+waxed preserved cores) is extremely useful for cores that need to be tested without compromising their wettability states. Additionally, the CT scan data not only provides information about core heterogeneity along the scanned core interval but also produces high resolution images to view fractures, stylolites and sedimentary structures.

## INTRODUCTION

The full characterization of cored intervals is often overlooked and random core sampling is usually acquired for critical core analysis measurements. This can lead to unrepresentative selection of the core samples and raises questions about the effectiveness of the core data in the reservoir model and its calibration (Dernaika et. al, 2015). Traditional laboratory measurements may not produce reliable results for every testing condition or every type of reservoir rock and hence the continued development of laboratory methods is required to help characterize and understand challenging reservoir behaviors (Dernaika et., al, 2010, Serag et. al, 2010). Recently, digital imaging technology has been extensively used in the oil industry to obtain fast and reliable core data from reservoir rock samples.

The Digital Rock Analysis (DRA) technology has made a strong contribution to reservoir core characterization through the application of Dual Energy X-Ray CT Scanning (Siddiqui and Khamees, 2004, Walls and Armbruster, 2012, Al Ohiwan et. al, 2014).

In this study, carbonate and clastic core samples (a total of 30 m) were CT scanned to see the mineralogical effects on the CT data and some useful applications of Dual Energy whole-core ct scanning are illustrated.

## METHODOLOGY

The whole core CT data used in this study was acquired using a fourth generation medical CT scanner (Figure 6). The cores were imaged by the Dual Energy technique, and the bulk density and Zeff were calculated in each slice at 0.5 mm spacing along the core lengths. The Dual Energy technique provides two distinct 3D images by using a high-and a low- energy settings. The high energy images are more sensitive to bulk density and the low energy setting images are more sensitive to mineralogy.

## SUMMARY AND CONCLUSION

- DECT provides crucial data for representative selection of core plug samples to characterize heterogeneous reservoirs where visual inspection of cores proves insufficient.
- Dual energy CT (DECT) scanning is a fast, powerful, and non-destructive tool for characterization of reservoir core intervals identify mineralogy variations along reservoir core lengths without compromising their wettability states.
- DECT derived bulk density can be compared with wireline bulk density (RHOB).
- DECT improves sedimentological description of cores, detection of fractures, stylolites, and formation boundaries.
- CT textures can help identify facies changes in a single mineralogy reservoir.
- Percentage of vuggy porosity (%) can be calculated using CT image sin vuggy carbonate reservoirs.

## REFERENCES

Al-Owihan, H., Al-Wadi, M., Thakur, S., Behbehani, S., Al-Jabari, N., Dernaika, M. and Koronfol, S., (2014), "AdvancedRock Characterization by Dual-Energy CT Imaging: A Novel Method for Complex Reservoir Evaluation" paper IPTC17625 presented at the International Petroleum Technology Conference held in Doha, Qatar, 20-22 January.

Dernaika, M.R., (2010), "Combined Capillary Pressure and Resistivity Index Measurements in Tight Gas Sands Using Vapor Desorption Method", paper SPE 132097 presented at the SPE Deep Gas Conference and Exhibition held in Manama, Bahrain, 24–26 January.

Dernaika, M. R., Naseer Uddin, Y., Koronfol, S., Al Jallad, O., Sinclair, G. (2015) "Multi-Scale Rock Analysis for Improved Characterization of Complex Carbonates" SCA2015-034

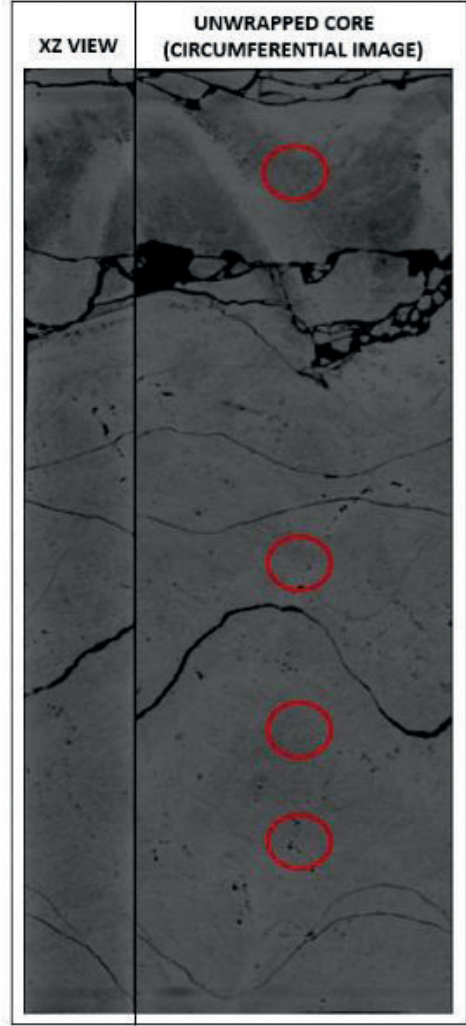
Serag El Din, S. Dernaika, M.R. Al Hosani, I., Hannon, L., Skjæveland, S.M. and Kalam, M. Z., (2010), "Whole Core Versus Plugs: Integrating Log and Core Data to Decrease Uncertainty in Petrophysical Interpretation and STOIP Calculations", paper SPE 137679 presented at the Abu Dhabi International Petroleum Exhibition & Conference held in Abu Dhabi, UAE, 1–4 November.

Siddiqui, S., Khamees, A.A. (2004) "Dual-Energy CT-Scanning Applications in Rock Characterization" SPE-90520-MS presented at the SPE Annual Technical Conference and Exhibition, 26-29 September, Houston, Texas.

Walls, J., Armbruster, M., (2012), "Shale Reservoir Evaluation Improved by Dual Energy X-Ray CT Imaging" Technology Update. JPT, November.

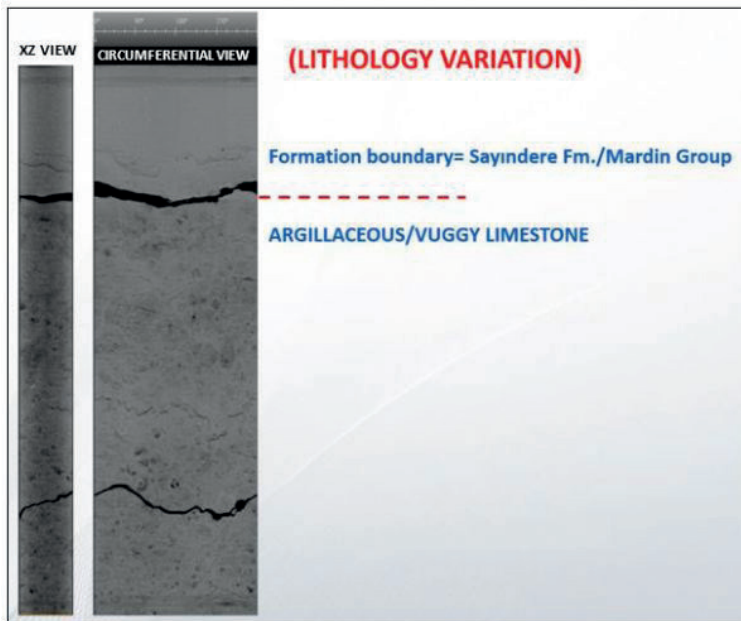
Keywords: computed tomography, digital rock physics

Figure 1.



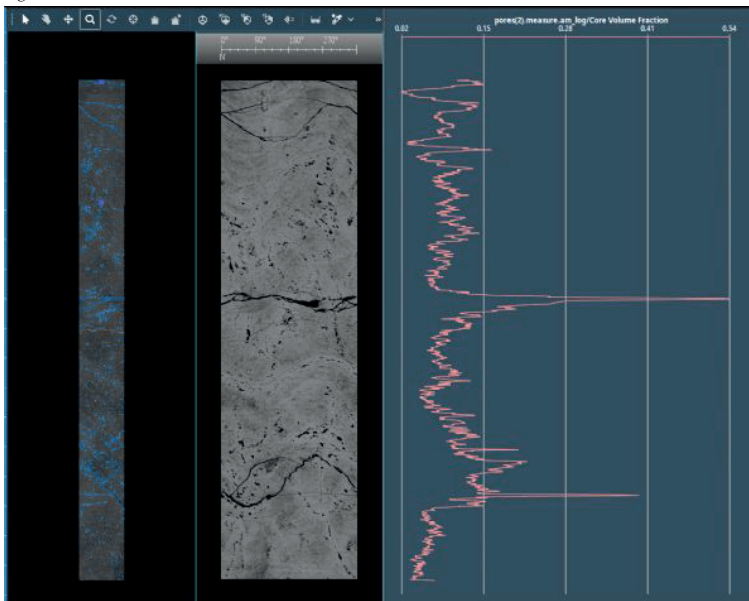
Core plug sampling of a scanned carbonate core sample based on the CT image (red circles showing selected core plug locations)

Figure 2.



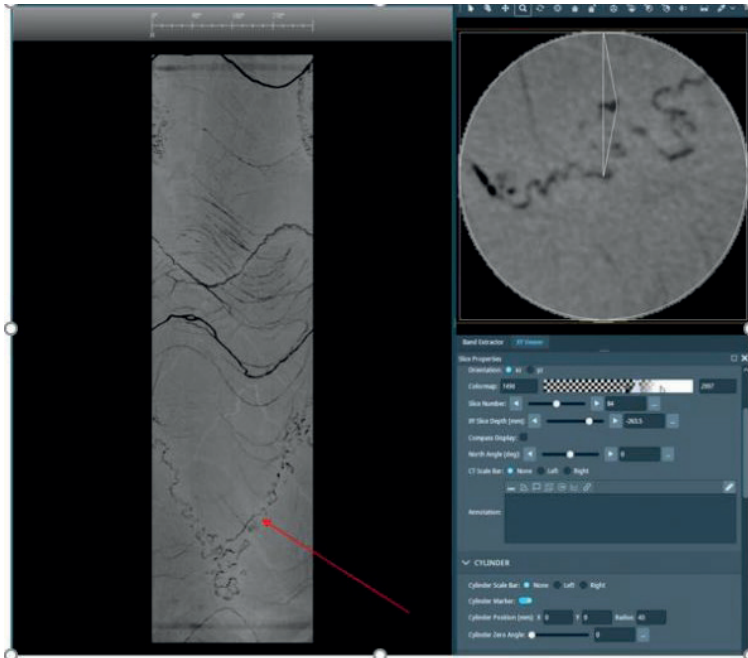
Detection of formation boundary based on the CT image contrast

Figure 3.



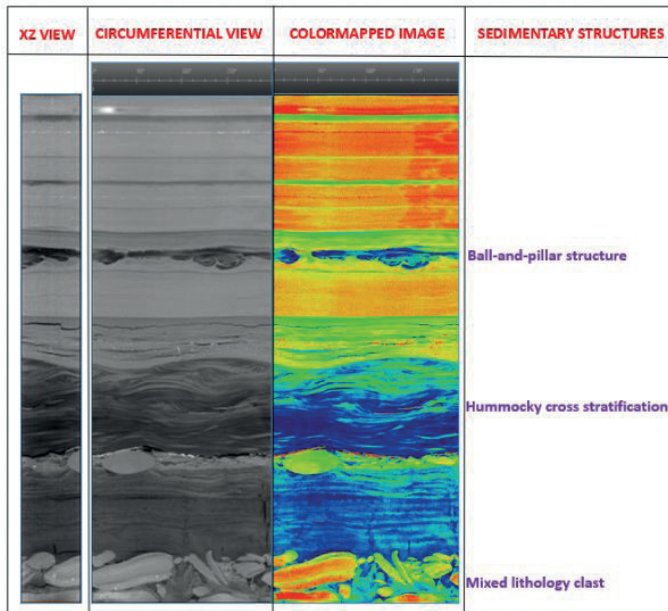
Vuggy porosity calculation by segmentation method in a vuggy reservoir (average whole porosity is calculated 11 % from the CT image). Segmented image showing segregated blue pore space on the far left, circumferential image of the core in the middle, and porosity log showing percent of pores along the scanned core interval on the far right)

Figure 4.



Identification of stylolites in a carbonate core (red arrow).

Figure 5.



Identification of sedimentary structures in a clastic core

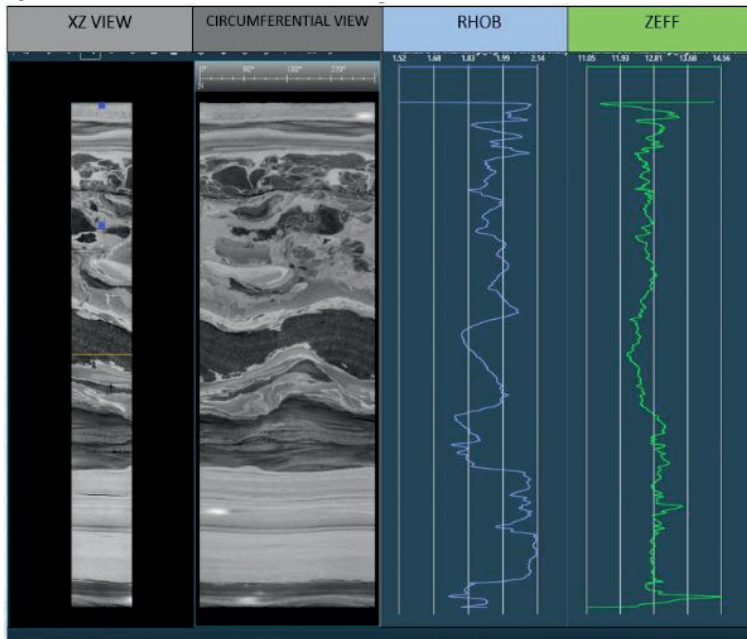


Figure 6.



Fourth generation medical CT scanner used in this study

Figure 7.



Continuous whole-core scans at 0.5 mm (500 micron) spacing and derived bulk density (RHOB) and effective atomic number (Zeff) logs along the scanned core interval

# Repurposing Pipelines for Hydrogen and Hydrogen Blend Service



Nicholas Waple<sup>1</sup>, Callum Peace<sup>2</sup>, Harry Cotton<sup>1</sup>, Hooman Haghighi<sup>3</sup>

<sup>1</sup>Wood Plc Staines / UK

<sup>2</sup>Wood Plc Perth, / Australia

<sup>3</sup>Wood Plc Aberdeen / UK

## 1. INTRODUCTION

The drive for energy transition is currently underway, with many projects looking to convert natural gas infrastructure for hydrogen service, as well as to blend hydrogen into existing gas networks. Limited international codes and standards exist which address hydrogen embrittlement concerns, with material requirements which impact the feasibility of repurposing pipelines for hydrogen service.

The feasibility of pipeline repurposing for hydrogen service is critical to the energy transition. Careful consideration of code requirements, and further research and development currently ongoing is required in order to remove over-conservatism in design maximise the achievable energy flow rate when repurposing to hydrogen service.

## 2. METHODS

This paper presents an overview of the key integrity challenges for the repurposing of pipeline infrastructure for hydrogen and hydrogen blend service and the potential blockers with respect to current code compliance, based on studies of international code requirements and recent repurposing study work. Case studies have been investigated to quantify the impact of repurposing onshore and offshore pipelines for hydrogen service.

## 3. FINDINGS

### 3.1 Material Review

There are significant challenges associated with designing and repurposing pipelines for hydrogen service due to the risk of hydrogen embrittlement. This phenomenon may occur in certain materials, such as carbon steel when exposed to hydrogen in a pressurized environment and result in material to become brittle and prone to cracking, most notably by increasing fatigue crack growth rates, and degrading the material effective fracture toughness, in effect reducing allowable safe design stresses and hence maximum allowable operating pressures.

Table 1: Summary of Failure Mechanisms

#### 3.1.1 Fatigue Cracking

The presence of hydrogen can accelerate the growth of pre-existing cracks under cyclic stress and reduce fatigue life. Some research has shown that the rate of fatigue crack growth in hydrogen can be up to 10 times higher than in air, with some reports suggesting

a factor of 30 or more. The line pipe strength/grade and microstructure appear have little impact on fatigue, but fatigue is increased by lower cycle frequencies. This may have significant implications for the design life and allowable operating conditions of existing pipelines repurposed for hydrogen service, particularly for aging pipelines or those subjected to significant cyclic loading.

[Performance Evaluation of High Strength Steel Pipelines for High Pressure Gaseous Hydrogen Transportation, CRES Project No. CRES-2009-J02-01]

[Hydrogen Embrittlement Considerations for Distribution of Gaseous Hydrogen, Sandia National Laboratories, PRCI mtg, October 2018]

#### 3.1.2 Toughness Degradation

The presence of hydrogen can reduce effective toughness, which is a measure of a steel's resistance to the propagation of pre-existing cracks (e.g., fatigue cracks, planar weld flaws) under constant applied tensile stress. The toughness is measured using pre-cracked FM specimens that are loaded in a pressurized hydrogen environment. Research by the University of Grenoble tested X70 pipe under 85 bara hydrogen pressure using standard CTOD tests and found a significant reduction in toughness. Figure 1 presents a summary of the results of FM toughness testing in hydrogen environment. This reduction was substantial at 1% nitrogen (0.85 Bara hydrogen partial pressure), indicating that the negative impact of hydrogen is significant even in pipelines conveying methane/hydrogen mixtures with hydrogen content below 10%. However, the addition of 100 ppm oxygen diminished the detrimental effect of hydrogen, possibly by forming a barrier to hydrogen uptake at crack surfaces.

Fig. 1: Summary of results of FM toughness testing in hydrogen environment

[Influence of Hydrogen and Oxygen Impurity Content in a Natural Gas / Hydrogen Blend on the Toughness of an API X70 Steel, DOI: 10.1115/PVP2018-84658, Conference: ASME 2018 Pressure Vessels and Piping Conference, July 2018: Laurent Briottet]

#### 3.2 Code Review

Transportation of hydrogen via pipelines is not new and exists internationally, most notably within both Europe and the USA. However, this experience is typically associated with the petrochemical industry transporting comparatively small volumes of hydrogen under low-stress conditions utilising low-strength grade steels when compared to typical hydrocarbon transmission

systems. In addition, when compared to natural gas and liquids, there is less available experimental and operating data with hydrogen, and although codes, standards and guidelines related to hydrogen transportation do exist, they are either conservative in their approach to materials and safety issues or neglect them altogether. International onshore/offshore pipeline codes and standards have been reviewed to determine their applicability to Hydrogen Service as presented in Table 2.

Table 2: Hydrogen Codes and Standards

[Repurposing Networks For Hydrogen, Conference: ADIPEC 2023. Paper ID: SPE-216844-MS, July 2023, C.Peace et al]

### 3.2.1 ASME B31.12

#### Prescriptive Design Method (Option A)

A “Low-Stress” design approach in line with Option A from ASME B31.12. This approach is considered to effectively be an interpretation of the petrochemical industry’s existing operational experience with hydrogen, rather than having a defined technical basis. This approach notably limits allowable design stresses to a maximum of 50% of yield strength (SMYS), with the steel SMYS degraded to an effective limit of approximately 52 KSI, effectively penalising the use of high strength material grades with little to no advantage in terms of pressure rating in using grades above X52. Material qualification to this approach requires restrictions to be applied to the linepipe and weld material hardness of 237 HBN (c.250 HV10), similar to that typical of Sour-hydrocarbon service.

Material testing in hydrogen is not strictly required subject to compliance with the above. However, in the case of repurposing pipelines it is unlikely to be possible to confirm full compliance with a potential need for destructive sampling and fracture mechanics testing in hydrogen as explained below for Option B approach.

#### Performance Based Design Method (Option B)

An alternative “High-Stress” design approach in line with Option B from ASME B31.12 employing fracture mechanics testing in order to quantify the impact of hydrogen embrittlement on the pipe steel and weld mechanical performance in order to technically justify design stresses following an Engineering Critical Assessment (ECA) approach up to that typical of hydrocarbon transmission pipelines. This Option allows for a design equivalent to that typical of hydrocarbon transmission pipelines (DF≤0.72) allowing for the full strength of higher strength grades (>X52) to be utilised in design. However, this method is subject to fracture mechanics testing of destructively collected linepipe and weld samples in hydrogen pressure environments to prove sufficient resistance to environmentally assisted cracking (effective toughness).

The acceptance criteria for the FM tests are determined by FM analysis taking account of cyclic and static

stress levels and size of defects in the pipeline based on manufacturing/construction Non-Destructive Testing (NDT) records and in line inspection including tools with crack detection capability.

From published test data, the levels of toughness demonstrated by Fracture Mechanics (FM) tests in hydrogen are variable depending on differences in metallurgy test procedures, parameters and interpretation of results. There is a need for more detailed testing standards defining requirements for FM testing in hydrogen and improved understanding of the necessary metallurgical characteristics (e.g. hardness, composition, micro-structure) for cracking resistance. This is the subject of a range of ongoing JIPs, notably including the DNV H2Pipe JIP.

[Fracture and Fatigue of Commercial grade API Pipeline steels in gaseous hydrogen, PVP2010-25825, July 18-22, 2010, Bellevue, Washington, USA, Chris San Marchi et al]

[Fracture Resistance and Fatigue Crack Growth of x80 Pipeline Steel in Gaseous Hydrogen, PVP2011-57684, July 17-21, 2011, Baltimore, Maryland, USA, Chris San Marchi et al]

[DVGW Project SyWeSt H2 “Investigation of Steel Materials for Gas Pipelines and Plants for Assessment of their Suitability with Hydrogen.”]

[Large Diameter Carbon Steel Pipe from EUROPIPE for Hydrogen Gas Transport, Technology for Future and Aging Pipelines (TFAP), 29-31 March 2022, Ghent Belgium, Christoph Kalwa.]

### 3.2.2 IGEM/TD/1

UK onshore gas transmission standard IGEM/TD/1 6th Edition includes a separate Hydrogen Supplement 2 (IGEM/TD/1S) including hydrogen blends. The design methodology of IGEM/TD/1 Supplement 2 is very similar to, and heavily influenced by ASME B31.12, with two design approaches.

#### Low Stress Design Approach

IGEM/TD/1 Supplement 2 provides a design considered approximately equivalent to an Option A design (i.e., DF≤0.5, SMYS de-rated to X52). IGEM/TD/1 Supplement 2 additionally limits longitudinal tensile stresses within the linepipe girth weld to a maximum of 180 MPa. Material qualification to this approach similarly to ASME B31.12 restrictions linepipe and weld material hardness to 250 HV10.

#### High Stress Design Approach

If sufficient material testing and qualification is carried out following the methodology outlined within ASME B31.12 Option B, IGEM/TD/1 Supplement 2 restrictions may be relaxed up to the allowable stresses specified for a natural gas pipeline to IGEM/TD/1, including a Design Factor (DF) up to 0.72 for grades up to X80.

It should be noted that both ASME and IGEM hydrogen

standards are applicable for onshore pipeline design only.

### 3.2.3 DVGW G 409 & G 464

The DVGW G 409 Technical Note has been published to address the conversion of high-pressure carbon steel pipelines (>16bar) from natural gas to hydrogen service (defined as  $\geq 98\%$  H<sub>2</sub> by volume), with supplementary guidance provided within DVGW G 464 on fracture-mechanical assessment for material qualification for steel pipelines in hydrogen service.

The guideline references and is strongly influenced by ASME B31.12, stating that fracture mechanical testing is required in order to technically justify the use of high grade steels (SMYS>360MPa), a high design factor (>0.5) or where significant fatigue loading is anticipated. This guideline recognises the limitations of testing methods specified within ASME B31.12 and supports the use of Elastic-Plastic Fracture Mechanics (EPFM) methods to ASTM E1820 which is well established within the offshore industry for sour service pipelines and is aligned with current industry best practices for hydrogen service.

### 3.5 Impact of Hydrogen Blends

ASME B31.12 excludes pipelines with a hydrogen content less than 10% by volume and considers hydrogen blends ( $\geq 10\%$ ) as equivalent to 100% H<sub>2</sub> regarding material qualification and design stresses.

This is in contrast with experimental test data currently available, which suggest the detrimental effect of hydrogen in reducing fracture toughness recorded in fracture mechanics (FM) tests is significant even with hydrogen fraction in nitrogen gas mixtures as low as 1% hydrogen, with a toughness reduction similar to that recorded in 100% hydrogen. In addition, the fatigue crack growth rate may be increased by a factor of more than 10 under hydrogen partial pressures below 6 Bara.

In addition, this does not align with many national regulations for natural gas pipelines. Table 3 below summarises code and standard limitations on blend concentration in comparison with regulatory limits.

Table 3: Blending Limit Comparison Summary

Based on these inconsistencies there is clear need for further research and development to provide a better understanding of these blending limits. There is currently ongoing research by such as the National Grid FutureGrid Project and DNV led HyReady and H2Pipe JIPs which will help clarify current uncertainties in the quantitative impact of low concentration hydrogen blends.

In practice the permissible blending ratio of hydrogen in pipelines designed for natural gas will depend on a range of factors, including material specification, pipeline integrity, design stresses, national regulations end user requirements, tracking /monitoring capabilities and limitations of pipeline facilities and equipment.

[Hydrogen Embrittlement Considerations for Distribution of Gaseous Hydrogen by Pipeline Chris San Marchi and Joe Ronevich, Sandia National Laboratories, PRCI mtg, October 2018, Pleasanton CA]

## 4. CASE STUDIES

Case studies have been investigated for the redesign and repurposing of both onshore and offshore pipelines for hydrogen service. Figure 2 presents Onshore case study examples of the code minimum wall thickness requirements, with natural gas codes in shades of blue, and hydrogen codes in shades of green. The case study selected wall thickness for natural gas transmission lines are presented in red.

Fig 2: Onshore Case Study – Wall Thickness Requirement

Figure 3 indicates the pressure drop associated with Hydrogen service under ASME B31.12 Option A, compared a Natural Gas pipeline of matching wall thickness designed to ASME B31.12 Option B using a 0.72 design factor. It is noted this assessment is based on Typical onshore pipeline operating pressures with X60 material grade.

Fig 3: Onshore Case Study – Reduce Design Pressure for Hydrogen Service

[Repurposing Networks For Hydrogen, Conference: ADIPEC 2023. Paper ID: SPE-216844-MS, July 2023, C.Peace et al]

## 5. ENERGY CAPACITY

Repurposing natural gas pipelines to hydrogen service results in a reduction in the design factor unless material performance data is available to justify the higher design factor. As well as this potential reduction in design factor and resulting de-rating of existing lines design pressure, differences in the volumetric energy densities and flow of natural gas and hydrogen result in significantly different energy flows for both energy carriers.

Hydrogen as an energy carrier has by far the highest gravimetric energy density, at 120-142 MJ/kg. The mass-based energy density (HHV-LHV) of hydrogen is roughly two to three times higher than that of methane or natural gas which is 50-55 MJ/kg. However, the volumetric energy density of hydrogen is comparatively low. Therefore, for practical transport purposes, the flowrate and density (operating pressure) of hydrogen should be maintained as high as allowable. Reduction in Maximum Allowable Operating Pressure (MAOP) results not only in a lower available pressure drop (and hence flowrate) but in lower mass density of transported fluid and potentially higher fluid velocity.

A range of cases were assessed using rudimentary models for different design codes and velocity limits as presented in Table 4.

Table 4: Comparison of Energy Ratio Capacities of ASME B31.12 Option A vs. Option B

## 6. CONCLUSION

There are still significant material and testing challenges in bridging the gap between low-stress design approaches reliant on historical operational data, and high-stress design methods justifying the use of carbon steel pipelines for high design stresses using high strength carbon steels. For the blending of hydrogen into gas networks, there are notable discrepancies between codes and standards, test data and government regulations as to the minimum allowable hydrogen blend ratio prior to introducing significant risk due to material effects.

Further research is ongoing within the industry to better understand the material effects of hydrogen and hydrogen blends on carbon steels, including the ongoing DNV H2 pipe JIP which could potentially improve future feasibility. Based on rudimentary calculations, comparing both energy Natural Gas (NG) and H2 carriers, repurposed pipelines can be capable of achieving circa 80-90% of the energy flow rate if design pressure can be maintained, or 50-60% if the design pressure is de-rated. If other operational restrictions are considered, such as flow velocity it can potentially have additional knock-on effect on the achievable flowrate and consequently to energy ratio.

Repurposing existing infrastructure for low-stress hydrogen transmission may be achievable, without destructive sampling and testing, in cases where documentation review confirms compliance with the material requirements including hardness limits of applicable hydrogen design codes such ASME B31.12. However, in most cases there will not be such compliance or original documentation will not be available to confirm it. In this situation destructive sampling and testing of the pipeline will be necessary including a requirement for FM testing in hydrogen.

System design is crucial to understand pipeline pressure requirements when repurposing to employ more low stress designs.

Keywords: Hydrogen, Pipeline Repurposing

Fig. 1: Summary of results of FM toughness testing in hydrogen environment

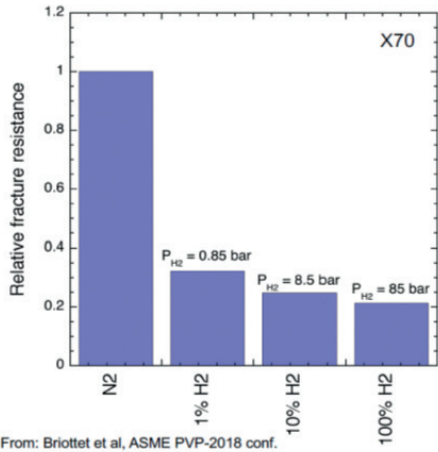


Fig 2: Onshore Case Study – Wall Thickness Requirement

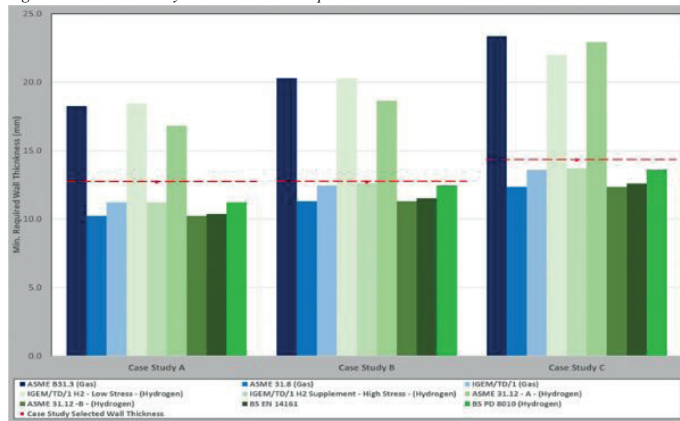


Fig 3: Onshore Case Study – Reduce Design Pressure for Hydrogen Service

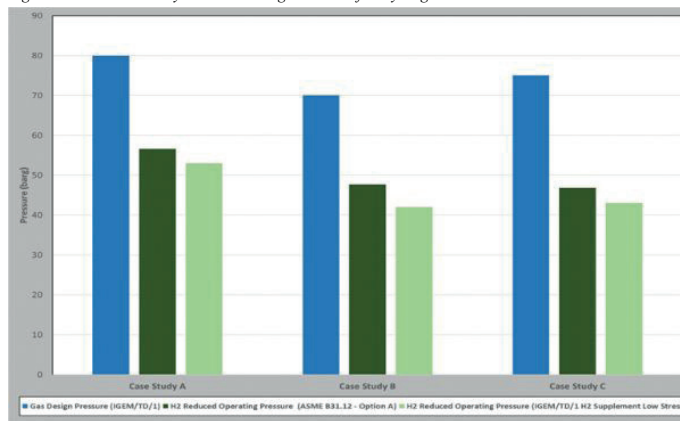


Table 1: Summary of Failure Mechanisms

Carbon Steel Failure Mechanism	Characteristics/Effects
Reduction in effective toughness	Hydrogen is absorbed at existing crack to assist crack propagation under static stress (i.e., reduce toughness).
Fatigue	Hydrogen is absorbed at existing crack to assist crack propagation under cyclic stress. Increase in fatigue crack growth rate by factor of 10 to 30 or more.
Corrosion	Blue hydrogen from hydrocarbon sources may be contaminated (CO <sub>2</sub> , water) to cause metal loss corrosion.
Hydrogen Induced Cracking(HIC) Hydrogen Stress Cracking (HSC, SSC)	Level of hydrogen absorbed by steel is much lower than sour service. Not a threat to pipelines complying with sour service requirements for hardness and steel chemistry
Reduction in tensile strength and ductility	Test data indicates effect is not significant degradation for elastic design DNV Joint Industry Practice (JIP) ongoing to produce a H <sub>2</sub> service stress strain curve.
Running Ductile fracture (Fracture Arrest)	Fast running fracture propagating along pipeline for some pipe lengths. Typically initiated by impact. Charpy impact requirements for natural gas pipelines are conservative for hydrogen.

Table 2: Hydrogen Codes and Standards

Code	H2 Service Within Scope	Hydrogen Embrittlement
ASME B31.12	✓	✓
IGEM/TD/1 Supplement 2	✓	✓
DVGW G 409 & G 464	✓	✓
AS/NZS 2885.1	X	X
ASME B31.3	✓	X
ASME B31.8	X	X
BS EN 14161	✓	X
BSI PD 8010-1	✓	X
CSA Z662:19	X	X
DNV-ST-F101	✓	X
EN 1594	✓	X
IGEM/TD/1 6th Edition	X	X
ISO 13623	✓	X
NEN 3650 / 3651	✓	X

Table 3: Blending Limit Comparison Summary

Source	H2 Blend Ratio	Comment
ASME B31.12	10% to 100% v/v	Considers 10% H <sub>2</sub> as equivalent to 100%. Scope excludes <10% v/v.
IGEM/TD/1 Supplement 2	Up to 100% v/v	Considers 10% H <sub>2</sub> as equivalent to 100%.
DVGW G 409	>=98% v/v	Effectively applicable to pure hydrogen with low level impurities only.
UK HSE “Injecting Hydrogen into the Gas Network	Up to 20% v/v	Considers concentrations of up to 20% v/v as “unlikely to increase risk from within the gas network”.
UK Gas Safety Management Regulations (GSMR)	Up to 0.1% v/v	Maximum allowable concentration in the UK gas transmission system.
International Regulatory Limits	0% to 10% v/v	Germany permits the addition of up to 10% H <sub>2</sub> into the national gas network. There is no known example of hydrogen being blended into the German transmission system at this concentration.

# Magnetotelluric System NORD

**Dmitrii Epishkin<sup>1</sup>, Denis Yakovlev<sup>2</sup>, Andrey Yakovlev<sup>3</sup>, Nikolay Palshin<sup>4</sup>, Nikita Zorin**

<sup>1</sup>STC Nord-West, Moscow / Russia

<sup>2</sup>STC Nord-West, Moscow / Russia; Nord-West Ltd., Moscow / Russia

<sup>3</sup>Nord-West Ltd., Moscow / Russia; Lomonosov Moscow State University, Moscow / Russia

<sup>4</sup>Nord-West Ltd., Moscow / Russia; Shirshov Institute of Oceanology RAS, Moscow / Russia



## SUMMARY

This work presents the testing results of a new magnetotelluric system NORD. The key features of the system are: wireless operation with options of real-time data processing and quality assessment, measuring complex impedance of electric lines, low self-noise, low power consumption, light weight, compactness, reliability, robust data processing algorithms. The receiver has a built-in calibration system as well as telemetry that allows to monitor the status of the device and identify common problems. At the moment, the NORD allows to obtain high-quality MT data in the range from 50 000 seconds up to 20 000 Hz. We carried out a large number of field tests and comparisons with equipment from leading manufacturers, which showed excellent performance of the system. Also in recent years, a few large-scale production works have been carried out using this system.

## INTRODUCTION

The use of high-quality modern equipment is one of the important components of the successful implementation of the magnetotelluric (MT) method, which is the main electromagnetic tool of petroleum exploration. A number of review papers and textbooks discuss land MT instrumentation (Simpson F, Bahr K. Practical Magnetotellurics, 2005, Cambridge University Press, Cambridge; Ferguson IJ, Chave AD, Jones AG, Mackie R, Rodi W. Instrumentation and field procedures. In: Magnetotelluric method, 2012, Cambridge University Press, pp 421–479). Other reviews are focused on magnetic (Poliakov SV, Reznikov BI, Shchennikov AV, Kopytenko EA & Samsonov BV. The range of induction-coil magnetic field sensors for geophysical explorations, 2017, Seismic Instruments 53: 1-18) and electric (Lu K, Macnae J. The international campaign on intercomparison between electrodes for geoelectrical measurements, 1998, Explor. Geoph. 29: 484-488) field sensors.

At present, a number of requirements are imposed on magnetotelluric systems. The system should have low level of self-noise, wide frequency range, the receiver input impedance should be sufficiently high to minimize the distortions of electric signal associated with poor grounding conditions. The equipment should be reliable, robust and able to operate in various climatic conditions; it also should be as simple as possible to use. We focused on these requirements when developing the station.

The NORD magnetotelluric system is manufactured by Nord-West Ltd., Russia, and consists of 3 main parts: 1) 5-channel receiver 2) magnetic and electric field sensors

3) software for communication with the station and for data processing. This work describes the distinctive features of the NORD system and presents the results of testing.

## MAIN FEATURES OF THE SYSTEM

NORD has a number of features that distinguish it from other magnetotelluric systems:

- An innovative feature of the NORD receiver is that it has the ability to measure the overall complex impedance of the grounded dipoles, which include the capacitive effects in the wires. This allows taking less biased electric field measurements in the regions with poor grounding conditions.
- The station has the ability to process data in real-time without stopping the record. It is also possible to view telemetry, time series, spectra and coherences in real-time, which allows you to quickly estimate the quality of the data.
- All interaction with the station is carried out via Wi-Fi, which increases the reliability of the device in the field. Operation of the system is carried out by any Android / iOS / Windows / Linux – based device with a Wi-Fi module and an Internet browser.
- The small dimensions and weight of the receiver make it possible to adapt it for marine measurements (Epishkin D, Palshin N, Yakovlev A, Yakovlev D. Technology of marine magnetotelluric sounding in transition zone. - Paper presented at the 24th EM Induction Workshop, Helsingor, Denmark, 13-20 August 2018).
- For advanced processing of raw time series we have developed EPI-KIT (Epishkin DV. Improving magnetotelluric data-processing methods, 2016, Moscow Univ. Geol. Bul. 71(5):347–354) — a modern and universal software for processing of MT and CSEM data. This software can process data received by equipment from a number of manufacturers, which allows you to combine different types of equipment in one project.

## RECEIVER

The first component of the NORD system is a modern digital receiving unit (Figure 1), specially designed to register the EM field signals in wide frequency range (Table 1). The receiver has 2 electric and 3 magnetic channels, each one equipped with a separate 32-bit ADC with a base sampling rate of 2400 Hz and 24-bit ADC with a base sampling rate of 312.5 kHz for radio-magnetotellurics (RMT) or audio-magnetotellurics (AMT). It is possible to save the time series



simultaneously at 5 sampling rates: 15 Hz, 150 Hz, 2400 Hz, 78.125 kHz, 312.5 kHz. The sampling rate schedule is easily configurable, and allows to control the final size of raw data files.

High accuracy of the acquired MT or CSEM data is ensured by low internal noise level ( $\sim 3.5 \text{ nV}/\sqrt{\text{Hz}}$  for AMT frequency range) and modern ADCs of NORD receiver, combined with using robust data processing algorithm implemented in the EPI-KIT software.

### ELECTRIC FIELD SENSORS

NORD system is supplied with NW-4 sensors, which is a special type of compact, accurate, environmentally sound and relatively inexpensive non-polarizable graphite electrodes with low self-noise level (Figure 2).

### MAGNETIC FIELD SENSORS

NORD system includes IMS induction coils (Table 2): low-noise magnetic field sensors with smooth and stable frequency characteristics. There are three types of sensors: IMS-5 – high-frequency sensors for AMT (0.1 Hz – 20 000 Hz), IMS-10 – classic MT band sensors (0.00002 Hz – 1000 Hz), IMS-15 – broadband sensors which allows obtaining a single AMT+MT (BBMT) curve without changing different types of sensors (0.00002 Hz – 10 000 Hz).

### OPERATION AND DATA PROCESSING SOFTWARE

Device control and status monitoring, as well as data processing, management and transferring to and from NORD is implemented by wireless network. The control program for Android has great functionality and provides the ability to carry out operational processing of NORD data in real time without interrupting the record (Figure 3). High-speed Wi-Fi connection allows downloading an average overnight MT record (50-70 MB for conventional schemes of signal sampling) within several seconds. Connection with the NORD receiver could be established either from a PC or a smartphone.

For processing of raw time series data acquired by NORD one should use EPI-KIT (Figure 4) — a modern and universal software solution for processing of MT and controlled-source electromagnetic (CSEM) data. At the bottom of the EPI-KIT software there is a solid mathematical kernel based on the correlation method and robust statistics (Epishkin DV. Improving magnetotelluric data-processing methods, 2016, Moscow Univ. Geol. Bul. 71(5):347–354). The EPI-KIT interface is practical and simple, while the implemented code supports the technology of parallel computation on graphical accelerators (GPU), which significantly reduces the processing time. The optimized computational routine allows working with the EPI-KIT software both on simple laptops and powerful multi-core computing systems. Apart of the NORD data files, EPI-KIT is also able to process the time series acquired

by receivers of Phoenix Geophysics, Metronix, LEMI and other manufacturers.

### SELF-NOISE TESTING

The measured internal noise level of the NORD receiver is shown in Figure 5 in orange. Note that it is characterized by two different noise floors depending on the type (high- or low-frequency) of the employed input circuit, however both of these noise floors are lower than the typical measured signal.

For all types of inductive magnetic sensors, we have also carried out numerous parallel tests, on the basis of which the self-noise of each IMS sensor was calculated. Also, for some sensors self-noise measurements were carried out in a shielded camera. The noise levels obtained by both methods agree with each other. Tests have shown that the magnetic coils have a stable and predictable noise level. Figure 6 shows results of the self-noise measurements for different types of IMS coils.

For the electrode field testing we used three types of widely used non-polarizable electrodes: graphite (NW-4 manufactured by Nord-West Ltd.), Cu-CuSO<sub>4</sub> and Pb-PbCl<sub>2</sub> (both manufactured by internationally recognized companies). We have chosen 8 brand-new electrodes of each type, properly serviced before use. To estimate the noise, a parallel test technique was applied. Electrodes of each type were grouped into pairs. Each pair formed an electrical line  $\sim 1$  meter long. All electric lines were located in parallel at a small distance from each other. To study the stability of the characteristics of the electrodes, the signals were recorded periodically for 2 weeks. The testing results are given in Figure 7. The highest noise level was consistently observed for Cu-CuSO<sub>4</sub> electrodes. Graphite and Pb-PbCl<sub>2</sub> electrodes both show noticeably better results quite similar to each other; but the noise level of graphite electrodes is slightly lower in the entire frequency range.

### SYNCHRONIZATION TESTING

Another important requirement for MT units is the accurate time synchronization. To check the NORD receivers' synchronization accuracy we developed a special test. The same sinusoidal signal with a frequency of several hundred Hz was applied simultaneously to several receivers, and for each moment of time the phase difference in degrees ( $\Delta\phi$ ) between the registered signals at the given frequency was calculated. Next, the time shift  $\Delta t = \Delta\phi / (360f)$  was calculated. Figure 8 shows an example of a two-hour observation of time synchrony accuracy between two NORD receivers. During the entire observation period, the synchronization accuracy between instruments was better than 60 ns, which is sufficient for synchronized processing of time series at frequencies up to 100 kHz.

**ELECTRIC LINES CALIBRATION TESTING**

NORD receiver can estimate the contact resistance of each grounded electrode separately and has the unique ability to measure the total complex response of grounded electric lines, which include the capacitive effects of wires and electrodes. This allows taking unbiased electric field measurements in the regions with poor grounding conditions by correcting the measured data for the distortion caused by high electrode contact resistance (ECR) effects (Zorin NI, Epishkin DV. Effect of electrode contact resistance on electrical field measurements, 2022, Izvestiya, Physics of the Solid Earth. 58(5):727–733).

Figure 9 shows an example of 4 MT curves taken at the same survey site but with different electrode contact resistances (1 kOhm is rather good, while 12 kOhm is definitely a bad contact resistance value for high-frequency MT measurements) and different data processing options (with or without the ECR-correction procedure). As could be clearly seen from the figure, the uncorrected MT curve measured with poorly grounded electrodes is greatly distorted, while all the other curves stay very close to each other.

**TESTING IN COMMERCIAL SURVEYS**

NORD system is being actively tested for several years, and dozens of pilot instruments have been already used in commercial MT and CSEM projects in Ural Mountains, Taymyr Peninsula, Siberia and Kazakhstan. To date, thousands of measurements have been carried out using the NORD system in various climatic conditions.

As a demonstration of the system’s capabilities, Figure 10 shows two measurement results. The first result (Figure 10, left) was obtained in Kamchatka (eastern part of Russia). This measurement was carried out in the MT mode. For 3 days of recording it was possible to obtain high-quality curves in the period range from 0.001 seconds to 30 000 seconds.

The second result (Figure 10, right) was obtained in the central part of the East European Plain. In this example, the recording was carried out in the BBMT mode. With 12 hours of data, high-quality results were obtained in the range from 0.0001 seconds to 1000 seconds

**CONCLUSIONS**

When making a new MT/CSEM instrument, we were resting upon more than 25-year experience of Nord-West company in carrying out field electromagnetic exploration and scientific research. This allowed to make a state-of-the-art, accurate, robust, lightweight, user friendly, universal and highly effective system NORD, consisting of a receiver, magnetic/electric sensors and associated software. Self-noise testing and thousands of performed measurements have already proved that NORD is an accurate and reliable field instrument, perfectly suited for both commercial and academic projects.

Keywords: Electromagnetic, instrumentation

Figure 1. Receiver NORD



Table 1. Technical characteristics of the NORD receiver

Number of channels	2 electric + 3 magnetic
Frequency range	DC - 35 kHz
ADC (per channel)	32 bit + 24 bit
Sampling frequencies	312.5 kHz, 78.125 kHz, 2400 Hz, 150 Hz, 15 Hz
Input resistance	10 MΩ
Input capacitance	< 0.5 nF
Max. input voltage	±600 mV (electric channels) ±2500 mV (magnetic channels)
Self-noise level	~ 3.5 nV/√Hz
Data transfer interface	Wi-Fi 802.11n
Tyme sync accuracy	±30 ns (RMS)
Power consumption	6 - 8.5 W
Power supply voltage	12 V
Weight	1.8 kg
Dimensions	20x10x13 cm
Temperature range	-40... +85 °C

Figure 2. Graphite electrode NW-4

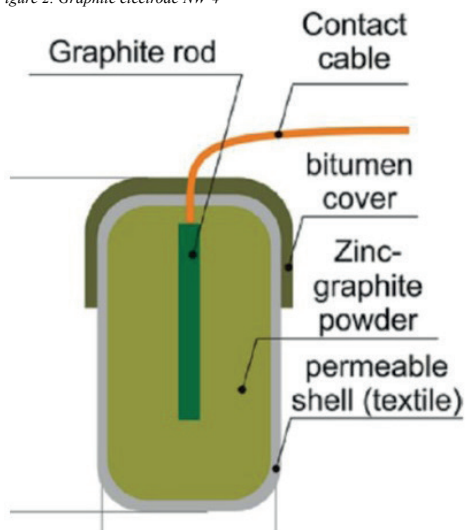


Table 2. Technical characteristics of the IMS magnetic coils

	IMS-5 coil	IMS-10 coil	IMS-15 coil
Methods	AMT, CSEM	MT, CSEM	BBMT, CSEM
Frequency range	0.1 Hz - 20 kHz	0.02 mHz - 1 kHz	0.02 mHz - 10 kHz
Output sensitivity (low frequencies)	0.2 V/(nT•Hz); < 5 Hz	0.7 V/(nT•Hz); < 2 Hz	0.7 V/(nT•Hz); < 2 Hz
Output sensitivity (high frequencies)	0.8 V/nT; > 5 Hz	1.6 V/nT; > 2 Hz	1.6 V/nT; > 2 Hz
Power consumption	0.96 W	1.2 W	1.7 W
Length	55 cm	105 cm	105 cm
Diameter	6 cm	7.6 cm	6 cm
Weight	3 kg	7 kg	5.5 kg

Figure 3. NORD mobile application for receiver control, data visualization, express processing and transfer

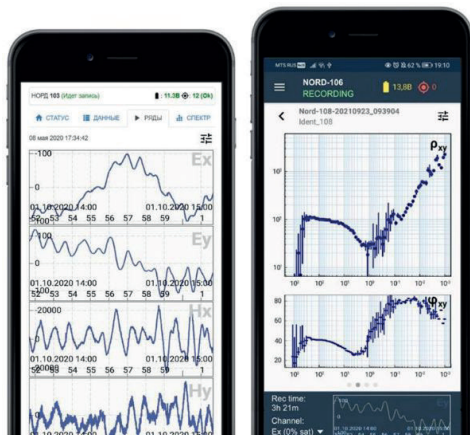


Figure 4. Robust MT data processing in the EPI-KIT software

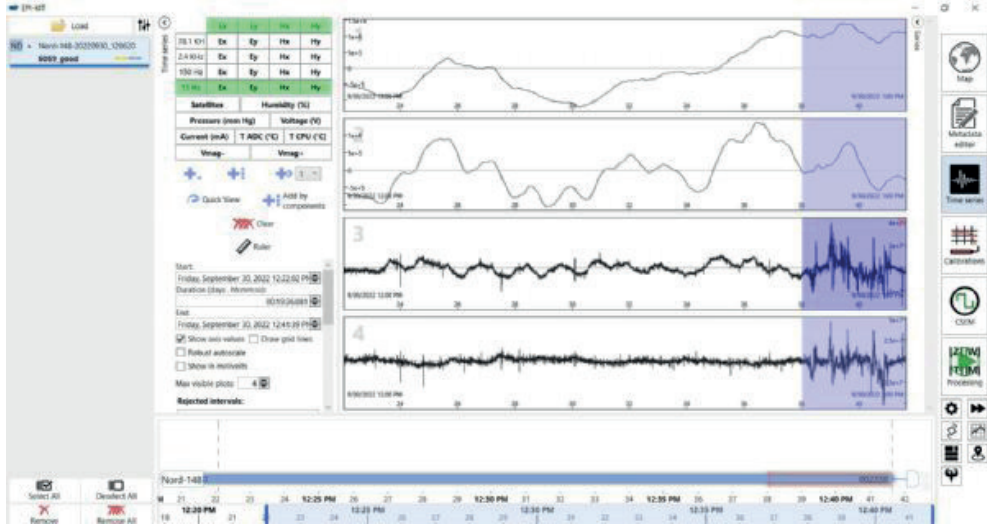


Figure 5. Self-noise level of the NORD receiver

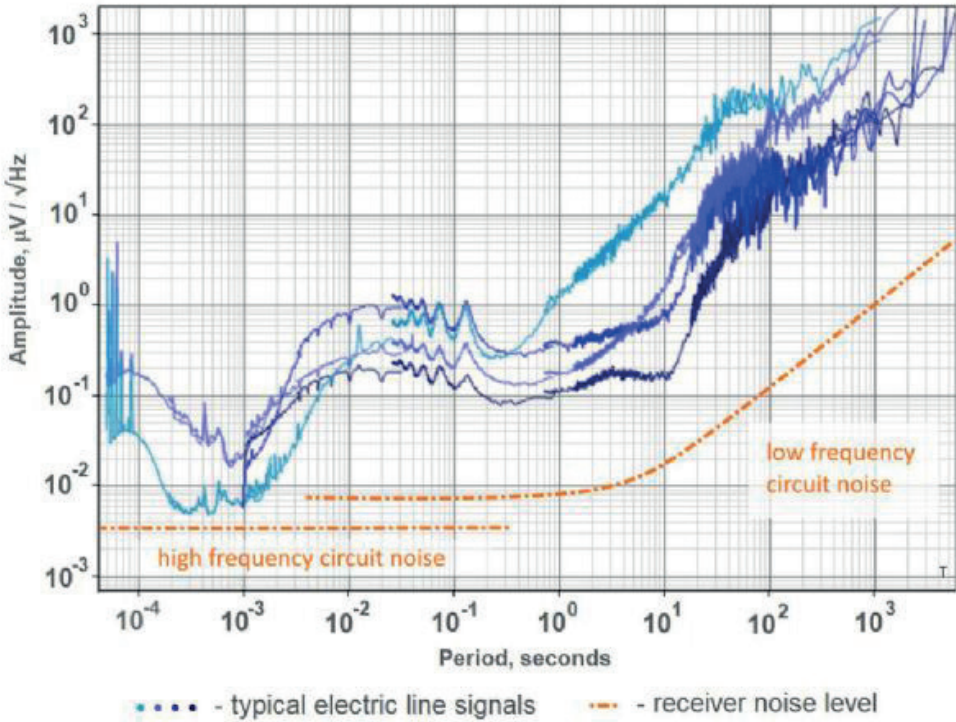


Figure 6. Self-noise level of the IMS magnetic coils

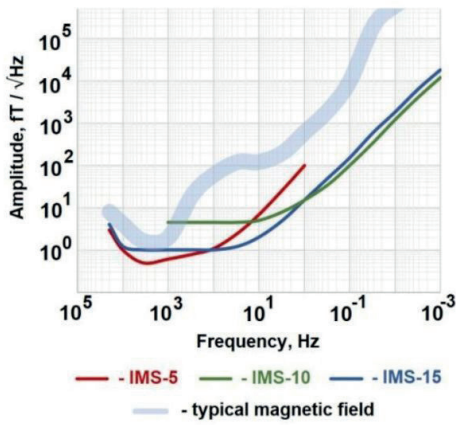


Figure 7. Self-noise level of graphite (NW-4) and other electrodes

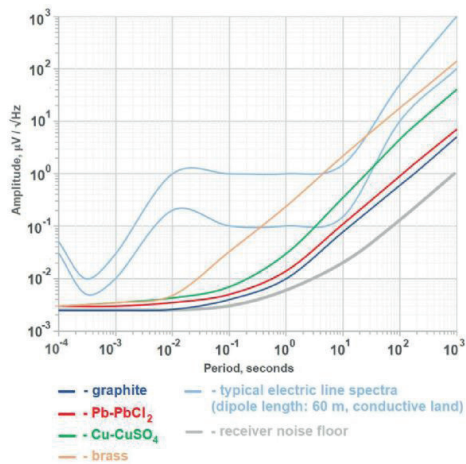


Figure 8. Time shifts ( $\Delta t$ ) between signals from two NORD stations synchronized by GPS

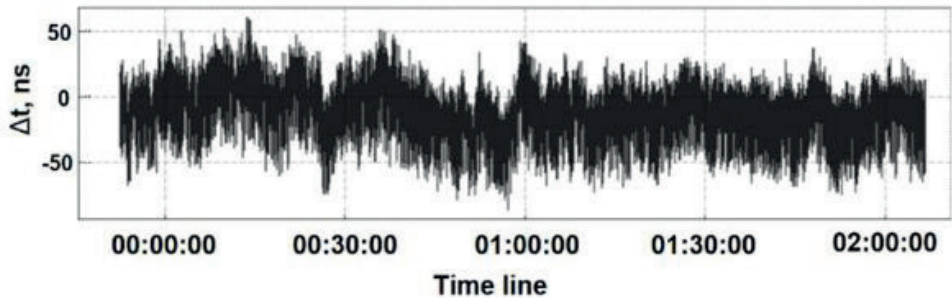


Figure 9. Correction of the measured data biased by high electrode contact resistance

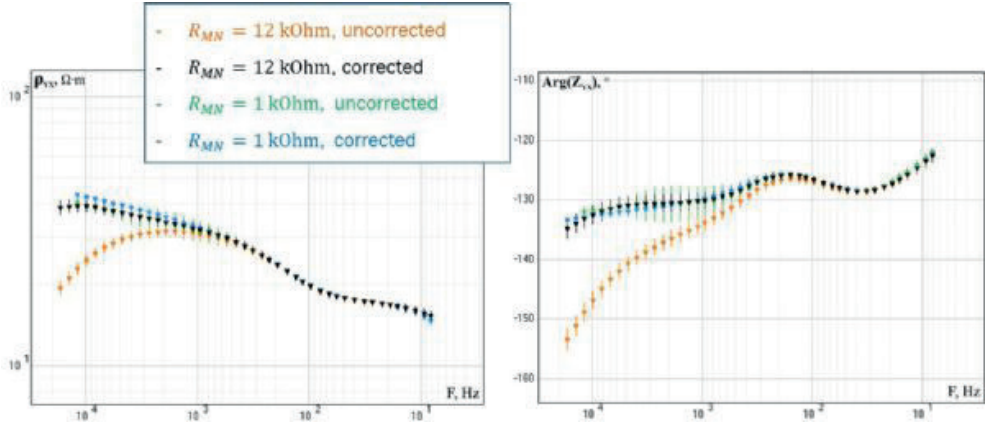
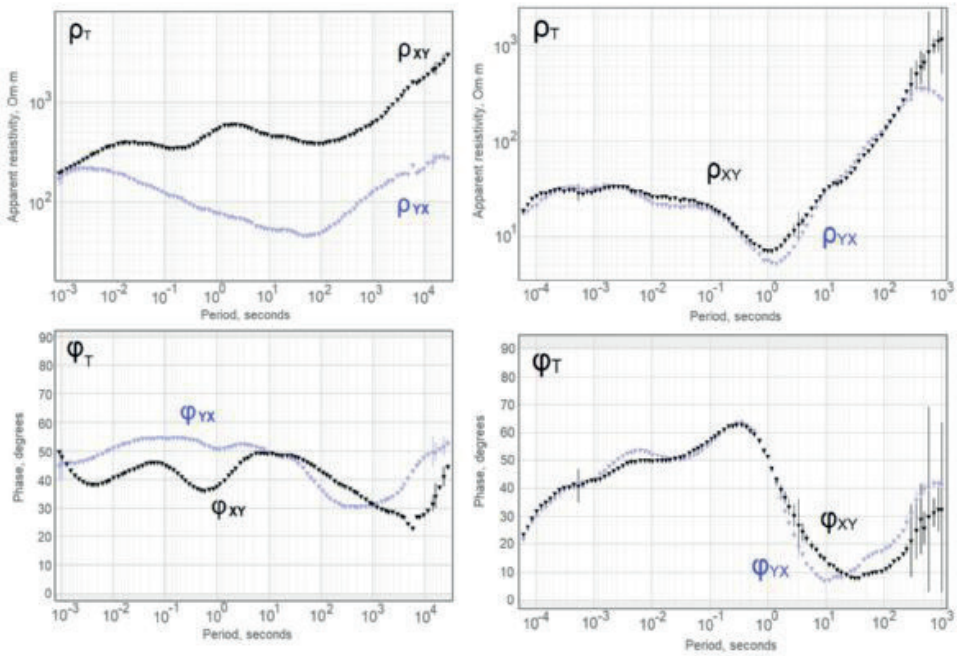


Figure 10. Processing results of a 3-day record at Kamchatka region with the IMS-10 magnetic coils (left) and a 12-hours record at the East European Plain with the IMS-15 magnetic coils (right)



# Integrated end-to-end Carbonate Acidizing Workflow

**Jakub Witek, Edmund Eswein**

SLB, RPS (Reservoir Performance Stimulation), EUR - Romania



## INTRODUCTION

An inventive end-to-end workflow has been designed for the purpose of optimization of stimulation treatment in high-temperature and high-pressure (HTHP) carbonate reservoir. The workflow is focusing on adding value through utilizing an advanced engineering approach, combined with lab testing, industry leading simulators and detailed evaluation of reservoir parameters and suitable stimulation technologies. Proposed process allows to understand the reservoir and calibrate the simulations results to its individual properties, which will be presented in a case history presentation, demonstrating significant production increase results.

## METHODS

One of the European Oil and Gas operators selected a candidate well in Continental Europe for a stimulation feasibility study. We responded with a systematic engineering plan and candidate assessment to maximize the well production potential and minimizing technical risks by utilization of fit-for-purpose technologies.

Scope of the technical study incorporated latest digital and technological advancements in carbonate reservoir stimulation present on the market, whereby key parameters related to the reservoir and well information were carefully evaluated.

To be able to properly analyze the data, a reservoir model was generated using an advanced matrix stimulation simulator. It was important to start a workflow review with a default set of data related to the candidate selection and formation damage characteristic, including quality log data, production history, well test results and summary of previous stimulation services. This is extremely important to be able to optimize critical model parameters. In collaboration with our Client Support Laboratory in Sugar Land, Advanced Core flow tests with 3D scans of wormhole geometries were used to further calibrate the simulator's fluid-rock interaction parameters. Various skin and permeability profiles were validated and subjected to iterations in the simulator with different fluids and treatment schedules.

## FINDINGS

Optimum fluids were chosen based on a risk analysis, careful review of the drilling records, mud type, workover history, and petrophysics in order to achieve key stimulation objectives. During the well candidate review it has been noticed that a combination of various fluids might be required for different purposes. Initially, it has been observed, that one of the main existing skin damages was caused by oil-based drilling mud. Due to that reason a special treatment fluid had to be selected to address the oil-based mud damage. Upon evaluation

of possible matrix acidizing and acid fracturing fluid systems, use of any standard acidizing fluid in

HTHP environment would have an impact on their effectiveness. Analysis of well and reservoir conditions indicated that the use of non-modified emulsified organic acids is not recommended. Moreover, chelating based fluids were declined due to economical reasons. Therefore, the main recommendation, also due to the harsh temperature environment, was to select an acid system with a retardation mechanism. A novel single-phase retarded acid was chosen as it has a high dissolution capacity, significantly retarded reaction kinetics along lower friction pressure characteristics compared to other retarded and conventional acid systems. Moreover, it has been observed that usually a single-phase retarded acid is up to 30% more efficient during the acid fracturing and up to 44% more efficient during matrix acidizing treatments compared with the traditional non-retarded acids. This means that with the help of the new retarded acid system, the same production increase can be achieved by using a lower volume of raw acid, lower volume of water needed for dilution, and lower volumes of chemicals will be required for the treatment (Abdrzakov et al. 2018).

Due to excessive production interval length and heterogeneity, use of diverters was highly recommended to maximize vertical coverage during the stimulation treatment. A polymer-free viscoelastic surfactant-based diverter was selected to alter the injection profile. This fluid can significantly simplify the process by continuously injecting acid into the formation. The acid will viscosify in situ and temporarily block the existing channels by forming a temporary barrier in the wormhole, to divert itself to undissolved areas. After the acidizing treatment, the diverter system breaks with no remaining damage upon contacting solvents or hydrocarbons.

The next step to validate the fluid selection was to perform individual Acid Core Flow tests to obtain an acid performance curve which presents a means of calibration of the acid-to-rock interaction. While performing general acidizing workflow this step is usually skipped, as it is time consuming and requires availability of core material. For majority of matrix acidizing treatment, such a performance test can validate the stimulation model by optimizing pumped volume of the fluids with the injection rate and regime of created wormhole (Fredd and Fogler 1996). Computer 3D tomography scanning is essential at this stage to view obtained results (wormhole geometry) and to optimize the treatment parameters. Obtained acid performance results data was used in a Matrix Acidizing Simulator to calibrate the acid and rock interaction of the model. Once the calibration is completed, the validation of the entire model can be performed based on analyzing

previous acidizing treatments of offset wells. This approach can compare and match the simulated post-skin with actual post-treatment skin obtained from the well test results (Abdrzakov et al. 2022).

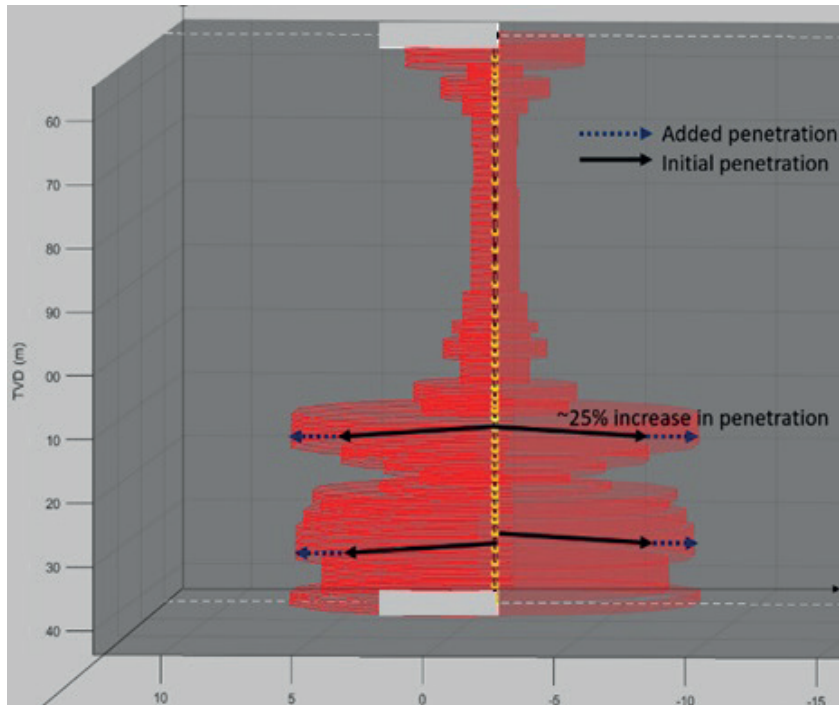
The optimized fluid selection has been further run in the Advanced Simulator to include individual well construction and to treat properly expected damage mechanisms by utilizing CT wellbore cleanup, CT acid matrix stimulation, and also a high-rate bullhead acidizing treatment.

## CONCLUSION

To conclude, the designed treatment using the above workflow and considering specifics of the well damage was successfully implemented. The final step of the workflow was to analyze and evaluate the post-stimulation results of the treatment using nodal analysis for skin post-treatment comparison. The post injection production analysis showed a significant increase in productivity index, without issues in cleanup. The proposed acidizing workflow has been proposed for a further well candidate in the same field and other places across in Europe with outstanding results.

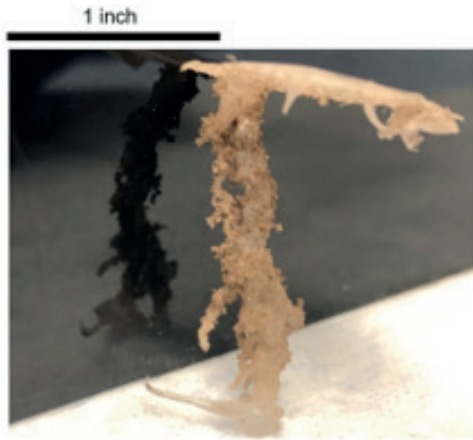
Anahtar Kelimeler: Carbonate acidizing workflow, acid design optimization

*Acid Optimization*



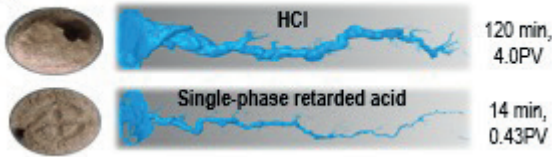


Acid Wormhole

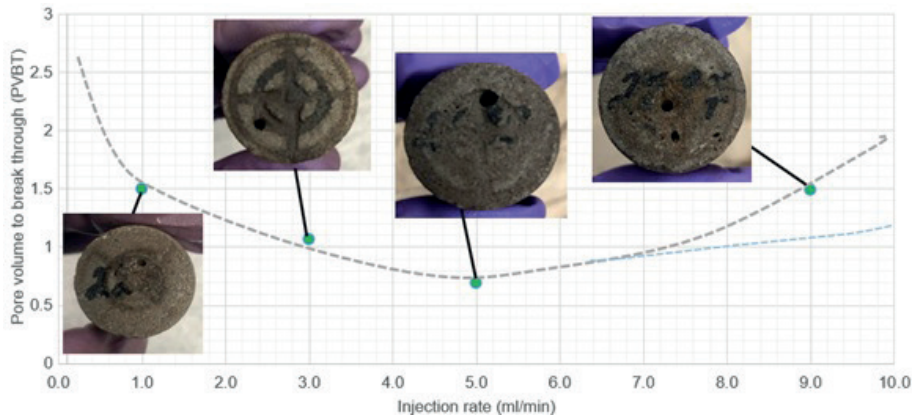


Acid Comparison

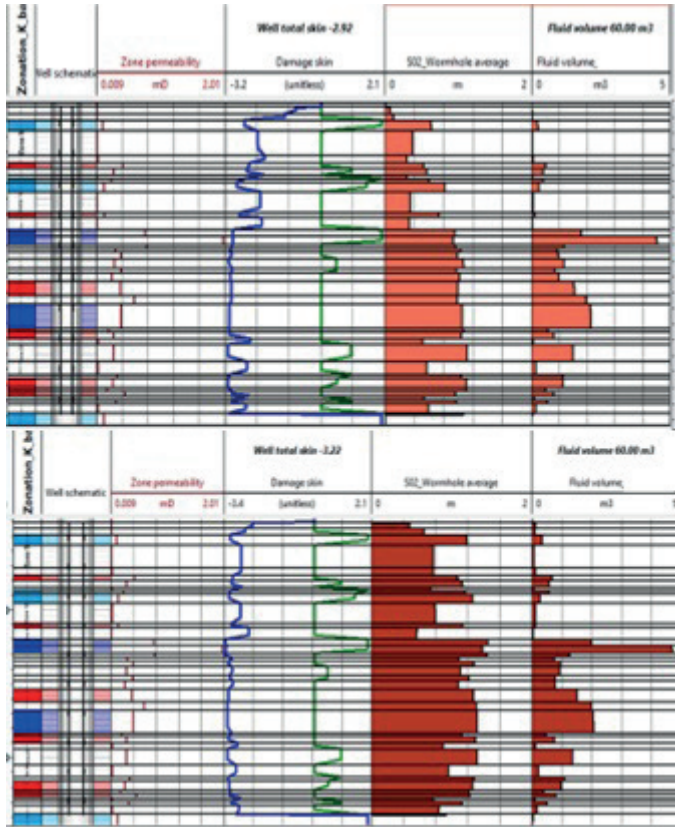
Deep Penetration



PVBT



Treatment Comparison





**Petrol Sistemleri Analizi, Havza Modellemesi  
ve Jeokimya**  
*Petroleum Systems Analysis, Basin Modeling,  
Geochemistry*

---



# A Case Study of the Regional 3-D Basin Modeling in Amu Darya and Afghan-Tajik Basins

**Yücel Deniz Erdal<sup>1</sup>, Zeynep Adıgüzel<sup>1</sup>, Şikrü Gökhan Köse<sup>1</sup>, Hasan Güney<sup>2</sup>, Helby Ellen<sup>2</sup>, Ayodeji Temitope Ajayi<sup>2</sup>, Mustafa Demirci<sup>1</sup>, Emrah Dölek<sup>1</sup>**

<sup>1</sup>TPAO

<sup>2</sup>Dragon Oil Ltd



## ABSTRACT

Amu Darya and Afghan-Tajik basins are prolific hydrocarbon basins with approximately 400 producing fields of Jurassic to Tertiary age reservoirs. Amu Darya basin is located mostly in Turkmenistan, Uzbekistan and extends marginally into Northern Iran and Afghanistan. Adjacent and to the East is the geographically smaller Afghan-Tajik basin separated by the southwest Gissar high. Afghan-Tajik basin marginally covers east of Turkmenistan and extends into Uzbekistan, Afghanistan, Tajikistan and Kyrgyzstan. Both basins were formed as a single rift basin during Mesozoic period, having similar geological and depositional histories as well as petroleum systems from Mesozoic to Cenozoic period with approximately 10 km sedimentary sequences. The single rift basin was subsequently exposed to compression from Late Oligocene to recent times widely known as the Alpine Orogeny phase. The result is a separation into two sub basins marked by the Gissar Range, a mountain range in Turkmenistan, Tajikistan and Uzbekistan.

Most of the discovered and productive hydrocarbons in both basins are from the Lower to Upper Jurassic clastics and carbonate reservoir with a Middle to Upper Jurassic shales as source rocks and Upper Jurassic salt as an effective seal. Dragon Oil Ltd and TPAO G&G team's studies confirmed the existence of this petroleum system in the Sanduqli and Mazar-i-Sharif blocks located in Afghanistan with several prospective areas for drilling new wells in the block. The aim of this study is to reduce exploration risks of generated prospects by calibrating the regional basin modeling study with the production fields in both basins and to have a better understanding of the petroleum systems, kitchen areas and possible charge mechanisms.

The regional basin modeling area approximately covers 75,000 km<sup>2</sup> in southeast Turkmenistan, southwest Uzbekistan, southeastern Tajikistan, and northern Afghanistan. A detailed 3-D basin model was constructed with 18 layers by using 11 structural depth maps, interpreted fault surfaces, topographical map of the area, formation tops of 50 wells, available temperature data and literature information. Initially, a structural model that reflects the depositional history of the basin through geological history was created. Lithologies, facies, source rock properties, and kinetics were assigned to related layers. Subsequently, boundary conditions that include paleo and present-day heat flows, paleo-water depths, sediment-water interface, temperatures were defined. Simulations were performed on basin and petroleum system modeling software in which models were calibrated with observed real data. As a result of the study, temperature, maturity, generation, expulsion, and transformation ratio maps of the source rocks as

well as hydrocarbon migration-accumulation maps were obtained which match with discovered fields very well.

The results show that source rocks are mostly in wet gas and dry gas maturity windows whereas they are in oil window within the edges of the study area. Onset of hydrocarbon expulsion of the Jurassic source rocks occurred in Cretaceous. The details and results of this 3-D basin and petroleum system model confirm the hydrocarbon charge-migration to the generated prospects in the Sanduqli and Mazar-i-Sharif blocks and to the production fields in the Amu Darya and Afghan-Tajik basins. This study reduced the risk and uncertainties of the prospects in the Sanduqli and Mazar-i-Sharif blocks and helped to better understand the petroleum systems, revealing the hydrocarbon prospectivity of the area.

## GİRİŞ

Amu Darya ve Afgan-Tajik Basenleri Asya Kıtası'nda yer almakla birlikte Türkmenistan, Özbekistan, Tacikistan ve Afganistan ülke sınırlarının içerisinde toplamda 500.000 km<sup>2</sup>'nin üzerinde bir alanı kaplamaktadır. Zengin hidrokarbon potansiyeli barındıran bu basenlerde Jura – Tersiyer yaşlı rezervuarlardan hidrokarbon üreten 400 civarında saha bulunmaktadır. Amu Darya Baseni'nin büyük bir kısmı Türkmenistan sınırları içerisinde kalsa da doğu ve güneydoğu kısımları diğer ülke sınırlarına düşmektedir. Amu Darya ve Afgan-Tajik Basenleri'nin Mezozoyik Dönemi'nden günümüze kadar geçirdiği jeolojik evrim ve ilişkili petrol sistemleri birçok uzman tarafından çalışılmıştır (Ulmishek,2004; Klett ve diğerleri, 2006; Ismagulova ve diğerleri, 2016; Sabawon,2017; Carneille, 2018; Gagala ve diğerleri, 2020). Bu basenler genişleme rejimi etkisi altında yekpare bir rift baseni olarak Mezozoyik döneminde oluşmuştur. Geç Oligosen ve Miyosen dönemlerinde Alpin Orojenezi neticesinde oluşan sıkışma rejiminin etkisiyle iki basen birbirinden Gissar Yükselimi ile ayrılmıştır. Bu nedenle iki basenin Neojen öncesi petrol sistemi elemanları oldukça benzerlik göstermektedir. Bu bölgede, Alt – Orta Jura klastik istif içerisinde ve Üst Jura yaşlı şeyl birimlerinin içerisinde 2 adet önemli kaynak kaya bulunmaktadır. Potansiyel rezervuar seviyeleri ise Jura yaşlı klastik ve karbonat çökelleri ile Hauterivian yaşlı klastikler oluşturmaktadır. Üst Jura yaşlı evaporatik Gaurdak Formasyonu bölgesel bir örtü kaya olarak Mezozoyik petrol sistemlerine katkı sunmaktadır (Figure 1; Klett ve diğerleri, 2006).

Geçmişten günümüze Amu Darya ve Afgan-Tajik Basenleri'nde çok sayıda ve nitelikli petrol ve doğalgaz arama faaliyeti yürütülmüş, bu çalışmalar sonucunda birçok saha keşfedilmiştir (Demirer ve Batı, 2017). Keşif yapılan sahaların çoğunluğu Mezozoyik petrol

sistemleri ile ilişkilidir. Öte yandan bu çalışmaya konu olan Amu Darya Baseni'nin güney doğu ucu ile Afganistan'ın kuzey ve kuzey batısında bulunan bu alanlarda sınırlı sayıda kuyu açılmış, test edilmemiş birçok yapı bulunmaktadır.

Bu çalışmanın amacı petrol sistemlerini, kaynak kaya mutfak alanlarını ve olası hidrokarbon şarj mekanizmalarını detaylı bir şekilde tanımlayarak arama risklerini en aza indirmek ve bölgenin hidrokarbon potansiyeline ışık tutmaktır. Bu çalışmada on bir adet bölgesel yapı haritası, topoğrafya haritası, fay yorumları ile mevcut kuyu verileri kullanılarak on sekiz katmanlı detaylı bir basen modeli oluşturulmuştur (Şekil 2). Çalışma alanı yaklaşık 75.000 km<sup>2</sup>'lik bir alanı kapsamaktadır. Basen ve petrol sistemi modelleme yazılımı (PetroMod 2019.1) kullanarak mevcut tüm veriler ile literatür verileri entegre edilmiş, model verileri ile gerçek veriler kalibre edilmiştir.

## DATA VE YÖNTEM

Üç boyutlu basen ve petrol sistemi modellemesinin temel amaçlarından biri, geçmişten günümüze basenin ve petrol sisteminin geçirdiği jeolojik evrimi anlamaktır. Model oluşturmak için yapı haritaları, faylar, kuyu verileri, 'model sınır koşulları' olarak tanımlanan diğer parametreler ile literatürden elde edilen veriler modele entegre edilir.

Bu çalışmada üç boyutlu jeolojik model oluşturmak amacıyla toplam elli kuyu verisi, sismik ve jeolojik verilerin yorumlanmasıyla oluşturulan on bir adet derinlik yapı haritası ve otuz bir tane fay yorumu kullanılmıştır. Yapı haritalarının üçü Jura, üçü Kretase ve beş tanesi Tersiyer dönemine aittir. Mevcut olmayan derinlik yapı haritalarına ait katmanlar ise kuyu verileri kullanılarak oluşturularak, üç boyutlu model geometri kurulmuştur.

Basenin jeolojik tarihçesi ve kuyulardan elde edilen verilere uygun olarak günümüz ve geçmiş dönem ısı akışı verileri (present day and paleo-heat flow), sediman-su etkileşim sıcaklığı (sediment—water interface temperature), geçmiş dönem su derinlikleri (paleo-water depth) gibi veriler sisteme tanımlanmıştır. Sonrasında ise sıcaklık, olgunluk, kaynak kaya parametrelerine dair kalibrasyonlar yapılarak model çalışması tamamlanmıştır.

## SONUÇLAR

Basen analizi ve petrol sistemi modellemesinde kullanılan iki Jurassic yaşlı kaynak kayanın olgunluk profilleri oluşturulmuştur. Bunlardan yaşlı olan Baysun Formasyonu içerisinde organik maddece zengin seviyelerdir ve tip III kaynak kaya olarak değerlendirilmiştir. Daha genç olan Kugitang Formasyonu'nda kaynak kaya seviyeleri içermektedir ve bu seviyeler tip II kaynak kaya olarak değerlendirilmiştir. Her iki kaynak kayanın da çalışma alanının derin olan orta alanlarında kuru gaz olgunluk penceresinde olduğu, gömülmenin nispeten daha az olduğu çalışma alanının kenarlarında ise erken

olgun petrol penceresine kadar düştüğü görülmüştür. Kaynak kaya tipinden kaynaklanan kinetik değişimler sebebiyle, tip III olan Baysun Formasyonu içerisindeki kaynak kaya seviyelerinin potansiyelinin önemli bir kısmını günümüze kadar tükettiği ancak, olgunluğun nispeten daha düşük olduğu yerlerde kaynak kayanın potansiyelini koruduğu düşünülmektedir. Derin alanlarda, Kugitang Formasyonu içerisindeki tip II kaynak kaya seviyelerinin Üst Kretase sonunda tükenmiş olduğu düşünülmektedir. Olgunluğun daha düşük olduğu alanlarda ise, türüm-atım zamanlamaları daha geç olabilmektedir. Bu bilgiler ışığında, derin alanlarda Kretase ve öncesi yapılar daha pozitif olarak değerlendirilebilir. Daha geç olgunlaşan alanlarda ise daha genç yapıların pozitif olabileceği değerlendirilebilir. Çalışma alanının büyüklüğünden dolayı, türüm-atım ve yapı oluşum zamanları farklılık gösterdiği için, prospektlerin petrol sistemleri noktasal bazda değerlendirilmelidir.

Çalışma alanındaki rezervuar kayalardan biri olan Kugitang Formasyonu'nun üzerindeki Gourdak Formasyonu'nun evaporitlerinin yüksek sıcaklık altında hidrokarbonlar ile tepkimeye girme olasılığı vardır. Bu sebeple söz konusu seviyelerde termokimyasal sülfat indirgenmesi (TSR) çalışılmıştır. Basenin derin kısımlarında, rezervuar sıcaklığının 120oC üzerinde olduğu görülmüştür. Bu alanların TSR açısından riskli olarak düşünülmektedir.

Bu çalışmada, 75.000 km<sup>2</sup> lik geniş bir alanda yürütülen üç boyutlu basen ve petrol sisteminin kalibre edilmiş sonuçları değerlendirilecek; model çıktıları ile bölgenin arama riskleri ve hidrokarbon potansiyeline ışık tutulacaktır.

## REFERANSLAR

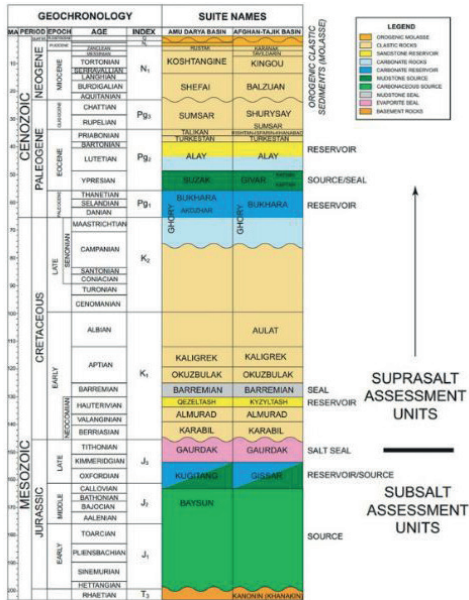
- Carmeille, M., Bourillot, R., Brunet, M. F., Pellenard, P., Fürsich, F., Schnyder, J., Barrier, E., Blanpied, C., Sidorova, I., 2018. Architecture And Sedimentary Evolution Of The Southwestern Gissar Carbonate Platform (Uzbekistan) During The Middle–Late Jurassic. *Marine and Petroleum Geology* Volume97, 437-465.
- Demirer, A., & Batı, Z., 2017. 132 Hydrocarbon Potential And Exploration History Of Northern Afghanistan 260–261. Ankara; TMMOB Jeoloji Mühendisleri Odası.
- Gagala, L., Ratschbacher, L., Ringenbach, J. C., Kufner, S. K., Schurr, B., Dedow, R., 2020. Tajik Basin and Southwestern Tian Shan, Northwestern India-Asia Collision Zone: 1. Structure, Kinematics, And Salt-Tectonics in the Tajik Fold-and-Thrust Belt of the Western Foreland of the Pamir. *Tectonics* Volume 39 Issue 5.
- Klett, T. R., Ulmishke, G. F., Wandrey, C. J., Agena, W. F., 2006. U.S. Geological Survey Afghanistan Ministry Of Mines And Industry Joint Oil and Gas Resource Assessment Team. 2006. Assessment of Undiscovered Technically Recoverable Conventional Petroleum Resources Of Northern Afghanistan. U.S. Geological Survey Open File Report, 2006-1253.
- Sabawon, A., Kurihara, M., Moriya, S., Kamata,

H., 2017. Hydrocarbon Generation and Expulsion Modeling of Jurassic-Cretaceous Petroleum System of the Amu Darya Basin, Northern Afghanistan. Journal of the Japanese Association for Petroleum Technology.

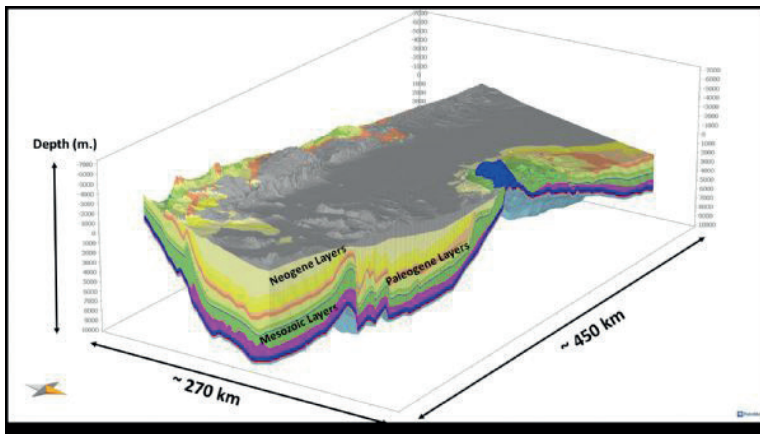
Ulmishek, G. F., 2004. Petroleum Geology And Resources of the Amu Darya Basin, Turkmenistan, Uzbekistan, Afghanistan, and Iran. U.S. Geological Survey Bulletin, 2201-H.

Keywords: Amu Darya Basin, Afghan-Tajik Basin

Şekil 1. Amu Darya ve Afgan-Tajik Basenleri'nin Kronostratigrafisi (Klett ve diğerleri, 2006).



Şekil-2. Çalışma alanında oluşturulmuş 18 katmanlı bölgesel 3 boyutlu model görşeli



# Exploring Hydrocarbons in 1.75 Billion-Year-Old Pre-Cambrian Deposits of South Africa Using Environment Friendly SDDT Technology



**Ongun Yoldemir, Joerg Enge**  
Pytheas Ltd., Berlin / Germany

## INTRODUCTION

The Greater Karoo basin in South Africa has long been recognized for its substantial coal potential, but previous attempts at hydrocarbon (HC) exploration have been largely unsuccessful, with only shallow biogenic gas and helium discoveries. As a result, exploration efforts shifted towards offshore areas. Other regions, apart from Karoo, consist of billions of years old Pre-Cambrian groups, primarily characterized as glacial sediments, volcanics, and basement rocks such as granite, dolerite, and gneiss. Recently, our group has been approached by various individuals to initiate an HC exploration project in the Soutpansberg basin, located northeast of the country, due to reports of oil and gas seeps known to the locals.

We have commenced a comprehensive study to understand the nature and depositional history of the Soutpansberg basin units. The sedimentary units within the basin have been dated to approximately 1.7-1.6 billion years old. Our research, along with previous studies, suggests that the basin likely formed either as a half graben before tectonic movements further fragmented Gondwana into the continents that later became Antarctica, Australia, and India. An alternative theory proposes that the basin originated as a failed rift, potentially serving as a precursor to future rifting events. Utilizing virtual density profiles, we were able to partially map the basin while distinguishing sedimentary sequences and formations previously identified in earlier studies. Both our virtual differential density profiles and field studies conducted by previous researchers indicate the presence of fluvial, lacustrine, and flood plain sedimentary systems within the basin. The sedimentary deposits exhibit well-developed sandstones, often medium to coarse-grained with high porosity, along with shales, sandy shales, and mudstones that act as local sealing rocks.

Considering the ancestral forms of blue-green algae discovered in the Fig Tree Group silicified shales, dating back 3 billion years, the presence of sediments as young as 1.7-1.6 billion years old, potentially deposited in lacustrine environments, appears to address the issue of source rocks. Global studies have revealed that blue-green algae or similar bacterial algae flourished extensively between 1.8 billion and 500 million years ago, covering vast areas during that time. Preserved organic matter from these organisms serves as an excellent source for various hydrocarbons, primarily oil. Favorable conditions, including source rocks, reservoirs, burial, heat flux, and sufficient time, indicate the existence of a promising hydrocarbon system within the Soutpansberg basin

## METHODS

In this study, we employed an innovative technology known as Satellite-derived Density Tomography (SDDT) to investigate the area. We extracted Vertical Density Tomography (VDT) logs from a 3D cube generated using SDDT technology, which were then calibrated with actual well data from the nearby Pande field in Mozambique to correlate hydrocarbon indicator (HCI) data within our study area. The data cubes were derived from satellite images, and the 1D vertical differential density tomography logs (VDDT) displayed the vertical density changes from the surface up to a depth of 10 kilometers. These logs provided bulk density values for the rock units, forming the lithological column. Derivatives of the original bulk density data were created to differentiate fluid density changes vertically. By studying and correlating the VDDT profiles with the well data, we were able to identify sequence boundaries, unconformities, and overall density changes over significant distances.

The VDDT logs were calibrated using well data exhibiting similar HCI figures from an oil and gas field. By combining the knowledge gained from previous studies and the density profiles generated at virtual wells, we successfully mapped the recognized units. HCI indicator curves were used to define and map reservoir zones, as well as to understand potential migration pathways through lateral density slices at different depths, allowing for the identification of major fault systems within that interval. These depth slices also aided in defining shale-rich zones that could be associated with lacustrine lakes, serving as potential source areas (kitchen areas).

## CONCLUSIONS

As a result of these comprehensive studies several depth maps of the identified sequences and HCI maps of different levels were created. Using these data an exploration strategy has been developed, highlighting high-potential areas for drilling. The HCI maps were created mainly in four different levels up to the depth of 5000 meters for the ease of planning, drilling and production in the case of discovery. All four levels of HCI were prepared for drilling with four different scenarios for drilling and production. A twenty year of drilling, completion and production program and resource estimations were made. The program included the construction of collection centers and production facilities but ruled out the target consumer system. The program as well as the prepared locations and their programs were sent to the authorities for approval. After the environmental studies required by law, the prospects were accepted by the authority, (PASA, petroleum agency of South Africa) who is responsible



for permitting, and controlling, the exploration and production of hydrocarbons in South Africa. The preparations for drilling are being pursued as of today while there are no conventional drilling rigs available in the country. Rigs designed for mineral exploration are going to be adapted to drill oil and gas wells and get equipped with hazard prevention measures and equipment. After the approval by PASA, a state agency for investment joined to the project.

The project is currently ongoing with the support and involvement of South African investment agency. Any further developments that occur during the period leading up to the presentation of this paper will be incorporated into the final output.

Keywords: Pre-Cambrian deposits, HC exploration

# Pitfalls in Basin Modeling - A Case Study From the Eastern Black Sea

**Turan İscimen**

Türkiye Petrolleri A. O.



## INTRODUCTION

Basin modeling deals with four-dimensional forward modeling as constructing the paleogeological settings, depositional environments, and paleo-boundary conditions such as paleodepth, paleotemperature, and in general the traceable historical conditions. These models provide essential insights for basin evolution, development, determining the kitchen areas, source rock maturation, and timing of hydrocarbon migration and accumulation. However, data scarcity and lack of sufficient amount of measured or available data might lead misinterpretations about the significant outcomes of the model. Therefore, modelers need to be aware of the certain pitfalls and availability of different possible scenarios. In this edition, I provide major pitfalls from a four-dimensional basin model located at the eastern Black Sea Basin.

Black Sea Basin is assumed to be formed as a back-arc basin during early-mid Cretaceous. Furthermore, eastern Black Sea sub-basin is thought to be opened during Aptian-Albian ages (Hippolyte et al., 2018; Nikishin et al., 2015a; Nikishin et al., 2015b). General timing for the petroleum system covers whole Cenozoic, so the model basement rock is assumed as Upper Cretaceous Yemislıcaı Volcanics. In other words, the basin evolution is modelled starting from post volcanic activity period (Figure 1).

The brief geological history of the basin and the study area as follows: During post Cretaceous, the basin was at the last stage of the opening phase and it gradually ceased with deposition of Paleocene sediments at local depressions. Within the Early Eocene the basin has started to go into NE-SW compressional regime and Kuma Fm. source rock was deposited where sedimentation rate is slow at the deeper parts of the basin (Hippolyte et al., 2018; Sosson et al., 2017). On the other hand, deep water conditions cause creation of accommodation space and the sedimentation rate increased during Oligo-Miocene. At the deeper parts, where sedimentation rate is relatively slower, Maikop source rock levels were deposited widespread through the study area. The beginning age of Sarmatian coincides with onset of active compressional stress regime and major tectonic activity, which forms the NE-SW trending faulted structures (Meredith and Egan, 2002). The effect of compressional tectonics ceases through time and the Plio-Pleistocene sequence deposited as less distorted, over a highly deformed Oligo-Miocene megasequence.

## SCOPE AND AIM

The aim of this study is to find out the major basin modeling pitfalls, which a basin modeler can encounter with as studying on the models and interpreting the

model results. In order to achieve that aim I have built a four-dimensional model and interpreted the model results.

## METHODOLOGY

The four-dimensional basin model is constructed in Petromod v2021 software. Key seismic surfaces, available relative and exact ages, boundary conditions (paleoheat flow, paleodepth, paleo-temperatures), available pyrolysis data, vitrinite reflectance values, and findings of unpublished and published scientific reports were used as inputs for the model. The model is calibrated with respect to porosity, pressure, temperature, and maturity. After the calibration process, I generated the base model and I run the model several times with different configurations as keeping the most of the parameters the same except one. By this approach, I expected to reveal the reasons of having distinct results while changing one parameter. In the end, I have found out five major pitfalls, which may have crucial effects on the model results. These five major pitfalls related with this model are presented below in the results part.

## RESULTS

### 1. The critical time, availability of petroleum system elements and it's spatial distribution among the study area

Critical time is the onset of petroleum expulsion following all of the petroleum system elements (source rock, reservoir rock, trap formation, overburden, and seal rock) are in place. The model comprises both thermogenic and biogenic source intervals starting from Eocene to Pleistocene. Their spatial distribution differ from each other according to the paleo depositional conditions. Critical timing could be uncoupled with maturity and kerogene transformation ratio for a source rock depending on the spatial distribution of burial rate and heat flow. Therefore, the modeler needs to be cautious about the hydrocarbon generated areas and their vicinity of the potential structural traps and reservoirs.

Briefly, in this case, kitchen area lies at the northern parts of the study area, but generation and expulsion mostly occur prior to and concurrent with major compressional tectonics. On the contrary, the source intervals at the southern parts, are relatively less mature and thinner. Moreover, at the southern regions, hydrocarbon generation and expulsion timing occurs at more favorable periods that is post-tectonic activity. However, NE-SW trending structures are located at the northern parts and missing at the southern parts. In other words, the hydrocarbon that was generated at the

southern parts, mostly become dispersed and cannot migrate into the larger structures. Moreover, formation of trap mechanisms happened to be Late Serravalian to Tortonian (Sarmatian), but onset of hydrocarbon expulsion starts in Oligocene, before trap formation at the northern areas. Therefore, in such cases, the modeler needs to elaborate the time span between onset of hydrocarbon generation, expulsion and trap formation. Furthermore, one needs to calculate the residual potential of the kitchen areas for post critical time period.

## 2. Regional tectonics and characteristics of faults

Active compressional tectonic regime is modeled through Sarmatian, and most of the sediments or layers below Pliocene, was shaped between 12.7 Ma to 5.3 Ma. The model faults, which cut through the Cenozoic sequence, provide upward migration from the Maikopian sequence. In this model, two end members (open and closed faulting scenarios) were applied to the model faults. The closed faults block both vertical and horizontal fluid flow. So the hydrocarbons become scattered and dispersed through large pile of sedimentary formations. On the other hand, if the faults are assumed to be open, hydrocarbons expelled from deeper sediments can migrate through the discontinuities and trapped if the reservoir and sealing conditions are met. In short, the open fault scenario provides more favorable results with respect to hydrocarbon accumulation.

## 3. Outflow and influx (migration) of hydrocarbons

Model boundary can be simulated as open or closed for fluid flow. If the model boundaries are open hydrocarbon can migrate outside and inside of the model through the boundaries. Conversely, closed boundary prevent both influx and outflow. In this case, when the model boundaries are closed, more hydrocarbon can be trapped within the system and the accumulations associated with the model border increase. So, modeler can understand the relative amount of hydrocarbon outflow is greater than the influx through the borders. Furthermore, closed boundary conditions cause more hydrocarbon accumulations within the model.

## 4. The effect of physical characteristics of reservoir facies on possible reservoirs and hydrocarbon accumulations

When there are fewer wells with limited pressure data, the modeler had better control over the other parts of the study area with respect to pressure gradients. Theoretically, the pressure gradient is expected to increase with greater depths, although the porosity and permeability of the rock lithology mix are decider agents for the pressure gradient. Pressure and porosity calibrations are pretty much straight forward, in case of adequate data points. However, lack of sufficient data requires making assumptions, additional model runtime, and trial and error process.

If the porosity and permeability of a chosen lithology mix is taken as default physical values, the reservoir properties can be miscalculated. In this model, when the reservoir layer parameters are used with default porosity and permeability values according to the lithology mix, in that case, the reservoir capacity would be overestimated for the so-called reservoirs. Moreover, unrealistic hydrocarbon accumulations could be present in favorable structures. On the other hand, when the reservoir layers are modeled with measured data, which has lower porosity and permeability, the reservoir quality of the so-called reservoir layers are diminished. However, the second case is more realistic and accurate according to the prognosed pore pressure gradient. To sum up, the modeler should be aware of that the default values of reservoirs could lead to misinterpretations and they are needed to be corrected according to the expected pressure gradient.

## 5. The effect of facies distribution and stacking patterns of similar formations on hydrocarbon accumulation and migration

When similar facies vertically stacked on top of each other, they form a larger, homogeneous mass either it is a reservoir or seal rock. The homogeneous mass act as a single geobody, which amplifies either reservoir or seal rock properties. Therefore, the modeler needs to elaborate on the vertical resolution and facies distribution through the model.

When the reservoir facies are vertically stacked together, according to flowpath and invasion percolation migration methods, the fluids can easily move upward direction. The upward movement continues until the fluids come across a sealing layer and then it starts to accumulate. In that case, two models were run in order to decipher the effect of facies distribution and stacking patterns of similar formations. The first model comprises large single homogeneous geobodies, conversely the latter constitutes reservoir-seal intercalations. In the first case, I observed that hydrocarbon accumulation potential of uppermost reservoirs are overestimated, although the underlying reservoirs might be underestimated. The reservoir layers of the second model, on the contrary, could hold more hydrocarbon entrapments at each layer bounded by seal rock facies. Therefore, the modeler needs to optimize vertical thickness of the layers considering reservoir and seal capacities.

## CONCLUSION

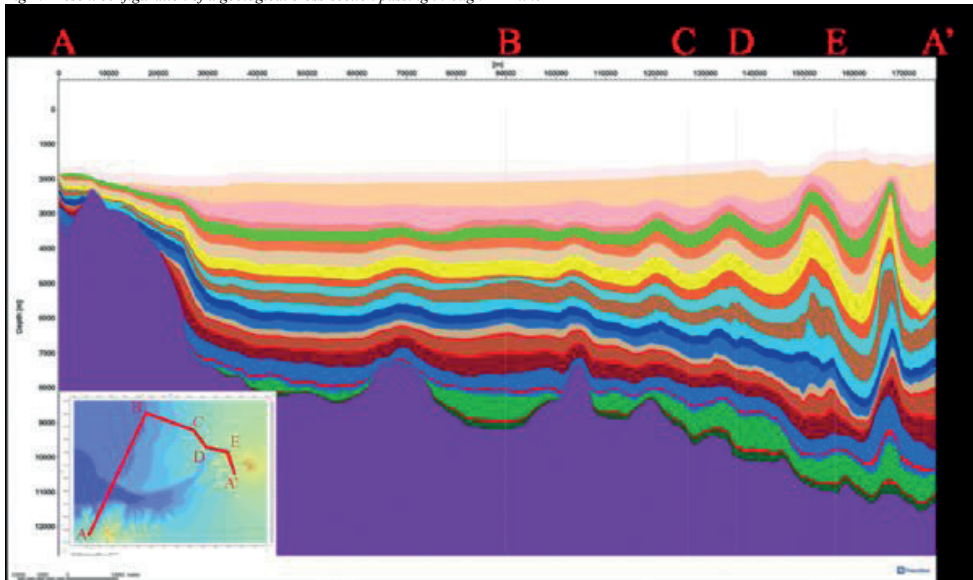
To sum up, availability of more data points narrows down the possible scenarios and provide more solid and reliable results. On the other hand, having less data points cause infinitely many possible scenarios, which requires modeler's detailed elaboration, model runtime, and trial-error process.

## REFERENCES

- Hippolyte, J.-C., Murovskaya, A., Volfman, Y., Yegorova, T., Gintov, O., Kaymakci, N., & Sangu, E. (2018). Age and geodynamic evolution of the Black Sea Basin: Tectonic evidences of rifting in Crimea. *Marine and Petroleum Geology*, 93, 298–314. <https://doi.org/10.1016/j.marpetgeo.2018.03.009>
- Meredith, D. J., & Egan, S. S. (2002). The geological and geodynamic evolution of the eastern Black Sea Basin: Insights from 2-D and 3-D tectonic modelling. *Tectonophysics*, 350(2), 157–179. [https://doi.org/10.1016/s0040-1951\(02\)00121-x](https://doi.org/10.1016/s0040-1951(02)00121-x)
- Nikishin, A. M., Okay, A. I., Tüysüz, O., Demirer, A., Amelin, N., & Petrov, E. (2015a). The Black Sea basins structure and history: New model based on new deep penetration regional seismic data. part 1: Basins structure and fill. *Marine and Petroleum Geology*, 59, 638–655. <https://doi.org/10.1016/j.marpetgeo.2014.08.017>
- Nikishin, A. M., Okay, A., Tüysüz, O., Demirer, A., Wannier, M., Amelin, N., & Petrov, E. (2015b). The Black Sea basins structure and history: New model based on new deep penetration regional seismic data. part 2: Tectonic history and Paleogeography. *Marine and Petroleum Geology*, 59, 656–670. <https://doi.org/10.1016/j.marpetgeo.2014.08.018>
- Sosson, M., Stephenson, R., & Adamia, S. (2017). Tectonic evolution of the Eastern Black Sea and caucasus: An introduction. *Geological Society, London, Special Publications*, 428(1), 1–9. <https://doi.org/10.1144/sp428.16>

Keywords: basin modeling, Black Sea

Fig 1: Present configuration of a geological cross-section passing through A-A' line



# Rock Eval Piroliz Analizi ile Kinetik Parametrelerin Karakterizasyonu ve Silüriyen Yaşlı Dadaş Formasyonu'nun Kinetik Parametrelerinin Belirlenmesi Projesi



**Cihan Can<sup>1</sup>, Zeynep Özlem Cihan<sup>1</sup>, Şükrü Gökhan Köse<sup>2</sup>, Yücel Deniz Erda<sup>2</sup>**

<sup>1</sup>Türkiye Petrolleri Anonim Ortaklığı Ar-Ge Merkezi Daire Başkanlığı

<sup>2</sup>Türkiye Petrolleri Anonim Ortaklığı Arama Daire Başkanlığı

## ÖZET

Türkiye Petrolleri Anonim Ortaklığı'nca deniz ve kara alanlarında yürütülen konvansiyonel ve ankonvansiyonel hidrokarbon arama faaliyetlerinde önemli bir yer tutan petrol sistemi ve basen modelleme çalışmaları ile petrol sisteminin zaman içerisindeki dinamik yapısı incelenerek, basenin petrol ve doğalgaz üretme potansiyeline yaklaşımda bulunmaktadır.

Kaynak kayalar, basenin geçirmiş olduğu gömülme ve termal tarihçesine bağlı olarak, belirli jeolojik dönemlerde hidrokarbon üretme potansiyeline sahiptirler. Türümü gerçekleşen bu hidrokarbonların türüne, miktarına ve zamansal dağılımına matematiksel modelleme yöntemleri ile yaklaşımda bulunmaktadır. Kerojenlerin hidrokarbona dönüşüm davranışı, kaynak kaya içerisindeki organik maddenin türüne göre farklılık göstermektedir. Kaynak kayanın içerdiği kerojen moleküllü, farklı ısı enerjisi seviyelerinde farklı hidrokarbon moleküllerine dönüşmektedir. Bu dönüşümün hızı, oranı ve ortaya çıkan hidrokarbon bileşenlerin miktarı kerojenin kinetik özellikleri ile tariflenir.

## DENEYSEL ÇALIŞMA

Ar-Ge Merkezi Jeokimya Müdürlüğü'nde bulunan Piroliz ve Kinetik Analizleri Laboratuvarı'nda kayalarındaki hidrokarbon potansiyeli, termal olgunluk, kerojen tipi ve organik malzeme zenginliği ile beraber kaynak kaya seviyeleri tayin edilebilmektedir. Dadaş Formasyonu'nu kesen kuyulardan basenin farklı lokasyonlarında açılan; 14 farklı kuyudan seçilen olgunlaşmamış-olgun aralığında, düşük-yüksek TOC değerlerine sahip seviyelerden 19 adet örnek seçilerek Rock Eval 7S cihazı ile 5-10-15-25°C/dakika sıcaklık artış hızına tabi tutularak, kinetik parametrelerinin saptanması amacı ile analizler yapılmıştır. Elde edilen veriler Basen Analizi Müdürlüğü'nce 2 adet kuyunun modellemesinde kullanılmıştır.

## SONUÇLAR

Çalışma sonucunda, 14 kuyu için basen modellemesi çalışmalarında kullanılacak kinetik enerji parametreleri üretilmiştir. Bu üretilen dotalar aracılığıyla, kuyular ile kerojen dönüşümü için enerji gereksinimleri arasında korelasyonlar yapılabilmektedir. Ayrıca, kinetik parametrelerin de işleneceği bir adım olarak değerlendirilen bu proje vasıtasıyla, TPAO ARGEM bünyesinde yeni bir değerlendirme yöntemi kazandırılarak yapılacak basen modellemesi çalışmalarına sağlam bir alt yapı oluşturulmasına

yardımcı olunmuştur.

The Characterization of Kinetic Parameters by Rock Eval Pyrolysis Analysis and Determination of Silurian Aged Dadas Formation Kinetics

## SUMMARY

Turkish Petroleum Corporation operates conventional and unconventional hydrocarbon exploration activities, in which petroleum system and basin modelling studies occupy an important place. According to these studies, the dynamic structure of petroleum system is examined and an estimation of petroleum and natural gas production potential is predicted.

Source rocks have a hydrocarbon production potential at some specific geological times according to burial and thermal history of a basin. Mathematical modelling tools are preferred to be used according to the type, amount and distribution of the hydrocarbon. The conversion behaviour of kerogen to the hydrocarbon changes according to the organic material type in a source rock. A kerogen molecule in the source rock converts into different hydrocarbon molecules based on different heating levels. This conversion rate, ratio and the amount of produced hydrocarbons are described as kinetic parameters of kerogen.

## MATERIALS AND METHODOLOGY

The source rock levels, hydrocarbon potential, thermal maturity, kerogen type and organic material richness of a rock is determined in Pyrolysis and Kinetic Analysis Laboratory at Turkish Petroleum Corporation Research and Development Center. In this study, 19 cutting samples from 14 different wells which are penetrated Dadas Formation, are immature – mature samples with low and high TOC values. They are analysed in Rock Eval 7S device with a temperature ramp of 5 to 25°C with an increment of 5°C in order to determine reaction kinetics. Collected data in this project are used for modelling 2 different wells at Turkish Petroleum Corporation Basin Analysis Department.

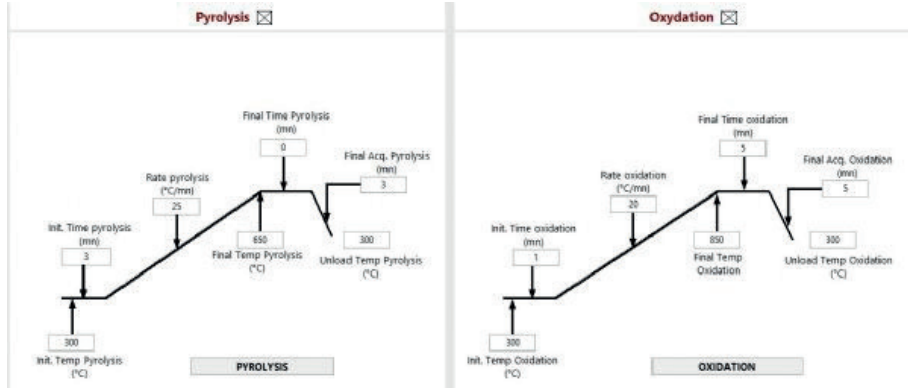
## RESULTS

At the end of this study, kinetic parameters are produced for 14 different wells in order to be used at basin modelling projects. By the help of this data, important correlations can be established according to the wells and their energy requirements for kerogen transformation. Furthermore, a strong infrastructure for basin modelling studies is aimed by TPAO R&D Center

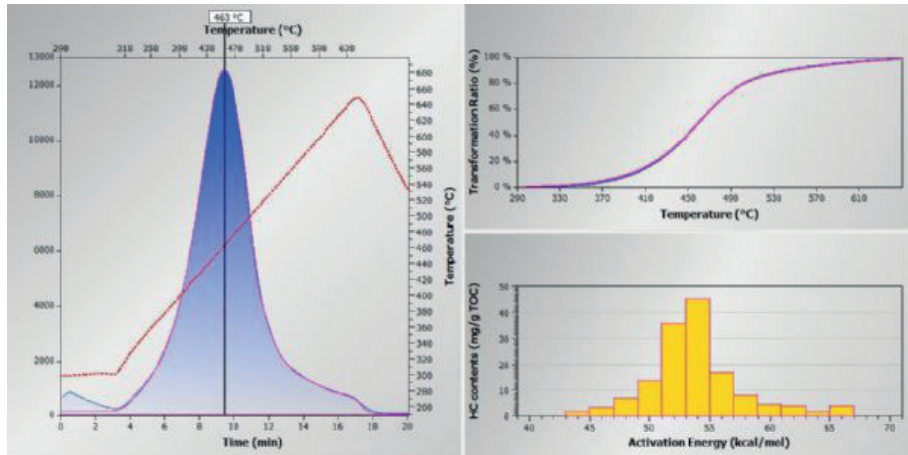
with gaining a new interpretation tool in which these newly-produced kinetic parameters will be used.

Anahtar Kelimeler: kinetik parametre, basen modellemesi

Şekil 1. Piroliz ve oksidasyon sıcaklık programları



Şekil 2. Bir kayaç numunesine ait kinetik analiz ve dönüşüm grafikleri



# Doğu Trakya Havzası Basen ve Petrol Sistemi Modellemesi (Basin and Petroleum System Modeling in the Eastern Thrace Basin)



**Esra Yalçın Yılmaz, Şükrü Gökhan Köse**  
TÜRKİYE PETROLLERİ A.Ö.

Türkiye'nin kuzeybatısında yer alan Tersiyer Trakya Havzası, kara alanlarındaki en önemli hidrokarbon arama bölgelerinden birisidir ve Türkiye'nin en fazla doğal gaz üreten kara bölgesidir. Günümüzde, Türkiye'nin kara gaz üretiminin yaklaşık %90'ı Trakya Havzasından sağlanmaktadır. Temel birimler üzerine gelen 9000 m'ye kadar ulaşan Eosen- Pliyosen sediman istifleri hem termojenik gaz hem de biyojenik gaz üretmektedir. Tersiyer istifi içerisindeki farklı seviyelerde rezervuar ve örtü birimleri de yer almaktadır. 2016 yılında keşfedilen Türkiye'nin ilk volkanik rezervuarı da Doğu Trakya Baseni'nde bu çalışma alanı içerisinde yer almaktadır. Trakya Havzası'nda, yapısal ve stratigrafik kaplanlarla birlikte, bunların kombinasyonları da var olabilmektedir. Bu çalışmada, 2 ve 3 boyutlu havza modellemesi ve petrol sistemi değerlendirmesi için derinlik haritaları (yapısal haritalar), fay yorumları, stratigrafi, kuyu logları ve jeokimyasal veriler entegre edilmiştir. Çalışma alanı Petrol Sistemi Modellemesi, Doğu Trakya Havzası'ndaki kaynak kaya olgunlukları, mutfak alanları, hidrokarbon türümü, atımı, dönüşüm oranları ve göç yollarının belirlenmesi gibi aramacılık açısından büyük önem arz eden sonuçlar ortaya koymuştur. Gömülme tarihesi ve termal tarihe modelleri oluşturulmuş, ölçülmüş veriler ve model sonuçlarıyla kalibre edilmiştir. Çalışma alanında, gömülme tarihesiyle uyumlu olarak kuzeydoğudan güneybatı yönüne doğru kaynak kayanın olgunluğunda ve termojenik hidrokarbon türüm ve atım miktarlarında önemli bir artış vardır. Kaynak kayaların olgunluk pencereleri, güneybatından kuzeydoğuya doğru kuru gaz olgunluk penceresinden, olgunlaşmamış pencereye kadar değişkenlik göstermektedir. Bu çalışmamız petrol sisteminde volkanik ve resifal rezervuarları içermekle birlikte Hamitabat, Ceylan ve Mezardere kaynak kayalarının potansiyellerini de değerlendirmek için yapılmış yayınlanan ilk 3 Boyutlu basen modelleme çalışmasıdır. Çalışmamız sonucunda, Doğu Trakya Baseni'nde kaynak kayaların potansiyellerinin termojenik petrol sistemi içinde daha iyi anlaşılması ve farklı alanlarda değişen parametrelerin arama çalışmaları açısından önemi ortaya konulmuştur.

The Thrace Basin is one of the major onshore hydrocarbon exploration region of Türkiye. The Tertiary sediment units on the basement rocks reaches up to 9000 m includes different plays in these sediment sequences including both thermogenic and biogenic gases. In this study, geophysical, geological and geochemical data are integrated for 2 and 3-dimensional basin modeling and petroleum system evaluation. The regional burial history and thermal history models are created, then calibrations are made with available data. In the study area, there are a significant increase in the maturity and the thermogenic hydrocarbon generation amounts of the source rock from northeastern to southwestern margin

based on the burial history. The maturity windows of the source rocks are dry gas to immature window from the southwest to northeast. As a result of this study, the maturity amount of the source rocks, the thermogenic petroleum systems, and migration pathways have been revealed on a regional scale to better understand the importance of variable parameters in different regions for exploration studies in the Eastern Thrace Basin.

## GİRİŞ

Trakya Baseni, içerisinde barındırdığı hidrokarbon potansiyeli açısından önemli bir alan olup, daha önce birçok çalışmacı tarafından petrol sistemlerinin detaylarına yönelik araştırmalar yürütülmüştür (Gürgey ve diğerleri, 2005; Huvaz ve diğerleri, 2005; Siyako ve diğerleri, 2008; Köse ve diğerleri, 2018, Gürgey ve Bati, 2018; Yalçın ve diğerleri, 2021). Trakya Baseni'nde termojenik petrol ve doğalgaz bulgularının yanında, biyojenik gaz sistemlerinin varlığı da kanıtlanmıştır. Ayrıca, Trakya Baseni'nde yer alan sahalarındaki gaz örneklerinin moleküler ve izotopik kompozisyonları ile bu gazları türeten kaynak kayaların kökeni ve korelasyonu üzerine detaylı çalışmalar da yapılmıştır (Hoşgörmez ve diğerleri, 2005; Hoşgörmez ve Yalçın, 2005).

Trakya Baseni'nde yapılan birçok çalışmada Hamitabat ve Mezardere formasyonlarının kaynak kaya potansiyelleri ortaya konulmuş, yer yer Ceylan Formasyonu, Osmançık ve Danişen Formasyonlarının da kaynak kaya olabileceği alanlar çalışılmıştır. Ayrıca, Tersiyer istifi içerisindeki farklı seviyelerde rezervuar ve örtü birimleri yer almaktadır. Farklı yaşlarda yapıların bulunduğu basende yapısal ve stratigrafik kaplanlarla birlikte bunların kombinasyonları da bulunmaktadır.

Bu çalışmada Eosen – Oligosen yaş aralığında bulunan olası kaynak kayaların termojenik gaz potansiyelleri ve petrol sistemleri değerlendirilmiştir.

## DATA VE YÖNTEM

DATA ve Yöntem: Basenin günümüz geometrisi ve geçmişteki çökelim tarihesinin modellenmesi için, temelden yüzeye kadar olan formasyonlarına ait yapı haritaları ve fay yorumları (TPAO Arama Grubu - Trakya Projesi, 2021) ile çalışma alanı içerisindeki 131 kuyunun verisi değerlendirildi. Bunlardan 34 kuyunun formasyon girişleri, jeolojisi haritası ve topoğrafya haritası kullanıldı. Gömülme tarihesine uygun olarak model kronostratigrafisi oluşturuldu. Isı tarihesi için önemli olan sınır koşulları olarak Isı Akısı (HF – Heat Flow), paleo suderinlikleri (PWD - paleo water depth), su-sediman etkileşim sıcaklıkları (SWIT - Sediment water interface temperature) çalışma alanı için

tanımlanmıştır. 31 kuyuya ait sıcaklık verisi BHT (kuyu dibi sıcaklığı), 6 kuyunun olgunluk verisi (vitritite relectance %Ro), ve 12 kuyunun kaynak kaya verileri (TOC ve HI) model kalibrasyonu için kullanıldı. Bu çalışmada kullanılan iş akışı Şekil 1'de özetlenmiştir. Basen ve petrol sistemi modellenmesi yapılırken ölçülmüş verileri modele kalibre etme işlemi oldukça önem arz etmektedir. Bu çalışmada olgunluğa karşı derinlik ve sıcaklığa karşı derinlik grafikleri çizdirilerek kalibrasyon işlemleri yapılmıştır. Şekil 2'de kalibrasyon işlemleri sonrasında, çalışma alanı içerisindeki bir nokta üzerine çizdirilmiş sıcaklık ve olgunluk verileri görülmektedir.

## SONUÇ

Çalışma alanı ve 3 Boyutlu günümüz basen geometrisi Şekil 3'te gösterilmiştir. Basen analizi çalışmalarında modellenen alan üzerinde Hamitabat, Ceylan ve Mezardere Formasyonlarına ait kaynak kayalarının olgunluk pencereleri değerlendirilmiştir. Olgunluk haritalarında elde edilen sonuçlara göre;

1. Hamitabat Formasyonu çalışma alanındaki kuzeydoğu kuşağı boyunca (gömülmenin az, basenin sığ olduğu kısımlar) olgunlaşmamış ve erken olgun zonlarda yer almakta olup, olgunluk dereceleri düşüktür. Bu alanlarda Transformation Ratio – hidrokarbon dönüşüm oranı - (TR%); dolayısı ile hidrokarbon türüm ve atım miktarları oldukça düşüktür. Bu dönüşüm oranı değerleri petrol sistemi açısından düşüktür ve yüksek miktarda hidrokarbon türümünü desteklememektedir.
2. Hamitabat Formasyonu çalışma alanındaki güneybatı alanlarda (basenin derinleştiği ve gömülmenin yüksek olduğu alanlarda) ıslak gaz – kuru gaz olgunluk pencerelerine ulaşmaktadır. Bu alanlarda artan olgunluk derecelerine bağlı olarak hidrokarbon dönüşüm oranları, hidrokarbon türüm ve atım miktarları göreceli oldukça yüksek seviyededir.
3. Ceylan Formasyonu ise çalışma alanının büyük bir kısmında olgunlaşmamış – erken olgun zonda olsa da güneybatı istikametinde gaz zonuna erişecek kadar gömülmektedir. Ancak kaynak kaya potansiyeli olarak göreceli olarak Hamitabat Fm. kaynak kayasından düşük değerlere sahip olması nedeniyle hidrokarbon türüm ve atım miktarları Hamitabat Formasyonuna göre göreceli olarak düşüktür.
4. Mezardere Formasyonu çalışma alanının çok büyük kısmında olgunlaşmamış, erken olgun pencerededir. Diğer kaynak kayalara nazaran daha az gömülmüş olan bu seviyedeki hidrokarbon dönüşüm oranları ve türüm atım miktarlarının düşük olması beklenmektedir.

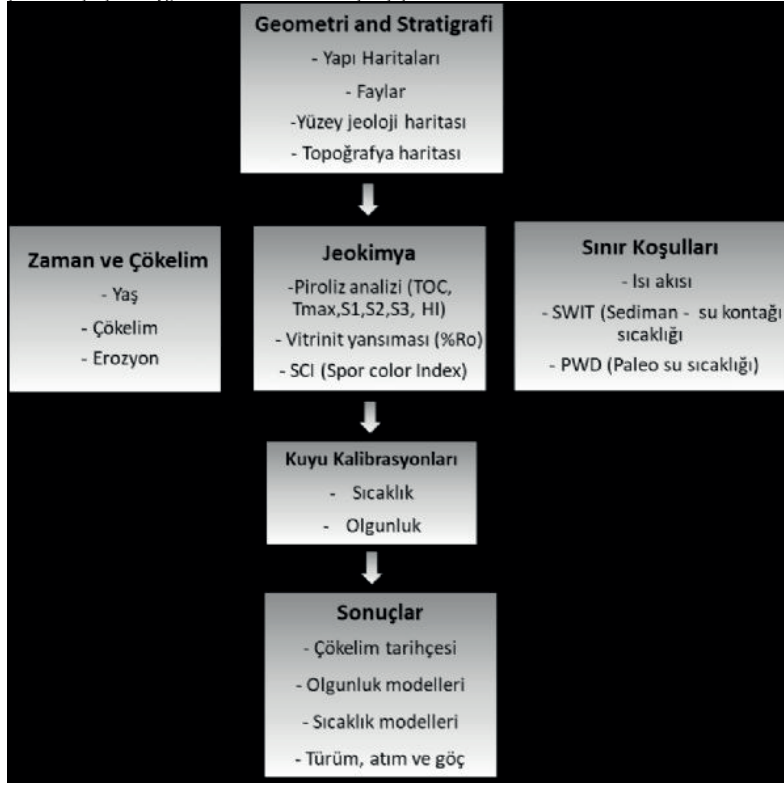
Özetle çalışma alanının kuzey kuşağında gömülme miktarının düşük olması nedeniyle kaynak kayalar düşük olgunluk derecelerine sahiptir. Güney batı doğrultusunda kaynak kayalara ait olgunluk dereceleri artarak sırası ile erken, orta, İleri olgun zonlara erişmekte; basenin en çukur alanlarında ise ıslak gaz ve kuru gaz olgunluk pencerelerine ulaşmaktadır. Bu çalışmada Trakya Havzasında olası Hamitabat, Ceylan ve Mezardere Formasyonları içerisindeki kaynak

kayaların potansiyelleri 3 boyutlu petrol sisteminde değerlendirmiştir. Ayrıca, çalışma alanında da petrol sistemi içinde volkanik ve resifal rezervuarlar da modellenmiştir. Çalışmamız sonucunda, alandaki kaynak kayaların olgunluk miktarları ile termojenik petrol sistemlerinin daha iyi anlaşılması ve farklı alanlarda değişen parametrelerin arama çalışmaları açısından önemi ortaya konulmuştur.

Anahtar Kelimeler: Thrace Basin, Basın Modeling

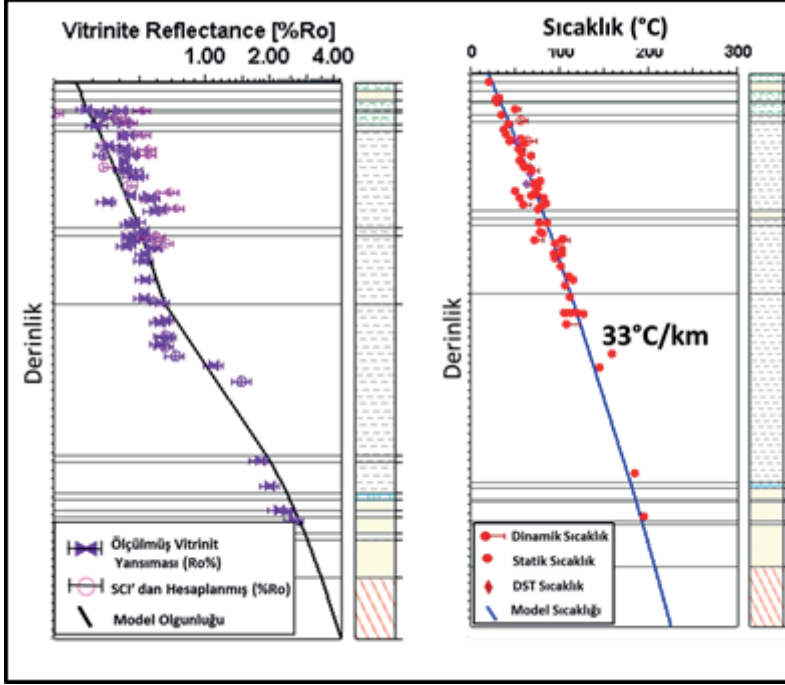


Sekil 1: Bu çalışmada uygulanan Basen Modellemesi İş akışı şeması



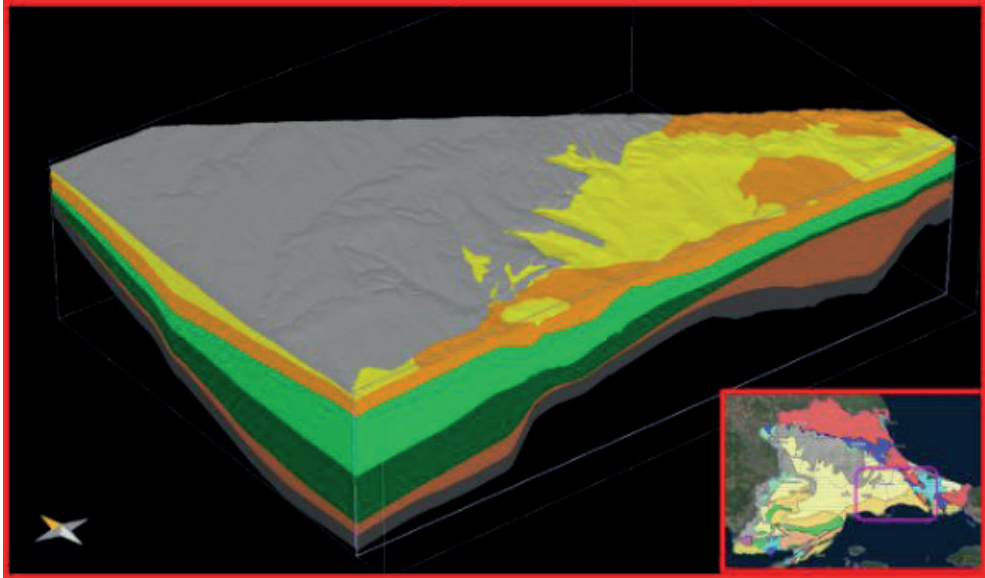
Bu çalışmada uygulanan Basen Modellemesi İş akışı şeması

Şekil 2: Çalışma alanında kyu verisi olan kuyulara ait Derinliğe karşı olgunluk ve sıcaklık Kalibrasyonları



Çalışma alanında kyu verisi olan kuyulara ait Derinliğe karşı olgunluk ve sıcaklık Kalibrasyonları

Şekil 3. Çalışma alanı ve 3 Boyutlu Model Geometrisi



Çalışma alanı ve 3 Boyutlu Model Geometrisi

# Dolomitleşme Sıcaklığının ve Zamanlamasının Rezervuar Kalitesine Etkisi Nedir? Örnek Çalışma: GDA Bölgesindeki Mardin Grubu Dolomitlerinin Kümelenmiş İzotop Sıcaklıkları



**Deniz Atasoy<sup>1</sup>, Aynur Geçer Büyükkutku<sup>2</sup>, Arzu Aktosun<sup>3</sup>**

<sup>1</sup>Türkiye Petrolleri Anonim Ortaklığı, Arama Daire Başkanlığı, Ankara / Türkiye

<sup>2</sup>Ankara Üniversitesi Jeoloji Mühendisliği, Ankara / Türkiye

<sup>3</sup>Türkiye Petrolleri Anonim Ortaklığı, Argem Daire Başkanlığı, Ankara / Türkiye

What is the Effect of Dolomitizing Timing and Temperature on Reservoir Quality?

A Case Study: Clumped Isotope Signals of Mardin Group Dolostones in SE Anatolia

Key Words: Mardin Group, clumped isotopes

Approximately half of world's carbonate reservoirs are dolostones. Broadly speaking, dolomitized reservoirs are better in comparison to limestone reservoirs. It is known that two moles of calcites convert to one mole of dolostone during dolomitization processes. These event can occur at various phases and conditions from depositional or near surface environment (reflux, evaporative and mixing dolomitization) throughout burial history to reservoir condition (late dolomitization an hydrothermal dolomitization).

Theoretically, dolomitization reaction results in porosity increment on existing porosity of primary carbonates up to 11%. However, early formed dolostone crystals tend to be grown during continuous burial event with increasing temperature and depth.

To date, carbonate oxygen isotope geothermometry has been widely applied to determine formation temperature of dolomitized rocks. In order to estimate the dolomitizing temperature, oxygen isotopic composition of dolomitizing fluid ( $\delta^{18}\text{O}_{\text{fluid}}$ ) must be well constrained. Unfortunately, it is really difficult to define certain values and thus assumptions give wide range of  $\delta^{18}\text{O}_{\text{fluid}}$  in most cases.

Clumped isotopes have been utilized to solve long standing geological problems to carbonates. Based on thermodynamic relationship, the technique basically focuses on abundance of chemical bonds which are between heavy ( $\delta^{18}\text{O}$ ) and rare ( $\delta^{13}\text{C}$ ) isotopes and is temperature dependent. With a measurement of  $\Delta_{47}$  parameter, this new generation paleothermometry provides not only dolomitizing temperature but also knowledge of oxygen isotope composition of dolomitizing fluid ( $\delta^{18}\text{O}_{\text{fluid}}$ ) independently. Under reservoir conditions, varying temperature values can give rise to trigger recrystallization event which may drive poroperm values of dolostones.

Mardin Group is one of most prolific reservoir in SE Turkey. In this work, clumped isotope technique was used to two dolomitic reservoirs of Mardin Group taking place at the similar depth of ~3 km from different locations. The main purpose of the study is to to serve decode timing and depth of dolomitization/ recrystallization events using one dimensional (1D) basin model.

In the Diyarbakır Basin, dolomitization at Well A occurred at ~60°C, reflecting early dolomitization stage and highly lower values when compared to modern day well temperature (~85°C) and maximum burial temperature ~110°C constrained by vitrinite reflectance data. The result indicates that the dolomitization event did not proceed during ongoing burial/thermal history. Obtained temperature values converts into depths of between 1.1 km and 1.6 km and completes the partial recrystallization stage in the ages of Late Cretaceous to Late Paleocene. The reconstructed  $\delta^{18}\text{O}$  value of the dolomitization fluid was calculated from 3 to 4.7‰ which was interpreted to be slightly modified of original Cretaceous marine waters.

In the Silopi Sub-Basin, dolomitization recorded up to ~125°C as blocking temperatures, showing late dolomitization process and higher temperature values to current borehole condition (~100°C). It is most likely that reservoir dolostones would have been deeper buried with respect to its present depth. Thus, clumped isotopes record elevated values where maximum burial depth was experienced.  $\Delta_{47}$  signatures of dolostone samples translate into a time for late dolomitization of Early-Middle Miocene and depth of between 2.2 km and 3.4 km.  $\delta^{18}\text{O}_{\text{fluid}}$  ranges between 3.3 and 6.1‰ was characterized as deeply-seated dolomitization fluid that may enlarge size of dolostone rhombs in this case.

It is concluded that although low T dolostones reflect a better reservoir characteristic with more porous texture in Diyarbakır Basin, high T dolostones display interlocked dolomite crystals that cause reduced porosity values of reservoir rock in Silopi Sub-Basin (Şırmak).

Dolomitleşme sıcaklığının ve zamanlamasının rezervuar kalitesine etkisi nedir?

Örnek Çalışma: GDA Bölgesindeki Mardin Grubu dolomitlerinin kümelenmiş izotop sıcaklıkları

Anahtar Kelimeler: Mardin Grubu, kümelenmiş izotoplar

## GİRİŞ

Karbonat rezervuarları litolojik olarak kireçtaşlarından ( $\text{CaCO}_3$ ), dolomitik kireçtaşlarından ve dolomitlerden  $\text{CaMg}(\text{CO}_3)_2$  meydana gelmektedir (MacDonald vd. 2015). Dünyanın her yerinde jeolojik zaman boyunca dolomit oluşumları gözlemlenmesine rağmen, güncel okyanuslarda dolomit depolanmaları sıklıkla şahit olunmamaktadır. Dolomitlerin deniz suyu sıcaklıklarında çökelediği bilgisine sahip olunmasına

karşılık, laboratuvar koşullarında dolomit mineralinin elde edilmesi henüz başarısızdır. Dolomitler hala gizemli bir mineral olmasının yanı sıra, karbonat rezervuarlarının %50'sini oluşturmaları onları oldukça popüler kılmaktadır (Warren 2000).

Dolomitler, birincil dolomitler veya dolomitleşme reaksiyonları ile ikincil bir mekanizmayla meydana gelmektedir. Dolomitlerin büyük bir bölümünün kireçtaşlarının çökeliminden sonra ikincil olarak meydana geldikleri, yalnızca Holosen'de dolomitlerin birincil dolomit olabilecekları düşünülmektedir. Dolomitlerin ikincil oluşum mekanizması “ dolomitleşme” olayı olarak tanımlanmaktadır. Bu diyajenetik süreç rezervuar kayacın depolanmasında itibaren sin-depolanma (evaporitik ve tekrar akış dolomitleşmesi) diyajenez, karışım zonu diyajenez, gömülme diyajenez ve tektonik kontrollü diyajenez ile meydana gelmektedir (MacDonald vd. 2015).



Jeolojik zaman boyunca dolomitlerin büyük bir çoğunluğu depolanması sonrası gömülme sürecinin başlamasıyla oluşmaktadır. Gömülme boyunca rezervuar koşulları altında artan sıcaklık organik değişimlere (organik maddenin olgunlaşma derecesini) ve dolomitleşme, rekristalizasyon vb. gibi inorganik değişimlere sebebiyet vermektedir (Macdonald vd. 2018). Dolomitleşme sürecinde, iki mol kalsitin bir mol dolomit dönüşmesi rezervuar kayacın (%11 kadar hacim kazandırmaktadır) gözeneklilik ve geçirgenlik değerlerinin değişmesine neden olmaktadır. Bu nedenle, rezervuar kayaç olan dolomitlerin paleosıcaklık değerlerinin güvenilir yöntemlerle belirlenmesi rezervuar karakterizasyon çalışmalarında önemli bir yer tutmaktadır.

Paleosıcaklıklar sedimanter basenlerin diyajenez ve termal süreçlerinin anlaşılması için önemli bir faktördür. Dolomitlerin oluşum mekanizmalarındaki bilinmeyenlerle birlikte dolomitlerin (oluşum ve/veya yeniden kristallenme) paleosıcaklıkları ve dolomitleşmeyi gerçekleştiren suların kökeninin belirlenmesi hususları bakımından belirsizlikler halen tartışılmaktadır.

Dolomitleşme aşamalarının düşük sıcaklıkta tamamlandığında dolomitlerin daha iyi rezervuar özellikleri sergilediği, diğer yandan yüksek sıcaklık altında dolomitlerinin var olan gözenekliliklerini kaybetmesiyle rezervuarın bu açıdan negatif etkilendiği ileri sürülmektedir. Bazı istisnaların bu genellemeyi teyit etmediği bilinmektedir (MacDonald vd. 2015).

Yeni nesil bir jeotermometre olan kümelenmiş izotopların (clumped isotopes) temelini termodinamik bazlı değişim sergileyen C ve O izotoplarının aralarında kurmuş oldukları bağ sayıları oluşturmaktadır (Eiler 2007). Sıcaklığın düşük olduğu koşullarda termodinamik duraylılık sebebiyle  $\delta^{13}\text{C}$  ve  $\delta^{18}\text{O}$  izotopları bir araya gelip kümelenirken, sıcaklığın artmasıyla bu izotoplara ait bağların sayısı azalmaktadır. Karbonatların oluşum sıcaklıklarındaki ağır ve nadir izotoplarının ( $^{13}\text{C}^{18}\text{O}^{16}\text{O}$ ) kurmuş oldukları bağların, bahse konu olan izotopların 1000 oC'lik koşullarda

sergilediği rastgele dağılım konumdaki bağlara oranı  $\Delta_{47}$  parametresi olarak tanımlanmaktadır (Eiler 2007).  $\Delta_{47}$  parametresi karbonatın kendisinin ( $\delta^{18}\text{O}_{\text{miner}}$ ) ve çökeliyi sağlayan suyun oksijen izotop değerlerinden ( $\delta^{18}\text{O}_{\text{su}}$ ) ilintisiz olarak sıcaklıklar değerlerinin ölçülmesini sağlamaktadır.

Tekniğin öncü çalışması olan Ghosh vd. (2006)'dan beri, kümelenmiş izotop yöntemi başarıyla kullanılarak dolomitler ve dolomitleşme hakkında yayınlar yapılmıştır (MacDonald vd. 2015, Swart vd. 2016, MacDonald vd. 2018). Dolomitler kireçtaşlarına göre yeniden düzenlenmeye (yüksek sıcaklıklarda  $\Delta_{47}$  değerlerinin yanıtıcı biçimde değişmesi-reordering) daha dirençli olduğu bilinmektedir. Bu nedenle, 25 °C'den 300 °C'ye kadar sahip dolomitlerin sıcaklıklarının analiz edilebileceği ortaya çıkarılmıştır (Bonifacie vd. 2017).

Bu çalışmanın amacı, Diyarbakır (Kuyu A) ve Şırnak (Kuyu C) çalışma alanlarında Güneydoğu Anadolu Bölgesi'nin (GDA) en üretken seviyelerin biri olan Geç Kretase yaşlı Mardin Grubu'na ait dolomitlerin i) dolomitleşme sıcaklıklarının ölçülmesini, ii.) dolomitleşmenin gerçekleştiği zaman ve derinlik bilgisinin ortaya çıkarılmasını iii.) dolomitleşme sularının  $\delta^{18}\text{O}_{\text{su}}$  değerlerinin hesaplanmasını ve dolomitleşmenin rezervuar üzerine etkisinin anlaşılması hedeflemektedir.

Şekil 1. Lokasyon haritası

İki çalışma alanının seçilmesi ve karşılaştırılacak olmasının nedeni, dolomitleşme olayı Diyarbakır çalışma alanında rezervuarı olumlu etkileyerek bir rezervuar sistemi gelişmesine imkân tanırken, Şırnak çalışma alanında, dolomitleşmenin rezervuarı negatif yönde etkilediği gözlemlenmektedir.

## YÖNTEMLER

Toz haline getirilmiş dolomit örnekleri 8 mg olarak tartılarak bakır numune kaplarına yerleştirilerek ortak asit yöntemi ile 90 °C sıcaklıkta 30 dakika boyunca reaksiyona sokulmaktadır. Gaz saflaştırma ünitesinde Murray vd. (2016) tarafından belirtilen 45 dk'lık bir proses ile dolomit numunelerinden saf  $\text{CO}_2$  gazı elde edilmektedir. Bu gaz bir deney tüpü içine hapsedilerek University of Miami (RSMAS) Kararlı İzotop Laboratuvarı'nda yer alan yeni nesil kütle spektrometresine (MAT 253) transfer edilerek ölçülmüştür.

Bu cihaz geleneksel kütle spektrometrelerinde olduğu gibi 44 ( $^{12}\text{C}^{16}\text{O}^{16}\text{O}$ ), 45 ( $^{13}\text{C}^{16}\text{O}^{16}\text{O}$  ve  $^{12}\text{C}^{16}\text{O}^{17}\text{O}$ ), 46 ( $^{12}\text{C}^{16}\text{O}^{18}\text{O}$ ,  $^{13}\text{C}^{16}\text{O}^{17}\text{O}$  ve  $^{12}\text{C}^{17}\text{O}^{17}\text{O}$ ) ölçümlerini gerçekleştirirken, ayrıca bünyesinde yer alan çoklu kolektör sayesinde 47 ( $^{13}\text{C}^{18}\text{O}^{16}\text{O}$ ,  $^{12}\text{C}^{18}\text{O}^{17}\text{O}$  ve  $^{12}\text{C}^{17}\text{O}^{17}\text{O}$ ), 48 ( $^{12}\text{C}^{18}\text{O}^{18}\text{O}$ ,  $^{13}\text{C}^{17}\text{O}^{18}\text{O}$ ) ve 49 ( $^{13}\text{C}^{18}\text{O}^{18}\text{O}$ ) ölçmektedir (Swart vd. 2016). Analizler sırasında kütle 48 ve 49 değerleri sürekli takip edilmektedir. Bu sayede, analizlerin güvenilirliği tespit edilmektedir.

Bu çalışmada Swart vd. (2019) tarafından önerilen ve asit düzeltme katsayısına ihtiyaç duyulmayan

bir sıcaklık formülü kullanılmıştır (Sıcaklık değeri formülde Kelvin cinsindedir).

$$\Delta_{47} = 0.0393 (\pm 0.00179) * (10^{6/T2 + 0.158 (\pm 0.0088) (R2) = 0.98})$$

Ölçülen sıcaklık değerleri Horita (2014)'ün formülüne yerleştirildiğinde, dolomitleşmeyi gerçekleştiren dolomitleşme sularının ( $\delta 18O_{su}$ ) değerleri rahatlıkla hesaplanmaktadır.

$$103 \ln \alpha_{dol} - su = 3.140 (\pm 0.22) * 106 / T2 - 3.14 (\pm 0.11)$$

## BULGULAR

Bu çalışma kapsamında, Diyarbakır (Kuyu A) ve Şırnak (Kuyu C) çalışma alanından örneklenen 8 adet dolomit numunesinin kümelenmiş izotop sonuçları ve  $\delta 18O_{su}$  (%) değerleri Tablo 1'de yer almaktadır. Kıyaslama da kullanılmak üzere, Kuyu C analizleri Atasoy vd. (2022)'nin çalışmasından alınmıştır.

Sedimanter basenlerde gömülme sıcaklıkları organik maddenin uygunluğu ve kaynak kayanın hidrokarbon türümü ile ilgilidir. Organik maddenin uygunluk derecesi, sıklıkla petrografik bir teknik olan vitrinit yansımaları yöntemiyle belirlenmektedir (Hunt 1996). Özellikle vitrinit yansımaları verisinden üretilen EasyRo modeliyle maksimum gömülme sıcaklıkları hesaplanmaktadır (Sweeney ve Burnham 1990). Bu kapsamda, Kuyu A için rezervuar seviye olan 2700 m başında yer alan Ro değeri yaklaşık 0.7 olduğu görülmektedir (Şekil 2). Şırnak çalışma alanında yer alan Kuyu C için Ro veri seti bulunmamaktadır.

## TARTIŞMA

Kuyu A için 1B basen modeline göre, ince kristalli dolomitlerin dolomitleşme sıcaklıkları en düşük sıcaklık olan 54.1°C için 1100 m, en yüksek sıcaklık için 66°C 1630 m gömülmenin gerçekleşmesi gerekmektedir. 1020 m de gerçekleşen gömülme olayı Geç Kretase'de, 1630 m de meydana gelen gömülme olayı Geç Paleosen'de meydana gelmektedir (Çizelge 3).

Şekil 3. Kuyu A'nın 1B termal tarihçesi ve dolomitleşme senaryosu

Dolomitleşme öncesi Derdere Formasyonu'nun ilksel karbonatlarının çökelimini sağlayan suların ortalama sıcaklıkları 35°C olarak kabul edilmektedir. Bu kapsamda, Derdere Formasyonu rezervuar kayaçlarının yaklaşık 60 °C olan kümelenmiş izotop sıcaklıkları "erken-sığ gömülme dolomitleşmesi ve kısmi kristallenme" sıcaklıkları olarak yorumlanmaktadır. Kuyu A'nın rezervuar seviye için kuyu loglarından elde edilen güncel kuyu sıcaklığı 80-85 °C olarak ölçülmüştür. Diğer yandan, Sweeney ve Burnham (1990)'nin formülü kullanılarak elde edilen maksimum gömülme sıcaklığı 110°C'dir. Bu sıcaklık değerleri, kümelenmiş izotop sıcaklıklarıyla değerlendirildiğinde, organik maddenin türüm-atım prosesinden önce dolomitleşme süreci rezervuarda sonlanmaktadır.

Şırnak çalışma alanında Mardin Grubu'ndan örneklenen beş adet dolomit örneğinin sıcaklık değerleri yeniden

kristallenme sıcaklığı olarak değerlendirilmektedir (Çizelge 4). Üretilen 1B basen modelinde, Mardin Grubu erken dolomitleşme aşamasına geçmesi için Geç Kretase'de 400 m'lik bir sığ bir gömülmeye ihtiyaç olduğu görülmektedir.

Şekil 4. Kuyu C'nin bir boyutlu gömülme tarihçesi ve dolomitleşme evreleri

Yeniden kristallenmenin başlangıcı olduğu düşünülen 75 °C sıcaklık değeri için bu diyajenetik sürecin Orta Eosen'de 1700 m derinlikte başlamış olması öngörülmektedir. Kümelenmiş izotop yöntemiyle ölçülen dolomitlerinin yaklaşık 92 °C olarak ölçülen sıcaklıkları yeniden kristallenmenin (Erken Miyosen) 2.2 km m derinlikte sonlandığını belirtmektedir (Şekil 4). Dolomitleşme sıcaklıkları kuyudan ölçülen log sıcaklığı olan 100 °C altında olduğu gözlemlenmektedir. Genel olarak, kuyuların güncel sıcaklıklarının dolomitleşme sıcaklıklarından daha yüksek olduğu söylenmektedir. Bu çıkarımın aksine, Kuyu C'den alınan numunelerin kuyu sıcaklıklarının üzerinde yer aldığı gözlemlenmiştir. En yüksek kümelenmiş izotop sıcaklık değeri (~125 °C) kuyu sıcaklığından 30 °C daha yüksektir. Bu dolomit numunesini sıcaklık değeri yaklaşık Orta Miyosen (Langhian) ~3.5 km'ye kadar gerçekleşen gömülme ile kazandığı ortaya çıkarmaktadır. Termal gradyanın 30 °C/km olduğu sahada, kuyu sıcaklığı ve kümelenmiş izotop sıcaklığındaki (~30 °C) farkın izah edilebilmesi için Kuyu C'nin yer aldığı sahanın maksimum gömülmeye ulaştıktan sonra, ~1 km kadar Miyosen'de Cudi Bindirmesi ile yükseldiği düşünülmektedir. Bu alanda, dolomitleşme süresi Miyosen'e kadar devam etmiştir. Bu süreç dolomit kristallerinin büyümesine neden olarak rezervuarda var olan gözenekliliğin azalmasına neden olmaktadır.

Kretase dönemi deniz sularının  $\delta 18O_{su}$  değerlerinin -2.5‰'den ‰ +1.5‰'e varan değerler aldığı bilinmektedir (Veizer vd. 1999). Diyarbakır çalışma alanı için hesaplanan dolomitleşme suları +3-4.7‰ arasında değer almaktadır. Bu değerler, ilgili karbonatların evaporitler içermemesi nedeniyle, çökelim ortamında yoğun buharlaşmaya maruz kalmayarak gömülme ile artmasıyla açıklanmaktadır. Kayaç-gözenek sıvısı arasında yaşanan reaksiyonda, 16O izotopları kayaya transfer olurken, 18O izotopları gözeneklerde yer alan dolomitleşme sıvılarında katılmaktadır. Şırnak çalışma alanında ise  $\delta 18O_{su}$  değerlerinin ‰ +6.1'e varan değerler alması, dolomitleşme sularının derin gömülme sonucu modifiye olmasıyla izah edilmektedir.

## SONUÇLAR

Diyarbakır çalışma alanında Mardin Grubu ince kristalli dolomitlerin dolomitleşmesi 1.1 ve 1.6 km derinlikte, Geç Kretase-Geç Paleosen döneminde sonlanmaktadır. Buna karşılık, Şırnak çalışma alanında Kuyu C tarafından penetre edilen Mardin Grubu karbonatları geç diyajenetik iri kristalli dolomitlerin kümelenmiş izotop sıcaklıkları 91.5°C-125.0°C arasında değerler aldığı görülmüştür. Bu değerler, kümelenmiş izotopların dolomitlerin yeniden kristallenme sıcaklıklarını kaydettiklerini ortaya çıkarmaktadır.

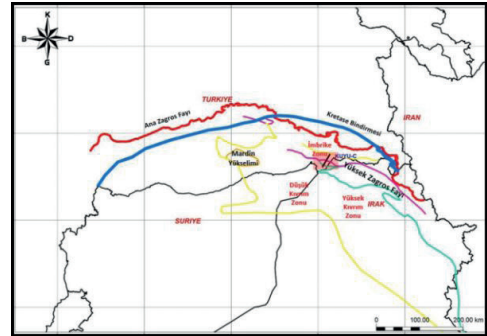
Diyarbakır çalışma alanında, dolomitleşme ve rekristalizasyonun düşük sıcaklıklarda ve sığ derinliklerde sonlandırmasıyla, dolomitler sahip oldukları gözeneklilikleri yeterince kaybetmemektedir. Diğer yandan, Şırnak çalışma alanında dolomit kristalleri yüksek sıcaklıklar altında ve oldukça derin gömülme koşullarında büyümektedir. Mevcut olan kristal arası gözenekliliğin kaybolması rezervuarın var olan porozitesinin azalmasına neden olmaktadır.

## REFERENCES

- Atasoy, D. Büyükkutku, A. Geçer, A. Aktosun, A. Güneydoğu Anadolu Bölgesi Mardin Grubu dolomitlerinin dolomitleşme yaşlarının ve derinliklerinin kümelenmiş izotoplar ve 1B basen modeli kullanılarak belirlenmesi. 2022. Yerbilimleri 1301-2894-2687-2978 V.43 doi: 10.17824/yerbilimleri.1095003 %U 10.17824/yerbilimleri.1095003
- Bonifacie, M. Calmels, D. Eiler, J. M. Horita, J. Chaduteau, C. Vasconcelos, C. Bourrand, J. J. 2017. Calibration of the dolomite clumped isotope thermometer from 25 to 350 °C, and implications for a universal calibration for all (Ca, Mg, Fe) CO<sub>3</sub> carbonates. *Geochimica et Cosmochimica Acta*, 200, 255–279.
- Eiler, J. M., 2007. "Clumped-isotope" geochemistry-The study of naturally-occurring, multiply substituted isotopologues. *Earth and Planetary Science Letters*, 262, 309-327.
- Ghosh, P., Adkins, J., Affek, H., Balta, Guoand W., Schauble, E.A., Schrag, D. and Eiler, J.M., (2006) C-13-O-18 bonds incarbonate minerals: A new kind of paleothermometer. *Geochim. Cosmochim. Acta*, 70, 1439–1456.
- Horita, J. 2014. Oxygen and carbon isotope fractionation in the system dolomite–water–CO<sub>2</sub> to elevated temperatures. *Geochim. Cosmochim. Acta*, 129, 111–124
- Hunt, J. M. (1996). *Petroleum Geology and Geochemistry*. 2nd edition. New York: Freeman and Company, 144p.
- MacDonald, J., John, C. & Girard, J.-P., 2015. Dolomitization Processes in Hydrocarbon Reservoirs: 544 Insight from Geothermometry Using Clumped Isotopes. *Procedia Earth and Planetary Science*, 13, 265-268
- MacDonald, J. M., John, C., and Girard, J. P., 2018. Testing clumped isotopes as a reservoir characterization tool: a comparison with fluid inclusions in a dolomitized sedimentary carbonate reservoir buried to 2–4 km. In: Lawson, M., Formolo, M.J., and Eiler, J. M., (eds.) *From Source to Seep: Geochemical Applications in Hydrocarbon Systems Series: Geological Society of London. Special Publications*, 468, 189-202.
- Swart, P.K. Cantrell, D.L. Arienzo, M.M. and Murray, S.T. 2016. Evidence for high temperature and δ<sup>18</sup>O-enriched fluids in the Arab-D of the Ghawar Field, Saudi Arabia. *Sedimentology*, 63; 1739–1752.
- Swart, P.K. Murray, S.T. Staudigel, P.T. and Hodell, D.A. 2019. Oxygen isotopic exchange between CO<sub>2</sub> and phosphoric acid: implications for the measurement of clumped isotopes in carbonates. *Geochem., Geophys. Geosyst.*, 20; 1–21.
- Sweeney, J.J. and Burnham, A.K. 1990. Evaluation of a Simple Model of Vitrinite Reflectance Based on Chemical Kinetics. *Aapg Bull.* 74; 1559–1570.
- Veizer, J. Ala, D. et al. 1999. Sr-87/Sr-86, delta C-13 and delta O-18 evolution of Phanerozoic seawater. *Chemical Geology*, 161; 59–88.
- Warren J. (2000) Dolomite: Occurrence, evolution and economically important associations. *Earth Science Reviews*, 52, 1-81.

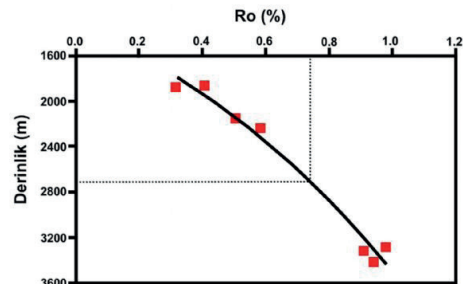
**Anahtar Kelimeler:** Mardin Grubu, kümelenmiş izotoplar

Şekil 1



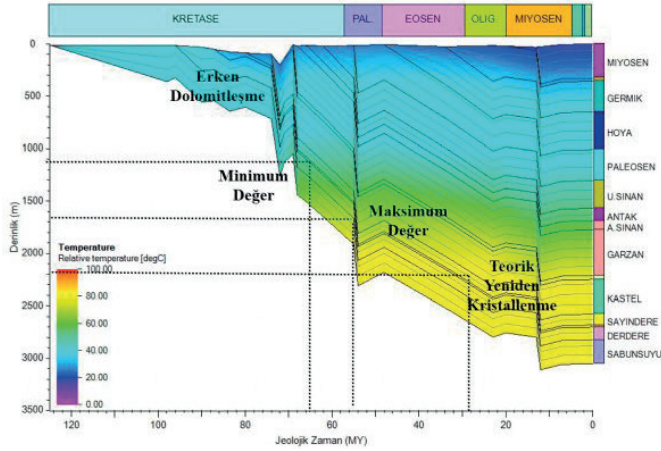
Lokasyon haritası

Şekil 2



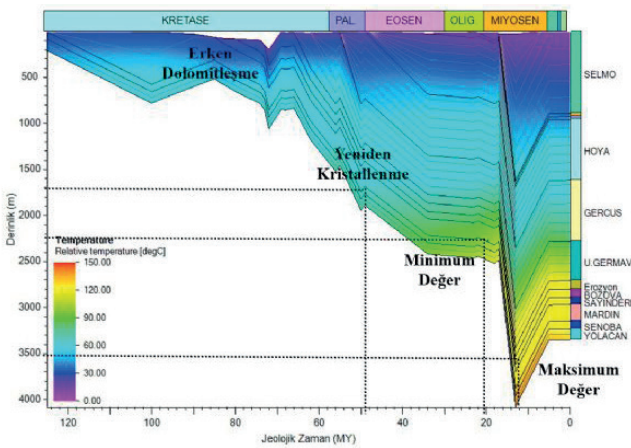
Derinlik ve Ro arasındaki ilişkiyi gösterir grafik (Kuyu A)

Şekil 3.



Kuyu A'nın 1B termal tarihçesi ve dolomitleşme senaryosu

Şekil 4.



Kuyu C'nin bir boyutlu gömülme tarihçesi ve dolomitleşme evreleri

Tablo 1.

Örnek No	Kuyu Adı	Örnek Derinliği (m)	$\Delta 47$ (%)	Sıcaklık (oC)	$\delta 18O_{su}$ (‰)
1	C	3010	0.451	92.54	3.32
2	C	3044	0.405	124.96	6.12
3	C	3074	0.453	91.47	5.35
4	C	3102	0.422	112.42	5.36
5	C	3148	0.430	106.50	5.03
6	A	2714	0.505	66.03	4.72
7	A	2716	0.510	60.18	3.99
8	A	2718	0.502	54.08	3.02

Kümelennmiş izotop analiz sonuçları

# Conceptual Risk Modeling for Biogenic Gas Fields

**Yücel Deniz Erdal**

TPAO



## ABSTRACT

TPAO's recent biogenic gas discovery in the western Black Sea has taken attention due to its size and also the concept. Biogenic gas is a product of bacterial and archaeal anaerobic fermentation of organic matter. This process requires more elusive conditions than thermogenic sources and as a result, the amount of biogenic gas discoveries are less common than thermogenic natural gas discoveries. Main factors that offer viable conditions for biogenic gas generation are rich organic matter content, optimum burial and redox conditions. While organic matter is crucial as a material for hydrogen rich products, last two factors together are as important as the first since they promote preservation of organic matter by protecting the material from oxidation before burial. Here, we investigate factors that control the biogenic gas generation probability in the sediments in terms of controlling surrounding conditions and hydrocarbon generation timing.

We will present a synthetic model where we introduce the concept of chance mapping for biogenic gas exploration in basin analysis discipline. We used the same concepts with a three-dimensional model in the western Black Sea region where TPAO made a significant discovery. Using a temperature, maturity, effective porosity and pressure calibrated model, we correlated biogenic gas accumulations with our chance mapping. However, due to the data restrictions, this synthetic model is used to demonstrate the concept that was proven in the previous studies.

There has been published studies that tested concepts for chance mapping for biogenic gas. Here, we create chance maps according to heating rate values and evaluate the area to address which areas the heating rate values lie between 7 and 18°C/My. Between 18 and 24°C/My is lower potential for biogenic gas accumulations and over 24°C/My is taken as a risk for fast pasteurization. Next step is to evaluate one-dimensional temperatures to see if the temperature concept is also working through geologic times. Appropriate amount of heating rate alone does not require that there is enough temperature to provide the optimum conditions to the microorganism to populate, therefore chance maps need to be created to define the proper areas for biogenic gas generation.

## INTRODUCTION

Biogenic gas generating microorganisms (methanogenic organisms) were affiliated with bacteria, though, due to the composition of their cell wall and cell membrane, today, they are known to be under archaea domain. Bacteria and archaea are two different major domains under prokaryotes. For transformation of organic matter into biogenic gas, on the other hand, presence of both archaea and bacteria is crucial. Anaerobic fermentation

of organic matter occurs in four steps: hydrolysis, acidogenesis, acetogenesis, and methanogenesis (Lee et al., 2014). First three stages are bacterial processes and the last stage where the actual biogenic gas occurs is an archaeal process that methanogens turn C, H, and O compounds into biogenic methane (Silva et al., 2015).

## METHODS

For prediction of biogenic gas generation, there are two models: The Clayton Concept, where Clayton (1992) introduced a heating rate dependent model and a temperature dependent model that relies on optimum conditions for a microbial activity, which is also taken into account in basin modeling simulations.

In the Clayton Concept, sedimentation rate is a function of preservation of the organic matter along with geothermal gradient, which provides enough temperature for organisms to populate. Either two factors must be favorable for biogenic gas generation. If the geothermal gradient is too low, microorganisms would not have enough temperature to populate in time and in the opposite case, organisms would disappear earlier due to high temperatures. As seen in the Figure 1, if one of the elements are low, the other can compensate due to the formula of heating rate which is a function of geothermal gradient and the sedimentation rate. In his study, Clayton (1992) demonstrated that all discovered biogenic gas lies between the heating rate range of 7-18°C/My, however as it is a relatively old concept, we sought to have more prospective ranges and investigated over 18°C/My heating rates as high pasteurization risk, but still may have a potential. Less than 7°C/My, on the other hand, accepted as too cold to sustain enough population of microorganisms.

In the temperature dependent model, a similar process, anaerobic digestion of organic wastes was thought to be a start point for biogenic gas generating microorganisms in sediments. This type of process is run at mesophilic (30-40°C) and thermophilic (50-60°C) temperatures (Leven et al., 2007). Thus, for our models, we used a Gaussian distribution with a mean of 40°C for maximum methanogenic organism population and effective between 10-70°C (30-50°C interval is the most effective) by using Schneider et al. (2016)'s concept (Figure 2).

## SUMMARY

In this study, by applying the criteria stated above, we used basin analysis principles to create chance maps according to heating rate. Next step is to evaluate one-dimensional temperatures to check if the temperature concept is also working since sufficient heating rate does not mean that we have the necessary temperature to



provide the optimum conditions to the microorganism. Here, we reveal what concept provided the best fit for the basin and petroleum system model of the biogenic gas discovery in the western Black Sea region.

## REFERENCES

Clayton, C., 1992, Source Volumetrics of Biogenic Gas Generation, in R. Vialy (ed.), Bacterial Gas: Editions Technip, Paris, p. 191-204.

Lee W, Chua A, Yeoh H, Ngho G. A review of the production and applications of waste-derived volatile fatty acids. Chem Eng J. 2014;235(1):83–99. <https://doi.org/10.1016/j.cej.2013.09.002>

Leven, L. (2007). Effect of process temperature on bacterial and archaeal communities in two methanogenic bioreactors treating organic household waste. FEMS Microbiol Ecol, 59, 683-693. <https://doi.org/10.1111/j.1574-6941.2006.00263.x>

Schneider, F., Dubille, M., & Montadert, L. (2016). Modeling of microbial gas generation: Application to the eastern Mediterranean “Biogenic Play”. Geologica Acta, 14(4), 403-417. <https://doi.org/10.1344/GeologicaActa2016.14.4.5>

Silva D, Cantão E, Mezzari P, Ma J, Nossa W. Assessment of bacterial and archaeal community structure in swine wastewater treatment processes. Microb Ecol. 2015;70(1):77-87. <https://doi.org/10.1007/s00248-014-0537-8>

Keywords: Basin modeling, Biogenic gas

Figure 1. Sedimentation rate over average geothermal gradient graphic according to the Clayton (1992) concept.

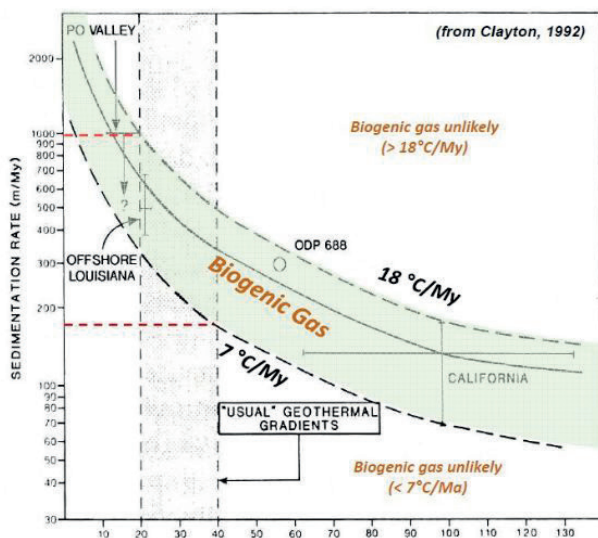
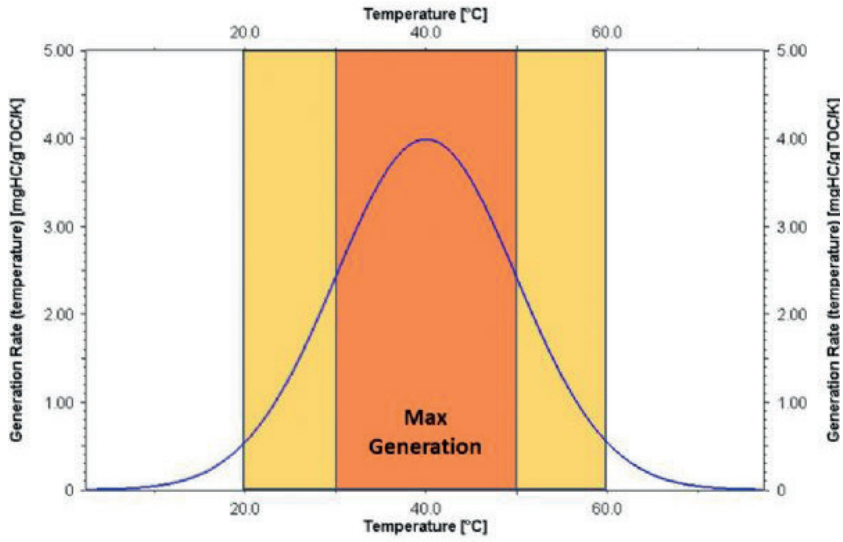


Figure 2. Temperature dependant biogenic gas generation model created by values modified from Schneider et al. (2016).



# Investigation the impact of Messinian Event in the Eastern Black Sea from a Biogenic Gas System Perspective

**Mehmet Hazar, Yücel Deniz Erdal, Şükrü Gökhan Köse**  
Türkiye Petrolleri Anonim Ortaklığı, Ankara / Türkiye



## ABSTRACT

Biogenic gas, which is an outgrowth of the decomposition of organic matter, has been evaluated as a lucrative hydrocarbon resource especially after recent discoveries both in the eastern Mediterranean and the Black Sea basins. Messinian Salinity Crisis is a geological phenomenon partial or almost complete drying-up of the Mediterranean Sea until the Zanclean flood. Impact of this event has been subject of numerous scientific researches for the vicinity of the Mediterranean Sea, however its outcomes for the Black Sea has not been concretized specifically for the aspect of biogenic gas generation. Differentiation of the biogenic gas potential during Messinian Event throughout a sample cross section from distinctive locations is a worthwhile method mentioned in the scope of this study.

## INTRODUCTION

The Black Sea is a marginal sea lying between Europe and Asia, east of the Balkans, south of the Eastern European Plain, west of the Caucasus, and north of Anatolia. It is supplied by number of rivers such as Danube, Dnieper, Kızılırmak and Don. Although six countries have a coastline on the sea, drainage basin of the Black Sea encompasses areas belonging to 24 different countries. In this respect, the Black Sea is an important marginal sea ultimately drains into the Mediterranean Sea of the Atlantic Ocean via the Turkish Straits.

The Black Sea and surrounding regions host a well-known source rock called Maykop Formation. Since the water chemistry of the Black Sea Basin has its unique composition throughout Cenozoic, Maykop Formation is not the only potential source rock, instead it is just the one of many potential source rock intervals. While the Black Sea basin appears as one single basin, through Mid-Black Sea High that includes the Andrusov Ridge, Tetyaev High, and Archangelsky High, these two sub-basins, western and eastern Black Sea basins, are differentiated in terms of both opening ages and provenance of their sediments. Although both basins differ in details, it is a well-known fact that both basins reside to thick Cenozoic sediments.

Biogenic gas refers to natural gas that is the byproduct of the microbial decomposition of biological and organic matter. For instance, methane soil gas on Earth is typically biogenic gas resulting from the decomposition of organic soil zones, landfills, marshes, and swamplands. The biogenic gas concept has been a worth-mentioning subject especially after substantial hydrocarbon explorations around diverse territories around the world. Some of these basins are the Tobago Basin, NW South America, Zohr Field, Egypt in the eastern Mediterranean and recently, Turkey's discovery

Sakarya Gas Field in the western Black Sea. There are certain findings that address the possibility of biogenic gas occurrence in any sedimentary basin. One and the most important finding about biogenic gas is that the origin of the gas is not likely to derive from a mature source rock. That is because, in such systems, preservation of the organic matter plays a key role. The organic matter should not be oxidized and/or exhumed during geologic time. Along with this, such sedimentary layer has to host high amount of organic matter to be considered as prolific. Although, the amount of organic matter and the preservation of it are important key factors, the presence of bacteria in such environments is a must for the generation of biogenic gas. These bacteria meet the fermentation into high organic matter environment in certain conditions, such as anoxia, preservation, and mild temperatures (theoretically, between 40 °C and 70 °C) (Figure 1). This event is called methanogenesis, the bacteria here is focused on producing hydrogen and carbon dioxide, and while doing this, it generates methane from sulfate reduction of hydrogen.

Turkey is surrounded by deep waters in which there is thick and young sedimentary bodies. Though we know little about the complex offshore stratigraphy of the region, we continue developing hypothesizes and through the discovery process, we can increase our learning curve without doubt.

## DISCUSSIONS AND OUTPUTS OF THE STUDY

Hereby, we present our biogenic expectations in the eastern Black Sea during Plio-Miocene. We know that a working biogenic system requires a certain range of heating rate along with the presence of bacteria (Figure 2). We are also aware of a hiatus during Messinian. Messinian Salinity Crisis (MSC) caused a dramatic change in water level of the Mediterranean Sea and it can be detected at the Black Sea basin from erosional surfaces. We discuss the potential of having such environments where there are all expectations meet in terms of biogenic gas occurrences and where one or more of the elements of biogenic gas could be missing. Thus, we used seismic stratigraphic surfaces in a geologically calibrated basin analysis model to better understand how the biogenic system in the eastern Black Sea could react to the objected hiatus. With the available biogenic gas kinetics from literature data, we aimed to have an insight of possible timing and productivity of the biogenic system in this region. We also present what uncertainties and biases one should expect in future projects.

According to this study it can be clearly observed that timing of biological activity and its gas producing potential are directly stimulated from end of Messinian

scraping. Secondly, the post Messinian sediments that follow transgression play a decisive role with respect to continuity of biogenic productivity of pre Messinian organic rich intervals. Thirdly, sedimentation rate is a function that measures the potential of biogenic activity, therefore in order to be more precise determination, it should be defined in detail by using palynological and paleontological studies. The last but not the least, although this study focus on a localized area, outcomes can be administered the whole Eastern Black Sea particularly for biogenic gas potential.

**REFERENCES**

Clayton, C., 1992, Source Volumetrics of Biogenic Gas Generation, in R. Vialy (ed.), Bacterial Gas: Editions Technip, Paris, p. 191-204

Katz, B., 2011, Microbial Processes and Natural Gas Accumulations: The Open Geology Journal, v. 5/1, p. 75-83.

doi:10.2174/1874262901105010075

Maurand N., A. Pujol, A. Ravin, S. Wolf, M. Dubille, P. -Y. Filleaudeau, and B. Lebreuilly, 2020, Modelling Biogenic Gas Generation and Migration – Application on the Levantine Basin, from oral presentation given at 2019 AAPG Africa Region, The Eastern Mediterranean Mega-Basin: New Data, New Ideas and New Opportunities, Alexandra, Egypt, September 6-7, 2019

Mayer J., R.F. Sachsenhofer, C. Ungureanu, A. Bechtel, R. Gratzler, M. Sweda and G. Tari, Petroleum Charge and Migration in The Black Sea: Insights from Oil and Source Rock Geochemistry, Journal of Petroleum Geology, Vol. 41(3), July 2018, pp 337-350

Olaru R., Krézsek C., Rainer T. M., Ungureanu C., Turi V., Ionescu G. and Tari G., 3D Basin Modelling of Oligocene – Miocene Maikop Source Rocks Offshore Romania And in The Western Black Sea, Journal of Petroleum Geology, Vol. 41(3), July 2018, pp 351-366

Rice, D.D., 1992, Controls, Habitat, and Resource Potential of Ancient Bacterial Gas in R. Vialy (ed.), Bacterial Gas: Editions Technip, Paris, p. 91-118.

Sachsenhofer R. F., Popov S. V., Akhmetiev M. A., Bechtel A., Gratzler R., Groß D., Horsfield B., Rachetti A., Rupprecht B., Schaffar W. B. H., and Zaporozhets N. I., The type section of the Maikop Group (Oligocene–lower Miocene) at the Belaya River (North Caucasus): Depositional environment and hydrocarbon potential, AAPG Bulletin, v. 101, no. 3 (March 2017), pp. 289–319

Schneider F., Matthieu D., Montadert L., Modeling of microbial gas generation: application to the eastern Mediterranean “ Biogenic Play “ Microbial gas generation model applied to offshore Lebanon, Geologica Acta, Vol.14, N° 4, December 2016, 403-417

Simmons M. D., Tari G. C. & Okay A.I., Petroleum geology of the Black Sea: introduction, Geological Society, London, Special Publications, 464, 1–18. First published online May 4, 2018, <https://doi.org/10.1144/SP464.15>

Keywords: Basin and Petroleum System Modeling, Biogenic gas systems

Figure 1. Working Principle of Biogenic Gas Generation Kinetic: Temperature vs Generation Rate Graph modified from PetroMod2019.1 Kinetics Editor

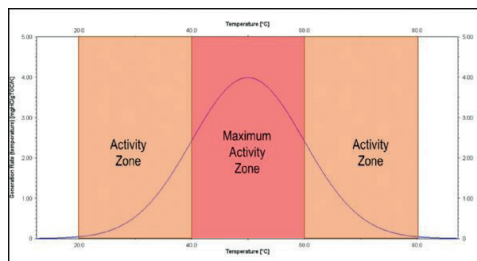
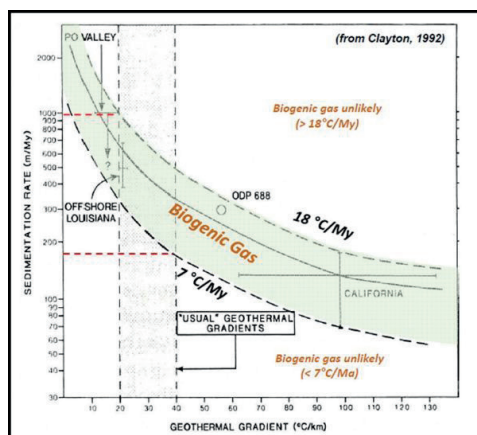


Figure 2. Clayton Concept of Biogenic Gas Generation Zone at geothermal gradient vs sedimentation rate diagram: Examples from existing fields modified from Maurand et al., 2020





**Petrol ve Dođal Gaz Endüstrisinde İş Sađlıđı,  
Güvenliđi ve Çevre**

*Health, Safety and Environment in the Oil  
and Gas Industry*

---



# Batı Karadeniz'deki Petrol Platformlarının Gemi Trafikğine Olan Etkisi ve Oluşabilecek Kaza Sonrası Petrol Yayılımı



Ersan Başar<sup>1</sup>, Mehmet Kerem Kemerli<sup>2</sup>

<sup>1</sup>Karadeniz Teknik Üniversitesi, Deniz Bilimleri Fakültesi

<sup>2</sup>MEKE Deniz Teknolojileri A.Ş.

Batı Karadeniz gemi trafiğinin yoğun olduğu ve 6 kıyıdaş ülkenin ihracat ve ithalatında kullandığı yoğun bir denizdir. Bu su alanı deniz ticareti ile deniz canlı kaynaklarından yoğun olarak yararlanan ekonomik ve ekolojik değeri yüksek olan bir bölgedir. Son yıllarda Karadeniz'in ulaşım ve canlı kaynakları yanı sıra yer altı kaynakları da önem teşkil etmiştir. Özellikle petrol arama çalışmalarına önem verilmiştir. Petrol arama alanları gemi trafiğinin yoğun olduğu Batı Karadeniz'in kuzey güney geçiş alanlarında bulunması platform ve gemi kaza risklerini artırmaktadır. Aynı zamanda platformlardan kaynaklanabilecek bir kaza sonrasında dağılacak olan petrol çevresel açıdan önemli riskler ve sorunlar doğuracağı gerçektir.

Yapılan çalışmada, Karadeniz'deki petrol arama alanlarındaki gemi trafik rotaları belirlenmiş ve bu rotaları üzerindeki riskli alanlar ortaya koyulmuştur. Daha sonra bu bölgelerde oluşabilecek bir platform gemi kazası akabinde oluşacak petrol dağılımı alanı ve bütçesi simülasyon yolu ile tespit edilmiştir.

Gemi trafiği açısından başta Sinop ve Ereğli açıkları, riskli alanlar oluşturduğu anlaşılmıştır. Petrol kirliliği açısından ise Batı Karadeniz'de en önemli risk alanları Kefken kıyıları olarak tespit edilmiştir.

The western Black Sea is a busy sea where ship traffic is intense and used by 6 riparian countries for export and import. This water area is a region with a high economic and ecological value, which is extensively exploited from marine living resources by sea trade. In recent years, in addition to the transportation and living resources of the Black Sea, seabed resources have also become important. In particular, importance has been given to oil exploration. Oil exploration areas being located in the north-south transition areas of the western Black Sea, where ship traffic is heavy, increases the risks of platform and ship accidents. The oil that will spread after an accident that may arise from the platforms in the same area will create significant environmental risks.

In the study, the ship traffic routes in the oil exploration areas in the Black Sea were determined and the risky areas on these routes were revealed. Then, the oil distribution area and budget that will occur after a platform ship accident that may occur in these regions have been determined by simulation.

In terms of ship traffic, it has been understood that the Sinop and Ereğli offshore areas constitute risky areas. In terms of oil pollution, the most important risk areas in the western Black Sea were identified as Kefken coasts.

## AMAÇ

Karadeniz'de kıyısı bulunan ülkeler hidrokarbon kaynaklarını en etkin bir şekilde kullanmak amacı ile petrol arama çalışmalarına dünyadaki büyük petrol

firmaları ile yaptıkları ortaklıklar sonucunda başlamıştır. Petrol arama çalışmaları esasında sondaj platformları kurulmakta olup bu platformlar gemi trafik rotaları üzerinde yer almaktadır [1]. Petrol alanlarında petrol bulunup çıkarılmaya başlandığında yoğun olarak tanker trafiğinin de artacağı açıktır. Bundan dolayı gemi trafik hatları üzerinde bulunan platformlarının gemi kazlarına açık olması riskleri artırmaktadır [2]. Bu alanlarda oluşabilecek kazalar sonrasında petrol dağılımlarının belirlenmesi amacı ile yapılan bu çalışmada riskli alanlar tespit edilmeye çalışılmıştır.

## YÖNTEM

Karadeniz son yıllarda artan gemi trafiği ve eklenen petrol arama çalışmaları ile kazalar sonrasında oluşabilecek petrol kirliliğini riskleri açısından önem taşımaktadır. Yapılan çalışmada petrol platformlarının olduğu veya tahmini olacağı bölgelerde simülasyonlar çalıştırılmış ve petrolün yayılım alanları tespit edilmiştir.

GNOME, NOAA (National Oceanic and Atmospheric Administration) tarafından 1999 yılında geliştirilen petrol yayılımının zamansal ve alansal olarak dağılımını tespit etmeye yarayan bir simülasyondur [3]. Bu simülasyona rüzgâr, akıntı, gelgit değerleri uygun formatlarda girildikten sonra petrolün yüzeydeki hareketini hesaplayarak sonuca gitmektedir [4]. Marcator projeksiyonlu seyir haritaları kullanılarak sayısal hale getirilmiştir. Yüzey akıntıları her iki yöndeki akıntı hızları m/sn olarak girilmiştir. İki boyutlu olarak girilen bu akıntı modelinde yönler (-) ve (+) olarak belirtilmiştir. Simülasyonda rüzgâr hızı 5 knot seviyesinde NW yönünde alınmıştır.

## BULGULAR

Yapılan çalışma sonrasında 2 senaryoda petrolün alansal ve zamansal dağılımı tespit edilmiştir. Senaryo 1 Karadeniz'in güney batı bölgesinde Türkiye'nin Çaycuma ilçesi açıklarında çalıştırılmıştır (şekil 1). Petrol genişleyen bir dağılımı göstermemiş olup yoğun olarak belli bir noktada toplandığı tespit edilmiştir. Petrol 1. senaryoda Türkiye kıyılarına ulaştığı tespit edilmiştir. Senaryo 2 Sinop açıklarında çalıştırılmıştır. Simülasyonun çalışması ile yakıtın Sinop açıklarında akıntı etkisi ile genişleyerek dağıldığı ve kıyıya ulaşmadığı tespit edilmiştir (şekil 2).

## SONUÇLAR

Her geçen gün artan tanker trafiği yoğun olarak gemi trafiği üzerinde baskı oluşturmaktadır. Bu baskı sonucundan da petrol ve petrol türevi taşıyan tankerin oluşturduğu risk de buna bağlı olarak artmaktadır. Bu tankerlerin boylarının ve kapasitelerinin büyümesi

sonucunda da manevra kabiliyetlerinde azalma olmakta bunun da kaza risklerini artırdığı bilinmektedir. Aynı zamanda petrol platformlarının da sayılarının artması koruma önlemlerinin en üst düzeyde alınması gerçeğini ortaya koymaktadır.

Yapılan çalışma sonrasında gemi trafiği açısından Sinop ve Kefken açıklarının riskli olduğu anlaşılmıştır. Sinop ve Ereğli açıklarında oluşabilecek bir kaza sonrasında yakıtın kıyıya vurma riskinin az olduğu açıkta daha uzun süre kalacağı anlaşılmaktadır.

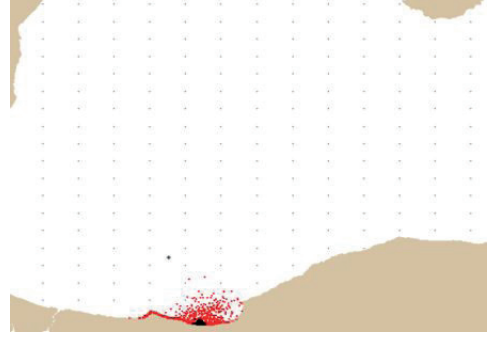
Kaza sonrasında yayılan yakıtı hızlı bir şekilde müdahale edilmesi çok önemlidir. Bu bölgelerde müdahale, bariyer kullanarak yayılımın kontrol altına alınması şeklinde yapılarak çevresel kirliliğin en aza indirilmesinde ve temizleme operasyonlarının yapılabilmesini başarı ile sağlayacaktır. Oluşabilecek petrol sızıntılarında kullanılmak üzere hazır bekletilecek olan malzeme ve ekipmanların depolanacağı yer uygun olarak seçilerek platformlarda depolanması sağlanması yararlı olacaktır. Yine aynı şekilde bu kaza alanlarına en kısa sürede ulaşabilecek ve operasyonları yürütebilecek kabiliyete gemilerin bulunması gerekmektedir. Karadeniz’de petrol araması yapan ve ileride kurulması düşünülen platformlar gemi geçiş rotaları üzerinde olduğu gerçeği unutulmamalıdır. Bundan dolayı gerekli önlemlerin alınması oluşabilecek kazaların etkilerini en aza indirmek açısından önemli olduğu anlaşılmaktadır.

#### KAYNAKÇA

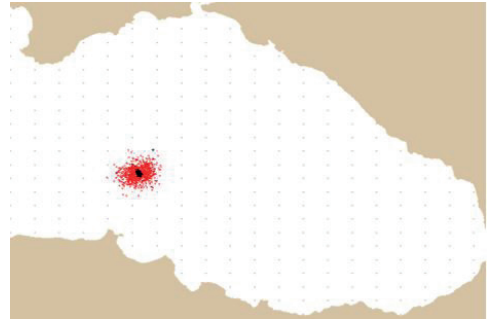
- [1] Başar, E. ve Erol, S. Karadeniz’deki Tanker Trafikinin Belirlenerek Tahmini Kaza Alanlarının Tespiti, Kıyı Alanları Konferansı, pp.1401-1408, Cilt 3, Trabzon, Nisan 2010,
- [2] Başar, E., (2010) ‘Weathering and Oil Spill Simulations in the Aftermath of Tanker Accidents at the Junction Points in the Marmara Sea’, Fresenius Environmental Bulletin, 19(2), pp.260-265.
- [3] GNOME, 2001a. User’s Manual, General NOAA Oil Modeling Environment, NOAA HAZMAT U.S. Coast Guard National, 77.
- [4] GNOME, 2001b. User’s Guide and Examples, General NOAA Oil Modeling Environment, NOAA HAZMAT U.S. Coast Guard National, 21.

Anahtar Kelimeler: Gemi kazası, Petrol kirliliği

Şekil 1. Filyos Petrol Dağılımı



Şekil 2. Sinop Açıkları Petrol Dağılımı





# Analysis of Spreading of Oil Spill on The Sea Surface During Gravity-Viscous and Surface Tension-Viscous Regimes



Metehan Erdoğan<sup>1</sup>, İsmail Durgut<sup>2</sup>

<sup>1</sup>SLB

<sup>2</sup>Orta Doğu Teknik Üniversitesi

We have discussed the effect of surface tension regime on oil spreading on the quiescent water in this study. We have treated the oil spreading diffusion alike by using advection-diffusion equation (ADE). We have derived a new form of diffusion coefficient including the surface tension regime after gravity viscous regime for oil spreading. An empirical parameter has been introduced into the diffusive length definition which can be used in the numerical solutions. An earlier numerical solution to the spreading of instantaneously released oil on the sea surface has been evaluated since it provides the slick's progress in only gravity-viscous regime without surface tension regime. It is compared with Nihoul's analytical solution and its asymptotic expansions to observe surface tension effect. In addition, we investigated the analytical solution by providing a wide range of spill volume, drag coefficient and surface tension values to understand their influences on the spreading. Implementation of the surface tension regime will help numerical solutions to describe oil spreading accurately.

## 1. INTRODUCTION

Offshore oil spills occur from the failure of transportation systems like tankers and pipelines and blowouts of wells. After that, they interact with seawater and air. They spread, move, evaporate and disperse into sea surface. Their extent on and in the sea through the processes should be estimated accurately for mitigation and prevention plans against spill's impact. Oil spreading is one of these processes where oil expands on the sea because of oil and water interactions. Oil spreading causes slick area and thickness changes in time. Main purpose of oil spreading calculations is finding out them in a specified time. Slick area and thickness are input parameters for the computations of other processes like evaporation. Therefore, their precise estimation will help to understand oil spill fate through combination of all processes.

Oil spreading follows three regimes which are gravity-inertia, gravity-viscous and surface tension viscous regimes, respectively (Fay 1969). One resisting and one supporting forces specify the regimes taking place. Gravity and surface tension accelerate it while inertia and viscosity retard it.

Many analytical solutions have been suggested for oil spreading with some modifications in time. (Fay, 1969; Hoult, 1972; Mackay et al., 1980a, 1980b; Lehr et al., 1984; Johansen, 1984; Elliott et al., 1986; Venkatesh et al., 1990; Daling et al., 1997; Chebbi, 2014; Brönnner et al., 2018). Later, thanks to the computational advances, oil spreading has been modeled with numerical solutions. Numerical models made easier to analyze slick in time and space in a sophisticated way. Some examples to oil spreading numerical solutions are discussed in Al-

Rabeh et al. (1989); Zhang et al. (1997), Cekirge et al. (1997), Tklich et al. (2003), Di Martino and Peybernes (2007); and Guo et al., (2014). Furthermore, Arkhipov (2008) has introduced a numerical technique employing Lagrangian random walk of particles placed into the grids for surface spreading under only gravity-viscous regime. Durgut and Reed (2017) has benefitted from similar numerical scheme by Voronoi diagrams instead of using grid. Their numerical solution also provides oil spreading under gravity viscous regime without surface tension regime. One of the aims of this study is to show how surface tension regime can affect the spreading of oil spill by comparing the exact solution with Durgut and Reed solution (2017). Another aim is to introduce an empirical parameter that can be used to define surface tension viscous regime in oil spreading algorithms of Arkhipov (2008) and Durgut and Reed (2017).

## 2. MATERIAL AND METHODS

Oil spreads in three regimes under the oppositely working forces which are inertial and viscous, and gravitational and surface tensional. Nihoul (1984) has built the force interactions with Eqn. 1 by neglecting inertial force which is valid for the first few hours of oil release. In original version of Eqn. 1, wind/current advection which is another oil surface expansion effect is included. The original equation is advection-diffusion equation (ADE), so it treats the spreading diffusion alike. However, it is neglected in Eqn.1. It means that surface expansion is assumed to be on the quiescent sea. Slick shape becomes circular with the assumption.

(Eqn.1)

where  $h$ ,  $t$ ,  $\rho_o$ ,  $\rho_w$  and  $Q$  represent slick thickness (m), time (s), oil density (kg/m<sup>3</sup>), water density (kg/m<sup>3</sup>) and sink/source term (m/s), respectively.  $g$ ,  $k$ ,  $\gamma$  and  $\psi$  which are regime force parameters denote gravitational acceleration (m/s<sup>2</sup>), drag coefficient (kg/m<sup>2</sup>s), surface tension (kg/s<sup>2</sup>) and surface tension variation term ( $\psi=0$  at the center, whereas  $\psi=1$  on the edges). On RHS of equation, the first term inside the gradient corresponds to gravity viscous regime, whereas the second term expresses surface tension viscous regime.

Deleersnijder and Loffet (1985) has stated time dependent radius of circular-shaped slick by suggesting self-similarity solution to Eqn. 1.

(Eqn.2)

where

(Eqn.3)

(Eqn.4)

Eqn. 2 corresponds to the exact solution of slick radius

for Nihoul's equation when oil spreads on the calm sea. Its log-log plot exhibits three different behaviors with time (Fig.1). Fig. 1 demonstrates there are two straight lines with the different slopes and one transition region between them. First straight line region represents gravity viscous regime while second one demonstrates surface tension regime. So, two asymptotic expansions for these two straight lines can be proposed to approximate to the exact solution. When  $aR^2 \ll 1$  where the gravity and viscosity forces are dominant, the asymptotic equation is:

(Eqn.5)

When  $aR^2 \gg 1$  where gravity is replaced with surface tension, the equation can be expressed as:

(Eqn.6)

The average thickness can be calculated from circle volume formula as:

(Eqn.7)

Arhipov (2008) suggested a numerical solution for instantaneous oil spill on the calm water in gravity-viscous regime without surface tension regime. The solution employs particle random walk on the grids following Gaussian distribution. In the solution, Eqn. 1 is converted to Eqn. 8. The multiplier of gradient of the thickness in Eqn. 1 can be defined as diffusion coefficient in Eqn. 8.

(Eqn.8)

where

(Eqn.9)

The particle's interactions with each other make the random walk space dependent and disturb the normal distribution resulting in high variance. Arhipov has defined a new parameter " $\lambda$ " into standard deviation for each time step to fit the distribution into Gaussian distribution. Now, the step length becomes:

(Eqn.10)

The step length represents the distance which the particles can take for a given time interval. The particles are distributed to new location at time  $t+\Delta t$  from the current position at time  $t$ . They follow the normal distribution where variance is zero and mean is one (Eqn. 11).

(Eqn.11)

Durgut and Reed (2017) have used the similar numerical scheme, but it slightly differs from Arhipov's solution. Firstly, instead of grids, Voronoi cells created by Voron++ are assigned to the each particles. The reason to use the Voronoi diagram is to reduce the solution dependency on the numerical parameters like number of particles, time step, etc. Secondly, the particle thicknesses are computed through volume of each particles per surrounding cell areas.

Arhipov (2008) and Durgut and Reed (2017) studies use diffusion length as it is stated in Eqn. 9 for only gravity-viscous regime. We have discussed to extend the diffusion length for both gravity viscous and surface tension regimes in Durgut et al. (2020). As a result, Eqn.

1 was converted into Eqn. 12 instead of Eqn. 8 without neglecting the surface tension (Deleersnijder and Loffet (1985)). The multiplier of thickness gradient in Eqn. 12 can be accepted as new diffusion coefficient placed into the step length.

(Eqn.12)

(Eqn.13)

We defined the step length in a similar way as Arhipov did. " $\alpha$ " (Eqn. 13) corresponds to Arhipov's empirical parameter, " $\lambda$ " for gravity-viscous term (Eqn. 10). " $\beta$ " coefficient is introduced to lower the variance of Gaussian distribution in solution for surface tension-viscous term.

### 3. RESULTS AND DISCUSSION

We compared the results of the analytical solution, asymptotic expansions and earlier algorithm formed by Durgut and Reed (2017). We also created a base scenario to evaluate the release parameters' effect on the slick behavior. The input parameters for this scenario are volume of released oil, surface tension and drag coefficient taken as 100 m<sup>3</sup>, 0.025 kg/s<sup>2</sup> and 0.003 kg/m<sup>2</sup>s, respectively. Oil and water densities are 890 and 1025 kg/m<sup>3</sup>, respectively.

Nihoul's exact solution, asymptotic solutions and the algorithm of Durgut and Reed (2017) are compared in Fig. 1. Fig. 1a and 1b depict that there is discrepancy between the analytical solution and the algorithm when surface tension regime takes place. They prove why adding surface tension to the available algorithm is so important for spreading of the spill. The algorithm follows the exact solution well until the transition between the regimes. After that, it follows the extended line of first asymptotic solution. So, the algorithm employing only gravity viscous regime tends to underestimate the slick area, in turn, to overestimate the thickness in surface tension viscous regime.

Unlike consensus, neglecting surface tension regime causes the erroneous prediction of the slick area. Small spills can directly start to propagate in surface tension regime or undergo it in early times of release due to thin layer of oil. Large spills can progress under the gravity-viscous regime at the beginning of the release, but after a while, surface tension becomes more and more dominant than gravity force. The extent of large spills cannot be accurately estimated by modeling only gravity regime in the long-term prediction. Therefore, gravity viscous regime is not enough to determine the spill spreading in all spill scenarios. The inclusion of surface tension regime term into the calculations of spill area is inevitable. So, new step length defined in Eqn. 13 can be used to describe oil spreading more realistically in particle based numerical algorithms of Nihoul's equation. Using it provides consistent results as it is discussed in Durgut et al. (2020).

Inclusion of surface tension parameter in random walk numerical solutions requires determination of " $\alpha$ " and " $\beta$ " coefficients in Eqn. 13 to provide best match with exact solution. " $\alpha$ " is provided as 0.34 by Arhipov

(2008). “ $\beta$ ” is determined through sensitivity analysis. Sensitivity analysis is performed in a variety of  $\beta$  range. They are shown in Figure 2 and Table 1. Most accurate results are obtained when  $\beta=0.35$ . So, we suggest to use this value for numerical solutions for oil spreading to describe surface tension regime.

Also, we observed how spreading of oil can be affected from the release parameters. The effect of volume can be seen from Fig. 2a and 2b. Initial radius and slick thickness increase with increasing volume. However, after hours, the slicks cover the same area regardless of release volume when their other properties are same. This interesting phenomenon can be explained as a result of differences of spreading rates in the regimes. A slick spreads more slowly under the effect of gravity force than surface tension. Since surface tension regime starts earlier for smaller spills, these spills have higher spreading rates for longer period of time. Therefore, they converge to same radius with larger slicks, even if their initial radius is smaller. However, they form thinner layer on the calm sea. Moreover, drag coefficient is directly proportional to the frictional force against the spreading. A slick experiencing higher friction resists spreading more and tends to move less, resulting in lower radius and higher thickness in every stage in Fig. 3a and 3b. However, logarithmic change rates of radius and thickness in logarithmic time are preserved. In Fig 4a and 4b, surface tension affects the duration of regimes. Lower surface tension force prolongs the gravity viscous regime. 4. CONCLUSION

Effect of surface tension regime was observed on the spreading of oil in this study. An algorithm investigating oil spreading under gravity viscous regime was compared with analytical and asymptotic solutions. The comparison emphasizes that the algorithm neglecting surface tension regime can estimate the progress of slick inadequately in the long term prediction scenarios. So, we have defined new step length to consider surface tension regime for particle movement in Gaussian random walk method of Nihoul’s equation. This study also reveals that the slick behavior can change in gravity viscous and/or surface tension viscous regimes with respect to release parameters.

Keywords: Oil slick spreading; Oil spill modeling; Gravity-viscous spreading; Surface tension-viscous spreading;

Equation 1-2-3-4-5-6-7

$$\frac{\partial h}{\partial t} = Q + \nabla \cdot \left[ \frac{(\rho_o - \rho_w)}{\rho_w} g \frac{\rho_w}{k} h^2 \nabla h - \frac{\gamma}{k} h \nabla \varphi^2 \right] \quad (1)$$

$$R^2 = \frac{1}{\alpha} \arctan(\alpha R^2) = \frac{4\gamma}{k} t \quad (2)$$

$$\alpha = \frac{2\pi}{3V} \left( \frac{2\gamma}{g \rho_w} \right)^{1/2} \quad (3)$$

$$g' = \frac{(\rho_w - \rho_o)}{\rho_w} g \quad (4)$$

$$R = \left[ \frac{27V^2}{2\pi^2} \frac{g' \rho_w}{k} t \right]^{1/4} \quad (5)$$

$$R = \left( \frac{4\gamma}{k} t \right)^{1/2} \quad (6)$$

$$h_{max} = \frac{\gamma}{\pi R^2} \quad (7)$$

Denklemlerin yerleri bildiri içinde belirlendi, parantez içinde verildi.

Equation 8-9-10-11-12-13

$$\frac{\partial h}{\partial t} = \nabla(D(h)\nabla h) \quad (8)$$

$$D(h) = \frac{g' \rho_w}{k} h^2 \quad (9)$$

$$\sigma = \sqrt{2\lambda D(h)\Delta t} = \sqrt{2\lambda \frac{g' \rho_w}{k} h^2 \Delta t} \quad (10)$$

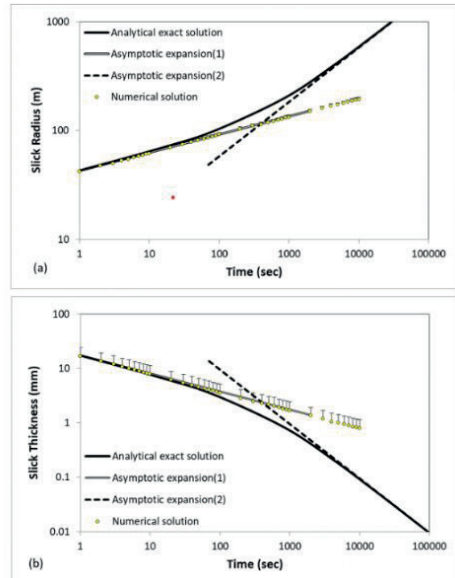
$$X^{i+\Delta t} = X^i + N(\mu, \sigma^2) D_x \quad (11)$$

$$\frac{\partial h}{\partial t} = Q + \nabla \cdot \left[ \frac{g' \rho_w}{k} h^2 \nabla h + \frac{2\gamma}{k} \left( \frac{h}{h_{max}} \right)^2 \nabla h \right] \quad (12)$$

$$D_x = \sqrt{\left[ 2\alpha \frac{g' \rho_w}{k} + 2\beta \frac{2\gamma}{k h_{max}} \right] h^2 \Delta t} \quad (13)$$

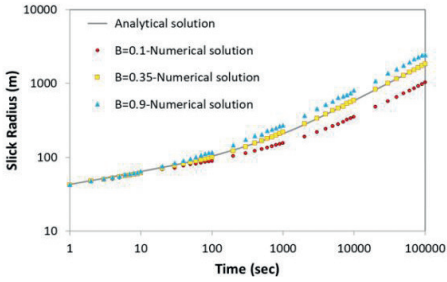
Denklemlerin yerleri bildiri içinde belirlendi, parantez içinde verildi.

Figure 1: Time development of a) slick radius and b) slick thickness for a base case scenario.



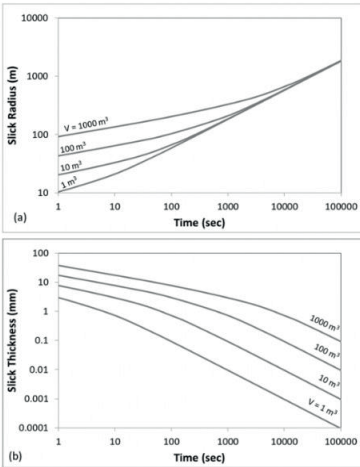
Results and Discussion kısmına eklenebilir.

Figure 2: Sensitivity analysis of numerical solution with changing  $\beta$



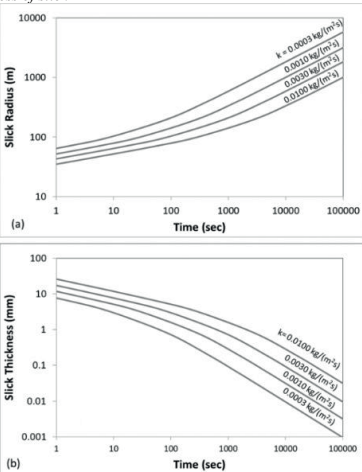
Results and Discussion kısmına eklenebilir.

Figure 3: Effect of different spill volumes on a) radius and b) thickness of slick



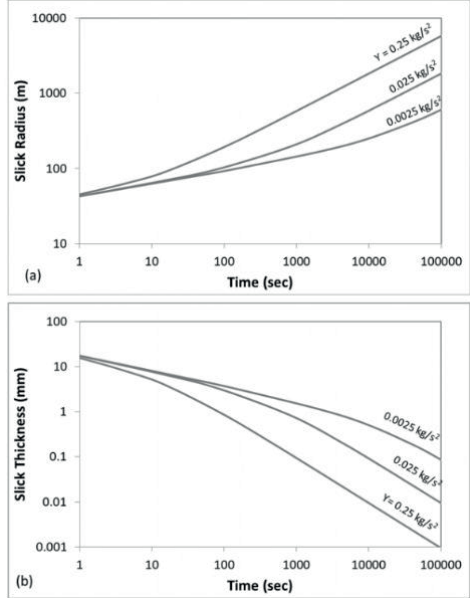
Results and Discussion kısmına eklenebilir.

Figure 4: Effect of different drag coefficients on a) radius and b) thickness of slick



Results and Discussion kısmına eklenebilir.

Figure 5: Effect of different surface tensions on a) radius and b) thickness of slick



Results and Discussion kısmına eklenebilir.

Table 1: Numerical solution accuracy with respect to Beta coefficient

Beta	Accuracy (%)
0.1	80.22
0.2	88.69
0.3	95.86
0.325	96.47
0.34	97.62
0.35	97.76
0.36	97.33
0.4	95.29
0.5	90.87
0.6	87.48
0.7	85.04
0.8	82.87
0.9	81.41

Results and Discussion kısmında Figure 2den hemen sonra koyulabilir.

# Petrol Döküntülerinde Risk Değerlendirmesi ve Acil Müdahale Planlarının Önemi

**Pelin Dođruvol, Müge Bıyıkhođlu, Ayşe Tuna İşsever**  
Meke Marine Teknoloji A.Ş., İstanbul / Türkiye



Denizcilik faaliyetlerinden kaynaklanan petrol kirlilikleri, deniz ekosistemi üzerinde zararlı etkilere neden olmakta ve ülkelere ciddi boyutta ekonomik zararlar vermektedir. Ülkemiz kıyı suları artan tanker taşımacılığı ve meydana gelen gemi kazaları nedeniyle petrol kirliliđi açısından büyük risk altındadır. Kazaların doğal yaşam, balıkçılık, sosyo-ekonomik ve rekreasyonel faaliyetler üzerinde uzun vadeli zararlı etkileri göz önünde bulundurulduğunda, petrol döküntüsüne müdahale edilmesi çeşitli kararların oldukça hızlı şekilde alınmasını gerektirir. Bu şekilde hızlı kararların alınması müdahale edecek olanların durumun değerlendirilmesi açısından yeterli derecede hazırlıklı olması, herhangi bir tereddüt duymadan hayati önem taşıyan kararları alabilmesi ve uygun kaynakları doğru yönetebilmesi durumunda sağlanabilir. Etkin ve etkili bir müdahale göz önüne alınarak hazırlanmış bir acil müdahale planı bu hedefin elde edilmesinde en önemli adımı oluşturacaktır.

Risk Değerlendirmesi ve Acil Müdahale Planı'nda petrol kirliliđinden korunmak veya petrol kirliliđinden korunmanın mümkün olmadığı durumlarda, deniz ortamında oluşabilecek petrol döküntülerine müdahale metotları ve temel ilkeleri belirlenir. Aynı zamanda, bu planlarda uygulanabilir prosedürler oluşturulur ve bir petrol döküntüsünde müdahale operasyonunda takip edilmesi gerekli haberleşme sıralaması, yetki kademeleri ve ilgili kişilerin sorumlulukları ulusal düzenlemeler dikkate alınarak açıklanır.

Bu çalışmamızda, petrol döküntülerine hazırlıklı olmak için oluşturulan Risk Değerlendirmesi ve Acil Müdahale Planları'nın önemi ve kapsamı gereken süreçler ortaya konulacaktır.

Oil pollution from maritime activities causes harmful effects on the marine ecosystem and causes serious economic damage to countries. The coastal waters of our country are under great risk in terms of oil pollution due to increasing tanker transportation and ship accidents. Considering the long-term detrimental effects of accidents on wildlife, fisheries, socio-economic and recreational activities, responding to an oil spill requires various decisions to be taken very quickly. Such rapid decision-making can only be achieved if responders are adequately prepared to assess the situation, can make vital decisions without hesitation, and can properly manage available resources. An emergency response plan prepared with an efficient and effective response in mind will be the most important step in achieving this goal.

In the Contingency Plan, the methods and basic principles of response to oil spills that may occur in the marine environment are determined in order to prevent oil pollution or in cases where it is not possible to prevent oil pollution. At the same time, applicable

procedures are established in these plans and the communication sequence to be followed in an oil spill response operation, the levels of authority and the responsibilities of the relevant persons are explained taking into account national regulations.

In this study, the importance of Contingency Plans created to be prepared for oil spills and the processes that they should cover will be revealed.

**Keywords:** Risk assessment, emergency response, oil spill

## AMAÇ

Günümüzde tanker trafiđinin yoğunluđu, hidrokarbon arama projeleri, endüstri ve rafineri atıkları denizlerimiz için petrol kirliliđi açısından tehdit oluşturmaktadır. Denizde uzun süre kalabilme potansiyeline sahip petrolün herhangi bir döküntü olması durumunda, uçucu kısmı uçmakta, bir kısmı rüzgar ve akıntının etkisiyle kıyılara vurmakta, bir kısmı mikrobiyal degradasyona uğramaktadır. Geri kalan kısmı ise deniz dibine çökerek sedimanda birikme göstermektedir. Petrol ve türevleri balıklar, çift kabuklu yumuşakçalar, karidesler, algler, deniz kuşları gibi birçok deniz canlısına etki ettiđinden denizlerde ciddi bir çevresel problemlere neden olmaktadır. Bu etkiler göz önüne alındığında, petrol döküntüne karşı hazırlıklı olmak ve gerekli önlemleri almak büyük önem taşımaktadır. Bu hazırlığın en önemli parçası bir proje veya tesisin petrol döküntüsü risklerini dikkate alarak uygun bir döküntüye müdahale prosedürü geliştirmektir. Bu çalışmamızın amacı meydana gelebilecek olası petrol döküntüleri için acil müdahale planlama sürecinin önemini ortaya koymaktır.

## YÖNTEM

Risk Değerlendirmesi ve Acil Müdahale Planı'nın önemini ortaya konmasında konu özelinde ulusal ve uluslararası literatürden ve uzun yıllara dayalı tecrübemizle oluşturduğumuz yazılı, sözlü ve görsel kaynaklarımızdan faydalanılacaktır. Böylece bu konu hakkında yayınlanmış ve yayınlanmamış çalışmalar bir araya getirilerek, tüm faydalı bilgiler bir bütün olarak sunulacaktır.

## BULGULAR

Petrol döküntüsüne müdahale konusunda dünyada ve ülkemizde yapılan çalışmalar incelendiğinde Risk Değerlendirmesi ve Acil Müdahale Planları'nın hazırlıklı olma konusunda önemli yer tuttuđu görülmüştür. Acil müdahale planlarının temelini oluşturan en önemli unsur risk değerlendirmesidir. Kaza olasılıklarının değerlendirilmesinde tesisten ve projeden kaynaklanan risk faktörleri ele alınır. Bu

amaçla tesisin veya projenin yapısı, işletimi, kaynakları ve sürecine ait veriler değerlendirilir. Çevresel risklerin değerlendirilmesinde ise kaza sırasında ve sonrasında zarar görebilecek jeolojik, biyolojik, ekolojik ve sosyo-ekonomik yapılar belirlenerek incelenir.

Risk Değerlendirmesi ve Acil Müdahale Planı'nın içeriği oluşturulurken aşağıda belirtilen amaçları kapması gerektiği belirlenmiştir.

- Tesis veya proje faaliyetleri sırasında bir arızadan doğabilecek bir döküntüyü veya döküntü tehlikesini kontrol altına almak için izlenecek yolları belirlemek,
- Zamanında yapılan bir sınırlamayla dökülen petrolün kaynaktan uzaklaşmasını en aza indirmek,
- Zamanında yapılan bir sınırlama ve temizlik müdahalesiyle ana döküntünün çevresel etkisini en aza indirmek,
- Uygun ekipman ve izlenecek yöntem seçimi ile temizlik müdahalesinin faydasını azami seviyeye çıkarmak,
- Eğitimli ve deneyimli işlevsel ekipler ile müdahalenin faydasını azami seviyeye çıkarmak,
- Olası petrol yayılımlarına karşı savunmasız olan, çevresel olarak hassas yaşam alanlarının korunmasını sağlamak.

## SONUÇ

Deniz kirliliğinin en etkili sebeplerinden biri olan petrol döküntüsü denizel ekosistem açısından ciddi bir tehlike oluşturmaktadır. Petrol döküntüsünün önlenmesi ve olası bir petrol kirliliğine karşı hazırlıklı olunması yönünde yürütülen çalışmalar geleceğimiz açısından büyük önem taşımaktadır. Son yapılan araştırmalar da göstermektedir ki petrol kirliliği önlem alınmadıkça tehdit olmaya devam edecektir. Bu çalışma ile petrol döküntüsü için alınabilecek önlemlere ve olası bir döküntü anında yapılması gerekenlere ışık tutulmaya çalışılmıştır. Mevcut çalışmanın gelecekte yapılacak araştırmalar için de kaynak oluşturacağı düşünülmektedir.

## KAYNAKÇA

MEKE Marine Teknoloji (2014-2023), Risk Değerlendirmesi ve Acil Müdahale Planları, İstanbul.

IOPF (2014), Technical Information Papers 16: Contingency Planning for Marine Oil Spills.

Doğruyol, P., 2019. Haliç Sedimanlarında Mikroplastik Kirliliğinin Araştırılması, İstanbul Üniversitesi-Cerrahpaşa Lisansüstü Eğitim Enstitüsü, Yüksek Lisans Tezi, İstanbul.

Anahtar Kelimeler: Risk değerlendirme, acil müdahale

# Büyük Gemi Kazaların Önlenmesi ve Çıkarılan Dersler

**Mehmet Kerem Kemerli**

ISCO (International Spill Control Organization)



Dünya ticaretinde çok önemli yer tutan deniz taşımacılığında teknoloji ve ihtiyaçlar özellikle petrol tankerlerinin boylarını 400 (dört yüz) metrelerin üzerine hacimlerini de 500 (beş yüz) DWT boyutlarına ulaştırmıştır. Okyanuslarda yılda iki milyar (2.000.000.000) tonun üzerinde petrol taşınmaktadır. Mevcut koşullar haliyle denizlerimizde kaza risklerini artırmaktadır. Bu riskler kimi zaman doğa kaynaklı kimi zamansa insan kaynaklı olarak karşımıza çıkmaktadır. Sonuç olarak bu kazalar doğanın kirlenmesine neden olmaktadır.

Kazaların önlenmesi için tedbirler almak mümkündür. Kaza sonrası temizlik ve kurtarma operasyonlarından çıkarılan dersler hem alınacak tedbirleri şekillendirmesi açısından hem de temizlik operasyonlarının ve tazmininin daha düzenli ve etkin yapılması açısından çok önemlidir. Pek çok kaza uluslararası kuralların değişmesini sağlamıştır.

Bu çalışmamızda, dünyadaki önemli kazaların oluş şekilleri ve temizlik operasyonları incelenmiştir. Görülen ve görülmeyen, kısa ve uzun vadeli verdiği zararlar göz önüne serilmeye çalışılmıştır. Kazaların ve temizleme operasyonlarının yerel ve uluslararası ortamlarda yol açtığı kanun ve düşünce sistematiği değişikliklerine değinilmiştir. Literatür açısından doğru bilinen yanlışlar gözler önüne sunulmuş ve kazalar sonrası uygulanan uluslararası aksiyonlar gösterilmiştir.

The technology and the needs in maritime transportation, which has a very important place in world trade, have increased the lengths of oil tankers to over 400 (four hundred) meters and their volumes to 500 (five hundred) DWT. Over two billion (2,000,000,000,000) tons of oil is transported annually in the oceans. Current conditions increase the risks of accidents in our seas. These risks are sometimes of natural origin and sometimes of human origin. As a result, these accidents cause pollution of nature.

It is possible to take measures to prevent accidents. The lessons learned from post-accident cleanup and rescue operations are very important both in terms of shaping the measures to be taken and in terms of making cleanup operations and compensation more organized and effective. Many accidents have led to changes in international rules.

In this study, the occurrence patterns and cleanup operations of major accidents in the world are analyzed. The short and long term damages, both seen and unseen, have been tried to be revealed. The changes in laws and thinking that accidents and cleanup operations have caused in local and international environments have been addressed. The misconceptions in the literature are presented and the international actions taken in the aftermath of accidents are illustrated.

## AMAÇ

Gemiler, tasarım hatalarından, insan hatalarından, mekanik hatalardan, ekstrem meteorolojik ve/veya oşinografik doğa olaylarından kaynaklı kazalar yaşayabilirler. Kaza sonucu yaşanan kurtarma çalışmaları, kazanın sebebiyet vermediği kirliliklerin olmasına yol açabilir. Kurtarma çalışmaları sırasında da bazen mekanik hatalar çoğu zaman da kritik karar hataları kirliliklere sebep olmaktadır. Kirlilikler de doğrudan ve dolaylı olarak insan hayatına kolay geri dönülemez zararlar vermektedir.

Bu çalışma ile endüstriyel anlamda gemi inşa, armatörlük, acentelik, gemi işletme, taşımacılık, pilotaj, römorkaj, gemi kurtarma, acil müdahale, iletişim, kıyı emniyeti, çevre, turizm, doğal hayat, deniz sektörlerinin gelişiminin nasıl bir parçası olduğu anlatılmıştır. Uluslararası destek ve kuralların faydaları gösterilmeye çalışılmıştır.

## YÖNTEM

Yıllar içerisinde olan kazaların ve temizleme operasyonlarının incelenmiş ve sebep sonuç ilişkileri ortaya konulmuştur.

## BULGULAR

Yapılan araştırmalar sonucunda aşağıda yer alan bulgular belirlenmiştir.

- Kazaların sebepleri,
- Yanlış metodoloji seçimi yüzünden kurtarma yerine kazanın veya kirliliğin büyümesi,
- Kirliliğin önlenmesi amacıyla yapılan çalışmaların ne gibi sonuçlar verdiğinin ortaya çıkartılması,
- Yeni temizlik metodlarının geliştirilmesi,
- Görülen aksaklık veya eksiklikler üzerine uluslararası kural ve kanunların güncellenmesi veya yeni kanunların çıkartılması.

## SONUÇ

Dünya'da artan deniz trafiği ve insan hatalarından oluşan kaza ve sonrasındaki kirliliklerin önlenmesi, önlenememesi halinde ise en verimli şekilde temizliğinin yapılabildiği şekilde tazmin edilmesine yönelik kuralların şeffaf ve herkes için geçerli olmasının nasıl sağlandığı gösterilmektedir.

Kirliliğe Acil Müdahalenin önemi, kirliletiçi tipi, kazanın olduğu coğrafyaya göre doğru müdahale tekniklerinin kullanılması, müdahale sırasında planlama, lojistik ve finansın ne kadar önemli olduğu gözler önüne serilmektedir. Uluslararası tazmin müessesesinin müdahalenin verimini nasıl arttırdığı anlaşılmıştır.

Bu çalışmanın deniz kaynaklı kirlenici kazalarının önlenebileceğinin ve her olaydan ders çıkartılarak bir sonraki olayda daha verimli çalışmanın mümkün olacağını gösterilmesine ışık tutacağı düşünülmektedir.

Anahtar Kelimeler: Gemi kazası, petrol kirliliği



# Petrol ve Doğal Gaz Üretim Faaliyetleri Sonucu Oluşan Atıksuların Membran Teknolojileri İle Yönetimi



İsmail Koyuncu<sup>1,2</sup>, Recep Kaya<sup>1,2</sup>, Börte Köse Mutlu<sup>1,2</sup>, Hale Özgün<sup>1,2</sup>, M. Evren Erşahin<sup>1,2</sup>, Mahmut Altınbaş<sup>1,2</sup>, Sema Sayılır<sup>2</sup>, Şebnem Doğa Atay-Balı<sup>3</sup>, Pelin Hoşhan<sup>3</sup>, Esra Eren<sup>3</sup>, Cumali Kınacı<sup>1,2</sup>

<sup>1</sup>Çevre Mühendisliği Bölümü, İstanbul Teknik Üniversitesi, İstanbul / Türkiye

<sup>2</sup>Prof. Dr. Dincer Topacık Ulusal Membran Teknolojileri Uyg-Ar Merkezi, İstanbul Teknik Üniversitesi, İstanbul / Türkiye

<sup>3</sup>Türkiye Petrolleri Anonim Ortaklığı, Ankara / Türkiye

## ÖZET

Petrol ve doğalgaz üretim atıksuyunun çevreye zarar vermeyecek şekilde bertarafı oldukça önemli olmakla birlikte artırılması güç atıksu sınıfına girmektedir. Membran prosesler, üretim atıksuyunun ileri derecede arıtılmasında en uygulanabilir alternatiftir. Bu çalışmada, mikrofiltrasyon, ultrafiltrasyon, membran biyoreaktör, nanofiltrasyon ve ters osmoz gibi eşitli membran prosesler karşılaştırılmalı olarak test edilerek en uygun proses konfigürasyonu oluşturulmuş ve TPAO Trakya Bölgesi kuyularında oluşan üretim atıksuyu desarj standartlarına uyacak şekilde bir pilot tesis çalışması ile ileri derecede arıtılabilmektedir.

## ABSTRACT

The disposal of waste water from petroleum and natural gas production in an environmentally harmless manner is of great importance; however, treating it proves to be challenging due to its classification as difficult-to-treat industrial wastewater. Membrane processes are the most feasible alternatives for advanced treatment of production wastewater. In this study, various membrane processes such as microfiltration, ultrafiltration, membrane bioreactors, nanofiltration, and reverse osmosis were compared and tested to establish the optimal process configuration. Through a pilot plant study, the most suitable process configuration was developed and successfully applied to achieve advanced treatment of production wastewater generated from wells in the TPAO Thrace Region, in accordance with discharge standards.

Anahtar Kelimeler Petrol Üretim Atıksuyu, Atıksu Geri Kazanımı, Membran Biyoreaktör, Ters Osmoz, Çevre Kirliliğini Önleme, Sürdürülebilirlik

## AMAC

Petrol ve doğalgaz üretim atıksuyunun çevreye zarar vermeyecek şekilde bertarafı önemle üzerinde durulması gereken bir konudur. Üretim atıksularının bertarafı amacıyla sıkça kullanılan yeraltına enjeksiyon yöntemi, atıksuların yeraltı sularında, yüzeysel sulara ve aynı zamanda toprakta çevre kirliliğine sebep olur. Bu sebeple, üretim atıksuyunun arıtılması gerekir. oluşturduğu olumsuz çevresel etkilerinin önlenmesi amacı ile arıtılması gerekmektedir. Arıtılması oldukça zorlu olan üretim atıksuyunun verimli, ekonomik ve ileri derecede arıtılmasını sağlayacak arıtma teknolojisinin geliştirilmesi önemlidir. Bu amaçla, Türkiye Petrolleri Anonim Ortaklığı (TPAO) Genel Müdürlüğü'ne

bağlı Trakya Bölge Müdürlüğü bünyesindeki üretim sahalarında oluşan petrol ve doğalgaz üretim atıksularının arıtılmasında Membran Biyoreaktör (MBR), Mikrofiltrasyon (MF), Ultrafiltrasyon (UF), Nanofiltrasyon (NF) ve Ters Osmoz (TO) gibi çeşitli arıtma membran prosesi alternatifleri karşılaştırılmış ve sonuçları karşılaştırılmalı olarak değerlendirilmiştir.

## GEREÇ VE YÖNTEM

Çalışma kapsamında ilk olarak, Trakya bölgesinde petrol ve doğalgaz üretim faaliyetleri sonucu oluşan atıksuyun karakterizasyonu yapılmıştır. Bu kapsamda, her bir kuyudan alınan numuneler mevsimler süresince analizlere tabi tutulmuştur. Ardından, laboratuvar ölçekli arıtılabilirlik deneylerine geçilmiştir. Ön arıtma amaçlı Ardışık Kesikli Reaktör (AKR), MBR, MF ve UF kullanılarak, ileri arıtma için ise NF ve TO prosesleri tercih edilmiştir. MBR ve yüksek basınçlı hücreli membran sistemi (MF/UF/NF/TO deneyleri için) kullanırken, Veri Tabanlı Kontrol ve Gözetleme Sistemi (SCADA) yardımı ile sistemler bilgisayardan kontrol edilmiş ve elde edilen tüm veriler bilgisayarda otomatik olarak depolanmıştır. Yüksek basınçlı sistemde, farklı gözenek çapına sahip membranlar, aktif karbon eklentisinin etkisi ve işletme basıncının etkisi gözlemlenerek optimizasyon yapılmıştır.

Tüm arıtılabilirlik çalışmalarında, arıtma veriminin hesaplanabilmesi için giriş ve çıkış suyu numunelerinde KOİ, TKN, TP, anyon, katyon ve ağır metal analizleri gerçekleştirilmiştir. Ayrıca kullanılan membranların SEM görüntüleri çekilmiş, EDS ile yüzeyinde tutulan maddelerin analizi ve temas açısı analizleri gerçekleştirilmiştir.

## BULGULAR VE SONUÇ

Laboratuvar ölçekli yürütülen deneylerde elde edilen sonuçlar doğrultusunda üretim atıksuyuna uygun arıtma prosesleri seçilmiş ve bu prosesler ile pilot ölçekli bir arıtma tesisi projelendirilmiştir. Hamitabat Bölgesine kurulan pilot tesis, karma olarak çeşitli kuyulardan toplanan atıksuyu aylar boyunca arıtmıştır.

Yapılan çalışmalar sonucunda, tesisin toplam su geri kazanım oranının ortalama %75 olduğu gözlemlenmiştir. UF ile yürütülen çalışmalarda ise ortalama akı değerinin 20 L/m<sup>2</sup>/sa iken MF ile yürütülen çalışmalarda ortalama akı değeri bu değer yaklaşık beş katı olmuştur. TO prosesinde ise ortalama 12,5 L/m<sup>2</sup>/sa olmuştur. İleri arıtmanın son aşaması olan TO ünitesinde iyonlar üst düzeyde bir verim ile tutulabilmiş ve desarj

suyu iletkenliđi 900  $\mu\text{S}/\text{cm}$  olarak elde edilmiřtir. Organik kirlilik giderim verimleri incelendiđinde ise Su Kirliliđi Kontrol Yönetmeliđi'nin sektöre özgü desarj standartları incelendiđinde sınır deđerlerin sađlanabildiđi görölmüřtür.

#### Teřekkür

Bu proje TÜBİTAK tarafından KAMAG Projeleri kapsamında 107G091 Proje numarası ile desteklenmiřtir. Arařtırmacılar, destekleri için TÜBİTAK'a teřekkür ederler. Ayrıca, çalıřma boyunca numune temini, önemli analizlerin gerçekleřtirilmesi dahil tüm destekleri için TPAO'ya teřekkürlerimizi sunarız.

# Petrol ve Doğalgaz Sektörünün İklim Değişikliğine Etkileri

**Murat Cilingiroğlu**

Sinerji Çevre Hizmetleri Denetim Danışmanlık Mühendislik Ltd Şti, Ankara



İklim değişikliğinin yoğun etkileri ve ön görülen olumsuz senaryolar, bu konuda uluslararası düzeyde daha keskin adımların atılması gerekliliğini doğurmuştur. Gelişmelerin bir sonucu olarak; Paris Anlaşması, 2015 yılında kabul edilmiş ve 175 ülke temsilcisiyle birlikte ülkemizde ilgili anlaşmayı imzalamıştır. Anlaşma; iklim değişikliğine sebebiyet veren sera gazlarında önemli paya sahip petrol endüstrisini ve fosil yakıtların kullanımını da tartışılır hale getirmiştir.

Bildiri içeriğinde öncelikle; dünya çapındaki enerji şirketleri ve fosil yakıt arama, üretim - rafinasyon prosesleri ile ilgilenen kuruluşların sera gazı emisyonları konusunda aldığı aksiyonlar, mevcut durumlarının değerlendirilmesi, önlem planları ve yol haritaları incelenecektir. Ülkemiz özelinde ise, petrol ve doğalgaz sektörünün amiral gemisi TPAO kurumunun 2021 yılı itibarıyla başlatmış olduğu kurumsal karbon ayak izi çalışmaları açıklanarak Türk Standartları Enstitüsü (TSE) tarafından doğrulanmış sera gazı raporuna esas sonuçlar hakkında bilgi verilecektir.

Bu bilgiler ışığında, TPAO'nun uluslararası rakipleri ile kıyaslanabilmesi sağlanarak, kurum tarafından atılan ve/veya atılması planlanan adımların neler olduğu açıklanacaktır. Böylelikle ülkemiz petrol – doğalgaz sektörünün sürdürülebilirlik ve iklim değişikliği alanında dönüşümü için yol haritasına ilişkin yaratılan pozitif etkinin ortaya konulması hedeflenmektedir.

The intense effects and predicted negative scenarios about Climate Change, has requires more strict movements internationally. As a conclusion of this improvements; Paris Agreement was adopted by representative of 175 country which one of them is ours, on 2015. According to this agreement, oil industry and use of fossil fuels which causes climate change is Greenhouse gases, have also become debatable.

In the content of the notice's first beggining, The actions taken by worldwide energy companies and organizations dealing with fossil fuel exploration, production - refining processes, evaluation of their current situation, precautionary plans and a course of action will be examined. This comprehensive appraisal will encompass the evaluation of their extant circumstances, preventive measures implemented, and the strategic blueprints that they have devised. On the domestic front, particular attention will be directed towards TPAO, the flagship institution in the petroleum and natural gas sector. Detailed elucidation will be provided regarding TPAO's corporate carbon footprint initiatives, which were inaugurated as of the year 2021. Furthermore, insight will be disseminated regarding the outcomes based on the greenhouse gas report, duly authenticated by the Turkish Standards Institute (TSE).

Given this information, an elucidation of the steps taken by the institution, or those that are planned to be taken,

will be provided to facilitate a comparison between TPAO and its international counterparts. Consequently, the objective is to articulate the positive influence generated in relation to the roadmap for sustainability and climate change transformation in the petroleum and natural gas sector of our nation.

## GİRİŞ

2020 sonrası iklim değişikliği rejiminin çerçevesini oluşturan Paris Anlaşması, 2015 yılında Paris'te düzenlenerek kabul edilmiştir. COP 21'de, 2020 sonrası için ilk kez küresel ölçekte bütün ülkeler sera gazı emisyon azaltımı taahhüdünde bulunmuşlardır. Anlaşma, 5 Ekim 2016 itibarıyla, küresel sera gazı emisyonlarının %55'ini oluşturan en az 55 tarafın anlaşmayı onaylaması koşulunun karşılanması sonucunda, 4 Kasım 2016 itibarıyla yürürlüğe girmiştir. Ülkemiz, Paris Anlaşması'nı, 22 Nisan 2016 tarihinde, New York'ta düzenlenen Yüksek Düzeyli İmza Töreni'nde 175 ülke temsilcisiyle birlikte imzalamış ve Ulusal Beyanımızda Anlaşma'yı geliştirmekte olan bir ülke olarak imzaladığımız vurgulanmıştır. Bu anlaşma ve dünyada da iklim krizinin çok daha sık gündeme gelmesi ve gittikçe toplumlar üzerindeki etkilerini de artırması sera gazlarında önemli paya sahip petrol endüstrisini ve fosil yakıtların kullanımını da tartışılır hale getirmiştir.

## GELİŞME

Bu kapsamda sözlü yapılması planlanan bildiriye, fosil yakıtların dünyadaki rezervleri, toplam sera gazına etkileri, enerji şirketlerinin ve fosil yakıt arama, üretim ve rafinasyon prosesleri ile ilgilenen kuruluşların iklim değişikliği ile mücadelede mevcut durumları, hangi önlemler aldığı, daha nasıl bir yol izlemesi gerektiği ve süreç çıktılarının paylaşılması öngörülmektedir. Petrol sektörü, küresel sera gazı emisyonlarının önemli bir kaynağıdır ve iklim değişikliğiyle mücadele çabalarıyla yakından ilişkilidir. Fosil yakıtların üretimi, rafinajı ve tüketimi, sera gazlarının atmosfere salınımına neden olur. Ancak, son yıllarda Türkiye'nin enerji sektöründe çevreye duyarlılık ve sürdürülebilirlik odaklı politikalara ağırlık verdiğini görmekteyiz. Ülkemizde petrol ve doğalgaz sektörünün amiral gemisi TPAO kurumu da bir ilke imza atarak 2021 yılı Kurumsal Karbon Ayak İzi hesabını yaparak raporlamış ve TSE kurumu tarafından da doğrulama çalışmalarını tamamlamıştır. Bu aşamadan sonra oluşan sera gazı emisyonlarını her yıl hesaplayıp raporlamak ve azaltım politikalarını belirleyerek kararlılık ve disiplinle uygulamayı hedef haline getirmiştir. Bu raporun çıktıları, diğer uluslararası şirketlerle karşılaştırılması, hedefler ile ilgili bilgilendirme yapılması da bu sunum içeriğinde

yer almaktadır. Bu zincirin ilk halkasını oluşturan çevre dostu hareketin, Türkiye’de de petrol ve doğalgaz sektöründe sera gazlarının hesaplanması, raporlanması ve azaltım kısmında indikatör görevi gerçekleştireceği aşikardır.

## SONUÇ

Küresel ısınma, iklim değişikliğinin başlıca aktörü olan bu gazlar, sera etkisi yaratarak dünya genelinde sürece negatif katkıda bulunurlar. Bu doğrultuda sera gazı ve etkileri, doğal gaz ve ham petrol arama, üretim süreçlerinde oluşan sera gazı kaynakları ile petrol şirketlerinin karşılaştırmalı sera gazı sonuçları üzerinden değerlendirmeler yaparak, katılımcıların iklim değişikliği ve sera gazı konularında bilinç seviyelerinin artırılması hedeflenmektedir.

Anahtar Kelimeler: iklim değişikliği, sera gazı

# Türkiye Petrolleri Anonim Ortaklığı (TPAO)'nda Sera Gazı Emisyon Hesaplama Çalışmaları

**Fatma Salcı, Erkan Buzpınar, Hatice Selcen Köse, Pınar Aydoğdu, Elif Gökçek Küllük, Şebnem Doğa Atay Bali, Muhammet Mustafa Çelebi, Galip Yılmaz, Ali Sercan Malgaz**

Türkiye Petrolleri Anonim Ortaklığı, İş Güvenliği ve Çevre Koruma Daire Başkanlığı, Çevre Koruma Müdürlüğü, Ankara / Türkiye



1954 yılından itibaren Türkiye'nin ulusal petrol şirketi olarak hidrokarbon arama ve üretim faaliyetlerini yürüten Türkiye Petrolleri Anonim Ortaklığı (TPAO), çevre bilinci ve yüksek farkındalığı ile çevresel çalışmalarını planlayıp yürütmekte ve geliştirmektedir.

Karada ve denizdeki faaliyet planlamalarında, çevresel çalışmaları da planlayıp takip eden TPAO; sıfır atık uygulamaları operasyonel atıkların yönetimi, çevre eğitimi, çevresel denetim, çevre mevzuatının takibi vb. çalışmalarını geliştirerek yürütmektedir. Son dönemde iklim değişikliği etkilerinin kendini iyice hissettirmeye başlaması ile ülke çevre politikalarına paralel çalışmalar planlayan TPAO, karbon ayak izi ve su ayak izi hesaplama çalışmalarına ve azaltma önlemleri geliştirmeye başlamıştır.

Bu bildiri ile TPAO'da yürütülen ve geliştirilen karbon ayak izi hesaplama çalışmalarından ve karbon ayak izi azaltım adına yapılan çalışmalardan bahsedilecektir.

Turkish Petroleum Corporation (TPAO), performing hydrocarbon exploration and production activity regarding with high environmental awareness, plans and improves its environmental studies since 1954.

TPAO, which also improves and monitors environmental studies considering with zero waste practices, operational waste managements, trainings, environmental audits, following environmental legislations on off shore and onshore operations. Recently, carbondioxide emission effects all over the world, therefore TPAO plans to calculate carbon dioxide footprint and also follow green house effect policies, and develop mitigation steps.

In this paper, TPAO carbon footprint calculations steps and mitigation steps will be mentioned.

## TPAO VE ÇEVRE

İş Güvenliği ve Çevre Koruma Daire Başkanlığı; 1989 yılında İş Güvenliği Koordinatörlüğü olarak TPAO içinde faaliyetlerine başlamıştır. 1991 yılında geliştirilerek İş Güvenliği Grup Başkanlığı olarak kurulmuş, 1992 yılında çevre koruma çalışmalarını da yürütmek üzere görevlendirilerek İş Güvenliği ve Çevre Koruma Grup Başkanlığı adı altında yapılandırılmıştır. 1995 tarihinde Genel Müdürlük ve Bölge Müdürlüklerindeki Sağlık Üniteleri ile Genel Müdürlükteki sivil savunma amaçlı olmayan yangından korunma çalışmaları ve Bölge Müdürlüklerindeki İtfaiye birimlerinin İş Güvenliği ve Çevre Koruma Grup Başkanlığı'na bağlanması ile çalışma ve yetki alanı genişletilmiş, 2004 yılında Grup Başkanlıkları Daire Başkanlıklarına dönüştürülmüştür. Karada olduğu gibi deniz alanlarında da artan faaliyetlere paralel şekilde nitelikli personel sayısını arttıran TPAO İş Güvenliği

ve Çevre Koruma Daire Başkanlığı, alt işverenlerle de gerekli koordinasyonu sağlayarak çevresel çalışmalarını sürdürmektedir.

## TPAO'da Çevre Koruma Çalışmaları

Çevre Koruma Müdürlüğü; Ortaklığımız hidrokarbon arama, sondaj, üretim hedeflerini gerçekleştirirken insan sağlığı, çevre sağlığı ve doğal dengenin korunmasına yönelik çalışmaları yürütmekten sorumlu bir birimdir. TPAO faaliyet alanları kapsamında, TS EN ISO 14001 Çevre Yönetim Sistemi temelli TPAO Entegre Yönetim Sistemi standart ve uygulamaları kapsamında, ulusal ve uluslararası çevresel standartları dikkate alarak yürütülen çevre koruma çalışmaları aşağıdaki ana başlıklar altında toplanabilir:

- Operasyonel Takipler (ankonvansiyonel projeler, OBM sondajı vb. projelerde İGÇK koordinasyonu ve saha görevleri)
- Tehlikeli Atık Yönetimi (kara ve deniz sondaj, üretim, kth, tıbbi, laboratuvar vb operasyonel atıklar) Çalışmaları
- Sıfır Atık (kağıt, plastik, ambalaj atıkları, organik atıklar vb.) Yönetimi Çalışmaları
- Ulusal ve Uluslararası Mevzuat Çalışmaları (ÇED, Ek-50 formları vb.)
- Eğitim, Denetim ve Tatbikatlar
- Kalite ve Yönetim Sistemleri ve Standartların Uygulama Takipleri
- Çevresel Farkındalığın Geliştirilmesi Çalışmaları
- Sera Gazı Emisyon Hesaplama Çalışmaları

## GELİŞTİRİLEN ÇEVRESEL ÇALIŞMALAR

TPAO olarak Sürdürülebilir Kalkınma Amaçlarını rehber alan ve düşük karbonlu enerjiye öncülük eden sorumlu bir şirket olarak, sahalarla yürütülen emisyon ölçümü çalışmalarını takiben, 2022 yılında ISO 14064-3:2019 standardı kapsamında; enerji, operasyon, proses ve diğer misyon kaynaklarından meydana gelen karbon ayak izlerinin hesaplanması çalışmaları yürütülmüştür.

Bu kapsamda 2022 yılında hizmet alım ihalesi yapılarak şirketimizin karbon ayak izi hesaplanması çalışmalarına başlanmıştır. Karbon ayak izi çalışmalarıyla TPAO tarafından 2021 yılında gerçekleştirilen faaliyetler sırasında doğrudan veya dolaylı olarak salınan sera gazı envanteri belirlenmiş ve hesaplanarak raporlanmıştır. Öncelikli olarak Bölge Müdürlüklerinin ve alt yüklenicilerin de katılım sağladığı geniş kapsamlı bir eğitim ve çalıştay programı gerçekleştirilmiştir. Adıyaman, Batman ve Trakya Bölge Müdürlüklerinde

kulelerde ve üretim kamplarında ve Kıyı Lojistik Merkezi'nde tespitlerde bulunulmuştur. Saha çalışmaları tamamlandıktan sonra her birim için hazırlanan Veri Şablonları ilgili birimlere gönderilerek gerekli verilerin temini çalışmalarına başlanmıştır. Elde edilen veriler kullanılarak Danışman Firma tarafından hesaplamalar yapılmıştır. Tüm analiz ve hesaplamaları içeren Rapor, ISO 14064-1:2019 standardının tüm gerekliliklerini kapsayacak şekilde ilgili Firma tarafından hazırlanarak ISO 14064-3:2019 Standardı kapsamında doğrultama yapılması için TSE Kurumu'na sunulmuştur. Doğrultama çalışmalarından önce Standart kapsamında prosedür ve talimatlar hazırlanmıştır. Ayrıca Genel Müdürlük Olur'u alınarak ilgili birimlerden oluşan bir «Sera Gazı Çalışma Komitesi» kurulmuştur. Doğrultama denetimleri TSE tarafından 05.12.2022 - 09.12.2022 tarihleri arasında gerçekleştirilmiştir. Program kapsamında Genel Müdürlük, Batman Bölge Müdürlüğü, Taşucu Kıyı Lojistik Merkezi ve sondaj gemisinde saha ziyaretleri yapılmıştır. Nihayetinde ilgili raporun doğrulanması gerçekleştirilmiş ve 2021 yılı TPAO Kurumsal Karbon Ayak İzi hesaplanmıştır (Tablo-1).

#### TABLE

2021 yılı içerisinde TPAO tarafından 17.998.009,150 BBL (2.861.468,993 m<sup>3</sup>) ham petrol, 311.896.092 m<sup>3</sup> (1.892.016,735 BBL) doğalgaz üretilmiştir. Toplamda ise 19.890.025,89 BBL ürün üretilmiştir. Yapılan hesaplama göre standardın tanımladığı 5 kategori toplamında kurum tarafından 11.063.459,0623 tCO<sub>2</sub>e salını gerçekleşmiştir. Bu kapsamda 1 BBL ürün başına 0,556 tCO<sub>2</sub>e, 3700 TPAO çalışanı üzerinden personel başına 2.990,1241 tCO<sub>2</sub>e olarak hesaplanmıştır. Kurumun, belirlenen kuruluş ve raporlama sınırları içinde hesaplanan sera gazı emisyonları TS EN ISO 14064-1 (2019) Standardı kapsamında TSE tarafından Makul Güven Seviyede doğrulanmıştır. TPAO sınırları içerisinde sera gazlarının biyolojik olarak uzaklaştırılması ve fiziksel olarak tutulması ve depolanması söz konusu değildir. Ağaçlandırma faaliyeti kaynaklı emisyon uzaklaştırmaları oldukça sınırlı bir azaltım sağlayacak nitelikte olduğundan hesaplanmamıştır. Sera gazının azaltılması için; Petrol endüstrisi özelinde azaltım metodları belirlenmesinde sergilenmesi gereken yaklaşım, sektöre özgü ayrı uzmanlıkların ortak çalışmasını ve uzmanlığa sahip kişilerin değerlendirmelerini gerektirmektedir. Bu nedenle yapılabilecek öneriler sınırlı kalmakla birlikte aşağıdaki temel konulara dikkat edilmesi gerekmektedir;

- Emisyon azaltımlarının belirlenmesi, genel kabul görmüş ilkelere ve sağlam teknik hususlara dayanmalıdır.
- Sera gazı raporuna dahil olan ve emisyon karnesini çıkaran bilgilerin güven seviyesi yükseltilmeli ve en doğru veri ile elde edilmiş raporlara dayalı yaklaşımlar sergilenmelidir.
- Petrol sahası özellikleri; yaş ve diğer faktörler önerilerin uygulanabilirliğini etkileyeceğinden sahaya özgü değerlendirmeler yapılmalıdır,

- Maliyet analizleri yapılması, planlanan yatırımlar için önem arz etmekle birlikte objektif değerlendirme yapılmasının önüne geçmemelidir. Bu doğrultuda kuruma ait petrol sahalarında yapılan örnekleme gözlemler ve literatürde yer alan öneriler dikkate alındığında sera gazı azaltım girişimleri aşağıdaki alt ailelere ayrılabilir;

#### Karbon Tutma ve Jeolojik Depolama

##### Flare Azaltma

##### Yakıt Değişirme

Tüm bu bilgilerin ışığında Temel Yıl olan 2021, Kurumsal Karbon Ayak İzinin önümüzdeki yıllara ışık tutacak ve karşılaştırma yapılabilecek bir yıl olması nedeniyle azaltım hedeflerinin Sera Gazı Çalışma Komitesinde nicel rakamlar ve stratejilerle belirlenmesi ve sahaya tatbik edilmesi önem arz etmektedir. TPAO'nun faaliyet alanının sürekli genişlemesi, yeni kuyuların açılması, yeni sahaların keşfi, çok fazla alt işverenle çalışılması gibi nedenler envanter listesinin sürekli değişmesine neden olmaktadır. Önümüzdeki süreçte bu zorlukların üzerinden gelinerek en doğru veriye ulaşılması amaçlanmaktadır. Veri akışlarının iyileştirilmesi ve düzenli kontrollerinin de sağlanmasıyla beraber 3'er aylık dilimlerde sera gazı izleme ve hesaplamaların gerçekleştirilmesi, azaltım hedefleri açısından değerlendirmeler yapılması, envanterin tamlik ve doğruluk kontrollerinin takibi de hem sera gazı sürecinin yönetilmesi hem de azaltım hedeflerine daha sağlıklı ulaşılması açısından önemli olup, bu konuda iyileştirme çalışmaları devam etmektedir. Operasyonel ve teknik çalışmaların yanı sıra, çalışan personelin ve alt yüklenici personelin farkındalık ve bilincinin artırılması amacı ile eğitimler ve organizasyonlar düzenlenmekte, planlı ve plansız denetimlerle eğitimlerin uygulamaya aktarılması durumu gözlemlenmektedir. TPAO Çevre Koruma Müdürlük ve şefliklerindeki uzman personelin bilgilerinin güncellenmesi ve tüm personelin çalışma koluna göre bilgi düzeyinin artırılması çalışmaları sürdürülmektedir.

#### SONUÇ

Sektöründe çevresel bakışı ile öncü ve lider olan TPAO, güçlenen kadrosu, yaptığı işbirlikleri ile, yeni açılımlarında ve uygulamalarında da yeni yüzyıl ve yeni dünyaya uyumlu şekilde çevresel faaliyetlerini yürütmeyi temel prensip olarak benimsemiştir.

Anahtar Kelimeler: Karbon Ayak İzi, Sera Gazı Envanteri

Tablo 1: TPAO Kategori I ve Kategori II Emisyonların Dağılımı Özet Tablosu

Tablo 1: TPAO Kategori I ve Kategori II Emisyonların Dağılımı Özet Tablosu

TPAO GENELİ ANA KATEGORİ VE ALT KATEGORİ EMİSYONLARIN DAĞILIMI ÖZET TABLO					
Alt Kategori	CO <sub>2</sub> (tCO <sub>2</sub> e)	CH <sub>4</sub> (tCO <sub>2</sub> e)	N <sub>2</sub> O (tCO <sub>2</sub> e)	GAZLAR (tCO <sub>2</sub> e)	TOPLAM (tCO <sub>2</sub> e)
KATEGORİ 1	560.864,8707	524,0306	1,064,0748	1.313.545,8290	1.875.998,8051
KATEGORİ 2	151.262,1863	0,0000	0,0000	0,0000	151.262,1863

TPAO Kategori I ve Kategori II Emisyonların Dağılımı Özet Tablosu







**Petrol ve Doğal Gaz Politikaları, Hukuki ve  
Ekonomik Gelişmeler**

*Oil and Gas Policies, Legal and Economic Developments*

---



# Türkiye'deki Petrol ve Doğal Gaz Arama ve Üretim Faaliyetlerinin Teknik ve Ekonomik Analizi

## Technical and Economic Analysis of Oil and Natural Gas Exploration and Production Activities in Turkey



**A. Uğur Gönülalan**

UG Enerji Danışmanlık

Kapitalizm sınırsız büyüme/genişleme eğilimine ve dinamiğine sahiptir. Ancak dünyanın doğal kaynakları sınırlı olup, sınırsız büyüme doğal kaynakların hızla tükenmesine neden olmaktadır. Kapitalizmin sanayisi fosil enerjilere (kömür, petrol, doğal gaz) dayanmaktadır. Bu nedenle enerji maliyetinin ucuz olması gerekmektedir. Enerjinin pahalı olması üretimi zora sokmaktadır. Enerji olmadan hiçbir şey olmaz, enerji her şeydir.

Türkiye'de 2021 sonuna kadar kümülatif olarak 17,487 milyar m<sup>3</sup> doğal gaz üretimi 1,162 milyon varil (165,24 milyon ton) ham petrol üretimi yapılmıştır (MAPEG, 2021).

2021 yılı sonu itibarıyla, Ülkemizde 4168 (TPAO 2.976) ekip/ay saha jeolojisi, karalarda 187.400 (TPAO tarafından 107.467) km<sup>2</sup> 2B ve 23.215 (TPAO tarafından 17.717) km<sup>2</sup> 3B sismik veri toplama çalışması yapılırken, denizlerde 202.426 (TPAO tarafından 160.670) km<sup>2</sup> 2-B, 93.419 (TPAO tarafından 89.493) km<sup>2</sup> 3B sismik veri toplanmıştır (MAPEG, 2021).

Türkiye'de 1934-2021 yılları arasında, toplam 5.341 adet kuyu açılmış olup 10,127 milyon metre sondaj yapılmıştır. 2021 yılı içinde 33 şirket arama-üretim faaliyetlerinde bulunmuştur. Ülkemizde 1954-2021 yılları arasında arama-üretim faaliyetlerini gerçekleştiren yerli ve/veya yabancı şirketler Doğrudan Yabancı Sermaye Yatırımı (DYY), cari fiyatlarla toplam 17,805 milyar dolar yatırım yapmışlardır.

Bu endüstrinin lokomotifini olan ulusal kuruluşumuz TPAO, 1954-2021 döneminde 11,777 milyar dolar yatırım gerçekleştirmiş olup yabancı/yerli şirketler ise 6,028 milyar dolar harcama yapmışlardır.

Ülkemizde 2002 yılında yurtiçi yerli ve yabancı yıllık yatırım tutarı 100 milyon dolar civarında iken büyük bir sıçrama göstermiş 2003-2021 yılları arasında oldukça yoğun yatırımlar yapılmıştır. Toplam yatırım tutarı 13,336 (TPAO yatırımı 8,600, yerli ve/veya DYY yatırım tutarı 4,736) milyar dolardır.

Bu yatırımlara bağlı olarak Rezerv, Üretim, Yatırım/Rezerv, YKRO (Yerine Konulabilir Rezerv Oranı), analizlerinin ekonomik büyüme verilerinin dikkate alındığı bir yaklaşım yapılmıştır.

Bu çalışmanın da Cumhuriyet tarihinin en yüksek yatırım tutarlarının gerçekleştirildiği 18 yıl (2003-2021) ile önceki yıllar karşılaştırılmıştır.

Öncelikle 1954-2021 ve 1984-2002 yatırım durumları sunulmaktadır. Ardından arama-üretim faaliyetleri için tespit ve önerilerde bulunulmuştur.

Anahtar Kelimeler; Petrol-Gaz, Arama-Üretim, Teknik ve Ekonomik Analiz

### ABSTRACT

The Capitalism has unlimited growth, expansion tendencies and dynamics. However, the world's natural resources are limited. Unlimited growth is based on the limit of natural resources. The industry of capitalism is based on fossil energies (coal, oil, natural gas). Therefore, the energy cost should be cheap. Expensive energy makes production difficult. Because without energy, nothing can happen, energy is everything.

Cumulative natural gas production of 17,487 billion m<sup>3</sup> and 1,162 million barrels (165.24 million tons) of crude oil was produced in Turkey until the end of 2021 (MAPEG, 2021).

As of the end of 2021, 4168 (TPAO 2.976) crew/month field geology in our country, 187,400 (107.467) km<sup>2</sup> 2D by TPAO and 23,215 (17.717) km<sup>2</sup> by TPAO 3D seismic data acquisition studies were carried out on land, while 202,426 (by TPAO 160.670) km<sup>2</sup> in marines were carried out. 2D, 93,419 (89,493 by TPAO) km<sup>2</sup> of 3D seismic data acquired (MAPEG, 2021).

Between 1934-2021, a total of 5,341 wells were drilled in Turkey and 10,127 million meters of drilling was done. 33 companies engaged in exploration and production activities in 2021. While carrying out exploration and production activities in our country between 1954-2021, domestic and/or foreign companies invested 17.805 billion dollars at current prices in this period.

Our national corporation TPAO, which is the locomotive of this industry, invested 11,777 billion dollars in the same period (1954-2021), and foreign/domestic companies spent 6,028 billion dollars. While the annual domestic and foreign investment amount was 100 million dollars in 2002 in our country, the investments were made with a great leap in the following years with the aim of great activity between 2003 and 2021. The total amount of this is 13,336 (TPAO's invested 8,600, foreign/domestic companies investment is 4,736) billion dollars.

Depending on these investments, an approach has been made according to the economic growth calculations of the technical and economic analysis for Reserve, Production, Investment/Reserve and YKRO (Replaceable Reserve Ratio). This approach is the subject of this paper and the last 18 years (2003-2021), which had the highest investment amounts in the history of the Republic, were compared with the previous years. First of all, the investment situations of 1984-2002 and 1954-2021 are presented. Afterwards, determinations and suggestions were made for exploration-production activities.

## 1. GİRİŞ

Enerji, bir ülkenin ekonomik ve sosyal gelişiminin en temel ve sürükleyici gereksinimlerinden biridir. Bu bakımdan, “Enerji Güvenliği”, ekonomik güvenliğin ve ulusal güvenliğin yaşamsal unsurlarındandır.

## 2. ÜRETİM

Ülkemizde 2021’de 415,036 milyon m3 doğal gaz üretilmiştir. Türkiye’nin doğal gazda ithalata bağımlılığı geçen yıla göre azalmış ve %98,9 olmuştur (Sarıyıldız 2021).

Doğal gaz tüketimi 2020 yılında toplam 48,6 milyar m3 olurken, doğal gaz ithalatı yaklaşık 48,1 milyar m3 seviyesinde gerçekleşmiştir. Türkiye’nin doğal gaz arzında ithalata bağımlılığı 2019’a göre artarak %99,1 olmuştur.

1976’dan 2021’e kadarki süreçte yıllık bazda doğal gaz üretimlerimiz Şekil 1’de gösterilmektedir. 45 yıllık süreçte 29 farklı şirket tarafından, 2021 yılı sonu itibarıyla kümülatif olarak toplam 17,487 milyar Sm<sup>3</sup>’lük üretim gerçekleştirilmiştir. Bu üretimin yaklaşık %30’u yabancı sermayeli şirketler tarafından yapılmıştır. Üretilen doğal gazın bugünkü BOTAŞ toptan satış fiyatı üzerinden değerlendirecek olursak yaklaşık olarak 4 milyar dolara karşılık gelmektedir. Kalan üretilebilir gaz rezerv miktarı 3,107 milyar m3 dür.

Uygulanmakta olan ikincil üretim yöntemleri ve keşfedilen yeni sahalardan gelen üretimle birlikte 2007 yılından itibaren petrol üretimimizde az da olsa sürekli bir artış eğilimi vardır. 2021 yılı petrol üretimi 3,4 milyon ton olup günlük 69.332 varildir.

Cumhuriyetin kuruluşunu takiben hükümet, Türkiye sınırları içinde yer alan petrol kaynaklarının bizzat kendi bünyesinde araştırılmasını ilke olarak kabul etmiş ve ilk olarak jeolojik etütlere başlanmıştır. Ancak konu ile ilgili bir tecrübe ve deneyim olmadığı için başarılı sonuçlar alınamamıştır. Akabinde Güneydoğu Anadolu’da Batman’ın güneyinde 1940 yılında açılan Raman-1 kuyusunda petrole rastlanırsa da ticari anlamda petrol keşfi 1945 yılında açılan Raman-8 kuyusu ile gerçekleştirilmiştir.

1954 yılında 6326 sayılı Petrol Kanunu’nun yürürlüğe konulmasıyla petrol arama ve üretim faaliyetleri yerli ve yabancı özel sermayeye de açılarak, yabancı petrol şirketlerinin Türkiye’ye gelmesinin yolu açılmıştır.

Petrol Kanunu’nun yürürlüğe girmesinden sonraki on yıllık dönemde, petrol arama faaliyeti tarihinde yaşanan iki sıçrama döneminden de artışı yaşanmıştır. Bu dönem içinde özel sermayeli şirketlerin de katkılarıyla yapılan jeolojik, jeofizik ve sondaj çalışmalarındaki artışlar sonucunda birçok yeni petrol sahası keşfedilmiştir.

Yapılan jeolojik ve jeofizik çalışmalarındaki artış sonunda sondaj faaliyetlerinde de artış olmuş ve birçok yeni petrol sahası keşfedilmiştir. Jeolojik ve jeofizik etütler 1958 yılında 164 ekip-ay jeoloji ve 157 ekip-ay jeofizik çalışma ile ilk sıçramasını yaparken (PİGM, 1982) sondaj faaliyeti de 1965 yılına kadar devamlı olarak artmıştır.

Bu sahalardan gelen üretimle beraber yerli petrol üretimi, 1969 yılında 3,6 milyon tona ulaşarak tüketimimizin %55’ini karşılamıştır.

Arama faaliyetlerindeki ikinci sıçrama dönemi ise 1980’li yıllarda yaşanmıştır. Bu dönemdeki yoğun arama faaliyetleri yeni keşiflere yol açmış, özellikle TPAO tarafından 1988 yılında Adıyaman’da yer alan Karakuş sahasının keşfiyle büyük üretim artışı yaşanmıştır. Üretim, 1991 yılında 4,45 milyon ton ile rekor seviyeye ulaşmıştır.

1991 yılında yurt içi ham petrol üretimi 85 bin varil/gün ile ülke tüketiminin ancak % 21’i karşılanabilmiştir.

Petrol üretimi, 1991’de zirve yapmasının ardından düşüşe geçmiş ve 2018 yılında 54.386 varil/gün mertebesinde gerçekleşmiştir. Uluslararası Enerji Ajansı’nın verilerine göre, yurt içinde üretilen ham petrolün toplam tüketimi karşılama oranı 1970’de %47 seviyelerinde gerçekleşirken söz konusu yurt içinde üretilen ham petrolün toplam tüketimi karşılama oranı sürekli düşüş eğilimi göstererek 1991 yılında %20’ye, 2018 yılında ise %8’lere kadar gerilemiştir (Şekil-2).

Ülkemizin hidrokarbon varlığını incelediğimizde, petrol sahalarımızın %7’sinin 25 milyon varil rezervden daha büyük, %93’ünün ise 25 milyon varilden daha küçük olduğu görülmektedir.

2021 yılı sonu itibarıyla Türkiye üretilebilir petrol rezervi, 411 milyon varil (58,34 milyon ton) olarak belirlenmiştir. 2021 yılında günlük ortalama 69.332 varil ham petrol üretimi gerçekleştirilmiştir. Yeni keşifler yapılmadığı takdirde, mevcut üretim miktarı dikkate alındığında, ham petrol rezervinin yaklaşık 19 yıllık ömrü bulunmaktadır.

## 3. ARAMA

Türkiye’nin her geçen gün artan petrol ve doğal gaz ihtiyacı ve söz konusu ihtiyacın yurt içi ve yurt dışı kaynaklardan karşılanması yönündeki çalışmalar artmış, yurt içi arama faaliyetleri yeterince aranmamış basenlere, özellikle de Akdeniz ve Karadeniz deniz alanlarına yönlendirilmiştir.

2021 yılında, Ülkemizde 21,9 (TPAO 10,4) ekip/ay saha jeolojisi çalışması gerçekleştirilmiştir. Karalarda 1.022,39 (TPAO tarafından 340,16) km 2B ve 2.522,07 (TPAO tarafından 2.422,48) km2 3B sismik veri toplama çalışması yapılırken, denizlerde 21.430,06 km2 3B sismik veri toplanmıştır (MAPEG, 2021).

### 3.1. Sondaj Öncesi Arama Faaliyetleri

Her geçen gün artan petrol ve doğal gaz ihtiyacının yurt içi kaynaklardan karşılanması yönündeki faaliyetler kapsamında, yeterince aranmamış basenlerde ve özellikle Akdeniz ve Karadeniz’deki deniz alanlarında son yıllarda yapılan çalışmalar büyük bir ivme kazanmıştır.

Ülkemizde bugüne kadar karaların %20’si, denizlerin ise %1’i aranabilmiştir.

1945 yılından 2021 yılına kadar yapılan arama

çalışmaları sonucunda 232 adet üretim sahası tespit edilmiş ve MAPEG tarafından tescil edilmiştir.

Tescil edilen üretim alanlarının %64'ü ham petrol (toplam 148 adet üretim sahası), %36'sı ise doğal gazdır (toplam 84 adet üretim sahası).

Toplamda 1.984 arama kuyusundan 232 adet üretim sahası keşfedilmesi ile hidrokarbon keşif başarı oranı %11,3 olarak belirlenmiştir.

### 3.2. Sondaj Faaliyetleri

Türkiye'de 1934-2021 yılları arasındaki 86 yıllık dönemde, toplam 5.341 adet kuyu açılmış olup yaklaşık 10.127 milyon metre sondaj yapılmıştır. Bu kuyuların %75'i Güneydoğu Anadolu'da, %17'si Trakya'da, %8'i ise diğer bölgelerde açılmıştır. Bugüne kadar açılan kuyu sayısı karalarda %98, denizlerde ise %2 civarındadır (Şekil-3).

2021 yılı sonu itibarıyla Türkiye'de 20 adet yerli ve 13 adet yabancı olmak üzere toplam 33 adet şirket arama ve/veya üretim faaliyetinde bulunmuştur.

## 4. YATIRIMLAR

Cumhuriyetin ilk birkaç kuşağı 1954 yılına kadar Osmanlı dış borçlarını ödemekle uğraştığı için, dış borçlanmaya ve yabancı sermayeye mümkün olduğunca uzak durmaya çalışmıştır. 1923-2004 arasındaki 81 yılda ülkemize 15,4 milyar \$ (DYY) girmiştir (Hazine Müsteşarlığı Raporları, Eğilmez, 2022).

2004 yılı sonrası DYY Toplamı 220 milyar \$'dır. Bunun 55,287 milyar \$'ı gayrimenkul, 164,713 milyar \$'ı gayrimenkul dışı yatırımdır (Ticaret Bakanlığı, Eğilmez 2022).

2005-2008 yılları arasındaki dönem, Türkiye ile AB'nin tam üyelik müzakerelerini ciddiyle yürüttüğü dönemdir ve DYY rekor kırmıştır. Bu dönemde yabancı sermaye girişinin yeniden sağlanabilmesi için, riskler düşürülmüştür (Eğilmez, 2022).

Petrol sektörüne baktığımızda; şirketlerin ülkemizdeki arama-üretim yatırımları 2002 yılında 100 milyon ABD \$ olan toplam yatırım tutarı, 2010 yılı sonu itibarıyla 13 kat artmıştır. 2016'da 2004 yılı seviyesinde yatırım yapılmış iken sonraki yıllarda tekrar artmıştır. 2021 sonu itibarıyla 2021 USD fiyatlarına göre 14,640 milyar dolar, cari fiyatlara göre 17,805 milyar USD arama üretim faaliyetleri için yatırım yapılmıştır.

TPAO, 2021 yılında 1,5 milyar \$'ı yurt içi, 895 milyon \$'ı yurt dışı olmak üzere toplamda 2,41 milyar \$ yatırım harcaması gerçekleştirmiştir. 2020 yılında görece yatay seyir izleyen yatırımlar, 2021 yılında Sakarya Doğal Gaz Sahası keşfi geliştirme faaliyetlerinin etkisiyle bir önceki yıla göre %63 artış göstererek 2,4 milyar \$'ı aşmıştır.

Aktif olan şirketlerin yatırımlarına bakılacak olursa yatırımın %80'i Türkiye Petrolleri Anonim Ortaklığı (TPAO) tarafından, %12'si yabancı sermayeli şirketler tarafından, kalan %8'i ise yerli sermayeli şirketler tarafından gerçekleştirilmiştir (Şekil-4).

Ülkemizde mevcut faaliyet gösteren şirketler bugüne kadar cari fiyatlarla 17,8 milyar \$ 'a yakın yatırım gerçekleştirmiştir.

## 5. PETROL ENDÜSTRİSİNİN YAPISI, YATIRIM, ÜRETİM, BÜYÜME GSYH VE EKONOMİSİ

Toplumun üretim biçim ve ilişkileri, ekonomik alışverişte; üretim kaynakları, biçimi, tüketim ve tasarruf ilişkileri, yatırım ilişkileri gibi ilişkiler bütünü EKONOMİK YAPI'yı oluşturur. Burada, piyasa, mal ve hizmetler yer alır (Eğilmez, 2022).

Dağlar, denizler, göller gibi insan elinin değmediği yapılara doğal yapı adı verilir.

Şekil-5'te görüldüğü gibi P&G endüstrisinin yapısı ise teknik, ekonomik, sosyal, siyasal ve hukuksal yapılar ile iç ve dış dünyadan etkilenmektedir. Hidrokarbon (P&G) yapısını etkileyen alanlarda sürdürülebilirlik sağlanmazsa kalıcı istikrar da sağlanamaz. Bunun için en iyi yöntem; yatırım ve geri dönüşler için projelendirme ve planlamadır.

### 5.1. İktisat Terimlerine Göre Kavramlar

#### 5.1.1. Ekonomideki büyüme,

Mili gelir artışından belirli bir zaman sürecince, misal bir yıl içinde üretilen mal ve hizmet miktarındaki artışı anlatır.

Bir ülkede üretilen mal ve hizmet miktarının zaman içinde artmasına iktisadi büyüme denir. İktisadi büyüme bir ülkede yaşayan insanların yaşam standartlarını sürekli biçimde yükseltmenin tek yoludur.

Son yıllarda, özellikle son birkaç yılda, TL'deki hızlı değer kaybı, TL ile hesaplanan GSYH'ye göre büyüme oranının \$'la verilen GSYH ve kişi başına gelire yansımadağı görülüyor.

#### 5.1.2. Gayrisafi Yurtiçi Hasıla (GSYH),

Ülkelerin ekonomik güçlerini karşılaştırmak için en çok başvurulan sıralama ölçütü GSYH büyüklüğü ve kişi başına gelirdir. Bir ülkede belirli bir dönem içinde (3 ay, 1 yıl) üretilen bütün nihai malların o yıla ilişkin ortalama piyasa fiyatları üzerinden toplanmasıyla oluşan toplam değere gayrisafi yurtiçi hasıla - GSYH diyorum.

Tablo-1'de GSYH'ye yıllar itibarıyla \$ cinsinden baktığımızda 1985 yılında 69 milyar \$ olan GSYH'nin 2019 yılında 749 milyar \$ olduğunu görüyoruz. 1985 – 2001 yılları arasındaki GSYH artışı 3,4 kat olmuştur. 2003- 2019 döneminde \$ cinsinden GSYH'de 3,1 kat artış olmuş. GSYH artış tutarının 2003-2019 döneminin bir önceki 17 yıla göre (1985-2001) yeterince başarılı olmadığı görülmektedir.

#### 5.1.3. Kişi başına gelir düzeyi,

Tablo-2'de kişi başına gelir konusu da GSYH ile aynı durumdadır. Burada da önceki döneme göre bir geri

gidişin söz konusu olduğunu görebiliyoruz (Eğilmez 2020).

### 5.1.4. İstihdam-İşsizlik,

Ülke ekonomisinin en önemli sorunu olan işsizlikte maalesef sorun çözülememiş, tam tersine büyütülmüş durumdadır.

1985-2002 döneminde ki 17 yılda % 8 olan ortalama işsizlik oranı, son 17 yıllık dönemde % 10,9'a yükselmiştir.

### 5.2.Ekonomik Kavramların Özeti

Büyüme-işsizlik ilişkisine bakıldığında işsizlik oranı artmıştır. İşsizlik oranındaki bu yükselişin büyümenin 'istihdam yaratmayan büyüme' kavramıyla uğraşılırken 'işsizliği artıran büyüme' kavramıyla mı uğraşılacaktır? (Eğilmez 2017).

Büyüme 1985 yılında 4,3 iken, 2002 yılında 6,4'e yükselmiş ve ortalama büyüme oranı 1985-2002=4,0 olmuştur.

Büyüme, 2002 yılında 6,4 iken 2019'da 0,5, ortalama 2002-2019=5,4'dir.

İşsizlik oranı ise, 1985 yılında 7,9 iken, 2002 yılında 10,3'e yükselmiş ve ortalama büyüme oranı 1985-2002=8,0 dir.

İşsizlik oranı, 2002 yılında 10,3 iken 2019'da 13,5, ortalama 2002-2019=10,9'dur (Eğilmez 2020) (Tablo-3).

GSYİH Kişi başı gelir; 2002'de 3.581 \$ iken 2019'da 9.093 \$ olmuştur. Artış oranı; 2002-2019= 2,5 'dir. 1985'de 1.330 \$ iken 2002'de 3.581 \$ olmuştur. Artış oranı; 2002-2019= 2,7'dir (Tablo-4).

Özetle GSYH çok az artmaktadır.

### 5.3. 2021 \$ Kuru, 2021 (2021=100 Endeksi)

#### Fiyatlarına Göre Yatırım-Rezerv-Üretim Analizi;

Çalışmada 2021 (2021=100 Endeksi) fiyatlarına göre hesaplar detaylı olarak yapılmış olup Tebliğin bütününde mevcuttur. Ancak genişletilmiş özetle kelime sayısı limiti nedeniyle konulamamıştır.

5.4. Cari Dolar Kuru Fiyatlarına Göre Yatırım-Rezerv-Üretim Analizi;

5.4.1. Türkiye'nin Arama Üretim Faaliyetleri Açısından 1954-2002 döneminde;

- Yatırımlar 28 misli artmış olup, yatırımın ortalama büyüme hızı % 5'dir.
- Üretilebilir rezerv artışı 10 misli olurken üretilebilir rezerv ortalama artış hızı %4,8'e ulaşmıştır.
- Üretim miktarındaki artış 13,67 misli olurken üretimin ortalama artış hızı % 5'e ulaşmıştır.

### 5.4.2. Türkiye'nin Arama Üretimi Faaliyetleri Açısından 2003-2022 döneminde,

Son yirmi yılda;

- Yatırımlar 20 kat artmış olup, yatırımın ortalama büyüme hızı % 17'dir.
- Üretilebilir rezerv artışı 1,42 misli olurken üretilebilir rezerv ortalama artış hızı %1,9'a ulaşmıştır.
- Üretim miktarındaki artış 1,4 misli olurken üretimin ortalama artış hızı % 2'ye ulaşmıştır.

### 5.4.3. TPAO'nun Arama Üretim Faaliyetleri Açısından 1954-2002 döneminde:

- Yatırımlar 34 misli artmış olup, yatırımın ortalama büyüme hızı %5'dir.
- Üretilebilir rezerv artışı 5,68 misli olurken üretilebilir rezerv ortalama artış hızı %3,6'ya ulaşmıştır.
- Üretim miktarındaki artış 16,26 misli olurken üretimin ortalama artış hızı % 6'ya ulaşmıştır.

### 5.4.4. TPAO'nun Arama Üretim Faaliyetleri Açısından 2003-2022 döneminde;

Son yirmi yılda;

- Yatırımlar 21 kat artmış olup, yatırımın ortalama büyüme hızı % 17'dir.
- Üretilebilir rezerv artışı 1,59'a ve üretilebilir rezerv ortalama artış hızı %2,5'a ulaşmıştır.
- Üretim miktarındaki artış 1,83 misli olurken üretimin ortalama artış hızı % 3'e ulaşmıştır.

## 6. TESPİT VE ÖNERİLER

1954-2021 arasında ülkemizdeki yatırım miktarı Cari Fiyatlara göre; 17,805 milyar \$, 2021 Dolar Kuru Fiyatlarına göre 14,670 milyar \$ olmuştur.

Bu yatırım ile belirlenen üretilebilir petrol ve doğal gaz rezerv toplamı 1,694 milyar varil petrol eşdeğeridir. Bu üretilebilir petrol ve doğalgaz rezervinin 1,264 milyar vpe'i üretilmiştir.

### 6.1. Dönemlerin yatırım açısından detaylı analizi

(Gönülalan, 2013);

(C ve D son yirmi yıllık dönemler analizidir);

#### 6.1.1. Türkiye'de Arama-Üretim Faaliyetleri İçin Toplam Yatırım;

- A- 1954-2002 dönemi 4,468 milyar \$
- B- 1954-2021 dönemi 17,805 milyar \$
- C- 1984-2002 dönemi 2,813 milyar \$
- D- 2003-2021 dönemi 13,367 milyar \$

### 6.1.2. TPAO'nun Arama Üretim Faaliyetleri Toplam Yatırım;

- A- 1954-2002 dönemi 3,177 milyar \$
- B- 1954-2021 dönemi 11,777 milyar \$
- C- 1984-2002 dönemi 1,984 milyar \$
- D- 2003-2021 dönemi 8,600 milyar \$

### 6.2. Son Yirmi Yılda 1 varil P&G Karşılığı Gerçekleştirilen Yatırım Açısından (Yatırım toplamı/Üretilbilir rezerv oranı) Karşılaştırması;

#### 6.2.1. Türkiye

- 1984-2002 Dönemi için 3,8 \$/V
- 2002-2021 Dönemi için 26,5 \$/V

#### 6.2.2. TPAO

- 1984-2002 Dönemi için 4,7 \$/V
- 2002-2021 Dönemi için 21,4 \$/V

#### 6.2.3. DYY

- 1984-2002 Dönemi için 9,8 \$/V dir.
- 2002-2021 Dönemi için 46,4 \$/V

### 6.3. Özet

#### 6.3.1. Türkiye'de toplam yatırımlar 1954-2002 döneminde Cari fiyatlarla toplam yatırımı 4,468 milyar \$ iken 2003-2021 döneminde 13,336 milyar \$ yatırım yapılmıştır.

- Son 20 yılda (2003-2021), 1954-2002 dönemine göre;
- 1) 3 kat fazla yatırım harcaması gerçekleşmiştir.
- 2) Rezerv oranlarına bakıldığında ise aynı dönemde 3 kat yatırıma karşı rezerv % 60 azalmıştır,
- 3) Üretim % 50 azalmıştır.

#### 6.3.2. TPAO açısından bakıldığında 1954-2002 döneminde Cari Fiyatlarla toplam yatırımı 3,177 milyar \$ iken, 2003-2021 döneminde 8,600 milyar \$ yatırım yapılmıştır. Son 20 yılda (2003-2021), 1954-2002 dönemine göre;

- 1) 2,7 kat fazla yatırım harcaması gerçekleşmiştir.
- 2) Rezerv oranlarına bakıldığında ise aynı dönemde 2.7 kat yatırıma karşı rezerv % 40 azalmıştır,
- 3) Üretim % 20 azalmıştır.

Sonuç olarak son 20 yılda yatırımların 3 kat fazlalığına rağmen yeterli rezerv ve üretim artışları sağlanamamıştır.

### 6.4. TPAO yatırımları açısından ekonomik izahı ise metre veya kuyu sayısı başına düşen yatırımlar Tablo-5'te verilmiştir.

1984-2002 dönemi ve 2003-2021 dönemleri içinde benzerliği olan 2 yıl 1986 ile 2011 yılının karşılaştırmasını yaptığımızda;

1986 yılında 104 kuyu 234 Bin metre sondaj yapılmış olup, TPAO yatırım tutarı cari fiyatlara göre 130,74 milyon dolar olmuştur. 104 kuyu sayısının gerçekleştiği 2011 yılında ise 199 Bin metre sondaj yapılmış olup, TPAO yatırım tutarı cari fiyatlara göre 579 milyon \$ olmuştur.

1986 yılında ortalama kuyu maliyeti 1,26 milyon \$ (559 \$/m) buna karşılık 2011 yılında ortalama kuyu maliyeti 5,67 milyon \$ (2.910 \$/m) olarak gerçekleşmiştir.

Sonuçta 2011 yılında 1986 yılına göre maliyetler yaklaşık 5 kat artmıştır.

Diğer taraftan Petrol Kanunu uygulamasında Türkiye kara alanları ruhsatlandırılması, hidrokarbon varlığına göre derecelendirilmelidir. 6326 ve 2808 sayılı eski yasalardaki bölge sisteminden 6491 sayılı Yeni Petrol Yasasına göre harita ölçek modeline geçilmiş olup, potansiyel alanların belirlenmesi amaçlı hangi paftanın(1:25000'lik ve/veya 1:50.000'lik), hangi önem derecesinde olduğu da belirlenmelidir.

Önem derecesine göre

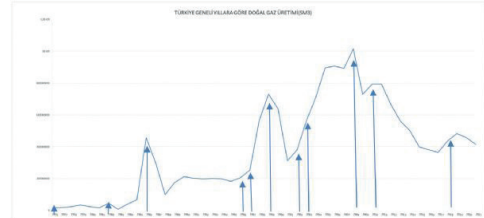
1. Petrol varlığı bilinen alanlar
2. Gaz varlığı bilinen alanlar
3. Petrol/Doğal gaz potansiyeli olabilecek alanlar
4. Henüz arama/araştırma safhasındaki alanlar olarak ayrılmalıdır.

Ruhsat süreleri önem derecelerine, arama dönemlerine göre 2 yıl, 4 yıl ve 6 yıl şeklinde düzenlenmelidir.

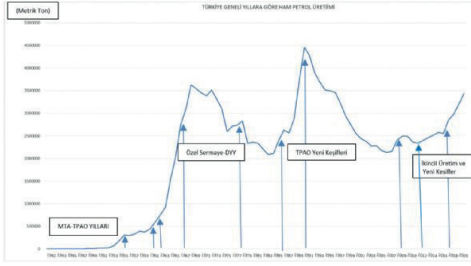
Kaynaklar Tablo-6'da verilmiştir.

Anahtar Kelimeler: Teknik ve Ekonomik Analiz

Sekil-1



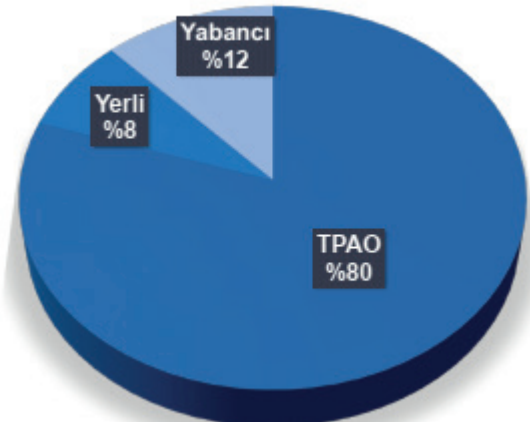
Sekil-2



Sekil-3



Sekil-4







Şekil-1: Yıllık doğal gaz üretimi (MAPEG, Sarıyıldız 2021'den Düzenleme AUG). Şekil-2: Yıllık ham petrol üretimi (MAPEG, Gül 2020'den Düzenleme AUG) Şekil-3: 1934-2021 arası Türkiye'de açılan petrol ve doğal gaz kuyularının sayısı ve metraji (MAPEG) Şekil-4: Şirketlere göre yatırım oranları (Sarıyıldız 2021) Şekil-5: Hidrokarbon arama-üretim ekonomik yapısı Tablo-1: Türkiye'de Yıllara Göre Büyüme Değerleri (Eğilmez 2020). Tablo-2: Türkiye'de Yıllara Göre Kişi Başına Düşen Gelir (\$) Değerleri (Eğilmez 2020). Tablo-3: Türkiye'de Yıllara Göre İşsizlik Değerleri (Eğilmez 2020). Tablo-4: Türkiye'de Yıllara Göre Ekonomik Özet Değerleri Tablo-5: TPAO'nun yatırımları Tablo-6: Kaynaklar

Tablo-1

Yıllar	Büyüme	Yıllar	Büyüme
1985	4,3	2002	6,4
1986	6,8	2003	5,6
1987	9,8	2004	9,6
1988	1,5	2005	9,0
1989	1,6	2006	7,1
1990	9,4	2007	5,0
1991	0,4	2008	0,8
1992	6,4	2009	-4,7
1993	7,9	2010	8,5
1994	-6,1	2011	11,1
1995	8,0	2012	4,8
1996	7,1	2013	8,5
1997	8,3	2014	5,2
1998	3,8	2015	6,1
1999	-3,4	2016	3,2
2000	6,6	2017	7,5
2001	-6,0	2018	2,8
2002	6,4	2019	0,5
<b>Ortalama</b>	<b>4,0</b>		<b>5,4</b>

Tablo-2

Yıllar	Kişi Başına Gelir (USD)	Yıllar	Kişi Başına Gelir (USD)
1985	1.330	2002	3.581
1986	1.463	2003	4.968
1987	1.636	2004	5.961
1988	1.685	2005	7.304
1989	1.959	2006	7.906
1990	2.682	2007	9.656
1991	2.621	2008	10.931
1992	2.708	2009	8.980
1993	3.004	2010	10.560
1994	2.184	2011	11.205
1995	2.759	2012	11.588
1996	2.928	2013	12.480
1997	3.079	2014	12.112
1998	4.442	2015	11.019
1999	4.003	2016	10.883
2000	4.229	2017	10.616
2001	3.084	2018	9.693
2002	3.581	2019	9.093
<b>Artış(Kat)</b>	<b>2,7</b>		<b>2,5</b>

Tablo-3

Yıllar	İşsizlik	Yıllar	İşsizlik
1985	7,9	2002	10,3
1986	8,0	2003	10,1
1987	8,1	2004	10,8
1988	8,4	2005	10,6
1989	8,6	2006	10,2
1990	8,0	2007	10,3
1991	8,2	2008	11,0
1992	8,5	2009	14,0
1993	8,9	2010	11,9
1994	8,6	2011	9,8
1995	7,6	2012	9,2
1996	6,6	2013	9,7
1997	6,8	2014	9,9
1998	6,9	2015	10,3
1999	7,7	2016	10,9
2000	6,5	2017	10,9
2001	8,4	2018	12,3
2002	10,3	2019	13,5
<b>Ortalama</b>	<b>8,0</b>		<b>10,9</b>

Tablo-4

Tablo-5

YILLAR	CARİ FİYATLARA GÖRE YATIRIM TUTARI(\$)	KUYU SAYISI	KUYU METRAJ(Metre)	KUYU SAYISINA GÖRE YATIRIM MİKTARI (\$)	KUYU METRAJINA GÖRE METRE YATIRIMI (\$)
1986	130,74 Milyon Dolar	104	234.000	1.250.000 Dolar	559 Dolar
2011	579 Milyon Dolar	104	199.000	5.567.000 Dolar	2.910 Dolar
2015	463 Milyon Dolar	53	88.000	8.736.000 Dolar	5.261 Dolar
2021	1.506 Milyon Dolar	112	250.000	13.446.000 Dolar	6.024 Dolar

Tablo-6

**Tablo-6****Kaynaklar:**

- Eğilmez, M., 2017, İşsizliği Artıran Büyüme, Ekim 16, 2017
- Eğilmez, M., 2020, Türkiye Ekonomisinin Son 17 yılı, T24, 03 Ocak 2020.
- Eğilmez, M., 2022, Türkiye'nin Yapısal Sorunları ve Çözüm Önerileri, Remzi Kitabevi.
- Gönülalan, A., U., 2012, Türkiye'de Petrol ve Doğalgaz Arama ve Üretim Yatırımlarının Kamu ve Doğrudan Yabancı Yatırımcı (DYY) Kapsamında (Yerli ve Yabancı Şirketler Açısından) İncelenmesi, Uluslar arası Enerji Kongre ve Fuarı, 04-05 Ekim 2012, Ankara.
- Gönülalan, A., U., 2013, Petrol Arama Üretim Faaliyetlerinin Petrol Kanunları ve Tasarıları Açısından İncelenmesi ve Sektörün Geleceğinin Değerlendirilmesi, Türkiye 19.Uluslararası Petrol ve Doğalgaz Kongre ve Sergisi, 15-17 Mayıs 2013, Ankara.
- Gül, S., Kalay, M., ve İbiş, H., 2020, Petrol Arama Ruhsatı Başvuru Prosedürü ve Türkiye'deki Petrol Arama Ruhsat Durumunun Değerlendirmesi, MAPEG Faaliyet Raporları
- Sarıyıldız, S., 2021, Kara ve Denizlerde Doğal Gaz Aramacılığında Ruhsatlandırma , TÜBA-Doğal Gaz Çalıştayı ve Paneli, 8-9 Ekim 2020-TÜBA DOĞAL GAZ RAPORU,
- TPAO, 2020 ve 2021, Faaliyet Raporu. <http://www.tpaogov.tr>.

# Current Status of Türkiye about Carbon Capture and Sequestration: A case study related to Carbon Capture and Sequestration in the Bati Raman Heavy Oilfield of Türkiye



Emre Özgür<sup>1</sup>, Şükürü Meray<sup>2</sup>

<sup>1</sup>Enerji ve Tabii Kaynaklar Bakanlığı

<sup>2</sup>Batman Üniversitesi

## ABSTRACT

With global warming, carbon capture and sequestration (CCS) has become an important action to minimize the negative effects of fossil fuels, factories, and other facilities on the environment. Currently, there is no direct carbon capture and sequestration for environmental reasons in Türkiye. Therefore, it is important to discuss current regulations and encouragements related to CCS in Türkiye. Bati Raman Heavy Oilfield of Türkiye is still under production since 1961. After the mid-1980s, a CO<sub>2</sub> injection enhanced oil recovery technique was implemented to increase oil production in the field. Thus, by capturing CO<sub>2</sub> in the factories, it is possible to sequester this CO<sub>2</sub> in the Bati Raman Heavy Oilfield. In this way, both negative environmental effects are minimized and the oil production in the Bati Raman Heavy Oilfield continues. In this study, current regulations related to CCS, current attitudes of factories to CCS arrangements, and other encouragement mechanisms about CCS in Türkiye were discussed by using the case study in the Bati Raman Heavy Oilfield of Türkiye.

## Potential CO<sub>2</sub> Sources for the CO<sub>2</sub> EOR application in the Bati Raman Heavy Oilfield

In the world, there are many CCS plans but at a certain level, these plans are canceled mainly due to budget deficits. Inconsistent and insufficient policy support is also one of the reasons for the cancelation of many CCS projects. Although there are approximately 40 years of underground CO<sub>2</sub> store experience in the Bati Raman Heavy Oil, it is not a complete CCS project (Ozgun, 2017). In the world, there are several CCS projects such as EOR or direct CO<sub>2</sub> sequestration. Figure 1 list the commercial-scale projects in operation in the world. Different than the Bati Raman Heavy Oilfield's CO<sub>2</sub>-EOR, the source of CO<sub>2</sub> in the fields in Figure 1 is obtained from the natural gas processing plant, onshore LNG plant, and synthetic natural gas plant. The highest CO<sub>2</sub> emissions occur at power plants, cement factories, oil refineries respectively in the world. CO<sub>2</sub>-EOR is the most widely used process with the highest potential for additional recovery. By considering the Batman Oil Refinery, and Kurtalan Cement Factory near the Bati Raman Heavy Oilfield, the CCS project might be applied for both oil recovery and carbon capture & sequestration purposes.

Oil refineries are responsible for significant CO<sub>2</sub> emissions all over the world. CO<sub>2</sub> emissions of oil refineries range according to the crude oil properties (API, sulfur content, and other content), refinery technology, and complexity. Jing et al. (2020) investigated the worldwide refineries and their CO<sub>2</sub>

emissions ranging from 0.74-ton CO<sub>2</sub>/ton crude oil to 5.69-ton CO<sub>2</sub>/ton crude oil with an average emission of 2.72-ton CO<sub>2</sub>/ton crude oil. By using the refinery data sets of Jing et al. (2020), it was found that Türkiye's refinery CO<sub>2</sub> emission is in the range of 3.02 ton CO<sub>2</sub>/ton crude oil. However, by considering Batman Oil Refinery's Nelson index (1.83, which is a very simple refinery and semi-finished products) (TUPRAS, 2021), and crude oil API gravity, it was predicted that the CO<sub>2</sub> emission in Batman Refinery is likely to be between 1.16-to-3.02-ton CO<sub>2</sub>/ton crude oil with an average of 2.37-ton CO<sub>2</sub>/ton crude oil. By using the methodology in Figure 2 (with Monte Carlo Statistical Simulation-Triangle Approximation), the minimum, mean and maximum daily/annual CO<sub>2</sub> emissions of the Batman Oil Refinery and Kurtalan Cement Factory were predicted. Figure 3 lists the predicted CO<sub>2</sub> emissions of Batman Oil Refinery by using the methodology in Figure 2. According to these estimations, daily CO<sub>2</sub> emissions of Batman Oil Refinery is quite enough for the application of CO<sub>2</sub>-EOR in the Bati Raman Heavy Oilfield. Moreover, the carbon capture at the Batman Oil Refinery and its storage in the Bati Raman Heavy Oilfield is likely to provide better air quality in the center of Batman Province.

Kurtalan Cement Factory might also provide the CO<sub>2</sub> needed for the continuation of CO<sub>2</sub>-EOR application in the Bati Raman Heavy Oilfield. It is very close to the pipeline sending CO<sub>2</sub> of the Dodan CO<sub>2</sub> Field to this oilfield, which is an advantage for the implementation CCS project integrated with the Bati Raman Heavy Oilfield. However, there should be an investment for carbon capture facilities (i.e., carbon capture, CO<sub>2</sub> purification systems, etc.) at the Kurtalan Cement factory. Kurtalan Cement Factory in Siirt, Türkiye was constructed in 1985. Its annual clinker production capacity was 590 thousand tons and its annual full capacity for cement production was nearly 740 thousand tons. According to the 2020 data, the facility has a production capacity of 776 thousand tons of clinker and 1.2 million tons of cement (Limak, 2020). The Kurtalan Cement Factory tries to minimize its wastes and CO<sub>2</sub> emissions during clinker and cement production.

The greenhouse gas emission of cement factories is approximately 5 % of anthropogenic greenhouse gas emissions (Kara et al., 2018). The chemical processes in the cement factories cause the release of huge amounts of CO<sub>2</sub> through the atmosphere. CO<sub>2</sub> emission in the cement factories varies depending on its raw material compositions, production facility types, technological updates, and energy resource types used in cement production. According to the literature survey in this study, CO<sub>2</sub> emitted for every tone of cement produced ranges from 0.55 to 1.1 tone with an average of 0.84

tones. In Türkiye, CO<sub>2</sub> emission in the cement factories ranges from 0.813 to 0.9-ton CO<sub>2</sub> per one ton of cement produced (Bektas, 2020). Although it is possible to reduce CO<sub>2</sub> emissions (below 0.5 ton/ton CO<sub>2</sub> cement) by updating cement production technology and using renewable energy resources for cement production, it is not likely to obtain zero-CO<sub>2</sub> emission in cement factories. However, underground CO<sub>2</sub> storage is an important alternative to store CO<sub>2</sub> released from cement factories. By using the annual cement & clinker production ranges of Kurtalan Cement Factory, the daily/annual CO<sub>2</sub> emissions of this factory were predicted by the methodology in Figure 2. The output results of the predicted CO<sub>2</sub> emissions of Kurtalan Cement Factory are listed in Figure 4. The lowest and maximum daily CO<sub>2</sub> emissions of Kurtalan Cement Factory are also enough for CO<sub>2</sub>-EOR application and further oil recovery in the Bati Raman Heavy Oilfield.

Overall, as listed in Figure 3 and Figure 4, both the Batman Oil Refinery and Kurtalan Cement Factory might provide enough CO<sub>2</sub> for the Bati Raman Heavy Oilfield after the depletion of the Dodan CO<sub>2</sub> Field. The current CO<sub>2</sub> sequestration facilities, CO<sub>2</sub> recycle facilities, and CO<sub>2</sub> sequestration experience since the mid-1980s are the best advantage for future possible CCS project(s) with Batman Oil Refinery and Kurtalan Cement Factory. The technical design and cost estimation of carbon capture facilities for the oil refinery and cement factory (i.e., carbon capture equipment, possible stop of production at the refinery and cement factory during the implementation of carbon capture facilities) should be conducted. The regulations and incentive mechanisms for CCS in Türkiye are also crucial for the companies (both oil companies, and CO<sub>2</sub>-source companies) to decide the investment on CCS application. Thus, in the following part, current regulations and incentive mechanisms and future suggestions in this study are discussed.

### Current Regulations and Incentive Mechanisms Related to CCS in Türkiye

In Türkiye, currently, there is not a commercial scale of CCS application. In Southeastern Türkiye, there are good experiences of underground CO<sub>2</sub> sequestration for CO<sub>2</sub>-EOR purposes in the heavy oilfields as in the Bati Raman Heavy Oilfield but the source of CO<sub>2</sub> in these applications is the natural CO<sub>2</sub> reservoirs. Hence, there is a lack of experience in carbon capture technologies. According to 2019 data, Türkiye's annual GHG emission was approximately 506.1 Mt CO<sub>2</sub> equivalent (TUIK, 2021) and this amount is in an increasing tendency.

Türkiye ratified several environmental agreements. For example, Türkiye became a party to UNFCCC United Nations Framework Convention on Climate Change in May 2004. Kyoto Protocol was ratified by Türkiye in May 2009. Paris Agreement was ratified in October 2021. Especially the participation of Türkiye in the Paris Agreement will make Türkiye release new regulations related to the reduction of carbon emissions. Generally, for GHG (i.e., CO<sub>2</sub>, H<sub>2</sub>S, etc.) emissions, there are upper

limits for different sectors. The companies try to keep their emissions below these upper limits because their emissions are controlled, and punishments are applied if the emissions are above the upper limits. However, this does not decrease Türkiye's GHG emissions. Most of the companies in Türkiye mention their carbon emission reductions and their environmental measures (i.e., tree planting, waste management, renewable energy preference, etc.) in their annual reports but unfortunately, they are not transparent about their annual CO<sub>2</sub> emissions. For this reason, it is crucial to forming a GHG emission database. This database should be transparent and can be reached by everyone, which is likely to form public pressure on the companies to cut their emissions as possible.

Although there are several prize systems for the companies' minimizing wastes and GHG emissions, there is no direct incentive mechanism in Türkiye. However, Turkish companies showing special care for the environment and lower GHG emissions are likely to obtain credits from EU green banks/ EU environmental projects.

For the implementation of a possible CCS project between the owner company of the Bati Raman Heavy Oilfield and the owners of Batman Oil Refinery and Kurtalan Cement Factory, the agreements should be signed between companies. There are no exact regulations for these agreements, and they can be determined completely between companies. However, there are some worries of the carbon source companies (i.e., Batman Oil Refinery, Kurtalan Cement Factory in this case):

- They do not have any obligations for carbon capture if their GHG emissions are below the upper GHG emission limit determined by Turkish laws & regulations
- Production stops during the implementation of carbon capture facilities in their sites
- Cost of carbon capture technologies (Carbon Capture Cost: 20-29 \$/ton CO<sub>2</sub>; Investment including carbon capture cost: 2096-2853 \$/kW (Akin, 2019) and technological upgrades for these systems

The biggest advantage of a carbon source company is to be a company having a profile respecting the environment and human health, which is also helpful to take credits from EU banks and funds from EU projects.

Briefly, currently, there is no obligation of Batman Oil Refinery and Kurtalan Cement Factory to provide CO<sub>2</sub> to the Bati Raman Heavy Oilfield and there is no regulation pushing them to invest in carbon capture and storage. However, after Türkiye's ratification on the Paris Agreement in October 2021, new regulations about carbon capture might be proposed in near future.

The owner company of the Bati Raman Heavy Oilfield needs a CO<sub>2</sub> source as soon as possible to keep the oil production at higher levels. CO<sub>2</sub>-EOR application has been applied since the mid-1980s in this field so there are many CO<sub>2</sub> injection wells, oil production wells, and CO<sub>2</sub> injection & recycle surface facilities. This is the biggest advantage of a feasible CCS project application.

Generally, for mature/depleted oil fields, the cost of CO<sub>2</sub> storage is approximately 1.3 \$/ton CO<sub>2</sub> and its monitoring costs range from 0.1 to 0.3 \$/ton CO<sub>2</sub> (Akin, 2019). Briefly, the owner company of the Bati Raman Heavy Oilfield should persuade the CO<sub>2</sub> source companies and feasibility studies should be conducted. Probably, the CO<sub>2</sub> source companies will expect the followings for CO<sub>2</sub> capture and its transportation to the Bati Raman Heavy Oilfield:

- The cost of carbon capture facilities on the oil refinery or cement factory should be supplied by the oilfield company.
- The cost of production loss during the implementation of carbon capture technologies should be financed mainly by the oilfield company.
- Additional price per ton of CO<sub>2</sub> might be expected from the oilfield company.

According to the meetings between the oilfield company and the Batman Oil Refinery & Kurtalan Cement Factory, Kurtalan Cement Factory hesitate to be a part of this CCS project due to the production stops during the implementation of carbon capture. However, the meetings are being held between the oil refinery and the oilfield company. The possible CCS project between the refinery and oilfield company will increase the air quality of Batman Province of Türkiye because the refinery is in the center of the city. This study (Figure 3) shows the Batman Oil Refinery might provide enough CO<sub>2</sub> for the CO<sub>2</sub>-EOR application in the Bati Raman Heavy Oilfield. The oilfield company should consider the following during the feasibility analysis for the CCS project with the Batman Oil Refinery:

- Daily/Annual CO<sub>2</sub> emissions rates of the Batman Oil Refinery should be estimated/measured at different production rates of the refinery.
- The cost of carbon capture technology implementation on the refinery should be estimated.
- The cost of refinery stops during the implementation of carbon capture should be estimated.
- The cost of a new possible CO<sub>2</sub> pipeline (8-10 km) between the refinery and oilfield should be estimated.
- The cost of current CO<sub>2</sub> injection/recycle systems' upgrade in the oilfield (which is crucial because the new houses are being built very close to oil/injection wells in the Bati Raman Heavy Oilfield) should be estimated.
- Monitoring technology should be implemented for detecting any CO<sub>2</sub> leakages.
- The oil production increase and its profit should be predicted with the continuation of CO<sub>2</sub>-EOR in the Bati Raman Heavy Oilfield by using CO<sub>2</sub> coming from the Batman Oil Refinery.

Although there are no direct sentences related to CCS, Turkish Petroleum Law.6491 states the environmental rules that should be obeyed in the oilfields. Thus, if CO<sub>2</sub> leakages in the Bati Raman Oilfield occur, the operations might be stopped and punishments to the oil company might be applied according to the Turkish Petroleum Law.6491. Apart from the Turkish

Petroleum Law, there is also secondary legislation "Turkish Petroleum Law Implementing Regulation" pointing to some technical parts related to underground storage besides the environmental part. However, it is also essential to bring new rules directly related to CCS applications as the CO<sub>2</sub>-EOR technique in Turkish Petroleum Law. Several incentive mechanisms related to CCS applications as CO<sub>2</sub>-EOR might also motivate other oil companies to implement CCS projects if their reservoirs are appropriate for CO<sub>2</sub>-EOR. In Türkiye, there is a huge experience about underground CO<sub>2</sub> sequestration as CO<sub>2</sub>-EOR. CCS application with CO<sub>2</sub>-EOR is a good start to finance and improve carbon capture technology and awareness in Türkiye.

## CONCLUSIONS AND POLITICAL IMPLICATIONS

In this study, the current status of Türkiye about CCS was discussed. Moreover, the possible CCS project between the owner of the Bati Raman Heavy Oilfield and the Batman Oil Refinery & Kurtalan Cement Factory was discussed in terms of both technical and regulatory aspects. The following concluding remarks were obtained in this study:

- The Dodan CO<sub>2</sub> reservoir is likely to be depleted within 1-2 years, so the urgent CO<sub>2</sub> source is essential for the continuation of CO<sub>2</sub>-EOR in the Bati Raman Heavy Oilfield. It is possible to provide this CO<sub>2</sub> by carbon capture at the nearest facilities (Batman Oil Refinery and Kurtalan Cement Factory).
- Both Batman Oil Refinery and Kurtalan Cement factory are likely to provide the essential CO<sub>2</sub> amount for the Bati Raman Heavy Oilfield.
- Batman Oil Refinery is in the center of Batman Province of Türkiye and for better air quality of Batman, the carbon capture at Batman Oil Refinery should be the obligation for both human health and environmental aspects.
- There is no regulation directly related to CCS in Türkiye. This depends on the agreement conditions determined by the companies.
- The CO<sub>2</sub> source companies do not have to capture GHG emissions if their GHG emissions are below the upper limits in the regulations.
- Regulations and incentive mechanics are essential to push the CO<sub>2</sub> source companies to capture CO<sub>2</sub> and its usage as CO<sub>2</sub>-EOR in the mature oil fields mainly in Southeastern Türkiye.

## REFERENCES

- Akin, S. (2019). AB Karbon Yakalama ve Depolama Direktifi Düzenleyici Etki Analizi Çalışması Bulguları. Low Carbon Turkey.
- Jing, L., El-Houjeiri, H. M., Monfort, J. C et al. (2020). Carbon intensity of global crude oil refining and mitigation potential. *Nature Climate Change*, 10(6), 526–532.

Kara, G., İbic, A., & Yagcioglu, E. (2018). Greenhouse Gas Emissions from Cement Industry. *Ulusal Çevre Bilimleri Araştırma Dergisi*, 1(2), 87–90.

Limak. (2020). Limak Group of Companies Annual Report 2020.

Russial, T. J. (2011). Carbon capture and storage – legal and regulatory framework. USEA.

Ozgun, E. (2017). Enhanced Oil Recovery Methods and Suggestions for Turkey. Chamber of Petroleum Engineers.

TUPRAS. (2021). Tüpraş 2020 Annual Report.

TUIK (2021). Greenhouse Gas Emissions Statistics, 1990-2019.

Keywords: CO2 Sequestration, Regulations

Figure-1, Commercial-scale CCS projects in operation (Russia, 2011)

Field Name	Location	CO <sub>2</sub> Source	Storage Formation	Year injection began	Mt CO <sub>2</sub> /year
Rangely	Colorado, USA	Natural gas processing plant	Oil-bearing EOR	1986	1.0
Sleipner	North Sea, Norway	Natural gas processing plant	Offshore subsea saline formation	1996	1.0
In Salah	Algeria	Natural gas processing plant	Depleted gas Reservoir	2004	1.2
Snohvit	Barent Sea, Norway	Onshore liquefied natural gas (LNG) plant	Offshore subsea saline	2008	0.7
Weyburn-Midale	Saskatchewan, Canada	Synthetic natural gas plant	Oil-bearing EOR	2000 Weyburn 2005 Midale	1.0

Figure-2, The methodology used to predict the ranges of annual CO2 emissions of Batman Oil Refinery and Kurtalan Cement Factory

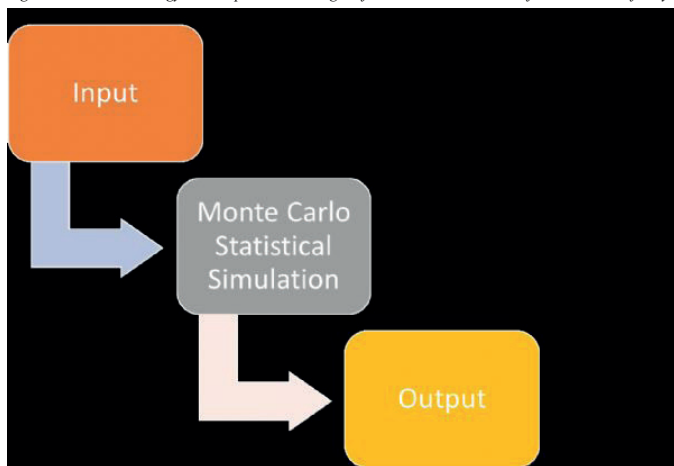


Figure-3, Predicted CO<sub>2</sub> emissions of Batman Oil Refinery

<b>Lowest CO<sub>2</sub> million m<sup>3</sup>/day</b>	<b>Mean CO<sub>2</sub> million m<sup>3</sup>/day</b>	<b>Maximum CO<sub>2</sub> million m<sup>3</sup>/day</b>
1.17	2.17	2.99
<b>Lowest CO<sub>2</sub> Mt/year</b>	<b>Mean CO<sub>2</sub> Mt/year</b>	<b>Highest CO<sub>2</sub> Mt/year</b>
0.768	1.42	1.96

Figure-4, Predicted CO<sub>2</sub> emissions of Kurtalan Cement Factory

<b>Lowest CO<sub>2</sub> million m<sup>3</sup>/day</b>	<b>Mean CO<sub>2</sub> million m<sup>3</sup>/day</b>	<b>Maximum CO<sub>2</sub> million m<sup>3</sup>/day</b>
0.505	0.811	1.092
<b>Lowest CO<sub>2</sub> Mt/year</b>	<b>Mean CO<sub>2</sub> Mt/year</b>	<b>Highest CO<sub>2</sub> Mt/year</b>
0.331	0.532	0.717



# Comparison Of Host Government Petroleum Contracts And Applicability For Türkiye Deepwater Offshore Licences



## **Fatih Vural**

Fatih Vural, Middle East Technical University, Petroleum and Natural Gas Engineering, Ankara / Türkiye

In the boundaries of sovereign nations, which has a legal dominion over of its geographical area, including natural resources, the vast majority of the World's energy sources are developed. If a country opens the resources for exploration and development which is referred to host country and the agreements signed between host country and National Oil Company (NOC), private companies or any combination of them to explore and/or develop petroleum licences are called as host government petroleum contract.

The fiscal system of host government contract is expected to encourage exploration and development activities, allow special incentives for some challenge fields and enable to provide fair sharing of economical incomes for Host Countries (HC) and International Oil Companies (IOCs).

Especially, expenditures and risk factors are very high for deepwater operations during exploration and development phases until reaching first commercial production for Operator that might be HC only, JV or an IOC. Therefore petroleum law, regulations, host government contracts and tender strategy should be arranged by considering items: geology (prospectivity of field, reserves, productivity and HC quality and type "gas or oil"), political stability of HC and abroad, legal system, fiscal system, transparency, market conditions and operational challenges. Deepwater Offshore Operations are the most challenge ones in exploration and also production stages. In order to start and continue such deepwater projects, HCs prefer to announce tender for opening offshore licences to investors. Before issuing such tenders, HC has to be sure about the status of above items to create an attractive atmosphere for potential bidders. Also tender strategy, financial terms/fiscal regime, contract methodology should be re-evaluated in every stages which are without discovery, after discovery, in exploration and production phases.

## **INTRODUCTION**

The petroleum law of Turkey published in 2013 and the regulations has been in effect since 2014. However there have been major changes in Turkey deepwater offshore activities after this year and some serious developments have taken place such as inclusion of 3 drillships in Turkish Petroleum (TPAO) Inventory, drilling one after another deepwater wells in Mediterranean and Black Seas, a gas discovery in the Black Sea, following potentials in the deepwaters and a deepwater service company established with own capital of TPAO.

As a result, petroleum contract type, tender strategy and fiscal regime of Turkey for deepwater operations should be re-examined and all related terms to be re-evaluated by considering current market conditions

and any changes in the neighbouring countries. The modern fiscal terms which are currently used by most of countries could be considered while making these evaluations. One of this modern term is royalty systems based on sliding scales as per daily production or cumulative production. A sample deepwater project economics will be run to understand and compare the economic impacts of this system.

## **HISTORY OF PETROLEUM LAW**

The Petroleum Law No. 792, which was passed in 1926, was the first Turkish legal legislation concerning petroleum. The Turkish State retained exclusive authority to perform petroleum exploration and development activities under Law No. 792. As a result, there were no incentives for foreign investment in the law. Petroleum Office was established under the Ministry of Trade on February 14, 1941 to carry out petroleum-related activities.

Petroleum Law No. 792 was replaced with Petroleum Law No. 6326 which came into force on 16 March 1954. The Turkish Petroleum Corporation ("TPAO") was established in the same year. TPAO's activities included petroleum exploration, drilling, development, refining, and transportation, as well as the purchase, selling, and distribution of petroleum and petroleum products. The new law made it possible for both domestic and international companies to participate in petroleum activities in Turkey. However, as progressive as Petroleum Law No. 6326 was at the time, it was not enough of an opportunity to attract the required levels of investment into Turkey's petroleum exploration and production activities. This was largely due to the persistence of legislative constraints and bureaucratic roadblocks. As a result, the Turkish legislative tried to replace the Law with a new one that could respond to the investors' needs while also providing incentives.

In 2003 and 2005, Petroleum Market Law and Liquefied Petroleum Market Law were enacted respectively.

The Turkish Parliament passed Turkish Petroleum Law No. 5574 on January 17, 2007, in order to create a more transparent and competitive legal and regulatory system. The Turkish President, on the other hand, vetoed the law, claiming that it did not adequately safeguard Turkey's national interests. The following were the reasons for the veto, and it should be remembered that much of the issue was about the country's national interests.

On June 11, 2013, the new Turkish Petroleum Law No. 6491 took effect, replacing the previous Petroleum Law No. 6326, which was enacted in 1954. The new Petroleum Law aims to ensure that the Turkish Republic's petroleum resources are explored, established, and generated in a timely, reliable, and

efficient manner consistent with national interests. The new Petroleum Law's key goal is to eliminate barriers to attracting foreign investment. As a result, the Law seeks to eliminate bureaucracy, simplify application processes, create incentives for exploration and development activities, lower prices, and create a more competitive climate. The major rights and incentives are in the new law (Akin Law Office, 2014):

a) Income Tax: The amount of the income tax deductions owed on the petroleum right holder's net income and the income tax withheld on behalf of its owners will not exceed 55 percent.

b) Tax exemption: Oil and gas field machinery manufactured and sold locally is excluded from customs duty, levies, and stamp tax. The exemption can continue even if the materials that are subject to exemption are transferred from one petroleum right holder to another with the approval of the General Directorate.

c) Exemption from Certification of Compliance for Imported Goods: Materials that a petroleum right holder has imported to use in petroleum operations that have been licensed by the General Directorate are not subject to a Turkish Standards Institute compliance evaluation.

d) Foreign employees: Excluded from normal work laws for a six-month duration and can work in Turkey if they receive a residence permit.

e) Permission to Build a Pipeline: An operation license holder can be given permission to construct a pipeline to transport the petroleum it produces upon request.

f) Right to Repatriation of Registered Capital: The new Law also eliminates restrictions on capital repatriation. By filing an application with the General Directorate, the holder of a petroleum right can transfer their cash funds and rights thereto, as well as economic assets, tax-free, either in cash or in kind, and after putting aside the amount needed for the payment of any taxes, duties, charges, and royalties owed to the State.

g) Right to keep the income in return for exportation of petroleum outside Turkey: The foreign currency produced by the petroleum export can be kept by the holder of a petroleum right abroad. This number will be deducted from remittances of capital imported into Turkey and transfers of net values in excess of it.

h) Right to Export Petroleum Products: Petroleum right holders are allowed to export a certain percentage of the petroleum and natural gas generated in fields discovered after January 1, 1980 (35 percent onshore and 45 percent offshore). The remaining portion, as well as the entire amount of petroleum and natural gas generated in fields discovered prior to January 1, 1980, must be kept for domestic use. The process and principles for redetermination and application of these ratios are controlled by the Council of Ministers.

As mentioned above, Turkish Petroleum Law (No:6491) was published on 30th of May, 2013. The Petroleum Regulation was also renewed in 2014. The former version of Petroleum Regulations was published in 1989 and it had been effective till 2014. Main objective of new Petroleum Law and Regulations is to regulate

upstream activities and explore Turkey's remaining oil and gas potential effectively. General Directorate of Mining and Petroleum Affairs is the Competent Authority in Turkey which regulate all oil and gas exploration and production activities and dedicate licences. As per decree-law (662), one of major duty of General Directorate of Mining and Petroleum Affairs is to establish an investment environment for foreign investors. Also there are some other defined works in the decree-law (662) for General Directorate of Mining and Petroleum Affairs (MAPEG, 2011) related with IOCs:

1. To ensure that domestic and foreign investors make their oil exploration and production investments in a competitive, transparent, safe and stable environment within a program,

2. To open the fields that are determined as potential in terms of oil to auction and to give exploration license,

3. To examine the applications of companies for Concessionaire.

Licence period for offshore exploration fields was settled as eight years. If Concessionaire completed work program and guaranteed one exploration well and %2 performance bond, licence period might be extended as 3 years more. If Concessionaire completed work program in extension period and guaranteed drilling of another well and new work program, it might be extended another 3 years more. The limit of extension period is 9 and 14 years for onshore and offshore licences respectively. If a discovery was occurred, two more years extension might be added to exploration period for well tests and commercial evaluations. Royalty ratio is %12.5 of produced oil. In the petroleum law, maximum tax ratio is limited with %55 as (MAPEG, 2013) "Obligated to pay petroleum right holders on their net income, the total withholding taxes and income taxes on behalf of their shareholders cannot exceed 55 percent.". %45 of produced oil and gas can be exported by Concessionaire, but rest of oil&gas has to be sold in local market. After exploration period, production licence is issued for 20 years and it can extended two times not more than 10 years by considering production program.

### **Proposed Improvements for Turkish Petroleum Law:**

However draft Petroleum Law in 2011 was prepared by including some major changes in the royalty system (Aydin, 2011). The first one was that a royalty regime in accordance with production rates, API gravity, water depth and implementation of secondary enhanced oil recovery. The second one is that %50 of royalty shall be transferred to the account of province. Also %5, %10, %20 and %30 less royalty would be collected for 0-500m, 501-1000m, 1001-1500m and more than 1500m water depths respectively. Moreover 50% less royalty would be applicable for 16 API or less gravity oil and %25 less royalty for enhanced recovery methods. Unfortunately above desirable terms and conditions were not enacted with new Petroleum Law.

Turkish Petroleum Corporation (TPAO/TP) is the State Oil Company who manages most of exploration and production activities in onshore and offshore areas. Also there are some other private local and international petroleum companies which continue to produce gas and oil and sell their products in local market generally.

As of January 1, 2016, Turkey's proven oil reserves were estimated by the Oil & Gas Journal (OGJ) at 312 million barrels, located mostly in the country's southeast region (Energy Information Administration, 2017). In recent years the production has been increased to more than 50,000 b/d, 150,000 b/d with international projects.

Turkey's overall intake of liquid fuels averaged about 680,000 b/d in 2019. More than 90% of the overall supply of liquid fuels comes from imports. Much of Turkey's crude oil was imported from Iraq and Iran, which together accounted for slightly more than 60% of the country's crude oil.

Most of Turkey's proved oil reserves are in the Batman and Adiyaman Provinces in the southeast and in Thrace in the northwest. In 2015, Turkey produced an estimated 62,000 b/d of petroleum and other liquids, accounting for about 7% of Turkey's oil consumption.

Turkish natural gas reserves are projected to be 177 billion cubic feet as of January 1, 2016 (Bcf).

Turkey is a major natural gas user and is becoming an effective transit state for natural gas. Turkey is one of the few countries in Europe where the consumption of natural gas continues to show strong growth. Increasing demand in Turkey has helped build several pipelines to carry natural gas into the country, and although little natural gas has been made available for export, new supplies have been contracted and new pipelines are under development to increase Turkey's natural gas imports and exports.

### **CHANGED CONDITIONS FOR TURKIYE OFFSHORE ACTIVITIES**

Turkey had not existing petroleum and gas resources in the offshore till last quarter of 2020. First biggest discovery was announced as 405 billion m3 in Blacksea, Sakarya Block, October, 2020. Turkey needs to create the proper constitutional framework for exploration fields in Black Sea and Mediterranean in the Turkey and North Cyprus Economical Zone which overlap with Greece and South Cyprus zones.

It should be re-considered some special terms for offshore licences after the discovery in Black Sea other than licence period if more IOCs are expected to show their interest despite current oil prices. All petroleum contracts should be re-evaluated and considered some attractive terms for IOCs in case of continuation of current low oil price trend especially for deepwater operations. Therefore Turkish Petroleum Law and Regulations might be recovered by authorities to settle more attractive fiscal regime in the region. By the way the well-known IOCs may show more interest to Turkey than any other region in the world and other countries in east Mediterranean and Black Sea. If IOCs show interest

and accept to make investment for deepwater projects in Turkey, it would be very easy solution to decrease operational costs and sharing of risks for exploration operations.

After attracting IOCs and receiving their interest and Turkey decide to announce tender for potential licence fields, there must be in a climate transparency meet the highest standard of international practice. In the petroleum law, regulations and contract terms should be in compatible each other. Duration, extension and relinquishment rules should be simpler, clear and understandable for any parties. Licence fields should be awarded in order, not all in one.

The fiscal regime terms might be regulated by decreasing maximum tax ratio as %52 which will be equal tax in Israel. Also it can be decreased more or arranged as per R factor based. For gas reservoirs, %12,5 royalty rate can be decreased by considering higher expenditures of gas projects than oil. By decreasing tax ratio, a training fee might be applicable to support nationalization activities and train drilling and marine crew for deepwater offshore operations. Although the fiscal terms would re-evaluated and made more attractive for IOCs, %45 of exportation rate can be decreased by considering oil and natural gas requirements in domestic market in Turkey. Fiscal regime could be separated for onshore and offshore projects, also some separation could be applicable for the projects in Black Sea and Mediterranean.

### **AN OFFSHORE PROJECT FISCAL REGIME COMPARISON WITH SOME IMPROVEMENTS**

As per the sample project summarized in the table, it describes a deepwater project as 23 years project life and 20 years production life. The project is covering 1 exploration, 1 appraisal and 40 development wells. Exploration and appraisal wells will not be completed as producer wells. Deepwater exploration well cost is 60 MM USD and Appraisal Well is 40 MM USD, so 100 MM USD is assumed in 2020. Then development wells will be drilled in future years till 2030. First commercial production will be in 1st quarter of 2023 and plateau production will be in 1st quarter of 2030. Total expenditure for wells is estimated 1.8 Billion USD in 10 years. For surface facilities, pipelines, LLIs and constructions, it is estimated as 19 Billion USD. Total expenditure is estimated as 22 Billion USD and 21 Billion USD will be spent in first 10 years which is a large investment amount.

According to draft petroleum law in 2011, it was planned to add some major changes such as a royalty regime in accordance with production rates, API gravity, water depths and implementation of enhanced secondary oil recovery.

IOC will not pay high royalty rates for initial production phases, however HC will receive almost same income "especially in the later phases of the project".

According to draft version of petroleum law in 2011, the Turkish Government aimed to increase oil investment

activities and oil/gas production without any knowledge about a discovery that may come from deepwater operations in the following years. However the draft version was not enacted with this incentive options, fixed royalty rate (12.5%) is still applicable and there is no incentives for deepwater operations in the law.

The thesis focused on possible attractive and desirable fiscal regimes for deepwater operations in Turkey. The deepwater offshore activities are increasing with Fatih, Yavuz and Kanuni Drillships. After drilling eight deepwater wells in Mediterranean in last three years, Tuna-1, Türkali-1 and Türkali-2 deepwater wells were drilled in the Black Sea. Sakarya Gas Block was also discovered with Tuna-1 well. During last 60 years, more than 1 billion oil and five hundred billion cubic feet of gas was produced (Özgür, 2015). Most of production was made from south east part of Turkey. Petroleum Law was updated several times between 1954-2013 as per requirement of petroleum sector. Although two production peaks (1969 and 1990) were observed in this period, production trends decreased year by year till last two years. On the other hand a new production peak may occur due to deepwater activities. Also, drilling activities has reached the highest level in the European Countries.

## CONCLUSION

As a summary, petroleum law and regulations of Turkey for offshore licences should be re-evaluated by considering current oil and gas market situation in the world and abroad, increasing offshore activities in East Mediterranean, the gas discovery of Turkey in the Black Sea. After a discovery, most of the countries prefer to use Production Sharing Agreement if they are not rich oil countries. If a concession is preferred for offshore, sliding scale royalty system could be selected for offshore activities. In the sliding scale, government can determine each ratio for different production level or it could biddable for IOCs. Therefore all tenders, petroleum laws and regulations should be reviewed and examined by Turkish Authorities/Law Makers attentively to increase total profit of Turkey in the long run, decrease project expenditures during exploration phase and create more attractive biddable atmosphere for IOCs.

Keywords: Host Government Petroleum Contract, Fiscal Systems



## **Petrol ve Doğalgaz Sektörü'nde Sürdürülebilirlik**

*Sustainability in the Oil and Gas Industry*

---



# Evaluation of Sustainability Aspects of CO<sub>2</sub> Sequestration in Depleted Shale Reservoirs Using Data Analytics



Kanan Aliyev<sup>1</sup>, Emre Artun<sup>2</sup>, Burak Kulga<sup>2</sup>

<sup>1</sup>Politecnico di Torino

<sup>2</sup>Istanbul Technical University

## ABSTRACT

This study aims to investigate the economic and environmental impacts of carbon-dioxide sequestration in shale reservoirs by estimating the net present value (NPV) and carbon footprint (CF) across various scenarios, considering reservoir properties, gas production, and carbon dioxide (CO<sub>2</sub>) injection data. Additionally, we present the findings of an analysis that explores the impact of reservoir and operational parameters. We found out that the application of carbon sequestration in shale reservoirs is a promising approach for reducing carbon emissions and mitigating global warming. Prolific gas production wells would be better candidates to avoid negative NPV due to the significant cost of the carbon sequestration operation. We also identified several key variables affecting the economic and environmental potential of CO<sub>2</sub> sequestration in shale formations, including stimulated reservoir volume (SRV) fracture permeability, original gas in place, initial reservoir pressure, reservoir's fracturing pressure, injection pressure constraint, horizontal wellbore length, and total production time.

## INTRODUCTION

The average global temperature has risen since the Industrial Revolution due to the increase in greenhouse gases, particularly carbon dioxide, which has increased by 47% [1]. Storing carbon dioxide in subsurface formations (geo-sequestration) is a possible solution to reduce its amount in the atmosphere [2]. The majority of studies on geo-sequestration has focused on depleted oil/gas reservoirs, saline aquifers, and unmineable coal seams. Only with the advent of hydraulic fracturing and horizontal drilling, depleted shale reservoirs gained popularity and became the focus of CO<sub>2</sub> sequestration. Sequestration capacity of shale reservoirs have been investigated for various formations such as Marcellus shale [3] and New Albany Shale [4,5] which demonstrated considerable amount of potential capacities. It was shown that CO<sub>2</sub> shows enhanced sorption and interactions with shale minerals, while preferentially sorbing over CH<sub>4</sub> in mixed gas systems. These findings suggest potential opportunities for CO<sub>2</sub>-based enhanced gas recovery in depleted shale gas reservoirs, offering a dual benefit of reducing CO<sub>2</sub> emissions and maximizing natural gas production [6]. More comprehensive volumetric capacity estimation studies were completed [7], with total bulk volume, total porosity, storage efficiency, and CO<sub>2</sub> density being the key parameters.

Numerical reservoir simulation studies that focus on shale formations incorporate dual-porosity/dual-permeability approach, multi-fractured horizontal wells

(MFHW), gas desorption/sorption, and diffusion flow [5]. Simulations showed that significant portion of the injected CO<sub>2</sub> can be trapped as an adsorbed phase in the shale, leading to incremental gas recovery. Additionally, CO<sub>2</sub>-EGR with adsorbed phase trapping holds promise as an effective method for carbon sequestration [8]. Further simulation studies revealed that, due to the effect of stress-dependent permeability, there is a minor reduction in cumulative gas injection in all measures for reservoir permeabilities. Moreover, a notable positive correlation was observed between gas sorption with CO<sub>2</sub> storage response in high-permeability shale reservoirs. These highlighted the potential of utilizing depleted shale gas reservoirs for sustainable sequestration [9]. Alternative modeling approaches, such as surrogate reservoir models were used to investigate economic feasibility of CO<sub>2</sub> sequestration in depleted shale formations and identify major cost drivers [10]. Results showed that transportation and injection costs were major cost contributors, while post-injection site care and pore space acquisition were minor drivers.

Experimental studies were performed to understand the adsorption and displacement behaviors of methane (CH<sub>4</sub>) and carbon dioxide (CO<sub>2</sub>) [11,12]. These experiments suggested that injecting CO<sub>2</sub> after partial desorption of CH<sub>4</sub> improves both CH<sub>4</sub> recovery and CO<sub>2</sub> sequestration. [11] CO<sub>2</sub> adsorption increased with higher pressures and lower temperatures. Altering the shale volume affected adsorption which indicated the potential for CO<sub>2</sub> storage in unconventional shale reservoirs. [12]

Existing studies suggest that shale reservoirs have great CO<sub>2</sub> storage capacity, while there are uncertainties surrounding the economic and environmental aspects of the global application of CO<sub>2</sub> sequestration in shales. This study examines the economic and environmental impacts of implementing carbon sequestration directly after gas production in fractured shale reservoirs. We also explore the impact of parameters, such as matrix and fracture properties, reservoir thickness, temperature, pressure, injection pressure, total production time, etc. on sustainability aspects.

## METHODOLOGY

The dataset employed consists of 2547 unique numerical-simulation scenarios that were run using a state-of-the-art reservoir simulator, PSU-SHALECOMP, which is a compositional dual-porosity, dual-permeability, multi-phase reservoir simulator [13]. The simulator incorporated the effects of water presence in the micropore structure, matrix shrinkage and swelling.

CO<sub>2</sub> sequestration was performed with a constraint of the injection rate after an initial gas recovery phase until a specified limit of the fracturing pressure was reached [13]. Furthermore, detailed records of production and injection rates were collected, encompassing a total of 22 periods consisted of 11 distinct production or injection periods, with 12 recording points for each phase, ensuring approximately equal intervals between these measurements. Each scenario has 27 reservoir and operational characteristics, which are considered as input parameters. Our analysis focuses on the evaluation of net present value (NPV) and carbon footprint (CF) which are the target variables.

**Step 1: Net Present Value Estimation.** In this step, the produced methane and injected carbon dioxide volumes are used to estimate the economic value of the carbon sequestration project. The profitability of a given scenario was analyzed via net present value (NPV). For gas price, we used the gas price of 5.39 USD/MCF (average price of the last 21 years in the North America market [14]). A discount rate of 10% per year ( $D=0.1$ ) was applied to all calculations. The cash flow analysis was performed using assumed associated costs from a thorough analysis of published papers. A list of capital costs has been provided Fig. 1 with their assumed cost values [15]. To determine the total expenditure due to hydraulic fracturing, cost of injected proppant, chemicals and equipment was considered [16]

**Step 2: Carbon Footprint Estimation.** To estimate the carbon footprint for all scenarios, we used The Oil Production Greenhouse Gas Emissions Estimator (OPGEE) developed by Stanford University [17]. This tool is based on the traditional way of carbon footprint estimation (i.e., life-cycle assessment), which involves adding up as many of the emissions' pathways. In the context of oil and gas production, these pathways typically include exploration, drilling and development, production, surface processing, transportation, and utilization of the fluid [17]. For this study, these six stages were investigated to estimate the carbon footprint for each scenario, considering that sources of the emission were different in these stages based on their operational objectives.

**Step 3: Exploratory Data Analysis.** During the exploratory data analysis phase of our study, we utilized various data analytics techniques to gain insights into estimated NPV and CF values. To achieve this goal, two effective visualization tools were employed: histogram and box plot. These enabled us to identify any patterns or outliers within distribution characteristics in relation to NPV and CF values. Furthermore, a statistical summary was performed for a greater understanding of average, minimum and maximum output values as well as central tendencies for each variable under examination. This allowed us to understand the impact of carbon sequestration in depleted shale reservoirs on economic and environmental parameters. We extended the application of these visualizations to the input parameters. We generated scatter plots to gain insights into the relationships and dependencies between input variables and the NPV and CF values. To further

quantify these dependencies, statistical measures such as Pearson and Spearman correlations were used. These measures helped us to both identify the direction and quantify the strength of the relationships between input and target variables. Pearson correlation coefficient assessed the linear correlation between variables, while the non-linear relationships were evaluated by Spearman's rank correlation coefficient [18].

## RESULTS AND DISCUSSION

Fig. 2 shows the distribution of the mean contributions of all scenarios to the carbon emissions. According to these results, a great majority of the emissions come from surface processing. Then, comes the production, transportation and maintenance operations.

As depicted in Figure 3-a, negative carbon footprints were estimated in nearly 99% of all scenarios, suggesting that the amount of injected CO<sub>2</sub> exceeds the amount of CO<sub>2</sub> emitted into the atmosphere during natural gas production. These results validate that depleted shale reservoirs can be a viable option for CO<sub>2</sub> storage. Initially, it was also hypothesized that CO<sub>2</sub> sequestration in depleted shale formations would result in positive NPV, indicating economic sustainability of the operation. However, as shown in Figure 3-b, approximately 40% of all scenarios resulted in negative NPV, making sequestration economically unattractive in shale reservoirs. Nevertheless, in the remaining scenarios, positive NPV values were estimated, highlighting the importance of considering the expected natural gas production and gas price before implementing carbon sequestration. The statistical summary in Figure 4 shows that the average and median values for NPV are 6.26 and 2.44 M USD, respectively. Since NPV values exhibit positive skewness as represented in Figures 3-b and 3-d, interpreting our findings based on the median value would be more appropriate. Therefore, it can be concluded that in the scenarios where CO<sub>2</sub> sequestration is economically feasible, the expected returns range from approximately 2.44 to 40 M USD for the majority of scenarios (45.11%). In these scenarios, the estimated CF values range between -0.16 and -1.39 Mton. Based on the analysis of these numbers, companies can make diverse decisions regarding the implementation of CO<sub>2</sub> sequestration after natural gas production, taking into account their individual strategies. However, it is evident that higher returns from gas production can make it a more attractive and viable option for reducing CO<sub>2</sub> emissions in the atmosphere.

In the second part of the analysis, we investigated the relationships and dependencies between variables. Based on our observations of the variable distributions, we found several examples that indicated a potential degree of relationship between the input and target variables. Among the input variables, SRV and natural fracture permeability, SRV and natural original gas in place, initial pressure, and fracture pressure emerged as the top variables with stronger correlations to estimated NPV compared to the rest of input variables (Figure 5). For the estimated carbon footprint (CF), the most



influential variables included total production time, stimulated reservoir volume (SRV) and natural fracture permeabilities, SRV and natural original gas in place and injection constraint (Figure 6). Similar distributions in histograms and nearly linear relationships in scatter plots supported these findings. By applying correlation measures, we were able to quantify the degree of association between the input variables and our estimated outputs, as presented in Figure 7. Hence, these statistical measures also showed that input variables highlighted above exhibited noteworthy relationships with the NPV and CF values.

## CONCLUSIONS

**The main conclusions from this study are given below:**

1. NPV and CF have a skewed distribution, which is reasonable due to the higher gas storing capacity of some formations compared to others.
2. Although in most scenarios (roughly 60%), a positive Net Present Value was estimated, there are cases where application of the carbon sequestration operation appears not economically attractive due to higher costs.
3. Carbon sequestration operations can significantly cut down the profits obtained from natural gas production from the fractured shale reservoirs. Therefore, it would be more appropriate to apply these operations in wells where a greater amount of natural gas production is expected, such that the cost of carbon sequestration will not lead to negative NPV.
4. The application of carbon sequestration in fractured shale reservoirs can be a good alternative for mitigating global warming, considering that in the majority of scenarios, the amount of injected CO<sub>2</sub> is greater than that of CO<sub>2</sub> generated during the production operation.
5. Results obtained from the univariate and bivariate analysis made it clear that there is a correlation between some of the input parameters and estimated parameters. Fracture permeability, production and injection constraints, original gas in place, initial pressure, fracture pressure, horizontal wellbore length, and total production time were these input parameters.
6. To improve upon these estimations and gain a more comprehensive understanding, future research can investigate additional factors, collect more extensive data, conduct more detailed analysis of carbon emissions and operation costs, and include risk and uncertainty analysis.

## REFERENCES

1. Tucker, O. 2018. Introduction. In: Carbon Capture and Storage. London: IOP Publishing
2. Metz, B. et al. eds., 2005. Summary for Policymakers. In: Carbon Dioxide Capture and Storage. s.l.:Cambridge United Press, pp. 7-8.
3. Tao, Z., Clarens, A. 2013. Estimating the Carbon Sequestration Capacity of Shale Formations Using Methane Production Rates. *Environ. Sci. Technol.* 47 (19):11318-11325 <https://doi.org/10.1021/es401221j>
4. Chen, Z., Liao, X., Zhao, X., Dou, X., Zhu, L. 2016. Development of a Trilinear-Flow Model for Carbon Sequestration in Depleted Shale. *SPE Journal*, 21 (04): 1386-1399 <https://doi.org/10.2118/176153-PA>.
5. Liu, F., Ellett, K., Xiao, Y., Rupp, J. 2013. Assessing the feasibility of CO<sub>2</sub> storage in the New Albany Shale (Devonian–Mississippian) with potential enhanced gas recovery using reservoir simulation. *International Journal of Greenhouse Gas Control*, 17:111-126, <https://doi.org/10.1016/j.ijggc.2013.04.018>
6. Schaefer, H.T., Davidson, C.L., Owen, A.T., Miller, Q.R.S., Loring, J.S., Thompson, C.J., Bacon, D.H., Glezakou, V.A., McGrail, B.P. 2014. CO<sub>2</sub> Utilization and Storage in Shale Gas Reservoirs: Experimental Results and Economic Impacts, *Energy Procedia*, 63: 7844-7851 <https://doi.org/10.1016/j.egypro.2014.11.819>
7. Goodman, A., Hakala, A., Bromhal, G., Deel, D., Rodosta, T., Frailey, S., Small, M., Allen, D., Romanov, V., Fazio, J., Huerta, N., McIntyre, D., Kutchko, B., Guthrie, G., 2011. U.S. DOE methodology for the development of geologic storage potential for carbon dioxide at the national and regional scale. *International Journal of Greenhouse Gas Control*. 5 (4):952–965. <https://doi.org/10.1016/j.ijggc.2011.03.010>
8. Mohagheghian, E., Hassanzadeh, H., Chen, Z. 2019. CO<sub>2</sub> sequestration coupled with enhanced gas recovery in shale gas reservoirs. *Journal of CO<sub>2</sub> Utilization*,34:646-655 <https://doi.org/10.1016/j.jcou.2019.08.016>
9. Armin Shirbazo, Amin Taghavinejad, Saber Bagheri, 2021. CO<sub>2</sub> Capture and Storage Performance Simulation in Depleted Shale Gas Reservoirs as Sustainable Carbon Resources. *Journal of Communications (Institute of Construction Materials)*
10. Tayari, F., Blumsack, S., Dilmore, R. & Mohaghegh, S. D., 2015. Techno-economic assessment of industrial CO<sub>2</sub> storage in depleted shale gas reservoirs. *Journal of Unconventional Oil and Gas Resources*, 11:82-94. <https://doi.org/10.1016/j.juogr.2015.05.001>
11. Huo, P., Zhang, D., Yang, Z., Li, W., Zhang, J., Jia, S. 2017. CO<sub>2</sub> geological sequestration: Displacement behavior of shale gas methane by carbon dioxide injection. *International Journal of Greenhouse Gas Control*, 66:48-59. <https://doi.org/10.1016/j.ijggc.2017.09.001>
12. Fakher, S., El-Tonbary, A., Abdelaal, H., Elgahawy, Y., Imqam, A. 2020. Carbon Dioxide Sequestration in Unconventional Shale Reservoirs Via Physical Adsorption: An Experimental Investigation. Paper presented at the SPE Europec, Virtual, 1-3 December, <https://doi.org/10.2118/200537-MS>
13. Kulga, B., 2014. Analysis of the efficacy of carbon dioxide sequestration in depleted shale gas reservoirs, Ph.D. Dissertation, The Pennsylvania State University, University Park, Pennsylvania

14. EIA (2022) Energy Information Administration - EIA - Official Energy Statistics from the U.S. Government <https://www.eia.gov/naturalgas/data.php#prices> Accessed March 1, 2022.

15. Celik, D., Bolat, F., Guler, M.I., Artun, E. 2021. Designing carbon sequestration in a depleted oil reservoir considering sustainability aspects. Kadir Has University, 4th Graduate Student Conference on Energy and Sustainable Development (GCESD), 8 October, Virtual

16. Gou, B., Guo, J. & Yu, T., 2018. Modeling of quantifying proppants for stimulation reservoir volume fracturing in a shale hydrocarbon reservoir. Journal of Geophysics and Engineering, 14(5):1-13. <https://doi.org/10.1088/1742-2140/aac4bc>

17. Brandt, A.R., Masnadi, M.S., Rutherford, J.S., ElHoujeiri, H.M., Quinn, L. Kourosh, V. Chen, Y., Duffy, J. 2022. Oil Production Greenhouse Gas Emissions Estimator OPGEE v3.0b User Guide & Technical Documentation, Stanford University, Stanford, California.

18. Mishra, S., Datta-Gupta, A. 2017. Applied Statistical Modeling and Data Analytics: A Practical Guide for the Petroleum Geosciences, 1st Edition. Elsevier, Amsterdam, The Netherlands, 235 pp.

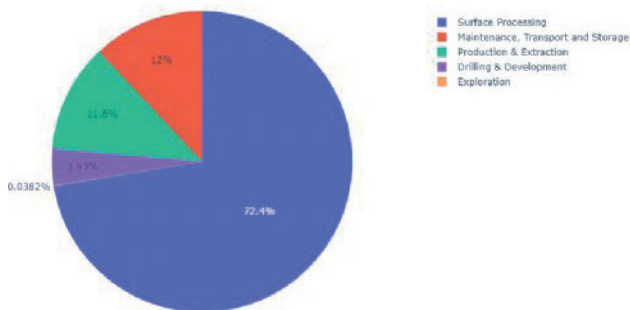
Keywords: CO<sub>2</sub> sequestration, sustainability

Figure 1

Item	Cost	Unit
Drilling & Completion (Vertical well)	250	\$/ft
Drilling & Completion (Horizontal well)	650	\$/ft (after vertical section)
Other production well surface equipment	200,000	\$/well
Other injection well surface equipment	300,000	\$/well
General construction for a well	100,000	\$/well
Gas-handling facility	10,000,000	for 100,000,000 scf/day capacity

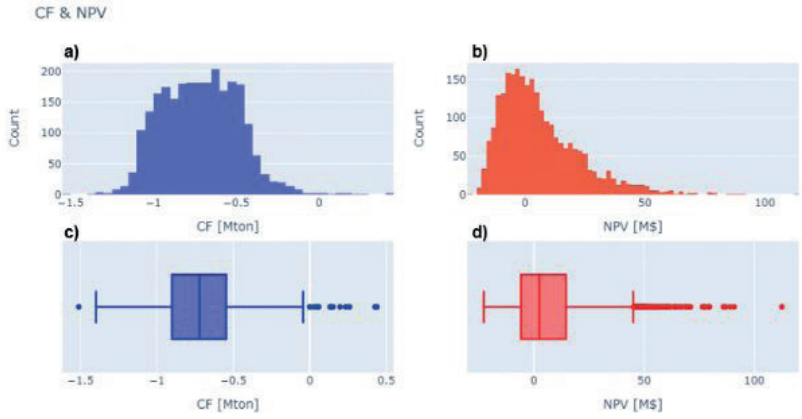
Cost assumptions for CAPEX

Figure 2



Distribution of carbon-emission contributions in a sequestration project after natural gas production from shale reservoirs.

Figure 3



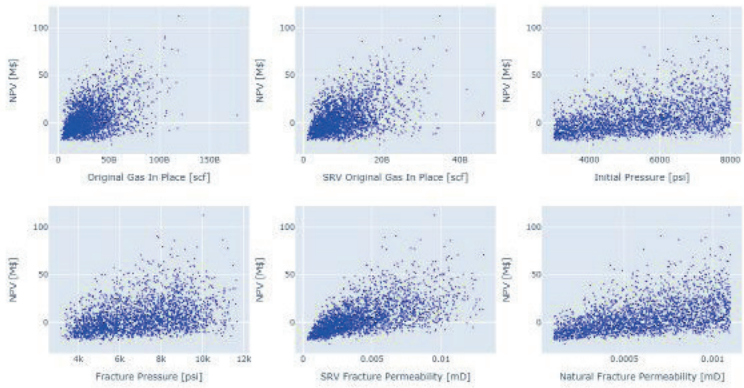
Distributions of carbon footprint and net present value, (a) Histogram of carbon footprint, (b) Histogram of net present value, (c) Box plot of carbon footprint, (d) Box plot of net present value

Figure 4

	Count	Mean	Std	Min	25%	50%	75%	Max
NPV (M USD)	2547	6.26	16.70	-22.69	-5.81	2.44	14.53	112.52
CF (Mton)	2547	-0.72	0.23	-1.51	-0.9	-0.72	-0.55	0.44

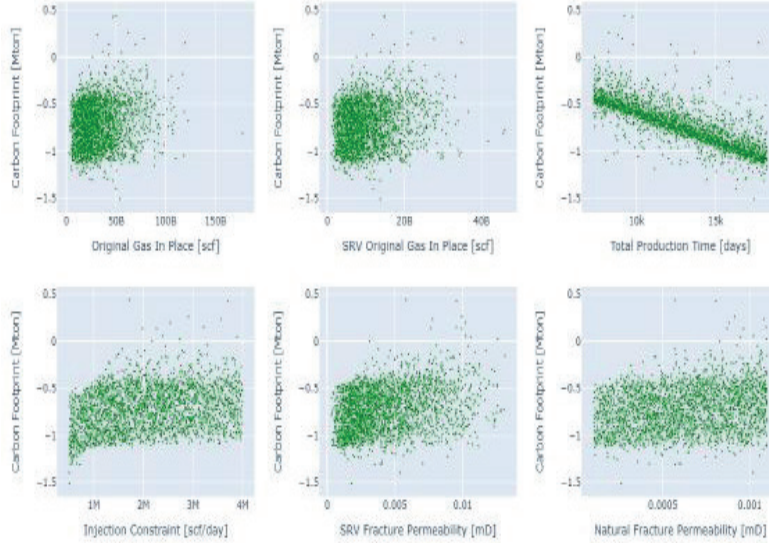
Statistical summary of the target variables

Figure 5



Scatterplots for net present value (M USD) as the target variable.

Figure 6



Scatterplots for carbon footprint (kton) as the target variable.

Figure 7

	NPV		Carbon Footprint	
	Pearson	Spearman	Pearson	Spearman
SRV Fracture Permeability	0.600*	0.654*	0.298*	0.288*
Natural Fracture Permeability	0.478*	0.514*	0.224*	0.211*
SRV Original Gas in Place	0.458*	0.422*	0.176*	0.154*
Original Gas in Place	0.456*	0.413*	0.170	0.142
Initial Pressure	0.413*	0.433*	-0.010	-0.010
Fracture Pressure	0.352	0.378	-0.001	-0.002
Area	0.322	0.288	0.117	0.100
Injection Constraint	0.313	0.354	0.270*	0.267*
Horizontal Wellbore Length	0.257	0.250	0.178	0.164
Reservoir Width	0.256	0.251	0.158	0.145
Reservoir Length	0.210	0.178	0.030	0.031
Hydraulic Fracture Length	0.180	0.148	0.035	0.034
Natural Matrix Porosity	0.122	0.110	0.072	0.070
Thickness	0.094	0.086	0.135	0.115
Lagmuir Pressure of CO <sub>2</sub>	0.047	0.046	-0.003	-0.004
SRV Fracture Spacing	0.029	0.016	-0.006	-0.004
Natural Fracture Porosity	0.017	0.021	0.014	0.007
SRV Fracture Porosity	0.016	0.021	0.005	0.003
Total Production Time	0.016	-0.022	-0.810*	-0.847*
Lagmuir Volume of CH <sub>4</sub>	0.012	0.002	0.020	0.013
Natural Fracture Spacing	0.011	-0.003	-0.002	-0.001
Lagmuir Pressure of CH <sub>4</sub>	-0.013	-0.008	0.010	0.009
Water Saturation in Matrix	-0.014	-0.015	0.003	-0.001
Lagmuir Volume of CO <sub>2</sub>	-0.015	-0.014	0.051	0.035
Production Constraint	-0.030	-0.015	-0.110	-0.103
Initial Temperature	-0.073	-0.078	0.110	0.097
Natural Matrix Permeability	-0.077	-0.069	-0.029	-0.019

Pearson and Spearman correlation results (\*: input parameters ranked within top five in terms of impact)

# Sustainability in Energy From Oil & Gas to Geothermal Energy



**Harun Yarm**

Turkler Geothermal Energy Exploration and Production Co.

Today, sustainability studies are tried to be carried out in every field. With the increasing energy need, the importance of sustainability in the field of energy is increasing. The aim of this study is to study the use of existing abandoned oil and gas wells to obtain geothermal energy in sustainability perspective. Researches shows that abandoned oil wells can be used for geothermal energy harnessing and there are more than 20 – 30 million abandoned oil wells in the earth (Groom,2020). It is critical to determine the thermal capacity of the abandoned wells and decide the proper usage technique and area of the energy potential. Thermal utilization techniques and their differences from each other are stated in this study. Geothermal energy can be used for electricity generation, heating (greenhouse and housing), thermal and health tourism, industrial mineral extraction, fishing and drying. Turkey has considerable potential in the field of geothermal energy and the use of abandoned oil wells as a geothermal energy source.

## 1. INTRODUCTION

Sustainability is the ability to meet the requirements of the present without compromising the capacity of future generations to satisfy their own needs. It is a combination of environmental protection, social accountability, and economic development.

Sustainability is essential for the health of the planet and the development of a prosperous society. It guarantees that resources are not exhausted more quickly than they can be restored and that the well-being of all individuals is prioritized. It is imperative to focus on sustainability in order to guarantee a better future for us and future generations.

Sustainability is one of the most important issues for the protection of nature today. Considering that our age is the age of consumption, sustainability, which is the opposite of this in many areas, is of great importance. The use of everything that is used for a purpose and has expired (from large-capacity things such as machinery, equipment, to packaging) either as it is or for a different purpose by going through some modification and improvement stages, makes that material no longer a waste. Contributing to the protection of nature and thus to the economy is now more important than ever, thanks to each end-of-life material that has gained a new usage area.

## 2. DIMENSIONS OF SUSTAINABILITY

Sustainability has three dimensions as environmental, social and economic benefits.

Environmental sustainability is the management of natural resources and ecosystems in a manner that meets human requirements. This includes measures

to reduce greenhouse gas emissions, water and energy conservation, and pollution prevention. There are a variety of ways to support environmental sustainability, ranging from promoting renewable energy sources to reducing waste.

Social sustainability is the practice of addressing the social and economic well-being of individuals and communities through the promotion of equity and inclusion, including measures such as access to education, health care, equal opportunity, and human rights. In other words, social sustainability is the promotion of a just and equitable society.

The objective of economic sustainability is to promote economic growth over a sustained period of time while simultaneously contributing to social and environmental well-being. This can be achieved through a variety of activities, such as fostering small business development, investing in environmentally friendly infrastructure, and generating new employment opportunities. Economic sustainability is the promotion of shared prosperity for all individuals while safeguarding the environment.

## 3. ENERGY DEMAND AND SUPPLY

After the industrial revolution, the need for energy and dependence on energy gradually increased. This energy need, which has increased in the process, has been tried to be obtained from many different sources, different energy sources such as hydropower, wind, solar, nuclear, geothermal, biofuels and etc. have been discovered with the developing technology day by day and their use have become widespread. Figure 2 shows increment of the primary energy consumption in the world after especially after industrial revolution.

Direct primary energy consumption decreases when covid-19 pandemic starts in 2020 and increases after the normalization in the World. Researches Show that energy demand dramatically increased in millennium age and pass 160.000 TWh at 2022 that can be seen on Figure 3.

With the millennium age, reducing the carbon footprint has become important and therefore sustainability in energy has gained importance. Research and studies on the importance of sustainability in meeting energy needs were emphasized. As a result, the share of renewable energy sources has started to increase in meeting the increasing energy needs with the millennium age.

## 4. HIDDEN ENERGY POTENTIAL IN OIL FIELDS

Sustainability, which is important in every field of human life, is also of great importance in the field of energy, where the most investment is made. For

example, oil and natural gas wells that have been used for hydrocarbon production and have now completed their service life or that have failed due to some reasons and cannot be used, can be used as a direct or indirect geothermal energy source if it is geologically and technically appropriate. In this way, there is no need to drill another well in the same region for the purpose of geothermal energy source, and an abandoned well can serve humanity again with a new and different purpose after the necessary studies. The energy needed in all areas of life is obtained from a green energy source, thus protecting nature. In addition, a serious economic gain can be obtained from the drilling investment required to reach the geothermal energy source in that region. Considering that half of the installation cost of a geothermal power plant and the cost of drilling for various heating solutions such as greenhouse cultivation and city heating, the cost of drilling varies between 50% and 70% of the total investment budget, it can be better understood how important drilling costs are.

James P. Williams at al estimate abandoned well amount for U.S. as 4 million and for Canada as 370.000 at 2020. 2 Abandoned well amount in U.S. can be estimated due to public data and regulations but it is not possible yet in next largest oil and gas producers, Russia, Saudi Arabia and China. According to the Cheng at al. (2014) there are 20 – 30 million abandoned oil wells in the World. 3

## 5. GEOTHERMAL POWER PRODUCTION FROM ABANDONED WELLS

There are two alternatives to produce geothermal energy with oil wells. One of them to convert abandoned oil wells for geothermal energy harnessing and the other one is producing oil and heat at the same time from the oil wells. Depth of the oil wells and the geothermal gradient makes it is possible to produce heat from the produced water with oil. Although the geothermal gradient varies from place to place, it averages 25–30 oC/km. In addition to this brine mining which means the extraction of any desirable compounds or elements, one another way of using the abandoned wells. Obtaining lithium from brine is a technology on which many researches and investments have been carried out recently.

There are different types of well abandonment in onshore and offshore wells. Possibility of re-usage of abandoned wells are related to abandonment strategies of them. Most suitable technique would be decided according to the thermal potential of the well and its structure. Mahmoud Khalifeh and Arild Saasen (2020) simplified schematics of well barrier in oil wells in Figure 6. 5

Geothermal Energy harnessing done with Enhanced Geothermal Systems (EGS) by open loop or closed loop configurations. This configurations are simplified in Figure 7.

Open loop configuration gathers higher enthalpy than closed loop configuration due to direct contact between working fluid with hot rock and larger heat transfer area. This concept works only with minimum two wells

which are very close to each other. In addition that, providing flows paths between injection and extraction with fracking and etc. is very crucial. Alimonti C. et al. (2016) says “In addition, to provide flow paths from the injection wells to the extraction wells, additional fracking maybe needed. Aside for imposing additional costs, fracking is a delicate process that needs to be conducted carefully. Incorrect fracking process may lead to the loss of the injected fluid and, in the case of toxic injected fluid, may result in a severe environmental pollution.” 6

The closed loop configuration gathers less enthalpy compared to the open loop system due to o direct contact between working fluid with hot rock and less heat transfer area. As it is stated by Kurnia J.C. et al. (2021) closed loop configuration does not require any additional drilling or fracking since the existing well serves as a wellbore or bore-hole heat exchanger. There are two types heat exchangers commonly use as closed-loop system. Those are double pipe heat exchangers and U-type exchangers as shown in Figure 8. 8a

## 6. GEOTHERMAL ENERGY CAPACITY DETERMINATION AND STUDIES

Oil and natural gas fields have a certain life span, although EOR techniques are applied to continue production, the field is abandoned for production after the existing reserve is produced and consumed or if production is no longer feasible. However, when geothermal energy reservoir management is done correctly, it is a renewable and sustainable energy source. With the right production and injection techniques, the right reservoir management and feeding strategy, it has an inexhaustible reserve.

Electricity generation, heating (greenhouse and housing), thermal and health tourism, industrial mineral extraction, fishing and drying are main areas that geothermal energy can be used. When the thermal energy capacities of abandoned wells are determined, it can be decided for what purpose these wells can be used. Since many data such as geological formation, temperature and flow information are known, the thermal energy capacities of the wells can be easily calculated. Since all these studies have already been carried out, there will be no additional costs for determining the thermal energy capacity. In the light of the data obtained, ones can decide the right usage area of the geothermal energy potential by using the Lindal categorization stated in Figure 9. 8

Many studies have been carried out in the world for the acquisition of geothermal energy from abandoned wells. According to the announcement of The U.S. Department of Energy (DOE) there are 4 investments to use abandoned wells for geothermal energy in Texas, Colorado and Oklahoma. 9 It is known that many projects are carried out in Slovenia, Croatia and France for utilization of abandoned wells. 10 - 11

## 7. POTENTIAL OF TÜRKİYE

Turkey has high thermal energy capacity that can be used from green house heating and tourism to electrical energy production. Although proven high enthalpy sources widely in western side of the Türkiye, on the contrary hydrocarbon reservoirs and consequently abandoned oil wells are mainly in southeastern part. According to the studies of The Institute of Mineral Research and Exploration (MTA) Geothermal resources and applications map of Türkiye (Fig. 10) has been published by The Institute of Mineral Research and Exploration (MTA) after long technical work and applications. 12

Baba et al. (2019) point out that there are several oil wells that abandoned due to several reason and the temperature of those wells varies from 41 oC to 137 oC. The map that contains the abandoned wells and surface temperature distribution of the southeastern part of Türkiye is stated in Baba et al.'s (2019) study named as "Use of abandoned oil wells in geothermal systems in Turkey". 13

Baba et al. published one more map that potential geothermal applications in the southeastern of Türkiye is shown. 14a

## 8. CONCLUSION

Sustainability is one of the most important issues for the protection of nature and crucial that urgent attention and action should be taken by the every part of society. Environmental, social and economic benefits are three main dimensions of sustainability. The requirement for energy increases with developments in technology. The modern world needs more energy than ever before, and this need will continue to increase. For this reason, the value of sustainability studies in the field of energy is increasing day by day and becomes invaluable. Geothermal energy is green energy. In other words, it is renewable and more sustainable than fossil fuels. Moreover, there are wide range of using are of geothermal energy sources in the earth. The thermal energy capacity of the world is too high to be ignored. At that point, abandoned oil wells might have the potential of thermal energy that is hidden for certain time period. Thermal energy harnessing can be done by several techniques from abandoned oil wells if the well is technically suitable and has the thermal energy potential. In addition, a serious economic gain can be obtained from the drilling investment required to reach the geothermal energy source by using already existed abandoned oil wells. Researches shows that there are plenty of abandoned wells around the world and those wells could be used again to serve for thermal energy purpose for society. There are already several applications on going in U.S., France, Slovenia and etc. for utilization of abandoned wells for thermal energy harnessing. There are several abandoned oil wells in Türkiye also than can be considered for that purpose. More academic researches and technic studies should be carried out to discover the hidden thermal power in abandoned oil wells and to be used for the benefit of society.

## REFERENCES

- Groom N (2020-06-17). "Special Report: Millions of abandoned oil wells are leaking methane, a climate menace". Reuters.
- <https://ourworldindata.org/energy-production-consumption#primary-energy-consumption>
- James P. Williams, Amara Regehr, and Mary Kang (2021) Methane Emissions from Abandoned Oil and Gas Wells in Canada and the United States. *Environmental Science & Technology* 2021 55 (1), 563-570 DOI: 10.1021/acs.est.0c04265
- Cheng W, Li T, Nian Y, Xie K (2014b) An analysis of insulation of abandoned oil wells reused for geothermal power generation. *Energy Procedia* 61:607–610. <https://doi.org/10.1016/j.egypro.2014.11.1181>
- Jade Boutot, Adam S. Peltz, Renee McVay, and Mary Kang (2022) Documented Orphaned Oil and Gas Wells Across the United States. *Environmental Science & Technology* 2022 56 (20), 14228-14236 DOI: 10.1021/acs.est.2c03268 <https://pubs.acs.org/doi/10.1021/acs.est.0c04265>
- Khalifeh M, Saasen A. Introduction to Permanent Plug and Abandonment of Wells. Vol 12. Gewerbestrasse 11, 6330 Cham, Switzerland: Springer Nature Switzerland AG; 2020. <https://doi.org/10.1007/978-3-030-39970-2>
- Alimonti C, Berardi D, Bocchetti D, Soldo E. Coupling of energy conversion systems and wellbore heat exchanger in a depleted oil well. *Geotherm Energy*. 2016;4(1):11. <https://doi.org/10.1186/s40517-016-0053-9>
- 8a. 8b. Kurnia, J.C. et al. (2021). Geothermal energy extraction using abandoned oil and gas wells: Techno-economic and policy review. *Int J Energy Res*. 2021;1–33
- <https://www.energy.gov/sites/default/files/2019/06/f63/GeoVision-full-report-opt.pdf>
- <https://www.energy.gov/eere/articles/doe-awards-84-million-accessing-geothermal-potential-abandoned-oil-and-gas-wells>
- <https://www.thinkgeoenergy.com/plans-in-motion-to-utilise-geothermal-from-abandoned-oil-wells-in-slovenia/>
- <https://www.thinkgeoenergy.com/how-could-geothermal-energy-be-derived-from-oil-wells/>
- <https://www.mta.gov.tr/en/arastirmalar/jeotermal-enerji-arastirmalari>
- 14a. Baba A, Saroglu F, Akkus I et al (2019) Geological and hydro geochemical properties of geothermal systems in the southeastern region of Turkey. *Geothermics* 78:255–271. <https://doi.org/10.1016/j.geothermics.2018.12.010>

Keywords: Abandoned oil well, Sustainability

Fig. 1 Three Dimensions of Sustainability

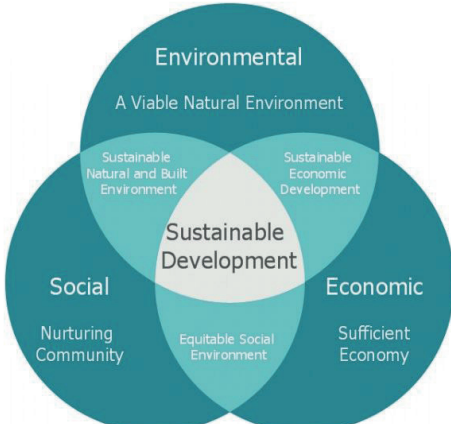
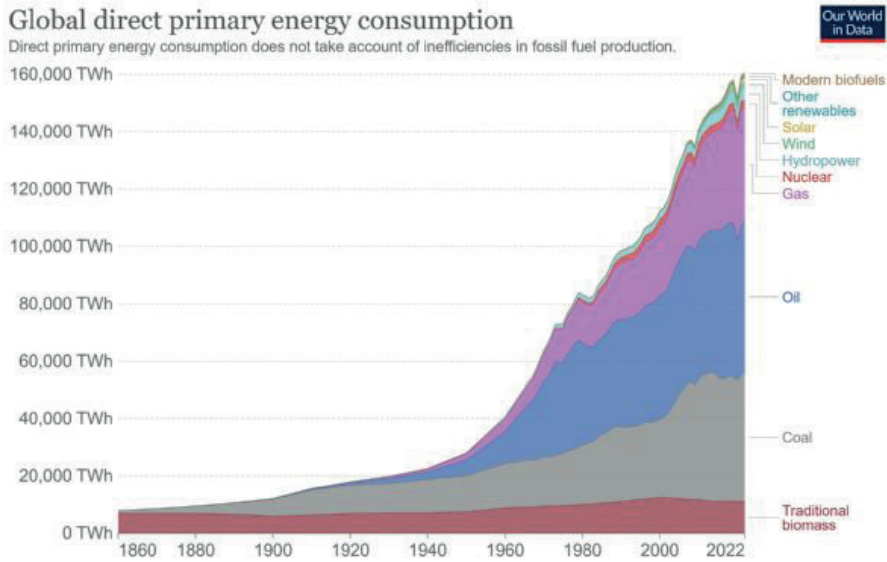


Fig. 2 Global Direct PE Consumption 1



Source: Energy Institute Statistical Review of World Energy (2023); Vaclav Smil (2017)  
 OurWorldInData.org/energy • CC BY



Fig. 3 Global Direct PE Consumption 2 1

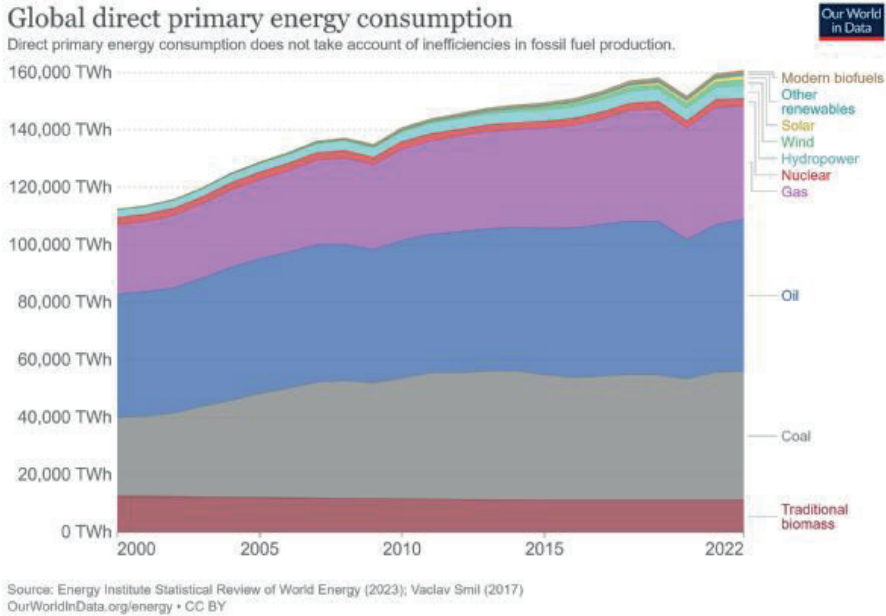


Fig. 4 Global Direct PE Consumption Sources 1

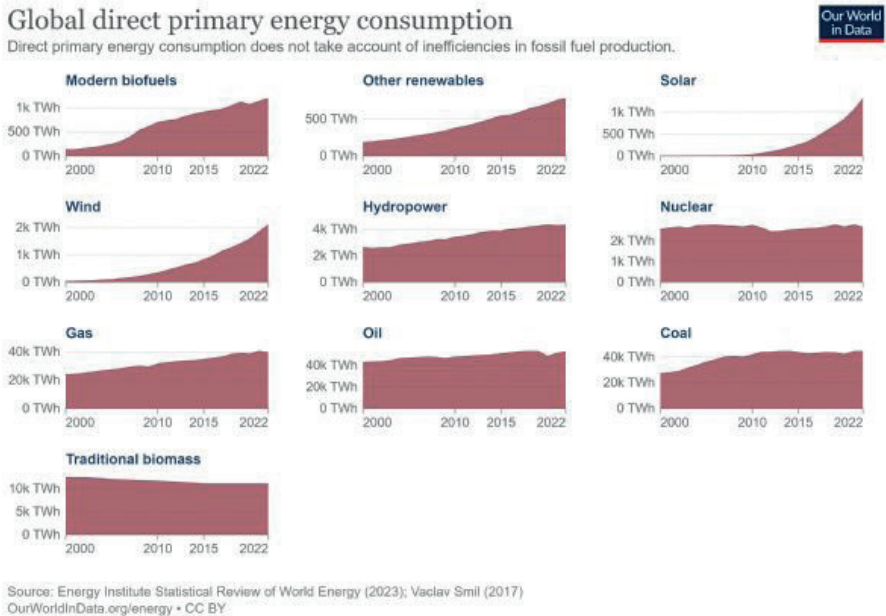


Fig. 5 Distribution of documented orphaned oil and gas wells across the U.S. based on state databases as of April 2022 (left) and September 2021 (right).<sup>4</sup>

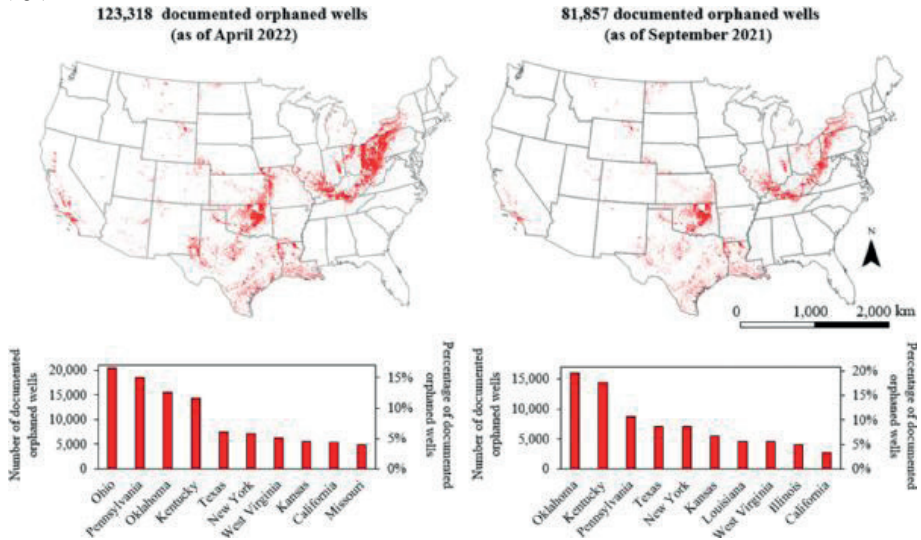


Fig. 6 Simplified well schematics of well barrier 5

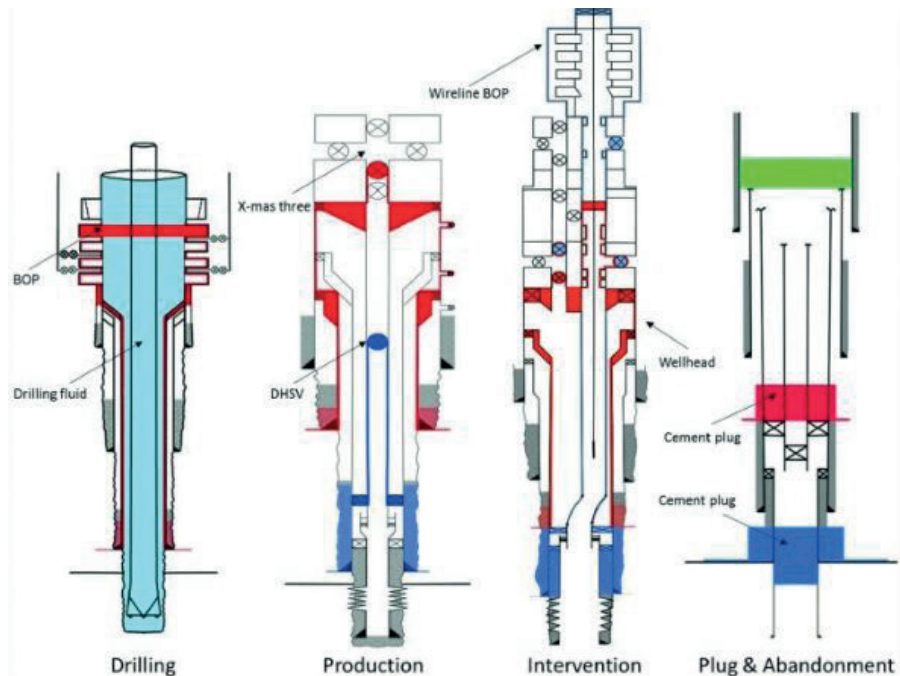


Fig. 7 Simplified schematics of (A) open loop and (B) closed loop geothermal energy extraction

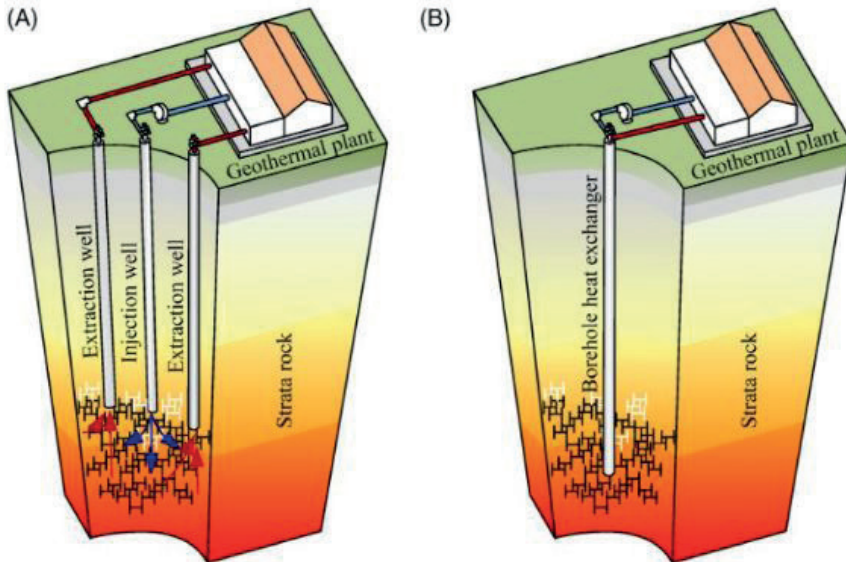


Fig. 8 Simplified schematics of (A) double pipe and (B) U-tube heat exchanger

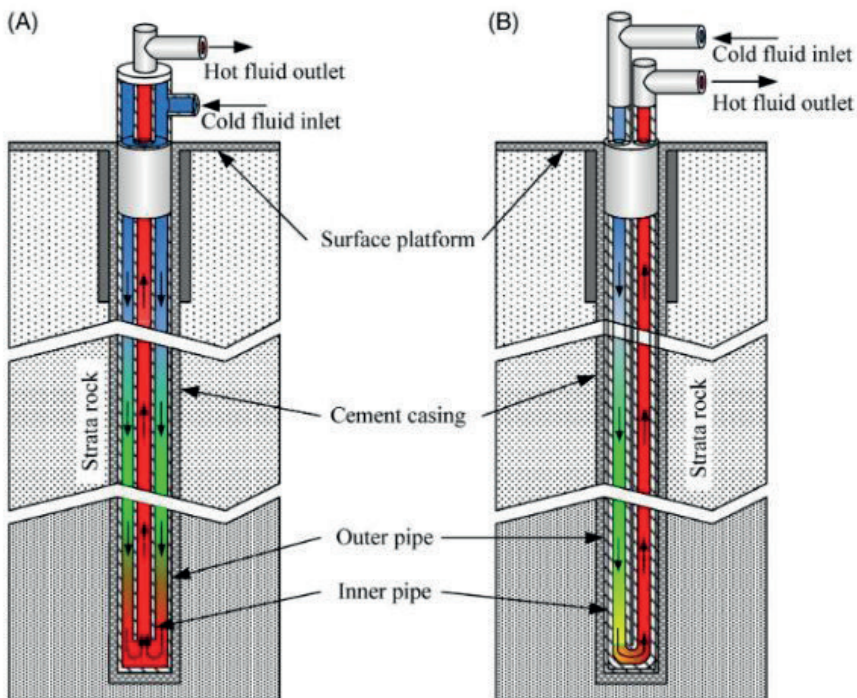


Fig. 9 Modified Lindal Diagram 8

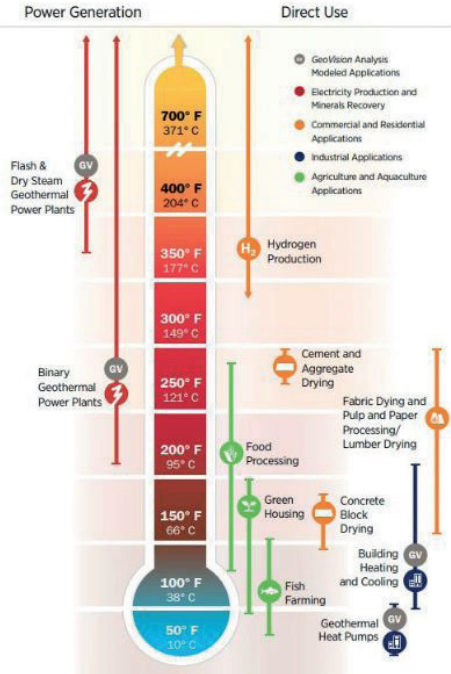


Fig.10 Geothermal resources and applications map of Turkey (MTA) 12

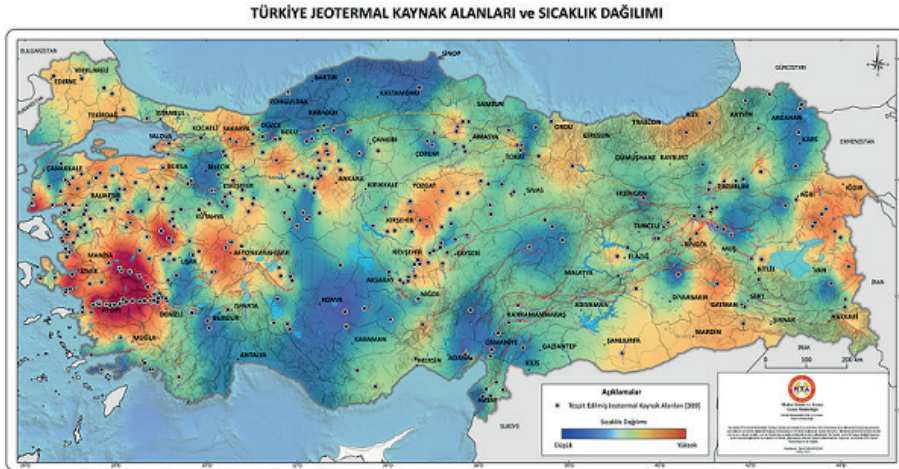


Fig.11 Surface temperature distribution of geothermal fluid in the southeastern region 13

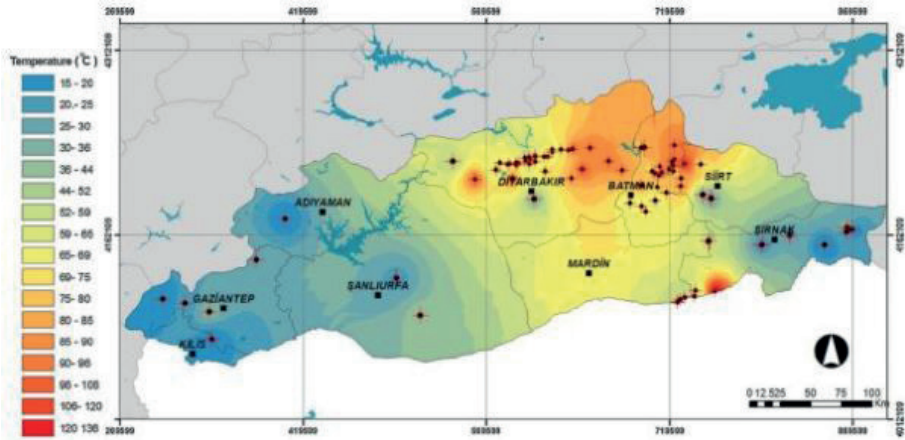
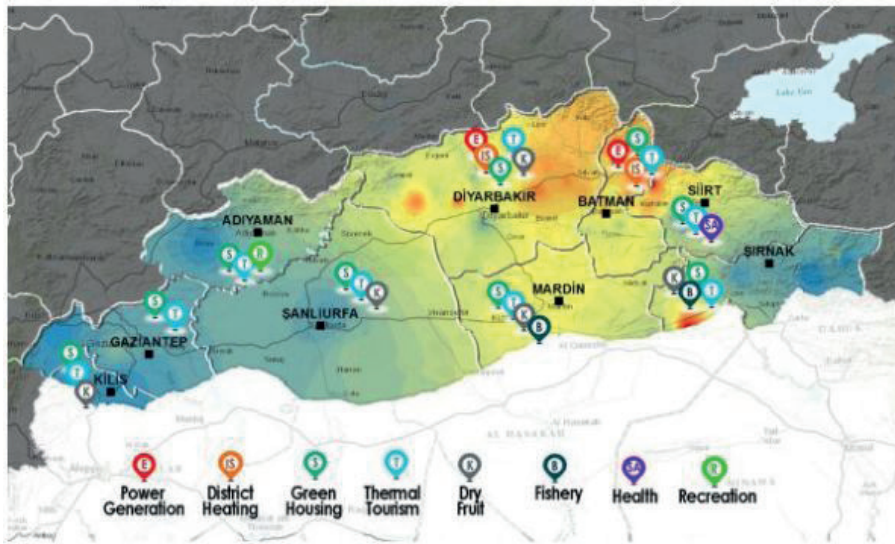


Fig.12 Potential geothermal applications in the southeastern region 13a



# Modüler Çelik Yapılar, Petrol ve Gaz Sahalarında İdeal Çözüm

## Mert Özdemir

Dorçe Prefabrik Yapı ve İnşaat Sanayii Ticaret A.Ş.



### ABSTRACT

The using of light gauge steel in oil fields offers a range of advantages and provides solutions that match the demands of the energy industry. With its high strength, durability, easy installation, flexible design and modification options, portability and recycling capability, corrosion resistance makes light steel the building material of choice in oil fields. These benefits provide significant contributions to the industry by enabling the construction of efficient and reliable oil production facilities. It also supports the future of the energy sector by taking an environmentally friendly and sustainable approach.

Modüler çelik yapılar petrol ve gaz sahaları için önemli avantajlar sunuyor. Hava sıcaklığının sıfırın altında ve üstünde 50 dereceyi bulduğu bölgelerde bile projelerin hızlı ve zamanında tamamlanmasını sağlıyor.

Petrol ve gaz sektöründe yer alan binalar söz konusu olduğunda alınması gereken birçok önlem bulunuyor. Üst düzey güvenlik önlemleri, ağır mevzuat gereksinimleri, zor çalışma koşulları gibi sebeplerle bu proje sahaları çalışması en güç ve tehlikeli sanayi kollarından biri olarak kabul ediliyor.

Modüler çelik yapıları, petrol ve gaz endüstrisinin ihtiyacı olan binaların mukavemetli ve hızlı yapılmasını sağlıyor. Endüstrinin beklentilerini karşılayan bu yapılar, BIM kullanılarak tasarlanırken tamamen özelleştirilebiliyor. İş verenler açısından bu durum, proje planlama, geliştirme ve inşaat aşamalarında zamandan ve maliyetten tasarruf yapmasını sağlıyor.

Suudi Arabistan'daki rafineri ve terminal projesi 7 ay gibi kısa bir sürede tamamlandı

Suudi Arabistan'ın Jazan bölgesindeki Rafineri ve Terminal projesi kapsamında yer alan, 8.500 kişilik kampın mühendisliği ve üst yapı işleri gerçekleştirildi. Prefabrik Hafif Çelik Yapı sisteminin kullanıldığı bu proje; 7 ay gibi kısa bir sürede, Dünya'nın en büyük petrol firmalarından olan Saudi Aramco'nun kapsamlı ve zor standartlarında tamamlandı. (1)

### Rusya'da -50 derecede gaz işleme tesisi inşa edildi

Rusya'nın Amur Bölgesinde, Amur Gaz İşleme Tesisi çalışanları için 18 bin işçi konaklama kampı "Prefabrik Modüler Hafif Çelik Bina" sistemiyle tamamlandı. Projenin tamamlanma aşamalarında, hava sıcaklığı sıfırın altında 50 dereceleri bulmuştur. (2)

### Ras Laffan Sanayi Bölgesi İşçi Konaklama Kampı

Ras Laffan, Katar'ın başkenti Doha'nın 50 km kuzeyinde yer alan bir endüstri bölgesi olarak Katar'ın sivilleştirilmiş doğal gaz ve sıvı gaz üretiminin

merkezi. LNG sektöründe dünyanın en büyük üretim üssü olan Ras Laffan sanayi şehrinin 3.550 kişilik işçi yaşam destek kamplarını mühendislik, üstyapı dahil olacak şekilde tamamlamıştır. (3)

### Hafif çelik modüler kamplar, çevrecidir

Petrol ve gaz endüstrisinde sahaların endüstriyel tesis inşaatı ve tesislerde çalışan işçiler için modüler işçi kampları hafif çelik yapı sistemi kullanılarak yapılmaktadır. Hafif çelik prefabrik modüler kamplar, yüksek karbon salımlı petrol ve gaz sahalarında, yapının geri dönüştürülebilir hammadde içeriği ve inşaat sürecinin sahada minimize edilmiş sürelerde tamamlanması gibi özellikleri sayesinde düşük karbon ayak izine sahiptir ve bu sahalarda önemli bir avantaj sağlamaktadır. (4)

Modüler Yapıların petrol ve gaz sektörü için sunduğu avantajlar

### Modüler çelik yapılarıyla petrol ve gaz sektörüne yönelik sunduğu bazı avantajlar şöyledir.

- Yangın güvenliği: Çelik yapılar diğer yapı türleriyle kıyaslandığında yangına ve patlamaya karşı önemli avantajlara sahiptir.
- Kolaylıkla genişletilebilir yapılar: Çelik binalar, gerektiğinde kolaylıkla genişlemeye imkân sağlayacak şekilde tasarlanmıştır. İhtiyaç duyulduğunda kapasite arzu edildiği kadar artırılabilir.
- Yüksek mukavemet: Modüler çelik binalar, petrol ve gaz endüstrisinin ihtiyaç duyduğu güç ve dayanıklılığı sağlarken en zorlu coğrafi koşullarda bile kalitesinden ödün vermez.
- Uygun havalandırma koşulları: modüler çelik yapılarındaki havalandırma sistemi, gaz ve petrol endüstrilerindeki katı zorunlulukları karşılayacak şekilde tasarlanmaktadır. (4)

### ENERJİ VERİMLİ ÜRETİM

Volümetrik (hacimsel) modüler çözümleri, inşaat sürelerini kalite ve güvenlikten (emniyetten) ödün vermeden kısaltmaktadır. Geleneksel inşaat yöntemlerine kıyasla enerji veriminin daha yüksek olmasının önemli sebeplerinden biri imalat sürecinin fabrika ortamında kontrol altında tutulmasıdır. Şantiyenin fabrikaya taşınmasıyla sahada ekipman, makine ve iş gücüne duyulan ihtiyaç önemli ölçüde azalmaktadır.

## DAHA AZ ATIK

Transparency Market Research verilerine göre, küresel inşaat atıklarının 2025 yılına kadar yıllık 2,2 milyar tona ulaşması bekleniyor. Volümetrik modüler inşaat projelerinde tasarım ve imalat süreçleri kontrollü bir fabrika ortamında yönetilip gerçekleştiği için inşaat atıkları minimize edilebiliyor. Geri dönüştürülebilir malzeme tercihleriyle de daha az atık politikası benimsenmiş olunuyor.

## MODERN İNŞAAT YÖNTEMLERİ (MODERN METHODS OF CONSTRUCTION – MMC)

Volümetrik (hacimsel) modüler çelik yapılarının üretim süreçlerinin imalat ve Montaj için Tasarım (Design for Manufacturing & Assembly- DfMA) ve Yapı Bilgi Modellemesi (Building Information Modeling – BIM) gibi modern inşaat yöntemleri kullanılmasıyla malzeme gereksinimi net olarak belirlenirken harcanan zaman ve hata riski en aza indiriliyor.

- Volümetrik (hacimsel) modüler yapı çözümleriyle, Yeşil Bina ve Sürdürülebilirlik kapsamında BREAM, LEED ve DGNB gibi üst düzey sertifikasyon ve standartların entegrasyonunu çok daha etkili ve verimli gerçekleştirebiliyor. -50 derecelere varan sert hava koşullarının hüküm sürdüğü Kazakistan'ın maden sahalarında konaklama şehirlerinden, +60 derece hava koşullarına sahip Katar'da yer alan ve 4,000 kişi kapasiteli bölgenin en büyük pandemi kompleksini tamamlamış bir şirkettir. Aynı şekilde İsviçre'deki modüler anaokullarından, Doğu Anadolu'nun çeşitli bölgelerinde yer alan ve yüz binlerce mültecinin konakladığı entegre mülteci tesislerine kadar birçok farklı projeye ve sektöre hizmet etmektedir. (4)

## NEDEN YAPI BİLGİ MODELLEMESİ KULLANILIYOR?

Yapı Bilgi Modellemesi (BIM), mimar ve mühendislere binaları ve altyapıyı daha verimli bir şekilde planlama, tasarlama, inşa etme ve yönetme imkânı sağlıyor. Oluşturulan sanal model, ön tasarımdan inşaat dokümantasyonuna, tedarik ve imalattan gerçek inşaat sürecine ve hatta inşaat sonrası bina yönetimine kadar olan süreci destekliyor. Bu sayede tasarımdan yıkımına kadar tüm yaşam döngüsü de ortaya çıkıyor.

## PETROL SAHALARI VE ÇELİK YAPILAR (ÖZET)

Petrol sahaları, enerji endüstrisinin önemli bir parçasını oluşturur ve dünya genelinde enerji üretimine önemli katkılar sağlar. Bu sahalarda yapılan tesislerin ve ekipmanların dayanıklılığı ve güvenilirliği, verimli ve sürdürülebilir bir üretim süreci için hayati öneme sahiptir. Hafif çelik, son yıllarda petrol sahalarında kullanımı giderek artan ve birçok avantajı olan bir yapı malzemesidir.

## YÜKSEK MUKAVEMET VE DAYANIKLILIK

Hafif çelik, yoğun mukavemet özellikleri sayesinde ağır iş yüklerini taşıma kabiliyetine sahiptir. Petrol sahalarında kullanılan yapılar ve ekipmanlar genellikle ağır yüklerle karşı karşıya kalır. Hafif çelik, yüksek dayanıklılığı sayesinde bu yüklerle başa çıkabilir ve uzun ömürlü yapılar oluşturur. Ayrıca, çelik yapıların depreme karşı sağlam direnç gösterme özelliği, petrol sahalarındaki güvenlik açısından da kritik bir avantajdır.

## KOLAY VE HIZLI KURULUM

Hafif çelik, diğer yapı malzemelerine göre daha hızlı ve kolay bir şekilde kurulabilir. Önceden üretilmiş çelik elemanlar, sahada montajı yapılacak yapıya göre ölçülendirilerek hazırlanır ve sahaya getirilir. Bu, inşaat sürecinin hızlanmasına ve zamanında projelerin tamamlanmasına katkı sağlar. Petrol sahalarında, hızlı ve etkili bir şekilde üretim yapmak, maliyetleri düşürmeye ve iş sürekliliğini sağlamaya yardımcı olur.

## ESNEK TASARIM VE MODİFİKASYON

Hafif çelik, esnek bir yapı malzemesidir ve çeşitli tasarım seçenekleri sunar. Petrol sahalarındaki tesislerin bazen mevcut alanlara uygun olarak tasarlanması gerekir. Hafif çelik, farklı tipteki yapıları kolayca inşa etmeye olanak tanır ve mevcut tesislerde yapılacak modifikasyonları destekler. Bu, saha koşullarına uygun özelleştirilmiş yapılar oluşturmak için büyük bir avantajdır.

## TAŞINABİLİRLİK VE GERİ DÖNÜŞÜM

Hafif çelik, beton veya diğer yapı malzemelerine kıyasla daha hafif bir yapıya sahiptir. Bu, parçaların taşınabilirliğini ve sahada kolay montajını kolaylaştırır. Aynı zamanda, petrol sahaları gibi geçici projelerde, yapıların sökülüp başka yerlerde kullanılabilir olması önemlidir. Hafif çeliğin geri dönüşüm kabiliyeti sayesinde, eski yapılar geri dönüştürülerek çevre dostu bir yaklaşım benimsenmiş olur.

## KOROZYON DİRENCİ

Petrol sahaları, zorlu çevresel koşullara maruz kalır ve korozyon riski yüksektir. Hafif çelik, dayanıklı bir kaplama veya paslanmaz çelik kullanılarak korozyona karşı korunabilir. Bu da yapıların ömrünü uzatır ve bakım maliyetlerini azaltır.

## SONUÇ

Petrol sahalarında hafif çeliğin kullanımı, bir dizi avantaj sunar ve enerji endüstrisinin taleplerine uygun çözümler sunar. Yüksek mukavemeti, dayanıklılığı, kolay kurulumu, esnek tasarım ve modifikasyon seçenekleri, taşınabilirlik ve geri dönüşüm kabiliyeti ile korozyon direnci, hafif çeliği petrol sahalarında tercih edilen yapı malzemesi yapar. Bu avantajlar, verimli ve güvenilir petrol üretim tesislerinin inşasını sağlayarak

endüstriye önemli katkılar sunar. Aynı zamanda, çevre dostu ve sürdürülebilir bir yaklaşım benimseyerek enerji sektörünün geleceğini destekler.

#### KAYNAKÇA

1. A.Ş., Dorçe Prefabrik Yapı ve İnşaat Sanayi Ticaret. Dorçe Prefabrik Yapı ve İnşaat Sanayi Ticaret A.Ş. Dorçe Prefabrik Yapı ve İnşaat Sanayi Ticaret A.Ş. [Çevrimiçi] <https://www.dorce.com.tr/projeler/cizan-rafineri-ve-terminal-projesi-8500-kisilik-isci-konaklama-kampi/>.
2. Dorçe Prefabrik Yapı ve İnşaat Sanayi Ticaret A.Ş. Dorçe Prefabrik Yapı ve İnşaat Sanayi Ticaret A.Ş. [Çevrimiçi] <https://www.dorce.com.tr/projeler/amurgaz-isletme-tesisi-17250-kisilik-yerlesim-kampi/>.
3. Dorçe Prefabrik Yapı ve İnşaat Sanayi Ticaret A.Ş. Dorçe Prefabrik Yapı ve İnşaat Sanayi Ticaret A.Ş. [Çevrimiçi] <https://www.dorce.com.tr/projeler/ras-laffan-sanayi-sehri-3-550-kisilik-kamp-insaati/>.
4. Dorçe Prefabrik Yapı ve İnşaat Sanayi Ticaret A.Ş. Dorçe Prefabrik Yapı ve İnşaat Sanayi Ticaret A.Ş. [Çevrimiçi] [www.dorce.com.tr](http://www.dorce.com.tr).

Anahtar Kelimeler: Modüler çelik yapılar, Modular building

*Aktogay Bakır Madeni Genişletme Projesi – İşçi Konaklama Kampı*



*örnek*

*Amur Gaz İşletme Tesisi 17.250 Kişilik Yerleşim Kampı*



*örnek*

*Ras Laffan Sanayi Bölgesi İşçi Konaklama Kampı*



*örnek*

*Suudi Arabistan/Cizan Rafineri ve Terminal Projesi – 8.500 Kişilik İşçi Konaklama Kampı*



*örnek*





## **Petrol, Dođal Gaz, LPG ve LNG Pazarı**

*Oil, Gas, LPG and LNG Market*

---



# LPG'nin Günümüzde Konvansiyonel ve Alternatif Kullanım Alanları



**Can Toydemir<sup>1</sup>, Lpg Dairesi<sup>2</sup>, Yasin Ersöz<sup>3</sup>**

<sup>1</sup>Milangaz (Likitgaz Dağıtım ve Endüstri A.Ş.) İstanbul

<sup>2</sup>EPDK

<sup>3</sup>Tüpraş

LPG, known as Liquid Petroleum Gas, is mostly obtained as a by-product from natural gas sources and plays an important role in world energy trade due to its ability to be liquefied and transported without the need for pipelines.

Although the use of cylinder, bulk gas and autogas in the world constitutes an important part of LPG consumption, LPG is an important raw material alternative to naphtha, especially in PHD plants in the petrochemical sector.

While the use of conventional LPG cylinders continues to increase, especially in underdeveloped and developing countries, its importance has started to decrease over the years due to the widespread natural gas network and access in developed countries and our country. However, earthquake, flood, etc. The fact that tubed LPG is an easily transportable and accessible energy source in disasters has repeatedly proven that LPG is not only a good day but also a bad day friendly.

Bulk gas, on the other hand, is a serious alternative and primary fuel to fuels such as coal and fuel oil in industrial facilities and businesses where natural gas does not reach, both with its ease of operation and with its environmentalist feature.

Especially because of its low emission value compared to diesel and gasoline, gasoline substitute product is used as an alternative vehicle fuel to diesel in many countries of the world, including our country, and it assumes the position of an important transition fuel for the automotive sector, which is on its way to advanced technology vehicles.

Especially in industrial facilities, Synthetic LPG is an ideal fuel for backing up natural gas. Thanks to air LPG mixers, natural gas can be used safely as an alternative, with a quick transition from natural gas without making any changes to the burning devices.

Ülkemizde 2005 yılında yayımlanan 5307 sayılı LPG kanunu ile düzenlenmiştir. Bilindiği üzere, 5307 sayılı Sıvılaştırılmış Petrol Gazları (LPG) Piyasası Kanunu yurt içi ve yurt dışı kaynaklardan temin edilen sıvılaştırılmış petrol gazlarının (LPG) güvenli ve ekonomik olarak rekabet ortamı içerisinde kullanıcılara sunumuna ilişkin piyasa faaliyetlerinin şeffaflık, eşitlikçi ve istikrarlı biçimde sürdürülmesi için gerekli düzenleme, yönlendirme, gözetim ve denetim faaliyetlerini yerine getirmek üzere EPDK (Enerji Piyasası Düzenleme Kurulu) görevlendirilmiştir.

Rafinerici lisansı sahiplerinin, 2022 yılı toplam LPG üretimi geçen yıla göre %8,53 artarak 1.100.359 ton olmuştur.

Rafinerici, dağıtıcı ve işleme lisansı sahiplerince 2022 yılında yapılan LPG ithalatı, geçen yıla göre %3,26 artarak 3.205.122 ton olmuştur.

2022 yılında 16 farklı ülkeden/bölgeden LPG ithalatı yapılmış olup en çok ithalat yapılan ilk 5 ülke Cezayir, ABD, Rusya Federasyonu, Kazakistan ve Norveç olmuştur.

Rafinerici ve dağıtıcı lisansı sahiplerince 2022 yılında yapılan LPG ihracatı, geçen yıla göre %88,76 artarak 409.898 ton olmuştur.

2022 yılında 16 farklı ülkeye/bölgeye LPG ihracatı yapılmış olup en çok ihracat yapılan ilk 5 ülke Lübnan, Tunus, İsviçre, Yunanistan ve K.K.T.C. olmuştur.

Dağıtıcı lisansı sahiplerince 2022 yılında 611.518 ton tüplü LPG, 163.736 ton dökme LPG, 3.098.039 ton otogaz olmak üzere toplam 3.873.293 ton LPG satışı yapılmıştır.

2022 yılı satış rakamları bir önceki yılın satış rakamları ile karşılaştırıldığında, tüplü LPG satışı %12,55 azalmış, dökme LPG satışı %68,16 artmış ve otogaz satışı %0,62 azalmış olup toplam LPG satışı %1,04 azalmıştır.

2022 yılında tüplü LPG %15,79, dökme LPG %4,23 ve otogaz %79,98 pazar payına sahip olmuştur.

Dağıtıcı lisansı sahiplerince 2022 yılında 47.733 ton Standardize (kokusuz) LPG satışı yapılmıştır. (2)

LPG Piyasası Kanununda Teknik düzenleme, "LPG'nin niteliği ile LPG faaliyetlerinde kullanılan mekân, aksam ve hareketlerin tanımlanmasında TSE standartları ve diğer mevzuatla getirilen düzenlemeleri," şeklinde tanımlanmıştır.

LPG Piyasasında Uygulanacak Teknik Düzenlemeler Hakkında Yönetmelikte " Piyasaya arz olunacak LPG'nin, sırasıyla TS, EN veya ISO standartlarına uygun olması zorunludur." hükmü yer almaktadır.

TSE tarafından yayımlanan ve piyasaya arz edilen LPG'nin özelliklerini belirleyen yürürlükte iki adet standart bulunmaktadır. Bunlar;

• Otogaz LPG için: TS EN 589 + A1 Otomotiv Yakıtları - LPG - Özellikler ve Deneysel Yöntemleri

• Diğer LPG türleri için (Karışım LPG, Ticari Propan, Ticari Bütan): TS 2178 Petrol Ürünleri - Yakıtlar (Sınıf F) - Sıvılaştırılmış Petrol Gazları (LPG)

Bu standartlarda belirtilen bazı önemli kriterlerle değinmekte fayda olacaktır.

Motor oktan sayısı bir yakıt sıkıştırılabilirliğini, dolayısıyla enerjisinin içten yanmalı motorlardaki verimini temsil etmektedir. Yüksek oktan sayısı, yüksek verim ve daha ekonomik enerji kullanımı anlamına gelmektedir.

Toplam dien içeriği çift bağ içeren hidrokarbonların içeriğini göstermektedir. Yüksek dien içeriği kalıntı problemlerine sebep olabilmekte ve aynı zamanda oktani düşürmektedir.

1,3 bütadien kanserojen olduğu için AB etiketleme regülasyon kurallarına göre belirtilmesi gerekmektedir. FCC ve coker ünitelerinden proses doğası gereği oluşmaktadır. 1,3 bütadien giderimi Selective Hydrogeneation Unit (SHU) ünitesi ile ayarlanmaktadır.

Doymamış hidrokarbonların azaltılması rafineri verimliliğini düşüren ve rafineri operasyonları gereği çok fazla değiştirilemeyen bir parametredir.

Yakıt içindeki kükürt yanma sonrası hidrojen sülfür ve sülfür oksit gibi korozif etkisi olan bileşenlere dönüşmektedir. Ham petrol içerisinde bulunan kükürt ve merkaptan, damıtma işlemlerinden sonra LPG'nin içinde bir miktar kalır. Ürün olarak satılmadan önce kirli LPG'nin, LPG merox ünitelerinde kükürtten temizlenmesi gereklidir. LPG merox ünitelerinin amacı üretilen LPG'nin H<sub>2</sub>S'ten arındırılması, merkaptanların tatlılaştırılması ve ekstraksiyonla giderilmesidir. İlk olarak LPG içerisinde ki H<sub>2</sub>S tehlikeli ve zararlı olduğundan merkaptan ekstraksiyonundan önce ortamdaki uzaklaştırılır. Merkaptan ekstraksiyonu bir petrol fraksiyonunun kostik çözeltisi kullanılarak disülfürülenmeyip merkaptan giderilmesidir.

Bakır şerit korozyon testi, taşıma, depolamadaki bakır veya bakır alaşımıyla bağlantılı parçalarının ve yardımcı ekipmanların hidrojen sülfür varlığında zarar görmesinin önüne geçilmesi için yapılır. Bu limit ayrıca hidrojen sülfürün sağlık ve güvenliği tehdit edecek limitlerde mevcut olmasının önüne geçmektedir. Yakıtların korozif etkisinin tespitini yapar.

LPG içerisinde korozif bir kirlilik olmaması için prestele filtreler vardır.

En önemli kriterlerden biri buharlaşma kalıntısı olup, LPG içerisinde kalıntı olması, yakıt filtrelerini, basınç regülatörlerini, yakıt karıştırıcılarını ve kontrol selenoidlerini aşındıracak ya da tıkayacak tortular oluşmasına sebep olabilir.

Su içeriğine sahip bir yakıt, yakıt tankında demir oksit partiküllerinin oluşmasına sebep olabilmektedir. Su ihtiva etmesi durumunda LPG'nin genleşmesi sırasında su yoğunlaşır ve depolama tankında korozyona sebep olabilir. Ayrıca su ve nem filtrelerde tıkanmaya da sebep olabilmektedir. LPG Merox üniteleri ile ayarlanır. (3)

LPG havadan daha ağır olduğu için büyük miktarlarda birikme ve hava ile yer değiştirme eğilimindedir. Büyük miktarlarda birikmesi durumunda oksijen eksikliğine sebep olarak solunumu etkileyebilir. LPG renksiz ve kokusuz olduğu için bu tür birikimler fark edilmez. Bu sebeple bir sızıntı meydana gelir gelmez tespit edilebilmesi için kendine özgü bir koku verilir.

EN 589 Ek A'da tarif edilen işleme göre LPG, deneye tâbi tutulduğunda, kokusu, kendine has (ayırt edilebilir ve hoş olmayan) olmalı ve havadaki derişimi alt parlama sınırının % 20'sinden daha az iken kokusu fark edilebilir olmalıdır. Böylece, hoş olmayan bu koku uyarıcı işlev görecektir. Etil merkaptan dozajlama sistemi ve LPG merox üniteleri ile ayarlanır. Merkaptan içeriğine göre daha sonra yapılacak etil merkaptan dozajlama oranı ayarlanır. 2010 sonrası EPDK tarafından atılan bir çok daha denetiminde dağıtıcı firmaların bu konuda teknik

düzenlemelere uygun olarak çalışıp çalışmadıkları denetlenmiş ve bazı yaptırımlar uygulanmıştır.

Otogaz için Yazlık LPG, Kışık LPG farkı; TS EN 589 standardında, yılın her bir dönemi ile ilgili mevsimsel sınırların ulusal şartlara göre belirlenmesine imkân tanımak üzere, en düşük buhar basıncı için A, B, C, D ve E olmak üzere beş tip verilmiştir. Her ülke, bu standarda ek olarak verilen millî bir ekte, bütün bir yıl boyunca en az 150 kPa (gösterge) buhar basıncını elde etmek için hangi tipin/tiplerin kabul edildiğini belirtmeli ve seçilen tiplerin kullanılacağı tarihleri ayrıntılı olarak belirtmelidir.

Bu standarda göre kış mevsiminde (31 Ekim-1 Nisan arası), Türkiye'de piyasaya "Tip B" otomotiv yakıtı LPG verilmesi gereklidir. Bu standartlara uygun otogaz, daha kolay buharlaşabilmekte ve kışın soğuk hava koşullarında aracın LPG ile çalışmasını kolaylaştırmaktadır. Bu şartın sağlanması için de otogazda, propan oranı artırılmaktadır

LPG nin imal ve depolamasında farklı deniz yapıları ve karar tesisleri bulunmaktadır.

Deniz ikmal tesisleri için Jetty (İskele); Gemi hareketinin yüksek olduğu, uzun tahliye sürelerinin gerektiği, rafineri ve büyük liman işletmelerinde yaygın olarak tesis edilmektedir.

Dolfin (Platform); İskele uygulamasını yapılamadığı batimetrik deniz koşullarda, daha düşük yatırım bedeli ile yapılabilmektedir.

CBM; Şamandıra sistemleri ise Jetty ve Dolfin'e göre ilk yatırım maliyeti daha düşük, işletme ve bakım masrafları daha yüksek, tasarımı gemi kapasitelerine göre sınırlandırılmış, oldukça kullanışlı ikmal yapılarıdır.

Bu tesislere ikmal yapılan LPG gemileri ise 3 grupta incelenebilir. 1)Basınçlı Gemiler; Atmosferik sıcaklık ve bu sıcaklığa karşılık gelen buhar basıncında ürünün taşındığı (17,5 bar - 5.000 ton) 2)Yarı Soğutmalı Gemiler; 0°C'da ve bu sıcaklığa karşılık gelen buhar basıncında LPG taşındığı (5.000-25.000 ton) 3)Tam Soğutmalı Gemiler; Propan ve Butan'ın buharlaşma sıcaklığının az üstünde taşındığı gemiler (5.000-60.000 ton)

LPG terminallerinde belli bazı kabuller ve operasyonel uygulamalar mevcuttur.

LPG Tedarikçisi ile yapılan uluslararası anlaşmalara göre talep edilen LPG miktarı ve zamanlaması tedarikçisi ile beraber yıllık programlanır. Tedarikçi kendi gemisi veya anlaşmalı Shipper LPG'yi ilgili yükleme limanından gemiyi tedarik ettirir. Yüklenen LPG Miktarı (OBQ - On Board Quantity) birinci sınıf bağımsız gözetim firması tarafından yükleme limanında hesaplanır ve geminin konşimentosu (B/L - Bill of Lading) bu değere göre düzenlenir.

Geminin yükleme limanından ayrılıp tahliye limanına varmasını müteakip, tahliye öncesinde LPG miktarı birinci sınıf gözetim firması tarafından tespit edilir. Bununla beraber gemi tanklarından alınan numuneler, akredite laboratuvarlarda test edilerek ürünün ulusal standartlara uygunluğu teyit edildikten sonra tahliye

gerçekleşir.

Yukarıda belirtildiği şekilde birinci sınıf bağımsız gözetim firması tarafından yapılan gemi ölçümleri ile gümrük beyannamesi arasında %0,5'den daha büyük fark olması halinde Gümrük mevzuatına uygun olarak cezai v.b. yaptırımlar uygulanır.

Bakanlık tarafından yayımlanan Savaş Tebliği ile birlikte ithalat yapılan bütün terminallerde tahliye edilen LPG miktarı sayaç ile tespit edilmeye başlanmış, sayaç ile gemi ölçümü arasındaki farkın 0,5'den içinde olması halinde sayaç değeri, dışında olması halinde ise gemi değeri ithal stok değeri olarak dikkate alınmaya başlanmıştır.

LPG genellikle ikmal büyüklüğüne bağlı olarak üretim tesisleri dışında atmosferik sıcaklıkta, o sıcaklıktaki buhar basıncına göre tasarlanmış basınçlı küresel ya da silindirik tanklarda stoklanır. Propan için tasarım basıncı 17,5 bar olmakla birlikte ürün kompozisyonuna göre (%30Propan + %70Butan) bu basınç değeri 10,5 bar'a kadar düşebilir.

Ayrıca yerel mevzuatların izin verdiği emniyet mesafeleri dikkate alınarak küresel ve silindirik tanklar örtülü şekilde de inşa edilebilir. Bu durumda yer üstü tanklarına göre emniyet mesafeleri ciddi miktarda azalmaktadır.

LPG yine kayaç yapıları uygun bölgelerde yer altı mağaralarında da stoklanabilmektedir. (Örneğin Lavera/ Fransa)

Özellikle doğalgaz yataklarından büyük miktarda üretim yapılarak gemilerle LPG nin taşınması imkan veren ülkelerde LPG soğutmalı (refrigerated) düşey silindirik tanklarda çok daha büyük hacimlerde stoklanmaktadır. (20.000 m3 ve üstü).

Bu gibi tesislerde buharlaşan LPG'nin (boil-off) tekrar prosese sokulabilmesi için yüksek kapasiteli kompresörler kullanılmaktadır.

LPG stok tanklarında saklanan LPG, Otogaz ve Dökmegaz müşterilerine LPG kamyon tanker veya yarı römorkta karayolu ile taşınır. Yine tüp dolum tesislerinin de ihtiyacı olan LPG benzer tankerler ile sevk edilmektedir.

Dağıtım şirketlerinin kullanmış olduğu tankerler (motorlu araç, basınçlı tank ve donanımları) TS 1445 – Sıvılaştırılmış Petrol Gazları LPG – Taşıma kuralları standardı ve/veya Tehlikeli Malların Karayolu ile Uluslararası Taşımacılığı Anlaşması (ADR) mevzuatına uygun olmak zorundadır.

Tankerler karayolunda seyir halindeyken ADR Mevzuatı, Karayolları Trafik Kanunu, Karayolları Trafik Yönetmeliği, Tehlikeli Maddelerin Karayoluyla Taşınması Hakkındaki Yönetmelik ve sair mevzuatlara uymak zorundadır.

Tanker üzerinde yer alan tesisat ve aksesuarlar, LPG ile çalışmaya uygun, çalışma esnasında ya da çalışmıyorken sızdırmayan ürünlerle donatılmış olmalıdır. Pompanın, çalışma esnasında istasyonda kurulu otogaz tankının sahip olduğu karşı basıncı yenebilmesi gerekmektedir.

Tanker üzerinde yer alan pompa elektrik, yardımcı

mekanik shaft ya da hidrolik kaplin tahriki aracılığı ile çalıştırılabilir.

Genel olarak, tankerlerde kullanılan LPG pompaları kademeli, santrifüj veya dişli tip üç farklı tipte kullanılmaktadır.

İşin emniyetli şekilde yapılması için ilgili standart ya da mevzuatlarda belirtilen periyodik bakımların zamanında yapılması gerekmektedir.

Tankerden otogaz tankının dolumu öncesi, dolum esnasında ve dolum sonrasında standartlarda belirtilen referans talimatlara uygun olarak boşaltım işlemi yapılmalıdır.

## LPG'NİN KULLANIM ALANLARI

### 1. Evsel ve Ticari Kullanım

Dünya çapında birçok evde çok çeşitli uygulamalar için LPG kullanılmaktadır. Pişirme ve ısıtmanın yanı sıra, LPG aynı zamanda güç üretmek, giysileri temizlemek ve çim biçmek gibi farklı amaçlarla da kullanılmaktadır. LPG, şebeke bağlantısına gerek kalmadan şebeke gazının tüm avantajlarını sağlar. LPG, geleneksel pişirme yakıtlarına (yakacak odun, odun kömürü veya tezek gibi) modern bir alternatif sağlayabilir, hava kirliliğinin azaltılmasına katkıda bulunur. Isıtma, odun yerine kullanılarak ağaç kesiminin, tezek yerine kullanılarak gübre israfının önüne geçilmesine imkân vermektedir.

2000 yılında 4.5 milyon ton toplam LPG pazarın 2.1 milyon tüplü pazar, hızla yayılan doğalgaz kullanımı nedeniyle %70 mertebesinde gerileyerek günümüzde 600 bin ton seviyesine gerilemiştir.

70 civarındaki dağıtım firması olmasına rağmen tüplü pazar ilk 5 dağıtım firması tüplü pazarın %95'ine sahiptir.

Tüplü pazar FMCG pazar özelliklerine sahip olmaya başlamış ve özellikle doğrudan dijital platformu ile satışlar hızla artmaktadır.

### 5307 sayılı 2005 tarihli LPG kanunu ile düzenlenen piyasada;

- Fiyat serbest oluşmakta ve tavan fiyat her il bazında dağıtım firmaları tarafından EPDK sayfasında yayımlanmaktadır.

- Münhasır bayilik ve depozito sistemi sektörün en önemli unsurlarındandır

- Dağıtım firmalarının birbirlerinin tüplerini doldurması yasaktır.

- Pazar payı %2'nin üstünde olan dağıtım firmaları için 20 günlük satış karşılığı zorunlu stok bulundurulması gerekmektedir.

- Ürünün emniyetli kullanımı gereği 2 kg üstündeki tüplerin firmaların LPG yetkili personel belgesine sahip bayi ve bayi elemanları ile teslimi ve montajı kuralı vardır.

- Tüpler gövdesinde dağıtım firmasının tescilli markasını kabartma olarak bulunması gereklidir.

- LPG tüp dolumu yapan firmalar, doldurdıkları veya doldurttukları ve yetkili bayileri vasıtasıyla veya doğrudan doğruya tüketiciye intikal ettirdikleri tüplerin kullanılmak üzere bulundurdıkları yerlerde infilakı, gaz kaçırmayı, yangın çıkarması sonucu verecekleri bedeni ve maddi zararları karşı sorumluluklarının teminatı olarak Tüpgaz Zorunlu Sorumluluk Sigortası yaptırmak zorundadırlar.

- Kullanılmak üzere bulunduran tüp gazın neden olduğu kaza, işyerinde bulunan yanıcı, parlayıcı, patlayıcı maddelerin de zarar vermesine yol açarsa, tazminat ödemelerinde Tüpgaz Sorumluluk Sigortasına öncelik verilir; bu sigortanın limitlerinin yetersiz kalması halinde Tehlikeli Maddeler ve Tehlikeli Atık Sorumluluk Sigortası, limitleri dahilinde işlemeye başlar.

## 2. ULAŞIMDA KULLANIMI

Dünya LPG Birliği (WLPGA) 2016 yılı sonu verilerine göre, dünyada ulaşım için 26,7 milyon ton LPG tüketilmiştir. Bu rakam, aynı yılda dünyadaki toplam LPG tüketiminin yaklaşık %9'una denk gelmektedir. LPG, binek araçlarda kullanımı açısından, dünya çapında birçok ülkede en önde gelen alternatif yakıt durumundadır. Türkiye ise otogaz tüketimi konusunda en önemli ülkelerden biri olup otogaz tüketiminde dünyada ikinci; Avrupa'da ise birinci durumdadır. WLPGA 2016 yılı sonu verisine göre dünyadaki otogazın %12'si Türkiye'de tüketilmiştir.

LPG'li araç sayısına bakıldığında ise, Türkiye dünyada açık ara birinci sıradadır. Türkiye'de, Türkiye İstatistik Kurumu (TÜİK) 2017 yılı sonu verilerine göre 4,6 milyon LPG'li araç bulunmaktadır. 4,6 milyon araç ile Türkiye'de en çok tercih edilen binek otomobil yakıtı oto gaz durumundadır ve Türkiye'deki araçların %38,4'ü otogazlıdır. LPG, dünya çapında birçok ülkede önde gelen alternatif yakıttır. 4 Karayolu taşımacılığında çevresel etkilerin azaltılmasına katkıda bulunur. WLPGA'ya göre LPG'nin deniz araçlarında kullanımı da gün geçtikçe artmaktadır. Özellikle LPG taşıyan gemilerde yakıt olarak LPG kullanılması da bir sektör standardı haline gelmektedir.

## 3. ENDÜSTRİYEL KULLANIM

Doğal gazı erişimi olmayan hatta şebeke elektriğine erişimi olmayan bölgelerde kurulan işletmeler için LPG ideal bir yakıttır. LPG işletmelerde mekan, proses ve su ısıtma, metal işleme, kurutma, gıda üretimi, petrokimya, sanayi fırınları çoğunlukla dökme gaz tesisleri aracılığıyla kullanılmaktadır. Yine Endüstriyel kuruluşlarda hem iç hem dış mekanda kullanılabilme imkanı nedeniyle LPG'li forkliftler özellikle dizel forkliftlere alternatif olarak tercih edilmektedir.

2000 yılında 1 milyon ton seviyesine ulaşan Dökme gaz pazarı doğalgazın hızlı yayılımı ve fiyat avantajı nedeniyle %94 seviyesinde daralmıştır.

- B2C sözleşme yapılması zorunluluğu vardır.

- Dağıtıcı veya kullanıcı tarafından kurulmuş, Teknik

Düzenlemeler yönetmeliğine uygun tesisler olmalı ve yıllık periyodik kontrolleri yapılmalıdır.

- Dağıtıcılar LPG ikmalini mülkiyeti ya da tasarrufu altında tescilli markasını, unvanını ve amblemini taşıyan ADR onaylı araçlar ile yapmalıdır.

- Dökme gaz Pazarında faaliyet gösteren 10 dan az dağıtım firması vardır.

- Propan arzı teknik altyapının yetersizliğine bağlı olarak sınırlıdır.

- LNG'ye göre 1/5 mertebesinde daha düşük ilk yatırım gerektirmektedir.

- Fiyat serbest oluşmakta ve tavan fiyat her il bazında dağıtım firmaları tarafından EPDK sayfasında yayımlanmaktadır.

- Sürecin her safhasında MMO tarafından eğitim almış ve sertifikalandırılmış personel kullanılma zorunluluğu vardır.

## 4. AEROSOL ENDÜSTRİSİ

Aerosollar içeriğinde emülsiyonlaştırıcılar, parfümler vb. ile birlikte aktif bir itici maddeyi barındırır. Çevre dostu olan LPG, daha önce aerosol endüstrisi tarafından kullanılan ve ozon tabakasına zararlı CFC gazlarının yerine geçmiştir. Standardize edilmiş LPG, aerosol üretiminde itici gaz olarak önemli bir hammaddedir.

## 5. SOĞUTMA ENDÜSTRİSİ

Saf, kuru "izo propan" (soğutucu tanımlayıcı R-290a) ve izo butanın (R-600a) soğutucu olarak kullanılması, ozon tabakasının korunması ve küresel ısınmanın önlenmesine olumlu yönde katkı sağlamakta birlikte ve geleneksel soğutma ve iklimlendirme sistemlerinde R-12, R-22, R134a ve diğer klorofluorokarbon veya hidroflorokarbon soğutucular için fonksiyonel bir alternatif olarak kullanılabilir.

## 6. TURİZM AMAÇLI

Ülkemizde öncelikle Kapadokya bölgesinde yaygın olarak uçuş yapan sıcak hava balonlarının yakıtı propandır. Balonların sepetlerinde bulunan paslanmaz çelikten mamul tüpler propan ile doldurularak, balonun altında bulunan özel brülörlerde likit fazında yakılarak yüksek bir ısı elde edilerek balonun içindeki havanın ısınması ve ısınan havanın yükselerek balon kubbesi ile birlikte sepeti yerden kaldırmasını sağlar

## 7. TARIMSAL KULLANIM

LPG, çiftlik ürünlerinin üretimini ve kalitesini artırmak için kullanılmasının yanı sıra çiftliklerde çeşitli uygulamalar için temiz ve şebekeden bağımsız olarak enerji erişimi olanağı sağlar. LPG tarımsal alanda;

- Kuluçka makineleri için sabit sıcaklık kontrollü ısıtma
- Tavukçuluk, seralar ve fidanlıklar için alan ısıtması
- Kimyasallar olmadan alev, yırtıcı ve zararlı kontrolü
- Seralarda bitki büyüme artırımı için CO2 üretimi

- Maliyetleri ve emisyonları azaltmak için makinelerde dizel yakıtı ikame olarak
- Su ısıtma sistemleri
- Sulama sistemleri
- Pamuk, tahıl, fındık ve meyve gibi kuru ürünlerin imalatı
- Zararlı ve Kemirgen mücadelesi için kullanılmaktadır.

## 8. SNG KULLANIMI

Sentetik Doğalgaz; yakma cihazları herhangi bir değişikliğe gerek olmadan, emniyet, verimlilik ve emisyon kriterlerinde önemli bir sapma yaşanmaksızın doğalgaz yerine LPG'nin hava ile karıştırılarak kullanılmasıdır. Basit olarak Sentetik doğalgaz LPG'nin doğalgazın ısı karakteristیکlerini sağlayacak şekilde hava ile uygun oranda karıştırılmasından ibarettir.

Özellikle doğalgaz kesintilerinin yaşanabileceği durumlarda SNG sistemleri cam, seramik gibi 7/24 çalışması gereken endüstrilerde işletmelerde son derece değerli bir yatırımdır.

SNG sistemlerinde LPG'nin stoklanması için tercihan toprakaltı LPG tankları tercih edilir. Böylece yangın tesisatları ile yapılacak ciddi yatırımların da önüne geçilmiş olur. Tüketim ve ikmal güvenliği dikkate alınarak stoklama kapasitesi yaklaşık 2-3 gün olarak belirlenir ve bu kapasiteye uygun tank veya tanklar tesis edilir. Tanklardan LPG sıcak sulu buharlaştırıcılara basınç farkıyla ya da gerektiğinde hız kontrollü LPG pompaları ile sevk edilir. Genellikle buharlaştırıcıların Fakirleştirici LPG giriş basıncına uygun olarak 4-5 bar aralığında çalıştırılması tercih edilir. İdeal olarak bir fakirleştiriciye bir buharlaştırıcı kapasite seçimleri yapılmaya çalışılsa da, buharlaştırıcı imalatları ile ilgili geometrik ve tasarımsal sınırlar nedeniyle bir fakirleştirici ya da birden fazla fakirleştirici sisteminin birden fazla bazen 3-4-5 buharlaştırıcı ile beslenmesi gerekebilir. Bu durumda özellikle buharlaştırıcı yerleşimi, buharlaştırıcı gaz çıkış hatları ve basınç düşümü hesapları son derece kritiktir. Zira uygun tasarlanmamış yerleşim ve boru tesisatı durumunda, sistem bazı buharlaştırıcılardan kapasitesinin üzerinden gaz çekişine neden olabilecek bu da o buharlaştırıcılarda gaz sıcaklığının düşerek sisteme likit LPG yürütmesine neden olabilecektir. Bu nedenle dengeleme vanaları ve gaz sıcaklığına bağlı buharlaştırıcı sıcak su kontrol vanalarının sistemde bulunması dikkate alınmalıdır.

Sonuç olarak; LPG geçmişten geleceğe, yaşamın geniş bir alanında enerji ihtiyacı karşılamaya devam edecektir. Özellikle taşınabilir ve kolay erişilebilir bir yakıt olması nedeniyle, ülkelerin enerji politikaları içinde LPG'ye gerekli önem verilmeye devam edilmeli ve ana yakıt, ikame yakıt, geçiş yakıtı ve acil durum yakıtı olarak LPG'nin sektörel konumlandırılmaları mutlaka orta ve uzun vadeli projeksiyonlar ile ele alınmalıdır.

Anahtar Kelimeler: LPG, Dökmegaz

# Kahramanmaraş Depremlerinin Türk Akaryakıt Piyasasına Etkisi

**Sinem Okumus, Aysun Korucan**

Enerji Piyasası Düzenleme Kurumu, Petrol Piyasası Dairesi Başkanlığı, Ankara / Türkiye



## ÖZET

Türkiye’de 6 Şubat 2023’te dokuz saat arayla meydana gelen depremler, 50.000’den fazla insanın ölümüne, binlercesinin yaralanmasına, milyonlarca insanın deprem bölgesinden tahliyesine ve altyapının zarar görmesine neden olmuştur. Deprem ve benzeri doğal afetlerde, afetzedelerin kurtarılması ve ihtiyaçların afet bölgelerine ulaştırılması için kesintisiz akaryakıt arzı vazgeçilmezdir. Bu nedenle, akaryakıt tedarikinin titizlikle izlenmesi akaryakıt ikmali açısından büyük önem taşımaktadır. Afetler sonrası kaotik ve beklenmedik koşullarda, gerçek zamanlı piyasa verilerine erişimiye, devlet kurumlarının anlık kararlar alması adına çok değerlidir. Depremler sonrasında yürütülen arama kurtarma çalışmalarında, dünyada tek olan Türk akaryakıt izleme sisteminden elde edilen gerçek zamanlı akaryakıt verilerinden yararlanılmıştır. Sistemlerden elde edilen veriler, Enerji Piyasası Düzenleme Kurumu’na (EPDK) depremlerin piyasa üzerindeki etkilerini analiz etme ve değerlendirme konusunda yol gösterici olmuştur. Bu çalışma, Türkiye akaryakıt piyasasının depremlerden ciddi şekilde etkilendiğini, ancak etkinin bölgeden bölgeye değiştiğini göstermektedir. Çalışmadan elde edilen veriler, depremlerin ilk gününde depremezdelelerin panikle istasyonlara koşmasında depremden az etkilenen bölgelerdeki akaryakıt satışlarında önemli artışa neden olduğunu ortaya koymaktadır. Öte yandan, depremden daha fazla etkilenen bölgelerdeki satışlarda benzer bir artış gözlenmemiştir. Dahası deprem sonrası günlerde bazı bölgelerde ulaşım altyapısının ve akaryakıt istasyonlarının yıkılması nedeniyle bu bölgelerde benzinin tükenmesi riski baş göstermiştir.

**Anahtar Sözcükler:** Akaryakıt İzleme Sistemi, Kahramanmaraş Depremleri

## ABSTRACT

The earthquakes hit Turkey nine hours apart on February 6, 2023 killed more than 50,000 people, injured thousands more, caused millions of people to flee the earthquake zone and damaged infrastructure. In force majeure situations, the uninterrupted supply of fuel is indispensable for rescuing victims and delivering supplies to disaster areas. Therefore, meticulous monitoring of fuel supply is of great importance for fuel supply. In chaotic and unexpected conditions after disasters, access to real-time market data for uninterrupted fuel supply is invaluable for government bodies to make instant decisions. In the search and rescue operations, real-time fuel data obtained from the Turkish fuel monitoring system, unique in the world, was utilized. The data obtained from this system guided the Energy Market Regulatory Authority (EMRA) in

analyzing and evaluating the effects of earthquakes on the market. This study reveals that the Turkish fuel market is severely affected by earthquakes, but the impact varies from region to region. The data from the study exhibits that on the first day of the earthquakes, victims rushed to fuel stations in a panic, which led to a significant increase in fuel sales in less affected regions. On the other hand, a similar rise in fuel sales was not observed in the regions more affected by the earthquakes. Moreover, due to the collapse of infrastructure and fuel stations in some regions in the days following the earthquakes, these regions faced the risk of running out of gasoline.

**Keywords:** Fuel Monitoring System, Kahramanmaraş Earthquakes

## 1. GİRİŞ

6 Şubat 2023 tarihinde, iki yıkıcı deprem (Kahramanmaraş depremleri) Türkiye’nin güneydoğusundaki 10 ili vurmuştur. Büyük can kayıplarının yanı sıra, birçok altyapı, kültürel miras, doğal gaz iletim boru hatları ve hastane ve okul gibi kamu binaları ciddi şekilde tahrip olmuştur. Depremler nedeniyle, Adana, Adıyaman, Diyarbakır, Gaziantep, Hatay, Kahramanmaraş, Kilis, Malatya, Osmaniye ve Şanlıurfa’da üç ay süreyle olağanüstü hal ilan edilmiştir.

Depremlerin ardından 200.000’den fazla bina çökmüş ve çok sayıda insan enkaz altında kalmıştır. Ölü sayısını aşırıya indirmek ve yıkılan binalardan yaralıları kurtarmak için arama ve kurtarma ekipleri görevlendirilmiştir. Hayat kurtarmak, depremezdeleleri tahliye edip hayatlarını kolaylaştırmak için konteyner, çadır, gıda ve su gibi bazı temel ihtiyaçların sağlanması devlet ve hayır kurumları için öncelik haline gelmiştir. Bu nedenle, deprem bölgesinde zamana karşı yarışan kuruluşlar için sürekli akaryakıt tedariki hayati önem kazanmıştır.

Kaotik koşullar altında, akaryakıt satışları ve stoklarına ilişkin gerçek zamanlı piyasa verileri acil karar alma süreçleri için çok değerli hale gelmiştir. Devlet kurumlarına akaryakıt stokları ve satışları hakkında saatlik ve günlük veri sağlamak için akaryakıt istasyonları ve depolama tesislerindeki otomasyon sistemlerinden oluşan akaryakıt izleme sistemi kullanılmıştır. Bu sistem, vergi ve akaryakıt kaçakçılığını önlemek amacıyla tüm piyasa faaliyetlerini izlemek için kurulmuş olsa da, yıkıcı depremlerden sonra Türkiye’nin gerçek zamanlı piyasa verileri kullanılmaya başlamıştır.

Bu çalışma, depremlerin Türkiye akaryakıt piyasasını nasıl etkilediğini ve kurumların anlık kararlar için gerçek zamanlı akaryakıt verilerini nasıl kullandığını göstermeyi amaçlamaktadır.



## 2. KAHRAMANMARAŞ DEPREMLERİNİN TÜRK AKARYAKIT PİYASASINA ETKİSİ

Depremlerin ardından ölü ve yaralı sayısının yüksek olmasının yanı sıra, bölgedeki binaların çoğu, doğal gaz iletim hatları, bazı akaryakıt istasyonları, karayolları, demiryolları ve birkaç depolama tesisi ağır hasar görmüştür. Ülkenin akaryakıt tüketiminin %11'ini karşılayan 1.800'den fazla akaryakıt istasyonu depremlerden etkilenmiştir. Arama kurtarma çalışmalarında, depremlenmeden tahliyesinde ve ısınma ihtiyaçlarının karşılanmasında motorin ve benzine erişim hayati önem arz etmiştir.

Kimi depremlenmeden korku ve panikle bölgeyi terk etmek, kimlerinin arabasında ısınmak, ambulans ya da vinçlerinse arama ve kurtarma için istasyonlara akın etmeleri nedeniyle depremlerin ilk günlerinde bölgede ikmal sorunları baş göstermiştir. Akaryakıt ve vergi kaçakçılığının önlenmesi amacıyla kurulan izleme sistemi deprem sonrasında kuruluş amacından farklı bir amaca hizmet etmiştir. Deprem bölgesinde hasar tespitinin yapılabilmesi ve akaryakıt faaliyetlerinin sürdürülebilmesi için ülke genelinden gerçek zamanlı akaryakıt verilerinin alınarak hızlı bir şekilde işlenmesi kurtarma ekipleri ve birçok devlet kurumu için elzem hale gelmiştir.

### 2.1. Akaryakıt İzleme Sistemi

Türkiye'nin petrol zengini bölgelere yakınlığı, akaryakıtların yüksek vergilendirilmesi, akaryakıt harici ürünlerin taşıması ve yetersiz denetim/izleme mekanizmaları geçmişte Türkiye'deki kaçakçılık faaliyetlerini artıran başlıca faktörlerdir (Yalta ve Yalta, 2016). Bu sorunlarla başa çıkmak için 2007 yılında 5015 sayılı Petrol Piyasası Kanunu (PPK) değiştirilerek akaryakıt istasyonlarına otomasyon sistemi kurulması zorunluluğu getirilmiştir.

Otomasyon sistemiyle yeraltı ve yerüstü tankları izlenirken, tankta bulunan yakıtın hacmi, sıcaklığı, tanka giren ve çıkan yakıt miktarı gibi bilgiler anlık olarak sistem kullanıcılarına gönderilmektedir. Akaryakıt dağıtıcıları bu verileri webservis aracılığıyla EPDK'ya göndermektedir. Böylelikle, EPDK lisans sahiplerinin yükümlülüklerini kontrol edebilmekte ve akaryakıt faaliyetlerini izleyebilmektedir.

Bayi otomasyon sistemine ek olarak, 2017 yılında PPK'ya yapılan ilavelerle depolama tesisleri de izleme sistemine dâhil edilmiştir. 2018 itibarıyla rafineri ve depolama tesislerindeki tüm akaryakıt faaliyetleri EPDK tarafından detaylı olarak izlenebilmektedir. Ayrıca webservis aracılığıyla gönderilen saatlik ve günlük verilere ek olarak, EPDK akaryakıt istasyonları ve depolama tesislerine uzaktan bağlanarak gerçek zamanlı akaryakıt stoklarını ve satışlarını izleyebilmektedir. Bu kapsamda, piyasa oyuncularından büyük miktarda veri alınarak depolanmaktadır.

Depremler sonrasında, 100 depolama tesisi, 38 dağıtıcı ve 12.000den fazla bayiden alınan gerçek zamanlı veriler kullanılarak;

- Akaryakıt tesislerinde hasar tespiti,

- Akaryakıt sıkıntısı yaşayan illerin tespiti,
- İletim yollarında meydana gelen hasarlar nedeniyle yeni ikmal yollarının belirlenmesi,
- Afet bölgelerinde arz-talep dengesinin takibi yapılmıştır.

### Şekil 1

Piyasanın temellerini gösteren harita Şekil-1'de verilmiştir. 43 milyon ton/yıl (860 bin varil/gün) petrol işleme kapasiteli beş rafineriden (EPDK, 2023b) üçü Ege ve Marmara bölgesinde kurulmuştur. Kıyı şeridindeki rafineriler, deniz yoluyla yapılan ithalattan beslenirken Orta ve Güneydoğu Anadolu bölgelerindeki rafinerilerde boru hattı ve kara tankerleriyle petrol tedarik edilmektedir. Petrol, Kırıkkale rafinerisine ağırlıklı olarak Türkiye'nin Akdeniz'deki petrol merkezi Ceyhan'dan boru hattıyla iletilirken (IEA, 2021), Batman rafinerisine karayolu tankerleri ve Ceyhan'dan (Dörtöl) Batman'a uzanan boru hattıyla gönderilmektedir.

Son yıllarda, Star Rafinerisi'nin faaliyete geçmesi ve TÜPRAŞ İzmit Rafinerisi'nde Fuel Oil Dönüşüm Projesi'nin sonlanmasıyla rafinerilerin üretimi artmıştır. Ancak rafineri üretimi Türkiye'nin sürekli artan petrol talebini karşılamakta yetersiz kalmıştır. Bu nedenle, denizyoluyla büyük miktarlarda petrol ürünü (motorin, LPG, havacılık yakıtları vb.) ithal edilmektedir. Petrol ürünleri, kıyı bölgelerindeki son kullanıcılara ağırlıklı olarak deniz taşımacılığıyla, iç kesimlerdeki tüketicilereyse boru hattı, karayolu ve demiryolu taşımacılığıyla ulaştırılmaktadır. Deprem bölgesine detayları Tablo-1'de verilen dört il ve taşıma yollarıyla ikmal yapılmaktadır.

Tablo 1

Normal koşullarda, deprem bölgesine akaryakıt temini boru hattı, kara, deniz ve demiryoluyla yapılmaktadır. Depolama tesislerinin Diyarbakır, Hatay, Mersin ve Malatya'ya dağılmasına karşın yüksek miktarda akaryakıt depolanması Hatay ve Mersin'de yapılmaktadır. İki ilde depolanan akaryakıtlar, İç Anadolu Bölgesi'nin güneyine, Güneydoğu Anadolu Bölgesi'ne ve Doğu Anadolu Bölgesi'nin bazı kesimlerine taşınmaktadır.

### 2.2. Depremin Etkileri

Bu çalışmada, Kahramanmaraş depremlerinin akaryakıt piyasası üzerindeki etkileri, izleme sistemi ve piyasa oyuncularından alınan veriler kullanılarak incelenmiştir. Çalışmada motorin ve benzin verileri kullanılırken, izleme sistemine dâhil olmayan LPG verileri kullanılmamıştır. İzleme sistemi, güncel akaryakıt verilerini derleme ve analizler etmek için tasarlanmasa da, depremler ardından gerçek zamanlı verilerin edinimi ve kullanımı önem kazanmıştır.

Depremlerin ve sayısız depremlerin ardından, 10 ildeki durumu izlemek için depolama ve bayi otomasyon verileri kullanılarak tesislerde ne kadar akaryakıt stoku

olduğu ve kalan stok ile günlük tüketim alışkanlıkları doğrultusunda afet bölgelerinde acil akaryakıt ihtiyacı belirlenmiştir.

Afet bölgesinde altyapının (demiryolları, karayolları ve iletim hatları) hasar görmesi, bazı tesislerin yıkılması akaryakıt dağıtımını ve satışlarını olumsuz etkilemiştir. İzleme sisteminden elde edilen verilerden depremlerin, altyapı, akaryakıt satışları ve arzı üzerinde etkileri olduğu tespit edilmiştir.

### 2.2.1. Altyapıya Etkisi

Deprem bölgesindeki tesislerin ilk hasar kontrolü EPDK tarafından izleme sistemiyle gerçekleştirilmiştir. Depremlerin ardından, elektrik kesintileri ve internet bağlantı kayıplarına rağmen veri sağlayıcıların çoğunun günlük veri gönderebilmesi, EPDK'nın deprem bölgelerindeki akaryakıt stoklarını kontrol edebilmesini ve acil durum yönetiminde bulunabilmesini sağladı. Depremin en çok etkilediği Hatay, Adıyaman, Kahramanmaraş ve Malatya'da dahi dağıtıcılar istasyon tanklarının %93'ünden EPDK'ya veri gönderilebilmiştir.

Cumhurbaşkanlığı Strateji ve Bütçe Başkanlığı'nın (SBB) Deprem Sonrası Değerlendirme Raporu'na (DSDR) göre, hasarın yaklaşık 355 milyon TL (18,8 milyon USD) olduğu öngörülmüştür (SBB, 2023). Piyasada çoğunlukla akaryakıt istasyonlarında oluşan hasar il bazlı olarak Şekil 2'de verilmiştir. Yapılan ilk hasar tespitine göre, bazı petrol istasyonları tamamen veya kısmen yıkılmıştır. Ayrıca, bazı yeraltı depolama tankları ve bağlantı parçaları çökmüştür. Şekil 2'de görüldüğü gibi, hasarın yaklaşık %89'u Hatay, Kahramanmaraş, Malatya ve Adıyaman'da meydana gelmiştir.

Afet bölgesindeki akaryakıt faaliyetleri, otoyol ve karayollarında meydana gelen yıkımlar nedeniyle olumsuz etkilenmiştir. Ulaştırma ve Altyapı Bakanlığı tarafından yapılan açıklamaya göre, 1.275 km demiryolu hattı, 446 köprü ve 175 tünel depremlerden önemli ölçüde etkilenmiştir (Artymiuk, 2023). DSDR'ye göre, hasarlı demiryollarının onarımı ve inşası için 17,4 milyar TL (922 milyon USD) gerekmektedir (SBB, 2023).

#### Şekil 2

Depremlerden zarar gören Türkiye'nin sırasıyla üçüncü ve yedinci büyük Mersin ve Hatay (İskenderun) limanları deprem sonrası faaliyetlerini askıya almıştır (Rubenstone, 2023). Depremler nedeniyle yaklaşık 38 milyon TL (2 milyon USD) hasar oluşmuştur (SBB, 2023). Bölgedeki lojistik altyapının önemli ölçüde yıkılması petrol faaliyetlerini aksatmıştır. Hasar gören limanlarda yürütülen faaliyetler yakın limanlara yönlendirilmiştir (Johnson, 2023).

Coğrafi ve altyapı kısıtlamaları nedeniyle, karayolu taşımacılığı deprem bölgesi için her zaman vazgeçilmez olmuştur. Mersin ve Hatay'da depolanan akaryakıt, karayolu tankerleriyle Doğu ve Güneydoğu Anadolu bölgelerinin iç kesimlerine taşınmaktadır. Bu bölgelerde, Mersin-Gaziantep ve Hatay-Gaziantep

arasındaki en kısa güzergâh üzerinde yer alan Nurdağı otoyolu, depremler sonrasında kullanılamaz hale geldiğinden Hatay ve Adana dışındaki illere akaryakıt sevkiyatı tamamen durmuştur.

Deprem bölgesindeki karayolları, demiryolları ve limanların tahrip olması, rafineri ve dağıtıcıların bölgeye akaryakıt sevkiyatını zorlaştırmıştır. Bu nedenle, akaryakıt ikmalinde alternatif güzergâhlar kullanılmıştır. Örneğin, Karadeniz ve İç Anadolu Bölgelerinden Doğu ve Güneydoğu Anadolu bölgelerinin iç kesimlerine karayolu taşımacılığıyla akaryakıt gönderilmiştir.

### 2.2.2. Akaryakıt Teminine Etkisi

İki deprem ve çok sayıda artçı, 2022 yılında Türkiye'nin toplam akaryakıt satışının %11,46'sının yapıldığı 10 ilde büyük bir yıkıma neden olmuştur. Bu illerde akaryakıt istasyonu ve depolama tesisi sayılarıyla satış miktarlarını gösteren Tablo 2'e göre, toplam akaryakıt istasyonlarının %15,14'ü ve depolama tesislerinin %9,6'sı bu illerde bulunmaktadır. Depolama kapasiteleri sınırlı olan bu tesislerin çoğunun Hatay'da bulunması, deprem bölgesine farklı alternatiflerle akaryakıt temini yapıldığının göstergesidir.

#### Tablo 2

Şekil 3 ve 4, depremlerin akaryakıt ikmal ve depolanması üzerindeki anlık etkilerini ortaya koymaktadır. Şekil 3 ve 4'te mavi çubuklarla gösterilen miktarlar il bazında 6 ve 7 Şubat günlerinde gün başı benzin ve motorin stoklarını gösterirken, turuncu ile gösterilen çubuklar yine il bazında anılan günlerde yapılan akaryakıt satışlarını ifade etmektedir. Şekil 3'te verilen mavi çubukla gösterilen gün başı stok miktarlarına göre, depremlerin ilk iki gününde neredeyse tüm illerde motorin talebini karşılayacak kadar stok olduğu görülmektedir. Bununla birlikte, Şekil 4'e göre 7 Şubat'ta Gaziantep, Hatay, Kahramanmaraş ve Kilis'te gün içerisinde yapılan satışlara göre benzin stoklarının endişe verici seviyelerde olduğu ve olası arz krizini önlemek için ek tedbirlerin alınması gerektiğini göstermektedir. Nitekim EPDK birçok dağıtıcıyı bölgeye akaryakıt tedariki için yönlendirmiştir.

#### Şekil 3

Motorin için Adıyaman, Hatay, Kahramanmaraş ve Malatya'da ve benzin içinse Adıyaman, Hatay, Kahramanmaraş, Osmaniye ve Malatya'da, 6 Şubat'ın başındaki akaryakıt stokları ile 6 Şubat'taki satışlar arasındaki fark ile 7 Şubat'ın başındaki stokların eşit olmaması bu illerdeki istasyonlarda veri gönderiminde sorun yaşanmış olabileceğini, dolayısıyla depremin yıkımını işaret etmektedir(5).

#### Şekil 4

Şekil 3 ve 4'de Adana ve Hatay dışındaki illerde demiryolu ve karayolu hasarının piyasa üzerindeki etkisi görülmektedir. Depremlen etkilenen illerin çoğunda 7 Şubat'ın başında benzin stok seviyesinin 7 Şubat'taki satışlara eşit olması arz sorununa işaret etmekte olup, istasyonlardaki stoklar tükenmeden önlemlerin alınması için yetkililere uyarı niteliğindedir.

### 2.2.3. Akaryakıt Satışlarına Etkisi

Depremlerin piyasa üzerindeki etkilerini değerlendirmek amacıyla, izleme sistemlerinden alınan günlük motorin ve benzin satışları derlenmiş, Türkiye'deki tüm akaryakıt satışları ayrıntılı bir şekilde incelenmiş ve etkinin bölgeden bölgeye değiştiği tespit edilmiştir. Marmara ve Ege Bölgelerinde depremlerin etkisinin az olmasından, yanıltıcı bir değerlendirme yapmamak için bu çalışmada sadece deprem bölgesindeki akaryakıt faaliyetleri dikkate alınmıştır.

Öncelikle, depremden etkilenen iller için 30 Ocak ile 13 Şubat 2023 (depremden bir hafta önce ve sonrası) dönemi akaryakıt satışları otomasyon sistemi verileri doğrultusunda derlenmiştir. 31 Ocak tarihi satışları başlangıç noktası alınarak bu tarihte yapılan satışlar 100 birim kabul edilerek diğer gün satışları hesaplanmıştır. Bu şekilde, mevsimselliğin ve farklı günlerin akaryakıt satışları üzerindeki etkilerinin ortadan kaldırılması amaçlanmıştır.

Deprem bölgesinde yapılan motorin ve benzin satışları Şekil 5 ve 6'da verilmiştir. 6 Şubatta motorin ve benzin satışlarının deprem öncesine göre sırasıyla %248 ve %560 arttığı tespit edilmiştir. Artışın motorinde bayi pompa satışından (%86) ve tankerle yapılan satıştan (%14), benzindeyse sadece pompadan yapılan satıştan kaynaklandığı gözlenmiştir.

Depremlerin Adana, Gaziantep, Osmaniye ve Şanlıurfa illerindeki etkisi diğer illere kıyasla daha dikkat çekicidir. Bu illerin aksine, Hatay, Kahramanmaraş ve Adıyaman gibi ağır hasarlı illerde satışlar nispeten sabit kalmıştır. Şekil 5 ve 6'da görüldüğü üzere, depremin ikinci günü olan 7 Şubat'ta benzin satışları genel olarak düşmüştür. Bu durum, söz konusu illerde yeterince benzin ve motorin stoku bulunup bulunmadığı, depremin ilk günü insanların istasyonlara akın etmesine yol açan panik ortamının daha sonra ortadan kalkıp kalmadığı gibi önemli soruları da gündeme getirmiştir.

#### Şekil 5

Arama kurtarma çalışmalarında iş makineleri, ambulanslar, kurtarma ekipleri ve aydınlatma ekipmanlarının tükettiği motorinin, afetten etkilenen tüm illerde normalden daha fazla olması beklenirken, Şekil 5'deki verilere göre Adıyaman, Hatay ve Kahramanmaraş'ta bu durum gözlenmemiştir.

#### Şekil 6

Türkiye İstatistik Kurumu'nun istatistiklerine göre, Ocak 2023 itibariyle Türkiye'deki toplam araçların %11,9'una karşılık gelen 3,14 milyon motorlu taşıt afet bölgelerinde kayıtlıdır. Bu araçların %46,4'ü otomobil olup tükettiği yakıt türleri motorin (%36,9), LPG (%35,1) ve benzindir (%26,8) (TÜİK, 2023). Buna göre, Şekil 5 ve 6, motorin ve benzinin ağırlıklı olarak diğer illere seyahat için kullanıldığını göstermektedir.

### 3. SONUÇ VE DEĞERLENDİRME

Kahramanmaraş depremleri, Türkiye'nin güneydoğusundaki 10 ili vurarak büyük yıkıma yol açmıştır. Depremler, 50.000'den fazla insanın ölümüne

ve binlerce insanın yaralanmasına neden olmuştur. Büyük can kayıplarının yanı sıra birçok altyapı, kültürel miras, doğalgaz iletim hatları, hastane gibi kamu binaları ağır hasar görmüştür. Hayatın durma noktasına geldiği bu illerde, insani ihtiyaçların yanı sıra, idari makamların kesintisiz akaryakıt tedarikini sağlamaya odaklanmaları ve bir tedarik krizi durumunda derhal harekete geçmeleri elzemdi. Bu noktada, vergi ve akaryakıt kaçakçılığını önlemek amacıyla akaryakıt istasyonları ve depolama tesislerine kurulan otomasyon sistemlerinden gelen veriler kullanılmıştır.

Depremler, gerçek zamanlı piyasa verilerinin mücbir bir durumda ne kadar hayati olabileceğini ortaya koymuştur. Bu sistemlerin verileriyle yetkililer, tesis ve istasyonlardaki akaryakıt stok miktarını anlık olarak tespit edebilmiş ve deprem bölgelerindeki istasyonlara akaryakıt ikmali yapılabilmıştır. Demiryolu hattı, köprü ve tünelin ağır hasar gördüğü göz önünde bulundurulduğunda, afet bölgesine akaryakıt tedariki için diğer alternatifler devreye sokulmuştur.

Bayi otomasyon sistemi verilerine göre, depremlerin ardından bazı iller birkaç gün boyunca stoksuza kalma tehdidiyle karşı karşıya kalmıştır. Nispeten daha az hasarlı illerde, depremin olduğu gün satışlarının deprem öncesine kıyasla artması, insanların panikle kargaşa ortamındaki davranışlarını göstermektedir. Buna karşılık, ağır hasar gören illerde, başta motorin olmak üzere akaryakıt satışlarının değişmediği, bu bölgelerdeki istasyonların çoğunun kullanılamaz hale gelmesi nedeniyle felaketin boyutunu ortaya koymaktadır. Birçok il benzinin tükenmesi riskiyle karşı karşıya kalmış ve bu durum yetkililerin benzin tedarik planlarını değerlendirirken göz önünde bulundurmaları gereken endişe verici bir durumdur.

Depremlerin piyasaya etkisi değerlendirirken günlük olarak izlenmeyen LPG çalışmaya dâhil edilmemiştir. İleriki çalışmalarda LPG'de dikkate alınarak depremlerin piyasa üzerindeki etki analizi yapılabilir.

Tüm bu yorum ve çıkarımlar gerçek zamanlı akaryakıt piyasası verileri sayesinde yapılabilmış ve bu veriler kullanılarak olası bir akaryakıt tedarik krizi yönetilebilmiştir. Ülke yakın zamanda yeni depremlere gebe olduğundan, bu felaketlerden önce acil durum planları oluşturmak kritik önem taşımaktadır. İstanbul gibi olası deprem bölgelerinde, etkiler tüm ülkeye yayılabilir ve akaryakıt krizi yönetimi çok daha zor olabilir. Bu nedenle, eldeki verilerden ve tüm olanaklardan yararlanarak acil eylem planlarına odaklanmak ve olası deprem bölgeleri özelinde çalışmalar yapmak, bu tür felaketlerin akaryakıt piyasasındaki yıkıcı etkilerini asgariye indirmek açısından önemlidir.

#### KAYNAKÇA

Artymiuk, Simon (2023). "Turkey and Syria battle impact of 7.8-magnitude earthquake". IRJ. Erişim 16.06.2023. <https://www.railjournal.com/infrastructure/turkey-and-syria-battle-impact-of-7-8-magnitude-earthquake/>.

EPDK (2023a). Petrol Piyasası Sektör Raporları. <https://www.epdk.gov.tr/Detay/Icerik/3-0-107/yillik-sektor-raporu> (12.04.2023)

EPDK (2023b). Petrol Piyasası Rafinerici Lisansları. <https://lisans.epdk.gov.tr/epvys-web/faces/pages/lisans/petrolRafineri/petrolRafineriOzetSorgula.xhtml> (27.05.2023)

IEA (2021). "Turkey 2021 Energy Policy Review". [https://iea.blob.core.windows.net/assets/cc499a7b-b72a-466c-88de-d792a9daff44/Turkey\\_2021\\_Energy\\_Policy\\_Review.pdf](https://iea.blob.core.windows.net/assets/cc499a7b-b72a-466c-88de-d792a9daff44/Turkey_2021_Energy_Policy_Review.pdf) (06.15.2023)

Johnson, Thomas (2023). "Infrastructure damage highlights severe impact of Turkey and Syria earthquakes". Erişim 18.06.2023. <https://www.newcivilengineer.com/latest/infrastructure-damage-highlights-severe-impact-of-turkey-and-syria-earthquakes-13-02-2023/>

Rubensone, Jeff (2023). "Uneven Code Enforcement Seen in Earthquake-Damaged Buildings in Turkey". ENR. Erişim 16.06.2023. <https://www.enr.com/articles/55904-uneven-code-enforcement-seen-in-earthquake-damaged-buildings-in-turkey>.

SBB (2023). Türkiye Earthquakes Recovery and Reconstruction Assessment. <https://www.sbb.gov.tr/wp-content/uploads/2023/03/Turkiye-Recovery-and-Reconstruction-Assessment.pdf> (10.06.2023)

TÜİK (2023). "Road Motor Vehicles, December 2022". <https://data.tuik.gov.tr/Bulten/Index?p=Motorlu-Kara-Tasitlari-Aralik-2022-49436#:~:text=T%C3%BCrkiye'de%202022%20y%C4%B1n%C4%B1%20sonu,ya%C5%9F%2014%2C8%20olarak%20hesapland%C4%B1> (15.06.2023)

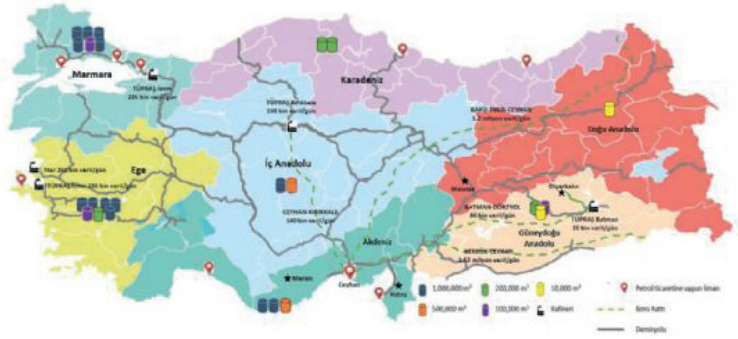
Yalta, A. T. & Yalta, A. Y. (2016). The dynamics of fuel demand and illegal fuel activity in Turkey. *Energy Economics*, 54, 144-158. <https://doi.org/10.1016/j.eneco.2015.11.026>

## DİPNOTLAR

- (1)2022 yılı benzin ve motorin satışları.
- (2)Havacılık yakıtı depolanan ve havalimanında bulunan tesis.
- (3)EPDK lisans verilerine göre yazarlar tarafından hesaplanmıştır.
- (4) Gün başı stok miktarı.
- (5)Mevcut durumda otomasyon sistemi kapsamında dağıtıcılardan satış ve dolum verileriyle birlikte gün başı stok seviyesi de EPDK'ya bildirilmektedir. Bu nedenle, ilgili günün gün başı stok, dolum ve satış verileri kullanılarak gün sonu stoku hesaplanabilmektedir. Bir önceki güne ait gün sonu stok verileri, bir sonraki günün gün başı stok verileri ile karşılaştırılarak veri tutarlılığı kontrol edilmektedir.

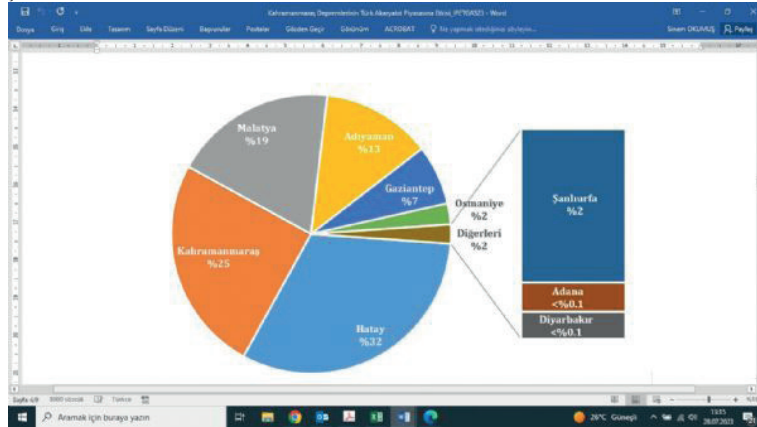
Anahtar Kelimeler: Akaryakıt İzleme Sistemi, Kahramanmaraş Depremleri

Şekil 1



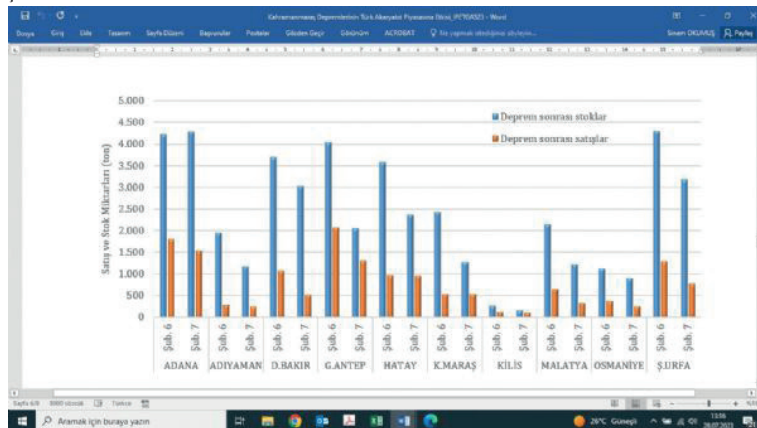
Türk Petrol Piyasasının Temelleri (Yazarlar tarafından çizilmiştir)

Şekil 2



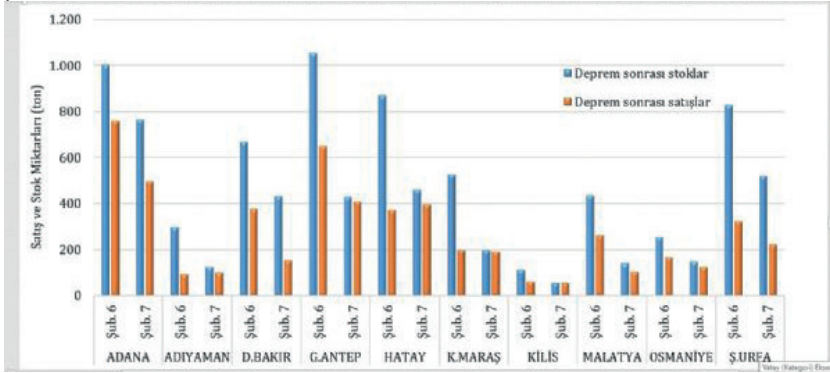
Türk Petrol Piyasasında Oluşan Hasarlar (SBB, 2023)

Şekil 3



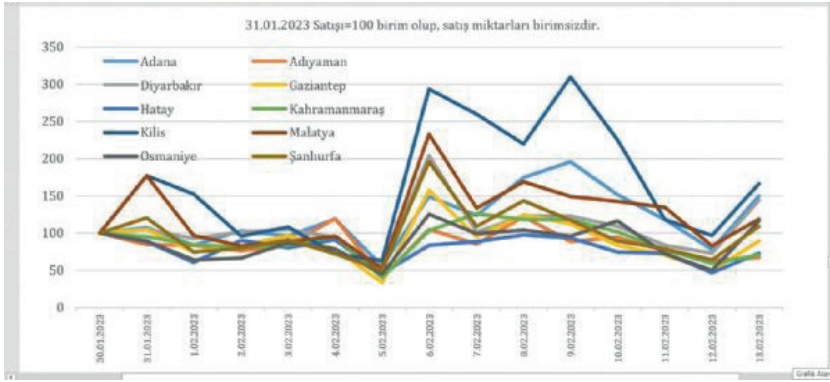
Deprem Öncesi ve Sonrası İstasyonların Motorin Stok(4) ve Satışları (İzleme sistemi verilerine göre yazarlar tarafından oluşturulmuştur)

Şekil 4



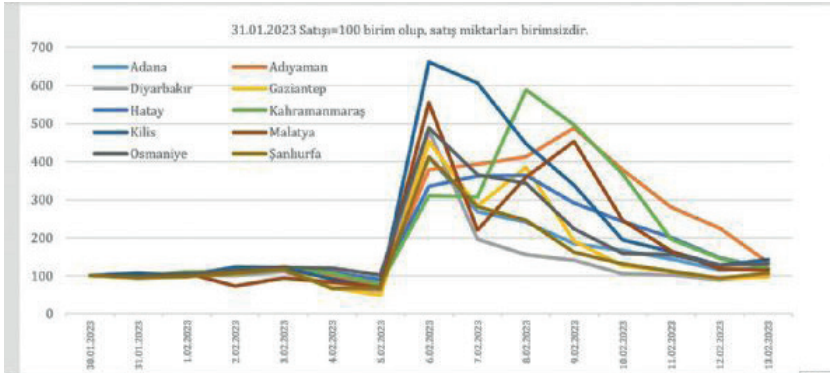
Deprem Öncesi ve Sonrası İstasyonların Benzin Stok(4) ve Satışları (İzleme sistemi verilerine göre yazar tarafından oluşturulmuştur)

Şekil 5



Deprem Öncesi Ve Sonrası Bayilerin Motorin Satışları (İzleme sistemi verilerine göre yazar tarafından oluşturulmuştur)

Şekil 6



Deprem Öncesi Ve Sonrası Bayilerin Benzin Satışları (İzleme sistemi verilerine göre yazarlar tarafından oluşturulmuştur)

*Tablo 1*

Ulaşım Türü	Diyarbakır	Hatay	Mersin	Malatya
Demiryolu	X	X	X	
Denizyolu		X	X	
Karayolu		X	X	X

*Depremden Bölgesine Yapılan Akaryakıt İkmali (Yazarlar tarafından hazırlanmıştır)*

*Tablo 2*

İl	İstasyon Sayısı	Depolama Tesisi Sayısı	Depolama Kapasitesi (m3)	Akaryakıt Satışı(1) (2022) (ton)
Adana	295	1(2)	2.568	644.557
Gaziantep	252	1(2)	677	552.823
Şanlıurfa	288	-	-	329.166
Diyarbakır	216	1	9.256	282.625
Hatay	238	5	249.177	489.229
Kahramanmaraş	197	-	-	290.895
Malatya	132	1	4.980	183.149
Adıyaman	144	-	-	142.180
Osmaniye	95	-	-	128.038
Kilis	22	-	-	26.511
Toplam	1.879	9	266.658	3.069.172
Genel Toplam	12.413	94	14.791.209(3)	26.787.937
%	%15,14	%9,6	%1,8	%11,46

*6 Şubat 2023 İtibarıyla Deprem Bölgesindeki Akaryakıt Tesisleri ve 2022 Yılı Akaryakıt Satışları (Petrol Piyasası Sektör Raporları (EPDK, 2023a), Lisans Sayıları (EPDK, 2023b) ve Turkey 2021 Energy Policy Review (IEA, 2021))*







## **Rezervuar alıřmaları**

*Reservoir Studies*

---



# Minimization Of The Noise In The Calculated Pressure Derivative Data For The Interpretation Of Transient Tests

**Doğuhan Coşar, Çağlar Sınayuç**

Petroleum and Natural Gas Engineering, Middle East Technical University, Ankara / Türkiye



Well tests are conducted to estimate essential reservoir parameters like permeability and skin factor. Pressure data is recorded at regular intervals during these tests, which are crucial for predicting the production potential of oil or gas. Analyzing pressure changes provides insights into the reservoir's characteristics and its ability to produce hydrocarbons over time.

Three different cases of drawdown tests are examined, and derivative curves are plotted using data points separated by specific intervals, ranging from 0.10 to 0.50 of a log cycle. This interval selection is vital to avoid excessively noisy derivative values during differentiation. A novel method is developed to determine the log cycle interval that minimizes noise while maintaining the integrity of the derivative curve. Additionally, second and third derivatives are calculated for each log cycle interval to identify the most suitable one.

The log cycle interval helps identify early, middle, and late-time regions, representing different flow regimes in both cases. The data from the middle time region is selected for the estimation process, as it offers the best estimates of permeability. These results are then compared with those obtained from KAPPA's Saphir Module, an industry-standard PTA (pressure transient analysis) module. The Python code used for estimation is found to provide more accurate estimations of permeability and skin factor and can handle noises up to  $\pm 2.5\%$ .

**Keywords:** Pressure Transient Analysis, Derivative Plots

## STATEMENT OF THE PROBLEM

In petroleum engineering, determining reservoir parameters such as permeability, porosity, and skin factor is of utmost importance. Accurate determination of these parameters is essential for conducting feasibility analyses because significant amounts of money are invested in the discovery and development of reservoirs. Well testing provides valuable data for evaluating and optimizing production, making the accuracy of this data critical for decision-making and feasibility assessments. To make informed decisions, it is crucial to have a clear understanding of reservoir parameters, especially permeability and skin factor.

Despite efforts to ensure the reliability of well test data, uncertainties persist due to factors like multiphase flow measurement and complex fluid flow dynamics. These uncertainties introduce noise in the data, necessitating their elimination to make the most informed decisions.

Derivative plots offer valuable insights into reservoirs, but calculating pressure derivatives is a delicate process as it can easily amplify the existing noise in the data.

Various new methods are employed to estimate these parameters, incorporating recent technological advancements to enhance accuracy and minimize predictive errors.

## METHODOLOGY

### i) Noise Elimination of Derivative Plots

In 1983, Bourdet et al. introduced derivative plots, which were regarded as the most valuable diagnosis tool at that time, as mentioned by Horne (1995).

Calculating pressure derivatives is a delicate procedure due to the risk of amplifying noise in the data. Several differentiation methods can be employed, and one such method involves numerically differentiating adjacent points using Eq 1. However, this approach is rarely used in well test analysis because it leads to very noisy derivative values.

$$\left( \frac{\partial P}{\partial t} \right)_i = t_i \left[ \frac{((t_i - t_{i-1})) \Delta p_{i+1}}{(t_{i+1} - t_i)(t_{i+1} - t_{i-1})} + \frac{((t_{i+1}) + t_{i-1}) - 2t_i}{(t_{i+1} - t_i)(t_i - t_{i-1})} \Delta p_i - \frac{((t_{i+1}) - t_i) \Delta p_{i-1}}{(t_i - t_{i-1})(t_{i+1} - t_{i-1})} \right] \quad \text{Eq 1}$$

Eq 1

It is suggested in the literature that numerical differentiation with respect to natural logarithm of time by using Eq 2 would reduce the noise in the derivative calculation compared to the previous method.

$$A = \ln \left[ \frac{(t_i/t_{i-1}) \Delta p_{i+1}}{(t_{i+1}/t_i)} \right] / \ln \left[ \frac{(t_{i+1}/t_i)}{(t_{i+1}/t_{i-1})} \right]$$

$$B = \ln \left[ \frac{((t_{i+1}) - t_{i-1}) / (t_i^2)}{(t_{i+1}/t_i) \ln(t_i/t_{i-1})} \right] \Delta p_i / \ln \left[ \frac{(t_{i+1}/t_i)}{(t_{i+1}/t_{i-1})} \right]$$

$$C = \ln \left( \frac{(t_{i+1}/t_i) \Delta p_{i-1}}{(t_{i+1}/t_{i-1})} \right) / \ln \left( \frac{(t_i/t_{i-1})}{(t_{i+1}/t_{i-1})} \right)$$

$$\left( \frac{\partial P}{\partial t} \right)_i = \left( \frac{\partial P}{\partial \ln t} \right)_i = A + B - C$$

where Eq 2

Using data points that are at least 0.2 of a log cycle apart instead of adjacent points while differentiating with respect to the natural logarithm of time can result in further noise reduction. However, this method has a limitation: it may lead to a lack of data during the first and last differentiation intervals. So the third differentiation method is

$$\left( \frac{\partial p}{\partial t} \right)_i = \left( \frac{\partial p}{\partial \ln t} \right)_i = A + B - C$$

where

$$A = \ln \left( \frac{(t_i/t_{i-k}) \Delta p_{i+j}}{(t_{i+j}/t_i) \ln(t_{i+j}/t_{i-k})} \right)$$

$$B = \ln \left( \frac{(t_{i+j}) - t_{i-k}}{[(t_i)]^2} \Delta p_i \right) / \ln \left( \frac{(t_{i+j}/t_i)}{(t_{i+j}/t_{i-k})} \right)$$

$$C = \ln \left( \frac{(t_{i+j}/t_i) \Delta p_{i-k}}{(t_{i+j}/t_{i-k}) \ln(t_i/t_{i-k})} \right)$$

$$(i+j)/t_{(i-k)})$$

Eq 3

$$\ln [t_{(i+j)}] - \ln [t_i] \geq 0.2$$

$$\ln [t_i] - \ln [t_{(i-k)}] \geq 0.2$$

where

Horne (1995) mentioned that the differentiation interval could be substituted with values ranging from 0.1 to 0.5, depending on the specific case.

During the differentiation of late-time data, the distance between data points becomes larger than the last data point and the previous differentiation point. This phenomenon, known as the end effect, prevents smoothing on the right side and may distort the shape of the derivative curve. Bourdet et al. (1989) proposed a solution to this issue by introducing a pseudo point to the right and fixing it. The difference ( $\Delta X$ ) between the pseudo point and the point before it should be greater than or at least equal to this length.

A Python code was developed to process pressure and time data. It calculates derivative values using data points separated by a proportion of a log cycle, ranging from 0.10 to 0.50, with increments of 0.01. As a result, 41 different derivative values with various separation intervals are computed.

### ii) Selecting the Smoothest Derivative Plot

The aim is to find the best log cycle interval among the 41 different intervals (between 0.10-0.50), the one that eliminates the most amount of noise without overly smoothing the derivative plot. In order to be able to do that Python is used. Second and third derivative values are calculated for every one of the 41 different derivative values. Number of sign changes in the second and third derivatives are calculated separately and divided to the total number of data points.

For example when using 0.26 log cycle intervals,

Number of sign changes is 2 for the second derivative values and 8 for the third derivative values, meaning that there are 8 different inflection points. There are 53 data points in total and the ratio for the second derivative is:

$$(\text{Number of sign changes})/(\text{Number of data points}) = 2/53 = 0.03774$$

And the ratio for the third derivative is:

$$8/53 = 0.15094$$

0.31 interval has the lowest sum of ratios among the all 41 second derivative values and all 41 third derivative values meaning that it is the smoothest of them. For all three of the cases, it is proven that the best intervals are the ones that have the smallest sum of sign change ratios of second and third derivatives.

### iii) Determination of the Middle Time Region

In the early time region, the flow behavior in and around

the wellbore, including effects like wellbore storage and formation damage/stimulation, plays a dominant role in the fluid flow. As time progresses, the flow is expected to transition to infinite-acting behavior in the middle time region, assuming a homogeneous reservoir. In this region, the pressure derivatives are expected to be horizontal.

Having identified the optimal log cycle interval that provides a derivative plot with minimal noise and appropriate smoothing, our focus is now on determining the middle time regions. These regions are crucial for obtaining the most accurate estimates of permeability ( $k$ ) and skin factor ( $S$ ).

For all drawdown cases, infinite acting radial flow is observed during the middle time regions, resulting in horizontal derivative curves. Specifically, the first derivative values remain relatively constant, and the second derivative values approach zero.

To identify the middle time regions, Python is employed once again, and all three derivatives (first, second, and third) are analyzed. We locate the region that follows a specific inflection point, where the first derivative values are relatively constant and the second derivative values fall within the range of -100 to +100. This constraint is incorporated into the Python code to facilitate the selection of points that come after the inflection point.

Figure 1 Middle Time Region Estimation for Drawdown Case I. Cosar(2022)

Up to this point, we have identified the flow regions of early time, middle time, and late time, as depicted in the figure above. The semi-log plot provides a clear indication that the time region estimations are precise for Drawdown Case I.

### iv) Permeability and Skin Factor Estimation

Once more, Python is employed to estimate the permeability and skin factor using the graphical analysis method, utilizing the data points obtained from the middle time region estimation.

A semilog plot of pressure ( $P$ ) versus time ( $t$ ) is generated using Python. A best-fitting line is drawn through the points corresponding to the middle time region. By calculating the slope of this line, referred to as “ $m$ ,” the permeability can be estimated using the following equation

$$k = -162.6 (Q \times B \times \mu) / (m \times h)$$

Eq 4

In order to estimate the skin factor,  $S$ , following equation is used.

$$s = 1.151 [(P_i - P_{1hr}) / |m| - \log [k / (\phi \mu c_t r_w^2)]] + 3.2274$$

Eq 5

It should be noted that for the  $P_{1hr}$  value, the point on the semi-log straight line should be used rather than the measured  $P$  value at 1 hour.

**RESULTS**

The study demonstrates that the noise in derivative plots can be eliminated by identifying the optimal log cycle interval and using it during pressure derivative calculations. Pressure derivatives are considered highly valuable for diagnosing well test analysis. By improving the accuracy of time region identifications, the estimations of permeability and skin factor are enhanced. These stand correct for three different drawdown tests.

The estimation process utilizes a graphical analysis method, which results in minimal error and performs calculations rapidly, completing them within seconds.

It is shown that the Python code written can estimate permeability and skin factor in three different drawdown cases more accurately than KAPPA’s Saphir Module, an industry standard Pressure Transient Analysis tool, as can be seen from Table 1.

Table 1 Absolute Error Percentages of Different Methods

Case Graphical Analysis Method KAPPA’s Saphir Module

Drawdown I 0.915% 1.243%

Drawdown II 1.946% 3.900%

Another drawdown test data with known parameters( $k=40$  md,  $S=+2.90$ ) had been generated and to test the methods tolerance to noise, random artificial Gaussian noise of  $\pm 0.5\%$ ,  $\pm 1\%$ ,  $\pm 1.5\%$ ,  $\pm 2\%$ ,  $\pm 2.5\%$ ,  $\pm 3\%$  is added to the Drawdown Case III pressure data. The Python code had been run 20 times for each case. Confidence interval of 95% is used for the calculations. It is seen that the Python code can handle noises up to  $\pm 2.5\%$ .

Table 2 Permeability and Skin Factor Estimations with Randomly Added Noises

Parameter	$\pm 0.5\%$	$\pm 1\%$	$\pm 1.5\%$	$\pm 2\%$	$\pm 2.5\%$	$\pm 3\%$
k(md)	39.365	39.893	39.825	41.424	40.746	37.050
S	2.758	2.973	2.833	3.133	3.086	2.170

**CONCLUSION**

Well testing provides valuable data for evaluating and optimizing production, making it a crucial aspect of reservoir management. The accuracy of this data is essential for understanding the reservoir’s characteristics and making informed decisions accordingly.

Flow period identification is the initial and arguably the most critical step in well test analysis. Derivative plots, which are diagnostic plots, play a vital role in this identification process, and their reliability directly impacts the accuracy of permeability and skin factor estimates.

Although pressure and flow rate measurement technology has improved, some level of noise persists in most well test data and must be addressed before performing reservoir characterization and parameter estimation processes.

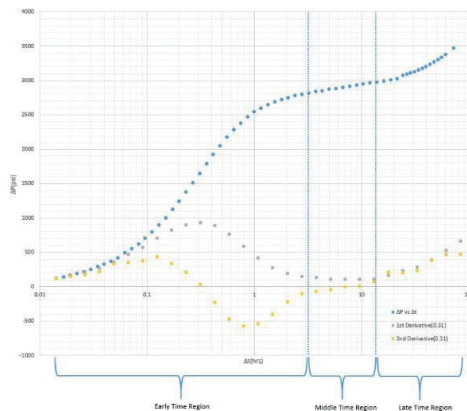
The Python code developed in this context has

demonstrated the ability to handle noise up to  $\pm 2.5\%$ .

It also provides more accurate estimations of permeability and skin factor compared to an industry standard PTA software tool, KAPPA’s Saphir Module.

Keywords: Derivative Plots, Pressure Transient Analysis

Middle Time Region Estimation for Drawdown Case I



Absolute Error Percentages of Different Methods

Case	Graphical Analysis Method	KAPPA’s Module	Saphir
Drawdown I	0.915%	1.243%	
Drawdown II	1.946%	3.900%	

Permeability and Skin Factor Estimations with Randomly Added Noises

Parameter	$\pm 0.5\%$	$\pm 1\%$	$\pm 1.5\%$	$\pm 2\%$	$\pm 2.5\%$	$\pm 3\%$
k(md)	39.365	39.893	39.825	41.424	40.746	37.050
S	2.758	2.973	2.833	3.133	3.086	2.170

Known Parameters:  $k=40.000$  md,  $S=+2.900$

# Integrating Various Sources Of Indicators And Water Measurements Data Of Different Degree Of Uncertainty To Understand Aquifer Encroachment And Resulted Water Breakthrough To Gas Producers



**Murat Zhiyenkulov<sup>1</sup>, Michael Nashaat<sup>2</sup>, Hassan Kolivand<sup>2</sup>, Oleh Lukin<sup>1</sup>, Abdurrahman Shah<sup>2</sup>, Kassem Ghorayeb<sup>2</sup>, Viacheslav Filatov<sup>3</sup>, Denys Grytsai<sup>3</sup>**

<sup>1</sup>Schlumberger, Kyiv / Ukraine

<sup>2</sup>Schlumberger, Abu Dhabi / UAE

<sup>3</sup>Ukrgezvydobuvannya, Kyiv / Ukraine

## ACKNOWLEDGEMENT

This study was presented at the SPE Eastern Europe Subsurface Conference, November 23–24, 2021. Full paper is available at SPE library with number SPE-208556-MS

## INTRODUCTION

Opishnyanske Field is a mature Ukrainian gas field that began producing in 1972 from three formations: Visean, Serpukhovian, and Bashkirian. A reservoir simulation study was implemented to understand the movement of the water in the reservoir and to maximize the field recovery. Some wells showed high water production at their late life, and this was the key question that we wanted to understand. If this was a water breakthrough, which means that the aquifer water swept the gas in the reservoir and reached these wells, then there is little potential left in this field. If this was not a water breakthrough, there could still exist some un-swept areas to be produced. The second key question was to understand the aquifer strength and direction to be integrated into the simulation model.

The field has different sources of data that could be used to understand the water movement in the reservoir, which are:

- Observed production data.
- Water analysis reports (surface water salinity and density measurements, Fig 1).
- Production logging data.
- Pressure data and geological maps to understand the communication between the wells.

Although different sources of data are available, each one has a level of inaccuracy, which was the key challenge. The field also has some other challenges, such as:

- Commingled production.
- Contradiction between the observed water/gas ratio (WGR) and water analysis data.
- Limited water analysis data points in some wells.
- Issues with back allocation of the observed data.

Integrating all the available data had a significant effect on understating the water behavior. Data analysis and integration resulted in excluding all the data anomalies and reaching a good understating regarding:

- The wells that are showing a water breakthrough

- Aquifer strength and direction

## METHODOLOGY

The main data analysis technique was to integrate all the sources of data to detect and exclude the outliers. These sources of data are as below:

- Observed production data.
- Water analysis data (Surface water salinity and density measurements).
- Production logging data.
- Pressure data and geological maps to understand the communication between the wells.
- Completion events to highlight the commingled production.

It was critical to have ability to plot, visualize and analyze all the data, including non-numerical data too (such as produced water type) to allow integrated data analysis.

## DEFINING WATER SOURCES

All the output of Water analysis reports was converted into numerical representations, which makes it easy to chart them and use them in the analysis next to the other sources of data. The water sources are assigned numerical probability values between zero (0) and one (1.0). A probability of 1 means a confirmed reservoir water, while a probability of 0 means a condensate water confirmed by the sampling report (Fig 2, top left plot).

- A probability of 0 means a Condensate water that was vaporized in the gas, which means there is no water breakthrough.
- A probability of 1 means a confirmed reservoir water. It indicates that there is a water breakthrough.

If the source of water is not mentioned in the report, then based on the water density and solids content the probabilities of 0.3 or 0.7 is assigned as described in Fig 3.

## WATER BREAKTHROUGH ANALYSIS

Once water source probabilities are assigned, follow the steps below.

1. Create dynamic wells showing the producing interval and load the available data to it. Available water analysis reports were translated into numerical representation

to be loaded as discrete logs (like water source probabilities) and used in the analysis (Fig 4, Fig 5).

2. Start the analysis with non-commingled communicated wells for each formation. This gives a good understanding about the water movement of each compartment in each formation separately which then used to understand the behavior of commingled wells producing from more than one formation.

3. For each well, compare the three sources of data (water analysis data, observed Gas Water Ratio, and Production logging data) for the same producing interval to:

- Exclude Data Anomaly.
- Decide the breakthrough time of each well.

4. For each compartment, compare the trend of the nearby wells in the same formation/ compartment to exclude the anomaly well data which could be due to the data back allocation issues.

5. Map the breakthrough of each compartment and then conclude the water movement and direction.

### BREAKTHROUGH SIGNATURE

We use the following criteria to determine whether there is a reservoir water breakthrough or not:

1. An increase in both the water rate and the WGR: some wells show high WGR at the end of their life as the gas production becomes very low and the water production becomes almost constant due to inaccurate water measurement. In this case, considering only the WGR, one would conclude that there is a water breakthrough, whereas this is because of the inaccurate measurement of water at very low gas rates. Therefore, it is important to see a clear increase in both the water rate and the WGR to confirm breakthrough of a reservoir water.

2. Confirmed/continuous water salinity measurements: it is important to have a continuous water salinity confirming that this is reservoir water. Some wells show a single sample indicating reservoir water samples, while all other samples are indicating a condensate water. This single reservoir sample could be measurement inaccuracy. Therefore, it is important to have many samples confirming reservoir water.

3. Confirmed by production logging data: Having a production log confirming that there is a water saturation at the reservoir level is a good confirmation that this well is flushed by water and this is mostly a breakthrough.

4. An agreement with nearby wells that are producing from the same zone: integration with the surrounding wells is vital information, as it does not make sense to have a breakthrough in the shallowest well, while there is no breakthrough in the surrounding deeper wells producing from the same formations.

Fig 4 shows a good example of a clear breakthrough where the above criteria are applied, while Fig 5 shows there is no breakthrough.

### LIMITATIONS AND DATA CHALLENGES

Our approach allowed us to plot, visualize and analyze all the data, including non-numerical data too (such as produced water type) to perform an integrated data analysis.

However, we still had several challenges, such as:

- Data inaccuracy, especially with old data. For example, in Fig 5 we observed two data points with non-zero probability (could be reservoir water due to parameters measured in lab), whereas as all other points have zero probability (confirmed by lab analysis).

- Limited water analysis data points in some wells, we see water production in some wells, but water sample analysis was not performed.

- Contradiction between the observed water/gas ratio (WGR) and water analysis data.

- Commingled production, wells producing from several formations same time.

- Issues with back allocation of the observed data.

### RESULT

Integrating all the available data had a significant effect on understating the water behavior and the following was concluded:

- Detecting the wells that showed a breakthrough which was categorized based on the available data to high, mid and low probability.

- Understanding the behavior of each compartment/ formation separately which helped to better interpret the observed dynamics of the commingled producers.

- Declaring the aquifer movement and direction Based on this analysis, the water breakthrough was excluded as a reason behind the well shut in for many wells. Another clear reason came strongly which is the salt precipitation around some wells due to water evaporation in addition to reservoir energy.

These results guided the simulation model to get a good match to the confirmed water production which then used to maximize the recovery.

Keywords: water breakthrough analysis in gas wells

Figure 1: Sample of the water analysis report.

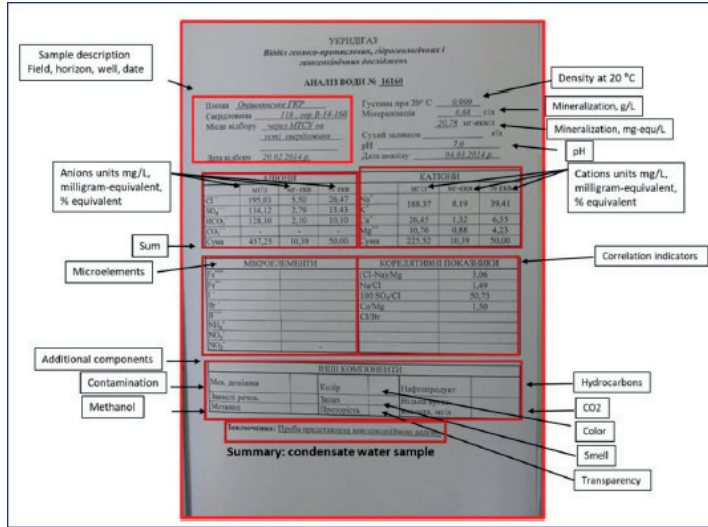
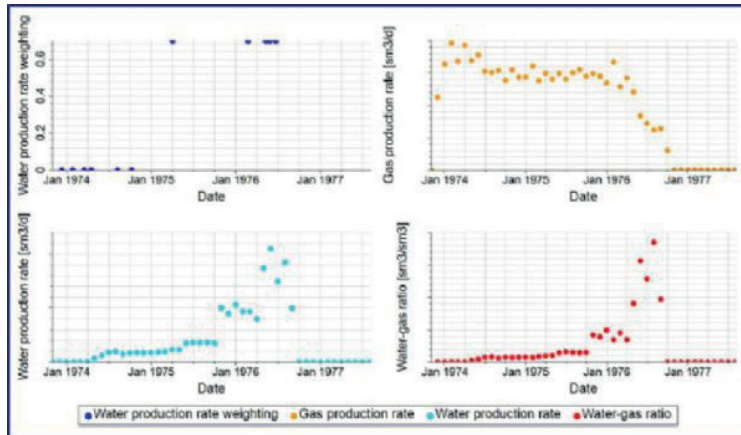


Figure 2: example of the observed data and the numerical representation of the water analysis reports.



Clockwise from top left: water source probability, gas rate, WGR and water rate for a sample well.

Figure 3: flowchart to assign water source probability if it is not specified in the water analysis report.

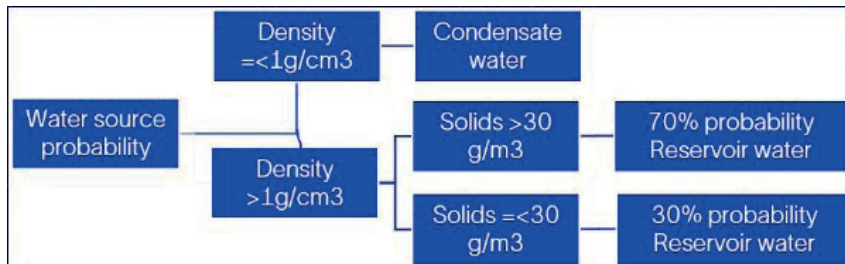
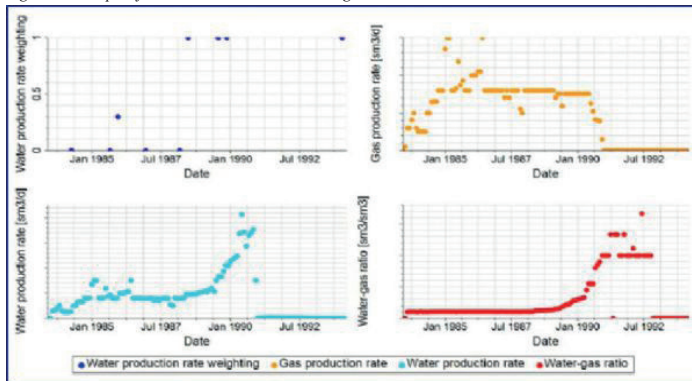


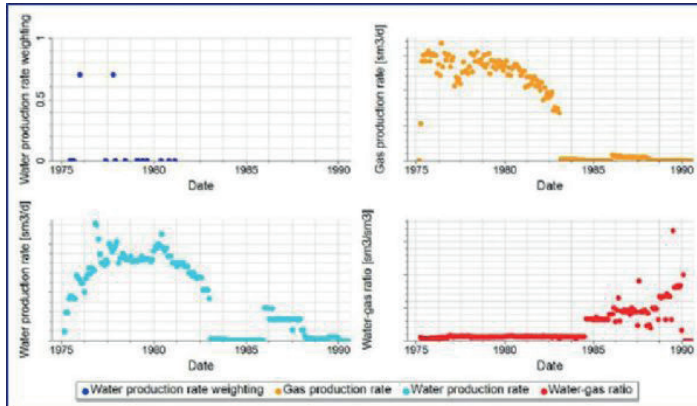


Figure 4: Example of a well with a water breakthrough.



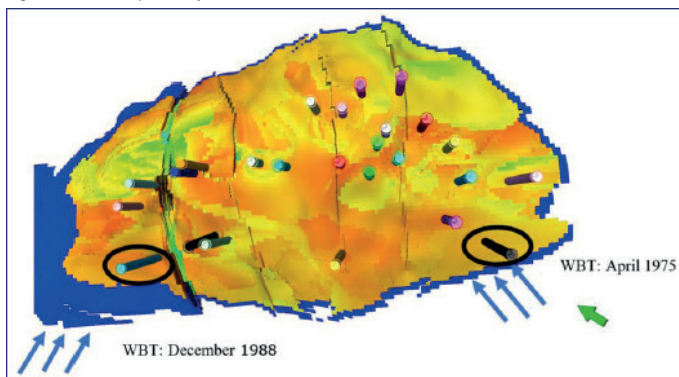
Clockwise from top left: water source probability, gas rate, WGR and water rate for a sample well. Water rate starts increasing sharply after 1988 and water probability shows 1. This means that water breakthrough occurred in this well.

Figure 5: Example of a well without a water breakthrough.



Clockwise from top left: water source probability, gas rate, WGR and water rate for a sample well. There is some water production in this well between 1975 – 1985, but water analysis reports confirm that this water a condensate water. Hence probability = 0. Two water sample points have higher probability, possibly due to sample contamination.

Figure 6: Water analysis workflow conclusions.



# Unlocking New Reservoir Zones at Shallow Depth Based on Integrating Post-Hydraulic Fracture Performance with Reservoir, Petrophysics and Geology Data



**Murat Zhivenkulov<sup>1</sup>, Michael Nashaat<sup>2</sup>, Hassan Kolivand<sup>2</sup>, Yerlan Seilov<sup>1</sup>, Abdurrahman Shah<sup>2</sup>, Kassem Ghorayeb<sup>2</sup>, Roman Madatov<sup>1</sup>, Svetlana Grytsai<sup>3</sup>, Viacheslav Filatov<sup>3</sup>**

<sup>1</sup>Schlumberger, Kyiv, Ukraine

<sup>2</sup>Schlumberger, Abu Dhabi, UAE

<sup>3</sup>Ukrzavvydobuvannya, Kyiv, Ukraine

## ACKNOWLEDGEMENT

This study was presented at the SPE Eastern Europe Subsurface Conference, November 23–24, 2021. Full paper is available at SPE library with number SPE-208517-MS.

## INTRODUCTION

Skhidno-Poltavske Field is a Ukrainian gas field producing mostly from commingled wells. These commingled wells have no information about the production split and the pressure data measured for each formation separately. This was one of the main challenges to study the field and understand the potential of each individual formation. Many wells were hydraulically fractured (HF) and showed a wide range of production and pressure performance after the stimulation.

Six of these HF wells showed atypical pressure and production behavior after the HF compared to the rest of the wells (Fig 1). The main challenge in the reservoir simulation study was to understand whether these HF wells reached isolated lateral segments of the same producing zones or accessed other reservoir zones by/through vertical propagation of the hydraulic fracture plane.

Understanding the pressure and production performance of these wells and comparing them to the other wells was the key to revealing their behavior (Fig 2). This was integrated with the petrophysical data to understand the potential formations and the uncertainty range of their properties. The geomodeling was the destination to translate these uncertainties into different realizations that were all dynamically tested to generate the most probable realization.

The integration between different domains resulted in unlocking an overlooked productive zone that was out of consideration. This increased the reserves of this field and extended its life. One of the study recommendations was to test and develop this formation through perforating the existing wells or drilling new wells targeting the overlooked productive zone.

## METHODOLOGY

The following workflow was implemented:

- Build a geological model integrating all subsurface data in one place.
- Study the pressure behavior of the non-commingled wells to understand the pressure behavior of each

formation separately.

- Categorize the commingled wells based on its pressure behavior to understand the most contributing formation and guide the static model.
- Compare the pressure behavior of the HF wells with the individual formations/zones/intervals performance to understand the apparent fracture extension and propagation.
- Study the pressure and production of abnormal wells and the communication between them.
- Generate different geological realizations for the possible formations that could be the reason behind this abnormal behavior which could be either:
  - o Scenario 1: Existing producing formation where the HF reached to isolated lateral segments within Moscovian formation.
  - o Scenario 2: Vertical communication with shallower un-depleted zones (Kassimovian layer)
- Use the reservoir simulation to test these realizations and came up with the most representative scenario.

## DISCUSSION

Integrating all the available pressure and production data with the geological realizations resulted in the following.

## CONCLUSIONS

- Scenario 1: one realization was generated to extend the continuity of one of the existing formations, but it could not match the behavior of the HF abnormal wells. This solution was disqualified due to this reason in addition to some other RE evidence (Fig 3, 4).
- Scenario 2: Petrophysical data showed one upper formation that had never produced. One realization was generated to simulate the vertical propagation of the HF towards this new formation. This formation is not extended everywhere, so analyzing the pressure data of this abnormal wells and its communication guided the static model. This scenario showed a very good match to the pressure and production behavior of these abnormal wells after the HF (Fig 5, 6).

## RESULTS

To summarize the study, in Scenario 1 a geomodeler created a new model where all sandbodies observed

at wells were connected together within each sub-formation of Moscovian formation. This is presented in Figure 3, where red dots are wells and yellow area is a sand connecting these wells. Despite having more sand and more GIIP in this scenario, reservoir pressures from simulation were below measured pressures, which indicates that model has lower GIIP volumes than in reality, as displayed in Figure 4.

In Scenario 2, similar to scenario 1, the low porosity sands were connected together within each sub-formation of Kassimovian formation. Then a reservoir engineer added additional connection from Moscovian formation to Kassimovian formation by extending hydraulic fractures vertically in 6 wells that show atypical pressure and production behavior. This is presented in Figure 4. When this scenario was simulated, it produced much better reservoir pressure match as displayed in Figure 6.

Kassimovian formation is tight, hence was not developed by the operator. However, behavior of 6 hydraulically fractured wells and their analysis in this study indicate that Kassimovian formation can produce if hydraulically fractured. Connecting Kassimovian formation to Moscovian formation produced better history match results and increased GIIP in the simulation model by 15%.

Keywords: reservoir modeling and history matching of hydraulic fracture impact

Figure 1: production performance of the hydraulically fractured wells compared with other wells

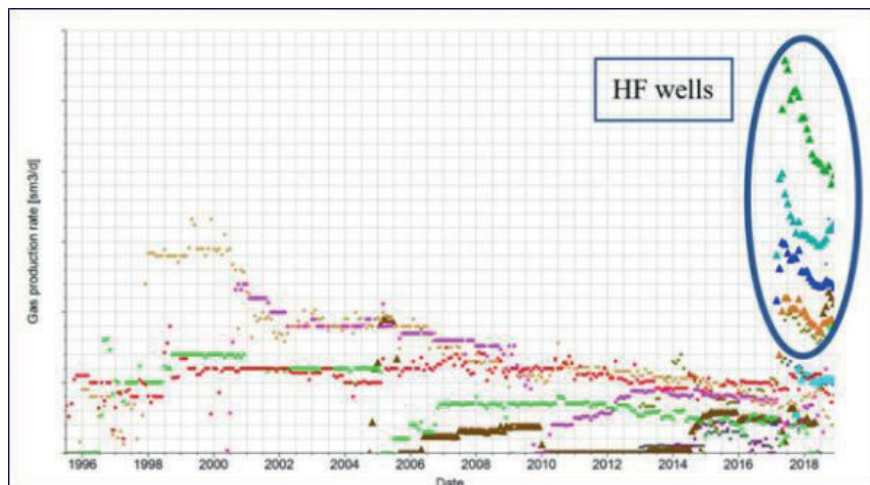


Figure 2: Location map showing the atypical well locations

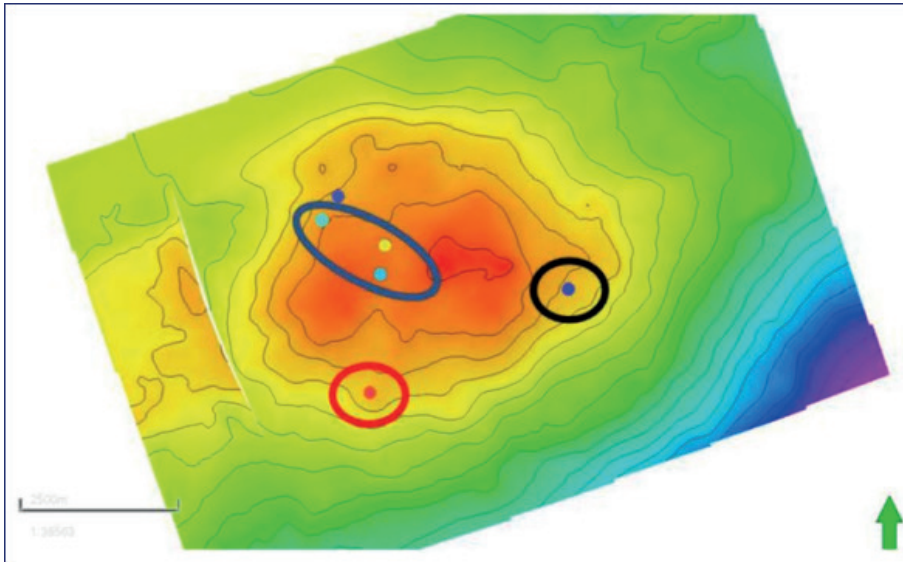


Figure 3: Scenario 1: Comparison of initial and new sandstone distributions in Moscovian intervals. Analogs from India

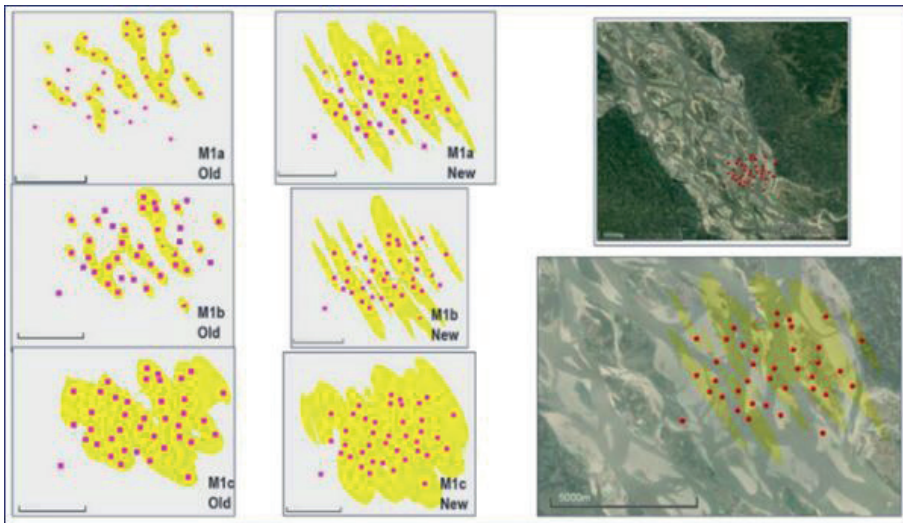
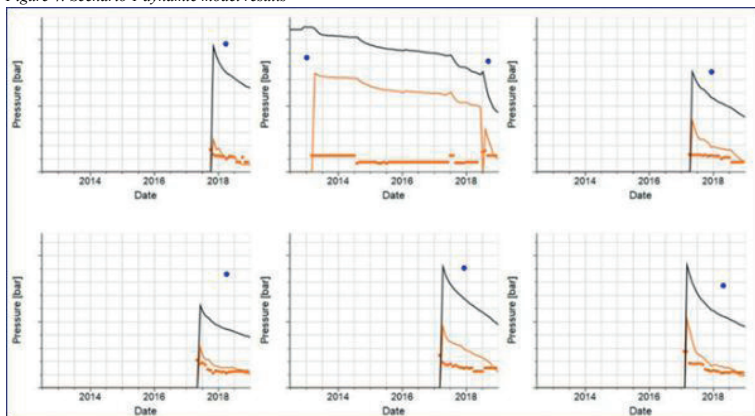


Figure 4: Scenario 1 dynamic model results



Simulation pressures are below measured pressures, which indicates that model has lower GIIP volumes than in reality. Blue dot – measured reservoir pressure, black line – simulated reservoir pressure. Orange dots and line – measured and simulated well BHPs.

Figure 5: Scenario 2: Initial and alternative sandstone distributions for K5 horizon. Yellow indicates mouth-deltaic sandstones, red mostly channelized sandstones

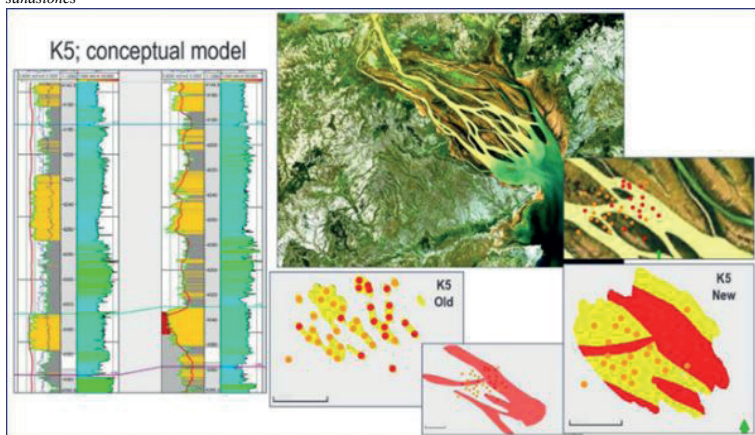
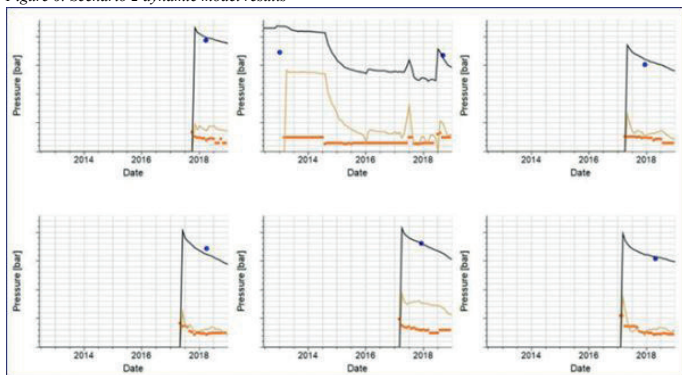


Figure 6: Scenario 2 dynamic model results



These plots show better match between simulation and measured pressures. Blue dot – measured reservoir pressure, black line – simulated reservoir pressure. Orange dots and line – measured and simulated well BHPs.

# Analysis of the Effect of Salt Zones on Gas Production from Gas Hydrates in the Mediterranean Sea



Sükrü Meray<sup>1</sup>, Lin Chen<sup>2</sup>

<sup>1</sup>Department of Petroleum and Natural Gas Engineering, Batman University, Türkiye

<sup>2</sup>Institute of Engineering Thermophysics, Chinese Academy of Sciences, Beijing 100190 /

School of Aeronautics and Astronautics, University of Chinese Academy of Sciences, Beijing 100049 / China

## ABSTRACT

Recently, gas hydrates have become very popular due to their huge reserve potential all around the world. It is known that the Mediterranean Sea has gas hydrate potential (in the ranges of trillion cubic meters of methane-CH<sub>4</sub>). There is a high possibility of the existence of salt layers in the Mediterranean Sea because of the Messinian Salt Crisis. The effect of salts on gas hydrate production behavior in the Mediterranean Sea has not been investigated so far. Similarly, in Gulf of Mexico, salt zones near gas hydrate stability zone were detected. In this study, by using ODP (Ocean Drilling Program) Leg 160-161 and DSDP (Deep Sea Drilling Program) Leg 13-42A drilling and coring data, pore water salinity change with depth was taken into consideration. By using the python codes written, GHSZ (Gas Hydrate Stability Zone) thicknesses of the Eastern and Western Mediterranean Sea were estimated and their maps were drawn. Finally, according to the drilling and coring data of ODP Leg 160-161 and DSDP Leg 13-42A, gas hydrate production simulations from gas hydrates in different cases in the Mediterranean Sea were conducted with TOUGH + HYDRATE. It was found that salt formations near gas hydrates provide higher heat flux through gas hydrate sections during depressurization. This caused a higher gas production rate under the conditions of the Mediterranean Sea.

## 1. INTRODUCTION

Gas hydrates are ice-like structures formed by gas molecules and water molecules at low temperature and high-pressure conditions. These conditions exist in both permafrost and marine environments. According to Chong et al. [1], the amount of technically recoverable natural gas from gas hydrates is approximately 300 tcm (standard trillion cubic meter). Because of this potential, tremendous efforts have been made for gas hydrate explorations and production since 2002. Many gas hydrate production trials (depressurization, thermal injection, CH<sub>4</sub>-CO<sub>2</sub>/N<sub>2</sub> replacement) were implemented in Canada, USA, Japan, and China [2].

Although gas hydrate production technologies are still at the stage of research & development (R&D), gas hydrates might be near-future energy resources in the world. Thus, it is important to explore gas hydrates and to develop new novel exploration and production technologies for feasible gas production from gas hydrates. However, initially, the identification of gas hydrates and production potentials in a certain area is essential so it is possible to design drilling and production trial processes. Meray and Longinos [3-4] analyzed the gas hydrate potential of the Mediterranean Sea in detail

and it was found that the Mediterranean Sea has huge gas hydrate potentials (~technically recoverable 98.16 tcm). In all numerical simulations conducted with HydrateResSim by Meray and Longinos [3], the salinity of pore water in the Mediterranean Sea was taken as 3.8 % wt. as an average. The Mediterranean Sea has a unique geological history. Due to the Messinian salinity crisis in the Mediterranean Sea in its geological history, many salt formations and evaporites exist in the Mediterranean Sea [5]. This caused a pore water salinity gradient with depth in the Mediterranean Sea. Moreover, thick, and thin salt formations exist within/near gas hydrate stability zone of the Mediterranean Sea. According to Max et al. [6], the thermal conductivity of salts is higher than sediments, so the heat flux created by neighbor salt formation strains gas hydrate formations. Thus, in this study, it is aimed to analyze the effect of salt zones on gas hydrate production potential in the Mediterranean Sea by using the drilling and coring data collected in ODP 160-161 and DSDP Leg 13-42A [7-10].

## 2. MATERIALS AND METHODS

In this study, by relying on the drilling and coring data (i.e., pore water salinity gradient, geothermal gradient, pore pressure gradient) obtained during ODP Leg 160-161 and DSDP Leg 13-42A [3-4,7-10], GHSZ thickness maps of the Eastern and Western Mediterranean Sea were prepared in this study. In order to prepare these maps, bathymetry data was obtained from TOPEX [11]. Moreover, HEP software developed by Meray [12] was used to predict gas hydrate properties and equilibrium conditions.

In this study, it was also aimed to investigate the effect of heat flux coming from salt formations on gas production from near gas hydrate formations in the Mediterranean Sea. For this reason, in this study, the most widely used gas hydrate simulator TOUGH + HYDRATE was chosen for numerical modelling. TOUGH + HYDRATE (v1.5) is a numerical code developed by Lawrence Berkeley National Laboratory. It is commonly used to simulate gas production (i.e. depressurization, thermal stimulation, chemical injection or their combination) from gas hydrates. With this simulator, it is possible to model the non-isothermal gas release, phase behavior and flow of fluids and heat under conditions typical of common natural CH<sub>4</sub>-hydrate deposits [13].

The simulation parameters (i.e., porosity, geothermal gradient, pore water salinity, pressure gradient, thermal conductivity, grain size, etc) used in this study were selected mainly by relying on the drilling and coring data obtained from the scientific drilling programs in the Mediterranean Sea [7-10, 14]. Thus, these data sets

mimic the Mediterranean Sea conditions. However, for more precise data sets, special gas hydrate exploration projects (i.e., LWD, coring data, seismic, etc) targeting gas hydrates in the Mediterranean Sea are essential in future.

### 3. RESULTS AND DISCUSSIONS

According to ODP Leg 160-161 and DSDP Leg 13-42A [8-10] drilling and coring data, in the Western Mediterranean Sea, geothermal gradient is higher than 50°C/km. For instance, at some sites (Site 371, 372, 373), geothermal gradient varies from 63°C/km to 83.1°C/km between seafloor and 150 mbsf (meter below seafloor). Moreover, between these depth intervals, pore water salinity increases from 3.8% wt. to 7.1 % wt. (weight) with depth [10]. By accounting all these parameters, GHSZ thickness map of the Western Mediterranean Sea was obtained as shown in Figure 1-a. Hence, it was found that the maximum and average GHSZ thickness in the Western Mediterranean Sea are ~181.8 m and ~100.6 m, respectively.

In the Eastern Mediterranean Sea, the geothermal gradients are less than 50°C/km and gas source potential is extensive [7, 9, 10]. For instance, at Site 374, the geothermal gradient varies from 24°C/km to 32.5°C/km between seafloor and 250 mbsf. Interestingly, pore water increases from 3.8 % wt. to 14.3 % wt. at this depth intervals of Site 374 in the Eastern Mediterranean Sea. Hence, by considering these gradients for the first time, GHSZ thickness map of the Eastern Mediterranean Sea was obtained in this study as shown in Figure 1-b by the help of python codes written in this study. It was found that the maximum and average GHSZ thickness in the Eastern Mediterranean Sea are ~519.6 m and ~235.2 m, respectively.

Due to the Messinian Salt Crisis, salt formations and evaporites exist all over the Mediterranean Sea. According to X diffraction analysis of salt core samples obtained during DSDP Leg 42A [10, 14], NaCl % wt. is generally between 89.3 % to 98.4. For instance, in Figure 2-d, halite sample collected from Site 376 in the Eastern Mediterranean Sea was shown. The distance of these salt formations to seafloor and the bottom of GHSZ range all over the Mediterranean Sea. Thus, in this study, several numerical gas production simulations from the Eastern and Western Mediterranean Sea gas hydrates were conducted to investigate the effect of this distance and high thermal conductivity of salts on gas production. TOUGH + HYDRATE (v1.5) was used in this study for these simulations. Figure 2 shows the lithological distribution of the cases simulated in this study. In Table 1, the parameters used in numerical simulations are shown. In Table 2, the cases simulated with TOUGH + HYDRATE were listed.

In the gridding process of the cases in Figure 2 and Table 2, a half of section of a cylindrical reservoir with a diameter of 500 m was gridded. Along z axis, 0.5 m cartesian grids in gas hydrate section were selected. Along the radial axis, 100 logarithmic grids were selected. Before starting gas production simulations

from the gas hydrate reservoirs in the conditions of the selected cases, initialization process was implemented so gas hydrate stability conditions were preserved. After that, depressurization along gas hydrate sections (10 m-thick) was simulated for every case in this study.

In Figure 3, Case 1 and Case 2 were simulated for Site 124 in the Western Mediterranean Sea. The distance between the halite section and gas hydrate section in Figure 2-a is nearly 330 m. In order to understand the effect of halite section on gas hydrate production, Case 1 assumes that halite section exists below 3146 mbsl (meter below sea level) but Case 2 assumes this section is a non-halite section. As seen in Figure 3, there is almost no difference in gas production between Case 1 and Case 2. Thus, the halite section 300 m-away from gas hydrate section does not affect gas hydrate production behavior.

Similarly, in Case 3 and Case 4, the effect of halite section on gas hydrate production was investigated for Site 374 in Figure 2-b. The distance between gas hydrate section and halite section is nearly 360 m. As seen in Figure 4, due to high distance of halite section to gas hydrate section, there is almost no effect of halite section on gas hydrate production for the cases of Site 374.

As seen in Figure 2-c and Table 2, the hypothetical gas hydrate reservoir in the conditions of the Eastern Mediterranean Sea was simulated. Different than Case 1-4, this time, halite was chosen at just below gas hydrate section in Case 5-7. The purity of gas hydrate sections varies so their thermal conductivity values vary. Thus, in Case 5-10, different thermal conductivities were chosen to investigate the effect of this on gas hydrate production. As seen in Figure 5, higher gas production from gas hydrates was observed if the thermal conductivity of bottom boundary is higher. For instance, in Case 5 and Case 6, the thermal conductivity is 5.3 W/m.K and 3.5 W/m.K, respectively. On the 1000th day of gas production from gas hydrates, 4 % of higher gas production was obtained for Case 5. Moreover, gas production was faster in Case 5 than Case 6 due to higher heat flux from bottom boundary. Thus, it is important to identify the lithology of boundary formations of gas hydrates and to measure their physical and chemical properties (i.e., thermal conductivity).

As an example, pressure, temperature, and gas hydrate saturation changes of Case 5 during gas production at a depressurization pressure of 4 MPa are shown in Figure 6. Gas hydrate dissociates both radially and axially as seen in Figure 6. Especially, the heat flux from upper and lower boundaries provides gas hydrate dissociation axially. This is due to temperature reduction up to 2 °C in gas hydrate section during endothermic gas hydrate dissociation.

### 4. CONCLUSIONS

In this study, gas in-place estimations in the potential gas hydrates of the Mediterranean Sea were made by Monte Carlo simulations by considering pore water salinity gradient. ODP Leg 160-161 and DSDP Leg

13-42A data sets were useful to make these estimations and to prepare GHSZ thickness map of the Eastern Mediterranean Sea. Moreover, salt formations are commonly seen in the Mediterranean Sea due to the Messinian Salt Crisis. Thus, in this study, for the first time, the effect of salt formations near/within GHSZ on gas hydrate production behavior. The numerical simulations of these were conducted by using TOUGH + HYDRATE. The following concluding remarks were obtained in this study:

- Average GHSZ thickness in the Eastern and Western Mediterranean Sea are nearly 235.2 m and 100.6 m, respectively.
- Pore water salinity gradients in the Mediterranean Sea due to Messinian Salt Crisis reduces GHSZ thicknesses.
- Salt (halite) formations near gas hydrates promote gas hydrate production due to their higher thermal conductivities.

## 5. ACKNOWLEDGEMENTS

This work was partially supported by the Start-up Program of the Chinese Academy of Sciences and the CAS from 0 to 1 fund (No. ZDBS-LY- JSC018; Prof. Lin CHEN).

## 6. REFERENCES

- [1] Chong, Z. R., Hern, S., Yang, B., Babu, P., Linga, P., and Li, X., Review of natural gas hydrates as an energy resource: Prospects and challenges. *Applied Energy*. 162 (2016) 1633-1652.
- [2] Collett, T.C., Gas Hydrate Production Testing-Knowledge Gained. The Offshore Technology Conference, Houston, Texas, USA, 6-9 May 2019 (OTC-29516-MS).
- [3] Mery, S., Longinos, S.N., Does the Mediterranean Sea have potential for producing gas hydrates? *Journal of Natural Gas Science and Engineering*. 55 (2018) 113-134.
- [4] Mery, S., Longinos, S.N., The Gas Hydrate Potential of the Eastern Mediterranean Basin. *Bulletin of The Mineral Research and Exploration*. 160, 117-134.
- [5] Montadert, L., Letouzey, J., Mauffret, A., Messinian Event: Seismic Evidence. Publication date: May 2007. Doi: 10.2973/dsdp.proc.42-1.154.1978. Retrieved from (Accessed on October 29, 2019): [www.deepseadrilling.org/42\\_1/volume/dsdp42pt1\\_54.pdf](http://www.deepseadrilling.org/42_1/volume/dsdp42pt1_54.pdf)
- [6] Max, M.D., Johnson, A.H., Dillon, W.P, Economic Geology of Natural Gas Hydrate. Springer (2006), ISBN-10 1-4020-3971-9.
- [7] ODP Leg 160, Mediterranean Sea I: The Eastern Mediterranean Sites 963-973, 3 March-3 May 1995. Retrieved from (Accessed on October 22, 2019): [www-odp.tamu.edu/publications/leg\\_ndx/160index.htm](http://www-odp.tamu.edu/publications/leg_ndx/160index.htm)
- [8] ODP Leg 161, Mediterranean Sea II - The Western Mediterranean Sites 974-979, 3 May-2 July 1995. Retrieved from (Accessed on October 22, 2019): [www-odp.tamu.edu/publications/leg\\_ndx/161index.htm](http://www-odp.tamu.edu/publications/leg_ndx/161index.htm)
- [9] DSDP Volume XIII Table of Contents. Publication date: May 2007, Doi: 10.2973/dsdp.proc.13.1973. Retrieved from (Accessed on October 29, 2019): [www.deepseadrilling.org/13/dsdp\\_toc.htm](http://www.deepseadrilling.org/13/dsdp_toc.htm)
- [10] DSDP Volume XLII Part 1 Table of Contents. Publication date: May 2007, Doi: 10.2973/dsdp.proc.42-1.1978. Retrieved from (Accessed on October 29, 2019): [http://deepseadrilling.org/42\\_1/dsdp\\_toc.htm](http://deepseadrilling.org/42_1/dsdp_toc.htm)
- [11] TOPEX. Extract XYZ Grid - Topography or Gravity. Retrieved from (Accessed on December 15, 2019): [https://topex.ucsd.edu/cgi-bin/get\\_data.cgi](https://topex.ucsd.edu/cgi-bin/get_data.cgi)
- [12] Mery, S., Analysis of the Black Sea gas hydrates. PhD Thesis (2017), Middle East Technical University, Ankara, Turkey.
- [13] Moridis, G., User's Manual for the Hydrate V1.5 Option of TOUGH+ V1.5: A Code for the Simulation of System Behavior in Hydrate-bearing Geologic Media. Earth Sciences Division, Lawrence Berkeley National Laboratory, Berkeley, CA 94720, August 2014.
- [14] Kuehn, R., Hsü, K.J., Chemistry of Halite and Potash Salt Cores, DSDP Sites 374 and 376, Leg 42A, Mediterranean Sea. Publication date: 2007, Doi: 10.2973/dsdp.proc.42-1.124.1978. Retrieved from (Accessed on October 29, 2019): [www.deepseadrilling.org/42\\_1/volume/dsdp42pt1\\_24.pdf](http://www.deepseadrilling.org/42_1/volume/dsdp42pt1_24.pdf)

Keywords: gas hydrates, Mediterranean Sea



Figure 1: GHSZ thickness map of a) the Western Mediterranean Sea b) the Eastern Mediterranean Sea

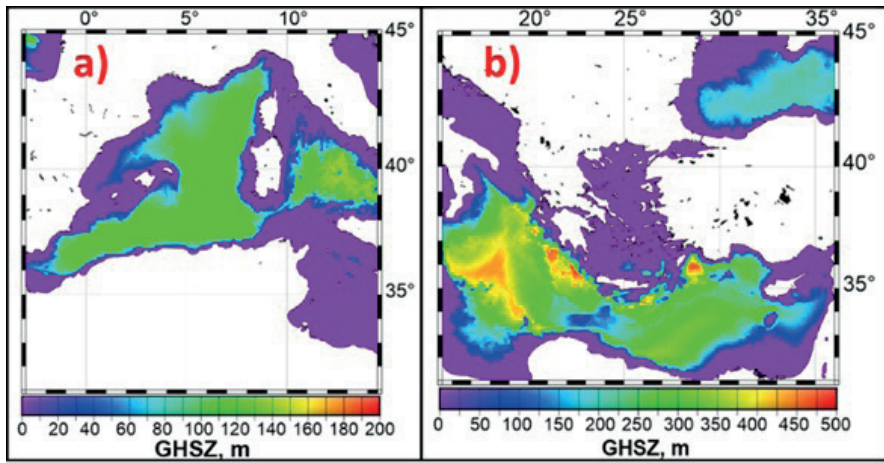


Figure 2: a) Site 124 b) Site 374 c) Hypothetical Reservoir in Table 1 d) Halite sample collected from Site 376 in the Eastern Mediterranean Sea [7-10]

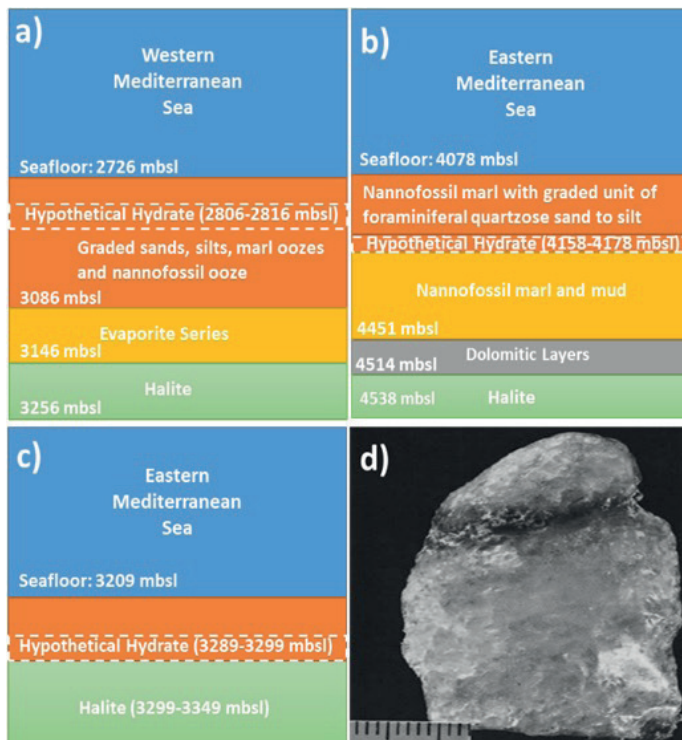


Figure 3: Cumulative CH<sub>4</sub> production in Case 1 and Case 2 at a depressurization pressure of 4 MPa

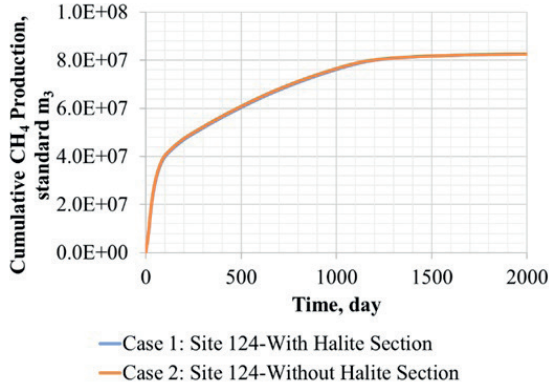


Figure 4: Cumulative CH<sub>4</sub> production in Case 3 and Case 4 at a depressurization pressure of 4 MPa

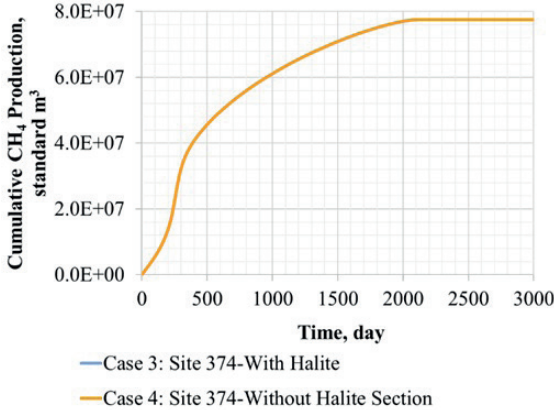


Figure 5: Cumulative CH<sub>4</sub> production in Case 5-10 at a depressurization pressure of 4 MPa

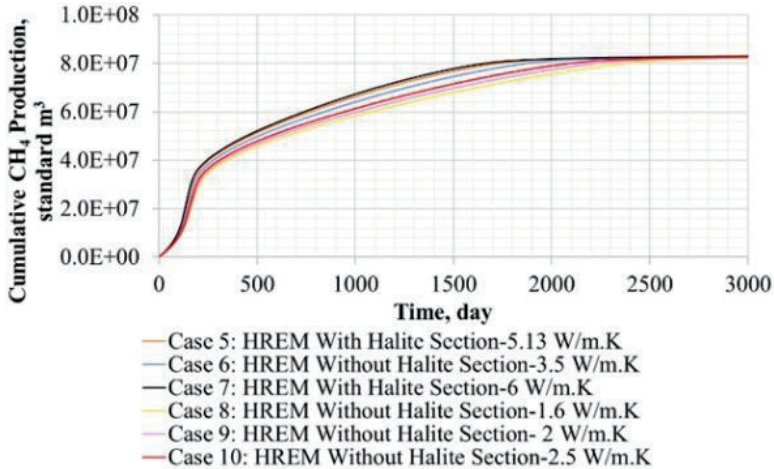


Figure 6: Pressure, temperature, and gas hydrate saturation change during gas production for Case 5 a) at the beginning b) 420th day c) 1800th day

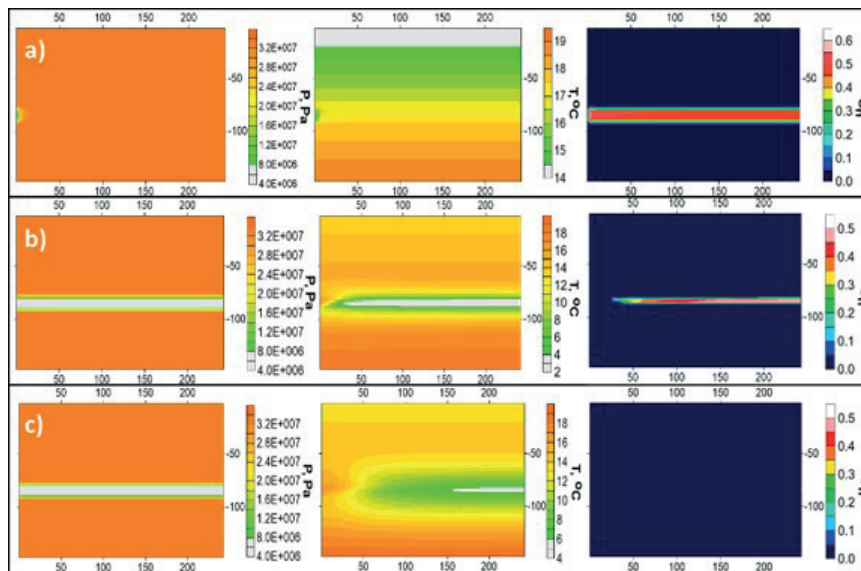


Table 1: Numerical simulation parameters for the Mediterranean Sea [3-4, 7-10, 14]

Parameter	Site 124 in the Western Mediterranean Sea	Site 374 in the Eastern Mediterranean Sea	Hypothetical Reservoir in the Eastern Mediterranean Sea (HREM)
Pressure at Seafloor, psia	3985.6	5956.5	4691
Temperature at Seafloor, oC	11.9	13.37	13.38
Salinity at Seafloor (% wt)	3.8	3.8	3.8
Pressure Gradient Below Seafloor, psi/ft	0.46	0.46	0.46
Salinity Change (% wt/m)	0.01694	0.0147 to 150 mbsf; 0.0411	0.0262
Geothermal Gradient, oC/m	0.063	0.0325 (0-109 mbsf); 0.0276 (109-161.5 mbsf); 0.0261 (161.5-209 mbsf); 0.0242 (210-256.5 mbsf)	0.0335
Porosity, %	50	50	50
Hydrate Saturation, %	50	50	50
Intrinsic Permeability (k <sub>x</sub> =k <sub>y</sub> =k <sub>z</sub> ), md	1000	1000	1000
Capillary Pressure Parameters of Van Genuchten	λ:0.46; Sirw:0.1; 1/Po: 10 kPa; Pmax:1000 kPa; Smaxw: 1.0	λ:0.46; Sirw:0.1; 1/Po: 10 kPa; Pmax:1000 kPa; Smaxw: 1.0	λ:0.46; Sirw:0.1; 1/Po: 10 kPa; Pmax:1000 kPa; Smaxw: 1.0
Relative Permeability Parameters of Modified Stone Equation	Sirw:0.1; Sirg:0.01; n:3.855; ng:2.5	Sirw:0.1; Sirg:0.01; ng:2.5	Sirw:0.1; Sirg:0.01; n:3.855; ng:2.5

*Table 2: Cases simulated with TOUGH + HYDRATE in this study*

Case	Location	Lower Boundary
1	Site 124	With Halite Section: 5.13 W/m.K
2	Site 124	Without Halite Section: 3.5 W/m.K
3	Site 374	With Halite Section: 5.13 W/m.K
4	Site 374	Without Halite Section: 3.5 W/m.K
5	HREM	With Halite Section: 5.13 W/m.K
6	HREM	With Halite Section: 3.5 W/m.K
7	HREM	With Halite Section: 6.0 W/m.K
8	HREM	Without Halite Section: 1.6 W/m.K
9	HREM	Without Halite Section: 2.0 W/m.K
10	HREM	Without Halite Section: 2.5 W/m.K

# Estimation of Missing Well-Log Sections Using Machine Learning Assisted Multivariate Imputation: A Case Study

Emre Artun<sup>1</sup>, Serhat Canbolat<sup>2</sup>, Elif Cihan Yıldırım<sup>2</sup>, Cansu Açıkğöz<sup>2</sup>, Onur Yürüker<sup>2</sup>

<sup>1</sup>Istanbul Technical University

<sup>2</sup>Turkish Petroleum Corporation



Collecting high-quality data in upstream operations is crucial because it can have a significant impact on future exploration and development decisions. Low-quality data can create statistical bias and decrease accuracy and precision in modeling studies. Machine learning applications that utilize petrophysical data also require high-quality and complete data sets. While well logs typically provide comprehensive spatial data related to the reservoir, variations in logging practices, occasional failures in logging equipment and well-specific issues in logging operations result in inconsistency in measured well logs. In this study, multivariate imputation by chained equations (MICE) was applied to estimate missing log values in a fractured carbonate reservoir in south-eastern Turkey. Preliminary modeling efforts and examples from the literature suggested using the random forests algorithm. MICE method that utilizes random forests as the internal machine learning algorithm was successfully applied to estimate missing log measurements in the three flow units of the reservoir (FU1, FU2, and FU3) at depths where a given type of log measurement was not available. Univariate analyses of all log measurements and well-based mean values showed that statistical features of logs were not altered significantly after the imputation.

## INTRODUCTION

In data-driven modeling efforts, missing data is an important data-quality problem that must be addressed properly. Three different types of missing data can be defined according to the dependability of data points of the missing variable (Rubin 1976):

- 1) Missing Completely at Random (MCAR): Missing data points are purely random and they do not depend on any other variable.
- 2) Missing at Random (MAR): Missing data points depend on some other variable in the data set
- 3) Missing not at Random (MNAR): Missing data points depend on the missing values themselves

While MCAR data would cause only information loss for the analysis, modeling with MAR and MNAR data can introduce significant bias to the analysis. Dealing with missing data is a common challenge when working with well log data sets. Missingness can be due to a number of reasons and missing data can be classified in any of the groups above. While it is typical to filter out depth levels that contain missing values, this can reduce the amount of information available for training and validating data-driven models. Especially, in the case of MAR and MNAR, imputation methods should be applied to estimate the missing points to complete

the data set in a reasonable way. On the other hand, imputing values can still introduce bias and impact the statistical distribution of the data (McDonald, A. 2022). Because of this, imputation should be performed by paying attention to the statistical features of the data set before and after the imputation.

Due to their resolution, availability and size, well logs can be highlighted as an indispensable type of data in subsurface modeling studies, including machine learning applications. When developing machine learning models, poorly understood data quality can negatively impact the predictive power of the algorithm, leading to incorrect results and conclusions (McDonald, 2021). Data quality issues within well log data can vary considerably between wells (Xu et al., 2019) and can be affected by incomplete data sets, erroneous values and inconsistency. Incomplete data was considered as one of the most problematic data-quality issues faced by petrophysicists (McDonald, 2021; Storey, 2016).

To estimate missing well logs, univariate (donor-based) or multivariate (model-based) imputation techniques can be utilized. Several studies have been conducted to demonstrate varying application of model-based imputation to well log data. These studies utilize machine learning algorithms to estimate the missing log type from other logs. To assess the impact of missing data on machine learning models, McDonald (2022) conducted a study using three commonly used algorithms, namely support vector regression, random forests, and artificial neural networks, for prediction purposes. The results showed that the performance of all three algorithms decreased with the decrease in the training data set size. Artificial-neural-network model was affected the most and the prediction results were highly variable with different data sets. In contrast, the random forests algorithm's results were the least affected and the most stable. In a similar study to predict density, neutron porosity, and sonic logs, neural-network based and tree-based algorithms were compared with respect to computational complexity, run time and prediction performance (Simoies et al. 2023). While all algorithms resulted in successful predictions, tree-based eXtreme Gradient Boosting (XGBoost) was highlighted as an efficient and robust algorithm for these applications. Tree-based methods have been proven to be successful in well-log imputation in other studies as well (Maldonado-Cruz et al. 2023).

In this study, we estimate the missing well logs of an oil field in south-eastern Turkey using a machine learning assisted multivariate imputation method. The field under consideration has been producing from three different fractured carbonate reservoirs (flow units FU1, FU2, and FU3) since 1990. The predictive model for

imputation was built using the raw log measurements from 48 wells after quality-checking, cleaning, and exploring the data by focusing on the perforation intervals. Missing log values in all three flow units were estimated with this multivariate imputation method. Quality of the imputation is evaluated through pre- and post-imputation distribution comparisons and summary statistics of individual wells. The results emphasize that multivariate imputation using random forests can be an effective method to achieve more complete petrophysical data sets in carbonate reservoirs.

### EXPLORATORY DATA ANALYSIS

The following logs were available in the data set; Caliper (CALI), Spontaneous Potential (SP), Sonic (Compressional Slowness) (DT), Laterolog Deep (LLD), Laterolog Shallow (LLS), Micro-spherically Focused Log (MSFL), Photoelectric Factor (PEF), Bulk Density (RHOB), Gamma Ray (GR), Gamma Ray Total Counts (GRTC), Neutron Porosity (NPHI). The log parameters for the wells were subjected to quality control, and erroneous measurements were removed from the data set. For better visualization, natural-log-transformation was applied to logs with lognormal distribution, such as LLD, LLS, and MSFL. Table 1 shows the number of wells (out of the total number of 48), in which the given log type was not available at all. The table reveals that for some log types, nearly half of the wells had missing data. In addition to full unavailability of a given log type in a given well and formation, there were also missing log measurements within a well. Figure 1 shows the distribution of missingness in the log measurements for each flow unit. Each column represents a type of log. Blue boxes indicate the availability of that log measurement and maroon boxes indicate that it is not available. The numbers on the left show the number of depth measurements for each missing/present log combination in that row. While distribution patterns are similar for each flow unit, the large proportion of missing logs should be recognized for further modeling studies. There are only two depth points in FU1 formation where no logs were taken, while this number is around 400 in FU2 and FU3 (1 well). However, on the good side, the number of measurements with different types of logs is quite high in each flow unit. This suggests that the amount of information that span across all wells can be considered for data imputation.

A practical approach used in data mining studies is to estimate missing data by assigning the mean value of the variable to the missing data point (also known as, donor-based, univariate imputation). For instance, if we were to analyze data from 48 wells in the reservoir, but Gamma Ray log is not available in 3 wells, we may substitute the missing wells with mean Gamma Ray value of the remaining 45 wells, rather than excluding those wells from the analysis. This approach assumes that the mean value would represent the variability in the data. In the first attempt for data exploration, the following steps were performed:

1) Available log measurements in perforation intervals were averaged for each well and for each flow unit (FU1, FU2 and FU3).

2) Mean imputation was applied to estimate average log value for each well and for each flow unit.

Through univariate data visualization, we examined the distributions of each log type according to formations, checked for similarities and differences between the flow units, and performed a quality-check of the log measurements. This helps identify data objects with characteristics that are considerably different than most of the other data objects in the data set (i.e., outliers) (Tan et al., 2016). Such analysis can be achieved by using box-and-whisker plots, which are designed to visualize the distribution of variables along with some key statistical features (Tukey, 1977):

- The lower and upper bounds of the box show the Q1 and Q3 values of the variable in the data set.
- The line in the middle of the box shows the median value,
- The line extending from the bottom of the box is bounded by the value obtained by subtracting  $1.5(Q1-Q3)$  from Q1,
- The line extending from the top of the box is bounded by the value obtained by adding  $1.5(Q1-Q3)$  to Q3,
- Values outside these limits are called outliers (i.e., values outside the normal distribution of the data) and are highlighted in the plots as dots.

Figure 2 shows the box-and-whisker plots of all log parameters averaged for each well according to perforation intervals for each flow unit. As can be seen in these plots, there is not a large variation among the flow units. Depending on the horizontal and directional wells and perforation thicknesses, there are outliers compared to the general distribution in the wells. The overall range of CALI logs decreases reflecting the decrease in well diameter in deeper formations. SP logs decrease slightly with depth, while NPHI logs show parallelism with an increase in depth. Resistivity logs (LLD, LLS, and MSFL) generally decrease with depth due to the overall increase in water saturation and decrease in hydrocarbon saturation.

Multivariate Imputation by Chained Equations (MICE)

It's important to note that while the patterns of missing log counts in all flow units are similar, the number and types of missing logs can vary significantly between them. This suggests that different flow units may require different approaches for handling missing log data, and that any predictive model should take into account the specific characteristics of each formation. Additionally, the high number of measurements with different types of logs in each formation is promising for the development of a predictive model that can accurately impute missing log data.

Missing data can be classified based on the structure of the data (van Buuren 2018). When variables are missing completely at random (MCAR), which means that they are missing independently and without any specific

reason, multivariate imputation by chained equations (MICE) has been found to be an effective approach (van Buuren and Groothuis-Oudshoorn in 1999). This method can be explained in four steps (Azur et al. 2011), and can be illustrated as shown in Figure 3:

1. Donor-based mean imputation is performed by assigning mean values to each missing data point. These mean values can be thought of as placeholders.
2. For a single variable (say,  $y$ ), the placeholders are deleted and considered as missing data again
3. A model is developed for the variable  $y$  using the available values from other variables to estimate the missing values in  $y$ . These estimated values are then saved for use in estimating other variables.
4. Steps 2 and 3 are repeated for all variables with missing data. After completing all variables, one cycle is completed. In step 4 the process can be repeated for a designated number of cycles, and the estimated values are then assigned as imputed data.

Different machine learning or statistical methods can be used in the development of the model in step 3. Random forest algorithm stands out as a powerful machine learning algorithm for the estimation of a single output variable. In the estimation of missing log values, this algorithm has been successfully applied (McDonald, 2022). Tree-based methods in general result in satisfactory predictions in petrophysical machine learning studies performed with petrophysical data. Therefore, random forests algorithm was chosen for the log-data imputation application. Random forests is an ensemble learning algorithm that combines the predictions of multiple individual decision trees. The final prediction is determined by aggregating the predictions of all the trees, typically through averaging in regression problems. In this study, randomForest package (Liaw and Wiener, 2002) in R statistical computing environment (R Core Team, 2021) was used to train the random forest models. As a pre-processing step, natural-log-transformation was applied to logs with lognormal distribution, such as LLD, LLS, and MSFL. Number of trees to grow was set as 500 and number of variables randomly sampled as candidates at each split was set as 10. Before performing the MICE methodology on the whole data set, preliminary machine-learning models have been developed with the available log measurements in the following structures to test the random forest algorithm:

- Estimation of PEF log from other logs and X, Y, depth
- Estimation of LLD log from all other logs except LLD, LLS, MSFL and X, Y, depth
- Estimation of LLS log from all other logs except LLD, LLS, MSFL and X, Y, depth
- Estimation of MSFL log from all other logs except LLD, LLS, MSFL and X, Y, depth
- Estimation of NPHI log from other logs and X, Y, depth
- Estimation of GR log from all other logs except GRTC and X, Y, depth.

Figure 4 shows the cross-plots of the predictions of these 6 models. The points on the line in the middle indicate that the prediction was completely correct, while the points moving away from the line indicate that the prediction differed from the actual value, and as the distance from the line increases, the error rate also increases. The dark gray points represent the measurements used in the training (model development) stage, while the blue ones represent the measurement points that was not included in the model training data during the development stage. Overall, we can see that all models can make log predictions within acceptable accuracy levels. These experiments show that the random forests algorithm can be used to predict missing log values, thus can be considered as a reliable learning algorithm in the MICE application. These tests are important since we will not be able to validate the predictions for the missing values.

For each flow unit, MICE methodology assisted with random forests algorithm was applied with 10 iterations. In this study, mice package (van Buuren and Groothuis-Oudshoorn, 2011) in R statistical computing environment (R Core Team, 2021) was used. Same hyperparameters as in the preliminary models outlined above were used. As a result of this process, a prediction was made for each measurement point where the log value was missing. Thus, all log types were obtained as real or predicted for all wells and formations. Figure 5 shows the density (frequency) distributions of all log types before and after prediction in each of the three formations. These distributions show us that the overall distribution of log parameters did not change significantly after applying the data imputation method. Figure 6 shows sample log sections from different wells that show actual log measurements and imputed log measurements for the missing sections. By analyzing missing sections, we can see that imputed log values are within reasonable ranges. Since we cannot validate these predictions of missing values, statistical features and qualitative assessments are the only ways to comment on the overall quality of the imputation method.

Imputed log values are averaged for each well and for each flow unit. The histogram distributions of these values are shown in Figures 7, 8, and 9 for each of the three flow units, respectively. The histograms on the left show the distributions when univariate mean imputation was applied for missing log values. The histograms on the right show the distributions obtained after missing values were estimated using the multivariate data imputation method. These comparisons show that there were no dramatic changes in the histograms after the data imputation method. However, since the multivariate imputation method considers multiple variables (logs) covering a spatially large area, we can comment that they are more reliable than the univariate mean imputation. Figure 10 shows the box plots created with the values obtained after the imputation. When compared with the box plots created using raw data (Figure 2), we can see that the general distributions of the parameters are similar. Outlier points remained the same, which shows that the imputation process has not

produced new outliers in the data set. These findings demonstrate that the imputation process has been successfully completed.

## CONCLUSIONS

In this study, multivariate imputation using chained equations methodology was applied to estimate missing well log sections in a fractured carbonate reservoir in south-eastern Turkey. The methodology was applied to three flow units separately in a data set with 48 wells. Following are the key conclusions drawn from the study:

- 1) Random forests algorithm can be used to train machine learning models for estimation of well logs from other available log types and spatial coordinates.
- 2) Density distributions and well-based summary histograms for each of the three flow units revealed that statistical features of well logs have not changed significantly.
- 3) Because of inclusion of multiple log types in model building, multivariate imputation using random forests can be a reliable methodology for estimating missing well log sections.
- 4) Data quality and proportion of missing data play an important role in the success of the methodology presented in this study. More research is needed to determine acceptable levels of missingness in the data set. This uncertainty and difficulty of validation can be considered as the main limitations of this methodology.

## ACKNOWLEDGEMENTS

Authors would like to express gratitude to Turkish Petroleum Corporation for providing support during this study.

## REFERENCES

- Azur, M., Stuart, E. A., Frangakis, C., and Leaf, P. J., 2011. "Multiple Imputation by Chained Equations: What Is It and How Does It Work?" *Int. J. Methods Psychiatr. Res.* 20 (1): 40–49.
- Liaw, A., Wiener M., 2002. "Classification and Regression by randomForest." *R News*, 2(3), 18-22. <https://CRAN.R-project.org/doc/Rnews/>
- Maldonado-Cruz, E., Foster, J.T., Pyrcz, M.J. 2023. "Sonic Well-Log Imputation Through Machine-Learning-Based Uncertainty Model/Sonic-Well-Log-Imputation-Through-Machine-Learning" *Petrophysics* 63(2):253-270 <https://doi.org/10.30632/PJV64N2-2023a7>
- McDonald, A., 2022. "Impact of Missing Data on Petrophysical Regression-Based Machine Learning Model Performance." In *SPWLA 63rd Annual Logging Symposium Proceedings*. SPWLA-2022-0125. 11-15 June. Stavanger, Norway.
- McDonald, A., 2021. Data Quality Considerations for Petrophysical Machine Learning Models. *Petrophysics*, 62(6): 585–613. <https://doi.org/10.30632/PJV62N6-2021a1>

R Core Team, 2021. "R: A language and environment for statistical computing". R Foundation for Statistical Computing, Vienna, Austria. <https://www.R-project.org/>

Rubin, D.B. 1976. "Inference and Missing Data" *Biometrika* 63(3):581-592. <https://doi.org/10.2307/2335739>

Simoes,V., Mainar, H., Abubakar, A., Zhao, T. 2023. "Comparative Study of Machine-Learning-Based Methods for Log Prediction" *Petrophysics* 63(2):192-212. <https://doi.org/10.30632/PJV64N2-2023a4>

Storey, M. C., 2016. Demystifying Log Quality Control. Society of Petroleum Engineers - SPE Asia Pacific Oil and Gas Conference and Exhibition 25-27-October). doi:10.2118/182313-ms.

Tan, P., Steinbach, M., Karpatne, A., Kumar, V., 2016. *Introduction to Data Mining*, Pearson, London, England.

Tukey, J. W, 1977. *Exploratory Data Analysis*. Addison-Wesley, Reading, Massachusetts.

Xu, C., Misra, S., Srinivasan, P., and Ma, S., 2019. "When petrophysics meets big data: What can machine do?" SPE Middle East Oil and Gas Show and Conference, MEOS, Proceedings, 2019-March (MI). doi:10.2118/195068-ms.

van Buuren, S., 2018. *Flexible Imputation of Missing Data*. 1st ed. Chapman & Hall/CRC Interdisciplinary Statistics.

van Buuren, S., Groothuis-Oudshoorn, K., 2011. "mice: Multivariate Imputation by Chained Equations in R." *Journal of Statistical Software*, 45(3), 1-67. doi:10.18637/jss.v045.i03.

van Buuren, S., and Groothuis-Oudshoorn, K., 1999. "Flexible Multivariate Imputation by MICE." *TNO Prevention; Health*.

Keywords: Well Logs, Multivariate Imputation



Figure 1. Distribution pattern of missing logs in each flow unit.

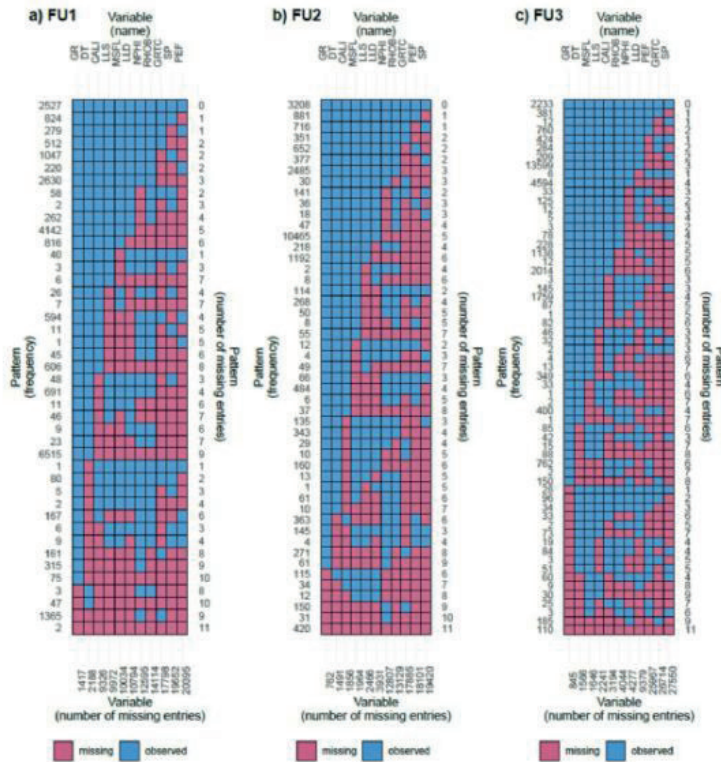


Figure 1. Distribution pattern of missing logs in each flow unit.

Figure 2. Box plots showing the distribution of averaged log values by flow unit.

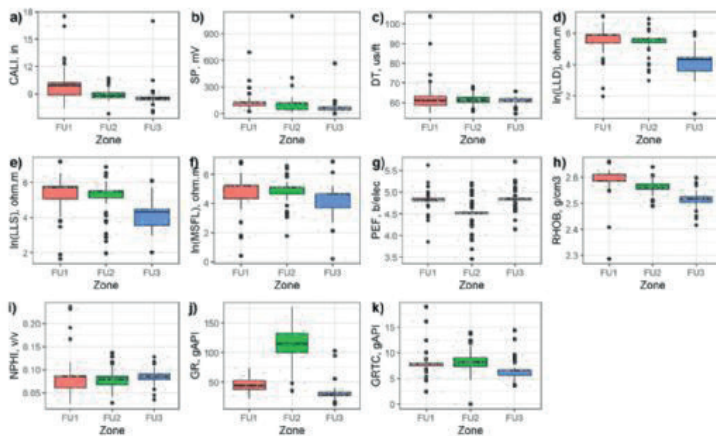


Figure 2. Box plots showing the distribution of averaged log values by flow unit.

Figure 3. Multivariate imputation by chained equations: an example application.

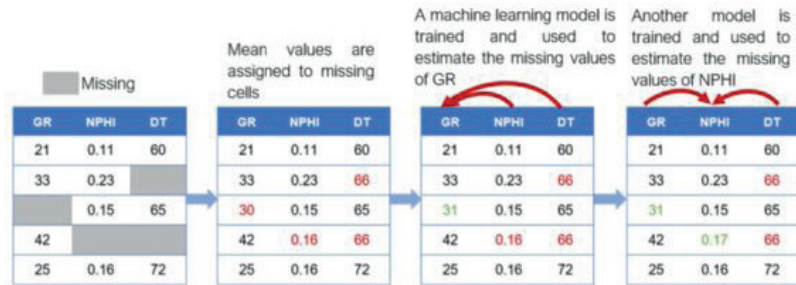


Figure 3. Multivariate imputation by chained equations: an example application.

Figure 4. Results of random forest algorithm for imputing missing logs from other log types and spatial properties a) LLS, b) LLD, c) MSFL, d) PEF, e) NPHI, f) GR.

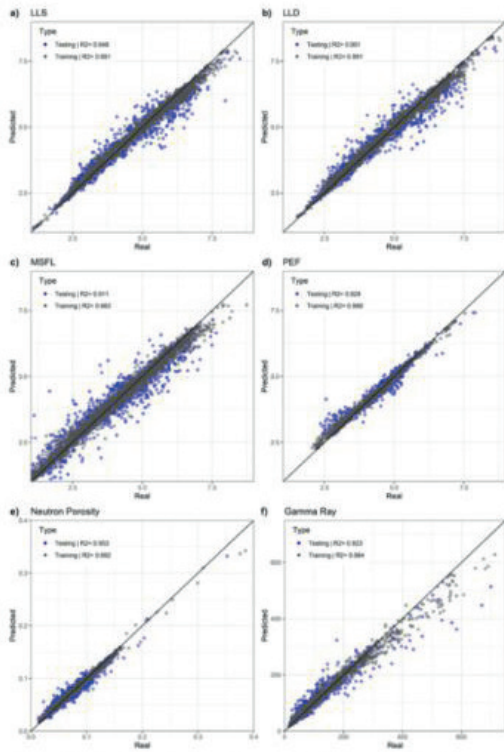


Figure 4. Results of random forest algorithm for imputing missing logs from other log types and spatial properties a) LLS, b) LLD, c) MSFL, d) PEF, e) NPHI, f) GR.

Figure 5. Parameter distributions before and after the multivariate imputation by chained equations (MICE) method.

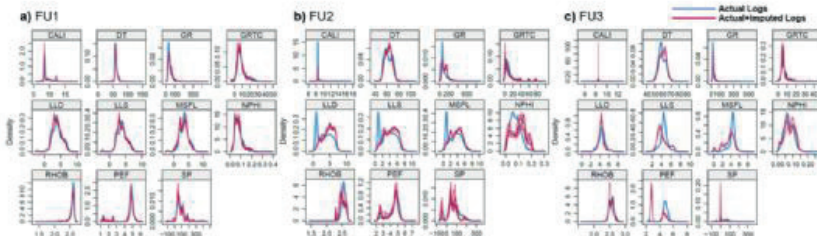


Figure 5. Parameter distributions before and after the multivariate imputation by chained equations (MICE) method.

Figure 6. Sample log sections from different wells that show actual log measurements and imputed log measurements for the missing sections.

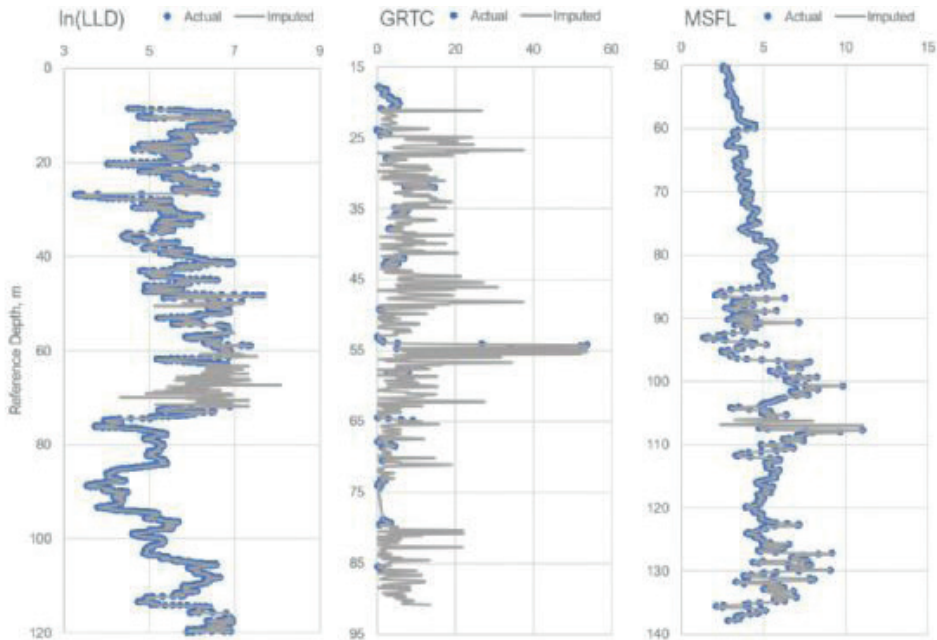


Figure 6. Sample log sections from different wells that show actual log measurements and imputed log measurements for the missing sections.

Figure 7. Histograms of average log values in wells in FU1 after multivariate imputation using chain equations: a) distribution before data imputation, b) distribution after data imputation.

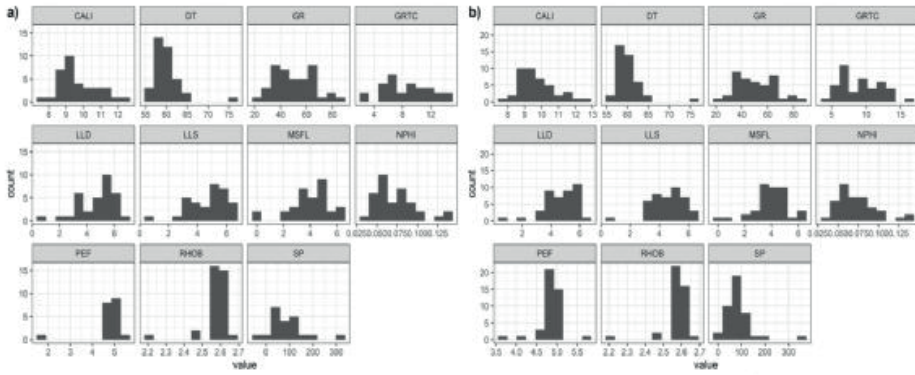


Figure 7. Histograms of average log values in wells in FU1 after multivariate imputation using chain equations: a) distribution before data imputation, b) distribution after data imputation.

Figure 8. Histograms of average log values in wells in FU2 after multivariate imputation using chain equations: a) distribution before data imputation, b) distribution after data imputation.

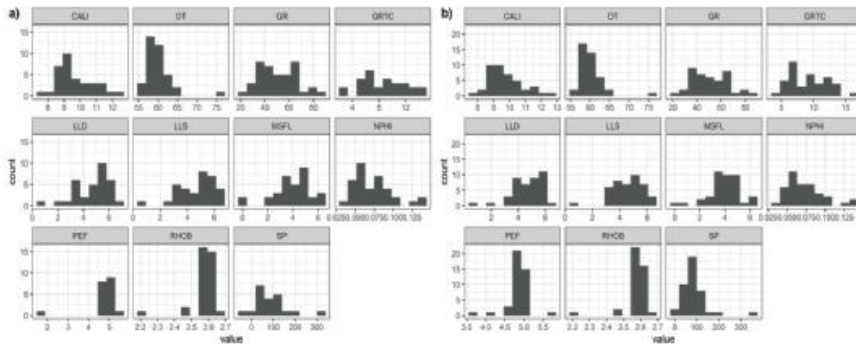


Figure 8. Histograms of average log values in wells in FU2 after multivariate imputation using chain equations: a) distribution before data imputation, b) distribution after data imputation.

Figure 9. Histograms of average log values in wells in FU3 after multivariate imputation using chain equations: a) distribution before data imputation, b) distribution after data imputation.

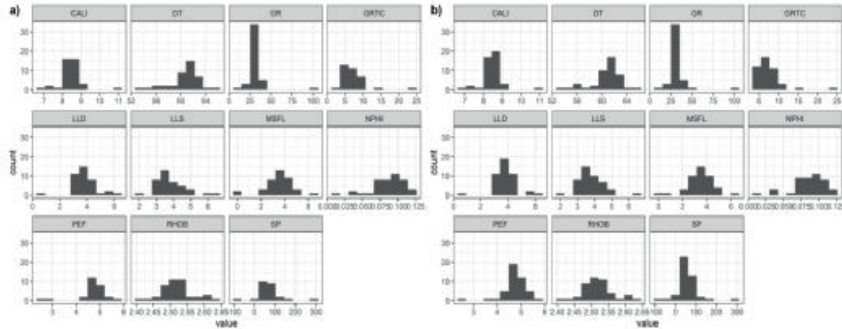


Figure 9. Histograms of average log values in wells in FU3 after multivariate imputation using chain equations: a) distribution before data imputation, b) distribution after data imputation.

Figure 10. Box plots showing the distribution of mean log values obtained after data imputation for each formation.

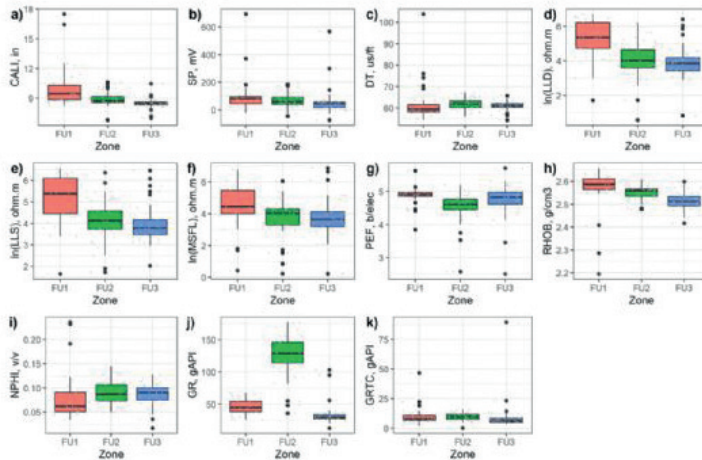


Figure 10. Box plots showing the distribution of mean log values obtained after data imputation for each formation.

Table 1. Number of wells with missing logs by log type in each flow unit.

ZONE	CALI	SP	DT	LLD	LLS	MSFL	PEF	RHOB	GR	GRTC	NPHI
FU1	9	20	8	19	18	18	24	12	1	25	15
FU2	6	20	8	20	17	18	23	10	1	18	13
FU3	7	25	10	18	18	18	23	11	3	18	14

# Coal Bed Methane Characterization for Gas Production Recovery Optimization - Zonguldak, Turkey



**Sofiane Belhocine, Ahmet Ergün Mengen, Muhammed Emin Bulguroğlu, Rabah Boudissa**

Unconventional department, Turkish Petroleum Corporation (TPAO) - Ankara / Türkiye

## 1. INTRODUCTION

As the worldwide energy demand has continued to increase for the last decade, Turkish Petroleum Corporation (TPAO) has taken initiatives to find more opportunities and expand her recoverable reserves portfolio from complex unconventional resources. TPAO has expanded her exploration and development activities to unconventional resources. One of the major promising gas resources found in Turkey are the coal bed methane plays located in the northern part of Turkey (Zonguldak & Amasra Black sea area). Zonguldak area as displayed in Figure 1 below contains too many shallow wells for mining purposes.

This paper demonstrates the integrated multidisciplinary work, which has been developed to construct a reservoir model and come up with most optimal development scenarios to evaluate the project value. The main challenges were the data quality, quantity, and very limited number of tested wells in the target zones. The static modeling, properties prediction, volumetric estimates and dynamic modeling are highly challenging in this context

Considering the clustered data coverage across the study area and the absence of any seismic guidance; surface geology, borehole image logs and mines data were integrated for sedimentological structures analysis that provides first depositional trends (Coal, shale, sandstone and limestone). Coal and cleat petrophysical data have been derived from literature in which the information belongs to the coal bed reservoirs having the similar methane adsorption trends and obtained from the available limited core data analysis and been subject to carrying out uncertainty analysis later. In the absence of special core analysis data (SCAL), Corey correlations dependent SCAL curves have been constructed based on analogs for shale and coal formations.

A full reservoir characterization study was also achieved by integrating all available geological data with the extensible dynamic data (gas adsorption, PVT analysis and hydraulic fracture/ post fracture data).

Firstly, the gas in place from dynamic model has been validated with the ones estimated from the geological model (an error of less than 3% has been achieved in terms of differences, which is considered as a very acceptable error margin). Then we put in place the below forecast scenarios to optimize the field development plan, this was based on different technical criteria (limited pilot area, thin coal bed seams (average of 3m) & area topography):

- ♣ 1 Well with 2 stages hydraulic fracture
- ♣ 2 Wells with 2 stages hydraulic fracture for each well
- ♣ 3 Wells with 2 stages hydraulic fracture for each well

♣ 4 wells with 2 stages hydraulic fracture for each well

♣ 5 wells with 2 stages hydraulic fracture for each well

As results & among the tested forecast scenarios, a pattern of five (5) wells can lead to higher gas production and higher gas recovery with 2 stages hydraulic fracture for each well.

## 2. CBM DYNAMIC MODELING WORKFLOW

In the aim of performing the full development plan for Zonguldak sector, the workflow below has been carried out step by step (Fig 2):

- ♣ Static model QC
- ♣ Dynamic model extraction from the full fine geological model
- ♣ Property distribution for Coal, shale matrix and fracture system
- ♣ Fluid Modeling (blackoil sets of correlations for a dry gas system)
- ♣ Adsorption data for both coal and shale system
- ♣ Compressibility data (from analogs)
- ♣ Well planning, completion and hydraulic fracture data
- ♣ Forecast scenarios optimization

### 2.1 PVT analysis

The type of gas in Zonguldak region is mostly methane with low concentrations of other hydrocarbon and non-hydrocarbon components. A gas chromatography has been performed on an early drilled well and has showed the composition highlighted in Table 1. Another gas chromatography has been carried out after a limited flow back period and has confirmed the same gas composition with more than 95% methane. (Table 1)

Based on the above gas chromatography and a gas gravity of 0.6 (air), a Blackoil PVT Model has been developed for CBM Zonguldak field using Petrel inside built-in correlations (Figure 3 below). Figure 3 highlights the gas formation factor and gas viscosity variation with pressure changes. References (1, 2, 3, 4, 5, 6).

♣ Initial Gas FVF = 0.0067  $\text{m}^3/\text{m}^3$

♣ Initial gas viscosity = 0.016 cP

### 2.2 Adsorption Data

Several lab experiments for the total gas content and gas desorption had already been done for Zonguldak and other coal bed methane plays. Table 2 describes the recent adsorption data done on some CBM samples from Zonguldak area (2019).

Gas adsorption studies done on the coal samples from Karadon field within Zonguldak province.

Methane adsorption at 30 °C using GAI-100 system and 99.95% pure methane

(our chromatography study has shown more than 95% methane)

Measure delta pressure due to gas adsorption

Modeled using Langmuir Isotherm adsorption function:

Gas adsorption measured at different pressures

Modeled using Langmuir isotherm adsorption

$$V=(V_{L,P})/(P_{L+P})$$

VL: Langmuir volume value (scf/ton) (at high pressure)

PL: Langmuir pressure (psia) (half of volume is adsorbed)

V: Gas amount in the coal (scf/ton)

P: Corresponding pressure range value (psia)

Same analysis has shown that the average ASH (minerals) is 10% and moisture (water) is around 3%. Those values in addition of coal density estimated at 1600 kg/sm<sup>3</sup> (1.6 g/cc) have been used for gas in place estimation as well as for the gas production forecast scenarios.

Zonguldak shale may have also potential for adsorbed gas with lower gas content based on the literature survey. We expect some gas adsorbed on the shale surfaces which may contribute to Zonguldak total gas production. As no laboratory experiment was performed on shale samples so far, a default low gas content has been assigned for shale layers with a lean gas adsorption displayed in Figure 5.

### 2.3 SCAL Data

In the absence of SCAL data for Zonguldak coal and shale facies, some analogs have been used for both shale and coal systems as shown in Figure 6 below.

For the coal's cleat system and shale-fractured system, a straight-line relative permeability curves have been used with a 100% water saturation of the fractured zones shown in Figure 7.

### 2.4 Data & Results

The next step consists in determining the gas in place potential for the study area. We have used a gradient of pressure of 0.43 psi/ft, gas water contact on top of structure (cleat and shale fractures filled with water). Table 3 summarizes the values used for the dynamic modeling study.

The estimation of volumes in place was mainly based on the adsorbed gas in both shale and coal surface (in absence of laboratory measurements and test data, the free gas volume has been removed from the total gas volumes considering only the adsorbed gas in the coal and the shale).

The below table highlights the gas in place for our total sector and by facies (coal and shale). Note that the gas

in place is only the adsorbed part of it (from literature the free gas can present 2% only from total gas in place for CBM plays).

The big part of gas in place in the sector of study is the shale facies, this is due to the thick shale layers we have seen in the stratigraphy of the old exploration wells. The average coal layers in this sector is around 3m where the average shale layers thickness is more than 10m. Adsorption laboratory experiment for shale will be considered to confirm the presence of adsorbed gas in that shale.

Several scenarios have been tested, starting from 1 well to 5 wells with 2 stages hydraulic fracture stages for each well, the idea for 5 wells spot as displayed in Figure 8 is to help dewatering the system in a short period, get gas desorbed from the coal and achieve higher peak gas production rate in a short period of production time.

Due to very low coal and shale permeabilities, wells can't produce at economic rates without the hydraulic fractures, all the forecast scenarios are considering hydraulic fractures. Due to model size, Petrel inside built correlations for hydraulic fracture have been used to honor the effect of hydraulic fracture on the wells. Input hydraulic fracture data (Width, conductivity, half length and height) have been simulated using frac tool and the output were integrated in the dynamic model and converted into transmissibility and productivity index multipliers to honor the hydraulic fracture effect.

Figure 9 below summarizes the production performance results of simulating the 5 scenarios with two stages hydraulic fracture:

- ♣ 1 Well with 2 stages hydraulic fracture
- ♣ 2 Wells with 2 stages hydraulic fracture for each well
- ♣ 3 Wells with 2 stages hydraulic fracture for each well
- ♣ 4 wells with 2 stages hydraulic fracture for each well
- ♣ 5 wells with 2 stages hydraulic fracture for each well

The below table (Table 5) summarizes the production rates and cumulative volumes as well as the pick gas rate for each forecast scenario.

### 3. CONCLUSION

- ♣ 5 wells spot scenario with 2 stages hydraulic fractures for each well can produce 946 MM sm<sup>3</sup> of gas in 20 years with a peak gas rate of 174k sm<sup>3</sup>
- ♣ The major total gas production is obtained from the coal zones (Shale production represents less than 5% of total gas production due to low gas content in shale).
- ♣ Lower gas production observed in scenarios with less production wells (1, 2 and 3 wells) is due to the de-watering period which takes more time compared to 4 and 5 wells scenarios
- ♣ Targeting deep zones in Zonguldak where the gas content is higher compared to the shallowest part (hydraulic fractures can enhance the total system conductivity and connect the cleat fracture system to the wells)

♣ Reducing the bottomhole flowing pressure with a presence of downhole water pumps will help to decrease the de-watering period and reach a peak production rate in less than 5 years.

#### 4. RECOMMENDATION

♣ Further laboratory analyses are required to understand Zonguldak coal: Adsorption at different depths, reservoir pressure, cleat permeability, cleat compressibility.

♣ Installing a downhole, water pump will help achieve a low BHP values and improve the de-watering phase.

♣ Spot well strategy can help draining more water at the first stages of production and therefore allows more gas to be desorbed from the coal seams.

♣ Analyses are also required for shaly layers to understand the mineralogy, gas adsorption potential and petrophysical parameters.

♣ A DFIT or DST are required to understand reservoir pressure and formation permeability and how they vary with depths for the different coal layers.

#### 5. REFERENCES

♣ Hall, H.R., and Yarborough, L.: 'A new equation of state for Z-factor calculation,' OGJ (June 18, 1973).

♣ Piper, L.D., McCain, W. D., Jr., and Corredor, J.H.: 'Compressibility Factors for Naturally Occurring Petroleum Gases.' Paper SPE 2668 presented at the 1993 SPE ATCE: SPE Reprint Series No. 52 (1999)

♣ Carr, N. L., Kobayashi., and Burrows, D.B.: 'Viscosity of hydrocarbon Gases Under Pressure,' Trans. AIME (1954) 201, 264-272

♣ Meehan, D.N.: 'Improved Oil PVT Property correlations,' Oil and Gas Journal, 78(43): 64-71, (October 1980)

♣ Meehan, D.N.: 'A Correlation For Water Compressibility,' Pet. Eng. Int., (Nov, 1980) 125-126

♣ Kestin, Khalifa, & Correia, 'Effect of Pressure on the Viscosity of Aqueous NaCl Solution in the Temperature Range 20-150 C.' J. Chem. Phys. Ref. Data, Vol 10, No, 1, 1981, P71

♣ T.L. Hower, SPE, Malkewics Hueni Associates, Inc., 'Coalbed Methane Reservoir Simulation: An evolving Science' – SPE 84424

♣ Sinayuç, C., and Gümrah, F. (2009) Modeling of ECBM recovery from Amasra coalbed in Zonguldak Basin, Turkey, International Journal of Coal Geology, 77, 162-174

♣ Yalçın, M.N., Schenk, H.J., and Schaefer, R.G. (1994). Modeling of gas generation in coals of the Zonguldak basin (northwestern Turkey). International Journal of Coal Geology, 25, 195-212

♣ Yalçın M.N., İnan, S., Gülbin, G., Mann, U., and Schaefer, R.G (2002). Carboniferous coals of the Zonguldak basin (northwest Turkey): Implications for coalbed methane potential. American Association of Petroleum Geologists bulletin, 86 (7), 1305-1328



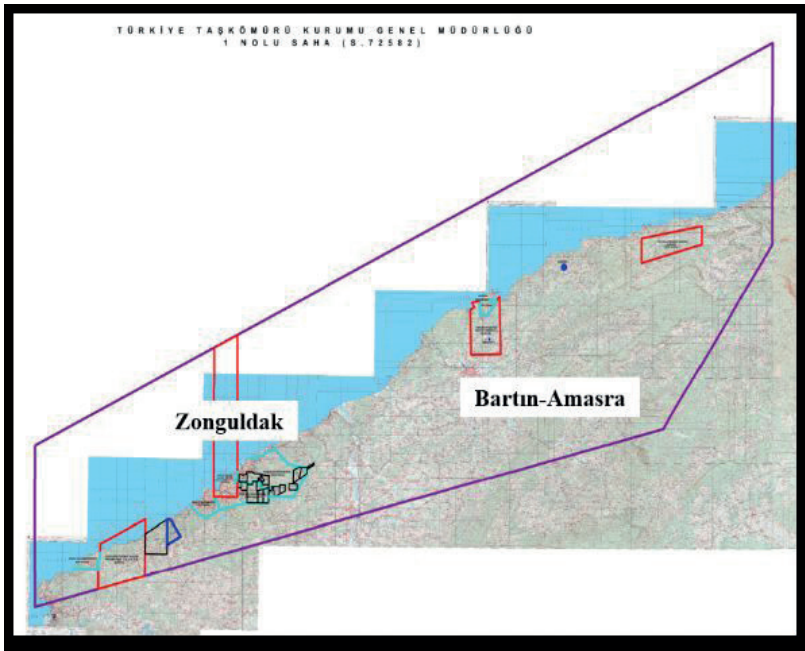


Figure 1

CBM Dynamic Modeling workflow

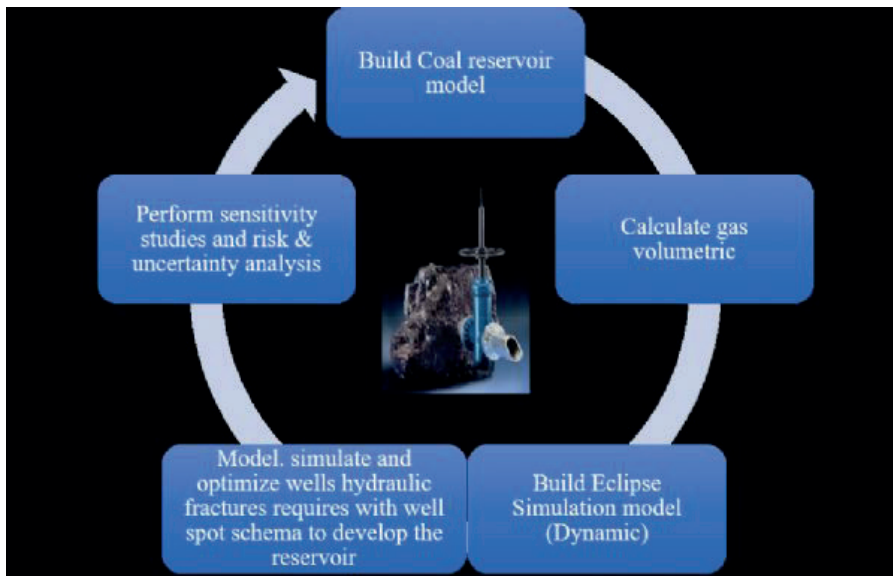


Figure 2 This describes the different steps we have followed in order to build a dynamic model and come up with the most economic development scenario to optimize our gas production.

Component	Analysis 1 (%)	Analysis 2 (%)
O2	0.004	0
N2	1.44	0
CO2	0.126	4.96
C1	95.21	95.01
C2	2.182	0
C3	0.742	0
iC4	0.114	0
nC4	0.132	0
iC5	0.027	0
nC5	0.019	0
C6+	0.004	0

Table 1

PVT Model for Zonguldak CBM project

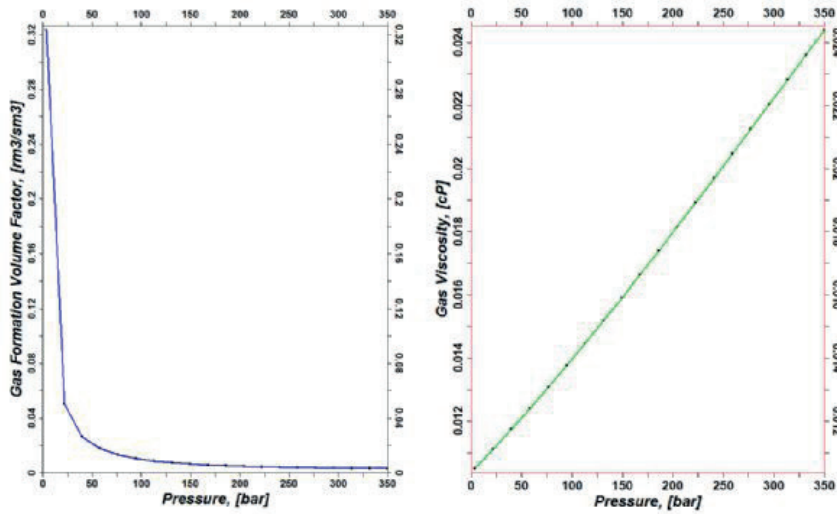


Figure 3

Langmuir Coal isotherm adsorption Data – Coal

Pressure (Psia)	Methane Storage Capacity (scg/ton) - Sample 1
14.7	0
114.7	125.44
214.7	211.15
314.7	273.42
514.7	357.86
104.7	465.72
2014.7	458.37
5014.7	613.71
V1 (scf/ton)	666.67
P1 (psia)	431.47

Table 2

Langmuir coal isotherm adsorption

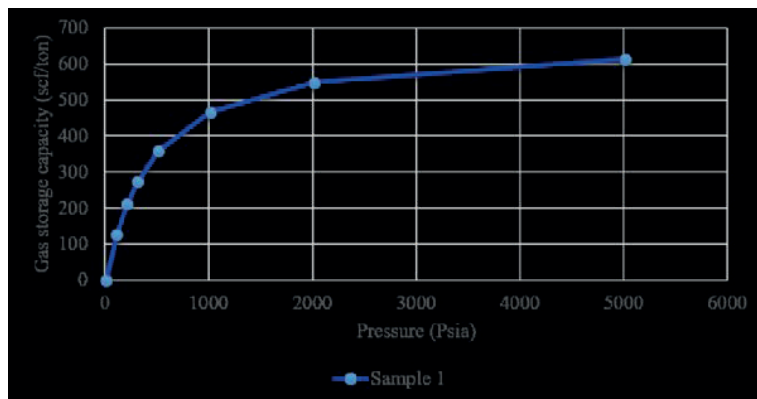


Figure 4 The release of Coal adsorbed gas is commonly described by a pressure relationship called the Langmuir Isotherm. It is the total adsorbed gas content versus pressure. As pressure increase to infinite the volume of adsorbed gas approaches the Langmuir maximum volume.

Shale Langmuir shale isotherm adsorption

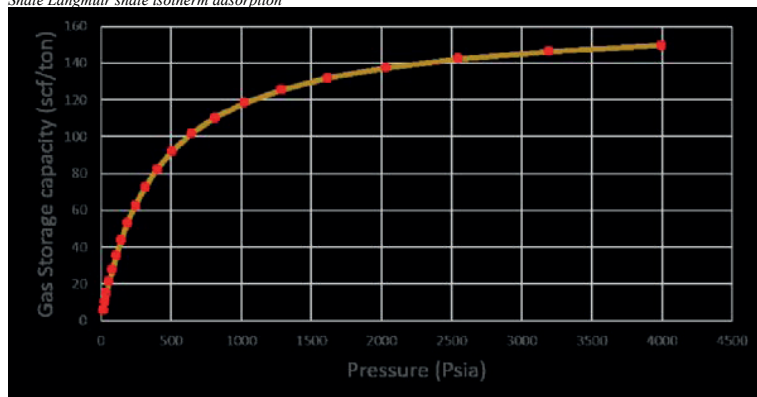


Figure 5 Figure 4 The release of shale adsorbed gas is commonly described by a pressure relationship called the Langmuir Isotherm. It is the total adsorbed gas content versus pressure. As pressure increase to infinite the volume of adsorbed gas approaches the Langmuir maximum volume. The total content of gas in shale is considered much lower than the one in the coal.

Shale & Coal SCAL data (Relative permeability curves, system gas/water)

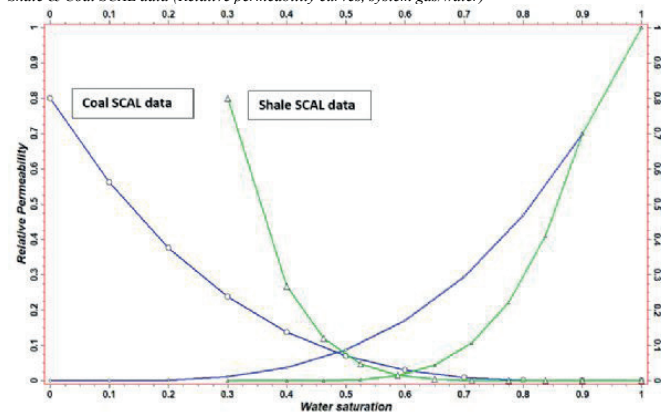


Figure 6

Cleat and Frac system relative permeability curves

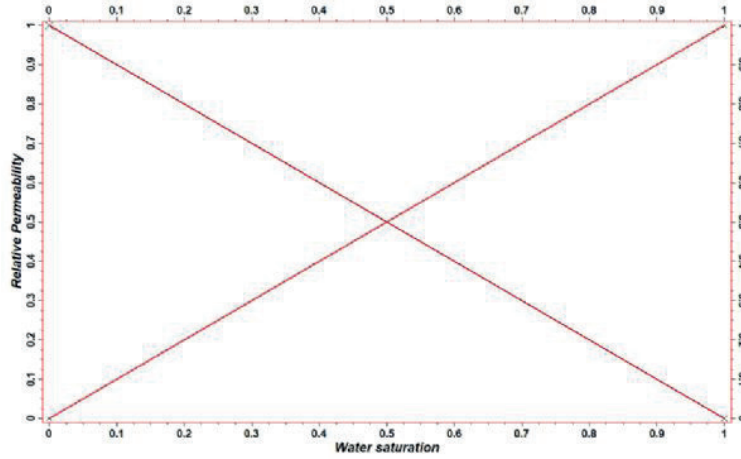


Figure 7 The relative permeability curves will determine how water and gas would flow in reservoir conditions, usually in the natural fracture system straight lines are used to estimate the relative flow of water and gas.

CBM Dynamic Data Summary

Data	Value	Source
Coal Density (g/cc)	1.6	
Coal Langmuir volume (scf/t)	667	
ASH content (%)	10	
Moisture Content (%)	.	
Pressure gradient (psi/ft)	0.43	
Average Initial reservoir pressure (Psia)	1842	
Initial water saturation (%)	100	
Average Fracture spacing (m)	10	
Cleat permeability (md)	2	
Cleat porosity (%)	2	
Coal relative permeability	Curve	Analog
Cleat relative permeability	Straight line	
Shale Data	Analog	Petrel default
Coal compressibility (psia-1)	1.38E-6	Analog
Gas gravity	0.6	Assumption
Water salinity (ppm)	20000	Analysis
Completion	7in wellbore with 2 stages hydraulic fracture using correlations	
Production control	Minimum BHP 10 bars (water pump)	

Table 3 Table describes all the data which have been used in the dynamic model and the different sources of these data. ASH: Ash is part of coal that does not adsorb gas Moisture: Moisture competes with methane for adsorption sites on the surface of coal BHP: Bottom hole Pressure

CBM Gas in Place Estimation

	Gas in place (MM sm <sup>3</sup> )	Percentage (%)
Coal	1929.41	37.23
Shale	3252.81	62.77
Field	5182.22	100

Table 4 CBM: Coal Bed Methane MM: Millions

Sector Model with the 5 vertical wells schematic

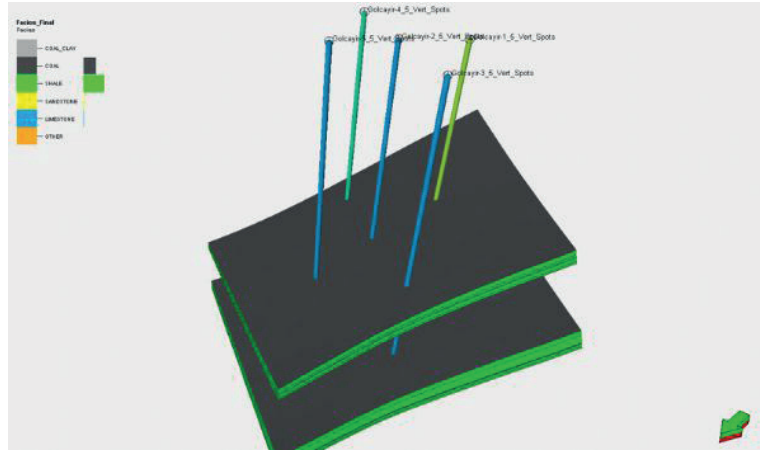


Figure 8

20 years results of the 5 forecast scenarios

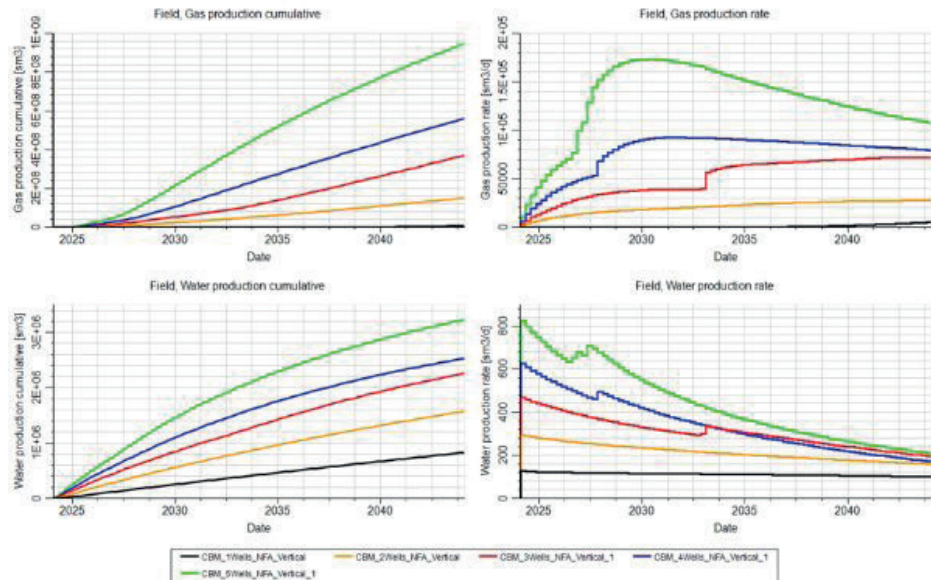


Figure 9

*20 years-production results for the five (5) wells forecast scenarios*

Case	Pick gas rate (sm <sup>3</sup> /d)	Initial water production rate (sm <sup>3</sup> /d)	Gas cumulative @ 1 year (MM sm <sup>3</sup> )	Gas cumulative @ 2 years (MM sm <sup>3</sup> )	Gas cumulative @ 3 years (MM sm <sup>3</sup> )	Gas cumulative @ 4 years (MM sm <sup>3</sup> )	Gas cumulative @ 5 years (MM sm <sup>3</sup> )	Gas cumulative @ 2042 (MM sm <sup>3</sup> )
1 Well	5500	127	0.2	0.5	0.8	1	1.2	10.8
2 wells	28200	293	1.5	5.1	9.7	15.3	21.5	155
3 wells	73000	467	2.7	2.7	19	30.8	44	372
4 wells	93400	627	5.01	5.01	33.3	53	81.5	560
5 wells	174000	829	8.4	8.4	55.5	95.6	161.6	946

*Table 5*

# Assessing CO<sub>2</sub> Enhanced Geothermal Potential and CO<sub>2</sub> Storage in a Red Sea Rift Basin, Al Wajh: A Comprehensive Reservoir Model and Simulation Study



**Bora Yalcin, Justin Ezekiel, Martin Paul Mai**  
King Abdullah University of Science and Technology

The transition towards a Net Zero Carbon Economy in response to the growing global demand for energy presents significant socio-economic challenges, such as equitable access to affordable clean energy solutions. Geothermal energy, as a renewable energy source, has gained attention as a viable alternative to fossil fuels. Utilizing supercritical CO<sub>2</sub> for geothermal heat extraction, CO<sub>2</sub> plume geothermal (CPG), offers advantages such as enhanced mobility while enabling CO<sub>2</sub> sequestration. The integration of CO<sub>2</sub> capture, utilization, and storage (CCUS) in geothermal reservoirs aligns with circular carbon economy models and supports the goals of sustainable energy development. The geothermal potential of deep saline aquifers, particularly in the young and high-heat-flux Red Sea rift basins of western Saudi Arabia, holds promise for geothermal heat extraction and CO<sub>2</sub> storage. However, accurately assessing the geothermal and carbon storage potential requires comprehensive characterization of unknown parameters specific to the target aquifer units. These parameters include gross rock volume (GRV), recoverable energy, heat capacity, porosity, and temperature. This study presents a detailed reservoir model developed using advanced geostatistical techniques and a state-of-the-art CO<sub>2</sub> fluid flow simulator, aiming to constrain uncertain parameters and provide accurate estimates of recoverable geothermal energy and CO<sub>2</sub> storage capacity of the target aquifers. Through simulation and analysis, the study identifies the volumetric and spatial arrangement of high-permeable submarine channel sands as critical factors affecting reservoir production performance. Our Injection production simulations of CPG activities reveal the rock volumetrics that can economically recover the desired amount of geothermal heat energy. Our findings highlight the potential to produce 790 TWh of geothermal energy in a 40-year injection-production scenario and store 76.5 Giga-tonnes of CO<sub>2</sub> in the Burqan and Umluj units of the Al Wajh basin. This work contributes to the understanding of geothermal reservoirs, particularly in syn-rift submarine clastic systems. It provides valuable insights for future research in detailed reservoir modeling and simulation studies, offering a stepping stone toward the sustainable harnessing of CPG energy in the renewable energy sector.

## INTRODUCTION

The combination of CO<sub>2</sub> plume geothermal (CPG) technology with CO<sub>2</sub> storage is pivotal for sustainable energy development. Geothermal energy, a clean renewable source, offers a promising alternative to fossil fuels in the journey to a Net Zero Carbon Economy. In Saudi Arabia, where energy demand is soaring,

geothermal energy is crucial for diversifying the energy mix. The Red Sea basins in western Saudi Arabia hold geothermal potential due to their youth and high-heat-flux characteristics. These basins offer a chance to extract geothermal heat and store CO<sub>2</sub> concurrently. Utilizing supercritical CO<sub>2</sub> for heat extraction enhances efficiency and enables carbon sequestration, contributing to reducing CO<sub>2</sub> emissions. Integrating CO<sub>2</sub> capture, utilization, and storage in geothermal reservoirs aligns with sustainable energy goals. The CPG approach in Saudi Arabia's Red Sea basins taps into geothermal potential, harnesses clean energy, and sequesters CO<sub>2</sub>, significantly advancing climate goals and regional renewable energy sectors.

Accurately assessing geothermal potential requires understanding parameters unique to the target aquifers. Estimating gross rock volume, recovery factor, heat capacity, porosity, and temperature are essential. Current assessments based solely on basin extent and aquifer thickness are limited by assumptions, leading to uncertainties. Detailed studies are needed to refine estimates in clastic sedimentary aquifers, considering geological complexities and inter-well dimensions. However, a gap exists between basin-scale and inter-well dimension assessments. Furthermore, existing studies address channel dimensions but not their variations along basins.

This study comprehensively assesses geothermal energy potential in Al Wajh basin's Burqan and Umluj units. Advanced geostatistical techniques and a state-of-the-art CO<sub>2</sub> fluid flow simulator create a robust reservoir model. Integrating geological data and well information, we develop a 3D model representing the reservoir accurately. Our specialized flow simulator accounts for CO<sub>2</sub> dynamic properties, allowing analysis of geothermal potential and energy extraction.

Our methodology involves structural and geostatistical modeling, and simulation setup. A structural model determines aquifer volume, while a trend model captures submarine channel distribution (Mohriak et al., 2014; Slatt and Rodriguez, 2013; Hofstra et al., 2017). Multiple-Point Statistics (MPS) improves facies spatial representation. Our simulation setup configures the geothermal scheme and fluid model, including mutual solubility and heat exchange. Flow simulations using various geostatistical methods are evaluated, and a 500-year simulation observes natural heat recovery.

We constrained heat-recovering rock formations using flow results from distinct submarine clastic units. A Monte Carlo simulation evaluates energy extraction and CO<sub>2</sub> storage capacity in these formations. This study presents an initial CPG potential assessment for Al Wajh, supporting its growth as a tourism center with affordable decentralized energy.

## METHODS

In the domain of reservoir modeling, two primary methods for representing categorical data such as facies or rock types are sequential indicator simulation (SIS) and multiple point statistics simulation (MPS) (Deutsch and Journel, 1992; Mariethoz and Caers, 2014). SIS, relying on variogram models, encounters limitations when spatial dependencies exhibit significant variations, especially in cases of environmental transitions that challenge the capture of complex geometries. In contrast, MPS, a non-parametric technique, utilizes training images to generate random fields, accommodating shifting facies geometries and facilitating adaptable modeling, such as the widening of channel widths and lobes (Mariethoz and Caers, 2014; Tahmasebi et al., 2018). We opt for MPS due to its capability to effectively represent intricate channel complexities. Below, we outline the process of integrating well data, channel dimensions, and trend models to construct the MPS simulation model for the distribution of submarine clastic rock types in the Burqan and Umluj units.

Our analysis of the AWSO-1 well data employs Petrel software to identify distributions of sand, silt, and shale at specific depths. This two-dimensional trend model extends into a three-dimensional aquifer reservoir model using the Euclidean distance to slope attribute. Through the application of a parameterized Gaussian-like function, we generate a three-dimensional probability cube that represents the distribution of channel volume. This function centers around the presumed location of AWSO-1, which marks the highest channel volume along the slope, gradually tapering towards both the slope and basin. To account for uncertainties, we present variations in the span of sand distribution using the deterministic model discussed in the uncertainty quantification section.

Channels within shale backgrounds typically feature sand concentrated along their axis, with finer sediments off-axis. AWSO-1's recorded sand percentage of 57% guides the scaling of the channel volume percentage in proportion to the peaked sand facies probability cube. We assign one-quarter of the sand facies to the silt probability and allocate the remaining portion to the shale probability, thereby maintaining consistency with well statistics. This approach aligns with previous research (Alpak et al., 2013; Slatt and Sanderson, 2013), where the sum of sand, silt, and shale probability cubes equals 100%. The sum of sand and silt probability cubes effectively mirrors the channel volume percentage trend, exerting an inverse influence on the shale probability cube.

Upon calibration with AWSO-1 well data and leveraging insights from prior work (Alpak et al., 2013), we derive sand, silt, and shale probability cubes for the Umluj and Burqan formations. For the purpose of multiple-point statistics simulation, we utilize a training image that molds a channel object, emulating the geometry of syn-rift submarine channels (Leppard and Slatt, 2006; Slatt and Sanderson, 2013). This user-defined object, initially non-dimensional, structures the channel axis with sand and the off-axis with silt, while maintaining shale as the

background. Integrated with AWSO-1 data, this object dictates channel orientation, width ratios, and thickness.

## FINDINGS

A deterministic trend model we developed influences the distribution of rock types in our study area. This model incorporates factors such as the distance to the slope and the percentage of each facies that fit into the AWSO-1 well data. While this model represents the submarine clastic facies and helps constrain the sand distribution within the basin, it is essential to acknowledge that numerous possibilities may deviate slightly from the current deterministic model. To account for this uncertainty, we performed an uncertainty quantification analysis, allowing for potential variations in the extent of sand content. This analysis enabled us to explore scenarios where the sand content range could be narrower or wider than the base case Gaussian fit, providing a more comprehensive understanding of the potential variability in the rock-type distribution. This model provides us to model spatial changes in the facies percentage along and across the basin that creates locally varying mean and overcomes mean stationarity in the model area. However, we build the trend model based on a global data set for submarine channel distribution along the slope to the basin which agrees with the conceptual understanding of this regard. Although our model honors limited observations and geological complexities of such submarine clastic units, we lack adequate data from the actual reservoir rock. Therefore we would like to emphasize that we can further reach close to the ground truth with only actual subsurface data from Al Wajh basin units.

The incorporation of submarine channel size and geometry, derived from an analogous present environment, played a crucial role in controlling the lateral facies variations. By utilizing this information, we constructed training images that successfully assimilated well data and facilitated the arrangement of facies across the basin. This approach enabled us to effectively prescribe a non-stationary spatial dependence of facies, adjusting the channel width to transition from narrow channels on the upper and middle slopes to wider fan lobes on the middle to the toe of the slope. We further validated the results of our training image-based multiple-point statistics (TI-MPS) model by comparing flow simulation and recovery outcomes with variogram-based algorithms. Our findings indicate that at the sub-sector scale (800 by 800 meters lateral boundary with 500-meter well spacing), our method strikes a balance between the narrow channel and layer cake representations. While this verification instills confidence in the current model, it is important to note that the training image we used relies on statistical data that is adopted from another basin which we assume was analogous. To enhance the robustness of geostatistical models, future investigations should encompass actual subsurface data, including 3-D seismic surveys and additional well data.

We overcome 1st and 2nd-order stationarity for the

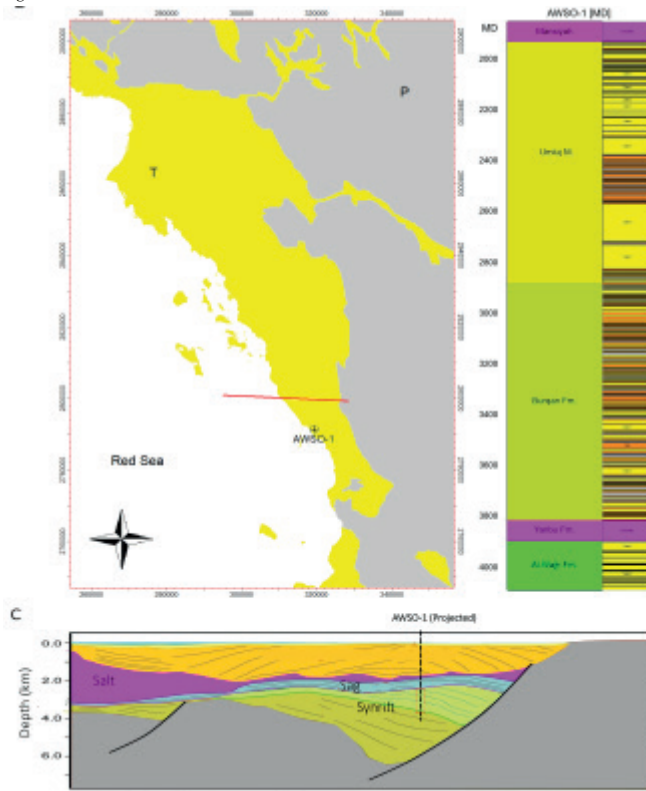


rock-type model with trend model and TI-based MPS simulations, respectively. We build such a rock-type distribution model to condition--assign-- porosity and permeability distributions that represent each of that rock-type. This way we generate a porosity and permeability model of the submarine clastic aquifers that those properties are conditioned to the associated rock types' spatial continuity in a fully nonstationary model. From shale to channel sand the range of permeability value has 4 orders of magnitude difference that suggests a large anisotropy in the reservoir system with realistic hence complex spatial arrangement of those permeability values. In an injection production scenario, the fluid flow in a heterogeneous reservoir is predominantly controlled by the permeability tensor of the system. Our model is highly robust regarding its heterogeneous permeability distribution representation in space by this explained method.

We designed the simulation setup in this study, including well-spacing, injection-production perforation depths, CO<sub>2</sub> injection rates, and a 7-year first injection stage to achieve 95% or more CO<sub>2</sub> saturation in the production well. The goal was to optimize the economic injection-production scenarios in a CPG energy production venture in thick heterogeneous saline aquifers. Therefore we have a well spacing of around 500 meters in lateral distance and 400 meters at maximum depth difference between injection and production well perforations. Our flow simulations and resultant heat recovery factors from alternative realizations of the geostatistical model based on the same well data show that we achieve similar heat recovery results based on variogram models or MPS models. This implies that, in an inter-well dimension of the model boundary with adequate well data of porosity and permeability, we achieve similar results with standard geomodeling methods versus the advanced geomodeling methods. However, for a full-field model, that is in a larger reservoir dimension, with changing local mean and spatial dependence, standard modeling methods lose their capability to represent reservoir heterogeneity. Therefore for field development planning, or a potential energy recovery assessment of a frontier reservoir, a full-field model may need to be carried out by training image-based MPS models with trend models incorporated in it.

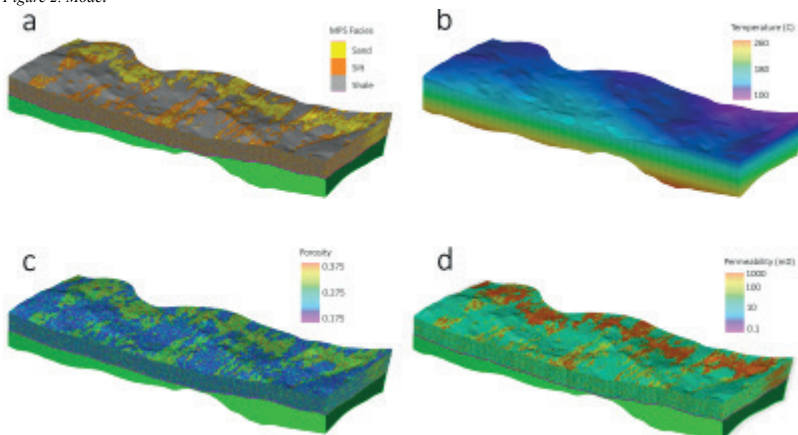
Keywords: modelling and simulation

Figure 1. Model Area



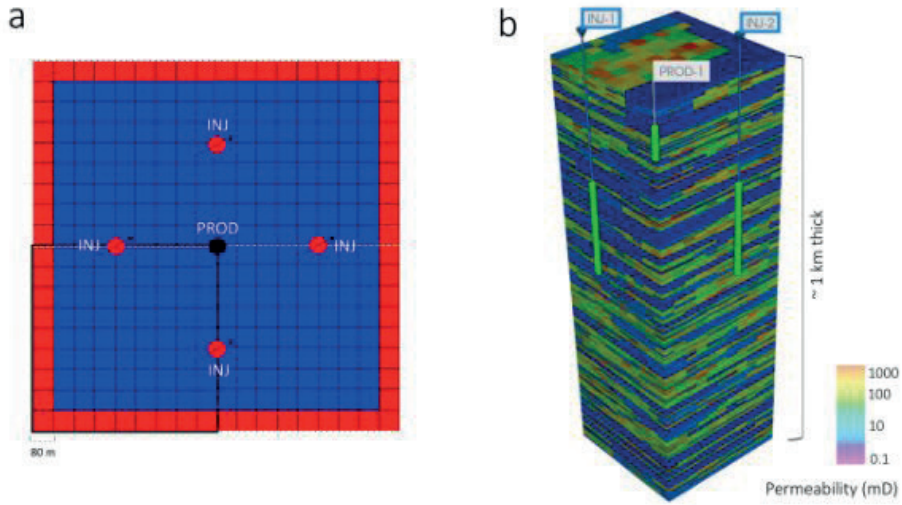
(a) Surface geology map of Al Wajh basin. The red line is the seismic section location. (b) The digitized version of the lithology log of the AWSO-1 well. (c) Seismic section and interpretation of the Al Wajh basin. The well is projected to the seismic line. The red box on the well projection shows the section of syn-rift submarine clastics (Burqan and Umluj units).

Figure 2. Model



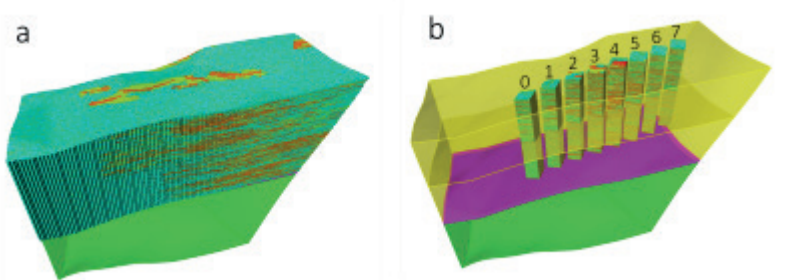
(a) MPS Simulation realization (b) The temperature model with temperature gradient 32 C/1000 m and with an average surface temperature of 30 C. (c) Porosity distribution model informed with MPS simulation rock-type distribution. Porosity ranges for each rock type, sand silt, and shale is randomly distributed to associated rock-type in the model area. (d) The permeability distribution model of the corresponding rock types. Porosity and permeability values are adopted from submarine rock types

Figure 3. Simulation Setup



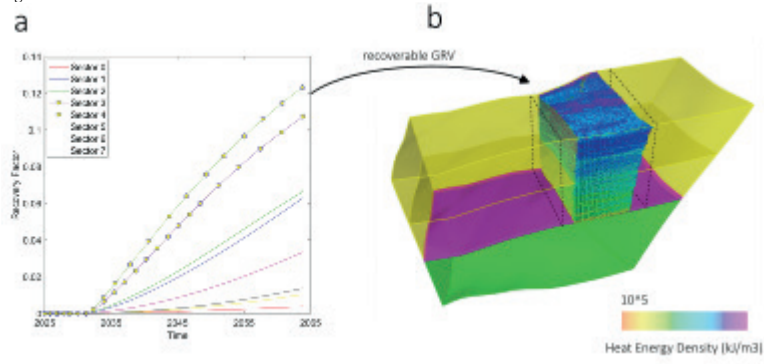
(a) Injection and production wells configuration and boundary condition of the around well simulation setup. (b) We use a quarter representation of the inverted five-spot well configuration for simulation purposes. In this image we display 2 injectors and 1 producer where injectors are perforated (perforations are marked as bright green circles on the well path) 200 meters continuously in the middle of the aquifer unit Umluj and producer is perforated on the top of the aquifer selectively where only the perforations includes the sandy units.

Figure 4. Simulation in subsectors



(a) We cropped the full field model 12 km length to 6 km width where the AWSO-1 well is located in the middle of this sector area. (b) We then further cropped sub-sectors with the same dimension around well simulations we conducted in the earlier sections. We cropped 8 different sub-sectors to evaluate the recovery factors for each to constrain above 10% recovery factor thresholds. As we prescribed the changing channel width and changing channel sand volume percentage according to the distance to slope each sector has a different sand percentage and spatial dependence on other rock-types. Moreover, the top of the reservoir is colder, towards the up-dip, proximal to the slope and it is hotter, towards the down-dip, to the basin-ward direction. Consequently, every sector carries a different amount of geothermal energy and has different reservoir property distribution.

Figure 5. Simulation Results



a) The time (the 40 years injection production) versus the heat recovery factor graph. Only Sectors 3 and 4 are able to achieve a reservoir performance above 10% heat energy recovery. The other sectors fall behind the 10% recovery factor threshold. (b) The reservoir volume with a sand percentage above 41% (the base case for a 10% recovery factor for heat production).

# Calculation of Natural Gas Viscosity of a Gas Reservoir Using Correlations and Comparison with Manual Readings Through Well Known Charts



**Abdullah Gürkan İscan**

Department of Petroleum and Natural Gas Engineering, Faculty of Engineering, Cyprus International University, Lefkoshia, Turkish Republic of Northern Cyprus

## **1. ABSTRACT**

It is very crucial to comprehend the properties of natural gas. Natural gas is very sensitive to pressure and temperature. The measurements of natural gas PVT properties (Pressure Volume Temperature) are carried out at laboratory conditions by means of tedious experiments. These tests are conducted at various pressure and temperature points for each measurement. Therefore, acquisition of data is cumbersome and time consuming. In this study, the viscosity of a Caspian region gas reservoir gas viscosity was calculated at different pressure values at different SG (specific gravity) using the correlations of (Lee et al., 1966). A temperature sensitivity was carried. In addition, the classical manual viscosity reading was implemented using the charts presented in (Carr et al., 1954) and (Katz et al., 1959). The calculated values were compared with the manually read viscosities. A very good match was obtained using the chart of (Carr et al., 1954) while a reasonable match was obtained using the charts of (Katz et al., 1969). For the direct calculation of viscosity, the gas compressibility calculations are required at each pressure and temperature. The required gas compressibility was calculated as per (İscan, 2021). (Carr et al., 1954) and (Katz et al., 1959) presented charts to manually read the gas viscosity as a function temperature, pressure and specific gravity. These charts are useful; however, one has to look up for each temperature, pressure and specific gravity one by one for each reading of viscosity which is a long process for readings at various temperature, pressure and specific gravity points. Moreover, the charts are available for specific gravity range of 0.6 to 1 at 0.1 specific gravity increment in (Katz et al., 1959). Therefore, for specific gravity values falling in between of these 0.1 increments, the engineers need to read a couple of charts and then make linear interpolation. Especially, when hundreds of pressure points at different temperature ranges are considered in modern reservoir analysis either by means of simulation or well testing, practical calculations would be required. In addition to the chart methods, there are commercial special PVT software products which are expensive and sometimes difficult to access in practical engineering and academic environment. (Lee et al., 1966) proposed a set of equations for direct calculations of natural gas viscosity as a function of various parameters such as density, temperature, molecular weight, specific gravity and compressibility. This study will facilitate direct, accurate and practical calculation of gas viscosity at different pressure, temperature, gas compressibility and specific gravity to further improve reservoir surveillance as a compact and practical application. It is presumed that this study will mitigate the difficulties

in gas viscosity determinations as a compact in-house applicable tool which every engineer can apply to generate their own file independently without having need to access expensive resources. This study will provide a quick and practical tool for in-house quality control (q/c) of various types of reservoir engineering work done by service companies as well as well test interpretation where gas viscosity is a predominant parameter in the calculation of permeability and skin.

## **2. THE STATEMENT OF THE PROBLEM AND THE OBJECTIVE**

Viscosity plays a significant role in all oil and gas reservoir fluid dynamics as well as flow equations, transmissibility and permeability times thickness products and well test interpretations. Therefore, accurate calculation of the gas viscosity is particularly a dominant step. The gas viscosity can be identified using some charts in the literature by entering the pressure and temperature one by one. However, each reading is made at specific temperature and pressure points. Moreover, the accuracy of the decimal points is important which cannot be resolved through chart readings. In addition to the chart methods, there are commercial special PVT software products which are expensive and sometimes difficult to access in practical engineering and academic environment. Hence, an automated, economic and practical Microsoft Excel(R) based gas viscosity calculation procedure is very helpful not only in dynamic and static reservoir modeling but also on field or facility gas property surveillance. The calculation methodology applied in this paper is totally based on mathematical equations which combine several gas properties from gas compressibility to pseudo critical properties. The gas viscosities were also read through the charts in the literature to validate the accuracy of the calculations. The calculated and the manually read values match very well.

As a practical quality control(q/c) in our daily reservoir engineering routine, it is a common practice to work with several service companies in the interpretation of the well tests for which the operating companies dedicate significant budgets. As a reservoir engineer one of our first quality control (q/c) items in a gas well test interpretation report is the gas viscosity. Because, this gas viscosity has direct impact on permeability and skin which are some of the major deliverables of a well test. If the operating company reservoir engineer has a practical calculation tool in hand, it will be a very quick and value adding q/c action in the validation of the reports. Several examples can be elaborated to emphasize the significance of gas viscosity determination in various reservoir and production engineering activities from

reservoir simulation to production rates.

As it was summarized above, it is presumed that this study will mitigate the difficulties in gas viscosity determinations as a compact in-house applicable tool which every engineer can apply in order to generate their own file independently without having need to access expensive resources.

The objective of this study is to calculate the gas viscosity of a Caspian region gas reservoir sample using the correlations of (Lee et al., 1966) and comparing the calculated viscosity to the classical manually read values from the charts of (Carr et al., 1954) and (Katz et al., 1959). This study will facilitate direct, accurate and practical calculation of gas viscosity at different pressure, temperature, gas compressibility and specific gravity to further improve reservoir surveillance. In reservoir simulations and well test interpretations, major physics phenomenon relies on equations including the term viscosity. Therefore, a generic and practical approach was validated with different chart approaches.

### 3.METHODOLOGY

A systematic way to calculate natural gas viscosity plays a dominant role in flow of natural gas in porous media. As the gases are very sensitive to pressure changes, the viscosity varies at different pressure values of the porous media.

(Lee et al., 1966) studied the density and viscosity properties of different natural gas samples for a pressure range of 100 to 8000 psia and a temperature range of 100 to 340F. In their study, a correlation was proposed to calculate the viscosity as a function of pressure, temperature, compressibility factor, molecular weight and specific gravity. (Katz et al., 1959) presented the viscosity versus reservoir temperature charts as functions of reservoir pressure traverse curves for a gas specific gravity range of 0.6 to 1. The understanding of viscosity is indispensable to study the flow of fluids in porous media or pipes. (Carr et al., 1954) studied the viscosity of hydrocarbon gases under pressure. In their study, the gas viscosity to viscosity at atmospheric conditions was plotted with respect to temperature at different pseudo reduced pressure traverses.

(Lee et al., 1966) proposed a set of equations to calculate the gas viscosity using Equations 1 to 6.

$$Mg=28.967\gamma \text{ (Eq.1)}$$

$$\rho=(PMg)/zRT=0.00149406(PMg)/zRT \text{ (Eq.2)}$$

$$K1=c((0.00094+2X10^{(-6)} Mg)T^{1.5})/((209+19Mg+T)) \text{ (Eq.3)}$$

$$X=3.5+986/T+0.01Mg \text{ (Eq.4)}$$

$$Y=2.4-0.2X \text{ (Eq.5)}$$

$$\mu g=K1 \exp(X\rho^Y) \text{ (Eq.6)}$$

The sequence of the calculation procedure needs to follow the calculation of the molecular weight of the gas which is a function of the specific gravity and the molecular weight of the air (Eq.1). The density term is very vital as the pressure and the gas compressibility

terms are in the density calculation (Eq.2). One of the main parameters changing with pressure temperature is the gas compressibility the "z". This parameter changes with pressure and temperature and it is an input parameter for the calculation of viscosity. The "z" gas compressibility factor calculations which were used in this study were discussed in (Iscaan, 2021) which uses the approach of the compressibility equations of (Dranchuk and Abou Kassem, 1975) and manual readings through the charts of (Standing and Katz, 1942). The z factor calculation is especially essential in gas reserves calculations and gas volumetrics. A very common way pressure/compressibility vs cumulative gas production requires accurate and successive calculations of the compressibility at various pressure points.

The viscosity of the gas was calculated using the equations given above in unit of cp. The original equation yields the results in micropoise. In the equation for K1 (Eq.3), the numerator was taken in to  $10^{-4}$  parenthesis to have viscosity in centipoise. The "X" and "Y" are internal correlation parameters which are functions of the molecular weight and the temperature (Eq.4 & Eq.5). The gas viscosity term is calculated through (Eq.6).

The determination of the viscosity by manual reading through the charts (Figure 1) of (Carr et al., 1954) is summarized below which has been applied in this study.

The molecular weight of the gas is calculated using the specific gravity of the gas. Then, the molecular weight of the gas is entered over the abscissa of the figure above (Figure 1). The corresponding reservoir temperature curve is intersected by moving vertically parallel to the ordinate. After having intersected the temperature curve, the viscosity at 1 atm is read over the ordinate. If the CO<sub>2</sub>, H<sub>2</sub>S and N<sub>2</sub> concentrations are known, the corresponding viscosities are read similarly. Once the viscosity at 1 atm is determined by manual reading, the next step is the calculation of the pseudo reduced temperature and the pseudo reduced pressure. Pseudo reduced temperature is defined as reservoir temperature divided by the critical temperature where both temperature values need to be in unit of Rankine. The pseudo reduced pressure is calculated by dividing the reservoir pressure by the critical pressure of the gas in units of psi. Both the pseudo reduced temperature and pressure values are dimensionless as they are ratios. Then, the pseudo reduced temperature is entered over the abscissa of the chart above (Figure 2), and it is moved vertically until intersecting the pseudo reduced pressure. It is moved horizontally parallel to the abscissa to intersect the viscosity ratio axis where the corresponding viscosity to the viscosity at 1 atm ratio is found. This ratio is multiplied by the viscosity at 1 atm which had been read manually in a previous step. As it is discussed here, this is a process at a single temperature, pressure and specific gravity point. It can be inferred that doing this type of reading for a couple of points can be practical. However, when various pressure points are considered a more practical and direct calculation method would be more efficient as described by (Lee et al., 1966).

#### 4.RESULTS, FINDINGS AND DISCUSSION

The calculations of the viscosity using the equations which were proposed by (Lee et al., 1966) made it possible to calculate and plot the density as a function of pressure and temperature.

The density of the gas was calculated at 200 F and three different specific gravity points from 0.6-0.8. It is clearly observed that the density of the gas increases with increasing pressure. In addition, it is observed that the density increases at constant pressure with increasing specific gravity (Figure 3).

The density was also calculated at constant specific gravity of 0.65 at three different temperature points with respect to pressure.

It is observed that the density decreases at constant pressure with increasing temperature (Figure 4).

After having calculated and observed the behavior of density, the interim parameters of X and Y were calculated leading to the gas viscosity. The physical reading of the viscosity values were carried at 200 F and 0.8 specific gravity using the viscosity charts of (Carr et al., 1954) (Figure 1) and (Katz et al., 1959). The error percentages were calculated as calculated vs read.

$$\text{Error}\% = \frac{(\text{Calculated} - \text{Manual})}{\text{Calculated}} \times 100$$

It is observed that the error percentage interval in manual reading of Katz is from 4 to 18 % while the error percentage interval is from -1.9 to 4 % through the manual reading of (Carr et al., 1954). The manual readings are with rulers and eyes. As the charts do not have decimal resolution as well the calculations, there might be some human error regarding the manual reading.

The viscosity of the gas matches very well as seen above using (Carr et al., 1954). In addition to the plot above (Figure 5), the manual vs calculated viscosity values were plotted with respect to each other at increasing pressure points to see how the point correlate with each other. The objective of this plot is to be able to quantify the correlation and the regression coefficient.

A regression coefficient of 99.81 was obtained at 200 F and SG of 0.8 in the cross plot of manual vs calculated (Figure 6) which shows very good match. This regression shows quite sufficient level of accuracy between the manually read and the calculated values of viscosity. The linear correlation equation was provided which facilitates to quantify the direct relationship between the calculated and the manual viscosity.

The manually read viscosity deviates from the calculated one above 2,000 psi in (Katz et al., 1959). However, the viscosity values are still reasonably close enough to each other. The maximum error percentage reaches up to 18% above 6,000 psi (Figure 7).

#### 5.CONCLUSION

This study brings together the conventional manual readings of viscosity with the calculated approach. The good match between them was showed through various charts. In modern reservoir studies, dealing

with too many pressure and temperature points and the corresponding viscosity values are needed especially in gas reservoir engineering. Therefore, a systematic and practical way of calculation would facilitate the practical work of the engineers rather than dealing with charts and reading the values by means of tedious and time-consuming ways. This study will facilitate the direct calculation of big data viscosity calculations in several reservoir and practical field applications at different temperature, pressure and specific gravity ranges. The calculation methodology applied in this paper is totally based on mathematical equations which combine several gas properties from gas compressibility to pseudo critical properties. The gas viscosities were also read through the charts in the literature to validate the accuracy of the calculations. The calculated and the manually read values match very well. It is presumed that this study will mitigate the difficulties in gas viscosity determinations as a compact in-house applicable tool which every engineer can apply in order to generate their own file independently without having need to access expensive resources.

This study will provide a quick and practical tool for in-house quality control of various reservoir engineering work done by service companies as well as well test interpretation where gas viscosity is a predominant parameter in the calculation of permeability and skin.

1. The gas viscosity was calculated at a temperature range between 170 to 200 F and pressure range of atmospheric to 6,000 psi.
2. Manual viscosity readings were carried out using well known charts of (Katz et al., 1959) and (Carr et al., 1954). The viscosity was calculated using the correlations of (Lee et al., 1966).
3. Very good matched were obtained with regression coefficients of 0.99 in comparison of the manual readings with respect the calculated ones. Nevertheless, the (Carr et al., 1954) charts yielded closer relation with the calculated ones than the (Katz et al., (1959) chart readings.
4. The gas viscosity increases with increasing pressure at constant temperature.
5. The density increases with increasing specific gravity at constant pressure and temperature.
6. The density of the gas increases with increasing pressure at constant temperature.

#### 6.NOMENCLATURE

Mg: Molecular weight, g/mole

$\rho$ : Density, g/cc

P: Pressure, psi

R: Gas law constant, J/(g mol-K)

T: Temperature, R and F

z: Gas Compressibility Factor

X: Internal Parameter For K1 and viscosity

Y: Internal Parameter For K1 and viscosity

SG: Specific Gravity of Gas

$\mu_g$ : Gas Viscosity, cp

## 7. REFERENCES

1. Lee, A.L., Gonzales, M.H., AIME, J.M., & Eakin, E.B. (1966). The viscosity of natural gases. Journal of Petroleum Technology, August, 997-1000.
2. Carr, N.L., Kobayashi, R., Burrows, D.B. (1954) Viscosity of hydrocarbon gases under pressure. Petroleum Transactions AIME, Article SPE-297G, 47-55.
3. Katz, D.L., Cornell, D., Vary, J.A., Kobayashi, R., Elenbaas, J.R., Poettmann, F.H., & Weinaug, C.F. (1959). Handbook of Natural Gas Engineering. Mc Graw Hill Book Company Inc.
4. Iscan, A.G. (2021). Calculation of gas compressibility z- factors of a caspian region gas well and their comparison with common chart read method. International Aegean Scientific Research Symposium Proceedings Book, ISBN 978-605-74014-2-7, 153-162.
5. Dranchuk, P.M., & Abou-Kassem, H. (1975). Calculation of z factors for natural gases using equations of state. The Journal of Canadian Petroleum Technology. July 14 (PETSOC-75-03-03):34-36.
6. Standing, M.B., & Katz, D.L. (1942). Density of natural gases. American Institute of Mining and Metallurgical Engineers, 140-149.

Keywords: Gas Density, Gas Viscosity

*Equations To Calculate Viscosity*

$$Mg = 28.967\gamma \quad (\text{Eq.1})$$

$$\rho = \frac{PMg}{zRT} = 0.00149406 \frac{PMg}{zRT} \quad (\text{Eq.2})$$

$$K_1 = \frac{(0.00094 + 2 \times 10^{-6} Mg) T^{1.5}}{(209 + 19Mg + T)} \quad (\text{Eq.3})$$

$$X = 3.5 + \frac{986}{T} + 0.01Mg \quad (\text{Eq.4})$$

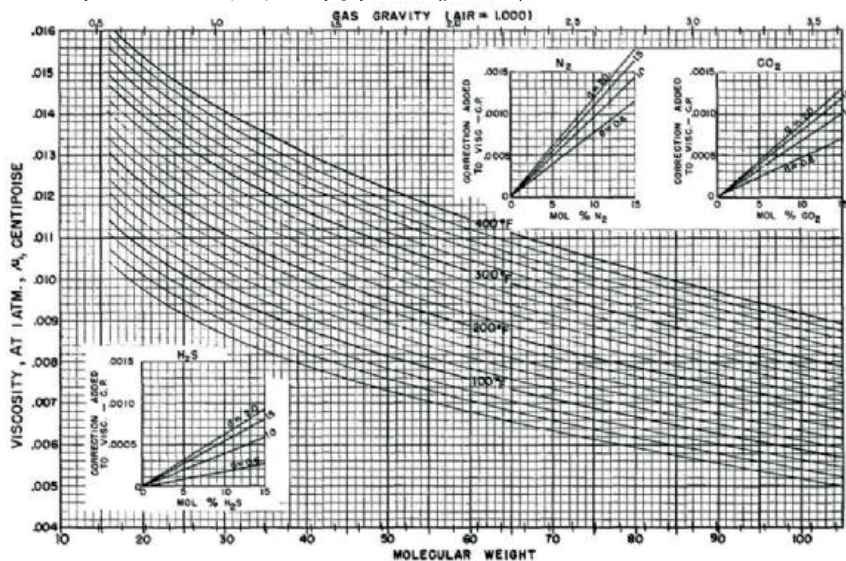
$$Y = 2.4 - 0.2X \quad (\text{Eq.5})$$

$$\mu_g = K_1 \exp(X\rho^Y) \quad (\text{Eq.6})$$



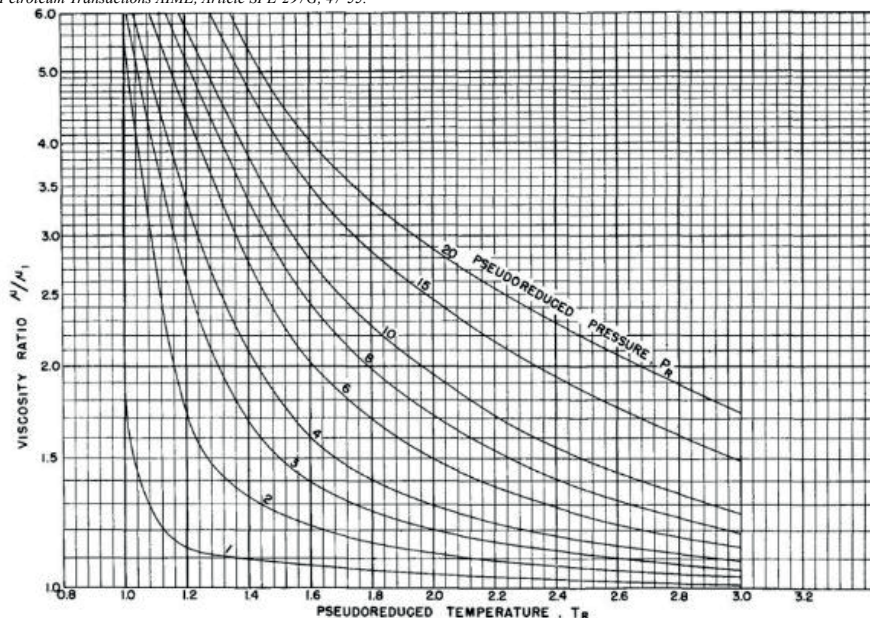
Figure 1 The viscosity at one atm chart after Carr et al.,(1954)

(Carr,N.L.,Kobayashi,R.,Burrows,D.B.(1954).Viscosity of hydrocarbon gases under pressure. Petroleum Transactions AIME, Article SPE-297G, 47-55.



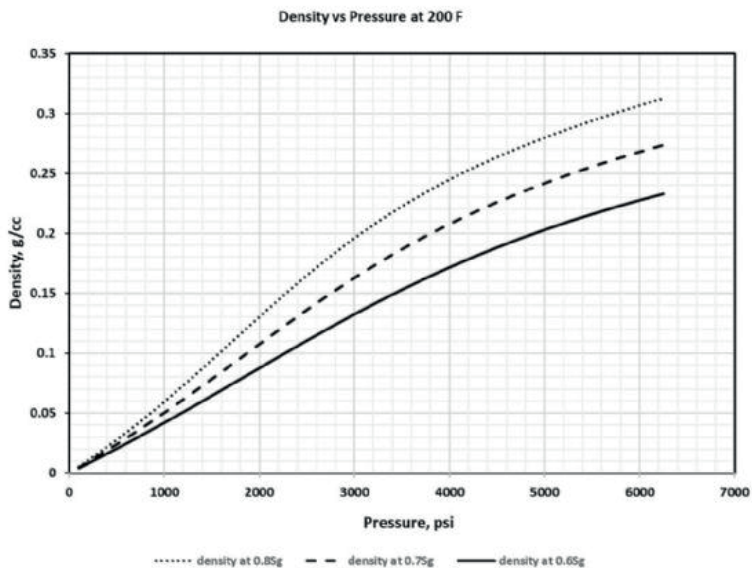
The determination of the viscosity by manual reading through the charts (Figure 1) of (Carr et al.,1954) is summarized below which has been applied in this study. The molecular weight of the gas is calculated using the specific gravity of the gas. Then, the molecular weight of the gas is entered over the abscissa of the figure above (Figure 1). The corresponding reservoir temperature curve is intersected by moving vertically parallel to the ordinate.

Figure 2 The viscosity ratio chart after Carr et al.,(1954) (Carr,N.L.,Kobayashi,R.,Burrows,D.B.1954).Viscosity of hydrocarbon gases under pressure. Petroleum Transactions AIME, Article SPE-297G, 47-55.



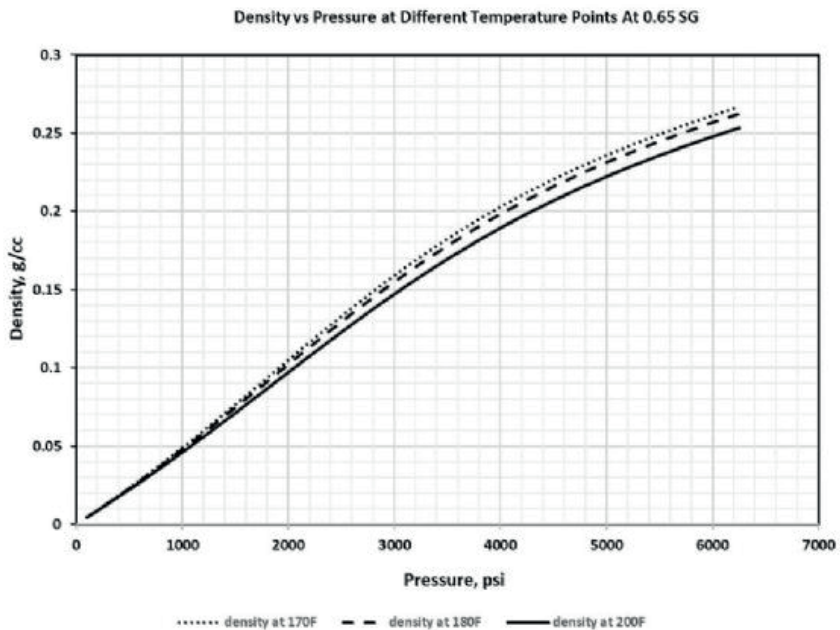
The pseudo reduced temperature is entered over the abscissa of the chart above (Figure 2), and it is moved vertically until intersecting the pseudo reduced pressure. It is moved horizontally parallel to the abscissa to intersect the viscosity ratio axis where the corresponding viscosity to the viscosity at 1 atm ratio is found. This ratio is multiplied by the viscosity at 1 atm which had been read manually in a previous step.

Figure 3 Density vs Pressure of the Gas at constant 200 F and different SG



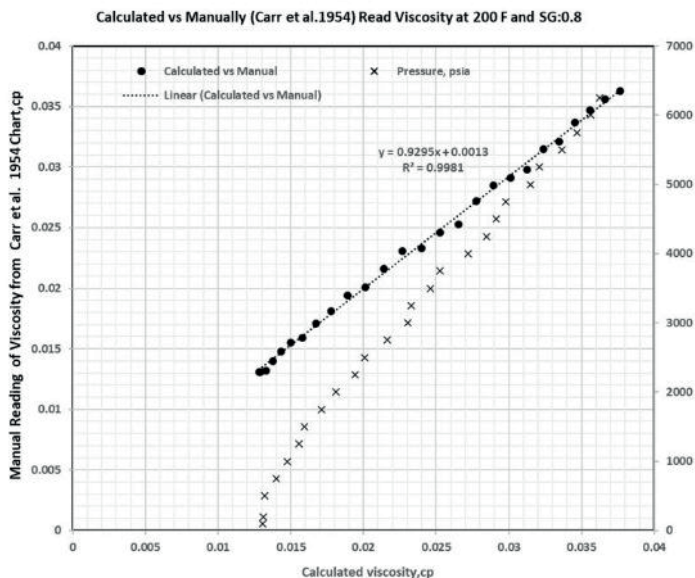
The density of the gas was calculated at 200 F and three different specific gravity points from 0.6-0.8. It is clearly observed that the density of the gas increases with increasing pressure. In addition, it is observed that the density increases at constant pressure with increasing specific gravity (Figure 3).

Figure 4 Density vs Pressure of the Gas at SG:0.65 at different temperature



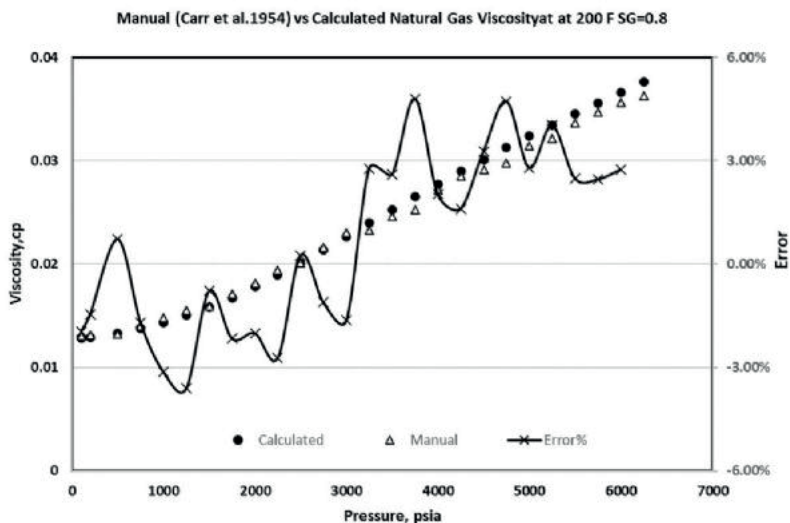
It is observed that the density decreases at constant pressure with increasing temperature (Figure 4).

Figure 5 Manually Read vs Calculated Viscosity at Constant Temperature, SG and ranging Pressure



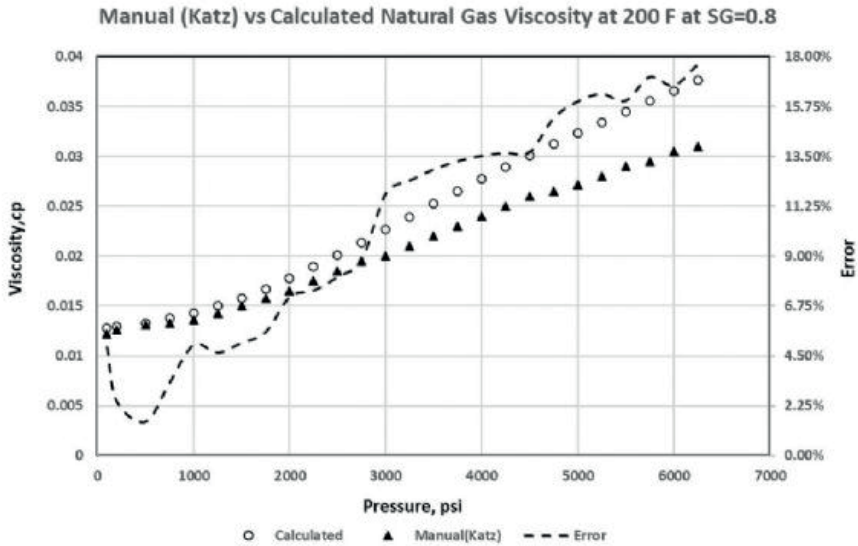
A regression coefficient of 99.81 was obtained at 200 F and SG of 0.8 in the cross plot of manual vs calculated (Figure 5) which shows very good match. This regression shows quite sufficient level of accuracy between the manually read and the calculated values of viscosity. The linear correlation equation was provided which facilitates to quantify the direct relationship between the calculated and the manual viscosity.

Figure 6 Viscosity Comparison of Manual Reading from (Carr et al.1954) vs Calculated and the Error% Between Them



The viscosity of the gas matches very well as seen above using (Carr et al.,1954). In addition to the plot above(Figure 6), the manual vs calculated viscosity values were plotted with respect to each other at increasing pressure points to see how the point correlate with each other.

Figure 7 Viscosity Comparison of Manual Reading From (Katz et al., 1959) vs Calculated and the Error% Between Them



The manually read viscosity deviates from the calculated one above 2,000 psi in (Katz et al., 1959). However, the viscosity values are still reasonably close enough to each other. The maximum error percentage reaches up to 18% above 6,000 psi (Figure 7).

# An Integrated Approach to Carbonate Reservoir Characterization: A Case Study from SE of Turkey



Mustafa Kamil Yüksek<sup>1</sup>, Ashhan Deliktaş<sup>1</sup>, Attila Aydemir<sup>2</sup>

<sup>1</sup>Türkiye Petrolleri Anonim Ortaklığı

<sup>2</sup>Atilim University

## SUMMARY

Pre-stack inversion, Neural Network Inversion (NNI) and the rock physics analysis were conducted on the complex oil-bearing carbonate reservoir, the Cretaceous age Derdere Formation, located in SE of Türkiye. Through the utilization of cores samples, PEF logs and elastic property logs, localized rock physics relationship was established to discern the elastic behavior of the producing facies within the Derdere Formation. Inverted acoustic impedance (AI) and shear impedance (SI), computed  $\lambda\rho$  and  $\mu\rho$  relationships, VP/VS ratio and porosity cubes derived from NNI were employed to thoroughly characterize the intricate nature of the carbonate reservoir. By cross plotting the computed  $\lambda\rho$  and  $\mu\rho$ , hydrocarbon-bearing facies were identified and correlated with actual production data. The study reveals that fracture and the interplay of different porosity types within the reservoir contributed to variation in elastic responses. These techniques have yielded significant insights into the elastic properties and reservoir characteristics of the studied carbonate reservoirs.

## INTRODUCTION

Siliciclastic sediments such as the sandstone, siltstone, conglomerate and shale are primarily composed of silicate and a wide range of minerals such as quartz, clay minerals and organic fragments (plants or residues of other organic materials, etc.). Sandstone is the main reservoir for the hydrocarbons and it demonstrates four basic pore types (Pittman, 1979). The primary porosity type of sandstone reservoir is the interparticle porosity, which reflects its depositional texture and fabric, and there is a linear correlation between the porosity and permeability for clean sandstone reservoirs. Carbonate rocks, on the other hand, are composed of mostly mono-mineralogical composition, which is either calcium carbonate or dolomite. However, the carbonate porosity types are diversified (Choquette and Pray, 1970). Carbonate diagenesis, pore type and pore properties (i.e., pore structure, pore geometry etc.) have important effects on the elastic properties of the rock (Eberli et al., 2003; Weger et al., 2009). During the dolomitization process; while the mineral density is increased, seismic velocity and porosity may change. The first-degree dolomitization creates more dense rock frame (in comparison to a calcite rock frame) and increases porosity. This process also creates low impedance with the higher porosity. In contrast, the second-degree dolomitization increases the size of the dolomite crystals and kills the porosity. This process causes high velocity and density, resulting the high acoustic impedance with low porosity and changes the permeability. At the end, complex and heterogenetic

reservoir occurrences are observed in carbonate rocks. For these reasons, successful hydrocarbon exploration and effective production from the carbonate rocks mainly depend on the precise approximation on the porosity and permeability prediction.

Since the porosity type mainly controls the elastic properties of the reservoir rock and pore characteristics are more complex, the linear relationship between the porosity and permeability may not be applied onto the carbonate reservoirs. This difference is also one of the main reasons why the most of the rock physics theory work for siliciclastic rocks and are not generally applicable to the carbonate rocks.

Efficient hydrocarbon exploration and effective production from the carbonate reservoirs require quantitative/integrated workflows due to the heterogeneity and complexity of the carbonate rocks. Accurate porosity and facies prediction are crucial for understanding of fluid flow in the tight carbonate reservoirs. Due to diversity in the pore structure, pore geometry, diagenesis and mineralogy, the qualitative interpretation approach could be misleading and result in ineffective well proposals targeting the carbonate reservoirs. In this case study, we suggested an integrated approach to characterize the Cretaceous carbonate reservoir rock, Derdere Formation in the southeast of Turkey (Figure 1).

## DATA AND METHODS

In this study, well log data from 22 wells, 3D seismic data (146 km<sup>2</sup>) and 4 sets of VSP data from Well-B, Well-C, Well-I and Well-15 (Figure 1) were used to conduct the elastic inversion method and petrophysical analysis to characterize the Derdere Formation. 3D seismic is a zero-phase data and a pre-stack gather conditioning workflow is applied on the seismic data.

In the first stage, we conducted a seismic data analysis and processing workflow which involved the creation of three distinct sets of seismic stacks with different offsets: the near offset range (20-100), moderate offset range (100-200) and the far offset range (200-300). Trim statistics and AVO-friendly radon transform filtering were also applied to improve the flattening of gathers and to improve the Signal/Noise (S/N) ratio. These offset-dependent wavelets, essential for the inversion process, were derived using a statistical method.

Ozdemir et al. (2001) initially introduced the pre-stack acoustic impedance (AI), shear impedance (SI) and density inversion. Later, Hampson et al. (2005) proposed an innovative approach for the simultaneous pre-stack inversion. To increase the accuracy of the porosity prediction and facies distribution, property

logs and inverted seismic attributes were used as the input data for the Neural Network Inversion (NNI). For the pre-stack inversion, we constructed geo-statistical AI, SI (Shear Impedance) and  $\rho$  (Density) background models using the well log data. In cases where S-wave velocity data were unavailable or missing for certain wells, S-wave velocity was determined using a mudrock line (Figure 2) to construct the SI model. To suppress the noise and improve the quality of the inversion, the models have been subjected a lateral filtering process. The porosity model was also constructed with the same method (Ozer et al., 2023). Facies logs were created using Photoelectric Factor Logs (PEF) for the Derdere Formation which was previously subdivided into three facies as the calcite, dolomite and dolomitic calcite, using the analysis of nine cores. In the following stage, we aimed to extract the elastic properties, facies distribution and geofluid types to characterize the carbonate reservoir to reduce the well placement risk and enhance the production.

### ROCK PHYSICS ANALYSIS

Rock physics analysis uses the elastic properties of the carbonate reservoirs. Reservoir characterization, lithology and fluid type discrimination for the carbonate reservoir, Inverted AI and SI, and computed  $\lambda\rho$  and  $\mu\rho$  relationships together with the computed VP/VS ratio have been used to determine the rock properties (Pickett, 1963; Gardner et al., 1974; Goodway et al., 1997; Ozdemir et al., 2006). Due to the complexity of the carbonate reservoir, inverted results and well logs were calibrated with the laboratory data to understand the elastic properties of the production zones for the each well. The oil has been produced from the matrix or fractures, or a combination of both in the investigated carbonated reservoir. It is known that fractures cause anisotropy and affect the elastic properties of the carbonate rock.

We constructed a cross-plot of the computed  $\lambda\rho$  and  $\mu\rho$  logs, resulting in the identification of the most prominent hydrocarbon anomaly. At the right side of Figure 3, three zones are selected on the  $\lambda\rho$ - $\mu\rho$  cross plot. Green and light-green colors represent the non-producing zones. Red marks indicate the potential production (expected) zones. When these zones are selected and reflected in the well logs, a noteworthy level of congruence was observed with the existing production data. Colors differentiate the producing and non-producing carbonate zones and also red mark indicates that there is potential for another zone where the DST operation was not performed. When the production expected values were chosen on the cross plot and compared to the production zone for Well F, it has shown that the results are well-consistent (Figure 3).

### PRESTACK INVERSION AND NEURAL NETWORK RESULTS

Selected areas on the computed  $\lambda\rho$ ,  $\mu\rho$ , VP/VS ratio and porosity sections on the Well A and Well F locations, and their cross-correlation are seen in Figure 4. Previously

completed lithofacies descriptions from nine cores indicate that there are three facies (producing facies) for the Derdere Formation with different elastic properties. To investigate and characterize these facies, the inverted and computed results were cross-plotted (Figure 4). In the  $\lambda\rho - \mu\rho$  display, the Well A and Well F locations were selected (Figure 4-A). Four producing zones were found in the selected areas on the section and these zones were color-coded (Figure 4-A, at the right side). The color-coded zones were reflected in the section (Figure 4 -A, at the left side). VP/VS ratio and porosity sections were taken from Well A and Well F locations are seen at the right side of Figure 4 -B. The first section indicates the computed VP/VS ratio cubes and the second is the porosity from NNI. When producing values are selected on the cross plot (Figure 4 -B, at the right side) and reflected in the sections, corresponding zones demonstrate the producing facies. These results match with the production data of Well A and Well F. Representative colours in the section illustrate the producing facies. These findings were corrected with the production data. However, PEF logs and nine core descriptions indicate that there are three main facies for the Derdere Formation. These differences can be explained as follows: in addition to the effects of the three facies on the elastic properties, a combination of the different porosity types developed together in the reservoir levels create an extra influence. Furthermore, we interpreted that, since we are producing oil from the matrix, fracture and matrix + fracture porosities, these four main areas on the cross plot not only define the three facies of the Derdere Formation but also characterize the elastic responses of the combined porosity types of the reservoir that produce oil.

### CONCLUSIONS

Pre-stack inversion, NNI, rock physics analysis and further investigation of selected areas in Wells of A and F confirmed the presence of producing facies with different elastic properties. The study revealed that the oil has been produced from the matrix, fractures or from the combination of both, that create anisotropy and affect the elastic properties of the rock. By cross-plotting the computed  $\lambda\rho$  and  $\mu\rho$ , the hydrocarbon-bearing facies are identified and correlated with the production data. Fractures and the combination of porosity types in the reservoir affect the elastic responses. The detection of four facies on the cross plot helps to map out the bypassed zones and will be utilized with successful well placement in the near future. In case of well confirmation, this will enhance the effective oil production.

### REFERENCES

- CHOQUETTE, P. W., AND L. C. PRAY, 1970, GEOLOGICAL NOMENCLATURE AND CLASSIFICATION OF POROSITY IN SEDIMENTARY CARBONATES: AAPG BULLETIN, V. 54, P. 207-250

EBERLI, G. P., BAECHLE, G. T., ANSELMETTI, F. S., AND INCZE, M. L., 2003, FACTORS CONTROLLING ELASTIC PROPERTIES IN CARBONATE SEDIMENTS AND ROCKS: THE LEADING EDGE, V. 22, NO. 7, P. 654-660

GARDNER, G., GARDNER, L., AND GREGORY, A., 1974, FORMATION VELOCITY AND DENSITY—THE DIAGNOSTIC BASICS FOR STRATIGRAPHIC TRAPS: GEOPHYSICS, V. 39, NO. 6, P. 770-780.

GOODWAY, W., CHEN, T. AND DOWNTON, J., 1997, IMPROVED AVO FLUID AND LITHOLOGY DISCRIMINATION USING LAME PETROPHYSICAL PARAMETERS; "AP", "MP", AND "A/M FLUID STACK", FROM P AND S INVERSION: 67TH SEG TECHNICAL PROGRAM, EXPANDED ABSTRACT AV 2.7, 183-186.

HAMPSON, D.P., RUSSELL, B.H. AND BANKHEAD, B., 2005. SIMULTANEOUS INVERSION OF PRE-STACK DATA: 74TH SEG ANNUAL INTERNATIONAL MEETING, EXPANDED ABSTRACT, SI 1.2, 1633-1638.

OZDEMIR, H., RONEN, S., OLOFSSON, B., GOODWAY, B., YOUNG, P., (2001). SIMULTANEOUS MULTICOMPONENT AVO INVERSION. SEG TECHNICAL PROGRAM EXPANDED ABSTRACTS. 20. 269-272. 10.1190/1.1816589.

OZDEMIR, H., HANSEN, J.W. AND TYLER, E., 2006. ROCK AND RESERVOIR PARAMETERS FROM PRE-STACK INVERSION OF SURFACE SEISMIC DATA. FIRST BREAK, 24, 83-87.

OZER, Z., KAMACI, Z., AYDEMIR, A., 2023. INNOVATIVE 3D MODELING OF AN OLD OIL FIELD FOR SUSTAINABLE PRODUCTION: CASE STUDY OF KATIN-BARBES OIL FIELD (KBOF), SE ANATOLIA- TURKEY. MARINE AND PETROLEUM GEOLOGY, 154: 106341.

PICKETT, G. R., 1963, ACOUSTIC CHARACTER LOGS AND THEIR APPLICATIONS IN FORMATION EVALUATION: JOURNAL OF PETROLEUM TECHNOLOGY, V. 15, NO. 06, P. 659-667.

PITTMAN, D.E., 1979, POROSITY, DIAGENESIS AND PRODUCTIVE CAPABILITY OF SANDSTONE RESERVOIRS. SEMP SPECIAL PUBLICATION. NO. 26 P. 159-173.

WEGER, R. J., EBERLI, G. P., BAECHLE, G. T., MASSAFERRO, J. L., AND SUN, Y.-F., 2009, QUANTIFICATION OF PORE STRUCTURE AND ITS EFFECT ON SONIC VELOCITY AND PERMEABILITY IN CARBONATES: AAPG BULLETIN, V. 93, NO. 10, P. 1297-1317.

Keywords: Seismic Petrophysics, Carbonate Reservoir Characterization

Figure 1

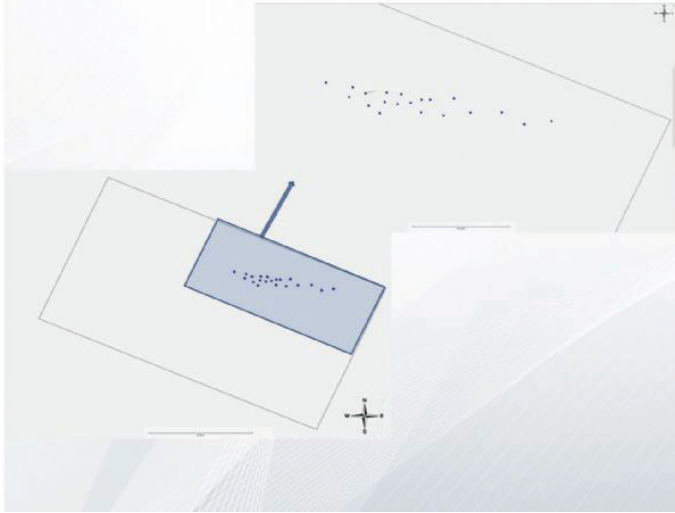


Figure 1. Study Area and well locations

Figure 2

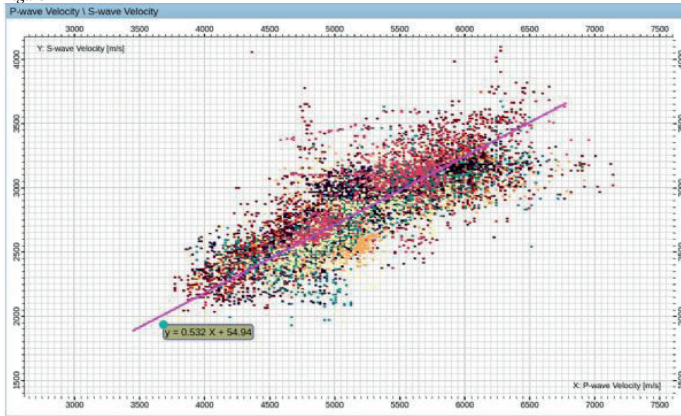


Figure 2. P-wave and S-wave velocity relationship.



Figure 3

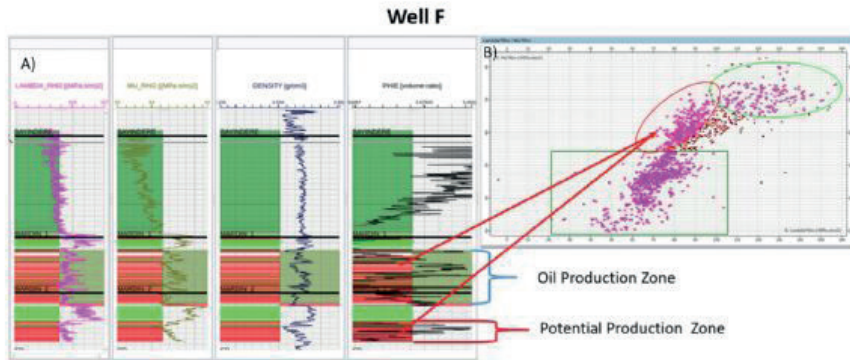


Figure 3. A) LamdaRho ( $\lambda\rho$ ), MuRho ( $\mu\rho$ ), Density and Porosity logs, respectively (from left to right). B)  $\lambda\rho$  versus  $\mu\rho$  crossplot. Three zones selected on the crossplot. The green and light green zones are represented non-producing intervals. Red marks represent the potential production (expected) zones.

Figure 4

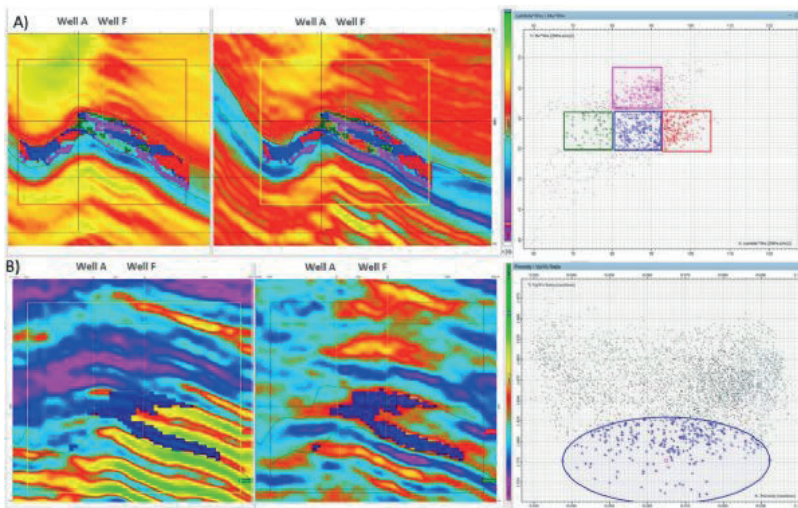


Figure 4. A) LamdaRho ( $\lambda\rho$ ) (left section), MuRho ( $\mu\rho$ ) (right section) and  $\lambda\rho$ - $\mu\rho$  cross plot, respectively. B) VP/VS ratio (left section), Porosity (right section) and VP/VS - Porosity cross plot, respectively. Values corresponding to hydrocarbon-bearing zones are selected on the cross plots and highlighted onto the sections. For  $\lambda\rho$ - $\mu\rho$  cross plot, colored areas represent four elastic faciesses within the Derdere Formation. Blue circled areas on the VP/VS-Porosity cross plot demonstrates production values. The selected areas were reflected to the sections.

# Physics-Informed Neural Networks for Solving Partial Differential Equations: Applications and Challenges



**Amir Shamsa, Mehdi Paydayesh, Maria Perezhogina**  
Slb, Digital and Integration

Physics-informed neural networks (PINNs) are an emerging class of deep learning models that provide an alternative approach to solving partial differential equations. By incorporating knowledge of the underlying physics, PINNs can overcome the limitations of traditional data-driven models while maintaining the advantages of deep learning techniques. In this study, we implement PINNs for a variety of applications and demonstrate their effectiveness in solving the heat equation and pressure diffusion problem. Associated challenges and limitations, including the need for good initialization and architectural engineering and issues with specific types of equations or domains are also discussed.

## INTRODUCTION

Partial differential equations (PDEs) are widely used to model complex physical systems in various domains, such as fluid dynamics, heat transfer, and electromagnetism. Solving PDEs accurately and efficiently is essential for understanding these systems and making predictions. Traditional methods for solving PDEs, such as finite element methods and finite difference methods, can be computationally expensive, especially for multi-dimensional problems (Trefethen 2000). On the other hand, data-driven approaches, such as deep learning, often struggle with a lack of data or the complexity of the underlying physical system (Goodfellow, Bengio, and Courville 2016). Physics-informed neural networks (PINNs) provide a promising alternative by leveraging the power of deep learning while incorporating physics-based knowledge (Raissi, Perdikaris, and Karniadakis 2019).

### PINN Implementation for Different Models

PINNs were implemented for various applications, including:

- radioactive decay
- logistic function
- Un-damped oscillator
- damped oscillator
- Bernoulli model.

To utilize PINNs for various applications, we employed a feed-forward deep neural network with multiple hidden layers. Each layer consisted of a specific number of neurons and utilized the ReLU activation function. Neural Network Architecture:

- Input Layer
- Hidden Layers, three layers with [h1, h2, h3] neurons as hyperparameters
- Optimizer (SGD, Adam)
- Output Layer

For single-trend ODEs (Ordinary Differential Equations), such as radioactive decay, PINNs outperform traditional neural networks right from the initial iterations. However, as the model complexity increases from the logistic function to oscillators, appropriate initialization and increased iterations become crucial. For the Bernoulli model, which is the most complicated in this series, changing the neural network architecture was necessary in addition to appropriate initialization. The Adam optimizer was chosen for training due to its adaptive learning rate properties with a learning rate starting from 0.001, which was reduced based on validation loss plateaus. The model's convergence was monitored using a separate validation set, and early stopping mechanisms were implemented to prevent overfitting.

Hyperparameter tuning is crucial in training the neural networks. For our implementations, we utilized a grid search approach over various hyperparameters. The learning rate, batch size (32(or 64) in our experiments), and the hyperparameter  $\lambda$ , which balances residual and boundary losses, were systematically varied.

To determine convergence, we monitored the loss during training. Once the decline in loss values became negligible or the loss value plateaued for a significant number of epochs, we deemed the model to have converged. Typically, our models showed signs of convergence between 500 to 1500 epochs, depending on the complexity of the application. It's important to note that for complex applications like the Bernoulli model, this architecture was adjusted with additional hidden layers and neurons to capture the intricate relations.

### Solving the Heat Equation with a PINN

The heat equation is a fundamental PDE in heat transfer problems; it describes the distribution of heat in a physical system over time. It can be stated as:

$$\frac{du}{dt} = k \nabla^2 u$$

where

$u$  is the temperature

$t$  is time

$k$  is the thermal conductivity

$\nabla^2$  is the Laplace operator.

A PINN was used to solve the equation by employing a neural network to approximate the temperature distribution and training the network by minimizing a loss function that enforces the heat equation and boundary conditions.

Residual loss is the error resulting from the discrepancy between the predicted and actual heat equation, represented as:

$$L_{res} = |\frac{du}{dt} - k \nabla^2 u|^2$$

This loss ensures that the model solution abides by the physics of the heat equation.

The loss function plays a pivotal role in training the neural network. It quantifies the difference between the predicted output of the neural network and the expected output. In our implementations, we used a combination of residual loss and physics (with boundary and initial conditions) loss.

The weights of each loss in the total loss function were chosen based on hyperparameter tuning. We used a grid search approach on the lambda ( $\lambda$ ) values ranging from 0.01 to 10 to balance the importance of residual and boundary losses. The best  $\lambda$  value was selected based on the model's performance on the validation set.

To determine convergence, we monitored the loss during training. Once the decline in loss values became negligible or the loss value plateaued for a significant number of epochs, we deemed the model to have converged. Typically, our models showed signs of convergence between 500 to 10000 epochs, depending on the complexity of the application.

The results showed that PINNs can provide accurate solutions (Fig. 1 and Fig. 2), demonstrating their effectiveness in solving PDEs for this type of problem.

Fig. 1—The two images on the left represent the exact solution to the heat equation. The third image depicts the training data for the neural network, while the image on the right shows the training data, initial condition (IC), and boundary condition (BC) set up for the PINN.

Fig. 2—Both a standard neural network and a PINN were used to solve the heat equation. The left four plots illustrate the temperature and residuals obtained from the neural network after 100 epochs (iterations) and 1,000 epochs. The right four plots row show the temperature and residuals from the PINN after 100 and 1,000 epochs. Comparison with the exact solution in Fig. 1 shows that the PINN outperforms the standard neural network in capturing the exact solution.

Solving the Pressure Diffusion Equation with a PINN  
The pressure diffusion problem is relevant in fluid flow through porous media. The PDE that describes the diffusion of pressure in a fluid system over time is:

$$\frac{dp}{dt} = D \nabla^2 p$$

where

$\frac{\partial p}{\partial t}$  is the rate of change of pressure (p) over time (t)

D is the diffusion coefficient characterizing the medium

$\nabla^2$  is the Laplace operator

measuring pressure changes in space

$\nabla^2 p$  is the application of the

Laplace operator to the pressure (p).

To solve the pressure diffusion equation using a PINN, the first step is defining the neural network architecture that approximates the pressure distribution. Inputs to the neural network are spatial coordinates (x,y,z) and time t, and the output is the pressure p.

The network can be trained by minimizing a loss function that consists of two parts:

- residual loss

$$L_{res} = \left| \frac{dp}{dt} - D \nabla^2 p \right|^2$$

which enforces the pressure diffusion equation at all points in the domain

- boundary loss

$$L_{bc} = |p(x,y,z,t) - p_{bc}(x,y,z,t)|^2$$

which enforces the boundary conditions of the problem and where  $p_{bc}(x,y,z,t)$  is the known pressure distribution at the boundary. The total loss function is given by:

$$L = [\lambda L]_{res} + L_{bc}$$

where  $\lambda$  is a hyperparameter that balances the importance of the residual and boundary losses.

For this problem, convergence was assessed based on the change in loss over 10,000 epochs. Convergence plots, depicting the decline in the loss function over the epochs, are provided in the supplementary material. The same hyperparameter tuning approach as described earlier was used.

The results (Fig. 3) demonstrate that PINNs can effectively solve the pressure diffusion problem, further validating their applicability in solving PDEs.

Fig. 3—Pressure estimates (black dots) obtained from a standard neural network (top row, left) and a PINN (top row, right) are compared with a synthetic solution (red dots) created via flow simulation. The PINN shows a better match from 2030 onward, where the neural network has not seen the data (test set). The bottom row illustrates another comparison between the PDE pressure solution (bottom left) in a water injection scenario and the PINN solution via flow proxy modelling (bottom middle). The bottom right figure displays the difference pressure difference between the two, with an error of  $\pm 1\%$ . The PINN offers a faster single-loop solution incorporating physics laws than the PDE numerical flow solver.

## CONCLUSION

PINNs are well-suited for solving PDEs where physics-based models are important but may be incomplete or inaccurate, and where data-driven models are limited by a lack of data or the complexity of the underlying physical system. However, PINNs might not work “straight out of the box,” and several challenges need to be addressed:

- Good initialization and architectural engineering are required for optimal performance.
- PINNs may struggle with certain types of equations or domains, such as stiff equations, equations with discontinuities, or nonlinear equations with chaotic solutions.

Despite these challenges, the results so far have been promising, and PINNs have the potential to become a valuable tool for solving PDEs in various domains.

**ACKNOWLEDGMENTS**

The authors are grateful to SLB for supporting this publication.

**REFERENCES**

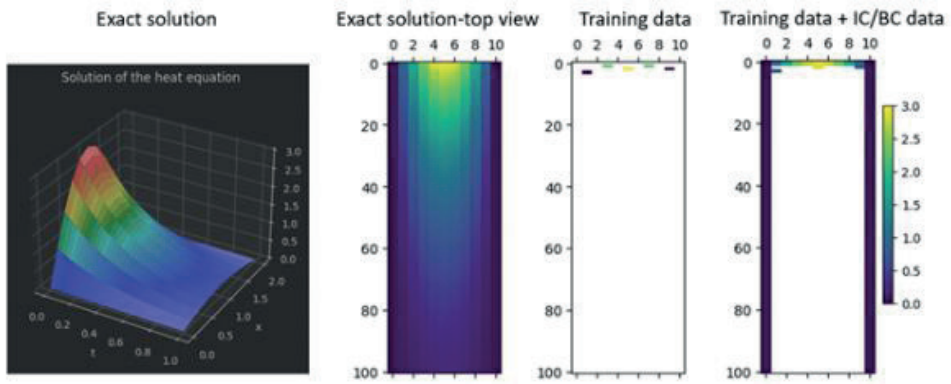
Goodfellow, I., Bengio, Y., and Courville, A.: Deep Learning, MIT Press (2016).

Raissi, M., Perdikaris, P., and Karniadakis, G. E.: "Physics-informed neural networks: A deep learning framework for solving forward and inverse problems involving nonlinear partial differential equations," *Journal of Computational Physics* (2019) 378, 686–707.

Trefethen, L. N.: Spectral methods in MATLAB, SIAM (2000).

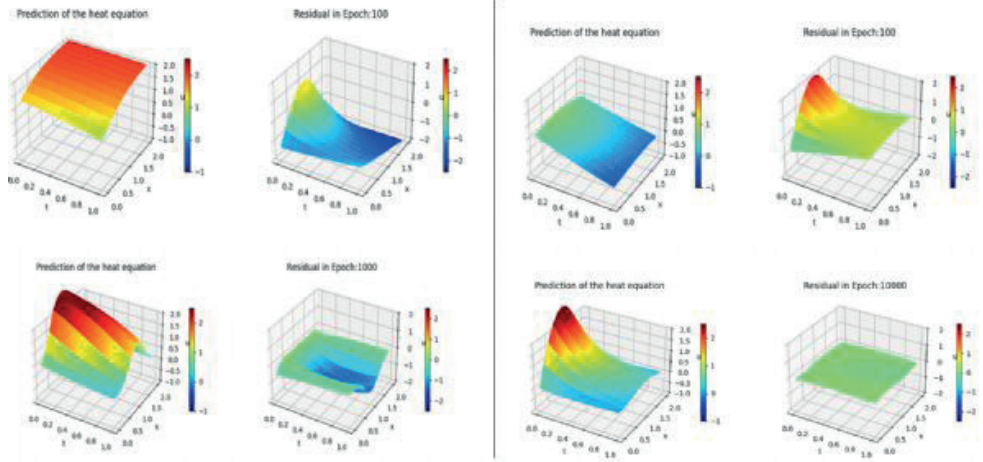
Keywords: Machine Learning, Physics-Informed Neural Network

Fig. 1



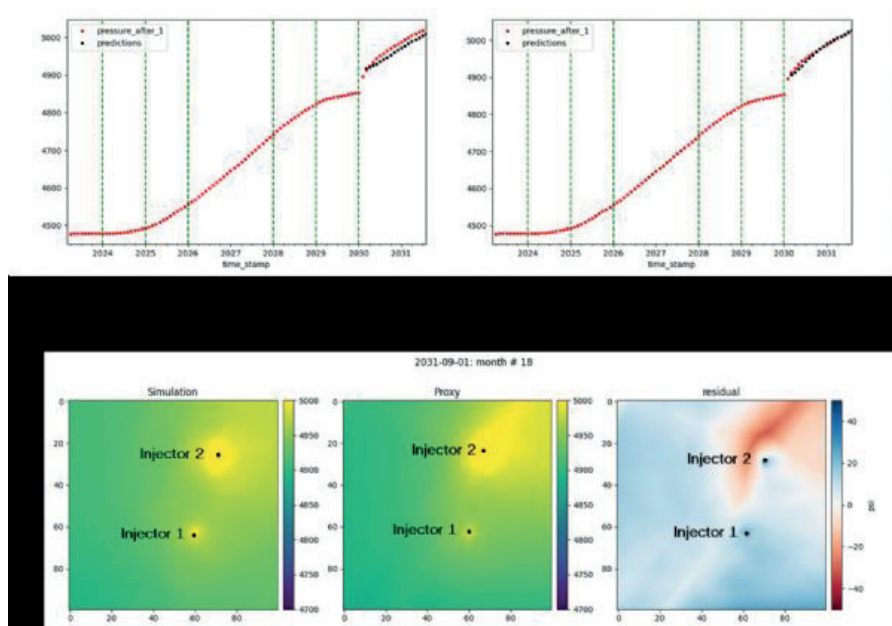
The two images on the left represent the exact solution to the heat equation. The third image depicts the training data for the neural network, while the image on the right shows the training data, initial condition (IC), and boundary condition (BC) set up for the PINN.

Fig. 2



Both a standard neural network and a PINN were used to solve the heat equation. The left four plots illustrate the temperature and residuals obtained from the neural network after 100 epochs (iterations) and 1,000 epochs. The right four plots show the temperature and residuals from the PINN after 100 and 1,000 epochs. Comparison with the exact solution in Fig. 1 shows that the PINN outperforms the standard neural network in capturing the exact solution

Fig. 3



Pressure estimates (black dots) obtained from a standard neural network (top row, left) and a PINN (top row, right) are compared with a synthetic solution (red dots) created via flow simulation. The PINN shows a better match from 2030 onward, where the neural network has not seen the data (test set). The bottom row illustrates another comparison between the PDE pressure solution (bottom left) in a water injection scenario and the PINN solution (bottom middle). The bottom right figure displays the pressure difference between the two, with an error of  $\pm 1\%$ . The PINN offers a faster single-loop solution incorporating physics laws than the PDE numerical solver.

# Integrated Reservoir Characterization of Fractured Carbonates: Garzan Limestone Case



**Ufuk Durmus**

Turkish Petroleum Corporation (TPAO), Ankara / Türkiye

## SUMMARY

In this study, I characterize producing Garzan limestone formation in Southeastern Turkey. Due to highly active tectonics in the area of interest, natural fractures can be found inside carbonates aligned with the regional stress direction. I utilize available core measurements, dipole sonic logs, and legacy stack seismic data to understand the Garzan reservoir and differentiate between oil-producing and non-producing facies in the field. With the help of dipole sonic data and the rock physics modeling, I also show that Garzan carbonate has HTI anisotropy and the fractures can be the primary driver for oil production.

## INTRODUCTION

Garzan limestone formation is one of the main oil reservoirs in Southeast Turkey. Maastrichtian Garzan formation is comfortably underlain by Kiradag formation. Kiradag formation is composed of laminated sand layers and silty shales, while Garzan is bioclastic limestone with high fossil content. Garzan formation has three geologic facies in the area of interest, and the aim is to delineate the best-producing upper facies.

The dataset consists of 15 wells, some reported vertical core measurements, and legacy stack seismic data from the year 2005. The challenging part is to work with the limited dataset to characterize this geologically-complicated reservoir. Only one well has dipole sonic log measurements, and another well has isotropic core measurements from the reservoir interval.

First, I run model-based post-stack inversion to obtain P-impedance from the legacy seismic data. Second, I process dipole sonic logs from Well W-3 to invert for fast and slow shear moduli. Following that, I build an anisotropic rock physics model to understand the effect of fractures and mineralogy content on elastic properties.

## THEORY AND METHODOLOGY

Vertical-fractured rocks yield horizontal transverse anisotropy (HTI). Consequently understanding anisotropy plays an important role in the processing, interpretation, and inversion of seismic data. The stiffness matrix of HTI anisotropy is provided in Equation 1. One should note that five independent stiffness coefficients control the HTI media.

S-impedance and density cannot be estimated from the available seismic data because there is no prestack seismic data. The anisotropy analysis cannot be made from the seismic data either. Naturally, isotropic P-impedance inversion is run with the legacy stack data. In this work, I utilize model-based post-stack seismic

inversion for P-impedance (Russell, 1988).

The dipole sonic log from Well W-3 is processed and the Thomsen anisotropy parameter  $\gamma$  is estimated using shear slowness recorded in two different azimuth directions. The measured shear velocities can be used to compute  $C_{ij}$  coefficients with the following Equations 2 and 3.

Here  $\gamma$  is Thomsen (1986)'s parameter to estimate anisotropy. Intuitively, S-wave anisotropy can be understood from the anisotropy parameter  $\gamma$ .

To model anisotropy in the reservoir laterally, I build a rock physics model and estimate elastic parameters. First a rock matrix model was built by using Hill (1963)' average equation, and then vertically aligned a set of fractures was added into the medium by utilizing Hudson (1981) model. Elastic moduli of the minerals needed for this study are provided in Table 1.

## POST STACK INVERSION AND FACIES DEFINITION

The legacy (2005) stacked seismic data is inverted to acoustic impedance (AI) using a model-based algorithm (Russell, 1988). Isotropic AI inversion enables the lithology separation in Garzan formation with three different facies, Kiradag formation, and Beloka formation (Figure 1). Garzan facies can be subcategorized as F1, F2, and F3 zones from the acoustic impedance. The target upper facies (F1) of Garzan formation is relatively low impedance plotted in light blue. Stiff Garzan facies (F2) below F1 has high impedance values as expected from a limestone formation plotted in purple. The third Garzan facies (F3) is a transition from Garzan to Kiradag formation, which is a clastic formation with low impedance plotted in yellow and red colors. Well X-1,2,3 produce oil from low-impedance upper facies (F1), while Well Z-1 is a dry well. The producing wells (X-1,2 and 3), the dry well Z-1, and a prospect drilling location are annotated on the AI section in Figure 1. Judged from the AI results at the dry well (Z-1), it is likely that the planned well will penetrate into the oil-producing facies of Garzan limestone at the planned location.

## ANISOTROPY MODELING

The dipole shear sonic logs processed to seismic velocities in two directions were used to estimate the anisotropic behavior in the reservoir zone. Figure 2 shows the measured well log data in one well (W-3) with the well log interpretations total porosity ( $\Phi T$ ) and water saturation ( $S_w$ ). The lithology interpretations show agreement with the computed anisotropy parameters. The type of anisotropy can be interpreted

as summarized in Table 2. An anisotropic rock physics model was calculated to understand the anisotropy caused by fractures. Voigt-Reuss and Hashin-Shtrikman bounds are computed from Garzan to Kiradag formations using Equations 5 - 12.

Here,  $K_{eff}$ ,  $K_{hs-}$  and  $K_{hs+}$  are the effective bulk modulus, lower bound of HS and upper bound of HS, respectively.  $\mu_{eff}$ ,  $\mu_{hs-}$  and  $\mu_{hs+}$  represent the same notation for shear modulus.  $N$  is the number of elements.  $v_i$  is volume fraction of each element. Hashin and Shtrikman (1963) provides the narrowest possible bounds for a multi-phase composite.

To see the effect of mineralogy on shear modulus, well data is plotted with the various model bounds (Figure 3). It can be clearly observed that non-producing facies including Kiradag formation is mostly inside the mineral bounds for shear modulus. However, producing zone is violating the lower bound with the effect of fractures and hydrocarbon saturation, which makes the rock matrix softer.

Now that the dipole sonic log measurements provide us with anisotropy estimation. The role of fracture density and mineralogy in the reservoir can be further investigated using the anisotropic rock physics model given in Figure 4. To quantitatively visualize the anisotropy, I use the histogram and the probability density function with 0.021 mean and 0.0262 standard deviation. As the fracture density increases in the model, the anisotropy parameter of  $\gamma$  also increases with almost the same values. This is important because the relationship between anisotropy and the amount of cracks in the reservoir can be established. The anisotropy parameter  $\gamma$  ranges from 0 to 0.14 in the reservoir facies and crack density can be estimated from this. Even though the core data measurements from Well X-2 are limited and isotropic, it still shows a good match with the well logs from Well W-3.

## DISCUSSION & CONCLUSION

Not only matrix porosity but also fracture density is crucial in permeability and therefore good reservoir quality in the Garzan limestone formation. In this study, a direct relationship between producing facies and fractures is found by using dipole sonic logs and a rock physics model. Hydrocarbon saturation within the reservoir has a great impact on bulk modulus, and the vertically aligned fractures within the reservoir increase the shear-wave-controlled anisotropy parameter  $\gamma$ . The fracture density within the formation lowers the value of both isotropic and anisotropic shear modulus. This influence can also be seen in the acoustic impedance results, which help us separate different facies and differentiate between producing and non-producing zones in the field.

## ACKNOWLEDGMENTS

I wish to thank Turkish Petroleum Corporation for using the dataset and allowing me to publish this work. I am also grateful to Huseyin Ozdemir for reviewing the

manuscript.

## REFERENCES

- Hashin, Z., and S. Shtrikman, 1963, A variational approach to the theory of the elastic behaviour of multiphase materials: *Journal of the Mechanics and Physics of Solids*, 11, 127–140.
- Hill, R., 1963, Elastic properties of reinforced solids: Some theoretical principles: *Journal of the Mechanics and Physics of Solids*, 11, 357–372.
- Hudson, J. A., 1981, Wave speeds and attenuation of elastic waves in material containing cracks: *Geophysical Journal of the Royal Astronomical Society*, 64, 133–150.
- Mavko, G., T. Mukerji, and J. Dvorkin, 2009, *The Rock Physics Handbook*: Cambridge University Press.
- Reuss, A., 1929, Berechnung der Fließgrenze von Mischkristallen auf Grund der Plastizitätsbedingung für Einkristalle.: *ZAMM - Zeitschrift für Angewandte Mathematik und Mechanik*, 9, 49–58.
- Russell, B. H., 1988, *Introduction to Seismic Inversion Methods*: Society of Exploration Geophysicists.
- Thomsen, L., 1986, Weak elastic anisotropy: *Geophysics*, 51, 1954–1966.
- Vanorio, T., M. Prasad, and A. Nur, 2003, Elastic properties of dry clay mineral aggregates, suspensions and sandstones: *Geophysical Journal International*, 155, 319–326.
- Voigt, W., 1910, *Lehrbuch der Krystalloptik: (mit Ausschluss der Krystalloptik)*: BG Teubner-Verlag, Leipzig.

Keywords: fractured carbonates, anisotropy

Equation 1

$$C^{(HM)} = \begin{pmatrix} C_{11} & C_{13} & C_{13} & 0 & 0 & 0 \\ C_{13} & C_{33} & C_{23} & 0 & 0 & 0 \\ C_{13} & C_{23} & C_{33} & 0 & 0 & 0 \\ 0 & 0 & 0 & C_{44} & 0 & 0 \\ 0 & 0 & 0 & 0 & C_{55} & 0 \\ 0 & 0 & 0 & 0 & 0 & C_{55} \end{pmatrix}, \quad (1)$$

where  $C_{23} = C_{33} - 2C_{44}$ .

Equations 2-4

$$C_{44} = \rho_b V_{S1}^2, \quad (2)$$

$$C_{55} = C_{66} = \rho_b V_{S2}^2, \quad (3)$$

where  $\rho_b$  bulk density, S1 and S2 are shear velocities in two directions.

The anisotropy can be readily estimated from Equation 4.

$$\gamma = \frac{C_{44} - C_{55}}{2C_{44}}. \quad (4)$$

Table 1: Elastic moduli and densities of minerals ( $a = \text{Mavko et al. (2009)}$ ,  $b = \text{Vanorio et al. (2003)}$ )

Minerals	K (GPa)	$\mu$ (GPa)	Density (g/cm3)
Calcite (a)	70.2	29	2.71
Clay (b)	12	6	2.55

Equations 5-12

$$M_V = \sum_i^N f_i M_i \quad (5)$$

$$\frac{1}{M_R} = \sum_i^N f_i \frac{1}{M_i} \quad (6)$$

$$M_{VRH} = \frac{M_V + M_R}{2} \quad (7)$$

where  $f_i$  is the volume fraction of various composites,  $M_i$  is the Bulk and Shear moduli of each composite, and N is the number of composites. The stiffest and the softest bounds can be estimated by using Voigt (1910) and Reuss (1929) bounds, respectively.

$$K_{HS}^- \equiv \Lambda(\mu_{min}) \leq K_{eff} \leq \Lambda(\mu_{max}) \equiv K_{HS}^+, \quad (8)$$

$$\mu_{HS}^- \equiv \Gamma(\zeta(K_{min}, \mu_{min})) \leq \mu_{eff} \leq \Gamma(\zeta(K_{max}, \mu_{max})) \equiv \mu_{HS}^+, \quad (9)$$

where the functions  $\Lambda$ ,  $\Gamma$  and  $\zeta$  are calculated as follows

$$\Lambda(\mu) \equiv \left( \sum_{i=1}^N \frac{v_i}{K_i + \mu} \right)^{-1} - \mu, \quad (10)$$

$$\Gamma(\zeta) \equiv \left( \sum_{i=1}^N \frac{v_i}{\mu_i + \zeta} \right)^{-1} - \zeta, \quad (11)$$

$$\zeta(K, \mu) = \frac{\mu}{6} \left( \frac{9K + 8\mu}{K + 2\mu} \right). \quad (12)$$



Table 2: Anisotropy classification using stiffness coefficients

Cij Relationships	Media
$C44 = C55 = C66$	Isotropic
$(C44 = C55) < C66$	VTI
$C44 > (C55 = C66)$	HTI

Figure 1

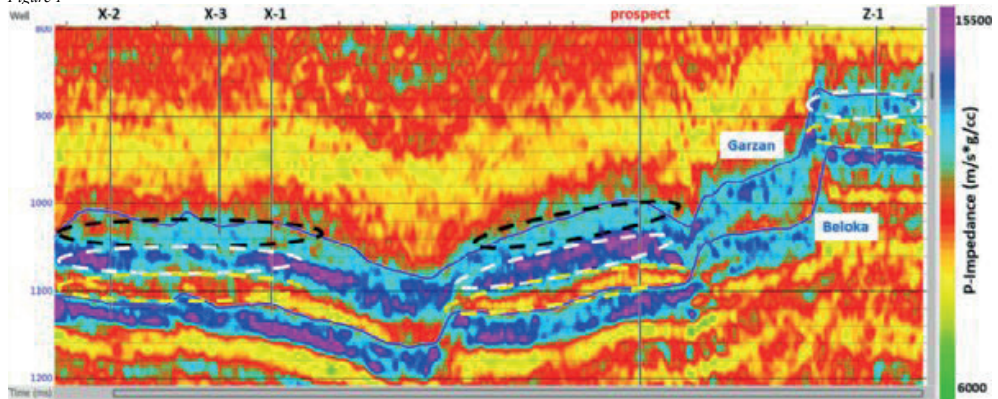


Figure 1: P-impedance inversion result section shown in arbitrary line covering Well X-1,2,3, Well Z-1, and the prospect well. Garzan limestone and underlying Beloka limestone horizons are displayed on top. The producing facies (F1) of Garzan limestone is marked with the black ellipse. The non-producing facies (F2) and Kiradag formation (F3) are shown with white and yellow ellipses, respectively. The dry Well Z-1 does not exhibit good producing facies based on AI results.

Figure 2

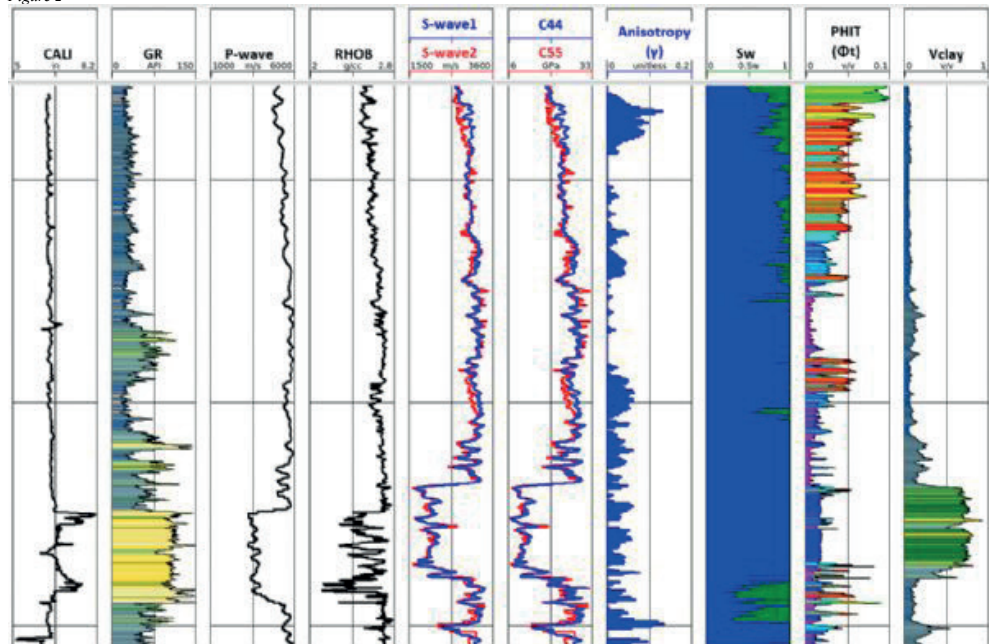


Figure 2: Well logs from Well W-3 in which dipole sonic logs are acquired. The logs shown here cover 250 meters with sampling rate of 0.5 foot (0.1524m), and anisotropy estimated from the dipole sonic logs is compatible with water saturation.

Figure 3

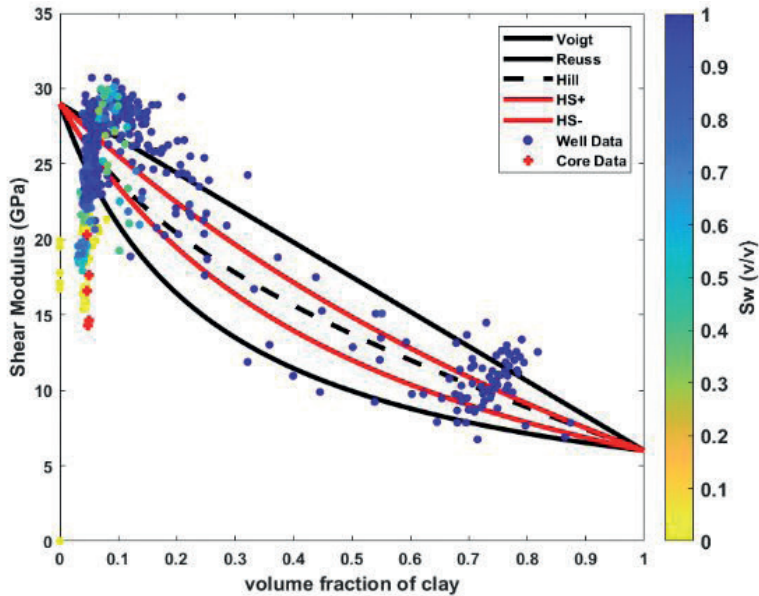


Figure 3: Different types of bounds are calculated for calcite and clay mineral mixtures. The calculated shear modulus from Well W-3 and core data from Well X-2 are shown on top of the bounds. The well data is color-coded by water saturation.

Figure 4

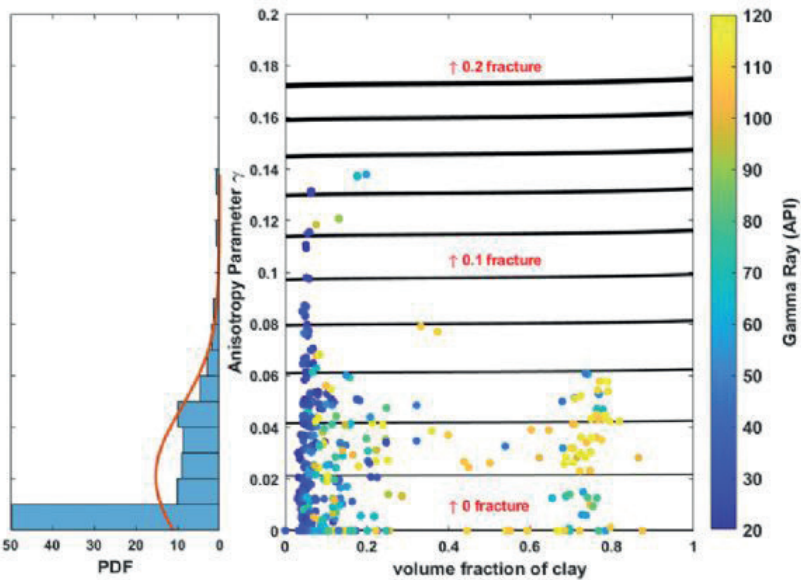


Figure 4: Probability density function of anisotropy  $\gamma$  calculated from dipole sonic log (on the left). Change of anisotropy  $\gamma$  with volume fraction of clay, juxtaposed by the effect of fracture density on anisotropy from the rock physics model (on the right). Each black bar represents 2% fracture density change in the model. The well data is color-coded by Gamma Ray values.

# Unlocking New Discovery in Thrace Basin, Turkey: Probabilistic Neural Network Application to estimate NPHI and Acoustic Impedance Cross Plotting for Hydrocarbon Mapping



**Sait Baytok, Ergin Karaca**

Turkish Petroleum Offshore Technology Center (TP-OTC)

## ABSTRACT

In this study, we propose a relationship between neutron porosity and acoustic impedance for direct hydrocarbon determination. Rock physics analysis indicates that acoustic impedance and neutron porosity successfully predict hydrocarbon-bearing intervals. Therefore, generating these two properties using various methods offers an opportunity to map hydrocarbons in the area. To integrate well-logs and seismic data, we used model-based post-stack seismic inversion to generate acoustic impedance and multi-attribute transform and neural network applications to generate neutron porosity. We derived a statistical relationship by analyzing a set of training data at well locations. Our approach was proven reliable based on consistent results between wells and seismic data. Overall, our study suggests that multivariate geostatistical techniques, including the proposed neutron porosity and acoustic impedance relationship, can effectively support hydrocarbon exploration and development in the Thrace Basin.

## INTRODUCTION

The Tertiary Thrace Basin in Turkey has been explored for gas since the 1960s, with limited studies on reservoir geophysics (Baytok et al., 2016; Baytok et al., 2017; Sele, 2014; Arpacı and Özdemir, 2020). Geologically, it is a triangular-shaped basin with pre-Tertiary crystalline rocks of the basement and overlying Tertiary sedimentary rocks that contain formations deposited in various environments (Turgut and Esseller, 2000; Less et al., 2011). The main targets are carbonate deposits located on top of Palaeozoic highs, especially in the northern and eastern parts of the basin (Aydin and Nur, 1982; Less et al., 2011). This study utilized multiattribute transform and model-based seismic inversion methods to predict NPHI and AI properties for prospect identification. Our approach using AI and NPHI proved reliable, with consistent results at three post-study drilled wells and a new discovery in the first well (Baytok et al., 2016; Baytok et al., 2017; Sele, 2014; Arpacı and Özdemir, 2020).

## ROCK PHYSICS ANALYSIS

No shear sonic logs or prestack seismic data were available for useful rock physics analysis in the reservoir characterization of the field. Instead, a poststack seismic approach was employed. The combination of NPHI and AI proved to be the most effective reservoir indicator. In Figure 1, the NPHI-AI crossplot at five wells reveals that producers are characterized by low NPHI values below 0.15. The presence of hydrocarbons is indicated

by resistivity logs and neutron-density crossovers. Hydrocarbon-bearing intervals can be defined by holding NPHI values between 0 and 0.15 and AI values between 5000 and 9000 m/s x g/cm<sup>3</sup> (Figure 1).

## MODEL-BASED POSTSTACK SEISMIC INVERSION (MBSI)

The main objective of seismic inversion is to convert a seismic section into a rock property section, enabling the determination of dry rock and reservoir fluid properties. This, in turn, allows for the tracking of reservoirs away from wellbores. To achieve this, we utilized model-based seismic inversion (MBSI) to invert poststack 3D land seismic data to AI. The background model was generated using data from 34 wells and four picked horizons. Figure 2 (top) shows an arbitrary seismic line passing through both dry and gas wells, along with the corresponding inverted AI (middle).

NPHI prediction using Multiattribute Linear Regression and Neural Networks

Multiattribute transforms predict a single dependent variable using one or more independent variables. We used a method to predict NPHI logs at 11 wells using a subset of 24 seismic attributes, expanded using nonlinear transforms (Table 1). Linear regression and multivariate linear regression were problematic, so we used a convolutional operator with an operator length of 18 points and stepwise regression to select eight attributes with a 72% correlation to NPHI logs. The PNN is chosen in this study due to its mathematical simplicity and consistent estimator. After PNN training, the correlation between actual and predicted NPHI values improved up to 0.82. The NPHI arbitrary section derived from PNN analysis is shown in Figure 2 (bottom).

The study resulted in a gas discovery in the target structure. Comparison of the inverted AI and NPHI to well data was done, but due to confidentiality, only the results of post-study wells can be presented. A shallow well drilled at the easternmost part far from the target structure targeting a sandstone lens showed low probability of hydrocarbons. The first exploration well drilled in the target structure showed NPHI values below 0.15, which was proven by post-well log measurements, leading to the development of a new play concept. Seismic crossplots of NPHI values below 0.15 within the range of AI values between 5000 to 9000 m/s x g/cm<sup>3</sup> indicate potential.

## CONCLUSIONS

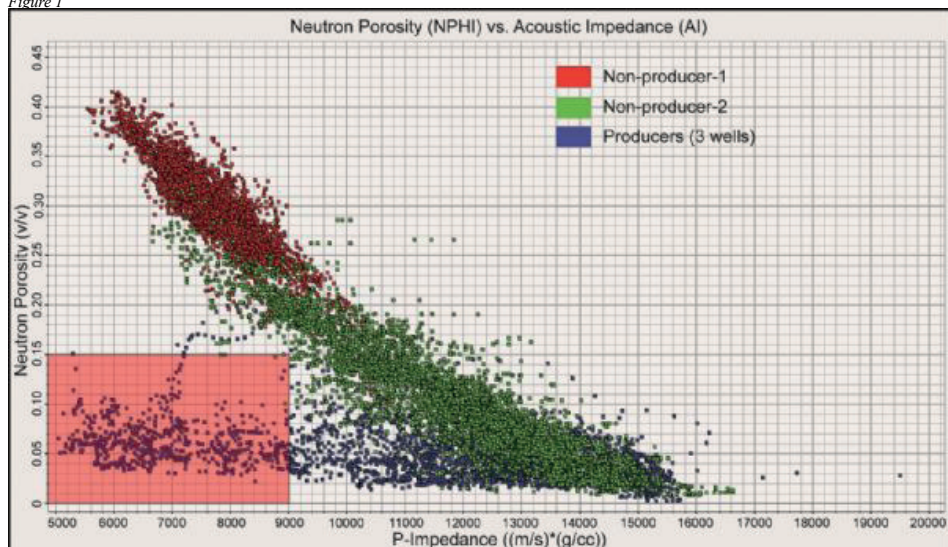
We utilized multivariate geostatistical techniques and model-based seismic inversion to predict NPHI and AI values, respectively, from seismic data to identify potential hydrocarbon bearing intervals. Our results were validated with a successful discovery and matching log measurements. Due to the unavailability of prestack seismic gathers, we relied on poststack inversion and sample-based seismic attributes. We employed a multiattribute transform and neural networks for NPHI prediction, achieving a higher correlation with a PNN network. NPHI was found to be the most significant factor in determining hydrocarbon potential, with AI providing complementary information. Our study demonstrates the successful application of multivariate geostatistical techniques and crossplotting of NPHI and AI values to identify potential hydrocarbon-bearing intervals.

## ACKNOWLEDGEMENTS

The authors thank to TPAO for permitting to show the well and seismic data. We greatly appreciate the contributions of our colleagues at the TPAO data processing center and the project team of the study area through their presentations and personal communications. The comments from anonymous reviewers and Hüseyin Özdemir helped to improve the content of the paper.

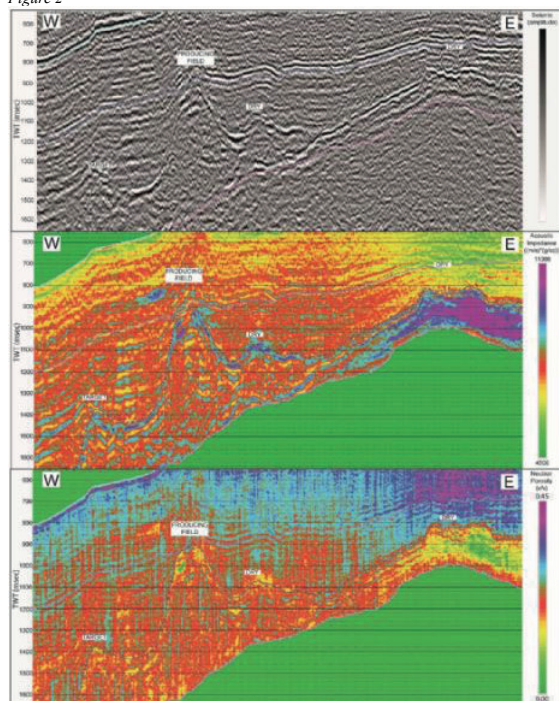
Keywords: PNN, Multiattribute

Figure 1



NPHI vs. AI rock physics template. Red and green dots represent the data from dry wells while blue from 3 different producers. Red rectangle contains values that describe hydrocarbon bearing intervals in which NPHI values are between 0 to 0.15 and AI values between 5000 to 9000 ((m/s)\*(g/cc)).

Figure 2



West-East oriented cross-sections from seismic data (top panel), AI from MBSI (middle panel) and NPHI from multi-attribute and PNN application. Target structure, production field, and two dry structures from west to east can be seen, respectively.

Table 1

Attribute	Nonlinear transforms
Amplitude Envelope	Natural Log Exponential Square Inverse Square root
Amplitude Weighted Cosine Phase	
Amplitude Weighted Frequency	
Amplitude Weighted Phase	
Average Frequency	
Apparent Polarity	
Cosine Instantaneous Phase	
Derivative	
Derivative Instantaneous Amplitude	
Dominant Frequency	
Filter 5/10 - 15/20	
Filter 15/20 - 25/30	
Filter 25/30 - 35/40	
Filter 35/40 - 45/50	
Filter 45/50 - 55/60	
Filter 55/60 - 65/70	
Instantaneous Frequency	
Instantaneous Phase	
Integrate	
Integrated Absolute Amplitude	
Quadrature Trace	
Second Derivative	
Second Derivative Instantaneous Amplitude	
Seismic Inversion	

Complete list of attributes used in multiattribute analysis and list of nonlinear transforms.

# Utilizing Seismic Amplitude Information and Extending The Value of The Seismic Beyond Structural Imaging

Omar Aly<sup>1</sup>, Aya Ibrahim<sup>1</sup>, Tarek Nafie<sup>1</sup>, Ahmed Hassan<sup>1</sup>, Mohamed Fekry<sup>1</sup>, Amin Al Maktari<sup>2</sup>, Aref Al Shadadi<sup>2</sup>, Mohammed Ali Al Rawqi<sup>2</sup>

<sup>1</sup>slb

<sup>2</sup>SEPOC



## INTRODUCTION

This study aims to understand the reservoir properties distribution of the Alif formation from seismic data and enhance the seismic interpretation model for well planning support. The objective is to minimize drilling risk associated with the high rapid spatial heterogeneity and compartmentalization of the current reservoir rocks. Seismic inversion and Rock physics are powerful tools that deliver information about intra-well rocks elastic attributes and reservoir properties such as porosity, saturation, and rock lithology classification.

The study focuses on the surface Seismic and Rockphysics Inversion study conducted on the current project to characterize the reservoir properties of the Alif formation from the seismic data. The current reservoir rocks are affected by complex faulting systems and high horizontal and vertical heterogeneity of their reservoir properties distribution, which is difficult to resolve using seismic imaging techniques alone. To better characterize the reservoir rocks in terms of reservoir properties such as Effective Porosity, Water Saturation, and Rock Classification, it is crucial to go beyond seismic imaging techniques.

Geophysical logs, including sonic and density logs, measure rock properties near the borehole. Reliability of these logs is affected by borehole diameter, shape, and drilling fluid invasion. Acoustic well logs need to be conditioned before using them in geophysical analysis, as errors will propagate through subsequent processes. Surface seismic data quality is impacted by residual noise, multiples contamination, and improper amplitude balancing.

The studied area lies in the middle of the Marib – Shabwa Basin, which is one of the main sedimentary basins with proven commercial quantities of oil and gas. The main reservoir, Alif, is characterized by rapid spatial heterogeneity and compartmentalization. Understanding these reservoir properties has a significant impact on rock types, fluid flow characteristics, and permeability and production from the reservoir.

Pre-stack inversion is considered an ideal technique for intra-well reservoir properties prediction compared to classical-traditional seismic AVO attributes and/or conventional geostatistical techniques based on Kriging and Co-Kriging techniques. However, it leads to the conversion of reservoirs into non-reservoirs and vice versa, making petrophysical predictions inaccurate. (Ray and Chopra, 2016).

## METHODS AND WORKFLOWS

A good quality acoustic logs (Compressional Sonic, Shear Sonic, and Density) is essential for seismic

inversion and rock physics work. These logs measure the rock properties a few inches from the borehole, and their reliability is affected by large and rapid variations in the diameter and shape of the borehole cross-section and the process of drilling fluid invasion. The first step in well data manipulation is acoustic well logs conditioning, which involves using other recorded logs that are not affected by bad hole conditions and the process of drilling fluid invasion to condition and edit suspicious intervals on an acoustic log.

The first pass of log conditioning involves minor editing to correct for obvious defects such as cycle skips and erroneous extremely low readings on the sonic logs caused by bad hole conditions. For the Density Log, Borehole wash-out zones are identified, and Caliper log readings and the degree of conformity between various log curves are used as major indicators for the density log quality. Subsequent conditioning passes involve a wide range of multivariate statistical regression relationships based on other recorded correlation logs that are not affected by bad hole conditions.

The second step involves a wide range of multivariate statistical regression relationships based on other recorded correlation logs that are not affected by bad hole conditions. Direct logging measurements of the rock matrix provided by natural Gamma-Ray and Deep Resistivity tools minimize invasion influences, which normally affect the reliability of the measurements. Therefore, Gamma-Ray and Deep Resistivity can be used to train a Multivariate statistical Regressions to generate synthetic readings for the Sonic and Density logs to replace the suspicious intervals.

Quality control of the acoustic logs is checked through cross-plotting, with very good agreements between the edited logs cross-plotting with standard Rock-physics templates. Cross-plots analysis of the Acoustic Impedance versus Rhob and Vp/Vs indicate major improvements in the clustering of the rock lithology classes with respect to the rock physics template iso-lines after log conditioning, adding measures of confidence on the reliability of the current acoustic/elastic logs for the subsequent inversion work.

In summary, the proposed workflow for seismic pre-Stack simultaneous Deterministic seismic inversion computes elastic properties, including Acoustic Impedance, Vp/Vs, and Density based on the input angle stack. The first step is Surface Seismic to Well Tie analyses using Deterministic Wavelet Extraction, which estimates embedded wavelets in the seismic data by matching the seismic reflectivity with the well log reflectivity and tie the well to the seismic data. The quality of extracted wavelets is examined through several statistical tests, and the best results are obtained for the angle ranges 5° to 15°, 13° to 23°, 21° to 31°,

and 29° to 39°.

For seismic inversion to absolute acoustic/elastic properties, low frequency information missing in the seismic data is required. Low frequency models for acoustic impedance and shear impedance logs are supplied in the form of low frequency models for acoustic impedance and shear impedance logs and created in a structural model frame constructed using the interpreted seismic horizons after spatial smoothing. The calibrated acoustic and elastic properties of the current three wells were interpolated in dual conformity to the received three interpreted seismic horizons. Determination of the extreme low frequency component is achieved based on trials, with a low frequency cut-off of 0-11 Hz being the most adequate for the current data.

The current pre-stack simultaneous inversion produces primary outputs such as Acoustic-Impedance Vp/Vs and Density acoustic/attributes. To ensure the reliability of the results, visual inspections are conducted at each well location and high correlation coefficients between the inverted traces and their corresponding well logs are calculated. This provides high levels of confidence in the reliability of the current deterministic inversion results for subsequent reservoir properties prediction steps.

The Relative Acoustic Impedance Inversion is an iterative inversion technique that involves minimal data manipulation and requires minimal data manipulation. It is decided to produce relative acoustic impedance maps at the top of the reservoir level (top Alif Formation) and compare it with its corresponding pre-stack inversion attributes to check consistency. Good agreements between the relative acoustic impedance and pre-stack inversion attributes are obtained, providing a high level of confidence in the reliability of the current deterministic inversion results.

To build up a Petro-Elastic Rock Physics Model for Porosity and saturation estimation from well acoustic/elastic logs, a multivariate statistical regression relationship between the different acoustic/elastic logs attributes of the current reservoir rocks and petrophysical properties is established. The obtained Full-Elastic multivariate statistical regression relationship is then used to predict the Porosity and saturation from the elastic attributes for the current reservoir rocks.

For quality control of the estimated Petro-Acoustic/Elastic Porosity and saturation logs output from Multivariate Statistical Regression at the current well locations are compared with its corresponding petrophysical porosity logs. The close similarities between them add measure of confidence that it will be possible to predict the Effective Porosity and saturation of the current reservoir rocks from the inversion data output.

The workflow used for rock lithology classification of the current reservoir rocks based on its acoustic/elastic signature is described. Lithology Prediction is a rock physics-based workflow that integrates well logs, high end seismic inversion, Petrophysical data, and Rock Physics analysis to provide an estimate of the most

probable lithology and the uncertainty associated with the prediction. Relationships observed at the wells between the physical properties estimated by seismic inversion, i.e., Acoustic impedance and Vp/Vs, and observed lithology can be used to convert the inversion results to lithology cubes.

The current reservoir rocks are classified into three classes: HC-Sand, Brine Sand, and Shale, using the following Petrophysical Cut-Offs. The Probability Density Function Pdfs are derived for these three rock classes, and a 1D comparison between the logs and the predicted litho-flags along with the probability of the occurrence of each class is generated.

The PDF analysis technique is used to measure the level of confidence in the lithology prediction. However, uncertainties from well log, petrophysical data, noise, and multiples in surface seismic data affect the level of confidence in the lithology prediction. As an industry standard procedure, Statistical Probability Density Functions (PDF) are generated for the various predicted lithofacies using Bayesian inversion techniques.

By using the above-mentioned PDFs statistical results and the Petrophysical Cut-Offs, it becomes possible to convert the current inversion attributes into Lithology cubes and compute its probabilities for the current reservoir rocks. However, it should be emphasized that the Lithology Prediction results cannot be interpreted as a stand-alone product but should be interpreted in conjunction with its probability results (level of confidence in the prediction) for each class.

## QUALITY CONTROL OF THE RESULTS

### Blind Well Testing and Attributes Maps (Findings)

In order to ensure quality control of inversion results, blind well testing was conducted, as well as the inversion acoustic/elastic attributes and predicted reservoir properties attributes maps to check the consistency of the results. A well that was not used in the current inversion project, was used for blind well testing. The faulted zone around the fault plan causes rapid lateral variations of seismic amplitudes fidelities, resulting in wave scattering/diffraction and potential mode conversions between compressional, converted shear, and Rayleigh waves. This phenomenon is specific to seismic waves and is characterized by changes in the seismic amplitudes response of seismic reflectors.

Seismic data imaging techniques around faulted zones impose limitations on the reliability of seismic amplitudes responses fidelities. To confirm these observations, a seismic to well tie assessment using deterministic wavelet extractions was performed around the blind well location. Although it is not possible to extract a stable seismic wavelet at the exact well location, it is possible to extract a stable wavelet from around the well location away from the faulted zone.

Due to limitations imposed by seismic data imaging techniques around faulted zones, the 1D-Qcs of the inversion results were performed at both the exact well

location and the best location. Visual inspection of inversion attributes and reservoir properties predictions versus their corresponding logs generally indicates improvements in the match at the best well location.

For further QC of inversion attributes and predicted reservoir properties, maps at the top of the Alif formation were produced. Zones with low AI and  $V_p/V_s$  correspond to high hydrocarbon probabilities, effective porosity, low  $S_w$ , and the vice versa. This consistency adds a measure of confidence to the results. The blind well is shown to be located outside the predicted sweet spot which is consistent with the drilling results.

To demonstrate the value of the current seismic reservoir characterization study, an arbitrary line passing by the studied wells was shown to show the conventional seismic image versus the corresponding acoustic/elastic attributes and reservoir properties prediction attributes results. This highlights the valuable information about the current reservoir that can be obtained beyond conventional seismic imaging.

## SUMMARY AND CONCLUSIONS

This paper shows how to bridge the geophysical information given by seismic data into Petrophysical Reservoir Property geological insights through seismic inversion and rock physics techniques.

The provided Acoustic/Elastic and Petrophysical logs for the current studied wells are then used in the current Rock physics modeling. A series of Rockphysics models is built using Multiwell cross-plots between the inversion elastic attributes namely, Acoustic Impedance and Shear Impedance versus the reservoir attributes namely, Effective Porosity and Water Saturation. All the inversion acoustic/elastic properties have been simultaneously used in a full solution as inputs to generate a multivariate statistical regression with maximum correlation and minimum mean square error.

Reservoir rocks are classified into three classes: HC-Sand, Brine-Sand, and Shale, using Petrophysical Cut-Offs. Inversion-driven Lithology Prediction uses relationships between inversion Acoustic/Elastic attributes and rock type. Deterioration in these attributes generates uncertainty in lithology Prediction. 1D-QC results show good correlation between logs classification and predicted litho-classes, adding confidence to the results.

In summary, extensive Quality Controls of the current seismic reservoir characterization results have been performed, including the following:

(1)- For Quality Control of the inversion acoustic/elastic attributes results, the inverted acoustic/elastic properties traces at each of the current wells locations are visually compared with its corresponding well logs. In addition, the inverted traces at the well's locations are cross correlated versus its corresponding well logs and its correlation of coefficients are calculated. The obtained very good coefficients between the inverted traces and its corresponding well logs give high level of confidence on the reliability of the current deterministic

inversion results to be used for the subsequent inversion driven reservoir properties Prediction steps.

(2)- For further Quality Control of the pre-stack inversion results, Relative Acoustic Impedance and Pre-Stack Inversion Attributes Maps at Top Alif Formation are generated. The produced attributes are showing very good agreements between the relative acoustic impedance and pre-stack Inversion attributes (AI,  $V_p/V_s$  and Density). This quality control of the inversion results added measure of confidence that there are no artifacts and/or relics are introduced in the pre-stack inversion attributes results.

(3)- Additionally, quality control of the inversion driven Predicted Petro-Acoustic / Elastic Effective Porosity and Water Saturation logs output form Multivariate Statistical Regression at the current studied wells locations are compared with its corresponding petrophysical logs. The close similarities between the Predicted Effective Porosity and Water Saturation logs and its corresponding Petrophysical logs adds measure of confidence that it will be possible to predict both the Effective Porosity and Water Saturation of the current reservoir rocks from the inversion data output.

(4)- Meanwhile, the results of the 1D – Quality Control of the well correlation between Petrophysical logs classification and predicted litho-classes indicated very good between the logs classification and predicted litho-classes. The close similarities between the logs classes and its corresponding predicted litho-classes well logs add measure of confidence at the obtained results.

(5)- For a more robust quality control of the results, a Blind Well Testing is performed. It is evident that there are very good similarities between the inversion attributes and the reservoir properties Prediction s versus its corresponding logs. Blind well testing is considered as the ultimate QC to appraise the seismic reservoir characterization results.

It is evident that the current Seismic and Rock Physics Inversion study has provided invaluable information regarding the Petro-Elastic and the Reservoir Properties attributes characterization of the reservoir units distribution all over the studied area. The obtained deterministic Petro-Acoustic/Elastic Reservoir Properties attributes are providing more accurate results with regards to the identification of the reservoir Geo-Bodies and for better definition of the hydrocarbon saturated sandstone reservoirs characterization. This should avoid pitfalls that can arise from using only classical-traditional AVO attributes analysis that are based only on seismic amplitudes analysis and mapping. Another advantage, in using the Seismic and Rock Physics Inversion attributes results for seismic reservoir characterization, lies on that fact that these attributes are driven from the integration of seismic and well logs data which can better define the inter-wells reservoir elastic properties distribution heterogeneities on basis of physical measurements obtained from the inverted seismic amplitudes rather than using conventional Geostatistical Co-Kriging techniques which is usually used to propagate the inter wells reservoir properties



into the 3D-Model grid.

Keywords: Seismic Inversion, Rock physics

*Beyond seismic image attributes*

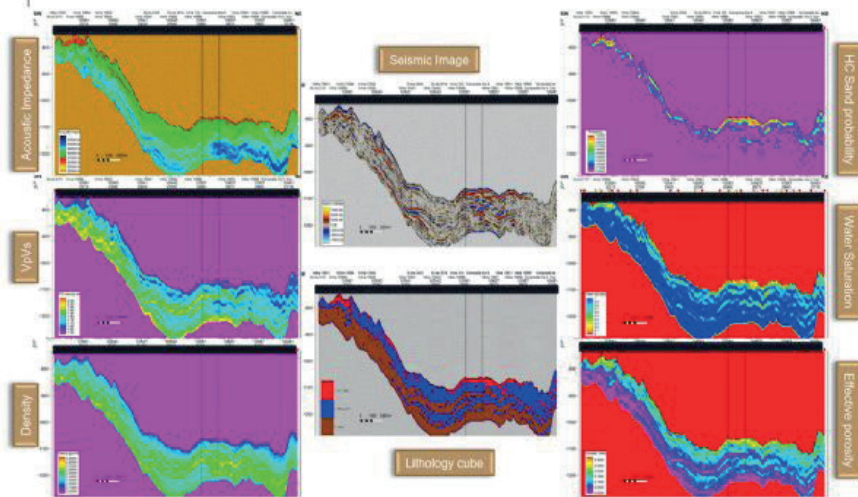
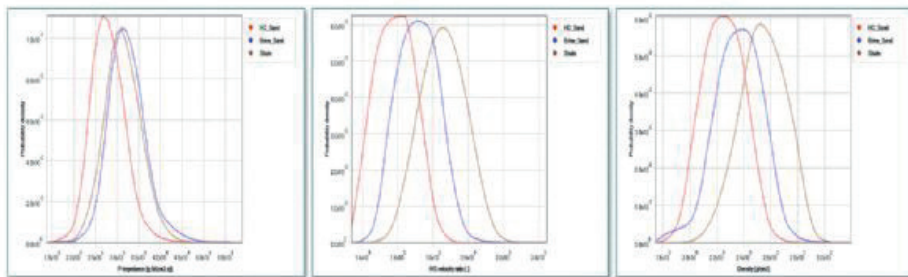
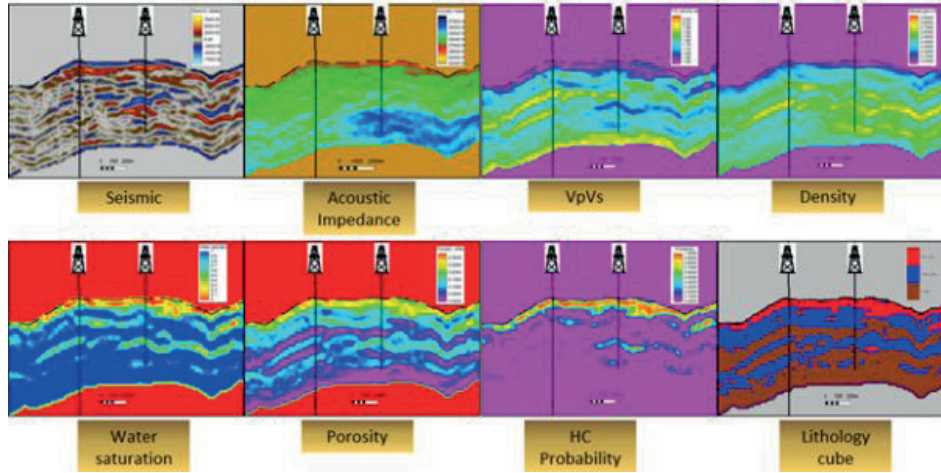


Figure 24: Example for going Beyond Seismic Image: from Seismic Imaging to Reservoir Acoustic/Elastic attributes and Reservoir Properties Predictions.

*PDF Analysis and Rock class classification*





Seismic well tie and wavelet extraction

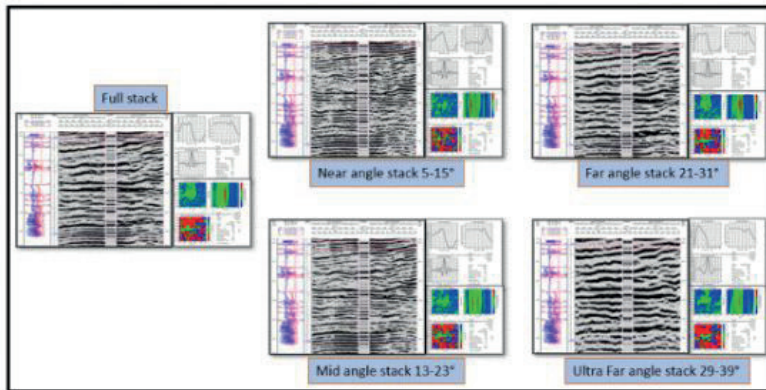


Figure 6: Example of Seismic to Well Tie and Deterministic Wavelets Extraction Results

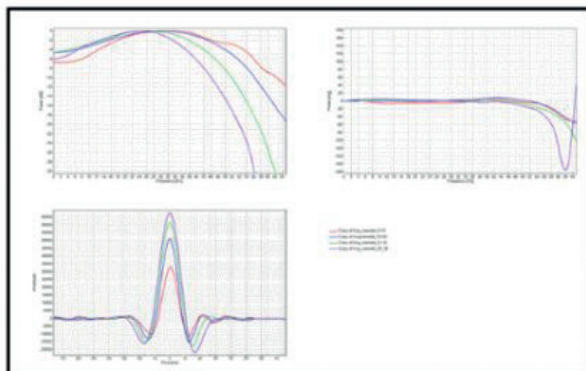


Figure 7: Average Extracted Wavelets from the different Angle Stacks: Time and Frequency Domains Diagnostics

Stratigraphic column and location map of Marib basin

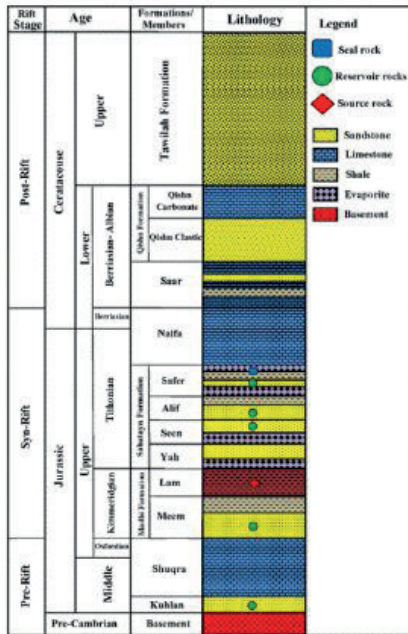


Figure 1: Stratigraphic column of Marib Basin



Figure 2: Location Map of Marib Basin

Well log conditioning crossplot analysis

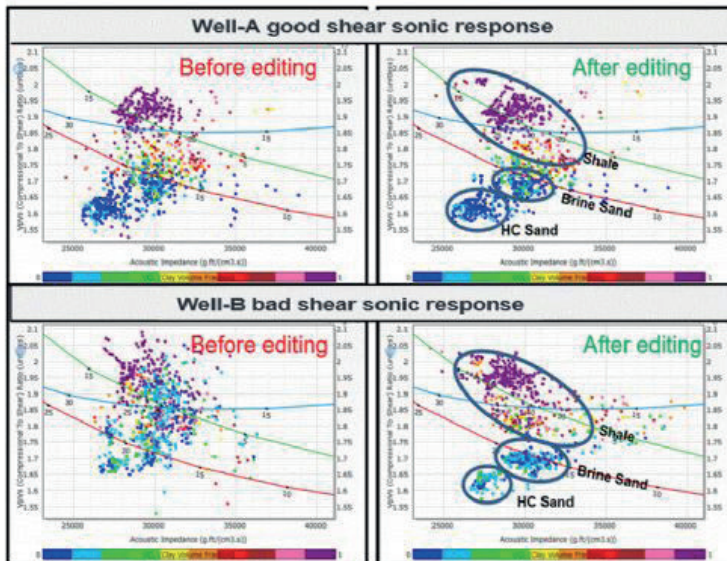


Figure 4: Cross-plots of the Acoustic Impedance versus the Vp/Vs Color coded by Vcl (before and after conditioning). Notice the improvements in the clustering of the rock classes with respect to the rock physics template iso-lines IN Well B, after log conditioning.

# Seismic Reservoir Characterization of Hydrocarbon-Bearing Sandstones, In A Producing Field, Thrace Basin



**Taner Arpacı**

Türkiye Petrolleri Anonim Ortaklığı (TPAO)

## SUMMARY

Thrace basin has high potential gas reservoirs. However, main production has been from small sand patches/lenses. It is necessary to conduct detailed reservoir characterization studies to map hydrocarbon bearing sandstones. AVO attributes and inverted elastic rock parameters inverted from seismic data are utilized for clastic reservoirs for the detection of new potential bypassed zones. Seismic inversion results showed agreement with the available well data. The analysis indicated a small gas-bearing bypassed sandstone lens confirmed by drilling.

## INTRODUCTION

Thrace basin is situated in NW corner of Turkey. The gas production is mainly made in Oligocene Osmancık formation. The depositional environment of Oligocene formations is a fluvial and deltaic system. The Osmancık formation forms delta-front facies of this deltaic deposition. The stratigraphic section mostly consists of clastic facies and minor carbonates. Faults in the basin form seals for structural hydrocarbon traps (Huvaz et al., 2005; Siyako, 2006).

AVO anomalies or attributes from CDP gathers and elastic parameters inverted by prestack inversion method provided an understanding of gas bearing sandstone properties in the basin. Main producers are small gas pockets in the field under study. Inverted rock properties such as impedances,  $V_p/V_s$  ratio and  $\lambda\rho$  show a good match with production intervals. In other words, these parameters are considered as pore fluid indicators for reservoir rocks. The main concern of the use of these indicators is to reduce the risk of drilling dry wells.

## DATA SETS AND DATA PREPARATION

12 drilled wells were available for the field study (Figure 1, left). All wells include full set logs including P-sonic and density logs. However, shear sonic log is only available at Well-C. Using a crossplot of p-velocity versus s-velocity in Well-C, a linear relation was extracted. Using this equation, s-sonic logs for other wells were computed. The estimated shear sonic logs were used for low frequency model building. Spikes and bad signals were eliminated to increase the reliability of the initial model.

Seismic data volume includes 3D vibroseis seismic data, cropped from a merged data set, covering about 190 km<sup>2</sup>. Trim statics and mild parabolic radon transform filtering were applied to improve the S/N ratio of the CMP gathers.

## RESERVOIR CHARACTERIZATION

Acoustic impedances (AI), shear impedances (SI) and density logs (RHOB) from eleven wells were utilized for prestack seismic inversion. Wells-A, B, D, E on the south of the study area and Well-1 and 2 on the north are the producers. Well-C is a gas-show well and Wells-F, G, H, I and Well-3 are dry wells. Well-X was the target well with a prospect which is stratigraphically trapped. Figure 1 (right) indicates a composite stack, i.e., a random line section across Well-1, 2, 3 and X. Yellow ellipses represent drilled prospects in Well-1, 2 and 3. Well-1 and Well-2 produces gas fluid with a high amount of water while the target zone drilled at the location of Well-3 only has water. The target prospect in this study was the zone shown with a white ellipse in Well-X location. There is natural gas production at about 750 ms at Well-1 and Well-2.

AVO analysis indicate an important DHI in the Osmancık Formation which is composed of alternating clastic sediments (Shuey, 1985). Intercept x gradient ( $I \times G$ ) attribute shows a clear positive anomaly at the target depth of Well-X (Figure 2, A). The crossplot of intercept versus gradient (Figure 2, B) and selecting data points falling in a zone with negative intercept and gradient (Figure 2, C) help us to understand the AVO behaviour in the producing and non-producing reservoir zones (Figure 2, D). One of the good producers, Well-B, shows a clear anomaly while this anomaly is weaker at low producer, Well-1. Moreover, non-producing Well-3 does not show an AVO indication. These results show that AVO is a reliable tool and sensitive to the presence of hydrocarbon fluid.

Prestack inversion was utilized to distribute rock properties all over the field (Hampson, D.P., Russell, B.H. and Bankhead, B., 2005). Although log data provides higher resolution than seismic data, elastic rock properties represent variations only at well location. Also, stack seismic data does not contain information from other than zero offset reflections, resulting the loss of fluid identification. To detect hydrocarbon fluid, AI and SI were generated (see, for example, Özdemir, H., Hansen, J.W. and Tyler, E., 2006). The angle band stacks 0o-15o, 15o-30o, and 30o-45o and extracted wavelets from each angle stack were used as input for simultaneous prestack inversion scheme. Using created AI and SI from prestack inversion,  $VP/VS$  ratio,  $\lambda\rho$  and  $\mu\rho$  were also computed.  $VP/VS$  ratio and  $\lambda\rho$  are hydrocarbon indicators while  $\mu\rho$  shows the lithology changes (see, for example, Özdemir, Murineddu and Khazanehdari, 2005).

Figure 3 shows a horizon map of inverted rock properties representing hydrocarbon producing intervals at Well-1, 2 and 3. While producing wells, Well-1 and 2, have low  $VP/VS$  ratio and  $\lambda\rho$ , non-producing Well-3 indicates

higher values. Although distance between these wells are not more than 200 m., inversion results are found very successful to discriminate hydrocarbon bearing zones with high water volume and water bearing zone.

The AVO attributes and the prestack impedance inversion results are calibrated at the available wells helped to identify the bypassed sand lenses. Well X was drilled and high amount of gas volume was discovered. The measured logs including compressional velocity, shear velocity and density are shown in Figure 4, left. The entrance of the Osmancik Formation (Tyoy) and top/base reservoir markers are indicated in this well section. In Figure 4 (right panel), real prestack seismic gathers, generated AVO model at reservoir interval (using Zoeppritz's (2019) equations, measured log data and seismic wavelet) and gradient analysis of real and synthetic gathers are given. Both intervals show AVO class III anomaly.

The acoustic impedance (AI, P-impedance) and VP/VS ratio crossplots are frequently used in reservoir characterization studies to discriminate lithology variations and hydrocarbon zones due to different behaviour of elastic properties (Goodway, Chen and Downton, 1997). A crossplot created using measured well logs (Figure 5A) showed clear differentiations for the lithology types and the reservoir zone. Each zone was identified with different colours (Figure 5B): (1) Red color represents sandstone and siltstone alternations, (2) dark and light grey coloured zones indicate siltstone and shalestone alternations with dominant siltstone (dark) or shale (light), (3) purple zone is limestone and (4) yellow colour illustrates gas bearing sandstone. When AI and VP/VS ratio were plotted using outputs from seismic inversion, due to the presence of thin layers, lithology and gas bearing sand pocket were not detected clearly. However, when the zones were selected using the same shapes and colors in the crossplot of well logs (Figure 5C), the response of both seismic (Figure 5D-1) and well logs (Figure 5D-2) become similar. In other words, when the cut-offs from AI and VP/VS ratio crossplot of well logs were specified, the expected results of inversion become easier to be evaluated.

## CONCLUSIONS

Pore fill and lithology variations from the prestack inversion results were calibrated at the existing gas producing and non-producing wells. The results show that AVO and inversion are significant tools to detect gas bearing sandstone reservoirs. The later drilled well, Well-X, was achieved after the confirmation of the reliability of inversion outputs and AVO classification. AVO class III anomalies and low  $\lambda\rho$  and VP/VS ratio values from inversion results could be useful to step out new potential hydrocarbon filled areas.

## REFERENCES

Goodway, W., Chen, T. and Downton, J., 1997, Improved AVO fluid and lithology discrimination using Lamé petrophysical parameters;  $\lambda\rho$ , " $\mu\rho$ ", and " $\lambda/\mu$

fluid stack", from P and S inversion: 67th SEG Technical Program, Expanded Abstract AV 2.7, 183-186.

Hampson, D.P., Russell, B.H. and Bankhead, B., 2005, Simultaneous inversion of pre-stack data: 74th SEG Annual International Meeting, Expanded Abstract, SI 1.2, 1633-1638.

Huvaz, O., Sarikaya, H. & Nohut, Ö.M., 2005, Nature of a regional dogleg pattern in maturity profiles from Thrace basin, northwestern Turkey: A newly discovered unconformity or a thermal anomaly. AAPG Bulletin, 89, 1373-1396.

Özdemir, H., Hansen, J.W. and Tyler, E., 2006, Rock and reservoir parameters from pre-stack inversion of surface seismic data. First Break, 24, 83-87.

Özdemir, H., Murineddu, A. and Khazanehdari, J., 2005, Pore-fill and pressure changes from 4D seismic data: Geological Society of Great Britain Petroleum Group Int. Conference, Bright or Dim?; and Petroleum Exploration Society of Great Britain PESGB Meeting, PETEX'2006. Extended Abstracts.

Shuey, R.T., 1985, A simplification of Zoeppritz Equations: Geophysics, 50, 609-814.

Siyako, M., 2006, Lignitic sandstones of the Trakya Basin. Bulletin of the Mineral Research and Exploration, 132, 63-72.

Zoeppritz, K., 1919, On reflection and propagation of seismic waves: Gottinger Nachrichten, 1, 66-84.

Keywords: AVO, Seismic Inversion

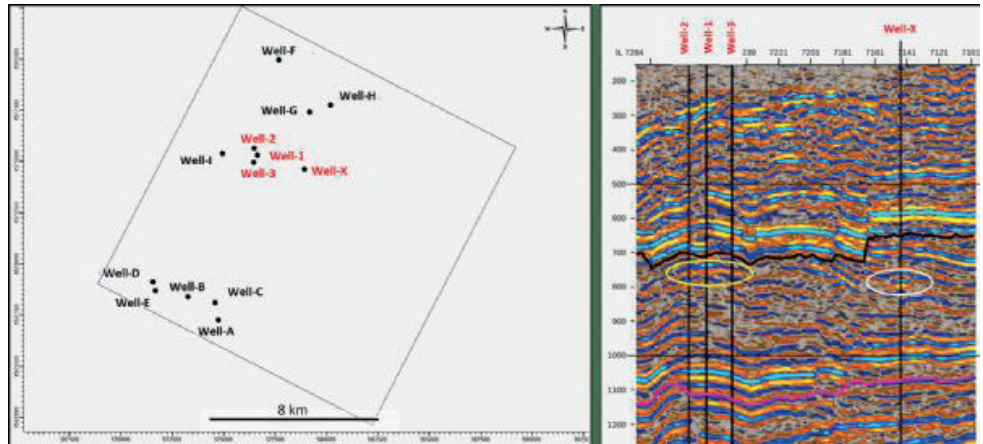


Figure 1. Time base map of the field with annotated wells (left) and an arbitrary seismic stack section passing through Well-1, Well-2, Well-3 and Well-X (right). Yellow ellipse illustrates targetted zone at Well 1, 2 and 3, resulting success in Well-1 and 2. White ellipse indicates target zone at Well-X.

AVO Attribute

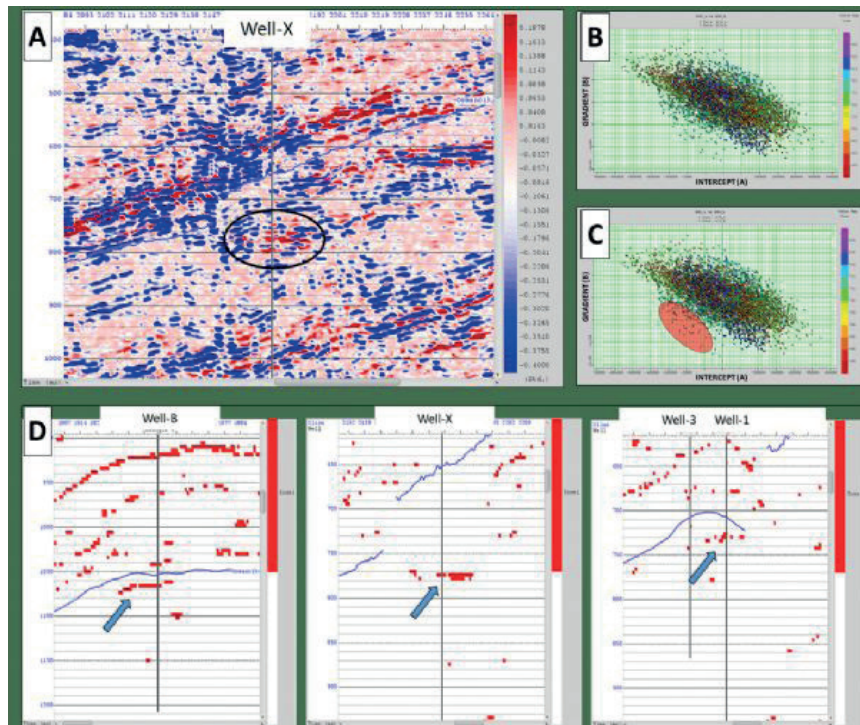


Figure 2. (A) AVO product (I x G) at Well-X location, (B) Intercept versus Gradient crossplot, (C) selected AVO III class zone and (D) Cross-section of the selected zone at Well-B, Well-X and Well-1 and 3 locations are shown in the figure. AVO product is positive and crossplot of I and G help us to specify data points representing class-III zone (negative intercept and gradient). These zones are mapped on cross-sections around wells indicated with blue arrows.

Rock Property Maps

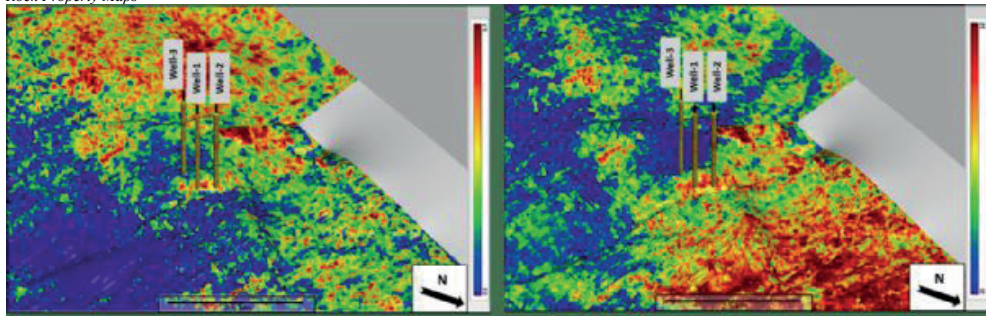


Figure 3. Inverted rock property maps,  $VP/VS$  ratio (left) and  $\lambda\rho$  (right), of gas producing Well-1 and 2 and non-producer Well-3. Although wells are close to each other, producing zone can be discriminated clearly.

AVO Model

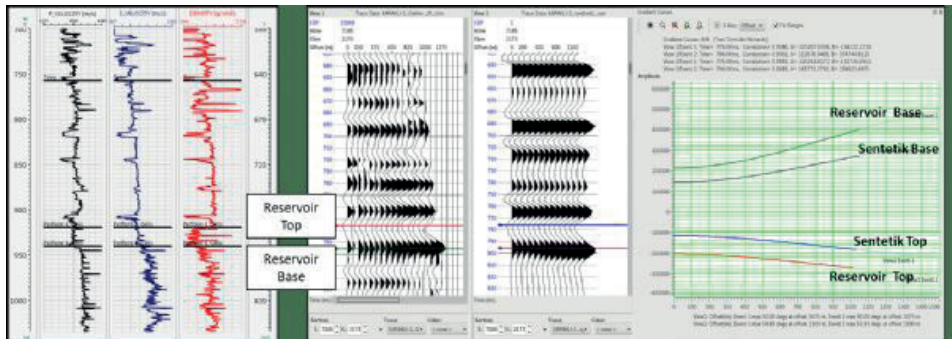


Figure 4. Measured P-wave, S-wave and RHO (on the left panel) and real gathers, synthetics and gradient analysis at Well-X location are shown on middle panel and right panel, respectively.

Rock Physics

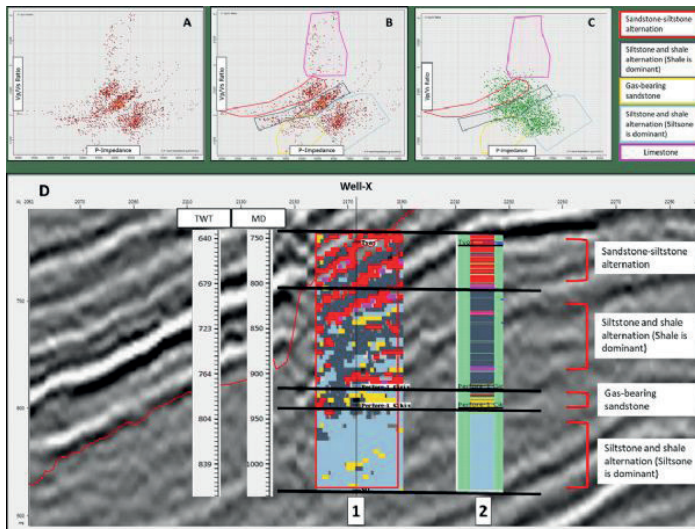


Figure 5. (A) AI and  $VP/VS$  ratio crossplot from logs at Well-X, (B) selected lithology and hydrocarbon zones, (C) AI and  $VP/VS$  ratio crossplot from inversion outputs and (D) reflecting the same zones from both logs (1) and inversion (2) crossplots on the seismic section are shown.

# Multiple Approaches to Reservoir Characterization of Gas-Bearing Sandstone: a Case Study from the Thrace Basin, Turkey



**Mustafa Kamil Yüksek**

Türkiye Petrolleri Anonim Ortaklığı

## SUMMARY

AVO attributes, pre-stack inversion to rock properties and rock physics analysis have been used to characterize the gas-bearing sandstone reservoir in the Osmancik Formation in the northwest of the Thrace Basin, the European part of Türkiye. 3D seismic data and well logs (from both producing and non-producing wells) were used for pre-stack inversion and rock-physics analysis. The results of these analyses were used to identify the characteristic properties of the reservoir zones and calibrated at the producing and the dry wells. Understanding of the elastic behaviour of the gas-bearing sandstones from the rock physics analysis helped to determine the hydrocarbon effects on the seismic data and helped to identify the possible bypassed sand pockets in the study area.

## INTRODUCTION

Triangular-shaped Thrace Basin, located to the northwest of Türkiye, contains one of the most prolific hydrocarbon-bearing reservoirs (Demir et al., 2011). Oil and gas wells have been producing from Eocene and Oligocene age carbonate and sandstone reservoirs in the basin. Osmancik Formation is the main gas producing sandstone reservoir in the northwestern part of the basin. The formation was deposited in a deltaic environment as a result of a continuous sandstone-shale succession. It contains Oligocene age fossils (Saner, 1908). The Osmancik Formation, mostly composed of small sand patches/lenses is the main subject of this study. It is important to characterize the stacked elastic properties of the formation to enhance productions and to explore new gas-bearing sand patches/lenses.

Pre-stack inversion, AVO analysis and rock physics studies are the main methodologies for the reservoir characterization. Previous pre-stack acoustic impedance (AI), shear impedance (SI) and density inversion was introduced by Ozdemir et al. (2001), and Hampson et al. (2005) suggested a new approach for the simultaneous pre-stack inversion. Amplitude variation with offset (AVO) analysis have been used to estimate reservoir rock properties that can be utilized for the hydrocarbon and fluid detection, and lithology discrimination. Several authors have proposed many equations to analyze the AVO effects. Aki and Richard (1979) proposed 3-term approximation to Knott-Zoeppritz equations. Later on, Shuey (1985) proposed a simplified arrangement of Zoeppritz equations that is currently used for the AVO analysis. AVO analysis is one of the essential Direct Hydrocarbon Indicator (DHI) tool for the elastic reservoirs of the Thrace Basin, particularly for the Osmancik Formation. However, AVO anomalies need to be calibrated with the well log data to reduce the exploration risk (ie., Arpacı and Ozdemir, 2020).

This study focused on the northwest of the Thrace Basin where the hydrocarbon production is limited due to the shallowness of the reservoir and more complex lithology compared to the southeastern part of the basin where the reservoirs are in the moderately depth or deeper. In this paper study we used the rock properties like inverted acoustic impedance (AI), computed P-wave velocity (VP) and S-wave velocity (VS) ratio (VP/VS), and AVO attributes (product (AxB) and scaled Poisson ratio) to help for mapping the hydrocarbon-bearing zones.

## DATA AND METHODS

Well log data from five wells (A, B, C, D, and E), 3D seismic data and a set of VSP data from Well C have been used to conduct the seismic inversion and the reservoir characterization. Figure 1 shows a seismic section crossing three wells (left) and well locations in map view (right). The elastic properties of the Osmancik Formation were computed from the measured Vp, Vs and density ( $\rho$ ) logs. The VP-VS crossplot at from Well A, Well C and Well D were used to estimate the mudrock line in the area. Then, this estimated mudrock line was used to calculate the Vs velocities for the remaining wells having no shear sonic logs.

3D seismic data set (600 km<sup>2</sup>) is a zero phased data and a seismic gather conditioning workflow and AVO analysis were applied before pre-stack inversion. Trim statistic and AVO friendly radon transform filtering were also applied to improve flattening and Signal/Noise (S/N) ratio of the seismic gathers. In addition, AVO analysis was applied to the gathers before and after the trim statistic and Radon applications were performed for the quality control. The near, middle and far offset stacks were created. The offset dependent wavelets used in the inversion process were extracted by a statistical method. The synthetic seismic traces have been created at the wells and well-ties were assessed using the near offset data while double-checks were being made at the other offsets. AI, SI and  $\rho$  background models were created from the existing well log data and they have been smoothed for pre-stack inversion.

## AVO AND PRESTACK INVERSION RESULTS

Goodway et al., (1997) proposed a method to characterize the reservoir rocks based on the change in reservoir's elastic behaviour. LambdaRho ( $\lambda\rho$ ) and MuRho ( $\mu\rho$ ) computed from AI and SI were cross-plotted to discriminate reservoir zones from the other lithologies.

AVO attributes and the rock properties computed after pre-stack inversion ( $\lambda\rho$ ,  $\mu\rho$  and VP/VS) were investigated for the target zones in the Osmancik Formation. Note that, Well A, B, C, and D are the



gas producing wells and Well E is dry well. X is the proposed well.

AVO attributes and the inverted rock properties of random sections across the existing wells and the proposed well were created to illustrate the responses of the producing, non-producing and the prospect zone. Figure 2 shows the random or the arbitrary lines from the inverted AI, and computed  $\lambda\rho$  and  $Vp/Vs$  sections after the pre-stack inversion with the  $A \times B$  and  $(A+B)/2$  (scaled Poisson's ratio) computed after AVO analysis. The producing horizons of the Osmancik Formation demonstrate none-continues sharp decrease in AI, acoustic impedance,  $VP/VS$  ratio and  $\lambda\rho$  in respect to non-producing and surrounding zones. Product of  $A \times B$  demonstrates positive stack pattern where the scaled poison ratio shows positive and negative stack pattern (European polarity) compared to the surrounding zones. Both patterns are considered as the direct hydrocarbon indicators (DHI). In contrast, in the non-producing well (Well E), the prospect zone has higher AI,  $VP/VS$  ratio and  $\lambda\rho$  values in respect to producing wells and Well X. The proposed well (Well X) has similar properties at the production zones when compared to the producing wells.

## ROCK PHYSICS ANALYSIS

Understanding the fluid effects on the acoustic properties is an important step for the reservoir characterization. Inverted AI and SI, and computed  $\lambda\rho$  and  $\mu\rho$  relationships together with the computed  $VP/VS$  ratio have been used for the reservoir characterization and lithology discrimination (Pickett, 1963; Gardner et al., 1974; Goodway et al, 1997; Ozdemir et al., 2006). To investigate this rock physics approach to production zones and target zones, often the AI- $VP/VS$  ratio crossplot is used. The characteristic responses of the production zones are utilized to differentiate the hydrocarbon bearing zones away from the drilled locations. Figure 3 shows AI- $VP/VS$  crossplots for the existing producing (Figure 3a and b), the non-producing (Figure 3c) and the proposed well (Figure 3d). The inverted AI and computed  $VP/VS$  ratio values at the producing zone are between 4200 to 4800 (m/s)\*(gr/cc) and between 1.9 to 2.7, respectively. There are two gas producing zones (upper and lower reservoirs) for Well A and Well B (Figure 3a and b). The crossplots of Well A and Well B display the purple and green colors to highlight the respective producing values for the upper and lower reservoirs. Red area is used to project the corresponding production values on the non-producing Well E (Figure 3c) and proposed Well X (Figure 3d). When the producing values selected on the crossplots (Figure 3, left side) and projected to the inverted results on the sections (Figure 3, right side), they correspond to gas production zones on the wells' location (Figure 3 a and b). The similar properties are not observed at the target zone in the non-producing Well E. The top of anomalous zone in the Osmancik Formation is a coal bedding zone. For the proposed Well X, the  $VP/VS$  ratio is between 1.9 to 2.4 and the AI is 4500 to 4800 (m/s)\*(gr/cc), respectively, both indicate hydrocarbon anomaly in

the reservoir level of the Osmancik Formation (Figure 3d). The sections on the right side of Figure 3 illustrate that when expected gas producing values are selected on the cross plot and projected onto the inverted results, it becomes obvious that producing and the expected values indicate the same zones of interest. The dry well shows no anomalies at the expected pay zones while the prospect well has two consecutive anomalous zones in the Osmancik Formation that may indicate possible producing zones.

## CONCLUSIONS

Inverted AI, computed  $\lambda\rho$  and computed  $VP/VS$  ratio results, and AI- $VP/VS$  crossplots clearly differentiate the gas reservoir for producing wells and indicate potential gas bearing zone for the proposed well. The results are consistent with the production data. The AVO attributes and the inversion results demonstrate DHI anomaly in the gas bearing levels only. The 3D cubes computed from the crossplot analysis have a good correlation with the gas producing zones in the Osmancik Formation at the pay wells. These findings strongly indicate that the proposed well X has gas bearing zone in the Osmancik Formation.

## REFERENCES

- Aki, K, And Pg Richards, 1980. Quantitative Seismology: Theory And Methods. Wh Freeman And Co. P 119-183
- Arpaci, T. & Ozdemir, H.,2020. Step-Out Well Positioning Using Hydrocarbon Indicators From Seismic Inversion: A Case Study. First Break. 38. 43-51.
- Demir, D., Bilim, F., Aydemir, A., Ates, A. 2012. Modelling Of Thrace Basin, Nw Turkey Using Gravity And Magnetic Anomalies With Control Of Seismic And Borehole Data. Journal Of Petroleum Science And Engineering, 86-87, 44-53.
- Gardner, G., Gardner, L., And Gregory, A., 1974, Formation Velocity And Density—The Diagnostic Basics For Stratigraphic Traps: Geophysics, V. 39, No. 6, P. 770-780.
- Goodway, W., Chen, T. And Downton, J., 1997, Improved Avo Fluid And Lithology Discrimination Using Lame Petrophysical Parameters; " $\lambda\rho$ ", " $\mu\rho$ ", And " $\Lambda/M$  Fluid Stack", From P And S Inversion: 67th Seg Technical Program, Expanded Abstract Av 2.7, 183-186.
- Hampson, D.P., Russell, B.H. And Bankhead, B., 2005. Simultaneous Inversion Of Pre-Stack Data: 74th Seg Annual International Meeting, Expanded Abstract, Si 1.2, 1633-1638.
- Ozdemir, H., Ronen, S., Olofsson, B., Goodway, B., Young, P., (2001). Simultaneous Multicomponent Avo Inversion. Seg Technical Program Expanded Abstracts. 20. 269-272. 10.1190/1.1816589.
- Ozdemir, H., Hansen, J.W. And Tyler, E.,2006. Rock And Reservoir Parameters From Pre-Stack Inversion Of Surface Seismic Data. First Break, 24, 83-87.

Pickett, G. R., 1963, Acoustic Character Logs And Their Applications In Formation Evaluation: Journal Of Petroleum Technology, V. 15, No. 06, P. 659-667.

Saner S., Batı Ponditler'in Komşu Havzaların Oluşumlarının Levha Tektoniği Kuramıyla Açıklanması, 1980. Kb Türkiye, Maden Tetkik Ve Arama Dergi, 93/94, 1-20,

Shuey (1985), Shuey, R. T. (1985). A Simplification Of The Zoeppritz Equations. Geophysics, 50(4), 609-614.

Keywords: Seismic inversion, Thrace Basin

Base Map and Seismic

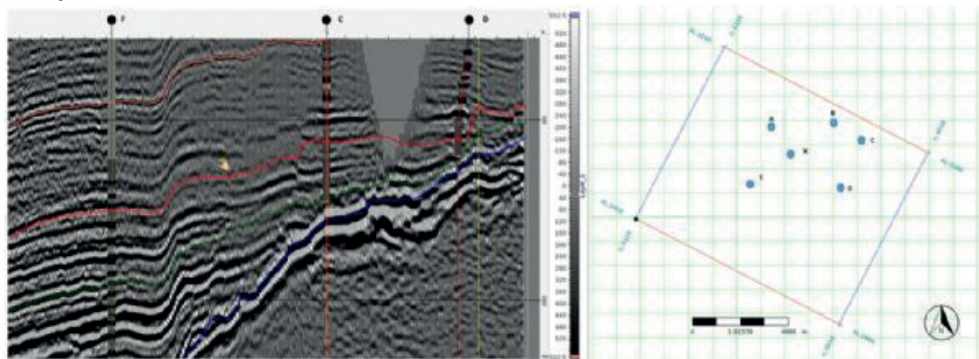


Figure 1. Seismic to well tie correlation (left). C and D are producing wells from Osmancik Formation and E is a dry well. Horizons from top to bottom are Osmacik Fm (orange colour), Reservoir facies of the Osmancik Fm (red colour) and Mezardere Formation (Blue). Well locations on the study area (right). A, B, C, D, are producing wells, E is the dry well and X is the prospect.

AVO Attributes and Inversion Results

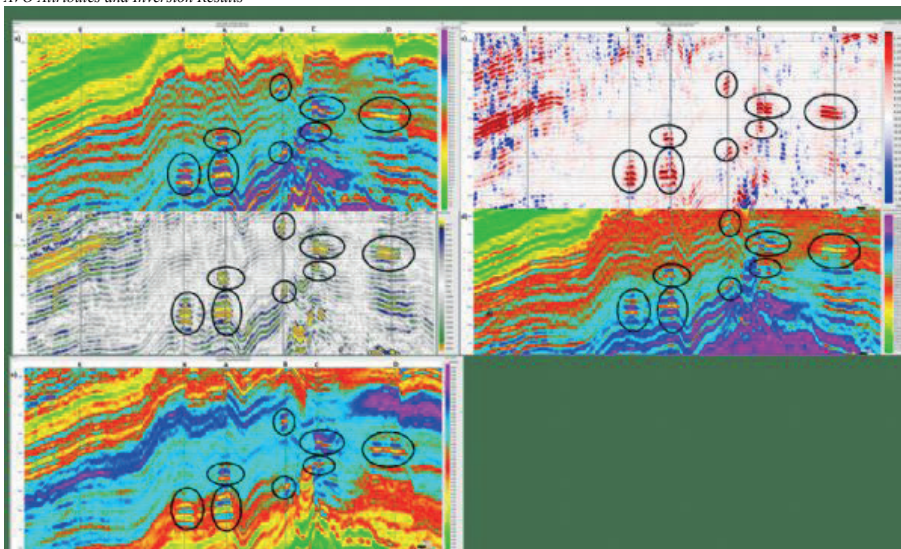


Figure 2. AVO attributes and inversion results for the Osmancik Formation across the producing (A, B, C and D), non-producing (E) wells and proposed (X) well. Pre-stack inversion results are  $\lambda_p$  (a) and scaled poisson ratio (b). AVO attributes are the product  $A \times B$  (c), AI (d) and VP/VS ratio (e).. Anomalies of the hydrocarbon bearing zones and target zones are highlighted on each section.

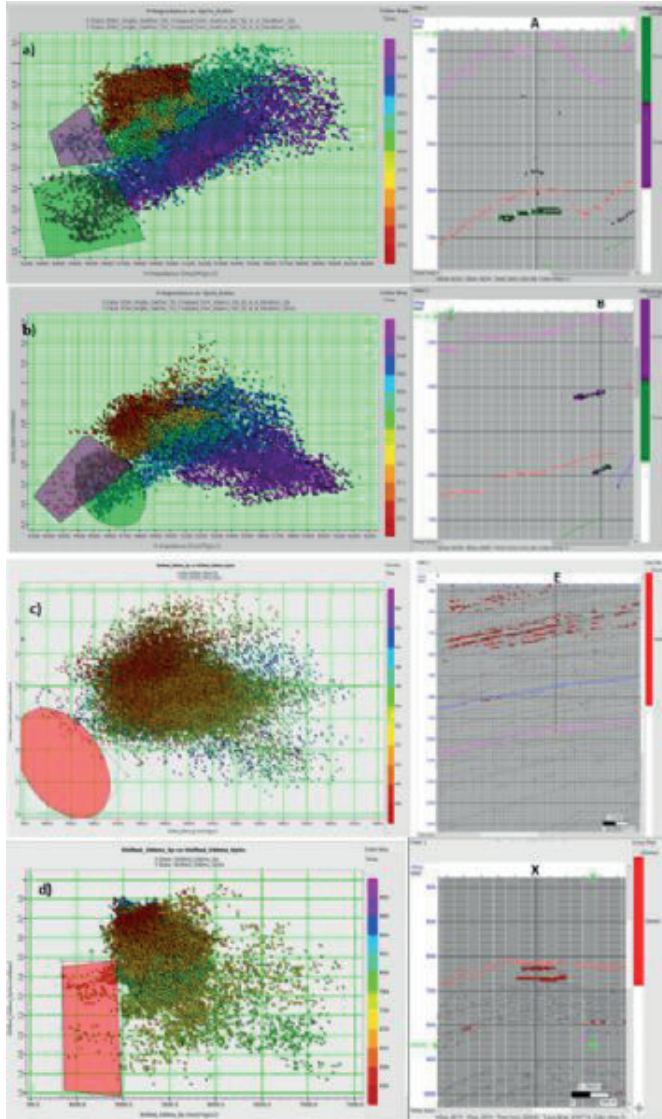


Figure 3.  $Al-V_p/V_s$  crossplots at the producing wells Well A (a) and B (b) with two producing zones, non-producing Well E (c) and proposed well (d). Values corresponding to producing zones are selected and highlighted on the crossplots. Purple and green areas represent production zones in the producing wells (a and b). Red areas represent gas expected values. There is no anomaly for dry well (c). Two consecutive zones show anomaly for the proposed Well X (d).

# The Critical Role of Velocity in Pore Pressure Estimations and the Impact of the Centroid Effect

**Ergin Karaca**  
TP-OTC



This study examines changes in pore pressure estimations relative to enhancements in seismic velocity for the most accurate pore pressure scenarios, as well as giving a special focus on the role of the Centroid Effect in specific geological contexts. A precise calculation of pore pressure is key to maintaining safety in drilling procedures. Inaccurate estimates can lead not only to dangerous blowouts but also to additional issues such as well kicks, lost circulation, stuck pipe, excessive costs, and borehole instability. Seismic velocity is one of the crucial parameters for pore pressure estimations in wildcat fields where no offset wells are present. Hence, a more accurate seismic velocity tends to yield the most realistic pore pressure estimations. Many pore-pressure prediction techniques prioritize shale properties such as velocity and resistivity, neglecting the significant mismatch in pore pressures between shale and sand formations, particularly in a tilted and hydraulically connected permeable sandstone reservoirs. Improving seismic velocity and accounting for the “Centroid Effect” to such reservoirs can lead to more accurate pore pressure estimations, ensuring safe drilling operation windows and mitigating associated risks and costs.

## INTRODUCTION

The prediction of pore pressure is a fundamental aspect in the safe and efficient planning and execution of drilling operations in the oil and gas industry. An accurate assessment of pore pressure helps prevent potential drilling hazards such as blowouts and wellbore instabilities, and optimizes operational costs (El-Werr, 2017). Seismic velocity data is critical for predicting pore pressure, particularly in areas where offset well data is insufficient, such as wildcat fields. The ability to generate more accurate seismic velocities can enhance pore pressure predictions, leading to safer and more consistent wellbore quality in cost effective manner (Bahmaei, 2020). This can be further improved by re-picking the velocity from pre-stack gathers near the prospect well. If this approach doesn't provide sufficient accuracy, pre-stack inversion can be performed to further enhance the seismic velocities (Chopra, 2006; Tingay, 2011). The improved velocities can then be used for estimating potential vertical pore pressure variations and potential pressure ramps with better accuracy, contributing to the optimization of drilling practices. Tilted permeable sand layers for instance can present pressure ramp which departs vertical expected pore pressure trends. Consequently, the fluid movement along this pathway can elevate pressures at the top of the structure, which is frequently a targeted location for exploration drilling (Young, 2005).

This paper focuses on improving the accuracy of pore pressure predictions by enhancing seismic velocity

measurements, particularly accounting for the centroid effect in the presence of dipping sandstones.

## METHODOLOGY

The process of predicting pore pressure requires assessing pore pressure based on alterations in the properties of rock, particularly variations in sonic velocity or resistivity (Mouchet and Mitchell, 1989; Bell, 2002; and Sayers, 2006). The main aim of a pore-pressure prediction is to accurately determine pore pressure from the available seismic velocity before drilling (Sayers et al., 2002). In absence of offset wells, the existing seismic velocities are the only data where they should be carefully quality controlled to ensure that they reflect the subsurface information and also to avoid erroneous velocity picks caused by residual multiple energy in the seismic signal (Tingay, 2011). Figure (1) illustrates the variability of seismic velocity based on velocity picking from semblance data. Therefore, making detailed and dense velocity selections near prospect wells can provide significantly more accurate velocity data for pore pressure estimations.

Furthermore, using pre-stack inversion to obtain more accurate seismic velocities is another method for estimating pore pressures. Figure (2) compares pore pressure estimations calculated from seismic velocity (represented by a dashed line) and those generated from pre-stack inversion (represented by a solid line). This method offers more precise predictions, accurately following the pore pressures of shales.

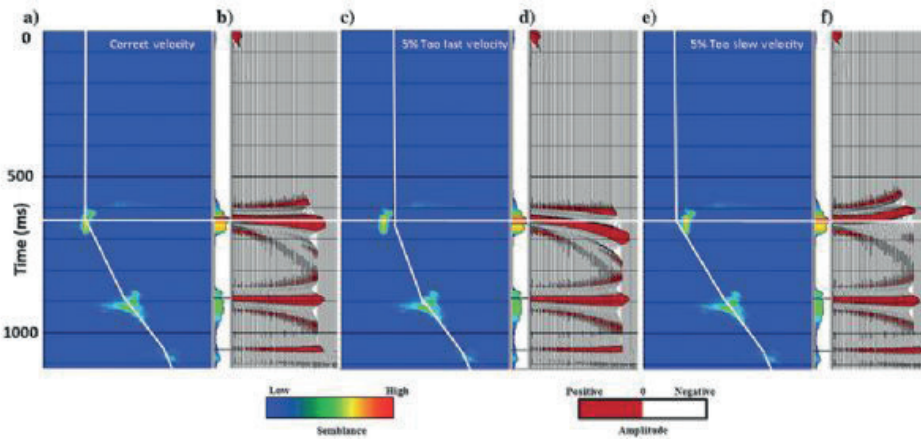
Finally, the centroid effect should be the most important concern when providing the final pore pressure profile from seismic velocity in cases where tilted and hydraulically connected permeable sandstone reservoirs are present. Figure (3) illustrates how the sand pressure gradient deviates from the shale pressure gradient in such reservoirs, highlighting the significance of this method.

## CONCLUSION

In conclusion, this study highlights the crucial role of velocity in accurate pore pressure estimations and emphasizes the significance of considering the centroid effect in tilted and hydraulically vertically connected permeable sandstone reservoirs. By improving seismic velocity through methods such as re-picking and pre-stack inversion, and incorporating the calculation of the centroid effect to account for non-uniform pressure distribution, more precise and reliable pore pressure predictions can be achieved which, enhances drilling safety and minimizes potential risks during drilling operations.

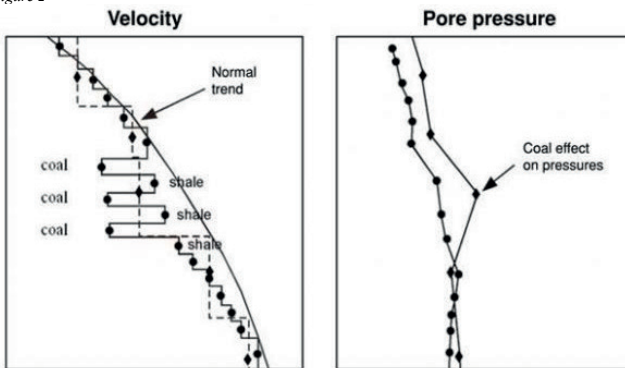
Keywords: Pore Pressure, Seismic Velocity

Figure 1



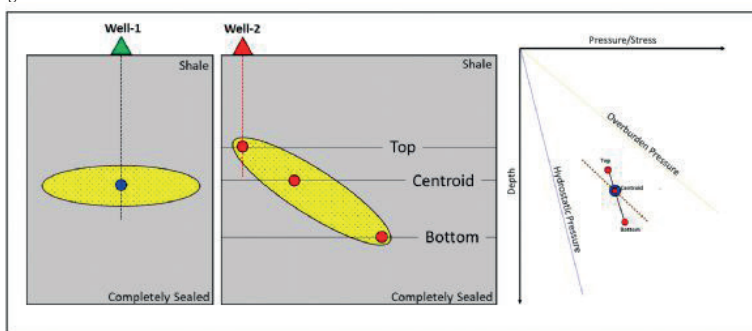
Selecting velocity in semblance panels (on the left) with corresponding NMO corrected gathers (Verma and Marfurt, 2016)

Figure 2



The comparison between stacking velocities (indicated by a dashed line) and inversion velocities (solid line) through a thin layer of coal seams demonstrates the enhanced resolution provided by inversion (from Chopra, 2006 after Huffman, 2002).

Figure 3



Centroid effect on tilted and hydraulically connected permeable sandstone reservoirs (Updated from Zoback (2010))

# Güneydoğu Anadolu Bölgesi Diyarbakır Yöresi Tektonik Süreçlerinin Bir Üretim Sahasına Etkisi



**Canberk Güzelcan, Aşlıhan Deliktaş, Berat Niran Taşdemir, Cansu Güner Çiçek, Ceyda Çetinkaya Kayrın**

TPao Genel Müdürlüğü, Üretim Daire Başkanlığı, Söğütözü Mah. Şht. Öğretmen Aybüke Yalçın Cad. No:10, 06100, Çankaya / Ankara / Türkiye

## ÖZ

Barbeş Sahası, Türkiye'nin Güneydoğu Anadolu Bölgesi, Diyarbakır il sınırları içerisinde yer almaktadır. Sahanın keşfi 1972 yılında gerçekleşmiş ve 2012 yılında Türkiye Petrolleri Anonim Ortaklığı (TPAO) tarafından devralınmıştır. Üretilen toplam petrol miktarı 26,8 milyon varil, günlük net petrol üretimi 580.6 varil/gün ve güncel su oranı %97'dir.

Bu çalışmada, TPAO tarafından arama ve üretim faaliyetleri yürütülen Barbeş Sahası'ndaki üretim dağılımını homojen hale getirmek ve üretimi arttırmak adına, fay ve çatlak sistemlerinin baskın rol oynamasından ötürü çatlak karakterizasyonu yapılmış ve iki farklı çatlak seti tespit edilmiştir. Sismik veriler ve daha önceki çalışmacıların literatür örnekleriyle de karşılaştırma yapılarak çatlakların iki farklı fay sistemine bağlı olduğu görülmüştür. Yapılan analizlerle Doğu-Batı eksenli çatlakların rezervuar seviyeye su getirdiği; Kuzey-Güney eksenli çatlakların ise petrol getirdiği gözlenmiştir.

Sahada yapılacak yeniden tamamlama operasyonları ve açılacak yeni kuyular planlanırken, çalışma sonucunda elde edilen bulguların dikkate alınması önerilmiştir.

## ABSTRACT

The Barbeş Field is located in the Southeast Anatolia Region of Turkey, within the borders of Diyarbakır province. The discovery of the field took place in 1972 and was acquired by the Turkish Petroleum Corporation (TPAO) in 2012. The total produced amount of oil is 26.8 million barrels, with a daily net oil production of 580.6 barrels/day and a current water cut of 97%.

In this study, in order to homogenize the production distribution and increase production in the Barbeş Field, where exploration and production activities are conducted by TPAO, crack characterization was carried out due to the dominant role of fault and fracture systems, and two different fracture sets were identified. By comparing seismic data with previous studies and literature examples, it was observed that the fractures are associated with two different fault systems. The analyses revealed that the East-West-oriented fractures bring water to the reservoir level, while the North-South-oriented fractures bring oil.

During the planning of recompletion operations and the drilling of new wells in the field, it is recommended to take into account the findings obtained from this study.

## GİRİŞ

Barbeş Sahası, Türkiye'nin Güneydoğu Anadolu Bölgesi, Diyarbakır il sınırları içerisinde yer almaktadır.

Coğrafi olarak Güneydoğu Toros Dağları'nın güneyinde yer almaktadır. Saha genelinde hedef formasyon olan Derdere Formasyonu, Alt Otokton İstif'te yer almakta olup, Geç Kretase yaşlı dolomitik kireçtaşlarından oluşmaktadır.

Bölgede iki farklı tektonik unsurun yapısal jeolojiye etkisi gözlenmektedir. Arap Plakası'nın, Güneydoğu'dan Kuzeybatı'ya doğru Avrasya Plakası'nın altına dalması, Bitlis-Zagros Kenet Kuşağı boyunca bindirme özelliği gösteren makro ve mikro fayların oluşumuna sebep olmuştur. Bu fayları oluşturan tektonik hareket, Barbeş Sahası'na Güney-Güneydoğu yönünden sıkıştırıcı bir etki yaratmaktadır. Öte yandan bölgenin kuzeydoğusundan güneybatısına uzanan Doğu Anadolu Fay Zonu, Barbeş Sahası'nı kuzeyden sınırlamaktadır. Doğu Anadolu Fay Zonu, sol yönlü doğrultu atımlı bir fay olduğundan, bölgede makaslama gerilmesi yaratmaktadır. Sonuç olarak Barbeş Sahası, kuzeyden makaslama gerilmesi ve güneyden sıkışma gerilmesi etkisi altında kalmıştır ve farklı yönelimlere sahip çatlak ve fayların üretime farklı etkileri olduğu olduğu gözlenmiştir.

## AMAÇ

Bu çalışmada, arama ve üretim ruhsatı Türkiye Petrolleri Anonim Ortaklığı'na (TPAO) ait olan Barbeş Sahası'nda, kuyular arası üretim oranlarının homojen olmamasının nedenleri ortaya konmak istenmiştir. Saha genelinde çatlak ve fay sistemlerinin baskın rol oynaması nedeniyle, çatlak karakterizasyonu çalışmasının aydınlatıcı olabileceği düşünülmüştür. Bu sebeple sahada görüntü logu alınmış olan 7 kuyuda çatlak karakterizasyon çalışması yapılmıştır. Yapılan bu çatlak analizlerinden yola çıkarak, çatlakların oluşum mekanizmasını anlamak ve yönelimlerine göre rezervuar üzerindeki etkilerini tespit etmek amacıyla bölgenin tektonik karakteri de incelenmiştir.

## GEREÇ VE YÖNTEM

Barbeş Sahasında farklı tektonik etkilerle oluşmuş kırık ve çatlakların karakterizasyonu için sahada yer alan kuyulardan 7 tanesinde bulunan görüntü logları, analiz için kullanılmıştır. Kuyu loglarının yorumlanması için Schlumberger Techlog programından faydalanılmıştır. Öncelikle elektriksel logların "LQC" (Log Quality Control) veri seti oluşturulup, kullanılan kuyu loglarının birbirleriyle korele edilmesi; sonrasında görüntü logları üzerinde "Dip Picking" adı verilen çatlak, fay, tabaka sınırı, yıkıntı tespit ve sınıflandırma işlemi uygulanmıştır.

Kuyu logları üzerinde yapılan incelemeler sonrasında sismik veriler, Schlumberger

Petrel programı üzerinde incelenmiş; fay ve çatlaklar, üç boyutlu sismik kesit üzerinde “Ant Tracking” yöntemi kullanılarak yorumlanmıştır.

Yapılan uygulamalar sonrasında, daha önceki çalışmacıların literatür örnekleriyle karşılaştırmalar yapılmış ve analiz sonuçları arasında bir uyum görülmüştür.

## BULGULAR VE SONUÇ

Tüm logların ve kuyu operasyonlarının, derinliğe ve formasyona bağlı olarak denetirilmesi ile bölgenin jeolojik özellikleri bir araya getirilerek iki farklı stres rejiminin yarattığı; temelde dağınmık, detaylı incelemeler sonucu iki farklı çatlak setinin oluştuğu gözlenmiştir.

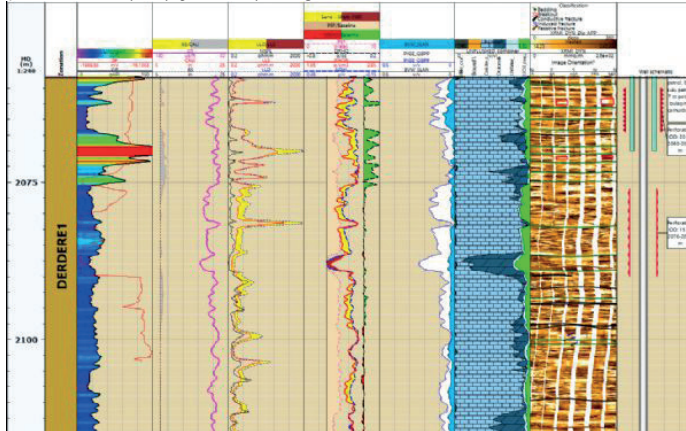
Önceki çalışmalarla benzer şekilde sismik kesitte de iki farklı stres rejiminin sebep olduğu bindirme fayları ve doğrultu atımlı faylarla birlikte, bu faylarla benzer yönelimde ve özellikte çatlak setlerinin oluştuğu gözlemlenmiştir.

Gelinen son noktada, yapılan yorumlamalar ile üretim verileri bir araya getirilmiş, sahadaki üretim kuyularının lokasyona bağlı olarak hangi özellikteki fay-çatlak sistemi üzerinde yer aldığı belirlenerek bindirmeye veya makaslamaya bağlı gelişen süreksizliklerin, üretim adına pozitif veya negatif etkileri ortaya konmuş ve olası yeni kuyu önerileri bu değerlendirmeye göre belirlenmeye çalışılmıştır.

Çalışmalar neticesinde, rezervuar seviyede görülen Doğu-Batı yönelimli çatlakların doğrultu atımlı fayla ilişkili olup su getirdiği; Kuzey-Güney yönelimli çatlakların ise bindirme faylarıyla ilişkili olup petrol getirdiği ortaya konulmuştur. Dolayısıyla yeniden tamamlama operasyonlarında bu bulguya dikkat edilmesi ve açılacak yeni kuyuların türleri ve lokasyonlarının buna göre tasarlanması önerilmiştir.

**Anahtar Kelimeler:** Doğal çatlaklı karbonatlar, çatlak karakterizasyonu

*Çatlak karakterizasyonu yapılan bir kuyu örneği*



# Three Dimensional Reservoir Characterization of Dodan Field as a Candidate Underground Gas Storage (UGS)



**Nilsu Kustak<sup>1</sup>, Diethard Kratzer<sup>2</sup>, Robert Rieger<sup>2</sup>, Claudia Steiner – Luckabauer<sup>2</sup>, Ceyda Çetinkaya Kayrın<sup>1</sup>, Fevzi Mert Türresin<sup>3</sup>, Hasan Çağlar Üsdün<sup>3</sup>**

<sup>1</sup>TPAO Production Department, Söğütözü Mah. Şht. Öğrt. Aybüke Yalçın Cad. No: 10 Çankaya, Ankara / Türkiye

<sup>2</sup>HOT Energy Group, Parkstrasse 6 8700 Leoben, Austria

<sup>3</sup>TPAO Research and Development Center, Söğütözü Mah. Şht. Öğrt. Aybüke Yalçın Cad. No: 10 Çankaya, Ankara / Türkiye

## INTRODUCTION

The Dodan carbon dioxide gas field, discovered in 1965, is located in the southeastern part of Turkey, northeast of Batman City and Batı Raman Oilfield where immiscible CO<sub>2</sub> flood is applied as an EOR application since 1986. The Dodan field is a northwest-southeast trending anticline and shows a classic representation of Miocene compressional structures in the Bitlis-Zagros Suture (Fig.1). The field size is about 10 by 2 km.

The main reservoirs in the field can be classified as complex-lithology, fractured carbonate reservoirs of the Garzan Formation (limestone) and Mardin Group (dolomitic limestone). Core plug porosity and permeability shows average values of 2.59% and 0.13 mD in Garzan reservoir and 3% and 0.25 mD in the Mardin reservoir. Average depth of Garzan reservoir is 1830 m, the net thickness is about 20 m. Average depth of Mardin reservoir is about 2050 m with a net thickness of about 210 m. The field was developed by 24 wells with about 750 m spacing. Production mechanism of the field is gas expansion and water drive. The cumulative gas production from Garzan Formation is 65.608 MMMscf and the cumulative water production is 539.8 Mscf by the end of 2022. From Mardin Group, the cumulative gas production is 231.686 MMMscf (6560.63 million cubic meters) and the cumulative water production is 3127.6 Mscf by the end of 2022.

The producible gas in reservoirs is about to finish and the existing process facility is close to the end of its design and economic life. A possible option is to convert the field into a gas storage, which requires predicting the amount of CO<sub>2</sub> that can be reinjected. In this respect, the aim of the study was to define the areal and vertical extent, properties and continuity of the reservoir, and most importantly an estimation of the storage capacity. Main challenges of the study were the poor data situation to develop a sound structural model, the very low porosity/permeability conditions in the reservoir and the lack of hard data to develop a representative fracture model.

## STRUCTURAL MODELLING

The anticline of the Dodan field is likely to be associated to a breakthrough fault-propagation fold. This fold type is generally asymmetric with steeper and narrow forelimbs (SW flank) than their corresponding backlimbs (NE flank) and shows additional faults cutting through the fault-propagation fold (Fig. 2). The Dodan fold shows the separation of a part of the

forelimb as a small span. Main evidence for this type of fault-propagation fold is the repetition of strata encountered in two wells.

Due to the complex geological structure and the sparse input data a standard modelling workflow could not be applied. Available vintage 2D seismic data (10 lines) is of poor quality and just two seismic lines directly cross the anticline and provide useful information of the reservoir structure and faults (Fig. 3). Considering the relatively high uncertainty of the seismic interpretation, available well markers represent the most reliable structural input. Thus, the structural model was developed according to the workflow sketched in Fig. 4. Based on the concept of a fault-propagation fault, depth structure maps were created and converted to time domain by a simple velocity model derived from check shot data. Later maps were constrained by seismic horizon and fault interpretations and used as trend maps in 3D geological modelling. This workflow ensures that all available input data were honored with a high weight put on the well marker set.

Horizons, faults and isochore maps were used to set up fine and coarse scaled reservoir grids with Garzan and Mardin sub-zones established. Fig. 5 displays a perspective view of the reservoir zone model.

## FORMATION EVALUATION

The petrophysical evaluation started with the attempt to explain the gas effect on wireline logs and consequently the estimation of porosity as well as permeability from wireline logs. The result is that the type of gas present (CO<sub>2</sub>) is not primarily influencing the signature on wireline logs. However a combination of low matrix porosity, fracture signatures, mud filtrate invasion and depth of investigation dictates the physical log reading. Especially the resistivity readings are strongly biased from the combination of all those influence parameters. This makes it challenging to estimate water saturation in a meaningful way for low porous reservoir sections. Based on the gained understanding of the physical log response to the reservoir rock, porosity, water saturation and permeability were estimated. Core data and test data were key input to conclude on the current in situ log behavior. The complex natural environment can be subdivided into two groups which are a) a poor / tight reservoir rock and b) a reservoir rock of moderate reservoir quality. Both types show fractures. The outcome was implemented into the static model as described below.



## PROPERTY MODELLING

Characterizing the reservoir in 3D space follows standard technical approaches and is separated in matrix and fracture properties. According to sedimentological studies the main depositional environment categories lagoon, back shoal, shelf margin and open shelf are dominant in the Garzan Formation. A prograding system from lagoonal environment at the base, to back shoals, shelf margin and open shelf in the upper part is suggested. Also a lateral transition from SW to NE (deepening in the SW) was recognized. Depositional environment modelling was controlled by probability maps and vertical proportion curves. Fig. 6 shows the depositional environment model characterizing the transition from lagoon to shelf margin and open shelf.

Stochastic porosity modelling constrained by the depositional environment model was applied in the Garzan Formation. No areal driver for porosity distribution was available for the Mardin Formation. Model average porosity is very low in the Garzan Formation (3.4%) and as well in the Mardin Formation sub zones Karababa (3.3%), Derdere (2%) and Sabunsuyu (1.6%).

Core analysis was conducted in the field but core plug porosity and permeability do not show a distinct relationship. Due to the limited range of the permeabilities and the bias of fracture permeability on low porosities, the uncertainty is high in this data set. Therefore, three equations representing a low, base and high case scenario are defined to cover the uncertainty. Stochastic modelling was applied for creating the permeability model. Average horizontal permeability is extremely low in Garzan (0.01 mD), Karababa (0.2 mD), Derdere (0.01 mD) and Sabunsuyu 0.0005 mD).

The water saturation model was derived from a saturation height model approach based on petrophysical logs while honoring SCAL measurements as good as possible. Since almost all SCAL measurements in Dodan have been affected by micro scale fractures in the core plugs, interpreted water saturation logs were used as the basis for building the saturation height model. Average water saturation is relatively high in Garzan (49%), Karababa (56%), Derdere (67%) and as well Sabunsuyu (76%). Finally, volume calculation was applied which results in a total matrix GIIP of about 602 MMMscf.

## FRACTURE MODELLING

High variability in production data indicates that fractures play major a role in the Dodan field. XRMI data provides the main input for the discrete fracture model; unfortunately just three wells with XRMI data are available. Logged intervals in the reservoir sections are relatively short and data quality is limited in several intervals. Considering the field size and the total available length of image logs, the reservoir is highly under-sampled. The development of a fractured reservoir is primarily related to its tectonic history. In the Dodan field, most of the occurring fractures are most likely related to the folding and faulting of the brittle

limestone and dolomite strata.

Fig. 9 (left) shows the conceptual model of the Dodan fold anticline with the expected fracture pattern. Fracture data for all wells and all open fractures and bedding dips in Garzan, Beloka and Mardin is shown in a dip azimuth rose plot Fig. 9 (right). Beddings and laminations associated to the backlimb strata of the anticline are colored in orange. The longitudinal fracture set is colored pink, conjugate fractures in yellow and the transversal fractures in brown. Fracture intensity logs were computed for all open fractures and separately for the three defined fracture sets.

No driver for the prediction of the areal fracture distribution (e.g. 3D seismic) is available. Thus, three conceptual scenarios were developed to control the population of the fractures in the model.

- Conceptual fracture intensity trend

The structural style of the reservoir and the brittleness of the present carbonate rocks suggest that fracturing might be increased along the crest of the folded anticline. Wells with available fracture intensity logs show a distinct NW-SE trend. Based on this conceptual approach a fracture intensity trend property was modelled and used to guide the interpolation of the upscaled fracture intensity logs for each fracture set (Fig. 10, A).

- Fracture probability log

The fracture probability log is defined as the difference between the deep reading resistivity log and the shallow reading resistivity log referenced to the deep reading resistivity log. The resulting curve describes a trend which might be related to the probability of fractures occurring. The higher the difference and the higher the absolute values, the more probable the fracture imprint is. No conclusion can be made about the fracture density, angle or aperture. The fracture probability log was modelled in 3D space and used to control the fracture intensity distribution for the three defined fracture sets (Fig. 10, B).

- Fracture index

The fracture index is calculated from the normalized average of the surface curvature and the distance to fault properties. It is also a conceptual approach and combines the effects of the surface curvature and the distance to fault on the fracture occurrence. Similar to the previously applied workflow, the fracture index property was used as a driver in modelling the fracture intensity for the three fracture sets (Fig. 10, C).

Fracture intensities were modelled and steered by the three conceptual fracture distribution scenarios. Discrete and implicit fracture models were set up to distribute the fractures in 3D space. Fracture aperture data, derived from XRMI interpretations and thin section analysis, provides the main input for the fracture permeability estimation. Fracture length is uncertain and hard to determine and was thus estimated. The modelled fracture permeability was calibrated to well test permeability in six wells. Scoping simulation runs however revealed that the fracture permeability in the conceptual models is too low for the Garzan and the Karababa Formation.

Although all available data was integrated in the fracture models the production behaviour of some wells cannot be matched. Based on results of scoping simulation runs an alternative conceptual fracture intensity model was designed and used to set up a fracture model. This fracture model will be tested in simulation runs and iterated in a future project phase.

## DISCUSSION AND RESULTS

Reservoir characterization of Dodan field was challenging as Dodan field is a complex natural environment with fractures. In addition, it was a low porosity-permeability environment with the poor data for the structural model and lack of data for the fracture model. To overcome those conditions, different methods were studied and unconventional solutions were applied. The field was subdivided into two groups as poor / tight reservoir rock and moderate reservoir rock, both with fracture imprint. Petrophysical evaluation was conducted using a deterministic workflow for both Garzan and Mardin Formation. The matrix properties such as porosity, permeability and water saturation are defined in the grids. Porosity logs were upscaled and then for modelling porosity into 3D grid, Garzan Formation is analysed for each depositional environment separately however Mardin Group is analyzed together as Derdere and Sabunsuyu Formations are under-sampled by well data. Uncertainty was high on permeability data because of the limited range and fracture permeability estimation, therefore low, base and high case scenarios are defined to cover the uncertainty. For the water saturation model, a deterministic approach was used based on the interpreted water saturation log. Although the high variability in production data shows that fractures play a role in the field, there were only three wells with XRMI data and no input for the prediction of areal distribution in order to create discrete fracture model. Therefore, fracture characterization was done from borehole image logs and conceptual approaches, such as fracture intensity trend, fracture probability log and fracture index, were used for the prediction of areal fracture distribution. As a result of the 3D reservoir characterization study, the estimated fracture volume is about 10 MMMscf which is about 1.7% of the matrix volume and considering a matrix volume of about 602 MMMscf, the total GIIP volume results in 612 MMMscf.

## REFERENCES

KAYMAKCI, N., INCEÖZ, M., ERTEPINAR, P. and KOÇ, A. (2010): Late Cretaceous to Recent kinematics of SE Anatolia (Turkey). Geological Society London, Special Publications, 340, 409-435.

Keywords: 3D Geological Modelling, Reservoir Characterization

Fig. 1 Tectonic position of the Dodan field in the Bitlis-Zagros Suture.

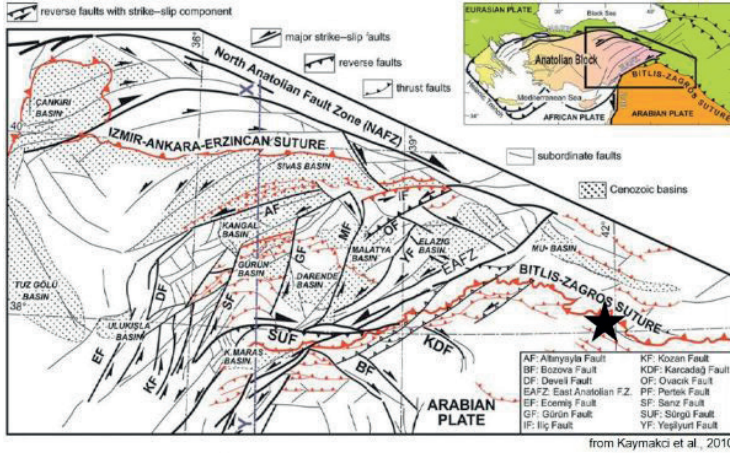
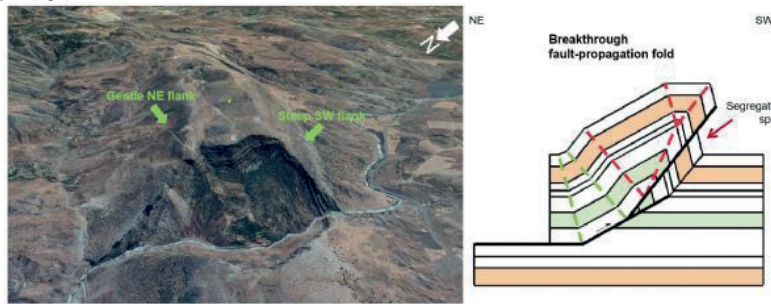


Fig. 2 Perspective satellite image of the Dodan field anticline highlighting the steep forelimb and gentle backlimb (left). Breakthrough fault-propagation fold (right)



Perspective satellite image of the Dodan field anticline highlighting the steep forelimb and gentle backlimb (left). Breakthrough fault-propagation fold. Parts of the forelimb are split of as span and additional kink bands occur at the backlimb (right).

Fig. 3 Limited data quality of line DD5325 with horizon and fault interpretations and the field base map (lower left).

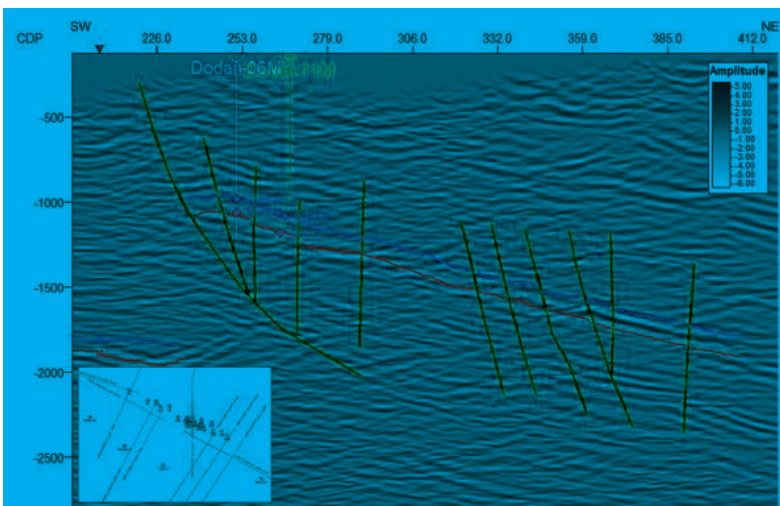


Fig. 4 Applied workflow in establishing the 3D geological model

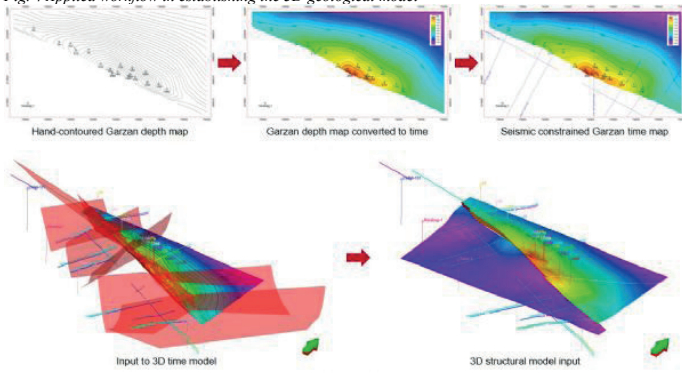


Fig. 5 Perspective view of the reservoir zone model.

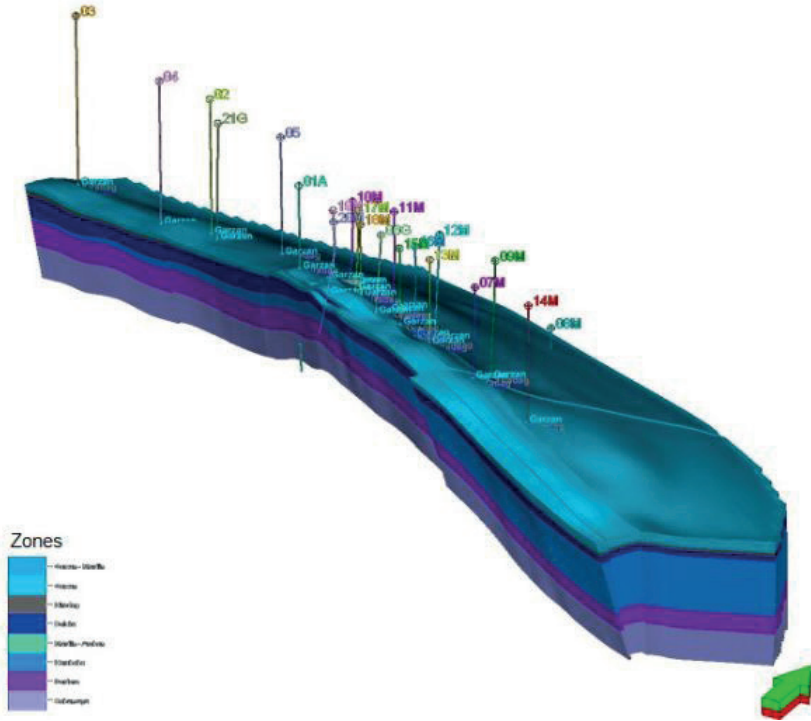


Fig. 6 Depositional environment model of Garzan Formation. A and B shows the probability map and vertical trend, C the final model.

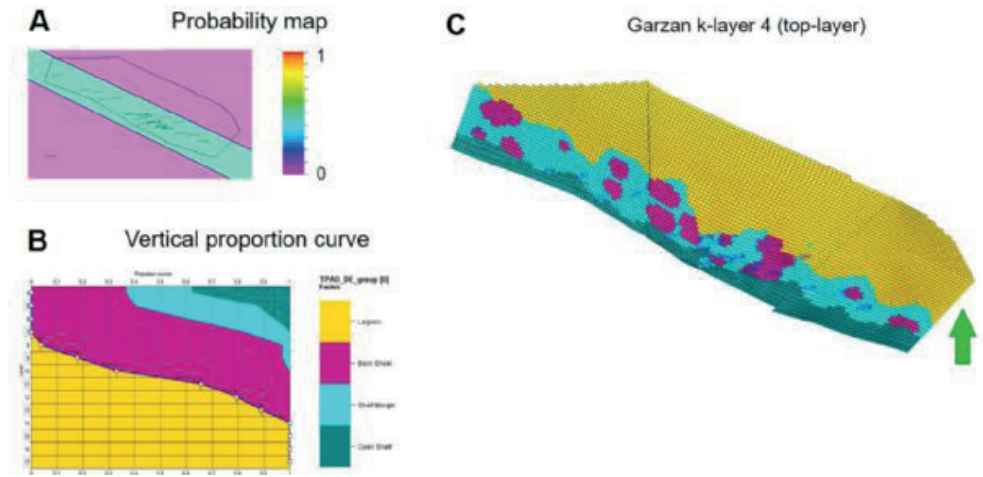


Fig. 7 Porosity distribution in Garzan and Mardin sub zones top layers.

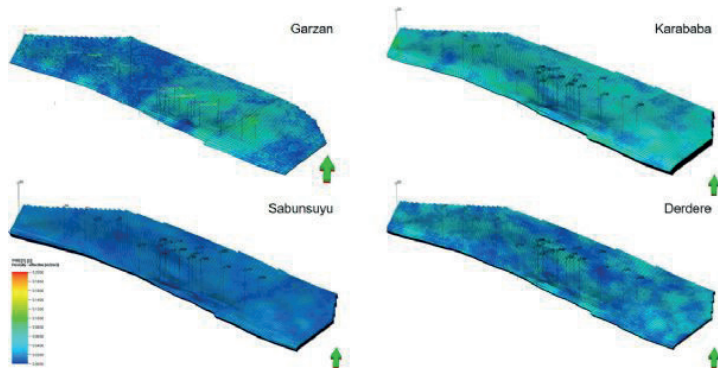


Fig. 8 Horizontal permeability distribution in Garzan and Mardin sub zones top layers.

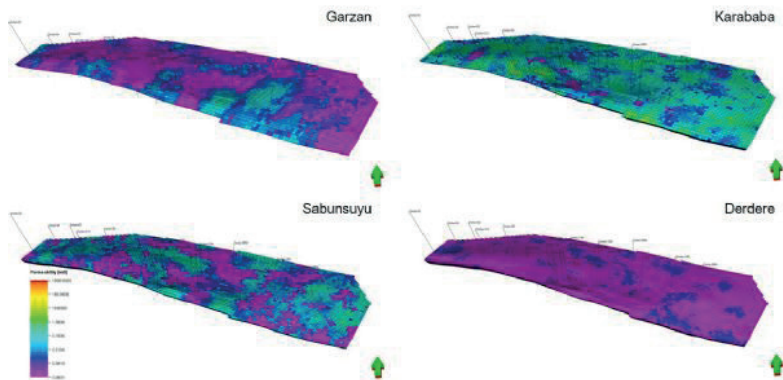


Fig. 9 Conceptual model of fracturing in the Dodan fold anticline (left). Dip azimuth rose diagram (right) of all open fractures (longitudinal (pink), conjugate (yellow) transversal (brown)). The orange set represents the bedding dips and laminations

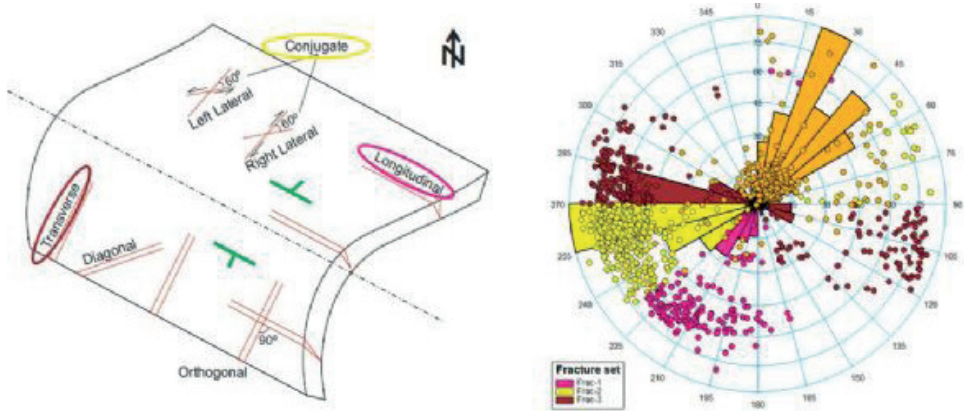
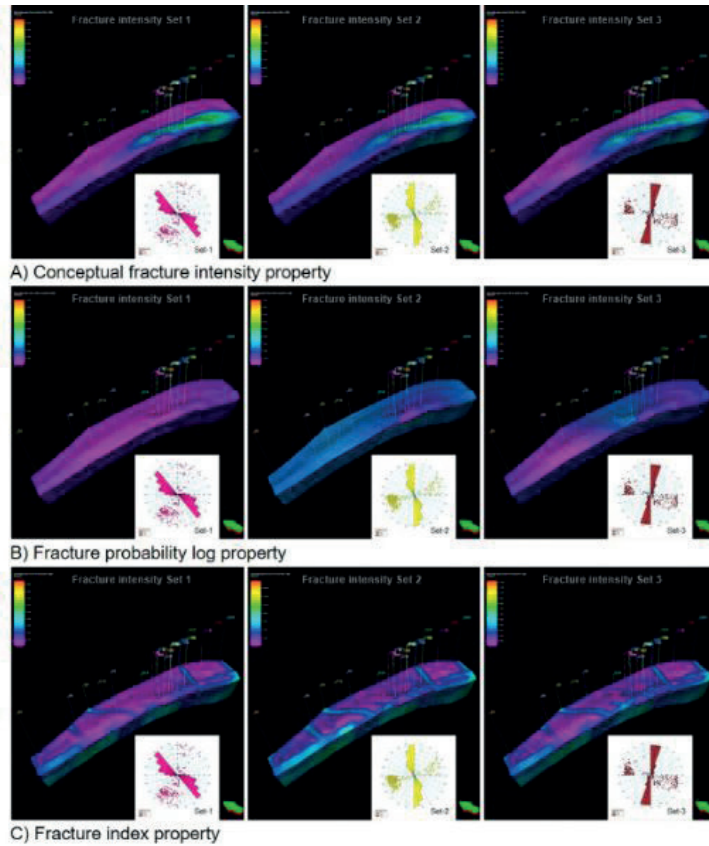


Fig. 10 Fracture intensity distribution scenarios. Conceptual fracture intensity property (A), fracture probability log property (B) and fracture index property (C).



# Bypass Pay Identification and Hydrocarbon Quantification with Advanced Pulsed Neutron Behind Casing as a Result of Logging Optimization and Data Analysis



Yernur Akashev<sup>1</sup>, Samira Ahmad<sup>1</sup>, Chiara Cavalleri<sup>1</sup>, Sviatoslav Yuras<sup>2</sup>

<sup>1</sup>Schlumberger; Digital and Integration; Analysis and Interpretation

<sup>2</sup>UkrGasVydobuvannya

## ACKNOWLEDGEMENT

This study was presented at the SPE Eastern Europe Subsurface Conference, November 23–24, 2021. Full paper is available at SPE library with number SPE-208512-MS

## INTRODUCTION

Oil and gas companies often face challenges with wellbore stability during drilling, exploration, appraisal, and production. The challenges with well stability are mainly related to the complex geological structure and geomechanical restrictions, combined with lack of original well data or models to properly understand the reservoir properties. In the Dnieper-Donets Basin (DDB), Ukraine, hydrocarbon prospects and plays typically have no geomechanical models and wells are drilled with water-based mud. Drilling commonly leads to washouts and poor borehole conditions. In such cases, core and open hole logging data will not be recorded because of the high operational risk.

Consequently, characterization of geological and geophysical properties of the reservoir is insufficient to enable confident decisions for further well testing and development. Although logging-while-drilling (LWD) technologies are available, these services can be expensive and usually not foreseen during the planning of vertical wells or wells with low deviation.

This paper presents three case studies in different fields within the Dnieper-Donets Basin (DDB), where the operator encountered challenges in acquiring open hole logging data and where advanced pulsed neutron logging (PNL) technology was deployed behind casing to help address evaluation challenges and drive the definition of positive production tests results.

1. Case Study A: Enabling a standalone cased hole evaluation and highlighting new potential reservoir zones otherwise overlooked due to absence of open hole logs.

The Well “A” is located in Dnieper-Donets Basin (DDB). The target formation is the Visean sandstone, with variable reservoir properties and quality, and producing gas across the field. This well was drilled to more than 4000m total measured depth. While drilling the deviated section of this well, a lot of technical issues were encountered. Amongst them were drilling bit stuck, borehole washout, bits damage. These issues occurred, before the second and third sections could finally be drilled.

After a series of technical difficulties encountered, the only data that could be acquired in the open hole section of the well were gamma ray, deep resistivity, SP, and

caliper logs. Unfortunately, the caliper data did not even cover the entire open hole interval.

In this well, the advanced PNL technology was logged behind multiple well sections and casing configurations: in presence of double casings (140 mm and 168 mm outer diameter – OD - casings), and triple casings (168 mm, 245mm, and 324 mm OD). The well was filled with water-based mud of 1.05g/cm<sup>3</sup> at the time of logging. The main target zones were encountered in the bottom section of the well, with 140 m OD.

2. Case Study B: Finding by-passed hydrocarbon intervals that were missed from log analysis based on conventional open hole logs for current field operator. The second case study focuses on the formation evaluation performed in a deviated appraisal-development well in the DDB basin. In general, the reservoirs in the field have porosity ranging between 6 to 15p.u. and the permeabilities are generally low, just above 0.1mD. The target formation in well “B” is the Middle Carboniferous, Moscovian formation, which consists mostly of sandstone with shale and carbonate cement, siltstone, and some clay minerals.

The information provided by the sonic and neutron logs did not cover the main target reservoir and were not sufficient to describe the main rock properties and fluids. Additional measurements to quantify lithology, porosity, and gas saturations were required. At this purpose, an advanced PNL logging technology was recorded across main 127 mm OD section of the well filled with water-based mud of 1.07g/cm<sup>3</sup> density. The cased hole logs acquisition and prompt data analysis addressed the main evaluation challenges and filled the large gap existing because of limited and partial open hole logging. This approach has been beneficial to collect critical formation parameters and define additional and by-passed pay; hence to select the best hydrocarbon intervals for further stimulation.

3. Case Study C: Identifying gas saturated reservoirs and providing solid lithology identification that previously was questioned from drilling cuttings in an unconventional reservoir.

The third case study is well “C” targeting the Lower Visean formation in DDB, with a total depth of more than 4000 m. The main horizons consist of carbonates, shales, sandstone, argillites, and marls. The open hole was logged with typical local logging suite including gamma ray, neutron log, resistivity log, spontaneous potential, caliper, monopole sonic log, caliper, micro-resistivity, and inclinometer.

With only a vintage and limited set of open hole logs, the complex mineralogy and high organic shale content posed additional challenges to build a robust petrophysics model. According to previously logged

data, there are also evidences of thin beds and layered formation further complicating standard formation evaluation. From the core analysis, we have also discovered the presence of shale intervals rich in organic matter as well as low porosity carbonate rock.

A logging plan was agreed to perform the evaluation using the advanced PNL logging technology. This gave access to high-resolution spectroscopy and in-situ Total Organic Carbon (TOC), sigma, neutron porosity, and FNXS behind casing. The comprehensive cased hole formation evaluation started with detailed mineralogy, matrix properties, and corrected porosity as inputs to the petrophysical computation. Pulsed neutron logging was recorded behind single casing 178 mm OD, with the borehole filled with water base mud.

## METHODOLOGY

### Advanced Pulsed Neutron Logging (PNL)

The advanced PNL technology (Figure 2) integrates a high-output pulsed neutron generator (PNG), two LaBr3:Ce gamma ray detectors, and a deep YAP (YAlO3) detector. The pulsing scheme of the tool is optimized to enable self-compensated outputs and higher precision to be delivered. (Rose et al., 2015). A unique feature of the advanced PNL technology, is the ability to log both time and energy domain simultaneously, with significant time saving. Both time and energy domain measurements can be used as input to the multi-mineral solver to build a robust petrophysical model and solve for the petrophysical properties.

### TIME DOMAIN LOG ACQUISITION MODE

The time domain data acquisition delivers formation capture cross-section (sigma), hydrogen index (HI) and a new formation property, inelastic gas known as fast neutron cross section (FNXS), which is used for gas quantification. The acquisition mode is also known as GSH Mode; a short term for Gas-Sigma-Hydrogen Index. Formation sigma and neutron porosity (HI) measurements are automatically corrected for borehole effects (casing, tubing, annular fluids, changes in borehole fluids or gas filled sections). This self-correction advantage is achieved through design, measurements, characterization, and a devised algorithm (Rose et al., 2015).

In addition to traditional PNL methods based on neutron counts ratio or sigma logs, the advanced technology deployed in the case studies, deliver an independent measurement, the fast neutron cross section (FNXS), which is highly sensitive to gas largely independent of hydrogen index and formation salinity. The physical processes leading to the detected inelastic gamma rays were modeled explicitly using Monte Carlo techniques in a wide range of formation and borehole conditions. It was found that the inelastic gamma ray response is dominated by FNXS and thus can be described approximately by FNXS measurement. This approximation can be improved by introducing additional formation properties such as bulk density and atomic density (Rose et al., 2015).

## ENERGY DOMAIN MODE

The energy-domain mode delivers spectroscopy outputs including dry-weight elemental mass fractions, total organic carbon (TOC), lithology, and matrix properties through spectral deconvolution and closure. The energy-domain mode also provides carbon-oxygen ratio that is useful to quantify oil saturation in formations with fresh water or unknown formation salinity. The spectroscopy analysis for the slim pulsed-neutron tool is made separately for the near and the far LaBr3:Ce detectors, and then combined based on the variance-weighted-average of the two. (Rose et al., 2015).

A detailed mineralogical quantification from spectroscopy-derived dry-weight elemental logs was done using a machine learning algorithm (Craddock et al., 2021). This algorithm is based on variational autoencoder (VAE) formulations, comprising an input(s), encoder, decoder, output(s), and a heteroscedastic loss function that optimizes the mapping (coefficients) between the input(s) and output(s) and provides an estimate of uncertainty on the output(s) values. The inputs are a set of spectroscopy-derived dry-weight elemental concentrations, and the outputs are a set of estimated mineral concentrations and a set of reconstructed dry-weight elemental concentrations. The reconstruction of original dry-weight elemental concentrations validates that the estimated mineralogy is at least a valid solution within the constraints provided by the spectroscopy-derived elemental measurements as shown in Figure 4.

## RESULTS

### Standalone Cased Hole Formation Evaluation: Case Study Well A

Looking at the GR and RES in Figure 5, the sand with high resistivity shows good gas zone prospect. Using the advanced PNL, FNXS (independent gas indicator) and FNXS matrix crossover, the good gas zones is easily identified against a low porosity gas sandstone.

Figure 6 is a focused display of the results in the lower Viséan Sandstone. The advanced PNL shows clearly that this interval is a low porosity (average 9 p.u.), gas-filled sandstone.

The porosity is computed using a multi mineral solver with the following log inputs: neutron porosity (TPHI), FNXS, and the mineral dry weight fractions from the elemental spectroscopy analysis for matrix correction, together with the measurements' uncertainty. Formation sigma (SIGM) was used as part of the model as additional quality control. All crossover indicators agree to confirm the presence of dry gas; this includes review of FNXS vs. FNXS matrix crossover.

In Figure 7, the yellow highlights on the FNXS vs TPHI crossplot are the gas interval in the sandstone interval.

### Identification of Bypass Pay: Cased Study Well B

The advanced PNL technology was recorded in GSH-



LITH mode. The interpretation of the advanced PNL logs enabled finding bypassed pay and quantification of the hydrocarbon volume and saturation with a high level of certainty. The analysis of the data and log responses to formation was performed in real-time. The advanced PNL results are displayed in Figure 8.

While recording the advanced PNL, an additional sandstone reservoir was discovered at the top of the agreed logging interval marked as TLI in the depth track in the plot above. The presence of additional sands with hydrocarbon potential just above the main target zones was immediately discussed and the logging interval was extended to enable a complete evaluation of the recently discovered gas zone.

Other zones of interest were successfully characterized as shown in Figure 9.

By extending the logging interval additional sand units with different rock quality were encountered. Of those, the sand interval at X350m was proven to be a good gas saturated formation with porosity ~11.2 p.u. and average gas saturation 62.5%. The additional sand interval at X200m is also gas saturated and has similar rock quality with higher water saturation compared to the previous sand based on the log's response and interpretation. A well test in pilot hole well "B" was performed across this sand at X200m flowing both gas and water confirming the log results. In our case in well "B" was tested interval X350 and confirmed gas saturation with good production rate.

## UNCONVENTIONAL PETROPHYSICAL EVALUATION

### Case Study Well C

The analysis of elemental spectroscopy log outputs, in addition to providing standard and advanced mineralogy, discovered the presence of shale intervals rich in organic matter as well as low porosity carbonate rock. The complex mineralogy and high organic shale content posed additional challenges to build a robust petrophysics model, when only based on vintage and limited set of open hole logs. In addition, according to previously logged data, there are also evidences of thin beds and layered formation further complicating standard formation evaluation approaches.

The mineralogy and matrix properties measured with the advanced PNL were also used to derive a matrix corrected porosity together with neutron porosity also measured. The integrated evaluation successfully identified the hydrocarbon bearing intervals within a low porosity carbonate sequence and the organic rich shale. For the first time in the field, it was possible to isolate and characterize new targets and apply a novel accurate approach for lateral landing target selection and development. The carbonate zone (interval X120m – X200m in the log plot) and gas shale above (interval X100m – X120m) was considered for further investigation and evaluation prior development and potential production.

## CONCLUSIONS

During the performance of production tasks, we have encountered various obstacles, geological, technical operational challenges, etc. However, with the development of the new advanced PNL technologies, this makes it possible to address our formation evaluation challenges and reduce risks in making important decisions.

The proposed methodology was tested in several wells, both in open hole and behind casing. The results showed the robustness and effectiveness of using the advanced pulsed neutron logging (PNL) technologies in multiple cases:

1. For Case Study A - enabled a standalone cased hole evaluation and highlighted new potential reservoir zones otherwise overlooked due to absence of open hole logs.
2. For Case Study B - found by-passed hydrocarbon intervals that were missed from log analysis.
3. For Case Study C - identified gas saturated reservoirs and provided solid lithology identification that previously was questioned from drilling cuttings in an unconventional reservoir.

We introduced three different cases, where we have encountered different types of reservoirs and its associated challenges, however, with the use of the latest advanced PNL behind casing, this allowed us to obtain the necessary geological information such as:

- Mineralogy.
- Porosity.
- Gas saturation.
- Total organic carbon content.
- Bypass Pay Identification and Hydrocarbon Quantification.
- Inputs for making effective completion decisions.

Well tests and special coring analysis verified the accuracy of the advanced PNL logging data interpretation results. Advanced PNL behind casing gives us a new possibility to better understand our reservoirs and provided us with the very critical information for our well completion and field development planning.

Particularly, this work describes in detail the application of the alternative methodology and interpretation workflows through casing when open hole logging was missing due to operational risks or was limited in accuracy and data quality due to difficult borehole conditions, or not sufficient to properly evaluate formation properties. The relevant examples presented illustrate the effectiveness of this approach in exploration or mature fields in Ukraine.

Keywords: Advanced Pulsed Neutron Logging, Standalone Cased Hole Formation Evaluation

Figure 1: Dnieper-Donets Basin (DDB) (source - <https://www.usgs.gov/media/images/dnieper-donets-basin>).

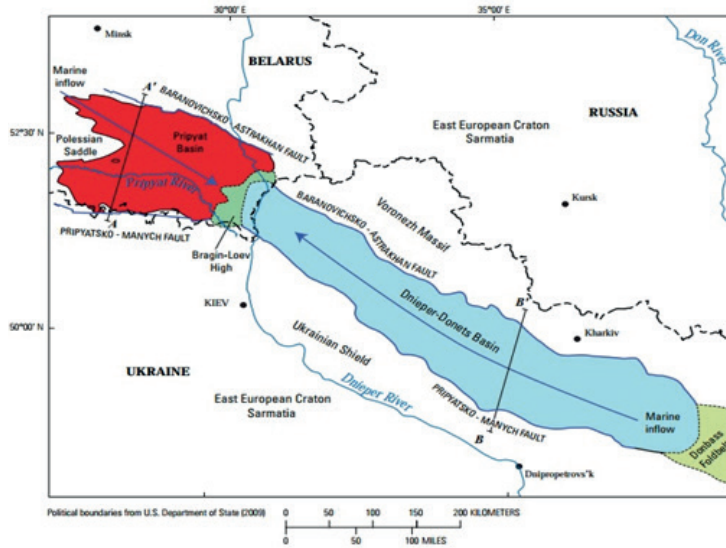


Figure 10: Advanced PNL high resolution spectroscopy results with advanced mineralogy (VAE) results against core XRD. Refer to Nomenclature section at the end of the paper for the curve description.

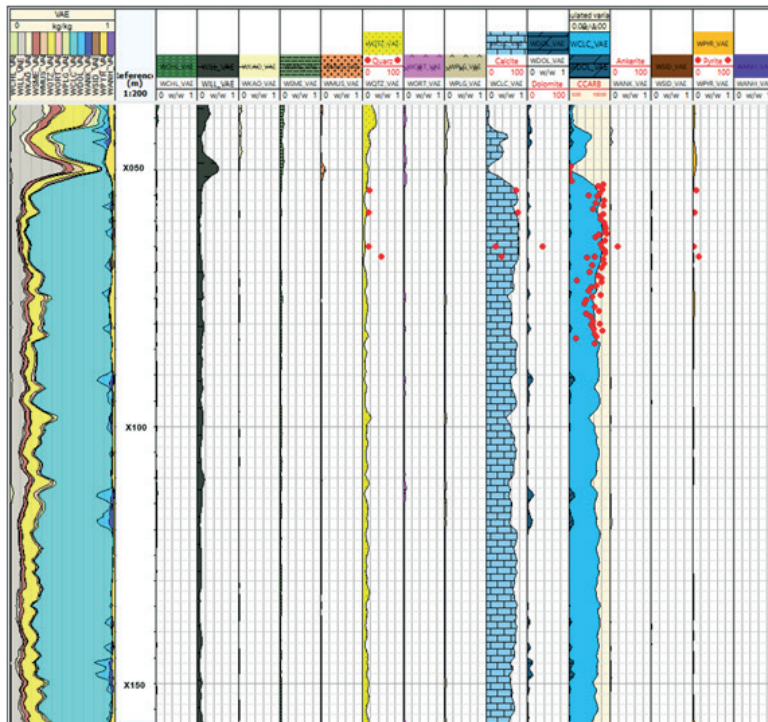


Figure 11: Advanced PNL results with DWTOC vs TOC core displayed in the final track. Delta Log R (sonic) displayed in green, DWTOC (advanced PNL results from spectroscopy) in black with pink shaded, and the TOC (core) in red circle. The DeltaLogR and

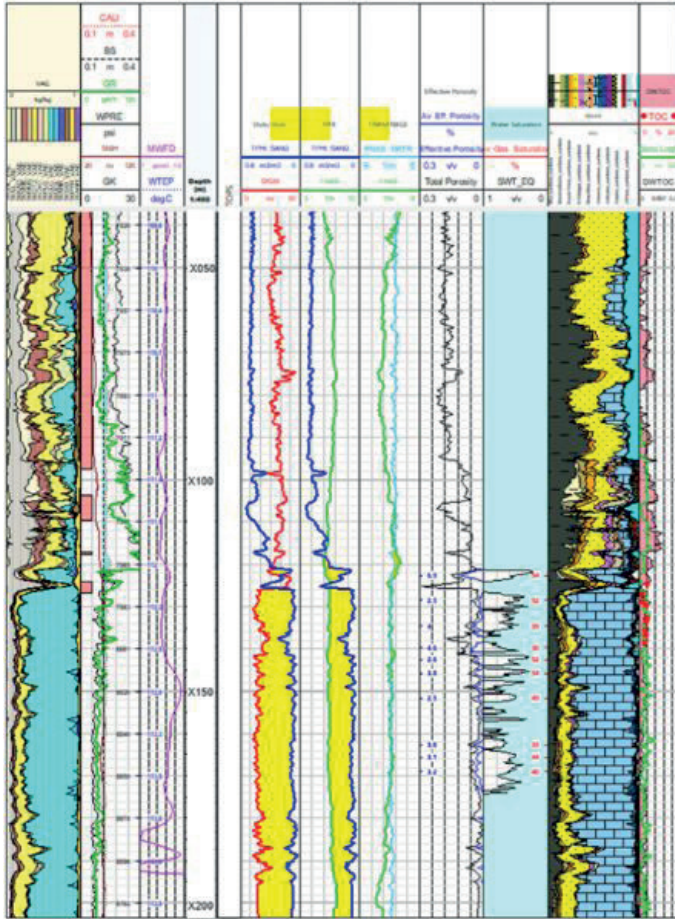


Figure 2: Advanced PNL Technology

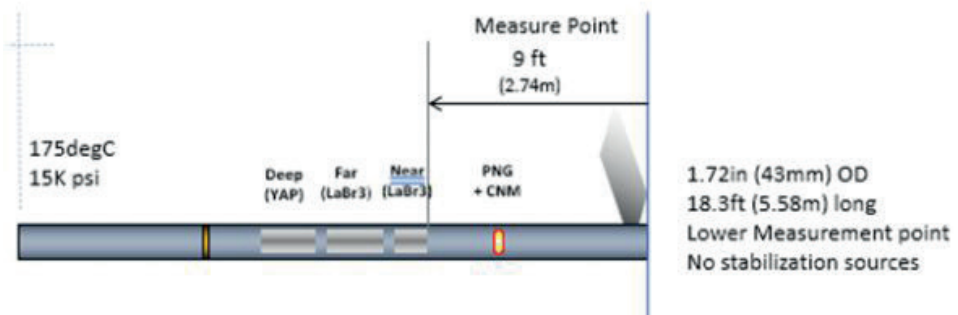


Figure 3: Advanced PNL Logging Mode

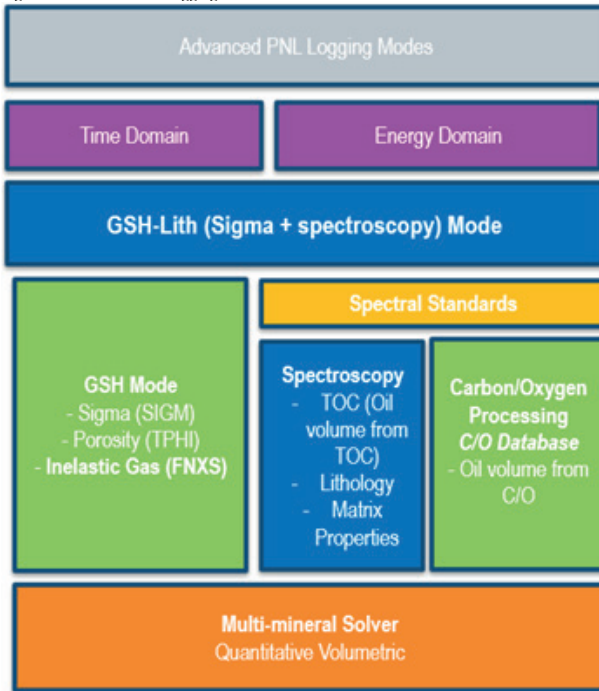


Figure 4: Advanced Mineralogy – Variational Auto Encoders (VAE). Top left is a description on the processing workflow for the advanced spectroscopy. Top right is the gamma ray spectrum recorded by the advanced PNL spectroscopy that includes a capture

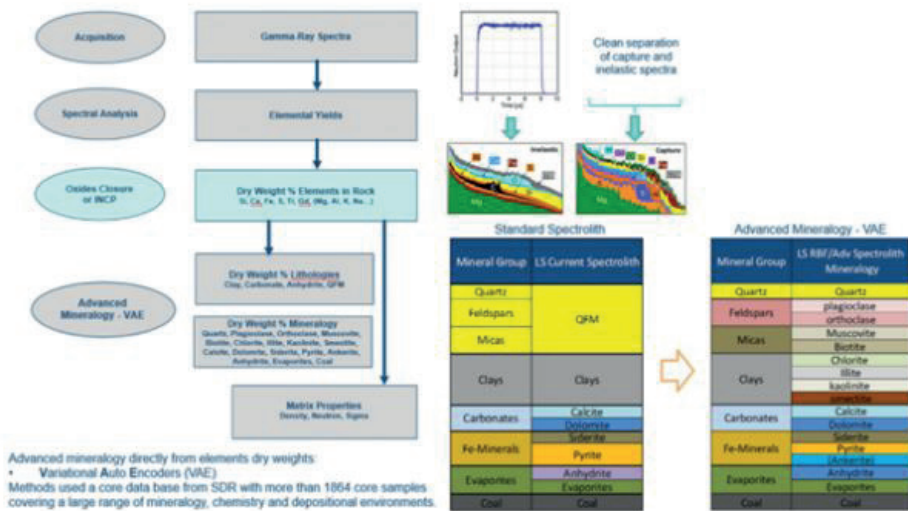


Figure 5: Well "A" Advanced PNL results. There are several sand intervals across X050m, X100m, X150m and X200m.

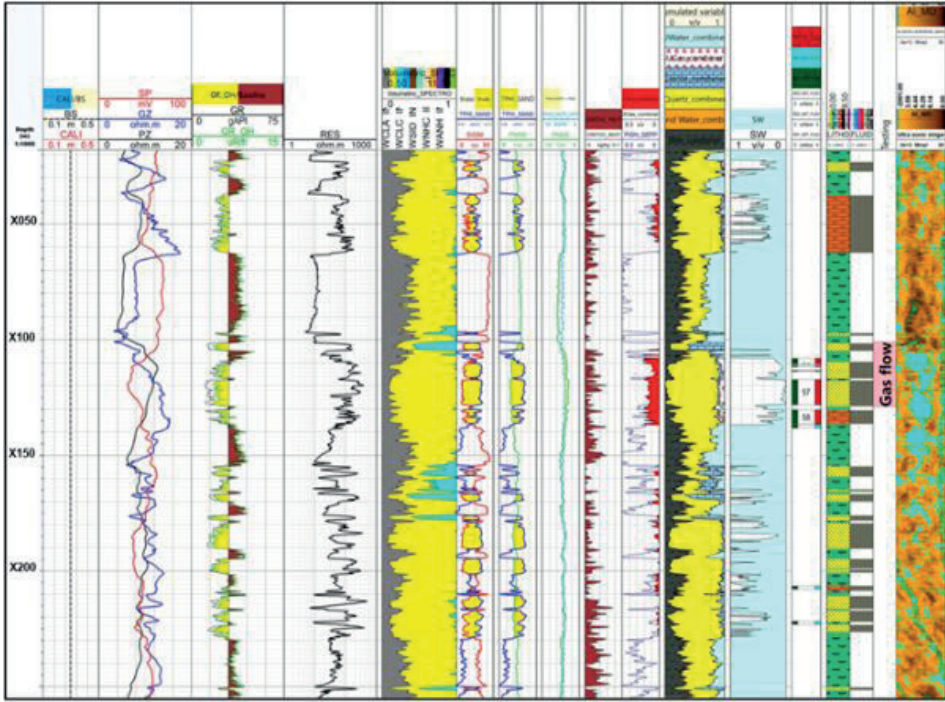


Figure 6: Well "A" Advanced PNL results focus in the Lower Visean Sandstone, low porosity – gas saturated sandstone interval with average 9p.u. Refer to Nomenclature section at the end of the paper for the curve description.

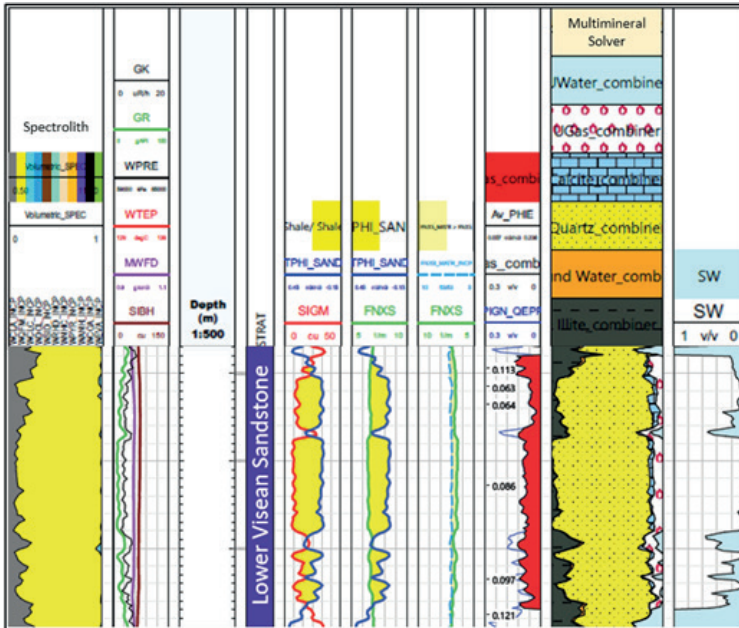


Figure 7: Well "A" FNXS vs. TPHI crossplot

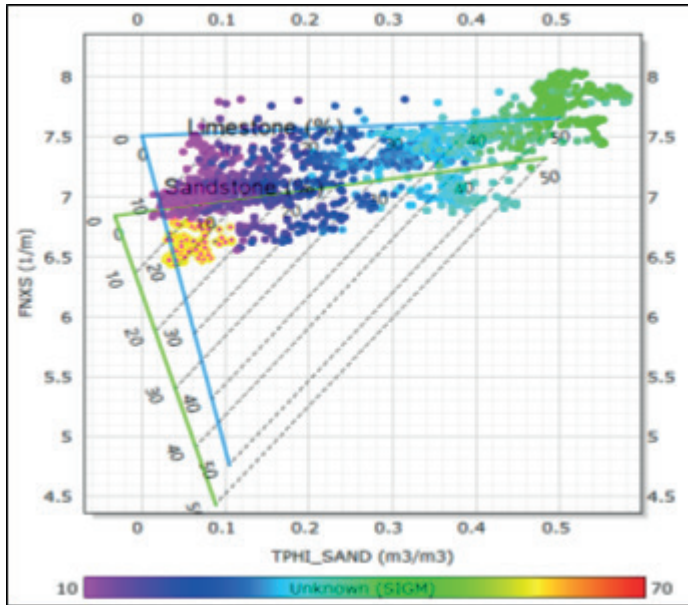


Figure 8: Well "B" Advanced PNL Results displaying the agreed top logging interval. It is evident that there is a potential hydrocarbon sand above the "agreed" top logging interval, marked TLI on the depth track. Refer to Nomenclature section at the

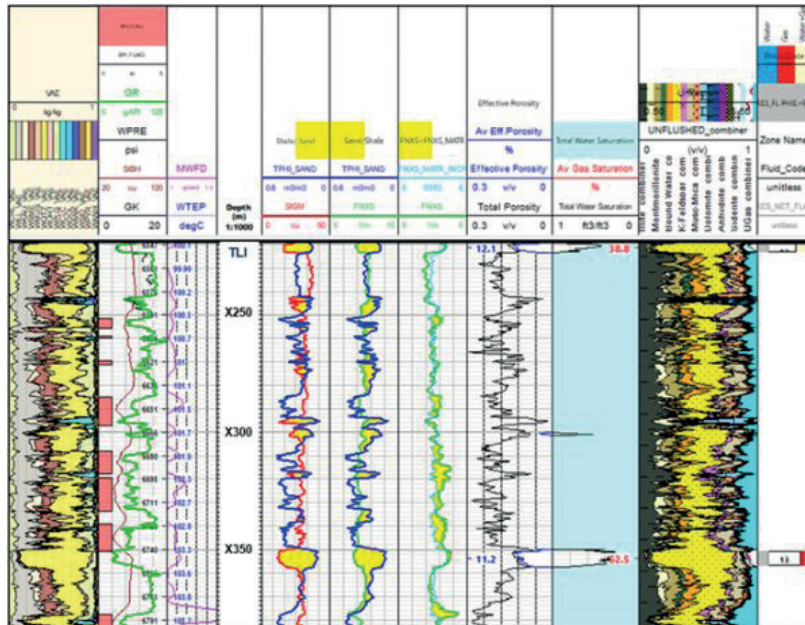
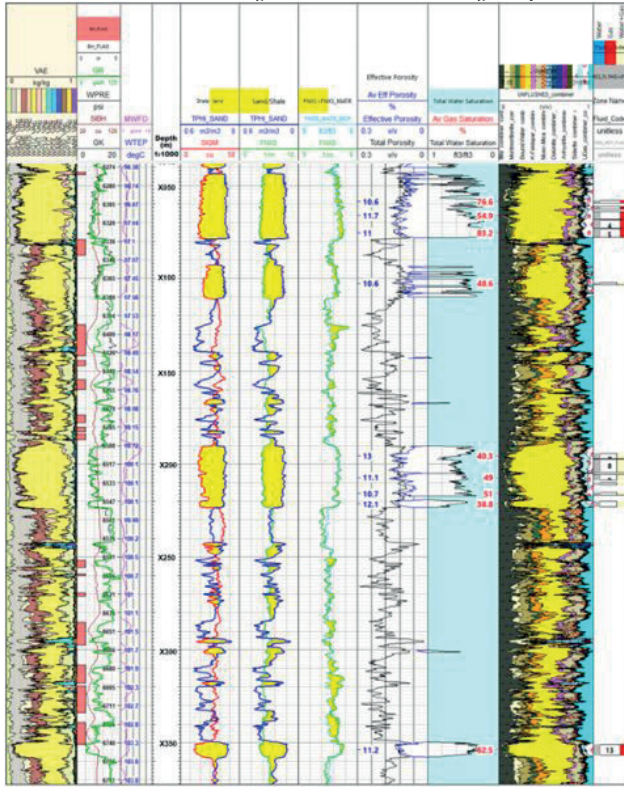


Figure 9: Well "B" Advanced PNL results with added logging interval at the top. There are 3 additional sands above the agreed logged interval. The advanced PNL result shows at X200m; gas + water interval, at X100m, higher clay content with gas interval



# Sub-Seismic Fault and Fracture Analysis Using Conventional and Image Logs: A Case Study In Bozhüyük Field, Southeast Turkey



**Çansu Güner Cicek<sup>1</sup>, Onur Yürüker<sup>1</sup>, Osman Merety<sup>2</sup>, Ceyda Çetinkaya Kayrın<sup>1</sup>**

<sup>1</sup>TPAO, Production Department, Söğütözü Mahallesi Şht. Öğretmen Şenay Aybüke Yalçın  
Caddesi No: 10 06530 Çankaya Ankara / Türkiye

<sup>2</sup>TPAO, Exploration Department, Söğütözü Mahallesi Şht. Öğretmen Şenay Aybüke Yalçın  
Caddesi No: 10 06530 Çankaya Ankara / Türkiye

## INTRODUCTION

Reservoir management in naturally fractured carbonate reservoirs poses challenges for accurate reservoir modelling. The southeast of Turkey is characterized by tectonic activity and predominantly consists of naturally fractured oil-producing reservoirs. The spatial distribution of fractures plays a crucial role in reservoir simulation and affects the flow units. Fractures can lead to water influx, impacting oil production and complicating recovery from the matrix. Hence, a detailed examination of fracture distribution and fault modelling is essential for heterogeneous fractured carbonate reservoirs.

In the East Anatolian Fault Zone, the north-south directional contraction is provided by both thrust and strike-slip faults. This stress system works within the fields around the Adıyaman Fault Zone. The field of this study, Bozhüyük, is located in the Adıyaman region, southeast Turkey. Hydrocarbon production in the Bozhüyük Field occurs from carbonate reservoirs, which have matrix porosity and naturally occurred fractures. There are five different oil-producing formations spatially distributed in the area. The Bozhüyük Field is tectonically active; therefore, all the wells planned to drill vertically have some deviation towards fault zones. Moreover, most the wells have loss or duplication at some part of the formations, which are recognized from conventional and image logs.

Bozhüyük Field was discovered in 2012 from two dimensional seismic data and field studies. The field is a thrust-related anticline with internal deformation characterized by thrust, strike-slip and oblique-slip normal faults. Bozhüyük Fault, a Middle Miocene-aged thrust fault with left-lateral strike-slip component, limits the field in the northwest-southeast direction. Moreover, there are many Cretaceous-aged reactivated faults with changed stress regime within the field. There is three-dimensional (3D) seismic data recorded in 2019, seven years after the first well was drilled in the field. This 3D seismic cube covers the entire area; however, it was effected by the Atatürk Dam, which is the western border of the field. The vertical seismic resolution is approximately fifteen meters, and this quality is not enough to detect some of the Cretaceous-aged faults, which have a throw length smaller than fifteen meters.

During the development stage of the field, a deviated well was planned and drilled towards the dam at the west part of the field. Due to lack of the seismic data, the well cut the formations at unexpected depths and intersected four faults with different thrown amounts,

unfortunately. Although the image log recorded after drill process shows too many conductive fractures, the expected production rate could not be achieved. Many of the faults and fractures in the Bozhüyük Field are thought to transport aquifer water throughout oil production levels. Therefore, only seismic data and field geology are not sufficient to structural modelling of such a fractured and tectonically active field. It is necessary to establish a more detailed structural model in order to increase the oil production with enhanced oil recovery. By having a better understanding of the distribution of fractures within the reservoir, decisions that are more accurate can be made about well placement and production strategies, leading to better reservoir performance and management.

The aim of this study is to combine the fault and fracture system with the structural model based on conventional logs and borehole image data.

## MATERIALS AND METHODS

In this study, conventional and image logs were used to detect sub-seismic faults and fractures. Nineteen well log data were interpreted by considering fault and fracture systems. Formation and facies thicknesses and their distributions were considered to recognize any sub-seismic fault.

Twenty-one wells, aiming at the Cretaceous-aged reservoirs, were drilled in the Bozhüyük Field. Since the region is tectonically active, some of the wells, which were planned to drill vertically, have inclinations toward possible fault zones.

In Figure-1, the continuity of the Karaboğaz Formation can be observed from northwest to southeast direction with gamma ray log (GR). The rightmost well, B-4 is the reference one. Although there is no time gap of deposition between Sayındere, Karaboğaz and Karababa-C (KBB-C) Formations, different thickness and GR responses can be seen obviously. When the possible fault points were combined, it is thought that there is a northwest-southeast trending fault, which is compatible with the general stress regime of the area.

Image log interpretation is another method to recognize the fault and fracture in the wells. They help to identify any natural or induced fracture in the formations along the wellbore path. The conductive fractures are represented as black color in borehole images and they help to communication between matrix and porous media. On the other hand, resistive fractures are white in color and filled with calcite mineral. Also, the



borehole images are important way to identify small faults where seismic resolution or standard well logs are not sufficient. The main difference between fault and fracture identification in borehole image is that fault has some throw amount can be seen from bedding planes and fractures do not have this feature. In Figure-2, there are a few examples of faults identified from image logs.

In addition to the determination of faults from conventional and image logs, all fractures were also processed. The conductive fracture distribution among the field is consistent with the active stress regime in the field. They are both fold and fault related fractures.

## FINDINGS AND CONCLUSIONS

Conductive fracture distribution among the field shows that some fractures are related with folding mechanism. These are perpendicular to maximum stress direction, which is determined from the induced fractures. These conductive fractures are in the apex area and shows east-west direction. On the other hand, some of these fractures are related with faulting mechanism. They are almost parallel to fault directions and located inside of the fault zones. Therefore, this type of fractures are mostly seen when the well cuts a fault. In the Bozhüyük Field; among nineteen well, seventeen of them are cutting at least one fault. Therefore, most of the conductive fractures shows parallel direction to faulting system

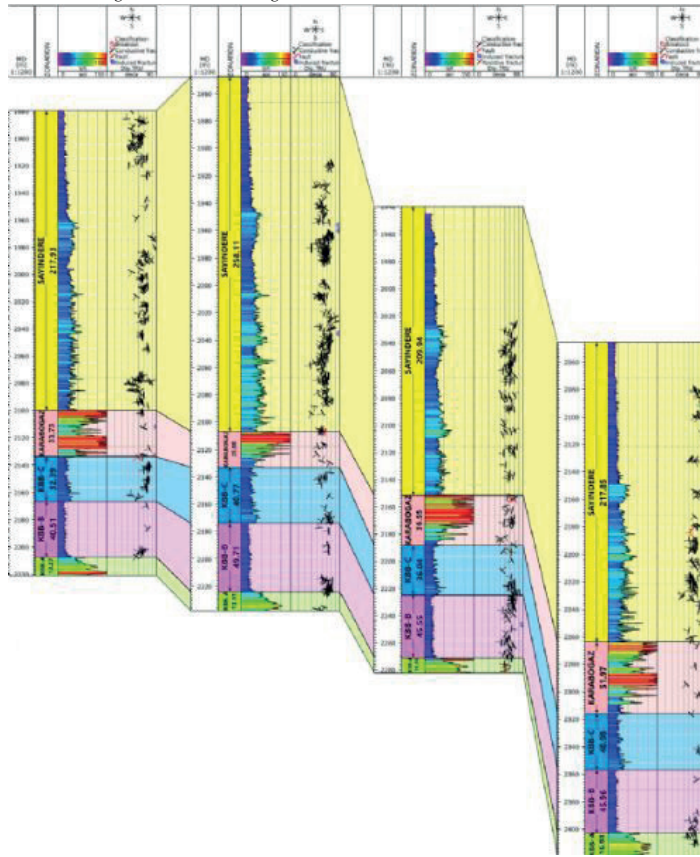
The maximum stress direction of the field is approximately north to south direction according to induced fractures determined from image logs. Most of the Cretaceous-aged faults are making approximately 30-35° angle with maximum stress direction of the field.

Due to the fact that 3D seismic data were obtained towards the end of the field development, only the last three production wells were drilled directionally in the aim of cutting conductive fractures. Two of them performed as expected. In the further stages of the study as simulation part, the compatibility of the flow zones and fractures will be examined.

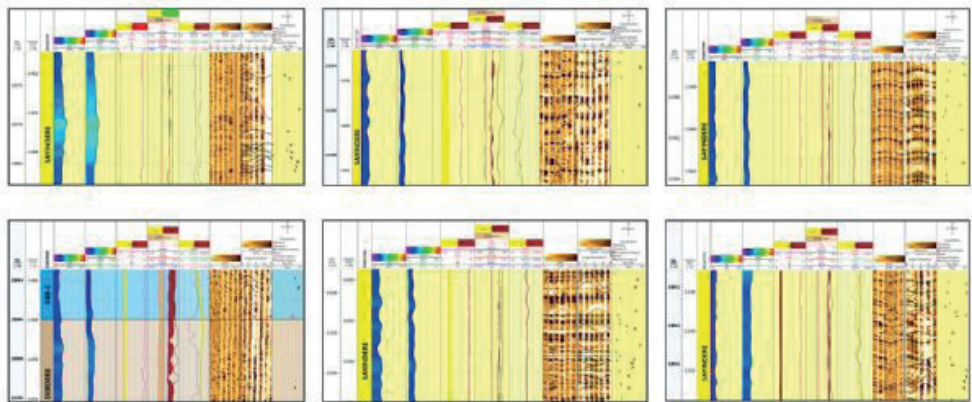
As a result of this study, formation maps and fault polygons have been renewed to be used in the structural model of the field, based on the fault and fracture systems determined from conventional and image logs (Figure-3). In this way, it is predicted that more accurate production simulations can be made.

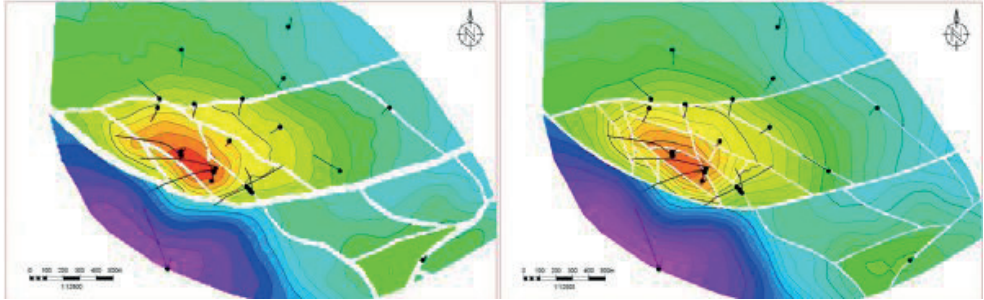
Keywords: Fracture Interpretation from Image Logs, Structural Reservoir Modeling

Conventional Log Correlation in Karaboğaz Formation



Fault Examples on Image Logs at Different Wells





# Reservoir Saturation Monitoring over time: Case Studies from Karacali Gas Field and Bati Raman Heavy Oil Field



**Uğur Yüce**  
TPAO

## INTRODUCTION

Reservoir surveillance is a vital step to support the production strategies and create a road map for the operational plans throughout the life of hydrocarbon producing fields. To do that, pulse neutron logging is available to fill the gaps. Pulsed neutron logging (PNL) running behind the casing has numerous applications in the industry including reservoir monitoring, effect of steam-gas injections, water-hydrocarbon contact determination, formation evaluation of old wells, missing logged intervals, previously bypassed zone determination and tracking the reservoir depletion profiles.

## METHODS

Neutrons sent from the source passing quickly from casing and cement. Upon reaching the formation, they collide with the elements present and are mainly absorbed by the chlorine atoms in the formation water. As a result, the neutrons lose energy and transition to a lower energy state, emitting gamma rays that is detected by the receiver(Ref.1).

Tau is the time required for the thermal neutron to loose its energy thermal decay time constant in microseconds; capture cross section is calculated in the equation (Formula-1);

$\Sigma$  is the capture cross-section for thermal neutrons per cc of a medium(Ref.2). It can be observed from Table-1 there is a distinct difference in capture cross section between hydrocarbons and saline formation water. Neutron absorption process takes more time in hydrocarbon bearing zones compared with the saline formation water bearing zones due to high chlorine content of saline water. As a result,  $\Sigma$  becomes lower in hydrocarbon reservoirs.

Due to the close values between fresh water and hydrocarbons, ideal conditions(Ref.4) for water saturation calculation from PNL are mainly formation water salinity (>100Kppm), reservoir porosity (>10%) and reservoir should be clean (Volume of shale (Vshale) is around 0). The reservoir characteristics need to be understood before the parameter selection. This step is critical when calculating water saturation behind casing.

The formula used to calculate water saturation ( $S_w$ ) from pulsed neutron log data is shown on Formula-2(Ref.5);

For the parameters needed for  $S_w$  is shown in Table 2.

## FINDINGS AND CONCLUSIONS

Osmancik Formation of Karacali Field is a shaly sand reservoir in Thrace Basin. In Well-A, the lack of zonal isolation behind the casing due to the poor cement

integrity and producing intervals in nearby wells correlatable with the candidate perforation intervals required to confirm whether the initial water saturation is kept in the promising interval. PNL run in this well as a first step to understand the current potential of the interval. After the PNL processing, it is observed on Figure 1 that water saturation still exists although the casing is free of cement shown on Figure 2. Then, remedial cement for the free pipe is planned. CBL is run to see the effectiveness of the remedial job. The comparison for the remedial cement job is shown on Figure 1, representing an effective remedial program created a satisfied zonal isolation. The well is perforated and started to produce gas with no issue.

On the other side, Garzan Formation of Bati Raman Field is a naturally fractured vugy carbonate rock located in the Southeastern Türkiye. In order to track the depletion profile and make a decision about the remaining perforation intervals in Well-B, a PNL logging program were performed. The comparison of water saturation fractions are shown on Figure 3. It can be observed that in most intervals except top of the reservoir bulk volume water fractions increased significantly from 1988 to 2019 representing a depletion profile of the producing reservoir at the corresponding intervals. Table 3 shows parameters selected for the calculation.

In the first case study, although the field salinity parameter is not quite high for the pulsed neutron logging application in Well-A, the big difference between oil and gas allowed a satisfied formation evaluation. The current gas saturation confirmed when compared with initial gas saturation in Well-A eased the decision making process in the field. The approach is then distributed nearby wells to reveal by-passed zones to increase production.

In the second case study, the reservoir parameters are suitable to create a representative water saturation profile in Well-B since formation water salinity and effective porosity are quite high for the water saturation estimation from the pulsed neutron logging. As a result of the field application in this well, the depletion profile for open and remaining perforations were determined in Well-B. Based on that information, new wells are planned accordingly in that region of the field.

Pulsed neutron logging tools are easy to operate in the production fields. It is an effective tool for the reservoir management studies. By establishing the reservoir parameters for each producing fields, it can be moved for further studies in the field development plans.

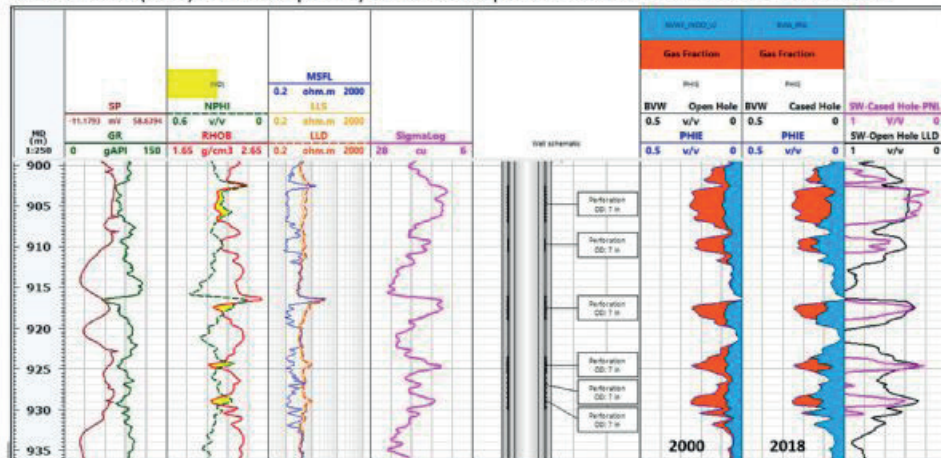
REFERENCES

- 1.) Morris, C., Aswad, T., Morris, F., and T. Quinlan. "Reservoir Monitoring with Pulsed Neutron Capture Logs." Paper presented at the SPE Europec/EAGE Annual Conference, Madrid, Spain, June 2005. doi: <https://doi.org/10.2118/94199-MS>
- 2.) Clavier, C., Hoyle, W., and D. Meunier. "Quantitative Interpretation of Thermal Neutron Decay Time Logs: Part I. Fundamentals and Techniques." J Pet Technol 23 (1971): 743–755. doi: <https://doi.org/10.2118/2658-A-PA>
- 3.) Techlog64 2022.2, "Sigma Interpretation", Guru Documentation, Schlumberger
- 4.) Al-Nasser, M. N., Ma, S. M., Al-Mushrafi, N. M., Al-Muthana, A. S., Riley, St., and Abel I., G., "Quantifying Gas Saturation with Pulsed Neutron Logging—An Innovative Approach." Paper presented at the SPE Reservoir Characterization and Simulation Conference and Exhibition, Abu Dhabi, UAE, September 2013. doi: <https://doi.org/10.2118/166025-MS>
- 5.) Tugan, M. F., Yuce, U. "Discovery of New Horizons in a 36 Years Old Conventional Oil and Gas Play by Utilization of State-of-the-Art Formation Evaluation Approaches: A Case Study from the Thrace Basin, Turkey" Paper presented at the SPWLA 60th Annual Logging Symposium, The Woodlands, Texas, USA, June 2019. [https://doi.org/10.30632/T60ALS-2019\\_N](https://doi.org/10.30632/T60ALS-2019_N)

Keywords: Reservoir Saturation Monitoring, Pulsed Neutron Logging

Figure-1

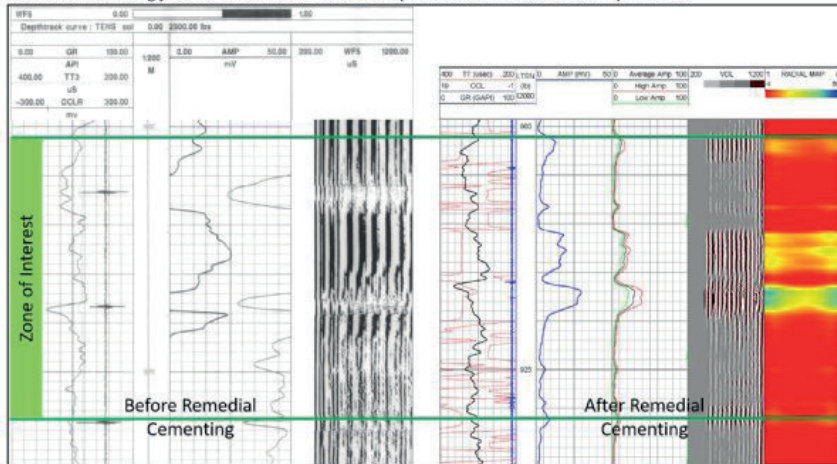
**Figure 1.** Water saturation comparison in proposed intervals between 2000 and 2018 in Well-A. Bulk Volume Water Fraction (BVW) in effective porosity calculated in open hole vs cased hole shown on Track 7 and 8.



Water saturation comparison in proposed intervals between 2000 and 2018 in Well-A. Bulk Volume Water Fraction (BVW) in effective porosity calculated in open hole vs cased hole shown on Track 7 and 8.

Figure-2

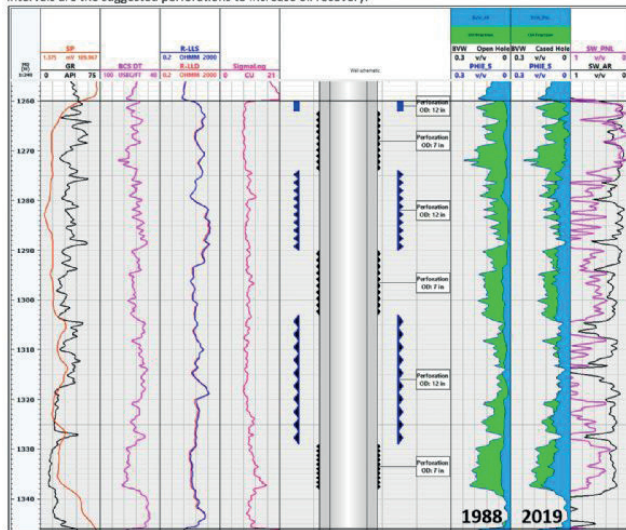
**Figure 2.** Remedial cementing job in the zone of interest in Well-A. The comparison between before and after remedial cementing job shows a zonal isolation is improved after the work over operation.



Remedial cementing job in the zone of interest in Well-A. The comparison between before and after remedial cementing job shows a zonal isolation is improved after the work over operation.

Figure-3

**Figure 3.** Water saturation comparison between 1988 and 2019 in open and remaining intervals in Well-B. Blue intervals are the suggested perforations to increase oil recovery.



Water saturation comparison between 1988 and 2019 in open and remaining intervals in Well-B. Blue intervals are the suggested perforations to increase oil recovery.

Formula-1

**Formula 1.** Sigma calculation

$$\Sigma = 4550/\tau \text{ in cross section unit (c.u.)}$$

Sigma calculation formula

Formula-2

**Formula 2. Water saturation calculation behing casing**

$$S_w = \frac{(\Sigma_{log} - \Sigma_{matrix}) - \varphi_e(\Sigma_{hydrocarbon} - \Sigma_{matrix}) - V_{shale}(\Sigma_{shale} - \Sigma_{matrix})}{\varphi_e(\Sigma_{water} - \Sigma_{hydrocarbon})}$$

Water saturation calculation formula behing casing

Table-1

Quartz	4.3
Calcite	7.3
Dolomite	4.8
Shale	20-60
Gas	1-16
Oil	16-23
Fresh Water	22
Formation Water	19-128

Capture Cross Section (c.u.) of Some Materials

Table-2

Data	Data Source
$\Sigma_{matrix}$	Based on XRD-XRF analysis and sedimentological description
$\Sigma_{hydrocarbon}$	Based on Hydrocarbon PVT Properties
$\Sigma_{formationwater}$	Based on equivalent formation water salinity and pressure
$\Sigma_{shale}$	Based on log readings in a shale interval
$\varphi_e$	Effective Porosity estimated from well logs and calibrated with core data if possible
$V_{shale}$	Shale Volume estimated from well logs and calibrated with core data if possible

Parameter Descriptions

Table-3

Data	Well A	Well B
$\Sigma_{matrix}$	5.9	5.1
$\Sigma_{hydrocarbon}$	10	20
$\Sigma_{formationwater}$	55	95
$\Sigma_{shale}$	20	15
$\varphi_e$ (v/v)	0.12	0.10
$V_{shale}$ (v/v)	0.35	0.03

Parameter Selection

# Raman Sahası Garzan Formasyonu Hedefli Rezervuar Karakterizasyonu ve Saha Geliştirme Çalışması

## Raman Field Garzan Formation Targeted Reservoir Characterization and Field Development Study



**Merve Benzek, Ceyda Çetinkaya Kayrın, Safiğül Tuba Kamanlı, Melahat Aşlı Akdere**

ITPAO Genel Müdürlüğü, Üretim Daire Başkanlığı, Söğütözü Mah. Şht. Öğretmen Aybük Yalçın Cad. No:10, 06100, Çankaya/Ankara / Türkiye

Türkiye'nin en büyük ikinci petrol sahası olan Raman Sahası, Güneydoğu Anadolu Bölgesi Batman ili sınırları içinde yer almaktadır. 1945 yılında kazılan Raman-8 kuyusu ile Türkiye'de ilk petrol keşfi ilan edilmiştir. 1945 yılından günümüze kadar Raman Sahası'nda toplam 308 kuyu kazılmıştır ve sahanın kümütaltif petrol üretimi 116 milyon varile ulaşmıştır. Sahada birincil rezervuar kaya Mardin Grubu platform kireçtaşları, ikincil rezervuar kaya Garzan Formasyonu resifal biyoklastik kireçtaşlarıdır. Saha sınırları birincil rezervuar kaya için netlik kazanmışken ikincil rezervuar kaya için durum aksidir. Bu yüzden Garzan Formasyonu hedefli saha geliştirme çalışması sahanın üretimi artırmak için öncelik taşımaktadır. Bu çalışmada da bu amaç doğrultusunda kuyu logları korelasyonu temelli bölgesel sınıflandırmalar ile önceki çalışmalardan gelen sismik yorum sonuçları ve sedimentolojik tanımların entegrasyonu yapılmıştır. Çalışmanın sonuçlarına göre Raman Sahası'nda Garzan Formasyonu hedefli 21 tane yeni kuyu yeri belirlenmiş, kazılmış ve petrol üretimi ile sonuçlanmıştır. Yeni kuyu sondajlarına ek olarak sahadaki eski kuyular için de yeniden tamamlama operasyonları hazırlanmıştır.

Raman Field, which is the second largest field in Turkey, is located within the borders of Batman province in the Southeastern Anatolia Region. The first oil discovery in Turkey was declared with the Raman-8 well drilled in 1945. 308 wells have been drilled in the Raman Field since 1945 and the cumulative oil production is 116 million barrels. In the Raman Field, the primary reservoir rock is the platform limestones of the Mardin Group while the secondary reservoir rock is the reefal bioclastic limestones of the Garzan Formation. While the reservoir boundaries are definite for the Mardin Group, it is reversed for the Garzan Formation. Therefore, the Garzan Formation targeted field development work to increase the production of the field has priority. In this study, for this purpose, regional classifications based on well logs correlation with seismic interpretation results and sedimentological definitions from previous studies are integrated. According to results of the study, totally 21 wells locations were decided, drilled and completed with oil produced. In addition to new wells drilling, workover operations for the old wells in the field were planned.

### GİRİŞ

Raman Petrol Sahası, yapısal olarak Türkiye'nin güneydoğusunda yer alan, doğu-batı doğrultulu bir antiklinalden oluşmaktadır. Raman yapısı olarak isimlendirilen bu antiklinal güneydeki dik yamaç

boyunca uzanan büyük bir ters fay ile sınırlanmıştır. Yapısal olarak topoğrafik kontrol altındaki Raman antiklinali, kuzeyde yer alan Toros-Zagros sıradağlarının kuşağındadır.

Raman yapısı içinde rezervuar birimler Kretase yaşlı Mardin Grubu'nun platform kireçtaşları ve Garzan Formasyonu'nun resifal biyoklastik kireçtaşlarıdır. Sahada üretim bu iki rezervuar kayadan gerçekleşmektedir. Sahanın birincil rezervuar birimi Mardin Grubu iken ikincil rezervuar birimi Garzan Formasyonu'dur. Mardin Grubu saha boyunca rezervuar özelliği gösterirken Garzan Formasyonu sahanın sadece doğu bölgesinde rezervuar özelliği göstermektedir. Mardin Grubu'ndan üreten kuyuların dağılımı ile yapının yüksekliği arasında doğrusal bir ilişki vardır. Bu yüzden yapının düşük yerleri olan sahanın kuzeydoğusunda Mardin Grubu'ndan üretim yapılamamaktadır. Sahanın sınırı petrol-su kontağı ile belirlenebilmektedir. Fakat Garzan Formasyonu için yapısal etkinin yanı sıra stratigrafik yayılım da rezervuarın sınırı için önemli bir faktördür.

### AMAÇ

Olgun bir petrol sahası olan Raman Sahası'nda üretimi artırmak için saha geliştirme çalışmaları kapsamında Garzan Formasyonu odaklı çalışma yürütmek öncelikli bir ihtiyaçtır. Çünkü rezervuar sınırları Mardin Grubu için kesinleşmişken Garzan Formasyonu için belirsizlik ihtiva etmektedir. Bu durum, Garzan Formasyonu hedefli rezervuar karakterizasyon çalışması yürütmeye motivasyon oluşturmuştur.

### ÇALIŞMA ALANI, VERİ VE YÖNTEM

Garzan Formasyonu sahanın sadece doğu bölgesinde rezervuar özelliği gösterdiği için çalışma alanı Raman Sahası'nın doğu bölgesini içermektedir.

Kullanılan veriler kuyu kesinti örnekleri ve karot tanımları, kuyu logları yorumları ve korelasyonları, üretim testleri ve üretim bilgilerinden oluşmaktadır.

Çalışma kuyu logları korelasyonu temellidir. Korelasyon sonuçları önceki çalışmalardan gelen sismik yorum sonuçları ve sedimentolojik tanımlamalar ile karşılaştırılmıştır. Çalışmadaki mevcut veriler ile saha içi rezervuar fasiyesinin alansal dağılımı ve çatlak gelişimi yorumları yapılarak saha içi rezervuar sınıflandırması sunulmuştur.



## BULGULAR

Çalışma alanı rezervuar oluşum mekanizmasına göre kuzey ve güney bölgesi olarak iki ana bölgeye ayrılmıştır. Bu iki bölge arasındaki en temel fark sahanın kuzeyinde fasiyes çökeli, güneyinde de çatlak oluşumu kontrolünün olmasıdır (Şekil-1).

Birinci bölge, sahanın kuzey-kuzey doğu kesiminde kalan alandır. Rezervuar fasiyesi kıyı arkası ya da kıyı önü çökel ortamından oluşmuş biyoklastik kireçtaşlarıdır. Rezervuar özelliklerine göre bu kuzey alan da kendi içinde A, B ve C isimlendirmesi ile üç ana alt bölgeye ayrılmıştır. Şekil-2'de her bir bölgeden temsili kuyuların A bölgesinden C bölgesine doğru oluşturulmuş kuyu loglarının korelasyonu gösterilmiştir. Rezervuar seviye A ve C bölgesinde Garzan Formasyonu girişinden yaklaşık 5-10 m. sonra, B bölgesinde ise hemen sonra kesilmektedir. Rezervuar fasiyesin maksimum kalınlığı A bölgesinde 20 m., B bölgesinde 35 m. ve C bölgesinde 5 m.'dir (Şekil-1). Rezervuar paket A ve B bölgesinde dikey yönde devamlı, tek parça ve gözeneklilik değerleri yüksek bir paket iken C bölgesinde bu poroz paket devamsız ve kil bantlarının ardalanması ile bölünmektedir. Bu rezervuar paketlerin hesaplanan ortalama etken gözeneklilikleri A ve B bölgesi için %5 ile %20 arasında, C bölgesinde %5 ile %12 arasında değişmektedir.

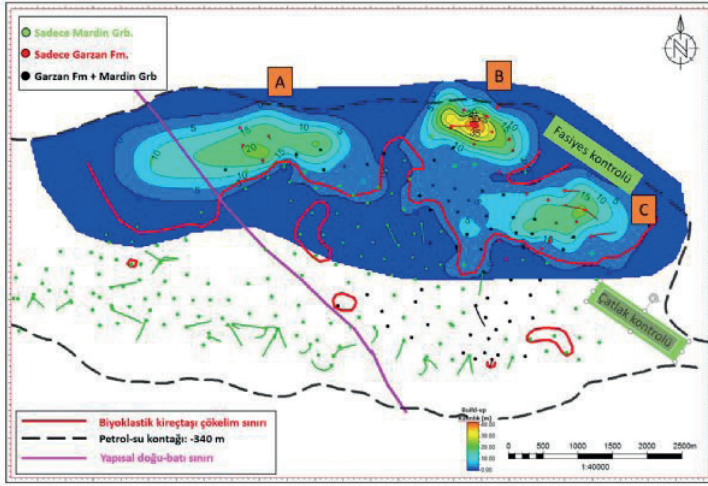
İkinci bölge olan sahanın güney kesiminde ortalama matriks porozite yaklaşık %5 olup sahanın etken gözeneklilik alt eşik değeri (cut-off) %8'den küçüktür. Üretim sadece çatlak porozitesinden gerçekleşmektedir. Çatlaklı zon sıklıkla Garzan Formasyonu'nun tabanına yakın aralıklardadır.

## SONUÇ

Sonuç olarak Raman Sahası'nda Garzan Formasyonu'nun rezervuar özellikleri kuyu logları korelasyonu temelli bir çalışma ile bölgesel sınıflandırma ile yeniden tanımlanmıştır. Çıkan sonuçlar daha önce yapılmış olan sismik yorum sonuçları ve sedimentolojik çalışmalar ile karşılaştırılmış ve uyumlu oldukları görülmüştür. Elde edilen yeni bilgiler ışığında Garzan Formasyonu hedefli yeni kuyu yerleri birinci bölgede belirlenmiştir. Toplam 22 tane kuyu kazılmış ve bunlardan 21 tanesi olumlu üretim ile sonuçlanmıştır. Bu kuyuların Temmuz 2023 itibari ile günlük üretimi ortalama 864 varil, kümülatif petrol üretimi ise 1.633,300 varildir (Şekil-3). Çalışma kapsamında ikinci bölgedeki eski kuyular için de yeniden tamamlama operasyonları hazırlanmıştır.

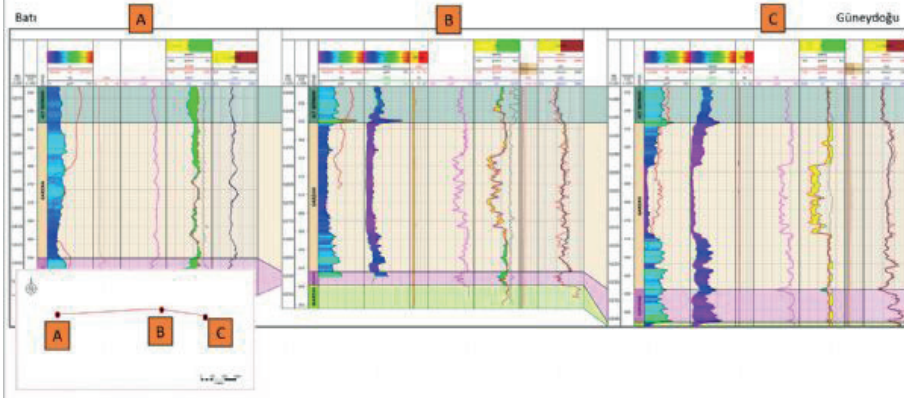
Anahtar Kelimeler: Raman Sahası, rezervuar karakterizasyonu

Şekil-1:



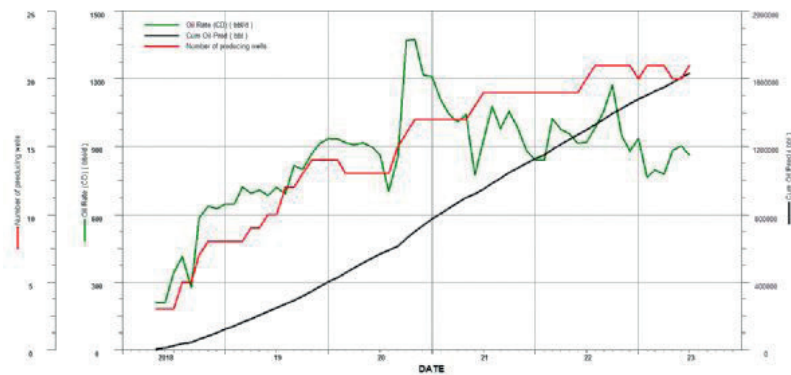
Raman Sahası'nda Garzan Formasyonu rezervuar fasiyes kalınlık haritası

Şekil-2:



Raman Sahası'nın kuzey-kuzey doğu bölgesinden temsili kuyuların kuyu logları korelasyonu

Şekil-3:



Raman Sahası'nda 2018-2023 yılları arasında kazılmış Garzan Formasyonu hedefli kuyulara ait üretim grafiği

# 3D Geological Modeling Study of the Garzan Formation in Cakilli Field

**Safigül Tuba Kamanlı, Elvan Aydın**  
Turkish Petroleum Company



## INTRODUCTION

Numerical reservoir modeling is the most sophisticated tool to be a vital input for the field development plans and to facilitate decision-making steps for the investment plans. This study presents the workflow for geological modeling of Cakilli Field to select best infill well locations and optimum water flooding scheme in order to maximize oil production.

Cakilli Field is located in the southeastern part of Turkiye (Figure-1) was discovered in 2015. The field has been developed with new appraisal and production wells for 8 years. Currently, the field has an average oil production of 7,000 bbl/d from 30 producer wells with an average of 56% water cut.

Late Cretaceous (Maastrichtian) aged reservoir rock is the Garzan Formation in Cakilli Field. Based on sedimentological studies, it has been concluded that upper part of the Garzan Formation is bioclastic limestone having primary porosity. Due to the diagenetic effects (in this case meteoric), primary porosities are enlarged, creating vuggy porosities and high permeabilities. Lower part of the formation is shaly-marly showing deepening in the sequence (Yetim, S.M.et al., 2017).

## METHODS

The Garzan Formation is divided into two zones based on production data, sedimentological studies and petrophysical interpretations. Upper zone is a clean zone and it has high vuggy porosity. Lower part of the zone is a non-reservoir unit due to the high clay content (Figure-2 and Figure-3).

Spectral Decomposition is a method employed to aid in the interpretation of seismic data. According to the Spectral Decompositional Model, the field is bounded by the facies polygon (Figure-4). Çakılı-A located at facies boundary was drilled. As a result of drilling appraisal well, the effective porosity in the well was calculated, about 2%. It is confirmed that there is a good agreement about the facies polygon between seismic interpretation and field observation from the drilled wells.

Before creating a 3D geological modeling of the field, the construction of grid cell and fault modeling is required. In order to assist flow among wells and decrease run time speed in the simulator, grid cells of the geological model were decided to be as 40x40 m in X and Y direction. Vertical variations in the petrophysical properties were captured in the model by dividing Zone1 and 2 into 70, 5 layers, respectively (Figure-5).

Petrophysical reservoir properties have been distributed in a three-dimensional domain using geostatistical methods in the geomodel. Effective porosities calculated

from open hole well log interpretation is upscaled in the Z-direction. In this study, upscaled effective porosity values were distributed using variogram models (Figure-6) by applying Sequential Gaussian Simulation (SGS).

Net to gross (NTG) model was created by using porosity and permeability relation obtained from routine core analysis. Oil water contact was determined according to production data and interpreting well logs. Water saturation model was constructed as a function of depth.

## FINDINGS AND CONCLUSIONS

After property modeling, initial oil in place volume (STOIIP) was calculated as 67 million stb. As a result of the decrease in the field pressure, maintaining pressures and increasing oil recovery requires operational interventions to the field. Enhanced oil recovery strategies can be adapted to the field based on the geomodel.

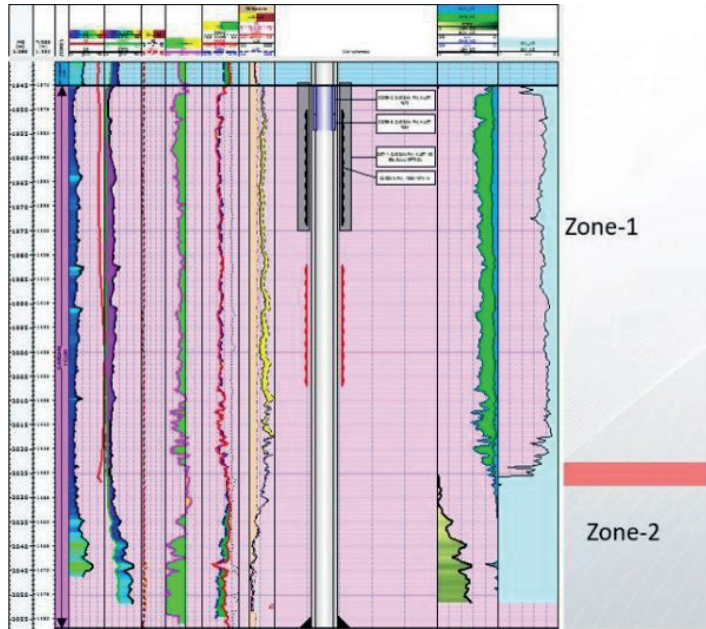
In the field, the location of in-fill and step-out wells was chosen efficiently with the aid of the geomodel. Therefore, this model will be updated based on new data and certain changes can be expected in oil in-place.

## REFERENCES

Yetim, S.M., Güray, A., Çevik, T., 2017, Cakilli-2 Kuyu Değerlendirme Sunumu, TPAO ARGEM.

Keywords: 3D Geological Model, Garzan Formation Facies

Figure 2



Reservoir Levels

Figure-1:



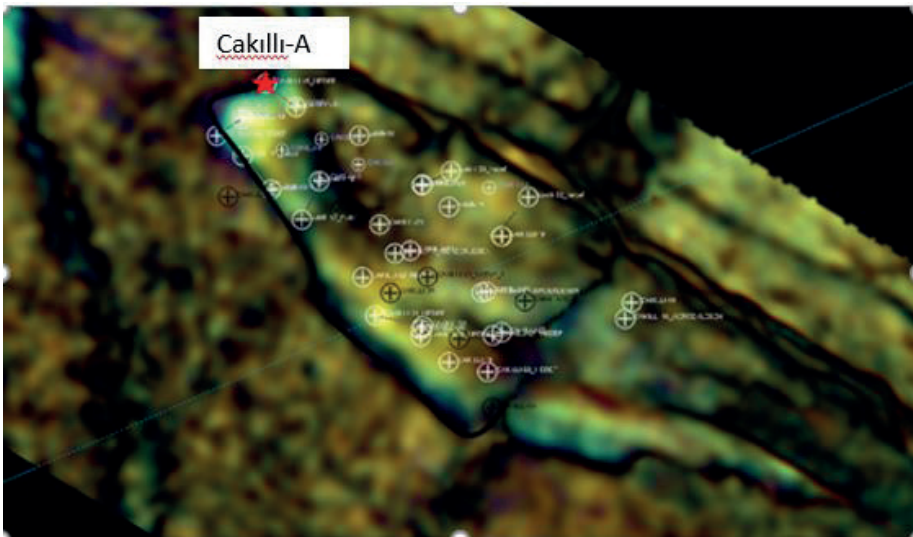
Location of the Çakılı Field

Figure-3:



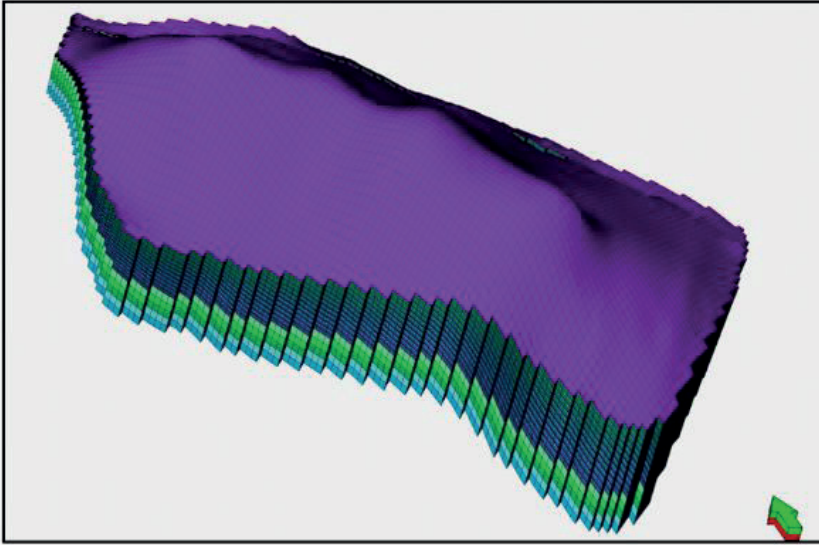
Vuggy Porosity Filled with Hydrocarbon on Cakilli-3 Core (TPAO AR-GEM taken by Ugurlu, I.O, 2017)

Figure-4



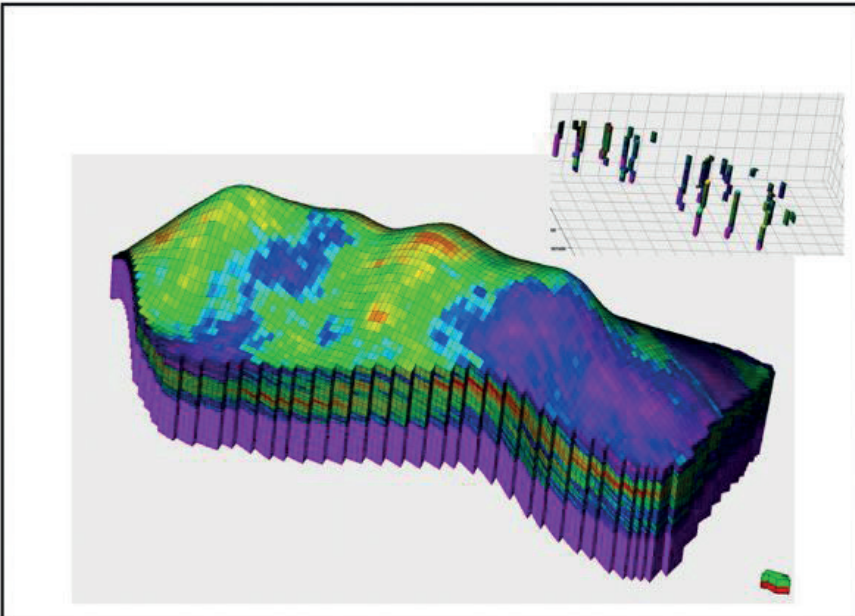
Spectral Decompositional Model of the Cakilli Field

Figure-5



3D Modeling of the Zones

Figure-6:



Upscaled Porosity Logs and Distributed Porosity Modeling

# Elastic Response of Porous Rock to Accumulated Slip on Strike Slip Fault Networks in Geo-Reservoirs

**Bora Yalcin, Olaf Zielke, Martin Paul Mai**  
King Abdullah University of Science and Technology



Subsurface reservoirs are generally highly fractured, whereby fractures constitute a natural fluid flow path and define the preferential flow direction. Slip accumulated during the faulting process alters also the petrophysical properties of the host rock. Although the mechanical alteration of the host rock, and related porosity and permeability changes, due to fault slip has been previously described, a predictive physics-based model has not been scaled with fault length in reservoirs to provide an initial porosity permeability alteration model yet. In this study, we develop a predictive model to quantify how accumulated fault slip changes porosity and permeability in a porous medium, by combining deformation modeling based on triangular dislocations and linearized poro-elasticity equations. We applied our model the Ghawar field fault map and rock-types. We conducted a Monte-Carlo simulation, varying fault roughness and accumulated slip, to quantify the corresponding variation in porosity and permeability using a 5 km long strike-slip fault and three different rock-types. Our Monte-Carlo simulation shows that long-term accumulated slip on rough strike-slip fault surfaces change porosity by  $\pm 1\%$ , leading to an absolute permeability change of up to 22.5%. We further used these results as a benchmark for the elastic response of porous rocks to accumulated slip scaled to certain fault length. Using these benchmark results for Ghawar field reservoir rocks, we determined the slip-related porous medium permeability changes for every fault on the Ghawar fault map, accounting for their length, location, and orientation. In doing so, we found that fault roughness, slip amount, and shear sense all affect the medium's permeability, creating substantial permeability anisotropies. Locally, these anisotropies are further enhanced by superposition of permeability changes of individual faults that constitute the fault system. We suggest the resulting permeability distribution model should be used as the initial permeability model for porous media in fractured reservoirs.

## INTRODUCTION

Subsurface reservoirs, known for their economic significance, host hydrocarbons and latent heat and have been extensively studied (Dake, 1983). The parameters governing fluid flow within these reservoirs, notably porosity and permeability, are often treated as homogenous and isotropic, yet the actual conditions are far more intricate (Cheng et al., 2016). The presence of fracture networks in these reservoirs, which significantly modify fluid flow pathways and rock properties, adds complexity to the picture (Ozkaya et al., 2019). While qualitative observations exist, predictive modeling of the interactions between fractures and rock alterations remains a challenge (Farrell et al., 2017; Flodin and

Gudmundsson, 2005; Micarelli et al., 2006).

Current models fall short in integrating both the mechanical and chemical effects of fault mechanics, often lacking universal fracture scaling rules and effective parameterization (Aydin and Borja, 2018). To address this gap, our study focuses on quantifying changes in porosity and permeability due to accumulated fault slip. We achieve this by incorporating dislocation theory and poro-elastic formulations (Zimmerman et al., 2017) to compute the impact of fault slip on porosity and permeability for various rock types and fault properties.

Our methodology involves deriving the change in porosity resulting from fault slip and then translating this change into permeability alterations. The model is applied to a strike-slip fault case study, examining different types of reservoir rock. Through numerical experiments, we simulate the strain-induced changes in permeability within faulted porous media. By scaling these findings to a real reservoir sector model, we demonstrate the alterations in permeability distribution based on variations in fault and rock properties. This study bridges the gap between qualitative observations and predictive modeling, offering valuable insights for improved reservoir management.

## METHOD

Our formulation relates volumetric strain due to slip on a fault surface, to porosity change in the surrounding porous medium. We parameterize the displacement that accumulated over time along the fault as a single, non-uniform distribution of slip. This slip distribution is then used to compute the corresponding deformation of the porous, elastic medium. By modifying the linearized poro-elasticity equations of (Zimmerman, 2017), we develop an expression that links slip-induced strain to porosity changes. The derivation assumes that the difference in deformation (elastic behaviour) between porous and non-porous materials is represented by pore space deformation (assuming an otherwise identical host rock composition). However, the derivation carries the limitation of not explicitly calculating the grain strain component of the bulk strain for the faulted porous material. Therefore, we constrain the grain strain with the Biot constant (Biot, 1957; Detournay, 1993). Finally, we converted the change in porosity to a change in permeability, using established power-law relations.

## RESULTS

We parameterized the fault roughness and the amount of accumulated slip affecting mechanical deformation, then correlated them with fault length. Since deformation is linearly proportional to dislocation (accumulated slip in this case), it also scales with fault length. This

relationship provides a general approach for reservoirs characterized by faults of varying length. Our method comes at lower computational cost than applying the physical model and uncertainty analysis for all faults in the reservoir. Fault lines on the fault map are traces of faults at the depth of the reservoir. Therefore, it is appropriate to position the center of the penny shaped faults embedded on the thin reservoir horizon and then enforce accumulated slip on the fault surface. We have not considered horizontal or vertical transitions in the reservoir from one rock type to another. Moreover, our model has not considered either the burial history and related changes in the reservoir rock properties or the other alterations such as chemical alterations. This method assumes the strike-slip fault growth --hence the slip accumulation-- happens after lithification is completed without chemical alterations.

To couple the chemical alterations with mechanical alterations one needs burial and diagenesis history. The diagenesis or fluid migration history through fractures and porous media is unique for each reservoir and needs targeted studies to for calibration, which is beyond the scope of this work. For example there are existing solvers with multi-physics coupling capability for fault related chemical precipitation/dissolution and mechanics of porous material (Poulet,2017), but these require as input the paleo fluid chemistry, paleo stress and paleo temperature.

The numerical experiments carried out in this paper offer a clear understanding of how slip-related poro-elastic deformation affects the petrophysical properties of reservoir rocks. The slip-induced poro-elastic deformation and resultant porosity/permeability change can be quantified with known initial porosity, permeability, bulk modulus, shear modulus and length of the faults in the reservoir. It is known that faults have rough surfaces and including this information in the model shows that fault roughness redistributes and amplifies the strain, and hence the change in porosity/permeability. Experiments in this study suggest that slip-induced poro-elastic deformation and the resulting porosity/permeability change are most prominent close to the fault surface. This deformation is spatially distributed all along the fault on deformed spaces. The numerical experiments for different rock types indicate that based on different initial porosity and permeability, enforcing the same fault slip may result in significantly different permeability changes around it. These numerical experiments for different stiffness values indicate that a lower bulk modulus results in a higher porosity change when enforcing the same slip-boundary condition. Similarly, a lower shear modulus means less strain -and hence less stress for elastic behavior- for any given slip discontinuity; this means for the same slip on fault, the rock deforms less and hence the absolute change in porosity would be less.

For complex fault networks we see that combination of shear sense and fracture intensity creates permeability anisotropy in the porous medium. The combination of deformation caused by intermediate length faults in the reservoir accumulates to large permeability anisotropy.

To capture such deformation and related permeability variation in the reservoir propose this new method, which in fact is straightforward to apply since only fault map and rock properties are needed. We conjecture that our proposed approach is promising to build better static reservoir models.

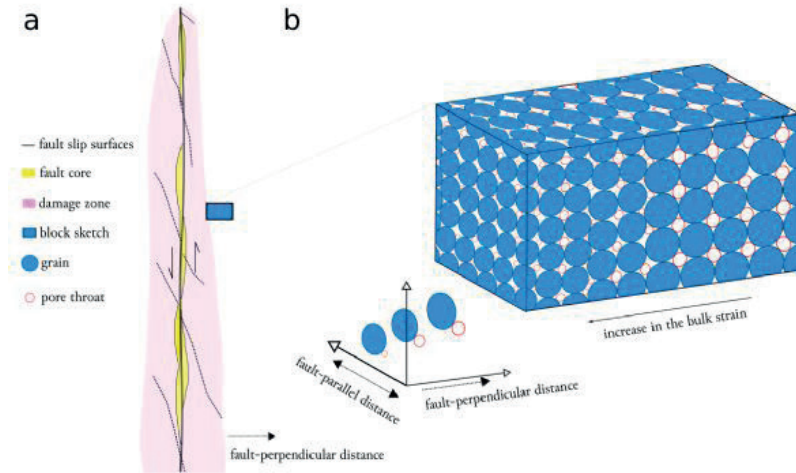
## CONCLUSION

This paper presented a generalized solution for slip-induced poro-elastic deformation and its effects on the fault-surrounding --porous media-- permeability. We integrated this new formulation with triangular dislocation solution and showed the resultant porosity and permeability profiles for several known rock types with possible uncertainty ranges. Our numerical experiments document that, for any fault length, slip-induced poroelastic deformation can be modelled with known petrophysical and rock mechanical parameters of target reservoir. To demonstrate that, we scaled up the single fault porous medium interaction to a complex fault network for a known reservoir rock-types and its faults. Results show that complex fault arrangements, with their shear sense and intensity, generate sensible permeability anisotropy in the reservoir. In fact, this physical model application is a necessity to increase the reliability of the porosity and permeability property distribution models for all fractured reservoirs. We developed a complete workflow that can be implemented on any reservoir with its rock properties and fault map.

Keywords: Triangular-dislocation, Poro-elasticity

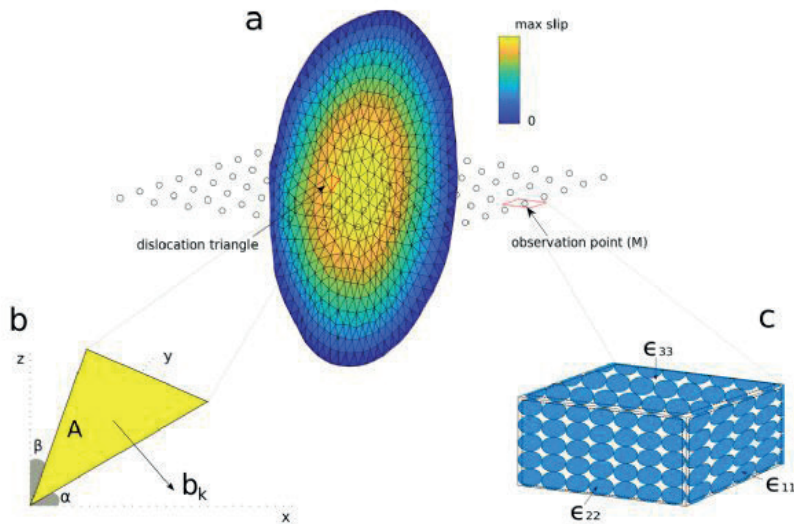


Figure 1. Conceptual Sketch



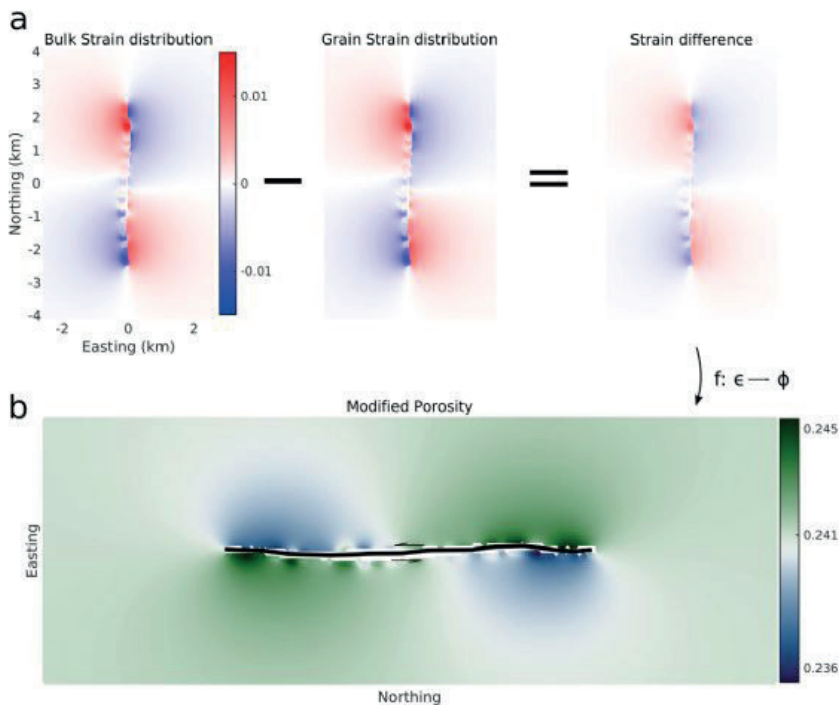
(a) Map view of the conceptual architecture of a strike slip fault, comprising a main fault-slip plane, a fault core, small-scale fractures, and an intensely fractured damage zone. (b) Close-up view of a 3D block diagram depicting beyond the damage zone. Conceptually, the off-fault media is created due to repeated slip-induced inelastic and elastic deformation. With decreasing distance to the slip plane, grain-size and pore-dimensions are changing due to accumulated strain.

Figure 2. Model Setup



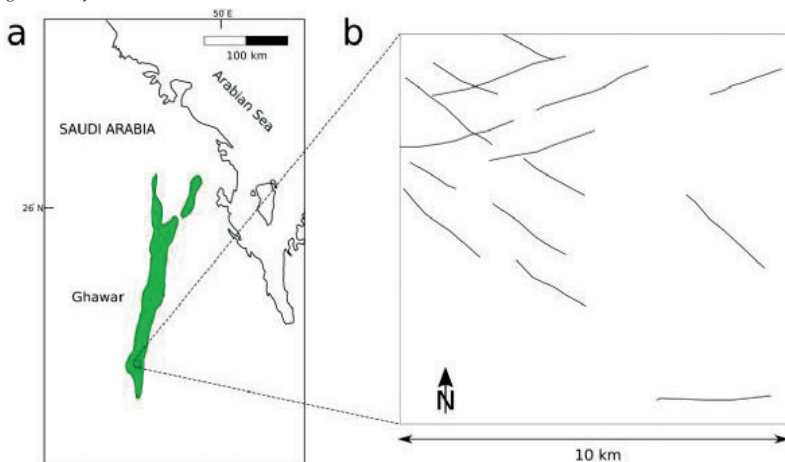
(a) Model setup showing the circular fault, discretized by a triangular mesh and embedded in an elastic full-space, on which the tapered slip distribution is resolved. Observation points are defined on a fault-perpendicular plane at the depth level of the center of the circular fault. In the calculations, the faultsurface mesh and observation-point spacing are much denser than displayed here. (b) Each triangular dislocation mesh describes a discontinuous slip amount which lies on plane A. Plane A bounded by three vertices  $A_0, A_1, A_2$  on which vertices the slip has a vertical component with  $\beta$  angle and horizontal component  $\alpha$ . The amount of slip is described with Burger's vector  $b_k$  (c) Conceptual 3D view of the bulk volume composed of grains (blue spheres) and pores (white space between grains). The applied 2D dislocation function on the geometrically rough fault determines the components of the slip-induced strain for every observation point. We use the volumetric strain to calculate the change in porous volume.

Figure 3. Model Formulation



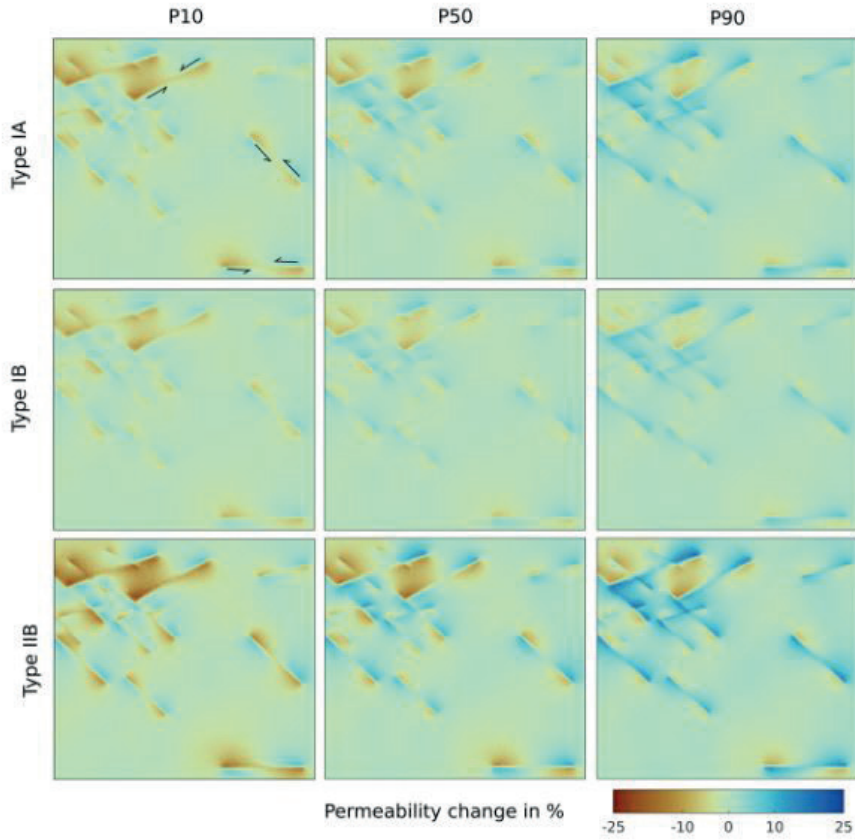
(a) Graphical demonstration of the model formulation and workflow. We subtract the volumetric grain strain from volumetric bulk rock strain to obtain the pore strain at observation points. We then use initial porosity to calculate modified porosity values on the reservoir rock. (b) The highly affected region, that is the highest change in porosity; from fault slip related deformation is closest to fault. A large number of observation points are only minimally affected by this deformation which means the sensible alteration in porous media is local. Note that we used Type-IA rock type petrophysical and rock mechanical properties with a 5 km long fault embedded on the medium for this realization is as follows; the grain strain to bulk strain ratio is  $\epsilon_g/\epsilon_b = 0.473$  and the fault roughness parameters are  $C = 0.005$ ,  $H_{dip} = 0.8$ ,  $H_{strike} = 0.8$ .

Figure 4. Study Case



(a) Approximate geographic location of the Ghawar field. (b) Map view of a 10 by 10 km sector showing mapped faults in the Haradh section of the Ghawar reservoir.

Figure 5. Results



For three different rock types (Type-IA, Type-IB and Type-IIB) we show P10, P50 and P90 cases of permeability change due to accumulated slip on reservoir faults. The change in permeability in the porous media is normalized and displayed as percentage change. The highly fractured northwest corner and shows stronger permeability change based on left lateral shear sense (marked on upper left corner map) on the strike-slip faults. This realization shows combination of the faults orientation and spacing can create substantial anisotropy in the permeability pattern on the reservoir.

# Navigating Complex Carbonate Reservoirs: Use Cases from a Novel Integrated Well-Placement Workflow

**Kemal Çağrı Hekimoğlu<sup>1</sup>, Melike Özkaya Türkmen<sup>2</sup>, Onur Yürüker<sup>2</sup>,  
Batur Alp Aydın<sup>2</sup>, Osman Meretz<sup>2</sup>, Ceyda Çetinkaya Kayrın<sup>2</sup>**

<sup>1</sup>Geolog

<sup>2</sup>Türkiye Petrolleri Anonim Ortaklığı



## INTRODUCTION

A novel approach and use cases for geosteering are presented in this paper using data from Southeast Türkiye, where the structural complexities and diagenetic processes in carbonate reservoirs make it challenging to efficiently exploit hydrocarbon deposits. Petrophysical log data is integrated with surface mineralogy for rock classification, establishing expected responses from surface data, to generate a vendor-independent geosteering workflow standardizing real-time data QC procedures and steering decisions. The paper highlights the challenges faced in the region, including homogeneous gamma/resistivity responses from clean carbonate reservoir rocks, campaign being the first attempt of drilling laterals in this field, circulation loss in the lateral section, unexpected faults along the trajectory, unstable stress state in the vicinity of the faults, and eventually complex well trajectory.

Although all AML (Advanced Mud Logging) work was conducted by the same service company, three different vendors provided the directional drilling, LWD & MWD services throughout the campaign, each utilizing their own tools and software. This paper introduces and discusses the sequential decision-driven approach to the geosteering process with a focus on the integration of AML techniques, subsequently presenting five case studies to exemplify the framework. The case studies examined in this paper were conducted on wells drilled within the K, GK, and B fields. These fields were formed as a result of two significant tectonic events that occurred during the Cretaceous and Miocene eras and are bordered by strike-slip faults while being divided into blocks by normal faults. The study primarily focuses on three carbonate reservoirs that were deposited during the Late Cretaceous period. According to their depositional sequences, these reservoirs are the KBB-C Member, the KB Fm, and the SD Formation (Yilmaz and Turesin, 2022). Since the reservoir properties of all these formations are moderate to low, economic oil production is mainly achieved through fractures.

## METHODS

Geosteering encompasses a multifaceted and interdisciplinary approach that incorporates the collaboration of various disciplines including drilling, geology, and directional. Some specific challenges related to geosteering which are addressed with the proposed workflow include data integration, communication and alignment, decision-making, and risk management. To overcome these challenges, the operational workflow introduces separate work paths where each domain works on its own datasets and the integration process is carried out through team

collaboration with the operator's oversight. This results in the domain experts independently generating their own models, and exchanging perspectives from their specialized domains under the guidance of the operator G&G team.

## PRE-DRILL PLANNING PHASE

Prior to drilling, a dedicated pre-well model is constructed for each well using a combination of log data, rock geochemistry measurements, and seismic interpretations. The workflow steps are followed as described in (Fig.1) during the pre-well modeling process. This model is used to estimate the rock properties and establish analogs to be followed during drilling. Upon commencement of the geosteering project, the operator establishes the target formation zones in relation to the respective well objectives. The operator designates and compiles all pertinent offset well datasets from the selected offset wells and disseminates them to the directional drilling and AML teams for utilization as INPUT datasets in the construction of the geosteering models

Each of the three directional drilling service providers employed proprietary software and techniques to process the INPUT data. In the example case histories presented in this study, a minimum of some variation of a triple-combo log dataset was available for pre-drill work. All service providers employed a combination of model-based, strat-based, and multi-well reactive geosteering approaches. Due to the focus of this paper on optimizing the utilization of AML techniques, vendor-specific internal processes will not be discussed in detail. The general operational workflow will be defined instead.

The drilling and G&G teams, along with the directional drilling team, collaborate to develop the well design, well trajectory plan, and drilling program. As part of this planning process, the AML team is consulted for certain details, such as the drilling mud type and specifications, to ensure the effective operation of the advanced surface equipment. The AML team collates the provided datasets into relevant sub-datasets to generate a visual correlation of the offset wells. Log responses within the target formation zones, as provided by the operator, are flagged, which will help match relevant surface data indications later on. After establishing an AML solutions package, a Quality Risk Analysis, Mitigation, and Contingency Plan (QRAMCP) is generated to detail potential AML data risks and list control measures. The risk categorization used in the QRAMCP to describe the risk level is shown in (Fig.2). Potential risks identified with regard to the AML service scope used in the lateral well campaign are detailed in (Fig.3). These measures

are discussed among all domains involved to determine if critical aspects of the well program can be optimized to match requirements.

The primary objective of the lateral wells campaign under consideration is to position the laterals within the zones of the highest porosity. Historically, mud gas measurements have been employed as a complementary dataset to achieve this goal. However, standard mud gas measurement techniques may not be reliable, especially when diesel is added to the drilling fluid system or oil-based mud is used. In such cases, the hydrocarbons present in the mud system can obscure the formation gas measurements and the increased solubility of hydrocarbon gases in the mud may complicate the extraction of mud gas. To address these limitations, AMG technology was used as a quality control and correction method for mud gas concentrations, increasing the confidence in mud gas data and permitting its real-time use to support steering decisions.

The cuttings available in the operator's repository from the relevant depths of the offset wells undergo a visual evaluation for both physical quality and quantity. After acquiring the ACA measurements, a data quality check is applied which involves dynamic depth-matching the ACA data by correlating the calculated gamma log from elemental measurements to the downhole gamma log.

An available alternative dataset such as Elemental Concentration Logs may be used to increase depth confidence where trend changes are observed if a target zone where limited or not legacy cuttings data is found. An additional benefit to this type of utilization is the ability to calibrate the ECL data using direct rock measurements.

The AML team leverages their knowledge of the local geology, equipment technical specifications, and experience with local operational practices to identify marker elemental indicators from the ACA measurements. This step is crucial in the workflow to ensure that the selected markers are elements/ratios which are geologically relevant, expected to be measured at concentrations above the equipment limit-of-detection, have trend variations within the measurement sensitivity of the equipment, and are unaffected by operational factors such as mud additives or sample cleaning procedures. Using these proxies, the team generates a multi-well stratigraphic correlation log to construct the AML geosteering model, which describes expected elemental marker responses and serves as a roadmap during drilling.

## DRILLING PHASE

The first data that becomes available at the surface during drilling operations is either ACA or LWD (Logging While Drilling), depending on the drilling speed (ROP) and the tool offset. In simple terms, when the time required to drill the tool offset distance is more than the time it takes for the newly drilled rock to reach the surface, be processed and analyzed, ACA data will be available earlier than LWD data, and vice versa. Within the proposed workflow, as shown in (Fig.4),

ACA is utilized for different purposes based on this aspect. When ACA data is available earlier, it is used immediately to determine the current stratigraphic position, and LWD data is used for validation purposes. Conversely, when LWD data is available earlier, depending on the confidence level in the LWD data interpretation, the ACA may either be used only for validation after the geosteering decision has been made or in a low-confidence scenario, ACA data may be utilized to make a more informed decision.

## SEQUENTIAL DECISION-MAKING

Geosteering is a process that involves making decisions in a sequential manner. To ensure that the subsequent decisions are informed and accurate, it is essential to validate the accuracy of prior decisions. This means that geosteering is a continuous process of decision-making, where each step builds upon the previous one to achieve optimal results. In this regard, AML data plays a critical role in validating prior decisions and ultimately supporting subsequent decisions, even if it is obtained after LWD data. If multiple incorrect sequential decisions are made without validation, the resulting eventual error can increase exponentially. This is because each incorrect decision can compound the error of the previous decisions, leading to an accumulation of errors over time. Without validation, there is no way to ensure that the initial decision is correct. In this way, each incorrect decision increases the likelihood of subsequent incorrect decisions, leading to an exponential increase in the eventual error. The sequential decision-making process involved in the geosteering work utilized during the campaign is illustrated in (Fig.5).

A set of anticipated faults can be delineated prior to drilling through the use of local geologic knowledge and available seismic interpretations. However, in highly fractured carbonate settings, such as the study area, unexpected sub-seismic faults may be encountered during drilling, which can result in deviation of the wellbore from the target zone. Assessment of the new stratigraphic position of the well and the amount of the ensuing displacement using only homogeneous features in LWD gamma and resistivity log responses poses a significant challenge.

Azimuthal resistivity/gamma-ray image logs were utilized to calculate the formation-dip angles. The calculated dip is then extrapolated under the assumption that there will be no significant changes in the formation-dip angle ahead of the bit.

To ensure that each team member is assigned a clear role in the decision-making process, a RACI Matrix is utilized. This matrix is updated before each well to ensure that the information is up-to-date and relevant to the specific well.

### ADVANCED CUTTINGS ANALYSIS (XRF AND XRD)

Drill cuttings are cleaned and processed according to internal procedures before being analyzed with an Energy Dispersive X-Ray spectrometer (ED-XRF) for inorganic elemental analysis and with an X-ray diffractometer (XRD) for mineral composition evaluation on rock powder. The analytical methods result in data for 32 elements: 10 major elements reported as oxides in percentage by weight and 22 trace elements reported as parts per million, representatives of sedimentary rocks.

Furthermore, to ensure optimum depth allocation of the samples and to confirm the absence of sample mixing along the borehole, a comparison between the MWD Gamma Ray and the Chemical or Synthetic Gamma Ray (CGR) is used.

### ADVANCED MUD GAS (AMG)

AMG system utilized a process that involves tying a mud-gas sample line into the inlet and outlet of the mud system and using a constant-volume degasser to extract the hydrocarbons in a stable, constant-flow environment. The mud gas is then measured at the end of the return flow line coming from the wellhead and at the intake of the mud pumps in the active pits. This difference between inlet and outlet mud gas volumes is used to measure the net gas from the formation, which is called the Gas-In vs Gas-Out recycling monitoring, a crucial component of the AMG system.

## FINDINGS

### Case Study-1: K-48 Geochemical Analysis

K-48 well was the first well drilled in the lateral campaign utilizing the AML workflow. The well's primary target was the shallower, higher porosity zone within the KBB-C formation. KB Formation is considered a secondary target.

XRF / XRD measurement results of cuttings analysis from the offset K-47 well were incorporated into available literature and petrophysical logs to characterize (1) the geochemical differences between the KB and KBB-C formations, (2) chemical signatures from intervals identified as analogs for porous zones according to downhole logs

Ternary plots were used to visualize the geochemical similarity of the porous zones when compared to K-47 analogs, shown in (Fig.6).

### Case Study-2: Fracture / Fault Identification Using Geochemical Proxies

The identification of fractures and faults is crucial for successful hydrocarbon exploration and production, particularly in highly fractured carbonate reservoirs. In these types of reservoirs, hydrocarbon production is

supported by fracture networks, making the detection of these features a critical.

One technique used to detect fractures and faults involves analyzing minor and trace elements associated with hydrothermal regimes. By identifying geochemical anomalies in elements such as Sr, Cl, Ti, As, Ni, S, Pb, and Zn, indirect indications of fracture and fault systems can be obtained. However, it is important to note that the mineral species associated with fractures and faults can vary significantly based on specific fault conditions, surrounding fluid composition, and syn- and post-faulting pressure/temperature conditions. Therefore, geochemical proxies are not a one-size-fits-all solution.

As part of the fracture/fault identification process through the interpretation of geochemical proxies, flags are generated for each identified feature.

By using a multi-faceted approach that incorporates geochemical proxies, high-resolution borehole image logs, and other data sources, a more comprehensive understanding of the subsurface can be obtained. This, in turn, leads to more accurate assessments of the potential for hydrocarbon production.

The fractures/faults identified through ACA provide information where image log data may not be available, such as in "bad hole" conditions or limitations caused by hole conditions or tool offset. These insights are then cross-referenced with other data sources, such as mud losses and mud gas concentrations, to evaluate potential pay zones.

During the initial phase of the drilling campaign, high-resolution borehole image log data for K-48 well was made available. To assess the reliability of geochemical proxies for identifying fractures and faults, the interpreted conductive and resistive fractures from the borehole image logs were compared with the fracture/faults identified from ACA. After analyzing the data, it was found that Pb and As elemental concentrations tracked the resistive and conductive fracture counts well, demonstrating a strong correlation between the geochemical dataset and the data from the image logs (Fig.7).

### Case Study-3: Cavings Depth Allocation using Hierarchical Clustering and Principal Component Analysis

Another advantage of having onsite ACA available is the possibility to analyze cavings alongside cuttings samples. A combination of hierarchical clustering and principal component analysis (PCA) was used to match the geochemical signature of the cavings to the cuttings samples to determine their depth of origin.

During the drilling of the K-48 well, cavings samples were collected at two different times. The cavings were analyzed with the same procedure as the cuttings samples collected from the same well and analyzed using XRF and XRD. Hierarchical clustering analysis was used to match the geochemical signature of the cavings samples to the cuttings samples in order to determine the approximate depth from which the cavings samples

originated within the wellbore. To optimize our analysis, PCA technique was also employed to reduce the dimensionality of the dataset and identify patterns in the data. A three-dimensional scatter plot was constructed to better visualize the relationships between the cavings and cuttings samples, plotting PCA component-1 on the X-axis, PCA component-2 on the Y-axis, and using PCA component-3 as the color identifier (Fig.8). By combining hierarchical clustering and PCA analysis, it was possible to more accurately allocate the depth of the cavings samples and gain a better understanding of the properties of the subsurface encountered during drilling. This information was used to support decisions on drilling and production activities.

#### **Case Study-4: Improving ECL Data Accuracy Using ACA Data**

In this study, during one particular well, a challenge was encountered where an old well with limited cuttings samples available within the target zones was the only available offset well for modeling. To overcome this challenge, Elemental Concentration Log (ECL) data from the well was used, which had a high sampling frequency but lower precision and accuracy due to measurement ambiguities.

To eliminate these limitations, a simple methodology was utilized to calibrate the ECL data using more accurate data, specifically the ACA data in the form of XRF measurements. This calibration process enabled the improvement of the accuracy of the ECL Data concentrations and ultimately resulted in a more accurate dataset with a high sampling frequency to be used for geosteering modeling. The adjusted concentrations of ECL data are plotted together with the ACA data on a composite log using the same data scales (Fig.9). The standard deviation and coefficient of variation of the adjusted ECL data are also calculated and compared with the ACA data to evaluate the calibration accuracy. The calibrated dataset is then used to generate the stratigraphical model (Fig.10). Overall, the methodology presented in this study, although a simple process, proved to be an effective approach to integrating downhole and surface data by calibrating datasets with different sampling rates and accuracy levels.

#### **Case Study-5: K-44 Lateral Well Geosteering Process and Results**

K-44 well was drilled as a producer targeting a relatively higher porosity zone within the main target of KBB-C Formation. The SD Formation was also planned to be crossed during the curve section of the well as a secondary target. Before drilling, 309 cuttings samples were analyzed with XRF from two offset wells, K-20 and K-28. The XRF data from the offset wells were depth-synchronized with downhole logs and quality-controlled. A geosteering model was generated based on this data. The AMG data quality plot in (Fig.11) shows that the system effectively cleaned the data from crude

oil contamination within the mud system, providing high confidence mud gas show zonation. Of the available offset wells, K-28 well provided the closest similarity and was predominantly used to support stratigraphic position decisions. The results of the geosteering work are discussed under the titles of the three prominent formations crossed during the drilling of the curve, landing, and lateral sections of the well.

K-44 lateral well's final geosteering model shown in (Fig.12), visualized all points discussed in the case study. The process utilized during the lateral well was successful in providing detailed stratigraphic information for the SD, KB, and KBB-C formations. The integration of XRF data from offset wells and AMG data effectively supported stratigraphic position decisions, providing a high degree of confidence in the resulting geosteering model. The identification of faults and lateral heterogeneity within the formations was made possible through the analysis of geochemical parameters. The results of this case study demonstrate the benefits of utilizing advanced techniques such as geosteering and XRF analysis for successful drilling operations in complex reservoirs.

#### **CONCLUSIONS**

This paper presents a novel workflow for optimizing well placement within highly fractured carbonate reservoirs, using a combination of rock and reservoir fluid geochemistry measurements, and petrophysical log data. Several phases are discussed throughout the workflow, including pre-drill planning, and drilling, with a focus on data integration, communication and alignment, decision-making, and risk management.

Five case studies are presented in this paper to demonstrate the application of the workflow in a multi-well field in Adiyaman, Turkiye. The case studies cover various aspects of the workflow, including geochemical analysis, fracture/fault identification, cavings depth allocation, data accuracy improvement, and geosteering results.

Using the workflow, we have been able to establish communication standards between multiple disciplines and service providers, define operational processes to minimize interpretation uncertainty, compile a comprehensive risk analysis and QC factors for AML data accuracy, address geosteering-related uncertainties, and suggest mitigation strategies. Ultimately, the presented workflow provides an effective and efficient approach to achieve optimal results in formation evaluation and well placement, leading to better reservoir management and improved economic outcomes for operators.

**Keywords:** geosteering, onsite-geochemistry

Fig.1 Pre-drilling / Planning Phase of the proposed workflow

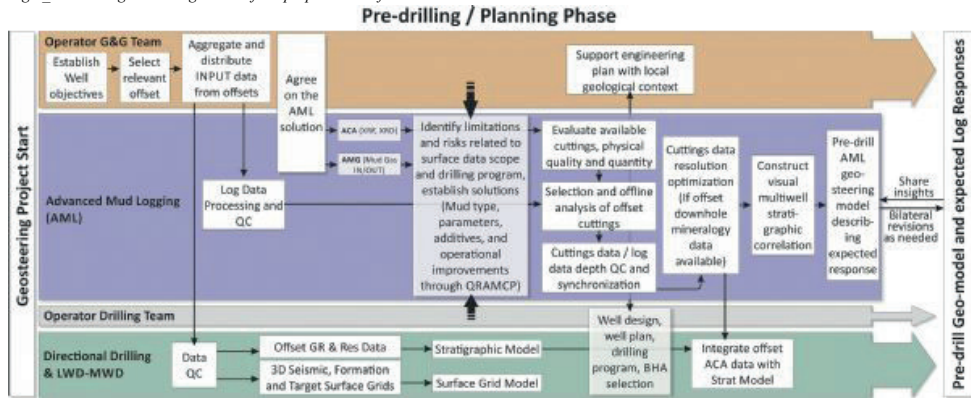


Fig.2 AML Risk Categorization

$R = L \times M$

		Magnitude				
		Insignificant	Minor	Moderate	Major	Catastrophic
Likelihood	Almost Certain	5	10	15	20	25
	Likely	4	8	12	16	20
	Possible	3	6	9	12	15
	Unlikely	2	4	6	8	10
	Rare	1	2	3	4	5

Fig.3 AML Quality Risk Analysis, Mitigation, and Contingency Plan

CATEGORY	HAZARD	INITIAL RISK			CONTROL MEASURES		RESIDUAL RISK			CONTINGENCY PLAN
		Likelihood	Magnitude	Risk Level	Current and Planned Prevention Measures to reduce Likelihood	Current and Planned Mitigation Measures to reduce Magnitude	Likelihood	Magnitude	Risk Level	
AMG	Data acquisition	2	4	8	Routine maintenance and inspection performed to all components of AMG-GS	Availability of spares for all mission-critical equipment. Failure reporting procedures and 24/7 remote technical assistance.	1	2	2	Inform the client of the situation.
AMG	Drilling fluid	3	4	12	Lab tests were conducted to assess maximum operable viscosity; information was passed on to TRAQ's Drilling and R&D dept.	High-flow CVD reducers were sent to the rig site to increase the extraction efficiency in higher viscosity muds.	2	2	4	Revert to conventional Gas-OIL only setup without AMG.
AMG & ACA	Total mud losses	1	5	5	-	-	1	5	5	Inform client and standby for action.
ACA	Geological uncertainties	3	4	12	Multiple offset wells are analyzed and integrated into the model.	Utilize AMG-GS data to establish if the target zone is penetrated.	3	2	6	Involve the client to elaborate on the local heterogeneity.
AMG & ACA	Continuous mud losses	4	4	16	-	Continuous MWD-GR vs. XRF GGR correlation for depth QC. High-accuracy mudflow sensor (EMFC) planned to be utilized on upcoming wells to evaluate the precise level of losses as quickly as possible.	4	2	8	Involve the client to reassess the interpretation referring to prior experiences within the field.
ACA	Hole stability	3	5	15	-	"Selective Analysis" procedure is to be followed whenever sample mixing is suspected with the support of the WSGs.	3	3	9	Inform the client and generate a synthetic cleaned dataset using measurements from most likely break-out intervals.



Fig.4 Drilling and Post-Drilling Phase of the proposed workflow

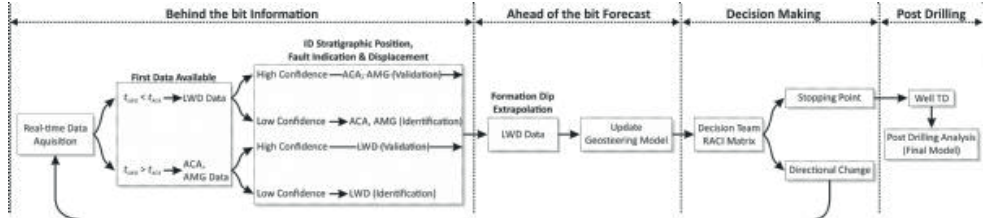


Fig.5 Sequential Decision Making Workflow

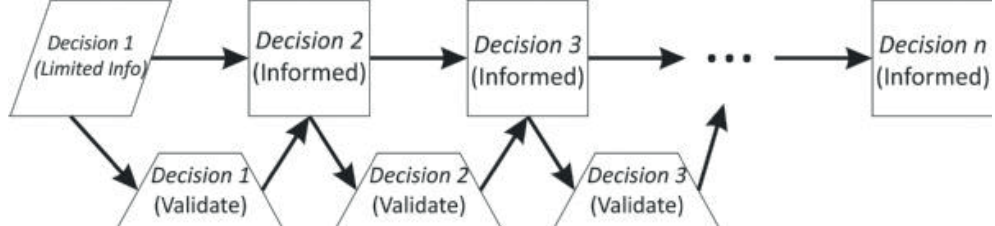


Fig.6 Geochemical ternary plot showing the comparison between similar zones from the KB and KBBC Formations of K-47 and K-48 wells

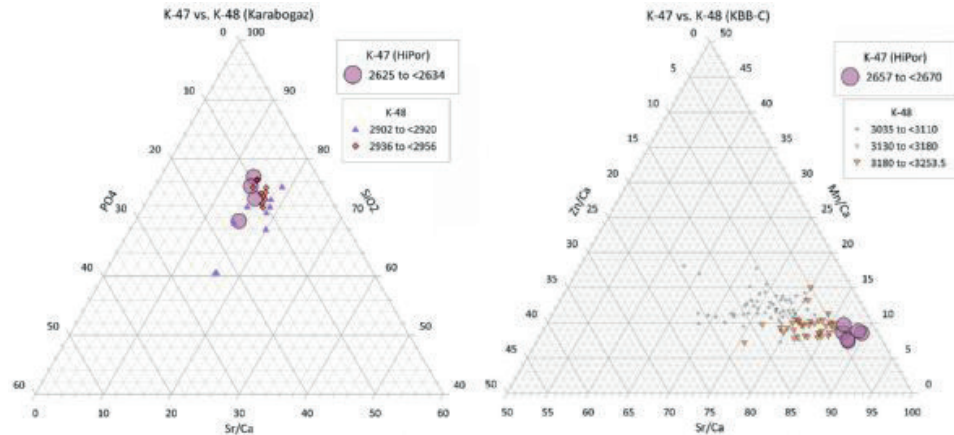


Fig.7 Log comparison of fracture counts from high-resolution image log and ACA data

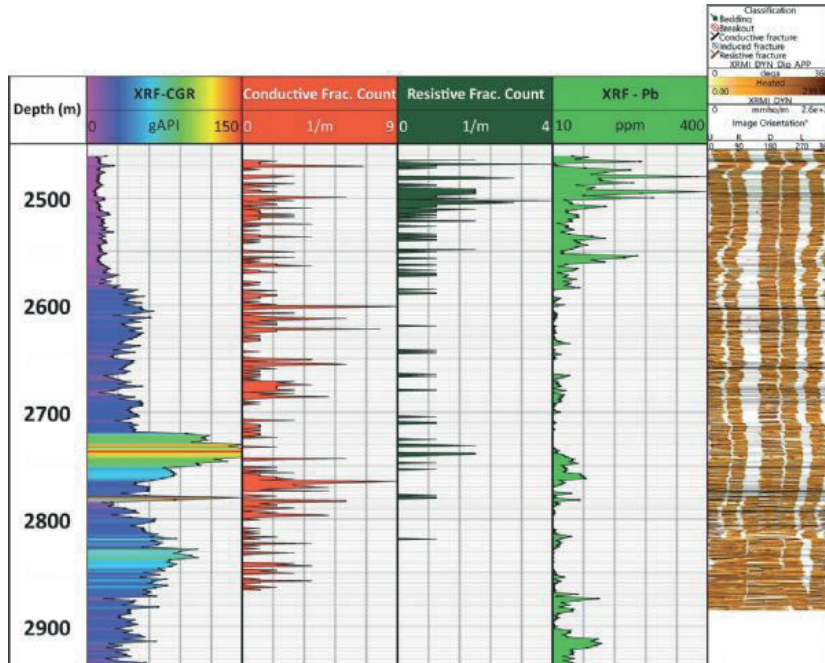


Fig.8 Scatter plots visualizing the relationship between cavings and cuttings using three PCA components

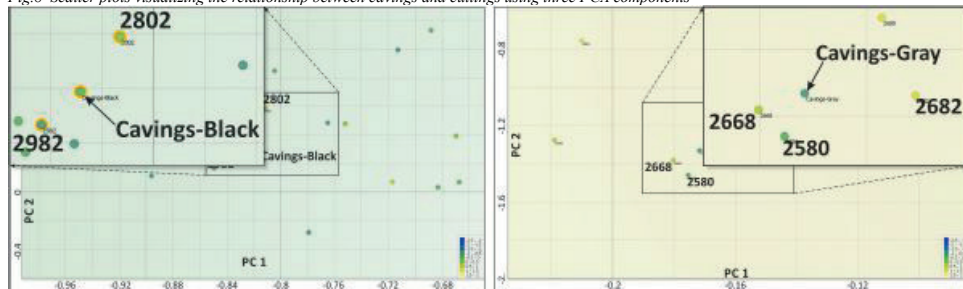


Fig.9 Log showing the ACA vs. calibrated ECL data comparison

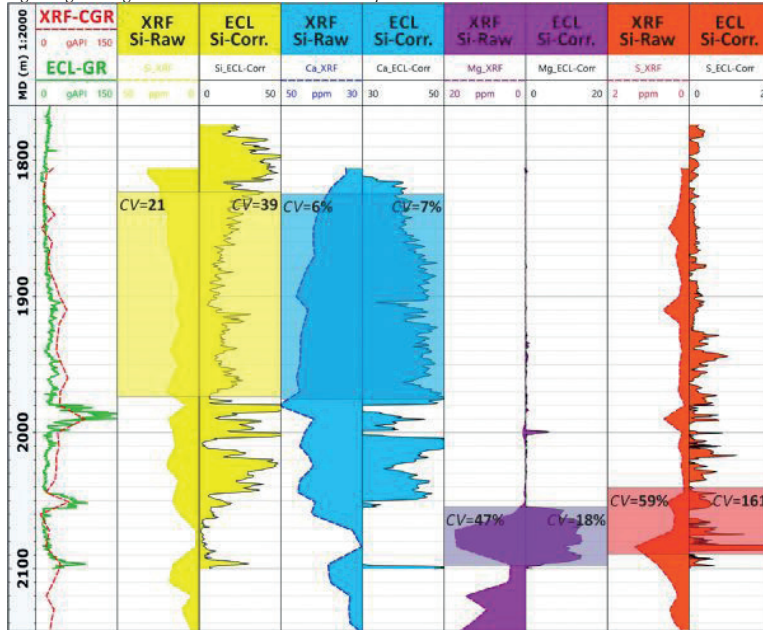


Fig.10 Example stratigraphic model created for B-53 well, using calibrated the calibrated ECL dataset

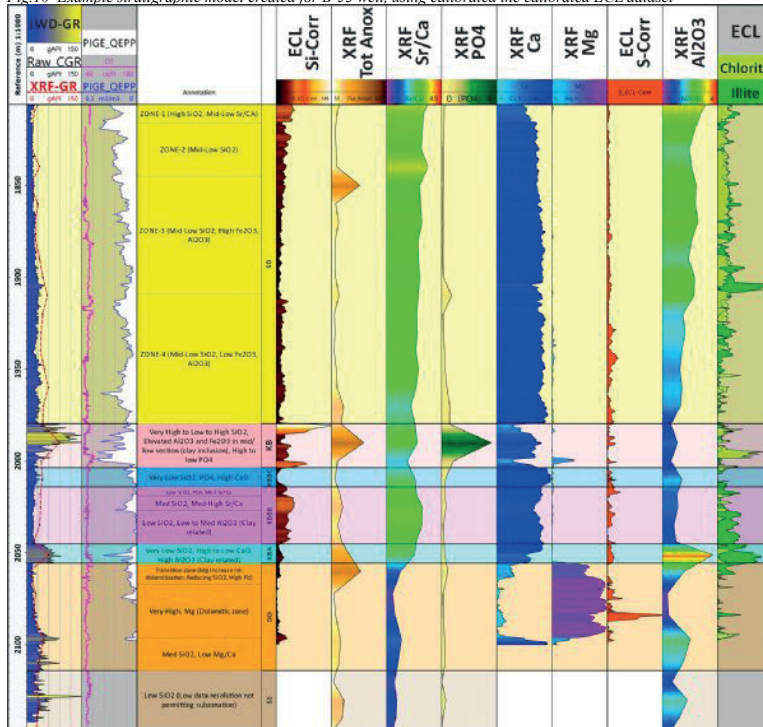


Fig.11 K-44 Well Lateral AMG Data Quality Plot

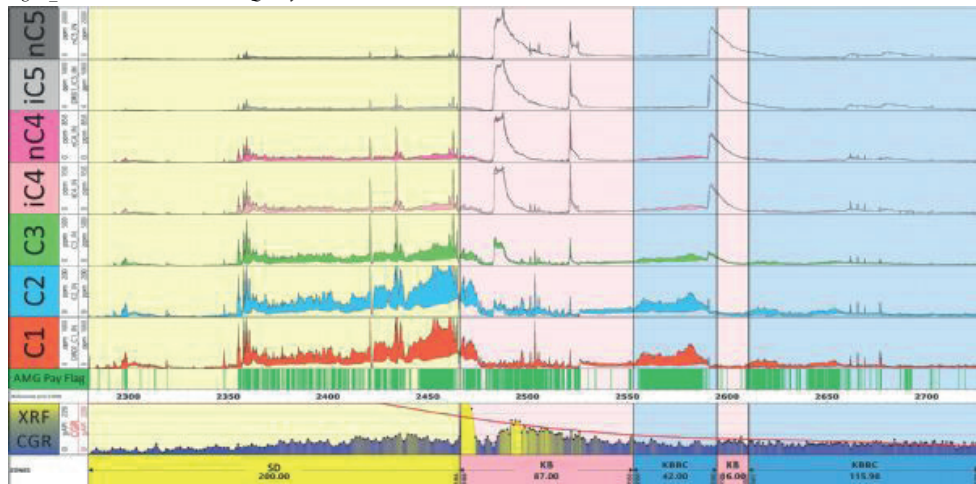
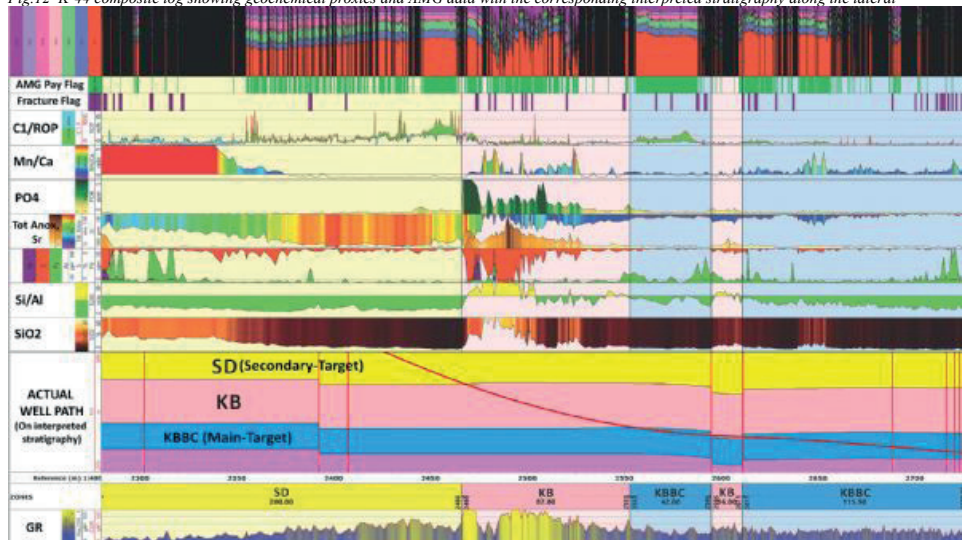


Fig.12 K-44 composite log showing geochemical proxies and AMG data with the corresponding interpreted stratigraphy along the lateral



# Güneydoğu Anadolu Bölgesi'nde Petrol Üretilen Rezervuar Birimler



**Erhan Yılmaz<sup>1</sup>, Fevzi Mert TÜRESİN<sup>2</sup>**

<sup>1</sup>Jeoloji Mühendisi

<sup>2</sup>Türkiye Petrolleri A.O.

## ÖZET

Bu çalışma, 2021 yılında TPAO AR-GE Merkezi'nde yapılan ve 2022 yılında kitaplaştırılan "Güneydoğu Anadolu Bölgesi'nde Petrol Üretilen Rezervuar Birimlerin Stratigrafisi, Sedimentolojisi, Paleocoğrafik Yayılımları ve Rezervuar Özellikleri" konulu çalışmanın genel bir özeti kapsamaktadır.

Güneydoğu Anadolu Bölgesinde yaşları Geç Ordovisiyen'den Geç Paleosen'e kadar değişen 18 farklı birimden petrol üretilmektedir. Rezervuar birimler Adıyaman, Diyarbakır, Batman, Nusaybin ve Şırnak olmak üzere beş ana bölgede yer almaktadır. Petrol sahalarının büyük bir kısmı ağır ve orta sınıfı petrol içermekte olup, ham petrolün API gravite değerleri oldukça değişkenlik göstermektedir. Çalışmada petrol üreten rezervuar birimler önem derecelerine göre birinci, ikinci ve üçüncü derecede önemli rezervuarlar olmak üzere üç alt sınıfta gruplandırılmışlardır.

Anahtar kelimeler: GDA, Rezervuarlar

## ABSTRACT

THIS STUDY INCLUDES A GENERAL SUMMARY OF THE STUDY ON "STRATIGRAPHY, SEDIMENTOLOGY, PALEO GEOGRAPHICAL DISTRIBUTION AND RESERVOIR CHARACTERISTICS OF PETROLEUM PRODUCING RESERVOIR UNITS IN THE SOUTHEASTERN ANATOLIA REGION", WHICH WAS MADE BY TPAO AR-GE CENTER IN 2021 AND PUBLISHED AS A BOOK IN 2022.

OIL IS PRODUCED IN THE REGION FROM 18 DIFFERENT RESERVOIR UNITS, WHOSE AGES RANGE FROM LATE ORDOVICIAN TO LATE PALEOCENE. RESERVOIR UNITS ARE LOCATED IN FIVE MAIN REGIONS: ADIYAMAN, DIYARBAKIR, BATMAN, NUSAYBIN AND ŞIRNAK. MOST OF THE OIL FIELDS CONTAIN HEAVY AND MEDIUM GRADE OIL, AND API GRAVITY VALUES OF CRUDE OIL VARY WIDELY. IN THE STUDY, THE OIL PRODUCING RESERVOIR UNITS ARE GROUPED INTO THREE SUB-CLASSES ACCORDING TO THEIR IMPORTANT AS FIRST, SECOND AND THIRD DEGREE RESERVOIRS.

## GİRİŞ

İnceleme alanı batıda XIII. Bölge doğusu (Kahramanmaraş-Musabeyli hattı doğusu), doğuda İran, güneyde Suriye ve Irak, kuzeyde yaklaşık Miyosen bindirmesi ile sınırlanmış alanları kapsamaktadır (Şekil-1).

Bölgede petrol üretilen rezervuar birimlerinin rezervuar

fasiyesleri, özellikleri ve paleocoğrafik yayılımlarının ortaya konulması, rezervuarların sınıflandırılması bu çalışmanın ana amacını oluşturmaktadır.

Çalışmada yerli ve yabancı şirketlerin 2020 öncesi yayınlanmış/yayınlanmamış veriler derlenip, üretilen yeni verilerle birlikte değerlendirilmiş, yapılan çalışmalar aşağıda özetlenmiştir:

- Temel karot analizleri (15.618 adet),
- Petrol analizleri (7.914 adet), petrolün formasyonu, kaynak kayası ve petrol gruplarına yaklaşım,
- Petrografik analizler (15.886),
- SEM analizleri,
- Kuyu verileri ve kompozit loglar (3.301 adet),
- Kuyu bitirme raporları (1.035 adet),
- Elektrik log verileri (1.597 adet),
- Log değerlendirme raporları (179 adet),
- Üretim bilgileri (194 saha),
- Makro ve mikrofotograf çekimi (753 adet)
- Teknik rapor ve makale (543 adet),
- Çökel ve rezervuar fasiyeslerinin özelliklerinin belirlenmesi,
- Her birimin ve petrol sahalarının rezervuar özellikleri belirlenmesi,
- Diyajenetik mekanizmaların oluşum zamanları belirlenerek rezervuar özelliklerine etkilerinin saptanması,
- Litolojik-sedimentolojik logların hazırlanması,
- Birimlerin ayrıntılı fasiyes dağılım haritaları hazırlanması,
- Teknik raporun yazılması.

## STRATİGRAFİ

GDA Bölgesi'nde otokton birimler yaşları Prekambriyen'den Güncel'e değin uzanan, karasaldan derin denize kadar değişen ortam koşullarında çökelmiş karbonat ve silisiklastik kayalardan oluşmuş, 12 ayrı grup altında toplanan 59 formasyon, 6 üye ile hiçbir gruba dahil edilmemiş 3 formasyon ile temsil edilmektedir.

Prekambriyen-Paleozoyik yaşlı istif 5 grup altında toplanan 14 formasyon ile hiçbir gruba dahil edilmemiş 2 formasyondan oluşmaktadır. Bunlar, yaşlıdan gence doğru, Telbesmi Formasyonu; Derik Grubu (Sadan, Zabuk, Koruk, Sosink formasyonları); Habur Grubu (Seydişehir, Bedinan formasyonları); Yurteri Formasyonu; Diyarbakır Grubu (Dadaş, Hazro, Kayayolu formasyonları); Zap Grubu (Yığınlı, Köprülü, Belek formasyonları), Tanin Grubu (Kaş, Gomaniibrik

formasyonları) şeklinde sıralanırlar (Şekil-2).

Otokton istifinin büyük bir bölümü Mesozoyik yaşlı çökel kayalardan oluşmaktadır. Bölgenin en önemli kaynak ve rezervuar kayaları Mesozoyik yaşlı birimlerden oluşmaktadır. 5 grup altında toplanmış ve 33 formasyona ayrılmıştır. Bunlar Çiğli Grubu (Yoncalı, Uludere, Uzunçeçit formasyonları); Cudi Grubu (Çanaklı, Bakük, Girmeli, Çamurlu, Telhasan, Dinçer, Kozluca, Yolaçan, Latdağı, Şenoba formasyonları); Mardin Grubu (Areban, Sabunsuyu, Derdere, Karababa formasyonları); Adıyaman Grubu (Karaboğaz, Ortabağ, Sayındere, Beloka formasyonları) ile Şırnak Grubu (Kastel, Bozova, Kıradağ, Terbüzek, Besni, Haydarlı, Garzan, Üçkiraz, Sinan (Alt), Germav (Alt), Nusaybin, Antak formasyonları)dur (Şekil-3).

Senozoyik yaşlı otokton istif değişik ortam koşullarında çökelmiş karbonat ve silisiklastik kayalardan oluşmuş 3 ayrı grup altında toplanan 15 ayrı formasyon ile hiçbir gruba dahil edilmemiş Şelmo Formasyonu ile temsil edilmektedir (Şekil-4). Grupları oluşturan formasyonlar Germav (Üst), Sinan (Üst), Kayaköy, Antak, Belveren, Becirman, Gerçüş formasyonları (Şırnak Grubu); Kavalköy, Hoya, Gaziantep, Havillati, Germik formasyonları (Midyat Grubu) ile Kapıkaya, Fırat, Lice formasyonlarıdır (Silvan Grubu).

## REZERVUAR BİRİMLER

GDA Bölgesi petrol arama çalışmaları bakımından Türkiye'nin en önemli bölgesini oluşturmaktadır. Türkiye'de petrol sahalarının önemli bir kısmı ikinci veya üçüncü kuyularda keşfedilmiştir. Adıyaman, Çemberlitaş ve Karakuş sahaları bunun en güzel örnekleridir. Geçmişte yeraltı verilerinin yetersiz olması nedeniyle uygun konumda olmayan veya teknik nedenlerle terk edilen kuru kuyuların açıldığı alanlarda, yeni verilerin ışığında daha sonra açılan kuyularda olumlu sonuçlar alınmıştır.

2019 yılı Aralık ayı sonuna kadar Türkiye'de petrol üretilen sahalarının yaklaşık %98'i GDA Bölgesi'nde bulunmaktadır. Yabancı ve yerli şirketler tarafından toplam 194 sahadan 1.106.622.022 varil ham petrol üretimi yapılmıştır. Üretiminin yaklaşık %57,91'i milli şirketimiz TPAO tarafından gerçekleştirilmiştir. TPAO dışındaki üretimin çok büyük bir bölümü, %41,54'ü yabancı şirketler tarafından yapılmıştır. Diğer yerli şirketlerin üretim oranı ise %0,55 olmuştur.

En fazla üretim yapan petrol sahası 1961 yılında Batman ilinin yakın güneyinde TPAO tarafından keşfedilen Batı Raman sahasıdır. Sahadan 2020 yılına kadar 127.012.085 varil petrol üretilmiştir. Batı Raman sahasını Raman, Şelmo, Beykan, Kurkan, Karakuş, Batı Kayaköy, Garzan, Kuzey Karakuş ve Kayaköy sahaları takip etmiştir. Toplam üretimin %63,64'ü bu 10 sahadan yapılmaktadır.

Petrol sahalarının büyük bir kısmı ağır ve orta sınıfı petrol içermekte olup, ham petrolün API gravite değerleri değerleri 8,00-72,40; kükürt oranı %0,00-7,09 arasında değişmektedir.

Ülkemizdeki ham petrol sahalarının üretim derinliği 865 (Direktili sahası) ilâ 3.541 metre (Kayayolu sahası)

arasında değişmektedir. Ortalama üretim derinliği 1.750 metre civarındadır.

GDA Bölgesi'nde yaşları Geç Ordovisiyen'den Geç Paleosen'e kadar değişen 18 ayrı rezervuar birimden petrol üretilmektedir. Rezervuar birimlerin hemen hemen tamamı yapısal kapan özelliğindedir. Sadece Garzan Formasyonu bazı alanlarda yapısal kapan özelliği ile birlikte stratigrafik kapan özelliği de göstermektedir. Rezervuar birimler Adıyaman, Diyarbakır, Batman, Nusaybin ve Şırnak olmak üzere beş ana bölgede yer almakta olup, üretimin tamamına yakın bir kısmı (%99,34'ü) 14 ayrı rezervuar birimden oluşan Kretase yaşlı karbonatlardan yapılmaktadır (Şekil-5). Daha derindeki Paleozoyik yaşlı kumtaşları ile daha sığdaki Sinan Formasyonu Üst Üyesi karbonatları ile Gerçüş, Antak ve Kastel formasyonlarından az miktarda petrol üretilmektedir. 2019 yılı Aralık ayı sonuna kadar keşfedilen sahalarından 68'i Adıyaman, 41'i Batman, 77'si Diyarbakır, 7'si Nusaybin ve 1'i de Şırnak Bölgesi'nde yer almaktadır.

Rezervuar birimleri önem derecelerine göre birinci, ikinci ve üçüncü derecede önemli rezervuarlar olmak üzere üç alt sınıfta toplamak mümkündür. Birinci derecede önemli rezervuar birimleri Derdere, Karababa, Garzan, Sinan (Alt Üyesi) formasyonları oluşturmaktadır. Yurteri, Hazro, Sabunsuyu, Karaboğaz, Sayındere, Nusaybin, Beloka, Sinan (Üst Üyesi) formasyonları ikinci derecede; Kastel, Bozova, Antak, Gerçüş, Germav formasyonları üçüncü derecede önemli rezervuar birimlerdir.

## YURTERİ FORMASYONU

GDA Bölgesi'nde Orta-Geç Ordovisiyen yaşlı çökelilerin en üst seviyelerinde yer alan ve genel anlamda üste doğru derinleşme gösteren Hırnansiyen yaşlı buzul etkili denizel çökeliler (Yurteri Formasyonu) diyamiktik-konglomeratik kumtaşı, kumtaşı, silttaşı ve şeyl litoloji topluluğundan oluşmaktadır.

Bu çökeliler içerisinde, özellikle Yurteri Formasyonu'nun en alt seviyesinde yer alan kumtaşları iyi-çok iyi bir rezervuar özelliği sunmaktadır. Ortalama porozite %14,53; permeabilite 30,35 mD'dir.

Üretilen petrolün ortalama API gravite değeri 39,84; kükürt oranı %0,13'dür. Kaynak kayası Dadaş Formasyonu olup, Grup III petroleri içerisinde yer almaktadır.

2020 yılına kadar 15 sahadan diğer birimlerle birlikte 4.800.594 varil petrol üretilmiştir. Altınakar Sahası'ndan Karababa Formasyonu C Üyesi ve Çikşor Sahası'ndan da Derdere Formasyonu ile birlikte üretim gerçekleştirilmiştir

## HAZRO FORMASYONU

Sadece Diyarbakır ili Hazro yöresinde mostra veren Hazro Formasyonu iki klastik ve bunların arasında anahtar seviye özelliği taşıyan bir karbonat seviyeden oluşmaktadır.

Şeyl, silttaşı, kumtaşı ve marn litoloji topluluğu ile

temsil edilen Alt klastik üyede gelişen kum oluşukları iyi bir hazne kaya özelliğine sahiptirler. Kumtaşlarının porozite değerleri %0,01-30,00; permeabilite değerleri 0,01-332,79 mD arasında değişmektedir. Ortalama porozite %10,60; permeabilite değeri 16,40 mD'dir.

Üretilen petrolün ortalama API gravitesi 46,02'dir. Kaynak kayası Dadaş Formasyonu olup, Grup III petroleri içerisinde yer almaktadır.

2020 yılına kadar 4 sahadan 1.300.305 varil petrol üretilmiştir.

### SABUNSUYU FORMASYONU

Sabunsuyu Formasyonu gel-git düzlüğü, şelf lagünü ve sığ karbonat platformu ortam koşullarında çökelmiş dolomit, dolomitik kireçtaşı ve kireçtaşlarından oluşur. Egemen litoloji dolomittir. Şırnak-Hakkari arası hariç sürekli gelişim göstermiştir.

Gel-git düzlüğü çökelleri algal lamineal anhidrit ile algal dolomikrit (stromatolit) ara bantları içeren dolomikrit/dolomikrosparitlerden oluşmaktadır. Ortalama görsel porozite oranı XII. Bölge güney alanlarında %10-25; XI. Bölge Diyarbakır kuzey alanlarında %5-20 arasında değişim göstermektedir. Bu dolomitler XII. Bölge'de petrol/su dokanağının altında kalması nedeniyle petrol üretme potansiyeline sahip değildirler. XI. Bölgede Sabunsuyu Formasyonu'nun sığ denizel kökenli dolosparitleri ile birlikte üretime katkı sağlamaktadırlar.

Genelde formasyonun üst seviyelerinde gözlenen sığ denizel çökeller kavkılı, küçük bentik foraminiferli çamurtaşı/vaketaşı; biyoklastik vaketaşı/istiftaşı; peloidli, biyoklastik istiftaşı/tanetaşı fasiyesleri ile bu fasiyeslerin dolomitleşmesi sonucu oluşmuş dolosparitlerden oluşmaktadır.

Kavkılı, küçük bentik foraminiferli çamurtaşı/vaketaşları Güney Kıvrım-11 kuyusunda rezervuar özelliği taşımakta olup, ortalama %12,07 poroziteye, 1,63 mD geçirgenliğe sahiptir.

Peloid-intraklastik, biyoklastik istiftaşı/tanetaşlarında ortalama porozite %11,37; permeabilite 0,31 mD'dir.

Sığ denizel çökellerinin tamamen dolomitleşmesi sonucu oluşan dolosparitlerin ortalama porozitesi %10,79; permeabilitesi 12,97 mD'dir. Beykan Sahası'nda %17,78 ile en yüksek ortalama poroziteye sahiptir. X. ve XI. Bölge kuzey alanlarında bu dolomitlerden üretim yapılmaktadır.

Üretilen petrolün API gravite değerleri 24,50-36,50 arasında değişmektedir. Kaynak kayasını Dadaş Formasyonu, Cudi Grubu'nun Şenoba Formasyonu oluşturmakta, Grup I ve III petroleri içerisinde yer almaktadır. Ayrıca, birimin tektonizma sonucu Derdere Formasyonu ile karşı karşıya geldiği bazı alanlarda (Ozan Sungurlu, Bozhüyük sahaları) kaynak kayasını Derdere Formasyonu oluşturmakta, Grup II içinde yer almaktadır.

2020 yılına kadar 8 sahadan diğer birimlerle birlikte 178.557.355 varil üretim yapılmıştır. Sivritepe Sahası'ndan sadece Sabunsuyu Formasyonu'ndan üretim yapılırken, 6 sahada Derdere Formasyonu;

I sahada Sayındere, Karaboğaz, Karababa, Derdere formasyonları ile birlikte üretim gerçekleştirilmiştir.

### DERDERE FORMASYONU

GDA'da geniş yayılıma sahip Derdere Formasyonu kireçtaşı, dolomitik kireçtaşı ve dolomitlerden oluşur (Şekil-6, 7). Şırnak-Hakkari arasındaki alan hariç sürekli yayılım gösterir. Birçok üretim sahasının rezervuar kayasını oluşturmaktadır. Aynı zamanda kaynak kaya potansiyeline de sahiptir.

Altın üstte doğru platform içi çukurluk, karbonat kum sığlığı, lagün ve gel-git düzlüğü ortam koşullarında çökelmiş karbonatlardan oluşmaktadır (Şekil-8, Tablo-1).

Platform içi çukurluğu çökelleri az sferli, biyoklastik vaketaşı/istiftaşı; organik maddece zengin, sferoidal fosilli vaketaşı/istiftaşı; plankton-sferli, kavkılı çamurtaşı/vaketaşı/istiftaşı ve bu fasiyeslerin dolomitleşmesi sonucu oluşmuş dolomikrosparit/dolosparitlerden oluşur.

Az sferli, biyoklastik vaketaşı/istiftaşlarının genelde rezervuar özellikleri yoktur. Bazı alanlarda (Beykan, Kurkan, Yeniköy sahalarında) %10-15 arasında değişen oranlarda görsel porozite içermekte, petrol üretimine katkı sağlamaktadır (Şekil-9).

Plankton-sferli, kavkılı çamurtaşı/vaketaşı/istiftaşlarının porozite değerleri %0,05-32,01; permeabilite değerleri 0,01-68,29 mD arasında değişmektedir (Tablo-2). XI. Bölge'nin kuzeydoğusunda, Diyarbakır kuzey sahalarında iyi bir rezervuar özelliği göstermektedir. En yüksek ortalama poroziteye Güney Sarıcak (%13,57) ile Beykan (%12,90) sahalarında ulaşmaktadır. Bu fasiyesin tamamen dolomitleşmesi sonucu oluşmuş dolomikrosparit/dolosparitlerin ortalama porozitesi %14,99; permeabilitesi 15,65 mD'dir. Diyarbakır sahalarında üretime katkı sağlarlar (Şekil-10).

Birimin genelde üst seviyelerinde yer alan sığ denizel karbonatlar intraklast-peloidli istiftaşı/tanetaşı; intraklast-peloidli, biyoklastik istiftaşı/tanetaşı; oolitik tanetaşı; biyoklastik vaketaşı/istiftaşı; kavkılı, küçük bentik foraminiferli çamurtaşı/vaketaşı ve bu çökel fasiyeslerin dolomitleşmesi sonucu oluşan dolomikrosparit/dolosparitlerden oluşmaktadır.

İntraklast-peloidli istiftaşı/tanetaşlarının porozite değerleri %0,04-31,66; permeabilite değerleri 0,01-251,96 mD arasında değişmektedir (Şekil-11; Tablo-2). Diyarbakır kuzeyinde ve batı alanlarında (Doğu Beşikli), XII. Bölge güneybatı alanlarında (Yakacık, Beşikkaya) rezervuar özelliği taşımaktadırlar.

Biyoklastik vaketaşı/istiftaşları ortalama %7,29 porozite; 14,28 mD permeabiliteye sahiptir. Diyarbakır'ın kuzey alanlarında (Yeniköy, Güney Kıvrım, Karacan sahaları) en yüksek ortalama poroziteye sahiptirler.

Sığ denizel kireçtaşlarının dolomitleşmesi sonucu oluşmuş dolomikrosparit/dolosparitlerin görsel porozite değerleri %1-25 arasında değişim gösterir (Şekil-12). Çatlaklanmanın etkili olduğu bindirme alanlarında (Ozan Sungurlu, Cendere, Güney Karakuş, Kuzey

Karakuş, Karakuş, Doğu Beşikli) çatlaklı rezervuarlar için tipik örnek oluşturur. Dolomitler diğer çökel fasiyeslere göre birinci derece rezervuar özelliğine sahiptir. Birçok alanda en üretken ve potansiyel rezervuar zonları oluşturur. Ortalama porozite %12,60; permeabilite 50,20 mD'dir.

Gel-git düzlüğü çökelleri genelde rezervuar özelliği olmayan kireç çamurtaşı, algal çamurtaşı (bağlamtaşı) ve dolomikrit/dolomikrospartitlerden oluşmaktadır.

Üretilen petrolün API gravite değerleri 12,00-43,06 arasında değişmektedir (Tablo-3). Kaynak kayası Dadaş Formasyonu, Cudi Grubu (Şenoba, Çamurlu, Bakük formasyonları) ile kendisidir. Üretilen petrol Grup I, II, III, I+II ve II+III içinde yer almaktadır.

2020 yılına kadar 81 sahadan diğer formasyonlarla birlikte 616.662.751 varil üretim yapılmıştır. 31 sahada Sinan (Alt Üyesi), Yurteri, Garzan, Hazro, Karababa, Karaboğaz, Kastel, Sabunsuyu, Sayındere formasyonlarından biri veya birkaçı Derdere Formasyonu ile birlikte üretime katkı sağlamıştır (Tablo-2).

### KARABABA FORMASYONU

Karababa Formasyonu çört ara seviyeli kireçtaşı, dolomitik kireçtaşı ve organik maddeli kireçtaşlarından oluşan bir karbonat istifidir. Sabunsuyu ve Derdere formasyonlarına nazaran düzensiz olarak yayılım göstermektedir.

Koyu renkli, organik maddeli, fosfatlı, planktik foraminiferli kireçtaşları "A Üyesi"; daha az organik madde içeren, koyu renkli, silisleşmeli, çört nodül ve ara bantlı, sferli, planktik foraminiferli, ince bentik kavkılı kireçtaşları "B Üyesi"; makro kavkılı, sığ denizel kireçtaşları "C Üyesi" olarak adlandırılmaktadır.

A Üyesi'nin herhangi bir rezervuar özelliği yoktur. GDA'nın en önemli kaynak kayalarından biridir.

B Üyesi bölge geneline rezervuar olarak çok önem taşımamaktadır. Yoğun çatlaklanmaların geliştiği alanlarda (Adıyaman Bölgesi) çatlaklı karbonat rezervuarı olarak davranmakta, üretime katkı sağlamaktadır.

### C Üyesi

C Üyesi biyoklastik vaketaşı-istiftaşı çökel dokusundaki kireçtaşları ile temsil edilir. Yayılım alanı Karababa Formasyonu'nun geliştiği şelf içi çukurluğun boyutu ile sınırlıdır.

Biyoklastik vaketaşı/istiftaşı ve sfer-planktik foraminiferli, biyoklastik vaketaşı/istiftaşı çökel fasiyeslerinden oluşur.

Orta ve üst seviyelerini oluşturan biyoklastik vaketaşı/istiftaşı önemli derecede rezervuar özelliğine sahiptir. XI. Bölge batısı ile XII. Bölge'de üretilen petrolün bir bölümü C Üyesi'nin bu fasiyesten yapılmaktadır. Porozite değerleri %0,01-29,23; permeabilite değerleri 0,01-43,43 mD arasında değişmektedir. C Üyesi'nin rezervuar özelliklerini diyajenez ve tektonik kontrol

eder. Genelde iyi porozite gelişimi gözlenmesine rağmen matriks porozite ve çatlak gelişiminin yoğun olmadığı alanlarda permeabilite sorunu ortaya çıkmaktadır. Permeabilite genelde düşük olup, çoğunlukla 1 mD'den azdır. Bazı alanlarda dolomitleşme sonucu oluşan dolospartit rezervuar özelliği taşımaktadır. Dolomitlerin ortalama porozitesi %9,98; permeabilitesi 11,26 mD'dir.

Çatlak sisteminin iyi gelişmediği sfer-planktik foraminiferli, biyoklastik vaketaşı/istiftaşı genelde rezervuar özelliğine sahip değildir.

Karababa Formasyonu yayılım alanının batısında ve doğusunda farklı fasiyeslerde çökelmiştir. Klasik Karababa A, B ve C diziliminden farklılık göstermekte ve üyelerine ayırlanamamaktadır. Sığ denizel-lagün koşullarında çökelmiş Murciella'lı, küçük bentik foraminiferli, kavkılı çamurtaşı/vaketaşı/istiftaşı ve pellet-peloidli, biyoklastik istiftaşı/tanetaşı fasiyeslerinden oluşur:

Murciella'lı, küçük bentik foraminiferli, kavkılı çamurtaşı/vaketaşı/istiftaşı diyajenez sonucu rezervuar özelliği kazanmıştır. Batı Yemişlik, Çelikli, Güney Raman, Mermer, Raman, Yemişlik sahalarında bu çökel fasiyesten üretim yapılmaktadır. Porozite değerleri %0,11-38,53; permeabilite değerleri 0,01-404,92 mD arasında değişmektedir. Bazı seviyelerin dolomitleşmesi sonucu oluşan dolomitler özellikle fasiyesin üst seviyelerinde ara bantlar halindedir. Ortalama porozitesi %4,74; permeabilitesi 6,11 mD'dir.

Pellet-peloidli, biyoklastik istiftaşı/tanetaşları ara bantlar halinde ve kalınlıkları çok azdır. Genelde çimentolanma yaygındır. Bu nedenle zayıf rezervuar özelliği gösterirler.

Üretilen petrolün API gravite değerleri 10,80-43,00 arasında değişmektedir. Kaynak kayasını Karababa (A Üyesi), Beloka (Dirik Üyesi), Derdere ve Dadaş formasyonları ile Cudi Grubu oluşturur. Grup I, II, II+III petroleri içerisinde yer alır.

2020 yılına kadar 63 sahadan diğer formasyonlarla birlikte Karababa Formasyonu'ndan 336.699.430 varil petrol üretimi yapılmıştır. 46 sahada Germav (Alt), Kastel, Sayındere, Karaboğaz, Derdere, Sabunsuyu, Garzan, Beloka (Bada), Yurteri formasyonlarından biri veya birkaçı Karababa Formasyonu'na eşlik etmişlerdir.

### KARABOĞAZ FORMASYONU

Derin denizel, sakin ve anoksik ortam koşullarında çökelmiş Karaboğaz Formasyonu, genelde üste doğru derinleşen, koyu renkli, çörtlü-çört ara bantlı, fosfatlı, glokonili ve organik maddece zengin karbonatlı kayalardan oluşmuştur. Çört oranı yer yer %50-70 dolaylarına kadar yükselir.

Karaboğaz Formasyonu rezervuar kayadan çok kaynak kaya olarak daha çok önem taşımaktadır. Bazı alanlarda, kaynak kaya özelliğinin yanında rezervuar kaya olarak da davranabilmektedir. Ancak, üretken olabilmesi için rezervuar fasiyeslerinin mutlaka çatlaklanmanın oluşturduğu drenaj sistemi ile permeabilitesinin iyileştirilmesi gerekmektedir.



Karaboğaz Formasyonu genel olarak altta pelajik kireçtaşı ara seviyeli fosfatlı, biyoklastik kireçtaşları, üstte çört ara seviyeli, planktonlu, zengin organik maddeli kireçtaşları olmak üzere iki temel litofasiyesten oluşmaktadır.

Fosfatlı, biyoklastik vaketaşı/istiftaşları birimin rezervuar fasiyesini oluşturur. Bu fasiyesinin üretken olabilmesinde erime sonucu oluşmuş porozite ile birlikte çatlak sistemlerinin de gelişmesi oldukça önemlidir. Porozite değerleri %0,29-20,51 arasında değişim göstermektedir. Permeabilite değerleri çatlaklanmanın olmadığı alanlarda 1 mD'den düşüktür. Çatlaklanmanın olduğu alanlarda 123,90 mD'ye kadar çıkmaktadır. Karakuş, Kuzey Karakuş, Güney Karakuş, Cendere, Ozan Sungurlu, Tokaris, Beşikli üretim sahalarında üretilen petrolün çoğunlukla çatlaklı rezervuar zonlarından elde edilmektedir. Dolomitleşme bazı sahalarda bu fasiyesin kısmen veya tamamen dolomitleşmesine neden olmuştur. Ancak, kalınlıkları genelde az olup, birkaç metreyi geçmemektedir. Dolomitik dolosparit karakterindeki bu dolomitlerde porozite %7,47-12,23; permeabilite 0,03-0,32 mD arasında değişmektedir.

Üretilen petrolün API gravite değeri 10,40-36,20 arasında değişim göstermektedir. Kaynak kayası hem kendisi, hem de Derdere ile Karababa (A Üyesi) formasyonlarıdır. Grup II petrolerinin içinde yer almaktadır.

2020 yılına kadar 38 sahadan diğer formasyonları ile birlikte 203.139.312 varil petrol üretimi yapılmıştır. 37 sahada Sayındere, Karababa, Derdere, Sabunsuyu formasyonları Karaboğaz Formasyonu'na eşlik etmişlerdir.

### SAYINDERE FORMASYONU

Sayındere Formasyonu genellikle yeknesak bir litolojiye sahip olup, derin denizel çökellerle temsil edilmektedir. Bazı alanlarda, taban kesimlerini daha koyu renkli, organik karbonca zengin killi kireçtaşları oluşturmaktadır. Ayrıca, XII. Bölge'nin batı alanlarında (Adıyaman batısı, Gölbaşı-Tut, Araban-Bozova) Saytepe Üyesi olarak adlandırılan yer yer killi kireçtaşları ile ardalanmış kalsitürbüditik kireçtaşları ile temsil edilen yamaç fasiyesi bulunmaktadır.

Çatlaklanmalar haricinde (Şambayat, Altıntop sahaları gibi) rezervuar özelliğine sahip değildir. Özellikle taban kesiminde yer alan ve A litofasiyesi olarak adlandırılan organik maddece zengin kireçtaşları kaynak kaya bakımından önem taşımaktadır. Çatlaklanmanın yaygın olmadığı alanlarda iyi bir örtü kaya özelliği göstermektedir.

### Saytepe Üyesi

Saytepe Üyesi planktik foraminiferli, killi kireçtaşları ile ardalanmış bentik foraminiferli, biyoklastik kireçtaşlarından (kalsitürbüdit) oluşmakta, yukarı doğru derinleşen bir karbonat yamacını temsil etmektedir.

Yayılmına bağlı olarak Adıyaman ili batısında kalan

alanlarda ve Bozova civarında rezervuar özelliği taşımakta, üretime katkı sağlamaktadır.

Saytepe Üyesi'nin karbonatları biyoklastik tanetaşı, biyoklastik vaketaşı/istiftaşı ve sfer-planktik foraminiferli, kavkılı vaketaşı/istiftaşı çökel fasiyesleri ile temsil edilmektedir. Bu üç çökel fasiyesten ikisi rezervuar özelliği sunmaktadır.

Rezervuar fasiyeslerden biyoklastik tanetaşlarının porozite değerleri %0,20-16,67; permeabilite değerleri 0,01-8,21 mD arasında değişmektedir.

Birinci derece rezervuar fasiyesi oluşturan biyoklastik vaketaşı/istiftaşlarının porozite değerleri %2,50-24,52; permeabilite değerleri 0,01-14,64 mD arasında değişir. Maksimum ortalama poroziteye %17,60 ile Bozova Sahası'nda ulaşmaktadır.

Üretilen petrolün API gravite değerleri 9,70-42,00 arasında değişmektedir. Kaynak kayasını hem kendisi hem de Dadaş, Derdere, Karababa (A Üyesi), Karaboğaz formasyonları ile Cudi Grubu oluşturur. Genelde Grup I, II, III petrolerinin içinde yer alır. Araban Sahasında ise Grup I+II içerisinde yer alır.

2020 yılına kadar 38 sahadan diğer formasyonlarla birlikte Sayındere Formasyonu'ndan 180.001.480 varil petrol üretim yapılmıştır. 27 sahada Sayındere Formasyonu Karaboğaz, Karababa, Derdere, Sabunsuyu formasyonlarına eşlik ederek üretime kısmi katkı sağlamıştır.

### BELOKA FORMASYONU

X. Bölge'nin merkezi alanları ile Nusaybin-Cizre arasında yayılım gösteren Beloka Formasyonu "Bada" ve "Dirik" şeklinde iki üyeden oluşmaktadır. Her iki üye de petrol aramacılığı açısından önemlidir. Yayılım alanının kuzey kesimlerinde Bada Üyesi'nden, güney alanlarda (Güney Diñçer) Dirik Üyesi'nden üretim yapılmaktadır. Dirik Üyesi aynı zamanda yayılım alanının kuzey kesimlerinde kaynak kaya özelliğine de sahiptir.

### Bada Üyesi

Bada Üyesi şelf kenarı yükseltisi-lokal karbonat yığılım kompleksinden ve iyi bir rezervuar özelliği gösteren iki ayrı fasiyesten oluşmuştur.

Birinci derecede rezervuar fasiyesi oluşturan biyoklastik istiftaşı/tanetaşı/moloztaşlarının porozite değerleri %2,50-27,76; permeabilite değerleri 0,05-289,380 mD arasında değişmektedir.

İkinci derecede önemli rezervuar fasiyesi olan biyoklastik vaketaşı/istiftaşı/moloztaşlarının porozite değerleri %0,32-25,40; permeabilite değerleri 0,01-290,13 mD arasında değişir.

Dolomitleşme bazı sahalarda çok etkili olmuş, rezervuar fasiyeslerinin kısmen veya tamamen dolomitleşmesine neden olmuştur. Dolosparit karakterindeki dolomitlerin porozite değerleri %2,09-31,97; permeabilite değerleri 0,04-4.168,80 mD arasında değişmektedir.

Üretilen petrolün API gravitesi 11,35-35,60 arasında

değişmektedir. Bada petrolü hem kendisinden (Dirik Üyesi'nden), hem de Derdere Formasyonu'ndan türemiş, Grup II petrolerinin içinde yer almaktadır.

2020 yılına kadar 7 sahadan Garzan Formasyonu ile birlikte 18.939.222 varil petrol üretimi yapılmıştır.

### Dirik Üyesi

Dirik Üyesi düşük enerjili, açık şelf-sığ havza koşullarında çökelmiş üç ayrı fasiyesten oluşmaktadır.

Güney Dinçer Sahası'ndan dolomitlerle birlikte üretim yapılan killi, sfer-planktonlu, ince kavkılı vaketaşı/istiftaşlarının (kalsisilit/kalkarenit) porozite değerleri %0,02-42,91; permeabilite değerleri 0,001-3.912,00 mD arasında değişmektedir. Hidrotermal sularının etkisi ile lokal olarak gelişen dolomitleşme bazı kuyularda (Güney Dinçer-16) çok etkili olmuş, fasiyesin tamamen dolomitleşmesine neden olmuştur. Dolosparit karakterindeki dolomitlerin porozite değerleri %2,09-30,06; permeabilite değerleri 0,01-1658,34 mD arasında değişmektedir.

Üretilen petrolün API gravitesi 11,80-17,09 arasında değişmektedir. Kaynak kayası Cudi Grubu olup, Grup I petroleri içinde yer almaktadır.

2020 yılına kadar Dirik Üyesi'nden sadece Güney Dinçer Sahası'ndan 7.747.601 varil petrol üretim yapılmıştır.

### KASTEL FORMASYONU

Kastel Formasyonu, genel olarak şeyl ve marnlarla ardalanan türbiditik kökenli silttaşı, kumtaşı ve çakıltaşlarından oluşur.

Kumtaşları bazı seviyelerde rezervuar özelliğine sahiptirler. %5-10 oranında görsel porozite içermektedir. Bazı alanlarda porozite oranı %14-17'ye ulaşmaktadır.

Üretilen petrolün API gravite değerleri 12,00-41,10 arasında değişmektedir. Kaynak kayasını Sayındere, Karaboğaz, Karababa (A Üyesi), Derdere, Dadaş formasyonları oluşturmaktadır. Adıyaman Sahası'nda Grup II, Diyarbakır kuzey alanlarında Grup III petroleri içinde yer almaktadır.

2021 yılına kadar Adıyaman, Akgün, Doğu Hasancık, Beykan sahalarından 469.078 varil petrol üretimi yapılmıştır.

### BOZOVA FORMASYONU

Bozova Formasyonu çok yeknesak bir litolojiye sahip olup, derin denizel killi kireçtaşı ve marnlardan oluşmaktadır.

Görsel olarak porozite içermezler, rezervuar özellikleri yoktur. Ancak, bazı alanlarda Doğu Yananköy, Yananköy, Doğu Sadak, Kedil sahalarında olduğu gibi çatlaklanma ile rezervuar özelliklerine sahip olabilmektedirler. Ayrıca, yer yer etkin dolomitleşme ile Kedil-1 kuyusunda olduğu gibi diyajenetik olarak dolomikrosparit/dolosparite dönüşebilmekte ve çatlaklanma özelliği gösterebilmektedir. Dolosparitlerin

porozite değerleri %3,08-5,38; permeabilite değerleri 0,01-0,15 mD arasında değişmektedir.

Üretilen petrolünün API gravite değerleri Yananköy Sahası'nda 10,40-10,80 arasında değişim gösterirken; X. Bölge'de, Kedil-1 kuyusunda 25,20-28,00 arasında değişim göstermektedir. Kaynak kayasını Doğu Yananköy, Yananköy sahalarında Sayındere, Karaboğaz, Karababa, Derdere formasyonları oluşturmakta, Grup II petroleri içinde yer almaktadır. Kedil-1 petrolü Cudi Grubu birimlerinden türemiş olup, Grup I petroleri içinde yer almaktadır.

2020 yılına kadar 2 sahadan Germav Formasyonu Alt Üyesi ile birlikte Bozova Formasyonu'ndan 1.002.836 varil petrol üretimi yapılmıştır.

### GARZAN FORMASYONU

Kireçtaşı, killi kireçtaşı ve dolomitlerden oluşan Garzan Formasyonu X. Bölge'nin şelf alanının büyük bir kesiminde yayılım göstermektedir. Açık şelf, karbonat kum sığlığı ve şelf lagünü olmak üzere 3 ana ortama ait farklı fasiyelerden oluşur.

Açık şelf çökellerini oluşturan killi, sfer-planktonlu, kavkılı vaketaşı/istiftaşları genelde kesif ve kötü poroziteli olup, rezervuar olarak önemi yoktur.

Karbonat kum sığlığı çökelleri Garzan Formasyonu'ndan petrol üretiminin yapıldığı fasiyesleri içerir. Yüksek porozite ve permeabilite değerleri ile birinci, ikinci, üçüncü, dördüncü derecede rezervuar fasiyesler olarak önem taşırlar. Sığ karbonat şelfinin şelf kenarı ile şelf lagünü içinde düzensiz taban topoğrafyasına bağlı olarak gelişmiş sığlıklar ve civarlarında çökelmiş fasiyeslerle temsil edilir. Sığlık alanları düzensiz yayılım göstermektedir. Sığlık çökelleri iri bentik foraminiferli istiftaşı; biyoklastik istiftaşı/tanetaşı/moloztaşı; biyoklastik vaketaşı/istiftaşı/moloztaşı; iri bentik foraminiferli, biyoklastik vaketaşı/istiftaşı ve küçük bentik foraminiferli, biyoklastik vaketaşı/istiftaşı fasiyelerinden oluşmaktadır.

Biyoklastik istiftaşı/tanetaşı/moloztaşlarının porozite değerleri %0,60-29,10; permeabilite değerleri 0,01-3.397,80 mD arasında değişmektedir. Genelde 2. derecede rezervuar fasiyesidir. Ancak, çimentolanmanın daha az olduğu alanlarda (Arıkaya, Batı Haznemir, Çakıllı, Demirkuyu, Germik, Güney Garzan, Raman, Tura) 1. derecede rezervuar fasiyesidir.

Biyoklastik vaketaşı/istiftaşı/moloztaşlarının porozite değerleri %0,04-39,73; permeabilite değerleri 0,01-2.221,00 mD arasında değişmektedir. Bölge genelinde birçok alanda birinci derecede rezervuar fasiyes özelliğindedirler.

İri bentik foraminiferli, biyoklastik vaketaşı/istiftaşlarının porozite değerleri %0,04-25,63; permeabilite değerleri 0,01-346,74 mD arasında değişmektedir. Üçüncü derecede rezervuar fasiyesidir.

Küçük bentik foraminiferli, biyoklastik vaketaşı/istiftaşları lokal erime boşluklarının dışında zayıf matris porozite ve düşük geçirgenlik özelliği ile dördüncü derecede rezervuar fasiyesi oluşturur.

Dolomitleşme bazı alanlarda etkili olmuş, sığlık çökellerinin kısmen veya tamamen dolomitleşmesine neden olmuştur. Dolosparitler şeklindeki dolomitlerin porozite değerleri %1,40-22,42; permeabilite değerleri ise 0,03-819,41 mD arasında değişmektedir.

Şelf lagünü çökelleri küçük bentik foraminiferli çamurtaşı/vaketaşı fasiyesi ile temsil edilir. Düşük porozite ve permeabilite olmaları nedeniyle rezervuar özelliği taşımamaktadırlar.

Üretilen petrolün API gravite değerleri 10,00-35,50 arasında değişmektedir. Yayılım alanının Batı Raman-Raman-Çakılı-Batı Kentalan hattı boyunca kaynak kayasını Cudi Grubu birimleri oluşturmada, Grup I petrolerinin içerisinde yer almaktadır. Yayılım alanının kuzey kesimlerinde, kaynak kayasını Sayındere, Derdere, Beloka (Dirik Üyesi) formasyonları oluşturur, Grup II petroleri içinde yer alır. Bastokan, Garzan, Germik, Güney Garzan, Günyayla, Reşit, Kurtalan (Tilan), Toytepe kuyularının petroleri Cudi Grubu, Derdere ve Beloka (Dirik Üyesi) formasyonlarının türettiği bir karışım petrolü olup, Grup I+II sınıfı içinde yer almaktadır. Haznemir-1 kuyusu petrolü diğer petrolerden farklılıklar göstermekte kaynak kayasını Beloka (Dirik Üyesi), Derdere ve Dadaş formasyonları oluşturmada, Grup II+III karışım petroleri sınıfında yer almaktadır.

2020 yılına kadar 23 sahadan diğer formasyonlarla birlikte Garzan Formasyonu'ndan 325.151.885 varil petrol üretimi yapılmıştır. 8 sahadan Sinan (Alt ve Üst üyeleri), Germav (Alt Üyesi), Beloka (Bada Üyesi), Derdere formasyonlarından biri veya birkaçı Garzan Formasyonu'na eşlik etmektedir.

## SİNAN FORMASYONU

Sinan Formasyonu gayri resmi olarak "alt Sinan" ve "üst Sinan" olarak ikiye ayrılmıştır.

### Sinan Formasyonu Alt Üyesi

Orta-Geç Maastrichtiyen yaşlı Sinan Formasyonu Alt Üyesi X. ve XI. bölgelerin kuzey alanlarında, üste doğru sığlaşma özelliği gösteren gel-git düzlüğü/sığ denizel ortam koşullarında çökelmiş şeyl, marn, dolomit, dolomitik kireçtaşı ve kireçtaşı litoloji topluluğundan oluşmaktadır.

Gel-git düzlüğü çökelleri yer yer evaporit, çamurtaşı/şeyl ve kumtaşı ara bantları içeren dolomikrit/dolomikrosparitlerden oluşmaktadır. Birimin en üst seviyelerinde yer alan bu dolomitlerin porozite değerleri %0,18-22,23; permeabilite değerleri 0,01-178,34 mD arasında değişim göstermektedir. Dilimalan, Dodan, Halkış, Köşeler, Malahermo, Özlüce, Şelmo ve Taşpınar sahalarında rezervuar özellikleri gösterirler.

Yayılım alanının güney ve güneydoğusunda gözlenen şelf lagünü çökelleri Loftusia'lı vaketaşı/istiftaşı ile kavkılı, küçük bentik foraminiferli çamurtaşı/vaketaşı fasiyesleri ile temsil edilmektedir. Genelde rezervuar özelliğine sahip değildirler. Ancak, bazı alanlarda tamamen dolomitleşerek rezervuar

özelliği kazanmışlardır. Dolomikrosparit/dolosparit karakterindeki bu dolomitler Batı Şelmo, Şelmo ve Özlüce sahalarında %1,09-18,08 porozite; 0,01-11,40 mD geçirgenliğe sahip olup, üretime katkı sağlamaktadırlar.

Şelf lagünü içinde ve platform kenarında herhangi bir bariyer oluşturamayacak kadar küçük ölçekli sığlık alanlarda iri bentik foraminiferli, biyoklastik vaketaşı/istiftaşı/moloztaş ve biyoklastik istiftaşı/tanetaşlarından oluşan karbonatlar çökelmiştir. Bu karbonatlarının rezervuar özelliğini diyajenez kontrol etmektedir. Dolomitleşmenin yoğun olduğu alanlarda (Batı Silivanka, Batı Şelmo, Güney Şelmo, Halkış, Malahermo, Özlüce, Şelmo) dolosparitlerden oluşan bu dolomitler en önemli rezervuar seviyeleri oluştururlar. Porozite değerleri %0,32-28,89; permeabilite değerleri 0,03 ilâ 32,30 mD arasında değişmektedir.

Üretilen petrolün API Gravite değerleri 19,00-70,00 arasında değişmektedir. Kaynak kayasını Derdere, Beloka (Dirik Üyesi), Sayındere, Dadaş formasyonları oluşturmada, Grup II ve II+III petroleri içerisinde yer almaktadır.

2020 yılına kadar 6 sahadan Garzan ve Derdere formasyonları ile birlikte Sinan Formasyonu Alt Üyesi'nden 93.526.522 varil üretim yapılmıştır.

### Sinan Formasyonu Üst Üyesi

X. Bölge'nin kuzeybatısında dar bir alan ile X. Bölge'nin kuzeyinde yayılım gösteren Orta Paleosen yaşlı Sinan Formasyonu Üst Üyesi genel anlamda üste doğru sığlaşan bir karbonat istif özelliğindedir. Şeyl-marn ara bantları içeren kireçtaşı-dolomit ardalanmasından oluşur.

Regresif özellikli Sinan Formasyonu Üst Üyesi'nin karbonatları gel-git düzlüğü, şelf lagünü, şelf kenarı karbonat yığışım kompleksi (sığlık-sığlık yamacı) ve açık şelf-yamaç ortamlarına ait fasiyeslerden oluşmaktadır.

Gel-git düzlüğü çökelleri yer yer şeyl ve evaporit ara bantları içeren dolomikrit/dolomikrosparitlerden oluşmaktadır. Birimin en üst seviyelerinde yer alan bu dolomitlerin porozite değerleri %0,98-51,23; permeabilite değerleri 0,01-51,77 mD arasında değişmektedir. Silivanka Sinan Sahası'nın üretim seviyesini oluştururlar.

Şelf lagünü çökelleri küçük bentik foraminiferli çamurtaşı/vaketaşı fasiyesi ile temsil edilmektedir. Silivanka, Silivanka Sinan ve Batı Silivanka sahalarında gel-git düzlüğü dolomitleri ile birlikte rezervuar seviyeleri oluştururlar. Ancak, ortalama poroziteleri dolomitlerden daha azdır.

Şelf kenarı karbonat yığışım kompleksi (sığlık-sığlık yamacı) çökelleri yeşil algli, peloidli, bentik foraminiferli, biyoklastik vaketaşı/istiftaşı; bentik foraminiferli, intraklast-peloidli istiftaşı/tanetaşı; peloid-intraklastlı, yeşil algli, biyoklastik istiftaşı/tanetaşı ve bentik foraminiferli, algli, mercanlı istiftaşı (bağlamtaşı) fasiyeslerinden oluşmaktadır. Çimentolanmanın etkin olmadığı alanlarda (Yanarsu

Sahası) rezervuar özelliğine sahiptirler, üretime katkı sağlarlar. Bu fasiyeslerin porozite değerleri %0,11-27,63; permeabilite değerleri 0,01-136,56 mD arasında değişmektedir.

Açık şelf-yamaç çökelleri hemi-pelajik killi kireçtaşlarından oluşmakta, rezervuar özelliği taşımamaktadırlar.

Üretilen petrolün API gravite değerleri 12,05-21,50 arasında değişmektedir. Petrolün kaynak kayasını Sayındere, Beloka (Dirik Üyesi), Derdere formasyonları ile muhtemel Cudi Grubu'nun Şenoba Formasyonu oluşturmakta, Grup II ve I+II petrolleri içerisinde yer almaktadır.

2020 yılına kadar sadece 2 sahadan Garzan Formasyonu'yla birlikte toplam 1.180.771 varil petrol üretimi yapılmıştır.

### GERMAV FORMASYONU

GDA'da "Alt" ve "Üst" şeklinde gayri resmi olarak iki üyeye ayrılan Germav Formasyonu, orta-Geç Maastrichtiyen dönemi başlangıcından Geç Paleosen sonuna kadar geçen zaman aralığında çökelmiş denizel kırıntılı çökellerden oluşmaktadır.

Germav Formasyonu'nu oluşturan litolojilerin genelde rezervuar özellikleri yoktur. Ancak, bazı alanlarda Doğu Yananköy, Yananköy, Mağrip, Kurtalan, Kedil sahalarında Germav Formasyonu Alt Üyesi'nde gözlemlendiği gibi çatlaklanma ile rezervuar özelliklerine sahip olabilmektedirler.

Germav Formasyonu Alt Üyesi çatlaklarından üretilen petrolün API gravite değeri 15,00-38,50 arasında değişmektedir. Kaynak kayası Sayındere, Beloka (Dirik Üyesi), Karaboğaz, Karababa (A Üyesi), Derdere, Şenoba formasyonu olup, Grup I, II ve I+II petrolleri içerisinde yer alır.

2020 yılına kadar 5 sahadan diğer formasyonlarla birlikte toplam 18.646.656 varil petrol üretimi yapılmıştır. Sadece Kurtalan Sahası'ndan Germav Formasyonu Alt Üyesi'nden üretim yapılırken, diğer dört sahada Bozova, Garzan, Karababa formasyonları üretime eşlik etmişlerdir.

### NUSAYBİN FORMASYONU

X. Bölge'nin güneyinde yer alan sahalarda yayılım gösteren Nusaybin Formasyonu düşük eğimli karbonat yamacında (ramp) çökelmiş kireçtaşı, dolomit ve marnlardan oluşmaktadır.

Karbonat kum sığılı (ramp crest) çökelleri peloidli, biyoklastik tanetaşlarından oluşmakta, iyi kalitede bir rezervuar özelliği sunmaktadır. %17,39 ortalama poroziteye ve 78,66 mD permeabiliteye sahiptirler. Bazı alanlarda (özellikle İkiztepe Sahası) dolomitleşme olumlu yönde etki yaparak porozitenin artmasına neden olmuştur. Fasiyesin bazı seviyelerinin dolomitleşmesi sonucu oluşan dolomikrosparit/dolosparitlerin ortalama porozitesi %17,72; permeabilitesi 208,29 mD'dir.

Sıhık önü (yamaç-outer ramp) çökelleri fosfat pelletli, biyoklastik istiftaşı; planktik foraminiferli,

peloidli, biyoklastik istiftaşı ve killi, kavkılı, planktik foraminiferli vaketaşı-istiftaşı fasiyeslerinden oluşmaktadır.

Fosfat pelletli, biyoklastik istiftaşlarının genelde rezervuar özellikleri yoktur. Ancak dolomitleşme ile (İkiztepe sahası gibi) rezervuar özelliğini kazanabilmektedirler.

Planktik foraminiferli, peloidli, biyoklastik istiftaşlarının ortalama porozitesi %20,09; permeabilitesi 51,48 mD'dir. Bölgede ikinci derece önemli rezervuar fasiyesi oluşturur.

Killi, kavkılı, planktik foraminiferli vaketaşı-istiftaşlarının genelde rezervuar özelliği taşımazlar, yer yer zayıf-çok zayıf rezervuar özellikleri gösterirler.

Petrolün sahalarda bazında API gravitesi 11,20-15,61 arasında değişmektedir. Grup-I petrollerinin içinde yer alan petrolün kaynak kayasını Cudi Grubu birimleri oluşturmaktadır.

2020 yılına kadar 4 sahadan 15.476.658 varil petrol üretimi yapılmıştır.

### ANTAK FORMASYONU

Genelde, X. ve XI. bölgelerin kuzeyinde yayılım gösteren Antak Formasyonu karasal kökenli klastik bir birimdir. Çamurtaşı/şeyil, silttaşı, kumtaşı, çakıltaşı ve dolomitlerden oluşur.

Antak Formasyonu'ndan ekonomik petrol üretiminin yapıldığı tek saha olan Kurkan Sahası'nda olduğu gibi rezervuar özelliği taşıyan dolomit, çakıltaşı ve kumtaşı seviyeleri bulunmaktadır. Kumtaşlarının porozite değerleri %3,15-9,97; permeabilite değerleri 0,01-2,56 mD arasında değişir. Dolomitlerin porozite değerleri %1,19-13,09; permeabilite değerleri 0,03-0,10 mD arasında değişmektedir.

Üretilen petrolün API gravite değeri 19,00'dur. Kaynak kayasını Dadaş Formasyonu oluşturmakta, Grup III petrollerinin içerisinde yer almaktadır.

2021 yılına kadar sadece Kurkan Sahası'ndan 9.183 varil petrol üretimi yapılmıştır.

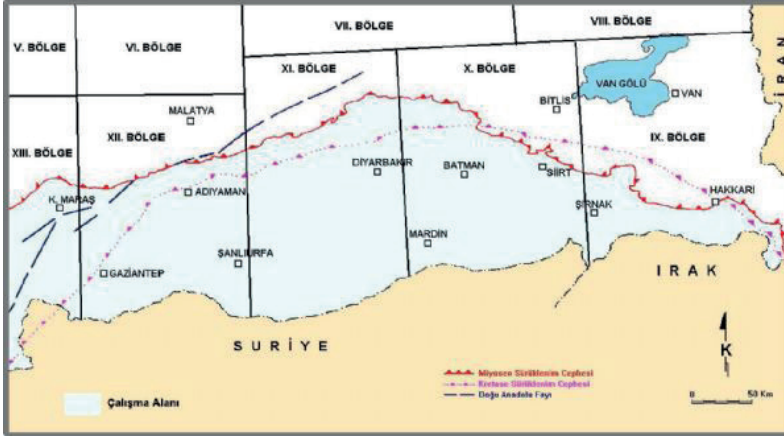
### GERÇÜŞ FORMASYONU

Gerçüş Formasyonu genellikle karasal kırmızı renkli klastik çökellerden oluşmuş bir birimdir. Çoğu yerde alt seviyelerde şeyiller ile ardalanan ve yer yer baskın olarak bulunan ince dolomit ve evaporit ara bantları da gözlenir. Bu dolomitler Dirsekli Sahası'nda olduğu gibi rezervuar özellikleri sunmakta ve bu seviyelerden petrol üretimi yapılmaktadır. Dolomikrit/dolomikrosparit karakterindeki bu dolomitler %5-18 arasında değişen oranlarda görsel porozite içermektedir.

Dirsekli Sahası'ndan üretilen petrolün API gravitesi 21,30-22,00 arasında değişmektedir. Kaynak kayasını muhtemelen Cudi Grubu oluşturmakta, Grup I petrolleri içerisinde yer almaktadır.

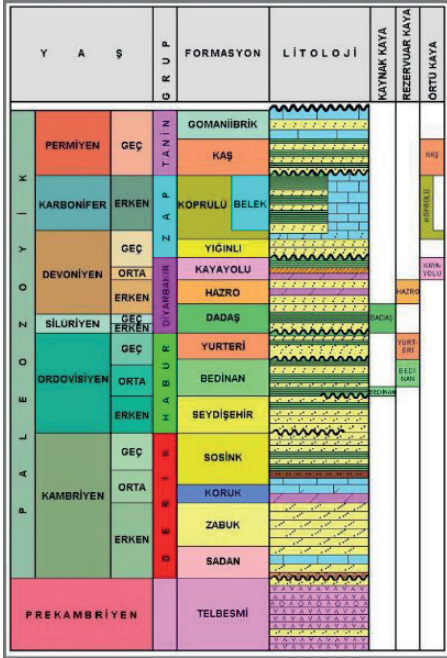
2020 yılına kadar Dirsekli Sahası'ndan sadece Gerçüş Formasyonu'ndan 43.000 varil petrol üretimi gerçekleştirilmiştir.

Şekil-1



Şekil-1. Çalışma alanı lokasyon haritası.

Şekil-2

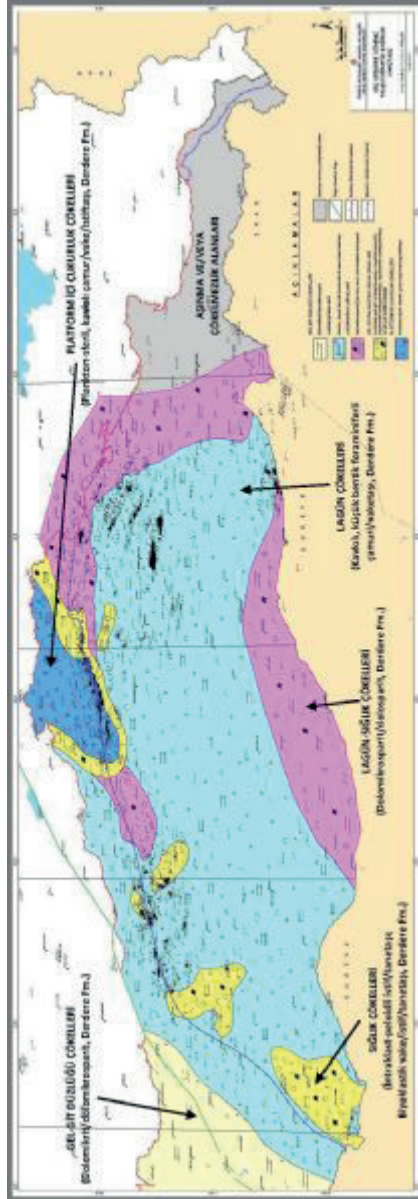


Şekil-2. Güneydoğu Anadolu Bölgesi Prekambriyen-Paleozoyik yaşlı otokton birimlerin geliştirilmiş stratigrafisi.





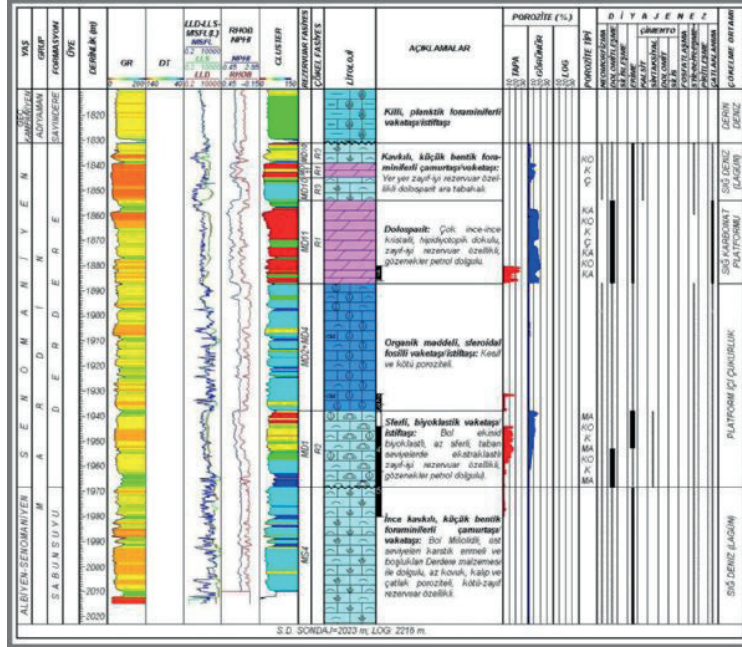
Şekil-7



Şekil-7. Mardin Grubu birimlerinden Dardere Formasyonu'nun Geç Dardere dönemindeki paleocoğrafik dağılımı.

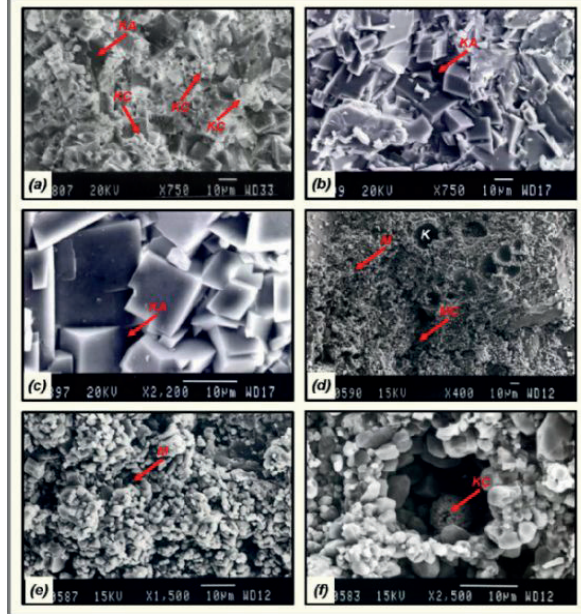


Sekil-8



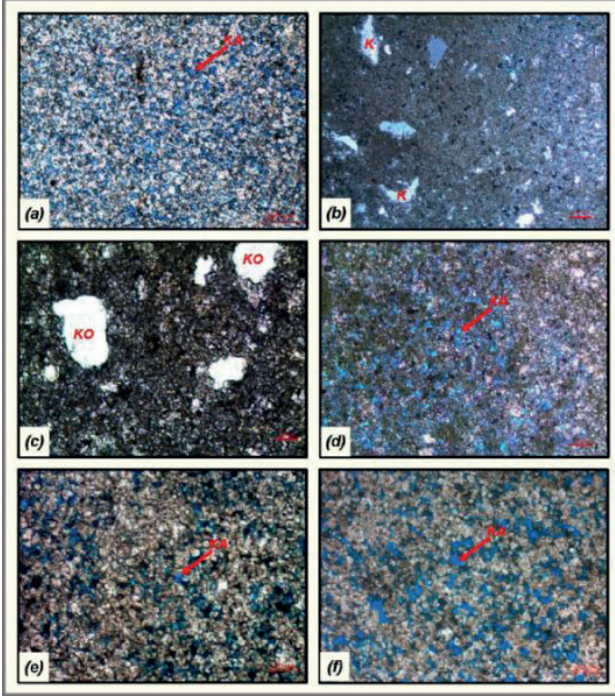
Sekil-8. Dardere Formasyonu'nun Yeniköy-36 kuyusunda çökel fasiyes, diyajenez ve rezervuar özellikleri.

Sekil-9



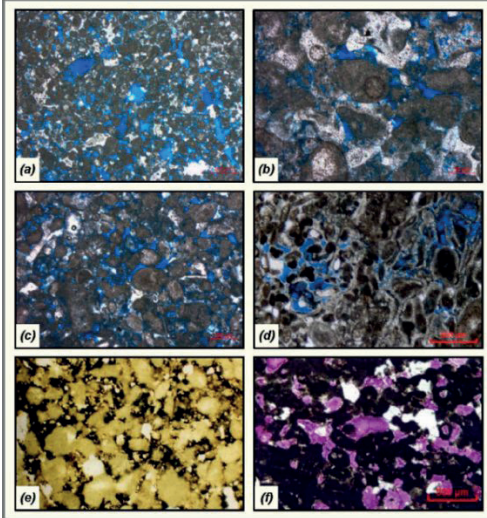
Sekil-9. Dardere Formasyonu karbonatlarının taramalı elektron mikroskop (SEM) görüntüleri (KA: Kristal arası porozite, K: Kalıp porozite, M: Matris (mikro) porozite, KÇ: Kalsit çimento). (a) Dolomitlerde kristal aralarında kısmi kalsit çimento, Didan-1, (b) (c) İnce-orta kristalli dolomitlerde kristal arası gözenekler, Ozan Sungurlu-1A, (d) (e) (f) Dardere Formasyonu'nun tabanında yer alan ve rezervuar özelliği sunan az sferik, biyoklastik vakaştaşı/istifişi çökel fasiyesinde gözenek matris, kalıp ve mikroçatlak tipindeki gözenekler ile kalıp boşluğunda gelişen ve poroziteyi olumsuz etkileyen kısmi kalsit çimento, Yeniköy-36.

Şekil-10



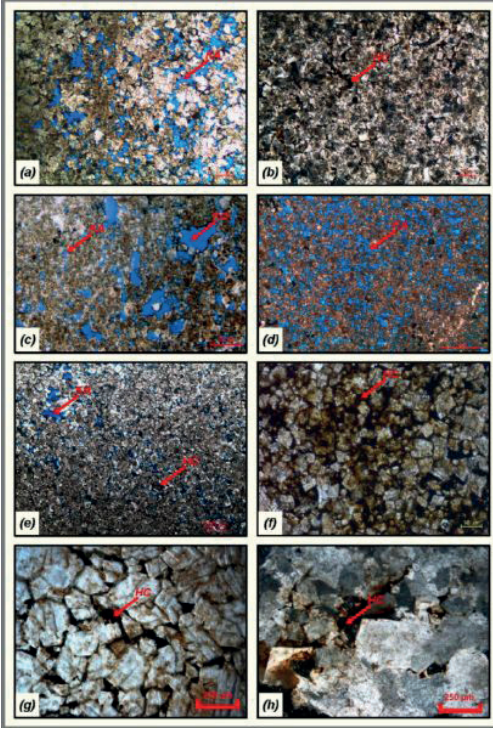
Şekil-10. Derdere Formasyonu'nun platform içi çukurluk-yamacı ortam koşullarında çökelmiş, plankton-sferli, kavkılı çamurtaşı/vaketaşı/istiftaşı çökel fasyesinin diyajenezi sonucu oluşmuş dolomikrosparit/çok ince kristalli dolosparitlerin mikrofotografları (Mavi alanlar poroziteyi (KA: Kristal arası, KO: Kovuk) göstermektedir). (a) Beykan-61, (b) Hoşan-3 (c) Güney Kırtape-11, (d) Hoşan-3, (e) Hançerli-6, (f) Camveren-1.

Şekil-11



Şekil-11. Derdere Formasyonu'nun karbonat kum sığığı çökel fasyeslerinden intraklast-peloidli istiftaşı/tanetaşı çökel fasyesinin mikrofotografları. Kalsit çimentolanma taneler arası boşluk alanlarını tamamen dolgulayamamış ve ilksel tane arası porozite kısmen korunmuştur (Mavi ve pembe alanlar poroziteyi, kahve renkli alanlar petrol dolgularını göstermektedir). (a) (b) (c) Barbeş-25, (d) Doğu Beşikli-2, (e) Çukurtaş-4, (f) Yakacık-1.

Şekil-12



Şekil-12. Derdere Formasyonu'nun birinci derece önemli rezervuar seviyelerini oluşturan dolosparitlerin mikrofotografı (Mavi alanlar poroziteyi (KA: Kristal arası; KO: Kovuk), kahverenkli alanlar petrol dolgularını (HC) göstermektedir). (a) Cendere-9, (b) Çemberlitaş-5, (c) Doğu Beşikli-2, (d) Yeniköy-36, (e) Karakuş-5, (f) Hasankeyf-1, (g) Reşan-5, (h) Yolacı-3.

Tablo-1. Mardin Grubu karbonatlarının XII. ve XI. bölgeler ile X. Bölge batı alanlarında çökelme evreleri ve çökelme fasiesleri.

ÇÖKELME EVRESİ	FORMASYON	ÇÖKELME FASİYESLERİ	ÇÖKELME ORTAMI			
III	REGRESİF	KARABABA	C ÜYESİ	BIYOKLASTİK VAKETAŞI/İSTİFTAŞI	SİĞ KARBONAT PLATFORMU	OKSİK
	DURAYLI		B ÜYESİ	SFER-PLANKTİK FORAMİNİFERLİ, BIYOKLASTİK VAKETAŞI/İSTİFTAŞI	PLATFORM İÇİ	ANOKSİK-OKSİK
	TRANSGRESİF		A ÜYESİ	ORGANİK MADDELİ, PLANKTİK FORAMİNİFERLİ VAKETAŞI/İSTİFTAŞI	ÇUKURLUK	ANOKSİK
II	REGRESİF	DERDERE	KIREÇ ÇAMURTAŞI	GEL-GİT DÜZLÜĞÜ	OKSİK	
			ALGAL ÇAMURTAŞI/BAGLAMTAŞI	KARBONAT KUM SİĞLİĞİ		
			DOLOMİKİRİT/DOLOMİKROSPARİT			
			INTRAKLAST-PELOİDLİ İSTİFTAŞI/TANETAŞI			
			INTRAKLAST-PELOİDLİ, BIYOKLASTİK İSTİFTAŞI/TANETAŞI			
	OLİTİK TANETAŞI					
BIYOKLASTİK VAKETAŞI/İSTİFTAŞI	LAGÜN					
KAVKILI, KÜÇÜK BENTİK FORAMİNİFERLİ ÇAMURTAŞI/VAKETAŞI	LAGÜN-KARBONAT KUM SİĞLİĞİ					
DOLOMİKROSPARİT/ÇOK İNCE-İNCE-ORTA KRİSTALLİ DOLOSPARİT	PLATFORM İÇİ	ANOKSİK				
TRANSGRESİF	ÇOK İNCE-İNCE KRİSTALLİ DOLOSPARİT	ÇUKURLUK	OKSİK			
PLANKTON-SFERLİ, KAVKILI ÇAMURTAŞI/VAKETAŞI/İSTİFTAŞI	PLATFORM İÇİ	ÇUKURLUK	ANOKSİK			
ORGANİK MADDELİ, SFERLİ ÇAMURTAŞI/VAKETAŞI/İSTİFTAŞI						
AZ SFERLİ, BIYOKLASTİK VAKETAŞI/İSTİFTAŞI						
I	REGRESİF	SABUNSUYU	DOLOMİKİRİT/DOLOMİKROSPARİT	GEL-GİT DÜZLÜĞÜ	OKSİK	
	DURAYLI		BIYOKLASTİK İSTİFTAŞI/TANETAŞI	ŞELF LAGÜNÜ (SİĞLİK)		
			KAVKILI, PELOİDLİ İSTİFTAŞI/TANETAŞI	ŞELF LAGÜNÜ (SİĞLİK)		
			BIYOKLASTİK VAKETAŞI/İSTİFTAŞI	ŞELF LAGÜNÜ (SİĞLİK)		
	ÇOK İNCE-İNCE-ORTA KRİSTALLİ DOLOSPARİT		ŞELF LAGÜNÜ (SİĞLİK)			
	ALGAL DOLOMİKİRİT/DOLOMİKROSPARİT (DOLOMITLEŞMİŞ ALGAL DOLOMİKİRİT/DOLOMİKROSPARİT)	GEL-GİT DÜZLÜĞÜ				
	TRANSGRESİF	AREBAN	KUMLU DOLOMİKİRİT	KIYI ÇİZGİSİ		
KUMTAŞI						
ŞEYL						

Tablo-2. Derdere Formasyonu çökel/litofasiyeslerinin tapa porozite ve permeabilite değerleri.

FASİYES	FASİYES NO	POROZİTE (%)			PERMEABİLİTE (smv, mD)			VERİ SAYISI
		MIN.	MAX.	ORT.	MIN.	MAX.	ORT.	
AZ SFERLİ, BİYOKLASTİK VAKETAŞI/İSTİFTAŞI	MD1	0,19	17,13	8,79	0,01	2,23	0,24	83
ORGANİK MADDECE ZENGİN, SFEROİDAL FOSİLLİ VAKETAŞI/İSTİFTAŞI	MD2	0,01	17,47	1,63	0,01	13,39	0,35	184
ÇOK İNCE KRİSTALLİ DOLOSPARİT	MD3	1,86	6,02	2,91	0,02	0,08	0,05	7
PLANKTON SFERLİ, KAVKILI ÇAMURTAŞI/VAKETAŞI/İSTİFTAŞI	MD4	0,05	32,01	7,10	0,00	68,29	0,91	387
DOLOMİKROSPARİT/ÇOK İNCE-İNCE KRİSTALLİ DOLOSPARİT	MD5	1,04	30,37	14,99	0,00	330,00	15,65	207
İNTRAKLAST-PELOİDLÜ İSTİFTAŞI/TANETAŞI	MD6	0,04	31,66	8,07	0,01	251,96	4,62	166
İNTRAKLAST-PELOİDLÜ, BİYOKLASTİK İSTİFTAŞI/TANETAŞI	MD7	0,66	10,82	6,50	0,02	26,00	1,04	39
OOLİTİK TANETAŞI	MD8	2,18	9,18	6,83	0,03	1,85	0,51	7
BİYOKLASTİK VAKETAŞI/İSTİFTAŞI	MD9	0,01	32,19	7,29	0,01	673,00	14,28	135
KAVKILI, KÜÇÜK BENTİK FORAMİNERLİ ÇAMURTAŞI/VAKETAŞI	MD10	0,01	26,70	8,62	0,01	1.122,00	6,54	257
DOLOMİKROSPARİT/ÇOK İNCE-İNCE-ORTA KRİSTALLİ DOLOSPARİT	MD11	0,09	31,20	12,60	0,01	1.733,98	50,20	645
KİREÇ ÇAMURTAŞI	MD12							0
ALGAL ÇAMURTAŞI (BAĞLAMTAŞI)	MD13	1,15	2,91	1,81	0,01	0,04	0,03	3
DOLOMİKRİT/DOLOMİKROSPARİT	MD14	7,61	35,91	27,14	0,06	88,49	31,70	11
ANHİDRİT	MD15	3,76	3,76	3,76	0,10	0,10	0,10	1
<b>DERDERE FORMASYONU GENELİ</b>		<b>0,01</b>	<b>35,91</b>	<b>9,44</b>	<b>0,01</b>	<b>1.733,98</b>	<b>20,38</b>	<b>2.132</b>

Tablo-3. Dardere Formasyonu'nun genel rezervuar özellikleri.

REZERVUAR BİRİM	DERDERE FORMASYONU		
<b>I. REZERVUAR TANIMI VE FİZİKSEL ÖZELLİKLERİ</b>			
KEŞİF KUYUSU	Kayaköy-2		
KEŞİF TARİHİ	1961		
ÜRETİME BAŞLAMA TARİHİ	Mayıs 1961		
YAPI	Antiklinal		
KAPAN	Yapısal		
LİTOLOJİ	Dolomit+Kireçtaşı		
YAŞ	Senomanyen		
SONDAJ DERİNLİĞİ (m)	1.439 (Yatır)-4.330 (Kayayolu)		
SU/PETROL KONTAĞI (-m)	491 (Yatır)-2.490 (Kayayolu)		
ORTALAMA GÖZENKLİLİK (%)	4 (Karadut; Bölükayla)-20 (Kartaltepe)		
ORTALAMA GEÇİRGENLİK (mD)	0,25 (Yerigüzel)-5.400 (Bostanpınar)		
ORJİNAL SU DOYMUŞLUĞU (%)	15 (Bektaş, Güney Şahaban)-65 (Tokaris)		
<b>II. ÜRETİM SAHALARI</b>	Adıyaman, Akpınar, Alçık, Alibey, Bahçecik, Barbeş, Batı Fırat, Batı Gökçe, Batı Kayaköy, Batı Malatepe, Batı Migo, Bayısu, Bektaş, Beyaz Çeşme, Beykan, Bostanpınar, Bozhüyük, Bölükayla, Canveren, Cendere, Çemberlitaş, Çıksor, Çobantepe, Didan, Dirsekli, Dodan, Doğu Beşikli, Doğu Çemberlitaş, Doğu Sadık, Doğu Yatır, Doğu Yeniköy, Eskitaş, Göküçü, Güney Beykan, Güney Hazro, Güney Karakuş, Güney Kayaköy, Güney Kırtepe, Güney Kurkan, Güney Sarıcak, Güney Sarık, Güney Şahaban, Güneydoğu Şahaban, Haçerli, İkizce, Karaali, Karacan, Karadut, Karakilise, Karakuş, Kartaltepe, Kastel, Katin, Kayaköy, Kayayolu, Kervan, Köprü, Köşeler, Köşk, Kurkan, Kuzey Karakuş, Kuzey Migo, Malatepe, Mehmeddere, Miyadin, Ozan Sungurlu, Petek, Piyanko, Sarıcak, Sebyan, Sinca n, Şahaban, Tokaris, Ulaş, Varınca, Yalankoz, Yatır, Yeniköy, Yerigüzel, Yeşildere, Yolaçan		
<b>III. REZERVUAR FASİYESLERİ</b>	<b>Porozite (%)</b>	<b>Permeabilite (mD)</b>	<b>Porozite Tipi</b>
Az sferli, biyoklastik vaketaşı/istiftaşı (MD1)	8,79	0,24	Matriks, mikrokalıp, çatlak
Plankton-sferli, kavrılı çamurtaşı/vaketaşı/istiftaşı (MD4)	7,10	0,91	Matriks, kovuk, çatlak, stilolit
Dolomikrosparit/çok ince-ince kristalli dolosparit (MD5)	14,99	15,65	Kristal arası, kovuk, çatlak
İntraklast-peloidli istiftaşı/tanetaşı (MD6)	8,07	4,62	Tane arası, tane içi, kovuk, kalıp
İntraklast-peloidli, biyoklastik istiftaşı/tanetaşı (MD7)	6,50	1,04	Tane arası, tane içi, kovuk, kalıp
Oolitlik tanetaşı (MD8)	6,83	0,51	Tane arası, tane içi, kovuk, kalıp
Biyoklastik vaketaşı/istiftaşı (MD9)	7,29	14,28	Matriks, kovuk, kalıp, tane içi, çatlak
Kavrılı, küçük bentik foraminiferli çamurtaşı/vaketaşı (MD10)	8,62	6,54	Tane içi, kovuk, kalıp
Dolomikrosparit/çok ince-ince-orta kristalli dolosparit (MD11)	12,60	50,20	Kristal arası, kovuk, kalıp, çatlak
<b>IV. AKIŞKAN ÖZELLİKLERİ</b>			
API GRAVİTESİ (°)	12,00 (Araban)-41,37 (Beyaz Çeşme); Ortalama: 29,70		
KÜKÜRT ORANI (%)	0,20 (Göküçü, Güney Kırtepe, Karacan)-4,70 (Didan); Ortalama: 1,02		
FORMASYON SUYU TUZLULUĞU (ppm)	1.000 (Yerigüzel)-215.000 (Kayayolu)		
<b>V. PETROLÜN KÖKENİ</b>			
PETROL GRUBU	I; I+II; II; II+III; III		
KAYNAK KAYA	Dardere; Cudi; Dadaş		
<b>VI. ÜRETİM BİLGİLERİ (01.01.2020)</b>			
KÜMÜLATİF PETROL ÜRETİMİ (stb)	616.662.751		
2019 YILI ÜRETİMİ (stb)	10.099.444		
<b>VII. ÜRETİM YAPAN DİĞER BİRİMLER</b>	Sinan (Alt), Garzan, Kastel, Sayındere, Karaboğaz, Karababa, Sabunyu, Hazro, Yurteri		

# Rezervuar Kompartmanlarının Belirlenmesinde Jeokimyasal Yaklaşım: Çakıllı Sahası Geochemical Approaches for Determination of Reservoir Compartments: Çakıllı Field



**Hüsnü Corbacıoğlu, Serdar Doğan, Yağmur Sümer Görenekli, Samet Öksüz**  
Türkiye Petrolleri A.O. Ar-Ge Merkezi Jeokimya Müdürlüğü Ankara / Türkiye

Petrol rezervuarlarında bulunan akışkanların (su, petrol, gaz) bileşimleri hem yanıl hem de dikey yönde heterojendir. Rezervuar jeokimyasının asıl amacı da bu heterojenliğin nedenlerinin belirlenmesi ve bu bilgilerin üretim ve geliştirme stratejilerinde uygulanmasıdır. Bu anlamda rezervuar jeokimyası, rezervuar jeolojisi ile mühendislik arasında bir bağdır. Rezervuar jeokimyası çalışmalarının temelini jeokimyasal örnekleme ve analizler oluşturmaktadır.

Çakıllı Sahası, Türkiye Petrolleri A.O. tarafından yeni üretime başlanmış sahalardandır. Çakıllı Sahası'ndan 18 adet petrol üretimi yapan kuyudan petrol numuneleri alınarak rezervuar jeokimyası çalışması yapılmıştır. Bu çalışmalar sonucunda çalışılan alandaki petrolerin bileşimindeki farklılıklar tespit edilerek haritalanmış, kompartmanlaşma, rezervuar devamlılığı, sahadaki petrol dolun yönü konularına yaklaşımlarda bulunulmuştur. Bu değerlendirmeler sonucunda, Çakıllı Sahası'nda 6 farklı rezervuar devamlılık alanı (kompartmanı) tespit edilmiştir.

The compositions of fluids (water, oil, gas) in petroleum reservoirs are heterogeneous both laterally and vertically. The main objective of reservoir geochemistry is to determine the causes of this heterogeneity and to apply this knowledge in production and development strategies. In this sense, reservoir geochemistry is a link between reservoir geology and engineering. The basis of reservoir geochemistry studies is geochemical sampling and analysis.

Çakıllı Field is one of the fields where production has recently started by Türkiye Petrolleri A.O. Reservoir geochemistry studies were conducted by taking oil samples from 18 oil producing wells in Çakıllı Field. As a result of these studies, we identified and mapped the differences in the composition of the oils in the field, and approached the issues of compartmentalization, reservoir continuity and the direction of oil filling in the field. As a result of these evaluations, we identified 6 different reservoir continuity areas (compartments) in Çakıllı Field.

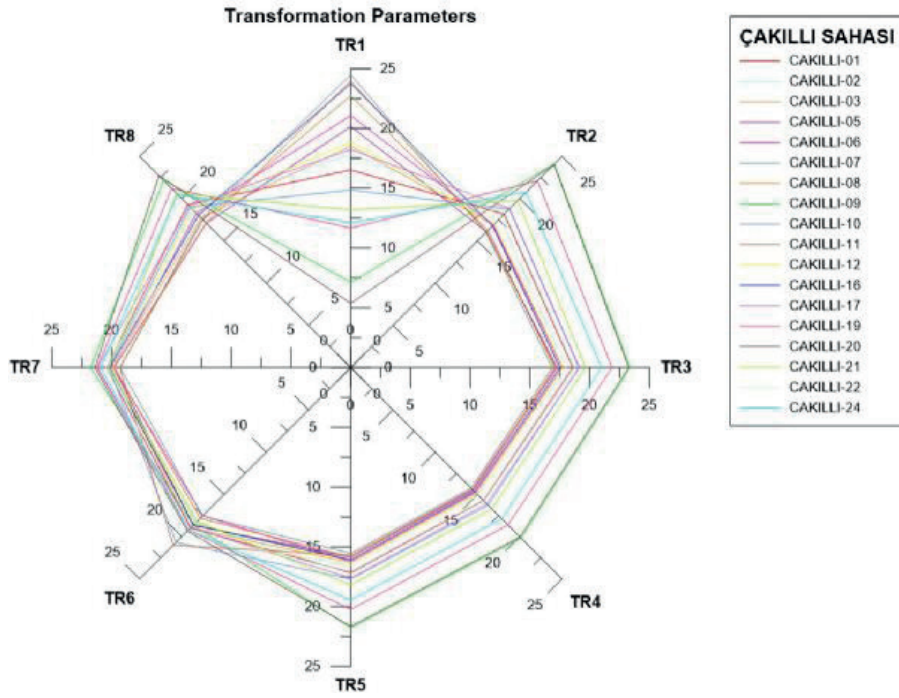
## ANALİZ VE DEĞERLENDİRME YÖNTEMLERİ

Alınan petrol örneklerinin hafif uçlarını kaybetmemesi için özel teknikler kullanılmış ve soğuk zincir transfer yöntemi ile laboratuvara taşınması sağlanmıştır. Bu örnekler üzerinde API gravite, Gaz Kromatografi, Gaz Kromatografi-Kütle Spektroskopisi analizleri uygulanmıştır. Bu analizlerden elde edilen veriler çeşitli yıldız diyagramları ve istatistiksel yöntemler kullanılarak değerlendirilmiştir.

## SONUÇLAR

Yapılan inter-alkan, halpern ve istatistiksel çalışmalar sonucunda çalışılan alandaki petrolerin bileşimindeki farklılıklar tespit edilerek haritalanmış, kompartmanlaşma ve rezervuar devamlılığı konularına yaklaşımlarda bulunulmuştur. Bu değerlendirmeler sonucunda, Çakıllı Sahası'nda 6 farklı rezervuar devamlılık alanı (kompartmanı) tespit edilmiştir. Bu kompartman içi alanlarda, kuyu yoğunluğu ve veri kalitesi göz önüne alınarak, üretimi geliştirme faaliyetleri açısından önemli risk düşümü sağlanabilecektir.

Anahtar Kelimeler: Jeokimya, rezervuar



Çakıllı Sahası Halpern Grafiği

# Improved Permeability Prediction of a Heterogeneous Carbonate Reservoir Using Pore-Space and Pore Type Characterization



**İbrahim Olgun Uğurlu**

Turkish Petroleum Corporation, Ankara, TP R&D Center/Sedimentology&Reservoir Geology Department

Carbonate reservoirs are known as heterogeneous reservoirs due to containing a variety of pore types caused by depositional setting and the diagenetic process (Weger et. Al, 2009, Arifianto et.al, 2018). The purpose of this study is to quantify pore-space geometry in thin sections and develop an empirical diagenesis coefficient (D) for different pore types based on their contribution to the fluid flow. In this study, 87 core plugs were taken from a carbonate reservoir, and these core plug samples were cleaned in a Soxhlet extraction apparatus using hot toluene and methanol for porosity/permeability measurements. 2 thin section samples were prepared from the end trims of each core plug and the samples were epoxy impregnated for further digital image analysis (DIA). Parameters of pore-space geometry such as thin section porosity (TSP, %), dominant pore size (DOMsize), tortuosity (PoA), and aspect ratio (AR) are calculated using the DIA in epoxy impregnated thin sections and major/minor pore types are determined for each thin section. Reservoir characterization method based on through Flow Zone Indicator (Amafeule, 1993) is used to delineate flow units (Figure 1). 5 different flow units are determined and every flow unit has distinctive depositional texture and diagenetic process. Aforementioned pore-space parameters are calculated for these five distinctive pore facies (Figures 2, 3, 4, 5, and 6). Different pore types such as matrix-leached intergranular porosity, separate & touching vugs, matrix porosity, and microporosity are identified in the thin sections, and diagenesis coefficients are appointed to them accordingly (Lucia, 2007, Tonietto et. al, 2014) (Figure 7 and 8). Pore-space parameters and diagenesis coefficients are linked to the permeability of the core plug samples and the best predictors of permeability are determined using multivariate regression analysis. The correlation between the permeability of the core plug samples and pore-space parameters resulted in a coefficient of determination of  $R^2=0.69$  (Figure 9 and Table 1). Thus, pore space parameters alone are able to explain 69% of the variation of permeability. However, pore-space parameters do not take into account that each pore type has a different contribution to the fluid flow, so there is a need to develop diagenesis coefficient (D) to account for this phenomena. Combining these parameters with diagenesis coefficient improves the coefficient of determination permeability estimates from 0.69 to 0.81 (Table 2). Based on the multivariate regression analysis of the different parameters, it is inferred that the best predictors of permeability are PoA (tortuosity), TSP (thin section porosity, %) DOMsize (dominant pore size), and diagenesis coefficient (D). Different pore facies (PF) identified in the thin sections were integrated with log effective porosity and results reveal that intervals with the highest log effective

porosity contains PF1&PF2 that have the highest value of flow units (Figure 10).

## INTRODUCTION

Pore characteristics of a rock is dependent on the type and geometry of the pore system and they are the key to improving reservoir description and exploitation (Chehrizi et. al, 2010) Digital image analysis (DIA) is a well-known method of quantifying pore geometry of a rock from images of thin sections (Anselmetti et. al, 1998, Weger. et., al, 2009). The DIA has been used to characterize pore space quantitatively from blue-dyed epoxy impregnated thin sections and thin section porosity (%), dominant pore size (DOMsize), aspect ratio (AR), tortuosity (PoA) can be derived from thin sections using the DIA based pore space quantification (Anselmetti et. al, 1998, Weger et. al, 2009). The aim of this study is to determine the DIA-based pore space parameters and produce an empirical diagenesis coefficient based on pore types and correlate these parameters with permeability.

## METHODOLOGY

In this study, 87 core plugs (all having a diameter of 1.5 inch) were taken from a carbonate reservoir, and these core plug samples were cleaned in a Soxhlet extraction apparatus using hot toluene and methanol for porosity/permeability measurements. 2 thin section samples were prepared from the end trims of each core plug and the samples were epoxy impregnated for further digital image analysis (DIA). The concept of Rock quality Index (RQI) and Flow Zone Indicator (FZI) were applied to classify core data in hydraulic flow units (HFU). 5 different flow units were identified to divide reservoir rock in the studied core intervals and pore geometry and pore type of each flow unit was established. Pore geometry data, which is the thin section porosity (%), dominant pore size (DOMsize), aspect ratio (AR), and tortuosity (PoA) was calculated using an open-source software (Image-j) from blue-dyed epoxy impregnated thin sections. Since every unique pore type has different contribution to the fluid flow (Lucia, 2007, Tonietto et. Al, 2014), the influence of the pore type was evaluated and numerical value for each pore type was produced as a diagenesis coefficient (D). Pore type (Lucia, 2007) of all thin sections were studied by petrographical observation and major/minor pore types were identified for each thin section. Pore geometry parameters combined with diagenesis coefficient were used to estimate permeability and multivariate regression analysis were used to determine the best predictors of permeability.



## RESULTS AND DISCUSSION

In this study, pore space geometry and pore type based diagenesis coefficients are used to quantify pore system to predict permeability of a heterogeneous carbonate reservoir. Based on the study dealing with the quantitative characterization of the type and geometry of the pore space, the following conclusions can be drawn:

- The correlation between the permeability of the core plug samples and pore-space parameters (thin section porosity (TSP, %), dominant pore size (DOMsize), tortuosity (PoA), and aspect ratio (AR)) resulted in a coefficient of determination of  $R^2=0.69$  (Figure 9 and Table 1).
- Combining the pore space parameters with diagenesis coefficient improves the coefficient of determination permeability estimates from 0.69 to 0.81 (Table 2).
- Based on the multivariate regression analysis of the different parameters, it is inferred that the best predictors of permeability are PoA (tortuosity), TSP (thin section porosity, %), DOMsize (dominant pore size), and diagenesis coefficient (D).
- Different pore facies (PF) identified in the thin sections were integrated with log effective porosity and results reveal that intervals with the highest log effective porosity contains PF1&PF2 that have the highest value of flow units (Figure 10).
- Quantifying pore space geometry alone is not able to explain permeability variation very well in a heterogeneous carbonate reservoir as carbonate rocks commonly contain a variety of pore types that can have different contribution to the fluid flow.
- This study can be improved by using more advanced imaging techniques such as computed tomography and providing more data (more core plugs) for multivariate regression analysis.

## REFERENCES

- Amaefule J., Altunbay M., Tiab D., Kersey D., and Keelan D., 1993 Enhanced reservoir description using core and log data to identify hydraulic flow units and predict permeability in uncored intervals/Wells SPE 26436 205–220
- Anselmetti, F. S., and G. P. Eberli, 1999, The velocity-deviation log: A tool to predict pore type and permeability trends in carbonate drill holes from sonic and porosity or density logs: AAPG Bulletin, v. 83, p. 450–466.
- Arifianto, I., Surjono, S.S., Erlangga, G., Abrar, B., Yogapurana, E., 2018. Application of flow zone indicator and Leverett J-function to characterize carbonate reservoir and calculate precise water saturation in the Kujung formation, North East Java Basin. *Journal of Geophysics and Engineering*, 15(4): 1753–1766
- Chehrizi, A., Rezaee, R., Rahimpour, H., 2011. Pore-facies as a tool for incorporation of small-scale dynamic information in integrated reservoir studies. *J. Geophys. Eng.* 8 (2), 202e224.

Eberli, G., P., Baechle, G., T., Weger, R., Massaferro, J., L., 2004, Quantitative discrimination of effective porosity using digital image analysis- implications for porosity– permeability transforms, 66th Eage Conference & Exhibition, Paris.

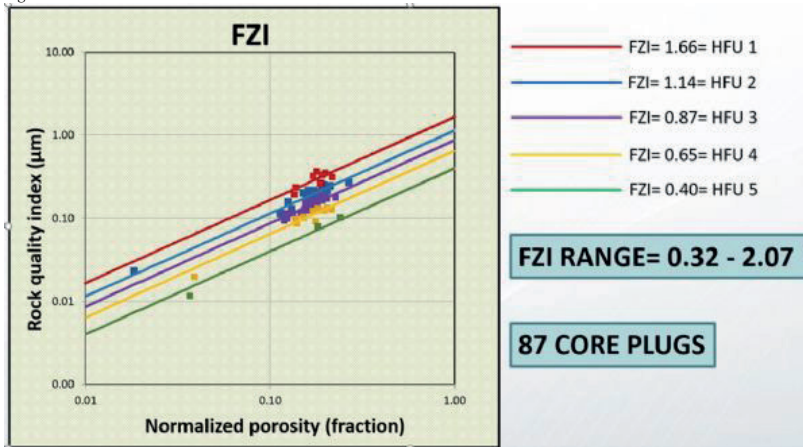
Lucia, F. J., 2007, Carbonate Reservoir Characterization; An Integrated Approach (Second Edition), Springer Berlin Heidelberg, 336 p.

Tonietto, S., N., Smoot, M., Z., Pope, M., C., 2014, Pore Type Characterization and classification in Carbonate Reservoirs: AAPG Annual Convention and Exhibition, Houston, Texas, April 6-9.

Weger, R., J., Eberli, G., P., Baechle, G., T., Massaferro, J., L., Sun, Y., 2009, Quantification of pore structure and its effect on sonic velocity and permeability in carbonates: The American Association of Petroleum Geologists, v. 93, no.10, p. 1297-1317, doi: 10.1306/05270909001.

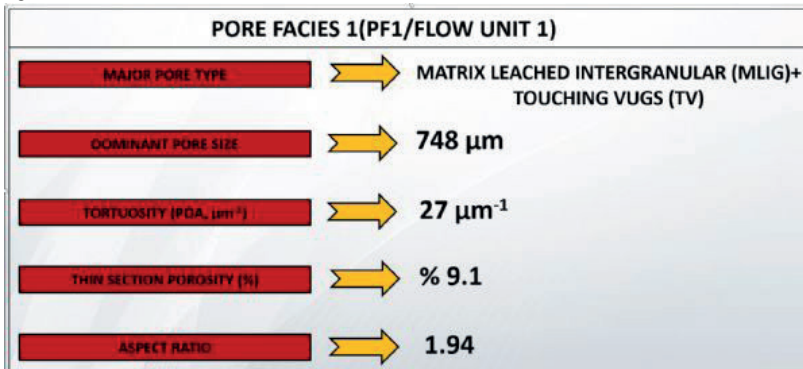
Keywords: permeability, pore space characterization

Figure 1.



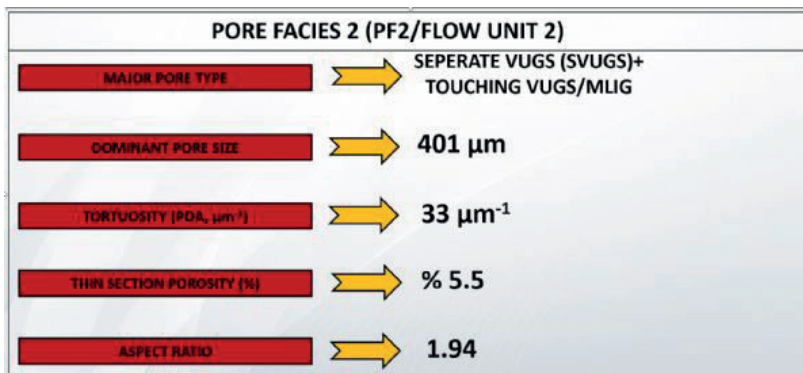
Delineation of 5 distinctive flow units

Figure 2.



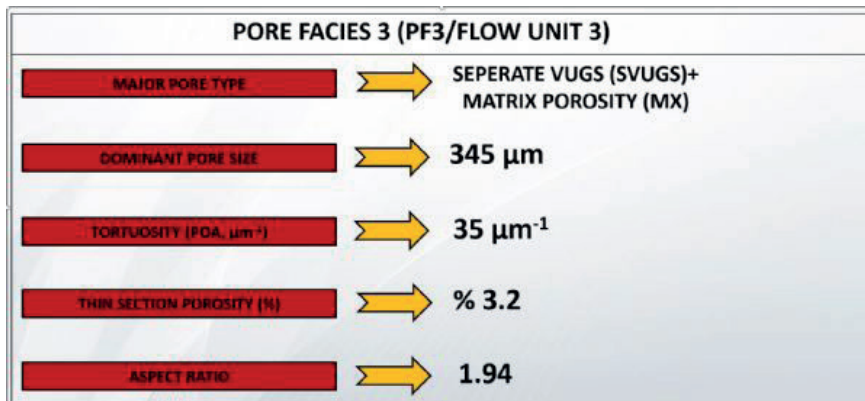
Pore-space parameters and pore types of Pore Facies 1 (PF1, Flow Unit 1).

Figure 3.



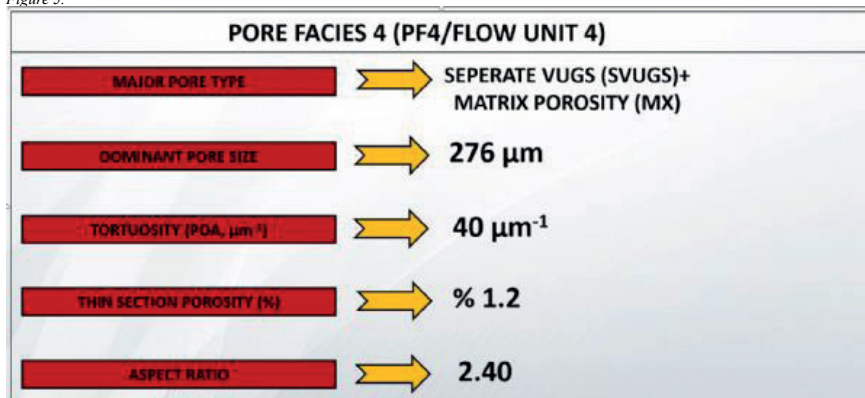
Pore-space parameters and pore types of Pore Facies 2 (PF2, Flow Unit 2).

Figure 4.



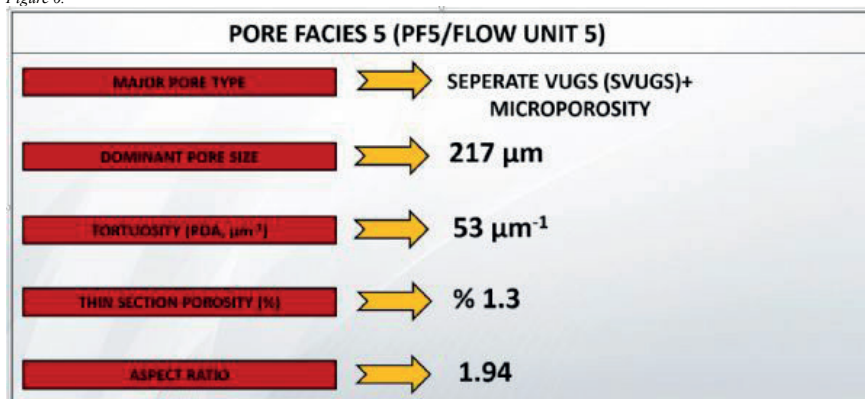
Pore-space parameters and pore types of Pore Facies 3 (PF3, Flow Unit 3).

Figure 5.



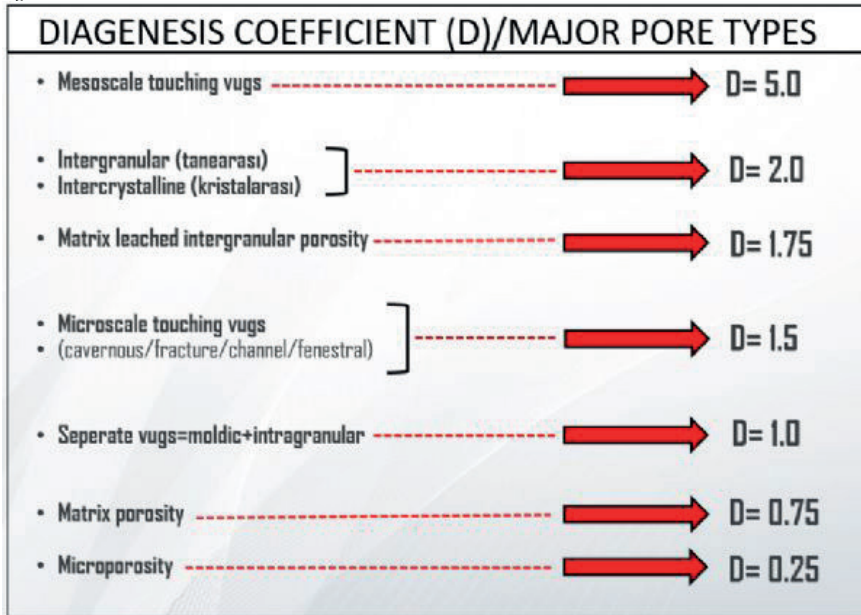
Pore-space parameters and pore types of Pore Facies 4 (PF4, Flow Unit 4).

Figure 6.



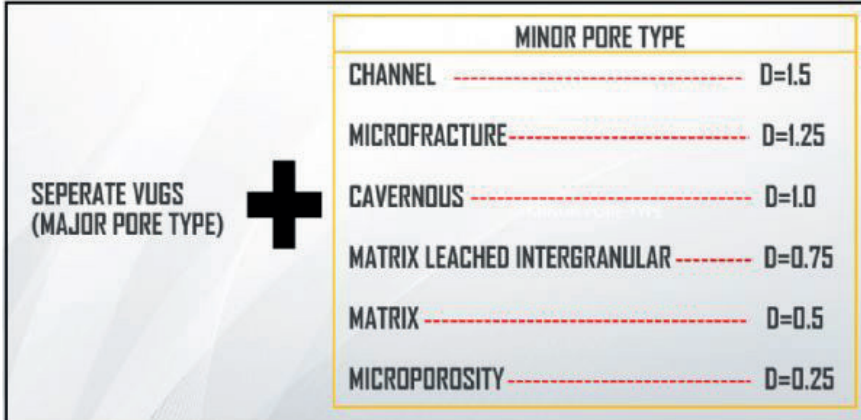
Pore-space parameters and pore types of Pore Facies 5 (PF5, Flow Unit 5).

Figure 7.



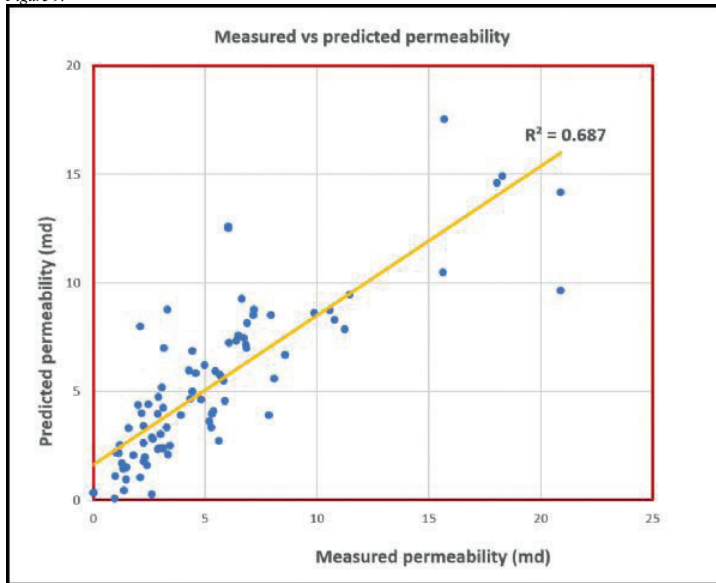
Diagenesis coefficients (D) based on major pore types

Figure 8.



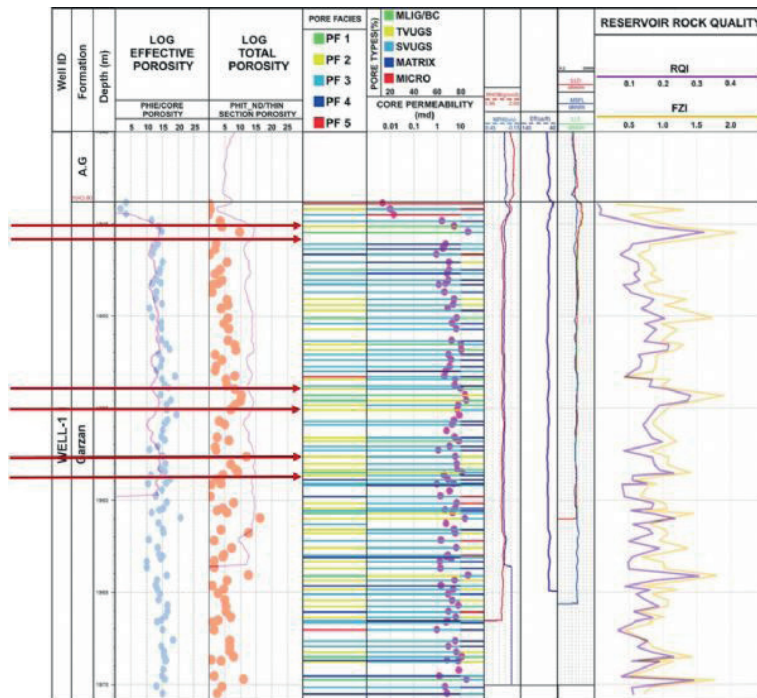
Subdivisions of diagenesis coefficients (D) (when the major pore type is seperate vugs but minor pore types are different)

Figure 9.



Predicted vs. measured permeability showing coefficient of determination of 0.687.

Figure 10.



Integration of pore facies/pore types with wireline logs, the best pore facies (PF1&PF2) corresponds to the highest log effective porosity intervals (intervals between red arrows).

Table 1.

SUMMARY OUTPUT								
<b>Regression Statistics</b>								
Multiple R	0,828833387							
<b>R Square</b>	<b>0,69</b>							
Adjusted R Square	0,671694773							
Standard Error	2,55733965							
Observations	87							
<b>ANOVA</b>								
	<i>df</i>	<i>SS</i>	<i>MS</i>	<i>F</i>	<i>Significance F</i>			
Regression	4	1176,879376	294,2198439	44,98783943	6,08403E-20			
Residual	82	536,2788591	6,539986087					
Total	86	1713,158235						
	<i>Coefficients</i>	<i>Standard Error</i>	<i>t Stat</i>	<i>P-value</i>	<i>Lower 95%</i>	<i>Upper 95%</i>	<i>Lower 95,0%</i>	<i>Upper 95,0%</i>
<b>Intercept</b>	-0,486306822	2,511206931	-0,193654619	0,846925233	-5,48189737	4,509283726	-5,48189737	4,509283726
<b>PoA</b>	0,021732899	0,023584595	0,921487055	0,35949943	-0,025184373	0,068650171	-0,025184373	0,068650171
<b>aspect ratio</b>	-0,6300061	1,289318345	-0,488635023	0,626404398	-3,194871011	1,934858811	-3,194871011	1,934858811
<b>DOMsize</b>	0,002262596	0,000829064	2,729097462	0,007769335	0,000613324	0,003911868	0,000613324	0,003911868
<b>thin section porosity</b>	0,99199915	0,098566378	10,06427514	0,00000000000000056	0,795919225	1,188079075	0,795919225	1,188079075

Multivariate regression analysis results for all of the pore-space parameters

Table 2.

SUMMARY OUTPUT								
<b>Regression Statistics</b>								
Multiple R	0,90							
<b>R Square</b>	<b>0,81</b>							
Adjusted R Square	0,80							
Standard Error	2,007613149							
Observations	87							
<b>ANOVA</b>								
	<i>df</i>	<i>SS</i>	<i>MS</i>	<i>F</i>	<i>Significance F</i>			
Regression	4	1382,656369	345,664092	85,76186253	1,71027E-28			
Residual	82	330,5018657	4,03051056					
Total	86	1713,158235						
	<i>Coefficients</i>	<i>Standard Error</i>	<i>t Stat</i>	<i>P-value</i>	<i>Lower 95%</i>	<i>Upper 95%</i>	<i>Lower 95,0%</i>	<i>Upper 95,0%</i>
<b>Intercept</b>	-7,405438078	1,27491846	-5,8085582	0,0000001157	-9,941657029	-4,869219128	-9,941657029	-4,869219128
<b>PoA</b>	0,032167507	0,017543985	1,83353483	0,0703514367	-0,002733067	0,067068081	-0,002733067	0,067068081
<b>thin section porosity</b>	0,849944216	0,079886002	10,6394637	0,0000000000	0,69102551	1,008862921	0,69102551	1,008862921
<b>DIAGENESIS COEFFICIENT</b>	6,048177931	0,843266031	7,17232487	0,0000000003	4,370653167	7,725702696	4,370653167	7,725702696
<b>DOMsize</b>	0,002293319	0,000640564	3,58015504	0,0005804218	0,001019033	0,003567606	0,001019033	0,003567606

Multivariate regression analysis showing best predictors of permeability. PoA (tortuosity), Thin section porosity (TSP%), dominant pore size (DOMsize), and diagenesis coefficient (D) are the best predictors of permeability (with R2 of 0.81)

# Use of Reservoir Geochemistry in High Water Cut Production: A Case Study in The Karakuş Field



**Placido Franco<sup>1</sup>, Roberto Galimberti<sup>1</sup>, Alara Dişpençe<sup>2</sup>, Onur Acılar<sup>2</sup>, Esra Eren Tokoğlu<sup>3</sup>, Sinem Artan Ercengiz<sup>3</sup>, Onur Yürüker<sup>4</sup>, Ceyda Çetinkaya Kayrın<sup>4</sup>, Tufan Tıgıl<sup>4</sup>**

<sup>1</sup>Geolog Technologies, Via Monte Nero 30, 20098, San Giuliano Milanese

<sup>2</sup>Geolog Turkey, Mutlukent Mah. 1972 Cad. No:7A Çankaya / Ankara / Türkiye

<sup>3</sup>TPAO Genel Müdürlüğü, Ar-Ge Merkezi Daire Başkanlığı, Söğütözü Mah. Şht. Öğretmen

Aybüke Yalçın Cad. No:10 Çankaya / Ankara / Türkiye

<sup>4</sup>TPAO Genel Müdürlüğü, Üretim Daire Başkanlığı, Söğütözü Mah. Şht. Öğretmen Aybüke

Yalçın Cad. No:10 Çankaya / Ankara / Türkiye

## INTRODUCTION

Organic geochemistry is an established discipline commonly employed in oil and gas business. The most important and well recognized applications are within exploration and appraisal stage, where it has been used to address source rock identification and characterization (both in terms of maturity and type of organic matter), oil-oil and oil-source correlations, mostly aimed to reconstruct migration pathways and integrate basin studies (Tissot and Welte, 1984). More recent applications of organic geochemistry have been successfully applied to development geology and production engineering, providing the grounds for what today represents a mature discipline commonly referred to as reservoir geochemistry. Reservoir geochemistry tools have been applied to compartmentalization identification (Slentz, 1981), assessment of producing/non-producing intervals (Maness and Price, 1977), and to characterize fluid distribution in the reservoir. All reservoir geochemistry applications rely in the so-called petroleum fingerprinting technique, consisting of the high-resolution analysis, generally via gas chromatography (GC), to assess the unique chemical composition of each oil pool as consequence of specific processes happening during migration, accumulation, and residence in the reservoir (Van Bergen et al., 2018). Reservoir geochemistry methodologies have established an outstanding track-record of successful applications, proving to deliver results in agreement with classic methodologies, with big advantages in terms of costs and practical convenience (McCaffrey et al., 2012).

The most common reservoir geochemistry application in development stage is probably the compartmentalization assessment. In fact, a detailed knowledge of reservoir continuity is essential in successful oil field development and management programs, as it provides critical information for determining well spacings for primary production, and for planning secondary and tertiary recovery programs (Hwang et al., 1994). Although there is no one standard interpretation, since all geochemistry studies need to be placed within the proper geological and reservoir engineering context, some basic rules apply (Van Bergen et al., 2018).

• Oils from a single and connected reservoir have nearly identical fingerprints, whereas oils from separate reservoirs usually have subtle but consistent differences in their fingerprints (provided sufficient time for complete mixing).

• Although different fingerprints strongly support compartmentalization, identical compositions do not necessarily imply reservoir continuity.

• If a geochemical fingerprint from a single well remains stable over time, it is assumed that the well draws from a single, well mixed hydrocarbon pool.

Fingerprints deriving from the geochemical analysis of fluids from different wells, reservoirs, or even fields, can be systematically compared by means of chemometric techniques to identify significant differences that, once properly integrated in the context, can support the identification of flow barriers/separate compartments.

The described application deals with static reservoir modelling and the understanding of fluid distribution within a field in non-perturbated conditions. Once field production and oil commingling practice are put in place, it is often necessary to back-allocate production to the distinct hydrocarbon units, also called endmembers (EMs), as well as to monitor production evolution. This is valid when dealing either with multiple well flows converging into the same pipeline (multiwell lateral allocation) or with multiple reservoir/layers simultaneously produced at the well head (multilayer vertical allocation). The described process is known as production allocation and is extremely important both for fiscal and surveillance/monitoring purposes.

Production allocation techniques based on geochemistry methods use the geochemical variability between single EMs as baseline to deconvolute the commingled oil into contributing distinct flow zones. For this task, it is necessary to have access to pure EMs and commingled oils; these are GC-fingerprinted, and the resulting data processed using mixing models and deconvolution algorithms (Sandoval et al., 2022). Quantitative production allocation based on this approach delivers accurate results, with the big advantage of being the only feasible option where budget restrictions prevent the application of more expensive methodologies such as multiphase flowmeters or Production Logging Tests. The main limitation of the described tool is represented by the need to have enough chemical diversity among the hydrocarbon pools to allocate. Moreover, the number of EMs in the system and their compositional variance strongly influence results accuracy, requiring a “feasibility” phase to evaluate the applicability to the specific scenario under investigation.

The above considerations clearly highlight how reservoir compartmentalization assessment and

production allocation are deeply correlated aspects: understanding the fluid spatial and chemical distribution across the field is pivotal to identify proper EMs and effectively contributing zones to consider in allocation calculations.

The present paper deals with a reservoir geochemistry preliminary pilot study on few wells of the Karakuş Field, aimed to improve the understanding of both fluid distribution (reservoir continuity) and multilevel production allocation.

The study area has an autochthonous sequence of the Arabian platform (stratigraphy sequence is reported in Figure 1). Amongst the intersected units, Germav, Kastel, and Sayindere Fms act as cap rocks, whereas the fractured levels of Sayindere, Karaboğaz, Karababa-C, and Derdere Fms are reservoirs. The spheroidal units in lower levels of Derdere, Karababa-A, and Karaboğaz Fms can be considered source rocks for the oil in Karakuş field. Production is conducted from all these reservoirs. The sedimentation of carbonate rocks exhibiting source rocks and reservoir rocks characteristics was a result of successive transgression and regression phases. The lithology of Derdere Fm inner platform is limestone and dolomitic limestone, and Derdere Fm is the field primary reservoir. The semi-closed basins created after the sedimentation of Derdere Fm were filled with Karababa Fm. Karababa-C member of Karababa Fm, which is located at the upper levels, consists of shallow marine bioclastic wackestones and acts as the secondary reservoir in the field. On top of Karababa, Karaboğaz Fm was deposited, which contains anoxic, deep marine, cherty limestones rich in organic matter and acts both as source rock and reservoir rock. In a compatible manner, Sayindere Fm, consisting of deep marine limestones, was deposited on top of Karaboğaz Fm. The fractured intervals at lower levels of the formation particularly exhibit reservoir characteristics.

Karakuş Field was affected by two distinct tectonic phases that occurred in the Cretaceous and Miocene. The field was divided into blocks by the compressional regime occurred in the Cretaceous, that resulted in reverse faults and thrusts, and the left-lateral movement of the Adıyaman fault occurred in the Miocene together with the parallel synthetic strike-slip faults. As a result of seismic analysis, it was determined that the specified faults were almost in vertical direction and were cutting through all formations from Sayindere to Derdere. Analysis of cores indicated that matrix porosity and permeability of the secondary reservoirs of the field were significantly low. Therefore, the prevailing opinion is that the most significant factor providing the flow in the field is the fault and fracture developments. However, the presence of a potent aquifer in the field leads to high water cuts through these faults and fractures during production.

## METHODS

To deliver meaningful fingerprinting data, a reliable sampling strategy and appropriate sample selection are critical. In general, to understand fluid connectivity,

both between multiple layers in the same well or within the same formation across multiple wells, relevant fluids from target zones, often obtained from MDT/DST samples, are analyzed, and compared. However, when dealing with production allocation/reservoir surveillance and management projects, continuous sampling multiple times per well per year is required (time-lapse geochemistry).

In the present study, oil samples from a total of nine wells and sampled at the wellhead have been GC-fingerprinted to assess potential geochemical differences to use for reservoir compartmentalization assessment and subsequent production allocation. Production oils from wells completed and producing from single formations, as well as archive DST oils, were used as EMs, while oils potentially produced from multiple layers were analyzed and interpreted to deliver production allocation for each single well.

Pure EMs and production oil samples were analyzed through gas chromatography-mass spectrometry (GC-MS) operating in Single Ion Monitoring (SIM) mode and targeting the alkylbenzene components in the molecular range C8-C12 (Sandoval et al., 2022). Alkylbenzenes are selectively analyzed because they are believed to represent a molecular class which is extremely sensitive to reservoir condition variations, therefore they are very well suited for reservoir geochemistry applications (Mohamed et al., 2000). This is probably due to their chemical structure: the aromatic ring combined with lateral alkyl chain(s) yields a unique polarity responsible for interactions with water and rock matrix during expulsion, migration and accumulation process. At the same time, these low molecular weight compounds are very mobile within the oil column, being readily homogenized in a continuous reservoir. To minimize sample alteration due to analytical pre-treatment, especially in the lighter fraction, all oil samples were directly weighed, dissolved in dichloromethane solvent, and directly analyzed without further sample handling. Each sample is analyzed multiple times to assess analytical reproducibility. For each target compound, chromatographic peak height is registered, several peak ratios between closely eluting peaks are calculated and used for subsequent chemometric analysis. A typical GC-MS fingerprinting chromatogram is reported in Figure 2. Analyzed alkylbenzenes start with ethylbenzene and xylenes (C8-alkylbenzenes) and extend to butylbenzene (C10-alkylbenzenes); in the middle, all alkylbenzene isomers deriving from different distribution of the lateral aliphatic chain are analyzed.

The four algorithms utilized in this study to process petroleum fingerprinting data were hierarchical cluster analysis (HCA), principal component analysis (PCA), k-means analysis, and an original, in-house developed algorithm for oil deconvolution/unmixing [Sandoval et al., 2022]. The first three methodologies are fundamental to assess flow compartmentalization; they allow qualitative or semi-quantitative comparison between datasets, with the aim to highlight geochemical differences and to correlate oil samples. The last statistical tool, used to carry out production



allocation, allows deconvolution of a mixed fingerprint (commingled oil sample) into the original, distinct EMs (provided sufficient geochemical differences).

## FINDINGS

The entire study has been divided into two main stages. The first one consists of the fingerprinting of the EM oils representative of the different productive levels to allocate. The aim is to highlight geochemical differences to use for the subsequent phase, i.e., unmixing of produced oil samples resulting from commingled production. Therefore, this specific case study refers to a multi-level allocation, meaning that, for each well, production is allocated to the different productive reservoirs it drains from. Additionally, fingerprinting data can highlight differences in hydrocarbon composition within the same reservoir in different wells across the field, indicating possible presence of compartmentalization and hydrocarbon pool discontinuity (which represents a key information for reservoir engineering and production purposes).

Figure 3 and Table 1 summarize well distribution across the field, as well as producing zones for each well and type of oil.

The investigated scenario presented several challenges.

- Preliminary classic exploration geochemistry data (saturate biomarkers and aromatics) shows very poor distinction between oil samples from different wells and reservoirs, suggesting same origin and very similar maturity (data not shown), as well as a very complex reservoir geochemistry scenario (multiple reservoir oils to fingerprint, all geochemically similar).
- Most of the analyzed samples from nowadays production have >95% water cut. Therefore, significant practical challenges in retrieving enough oil matrix from the water were encountered. In some cases, no oil was retrieved from the production samples (K-11 and K-25 wells).
- Oil alteration due to water washing (high water volume in the sample must be considered as potential source of error. In some samples, oil alteration was evident from fingerprinting data. Therefore, caution is required during data interpretation).
- To compensate for lack of samples/insufficient quality, archive samples from relevant wells were analyzed.
- No PLT or other metering data are available to support/validate geochemical allocation results.
- Recent earthquake in the Adiyaman region likely impacted production, therefore additional unknowns are present whether given formations are still producing.

Fingerprinting results are reported in Figure 4.

The first, most important finding is that it is possible to distinguish Karababa-C from Derdere oils in terms of geochemical composition. Unfortunately, no Sayindere oil was available for fingerprinting, since production from well K-11 (pure Sayindere producer) delivered >99% water cut, and it was impossible to recover enough oil. Also, no archive/DST Sayindere oil was

available.

Fingerprints from K-14 and K-27 oils, both taken from the archive, delivered very similar fingerprints. At the time of sampling, K14 was solely producing from Derdere, while K27 was a mixed Karababa-C and Derdere producer. This result might suggest that at the time, production from Derdere Reservoir in K27 well was predominant. Moreover, K14 fingerprint was used as EM for subsequent production allocation calculations in other wells producing from multiple layers.

Fingerprints from K-06 and K-46 (Karababa-C producers) are quite different. This highlights a possible reservoir discontinuity for such reservoir between the two wells. This is expected, since K-06 and K-46 are located, respectively, in the eastern and western parts of the field, very far from each other. Moreover, fresh oil from K-27 well (nowadays Karababa-C producer) delivers oil very similar to K-06 (reported in Figure 4 as K-27 W), suggesting both wells access the same oil pool.

As concerns mixed oil samples from K-03 and K-21 wells (K-25 well was not evaluated since it yields >99% water cut), these were allocated for Derdere and Karababa-C percentage contribution using the unmixing algorithm described in Sandoval et al., 2022. (Sayindere input in K-21 was assumed marginal, since no EM was available) Since two possible EMs for Karababa-C Reservoir are available (K-06 and K-46), the choice of which one to use for unmixing commingled production has been carried out based on well location and relative proximity (see Table 2 for allocation results).

## CONCLUSION

Based on the discussed findings, the main study conclusions can be summarized as follows.

- Very high water cut production makes oil retrieval difficult, with alteration due to water washing that cannot be ruled out and potentially able to strongly affect interpretation.
- Despite the field uniqueness and complexity, qualitative to semi-quantitative information was obtained and carefully interpreted to better understand reservoir management aspects.
- Inferences can be made based on the locations of the wells, (such as the compartmentalization effect observed in the K-06 and K-46 reservoirs).
- The discovery well in the field, K-03, has the highest cumulative oil production and is exclusively producing from the Derdere Formation.
- K-21 well produces almost entirely from Karababa-C, even if some Derdere contribution is expected. A possible explanation could be that minor faults do not extend to Derdere and the aquifer, even if not distinguishable in seismic data.
- In the studied K-27 well, which intersects the fault zone covering both the Derdere Formation and Karababa-C Formation, the oil coming through the fractures is essentially from the Karababa-C Formation.

Overall, the present study proves that cost-effective laboratory techniques based on organic geochemistry tools can deliver meaningful information for reservoir management and production engineering. Being a pilot study, only a limited number of wells has been evaluated and obtained information still need to be better evaluated and integrated with available subsurface data and operator models. Further, considering the peculiarity of this field (very high water cut affecting sample quality), caution is required when inferring conclusions from geochemistry data. However, the implementation and extension to further wells in the field is straightforward and easy to accomplish.

Moreover, the adoption of reservoir geochemistry in more recent and productive fields, where limitations due to sampling and oil availability are not present, the described methodology as standard surveillance and monitoring tool would deliver its best potential, especially when applied at early stages of development and production to carry out production allocation on routine basis, as well as to better model fluid distribution across the field.

In addition, from a methodological point of view, the following points could be implemented as part of research activity.

- Extending the fingerprinting program to heavier alkylbenzenes, as well as to other molecular classes (aromatics, biomarkers, diamondoids, etc...) to include more geochemical variability. This might actually require to use different instruments, such as GC-MS/MS or multidimensional gas chromatography (MDGC).
- Implement automatic scoring algorithms to recognize those geochemical variations indicative of actual flow barriers and compartmentalization, as well as to automatically select the most relevant ratios for allocation computation.
- Understanding the geochemical processes responsible for alkylbenzene distribution in the reservoir and how to potentially use these compounds as paleoenvironmental indicators.

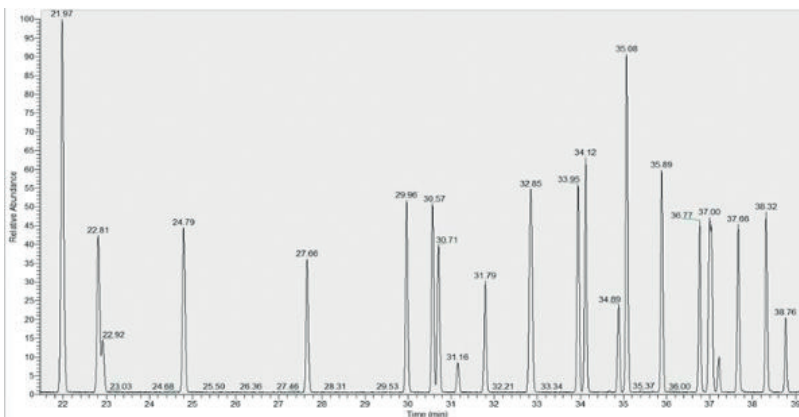
Keywords: Reservoir geochemistry, petroleum fingerprinting

Figure 1.

AGE	FORMATION	LITHOLOGY	REMARKS
Upper Miocene	Şelmo	[Pattern: Blue dots]	Conglomerate
Eocene	Midyat	[Pattern: Yellow and black bricks]	Limestone, Marl, Chert
Upper Cretaceous, Paleocene	Germav	[Pattern: Green dashes]	Shale, Marl, Limestone bands
Upper Cretaceous	Kastel	[Pattern: Grey dashes]	Shale, Marl
	Sayındere	[Pattern: Blue squares]	Shaly Limestone
	Karaboğaz	[Pattern: Orange and black bricks]	Limestone, Chert
	KBB-C	[Pattern: Green and black bricks]	Limestone
	KBB-B	[Pattern: Pink and black bricks]	Limestone, Chert
	KBB-A	[Pattern: Yellow and black bricks]	Shaly Limestone
	Derdere	[Pattern: Purple and black bricks]	Limestone, Dolomite

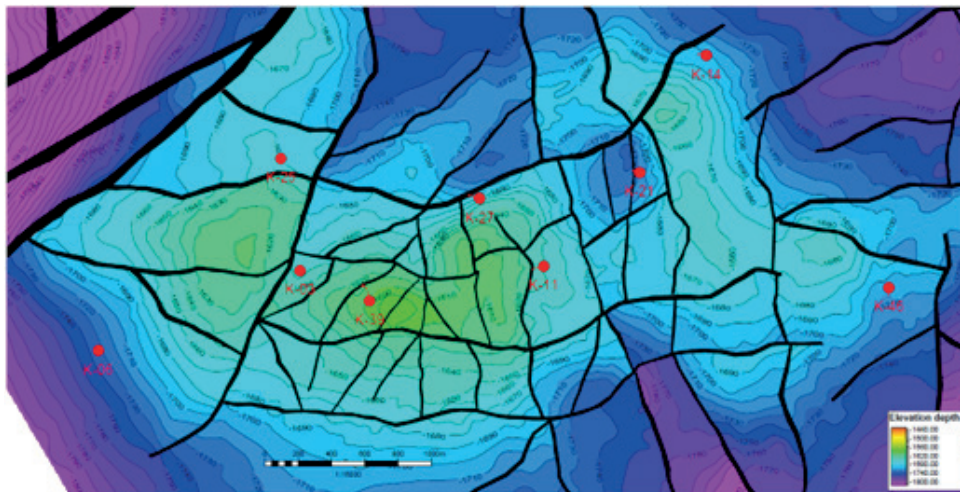
General stratigraphy for the cretaceous carbonates in the Karakuş Field.

Figure 2.



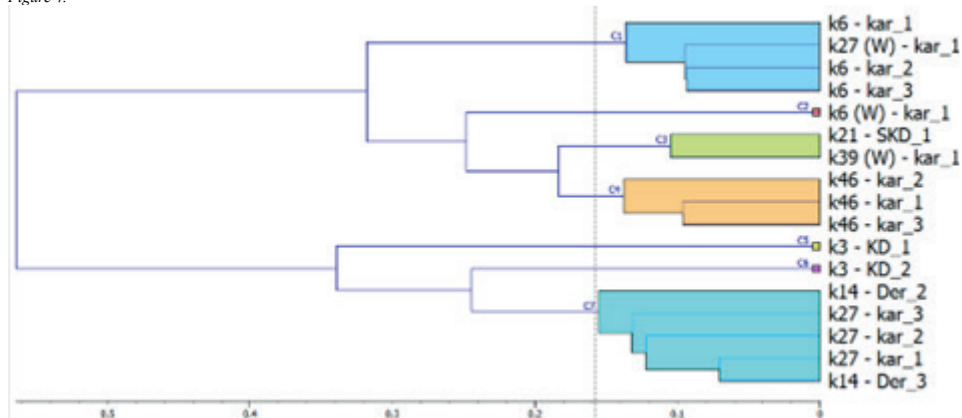
Example of GC-MS total ion chromatogram for alkylbenzene analysis in a crude oil sample.

Figure 3.



Geological map of the Karakuş Field, with the location of the wells object of the present study.

Figure 4.



Optimized HCA for the oil samples in the Karakuş Field reservoir geochemistry pilot study.

Table 1.

Well	Producing Formation	Type of oil
K-11	Sayindere	EM
K-06	Karababa-C (A and W)	EM
K-27	Karababa-C (W) or Derdere+Karababa-C (A)	EM
K-39	Karababa-C (W)	EM
K-46	Karababa-C (W)	EM
K-14	Derdere (A)	EM
K-03	Karababa-C+Derdere	Commingled
K-25	Karababa-C+Derdere	Commingled
K-21	Karababa-C+Derdere+Sayindere	Commingled

Summary of the oil samples/wells analyzed in the present study. In some wells, both oils from the production plant (W) and the archive (A) are available.

Table 2.

Well	Karababa-C (%)	Derdere (%)
K-03	0	100
K-21	98	2

*Production allocation of multilevel producing wells (K-03, K-21). Wells K6 and K21 were used as Karababa-C EM to allocate, respectively, wells K-03 and K-21.*

# Genetik Ters Çözüm ve Sismik Nitelik Kombinasyonu ile F3 Blok Kuzey Denizi Potansiyel Hidrokarbon Alanlarının Belirlenmesi

## A Combination of Genetic Inversion and Seismic Attributes for Prospect Identification in F3 Block, North Sea



**Süleyman Alemdar<sup>1</sup>, Ertan Pekşen<sup>2</sup>**

<sup>1</sup>Türkiye Petrolleri A.O., Arama Daire Başkanlığı, Ankara;Kocaeli Üniversitesi Fen Bilimleri Enstitüsü, Jeofizik Mühendisliği Ana Bilim Dalı,Kocaeli / Türkiye

<sup>2</sup>Kocaeli Üniversitesi Fen Bilimleri Enstitüsü, Jeofizik Mühendisliği Ana Bilim Dalı, Kocaeli / Türkiye

### ABSTRACT

In this study; using the post-stack seismic data (up to 1900 m) and well log (four wells) within the Pliocene aged units of the North Sea Dutch Sector area; the combination of neural network and genetic algorithm methods which is called as a genetic inversion (GI) method was used as the main seismic attribute from the volume attributes of the Schlumberger patented Petrel software. This attribute is more effective than classical inversion methods in terms of both data input and run time for the process.

Acoustic impedance log created for all wells in study area, then the correlation coefficient between acoustic impedance log and effective porosity logs checked. The results show that there is a relationship between acoustic impedance and effective porosity. Therefore, acoustic impedance cube created using genetic inversion. Genetic inverted acoustic impedance cube then used an input to create genetic inverted effective porosity cube. The result shows correlation = 0.8478655 and

F02-01 (Correlation = 0.916886, Samples = 144)

F03-02 (Correlation = 0.877023, Samples = 112)

F06-01 (Correlation = 0.7763297, Samples = 147)

F03-04 (Correlation = 0.7061655, Samples = 119)

Further, seismic attributes such as; Root Mean Square amplitude (RMS) (high amplitude values), Relative Acoustic Impedance (RAI), Instantaneous Frequency (IF), Envelope and Sweetness were applied to identify possible prospective areas. High amplitude values from RMS, polarity change of RAI, low values of IF, high values of Envelope and Sweetness represents a good reservoir quality.

As a result, applied seismic attributes and genetic inversion combination can be used to delineate possible good reservoir quality areas that can be considered as a new prospect.

Keywords; Genetic Inversion, Seismic Attributes

### 1 AMAÇ

Çalışma alanı (şekil 1.1) Hollanda açık deniz sediman çökelimlerinde birçok kanıtlanmış, petrol ve gaz arama faaliyetleri de gerçekleştirilen orta Paleozoyik yaşlı hidrokarbon sistemini içermektedir. Bu petrol sistemi içerisinde kalın Permiyen Zechstein tuz tabakası yapısal ve stratigrafik olarak etkili ekonomik hidrokarbon içeren kapanlar sunmaktadır. Fluvio-deltaik

sedimanter sistemler, verimli hidrokarbon rezervuarları oluşturabildikleri gibi yeralında karşılaşılan en karmaşık ve heterojen olanlar arasındadırlar. Alandaki olası potansiyel rezervuarların belirlenmesi amacıyla bir çok çalışma yapılmış fakat genetik ters çözüm uygulaması yapılmamıştır.

Genetik ters çözüm (GI) kullanmanın avantajları arasında; yalnızca geleneksel akustik/elastik empedans ters çözümü ile sınırlı olmayıp, aynı zamanda herhangi bir petro-fiziksel nitelik/parametreye genişletilebilmesi, herhangi bir seviye yorumu, fay yorumu ya da dalgacık çıkarımına model temelli ters çözüm yöntemlerinde olduğu gibi ihtiyaç duymaması, başlangıç modeli için kuyu loglarına ihtiyaç duyması sayılabilir. Ayrıca, GI işlemi, sismik küp gelişimini ve kayaç özelliğini bağlayan doğrusal olmayan çoklu iz operatörünü kurduktan sonra, bu operatör sadece üst ve taban yüzeyleri tarafından tanımlanan aralıkta türetilmiş olsa bile küpün her yerine model olarak uygulayacaktır.

Bu çalışmanın amacı sinir ağı ile genetik algoritma kombinasyonundan oluşan ve sismik küpü veya ilgili sismik niteliğini karşılık gelen bir log özelliğine dönüştürmek için doğrusal olmayan çok izli bir operatör kullanan Schlumberger patentli Petrel yazılım programı içerisindeki hacim niteliklerinden GI niteliğini kullanarak akustik empedans kübü, efektif porozite kübü oluşturmaktır. Oluşturulan bu küpler arasında efektif porozite-akustik empedans korelasyonunu test etmek ve sonrasında potansiyel rezervuar olabilecek noktalara ait poroziteyi tahmin etmek için, tüm sismik hacim boyunca empedans modelini hesaplamaktır. Daha sonra, kuyu logu verilerinden empedans ve efektif porozite arasındaki ilişkiyi kurarak empedans ters çözüm modelini efektif porozite modeline dönüştürmektir.

Ayrıca, bu çalışma ile elde edilecek efektif porozite modeli ve ortalama karekök genliği (Root Mean Square), görece akustik empedans (Relative Acoustic Impedance), anlık frekans (Instantaneous Frequency), zarf (Envelope), yumuşatıcı (Sweetness) sismik nitelikleri kombine edilerek olası prospektif alanların tespiti amaçlanmıştır.

Anahtar Kelimeler; Genetik Ters Çözüm, Sismik Nitelikler

## 2 YÖNTEM

### 2.1. Veri

Üst Jura-Alt Kretase tabakalarında petrol ve gaz aramak için F3 bloğunda yaklaşık 375 kilometrekare alanı kapsayan üç boyutlu sismik veri, 650 boyuna hat (inline) ve 950 kesen enine hat (crossline) olarak toplanmıştır. Sismik veri setini oluşturan hatlar ve kesen hatlar arası artış 1 hat, bin ölçüsünde (bin size) 25metre/hat x 25metre/hat, toplam iki yol zamanlı veri süresi 1,848 milisaniye (1900m), örnekleme aralığı 4 milisaniyedir. Çalışma alanı içerisinde dört adet dikey kuyu mevcuttur. Kuyuların isimleri F02-1, F03-2, F03-4 ve F06-1 ve son derinlikleri sırasıyla 3128m, 2150m, 3150m, 3530m şeklindedir. Tüm kuyularda sonik ve GR (Gamma Ray) logları mevcut olmakla birlikte yalnızca F02-1 kuyusu ve F03-2 kuyusunda yoğunluk logu mevcuttur.

Sismik veriye ait enine ve boyuna (yorumlu-yorumsuz) hat görüntüsü, zaman dilimi görüntüsü ve F02-1, F03-2, F03-4 ve F06-1 kuyuları arası mesafe şekil 2.1 de gösterilmiştir.

Potansiyel prospekt lokasyonu, sismik stratigrafinin belirlenmesi ve tabakalar arası ilişkisinin kurulması, formasyonlara ait fiziksel ve petrofiziksel özelliklerin belirlenmesi ile belirlenmektedir. Formasyona ya da rezervuara ait bu fiziksel ve petrofiziksel özelliklerin belirlenmesinde çeşitli yorum araçları-yazılımlar ve matematiksel-fiziksel eşitlikler kullanılmaktadır. Bu araçlar sismik nitelikler (seismic attributes) olarak adlandırılmaktadır. Bu çalışmada kullanılan sismik nitelikler arasında genetik ters çözüm (Genetic Inversion), göreceli akustik empedans (Relative Acoustic Impedance), ortalama karekök genlik (Root Mean Square), yumuşatıcı (Sweetness), zarf (Envelope), anlık frekans (Instantaneous Frequency), yapısal yumuşatma (Structural Smoothing) nitelikleri sayılabilir. Sismik nitelik ve genetik ters çözüm sonuçlarının analizi amacıyla IL 191 ve XL 1193 hatları ile düşey (Z) -524 ms seçilmiştir.

### 2.2. Ortalama Karekök Genliği RMS (Root Mean Square)

Bu nitelik genel anlamda seçilen veri kümesi içerisindeki değişim oranının istatistiksel olarak hesaplanmasına dayanır. Hesaplama öncesi genlik değerlerinin belirlendiği N örnek açıklığında seçilen pencere ile sismik izden sonuç elde edilmektedir. Genliklerin karelerinin toplamının, kullanılan pencerede yer alan iz sayısına bölünmesinden elde edilmekte olup bir N veri küme değeri için hesaplama şu şekildedir;

$$XRMS = x = \sqrt{(1/N) \sum_{i=1}^N x_i^2} \quad (2.1)$$

Ortalama karekök genliğin yüksek değerleri, potansiyel rezervuar olabilecek kumlar gibi yüksek poroziteye sahip litolojileri temsil etmekle birlikte, ilgilenilen bölgede direkt hidrokarbon belirteci olarak da kullanılabilir. Çalışmada seçilen pencere değeri 9'dur.

### 2.3. Görece Akustik Empedans RAI (Relative Acoustic Impedance)

Bu sismik nitelik; formasyon sınırlarını, uyumsuzluk yüzeylerini ve süreksizliklerini gösterir, ayrıca formasyondaki porozite ve rezervuar içindeki sıvı içeriğinin varlığı ile ilgili bilgi verir. Görece akustik empedans, düzenli olarak örneklenen genlik değerlerinin bir toplamıdır. Potansiyel, düşük frekanslı gürültüyü azaltmak için, sismik izi entegre ederek, sonucu yüksek geçişli (Low-cut frequency) bir Butterworth filtresinden geçirilerek hesaplanır.

Çalışmada seçilen yüksek geçişli süzgeç (Low-cut frequency) değeri 10.5 Hertz'dir.

### 2.4. Yumuşatıcı Nitelik (Sweetness)

Bu sismik nitelik, zarf ve anlık frekans niteliklerinin birleşik uygulanmasıdır ve sismik verilerde genel enerji değişimlerinin tanımlanması için kullanılır. Kil ve kumlu birimlerin ayrımında da bir belirteç olan yumuşatıcı nitelik (sweetness attribute) belli bir frekansa karşılık gelen genlik değerinin frekans kareköküne oranlanmasıyla hesaplanır. Klastik seviyelerde nitelik; yüksek genlik değerleri ve düşük frekanslar ile tanımlanır. Çalışmada seçilen pencere değeri 34'tür.

### 2.5. Zarf (Envelope)

Fazdan bağımsız olarak analitik sinyalin ( karmaşık iz) toplam anlık enerjisi olarak tanımlanan bu sismik nitelik 'Anlık Genlik', 'Büyükçük' veya 'Yansıma gücü' olarak da bilinir. Zarf genliğinin karesi, f (gerçek) ve g (sanal) sismik iz bileşenlerinin karelerinin toplamına eşittir. Yüksek zarf değerleri, gaz birikiminden dolayı oluşan parlak nokta belirteci olabileceği gibi, sediman sekans sınırlarını da belirtebilmektedir. Çalışmada seçilen pencere değeri 10'dur

### 2.6. Anlık Frekans (Instantaneous Frequency)

Bu özellik jeolojik aralıkların döngüselliğini ölçmeye yardımcı olup, düşük anlık frekans değerleri hidrokarbon potansiyelini temsil edebilmektedir. Fazın zaman türevi,  $w=d(\text{faz})/dt$ . Anlık frekansın zaman türevi faz ivmesi olarak adlandırılır. Anlık fazın zamansal değişim oranından (zaman türevi) hesaplanır. Yüksek frekans değerleri keskin arayüzleri veya ince şeyl tabaka varlığını, düşük frekans değerleri ise, yüksek poroziteli tabakaları göstermektedir. Ayrıca, anlık frekans faz ve genlikten bağımsızdır ve hidrokarbon, kırık bölgelerinin tespiti, kalınlık değişimi ve litolojideki yanal değişimler gibi rezervuar kaya özelliklerini göstermede faydalıdır. Çalışmada seçilen pencere değeri 34'tür.

### 2.7. Yapısal Yumuşatma (Structural smoothing)

Üç boyutlu Gaussian süzgeciyle uygulanan hızlı hacimsel bir sinyal işlemi olan yapısal yumuşatma veriye, sismik yansıtıcıların devamlılığını ve sinyal/gürültü oranını arttırmak amacıyla uygulanmaktadır.

Çalışmada seçilen süzgeç değerleri sigma x (2.5), sigma y (2.8) ve sigma z (1.6) şeklindedir. Herhangi bir kenar güçlendirme işlemi uygulanmamıştır.

### 2.8. Genetik Ters Çözüm (Genetic Inversion (GI))

Genetik ters çözüm (GI), sinir ağı ve genetik algoritma kombinasyonu ile başlangıç kuyu konumundan uzakta rezervuar parametre tahmin etme yaklaşımıdır. Schlumberger yazılım firmasına ait Petrel sismik yorumlama programı içerisinde bulunan hacim niteliklerinden genetik ters çözüm yöntemi diğer geleneksel ters çözüm yöntemlerinden farklı olarak, genetik ters çözümde bir ön modele, seviye yorumuna, fay yorumuna veya herhangi bir girdi dalgacığına gerek duyulmaz. Yalnızca yığıma sonrası (post-stack) sismik veri ve kontrol GI'da kullanılan sinir ağı, bir sigmoid aktivasyon fonksiyonu ve gizli katman ilişkisi ile şu şekilde karakterize edilmiştir;

- Aktivasyon fonksiyonu (sigmoid function),

$$f(x)=1/(1+e^{(-x)}) \quad (2.2)$$

- Girdi/Gizli katman ilişkisi:

$W_{0,n}$  girdi tabaka,  $w_{0,p+1}$  gizli tabakalardan birini temsil etmek üzere,

$$\gamma(\text{gizli\_tabaka})=f(\sum_{i=1}^n (i-1)^{(n-1)})$$

$$\llbracket y(\text{girdi}), i * w(\text{girdi}), i + w(\text{girdi}), n \rrbracket, \quad (2.3)$$

Sinir ağı (Neural Network), ortak çok katmanlı bir ağ olmakla birlikte genetik ters çözüm (GI) modülü durumunda bir veya daha fazla gizli katman eklenerek genetik ters çözüm işlemi gerçekleştirilmektedir (Şekil 2.2).

GI algoritması, hata fonksiyonunu tahmin etmek için sentetik veri kümesi hesaplayarak düz çözüm modelleme adımından geçmemektedir. Sürecin kendisi, sismik küp vektör alanından nitelik alanına gitmek için doğrudan bir fonksiyon oluşturmaya çalışmaktadır. Geleneksel bir ters çözüm şeması her yinelemede (iterasyonda) (modelleme, hata fonksiyonu hesaplama, geri yayılma, model yeniden tahmin vb.) her şeyi aynı anda yaparken, sinir ağı sürecinde modelleme kısmı tümüne göre hesaplanan bir uygunluk fonksiyonu sonunda yapılır. Genetik ters çözüm işlemi, sismik küp genişliğini ve kayaç özelliğini bağlayan doğrusal olmayan çoklu iz operatörünü kurduktan sonra, bu operatör sadece üst ve taban yüzeyleri tarafından tanımlanan aralıkta türetilmiş olsa bile küpün her yerine model olarak uygulayacaktır.

GI işlemi esnasında her bir girdi rastgele oluşturulmuş bir ağırlık alır. Sinir ağı ile eğitilen kuyularda ölçülen ve tahmin edilen log değerleri arasındaki en küçük kare hatasına göre hesaplanan bir uygunluk fonksiyonu elde edilir. Genetik kısım, ilk nesil bireyler için en uygun değeri seçerek yeni nesil bireyler oluşturmak için kullanılır. Birinci nesilden seçilen değerlerin yarısını ve ikinci nesilden geri kalanını olarak yeni nesil ağırlıkların çaprazlanması (Şekil 2.2), yeni optimize edilmiş bir operatör verir. Mutasyon aşamasında (Şekil 2.2), ağırlık faktörleri rastgele değiştirilir.

Çalışmada genetik ters çözüm akustik empedans ve efektif porozite kübü oluşturulması amacıyla seçilen parametreler Şekil 2.3'te gösterilmiştir.

### 3 BULGULAR

Yöntem kısmında tanımlanan sismik nitelikler seçilen operatör-pencere değerleri ile sismik veriye uygulanmış ve elde edilen sonuçlar prospektif alan ve rezervuar karakterizasyonu için analiz edilmiştir. 3B sismik veriye yapısal yumuşatma uygulanarak verideki sinyal/gürültü oranı artırılmış ve yanal devamlılıklar daha iyi görüntülenmiştir (Şekil 3.1.).

Sismik nitelik ve genetik ters çözüm sonuçlarının analizi amacıyla IL 191 ve XL 1193 hatları ile düşey (Z) -524 ms seçilmiştir.

Yapısal yumuşatma uygulaması sonrasında sismik veri ortalama karekök genliği niteliği ile analiz edilerek yüksek genlikli noktalar tespit edilmiştir. Şekil 3.3'de sismik veriye ait yapısal yumuşatma ve yüksek genlikli olası potansiyel alanları gösterilmiştir.

Sismik veriye uygulanan karekök ortalama genlik niteliği ile elde edilen yüksek genlikli noktalar ile korelasyon kontrolü amacıyla; formasyon sınırlarını, uyumsuzluk yüzeylerini ve süreksizliklerini gösteren, formasyondaki porozite ve rezervuar içindeki sıvı içeriğinin varlığı ile ilgili bilgi veren görece akustik empedans niteliği uygulanmıştır. Uygulanan diğer bir sismik nitelik de gaz birikiminden dolayı oluşan parlak nokta belirteci olabileceği düşünülen zarf genişliğidir. Yüksek zarf değerleri, ve görece akustik empedans değerleri ve olası potansiyel alanlar (siyah yuvarlak) Şekil 3.4'de gösterilmiştir.

Sismik veriye düşük frekans değerlerinin, kumca zengin (yüksek poroziteli) tabakaları temsil ettiği anlık frekans niteliği ve yüksek genlik değerleri ve düşük frekansları temsil eden yumuşatıcı (sweetness) niteliği uygulanmıştır. Düşük frekans değerleri beyaz yuvarlak ile, yüksek yumuşatıcı nitelik değerleri ise siyah yuvarlak ile Şekil 3.5'te gösterilmiştir.

### Genetik Ters Çözüm (Genetic Inversion)

Çalışma alanında bulunan dört adet kuyuda akustik empedans (AI) logu empedans=hız x yoğunluk formülü ile hesaplanmıştır. Yapısal yumuşatma uygulanmış sismik veri girdi olarak kullanılmış, tüm kuyular seçilmiş ve AI logu, global kuyu logu olarak seçilmiştir. Elde edilen sonuç, AI ve efektif porozite arasındaki korelasyonu yani AI arttığında rezervuardaki porozitenin azaldığını göstermiştir. AI ve porozite arasındaki ilişki, AI logu ve porozite logu ile kuyu bazlı olarak çapraz çizdirilerek korelasyon katsayısı olarak gösterilmiştir (Şekil 3.6). AI ve porozite arasındaki korelasyon, AI genetik ters çözüm küpünün dört kuyu için efektif porozite logları ile eğitilebileceğini göstermiştir. Bu ilişki sonucu, genetik ters çözüm için girdi verisi olarak AI ters çözüm kübü, global kuyu logu olarak efektif porozite logu (PHIE) seçilmiştir. AI kübü efektif porozite logu ile eğitilmiş ve genetik ters çözüm işlemi sonrasında tüm kuyulara ve genele ait korelasyon değerleri ve beklenen log şu şekilde elde edilmiştir;

$$\text{Korelasyon} = 0.847$$

$$F03-2 (\text{Korelasyon} = 0.878 \text{ Örnek} = 429)$$



F02-1 (Korelasyon = 0.917 Örnek = 389)

F06-1 (Korelasyon = 0.776 Örnek = 366)

F03-4 (Korelasyon = 0.706 Örnek = 417)

Tüm kuyular için, genetik ters çözüm ile elde edilen efektif porozite kübü ile girdi olarak kullanılan efektif porozite logları arasındaki ilişki, akustik empedans hesaplamasında kullanılan yoğunluk ( $R_{hob}$ ) ve hız logları, genetik ters çözüm ile elde edilen AI ve hesaplanan AI, ortalama karekök genlik sismik görüntü, yapısal yumuşatma uygulanmış sismik görüntü şekil 3.7'de gösterilmiştir.

GI sonucu elde edilen efektif porozite kübüne ait analiz edilmiş olan IL 191, XL 1103 sayılı hatlara ait görüntü şekil 3.8'da gösterilmiştir.

#### 4 SONUÇLAR

Tüm sismik nitelikler küp olarak elde edilmiş, prospektif alanların belirlenmesi ve rezervuar karakterizasyonu amacıyla, opasite değeri uygulanarak yüksek veya düşük değerler ortaya çıkarılmış ardından bu noktalara ait boyuna (inline-IL) 191 ve kesen (crossline-XL) 1103 sismik hatları incelenmiştir. Sonuç olarak;

Ortalama karekök genliği sismik nitelik kübü 0-14000 genlik aralığında değerler içermektedir. Yüksek genlik değerlerine ulaşılan noktalarda olası hidrokarbon varlığından bahsetmek olasıdır,

Zarf nitelik kübü 0-31180 genlik aralığında değerler içermektedir. Gaz birikiminden dolayı oluşan parlak nokta belirteci olabileceği düşünülen zarf genliği incelenen alanda 17500 ve üzeri yüksek zarf değerleri göstermektedir,

Formasyondaki porozite ve rezervuar içindeki sıvı içeriğinin varlığı ile ilgili bilgi veren görece akustik empedans niteliği kübü -25000 ile 36500 genlik aralığında değerler içermektedir. Prospektif olabileceği düşünülen alanda pozitif-negatif empedans dönüşümü gözlenmiştir,

Düşük frekans değerlerinin, kumca zengin (yüksek poroziteli) tabakaları temsil ettiği anlık frekans niteliği kübü 0-221 Hz aralığında değerler içermektedir. Prospektif olabileceği düşünülen alanda 20-30 Hz düşük anlık frekans değerleri gözlenmiştir,

Yüksek genlik değerleri ve düşük frekansların ilişkisini temsil eden yumuşatıcı (sweetness) nitelik kübü 0-5200 aralığında değerler içermektedir. Prospektif olabileceği düşünülen alanda 2500 ve üzeri yüksek değerler gözlenmiştir.

Akustik empedans ve efektif porozite arasındaki çapraz ilişki F03-04 kuyusunda %67, F03-02 kuyusunda %83, F02-01 kuyusunda %66, F06-01 kuyusunda ise %70 olarak hesaplanmıştır.

AI ve porozite arasındaki korelasyon, AI genetik ters çözüm küpünün dört kuyu için efektif porozite logları ile eğitilebileceğini göstermiştir. Bu ilişki sonucu, genetik ters çözüm için girdi verisi olarak AI ters çözüm kübü, global kuyu logu/nitelik (Global well log/Attribute) olarak efektif porozite logu (PHIE) seçilmiştir.

AI kübü, efektif porozite logu ile eğitilmiş ve genetik ters çözüm işlemi sonrasında tüm kuyulara ve genele ait korelasyon değerleri şu şekilde elde edilmiştir;

Korelasyon = 0.847

F03-2 (Korelasyon = 0.878 Örnek = 429)

F02-1 (Korelasyon = 0.917 Örnek = 389)

F06-1 (Korelasyon = 0.776 Örnek = 366)

F03-4 (Korelasyon = 0.706 Örnek = 417)

Genetik ters çözüm niteliği ile AI kübü ile efektif porozite (ters çözüm operatörü) arasında mantıksal bir ilişki kurularak olası prospektif noktalara ait rezervuar parametrelerinin çıkarımı sağlanmıştır.

Elde edilen sonuçlar, arama, üretim ve saha geliştirme amacıyla rezervuar karakterizasyonunu geliştirmek için genetik ters çözüm ve sismik nitelik kombinasyonunun kullanılabilirliğini göstermektedir.

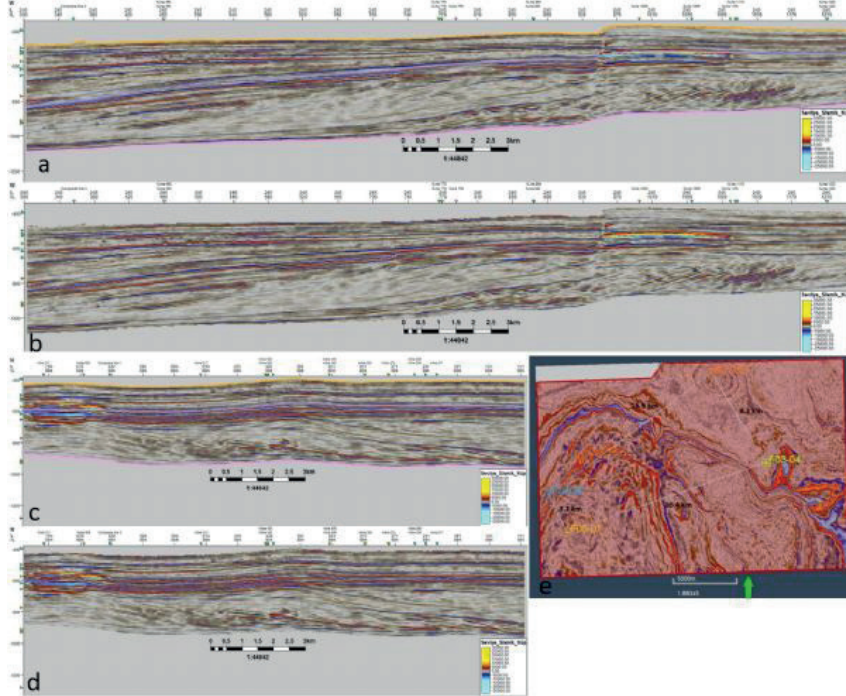
Anahtar Kelimeler: Genetik Ters Çözüm, Sismik Nitelikler

Şekil 1.1



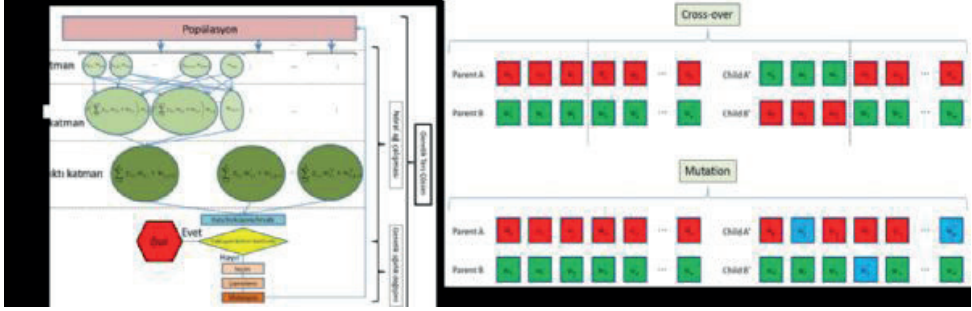
Kırmızı kare içerisinde çalışma alanı F3 blok sismik verinin kapladığı alan ve konumunun gösterimi. Çalışma alanı, Hollanda'nın Kuzey Deniz açıklarında, doğu kısmında Danimarka ve batısında İngiltere'ye yer almaktadır.

Şekil 2.1.



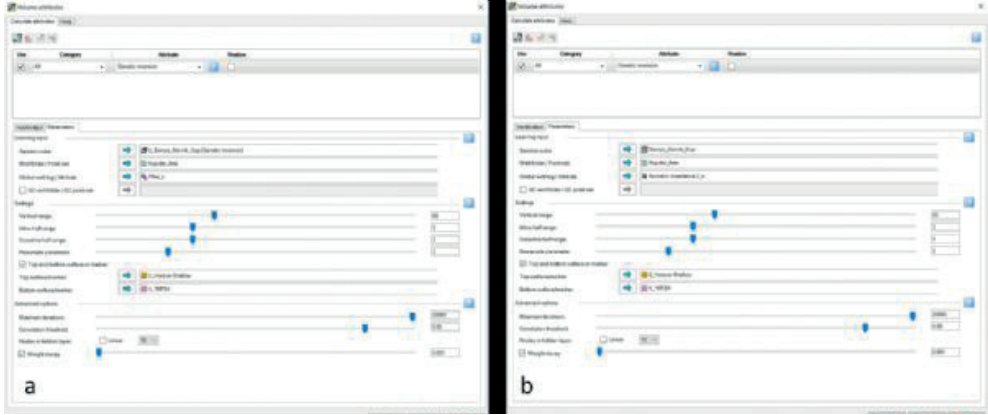
Çalışma alanı F3 blok sismik verisinin alt (mor) ve üst (turuncu) seviyelerinin gösterimi a) boyuna (inline-IL) 245 yorumlu, b) boyuna (inline) 245 yorumsuz, c) kesen (crossline-XL) 884 yorumlu, d) kesen (crossline) 884 yorumsuz ve e) 4 adet kuyu lokasyonu ve sismik zaman dilimi gösterimi.

Şekil 2.2.



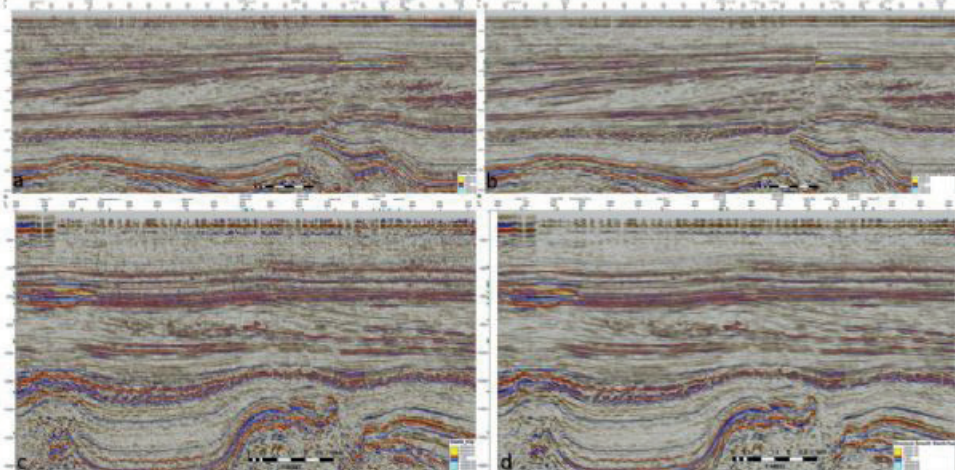
Genetik ters çözüm algoritması (Petrel Guru) ve Çaprazlama (cross-over) ve mutasyonun (mutation) çalışma prensibi (Petrel)

Şekil 2.3.



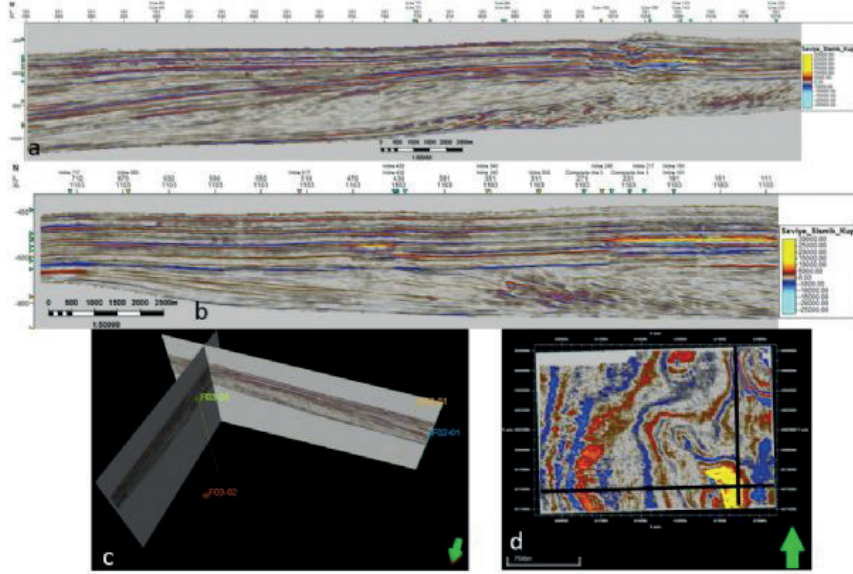
GI işlemi için seçilen parametre değerleri a) efektif porozite genetik ters çözüm b) akustik empedans GI

Şekil 3.1.



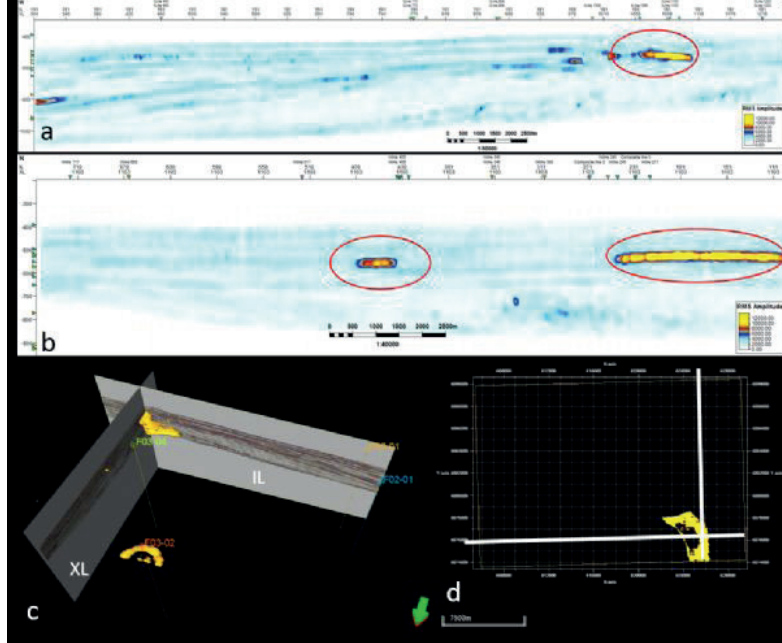
F3 blok sismik verisinin a) boyuna (inline-IL) 245 ham, b) boyuna (inline) 245 yapısal yumuşatma uygulanmış, c) kesen (crossline-XL) 884 ham, d) kesen (crossline) 884 yapısal yumuşatma uygulanmış halinin gösterimi.

Şekil 3.2.



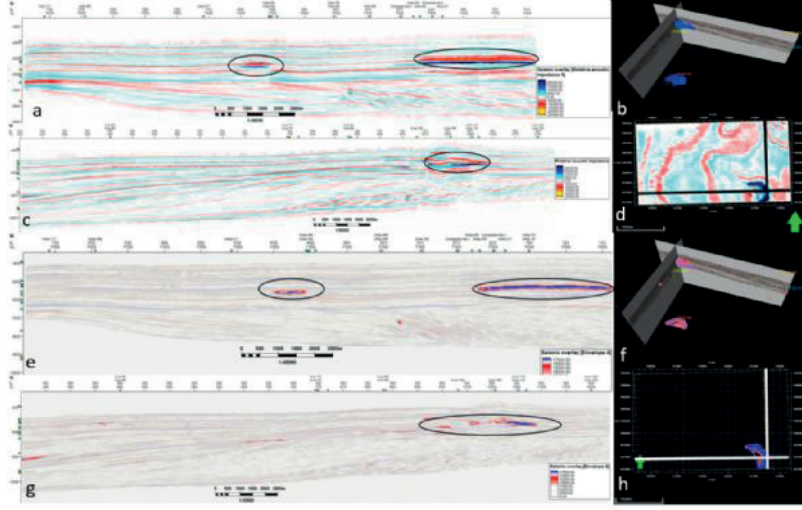
Sismik nitelik ve GI sonuçlarının analizi amacıyla kullanılan a) boyuna (inline-IL) 191 yapısal yumuşatma uygulanmış b) kesen (crossline-XL) 1103 yapısal yumuşatma uygulanmış, c) 3B pencerede IL 191 ve XL 1103 gösterimi d) -524 ms zaman dilimi gösterimi.

Şekil 3.3.



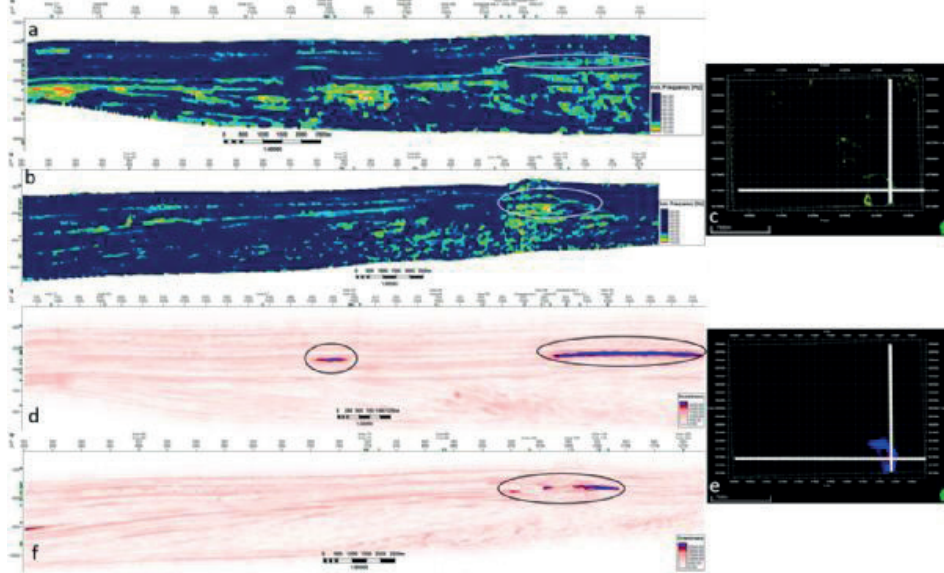
Sismik veri ortalama karekök genişliği (RMS) niteliği ile analiz edilerek elde edilen yüksek genitli noktalar (kırmızı yuvarlak) a) boyuna (inline-IL) 191 RMS b) kesen (crossline-XL) 1103 RMS, c) Üç boyutlu pencerede IL 191 ve XL 1103 RMS gösterimi d) -524 ms RMS zaman dilimi gösterimi.

Şekil 3.4.



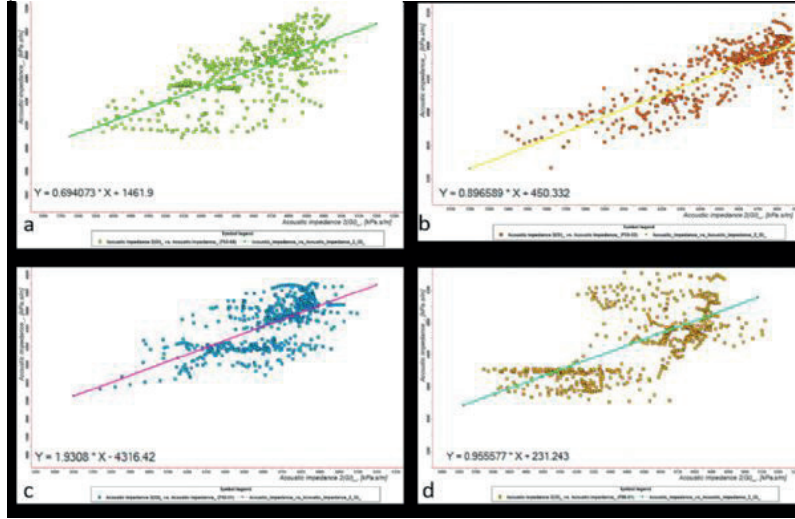
Sismik veri görece akustik empedans (RAI) niteliği ile analiz edilerek elde edilen yüksek ve düşük empedans değerleri ile yüksek zarf niteliği değerlerinin (siyah yuvarlak) gösterimi a) kesen (crossline-XL) 1103 RAI niteliği, b) 3B pencerede IL 191 ve XL 1103 RAI niteliği, c) boyuna (inline-IL) 191 RAI niteliği, d) -524 ms RAI niteliği zaman dilimi gösterimi, e) kesen (crossline-XL) 1103 zarf niteliği, f) 3B pencerede IL 191 ve XL 1103 zarf niteliği, g) boyuna (inline-IL) 191 zarf niteliği, h) -524 ms zarf niteliği zaman dilimi gösterimi.

Şekil 3.5.



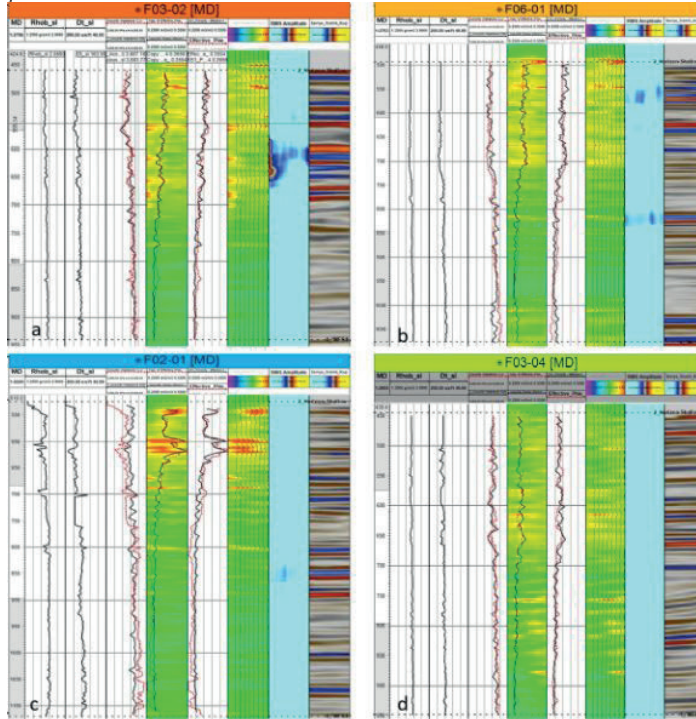
Sismik veri anlık frekans (IF) niteliği ile analiz edilerek elde edilen düşük frekans değerleri (beyaz yuvarlak) ile yüksek yumuşatıcı (sweetness) niteliği değerlerinin (siyah yuvarlak) gösterimi a) kesen (crossline-XL) 1103 IF niteliği, b) boyuna (inline-IL) 191 IF niteliği, c) -512 ms IF niteliği zaman dilimi gösterimi, d) kesen (crossline-XL) 1103 yumuşatıcı (sweetness), e) -512 ms zarf niteliği zaman dilimi f) boyuna (inline-IL) 191 yumuşatıcı (sweetness) gösterimi.

Sekil 3.6.



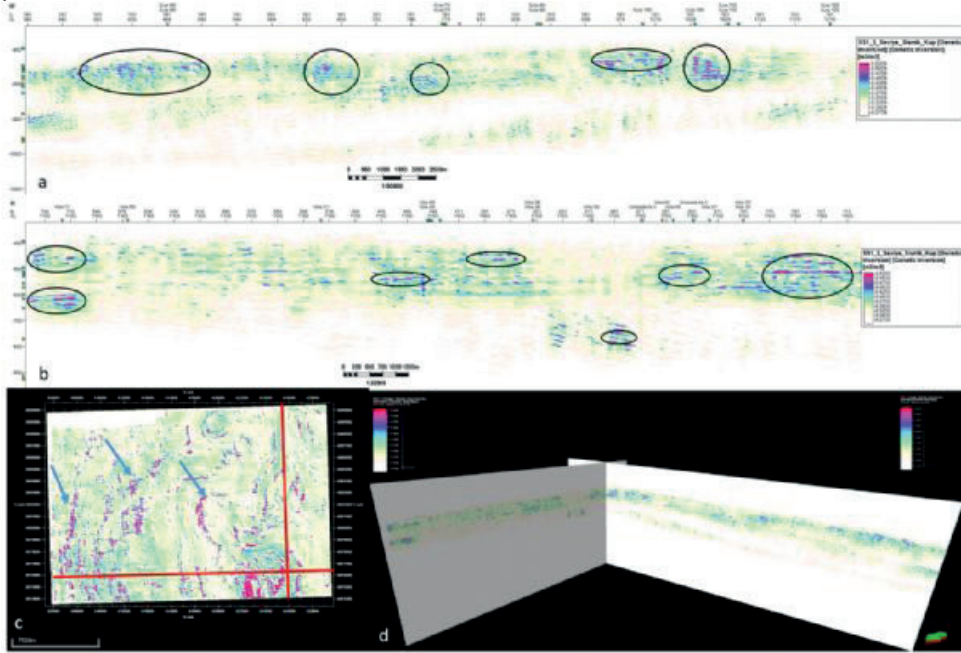
Akustik empedans ve efektif porozite arasındaki çapraz ilişki a) F03-04 kuyusuna ait çapraz korelasyon (%67) b) F03-02 kuyusuna ait çapraz korelasyon (%83) c) F02-01 kuyusuna ait çapraz korelasyon (%66) d) F06-01 kuyusuna ait çapraz korelasyon (%70)

Sekil 3.7.



Soldan sağa, yoğunluk logu, hız logu, hesaplanan akustik empedans (AI) (kırmızı kesik çizgi) üzerine genetik ters çözüm AI (siyah çizgi), GI efektif porozite görüntüsü üzerine efektif porozite logu (kırmızı kesik çizgi) üzerine GI efektif porozite logu, efektif porozite logu (kırmızı kesik çizgi) üzerine GI efektif porozite logu, GI efektif porozite görüntüsü, RMS görüntüsü, yapısal yumuşatma uygulanmış sismik veri görüntüsü a) F03-02 kuyusuna ait sonuçlar b) F06-01 kuyusuna ait sonuçlar c) F02-01 kuyusuna ait sonuçlar d) F03-04 kuyusuna ait sonuçlar

Şekil 3.8.



G1 sonucu elde edilen efektif porozite kübüne ait yüksek porozite değerleri (siyah yuvarlak) a) boyuna (inline-IL) 191 efektif porozite G1, b) kesen (crossline-XL) 1103 efektif porozite G1, c) -524 ms efektif porozite G1 zaman dilimi gösterimi, d) Üç boyutlu pencerede IL 191 ve XL 1103 gösterimi

# Yeraltı Doğalgaz Depolama Rezervuarları: Antropojen Sismisite, Deprem Tehlikesi ve Sürdürülebilirlik



Hüseyin Sadi Kuleli<sup>1</sup>, Ekrem Zor<sup>2</sup>, Mehmet Ergin<sup>2</sup>, Haluk Kunter<sup>3</sup>,  
Taner Teoman<sup>3</sup>, Haldun Bingöl<sup>3</sup>

<sup>1</sup>Seismo Analytics Inc.

<sup>2</sup>TÜBİTAK Marmara Araştırma Merkezi İklim Değişikliği ve Sürdürülebilirlik Başkan Yardımcılığı Yer Bilimleri Araştırma Grubu

<sup>3</sup>Belirti Mühendislik Danışmanlık ve Ticaret A.Ş

## ÖZ

Yeraltında hammaddelerin depolanması, yeryüzü depolama alanlarına göre daha ekonomik ve alan kullanımı açısından daha verimlidir. Yer altında her türlü endüstriyel veya atık madde (doğalgaz, CO<sub>2</sub>, hidrojen, zararlı atık) depolamak amacı ile oluşturulan, çeşitli rezervuar tipleri (tuz mağarası, kullanılmayan maden ocakları, jeolojik formasyon), için en önemli sürdürülebilirlik parametresi, deprem riskinin kestirilmesi ve deprem zararının azaltılmasıdır. Rezervuarların deprem riskini doğuran iki kaynak vardır: rezervuarda oluşan antropojenik (anthropogenic) sismisite ve rezervuardan uzakta oluşacak, depremlerin, rezervuar üzerindeki etkileri. Rezervuarlarda görülen antropojenik sismisite genellikle rezervuarın örtü kaya kısmında (caprock, seal) veya doğalgazın rezervuar a giriş veya tahliye kuyularında (wellhead) görülür. Burada gözlenen hasar uluslararası literatürde iki ana başlık altında incelenmektedir: “caprock Integrity” ve “wellhead Integrity”. Yapı sektöründe, deprem tehlikesinin kestirimi ve hedef yapının performansını dikkate alan “performans temelli” yaklaşımlar ile depreme dirençli yapı dizaynında büyük başarılar elde edilmiştir. Performans temelli yaklaşımlarda, kısaca hedef yapının, tahmin edilen deprem yükleri karşısında, performansının bilinmesi gerekir. Yer altında oluşturulmuş Jeolojik yapılarda ise performans hesaplamaları, rezervuarda sürekli olarak bazı verilerin gözlemesi ile rezervuar performansının sürekli olarak denetlenmesini gerekli kılar (reservoir structural health monitoring). Bu türlü yapılarda, deprem tehlikesi; rezervuarın içinde ve çevresinde yer alan, aktif faylar ile yapının örtükaya(caprock, seal) veya tüm kabuğunda (cavity) oluşan, çatlakların (fracture) ürettiği depremlerin, etkilerinin, toplamıdır. Bu çalışma, bu tür rezervuarlar için deprem tehlikesinin kestirilmesi ve en aza indirilmesi amacı ile uygulanabilecek, bir akış diyagramı (Workflow) tanımlama, girişimidir. Bu çalışmada gösterilen şekiller ve sonuçlar, referans olarak verilen çalışmalar ve yazarlardan alınmıştır. Bu proses kısaca, sismolojide, geniş uygulama alanları olan, üç görüntüleme (imaging) yönteminin, birbirlerini tamamlayıcı bir şekilde uygulanması esasına dayanır. Her üç yöntem için de antropojenik sismisite sonucunda gözlenen veriler kullanılmaktadır. Öyle ki bu metodlar, anlatım sırasına göre: rezervuarlarda oluşan deprem odak noktalarının haritalanması, rezervuar gerilme (stress) durumu ve yönelimi ve sismik tomografi yöntemidir

## ABSTRACT

This study proposes a workflow for the earthquake hazard assessment of all types of reservoirs (Salt cavities, depleted reservoirs, and geological formations), utilized for the purpose of storing various industrial materials (i.e., natural gas, CO<sub>2</sub>, hydrogen, and hazardous waste). Gas storage in subsurface facilities, which act essentially as reservoirs, leads to microseismic activities due to pore pressure fluctuations created by gas injection or depletion. This type of earthquake activity has been classified as anthropogenic seismicity in the seismology literature. Therefore, gas storage reservoirs have the capacity to create significant earthquake hazards due to this anthropogenic seismicity and their interactions with active fault systems in or around the reservoirs. Conversely, distant earthquakes could create hazards to such reservoirs due to stress changes caused by long-period waves. Performance-based structural design has been used in the construction sector for the mitigation of structural damage to buildings caused by earthquakes, which factors in the source of the earthquake and the earthquake tolerance of the structure. Therefore, the performance of the reservoirs must be measured and recorded taking into consideration the earthquake potential and the performance of the reservoir. In this study, we attempted to implement a “workflow” for different reservoir types to understand their fracture characteristics and assess their seismic hazards. This workflow will be based on the successive application of three complementary seismic imaging techniques. All techniques will use seismic data, which is monitored from induced or natural earthquakes. The techniques are classified in terms of their reservoir investigation methods. The first technique is reservoir delineation (mapping), which ensures the accurate location of induced earthquake hypocenters in oil and gas fields. The second technique determines the reservoir’s stress state and orientation. Finally, the required seismic tomography is applied for all reservoir types.

## 1. Yeraltı gaz rezervuarları için yakın ve uzak odaklı deprem tehlikesi

Yer altında, doğalgaz depolama işlemi için çeşitli Jeolojik yapılardan yararlanılmaktadır. Bu yapılar, önceden kullanılan ve halen üretim olmiyan terkedilmiş (depleted) gaz rezervuarları, doğrudan uygun olan akifer içine ve oluşturulan büyük hacimli tuz mağaralarıdır. Yeraltı gaz depolama tesisleri, ait oldukları jeolojik formasyona uygun olarak, bir rezervuar gibi davranırlar. Bu rezervuardaki endüstriyel veya doğal nedenler yada rezervuar dışında oluşan depremlerin, rezervuarı



oluşturan kayaçlardaki gözenekler (pore) üzerinde oluşturduğu basınç farkı nedeni ile oluşan jeomekanik duraysızlık (değişim) rezervuarda çatlakların (fracture) oluşumuna neden olmaktadır. Bu çatlakların, oluşması esnasında, mikro depremler üretilmektedir. Ayrıca, bu çatlak sistemi oluşurken, meydana gelen mikrosismik aktivite bir yandan da, ortamdaki pasif fayları uyatararak tekrar aktif hale geçmelerine neden olabilmektedir. Böylece oluşan bu karmaşık çatlak sistemi, belli bir kritik seviyeye ulaşması halinde rezervuarın özellikle, örtü kaya kısmında daha büyük depremlerin oluşmasına ve rezervuarın tümünde önemli hasarlara neden olmaktadır. Ayrıca, Bu rezervuarlar da oluşan, çatlak yapısı ve ürettiği mikrosismik aktivite ile bulunduğu bölgenin antropojenik sismisite etkinliği açısından da, önemlidir. Antropojenik sismisite, günümüzde endüstriyel faaliyetlere paralel olarak, artış göstermektedir (Ellsworth, 2013). Bu çalışmada, seçilen ilk örnek, Cesca ve dig., (2014) den alınmış, İspanya da 2013 yılında Valencia körfezinde yer alan, Castor (offshore) yeraltı gaz deposu çevresinde gözlenen sismik aktivite rezervuardaki enjeksiyonunun başlaması ile başlamıştır, deprem odaklarının alansal dağılımı enjeksiyon kuyusu ile ilişkisini gösterir ve sığ odaklıdır (Şekil, 1). Spanish Instituto Geográfico Nacional (IGN), un raporuna göre iki aylık süre içinde, 550 küçük deprem gözlenmiştir bu depremlerden, 17 tanesinin magnitüdü 3 den büyüktür, ve enjeksiyon duruktan 2 hafta sonra magnitüdü 4.3 Mw olan bir deprem meydana gelmiştir (Cesca ve dig., 2014). Bir diğer örnek ise, rezervuarda oluşmayan (çok uzakta), fakat rezervuarı etkileyen bir depremdir. Rezervuardan uzakta oluşan depremlerin, yerel sismisiteye etkisi konusunda bir çok çalışmadan söz edebiliriz, (Cannata ve dig., 2010, Brodsky & Prejean 2005, İtaba & Ryosuke 2011). Öyleki, Paris sedimentar baseninde yer alan, yer altı tuz mağarasının (Şekil, 2), dış kabuğunun aniden çökmesi öncesi ve sırasında görülen mikrosismik aktivite ile buradan 12,000 km uzakta Endonezya’da olan (M ~ 7.2 Kepulauan Talaud) arasındaki ilişki incelenmiştir (Jousset and Rohmer, 2012). Bu deprem kaynağından yayılan, uzun peryotlu dalgalar (yüzey dalgaları), rezervuar ile temasında ve sonrasında maximum dinamik stress artışı göstermiş, bunun sonucu olan dolomit tabakasında, bu stress artımı kritik seviyeye geçtiği için rezervuarın kabuğunda çökme oluşmuştur. Aynı zamanda, bu esnada çok fazla miktarda mikrosismik aktivite görülmüştür (Şekil, 3). Bu dalgaların geçişi sırasında kestirilen basınç değişimi, daha önceden hesaplanan rezervuarın çökmesi için gerekli olan basınç değişimine çok yakındır (Jousset & Rohmer, 2012). Aynı şekilde, rezervuar (cavern + overburden + brine system) için hesaplanan fundamental dalga peryodu aralığı, 10–20 s aralığındadır, Bu frekans aralığı, yüzey dalgaları ile çakışmaktadır (Jousset & Rohmer, 2012).

## 2. Deprem hasarı kestirimi ve zararlarının azaltılması metodları

Tarihsel gelişimi içinde, “deterministic” ve “probabilistic” kestirim yöntemleri, deprem tehlikesinin kestiriminde önemli roller oynamışlardır. Bu kestirimler

öncelikle seçilen etkin maksimum manyitude sahip bir deprem için (max credible magnitude), bu depremin odağından, hedef noktasına uzaklık, dikkate alınarak, yer hareketi (ivme, hız, yerdeğiştirme), daha önceden ölçülmüş veriler üzerinden (empirical) kestirilir. Bu kestirimde, öncelikle, deprem dalgalarının belli bir uzaklık için “sönümlenmesini” (attenuation) veren ampirik bağıntılar oluşturulur. Bu yöntemler çalışılan bölgenin jeolojik yapısı ve deprem kaynağının fiziksel özellikleri dikkate alınmadan uygulanır. Aynı şekilde, hedef yapının dinamik özellikleride (deprem karşısındaki davranışları) dikkate alınmaz. Öncelikle, yer altını homogen olmayan bir yapıda olması nedeni ile, sönümlenme eğrisi uzaklığa bağlı olarak azalmayabilir. Burada (Şekil, 4 c) deprem kaynağına daha uzak bölgelerde, yakın bölgelere nazaran daha yüksek ivme değerleri ölçülmüştür (Cranswick, ve dig., 2000). Bu örnek, sadece, bir hedef deprem seçerek bunun uzaklığa bağlı etkisinin hesaplanmasını temel alan klasik yaklaşımın yetersizliğini ortaya koymaktadır. Bu nedenle, bu çalışmada, her türlü yer altı yapısında deprem zararının azaltılması ve yapı sağlığının sürekliliğinin sağlanması için “performans temelli”, yapı dizaynı yaklaşımı önerilmiştir. Bu yaklaşımda, deprem zararının kestirilmesi için, ilk olarak, deprem kaynağının ve deprem dalgalarının yayındığı ortamın fiziksel özelliklerinin bilinmesi gerekir. İkinci olarak, deprem tehlikesine konu olan her türlü yapı, deprem dalgalarının “frekans içeriğine” karşı aynı şekilde tepki vermez ve özellikle “büyük yapıların (gökdelen, köprü, yer üstü petrol deposu)”, farklı elemanlarının, deprem dalgalarının farklı frekansları için, gösterdikleri tepki farklıdır. Bu nedenle yapının depreme karşı performansı hesaplanırken, deprem kaynağının özellikleri, üzerinde yer aldığı jeolojik yapının etkisi, bina yapımında kullanılan malzeme, yapının gelebilecek deprem dalgasının frekans içeriğinin bilinmesi gerekli kılabilir. Bu nedenle, performans temelli yaklaşımda, yapının deprem direnci, bir çok parametre dikkate alınarak hesaplanır. Yer içinde ve -yerkabuğun bir parçası- olan jeolojik yapıların deprem davranışları yer yüzünde inşaa edilen yapıların davranışlarından çok farklıdır. Böyle yapılar, depremler, diğer doğal olaylar yada, rezervuardaki, endüstriyel aktivitenin neden olduğu jeomekanik tepki nedeni ile, çeşitli yapıda sismik aktivite üretirler. Sözü edilen tüm bu sismik aktivite, sismoloji literatüründe “antropojen” (Anthropogenic) sismisite olarak adlandırılır. Bu yapılar, deprem tehlikesinin hesaplanabilmesi için, rezervuar dışındaki deprem kaynağının yanısıra, rezervuarda oluşacak antropojenik sismisiteye karşı rezervuarın, tepkisinin dikkate alınması gereklidir. Bu çalışmada verilen örneklerin tümü rezervuarda oluşan mikrosismik veriyi kullanılmaktadır ve referans verilen çalışmacılardan alınmıştır.

### 2.1 Rezervuar deprem tehlikesi kestirimi:

#### Antropojenik sismisite ve çatlak sistemi tanımlama (characterization)

Rezervuarlarda, depreme neden olan çatlak sisteminin tanımlanması ve haritalanması için, bu çatlak

sisteminin ürettiği, mikrosismik aktivitedeki her bir mikro depreme ait, kaynak parametreleri, (kaynak boyutu, sismik moment, stress drop...) ve yayıldığı ortamın jeofizik özelliklerinin, (sönümlenme, sismik hız, gibi ) kestirilmesi, gerekir. Rezervuardaki, bu deprem kaynaklarının yapısı ve diğer jeofizik verilerin kullanılması ile, bu rezervuarın jeomekanik yapısı ve depreme karşı göstereceği direncinde (performansı) modelleyebiliriz. Deprem kaynağının fiziksel özellikleri dediğimizde, rezervardan uzakta oluşan depremlerde, problem, bir tek fayın kaynak parametreleri kestirme iken, rezervuar içi depremlerde, birden fazla mikro depremin oluşturduğu bir çatlak yapısının (pattern) fiziksel özelliklerini kestirme problemine dönüşür (Kurison & Kuleli, 2021). Rezervuar, sismolojisinde birinci adım, bu çatlakların oluşumu esnasında ortaya çıkan, sismik aktivitenin gözlenmesidir. Bu sismik aktivite gözlenebilirse, sismolojinin temel metodları kullanılarak oluşan çatlakın, konumu, geometrik ölçüleri, ortaya çıkan enerji miktarı, üretim miktarı hesaplanabilir (Kurison & Kuleli, 2021). Bu hesaplamalarda ortaya çıkan en önemli problem, çatlakın konumu ve istasyonların konumlarının geometrik ilişkisinde kaynaklanan problemdir. Hedef çatlak sistemi, istasyonlara göre daha derindedir. Bu nedenle, çatlak sisteminin yer koordinatlarının belirlenmesinde, derinlik hesaplamasındaki hata payı (uncertainty) büyüktür. Bu problem, tüm rezervuar jeomekanik parametrelerin hesaplanmasında karşımıza çıkmaktadır. Bu problemde kaçınmanın iki metodu vardır. Öncelikle, yapacağımız gözlemler için sismik alıcı sistemlerini, bir kuyu vasıtası ile olabildiğince derine yerleştirmek ve farklı jeofizik metodları ayrı ayrı veya birlikte kullanmaktır. Böylece modelleme işlemindeki hata payını azaltabiliriz. Yeraltı yapılarında, çatlak yapısının kestirimi yapının performansını belirleyen en önemli parametredir. Öyleki, rezervuarın performansı, bu çatlak yapısının ne ölçüde tolere edileceği ile ilgilidir. Bu çalışmada, çatlak yapısının kestirimi için üç yöntem önerilmiştir. bu Yöntemler: Rezervuardaki deprem aktivitesine ait odakların dağılımının çok duyarlı olarak haritalanması, rezervuar stress dağılımının alansal olarak elde edilmesi ve rezervuardaki çatlak yapısının görülebilmemesini sağlayan "sismik görüntüleme" (Tomography) teknikleridir. Bu çalışmada örnek verilen, Yibal rezervuarı (Umman), hem gaz hemde petrol üreten bir rezervuardır, yüzeye yakın olan Natih formasyonundan "gaz", daha derinde olan Shuaiba dan "petrol" üretimi vardır. Antropojen sismisitenin olduğu bu rezervuar için, bu çalışmada önerilen her üç yöntem de uygulanmıştır (Kuleli ve diğ., 2009, Zhang ve diğ., 2009, Li ve diğ., 2011). Umman'daki bu üretim petrol sahasında, sismik olayların çoğu, azalan rezervuar basıncına yanıt olarak mevcut fayların yeniden aktivasyonundan kaynaklanmaktadır.

### 2.1.1 Rezervuarlarda deprem odaklarının haritalanması

Herhangi bir rezervuarda, antropojen sismisiteye neden olan çatlak sisteminin haritalanmasında, en önemli yöntem, bu sismik aktivitenin yerinin yeterli

duyarlılıkta belirlenmesidir. Rezervuarlarda oluşan bir çatlak, sismik kaynağın boyutuna bağlı olarak, bir tek sismik olaydan meydana gelebileceği gibi, bir çok sismik olayın belli bir geometride oluşması ile de meydana gelebilir. Her bir sismik bir olay için, yer bulma (location) işlemi, öncelikle uygun bir istasyon dağılımı olması ve sismik hız dağılımının çok iyi bilinmesini gerektirir. Petrol ve gaz sahaları, hız modellerinin genellikle değişen yüksek ve düşük değerlere sahip katmanlardan oluşturduğu tortul havzalarda bulunur. Çoğu standart deprem yer bulma algoritması bu tür modelleri yeterli duyarlılıkta kullanamaz. Ayrıntılı, katmanlı hız modellerinin kullanımı, yer bulma algoritmalarında, detaylı dalga seyahat süresi hesaplamaları gerektirir. Yibal rezervuarına ait bu veride, mikrosismik olaylar öncelikle, standart konum belirleme teknikleri ve geleneksel hız modelleri kullanılarak hesaplanmıştır. Bu hesaplama ile, deprem odaklarının geniş bir derinlik aralığında dağılmış olduğu görülmektedir (Şekil, 5 a). Bu nedenle, ikinci olarak, daha yüksek konum belirleme hassasiyeti için, daha uygun bir algoritma "NonLinLoc" (Lomax ve diğ., 2000) ve kontrol atışlarından elde edilen ayrıntılı hız modelleri kullanılmıştır (Şekil, 5 b). Enine kesitler, odak noktalarının büyük çoğunlukla gaz rezervuarında bulunduğunu ve petrol rezervuarlarında nispeten az olarak meydana geldiğini göstermektedir.

### 2.1.2 Mikrosismik depremlerin kaynak mekanizması ve stress kestirimi

Bu bölümde yine Yibal sahasına ait veriler kullanılmış ve Li ve diğ., (2011) nin sonuçları verilmiştir. Rezervuarlarda, efektif gerilme (stress) ve gözenek basıncı hesaplamalarında gerilme tensörünün belirlenmesi, rezervuar deprem güvenliği açısından çok önemlidir. Bu nedenle rezervardan elde edilen mikrosismik sinyallerin odak mekanizmaları, faylar üzerindeki hareket yönü, fayın geometrisini ve rezervuarın jeomekanik modellemesi için önemli olan gerilme tensorunu belirlerler. Antropojen depremlerin çoğu küçük magnitudüdür ve nispeten az sayıda istasyonda kaydedilir, bu yüzden azimut kapsama alanı ideal olmayabilir. Bu nedenle, odak mekanizmasını belirlemenin en doğru yolu, sismogramların tümü (P ve S dalgaları) kullanılan moment tensör ters çözümüdür (Li ve diğ., 2011; Song & Toksoz, 2011). Bu çalışmada gözlenen, İki (eşlenik) fay grubu vardır, başlıca, maksimum bölgesel yatay gerilme yönüne paralel uzanan KD-GB doğrultulu faylarda görülür (Şekil, 6). Odak mekanizmaları, KD-GB yönlü mavi okla gösterilen maksimum yatay gerilim yönünü tanımlar (Li ve diğ., 2011).

### 2.1.3 Rezervuarlarda sismik tomografi uygulaması

Bu yöntemi uygulamadaki amaç, rezervuardaki aktif olarak bulunan çatlak yapısının, yanal ve düşey hız dağılımı ile ne ölçüde bir ilişki göstereceğidir. Bu çalışmada kullanılan tomografi yöntemi, "Double Differences" (DD) yöntemini kullanan "sismik hız tomografisi"dir, buradaki şekil (Şekil, 7) ve sonuçlar Zhang ve diğ., (2009) dan alınmıştır. DD

tomografi yöntemi, ortak istasyonlarda gözlemlenen deprem çiftlerinin diferansiyel varış sürelerinin bir kombinasyonunu kullanır (Zhang & Thurber, 2003). Sismik aktivitenin odak yerleri ile mevcut fay izleri ile güçlü bir korelasyon göstermektedir. Bununla birlikte, ana aktif faylar boyunca önemli hız değişimleri görülmektedir (Şekil, 7). Çanak şeklindeki düşük hız anomalisi, muhtemelen gaz oluşumunun yer değiştirmesinden kaynaklanan iki kuzeydoğu-güneybatı fayında mevcuttur.  $V_p/V_s$  oranları, gaz üreten rezervuarın derinlik aralığı ile uyumlu olarak modelin daha sığ kısmında 1,75'ten küçükken, modelin daha derin kısmında 1,75'ten büyüktür. Rezervuar görüntüleme, rezervuar katmanları içindeki yapıları ve hız değişikliklerini belirlemede cesaret verici sonuçlar göstermektedir. Bu nedenle, antropojen sismisite verilerini kullanan 3 boyutlu sismik tomografi, rezervuar görüntüleme ve özellikle tahmini için büyük bir potansiyele sahiptir.

## SONUÇLAR

Bu çalışmada konu edilen yer altı, gaz depolama rezervuarları için, gaz arzında, en önemli sürdürülebilirlik parametresi, deprem zararlarına karşı direçli olmasıdır. Bu tür rezervuarlar, hem rezervuarın kendi ürettiği andropojenik hemde uzakta oluşan depremlerden etkilenir, o nedenle deprem tehlikesinin hesaplanması için her iki grup depremi de göz önünde bulundurulmalıdır. Rezervuarda, deprem tehlikesi kestirimleri ve rezervuarın bu tehlikeye karşı göstereceği performans, hem depolama işlemi başlamadan hemde depolama işlemi devam ettiği müddetçe geliştirilerek devam etmelidir. Kisaca, rezervuar, "yapısal health monitor" konseptine uygun, sürekli olarak monitör edilmelidir. Rezervuarda, sürekli olarak ölçülmesi (hesaplanması) gerekli verilerden en önemileri, sismik/mikrosisimik, gözenek basıncı, stress hali, sismik imajdaki değişimdir.

Doğalgaz depolama konusunda Türkiye "farklı nitelikte" doğalgaz depolama alanları (rezervuarları) oluşturarak, gaz arzında, süreklilik konusunda farklı seçenekler kullanmıştır Fakat Türkiye'nin sismotektonik olarak çok aktif bir coğrafik konumda olduğu düşünülürse, bu rezervuarlar için deprem güvenliği konusunda çok sayıda "özellikle çatlak sistemini inceleyen" (fracture mechanics) konularda bilimsel ve teknolojik çalışmalara ihtiyaç duyulacağı açıktır (Kurison C. Ve dig., 2021). Bunun yanı sıra, rezervuar güvenliği konusunda diğer önemli konu, özellikle doğal afetler ve rezervuarın bunlara tepkisini, sürekli gözleyerek ve bu gözlem verisini, anlık olarak değerlendirecek bir merkezinin oluşturulması gerekliliğidir. Ölçülen tüm veriler, gerçek zamanlı (real time) olarak değerlendirme merkezine iletilmeli ve burada gerçek zamanlı olarak değerlendirilmelidir.

## REFERANSLAR

1. Cesca, S.; Grigoli, F.; Heimann, S.; González, Á.; Buforn, E.; Maghsoudi, S.; Blanch, E.; Dahm, T., 2014. September–October seismic sequence offshore Spain: a

case of seismicity triggered by gas injection?, *Geophys. J. Int.*, V. 198, Issue 2, Pages 941–953,

<https://doi.org/10.1093/gji/ggu172>

2. Cranswick, E.; Ozel, O.; Meremonte, M.; Erdik, M.; Şafak, E.; Mueller, C.; Overturf, D.; Frankel, A., 2000. Earthquake Damage, Site Response, and Building Response in Avcılar, West of Istanbul, Turkey. *International Journal for Housing Science and its Applications*. 24.

3. Kurison, C., Kuleli H.S., 2021. Matrix permeability and flow-derived DFN constrain reactivated natural fracture rupture area and stress drop — Marcellus Shale microseismic example., *The Leading Edge*, 40 (9): 667–676.

4. Kurison C. and Ahmed M. Hakami, A.M., Kuleli S. 2021. Integration of Geoscience and Engineering Concepts to Account for NaturalFractures in Fluid Flow within Shale Reservoirs. SPE-204747-MS, SPE Middle East Oil & Gas Show and Conference, Manama, Bahrain.

5. Jousset, P.; Jérémy R., 2012. Evidence for remotely triggered microearthquakes during salt cavern collapse, *Geophys. J. Int.*, Volume 191, Issue 1, Pages 207-223 <https://doi.org/10.1111/j.1365-246X.2012.05598.x>

6. Kuleli, H.S.; Sarkar, S.; Toksoz, M.N.; Al-Kindy, F.; El Hussain I.; Al-Hashmi, S. 2009. Monitoring Induced Seismicity at an Oil/Gas Field. *Eos Trans. AGU*, 90(52), Fall Meet. Suppl., Abstracts, S31E-03.

7. Li, J.; H. Zhang, H.; Kuleli H.S.; Toksoz, N., 2011. Focal mechanism determination using high-frequency waveform matching and its application to small magnitude induced earthquakes. *Geophys. J. Int.*, 184 (3), 1261-1274. <https://doi.org/10.1111/j.1365-246X.2010.04903.x>

8. Lomax, A.; Zollo A.; Capuano P.; Virieux P., 2001. "Precise, absolute earthquake location under Somma-Vesuvius volcano using a new three-dimensional velocity model." *Geophysical Journal International* 146(2): 313-331.

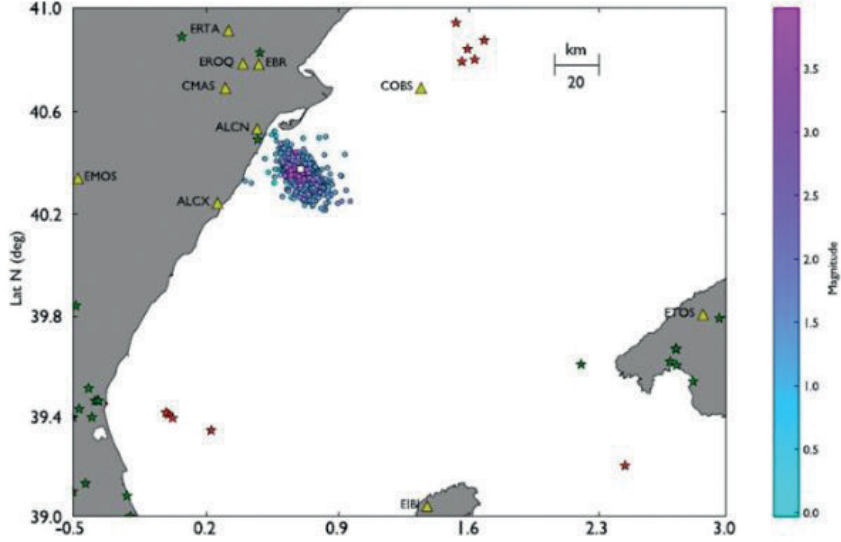
9. Song, F.; Toksoz, M., 2011. Full-waveform Based Complete Moment Tensor Inversion and Stress Estimation from Downhole Microseismic Data for Hydrofracture Monitoring *Geophysics*, 76(6): WC103. <https://doi.org/10.1190/geo2011-0027.1>

10. Zhang, H.; Sarkar S, Toksoz M.N, Kuleli H.S; Al-Kindy F., 2009. Passive seismic tomography using induced seismicity at a petroleum field in Oman. *Geophysics*. Nov;74(6): WCB57-69.

11. Zhang, H.; Thurber, C., 2006. Development and Applications of Double-difference Seismic Tomography. *Pure appl. geophys.* 163, 373–403. <https://doi.org/10.1007/s00024-005-0021-y>

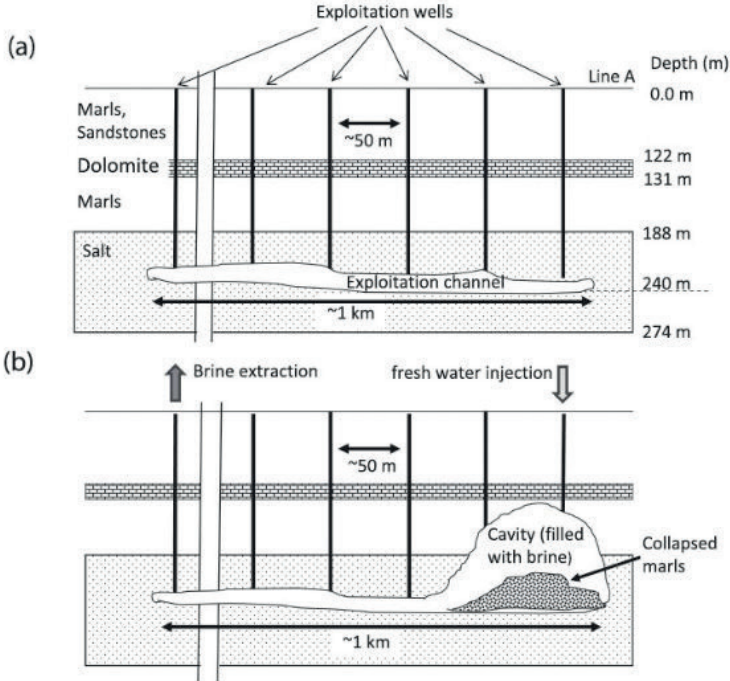
Anahtar Kelimeler: Doğalgaz depolama, rezervuar deprem tehlikesi

Şekil 1



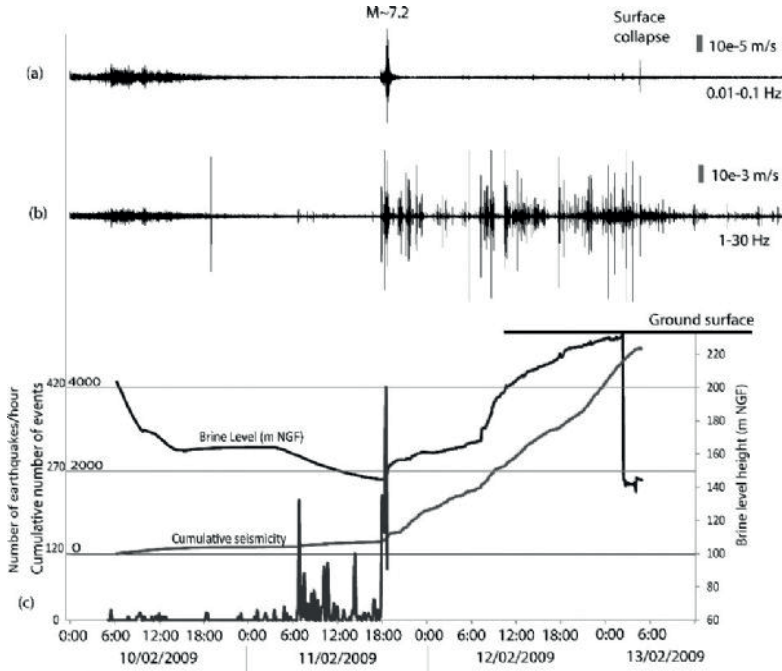
Şekil 1. Bölgedeki deprem istasyonları ve depremlerin merkez üssü dağılımı. Daireler: sismik aktivitenin merkez üssleri. Yeşil yıldızlar: Tarihsel sismisitenin merkez üssleri. Kırmızı yıldızlar: Operasyon öncesi aletsel depremselliğin merkez üssleri. Beyaz kare: Castor gaz enjeksiyon platformunun konumu. Üçgenler: Sismik istasyonlar (Cesca ve diğ., 2014).

Şekil 2



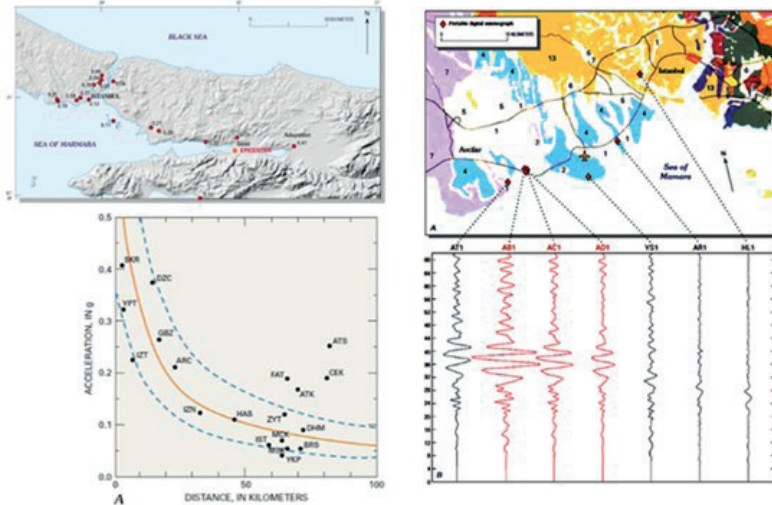
Şekil 2. Tuz mağarasının sematik gösterimi: bu mağara şeklinde görülen şarj-deşarj, (explotion) kuyuları vasıtası ile, su enjekte edilerek oluşturulmuştur. Tuzlu su çıkışının sağlandığı kayu şeklin üzerinde görülmektedir (Jousset & Rohmer,2012).

Şekil 3



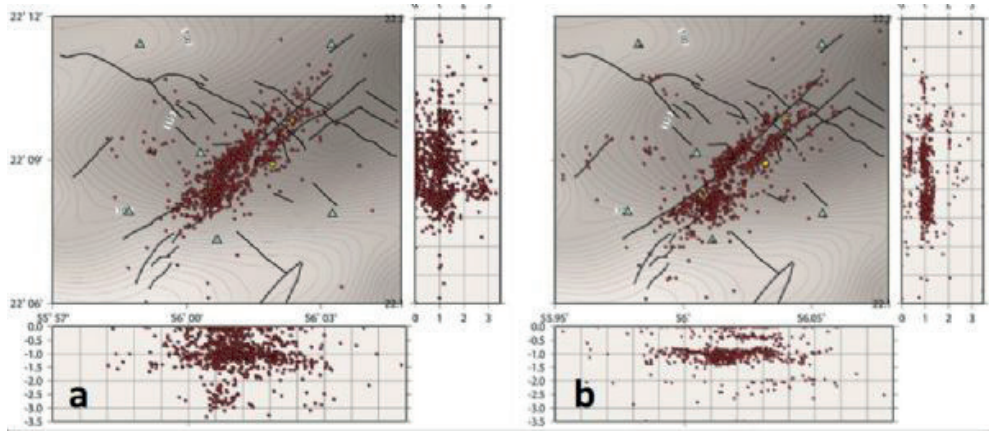
Şekil 3. (a)  $M \sim 7.2$  Kepulauan, Indonesia depreminin alçak-geçişli filtreye (0.01–0.1 Hz) ile filtrelenerek elde edilen uzun periyotlu tepkisi görülmektedir. (b) Aynı sismik kayıt, yüksek geçişli filtreleme (1–30 Hz) sonucu ve tuz mağarasındaki çökme olayının oluşması sürecindeki mikro sismik aktiviteyi göstermektedir (Jousset & Rohmer, 2012).

Şekil 4



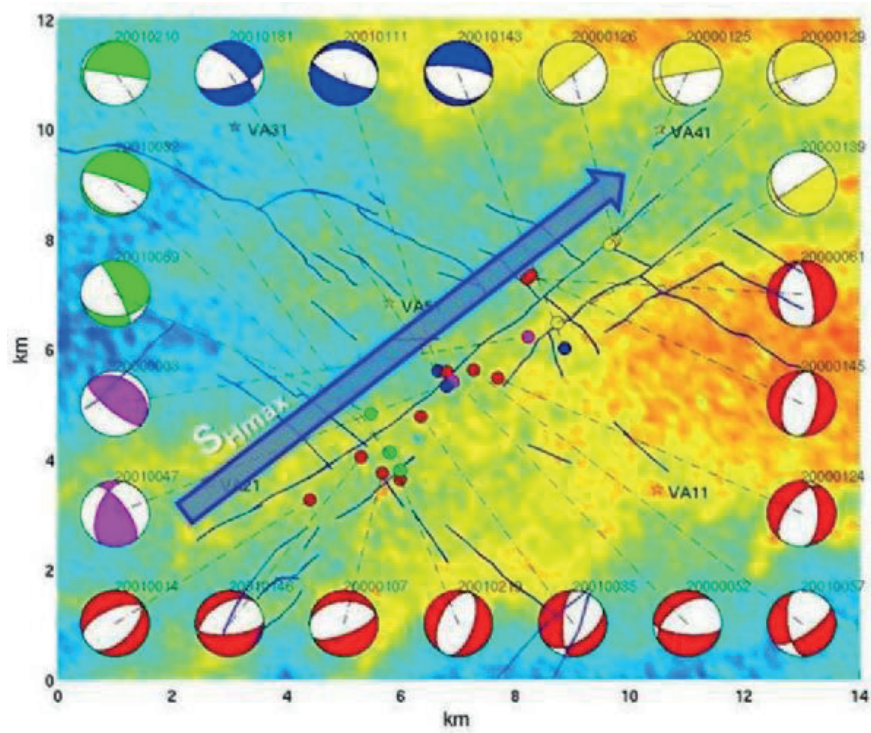
Şekil 4. İzmit depreminin (1992) İstanbul'un değişik semtlerinde ölçülen maksimum ivme sismogramları ve teorik sonumleme grafiği (Cranswick, ve diğ., 2000).

Şekil 5

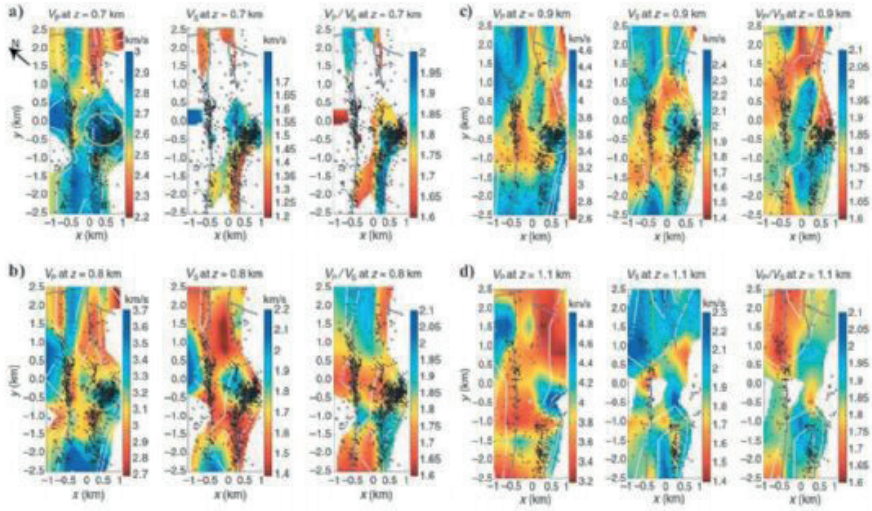


Şekil 5. a) Üst panel: Fay haritalarıyla birlikte sismik odaklar (epicenters). Altı panel: Düşey bir düzlem boyunca odakların derinlik dağılımı (hypocenters). b) geliştirilmiş hiz profiline göre hesaplanan sismik odak dağılımları (Kuleli ve diğ., 2009).

Şekil 6



Şekil 6. Farklı odak mekanizmaları birkaç renkte gruplandırılmıştır. Odak mekanizmaları, KD-GB yönlü mavi okla gösterilen maksimum yatay gerilim yönelimini tanımlar (Li ve diğ., 2011).



Şekil 7. a)  $z=0,7$  km, b)  $z=0,8$  km, c)  $z=0,9$  km ve d)  $z=1,1$  km derinliklerinde,  $V_p$ ,  $V_s$  ve  $V_p/V_s$  modellerinin, gösterimi. Sekillere, fay haritaları, ve her bir kesit grafiğininin 100 m derinliği için sismisite eklenmiştir (Zhang ve dig., 2009).







**Sedimentoloji, Stratigrafi ve ökelim Ortamları**  
*Sedimentology, Stratigraphy and Depositional Systems*

---



# Palaeoenvironmental Significance of Pithonellid Calcitarchs in SE Anatolia: a Discussion on the Use of the Term ‘Calcispheres’



Oğuz Mülayim<sup>1</sup>, İsmail Ömer Yılmaz<sup>2</sup>, Bruno Ferré<sup>3</sup>

<sup>1</sup>Turkish Petroleum Corporation, Adıyaman Directorate, Adıyaman / Türkiye

<sup>2</sup>Middle East Technical University, Department of Geological Engineering, Ankara / Türkiye

<sup>3</sup>2 rue Guy de Maupassant, F-76800 Saint Étienne du Rouvray / France

‘Pithonellid calcitarchs’ (middle? Cenomanian) are found in the organic-rich limestones of the Derdere Formation at SE Türkiye in the northern Arabian Platform. Unfortunately, little is known about the pithonellid calcitarchs in the Cretaceous strata of Türkiye. The diversity or occurrence of ‘pithonellid calcitarchs’ is extremely low in the study area. Three morphogroups of ‘pithonellid calcitarchs’ are distinguished in the study. In the literature, *Pithonella sphaerica* (Kaufmann, 1865) and *P. ovalis* (Kaufmann, 1865), both dominant in the pithonellid assemblages, and *Bonotocardiella conoidea* (Bonet, 1956), less abundant, are mentioned. The marked increase in pithonellids may be related to an early transgressive phase due to sea-level changes during the Cretaceous time, particularly evident in the Cenomanian (Upper Cretaceous). They represent a potentially useful correlative biomarker horizon in the successions of SE Türkiye. ‘Pithonellid calcitarchs’ have been interpreted as indicators of increased nutrient input and discussed in terms of paleoecology/palaeoenvironment and their association with roveacrinid crinoids. In the base of the Derdere Formation, a carbonate succession deposited under eutrophic conditions, there is a positive relationship between ‘pithonellid calcitarchs’ and nutrient input, as indicated by the low diversity or abundance of benthic and planktonic foraminifera. Platform drowning or possibly a mid-Cenomanian event (MCE1) and an anoxic bottom environment could be related to the abundance peak of ‘pithonellid calcitarchs’. In addition, the terminology of calcisphere is also discussed in this study. Nowadays, the term calcispheres is used inconsistently. To eliminate this confusion, the term ‘pithonellid calcitarchs’ is proposed to be used in both global and regional studies.

## INTRODUCTION

On a global scale, pithonellid calcitarchs represent an important, massive petrogenetic contribution to the Late Cretaceous carbonate factory. They are abundant in pelagic/hemipelagic and ramp/shelf carbonate sediments worldwide (Wendler et al., 2022a; 2002b). Pithonellid calcitarchs were abundant during the Cretaceous (Hart, 1991; Dias-Brito, 2000; Versteegh et al. 2009). There are several reports on the Cretaceous deposits of the Arabian Platform and adjacent areas: e.g., Iran (Adams et al., 1967), Israel (Bein and Reiss, 1976), southeastern Turkey (Cros et al., 1991), Jordan (Wendler et al., 2010), and northern Iraq (Hussein, 2017). Pithonellid calcitarchs cannot be used biostratigraphically because they have a wide stratigraphic range. However, they have the potential to be used for palaeoenvironmental

reconstruction, and therefore we used them to interpret the conditions that prevailed in southern Türkiye. In this study, we discuss the palaeogeographic implications of the pithonellid calcitarchs.

## CALCISPHERES AND PITHONELLID CALCITARCHA

The term ‘calcisphere’ is not formally recognized and has remained informal until recent times, although most authors use the term in various approaches, which are summarised below. Early scientific studies associated these essentially spherical calcareous microfossils with the benthonic foraminifera genus *Lagena* (Kaufmann, 1865). These pithonellid calcitarchs were then assigned to various foraminifera groups such as *Oligostegina*, *Fissurina*, *Orbulinaria*, *Pleurozonaria*, and *Stomiosphaera* (Colom, 1955). Dias-Brito (2000) summarised that other speculations classified them into tintinnida, calcareous algal spores, chlorophycean algal zoospores, unicellular algae, benthonic algal oogonia, oolitic structures, protozoa, planktonic protists, and planktonic ciliate organisms respectively. However, Wall and Dale (1968) initially suggested interpreting them as calcareous dinocysts. Later, Keupp (1979, 1987) pointed out the same relationship with Mesozoic calcisphaerulids. Wendler et al. (2002b) suggested several origins for *Pithonella ovalis* and *P. sphaerica*, including the possibility that they are skeletons of dinoflagellates with a vegetative coccoid life stage, which could explain their predominance over other calcareous dinoflagellates in the Cretaceous assemblages. In recent literature (Farzadi, 2006; Piryaeu et al., 2011; Hussein, 2017), the term *Oligostegina* is still commonly used for pithonellid microfossils in Iran and Iraq. Finally, analogous to the listing of *Acritarcha* for organic microfossils of unknown origin, Versteegh et al. (2009) proposed the new group *Calcitarcha*, which includes all calcareous microfossils with a central cavity of an unknown biological relationship. In the following, we have adopted the nomenclature proposed by Wendler et al. (2013) for pithonellid calcitarcha.

## MATERIALS AND METHODS

Micropaleontological studies were carried out on 71 thin sections of limestone samples (boreholes and outcrops) to characterise the pithonellid calcitarchs. Subsequently, microfacies textures were determined in the sedimentology laboratory of the Geological Engineering Department of Middle East Technical University (METU) with an Olympus CX31 polarising microscope using the nomenclature of Dunham

(1962) and following the standards of Flügel (2010). Carbonate rocks were classified using the comparison tables defined by Terry and Chilingar (1955) for visual estimation of percent composition. Facies analyses were performed using this semiquantitative method and Dunham classification. Species identification was performed using a scanning electron microscope (SEM) in the METU central laboratory. The SEM slabs, raw sample material, and processed samples analyzed for the present study are all located in the sedimentology laboratory of the Department of Geological Engineering (METU), Ankara (Turkey), under the registration code and numbers TPA.01-SAB1-9; the samples from the K1-1, Y-1, S-2, and S1-2 well sections are located at the Research and Development Centre (ARGEM) of the Turkish Petroleum Corporation (TPAO), Ankara (Türkiye), under the registration code and numbers TPA.01-K1-1, TPA.01-Y-1, TPA.01-S-2, and TPA.01-S1-2, respectively.

## RESULT

### Palaeoenvironmental Synthesis

The distribution of pithonellid calcitarchs was under the control of accompanying tectonic phenomena, climatic conditions, paleoceanographic changes, and facies-determining environmental factors (Brass et al., 1982; Dias-Brito, 1982; Hay, 1988; Woo et al., 1992). These conditions were highly favourable for opportunistic, r-selected pithonellids, allowing them to thrive and evolve. They thrived in oligotrophic, mesotrophic carbonate ecosystems in association with other pelagic organisms such as roveacrinid crinoids. The pithonellid calcitarchs were thermophilic planktonic organisms associated with fine-grained carbonates deposited in ramp/shelf environments. Therefore, their distribution was controlled by both latitudinal and environmental factors (Dias-Brito, 2000). The increasing abundance of *Pithonella ovalis*, *P. sphaerica*, and *Bonetocardiella conoidea* has been linked to the drowning of the SE Anatolian carbonate platform, as reported by Mülayim et al. (2019a, 2019b) at several sites in the region. Long-term sea-level rise has been extensively documented (Dias-Brito, 2000), and widespread drowning of Middle Eastern carbonate platforms has been noted for the middle Cenomanian (Ziegler, 2001; Sharland et al. 2001), with this drowning coinciding with that of the SE Anatolian carbonate platform (Mülayim et al., 2019a, 2019b). In the study material, the pithonellid calcitarchs are associated with small, simple morphologies of r-strategist planktonic foraminifera that are surface-dwelling species such as the genera *Heterohelix*, *Globigerinelloides*, and *Muricohedbergella* (Hart, 1980a, 1999; Jarvis et al. 1988; Leckie, 1987; Leckie et al., 1998, 2002; Keller and Pardo, 2004). The low salinity tolerance of *hedbergellids* (such as *Muricohedbergella planispira*) and the low oxygen tolerance of heterohelicids have been extensively documented (Hart, 1980b, 1999; Leckie, 1987; Leckie et al., 1998, 2002; Keller and Pardo, 2004; Mülayim et al., 2020). In the

study material, the pithonellid calcitarchs could be considered opportunistic forms by their association with small r-strategist planktonic foraminifera. The latter are cosmopolitan, opportunistic, and adapted to eutrophic environments as documented by Leckie (1987), Premoli Silva and Sliter (1994), Coccioni and Luciani (2004), and Caron et al. (2006).

The paleoecological significance of the roveacrinid crinoids and their connection to the pithonellid calcitarchs

The roveacrinid skeletons were not transported far, not even stirred up by bottom currents, and their crumbled, disarticulated pieces were locally dismantled and scattered in the (lower? to middle Cenomanian) mud-supported sediments of SE Türkiye (Mülayim et al., 2018). They are considered opportunistic organisms because their abundance is positively correlated with that of carbonate producers (pithonellid calcitarchs and heterohelicids) (Ferré, 1995; Ferré et al., 1997). In SE Türkiye, roveacrinid crinoids are more abundant along with pithonellid calcitarchs in the outer ramp environments (Mülayim et al., 2018). This relative rarity could be due to gradual environmental changes in the most likely progressive sedimentary environments of the basin, detrital input, and, less likely, nutrient depletion, resulting in restricted ecological niches and declining diversity (Ferré et al., 2005). In SE Türkiye, the mid-Cenomanian interval documents a peak in diversity and abundance of both pithonellid calcitarchs and roveacrinid crinoids. This quantitative aspect coincides with a global eustatic peak in sea level (Haq, 2014). Ferré (1995) demonstrated that the abundance peaks of roveacrinids, pithonellid calcitarchs, and planktonic foraminifera coincide. In the context of these paleoenvironmental conditions inferred from microfaunal associations, roveacrinid crinoids thrived in environments where they often developed abundant opportunistic populations that most likely fed on pithonellid calcitarchs (Ferré et al., 1997; Ferré et al., 2017; Mülayim et al., 2018). Their wide paleogeographic distribution and global (at least Tethysian-wide) dispersal reflect an early planktonic stage as echinoderm broods or juveniles. Later, they sank to the seafloor as benthonic (benthic-pelagic), bottom-dwelling adults, possibly swimming to escape predatory pressure (Ferré et al., 2016). They are thought to feed on pelagic sinking nutrients (as epibenthonic hemipelagic dredges), and their abundance levels correlate with blooms of calcareous dinocysts, pithonellid calcitarchs, and heterohelicids. Consequently, they can be used to complement sedimentary deposits as well as the eustatic context or highly productive events. While anoxic events have attracted much of the stratigraphic attention (Ferré et al., 2018), such roveacrinoid debris levels can be interpreted as one of the first stirrings of surface productivity and an anoxic bottom environment. This ecological coincidence has also been documented in SE Türkiye, where "middle" Cretaceous deposits are considered anoxic in some places (Mülayim et al., 2019a, 2019b), which is related to sea-level changes. Such accumulation beds have high potential value

as field marker beds for at least regional and even Tethysian wider, long-range correlation. At the very least, we can suggest that this underappreciated fossil group offers potential fossil signposts to detect even minor ecological disturbances and constrain some key crises.

## CONCLUSION

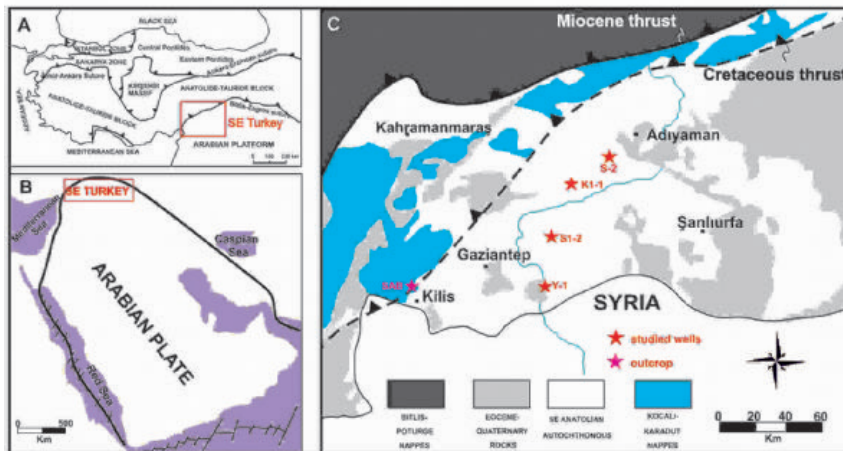
The pithonellid calcitarchs in SE Türkiye are characterized by low diversity: only three taxa are recorded. *Bonetocardiella conoidea*, *Pithonella ovalis* and *P. sphaerica* are good biomarkers for the middle? Cenomanian. The stratigraphic level with the highest occurrence of pithonellid calcitarchs can also be used as a correlative tool for the base of Derdere in petroleum exploration.

Pithonellid calcitarch were opportunistic Tethyan organisms that thrived in warm, saline, and CaCO<sub>3</sub>-rich surface waters. Therefore, they are a useful paleoceanographic tool for identifying Cretaceous pelagic carbonate ecosystems in the Tethys.

Being highly dependent on carbonate ecosystems, they could have thrived under changing water conditions and under the influence of fluctuations in relative sea level. It was the most opportunistic and, living in waters with varying nutrient levels and tolerating higher stress conditions.

Keywords: pithonellid calcitarcha, calcspheres

Fig.1



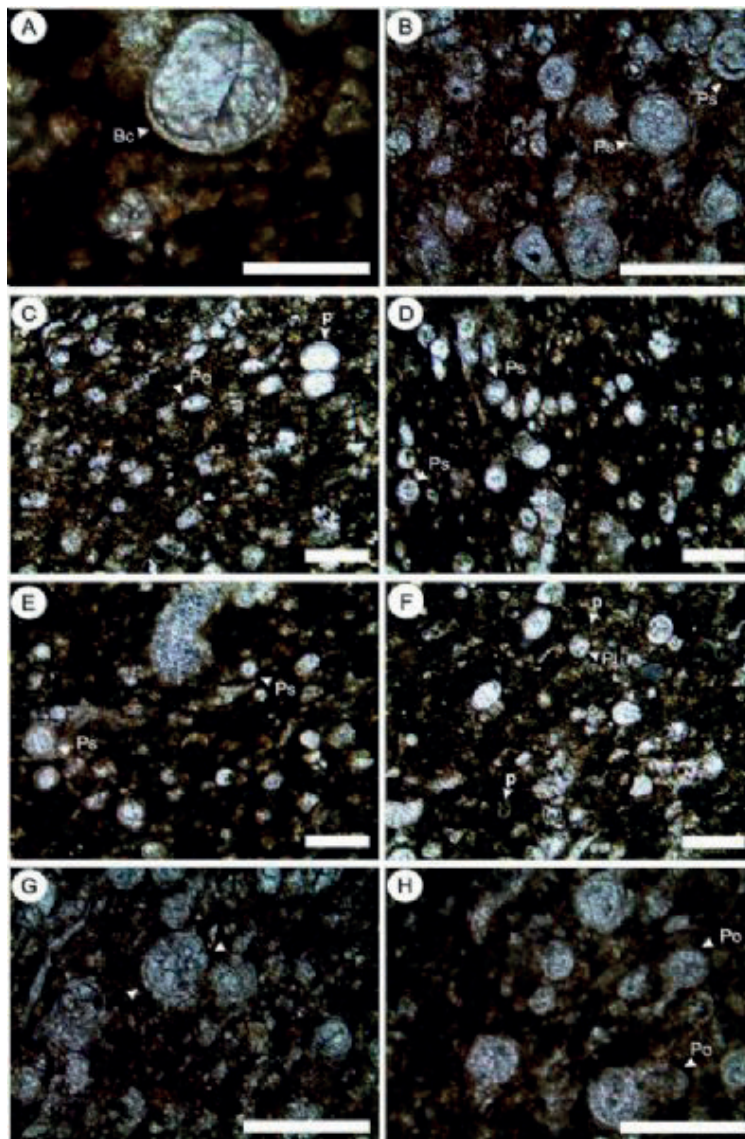
A. Location of the study area. B. Geographic location of SE Turkey in the northernmost part of the Arabian Platform (modified from Sharland et al. 2001; Şenel, 2002; Mülayim et al., 2019b). C. Simplified geological map of the northwestern part of SE Turkey and position of the investigated borehole sections (modified after Mülayim et al., 2019b).

Fig.2

System	Series	Stage	Formation	Member	Lithology	Microfacial texture	Depositional environment
CRETACEOUS	UPPER	Turonian	Karababa	Karababa-A	Planktonic foraminiferal wackestone/packstone		outer ramp, low energy
				Derdere-C	Peloidal wackestone/packstone Bioclastic wackestone/packstone		inner ramp, shallow marine
		Middle-Late Cenomanian	Derdere	Derdere-B	Dolomudstone Fine/medium/coarse crystalline dolomite mosaics		Recurrent deposition gaps, Dolomitization
				Derdere-A	Dark-brown organic-matter, pithonellid and roveacrinid rich Dolomudstone		outer ramp, low energy
	LOWER	Albian/ Early Cen.	Sabunsuyu		Dolomudstone		restricted shallow shelf, low energy
<b>Legend</b> Planktonic foraminifera (⊙)    Bivalves (⌢)    Algae (⌢)    Peloids (⌢)    Intraclasts (⌢)    Pithonellids (⌢) Benthonic foraminifera (⊙)    Gastropods (⌢)    Roveacrinids (⌢)    Drooping unconformity (⌢)							

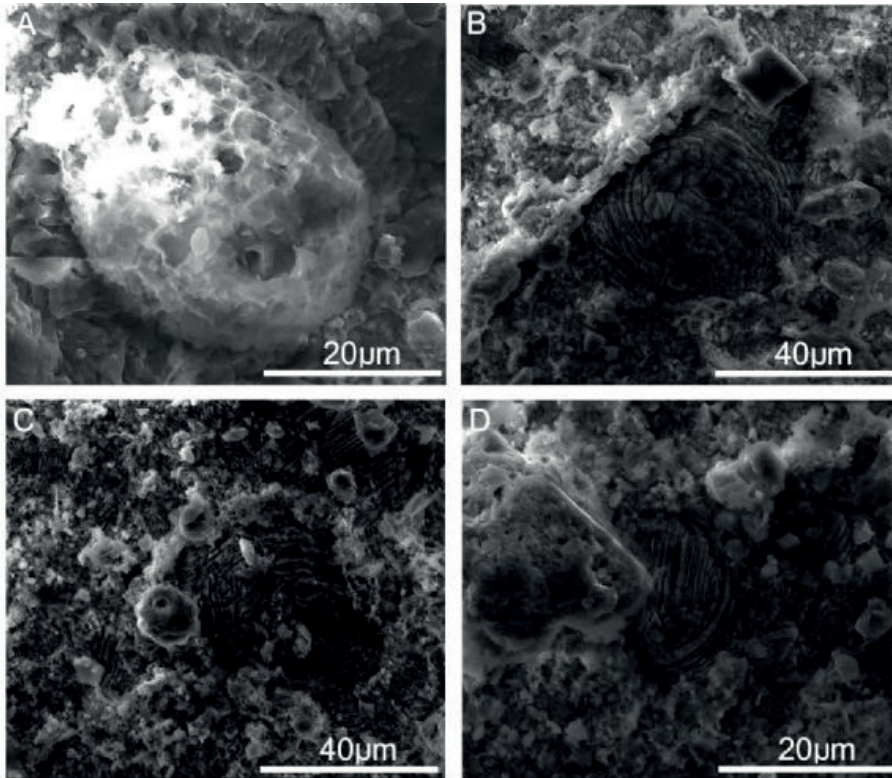
Synthetic stratigraphic columnar section of the respective Cretaceous lithostratigraphical units in the study area (modified from Mülayim, 2020; no vertical scale implied). Red square indicates the study interval.

Fig.3



Thin section photographs of pithonellid calcitarchs, Middle Cenomanian, study area, SE Turkey. A. Cone-shaped form, *Bonetocardiella conoidea*, Bc, core sample 370039. B. Thick-walled spherical form with typical pithonelloid crystal-orientation - *Pithonella sphaerica*, Ps; right middle and upper corner: organic walls are preserved, and the bottom on the middle, core sample 370034. C. Centre - *Pithonella ovalis*, Po, core sample 370025. D. left (10 o'clock above centre) and others on the left: *Pithonella sphaerica*, Ps, core sample 370030. E. left = very clear *Pithonella sphaerica* with nicely visible crystal orientation core sample 370022. F. multilayered form, the *Pithonella lamellata* form spectrum, an archeopyle, spiralling fine striations and perforations, p: planktonic foraminifers, core sample 370021. G. multilayered type, this type is different from the *Pithonella sphaerica* form spectrum by its darker appearance and the brownish crystals, core sample 370019. H: *Pithonella ovalis*, core sample 370005. Scale bar: 100  $\mu$ m and 200  $\mu$ m.

Fig.4



SEM photographs of pithonellid calcitarchs, middle Cenomanian, study area, SE Turkey. A. typical pithonelloid wall type. On the left and right sides of the sphere, the crystals are uniformly inclined towards a point of the sphere at around 11 o'clock, sample 2023. B. *Pithonella sphaerica* with a spiral crystal arrangement, sample 2011. C and D. *Pithonella sphaerica* with blocky cement infillings (the parallel lines are cleavage lamellae) samples 2002 and 2003, respectively



# Carbonate Sedimentology, Micropaleontological Analysis and Stable Isotope Geochemistry of the Garzan Formation at the Core of Gercus Anticline and Subsurface Extent, Batman, SE Turkey



**Damla Altıntaş<sup>1</sup>, İsmail Ömer Yılmaz<sup>2</sup>, Sevinç Özkan Altuner<sup>2</sup>**

<sup>1</sup>Türkiye Petrolleri Anonim Ortaklığı, Ankara / Türkiye

<sup>2</sup>Orta Doğu Teknik Üniversitesi, Ankara / Türkiye

## THE PURPOSE AND SCOPE

The Garzan Formation is one of the most prolific reservoirs in southeast Turkey. It crops out only in the center of the Gercus Anticline. A field study was conducted in July 2015 in order to examine the Garzan successions in situ. The study area is seated in Konak Village, near Gercus County, Batman. The Well F is located at the western side of the field study area. This well is studied to compare and contrast the sedimentological properties of the Garzan Formation at the outcrop with the subsurface extent.

## DATA SET AND METHODOLOGY

The upper part of the Garzan Formation is outcropped at the core of Gercus Anticline. One-hundred-and-forty-six-meter section was measured and sampled in Konak Section (Figure 1). A total of forty one samples were collected from closely spaced intervals at the lower part of the section. The sampling interval is diminished at the upper part of the section due to vegetation. The samples were cut and thin sections were prepared for sedimentological analyses. Each sample were drilled and the obtained powder was collected for isotope analysis. In order to understand the mineralogical composition of the samples, XRD analyses were performed on four samples.

In the Well F, the Garzan Formation was penetrated from top to bottom and one-hundred-and-seventy-one-meter thick strata were cut. A four-meter-thick core is recovered in the form of short columns and small pieces. Seven thin sections were prepared for petrographic analysis and two core plugs were obtained for routine core analysis.

## Structural Geology and Geomorphology of Gercus Anticline

Gercus Anticline, the part of a fault-propagation folding mechanism, is located at the high folded zone of the Bitlis-Zagros Fold and Thrust Belt. (Yildirim, 2003; Seyitoglu et al., 2017). It is one of the major asymmetrical anticlines plunging both east and west directions. The southern limb of the structure is bounded by a reverse fault (Figure 2 and Figure 3).

## Lithostratigraphic Units

The lithostratigraphic units in the Gercus Anticline is composed of Hoya, Gercus, Becirman, Germav and Garzan formations deposited from Cretaceous to Miocene. The Garzan Formation is the oldest rock unit

cropped out at the core of the anticline. The lithological properties of the each formation from bottom to top are given in the Figure 4.

## Sedimentological and Paleontological Analyses

In order to define the sedimentological, diagenetic and micropaleontological architecture of the Garzan Formation, 41 thin sections are described and classified in the Konak Section. A total of 34 thin sections of the cuttings and core slabs are defined in the Well F. The main biogenic components are the benthic foraminifers, rudist, echinoid, ostracod and pelecypod tests, corals, bryozoans, and dasycladacean algae. Detailed microfacies are defined and classified by the distribution of these components.

The rudist shoals (build-ups) are seated across the Garzan carbonate shelf. The shoals are subdivided into facies zones as lagoon, back-shoal, shoal, fore-shoal, slope and deep marine in the area of extent. Standard Microfacies (SMF) are applied for microfacies analysis. In the lagoon and backshoal facies zones, peloidal grainstone/packstone (SMF 16), whole fossil wackestone/floatstone (SMF 8) and packstone with abundant foraminifera or algae (SMF 18) facies are described. The shoal is represented by limestone with rudist and echinoid concentrations (SMF 12). Allochthonous bioclastic rudstone/packstone/floatstone (SMF 5) and SMF 18 facies with abundant larger benthic foraminifera are assigned to foreshoal facies. In the slope and deep shelf facies zones, microbioclastic peloidal calcisiltite (SMF 2) and pelagic mudstone/wackestone with Calcispherulid and planktic foraminifera (SMF 3) are observed. The micropaleontological analyses are conducted to classify the benthic foraminifers and the age of the Garzan Formation is defined as Maastrichtian in this study.

The diagenetic processes that affect the Garzan Formation in the area of interest are neomorphism, micritization, dissolution, cementation, compaction, mineralization, and partial dolomitization. The euhedral dolomite crystals are defined during the thin section analysis. Some of the dolomite crystals are differentiated as infill of stylolites. The total percentage of the dolomite in the total rock mineral composition ranges between 6-13% based on the XRD analysis. Channel, fracture, moldic, vuggy and intraparticle porosity types are described. The pore spaces are occluded by cement. Blocky calcite, drusy mosaic, and syntaxial cement overgrowths on echinoderm fragments are the main cement types. Micritic rims, stylolites, phosphate

nodules, and pyrite minerals are the other observed diagenetic features. At the contact of the Garzan and Germav formations, glauconite minerals are described.

### Geochemical Analysis

Forty one samples were analysed for stable isotopes from bulk rock samples ( $\delta^{13}\text{C}$  (‰) VPBD and  $\delta^{18}\text{O}$  (‰) VPBD) in the stable isotope laboratory of the Central Laboratory in the Middle East Technical University. The samples are powdered by microdrilling method by using hand dremel.

The carbon isotope values change between 0.68-4.13. The oxygen isotope value range between -6.88 to -2.78. The positive covariance of values in the cross-plots of the carbon and oxygen isotopes is an evidence for mixing of meteoric and marine water.

### CONCLUSION

The sedimentological examinations and the microfacies analyses reveal that the shallow marine depositional environment conditions allowed the deposition of the carbonate rock successions. The depositional sub-environments of the Garzan strata are defined as lagoon, back-shoal, shoal, fore-shoal, slope and deep marine. The microfossil analysis presents that the age of the Garzan Formation is defined as Maastrichtian based on the classification of the benthic foraminifers. The stable isotope measurements display the depositional and the diagenetic history of the rock unit. The diagenetic processes that influence the Garzan successions in the area of interest are observed as neomorphism, micritization, dissolution, cementation, compaction, mineralization and, partial dolomitization.

### REFERENCES

- Moore, C.H., 1989, Carbonate Diagenesis and Porosity: Developments in Sedimentology v. 46, Elsevier, Amsterdam, 338 p.
- Seyitoglu, G., Esat, K., and Kaypak, B., 2017, The neotectonics of southeast Turkey, northern Syria, and Iraq: the internal structure of the Southeast Anatolian Wedge and its relationship with recent earthquakes, Turkish Journal of Earth Sciences, 26: 105-126, Tübitak, 22 p.
- Siyako, M., Şeker, H., Bahtiyar, İ., Özdemir, İ., Kılınç, S., F., Arslan, M., D., Karaçay, A., Özsoy, S., and İşdiken, B., 2014, Batman, Beşiri, Kurtalan, Raman ve Gercüş Civarının Jeolojisi ve Hidrokarbon Olanakları, TPAO Report, No: 5546, p. 29.
- Tucker, M.E., and V.P. Wright, 1990, Carbonate Sedimentology: Blackwell Scientific Publications, Oxford, p. 482.
- Yildirim, A., 2003, Geomorphological Features Gercüş Anticlinal and Surrounding, Marmara Coğrafya Dergisi, No: 8, 14 p.

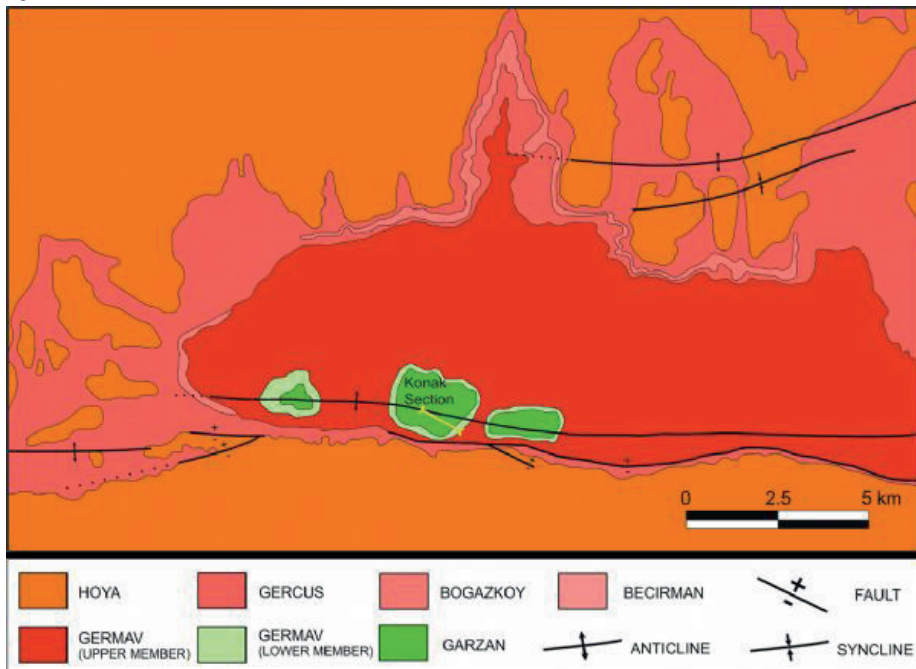
Keywords: Garzan Formation, Gercus Anticline

Figure 1



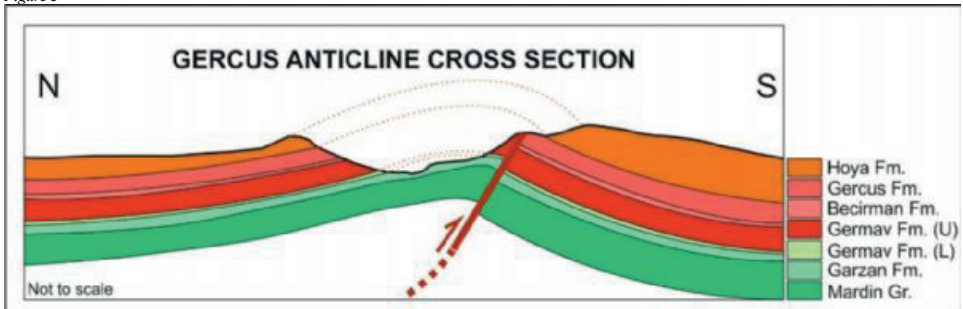
Konak Section (Google Earth satellite image).

Figure 2









The geological map of the Gercus Anticline (redrawn from Siyako et al., 2014).

Figure 3



The geological cross section of the Gercus Anticline (Not to scale).

Figure 4

AGE	UNIT	THICKNESS (m)	LITHOLOGY	DESCRIPTIONS	ENVIRONMENT	FIELD PHOTOS
MIO	Hoya	>100	Limestone	Yellowish white colored, fossiliferous, fractured	Restricted Shallow Marine	
PALEOCENE	Gercus <small>Bogazkoy Member</small>	300	Dolomitic limestone	Yellowish white colored, dolurinated	Aluvial Fluvial Sabhka Playa	
			Conglomerate	Reddish brown colored, channelized, composed of polygenic clasts		
			Gypsum	White colored, tough		
			Mari	Greenish gray colored, laminated, fishy		
PALEOCENE	Becirman	50	Claystone	Reddish brown colored, soft, sticky	Delta/ Shoreline	
	Limestone	Cream-white colored, fossiliferous, collitic				
CRETACEOUS	Germav (Upper)	375	Dolomite	Cream colored, micritic textured, with evaporite inclusions	Deep Marine	
			Sandstone	Yellow colored, thick and cross bedded, fossiliferous well sorted, carbonate cemented		
	Siltstone	Yellow colored, thin bedded, carbonate cemented				
	Shale	Dark grey, grey colored, laminated, fossil, carbonaceous				
CRETACEOUS	Germav(L)	50	Limestone	Yellowish cream colored, nodular, detritic, fossiliferous	Slope	
			Mari	Light grey beige colored, soft, microfossiliferous		
	Garzan	170	Argillaceous Limestone	Off-white colored, thin bedded		
CRETACEOUS	Mardin	300	Limestone	Cream, white colored, bioclastic, fossiliferous	Carbonate Platform	
			Dolomite	White to very light gray colored, moderately hard, fractured		

The lithostratigraphic units in the field study area.

# Gondwana Paleozoyik Buzulları ve GD Anadolu Paleozoyik Petrol Sistemlerine Olan Etkileri



**Nihat Bozdoğan<sup>1</sup>, Bayram Kara<sup>2</sup>**

<sup>1</sup>Sanko Enerji (PETAR)

<sup>2</sup>Çalık Petrol

## GİRİŞ

Geç Proterozoyik'ten Paleozoik'in sonuna kadar olan dönem boyunca, Gondwana kıtasının Arap Yarımadası ve onun bir parçası olan GD Anadolu ile Kuzey Afrika bölümü güney kutup bölgesindedir. Bu bölgelerin belli kesimleri, buzul etkisinde kalmıştır. Bu süre zarfında Arap Yarımadası'nın sedimanter birimlerinde Prekambriyen dönemine ait iki, Geç Ordovisiyen ve Geç Karbonifer-Erken Permiyen dönemlerine ait iki olmak üzere toplamda dört farklı döneme ait buzul olayının varlığı ve Paleozoyik çökellerine olan etkileri kaydedilmiştir (Bell and Spaak, 2007)..

Gondwana ve Arap Yarımadası üzerinde gelişen bu buzul olaylarından üç tanesi bölge Paleozoyik petrol sistemleri üzerinde çok etkili olmuşlardır (Şekil-1). Bu etki sadece rezervuar birimlerinin çökmesinde değil, aynı zamanda kaynak kaya fasiyeslerinin gelişmesinde, çökme ortamları ile yapıların oluşmasında ve örtü kaya oluşumlarında da etkileri olmuştur (Şekil-2).

Bu buzul olayının güney kutbu, o zamanlar Kuzey Afrika'nın batısında, günümüz Moritanya'sında bulunmakta olup buzul dönemlerine ait bu etkinin boyutları bölgelere göre büyük farklılıklar göstermektedir.

Prekambriyen buzul çökelleri Dünyadaki en eski iki ayrı buzullaşması olup yalnızca Infrakambriyen havzalarının korunduğu Umman'da bilinmektedir. Diamiktitlerin varlığı, Umman'da yeraltı çalışmalarında tesbit edilmiştir. Buzul çökellerinin mostralarna ise Güney Umman da rastlanmaktadır. Bölgede bu buzul çökellerinin oluşturduğu istifin, organik açıdan zengin şeyllerle örtülen bir karbonat ile sona ermektedir. Buzullu diamiktit biriminin en üstteki birkaç metresi, kırıntı destekli reworking konglomeralar ve çapraz tabakalı kumtaşları da dahil olmak üzere yeniden işleme ile uyumlu tortul özellikler gösterir. Diamiktitleri uyumlu olarak üzerleyen 2 m kalınlığı dolomit birimi ve en üstte ise stromatolitler bulunur. Bu karbonatlarda sıvı hidrokarbon kapanımlarına rastlanmaktadır. Ancak yeraltında, buzul tortullarında depolanmış ticari hidrokarbonlar yoktur. Bununla birlikte, örtü karbonatın üzerindeki organik açıdan zengin şeyllerin zayıf ve edilgenleşmiş kaynak kaya kalitesinde olduğu da tesbit edilmiştir. Bazı Umman sahalarında bu şeyillerin petrol oluşumuna katkılarının olduğuna inanılmaktadır (Bell and Spaak, 2007).

Prekambriyen dönemi için GD Anadolu bölgesi Umman'daki jeolojik sistem ile benzerlik göstermemekte olup Infrakambriyen havzaları gelişmediğinden bu buzulların etkisinden bahsetmek mümkün değildir.

Arap Yarımadası ve Kuzey Afrikada Geç Ordovisiyen (Geç Aşgilyen/Hürnansiye) buzullaşmasının varlığına ve etkilerine dair yaygın kanıtlar vardır.

Yeraltında buzullarla oyulmuş kanalların varlığı, saha çalışmalarında elde edilen gözlemler, parlatılmış ve çiziklenmiş buzul çakılları, sürüklenme izleri buzullarının etkilerini ortaya koymaktadır.

Arabistan'da yüzeyde ve yer altında kanalların ve tünel vadilerinin konumu, buzullu bölgenin batıda, Nubia ve Arap kalkanı bölgesinde olduğunu ve tortul taşınmasının günümüzün doğu ve kuzeydoğusuna doğru olduğunu göstermektedir.

Ordovisiyen'de buzul döneminin aniden sona ermesi ile Erken Silüriyen döneminde (Llandoveriyen) gelişen transgresyon ile kaynak kayaların çökmesi için ideal ortam koşullarını sağlamıştır. Kuzey Gondwana'nın büyük kısımlarında "hot shale" olarak tanımlanan, pirit ve radyoaktif elementler açısından zengin organik maddeli mukemmel kaynak kaya oluşumuyla sonuçlanması buzul döneminin bölge üzerinde oluşturduğu ikinci önemli etkidir. Bu Silüriyen kaynak kayası, kuzey Afrika ve Arap yarımadası ile GD Anadolu dahil Paleozoyik petrolerinin kaynağıdır. Katar'daki Kuzey Sahası için ana kaynak kayalardan biri olan ve Suudi Arabistan'daki Unayzah'daki petrol ve Ghawar, Khuff ve Unayzah'daki gaz ve Umman'daki Sahmah gibi bazı önemli petrol sahalarının da kaynak kayasıdır.

Silüriyen şeyilleri stratigrafik olarak daha genç rezervuarların (Devoniyen, Karbonifer, Permiyen) kaynak kayası olmakla birlikte, Silüriyen kaynak kayasının altında bulunan ve rezervuar özelliği taşıyan Ordovisiyen denizel kumtaşları için de (Ürdün'deki Risha sahası, Irak'taki Akkas sahası ve GDA daki Arpatepe, Çalıktepe, Altınakar gibi pekçok petrol sahasında olduğu gibi) kaynak oluşturmaktadır. Ancak Silüriyen kaynak kayasının altında bulunan buzul etkili, killi ve kaba klastik çökeller (diamiktit) hem yayılımları kısıtlı hem de rezervuar özellikleri taşımadıklarından potansiyelleri yoktur.

Gondwana kıtası son buzul dönemi olan Geç Karbonifer buzullaşmasının bölge petrol sistemlerine olan etkileri ağırlıklı olarak Orta Arabistan Yarımadasında kendini göstermiştir. Silüriyen depozisyonunun arkasından gelen akarsu ve denizel kumtaşlarının hakim olduğu bir çökel döneminden sonra bölge Karbonifer yaşlı Hersiniyen olayının etkisiyle karasallaşmıştır. Arap Levhasının ve de GD Anadolu'nun büyük bir bölümü bu dönemde yükselmiş ve de peneplenleşmiştir. Bu bölgesel uyumsuzluk yüzeyi daha sonra bir dizi buzul vadisi ve Geç Karbonifer'de buzul birikimleri ile şekillenmiştir. Yani Geç Karbonifer-Erken Permiyen döneminin buzul etkileri daha çok erozyonal bir paleocoğrafya oluşmasında etkili olmuştur. Suudi Arabistan'daki Unayzah klastikleri, bir dizi buzul ve buzul çevresi ortamını temsil eden diamiktitler ve bunlarla ara tabakalı şeyller, sıg denizel fluvial

kumtaşları ve konglomeralar ile karakterize edilir.

Orta Saudi Arabistan 'da, Geç Karbonifer buzul hareketlerinin Hersiniyen uyumsuzluğunun hemen üzerinde olmasından dolayı, Siluriyen şeyllerine kadar derinleşen aşımalar bu birimlerin yan yana gelmesine neden olarak Siluriyen kaynak kayasından rezervuar seviyeleri doğrudan beslenmiştir.

Esasında diamiktitler, Siluriyen şeyllerin üzerindeki birimlerde direk görülmezler. Geç Karbonifer'deki buzullaşma hemen bir sellenme ile de sonuçlanmamıştır. Ancak sığ denizel, fluviyal ve buzul çevresindeki kumtaşları Arabistan'da hem petrol hem de gaz için kanıtlanmış rezervuarlardır.

GD Anadolu bu dönemi çökelmezlikle geçirdiği için petrol potansiyeli açısından bu dönem buzullaşmasının kaynak kaya, kapanlanma, örtü kaya veya rezervuar kaya açısından petrol sistemine herhangi bir etkisi olmamıştır. Ancak doğrudan Dadaş formasyonu üzerine oturan Permian klavtikleri, derin vadilerle kazanıp bu vadiler içerisinde çökelen sığ denizel ve fluviyal temiz kumtaşları ile potansiyel taşıyacakları da muhtemeldir.

Bölgedeki en eski buzullardan iki tanesinde (Prekambriyen ve Ordovisiyen) olaylar, orijinal buzul sonrası taşkınla ilişkili denizel kaynak kayalarla sonuçlanırken, daha genç Karbonifer buzullaşmasında böyle bir olay gerçekleşmemiştir. Buzullaşmanın taban seviyesindeki bir artışla ilişkili olası bir görsel kaynak kayaya sahiptir. Karbonifer'in neden bir deniz taşkını kaynak kayası ile ilişkili olmamasının nedeni tam olarak anlaşılabilir. Ancak Karbonifer buzullaşmasının Neo-Tetis'in açılmasına yol açan ilk genişleme olayları ile de ilişkili olduğu düşünülmektedir.

Daha genç iki buzul olayının (Karbonifer ve Ordovisiyen) her ikisi de buzul etkisinin arkasından yeniden işlenmiş kumtaşı rezervuarlarına sahiptir. Umman'da ise diamiktit çökel paketlerinin tepesindeki kırıntı destekli ve yeniden işlenmiş klavtik rezervuarların mümkün olduğunu gösterir.

#### **Genç Ordovisiyen Buzullaşmasının Güneydoğu Anadolu Paleozoyik Petrol Potansiyeline Etkileri:**

GD Anadolu bölgesi jeolojik sistem olarak Gondwana Kıtası üzerinde Kuzey Afrika ve Arap Plakası ile benzer jeolojik özellikler taşımaktadır. Özellikle Arap Plakası kuzey ucunda yer almasından dolayı bu bölge ile daha da benzer özellikler taşımaktadır. Ancak kıta üzerinde yaşanan buzul olayları incelendiğinde bölgelere göre büyük farklılıklar da görülmektedir.

Geç Ordovisiyen buzullarının GD Anadolu Paleozoyik petrol potansiyeline etkisini üç başlık altında incelemek mümkündür. Öncelikle, buzulların ağırlıkları ve yüksek aşındırma güçleri dolayısıyla derin vadiler oluşturması veya mevcut kuzuma vadilerin daha da derinleştirilmesidir. Bu vadilerin üzerleri kaynak kayalarla örtüldüğünde kapalı sistem vadi kapanlarını oluşturacaktır. Ancak bu vadilerin iyi boylanmış ve yakanmış iyi rezervuar karakterine sahip temiz kumtaşları ile doldurulup rezervuar kayaların oluşmasını sağlamasıdır. İkinci olarak buzul dönemi

sonucunda aniden gelişen transgresyon etkisinde anoksik indirgeyici ortamların mükemmel seviyede kaynak kayaların oluşumuna olanak sunmasıdır. Son olarak ise buzul döneminin bitmesini takiben gelişen şeyillerin örtü kaya özellikleri kazanmasıdır.

GD Anadolu'da buzul çökelleri veya buzul etkili çökelere sadece Mardin-Derik bölgesindeki Kambriyen-Ordovisiyen mostralarının görüldüğü Mardin Yükselim alanında gözlenmiştir (Ghienne v.d. 2010). Bu istif yaklaşık 50 metre kalınlığında, 150 metre genişliğinde kanal yapısında görünümü olan mavimsi gri renkli, çakıllı şeyiller, kötü boylanmış, kahverengimsi çakıllı kumtaşları, buzul çakılları içeren konglomeralar ile diamiktitlerden oluşmaktadır (Şekil-3). İstif içerisinde gözlenen parlak ve çizilmiş çakılların varlığı ile "dropstone" karakterinde çakıl ve blokların görünmesi ve stratigrafik olarak bölgedeki en genç Ordovisiyen çökelleri olması bu kaba klavtik malzemenin buzul etkisi ile çökeltmiş bir istif olduğunu düşündürmektedir. Çökel grubunun yayılım alanı çok sınırlı olup yanal yönde korelasyonu yapmak ta zordur. Birim, altında bulunan Geç Ordovisiyen yaşlı kumtaşı ve şeyillerden oluşan Bedinan formasyonunun Bedinan-III üyesinin üzerine bir aşımın yüzeyi ile oturur.

Bu istif alttan eksik çökelerek, üstten ise aşınarak eksilmiş, transgresif bir çökel topluluğu yapısında olup tane boyu yukarıya doğru küçülmektedir. Kil ve silt içerisinde serpilmiş çakıllı diamiktitlerin oluşturduğu bu çökel topluluğunun herhangi bir rezervuar potansiyeli yoktur. Altındaki iyi boylanmış, yer yer çapraz tabakalı gelgit etkili kum barları ise iyi rezervuar özelliklerine sahiptir (Bedinan-III). Bölgedeki en genç Ordovisiyen çökeltimi olan bu birimin biyo- ve lithostratigrafik özellikleri gereği Bedinan formasyonunun dördüncü üyesi olarak tanımlanmaktadır. Bedinan-III üyesi ise, özellikle en üstünde bulunan beş metrelik seviyesi geniş yayılımı, %25 lere ulaşan porozite değerleri ve iyi boylanmış temiz kumtaşları özelliğiyle Paleozoyik petrol sisteminin önemli bir rezervuarıdır (Şekil-4).

Kayseri-Pınarbaşı bölgesinde arazi çalışmaları ile tanımlanan kaba klavtik istif Ordovisiyenin en genç buzul etkili çökelleri olarak tanımlanmış ve Halevikkere formasyonu olarak isimlendirilmiştir (Ghienne v.d. 2010). Mardin\_Derik'teki buzul etkili çökelde aynı isimle yayımlanmıştır. Şenalp ise 2018 de aynı yerdeki aynı çökel paketini sadece arazi gözlemlerine dayanarak Yurteri formasyonu olarak adlandırmak istemiştir.

Ordovisiyen sonu buzul çökelleri, GD Anadolu bölgesi ve Toros kuşağında başka mostralarda da gözlenmiştir. Amanos dağlarında, Kayseri Pınarbaşı, Silifke Taşucu, Adana Kozan ve Anamur bölgelerinde "dropstone" karakterinde kaba çakıllı, bloklu kumtaşı ve silttaşı şeklinde görmek mümkündür. Önceki çalışmalarda Siluriyen çökellerinin taban koglomerası olarak düşünülmüştür. Toros kuşağında, Arabistan'da ve Kuzey Afrika'da bu buzul dönemi çökellerinin üzerine mutlaka Siluriyen çökelleri gelirken, Mardin-Derik ve Ceylanpınar bölgesinde Siluriyen çökellerine rastlanılmamaktadır. Bunun sebebi, Mardin Derik bölgesinin Mardin-Kahta yükseliminin güney

bölgesinde kalması ve daha yüksek bir topografya üzerinde olmasıdır (Şekil-5).

Bu nedenledir ki Diyarbakır baseninde çökelen Ordovisiyen ve Siluriyen çökel grubu, daha korunmuş bir alanda buzul etkilerinden hiç etkilenmemiş denizel bir ortamda, tıpkı Kuzey Irak, Suriye, Kuzey Libya ve Arabistan'ın bazı bölgelerinde ve Ceylanpınar, Derindere, Mollacabir, Yarımcı, Handof, Çıksor, Sarık gibi onlarca kuyuda olduğu gibi ne buzul vadileri, ne de bu vadileri dolduran genç Ordovisiyen rezervuar birimleri oluşmamıştır (Şekil-6). 1500 metre kalınlığa ulaşan, Ordovisiyen çökelleri sakin denizel koşullarda dört regresif çevrimin etkisinde çökelişini tamamlamıştır.

Siluriyen çökelleri Ordovisiyen paleotopografyası üzerine kimi yerde diskordansla, kimi alanda uyumlu olarak tedrici geçişle gelmektedir (Şekil-7). Bu paleocografik taban yapısı dolayısıyla bazı alanlarda Erken Siluriyenin altında, bazı alanlarda ise Geç Ordovisiyen çökellerinin üst bölgelerinde eksiklikler ve aşınmalar görülmektedir (Kara ve Işık, 2021). Ancak bu düzensiz taban paleotopografyası tektonik gelişmelerin ürünüdür.

## SONUÇLAR

Gondwana kıtası Paleozoyik buzul dönemi olaylarının bölge ülkeleri petrol sistemleri üzerindeki etkileri incelendiğinde, Prekambriyen döneminde iki ve Geç Ordovisiyen ile Geç Karbonifer dönemlerine ait toplam dört adet buzul döneminden sadece Geç Ordovisiyen (Hirnantisiyen) buzullaşmasının GD Anadolu'da pasif etkili olduğu görülmektedir.

Diğer buzul dönemleri çökmezlik veya jeolojik sistemin farklı olmasından dolayı Prekambriyen ve Karbonifer havzaları gelişmemiş olup GD Anadolu'da herhangi bir etki bırakmamıştır.

Genel olarak değerlendirildiğinde bölgede hüküm sürmüş buzullaşma olayları Paleozoyik petrol sistemleri üzerinde şu konularda etkili olmuşlardır;

- Buzul hareketlerinin derin buzul vadiler oluşmasına veya mevcut vadilerin derinleşmesine sebep olarak kaynak kayalar ile rezervuar birimlerinin karşı karşıya gelmesine sebep olmuşlardır.

- Buzullar tarafından oluşturulan derin vadiler, buzullaşma döneminden sonra denizel, geçiş veya fluvial koşullar altında iyi yıkanmış, iyi boylanmış ve tabakalanma gösteren yüksek poroziteli rezervuar kumtaşları tarafından doldurulursa bu bölgeler vadi tipi kapanlar olarak aramacılıkta önemli potansiyel taşıyabilirler.

- Bu buzulların hızlı erimesini takiben üzerlerine gelen kaynak kayaların oluşmasına sebep olmuşlardır.

- Bu kaynak kayalar aynı zamanda kaliteli örtü kaya görevi de gördüklerinden petrol sistemlerini olumlu etkilemişlerdir.

Genç Ordovisiyen dönemi buzulları Mardin-Derik bölgesindeki Kambriyen-Ordovisiyen mostraları üzerinde tanımlanmıştır. 150 metre genişliğinde, 50

metre kalınlığında kanal yapısında görünen, buzuldenizel çökeltme ortamlarında oluşan, kil-silt matris içerisinde gelişen parlak ve çizikli çakılların, çakıllı kumtaşlarının ve diamiktillerin olduğu çökel grubunun rezervuar özelliği yoktur.

Bu birimin kronostratigrafik muadili olan ve Diyarbakır Baseninde geniş yayılıma sahip Bedinan-IV üyesi ise denizel ortamda çökeltmiş ve özellikle formasyon girişindeki ilk beş metrelik kısım ile 30 metre civarında toplam kalınlığı olan seviyeleri iyi rezervuar özellikleri taşımakta olup ancak bu kum gelişmelerinin de buzullarla ilişkisi yoktur.

Bölgenin yapısal durumu incelendiğinde petrol sistemlerini etkileyen derin buzul vadilerinin gelişmediği, açılma tektoniğinin oluşturduğu normal faylarla gelişen yarı graben veya grabenleşme sonucunda oluşan yapı modellerinin geçerli olduğu bilinmektedir (Şekil-8-11). Bu nedenle Ürdün'de ve Saudi Arabistan'da olduğu gibi vadilere yönelik yapılan arama stratejileri GD Anadolu için uygun değildir ve zaten bu alanda bir başarıda elde edilememiştir (Şekil-12).

Son olarak buzul erimelerinin arkasından gelişen hızlı deniz yükselmeleri, çok iyi kaynak kaya ve örtü kaya oluşumlarına sebep olmuşlardır. Tüm Kuzey Gondwana da olduğu gibi GD Anadolu bölgesinin en iyi kaynak kayalarından birisi olan Dadaş formasyonu böyle bir etki ile oluşmuştur. Paleozoyik buzullarının GD Anadolu petrol sistemleri üzerindeki tek etkisi bu şeyillerin çökeltmesi olmuştur.

## RESULTS

The effects of the Paleozoic glacial period of the Gondwana continent on the oil systems of the region are examined, it is seen that only the Late Ordovician (Hirnantian) glaciation was effective in SE Anatolia, out of four glacial periods two in the Precambrian period and two in the Late Ordovician and Late Carboniferous periods.

Other glacial periods did not have any effect in SE Anatolia due to the non-deposition or the difference of the geological system.

In general, the glaciation events that prevailed in the region had an impact on the Paleozoic oil systems on the followings;

- Glacial movements caused the formation of deep glacial valleys or the deepening of existing valleys, causing source rocks and reservoir units to come into contact.

- After glaciation period, if these incised valleys are filled with reservoir sandstones, with good porosity, well sorted and layered, deposited under normal marine conditions may have significant potential for exploration as valley-type traps.

- Rapid melting of the glaciers, may be followed by a transgression may cause deposition of the organic rich shales (source rock).

- These shales/source rocks may act as cap rock and has

a positive impact on oil systems.

These Late Ordovician glaciers were identified on the Cambrian-Ordovician outcrops in the Mardin-Derik region. The sediment group, which consists of bright and scratched pebbles, pebbly sandstones and diamictites, which are formed in a clay-silt matrix, appearing in the channel structure with a width of 150 meters and a thickness of 50 meters, formed in glacial-marine deposition environments, does not have a reservoir properties.

The Bedinan-IV member, which is the chronostratigraphical equivalent of this unit and has a wide stribution in the Diyarbakır Basin, was deposited in the marine environment, no relation with glaciers, and especially the first five meters of the the formation, total thickness is around 30 meters,have good reservoir characteristics.

When the region is evaluated structurally, deep glacial valleys that affect the oil systems do not develop, and that the structure models formed as a result of graben or semi-graben developed by normal faults under the extensional tectonics. For this reason, exploration strategies for valleys, as in Jordan and Saudi Arabia, are not suitable for SE Anatolia and till now there is not successful result in the area.

Finally, rapid sea rises due to glacial melting may resulted in very good source rock and cap rock formations in the area. The Dadaş formation, which is one of the best source rocks of the SE Anatolian region, was formed by such an effect. The only effect of Gondwana glaciers on the SE Anatolian oil systems was the deposition of these shales.

## REFERANSLAR

- Ghienne, J.F, Monod, O., Kozlu, H. and Dean, W.T. 2010. Cambriyen-Ordovician depositional sequence in the Middle East: A perspective from Turkey. *Earth-Science Reviews*, 101, 101-146.
- Bell, A., and Spaak, P. 2007. Gondwanan Glacial Events and their Influence on Petroleum Systems in Arabia. Search and Discovery Article No: 30047, Extended abstract prepared for 2006 AAPG International Conference, 4 p.
- Bozdoğan, N., Karabulut, N., Erten, A., İztan, H., Çubukçu, A. ve Korucu, M. 1994. Güneydoğu Anadolu Diyarbakır Bölgesi Paleozoyik Birimlerin Stratigrafisi ve petrol potansiyeli. *Türkiye 10. Petrol Kongresi*. 125-139.
- Haq, U.B. and Al-Qathani, A.M. 2005. Phanerozoic cycles of sea-level change on the Arabian Platform. *GeoArabia*, 10(20); 127-160.
- Kara, B., ve Işık, V., 2021. Reservoir Characteristics and Unconvantional Oil Potantional of Silurian aged Dadaş Shale in Southeast Turkey. *Journal of Petroleum Science and Engineering*, 200, doi:108365.
- Kara, B., 2021., Diyarbakır havzası Paleozoyik birimlerinin yüzey-yeraltı jeolojisi ve petrol potansiyeli. Ankara Üniversitesi Fen Bilimleri Enstitüsü Doktora

Tezi. 206 sayfa.

- Konert, G. Affi, A.M., Al-Hajri, A.M., and Droste, H.J. 2001. Paleozoic Stratigraphy and Hydrocarbon Habitat of the Arabian Plate, *GeoArabia*, 6(3); 407-442.
- Luning, S., Shahin, Y.M., Loydell, D., Al-Rabi, H.T., Masri, A., Tarawneh, B. and Kolonic, S. 2005. Anatomy of a World-Class Source rock. Distribution and Depositional Model of Silurian Organik Rich Shales in Jordan and implications for Hydrocarbon Potential. *The AASP Bulletin*, 89, No.10, 1397-1427.
- Monod, O., Kozlu, H., Ghienne, J.F., Dean, W.T., Gunay, Y., Le Herisse, A., Paris, F., and Robardet, M. Y.M. 2003. Late Ordovician glaciation in southern Turkey. *Terra Nova*, 15(4); 249-257.
- Şenalp, M., Bahtiyar, İ., Işıkalp, U., Uz, E. and Kaya, M., 2018. Sequence Stratigraphy and Sedimentology of the Paleozoic Succession on the Arabian Platform and Their Impact to Hydrocarbon Exploration in Southeast Turkey. TPJD Eğitim yayınları, Ankara.
- Yıldız, G. 2019. Reservoir Heterogeneity, Sedimentology, and Diagenesis of Ordovician Bedinan Formation, Southern Diyarbakır Basin, SE Turkey: Paleogeographic Implications. Master's Thesis, Middle East Technical University, Ankara.

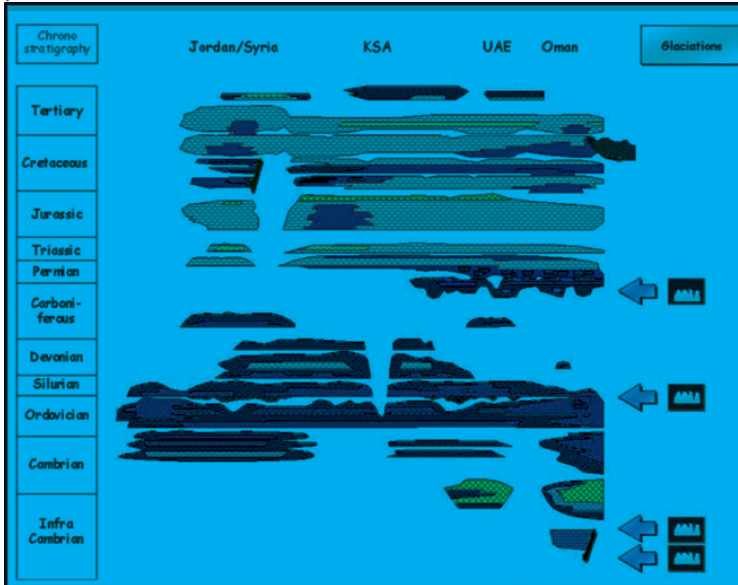
Anahtar Kelimeler: GD Anadolu, Paleozoyik Buzulları ve Petrol Sistemi

<sup>1</sup>Sanko Enerji (PETAR), nihath.bozdogan@sankoenerji.com.tr

<sup>2</sup>Çalık Petrol, bayram.kara@calikpetrol.com



Şekil-01



Gondwana Kitası Paleozoyik buzul dönemleri (Bell and Spaak, 2007)

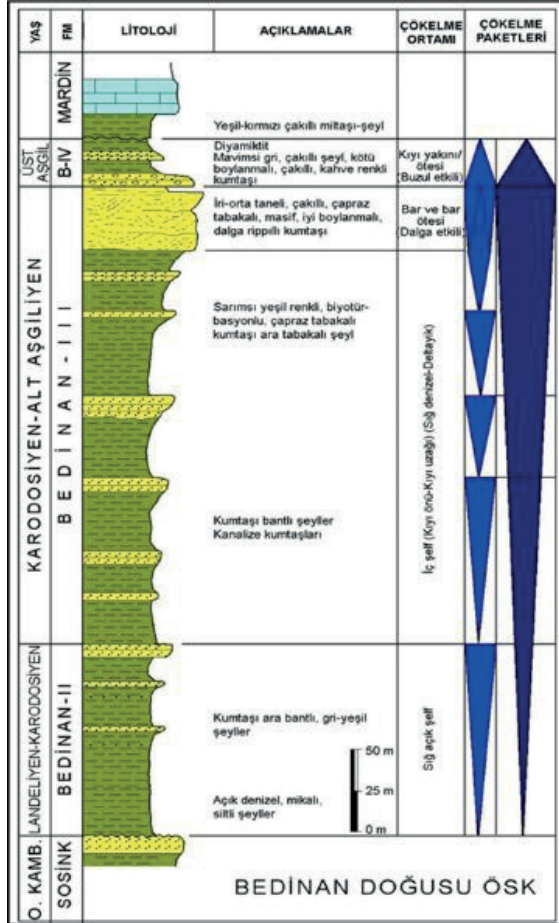
Şekil-02

MY	ERA	PERİYOD	ANA KAYA	REZERVUAR	ÖRTÜ	GÖMÜLME	TÜRÜM	GÖÇ	KAPAN	TEKTONİK EVRELER
0-2.3	SENOZOYİK	Holosen							ALPIN ORDOZİZİ MYOSEN BİNDİRİMESİ	7. TEKTONİK EVRE AÇILMA
2.3-0.2		Pleistosen								
0.2-0.02		Pliyosen								
23-5.3		Myosen				SELMO	TÜRKİYE SONU: 13.5 MY	GÖÇ SONU: 20 MY		
5.3-0		Oligosen					GERMİK HOYA	GÖÇ BAŞLANGIÇ: 44.5 MY		
0-66	MESOZOYİK	Eosen							ALPIN KRETASE BİNDİRİMESİ	6. TEKTONİK EVRE AÇILMA
66-0		Paleosen								
145-66		Kretase	ÖZÜMÜNÇÜK, YERİNE, FAYATLI, İZMİT, HATTA, KARADAG			BERNARİ DEREZİ, BELUKA, KARABAGA, DENDRE, BAKIRCIYI, AMBAR				
201-145		Jura								
252-201		Triyas					ULUDERE, GÖMÜNİBİRİK, FAS			
252-0	PALEOZOYİK	Permian							ALPIN KRETASE BİNDİRİMESİ	1. TEKTONİK EVRE AÇILMA
252-252		Karbonifer								
360-252		Devoniyen					KAYIYOLU			
444-360		Siluriyen					HAZRO			
444-444		Ordoviyen					DADAŞ			
444-444						BEİRMAN, SEYDİŞEHİR				

GD ANADOLU SİYERİBİRİK BAŞENTİ ERNEVİ MİLEZOYİK PETROL SİSTEMİ TABLOSU (Gökçen, 2021)

GD Anadolu Paleozoyik Petrol Sistemi (Kara, 2021)

Sekil-03

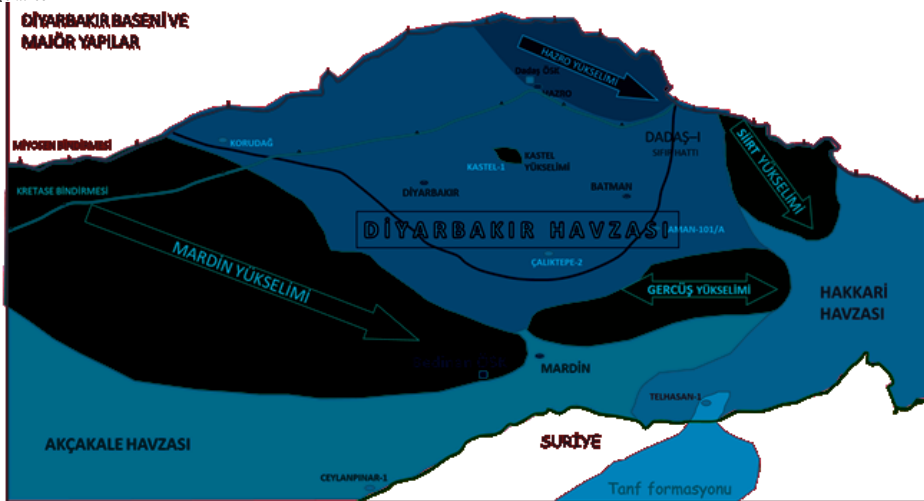


Şekil-04

YAS	GRUP	LİTOLOJİ	KALINLIK (m)	ÇÖKELME ORTAMI	AÇIKLAMALAR	GÖZENEK (%)			REZERVUAR KAYA BR	KAYNAK KAYA
						0	10	20 30		
ORTA ORDOVİSİYEN	DİYARBAKIR	D-I	100	BASEN	Kavilî karbonat ardalınamalı kahverengimsi yeşil					KK
	UR	B-IV	350	Kıymı seditli kıyî öneli kıyî ötesi, Sığ deniz	Kuvars arenit, Subarkoz, Dolomit çimento	30 mD		A		
		B-III	800	Kıyî öneli, Plaj yüzü, Yayıgı kumları, Sığ deniz	Kuvars arenit Subarkoz, Subiltarenit Karbonat çimentolu İnce-Orta taneli, İyî boylanmalı	25 mD		B		
	B-E	B-II	600	İç şelf	Silttaşı Çamurtaşı					KK
GEÇ ORDOVİSİYEN	H	B-I	400	Basen	Koyu gri mikali şeyiller					

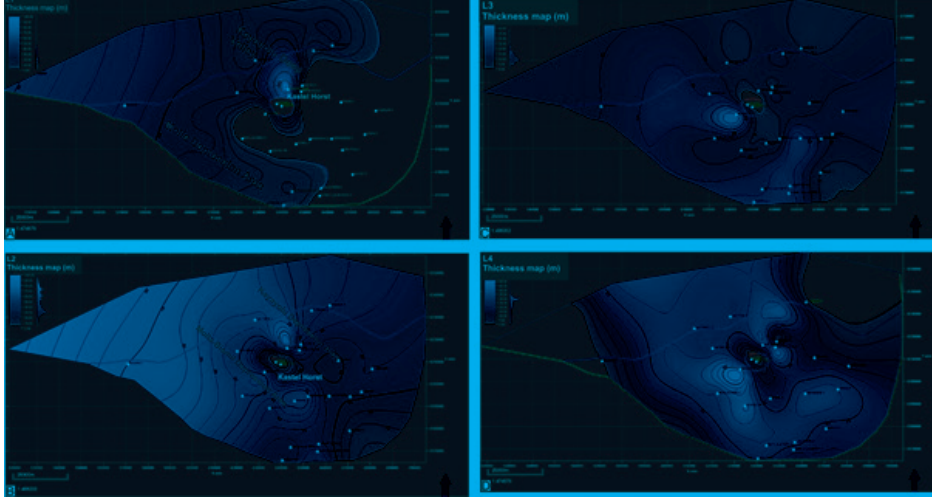
Bedinan formasyonu geliştirilmiş stratigrafik istifi ve rezervuar özellikleri

Şekil-05



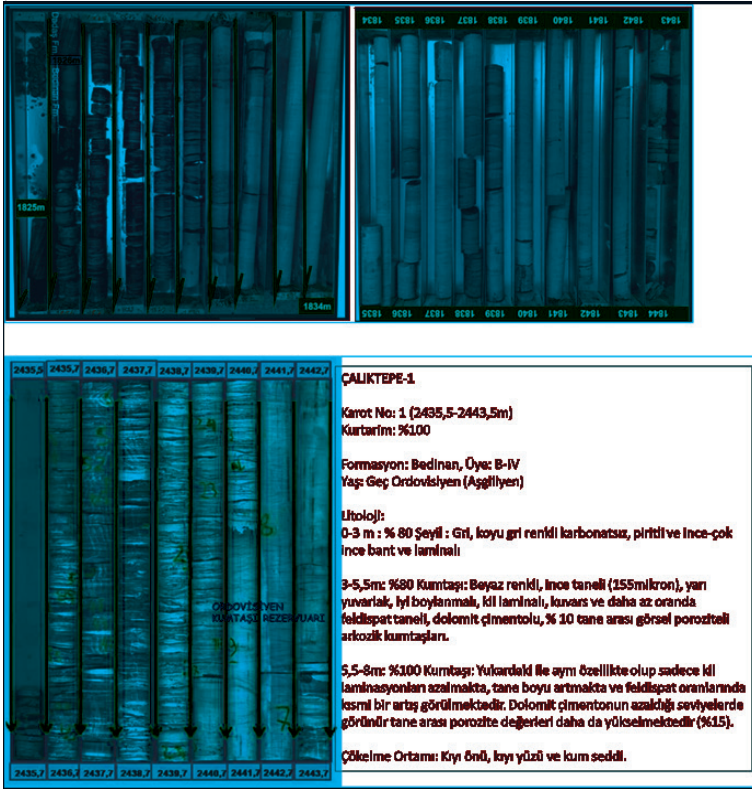
GD Anadolu Paleozoyik sedimanter basenleri ve major yapıları (Kara, 2021)

Şekil-06



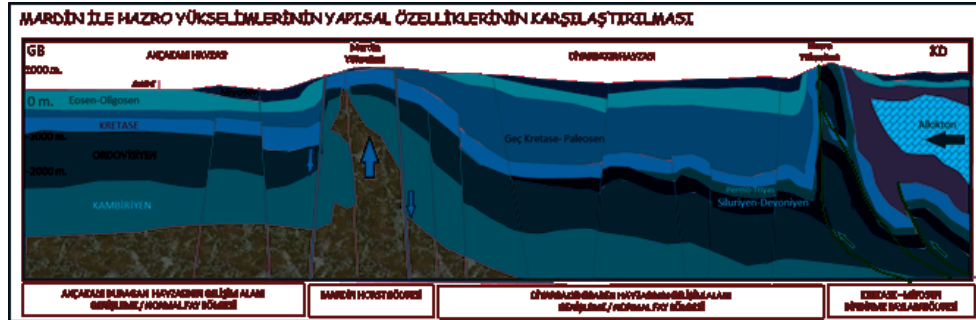
GD Anadolu Dadaş formasyonu alt üyesinin (Dadaş-1) litofasiyes birimlerinin bölgesel özellikleri (Kara ve Işık, 2021)

Şekil-07



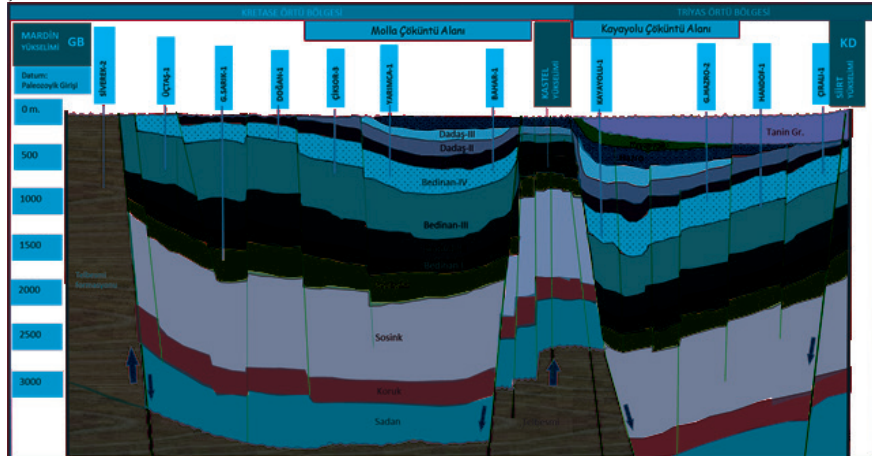
GD Anadolu Ordovisiyen-Sihriyen çökelleri geçiş özellikleri (Düzova-1 ve Çalıktepe-1) (Kara, 2021)

Şekil-08



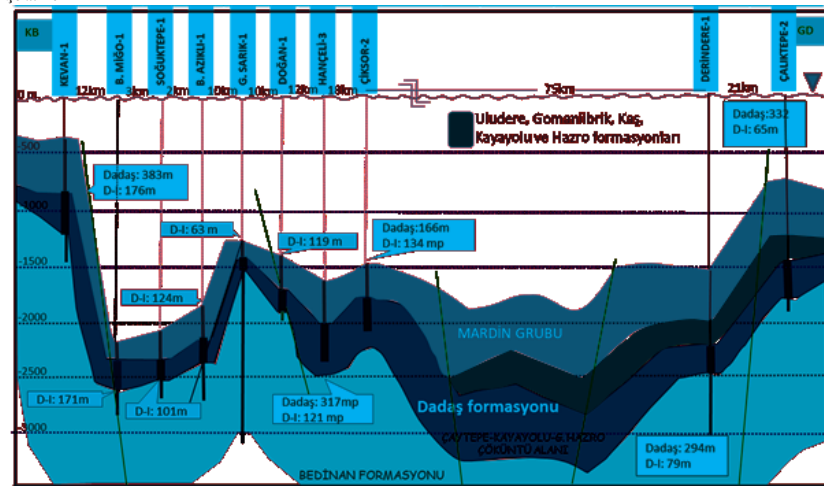
GD Anadolu bölgesi Paleozoik ana yapısal özellikleri (Kara,2021)

Şekil-09



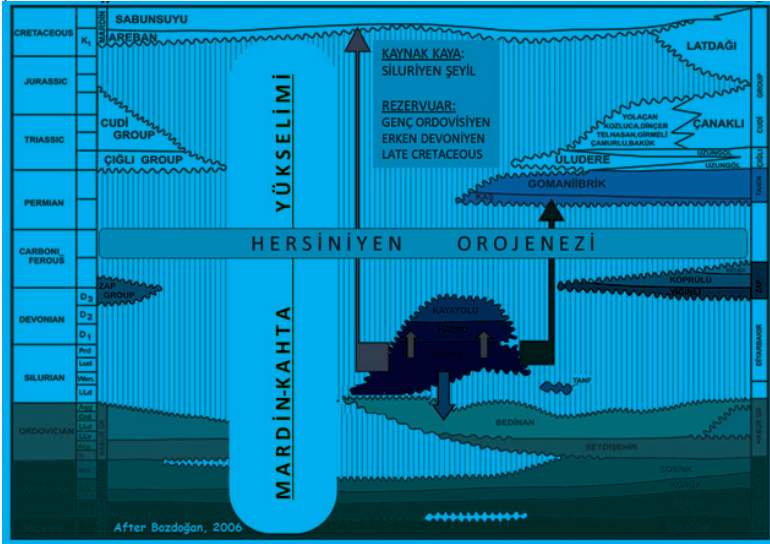
GD Anadolu bölgesi Diyarbakır Havzası Paleozoik çökelleri GB-KD yönlü jeolojik kesiti (Kara,2021)

Şekil-10



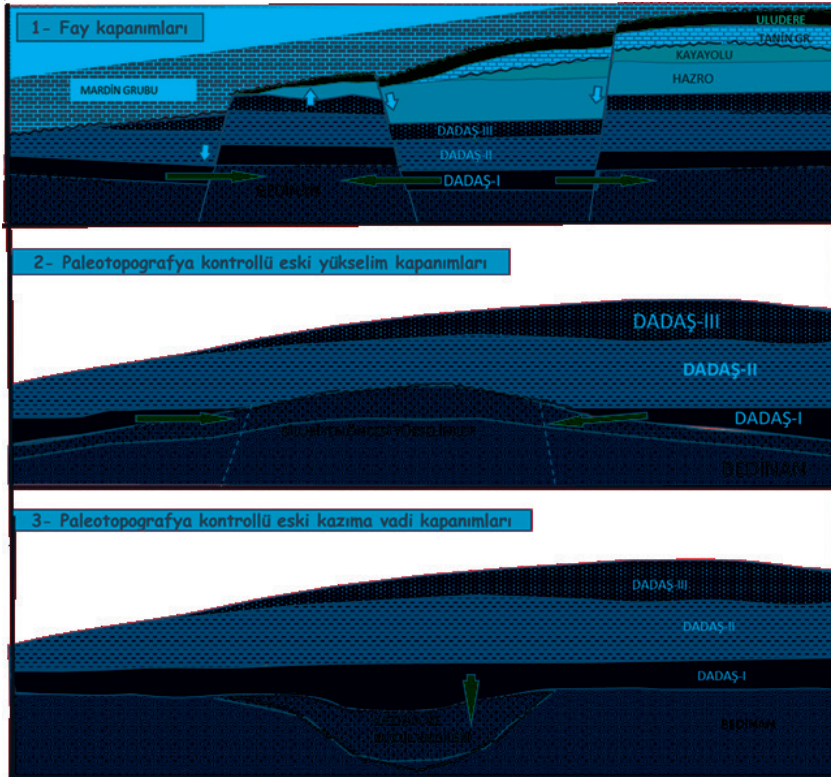
GD Anadolu Dadaş formasyonu yapısal özellikleri (Kara,2021)

Şekil-11



GD Anadolu Paleozoyik çökelleri zaman-stratigrafi ilişkisi ve Paleozoyik Petrol Sistemi.

Şekil-12



Geç Ordovisiyen Play Modelleri (Luning vd., 2003 den faydalanılmıştır).

# Sequence Sequence Analysis and Depositional Models of the Maastrichtian to Early Eocene Succession at the Gercus Anticline, Batman, Southeast of Turkey



**Mehmet Özen Gürbüz**

Turkish Petroleum Company, Ankara / Türkiye

The Southeastern Anatolian Platform became an active continental margin starting from the Late Cretaceous (Campanian). The South Atlantic Ocean started to open up which resulted in the closure of the Neo-Tethys Ocean. Thus, Southeastern Anatolia has reached the effect of a compressive tectonic regime that has existed until today (Şengör and Yılmaz, 1981). During the closing process of the Neo-Tethys Ocean, the sediment deposition in the northern part of the Southeast of Turkey was dominated by the terrigenous clastic sedimentary processes and shallow marine and coastal depositional environments were effective in the south. Thus, The Late Cretaceous – Early Eocene succession was deposited under the effect of regional tectonism and global sea level changes. The factors affecting platform initiation, architecture, facies distribution, depositional models, and sequence stratigraphic analysis of the Maastrichtian to the Early Eocene succession remain poorly understood. In this work, sedimentological and sequence stratigraphic analysis lead to a better understanding of the controlling factors for the deposition of the sequences from Late Cretaceous to Early Eocene in the Southeast of Turkey

In the study area, depositional sequences are classified into three main groups developed under the control of tectonism and global sea level changes. These sequences are listed below as:

Late Cretaceous (Maastrichtian) Sequence - Garzan and Lower Germav Formations

Early to Late Paleocene Sequence - Upper Germav Formation

Late Paleocene to Early Eocene Sequence – Upper Germav Formation, Becirman Formation, Gercüş Formation, Boğazköy Member of the Gercus Formation, and Hoya Formation

## LATE CRETACEOUS (MAASTRICHTIAN) SEQUENCE

Favorable conditions were created for the precipitation of shallow carbonates in the study area, which was under marine influence with the Maastrichtian transgression.

The Garzan Formation, outcropping in the core of the Gercüş Anticline, began to deposit on relatively high areas of irregular paleo-topography under these conditions.

Bioclastic limestones were deposited at paleohighs and adjacent environments. Mudstones and argillaceous mudstones/wackestones were developed at the paleotopographic lows. Lagoonal limestones were deposited in sheltered areas in the landward side of the bioclastic shoals under low depositional energy conditions.

The characteristics of the parasequences of the Garzan Formation in the shoal depositional areas are shallowing upper trends and rudist rudstones and/or grain-dominated packstones form the uppermost part of the cycles.

The primary porosity of these limestones, which were exposed to meteoric water diagenesis, increased in places with leaching and decreased in places due to the cementation that occurred as a result of meteoric diagenesis. Meteoric diagenesis and primary deposition facies have had an intense effect on the reservoir properties of the Garzan Formation.

As a result of the increase in the severity of the transgression during the Late Maastrichtian period, the Garzan Formation was followed by the Lower Germav Member of the Germav Formation with a sudden deepening. As a result, the limestones of the Garzan Formation deepen upwards in sequence scale and pass into clayey limestones and marl and shale lithology of the Lower Germav Member (Figure 1).

The maximum flooding surface (MFS) of the Late Cretaceous (Maastrichtian) Sequence was developed within the Lower Germav Formation. This MFS is rich in glauconites and phosphates characterized by dense planktonic fossiliferous level (condensed section) (Figure 1).

The succession, which turned into clayey limestone from marl/shale lithology as a result of regression after MFS, entered the shallowing trend, forming the end of the Late Maastrichtian sequence and transitioning to the Early and Late Paleocene period, which is a new sequence.

## EARLY TO LATE PALEOCENE SEQUENCE

The Early to Late Paleocene sequence is bounded below by the sequence boundary of the Cretaceous/Paleocene. Since the study area was located on the upper slope and basin of the platform, the succession is continuously visible. Possible erosional surface is expected in the northern parts, in the inner parts of the platform, on the sides close to the land.

The Early to Late Paleocene sequence starts with divergent turbiditic and pelagic marl and shale alternations of the lower parts of Upper Germav Member. The regressive succession which composes of shale and marl alternations on the lowermost part changes into siltstones and sandstones upwards (Figure 2).

The Upper Germav Member of the Germav Formation has started deposition in the deep sea/basin (prodelta) and has transitioned to platform slope as a result of regression. There is an increase in the shale/sandstone

ratio upwards. In the lower parts, turbiditic sandstones transit upwards into turbiditic channel sandstones. With the effect of shallowing, the delta distribution channels and the platform edge change to sandstones (lowstand delta). During this period, the platform and the platform slope were exposed (Figure 2).

#### LATE PALEOCENE TO EARLY EOCENE SEQUENCE

In the Late Paleocene, patchy reefs of the Becirman Formation were deposited on the delta distribution channels by sequence-scale transgression. These limestones started to deposit on the upper slope of the platform, on the platform edge, behind the platform edge and in front of the platform edge. The thickest limestones were deposited at the time of the maximum flooding, when the transgression reached its maximum level.

After this period, regression began at the sequence scale. With the increase of the clastic input, unfavorable conditions for the precipitation of carbonates were formed and the carbonates were not fully developed. With the effect of the regression, the depositional environment shifted from the platform edge to the platform interior and shoreline. Well sorted sandstones in front of the coast and near the coast, reaching 30-40 meters in thickness, were deposited. The progradation continued and was completely under clastics influence with fluvial/playa deposits.

With the transgression, the marine influence was again dominant in the study area and tidal deposits were formed. The carbonates of the Boğazköy Member of the Gercüş Formation were deposited in this sabhka environment. While mudstones and/or wackestones were predominate in subtidal parasequences, packstones and/or locally cross-bedded grainstones and algal limestones were deposited in the intertidal zone. In the supratidal environment, evaporites are the dominant lithology. These limestones are thought to have been dolomitized with the sabhka dolomite pattern (or seepage reflux) (Figure 3).

#### RESULTS

1. As a result of the sequence-stratigraphic studies, the Late Maastrichtian sequence was divided into 4 TST (Transgressive System Tract) and 4 HST (Highstand System Tract).
2. In the study area, the Garzan Formation gradually deepens upwards and passes into the Lower Germav Member of the Germav Formation.
3. The carbonates of the Garzan Formation cannot catch-up the relative sea-level rise and drowning unconformity was developed between the Garzan Formation and the Lower Germav Member of the Germav Formation.
4. Tidal channels were developed between the adjacent paleotopographic highs during the deposition of the Garzan Formation.
5. The cycles of the uppermost part of the succession

of the Garzan Formation where it gradually deepens and passes into Lower Germav Member compose of rudist and gastropod-bearing packstones; large benthic foraminiferal packstones and floatstones; bivalve, echinoderm floatstone; planktonics foraminiferal, bivalve floatstone, from bottom to top of the cycles, relatively.

6. The Garzan Formation and the Lower Germav Member of the Germav Formation belongs to the same depositional sequence, genetically.
7. On the other hand, the Upper Germav Member of the Germav Formation belongs to a completely different new depositional sequence, genetically.
8. The Paleocene Sequence consists of 1 early FSST (Early Falling Stage System Tract), 1 late FSST (Late Falling Stage System Tract) and 1 LST (Lowstand System Tract) depositional system tract, in which turbiditic shales are dominant on the lower part and the sandstone ratio increases upwards.
9. During the Early Paleocene, at the end of the late FSST period, the sandstones are thickening upwards and grain-sizes are increasing upwards. These sandstones thicken towards the east (on Ilisu sides). It is important for oil exploration to find sandstones (such as Kentalan Anticline) produced by the submarine fan, which reach serious thicknesses to the east and north of Mardin-Dargeçit.
10. During the Late Paleocene, the Lower Germav Member of the Germav Formation consists of deltaic and shore deposits. Patchy carbonates, which compose of nodular limestones, were deposited on delta sandstones by transgression. These carbonates do not have lateral continuity. This succession includes 2 TST (Transgressive System Tract), 2 HST (Highstand System Tract), and 2 LST (Lowstand System Tract).
11. During the Late Paleocene to Early Eocene, the Gercüş Formation and the Boğazköy member composes of 2 TST (Transgressive System Tract), 2 HST (Highstand System Tract), and 2 LST (Lowstand System Tract).

Keywords: Sequence stratigraphy, depositional models



Figure 1 – Depositional Model of the Late Cretaceous (Maastrichtian) Sequence

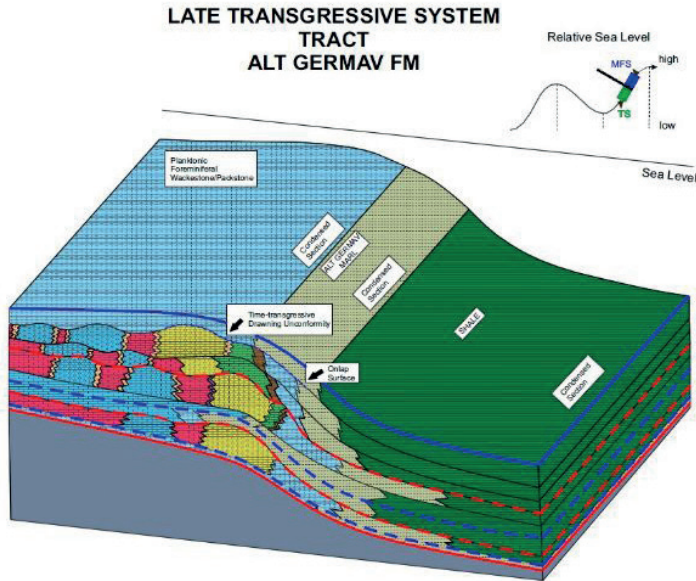


Figure 1 – Depositional Model of the Late Cretaceous (Maastrichtian) Sequence

Figure 2 – Depositional Model of the Early to Late Paleocene Sequence

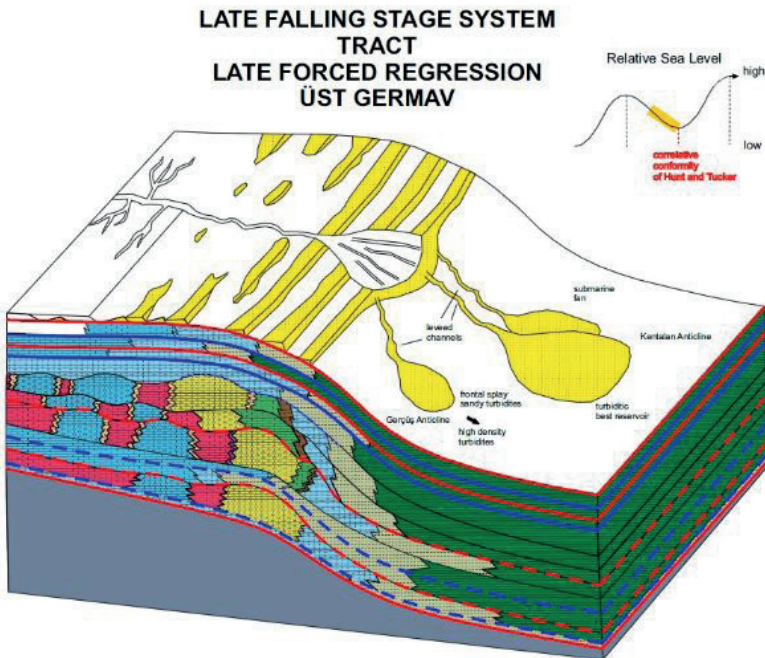


Figure 2 – Depositional Model of the Early to Late Paleocene Sequence



# Preliminary Results of Mineralogical, Organic Petrographical and Rock-Eval Pyrolysis Analyses of the Oligocene Formation in the Silivri (NE Thrace Basin)



Cüneyt Bircan<sup>1</sup>, Rıza Görkem Oskay<sup>2</sup>, Ali İhsan Karayığit<sup>3</sup>

<sup>1</sup>Balıkesir University, Department of Geological Engineering, Çağış-Balıkesir / Türkiye

<sup>2</sup>Hacettepe University, Başkent OSB Technical Sciences Vocational School, Sincan-Ankara / Türkiye

<sup>3</sup>Hacettepe University, Department of Geological Engineering, Beytepe-Ankara / Türkiye

## ABSTRACT

Thrace Basin hosts important natural gas fields of Türkiye, and these fields are mostly located in the central parts of the basin. Furthermore, small natural gas fields are also located in the north-eastern parts of the basin. This study presents primary results of mineralogy, organic petrography and Rock-Eval pyrolysis analyses of Oligocene formations cored in one natural gas production well in the north of Silivri (Istanbul) area. The mineralogical analysis show that quartz and clay minerals are the dominant phases, while calcite abundant phases in all studied formations. Furthermore, feldspars, dolomite and pyrite are minor phases. Huminite and liptinite groups macerals were commonly observed in all studied formation, whereas inertinite is generally rarely identified in the studied formations. The measured random huminite/vitrinite reflectance (%R<sub>v</sub>) values of Mezardere, Osmancık and Danişmen formations are %0.50-0.52, %0.45-0.51, and %0.43-0.44, respectively. The Rock-Eval pyrolysis of the studied formations are variable, and relatively high S<sub>1</sub> values are obtained from the Mezardere Formation. In addition, S<sub>2</sub> and hydrogen index (HI) values of Mezardere and Osmancık formations are relatively higher than Danişmen Formation, and S<sub>3</sub> values are generally high in all studied formations. Considering to abundance of carbonate minerals and the existence of possible perhydrous huminite macerals, the relatively high S<sub>3</sub> values and low Tmax values of the samples are expectable. Nevertheless, measured %R<sub>r</sub> TOC, HI, and S<sub>1</sub>+S<sub>2</sub> values of the samples from Mezardere and Osmancık formations could suggest that these formations have clear gas generation potential, while Danişmen Formation have very limited gas-generation potential in the study area.

## INTRODUCTION

The Thrace Basin hosts the most important in-shore natural gas fields in Türkiye, and has recently met the domestic natural gas demands of Türkiye. Since the late 1970s, several hydrocarbon exploration studies have been done in the basin. Several studies have been conducted in order to determine the hydrocarbon generation potentials of Tertiary basinal infillings in the Thrace Basin. These studies show that Eocene and Early Oligocene shales (e.g., Mezardere Formation) in the Tertiary basinal infilling are source rocks, while Late Oligocene coal seams might have limited gas generation potential (Çelik et al., 2017; Gürgey, 2009; 2015; Huvaz et al., 2005, 2007; Karayığit et al., 2021). Furthermore, Late Eocene marine and clastic sediments

and Late Oligocene sandstones and tuffite are reservoir rocks. Previous sedimentological and paleontological studies in the basin show that the Late Eocene (?)–Early Oligocene Mezardere Formation, or Mezardere shales, deposited under prodelta and shallow marine conditions, while delta front conditions were more common during deposition of the Osmancık Formation (Çelik et al., 2017; Gürgey and Batı, 2018; Siyako, 2006; Turgut and Eseller, 2000). The Late Oligocene Danişmen Formation, or lignitic sandstones, were deposited under delta plain and lacustrine conditions, and shallow conditions were also developed during this period of time. The previous studies were mostly focused on the central parts of the Thrace basin due to the presence of natural gas production fields, and data about the hydrocarbon generation potential of Oligocene formations in the north-eastern parts of the basin is limited to date. Therefore, this study focuses on mineralogical and organic petrographical features, and Rock-Eval pyrolysis analyses of Oligocene formations (Mezardere, Osmancık, and Danişmen) in the southeastern parts of the Thrace Basin.

## METHODS

A total of twenty-two shale samples were obtained from Oligocene formations from one deep natural gas production well, which is drilled in the north of Silivri (Istanbul) (Table 1). The mineralogical composition of samples was determined using X-ray diffraction (XRD) whole-rock analysis. The semi-quantitative mineralogical compositions of samples were determined using Rietveld based TOPAS 3 software. For organic petrographical analysis, polished blocs were prepared from selected fifteen samples using the cold-moulding method, and random vitrinite/huminite reflectance (%R<sub>r</sub>) measurement and maceral identification, under white incident light and blue-light excitation, were conducted on the polished blocks. Maceral identification was done according to the nomenclature of the International Committee for Coal and Organic Petrology (ICCP), while %R<sub>r</sub> measurements were done following ASTM D2798 (2014) and D7708 (2014). The Rock-Eval Pyrolysis and total organic carbon (TOC) analyses of selected samples were conducted using Rock-Eval 6 equipment, according to the procedure described by Espitalié et al. (1977) and Lafargue et al. (1998), and the accuracy of the results was cross-checked using IFP 160000 standard material.

## FINDINGS

The identified minerals using XRD analysis are quartz, clay minerals (smectite, illite, and chlorite), carbonate minerals (calcite and dolomite), feldspars, and pyrite in the studied formations (Table 1). Gypsum and halite are detected only in the Danişmen Formation. Clay minerals are the dominant phases in the studied formations, while quartz, calcite and feldspars are abundant phases (Table 1). Dolomite and pyrite are minor phases. Although detailed scanning electron microscopy analyses have not yet been conducted on the samples, the clay minerals are mostly observed as aggregates with mineral matter and macerals during organic petrography studies. These observations could suggest that the detected minerals are mostly clastic influxes from the Eocene formations (e.g., Soğucak limestone) or Strandja Massif since these units are composed of pre-Oligocene basement in the study area. Nevertheless, the existence of carbonate bands in the samples could also be indicator of a carbonate-rich deposition environment. Framboidal pyrite grains also indicate anoxic conditions during the Oligocene. Additionally, flaky graphite grains were observed during organic petrography studies, which are presumably derived from Paleozoic graphite schists within the Strandja Massif, and possible glauconite grains could be indicators of marine conditions.

Maceral compositions of the studied formations are almost similar, and huminite macerals, particularly ulminite, are the most commonly identified macerals in the studied formations. Sporinite and liptodetrinite are commonly identified liptinite macerals, while alginite was detected in a few samples from the Osmançık Formation. Inertinite group macerals are rare, and inertodetrinite and fusinite are common macerals in this group. The Danişmen Formation hosts a rich fungal flora according to previous palynological studies (Ediger, 1981; Ediger and Alişan, 1989), and as expected, funginite is also observed in the studied samples from this formation. The %R<sub>r</sub> values of the Mezardere, Osmançık and Danişmen formations are %0.50-0.52, %0.45-0.51, and %0.43-0.44, respectively (Table 2). Although the %R<sub>r</sub> values were measured mostly from the ulminite-B variety, %R<sub>r</sub> measurements also show the existence of low %R<sub>r</sub> ulminite-A variety is also existed in all studied formations. Such huminite grains are expected, particularly for Danişmen Formation, since gymnosperms were common elements of paleovegetation during the Oligocene in the Thrace Basin (Akgün et al., 2013; Batı, 1996; Çelik et al., 2017), and %R<sub>r</sub> measurements could be relatively lower due to the presence of H-rich compounds (Vu et al., 2013).

Rock-Eval pyrolysis analyses of the samples show that S<sub>1</sub>, S<sub>2</sub>, and S<sub>3</sub> values are variable, while TOC values of the studied formations are generally around %1.00 (Table 2). S<sub>1</sub> values of the samples from the Mezardere Formation are relatively higher than other studied formations, whereas S<sub>2</sub> values of the Mezardere and Osmançık formations are generally higher than 1.6 mg HC/g (Table 2). In all studied formations, S<sub>3</sub> and oxygen index (OI) values are slightly high (Table 2).

Furthermore, T<sub>max</sub> values of the studied formations are around 430°C, while hydrogen index (HI) values of the Osmançık and Mezardere formations are generally higher than 150 mg HC/g TOC (Table 2). The relatively high S<sub>2</sub> and HI values of the Mezardere and Osmançık formations could be related to the common presence of liptinite group macerals in the studied samples from these formations. Nevertheless, the relatively higher S<sub>3</sub> values of the studied formation could be related to the abundance of carbonate minerals in the studied samples. The HI values higher than 120 mg HC/g TOC could suggest that ulminite grains with lower %R<sub>r</sub> are likely perhydrous (Mansour et al., 2023). During the Rock-Eval pyrolysis analysis, breakdown of carbonate minerals and perhydrous huminite macerals could provide additional CO<sub>x</sub> into the pyrolysis atmosphere; in turn, S<sub>3</sub> could elevate, and the S<sub>2</sub> peak may also be suppressed (Spiro, 1991; Vu et al., 2013; Yang and Horsfield, 2020). Therefore, T<sub>max</sub> values of the studied samples, particularly from the Mezardere and Osmançık formations, are lower, while OI values are higher than expected. The %R<sub>r</sub>, TOC, and S<sub>1</sub>+S<sub>2</sub> values of the studied samples show that the Mezardere and Osmançık formations have medium to good source rock potential; nevertheless, lower %R<sub>r</sub> values than %0.60 could suggest that these formations have gas generation potential instead of liquid hydrocarbon, which is also in agreement with the production (PI), bitumen (BI) and quality (QI) indexes values of the studied samples (Table 2).

The reported measured %R<sub>r</sub> and T<sub>max</sub> values of the Mezardere Formation in the Thrace Basin are %0.45-0.75 and 421-457°C, respectively (Gürgey, 2015; Gürgey and Batı, 2018). Nevertheless, significantly higher %R<sub>r</sub> and T<sub>max</sub> values were reported from the central parts of the basin, where the Mezardere Formation has deeper burial depths than the study area. The reported measured %R<sub>r</sub> and T<sub>max</sub> values of the Mezardere from natural gas fields close to study area are around %0.50 and 430°C, respectively (Gürgey, 2015), which are close to the studied samples in this study. Furthermore, the reported %R<sub>r</sub> and T<sub>max</sub> values of Early Oligocene shales in the İhsaniye Formation, which is equivalent to the Mezardere Formation in the north-easternmost of the Thrace Basin, are between %0.29-0.31 and 406-434°C (Tulan et al., 2020). The results of this study and previous studies indicate that the Mezardere Formation could be the source of natural gas in the NE parts of the Basin, and the Osmançık Formation also has gas generation potential, at least in the study area. Furthermore, the Danişmen Formation seems to have limited gas generation potential. Overall, the Mezardere and Osmançık formations in the study area could be considered a source rock for producing natural gas in the study area. Considering the limited number of samples investigated from the Danişmen Formation, additional samples should be studied from this formation in order to have a better understanding of the hydrocarbon generation potential of the Danişmen Formation in the study area.

## CONCLUSION

Based on mineralogy, organic petrography, and Rock-Eval pyrolysis analyses, the maturity and hydrocarbon generation potential of the Mezardere, Osmancık and Danişmen formations in the study area are relatively different, and Rock-Eval pyrolysis analyses seem to be affected by the mineralogical and maceral compositions of the formations. The relatively higher TOC,  $S_2$ , and HI values of studied samples from the Mezardere and Osmancık formations are related to the common presence of huminite and liptinite macerals, while the relatively higher  $S_3$  values of all studied formations could be related to the abundance of carbonate minerals and the existence of prehydrous huminite macerals. Hence, Tmax values are relatively lower and OI values are higher than expected. Nevertheless, the measured TOC, HI, and  $S_1+S_2$  values of the studied samples from the Mezardere and Osmancık formations imply that these formations have medium to good source rock potential; however, the % $R_f$  values could suggest that these formations are more gas-prone. Furthermore, the Danişmen Formation in the study area has very limited gas generation potential. Overall, the Mezardere and Osmancık formations could be source rocks for producing natural gas in the study area. This study was based on a limited number of samples from the study area; therefore, further studies should be conducted with more samples in order to better understand the possible contributions of the Danişmen Formation.

## ACKNOWLEDGMENTS

This study is supported by Balıkesir University Scientific Research Projects Coordination Unit under project no: 2022/043

## REFERENCES

Akgün, F., Akkiraz, M.S., Üçbaşı, S.D., Bozcu, M., Kapan Yeşilyurt, S., Bozcu, A., 2013. Oligocene vegetation and climate characteristics in north-west Turkey: Data from the south-western part of the Thrace Basin. *Turkish Journal of Earth Sciences*, 22, 277-303.

American Society for Testing and Materials (ASTM) D7708–11, 2014. Standard Test Method for Microscopical Determination of the Reflectance of Vitrinite Dispersed in Sedimentary Rocks sec. 5, v. 05.06. Annual Book of ASTM Standards: Petroleum Products, Lubricants, and Fossil Fuels; Gaseous Fuels; Coal and Coke, ASTM International, West Conshohocken, PA, 10 p.

American Society for Testing and Materials (ASTM) D2798–11a, 2014. Standard Test Method for Microscopical Determination of the Vitrinite Reflectance of Coal sec. 5, v. 05.06 Annual Book of ASTM Standards: Petroleum Products, Lubricants, and Fossil Fuels; Gaseous Fuels; Coal and Coke, ASTM International, West Conshohocken, PA, 5 p.

Bati, Z., 1996. Palynostratigraphy and Coal Petrography of the Upper Oligocene Lignites of the Northern Thrace Basin, NW Turkey. Middle East Technical University

(Unpub. PhD Thesis, 233 pp.).

Çelik, Y., Karayigit, A.İ., Querol, X., Oskay, R.G., Mastalerz, Kayseri Özer, 2017. Coal characteristics, palynology, and palaeoenvironmental interpretation of the Yeniköy coal of late Oligocene age in the Thrace Basin (NW Turkey). *International Journal of Coal Geology* 181, 103–123.

Ediger, V.S., 1981. Fossil fungal and algal bodies from Thrace Basin, Turkey. *Palaeontographica Abteilung B* 179, 87–102.

Ediger, V., Alişan, C., 1989. Tertiary fungal and algal palynomorph biostratigraphy of the northern Thrace basin, Turkey. *Review of Palaeobotany and Palynology* 58, 139–161.

Espitalié, J., Laporte, J.L., Madec, M., Marquis, F., Leplat, P., Paulet, J., Boutefeu, A., 1977. Méthode rapide de caractérisation des roches mères de leur potentiel pétrolier et de leur degré dévoluton. *Revue de l'Institut français du pétrole* 32, 23–42.

Gürgey, K., 2009. Geochemical overview and undiscovered gas resources generated from Hamitabat petroleum system in the Thrace Basin, Turkey. *Marine and Petroleum Geology* 26, 1240–1254.

Gürgey, K., 2015. Estimation of oil in-place resources in the lower Oligocene Mezardere Shale, Thrace Basin, Turkey. *Journal of Petroleum Science and Engineering* 133, 543–565.

Gürgey, K., Bati, Z., 2018. Palynological and petroleum geochemical assessment of the lower Oligocene Mezardere formation, Thrace Basin, NW Turkey. *Turkish Journal of Earth Sciences* 27, 349–383.

Huvaz, O., Karahanoglu, N., Ediger, V., 2007. The thermal gradient history of the Thrace basin, NW Turkey: Correlation with basin evolution processes. *Journal of Petroleum Geology* 30, 3–24.

Huvaz, O., Sarikaya, H., Nohut, O.M., 2005. Nature of a regional dogleg pattern in maturity profiles from Thrace basin, northwestern Turkey: A newly discovered unconformity or a thermal anomaly? *AAPG Bulletin* 89, 1373–1396.

Karayigit, A.I., Oskay, R.G., Çelik, Y., 2021. Mineralogy, petrography, and Rock-Eval pyrolysis of late Oligocene coal seams in the Malkara coal field from the Thrace Basin (NW Turkey). *International Journal of Coal Geology* 244, 103814.

Lafargue, E., Marquis, F., Pillot, D., 1998. Rock-Eval 6 applications in hydrocarbon exploration, production, and soil contamination studies. *Revue de l'Institut français du pétrole* 53, 421–437.

Mansour, A., Gentzis, T., Tahoun, S.S., Ahmed, M., Gier, S., Carvajal-Ortiz, H., Neumann, J., Fu, X., Wang, J., 2023. Near equatorial paleoclimatic evolution and control on organic matter accumulation during the Cenomanian in the Abu Gharadig Basin, southern Tethys: Insights from palynology, organic petrography, and geochemistry. *International Journal of Coal Geology* 270, 104221.

Siyako, M., 2006. "Lignitic sandstones" of the Trakya

basin. Bulletin of Mineral Research and Exploration 132, 63–73.

Spiro, B., 1991. Effects of minerals on Rock Eval pyrolysis of kerogen. Journal of Thermal Analysis and Calorimetry 37, 1513–1522.

Tulan, E., Sachsenhofer, R.F., Tari, G., Flecker, R., Fairbank, V., Pupp, M., Ickert, R.B., 2020. Source rock potential and depositional environment of the lower Oligocene İhsaniye formation in NW Turkey (Thrace, Karaburun). Turkish Journal of Earth Sciences 29, 64–84.

Turgut, S., Eseller, G., 2000. Sequence Stratigraphy/ tectonics and depositional history in eastern Thrace Basin/ NW Turkey. Marine and Petroleum Geology 17, 61–100.

Vu, T.T.A., Horsfield, B., Mahlstedt, N., Schenk, H.J., Kelemen, S.R., Walters, C.C., Kwiatek, P.J., Sykes, R., 2013. The structural evolution of organic matter during maturation of coals and its impact on petroleum potential and feedstock for the deep biosphere. Organic Geochemistry 62, 17–27.

Yang, S., Horsfield, B., 2020. Critical review of the uncertainty of Tmax in revealing the thermal maturity of organic matter in sedimentary rocks. Int. J. Coal Geol. 225, 103500.

Keywords: Thrace Basin, organic petrography

Table 1

Formation	Sample ID	Quartz	Calcite	Dolomite	Pyrite	Feldspars	Gypsum	Halite	Clay Minerals
Danişmen	TRC-2	++	++		+	++			+++
Danişmen	TRC-3	++	++	+	+	++			+++
Danişmen	TRC-5	++	++	+		++			+++
Danişmen	TRC-6	++	++	+		++		+	+++
Danişmen	TRC-10	++	++	+		++			+++
Danişmen	TRC-15	++	++	+	+	++			+++
Osmancık	TRC-17	++	++	+	+	++			+++
Osmancık	TRC-25	+++	++	+	+	++			+++
Osmancık	TRC-28	++	++	++	+	++			+++
Osmancık	TRC-32	+++	++	+	+	++			+++
Osmancık	TRC-37	++	++	+	+	++			+++
Osmancık	TRC-39	++	++	+	+	++			+++
Osmancık	TRC-45	++	++	+	+	++			+++
Osmancık	TRC-48	++	++	+	+	++			+++
Mezardere	TRC-51	++	++	+	+	++			+++
Mezardere	TRC-53	++	++	+	+	++			+++
Mezardere	TRC-55	+++	++	+		++			+++
Mezardere	TRC-58	+++	++	+	+	++			+++
Mezardere	TRC-63	++	++	+	+	++			+++
Mezardere	TRC-69	+++	++	+	+	++			+++

Mineralogical compositions of the studied shale samples based on XRD (on crystalline basis) (+++ = dominant phase (> 20%), ++ = abundant phase (5–20%), + = minor phase (< 5%)

Table 2

Formation	Sample ID	TOC	S1 (mg HC/ g rock)	S2 (mg HC/ g rock)	S3 (mg CO2/ g rock)	Tmax (°C)	HI	OI	PI	BI	QI	%Rr	Std
Danişmen	TRC-2	0.89	0.13	0.97	1.67	429	109	188	0.12	0.15	1.2	0.43	0.02
Danişmen	TRC-6	0.79	0.13	0.99	1.86	433	127	238	0.12	0.16	1.4	0.44	0.03
Osmancık	TRC-15	0.96	0.17	1.47	1.77	426	152	182	0.10	0.18	1.7	0.45	0.03
Osmancık	TRC-17	0.97	0.14	1.47	1.51	432	153	157	0.09	0.15	1.7	0.46	0.03
Osmancık	TRC-25	0.88	0.19	1.24	2.35	427	141	267	0.13	0.22	1.6	0.46	0.03
Osmancık	TRC-28	1.01	0.15	1.64	1.83	435	162	181	0.08	0.15	1.8	0.45	0.03
Osmancık	TRC-32	0.66	0.13	1.03	1.12	432	156	170	0.11	0.20	1.8		
Osmancık	TRC-39	1.09	0.11	1.80	1.22	431	165	113	0.06	0.10	1.8	0.45	0.03
Osmancık	TRC-45	1.38	0.13	3.62	0.95	435	262	69	0.03	0.09	2.7	0.51	0.03
Osmancık	TRC-48	1.07	0.08	1.80	0.85	432	168	79	0.04	0.07	1.8	0.50	0.03
Mezardere	TRC-53	0.92	0.17	1.51	2.06	432	164	224	0.10	0.18	1.8	0.50	0.03
Mezardere	TRC-55	0.60	0.21	0.93	1.69	429	155	282	0.44	0.35	1.9	0.51	0.02
Mezardere	TRC-58	0.94	0.33	1.95	2.04	433	207	217	0.15	0.35	2.4	0.50	0.03
Mezardere	TRC-63	1.00	0.23	1.39	2.28	427	139	228	0.14	0.23	1.6	0.52	0.03
Mezardere	TRC-69	1.06	0.24	2.60	0.98	435	245	91	0.08	0.23	2.7	0.52	0.03

Rock-Eval pyrolysis parameters and measured %Rr values of the studied shale samples (TOC: total organic carbon, HI: hydrogen index, OI: oxygen index, PI: production index (S1/S1 + S2); BI: bitumen index (S1/TOC), and QI: quality index ((S1 + S2)/TOC)

# Güneydoğu Anadolu Bölgesi Üst Kretase Karbonat İstifinin (Adıyaman Grubu) Stratigrafisi, Foraminifer Biyostratigrafisi Ve Mikrofasies Özellikleri



**Recep Özkan**

Türkiye Petrolleri Anonim Ortaklığı

## AMAÇ

Adıyaman Grubu birimlerini kapsayan bu çalışma, Türkiye'nin en önemli petrol üretim bölgesi olan Güneydoğu Anadolu Bölgesi'ndeki Kretase sedimanter istifinin stratigrafik problemlerine gözüm getirmek amacıyla yapılmıştır. Ağırlıklı olarak Kampaniyen'de çökelen ve bölgede özellikle Adıyaman yöresinde yaygın olarak yüzeyleyen Adıyaman Grubu, hem kaynak hem de rezervuar birimleri kapsamından dolayı önemli bir sedimanter istiftir. Adıyaman Grubu birimleri, jeolojinin değişik disiplinlerinde yayınlanmış veya yayınlanmamış bir çok çalışmaya konu olmasına rağmen, bu birimlerde yapılan biyostratigrafik veriler sınırlıdır. Adıyaman Grubu istifinin çökeltme evriminin iyi anlaşılmasına katkı sağlaması için bu gruba yönelik detaylı biyostratigrafik çalışmanın yapılmasına gerek duyulmuştur.

Çalışmanın amacı; Arap Platformu'nun kuzey kenarında, Kretase karbonat platformunda gelişen Adıyaman Grubu birimlerinin; 1) litostratigrafik özelliklerinin belirlenmesi, 2) foraminifer topluluğunun ortaya çıkarılması ve foraminifere dayalı olarak yaş konaklarının belirlenmesi, 3) makro ve mikrofasies özelliklerine göre çökel ortamlarının tespit edilmesi, ve 4) sekans stratigrafisi bazlı çalışma yapılmasıdır.

## GEREÇ VE YÖNTEM

Bu çalışmada, Adıyaman Grubu birimlerinin en iyi yüzeylendiği alanlarda kesit ölçüm ve örnekleme çalışması gerçekleştirilmiştir. Bu bağlamda, Adıyaman İli sınırları içerisinde, Ünlüce Köyü civarında ölçülen İnşidere ve Akpınar Köyü civarında Saydere kesitlerinden derlenen örnekler ile birlikte önceki çalışmacılar tarafından Mardin İli, Evciler Köyü civarında ölçülen Evciler (Köylüoğlu, 1988) ve Siirt İli, Pervari İlçesi, Yapraktepe Köyü civarında ölçülen Körkandı (Perinçek, 1980) (Şekil 1) kesitlerinden alınan örnekler bu çalışmanın materyalini oluşturmaktadır.

Bölgede yapılan arazi çalışmasında Adıyaman Grubu birimlerinin alt-üst ilişkileri, kalınlıkları, yapısal durumu, mostra açıklık durumu v.b. durumları göz önünde tutularak kesit ölçmeye en uygun alanlar değerlendirilmiş ve belirlenmiştir. Buna göre, Adıyaman Grubu istifinin foraminifer içeriğini ortaya koymak ve stratigrafik çatusını kurmak amacıyla İnşidere ve Saydere yörelerindeki kesitlerin ölçülerek örnekleme kararı alınmıştır. Ölçüm esnasında, tabakaların litolojik tanımları yapılarak, fasies ve sekans stratigrafik bazlı gözlemler gerçekleştirilmiştir. Kesit ölçümünde Jakop çubuğu kullanılmıştır. Kesitler boyunca kireçtaşı tabakalarından örnekleme çalışması yapılmıştır. Bu kesitlere ilaveten daha önce Evciler ve Körkandı yörelerinde ölçülen kesitlerin kullanılmasına

karar verilmiştir.

Foraminiferlerin tespiti için kesitler boyunca derlenen toplam 233 adet örnekten hazırlanan ince kesitler incelenmiştir. İncelemelerde alttan aydınlatmalı ZEISS ImagerM2 model polarizan mikroskobu kullanılmıştır. Planktonik foraminiferlerin tanımlanmasında Robaszynski ve diğ. (1984), Premoli Silva ve Verga (2004) ve Cocconi ve Premoli Silva (2015) çalışmaları, bentik foraminiferlerin tayinlerinde ise Wannier (1980), Andreiff ve Neumann (1983) ve Fleury ve Özkan (2020) çalışmaları kullanılmıştır. Mikrofasies ve sekans stratigrafie yönelik çalışmalarda kesitler boyunca alınan örneklerden hazırlanan ince kesitler kullanılmıştır. Mikrofasies analizlerinde ve ortam yorumlarında Dunham (1962), Embry ve Klovan (1971) ve Flügel (2004) sınıflamaları kullanılmıştır. Sekans stratigrafik yorumlarda Van Wagoner ve diğ. (1988), Posamentier ve diğerleri. (1988) ve Catuneanu ve diğerleri. (2009, 2011) tarafından geliştirilen kavramlar izlenmiştir.

## BULGULAR VE SONUÇ

Adıyaman Grubu, artan üste doğru, Karaboğaz, Saytepe, Saydere, Sayındere, Beloka ve Sanlı formasyonları olmak üzere altı litostratigrafik birime ayrılmıştır. Bentik ve planktonik foraminiferlere dayanan ayrıntılı biyostratigrafik incelemelere göre, Adıyaman Grubu formasyonlarının geç Santoniyen-erken geç Kampaniyen stratigrafik aralığında çökelmiştir. Saytepe, Beloka ve Şanlı formasyonları bentik foraminiferler tarafından karakterize edilirken, Karaboğaz, Saydere ve Sayındere formasyonlarının çökeltme yaşlarının belirlenmesinde planktonik foraminiferler belirleyici olmuştur. Mikrofasies analizleri, pelajik fasieslerin baskın olduğu, derin şelf ortamından lagüne ortamına kadar uzanan geniş bir fasies kuşağında dağılımı 12 temsili mikrofasiesin tanımlanmasına imkan vermiştir. Sekans stratigrafisi çalışmasına göre, sekans stratigrafik yüzeyler ile ayrılan üç ardışık çökel istif tanımlanmıştır. Sekans sınırları, küresel sekans sınırları (Haq, 2014) ile karşılaştırılmıştır. Göreceli deniz seviyesi değişikliklerine foraminiferlerin bolluk ve çeşitlilik açısından tepkisi kaydedilmiştir. Bu çalışma, biyostratigrafik verilere dayanarak Adıyaman Grubu'nun stratigrafik yapısına yönelik yeni öneriler sunmaktadır.

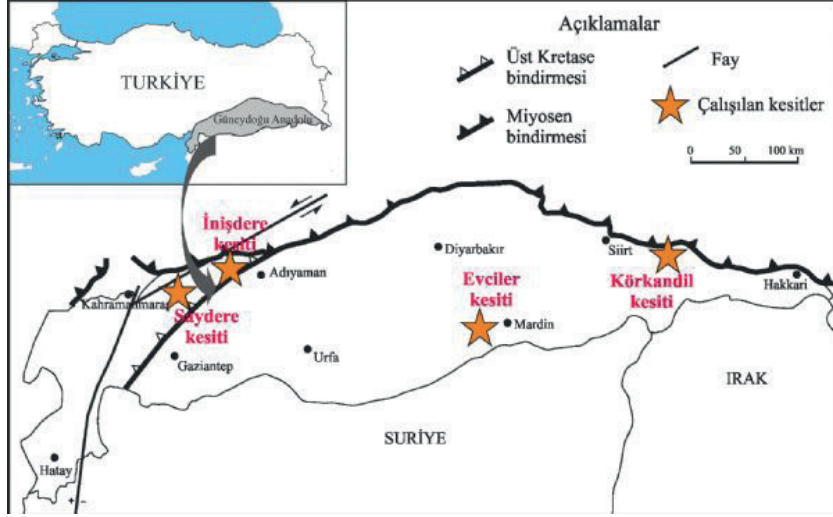
## YARARLANILAN KAYNAKLAR

Andreiff, P., Neumann, M., 1983. Siderolites praevidali, nouvelle espèce de foraminifere du Campanien stratotypique: Description et intérêt biostratigraphique. Revue de Micropaleontologie 26 (1), 3-14.



- Catuneanu, O., Abreu, V., Bhattacharya, J.P., Blum, M.D., Dalrymple, R.W., Eriksson, P.G., Fielding, C.R., Fisher, W.L., Galloway, W.E., Gibling, M.R., Giles, K.A., Holbrook, J.M., Jordan, R., Kendall, C.G.St.C., Macurda, B., Martinsen, O.J., Miall, A.D., Neal, J.E., Nummedal, D., Pomar, L., Posamentier, H.W., Pratt, B.R., Sarg, J.F., Shanley, K.W., Steel, R.J., Strasser, A., Tucker, M.E., Winker, C., 2009. Towards the standardization of sequence stratigraphy. *Earth-Science Reviews* 92 (1-2), 1-33.
- Catuneanu, O., Galloway, W.E., Kendall, C.G.St.C., Miall, A.D., Posamentier, H.W., Strasser, A., Tucker, M.E., 2011. Sequence Stratigraphy: Methodology and Nomenclature. *Newsletters on Stratigraphy* 44 (1), 173-245.
- Coccioni, R., Premoli Silva, I., 2015. Revised upper Albian-Maastrichtian planktonic foraminiferal biostratigraphy and magneto-stratigraphy of the classical Tethyan Cubbio section (Italy). *Newsletters on Stratigraphy* 48 (1), 47-90.
- Dunham, R.J., 1962. Classification of carbonate rocks according to depositional textures. In: Ham W.E. (Ed.), *Classification of Carbonate Rocks*. American Association of Petroleum Geologists Memoir, Tulsa, pp. 108-121.
- Embry, A.F., Klovan, J.E., 1971. A Late Devonian reef tract on northeastern Banks Island, Northwest Territories. *Bulletin of Canadian Petroleum Geology* 19 (4), 730-781.
- Fleury J.J., Özkan, R., 2020. *Metacuvillierina sireli* n. sp., a Campanian Rhapydioninidae (Foraminifera), from southeast Turkey, with new considerations on the endoskeleton and phylogenetic interpretation of the family. *Garnets de Geologie* 20 (9), 165-213.
- Flügel, E., 2004. *Microfacies of carbonate rocks: analysis, interpretation and application*. Springer, Berlin, Heidelberg, New York, 976 pp.
- Haq, B., 2014. Cretaceous eustasy revisited. *Global Planet Change* 113, 44-58.
- Köylüoğlu, M., 1988. Kasrık ve Şemikan fosfat yataklarını içeren Beloka Formasyonu'nun paleontolojisi ve stratigrafisi, Mardin-mazıdağı, GD Türkiye. *Türkiye Petrol Jeologları Derneği Bülteni* 1 (2), 141-151.
- Perinçek, D., 1980. IX. Bölge Hakkari – Yüksekova-Çukurca – Beytüşşebab – Uludere – Pervari dolayının jeolojisi. Technical report, TPAO Arama Grubu, Raporu 1481, Ankara, 80 pp.
- Posamentier, H.W., Jervy, M.T., Vail, P.R., 1988. Eustatic controls on elastic deposition. I. Conceptual framework. In: Wilgus, C.K., Hastings, B.S., Kendall, C.G.St.C., Posamentier, H.W., Ross, C.A., Van Wagoner, J.C. (Eds.), *Sea Level Changes-An Integrated Approach*. SEPM Special Publication, pp. 110-124.
- Premoli Silva, I., Verga, D., 2004. Practical manual of Cretaceous planktonic foraminifera. In: Verga, D., Rettori, R. (Eds.), *International School on Planktonic Foraminifera, 3rd Course, Cretaceous*. Universities of Perugia and Milan, Tipografia Pontefelcino, Perugia, 283 pp.
- Robaszynski, F., Caron, M., González-Donoso, J.M., Wonders, A.H., European Working Group on Planktonic Foraminifera, 1984. Atlas of Late Cretaceous Globotruncanids. *Revue de Micropaléontologie* 26 (3-4), 145-305.
- Van Wagoner, J.C., Posamentier, H.W., Mitchum, R.M., Vail, P.R., Sarg, J.F., Loutit, T.S., Hardenbol, J., 1988. An overview of sequence stratigraphy and key definitions. In: Wilgus, C.K., Hastings, B.S., Kendall, C.G.St.C., Posamentier, H.W., Ross, C.A., Van Wagoner, J.C. (Eds.), *Sea Level Changes-An Integrated Approach*. SEPM Special Publication, pp. 39-45.
- Wannier, M., 1980. La structure des Siderolitinae foraminifères du Crétacé supérieur. *Eclogae Geologicae Helvetiae* 73 (3), 1009-1029.
- Stratigraphy, Foraminiferal Biostratigraphy And Microfacies Of The Upper Cretaceous Carbonate Succession (Adiyaman Group) In The Southeast Anatolia
- Recep Özkan, PhD.
- Turkish Petroleum Corporation, Research and Development Center, 06530 Çankaya, Ankara, Turkey
- This study presents a stratigraphic framework for the Adiyaman Group succession developed on the northern margin of the Arabian Platform. This Upper Cretaceous carbonate sequence, distributed widely in outcrop and subsurface rocks in the southeast Anatolia region, is investigated in terms of lithostratigraphy, biostratigraphy, microfacies analysis and sequence stratigraphy. The sequence is divided into six lithostratigraphic units, which, in ascending order, are the Karaboğaz, Saytepe, Saydere, Sayındere, Beloka and Sanlı formations. A detailed biostratigraphic analysis, based on benthic and planktonic foraminifera examined in thin sections, revealed that the Adiyaman Group formations were deposited from late Santonian to early late Campanian time. While the Saytepe, Beloka and Sanlı formations are best characterized by benthic foraminifera, the planktonic foraminifera are useful as age diagnostic taxa for the Karaboğaz, Saydere and Sayındere formations. Microfacies analysis led to the identification of 12 representative microfacies, which are distributed in a wide facies belt ranging from basin to lagoon, with the pelagic facies being dominant. Sequence stratigraphic study allowed the recognition of three successive depositional sequences that separated by sequence stratigraphic surfaces. Sequence boundaries are correlated to global cycle boundaries. Response in terms of abundance and diversity of the foraminifera to relative sea-level changes is recorded. This study provides revisions in stratigraphic nomenclature that rely on precise biostratigraphic data
- Key words: Cretaceous, biostratigraphy
- Anahtar Kelimeler: Biyostratigrafi, Kretase

Sekil 1



Çalışılan stratigrafik kesitlerin lokasyon haritası.

# Palynological and Paleobiogeographical Findings from the Upper Ordovician Successions in the Central and Eastern Taurides



**Sinem Tanrıku<sup>1</sup>, Sevinç Özkan Altın<sup>2</sup>, Demir Altın<sup>2</sup>**

<sup>1</sup>Türkiye Petrolleri A. O. Arge-Merkezi

<sup>2</sup>Orta Doğu Teknik Üniversitesi-Jeoloji Mühendisliği Bölümü

## SUMMARY

Three measured sections from the Central and Eastern Taurides yielded a fairly diverse and fossiliferous Late Ordovician palynomorph assemblage.

## INTRODUCTION

Three stratigraphical sections were measured in the Central and Eastern Taurides yielding a fairly diverse and fossiliferous Late Ordovician palynomorph assemblage. Within these sections, Hırmanlı Yol-1 Section is in the Central Taurides, while Halevikdere Section and Pekmezli-3 Section are in the Eastern Taurides.

## LITHOSTRATIGRAPHY

Hırmanlı Yol-1 Section is a 33 m thick short section composed of fissile, dark gray shales and underlain by the glacio-marine conglomeratic sandstones. Measured part of the Halevikdere Section covering the Upper Ordovician beds is, again, a fairly short section (27 m thick). Halevikdere Section is composed of fissile, dark gray shales and overlain by the Silurian black shales and lydites. Pekmezli-3 section is 135 m thick and composed of fissile, gray to dark gray shales. Pekmezli-3 succession is underlain by glacio-marine conglomeratic sandy beds and is overlain by the Silurian black shales.

## PALYNOSTRATIGRAPHY

Palynomorph assemblages obtained from these three sections are quite similar in terms of diversity and preservation. All sections have relatively few numbers of chitinozoans when compared to the acritarch assemblages. *Lagenochitina baltica*, *L. prussica*, *Acanthochitina barbata*, *Desmochitina minor*, and *Armoricochitina nigerica* comprises the main chitinozoan assemblage in the sections. Paleogeographically, *Lagenochitina baltica*, *Acanthochitina barbata*, and *Desmochitina minor* are observed in the Baltoscandia, Laurentia and Northern Gondwana, whereas *Armoricochitina nigerica* is only known from the Northern Gondwana. Acritarch assemblages include mostly cosmopolitan species such as *Leiofusa fusiformis*, *Eipoikilofusa striatifera*, *Villosacapsula setosapellicula*, and *Multiplicisphaeridium* spp. including a few numbers of paleogeographically restricted taxa, which are *Dactylofusa cucurbita* and *Estiastra iranicum*. In addition to these marine palynomorph assemblages, early occurrences of some spores including, tetrads, dyads, and trilete spores are observed in the studied sections.

## RESULTS

All of these three sections yielded quite rich palynomorph assemblage including one of the earliest undoubted terrestrial spore data. Although most of the palynomorph assemblage is cosmopolitan, some paleogeographically important taxa are also observed in these Upper Ordovician strata.

Keywords: Ordovician, palynology

# Late Paleocene-Early Eocene Stratigraphy and Hydrocarbon Potential, Southeast of Turkey



**Mehmet Özen Gürbüz, Halil Şeker, İsmail Bahtiyar, Hasan Altınbay, Ali Can Diyarbakırlı, Mehmet Şahin, Deniz Atasoy, Mahir Kaya, Hasan Çağlar Üsdün, Fırat Göçmenoğlu, Sinem Artan Ercengiz, Yinal Neşes Huvaj**

Turkish Petroleum Company, Ankara / Türkiye

In the Southeastern of Turkey, during the closing process of the Neo-Tethys ocean, at the end of the Late Paleocene/Early Eocene, terrigenous sediments were dominant in the northern areas and coastal or shallow marine conditions prevailed in the south. Under the effect of this paleogeography, deltaic deposits were formed. In order to determine the importance of this sedimentary sequences in terms of hydrocarbon exploration, detailed studies were carried out with a large expert team within the borders of Gercüş District of Batman Province and Dargeçit District of Mardin Province. The results obtained with the stratigraphy of the Late Paleocene/Early Eocene succession, possible reservoir units, their reservoir properties, and the origins of the hydrocarbons are shared here.

In the Paleocene succession, alternations of sandstone and shale are dominant. Sandstone to shale ratio and grain size increase upwards. At the top, thick channel-fill sandstone layers with locally conglomerates are observed alternating with red-burgundy colored silt and mudstones. The deltaic succession observed in this section indicates that the basin is gradually filled up and that deltaic-fluvial progradations had taken place at the end. Nodular limestones with abundant macrofossils were deposited on the top of delta channels as a result of small-scale transgression. The thickness of these patchy carbonates vary from 1 to 10 meters and they do not show any lateral continuity. The thickness of these limestones increases from west to east. The reason why these limestones were not seen in the west was interpreted as the fact that the east was paleotopographically lower during the deposition that continued under the influence of the shallow marine environment. The western part was exposed during the same depositional period and was under continental influence. The sandstones are greenish gray, polygenic, fine-grained, well sorted, well-rounded, hard, calcite-cemented, trace fossil-bearing and calcarenitic. The sandstone layers thicken upwards and have a channel geometry with a thickness of 1-1.5 meters at the top. The delta-capped carbonates were developed on the top of deltaic channels and were interpreted as products of a maximum flooding surface (MFS). After this MFS, progradation was dominant in the succession and it shows a transition to Early Eocene deposits dominated by terrestrial sediments formed as a result of shallowing and exposure of Paleocene units. The Early Eocene sequence was dominated by terrestrial sediments and followed by the carbonates which were deposited in the tidal plain (sabhka) environment under marine influence with the transgression. These subtidal parasequences consist of dolomitic marl and dolomitic marl, intertidal parasequences include gastropod, bivalve packstone,

cross-bedded ooid grainstone and algal laminated organic matter-rich dolomites, and the supratidal deposits consist of evaporite and red mudstones. The part of the Early Eocene sequence, which consists of dolomitic marl, dolomite, and evaporite intercalations, is important because it contains reservoir and source rock levels. Dolomitic marls are cream, yellowish cream colored, hard, with evaporite bands and inclusions, the dolomites in the upper levels of the unit are cream colored, micritic in character, gray colored, hard, bivalve, gastropod-bearing and microfossilized towards the top. The external shapes of the fossils have been preserved, and the interiors were dolomitized. In places, in the upper parts of the dolomites, there are greenish gray, gray colored, soft, laminated algae rich levels. These levels are important to the source rock. In the uppermost parts, the dolomites are ooid-rich, macro and micro fossiliferous, locally cross-bedded grainstone or packstone. This type of dolomites have good reservoir rock characteristics. An increase in the rate of evaporite and red colored terrestrial mudstone is observed towards the top of the succession. As a result of thin section analysis; Orbitolites spp., macro shell and algae fragments Lockhartia spp., large benthic foraminifers as well as benthic foraminifers belonging to Miliolidae, Rotaliidae, Textulariidae families, macro shell (Mollusk) fragments and red algae fragments were observed. Of these fossil organisms, only Lockhartia spp., species spread throughout the Paleocene (Serra-Kiel, Hottinger et al., 1998). The deposition age of the measured successions was determined as Late Paleocene-Middle Eocene. It was determined that algal carbonates in the Early-Middle Eocene deposits have good-very good source rock potential (TOC: 1.88-9.55%, HI:41-310). It has been founded that the dolomitic packstones and grainstones in this sequence have porosity values over 20% (Permeability: 7.21-77.5 md). The delta sandstones found in the Late Paleocene sediments have porosity values over 20% in places (Permeability: 2-178 md). It was determined that the petroleum extract sample obtained from the sample taken from the delta sandstone was derived from a source rock of low maturity and clastic lithology in a poorly preserved "oxic" environment. In the light of these evaluations, it has been determined that this source rock does not show similar characteristics with the source rocks that have produced economic hydrocarbons in the Southeast of Turkey.

As a result, the importance of these units in terms of hydrocarbon exploration has been revealed as a result of field geology studies. If these are tracked in subsurface, hydrocarbon discovery can be made in adequate burial conditions and in suitable traps. The evaluation that the

source of the sample taken from the extract sample in the sequence has oxic and clastic lithology shows us that the delta deposits contain possible source and reservoir rocks together. In Figure-1, all findings are summarized in a regional stratigraphic section.

## RESULTS

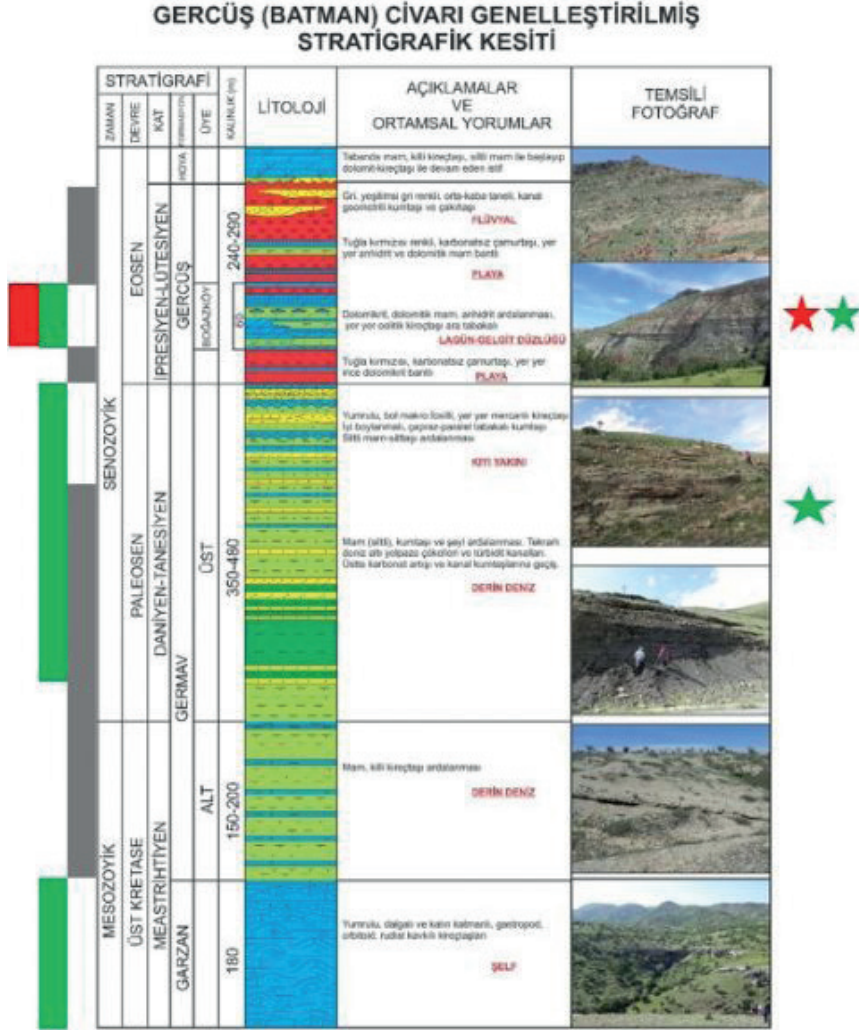
1. The Paleocene (Daniyen-?Early Selandiyen) succession consists of turbiditic shales below and the sandstone/shale ratio increases upwards.
2. Sandstones with increasing thickness and grain size in the Danian-?Early Selandian period are in reservoir rock potential in terms of petroleum production. These sandstones thicken towards the east. Towards the east and north of Mardin-Dargeçit, it is possible to find thick sandstones that are the product of submarine fan.
3. During the Late Paleocene, delta and shore deposits are dominant. Nodular limestones, which could not have lateral continuity, were deposited on delta sandstones by transgression.
4. It was observed that the facies of the Boğazköy Member of the Gercüş Formation deepened towards the east. Terrigenous mudstones and supratidal facies are dominant in the northwest, while intertidal and subtidal facies dominate to the south and east.
5. Algal boundstones in the Early Eocene tidal deposits have been identified as potential petroleum source rock under favorable burial conditions with high TOC values.
6. It has been determined by field and laboratory data that the deltaic succession of the Late Paleocene period and the tidal sediments of the Early Eocene period can be very good reservoirs.
7. As a result of the geochemical analysis of the extract sample taken from the sandstones in the Late Paleocene succession, it was determined that it was derived from a source rock containing terrestrial organic matter deposited in the anoxic environment. Among the known source rocks in Southeastern Anatolia, there is no source rock deposited in such an environment.

## REFERENCES

Serra-Kiel, J., L. Hottinger, ve diğ. (1998). "Larger foraminiferal biostratigraphy of the Tethyan Paleocene and Eocene." *Bulletin de la Société géologique de France* 169(2): 281-299.

Keywords: Stratigraphy, Hydrocarbon Potential

Figure 1 - Generalized stratigraphic section of the study area and evaluation of the units in the section in terms of source, reservoir, seal, and overburden rock (red columns: source rock; green columns: reservoir rocks; gray columns: overburden rock)



# Hydrocarbon Exploration And Potential Of Mannar Basin Of Srilanka, Using Environmental Free SDDT Technology



**Ongun Yoldemir**

Pytheas Ltd., Berlin / Germany

## INTRODUCTION

Srilanka is an island south east of India. The Island of Srilanka is composed almost entirely of crystalline rocks of Archean or pre-Cambrian age. In the extreme north these are overlain by limestones of Miocene or later age. At one point on the northwest coast a very small area of Jurassic rocks lies on the surface of the coastal plain. The ancient crystalline rocks resemble in many respects the Grenville series of the Canadian Shield. They are largely biotite gneisses, interstratified with which are at least two great beds of white crystalline limestone, often dolomitic, with associated beds of quartzite and of sillimanite-bearing rocks of undoubted sedimentary origin.

Due to its weak and import dependent economy the country is in great need of international exploration efforts. The authorities are in the phase of preparation for an international bidding process of the offshore basins surrounding the country.

The offshore investigations in Sri Lanka have identified three oceanic basins (i.e., the Mannar, Cauvery and Southern Basins) for possible oil and gas generation. These sedimentary basins recorded thick sedimentary successions from the Upper Jurassic to recent in age. The Cauvery and Mannar Basins contain a complex sequence of potential source rock beds from the Upper Jurassic to Neogene. An extensive kitchen source can be expected during the Upper Cretaceous.

Although the Indian sector of the Cauvery basin to the north has a lot of proven hydrocarbon occurrences at the Indian sector, there are no significant success stories at the Srilankan part of the Cauvery basin due to the lack of exploration efforts. On the other hand the Mannar basin to the west of the island has two small to medium scale gas discoveries.

The Mannar Basin is a frontier failed rift basin between India and Sri Lanka. The Sri Lankan part has an area exceeding 42,000 km<sup>2</sup>. Although the recent two gas discoveries have confirmed the existence of an active petroleum system in the Mannar Basin, a major portion of the basin is still poorly explored. The basin began to evolve since the Upper Jurassic and experienced two rifting events; an early Late Jurassic syn-rift phase associated with East-West Gondwana break up; and a later, earliest Cretaceous syn-rift phase associated with Antarctica separation from greater India around 142 Ma. Rifting was followed by a post-rift phase comprising a thermal sag period and an inversion period. Three potential source rocks intervals have been interpreted at Maastrichtian, Campanian, Albian-Aptian, and Late Jurassic stratigraphic levels. The Mannar basin together with other offshore areas of Srilanka is going to be open for bidding by the Petroleum Resources Development Secretariat (PRDS). Pytheas is asked to provide test

cases in order to enhance the understanding of the HC potential of the basin.

## METHODS

This study used a very new technology developed by Pytheas, where the Vertical density tomography logs extracted from the 3D cube obtained by SDDT technology and calibrated with actual well data to successfully solve the mystery created by prior unknown Late Cretaceous aged facies, which mislead all explorational strategy. The data cubes are calculated from satellite images. 1d data, obtained from the 3D data cube which is named as vertical differential density tomography log (VDDT) displays the vertical density changes from the surface up to 10 kilometers. The 1D vertical differential density tomography logs are the calculated bulk density values of rock units that create the lithological column. Since the original data is composed of bulk density values, derivatives of this data are created to be able to differentiate fluid density changes vertically. 1D differential density log is calculated at every pixel up to the depth of 10 kilometers. By studying and correlating the VDDT profiles after calibration with the actual well data, the sequence boundaries and/or unconformities with overall density changes are often recognized and correlated for long distances.

## FINDINGS AND CONCLUSION

The VDDT logs of the area are calibrated by the help of the actual wells which are Dorado-1 (gas show well), North Dorado-1 (dry well) and Barracuda-1 (gas well). Using the defined stratigraphy at the wells the stratigraphical model was created. Several EW and NS profiles were correlated. The unconformities that are related the rifting phases of the area were detected and mapped in the test area. The HCI distribution maps were created in order to reflect the potential of different stratigraphic levels, and summarized in two maps which are classified as relatively shallower targets and deeper hydrocarbon existences. Detailed (tighter grid) studies around Barracuda-1 allowed the definition of the structure that the well was drilled upon as well as potential zones of hydrocarbon existence that could be used to further develop the area. Other clusters of HCI were also defined and presented in the final work. The results show that the Mannar basin has significant hydrocarbon potential and needs to be further explored. Although the water depths of up to 1500 meters create a significant risk, today's offshore technology and need for further hydrocarbons in the area makes the plays worthy of exploring.

This study is presented by the generous permission of PRDS (Petroleum Resources Development Secretariat) of Srilanka.

Keywords: Offshore Srilanka, HC exploration





**Sismik Veri İşlem**

*Seismic Data Processing*

---



# Seismic Reprocessing for Carbon Storage

**Arindam Kanrar, Joseph Sutcliffe, David Barlass, Shona Joyce, James Bailey, Khaled Abdel Aleem Abdel Aleem, Rachel Little, Priyabrata Pradhan**  
SLB London / United Kingdom



## INTRODUCTION

To support the carbon storage (CS) licensing round and ongoing CS projects in the Central North Sea (CNS), SLB has performed a CS focused seismic-reprocessing project to reduce uncertainty in the identification and characterisation of potential carbon stores and associated containment risks in the area. The available geological datasets were used as the primary data source for a regional screening to rapidly assess the key criteria for geological storage locations across the CNS. The study focused on the carbon storage potential of the Paleogene within the CNS – namely the aquifer potential of Mey and Maureen sands. Interpretation of regional seismic and well data provided the basis for a series of common risk segment maps which have been further integrated with non-geological information to highlight areas of highest CS potential in the CNS.

## METHODS

### Play-based carbon storage screening technique

Established play-based techniques were updated for the key geological criteria required for carbon storage. Reservoir thickness maps, net to gross and depositional facies indicated areas of high, medium, and low risk (Figure 1) to assess the CS reservoir potential of an interval, as described by Barlass et al., 2023. The CS potential maps suggest that the northern sector of the study area towards the Outer Moray Firth consistently mapped as a high potential area for low-risk carbon storage, with the Palaeocene reservoirs offering significant storage potential. Palaeocene Balmoral and Andrew sands have the broadest low-risk CS zones.

### Carbon storage focused reprocessing

This initial phase of screening has been critical to highlight the areas and intervals for CS storage, leveraging the vast repository of geological data available in the area. It has directed the location and imaging focus of the seismic reimagining project. The resolution of the public-domain geological datasets, however, limit the accuracy of the containment analysis of CS plays. The study also emphasized the importance of detailed containment assessment on the new seismic dataset. Hence a high-resolution dataset is required to perform the detailed containment assessment. The East Mey area identified both shallow Palaeocene and deeper Jurassic reservoirs as potential storage targets. A reprocessing study was performed with 11 heritage towed-streamer surveys, acquired between 1993 and 2003 to provide this high-resolution dataset.

A reprocessing workflow was designed to provide

shallow and deep imaging with extra focus on producing a high-resolution dataset for overburden analysis. The workflow design focused on improved resolution for both shallow and deep targets, improved signal-to-noise ratio, multiple elimination, amplitude integrity preservation and the production of a single seamlessly merged image cube.

Denoise workflows were applied targeting various noise modes observed during the acquisitions. An adaptive deghosting approach (Rickett, 2014) was implemented to properly correct the wavelet phase and expand the usable frequency bandwidth by narrowing the source and receiver ghost notches, resulting in a broadband dataset for demultiple and imaging. A 3D general deterministic water-layer demultiple approach was implemented to predict the strong water-layer multiples. Residual longer period free-surface multiples were modelled using a 3D surface-related multiple elimination approach (Dragoset et al., 2008), coupled with a full-bandwidth adaptive subtraction workflow to subtract the multiple energy from the input data. Survey matching and merging techniques compensated for the amplitude, phase, timing, and frequency variations between the different legacy surveys and produced a uniform dataset as input to the migration process.

## FINDINGS

Figure 2 and 3 show an example of the 3D Kirchhoff prestack time migration (KPSTM) results with newly reprocessed data which clearly show an uplift in the imaging compared to the existing legacy data in both the shallow and deep sections. Compared with the legacy seismic image available, the newly processed data shows substantially improved imaging of the shallow gas chimneys and polygonal faults. Further depth imaging work was carried out with full-waveform inversion (FWI) (Jiao, K., 2015), reflection tomography, and Kirchhoff depth migration (KDM) to reduce the geological uncertainty and provide increased confidence in regional mapping and AVO analysis. FWI allowed detailed velocity updates at shallow depths which is highlighted in Figure 4, improving the depth image reliability, and providing direct insights into variations in lithology. Containment assessment was performed on the reprocessed dataset focusing on understanding and mapping potential CO<sub>2</sub> leakage pathways. The new reimagining and reinterpretation helped to identify type 1 and type 2 gas chimneys present in the study area.

## CONCLUSIONS

This project emphasizes the use of play-based carbon storage screening supported by focused CCS reimagining to confidently map and assess CO<sub>2</sub> storage potential

within the CNS. Regional geological data is an excellent source for rapid CS screening. We effectively identified high-potential CS areas and stratigraphic intervals in addition to identifying key containment risks by utilizing existing geological data. These risks were further evaluated and mitigated by using newly re-processed data that were reimaged to address the resolution and imaging challenges associated with the legacy imaging in the area. Seismic reprocessing, reimaging and associated interpretation have markedly updated and improved the quality of CS play maps over the study area. The broader bandwidth and resulting higher resolution reflectivity have allowed detailed identification and mapping of leak pathways, including pockmarks and small-scale faulting, improving seal integrity understanding in the study area.

## REFERENCES

- D. Barlass, A. Kanrar, H. Barnett, S. Joyce, K.A. Aleem, J. Bailey, D. Scarpellini, C. D'Aguanno, A. Cooke, C. Field, D. Wheeler, Dedicated carbon storage seismic reprocessing for Central North Sea CCS site selection: 84th EAGE Conference and Exhibition, Extended Abstracts Jun 2023, Volume 2023, p.1 - 5
- Rickett, J., Van Manen D.-J., Loganathan P., and Seymour N., (2014), Slanted-streamer data-adaptive de-ghosting with local plane waves: 76th EAGE Conference and Exhibition, Extended Abstracts DOI: 10.3997/2214-
- Dragoset, B., Moore, I., Yu, M., and Zhao, W. [2008] 3D general surface multiple prediction: An algorithm for all surveys. 78th Annual International Meeting, SEG, Expanded Abstracts, 2426-2430
- Jiao, K., Sun, D., Cheng, X. and Vigh, D. [2015] Adjustive full waveform inversion 85th Annual International Meeting, SEG, Expanded Abstracts, 1091-1095

## ACKNOWLEDGEMENTS

The authors thank SLB for the use of the seismic data and permission to publish this work.

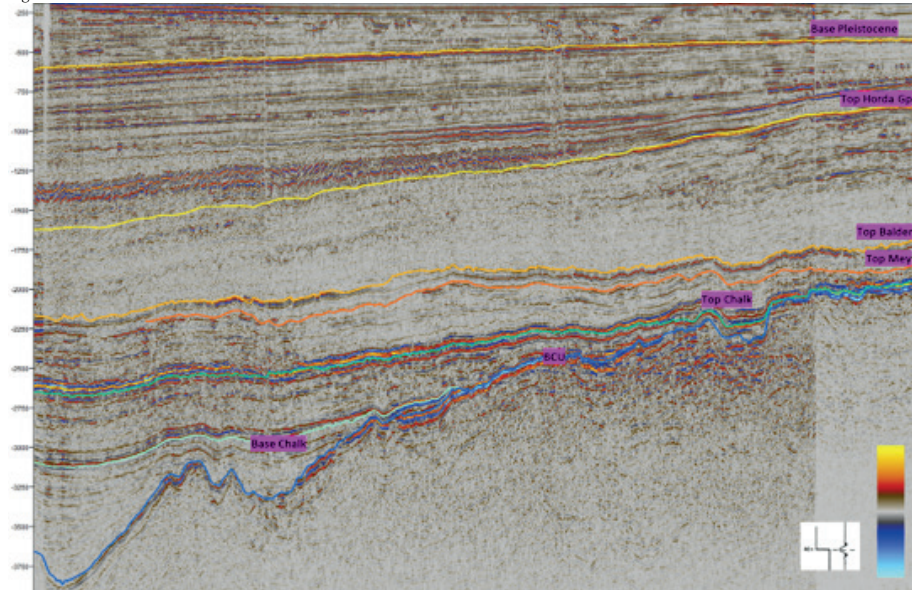
Keywords: Carbon Storage

Figure 1



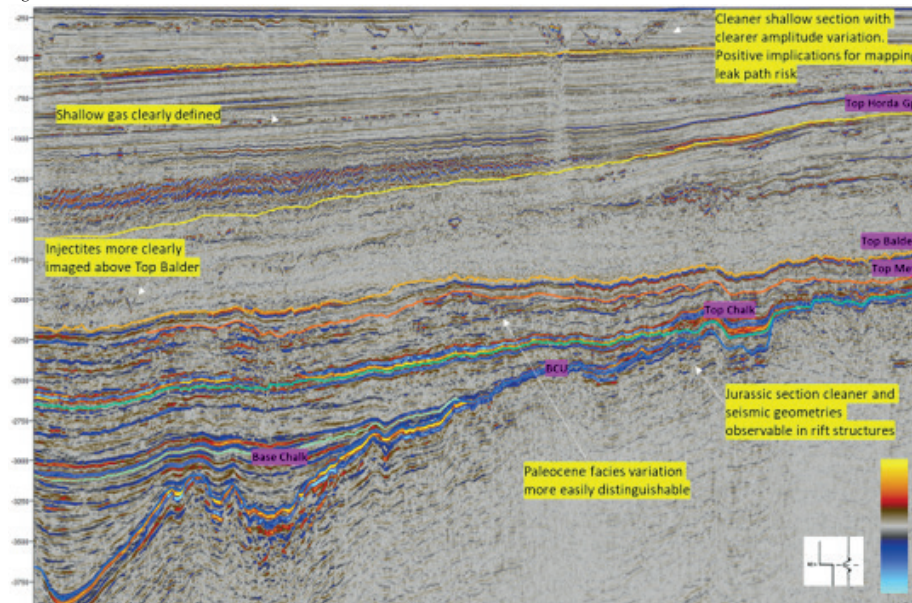
CS reservoir potential for Andrew member (left) and Captain sandstone member (right). Green represents area of low CS risk, yellow represents area of medium CS risk and red represents area of high CS risk.

Figure 2



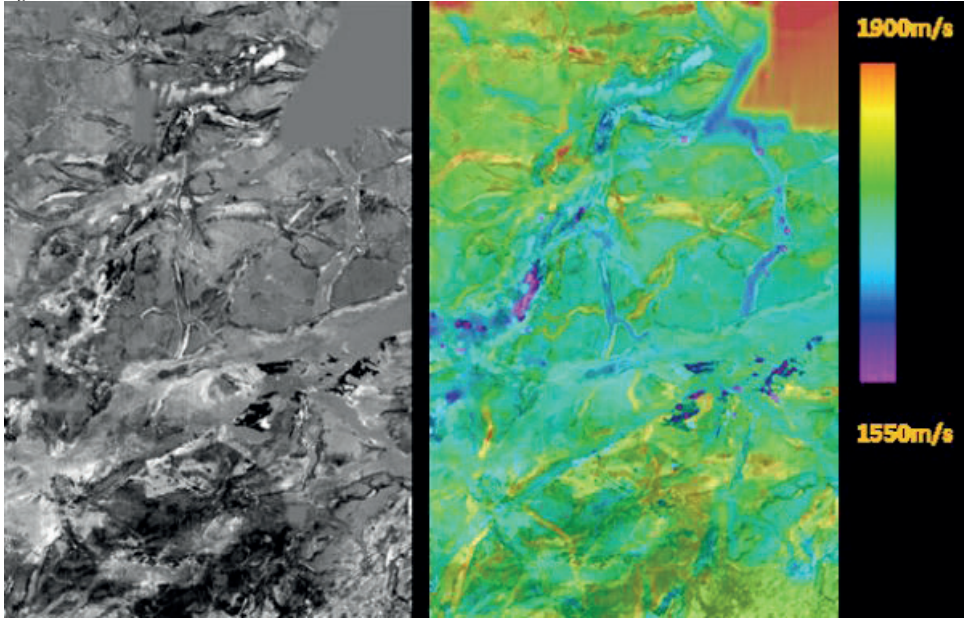
KPSTM stack image; legacy

Figure 3



Newly reprocessed and reimaged KPSTM stack. Note the improved resolution and imaging in the reprocessed and reimaged data in both the shallow and deep sections.

Figure 4



KPSDM depth slice capturing shallow Nordland geology (left). FWI velocity depth slice shows different geological packages corresponding to different velocity (right).

# Multi-Year Evolution of Processing Improvements to A 10 Day Delivery. The Edvard Grieg PP And PS Time-Lapse OBC Story



**Richard Ford<sup>1</sup>, Francesca Twynam<sup>1</sup>, Alice Ramsden<sup>1</sup>, Taylor Leitch<sup>1</sup>, Michael Hooke<sup>1</sup>, Per Eivind Dhelie<sup>2</sup>, Vidar Danielsen<sup>2</sup>, Arnstein Kvilhaug<sup>2</sup>, Knut Richard Straith<sup>2</sup>**

<sup>1</sup>slb, Crawley / UK

<sup>2</sup>Akerbp, Oslo / Norway

## INTRODUCTION

Reducing the turnaround time from acquisition to imaging for time lapse (4D) surveys supports closer to real-time analysis of the reservoir and therefore proactive rather than reactive planning for infill drilling and production. It also enables the potential for an increase in the frequency of acquisition, either a full repeat of the baseline survey or localized over a specific area of interest. This requires rapid delivery of final 4D interpretation volumes. However, processing sequence timelines for 4D seismic data have historically been on the order of months, by which time the subsurface interpretation of reservoir dynamics may differ from the current reality. The ideal situation is an interpretable 4D volume to be produced directly after acquisition without any compromise in the quality of, and confidence in, the data. The Edvard Grieg time-lapse seismic project comprises multiple vintages of ocean-bottom cable data acquired since 2008. Described here are the evolution of the processing workflows and project logistics that have led to high-quality PP and PS datasets being delivered less than 10 days after acquisition.

## Overview of 4D at Edvard Grieg

The Edvard Grieg oil field is located in the Norwegian North Sea on the Utsira High approximately 180 km west of Stavanger. The field was discovered in 2007 by exploration well 16/1-8, block 16/1. The field is in a continental half graben setting of Triassic age with the reservoir sitting at 1900 m. Four water injection wells provide the pressure support for the field, predominantly from the west, and oil is produced from 13 production wells. Monitoring of where the water is moving to, and when it will reach the production wells, is critical for planning infill wells for the remainder of the production cycle.

An ocean-bottom cable (OBC) 4D seismic acquisition and imaging campaign was launched in 2016 to capture the dynamic reservoir changes from production (first oil in 2015). Interpretation of the processed 4D signal between the 2008 and 2016 vintages was impaired by significant levels of background noise and ambiguous signal, with the fundamental challenge being the different acquisition geometries of the two surveys. The 2008 baseline was deployed with a cross-spread geometry while the 2016 monitor survey used inline shooting. To match the surveys prior to imaging, the 2016 data was decimated to match the 2008 data, and, in doing so, this reduced the signal-to-noise ratio. The 2016 survey was repeated in 2018, 2020 and 2022 using inline geometry characterised by a flip-flop shot carpet

of 25 m (inline) by 50 m (crossline) overlying ocean-bottom cables with receivers 25 m (inline) by 200 m (crossline). Water depth in the Edvard Grieg field is relatively constant at 100 m +/- 5 m. For successive acquisitions, the survey shape has changed depending on the 3D/4D interpretation requirements (see Figure 1). Additional challenges were the changing swath dimensions for each survey along with a new acquisition vendor from 2020 onwards.

## METHODS

### Processing sequence evolution

An updated processing sequence was introduced for the 2016-2018 4D comparison to improve turnaround relative to the legacy workflow. It relies on up/down deconvolution (UDD) as described by Ford et al., 2019. The process removes all free-surface multiples, source/receiver-side ghosts, and signature effects for a 1D medium (Amundsen et al., 2001; Wang et al., 2010). Hydrophone (P) and calibrated vertical particle velocity (Vz) components are combined by decomposition to the up and downgoing wavefields "just above" the seabed in the tau-p-q domain prior to spectral division. UDD is executed independently for each ray parameter trace and consists of a stabilised spectral division of the up-going by the down-going wavefields. The deconvolution result is band-limited with a dipole source field and a common wavelet for all 4D vintages. For the converted wave data, we follow the same principles as the pressure wave and apply radial/down deconvolution (RDD). In RDD, the upgoing radial (Vx and Vy geophone components rotated to the source-to-detector azimuth) undergoes spectral division with the downgoing wavefield decomposed from the combination of P and Vz (Twynam et al., 2020).

UDD provides several benefits. There is no interpretive adaptive subtraction of multiple models that can harm primary, and certain noise types (e.g., seismic interference, linear noise, direct arrival energy) are attenuated directly by UDD or with a tau-p-q mute reducing the overall number of processes required to obtain an interpretable volume. The UDD flow also accounts for water column variability, hence sail line timeshifts observed on the legacy workflow were not present after UDD. Turnaround was improved further by using reverse-time migration (RTM) to image the PP and PS data. The ability to transpose from receiver gathers to the image domain removes the necessity of sorting to offset/azimuth tiles and post-migration

stacking. The 4D of the updated UDD flow, derived in parallel with processing of the 2016-2018 through the legacy flow, and without a conventional denoise sequence, can be interpreted with similar confidence while being delivered significantly earlier (Figure 2).

### Processing milestones and project logistics

After the first UDD-based 4D was delivered ten days after last shot point for the 2016 to 2018 surveys, a post-mortem of the workflow and logistics led to improved planning and the addition of impactful processes to improve 4D repeatability. The workflow expanded to include shear noise attenuation and the calibration of sources to equalise their responses. One challenge for the 2020 survey was to deliver in-progress 4D datasets at the completion of each swath. Due to the different survey extents, areas not covered by the 2018 (largest area) survey were infilled using the 2018 data to create RTM volumes of equal fold and spatial extent. Three vintages of PP data, 2016, 2018 and 2020, were delivered after the last 2020 shot point for each swath with the 2020 contribution replacing the 2018 infill for the second swath. Data delivery included an attribute cube, a volume containing 4D attributes for all combinations of vintages, including RMS extractions, time shifts, and amplitude extractions windowed across target horizons (e.g., sum of energy, min/max amplitudes, timeshifts) for efficient time-lapse interpretation.

During 2020 processing, we accelerated the converted wave workflow including optimisation of PS RTM, vector fidelity (equalisation of the spectral response for  $V_x$  and  $V_y$ ) prior to rotation, co-processing with the PP data. An additional technical challenge was to identify the sources of strong 4D noise. Despite the good repeatability of receivers, the slow shear wave is significantly affected by short-period velocity variations in near surface. A 4D PS statics workflow was derived matching receiver stacks to a common (2018) PP vintage (in PS time) leading to a significant uplift of the 4D metrics. The 2022 4D campaign was the first time both PP and PS were delivered for four vintages in 10 days or less for each swath using the UDD/RDD workflows.

Processing flow improvements are not the only factor for rapid delivery. Careful planning and retention of experience from one monitor survey to the next are also important. Pre-project testing was performed to understand the effect of different processing scenarios including the impact of noise attenuation prior to UDD/RDD on the PP/PS 3D and 4D image. A dedicated point of contact with the acquisition vessel, organising resources (people/compute) and designating timeline milestones for every objective are crucial. Offshore communication was established between the team and on-board processors with early QC data transfers, which allowed the processing team to rapidly identify issues with acquisition. Through workflow tolerance testing we could inform and make recommendations on whether to reshoot source lines or redeploy cables.

## RESULTS

### Field development impact from workflow enhancements

The interpretation of a high-quality 4D product delivered in days as opposed to weeks or months has had a positive impact on field production optimisation and infill well campaign over the Edvard Grieg field. The dominant 4D amplitude effect observed on the PP allows an accurate tracking of the waterflood front advancement, demonstrating the connectivity pathways across the field whilst also highlighting pockets of un-swept oil (Figure 3). Amplitude softening effects around the poorer quality reservoir units have been interpreted as a gas out of solution response around key production wells. The converted wave dataset provides an independent wavefield measurement with a higher sensitivity to pressure effects and has been used to track pressure balance across the field both at the water injection and production sites. The converted wave does not transmit through fluids, and, therefore, unlike PP, does not register saturation-related changes (Figure 4). Joint interpretation of PP/PS 4D data, delivered simultaneously, allows for a separation of saturation-only versus pressure effects.

High correlation between the 4D results, infield intervention history and downhole production measurements allows for a better understanding of the full-field performance and reservoir flow simulation model with each additional vintage. The 4D results from 2018 and 2020 directly contributed to the location selection and positioning of three infill wells placed in 2020, whilst 2022 results are currently being integrated to inform three additional infill wells scheduled for 2023. All of these 4D interpretations rely on a high confidence in the signal processing workflow to preserve 4D signal fidelity whilst reducing noise content to achieve a low NRMS both at target and within the overburden (<6%).

The 4D monitoring campaign has contributed to the extension of the production plateau by more than two years with an increase in the recovery factor of approximately 10%, equivalent to an addition of 30-50 million barrels to the total recoverable reserve estimate.

## CONCLUSIONS

Edvard Grieg's highly repeatable two-year interval ocean-bottom multi-component monitoring programme and tailored processing sequence produces reliable, high-fidelity 4D results to inform the field development, infill well placement and intervention strategy. Multiyear collaborative workflow development and the application of the latest processing technology has optimised both the data quality and processing efficiency of the base workflow. This condensed reliable workflow, utilising UDD, RDD, and RTM imaging, facilitates the rapid turnaround of a 4D result within 10 days of data receipt. Streamlining of the PP and PS workflows to be delivered in parallel facilitates joint 4D interpretation and evaluation of the field's evolution with respect to



saturation changes and pressure.

**REFERENCES**

Amundsen, L., Ikelle, L. and Berg, L. (2001), Multidimensional signature deconvolution and free-surface multiple elimination of marine multicomponent ocean-bottom seismic data: *Geophysics*, 66, no. 5, 1594–1604.

Ford, R., Twynam, F., Caprioli, C., Hooke, M., Whitebread, R., Kristiansen, P., Boiero, D., Dhelie, P E., Danielsen, V. and Straith, K. R. (2019), Fast turnaround OBS time-lapse processing enabled by up down deconvolution: A North Sea case study: 89th Annual International Meeting, SEG, Expanded Abstracts, 5280–5284.

Twynam, F., Ford, R., Caprioli, P., Hooke, M., Whitebread, R., Dhelie P. E., Danielsen, V. and Straith, K. R. (2020), Improved reservoir monitoring with PP & PS time-lapse imaging utilising up/down deconvolution: An OBC case study from the Edvard Grieg field: Norwegian Petroleum Forum, Expanded Abstracts.

Wang, Y., Bale, R. Grion, S. and Holden, J. (2010), The ups and downs of ocean-bottom seismic processing: Applications of wavefield separation and up-down deconvolution: *TLE*, 29, 1258–1265.

**ACKNOWLEDGEMENTS**

The authors thank Aker BP and partners in PL338, OMV and Wintershall Dea, and SLB for permission to publish this work.

Keywords: 4D, Multicomponent

Figure 1

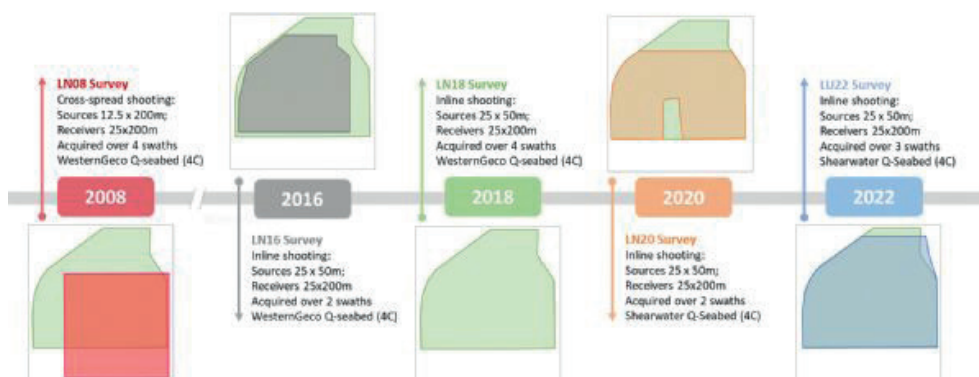


Figure 1 Survey outlines and acquisition information for all OBC surveys over the Edvard Grieg field with 2018 employed as a reference polygon.

Figure 2

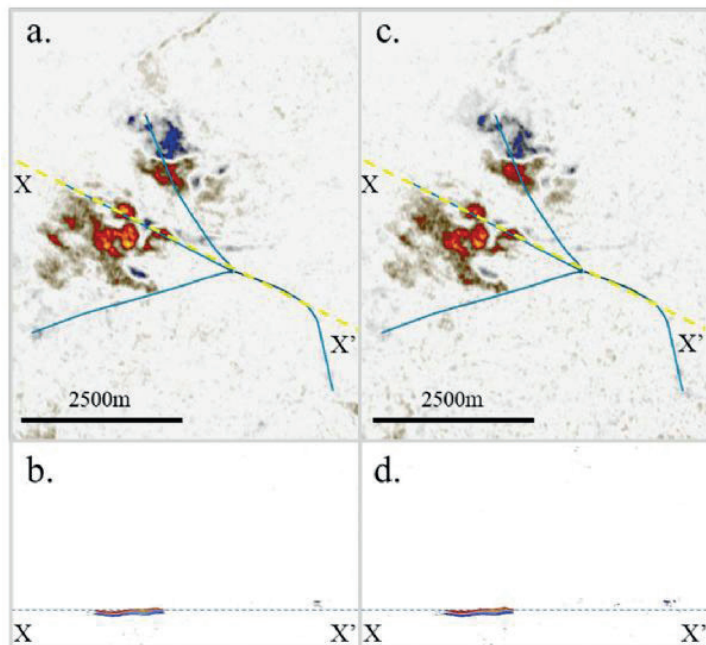


Figure 2 4D Timeslices at reservoir for 2018-2016 and 4D section view for the legacy (a and b) and UDD workflow (c and d). The globally matched volumes provide an almost identical interpretation.

Figure 3

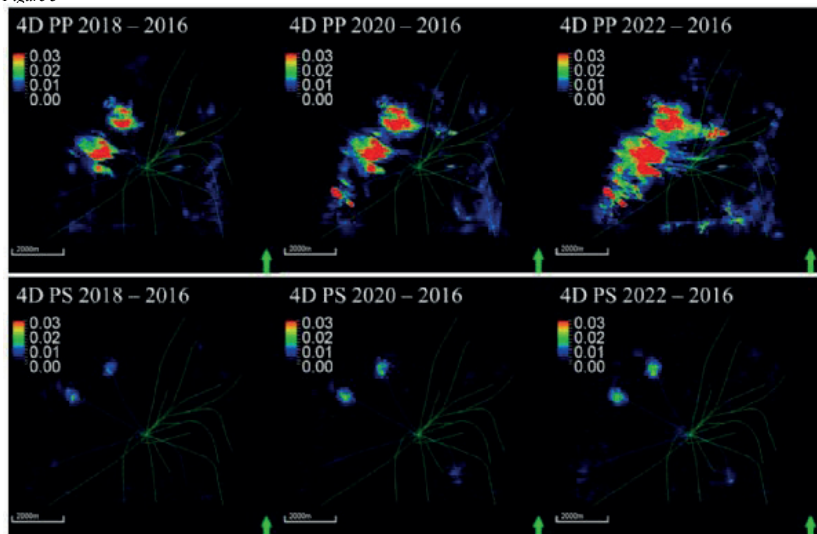
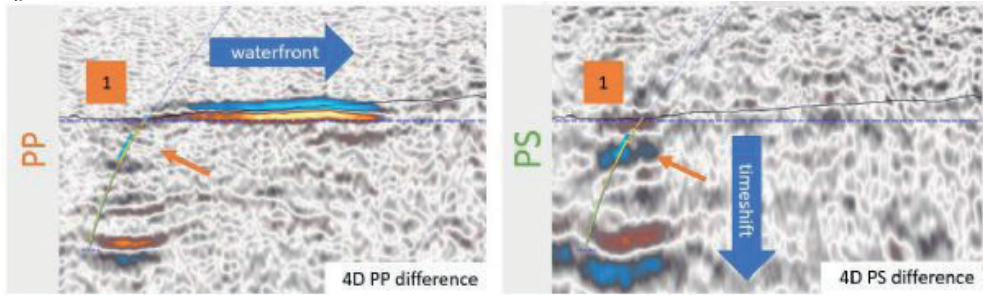


Figure 3 Two-, four-, and six-year 4D difference (2016 to 2022) sum of energy attribute extraction at reservoir for PP (top) and PS (bottom). The images highlight on the PP the water sweep from the westerly injector wells (blue) to the producing wells (green). Pressure-only effects independent of saturation changes can be seen on the PS 4D attribute plots at the source of water injection.

Figure 4



Demonstration of the difference in PP and PS 4D response in section view. The pressure increase between 2016 and 2018 shows as a timeshift on the PP and PS data, however, it is challenging to separate fluid and pressure effect on PP. The PS data highlights only the perforated zone pressure effects.

# Full Waveform Inversion And Modern Signal Processing Brings Imaging Uplift for Presalt Reservoirs in The Kwanza Basin

**Samuel Madden, Mina Matter, Alex Cooke, Amr Ghanem, Carina Lansky, Mahmoud Mahfouz, Deepak Rathee**  
SLB, London / United Kingdom



## INTRODUCTION

In deep-water Kwanza basin, offshore Angola, the pre-salt hydrocarbon potential remains under explored. This is, in part, due to the challenges associated with seismic exploration in this environment. The majority of seismic data in the area have limited offset and azimuth coverage, and this inhibits building an accurate velocity model, on which reliable pre-salt imaging is highly dependent, especially in the presence of strong contrasts associated with carbonate and salt formations. As a result, heritage seismic imaging in the area often suffers from distortion and poor focusing of pre-salt targets, resulting in interpretation uncertainty.

In this case study, we demonstrate how the application of contemporary signal-processing and imaging workflows to heritage data from the area can significantly improve the reliability of pre-salt interpretation. Key to these improvements are the latest developments in full-waveform inversion which include multidimensional objective functions and automated decision making. These techniques allow us to overcome some of the challenges associated with the overburden geology and acquisition geometry, using both early arrivals and reflections to simultaneously update all geological units, even in the presence of strong velocity contrasts.

Typically, seismic imaging in a complex salt environment requires rich azimuthal coverage and long offsets to illuminate the subsurface and enable building an accurate velocity model to be used with the appropriate imaging algorithm (Kang et al., 2021). Moreover, geometry of the salt, in offshore Angola, has variable complexity, and the majority of the data acquired to date is narrow-azimuth (NAZ) towed streamer. Previous studies performed in this area have shown that reliable subsalt images can be achieved with NAZ data, but an accurate velocity model is critical to success (Shmelev et al., 2016 and Branston et al., 2022). Herein we demonstrate the rejuvenation of multi-survey NAZ seismic surveys by applying broadband signal processing and focusing on velocity model building and depth imaging, using recent developments in full-waveform inversion (FWI) such as enhanced template-matching FWI (ETM-FWI) automation. This resulted in the reduction of structural uncertainties, and improved understanding of the depositional context at pre-salt targets, migration pathways and trapping styles. We show how improvements in model building contribute to a significantly improved image of the legacy seismic data.

More than 4.2 billion barrels of oil equivalent (IHS Markit EDIN) has been discovered (Cameia, Mavinga, Orca, etc.) in pre-salt plays over the outer Kwanza basin covering blocks 20 & 21 (Figure 1). Carbonate mounds (Aptian Microbialites) which are developed

on the basement highs overlain by salt are the key targets in the deep-water. Most of the exploration wells drilled so far had the uncertainty in the seismic imaging as one of the key challenges in successfully mapping pre-salt carbonate reservoirs and predicting accurate reservoir properties. Distortion and poor focusing of the seismic image associated with unresolved overburden heterogeneity complicates the understanding of deeper structure and fracture delineation.

The combination of uncertainty in the velocity model and strong contrasts associated with salt and carbonates make it challenging for FWI to converge when classic objective functions are used. Together with the acquisition geometry limitations, we identified the challenges in the target area with input data comprising three neighbouring surveys with limited overlap. Two surveys were acquired with 4800 m streamers towed at 7-m depth with sources towed at 5-m depth. The third orthogonal survey was acquired with an 8000 m maximum offset, an 8-m cable depth and a 6-m source depth. A spatially variant high-resolution anisotropic model was built by combining common-image-point (CIP) tomography (Woodward et al., 2008) to refine the model prior to FWI, ETM-FWI (Vigh et al., 2020a; Kang et al., 2020) was used to update sediment, salt, and carbonate velocities simultaneously. CIP tomography was used again below salt. Integrating these technologies improved imaging of the key target, despite the limitations of the acquisition geometry of the legacy dataset. Additionally, ETM-FWI enabled use of the full record to provide greater depth of penetration, updating the model globally without differentiating specific lithologies and eliminating the need to carry out interpretation-based salt geometry scenario testing.

The signal processing included 3D multi-cable adaptive deghosting to attenuate source and receiver ghost effects and broaden the useable frequency content of the input data. This was preceded by noise attenuation and followed by multiple attenuation workflows.

## METHODS

The multistage velocity model building (VMB) workflow can be broken into three main stages: Initial model building, post-salt and salt VMB, and pre-salt VMB.

The legacy velocity model consisted of a series of individual tilted-transverse isotropic (TTI) models for each of the adjacent surveys. The legacy model building was driven mostly by multiscale CIP tomography with geologic constraints (Zdraveva et al., 2013) to update the post- and pre-salt sediment regions of the model. The salt structure was introduced by iterative sediment and salt flood scenarios to interpret surfaces

representing top and base of salt. The starting Vp model for the reimaging was obtained by merging these legacy models. To help remove the short scale length variations and the inconsistency of salt/sediment models between surveys, the salt velocities were removed before structurally smoothing the single sediment model. In parallel, anisotropy functions were derived using previous experience in the area (Zdraveva et al., 2011 and Shmelev et al., 2016) and available well data. Kirchhoff depth migration (KDM), forward modelling and 1D ray-tracing analysis were used throughout to validate the model building stages.

Input model to FWI: FWI convergence issues can occur when there is a large difference between the recorded and modelled seismic waveforms, therefore the quality of the starting model is crucial. To address this, the low-wavenumber velocity component was updated through two iterations of CIP tomography, focused on the post-salt section, with a priori geological information to constrain the shape of the model update. The resultant model was used to build the salt model; top salt was interpreted using the second tomography image, followed by a salt flood with a constant velocity of 4500 m/s driven by well data and finally the base salt was interpreted using the salt flood image. The smoothed legacy velocity was inserted below base salt honouring the depth change due to the changing overburden sediment and salt geometry. Once all zones were put together, a smoothing was applied to remove the salt boundary to allow ETM-FWI updates to refine the salt geometry.

Post salt and salt model building: ETM-FWI with automatic decision making (Halliday et al., 2022) was used to update the entire velocity field simultaneously, avoiding 'locked in' errors associated with a layer-by-layer top-down approach. The approach depends on matching the local patterns between the recorded and modelled full shot record, decomposing the wavefield into its directionality (dip), phase, and frequency. It then classifies events according to criteria for adjustive FWI (Jiao et al., 2015) and least-squares FWI, providing additional measures to determine which objective function to use without manual intervention. This occurs for each iteration, and output quality control (QC) maps indicate the model update direction. Utilising ETM-FWI with automatic decision making ensures robust matching (Figure 2), even in the presence of strong velocity contrasts.

## RESULTS

The results demonstrated that this workflow was able to resolve velocity heterogeneity (Figure 3) by simultaneously updating the sediment, salt, and carbonate layers.

Figure 4 shows the uplift observed in the new seismic image compared to the legacy image. The image using the new model shows significant uplift around salt flanks and base-salt allowing for better understanding the syn-rift system located pre-salt and resulting in increased confidence.

With the acquisition limitations of narrow azimuth and relatively short offsets it was critical to build a robust low-frequency model, this was achieved using CIP reflection tomography on top of a conditioned legacy model, and salt model building via interpretation and insertion. This was followed by ETM-FWI with automated decision making to refine the entire model from post-salt, salt and the immediate pre-salt. This method determines which events require a travel-time-based objective function and which are within a suitable tolerance for a least-squares objective function without manual intervention. Repeating the reclassification for each iteration ensures that the model rapidly and robustly converges even in the presence of strong velocity contrasts. This method was able to alter the shape and velocity of the salt body whilst inserting shallow low velocity zones in the overburden.

Born Modelling Reflection FWI (RFWI) (Sun et al., 2018) was used to update the deeper pre-salt section where both the model accuracy and data signal-to-noise ratio deteriorated. The RFWI was used initially as an indicator of update direction, and combined with pre-salt scaling to accelerate convergence, before refining with further iterations of RFWI. The last step of the velocity model build was to apply an iteration of reverse-time migration surface offset gather (RTM SOG) tomography which was greatly assisted by the bulk corrections made by the RFWI.

## CONCLUSION

We demonstrated a successful application of a velocity model building workflow employing ETM-FWI to use the full shot record to update post-salt and salt velocities simultaneously, using an offset-limited, narrow-azimuth legacy dataset. This approach has accurately determined the contrasting carbonate and anhydrite layers surrounding the salt, simplifying and improving continuity and focusing of the base of salt and pre-salt reflectors.

Geological uncertainty was reduced via a combination of modern signal processing and velocity model building techniques. The offset and azimuth limitations of the heritage data were largely overcome by initially creating a robust low-frequency model with reflection tomography and then refining it with ETM-FWI. The deeper pre-salt low frequency model was further updated with RFWI and RTM SOG tomography, leading to a significant imaging uplift.

ETM-FWI with automated decision making was able to capture high-resolution velocity features in the overburden and adjust the salt shape and velocity, while Born modelling RFWI combined with RTM SOG Tomography was able to make effective updates in the pre-salt. The majority of data offshore Angola is narrow-azimuth streamer of a similar maximum offset and vintage. These results demonstrate that renewed value can be gained through modern techniques and lead to improved understanding of the pre-salt geology in the region.

**ACKNOWLEDGEMENTS**

We thank SLB multiclient and Agência Nacional de Petróleo, Gás e Biocombustíveis (ANPG) for permission to present the results. We also thank Olga Zdraveva, Suganda Tewari, Claire Field, and Shipra Mahat.

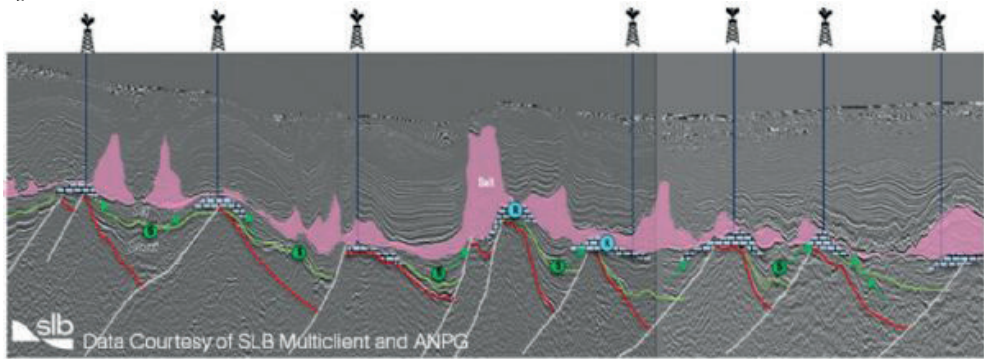
88th Annual International Meeting, SEG, Expanded Abstracts, 1283-1287.

Keywords: FWI, Reprocessing

**REFERENCES**

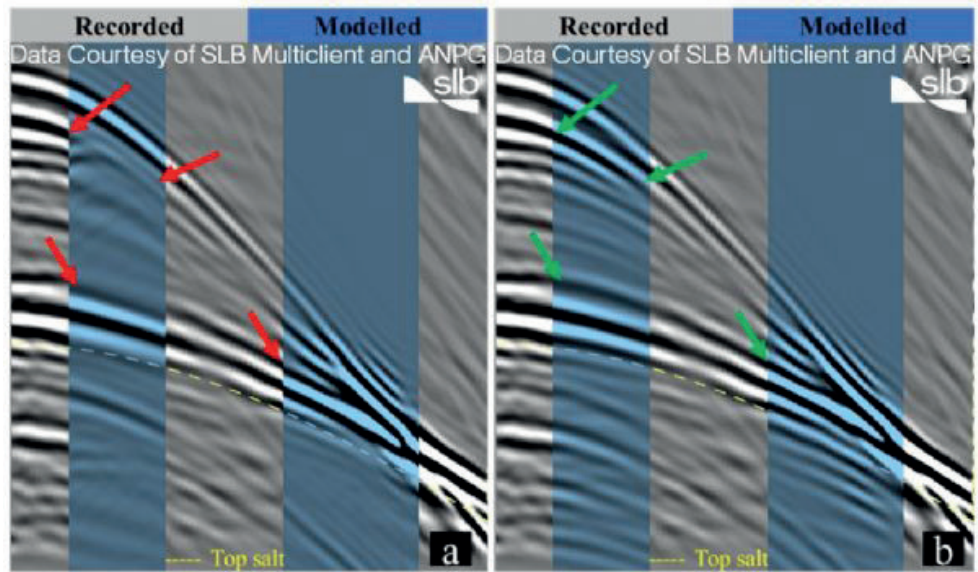
- Kang, W., Brand, N., Cheng, X., Vigh, D., Seymour, N. and Ishak, M., 2021, October. Reliability, Efficiency, and Robustness: Enhanced Template-Matching Full-Waveform Inversion Using Sparse Ocean-Bottom Node Data. In 82nd EAGE Annual Conference & Exhibition (Vol. 2021, No. 1, pp. 1-5). European Association of Geoscientists & Engineers.
- Shmelev, A.A., Cooke, A., Zdraveva, O. and Penwarden, J. [2016] High Resolution Model Building and Broadband Imaging in Deep Water Offshore Angola. 78th EAGE Annual Conference and Exhibition, Volume 2016, 1-5.
- Branston, M., Chapelle, M., Rathee, D., Ramsumair, R., Thompson, J., & Campbell, R. [2022] What is the Right Level of Acquisition Effort to Enable Successful, Cost-Effective Exploration? 83rd EAGE Annual Conference & Exhibition, Vol. 2022, 1-5.
- Woodward, M.J., Nichols, D., Zdraveva, O., Whitfield, P. and Johns, T. [2008] A decade of tomography. *Geophysics*, 73, no. 5, VE5-VE11.
- Vigh, D., Cheng, X. and Kang, W. [2020a] Full Waveform Inversion with OBN data collection via Mad Dog examples. 90th Annual International Meeting, SEG, Post-convention workshop.
- Kang, W., Reisdorf, A., Madden, S., Robertson, V., Chen, D., Chen, Z., Xu, J., Cheng, X. and Vigh, D. [2020] Salt Reshaping with Template-Matching Full-Waveform Inversion. 82nd EAGE Annual Conference & Exhibition Workshop Programme, Volume 2020, 1 – 5.
- Zdraveva, O., Hydal, S. and Woodward, M. [2013] Tomography with geological constraints: An alternative solution for resolving carbonates. 83rd Annual International Meeting, SEG, Expanded Abstracts, 4770-4774.
- Zdraveva, O., Woodward, M., Nichols, D. and Osypov, K. [2011] Building Anisotropic Models for Depth Imaging: Comparing different approaches. 12th International Congress of the Brazilian Geophysical Society, Extended Abstracts.
- Halliday, D., Bloor, R., Cheng, X. and Elbadry, M. [2022] Automated Decision Making for Full-Waveform Inversion. 83rd EAGE Annual Conference & Exhibition, Vol. 2022, 1-5).
- Jiao, K., Sun, D., Cheng, X. and Vigh, D. [2015] Adjustive full waveform inversion. 85th Annual International Meeting, SEG, Expanded Abstracts, 1091-1095.
- Sun, D., K. Jiao, X. Cheng, and D. Vigh, 2018, Keys to robust reflection based full waveform inversion:

Figure 1



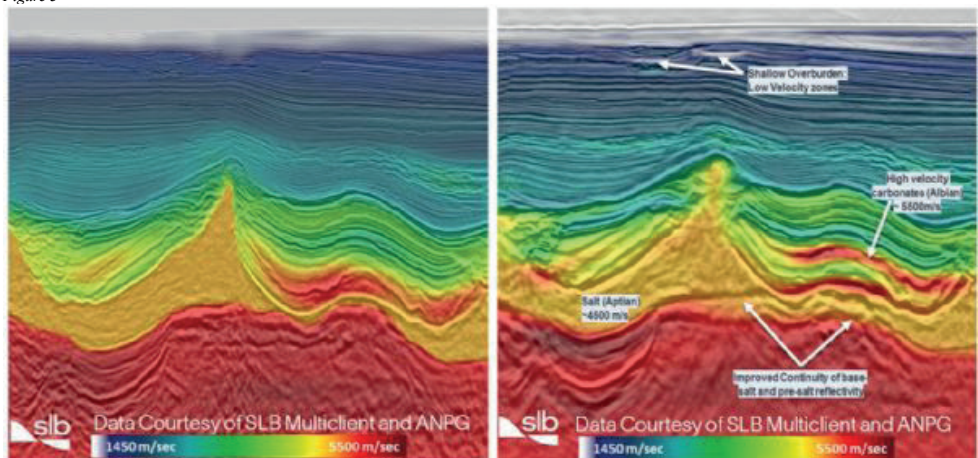
Pre-salt play section through deep water, Kwanza basin

Figure 2



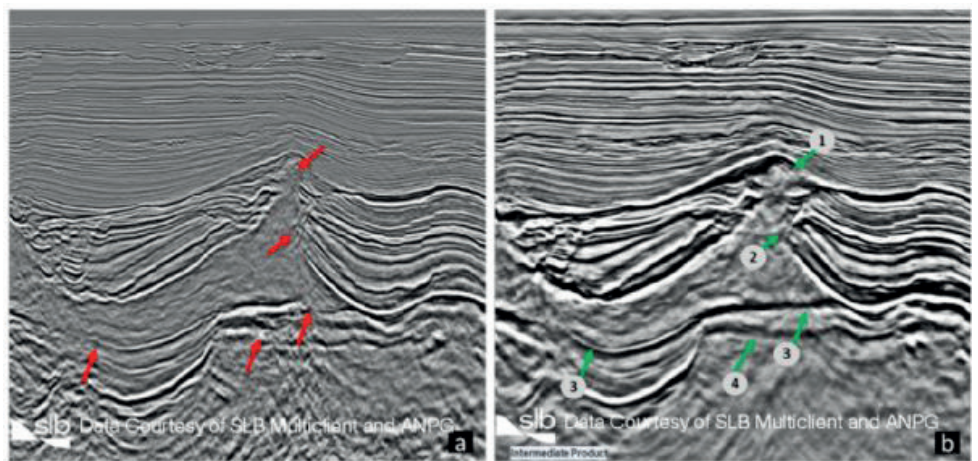
Interleaved shot QC. (a) Raw shots interleaved with modelled shots (blue shaded) using input model to FWI. (b) (c) Interleaved shot QC after ETM-FWI.

Figure 3



Legacy velocity model overlaid on the legacy KDM image (left) versus new velocity model overlaid on the new reprocessed KDM image (right). The salt shape and internal velocity has been altered as well as the shallow imaging benefiting from the insertion of low-velocity zones.

Figure 4



(a) legacy KDM image using legacy velocity model, and (b) reprocessed KDM image with the new velocity model. The green arrows on image (b) show improved definition of salt geometry (arrows 1 and 2), clear base salt reflector (arrows 3 and 4) and improved imaging of the pre salt reservoir section (arrow 4); compared to areas indicated by the red arrows on image (a).



# Dual-Source and Hexa-Source Time-Lapse OBC Acquisition And Imaging for the Edvard Grieg Field



**Richard Ford<sup>1</sup>, Francesca Twynam<sup>1</sup>, Alice Ramsden<sup>1</sup>, Taylor Leitch<sup>1</sup>, Michael Hooke<sup>1</sup>, Per Eivind Dhelie<sup>2</sup>, Vidar Danielsen<sup>2</sup>, Arnstein Kvilhaug<sup>2</sup>**

<sup>1</sup>slb, Crawley / UK

<sup>2</sup>Akerbp, Oslo / Norway

## INTRODUCTION

Optimising acquisition strategies has become increasingly important for operators to facilitate commercially viable reservoir monitoring 4D campaigns over maturing fields in the North Sea. Lundin Energy, (now Aker BP) have acquired four highly repeatable, inline geometry, ocean-bottom cable (OBC) surveys over the Edvard Grieg field with the same Q-Seabed recording equipment (receiver spacing 200 x 25 m) and source configuration every two years since 2016. In 2022, an additional hexa-source field test was acquired after the conventional dual-source production was complete, repeating a 1.8 by 8 km area, with 12 sail lines spaced 150 m apart and towing six source arrays. This patch test reduced acquisition time by more than 66% whilst also providing a denser shot carpet of 25 x 25 m compared to the conventional 50 x 25 m layout. This six-source gun array used a smaller gun volume (720 cu. inch versus 3147 cu. inch) and was towed at a shallower depth, 5 m compared to 8 m. To accommodate this higher shooting rate, the shot interval was reduced from the 4.5 seconds to 1.7 seconds. This resulted in the next shot energy sitting directly over the target reservoir zone. The objective of this hexa-source field test was twofold; firstly, to produce a reliable 4D difference (monitor minus baseline), replacing the conventionally acquired dual-source data with the hexa-source test patch to assess the 4D quality between the 2 source configurations, and secondly to optimise the processing workflow to produce a high-fidelity 3D image to evaluate the data quality of a hexa-source dataset.

## METHODS

### Hexa-source field test configuration; the benefits and challenges for 4D repeatability

In addition to the increase in operational efficiency and reduction in survey duration, bringing significant cost reduction, using a smaller source volume presents several additional operational, environmental and data quality benefits. The reduction in gun areal footprint, from 32 to 4-gun positions per array, provides a source which is closer to a point source and therefore there is less gun averaging for the input energy pulse. Controlled shot dithering was introduced and optimised for this field test to add a randomisation to each consequent shot firing time. The dither time was specified to be a minimum of +/-250 ms for this test, however the actual shot time variation ranged from 1.7 to 2.5 seconds providing a good spacing of each interfering shot and a truly random next shot distribution within the receiver domain. (See Figure 1) By decreasing the gun firing

interval and distance between adjacent shot lines, the hexa-source configuration allowed for a denser source geometry, doubling the spatial sampling, increasing fold, and therefore naturally improving the signal-to-noise ratio. Reducing the air gun pressure and utilising a quieter source also presents the opportunity to reduce the environmental impact of the survey.

However, with a quieter source also comes lower power and a lower peak-to-bubble ratio commonly considered a key metric for good high-quality source injection. Inadequate removal or different treatment of this bubble pulse energy between the two configurations posed a significant risk with the potential to significantly diverge the low-frequency component of the 4D signal present. The final factor to consider using a lower source volume is the reduction in penetration, particularly for the low frequencies. This was later modelled using finite-difference modelling to understand the impact. The change in source tow depth also has negative 4D implications by modifying the output spectra and moving the source ghost notch position and arrival time of the multiple energy. All of these source wavelet modification factors were closely evaluated and compensated in the co-processing of the conventional dual-source 2016 baseline versus the two 2022 monitor surveys.

### Pre-processing and imaging 3D/4D workflow

This hexa-source test provided a real field example dataset to demonstrate the effectiveness and 4D friendly nature of the iterative source separation with priors (ISSP) deblending method. The “true” reference for signal underneath the contaminating next shot energy was available from the conventional dual source dataset. The ISSP process applied was outlined by Kumar, R et al. (2021) and can be summarized as a generic data-driven iterative process that involves applying a coherency filter to the input data to estimate the signal. It hence assumes that most coherent energy in the data is signal. From this estimated signal an estimation of the coherent (interference) noise is made. By subtracting the estimated signal and noise from the input data we obtain a residual. Adding this residual to the estimated signal provides the input to the next iteration of the coherency filter. In the next pass, where the input is expected to contain less (interference) noise, we can lower the coherency threshold to obtain a better estimate of the signal. The subsequent next shot and prior shot noise was effectively removed from all four components without damaging primary signal amplitudes, see Figure 2.

Following the deblending application both conventional dual-source and hexa-source datasets were co-processed

through the verified 4D production sequence. This included source harmonisation with the application of calibrated marine source (CMS) to their individual far field signature target wavelets to remove shot-to-shot signature variability. A noise attenuation sequence was then designed to remove seismic interference energy, anomalous high-amplitude spikes and shear noise from the Z component.

Up/down deconvolution was applied to remove all free surface multiples, source/receiver side ghosts, water column effects and source signature. (Amundsen et al., 2001, Ford et al., 2019). In this 4D application a common target wavelet was input for both acquisition geometries to perform an initial source signature matching and both surveys were output to the same 50 x 25 m acquisition grid for further processing. In contrast for the 3D optimised volume the original dense source density (25 x 25 m) was preserved.

After selection of the equivalent spatial extents from the dual-source and hexa-source data for the 2016 baseline dataset and the 2022 monitor datasets, RTMs were run up to a maximum frequency of 50 Hz for the 4D volumes. Post migration, a frequency-variant global matching was applied to match the two 2022 monitors to the 2016 baseline and account for amplitude, phase, and timing differences. Following this, a sequence of post-stack conditioning including residual demultiple, 4D co-denoise, inverse amplitude Q compensation and footprint attenuation were applied. Surface attribute extractions were generated around the key target horizon to compare the 4D response between the two monitor volumes. The 3D image was generated with an optimised Kirchhoff Depth Migration, adjusting the offset-vector tile dimensions to account for the denser acquisition geometry.

## RESULTS

### 4D results and finite difference source modelling

The sum-of-energy attribute extracted from the 4D differences shown in Figure 3 demonstrates that the main areas of 4D signal within the northern area of the field can be fully reproduced using the hexa-source monitor 2022 survey with similar amplitude strength relative to the 2016 dual-source baseline and very little additional noise at the target reservoir. Considering the difference of input source signature and different source acquisition datums, the level of residual overburden difference in the 4D shows a good repeatability with an average NRMS of <7% for the overburden and reservoir section, only 1-2% higher than the highly repeatable conventional dual-source 4D result.

Finite difference modelling scenario testing was used to better evaluate the impact of the alternate source configuration on the sub-chalk character of the signal without the impact of the multiple and noise. Using the separate gun far-field source signatures, gun depth, shot geometry and Vp and density property fields, the earth response was modelled. This exercise demonstrated that

the overburden and reservoir target showed a similar signal response, however, the responses deeper than 2.2 seconds began to diverge. This divergent response could also be observed as a stronger residual 4D difference along the basement surface (see Figure 3).

## 3D RESULT

The secondary objective of this field study was to verify the signal content and strength for the smaller volume point hexa-source configuration. The lack of residual amplitude differences within the target zone on the 4D proves that at this depth, relative signal strength has been preserved to create a comparable image. Within the shallow overburden section some uplift in amplitude strength and event resolution is observed above 90 Hz. (See Figure 4) The addition crossline shot density also improves overall signal-to-noise ratio through the power of stack. The sharper focusing of small-scale geological features such as glacial scours and shallow gas pockets demonstrate some small benefits of resolution with this operationally efficient, cost-effective hexa-source pattern.

## CONCLUSIONS

Despite the source configuration differences between the conventional dual-source and the hexa-source geometries and the significant next shot contamination within the target reservoir zone, a comparable 4D difference was successfully reproduced. The application of ISSP deblending to the hexa-source data, demonstrated an excellent signal preservation suitable for further 4D interpretation work. Shallow time slices <800 ms demonstrate a small uplift in high-frequency event construction utilising the denser shot sampling and closer to a point-source configuration. Even with the smaller source volume, penetration to the reservoir level at 1.9 km shows equivalent imaging. This hexa-source field test demonstration tested the limits of deblending against a perfect baseline dual-source result and therefore verifies this alternate source configuration and workflow for future 4D acquisitions.

## REFERENCES

- Amundsen, L., Ikelle, L. and Berg, L. (2001), Multidimensional signature deconvolution and free-surface multiple elimination of marine multicomponent ocean-bottom seismic data: *Geophysics*, 66, no. 5, 1594–1604.
- Ford, R., Twynam, F., Caprioli, C., Hooke, M., Whitebread, R., Kristiansen, P., Boiero, D., Dhelie, P.E., Danielsen, V. and Straith, K. R. (2019), Fast turnaround OBS time-lapse processing enabled by up down deconvolution: A North Sea case study: 89th Annual International Meeting, SEG, Expanded Abstracts, 5280–5284.
- Kumar, R., Amin, Y., Mahdad, A., Bilsby, P., Narayan, A., Brouwer, W. G., Misbah, A. and Vassallo, M. (2021). Effects of dimensionality of transform domain

on multiple stages source separation with prior: First International Meeting for Applied Geoscience & Energy, SEG Expanded Abstracts, 76-80.

**ACKNOWLEDGEMENTS**

The authors thank Aker BP and partners in PL338, OMV and Wintershall Dea, and SLB for permission to publish this work.

Keywords: 4D, deblending

Figure 1

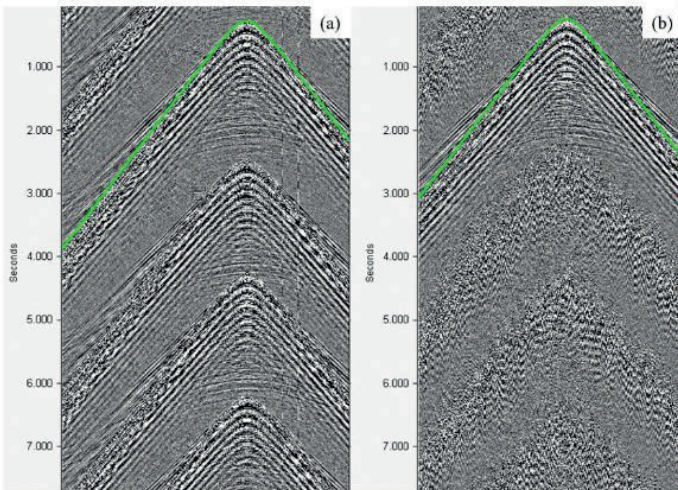


Figure 1 Raw shot (a) and receiver gather (b) demonstrating relative coherency of next shot energy repeating every 1.7 seconds in two domains. The green graph indicates the position of the direct arrival energy of the prime shot.

Figure 2

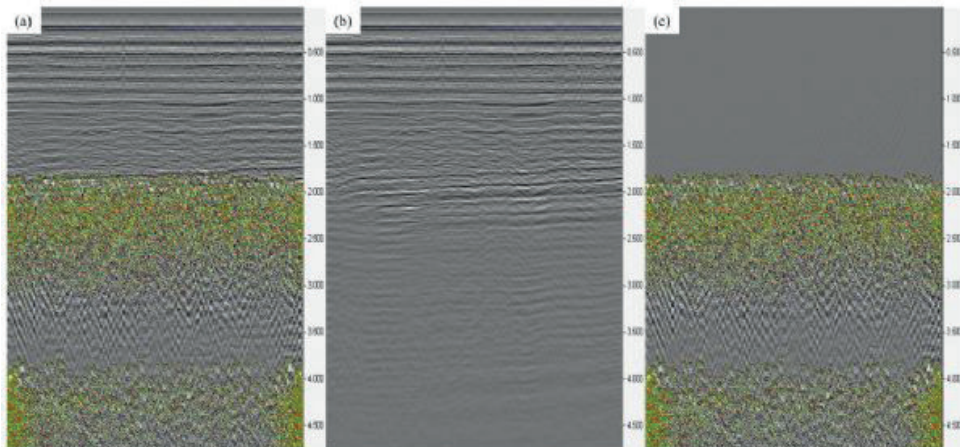


Figure 2 Pre-migration brute CMP stack of the P component before (a), after (b) and the difference (c) following the application of 3D ISSP. Note that the target reservoir interval for this field occurs at 1.9 seconds.

Figure 3

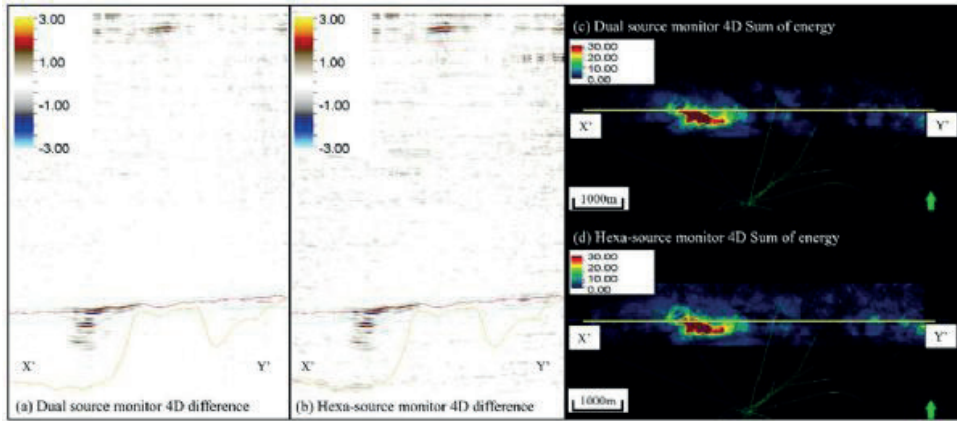


Figure 3 Comparison of 4D difference between the dual-source monitor (a) and hexa-source monitor (b) minus the dual source 2016 baseline vintage. To the right, the sum-of-energy attribute extraction from an 80-ms window around the target shows good repeatability of main 4D signal around injector well site between the dual source monitor (c) and the hexa-source monitor (d). Top reservoir and basement surface interpretation are shown.

# Sismik Yansıma Veri İşlemi İçin Geliştirilen Yeni Bir Yazılımın (ATA-SIS) Tanıtımı



**Alican Pekivi<sup>1</sup>, Hulya Kurt<sup>2</sup>**

<sup>1</sup>Istanbul Teknik Üniversitesi; Maden ve Tetkik Arama Genel Müdürlüğü, İstanbul / Türkiye

<sup>2</sup>Istanbul Teknik Üniversitesi, İstanbul / Türkiye

## ABSTRACT

Seismic exploration has had a significant impact on the discovery and production rates of oil and gas reserves. Developments in the software industry over the past 50 years and intensive use of workstations allows the seismic data processing stages to be implemented entirely on the digital platform. Many companies in the oil and gas industry have developed their own seismic data processing packages. These packages need powerful workstations and this situation restricts access to professional software. In this project, it is aimed to develop a software that performs basic seismic data processing steps. This software differs from professional software with its easy use and easy access. In addition, the software is suitable for both workstations and office computers. Java programming language is used to write the software, and this programming language was compiled using the Eclipse 2022. Open GL library is used for seismic graphics and sections. The software is prepared on Windows platform and tested on different versions of Microsoft Windows and Linux.

## 1. GİRİŞ

Petrol ve doğal gaz aramacılığında kullanılan jeofizik yöntemlerin başında gelen sismik yansıma yöntemi veri toplama, işleme ve yorumlama olmak üzere üç aşamada gerçekleştirilir. Veri toplamada, denizde ve karada kullanılan farklı ekipmanlar tarafından üretilen kaynak sinyalinin yer altında yoğunluğu ve hızı farklı olan jeolojik katmanlardan yansımaları ile elde edilen sinyallerin kaydedilmesi sağlanır. Kaydedilen bu sinyalin verinin taban altı görüntüsüne dönüştürülmesi ve yoruma hazır hale gelebilmesi için, bir takım matematiksel aşamalardan geçmesi gerekmektedir. Ardaşık olarak uygulanan bu matematiksel işlem aşamalarının bütününe sismik veri işlem adı verilir (Dondurur, 2009). Veri yorumlamada ise veri işlem sonucu elde edilmiş yer altı modelinin yapısal, stratigrafik ve litolojik olarak yorumlanması yapılır.

Dünyada son 50 yıl içindeki teknolojik gelişmeler sismik yansıma yöntemlerinin de gelişimine olanak tanımıştır. 1960'lı yıllarla birlikte sismik veri toplama yöntemleri gelişmiş, kanal sayısı artışı ve araştırma alanlarının genişlemesi ile daha çok verinin kaydedilmesi gereksinimini doğmuştur. Daha önce analog olarak toplanan veriler bu yıllardan itibaren sayısal olarak toplanmaya başlamıştır. Bu gelişmeler hesap makineleri yerine bilgisayar kullanımı ve verilerin bilgisayar ortamında kaydedilmesini zorunlu hale getirmiştir. 1970'li yıllarda tamamen bilgisayar sistemlerine geçilmiş, dekonvolüsyon, hız analizi, NMO (normal kayma) düzeltmesi gibi bazı veri işlem algoritmaları geliştirilmiştir (Yılmaz, 2001). 1980'li yıllarda

bilgisayar ortamında hazırlanan 3 boyutlu yer altı modelleri hidrokarbon rezerv boyutu hesaplamalarında önemli bir yer almıştır. Bu hesaplamalardan elde edilen sonuçlar üretim maliyetlerini düşürmüştür. Günümüzde ise sismik yöntemler ile yeraltı modellerinin derinlik ortamında oluşturulabilmesi sondaj kuyusu açmak gibi pahalı yöntemlere olan gereksinimi azaltmıştır. (Yılmaz, 2001) Yaşanan bu teknolojik gelişmeler petrol ve doğal gaz sektöründeki arama firmalarının kendi sismik veri işlem yazılımlarını geliştirmesi için teşvik edici olmuştur. Halliburton Landmark firmasının Promax, CGG firmasının Geovation, Paradigm Geophysical firmasının Echos yazılımları bu tarz sismik veri işlem yazılımlarına örnek olarak gösterilebilir.

## 2. AMAÇ

Petrol ve doğal gaz aramacılığı için geliştirilen profesyonel sismik veri işlem yazılımları büyük veri setleri ile işlem yapabilmek için güçlü iş istasyonlarına ve aynı zamanda bu konuda tecrübeli personeli ihtiyaç duymaktadır. Bu durum, sismik veri işlem üzerinde çalışmalar yapan kişilerin profesyonel yazılımlara erişimini kısıtlamaktadır. Geliştirilmesine bu çalışma ile başlanan ATA Sismik Veri İşlem Programının amacı ulaşılması ve kullanımı kolay bir sismik veri işlem programının eksikliğinin giderilmesidir. Program, Türkçe dil desteği vermesi, Windows ve Linux tabanlı ofis bilgisayarlarına uyumlu olması ile profesyonel yazılımlardan ayrılmaktadır. Programın kullanımı sırasında kullanıcıların girmesi gereken parametre sayısı minimum düzeyde tutulmuş ve program hakkında tecrübesi olmayan kullanıcıların da kolayca uyum sağlaması hedeflenmiştir.

## 3. PROGRAMIN YAPISI

Program Java Programlama dilinde yazılmış ve Eclipse 2022 programında derlenmiştir. Sismik izlerin çizimlerinde açık kaynak kodlu uygulama geliştirme arabirimi olan OpenGL kütüphanesinden faydalanılmıştır. Program hem Windows hem de Linux işletim sistemleri ile çalışacak şekilde hazırlanmış, farklı Windows ve Linux sürümlerinde test edilmiş ve testleri geçmiştir.

Program, sismik ham veri yükleme işleminden migrasyon işlemine kadar birçok temel sismik veri işlem yöntemini gerçekleştirmektedir. Her veri işlem adımının altı harften oluşan kısa bir kodu vardır. Kullanıcı öncelikle hangi sırada ve hangi veri işlem yöntemini uygulayacağını belirleyerek akış şemasını oluşturur ve ilişkili parametreler girildikten sonra iş dosyası başlatılır. Program her veri işlem aşamasını sırayla uygular ve her aşamadan sonra elde edilen çıktı bir sonraki veri işlem aşamasının girdisi olarak

kullanılır. Programın işlem yapma süresi veri boyuna olduğu kadar girilen parametrelere de bağlıdır. Zira veri işleminde gerçekleştirilen hesaplamalara göre farklı işleme zamanı gerekmektedir.

### 3.1. Veri Tabanı ve Sınıflandırma

Program, kurulum esnasında SISMİK isimli bir klasör açar. Oluşturulan projeler kullanıcı isimleri ile bu klasörün altında yer alır. Proje klasörlerinin altında isimleri sırasıyla DATA, FORMAT, JOBS, LISTS, MONITOR, SCREENSHOTS ve TABLES olan yedi alt klasör yer alır. Bunlardan DATA sismik verilerin kaydedildiği klasördür ve genlik, başlık bilgileri ve veriye ait genel bilgileri içeren 3 adet dosya içerir. FORMAT projede kullanılan başlık bilgileri, SEG D ve SEG Y dosya formatlarının tanımlandığı dosyaların saklandığı; JOBS iş dosyalarının kaydedildiği; LISTS tamamlanan işlere ait log dosyalarının tutulduğu; MONITOR iş dosyalarının çalışması sırasında girdi ve çıktı verilerinin geçici olarak kaydedildiği; SCREENSHOTS alınan ekran görüntülerinin kaydedildiği ve TABLES ise sismik veri haricinde elde edilen bütün verilerin kayıt altında tutulduğu klasörlerdir.

### 3.2. Veri İşlem Aşamaları ve İş Dosyası Oluşturma

Programda geliştirilen veri işlem aşamaları halihazırda 29 modülü içeren 11 ana başlık altında toplanmıştır (Şekil 1). Programda ayrıca hız analizi, güdültülü kanalların sisteme tanıtılması, FK süzgeçlemesi için poligon oluşturulması gibi işlemlerin gerçekleştirilmesinde kullanılan yardımcı modüller de mevcuttur.

Şekil 1. Program üzerinden uygulanabilecek temel veri işlem aşamaları.

Kullanılacak veri işlem adımlarının ve parametre değerlerinin seçimi dört ana sütuna ayrılan "İş Dosyası Oluşturma" ekranında belirlenir. Şekil 2'de taslak olarak verilen bu ekranın en soldaki (a) kısmında hangi veri işlem adımının seçildiği ve bunların dizilimi, (b)'de seçilen veri işlem adımında girilecek parametreler, (c)'de iş dosyasının ve yerleştirileceği klasörün adı (d)'de ise seçim yapılacak mevcut veri işlem modülleri yer alır. Programda ayrıca sismik verilerin görüntülenmesi amacıyla oluşturulan bir alt programda veri işlem çıktılarının görüntülenmesi, odaklanarak büyütülmesi, küçültülmesi, genlik ayarlaması yapılması mümkündür. Sismik verilerin genlik ve frekans-dalga sayısı spekturumu gibi işlemlerinin görüntülenmesi de yine aynı alt programla sağlanabilmektedir.

Şekil 2. İş Dosyası Hazırlama ekranı taslak görüntüsü.

## 4. YÖNTEM VE GEREÇLER

Bu kısımda programın halihazırda mevcut 11 veri işlem adımı ve bu adımlara bağlı modüllerin kısaca tanıtımı yapılacaktır. Program çok kanallı sismik yansımaya verilerinin atış ortamından yığma sonrası zaman migrasyonu işlemlerine kadar temel veri işlem adımlarını içermekle birlikte bugünlerde geliştirilmesi halen devam etmektedir.

### 4.1. Sismik Veri ve Programa Yüklenmesi

Arazide toplanan sismik veri, Society of Exploration Geophysicists (SEG) derneği tarafından tanımlanan formatlarda binary olarak kaydedilir. Veri yükleme işlemi bu özel formattaki verilerin okunması ve programın dahili formatına çevrilmesi işlemidir. Programın SEGYIN ve SEG DİN modülleri SEG tarafından standart olarak kabul edilen SEGY ve SEG D formatlarındaki verilerin programa yüklenmesini sağlar. SEGY veri seti, metin formatında başlık bilgileri, binary formatında başlık bilgileri ve kanal bloğu olmak üzere 3 ana başlığa ayrılabilir. Başlık bloğu, ASCII formatında olup 40 satır, 80 sütundan oluşur ve 3200 byte yer kaplar (Norris ve Faichney, 2002). Binary başlık bloğu 400 byte uzunluğunda olup veriye ait genel bilgileri içermektedir. Kanal Bloğu, kanala ait bilgileri taşıyan blok ve genlik değerlerinin olduğu blok olarak iki parçaya ayrılır. SEG D formatı genel başlık blokları, kanal setleri, kanal bilgileri ve kanal genlik değerlerinden oluşur. Genel başlık blokları veriye ait genel bilgileri içerir. Kanal setleri, belirli kanallara ait bilgilerin yer aldığı bloklardır. Kanal bilgileri ve kanal genlik değerleri ise her kanalın kendine özgü bilgilerini taşımaktadır.

### 4.2. Veri Yönetimi

Sismik verilerin boyu, örnekleme aralığı, başlık bilgileri ile ilgili yenilenmeleri, bozuk olanlarının veriden çıkarılması gibi işlemler bu kısımda yer alır. Kayıt uzunluğunun hedef derinlik göz önüne alınarak yeniden belirlenmesinde LENGTH modülü; veri toplama sırasında bazı alıcılarda oluşan ve gerçek yansımaları bastıran gürültülerin veriden silinmesi amacıyla kullanılan TREDIT modülü kullanılmaktadır. Başlık bilgilerinin kullanılarak verinin istenilen kısmının seçilmesinde SELECT; her iz için ayrı uygulanan ve istenilen başlık değerinin, referans başlık değeri baz alınarak matematiksel olarak değiştirilmesinde HDRMAT modülü kullanılır. Belirli veri işlem aşamalarından daha iyi sonuç alabilmek için daha çok atış gruplarında olmak üzere veri setinde bir gruba ait sismik izlerin yerinin değiştirilmesinde REVERS modülü geliştirilmiştir. Veri işlem tamamlandığında aynı modül tekrar kullanılarak veri grupları eski haline getirilir. Gürültü bastırma bazı veri işlem aşamalarında sismik veri gruplarının ilk ve son kanallarında meydana gelen gürültülerden kaçınmak amacıyla veri grubunun başına ve sonuna sentetik kanallar eklenmiştir. Böylece veri işleminin gürültü oluşturan etkilerinin bu sentetik kanallar üzerinde kalması sağlayan TRADRM modülü geliştirilmiştir. Aynı modül ile sentetik kanallar geri kaldırılmaktadır. Son olarak CHANGE modülü ile istenilen başlık bilgilerinin başka bir başlık bilgisi referans alınarak değiştirilmesi işlemi gerçekleştirilir.

### 4.3. Geometri Tanımlama

Atış-alıcı koordinat bilgilerinin tanımlandığı kısımdır. İki boyutlu deniz sismik verilerinin teorik geometrik tanımlanmasının yapıldığı GEOM2D modülünde yakın ofset, toplam kanal sayısı, atış ve alıcı aralığı, ilk son atış numarası ve kaçan atış bilgilerinin sisteme

girilmisasağlanır. Modül her kanala ait atış numarası, uzaklık ve CDP (Common Depth Point/Ortak Yansıma Noktası) numarası gibi bazı başlıklar girilen verilere göre hesaplayarak güncelleme gerçekleştirir. Bir diğer modül olan NEMERGE modülünde P190 navigasyon dosyası kullanılarak her kanala ait atış numarası, kaynak alıcı uzaklığı, atış alıcı ve CDP koordinat bilgileri, alıcı derinliği gibi bazı başlıklar güncellenir. Bilindiği gibi P190, deniz sismisinde hazırlanan standart navigasyon dosyasının uzantısına verilen isimdir ve dosyada atış ve alıcıların koordinat ve derinlik bilgileri mevcuttur.

#### 4.4. Genlik Kazanımı

Ara yüzey düzensizlikleri, saçılma, soğurulma ve tekrarlı yansımalar gibi birçok etken kaynak sinyalinin genliğini etkilemektedir. Sinyaldeki genlik kaybının veriyeye tekrar kazandırılması için belirli matematiksel işlemlerden faydalanılır. Genlik kazanç kavramı, zamanla değişen ölçekleme yöntemidir (Yılmaz, 2001). TPOWER modülü zamana bağlı genlik düzenlemesi işlemini gerçekleştirir. Atış alıcı arasındaki mesafe (x), zaman (t) ile verilirse zamana bağlı genlik düzenlemes denklem 4.1(4.1)

şeklinde gösterilebilir. Burada  $S(x,t)$  genlik değerini, p kullanıcı tarafından belirlenen katsayıyı, t ise zamanı ms cinsinden temsil eder. Katsayı değeri ne kadar büyük seçilirse geç varışlardaki genlik değerleri o kadar artacaktır. Değişik uygulamalarda bu değer genel olarak 2 ve civarında seçilir (Claerbout, 1985). En sık kullanılan genlik düzenleme yöntemlerinden bir diğeri olan otomatik genlik kazancı AGCSIS modülü kullanılarak gerçekleştirilir. Yöntemin esası belirli bir pencere içindeki genlik değerlerini kullanarak ortalama değer hesaplamaya dayanır.

denklem 4.2(4.2)

Denklem 4.2'de N pencere boyu ve rms değerleri kullanıcı tarafından belirlenir.

#### 4.5. Sinyal İşleme

Bu kısımda ağırlıklı olarak kullanılan süzgeçleme işlemleri ile verinin genlik spektrumunda değişiklik yapılarak gürültünün veriden atılması sağlanır. Bu amaçla kullanılan FILTER modülünde belirlenen 4 köşe frekans değerine bağlı olarak oluşturulan süzgeç penceresi ile veride bant geçişli süzgeçleme işlemi uygulanır. Bu modülde kullanıcının seçimine bağlı olarak frekans veya zaman ortamında süzgeçleme yapılabilir. Modülde ayrıca pencere türü ve operatör uzunluğu gibi parametreler de opsiyonel olarak kullanılabilir. Bir diğer modül olan BUTTER'da diğerlerine göre daha geniş geçiş bölgesine sahip ve pencere fonksiyonu Denklem 4.3'de verilen Butterworth bant geçişli süzgeçlemesi uygulanır.

denklem 4.3 (4.3)

Denklemde FA alçak geçiren, FB yüksek geçiren frekans değerlerini, N alçak geçiren M ise yüksek geçiren filtrenin mertebesini ifade eder. Kullanıcı bu 4 değeri sisteme girerek süzgeçleme penceresini tasarlar. Verinin

frekans dalga sayısı ortamında süzgeçlenmesine olanak tanıyan FKFLTR modülünde giriş verisi önce zaman sonra uzaklığa bağlı Fourier dönüşümü alınarak frekans dalga sayısı ortamına geçilir. Oluşturulan F-K panelinde verinin atılacağı veya tutulacağı alan belirlenerek bir poligon oluşturulur. Kullanıcının seçimine göre poligonun içinde veya dışında kalan kısım sıfırlanır. Ters Fourier Dönüşümü işlemi iki kez tekrar edilir ve zaman uzaklık ortamına dönüş sağlanır. FKFANF modülünde frekans dalga sayısı ortamında süzgeçleme işlemi yapılmakla beraber klasik yöntemden farklı olarak kullanıcı süzgeçleme yapılacak frekans aralığını ve sismik hızı sisteme kendisi tanıtır. Bu parametrelere ait bir süzgeç poligonu program tarafından otomatik olarak tasarlanır ve veriyeye uygulanır. Bu kısımda olan diğer modüllerden RESAMP verinin örnekleme aralığını değiştirebilme imkanı verirken MUTETX ise verinin istenmeyen alanlarının atılması amacıyla kullanılır.

#### 4.6. Sıralama

Veri toplama işlemi sırasında ham veri atış ve alıcı grupları halinde sisteme sırayla kaydedilir, ancak bazı veri işlem aşamalarını uygulayabilmek için verinin farklı şekillerde sıralanması gerekmektedir. HDRSRT modülü kullanıcının belirlediği başlıklara göre verinin sıralanmasını sağlamaktadır. Sıralama yapan bir diğer modül olan CDPSTR hız analizi ve yığıma işlemleri için sismik verinin CDP ve kaynak alıcı uzaklığına göre sıralanmasını sağlar. Bu modül diğer sıralama modüllerden farklı olarak herhangi bir parametreye ihtiyaç duymaz ve veriyeye CDP ve kaynak alıcı uzaklığına göre otomatik olarak sıralar ve hız analizine hazır hale getirir.

#### 4.7. Hız Analizi ve Normal Kayma (Normal Move-Out, NMO) Düzeltmesi

Hız analizi, kaynak alıcı arasındaki mesafeden ötürü aynı noktadan yansıyan verinin farklı varış zamanlarında alıcılara ulaşmasını temel alarak tabaka hızlarının belirlenmesi işlemidir. Kaynaktan çıkan dalgacığın yansıma yüzeyinden alıcıya ulaşma zamanı  $t(x)$ , Denklem 4.4'de verilmiştir. Buna göre;

denklem 4.4 (4.4)

x kaynak ile alıcı arasındaki mesafeyi, V RMS hızını,  $t(0)$  ise başlangıç zamanını temsil etmektedir.

CDP gruplarına uygulanan normal kayma(NMO) düzeltmesi, sismik verilere uygulanan en önemli rutin süreçlerden biridir ve yığıma işlemi başta olmak üzere birçok veri işlem aşamasının öncesinde gerçekleştirilmesi gereklidir. Normal kayma (NMO) düzeltmesinin temel amacı, kaynak ile alıcı arasındaki mesafeden ötürü oluşan bu zaman farkını ortadan kaldırarak yansıma paketini yatay hale getirmektir. Bu amaçla hazırlanan VELNMO modülünde sismik veri gruplarına sabit hızla NMO uygulaması sağlanır. Kullanıcı hız bilgisini m/s cinsinden sisteme tanıtır. NMOCOR modülünde ise kullanıcının semblans haritası üzerinden işaretlediği hız ve düşey çift-yol alış zaman değerleri kullanılarak NMO düzeltmesi uygulanmaktadır.

#### 4.8. Yığma

Yığma modülüolan TSTACK sismik veri gruplarının toplanması ve bir iz haline getirilmesini sağlar. Bu işlem genelde NMO düzeltmesi uygulanmış CDP verilerinin toplanarak sinyal gürlütlü oranının artırılması için kullanılmaktadır. Yapılan bu işlem sonrasında toplanan sismik izler yanyana getirilerek yığma (stack) olarak adlandırılan ve yer altı modelini yansıtan sismik kesit elde edilir.

#### 4.9. Migrasyon

Sismik migrasyon, kesitteki eğimli yansımaları gerçek yerlerine taşıyan ve saçılma enerjisini yok eden dalga denklemi kuramlı bir işlemdir. Bu amaçla oluşturulan MIGTIM modülünde sismik hız değerleri ve apertur genişliği bilgileri kullanılarak yığma sonrası Kirchoff Migrasyonu uygulanır.

### 5. BULGULAR

Bu kısımda gerçek sismik veriler kullanılarak programın bazı veri işlem yöntemleri ve modüllerinin kullanımına yönelik görsel örnekler sunulacaktır. Bu görsel örneklerin hazırlanmasında Marine Geoscience Data System veritabanından akademik çalışmalarda kullanılmak üzere elde edilen veriler kullanılmaktadır.

#### 5.1. Veri Seçilmesi

Program üzerinden ‘Veri Yönetimi’ başlığı altında bulunan modüller aracılığı ile sismik verinin başlık bilgileri güncellenebilir ve istenilen veriler seçilebilir. 2B sismik SEG D yansıma verileri okutulmuş ve sadece ilk kanallardaki izler seçilerek tek kanallı sismik yansıma kesiti elde edilmiştir (Şekil 3).

#### 5.2 Süzgeç Uygulaması

600 kanallı ham sismik atış verisine Butterworth süzgeç uygulanmış ve sonuçlar karşılaştırılmıştır(Şekil 4). Veriyi düşük frekanslı gürlütlülerden arındırmak için süzgeç penceresinin alçak frekans sınır değeri 8 Hz olarak belirlenmiştir. Sonuç incelendiğinde düşük frekanslı gürlütlülerin atıldığı ve yansıma hiperbollerinde neredeyse hiç kayıp yaşanmadığı görülmüştür (Şekil 4a). Verinin genlik spektrumunu incelendiğinde düşük frekanslı değerlerin baskın olduğu ve diğer frekans değerlerini maskeleyiği görülmektedir. Süzgeçleme sonrası ise düşük frekanslı değerler parametrelere uygun olarak baskılanmış ve yüksek frekanslı değerler belirgin olarak ortaya çıkmıştır.

Şekil 3. Her atışın ilk kanalındaki izlerini seçerek oluşturulan tek kanallı sismik yansıma kesit

Şekil 4. Sismik atış verisinin (a) Süzgeçleme işlemi öncesi(b) sonrasındaki gösterimi. (c) Süzgeç uygulamadan ve uygulamadan sonraki iki veri arasındaki fark. (d) Süzgeçleme işlemi öncesi (e) sonrası genlik spektrumlarının gösterimi.

#### 5.3. Genlik Kazanımı

Genlik kazanımı için yapılan örnek çalışmada denklem 4.1 kullanılmıştır ve p değeri 1.4 ve 2.4 olarak seçilerek işlem yapılmıştır. Şekil 5’de verilen genlik kazanımı sonuçları incelendiğinde p değerinin artmasıyla sığ kesimdeki genlik değerlerinin azaldığı ve geç varışların genlik değerlerinin daha çok güçlendiği gözlenmektedir.

#### 5.4. Mute (İstenmeyen Alanların Atılması) İşlemi

Sismik verilerde birincil yansımalar dışında kalan direkt ve kırılma varışlarını veriden atmak amacıyla mute uygulaması MUTETX modülü yardımıyla gerçekleştirilmiştir. Kullanıcı bu işlemi yapabilmek için Picker isimli interaktif modülü kullanarak sismik veri üzerinde işaretlemeler yapar ve gürlütlü alanları belirler (Şekil 6).Bu işaretlemeler belirli aralıklarla yapılabilir ve veri işlem esnasında interpolasyon yöntemi ile verinin tamamına uygulanır.

Şekil 5. (a) Genlik düzeltmesi öncesi (b) P= 1.4 için genlik düzeltmesi (c) P=2 için genlik düzeltmesi

Şekil 6. (a) Mute yapılacak sismik atış verisi (b) Verinin muteişlemiuygulanmış hali.

#### 5.5. FK Süzgeçleme İşlemi

Bu süzgeçleme işleminde FKFLTR modülüçalıştırılmış ve veri frekans dalga sayısı ortamına aktarılmıştır (Şekil 7). Oluşturulan panelde veriden atılacak veya tutulacak alanlar sırasıyla belirlenen poligonun içerisinde ve dışarısında kalan kesimler olarak belirlenmiştir.

Şekil 7. (a) FK süzgeçleme öncesi,(b) sonrası ve ve(c) iki veri arasındaki fark (db) FK süzgeçleme için poligon oluşturulması (ec) Süzgeçleme sonrası verinin FK spektrumunu.

#### 5.6. Hız Analizi ve NMO Düzeltmesi

Hız analizi yapabilmek için HIZ isimli interaktif bir modül çağrılır. Hız analizi yapılacak sismik veri ve hız verisinin kaydedileceği dosya ismi sisteme girilir ve program başlatılır. Program veri setini kullanarak bir semblans haritası elde eder (Şekil 8a).Kullanıcı semblans haritası üzerinden yansıma hiperbollerine uygun hız ve sıfır ofset zamanını belirler.Seçilen bu değerler ile interaktif olarak CDP grubunun NMO düzeltme değerleri olarak hesaplanır ve programda gösterilir. Hız analizi CDP gruplarına istenilen aralıklarla uygulanabilir. Kaydedilen hız dosyası NMO düzeltmesinin bütün CDP gruplarına uygulanması için kullanılır(Şekil 9).

Şekil 8. (a) Semblans haritası üzerinde hız işaretlenmesi, (b) NMO öncesi (c) NMO sonrası CDP kaydı

Şekil 9. Üç CDP grubunun NMO düzeltme işlemi (a) öncesi ve (b) sonrası

### 6. SONUÇLAR

Proje kapsamında hazırlanan yazılımın genel amacı, sismik endüstri piyasasında ulaşılması ve kullanılması



kolay bir sismik veri işlem programının eksikliğini gidermektir. Program, temel veri işlem aşamalarının çoğunu uygulayarak sismik ham verinin migrasyon kesitine dönüştürülmesine kadar uzanan işlemleri desteklemektedir. Ayrıca bu yazılımın, ileriki dönemlerde geliştirilen farklı algoritmalarla daha da zenginleştirilmesi ve ileri düzey veri işlem aşamalarını da gerçekleştirebilmesi amaçlanmaktadır.

#### REFERANSLAR

Claerbout, JF, (1985), Imaging the Earth's Interior, Blackwell Sci. Pub

Dondurur D, (2009), Deniz Sismiğinde Veri İşlem, TMMOB Jeofizik Mühendisleri Odası, Ankara

Norris M, Faichney A, (2002), SEG Y rev 1 Data Exchange Format, SEG Technical Standart Committee, 2-19

Yılmaz, Ö, (2001), Seismic Data Analysis. SEG

Anahtar Kelimeler: sismik, yazılım

*Denklem 4.1 den denklem 4.4e kadar*

$$G(x,t) = S(x,t)t^p \quad (4.1)$$

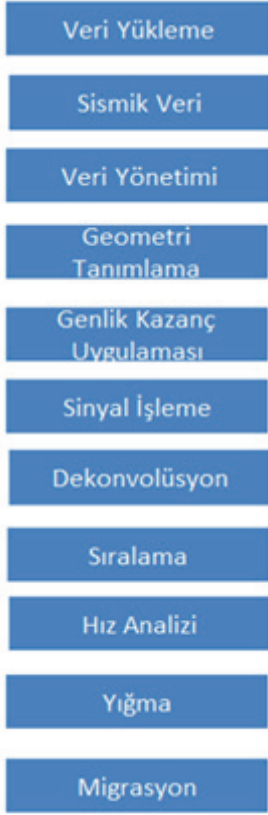
$$G(t) = \frac{\text{rms}}{N * \sum_{i=0}^N |x_i|} \quad (4.2)$$

$$A(F)^2 = \frac{F^{2N}}{\left(1 + \frac{F^{2N}}{FA}\right) * \left(1 + \frac{F^{2M}}{FB}\right)} \quad (4.3)$$

$$t(x)^2 = t(0)^2 + \frac{x^2}{v^2} \quad (4.4)$$

*Yöntem ve Gereçlerde yer alan denklemlerin resim formatında alt alta gönderilmiştir.*

Şekil 1. Program üzerinden uygulanabilecek temel veri işlem aşamaları.



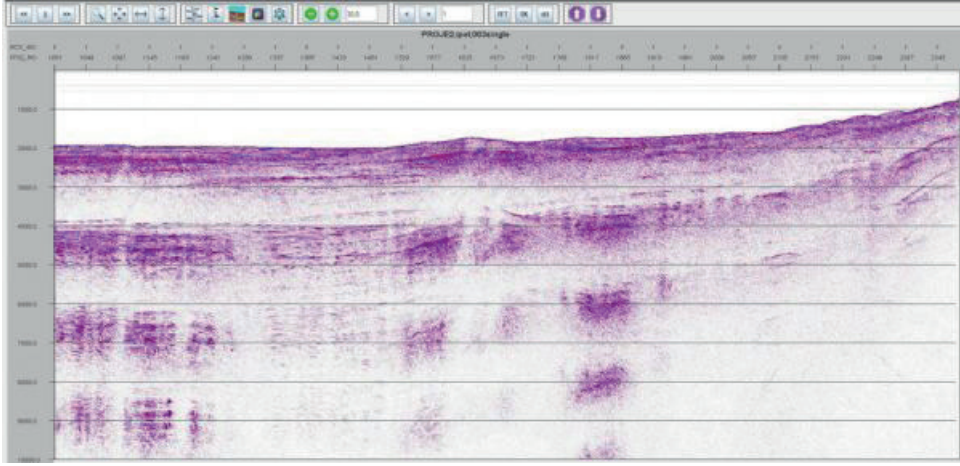
3.2Veri İşlem Aşamaları ve İş Dosyası Oluşturma başlığı altında kullanılmaktadır.

Şekil 2. İş Dosyası Hazırlama ekranı taslak görüntüsü.

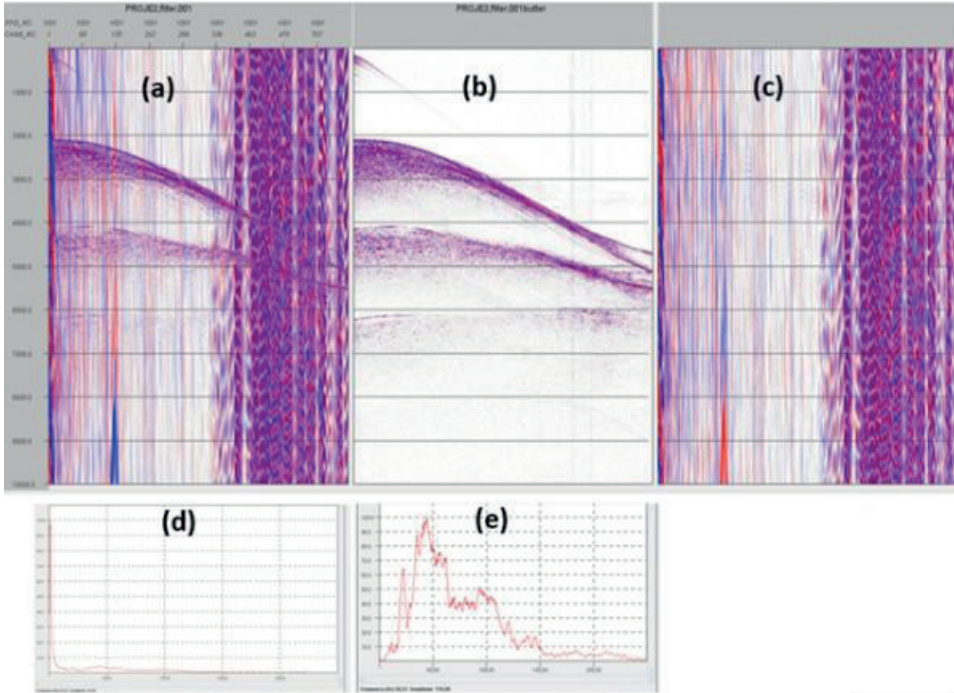
İş Dosyası Hazırlama Ekranı			
(a) Modül seçimi	(b) Parametre seçimi	(c) Klasör belirleme	(d) Modül menüsü
<input type="text"/>	<input type="text"/>	<input type="checkbox"/> <input type="text"/>	<input type="text"/>
<input type="text"/>	<input type="text"/>	<input type="checkbox"/> <input type="text"/>	<input type="text"/>
<input type="text"/>	<input type="text"/>		<input type="text"/>
<input type="text"/>	<input type="text"/>		<input type="text"/>
			<input type="text"/>
			<input type="text"/>
			<input type="text"/>

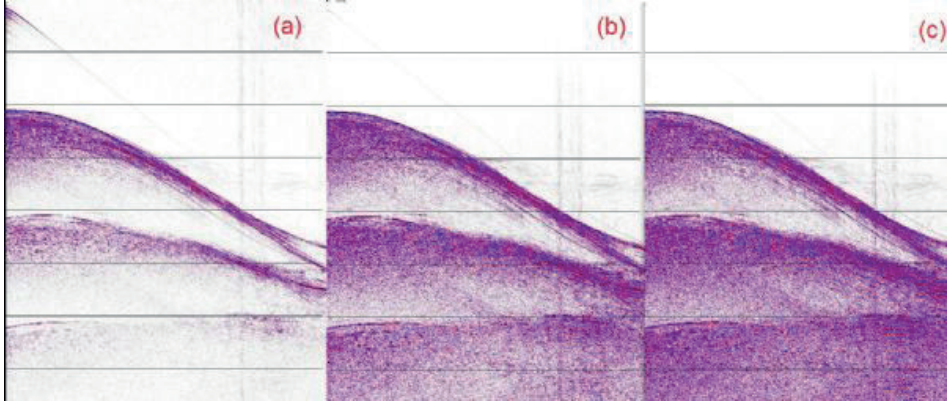
3.2Veri İşlem Aşamaları ve İş Dosyası Oluşturma başlığı altında kullanılmaktadır.

Şekil 3. Her atışın ilk kanalındaki izleri seçerek oluşturulan tek kanallı sismik kesit

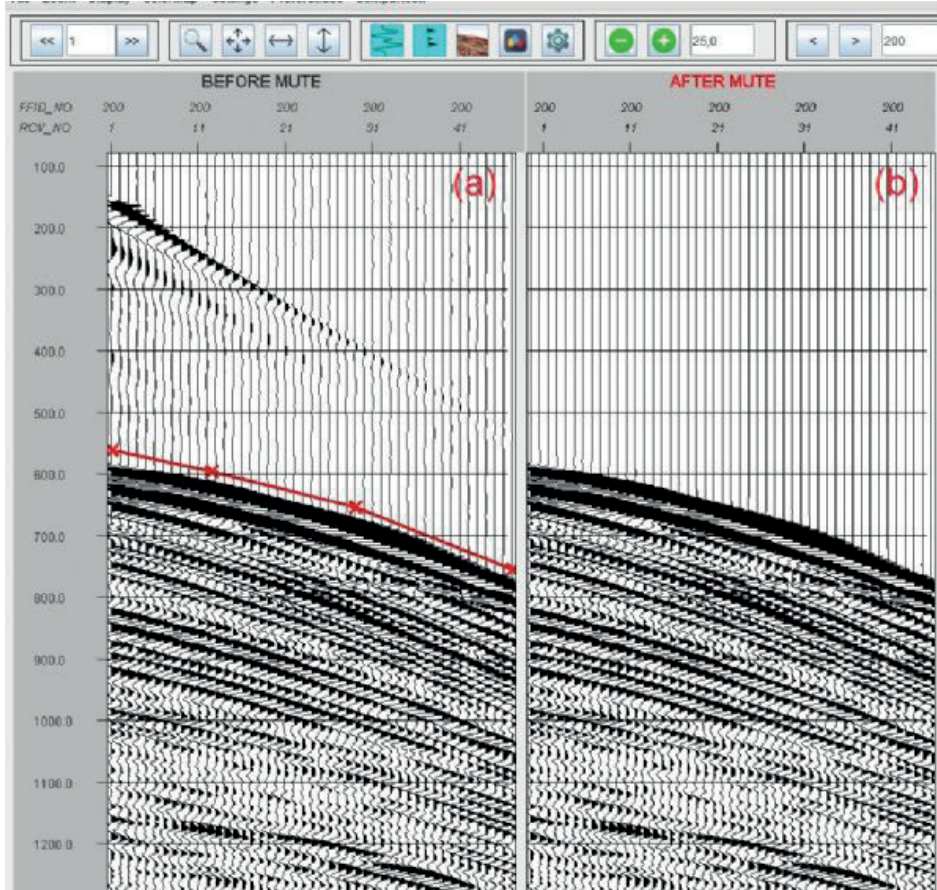


Şekil 4. Sismik atış verisinin (a) Süzgeçleme işlemi öncesi (b) sonrasındaki gösterimi. (c) Süzgeç uygulamadan ve uyguladıktan sonraki iki veri arasındaki fark. (d) Süzgeçleme işlemi öncesi (e) sonrası genlik spektrumlarının gösterimi.

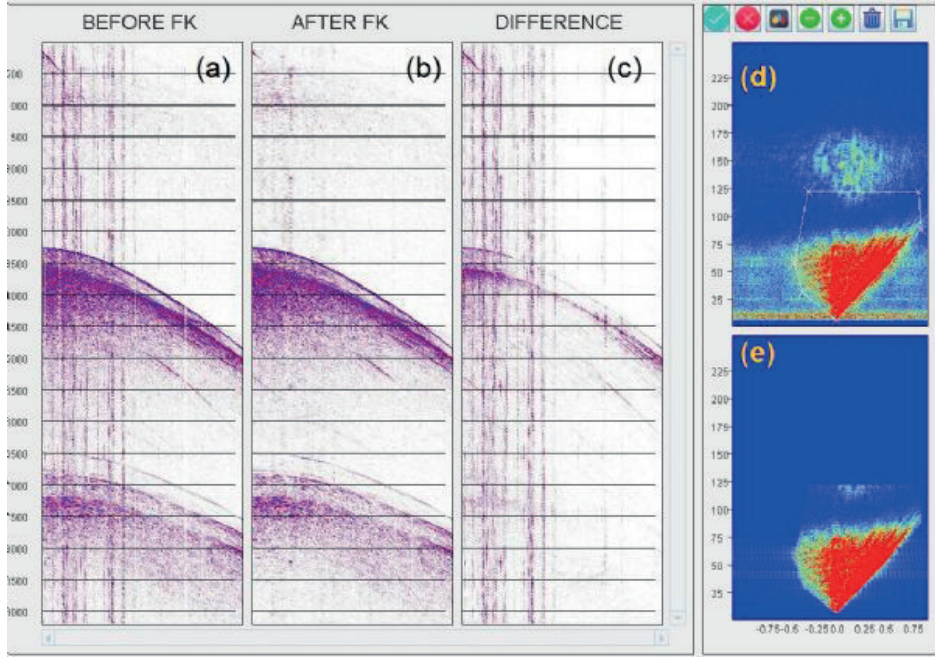


Şekil 5. (a) Genlik düzeltmesi öncesi (b)  $P=1.4$  için genlik düzeltmesi (c)  $P=2$  için genlik düzeltmesi

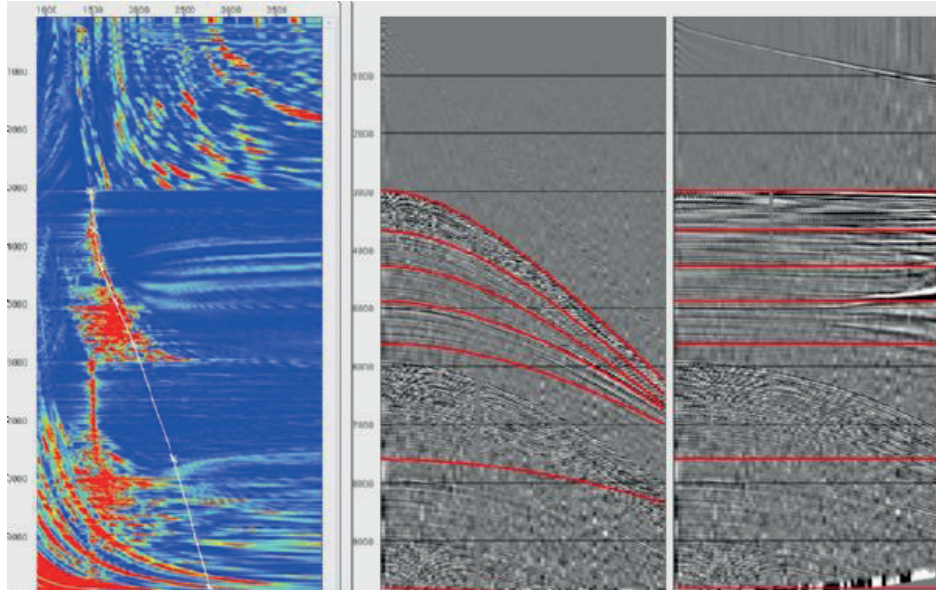
Şekil 6. (a) Mute yapılacak sismik atış verisi (b) Verinin mute işlemi uygulanmış hali.



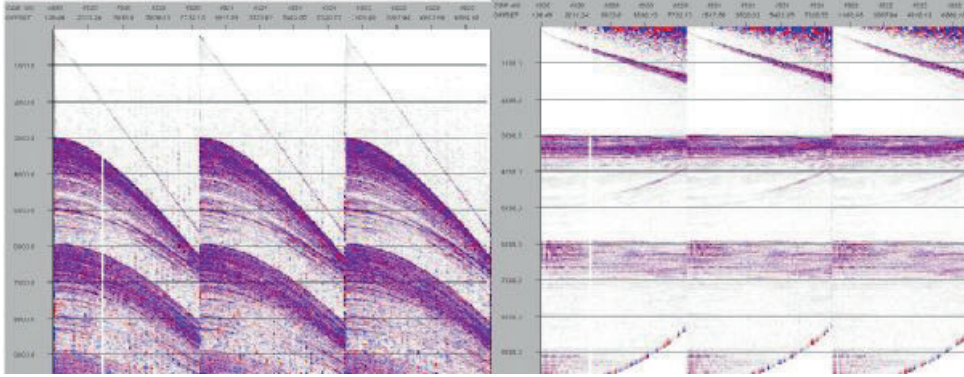
Şekil 7. (a) FK süzgeçleme öncesi, (b) sonrası ve (c) iki veri arasındaki fark (d) FK süzgeçleme için poligon oluşturulması (e) Süzgeçleme sonrası verinin FK spektrumu.



Şekil 8. (a) Semblans haritası üzerinde hız işaretlenmesi, NMO öncesi ve NMO sonrası sismik kesit



Şekil 9. Üç CDP grubunun NMO düzeltme işlemi (a) öncesi ve (b) sonrası



# An Acoustic Wave Equation with the Effects of Reflectivity

Jiayong Bai, Orhan Yilmaz  
AspenTech



## INTRODUCTION

Seismic modeling simulates wave propagation in terms of physical properties. It is used to generate seismic data. It is also used for survey design and evaluation. Seismic migration such as reverse-time migration (RTM) (Baysal et al., 1992) reverses the forward modeling process, re-locates seismic events where they occur, and generate an image of the subsurface. It is noticed that seismic modeling, based on wave equation, is an essential part of RTM.

The large variations of velocity or density could result in very strong reflections, which could greatly affect seismic wavefields. However, seismic modeling and migration commonly ignore the effects of reflectivity caused by velocity and density. The ignorance could result in inaccurate wavefield extrapolation. Particularly, this could be an essential problem when predicted seismic data is compared to field data for optimizing velocity in full-waveform inversion or is used for optimizing migration image in least-squares RTM. Note that historically the reflectivity has been used in many ways. For example, linearized Born modeling is the solution to a wave equation with a virtual source, a background wavefield after scattering by the first-order reflectivity and a second derivative in time (Panning et al., 2009). Whitmore et al. (2020) introduced a wave equation with the effects of reflectivity caused by acoustic impedance for modeling, and Yang et al. (2021) used the equation for the simultaneous inversion of velocity and reflectivity.

We present an acoustic wave equation which includes the effects of reflectivity caused by both velocity and density. The equation is solved through time-domain finite-difference (FD) methods. The spatial and temporal sampling conditions are determined for the FD solutions to avoid numerical instability. The acoustic wave equation is tested in seismic modeling with SEAM model to illustrate how the effects of reflectivity could affect seismic wave propagation in both amplitude and in phase. The equation is also applied in RTM with Volve field dataset to show the influences of reflectivity on migration images and how strong reflectivity caused by large variations of velocity or density could affect illumination in seismic migration.

## THEORY

We get the following seismic wave equation from the momentum equation for a continuum and stress-strain relationship.

$$\rho (\partial^2 u) / (\partial t^2) = \nabla (\nabla \cdot u) + \nabla \mu : [\nabla u + (\nabla u)^T] + (\lambda + 2\mu) \nabla \nabla \cdot u - \mu \nabla \times \nabla \times u, \quad (1)$$

where  $\rho = \rho(x)$  is the density at the position  $x$ ,  $\lambda$  and  $\mu$  are Lamé parameters,  $u = u(x, t)$  is the displacement vector at

$x$  and time  $t$ ,  $\nabla$  is the gradient of a scalar field,  $\nabla \cdot$  is the divergence of a vector field,  $\nabla \times$  is the curl of a vector field, and  $T$  means transpose. In inhomogeneous media, the gradients of Lamé parameters are nonzero. Without ignoring the gradients, mathematical manipulation eventually results in the following wave equation

$$1/V^2 (\partial^2 P) / (\partial t^2) = \nabla^2 P + 4 \nabla V / V \cdot \nabla P + 2 \nabla \rho / \rho \cdot \nabla P, \quad (2)$$

where  $P = \nabla \cdot u$ , and  $V = \sqrt{(\lambda + 2\mu) / \rho}$  is the P-wave velocity. Note that the effects of reflectivity are included through the gradient of wavefields multiplied by the normalized gradients of velocity and density. Ignoring the gradients of velocity and density in Equation 2 reads

$$1/V^2 (\partial^2 P) / (\partial t^2) = \nabla^2 P. \quad (3)$$

This scalar wave equation is commonly used for seismic modeling and RTM in isotropic media.

We solve Equation 2 through the second-order time-domain FD methods. We assume that the spatial sampling rate for the FD methods is  $V_{\min} / (n \times f_N)$ , where  $V_{\min}$  is the minimum velocity, and  $n$  is the number of points needed to cover the Nyquist frequency  $f_N$  for nondispersive propagation. To avoid or minimize numerical dispersion effects, the temporal sampling  $\Delta t$  is chosen to be  $\Delta t \leq 2 / (V_{\max} \times \sqrt{\Lambda})$  with  $V_{\max}$  being the maximum velocity and

$$\Lambda = 1 / [\Delta x]^2 \sum_{i=-N}^N \|w_i^x\| + 1 / [\Delta y]^2 \sum_{i=-N}^N \|w_i^y\| + 1 / [\Delta z]^2 \sum_{i=-N}^N \|w_i^z\| + 4 / V_{\min} ((g_{\max}^x) / \Delta x \sum_{i=-N}^N \|b_i^x\| + (g_{\max}^y) / \Delta y \sum_{i=-N}^N \|b_i^y\| + (g_{\max}^z) / \Delta z \sum_{i=-N}^N \|b_i^z\|) + 2 / \rho_{\min} ((s_{\max}^x) / \Delta x \sum_{i=-N}^N \|b_i^x\| + (s_{\max}^y) / \Delta y \sum_{i=-N}^N \|b_i^y\| + (s_{\max}^z) / \Delta z \sum_{i=-N}^N \|b_i^z\|), \quad (4)$$

where  $\Delta x$ ,  $\Delta y$ , and  $\Delta z$  are the spatial sampling rates along the  $x$ -,  $y$ -, and  $z$ -axes, respectively,  $w$  values are the FD coefficients of the 2nd-order partial derivatives in the  $x$ -,  $y$ -, and  $z$ -directions with  $(2N)$ th-order accuracy,  $b$  values are the FD coefficients of the 1st-order partial derivatives in the  $x$ -,  $y$ -, and  $z$ -directions with  $(2N)$ th-order accuracy,  $g_{\max}^i$  is the maximum gradient of velocity in the  $i$ -direction,  $\rho_{\min}$  is the minimum density, and  $s_{\max}^i$  is the maximum gradient of density in the  $i$ -direction.

## EXAMPLES

We test Equation 2 in seismic modeling with a section of SEAM model. As shown in Figure 1, the section consists of two salt structures. A Ricker wavelet with the peak frequency of 15 Hz is used. Wavefield snapshots and synthetic data produced from Equation 2 and 3 are displayed in Figure 2. When Equation 2 is solved with constant density, the effects of reflectivity caused by

density are not included.

We observe that the effects of reflectivity caused by velocity impact the wavefields and synthetic data both in amplitude and in phase. For example, the wavefronts indicated by the red arrows in Figure 2(a) and (c), the seismic events (indicated by the red arrows) of water bottom and the events indicated by the green arrows in Figure 2(b) and (d) confirm the observation. When the effects of reflectivity caused by velocity and density are included, the snapshots in Figure 2(a) and (e) and synthetic data in Figure 2(b) and (f) still support the observation.

We also observe that the effects of reflectivity caused by density impact the wavefields and synthetic data only in amplitude. For example, the amplitudes of the wavefront indicated by the green arrow in Figure 2(e) and large-offset seismic event indicated by the yellow arrow in Figure 2(f) are much larger than the ones in Figure 2(c) and (d), respectively.

In general, the effects of reflectivity caused by velocity and density produce additional wavefronts in the snapshots and bring up weak signals at later time in the synthetic data. Note that the seismic energy beneath the salt bodies in Figure 2(c) and (e) are weaker than the one in Figure 2(a). This indicates that the large variations of velocity and density prevents the penetration of energy through the salt bodies. The effects of reflectivity caused by density further reduce the penetration. Therefore, the signals beneath the salt bodies in Figure 2(e) are weaker than the ones in Figure 2(c).

Equation 2 is also used in RTM with the Volve OBC dataset. The dataset is sorted to common receiver gathers. We migrate the receiver gathers along a receiver line. Figure 3(a) is obtained from Equation 3, while Figure 3(b) is produced from Equation 2 with constant density. Both images are compensated by their source illuminations. As indicated by the black rectangles and ovals in Figure 3, the seismic events close to the water bottom are different. The structures highlighted by the green rectangles are also different. The blue oval in Figure 3(b) clearly shows an uplift along the seismic event indicated by the yellow arrow. The blue arrows in the crossline section indicate that the event is more continuous in Figure 3(b) than in Figure 3(a). The velocity contrast along the event is very large. On the one hand, since the large contrast reduces energy penetration, the signals below the event in Figure 3(b) are weaker when compared to the ones in Figure 3(a). On the other hand, the signals from 750 meters down to the strong event are enhanced in Figure 3(b) when compared to the scalar wave equation 3, shown in Figure 3(a).

## CONCLUSIONS

We present an acoustic wave equation with the effects of reflectivity caused by velocity and density for wavefield extrapolation in isotropic media. The spatial and temporal sampling criteria are determined to avoid numerical artifacts and instabilities for the FD solutions of the equation. The effects of reflectivity caused by

velocity affect seismic wavefields and synthetic data both in amplitude and in phase, while the effects of reflectivity caused by density affect the wavefields and synthetic data only in amplitude. Strong reflectivity caused by large variations of velocity or density due to, for example, salt bodies could prevent the penetration of energy through the bodies. As a result, the illumination beneath the large variations could be poor when the equation is applied in the migration of Volve field dataset.

## ACKNOWLEDGEMENTS

We thank SEG for SEAM model. We also thank Equinor and the Volve license partners for the Volve field dataset.

## REFERENCES

- Baysal, E., Kosloff, D.D. and Sherwood, J.W.C. [1992] Reverse time migration. *Geophysics*, 1514–1524.
- Panning, M.P., Capdeville, Y. and Romanowicz, B.A. [2009] Seismic waveform modelling in a 3-D Earth using the Born approximation: potential shortcomings and a remedy. *Geophys. J. Int.*, 161–178.
- Whitmore, N.D., Ramos-Martinez, J., Yang, Y. and Valenciano, A.A. [2020] Seismic modeling with vector reflectivity. 90th Annual International Meeting, SEG, Expanded Abstracts, 2709–2713.
- Yang, Y., Ramos-Martinez, J., Whitmore, D., Huang, G. and Chemingui, N. [2021] Simultaneous inversion of velocity and reflectivity. 91st Annual International Meeting, SEG, Expanded Abstracts, 577–581.

Keywords: Seismic modeling and migration, wave equation



Eqn 1

$$\rho \frac{\partial^2 \mathbf{u}}{\partial t^2} = \nabla \lambda (\nabla \cdot \mathbf{u}) + \nabla \mu \cdot [\nabla \mathbf{u} + (\nabla \mathbf{u})^T] + (\lambda + 2\mu) \nabla \nabla \cdot \mathbf{u} - \mu \nabla \times \nabla \times \mathbf{u}, \quad (1)$$

Image of Equation 1

Eqn 2

$$\frac{1}{V^2} \frac{\partial^2 P}{\partial t^2} = \nabla^2 P + 4 \frac{\nabla V}{V} \cdot \nabla P + 2 \frac{\nabla \rho}{\rho} \cdot \nabla P, \quad (2)$$

Image of equation 2

Eqn 3

$$\frac{1}{V^2} \frac{\partial^2 P}{\partial t^2} = \nabla^2 P. \quad (3)$$

Image of equation 3

Eqn 4

$$\Lambda = \frac{1}{\Delta x^2} \sum_{i=-N}^N \|w_i^x\| + \frac{1}{\Delta y^2} \sum_{i=-N}^N \|w_i^y\| + \frac{1}{\Delta z^2} \sum_{i=-N}^N \|w_i^z\| + \frac{4}{V_{min}} \left( \frac{g_{max}^x}{\Delta x} \sum_{i=-N}^N \|b_i^x\| + \frac{g_{max}^y}{\Delta y} \sum_{i=-N}^N \|b_i^y\| + \frac{g_{max}^z}{\Delta z} \sum_{i=-N}^N \|b_i^z\| \right) + \frac{2}{\rho_{min}} \left( \frac{s_{max}^x}{\Delta x} \sum_{i=-N}^N \|b_i^x\| + \frac{s_{max}^y}{\Delta y} \sum_{i=-N}^N \|b_i^y\| + \frac{s_{max}^z}{\Delta z} \sum_{i=-N}^N \|b_i^z\| \right), \quad (4)$$

Image of equation 4

Figure 1

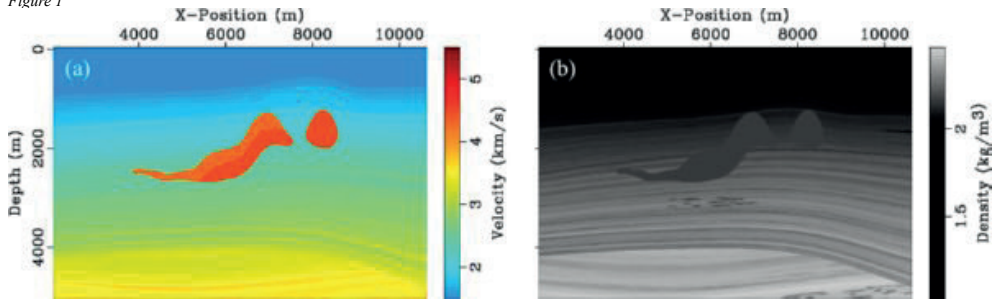


Figure 1 Velocity (a) and density (b) of SEAM model.

Figure 2

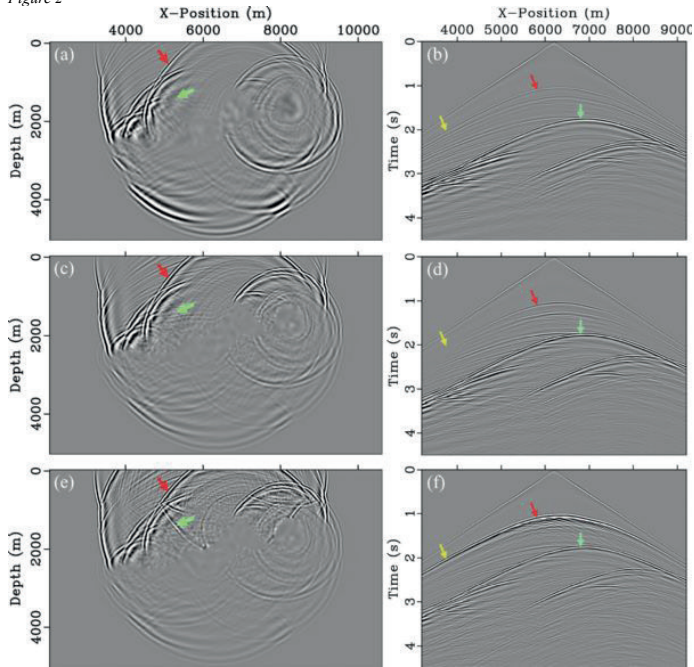


Figure 2 SEAM model. Wavefield snapshot (a) and synthetic data (b) generated from Equation 3. The same snapshot (c) and synthetic data (d) generated from Equation 2 with constant density. Snapshot (e) and synthetic data (f) generated from Equation 2 with variable density shown in Figure 1(b).

Figure 3

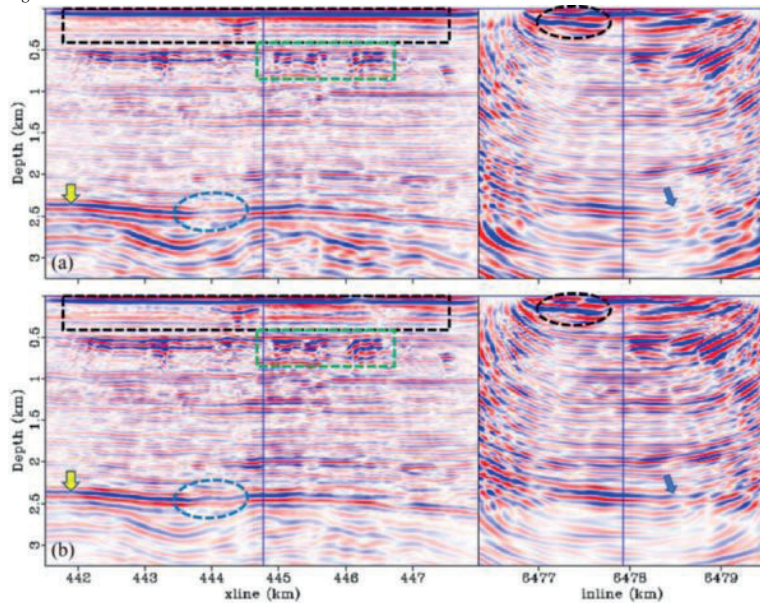


Figure 3 Volve field dataset. (a) Migration image obtained from Equation 3. (b) Migration image obtained from Equation 2 with constant density.



## **Sismik Veri Toplama**

*Seismic Data Acquisition*

---



# Vibratör Harmonikleri - Sinyal mi Gürültü mü ? Vibrator Harmonics - Signal or Noise ?



**Orhan Güreli**

RR Sismik Mühendislik AŞ., Ankara / Türkiye

In the conventional vibroseis method, the signal processing algorithms, including cross-correlation and deconvolution, are applied to convert the raw shot data into a seismic section. Vibrators are the best of the seismic sources and are widely used in exploration worldwide.

The vibroseis seismic data quality is directly related to sweep signal harmonics. In other words, if the harmonic noise level increases, seismic quality decreases.

In conventional vibrators, harmonic distortion is generated as a result of nonlinear coupling of vibrators and considered as coherent noises and consequently effects of these harmonics, contaminations are subject to the elimination from the field records. Over the years, different formalisms, using sweep parameters and phases, are proposed for the attenuation of these effects.

In this study, a new algorithm is developed using harmonic components of the signal sweep as an auxiliary source, instead of striving to eliminate them, in order to broaden the frequency bandwidth of the seismic imaging.

Our approach is tested on synthetic and real data and results are discussed.

Keywords: Sweep, Harmonic.

## ÖZ

Geleneksel vibrosismik yöntemde, ham arazi kayıtlarını bir sismik kesite dönüştürmek için çapraz korelasyon ve ters evrişim dahil olmak üzere birçok veri işlem aşamaları uygulanır. Vibratörler, sismik kaynakların içinde en iyisidir ve dünya çapındaki sismik ekiplerinde yaygın kaynak olarak kullanılır.

Vibrosismikte sismik veri kalitesi, doğrudan sweep sinyali ve harmonikleri ile ilgilidir. Yani harmonik gürültü seviyesi artarsa sismik kalite düşer.

Konvansiyonel vibratörlerde, vibratörlerin doğrusal olmayan yer ile temasından dolayı harmonikler oluşur ve sweep parametresine bağlı bir gürültü olarak değerlendirilir. Dolayısıyla bu harmoniklerin yani gürültülerin etkileri saha kayıtlarından elimine edilir. Yıllar içinde, bu etkilerin hafifletilmesi için farklı sweep parametreleri ve proses aşamalarında farklı işlemler uygulanmıştır.

Bu çalışmada, sismik kesitlerin frekans bant genişliğini genişletmek için sweep sinyalinin harmonik bileşenlerini ortadan kaldırmaya çalışmak yerine bu harmoniği sinyal olarak kullanan yeni bir algoritma geliştirilmiştir.

Bu yaklaşımımız sentetik ve gerçek veriler üzerinde test edildi ve sonuçları gösterilecektir.

Anahtar Kelimeler: Sweep, Harmonik.

## GİRİŞ

Petrol, Doğalgaz, Jeotermal ve Maden Aramacılığında Jeofizik bir yöntemi olan "Sismik Yansıma Yöntemi" yaygın olarak kullanılır. Sismik yansıma yönteminde kaynak olarak yaygın bir şekilde Vibratör denilen yeri titreştirerek dalga gönderen bir araç kullanılır. Bu Vibratörler sinyal (bu sinyal sweep olarak isimlendirilir) üretirken, harmonik denilen gürültüleri de üretir.

Bir vibratör grubu (Bir atış noktasında genelde 4 adet vibratör kullanılır, buna vibratör grubu denir) kullanılarak elde edilen sismik verilerin harmonik bozulmaları iyi bilinen bir olaydır. Kaydedilen ham verilerdeki bu harmonikler, kayıtlarda harmonik hayaletler olarak bilinen kaynak (Vibratör grubu) ile ilişkili gürültü dizileri ile sonuçlanır (Wei, Phillips, ve Hall, 2010).

Harmonikler, vibratörlerin mekanik aksamına bağlı olarak doğrusal olmayan etkilerinden ve özellikle yakın yüzeyde (Walker, 1995; Lebedev ve Beresnev, 2004) oluşur. Sismik veri toplama (Silverman, 1979; Rozemond, 1996) ve veri işleme aşamasında bu harmonikleri ortadan kaldırmaya çalışan birçok teknik geliştirilmiştir (Eisner, 1974; Abd El-Aal, 2011; Jianjun, Jie, Yong, ve Xiling, 2012).

Temel sweep'ten (Fundamental sweep) elde edilen ham verilerdeki harmonikleri zayıflatmak için çeşitli teknikler geliştirildi ve bu durum da veri kalitesini artırdı (Sorkin, 1972; Meunier ve Bianchi, 2003; Gang ve Yuan, 2014).

Faz kaydırma yöntemi, harmonik bozulma etkisinin giderilmesinde yaygın olarak kullanılan bir yöntemdir. Her sweep,  $\theta = 360 / N$ 'ye eşit bir başlangıç faz ( $\theta$ ) kayması ile üretilir, burada N, kayıt başına düşen sweep sayısıdır (Sorkin, 1972; Abd El-Aal, 2010; Wuxiang, 2010; Yongsheng vd., 2011). Böylece sweep frekansı kullanılarak harmonik gürültüler elimine edilmeye çalışılır.

Yukarıda görüldüğü gibi, farklı yazarlar çalışmalarında harmonikleri bir gürültü olarak değerlendirmişler ve bunları ortadan kaldırmak için çeşitli yöntemler geliştirmişlerdir. Bu yazarlara göre harmonikler istenmeyen gürültü olarak kabul edilir ve kayıtlardan çıkarılması gerekir.

Harrison (2011 ve 2012) çalışmasına göre, Gabor dönüşümü kullanılarak Vibratörün ürettiği sweep ile ilgili temel ve harmonik bileşenleri ayrıştırılmasını sağlamıştır. Ayrıca yeni bir yaklaşım ve harmoniklerin ek bir sinyal olarak kullanılması konusunda öncü bir çalışma oluşturmuştur. Sığ ve ince tabakaların sismik görüntülemesi için harmoniklerin ve bunlarla ilişkili yüksek frekans içeriklerinin kullanılabilirliğini önermektedirler. Uygulamalarında temel sweep'in harmonik bileşenlerden kaldırılmadığı unutulmamalıdır.

Bu noktada harmonikler sadece istenmeyen bir gürültü olarak değil aynı zamanda, amaca uygun yüksek frekanslı bir sismik kesit elde etmede de kullanılabilir. Bu makalede, harmoniklere gürültü olarak değil, sinyal olarak kullanılması anlatılmıştır. Bu teknikte sweep'ler 0 ve 180 derece fazlı üretilmektedir. Böylece farklı fazlı sweep'ler hem toplanmış, hemde bir birinden çıkarılmıştır. Böylece iki ayrı kayıt elde edilmiştir. Bu kayıtlardan bir tanesi, temel frekanslı (f1-f2), diğeri ise iki kat frekanslı (2f1-2f2) olmuştur.

### SWEEP SİNYALİNİN ELDE EDİLiŞİ

Sweep; Vibratör tarafından yere gönderilen sinyaldir. Vibratörler yere daha önceden belirlenmiş frekans aralığında (f1'den f2'ye doğru artan veya azalan) ve belirli bir sürede (sweep süresi) yeri titreştiren makinalardır.

#### Harmoniklerin Analizi

Seriff ve Kim (1970) ifade ettiği üzere sweep ve harmoniklerinin teorik kısımlarını anlatmıştır. Sweep denilen sinyal, düşükten yükseğe doğru frekansı değişen bir sinüs dalgası şeklindedir.

Seriff and Kim (1970) tipik linear bir sweep'i  $S_1(t, \theta)$  aşağıdaki formülle açıklamıştır.

$$S_1(t, \theta) = \alpha_1 \sin[2\pi(f_1 + Qt)t + \theta], 1$$

burada  $\alpha_1$  ve Q birer sabittir. Q sabiti ise aşağıdaki gibidir

$$Q = (f_2 - f_1) / T, 2$$

Sweep  $S_1(t, \theta)$ 'nin kth harmonik bozulma formülü ise aşağıdaki gibidir

$$S_k(t, k\theta) = \alpha_k \sin[2\pi k(f_1 + Qt)t + k\theta], 3$$

burada  $\alpha_k$  sinyal genliği, f1 sweep başlangıç frekansı, f2 sweep bitiş frekansı, T sweep süresi, k harmonik derecesi,  $\theta$  sweep başlangıç fazı,  $k\theta$  k.cı harmonik fazı t ise zamandır.

Tablo 1'de üç farklı sweep harmonikleri karşılaştırılmıştır. Sweep\_A ile Sweep\_B'nin bütün parametreleri aynı, sadece başlangıç fazı farklıdır. Sweep\_A ile Sweep\_C'nin bütün parametreleri aynı, sadece başlangıç ve bitiş frekanslar farklıdır, yani iki katıdır.

$$Sweep\_A = H_1 + H_2 + H_3 + H_4 + \dots + [H]_k, 4$$

$$Sweep\_B = [-H]_1 + H_2 - H_3 + H_4 - \dots + [\pm H]_k, 5$$

$$Sweep\_C = H_2 + H_4 + \dots + [H]_k, 6$$

Sweep\_C'nin H\_2, H\_4, gibi harmonikleri ile diğer Sweep'lerin harmoniklerinin arasında genlik farkı vardır. Genlikler kendi içinde normalize edildiğinde fark kaybolmaktadır. Bu yüzden bu çalışmada genlikler ihmal edilmiştir.

Eğer Formül 4'te Sweep\_A ve Formül-5'te verilen Sweep\_B birbirleri ile toplanırsa tek sayılı harmonikler ve temel sweep elimine edilmiş olur.

$$Sweep\_A + Sweep\_B = Sweep\_A + Sweep\_B$$

$$B = 2H_2 + 2H_4 + \dots + \text{çift sayılı harmonikler}, 7$$

Eğer Sweep\_B, Sweep\_A'dan çıkarılırsa çift sayılı harmonikler elimine edilmiş olur.

$$Sweep\_A - Sweep\_B = Sweep\_A - Sweep\_B$$

$$B = 2H_1 + 2H_3 + \dots + \text{tek sayılı harmonikler}, 8$$

burada Sweep\_(A+B) ve Sweep\_(A-B) korele edilmemiş yeni sweep'lerdir.

Her bir sweep kendi Temel sweep (Fundamental sweep)'i ile korelasyon yapılır ve atışlar elde edilir. Bunlar da kayıt olup "Record" olarak isimlendirilir.

$$Record\_A = H_1 \otimes Sweep\_A, 9$$

burada H\_1; Sweep\_A'nın Temel sweep'i, Record\_A; Sweep\_A'nın H\_1 ile korelasyonundan elde edilen kayıt,

$$Record\_B = H_1 \otimes Sweep\_B, 10$$

burada H\_1; Sweep\_B'nin Temel sweep'i, Record\_B; Sweep\_B'nin H\_1 ile korelasyonundan elde edilen kayıt,

$$Record\_C = H_2 \otimes Sweep\_C, 11$$

burada H\_2; Sweep\_C'nin Temel sweep'i, Record\_C; Sweep\_C'nin H\_2 ile korelasyonundan elde edilen kayıt,

$$Record\_A - B = H_1 \otimes Sweep\_A - B, 12$$

$$Record\_A + B = H_2 \otimes Sweep\_A + B, 13$$

burada Record\_(A-B), Sweep\_A veya Sweep\_B'nin H\_1 olan Temel sweep'i ile  $[Sweep]_{(A-B)}$ 'nin korelasyonu ile elde edilir. Record\_(A+B) ise Sweep\_C'nin H\_2 olan Temel Sweep'i ile  $[Sweep]_{(A+B)}$ 'nin korelasyonundan elde edilir. Formül-9, 10, 11, 12 ve 13'teki  $\otimes$  korelasyon operatörünü temsil eder. Record\_A, Record\_B, Record\_C, Record\_(A+B) ve Record\_(A-B) "Raw shot" tabir edilen ham kayıtlardır. Şekil 1'de sentetik olarak üretilen temel sweep ve harmonikleri görülmektedir. Burada H\_1-Temel sweep ve harmonikleri (H\_2, H\_3 ve H\_4) zaman ortamında (üstte), toplanmış durumu (ortada) ve aynı eksende karşılaştırmaları (altta) görülmektedir.

### SENTETİK VERİ ÜZERİNDE HARMONİK ANALİZİ

Aşağıda verilen parametrelere göre 3 adet sweep sentetik olarak üretildi. Temel sweep ile birlikte kıyaslamak için üç adet harmonik'te (Temel sweep-H\_1, H\_2, H\_3 ve H\_4) birlikte üretildi.

Sentetik veri için aşağıdaki sweep parametreleri kullanıldı.

Sweep\_A: 12-64 Hz, 8 sn sweep boyu ve 0 derece başlangıç fazı,

Sweep\_B: 12-64 Hz, 8 sn sweep boyu ve 180 derece başlangıç fazı,

Sweep\_C: 24-128 Hz, 8 sn sweep boyu ve 0 derece başlangıç fazı,

Şekil 2'de verilen temel sweep'ler için yukarıda verilen Sweep parametreleri kullanıldı. Sentetik olarak üretilen Sweep\_A, Sweep\_B, Sweep\_C, Sweep\_(A+B) and Sweep\_(A-B) analizleri görülmektedir.

Sweep\_A ve harmoniklerinin başlangıç fazı sıfır (0) derece, Sweep\_B'nin Temel sweep'i ve tek sayılı harmoniklerinin başlangıç fazı 180 derece, çift sayılı harmoniklerin başlangıç fazı ise sıfır (0) derecedir. Sweep\_C'nin ise giriş fazı sıfır (0) derece olup sadece başlangıç ve bitiş frekansları Sweep\_A ve Sweep\_B'ni başlangıç ve bitiş frekanslarını iki katıdır.

## GERÇEK VERİ UYGULAMASI

### Veri toplama çalışması:

2020 yılında, Arar Petrol AS (ARAR) tarafından Osmaniye ili sınırları içinde sismik programı kapsamında bu test çalışması yapıldı. Bunun için birbirini takip eden 28 farklı atış noktasında Sweep\_A, Sweep\_B ve Sweep\_C yukarıda verilen parametrelerle ayrı ayrı sweep'leri üretildi ve kayıt edildi. Her bir atış, 20 m aralıklarla yüzeye çakılmış 500 adet alıcılar (jeofonlar) ile kaydedildi.

Şekil 3'te:  $[[Record]]_A$  ve  $[[Record]]_B$  ham arazi kaydı ve spektrumu görülmektedir. Sweep\_A ile Temel sweep'i-H\_1'in Formül(9)'daki denkleme göre korelasyonu ile elde edilmiştir. Sweep\_B ile Temel sweep-H\_1'in Formül-10'daki denkleme göre korelasyonu ile elde edilmiştir.

Şekil 4'te  $[[Record]]_{(A-B)}$  ve  $[[Record]]_{(A+B)}$  ham arazi kaydı ve genlik-frekans spektrumu görülmektedir.  $[[Record]]_{(A-B)}$ , Sweep\_A ve Sweep\_B'nin farkı Formül 12'deki denklemler kullanılarak elde edilmiştir.  $[[Record]]_{(A+B)}$ , Sweep\_A ve Sweep\_B'nin toplanması Formül-13'deki denklemler kullanılmıştır. Proseste bu arazi kayıtları kullanılmıştır.  $[[Record]]_{(A-B)}$  ile Şekil 3'teki  $[[Record]]_A$  ve  $[[Record]]_B$  ile benzerlik göstermektedir.

Şekil 5'te  $[[Record]]_{(A+B)}$  ve  $[[Record]]_C$  ham arazi kaydı ve genlik-frekans spektrumu görülmektedir. Bu kayıtlardan  $[[Record]]_C$ , Sweep\_C ile Temel sweep-H\_2'in Formül 11'deki denkleme göre korelasyonu ile elde edilmiştir.  $[[Record]]_{(A+B)}$  ve  $[[Record]]_C$  incelendiğinde hem arazi kayıtların hem de spektrumları oldukça birbirlerine benzemektedir.

Tablo 2'de Temel veri işlem iş akışı görülmektedir. Tüm verilerin prosesleri bu tabloya göre yapılmıştır.

Şekil 6'da  $[[Record]]_A$ 'dan elde edilen  $[[Stack]]_A$  ve  $[[Record]]_B$ 'den elde edilen  $[[Stack]]_B$  proses kesiti ve spektrumu görülmektedir.  $[[Record]]_A$  ve  $[[Record]]_B$  ayrı ayrı proses edilerek ve  $[[Stack]]_A$  ve  $[[Stack]]_B$  kesitleri elde edildi. Bu kesitler ve spektrumları incelendiğinde oldukça benzer olduğu görülür.

Şekil 7'de  $[[Record]]_{(A-B)}$ 'den elde edilen  $[[Stack]]_{(A-B)}$  ve  $[[Record]]_{(A+B)}$ 'den elde edilen  $[[Stack]]_{(A+B)}$  proses kesiti ve spektrumu görülmektedir. Kesitler incelendiğinde frekans içeriğindeki farklılık çok belirgin olarak görülmektedir. Bu farklılık frekans spektrumlarında da görülmektedir. Bu farkın sebebi Temel sweep ve tek sayılı harmoniklerin elimine edilmesidir. Temel sweep'in elimine edilmesi ile veri yüksek frekanslara kaymıştır. Böylece yüksek frekanslı

kesit elde edilmiştir. Bu yeni işlem ile ayrımlılık artmış ve ince tabakaları kesitlerde daha görünür hale gelmiştir.

Bu yeni teknik ile aynı veriden iki ayrı kesit elde etmek mümkün olmuştur. Bu kesitlerden bir tanesi konvansiyonel kesit ( $[[Stack]]_{(A-B)}$ ) aynı zamanda bazı harmonikleri elimine edilmiş olup diğeri ise yüksek frekanslı kesit ( $[[Stack]]_{(A+B)}$ ) olup bu kesitten bazı harmonikler elimine edilmiş olur.

Yüksek frekanslı sweep sinyali sahada vibratör tarafından üretilmesi bile, bu yeni vibrosismik veri toplama tekniği ile yüksek frekanslar üretiliyormuş gibi bir sismik kesit elde etmek mümkündür.

Şekil 8'de  $[[Stack]]_{(A+B)}$  ile  $[[Record]]_C$ 'den elde edilen  $[[Stack]]_C$  proses kesiti ve spektrumu görülmektedir.  $[[Stack]]_C$ ,  $[[Stack]]_{(A+B)}$  kıyaslamak amacıyla üretilmiştir.  $[[Stack]]_C$ ,  $[[Stack]]_{(A+B)}$  parametreleri ile sahada üretilmiştir. Kesitler ve spektrumları karşılaştırıldığında birbirinin aynı oldukları açıkça görülmektedir. Bu sonuç bize gösteriyor ki sahada  $[[Stack]]_C$  üretilmesi bile aynı kesiti bu teknik ile üretmek mümkün olmaktadır.

## SONUÇLAR

Vibratör tarafından üretilen harmonikler, geleneksel olarak, sismik veri toplama ve veri işleme aşamaları sırasında kayıtlardan ve kesitlerden elimine edilmek istenen gürültü olarak görülmüştür. Bu araştırma çalışmasında, temel sweep olmaksızın daha yüksek harmonik frekansların sığ, ince reflektör katmanlarını görüntülemek için kullanılabilirliği gösterilmiştir. Ayrıca, vibrosismik verilerdeki harmonikleri kullanmak için yeni bir yaklaşım sunulmuştur. Bu teknik bize iki farklı kesit elde etmemizi sağlamıştır. Böylece bu yöntem hem geleneksel parametrelere göre elde edilen kesitleri, hemde yüksek ayrımlılıklı kesitleri sunmuştur.

## REFERANSLAR

- Abd El-Aal, A. E. K. (2010). Eliminating upper harmonic noise in vibroseis data via numerical simulation. *Geophys. J. Int.* (2010) 181, 1499–1509. doi: 10.1111/j.1365-246X.2010.04594.x
- Abd El-Aal, A. E. K. (2011). Harmonic by harmonic removal technique for improving vibroseis data quality. *Geophysical Prospecting* (59): 279-294.
- Eisner, E. (1974). Method for determining optimum seismic pulse. US Patent. 3,815,704.
- Gang, M. Y., ve Yuan, Z. (2014). Harmonic noise removal on vibroseis slip-sweep data based on Model method. CPS/SEG Beijing 2014 International Geophysical Conference.
- Harrison, C. B., Margrave, G. F., Lamoureux, M. P., Siewert, A., ve Barrett, A. (2011). Harmonic decomposition of vibroseis sweeps using Gabor analysis. CREWES Research Report 2011.
- Harrison, C. B., Margrave, G., Lamoureux, M., Siewert, A., Barrett, A., ve Isaac, L. H. (2012). Towards using harmonic "contamination" as signal for thin reflectors.

CREWES Research Report - Volume 24

Jianjun, X., Jie, Y., Yong, G., ve Xiling, C. (2012). Suppressing harmonics based on singular value decomposition in time frequency domain. SEG Technical Program Expanded Abstracts, 1052-3812, DOI <http://dx.doi.org/10.1190/segam2012-0119.1>

Lebedev, A. V., ve Beresnev, I. A. (2004). Nonlinear distortions of signals radiated by vibroseis sources. *Geophysics* 69(4): 968-977.

Meunier, J., ve Bianchi, T. (2003). Method of reducing harmonic noise in vibroseis operations. U.S. patent, 6 603 707.

Rozemond, H. J. (1996). Slip-sweep acquisition. SEG meeting, Denver, Colorado, USA, SEG. Extended Abstracts: 64-67.

Seriff, A.J. ve Kim, W. H. (1970). The effect of harmonic distortion in the use of vibratory surface sources. *Geophysics* 35(2), 234-246.

Silverman, D. (1979). Method of three dimensional seismic prospecting. U.S. Patent. 4,159,463.

Sorkin, S. A. (1972). Sweep signal seismic exploration U.S. Patent. 3,786,409.

Yongsheng, S., Changhui, W., Mugang, Z., Xuefeng, Z., Zhenchun, L., Fenglei, L., ve Lieqian, D. (2011). A method for harmonic noise elimination in slip sweep data. SEG Technical Program Expanded Abstracts, 30. 10.1190/1.3627600.

Walker, D. (1995). Harmonic resonance structure and chaotic dynamics in the earth-vibrator system. *Geophysical Prospecting* 43: 487-507.

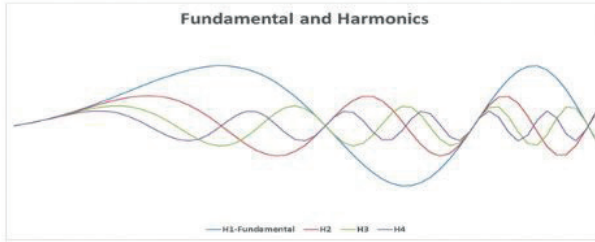
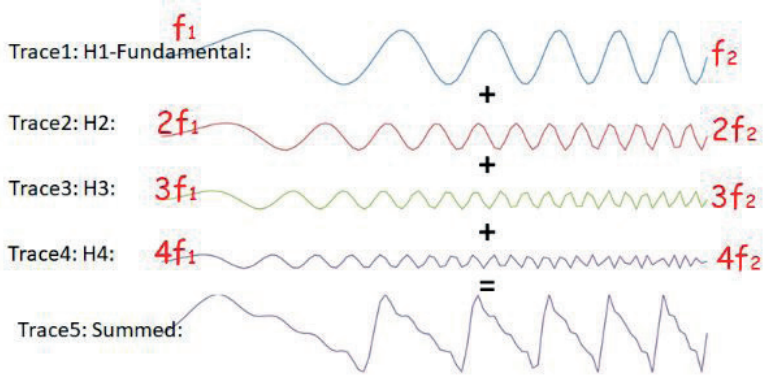
Wei, Z., Phillips, T.F., ve Hall, M.A. (2010). Fundamental discussions on seismic vibrators. *Geophysics*, 75, No. 6, W13-W25. <http://dx.doi.org/10.1190/1.3509162>.

Wuxiang, C. (2010). To attenuate harmonic distortion by the force signal of vibrator. SEG Denver Annual Meeting.

Anahtar Kelimeler: Sweep, Harmonik

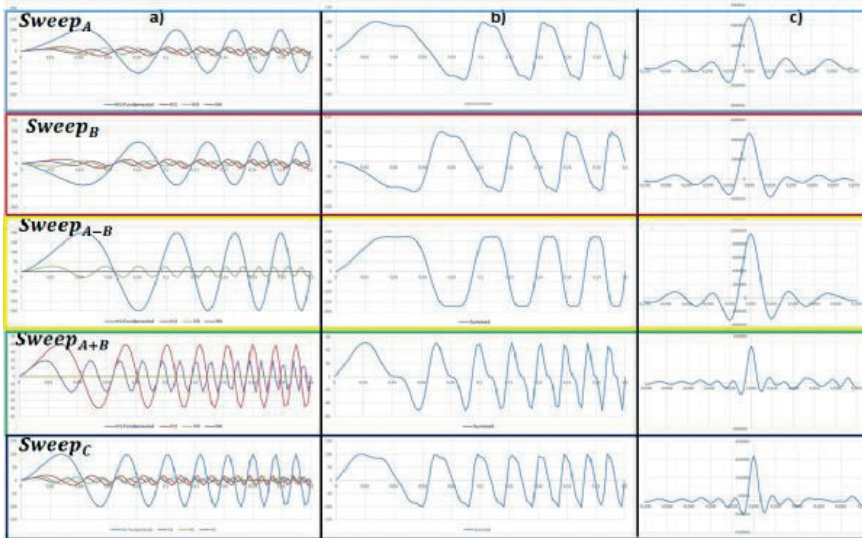


Şekil-1



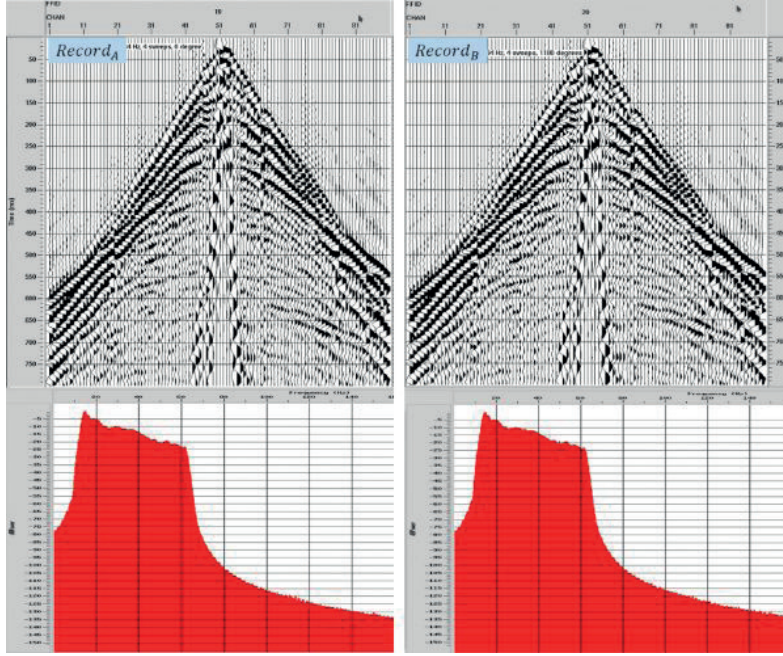
Şekil 1: İz-1: Temel sweep-H\_1 genliği- $\alpha_1 = 100$  birim, İz-2: Birinci harmonik-H\_2 genliği- $\alpha_2 = 50$  birim, İz-3: İkinci harmonik-H\_3 genliği- $\alpha_3 = 33$  birim, İz-4: Üçüncü harmonik-H\_4 genliği- $\alpha_4 = 25$  birim, İz-5: Temel sweep  $S(t,0^\circ)$  ve harmoniklerinin toplamı. Temel sweep ve harmoniklerin birlikte görünüşü (altta)

Şekil-2



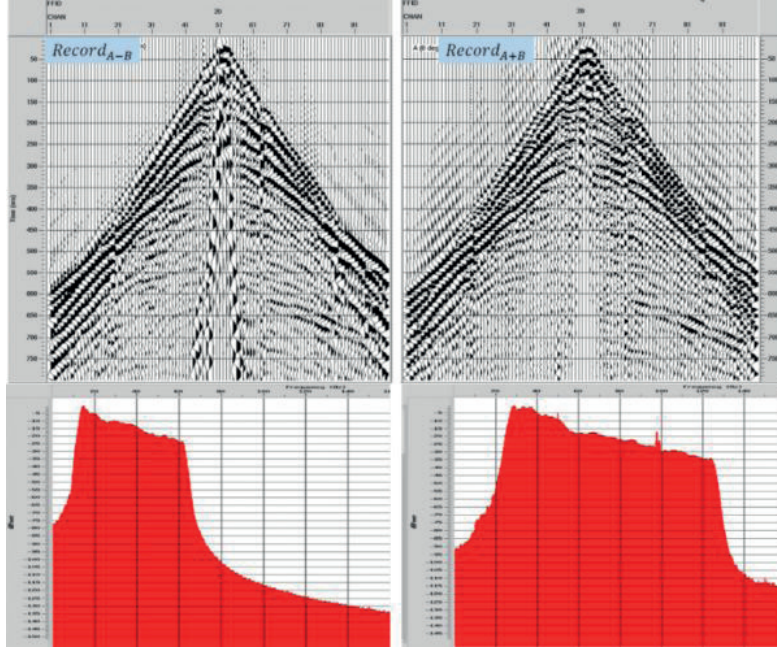
Şekil 2: Sweep\_A, Sweep\_B, Sweep\_(A+B), Sweep\_(A-B) ve Sweep\_C analizi, a) Her bir sweep'in Temel sweep ve harmoniklerinin görünüşü, b) Her bir Sweep'in Temel sweep ve harmoniklerinin toplamının görünüşü, c) Sweep\_A, Sweep\_B, Sweep\_C, Sweep\_(A-B)'nin temel sweep'leri ile korelasyonu ve Sweep\_(A+B)'nin birinci harmonik ile korelasyonu.

Şekil-3



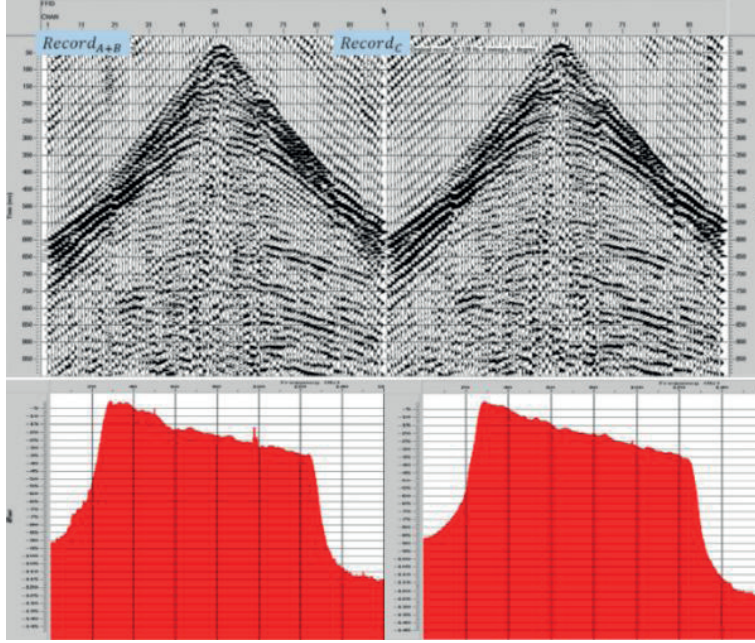
Şekil 3: [(Record)]\_A ve [(Record)]\_B ham arazi kayıtları ve genlik-frekans spektrumu.

Şekil-4



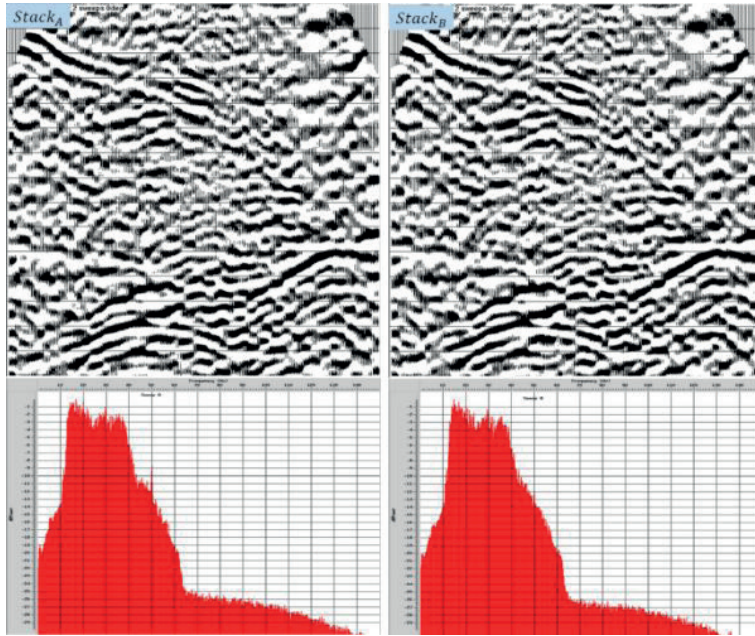
Şekil 4: [(Record)]\_(A-B) ve [(Record)]\_(A+B) ham arazi kayıtları ve genlik-frekans spektrumu.

Şekil-5



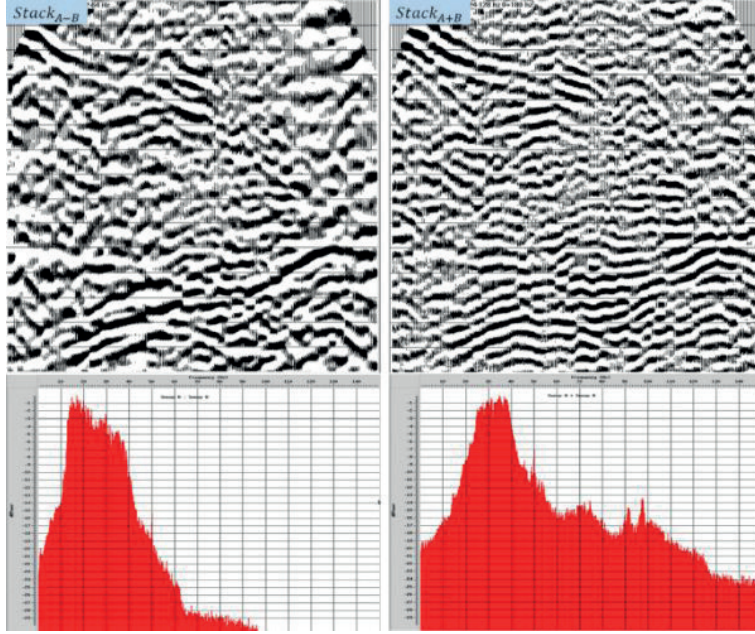
Şekil 5: [[Record]]\_(A+B) ve [[Record]]\_C ham arazi kayıtları ve genlik-frekans spektrumu.

Şekil-6

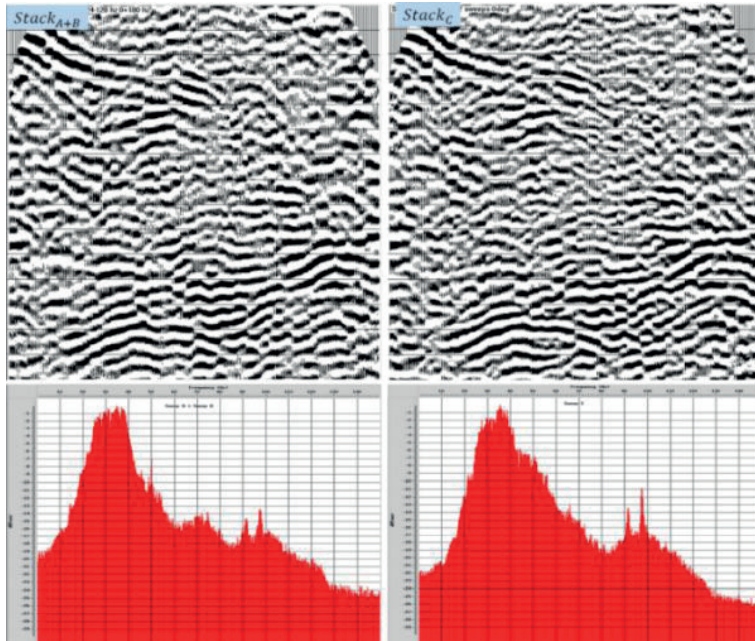


Şekil 6: [[Stack]]\_A ve [[Stack]]\_B proses kesiti ve spektrumu.

Şekil-7

Şekil 7:  $[(Stack)_{(A-B)}$  ve  $[(Stack)_{(A+B)}$  proses kesiti ve spetrumu.

Şekil-8

Şekil 8:  $[(Stack)_{(A+B)}$  ve  $[(Stack)_{(C)}$  proses kesiti ve spetrumu.

Tablo 1

Harmonik derecesi	$\theta$ (derece)	$k\theta$ (derece)	$k(f_1 \text{ to } f_2)$	$S_k(t, k\theta)$	Sweep <sub>A</sub> ( $\theta=0^\circ$ ) $f_1 \text{ to } f_2$	Sweep <sub>B</sub> ( $\theta=180^\circ$ ) $f_1 \text{ to } f_2$	Sweep <sub>C</sub> ( $\theta=0^\circ$ ) $2f_1 \text{ to } 2f_2$
k=1	0	0	$f_1 \text{ to } f_2$	$H_1 = S_1(t, 0)$	H <sub>1</sub>		
k=1	180	180	$f_1 \text{ to } f_2$	$-H_1 = S_1(t, 180)$	+	-H <sub>1</sub>	
k=2	0	0	$2f_1 \text{ to } 2f_2$	$H_2 = S_2(t, 0)$	H <sub>2</sub>	+	H <sub>2</sub>
k=2	180	360=0	$2f_1 \text{ to } 2f_2$	$H_2 = S_2(t, 2 \times 180)$	+	H <sub>2</sub>	+
k=3	0	0	$3f_1 \text{ to } 3f_2$	$H_3 = S_3(t, 0)$	H <sub>3</sub>	+	
k=3	180	540=180	$3f_1 \text{ to } 3f_2$	$-H_3 = S_3(t, 3 \times 180)$	+	-H <sub>3</sub>	
k=4	0	0	$4f_1 \text{ to } 4f_2$	$H_4 = S_4(t, 0)$	H <sub>4</sub>	+	H <sub>4</sub>
k=4	180	720=0	$4f_1 \text{ to } 4f_2$	$H_4 = S_4(t, 4 \times 180)$		H <sub>4</sub>	

Tablo 1: Sweep, faz ve harmonik ilişkisi

Tablo 2

Basic processing of field data					
	Stack <sub>A</sub> :	Stack <sub>B</sub> :	Stack <sub>C</sub> :	Stack <sub>A+B</sub> :	Stack <sub>A-B</sub> :
Input data:	Record <sub>A</sub>	Record <sub>B</sub>	Record <sub>C</sub>	Record <sub>A+B</sub>	Record <sub>A-B</sub>
Number of Shots	28	28	28	28	28
Data type	Uncorrelated data	Uncorrelated data	Uncorrelated data	Uncorrelated data	Uncorrelated data
Pilot sweep for cross-correlation	H <sub>1</sub> of Sweep <sub>A</sub> H1: 12-64 Hz	H <sub>1</sub> of Sweep <sub>B</sub> H1: 12-64 Hz	H <sub>2</sub> of Sweep <sub>C</sub> H2: 24-128 Hz	H <sub>2</sub> of Sweep <sub>C</sub> H2: 24-128 Hz	H <sub>1</sub> of Sweep <sub>A</sub> H1: 12-64 Hz
Geomety	yes	yes	yes	yes	yes
Deconvolution	yes	yes	yes	yes	yes
Elevation statics	yes	yes	yes	yes	yes
Velocity analysis-1	yes	yes	yes	yes	yes
Residual static-1	yes	yes	yes	yes	yes
Bandpass filter	yes	yes	yes	yes	yes
Normal Move Out (NMO)	yes	yes	yes	yes	yes
Common Mid Point (CMP) Stack	yes	yes	yes	yes	yes

Tablo 2: Temel veri işlem iş akışı.

# Innovative Distributed Acoustic Sensing Technology and Applications in Borehole Seismic

**Rafael Guerra**

SLB Wireline, Bucharest / Romania



## INTRODUCTION

For decades, borehole seismic surveys have consistently demonstrated their ability to bridge the scale gap between logs and surface seismic data, helping geoscientists calibrate and integrate seismic data processing and reservoir geophysical studies. This is achieved through direct in-situ measurements of travel times and of the seismic response; accurate calibration of velocity, anisotropy and anelasticity; quantitative seismic phase and amplitude at normal incidence and functions of offset and azimuth, for both P and S waves; higher resolution imaging around the wells, time-lapse seismic and microseismic monitoring. Borehole seismic also provides valuable stand-alone solutions where surface seismic is of poor quality, non-existent or is not cost effective due to the small size of the reservoirs.

Both microseismic and advanced VSP applications benefit from larger receiver array antennas. However, larger geophone arrays are slow to rig up and rig down, expensive to manufacture and maintain, and prone to downhole failure which can lead to costly downtime on expensive drilling rigs. Geophone arrays are not practical for time-lapse (4D) VSP monitoring in most completed wells due to poor coupling and data quality when recording inside the tubing and the need to shut down injection or production for several days. In addition, for long-term monitoring of induced seismicity, conventional digital geophone arrays can require regular maintenance, which can affect overall project feasibility and economics.

Distributed Acoustic Sensing (DAS) technology, using fiber optics as a passive sensor, has changed the borehole seismic landscape and beyond, introducing multi-physics applications and overcoming many of the limitations of conventional geophone tools mentioned above, while introducing some new ones. Its advantages include the versatility of deployment options, its reliability, high data density and real-time measurements, which explain its rapid adoption by the industry. DAS borehole seismic data can now be efficiently acquired over a wide range of fiber-optic deployments, including disposable fiber, slickline, coiled tubing, wireline or permanent installations. On wireline conveyance, DAS fibre-optic technology can be used with any tool string and acquire VSP data in minutes, eliminating the need for a dedicated geophone array and saving 12 hours or more of expensive rig time. When permanently installed, DAS provides passive downhole sensing operated from surface, cost effectively and on-demand, with no production deferral necessary while acquiring data, and with low operational risk and reduced HSSE exposure. The surface DAS laser interrogator systems have made continuous progress. For example, the latest interrogators allow two wells to be recorded simultaneously using a single low-

power DAS box, with maximum pulse frequency rate (PFR), wide dynamic range and no need for specially engineered fibers to achieve equivalent detection of very weak dynamic strain signals.

In addition, recent advances in downhole DAS seismic data processing, including flow-noise attenuation, full integration with surface seismic workflows, the use of elastic full waveform inversion (eFWI), and the application of machine learning automation and data streaming in microseismic projects, have brought a step change in the DAS data analysis.

Here, after a brief technical background, we will look at selected case studies to see how some of these DAS technology breakthroughs are driving a re-evaluation of borehole seismic methods, both in the oilfield and beyond, for example in CO<sub>2</sub> sequestration or geothermal monitoring.

## METHODS

DAS interrogator systems use laser light and the Rayleigh scattering effect to measure optical phase leads or lags in backscattered light due to local elastic shrinkage or elongation of the optical fibers caused by acoustic motion. The measured phase leads or lags are directly proportional to the relative fiber elongation or dynamic strain. Since laser pulses do not have infinite resolution, the measurement is made over a gauge length (GL), which for seismic applications is typically on the order of 10 m. This dynamic strain measurement is a moving average, within the GL window, along the optical fiber and effectively creates a filter in the wavenumber domain. This conditions the DAS directivity response to P and S seismic waves, which must be compensated for during data pre-processing for more advanced seismic applications (Sayed et al., 2020). The latest interrogator performance measured according to SEAFOM MSP-02 (using GL=6.4 m, standard single-mode fiber with a one-way insertion loss of 0.2 dB/km) allows two wells or fibers to be read simultaneously using a single low-power (100 W) DAS box, with maximum PFR = 20 kHz over 5 km, resulting in a wide dynamic range of 135 dB@10Hz and 155 dB@1 Hz, without the need for specially designed fibers, to achieve equivalent detection of very weak dynamic-strain signals (1.5  $\mu\text{e}\cdot\text{Hz}^{-1/2}$ ) at the front of a 5 km fiber. See Figure 1. A single DAS box can simultaneously acquire two fibers in a well, with different gauge lengths and sampling rates to suit each application, which may have different bandwidth requirements. For example, well integrity and flow-profiling applications analyze the spectrum from ~ 2 Hz to >1 kHz, microseismic monitoring from ~ 20 Hz to 800 Hz, seismic monitoring from ~ 2 Hz to ~120 Hz, and low frequency strain and temperature monitoring from ~ 0.001 Hz to 2 Hz.

In the mid-2000s, a prototype optical telemetry system based on a wireline heptacable with single-mode fibers was developed (Varkey 2008). Since 2013, this cable has been used to record several VSPs onshore and offshore (Frignet and Hartog, 2014) in combination with a variety of open-hole and cased-hole logging tools. Two challenges quickly emerged: ensuring cable coupling to the borehole wall, and the ability to manufacture high-strength hybrid cables that would allow logging of the deeper or most complex wells. The former is key in vertical wells, and cable slack was used to increase the number of contact points between the cable and the borehole wall. The latter is key in deep and/or highly deviated wells to allow high force pulling and release of stuck tools or cables. The first hybrid logging cables tested since the end of 2013 had a Safe Working Load (SWL) of 10-13 klbf [44-58 kN], but finally in 2021 the first hybrid high-strength torque-balanced wireline logging cables were commercialized with a SWL = 18 klbf [80 kN], capable of conveying any wireline logging tool, including geophone array tools. Other types of fiber optic conveyance are comparatively much less challenging to manufacture (cemented fibers permanently installed or clamped to tubing semi-permanently, conveyed on coiled tubing, coaxial logging cables or slickline).

## RESULTS

DAS seismic and microseismic data have been successfully recorded in various types of fiber-optic cable deployments: cemented, strapped to tubing under flow, coiled tubing, coaxial wireline cable and hybrid wireline heptacable (Figure 3).

For microseismic applications, most published examples correspond to fiber-optics cemented behind the casing in monitor wells, as shown in Figure 3a where DAS data (labelled hDVS – heterodyne Distributed Vibration Sensing) are compared with geophones clamped in the same monitor well (Molteni and Williams, 2016). Excellent DAS microseismic data have also been obtained using hybrid coiled tubing wireline cables deployed in monitor deviated/horizontal wells and relying solely on gravity for coupling, as shown in Figure 3d (Wilson, 2021, SLB published data). Single-component (1C) DAS axial strain measurements, unlike 3C geophones, do not allow the azimuth of microseismic events to be determined, only the distance of the event from the borehole and its depth, and an approximate event magnitude. This may not be a limitation in some applications where depth is the primary parameter of interest, such as in monitoring the integrity of reservoir seals. To our knowledge, there are currently no published examples of microseismic events mapped using DAS fibers deployed in live flowing wells. However, this is not the case for DAS VSPs using active seismic sources.

In an offshore oil producing field, four wells instrumented with fiber-optic cables clamped to tubing were used to acquire DAS 3DVSP data along with six airguns deployed from a supply vessel (Figures 3b and 4). The main objective was to verify the

applicability of the technology in a producing field that had a deltaic reservoir formed by thin clinoform sands. The results showed that the DAS 3D VSPs can be acquired even in high-noise producing wells, as long as a rigorous processing sequence is applied (Ali et al, 2021). Production related noise was dominant in lower frequencies up to 35 Hz and was distributed over a range of velocities in the shot domain. Tau-p and FX infinite-impulse-response dip filters were used to remove the very low velocity components of this noise. Tau-p domain denoising was also used to attenuate the constant velocity noise. The operator concluded that it was possible to improve the geological knowledge, due to the higher resolution of the DAS VSP depth images and by incorporating a multi-scale integration approach (Liborio et al., 2023). The results showed potential for 4D DAS time-lapse studies and a monitoring survey was planned.

Not all wells have optical fibers installed and wireline or coiled tubing (CT) conveyance can then be used to acquire DAS VSP data on demand, for example if a surface seismic survey is planned in the area. Real-time downhole CT logging services have introduced multi-mode and single-mode fiber inside the CT, enabling the possibility of DAS seismic acquisition. In a CO<sub>2</sub> storage research project onshore Japan, a CT walkaway DAS VSP was recorded in a highly deviated well using vibroseis sources. The tube wave noise was very strong but could be handled during data processing (Figure 3c). The conclusion was that cost-effective seismic monitoring of CO<sub>2</sub> storage could be achieved with the DAS CT method without drilling a new observation well (Kimura et al., 2017; Kobayashi et al., 2020).

For exploration and appraisal wells, while some operators record seismic while drilling on LWD, the most common situation is to wait until the final phase of drilling to record borehole seismic data on wireline along with other logs. At this point, there are often multiple casing strings that are not cemented, making it impossible to record quality VSP data up to shallow depths. Using conventional geophone arrays, each survey takes approximately 12 hours from rig up to rig down. Hybrid logging cable technology allows the elimination of the extra seismic run, as DAS VSPs can now be acquired during any other logging run. Onshore Colombia, an operator successfully acquired a wireline DAS vibroseis VSP in 1 h in an S-shaped well, with approximately 3 m of cable slack (Figure 3e) during an intermediate sonic run (Martinez et al., 2020). Offshore Norway, an operator acquired a wireline DAS VSP during a formation tester run in a vertical well with 20-30 m of cable slack (Figure 5a), with a reduced number of shots and saving 12 h of operational time compared to a dedicated geophone array run, also minimizing the impact on marine biodiversity and reducing the greenhouse gas emissions by an estimated 33 tonnes (Guerra et al., 2020). Similarly, offshore UK, another operator acquired a wireline DAS VSP during a sonic run in a deviated well in less than 1 hour, this time using the new high-strength hybrid logging cable with a safe working load of 18 klbf [80 kN] (Figure 5b).

Only 5 ft of cable tension relief was applied. Again, a reduced number of shots was required (30 versus 3000), reducing the total operating time by 12 hours, minimizing the impact on marine biodiversity and reducing CO<sub>2</sub> emissions (Guerra et al., 2023).

One of the challenges faced by DAS microseismic monitoring projects is the large size of the recorded files, due to the fine spatial and temporal sampling used, and the long fiber antenna. Currently, microseismic events can be detected automatically in the field, using both standard methods and machine learning. The short data segments of interest are extracted and further processed in the field using resampling and compression algorithms, before being streamed in near real-time to the cloud for remote automated interpretation and integration with other data. This workflow has been successfully applied to an onshore USA geothermal project (Figure 6). It is also possible to provide email alerts with the mapped location of any event that exceeds a pre-defined threshold, and to implement a traffic light system, if required by local regulations.

## CONCLUSION

Through a series of case studies, we have seen how Distributed Acoustic Sensing (DAS) technology, which uses fiber optic as a passive sensor, is changing the borehole seismic landscape by overcoming many of the limitations of conventional geophone tools. Its advantages include the versatility of deployment options, its reliability, high data density and real-time measurements, which explain its rapid adoption by the industry. DAS borehole seismic data can now be efficiently acquired over a wide range of fiber-optic deployments, including disposable fiber, slickline, coiled tubing, wireline or permanent installations. On wireline conveyance, DAS fibre-optic technology can be used with any tool string and acquire VSP data in minutes, eliminating the need for a dedicated geophone array and saving 12 hours or more of expensive rig time. When permanently installed, DAS provides cost-effective, on-demand, surface-operated, passive downhole sensing without the need to interrupt production during data acquisition, with low operational risk and reduced HSSE exposure. The DAS surface laser interrogator systems have continued to evolve, with the latest interrogators allowing two wells to be recorded simultaneously using a single low power DAS box, with maximum pulse frequency rate (PFR), wide dynamic range and no need for special fibers, to achieve equivalent detection of very weak dynamic strain signals.

## REFERENCES

Ali, S., Miranda, F., Spadavecchia, E. and Aguilar, C. [2021] Processing of a large offshore 3DVSP DAS survey in a producing well. SEG/AAPG/SEPM First International Meeting for Applied Geoscience & Energy

Dean, T., Cuny, T. and Hartog, A. [2017] The effect of gauge length on axially incident P-waves measured using fibre-optic distributed vibration sensing.

Geophysical. Prospecting 65

Frignet, B. and Hartog, A. [2014] Optical Vertical Seismic Profile on Wireline Cable. SPWLA-2014-FFFF

Guerra, R., Cuny, T., Kimura, T., Rufino, R., Danielsen, J. and Kamp, W. [2020] hDVS/DAS VSP Recorded While Logging Formation Tester in Vertical Well, Offshore Norway: 82nd EAGE

Guerra, R., Bajwa, H., MacLeod, P. and Sanger, K. [2023] Ultra-strength fibre optics logging system acquires DAS VSP in minutes, offshore UK: 84th EAGE Conference & Exhibition.

Kimura, T., Chen, Y., Kobayashi, Y., Xue, Z. and Adachi, K. [2019] DAS VSP Acquisition Through Coiled Tubing Fiber-Optic Cable. 5th EAGE Borehole Geophysics Workshop

Kobayashi, Y., Uematsu, Y., Mochiji, S. and Xue, Z. [2020] A field experiment of walkaway distributed acoustic sensing vertical seismic profile in a deep and deviated onshore well in Japan using a fibre optic cable deployed inside coiled tubing. Geophysical Prospecting, 68(2), pp.501–520

Liborio, C., M. Fervari, Mariotti, M., A. Cerliani, Miranda, F. and Ferla, M. [2023] Closing the gap between seismic and well data with 3D DAS VSP: an integrated workflow. 84th EAGE Conference & Exhibition

Martinez, A., Useche, M. and Guerra, R. [2020] Use of Fiber Optics Acoustics to Improve Drilling Efficiency and Well Placement. Offshore Technology Conference, Houston, TX

Molteni, D., Williams, M. and Wilson, C. [2016] Comparison of Microseismic Events Concurrently Acquired with Geophones and hDVS. 78th EAGE Conference & Exhibition

Sayed, A., S. Ali, and R. R. Stewart [2020] Distributed Acoustic Sensing (DAS) to velocity transform and its benefits. SEG Technical Program Expanded Abstracts

Varkey, J., Mydur, R., Sait, N., Wijnberg, W., Kunathikom, S. and Darpi, M. [2008] Optical fiber cables for wellbore applications, Patent US7324730 B2

Varkey, J., Grisanti, M., Kim, D. and Huang, Q. [2019] Cladding for an electro-optical device. Patent US11668872

Keywords: borehole geophysics, DAS (distributed acoustic sensing)



Figure 1: Lab based SEAFOM measurements at the front of a 5 km standard single mode fiber using (a) Sintela DAS interrogator and (b) DAS wave-number filters as functions of GL and velocity for axial P-waves (Dean et al., 2016).

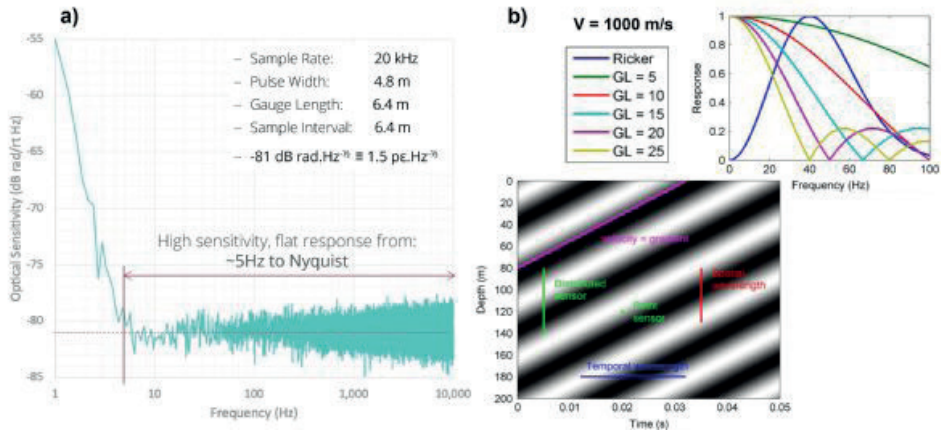


Figure 2: (a) High-strength torque balanced hybrid heptacable and (b) hybrid collector to enable electrical and optical signals to pass from the rotating cable drum to the instrument cabin (Varkey et al., 2019).

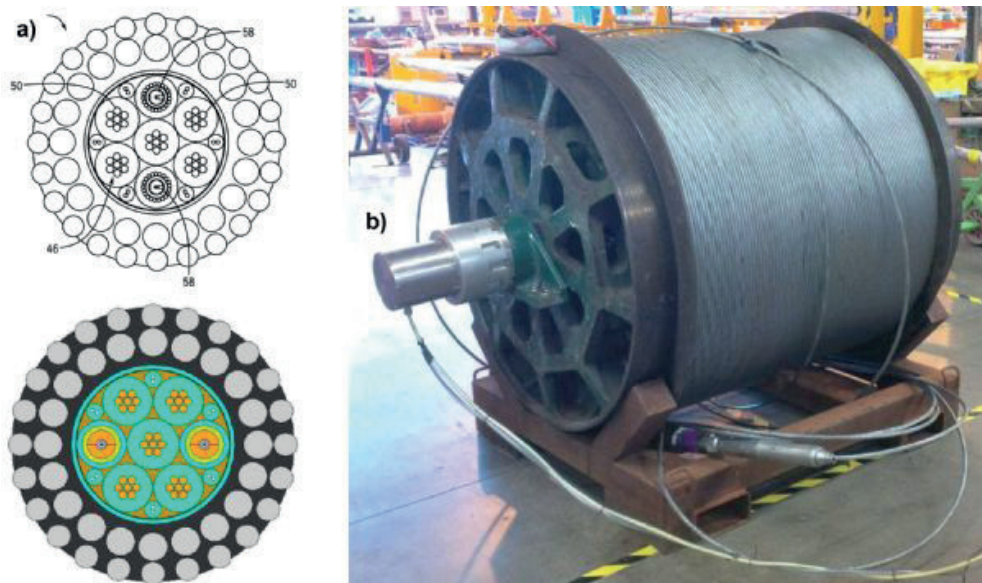


Figure 3: DAS seismic and microseismic data recorded in various types of fiber-optic cable deployments: (a) cemented, (b) strapped to tubing, (c) coiled tubing, (d) coaxial cable and (e) hybrid wireline heptacable. See text for reference list.

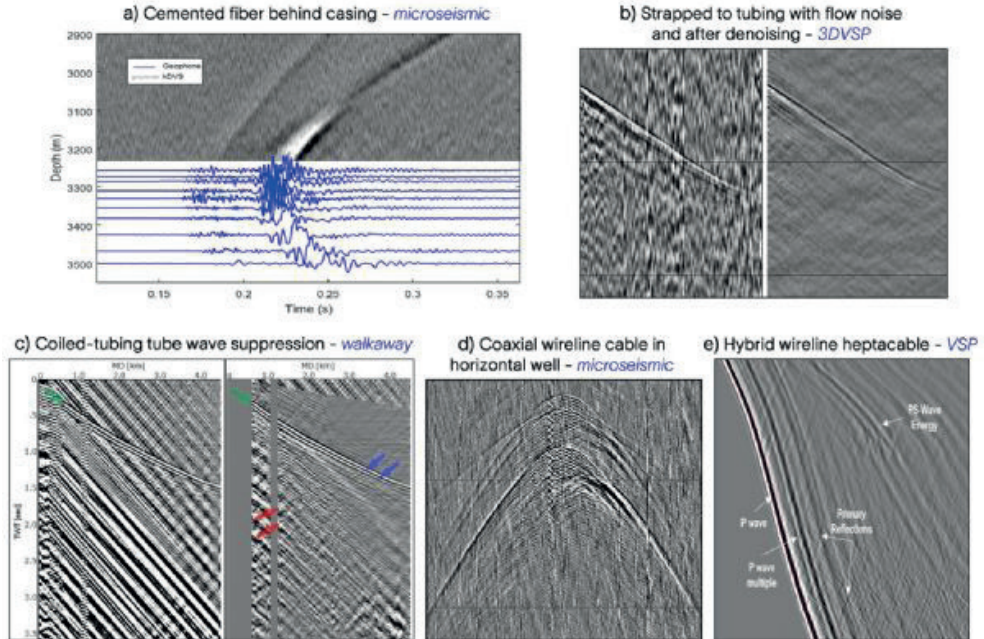


Figure 4 - DAS 3DVSP acquired in 4 producers, with 10,000 shots; (b) Oil flow noise before and after noise attenuation along with the RTM 3DVSP image (Ali et al., 2021); (c) 3D PSDM and 3DVSP DAS interpretations compared (Liborio et al., 2023).

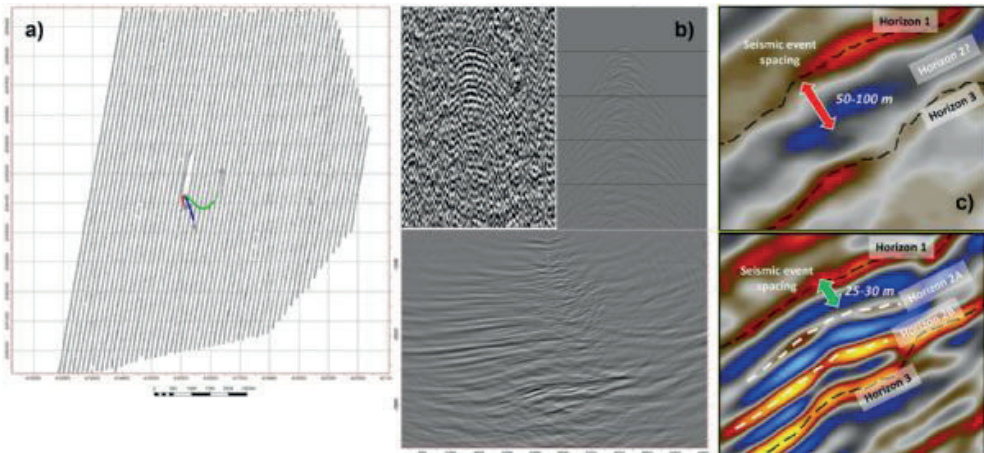


Figure 5: (a) ZVSP acquired in vertical well offshore Norway using hybrid logging cable during formation tester run, compared to geophone VSP and (b) ZVSP acquired in deviated well offshore UK using high-strength hybrid logging cable during sonic run

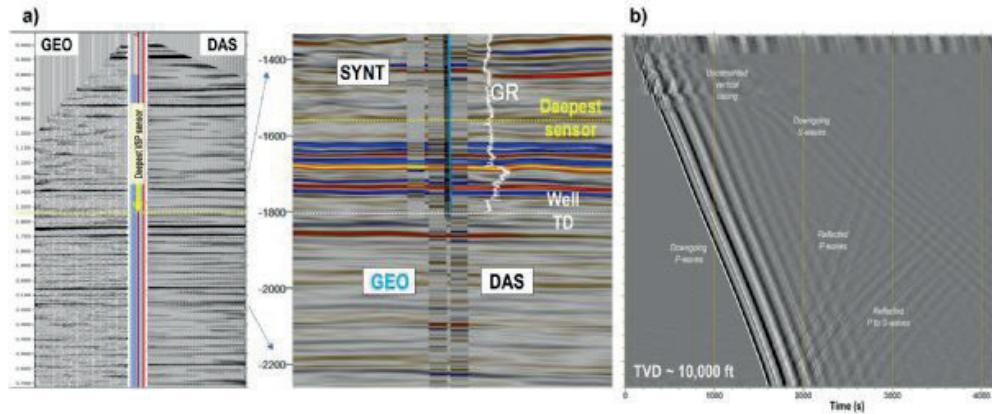
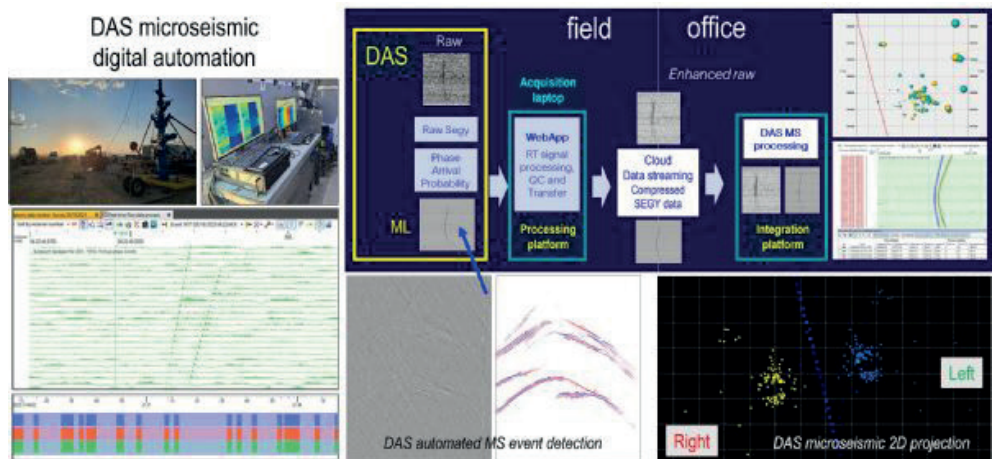


Figure 6 - Example of DAS automation during geothermal monitoring project, onshore USA (Mizuno, 2023, SLB published data). As there is no azimuthal information in 1C DAS data, the projection plane must be defined a priori.



# Low Frequency Single Geophone Versus Standard Geophone Array; A Field Test Study in the SE Turkey

**Yılmaz Sakalhoğlu, Zhao Mingqiu, Chen Xin**  
BGP Inc. CNPC Abu Dhabi



## SUMMARY

A field test was carried out in the SE Turkey to compare 2D seismic data acquired using single low frequency geophone (4.5-Hz) and a standard twelve-element geophones (10-Hz) inline array. Shallow layers data quality is good but deep reflections are fuzzy in the conventional data recording. The aim of this test study was to illuminate a deep target (1.5 - 1.6 sec) reservoir by the recording of broadband data. The main results of this field study are as follows; (1) 10-Hz standard geophone type output sensitivity is 110 v/inch/s lower than 4.5-Hz geophone type sensitivity; (2) 10-Hz geophone has a fall off in amplitude below its natural frequency of 12 dB/oct. and signal is -3 dB down at 10-Hz; (3) Field records showed that surface noises effects are less with 10-Hz geophone type due to inline arrays but there is high frequency noises which are dominated on shot records; (4) Low frequency geophones data shows consistently strong amplitudes on the deep reflections; (5) Amplitude-frequency spectrum analysis shows that low frequency geophones provided 8-dB higher amplitude at 4.5-Hz; (6) Deep reservoirs have stronger signal amplitudes with 4.5-Hz geophone type and low frequency contents of the data provide better deep data imaging, and useful for the P-impedance inversion processing.

## INTRODUCTION AND FIELD TEST

Low frequency seismic data recording is considerably growing in land seismic data acquisition. There are numerous recorded field data in which low frequency components of the reflected waves show surprising imaging capabilities. Advances in land data acquisition equipment and techniques allow us to use modern vibrators which are emitting low frequency sweep and also low natural frequency geophone types to improve deep data imaging. In the past often low frequency components are filtered during the processing stage. Besides, geophone type is a critical parameters of seismic data recording especially for the capturing of low frequency components of the signal. We demonstrate comparison of 4.5-Hz geophone data to 10-Hz standard geophone data and present how deep reservoirs data quality improved by the implementation of the low frequency data recording.

Generally 10-Hz natural frequency geophone types and 8-Hz vibroseis sweep start frequency are used in land seismic data acquisition. This test study presents how low frequency data recording is possible with single 4.5-Hz natural frequency geophone type and 5-Hz sweep signal start frequency with standard vibrators and how much better would it really be to use 4.5-Hz single geophone type to improved data quality in the foreland areas of South East Turkey? The study area is located at

the foothills of the over thrust zones of SE Turkey and about 20-km Eastern side of Diyarbakir City. Surface condition is partly undulated, covered with clastics sand stones and river beds. The main purpose of this study is to record better data from Palaeozoic age sand stones reservoirs and to get better data imaging on P-impedance inversion sections for the reservoir characterisation. A 20-km long 2D test line has designed to record better data from deep target horizons. Two receiver lines laid out with 50-m receiver group interval and 50-m lateral apart each other. Line-A equipped with single 4.5 Hz geophone type and Line-B equipped with twelve elements, standard 10-Hz geophones type in inline array. Source line laid out in the mid-way between the receiver lines with 50-m shot group interval. Location of the study area and a schema of the receivers and shot lines layout is shown in the Figure 1. Active recording channel number is 200, maximum fold number is 100. Linear sweep signal imparted with 5-84 Hz sweep signal band and 16-seconds length.

This field study is the first low frequency data recording in the SE Turkey. The main objective of the survey area was to illuminate a deep target at about 1.5 – 1.6 seconds. Shallow layers data quality is good but deep Paleozoic age target horizons are fuzzy in the standard data recording techniques. We were expected that a 4.5-Hz geophone type and sweep starting from 5-Hz may help to record better data from deeper targets.

## Comparison of Low Frequency Geophone Data to Standard Geophone Data

The natural undamped frequency of the geophone type is a important factor for low frequency data recording and have a great influence on data quality. For this reason, we have tested two types of vertical component geophones currently used in the over thrust zones and platform areas of SE Turkey. Type-A; Single geophone element with 4.5-Hz natural frequency, and output sensitivity is 0.810 v/inch/s. Type-B; natural frequency 10-Hz with twelve geophone elements in a string and inline array length 25-m. Type-B geophones are named as standard geophone and output sensitivity is 0.689 v/inch/s. 10-Hz geophone has a fall off in amplitude below its natural frequency of 12-dB/Oct. Signal will be -3dB down at 10-Hz. The tested geophone types characteristics and amplitude – frequency response curves are shown in the Figure 2. Low frequency geophones are always useful for low frequency data recovery, but mind also sensitivity especially when using single geophones. Based on the penetration of the 5-Hz start frequencies of the sweep signal and recording of low frequency components of the data, we analyzed seismic data quality acquired in the tested 2D lines. We demonstrate comparison of 4.5-Hz geophone type

stack data to the 10-Hz geophone type data and present deep target horizons data quality improvement by the acquiring of low frequency data.

A preliminary comparison carried out on raw field data with amplitude-frequency spectrum and vertical resolution analysis of both geophone types data. Raw field data shows that surface noises effects are less with standard geophones due to inline arrays but there is high frequency noises which are dominated on shot records. Low frequency geophones data shows consistently strong amplitudes on the deep sections of the field records. In the light of amplitude-frequency spectrum analysis, we understood that low frequency geophones provided 8-dB higher amplitude at 4.5-Hz. The upper stack section with 4.5-Hz geophone data in Figure-3 shows where reflections amplitudes continuity, consistency and strength at deep targets are significantly improved compared to the bottom side 10-Hz standard geophone data. This improvement can be attributed to the recording of low frequencies.

One another advantages of low frequency data recording is seen on P-impedance inversion processing stage. As shown in Figure 4, P-impedance inversion section with 4.5-Hz geophone data presents better imaging of the sandstones reservoir description in the deep targets at about 1.5-1.6 seconds. Lateral continuity of the reflections and also vertical resolution of the data especially in deeper parts are improved with low frequency data recording. But deep parts of the P-impedance inversion section with 10-Hz geophone data are not as good as 4.5-Hz geophone data.

## CONCLUSIONS

There are significant advantages of using low frequency geophone type and recording of the low frequency data in the SE Turkey in processing stage and also in reservoir characterization studies. Deeper targets have stronger reflections by the using of 4.5-Hz geophone type and 5-Hz sweep start frequency. Low frequency contents of the data provide better deep data which standard data recording provides fuzzy data imaging. Low frequency geophones are provide coherency with deep targets and useful for the P-impedance inversion processing.

## REFERENCES

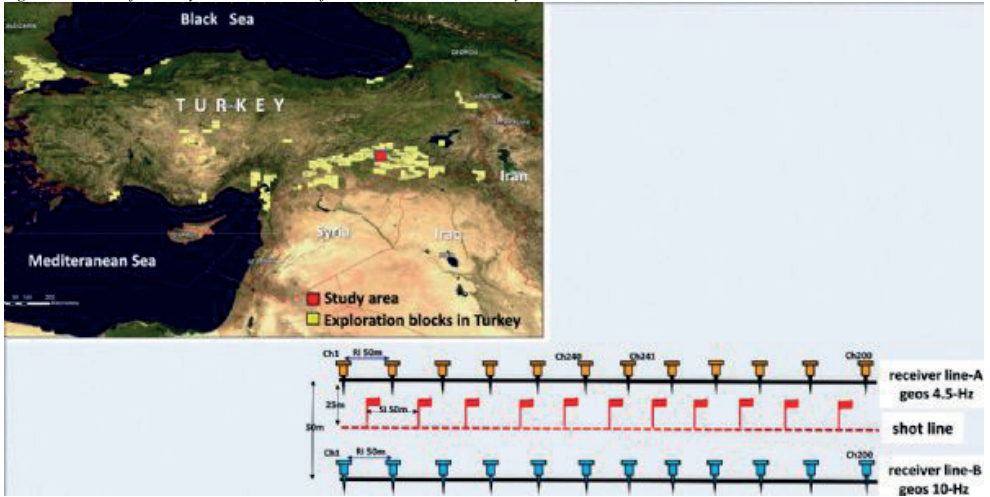
Archer, J., Bell, L., Hall, M., Margrave G., Hall, K., and Bertram, M., (2012), Obtaining low frequency seismic data, onshore and in shallow water: First Break, 30, 78-87.

Gureli O., Sefunc A., Basar H.S., Akdeniz, A., and Kayiran T., (2000), "Variation Of Amplitude With Sweep Parameters" 1th Turkish International Oil and Gas Congress and Exhibition-TURKIOG, 41-43.

Peter Maxwell, Malcolm Lansley (2011), What receivers will we use for low frequencies? SEG San Antonio 2011 Annual Meeting.

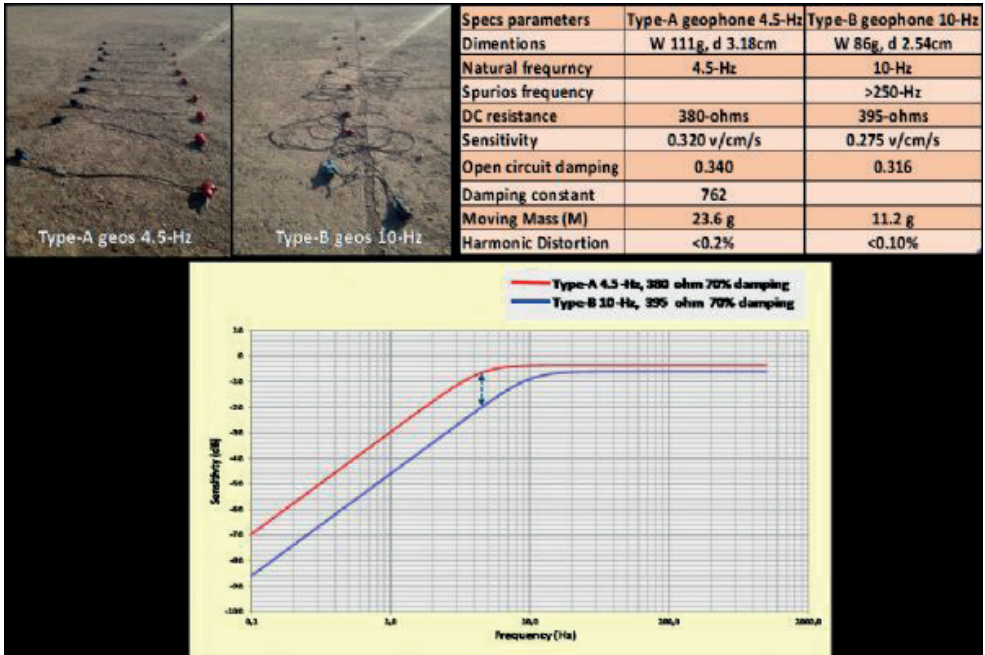
Sakallioğlu Y., Gureli O., and Basar H.S., (2012), Vibrosismik text book, Altan Press, 396 pages.

Figure 1 Location of the study area and schema of the receiver and shot lines layout.



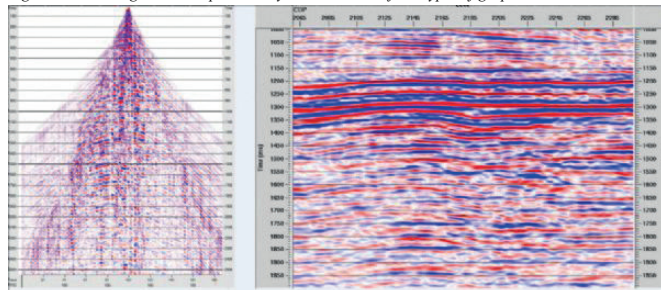
Introduction and field test basligi altindaki paragraftan sonra yerlestir

Figure 2 Geophones field layout, characteristics and amplitude – frequency response of the geophone type-A and type-B.

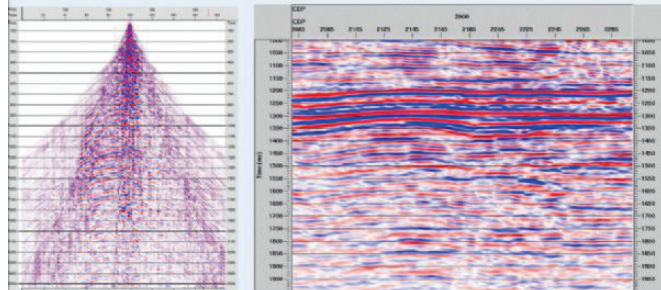


Comparison of Low Frequency Geophone Data to Standard Geophone Data basligi altindaki paragraftan sonra yerlestiriniz.

Figure 3 Raw shot gathers and preliminary stack sections of two types of geophone data.



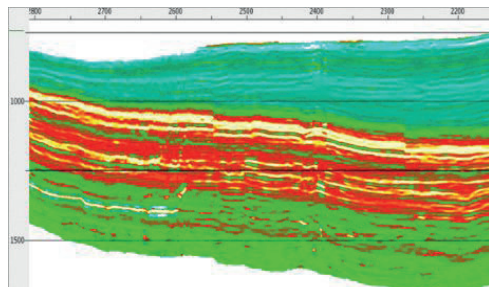
a) Raw shot gather and stack data from type-A 4.5-Hz geophones.



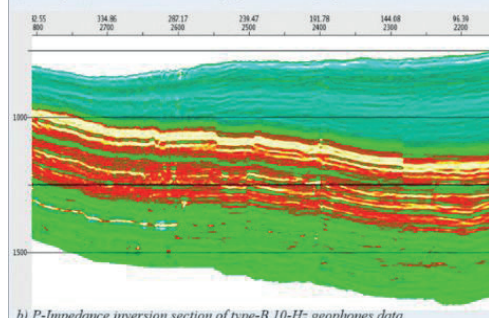
b) Raw shot gather and stack data from type-B 10-Hz geophones.

Comparison of Low Frequency Geophone Data to Standard Geophone Data baslignin son paragrafi altına yerlestiniz.

Figure 4 Comparison of the P-impedance inversion sections of type-A and type-B geophones data.



a) P-Impedance inversion section of type-A 4.5-Hz geophones data.



b) P-Impedance inversion section of type-B 10-Hz geophones data.

Conclusions dan once yerlestiniz.







## **Sismik Veri Yorumlama ve Analizi**

*Seismic Data Interpretation*

---



# Seismic Facies Analysis: From Basin to Prospect, From Visualisation to Value



Simon Mann<sup>1</sup>, James Ostriko<sup>2</sup>, Stefane Gesbert<sup>3</sup>

<sup>1</sup>Shell Global Solutions, London / UK.

<sup>2</sup>Shell International Exploration and Production, Houston / USA.

<sup>3</sup>Shell Global Solutions, Netherlands

## INTRODUCTION

Seismic facies analysis is a fundamental tool for interpreting seismic data within the exploration evaluation workflow. The aim is to convert geophysical data into a geological model that can then be used to evaluate the chance of finding hydrocarbons and the potential range of in-place volumes. Seismic facies can be characterized using multiple seismic attributes. Each attribute is a “filter” that discards part of the data to highlight features of geological interest. In this paper, the definition of ‘seismic facies’ is not restricted to geological facies only, rather “a group of seismic amplitude variations with characteristics that differ distinctly from those from other facies” (3).

Figure 1. Camouflaged snake (Thayer 1915)

## METHOD

Seismic attributes can be used to identify and constrain various important subsurface parameters: e.g., stratigraphy, structure, rock properties, fluid type and more. Specific examples include (1) Amplitude extractions, for example peak, trough, envelope & AVO for elastic impedance contrasts, (2) Waveform/frequency extractions, for example spectral decomposition for bed spacing, bed thickness and stratigraphy, (3) Continuity extractions, for example coherency, dip/azimuth & chaos for structural geology (faults, fractures) and stratigraphy (lateral strata continuity and facies changes) and (4) Configuration extractions, for example dip, curvature, instantaneous phase, and more generally reflector stacking patterns for bedding patterns, depositional processes, erosion & paleo-topography.

Figure 2. What are Seismic Attributes?

The wavelength of seismic data limits the ability to detect and resolve features. Seismic detection is the ability to identify that some features exist, typically below  $\frac{1}{4}$  wavelength. Seismic resolution is the ability to distinguish between two features and typically exists above  $\frac{1}{4}$  wavelength. Below  $\frac{1}{30}$  wavelength there simply is not enough data to resolve any features.

Figure 3. Resolution, Detection and Broadband.

Seismic Facies Analysis using seismic attributes can be applied at various scales: from basin understanding to play mapping; lead identification and through to prospect maturation. Historically the resolution of the seismic data tracks the workflow: from regional, sparse, full stack, legacy 2D deployed for basin understanding; through to 3D seismic data in zones of interest for play mapping and lead identification; and finally, multi-dimensional seismic attribute interpretation on modern broadband 3D or repeat 3D (4D) data. As global

coverage of seismic data increases, mega-merge 3D datasets are being created which can occasionally span an entire basin. This allows for improved basin and play understanding, while identifying more leads within a broad regional context, and better understanding their risk profile and constraining their potential volumes. Figure 4. PBE and Seismic Attributes, from basin to play, from lead to prospect.

## FINDINGS

At basin scale, modern extraction tools can semi-automatically interpret 10s to 100s horizons across large datasets. These grids can be used to constrain basin fill and burial history. When coupled with attributes such as waveform classification and spectral decomposition, stratigraphic, geomorphological, and EOD interpretation can be made.

Figure 5. Basin Fill - Depositional Environment.

At play scale, single reservoir / seal pairs can be seismically “sculpted” across a basin and interpreted. Well data can then be integrated to constrain and calibrate the interpretation, for example, biostratigraphic information for EOD and GDE setting and various log data for geological facies. This integration of well data with seismic geomorphology helps to translate qualitative regional work into quantitative predictions. For example, EOD polygons can be created (e.g., Lower Delta Plain) that contain risk prediction (number of wells that have found reservoir) and rock property prediction for use in volumetrics (e.g., bed thicknesses, widths, NTG, porosities, etc.)

Figure 6. Play Definition - Reservoir Extent

At lead level, screening various qualitative and quantitative seismic attribute volumes directly supports lead identification. Whether a quantitative QI attribute volume for identifying reservoir rocks and potential Direct Hydrocarbon Indicators, or a more qualitative seismic geomorphological attribute volume for constraining potential stratigraphy traps.

Figure 7. Lead Refinement: channels and lobes

Once down to prospect scale, more quantitative seismic facies analysis can help to constrain prospect risk and volumetrics. For volumetrics the main impact is on GRV, where commonly hydrocarbon column height has the main impact and can occasionally be constrained via seismic observations. In addition, certain seismic responses can only be explained by the presence of hydrocarbons, in this scenario the POS can be modified accordingly.

Figure 8. Application of Seismic Facies Analysis to Prospect Risk and Volumes

CONCLUSIONS

Seismic facies analysis is an integral tool for interpreting seismic data within the exploration evaluation workflow. Analysis can be applied at various scales: from basin understanding to play mapping; lead identification and through to prospect maturation. As technology improves across seismic acquisition, processing and interpretation, the application of this workflow will continue to be a core component of the exploration evaluation workflow.

Keywords: Seismic Facies Analysis, Seismic Attributes

Figure 1. Camouflage Snake (Thayer 1915)



Figure 2. What are Seismic Attributes

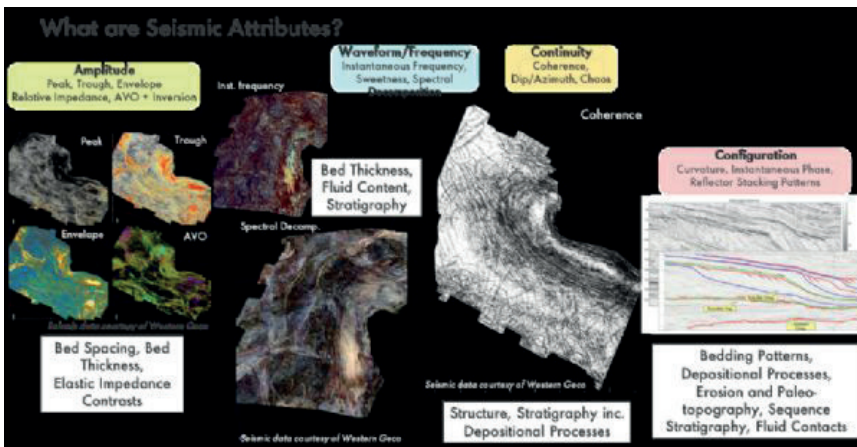


Figure 3. Resolution Detection & Broadband

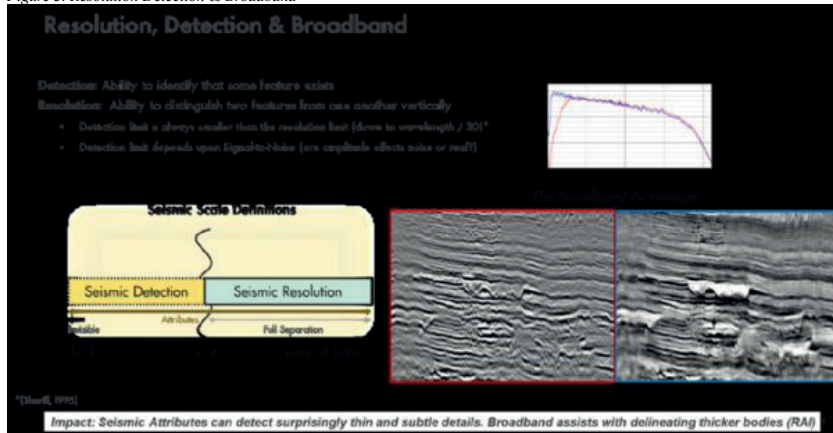


Figure 4. PBE and Seismic Attributes, from basin to play, from lead to prospect

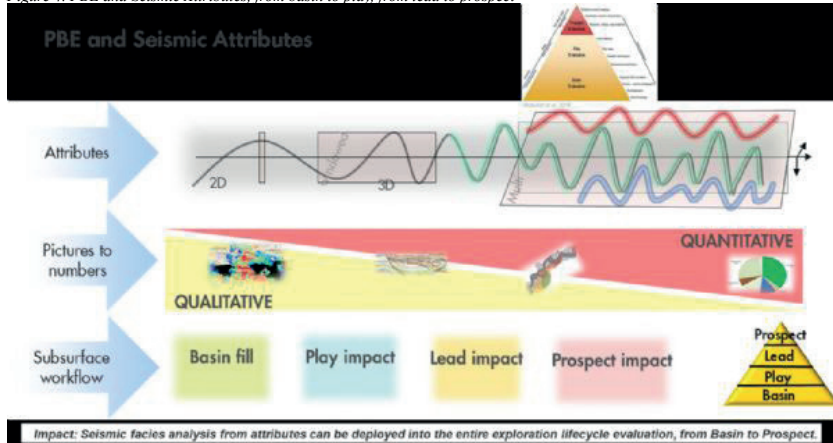


Figure 5. Basin Fill - Depositional Environment

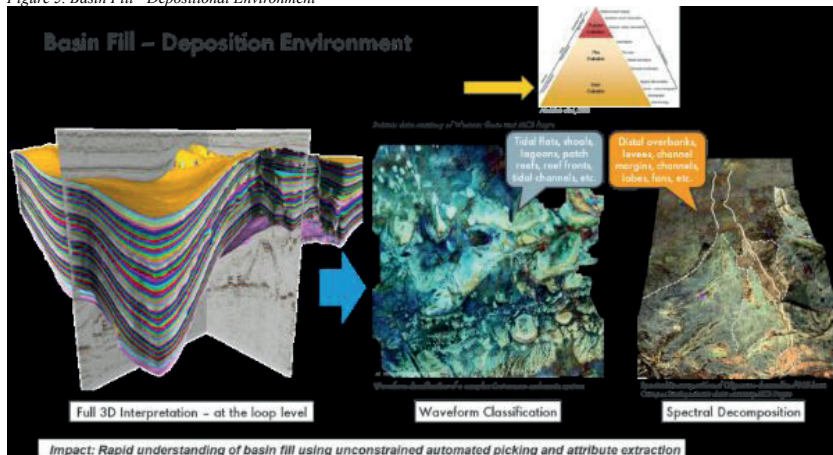


Figure 6. Play Definition - Reservoir Extent

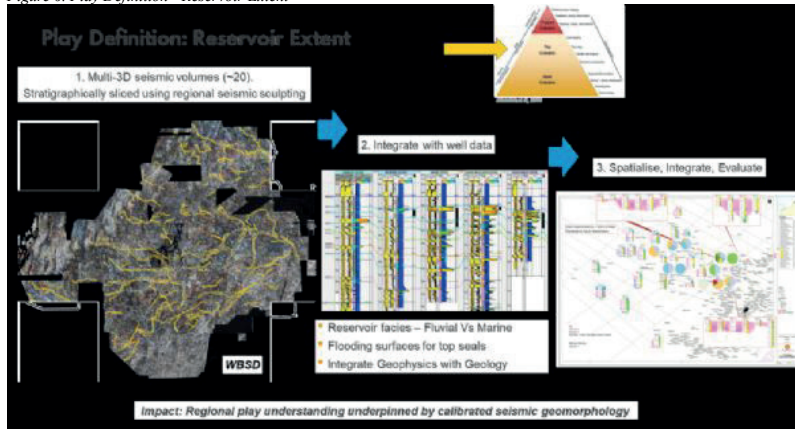


Figure 7. Lead Refinement, Channels and Lobes

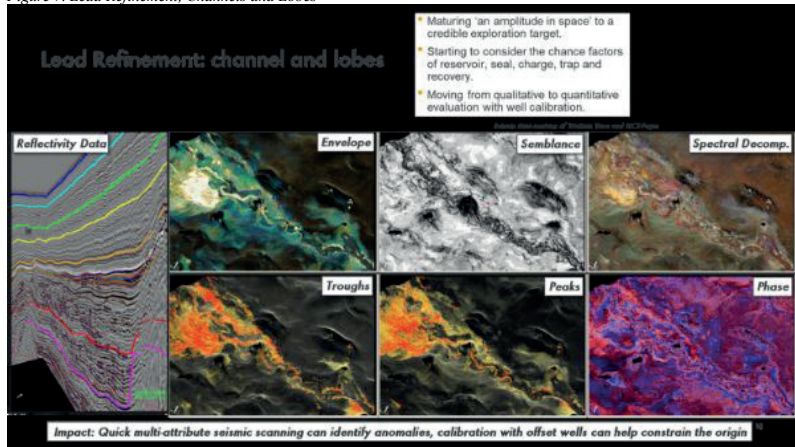
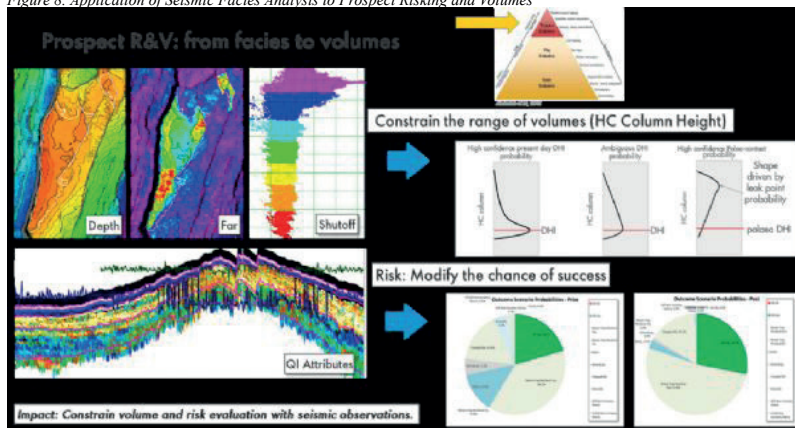


Figure 8. Application of Seismic Facies Analysis to Prospect Risking and Volumes





**Sondaj Mühendisliđi**

*Drilling Engineering*

---





# Planning and Execution of A Horizontal Well in Southeast Anatolian Field: Advanced Processes and Technologies for Drilling and Logging



Ihsan Kaya<sup>1</sup>, Davide Di Tommaso<sup>2</sup>, Inan Sare<sup>2</sup>, Shahbazi Kaveh<sup>2</sup>

<sup>1</sup>TPAO

<sup>2</sup>Weatherford

## INTRODUCTION

Many wells were drilled in the oil rich carbonate reservoirs of the Southeast Anatolian region, but the paper will discuss and present the drilling of the first horizontal well in the specific field, from planning to execution. It will show how the lessons learned from previous horizontal wells in similar formation helped to predict some of the key directional drilling challenges and choose the most suitable technologies and procedures to reach and drill in the carbonate pay-zone.

Most recent processes and technologies were used: from drilling engineering for bottom hole assembly (BHA) optimization to novel push-the-bit rotary steerable system (RSS), from geosteering technique to advanced logging while drilling (LWD) measurements, from pre-drill modelling to real time monitoring using web-based platforms.

The robust drilling engineering processes not only allowed drilling safely to total depth, but also delivered benchmark performances across the way.

## METHODS

After some discussion between operator and service company three key risks were identified, based on the experience in previous wells with same stratigraphy (figure 1), and listed below:

- Losses in the lower Germav formation.
- High lateral and stick-slip vibration with consequent steering control and BHA damage when drilling the Garzan formation, especially in the horizontal section.
- Low contrast in logging measurements which makes it difficult to find the right LWD tool to characterize the formation layers within the reservoir and place the well in the most favorable one for production.

The Drilling Engineering quality process was followed to enable the operator to safely achieve its drilling schedules while ensuring accurate well positioning by means of directional drilling and geosteering service:

**Design.** This stage initiates the workflow by establishing and aligning the scope of work, project requirements and key performance indicators (KPIs). A risk assessment was conducted to identify and communicate all risks, as well as establish the control measures and contingency plans.

During this stage the service provider performed anti-collision study, modelling for torque and drag and hydraulic using multiple combinations of parameters (figure 2), and advanced vibration analysis, using different assembly options as inputs, to establish best configuration, stabilization and drilling parameters

based on the drilling program from Operator (figure 3). In parallel a pre-job feasibility study, based on offset well data, was incorporated into the meeting for validation of the technologies required, to discuss any uncertainties, and to establish a well placement strategy with the Operator.

Based on those analysis some solution to the key risks and challenges were proposed:

- Modify well architecture to add an extra 11-3/4" liner to isolate loss zone from mobile formations in Upper Germav (figure 4).
- Use of push-the-bit rotary steerable (RSS), with full collar rotation, to reduce stick-slip while providing greater rate of penetration (ROP), lower surface torque and smooth dog-leg severity (DLS).
- Use of an advanced LWD spectral and azimuthal gamma ray, highly sensitive even in a low contrast like this, together with LWD sonic, to determine top of Garzan in the 10 5/8" section and as main geosteering tool in the 8 1/2" section until total depth of the well.

## EXECUTION

The second stage of the process covers the execution of the drilling program, whereby the drilling engineering team monitored the services in real time, to optimize drilling performance, and to identify and mitigate hazards. Directional and logging while drilling data, specifically near bit inclination and gamma ray, spectral azimuthal gamma ray and sonic, were monitored and analyzed by geosteering specialists against the model to correlate and get bedding dip from the image to position the well in the right interval (figure 5). During this phase, digitalization and automation solutions were critical to gather, consolidate and process data from multiple sources, using Weatherford built-in intelligence to expand the analytical capacity of the drilling engineers. For this scope a proprietary web-based platform, called Centro, allowed faster and smarter decisions during the execution phase (figure 6).

## EVALUATION

Once the directional drilling work is completed, the drilling engineer evaluates the service performance by benchmarking against previously established KPIs, documenting on-the-job knowledge gains, and customizing the end-of-well report, as required. Lesson learned and suggestion are also included for future use.

## OPTIMIZATION

During this last phase, the service company's drilling

engineers study post-well analytics. They use the data to establish further optimization solutions for implementation in future well designs, with the goal to improve drilling performance on a field-wide scale.

In summary, the approach to consistently deliver quality directional drilling solutions was based on three guiding pillars: novel RSS and LWD technologies, robust drilling engineering quality process, and an agile digitalization and automation platform. Solutions for the key risks listed above were:

- Modify well architecture to add an extra 11-3/4" liner to isolate loss zone from mobile formations in Upper Germav.
- Use of push-the-bit rotary steerable (RSS), with full collar rotation and Anti stick Tool, to reduce stick-slip while providing greater rate of penetration (ROP) and lower surface torque.

Besides the processes some of the most recent and advanced technologies were used to drill and log the well. Below there is a brief description of each of them (figure 7).

Rotary-Steerable Systems has plenty of benefits eliminating time spent orienting tool face (controls it automatically especially in harsh conditions), increasing rates of penetration while rotary drilling, as compared to sliding with a Motor, improving hole quality reduces wellbore drag, which can cause and increase shocks, vibration and stick-slip, reducing chances of the drillstring becoming stuck due to constant rotation whilst drilling. The main advantage of this novel Push-the-Bit Rotary-Steerable System is the proportional steering control with its three independent pads, resulting in smoother wellbore profiles with no transition legdes, or immediate changes in dogleg severity that result from the transition from rotating to sliding modes (constant dogleg). It also provides near bit inclination and total gamma ray at only 2 meters from the bit to take extremely timely decision.

The LWD Spectral Azimuthal Gamma Ray sensor uses scintillation detectors mounted in pockets on the drill collar to provide high-precision total gamma ray measurements, high-quality real-time 16-bin borehole image logs and accurate measurements of potassium (K), uranium (U), and thorium (Th) content in the formation. The high-precision total gamma ray log increases certainty in well-to-well correlations and shale volume calculations, while the gamma ray borehole images guided real-time geosteering decisions and provide formation structural dip information.

The LWD Sonic tool in use is a next generation acoustic device, being the first LWD sonic tool to deliver clear, accurate, and reliable compressional and shear wave travel-time data in real time, without the requirement for significant post processing and correction. That is achieved by means of a high-output transmitter and unique attenuator design combined with advanced acquisition modes and real-time downhole processing techniques for accurate, reliable data. Main applications are porosity evaluation and geomechanic parameters used as inputs for completion. If required, the tool can be

configured in azimuthal acquisition mode to acquire up to 16-bin compressional and shear curves for anisotropy analysis and advanced geosteering application.

## FINDINGS

In the 12.25" section a 9-1/2" Push-the-Bit Rotary Steerable System (Magnus RSS®), with near bit gamma ray and inclination, was made up with the HEL MWD, including directional and gamma ray sensors at 2.4 m from the bit, to drill at total of more than 600m. The RSS was used to build the angle and later set on autopilot mode to hold a30° inclination. ROP was limited to 13 m/hr to drill until lower Germav was intercepted and until section TD. Some back-reaming was necessary during the run after some pack-offs and torque increase episodes were observed.

In the 10 5/8" section the drilling and geosteering utilized a 8" Mud Motor along with 6.75" Spectral Azimuthal Gamma Ray (SpectralWave®) and Sonic (ShockWave®) to drill the section, build and enter the Garzan formation. The main contribution of the LWD in this section was to identify the two gamma ray markers forecasting the top of Garzan formation, even if the real time geochemistry and X-ray fluorescence (XRF) could not, due to its sampling nature and lower resolution. Based on this data, after inclination was built, the original trajectory was revised: TPAO and Weatherford team monitored the model and constantly revised the projected top of Garzan formation maintaining the tangent of 80°. When agreed and confident that the top of Garzan was 2m below the bit in TVD, sliding was started to try and land the well with 3.5 deg/30m dogleg. The transition area from the lower Germav formation into the top of Garzan proved to be difficult formation for sliding, but inside Garzan was immediately different with less weight on bit being required and the assembly sliding easily with a good ROP of 8-10 m/hr. After reaching 85° inclination, the casing depth was defined, and section could end. After completion of the 10 5/8" section, borehole enlargement operation was performed without any issues, proving good hole conditions.

In the 8 1/2" section the drilling was planned to begin from the curve section utilizing a 6.75" Push-the-Bit Rotary Steerable System (Magnus RSS®), with the same Spectral Azimuthal Gamma Ray (SpectralWave®) and Sonic (ShockWave®) tools used in the previous section. The objective of the well was to start drilling 8 1/2" section according to the most recent agreed plan and stay into the Garzan formation from 9 5/8" casing shoe depth and continue to drill horizontally using geosteering until total depth of the well was reached. Operations on the well began from about 150 m before entering Garzan formation in the 10 5/8" section until total depth for the section was reached. Initially the RSS was set on autopilot mode at 87° target inclination and the ROP was controlled at 5m/hr for hole cleaning and accurate Geo-steering purpose. Well Placement and drilling operations in the 8 1/2" lateral section were postponed due to the earthquake that hit Turkey during the night between the 5th and 6th of February. On

February 24th the operations were resumed for drilling the 8 1/2" lateral section in Garzan formation. The torque and stick-slip were initially high, as they were prior to drilling being suspended, but after increasing the RPM, the torque decreased, even if increasing sporadically. After about 150 m of drilling, decision was made to pull out to check the BHA and revise mud system considering the 16 days operation suspension, but BHA was found in good condition but changed for the next run. The drilling was resumed at a controlled ROP of 6 m/hr in the horizontal section to improve hole cleaning and was completed when planned total well depth was reached. Over a total of 500 meters were successfully drilled within the target zone.

Figure 8 shows the LWD dataset, including near bit inclination and total gamma ray, spectral gamma ray (Uranium, Thorium and Potassium concentrations), gamma ray image, compressional slowness. LWD dataset was used to forecast and confirm positions of formation tops, to take decisions about trajectory to follow, by comparison with the modelled data from offset wells. LWD gamma ray image was processed in real time to get formation bedding dips to modify the geometry of the model and optimize well placement using geosteering.

## CONCLUSIONS

The combination of the novel push-the-bit, along with the other mitigations put in place at planning stage with lubricant and anti-slick device, proved effective in minimizing torque and stick slip vibration allowing optimization of rotations per minute (RPM) for effective hole cleaning. The subsequent logging run did not encounter hole problems, which indicates clean and good quality in gauge hole. The advanced LWD sensor provided spectral gamma ray and good quality image for accurate dip picking and structural interpretation of the formation. The sensor, at only 6.7 meters from the bit, enabled to accurately identify markers in both sections in a timely manner. Variations of Uranium and Potassium were found as good indicators of the top and inside Garzan formation and compared with X-ray fluorescence (XRF) data onsite. The correlation with total and spectral gamma ray, and the real time bedding dips evaluation were the main geosteering measurements to provide inputs to the directional driller for sending downhole commands to the RSS and accurate position the wellbore in the pay zone.

The advancements in directional drilling technology have significant impact on the life of the well, beyond drilling to the completions phase as well; this handshake between the service providers' offerings and the customers' objectives has been facilitated by adoption of digitalization and automation processes throughout all phases of the drilling engineering quality process: design, execute, evaluate and optimize. While there are multiple RSS providers, only a few can offer comprehensive drilling solutions to operators globally, based on a wide range of tool sizes, operational reliability, seamless BHA integration, remote capability,

global experience, and a sound drilling engineering quality process.

Keywords: drilling engineering process, directional drilling

Figure 1

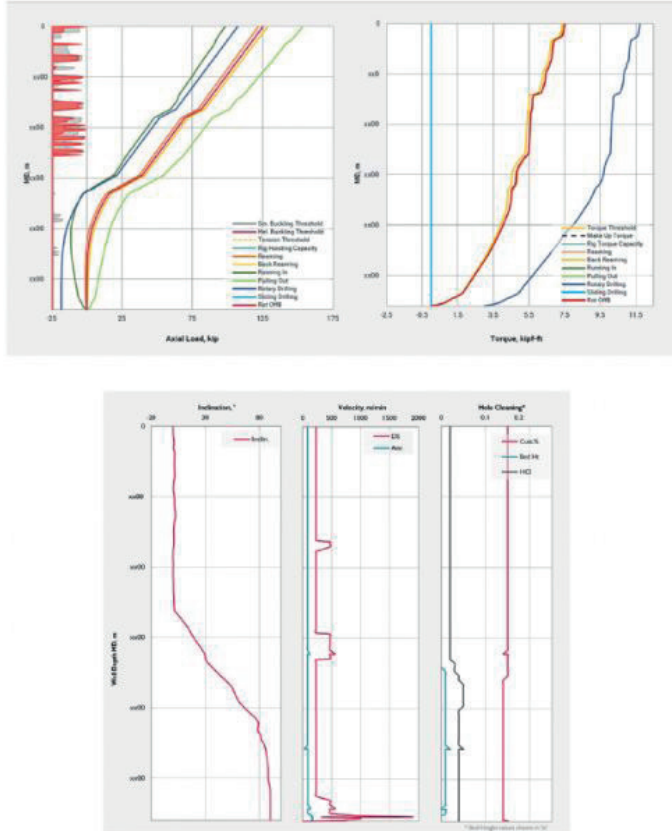
YAŞ (AGE)	FORMASYON (FORMATION)	LİTOLOJİ (LITHOLOGY)	AÇIKLAMALAR (DESCRIPTION)
MİYOSEN	LAHTI		Şeyl, Çakıllaşı, Kumtaşı
	ŞELMO		Kumtaşı, Çakıllaşı, yer yer şeyl ara bantlı
EÖSEN-ÖDÜSSEN	GERMİK		Şeyl, Jips, Dolomit
	HOYA		Kireçtaşı, Dolomit
PALEOSEN	GERCÜŞ		Konglomera, Killi Kireçtaşı, Şeyl, Marn, Kumtaşı
	UST GERMAV		Şeyl, Kumtaşı, Marn
	ALT GERMAV		Şeyl, Kumtaşı, Marn
ÖZEA MALEST BİRHİTİ N	GARZAN		Kireçtaşı, Biyoklastik Kireçtaşı

→	Shale, Sandstone, Conglomerate
→	Partly Shale, Sandstone, Conglomerate
→	Shale, Jips, Dolomite
→	Limestone, Dolomite
→	Conglomerate, Argillaceous Limestone, Shale, Marl
→	Shale, Conglomerate, Marl
→	Shale, Conglomerate, Marl
→	Limestone, Bioclastic Limestone

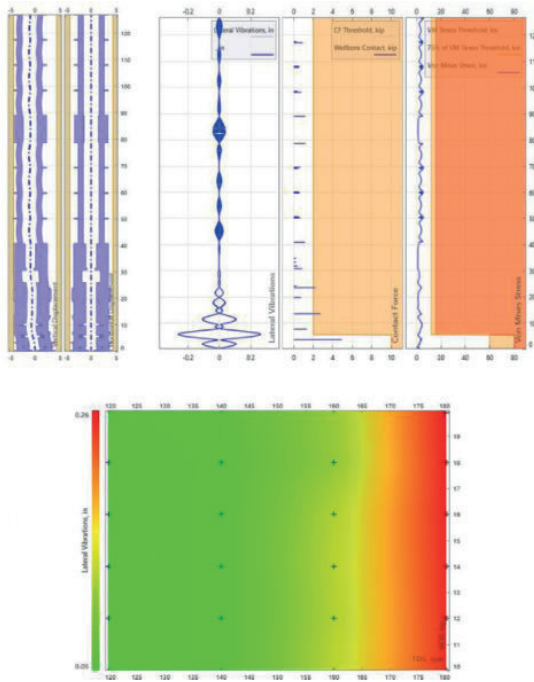
Prognosed stratigraphy of the well

Figure 2



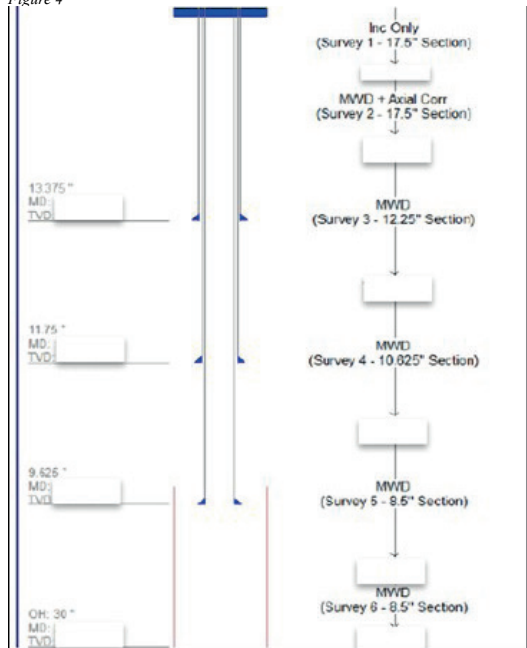
Two screen shots from pre-drilling modelling analysis. Torque and drag analysis on top and hydraulic analysis at bottom.

Figure 3



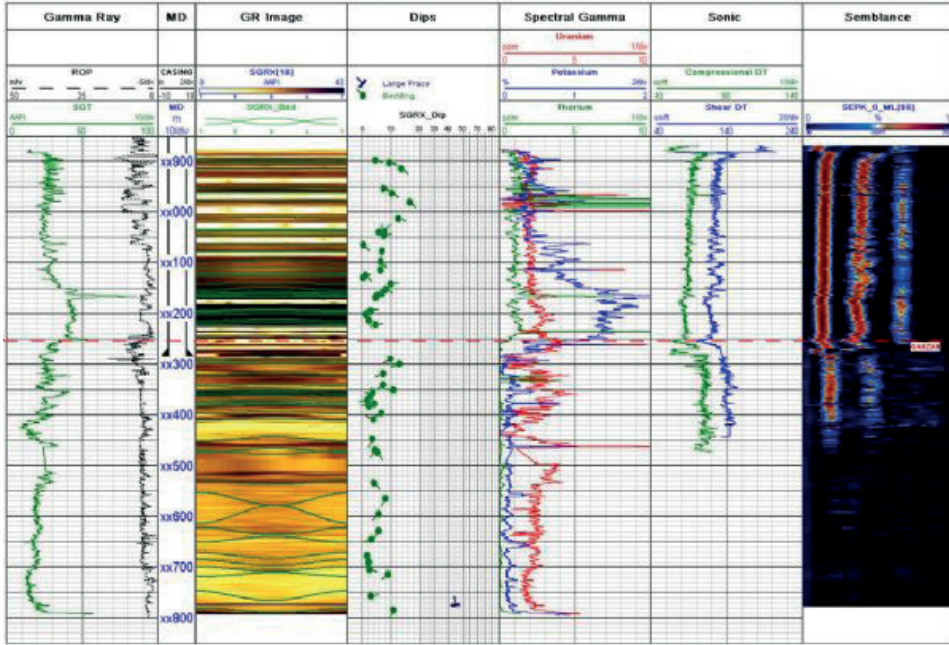
Two examples of BHA vibration analysis performed during design stage. Top: static and vibration analysis; bottom: critical rotary speed map.

Figure 4



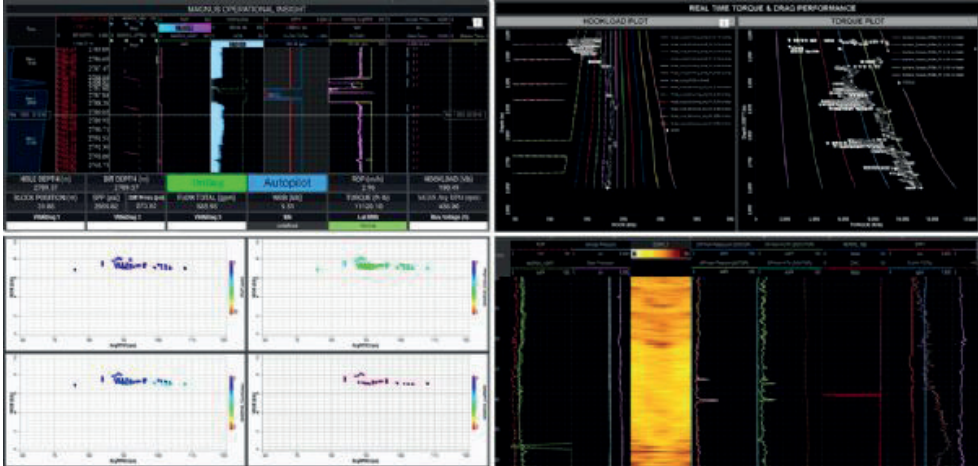
Well architecture.

Figure 5



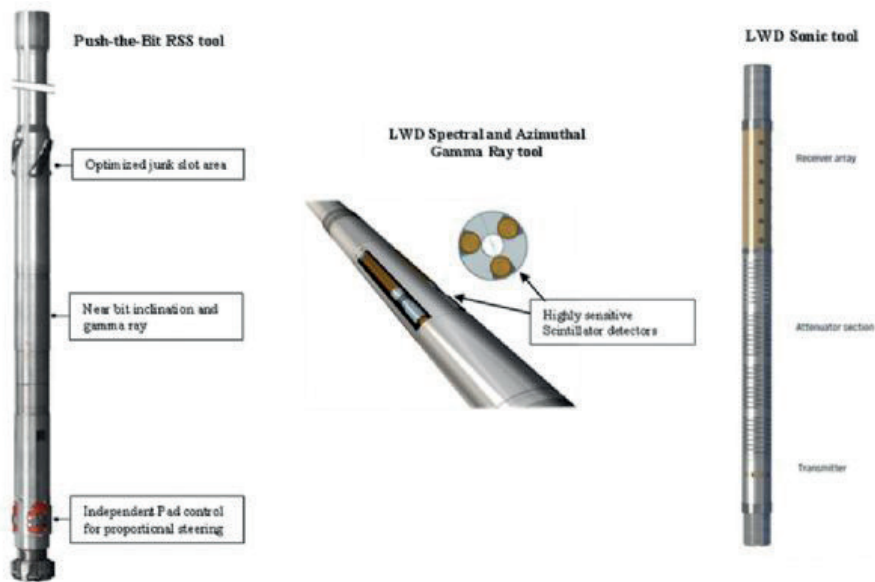
LWD dataset acquired in the 10 5/8" and 8 1/2" sections of the well with dip interpretation of bedding from gamma ray (GR) image.

Figure 6



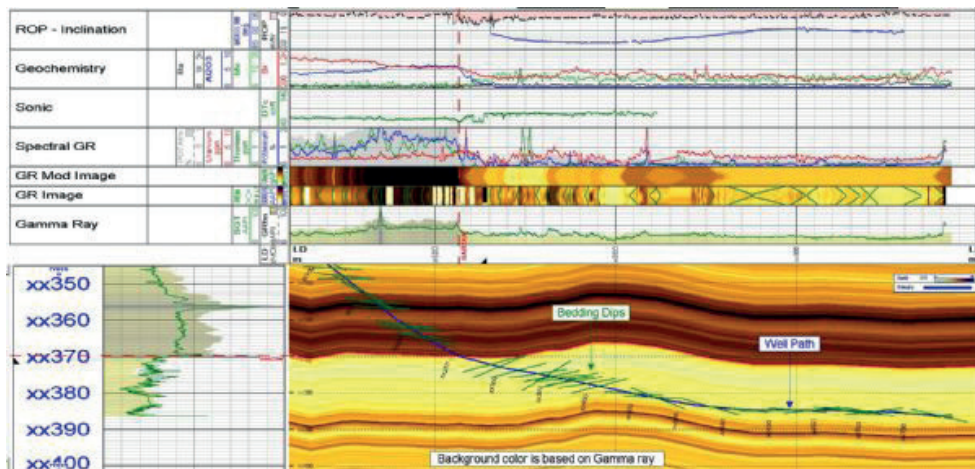
Four examples of dashboards of Centro, real time web-based platform, from the well: Magna RSS operational parameters (top left), Real time versus prognosed torque and drag (top right), Cross-plot of drilling parameters for performance optimization (bottom left) and LWD logs (bottom right).

Figure 7



Push-the-Bit Proportional Steering RSS (left), LWD Spectral and Azimuthal GR (center) and Sonic (right) tools included in the BHAs used to drill the well.

Figure 8



Screen capture of the geosteering software in the horizontal section at the end of well. Earth model color is based on gamma ray variation (yellow=low gamma ray; black=high gamma ray). Real time dips are represented as green segments. Note the spikes in the gamma ray sensors used as markers in both sections.

# Experimental Investigation of The Effect of Type And Concentration of Polymers On The Rheological Properties Of Drilling Fluids



**Mehmet Soylu**

Department of Petroleum and Natural Gas Engineering, Middle East Technical University, Ankara / Türkiye

## ABSTRACT

Precise control and proficient management of the drilling fluid rheology are of paramount importance not only in establishing wellbore stability and ensuring successful operations but also circumventing numerous predicaments such as lost circulation, pipe sticking, kicks, and blowouts. A plethora of research and design endeavors have been undertaken to explore numerous components to adjust and maintain the drilling fluid rheology to obtain optimality within operations, leading to the eventual evolution of numerous flow models and drilling fluid compositions. One key component in a myriad of drilling mud compositions may be given as polymers, which can be used to modify the mud rheology in multitudes of manners. Polymers, however, show behavior affected by many factors, such as temperature, mixing order, and mixing time.

This study experimentally investigated the effect of adding four polymers at different concentrations on the drilling fluid rheology. The polymers of interest include high and low viscosity Poly-anionic Cellulose variants, Xanthan Gum, and Polyacrylate Copolymers. A polymerized base fluid was prepared, and different concentrations of each polymer were added. The drilling fluid rheologies were evaluated under elevated temperatures, and the impact of each polymer was discussed within the scope of Bingham Plastic model.

## STATEMENT OF THE PROBLEM

Keeping the drilling fluid rheology optimal will affect multiple aspects of any drilling operation, and polymers are a vital component in many drilling fluid compositions. While the influence of polymers is predictable, their behavior may change with increasing temperature, changing compositions, and mixing order.

Considering that underground temperatures inherently grow higher than surface temperatures with increasing depth, measurements taken at room temperature may not reflect reality. Moreover, a specific composition, as well as a specific set of mixing workflow, is required to isolate the individual impact of a polymer, as these factors also impact the resultant rheological properties. As such, this study aims to experimentally test the effects of polymers on drilling fluid rheology through a series of experimental measurements conducted at 120°F.

## EXPERIMENTAL SETUP

The materials used in the experimental processes were provided by GEOS Drilling Fluids & Waste Management Solutions Inc. A brief list of the materials

may be given:

- **GEOBEN NT:** GEOBEN NT is a nontreated bentonite meeting the API 13A SEC 4 specifications [1].
- **Polyanionic Cellulose (PAC):** Herein, two PAC variants of low and high viscosities, REOPAC LV and REOPAC HV, respectively, were provided [1]. REOPAC LV is commonly used to control fluid loss, whereas the REOPAC HV is used both as a fluid loss control agent and a viscosifier [1].
- **REOZAN D:** REOZAN D is a xanthan gum, and it is a highly effective viscosifier [1].
- **HOTTROL NP:** HOTTROL NP is a sodium polyacrylate copolymer of medium molecular weight, and this additive is mainly used to reduce fluid loss in freshwater and seawater muds [1].
- **Caustic Soda:** 25% caustic soda was provided and used to maintain the pH of the drilling fluids within the working region of the additives, mainly around 9.5.

Experiments were carried out at Drilling Fluids Laboratory, Petroleum and Natural Gas Engineering Department, METU. The main laboratory equipment used in experimental research may be briefly illustrated as follows:

- **Multimixer:** 110V multimixer with five mixing slots was utilized to prepare the suspensions. Once the fluid-filled jars are attached, the blades will automatically mix the liquid.
- **Ofite Portable Roller Oven:** Once the mixed mud samples were ready, each sample was aged in the roller oven at 120 °F for 16 hours. The oven provides constant rotation to prevent settling and automatically heats the samples to a specified temperature.
- **Fann35Sa Viscometer:** Before the start of experiments, the calibration of viscometer was checked with a special calibration fluid provided by GEOS Energy Inc, whereas the rotation count was checked with a tachometer. Once the calibration process was completed successfully, the viscometer was used to obtain the rheology measurements.

## METHODOLOGY

With the given materials, a base drilling fluid composition was prepared and used as a reference for the polymer tests. The composition of the base fluid is shown in Table 1.

The base fluid composition was kept constant across the polymer tests, and different concentrations of REOPAC LV, REOPAC HV, REOZAN D, and HOTTROL NP were added according to Test 1, Test 2, and Test 3 conditions as provided in Table 2.



The schedule of the experiments was relatively uniform and may be given as follows:

- Hydration of Bentonite (16 Hours)
- Preparation of the drilling fluid samples
- Aging the samples in a roller oven (16 hours)
- Rheology Analysis

The bentonite was hydrated via tap water, and once an adequate bentonite suspension at the correct pH range was obtained, the suspension was sealed airtight and aged for 16 hours. The properties of the tap water used in the experiments are regularly measured in nearby pumping and measurement stations, and measurement results, as well as the average properties and average deviations of the properties of the tap water through the experiments, are provided in Table 3 and Table 4, respectively [2].

The hydrated bentonite was then incorporated with the rest of the components given in Table 1 and Table 2 to prepare the base fluid. Each component was added with the order given in Table 1 (from top to bottom), and each component was added over five minutes of continuous stirring. Periodically, the walls of the jar were scraped with a spatula to incorporate all the chemicals. Throughout this step, the pH of the solution, as well as the incorporation of the polymers, was carefully monitored. Once the drilling fluids samples were prepared, they were thermally aged in a roller oven for 16 hours at 120°F.

For the polymer tests, a batch of base fluid was prepared for at least three jars to keep the initial chemical concentrations and mixing conditions uniform. Then, desired amounts of polymers were slowly added and incorporated into the solution. Each concentration of the polymer was added after the order of the base fluid was completed, and each concentration was again added over five minutes of continuous stirring. The pH was again monitored and increased with caustic soda when needed. Polymer samples were also aged in a roller oven for 16 hours.

Once the samples were ready for analysis, the Fann35Sa viscometer available at METU Drilling Fluids Laboratory was used to measure the viscometer readings and the gel strengths of drilling fluids. Aged samples were poured into a thermocup to keep the temperature stable at 120 °F, and viscometer readings were taken with R1B1 (Rod radius of 1.8415 cm, bob length of 1.7245 cm, bob height of 3.8cm, and a shear gap of 0.117cm) configuration [3]. Dial readings were recorded at six different speeds (600, 300, 200, 100, 6, and 3 rotations per minute (RPM, Q), and Bingham Plastic model was used to obtain the Plastic Viscosity and Yield Point from the 600 rpm ( $Q_{600}$ ) and 300 rpm ( $Q_{300}$ ) dial readings via the following equations:

$$\text{Plastic Viscosity } (\mu_p) = \theta_{600} - \theta_{300} \quad (1)$$

$$\text{Yield Point } (\tau_y) = \theta_{300} - \mu_p \quad (2)$$

The gel strength was also measured with the Fann35Sa viscometer. For the gel strength measurements, the sample was first stirred at 600 RPM for 10 seconds.

Then, the stirring was turned off, and the fluid was allowed to develop gel strength for 10 seconds, 10 minutes, and 30 minutes. After the waiting period, the viscometer was turned on at 3RPM, and the peak reading was recorded as the gel strength in lbf/100ft<sup>2</sup>.

## RESULTS

At all steps of the experiment, the viscometer readings were at six rpm settings, which were 600, 300, 200, 100, 6, and 3 RPM. The viscometer readings were then converted to the shear rate (in 1/s) and shear stress (lbf/100ft<sup>2</sup>) using the constants associated with the R1B1 configuration. With a rod radius of 1.8415 cm, bob length of 1.7245 cm, bob height of 3.8 cm, and a shear gap of 0.117 cm, the shear rate coefficient is obtained as 1.703, and the shear stress coefficient is found to be 1.067. The initial measurements were taken on the base fluid, and it was seen that both the shear stress and the shear rate increased with increasing RPM. This was the expected and logical result, and the readings were satisfactory.

Gel strengths of the base fluid were also evaluated, and it was observed that increasing the waiting time drastically increased the gel strength. The results suggested that while the rate of increase in the gel strength diminished after the 10-minute mark, the gel still developed strength.

The plastic viscosity and the yield point were also calculated using the Bingham-Plastic flow model, and the viscometer dial readings  $\theta_{600}=43$  &  $\theta_{300}=30$  were used to obtain the plastic viscosity as 13 cP and yield point as 17 lbf/100ft<sup>2</sup>.

The polymer samples were calculated in a similar manner, and all three concentrations of each respective polymer were properly aged and tested. For the sample with 1 lb/bbl REOPAC LV addition, the findings are provided in Table 4, Table 5, and Table 6.

REOPAC HV, HOTTROL NP, and REOZAN D were also experimentally tested in a similar manner. All polymers were tested for three concentrations, and their results were compared with the base fluid and the rest of the polymer-added samples. The results obtained suggest that:

- The experimental data and the rheology obtained by the Bingham-Plastic model were consistent with the expected behavior of the polymers.
- Compared to the base fluid, the addition of REOPAC LV has resulted in a yield point increase of up to 74 %, a plastic viscosity increase of up to 54%, and a gel strength increase of 25%. At the highest REOPAC LV concentration, the yield point was recorded as 30 lbf/100ft<sup>2</sup>, and plastic viscosity was obtained as 20 cP.
- Compared to the base fluid, REOPAC HV has demonstrated a yield point increase of up to 353 %, a plastic viscosity increase of up to 123%, and a gel strength increase of up to 350%. At the highest REOPAC HV concentration, the yield point was recorded as 77 lbf/100ft<sup>2</sup>, whereas the plastic viscosity was obtained as 29 cP.

- Compared to the base fluid, HOTTROL NP samples showed a yield point decrease of up to 12%, a plastic viscosity increase of up to 19%, and a slight gel strength decrease of up to 13.5%. At the highest HOTTROL NP concentration, the yield point was recorded as 15 lbf/100ft<sup>2</sup>, and plastic viscosity was obtained as 16 cP. These results were expected as HOTTROL NP is a fluid loss control agent and not a viscosifier.
- Compared to the base fluid, the addition of REOZAN D has resulted in a yield point increase of up to 206%, a plastic viscosity increase of up to 123%, and a gel strength increase of up to 238%. At the highest REOZAN D concentration, the yield point was recorded as 52 lbf/100ft<sup>2</sup>; plastic viscosity was obtained as 29 cP. While the results on REOZAN D showed some deviation from the expected results. Nevertheless, the overall behavior followed the expected pattern, the deviation of which is concluded to be within acceptable range.
- Fluid loss control additives mainly resulted in minimal alterations in the drilling fluid rheology. Conversely, the rheology-adjusting additives showcased drastic alterations in the rheological parameters.

## CONCLUSIONS

The study has conducted experimental investigations into the impact of polymers on drilling fluid rheology by using four different polymer types of different concentrations. The polymers of interest for the experimental study are as follows:

1. Low Viscosity Polyanionic Cellulose (REOPAC LV)
2. High Viscosity Polyanionic Cellulose (REOPAC LV)
3. Xanthan Gum (REOZAN D)
4. Sodium Polyacrylate Copolymer (HOTTROL NP)

The juxtaposition of the experimental findings with the theoretical background yields the following Conclusions:

1. Sodium Polyacrylate Copolymer (HOTTROL NP) exhibited the slightest alteration in drilling fluid rheology compared to the other three polymer samples. Furthermore, this polymer displayed the most negligible variation in rheological properties with increasing concentration. These were the expected findings as the HOTTROL NP was mainly used as a fluid loss control additive and not a rheology-adjusting agent.
2. Diverging from other polymers, the addition of HOTTROL NP resulted with a subtle reduction in the gel strength of the drilling fluid with increasing concentration. Given that the primary function of this polymer is not to influence the rheology, this slight variation appears to be a natural occurrence, remaining notably consistent with the base fluid's rheology for the majority. Notably, all HOTTROL NP samples had a slight elevation in the yield point, with the highest belonging to the 0.5 lb/bbl HOTTROL NP sample. Beyond the 0.5 lb/bbl mark, the yield point gradually diminished with increasing HOTTROL NP concentration. Conversely, the plastic viscosity is seen to have a consistent increase with increasing polymer

concentration. With all said, the magnitude of change at all parameters was significantly minimal compared to any of the other three polymers.

3. REOPAC LV, REOPAC HV, and REOZAN D all showed a constant increase in the rheological parameters with increasing polymer concentration of the respective polymer.

4. REOPAC LV has consistently increased the yield point, progressively escalating from 17 to 30 lbf/100ft<sup>2</sup> as the concentration was augmented to 2 lb/bbl. Simultaneously, the plastic viscosity of the drilling fluid exhibited a persistent rise, deviating from the base fluid's 13 cP to 20 cP. Additionally, a discernible trend of elevated gel strength was evident when compared to the base fluid.

5. REOZAN D and REOPAC HV demonstrated substantial alterations in drilling fluid rheology across all concentrations. As both of these polymers are used as viscosifiers to adjust the rheology, this was the expected result, and the elevated magnitude of change compared to REOPAC LV and HOTTROL NP is justified.

6. REOZAN D demonstrated notable modifications in the yield point, ranging from 17 lbf/100ft<sup>2</sup> of the base fluid to 52 lbf/100ft<sup>2</sup> at the highest polymer concentration. Similarly, the changes in plastic viscosity demonstrated elevated values, ranging from 13 cP of the base fluid to 29 cP at the highest polymer concentration. Moreover, the gel strength exhibited a consistent rise with the increasing polymer concentration, as observed under the specified temperature conditions.

7. Notably, the addition of REOPAC HV led to the most substantial alterations in the yield point, going from the 17 lbf/100ft<sup>2</sup> of the base fluid to an impressive 77 lbf/100ft<sup>2</sup> at the highest polymer concentration. The alterations in the plastic viscosity encompassed a similar trend and ranged from 13 cP of the base fluid to 29 cP at the highest REOPAC HV concentrations. Similar to REOZAN D, REOPAC HV showcased significant and consistent increments in the gel strength with progressive increments in the polymer concentrations under the specified temperature conditions.

## RECOMMENDATIONS

While this study has researched the impact of polymers at a relatively high temperature of 120°F, the time constraints and experimental set-up has presented a limitation to the upper limit of the experiment. Especially at geothermal reservoirs, the temperatures may be significantly higher. Hence, future studies may experiment with more elevated temperature ranges to see how the temperature affects these results. While the chemical compositions of the tap water used in this study have been analyzed and are available for further evaluation, the results could be made more readily repeatable if re-done with pure water. Depending on the given time and equipment constraints, the results obtained from this study may be revalidated and improved to cover a broader range of cases.

**ACKNOWLEDGEMENTS**

This project has been possible with the help of different parties. The chemicals used in the experiments, as well as valuable insight on the experimental methodology, have been provided by GEOS Energy Inc. Valuable friends, Cem Apaydın, Mücahit Kabadayı, and Oğuzhan Konuralp have given extensive effort in preparation and testing of the samples, and this study would not have been possible without their help.

**REFERENCES**

1. GEOS – Viscosifiers Catalogue. (2021). Geosdfc.com. <https://www.geosdfc.com/products/viscosifiers.php>
2. Aski Genel Müdürlüğü Su Analiz Sonuçları. (2023). Aski.gov.tr. <https://www.aski.gov.tr/TR/SuAnalizSonuclari.aspx>
3. Expotech USA. (n.d.). Fann Model 35 Viscometer Instruction Manual. Retrieved January 1, 2022, from <https://www.expotechusa.com/Manuals/Fann/35496.pdf>

Keywords: Bingham-Plastic Model, Drilling Fluid Rheology

Figure 1: The Multimixer and mixing jars



Figure 2: Exterior (up) and interior (down) of the Ofite Portable Roller Oven

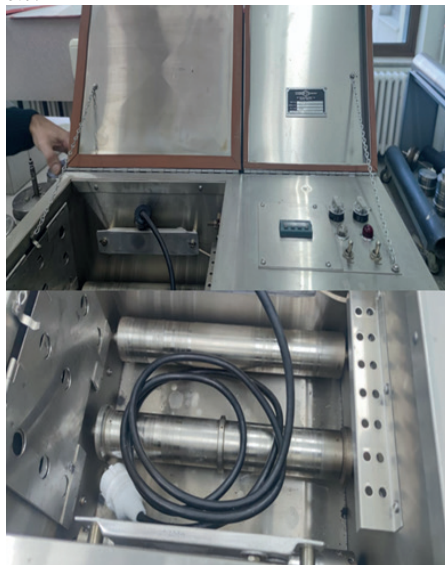


Figure 3: FANN35SA Viscometer without the rotor attachment



Figure 4: Workflow of the experiments

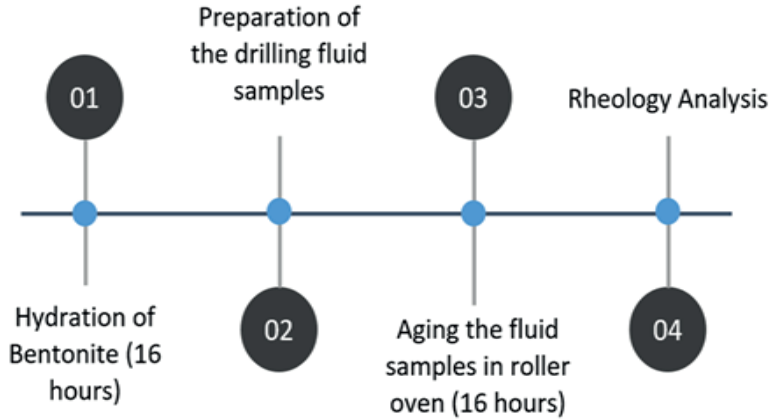


Table 1: The composition of the base fluid

Additive	Function	Amount
GEOBEN NT	Fluid Loss Control & Viscosifier	5 lb/bbl
REOPAC LV	Fluid Loss Control	1 lb/bbl
REOPAC HV	Fluid Loss Control & Viscosifier	0.5 lb/bbl
REOZAN D	Viscosifier	1 lb/bbl
GEOETHIN HT	Deflocculant	1 lb/bbl
HOTTROL NP	Fluid Loss Control	1 lb/bbl
CAUSTIC SODA	Alkalinity Control	As needed

Table 2: Tested polymer concentrations

Polymers	Test Concentration 1	Test Concentration 2	Test Concentration 3
REOPAC LV	1	1.5	2
REOPAC HV	0.5	1	1.5
HOTTROL NP	0.5	1	1.5
REOZAN D	0.5	1	1.5

Table 3: Measured properties of the tap water used in the experiment [2]

Parameter	Unit	Analysis Result
Residual Chlorine	(mg/l)	0.6
Conductivity	(25C,mS/m)	90.8
Ammonium	(mg/l)	<0.06
Nitride	(mg/l)	<0.006
Sulfate	(mg/l)	143
Iron	(µg/l)	12
Aluminum	(µg/l)	28
Coliform Bacteria	EMS/100ml	0
Escherichia Coli	EMS/100ml	0
Enterococcus	EMS/100ml	0

Table 4: Average Properties of the tap water used in the experiments [2]

Parameter	Unit	Average	Average Deviation
Residual Chlorine	(mg/l)	0.58	0.1
Conductivity	(25C,mS/m)	90.21	1.84
Ammonium	(mg/l)	<0.06	0
Nitride	(mg/l)	<0.006	0
Sulfate	(mg/l)	143	1.46
Iron	(µg/l)	16.83	12.78
Aluminum	(µg/l)	31.25	6.79
Coliform Bacteria	EMS/100ml	0	0
Escherichia Coli	EMS/100ml	0	0
Enterococcus	EMS/100ml	0	0

Table 5: Findings on the base fluid

Viscometer Speed (RPM)	Dial Reading	Shear Rate (1/s)	Shear Stress (lb/100ft2)
600	43	1021.8	45.881
300	30	510.9	32.01
200	24	340.6	25.608
100	16	170.3	17.072
6	4	10.218	4.268
3	3	5.109	3.201
Waiting Time	Gel Strength (lb/100ft2)	Rheological Parameters	Results for Bingham Plastic Model
10 seconds	4	Plastic Viscosity	13 cP
10 minutes	7	Yield Point	17 lb/100ft2
30 minutes	8	-	-

Table 6: Dial readings, shear rate (1/s), and shear stress (lb/100ft2) with respect to each viscometer setting for 1 lb/bbl REOPAC LV sample

Viscometer Speed, (RPM)	Dial Reading	Shear Rate (1/s)	Shear Stress (lb/100ft2)
600	53	1021.8	56.551
300	36	510.9	38.412
200	29	340.6	30.943
100	20	170.3	21.34
6	5	10.218	5.335
3	4	5.109	4.268

Table 7: Gel strengths (lb/100ft2) of REOPAC LV samples

Gel Strength	10-sec Gel	10-min Gel	30min Gel
Base Fluid	4	7	8
1lb/bbl	4	10	10
1.5lb/bbl	5	8	10
2lb/bbl	5	9	10

Table 8: Plastic viscosities (cP) and yield points (lb/100ft2) of REOPAC LV samples

	PV (cP)	YP (lb/100ft2)
Base Fluid	13	17
1lb/bbl	17	19
1.5lb/bbl	19	25
2lb/bbl	20	30

# A Synopsis on Pressure-While-Drilling Applications

**Korhan Kor**

TP-OTC Sakarya Gas Field Development Project



## 1. INTRODUCTION

Most non-productive times (NPTs) in an overall drilling sequence are directly related to the hole problems. The most significant problems encountered during drilling can be listed as lost circulation, formation kick, wellbore stability, differential sticking, and poor hole cleaning. These items are in a relationship with wellbore pressures, and have a high possibility of resulting in NPT events. Thanks to the pressure-while-drilling (PWD) tools introduced to the drilling industry in recent years, it is now possible to detect and understand the root causes of the mechanisms of the NPT events.

Most of the pressure-related major events occur if the operating mud weight (MW) envelope is exceeded. This envelope is also called a safe mud weight window (SMWW) and contains limits in terms of formation pore pressure (PP) and fracture gradient (FG). Regarding wellbore stability, this SMWW also contains another limit in terms of formation breakout pressure. A demonstration of a SMWW is shown in Figure 1.

The limits can be determined by offset wells analysis or can be calculated in a mechanical earth model (MEM) that is calibrated via a leak-off test (LOT) and/or formation integrity test (FIT). If the hydrostatic pressure through the drilling fluid in the well exceeds these limits, it is likely to occur at least one of the hole problems listed above.

## 2. APPLICATIONS

As general application, MW is measured at the surface in static conditions. Yet, the dynamic behavior of the mud is estimated via hydraulic models. PWD tools help measuring the pressure losses in the wellbore annulus, which unveils most of the key information about mud pressure-related events.

Common practices in challenging drilling environments where PWD can be used are applications for extended-reach drilling (ERD), underbalanced drilling (UBD), deep-water drilling, and high-pressure and high-temperature wells.

### 2.1. Annular Pressure (AP) Measurements

MW in the annulus that corresponds to a certain vertical depth is called equivalent mud weight (EMW). Since the calculation of EMW depends on the depth, the measurement accuracy is highly affected by the depth accuracy of the PWD sensor. It is also important to take the distance between the bit and the PWD sensor into consideration.

Another important aspect is the measurement sensitivity of the PWD sensor. The accuracy of a sensor can vary with the measurement range. The sensors for annular

pressure measurements can be used for various bore sizes. As well as tool sizes, the sensors are also available in various ranges. An illustration of the tool is shown in Figure 2.

### 2.2. Equivalent Circulating Density (ECD)

To maintain a safe operation, MW should be kept within the SMWW. If MW falls below the breakout limit, some caving will be observed at the shale shakers which will be an indication of a wellbore instability issue. If MW falls even below the PP limit, the formation fluid will influx into the well. If MW exceeds the FG, it is inevitable to face lost circulation. To avoid any of these hole problems, AP should be kept within SMWW. A sketch is given in Figure 3.

AP has two basic elements. The first one is the static pressure, which is granted via mud density gradient in the wellbore annulus. It is the MW that exactly corresponds to the depth across the PWD sensor. This density includes the effects of drilling cuttings and formation fluids. Hence, it is called equivalent static density (ESD). The second element is the pressure due to the vertical and rotational movement of the drill string. This also includes the effect of mud gelation, annular parasitic pressure losses, changes in the hole geometry, and all the other parameters that can have an effect on dynamic AP. This density is called ECD and defined as the effective density of the circulating mud associated with hydrostatic pressure plus frictional loss.

Rheological properties of the drilling fluid such as viscosity, yield point, gel strengths, etc., type of flow regime, and downhole temperature have individual effects on the dynamics of AP. Additionally, downhole pressure measurements are affected by the borehole size. If annulus size increases, the effect of dynamic pressure loss on ECD decreases. Another effective parameter is the rotary speed.

Shortly, ECD should be monitored constantly for challenging environments listed at the beginning to be sure that the dynamic MW stays in SMWW.

### 2.3. Formation Strength Test (FST)

FSTs are performed within a drilling sequence after a casing is cemented and before starting to drill a new section. The purposes of the FSTs are (1) to make sure about the integrity of the cement behind the casing shoe, (2) to gather data about the strength of the formation to update or calibrate the MEM, (3) to detect the resistance of the shoe against additional pressure.

There are two basic types of FSTs: FIT and LOT. FIT is performed for testing the strength of the casing shoe as well as the formation by increasing the bottom hole

pressure up to the required pressure. So, the formation is not fractured. Hence, FIT is preferred to be sure that the shoe and the total section depth will be able to be drilled as per design. LOT is to determine the leak-off point (LOP) of the new-drilled formation. It means that the drilling fluid is pumped continuously until a drop in the linear pressure trend is observed. LOP is commonly referred to as the initial pressure that differs from the expected trend when the formation is fractured. A sample is shown in Figure 4.

LOT is conducted to determine the fracture gradient of the formation of interest at shoe depth. This also means the result will deliver the maximum applicable MW that the casing shoe can hold against.

It's standard procedure to estimate the shoe strength by using the surface values obtained during the FST. This estimation is valid for both surface and downhole readings when water-based mud is used. However, some corrections should be made if synthetic oil-based mud (SOBM) are in use. Any incorrect adjustment of MW of an SOBM used in the calculation can cause an inaccurate characterization of the FG. This can create challenges in controlling pressures when drilling in narrow-margin environments.

### 2.3.1. Effect of Mud Compressibility

In deep-water wells where downhole temperatures are relatively low, the impact of mud compressibility is usually the most significant factor, causing MW of the fluid to increase with depth. This results in a higher downhole MW compared to surface. However, the exact amount of increase is hard to determine, as compressibility is not constant and depends on both pressure and temperature causing MW to change nonlinearly with depth. It has been suggested to use ESD while accounting for the impact of compressibility (Oort & Vargo, 2007).

### 2.3.2. Effect of Thermal Expansion

In HPHT wells, thermal expansion becomes more significant as the temperature rises with depth, causing the mud volume to expand and the density to decrease. This effect can be so strong that it cancels out the densifying impact of compressibility, resulting in a downhole MW that is lower than surface MW. It is challenging to anticipate the impact of thermal expansion on MW as it also depends on pressure and temperature. Adjusting surface MW to account for these changes will accurately reflect the actual downhole density experienced by the casing shoe during the FST. A PWD tool can be used to directly record a static mud pressure and obtain downhole MW (Oort & Vargo, 2007).

### 2.3.3. Effect of Gel Strength

During an FST, the entire amount of force applied from the surface is not felt as the exactly same amount in the downhole. It's possible to substantially overstate the

strength of the casing shoe based on surface data, which exhibits higher readings that don't accurately represent the actual shoe strength. This can lead to overestimating the available SMWW and inadvertently causing mud losses when drilling further. The variations observed in surface and downhole pressure can be ascribed to delays in pressure transmission and losses in the mud column. The thixotropic properties of the mud, including its gel strength, are especially significant in this context. To accurately consider the pressure change resulting from mud gelation, it's necessary to modify the surface pressure measured during the FST by incorporating the pressure loss caused by the effect of gel strength.

### 2.3.4. Effect of Cementing Unit Location

Most of the surface pressures measured during the FST are recorded at the cementing unit, which means the placement of the unit can influence how the FST pressure readings are interpreted. The cementing unit is frequently located on a platform beneath the reference point for the well. Not addressing this reference point and not adjusting for it can result in overestimating the FST pressure by an amount equal to the hydrostatic pressure created by the difference between the top of the mud column and the gauge's position at the cementing unit.

After calibrating the gauge and filling the lines with mud to the reference point, any subsequent pressure increases on the well during the FST will be added to the hydrostatic pressure on the gauge. The hydrostatic pressure at the start of the test can lead to higher pressure readings, which can cause an overestimation of the FST pressure.

To obtain an accurate test result from the relative point of reference for the well, the initial gauge pressure should be subtracted from the final FST pressure. However, this problem only occurs when surface pressures are used to calculate shoe strength, and it becomes irrelevant if downhole mud densities and recorded pressures are used.

## 2.4. Riserless Drilling

In riserless drilling, the drilling fluid and cuttings are discharged onto the seafloor near the wellhead. One of the major risks involved in drilling the riserless section is encountering a shallow water flow.

To ensure safe operations, a remotely operated vehicle with a camera is used to monitor any flow out of the wellhead. During connections, drill pipe is held steady and pumps are stopped to allow fluid oscillations to stabilize while observing for any signs of flow. Additional data are obtained using a PWD tool to detect any shallow water flows. If a flow is detected, unconsolidated sand may enter the wellbore leading to an increase in downhole pressure due to the weight of the additional solids in the annulus.

Often, these issues arise because of sands that are not consolidated and have high pressure at shallow depths below the seafloor. In severe cases, water flow can result

in losing the well. Large casings, which are a crucial support structure for the entire well, can be weakened due to extensive washouts. Keeping track of ECD helps to evaluate the depth and intensity of the water flow, and to determine whether it is significant enough to suspend drilling operations.

In typical hydraulic models, the impact of mud returns to the seafloor is often ignored. Using PWD measurements directly is an effective way to address this challenge. Changes in EMW and AP can have various causes such as ECD. PWD sensor reading is a cumulative measurement of all events happening. Understanding changes in EMW requires considering several factors, including dynamic conditions occurring far above the bit as well as those happening near the bit.

Gamma-ray (GR) tool may show a large washout, and it may not be accurate to assume that the interval is sand. A clean zone is the base for interpreting EMW during riserless drilling. EMW remains unaffected when drilling in a clean zone, even though there might not be a washout as seen by the caliper in the upper interval. For the lower clean zone, the hole may wash out beyond the depth that the GR sensor can detect. This may cause a significant increase in EMW. This increase is temporary and lasts only as long as the clean zone. After drilling the unconsolidated interval, EMW returns to its initial level. An example is shown in Figure 5.

When the clean zone is filled with fluid with a higher pressure than the normal seawater, a shallow water flow may occur. Figure 6 shows a depth-based log of a PWD sensor passing through a shallow water flow section. EMW shows a sharp increase, but it does not return to its baseline. Instead, the well keeps flowing while drilling ahead, and EMW remains higher than the seawater gradient, due to the weight of the solids carried in the shallow water flow mixture.

### 2.5. Well Control

Formation fluid or gas kick due to high formation pressures is a significant risk during drilling. When encountering gas kicks, the ECD response is mainly influenced by (1) the decrease in the density of the mud column due to the replacement of heavier fluid by less dense gas or fluid, and (2) the increase in AP losses caused by friction and inertia when moving the mud above the influx.

It is crucial to continuously monitor all drilling data to detect a downhole kick event. In Figure 7, PWD response to a gas influx is shown. When gas mixes with the drilling fluid, the density of the fluid and the AP decrease. After observing the decreasing ECD, a flow check was performed and confirmed the occurrence of a gas influx. Another observation was the increase in annular temperature, which occurred as the hotter formation fluid warmed the borehole.

Well control issues are especially dangerous if an influx occurs while tripping. Considering a kick occurs while tripping out, both the ESD and ECD just before the trip are greater than the PP. However, swab pressures via trip

may lower EMW below the PP, and the well may take an influx. While tripping back in, a decrease in pressure will be noted as the PWD sensor enters the swabbed-in light gas.

The mud-pulse PWD technology can only capture certain types of events. The tool cannot record any data during the rams are closed when there is no circulation, or during the tripping process. Additionally, the kill rates are usually too low to provide RT information. These points can be shortcomings for relying on only PWD data for well control events.

### 3. DATA MODES

In memory mode, the tool continuously records data in its internal memory. These data can be retrieved later when the tool is brought back to the surface. Memory-mode data are usually sampled at a higher frequency, which makes them more detailed but also more susceptible to noise. The recording gauges can be programmed to store data with typical settings being from 5 to 20 seconds.

RT mode involves linking the downhole pressure information with an MWD system, which can use either a mud pulse, electromagnetic, or surface hardwired system. The RT data is transmitted to the surface every 30 seconds or so. However, if a mud pulse system is used, data transmission can only occur when the pump flow rate exceeds a threshold. Electromagnetic or hardwired systems do not have this restriction.

In pumps-off mode, the memory data is analyzed within the PWD tool, and only a portion is transmitted to the surface when pulse-type MWD systems resume pumping. This mode is useful during connections or FST. The information can consist of either a continuous recorded pressure with the pumps off or a limited set of data.

### 4. INTERPRETATION

During connections several factors can impact the downhole pressure, which can be rotation, temperature, compressibility, cuttings, etc. Some of these factors are constantly changing and can cause the downhole pressure to fluctuate during connections. An issue hindering the interpretation of AP data is the range of formats. Depth-based logs are usually used for formation evaluation. Time-based format is more suitable for displaying RT information and interpreting memory-mode data after the event.

Figure 8 illustrates a standard time-based log format, where PWD data is presented along with other downhole and surface measurements. It is also crucial to have a presentation that shows the depth-based assessment of events with respect to the position of the BHA relative to the lithological boundaries. Figure 9 provides an illustration.



## 5. CONCLUSION

This paper demonstrates relying solely on monitoring surface pressures in RT can result in misinterpretation of events due to the complexity of the fluid and cuttings-filled column in the annulus. Using PWD measurements to monitor ECD can help interpret the complex events that may occur during drilling. An understanding of the events and causes can be attained by combining all the available information. The RT analysis of causes, signatures, and parameters suitable for monitoring is continuously evolving. Nevertheless, there are certain common events that have repeatable indications in both surface and downhole measurements. It is recommended to refer a simple interpretation guide for some of these common drilling events, highlighting the changes in ECD that are most frequently observed in RT time-based drilling logs.

## REFERENCES

- Aadnøy, B. S. (2009). *Advanced Drilling and Well Technology*. Society of Petroleum Engineers.
- Aird, P. (2019). *Deepwater Drilling: Well Planning, Design, Engineering, Operations, and Technology Application*. Elsevier Science.
- Gordon Technologies. (2022). <https://gordontechnologiesllc.com/gt-pwd/>
- Hutchinson, M., & Rezmer-Cooper, I. (1998). Using Downhole Annular Pressure Measurements to Anticipate Drilling Problems. SPE Annual Technical Conference and Exhibition.
- Naganawa, S. (2015). Optimum Hydraulics Design and Operation for Extended-Reach and Horizontal Geothermal Drilling. Proceedings World Geothermal Congress 2015.
- Oort, E. V., & Vargo, R. (2007). Improving Formation Strength Tests and Their Interpretation. SPE/IADC Drilling Conference.
- Rezmer-Cooper, I. M., Rambow, F. H. K., Arasteh, M., Nashem, M. N., Swanson, B., & Gzara, K. (2000). Real-Time Formation Integrity Tests Using Downhole Data. IADC/SPE Drilling Conference.
- Roy, S., Power, D. (2002). Using Real-Time Hydraulics Modeling to Complement Annular-Pressure-While-Drilling Data. AADE.
- Swanson, B. W., Elliott, G. S., Meier, J. L., & Easton, M. D. J. (1997). Measurement of Hydrostatic and Hydraulic Pressure Changes During HPHT Drilling on Erskine Field. SPE Offshore Europe.

Keywords: Downhole tools, Pressure-while-drilling

Figure 1: A safe mud-weight window (Naganawa, 2015)

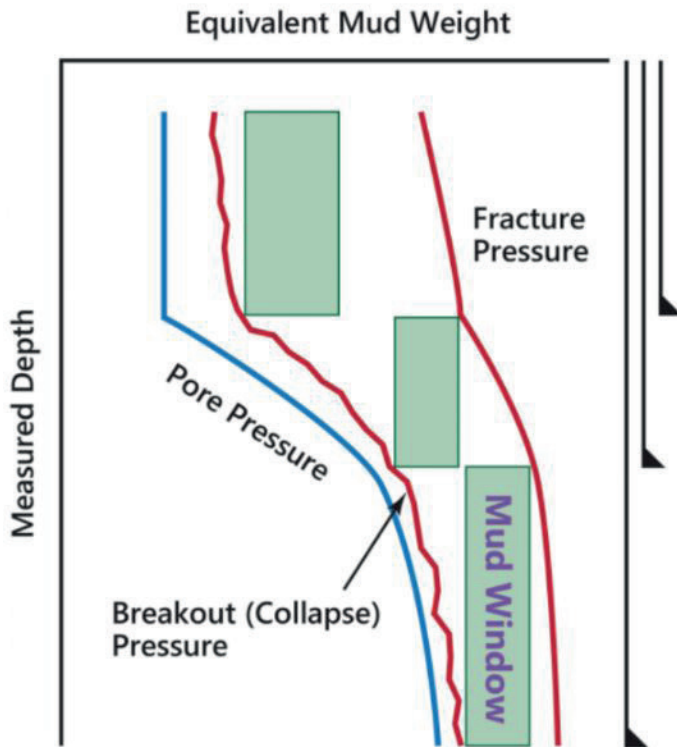


Figure 2: PWD tool (Aird, 2019)

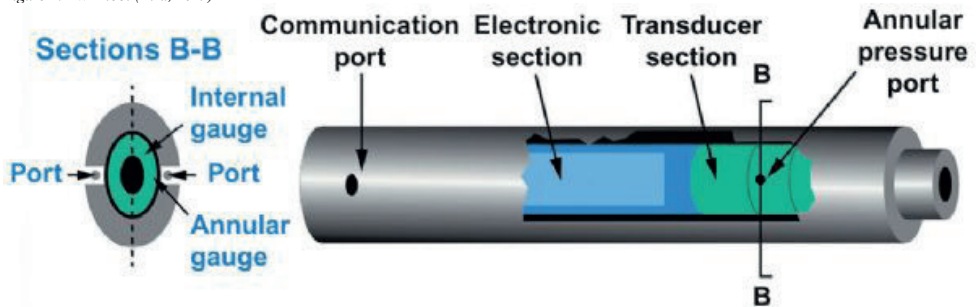


Figure 3: Annular pressure and hole problems (Naganawa, 2015)

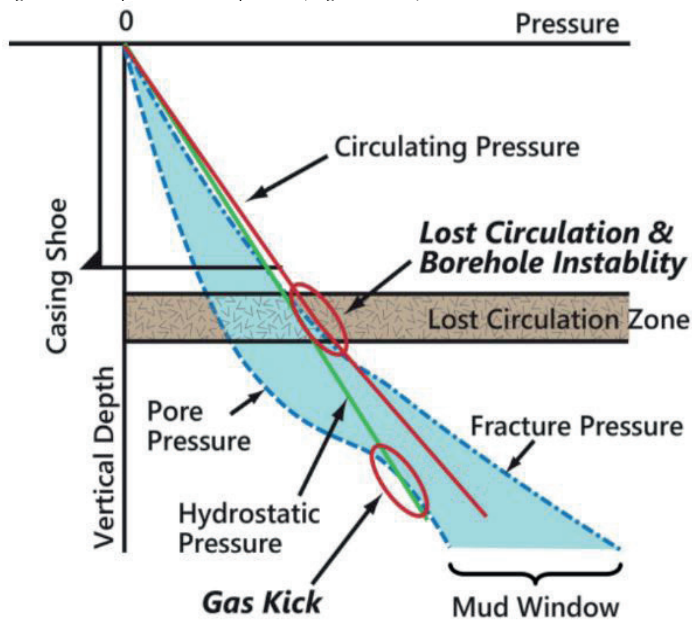


Figure 4: Sample FIT/LOT graph

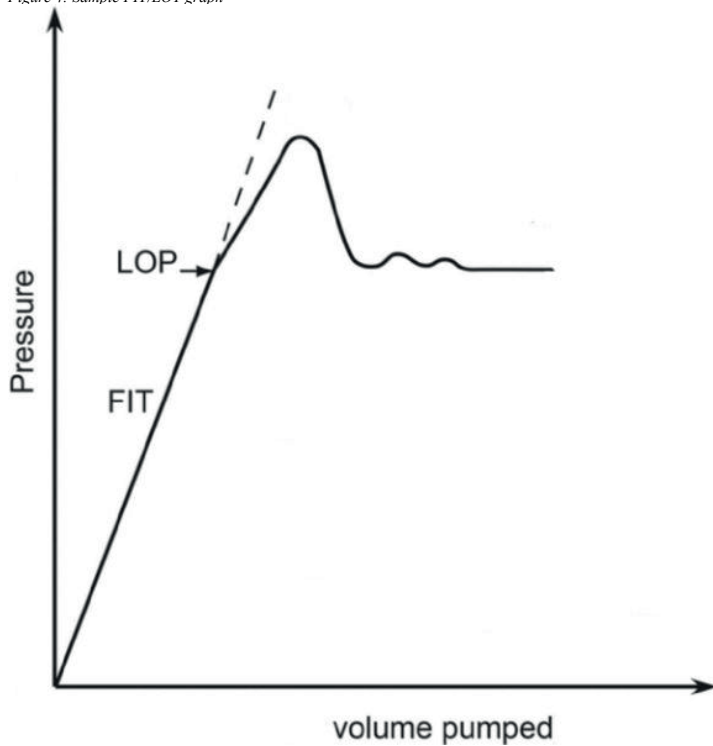


Figure 5: Non-flowing washout example (Aadnøy, 2009)

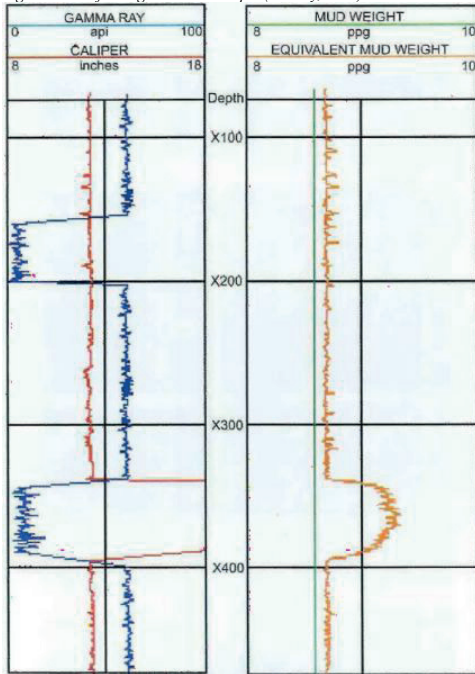


Figure 6: Shallow water flow example (Aadnøy, 2009)

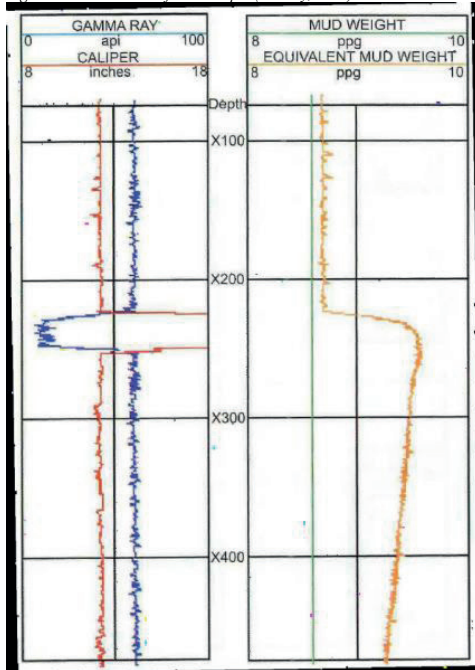


Figure 7: PWD response to a gas influx (Hutchinson & Rezmer-Cooper, 1998)

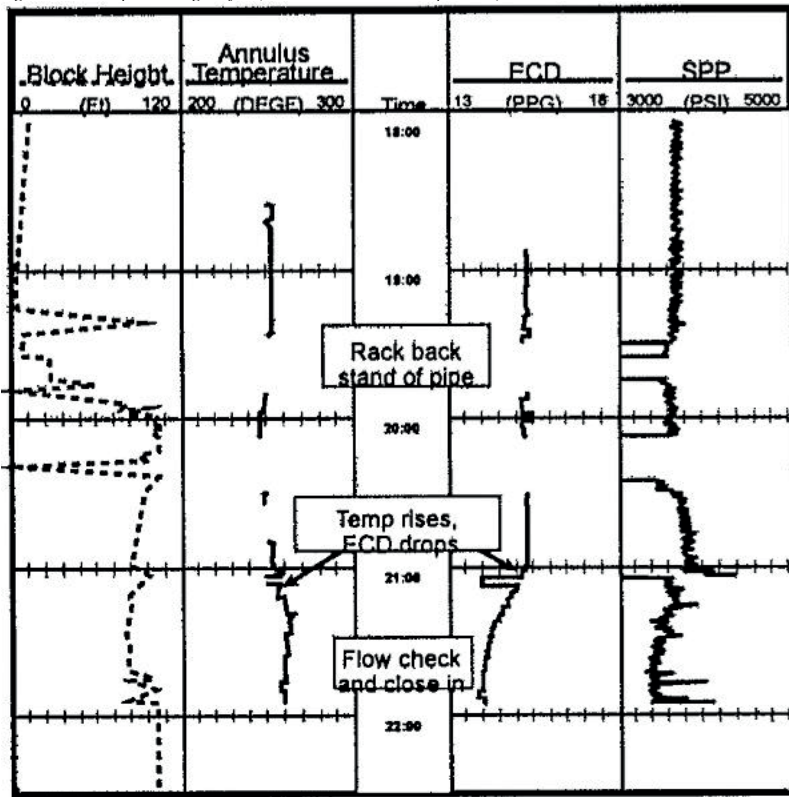


Figure 8: A time-based drilling log (Roy & Power, 2002)

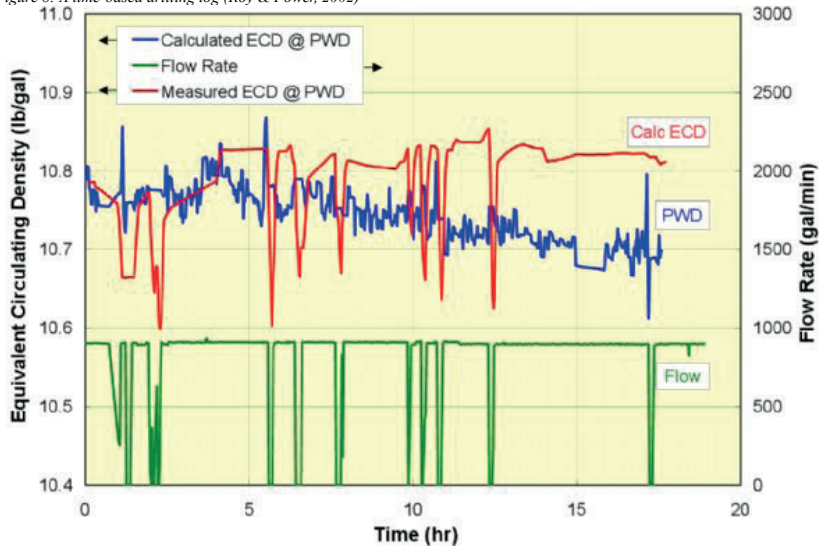
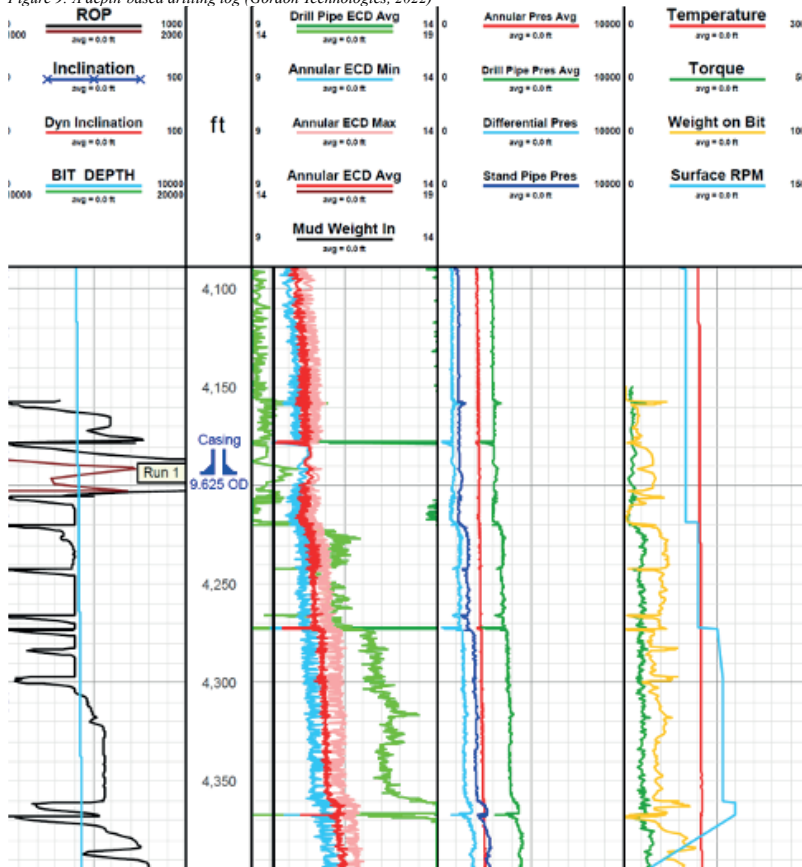


Figure 9: A depth-based drilling log (Gordon Technologies, 2022)



# Mature Field Development by Means of Rotary Steerable System and Reservoir Navigation Services, Turkey



Paolo Sudiro<sup>1</sup>, Melike Özkaya Türkmen<sup>2</sup>, Elif Cihan Yıldırım<sup>2</sup>,  
Batur Alp Aydın<sup>2</sup>

<sup>1</sup>Baker Hughes

<sup>2</sup>Türkiye Petrolleri Anonim Ortaklığı

## INTRODUCTION

The Adiyaman Region (SE Turkey) includes several small oilfields, hosted in reservoir rocks consisting of middle to upper Campanian shallow water and pelagic carbonates, belonging to the Mardin and Adiyaman Groups (Soylu et al., 2005). The shallow water Derdere and Karababa Formations and the pelagic Karaboğaz Formation host the main reservoir intervals and were also the source rocks of the local hydrocarbons. Reservoir thickness within the Derdere and Karababa Formations is about 10 m each and a maximum of 5 m in the Karaboğaz Formation. The area is tectonically complex, crossed by a dense network of high-angle faults, due to proximity to the East Anatolian Fault Zone (Yilmaz et al., 2006). The distribution of primary and secondary porosity, the latter of which was due to diagenetic processes, and the development of fractures control the reservoir quality.

Through the years, the local oilfields have been developed mostly by means of a dense array of vertical and low-angle wells, each one requiring a dedicated drilling pad and access road. This approach faced the well-known disadvantages commonly connected with this kind of field development (Joshi, 2003). Urban areas and areas submerged by the Atatürk Reservoir Lake were not accessible to drilling; only a limited interval of the reservoir layers were exposed to each wellbore, even if a single well could commonly intersect multiple overlying reservoir sections; vertical and low-angle wells could easily miss the more fractured intervals, reducing production. Moreover, areas used for the construction of drilling pads and access roads became unavailable for alternative economic activities and urban development.

Recently, the development strategy of the oilfields in the Adiyaman area has been revised to drill more high-angle and horizontal wells, in order to overcome these limitations. Rotary Steerable BHA (Bottom Hole Assembly) technology was selected for the accurate control of wellbore trajectory and dogleg severity, and geosteering helped in the assessment of the stratigraphic position of the wellbores and their placement in the optimal reservoir intervals. Moreover, by integrating the data from geosteering, the 3D geological field model could be improved with a level of detail that could not be achieved by relying only on low resolution seismic surveys and correlation of formation tops defined in vertical and low-angle wells.

## METHODS

The effectiveness of high angle wells in the field development depends on the accuracy and quality of

the wellbore trajectory and the optimal geological well placement in the reservoir. Issues like wellbore stability, risk of stuck BHA's, eventual wireline-logging runs and the completion program dictating tight dogleg severity constraints, also call for a very accurate control of the wellbores trajectory. Conventional steerable motor BHA, that alternate rotary and steerable mode drilling to follow the planned trajectory, cannot achieve this high level of positional accuracy and trajectory quality. Therefore, for the Adiyaman development project, Rotary Steerable Systems were deployed, in combination with logging while drilling tools measuring Multiple Propagation Resistivity and Azimuthal Gamma Ray for formation evaluation. The data measured by the logging tools were transmitted to surface and uploaded in the reservoir navigation software to update the geological model and assess the wellbore stratigraphic position and local structural trend, allowing to adjust the wellbore trajectory to reach the target interval and maintain the wellbore within it.

Almost 30 years of applications proved the advantages of Rotary Steerable Systems over conventional steerable motors. Drilling directional wells with conventional steerable motors is commonly resulting in tortuous wellbore trajectories, high local doglegs and increased risk of stuck BHA during slide-mode drilling. Moreover, alternating rotary and sliding mode drilling intervals, negatively affects the quality of formation evaluation logs, especially image logs. By means of Rotary Steerable Systems the continuous drillstring rotation reduces the risk of stuck BHA and improves the logs quality. Finally, the ability to steer a well without a motor, allows moving logging sensors closer to the bit, reducing the lag time between the drilling of the formation and the logging of the drilled interval. This improves the response time to changes in formation and minimize the chances of formation invasion by drilling fluids before logging.

Figure 1 displays an example of the RSS BHA type deployed for the project. It consists of a non-rotating sleeve with three radial pads, pushing against the wellbore wall to drive the bit in the required direction. A near bit inclination sensor allows the tool to self-adjust the wellbore trajectory to maintain the planned inclination. Trajectory changes are applied as needed by sending a downlink command from surface with an updated target inclination for the tool to follow. By opportunely modulating the force applied by each pad against the formation, and selecting the proper increments of inclination changes, the RSS can maintain the dogleg severity within the required limitations.

Due to the low resolution of the available seismic grid, coupled with the tectonic complexity of the area, position of the formation tops along the planned wellbore

trajectory had significant uncertainties. Moreover, local variations in porosity and fracture density could affect the thickness, or even the actual occurrence, of the target intervals. Several faults were also expected, which could offset the stratigraphic sequence, taking the wellbores out of the target interval and forcing trajectory changes to return to the target layers (Figure 2).

To help assessing the stratigraphic position of the wellbores and the interpretation of structural trends, reservoir navigation service was deployed. During geosteering operations, the reservoir navigation software is updated in real time with the logging data transmitted to surface by the downhole tools. Surface data, like total or chromatographic gas and XRF/XRD measurements, lithological descriptions and drilling parameters can also be added to the geosteering logs as needed. These data are plotted in MD and TVD/TVDSS formats. TVD/TVDSS logs are used for cross-well correlation between the actual well and the offset wells; MD logs, together with a geological interpretation, help visualizing the structural trend, the location and throw of faults, lateral thickness variations of stratigraphic intervals and the wellbore stratigraphic position.

If a high-resistivity reservoir is bound by low-resistivity shoulder beds, as it is commonly the case, geosteering can use downhole resistivity tools to maintain the wellbore within the target interval. By means of the differential response of resistivity measurements with different depths of detection, it is possible to detect an approaching boundary before the tool actually crosses it, allowing adjusting the wellbore trajectory and avoiding the reservoir exit. The resistivity response to nearby resistivity boundaries also allows following a selected target, like a reservoir boundary or the OWC, at a specific distance.

However, the resistivity profile of the reservoir formations in the Adiyaman oilfields poses additional challenges to the geosteering operations. The stratigraphic interval hosting the reservoir rocks consists of mainly calcite with little amount of other components like clays, chert or kerogen; therefore, there is no significant lithological difference between the reservoir layers and the shoulder beds (Soylu et al., 2005). This lithological uniformity leads to minimal resistivity contrast throughout the oil-bearing formations and, in some cases, to a reverse resistivity profile, with the oil-bearing formation having a lower resistivity than the shoulder beds. Therefore, the early warning of approaching shoulder beds, allowing adjusting the trajectory anticipating changes in formation dip, usually provided by resistivity measurements in standard geosteering applications, could not be applied to the present deployment. Navigation of the reservoir was based on correlation with offset wells to determine the wellbore stratigraphic position and dip picking on Gamma Ray image to assess the structural trends (Figure 2).

The adjustments made on the reservoir navigation model based on real time observation during geosteering provide also information for the interpretation of the structural trend along the wellbore, with a resolution

that could not be achieved by means of seismic data interpretation and correlation between wells. Figure 3 shows the 3D geological model before (A) and after (B) the drilling of the example well. The top of the reservoir was found several meters shallower than expected and the dip trend significantly differed from the one exported from the pre-well 3D model. Plotted on the pre-well 3D geological model, the actual wellbore is placed above the reservoir top. Moreover, a number of high angle faults were crossed that were not expected based on the interpretation of the pre-well data.

The structural information acquired during the navigation of the reservoir could be integrated in the 3D model to reprocess the reservoir top surface. Figure 3B shows the reprocessed top reservoir surface from the 3D model overlapping the top reservoir boundary mapped during geosteering. Despite the limited extension of the wellbore, having only a minor impact on the field 3D geological model, integrating more and longer wells would further improve the resolution of the 3D field model.

## RESULTS

The results from one of the wells drilled during the drilling campaign, shown in Figure 2, exemplify the issues posed by the local reservoir and the results achieved by use of horizontal drilling in connection with geosteering. As drilling progressed, the landing point was adjusted to accommodate significant differences in the TVD of the expected top markers. Similarly, wellbore trajectory was further revised multiple times while drilling the lateral section, due to the occurrence of unexpected subseismic faults, variations in the structural trend and lateral changes in the reservoir rock properties.

During the geosteering of the well presented in this case history, the following observations were made (list numbers refer to the same numbers in the geological interpretation in Figure 2):

1. Gamma Ray and Propagation Resistivity values gradually increased while the wellbore drilled down through the Sayıdere Formation, gradually building hole inclination following the planned wellpath. A sudden increase in Gamma Ray, accompanied by the encounter with a cherty limestone, marked the top of the Karaboğaz Formation. Correlation with the main offset well was always good, allowing confidently determining the wellbore stratigraphic position while cutting down through the sequence.
2. Once inside the Karaboğaz Formation, the log correlation and Gamma Ray image showed that the wellbore was still cutting down stratigraphy with a relatively steep angle and the top of the reservoir was coming shallower than expected. Therefore, the planned wellbore trajectory was abandoned and hole inclination was increased with higher DLS to land the wellbore in the target interval. At the entry point into the reservoir, Gamma Ray and Propagation Resistivity showed better correlation with a different offset well than the one picked for correlation of the initial part of the section



and the reservoir navigation model was adjusted accordingly.

3. Entry into the target layer was confirmed by a marked increase in Gamma Ray and faster ROP. Continued building inclination to land the well into the target interval.

4. The high-porosity layer inside the reservoir proved thinner than expected from correlation with the offset wells and the formation dip was also lower than expected from the pre-well geological model. Therefore, the wellbore entered into a tighter limestone with poor reservoir properties. Hole inclination was further increased to move back up in stratigraphy towards the better reservoir layer above.

5. Drilling continued up stratigraphy until the Gamma Ray increased marking the entry into the upper reservoir layer. Hole inclination was dropped to bring the wellbore to the middle of the target layer and then it was adjusted to maintain the stratigraphic position. The thickness of the high porosity interval within the target layer was estimated to be around 1.5 m locally.

6. Gamma Ray and Propagation Resistivity log trends remained steady, and the Gamma Ray image did not show any feature, over about 500 m MD of lateral section while drilling along the reservoir interval, until both the Gamma Ray and Resistivity suddenly increased.

7. A sinusoid on the Gamma Ray image showed that the formation dip had rapidly changed, becoming steeper, while the wellbore exited the target interval. Further changes in Gamma Ray image and Gamma Ray and Propagation Resistivity logs allowed identifying a sequence of faults taking the wellbore out of the reservoir into the lower Karaboğaz Formation, with a total estimated vertical displacement estimated of 13 m.

8. Hole stability problems arose after crossing the faulted area. In order to avoid the risk of a lost BHA, and having achieved the economical drain length, TD was called earlier than planned.

Despite the lack of strong resistivity contrast between the reservoir rock and the shoulder beds, which limit the full use of geosteering capability, and the challenges posed by uncertainties in the structural trend and local position of formation markers, the well was successfully landed and geosteered within the target interval of the reservoir formations, fulfilling the economic objectives and exposing the target formation to 95% of the drain section. The Rotary Steerable System allowed an accurate control of the wellbore trajectory, keeping the dogleg severity in the lateral section within the limit of  $1^{\circ}/30$  m.

#### ACKNOWLEDGEMENTS

The authors thank Türkiye Petrolleri A.O. and Baker Hughes for granting the permission to use the data presented in this paper.

#### REFERENCES

- Johnstone, J. A., and Gruenhagen, H. [2001] Using rotary closed-loop drilling to increase operational efficiency and reduce operational risk. Paper presented at the SPE Offshore Europe Oil and Gas Exhibition and Conference, Aberdeen, United Kingdom, September 2001. doi: <https://doi.org/10.2118/71840-MS>
- Joshi, S.D. [2003] Cost/Benefits of Horizontal Wells. Paper presented at the SPE Western Regional/AAPG Pacific Section Joint Meeting, Long Beach, California, May. 2003. doi: [10.2118/83621-MS](https://doi.org/10.2118/83621-MS)
- Soylu C., Yalçın M.N., Horsfield B., Schenk H.J. and Mann U. [2005] Hydrocarbon generation habitat of two Cretaceous carbonate source rocks in SE Turkey. *Journal of Petroleum Geology*, 28/1, 67-82. doi: [10.1111/J.1747-5457.2005.TB00071.X](https://doi.org/10.1111/J.1747-5457.2005.TB00071.X).
- Yilmaz, H., Over, S. and Ozden, S. [2006] Kinematics of the East Anatolian Fault Zone between Turkoglu (Kahramanmaraş) and Celikhan (Adiyaman), eastern Turkey. *Earth Planet Sp.* 58, 1463–1473. doi: [10.1186/BF03352645](https://doi.org/10.1186/BF03352645)

Keywords: Geosteering, RSS

Figure 1

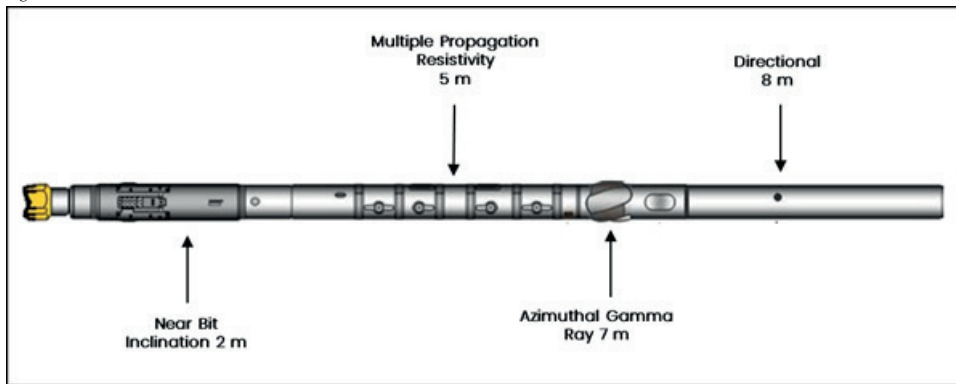


Figure 1 Example of a RSS BHA of the type used in the drilling campaign, with indication of sensor offsets typical of this kind of BHA. Actual sensor offsets could vary in different BHA's by adding additional components, like logging tools, stabilizers, flex subs, flex joints or a modular motor. The modular design of the RSS BHA also allows adding additional logging tools if required.

Figure 2

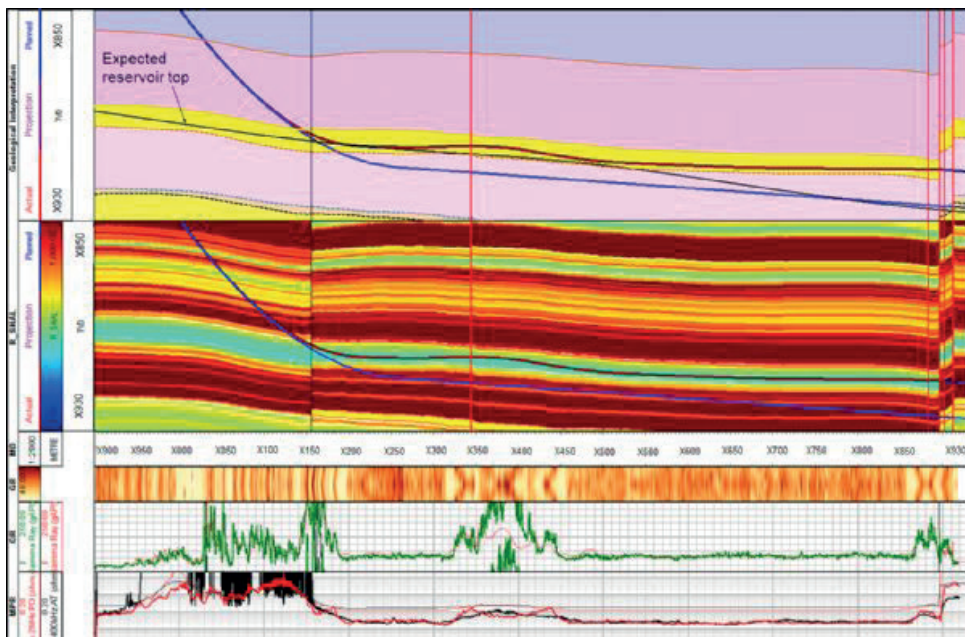


Figure 2. Cross section along one of the wells of the drilling campaign. From top to bottom: Track 1) Post-well geological interpretation with Actual wellbore trajectory (solid red) and Planned wellbore trajectory (solid blue). The yellow layer within the Karaboğaz Formation is the target interval. The vertical black line at X250 m MD from the beginning of the cross section marks the depth where the main offset well was changed. Track 2) Shallow resistivity gradient cross section with Actual wellbore trajectory (solid red). Track 3) Measured depth. Track 4) Gamma Ray image. Track 5) Real Time (solid green) and Offset (dashed red) Gamma Ray. Track 6) Real Time Shallow (solid red) and Deep (solid black) resistivity, Modelled Shallow (dashed red) and Deep (dashed black) resistivity. Numbers in the white squares in Track 1 are decision points explained in the main text.

Figure 3

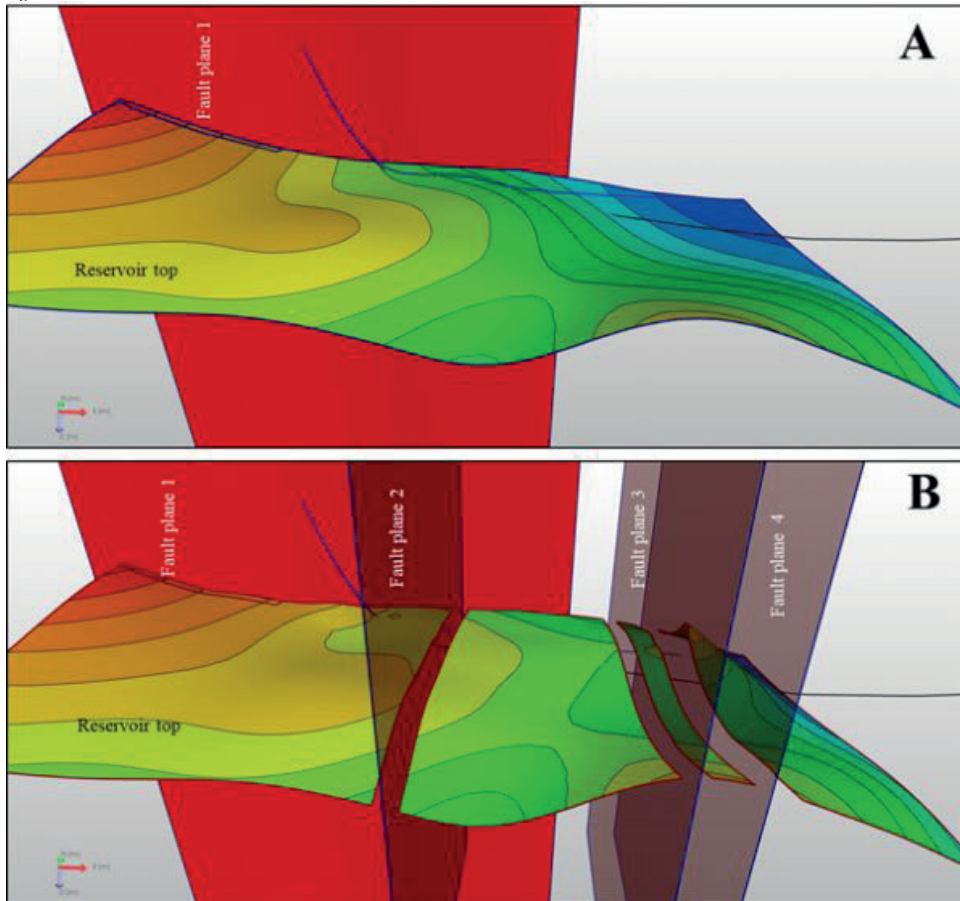


Figure 3. A) Pre-well 3D geological model from the same horizontal well shown in Figure 2, showing planned wellbore trajectory (solid black), pre-well reservoir top surface and a vertical fault (Fault plane 1) interpreted from seismic data, integrated with actual wellbore trajectory (solid blue) and three more high-angle faults detected during the drilling (Fault planes 2-4). B) Post-well 3D geological model with reprocessed reservoir formation top to fit the structural trend interpreted during the navigation of the reservoir.





**Türkiye GDA Kenet Kuşakları ve İlişkili Basenlerin  
Petrol Potansiyeli**

*Petroleum Potential of Southeastern Anatolia and  
Surrounding Areas*

---



# Paleo-Fayların 2023 Depremlerindeki Rolü ve Petrol Havza ile Yapılarına Etkisi

## The Role of Paleo-Faults in the 2023 Earthquakes and Their Effects on The Oil Basin and its Sturucture



**Doğan Perincek**

Emekli Profesör, Çalık Petrol Danışman, Çanakkale / Türkiye

**ÖZ**

Şubat 2023 depremi Ölü Deniz ve Doğu Anadolu Fayı (DAF) üzerinde gerçekleşmiş olsa da bu depremlerin dağılımını kontrol eden paleo-yapı ve paleo-fayların olduğunu öngörülmektedir. Bunlardan en belirgin olanı Bozova Fayıdır. Bozova Fayı ile yaklaşık aynı doğrultuda çok sayıda yapısal çizgisellik gözlenmiştir. KB-GD doğrultulu çizgisellikler DAF ve Ölü Deniz Fayı sisteminde sıçramalara, kesintilere, deprem odak noktalarının önünde engellere neden olmuştur. Engeller nedeniyle bazı alanlarda depremlerin yoğunlaştığı görülmüştür. Artçı depremlerin dizilimi kısmen KB-GD doğrultulu Paleo-fayların kontrolünde gelişmiştir. Artçı depremler Batıda Göksun ve Doğuda Lice dolayında ve Malatya Fay hattında engelle karşılaşmakta ve yön değiştirmektedir.

Arabistan Levhası KB-GD doğrultulu Kambriyen öncesi faylarla boydan boya, birçok kez kesilmiştir. Bu fay sistemi sonraki dönemlerde tekrar aktif olmuş ve Arabistan Kıtası üzerindeki petrol sahaları dahil birçok yapıyı kontrol eder duruma gelmiştir (Perincek vd., 2000 a, b, c, 2006). Yanal atım yönü farklı olsa da NAJD fay sistemi gömülü faylarının, Şubat 2023 depremlerinde kontrol edici rol aldığı görülmektedir. Suriye, Batı Suudi Arabistan ve Karacadağ volkanizması dahil Arabistan Levhasının birçok yerinde genç volkanizma olmuştur. Bu volkanizmanın Najd Fay sisteminin yeniden aktivitesi ile ilişkili olduğu düşünülmektedir.

Perincek vd. (1987) yaptıkları çalışmalarda Elâzığ, Lice, Adıyaman, Elbistan faylarını tanıtmışlardır. Elâzığ Fayı 2023 depreminde çok sayıda artçı deprem üretmiş ve hemen güneyindeki DAF segmentinin rolünü üzerine almıştır. Elâzığ Fayı Elâzığ Kenti yakınında başlamakta, Fırat Nehir yatağında atım yaptıktan sonra Malatya yakınlarının Kuvaterner örtü altında kaybolmaktadır. Elâzığ Fayı Şubat depremlerinde Malatya Fay engeli önünde çok sayıda artçı depremler yaratarak bölgedeki önemli belirgin hale gelmiştir (Perincek, 10-14 Nisan 2023).

Although the February 2023 earthquake occurred on the Dead Sea and the EAF, it is predicted that paleo-structure and paleo-faults control the distribution of these earthquakes. The most obvious of these is the Bozova Fault. Numerous structural lineaments were observed in approximately the same direction as the Bozova Fault. NW-SE lineaments have caused interruptions and barriers in the EAF and Dead Sea Fault system. The sequence of aftershocks was developed partially under the control of NW-SE trending Paleo-faults. Aftershocks encounter obstacles-barriers and change direction around Göksun in the west and Lice in the east and along the Malatya Fault line.

The Arabian Plate has been cut through several locations

by NW-SE trending pre-Cambrian faults. This fault system has been active again in the following periods and has come to control many structures including oil fields on the Arabian Continent (Perincek et al., 2000, 2006). Although the lateral slip direction is different, it is seen that the embedded faults of the NAJD fault system play a controlling role in the February 2023 earthquakes. Young volcanism has occurred in many parts of the Arabian Plate, including Syria, Western Saudi Arabia, the Karacadağ volcanism in Türkiye. This volcanism is thought to be related to the re-activity of the Najd Fault system.

Perincek et al. (1987) introduced the Elâzığ, Lice, Adıyaman and Elbistan faults in their studies. Elâzığ Fault produced many aftershocks in the 2023 earthquake and took over the role of the EAF segment just south of it. The Elâzığ Fault starts in the east of the Euphrates River, and after slipping on the riverbed, it disappears under the Quaternary cover near Malatya. In the February earthquakes, it has become significant in the region by creating many aftershocks in front of the Malatya Fault barrier.

### GİRİŞ

Anadol'unun en önemli aktif tektonik yapılarından biri olan Doğu Anadolu ve Ölü Deniz Fay Zonu'nda bir ay içinde peş peşe üç büyük deprem meydana gelmiştir. Kuzeydoğu-güneybatı uzanımlı, 550 km uzunluğundaki Doğu Anadolu Fay Zonu, batıya doğru hareket eden Anadolu Bloğu'nun güneydoğu sınırını oluşturmaktadır. Doğu Anadolu Fayı, Anadolu Levhası ile Arap Levhası arasındaki görelî hareketi sonucu oluşmuştur (Arpat ve Şaroğlu, 1975; Şengör ve Yılmaz, 1981; Perincek vd. 1987; Barka ve Kadinsky-Cade, 1988; Perincek ve Çemen, 1990; 1997). Toplam yanıl atım yaklaşık 15 ila 27 kilometre arasında değişmektedir (Arpat ve Şaroğlu, 1975)

Şubat depremlerinin ardından deprem odaklarının Bozova Fayı uzantısında sınırlandığı görülmüş, buradan hareketle önce KB-GD doğrultulu Bozova Fayı Çizgiselliği "B" daha sonra diğer çizgisellikler (G.B1, G.B2, G.B3, G.B4, K.B1, K.B2, K.B3) tanımlanmaya çalışılmıştır. Bu çalışmaya öncülük, kılavuzluk eden makaleler öncelikle kendi çalışmalarımız olmuştur (Perincek vd., 1987; Perincek ve Kozlu 1984; Perincek vd., 2000 a ve 2006).

Doğu Anadolu Fay Zonu, kuzeydoğuda Karlıova'dan başlayıp Kuzey Anadolu Fay Zonu'nda kesilmektedir. Doğu Anadolu Fay Zonu güneybatıya doğru devam ederken, fay sıçramaları, fay boyunca bükümler ve fay doğrultularındaki değişikliklere bağlı olarak birkaç farklı segment'e bölünmüştür (Arpat ve Şaroğlu, 1975;

Perinçek 1979 a, b; Şaroğlu vd., 1992; Duman ve Emre, 2013). Çelikhhan'ın güneybatısındaki Doğu Anadolu Fay Zonu'ndan sol yönlü bir fay ayrılarak batıya, Göksun'a doğru uzanır (Perinçek ve Kozlu 1984). 6 Şubat'taki ikinci 7,5 büyüklüğündeki deprem bu fay üzerinde meydana gelmiştir.

Doğu Anadolu Fay Zonu'nun Kuzeydoğuda Karlıova ile güneybatıda Türkoğlu arasındaki izi konusunda yerbilimciler mutabakat içindedir. Fakat Türkoğlu sonrasında fayın güneybatı ya da Güney yönünde nasıl devam ettiği konusunda üç farklı görüş vardır (Yönlü vd., 2017). Bu makalede ağırlıklı olarak, Perinçek ve Çemen (1990) tarafından kabul edilen görüş dikkate alınmıştır. Birçok yerbilimcinin katıldığı bu görüşe göre; Ölü Deniz Fay Zonu, Doğu Anadolu Fay Zonu ile Türkoğlu yakınlarındaki Karasu Fayı üzerinde birleşmektedir,

### SON DEPREMLERİN JEOLJİ BİLİMİNE GETİRDİĞİ YENİ BAKIŞ AÇISI

Şubat 2023 depremi Ölü Deniz ve Doğu Anadolu Fayı (DAF) üzerinde gerçekleşmiş olsa da bu depremlerin dağılımını kontrol eden paleo-yapı ve paleo-fayların olduğunu öngörülmektedir.

Şekil 1- 6 Şubat depremlerinin olduğu alanda Cumhuriyet tarihinin en büyük felaketi yaşanmıştır. Harita bölgedeki aktif fayları göstermektedir (Perinçek vd. 1987). Harita üzerine Şubat 2023 yılında olan depremler işaretlenmiştir. 7.7 büyüklükteki ilk deprem Pazarcık yakınında saat 4.17 de olmuş bunu 11 dakika sonra 4.28 de 6.6 (6.7) büyüklükteki Nurdağı depremi izlemiştir. İlk büyük depremden 9 saat 7 dakika sonra saat 13.24 de 7.6 büyüklükteki Ekinözü depremi olmuş bunu da 98 dakika sonra saat 15.02 de 6 büyüklükteki Göksün depremi izlemiştir. Söz konusu bu depremlerden 17 gün sonra 20 Şubat'ta Hatay ili Arslanyazı Köyü yakınında saat 20.04'te 6.4 büyüklüğünde bir deprem meydana gelmiştir. Bu depremden 3 dakika sonra, yine batıda Samandağ'ı yöresinde 5,8 büyüklükte deprem yaşanmıştır. Bölgede olan büyük (7.7, 6.6 ve 6.4) depremi takip eden depremleri bu depremlerin hemen batısında olması dikkati çekmektedir ve tesadüf değildir. Kırılmanın doğudan batıya olduğunu göstermektedir. Doğu Anadolu ve Ölü Deniz Fay Zonları genel doğrultusu Kuzeydoğu Güneybatı olduğu halde burada sözü edilen depremlerin önce doğuda ve hemen ardından batıda olmasının nedeni nedir. Bu makale bu doğu-batı diziliminin GD-KB doğrultulu paleo-fayların kontrolünde geliştiğini vurgulamak için kaleme alınmıştır. Bu yorumu desteklemek için çok sayıda veri derlenmiştir. Yukarıda verilen şekilde Güneydoğu – Kuzeybatı doğrultulu birçok fay görülmektedir. Bunlardan en önemlisi Bozova Fayı'dır. Ayrıca Suriye sınırları içinde üç fay Suriye jeoloji haritasından alınarak bu haritaya aktarılmıştır. Bozova Fayı Atatürk Barajının hemen güneyinde bulunan sağ yanal atımlı bir faydır (Perinçek vd., 1987; Çemen, 1990; Çemen vd., 1990; Perinçek ve Çemen, 1991). Bozova Fayı; Kuzeybatı yönde, Gölbaşı yakınında Doğu Anadolu fayının doğrultusunu belirgin bir

şekilde değiştirdiği noktadan geçmektedir. Sonrasında 7.6 büyüklükteki Ekinözü depreminin olduğu noktaya geçip Afşin yönünde uzanmaktadır. Daha kuzeybatıda Tavla Fayı'nın sonlandığı Göksu Fayı'nın başladığı alana ulaşmaktadır. Tavla ilçesi yakınında sözü edilen iki fay zonunun doğrultusundaki ani değişim dikkati çekmektedir. Özetle Bozova Fayı ve onun kuzeybatı devamındaki çizgisellik boyunca yer alan fayların doğrultularının değiştiği görülmektedir. Bozova Fayı paleo-fay olarak düşüncemizi sağlayan nedenler vardır ve günümüzden önce defalarca tekrarlanan aktivite gösterdiği bilinmektedir. Geç Miyosende sağ yanal atımlı faya dönüşmeden önce terse fay karakterli olduğu saha çalışmaları ile bilinmektedir. Bozova Fayı kuzeyindeki sol yanal atımlı Adıyaman fayı ile birlikte çalışarak, iki fayın arasında kalan alanın doğuya kaçmasını sağlamaktadır (Perinçek vd. 1987). Fayların birleşme alanında doğuya kaçmaya bağlı olarak, oluşan çökme alanında alüvyon birikmiştir. Benzer durum sağ yanal atımlı Kalecik Fayı ile sol yanal atımlı Lice Fayı çifti içinde söz konusudur. Burada 2017 -2018 yıllarında Samsat depremleri olmuştur. Bu depremlerin Lice-Kalecik fay çiftinin birlikte çalışması ile olduğu düşünülmektedir. Her iki fay çiftinin ortasında görülen turuncu oklara doğuya kaçışı temsil etmektedir.

KB-GD doğrultulu Bozova ve Kalecik faylarının Güneydoğu devamında Akçakale Grabeni bulunmaktadır. Çöküntü alanındaki alüvyon örtü tektonik aktivitenin yakın geçmişte de sürdüğünü göstermektedir. Akçakale çöküntü alanında Doğu-Batı gerilme iki yönlü turuncu oklarla işaretlenmiştir. Bozova Fayı, Suruç, Akçakale grabenleri Najd Fay Sisteminin etkisinde oluşmuştur. Suriye'deki Fırat Grabeni Najd Fay Sistemi'nin kontrolü altında gelişmiştir (Perinçek vd. 2000, 2006). Yoldemir ve Perinçek (1990) Pazarcık dolaylarında ve kuzeyinde yaptıkları çalışmada Paleosen döneminde şekillenmiş grabenin varlığından bahsetmektedir. Suudi Arabistan ve Suriye'de bilinen grabenlerin Najd Fayı'nın Geç Kretase dönemindeki aktivitesine bağlı olarak geliştiği bilinmektedir (Perinçek vd. 2006).

Şekil 2- Haritada deprem odaklarının dağılımı dikkate alınarak 8 çizgisellik tanımlanmıştır (B, G.B1, G.B2, G.B3, G.B4, K.B1, K.B2, K.B3). İkinci aşamada; bölgede bulunan Güneydoğu-Kuzeybatı doğrultulu faylar (Bozova ve Karacadağ fayları) ve Suriye'deki faylar ile çizgiselliklerin doğrultuları karşılaştırılmış ve olağanüstü bir uyumun olduğu fark edilmiştir. Rakka – Deyrizor alanında kalan Fırat Grabeni de söz konusu çizgisellikler ile aynı doğrultuda uzanmaktadır. Rakka batısında Fırat Nehri yatağında gözlenen ani doğrultu değişimleri; burada bir fay olabilir kanaati uyandırmış ve bu çizgisellik olarak haritaya işaretlenmiştir. Ayrıca deprem odaklarını farklı yönlerde sırlayan engeller, sarı kutularla işaretlidir. Engeller bazen bir fay ile (Malatya Fayı, Göksu Fay Zonu), bazen fay ve bindirme ile (Bingöl Güneybatısında Bitlis bindirme cephesi ve DAF'ında gözlenen bir sıçrama) bağlantılıdır. Bingöl Güneybatısında tanımlanan engel alanının doğrultusu ilk defa Perinçek vd. (1987), Perinçek (1990) tarafından tanımlanan Kozluk-Narlı Fayı ve Yüksekova Şemdinli



Fayı doğrultusu ile aynı olup Kuzeybatı-Güneydoğu uzanmaktadır. Bitlis ve Bingöl kuzeyinde deprem odaklarının dizilimi de dikkatleri çekecek ölçüde Kuzeybatı-Güneydoğu doğrultudadır. Çalışma yapılırken önce deprem odakları dikkate alınarak çizgiselliklerin konumu belirlenmiş sonra bunların Ölü Deniz ve Doğu Anadolu fayları ile kesiştiği yerlerdeki yukarıda belirtilen ilişkisi gözlenmiştir. Daha sonra Suriye'deki faylarla bağlantısı ortaya konmuştur. (Harita; Boğaziçi Üni. KRDAE).

Şekil 3- Suudi Arabistan'ın Batısında metamorfik temelin yüzeyletiği alanda Kambriyen öncesinde aktif olmuş KB-GD doğrultulu Najd Fay Sistemi sol yanal atımlıdır (Edgell, 1992; Perinçek vd., 2000 a; Perinçek vd., 2000 b; Perinçek vd., 2006). Ghawar petrol sahasının yüzeyde izlenen yapısal hatlar; Najd Fay Sistemine dahil edilen KB-GD doğrultulu çizgisellikler ile uyum içindedir (Saner vd., 2005; Perinçek vd., 2000 c). Ghawar petrol sahasında 3 D sismik yorum yapılırken KB-GD doğrultulu fay sistemi haritalanmıştır (Perinçek vd., 2000 c). Petrol sahasını etkileyen bu fay sisteminin Najd Fay Sistemi ile ilişkisi olduğu sonucuna varılıp; uydu ve radar görüntüleri, topografi haritaları, basılı yayınlar ve sismik veriler gibi farklı kaynaklar kullanılarak Suudi Arabistan doğusunda Katar'dan Suriye'de Şam'a kadar uzanan Doğu Najd Fay Sistemi haritalanmıştır (Perinçek vd., 2000 a; Perinçek vd., 2006). Najd Fayı ilk kez Prekambriyen 'de oluşmuş ve daha sonra muhtemelen Paleozoyik ve geç Jura dönemleri olmak üzere çeşitli kereler ve değişik şiddetlerde geç Kretase 'den geç Tersiyer döneme kadar sürekli yeniden etkinleşmiştir (Perinçek vd., 2006).

Batı Najd Fay Sistemi gibi Doğu Najd Sistemi de Miyosen Pliyosen döneminde tekrar aktif hale geldiğinde, volkanik çıkışlara neden olmuştur. Batı Suudi Arabistan'da olduğu gibi, Orta Suriye'de ve Şam dolayında da Doğu Najd Fayı'nın ürünü volkanik yaygıları bulunur; bunlar ve Karasu-Hassa Grabeni, Yazihan dolayındaki bazalt yaygıları da Karacadağ volkanizması ile aynı yaşta ve benzer birleşimdedir, Suudi Arabistan batı yarısında Geç Miyosen Pliyosen, Pleistosen, Kuvaterner yaşlı ve Najd Fayı ile bağlantılı olduğunu düşündüğümüz bazalt yaygıları bulunur (Haksal, 1981; Şaroğlu ve Emre, 1987; Tatar vd., 2004; Demir et al., 2007; Sevimli, 2009; Trifonov vd., 2011; Kavak 2013; Segev vd. 2014; Sevimli vd., 2017; Alohalı vd. 2022). Suriye'nin kuzey yarısında Türkiye sınırlarına yakın alanlarda özellikle Geç Miyosen, Pliyosen, Erken-Orta Pleistosen volkanizması yaygındır. Türkiye sınırlarına yakın alanda Suruç ve Cizre Güneyinde Pliyosen ve Pleistosen, Kilis Güneyinde ise Geç Miyosen ve Pleistosen yaşlı volkanit yaygıları görülür.

Şekil 4- Suriye'de Fırat Nehri boyunca yer alan Fırat Grabeni'nde yüzey ve sismik veriler kullanılarak faylar haritalanmıştır (Litak vd., 1997). Fırat grabeni Najd Fay Sisteminin en belirgin unsurlarından biridir. Fırat Grabenini sınırlayan fay sisteminin Güneydoğu Anadolu'daki uzantısı olan Bozova Fayı, Akçakale Grabeni "B", "G.B1", "G.B2" çizgisellikleri ile aynı doğrultudadır. (Sağ alt köşedeki harita; Perinçek vd.

2006 dan alınmıştır.) Palmyra yapısının oluşumunun da Najd Fay Sisteminin kontrolünde geliştiği belirtilmektedir (Perinçek vd., 2000 a, 2006).

Şekil 5- Kuveyt Mauddud petrol sahasında da Najd Fay Sisteminin izleri net olarak görülmektedir. Orijinal haritada yapıyı ortadan biçen KB-GD doğrultulu fay makalenin yazarı tarafından, sağ yanal atımlı gösterilmiş olsa da, sarı renk ile gösterilen yapı eksenine dikkate alındığında fayın sol yanal atımlı olduğu bariz bir şekilde görülmektedir ve sol yanal atımlı Najd Fayı ile uyum içindedir. Sismik kesitte ise söz konusu fay negatif çiçek yapısı özelliği gösterir. Soldaki sismik kesitin sağında gözlenen ters fay Najd Fay Sisteminin doğu batı sıkışma bileşeni ürünüdür. (harita ve kesit; Carman, 1996 yayınından değiştirilerek kullanılmıştır).

Perinçek vd., (2006) Katar ile Şam arasında haritaladıkları Doğu Najd Fay Sistemi boyunca grabenler olduğunu belirtmişlerdir. Doğu Najd Fay Sistemi boyunca; Azraq-Sirhan Grabeni, Kuzeybatı devamındaki İrbın Rift'i (Segev vd. 2014) ve Sirhan-Al Jawf fay zonu güneydoğusundaki An-Nafud Grabeni bulunur. Segev vd. (2014) Najd Fay Sistemi ile aynı doğrultuda olan ve Ölü Deniz Fay Sisteminin batısına geçen fayları haritalamışlardır. Söz konusu fayların Najd Fay Sisteminin devamı olduğu ve Ölü Deniz Fayı ile yanal yönde atıldığı düşünülmektedir. Pre-kambriyen de ortaya çıkan Najd Fay Sistemi Jura, Üst Kretase, Eosen-Oligosen ve Miyosende de tekrar aktif hale gelmiştir (Perinçek vd., 2000 a; Perinçek vd., 2006; Segev vd. 2014) ve bu makalede vurgulandığı gibi aktivitesini günümüzde de sürmektedir. Azraq-Sirhan Grabeni ile Neo-Tetis okyanusunun açılması sırasında (rift-drift) okyanus ortası sırta oluşan transform fay arasında ilişki kurulmuştur (Segev vd. 2014; şekil 3A). Azraq-Sirhan Grabeni'nin Kuzeybatı devamında Jebel Drouz yükseliminde birbirini üzerleyen Kuvaterner, Pliyosen, ve Miyosen yaşlı bazalt yaygıları bulunur (Segev vd. 2014). Ölü Deniz Fayı öncesi duruma dönmek için restorasyon yapılmış, doğusundaki blok 90km güneye kaydırılarak; Ölü Deniz Fayı batısındaki Fari'a Grabeni ile doğusundaki İrbid Grabeni (İrbın Rifti) ve ilgili Najd fayları çakıştırılmıştır (Segev vd. 2014). Böylece Najd Fayı'nın Ölü Deniz Fayı batısında devam ettiği gösterilmeye çalışılmıştır. Najd Fay Sistemi Ölü Deniz Fayından daha yaşlıdır, Miyosen ve günümüzde tekrar aktif olmuş ve bu fay sistemi ile ilgili tüm faylarda Miyosen, Pliyosen ve Kuvaternerde Türkiye'de Karacadağ dahil bazalt çıkışları gerçekleşmiştir. Najd Fay Sistemi Suriye ve İsrail'de Ölü Deniz Fay Sisteminin kestiği gibi Türkiye'de de Najd Sistemi içinde kalan faylar DAF ve Ölü Deniz Fayını kesmektedir. Buna en güzel örnek Bozova Fayıdır. Bu aşamada DAF sitemini kesen çizgiselliklerde atım miktarı Suriye'de olduğu gibi net bilinmemektedir. İlave çakışma gerekmektedir.

Şekil 6- Mavi ile işaretli çizgisellikler belirgin bir şekilde deprem odaklarını sınırlamaktadır. Ayrıca çizgisellikler Ölü Deniz ve Doğu Anadolu faylarının sıçrama yaptığı ya da boşluk oluşturduğu alanlarından geçmektedir. En önemlisi çizgisellikler Bozova ve Karacadağ fayları ile uyum içinde ve onların doğrultusunda uzanmaktadır. Çizgiselliklerin; bugüne kadar fark edilmeyen,

temelde mevcut paleo-fayların kontrolünde geliştiği düşünülmektedir. (Harita; Boğaziçi Üni. KRDAE).

Şekil 7- Elazığ Fayı Şubat 2023 depremleri sırasında Doğu Anadolu segmentinden daha fazla deprem üretmiştir. Elazığ Fayı; Bozova Fayı'nın Kuzeybatı devamı olan çizgisellik "B" hattında ve Sürgü (Çardak) Fayı'nda sonlanmaktadır. Bozova çizgiselliği olarak tariflediğimiz fayın Kuzeybatı tarafında 7.6 büyüklükteki Ekinözü depremi, 1544 tarihsel depremi; Güneydoğu ucunda ise 1003 ve 718 tarihsel depremleri bulunur. Bozova Fayının hemen kuzeyinde 2017 yılında 5.5 büyüklükte Samsat depremi olmuştur. Söz konusu çizgiselliğin "B"; Kuzeybatıda olan deprem odaklarını güneyden sınırladığı net olarak görülmektedir. "B", "G.B1" çizgisellikleri artıç depremler odaklarını Kahramanmaraş kuzeyinde ve batısında keskin bir şekilde sınırlar. (Harita; AFAD).

Şekil 8- Sol yanal atımlı Lice Fayı yüzey ve kuyu verileri kullanılarak Atatürk Barajı dolayından Lice ilçesine kadar uzandığı saptanmış ve adlanmıştır (Perinçek vd. 1987). Şubat 2023 depremleri sırasında Bingöl ile Lice arasında sarı ile gösterilen dikdörtgenin Güneybatısında deprem odak sayısında bir kümeleşme-yoğunlaşma görülmüştür. Söz konusu sarı hat Lice Fayının KD ucunda kalır, bu makalede deprem odaklarını sınırlayan engel olarak tariflenmiştir. Deprem odaklarının kümelendiği alanda, Miyosen bindirmeleri de Şarıyaj cephesine neredeyse paralel olarak KB dan GD ya döner. MTA aktif fay haritasında DAF'ın da Bingöl Kovancılar arasında, iki kez doğrultusunu değiştirdiği görülür (Şaroğlu vd. 1992; Duman ve Emre, 2013; Emre vd. 2013). Doğrultu değişimi sarı ile işaretlenen hat boyunca gerçekleşmiştir. 6 Eylül 1975 Lice depremi Bitlis Şarıyaj Zonu üzerinde Doğu Anadolu Fayı'nın 50 km kadar güneyinde oluşmuştur (Arpat, 1977; Eyidoğan,1983). Fay üzerinde düşey atımın yanı sıra sol-yanal atım da belirlendiğinden oblik bir fay konumundadır (Arpat, 1977; Eyidoğan, 1983). Bitlis Bindirme Zonu'nun depremi üreten kısmı Arpat (1977) tarafından depremin hemen ardından çalışılmış, arazi gözlemlerinde bazı yüzey kırıklarında sol yanal hareket saptamıştır. Arpat bu tespitine rağmen, depremin yerli istif içindeki ters faylarla bağlantılı olduğu sonucuna varmıştır (Arpat, 1977). Lice depremi; Atatürk Barajı yakınından Lice'ye kadar uzanan sol yanal atımlı Lice Fayı'nın (Perinçek vd. 1987) Bitlis Şarıyaj Zonu ile kavuşma alanında, haritada gösterilen sarı dikdörtgen engeli önünde olmuştur. Yazara göre eprem sol yanal atımlı Lice Fayı'nın ürünüdür. (Harita; Boğaziçi Üni. KRDAE).

Şekil 9- Haritada tarihsel dönem depremleri ve bölgedeki faylar görülmektedir (Emre vd., 2013). Ölü Deniz ve Güneydoğu Anadolu fay zonları boyunca Kuzeydoğu-Güneybatı dizilen (mavi dikdörtgen) "V" ve "X" şiddet arasında olan tarihsel depremlerin sayısı 6 adettir. Kuzeybatı-Güneydoğu dizilen (siyah dikdörtgen) tarihsel depremlerin sayısı ise 8 tane dir. Kuzeybatı-Güneydoğu dizili depremlerin sayısının fazlalığı dikkatimizi çekmekte ve depremlerin aynı doğrultudaki paleo-fayın ürünü olduğu düşünülmektedir. Söz konusu 8 tarihsel deprem "G.B2" olasılı fay olarak

tariflediğimiz hat yakınında kalmaktadır.

Şekil 10- Hatay Havaalanı'nın jeomorfolojik özellikleri çalışmasında sunulan morfolojik harita (soldaki harita Özşahin, 2010 yayınından alınmıştır) KB-GD doğrultulu Paleo-fay olarak yorumladığımız çizgisellikler ile ilgili önemli ipuçları vermektedir. Amanos Dağları'nın zirvelerinden geçen su bölümü çizgisi (açık mavi) yaklaşık KKD-GGB doğrultulu olarak Belen yakınlarına kadar uzanır. Belen ilçesi yakınında Amanos Dağları KB-GD doğrultulu "G.B3" çizgiselliğini tarafından kesilir. Haritada işaretli iki çizgisellik geçildikten sonra Amanos Dağlarının zirvelerini doğrultusu bariz bir şekilde değişir ve GB ya döner. İki çizgisellik arasında kalan alan içinde; Güneydoğuda Amik Gölü ve Kuzeybatıda Amanos Dağları "Belen Bloğu" kalır. Bu blok ok ile gösterildiği gibi Kuzeybatı yönünde kaymıştır. Karasu Grabeni Amik Gölü dolayında ovanın diğer bölgelerine göre çok daha geniştir. Bu genişlik Paleo-fay olarak düşünülen fayların kontrolünde gelişmiştir. Nisan 2023 kurultayında bölgede çalışan birçok yerbilimci son depremlerle oluşan yüzey kırığının Kuzeyden Amik Ovası'nın olduğu alana kadar uzandığını ve burada sonlandığını belirtmiştir. Bu sonlanma "G.B3" çizgiselliği kontrolünde gerçekleşmiştir. Sonlanmanın Paleo-fay olarak tanımlanan hatlar kontrolünde olduğu tarafımızdan kabul görmektedir. Belen Bloğu'nu güneyden sınırlayan çizgisellik önceki şekillerde tanımlanmamış olsa da deprem odaklarının dağılımı bu hat içinde ip ucu vermektedir. Ayrıca Belen Bloğu'nun morfolojide net görülen izleri, bu adlanmış çizgisellik için tartışması ipucu vermektedir. Perinçek vd., (1987) yayınında Belen ilçesi dolayında ve Güneyinde KB-GD doğrultulu iki fay görülmektedir. Bu faylar Burada verdiğimiz çizgisellikler ile aynı doğrultudadır. Amanos Dağları Belen dolayında KB-GD doğrultulu faylar haritalanmıştır (Günay; 1984) bu alanda aynı doğrultuda faylarla sınırlı bir grabenin varlığı da söz konusudur.

## SONUÇLAR

Bu makaledeki modelin başlangıcı 2023 Şubat depremleri sonrasında gözlenen ve yorumlanan KB-GD çizgisellikler ile şekillenmiştir. Önce 8 adet çizgiselliği (paleo-fay) gözlemlenmiş; daha sonra mevcut jeoloji haritalarında ve Başta yazarın kendi makaleleri başta olmak üzere çok sayıda makalede gözlenen veriler kullanarak model güçlendirilmiştir.

Mardin Yükseliminin Kuzeybatı devamının Güneybatı sınırı Bozova Fayı'nın doğrultusu (B çizgiselliği) ile uyum içindedir (Şekil 11). 8 adet çizgisellik ile aynı doğrultuda bulunan Karacadağ Fayı ile Yazihan Fayı çifti tezimizi destekleyen diğer bir fay çiftidir (Şekil 12). Karacadağ Fayı Arabistan kıtası üzerinde Yazihan Fayı ve Güneydoğu devamı Anadolu kıtası ve eklentileri üzerindedir

Ölü Deniz ve Doğu Anadolu Fay zonlarının üzerinde gerçekleşen 6 Şubat depremlerinin odakları bu fay zonlarına hemen hemen dik uzanan paleo-fay olarak tariflenen çizgisellikler tarafından kesilmektedir.

9 adet KB-GD doğrultulu olasılı fay "çizgisellik"

olarak tanımlanmıştır. Bunlardan 8 tanesi harflerle adlanmıştır (B, G.B1, G.B2, G.B3, G.B4, K.B1, K.B2, K.B3). Söz konusu çizgisellikler Suriye’de jeoloji haritalarında izlenen faylarla aynı doğrultudadır. 9 adet çizgisellik (paleo-fay) dışında başkalarının da olması beklenmektedir.

Paleo-fayların Kambriyen öncesi yaştaki Najd Fay Sisteminin ile ilgili olduğunu gösteren veriler vardır. Najd Fay Sistemi; Jura, Kretase, Miyosen döneminde ve Arabistan Levhasının kuzey kesiminde günümüzde de tekrar aktivite kazanmıştır. Güneydoğu Anadolu’da bulunan Bozova Fayı, Karacadağ Fayı, Hekimhan-Yazihan Fayı dolaylı olarak Najd Fay Sistemi etkisinde şekillenmiştir.

Söz konusu aktivitenin tekrarlanması Miyosen-Pliyosen döneminde volkanik aktivite ile sonuçlanmış bazalt yaygıları oluşmuştur. Karasu Grabeni alanında, Karacadağ dolayında, Yazihan Kuzeybatısında, Suriye’de Şam yakınında, Batı Suudi Arabistan’da görülen yaygın bazalt örtüleri Paleofayların aktivitesi ile ilgili ve aynı yaşlarda olduğu görülmektedir.

Arabistan kıtası üzerinde Najd Fay Sisteminin ürettiği çok sayıda graben vardır. Bunlardan en önemlisi Suriye’deki Fırat Grabenidir. Türkiye’de ise Akçakale ve Suruç grabenleri Fırat Grabeni gibi Najd Fay aktivitesi ile bağlantılı olarak oluşmuştur. Suudi Arabistan’da henüz tam olarak tanınmamış başka graben yapıları da bulunmaktadır (Perinçek vd., 2006)

NAJD Fay Sistemi Suriye ve İsrail’de Ölü Deniz Fay Sistemini kestiği gibi Türkiye’de de Najd Sistemi içinde yorumlanan 9 adet çizgisellik ve ilgili faylar DAF ve Ölü Deniz Fayını kesmektedir.

## KAYNAKLAR

Abdullah Alohali, A., Bertin, D., Silva, S., Cronin, S, Duncan, R., Saleh Qaysi, S and Moufti, M. R., 2022. Spatio-temporal forecasting of future volcanism at Harrat Khaybar, Saudi Arabia. *Journal of Applied Volcanology* 11:12, pp.1-21. <https://doi.org/10.1186/s13617-022-00124-z>.

AFAD, Afet ve Acil Durum Yönetimi Başkanlığı, Deprem ve Zarar Azaltma Genel Müdürlüğü, <http://www.deprem.gov.tr/>

Arpat, E. 1977. 1975 Lice Depremi, Yeryuvarı ve İnsan, Şubat 1977, 15-27.

Arpat, E., Şaroğlu, F., 1975. Türkiye’deki bazı önemli genç tektonik olaylar. *TJK Bül.* 18, 91–101.

Barka, A., Kadinsky-Cade, K., 1988. Strike-slip fault geometry in Turkey and its influence on earthquake activity. *Tectonics* 7 (3), 663–684.

BOUN KOERİ. 2023 Boğaziçi Üniversitesi, Kandilli Rasathanesi ve deprem araştırma enstitüsü (KRDAE) bölgesel deprem-tsunami izleme ve değerlendirme merkezi (BDTİM) <http://udim.koeri.boun.edu.tr/zeqmap/hgmmmap.asp#>

Carman, G. J., 1996. Structural Elements of Onshore Kuwait. *GeoArabia*, Vol. 1, No. 2, 239-266. Gulf PetroLink, Bahrain. <https://doi.org/10.2113/>

geoarabia0102239

Çemen, İ. 1990. Araban Tektonik Bloğu Doğu Kısımının Yapısal Jeolojisi ve Petrol Potansiyeli. TPAO rapor no: 2727.

Çemen, İ., Perinçek, D., Ediger, Ş. V., Akça, L. 1990. Güneydoğu Anadolu’daki Bozova doğrultu atımlı fayı: üzerindeki ilk hareket ters faylanma olan faylara bir örnek. *Türkiye 8. Petrol Kongresi*, 169-179

Demir, T., Westaway, R., Bridgland, D., Pringle, M., Yurtmen, S., Beck, A., and Rowbotham, G., 2007. Ar-Ar dating of late Cenozoic basaltic volcanism in northern Syria: Implications for the history of incision by the River Euphrates and uplift of the northern Arabian Platform. *Tectonics*, VOL. 26, TC3012, doi:10.1029/2006TC001959

Duman, T.Y., Emre, Ö., 2013. The East Anatolian Fault: geometry, segmentation and jog characteristics. *Geol. Soc. (Lond.) Spec. Publ.* 372.

Edgell, H.S., 1992, Basement tectonics of Saudi Arabia as related to oil field structures, in: Rickard, M.J. et al. (Ed.), *Basement Tectonics*. Kluwer Academic Publishers, Dordrecht, 169-193.

Emre, Ö., Duman, T.Y., Özalp, S., Elmacı, H., Olgun, Ş. ve Şaroğlu, F., 2013. Açıklamalı Türkiye Diri Fay Haritası. Ölçek 1:1.250.000, Maden Tetkik ve Arama Genel Müdürlüğü, Özel Yayın Serisi-30, Ankara-

Eyidoğan, H., 1983. Bitlis-Zağros bindirme ve kıvrımlı kuşağının sismotektonik özellikleri. Doktora Tezi, İstanbul Teknik Üniversitesi, Maden Fakültesi, 112s (yayımlanmamış).

Günay, Y., 1984. Amanos Dağlarının Jeolojisi ve Karasu Hatay Grabeninin Petrol Olanakları, TPAO Arama Grubu Başkanlığı Hakkari-Şariyaj Projesi, Ankara 1984.

Haksal, A., 1981. ‘‘Petrographie und Geochemie des Schildvulkans Karacadağ’’ (Südstonato-lien). Diplomarbeit (doktora tezi). Hamburg Üniv. Almanya.

Kalafat, D., Güneş, Y., Kara, M., Deniz, P., Kekovalı, K., Kuleli, H.S., Gülen, L., Yılmaz, M., Özel, N. M., 2007. A revised and extended earthquake catalogue for Turkey since 1900 (M  $\geq$ 4). Bogaziçi University Publication, 1-553.

Kavak, O., 2013. Diyarbakır ve Çevresinde Yer Alan Karacadağ Volkanitinin Genel Özellikleri. S. 361-372.

Korkmaz, H., Çetin, B., Özşahin, E., Karataş, A., Bom, A., 2011, Hatay Coğrafyası. <https://www.researchgate.net/publication/256704329>.

Litak, R., Barazangi, M., Beauchamp, W., Seber, D., Brew, G, sawaf, T. and Al-youssef, W., 1997., Mesozoic–Cenozoic evolution of the intraplate Euphrates fault system, Syria: implications for regional tectonics. *Journal of the Geological Society*, London, Vol. 154, 1997, pp. 653–666, 15 figs.

Özşahin, E. 2010 Hatay havaalanı’nın jeomorfolojik özellikler ve doğal risk açısından değerlendirilmesi. *Turkish Studies International Periodical For the Languages, Literature and History of Turkish or Turkic* Volume 5/4 Fall 2010, pp. 1390-1411

- Perincek, D., 1990, Stratigraphy of the Hakkari Province, Southeast Türkiye, Turkish Association of Petroleum Geologist Bulletin, Vol. 2/1, pp. 21-68, (in Turkish).
- Perincek, D., G. Eren, 1990, Origin of the Amik Basin within the strike-slip East Anatolian and Dead Sea fault zones, 8th Petroleum Congress of Turkey, pp.180-192, (in Turkish).
- Perincek, D., K. G Al-Hinai and S. Saner, 2000 a, Rejuvenation of the pre-Cambrian Najd Fault System and its importance in the oil province of Saudi Arabia, TURKIOG 1st Turkish International Oil & Gas Congress and Exhibition, 16-18 November 2000, Extended abstracts, pp.75-82
- Perincek, D., O. Duran, N. Bozdoğan, and T. Coruh, 1992, Stratigraphy and Palaeogeographical Evolution of the Autochthonous Sedimentary Rocks in the Southeast Turkey, Proceeding, Sungurlu Symposium, Turkish Petroleum Corporation - Turkish Association of Petroleum Geologists, pp. 274-305, (in English).
- Perincek, D., S. Saner and K. G Al-Hinai, 2000 b, Re-activation of the pre-Cambrian Najd Fault System and its importance in the oil province of Saudi Arabia, Exploration beyond 2000, Australian Society of Exploration Geophysicists (ASEG) 14th International Conference and Exhibition, Abstracts, p.11
- Perincek, D., S. Saner and K. G Al-Hinai, 2006, Rejuvenation of the Pre-Cambrian Najd Fault System and its importance in the oil province of Saudi Arabia. General Directorate of Mineral Research and Exploration Journal (MTA Dergisi). 132, s 91-99, Ankara, Turkey
- Perincek, D., S. Saner, A. Al-Ghamdi, J. Cole and R. Kamal, 2000 c, Surface to Subsurface Data Integration for an Improved Understanding of the Structural History of the Ghawar Field, Saudi Arabia. Geo2000, GeoArabia Volume 5, Number 1, Abstracts, p.82
- Perincek, D. 1979a. Geological investigation of the Çelikhansincik-Koçali area (Adıyaman province). İstanbul Üniversitesi, Fen Fakültesi Mecmuası Seri B, 44, 127-147.
- Perincek, D. 1979b. Interrelations of the Arabian and Anatolian plates. First Geological Congress on Middle East, Geological Society of Turkey, Ankara, Guide book for excursion B., 34 p.
- Perincek, D. and Kozlu, H., 1984. Stratigraphy and structural relations of the units in the Afşin-Elbistan-Doğanşehir region (Eastern Taurus), Geology of the Taurus Belt, Int. Symp., Tekeli, O. And Gönçüoğlu, M.C. (Eds.), Miner. Res. Explor. Inst., Ankara. September 26-29, 1983, p. 181- 198, Ankara-Turkey.
- Perincek, D. Günay, Y., Kozlu, H. 1987. New observations on strike-slip faults in east and southeast Anatolia. In Proceedings of 7th Biannual Petroleum Congress of Turkey. UCTEA Chamber of Petroleum Engineers and Turkish Association of Petroleum Geologists, Ankara, Turkey. 89-103.
- Perincek, D., 2023. Paleo-fayların 2023 Depreminde Rolü; Artçı Depremlerin İlerlemesini Durduran Engeller. (The Role Of Paleo-faults In The 2023 Earthquake; Barriers That Stop The Progression Of Aftershocks). Uluslararası Katılımlı 75. Türkiye Jeoloji Kurultayı 10-14 Nisan 2023 (75th Geological Congress of Turkey with International Participation April 10-14 2023, Ankara Turkey) Özler Kitabı, Sayfa 82 (Abstract book, P.82).
- Perincek, D., and Çemen, I., 1990. The structural relationship between the East Anatolian and Dead Sea fault zones in southeastern Turkey. Tectonophysics, 172, 331-340.
- Perincek, D., Çemen, İ. 1991. Late Cretaceous-Paleogene structural evolution of the structural highs of Southern Anatolia. Ozan Sungurlu Simpozyumu Bildirileri. 386-403
- Pınar, A., 1995. Rupture process and spectra of some major Turkish earthquakes and their seismotectonic implications. PhD Thesis, Boğaziçi University, İstanbul, 125 pp, (unpublished).
- Saner, S., K. Al-Hinai, and D. Perincek, 2005, Surface expressions of the Ghawar structure, Saudi Arabia. Marine and Petroleum Geology, pp. 1-15
- Segev, A., Lyakhovsky, V., Weinberger, R., 2014. Continental transform-rift interaction adjacent to a continental margin: The Levant case study. Earth-Science Reviews 139, 83–103. <http://dx.doi.org/10.1016/j.earscirev.2014.08.015>.
- Sevimli, U. İ., 2009. Yazihan (Malatya) batısının tektono-stratigrafisi. Doktora Tezi, Çukurova Üniversitesi, Fen Bilimleri Enstitüsü. 144 Sayfa.
- Sevimli, U. İ., Zorlu, K., Bağcı, U., 2017. Yazihan, (Malatya) Dolayının Neotektonik Özellikleri Volkaniklerin Petrografisi ve Jeokimyası. Kahramanmaraş Sütçü İmam Üniversitesi Mühendislik Bilimleri Dergisi. Cilt: 20, Sayı: 4, 143 -157.
- Sungurlu O., Perincek D., Kurt G., Tuna E., Dülger S., Çelikdemir E. and Naz H., 1985. Geology of the Elazığ-Hazar-Palu area (Hazar-Palu alanının jeolojisi). Bull. Turk. Ass. Petrol. Geol., (Petrol İşleri Genel Müdürlüğü Dergisi) 29: p,83-191.
- Şaroğlu ve ve Emre, Ü., 1987, Karacadağ volkanitlerinin genel özellikleri ve Güneydoğu Anadolu otoktonundaki yeri: Türkiye 7.Petrol Kongresi Bildiriler Kitabı, 384-391
- Şaroğlu, F., Emre, Ö., Kuşçu, I., 1992. The East Anatolian fault zone of Turkey. Ann. Tecton.6, 99–125.
- Şengör, A.M.C. and Yılmaz, Y., 1981. Tethyan evolution of Turkey: a plate tectonic approach: Tectonophysics, v. 75, p. 181-241.
- Şengör, A.M.C., Görür, N., Şaroğlu, F., 1985. Strike-slip faulting and related basin formation in zone of tectonic escape: Turkey as a case study. In: Biddle, K.T., Christie-Blick, N. (Eds.), Strike-Slip Deformation, Basin Deformation and Sedimentation. In: Spec. Publ., Soc. Econ. Paleontol. Mineral., vol.37, pp.227–264.
- Tatar, O., Piper, J.D.A., Gürsoy, H., Heimann, A., Koçbulut, F. 2004. Neotectonic deformation in the

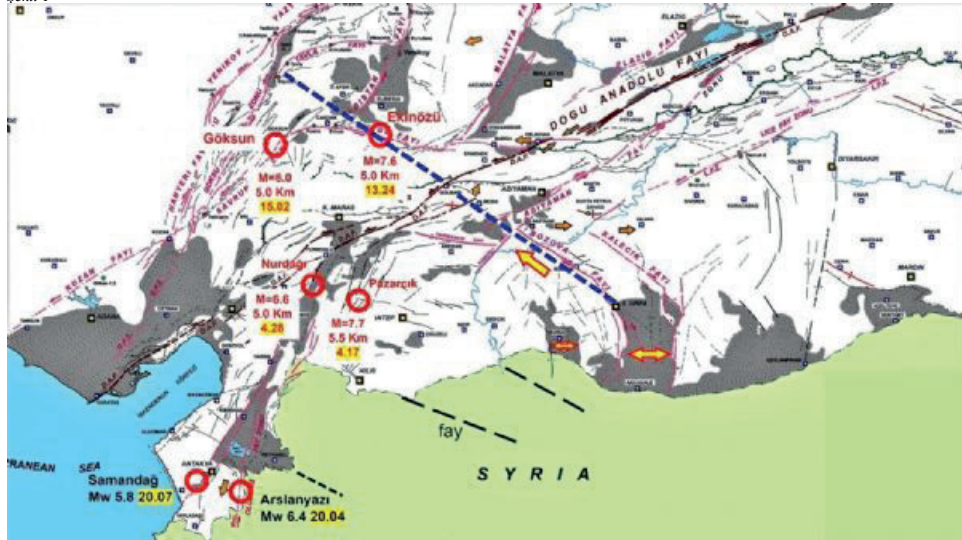
transition zone between the Dead Sea Transform and the East Anatolian Fault Zone, Southern Turkey: a palaeomagnetic study of the Karasu Rift Volcanism. *Tectonophysics* 385 pp. 17– 43. doi:10.1016/j.tecto.2004.04.005

Trifonov, V.G., Dodonov, A.E., Sharkov, E.V., Golovin, D.I., Chernyshev, I.V., Lebedev, V.A., Ivanova, T.P., Bachmanov, D.M., Rukieh, M., Ammar, O., Minini, H., Al Kafri, A.-M., Ali, O., 2011. New data on the Late Cenozoic basaltic volcanism in Syria, applied to its origin. *Journal of Volcanology and Geothermal Research* 199 (2011) 177–192. doi:10.1016/j.jvolgeores.2010.01.013

Yönlü, Ö., Altunel, E. and Karabacak, V., 2017. Geological and geomorphological evidence for the southwestern extension of the East Anatolian Fault Zone, Turkey. *Earth and Planetary Science Letters*, 469, 1-14.

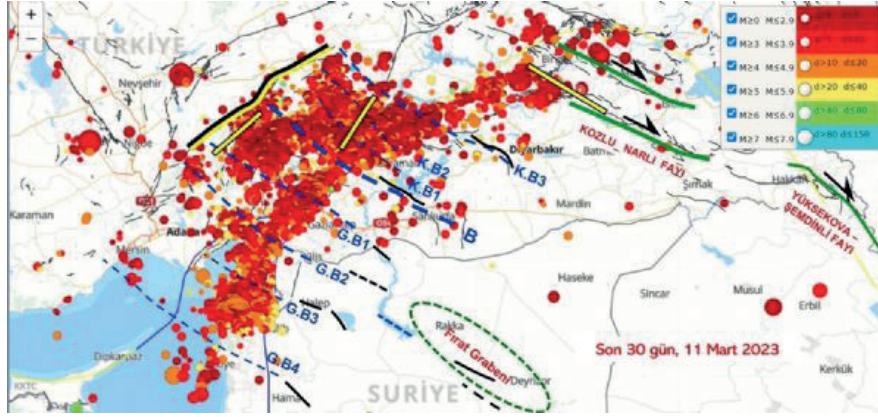
Anahtar Kelimeler: Doğu Anadolu Fayı -Ölüdeniz Fayı, Najd Fay Sistemi

Şekil 1



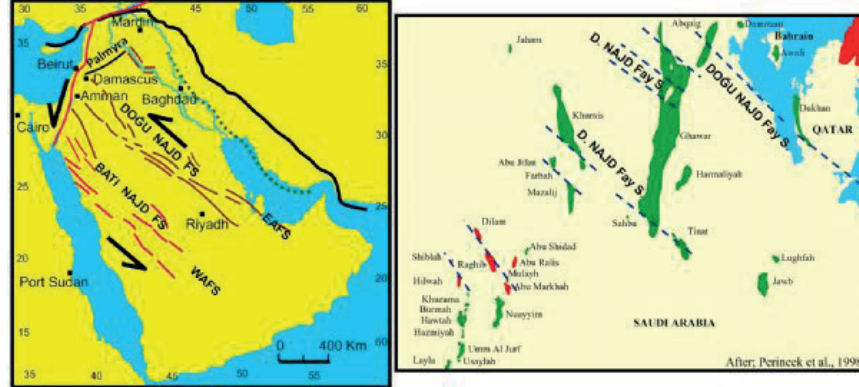
Metin içindeki Şekil 1 yazısı üstüne konacak

Şekil 2



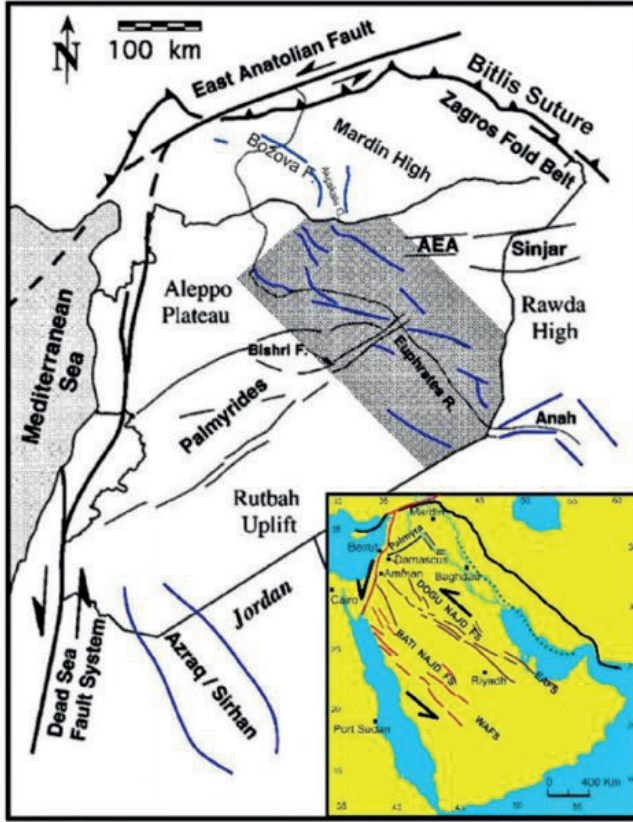
Metinde Şekil 2 yazısının üstüne

Şekil 3



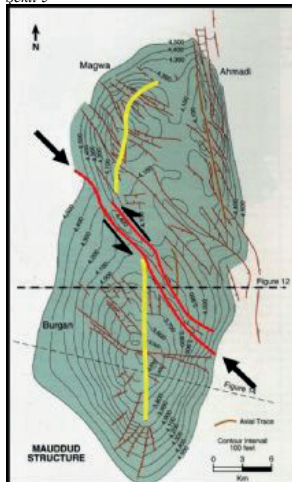
Şekil 3- Suudi Arabistan'ın Batısında metamorfik temelini yüzeylendiği alanda Kambriyen öncesinde aktif olmuş KB-GD doğrultulu Najd Fay Sistemi sol yanal atımlıdır (Edgell, 1992; Perinçek vd., 2000 a; Perinçek vd., 2000 b; Perinçek vd., 2006). Ghawar petrol sahasının yüzeyde izlenen yapısal hatlar; Najd Fay Sistemine dahil edilen KB-GD doğrultulu çizgisellikler ile uyum içindedir (Saner vd., 2005; Perinçek vd., 2000 c). Ghawar petrol sahasında 3 D sismik yorum yapılırken KB-GD doğrultulu fay sistemi haritalanmıştır (Perinçek vd., 2000 c). Petrol sahasını etkileyen bu fay sistemin Najd Fay Sistemi ile ilişkisi olduğu sonucuna varılıp; uydu ve radar görüntüleri, topografya haritaları, basılı yayınlar ve sismik veriler gibi farklı kaynaklar kullanılarak Suudi Arabistan doğusunda Katar'dan Suriye'de Şam'a kadar uzanan Doğu Najd Fay Sistemi haritalanmıştır (Perinçek vd., 2000 a; Perinçek vd., 2006). Najd Fayı ilk kez Prekambriyen'de oluşmuş ve daha sonra muhtemelen Paleozoyik ve geç Jura dönemleri olmak üzere çeşitli kereler ve değişik şiddetlerde geç Kretase'den geç Tersiyer döneme kadar sürekli yeniden etkinleşmiştir (Perinçek vd., 2006).

Şekil 4

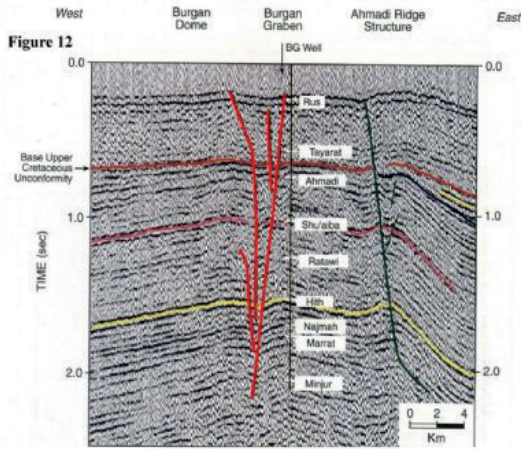


Metinde Şekil 4 yazısının üstüne

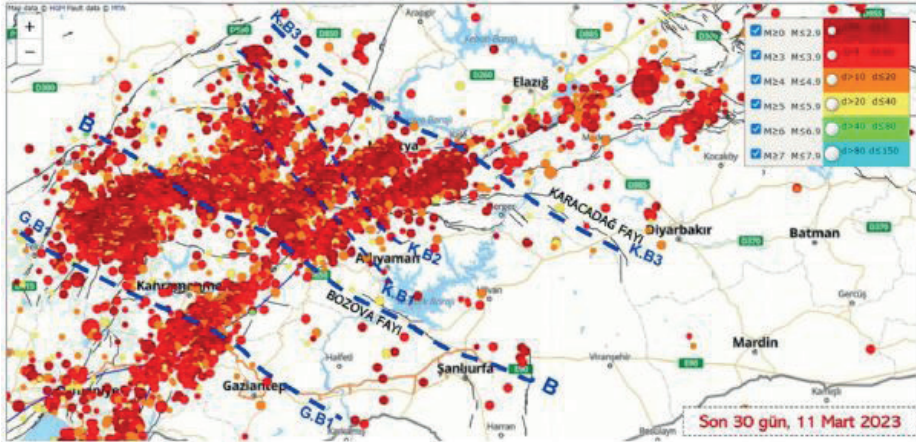
Şekil 5



Metin içindeki Şekil 5 yazısının üstüne

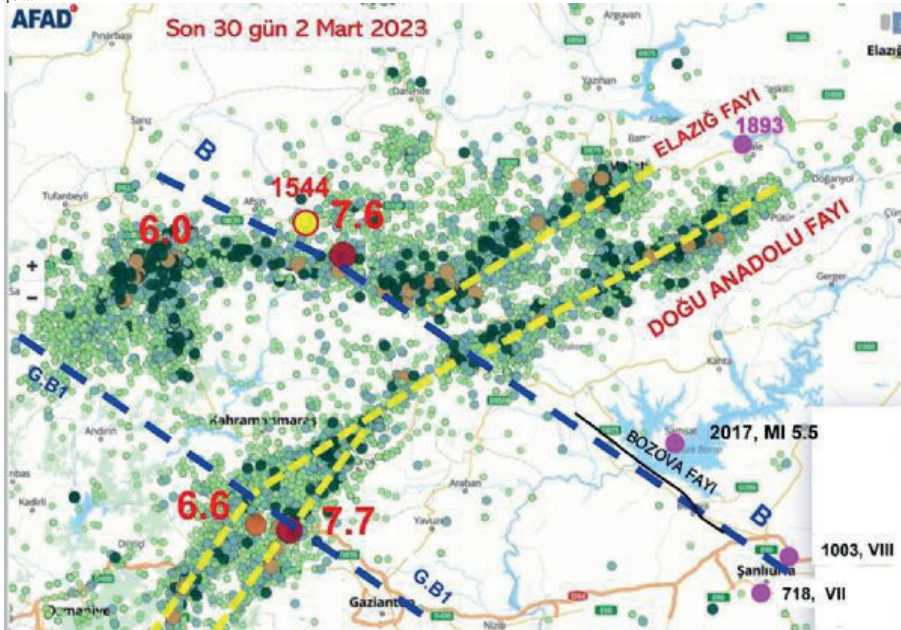


Şekil 6



Metin içinde Şekil 6 yazısının üstüne

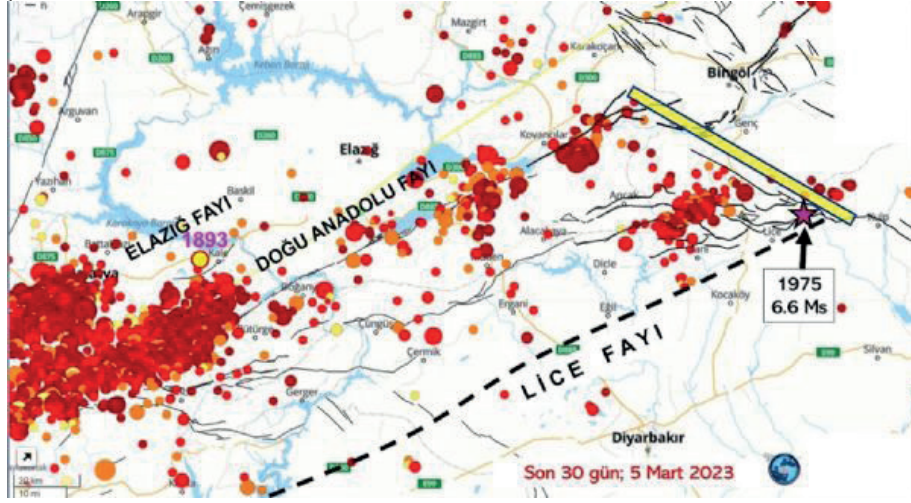
Şekil 7



Metin içinde Şekil 7 yazısının üstüne

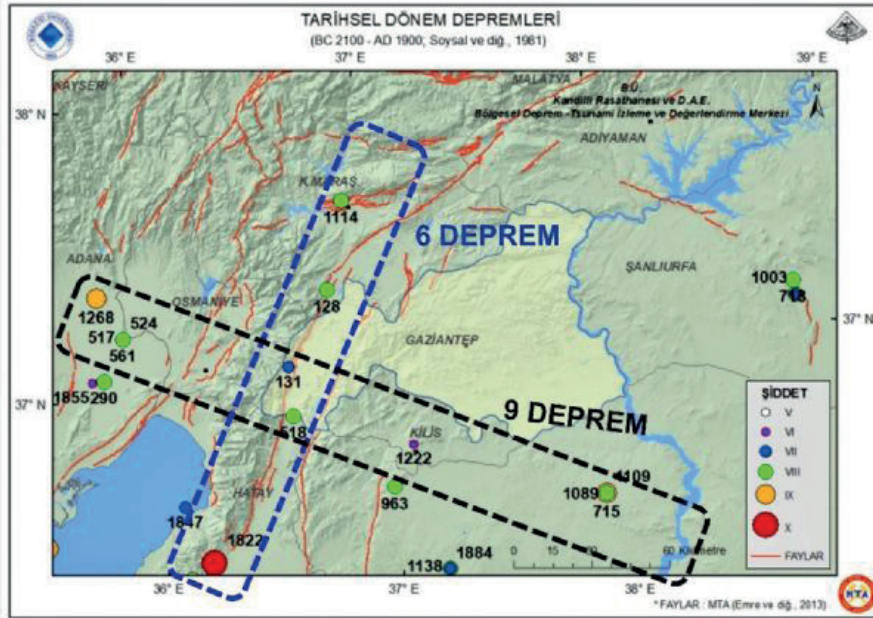


Şekil 8



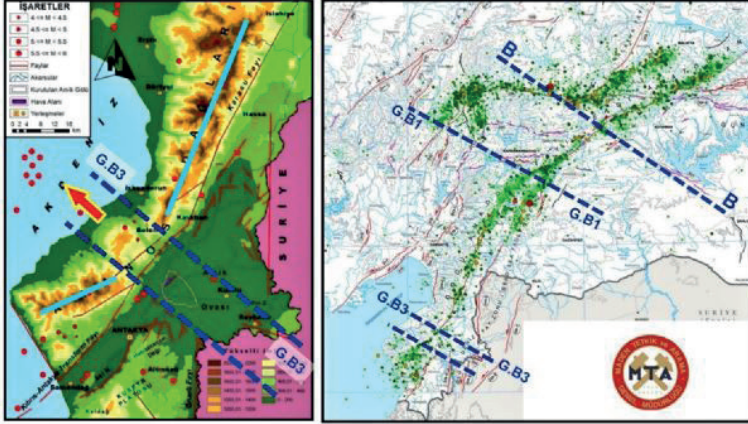
Metin içinde Şekil 8 yazısının üstüne

Şekil 9



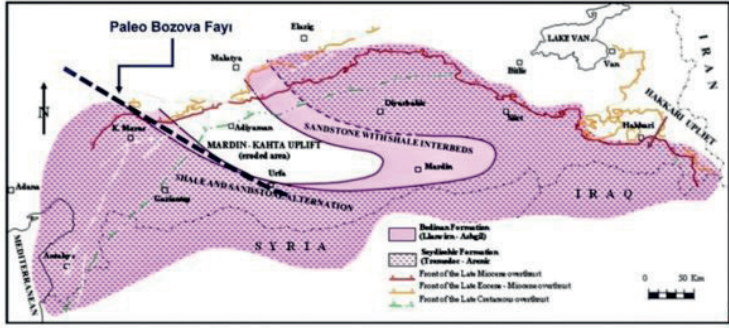
Metin içinde Şekil 9 yazısının üstüne

Şekil 10



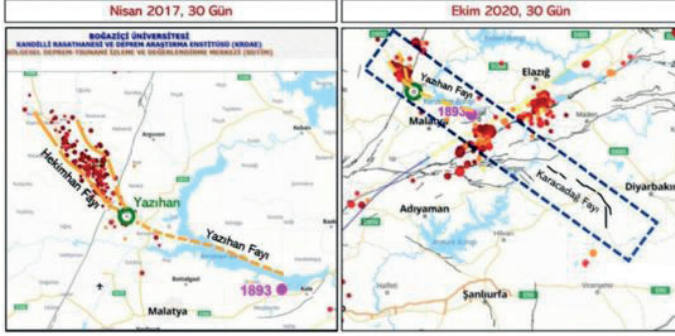
Metin içinde Şekil 10 yazısının üstüne

Şekil 11



Şekil 11- Ordovisiyen dönemi paleo-coğrafya haritası; Seydişehir ve Bedinan formasyonlarının dağılımını göstermektedir (Perinçek vd. 1992). Mardin-Kahta yükselimin Güneybatı sınırı Paleo-Bozova Fayı ile örtüşmektedir. Bozova Fayı'nın ilk oluşum yaşı Prekambriyen olan ve Jura, Kretase, Miyosen sonlarında tekrar aktif hale gelen GD-KB doğrultulu Najd Fay Sistemi (Perinçek vd. 2000 ve 2006) ile ilişkili olduğu düşünülmektedir. Bu harita ilişkiliyi destekleyen önemli bir veridir. ¶

Metin içinde SONUÇLAR kısmından iki önceki satıra



Şekil 12- Son altı yıldır Yazihan – Hekimhan arasında kalan akanda olan depremler dikkatle izlenmiştir. Söz konusu alanda aktif fay haritasında fay konmamış olsa da KB-GD doğrultusunda dizili depremleri faysız izaha etmek mümkün değildir. Alan çalışılmış ve Hekimhan Fayı, Yazihan Fayı olarak tanınmıştır. Fırat Nehri Yazihan Fayına ulaştığı noktadan ani yön değişimi göstermektedir. Ayrıca Karakaya Barajı gölü alanı Kuzeydoğusunda görülen alüvyon fan deltaları burada bulunan faylar için önemli bir veri desteği sağlamaktadır. (Harita ve deprem odakları kaynağı Boğaziçi Üni. KRDAE). Karacadağ da haritalan fayın genel doğrultusu KB-GD olup yaklaşık 35 km uzunluğundadır (Kavak, 2013).

Metinde SONUÇLAR kısmının bir satır öncesine

# Hoya Formasyonu'nun Petrol Sistemi Petroleum System of Hoya Formation



**Deniz Atasoy<sup>1</sup>, Aynur Geçer Büyükkutku<sup>2</sup>, Arzu Aktosun<sup>3</sup>, Fevzi Mert Türesin<sup>3</sup>,  
Hüsnü Çorbacıoğlu<sup>3</sup>**

<sup>1</sup>Türkiye Petrolleri Anonim Ortaklığı, Arama Daire Başkanlığı, Ankara / Türkiye

<sup>2</sup>Ankara Üniversitesi Jeoloji Mühendisliği, Ankara / Türkiye

<sup>3</sup>Türkiye Petrolleri Anonim Ortaklığı, Argem Daire Başkanlığı, Ankara / Türkiye

Middle-Late Eocene aged Hoya Formation covers widely surficial area of SE Anatolia. The formation is equivalent to Pila Spi Formation in Iraq which has produced oil from Taq Taq Oil Field since 2005. However, Hoya Formation has not produced any commercial amount of hydrocarbon yet, but it is expected that the formation contains an existing petroleum system where it was sufficiently buried. A subsurface data set derived from Well C penetrating through the formation was used to investigate HC potential of the Hoya Formation.

In this study, the formation was mainly subdivided into three members such as Upper Hoya Member, Middle Hoya Member and Lower Hoya Member from top to bottom. The Upper Member consists of mostly fine crystalline dolostones interbedded with anhydrite layers. Using wireline logs, the porosity and permeability values of dolostones were calculated up to 27% and 63.5 md respectively. In this unit, fine crystalline dolostones was characterized with a good reservoir when compared to porosity cut-off values of 8% and anhydrites were considered to be a seal rock. In addition to this, Middle Unit is composed of limestones and organic rich beds which contain Type II origin, immature (427°C) and with TOC content varied from 0.6% to 1%. In terms of lithology, the Lower Unit which is as similar as Upper Unit (anhydrite content is lower than Upper Member) was evaluated as another reservoir section that have high poroperms values up to 25% and 32.7 md

As a result of INPEFA log analysis, this part was evaluated as a product of a long term transgression. During this transgressive period, organic matters would have been preserved under anoxic conditions. Thus, interval of 1244-1272 m was determined as source rock section of the system. In spite of existence of the source rock, the organic materials are needed to be more buried in order to generate a commercial amount of hydrocarbon at this location.

In conclusion, Hoya Formation provides all the requirements of a petroleum system such as seal rock, reservoir unit and organic matter enriched rocks.

## GİRİŞ

Midyat Grubu'na ait Hoya Formasyonu, klastik litolojiden meydana gelen Gercüş Formasyonu'nun üzerine uyumsuzlukla gelmektedir (Perinçek vd. 1992). Hoya Formasyonu'nun üzerine ise uyumlu olarak, genellikle evaporitlerden oluşan Germik Formasyonu çökelmiştir (Şekil 1).

Hoya Formasyonu sınırlı sığ denizel ve yarı sınırlı görece derin şelf kenarı istif özelliği sergileyen Güneydoğu Anadolu (GDA) Bölgesi'nin bir kısmında

(genellikle güneyinde) yüzlek veren bir birimdir (Şekil 2).

## AMAÇ

Arap Platformu'nda Orta-Geç Eosen döneminde Hoya Formasyonu ile Jaddala ve Pila Spi formasyonları (Suriye, Irak), Dammam Formasyonu (Katar, Kuveyt, Suudi Arabistan) ve Pabdeh-Jahrum formasyonları (İran) çökelmiştir (Aqravi vd. 2010). Pila Spi Formasyonu'nda 2005 yılında TTOPCO (Genel Enerji ve Addax Petroleum Company) şirketi tarafından Taq-Taq Sahası'nda 23 API graviteli petrol keşfi gerçekleştirilmiştir (Al-Qayim ve Othman 2012).

Eosen yaşlı Pila Spi Formasyonu'ndan ve bu formasyonun derin eşleniği (basinal çökeller) olan şeyl, mam ve kilitaşı litolojili Jaddala Formasyonu'ndan, Pulkhana, Jambour, Kor Mor ve Taq Taq sahalarında hidrokarbon türünün erken aşamalarında oldukları için petrol üretimi gerçekleştirilmemektedir. Örneğin, Kuzey Irak'taki Qumar Sahası için yapılan çalışmada için ortalama TOC %2.4, S<sub>2</sub>: 11 mg/g kaya ve T<sub>max</sub>: 420 °C değerleri elde edilmiştir. Buna karşılık, Taq Taq Sahası'ndaki Pila Spi Formasyonu'nun kaynak kayası Paleosen yaşlı Aalij/Kolosh formasyonundaki organik maddece zengin seviyeleri ile ilişkilendirilmektedir (Baban ve Ranyayi 2013).

Türkiye-İrak sınırı yakınlarındaki Shaikan'da (Dohuk şehri yakınlarında) Pila Spi Formasyonu'ndan büyük petrol sızıntıları gözlemlenmektedir (Durham 2010). Bunun yanı sıra, bu çalışmada kullanılan Kuyu C'nin bulunduğu lokasyona yalnızca 30 km uzaklıktaki Tawke Petrol Sahası'nda, Pila Spi Formasyonu'nun yine rezervuar potansiyeli taşıdığı ifade edilmektedir (Aqravi vd. 2010).

TPAO tarafından kazılan Kuyu C'de, Hoya Formasyonu'ndan petrol emareleri gözlemlenmesi, bu formasyonun rezervuar potansiyeli hakkındaki umutların yeşertmesine neden olmuştur. Bu durum, Türkiye-İrak sınırında bu formasyonun yeterince gömüldüğü alanlarda, Hoya Formasyonu'nu oldukça prospektif hale getirmektedir. Bu nedenle, Hoya Formasyonu'nun hidrokarbon üretme potansiyeli bu çalışmanın ana konusunu teşkil etmektedir.

Çalışma alanında formasyonun giriş kotları, batıda yer alan Mardin Yükselimi'nde doğru yükselmektedir. Yükselimin üzerinde Eosen çökelleri yer almamaktadır. Diğer yandan, kuzeyde Gercüş, Germav ve Hermis antiklinallerinde Hoya Formasyonu aşınmış bulunmaktadır. Hoya Formasyonu Kuyu C'de -550 m kotunda iken, Silopi Baseni'nin olduğu alanda formasyonun girişi -2400 m kotuna kadar inmektedir (Şekil 3).

Hoya Formasyonu'nun gömüldüğü bu alanda Hoya Formasyonu'nun rezervuar özelliği sergileyip sergilememesi ve organik maddece zengin seviyelerin var olup olmaması bu çalışmanın temelini teşkil etmektedir. Bu iki petrol sisteminin elemanın birlikte olması bile, üretilen hidrokarbonun hapsolmesini sağlayarak örtüye görevini üstlenecek intervallerin varlığının belirlenmesi de ayrıca önem arz etmektedir.

## YÖNTEMLER

### Kuyu Logları

Kuyularda 12¼ inç ve dar daha kuyu çaplarında full-set log alınabilmektedir. Bu sebeple, yüzlerce kuyu tarafından penetre edilen Hoya Formasyonu'nun genellikle yüzeyde olması ve kuyu sondajın geniş çap ile (26 inç) başlanması nedeniyle bu formasyon gözümüze kadar petrofiziksel olarak değerlendirilememiştir. Bu formasyonun rezervuar özelliklerinin daha iyi anlaşılabilmesi için Kuyu C'nin sondajı bu durum gözetilerek dizayn edildiğinden dolayı, bu çalışmada tek bir kuyu verisi üzerinden yürütülmüştür.

Schlumberger (1974) tarafından rezervuar kayanın değerlendirilmesinde önemli bir kriter olan gözeneklilik kuyu logları kullanılarak hesaplanabilmektedir. Ortalama gözeneklilik logu (PHIA) aşağıda formüle yer aldığı üzere RHOB (yoğunluk logu) ve NPHI (nötron logu) logları kullanılarak hesaplanmaktadır. Daha sonra, gözenekliliğin hesaplandığı formasyonun kil miktarı (GR<sub>indeks</sub>) GR logunun minimum ve maksimum değerlerinin belirlenmesiyle tespit edilmektedir. Son aşamada, PHIE (etkin gözeneklilik) PHIA log değerlerinden GRindeks hesaplamasının çıkarılmasıyla elde edilmektedir.

$\rho_{ma}$ : Matrisin yoğunluğu (gr/cm<sup>3</sup>)

$\rho_{log}$ : Yoğunluk logundan okunan değer (gr/cm<sup>3</sup>)

$\rho_{akışkan}$ : Formasyon sıvısının yoğunluğu (gr/cm<sup>3</sup>)

$\Phi$  (RHOB) =  $\rho_{ma} - \rho_{log}$

$\rho_{ma} - \rho_{akışkan}$

PHIA (ortalama gözeneklilik) =  $\Phi_{RHOB} + \Phi_{NPHI}$

2

GR<sub>indeks</sub> (kil düzeltmesi) = GR<sub>log</sub> - GR<sub>min</sub>

GR<sub>mak</sub> - GR<sub>min</sub>

PHIE (etkin gözeneklilik) = PHIA \* (1 - GR<sub>indeks</sub>)

DT (Sonik) logu akustik dalgaların kuyu eksenine boyunca formasyonlardan geçiş zamanının ölçülmesi olarak tanımlanmaktadır (Wyllie vd. 1958). Formüle  $\Delta t_{ma}$  değeri kireçtaşları 156  $\mu$ sec/m için ve dolomitler için 143  $\mu$ sec/m değeri alınmaktadır.  $\Delta t_{sıvı}$  parametresi yerine petrol için 755  $\mu$ sec/m, tatlı su için 620  $\mu$ sec/m ve tuzlu su için 607  $\mu$ sec/m değerleri alınmaktadır (Spain 1992).

$\Phi$  (DT) =  $\Delta t_{log} - \Delta t_{ma}$

$\Delta t_{akışkan} - \Delta t_{ma}$

$\Delta t_{log}$ : Sonik logdan okunan değer ( $\mu$ sec/m)

$\Delta t_{ma}$ : Akustik dalganın matristen geçiş zamanı ( $\mu$ sec/m)

$\Delta t_{akışkan}$ : Akustik dalganın formasyondaki sıvılardan geçiş zamanı ( $\mu$ sec/m)

DT logu sadece matris gözenekliliği ölçmektedir (Al-Qayim ve Othman 2012). Bu nedenle, ikincil gözeneklilik değerlerinin hesaplanmasında PHIA logundan elde edilen değerler DT log gözeneklilik değerlerinden çıkarılmaktadır.

$\Phi_{ikincil\ gözeneklilik}$  (%) = PHIA - Gözeneklilik (DT)

Su doygunluğu gözenek hacminde yer alan formasyon suyu miktarının toplam gözenek hacmine oranı olarak tanımlanmaktadır (Asquith ve Krygowski 2004). Archie (1942)'nin önerdiği formül ile hesaplanmaktadır.

$S_{wn} = R_w \times a$

( $\Phi \times m \times R_t$ )

$S_w = S_u$  doygunluğu

n = Satürasyon katsayısı (2 olarak kabul edilmiştir)

$R_w$  = Formasyon sıcaklığındaki formasyon suyu rezistivitesi

$\Phi$  = Gözeneklilik

a = Eğrilik Katsayısı (1 olarak kabul edilmiştir)

m = Çimentolanma katsayısı (2 olarak kabul edilmiştir)

$R_t$  = Formasyon rezistivitesi (LLD logundan okunan değerler)

k = Geçirgenlik (md)

INPEFA (Integrated Prediction Error Filter Analysis) logu, negatif trendler karbonat birimlerde daha az şeyli bir litolojiyi ve azalan deniz seviyesi (regresyon) değişimini işaret etmektedir. Diğer yandan, pozitif trendler daha şeyli bir litolojiyi ve yükselen deniz seviyesi (transgresyon) hareketini göstermektedir (Nio vd. 2005). Negatifden pozitive veya pozitiften negatif trende geçişler dönüşüm noktaları olarak adlandırılmaktadır. Bu çalışma için CycloLog programı kullanılarak SGR logu INPEFA loguna dönüştürülmüştür. INPEFA logları las dosyası olarak kaydedilmiş ve Petrel (2021) programına transfer edilmiştir.

## PİROLİZ ANALİZLERİ

Piroliz analizleri organik jeokimyasal bir teknik olarak, organik maddenin termal olgunluğunun, kalitesinin ve miktarının belirlenmesinde kullanılmaktadır (Tissot ve Welte 1984).  $S_1$ ,  $S_2$ ,  $S_3$  ve Tmax değerleri analizlerden direk ölçülmektedir. Bu değerlerden TOC, HI, OI ve PI değerleri hesaplanmaktadır. 100 mg'lık organik maddece zengin örneklerin piroliz analizleri Rock Eval-6 Turbo cihazı ile TPAO Ar-Ge Merkezi Jeokimya Laboratuvarlarında gerçekleştirilmiştir.

## BULGULAR VE TARTIŞMA

Hoya Formasyonu'nun Üst ve Alt üyelerinde hâkim litolojisi dolomitlerden ve yer yer anhidrit bantlarından meydana gelmektedir. Bu dolomitler çoğunlukla unimodal öz şekilsiz-yarı öz şekilli, ince

kristalli dolomitler olarak tanımlanmaktadır. Orta Üye litolojisi genellikle fosilli vakaetişi bileşimine sahip kireçtaşlarında oluşmaktadır (Şekil 4).

Al-Qayim ve Ottoman (2012) tarafından Pila Spi Formasyonu gözeneklilik değerlerine göre 6 gruba ayrılmıştır. En iyi rezervuar özelliği sergileyen (PU 2) birimi oluşturan orta kristalli dolomitleri ortalama etkin gözeneklilik değeri %21.5 olarak hesaplanmıştır. Bir diğer çalışmada, Zakho kesitinde örneklenen kireçtaşlarının gözeneklilik değerlerinin %12.6-19.4 arasında değişen değerler almıştır (Zaidky ve Rashid 2021). Taq Taq Sahası'nda hidrokarbon üretimi gerçekleştirilen Pila Spi Formasyonu için gözeneklilik sınır değeri % 8.2 olarak belirlenmiştir (Al-Qayim ve Ottoman 2012). Bu değere paralel olarak, eşik değeri hesaplamasında teorik olarak en düşük geçirgenlik de 0.01 md olarak kabul edilmiş ve böylece Hoya Formasyonu için gözeneklilik eşik değeri %8 olarak belirlenmiştir (Şekil 5). Şekil 6, 7 ve 8'de yer alan petrol sistemi kolonunda hesaplanan efektif porozite değerlerinin (PHIE) üzerinde kalan kısımlar "rezervuar" ve altında kalan bölümler ise "Geçirimsiz Birim" olarak adlandırılmıştır.

Yapılan log değerlendirmelerine göre, Hoya Formasyonu Üst Üyesi'nin etkin gözeneklilik değerleri %27'e kadar çıkmaktadır (Şekil 6). Dolomitlerin gözeneklilik değerleri oldukça yüksek iken, özellikle üst kısımlardaki anhidrit tabakaları geçirimsizdirler. İyi bir örtü kaya özelliği sergileyecekleri düşünülmektedir

Egemen litolojisi kireçtaşlarından oluşan Orta Üye'nin etkin gözeneklilik değerleri % 18'e varan değerler almaktadır. Orta Üye'de ikincil gözeneklilik gelişimi (porozite-DT ve PHIA logları arasındaki fark) Üst ve Alt Üye'ye oranla daha düşüktür. Bu durum, ikincil gözenek gelişiminde en önemli etkenin dolomitleşme olduğunun göstergesidir (Şekil 7)

Alt Üye'nin etkin gözeneklilik değerleri Üst Üye ile benzer olarak, %25'e varan değerler almaktadır. Üst Üye'ye oranla daha az anhidrit seviyeleri içermesinden dolayı birimin büyük bir bölümü eşik değerin üzerinde kalmaktadır. Bu değerler ile Alt Üye'nin iyi bir rezervuar özelliği taşıdığı görülmektedir (Şekil 8).

Archie (1942) formülü baz alınarak gerçekleştirilen Hoya Formasyonu'nun geçirgenlik tahmini hesaplamalarına göre, dolomit egemen litolojiye sahip olan Üst Hoya (2.92-63.54 md) ve Alt Hoya (2.93-32.70 md) üyelerinin, Orta Hoya Üyesi'ne (0.73-9.13 md) oranla daha yüksek geçirgenlik değerleri sergilediği görülmektedir (Şekil 9).

Turkuaz renkli kısımlar Hoya istifinde tamamen suya doygun kesimlerin de var olduğunu işaret göstermektedir. Buna karşılık, yeşil pikler ise hidrokarbon doygun kısımlarında var olduğunu sergilemektedir. Özellikle Orta Üye ve Üst Üye'deki bu kısımlar sondaj sırasında hidrokarbon emareli olarak geçilmiştir (Şekil 9).

Hoya Formasyonu'nun kendi kaynak kayasının var olup olmadığını anlaşılması organik jeokimyasal bir çalışma yürütülmüştür (Tablo 1). Elde edilen piroliz analiz sonuçlarına göre, Orta Üye'de TOC değerleri % 0.6'den %1'e varan,  $S_2$  indeksi 2.5 ve 6.2 (mg HC/g

kaya) arasında değişen ve ortalama  $T_{max}$  değeri (427°C) olgun olmayan olarak kabul edilen Hoya Formasyonu kaynak kaya seviyelerine sahiptir (Şekil 10-11). Hoya Formasyonu çökelinin INPEFA log trendlerinden görüldüğü üzere, aşağıdan yukarıya 3 adet regresyon-transgresyon döngüsü yaşanarak gerçekleştiği tespit edilmiştir. Bu çalışmada, Alt Üye'nin depolanması sırasında uzun süreli bir regresyon yaşanırken, bunun aksine Orta Üye'nin çökeli esnasında uzun süreli bir transgresyon meydana geldiği bilinmektedir. Üst Üye ise iki adet transgresyon-regresyon döngüsünün ürünü olarak ortaya çıkmaktadır (Şekil 12).

Bahse konu olan organik maddece zengin seviyelerin çökeli ve Orta Üye kireçtaşlarının depolanması, uzun soluklu bir transgresyonun ürünü olarak karşımıza çıkmaktadır. Transgresyonun uzun süreli olması organik maddenin korunmasına ve oksik koşulların gelişmesine sebebiyet verdiği düşünülmektedir (Şekil 12).

## SONUÇLAR

Hoya Formasyonu'nun iyi bit kaynak kaya olarak türüm-atım yapılabilmesi için Kuyu C'nin bulunduğu alana nazaran, daha derin bir konumda bulunması gerekmektedir. Orta Üye'deki bu mevcut kaynak kaya seviyelerinin üzerine, Üst Üye'nin poroz dolomitleri iyi bir rezervuar kaya özelliği sergilemektedir. Yine Üst Üye'de yer alan anhidritlerin ise örtü kaya görevi üstlenmesi Hoya Formasyonu'nun kendi içerisinde bir petrol sistemi oluşturduğu gerçeğini gözler önüne sermektedir. Bunun yanı sıra, Hoya Formasyonu üzerine gelen evaporit dominant litolojiye sahip Germik Formasyonu'nda iyi bir örtü kaya özelliğinde olması beklenmektedir. Tüm bu bilgiler ışığında, daha derin gömüldüğü ve kapanma sahip olduğu alanlarda Hoya Formasyonu'ndan ekonomik anlamda bir keşif yapılabilmesi oldukça mümkün durmaktadır.

## REFERANSLAR

Al-Qayim, B. and Othman, D. 2012. Reservoir characterization of an intra-orogenic Carbonates platform: Pila Spi Formation, Taq Taq oil field, Kurdistan, Iraq. Geological Society of London Special Publications. 370. 139-168.

Aqrawi, A.A.M. Goff, J.C. Horbury, A.D. Sadooni F.N. 2010. The Petroleum Geology of Iraq. Scientific Press, Beaconsfield, UK, pp. 424.

Archie, G.E. 1942. The electrical resistivity log as an aid in determining some reservoir characteristics. 146(1):54-67

Asquith, G. and Krygowski, D. 2004. Chapter 4: Porosity Logs. In: Asquith, G., and Krygowski, D. (eds.), Basic Well Log Analysis, (Second edition). AAPG Methods in exploration 16, Tulsa, Oklahoma: 37-76.

Baban DH, Ranyayi KSM (2013) Potentiality of Paleocene source rocks and their contribution in generating the accumulated oil in the Eocene Pila Spi

Reservoir in Taq Taq Oil Field, Kurdistan Region/ Iraq.  
Arab J Geosci 6:4225–4237

Durham, L. 2010. Iraq potential faces a lot of ifs. AAPG Explorer, March Issue.

Nio, S.D. Brouwer, J. Smith, D. De Jong, M. and Bohm, A. 2005. "Spectral trend attribute analysis: application in the stratigraphic analysis of wireline logs, First Break", 71–75.

Spain, D. 1992. Petrophysical evaluation of a slope fan/basin fan floor complex: Cherry Canyon Formation, Ward County, Texas. American Association of Petroleum Geologists, Bulletin, 76; 805–827.

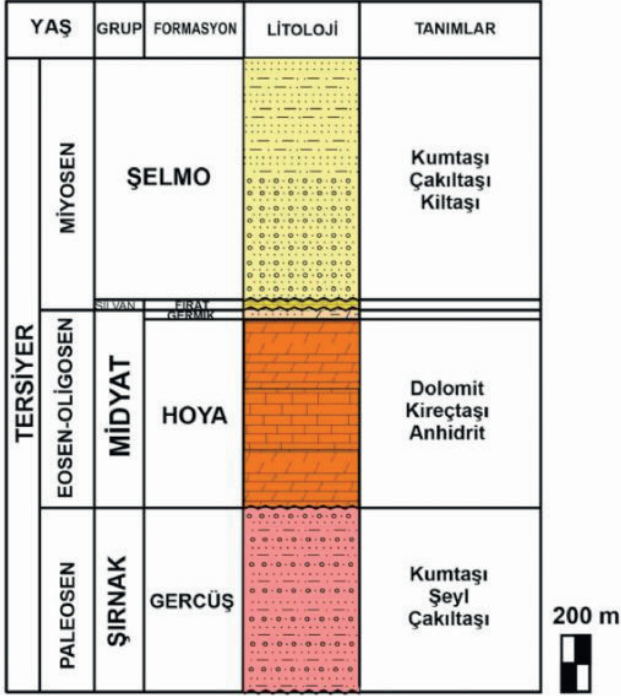
Tissot, B.P. and Welte, D.H. 1984. Petroleum formation and occurrence. Springer Verlag, 699p. New York.

Wyllie, M.R. J. Gregory, A.R. and Gardner, G.H.F. 1958. An experimental investigation of factors affecting elastic wave velocities in porous media: Geophysics, 23; 459-493.

Zaidky, R.H.S. Rashid, N.M. 2021. The Characteristics and Porosity Determination of Carbonate rock (Pila Spi formation), Bekhair anticline, Zakho, Kurdistan Region of Iraq. International Journal of Advanced Research in Science, Engineering and Technology. Vol. 8, Issue 8. ISSN: 2350-0328.

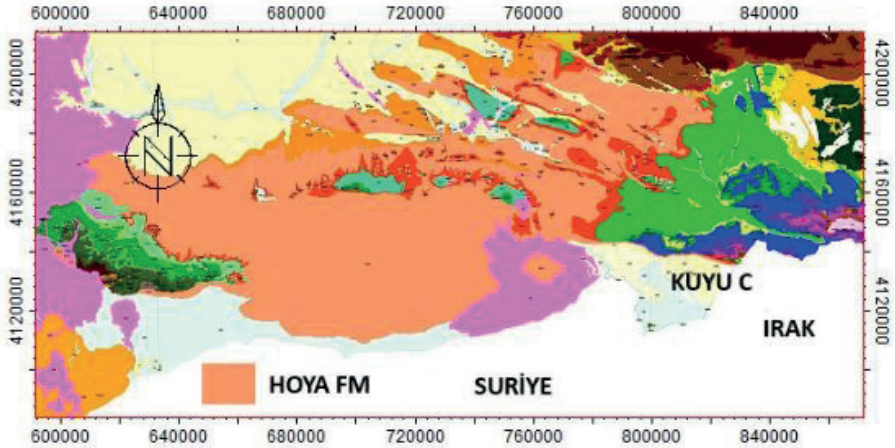
Anahtar Kelimeler: Hoya Formasyonu, Midyat Grubu

Şekil 1.



Hoya Formasyonu'nu gösterir stratigrafik kesit

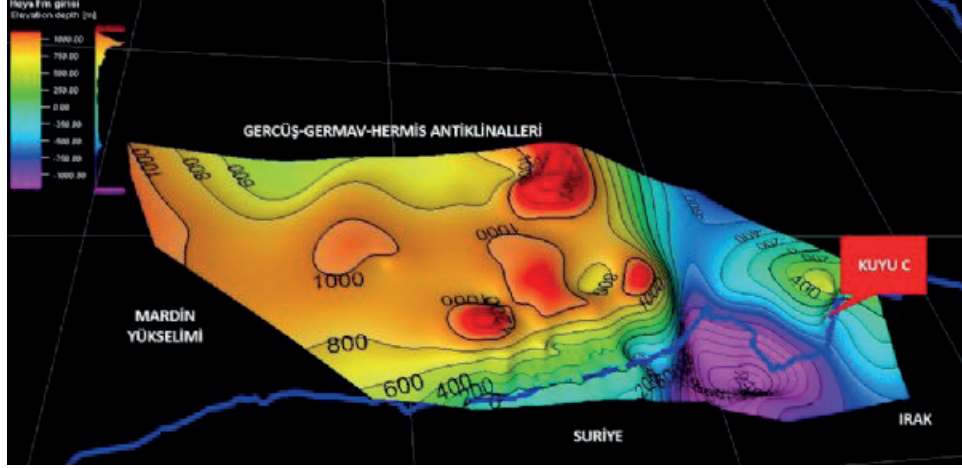
Şekil 2.



Çalışma alanı lokasyon haritası (Ölçek: 1/2.000.000)

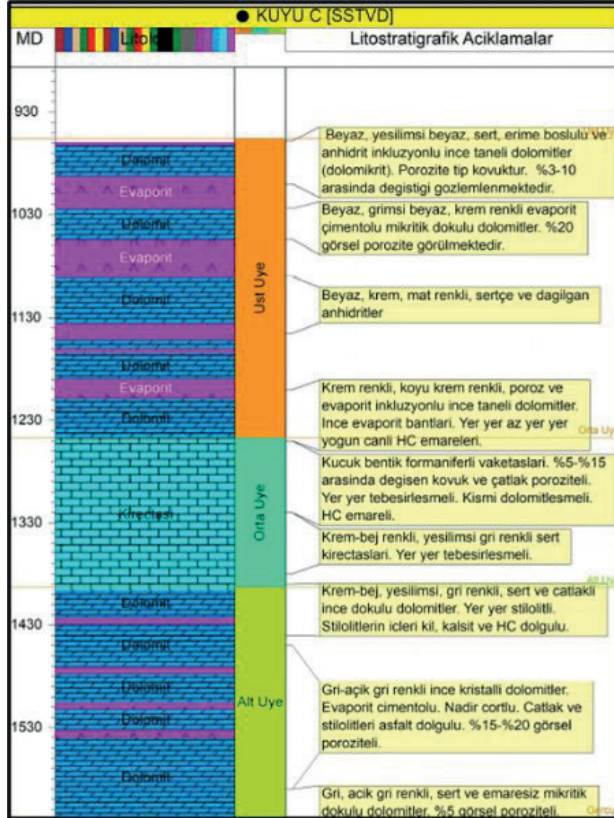


Sekil 3.



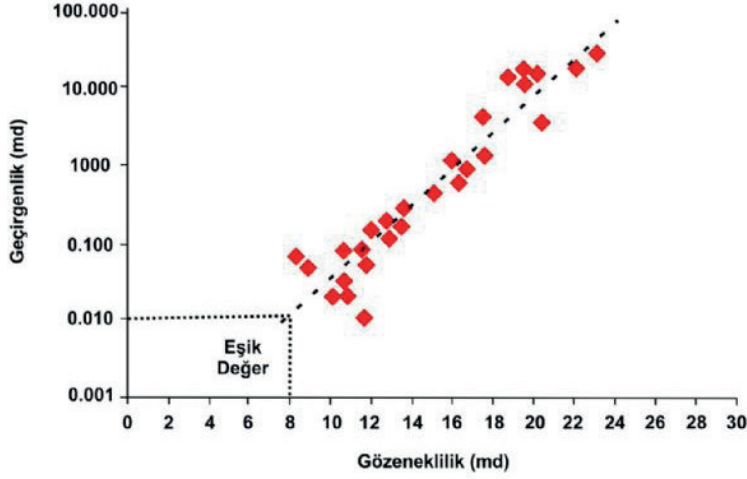
Hoya Formasyonu girişi haritası (Ölçek: 1/1.000.000)

Sekil 4.



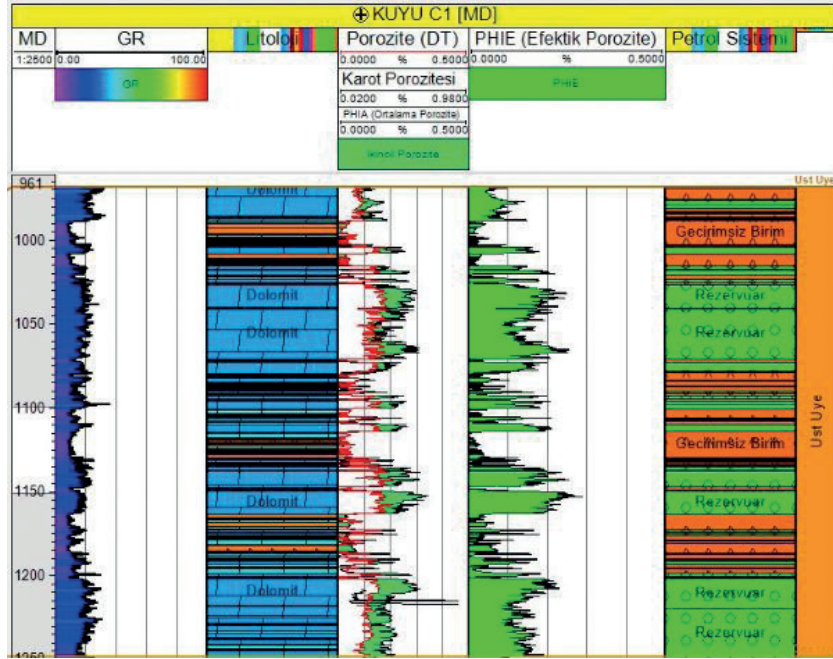
Hoya Formasyonu'nun litostratigrafisi (Ölçek: 1/1000)

Şekil 5.



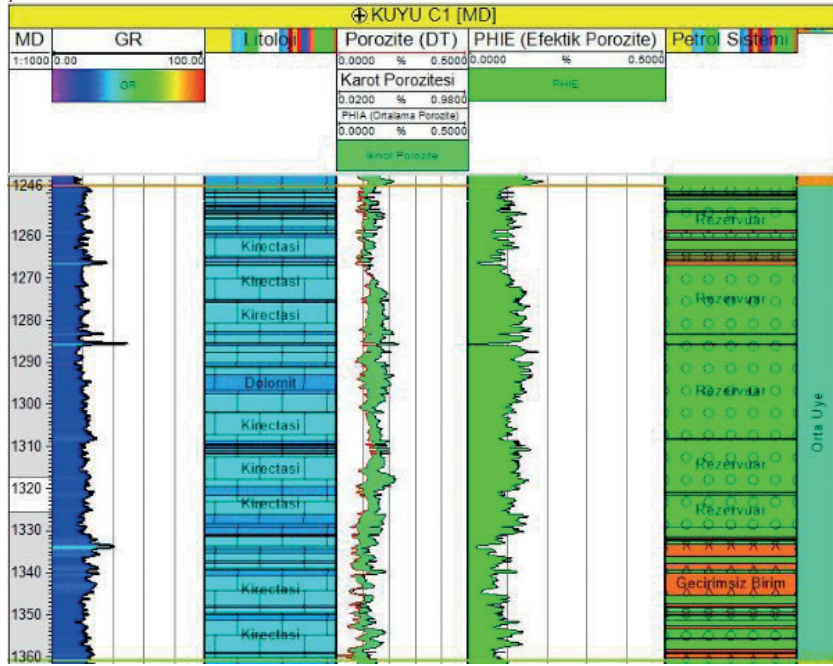
Hoya Formasyonu'ndan alınan karotun petrofizik değerleri ve belirlenen eşik değeri

Şekil 6.



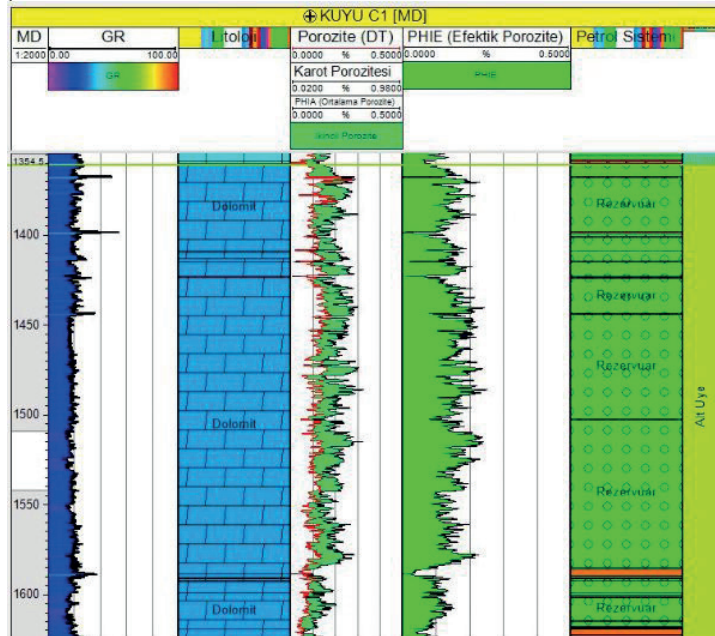
Üst Üye gözeneklilik logları ve petrol sistemi (Ölçek: 1/1750)

Şekil 7.



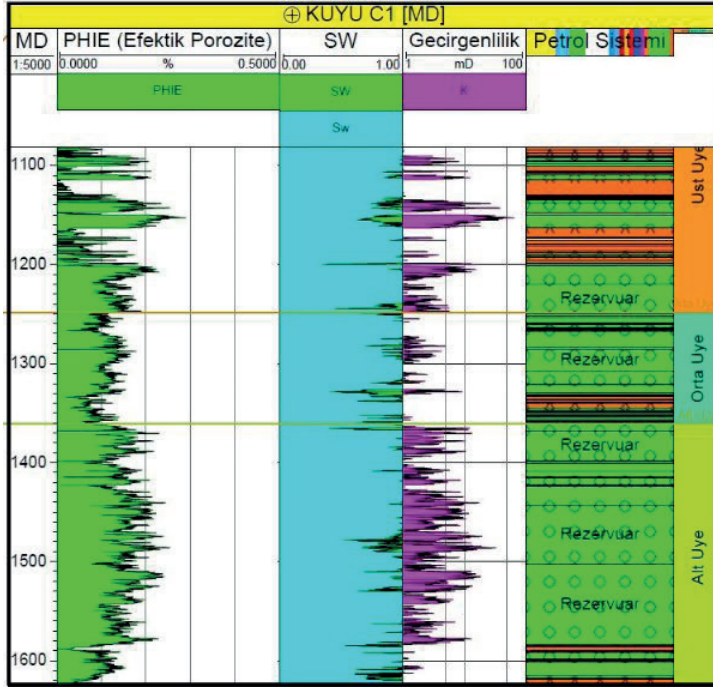
Orta Üye gözeneklilik hesaplamaları ve petrol sistemi (Ölçek: 1/1000)

Şekil 8.



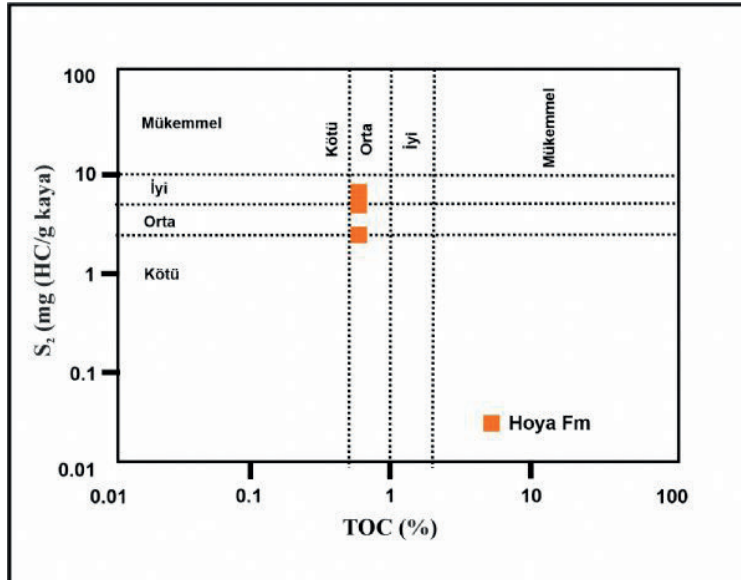
Alt Üye'nin gözeneklilik tahminleri ve petrol sistemi (Ölçek: 1/1750)

Şekil 9.



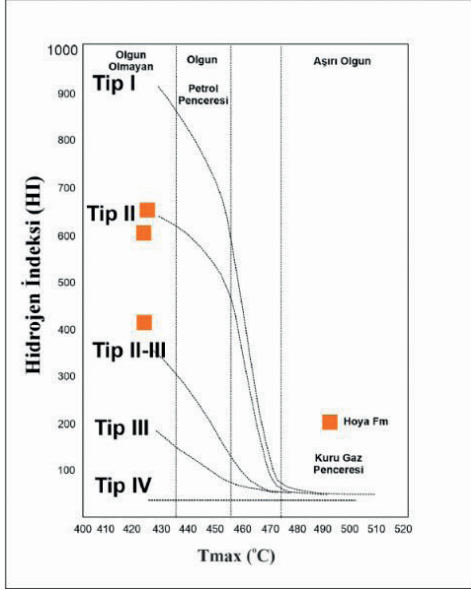
Geçirgenlik ve su saturasyonu hesaplamaları (Ölçek. 1/5500)

Şekil 10.



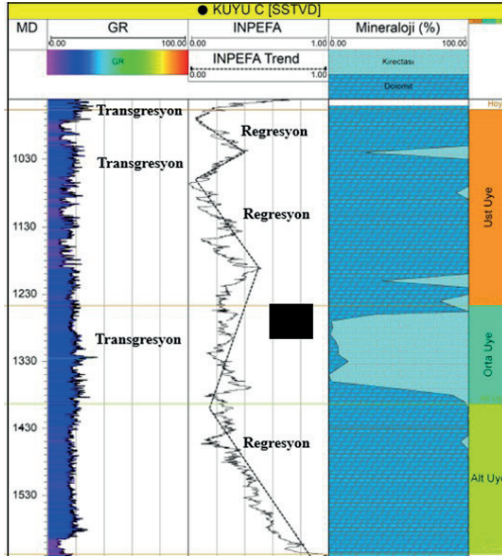
TOC ve  $S_2$  grafiği

Şekil 11.



HI ve Tmax karşılaştırılarak kerojen tipinin belirlenmesi

Şekil 12.



INPEFA logu ile deniz suyu değişimlerinin belirlenmesi (Şyah kutucuk kaynak kayalı seviyeyi temsil etmektedir. Mineraloji kısmında evaporitler göz ardı edilmiştir)

*Tablo 1.*

Parametreler	Açıklamalar
TOC	Toplam organik karbon (%)
Tmax	Piroliz boyunca maksimum HC üretme sıcaklığı
S1	Uçucu hidrokarbon miktarı (mg HC/ g kaya)
S2	Kalan HC üretme potansiyeli (mg HC/ g kaya)
S3	CO2 miktarı (mg HC/ g kaya)
HI	Hidrojen İndeksi = $S2 \times 100 / TOC$ (mg HC/g TOC)
OI	Oksijen İndeksi = $S3 \times 100 / TOC$ (mg CO2/g TOC)
PI	Üretim İndeksi = $S1 / (S1 + S2)$

*Piroliz analizinde kullanılan parametreler**Tablo 2.*

Derinlik	TOC	S1	S2	S3	Tmax	HI	OI	PI
1244	0.93	0.65	6.22	0.25	427	669	27	0.10
1246	0.87	0.56	5.29	0.35	424	608	40	0.10
1248-1272	0.61	0.23	2.49	0.48	425	408	79	0.08

*Hoya Formasyonu'ndan alınan örneklerin piroliz analiz sonuçları*

# Imprints of Late Paleozoic-Early Mesozoic Tethyan Evolution in The Northern Arabian Plate (SE Turkey) and Its Role in The Paleozoic Petroleum System



**Gökay Yıldız**

Çalık Petrol Arama Üretim Sanayi ve Ticaret A.Ş.

## ABSTRACT

Carboniferous hiatus, widely extensive across the Arabian Plate, is causally associated with the Hercynian (Variscan) orogeny. However, this epeirogenic tectonic activity occurred far from the Arabian Plate. Alternatively, Gondwana oriented subduction of the Paleo-Tethyan oceanic crust deciphered by metamorphism, arc-type granitic intrusions and structural deformations may be a strong alternative accounting for the Carboniferous paleostructures of SE Turkey (northern Arabian Plate). The Carboniferous compressional tectonism was followed by the initiation of the back-arc spreading of the Neo-Tethys Ocean in between Middle Permian and Triassic. The detachment of the Cimmerian Supercontinent from the eastern margin of Gondwana as a consequence of the opening of Neo-Tethys Ocean caused to extensional deformations along the Arabian Plate margin near regions. The technologies needed for the delineation of subsurface geology have been developed and advanced, which enables us to reveal the imprints of the Carboniferous compressional and the ensuing Permian-Triassic extensional deformations in SE Turkey. In conclusion, the imprints of the SW-, EW- directed compressive stress along the Gondwana margin during the Middle Carboniferous resulted in the development of retroarc foreland system in SE Turkey. The generation of angular unconformity between the disturbed Paleozoic units and the post-Carboniferous units created a path for hydrocarbon migration from the Silurian source rocks to younger reservoir levels. The following Permian-Triassic extensional tectonism ensuing the opening of the Neo-Tethys Ocean led to the development of NW and WNW-trending extensional normal faults. The horst structures bounded on both sides by the steeply dipping normal fault allow lateral hydrocarbon migration from the Silurian source rock to the Ordovician Bedinan Formation sandstones.

## MATERIALS AND METHODS

The studied methods are listed below;

- Horizon picking of the Paleozoic units and fault interpretation
- Impact of Eustacy on the distribution of the sedimentary units
- Geological analogies between the Arabian countries
- Chronostratigraphic and lithologic correlations
- Basin and facies analysis
- Evaluation of the variation in sediments thickness
- Subsidence analysis

The data repositories of Çalık Petrol Exploration and

Production Company including a collection of seismic section, wireline logs, well programs and completion reports were used in this study and listed below;

- Gamma ray and sonic log readings of nine wells and 397 km<sup>2</sup> 3D seismic data
- Cutting descriptions of the Paleozoic section penetrated in sixteen wells
- Well programs and well completion reports
- An interpretation software package for well correlation, structural modelling, property modelling and seismic interpretation

## RESULTS

Carboniferous compressional tectonism and its role in the Paleozoic Petroleum system

Gondwana-oriented subduction of the Paleo-Tethys oceanic crust during the mid-Carboniferous (Fig. 1) is a strong culprit accounting for the regional structural deformations (uplifting, faulting, folding), extensive deep erosion of the pre-Permian units and long-lasting nondeposition in southeast Turkey. Furthermore, the compressional stress culminated in the development of retroarc foreland basin system and “ Arch-Basin” geometry in that region (Fig. 2). The first unit sealing the mid-Carboniferous unconformity surface is the Middle Permian (Wordian-Capitanian) Kaş Formation. Therefore, the mid-Carboniferous unconformity surface is regarded as the pre-Kaş unconformity surface, and which corresponds to pre-Khuff and pre-Unayzah (Saudi Arabia, Kuwait, Bahrain, Qatar), pre-Al-Khlata (Oman), pre-Ga’ara (Iraq), and pre-Faraghan (Zagros, Iran) unconformity surfaces (Konert et al., 2001; Vaslet et al., 2005; Al-Husseini, 2006; Faqira et al., 2009; Tavakoli-Shirazi et al., 2012; Stephenson et al., 2017; Yıldız, 2022) in the Arabian plate.

Two arches, namely, Mardin-Kahta and Siirt initially formed by a possibly precursor event were rejuvenated by the Carboniferous compression. Repetitive re-activation related stratigraphic hiatus over the arches beclouds the prediction of the influence of the Carboniferous compression on the arches. Accordingly, deep well data from the interior part of the Diyarbakır Basin (located in between Mardin-Kahta and Siirt arches) where the significant portion of the Paleozoic units preserved, serve as a significant stratigraphic control to manifest the compression-related distortion on the arches. On this basis, stratigraphic correlation using wireline logs data from the Diyarbakır Basin to the crest of the Mardin-Kahta and Siirt arches by flattening the pre-Kaş unconformity surface (Fig. 2) revealed that the pre-Permian substrate displays the progressive erosion and angular truncation towards the arches. It manifests

vertical movement of the arches due to the impact of the Carboniferous compression (Yıldız, 2022).

The mid-Carboniferous compressional event had also a significant role in the petroleum system of southeast Turkey in terms of the distribution and thermal maturation of the Silurian source rock (Dadaş Formation) and oil migration. For instance, the fact that Silurian Dadaş Formation crops out beneath the pre-Kaş unconformity surface provides a path for oil migration into younger reservoir rocks (Fig. 2). Furthermore, the compression related angular truncation of the Silurian shales towards the arches confined the distributional area of the unit to a narrower area (Fig. 2) (Yıldız, 2022).

Permian-Triassic extensional tectonism and its role in the Paleozoic Petroleum system

Integration of the stratigraphic records and the structural architecture of southeast Turkey and the eustatic sea level changes provides a significant input to trace the exact time of initial spreading of Neo-Tethys Ocean and drifting of the peri-Gondwanan terranes (Cimmerides) along the Paleozoic margin of southeast Turkey. On this basis, despite the sharp decline in the global sea level from the Middle Permian (Roadian) to the Triassic (Haq and Al-Qahtani, 2005; Haq and Schutter, 2008; V'erard et al., 2015; Boulila et al., 2018), the transgressive Middle-Upper Permian units (Tanin Group) and the Lower Triassic units (Çiğli Group) deposited on the pre-Kaş unconformity surface after a significant erosion and nondepositional period. These units anomalously thicken towards the NE margin of SE Turkey. Furthermore, the interpretation of the high-resolution seismic sections crossing the Diyarbakır Basin revealed the NW and WNW trending normal fault penetrating up to the Triassic units (Fig. 3) (some re-activated during the Alpine orogeny). The polarity of the normal faults and the thickening trend of the syn-rift Permian to the Lower Triassic units with considerable facies change account for the NE-SW stretching and rifting during the Middle Permian to Triassic. The first unit sealing the subsided platform is the Wordian-Capitanian Kaş Formation, which displays that the initial spreading of the Neo-Tethys commenced most lately in the Wordian time along the northern margin of the Arabian Plate (Fig. 4). This inference is consistent with those in other regional studies (Stampfli and Borel, 2002; Domeier and Torsvik, 2014; Kavooosi, 2016; Fergusson et al., 2016; Zeng et al., 2019) for the initial spreading of the eastern Neo-Tethys Ocean (Fig. 4). However, the onset of the western Neo-Tethys (eastern Mediterranean) spreading between the Afro-Arabia and the Cimmerian terranes initiated in the Early Triassic and become more continuous during the Middle-Late Triassic/Jurassic (Fig. 4). The development of the extensional basin along the Paleozoic margin of southeast Turkey during the Middle Permian-Triassic culminated in the inversion of the early formed megastructure. For instance, the Siirt Arch upwarped by the mid-Carboniferous compression is the site of thick Permian and the Lower Triassic transgressive units, which clarify that the extensional phase inverted (negative inversion) the early-formed Siirt Arch. The Permian-Triassic extensional tectonism has significant

impact mostly on the Paleozoic petroleum system of southeast Turkey in terms of hydrocarbon migration, trapping mechanism and deposition of reservoir rocks. The extensional normal fault resulted in the development of en-echelon horst and grabens (Fig. 3), which allow the juxtaposition of the Ordovician Bedinan Formation reservoir levels and the Silurian source rock. Therefore, The oil discovered from the Ordovician reservoirs was laterally charged in the horst structures, where the reservoir was in direct contact with the downfaulted block of the Dadaş shales. The impermeable beds of the Dadaş shales in the downfaulted block prevent lateral and updip hydrocarbon migration (fault seal). Furthermore, the chronostratigraphic and lithologic equivalents of the syn-rift units of southeast Turkey in Saudi Arabia, Qatar, Kuwait, and Iran constitute the main hydrocarbon producing levels (e.g., North field, Qatar; Ghawar field, Saudi Arabia).

## CONCLUSION

- (1) Hercynian Orogeny occurred far from the Arabian Plate; therefore, the Gondwana-directed subduction of the Paleo-Tethys during the Middle Carboniferous may be considered as a culprit accounting for uplift, erosion and accordingly the development of "arch-basin" geometry in SE Turkey (northern Arabian Plate).
- (2) The early formed Mardin-Kahta and Siirt Arches are the two arches, uplifted and eroded due to the Mid-Carboniferous compression, and those are separated by the Diyarbakır Basin where the most significant portion of the Lower Paleozoic strata remained.
- (3) The mid-Carboniferous event confined the Silurian source rock (Dadaş Formation) into the narrower area (Diyarbakır Basin) by erosion over the Mardin-Kahta and Siirt arches and hence limits the Paleozoic potential area into the Diyarbakır Basin.
- (4) As a consequence of the mid-Carboniferous compression, the exposure of the Silurian organic-rich Dadaş shales beneath the mid-Carboniferous unconformity (pre-Kaş unconformity) surface provides a path for oil migration from the source rock into the younger reservoirs.
- (5) The mid-Carboniferous compression delayed the maturation process of the Silurian Dadaş shales by erosion and nondeposition of a considerable amount of strata, and additionally prevented the deposition of high reservoir quality levels, its equivalents in some of the Arabian countries (e.g. Saudi Arabia) contains a significant amount of oil and gas.
- (6) Despite the sharp decline in global sea level from the Middle Permian to the Triassic, the deposition of the Permian units (Kaş and Gominiibrik formations) with the thickening trend towards the NE edge of SE Turkey after a considerable hiatus manifests the extensional tectonism related subsidence as a result of the spreading of the Neo-Tethys ocean.
- (7) In SE Turkey, the first unit deposited on the mid-Carboniferous unconformity surface is the Wordian-Capitanian Kaş Formation; therefore, it is evident



that the Neo-Tethys ocean opened along the northern Gondwana margin (Paleozoic margin of SE Turkey) in the Wordian time at the latest.

(8) The Permian-Triassic extension-related NW-WNW trending normal faults inverted the Carboniferous Siirt Arch to the Siirt Trough, which is deciphered by anomalously thick the Permian and the Triassic units.

(9) The Permian-Triassic syn-rift units in SE Turkey constitute a potential reservoir level for hydrocarbon accumulation because its equivalents in other Arabian countries are world-class reservoirs and contain an immense quantity of hydrocarbons.

(10) The deposition of the syn-rift Permian-Triassic units caused an extra charge on lower-lying units, and hence provided the earlier maturation of the Silurian source rock in the Diyarbakır Basin.

(11) The vertical displacement of the Permian-Triassic normal faults caused the juxtaposition of the Silurian source rock (Dadaş Formation) and the Ordovician reservoir rock (Bedinan Formation), and hence provided a path for lateral oil migration from the source rock to the porous media.

(12) In the Diyarbakır Basin where the Silurian source rock exists, the development of the NW, WNW-trending, en-echelon horst blocks in response to the Permian-Triassic extension trap hydrocarbon in the Ordovician sandstone reservoirs as the impermeable Dadaş shales in the falling block cause oil accumulation in the horst structures.

## REFERENCES

Al-Husseini, M. I. (2004). Pre-Unayzah unconformity, Saudi Arabia. *GeoArabia*, 3, 15-59.

Boulila, S., Laskar, J., Haq, B.U., Galbrun, B., Hara, N., 2018. Long-term cyclicities in Phanerozoic sea-level sedimentary record and their potential drivers. *Global Planet. Change* 165, 128–136. <https://doi.org/10.1016/j.gloplacha.2018.03.004>.

Domeier, M., Torsvik, T.H., 2014. Plate tectonics in the late Paleozoic. *Geosci. Front.* 5 (3), 303–350. <https://doi.org/10.1016/j.gsf.2014.01.002>.

Faqira, M., Rademakers, M., Afifi, A.M., 2009. New insights into the hercynian orogeny, and their implications for the paleozoic hydrocarbon system in the Arabian plate. *GeoArabia* 14 (3), 199–228. <https://doi.org/10.2113/geoarabia1403199>.

Fergusson, C.L., Nutman, A.P., Mohajjel, M., Bennett, V.C., 2016. The Sanandaj–Sirjan Zone in the Neo-Tethyan suture, western Iran: zircon U–Pb evidence of late Palaeozoic rifting of northern Gondwana and mid-Jurassic orogenesis. *Gondwana Res.* 40, 43–57. <https://doi.org/10.1016/j.gr.2016.08.006>.

Haq, B.U., Al-Qahtani, A., 2005. Phanerozoic cycles of sea-level change on the Arabia

Platform. *GeoArabia* 10 (2), 127–160.

Haq, B.U., Schutter, S., 2008. A chronology of paleozoic sea-level changes. *Science* 322

(5898), 64–68. <https://doi.org/10.1126/science.1161648>.

Kavoosi, M.A., 2016. The Capitanian rifting phase and its impact on hydrocarbon distribution in the Zagros fold-thrust belt, SW Iran. In: *International Congress on Palaeozoic Straigraphy of Gondwana*. Perugia, Italy

Konert, G., Afifi, A., Al-Hajri, S., & Droste, H. (2001). Paleozoic Stratigraphy and Hydrocarbon Habitat of the Arabian Plate. *GeoArabia*, 6(3), 407-442.

Stephenson, M.H., Al-Mashaikie, S.Z.A.K., Kurukchi, W.M., 2017. Palynological assemblages across the hercynian unconformity in western Iraq. *Rev. Micropaleontol.* 60 (3), 417–432. <https://doi.org/10.1016/j.revmic.2016.05.005>.

Stampfli, G.M., Borel, G.D., 2002. A plate tectonic model for the Paleozoic and Mesozoic

constrained by dynamic plate boundaries and restored synthetic oceanic isochrons.

*Earth Planet. Sci. Lett.* 196 (1–2), 17–33. [https://doi.org/10.1016/S0012-821X\(01](https://doi.org/10.1016/S0012-821X(01)

00588-X.

Tavakoli-Shirazi, S., Frizon de Lamotte, D., Wrobel-Daveau, J.-C., Ringenbach, J.-C., 2012. Pre-Permian uplift and diffuse extensional deformation in the High Zagros Belt (Iran): integration in the geodynamic evolution of the Arabian plate. *Arabian J. Geosci.* 2329–2342. <https://doi.org/10.1007/s12517-012-0542-5>.

Vaslet, D., Le Nindre, Y.-M., Vachard, D., Broutin, J., Crasquin-Soleau, S., Berthelin, M., Al-Husseini, M. (2005). The Permian-Triassic Khuff Formation of central Saudi Arabia. *GeoArabia*, 10(4), 77-134. Retrieved from <https://hal.archives-ouvertes.fr/hal-00022202>

V'erard, C., Hochard, C., Baumgartner, P.O., Stampfli, G.M., Liu, M., 2015. 3D palaeogeographic reconstructions of the Phanerozoic versus sea-level and Sr-ratio variations. *J. Palaeogeogr.* 4 (1), 64–84. <https://doi.org/10.3724/SP.J.1261.2015.00068>.

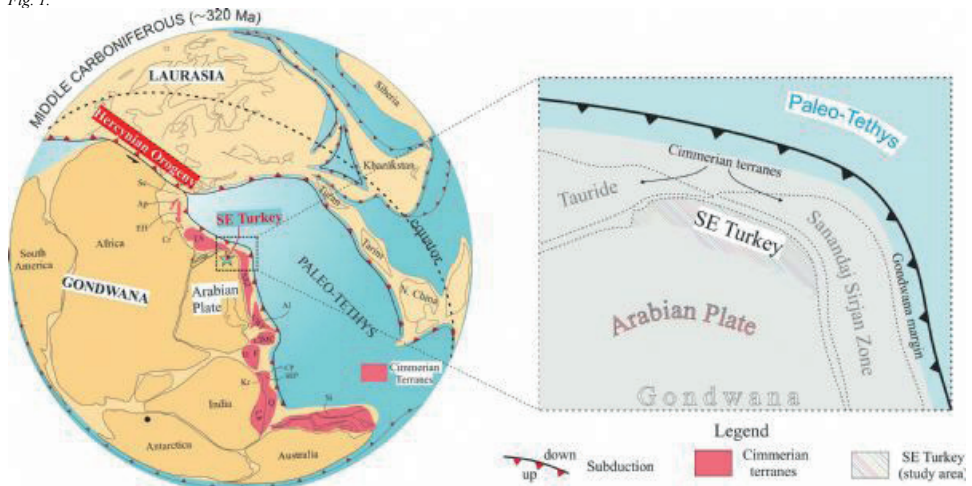
Yıldız, G., 2022. Late Paleozoic-Early Mesozoic paleotectonics of the northern Arabian Plate (SE Turkey) and its role in the Paleozoic petroleum system, Marine and Petroleum Geology, <https://doi.org/10.1016/j.marpetgeo.2022.105529>

Zeng, Y.-C., Xu, J.-F., Ducea, M., Chen, J.-L., Huang, F., Zhang, L., 2019. Initial rifting of

the Lhasa terrane from Gondwana: insights from the permian (~262 Ma) amphibolerich lithospheric mantle-derived yawa basanitic intrusions in southern tibet. *JGR Solid Earth* 124 (3), 2564–2581. <https://doi.org/10.1029/2018JB016281>.

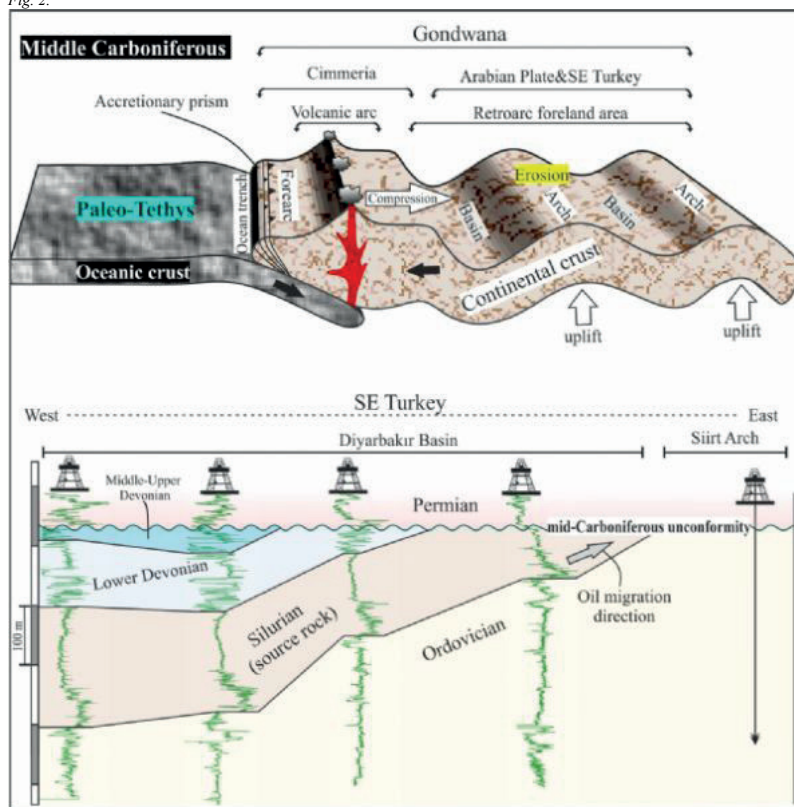
Keywords: Paleozoic petroleum system of SE Turkey, Tethyan geodynamics

Fig. 1.



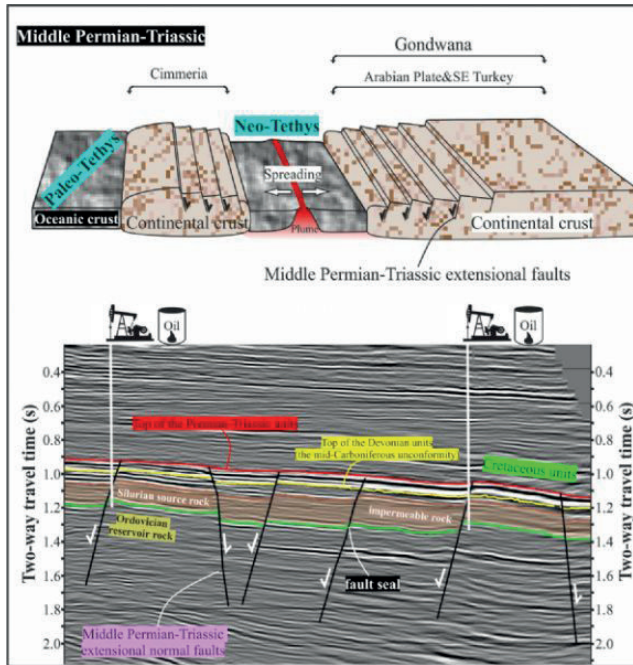
Paleogeographic reconstruction for the Middle Carboniferous (after Stampfli and Borel (2002)). Sc, Sicily; Cr, Crete; Ap, Apulia; EH, External Hellenides; TA, Tauride-Anatolide; SSZ, Sanandaj Sirjan Zone; NWI, Northwest Iran; Al, Alborz; CIMC, Central Iranian Microcontinents; H, Helmand; F, Farah; CP, Central Pamir; SEP, Southeast Pamir; Kr, Karakoram; Q, Qiangtang; Lh, Lhasa; Si, Sibumasu

Fig. 2.



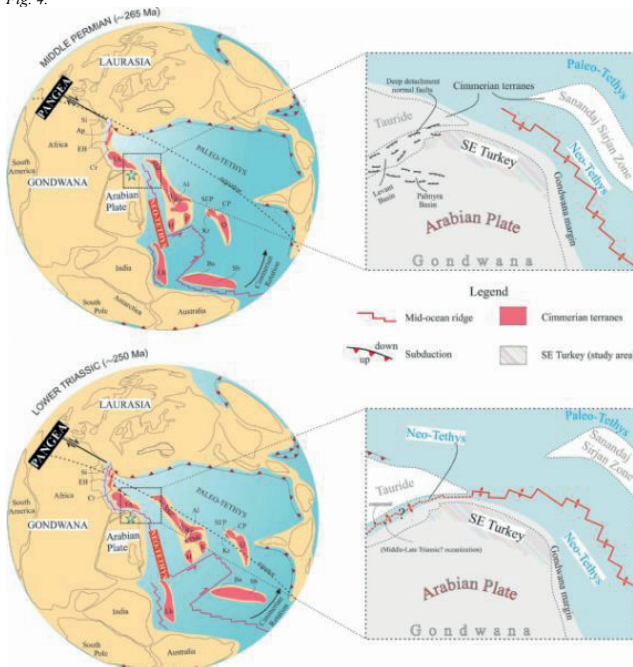
Geodynamic evolution of the northeast Gondwana margin during the mid-Carboniferous

Fig. 3.



Geodynamic evolution of the northeast Gondwana margin from the mid-Permian to the Triassic

Fig. 4.



Paleogeographic reconstruction for the Middle Permian-Lower Triassic (after Stampfli and Borel (2002))





**Üretim Mühendisliği**

*Production Engineering*

---



# Overcoming Complex Flow Assurance Issues with Respect to Gas Hydrate Formation in Deep-Water Well Testing Operations



**Yakov Shumakov, Ozgur Karacali**  
SLB;

## INTRODUCTION

Today many exploration, appraisal, and development well test operations are performed in new frontiers such as offshore deepwater environments, including the Black Sea. Deepwater well test and well clean-up operations are presenting unique challenges related to flow assurance aspects that are beyond the standard well test playbook. Many failures and operational issues related to flow assurance, such as the plugging of pipelines or tubing by wax or hydrates, have hindered the interpretability of data, thereby compromising the test objectives and significantly increasing the total costs of such well tests or leading to serious health, safety, and environment incidents.

Hydrate formation is one of the most common flow assurance issues during the well test and well clean-up operations in gas and gas-condensate reservoirs in a deepwater offshore environment. Low ambient temperature of the water column along the marine riser in combination with the high-water depth can cool down the produced fluid causing the hydrate formation. Several past experiences have shown that it is nearly impossible to perform a deepwater well test and achieve the test objectives without appropriate test design, equipment selection, and operations planning including the assessment and mitigation actions in place to reduce the risk of hydrate formation.

Well tests and well clean-ups are complex offshore operations that involve multiple expertise across different domains and services that include temporary surface well test packages, landing string and drillstem test string with specialized downhole tools and components, or permanent completion. Therefore, the risk assessment of hydrate formation and plan of mitigation actions must be performed in line with the detailed well test operation sequences and capabilities of the equipment used offshore. Today there is no single practical workflow available that would guide operators through the process of planning deepwater well test operations effectively with a detailed assessment of the risk of hydrate formation and a mitigation plan.

### **Risk assessment of hydrate formation**

While we try to keep hydrocarbons in the ground during drilling and completion operations, during clean-up, the well is put on production to recover all the non-hydrocarbon fluids lost in the formation, usually through temporary surface facilities installed on the rig or platform. This is either to test an exploration and appraisal well or to simply clean a well before connecting it to the production facilities.

During well clean-up and flowback operations, multiple non-reservoir types of fluids can be produced, including

completion brines, drilling fluids, and formation and vapor water. These fluids can cause multiple issues such as plugging, erosion, corrosion, and scale formation. At a certain operating condition, such fluids in combination with produced reservoir gas can form hydrates in the production system. The hydrates can plug the tubing or production lines at the surface, which will hamper or cease the operations completely, and it may take weeks to recover from this incident. Therefore, hydrate formation has always been considered one of the major risks during the well test and well clean-up operations performed in deepwater gas-bearing reservoirs.

The risk of hydrate formation is typically evaluated by considering two aspects: sensitivity of non-reservoir fluids containing water molecules in combination with the reservoir hydrocarbons to form hydrates and anticipated operating conditions in terms of pressures and temperatures along the production string and process plant at surface.

Gas hydrates are clathrate structures consisting of a water molecule lattice interconnected through hydrogen bonds, which creates different types of cavities that can enclathrate small non-polar or slightly polar molecules. Natural gas hydrates typically formed during the well test operations are a sub-class of these hydrates in which the enclathrated molecules are predominantly hydrocarbons. The encapsulated natural gas molecule is referred to as the hydrate former, and the most abundant natural gas hydrate former in nature is methane (CH<sub>4</sub>). There are several known hydrate structures, the most common being structure I and structure II (Sloan and Koh 2007).

When the well is opened for the first flow, different types of non-reservoir fluids are often produced from the well and reservoir in varying quantities; these fluids are often an inevitable consequence of the drilling and completion process. Each type of fluid, including completion brine, drilling mud filtrate, and formation water, in combination with reservoir hydrocarbons potentially can introduce the risk of hydrate formation. Most of the completion brines and drilling fluids contain salt, which is used to increase their density. Salt is a hydrate inhibitor and changes the thermodynamic stability of natural gas hydrate due to the fact that the resulting ions in the aqueous solution of the salt will reduce the chemical potential of liquid water; for sufficiently high concentrations of ions, the water will be more stable as liquid water rather than hydrate water (Fig.1). Therefore, the risk of hydrate formation with these fluids is relatively low in comparison with fresh water. However, it is important to remember that produced completion brine or drilling mud filtrates during the test can be mixed with other types of water with lower salinity, which increases the risk of hydrate

formation.

Natural gases also contain a small fraction of water vapor. Even an insignificant amount of vapor water present in the flow can be sufficient for hydrate formation. Since the vapor water is fresh, it introduces the highest risk of hydrate formations during the operations.

Today a new generation of multiphase transient wellbore flow simulation software coupled with a hydrodynamic reservoir simulator are used to simulate complex well and flow behavior during well clean-up or entire well test operations and to predict flowing operating conditions to assess the risk of hydrate formation (Shumakov et al., 2021). One of the key parameters influencing the well clean-up process is the volume of fluid losses in the formation that must be measured accurately while drilling or running in hole the lower and upper completions before conditioning the well for clean-up. With transient flow simulation, the initial part of well clean-up process can be optimized to achieve a piston displacement of wellbore volume by reservoir fluid, thus eliminating the mixing of the wellbore cushion with reservoir fluids, reducing the risk of a gas breakthrough and hence reducing the risk of hydrate formation.

Typically, it is assumed that the risk of hydrate formation persists for a short time during the cold restart process. During the flow, the wellbore is warmed up from a static temperature above the hydrate formation temperature by the produced hot reservoir fluid either during the initial period of well clean-up or opening the well for a flow after a long period of shut-in (Fig. 2). That may not be the case for deepwater wells where the risk of hydrate formation can remain high during the entire well test operation due to the significant cooling effect of produced fluid along the marine riser.

It is also assumed that the higher gas flow rate tends to maximize flowing wellhead temperature. However, in many cases, at the high gas velocity, significant fluid cooling may occur along the production string due to the domination of the extensive pressure drop related to friction and the Joule-Thomson effect. Therefore, it is possible during a deepwater well test to see a reverse effect with a decrease in the flowing wellhead temperature with the choke size increase.

Even though the transient wellbore simulator can accurately predict the flowing operating conditions during the deepwater well clean-up operations, the simulation results heavily depend on the input parameters and model description. The temperature effect is an inertial process. Therefore, accurate prediction of flowing fluid temperature can be complex, and it requires an accurate description of well events prior to the operations to predict the initial conditions along the wellbore and the reservoir. These events include fluid circulation during the drilling stage of the well with the fluid losses into the formation, fluid circulation during wellbore clean-out, running in the hole the completion, and fluid displacement prior to opening the well for the initial flow.

Another contributing factor, and one unique in deepwater wells, is related to the description of

heat transfer along the marine riser. The accurate calculation of heat transfer across the marine riser is a very complex process involving multiple effects, and it cannot be assumed as a static value, as used in steady-state simulators. Several attempts have been done in the past (Tang et al., 2019; Sarkar et al., 2013; Taxy and Lebreton, 2004) to calculate the actual heat transfer coefficient for drilling risers, but it is still quite unknown and varies from one manufacturer, size, and model of the riser to another. In general, to describe the heat transfer across the drilling or marine riser in a cold startup case such as a well clean-up operation, the following information is required:

- Temperature profile across the water column, considering seasonal changes
- Sea and air current with the depth, which includes a small fraction of marine riser from the water surface to rotary table exposed to the air
- Fluid properties inside the marine riser between the landing string and riser wall (heat capacity, heat conductivity, and fluid viscosity)
- Riser dimensions, model, and manufacturer

#### Mitigation measures to reduce the risk of hydrate formation

Thermodynamic hydrate inhibitors such as methanol or monoethylene glycol (MEG) are widely used inhibitors to prevent hydrate formation in the production string, pipelines, or temporary surface well test equipment during the test. Although the efficiency in preventing hydrate formation of both inhibitors is very similar, the selection of which product to use may not be simple as it must consider multiple factors:

- MEG
- MEG is easy to use and widely available in the market.
- High viscosity causes a bigger pressure loss due to friction and hence less injection capacity through the chemical injection lines.
- Viscosity is highly sensitive to temperature and therefore typically causes high uncertainty in injection capacity.
- MEG can cause salt precipitation.
- Methanol
- Methanol use is prohibited in some countries.
- Methanol is complex to handle, requiring an environmental guard system.
- The lower viscosity product typically requires higher injection volume in comparison with MEG.
- There is a loss of methanol to gas and condensate phases.

Deepwater well test operations are required to have a reliable chemical injection system in place to mitigate the risk of hydrate formation. The hydrate inhibitors can be injected at the seabed or below the mud line. The chemical injection system is complex and includes umbilical lines, fittings, and crossover with hoses;



backpressure circulation and check valves with fittings; and a chemical injection sub and chemical injection liner installed below mud line. The chemical injection is performed at surface using air-driven chemical injection pumps. The typical injection rate of hydrate inhibitors through the system is 1 to 2 liters/min of MEG or 2 to 3 liters/min of methanol. This volume is sufficient to prevent hydrate formation with a small volume of water typically produced during the test. However, in some exceptional cases, the chemical injection system can be customized to achieve a chemical injection rate of up to 15 liters/min of methanol.

### Early hydrate formation detection during the well test execution

Despite all the mitigation actions during the execution stage, there are still residual risks of hydrate formation due to some operational issues such as chemical injection pump failure or insufficient chemical injection rate in comparison with the volume of water produced. Therefore, early hydrate formation detection during the operations is essential to prevent a big incident from happening, such as plugging of the piping and tubing, which may take weeks to recover from.

During the flow of a mixture of reservoir hydrocarbons in combination with some water fractions in a hydrate formation region, the hydrates can form. The hydrates start to form from small hydrate shells that start to agglomerate and eventually form the hydrate plug. The hydrate deposition mechanism and duration of each stage depends on the flow production regime.

In the annular, slug, or in the churn flow regimes with substantial liquid presence in the gas flow, the hydrate forms a film at the water gas interface. This causes a pressure increase due to the change in flow area, and the pressure increases causes the hydrate film to crumple, freeing water and removing the flow restriction. This process repeats until the hydrates eventually plug the flow area. During the flow of the well, the hydrate deposition, in this case, can be easily detected by the abrupt and erratic behavior of the wellhead and bottomhole flowing pressures. An increase in the rate of hydrate inhibitor injection can prevent from hydrates from plugging the tubing.

As an example, Figures 3 and 4 show the behavior of wellhead and bottomhole flowing pressure at the time of hydrate formation in the tubing during the ultradeep water well test. During the flow of the well, it was decided to stop the methanol injection when, after a short while, hydrate formation was observed by increased pressure loss in the tubing and abrupt behavior of the wellhead and bottomhole flowing pressures. The resumption of methanol injection at 9 liters/min at the seabed prevented the hydrate formation.

In the annular, mist, or finely dispersed bubble flow regimes with very small liquid content in the gas-dominated flow, the hydrate typically forms on the entrained droplets, and annular film and quickly forms hydrate deposition on the wall forming a stenotic buildup.

During the flow of the well, the hydrate formation can be detected by monitoring the pressure gradient change in the tubing string and later in hydrate deposition as an apparent restriction in the string by monitoring wellhead and bottomhole flowing pressures. If hydrate formation is detected, it is recommended to increase the hydrate inhibitor injection and start choking back the well to be ready to shut in at any moment. Figures 5 and 6 show a field example of hydrate formation in gas-dominated flow with a small fraction of liquid present in the flow during the ultra-deepwater well test.

As was shown in the examples, the early detection of hydrate formation and prompt and correct actions can help to recover and prevent the hydrates from plugging the string.

### CONCLUSIONS

Over the course of 3 years, more than 25 well test operations have been successfully performed in deepwater environments. On these operations, we have successfully demonstrated our capabilities to flow test the wells in a very complex lithological environment comprising a multilayer system with little overburden, incompatible pressure regimes, intercalations of water zones, and low reservoir pressure.

All these elements related to the gas field development and water production could have seriously hampered the performed well test and well clean-up operations. Operating within the gas hydrate zone has enabled the confirmation of the tuning of the models used, has provided a higher visibility of the risks, and, finally, has resulted in better mitigation of the flow assurance issues that have arisen.

Conventional flow assurance operating strategies would not have allowed the results that have been achieved by the process described in this paper, which include faster well clean-up and achieving well test objectives.

A close and real-time collaboration between all parties has been a key element of success, from early design to detailed simulations with sensitivities and on-the-fly execution. Efficient communication at all levels of management, logistics, and execution delivered the required low latency between diagnostics and decisions leading to an efficient resolution of issues or modification of planned operations. A continuous improvement process has been delivering an optimized orchestration of the operations.

### REFERENCES

- Husebø, J., Erslund, G., Graue, A., and Kvamme, B. 2009. Effects of salinity on hydrate stability and implications for storage of CO<sub>2</sub> in natural gas hydrate reservoirs. *Energy Procedia*, 1 (1): 3731-3738. <https://doi.org/10.1016/j.egypro.2009.02.172>.
- Nagashima, K., Orihashi, S., Yamamoto, Y., and Takahashi, M. 2005. Encapsulation of Saline Solution by Tetrahydrofuran Clathrate Hydrates and Inclusion Migration by Recrystallization. *Journal of Physical*

Chemistry, B, Condensed Matter, Materials, Surfaces, Interfaces & Biophysical 109 (20): 10147-10153. <https://doi.org/10.1021/jp040680i>.

Sarkar, S., Moeleker, P., Kotikanyadanam, M., Chin, G., Schwing, A., Henkes, R., and Zabarar, G. 2013. Optimizing Operational Performance of Riser Systems Through Improved Understanding of Riser Thermal Behaviour. Paper presented at the International Petroleum Technology Conference, Beijing, China, 26-28 March. <https://doi.org/10.2523/IPTC-17185-MS>.

Shumakov, Y., Hollaender, F., and Zhandin, A. 2021. Fast, Environmentally Sound and Efficient Well Clean-Up Operations: Lessons Learned and Best Practices from Operations Around the World. Paper presented at the SPE Offshore Europe Conference & Exhibition, Virtual, 7-10 September. SPE-205419-MS. <https://doi.org/10.2118/205419-MS>.

Sloan, E. D. and Koh, C. A. 2007. CSMGem Hydrate Production Program, 1.10. Center for Hydrate Research, Dept. of Chemical and Petroleum-Refining, Colorado School of Mines, Golden, Colorado, USA.

Tang, H., Bailey, W., Stone, T., and Killough, J. 2019. A Unified Gas/Liquid Drift-Flux Model for All Wellbore Inclinations. SPE Journal 24: 2911-2928. <https://doi.org/10.2118/197068-PA>.

Taxy, S. and Lebreton, E. 2004. Use of Computational Fluid Dynamics to Investigate the Impact of Cold Spots on Subsea Insulation Performance. Paper presented at the Offshore Technology Conference, Houston, Texas, USA, 3-6 May. <https://doi.org/10.4043/16502-MS>.

Keywords: Deep water well test operations, hydrate formation and mitigation

Fig.1

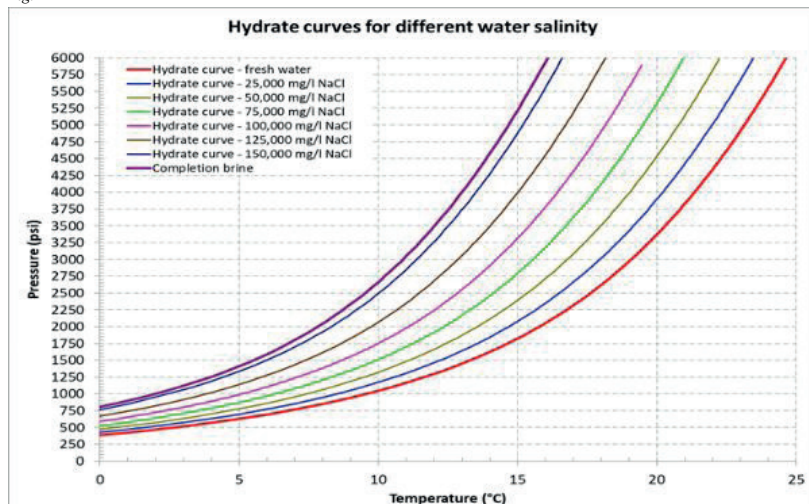


Figure 1. The graph illustrates the importance of knowing the salinity of the hydrate-forming water as it will indicate the stability of hydrate.

Fig.2

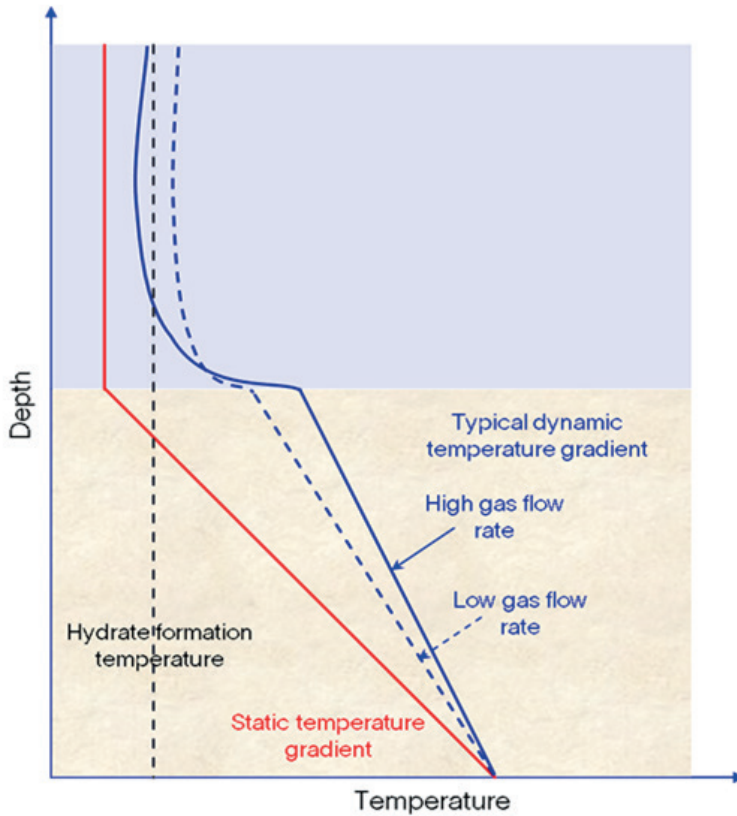


Figure 2. Visualization of static and dynamic temperature profile along the production string in comparison with hydrate formation temperature.

Fig.3

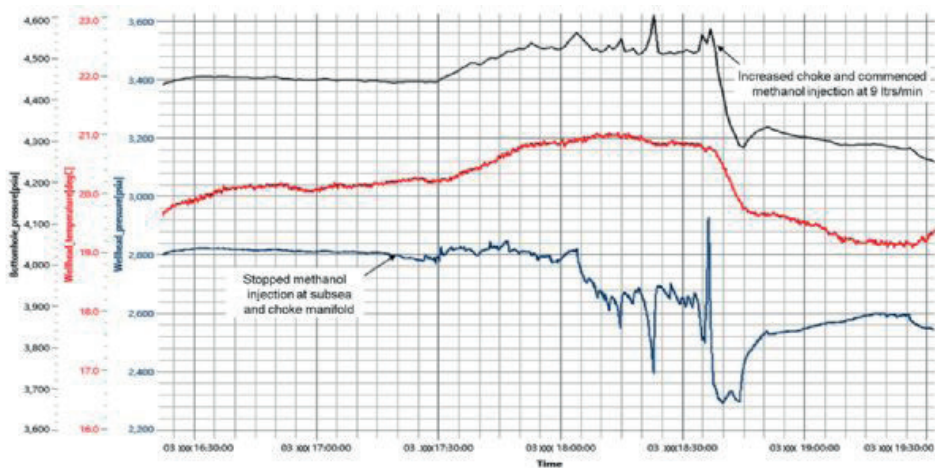


Figure 3. Detection of hydrate formation by monitoring wellhead and bottomhole flowing pressure behavior during a deepwater well test when the well produced in an annular flow regime with high water content in the flow.

Fig.4

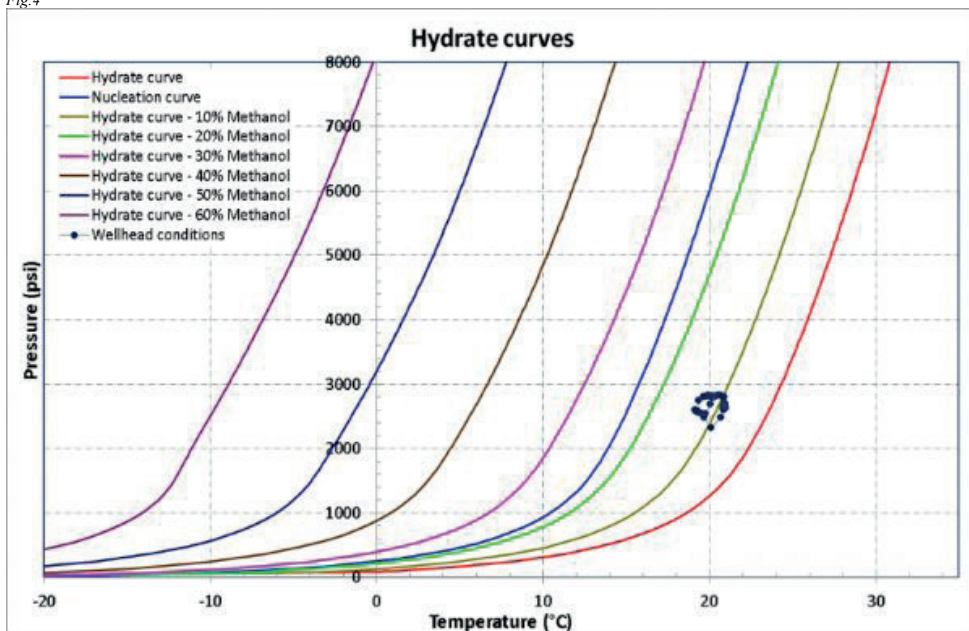


Figure 4. Operating conditions at the wellhead during the time of hydrate formation.

Fig.5

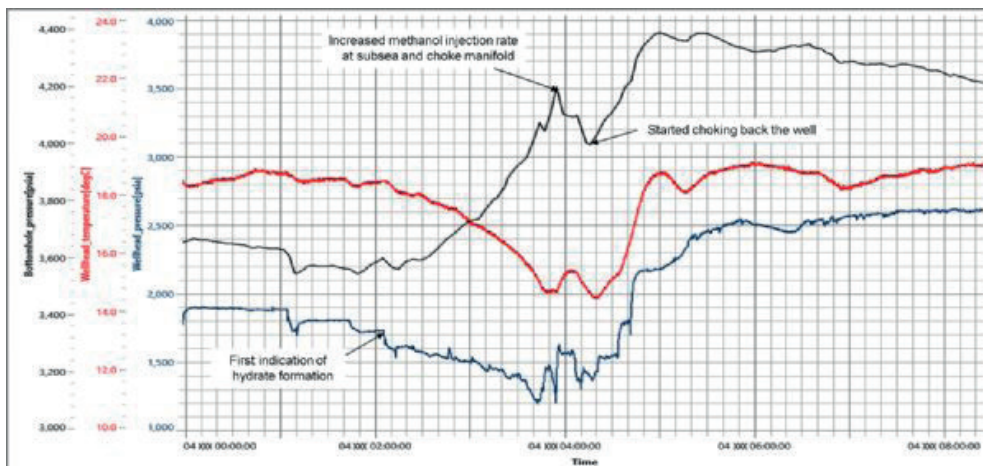


Figure 5. Detection of hydrate formation by monitoring wellhead and bottomhole flowing pressure behavior during a deepwater well test in gas-dominated flow with a small fraction of liquid.

Fig.6

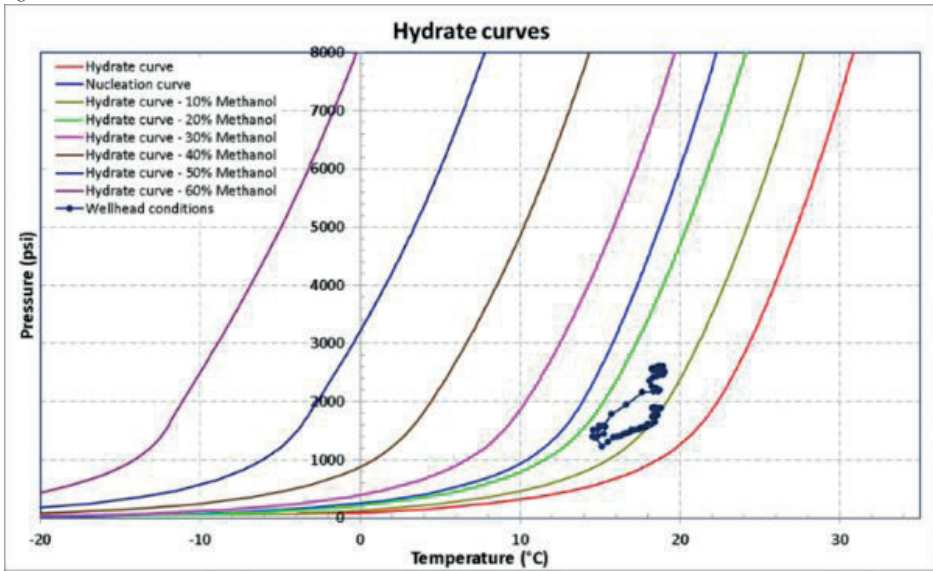


Figure 6. Operating conditions at the wellhead during the time of hydrate formation.

# Single Configuration Enables Seamless Workflow From Cleanup to Extended Well Test and to Production in a Harsh Environment



**Symon Thomas Shields**  
SLB, UK / Aberdeen

## OBJECTIVES/SCOPE

A recently completed series of operations on a land location from cleanup to production processing encompassed multiple Objectives: clean out solids in a perforated liner in a high H<sub>2</sub>S environment; regain access to a lower reservoir; acid stimulate and test the lower reservoir; and pre-condition the oil with a sweetening process, initially with a chemical scavenger and ultimately incorporating a stripping unit (NSCU) to be able to export the oil. These operations enable a proof of concept of the entire workflow from pore to process.

## METHODS, PROCEDURES, PROCESS

From the standard portfolio, slightly customized equipment, and designed solutions produced a robust and innovative well testing package. The design accounted for contingencies of all eventualities and enabled performing the clean-up and subsequent well-test with the same configuration seamlessly. This to be able to deploy a package suitable to handle the unpredictable clean up phase all the way to production that would only be required to install and commission once.

In Exploration type well testing, data collection is paramount, however in extended well testing practices the emphasis is on more leaning towards the returns. A combination of simulation software including chemical process simulator and steady state multiphase flow simulator with mechanical and chemical intervention resulted in an efficient reduction of H<sub>2</sub>S and Reid vapor pressure. These approaches have led to meeting the customers objectives of not only accurate and transparent returns but also paved the way for future more permanent solutions to be put in place.

The area was known for its rich H<sub>2</sub>S content and careful consideration had been taken to not only characterise the reservoir by flowing at certain rates but also to respect and protect the surrounding communities in the case of flaring gas that contains high quantity of H<sub>2</sub>S. Many different applications were considered from a technology and from a cost perspective.

A customer applied dispersion study dictated an engineering solution to attain acceptable SO<sub>2</sub> dispersion. This was achieved by a custom built 60 m flare and real time software modelling as well as monitoring.

This resulted in a safe operation that ensured cost and safety can go hand in hand.

## RESULTS, OBSERVATIONS, AND CONCLUSIONS

The fabrication of project specific pressurized tanks in addition to the implementation of a newly designed chemical sweetening process, and subsequent processing with the NSU, allowed for continuous operations from the clean-up to the extended well test that lasted more than 100 days. Digital enablement ensured additional safety in terms of intrinsic measurement with multiphase and Coriolis meters. Extensive data capture and real time monitoring and data transmission capabilities enabled remote decision making.

This unconventional approach to surface well testing led to a rigorous yet innovative design, and strict procedural controls were in place to deliver the project incident free from preparation to deployment.

This workflow did not only meet the clean up objectives but also ensured that quick cash returns in conditioning the oil to a commercial standard was realised. By implementing a single well testing package that could seamlessly ensure to uphold certain upfront agreed production standards, a proof of concept was created.

## NOVEL/ADDITIVE INFORMATION

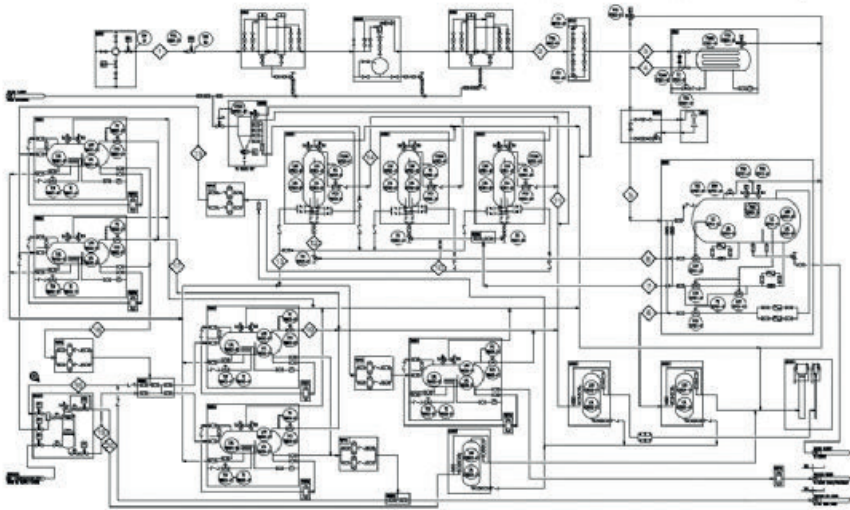
A novel H<sub>2</sub>S scavenger for surface well testing operations in combination with the right dosage procedure and injection method led to an efficient and cost-effective operation and was safer than conventional scavengers used previously.

Leveraging the expertise of different business lines to create from existing surface equipment a temporary solution while a more permanent production solution could be designed based on the results will de-risk some of the initial investments needed.

Integrating temporary equipment with existing or even customer equipment provided not only flexibility and cost savings but also expedited operations.

A platform of open discussion, sharing ideas, mutual trust, and alignment from both operator and service provider allowed for a seamless transition from the unpredictable clean up to the production process phase to allow robustness and efficiency.

Keywords: Single configuration, Pre-conditioning oil



Process flow diagram, detailing how the well test package used for the clean up seamlessly transition to an extended well test package without changing any of the components.

# ESP Malzeme Kullanım Ömürlerinin (Runlife) Adıyaman, Diyarbakır ve Batman Bölgelerinde İncelenmesi Investigation of ESP Equipments Runlife in Adıyaman, Diyarbakır and Batman Regions



**Ayhan Budak**

Türkiye Petrolleri A.O. Üretim D.B.

Electrical Submersible Pump (ESP) system has proven itself in the oil production industry. It is one of the highly efficient oil production systems with wide production range and application area.

Turkish Petroleum Co. (TPAO)'s first ESP application was made in 1985 in South Sahaban field and upon receipt of positive results the use of ESP has expanded rapidly. As of end of 2022, 323 ESP wells run in 3 different regions and in range of 125-9325 bpd gross production.

In this study, the technological advances of the ESP system, management, impact of the well conditions and properties on the materials runlife is aimed to be determined. Therefore 3787 ESP operation reports (2055 run and 1732 pull) and 4957 ESP downhole equipments recorded in this reports were examined, belong to the last 35 years (between 1987-2022).

ESP downhole equipment's runlife value were assessed and the results were compared separately for having different features regions Adıyaman, Diyarbakır and Batman.

## ÖZ

Elektrikli Santrifüj Dalğıç Pompa (ESP) sistemi, petrol üretim sektöründe kendini kanıtlamış, üretim aralığı ve uygulama alanı geniş, yüksek verimli petrol üretim tekniklerinden bir tanesidir.

Türkiye Petrolleri AO'nun ilk ESP uygulaması, 1985 yılında Güney Şahaban sahasında yapılmış ve olumlu sonuçlar alınması üzerine ESP kullanımı hızla yaygınlaşmıştır. 2022 yılı sonu itibarıyla Adıyaman, Diyarbakır ve Batman Bölgelerinde 323 adet kuyu ESP ile 125-9325 v/g aralığında üretim yapmaktadır.

Bu çalışmada, ESP sistemlerindeki teknolojik gelişmelerin, işletmeciliğin, kuyu şartlarının ve mayi özelliklerinin malzeme kullanım ömürleri üzerindeki etkilerinin tespit edilmesi hedeflenmiştir. Bu nedenle 35 yıllık süreçte (1987-2022 yılları arası) yapılan 3787 adet ESP operasyonu raporu (2055 iniş ve 1732 çıkış raporu) ve bu operasyonlarda kullanılan 4957 adet ESP yeraltı malzemesi (motor, pompa, intake ve seal) incelenmiştir. ESP malzemelerinin kullanım ömürleri, değişik kuyu ve mayi özelliklerine sahip olan Adıyaman, Diyarbakır ve Batman Bölgeleri için ayrı ayrı olarak değerlendirilip sonuçları karşılaştırılmıştır.

## GİRİŞ

Türkiye Petrolleri'nde ESP üretim sistemlerinin ilk kullanılması 1985 yılında Diyarbakır Bölgesinde, G.Şahaban sahasında olmuştur. Yüksek debili, derin ve

yüksek sıcaklıktaki kuyu şartlarına uygun üretim tekniği olduğundan, Adıyaman Bölgesindeki kuyularda 1989 yılında ESP uygulamaları başlamış ve olumlu sonuçlar alınmasıyla birlikte uygulama sayısı hızla artmıştır. 2022 yılı sonu itibarıyla, Adıyaman, Diyarbakır ve Batman Bölgelerinde bulunan değişik kuyu şartlarına ve mayi özelliklerine sahip 323 kuyuda ESP üretim sistemleriyle 125-9325 v/g debi aralığında üretim yapılmaktadır.

Petrol üreten şirketler, satın aldıkları malzemeyi mümkün olduğunca uzun süreyle kullanmak isterler. Bu sayede kuyularda görülen arıza sayısı azalacak ve neticesinde üretim kayıpları ve operasyon maliyetleri de azaltılmış olacaktır. Daha uzun süreli çalışma süresini (runlife) yakalayabilmek için teknoloji takip edilmekte ve yeni geliştirilen ürünler daha fazla maliyete katlanılarak satın alınmaktadır. Yeni bir uygulama veya ilk kez kullanılan bir malzeme hakkında karar verebilmek için 3-5 yıllık bir süreyle takip edilmesi gerekmektedir.

Petrol üreten firmaların beklentilerini çok iyi bilen üretici firmalar ise ESP üretim sistemlerini gerek yeraltı gerekse yerüstü ekipmanları olsun, teknolojik olarak sürekli yenilemekte ve geliştirmektedirler. Bu durum doğal olarak malzeme fiyatlarına artış olarak yansımaktadır.

Petrolü bulmak kadar düşük maliyetlerle üretmeninde önemli olduğu günümüzde, üç temel parametre, 1-uygun malzeme seçimi, 2-ışletmecilik ve 3-ekonomik analiz, dikkat edilmesi gereken unsurlar haline gelmiştir. Bu çalışmanın amacı, elimizdeki veriler ışığında, aşağıdaki soruların yanıtlarını bulmaktır.

- Daha fazla para ödeyerek aldığımız geliştirilmiş ürünler, gerçekten beklentilerimizi karşılayabiliyor mu?
- Kuyu şartları ve mayi özellikleri, malzeme kullanım ömrünü ne kadar etkiliyor?
- Yer üstü kontrol ekipmanları, malzeme kullanım ömrünü ne kadar etkiliyor?
- Malzeme seçiminde ne kadar isabetli kararlar veriliyor?
- İşletmecilik, malzeme kullanım ömrünü ne kadar etkiliyor?

Bu soruların cevaplarını verebilmek için; Adıyaman, Diyarbakır ve Batman Bölgelerinde 1987-2022 yılları arasında kapsayan 35 yıllık süreçte yapılan 3787 adet ESP operasyon raporu incelenmiştir. Bu üç bölge farklı kuyu şartlarına ve mayi özelliklerine sahip olduklarından, çalışma her bölge için ayrı olarak yapılmıştır. Çıkış Raporlarında yer alan 4957 adet ESP malzeme kaydı kullanılarak, motor (1111 adet), pompa (1614 adet), intake (607 adet) ve seal (1625 adet) için runlife değerleri hesaplanmıştır.



### 1-) ESP YER ALTI ARIZALARI ve DAĞILIMI

Yeraltı arızası nedeniyle yapılan toplam 1732 adet ESP çıkış operasyonunun, 1013 adedi Adıyaman, 453 adedi Diyarbakır ve 266 adedi Batman Bölgelerinde gerçekleştirilmiştir. Arıza dağılımı incelendiğinde (Tablo-1) %57'lik kısmının (980 adet) kablo+motor+pompa arızalarından oluştuğu görülmektedir. Arızaların %11,5'lik kısmını intake+seal+tubing oluştururken geriye kalan %31,5'lik kısmını yeniden tamamlama, ESP dizisi küçültme/büyütme, check valve arızası, bleeder valve arızası vb. nedenlerden dolayı yapılan operasyonlar oluşturmaktadır.

Üretici firmalara incelenmek üzere gönderilen az sayıda malzemelerin haricinde diğer arızalı malzemelerin açılarak iç kısımlarında ayrıntılı bir inceleme yapmamız mümkün olmadığından, arıza tespiti dışarıdan görsel ve elektriksel ölçme yöntemiyle yapılmaktadır. Bu yöntem bazen yanlış sonuçlar elde etmemize neden olabilmektedir. "Motor Arızası" olarak belirtilen arızaların bir kısmının asıl nedeni seal, pompa, intake ya da kablo olabilirken, aynı şekilde "Kablo Arızası" olarak belirtilen arızaların bir kısmının asıl nedeni ise motor ya da pompa arızası olabilmektedir.

### 2-) KUYU ŞARTLARI ve MAYI ÖZELLİKLERİ

ESP ile üretim yapılan kuyulardaki pompa derinlikleri, mayı özellikleri, kuyu dibi sıcaklıkları ve debileri, Adıyaman, Diyarbakır ve Batman Bölgelerinde farklılıklar göstermektedir (Tablo-2, Grafik-1, Grafik-2, Grafik-3 ve Grafik-4).

Adıyaman Bölgesi, ortalama 1836 m üretim derinliği ve ortalama 229 F mayı sıcaklığı ile en zorlu kuyu şartlarına sahiptir. Bu durum Diyarbakır Bölgesinde ortalama 1548 m ve 154 F ve Batman Bölgesinde ortalama 1517 m ve 162 F ile daha iyi bir durum göstermektedir.

Petrol gravitesine bakıldığında, Diyarbakır'ın 30,4 API ile en yüksek ortalamaya sahip olduğu görülmektedir. Gravite, Adıyaman'da ortalama 27 ve Batman'da 22,2 API değerindedir.

### 3-) ESP MALZEMESİ KULLANIM ÖMÜRLERİ (RUNLIFE)

Motor, Pompa, Intake ve Seal için Adıyaman, Diyarbakır ve Batman Bölgelerinde, 35 yıllık sürecin, daha fazla önem arzettiği için son 22 yıla ait bilgileri gösteren (2000-2022 yılları arası) "Yıl Sonu Runlife", "Dağılım" ve "Operasyon Sayısı" grafikleri hazırlanmıştır.

#### 3.1-) Motor Kullanım Ömürleri

ESP motorları için hazırlanan grafikler (Grafik-5, 6 ve 7) incelendiğinde; runlife (RL) değerinin sürekli olarak arttığı görülmektedir. 2000'de 2.16 yıl olan ortalama RL değeri, 2022'de 3.95 yıla yükselmiştir. Adıyaman'da 3.61 yıl, kuyu şartlarının daha uygun olduğu Diyarbakır'da 4.45 yıl ve Batman'da 4.19 yıla ulaşmıştır. 9 defa kuyuya indirilen ESP motoru bulunmakla beraber, en fazla RL değeri Diyarbakır

bölgesinde 1 defa kuyuya indirilen ve toplamda 23.10 yıl çalışan motora aittir.

#### 3.2-) Pompa Kullanım Ömürleri

ESP pompaları için hazırlanan grafikler (Grafik-8, 9 ve 10) incelendiğinde; runlife (RL) değerinin sürekli olarak arttığı görülmektedir. 2000'de 3.29 yıl olan ortalama RL değeri, 2022 yılında 5.58 yıla yükselmiştir. Adıyaman'da 5.11 yıl, kuyu şartlarının daha uygun olduğu Diyarbakır'da 6.21 yıl ve Batman'da 6.18 yıla ulaşmıştır. 12 defa kuyuya indirilen ESP pompaları bulunmakla beraber, en fazla RL değeri Diyarbakır'da 1 defa kuyuya indirilen ve toplamda 23.10 yıl çalışan pompaya aittir.

#### 3.3-) Intake Kullanım Ömürleri

ESP intake'leri için hazırlanan grafikler (Grafik-11, 12 ve 13) incelendiğinde; runlife (RL) değerinin sürekli olarak arttığı görülmektedir. 2000'de 2.46 yıl olan ortalama RL değeri, 2022 yılında 5.60 yıla yükselmiştir. Adıyaman'da 5.15 yıl, Diyarbakır'da 6.91 yıl ve Batman'da 4.97 yıl olarak gerçekleşmiştir. 11 defa kuyuya indirilen ESP intake bulunmakla beraber, en fazla RL değeri Diyarbakır'da 1 defa kuyuya indirilen ve toplamda 23.10 yıl çalışan intake'e aittir.

#### 3.4-) Seal Kullanım Ömürleri

ESP seal'leri için hazırlanan grafikler (Grafik-14, 15 ve 16) incelendiğinde; runlife (RL) değerinin sürekli olarak arttığı görülmektedir. 2000'de 1.42 yıl olan ortalama RL değeri, 2022 yılında 2.80 yıla yükselmiştir. Adıyaman'da 2.47 yıl, kuyu şartlarının daha uygun olduğu Diyarbakır'da 3.46 yıl ve Batman'da 3.06 yıla ulaşmıştır. 9 defa kuyuya indirilen ESP seal bulunmakla beraber, en fazla RL değeri Diyarbakır'da 1 defa kuyuya indirilen ve toplamda 23.10 yıl çalışan seal'e aittir.

### SONUÇLAR

ESP üretim dizisinin temel malzemeleri olan motor, pompa, intake ve seal runlife değerleri incelendiğinde, sürekli olarak bir artış olduğu görülmektedir. Özellikle 2011 yılına kadar daha yüksek artış ivmesi izlenirken, bu yıldan sonra ivmede azalma, hatta Batman ve Diyarbakır bölgelerinde negatif yönde trentler görülmüştür. Bu trent değişiminin nedenleri Diyarbakır bölgesinde Perenco firmasından devralınan kuyularda yapılan yeniden tamamlama, jel operasyonları, kullanım ömrünü doldurmuş pompaların yenileriyle değiştirilmesi, Batman bölgesi Raman sahasında yapılan jel operasyonlarına bağlı pompa değişiklikleri ve üretim artışı projesi kapsamında ESP ile üretilmeye başlanan kuyulardır.

Yazının giriş bölümünde ki sorularımıza cevap verecek olursak;

- Daha fazla para vererek aldığımız geliştirilmiş ürünler, gerçekten beklentilerimizi karşılayabiliyor mu? Motor, pompa, intake ve seal RL değerlerinde görülen sürekli

artış beklentilerimizi karşıladığını göstermektedir.

- Kuyu şartları ve mayi özellikleri, malzeme kullanım ömrünü ne kadar etkiliyor? Adıyaman, Diyarbakır ve Batman bölgelerindeki RL değerleri karşılaştırıldığında, çok net bir ayırım olduğu görülmektedir. Kuyu derinliklerinin sıg, sıcaklığın düşük, casing çaplarının dar ve üretim debisinin yüksek olduğu (daha iyi motor soğutması sağlıyor) Diyarbakır ve Batman bölgelerinde çok daha yüksek RL değerleri görülmektedir.

- Yer üstü kontrol ekipmanları, malzeme kullanım ömrünü ne kadar etkiliyor? ESP sistemine kesintisiz ve düzenli enerji verildiğinde arızalanma riski azalmaktadır. Bunu sağlamak amacıyla SWB (switchboard) kullanımı azaltılarak yerine VSD (variable speed driver) kullanım oranı artırılmaktadır. Bu sayede ESP dizisine düzenli enerji verilmekle birlikte aynı zamanda da kuyuda dizi değişikliği yapmadan daha geniş üretim aralığında çalışma imkânında kazanılmaktadır.

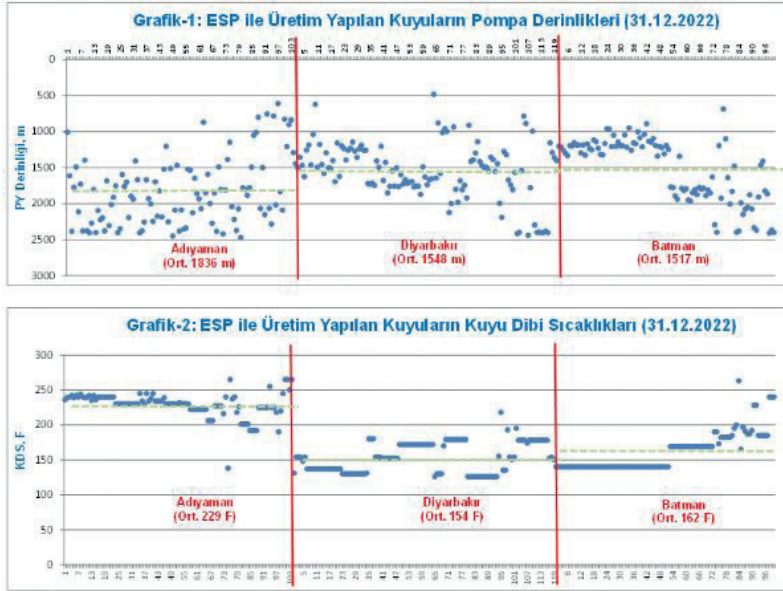
- Malzeme seçiminde ne kadar isabetli kararlar veriliyor? Nadiren de olsa yetersiz veriden kaynaklı hatalı dizaynlar yapılabilmektedir. Bu durumların çoğu önceden tahmin edilebildiği için, oluşabilecek sorunları engelleyecek tedbirler alınarak VSD ile geniş üretim aralıklarına sahip dizaynlar yapılmaktadır. Satın alınacak malzemeler ve tedarikçi firmalar seçilirken, en zor kuyu şartlarına uygun malzemeler ve ürünleri denenip olumlu sonuçlar alınmış firmalar tercih edilmektedir. Bu çalışma sonucunda malzemelerin RL değerlerinde görmüş olduğumuz sürekli artış, yapılmakta olan uygulamanın doğruluğunu göstermektedir.

- İşletmecilik, malzeme kullanım ömrünü ne kadar etkiliyor? İşletmeciliğin malzeme ömrü üzerinde çok etkili olduğu kesindir. Düzenli yapılan yerüstü kontrolleri, yük kartı takip ve yorumları, kuyu mayi seviyesi, üretim testi, numune analizleri vb. sayesinde muhtemel pek çok arıza oluşmadan tespit edilmekte ve gerekli önlemler alınmaktadır. İşletmeciliğin iyi yapılmadığı yerlerde çok daha fazla arıza görülecek ve malzeme RL değerleri düşecektir.

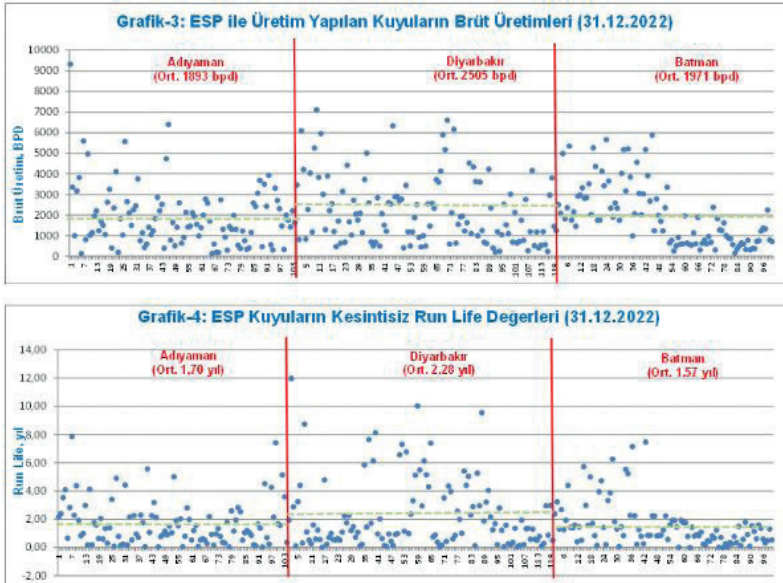
ESP sistemi malzeme seçimi, pompa dizaynı, iniş/çıkış operasyonu, işletmecilik, malzeme takibi, stoklama, sorunların incelenmesi, kendisini kanıtlanmış firmalarla çalışma, zamanında malzeme temini gibi pek çok konu başlığını barındırmaktadır. Bu konularda Adıyaman, Batman ve Diyarbakır bölgelerinde uygulanmakta olan dikkatli ve titiz çalışmanın olumlu sonuçlarının alındığı görülmektedir.

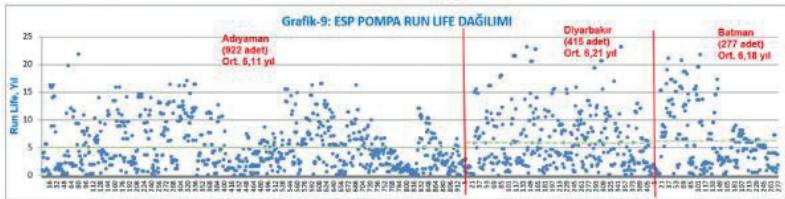
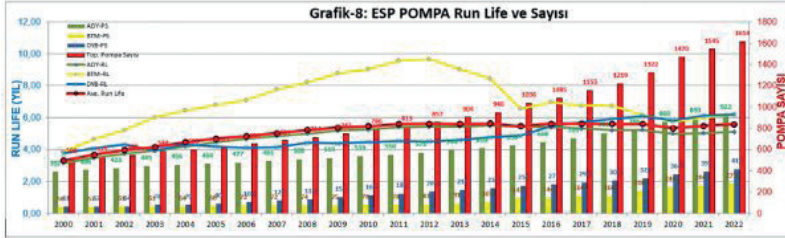
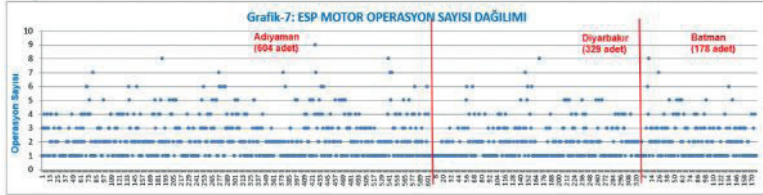
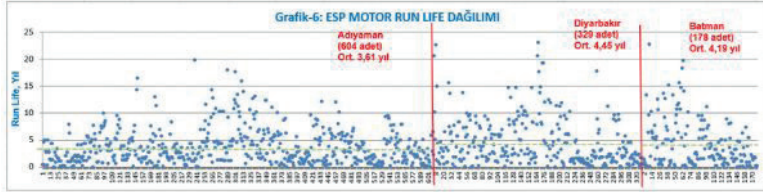
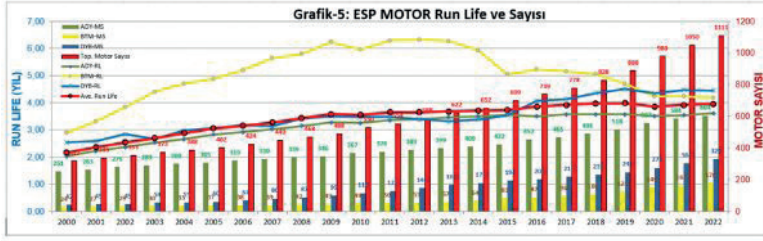
Anahtar Kelimeler: ESP RUNLIFE

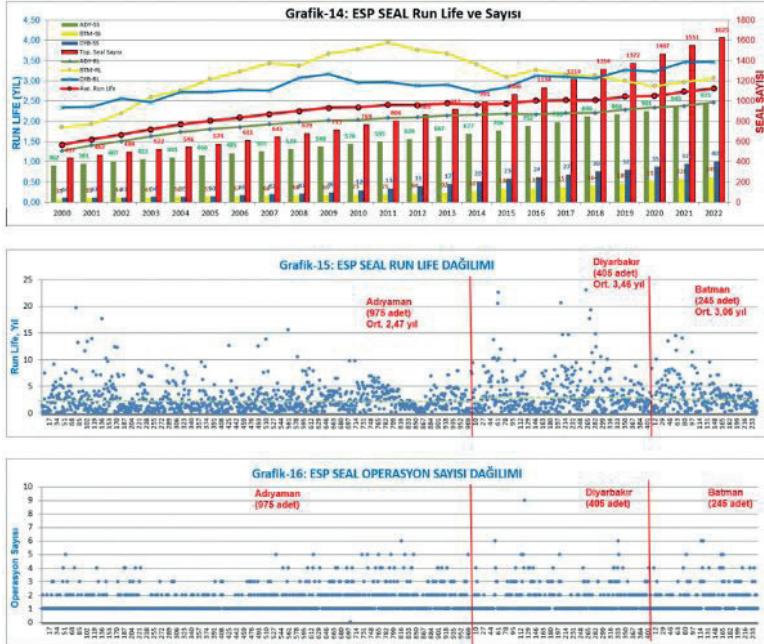
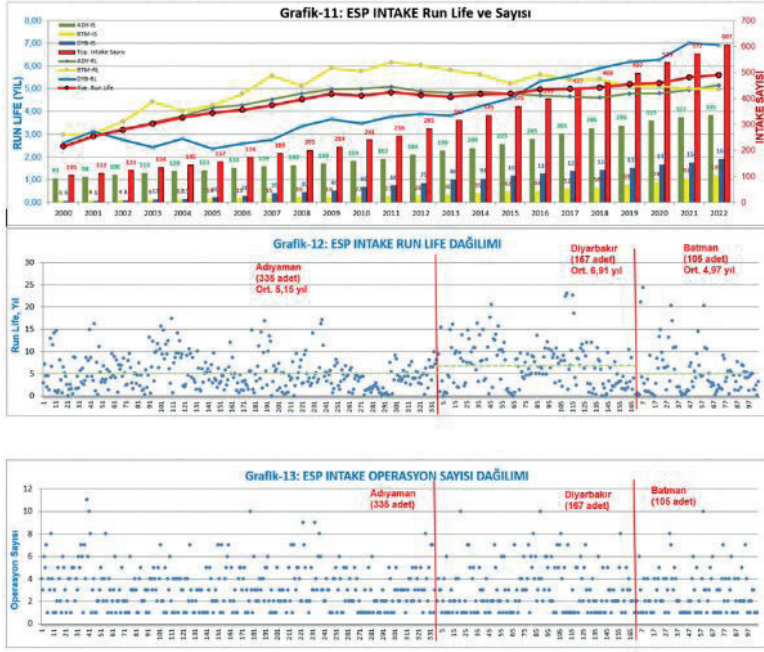
Grafik-1 &amp; 2



Grafik-3 &amp; 4







<b>Tablo-1: ESP Arızalarının Bölgelere ve Türlerine Göre Dağılımı (1987-2022)</b>															
	Arıza Sayısı	Kablo		Motor		Pompa		Intake		Seal		Tubing		Diğer	
		Arıza	Oran	Arıza	Oran	Arıza	Oran	Arıza	Oran	Arıza	Oran	Arıza	Oran	Arıza	Oran
Adıyaman	1013	249	25%	232	23%	91	9%	17	2%	5	0%	148	15%	271	27%
Batman	266	66	25%	67	25%	12	5%	1	0%	1	0%	8	3%	111	42%
Diyarbakır	453	102	23%	130	29%	31	7%	2	0%	5	1%	16	4%	167	37%
Toplam	1732	417	24%	429	25%	134	8%	20	1%	11	1%	172	10%	549	32%

<b>Tablo-2: Bölgelerin Kuyu Şartları ve Mayi Özellikleri</b>						
	Kuyu Sayısı	Ort. Üretim Derinliği, m	Ort. Mayi Sıcaklığı, F	Ort. Brüt Üretim, BPD	Gravite, API	Casing OD, inch
Adıyaman	104	1836 (750-2400)	229 (118-265)	1893 (125-9324)	27 (19-38)	6 <sup>5</sup> / <sub>8</sub> " - 9 <sup>5</sup> / <sub>8</sub> "
Diyarbakır	119	1548 (882-2450)	154 (126-218)	2505 (230-7100)	30,4 (24-38,5)	6 <sup>5</sup> / <sub>8</sub> " - 9 <sup>5</sup> / <sub>8</sub> "
Batman	100	1517 (689-2411)	162 (140-265)	1971 (3150-5650)	22,2 (18-42,5)	5" - 9 <sup>5</sup> / <sub>8</sub> "

# Wireless Monitoring of Artificial Lift Wells – Techno-Commercial Feasibility of GEOEM Wireless Well Monitoring



**Aastik Saluja, Nick Nazarovs**

Geo Pressure Systems Inc. (GEO PSI), Calgary / Canada

## ABSTRACT

With the ever-increasing need for cost-effective actionable data and the explosion of digital oilfield initiatives, O&G operators continuously search for innovative technology solutions that deliver significant value and operational performance.

The global conventional Brownfield Investment for 2023 is close to \$200 Billion, and further spending is estimated to remain stable toward the end of the decade.<sup>1</sup> With such a colossal investment, access to innovative yet cost-effective technologies will be vital in maximizing the NPV of existing well assets.

One such innovative solution supporting the industry's push toward increased digitalization is GEOEM, a wireless downhole monitoring solution developed as a high-performance, cost-effective alternative to wired-based systems.

With the help of pilot trial studies and successful commercialization in more than 150 wells onshore Australia, this paper seeks to support the proposition that downhole pressure monitoring solutions utilising wireless telemetry can be reliable and cost-effective.

## INTRODUCTION

Numerous studies have conclusively proven the advantages of real-time downhole data over derived values based on surface measurements or production and reservoir simulations. It is widely accepted that analysis uncertainties will be significantly less when using direct in-well measurements rather than indirect or modelled values. The reality is that direct, in-well real-time measurement is the best solution<sup>2</sup>.

Operators in Australia have historically adopted a strategy of installing a wired gauge system in every well. To date, there are approximately 15,000 wells drilled and completed that incorporate downhole gauges. Well depths vary from 450m to 1,400m and typically utilize 7" production casing. The well completions incorporate Progressive Cavity Pumps (PCP) as the primary form of artificial lift, although Linear Rod Pumps (LRP) are being deployed more frequently as wells age. Workovers can be frequent, as soon as six months after initial completion. However, there are now wells with expected pump run lives of more than five years. The mean time to workover (MTTW) is also continually increasing as refinements to well design, equipment design, well intervention practices and operation are rolled out, with MTTW expected to extend out to 6 years.

The key drivers for implementing a gauge in every well strategy is to maximize production, while at the same time protecting the pump, thereby maximizing production uptime. While the 'gauge in every well'

strategy has been phenomenally successful, the continuously changing well production profile over time poses challenges to well intervention and workover practices during later well life.

Intervention challenges exist because some reservoirs cannot hold suitable columns of kill fluid during workover activity, while often decreased production is a post-workover reality due to formation impairment. The decreased production is thought to occur due to the sensitivity of the reservoirs to nonnative kill fluids.

Due to these challenges, some Operators have moved towards snubbing-based workovers. However, snubbing equipment and practices preclude the ability to incorporate cabled downhole gauge solutions on the outside the production tubing. As such, while cable-based downhole gauges have been phenomenally successful and cost-effective, Operators have been motivated to identify a suitable wireless in-well monitoring solution that can be deployed during live well workovers.

## Technical Specifications

### What's different from a Wired System

The working principle of a wireless system is entirely different and highly complex from a conventional wired system, but this paragraph covers a basic outline of the working principle. The significant difference between the two systems is the inbuilt battery in the wireless tool that powers it for data capture & transmission. In this case, it is powered by a lithium battery to take measurements at pre-determined sampling intervals and sends them through a low-frequency electromagnetic (EM) signal that propagates through the overburden surrounding the well to the surface. A surface receiver connected to the ground aerial detects and decodes the EM signals and outputs the extracted measurements to the wellsite RTU or local data acquisition system using Modbus RS485 or other industry protocol.

Refer below Figure 1 for a visual schematic of the GEOEM working principle for Data Transmission. GEOEM uses the same Piezoresistive pressure and temperature transducer as wired gauge systems. Table 1 below summarises technical specifications of the GEOEM tool.

### Optimization of Battery Life- Longer Downhole Runs

The biggest challenge for wireless or battery-operated Downhole tools is to function for longer durations and provide Real-Time Data till a planned Workover is in place. While wire-based downhole gauge systems have access to unlimited power and, therefore, no

limitation on measurement frequency, wireless-based systems must delicately balance available battery current capacity, transmitter power requirements, and transmit frequency to meet the life of Well monitoring requirements.

Transmit frequency has a direct bearing on battery operating life. Simply put, the faster the transmit rate, the faster the battery depletes. GEOEM utilizes two methods of managing transmit rate. The first and most simplistic method is termed the ‘data-on-time’ ( $\Delta T$ ) mode, whereby the tool is programmed to transmit a reading at a fixed, user-specified time interval. Refer to Table 2, which highlights GEOEM Battery Life Estimation based on Sampling Rate ( $\Delta T$  Mode)

The second, more sophisticated method is termed the ‘data-on-demand’ ( $\Delta P$ ) mode, whereby the tool is programmed to transmit a reading only when in-situ pressure changes by more than “X” psi or after “Y” hours, whichever is sooner. In this mode, end users obtain data when they need it the most, i.e., during well startup, following pump speed changes and after well shutdowns. However, measurements are transmitted infrequently during pseudo-steady-state production conditions

This conserves battery life and, in so doing, greatly extends system operating life.

Table 3 below provides a theoretical estimation of the reduction in signal transmission due to the application of the  $\Delta P$  mode. For example, it illustrates that a 0.72 psi  $\Delta P$  trigger would decrease the total amount of samples sent in this period by 5,218 or 83.4% of total samples. This equates to a significant saving in battery life.

## CUSTOMER BENEFIT

The transition from wired to wireless downhole monitoring delivers a number of tangible customer benefits, including life-of-well cost savings, increased operational efficiency, improved gauge reliability, reduced HSE risk profile, better Environment Social Governance (ESG), higher local content, and simplified, circular supply chain.

Improved gauge reliability stems from the placement of the entire GEOEM system below the pump, remote from the shock and vibration induced by the rod string above the pump. Shock and vibration are the leading cause of wired gauge system failures, as the pressure gauge and instrument cable are also situated entirely above the pump.

Incorporating a GEOEM system in the PCP completion eliminates retrieving and installing downhole instrument cables, cable clamps, and tubing hanger cable penetration systems during Well workovers. This reduces Well re-completion times and, thus, reduces the kill fluid volume requirements and rig time—this improvement in operational efficiency results in direct rig cost savings.

A reduction in the HSE risk profile stems from the removal of gauge installation personnel from the rig floor after make-up of the GEOEM BHA. Furthermore,

the elimination of downhole instrument cable removes HSE exposure related to pinch points, sharp objects, manual handling, overhead equipment, and pressure testing.

In today’s world, a focus on ESG is essential. Wireless-based downhole monitoring systems improve clients’ ESG goals by eliminating the need for cable and clamps in the well. While cable and clamps can be reused during well workovers, they do eventually Favourable ESG have to be replaced, with replacement frequency dependent on severity of in-situ conditions. In worst-case scenarios, the cable and clamps are having to be replaced during every workover. Furthermore, it is not possible to recycle discarded instrument cable, due to the external thermoplastic encapsulation. The cable is instead dumped in landfills. In contrast, all components of the GEOEM system, except for the battery pack, can be reused throughout well life. Based on the bill of materials for a typical wired gauge system, use of a GEOEM system instead results in a carbon reduction of ~450kg per system, and no landfill.

Lastly, there are tangible life-of-well cost benefits. The cost benefits relate to both improved installation efficiency above and life-of-well reduction in equipment replacement costs described above.

## INSTALLATION SUCCESS

There have been 155 successful GEOEM installations in Australia on PCP and LRP completions. Refer to Table 4 below highlighting the Installation Summary and completion type details for installed GEOEM systems.

### Case Study 1 – Wired vs Wireless Data Accuracy

During the technology pilot phase, Operators wanted to validate the accuracy of wireless GEOEM gauges against traditional wired gauges. In two wells, a traditional wired gauge system was installed above the pump and a GEOEM gauge below the pump. Figure 2 below is a plot of pressure data acquired from both systems in one of the wells. The plot clearly shows that the pressure data received from the GEOEM gauge correlates precisely with the pressure data from the shallower-set wired gauge. The plot also demonstrates the much better resolution of the GEOEM pressure gauge data.

### Case Study 2 – Sample Management - $\Delta P$ & $\Delta T$

Data from another GEOEM pilot well was utilised to illustrate the power of the  $\Delta T$ , and  $\Delta P$  transmit management tools. The plot in Figure 3 below shows bottom-hole pressure data from a GEOEM gauge programmed to transmit readings whenever the pressure changed by more than two psi ( $\Delta P$ ) or after every 3-hours; whichever was sooner. In this mode, the GEOEM system transmitted a total of 4,512 pressure readings during the ~1-year period covered by the plot. Had the GEOEM gauge instead been programmed to transmit readings at fixed 1-hr intervals, using the



$\Delta T$  mode, it would have transmitted a total of 11,143 samples during the same period. Use of the  $\Delta P$  mode therefore resulted in a 59.5% reduction in the number of transmitted readings, significantly increasing battery run life.

### Case Study 3 – Production Optimization

Data acquired from another pilot study was also utilised to compare the flowing bottom hole pressure (FBHP) acquired from above-pump wired based gauges and below-pump GEOEM gauges. Production optimisation focuses on maximising drawdown and production uptime by not risking the pump-off condition. Installing GEOEM systems accomplishes this objective more effectively because it enables the annulus fluid level to be pulled down lower towards the pump inlet. While the data plot of this data is confidential, and cannot be distributed, it clearly demonstrated that after installing GEOEM systems in a number of wells, the Operator was subsequently able to apply a lower FBHP than was possible using wired gauges following previous well workovers. The higher drawdown applied resulted in increased gas production, boosting well NPV.

### Case Study 4 – Life of Well Cost Saving

Outside of the normal technical considerations comparing wired and wireless downhole monitoring solutions, the life-of-well cost saving should be a consideration. While wire-based solutions seem more cost-effective for initial well completions, ongoing equipment replacement costs and slower installation times over the life of the well are likely to outpace the initial completion and subsequent workover costs utilising GEOEM systems. Table 5 below highlights some life-of-well cost considerations.

A recent confidential study concluded that significant life of well savings could be achieved migrating from wired-based to wireless GEOEM systems. Based on a typical well, and typical number of workovers performed over the well life, the total cost for GEOEM systems would be ~75% of total cost for wired systems. These savings consider the extra rig time, and thus rig cost, incurred retrieving and re-installing wired gauges, and the far higher percentage of wireless gauge components that can be reused and recycled compared to wired gauge systems. While confidential in nature, 5-figure per well cost saving results in an 8-figure cost saving over the life of 1000+ wells.

### CONCLUSION

The above examples establish the techno-commercial viability of installing a Wireless monitoring solution in artificial lift Wells. Case Study 1 & 2 indicates the technical feasibility of this technology in line with the Operator's requirement of getting seamless data monitoring, while Case study 3 & 4 highlights the commercial viability, and production optimization, indicating overall value addition to the project.

### REFERENCES

- [1]- Palzor Shenga, Rystad Energy 2023, Commentary: 2023 Global Conventional Brownfield Investment to Near \$200 Billion < <https://www.hartenergy.com/ep/exclusives/commentary-2023-global-conventional-brownfield-investment-near-200-billion-204283>>
- [2]- Gonzalez, L. E., Chokshi, R. N., Gonzales, R. O., Adams, T (2016) Lessons Learned in Permian Gas-Lift Shale Wells: Dynamic Production Analysis With Downhole Gauge, Society of Petroleum Engineers, June 2016. Doi: 10.2118/180949-MS

Keywords: Wireless Monitoring

Figure 1: A visual schematic of the GEOEM working principle for Data Transmission

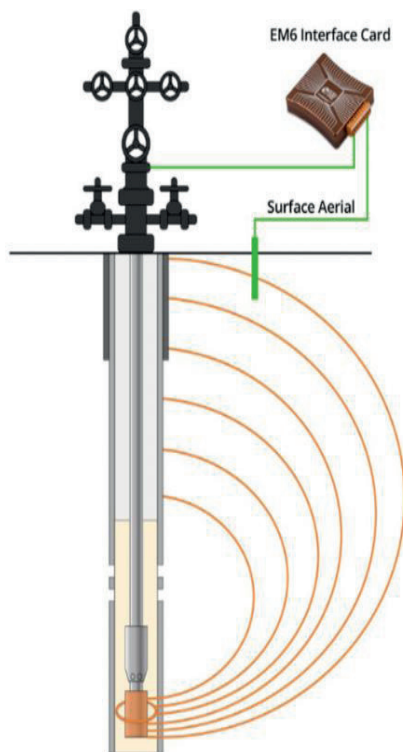


Table 1: Technical Specifications of GEOEM Wireless Monitoring System

Measurement	Pressure, Temperature, Vibration, Inclination
Maximum Pressure	Up to 10,000 psi
Maximum Temperature	Up to 125°C
Pressure Sample Rate	30 seconds - 1 Day
Temperature, Vibration Sample Rate	10 Minutes - 1 Week
Pressure Accuracy	0.05% Full Scale
Pressure Resolution	0.04 psi
Temperature Accuracy	±1°C
Temperature Resolution	0.1°C

Table 1 summarises technical specifications of the GEOEM tool.

Table 2: GEOEM Battery Life Estimation based on Sampling Rate ( $\Delta T$  Mode)

Sample Rate	Samples / Day	Battery Life / Months	Total Samples
30 Seconds	2,880	0.6	53,243
1 Minute	1,440	1.2	53,061
10 Minutes	144	11.4	49,984
30 Minutes	48	21.4	31,305
1 Hour	24	51.8	37,805
6 Hours	4	126.2	15,355
12 Hours	2	147.4	8,966
24 Hours	1	160.9	4,894

GEOEM Battery Life -  $\Delta T$  Sample Mode

Table 3: Showcasing theoretical estimation of transmitted samples for corresponding  $\Delta P$  values.

$\Delta P$ Trigger	Transmitted Records	% Samples Sent
Base Case, No Trigger	6,258	100%
0.14 psi	2,598	41.5%
0.72 psi	1,040	16.6%
1.45 psi	954	15.2%
2.9 psi	940	15%

GEOEM  $\Delta P$  Sampling

Table 4: Installation Summary and types of completion details for installed GEOEM systems

Total Installations	155
Total Days Deployed & Working	37,938
PCP Completions	134
LRP Completions	21
Longest Operating System	742 days
Deepest System Depth	1412.86m RKB
Maximum Well Deviation	80 degrees
Systems using $\Delta T$ Mode	133
Systems using $\Delta P$ Mode	22

GEOEM Installation Summary

Figure 2: Plot Showcasing Pilot well run with simultaneous Wired & Wireless pressure datasets.

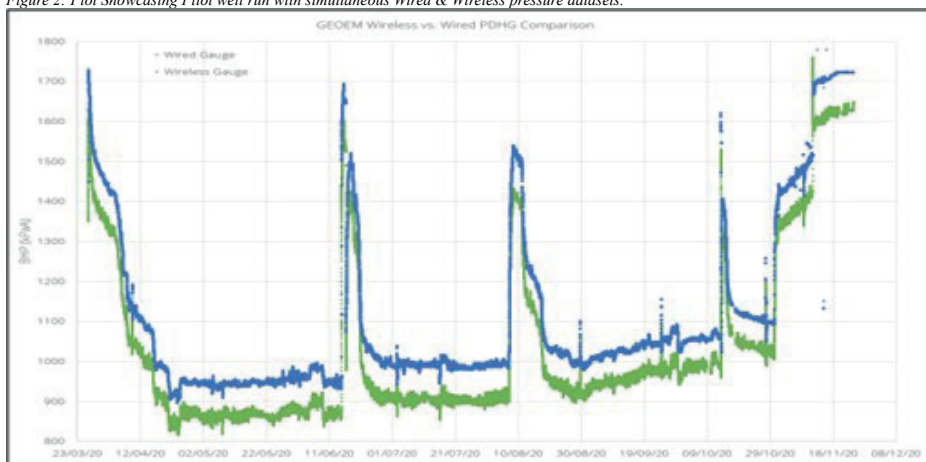


Figure 3: Plot showcasing a  $\Delta P$  &  $\Delta T$  run highlighting sample statistics and battery optimization.

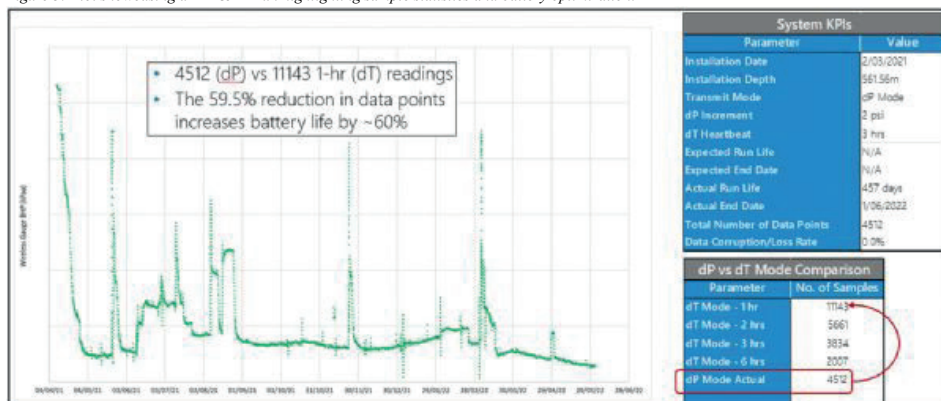


Table 5: Highlighting the Life-of-Well Cost-Saving Potential

Equipment on Workover	No Replacement Cable and Clamps
Wellhead and Tubing Hanger Cost	No Ports, No WHFT
Personnel Costs and Support	Decreased Personnel and Support Cost
Intervention Costs – RIH / POOH	Speed Increased
Intervention Costs - Fishing	No Fishing for TEC and Clamps

GEOEM Life-of-Well Cost Considerations

# Integrated Artificial Lift Optimization Workflow And New Technologies Implementation Helps Improving Reciprocating Rod Pumping Performance on Heavy Oil Fields, Onshore Romania



**Gheorghe Ditoiu, Vasile Mogos**

Endurance Lift Solutions International, Romania

## 1 INTRODUCTION

It is well known worldwide that producing heavy oil wells poses numerous operations challenges from artificial lift standpoint. In case of reciprocating rod pumping, challenges might include but not limited to low pump fillages/efficiencies, premature pump failures due to high solids content, subsurface equipment corrosion, gas interference/lock, plunger fall issues, etc.

Optimizing reciprocating rod lift performance in such conditions requires an integrated approach, operator – artificial lift contractor, and careful design and selection considerations for both surface and subsurface components to achieve maximum production rate and maximize the run life.

The presentation will focus on describing the integrated optimization workflow introduced lately and on the most effective reciprocating rod lift solutions and improvements implemented on heavy oil fields, onshore Romania, as result of the integrated optimization approach.

At the end it will also show the results related to mean time between intervention performance improvements got so far.

Following topics will be addressed in more details:

- Subsurface pump corrosion mitigation solutions.
- Dedicated pump designs and solutions for heavy oil applications.
- Optimizing operating parameters - pump stroke optimization.
- Rod pumps and pump components tracking solutions.
- Pumps KPI monitoring
- Fields Results

## 2 HEAVY OIL FIELD DATA

Reciprocating rod pumping system is being almost exclusively used for producing over 500 heavy oil wells on in Romania.

The wells produce 12 – 18 API oil density from shallow reservoirs, relatively low production rates and high content of produced solids. The reservoir depths vary from 200 to 500 m TVD but there are applications on different fields with reservoirs averaging 1000 m TVD. Most of the production and injection wells are vertical but there are slanted, and horizontal wells as well.

Figure 1: Heavy oil analysis

(Crude oil analysis report, well XY, April 2022)

The heavy oil reservoirs are exploited in both cold and thermal production (cyclic steam injection and

underground fireflood) and therefore the production parameters may vary greatly from well to well or, even in the same well, depending on reservoir conditions and production patterns.

Producing heavy oil together with associated water from the reservoir can create emulsions, which, due to elevated viscosities, can make things worse from the artificial lift performance perspective – particularly causing lower pump efficiencies on standard API pump designs, sucker rod string floating issues, lower subsurface equipment run life, etc.

Viscosity of emulsions can be substantially greater than the viscosity of either the oil or the water because emulsions behave as non-Newtonian fluids. This behavior is a result of internal droplet structure and structural viscosity. The viscosity of emulsions depends on several factors: viscosities of oil and water, volume percent of water in the liquid, oil or water droplet-size distribution, temperature, shear rate and amount of solids present in the produced liquid.

Microscopic and rheological analysis performed of different types of emulsions on the largest heavy oil field, onshore Romania, shows that the droplets sizes vary from 10 to 65  $\mu\text{m}$ . The appearance, colour and the droplet-size distribution, divided the samples in two categories (Figure 2) - brightness pictures with light colour, and water droplets sizes < 40  $\mu\text{m}$  and dark pictures and less bright, with water particle sizes > 50  $\mu\text{m}$ : - the emulsions from the West area have a brighter appearance than the East area, and are finely & medium dispersion - the emulsions from the East are medium & coarse dispersion. Fine emulsions have much higher viscosities than the corresponding coarse emulsions.

Figure 2 Microscopic analysis of emulsions on heavy oil field

(Technical report, ICPT Campina, 2022)

Figure 3 shows that the viscosity of the emulsion can be substantially higher than the viscosity of the oil or water at a given temperature. The emulsion viscosity increases initially with the increases of the water content, reaches a maximum at around 80 % water content then, the type of emulsion inverts from water in oil to oil in water and emulsion viscosity starts to drop sharply toward the water viscosity. Temperature has a significant effect on emulsion viscosity. Figure 3 below shows an example of the effect of temperature on emulsion viscosity. Emulsion viscosity decreases with increasing temperature (the data have been plotted on a semi log scale).

Figure 3 Viscosity of emulsions (Sunil L. Kokal, Saudi Aramco – 2006 Petroleum Engineering Handbook— Vol. I Crude Oil Emulsions)

The ratio of the viscosity of an emulsion to the viscosity of the virgin crude oil at the same temperature can be approximated by the following equation.

$$\mu_e/\mu_o = e^{5\Phi} (1 - 3\Phi + a\Phi^2)$$

where  $a$  is the factor for the type of emulsion,  $\mu_e$  is the viscosity of emulsion,  $\mu_o$  is the viscosity of clean oil at same temperature, and  $\Phi$  is water cut or fraction of water. The value of  $a$  varies depending on the type of emulsion: 7.3 for very tight emulsion, 5.5 for tight emulsion, 4.5 for medium emulsion, 3.8 for loose emulsion, and 3.0 for very loose emulsion.

Using the above equation and graph, the fluid viscosity for downhole conditions can be easily estimated and can provide a better image regarding the pumped fluid conditions.

Underground firefloods generate a lot of combustion gases that together with the associated free gas causes gas interferences/lock in the reaction wells and can negatively affect the standard pump design performances. The produced gas and water contain have high corrosion potential affecting the subsurface equipment especially pumps with standard metallurgies.

Furthermore, another effect of the underground fireflood is partial oxidizing of crude oil. The partially oxidized crude oil is denser and much more viscous than the original crude oil posing additional issues on recovery and artificial lifting performance.

### 3 INTEGRATED ARTIFICIAL LIFT OPTIMIZATION WORKFLOW

The optimization workflow implemented lately addresses the entire artificial lift system including both subsurface and surface equipment. It supposes a more involvement of the artificial lift service contractor in the Artificial Lift optimization activity. Presentation will highlight more the artificial lift contractor side in the optimization workflow.

The artificial lift contractor involvement in the optimization workflow can be split on 3 main parts: Pump shop services, AI optimization & engineering support, and inventory management & equipment supply.

Regarding pump shops services their quality and complexity have been constantly enhanced. Now, contractor pump shops, besides performing regular equipment maintenance, repairs, and inspections services, has been expanded and now the services include but not limited to reviewing pumps history, making recommendation for pump solution improvements, recording data, reporting pump findings and other critical information gathered. This information is then used for performing advanced root cause failure analysis at frequent failure wells or other regular pump and artificial lift optimization reviews.

On the Artificial Lift optimization & engineering support services side, depending on the application, contractor inputs might include:

- Selecting and proposing optimum Artificial Lift and/

or pump solution

- Optimizing Rod Pump Design and Operation
- Trouble shooting problematic wells
- Ensure Proper Operating Procedures
- Performing advanced pump Root Cause Failure Analysis

On the inventory management service side, contractors have taken over the whole parts and equipment inventory and optimize it continuously, based on the field requirements. Taking over and optimizing the inventory resulted in a significant reduction of the inventory-related costs for the company. On the other hand, having the AL inventory in their hands, the contractor was able to optimize the service quality and improve the response to requirements from the field.

Figure 4: Artificial Lift Integrated Optimization Workflow

### 4 SUBSURFACE PUMP CORROSION MITIGATION SOLUTIONS

Following numerous pump inspection findings and produced water and gases chemical analysis was concluded that wells are prone to severe corrosion on standard pump metallurgies. The corrosion of the pump components is mainly caused by the salinity of produced water and high CO<sub>2</sub> content both in water and gasses production.

Corrosiveness of the produced fluids it was found to be increased at high GOR wells. It also was found that the corrosion tendency is higher in the area of free level liquid/gas. As the reservoir low pressure and low static fluid level the corrosion affected mainly the pumps themselves and surrounding areas reducing the run life of the pumps, increased the operational end user cost, generated production loss due to downtime for interventions. Also, the losses in production occurred due to premature pump efficiency drop down.

Figure 5: Pump shop findings – Corrosion impact on standard pump metallurgies

(Interface Upstream Application– Reports and Data)

To mitigate corrosion impact on standard pumps metallurgies AL service contractor recommended (NACE 0176 RP) and then implemented solution with corrosion resistant metallurgies which mainly consisted in:

- Brass barrels chrome plated
- Spray metal plungers with Monel or nickel-plated on ID
- Stainless steel (AISI 316L) fittings
- Valves with silicon balls and tungsten carbide seats

Figure 6: Corrosion resistant pump metallurgies

## 5 DEDICATED PUMP DESIGNS AND SOLUTIONS FOR HEAVY OIL APPLICATIONS.

Conventional API pumps proved to not produce the wells efficiently in heavy oil applications onshore Romania. As result there have been designed specialty pumps for such conditions. The aim was to minimize the pressure drops across the pump, maximize fillage and ultimately increase pumping efficiency. In this respect the specialty pump designs might include oversized standing valves, Box end plungers, HI flow insert cages, energized valve, optimized plunger fit, etc. Some of those features will be detailed further below.

### 5.1 “THE” Specialty Pump

One of the specialty pumps developed for heavy oil applications is “THE pump”. This pump is built to move the maximum amount of fluid. It is a tubing type with a B13 heavy wall barrel, but unlike the API TH Pump, it doesn’t use a retrievable standing valve (SV) assembly. The SV is connected to the tubing at the lower end of the barrel, rather than being cup or mechanically anchored on to the seating nipple. In this way the SV assembly length is minimized for a lower pressure drops

The “THE” specialty pump uses an oversize positive SV called Big Dog Cage. It gives the pump intake a much larger flow area compared with standard TH pump SV for a minimized pressure drop.

“THE” pump is designed with box end plunger for a larger flow area through plunger ID and lower pressure drop.

Figure 7: 20-1.75-THE SV vs 20-175 TH API standard pump SV

(1.75” THE pump has 2.5 times larger intake area that 1.75” API TH standard pump).

### 5.2 Energized valves

For deviated wells and high GOR applications the solutions identified to mitigate gas interference and low pump efficiencies caused by delays in closing standard valves was by using energized valves.

The energized valves use a spring-loaded support that guides the ball as it moves upward, then returns it quickly directly to the seat on the down stroke.

Figure 8: Energized valves

### 5.3 BLAZE Technology

Another improvement implemented solution was introducing BLAZE technology for hardening surface pump parts and other artificial lift equipment like sucker rod couplings, guides, pump setting nipples, etc., prone to mechanical wear, corrosion, abrasion or heat.

BLAZE is a completely new and unique method of Thermal Boron Diffusion (TBD) using a proprietary chemical formula to produce a slick, hard intermetallic ceramic boride layer on metal surfaces. In contrast to other surface treatments on the market such as hard

chrome, tungsten carbide thermal spray and boronizing, BLAZE excels in all areas, such as:

- Reduced coefficient of friction – permanent lubricity regardless of load.
- Highly resistant to abrasion–intermetallic ceramic nature means no risk of bonding break down, no increase in brittleness, excellent impact resistance.
- Corrosion resistance–impervious to fracking acids, H<sub>2</sub>SO<sub>4</sub>, HCL, Phosphoric, Chlorides, H<sub>2</sub>S and others.
- The BLAZE layer is 100% uniform where is deposited regardless of the part configuration. The layer can encapsulate an item or can be applied in select areas only.
- The layer averages 005”-.006” deep but will not affect original dimensions or surface finish (Ra/RMS) of apart (i.e., a surface with a1-Ra will have a1-Ra after BLAZE treatment).
- BLAZE is comprised of a single-phase layer of only Fe<sub>2</sub>B which sets BLAZE apart from all other types of thermal boron diffusion and the basis of the improvements listed above.
- Chemistry and processes are environmentally benign; no hazardous waste is produced.

The treatment resulted in up to 400 % run life improvement of the specific treated part.

## 6 OPTIMIZING PUMP OPERATING PARAMETERS - PUMP STROKE OPTIMIZATION

One of the key elements in optimizing reciprocating rod pumping in heavy oil applications is pump stroke optimization. Three main category measures have been implemented for optimizing pump stroke on heavy oil fields, onshore Romania:

### 6.1 Well Automation

Well Automation, besides local, standard automation (RPC, VSD and related accessories), it includes real time data transmission and remote monitoring and optimization. Most reciprocating rod pumped wells are fully automated for optimizing production and minimizing equipment failures.

### 6.2 Linear Rod Pumping

After a comprehensive review of the specific literature and performing successful field trials, linear rod pumping units (LRP) have been selected for driving reciprocating pumps on heavy oil fields, onshore Romania.

These pumping units, being more flexible in operation (operate at lower SPM, SL can be adjusted easier, have lower inertial effect on pumps plunger, requires less power on startups, etc.) made them a better option versus conventional beam pumping units for producing shallow heavy oil wells.

Besides the above-mentioned advantages, LRP pumping units through their Pump of Controller have some others useful features such as:

- Automatic pumping speed control as function of pump fillage and/or pump submergence - this feature recommends them for cyclic steam injection wells where the production starts with high flow rate and becomes very low at the end of the process.
- Measurement of power consumption and total run time.
- Calculates pumping fluid.
- Possibility of setting a minimum and maximum value for pumping speed (in order to prevent sand flowing in the well).
- Basic data transmission (flow rate value, pumping speed, power consumption, surface and down hole dynamometer card, maximum and minimum pump and sucker rod load, failures, and events).
- Automatic restart after power failure.
- Individual adjusting of Upstroke and Downstroke speeds for a better pump fillage

Currently, over 90 % of the heavy oil wells, onshore Romania are equipped with linear pumping units.

### 6.3 Optimizing Reciprocating Rod Pumps Slippage and Fillage

Some sort of slippage is beneficial for reciprocating pump functioning as it provides proper plunger lubrication, preventing premature wear or plunger getting stuck.

Pump slippage is also helping plunger to have a normal and complete fall in pump, during downstroke, maximizing the pump fillage and pump efficiency.

Optimizing pump slippage on heavy oil fields onshore Romania has been done using 2 measures.

The first measure was to optimize the plunger fit. In practice it was found that a pump fit between -8 and -12 th inches is optimal for proper plunger lubrication, providing a minimal wear due to solids production and ensuring full plunger fall during downstroke.

The second measure to optimize further the pump slippage includes optimizing pumping speed during pumping cycle.

During upstroke high pump slippage is not beneficial. Since the standing valve is open, slippage replaces the fluid that would normally be entering the pump. As a result, less fluid will be entering the pump upon each upstroke.

Pump slippage during the downstroke does not impact the system efficiency. Due to a closed standing valve, downstroke slippage doesn't result in less fluid entering the pump.

Pump slippage during the downstroke is desirable. It ensures normal plunger falling, with closed standing valve and traveling valve, slippage increases the pressure between the two valves, causing the travelling

valve to open sooner. Opening sooner is generally better for pumping unit loading.

Optimizing pump stroke can have the following positive implications in optimizing artificial lift:

- Maximize the pump fillage and efficiency.
- Worn pumps can stay in the well longer with minor average SPM increase,
- Pumps with higher clearance (solids, etc.) are possible for lower fluid volume wells.
- Less strokes per day are required for the same production.
- Less strokes per day means less wear for the same production.

For poor pump fillages and gas interference optimizing pump stroke can be done manually by setting/resetting the pumping speed depending on the specific well conditions or autonomously based on algorithms that supposes counting "pump off" or low fillage events and then adjusting the speed accordingly. The advanced pump stroke optimization supposes upgrading standard Rod Pump Controllers configuration with a dedicated board and software to enable them performing the required optimization algorithms.

Figure 9: Rod Pump Controller autonomously reduces SPM (reduces speed on downstroke) to maximize pump fillage

(Autonomous, Self-Optimizing Pump Stroke Optimization (PSO) Equipment – Endurance Lift Solution International, Technology days, March 2018, Bucharest, Romania)

## 7 ROD PUMPS AND PUMP COMPONENTS TRACKING SOLUTIONS

Rod pumps and pump components tracking applications are essential tools for optimizing pump design. "Interface upstream" is the tracking application that is being used for tracking and optimizing pump designs in Romania.

The key benefits of it includes (Interface Upstream Application - User Manual, 2016, internal document):

Figure 10: 'Interface upstream' pumps and parts tracking application reports example

- WEB based, interactive user interface, allows access from anywhere.
- Capture, track, record, and help analyzing of rod pumps and pump components performance.
- Capture, track, and record well activities (interventions), pump inspection and failure analysis reports.
- Key performance indicators (KPI) monitoring and reporting capabilities.
- Operator is granted with access to it for a common source of information.
- Customizable to be compatible with client applications for tracking operations.

- It simplifies pump related data collection and streamlines pumps performance reporting and analysis.

## 8 PUMPS KPI MONITORING

Pump KPI monitoring is one of the standard procedures for measuring and monitoring rod pumps performance on heavy oil fields onshore Romania. There have been selected few relevant key performance indicators (KPI) and developed a dashboard for viewing and reporting the results. The pumps KPI are calculated monthly and displayed on the dashboard as actual values and cumulated average values to date (YTD). Targets are set at the beginning of the year and displayed together with the actual values for an easy comparison and analysis.

The pump key performance indicators selected for monitoring and analysis are followings:

- No of active PCP and RRP wells
- RRP interventions number
- PCP interventions number
- RRP PF-PC failures number (RRP failures due to pump components failures)
- PCP PF-PC failure numbers (PCP failures due to pump components failures)
- RRP PF-PC – MTBF (RRP Mean time between pump failures)
- PCP PF-PC – MTBF (PCP failures due to pump components failures)

Figure 11: Implemented Pumps KPIs monitoring dashboard example.

## 9 FIELD RESULTS

As result of integrated optimization approach conducted in a systematic way, implementing above mentioned pump and artificial lift solutions, optimizing pumping parameters, monitoring pump performance, etc, the RRP performance has been continuously improved.

Based on the Interface upstream application recordings, the Pumps Mean Time Between Interventions has increased from 233 days in 2010 up to 589 days in 2023 and continues to increase.

The annual number of interventions has decreased from 2515 to 976 in 2022 and continues to decrease.

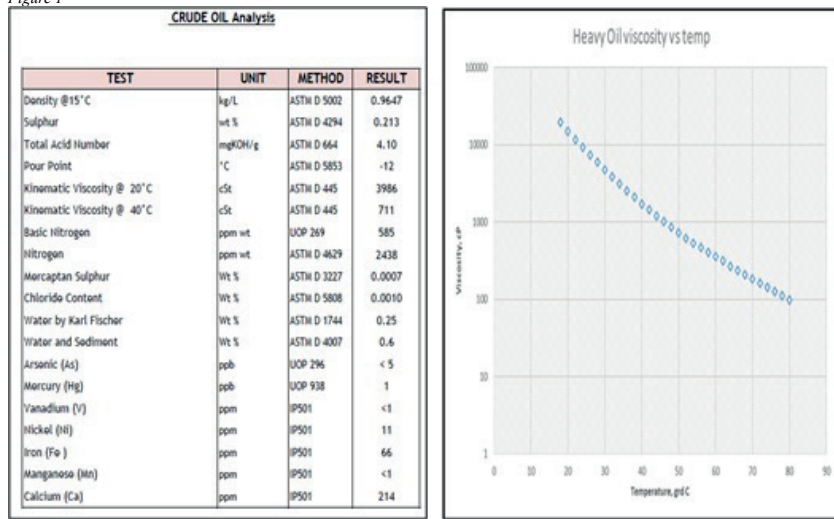
Figure 12: Heavy oil fields, on shore Romania – Pumps KPI variation 2010-2023

(Interface Upstream Application – Reports and Data)

Keywords: Reciprocating rod pumping optimization, Reciprocating rod pump solutions

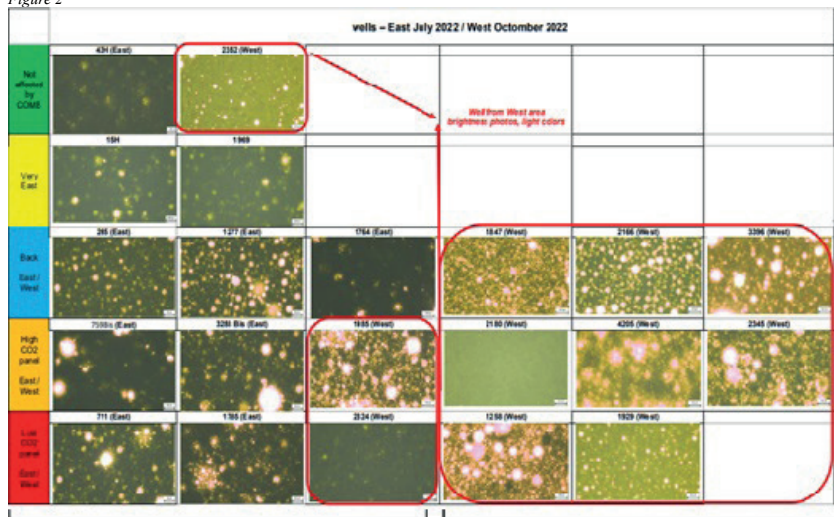


Figure 1



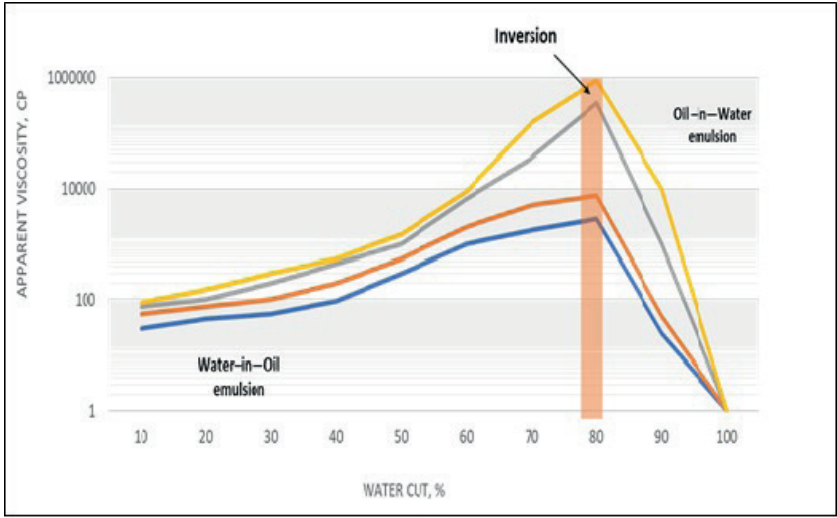
Heavy oil analysis

Figure 2



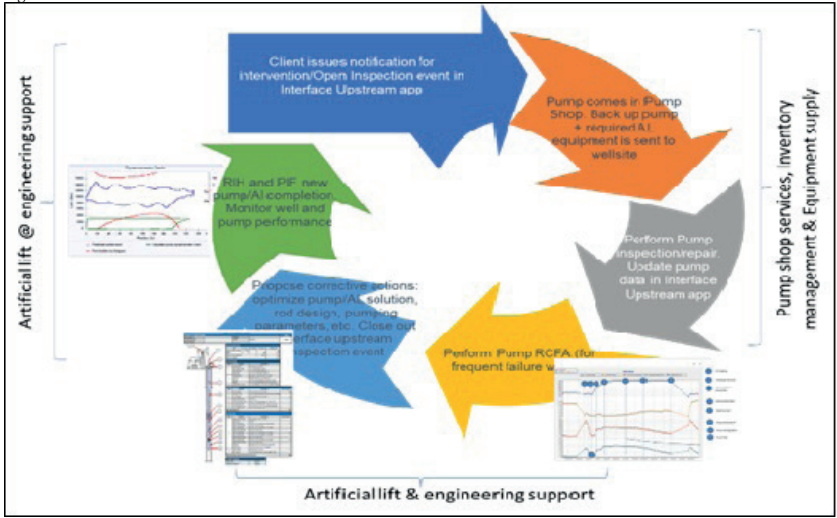
Microscopic analysis of emulsions on heavy oil field

Figure 3



Viscosity of emulsions

Figure 4



Artificial Lift Integrated Optimization Workflow

Figure 5



*Pump shop findings – Corrosion impact on standard pump metallurgies*

Figure 6



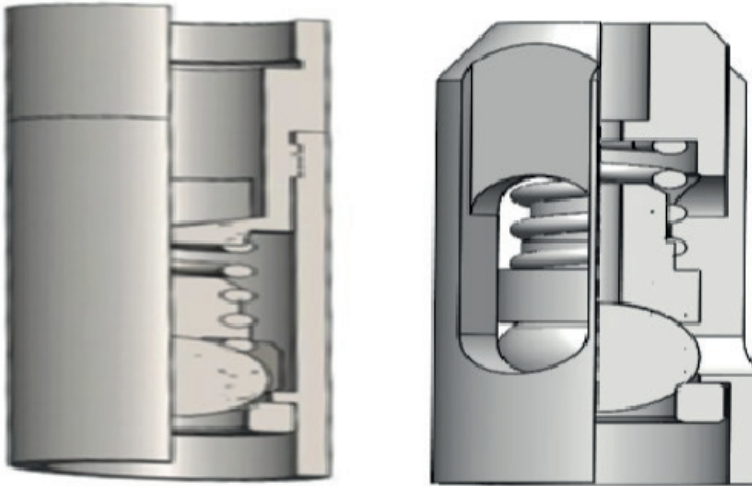
*Corrosion resistant pump metallurgies*

Figure 7



20-1.75-THE SV vs 20-175 TH API standard pump SV

Figure 8



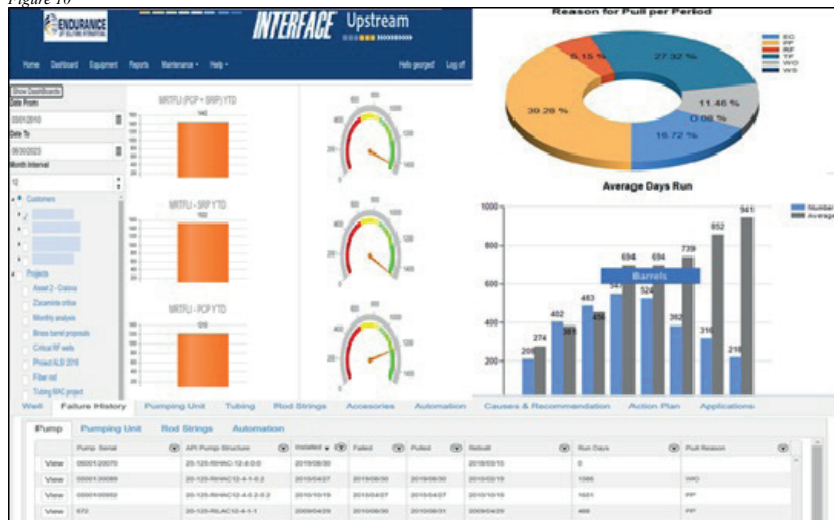
Energized valves

Figure 9



Rod Pump Controller autonomously reduces SPM (reduces speed on downstroke) to maximize pump fillage

Figure 10



'Interface upstream' pumps and parts tracking application reports example



# Açık Deniz Gaz Kuyularında Kum ve Su Kontrolü için Uygulanabilen Bazı Kimyasal Yöntemler

**Nazan N Topgüder**

Emekli, TPAO Araştırma Merkezi



Açık deniz gaz kuyuları üretime alındığında; özellikle gevşek yapılı (unconsolidated) formasyonlardan üretim yapılıyorsa kısa sürede kum üretimi ve bununla birlikte su üretimi de gündeme gelebilir. Üretim azalmasına sebep olan bu durumu önlemek için formasyonu stabilize ederek kum hareketliliğini önleyen ve bunu yaparken aynı zamanda formasyonun görelî geçirgenliğini de azaltarak su üretimini de azaltan kimyasal yöntemler geliştirilmiş ve birçok sahada uygulanmıştır.

Kum hareketliliği genel olarak tıkanma yaratarak üretim düşüşüne, kuyu tamamlama dizisinin ve diğer kuyudibi ekipmanının erozyonuna ve separatörler, boru hatları başta olmak üzere yüzey tesislerine zarar verir. Bu katı madde üretimini önleyen başlıca yolları 1) pasif kum kontrolü; yani seçici perforasyon, rezervuar yönetimi (üretim debisini sınırlandırmak, “kumsuz üretim debisi”ni saptamak) ve 2) aktif kum kontrolü; yani elekler, casing döşenmiş veya açık kuyularda gravel pack’ler veya kimyasal yöntemlerle formasyonun kendisinin konsolidasyonudur. Bu amaçla yaygın olarak kullanılan başlıca kimyasal yöntemler; formasyona adsorbe olarak konsolidasyon ve görelî geçirgenlik uyarlaması sağlayan polimer çözeltileri, ya da gevşek yapılı, dağılgan formasyonu doğrudan doğruya güçlendiren su bazlı reçineler olarak tanımlanabilir. Bu derlemede; gaz kuyularında kum ve su kontrolü için uygulanabilen bu kimyasal yöntemler hakkında genel bilgiler; problemin tespiti, uygun yöntemlerin saptanması için yapılacak laboratuvar çalışmaları, saha uygulaması tasarım çalışmaları ve dünyada yapılmış saha uygulamalarından örnekler verilecektir.

In offshore gas wells producing from unconsolidated sand formations; sand production along with water production may occur in quite a short time. As this phenomena reduces the production rate and the cumulative hydrocarbon production, chemical treatments to stabilize the sand production and also reducing water production rate by modifying the relative permeability of the formation are developed and applied in many fields around the world.

Sand production generally reduces production by plugging, causes erosion in well completion string and bottomhole equipment, and surface facilities such as separators and pipelines. There are mainly 2 ways to prohibit the fines production: 1) passive sand control; i.e. selective perforation, reservoir management (limiting the production rate, determining the proper production rate without sand) and 2) active sand control; i.e. screens, gravel pack in cased or open hole wells, or chemical treatments to consolidate the formation itself. The chemical treatments that are mainly used for this purpose are polymer solutions that are adsorbed by the formation to consolidate the formation along with the relative permeability modification (RPM) effect that reduces the water rate; or water soluble resins that

directly consolidate the formation.

This review paper covers background about these chemical treatments that are used for sand control and water rate reduction; determining the problem, laboratory tests to select the proper method to be applied in the field, field treatment design and examples of field treatments that are applied in different regions of the world.

## GİRİŞ

Rezervuar kayacı stabilitesinin zayıf olduğu üretim kuyularında aşırı su ve kum üretimi çoğunlukla karşılaşılan bir problemdir. Bu şartlar; yüksek su oranına, üretim kaybına, operasyonel problemlere ve sonuç olarak, yerinde gaz veya petrol rezervleri mevcut olsa dahi bu ekonomik olmayan şartlar nedeniyle kuyunun erken terk edilmesine sebep olur. Bu problemi önlemek amacıyla; kuyuda kum kontrolü için elekler, gravel veya frac pack’ler gibi mekanik yöntemlerle kum taneçiklerine karşı bir engel yaratarak kum üretimini önleme yoluna gidilir. Ancak çoğu zaman bu kum önleme sistemi verimsiz, yetersiz kalır; örneğin ince taneli parçacıklar varsa bunlar kum bariyeri tarafından yeterli kadar tutulamaz. Ayrıca kum üretimi; eleklerle mekanik zarar verebilir, tutma kapasitesinde kayıplara sebep olabilir. Bu durum özellikle, yüksek debiye sahip ve kum taneçiklerinin aşındırıcı etkisinin yüksek olduğu gaz kuyularında meydana gelir. Öte yandan, gravel pack’lerde veya elekler üzerinde kum taneçiklerinin birikmesi kuyunun akış davranışında bir skin etkisi yaratabilir.

Kum akışını kendi haline bırakarak üretim yapmak da bir seçenek olarak düşünülebilirse de; bu şekilde uzun süreli bir üretim, kuyunun yakın civarındaki kayacın dayanıklılığını daha da azaltarak boşlukların oluşmasına ve kuyuda su problemi de varsa bunu da aşırı hale getirerek kuyunun performansının iyice bozulmasına yol açar.

Tüm bu nedenlerden dolayı; kuyunun yakın civarındaki kayacı stabilize ederek kum üretimi problemini kaynağında önlemek en avantajlı yoldur. Burada kuyunun üretimini (veya enjeksiyon kuyusu ise enjektivitesini) azaltmadan kayacın stabilizasyonu için kimyasal yöntemler uygulanması başlıca seçeneklerden biridir.

Açık deniz gaz kuyularında görülen su/kum üretimi ile ilgili kritik derecede önemli problemleri önlemeye yaygın olarak kullanılan yöntem, kuyuları choke’layarak üretim debisini düşürmektir. Oysa suda çözünür polimerlerin enjeksiyonu ile hem su hem de kum üretiminin azaltılması mümkün olmaktadır. (Dupuis, et al. 2016)

Yüksek moleküler ağırlıklı suda çözünür polimerlerin geri-dönüştürülemez bir şekilde rezervuar kayacına adsorbe oldukları ve böylece iki-fazlı akış davranışını etkiledikleri bilinen bir gerçektir. Bu kimyasalların en belirgin etkilerinden biri de petrol veya gaz görelî geçirgenliği üzerinde çok daha az bir etki yaparken seçici olarak su görelî geçirgenliğini önemli ölçüde azaltmalarıdır. Bu özellik "RPM" (Relative Permeability Modification) olarak bilinmekte olup, üretim kuyularında su gelişini önleyici olarak da uygulanma olanağı sağlamaktadır. Öte yandan; gözenek cidarını kaplayan adsorbe olmuş polimer tabakası; bir kil stabilizörü gibi davranarak hem kil şişmesini hem de gevşek veya zayıf bağılı kumtaşlarında tanecik göçünü azaltmaktadır. (Zaitoun, et al. 2009)

Kum üretimini önlemede en iyi yöntem kumun rezervuarda kalmasıdır, çünkü yüzeyde olduğu kadar kuyu içerisinde de problem yaratacaktır. Bu amaçla kullanılan kimyasal yöntemlerden biri de epoxy reçinelerdir. Endonezya'nın offshore Mahakam sahasında (Mahardhini, et al. 2021) ve Avusturya'da bir gaz sahasında (Trujillo, et al. 2023) başarıyla uygulanmıştır. Laboratuvar testleri ile karışımın bileşimi, uygulama adımları ve enjektivite testi ile uygulama debisi belirlenir. Epoxy reçine; saptanan debiye göre enjekte edildikten sonra ötelenmiş ve reçine set olana kadar kuyu kapatılmıştır.

### KUM KONTROLU STRATEJİSİ

Gaz üretim kuyularındaki kum üretimi arttıkça, aşırı kum üretiminin kuyu stabilitesi ve yüzey tesisleri üzerindeki etkisini en aza indirmek için problemin saptanması, ölçülmesi ve gerekli önlemlerin alınması gerekir. Kum üretiminin yönetilmesinde genel olarak uygulanan pasif yöntemde; kumun yüzey tesislerine kadar ulaşmasından sonra yüzeyde önlem alınmasıdır. Burada amaç, mevcut ekipmanlarla kumu üretmek ve downtime sürelerini azaltmaktır (Kerya, et al. 2022).

Bu yaklaşım, iki ana süreçten oluşur; izleme (monitoring) ve iyileştirme (remediation). İki tür izleme yapılmaktadır: kum üretiminin izlenmesi ve korozyon/erozyon etkilerinin izlenmesi. Kum üretiminin izlenmesi, esas olarak ultrasonik kum detektörü ile yapılmıştır; korozyon/erozyon izlenmesi de bütün üretim akış hatları için ultrasonik testlerle yürütülmüştür. Etkin izleme sayesinde proaktif iyileştirme aksiyonlarının alınması mümkün olmaktadır. İyileştirme başlıca iki alanda yoğunlaşmaktadır: kuyulardaki kum üretimini en aza indirmek (MSFR/MASR -Maximum Sand Free Rate/ Maximum Allowable Sand Rate), su gelişini önleme, kum dayanıklılığını inceleme, vb. yoluyla) ve upgrading faaliyetleri ile yüzey tesislerinin bütünlüğünü ve güvenilirliğini artırmak.

İzleme kum ve erozyon etkilerinin izlenmesine odaklanır. İyileştirme bileşeni ise kuyudindeki kum üretimini en aza indirmek ve aynı zamanda yüzeydeki kum üretimini de yönetebilmeye odaklanır.

### KUM İZLEME

Kum izleme Ultrasonik Kum Detektörü ile yapılır. Bu amaçla, her bir offshore platformunda test başlıkları üzerine sensörler yerleştirilmiştir. Bu sensörlerden gelen kaba sinyaller, ana proses platformu üzerindeki server'a iletilir. Bu verileri yorumlamak için üretim test verisine ihtiyaç vardır. Bu üretim test verisi de üretkenlik endeksinden alınarak server'a iletilir. Böylece, Ultrasonik Test Detektörü, kuyu test separatörüne her bağlandığında kum üretiminin gerçek zamanlı olarak yorumlanabilmesine olanak sağlar.

#### Erozyon İzleme başlıca 3 kısma ayrılır:

1. Akış hattının gözlenmesi, kontrolü
2. Akış hattında Ultrasonik Test yapılması
3. Valf akış katsayısının izlenmesi

Kum üretimi; özellikle derin deniz kuyularından sürekli hidrokarbon üretimini riske eden en önemli faktörlerden biridir çünkü üretilen kum, pahalı kuyudibi ve denizdibi ekipmanlarını doldurabilir veya hasar verebilir ve bunlara müdahale etmek de teknik olarak çok zor ve yüksek maliyetli olabilir. Bu nedenle; kum üretiminin mümkün olduğu kadar önceden saptanması ve tedbir alınması için geliştirilen teknolojiler önem kazanmaktadır. Basınç ve sıcaklık sensör verilerini kullanarak kuyuya katı madde girişini ve kum kontrolunun etkilerini saptamak mümkün olmaktadır (Yamamoto, et al. 2023).

### POLİMER ÇÖZELTİLERİ İLE KUM KONTROLU

Kum kontrolü; kayaç yüzeyinin kayaç-akışkan etkileşimini uyarlayarak kayaç stabilizasyonunu sağlayacak bir ürünle muamele edilmesiyle de sağlanabilir. Bu amaçla kullanılan kimyasallardan biri de yeni bir polimer sistemidir. Bu sistem; su-bazlı bir polimerin kayacın yüzeyine adsorbe olarak ince bir film tabakası oluşturmasıyla meydana gelir (Dupuis, et al. 2016 ve Zaitoun, et al.2009). Adsorbe olan bu film tabakası; petrol veya gaz akışı için de gözenek merkezinde bir akış kanalı da bırakır. Böylece, su geçirgenliği önemli ölçüde azalırken; petrol veya gaz geçirgenliği korunmuş olur. Bu görelî geçirgenlik (RPM Relative Permeability Modification) etkisi sayesinde kum kontrolü etkisinin yanısıra su geçirgenliğinde azalma da sağlanabilir. Ayrıca polimerler, kuyuyu riske atmadan doğrudan enjeksiyon yapılabilmesine de olanak sağlar.

Kuyuya doğrudan doğruya (bullhead) enjeksiyon sırasında polimer çözeltisi doğal olarak öncelikle geçirgenliği yüksek zonlara yönelerek orada daha fazla ilerleyecektir. Çoğunlukla bu zonlar aynı zamanda kum ve su üretiminin esas kaynakları da olan yerlerdir. Böylece, mekanik düzeneklerle esas problem zonuna enjeksiyon yapmaya ihtiyaç olmaksızın, polimer çözeltisi kendiliğinden bu problemlili zonlara yönelerek optimizasyon sağlanmış olur.



Polimer teknolojisinin başlıca avantajları şöyle sıralanabilir:

- Doğrudan doğruya formasyona enjekte edilebilir
- Yerleştirme için özel ekipmana ihtiyaç yoktur
- Formasyon kirlenmesi riski düşüktür
- Kimyasal sistemin özelliklerinden dolayı kuyuda kendiliğinden optimize edilmiş yerleştirme olanağı vardı
- Kum kontrolü / Su kontrolü etkilerinin eş-zamanlı olarak sağlanması mümkün
- Açık ve uzun aralıklı formasyonlarda (potansiyel olarak yatay kuyular) da uygulama kolaylığı
- Su bazlı ve çevreci bir uygulama
- Mekanik kum kontrolü ekipmanlarıyla (elekler, gravel pack'ler, vb.) birlikte kullanılabilir

Uygulamanın başarısını artırmak için polimer, formasyonda mümkün olduğunca ileriye (3-5 m) gidecek şekilde enjekte edilir. Bu bakımdan uygulama, "gevşek ve derin" olarak nitelenmektedir ki bu özellikler polimer uygulamalarının esas avantajları olarak bilinmektedir.

#### LABORATUVAR ÇALIŞMALARI

Gevşek fakat formasyonda derinlere ilerleyebilecek bir kimyasal sistem istendiği için, uygulama tasarımı için yapılan laboratuvar çalışmalarında alışılagelmiş kayaç stabilitesi testleri yerine, flokülasyon testleri ve karot testleri yapılmıştır (Zaitoun, et al. 2009). Bu nedenle, kayaç yüzeyinin polimer filmi ile kaplanması amacıyla uygun olarak deneysel bir yöntem; flokülasyon (topaklanma) testleri geliştirilmiştir. Bu testlerde; belirli miktardaki kum örneği, topaklanma zamanını gözlemlemek için iki gözlem noktası olan dereceli bir tüp içerisinde bir polimer çözeltisi ile karıştırılmıştır. Tüp, kum ve polimer çözeltisinin karışması için 4 defa ters çevrilmiş ve çökeltme için bir süre bekletilmiştir. Topaklanma zamanı basit olarak, katı/sıvı arayüzeyinin bu iki gözlem noktasından geçiş zamanlarının ölçülmesiyle belirlenmiştir. Kaba bir yaklaşım olarak, en kısa topaklanma zamanının polimerin kumu kaplama etkisinin en yüksek olduğunu gösterdiği kabul edilebilir.

Testlerde kuyu temizleme sırasında dipten toplanan kum örnekleri kullanılmıştır. Referans olarak polimersiz bir örnek kullanılır ve aynı şartlarda yürütülen topaklanma testleri sonucunda görelî olarak polimer çözeltilerinin etkileri sınıflandırılabilir. Kullanılan polimer (Powelgel P321), su bazlı, sentetik bir kopolimerdir (Zaitoun, et al. 2020). Topaklanma testi sonucunda kumu kaplama özelliği bakımından uygun olduğu belirlenen polimer çözeltisi ile rezervuar karotlarında akış testlerine geçilir. Polimer çözeltisinin viskozitesi de ölçülerek, karot akış testine uygun polimer çözeltileri belirlenir.

Karot akış testleri ile; petrofiziksel veriler, polimer çözeltisinin enjektivitesi / kayaç içerisinde ilerleyişi, polimerin adsorpsiyonu, su geçirgenliğini azaltma etkisi ve polimer uygulaması sonrasında gaz geçirgenliğinin geri kazanılması gibi performans özellikleri belirlenir (Zaitoun, et.al. 2009 ve Dupuis, et al. 2016).

#### SAHA UYGULAMALARINDAN ÖRNEKLER

Saha uygulaması; seyreltik polimer çözeltisiyle (500 ppm) enjektivite testi yapıldıktan sonra, 3000 ppm'e kadar çıkan konsantrasyondaki esas polimer çözeltisinin enjeksiyonu, gaz geçirgenliğini korumak amacıyla nitrojen ile ötelemenin ardından kuyunun 24 saat kapatılması sonrasında kuyunun kademeli olarak tekrar üretime alınması adımlarını kapsar (Zaitoun, et al., 2020).

ENI'nin Adriyatik Denizi'ndeki offshore gaz kuyularında yapılan saha uygulamaları sonuçları; polimer uygulaması öncesi ve sonrasında kuyuların performansları Tablo-1'de verilmiştir (Dupuis, et al. 2016). Bu verilere göre kum üretimi ve su üretiminde önemli azalmalar sağlanmıştır.

Polimer ile kum kontrolü teknolojisi Endonezya'da da birçok offshore kuyusunda başarıyla uygulanmıştır (Zaitoun, et al. 2022). Güneydoğu Asya'daki birkaç sahada killi ve gevşek rezervuar kayacı nedeniyle aşırı kum üretimi görülmektedir. Bu kum üretimi kuyuda kum birikmesine, pompanın ve yüzey ekipmanının hasar görmesine, kuyunun sık sık kapatılmasına ve yüksek maliyetli kuyu temizleme operasyonlarına ve pompa değişimlerine sebep olur. Bu problemleri önleyici olarak polimerin adsorpsiyon özelliğinden yararlanılan polimer enjeksiyonu başarılı olmuştur. Polimerin RPM özelliği sayesinde; bir gaz kuyusunda polimer uygulamasından hemen sonra su üretimi % 70 azalmış, gaz üretimi 2 katına çıkmış; kum üretimi ise durmuştur. Polimer ile kum kontrolü uygulamalarından çıkarılacak dersler şöyle sıralanabilir:

- Teknoloji hem gaz hem de petrol kuyularında,
- Düşük veya yüksek geçirgenlikli kuyularda (10-5000 md)
- 30-90°C sıcaklıklarda,
- 1000-50,000 ppm TDS tuzluluklarda
- Düşük veya yüksek debili kuyularda (2500 b/d petrol veya saatte 50,000 SCM gaz kuyularında) uygulanabilir
- Uygulamanın etkinlik süresi petrol kuyularında 1 yıl, gaz kuyularında ise 2-4 yıldır
- Kuyuda tekrarlanacak uygulamanın etkinliği ilk seferki kadar olumlu etki yapar,
- Kayacı stabilize etmesi nedeniyle kuyu; daha yüksek debilerde de kum problemi olmadan üretim yapabilir,
- Kum kontrolü için polimer uygulaması; su yüzdesi 0 veya neredeyse %100 de olsa uygulanabilir,
- Kum kontrolü etkisinin yanı sıra birçok kuyuda olumlu bir yan etki olarak su üretiminde de bir azalma görülmüştür.

#### KUM KONTROLUNDA REÇİNELERİN KULLANIMI

Kum üretimini önlemede en iyi yöntem kumun rezervuarda kalmasıdır, çünkü yüzeyde olduğu kadar kuyu içerisinde de problem yaratacaktır. Bu amaçla kullanılan kimyasal yöntemlerden biri de epoxy reçinelerdir. Endonezya'nın offshore Mahakam

sahasında başarıyla uygulanmıştır (Mahardhini et al. 2021). Laboratuvar testleri ile karışımın bileşimi, uygulama adımları, enjektivite testi ile uygulama debisi belirlenir. Kimyasal karışımın bileşimi % 50 kimyasal reçine, %21 kimyasal sertleştirici (1) ve %29 kimyasal sertleştirici (2) olarak belirlenmiştir. Uygulama adımları ise; formasyonu uyarlamak için bir preflush, ardından kum konsolidasyonunu sağlayan kimyasal enjeksiyonu, dizel ile overflush ve dizel ile öteleme şeklindedir. Epoxy reçine; saptanan debiye göre enjektivite edildikten sonra ötelenmiş ve uygulama sonrası reçinenin formasyonda tam set olması için kuyu 2 hafta süreyle kapatılmıştır. Operasyonun başarısında formasyonun uygun preflush kimyasalları ile hazırlanmasını, enjektivite testinin ve operasyon sonrası temizleme ve üretime alma işlemlerinin rezervuarda ani basınç değişimi etkisi yaratmayacak şekilde yapılmasının kritik önemi vardır.

Diğer bir reçine uygulaması da, Avusturya gaz sahalarında karşılaşılan kum probleminin kontrolü için, sahanın ekonomik koşulları da dikkate alınarak; su-bazlı reçine (Internally Catalyzed Aqueous-Based Emulsion of Curable Epoxy Resin, ICABECER) uygulamasıdır (Trujillo, et al.2023).

Detaylı bir planlama ve saha uygulaması öncesinde yapılan laboratuvar testleri ile operasyonel riskler azalmış, maliyetler düşürülmüş ve çıktılar optimize edilmiştir. Yerleştirme tekniği ve öteleme tekniği ile rezervuar kayacı akış yollarında önemli bir tıkanma yaratmadan hedef üretim debilerine ulaşılmıştır. Uygulama öncesinde kum üretimi nedeniyle terk edilmesi planlanan kuyularda; kararlı bir gaz akışı ve azalan kum üretimiyle ekonomik şekilde gaz üretimi sağlanmıştır.

Saha uygulamasında öncelikle kumun kuyudan giderilmesi gerekir ki bu amaçla köpük kullanılarak önemli miktarda kum temizlenmiştir. Preflush 1 ve 2 sıvıları ile formasyon esas kum konsolidasyon adımına hazır hale getirilmiştir. Ardından kum konsolidasyon enjeksiyonu, (ICABECER) yapılıp nitrojen ile ötelenerek formasyona squeeze edilmiştir. Kuyudibi sıcaklığına bağlı olarak kuyu 4-7 gün kapatılarak reçinenin set olması beklenmiştir. Yaklaşık 1 hafta kapatılan kuyu; kademeli olarak üretime alınmış ve kum üretimine sebep olmayacak şekilde debi ayarlanmıştır. Uygulama sonrasında kuyu kum üretimi olmadan devreye alınmış ancak yaklaşık 6 ay sonrasında artan su üretimi nedeniyle yeniden kum üretimi başlamıştır.

## SONUÇ

Açık deniz gaz kuyuları üretime alındığında, özellikle gevşek (unconsolidated) yapıli formasyonlarda kum üretimi ve yanısıra su üretimi de kısa sürede gündeme gelerek, verimliliği azaltmakta hatta kuyunun terk edilmesine sebep olmaktadır.

Üretim azalmasına sebep olan bu durumu önlemek için formasyonu stabilize ederek kum hareketliliğini önleyen ve bunu yaparken aynı zamanda formasyonun görelî geçirgenliğini de azaltarak su üretimini de azaltan kimyasal yöntemler, özellikle polimer çözeltileri geliştirilmiş ve birçok sahada uygulanmıştır.

Sahanın ve formasyonun özelliklerine bağlı olarak yapılacak laboratuvar çalışmaları sonucunda seçilecek uygun kimyasallarla yapılacak başarılı saha uygulamaları ile kum ve su kontrolünü sağlayarak üretkenliği arttırmak mümkün olmaktadır.

## KAYNAKÇA

Dupuis,G., Bouillot,J., Zaitoun,A., Caremi,G. and Burrafato,G.: “Combined Water/Sand Control Polymer Treatments in Offshore Gas Wells”, SPE-179825-MS presented at the SPE EOR Conference at Oil and Gas West Asia held in Muscat, Oman, 21-23 March 2016.

Kerya,N., Leong,D.G. and Apiwathanasom,S.: “Sand Management Strategy in Offshore Gas Field in the Gulf of Thailand”, OTC-31499-MS presented at the Offshore Technology Conference Asia held in Kuala Lumpur, Malaysia, 22-25 March 2022.

Mahardhini,A., Yudis,P., Abidiy,I., Bawono,Y., and Pradityo,R.: “Successful Case of Resin-Based Chemical Sand Consolidation as a Remedial Sand Control Treatment” SPE-207942-MS presented at the Abu Dhabi International Petroleum Exhibition&Conference held in Abu Dhabi,UAE, 15-18 November 2021.

Trujillo,E.J.T., Santin,Y., Ukoha,O., Maier,R., Kiss,A., Moertl,M. and Zabel,D.: “Curing Sand Production Problems with an Aqueous-Based Resin Sand Consolidation Treatment to Optimize the Hydrocarbon Recovery Factor in Austrian Gas Fields”, SPE-214183-MS presented at the Gas & Oil Technology Showcase and Conference held in Dubai, UAE, 13-15 March 2023.

Yamamoto,K., Kanno,T., and Kumagai,K.: “Downhole Detection of Solid Inflow and Identification of Sand Control Failure Using Pressure and Temperature Sensing Data”, IPTC-23053-MS presented at the International Petroleum Technology Conference held in Bangkok, Thailand, 1-3 March 2023.

Zaitoun,A. and Pichery,T.: “New Polymer Technology for Sand Control Treatments of Gas Storage Wells”, SPE 121291 presented at the 2009 SPE International Symposium on Oilfield Chemistry held in The Woodlands, Texas, USA 20-22 April 2009.

Zaitoun,A. Templier,A. and Hernando,L.: “Gas Production Enhancement by Polymer Treatment” SPE-199312-MS presented at the SPE International Conference and Exhibition on Formation Damage Control held in Lafayette, Louisiana, USA, 19-21 February 2020.

Zaitoun,A., Salehi,N., Bouillot,J. Hernando,L., Wijaya,B.R., Reynold,W., Samosir,F.S., Pradipta,A., Witjaksana,A. and Kurniadi,W.: “Mitigating Sand Production by Polymer Injection in Indonesian Offshore Field”, SPE-210731-MS presented at the SPE Asia Pacific Oil & Gas Conference and Exhibition held in Adelaide, Australia on 17-19 October 2022.

Anahtar Kelimeler: Kum Kontrolu, Su Üretimini Azaltma

*Tablo 1- Uygulama Öncesi ve Sonrası Veriler (Dupuis, et al.)*

Kuyu	Önceki Gaz Debisi (kSm <sup>3</sup> /d)	Önceki Su Debisi (m <sup>3</sup> /d)	Kum Üretimi	Sonraki Gaz Debisi (kSm <sup>3</sup> /d)	Sonraki Su Debisi (m <sup>3</sup> /d)	Kum Üretimi
A-15S	26	4	Var	55	0.8	Yok
A-B8L	18	0.07	Var	49	0.1	Yok
B-65S	47	11	Var	40	4	Yok
C-4L	34	10	Yok	41	13	Yok
A-8S	18	0.85	Var	18	4	Var
D-15L	40	5.2	Var	46	6.1	Yok
E-6L	0	0	Su ve Kum Üretimi - Terk	103	14	Yok
F-6S	0	0	Su ve Kum Üretimi - Terk	21	2.8	Yok
F-10S	0	0	Su ve Kum Üretimi - Terk	25	12	Su ve Kum Üretimi - Terk





**Yapay Zeka ve Özdevimli Öğrenme**  
*Artificial Intelligence and Machine Learning*

---



# Machine Learning Assisted Forecasting of Field Performance: A Case Study



Emre Artun<sup>1</sup>, Serhat Canbolat<sup>2</sup>, Elif Cihan Yıldırım<sup>2</sup>, Cansu Açıkğöz<sup>2</sup>, Onur Yürüker<sup>2</sup>

<sup>1</sup>Istanbul Technical University

<sup>2</sup>Turkish Petroleum Corporation

## ABSTRACT

This paper presents a case study of a fractured carbonate reservoir in south-eastern Turkey, where machine learning is employed to forecast reservoir performance. The methodology includes four steps: 1) collecting, organizing and processing field data, 2) development of a forecasting model using real field data including raw and imputed well logs, reservoir properties from well log interpretations and operational characteristics, 3) estimation of spatial distributions of logs and reservoir properties, 4) applying the forecasting model throughout the reservoir area to identify potentially productive locations. This workflow was followed to identify potentially promising regions in the reservoir for infill drilling. Results showed that model-suggested areas were consistent with the current focus of the asset team.

## INTRODUCTION

With the advancement in data collection, storage and processing capabilities, all industries have been going through a digital transformation period in which data-driven models are extensively used to make predictions, forecasts and decisions. This era is also known as Industry 4.0 and data analytics and machine learning together represent the key set of methodologies followed to create valuable insights from data. Machine learning is broadly a modeling approach that relies on a collection of examples (data) of some phenomenon. The data may be generated in the nature (e.g., well measurements), or using modelling software (e.g., reservoir simulator outputs). The focus is to solve a regression or a classification problem that, once solved, we would understand a phenomenon better or to make a decision. Using a structured dataset that includes a set of observations, we utilize a machine learning approach to extract patterns within the data set. After proper validation, we use that as a model to make predictions, forecasts or to classify the dataset into certain groups.

Proper reservoir management requires using financial, technological and human resources while maximizing economic recovery of oil/gas (Satter and Thakur 1994). This can only be achieved by the effective use of available data, which is typically limited. High-resolution data is only available at well locations and there are a large number of uncertainties associated with the remaining parts of the reservoir. This creates major challenges for proper reservoir characterization and forecasting of reservoir performance. Machine learning can offer modeling protocols to make the best use of available data.

Machine learning-based performance forecasting models for hydrocarbon reservoirs can be broadly

divided into two groups: (1) proxy models that accelerate numerical-simulation-based forecasting and (2) models that are purely based on real (field) observations (Artun 2022). While proxy modeling helps to improve computational efficiency, the real value of machine learning algorithms becomes more evident when real data are used and other modeling approaches are not practical or possible at all. A common approach is to integrate all data in a systematic manner to solve reservoir management problems. For example, seismic data, well completion data, production performance can be used to train several machine learning models to improve the reservoir characterization and identify sweet spots in the reservoir (Thararoop et al. 2008, Ertekin 2021). Experimental data can be used to develop performance forecasting models for enhanced oil recovery processes such as steam-assisted gravity drainage (Canbolat and Artun 2022). Another approach follows a top-down modeling (TDM) procedure which includes a parametric representation that is very similar to reservoir simulation (Mohaghegh 2011, Mohaghegh et al. 2014). The TDM approach was also applied to unconventional reservoirs, including New Albany, Bakken, Huron, and Marcellus shale by incorporating reservoir properties as well as hydraulic-fracturing definitions as the controlling parameters for reservoir behavior (Kalantari-Dahaghi and Mohaghegh 2011, Mohaghegh et al. 2012, Esmaili and Mohaghegh 2016). Different machine learning algorithms were applied to unconventional reservoirs in many other studies (Schuetter et al. 2018, Al-Alwani et al. 2019, Kong et al. 2021).

In this study, a fractured carbonate reservoir in south-eastern Turkey was considered for integrating data into a performance forecasting model using machine learning. Well information, well logs and production histories were the available data. After quality check, and missing data imputation for well logs, a summary data set that includes properties of 48 wells was compiled. A neural network-based forecasting model was trained and tested using this data set. After estimating spatial distributions of reservoir properties throughout the field area, the forecasting model was applied to identify potentially promising locations for field development. This workflow was summarized in Fig. 1.

## Data Collection and Pre-Processing

In reservoir engineering related forecasting problems, the parameters of interest can be broadly divided into three groups (Artun 2022):

1. Reservoir characteristics (natural characteristics of the reservoir, which we typically do not have any control on such as porosity and permeability, etc.).

2. Operational (design) parameters (parameters that we can control in the field such as well location, completion interval, horizontal well length, etc.)

3. Performance indicators (volumetric, economic, or environmental performance characteristics of a given well or reservoir or field that we are interested in forecasting)

Considering this categorization, the following field data were compiled for a fractured carbonate reservoir in south-eastern Turkey:

Performance indicators:

Cumulative oil, gas and water production

Minimum, average and maximum oil rate observed

Minimum, average and maximum water-cut observed

### RESERVOIR CHARACTERISTICS

Raw well-log measurements: Caliper (CALI), spontaneous potential (SP), gamma ray (GR), gamma ray total counts (GRTC), sonic (DT), laterolog deep (LLD), laterolog shallow (LLS), micro-spherically focused log (MSFL), photoelectric factor (PEF), bulk density (RHOB), neutron porosity (NPHI), and conductivity (COND) from borehole image logs.

Reservoir properties interpreted from well logs: Water saturation calculated from Archie's equation (SWAR), water saturation calculated from capillary pressure as a function of depth (SWLAM), porosity (PORO) from NPHI and RHOB logs, permeability (PERM) as a function of porosity in calibration with the measurements on core samples, fracture intensity (NFRAC) and aperture (APERT) interpreted from borehole image logs, reservoir top (DTOP), reservoir thickness (ZONETHK), distance to the nearest fault (DFAULT), distance to the water-oil contact (DWOC)

Operational (design) parameters: Location of the well (X, Y), distance to the nearest active well (DWELL), perforation thickness (PERFTHK), well type (horizontal, vertical, deviated) (TYPE), first time of production (FIRSTPROD), duration of production (ACTIVEDAYS)

The field under consideration produces from three flow units. To integrate the information from all three flow units into a single well, a weighted average of mean values of well logs measurements, according to the perforation intervals in each flow unit, was calculated. If  $L_n$  is the average value of log measurements for the given well in the flow unit  $n$ ,  $n$  is 1, 2 or 3,  $PERFTHK_n$  is the perforation interval of flow unit  $n$ ,  $L_{well}$  is the weighted average of the log for the well is calculated as:

$$L_{well} = \frac{\sum_{i=1}^3 (L_i \cdot PERFTHK_i)}{\sum_{i=1}^3 PERFTHK_i}$$

The motivation behind this averaging is the lack of production history for each flow unit separately. As a result, the performance-forecasting model was designed as a well-performance forecasting model. The thickness of the flow units that the well is drilled through and perforation intervals were summed to be added to this

data set. Consequently, a summary data set, in which each of the 48 wells is an individual data object was designed.

### Development and Testing of the Performance Forecasting Model

As the choice of machine learning approach, artificial neural networks were selected due to highly non-linear and complex nature of the problem, which involves multiple input and output parameters. The parametric representation includes different types of input parameters such as reservoir properties, operational parameters related to wells, and geographical properties such as well locations, distances to nearby wells, faults and oil-water contact. These features of the problem made neural networks an ideal approach to extract the patterns between input and output parameters.

Parameters that follow a log-normal distribution such as permeability and resistivity logs, were transformed into their 10-base logarithm values before further modeling. Then, all parameters were scaled between 0 and 1. General architecture of the neural network is shown in Fig. 2. Two hidden layers shown in the figure is only for illustration. Number of layers and neurons were optimized during model training. To incorporate non-linearity into the model, logistic (sigmoid) function was applied in each neuron. As a result, 31 input parameters altogether were used to predict 9 output parameters that represent various performance characteristics of the well.

To optimize the model, the following model properties were varied, and 120,000 different models were trained and tested:

Number of wells used for training and testing (42, 43, or 44 wells for training)

Number of hidden layers (1, 2 or 3 layers)

Number of neurons in each layer (10-200 neurons in each layer and a total of 10-260 neurons)

Seed for random number generator for the distribution of wells and initialization of weights

Among the most successful models, 10 of them were selected as promising considering the variety in wells used for testing as well. Further analysis and visualization resulted in 4 models that can be used for forecasting (Table 1). As an example, real vs. predicted cross plots for the model with 79-23-18 neurons is shown in Fig. 3. In this model 4 wells were used for testing and the model was trained with the remaining 44 wells. Average R2 for training and testing were 0.99 and 0.90, respectively.

Table 1: Selected four models for the forecasting application.

The importance of variables was evaluated using the connection-weight approach, which takes into account the optimized weight values in the connection link (Olden and Jackson 2002). This approach calculates variable importance by considering the product of the raw input-hidden and hidden-output connection



weights between each input and output neuron. Finally, the product is summed across all hidden neurons. The variable importance chart in Fig. 4 shows that time-dependent parameters, such as first production time and active days, are the most important variables in production performance. These are followed by the reservoir properties, such as gamma ray total counts, distance to the oil water contact and neutron porosity.

### Identification of Sweet-Spots

To apply the forecasting model to the reservoir area, a grid system composed of 9801 grid points was defined (81x121,  $\Delta X = \Delta Y = 50$  m.). All spatial parameters were populated throughout the grid system using the second-order inverse distance weighting. Fig. 5 shows sample maps created as a result of this approach.

Models that were selected earlier were used to forecast the performance parameters in every single grid point. The reservoir characteristics and some of the geographical properties were obtained from the aforementioned populated values. For the following operational parameters, some assumptions were used to determine their values:

**DWELL:** For each grid point, the distance from the nearest well was calculated using Euclid's formula:

**TYPE:** Since the model was mostly trained with vertical wells, the proposed well also was selected as a vertical well, so a value of 1 is assigned to this variable.

**NPRFO:** It was assumed that the well was perforated in all three flow units, and the value of 3 was assigned to this variable.

**FIRSTPROD:** Current time is used as the first production time.

**ACTIVEDAYS:** This parameter indicates the duration of production for the proposed well. 0.5, 1 and 2 years were used separately to perform a short-term forecast and to see the changes with time.

Fig. 6 shows the map of forecasted minimum, average and maximum oil rate after 0.5, 1, and 2 years. The distributions do not change dramatically due to the short-term nature of the forecasts. South-eastern region of the field is shown with higher potential in terms of oil rate, with localized regions in the central and central-north of the field.

All grid points within the reservoir area were sorted in terms of oil production, average oil rate and average water cut. Top 100 with the most favourable performance metrics are shown in Fig. 7. These points show potentially high-performance regions in the field.

### CONCLUSIONS

A machine learning assisted workflow to design performance forecasting models for mature reservoirs was presented with a case study for a fractured carbonate reservoir.

A comprehensive data collection and pre processing study resulted in a summary data set which

includes one observation per well.

A comprehensive search for neural network design with 120,000 different configurations helped to find the most promising forecasting models.

Application of the model to the reservoir area revealed potentially promising regions for infill drilling.

### ACKNOWLEDGEMENTS

Authors would like to express gratitude to Turkish Petroleum Corporation for providing support during this study.

### REFERENCES

- Al-Alwani, M. A., L. Britt, S. Dunn-Norman, H. H. Alkinani, A. T. Al-Hameedi, A. Al-Attar. 2019. "Production performance estimation from stimulation and completion parameters using machine learning approach in the Marcellus Shale", In: Proceedings, 53rd U.S. Rock Mechanics/Geomechanics Symposium, 23–26 June, New York City, New York.
- Artun, E. 2022. "Machine learning assisted forecasting of reservoir performance", in Machine Learning Applications in Subsurface Energy Resource Management, pp. 185-206 ed. S. Mishra, CRC Press, Boca Raton, Florida.
- Canbolat, S., E. Artun. 2022. "Machine-learning approach for forecasting steam-assisted gravity-drainage performance in the presence of noncondensable gases" ACS Omega 7, 24, 21119–21130. doi:10.1021/acsomega.2c01939
- Ertekin, T. 2021. "The efficacy and superiority of the expert systems in reservoir engineering decision making process", Appl. Sci., 11, 6347. doi:10.3390/app11146347
- Esmaili, S., S. Mohaghegh. 2016. "Full field reservoir modeling of shale assets using advanced data-driven analytics", Geosci. Front., 7(1):11-20. doi:10.1016/j.gsf.2014.12.006
- Kalantari-Dahaghi, A. and Mohaghegh, S., 2011, "A new practical approach in modelling and simulation of shale gas reservoirs: application to New Albany Shale", Intl. J. Oil Gas Coal Tech., 4(2):103-133. doi:10.1504/IJOGCT.2011.038925
- Kong, B., Z. Chen, S. Chen, T. Qin. 2021. "Machine learning assisted production data analysis in liquid-rich Duvernay Formation", J. Pet. Sci. Eng., 200, 108377, doi:10.1016/j.petrol.2021.108377
- Mohaghegh, S.D., O. Grujic, S. Zargari, A. Kalantari, G. Bromhal. 2012. "Top-down, intelligent reservoir modelling of oil and gas producing shale reservoirs; case studies", Intl. J. Oil Gas Coal Tech., 5(1):3-28. doi:10.1504/IJOGCT.2012.044175
- Mohaghegh, S., A. Modavi, H. Hafez, M. Haajizadeh, S. Guruswamy, 2009, "Development of Surrogate Reservoir Model (SRM) for fast track analysis of a complex reservoir", Intl. J. Oil Gas Coal Tech., 2(1):2:23. doi:10.1504/IJOGCT.2009.023627

Mohaghegh, S. 2011. "Reservoir simulation and modeling based on artificial intelligence and data mining (AI&DM)", J. Nat. Gas Sci. Eng, 3(6):697-705 doi:10.1016/j.jngse.2011.08.003

Mohaghegh, S., Y. Al-Mehairi, R. Gaskari, M. Maysami, Y. Khazaeni, M. Gashut, A.E. Al- Hammadi, S. Kumar. 2014. "Data-driven reservoir management of a giant mature oilfield in the Middle East", In: Proceedings, SPE Annual Technical Conference and Exhibition, 27-29 October, Amsterdam, The Netherlands. doi:10.2118/170660-PA

Olden, J.; Jackson, D. 2002. "Illuminating the 'black-box': a randomization approach for understanding variable contributions in artificial neural networks", Ecol Model, 154, 135-150, doi:10.1016/S0304-3800(02)00064-9

Schuetter, J., S. Mishra, M. Zhong, R. LaFollette. 2018. "A data-analytics tutorial: Building predictive models for oil production in an unconventional shale reservoir", SPE J., 23(4):1075-1089. doi: 10.2118/189969-PA

Satter, A., G. Thakur. 1996. Integrated Petroleum Reservoir Management: A Team Approach, PennWell Books, Tulsa, Oklahoma.

Thararoop, P., Z. Karpyn, A. Gitman, T. Ertekin. 2008. "Integration of seismic attributes and production data for infill drilling strategies - A virtual intelligence approach", J. Pet. Sci. Eng., 63(1-4):43-52. doi:10.1016/j.petrol.2008.08.002

Keywords: Machine Learning, Forecasting

Figure.1 Workflow of the study

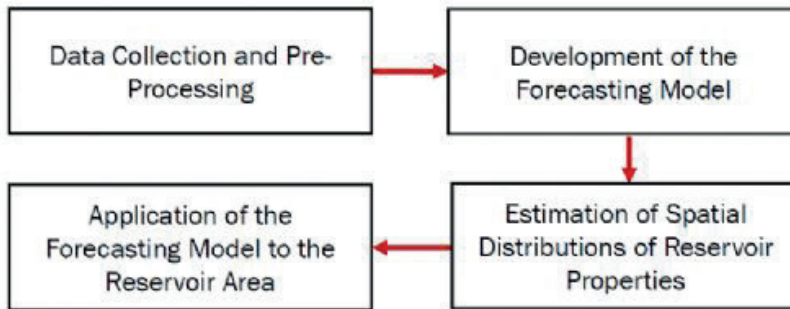


Figure 1: Workflow of the study

Figure.2 Architecture of the neural network design for the performance forecasting problem.

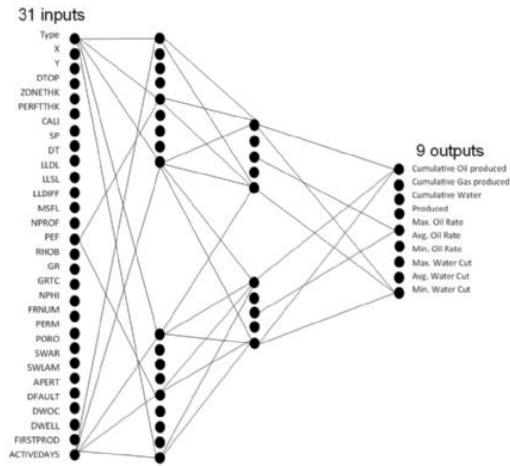


Figure 2: Architecture of the neural network design for the performance forecasting problem.

Figure.3 Real vs. predicted cross plots for 9 performance parameters that are predicted by the neural network with 79-23-18 neurons.

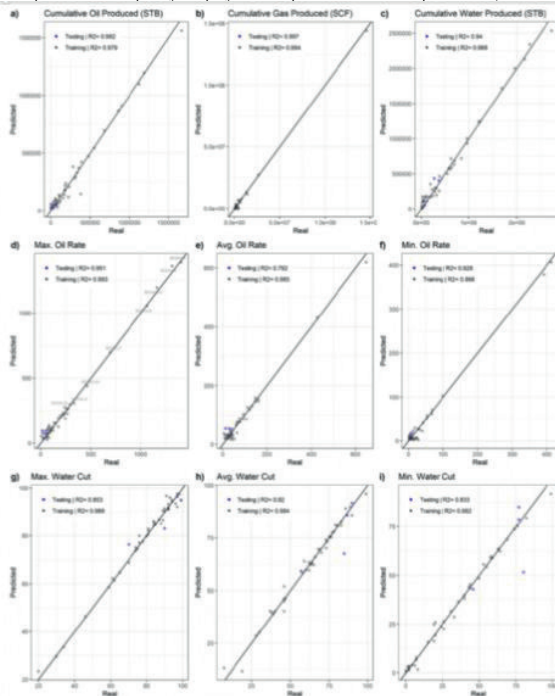


Figure 3: Real vs. predicted cross plots for 9 performance parameters that are predicted by the neural network with 79-23-18 neurons.

Figure.4 Variable importance plot for the neural network with 79-23-18 neurons.

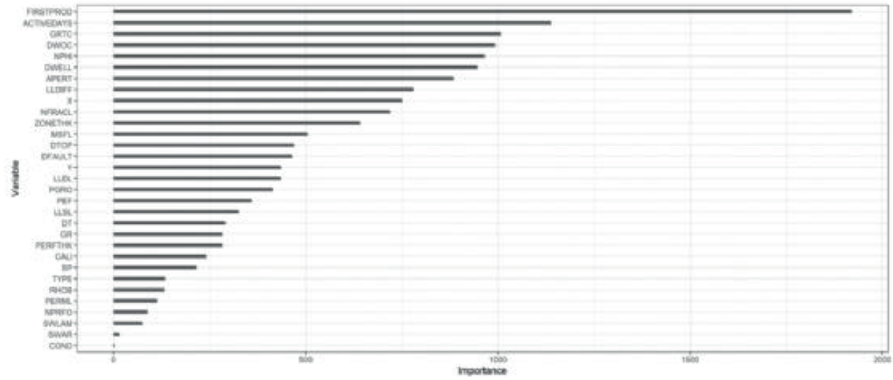


Figure 4: Variable importance plot for the neural network with 79-23-18 neurons

Figure.5 Sample distribution maps for averaged reservoir properties and well logs.

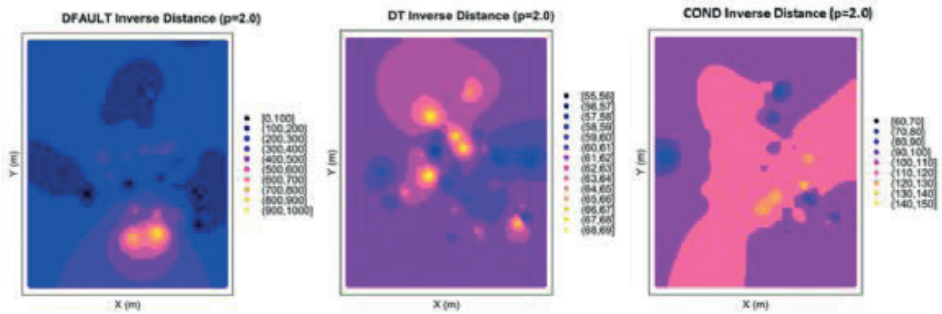


Figure 5: Sample distribution maps for averaged reservoir properties and well logs.

Figure 6 Map of forecasted minimum, average and maximum oil rate after 0.5, 1, and 2 years.

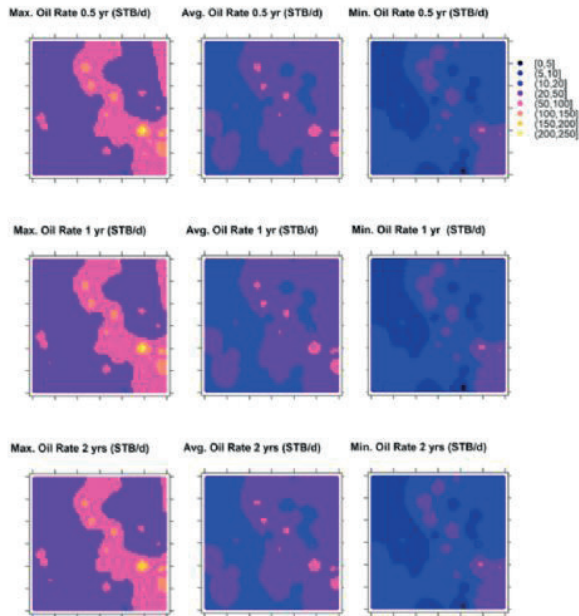


Figure 6: Map of forecasted minimum, average and maximum oil rate after 0.5, 1, and 2 years.

Figure 7 Map of top 100 locations for average oil rate, cumulative oil production and minimum water cut.

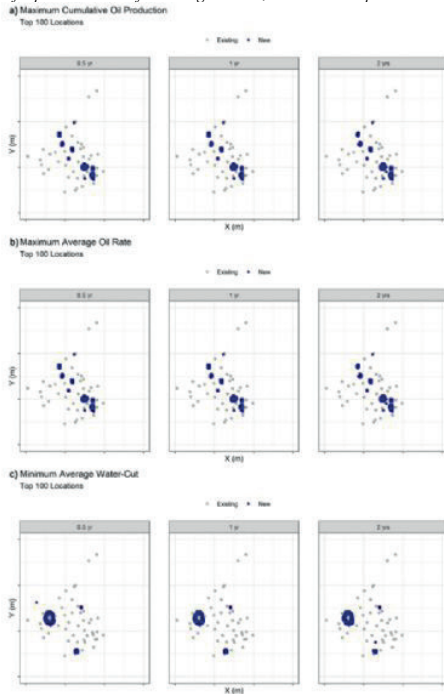


Figure 7: Map of top 100 locations for average oil rate, cumulative oil production and minimum water cut.

*Table.1 Selected four models for the forecasting application.*

No. of wells for Training	No. of wells for Testing	No. of hidden layers	No. of neurons in each layer	Seed	Avg. Training R2	Avg. Testing R2
44	4	3	79-23-18	10	0.99	0.90
44	4	2	65-35-0	980	0.99	0.84
43	5	3	91-24-15	980	0.99	0.83
44	4	3	68-37-10	500	0.98	0.81

# Determining Hydrocarbon-Bearing Volcanic Sediments using Neural Network Method – Based NPHI Cubes: A case Study

**Nur Göcer Ersay, Musa Çetin**  
Türkiye Petrolleri Anonim Ortaklığı



## SUMMARY

The exploration and identification of hydrocarbon fields play a crucial role in the petroleum industry. Traditional methods for reservoir evaluation often lack the resolution required to differentiate between producing and non-producing wells in areas with volcanic sediments. This study presents a methodology for determining hydrocarbon bearing zones in volcanic sediments using a neural-network based NPHI cube. The study has been conducted in the Thrace Basin, Türkiye where hydrocarbon is being produced from volcanic sediments. The relationship between the Neutron Porosity (NPHI) cube that was obtained from neural network (NN) and the Poisson Ratio (PR) cube which was obtained as a geomechanical parameter, has been proven to be beneficial in order to understand the study area and expanding the field's potential. Comprehending the correlation between these two parameters allows for more accurate determination of hydrocarbon accumulation locations and distinguish producing and non-producing wells. The results of the study were evaluated by comparing both cubes with the planned well data, hence demonstrating their usability.

## INTRODUCTION

Identification of hydrocarbon bearing zones accurately is essential for optimizing exploration and production strategies in petroleum industry. Seismic inversion is an effective method used for detection of hydrocarbon bearing zones within a field, however, traditional methods for reservoir evaluation often lack the resolution required to differentiate between producing and non-producing zones especially in reservoirs with volcanic sediments. In this study, a different methodology was proposed to address this challenge and to overcome the insufficiency of inversion studies by using neural network algorithms and geomechanical parameters. The study area is on the Thrace Basin where volcanic sediments are present (Figure 1). Previously drilled and blind wells that were used for the inversion are listed on Figure 1 with the prospective well location, Well-X. Main framework of the study was built upon pre-stack inversion analysis, which provided the acoustic impedance, shear impedance,  $V_p/V_s$  ratio, and related Lambda-Mu-Rho (LMR) cubes. Following the inversion analysis, Poisson's Ratio (PR) cubes were obtained by using the generated geomechanical cubes. The presence of fluid within pores has a direct influence on the PR rocks, making it possible to infer the nature of the pore fluid based on PR values. By examining the distinct correlation between PR and lithology, both the rock properties and the characteristics of the fluids present can be effectively determined (Zhao and Li, 2014). After the pre-stack inversion study,

the results have revealed areas within the field with potentially hydrocarbon bearing zones in volcanic sediments; however, a detailed resolution at the well log scale could not be achieved. Therefore, an NPHI cube was introduced to differentiate volcanic sediments from surrounding lithology, which was achieved with assistance of a neural network. NPHI can serve as a highly sensitive tool for obtaining average porosity information (Cannon, 2015). The neural network method plays a significant role in the analysis of seismic data and identification of hydrocarbon discoveries. A neural network model is an artificial neural network used to learn from and recognize patterns in large volumes of seismic data. This model processes the data, allowing for the identification and comprehension of intricate connections. In this study, Emerge module in the Hampson Russell software was used to create the neural network model. Emerge module within the Hampson Russell software uses geostatistical techniques to predict property volumes using well logs and attributes extracted from seismic data. The module enables the prediction of various properties, including NPHI which was specifically used in this study.

## MATERIALS AND METHOD

The outputs obtained from the seismic inversion study is shown in Figure 2. A crossplot zone along the line passing through Well-A and Well-B, reveals differences between two well locations. The target zone has been determined for these wells. However, it was observed that Well-E, despite not being a producing well, shows anomalies (Figure 3). Consequently, although the cubes enable the functionality, a detailed result cannot be obtained. To overcome this confliction, the seismic inversion results were accompanied by the PR cube, a geomechanical parameter. In an effort to understand the field, a difference was observed between wells that were used to generate pre-stack inversion results and those that did not. Due to its volcanic target nature within the field, the PR cube, in conjunction with the cross plot analysis, serves as an approachable parameter to determine the differences between producing and non-producing wells. Upon analyzing the obtained results, although a difference between wells was achieved, for a more detailed outcome and provide further elaboration, the NPHI cube obtained with assistance of neural network used with PR cubes cross correlation.

The neural network method was used to obtain the NPHI cube, by using well log data from three wells ( Well-C, E and F) located in the field (Figure 1). In addition to this, the best performing seismic attribute data from pre-stack inversion results, including the square of acoustic impedance cube, 1/Scaled Poisson Ratio cube, average frequency cube, frequency filter (15/20-25/30 Hz), and

amplitude weighted frequency cubes were used in neural network model to obtain the NPHI cube. The NPHI cube was generated by selecting the first three datasets with the lowest error. The verification error for all wells that were taken in the account in the operator length range is shown in the Figure 4. Wells with the lowest margin of error were chosen. Figure 4 also illustrates the selection of parameters and operators for the neural network method used. For the obtained cube with a correlation of 79%, it can be stated that the reliability decreases below 79% as we move away from the wells. It should be noted that it is appropriate to utilize other cubes when evaluating the results. The PR cube obtained from geomechanical properties is proven to be a significant parameter for reservoir oriented analysis and, when evaluated in correlation with the NPHI cube, reveals differentiation of the volcanic sediments with in the field.

## CONCLUSION

In conclusion, this study demonstrates the effectiveness of using a neural network based NPHI cube for determining hydrocarbon volcanic sediments where traditional methods for reservoir evaluation fails due to the lack of resolution. The methodology enables accurate differentiation between producing and non – producing wells, leading an improved reservoir characterization and resource estimation. Upon examining the reservoir geophysics results of the wells within the field, it has been observed that a difference can be obtained between producing and non-producing wells by using NPHI and PR cubes. In order to illustrate this differentiation, the study mainly focused on drilled wells, as depicted in Figure 5. As a result, it has been observed that the NPHI values with the range of 0.11-0.15, as well as the PR values with the range of 0.15-0.20, reflect the producing range along the field, based on the cross plot relationship between NPHI and PR cubes. The differentiation has been achieved throughout the utilization of the NPHI cube obtained by using neural network techniques; and the consistency of the results with the drilled wells has increased the confidence level in the study.

Furthermore, results have been presented for Well-x, which was a prospective well, also shows potential hydrocarbon bearing zones at the well location (Figure 6). It was later confirmed that following the well completion, the prospective interval of Well-X is in production.

## REFERENCES

- Zhao and Li (2014), Prestack Seismic Inversion and Seismic Attribute Analysis, Geophysical Exploration Technology.
- Cannon, S. (2015), Petrophysics: a practical guide. Hoboken, NJ: John Wiley & Sons.

Keywords: Seismic Inversion, Neutron Porosity



BaseMap

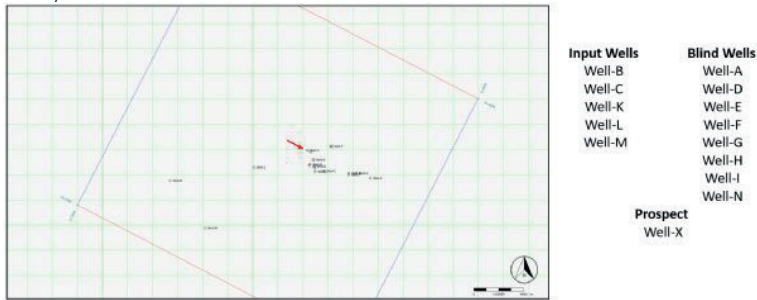


Figure 1. The basemap image of the study area. The wells used in the inversion study are Well-B, C, K, L, and M in sequential order. For the analysis, blind wells were used as Well-A, D, E, F, G, H, I and N. The verification well, Well-X is also located on the basemap with a red arrow.

LMR

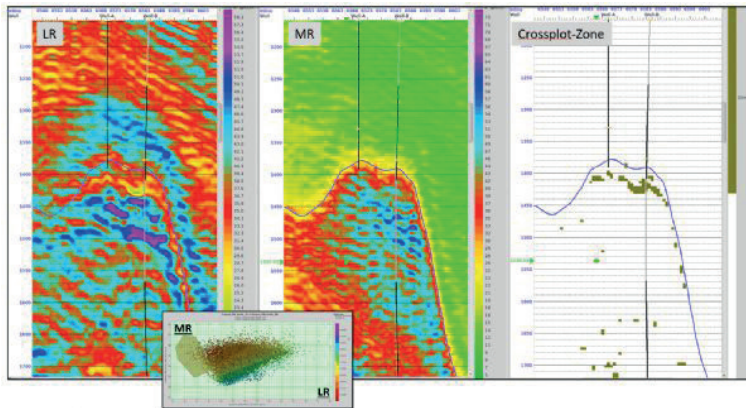


Figure 2. LR values (a), MR values (b), and the discriminative range (c) for target interval. By selecting the range where LR values are low and MR values are high, a crossplot zone (c) was created, showing anomalies along the line passing through Well-A and Well-B.

LMR-2

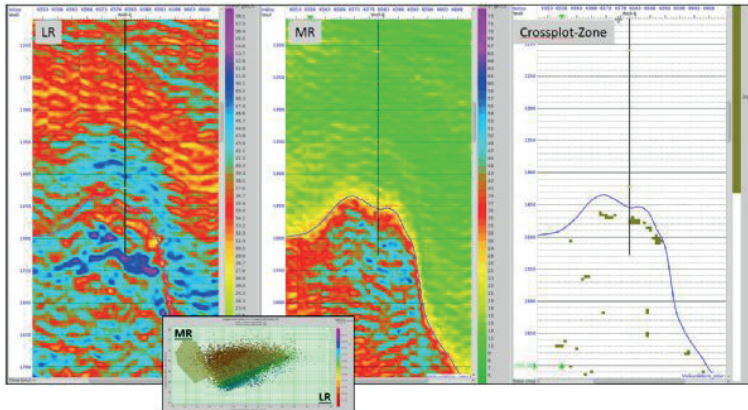


Figure 3. LR values (a), MR values (b), the discriminative range (c) for target interval. By selecting the range where LR values are low and MR values are high, a crossplot zone (c) was created, showing anomalies along the line passing through Well-E.

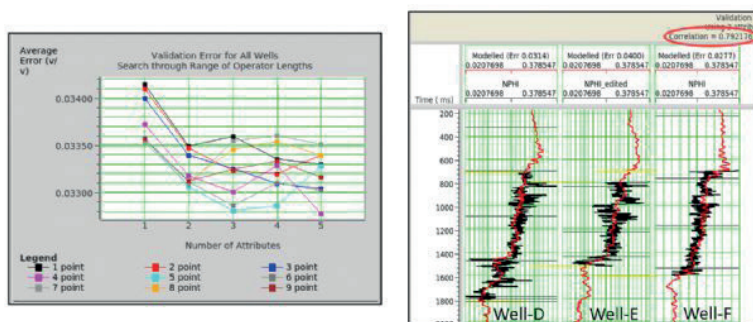


Figure 4. The operation length (a) and the verification error (b) for all wells Well- D, Well-E and Well-F.

NPHI cube

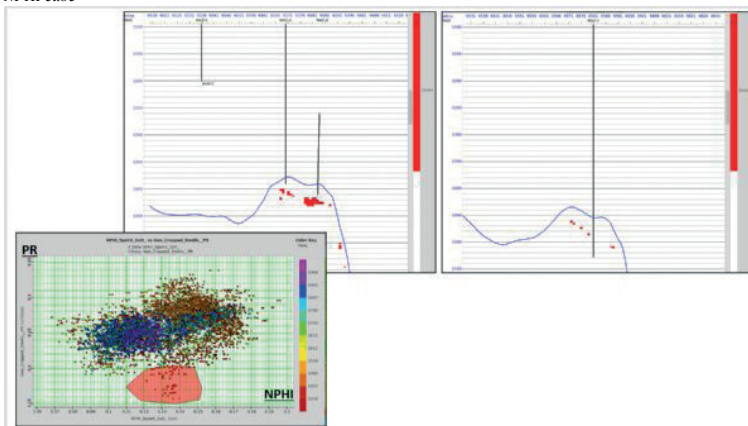


Figure 5. NPHI – PR cross-plot (a), the discriminative range (b) along the line passing through Well-A and Well-B, the discriminative range (c) along the line passing through Well-E. By selecting the range where NPHI values are between 0.11 – 0.15 and PR values are between 0.15-0.20.

NPHI

cube

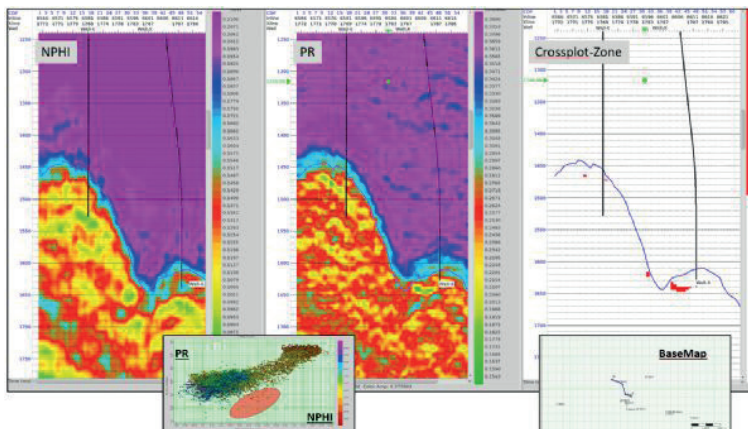


Figure 6. NPHI – PR cross-plot (a), NPHI values (b), PR values (c), the discriminative range (d) for target interval along the line passing through Well-X. By selecting the range where NPHI values are between 0.11 – 0.15 and PR values are between 0.15-0.20.

# Leveraging Edge Computing with Artificial Intelligence and Machine Learning for Subsurface Assets

**Afife Gozde Celik, Ratish Kumar Selvaraj**

SLB, Digital and Integration, London;Ankara



The process of making decision to respond on events occurring in subsurface equipment requires strong domain expertise and bias for action. Today limitless data is available from the equipment through controllers, however, comparing the equipment data with changing downhole flow condition is cumbersome to make right decision. Latency adds more challenges to respond if the equipment is in remote operating environment resulting in production loss and reduce total cost of ownership. Integral approach of applying data from the equipment and using multiple classical machine learning models for prediction of flow rate estimation real-time on well with Industrial Internet of things (IIoT) using edge computing to take an action at wellsite shall improve production optimization, increased equipment efficiency and reliability.

This presentation describes the workflow of machine learning algorithms with rule-based criteria, AI based workflows to improve the robustness of algorithm to improve ESP performance prediction based on real time virtual well flow condition. Also explains the application of advance edge computing device in the control the operation of ESP workflow to take remedial action with autonomy or minimum supervision.

## INTRODUCTION

ESP is an efficient and reliable artificial lift method that has evolved to become a critical component in many production operations and well productivity enhancement (Adesanwo et al. 2017). Therefore, it has become more important to anticipate, diagnose and control serious abnormal events in a timely manner. As the operation moves toward more complicated environments, the challenges posed to the ESP operation are also drastically increasing. ESP performance may decline without much warning and may abruptly reach the workover point leading to deferred oil production and unplanned replacement cost (Gupta et al. 2016). Traditionally, ESP monitoring relies on production engineers who are experienced with good interpretation skills (Diker et al. 2021), but this process may enlarge the response time and consequently become less effective. Therefore, a data-driven ESP smart alarm suite, integrated with a virtual flowmeter (VFM) deployed on the Edge has been adopted to enable real-time monitoring as proactive means to optimize performance, safeguard ESP health and minimize trips.

The provided Edge computing capability enables automated data acquisition, analysis, and alarm triggering, supporting real-time monitoring while avoiding latency issues or bandwidth limitations.

The overall smart alarm suite consists of eight different alarms, each targeting a specific potential suboptimal pump working condition.

## METHODOLOGY

This section explains the main workflow and methodology applied for the proposed smart alarm suite. Eight alarms are targeted in this suite as three standalone modules and five Edge-VFM-dependent alarms, each with a specific use case. Individual alarms can also be packaged separately if needed.

The attached Figure-1 summarizes the high-level workflow of the smart alarm suite.

### Motor Winding Temperature (MWT) Alarm

The MWT alarm are used to detect any abnormal changes in the motor winding temperature during the ESP operation.

In this alarm workflow, the MWT alarm consumes three different channels of ESP sensor data including MWT, ESP Drive Frequency, and the Average Amperage while having a Random Forest model trained based on three historical events tracked during operations. Subject matter experts (SMEs) manually labelled the training data following the logic that, when the MWT increases while the average amperage and the drive frequency stay constant, the alarm should be triggered. Additional features for the model include the one-hour rolling differences for each of the three data categories.

In the training process, the testing wells' data is split, in which 70% of records are fed into the train set, and 30% are fed into the test. The testing F1-score is close to 99%, demonstrating outstanding model accuracy. The model is packaged as an application programming interface (API). This API sits within a Docker container, a software packaging module that uses OS-level virtualization. The API is deployed for field testing, where the received field response enables future model re-training. Typically, we would like to implement machine learning model operationalization management (MLOps) for any model we deployed to improve the performance and gradually evolve the ML-based product, given the iterative nature of the ML-based tools.

## EMULSION ALARM

Emulsions are formed by non-soluble liquids agitated together, dispersing one into another, leading to increased viscosity of fluid produced. The formation of emulsions is detrimental to pump performance and affects fluid flow rates. There is also an increased potential for equipment failures, which may increase the cost of operation (Benedicte et al. 2017).The system is packaged as a self-sustained, containerized module that can be deployed as an on-premises service on gateways in the field. The modular nature of the emulsion detector allows for incremental modifications and expansions to field-specific deployments on wells.

The Emulsion detector module encompasses a machine learning model that is trained to capture the intricate underlying relationships between ESP signals that are indicative of emulsion formation. The model evaluates the timeseries data to output the emulsion identification probability and a binary value as an alarm indicator based on a preset probability threshold. These results are plotted over time and displayed on visualization dashboard accessible to engineers.

High frequency time series data are aggregated from ESP sensors and collected into a data store including pump intake and discharge pressures, motor temperature, vibration, frequency, etc. The historical emulsion events are identified by SMEs and the unique identification signatures are labeled and reviewed before being ingested into the model training pipeline. Features are generated on relevant signals using simple and complex descriptive statistics over rolling window calculations. These features help remove the temporal dependency of the sequential timeseries data, allowing for use of traditional machine learning techniques. The correlations between these features are assessed and considered to identify and discard non-relevant/non-descriptive features. From the remaining features, a subset is selected based on feature importance to further reduce the feature space and allow for a model that is made of more representative features.

The extent and feasibility of detection of emulsions is determined during the preliminary model development stage. During this stage, a model is developed on a subset of the data, the results are reviewed, evaluation metrics are established, and visualization dashboards are prototyped. On review, multiple machine learning models are built using the selected features, along with further feature reduction using techniques. Tree-based models like Random Forests prove to perform exceptionally well on these data, and after hyperparameter tuning to ensure the best fit using predefined evaluation metrics, a final model is selected and exported. The model is blind tested against time series data from a similar field as the original dataset; the selected key features, as well as model performance and emulsion detection probabilities are reviewed and interpreted.

An inference workflow is built using the exported model, and an API is designed to act as a wrapper to communicate with edge devices. The results are reviewed using an internal visualization dashboard to display trends in emulsion detection, probability scores over time and the detection threshold set by SMEs. This workflow is packaged as a containerized module to be triggered at a desired frequency by clients.

The current accuracy of the emulsion detector model is 94% using a probability threshold of 0.65. The edge response time of the emulsion alarm module is 5 seconds.

### GAS LOCKING (GLK) ALARM

Gas locking is one of the situations that the pump would ideally need to avoid during its operation. It is either

something like a gas slug causing the amount of gas at the pump intake to increase, or the pump to produce more head than it can (Dowling 2017).

In the present application, the GLK conditions are differentiated into three detectable categories: normal gas lock, gas lock when the pumping unit has proportional-integral-derivative (PID) controller, and suspected gas lock with emulsion potential. The normal gas lock (GLK Type 2 in our notation) is the condition when the intake pressure is consistently increasing because of the accumulation of gas. On the contrary, if the variable speed drive (VSD) has a PID module, the PID controller would automatically adjust the frequency when gas locking starts, leading to fluctuating frequency and intake pressure (GLK Type 1 in our notation). Another similar condition is that, if there is a potential of emulsion formulation, the intake pressure would still fluctuate even when at a constant frequency. This is the suspected gas lock condition, which ideally should be cross-checked against the previous specific emulsion alarm for confirmation.

The input data channels fed into the algorithm contain pump intake pressure, discharge pressure, and drive frequency. One issue during the alarm building is that there was only limited labeled data. Therefore, the detection algorithm is constructed as a hybrid pipeline. The benefits of using a hybrid pipeline are that it can serve as a first path for alarm triggering and it can generate a labeled dataset for future machine learning model training.

In the current hybrid workflow, the main detecting algorithm uses the rolling regression and the Pearson correlation calculations of the input data channels. The rolling regression is essentially a linear regression performed on the moving horizon, and the Pearson correlation is the correlation coefficient that measures the linear correlation between two sets of data. The rolling window is set as three hours based upon the offline testing results. It also removes potential false alarms associated with pump start-up by detecting ultra-low frequency points within the rolling window. As for the cutoff values used for this alarm, a machine-learning-based offline workflow is implemented. For example, one of the key cutoffs used in this pipeline is the value for pump intake pressure's rolling variance, and this threshold value is determined by a two-step workflow:

- Isolation forest algorithm implemented to remove outliers in the dataset
- K-Means clustering (with two clusters) to differentiate groups with high and low rolling variances. The high variance represents fluctuating intake pressure conditions, corresponding to gas locking under PID condition or suspected gas locking.

### EDGE-BASED VIRTUAL FLOWMETER (EDGE VFM)

Flowrate enables diagnosing multiple unfavorable conditions in the production system. However, it is not

available as frequently as required for these real-time workflows.

Several approaches to calculating real-time flow rates using trending ESP parameters have been attempted and documented. Most of approaches to calculating real-time flow rates using trending ESP parameters leverage the differential pressure across the pump and its relationship with the flow rate defined in the pump curves.

The proposed solution leverages a multiphase flow simulator adapted to run at the Edge to compute flowrates using the differential pressure across the pump and the one that occurs at the reservoir level. The first method uses calibrated pump curves to better represent the flow across the pump, and the second method uses a simplified inflow performance relationship (IPR) curve. The workflow described in the attached Figure -2 is entirely autonomous and manages the whole model lifecycle, including the calibration of both methods at the Edge.

The head-based method, which is the one with less uncertain variables, has shown the ability to keep its representativeness even when facing changes in frequency, fluid properties, flow conditions, and reservoir deliverability.

The combination of the two models enables further detection of problems that will be described in more detail in the next section.

Edge VFM Dependent Smart Alarms (Pump Wear, Pump Operating Condition, Pump Efficiency, Productivity Drop, Tubing Leak)

With the help of the Edge VFM deployment, the constructed wellbore models on the Edge will be calibrated whenever the sporadic data is fed into it. Therefore, the ESP pump performance curve is calibrated with updated pump rates and head derating factors. As the other component of the nodal analysis, the reservoir IPR model is also updated to reflect the current inflow condition. Two types of flow rates are yielded by the Edge VFM: head-based flow rate and IPR-based flow rate as mentioned.

In general, the calibration of the ESP and IPR components are not required to be synchronized, and the calibration of the pump performance curve happens more frequently. Therefore, the head-based flow rate is more up to date and is used in combination with the performance curve to estimate the following three alarms: pump wear, pump efficiency, and pump operating condition. The VFM calibration process will directly yield the updated pump derating factor, contributing to the pump wear alarm when compared against preset threshold value determined by SMEs. The head-based flow rate is compared against the operational envelope at the real-time current frequency to determine whether the pump is up thrusting or down thrusting. Additionally, the pump efficiency could be calculated in real time using the pump performance curve as well using the polynomial factors. These three metrics are calculated using physics-based rules on the Edge, enabling on-the-fly evaluation of the ESP operational

condition with which the traditional approaches could never have achieved.

In addition to the above three alarms, two others are also enabled using the Edge VFM. In these two use cases, both the head-based and IPR-based flow rates are utilized, and the joint trend contributes to the detection of the anomaly. The first alarm here is the tubing leak alarm. Theoretically, when the tubing leak happens, the pressure drop across the pump will decrease drastically, yielding a fast-decreasing pump head. When this abnormal pump head is fed to the Edge VFM, an increase in the head-based flow rate value will occur. On the other hand, as the pump intake pressure increases, the IPR-based flow rate calculation will decrease because of the decreased pressure drop inside the reservoir. Therefore, when a tubing leak occurs, we should expect a divergence in the two flow rates calculated by the VFM, where the head-based flow rate goes up and the IPR-based goes down. Figure-3 is an example of the testing case.

It shows that two flow rates calculated are diverging even at the beginning of the given period, indicating a developing tubing leak condition. Around early December 2021, the two flow rates are converging and the tubing leak indicator decreased one level. This matches the field remedial action taken at the same time period. This means that the tubing leak alarm is not only able to detect the leak event, but also the degree of the leak no matter whether the situation is improving or deteriorating.

A similar concept by using the two flow rates calculated could be applied to detect whether a productivity drop is developing in the reservoir. Theoretically when productivity is dropping, the skin factor in the IPR model should increase, leading to decreased pump intake pressure and flow bottomhole pressure. Given a stable reservoir pressure, the IPR-based flowrate value should increase if no calibration has been performed. On the other hand, the head-based flow rate will decrease as the pressure drop across the pump will increase.

## FINDINGS ON THE DEPLOYMENT OF THE EDGE

As the Edge is connected near to the data source, deployment at the Edge brings multiple benefits to the operations such as faster and deeper insights. It also allows for predictive analysis in near-real time, improving response times. This increased analytics capability in edge devices can power innovation to improve quality and enhance value.

The computing power from the Edge device in combination with fit to purpose instrumentation and production operations knowledge are the next step in reducing production losses and production optimization; the ESP surveillance was one of the firsts deployments that opened the window for different and innovative production workflows as in the following:

- Annular gas handling, which is an automated process to handle high gas wells to enhance production,

- Visual analytics to remotely monitor flares, including the flare gas volume measurement without the need for meters,
- Predictive health maintenance of horizontal pump systems with innovative sensors connected to the Edge,
- Multiphase flowmeters with real time monitoring and remote actions in combination with ESP Surveillance,
- Early events detection that affects ESP run life (smart alarms),
- Alerts and online set points report,

Remarkable results were achieved: 12-30% of oil production improvement, reduced field crew visits to the wells > 95%, and carbon footprint improvement, counting 4.4 km not traveled, and 0.75-ton CO<sub>2</sub> associated.

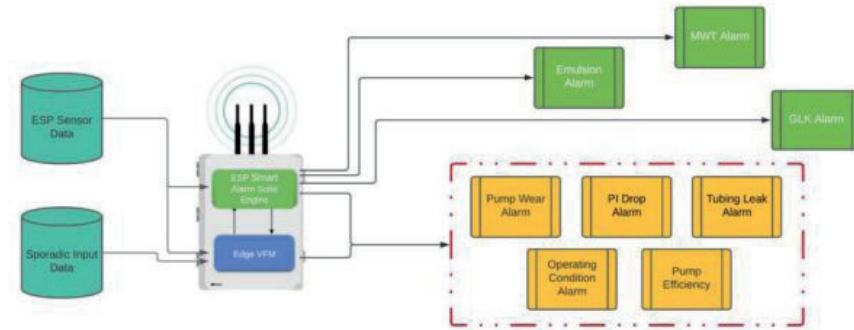
In late 2020, the first version of the smart alarms including Gas Lock detection, Motor Temperature was deployed over 300 oil producing wells in 2 different oilfields. In early 2022, the new version of the smart alarms was released.

## CONCLUSION

In this paper, a comprehensive ESP smart alarm suite is presented with the purpose of detecting early-stage anomalies during ESP operations, and to avoid unwanted events that may lead to deferred oil reduction. This presented workflow uses Edge computational powers with both data-driven and rule-based logics to fulfill its mission, and the successful incorporation of the Edge-based VFM provides valuable information regarding the real-time flowing conditions. Being able to evaluate the health condition of the ESPs in real-time has provided the end-users with a significant advantage to gain control of the field under operation and has saved precious time to perform required corrective actions to avoid any deteriorating potential.

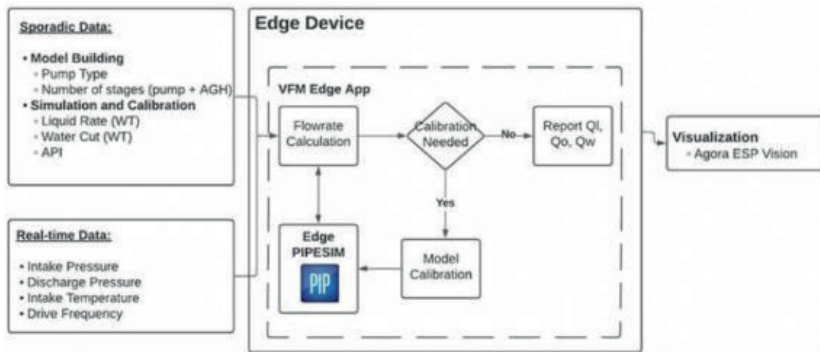
Keywords: artificial intelligence, edge computing

Figure-1



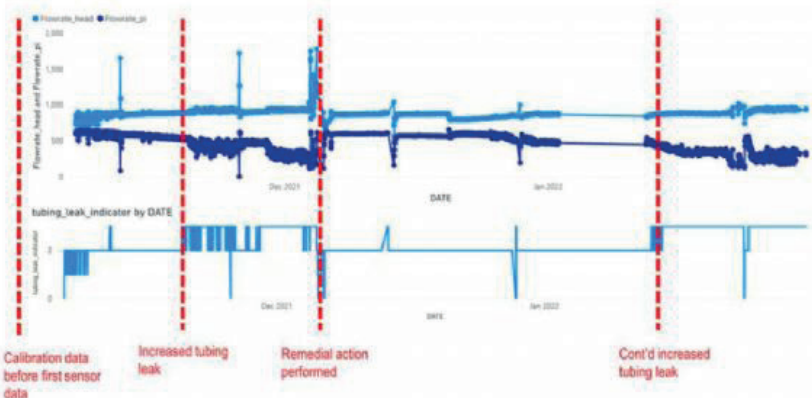
Overall workflow of the ESP smart alarm suite

Figure-2



Edge VFM Workflow

Figure-3



Edge VFM based tubing leak alarm testing result

# Prediction of Flow Rates from Using PLT p-T Measurements in a Horizontal Well By Machine Learning Methods



**Muharrem Hilmi Cevik, Murat Çınar**

Istanbul Technical University, Department of Petroleum and Natural Gas Engineering

## SUMMARY

The petroleum production process has a history of over a century, starting with vertical wells and evolving to include deviated and horizontal wells with technological advancements. Production Logging (PL) is a method used to determine fluid flow rates and distribution in petroleum wells. PLT measurements are obtained to assess production stages and rates in different zones. Traditional PL tools designed for vertical wells became inadequate for complex deviated and horizontal wells, leading to the development of new devices. PLT testing in horizontal wells can be challenging particularly if the flow rate is below 500 barrels per day and expensive.

Correlations between flow rate, pressure, and temperature can help predict flow rates. Horizontal wells enable high-flow oil and gas production, offering economic benefits. However, they also come with technical challenges like increased pressure drop and unbalanced flow profiles. Inflow Control Devices (ICDs), a result of advanced drilling technology, help resolve these issues.

Machine learning enables models to learn and improve from input data, making predictions and quick analyses. It has diverse applications, including image recognition and classification. The oil and gas industry's extensive data collection suggests increased use of machine learning in this field.

A commercial software was used to simulate a horizontal well reservoir system. The simulation involved modeling heat transfer, pressure and temperature distribution, and flow rates. The basic grid blocks in the I, J, and K directions are 162, 51, and 1, respectively. The well is positioned at the 26th grid block in the J direction and consists of 112 grid blocks in the I direction and the FlexWell option was used for better performance and production data. To simplify the model, the reservoir was simulated relative to the well rather than as a deviated well.

The goal is to predict each Inflow Control Device's contribution using machine learning techniques. A well reservoir model generates data on pressure, temperature, and flow rates. Machine learning models predict flow rates for high-choke and low-choke scenarios using this data. Synthetic data is created with CMOST module, and 4828 experiments were conducted in total.

The study aims to predict flow rates in six production zones using pressure and temperature data from two different PLT measurements (high-choke and low-choke). The goal is to find an alternative solution to PLT's limitations in low flow regions. Machine learning techniques are used to make flow rate predictions based on synthetic data generated from a well model with adjusted perforations using high-choke PLT data.

Machine learning techniques, including decision tree regression, linear regression, ridge regression, and random forest regression, were used to predict flow rates using pressure and temperature data. Decision tree regression and random forest regression performed the best. Predictions with high-choke data were nearly perfect. For low-choke, the test scores exceeded 90% but predictions were not as accurate. Nonetheless, the ML algorithms show promise for flow rate predictions.

The accuracy scores for low-choke are high, indicating that both algorithms can create effective machine learning models for synthetic scenarios. However, using only pressure or temperature parameters leads to higher error percentages in flow rate predictions using ML techniques. The Random Forest Regression (RFR) algorithm with temperature data yields the lowest error percentage. More parameters, particularly the pressure difference created by Inflow Control Devices (ICDs) in the wellbore, could improve the model's accuracy. For the High-choke situation, the ML algorithm shows promise, but more work is needed for generalization.

## METHODOLOGY

The relationship between pressure-temperature measurements and flow rates obtained from individual Inflow Control Devices (ICDs) has sparked the idea of using pressure-temperature (p-T) data to estimate flow rates in Production Logging Tool (PLT) operations for horizontal wells. In some instances, the reliability of flow rate data from PLT spinners is compromised due to tool sticking, resulting in flow rates being limited to approximately 500 RB/D. In such cases, estimating flow rates from p-T measurements becomes crucial for successful and cost-effective operations. Additionally, the possibility of cross-verifying spinner estimations (which require calibration) with flow rates derived from p-T data is considered practically useful. To achieve this, algorithms are developed using regression models.

The work is composed of three fundamental parts; 1) Developing a general model using real-world well configurations from the field. 2) Training the algorithm using synthetic data that is generated. 3) Testing the algorithm using actual measurements obtained from the field.

The available PLT measurements are from a horizontal well. However, the information is limited as there are no detailed data regarding the fluid properties or the reservoir. There are two distinct measurements: the first one was taken under high choke, resulting in a flow rate of 6,180 RB/D, and the second measurement was obtained under low choke, corresponding to a flow rate of 4,200 RB/D.

The modeled well has a total length of 10,304 ft, with an



actual vertical depth of 6,783 ft. The well is divided into six entrance zones, and each zone is equipped with 2.96 ft long ICDs to balance production. Although the well is primarily horizontal, there are deviations at certain points along its length. The specific section of the well to be modeled is depicted in Figure 1.

### PRODUCTION LOGGING DATA

The production log was conducted twice, using both high choke and low choke sizes, resulting in four sets of data: high choke-down survey for pressure, high choke-up survey for temperature, low choke-down survey, and low choke-up survey. Among these data sets, the high choke-down survey for pressure and the high choke-up survey for temperature were selected as they exhibited cleaner and less noisy measurements compared to the others. These data sets were used to create profiles for flow, pressure, and temperature. Figure 2 displays separate profiles for oil flow and water flow. For modeling purposes, a single-phase oil production model was adopted since water production is significantly lower and can be considered negligible.

The pressure profile, corresponding to the flow, is presented in Figure 3, indicating a total pressure difference of approximately 72 psi along the well. This pressure difference arises not only from friction but also from varying elevation differences from one zone to another. Figure 4 displays the temperature profile corresponding to the flow, showing an increase in temperature in the inlet zones due to the Joule-Thomson effect. As the flow moves towards the next inlet zone, the temperature tends to cool down due to heat losses in the wellbore. During oil production, temperature increases following pressure reduction due to the Joule-Thomson effect (Onur & Cinar, 2017). Though the change in temperature is minimal, it falls within the detection limits of current temperature sensors used in the industry. The slopes of the temperature usually exhibit a gradually decreasing pattern because of the increased flow rate between each pair of Inflow Control Devices (ICDs). As a result, temperature effectively identifies the productive zones or, in this case, the ICDs. The magnitude of the temperature change depends on fluid and reservoir characteristics, where the thermodynamic properties of the reservoir fluid dictate the rise. Furthermore, as the temperature rise is associated with pressure reduction, any parameter affecting pressure drawdown would influence temperature, indicating a correlation between flow rates and temperature.

The flow rate data obtained from the spinner or any other source tends to be noisy and challenging to simulate. For the sake of simplicity, the section of flow data before 7640 ft was excluded, and the average flow rate value was adopted between each pair of ICDs, as depicted in Figure 5.

### CMG MODEL

A commercial software called CMG was utilized to simulate the horizontal well-reservoir system. The input

data for the modeled reservoir are provided in Table 1. The simulation encompasses the analysis of heat transfer between the wellbore and the reservoir, the distribution of pressure and temperature throughout the well, and the calculation of flow rates.

The reservoir model consists of a total of 8262 grid blocks, with 162, 51, and 1 basic grid blocks in the I, J, and K directions, respectively. The well is positioned in the 26th grid block, which is at the center of the grid blocks in the J direction, forming 112 grid blocks in the I direction. The spacing of the well blocks is not even, and the FlexWell option was employed to enhance numerical performance and acquire production logging data from the software.

Additionally, the other grid blocks in the I and J directions are not evenly spaced but are arranged logarithmically. Figure 6 provides a 3D view of the reservoir model. For simplicity, to eliminate pressure differences caused by elevation, the well is not modeled as deviated, and the reservoir is instead modeled according to the well's position.

To enhance the precision of pressure and temperature measurements, a local grid refinement technique was implemented, creating 10 radial grids around the wellbore by dividing the parent blocks into child blocks, as depicted in Figure 7. Furthermore, to model the contribution obtained from the Inflow Control Devices (ICDs) in the actual field data, certain skin factors were assigned to the grid blocks of the ICDs in the CMG software. The skin factors, as presented in Table 2, were estimated based on high-choke flow rates since the specific ICD configuration data was not available for use.

### RESULTS

In this section, the objective is to use machine learning techniques to estimate the contribution of each Inflow Control Device (ICD). To achieve this, pressure, temperature, and flow rate data are generated using the CMG model. The generated pressure and temperature data are then utilized to obtain separate flow rate estimates for both high-choke and low-choke scenarios, employing machine learning algorithms. For each machine learning model, 70% of the data is used for training, and the remaining 30% is used for testing the model's performance.

### ESTIMATING FLOW RATE OF EACH ICD USING MACHINE LEARNING

Synthetic data is generated using the CMOST module, which is a part of the CMG simulator suite. The variables for the synthetic data are the permeability values of the grid blocks where each ICD is located. These permeability values range from 50 to 500 millidarcies (md) and are randomly assigned from a uniform distribution. As a result, a total of 4828 experiments were conducted to encompass various combinations of permeability values and their impact on the well's performance and flow rates.

### FLOW RATE ESTIMATION WITH HIGH-CHOKE PRESSURE DATA BY ML TECHNIQUES

The pressure dataset obtained from CMOST contains 107 rows and 4,829 columns. To utilize this data in ML techniques, we need two input values: one for the grid block and the other for the corresponding pressure data. To achieve this, the pressure values were combined into a single column instead of having separate columns, resulting in a new dataset with dimensions of 516,596 rows and 2 columns, as illustrated in Figure 8.

Similar to the pressure data, flow rate dataset was converted into a cumulative flow data set. Then, our dataset was transformed into 516,596 rows  $\times$  1 columns, as we will have an output value as the flow rate.

We trained these datasets as 70% train and 30% test size in the decision tree regression, linear regression, ridge regression and random forest regression module of the Python language. The random forest regression that gives the best results is shown in Figure 9. The accuracy scores of the test data for this method are presented in Table 3. In this table, the test and train scores are nearly identical, indicating that there is neither overfitting nor underfitting of the model. Prior to estimating the flow rate data, a standardization process was applied to the dataset.

In this case, the models were trained using three independent variables: grid block address, synthetic pressure, and synthetic flow rate data. The flow rate estimation results are almost perfect, particularly for decision tree regression and random forest regression. The reason behind these highly accurate estimations is that the model was specifically designed for high-choke pressure and flow rate conditions.

### FLOW RATE ESTIMATION WITH HIGH-CHOKE TEMPERATURE DATA BY ML TECHNIQUES

In this section, the same procedure is followed for estimating flow rate from pressure data. In this section, only decision tree regression and random forest regression as shown in Figure 10 are used as we get better results than the other two ML techniques. The accuracy score is as in Table 4. As evident from Figure 10, the flow rate estimation based on high-choke temperature data is reasonably well-matched, although not as perfect as the estimation from pressure data. The model's success in providing good results is primarily attributed to its tuning with high-choke data, which serves as the fundamental reason behind the accuracy achieved.

### FLOW RATE ESTIMATION WITH LOW-CHOKE PRESSURE AND TEMPERATURE DATA BY ML TECHNIQUES

In this section, synthetic data for pressure, temperature, and flow rate is generated by modifying only the flow rate parameter of the model previously obtained for

high-choke conditions. The flow rate parameter is set to 4200 RB/D, and the same procedure is replicated in this section. The aim is to estimate a low-choke flow rate using the pressure and temperature data with the help of the model trained on the newly generated synthetic data. Using random forest (RFR) results shown in Figure 11 and decision tree ML techniques, the accuracy of flow rate estimation based on both pressure and temperature data shows similar trends but is inconsistent. The model was not able to accurately replicate the measured flow rates. Table 5 presents the percentage of error in the estimated flow rates for each ICD. According to this table, the RFR algorithm's estimation using temperature data yielded better results compared to other estimations. For the 6th ICD, an estimation error could not be calculated due to the absence of raw data. However, when examining the 5th ICD, the RFR algorithm's error in estimating flow rate based on temperature data is significantly superior to other estimations. Consequently, it is evident that this study can be enhanced by incorporating new independent variables.

### CONCLUSION

The problem of overfitting and underfitting is a common challenge in machine learning techniques. However, in our study, we did not encounter this problem or managed to avoid it by utilizing random forest regression and decision tree regression. Moreover, we found that both algorithms were highly suitable for handling large datasets. These techniques establish non-linear relationships between independent and dependent variables. Each tree in the algorithms provides an individual estimate, and the results are then averaged, which leads to increased accuracy and reduced overfitting. Considering each interval for ICDs as a tree, these algorithms easily learn these intervals and produce high-accuracy results. The fact that the estimation of all synthetic data resulted in an accuracy score of over 90% indicates that these two algorithms are remarkably successful in estimating flow rates.

We employed the random forest regression and decision tree algorithms, trained with synthetic datasets, to estimate the PL high-choke and low-choke flow rates. The independent variables used for flow rate estimation were the location-pressure and location-temperature. High-choke flow rate estimation was carried out quite successfully. However, low-choke flow rate estimation was not as accurate as high-choke flow rate estimation. This discrepancy is attributed to the use of the high-choke simulation model to generate synthetic data, which might introduce inconsistency between PL measurements and synthetic data. To mitigate this inconsistency, we propose meticulously defining fluid parameters, incorporating ICD properties as inputs to the algorithms, and considering the temperature difference created by the time delay when measuring from the toe to the heel end in PL measurements.

REFERENCES

Onur, M., & Cinar, M. (2017). Analysis of sandface-temperature-transient data for slightly compressible, single-phase reservoirs. SPE Journal, 22(4), 1134–1155. <https://doi.org/10.2118/180074-pa>

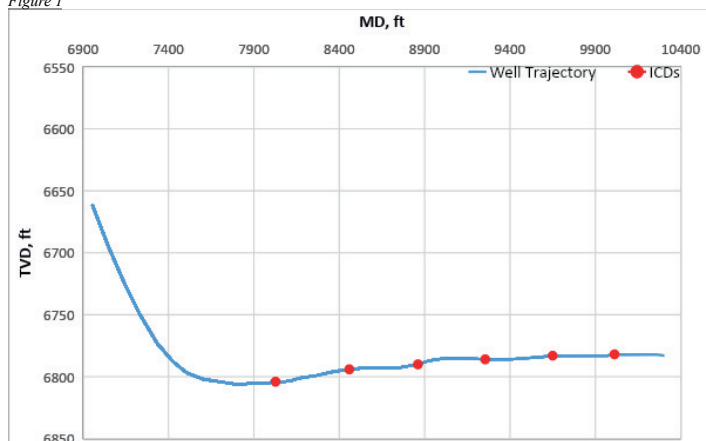
STARS. (2020). Computer Modelling Group LTD. Calgary, Canada

CMOST. (2020). Computer Modelling Group LTD. Calgary, Canada.

Python Software Foundation. (2023). Python Language Reference, version 3.11.4. Available at <http://www.python.org>

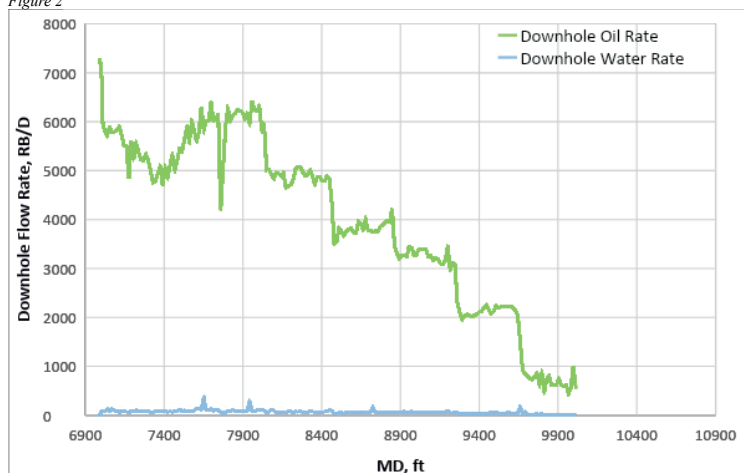
Keywords: Machine Learning, Production Logging

Figure 1



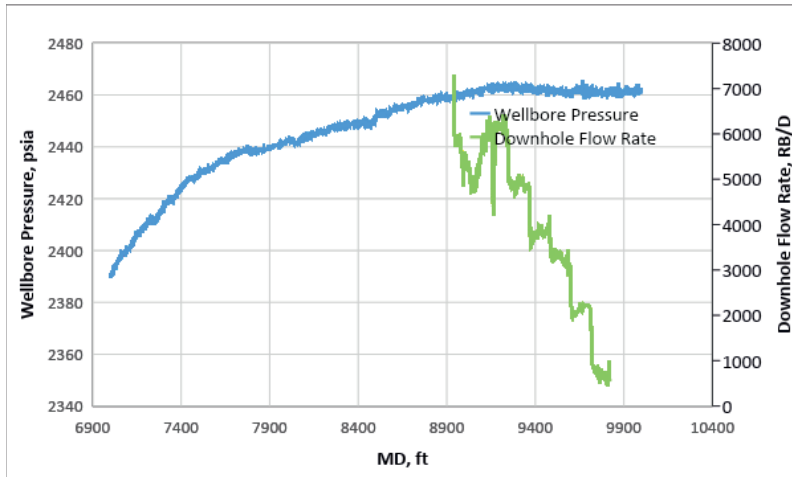
Modeled part of the well.

Figure 2



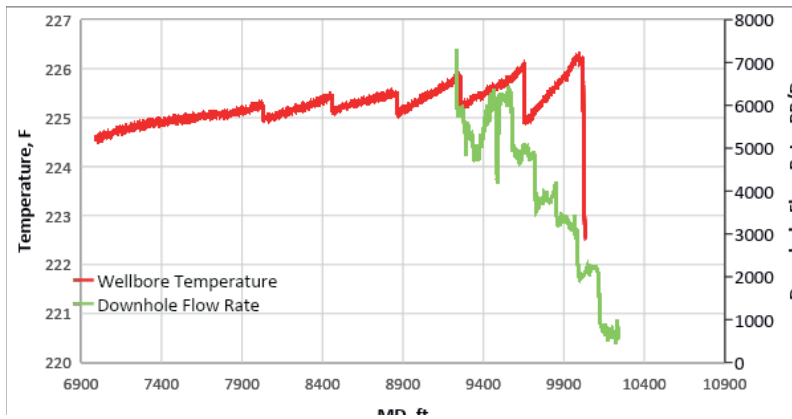
Flow profile of the well.

Figure 3



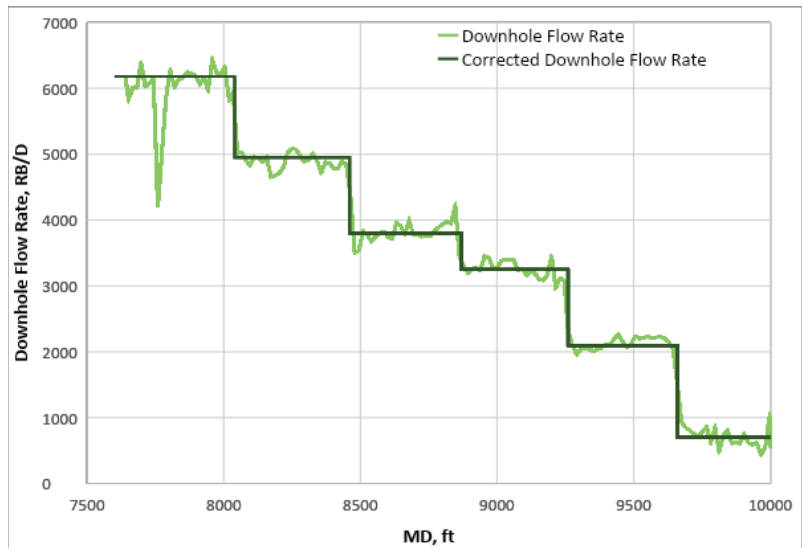
Flow profile and wellbore pressure.

Figure 4



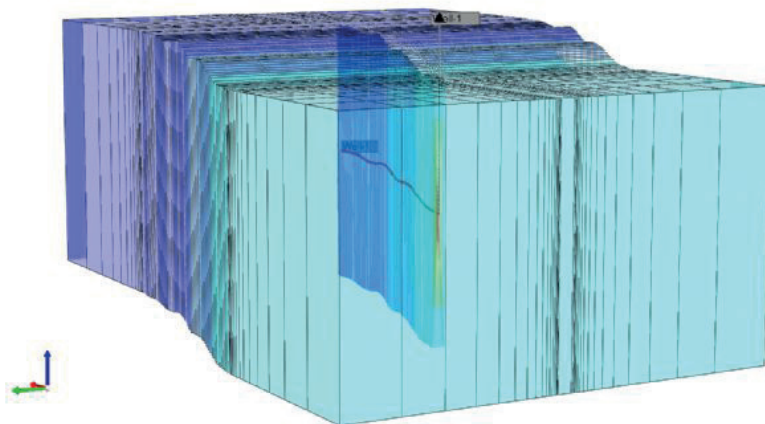
Flow profile and wellbore temperature.

Figure 5



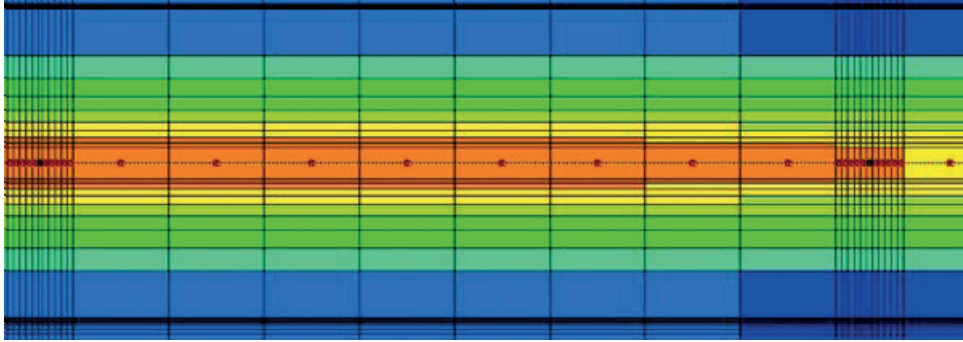
Corrected downhole flow rate.

Figure 6



The 3D view of the reservoir model.

Figure 7



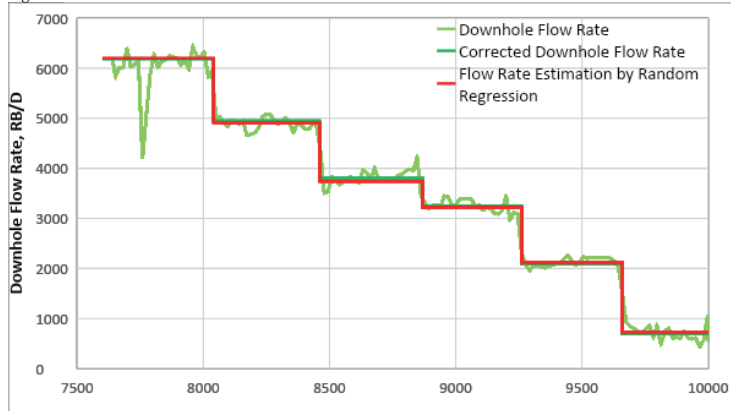
Local grid refinement.

Figure 8

grid_number	pressure, psi
0	15.29061
1	16.36766
2	17.36585
3	18.55517
4	19.67536
...	...
516591	1721.49300
516592	1721.48400
516593	1721.47500
516594	1721.46700
516595	1721.45600

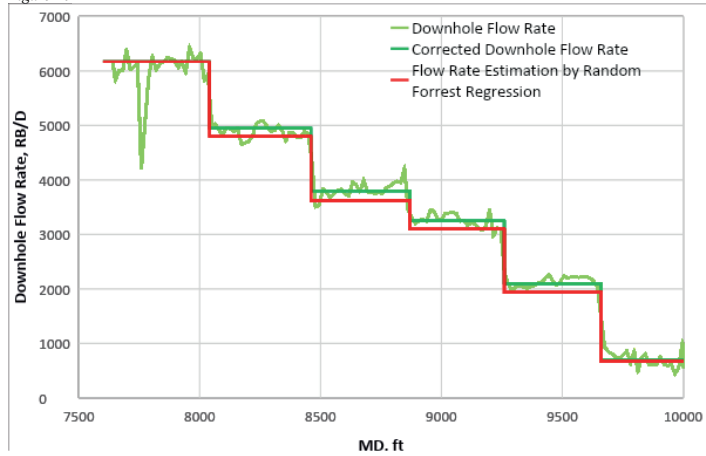
Pressure dataset.

Figure 9



Actual flow rate data and data obtained from pressure by random forest regression comparison.

Figure 10



Actual flow rate data and data obtained from temperature by random forest regression comparison.

Figure 11



Actual flow rate data and data obtained from low-choke temperature by random forest regression comparison.

Table 1

Input Data	Value
Reservoir Size, acre-ft	1,285,994
Initial Temperature, °F	218.39
Initial Pressure, psi	3343
Porosity, fraction	0.25
Permeability(l=J), md	350
Initial Oil Density, lb/ft3	46.8
Oil Viscosity, cp	1.84
Initial Oil FVF, RB/STB	1.23
Oil Saturation, fraction	1
Oil Compressibility, 1/psi	1.35E-05
GOR, f3/RB	421
Well ID, in.	4
Well Length, ft	2,251.46
Relative Roughness	0.0775

Input data used in reservoir modeling.

Table 2

ICD	Grid Block Address	Skin
1	36 26 1	0
2	56 26 1	0.3
3	75 26 1	8
4	93 26 1	2.1
5	113 26 1	3.4
6	132 26 1	10

Skin factors in each ICDs.



Table 3

ML Method	Accuracy Score
Decision Tree Regression	0.92
Linear Regression	0.87
Ridge Regression	0.87
Random Forrest Regression	0.95

Accuracy score of flow rate estimation of test data from pressure data for high-choke.

Table 4

ML Method	Accuracy Score
Decision Tree Regression	0.92
Random Forest Regression	0.92

Accuracy score of flow rate estimation of test data from temperature data for high-choke

Table 5

ICD No	Estimation Error by Pressure, RFR, %	Estimation Error by Pressure, DT, %	Estimation Error by Temperature, RFR,	Estimation Error by Temperature, DT %
1	1.94	1.7	1.94	1.7
2	20.3	20.7	18.7	19.7
3	12.3	13.6	5	9.3
4	28.37	30.2	18	25.3
5	62.8	63.7	56.2	23.7
6	-	-	-	-

Percentage of error of estimated flow rates

# Quantitative Interpretation Using Rock Physics Driven Convolutional Neural Network



**Ufuk Durmus**

Turkish Petroleum Corporation (TPAO), Ankara / Türkiye

## SUMMARY

In this study, the convolutional neural network is utilized to obtain elastic properties of the producing gas reservoirs in the Thrace Basin. I use a rock physics model for unconsolidated sands to create synthetic well logs and synthetic seismic data to train the network. Once the training is correctly done, the constructed convolutional neural network (CNN) is applied to the field data to predict the elastic parameters, which are crucial for subsurface characterization. I present the value of new machine learning techniques and how they improve accuracy compared to conventional seismic inversion results.

## INTRODUCTION

Machine learning applications have grown dramatically in the oil and gas industry in recent years, specifically in geophysics (Das et al., 2019). Estimating accurate elastic properties help us better develop the hydrocarbon fields. In this work, I have conducted both prestack simultaneous seismic inversion and rock physics-guided convolutional neural network (CNN) prediction and compared the results.

I use a land dataset containing 33 wells and three-dimensional (3D) angle gathers from a gas-producing field in Thrace Basin. There are two target formations in the area of interest. One of them is called Danisman formation, which is shale with interbedded sandstone. The other one is the underlying Osmancik formation, a sandstone reservoir. Our main interests are the lower sandy part of Danisman formation and the upper Osmancik formation. Since gas-bearing zones are composed of thin layers, obtaining a higher resolution of the subsurface properties such as P-impedance, S-impedance, and density is crucial in this field.

## THEORY & METHODOLOGY

First, I run deterministic simultaneous inversion using 28 wells and conditioned angle gathers from 0 to 45 degrees (Hampson et al., 2005). Following that, I apply CNN to predict the elastic properties of the reservoir rocks. For CNN training, I use 19 wells since they have suitable logs such as P-wave, density, pressure, temperature, clay volume, total porosity, and water saturation (Figure 1). To train the network, I first create synthetic wells using the Hertz-Mindlin rock physics model for unconsolidated sands. Hertz-Mindlin model is modified by Allo (2019) in a way that MSI values determine how soft (unconsolidated) or stiff (consolidated) the sandstone is. By adjusting the MSI values, I can match the real data for clastic formations. Using 19 field wells, I simulate 342 synthetic wells by varying porosity +0.05 and -0.05, clay volume +0.2,

and layer thickness %50 less and %200 more scenarios considering a realistic assumption for the field and calibrating the rock physics model (Table 1). I also define and constrain the geological facies with different reservoir cutoffs using porosity, V<sub>clay</sub> (volume of clay mineral), and S<sub>w</sub> (water saturation) parameters. With the synthetic well logs, I create synthetic angle gathers using Zoeppritz (1919) equations with 20 bins from 0 to 45 degrees in agreement with the PSTM seismic data (Figure 2).

As for the convolutional neural network, the method treats seismic data as image data for training and prediction. I use a 20 by 20 kernel size. Since the seismic data sampling rate is 4ms, the kernel size is defined as 20 horizontal (angle bins) and 80 vertical (4ms) for this work. The filter size of 3 by 3 is found to be the best fit for the network training. In addition to these, the number of epochs and hidden layers are determined to be 100. The number of convolutional layers is 2 for the training.

## RESULTS

The created synthetic well logs and seismic data are later utilized to train the convolutional neural network. In the training process, 30% of the synthetic wells are used for validation. Subsequently, the trained CNN with synthetic data is readily applied to the real angle gathers to estimate P-impedance, S-impedance, and density.

Well Y-1 is actively used for both seismic inversion and CNN prediction, while Well Y-4 is left blind to both analyses. To better understand and compare the results in the well locations, elastic properties are plotted in Figure 3. The measured well logs are filtered to 70Hz to be in the same frequency band with seismic and show its features better. It is evident that CNN results provide a better match with the real data in comparison with inversion results. Quantitatively, the correlation coefficient of P-impedance, S-impedance, and density from CNN results are %96.7, %96.2, %96.1 respectively, while the results from simultaneous inversion have %90.7, %89.9, %87.7 correlation, respectively at Well Y-1. When it comes to the blind well (Y-4), the correlation coefficient of P-impedance, S-impedance, and density from CNN are %88.3, %88.1, %85.5 respectively, however; the inversion shows %86.1, %86.6, %82.1 correlation respectively.

In addition, some of the wells in the area are shown in the arbitrary seismic section (Figure 4). It is observed that CNN resolves thin layers of the producing lower part of Danisman formation better than deterministic seismic inversion in both P-impedance and S-impedance results. It can also be seen that the separation between facies within Osmancik formation is improved with the CNN application. The convolutional neural network prediction provides less noisy and less model-biased

results compared to the simultaneous prestack inversion even if the former seems to be smoother than the latter.

## DISCUSSION & CONCLUSION

In this case study, I present a rock physics-driven convolutional neural network workflow to obtain elastic parameters and compare the results with deterministic seismic inversion. It can be concluded that CNN prediction provides similar in general and better results in some areas compared to seismic inversion. This could be an indication that the physics background integrated into CNN is important. Even though I use 9 wells less in CNN than inversion, this method is able to provide good-quality results. With the more accurate estimation of elastic properties, reservoir property estimation can also be enhanced to better understand the subsurface. The more knowledge we have, the better we understand and develop the field.

## ACKNOWLEDGMENTS

I wish to thank Turkish Petroleum Corporation for using the dataset and allowing me to publish this work.

## REFERENCES

- Allo, F., 2019, Consolidating rock-physics classics: A practical take on granular effective medium models: *The Leading Edge*, 38, 334–340.
- Das, V., A. Pollack, U. Wollner, and T. Mukerji, 2019, Convolutional neural network for seismic impedance inversion: *Geophysics*, 84, R869–R880.
- Hampson, D. P., B. H. Russell, and B. Bankhead, 2005, Simultaneous inversion of pre-stack seismic data: SEG Technical Program Expanded Abstracts, 1633–1637.
- Zoeppritz, K., 1919, VII b. *Über Reflexion und Durchgang seismischer Wellen durch Unstetigkeitsflächen*: *Nachrichten von der Gesellschaft der Wissenschaften zu Göttingen, Mathematisch-Physikalische Klasse*, 66–84.

Keywords: artificial intelligence, elastic properties

Figure 1: An example full set well logs from the field

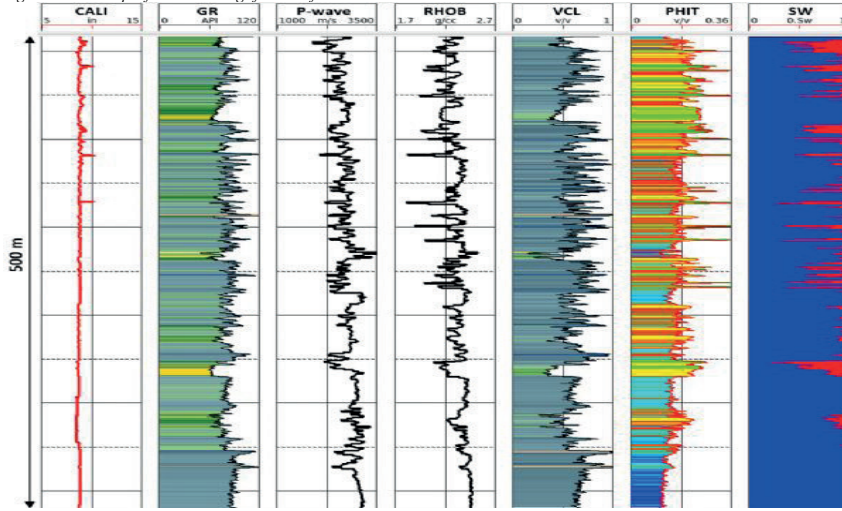


Table 1. Reservoir simulation parameters for synthetic well logs

Reservoir Properties	Scenarios
Layer Thickness	[0.5x 1x 2x]
Porosity	[-0.05 0 +0.05]
Clay Volume	[0 +0.2]

Figure 2: An example synthetic angle gathers created by synthetic well logs using Zoeppritz equations. The angle range is from 0 to 45 degrees with 20 bins same as field seismic data.

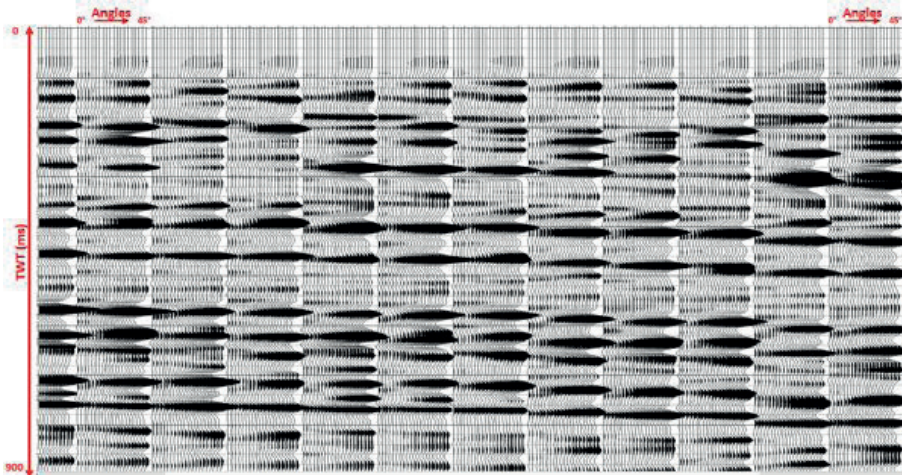


Figure 3: The CNN and inversion results plotted on top of measured logs at the well locations of Y-1 on the left and Y-4 blind well on the right. The red arrows indicate the improvement with CNN compared to the inversion results.

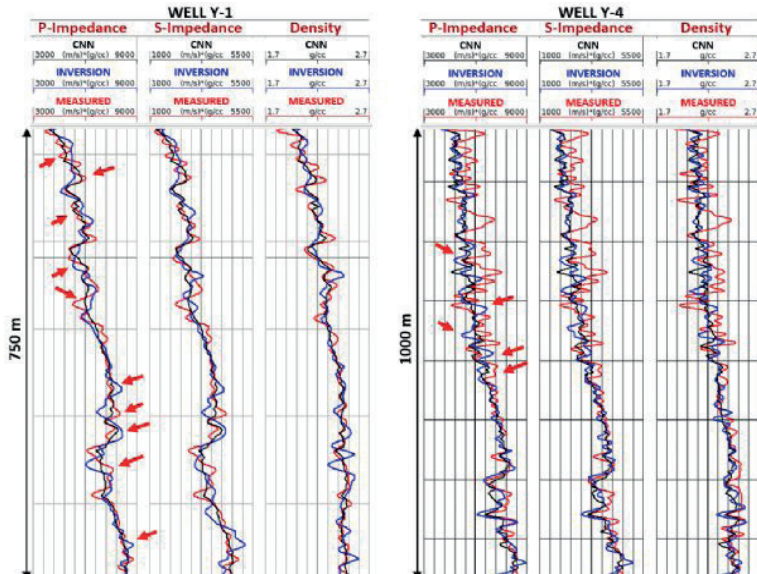
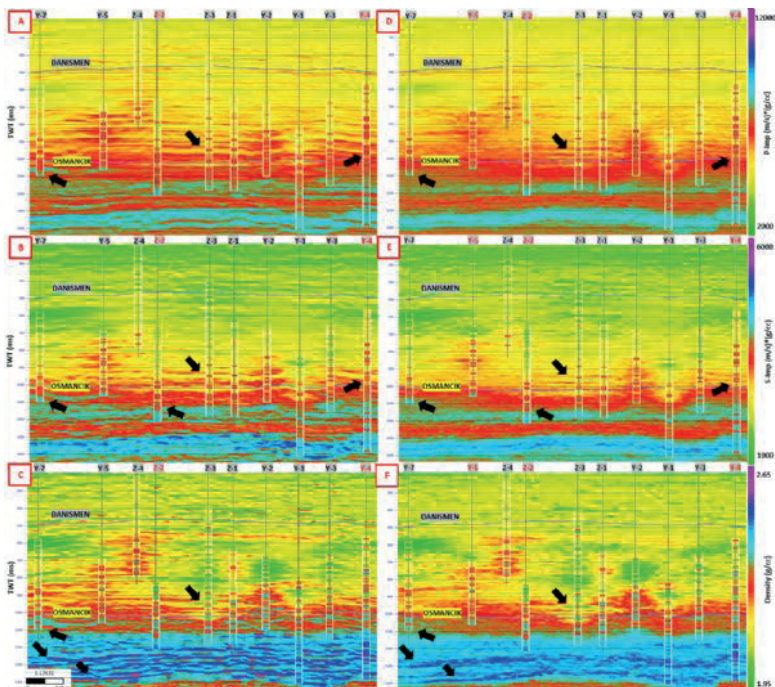


Figure 4: Arbitrary line crossing the wells in the area is shown in a) Inversion P-impedance section, b) Inversion S-impedance section, c) Inversion density section compared to e) CNN P-impedance section, f) CNN S-impedance section, f) CNN density



Black arrows indicate the areas where CNN application improve the results. Note that used wells annotated with black while blind wells are marked with red font. In these sections, the inversion has two blind wells and CNN has three blind wells.

# Implementing Adaptive Neuro-Fuzzy Inference System for Analysis of Heavy Oil Behavior Through Magneto-Rheology



**Uğur Özveren**

Department of Chemical Engineering, Marmara University, Goztepe Campus, 34722, Kadikoy / Istanbul / Türkiye

## ABSTRACT

Magneto-rheology, examining the response of materials to magnetic fields, is central to predicting viscosity alterations in heavy oil. This understanding holds paramount significance for petroleum engineering tasks, particularly in extraction and transportation, where fluid dynamics profoundly impact operational efficiency. The research harnesses the Adaptive Neuro Fuzzy Inference System (ANFIS), an advanced artificial intelligence methodology, to model viscosity variations in heavy oil under distinct magnetic and thermal conditions.

Using a comprehensive dataset, data was systematically partitioned for training and validation, ensuring an objective evaluation of the model's capabilities. When trained on essential magneto-rheological parameters, the ANFIS model effectively captured intricate relationships and predicted viscosity changes. Impressively, the model achieved an  $R^2$  value exceeding 0.999, underscoring its reliability and potential in modeling heavy oil magneto-rheological behavior. This achievement bridges the current knowledge gap and presents a cutting-edge approach with extensive industry applications.

## 1. INTRODUCTION

Petroleum remains a cornerstone of global energy, with heavy crude oil representing a significant fraction of recoverable reserves [1]. Its high viscosity, however, poses technical challenges in extraction and transportation. Numerous methods, such as dilution, heating, and the use of additives, have been deployed to mitigate these challenges. Although dilution with light hydrocarbons is common due to its efficacy, it has associated complications, including asphaltene precipitation, economic losses, and availability concerns. Heating, another method, involves elevating the oil's temperature to decrease viscosity. While effective, its efficiency is compromised in marine pipelines due to seawater's cooling effects. As alternatives exhibit shortcomings, magneto-rheology — the modulation of viscosity via magnetic fields — emerges as a promising solution. This technology can adjust heavy oil flow characteristics, eliminating chemical additives and presenting a more sustainable, economical approach. However, understanding the interaction between magnetic fields and heavy oil rheology demands powerful modeling techniques, making magneto-rheology a hot research topic in the quest for environmentally-friendly hydrocarbon extraction and transport.

Artificial intelligence (AI) offers transformative potential for modeling magneto-rheology in heavy oils, attributed to its predictive accuracy and adaptability.

The complex interactions between magnetic fields and heavy oil rheology align with AI's advanced analytical capabilities. With the capacity to process vast experimental data sets and uncover concealed data patterns, AI stands out as a superior modeling tool. This research aims to harness AI, specifically the ANFIS technique [2], to predict heavy oil viscosity changes influenced by magneto-rheology. Although magneto-rheology is extensively studied, a knowledge gap persists in its impact on heavy oil viscosity, and the application of ANFIS in this context remains unexplored. This investigation thus introduces a pioneering approach to understanding magneto-rheological behaviors in heavy oil via the ANFIS model, offering insights with profound implications for petroleum engineering.

## 2. MATERIALS AND METHODS

### 2.1. Data

This study seeks to address a pivotal knowledge void by employing the Adaptive Neuro Fuzzy Inference System (ANFIS), an advanced artificial intelligence technique, to model the variations in heavy oil viscosity ( $C_p$ ) due to magneto-rheology. The primary source for the dataset used is the exhaustive magneto-rheological compilation for extra heavy crude oil (8.5° API) curated by Ro et al. [3].

This collection contains 1200 instances, each capturing distinct conditions. These data points encompass varying parameters, such as Temperature (C), Magnetic Flux Density (T), and Speed (1/min), providing a robust foundation for the research analysis.

### 2.2. Adaptive Neuro-Fuzzy Inference Systems (ANFIS)

The research methodology harnesses the power of the Adaptive Neuro Fuzzy Inference System (ANFIS), a hybrid model merging the strengths of the Fuzzy Inference System (FIS) and the Artificial Neural Network (ANN). ANFIS stands out for its potential to model the nuanced viscosity changes in heavy oil due to magneto-rheological impacts, an area previously lightly treaded. The FIS within ANFIS plays a crucial role, as it offers a structured method to handle data that could be ambiguous, a challenge inherent when understanding magneto-rheological effects on oil viscosity. Concurrently, the ANN component learns from input data, formulating fuzzy rules essential for interpreting inputs and predicting the corresponding oil viscosity changes.

Integral to the ANFIS framework in this study is the incorporation of the Takagi-Sugeno inference

methodology. This method aids the system in crafting fuzzy rules based on the mappings between inputs (related to magnetic field parameters) and outputs (resultant oil viscosity changes). The architecture of ANFIS starts with an input layer, succeeded by the fuzzification layer, which associates each node with a linguistic term's membership value. This value is modifiable through a learning process, influenced by the back-propagation algorithm. Following this, the strength of each rule gets calculated in the subsequent layer, determined by multiplying specific membership values.

The next phase in ANFIS architecture is the normalization layer, tasked with adjusting all rule intensities. Proceeding further, the structure has an adaptive layer where a linear function is calculated, its coefficients altered by a multi-layer feed-forward neural network's error function. The concluding layer, the output layer, aggregates the net outputs from the preceding layer, resulting in the overall neuro-fuzzy system's output. This comprehensive system provides a methodological approach to understanding and predicting viscosity changes in heavy oil under magneto-rheological effects.

### 2.3. Statistical Performance Validation

The assessment of a model's capability to predict heavy oil viscosity changes relies on a range of statistical metrics. These errors, stemming from the comparison between forecasted and measured values, serve as crucial indicators of prediction accuracy.

For a comprehensive understanding of prediction accuracy, several metrics were examined. These include the correlation coefficient  $R^2$ , the Root Mean Square Error (RMSE), the Mean Absolute Percentage Error (MAPE).

## 3. RESULTS AND DISCUSSION

### 3.1. Correlation Matrix in Predicting Heavy Crude Oil Viscosity

During the exploratory data analysis phase to better understand the dynamics governing heavy oil viscosity, a correlation matrix was constructed. This analytical tool was meticulously designed to tease out the intricate relationships among key variables: Temperature (C), Magnetic Flux Density (T), and Speed (1/min). The primary goal of this endeavor was to determine how these specific factors, individually or in synergy, shape the Viscosity (Cp) of heavy oil.

The correlation matrix provided a clear numerical representation of the associations between Temperature (C), Magnetic Flux Density (T), Speed (1/min), and Viscosity (Cp). The results derived from the matrix were congruent with preliminary hypotheses, showcasing either minimal correlations or dominantly negative relationships among the selected parameters. Such findings emphasize the inherent complexity and often

elusive interactions between these variables, especially when contextualized within the broader realm of magneto-rheological effects on heavy oil viscosity.

### 3.2. Anfis Model

Magneto-rheology's potential in predicting heavy oil viscosity changes has been illuminated by the application of the Adaptive Neuro-Fuzzy Inference System (ANFIS). Developed through MATLAB® (R2023a) and utilizing the Fuzzy Logic Toolbox, the research focused on a comprehensive dataset of 1200 observations. The data partitioning strategy allocated 80% to the training phase and 20% to the validation phase. This distinction was strategically set to optimize the model's generalizability to new data and prevent overfitting—a concern in predictive modelling where the model's specificity to training data can impair its performance on unfamiliar datasets.

Within the training phase, the model sought correlations between heavy oil viscosity and three key parameters: temperature, magnetic flux density, and speed. This exploration yielded an impressive  $R^2$  value of 0.9987, suggesting a near-perfect alignment between the predicted values and the actual data. The test phase results were even more promising, with an  $R^2$  value of 0.999. Such high  $R^2$  values in both training and testing phases suggest an exceptional accuracy and reliability of the model. A close look at the probabilistic distribution showed a significant density in the lower viscosity range for both predicted and measured values, emphasizing the model's consistency in this range.

Performance metrics further spotlighted the ANFIS model's prowess. The training phase exhibited an RMSE of 3475.14676, signifying close alignment with real-world values, while the MAPE at 9.7051% indicated minimal deviation from the actual values. The testing phase metrics, including an RMSE of 3537.398408 and a MAPE of 11.9611%, affirmed the model's validity even when exposed to unseen data. These metrics, especially the proximity of  $R^2$  values to 1, reflect the model's capability to handle complex and exponential variations with precision.

In sum, the ANFIS model has demonstrated a pioneering capability in understanding the complexities of heavy oil viscosity through magneto-rheology. By integrating temperature, magnetic flux density, and speed as input variables, the model adeptly captures the intrinsic dynamics of the system. Beyond its academic significance, the results have vast implications for the energy sector, suggesting real-time applicability that can redefine control and optimization strategies in oil processing. The stellar performance of ANFIS in this study acts as a precursor to more groundbreaking work in the domain of heavy oil processing, holding vast promise for future endeavors.

## 4. CONCLUSIONS

This research successfully harnessed the Adaptive Neuro-Fuzzy Inference System (ANFIS) to model heavy

oil viscosity changes via magneto-rheology, addressing a significant knowledge gap. By strategically dividing the data, the study achieved exceptional  $R^2$  values for both training (0.9987) and testing (0.999) phases. The insights into the viscosity value distribution showcased a high density at lower ranges, with notable accuracy in the ANFIS model predictions when compared to measured values. While integrating temperature, magnetic flux density, and speed as inputs, the study advanced understanding of magneto-rheology's effects on heavy oil viscosity. Nonetheless, observed inconsistencies hint at areas for further refinement, paving the way for future research. Ultimately, this investigation not only fills a research void but also sets a promising trajectory for innovative solutions in heavy oil processing within the petroleum engineering sector.

#### REFERENCES

1. Souas, F., A. Safri, and A. Benmounah, A review on the rheology of heavy crude oil for pipeline transportation. *Petroleum Research*, 2021. 6(2): p. 116-136.
2. Haider, G.M., World oil reserves: problems in definition and estimation. *OPEC review*, 2000. 24(4): p. 305-327.
3. Roa, M., E. Aguilera, and R. Correa, Magneto-rheological dataset for an extra heavy crude oil (8.5° API) in the presence of a constant magnetic field. *Data in brief*, 2019. 24.

Keywords: Anfis, Crude Oil



# AI Seismic Interpretation: A Deeper Understanding of the Subsurface

**Luis Gomez Martinez, Abdulqadir Cader, Ryan Williams, Peter Szafian**  
Geoteric, London / UK



## INTRODUCTION

Artificial Intelligence assisted solutions are reshaping the way seismic interpretation is performed. Before the recent advances in AI technologies (such as deep learning) the best practices forming the backbone of seismic interpretation remained largely unchanged for many decades. These best practices and workflows are now being rewritten as it has been proven that the application of bespoke AI solutions to specific challenging and time-consuming interpretation tasks can yield results of completeness and accuracy that is far out of the reach of most interpreters (primarily due to the time pressure so common in a commercial environment).

## METHODS – AI SEISMIC INTERPRETATION

Some of the key parts of the seismic interpretation workflows are the mapping and correlating faults and horizons, along with defining geological features, such as channels or salt bodies. The first real success of applying AI into the E&P workflows was the detection of faults in the seismic cube. Faults can now be delineated in data of varying quality from a wide range of geographical areas and geological settings (Figure 1a). Calculating the locations of discontinuities is only the first step. The network of interconnected discontinuities must then be segmented and clustered into fault planes. This can be accomplished using an automatic fault plane extraction algorithm (Figure 1b).

Once a robust solution to identify faults had been developed, the next stage of the workflow involved horizon interpretation. We can easily identify every single peak and trough in a seismic cube, but accurately correlating individual horizon patches proved to be a much bigger challenge than detecting the discontinuities. A new solution was developed that is entirely aware of faults and understands the interplay between the faults and the horizons it is analysing (Figure 2). The fact that the horizons are aware of the faults means these objects are the perfect input to generate a watertight model.

And the latest stage of the AI seismic interpretation workflow involved creating a solution to identify and extract geological features such as channels, injectites, salt bodies, etc. The geoscientist can interpret some training examples representing the geological features, and those examples can be used to fine-tune the AI models, allowing the AI networks to account for geological details specific to the dataset.

## FINDINGS - EXAMPLES FOR NEW WORKFLOWS

The newly emerging and established AI solutions now allow new workflows to be developed, and new improved analyses to be undertaken, some of which will be discussed in this presentation. It is possible to build different AI networks with unique strengths: for example, some are superior at detecting small scale faults, while others perform better with large scale faults. When different AI fault networks are available it is possible to compare them and choose the best one(s) for the given structural setting or objective (Figure 3).

With the continuous developments in seismic acquisition and processing, the amount of information is increasing, as exemplified in the increasing number of available seismic volumes delivered to the interpreters. Time constraints and human limitations inevitably lead to underappraisal of a significant portion of the available information with data volumes sometimes left for years uninterpreted. Decisions may then be based on incomplete, imperfect, or simplified information. AI networks enable the fast, accurate and unbiased analysis of dozens of volumes, applying the same criteria and rigour to every voxel in every volume. For example, every partial stack – angle stacks, azimuth stacks – can now be processed with the same AI network, allowing the human interpreter to focus on comparing and interrogating the resulting AI fault volumes (Figure 4) to understand their significance.

By default, during manual fault interpretation we assign 100% confidence to every fault stick and associated fault surface, but AI networks provide a significantly more nuanced fault confidence distribution from 0 to 100%. This allows us to investigate the uncertainty around the structural model based on fault confidence results. Such enhanced understanding of the structural uncertainty can have significant consequences in a reservoir compartmentalised by faults, leading to alternative appraisal or field development plans (Figure 5).

And finally, how should a neural network be fine-tuned, or crafted to the interpreter's experience? Pre-trained AI networks can be fine-tuned by either a single interpreter, by the members of an asset team or even by multiple geoscientists across a company. The way you chose to do it is up to you, but we can share some of our insights from our study where geoscientists with different backgrounds, experience and fine-tuning strategies created their individual fine-tuned AI networks, using the same Foundation Network and focussing on the same target zone. The results were then combined to create a "corporate" AI fault network (Figure 6). Our findings confirmed the reliability and robustness of the pre-trained Foundation Network,

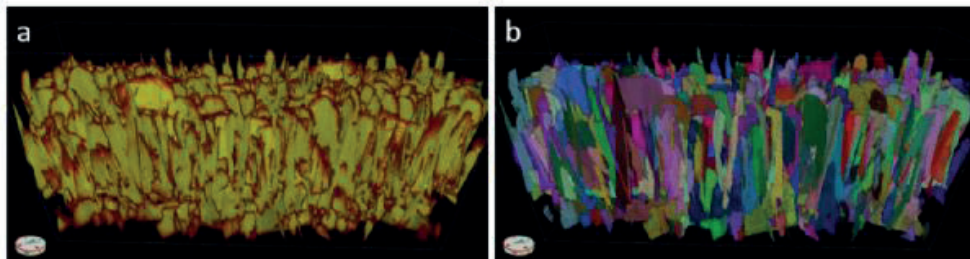
but also highlighted that by combining the AI with the knowledge of the Geoscientists, the latter can be preserved and transferred to other projects or data sets.

## CONCLUSIONS

These AI-based techniques significantly enhance the speed and quality of the interpretation of the subsurface. With the help of AI we can rapidly identify and extract faults, horizons and geobodies with unprecedented detail and accuracy. The time saved on manual interpretation can be used to better understand the geology and analyse feasible scenarios, enabling regional and field assessment to benefit from the most up to date information and ensuring high-quality exploration and development decisions.

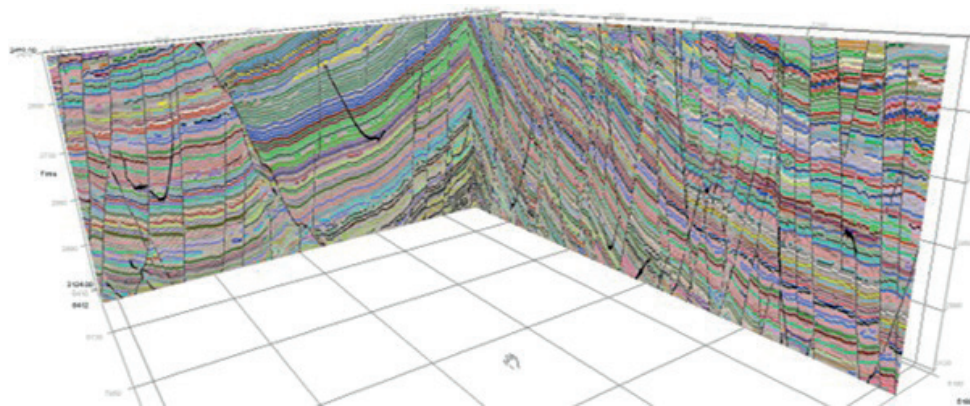
Keywords: Artificial Intelligence, Machine Learning

Figure 1



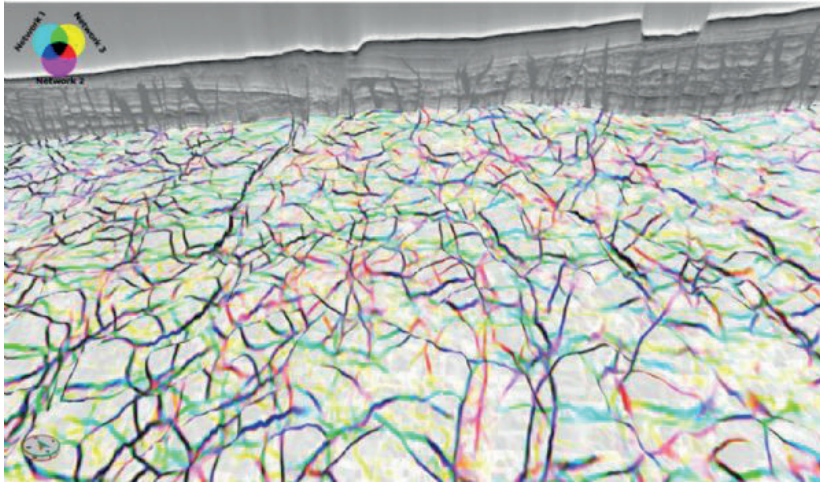
a) A completely interconnected, dense network of polygonal faults can be easily identified and extracted from the seismic data. b) However, segmenting the individual fault planes in this mesh requires the use of an automatic fault plane extraction algorithm.

Figure 2



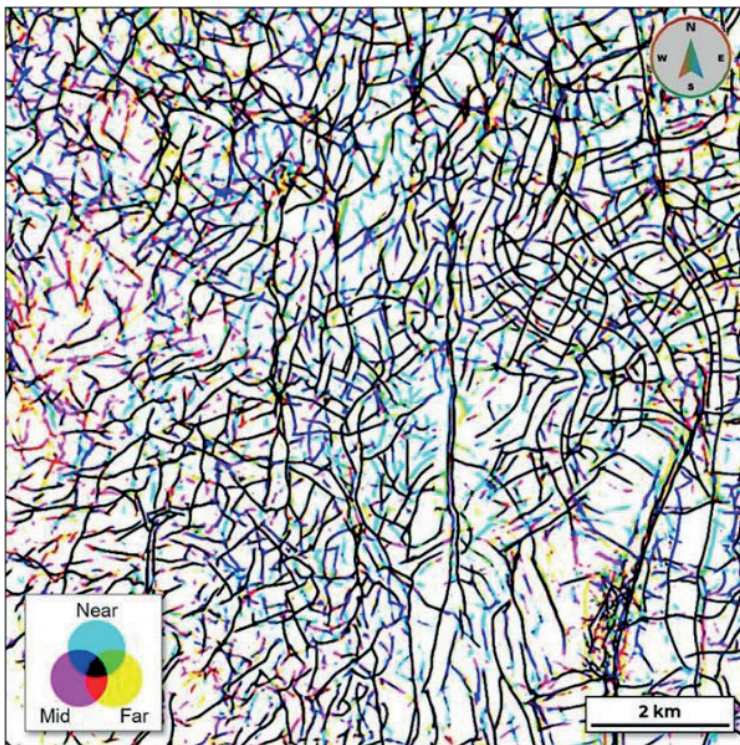
The AI assisted horizon interpretation identified and accurately mapped every horizon through faults and noise, without interpreter input or editing.

Figure 3



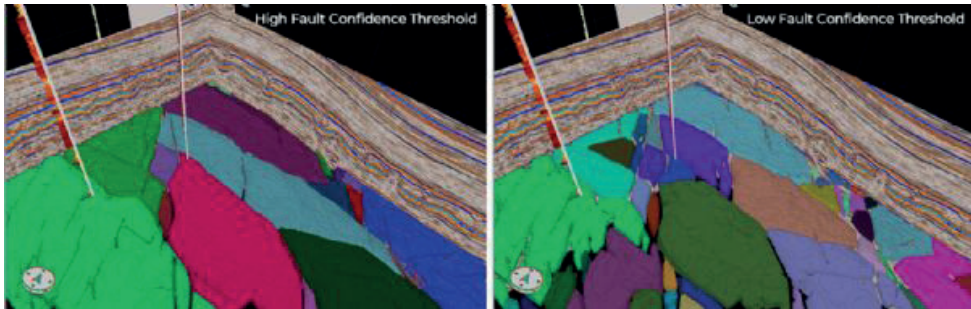
The results of three different AI fault networks combined into a CMY colour blend, draped over an AI horizon. Such data comparison workflows can help decide whether a single network is sufficient for our objectives or combining the results of different networks is more beneficial.

Figure 4



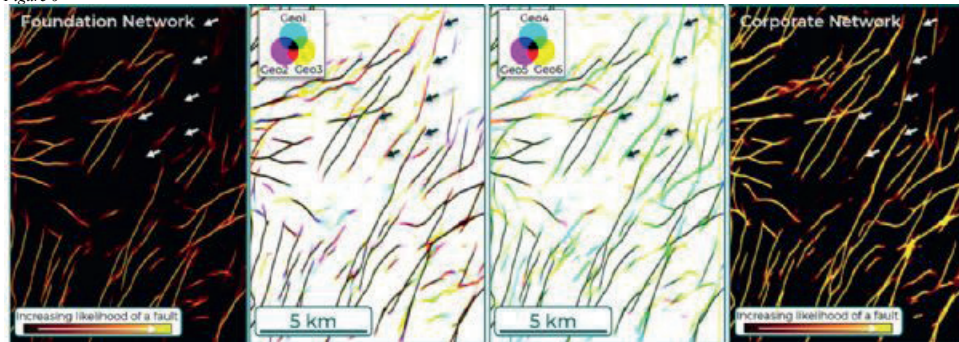
The near, mid, and far stacks were processed with the same 3D AI network. The three AI fault probability volumes were then co-visualised in a CMY colour blend. The colours indicate which angle stacks the faults were detected in; not all faults were imaged in all angle stacks.

Figure 5



Reservoir compartments extracted as geobodies between the top and base reservoir surfaces. AI Fault probability results were used to determine the extents of the individual compartments. When only high-confidence faults were considered (Left), the model suggests greater potential for reservoir communication. If the threshold for accepting a fault is set at lower confidence levels (Right), there is a higher probability of a more segmented reservoir with more limited communication between the segments.

Figure 6



Comparison between the results of the Foundation Network (left) and the individual, fine-tuned networks (middle left and right) confirms the presence of most initial faults, and shows that with fine-tuning, the geometry and lateral extent of the faults could be enhanced, while increasing the network's understanding of the data specific fault signals (arrows). The Corporate Network (right) successfully unified the Foundation Network and the knowledge of the interpreters.

# Leveraging AI in Automating Geophysical Feasibility Studies: A Leap Forward in CCS Monitoring

**Mehdi Paydayesh, Amir Shamsa, Maria Perezhogina**  
Slb, Digital and Integration



This paper delves into the transformational potential of artificial intelligence (AI) for automating the feasibility of various geophysical measurements for carbon capture and storage (CCS) monitoring. The focus is on 4D surface seismic, controlled source electromagnetics (CSEM), and gravity techniques. To address the drawbacks of existing methodologies, we propose an innovative AI-driven workflow that not only streamlines the process but also enhances the accuracy of feasibility predictions. In addition, we present a detailed discussion of the potential benefits of our approach, such as greater cost-effectiveness, increased accessibility, and reduced manual labour. Finally, we address the inherent challenges, such as data quality and model interpretability, and outline strategies for their mitigation. This research stands at the forefront of a paradigm shift in geophysical feasibility studies for CCS monitoring, potentially paving the way for broader and more effective implementation of CCS strategies in the battle against climate change.

## INTRODUCTION

Carbon capture and storage (CCS) has emerged as a crucial technological strategy to address the escalating global climate crisis. As a key solution to mitigating the increasing concentrations of greenhouse gases, CCS is not only integral to achieving global carbon neutrality but also offers a pathway to negative emissions, thus playing a pivotal role in the reversal of climate change. The criticality of CCS necessitates accurate and effective monitoring methods to ensure safe and efficient storage of carbon.

Within this context, geophysical measurements—particularly 4D surface seismic, controlled source electromagnetics (CSEM), and gravity techniques—are of paramount importance. These techniques provide a means to track and understand the behaviour of CO<sub>2</sub> within storage sites, ensuring that the stored carbon remains safely sequestered and aiding in the identification and mitigation of potential leakage incidents.

Feasibility studies that determine the suitability and potential effectiveness of these techniques for specific CCS sites are a vital prerequisite to successful CCS monitoring. The complexity and variability of geological storage sites make these feasibility studies an essential step in the CCS process, guiding the selection of appropriate monitoring techniques and informing monitoring strategy.

In this paper, we scrutinize the drawbacks of current feasibility study methodologies and propose an innovative, AI-driven workflow. This new approach aims to revolutionize the feasibility study process, harnessing the power of AI to improve efficiency, reduce

costs, and make CCS monitoring more accessible and effective.

## Overview of monitoring techniques

Each monitoring technique exploits different physical principles and responds to distinct subsurface properties.

- 4D seismic monitoring leverages changes in seismic data captured over time. Its efficacy lies in alterations of fluid saturation and pressure, both influenced by CO<sub>2</sub> injection. The typical modelling process involves computing fluid acoustic properties via thermodynamic relationships, applying a rock physics model to compute elastic properties, and creating a synthetic seismic response and seismic noise modelling. Geomechanical modelling and time-shift (due to injection) attribute calculation also form part of the common modelling steps

- CSEM generates electromagnetic fields using sources configuration and measures the subsurface response. The technique is sensitive to changes in subsurface electrical conductivity, potentially influenced by CO<sub>2</sub> injection. The modelling steps consist of using Archie's equation to compute resistivity, followed by modelling the CSEM response.

- Gravity monitoring measures changes in the Earth's gravitational field induced by CO<sub>2</sub> injection. Because CO<sub>2</sub> has a different density compared with native reservoir fluids, its injection leads to measurable shifts in the gravitational field.

The process of planning for these measurements involves multiple domains, including reservoir engineering, geophysics, rock physics, and geomechanics.

## Disadvantages of current feasibility study methodologies

The methodologies currently employed for conducting feasibility studies present a range of challenges that constitute substantial barriers to entry. These methodologies often require intricate manual input and expert knowledge in multidisciplinary fields. This complexity often translates into extended processing times, increased costs, and a high threshold for the required expertise.

For example, modelling a 4D seismic geophysical monitoring technique can take weeks or even months, depending on the complexity of the geological storage site. On average, it takes 3 months for a single iteration. This labour-intensive process includes several steps, such as flow simulation, rock physics modelling, and prediction, each requiring expert knowledge and significant computational resources. Furthermore, given the distinct physical principles and different subsurface

properties that each technique responds to, separate models must be created for 4D seismic, CSEM, and gravity monitoring, further multiplying the time and effort needed.

These challenges not only impede the efficiency of CCS monitoring but also its accessibility to organizations with fewer resources or limited technical expertise. There is a palpable need for a more streamlined, efficient, and accessible process. To address these challenges, we propose an AI-driven workflow for conducting feasibility studies. This multistage process integrates flow simulation, rock physics modelling, machine learning (ML), predictive analytics, and automated decision making.

### Key features of the workflow

**Use of an AI platform:** We employ a commercially available AI platform in the cloud, a powerful tool known for its capabilities in data science and ML. This platform enables leveraging high computational power, which is crucial for handling large datasets and running complex models. It also supports real-time project sharing, facilitating seamless collaboration among team members. This feature addresses the traditional challenge of information silos and improves the efficiency of the feasibility study process. We chose this specific platform for its wide array of features that integrate data ingestion, preprocessing, modelling, and visualization in a single, user-friendly environment.

**Tailored web application (app):** We have designed a bespoke web app, which serves as the user interface for our workflow. It automates standard quality control (QC) procedures and analyses, which not only reduces manual labour but also minimizes the potential for human error—a common challenge in traditional methodologies. Intuitive controls and visualizations make it easy for users to input data, run models, and interpret results, thereby increasing accessibility for nonexperts.

**Unified modelling of geophysical monitoring techniques:** to eliminate inefficiencies of running separate models for each technique, our workflow is designed to model geophysical monitoring techniques (4D seismic, CSEM, and gravity) concurrently, using a shared model. This unified approach increases efficiency and ensures consistency, because all techniques are modelled based on the same underlying data and assumptions.

**Iterative modelling:** The workflow is designed to be iterative, allowing users to define various scenarios and automatically rerun the flow model and all the consequent geophysical modelling. This feature is particularly useful for exploring different CO<sub>2</sub> injection strategies and evaluating their impact on geophysical responses—an area often identified as a bottleneck in traditional methodologies.

**Uncertainty quantification and risk maps:** Addressing the need for a more nuanced understanding of uncertainty, our workflow quantifies uncertainty and generates risk maps as part of the output. These tools

help users understand the uncertainty associated with the predictions and assess the risks of different CO<sub>2</sub> storage strategies. Users are thus empowered to make more informed decisions.

**Proxy modelling via ML:** To further optimize future run times, the workflow includes a proxy modelling component. This feature uses ML algorithms to generate simplified models (proxies) based on the results of previous, more complex models. The models are trained on preexisting data from the uncertainty quantification step and enable predicting the response of the geophysical methods of future CCS sites. These proxies can run much faster than the original models, making it feasible to perform large-scale simulations or real-time predictions.

**AI workflow advantages and challenges**  
The AI-powered approach offers tangible benefits, including efficiency, cost-effectiveness, and accessibility. Use of AI and ML algorithms can drastically reduce the time required for data processing and modelling, enabling real-time decision making and predictions. Instead of 3 months per iteration, workflows can be run in just minutes.

Automating labour-intensive processes can reduce operational costs by 75%. Moreover, the use of proxy modelling can help reduce future run times by 95%, leading to further cost savings. The tailored web app design and use of a shared model for all geophysical monitoring techniques make the workflow user-friendly and accessible, even for nonexperts.

However, potential challenges need to be addressed for successful implementation. The performance of AI and ML algorithms is heavily dependent on the quality of the input data. Hence, it is crucial to implement robust data validation and model calibration steps to ensure the accuracy and reliability of the output. We have incorporated automated standard QC procedures in our workflow to validate the input data.

As nonexperts begin to use the AI-powered system, there is a risk that analyses could be negatively affected by a lack of deep understanding of the underlying geophysical concepts and principles. This can lead to misinterpretation of results and poor decision making. We plan to provide comprehensive educational support and user training alongside the AI-powered workflow. This will include detailed documentation, tutorials, and case studies to help nonexperts understand the basic geophysical concepts, the working of the AI models, and interpretation of results. By providing the necessary support and resources, we aim to empower nonexperts to conduct deeper, more insightful analyses and make informed decisions.

By proactively addressing these challenges, we can unlock the full potential of AI in automating geophysical feasibility studies and make significant strides in CCS monitoring.

## CONCLUSION

This study underscores the transformative potential of leveraging AI to automate geophysical feasibility studies, marking a significant advancement in CCS monitoring. By integrating AI into these critical analyses, we can alleviate the labour-intensive, costly, and complex nature of conventional methodologies, thereby reducing barriers to entry and making CCS more accessible and efficient.

Our innovative, AI-powered workflow offers a unified modelling approach for key geophysical monitoring techniques to derive more consistent and comprehensive insights. With the integration of the selected AI platform, we have the capacity to handle large datasets and run complex models more efficiently. Additionally, our system's iterative modelling capability allows exploring various CO<sub>2</sub> injection strategies and their impacts on geophysical responses, thereby enhancing the flexibility and comprehensiveness of our analyses.

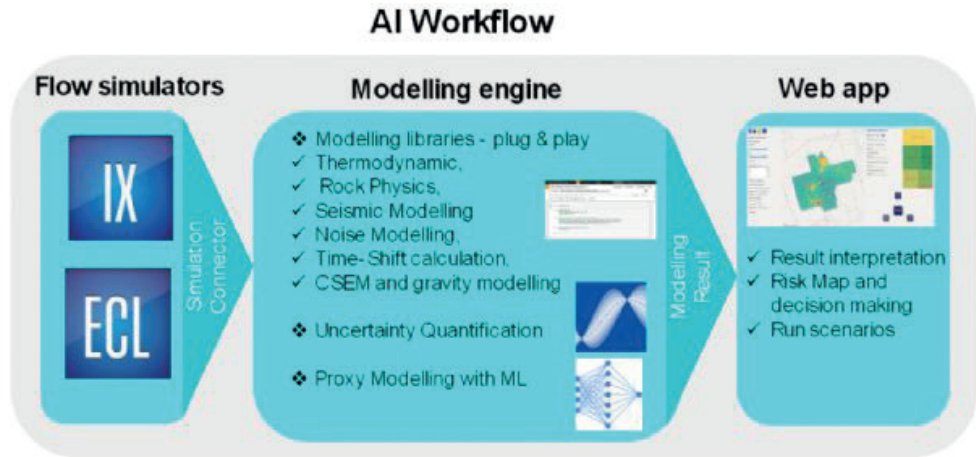
Incorporation of a proxy model powered by ML heralds a new era of large-scale simulations and real-time predictions. By leveraging historical modelling data, we can improve the accuracy of feasibility predictions and optimize future run times, demonstrating the remarkable potential of AI in this domain.

However, the journey toward fully automated, AI-powered geophysical feasibility studies is not without its challenges. Concerns over data quality, interpretability of AI models, and the need for expert oversight remain. As we continue to refine this AI-powered workflow, we remain cognizant of these challenges and are committed to addressing them, striving toward an efficient, cost-effective, and reliable solution that can reshape the landscape of CCS monitoring.

In conclusion, this research stands at the forefront of a new frontier in CCS and climate change mitigation. As we continue to refine and expand upon these AI-driven methodologies, we believe that they will play a crucial role in accelerating our global response to climate change, underscoring the immense potential and significance of AI in transforming the field of CCS and geophysics.

Keywords: AI automation, CCS monitoring

Fig. 1



*Leveraging an AI platform in the cloud, our workflow facilitates an end-to-end solution that seamlessly integrates flow simulators, multiphysics modelling, uncertainty quantification, and machine-learning-based proxy modelling. This comprehensive system delivers interpretable results, including risk maps, which enable end users to conduct detailed analyses and run various scenarios for dynamic result generation.*



# Yapay Zeka ile Sismik Hız Modellerinin Doğrudan Kestirimi: Eğitim Veri Seti ve Derin Ağ Eğitimi

**Moitaba Najafikhatounabad<sup>1</sup>, Hacer Yalım Keleş<sup>2</sup>, Selma Kadioğlu<sup>1</sup>**

<sup>1</sup>Ankara Üniversitesi, Müh.Fak., Jeofizik Mühendisliği Bölümü, Ankara / Türkiye

<sup>2</sup>Hacettepe Üniversitesi, Müh.Fak., Bilgisayar Mühendisliği Bölümü, Ankara / Türkiye



## ÖZET

Çalışmanın başlıca amacı, türev tabanlı sismik yansıma ters çözüm yöntemlerindeki doğruya çok yakın başlangıç hız modeli oluşturma zorlukları, yerel minimumlara takılma ve yüksek hesaplama maliyeti gibi sorunların üstesinden gelebilecek, birçok alanda çok başarılı sonuçlar vermiş olan, yapay zeka derin öğrenme yaklaşımı ile sismik atış kesitlerini girdi olarak alan ve profile ait iki boyutlu (2B) hız modelini çıktı olarak elde eden ağ tasarım yaklaşımını sunmaktır. Bu amaçla çok fazla sayıda yapay hız modelleri kümesi oluşturma, sismik atış kesitleri-hız modeli eğitim veri kümesini hazırlama, daha önce literatürde yapılmış çalışmalardaki 2B eğitilmiş evrişimli sinir ağları (convolutional neural network, CNN) ile hız modeli çıktılarını elde etme ve birbirleri karşılaştırmaları çalışmanın başlıca konularıdır.

Çalışmamızda antiklinal, senklinal, fay ve tuz domu içeren 4-8 tabakalı hız modellerini kapsayan toplam 18000 hız modeli oluşturuldu. Bu modellerinde binlerce tabaka, fay, antiklinal, senklinal ve tuz domu yapılarının oluşturulmasında matematik fonksiyonları kullanıldı ve özgün hız modellerinin oluşturulması sağlandı. Son olarak elde edilen hız modellerini kestirebilen yayınlanmış evrişimli sinir ağları (CNN) kullanan kodlayıcı – kod çözücü (encoder-decoder) derin ağ modelleri yaklaşımları ile ilgili PHYTON kodları hazırlandı ve derin öğrenme eğitim ve test işlemleri gerçekleştirildi ve edilen sonuçlar karşılaştırıldı.

Anahtar kelimeler: Sismik hız modeli kestirimi, yapay zeka

## ABSTRACT

The main objective of this study is to present a network design approach that takes seismic shot sections as input and obtains the two-dimensional (2D) velocity model of the profile as output with an artificial intelligence deep learning approach that can overcome the problems of derivative-based seismic reflection inverse solution methods such as difficulties in generating an accurate initial velocity model, getting stuck in local minima and high computational cost, which have yielded very successful results in many fields. For this purpose, the main topics of the study are creating a large number of artificial velocity model sets, preparing the seismic shot sections-velocity model training dataset, obtaining velocity model outputs with 2D trained convolutional neural networks (CNN) in previous studies in the literature and comparing them with each other.

In our study, a total of 18000 velocity models including 4-8 layer velocity models including anticlinal, synclinal, fault and salt dome were created. In these models, mathematical functions were used to create thousands

of strata, faults, anticlinal, synclinal and salt dome structures and unique velocity models were created. Finally, PHYTON codes related to encoder-decoder deep network modeling approaches using published convolutional neural networks (CNN) that can predict the velocity models obtained were prepared and deep learning training and testing processes were performed and the results were compared.

Keywords: Seismic velocity model estimation, artificial intelligence

## 1. GİRİŞ

Sismik yansıma yönteminde yeraltı gerçek hız modeline en yakın hız modelini belirlemek için ters çözüm yöntemleri kullanılmaktadır. Türev tabanlı yöntemler için iyi bir başlangıç hız modeli gerekmektedir. Başlangıç hız modeli ise türev tabanlı yöntemlerin başarı payını büyük ölçekte etkilemektedir. Bu yöntemler işlenmiş sismik veriler ile hız modelinden elde edilen sismik verileri çakıştırarak yenilemeli adımlar ile başlangıç hız modelinin parametrelerini değiştirir. Bu alanda en başarılı yöntem tam dalga şekli ters çözüm (TDT) yöntemidir. Ancak bu yöntem de başlangıç hız modeli ve döngü atlama, yerel minimumlara takılma ve yüksek hesaplama maliyeti gibi sorunlarla da karşılaşmaktadır. Bu sorunların giderilmesi için devam eden araştırmalarla birlikte yeni yöntemler de incelenmektedir. Bu yöntemlerden biri de yapay zeka derin öğrenme yöntemidir.

Derin öğrenme yönteminde, eğitim veri kümesi hazırlamak ve derin ağları eğitmek zaman alıcı olmasına rağmen, başlangıç hız modeli gereksiz, eğitilmiş bir ağ modeli ile sismik atış kesitlerinden hız modeli kestirebilmesi, hesaplama maliyetini ve insani hatayı azaltması açısından çok önem taşımaktadır. Bu nedenle, derin öğrenme yöntemlerinin sismik ters çözüm aşamasında kullanımı araştırmacılar tarafından irdelenen güncel bir araştırma konusudur. Denetimli derin öğrenme yönteminde her girdi için elde edilmesi planlanan çıktı, 'girdi-hedef' ikilisi şeklinde hazırlanmış bir veri kümesini gerektirmektedir. Bu bağlamda, etiketli gerçek verinin temini güç olduğundan, araştırmalar sentetik veriler üzerinde yapılmaktadır. Sentetik hız modelleri üretiminde gerçek yeraltı verileri referans alınmaktadır. Bununla birlikte 'zaman-uzam' boyutlu sismik atış kesitlerini girdi olarak uzamsal hız modelini kestirebilen katsayı kümesini elde etmek için uygun derin öğrenme ağının tasarlanması zorlu bir araştırma problemidir.

Canlıların sinir ağı sisteminden esinlenerek geliştirilen ilk matematiksel (yapay) sinir yapısı yaklaşık 80 yıl önce McCulloch ve Pitts tarafından (1943) tasarlanmıştır. Günümüzde, derin öğrenme yönteminin karmaşık

fonksiyonları ifadedeki başarısı pek çok alanda bu hesaplamalı yapıların kapsamlı araştırma yapmaya değer görülmesine neden olmaktadır. Derin modeller ile sismik ters çözüm gerçekleştiren araştırmalarda başlıca iki konu ele alınmaktadır; eğitim veri kümesi ve sinir ağı mimarisidir. İki boyutlu hız modeli eğiten ilk çalışmalarda sismik verilerin üzerinde hız analizi yapılarak eğitim veri kümesi 'CMP hız analizi – hız modeli' şeklinde hazırlanmıştır (Araya-Polo vd., 2018). Sonraki çalışmalarda sismik veriler üzerinde hız analizine yönelik herhangi bir işlem yapılmadan eğitim veri kümesi 'sismik atış kesiti– hız modeli' şeklinde hazırlanmıştır (Wu ve Lin, 2018, Liu vd., 2021; Li vd., 2020) (Şekil 1).

İzleyen bölümlerde gerçekçi yeraltı hız modelleri-atış kesitleri kümesini oluşturma ve denetimli derin öğrenme ağı ile eğitim ve test etme konuları sırasıyla sunulmuştur.

## 2. KARMAŞIK HIZ MODELLERİ-SİSMİK ATIŞ KESİTLERİ KÜMESİ OLUŞTURMA

Denetimli derin öğrenme yöntemi sismik verileri ile hız modelin arasındaki ilişkiyi öğrenerek sorunu çözmeye çalışmaktadır. Eğitim işleminin gerçekleşmesi için parametreleri farklı olan hız modellerine ait sismik verileri derin ağ modeline sunulmaktadır (Şekil1.). Bu süreçte sinir ağlarındaki katsayılar "sismik veriler-hız modeli" veri çiftinin arasındaki ilişkiyi öğrenme yönünde değiştirilir. Eğitim boyunca derin modelin çıktıları ile gerçek hız modellerin farkı, yanılğı enerjisi fonksiyonu ile hesaplanarak, parçalı türevlerin geri yayılım algoritması ile sinir ağların katsayılarına yanılarak onların değişim yönünün ve değerinin hesaplanmasında kullanılır (Rumelhart vd., 1986). Eğitim süresi bittikten sonra derin model daha önce görmediği sismik verilerine ait hız modeli ön kestirebilmesi hedeflenmektedir.

Çözülmesi hedeflenen problemin özelliklerine uygun derin ağ modelin tasarımı ve tasarlanan modelin derinliğine göre yeterli eğitim veri kümesinin hazırlanması denetimli derin öğrenme yönteminin başlıca gereksinimlerinden biridir. Ayrıca eğitim veri kümesi ele alınan problemin farklı parametrelerini kapsayacak şekilde hazırlanmalıdır. Eğitim veri kümesini sismik hız modelleri ve onlara karşılık gelen belirlenmiş atış ve alıcı aralıkları ile hesaplanan atış kesitleri oluşturmaktadır. Bu amaçla ilk aşama gerçek yeraltı modelleri oluşturmak, ikinci aşama modellere ait atış kesitlerini hesaplamaktır.

Hız modelleri yayınlanmış stratigrafik kaynaklar incelenerek 3 farklı tipte oluşturulmuştur:

- 1- Tabakalı (Ara yüzeyleri, hız değerleri ve tabaka kalınlığı farklı olan katman sayısı dörtten sekize dek değişen modeller)
- 2- Faylı (Atım ve açılıları farklı olan normal ve ters faylar ile kesilmiş tabakalı modeller)
- 3- Tuz domlu (en alt tabakanın farklı yerlerinde sokulum şeklinde yükselen, şekli ve hızı farklı olan ve üst tabakaları etkileyen tuz domları içeren modeller)

Hazırlanan iki boyutlu hız modelleri  $100 \times 100$  grid boyutlu olup tabaka hız değerleri 1500 m/s ile 4000 m/s arasında değişim göstermektedir. Hız değerleri derinlikle artacak şekilde rastgele seçilmişlerdir. Arayüzey veri seti için stratigrafik arayüzey şekillerine uygun olarak hazırlamak amacıyla trigonometrik fonksiyonlar, yuvarlatma fonksiyonları, polinomlar ve logaritmik fonksiyonlar gibi farklı matematiksel fonksiyonların biri veya birkaçı bir arada denetlenmiştir. Tabaka sayısı sabit olan her bir hız modelinin hazırlanması için ara yüzeyler ve onların derinlikleri rastgele olarak seçilmiş daha sonra tabakaların hız değerleri ilk tabakadan başlayarak rast gele bir şekilde belirlenmiştir. Hız modellerinin şeklini değiştiren arayüzeyler hazırlanan 116 adet arayüzey veri setinden rastgele olarak seçilmiştir.

Tabakalı hız modelleri hazırlandıktan sonra eğimi, yönü ve atım boyu rastgele bir şekilde seçilmiş fay parametreleri ile fay hatları oluşturularak faylı hız modelleri de hazırlanmıştır. Son olarak boyu, genişliği ve şekli farklı olan tuz domlarını oluşturmak için parametreleri rastgele bir şekilde seçilmiş dört farklı Gaussian fonksiyonu kullanılmıştır. Tuz domları hız modellerinin alt tabakalarında sokulum şeklinde yukarıya doğru çıkmıştır. Tuz domlarının hızı 4350 ile 4500 m/s arasında rastgele atanmıştır. Jeolojik dinamiği korumak için tabaka sayısına bağlı olarak tuz domun sokulum etkisi üst katmanlara yansıtılmıştır. Şekil 2'de test veri kümesine ait hız modellerinden bazı örnekler sunulmuştur. Her bir tabaka sayısı için sadece tabakalı, faylı ve tuz domu içeren modeller olarak (3 farklı tip) 1200 adet, toplam 3600 adet hız modeli hazırlanmıştır. Hazırlanan hız modellerin 1000 tanesi eğitim, 100'ü doğrulama (validation) ve diğer 100'ü ise test için ayrılmıştır. Toplam beş farklı tabaka sayısı olduğu için toplam 18000 ( $5 \times 3 \times 1200$ ) adet hız modeli oluşturulmuştur.

İkinci aşamada derin öğrenme ağına girdi olarak sunulacak sentetik sismik atış kesitleri hesaplanmıştır.  $100 \times 100$  grid hız modellerine ait atış kesitleri hesaplama geometrisi oluşturulmuştur. Buna göre, ilk gridden başlayarak 3 grid aralıkla 34 adet alıcı ve üçüncü gridden başlayarak 5 grid aralıkla 20 atış noktası yerleştirilmiştir. Modeller üzerindeki tüm atış noktalarına ait atış kesitlerinin hesaplanmasında zaman ortamında iki boyutlu akustik dalga yayılımı denklemi kullanılmıştır;

$$\left(\frac{\partial^2 P}{\partial t^2}\right)^2 - v^2 \left(\frac{\partial^2 P}{\partial x^2} + \frac{\partial^2 P}{\partial z^2}\right) = f(x,z) \quad (1)$$

Burada P akustik dalga alanı, v ortamın sismik dalga hızı, x ve z uzam koordinatı, t zaman ve f kaynak fonksiyonudur. Dalga denkleminin çözümü zaman ortamında sonlu farklar yöntemi ile hesaplanmıştır. Bu çalışmada sismik kaynak olarak merkez frekansı 20 Hz olan Ricker dalgacığı kullanılmıştır. Her bir alıcıda 1 saniye (s) boyunca sismik dalga alanı hesaplanmıştır. Sayısal hesaplamada dispersiyon olayını önlemek için minimum hız değerini (1500 m/s) ve kaynak frekansını (20 Hz) dikkate alarak  $\Delta x = 7$  metre (m) (Alford vd., 1974) ve hesaplamayı kolaylaştırmak için  $\Delta x = \Delta z$  olarak ayarlanmıştır. Elde edilen  $\Delta x$  ve maksimum hız değerine göre ideal zaman örnekleme aralığı 1 ms

(Lines vd., 1999) hesaplanmış ve dolayısı ile zamanda örnek sayısı 1000 adet olmuştur. Böylece her bir hız modelinde  $1000 \times 34$  boyutlu 20 atış kesiti elde edilmiştir.

### 3. DENETİMLİ DERİN ÖĞRENME AĞI

Bu bölümde sismik atış kesitlerini girdi olarak alıp onlara ait hız modellerini kestirebilen derin ağ modeli tasarımı, evrişimli sinir ağları (CNNs) kullanan kodlayıcı – kod çözücü (encoder-decoder) örneği üzerinde anlatılmıştır. Uçtan uca eğitilmesi planlanan sismik verilerinden hız modellerin elde edilmesi için tasarlanan derin modele girdi olarak zaman – uzam ortamında olan sismik atış kesitleri ve çıktı olarak da uzam-uzam ortamında olan hız modelleri sunulmalıdır.

Bu eğitimi gerçekleştirmek için tasarlanacak sinir ağı mimarisi ile ilgili Li vd. (2020) dikkate alınması gereken üç konuyu sıralamışlardır. Birincisi zaman serisi olarak sunulan sismik izlerden (dalga alanı) oluşan sismik kesitler ile hız modelinin arasındaki uzamsal ilişki özellikle yansıyan verilerde zayıf olmaktadır. Diğer bir deyişle, sismik kesitin boyutu hız modelin boyutu ile uyumsuzdur. İkincisi, karmaşık yapıya sahip hız modellerinde her bir atış için alıcılarda kaydedilen yansıma dalgasının hangi arayüzeyden geldiği net olarak belli değildir. Üçüncüsü, düşey eksen boyunca kaydedilen sismik iz zaman arttıkça sönümlenir. Sismik verilerin zamanla değişmesi kesitteki özelliklerin sabit çekirdeklerle çıkarılmasını zorlaştırır. Eğitim aşamasında hız modellerini oluşturabilmek için girdi verilerindeki özelliklerin çıkarılması ve farklı bir uzayda farklı boyutta bir görüntünün elde edilmesi için kodlayıcı-kod çözücü derin model tasarımı başarılı sonuçlar sunmuştur (Wu vd., 2018; Li vd., 2020; Liu vd., 2021).

Bu çalışmada Wu vd. (2018) tarafından önerilen 'InversionNet' adını verdikleri derin öğrenme ağ tasarımı ele alınmıştır. Li vd. (2020) InversionNet'e izleyen değişimleri uygulayarak daha iyi sonuçlar elde etmişlerdir;

1- Dördüncü katmanda Maxpooling işlemi yerine 2B evrişim (Conv2d) kullanmışlardır,

2- Kodlayıcıdan kod çözücüye geçiş yapan en küçük imgelerin boyutunu  $3 \times 3$  olarak ayarlamışlardır (Wu vd. (2018)  $1 \times 1$  'e dek düşürmüşlerdir).

Her iki çalışmada girdi verilerinin (sismik atış kesitleri) boyutu [20, 1000, 32] (sırayla atış sayısı, zaman ve alıcı sayısı) şeklinde kullanılmıştır. Yayınlanan her iki versiyonun parametre sayısı 42 milyondan büyüktür.

Bizim çalışmamızın özgünlüğünü oluşturan araştırma kapsamında InversionNet'in her iki versiyonunun kodları öncelikle PHYTON yazılım dilinde Pytorch kütüphanesi kullanılarak hazırlanmış ve daha sonra kodlayıcı – kod çözücü derin modellerin özelliklerini inceleme amacı ile Liv vd. (2020) tarafından yayınlan InversionNet'in tasarımında değişiklik yapılarak kod çözücü bölümünde deconv2d fonksiyonu yerine upsample + conv2d fonksiyonları kullanılarak imgelerin boyutu büyütülmüştür. Yeni InversionNet derin modelin parametre sayısı öncekilerin yarısına düşerek 20 milyon

olmuştur.

Hazırlanmış olan eğitim veri kümesi kullanılarak her üç derin model eğitilmiştir. Derin modellerin eğitilebilir potansiyelinin ölçülmesi için iki farklı yanlıgı enerjisi kullanılarak her bir model iki kere eğitilmiştir. Bir defa ortalama mutlak hata (MAE; L1) yanlıgı enerjisi olarak bir defa da L1'nin yanı sıra yapısal benzerlik (structural similarity – SSIM) yani L1+SSIM kullanılmıştır. Yapısal benzerlik fonksiyonu hız modellerin şeklinin diğer bir deyişle jeolojik yapıların kestirilmesinde katkıda bulunarak sonuçların daha iyileşmesinde yardımcı olmuştur.

Hazırlanan veri kümesinden 16500 veri çifti eğitim için ve 1500 veri çifti ise test için rastgele bir şekilde ayrılmıştır. Eğitim veri kümesinin %15 yani 2475 veri çifti doğrulama veri seti olarak ayrılmıştır. Elde edilen sonuçların karşılaştırılması için L1, ortalama karesel hata (MSE; L2), yapısal benzerlik metrikleri SSIM-(Wang vd., 2004) ve MSSIM-(Wang vd., 2003) kullanılmıştır.

### 4. SONUÇLAR

GÇalışmamızda Wu vd. (2018) tarafından tanıtılan daha sonra Li vd. (2020) tarafından ikinci versiyonu sunulan sismik atış kesitlerinden sismik hız modelini kestiren InversionNet'in üçüncü versiyonu tarafımızca geliştirilmiştir. Çalışmada üç farklı versiyon bir kez L1 yanlıgı enerjisi ve bir kez de L1+SSIM ile eğitilmiştir. Eğitim aşaması bittikten sonra eğitilmiş modeller test veri seti ile denenmiştir. Test aşamasındaki sonuçların yanlıgı ölçekleri (L1, L2, SSIM ve MSSIM) çizelge 1'de sunulmuştur. Her üç versiyonda elde edilen sonuçlara göre L1+SSIM yanlıgı enerjisi ile gerçekleşen eğitimin sonuçları daha başarılı olmuştur.

Elde edilen sonuçlara göre Li vd. (2020) yayınladığı versiyonun metrikleri Wu vd. (2018) tarafından yayınlanan modelden daha iyi olmuştur. Bu çalışma kapsamında hazırlanan InversionNet'in yeni versiyonunun parametre sayısı diğer iki modelin yarısı kadar olmasına rağmen her iki versiyona göre daha iyi sonuçlar sunmuştur. Sadece L1+SSIM ile eğitilen Li vd. (2020) sunduğu modelin L1 değeri yeni versiyondan az da olsa daha düşüktür.

Bu çalışma kapsamında hazırlanan InversionNet versiyonun test aşamasında kestirdiği hız modellerinden biri Şekil 3' te sunulmuştur. Eğitim aşamasında L1+SSIM yanlıgı enerjisi kullanılmıştır. Şekil 3' te görüldüğü gibi hız modelinin tabaka sayısı, ara yüzeylerin şekli ve en alt tabakada yukarıya doğru çıkan tuz domun şekli ve hız değeri  $L1 = 0.0031$  hata payı ile kestirilmiştir.

Elde edilen sonuçlara göre InversionNet derin modelin kod çözücü kısmında imgeleri büyütme için Upsample+Conv birleşimi dekonvülasyon fonksiyonun yerine kullanılırsa;

1- Parametre sayısı yarıya düşmektedir,

2- Modelin eğitilme potansiyeli daha da yükselmektedir.

## KAYNAKLAR

Araya-Polo, M., Jennings, J., Adler, A. and Dahlke, T. 2018. "Deep-Learning tomography", *Leading Edge*, 37(1), 58-66.

McCulloch, W. S. and Pitts, W. 1943. "A logical calculus of the ideas immanent in nervous activity", *Bull. Math. Biophys.*, 5, 115-133.

Li, Sh., Liu, B., Ren, Y., Chen, Y., Yang, S., Wang, Y. and Jiang, P. 2020. "Deep-learning inversion of seismic data", *IEEE Transactions on Geoscience and Remote Sensing*, 58(3), 2135-2149.

Liu, B., Yang, S., Ren, Y., Xu, X., Jiang, P. and Chen, Y. 2021. "Deep-learning seismic full-waveform inversion for realistic structural models", *Geophysics*, 86(1), R31-R44.

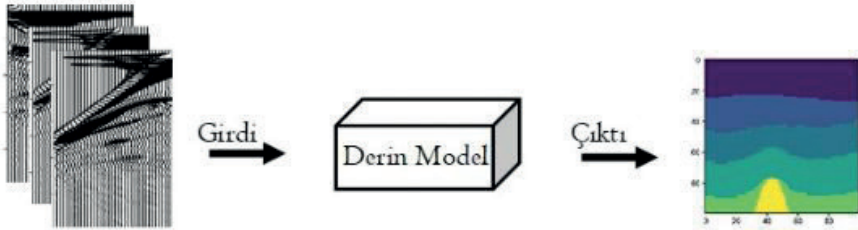
Wang, Z., Bovik, A. C., Sheikh, H. R. and Simoncelli, E. P. 2004. "Image quality assessment: From error visibility to structural similarity", *IEEE Transactions on Image Processing*, 13(4), 600-613.

Wang, Z., Simoncelli, E. P. and Bovik, A. C. 2003. "Multiscale structural similarity for image quality assessment", in *Proc. 37th Asilomar Conf. Signals, Syst. and Comput.*, 1398-1402.

Wu, Y., Lin, Y. and Zhou Z. 2018. "InversionNet: Accurate and efficient seismic waveform inversion with convolutional neural networks", In *Proc. SEG Tech. Program Expanded Abstr.*, pp. 2096-2100.

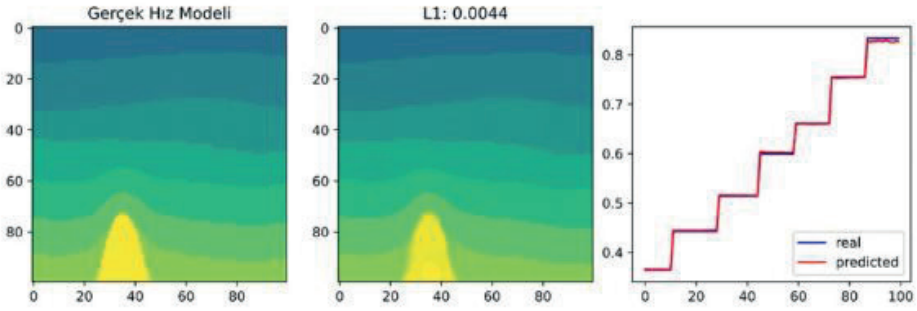
Anahtar Kelimeler: Sismik hız modeli kestirimi, yapay zeka

Şekil 1



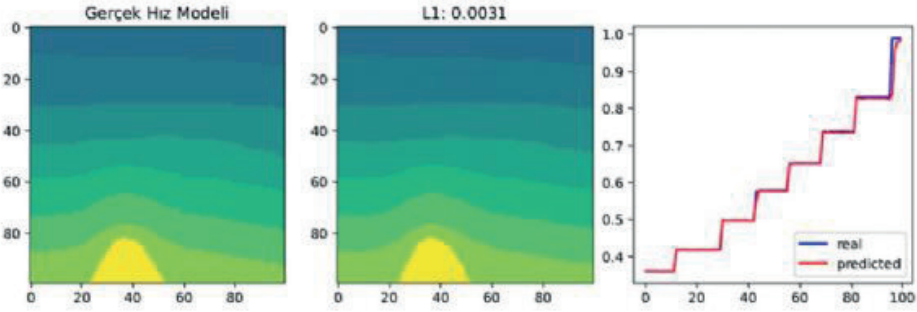
Tasarlanmış derin modelin eğitimi için sismik atış kesitleri girdi ve onlara ait hız modeli çıktı (target) olarak kullanılması

Şekil 2



Şekil 2. Test veri kümesindeki hız modellerinden bazı örnekler. İlk satırda 4, 6 ve 8 tabakalı modeller, ikinci satırda aynı tabaka sayıları için faylı modeller ve en alt satırda ise yine aynı tabaka sayıları için tuz domu içeren hız modelleri

Şekil 3



(a) karmaşık gerçek hız modeli, (b) Bu çalışmada sunulan InversionNet L1 + SSIM yanılığ enerjisi ile eğitilmiş model kestirimi ve (c) gerçek ve kestirilen hız modelleri için 50. grid üzerindeki ortak profil hız kesitleri karşılaştırması

Tablo 1

	Wu vd. (2018)		Li vd. (2020)		Geliştirilen Yeni versiyon	
	L1	L1+SSIM	L1	L1+SSIM	L1	L1+SSIM
L1	0.005533	0.005259	0.005375	0.004785	0.005037	0.004826
L2	0.000300	0.000281	0.000281	0.000250	0.000266	0.000247
SSIM	0.999985	0.999986	0.999986	0.999988	0.999987	0.999988
MSSIM	0.999998	0.999998	0.999998	0.999998	0.999998	0.999998

Wu vd. (2018) ve Li vd. (2020) tarafından yayınlanan InversionNet ve tarafımızdan geliştirilen son versiyona ait test aşamasındaki L1 ve L1+SSIM yanılığ enerjisi değerleri

# A Deep Dive Into The Black Box of Artificial Intelligence

**Orhan Kurt**

Geomatics Engineering Department, Kocaeli University, Kocaeli / Türkiye



## ABSTRACT

To solve any scientific problem by hard or soft computing (Artificial Intelligence, AI) method, a mathematical model is designed. The mathematical model consists of two parts. These are the functional and stochastic models. In many hard or soft computing methods, the stochastic models are chosen as a unit matrix (homogeneous-isotropic-uncorrelated). The functional models in both methods are established according to the Indirect Least Squares Method (LSM). Well, the data (scientific or engineering observations) are represented by some functions of the unknown parameters (the weights in AI). While the functional model is determined by an exact relationship in hard computing, while the defined relation between the data and the unknowns is artificially set based on some computation rules in soft computing. These computational rules in AI are defined as Artificial Neural Networks (ANN). The main contribution of this paper is to theoretically argue that the hard or soft computing methods are almost the same solution strategies. Also, the similarity of hard and soft computing methods would be numerically shown by means of a local geoid determination (GNSS leveling) problem for Ankara City. In this example, a third-degree polynomial model in hard computing with a deep learning model which has two hidden layers with two nodes activated by LU (Linear Unit or Identity) would be compared.

Keywords: Hard computing, black box of AI.

## OBJECTIVES

Soft Computing (SC) is the name of including some computational techniques (ANN: Artificial Neural Network, GA: Genetic Algorithm, Fuzzy Logic (FL), ... ) together according to types of problems. SC and Artificial intelligence (AI) definitions can be used instead of each other in the same means because AI uses the same SC techniques.

GA and FL are not solution strategies alone, they are supportive techniques for Soft and Hard Computing (HC). The general uses of them are to be used to prepare data (FL) before the computation or to develop the results (FA, GA) after the computation (SC or HC). So, the main frame of SC generally sets upon ANN. Furthermore, the functional models based on ANN constitute the core of Artificial intelligence (AI) containing Deep Learning (DL), Machine Learning (ML), and also all learning methods. For this reason, throughout all stages of this paper, AI (based on SC) would be represented via ANN. With the above short overview of AI, all discussions on ANN in the paper would be wrapped to AI as well.

The black box is just only to create a general functional model for a special scientific problem artificially. The solution of the artificial function is realized in the same way as in HC. On the way, the functional model is to be a linearized equation system by Taylor Expansion. The solution of the equation system is made by the Least Squares (LS) criterion (cost) function. While the non-linear equation systems are solved iteratively because needing initial values of the unknowns, the linear system does not require the initial values.

In order to better understand the main purpose of the study, the regional geoid determination problem (also named GNSS leveling) for the city of Ankara, which is a real surface determination problem, was chosen as a numerical example. Since surface fitting problems are suitable for all kinds of spatial problems, the selection of this problem also played a role.

The solutions to the selected problem were made by both polynomial and ANN methods in software developed in the C/C++ environment. In order to compare both methods, polynomial and ANN functional models (activated by LU) with equal unknowns were selected in both methods (Table-1, Figure-1).

The ANN functional model (named black box) has 2 nodes (latitude, longitude) in the input layer, 1 node (geoid height) in the output layer, and 2 hidden layers with 2 nodes activated by LU (Linear Unit or Identity activation function). The black box of the ANN functional model was created as an FCL-NN (Fully Connected Layer – NN), while the 3rd-degree surface polynomial was preferred in the polynomial functional model (Table-1, Figure-1). In the solution of both functional models, the numbers of unknowns ( $u=10$ ) are equal.

## MATERIALS - METHODS

The operating system and application software (for writing, image manipulation, compiling, drawing, etc.) used in the study were produced in the GNU environment (Table-2).

EGM08 spherical harmonic coefficients, Fortran programs that generate geoid height in WGS84 datum according to these coefficients are reached with the web pages of BGI (2023), ICEM (2023), NOAA (2023), and USNA (2023). The Geoid of Türkiye and the local geoid of Ankara are simulated by EGM08 for the surface determination problem.

A simple surface estimation problem has been selected for simplicity. Such a surface model can be used for every type of spatial estimation problem by changing the heights by any spatial dependent data (to be given as gravity, petroleum capacity, gas volume data, etc.).

The surface estimations of the polynomial and ANNs are performed via the simulated geoid undulations for Ankara. The software that constitutes the main objective of the study has been coded in C\C++ and Python environments by the author.

## CASE

The only distinction of ANN from HC is that its functional model is constituted artificially. A Neural Network (NN) is a sketch to derive any systematical relation between the unknown parameters (the synaptic weights) and data values (Figure-2, Table-3).

If an ANN functional model has equal or bigger two hidden layers, the model is accepted as a Deep Neural Network (DNN) (Figure 2). Connected to this definition, all NNs consisting of one hidden layer are defined as Feed forward NNs (FNN). The learning stage of a NN realize by back-propagation. That stage ensures the improvement of the random weights iteratively by means of well-defined learning data.

The sketch given in Figure-2 produces a DNN functional model, the arranged model according to the LU-activation function was given in Table-3. Since the arranged model is carefully inspected, it can be seen that the model represents a plane equation. That case was numerically also proved with computed coefficients for the 1st-degree polynomial function in this study. As a result, we can say that the achieved functional model always is a hyperplane if any linear activation function (given in Table-1) is used for any ANN even having infinite hidden layers. The hyperplane is a plane for the GNSS leveling problem selected for this paper (Figure-2, Table-3).

Regardless of how the functional model is obtained, the solution of any computation method according to LSM is performed in the same way (Table 4). According to Tables-3 and 4, solving the non-linear function with the linear solution method is a very important advantage, and this always ensures consistent results. The solution of the linear functional model of the DNN in a non-linear way creates a disadvantage, and the solution is inconsistent since depending on the initial random weights used in the learning phase.

## RESULTS

As a numerical example, the local geoid determination problem is designed for Ankara. 100 local geoid heights were simulated with EGM08 (Figure 3).

Latitude, longitude, and geoid height (B, L, N) data were used by translating them to the center of the data ( $x=B-B_0$ ,  $y=L-L_0$ ,  $z=N-N_0$ ). While  $N=f(x,y)$  is used in polynomial functions,  $N=N_0+z$  is taken in ANN functions. Learning with ANN is done with  $z=f(x,y)$  data. As a result of two successful trials, two statistically equivalent results are given in Table-5 (Figure-4, Table-5).

ANN solution after training with 100 data points (geoid heights) for Ankara.  $a_0$  is a random vector for the

initial values of the artificial functional model, and  $a_1$  is a trained vector by a software coded in C\C++ on Linux for the local geoid of Ankara (Figure-4, Table-5).

The ANN (Figure-2) functional model activated by LU always produces a plane equation although the solution of ANN is non-linear (Figure-5, Table-5,6).

## CONCLUSIONS

\* Polynomial surface models are non-linear, but their solutions are linear and consistent.

\* ANN surface models activated by LUs are linear, and their solutions have to be performed by the non-linear solution methods. Besides, ANN results are inconsistent because of the result's dependency on their initial values of the unknown parameters (synaptic weights of ANN) in the training stage.

\* Resolution of the ANN (consisting of the core of AI) is weaker than the hard computing method even though an ANN functional model is activated by a non-linear activation function.

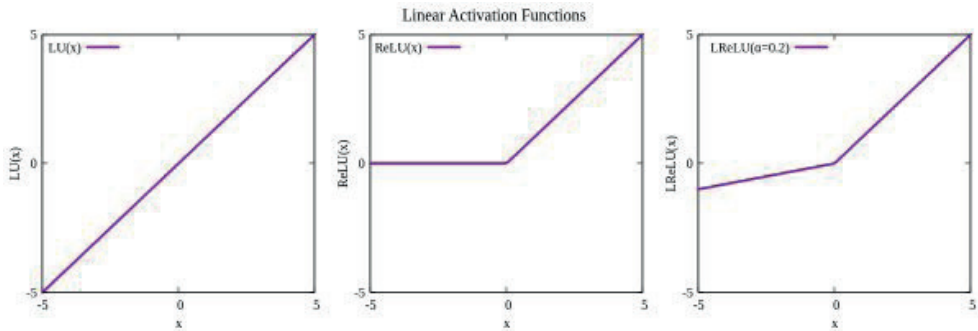
\* Methods of ANN (consisting core of many AI algorithms) should be used in discrete and without gaps (well-defined) data to be able to produce consistent results after training.

## ACKNOWLEDGMENT

We are very thankful to the anonymous heroic developers for their contributions to the GNU world.

Keywords: Hard computing, black box of AI

Figure-1



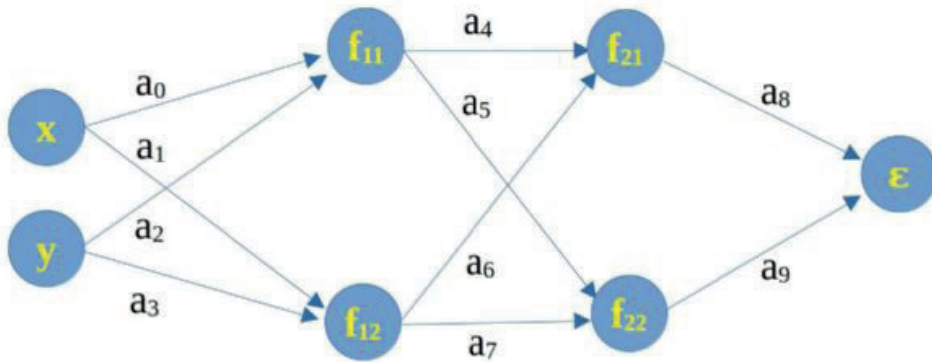
Linear activation functions (Table-1).

Table-1

Name	Abbreviation	Function	Derivative
Linear Unit	LU	$f(x)=\{x\}$	$f'(x)=\{1\}$
Rectified LU	ReLU	$f(x)=\{(x<0)?(0):(x)\}$	$f'(x)=\{(x<0)?(0):(1)\}$
Leaky ReLU	LReLU ( $\alpha=0.2$ )	$f(x)=\{(x<0)?(\alpha x):(x)\}$	$f'(x)=\{(x<0)?(\alpha):(1)\}$

Linear activation functions (Figure-1).

Figure-2



DNN sketch with LU activation function (Table-1, Figure 1) used in the proceeding for the local geoid determination for Ankara.

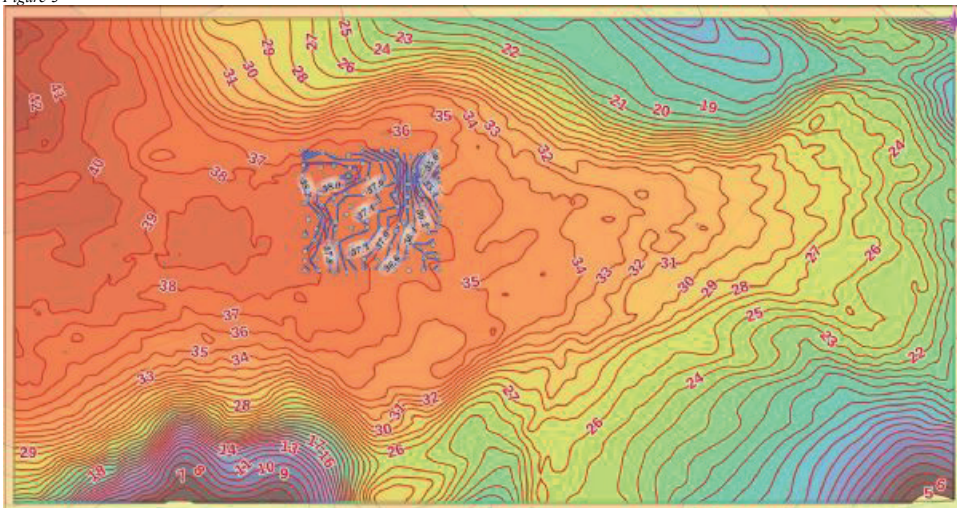


Table-2

Objective	Name	Web
Operating System	Linux Mint 21.2	<a href="https://linuxmint.com/">https://linuxmint.com/</a>
	Victoria	<a href="https://ubuntu.com/">https://ubuntu.com/</a>
	Ubuntu 22.04 jammy	
C/C++ Compiler	Code::Blocks IDE	<a href="https://www.codeblocks.org/">https://www.codeblocks.org/</a>
Python Compiler	Python 3	<a href="https://www.python.org/">https://www.python.org/</a>
	Geany IDE	<a href="https://www.geany.org/">https://www.geany.org/</a>
Image Manipulation	Pix 3.0.2	<a href="https://github.com/linuxmint/pix">https://github.com/linuxmint/pix</a>
	Drawing 1.0.2	<a href="https://maoschanz.github.io/drawing/">https://maoschanz.github.io/drawing/</a>
Office Tools	LibreOffice 7.5	<a href="https://www.libreoffice.org/">https://www.libreoffice.org/</a>
Plotting	GNU Plot 5.4	<a href="http://www.gnuplot.info/">http://www.gnuplot.info/</a>
	QGIS 3.32 Lima	<a href="https://qgis.org/en/site/index.html">https://qgis.org/en/site/index.html</a>
Geoid Simulation	EGM08 data and software (in Fortran)	BGI, <a href="https://bgi.obs-mip.fr/data-products/grids-and-models/egm2008-global-model/">https://bgi.obs-mip.fr/data-products/grids-and-models/egm2008-global-model/</a>
		ICEM, <a href="http://icgem.gfz-potsdam.de/home">http://icgem.gfz-potsdam.de/home</a>
		NOAA, <a href="https://vdatum.noaa.gov/download.php#download_geoid">https://vdatum.noaa.gov/download.php#download_geoid</a>
		USNA, <a href="https://www.usna.edu/Users/oceano/pguth/md_help/html/egm96.htm">https://www.usna.edu/Users/oceano/pguth/md_help/html/egm96.htm</a>
Data Manipulation	Sublime	<a href="https://www.sublimetext.com/">https://www.sublimetext.com/</a>
	Kate 21.12.3	<a href="https://kate-editor.org/">https://kate-editor.org/</a>
	Gedit 41.0	<a href="http://www.gedit.org">www.gedit.org</a>

GNU compilers, image and data manipulators, plotting tools, and simulation software and data.

Figure-3



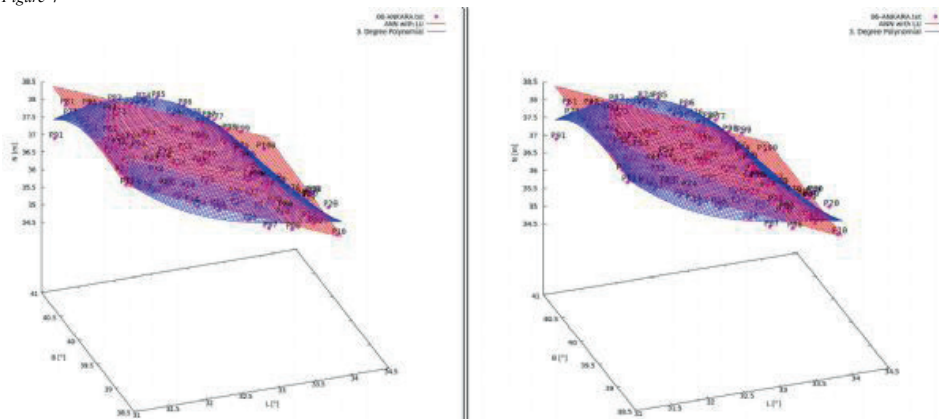
Geoid heights of Türkiye (1 m intervals in red) and Ankara (0.2 m intervals in blue) by EGM08.

Table-3

Source	Functional Model	Type
3th Degree Polynomial	$N = a_0 + a_1 x + a_2 y + a_3 x y + a_4 x^2 + a_5 y^2 + a_6 x y^2 + a_7 x^2 y + a_8 x^3 + a_9 y^3$	Non-linear (u=10)
DNN with LU (Figure-2)	$N = N_0 + (a_8 a_4 a_0 + a_8 a_6 a_1 + a_9 a_5 a_0 + a_9 a_7 a_1) x + (a_8 a_4 a_2 + a_8 a_6 a_3 + a_9 a_5 a_2 + a_9 a_7 a_3) y$	Linear (u=10)

3th Degree polynomial and DNN (Figure 2) surface functions (u: the number of unknown). (Note: The “ ” and “^” signs seen in Table-3 are used for subscript and superscript respectively. Where x=B-B\_0, y=L-L\_0, z = N-N\_0, B\_0=mean(B), L\_0=mean(L), and N\_0=mean(N).)

Figure-4



Two ANN solutions (in red) and 3th degree polynomial (in blue) for Ankara Geoid (Table-5).

Table-4

Non-Linear Hard Computing

```

y Data vector (n)
x Parameters (u)
f = n - u Degree of freedom
y = f(x) (known)
// Compute initials
x0= g(y0) (compute from some data)
loop max {d} > THRESHOLD{
A = df/dx (from know model)
l = y-f(x0) (from know model)
d = inv(ATA)*ATl (LSM)
x = x0 + RELAX * d //Updating
}
v = y - f(x)
σ = sqrt(vTv/n)

// Test for overestimation
T = |x|/σX
x significant unknowns for T<Zα
    
```

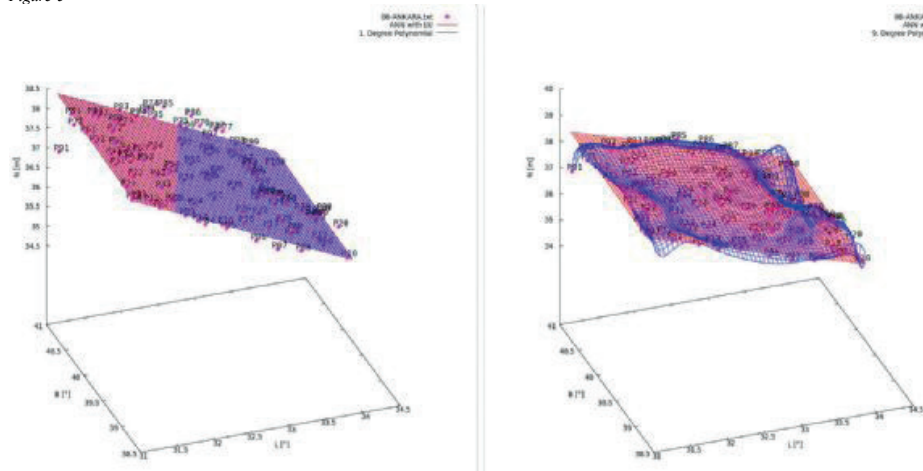
Non Linear Soft Computing (with ANN)

```

y Data vector(n)
x Synaptic Weights (u)
f = n - u Degree of freedom
y = f(x) (achieved from ANN)
loop { // Training
x0 (as random)
loop max {d} > THRESHOLD{// Back propagation
A = df/dx (according to ANN)
l = y-f(x0) (according to ANN)
d = inv(ATA)*ATl (LSM)
x = x0 + RELAX * d // Improve weights
}
v = y - f(x)
σ = sqrt(vTv/n)
x_min for (σ -> min)
}
// Scaling weights for overestimation
x = REGULARIZE * x_min regularized weights
    
```

Solution stages of Hard and Soft Computing (ANN) Method (coded in C/C++).

Figure-5



Comparisons the Polynomial functional models (1. and 9. degrees) with ANN functional models (Table-3).

Table-5

Initial input	Learned values	Initial input	Learned values
1. trial	1. trial	2. trial	2. trial
TRAIN: 100	L_0= 39.904714550000	TRAIN: 100	B_0= 32.604187760000
MAXITER: 1000	B_0= 32.604187760000	MAXITER: 1000	L_0= 39.904714550000
RELAX: 5e-02	N_0= 37.132465000000	RELAX: 5e-02	N_0= 37.132465000000
THRESHOLD: 1e-05	$\sigma_0 = \pm 0.5936$ m	THRESHOLD: 1e-05	$\sigma_0 = \pm 0.6032$ m
REGULARIZING: 1e-03	78. Train	REGULARIZING: 1e-03	7. Train
	1000. iteration		51. iteration
a_0 = {	a_A = {	a_0 = {	a_A = {
-1.0928726038e+00,	-9.3691932349e-01,	-2.8331532892e+00,	2.2768474467e-01,
-2.7933093527e+00,	-4.6064508499e+00,	4.1215282798e+00,	6.8499046448e+00,
-1.2451790941e+00,	-1.3954231820e+00,	-3.0108684491e+00,	-1.4146198984e-01,
-6.3666725907e+00,	-6.8587234585e+00,	-2.3593014678e+00,	1.2246936356e+00,
3.3068051247e+00,	-6.5416276831e+01,	-2.7707345646e+00,	4.3866410493e+00,
-2.9031792597e+00,	2.8048568237e+01,	1.7029994443e+00,	-2.6971108050e+01,
6.8680996233e+00,	1.3288740406e+01,	4.4206118269e+00,	1.1137615132e+01,
2.9577243300e+00,	-6.7681628747e+00,	1.0274382476e+00,	4.8969845558e+00,
2.4036817519e-01,	-2.2697488523e+01,	-2.3566447691e-01,	3.1423194279e-02,
1.0282156480e+00 ;	3.7386100482e-01 ;	-6.2855550851e-02 ;	-8.8635882876e-02 ;

Two ANN solutions results (a\_0: random initial vectors, a\_A: trained vectors) for Ankara Geoid (Figure-4).

Table-6

d = 1	d = 3	d = 6	d = 9
u = 3	u = 10	u = 23	u = 55
n = 100	n = 100	n = 100	n = 100
$\sigma_f = \pm 0.3490$ m	$\sigma_f = \pm 0.2264$ m	$\sigma_f = \pm 0.1338$ m	$\sigma_f = \pm 0.0906$ m
			a_P = {
			3.7334426831e+01,
			-4.1542837698e-01,
			-1.2896227039e-01,
			6.3612250964e-01,
			-7.3614606196e-01,
			-2.6460743086e+00,
			8.6461146933e-01,
			2.1175517835e+00,
			-2.4210604959e-01,
			-5.0526486739e-01,
			-1.9847874055e-01,
			4.3148973801e-01,
			3.1294790310e+00,
		a_P = {	2.2653053991e-01,
		3.7402374332e+01,	-5.9104746107e+00,
		-4.4954148349e-01,	-5.9647594364e-01,
		-8.2035566585e-01,	3.3566416332e+00,
		-4.6829919089e-01,	1.6907147292e-01,
		6.3270576373e-01,	-6.3056940881e-01,
		1.0733753415e-01,	6.0596315130e-01,
		-1.5169595437e-01,	-2.0647071615e+00,
		5.5059713651e-01,	-2.2710391819e+00,
	a_P = {	1.3420103024e-01,	-1.4488987799e+00,
	3.7357239718e+01,	-9.9895503263e-01,	5.0452568876e-01,
	-7.9379311647e-01,	-4.555040522e-01,	1.7005432691e+00,
	-1.8768310648e-01,	6.0767113143e-02,	-5.8416787442e-02,
a_P = {	-7.4383506695e-02,	7.2196609267e-02,	-3.9744603260e-01,
3.7132465000e+01,	5.0911658377e-01,	2.5119705280e-01,	5.1273657786e+00,
-8.4232910867e-01,	-9.3089046791e-02,	-5.3946659081e-01,	-4.9863198309e+00,
-1.2966071236e+04	-4.3910122844e-01,	-2.6150491458e-02,	-9.6161565031e+00,
};	-1.9082158132e-01,	2.3257676116e-01,	5.6022262409e-01,
	1.3950457404e-01,	-2.0669775998e-01,	5.3908552652e+00,
	-1.3912509820e-01};	8.0398652593e-01,	8.0229500150e-02,
		-7.7449003752e-01,	-1.3293504382e+00,
		6.5638922612e-01,	6.8514389873e-01,
		2.7659320268e-01,	7.5584575218e+00,
		-6.4989659743e-02,	4.4516817081e+00,
		3.0653938705e-01,	1.0877035292e+00,
		4.7143324487e-01,	-6.4940754436e-01,
		-1.1789657012e+00,	-7.8173647659e-01,
		9.2219440768e-01,	-8.6683724648e+00,
		-9.9895503263e-01};	1.0424541443e+01,
			1.3375309262e+01,
			-4.6544678571e-01,
			-1.1134380112e+00,
			-3.7796057101e+00,
			-1.1014628075e+01,
			-1.5611264612e+00,
			5.1928001919e-01,
			2.6886031467e+00,
			-5.8789140325e+00,
			-7.0525003595e+00,
			2.0564847531e+00,
			4.9728209210e+00,
			-5.0526486739e-01};

Polynomial functional models for 1,3,6, and 9 degrees (Figure-5).



**POSTER BİLDİRİLER**

***POSTER PRESENTATIONS***

---

---

---



**Bölgesel Jeoloji ve Tektonik**  
*Regional Geology and Tectonics*

---





# Babadağ ( Denizli ) Metabazik Birimlerinin Petrojenetik Karakteristikleri

Cihan Colak, Ali Kaya

Pamukkale Üniversitesi Mühendislik Fakültesi, Jeoloji Mühendisliği Bölümü, Denizli / Türkiye



## ÖZET

Güney Menderes Masifi'nin doğusunda yer alan Babadağ horstu, Çine Asması içerisinde yer alan Prekambriyen yaşlı çekirdek serisi ve onu üzerleyen Paleozoyik yaşlı örtü serisi birimleri ile temsil edilmektedir. Bu çalışmada, Denizli'nin güney-güneybatısında bulunan Babadağ bölgesindeki metabazik birimlerin petrojenetik özelliklerini açıklamayı amaçlamaktadır.

Çekirdek serisi içerisinde yer alan metabazik karakterdeki birimler petrografik ve jeokimyasal incelemeler sonucunda dört litolojiye ayrılmıştır. Bunlar Tip-I amfibolit, Tip-2 amfibolit, hornblend gabro ve granat amfibolit birimleridir.

Petrografik açıdan görece daha büyük albit porfiroblastları, titanit ve lökoksens bileşimi bakımından farklılık göstermesinin yanı sıra ana MgO, Ni ve Cr elementlerindeki yüksek değerler açısından Tip-I amfibolitler Tip-II amfibolitlerden ayrılmaktadır. Tip-I amfibolitlerin Ni ve Cr iz elementlerinin yüksek olması komatitik bazalttan türemiş olabileceğine işaret etmektedir.

Genel olarak tüm metabazik birimler E-MORB'dan OIB'ye doğru kıta içi bazaltlardaki fraksiyonlanma trendini göstermektedir. Toleyitik ve alkali okyanus adası bazaltları karakterindeki metabazik birimler modal olmayan yığın ergimesi modeline bağlı olarak granat lerzolit (derin) fasiyesine yakınsayan bileşimde jeodinamik izler taşıdığı görülmektedir.

Babadağ metamorfiklerindeki yer alan metabazik üyelerinden elde edilecek radyojenik izotop sonuçlarının yanı sıra manto kaynağı ve kabuksal etkileşim süreçlerinin modellenmesi ile sahanın jeodinamik evrim süreçleri önemli yönde detaylandırılacaktır.

## ABSTRACT

The Babadağ horst, which lies to the east of the Southern Menderes Massif, is represented by the Precambrian aged core series within the Çine Submassif and the overlying Paleozoic aged cover series units. In this study, we aim to explain the petrogenetic properties of the metabasic units in the Babadağ region, located in the south-southwest of Denizli.

The metabasic units in the core series are divided into four lithologies as a result of petrographic and geochemical investigations. These are Type-I amphibolite, Type-2 amphibolite, hornblende gabbro and garnet amphibolite units.

Petrographically, Type-I amphibolites differ from Type-II amphibolites in terms of relatively larger albite porphyroblasts, titanite and leucosene composition as well as high values in the main MgO, Ni and Cr elements. The high Ni and Cr trace elements of Type-I

amphibolite indicate that it may be derived from komatiitic basalt.

In general, all metabasic units show the fractionation trend of intracontinental basalts from E-MORB to OIB. The metabasic units in the character of tholeiitic and alkaline oceanic island basalts appear to have geodynamic traces with a composition converging to the garnet lerzolite (deep) facies based on the non-modal bulk melting model.

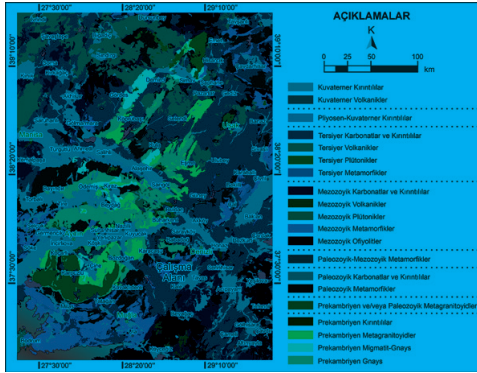
In addition to the radiogenic isotope results to be obtained from the metabasic members within the Babadağ metamorphics, the geodynamic evolution processes of the site will be detailed in a deterministic way by modelling the mantle source and crustal interaction processes.

**Keywords:** Metabasic, Babadağ (Denizli)

## GİRİŞ

Batı Anadolu'nun jeodinamik evrimi üzerinde etkili olan genişleme tektoniği, Menderes Masifi içerisinde yer alan doğu-batı uzanımı Simav, Gediz ve Büyük Menderes Grabenlerini meydana getirmiştir. Kuzeyinde Afyon zonu, batısında Kikladik çekirdek kompleksi, kuzeybatısında İzmir-Ankara zonu, doğu-güneydoğusunda ise Likya naplarının olduğu tektonik bindirme kuşakları ile üzerlenen Menderes Masifi, Pan-Afrikan temelli (çekirdek serisi) ve Paleozoyik-Erken Tersiyer yaşlı (örtü serisi) kayalar ile iki ana grupta temsil edilmekte olup Alpin orojenezine bağlı bölgesel metamorfizmanın etkilerini taşımaktadır (Candan ve diğ. 2011a; Candan ve diğ. 2011b; Koralay ve diğ. 2012). Menderes Masifi bölgesel olarak üç kola ayrılmakta olup kuzey Menderes, orta Menderes ve güney Menderes Masifleri ile temsil edilmektedir.

Çalışma alanı, güney Menderes Masifi kolunun doğu kanadındaki, kuzeyi Büyük Menderes Grabeni, batı-güneybatısı Karacasu Grabeni, doğu-kuzeydoğusu Çürüksu Grabeni, güneyi ise Tavas Havzası ile çevrelenen, Babadağ Horstudur (Şekil 1). Bölgede, Pan-Afrikan temelli (çekirdek serisi) ve Paleozoyik-Erken Tersiyer yaşlı (örtü serisi) kayalar grupları yayılım göstermektedir (Şekil 1).

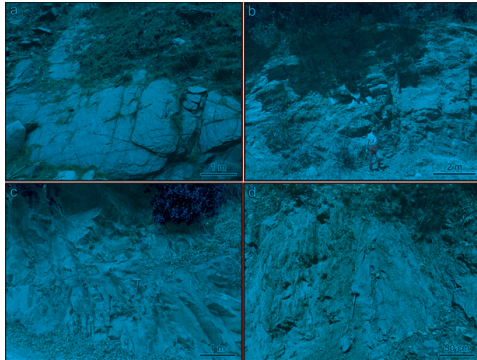


Şekil 1. 1/500.000 ölçekli Türkiye jeoloji haritası, İzmir ve Denizli paftaları, MTA, 2002, Ankara. Çalışma alanını gösteren yer bulduru haritası.

## GENEL JEOLJİ VE STRATİGRAFI

Babadağ metabazik birimleri dört grupta temsil edilmektedir. Bunlar, Tip-I amfibolit, Tip-II amfibolit, granat amfibolit ve hornblend gabrodan oluşmaktadır. Tip I amfibolitler açık soluk renkli olup Tip-II amfibolitlerden ayrılmakta olup daha az foliasyonludur. Tip-II amfibollerin foliasyonlu düzlemlerini kesen klivajlar bulunmaktadır (Şekil 2b). Çalışma alanı içerisindeki metabazik birimler yer yer sil ve dayk şeklinde yerleşim göstermekte ve granat albit mika şist birimlerini kesmektedir (Şekil 2). Bunun yanı sıra Çine gurubu içerisinde yer alan şistlerde de amfibolit bantlarına rastlanmaktadır.

Babadağ metamorfik birimlerinin çekirdek serisine içeren istif, tabanda milonitik gnays ve onu üzerleyen granat albit mika şist'tir. Granat albit mika şist birimleri içerisinde bant ve sil şeklinde amfibolitler yer almaktadır. İstifin üst kısımlarında ise siyah renkli muskovit kuvars şistler tabakalı bir görünümde yanal devamlılık göstermektedir. Çekirdek serisinin daha üst kısımlarında ise mika şistler gözlemlenmektedir (Şekil 3).



Şekil 2. Çalışma alanındaki granat albit mika şist birimi içerisinde yer alan Tip-I amfibolit amfibolit [a], Tip-II amfibolit [b], hornblend gabro [c], granat amfibolit [d] metabazik birimlerinin mostra görünimleri.

Yaş	Birim	Litoloji	Açıklamalar
Prekambriyen	Çine Gurubu	g	Mika Şist Muskovit Kuvars Şist
			Granat Amfibolit Hornblend Gabro Tip-II Amfibolit Tip-I Amfibolit Granat Albit-Mika Şist (gams) Milonitik Gnays (g)
Çekirdek Serisi			

Şekil 3. Babadağ metamorfik birimlerinin çekirdek serisine ait ölçeksiz stratigrafik sütun kesiti.

## PETROGRAFI

Babadağ metabazik birimlerini temsil eden Tip-I amfibolit, Tip-II amfibolit, granat amfibolit ve hornblend gabro birimleri için mineralojik-petrografik tanımlamalar sonucu benzerlikler ve farklılıklar ortaya konulmuştur.

Amfibolitler Tip-I ve Tip-2 Amfibolitler olmak üzere ikiye ayrılmıştır.

### Tip-I Amfibolit

Genel olarak nematoblastik dokusal özelliğini göstermesinin yanı sıra albit minerallerinin görece daha büyük ve eş boyutlu olduğu birimlerde nematoporfirogranoblastik dokudadır. Bununla birlikte belirgin ikizlenme göstermektedir. Ana mineraller amfibol, albit, epidot, klorit, kuvars minerallerinden meydana gelmektedir. Tali minerallerden ise titanit, lökoks, turmalin mineralleri bulunmaktadır. Titanit mineralleri, açık kahve renkli ve optik engebesi yüksek olup kuvvetli pleokroizma göstermektedir. Birim içerisinde birincil karbonat mineralleri de görülmektedir. Tip-I amfibolitler, Tip-II amfibolitlerden görece daha büyük albit porfiroblastlar içermesi ile titanit ve lökoks mineralleri bulunması bakımından ayrılmaktadır (Şekil 4a-4b).

### Tip-II Amfibolit

Amfibol mineralleri, uzamış ve çubuksu görünümündedir. Amfiboller mineralleri epidotlaşmış halde de bulunmaktadır. Albit mineralleri, porfiroblast halindedir. Epidot mineralleri, yüksek engebe göstermekte olup albit mineralleri içerisinde kapanım şeklinde bulunmaktadır. Klorit mineralleri soluk yeşik renktedir. Granat mineralleri, kalıntı halde bulunmakta olup neredeyse tamamen kloritleşmiştir (Şekil 4c-4d).

### Hornblend Gabro

Hornblend gabro birimi diğer metamorfiklere göre korunmuş magmatik dokusal özellik taşımakta olup plajiyoklaz ve hornblend bakımından fenokristal halde bileşim göstermektedir. Diğer metabazik üyelerle göre kuvars bileşimi de görece yüksektir. Ana mineraller amfibol, plajiyoklaz, granat, klorit, kuvars ve biyotit minerallerinden meydana gelmektedir. Tali minerallerden ise titanit, lökoks mineralleri

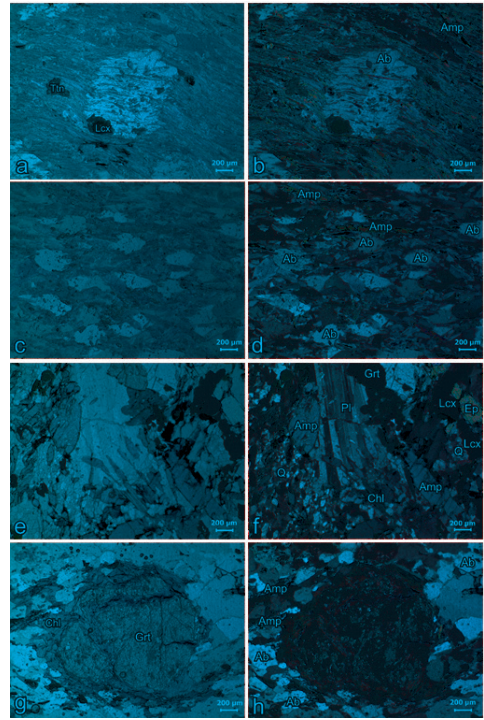
bulunmaktadır. Birim içerisinde demir kusmalarında yer yer görülmektedir. Birim içerisinde birincil karbonat mineralleri de görülmektedir (Şekil 4e-4f).

Amfibol mineralleri özşekilli bulunmanın yanısıra fenokristal halde olup dilinim yönleri belirginlik göstermektedir. Plajiyoklaz mineralleri, polisentetik ikizlenme göstermektedir. Granat mineralleri, yüksek engebeli ve paralel nikelde açık kahve renkte görülmektedir. Epidot mineralleri, amfibollerin alterasyonu şeklinde gözlenmektedir. Titanit mineralleri, açık kahve renkli ve optik engebese yüksek olup kuvvetli pleokroizma göstermektedir. Lökoksens mineralleri, titanit mineralleri ile birlikte bulunmaktadır. Klorit mineralleri, granat minerallerinde dönüşmüştür. Biotit mineralleri, az miktarda olup paralel nikelde sarı-kahve renkte eğik sönme sergilemektedir. Muskovit mineralleri, şistlere dokanak olan kısımlarında gözlemlenmektedir (Şekil 4e-4f).

### Granat Amfibolit

Granat amfibolit birimi özdeş albit minerallerinin yanı sıra görece daha büyük boyutlu granat minerallerinin bileşimine bağlı olarak nemato-porfirogranoblastik dokusal özelliğini göstermektedir. Ana mineraller amfibol, albit, granat, klorit, kuvars ve biyotit minerallerinden meydana gelmektedir. Tali minerallerden ise titanit, lökoksens mineralleri bulunmaktadır. Birim içerisinde birincil karbonat mineralleri de görülmektedir (Şekil 4g-4h).

Amfibol mineralleri, uzamış ve çubuksu görünümündedir. Albit mineralleri, özdeş porfiroblastlar halindedir. Bazı albitlerde ikizlenme görülmektedir. Granat mineralleri, görece büyük porfiroblast haldedir. Kloritleşme göstermektedir. Klorit mineralleri, soluk yeşil renktedir ve granat minerallerinden dönüşmüştür. Biotit mineralleri, görece az miktarda bulunmakta olup paralel nikelde sarımsı-kahverenkli. Biotitler kloritleşme göstermektedir. Titanit mineralleri, açık kahve renkli ve optik engebese yüksek olup kuvvetli pleokroizma göstermektedir. Lökoksens mineralleri, titanit mineralleri ile birlikte bulunmaktadır. Titanit mineralinden dönüşüm gösterdiği görülmektedir (Şekil 4g-4h).



Şekil 4. Metabazik birimlerin mikrofotografaları. Tip-I amfibolit [a-b], Tip-II amfibolit [c-d], hornblend gabro [e-f], granat amfibolit [g-h]. Paralel nikel (sol: a,c,e,g), haç nikel (sağ: b,d,f,h). Ab:Albit, Amp:Amfibol, Chl:Klorit, Ep:Epidot, Gr:Granat, Lcx:Lökoksens, Q:Kuvars, Pl:Plajiyoklaz, Tn: Titanit.

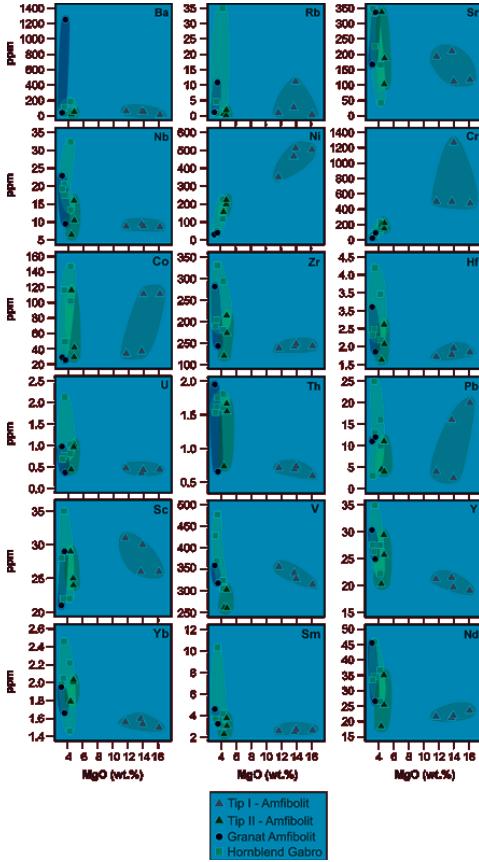
### JEOKİMYA

Tüm kaya ana-eser ve iz element ile nadir yer elementleri örnekleri ALS Geochemistry laboratuvarlarında hizmet alımı şeklinde yapılmış olup matematiksel normlara bağlı jeokimyasal ve jeotektonik sınıflandırma diyagramlarında değerlendirilmiştir.

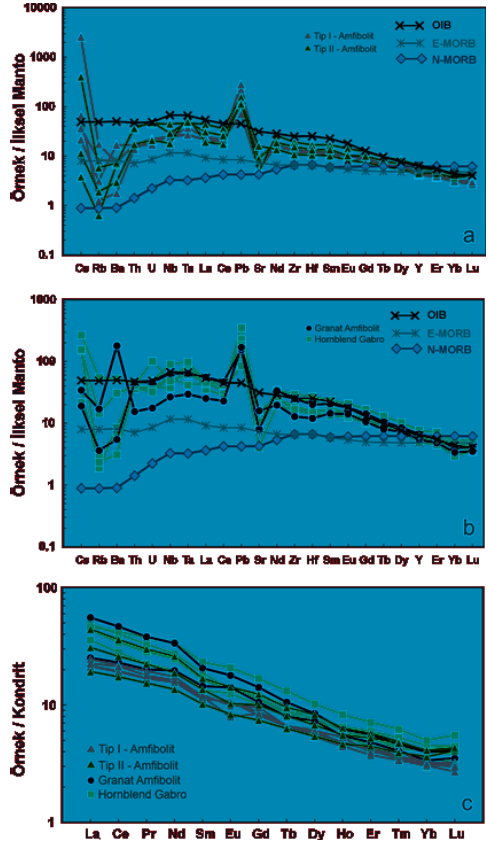
AFM diyagramına göre toleyitik seri içerisinde bulunmanın yanı sıra yüksek MgO içerikli amfibolitler ise toleyitik serinin daha bazik karakterdeki üyelerine işaret etmektedir (Şekil 5). Jensen (1976)'ya göre Tip-II amfibolit, granat amfibolit, hornblend gabro toleyitik seri içerisinde yüksek Fe-Mg içeriği gösterir iken Tip-I amfibolitler ise komatitik bazalt karakterindedir (Şekil 6). Le Bas vd. (1986) diyagramında genel olarak bazalt karakterindeki bölgede dağılım sergilemekte olup Tip-I ve Tip-II amfibolit birimleri toleyitik seri içerisindedir (Şekil 7).



E-MORB'dan OIB'ye giden trend sergilemektedir. Genel olarak Rb, Ba ve Sr elementleri negatif anomali gösterirken Pb elementi pozitif anomali sergilemektedir. Granat amfibolit ve hornblend gabro birimleri de amfibolit grubunda olduğu gibi Sun ve McDonough (1989)'a göre E-MORB'dan OIB'ye giden trend sergilemektedir (Şekil 10b). Sun ve McDonough (1989) kondrite göre normalize edilmiş örümcek diyagramlarında Tip-I amfibolit içerisinde negatif Eu anomaliği görülmektedir (Şekil 10c).



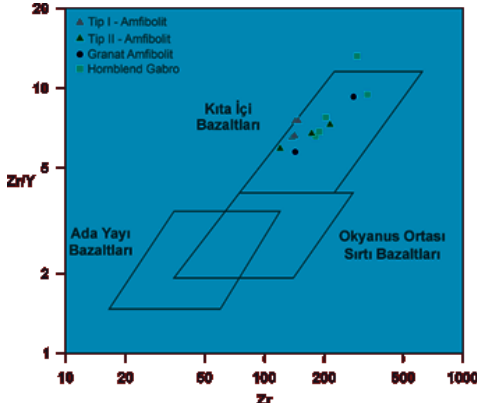
Şekil 9. MgO'e karşı Ba, Rb, Sr, Nb, Ni, Cr, Co, Zr, Hf, U, Th, Pb, Sc, V, Y, Yb, Sm, Nd tüm kaya iz elementlerin Harker (1909) diyagramlarındaki dağılımları.



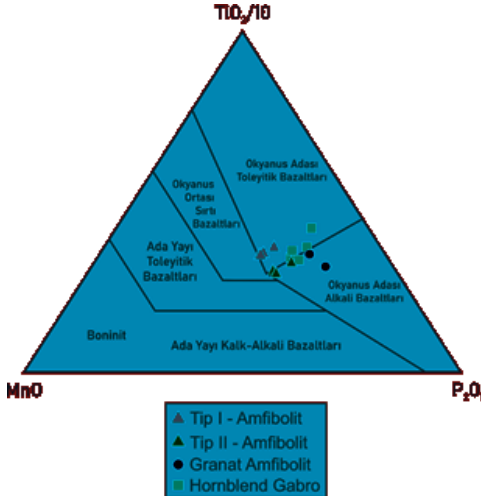
Şekil 10. Tip-I ve Tip-2 amfibolitlerin Sun ve McDonough (1989) ilksel mantoya göre normalize edilmiş örümcek diyagramı [a], hornblend gabro ve granat amfibolitlerin Sun ve McDonough (1989) ilksel mantoya göre normalize edilmiş örümcek diyagramı [b], Sun ve McDonough (1989) kondrite göre normalize edilmiş nadir yer elementleri örümcek diyagramı [c].

## TEKTONİK ORTAM

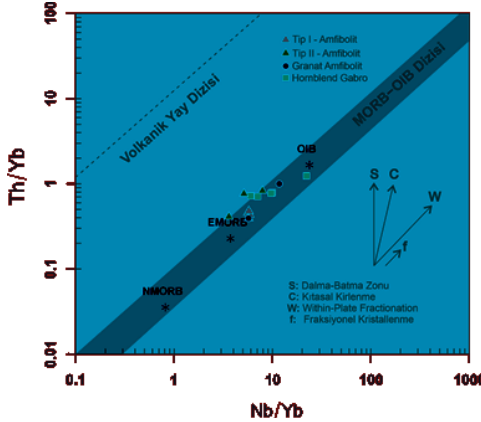
Pearce ve Norry (1979) diyagramında Tip-I ve Tip-II amfibolit, granat amfibolit ve hornblend gabro birimleri kıta içi bazaltları işaret etmektedir (Şekil 11). Mullen (1983) üçlü diyagramında metabazik birimler okyanus adası toleyitik bazaltları ile okyanus adası alkali bazaltları içerisinde dağılım sergilemektedir. Granat amfibolit üyesi ise okyanus adası alkali bazaltlara işaret etmektedir (Şekil 12). Pearce (2008) Th/Yb-Nb/Yb diyagramında kıta içi bazaltların fraksiyonlanma trendi içerisinde E-MORB'tan OIB'ye gidiş sergilemektedir (Şekil 13).



Şekil 11. Pearce ve Norry (1979) tektonik ortam diyagramındaki dağılımı.



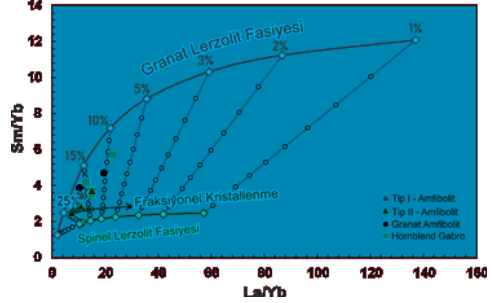
Şekil 12. Mullen (1983) tektonik ortam diyagramındaki dağılımı.



Şekil 13. Pearce (2008) tektonik ortam diyagramındaki dağılımı.

## JEOKİMYASAL MODELLEME

Babadağ metamorfitleeri içerisinde bulunan metabazik birimler, Frey (1980)'in ayrımlanma katsayılarına bağılı olarak modal olmayan yığınsal ergime modeline göre granat lerzolit (derin) ve spinel lerzolit (sığ) fasiyes içerisinde Gündüz ve Asan (2021)'in PetroGram programında projeksiyonlanmıştır. Buna göre Tip-II amfibolitten başlayan uç üye granat lerzolit fasiyesine yakınsayan türden ergime trendi sergilemektedir (Şekil 14).



Şekil 14. Babadağ metabazik birimlerinin Frey (1980) ayrımlanma katsayılarına göre modal olmayan yığınsal ergime modeli. Gündüz ve Asan (2021)'den PetroGram kullanılarak hazırlanmıştır.

## TARTIŞMA ve SONUÇLAR

Babadağ metamorfitleeri içerisinde yer alan metabazik birimler Tip-I amfibolit, Tip-II amfibolit hornblend gabro ve granat amfibolit litolojileri bakımından 4'e ayrılmıştır. Petrografik açıdan Tip-I amfibolitler görece büyük albit porfiroblastlar bulundurmanın yanı sıra titeni ve lökosen içeriği bakımında farklılık sergilemektedir. Tip-I amfibolitler, Tip-II amfibolitlere göre yüksek MgO, Ni, Cr değerlerine sahiptir. Tüm metabazik birimlerin E-MORB'tan OIB'ye giden bir trend ile uyumlu olduğu görülmektedir. Kıta içi bazaltlar içerisinde fraksiyon trendi gösteren metabazik birimler ilksel manto kaynağı bakımından derin fasiyes ergimesine işaret eden granat lerzolit fasiyesi boyunca gidiş göstermektedir.

Astenosferik manto içeriğinin yanı sıra litosferik manto ve delaminasyon izleri bakımından daha detaylı modellenme gerçekleştirilecek olup Sr-Nd radyojenik izotop verilerine bağılı manto ve kabuk karakteristikleri açısından değerlendirilecektir.

## KATKI BELİRTME VE TEŞEKKÜR

Yazarlar, YÖK 100/2000 Hesaplamalı Bilim ve Mühendislik Programı ile TÜBİTAK 2211/A Yurt İçi Doktora Burs Programı'nın sağlanmış oldukları burslar için ilgili kurumlara teşekkür etmektedirler. Bu çalışma, doktora tezi projesi (2021FEBE025) kapsamında Pamukkale Üniversitesi Bilimsel Araştırma Projeleri (BAP) Koordinasyon Birimi tarafından desteklenmektedir.

## KAYNAKLAR

- Bowen, N.L. 1928. The evolution of the igneous rocks. Princeton University Press, Princeton.
- Candan, O., Dora, O.Ö., Oberhänsli, R., Koralay, O.E., Çetinkaplan, M., Akal, C., Satır, M., Chen, F., Kaya, O., 2011a. Stratigraphy of The Pan–African Basement of The Menderes Massif And The Relationship With Late Neoproterozoic/Cambrian Evolution of The Gondwana, Maden Tetkik Ve Arama Dergisi, 142(142), 25-68.
- Candan, O., Oberhänsli, R., Dora, O.Ö., Çetinkaplan, M., Koralay, O.E., Rimmelé, G., Chen, F., Akal, C., 2011b. Menderes Masifi'nin Pan-Afrikan temel ve paleozoyik-erken tersiyer örtü serilerinin polimetamorfik evrimi”, Maden Tetkik ve Arama Dergisi, (142), 123-165.
- Fenner, C.N., 1929. The crystallization of basalts. American Journal of Science, 105, 225–253.
- Frey, 1980. The origin of pyroxenites and garnet pyroxenites from Salt Lake Crater, Oahu, Hawaii: trace elements evidence. Am. J. Sci. 280-A, 427-449.
- Erban, V., Janoušek, V., Farrow, C., ve ŠMÍD, J., 2003. Geochemical Data Toolkit (GCDkit): a key for magmatic geochemists to the treasury of data analysis, statistics and graphics in R. Geolines, 16, 25-26.
- Gündüz, M., ve Asan, K., 2021. PetroGram: An excel-based petrology program for modeling of magmatic processes. Geoscience Frontiers, 12(1), 81-92.
- Harker, A., 1909. The natural history of igneous rocks. Methuen, London.
- Irvine, T.N. Baragar ve W.R.A., 1971. A guide to the chemical classification of the common volcanic rocks. Canadian Journal of Earth Sciences 8, 523–548.
- Jensen, L.S., 1976. A new cation plot for classifying subalkalic volcanic rocks. Ontario Division of Mines Miscellaneous Paper 66.
- Koralay, O.E., Candan, O., Chen, F., Akal, C., Oberhänsli, R., Satır, M. ve Dora, O.Ö., 2012. Pan-African magmatism in the Menderes Massif: geochronological data from leucocratic tourmaline orthogneisses in western Turkey, International Journal of Earth Sciences, 101(8), 2055-2081.
- Kuno, H., 1968. Differentiation of basalt magmas. In: Hess, H.H., Poldervaart, A. (eds.), Basalts: The Poldervaart treatise on rocks of basaltic composition. Interscience, New York. 2: 623–688.
- Le Bas, M.J., Le Maitre, R.W., Streckeisen, A., Zanettin, B., 1986. A chemical classification of volcanic rocks based on the total alkali–silica diagram. Journal of Petrology 27, 745–750.
- McKenzie, D., O’Nions, R.K., 1991. Partial melt distributions from inversion of rare earth element concentrations. Journal of Petrology 32, 1021–1092
- MTA, 2002. 1/500.000 ölçekli Türkiye jeoloji haritası, İzmir, Denizli paftaları, Maden Tetkik ve Arama Genel Müdürlüğü, Ankara.
- Mullen, E.D., 1983. MnO/TiO<sub>2</sub>/P<sub>2</sub>O<sub>5</sub>: A minor element discriminant for basaltic rocks of oceanic environments and its implications for petrogenesis. Earth and Planetary Science Letters 62, 53–62.
- Pearce, J.A., Norry, M.J., 1979. Petrogenetic implications of Ti, Zr, Y and Nb variations in volcanic rocks. Contributions to Mineralogy and Petrology 69, 33–47.
- Pearce, J.A., 2008. Geochemical fingerprinting of oceanic basalts with applications to ophiolite classification and the search for Archaean ocean floor. Lithos 100, 14–48. Rollinson ve Pease 2021
- Sun, S.S., McDonough, W.F., 1989. Chemical and isotopic systematics of oceanic basalts: Implications for mantle composition and processes. In: Saunders, A.D., Norry, M.J. (eds.), Magmatism in ocean basins. Geological Society Special Publication 42. Geological Society, London. 313–345.
- Vermeesch, P., ve Pease, V., 2021. A genetic classification of the tholeiitic and calc-alkaline magma series. Geochemical Perspectives Letters, 19, 1-6.
- Whitney, D. L., ve Evans, B. W., 2010. Abbreviations for names of rock-forming minerals. American mineralogist, 95(1), 185-187.

# Complex Characterization Through Logging Data of a Heterogenous Faulted Zone



Constantin Laurian Ciuperca, Vladimir Andrei Hanumolo

Weatherford International, Wireline & IES services

## INTRODUCTION AND OBJECTIVES

The detection and complete characterization of faulted zones it is one of the targets of major importance during drilling and formation evaluation, as this interest area may generate significant geological hazard or risk during exploration and development of various well stages.

In general, crossing a fault zone it would create a variation of petrophysical parameters inferred from the geophysical logs as well as the local disturbance of the natural tectonic stress field.

Within the current abstract it is presented a case where a fault zone was comprehensively analysed by integrating borehole images, spectral gamma ray, laterolog and microlaterolog resistivities, density, photoelectric absorption factor, neutronic, temperature gradients and caliper data with borehole trajectory for a better understanding of the fault zone behaviour. The abnormal changes throughout the temperature gradients trend, over the fault area, were correlated with uranium content, breakout orientation, bedding walkout plot variation, fracture type and fracture density from borehole images, borehole inclination as well as with lithology.

## MATERIALS AND METHODS

### Geological Setting of the Area

The study area is located within the Arabian Platform, in the south-east of Turkey, close to Bitlis-Zagros Suture Zone (Fig.1).

### Method and Theory

The detailed interpretation of the high resolution microresistivity borehole image consisted in identification and comprehensive characterization of beddings, fractures, faults and as well as in-situ stress indicators.

Classification of the fractures was done based on their various intrinsic responses – darker or lighter than formation background or matrix.

Determination and classification of terminated and truncated features, identified thru the borehole high-resolution image as incomplete sinewaves of bedding and fractures, support fracture timing and geometry interpretation as well as sediment body analysis.

Present-day in-situ stress, which interferes with the borehole wall, is causing during the drilling stage different downhole damage mechanisms that are seen on the wellbore images as borehole breakouts and drilling induced fractures. The entire structural inventory features, that are picked from the wellbore wireline imagers, are generally

displayed in lower hemisphere Schmidt plot within group stereonet plots on azimuth for beddings, strike for fractures or faults and azimuth mirror for breakouts and induced fractures.

Fracture density calculation was done for the current analysis and plotted for both cumulative and separated to the 2 major fracture types, connected and non-connected.

Statistical definition of structural tilt and structural boundaries for distinct dip domains was presented in a dip vector azimuth plot (walk-away diagram). Each bed was drawn as an arrow pointing to its dip azimuth. The plot was built from the base of the study interval up-section, with the tail of each feature arrow placed at the head of the previous arrow (Fig. 2).

Temperature vs Depth crossplot is revealing different temperature gradient profiles that could be explained by the interference with the fault zone.

The borehole trajectory analysis was done by using tadpole display, with body situated on dip angle and tail points to down dip direction.

## CASE

Integrated analysis of well data

Firstly, the fault zone has been highlighted following the interpretation of the high resolution microresistivity borehole image data.

The actual faulted zone (3093.5-3108.5 m) begins with the occurrence of large breakouts, even though the fault interference and influence can also be observed in the adjacent formations.

Over this interval, a change in the azimuth of Pad 1 (blue curve on static images) and a rotation of the breakouts can be noted (Fig.3).

The influence of the fault zone it is extending as well towards the covering formation up to 3079m and in the one below, within the highly resistive carbonates, up to the depth of 3115m, as the temperature vs depth crossplot reveals.

Natural fracture orientation over 3079-3115m depth interval is quite scattered, not having a certain alignment with the minimum or maximum horizontal tectonic stress directions (Fig. 4), showing the predominance of conjugate type, fact which is also confirmed by the abundance of connected fractures.

From temperature vs depth cross-plot analysis were identified 3 distinct zones (Fig.5):

- Zone 1 – 3019-3079m – with positive trend +0.036°C/m (blue)
- Zone 2 – 3079-3115m – high variations in temperature trend (yellow)



- Zone 3 – 3115-3150m – with positive trend +0.0369°C/m (brown)

The penetration of the colder drilling fluid in the fault zone and in the near adjacent fractured formations it produced the rock cooling phenomena (Serra O., 2003).

Although the temperature gradient trend is the same in zones 1 and 3, due to the cooling of the rocks in the fault zone, the highest point in zone 1 (104.6 °C at 3079m) is lower than the lowest point in zone 3 (106.8 °C at 3115m).

Based on vector walkout plot, the fault zone showed the same NNE-SSW direction as the below highly resistive formation (green), the above near adjacent formation being oriented quite N to S starting with 3079m (yellow).

The faulted area, particularly the above near-adjacent fractured zone (in yellow in Fig.6), is characterized by high uranium values, element which is soluble in liquids and is usually accumulated or travelling within zones with higher secondary porosity. The uranium content decreases with the entry into the highly resistive zone below, which confirms the formation behaviour of acting as a seal.

Parallel analysis of the borehole trajectory in the fault zone and in the near-adjacent fault area is revealing a variation in the inclination of the borehole while the azimuth has been remaining constant (Fig.7).

**RESULTS AND CONCLUSIONS**

The precise characterization of faulted areas is a laborious process and requires the integration of as many geological and geophysical data as possible, for an accurate delineation of the zone and of near-adjacent areas where their influence is manifested.

In the presented case study, if the analysis is limited only to the triple combo log suite and borehole imaging data, there could be a temptation to delineate only the interval 3093.5-3108.5m as a fault zone, without considering the area of its influence in the near-adjacent zones, above and below.

The temperature measurements, analysed as gradients, is bringing a great value into showing how much is the influence of the fault zone on the adjacent formations.

Thus, the area where the temperature is not stabilized, marked by positive or negative variations, is considered the area where the fault manifests its influence (3079-3115m), unlike the stable areas where the trend can be determined with high accuracy (3019-3079m and 3115-3150m).

It can be noted the return to the same temperature gradient (+0.36 °C/m) with the exit from the abnormal temperature zone, the cooling of the formations by the drilling fluid in the fault zone causing no continuity between the two trend lines, the difference between them being 2.2 °C.

The increase in the uranium content in the fault area can be attributed both to the high mobility of the uranium that migrated from the rich uranium formation through

the fracture apertures, as well as to the seal formed by the highly resistive underlying formation that didn't allow further migration. As an argument for the migration of uranium along the fractures is the fact that the faulted zone belongs to structural zone 3 and not to zone 1, rich in uranium, as the vector walkout plot shows.

The natural fractures in the fault zone are conjugated, not observing a preferential orientation in the direction of the maximum horizontal tectonic stress, which is quite N-S as induced fracture reveals and breakouts confirmed.

Borehole inclination increases progressively from 6.8° in zone 1 to 8.1° in the fault zone where it stabilizes and then to 9.18° in zone 3, the azimuth remaining relatively constant.

This analysis highlights the usefulness of using the temperature log together with all the other geophysical and geological logs thru the process of properly and comprehensively characterizing the fault zone.

**REFERENCES**

Sarıfakıoğlu E., Dilek Y., Sevin M. (2017), New synthesis of the Izmir-Ankara-Erzincan suture zone and the Ankara mélange in northern Anatolia based on new geochemical and geochronological constraints, The Geological Society of America, Special Paper 525  
 Serra O. (2003), Well Logging and Geology, Editions Technip

Keywords: Fault zone, Temperature anomaly

Figure 1

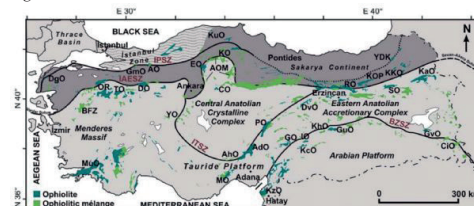


Figure 1 Simplified map of Turkey, showing the distribution of suture zones and major ophiolite complexes. BZSZ -Bitlis-Zagros suture zone (from Sarıfakıoğlu et al., 2017)

Figure 2

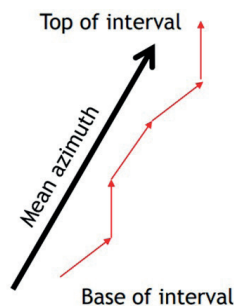




Figure 5

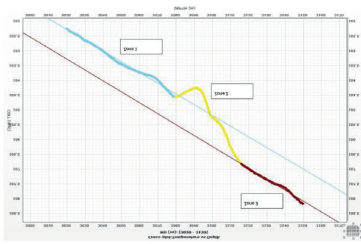


Figure 5 Temperature vs Depth crossplot

Figure 6

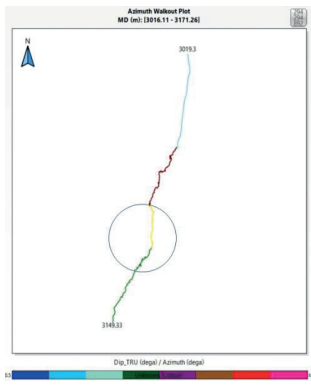


Figure 6 Vector walkout plot over fault and near-adjacent fault area

Figure 7

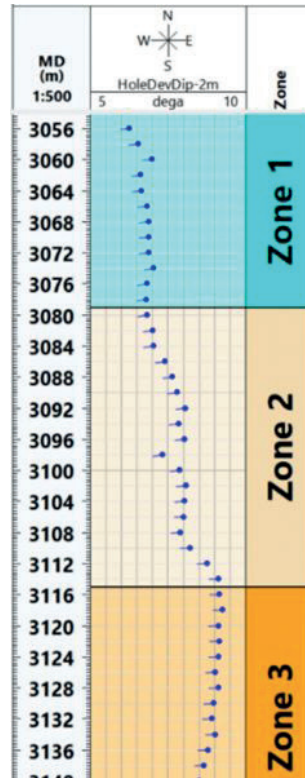


Figure 7 Borehole inclination variation over fault zone

---

---



## **Jeotermal Enerji**

---

---

---

# The Magnetotelluric Method in Geothermal Exploration: Case Studies



Nikita Zorin<sup>1</sup>, Dmitrii Epishkin<sup>1</sup>, Denis Yakovlev<sup>2</sup>, Andrey Yakovlev<sup>3</sup>, Nikolay Palshin<sup>4</sup>

<sup>1</sup>STC Nord-West, Moscow, Russia

<sup>2</sup>STC Nord-West, Moscow, Russia; Nord-West Ltd., Moscow, Russia

<sup>3</sup>Nord-West Ltd., Moscow, Russia; Lomonosov Moscow State University, Moscow / Russia

<sup>4</sup>Nord-West Ltd., Moscow, Russia; Shirshov Institute of Oceanology RAS, Moscow / Russia

## INTRODUCTION

Among the geophysical tools employed for investigation of geothermal systems, the electromagnetic (EM) methods could be very effective since the subsurface electrical conductivity is an important parameter characterizing a geothermal setting in a target area.

Electric resistivity of rocks containing small amount of clay could be described by the Archie relation:

$$\rho_s = F^2 \rho_f$$

where  $\rho_s$  is electric resistivity of the rock,  $F$  is porosity and  $\rho_f$  is electric resistivity of the pore fluid. In turn, the temperature dependence of electrical resistivity of fluid is:

$$\rho_t = \rho_{18} / (1 + \beta(t - 18))$$

where  $\rho_t$  is electric resistivity at  $t$  °C,  $\rho_{18}$  is electric resistivity at 18 °C,  $\beta$  is temperature coefficient, which is about 0.026 for the NaCl water solution. Thus, for example, increasing the temperature to 200°C will decrease rock resistivity in about 6 times, which makes the EM geophysical methods especially useful for geothermal exploration.

Many of high temperature zones (e.g. partially melted ones) and recharge areas (increased fracturing, high temperature and fluid mineralization) are characterized by reduced resistivity. Often hydrothermal processes result in forming clay caps. Clay mineral alterations resulting from the hydrothermal processes also have a low resistivity signature. The reliably identified low resistivity zones produced by brines and clays that cap a geothermal system represent attractive targets for EM exploration [e.g., Arnason et al., 2010; Muños, 2014; Patro, 2017].

## METHODOLOGY

Magnetotellurics (MT) is a passive geophysical method used to infer the Earth's resistivity structure from the measurements of the natural electric (telluric) and magnetic field components either at Earth's surface or at the seafloor. While being relatively cheap and absolutely safe for the environment, the MT method is characterized by high sensitivity to conductive structures and very broad span of imaged depths (roughly from ~100•n m to 10•n km for the regular modification, from ~10•n m to ~n km for the audio-frequency modification, and from ~n m to ~100•n m for the radio-frequency MT modification). As a result, magnetotellurics is especially useful when it is necessary to detect and image highly conductive zones over a wide range of depths in a region of geothermal significance.

Field magnetotelluric surveys carried out in geothermal areas have some specific features, compared to MT applied for deep (crustal and mantle) studies:

- 1) the depth of investigation is, as a rule, a few dozens of meters to 1-2 km;
- 2) requires high density of stations and the optimal location of survey lines (at least 5 stations over the given structure, extra stations beyond the boundaries of the exploration area);
- 3) the need to ensure high productivity of field work to reduce the cost of the survey;
- 4) the need to ensure the availability of quality data in the presence of cultural EM noise and / or low-level magnetotelluric signal

Below we give some examples of successful MT application in geothermal studies, performed by or in close cooperation with Nord-West Ltd.

## CASE STUDIES

### Jermaghybur geothermal field, Armenia

A detailed audio-frequency magnetotelluric (AMT) survey was carried out at Jermaghybur geothermal field, Armenia in 2003. The objective of the work was to clarify the structure and properties of the upper geothermal reservoir, determine the position and characteristics of the lower geothermal water reservoir. MT data were collected in the frequency range from 10 kHz to 0.1 Hz.

Resistivity cross sections (Figure 1) obtained from the AMT data inversion clearly show conductive zones corresponding to the upper geothermal reservoir, while variation of resistivity of the uppermost layer indicates different porosity. Several low resistive zones outlined at depth about 2 km were interpreted as the lower reservoir. Lower reservoir is more heterogeneous to compare with the upper one.

### Krafla and Hengill volcanos, Iceland

In 2005 - 2006 Nord-West participated in international project aimed at studying two geothermal fields in the vicinity of volcanoes Hengill and Krafl in Iceland. In both locations there are active geothermal power plants (Figure 2).

MT data were collected in the frequency range from 300 to 0.001 Hz. Additionally TDEM data were acquired by Iceland GeoSurvey (ÍSOR) at each MT site for accurate static shift correction.

The project had both practical goals (the results were used to set up the wells) and academic ones (studying the deep structure of the active zones of Iceland). Subsequently, the results of MT studies along with data from other methods were used to set up the IDDP-1 deep hole in the Krafla region (Iceland Deep Drilling Project), which was completed in 2009, revealing a magma chamber at a depth of about 2 km.

The resistivity structure of the crust in both survey areas is heterogeneous and deep low resistivity zones, interpreted as magma chambers, were revealed.

A typical resistivity cross section (see Figure 3) consists of three main types of rock: unaltered rocks on the upper part with resistivity of about 10-30 Ohm·m, a conductive altered clay cap with resistivity of about 2-10 Ohm·m (shown in red at Figure 3) and a resistive core below composed of chlorite-epidote metamorphic rocks.

The results obtained in cooperation with ÍSOR show that the regional deep structure of the crust in Iceland has features corresponding to the northeastern strike of the Mid-Atlantic Ridge, as well as transform tectonics (northwest strike).

### **Kamchatka Peninsula, Russia**

Kamchatka Peninsula is located in the Far East of Russia. The Pacific Ocean and the Sea of Okhotsk make up the peninsula's eastern and western coastlines, respectively. Kamchatka is famous for its volcanoes. The central valley of Kamchatka is flanked by large volcanic belts containing around 160 volcanoes, 29 of them are active. Thus, Kamchatka is a natural laboratory for studying volcanoes, and the geophysical studies there have both academic and practical importance.

Electromagnetic studies in the vicinity of Mutnovskaya GPP were carried out by Nord-West Ltd. in several phases, which took place between 2004 and 2014. The studies included both profile and array AMT and MT surveys accompanied by a limited amount of controlled-source EM exploration.

A broadband magnetotelluric (BBMT) survey at Ozernovsky block was carried out in 2018 and was aimed for estimating the geothermal prospects of the survey area and for proposing new exploration well sites location.

In 2016-2018 an MT survey was also carried out in the vicinity of Avacha volcano. The research was a part of a large interdisciplinary survey aimed at prospect assessment of the Avacha hydrothermal field. The specific objectives of the survey were (1) understanding of the geological structure and hydrothermal systems; (2) studies of the proposed zone of interaction of a deep thermal source and a near surface aquifer; (3) constructing of a resistivity model at the depth up to 10 km; (4) proposal for location of exploration wells and (5) preliminary assessment of the possibility and feasibility of developing geothermal resources in the survey area.

### **1. Mutnovskaya GPP**

Resistivity images obtained in the survey area showed a significant heterogeneity of rock properties at all depths. Special efforts were concentrated on better understanding of deep structure of the hydrothermal system. The deep part of the section corresponds to the resistive Mesozoic basement with a conductive sub-vertical channel connecting the upper crustal and near-surface conductive anomalies (see Figure 5). This sub-vertical asymmetric conductive zone was interpreted as a discharge zone and connected at depth to partially melted conductive zone corresponding to the magma chamber. Two resistive zones were also outlined: The northwestern one corresponds to volcanic and terrigenous metamorphosed rocks, while the southeastern one – to granodiorite intrusion.

The integrated interpretation of MT and logging data for one of the profiles along with the resulting conceptual model are given in Figure 6. In the central part of the model in the upper part of the subvertical discharge zone in depth interval from 300 to 1200 m a small highly resistive zone was distinguished. The existence of this zone was confirmed by drilling. This zone corresponds to hydrothermally altered silicified rocks, acting as a “cork” that prevents thermal fluids from reaching the surface. The model is supported by the absence of surface manifestations of hydrothermal activity in the area. At the same time the productive intervals in the well are at depth from 1600 to 2200 m, which is below “the cork”, while another well located nearby (650 m to southeast) entered the productive depth interval at 700 m. Approximately at the same depth a conductive lens was revealed. Its thickness is up to 250 m and width of about 1200 m. This is a natural hot water reservoir according to the integrated interpretation of geological, geophysical and logging data. The uppermost layer is a sequence of terrigenous and volcanic sediments.

Several locations of new exploration wells were proposed and our model was supported by drilling. One borehole is now used by the Mutnovskaya Geothermal power plant for commercial purposes.

### **2. Ozernovsky block**

Ozernovsky block is characterized by a number of thermal springs. Five wells were drilled in the area, which revealed highly mineralized geothermal waters with salinity of about 15 – 23‰ and temperature ranging from 60 to 115°C in the depth interval from 700 m to 1 km. BBMT data were acquired along seven profiles at 82 sites in frequency range from 104 to 10-3 Hz. The dimensionality analysis showed that impedances fit to 1D/2D ones for periods less than 10 s, while at longer period band 3D effects are significant. Impedances were rotated according to geological strike and bimodal 2D inversion was applied. Long period data were down weighted to reduce influence of 3D effects. The resistivity structure of the survey consists of a homogeneous uppermost layer corresponding to Quaternary terrigenous and volcanic deposits with resistivity of about 300 – 400 Ohm·m and thickness



ranging from 60 to 200 m. The second layer is characterized by low resistivity of about 1 - 30 Ohm•m and thickness ranging from 250 to 330 m and corresponds to fractured and hydrothermally altered Neogene rocks. More resistive (> 500 Ohm•m) and heterogeneous Neogene deposits occurring deeper are associated with the main hydrothermal circulation systems. The fractured zone is evidently identified as conductive zones (< 20 Ohm•m) at depth interval 400-800 m.

A large resistivity contrast between fractured hydrothermally altered rocks and host rocks makes interpretation of BBMT data efficient. Data analysis showed that elongated low resistive anomaly running from southwest to northwest divides survey area into highly resistive zones corresponding to intrusions. In the northern part of the survey area an isometric conductive anomaly was imaged. Both anomalies are interconnected by a relatively narrow conductive channel (Figure 7). The suggested spatial structure of anomalous zones is supported by geological data.

Figure 8 shows a resistivity cross section and its geological interrelation along a profile located in the northern part of the survey area, which crosses both conductive zones. Deep subvertical conductive zone represents a pathway of hot fluids, while two shallow conductive zones correspond to the abovementioned fractured and hydrothermally altered terrigenous and volcanic Neogene rocks.

Several locations of new exploration wells were proposed at the peripheral parts of the outlines anomalous zone, as the lowest resistivity usually corresponds to clay cap behind the reservoir.

### 3. Avacha volcano

5-component MT data were acquired in frequency range 400 – 0.01 Hz at 230 sites at regular array 500 x 500 m located at the Avacha volcano south-western slope. In addition, 5-component MT data in frequency range 400 - 0.0001 Hz were collected along 15 km profile at 8 sites. At the interpretation phase archive MT data available in the survey area were also used (Figure 9). Only principle components of impedance were available for archive data, which limits its value. Long period profile data were used for better understanding of the oceanic coast effect on the MT data.

The dimensionally analysis showed that impedances fit to 1D for periods less than 10 s, at period interval 10-100 s impedance are 2D and reflect elongated Avacha graben, while at longer periods 3D effects as well as coast oceanic effect were significant. Impedances were rotated according to geological strike and a bimodal 2D inversion was applied. Long period data were down-weighted to reduce the influence of 3D effects. In addition to a 2D inversion the 3D inversion was also used at initial steps of the multi-step interpretation procedure.

At the beginning a 3D regional inversion with homogeneous halfspace as starting model was carried

out with MT data in a wide period range. The 3D model obtained was used for constructing vertical slices corresponding to profiles. These slices were used as starting model for a 2D inversion along local profiles. The 2D inversion was carried out for limited range of periods: long period data affected by 3D effects were excluded from input data set.

Figure 10 shows resistivity cross section along MT profile (see Figure 9 for location) and geological interpretation. The main features revealed at the profiles are similar to that obtained along other MT profiles (MT array).

The common features are (1) north-eastern dip of resistive basement, (2) number of conductive zones at depth within Pg-N deposits at depth interval from 1 to 5 km, (3) a layer with anomalously low resistivity at the north-western part of profile at depth about 300 - 1000 m and (4) relatively resistive thin uppermost layer (Figure 10).

The most interesting element of the obtained resistivity image is a deep subvertical conductive zone at the north-eastern part of the model. This zone is interpreted as a possible geothermal fluids path. The conductive zone coincides with a low velocity zone. Alternative interpretation is a partially melted zone due to the reduced presence of fluids solidus temperature [Moroz and Gontovaya, 2018].

Several possible locations of exploration wells were proposed. The prospects for the development of geothermal resources in the survey area are estimated as high.

### CONCLUSIONS AND RECOMMENDATIONS

- MT is an environmental friendly and low cost geothermal exploration technology.
- The broad band span of depths that can be imaged using MT technology is one of advantages of the method;
- Geothermally altered and hot fluid saturated rocks are characterized by anomalously low resistivity which make them perfect targets for the MT method;
- MT could be applied both at a regional exploration phase for outlining areas with high geothermal prospects and at a detailed exploration phase for constructing a geothermal system model and estimation of its parameters;
- In most cases application of MT technology gives a possibility to reduce exploration drilling cost;
- If possible, a resistivity model should be interpreted together with all available geological and geophysical data including seismic, logging, and other EM data.

### REFERENCES

- Berdichevsky, M.N. and Dmitriev, V.I., 2008. Models and methods of magnetotellurics, Springer, 564 p.
- Árnason, K., Eysteinnsson H., Hersir, G.P., 2010. Joint 1D inversion of TEM and MT data and 3D inversion of MT data in the Hengill area, SW Iceland. Geothermics, V. 39, p. 13–34.

Moroz, Yu.F. and Gontovaya, L.I., 2018. Deep structure of south Kamchatka according to geophysical data, *Geodynamics & Tectonophysics*, V. 9 (4),

P. 1147–1161. doi:10.5800/GT-2018-9-4-0387.

Munoz G., 2014. Exploring for geothermal resources with electromagnetic methods. *Surv Geophys*, 35:101–122 DOI 10.1007/s10712-013-9236-0

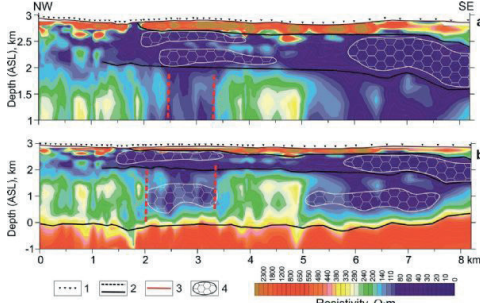
Palshin, N.A., Aleksanova, E.D., Yakovlev, A.G., Yakovlev, D.V. and Breves Vianna, R. Experience and prospects of magnetotelluric soundings application in sedimentary basins, *Geophysical Research*, 2017, V.18, No 2. P. 27-54 DOI: 10.21455/gr2017.2-2.

Patro, P. K., 2017. Magnetotelluric Studies for Hydrocarbon and Geothermal Resources: Examples from the Asian Region, *Surv. Geophys* V. 38, P.1005–1041 DOI: 10.1007/s10712-017-9439-x

Simpson, F. and Bahr, K., 2005. *Practical Magnetotellurics*, Cambridge University Press, 246 p.

Keywords: electromagnetic prospecting, geothermics

Figure 1. Resistivity cross sections at different scale along a typical profile crossing Jermaghbyur Geothermal Field



1 – AMT sites location; 2 - fault zones; 3 - geological boundaries; 4 – conductive zones corresponding to geothermal reservoirs.

Figure 2. Two survey areas in Iceland. Hydrothermal manifestation are shown as circles.

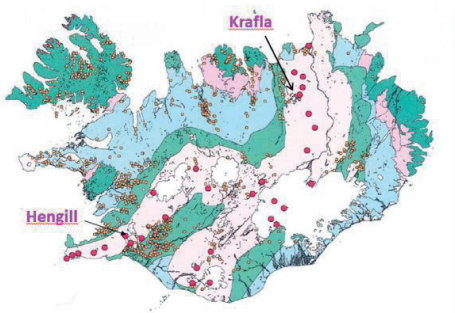


Figure 3. Typical resistivity section across a geothermal anomaly near the

Hengill volcano. Lithology is given according to wells as shown in brown-colored columns [Arnason et al., 2010].

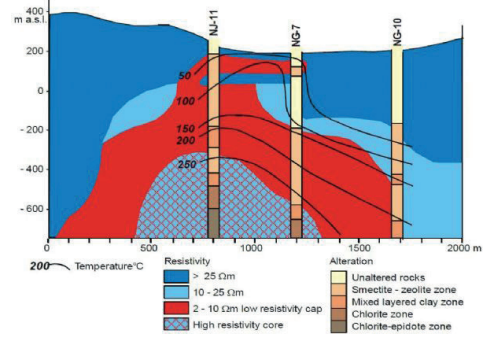
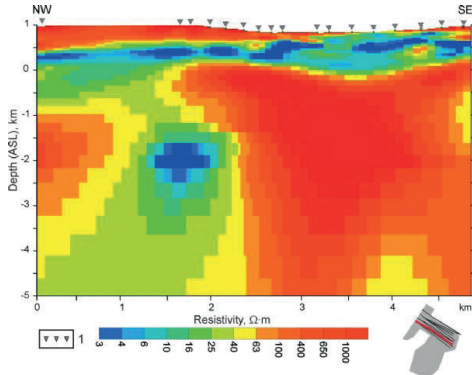


Figure 4. Location of the EM study areas in Kamchatka.



1 – Mutnovskaya geothermal plant, 2 – Avacha volcano, 3 - Ozernovskiy block.

Figure 5. Typical resistivity image of Mutnovskaya area, reflecting its deep heterogeneity.



1 - MT sites location, location of profile is given in the right corner.

Figure 6. Resistivity image (top panel) and conceptual model (bottom panel).

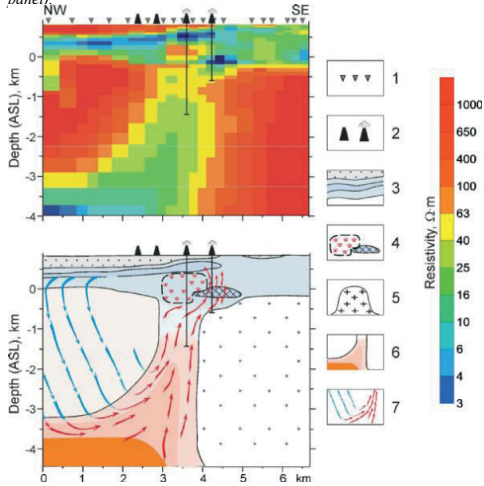
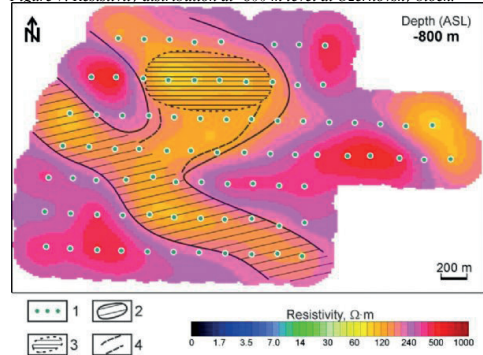
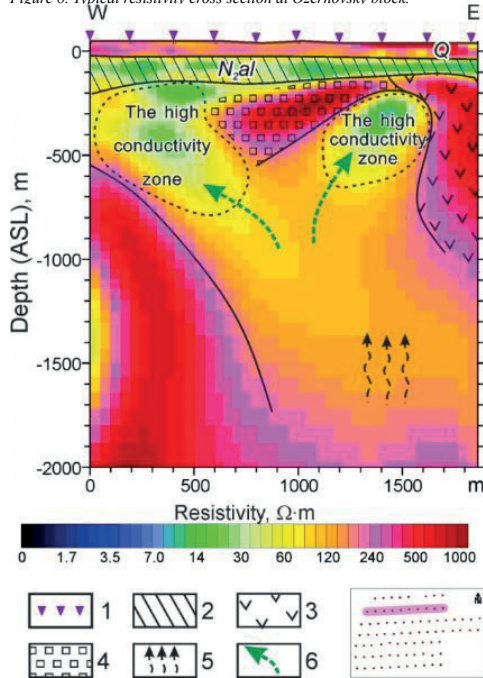


Figure 7. Resistivity distribution at -800 m level at Ozernovsky block.



1 - MT sites location, 2 - fracture zone, 3 - conductive anomaly, 4 - connecting channel.

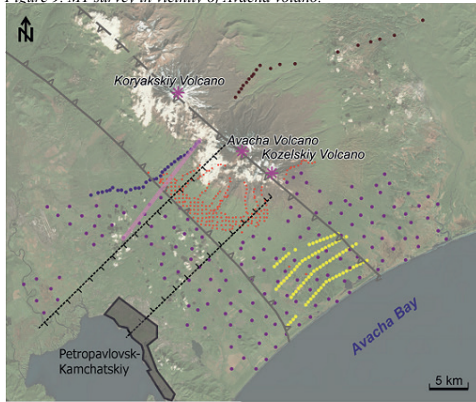
Figure 8. Typical resistivity cross section at Ozernovsky block.



1 - MT sites location, 2 - productive and empty wells, 3 - Neogenic volcanic and terrigenous sediments; 4 - conductive zones and hydrothermally altered rocks; 5 - granitite intrusion; 6 - hot fluid channel and possible partially melted deep zone; 7 - proposed fluid paths: blue is downward cold meteoritic fluid path and red is upward hot fluid path.

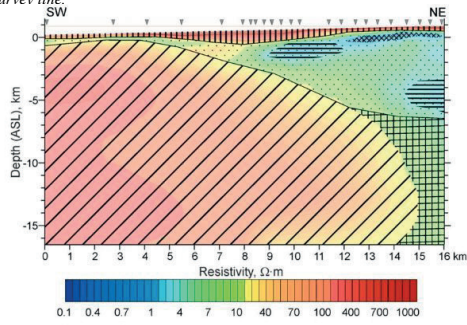
1 - MT sites location, 2 - fractured and geothermally altered Neogen rocks, 3 - resistive intrusions, 4 - consolidated Neogen rocks, 5 - possible heat flow, 6 - geothermal fluid paths.

Figure 9. MT survey in vicinity of Avacha volcano.



1 – archive MT data, 2 – array MT, 3 – MT profile, 4 – Petropavlovsk fault zone, 5 - Avacha graben

Figure 10. Resistivity section and geological interpretation along a survey line.



1 – MT sites, 2 – quaternary glacial, volcanogenic and terrigenous deposits, 3 – N-Pg formations, 4 – Craterous basement, 5 – conductive zones, 6 – zones with anomalously low resistivity (<0.5 Ohm·m), 7 – fractured subvertical zone – possible geothermal fluid path



**Petrol Sistemleri Analizi, Havza  
Modellemesi ve Jeokimya**

---

---

---

# Organofacies and Paleo-depositional Environment of the Northeast Java Basin, Indonesia: Hydrocarbon Generation and Expulsion Potentials Based on Hydrocarbon Geochemical Analysis



**Syahronidavi Al Ghifari**

Sivas Cumhuriyet Üniversitesi Mühendislik Fakültesi, Jeoloji Mühendisliği Ana Bilim Dalı,  
Sivas / Türkiye

Consumption requirements of energy in Indonesia reached 909.24 MBOE in 2021, an increase of 0.4% compared to 905.6 MBOE in the previous year (Ministry of Energy and Mineral Resources, 2021). The high level of demand compared with the income level of oil and gas needs, causing an energy crisis. Northeast Java Basin is included in a basin that has potential to do the exploration and exploitation of oil and gas. However, carried exploration activities are generally reservoir analysis, overburden, and migration, whereas evaluation of source rock is greatly simplified. Therefore, this research was conducted on source rock evaluation ranging from screening organic geochemical analysis and biomarker data. The study was conducted on wells SAG-1 to SAG-5, Northeast Java Basin, Indonesia. The purpose of this study was to determine the potential source rock, type of hydrocarbon and kerogen, maturity degree, depositional environment, relationship between decreased sedimentation and maturity, and knowing potential of hydrocarbons generation and expulsion. The method used in this research were total organic carbon analysis, rock-eval pyrolysis, gas chromatography and gas chromatography-mass spectrometry analysis. Based on the analysis, it is known that at the Miocene to Pliocene Tawun Formation and Tuban Formation potentially to be a potential source rock as biogenic source rock. The Eocene-Oligocene aged Ngimbang and Kujung Formations with kerogen type II/III and III can also be considered as potential SR's producing a mixture of oil and gas and also gas prone. The oil window is located at a depth of 2200 m. Ngimbang Formation depositional environment was a fluvial-deltaic one on the lower delta plain. Kujung Formation depositional environment was also on the delta plain, which was dominated mixed by shallow lacustrine and open marine conditions.

Keywords - Northeast Java Basin, Organic Geochemistry

## INTRODUCTION

The development levels of societies all over the world are evaluated by their energy use rates. Increasing usage rates and non-renewable properties of fossil fuels such as oil, coal, and natural gas, which have been used as a primary energy source for more than a century, have revealed the importance of energy security and sustainable energy concepts in recent years. The industrial and economic activities of the countries and the increase in their importance in national security have made the energy issue a focal point.

The increase in energy demand is mainly influenced by population intense, economic growth, energy prices and government policies. While the global energy consumption rate is increasing by 1-2% per year (<https://ourworldindata.org/energy-production-consumption>). Energy demand in Indonesia increases by an average of 3.5% every year (Agency for the Assessment and Application of Technology outlook energy, 2021). This increase in energy demand cannot be balanced with the current energy supply. Energy consumption needs in Indonesia are heavily dependent on non-renewable energy, which includes oil, coal, and natural gas. Energy consumption in Indonesia reached 909.24 MBOE in 2021, increasing by 0.4% compared to 905.6 MBOE in the previous year (Ministry of Energy and Mineral Resources, 2021). Meanwhile, the use of renewable energy has not yet been optimized.

The high level of exploitation that was not proportional to the level of exploration activities will cause an energy crisis. Therefore, it is necessary to explore potential wells, one of which is in the Northeast Java Basin. The Northeast Java Basin according to Satyana (2005) was a back-arc Tertiary sedimentary basin located on the southeastern boundary of the Eurasian Plate. The western part ends with the North Madura platform and the northern part were bounded by the Masalembu High (Fig.1).

The Northeast Java basin was generally dominated by subaerial sediments and shallow marine sediments, such as limestone. The stratigraphy of this basin consists of the Ngimbang, Kujung, Tuban, Tawun, Bulu, Wonocolo, Ledok, Mundu, Paciran and Tongue Formations (Fig.2). The source rock in the Northeast Java Basin is within a thick sequence, composed of fine clastic material and carbonate rocks. Based on research according to Waples (1985), it can be indicated that the degree of maturity of source rock in a certain area was deeper than the depth of 2000 m or equivalent to the Tuban Formation or the Kujung Formation. Based on this, from the Eocene to the Middle Miocene there was deposition of Tuban Formation, Kujung Formation, and Ngimbang Formation which functioned as effective source rocks (Bissada and Waples, 1991).

The research was conducted in Wells SAG-1 to SAG-5, Northeast Java Basin, Indonesia. The aim of the research is to determine the characteristics of the source rock in the study area, the formations with the potential to be active source rock, the characteristics of the depositional environment, the relationship between the sedimentation rate and the basin depression, and to evaluate the maturity level of the active source rock.

## MATERIAL AND METHODS

In this study, all samples were collected from SAG-1 well until SAG-5 well of the Northeast Java Basin, Indonesia. Hydrocarbon geochemical data includes total organic carbon, Rock-Eval pyrolysis (RE), thermal maturity, biomarkers, and carbon isotopes. Geochemical analysis was carried out at the Geoservices Indonesia laboratory. Organic carbon content was measured using the LECO CS-344 carbon/sulfur analyzer. The samples used are from wells SAG-1 to SAG-4. Rock Eval pyrolysis was carried out using the Delsi-Nermag Rock Eval II Plus TOC module. Rock Eval pyrolysis method consists of heating a programmed temperature (in a pyrolysis oven) in an inert atmosphere (helium) of a small sample (~100 mg) to determine it quantitatively and selectively. The samples used were from wells SAG-1, SAG-3 and SAG-4. The RE data analyzed were hydrogen index (HI), maximum temperature (Tmax), and oxygen index (OI) data. Biomarker data were obtained from Gas chromatography (alkanes and isoprenoids) and gas chromatography mass spectrometry analyzes (Steranes and terpanes). The samples used were from wells SAG-1, SAG-2 and SAG-5. Samples were extracted using dichloromethane in a Dionex ASE 350 accelerated solvent extractor at 75°C and 100 bar. After evaporation of the solvent to a total volume of 0.5 ml total solution in a Zymark TurboVap 500 closed cell concentrator, asphaltene were precipitated from a hexanedichloromethane solution (80:1) and separated by centrifugation.

## RESULTS

### Source Rock Evaluation

Analysis of the screening method was carried out on four wells in the Northeast Java Basin covering wells SAG-1 to wells SAG-4. Based on the results of the TOC analysis in well SAG-1, it was interpreted that the formations that have the potential to become source rock are the Tawun Formation, Tuban Formation, Kujung Formation and Ngimbang Formation. Based on HI and cross plot TOC data, it was indicated that Tawun Formation, Tuban Formation, Kujung Formation and Ngimbang Formation generally have the potential to produce gaseous hydrocarbons and oil mixed gas hydrocarbons. The dominant organic matter type was determined as type III in Tawun Formation SAG-1 well samples, type I, II/IIIb and type III in Tuban Formation, and kerogen type II/IIIb in Ngimbang Formation samples. The variation of Tmax with depth indicates that Ngimbang Formation is mature, while Tawun and Tuban Formations are immature.

The formations that have the potential to become source rock in well SAG-2 were Tawun Formation, Tuban Formation and Kujung Formation. Based on vitrinite reflectance data from SAG-2 wells, there were several samples that have reached an early maturity level, such as Tuban Formation and Kujung Formation. Based on the results of organic geochemical analysis in the SAG-3 well, it was interpreted that the formations that have the potential to become source rocks were the Kujung

Formation and the Ngimbang Formation. Based on the HI variation diagram with respect to depth and the HI vs TOC diagram of the SAG-3 well, it was interpreted that the Kujung Formation and Ngimbang Formation have the potential to generate hydrocarbons. According to the dominant kerogen types, the Kujung Formation includes kerogen types III and II/IIIb that produce oil or a mixture of oil and gas, while the Ngimbang Formation is included in kerogen type II and produces oil. The maturity level in the Kujung Formation ranges from immature to early mature, while the maturity levels in the Ngimbang Formation range from early mature to mature.

The results of the SAG-4 well screening analysis indicate that the Kujung Formation and Ngimbang Formation have the potential to become source rocks and produce hydrocarbons. According to the HI variation with depth and the HI-TOC diagram, SAG-4 wells in the Kujung Formation and Ngimbang Formation in general have low oil production potential with gas, mixed oil, and gaseous hydrocarbons. The kerogen type of the Kujung Formation was composed of either type II or type III. The kerogen type of the Ngimbang Formation was composed of type II, III or II/IIIb. Based on the Tmax data, it was interpreted that the maturity level of the Kujung Formation and the Ngimbang Formation in well SAG-4 were immature to mature.

### Biomarker Data

Gas chromatography (GC) analysis results were used to determine the paleo depositional environment, and n-alkane and isoprenoid data such as Pr/Ph ratio, Pr/nC17 ratio were used. In the gas chromatography-mass spectrometry (GC-MS) data the parameters used include the ratio of Tm/Ts, hopane, morethane/hopane ratio, C27 – C29 sterane diagrams. Based on the comparison ratio between Pr/Ph and Pr/nC17 and the graph of the hopane/sterane ratio with the Pr/Ph ratio, it is interpreted that the Tawun Formation was involved in reduction, the Tuban Formation in oxidation, the Ngimbang Formation in transition and the Kujung Formation in transition with mainly terrestrial supply. Based on the results of the analysis, it was interpreted that the Tuban Formation was included in a fluvial-deltaic depositional environment, due to the high composition of oleanane and bicadinans, while the low concentration of gammacerane.

The distribution of the Kujung Formation samples in the sterane triangle diagram shows that it is included in the transitional depositional environment, that is, the mixed shallow lake dominated and open marine area interpreted as a delta plain area. The Ngimbang Formation was included in a transitional depositional environment (lower delta plain). Determination of the origin of organic matter can be indicated based on ratio data for comparison between Pr/nC17 data and Ph/nC18 data. Based on this analysis, it was interpreted that the Tawun Formation was composed of kerogen which was predominantly reduced. The Tuban Formation, Kujung Formation and Ngimbang Formation generally originate



from terrestrial to transitional organic materials, which undergo a high oxidation process. Maturity level analysis based on the triterpane data parameter, namely the ratio of moretane/hopane with Tm/Ts. Based on these results, the Tuban Formation is in the immature to early mature stage, the Tawun Formation is in the immature stage, the Kujung Formation is in the early mature, and the Ngimbang Formation is in the early to peak mature stage.

## DISCUSSION

Based on the data and analysis results, it is interpreted that the average TOC values have the potential to become good source rocks, namely the Tawun Formation, Tuban Formation and Ngimbang Formation, while the Kujung Formation was included in the category of slightly potential source rocks. This is because the level of distribution of organic material varies in each well, depending on the conditions of the depositional environment. Generally, source rock will have a high content of organic matter if the sedimentation environment was anoxic. In addition, the sedimentation process must be fast with high transport energy. As a result of the dominant sedimentation process, plant remains do not undergo an oxidation process and will experience a faster decay process to form organic material. Besides that, the low TOC value was interpreted to mean that the TOC data analyzed comes from mature source rock and can also be interpreted due to the presence of sand material which will affect the low organic material composition. The average TOC data also explains that the SAG-1 well has the potential for drilling, while the SAG-3 and SAG-4 wells were interpreted that the source rock for the target in the drilling process that was the Ngimbang Formation. The SAG-2 well cannot be interpreted further because TOC data for the Ngimbang Formation was not available. Based on the oil maturity window data, it can be interpreted that the data below a depth of 2200 m in the SAG-1, SAG-3, and SAG-4 wells are the Kujung Formation and the Ngimbang Formation. The Ngimbang Formation and the Kujung Formation were active source rocks, while the Tawun Formation and Tuban Formation were biogenic source rocks which have shallow depths. Based on the Hydrogen Index (HI) data, it was interpreted that the Kujung Formation and the Ngimbang Formation produce hydrocarbons in the form of mixed oil and gas and gas prone with the kerogen type generally being type II/III and III (Fig. 3). The Tawun and Tuban Formations have the potential to produce gaseous hydrocarbons with kerogen type III when heated until they reach the maturity window (Fig. 3).

Analysis of the depositional environment in the Northeastern Java Basin, namely, in the Eocene Age sediment deposition process occurs with LST (lowstand system tract) conditions which were characterized by a decrease in sea level. As a result, sedimentary material will be deposited in the transition environment and the lower delta plain sub-environment, because the activity of the river begins to decrease and precipitates fine

material. During the Miocene, there was a process of sea level rise under the TST (transgressive system tract) conditions. As a result of the effect of rising sea water, it will cause the deposition of the Kujung Formation to be increasingly upward and will be increasingly influenced by increasingly dominant sea water. Based on the data and biomarker analysis of the Kujung Formation, it was interpreted that the depositional environment of the Kujung Formation was in a transition area which was dominated by supplies from terrestrial matters. Therefore, it can be indicated that the Kujung Formation being analyzed was the Kujung III Formation which is located at the bottom of the formation and has not experienced any uplift tectonic processes or the influence of eustasy.

Based on the results of the interpretation of biomarker data, the organofacies of the Ngimbang Formation and Kujung Formation were located in type d and e. Type d and e areas were included in the waxy transition area which has the characteristics of a small composition of sulfur elements, dominantly composed of organic material in the form of higher plants, resins, cuticles and bacteria, and dominantly produces hydrocarbons in the form of gas prone and mixed oil and gas (Fig. 4).

## REFERENCES

- Bissada, K.K., Peters, K.E., 1991, Exploration Geochemistry Seminar, Indonesia Petroleum Association.
- Brandsen P.J.E., Mathews S.J., 1992, Structural and Stratigraphic Evolution of the East Java Sea, Indonesia.
- Hunt, J.M., 1996, Petroleum Geochemistry and Geology, W.H. Freeman and Company, 2nd ed., San Francisco.
- Killops, S., Killops, V., 2005, Introduction to Organic Geochemistry, 2nd ed., Australia.
- Merrill, R.K., 1991, Source Rock and Migration Processes and Evaluation Techniques: AAPG, Treatise of Petroleum Geology, Handbook of Petroleum Geology.
- Mudjiono, R., Pireno, G.E., 2001, Exploration of The North Madura Platform, Offshore East Java, Indonesia, 28th Annual Convention Proceeding. Indonesian Petroleum Association.
- Pepper, A.S., P.J. Corvi., 1995, Simple Kinetic Model of Petroleum Formation Part I: Oil and Gas Generation from Kerogen, Elsevier Science Ltd, UK.
- Peters, K.E., Cassa, M.R., 1994, Applied Source Rock Geochemistry, The Petroleum System from Source to Trap: AAPG Memoir 60.
- Peters, K.E., Walters, C.C., Moldowan, J.M., 2005, Biomarkers and Isotopes in The Environment and Human History, Cambridge University, United Kingdom, 488 p.
- Pratiwi, R., 2015, Introduction to Petroleum Geochemistry and its Significance in Hydrocarbon Exploration, Semarang, Geoservices.
- Robinson., 1987, An Overview of Source Rocks and Oils in Indonesia, Proceedings Indonesian Petroleum Association, 16th Ann. Conv., 97-122.
- Satjana, A.H., 2010, Petroleum Geology of Indonesia: Current Knowledge, Regular HAGI Course. Surabaya.

Stach E., Mackowich M.T.H., Teichmuller M., Taylor H.G., Chandra D., Teichmuller R., 1982, Coal Petrology, Gebruder Borntraeger, Berlin.

Tissot, B. P., Welte, D. H., 1984, Petroleum Formtion and Occurrence, Springer-Verlag, New York.

Van, Bemmelen, R.W., 1949, The Geology of Indonesia. The Hague: Government printing Office.

Waples, D.W., Machihara, T., 1991, Biomarkers for Geologists–A Practical Guide to the Application of Steranes and Triterpanes in Petroleum Geology, Technology Research Center Japan National Corporation Chiba, AAPG Methods in Exploration no. 9.

Keywords: Northeast Java Basin, Organic Geochemistry

Northeast Java Basin, Indonesia

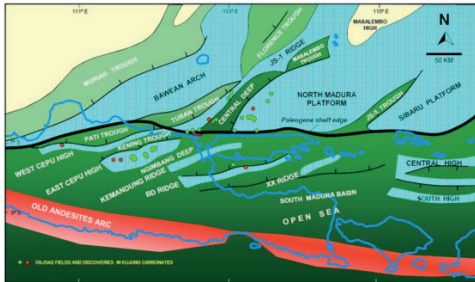


Fig. 1 Study area at Northeast Java Basin, Indonesia (Satyana, 2005)

Organofacies identification

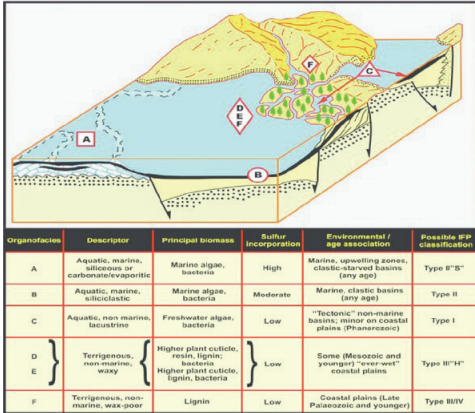


Fig 4. Interpretation of organofacies of the North East Java Basin based on well data SAG-1 to SAG-5

Stratigraphy of North East Java Basin, Indonesia

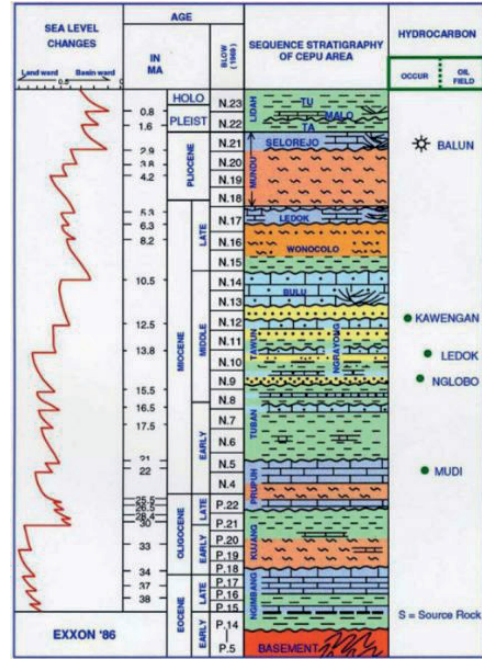


Fig 2. Stratigraphy of North East Java Basin, Indonesia (Nachrowi Koesoemo, 2003)

Tmax vs HI data at wells SAG-1 to SAG-4

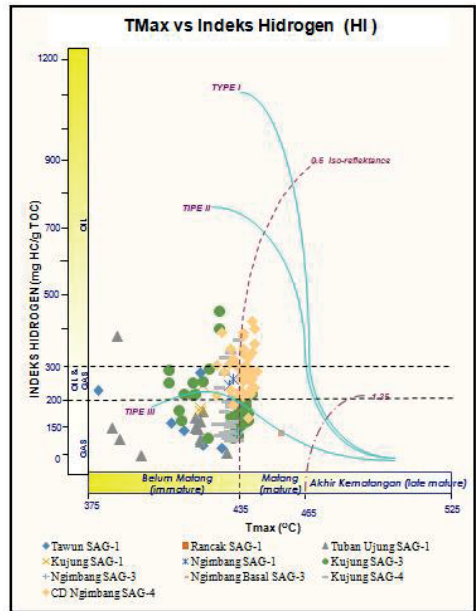


Fig 3. Distribution of Tmax data vs HI at wells SAG-1 to SAG-4

# Distribution Of Terpane and Sterane Biomarkers as Indicators of Organic Matter Input and Depositional Environments in Eocene Sediments Around Zara and Bozbel (Sivas-Türkiye)



**Nazan Yalçın Erik**

Sivas Cumhuriyet University, Sivas / Türkiye

Biological marker (biomarker) characteristics and depositional conditions of Eocene sediments around Zara-Bolucan northeast of Sivas Basin have been determined by means of detailed organic geochemical studies such as gas chromatography (GC) and gas chromatography-mass spectrometry (GC-MS) analysis. n-alkanes, isoprenoids, terpenoids and steroids were used to evaluate paleoenvironmental properties with biomarker data, especially, the marine environment features indicated by C23 tricyclic / C30 hopane, the C26 / C25 tricyclic terpanes, homohopane / C30 hopane and diasterane / regular sterane data. The Pr / Ph, Pr / n-C17 and Ph / n-C18 ratios indicate that there is marine organic matter input that predominantly deposited under reducing conditions. Also, the gammacerane index suggests that there was initially a low salinity environment. The significant terrestrial organic matter contribution is indicated by the isoprenoid and biomarker ratios, dominance of higher n-alkanes such as n-C29, n-C31, CPI, TAR values, n-C19/n-C31, relative abundance of C27-C28-C29 regular steranes. Suboxic to anoxic paleo-depositional conditions are confirmed by the isoprenoid and n-alkane ratios and Tm / Ts, C29Ts / C29 hopane ratios.

Keywords: Sivas Basin, Organic geochemistry

## 1. INTRODUCTION

The study area is located in the Sivas Basin in the northeast section which is one of the important sedimentary basins in Turkey (Görür et al., 1998; Fig. 1a). In this basin, the age of the sediments varies from Upper Cretaceous to Pliocene. The thickness of the basin fill is very variable and can reach up to 8000 m, mostly consisting of fine-grained sediments such as shale and limestone (Kurtman, 1973; Fig.1b and 1c). Many detailed studies on stratigraphic, structural geological features and petroleum geology have been carried out in the units in this basin. Organic geochemical evaluations of sedimentary organic matter provide information on the molecular composition of organic matter, maturation, type of organic matter, primary source and sedimentary facies characteristics (Tissot and Welte, 1984; Peters et al., 2005). The characteristics of the paleo-depositional environment are determined by using detailed organic geochemical data, especially biomarker features, in different sedimentary basin of the world (Zhang et al., 2015).

The Eocene and Miocene section hydrocarbon generation potential in the Sivas Basin has been mentioned by Özçelik and Altunsoy, 1996; Özçelik and Altunsoy, 1996; Altunsoy and Özçelik, 1998;

Özçelik, 2000; Yalçın Erik et al., 2015; Yalçın Erik, 2016. Sivas basin is an area that attracts attention in terms of hydrocarbon exploration in Turkey with its sediment thickness and structural-stratigraphic and sedimentological characteristics of the units, but has not been examined in sufficient detail. Although there is information that there is hydrocarbon potential in some studies conducted in this region, there is a need for detailed and comprehensive research. This study is important because it provides information that will contribute to hydrocarbon studies in the basin. The most important parameter that affects the source rock quality is its depositional environment characteristics that causes organic matter preservation and its amount in a basin that, in turn, defines the source rock hydrocarbon generation potential. Therefore, detailed organic geochemical analyses including biomarker data of the Eocene units, that contain important hydrocarbon source rock potential in the basin, are performed to evaluate depositional environment features.

## 2. GEOLOGICAL SETTING

The Ypresian aged (Eocene) Kozluca Formation has been formed by alternation of fine shales, marls, sandstones and clayey limestones. The formation is overlain by tuffite layers belonging to Bozbel Formation (Fig. 1). Lithological features and paleontological data indicate that this formation was deposited in deep marine conditions (Kurtman, 1973). The main facies of the Bozbel Formation are grey marls, reddish sandstones and subordinate conglomerates. Sandstones and marls of turbiditic origin are intercalated with volcanogenic layers. There is also an olistostrome bed made up of limestone blocks of Lutetian age (Gökçen, 1981; Fig. 1)

Fig.1

## 3. MATERIAL AND METHODS

Thirty-five organic rich shale, mudstone and carbonaceous shale outcrop samples of Eocene units were collected from around Zara-Bolucan region (Fig. 1). A systematic and detailed sampling guideline was followed based on vertical and lateral lithological changes of the Eocene sediments on two measured sections in the study area. Selected shale and carbonaceous shale samples (>0.5 TOC, wt.%) were extracted with organic solvents followed by bulk extracts Gas chromatography (GC) and Gas Chromatography-Mass Spectrometry (GC-MS) analyses on five samples. The aliphatic components obtained by chromatographic fractionation were done according to ASTM (D 5307-97, 2002) by Agilent 6850 instrument. Sterane and terpane ratios were computed by integration of peak heights

from the m/z 217, m/z 191 mass fragmentograms. n-alkanes and acyclic isoprenoids were described from mass fragmentogram of ion m/z 85. Biomarker analyses were performed in the research laboratories of Turkish Petroleum Corporation (TP Research Group, Ankara).

#### 4. RESULTS AND DISCUSSIONS

**4.1. Molecular geochemistry of organic matter**  
The extractable organic matter (EOM) amount of the investigated samples range from 29 to 141 mg/kg rock. The saturated fractions and hetero atomic components (Resin and Asphaltene) vary between 36% to 81% and 12% to 52%, respectively, while aromatic fractions range from 6% to 27%.

#### 4.2. N-alkanes and acyclic isoprenoids

The Gas Chromatography (GC) analysis has been used to determine paleo-environmental conditions of Eocene Bozbel and Kozluca Formation based on the distribution of n-alkanes and acyclic isoprenoids. These compound properties are very similar to each other in the investigated samples. n-alkane distribution of the studied samples comprise mainly n-C12 to n-C35 (lighter alkanes (<C12), possibly present in the formation but evaporated during sample acquisition, storage and extraction). Odd-Even carbon number Predominance (OEP) values and Carbon Preference Index (CPI25-35) (Bray and Evans, 1961) values of the Eocene samples range from 1.03 to 1.14 and 1.02 to 1.14, respectively. Long chain n-alkanes (n-C25–n-C35) are more dominant than medium chain (C21–C25) n-alkanes in the compositions of the samples, and C27, C29 and C31 are the most important components. The calculated n-C19/n-C31 ratios vary between 0.85 and 1.06, while, the n-C24+/n-C24- ratios are high (> 1) and TAR is more than 1.0 and range between 1.28 to 9.02. This wide range of values suggests various terrestrial to marine source organic matter input. This is also supported by predominance of C27, C29 and C31 n-alkanes (Peters and Moldowan, 1993; Peters et al., 2005). Phytane (Ph) values are higher than pristane (Pr) values in the studied samples, therefore the Pr / Ph ratios range from 0.52 to 0.82. Additionally, acyclic isoprenoid to n-alkane ratios of Pr/n-C17 and Ph/n-C18 range between 0.36 to 0.46 and 0.35 – 0.45, respectively and indicate anaerobic environment conditions (Peters et al., 2005).

#### 4.3. Terpanes and steranes

C24 tetracyclic terpane, C23 tricyclic terpanes, C29, and C30 hopanes, C27, and C29 regular steranes are considerable components (Fig. 2a, b), especially, the terpanes are prominent triterpenoid components of the Eocene sediments in the investigated area. The pentacyclic triterpanes are represented by hopanes and the homohopanes (Fig. 2a).

The C24 tetracyclic terpane to C23 triterpanes ratio varies according to organo-facies characteristics, with comparatively high ratios (1.39 – 2.76) in studied

source rocks with marine organic matter input (Peters and Moldowan, 1993). The relatively low C26 tricyclic to C25 tricyclic ratios (0.29 – 0.55) of the studied samples indicate a marine depositional environment conditions (Peters and Moldowan, 1993; Peters et al., 2005). C30 hopane and C29 norhopane ratios are generally close to each other in most of the studied samples, with C29/C30 hopane ratios in the range of 0.90 to 0.97. This values are generally associated with carbonaceous and clayey rocks, which is in agreement with the lithofacies identified for the studied samples. The C31-22R hopane/ C30-hopane ratio is generally higher Long chain n-alkanes (n-C25 – n-C35) are more dominant than medium chain (C21–C25) n-alkanes in the compositions of the samples, and C27, C29 and C31 are the most important components than 0.25 for marine environments and lower than 0.25 for lacustrine and deltaic environmental conditions (Peters et al., 2005). The C31-22R-hopane/C30-hopane ratios of the Eocene sediments range between 0.41 to 0.45, indicating a marine depositional environment.

Fig. 2

High C24 tetracyclic/C26 tricyclic ratio, medium-high norhopane/hopane ratio in the pentacyclic terpane composition of the investigated samples indicate marine carbonate facies and anoxic environment for Bozbel and Kozluca Formation samples. 18 $\alpha$ (H)-oleanane is quite low in the Eocene samples. Also, the gammacerane component was also determined at low values. The compositional ratios of regular steranes ( $\alpha\alpha$  20R) in the analyzed samples is C29>C27>C28. The predominance of the stigmastane (C29) component indicates an intense terrestrial organic matter input, whereas a dominance of cholestane (C27) and ergostane (C28) indicate a dominance of marine phytoplanktons and lacustrine algae, respectively (Peters and Moldowan, 1993).

#### 4.4. Paleodepositional conditions

Terpanes and steranes are the most important compounds that can give very specific information about the source and depositional environment of investigated organic matter (Tissot and Welte, 1984; Peters et al., 2005).

The C35/C34 homohopane and norhopane/C30 hopanes (C29H/C30H) values can be used to identify paleo-depositional facies characteristics (Peters et al., 2005). Moderate to high C35/C34 homohopane ratios indicate anoxic conditions of the paleo-depositional environment of Eocene sediments. The diasteranes/regular steranes ratio (diasterane index) for the analyzed samples show generally low values (0.36 – 0.91) and indicate carbonate rocks and anoxic depositional environment. The same conclusion can be reached by the dominance of 17 $\alpha$ (H)-22,29,30-trisnorhopane (Tm) over 18 $\alpha$ (H)-22,29,30-trisnorhopane (Ts), as well as the high values of C24 tetracyclic/C26 tricyclic terpane ratios (Peters et al., 2005). Especially, C24/C26 terpane ratios are related with a mixed organic matter of algal, bacterial and abundant terrestrial sources. This result is also supported by the C27, C28, and C29 regular sterane distributions. Also, the C31R homohopane/C30 hopane ratios (>0.25)

indicate that the Eocene sediments were deposited in a marine depositional environment. According to Yalçın Erik et al. (2015), organic matter in the Bozbel Formation is mainly Type-III kerogen (mainly gas prone), furthermore, continental palynomorphs are more abundant in the formation than dinoflagellates (Altunsoy and Özçelik, 1998; Yalçın Erik et al., 2015; Yalçın Erik, 2016). This is an important indicator for the marine depositional environment close to the shoreline and open for the continental material influxes (Tissot and Welte, 1984; Hunt, 1995).

Another widely used data in paleo-depositional evaluations is Pr / Ph values. The ratios of the Pr / Ph for the Eocene sediment extracts were generally low and ranged between 0.52 and 0.82 indicating anoxic, reduced marine carbonate depositional environment. Also, the Pr / n-C17 ratios ranged between 0.36 and 0.46 (< 0.5) indicating marine depositional environment. The cross plot of Pr / n-C17 versus Ph / n-C18 for the samples shows mixed (marine and terrestrial) source organic matters deposited under reducing condition with a less effect of biodegradation (Fig. 3b). Additionally, the Pr / Ph versus C31R homohopane / C30 hopane diagram and C26 / C25 tricyclic terpanes ratios (<0.9) indicate a carbonate and marine shale (Fig. 3a).

Fig. 3.

The majority of the analyzed samples show relatively similar concentrations of C29 with ~1 norhopane / C30 hopane ratios ranging from 0.90 to 0.97 (>0.6) and C35 / C34 values (>0.8) that indicate a marine environment with organic rich carbonates and evaporites (Waples and Machihara, 1991; Peters et al., 2005). Also, gammaceranes indicates that salinity was probably low to moderate at the paleo-deposition stage, and there likely were stratifications in water columns during deposition of the organic material in studied Eocene sediments. Plots of regular steranes C27 / (C27+C29) versus Pr / Ph ratio, and C27 / C29 versus Pr / Ph ratio suggests anoxic depositional condition and mixed organic matter (Fig. 4a and 4b).

Fig. 4.

## 5. CONCLUSIONS

The Eocene shale, mudstone and carbonaceous shale samples of Bozbel and Kozluca Formations are exposed around Zara and Bozbel regions and were analyzed for paleo-depositional environment characteristics. The detailed biomarker parameters such as Pr / Ph, n-C19 / n-C31, n-C24+ / n-C24- ratios, OEP, CPI, Tm / Ts ratio and high ratio of C29 regular steranes indicate that a mixed organic matter assemblage with a relatively higher percentage of terrigenous organic matter and low to intermediate percentages of algal and planktonic organic matter input. In this respect, all of the analyzed samples have Pr / Ph ratios of <1 and usually close to 1 CPI values (1.02-1.14) define algal / bacterial organic matter, which is typical of marine depositional conditions that indicate sedimentation under reducing conditions. Generally, the paleo-redox features of depositional environment are supported by the Tm / Ts

and Pr / n-C17 versus Ph / n-C18 diagram. The marine depositional environment conditions was supported by C26 / C25 tricyclic terpanes, C23 tricyclic / C30 hopane ratios and C31R homohopane / C30 hopane ratios. The low to moderate values of Pr / Ph and the gammacerane ratios indicate that a reducing, low to moderate salinity water column was present in paleo-depositional environment of the Eocene units in northeast Sivas Basin. Among the studied samples, the sterane / hopane ratio, the Ts/(Ts+Tm) ratio, 22S/(22S+22R) (C31) ratio and the distribution of intense peaks in the sterane and triterpane fields show immaturity-early maturity. Based on biomarker properties, it was interpreted that Eocene Kozluca and Bozbel formation were deposited in a marine depositional environment close to the shoreline and contained mixed aquatic and terrestrial organic matter.

## REFERENCES

- Altunsoy, M., Özçelik, O. Organic facies characteristics of the Sivas Tertiary basin (Turkey). *Journal of Petroleum Science and Engineering* 1998, 20(1-2), 73-85.
- Artan, Ü., Sestini, G. Sivas-Zara-Beyyınarı bölgesinin jeolojisi. *MTA Dergisi* 1971, 76, 80-98.
- Bechtel, A., Movsumova, U., Strobl, S.A.I., et al., Organofacies and paleoenvironment of the Oligocene Maikop series of Angeharan (eastern Azerbaijan). *Organic Geochemistry* 2013, 56, 51-67.
- Bray, E., Evans, E. Distribution of paraffins as a clue to recognition of source beds. *Geochim. Cosmochim. Acta* 1961, 22, 2-15.
- Gökçen, S. L. Zara-Hafik Güneyindeki Paleojen istifinin sedimentolojisi ve paleocoğrafik evrimi, *Yerbilimleri* 1981, 8, 1-21.
- Görür, N., Tüysüz, O., Şengör, A.M.C. Tectonic evolution of the Central Anatolian basins. *International Geology Review* 1998, 40, 831-850.
- Hunt, J.M., *Organic Geochemistry and Geology*: Freeman and Company, New York, 1995, 743 p.
- Kurtman, F. Sivas-Hafik-Zara ve İmranlı Bölgesi'nin jeolojik ve tektonik yapısı. *MTA Dergisi* 1973, 80, 1-33.
- Özçelik, O., Altunsoy, M., Bolucan (Zara-Sivas) yöresinde Oligosen yaşlı Selimiye Formasyonu kumtaşlarının sediment petroloji incelemesi, *Jeoloji Müh. Dergisi* 1992, 41: 131-137.
- Özçelik, O., Altunsoy, M., Clastic petrofacies, provenance and organic facies of the Bozbel Formation (Lutetian) in the Eastern Sivas Basin (Turkey). *Marine and Petroleum Geology*, 1996, 13.5: 493-501.
- Özçelik, O. Source rock Evaluation of Tertiary sediments in the Sivas Basin, Central Anatolia. *Bulletin of Faculty of Eng. Cumhuriyet Uni., Serie A, Earth Sciences* 2000, 17/1, 31-44.
- Peters, K. E., Moldowan, J. M. *The Biomarker Guide: Interpreting Molecular Fossils in Petroleum and Ancient Sediments*. Prentice-Hall, Inc, Englewood Cliffs, New Jersey, 1993.
- Peters, K. E., Walters, C.C., Moldowan, J.M. *The biomarker guide*. In: *Biomarkers and Isotopes in Petroleum Exploration*

and Earth History". vol. 2. Cambridge University Press, Cambridge, 2005.

Tissot, B.P., Welte, D.H. Petroleum Formation and Occurrence. Springer-Verlag, Berlin, 1984.

Waples, D.W., Machihara, T., Biomarkers for geologists—a practical guide to the application of steranes and triterpanes in petroleum geology. AAPG 9, 1991, 91.

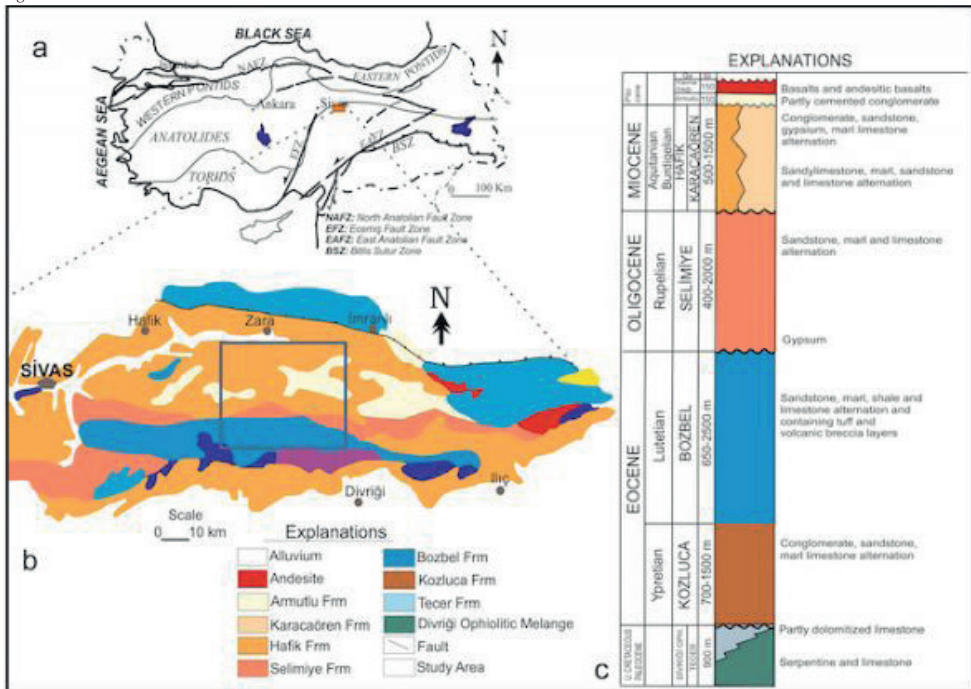
Yalçın Erik, N., Aydemir, A., Büyüksaraç, A. Investigation of the organic matter properties and hydrocarbon potential of the Sivas Basin, Central Eastern Anatolia, Turkey, using Rock-Eval data and Organic Petrography. Journal of Petroleum Science and Engineering 2015, 127, 148-168.

Yalçın Erik, N. Paleoenvironment characteristics and hydrocarbon potential of the Lower Miocene bituminous shales in Sivas Basin (Central Anatolia, Turkey). Journal of Arabian Earth Science 2016, 9-18.

Zhang, S., Wu, T., Zhang, S., et al., Organofacies and paleoenvironment of lower Carboniferous mudstones (Dishuiquan Formation) in Eastern Junggar, NW China. International Journal of Coal Geology 2015, 150–151,7–18.

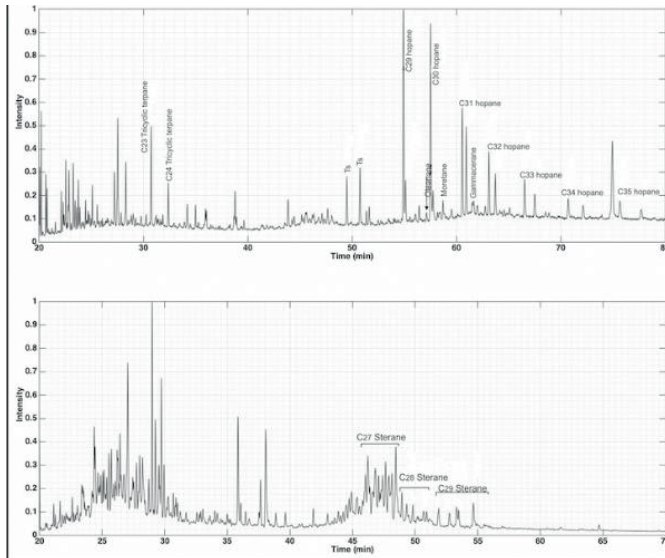
Keywords: Sivas Basin, Organic geochemistry

Fig.1



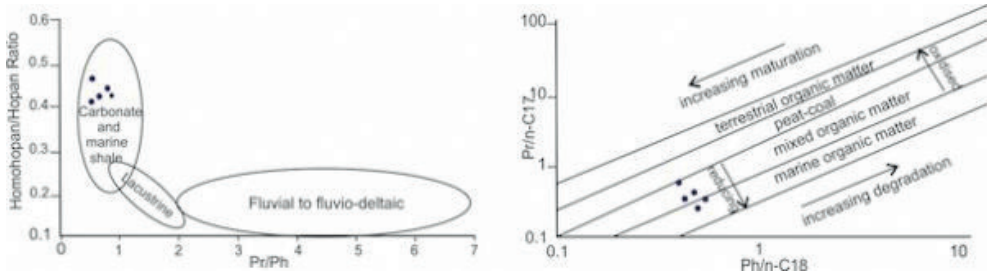
Location map, simplified geological map and stratigraphic section of the study area (modified from Özçelik, 2000).

Fig.2



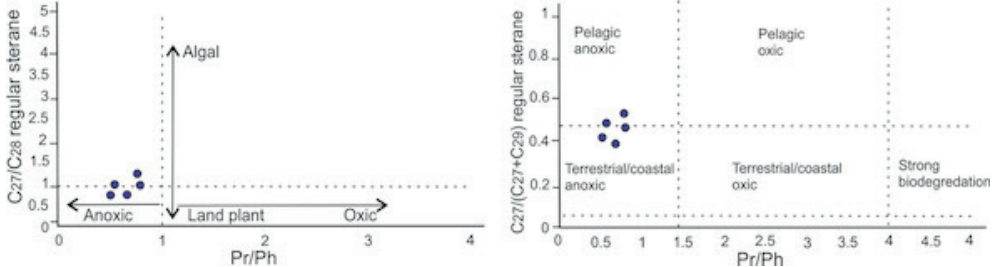
a) GC-MS chromatograms of a representative sample of the study area (a; m/z 191 and b; m/z 217)

Fig.3



Result of GC and GC-MS analysis data on diagrams; a) Homohopane / hopane ratio vs Pr / Ph ratio, b) Pr / nC17 vs Ph / nC18 ratio for Eocene sediments

Fig.4



Relationship between a) C27 / C28 regular sterane vs Pr / Ph ratios and b) C27 / (C27+C28+C29 regular sterane) vs Pr / Ph ratios for investigated samples.

---

---





## **Petrol, Dođal Gaz, LPG ve LNG Pazarı**

---



# COVID-19 Pandemisinin Türkiye'deki Enerji Tüketimine Etkisi

## Kıvanc Peker

Karadeniz Teknik Üniversitesi, Fen Fakültesi, Kimya Bölümü, Trabzon; Türkiye Enerji, Nükleer ve Maden Araştırma Kurumu (TENMAK), Nadir Toprak Elementleri Araştırma Enstitüsü (NATEN), Ankara



COVID-19 pandemisi sebebiyle tüm ülkeler, insanların iç içe bulunduğu okullar, iş yerleri, cafe ve eğlence mekanları gibi yerlerde insan yoğunluğunu azaltabilmek adına tedbirler almıştır. İnsan yoğunluğunun azaltılması başta ulaşım sektöründe tüketilen yakıtlar olmak üzere sanayi ve konutlarda elektrik ile doğal gaz tüketimlerinde azalmaya neden olmuştur. Pandemi tedbirlerinin yoğun olduğu dönemlerde küresel ölçekte elektrik tüketimleri %20-30 aralığında, benzin ve jet yakıtı talepleri sırasıyla 3.2 milyon varil/gün ile 3.0 milyon varil/gün dolaylarında düşmüştür. LPG/etan ve nafta talebi ise artan paketleme, hijyenik malzeme ve tıbbi satışlar sebebiyle neredeyse değişmemiştir. Türkiye'de 2020 yılı elektrik tüketim miktarı 2019 yılı elektrik tüketim miktarından yaklaşık olarak %1.7 oranında fazla iken, pandeminin ilan edildiği ve ilk kapanma kararlarının alındığı Mart ve Nisan aylarında elektrik tüketimi bir önceki yılın aynı dönemine kıyasla yaklaşık %15 düşmüştür. Doğal gaz tüketimi ise senelik olarak değerlendirildiğinde 2020 yılı tüketim miktarı 2019 yılı tüketim miktarından %3.8 fazladır. 2020 Mart-Mayıs aralığında kaydedilen tüketim miktarları bir önceki senenin aynı dönemlerine ait tüketim miktarlarına kıyasla %12-23 aralığında bir düşüş göstermiştir. Benzin, motorin, havacılık ve denizcilik yakıtlarında da kısıtlamalar ve kapanma kararları etkisini göstermiş olup en büyük düşüşü havacılık yakıtı tüketimi göstermiştir. Benzin, motorin ve denizcilik yakıtlarının tüketimlerinde %40'a varan düşüşler kaydedilmiştir. Tespit edilen en büyük düşüş ise Mayıs ayında %80'den fazla bir düşüş yaşayan havacılık sektöründe meydana gelmiştir. Bu verilerden de anlaşıldığı üzere insan hareketliliği ile enerji tüketimi birbirleriyle yakın ilişkilidir.

Due to the COVID-19 pandemic, all countries have taken measures to reduce human density in places such as schools, workplaces, cafes and entertainment venues where people are gathered. Reducing human density has led to a decrease in electricity and natural gas consumption in industry and home, especially in the fuels consumed in the transportation sector. During periods of intense pandemic measures, global electricity consumption decreased by 20-30%, and gasoline and jet fuel demands decreased by 3.2 million barrels/day and 3.0 million barrels/day, respectively. LPG/ethane and naphtha demand remained almost unchanged due to increased packaging, hygienic materials and medical sales. While the electricity consumption amount in 2020 in Türkiye was approximately 1.7% higher than the electricity consumption amount in 2019, electricity consumption decreased by approximately 15% compared to the same period of the previous year in March and April, when the pandemic was declared and the first shutdown decisions were taken. When natural

gas consumption is evaluated annually, the consumption amount in 2020 is 3.8% more than the consumption amount in 2019. Consumption amounts recorded in the March-May period of 2020 showed a decrease in the range of 12-23% compared to the consumption amounts of the same periods of the previous year. Gasoline, diesel, aviation and marine fuels were also affected by the restrictions and shutdown decisions, with aviation fuel consumption showing the biggest decrease. Up to 40% reductions were recorded in the consumption of gasoline, diesel and marine fuels. The biggest decrease detected was in the aviation sector, which experienced a decrease of more than 80% in May. As it can be understood from these data, human mobility and energy consumption are closely related to each other.

Keywords: COVID-19 Pandemic, energy consumption

## 1. GİRİŞ

Enerji, insan hayatı için en temel unsurlardan biridir ve sadece insan hayatı için değil, modern dünya için de vazgeçilmez bir unsurdur [1]. Sanayi üretimleri, ulaşım ve daha nice faaliyet sıkı sıkıya enerjinin varlığına bağlıdır [2]. İnsanların faaliyetleri, enerji tüketimi ile doğrudan ilişkilidir. Enerji üretim ve tüketim miktarları, insanların alışkanlıklarında veya günlük hayatlarında meydana gelen değişimlerden ve sanayi ürünlerine olan taleplerde yaşanan olumlu ya da olumsuz gelişmelerden aynı oranda etkilenmektedir. 2019'un sonlarında ortaya çıkan ve 2020'nin başlarında etkisini hissettirmeye başlayan Yeni Koronavirüs Hastalığı (COVID-19) sebebi ile kısa sürede insanların günlük hayatlarında ve alışkanlıklarında, küresel ekonomide, enerji tüketiminde, ulaşım sektöründe, karbon ayak izinde ve daha nice alanlarda büyük değişimler yaşanmıştır [3-6].

COVID-19, bulaşıcı bir hastalık olup ilk olarak 2019 senesinin Aralık ayında Çin'in Hubei eyaletinin Wuhan kentinde ortaya çıkmıştır [7-8]. Bulaşıcı bir hastalık olması sebebi ile ortaya çıktığı ilk andan itibaren hızla yayılmıştır. Hastalığın bulaştığı kişilerde çeşitli belirtilere rastlanmaktadır. Bu belirtiler arasında genel olarak yorgunluk, ateş, öksürük, nefes almakta güçlük çekme, koku ve tat alma yeteneklerinin geçici süreliğine kaybı vardır. Yeni tip koronavirüse maruz kalan kişilerin bir kısmında 1 ile 14 gün arasında hastalık belirtileri meydana gelirken, hastalandıkları halde belirti göstermeyen vakalara da rastlanmıştır [9].

COVID-19, esas olarak hasta olan bireylerle kurulan yakın temas sonucu bulaşmaktadır. COVID-19'a sebep olan yeni tip koronavirüslerin bulaştığı hastalar yani enfekte olan kişiler, nefes alma, hapsirme, öksürme ve hatta konuşma sırasında yaydıkları zerreciklerle sağlıklı

insanların da hastalanmalarına sebep olmaktadır [10-11].

Enfekte olan kişilerin bir kısmında belirti görülmemesi, süper taşıyıcı olarak adlandırılan bireylerin farkında olmadan sosyal hayatlarına devam etmesine ve Wuhan'da yaşadığı gibi hastalığın hızla yayılmasına neden olmuştur. Uluslararası seyahat gerçekleştiren ve farkında olmadan koronavirüs taşıyıcısı olan kişilerle birlikte hastalık Wuhan'dan tüm dünyaya kısa sürede yayılmıştır. Neredeyse tüm ülkelerden COVID-19'a ilişkin raporlar yayımlanmaya başlanmasıyla Dünya Sağlık Örgütü (WHO) 11 Mart 2020 tarihinde pandemi ilan etmiştir [12].

Dünya Sağlık Örgütü tarafından 11 Mart 2020 tarihinde pandemi ilan edilmiş olsa da hastalığın yayılması tüm hızıyla devam etmiştir. İnsanların işlerine gitmek için toplu taşıma araçlarını kullanması, iş yerlerinde kalabalık ortamlarda görev yapmaları, beslenme ve eğlence ihtiyaçları için birçok kişiyle ortak alanların kullanılması hastalığın yayılmasını hızlandırmıştır. İnsanların sosyal hayatlarının aynı şekilde devam etmesiyle ilk olarak Çin ve ardından İtalya, İngiltere, Almanya, Fransa, İspanya, Türkiye ve Amerika Birleşik Devletleri gibi birçok ülke salgının önüne geçebilmek adına sosyal hayatta kısıtlamalara gittiler. Pandeminin ilk tedbirlerinden olan bu kısıtlamalara zorunlu olmadıkça evden çıkılmaması, mesleği uygun olan bireylerin evden çalışması, mümkün olduğunca toplu taşıma araçlarının kullanılmaması ve kalabalık ortamlara girilmemesi tavsiyeleri örnek verilebilir. İlk tedbirlerin de yeterli sonuçlar vermemesi nedeniyle Çin, ABD, İngiltere, İtalya, İngiltere ve Türkiye gibi birçok ülkede "Lockdown" adı verilen geniş kapsamlı kapanmalara gidildi [13-15].

COVID-19 pandemisinin patlak verdiği ilk dönemlerde getirilen kısmi yasaklamalar ve ardından gelen geniş kapsamlı kapanmalar karayolları ve hava yolları gibi ulaşım yöntemlerinin kullanımını oldukça azaltmıştır. Fabrikalar ve iş yerleri çalışma kapasitelerini azaltarak insan yoğunluğunu düşürmeye çalışmıştır. Kamu ve özel sektörde uzaktan, vardiyalı çalışma yöntemleri geliştirilmiştir. Okullar ve üniversiteler önce tatil edilmiş ve ardından gerekli olan alt yapıya sahip olan ülkelerde uzaktan öğretime geçilmiştir. Sosyal hayatı kısıtlayıcı bu önlemler araçlarda yakıt tüketimi ile fabrikalar, işyerleri ve konutlarda da elektrik enerjisi ve doğal gaz tüketimini azaltmıştır [6, 16, 17].

## 2. KÜRESEL ETKİLER

Çin'in Wuhan eyaletinde Yeni Koronavirüs hastalığının patlak vermesinin ardından kısa süre sonra Japonya ve Güney Kore'de de vakalar görülmüş ve bunu Amerika Birleşik Devletleri ile Avrupa'da görülen vakalar izlemiştir. Orta Doğu ve Dünya'nın geri kalan kısımlarından da vakaların bildirilmesi ile birlikte kısa sürede COVID-19 pandemisi küresel ölçekte etkisini göstermiştir. 11 Mart 2020'de Dünya Sağlık Örgütü tarafından pandemi ilan edilmesiyle gidişatının kontrol altına alınabilmesi adına hükümetler tarafından art arda tedbirler yayımlanmıştır. Bu tedbirler; öncelikle

Wuhan'daki gibi vaka görülen bölgelerde karantina ilan etme şeklinde olmuştur. Bölgesel karantina ilan edilmesinin çözüm olmadığı anlaşılınca İtalya, İngiltere ve daha birçok ülkede kapanma kararları alınmıştır [6,16]. Sokağa çıkma yasağı, kutlama törenlerinin iptal edilmesi, okulların kapatılarak uzaktan eğitime geçilmesi, toplu taşıma araçlarında yolcu sayısına kısıtlama getirilmesi, iş yerlerinde vardiya uygulaması ve hava trafiğinin azaltılması getirilen diğer tedbirler arasındadır. Tedbirlerin sonucu olarak trafikteki araç sayısında önemli miktarda düşüş meydana gelmiştir ve dolayısıyla tüketilen yakıt miktarında kayda değer bir azalma gerçekleşmiştir. Aynı şekilde sanayide kullanılan gaz ve elektrik miktarlarında da alınan tedbirlerin kapsamına göre düşüşler gerçekleşmiştir. Tedbirlerin gevşetilmesi ile enerji tüketim miktarları zaman zaman önceki sene değerlerinin üzerine çıkmıştır.

### 2.1. Elektrik Tüketimi

COVID-19 pandemisi sebebiyle 2020 senesinde küresel ölçekte elektrik talebi yaklaşık olarak %1 düşmüştür. Lockdown olarak adlandırılan kapanma ve karantina kararları alınan dönemlerde ise tüketim miktarı bir önceki senenin aynı aylarına kıyasla %20 ile %30 arasında azalmıştır.

Hastalığın ilk olarak gözlemlendiği ülke olan Çin'de 2020 Şubat ayında önceki senenin aynı ayına kıyasla elektrik tüketiminde %10'luk bir düşüş kaydedilmiştir. Hastalığın zamanla yayılarak ABD'ye ulaşmasıyla birlikte alınan tedbirlerle ABD'de Mayıs ayında elektrik tüketiminde yaklaşık %10'luk bir düşüş meydana gelmiştir.

Dünya Sağlık Örgütü'nün 11 Mart 2020'de pandemi ilan etmesinin ardından Nisan ayına kadar Fransa, Almanya ve Birleşik Krallık'ta elektrik talebi %15'ten fazla düşmüştür. İtalya ve İspanya'da ise elektrige %25'ten fazla talep azalması olduğu tespit edilmiştir.

Mart ayının ortalarından Nisan ayının sonlarına kadarki süreçte ise Hindistan'da %20'yi aşkın bir düşüşe rastlanmıştır. ABD ve Avrupa'ya kıyasla daha az Covid-19 vakasına sahip olan Kore ve Japonya'da ise elektrik talebinde yalnızca %8 civarlarında bir daralma olmuştur [18].

### 2.2. Doğal Gaz Tüketimi

2020 senesinde COVID-19 pandemisi sebebiyle küresel ölçekte doğal gaz tüketimi 75 milyar metre küp azalmıştır. Bu miktar, 2019 senesi doğal gaz tüketiminin %1.9'u kadardır. Meydana gelen azalmanın büyük bir kısmı ise pandeminin ortaya çıktığı 2020 yılının ilk yarısında gerçekleşmiştir. Pandemi sürecinde doğal gaz tüketimi, fosil yakıtların tüketimine kıyasla daha az etkilenmiştir [18].

### 2.3. Petrol Tüketimi

Pandemi ile mücadele kapsamında alınan kısıtlama ve karantina kararları insanların faaliyetlerini oldukça fazla

azaltmıştır. İnsanların faaliyetlerinin azalması doğrudan hava, kara ve deniz ulaşım araçlarındaki yakıt talebini de aşağıya çekmiştir. Böylelikle benzin, motorin ve LPG gibi yakıtların tüketim miktarları “Lockdown” olarak adlandırılan kapanma dönemlerinde aşırı düşmüştür. 2020 yılı petrol talebi 2019 senesine göre 8,5 milyon varil / gün düşmüştür. Bu düşüş yaklaşık olarak %8,8’e denk gelmektedir. Ham petrol talebinde olan bu daralma ise günümüze kadar yaşanmış olan en büyük daralmadır. 2020 yılındaki hava yolcu trafiğinin 2019 yılı değerlerine göre %66 düşmesi sebebiyle jet yakıtı ve gazyağı talebi 3,2 milyon varil/gün (%41) azalmıştır. Benzin talebi ise 3 milyon varil/gün (%12)’den fazla düşmüştür. LPG/etan ve nafta talebi ise artan paketleme, hijyenik malzeme üretimi ve tıbbi ihtiyaçların karşılanması sebebiyle neredeyse değişmemiştir [18].

### 3. TÜRKİYE’DEKİ ETKİLER

Dünya Sağlık Örgütü’nün pandemi ilan ettiği 11 Mart 2020 tarihinde Türkiye’de ilk koronavirüs vakası tespit edilmiştir [19]. İlk vaka tespitinin hemen ardından spor karşılaşmalarının seyircisiz oynanması kararlaştırıldı, birkaç ülkeyle uçuşlar durduruldu, eğlence mekanları kapatıldı, okullar ve üniversiteler 3 hafta süreyle tatil edildi. 23 Mart itibari ile okullar ve üniversitelerde uzaktan öğretime geçildi ve bazı yaş gruplarına sokağa çıkma yasakları getirildi. Trafikte toplu taşıma araçlarında %50 kapasiteyle ulaşım sağlanması istendi. Bu tedbirleri kapsamlı kapanma kararları takip etti ve neticesinde insan hareketliliği neredeyse sıfırlandı. Böylelikle sanayi üretimi ve dolayısıyla elektrik, doğal gaz tüketimi kısıtlama kapsamının genişliğiyle orantılı olarak azaldı. İnsan hareketliliğinin ve dolayısı ile araç trafiğinin azalması ile araçlarda kullanılan benzin ve motorin gibi yakıt tüketimleri de önemli derecede düştü.

#### 3.1. Elektrik Tüketimi

Türkiye’deki elektrik tüketimi 2019 senesinde yaklaşık olarak 230 milyon kW iken 2020 senesinde elektrik tüketim miktarı Şekil 1’de gösterildiği üzere yaklaşık olarak %1,7’lik bir farkla 234 milyon kW olmuştur.

Pandeminin elektrik tüketimi üzerine etkisinin daha iyi anlaşılabilmesi adına sayısal veriler aylık olarak incelendi. 2020 Ocak ve Şubat aylarındaki elektrik tüketimi bir önceki senenin aynı dönem değerlerinden biraz fazla olup, Mart-Haziran ayları arasında ise önceki senenin değerlerinin altında kaldığı görülmüştür. 2019 senesi Mart ve Nisan aylarındaki elektrik tüketim miktarları aylık olarak yaklaşık 18.2 milyon kW iken, pandemi tedbirlerinin alındığı 2020 Mart ve Nisan dönemlerindeki elektrik tüketimi 2019 senesinin değerlerinden %15’e varan düşüşler yaşamış ve 15.3 milyon kW değerine gerilemiştir. 2020 Haziran ayından sonra pandemi tedbirlerinin gevşetilmesi ile sanayi ve sosyal alanlardaki faaliyetlerin artmasıyla senenin geri kalan kısmında elektrik tüketimi 2019 değerlerinin üzerine çıkmıştır. Aylık tüketim miktarları Şekil 2’de verilmiştir [20].

#### 3.2. Doğal Gaz Tüketimi

Türkiye’deki doğal gaz tüketimi 2019 senesinde yaklaşık olarak 45000 milyon Sm3 iken, 2020 senesindeki tüketim miktarı Şekil 3’te gösterildiği üzere bir önceki seneye göre yaklaşık %3,8’lik bir artışla yaklaşık 47700 milyon Sm3 olmuştur.

Pandemi tedbirlerinin ve kısıtlamaların doğal gaz tüketimi üzerine etkisinin daha anlaşılır olması için tüketim miktarları aylık olarak incelendi. Şekil 4’te görüldüğü üzere 2020 Ocak ve Şubat aylarında doğal gaz tüketim miktarları 2019 yılı Ocak ve Şubat aylarına kıyasla yaklaşık %10 fazladır. Pandemi tedbirlerinin alındığı ve kısıtlamaların yapıldığı 2020 Mart, Nisan ve Mayıs aylarında doğal gaz tüketim miktarları sırasıyla yaklaşık 4500, 3200 ve 2200 milyon Sm3 olmuştur. Bu değerler, bir önceki yılın aynı aylarına ait tüketim değerlerinden sırasıyla yaklaşık %12, %20 ve %23 oranlarında düşüktür. 2020 Haziran ve 2019 Haziran doğal gaz tüketim miktarları ise neredeyse eşittir. 2020 Haziran ayı itibari ile kısıtlamaların gevşetilmesiyle sanayi üretimi artmış ve senenin geri kalan aylarındaki doğal gaz tüketimi 2019 yılının tüketim miktarlarından fazla olmuştur [21].

#### 3.3. LPG Tüketimi

Türkiye’de LPG tüketiminin %80’i araç yakıtı olan otogaz formunda gerçekleştirilmektedir [22]. 2019 senesinde toplamda 4.2 milyon tonluk LPG kullanımı gerçekleştirilmişken bu tüketim oranı 2020 senesinde yaklaşık %7’lik bir daralma ile yaklaşık 3.9 milyon tona gerilemiştir. Tüketim değerleri Şekil 5’te verilmiştir.

2020 senesinde LPG tüketimindeki daralmanın pandemi kısıtlamalarının daha yoğun yaşandığı Mart – Haziran arasında olduğu belirlenmiştir. 2020 Ocak ve Şubat aylarındaki LPG tüketim miktarlarının yaklaşık 325.000 ton ile 2019 Ocak ve Şubat dönemlerinin LPG tüketim miktarlarının hemen üzerinde olmuştur. Bu durum, ilerleyen aylarda kısıtlama tedbirleriyle değişmiş ve 2019 verilerine göre 2020 Mart döneminde %12,5’lik, Nisan ayında %27’lik, Mayıs ayında %26’lık ve Haziran ayında ise %9’luk bir daralma gerçekleşmiştir. Daralmanın gerçekleştiği aylarda tüketim miktarları yaklaşık olarak 240.000 tona kadar gerilemiştir. Aralık ayının haricinde 2020 senesinin kalan aylarında ise LPG tüketimi 2019 tüketim miktarlarıyla hemen hemen aynı miktarda olmuştur. Tüketim miktarları Şekil 6’da verilmiştir [23].

#### 3.4 Yakıt Tüketimi

Türkiye’de, ithal edilen petrol işlenerek benzin, motorin, havacılık ve denizcilik yakıtları gibi fazlaca tüketilen yakıt türlerine dönüştürülür.

Yıllık toplam tüketimler incelendiğinde benzin ve motorin tüketimleri 2019 ve 2020 yıllarında neredeyse aynı kalmıştır. Benzin tüketimi 2019 senesinde yaklaşık 2.4 milyon ton iken, 2020 senesindeki tüketim miktarı önemsenmeyecek miktarda azalarak 2.36 milyon tona gerilemiştir. Motorin tüketimi ise 2019 senesinde 24.9 milyon ton iken, 2020 senesinde çok az bir

artış göstererek 25.2 milyon tona ulaşmıştır. Sayısal veriler Şekil 7'de verilmiştir.

2019 ve 2020 yılları içerisindeki benzin tüketimi aylara göre incelendiğinde 2020 Ocak ve Şubat aylarındaki benzin tüketim miktarlarının yaklaşık 180.000 ton değerle 2019 Ocak ve Şubat değerlerinin yaklaşık olarak %10 üzerinde olduğu tespit edildi. Her iki yılın Mart ayı tüketim değerlerinin ise neredeyse aynı miktarlarda olduğu ve 2020 Mart ayından itibaren pandemi kısıtlamaları sebebiyle tüketim miktarlarında aşırı düşüşlerin olduğu saptandı. 2019 Nisan, Mayıs ve Haziran benzin tüketimleri sırasıyla 188 bin, 198 bin ve 221 bin ton iken bu değerler 2020 Nisan, Mayıs ve Haziran aylarında sırasıyla 114 bin, 128 bin ve 211 bin ton olmuştur. Bu düşüşler, sırasıyla yaklaşık olarak %40, %35 ve %5'e denk gelmektedir. 2020 Temmuz ayı itibarı ile benzin tüketimi 2019 değerlerinin genel olarak üzerinde kalmıştır. Aylık tüketim miktarları ve oranları Şekil 8'de verilmiştir [24].

Motorin tüketim miktarlarının zamanla değişimi de benzin tüketim miktarlarının zamanla değişimine benzer bir davranış göstermektedir. 2020 Mart ayının sonuna kadar motorin tüketim miktarları 2019 yılının değerlerinin hemen üzerinde iken 2020 Nisan ayından itibaren tüketim miktarları 2019 yılı değerlerinin altına düşmüştür. 2019 Nisan ve Mayıs ayları motorin tüketimleri sırasıyla yaklaşık olarak 1.99 milyon ve 2.01 milyon ton iken bu değerler 2020 senesi aynı aylarda sırasıyla yaklaşık olarak 1.53 milyon ve 1.62 milyon ton olmuştur. Bu düşüşler sırasıyla yaklaşık olarak %23 ve %19'a denk gelmektedir. 2020 Haziran ayı itibarı ile tüketim miktarları 2019 değerlerinin üzerine çıkmıştır. Aylık tüketim miktarları ve oranları Şekil 9'da verilmiştir [24].

Havacılık ve denizcilik yakıtlarının 2019 ve 2020 yıllarındaki toplam tüketim miktarları incelendiğinde denizcilik yakıtlarının 2019 ve 2020 yıllarındaki toplam tüketim miktarları neredeyse eşit iken havacılık yakıtlarının tüketim miktarları 2020 senesi içinde 2019 yılı miktarına göre yaklaşık %40 oranında azalmıştır ve sayısal veriler Şekil 10'da verilmiştir.

2020 yılına ait havacılık yakıt tüketim değerlerinin tamamı 2019 yılı aylık tüketim değerlerinin altında kalmıştır. Hem yurt içi hem de yurt dışı uçuşların durdurulduğu / azaltıldığı 2020 Mart, Nisan ve Mayıs aylarındaki tüketim miktarları sırasıyla 71.900, 23.110 ve 19.081 ton olup bu değerler 2019 yılının aynı aylarında tüketilen yakıt miktarlarından sırasıyla yaklaşık olarak %27, %77 ve %81 daha az olmuştur. Nisan ve Mayıs aylarındaki aşırı düşüşler havacılık sektörünün pandemiden aşırı derecede etkilendiğinin açık bir göstergesidir. Pandemi ilan edilen 11 Mart 2020 tarihinden sene sonuna kadar havacılık yakıt tüketimi bir önceki senenin değerlerine göre yaklaşık %24 ile %81 oranları aralığında azalmıştır ve yakıt tüketim miktarları ile azalış oranları Şekil 11'de verilmiştir [24].

Denizcilik yakıtlarında ise 2020 Ocak, Şubat ve Mart aylarındaki tüketim miktarları önceki yıl tüketim miktarlarından %25 ile %30 arasında fazladır. 2020 Nisan ve Temmuz arasında 2019 yılı aynı dönem

tüketim miktarlarının altına düşmüştür. Bu dönemdeki düşüş oranları ise %22 ile %42 arasında olmuştur. Pandemi kısıtlamalarının hafifletilmesi ile yılın kalan aylarındaki denizcilik yakıt tüketimleri önceki yılın aynı dönem değerlerinin üzerine çıkmıştır. Sayısal veriler Şekil 12'de verilmiştir [24].

#### 4. SONUÇ

COVID-19 pandemisi sebebiyle tüm ülkeler, insanların iç içe bulunduğu okullar, iş yerleri, cafe ve eğlence mekanları gibi yerlerde insan yoğunluğunu azaltabilmek adına tedbirler almıştır. Böylelikle insan yoğunluğunun ve insanların birbirleriyle olan etkileşimlerinin en aza indirilerek virüsün hasta insanlardan sağlıklı insanlara bulaşmasının engellenmesi hedeflenmiştir. Tedbirler gereği uluslararası uçuşlar durdurulmuş, bireysel ve toplu taşıma amaçlarıyla kullanılan araçlarının trafikteki yoğunluğu azaltılmış, kamu ve özel kuruluşlarda vardiya usulü çalışma yapılmış, yeterli alt yapısı olan şirketler ve kamu kurumlarında uzaktan çalışmaya geçilmiş, okullarda ve üniversitelerde uzaktan öğretim uygulanmaya başlanmıştır. Böylece tüm dünyada insan yoğunluğu mümkün olduğunca azaltılmış ve virüsün yayılması kontrol altına alınmaya çalışılmıştır. İnsan yoğunluğunun azaltılması başta ulaşım sektöründe tüketilen yakıtlar olmak üzere sanayi ve konutlarda elektrik ile doğal gaz tüketimlerinde azalmaya neden olmuştur. Pandemi tedbirlerinin yoğun olduğu dönemlerde küresel ölçekte elektrik tüketimleri %20 -30 aralığında, benzin ve jet yakıtı talepleri sırasıyla 3.2 milyon varil /gün ile 3.0 milyon varil /gün dolaylarında düşmüştür. LPG/etan ve nafta talebi ise artan paketleme, hijyenik malzeme üretimi ve tıbbi ihtiyaçlar sebebiyle neredeyse değişmemiştir.

Küresel ölçekte etkili olan pandemi Türkiye'yi de etkilemiş ve özellikle kapanma kararlarının alındığı dönemlerde elektrik, araç yakıtları ve doğal gaz tüketimlerinde önemli düşüşlere sebep olmuştur.

Türkiye'de 2020 yılı elektrik tüketim miktarı 2019 yılı elektrik tüketim miktarından yaklaşık olarak %1.7 oranında fazla iken, pandeminin ilan edildiği ve ilk kapanma kararlarının alındığı Mart ve Nisan aylarında elektrik tüketimi bir önceki yılın aynı dönemine kıyasla yaklaşık %15 oranında düşmüştür. Doğal gaz tüketimi ise senelik olarak değerlendirildiğinde 2020 yılı tüketim miktarı 2019 yılı tüketim miktarından %3.8 fazladır. 2020 Mart-Mayıs aralığında kaydedilen tüketim miktarları ise bir önceki senenin aynı dönemlerine ait tüketim miktarlarına kıyasla %12-23 aralığında bir düşüş göstermiştir. Benzin, motorin, havacılık ve denizcilik yakıtlarında da kısıtlamalar ve kapanma kararları etkisini göstermiş olup en büyük düşüşü havacılık yakıtı tüketimi göstermiştir. Benzin, motorin ve denizcilik yakıtlarının tüketimlerinde %40'a varan düşüşler kaydedilirken, tespit edilen en büyük düşüş ise Mayıs ayında %80'den fazla bir düşüş yaşayan havacılık sektöründe meydana gelmiştir.

Bu verilerden de anlaşıldığı üzere insan hareketliliği ile enerji tüketimi birbirleriyle yakın ilişkilidir. Elde edilen verilerle hazırlanan bu bildiri, enerji

talebindeki daralmanın çevresel ve ekonomik etkilerinin araştırılmasına temel oluşturması amacıyla hazırlanmıştır.

## KAYNAKLAR

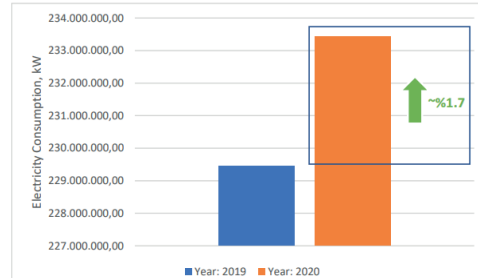
- [1] Peker, K. (2019). Energy utilization and policies in Turkey. *Journal of Engineering Research and Applied Science*, 8(1), 1033-1040.
- [2] Kaygusuz, K. (2020). Energy efficiency and renewables for industrial sector. *Journal of Engineering Research and Applied Science*, 9(1), 1386-1399.
- [3] Cheshmehzangi, A. (2020). COVID-19 and household energy implications: what are the main impacts on energy use?. *Heliyon*, 6(10).
- [4] Tian, X., An, C., Chen, Z., and Tian, Z. (2021). Assessing the impact of COVID-19 pandemic on urban transportation and air quality in Canada. *Science of the Total Environment*, 765, 144270.
- [5] Ibn-Mohammed, T., Mustapha, K. B., Godsell, J., Adamu, Z., Babatunde, K. A., Akintade, D. D., Acquaye, A., Fujii, H., Ndiaye, M.M., Yamoah, F.A., and Koh, S. C. L. (2021). A critical analysis of the impacts of COVID-19 on the global economy and ecosystems and opportunities for circular economy strategies. *Resources, Conservation and Recycling*, 164, 105169.
- [6] Rugani, B., and Caro, D. (2020). Impact of COVID-19 outbreak measures of lockdown on the Italian Carbon Footprint. *Science of the Total Environment*, 737, 139806.
- [7] Yuan, Z., Xiao, Y., Dai, Z., Huang, J., Zhang, Z., and Chen, Y. (2020). Modelling the effects of Wuhan's lockdown during COVID-19, China. *Bulletin of the World Health Organization*, 98(7), 484.
- [8] Ji, T., Chen, H. L., Xu, J., Wu, L. N., Li, J. J., Chen, K., and Qin, G. (2020). Lockdown contained the spread of 2019 novel coronavirus disease in Huangshi city, China: Early epidemiological findings. *Clinical Infectious Diseases*, 71(6), 1454-1460.
- [9] An, P., Song, P., Wang, Y., and Liu, B. (2020). Asymptomatic patients with novel coronavirus disease (COVID-19). *Balkan medical journal*, 37(4), 229.
- [10] Bandyopadhyay, S. (2020). Coronavirus Disease 2019 (COVID-19): we shall overcome. *Clean Technologies and Environmental Policy*, 22, 545-546.
- [11] Vella, F., Senia, P., Ceccarelli, M., Vitale, E., Maltezu, H., Taibi, R., Lleshi, A., Venanzi, R. E., Pellicano, G. F., Rapisarda, V., Nunnari, G. and Ledda, C. (2020). Transmission mode associated with coronavirus disease 2019: a review. *European Review for Medical & Pharmacological Sciences*, 24(14).
- [12] WHO, World Health Organization, Duyuru Tarihi 11 Mart 2020, <https://www.who.int/> (son erişim tarihi 08.07.2023 gg.aa.yyyy)
- [13] Kostoff, R. N., Briggs, M. B., Porter, A. L., Aschner, M., Spandidos, D. A., and Tsatsakis, A. (2020). COVID 19: Post lockdown guidelines. *International journal of molecular medicine*, 46(2), 463-466.
- [14] Nicola, M., Alsafi, Z., Sohrabi, C., Kerwan, A., Al-Jabir, A., Iosifidis, C., Agha, M., and Agha, R. (2020). The socio-economic

implications of the coronavirus pandemic (COVID-19): A review. *International journal of surgery*, 78, 185-193.

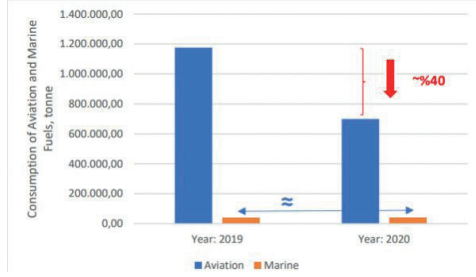
- [15] Di Domenico, L., Pullano, G., Sabbatini, C. E., Boëlle, P. Y., and Colizza, V. (2020). Impact of lockdown on COVID-19 epidemic in Île-de-France and possible exit strategies. *BMC medicine*, 18(1), 1-13.
- [16] Kirli, D., Parzen, M., and Kiprakis, A. (2021). Impact of the COVID-19 lockdown on the electricity system of Great Britain: a study on energy demand, generation, pricing and grid stability. *Energies*, 14(3), 635.
- [17] Santiago, I., Moreno-Munoz, A., Quintero-Jiménez, P., Garcia-Torres, F., and Gonzalez-Redondo, M. J. (2021). Electricity demand during pandemic times: The case of the COVID-19 in Spain. *Energy policy*, 148, 111964.
- [18] IEA, International Energy Agency, *Global Energy Review 2021*, <https://www.iea.org/> (son erişim tarihi 21.05.2023)
- [19] Göncüoğlu, M., Ayaz, N. D., Cengiz, G., Onaran, B., and Çufaoğlu, G. (2020). Emerging details about COVID-19 and chronology of the pandemic in Turkey. *Ankara Üniversitesi Veteriner Fakültesi Dergisi*, 67(3), 323-332.
- [20] EPDK, Elektrik Piyasası Aylık Sektör Raporu Listesi, Ankara, <https://www.epdk.gov.tr/Detay/Icerik/3-0-23/elektrikaylik-sektor-raporlar> (son erişim tarihi 08.07.2023 gg.aa.yyyy)
- [21] EPDK, Doğal Gaz Piyasası Aylık Sektör Raporu Listesi, Ankara, <https://www.epdk.gov.tr/Detay/Icerik/3-0-95/dogal-gazaylik-sektor-raporu> (son erişim tarihi 08.07.2023 gg.aa.yyyy)
- [22] EPDK, Sıvılaştırılmış Petrol Gazlarının (LPG) Farklı Kullanım Alanlarının İncelenmesi, Ankara, <https://epdk.gov.tr/Detay/Icerik/4-9338/lpgnin-farkli-kullanim-alanlari-ile-ilgili-%E2%80%9Ccsivi> (son erişim tarihi 08.07.2023 gg.aa.yyyy)
- [23] EPDK, LPG Piyasası Aylık Sektör Raporu Listesi, Ankara, <https://www.epdk.gov.tr/Detay/Icerik/3-0-105/lpgaylik-sektor-raporlari> (son erişim tarihi 08.07.2023 gg.aa.yyyy)
- [24] EPDK, Petrol Piyasası Aylık Sektör Raporu Listesi, Ankara, <https://www.epdk.gov.tr/Detay/Icerik/3-0-104/petrolaylik-sektor-raporu> (son erişim tarihi 08.07.2023 gg.aa.yyyy)

Anahtar Kelimeler: COVID-19 pandemisi, enerji tüketimi

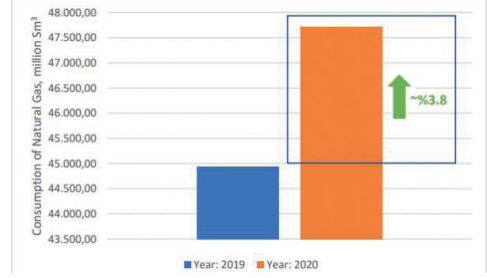
Şekil 1: 2019-2020 Yıllarında Türkiye'de'ki Toplam Elektrik Tüketimi



Şekil 10: 2019-2020 Yıllarında Türkiye'deki Toplam Havacılık ve Denizcilik Yakıtları Tüketimi



Şekil 3: 2019-2020 Yıllarında Türkiye'deki Toplam Doğal Gaz Tüketimi



Şekil 11: 2019-2020 Yıllarında Türkiye'de Aylara göre Havacılık Yakıtları Tüketimi



Şekil 4: 2019-2020 Yıllarında Türkiye'de Aylara göre Doğal Gaz Tüketimi



Şekil 12: 2019-2020 Yıllarında Türkiye'de Aylara göre Denizcilik Yakıtları Tüketimi



Şekil 5: 2019-2020 Yıllarında Türkiye'deki Toplam LPG Tüketimi



Şekil 2: 2019-2020 Yıllarında Türkiye'de Aylara Göre Elektrik Tüketimi

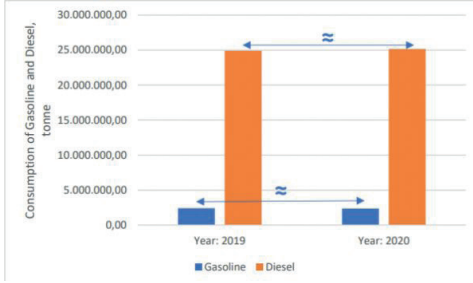


Şekil 6: 2019-2020 Yıllarında Türkiye'de Aylara göre LPG Tüketimi





Şekil 7: 2019-2020 Yıllarında Türkiye'deki Toplam Benzin ve Motorin Tüketimi



Şekil 8: 2019-2020 Yıllarında Türkiye'de Aylara göre Benzin Tüketimi



Şekil 9: 2019-2020 Yıllarında Türkiye'de Aylara göre Motorin Tüketimi



---

---



## **Petrol ve Dođal Gaz Tařımacılıđı ve Depolama**

---



# Küresel Enerji Talebinin Arktik Deniz’indeki LNG Gemi Trafikine Etkisi

**Arzu Bal, Ersan Başar**

Karadeniz Teknik Üniversitesi, Deniz Bilimleri Fakültesi



Dünyada nüfus artışı ve ekonomik büyümeyle birlikte enerjiye olan ihtiyaç ve talepler hızla artmaktadır. Artan enerji ihtiyacına karşı sıvılaştırılmış doğal gaz (LNG), küresel enerji taşımacılığının önemli bir unsuru haline gelmiştir. Bu noktada, Rusya, geniş doğal gaz rezervlerine sahip olması nedeniyle LNG taşımacılığı ve tedarikinde önemli bir rol oynamaktadır. Rusya, büyüyen uluslararası talebi karşılamak için boru hatları ve deniz terminalleri gibi LNG altyapısına önemli yatırımlar yapmaktadır. Buna ek olarak, Arktik, LNG taşımacılığı için stratejik bir konuma ve büyük bir potansiyele sahiptir. Zengin doğal gaz rezervlerine ve önemli pazarlara olan yakınlığıyla, Arktik, Rusya’nın LNG faaliyetlerini daha da genişletme fırsatları sunmaktadır. Özellikle küresel ısınmanın da etkisiyle Arktik bölgede deniz buzunun erimesine bağlı olarak açılan Kuzey Deniz Rotası (NSR) gibi yeni deniz yolları LNG taşımacılığında bu bölgede daha mümkün kılmaktadır. Bu çalışmada, Rusya’nın Sabetta limanından hareket eden LNG gemilerine ait 5 yıllık (2018-2022) veri seti, Census X-12 Yöntemi kullanılarak 2023, 2024 ve 2025 yıllarında NSR’deki LNG gemi trafiğinin tahmini yapılmıştır. Yapılan bu analiz sonucunda Rusya’nın Arktikte bulunan Sabetta limanına gelecek olan LNG gemi sayısında 2025 yılına gelindiğinde ortalama % 27.03’lük bir artış olacağı saptanmıştır. Küresel boyut da artan LNG talebine Rusya Arktik’de bulunan başta Yamal tanker terminalinden olmak üzere gemi trafiğinin artıracığı sonucu ortaya çıkmıştır.

With population growth and economic growth in the world, the needs and demands for energy are increasing rapidly. Liquefied natural gas (LNG) has become an important element of global energy transportation against the increasing energy demand. At this point, Russia plays a vital role in LNG transportation and supply due to its large natural gas reserves. Russia is making significant investments in LNG infrastructure such as pipelines and marine terminals to meet growing international demand. In addition, the Arctic has a strategic location and exciting potential for LNG transportation. With its proximity to rich natural gas reserves and important markets, the Arctic offers opportunities to further expand Russia’s LNG operations. Especially with the effect of global warming, new sea routes such as the Northern Sea Route (NSR), which was opened due to the melting of sea ice in the Arctic region, make LNG transportation more possible in this region. In this study, the LNG ship traffic in the NSR in 2023, 2024 and 2025 was estimated using the Census X-12 Method, a 5-year (2018-2022) data set of LNG ships departing from the Sabetta port of Russia. As a result of this analysis, it has been determined that there will be an average of 27.03% increase in the number of

LNG ships arriving at Sabetta port in the Arctic by 2025. It has also emerged that the global demand for LNG, which is increasing globally, will increase ship traffic, especially from the Yamal tanker terminal located in the Russian Arctic.

## AMAÇ

Küresel LNG tanker trafiği, Asya-Pasifik, Avrupa, Kuzey Amerika ve Orta Doğu dâhil olmak üzere farklı bölgelere ayrılmıştır. Asya-Pasifik bölgesinde Japonya en büyük LNG ithalatçısıdır ve Japonya’yı Çin, Güney Kore ve Tayvan takip etmektedir (CNOOC, 2021). Rusya, Asya LNG pazarına da doğalgaz tedarik etmektedir. Özellikle Çin gibi büyüyen ekonomiler, Rus doğalgazına olan talebi artırmıştır. Bu, Rusya’nın Asya LNG pazarındaki etkisini artırırken, bölgedeki enerji dengelerini de etkileyebilmektedir.

Asya-Pasifik bölgesindeki LNG’ye olan talep, nüfus artışı, kentleşme ve daha temiz enerji kaynaklarına doğru kayma gibi faktörlerden kaynaklanmaktadır (Nguyen ve Oanh, 2021).

Avrupa’da LNG’ye olan talep, enerji ihtiyacını çeşitlendirme, Rus gazına bağımlılığı azaltma ve iklim hedeflerine ulaşma ihtiyacı gibi faktörlerden kaynaklanmaktadır (European Commission, 2021). Ancak, Rusya, dünyanın en büyük doğal gaz rezervlerinden bazılarında ev sahipliği yapmaktadır ve ülke son yıllarda büyük bir LNG ihracatçısı haline gelmiştir. Öte yandan Avrupa, bölgenin enerji ihtiyacının önemli bir bölümünü oluşturan doğal gaz ile Rusya’nın kilit ihracat pazarlarından biridir. Avrupa bölgesi, son yıllarda LNG ithalatında önemli bir büyüme yaşamış ve İspanya, Fransa ve İtalya gibi ülkeler LNG’nin başlıca ithalatçıları haline gelmiştir (International Gas Union, 2021). Yeni LNG terminallerinin inşası da dâhil olmak üzere bölgede LNG altyapısının geliştirilmesi, LNG tanker trafiğinin büyümesine de katkıda bulunmuştur. Bu noktada, iklim değişikliği sebebiyle Arktik buzunun erimesi, Rusya’nın Kuzey Denizi Rotası üzerinden Avrupa’ya LNG ihraç etmesi için yeni fırsatlar sunarak Süveyş Kanalı üzerinden geleneksel nakliye yollarından daha kısa bir rota sağlamaktadır. Arktik üzerinden Rusya’dan Avrupa’ya LNG ihracatı, küresel LNG ticaretine yeni bir ivme kazandırma potansiyeline sahiptir. Rusya Enerji Bakanlığı’na göre, ülke 2035 yılına kadar Kuzey Deniz Rotası üzerinden yılda 80 milyon tona kadar LNG ihraç etme potansiyelinin bulunduğu bildirilmiştir (Russian Energy Ministry, 2020).

Bu çalışma, artan LNG talebi doğrultusunda Rusya’nın LNG arzını Arktik limanlarından sağlanması sonucunda NSR gemi trafiğinin nasıl etkileneceğinin belirlenmesi amaçlanmıştır. Hâlihazırda olan gemi trafiğinin hangi

oranda etkileneceği ortay koyulmaya çalışılmıştır.

## GEREÇ VE YÖNTEM

Rusya'nın Sabetta Limanı limanına gelen LNG gemilerine ait 5 yıllık (2018-2022) veri seti kullanılmıştır. Census X-12 Yöntemi uygulanarak 2023, 2024 ve 2025 yıllarında Sabetta Limanına kaç DWT LNG girişi yapılacağı tahmin edilmiştir.

Census X-12 ARIMA modeli, Bureau of Census birimi tarafından geliştirilen, zaman serisi verilerinin mevsimsel olarak düzenlenmesi için kullanılan istatistiksel bir yöntemdir. X-12 ARIMA modeli, bir zaman serisinin mevsimsel bileşenini belirlemek ve mevsimsellikten arındırmak için tek değişkenli zaman serisi analizi ve mevsimsel ayrışmanın bir kombinasyonunu kullanır. Model önce zaman serilerini üç bileşene ayırır: trend, mevsimsel ve düzensiz. Daha sonra kalan eğilim ve düzensiz bileşenleri tahmin etmek ve arındırmak için her bileşene ayrı ayrı ARIMA modelleri uygulanır. Son olarak, mevsimsellikten arındırılmış bir zaman serisi üretmek için ayarlanmış bileşenleri birleştirir. X-12 ARIMA modeli oldukça esnek ve çok frekanslı karmaşık mevsimsel modellerde dâhil olmak üzere çok çeşitli mevsimsel modelleri uygulayabilir. Ayrıca aykırı değerleri, eksik verileri ve zaman içindeki mevsimsel modeldeki değişiklikleri de uygulayabilir. X-12 ARIMA modelinin avantajlarından biri, model tarafından açıklanan değişkenlik yüzdesi, mevsimsel etkilerin büyüklüğü ve kalan düzensiz bileşenlerin büyüklüğü gibi ayrıntılı tanımlama yeteneğidir. Bu bilgiler, mevsimsel düzenlemenin etkinliğini değerlendirmek ve temel verilerle ilgili sorunları belirlemek için oldukça yararlıdır (Yamak & Erdem, 2017).

## BULGULAR

Bu çalışmada, 2011-2022 yılları arasındaki dünya genelindeki LNG ihracatı ile Rusya'nın boru hattı ve LNG tankerleri vasıtasıyla yapmış olduğu taşımacılık incelenerek gemi trafiğine olan etkileri belirlenmeye çalışılmıştır. Yapılan çalışma sonucunda Sabetta limanına gelen LNG DWT Miktarları 2023, 2024 ve 2025 tahmini Tablo 1 de verilmiştir. 2018-2022 yılları arasında her yıl ortalama 50000DWT lik 37 gemi bölgeye gelmişken 2023-2025 için yıllık 47 gemiye yükseleceği belirlenmiştir. Rusya tarafından gemiler vasıtası ile ihraç edilecek olan gaz Arktik bölgedeki tanker trafiğini artırması sonucunda bölgedeki trafiğin etkileneceği anlaşılmaktadır.

## SONUÇLAR

Dünyada her geçen gün enerjiye talep artmakta olup Rusya bu sektörde önemli bir aktör haline gelmektedir (Kropatcheva, 2014). Özellikle doğalgaz talebinde Avrupa'nın Rusya'ya olan bağımlılığı doğal gaz tedarikinde Rusya'yı söz sahibi yapmaktadır. Ratner (2022), yaptığı çalışmada bazı Avrupa ülkelerinin tamamen Rusya'dan yapılan doğal gaz ithalatına bağımlı

olduğunu söylemiştir. Ratner'a göre enerji Rusya'nın ekonomisinde önemli bir sektördür ve bu sektör içerisinde de doğal gazın kilit bir rolü bulunmaktadır.

Bu çalışmada yapılan Census X-12 yöntemi ile 2023-2025 yılları arasında Sabetta Limanına gelecek olan LNG tankerleri sayısının tahmini yapılmıştır. Yıllara göre değerlendirildiğinde en büyük artış %35,14 ile Nisan ayında, en düşük artış ise %18,60 ile Aralık ayında olduğu görülmektedir. Uygulanan Census X-12 yöntemine göre 2023 yılında 47 gemi 2024 yılında 45 gemi ve 2025 yılında ise 49 geminin Sabetta limanına gelmesi beklenmektedir. Bu tahminler yapılırken 2018-2022 yılları arasındaki LNG gemi trafiği göz önüne alınmıştır. Ancak, bu tahminlerde çok etkisi yaratabilecek siyasi ve ekonomik olaylara ek olarak doğal afetler gibi durumlar da beklenen gemi sayısında değişimler olabilir.

NSR, küresel LNG enerji talebine etki eden önemli bir faktördür. Bu yol, LNG nakliyatının maliyetlerini azaltabilir ve Rusya'nın LNG üretimini dünya pazarlarına daha etkili bir şekilde taşımasına yardımcı olabilir. Ancak çevresel endişeler, güvenlik sorunları ve jeopolitik faktörler, NSR'nin kullanımını etkileyebilir ve uluslararası ilişkilerde sorunlara yol açabilir. Enerji kaynaklarına daha kolay erişim ve ticaret fırsatları gibi olumlu yönlerden çevresel riskler ve jeopolitik gerilimler gibi olumsuz yönlerine kadar geniş bir yelpazeyi kapsayabilir. Bu nedenle, Arktik bölgesindeki gemi trafiği artışının yönetimi ve denetimi önemlidir.

## KAYNAKÇA

- CNOOC. (2021). China National Offshore Oil Corporation. Retrieved from <https://www.cnooc.com.cn/office/publish/site1/index.html>
- European Commission. (2021). LNG in Europe: Key Facts and Figures. Retrieved from [https://ec.europa.eu/energy/sites/ener/files/quarterly\\_report\\_on\\_european\\_gas\\_markets\\_q2\\_2020\\_0.pdf](https://ec.europa.eu/energy/sites/ener/files/quarterly_report_on_european_gas_markets_q2_2020_0.pdf)
- International Gas Union. (2021). Global Gas Report 2021. Retrieved from <https://www.igu.org/global-gas-report-2021/>
- Kropatcheva, Elena. (2013). He who has the pipeline calls the tune? Russia's energy power against the background of the shale "revolutions". *Energy Policy*. 66.10.1016/j.enpol.2013.10.058
- Nguyen, T. T. L., & Oanh, T. K. T. (2021). The development of liquefied natural gas (LNG) markets in Asia-Pacific region: Current status, prospects and challenges. *Energy Reports*, 7, 239-246
- Yamak R. ve Erdem F.H. (2017), "Uygulamalı Zaman Serisi Analizleri Eviews Uygulamalı", Trabzon: Celepler Matbaa Yayın ve Dağıtım.
- Anahtar Kelimeler: Gaz taşımacılığı, Kutup*

**Yıllara göre Ortalama Gelen gemi sayısı (2018-2022)  
ve Ortalama Gelecek gemi sayısı (2023-2025)**

Aylar	Ortalama Gelen gemi sayısı (2018-2022)	Ortalama Gelecek gemi sayısı (2023-2025)
Ocak	34	45
Şubat	35	45
Mart	40	51
Nisan	38	49
Mayıs	36	47
Haziran	34	44
Temmuz	33	43
Ağustos	33	42
Eylül	36	46
Ekim	38	47
Kasım	39	48
Aralık	42	50
Toplam Ortalama	37	47

---

---





## **Rezervuar Çalışmaları**

---



# Optimizing Oil Production in Naturally Fractured Carbonate Reservoirs with Gas Coning under Gas Production Constraint



**Abdulmalik Ibragimov<sup>1</sup>, Kamshat Ussenova<sup>2</sup>, Murat Zhiyenkulov<sup>2</sup>**

<sup>1</sup>KMG Karachaganak

<sup>2</sup>SLB

Gas coning is a frequent issue in naturally fractured carbonate reservoirs with a gas cap and an oil rim, leading to decreased oil production and early well abandonment. This paper proposes a production optimization approach for wells experiencing gas breakthrough in such reservoirs to improve ultimate oil recovery. The authors developed a numerical model that incorporates the effects of gas coning and breakthrough on a well productivity in the Karachaganak field. Using this model, authors optimize production rates to maximize oil recovery while adhering to gas production constraints. The research is focused to demonstrate that the most effective production strategy for a well is to operate intermittently. Additionally, the frequency of a well's uptime and downtime will progressively decrease over time as the fractured zone of a reservoir is depleted. The suggested production optimization approach can enhance oil recovery in naturally fractured tight carbonate reservoirs while reducing the impact of gas coning and gas breakthrough. The outcomes of this study can guide field development plans and optimize production strategies for comparable tight fractured carbonate reservoirs.

Keywords: Carbonate Reservoirs

---

---



## **Sedimentoloji, Stratigrafi ve Çökelim Ortamları**

---

---

---

# Evaluation of Paleo-depositional Environment Properties of Miocene coals of Divriği-Selimoğlu Region (Sivas-Türkiye) Using Organic Geochemical and Organic Petrographic Properties



**Harun Cakır, Nazan Yalçın Erik**  
Sivas Cumhuriyet University, Sivas

In this study, the organic geochemical and organic petrographic properties of the Upper Miocene Divriği-Selimoğlu coal deposits located in the south of the Sivas Basin were examined in detail, and the paleo-depositional environment and maturity levels were evaluated. Divriği-Selimoğlu coal field consists of sedimentary rocks containing thin, discontinuous coal seams within the Güneşevler Formation. The coal-bearing unit comprises mainly coal, carbonaceous shale, sandstone, clay, and organic-matter-rich clay horizons. Geochemical results are based on total organic carbon (TOC) content, Rock-Eval pyrolysis (RE), Gas Chromatography (GC), Gas Chromatography-Mass Spectrometry (GC-MS) and proximate analyses, whereas petrographic data include vitrinite reflectance (Rr), and maceral composition. According to petrographic evaluations, it was observed that huminite group was dominant and ulminite macerals were abundant. The TOC contents of investigated samples are 9.46-52.88 wt.%, whereas Tmax, Hydrogen Index (HI) and Oxygen Index (OI) values are 406-441 °C, 150-380 mg HC/g rock and 2-5 mg CO<sub>2</sub>/g rock, respectively. The dominant kerogen types are Type II-III (oil and gas) and Type-III (gas) kerogen. Petrographic, organic geochemical assessments and biomarker data indicate that thin and lenticular coal seams were deposited in the lower levels of the Upper Miocene coaly sequence in a lacustrine environment, but in the middle and upper levels in a lacustrine and deltaic system, in a small shallow lake environment with alluvial and fluvial effects.

## 1. INTRODUCTION

In recent years, young coal formations, which offer similar characteristics to the coals considered in this study, have attracted the attention of researchers in terms of organic geochemical, organic petrographic evaluations and hydrocarbon generation potentials, and it has been stated that they have oil generation potentials by the burial effect of humic organic materials in the diagenesis process (Wilkins and George, 2002; Petersen et al., 2009; Dai et al., 2018; Littke and Zieger, 2019; Dai et al., 2020; Zamani et al., 2023).

Lignite basins in Turkey cover an area of approximately 110,000 km<sup>2</sup>, of which 2% are Eocene, 6% Oligocene, 41% Miocene and 51% Pliocene (Tuncalı et al., 2002). The lignite-bearing basins display the characteristics of different geological settings, of which grabens and half-grabens are the most common ones especially in western Anatolia (Fig.1a). As in the coal field in this study, lignites in Turkey generally occur in tectonically active basins together with volcanic-clastic and carbonates deposited in lacustrine and fluvial environments. In

addition, the veins do not have a wide geographical distribution due to faults limiting the coal formation environments. The coal veins in these basins are generally Paleogene (Eocene, Oligocene) and Neogene (Miocene, Pliocene) in age (Tuncalı et al., 2002) (Fig. 1a). Apart from this, although there are coal formations with a narrow distribution area in many areas (Kangal, Divriği, Gemerek-Yeniçubuk, Gürün, Suşehri, Hafik and Şarkışla regions) in the Sivas Tertiary Basin, except for the Kangal-Kalburçayırı and Etyemez fields, they are used locally or are not economically evaluated due to their reserves (Fig.1b).

## 2. GEOLOGICAL SETTING

The area where the study was carried out in terms of coal is in the south of Divriği district of Sivas Province (Fig. 1b). The geological units in the study area were distinguished by Yılmaz and Yılmaz (2004) as relative autochthonous rocks, allochthonous units and cover units according to their relations with each other. In the area between Divriği-Sincan-Kangal, Paleozoic aged and low-metamorphic clastic rocks at the base and Lower Carboniferous-Campanian aged platform limestones are defined as relatively autochthonous (Yılmaz and Yılmaz, 2004). Allochthonous units consisting of mixed ophiolitic (Campanian-Maastrichtian) and ophiolitic sequence (Jurassic) overlie the relative autochthonous rocks tectonically. Kangal Formation and Munzur Limestone are in a relatively autochthonous position, tectonically overlain by the Yeşiltaşayla complex and Güneş Ophiolite (allochthonous units), and they predominantly represent the remains of an oceanic crust. Maastrichtian-Quaternary units were overlain by the angular unconformity over the relative autochthonous rocks and allochthonous units in the study area in a post-collisional period. Of these, the Maastrichtian-Lower Pliocene aged units represent the Paleotectonic and Neotectonic transition period, and the Upper Pliocene-Quaternary aged units represent the Neotectonic phase (Yılmaz and Yılmaz, 2004).

Selimoğlu coal field consists of sedimentary rocks containing thin, discontinuous coal seams within the Upper Miocene Güneşevler Formation. Only one coal seam alternating with limestones is operated by the underground and open pit mining methods. The coals investigated in this study have a bright appearance with variable thickness, not much lateral extension, and are seen in an area of approximately 50 km<sup>2</sup> with a thickness of 1.0-1.5 m (Fig.2a). The coal seams cropping out in the area are folded, fractured and thin, irregularly bedded and generally intercalated with clay and carbonate shales, depending on the regional technology and depositional environment (Fig. 2b).

### 3. MATERIAL AND METHOD

Five coal, eight bituminous shale and three shale samples were taken from the coal mine in Selimoğlu-Divriği coal field. The bulk coal samples were air dried, milled (<0.250 mm), and split to obtain representative samples for analysis. Proximate and ultimate analyses were performed for the coal samples following the ASTM standard procedures (ASTM, 1991). In this study, chemical and elemental analyzes of coals were made in MTA, MAT Department (Ankara). The data on the organic matter richness, organic matter type, diagenetic process and hydrocarbon generation potential of the coal and organic matter-rich carbonate shale samples were evaluated by Rock-Eval pyrolysis analysis (RE). The results of the RE pyrolysis analysis were interpreted according to Peters (1986) and Lafarque et al., (1998). Extracts from the two samples Güneyevler Formation were analyzed by Gas Chromatography (GC) and Gas Chromatography-Mass Spectrometry (GC-MS). Organic geochemical analyzes were made at TP Research Center (TP AR-GE, Ankara).

### 4. RESULTS AND DISCUSSION

#### 4.1. Chemical Composition

According to the elementary analysis evaluation, the carbon, hydrogen, and oxygen content of the samples were determined as 45.01%, 3.31% and 4.71% respectively. The common characteristics of the coal vary in the range of 12.66 to 14.81% moisture (Mad), 11.06 to 90.2% ash yield (Ad), 9.49 to 48.03% volatile matter (daf), 0.31 to 44.22 fixed carbon, 734 to 7257 Kcal/kg calorific value. Hence, this high volatility lignite coal has low to moderate moisture and low S content (1.68-8.52%), moderate ash yield, and high calorific value. The evaluation of rank in coals and carbonaceous shales was done using vitrinite reflectance (Rr), Tmax (from Rock-Eval pyrolysis), biomarker data and volatile matter content. The coal was determined to be "Sub-Bituminous A", based on chemical composition and huminite reflectance (0.38-0.61%).

#### 4.2. Petrographic Characteristics

According to the petrographic evaluations of the studied coals, it was observed that the huminite group was dominant (64-72%, average 66%) and ulminite macerals were abundant in them. There are atrinite and densinite in the humodetrinite group, and gelinite and corphuminites in the humocollinite sub-group. The macerals of the liptinite group (3-7%, average 4%) are sporinite, cutinite, alginite and liptodetrinite; Fusinite and inertodetrinites constitute the inertinite group (0.1-4%, mean 3). Mineral matter (14-28%, average 24%) is composed of pyrite and other minerals (calcite, clay minerals and quartz) (Fig. 3).

#### 4.3. Organic Geochemical Properties

Total Organic Carbon (TOC, wt.%) analysis of investigated coal samples was performed on eight

samples and it ranged between 9.46-52.88%. These results show that the samples taken from the Divriği-Selimoğlu coal-bearing unit are generally rich in organic matter content (TOC > 0.5%) and can be considered as source rock (Peters and Cassa, 1994). S<sub>2</sub>, hydrogen index and oxygen index values in Divriği-Selimoğlu samples were determined between 25.1-193.053 mg HC/g rock, 150-380 mg HC/g TOC, 2-350 mg CO<sub>2</sub>/g TOC, respectively. Production Index values vary between 0.02-0.05. The pseudo-van Krevelen diagram (HI vs. OI) shows organic type and relative hydrocarbon potential and, crudely, the course of maturation (Fig. 4a). The pyrolysis data (HI vs. Tmax) indicated that the analyzed samples are generally plot in the early to relatively immature-early mature zone of mixed Type III-II and predominantly Type III kerogens as indicated by the HI values in the range of 150–380 mg HC/g TOC (Fig. 4b). This HI values suggest that the sediments may be expected to generate mainly gas and limited amount of liquid hydrocarbons. More so, shale and carbonaceous shale samples with Hydrogen Index <200 mg HC/g TOC that contain a Type III vitrinitic kerogen would be expected to generate gas, while samples with HI values higher than 200 mg HC/g TOC can generate some oil and perhaps, their main generation products are gas and condensate (Hunt, 1995).

The presence of liptinitic macerals is most apparent to the oil and gas prone nature of the analysed samples of mainly Type III-II and Type III kerogens (Fig. 4a and 4b). Organic matter amount, organic matter type as well as organic maturation evaluation were made in samples rich in coal and organic matter. In addition, the Tmax values ranging from 406 to 441 oC indicate immature, early mature properties of the organic matter. These values were also supported by huminite reflectance values (avr. 0.54%). Overall, 20S/(20R+20S), 22S/(22R+22S) homohopane, and moretane/hopane ratios that reflect the maturity of organic matter are indicative of immature and mature organic matter.

#### 4.4. Molecular geochemistry

The extractable organic matter (EOM yield) was relatively high especially coal samples for the Divriği-Selimoğlu samples (44 to 13640 ppm). Intermediate and low values were determined for carbonaceous shale (602.6 to 9237.6 ppm) and shale samples (1910.4 to 5866.1 ppm) relative to coals.

##### 4.4.1. n-Alkanes and acyclic isoprenoids

The n-alkanes distribution of the studied coal and organic matter rich samples from the Güneyevler Formation comprise mainly from n-C<sub>7</sub> to n-C<sub>35</sub> (Fig. 4). Alkanes within the range between n-C<sub>23</sub> and n-C<sub>33</sub> account for the significant fraction of the chromatographic distribution of the analyzed samples. Odd n-alkanes predominate over even n-alkane with significant relative abundance of n-C<sub>27</sub>, n-C<sub>29</sub> and n-C<sub>31</sub> in investigated samples. This gives a relatively high carbon preference index (CPI; 3.06). Pristane to phytane ratio (Pr/Ph) for all the analyzed samples



is above 1.00. The coal samples have Pr/Ph ratio ranging from 6.09 to 12.38 with an average of 9.92. All the analyzed coal samples show a relatively low concentration of n-heptadecane (n-C17) compared to pristane, hence, Pr/n-C17 ratio ranges from 8.55 to 15.49 with an average of 13.25 and the Ph/n-C18 ratio ranges from 1.06 to 2.10 with an average of 1.50.

#### 4.4.2. Terpanes and steranes

The m/z 191 chromatograms of the analyzed samples from the Güneyevler Formation shows predominance of the C30-hopane, C29-norhopane, 17 $\alpha$  (H)-trisorhopane (Tm), C31 homohopane and a lesser extent amount of homohopanes (C32–C35), with relatively low amounts of tricyclic and tetracyclic terpanes (Fig.4). The C31 homohopane/C30 hopane ratio ranges from 0.36 to 1.42. Homohopane distribution is dominated by C31 homohopane and decreased in a cascading pattern from C31 to C35 homohopane (Fig. 4). The concentrations of tricyclic terpane and tetracyclic terpane in the analyzed samples are low. A relatively lower C24 tricyclic terpane composition was determined compared to the C23 tricyclic terpanes in half of the eight samples analyzed. Higher amount of C29 steranes, compared to other steranes, in the range of 34.29% to 68.21% also supports dominance of terrestrial source with varying marine and lacustrine influences.

The studied coal, shale and carbonaceous shale from the Güneyevler Formation have high concentration of steranes and diasteranes (Fig.4). The result reveals a higher concentration of C29 sterane (from 36.02 to 80.59%) compared to C28 (from 9.31 to 17.52%) and C27 (from 7.29 to 46.46%) in the analyzed samples. The relative high percentages of C29 steranes over the C27 steranes give C27/C29 regular sterane ratio which is generally >1 (0.06-1.68).

## 5. CONCLUSIONS

The fact that the region in the Divriği-Selimoğlu coal basin is covered with young sediments and volcanic rocks makes it difficult to follow the lateral continuity of the coal-bearing deposits locally. Although the operated coal seam is thin (1.0-1.5 m) in the region, it is of great importance as a local energy source due to its high heat value. Due to the intense effect of tectonism, faults and folds in the region, the coal mining and production phases are interrupted for many times or due to economic reasons.

Total Organic Carbon values of Divriği-Selimoğlu samples vary between 9.46-52.88%, indicating that these sediments are rich in organic matter content (TOC > 0.5%) and can be considered as hydrocarbon source rock. However, organic matter richness alone is not a sufficient parameter for hydrocarbon formation. Although some maturity changes are observed due to volcanic effects in the region, it is observed that the coals are generally not mature enough for hydrocarbon generation. Most of studied samples are immature-early mature and few samples are mature. Coal-bearing

Güneyevler Formation has different organo-facies and mainly has gas generation potential, but their maturation is not sufficient to derive hydrocarbons.

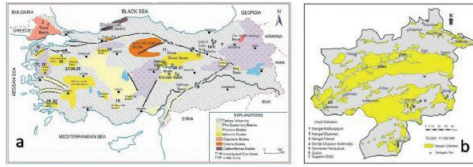
Petrographic, organic geochemical assessments and biomarker data indicate that thin and lenticular coal seams were deposited in the lower levels of the Upper Miocene coaly sequence in a lacustrine environment, but in the middle and upper levels in a lacustrine and deltaic system, in a small shallow lake environment with alluvial and fluvial effects.

## REFERENCES

- ASTM, 1991. Annual book of ASTM standards, Gaseous Fuels; Coal and Coke, 1916 Race Street, Philadelphia, PA 19103, 05.05, 520p.
- Dai S, Guo W, Nechaev VP, French D, Ward CR, Spiro BF, Finkelman BF. 2018. Modes of occurrence and origin of mineral matter in the Palaeogene coal (No. 19 – 2) from the Hunchun Coalfield, Jilin Province, China. *Int J Coal Geol* 189:94–110
- Dai, S., Bechtel, A., Eble, C. F., Flores, R. M., French, D., Graham, I. T., & O'Keefe, J. M. 2020. Recognition of peat depositional environments in coal: A review. *International Journal of Coal Geology*, 219, 103383.
- Hunt, J.M., 1995. *Petroleum Geochemistry and Geology*, W.H. Freeman and Company, New York, pp: 743.
- Lafarque, E., Marquis, F., Pilot, D., 1998. Rock-Eval 6 applications in hydrocarbon exploration, Production, and soil contamination studies. *Revue De L'Institut Français Du Petrole*, 53, 4.
- Littke R, Zieger L. 2019. Deposition, diagenesis and petroleum generation potential of Pennsylvanian coals and coal-bearing strata in Western Germany: a review. *Z der Deutschen Gesellschaft für Geowissenschaften* 170:289–309
- Peters, K.E. and Cassa, M.R. 1994. Applied Source-Rock Geochemistry. In: Magoon, L.B. and Dow, W.G., Eds., *The Petroleum System. From Source to Trap*, American Association of Petroleum Geologists, Tulsa, 93-120
- Peters, K.E., 1986. Guidelines for evaluating petroleum source rock using programmed pyrolysis. *American Association of Petroleum Geologists Bulletin* 70, 318-386.
- Petersen, H.I., Lindström, S., Nytoft, H.P., Rosenberg, P., 2009. Composition, peat-forming vegetation and kerogen paraffinicity of Cenozoic coals: Relationship to variations in the petroleum generation potential (Hydrogen Index). *International Journal of Coal Geology* 78, 119-134.
- Tuncali, E., Çifci, B., Yavuz, N., Toprak, S., Köker, A., Aycik, H., Gençer, A., Sahin, N., 2002. Chemical and Technological Properties of Turkish Tertiary Coals. *Mineral Research & Exploration General Directorate*, 402 p. ISBN-6595-46-9
- Wilkins, R.W.T., George, S.C., 2002. Coal as a source rock for oil: a review. *Int. Jour. Of Coal Geol.*, 50, 317–361.
- Yılmaz, H., Yılmaz, A. 2004. Divriği (Sivas) yöresinin jeolojisi ve yapısal evrimi. *Türkiye Jeoloji Bülteni*, 47(1), 13-46.

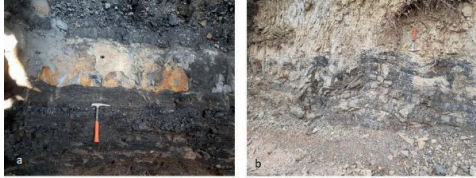
Keywords: Divriği, Organic Geochemistry

Fig.1



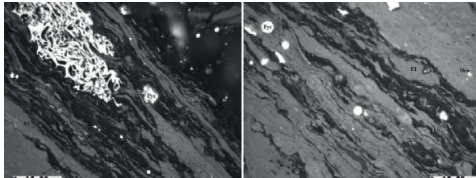
(a) Surface geological map with coal fields in Türkiye and (b) coal formations in Sivas Basin

Fig.2



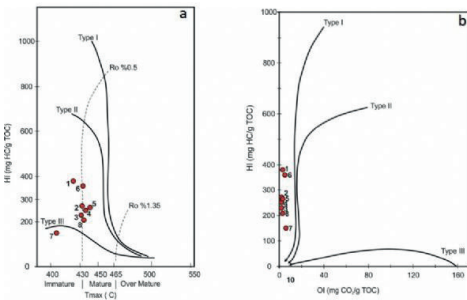
Major coal seam in Divriği-Selimoğlu coal mine, b) The coal layer-limestone alternation observed on the surface around Selimoğlu village is affected by regional tectonism

Fig.3



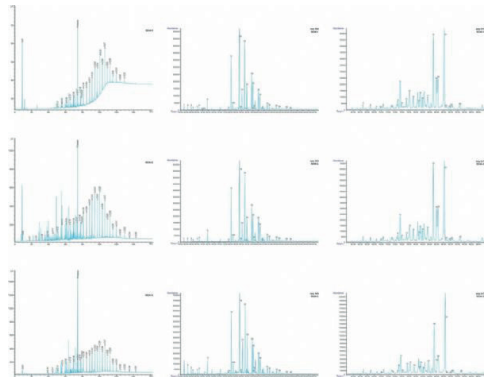
Microphotographs showing some of the common macerals (UL=ulminite, Den=densinite, fusinite) and Pyr=pyrite in the examined coal samples.

Fig.4



Distribution of investigated coal samples in (b) Modified Van Krevelen diagram, (a) HI-Tmax diagram.

Fig.5



The mass fragmentograms of m/z 85 (left), m/z 191 (center) and 217 (right) of saturated hydrocarbon fractions of the Divriği-Selimoğlu coal bearing unit samples.

# A New Depositional and Stratigraphic Framework for Jurassic Marrat Formation: Implications in Reservoir Management in Greater Burgan Field, Kuwait



Bashar Alenezi<sup>1</sup>, Kalyan Datta<sup>1</sup>, D. Saucier<sup>2</sup>, L. Faisal<sup>2</sup>, R. Former<sup>2</sup>

<sup>1</sup>GEOS Enerji A.Ş., Ankara

<sup>1</sup>Kuwait Oil Company (KOC)

<sup>2</sup>British Petroleum (BP)

A new depositional and stratigraphic framework proposed for Middle Marrat reservoirs of Marrat Formation has been designed to improve the reservoir management and development plan in the Greater Burgan Field to a great extent. The interpretation of depositional units and the consistent description of facies and facies associations were proposed for Middle Marrat, which provides a deeper understanding of reservoir depositional elements. The updated, and simplified, reservoir stratigraphy which integrates 3D seismic, well-log, core and production data, will support more effective future water flood management and depletion planning. Integration of this new framework with rock quality data has enabled the description of novel connectivity and sweep scenarios which can be tested against future surveillance data to ensure that “the right volume is being injected in the right places”. This novel depositional and stratigraphic framework will provide primary input for both reservoir management and the next generation 3D geocellular and simulation models.

## INTRODUCTION

The Middle Marrat reservoir of Kuwait was deposited during the Lower Jurassic Pliensbachian to Toarcian period, approximately 175-185 Ma, in a low-angle carbonate ramp setting on the neo-Tethys passive margin (Sharland et al., 2001). It comprises stacked shallow marine grainstone shoals and finer grained lagoonal and ramp sediments. The depositional architecture is overprinted by a range of diagenetic processes both reducing and enhancing reservoir quality. The type section for the Jurassic interval and Middle Marrat member has been provided by Yousif and Nouman (1997) and Sharland et al., 2001).

The Greater Burgan Field has three different structural culminations i.e. Burgan, Magwa and Ahmadi (Figure 1). Exploration and development activities in Middle Marrat of Greater Burgan Field is continuing since early 1980s. Drilling and production in Magwa field continued from that time, whereas Burgan exploration was halted intermittently and was finally development activities started from 2018. Ahmadi culmination was found to be unproductive. So far more than 80 wells have been drilled in Marrat Formation of Greater Burgan Field. With continuing development of both Magwa and Burgan structures in Greater Burgan Field, a need for revision of the existing depositional and stratigraphic

framework was felt in order to support reservoir management, infill drilling and future water injections.

## Depositional Model:

Twenty-two Middle Marrat cores (~5500ft of core) were interpreted during this study and used to develop a thorough understanding of depositional facies, facies associations and depositional environments (Figure 1).

Figure 1 Location map showing distribution and condition of Marrat cores

These data were integrated with available petrography, well logs, dynamic, and seismic data and used to develop a facies scheme and depositional models. Two depositional models have been developed, both of which are consistent with core data and the limited biostratigraphic data (Alsahlan et al., 2010; Al-Moraikhi et al., 2014; Kadar et al., 2015) which confirm a shallow water carbonate ramp setting: 1. “Ramp Barrier Model” which implies that the Middle Marrat member over Greater Burgan formed a barrier which created a land-attached subtidal lagoon behind it which progressively passes onto tidal flats and sabkha environments towards West Kuwait. This model, in the context of a very low angle carbonate ramp, would have resulted in relatively large-scale low-energy facies belts (i.e. all but shoal) and relatively narrow and disconnected shoal belts.

2. “Ramp Bank Model” which predicts one or more isolated banks or islands in an otherwise mid-ramp setting, with each island forming on a relative bathymetric high, formed by local depositional or structural effects, or possibly a combination of the two. Based on modern analogues (e.g. Turks and Caicos Islands of the Great Bahama Bank), the shoals of the windward margin are shown as having higher energy than the leeward margin.

It is important to stress out that both models are thought to be valid for the Middle Marrat member and most likely occurred in various proportions at different times and over different areas of Kuwait, with the ramp barrier model seen as dominant, based on the regional correlation work and the ramp bank model seen as more localized and episodic.

Core-based Facies and Facies Associations  
A key element of this work has been to develop

a common description of reservoir facies, their characteristics, associations and spatial distribution. The objective was to deliver

- A systematic and consistent description of facies and facies associations
- Identification of key stratigraphic surfaces
- Integration of core data with petrographic and well-log data

The new depositional scheme (Figure 2) is consistent across all the studied wells and enables more effective comparisons of different vintages of core.

Figure 2: Middle Marrat depositional scheme showing depositional settings, genetic elements and facies associations.

It is not possible to replicate the high-resolution core interpretation of facies in well log interpretation because the conventional suite of logs cannot discriminate between the various types of carbonate facies. More specifically, the absence of clay minerals means that gamma-ray log responses are indistinct, whilst both sonic and density-neutron log responses, which can be impacted by minor diagenetic changes, can be similar in different but related core facies associations. Consequently, the interpretation in uncored wells focused on identifying groups of facies associations which can be easier to discriminate, guided by detailed correlation work and the prevalent conceptual depositional model for the zone of interest.

**Stratigraphic Framework (Reservoir Zonation)**  
Following are the Key Stratigraphic Framework Insights:

- The study provides a new single common stratigraphic framework across Magwa and Burgan domes linked to core observations and depositional facies interpretation.
- Simpler model than previous frameworks with clearly defined criteria for each top

A number of studies have attempted to apply this detailed sequence stratigraphic framework, although the consistency of the underlying data, such as core descriptions, and the lack of a chronostratigraphic framework introduces significant uncertainty into the application of this framework. The origin and exact equivalency of the various reservoir picks were not fully understood leading to difficulties in integration and extrapolation. The detailed sequence stratigraphic model previously built (see Al-Jadi et al, 2015) appears to have been used to inform the static reservoir model (Al-Jadi et al, 2015) and to predict lateral facies variation via the genetic sequences. This stratigraphic model was developed to support their conceptual depositional model for the Middle Marrat, based on the description of 7 cored wells and integrated with wireline log data from 26 wells.

In the present work, the Marrat wells have been interpreted with the aim of linking chronostratigraphic surfaces as opposed to lithostratigraphic surfaces. The benefit of a chronostratigraphic approach is that it recognises lateral changes in facies and it doesn't assume that, for example, all shoal bodies at a similar depth with a similar well-log signature connect to one another. Recognition of this complexity can be very important for understanding and predicting fluid-flow in the subsurface, a. Intra-reservoir flow pathways can be complicated by subtle permeability contrasts found at changing facies boundaries. It is therefore necessary to recognize the potential for these events to understand how a reservoir might perform.

The new pick framework reflects integration of insights from seismic, well-log and core data. The workflow used to define this reservoir framework is summarized in Figure 3.

Figure 3: Pick framework interpretation methodology

The new framework is illustrated on a correlation of all available cored wells in Figure 4. The tops start at "00" at the base (Top Lower Marrat) and end at "100" at the top Middle Marrat. Each stratigraphic top caps a zone of the same number, for instance top 100 (top Middle Marrat) caps zone 100 which overlies top 90 and zone 90.

- Zone 10 is dominantly lagoonal but possibly less restricted with mid/outer ramp facies interpreted in South Burgan
- Zone 20 is also dominantly lagoonal with possibly less restriction in South. It contains well-developed tidal flats with poor reservoir quality. This zone is capped top 20 which correlates with a key Arabian Plate major flood surface (MFS), the Early Jurassic (middle Toarcian) J10 MFS (Sharland et al., 2001)
- Zone 40 follows the J10 MFS with open ramp facies dominating. Outer ramp facies are widespread at the base prograding gently into mid ramp towards the top of this zone. A few sparse dolomitised mid ramp intervals lead to isolated pockets of minor porosity development.
- Zone 50 shows continued progradation with dominance of lagoonal deposits in North and open ramp facies in the South. Roughly layered bands of dolomitization hint at higher frequency surfaces most likely corresponding to very low relief prograding clinoforms (Figure 6).

Figure 4: Cored well correlation – and schematic illustration of prograding clinoform geometries

- Zone 60 marks a flood back indicated by outer ramp facies in South, followed by progradation with dominance of lagoonal deposits in North and open ramp facies in the South. Lateral transition from lagoon to shoal to open ramp facies, combined with layered bands of dolomitization, hint at likely low-relief prograding clinoforms (Figure 6)

- Zone 70 points to a landward shift in facies and establishment of a major shoal belt across the area, with highest energy and thickest shoals in North and lower energy thinner shoals in South. Tidal flats and low energy shoals dominate in South Burgan.
- Zone 80 follows with an apparent filling up of accommodation space with tidal flats capped by anhydrite-rich sabkha deposits and evidence of surface exposure. Note thicker and more continuous sabkha deposits in South.
- Zone 90 is marked by a floodback and establishment of dominantly lagoonal environment across the area. Two distinct, thin and laterally continuous sheets provide some reservoir quality, one over Magwa and the other over Burgan with minor overlap around the saddle area.
- Zone 100 completes the sequence another floodback and re-establishment of dominantly lagoonal environment across the area. Minor intervals of dolomitized lagoon provide some reservoir quality, mostly limited to the Magwa dome.

#### Comparison with Previous Stratigraphic Framework

The new pick set differ significantly however from past pick sets (Al-Jadi et al., 2015) in that it is rooted in an integrated interpretation of core-derived depositional elements combined with observations from seismic, petrography, and dynamic data. Other key differences relate to the definition of top criteria and importantly how they correlate across the Greater Burgan area. Most of these changes concern zones 50 and 60 (~MM500 to MM820) where many secondary reservoir intervals are now the focus of drilling and development. The new pick set provide an alternative view on lateral reservoir connectivity which can be tested with future infill drilling and data acquisition.

Reservoir Depositional Elements (RDE) Maps  
Reservoir Depositional Elements are the depositional elements (e.g. carbonate shoal bodies or channel fills) that control reservoir dynamic behaviour during production. The length-scales and geometries of carbonate depositional elements are not as well constrained as clastic ones and tend to focus on shoal bodies exclusively, but these only account for part of the reservoir intervals of the Middle Marrat. Therefore, shoal dimensions have been estimated using data from analogue databases and a number of published ancient and modern analogues. The main shoal depositional elements applicable to the Middle Marrat main reservoir interval are elongate shoal bars; small tide-influenced channels; ebb-tide and flood-tide deltas. Dimensions for the other facies associations (lagoon, tidal flats, etc) are not as well constrained but the depositional context leads us to expect very large regional depositional belts. Figure 6 shows a cartoon with expected reservoir architectures across the range of reservoir intervals and ranges of reservoir permeability (based on RCA data) and quality of sweep (notional).

Figure 5: Reservoir architecture cartoons vs average permeability and expected quality of sweep

Reservoir Depositional Element (RDE) maps aim to capture a 2D description of the distribution, stacking patterns and boundaries between depositional elements and any relevant diagenetic or syn-depositional structural features. They honour data (core, well-log or seismic) but are model driven between data points and may be drawn to specifically emphasize features of interest, such areas of dolomitization, anhydrite etc., which may impact the reservoirs dynamic behaviour. They are a key integration tool; helping to communicate the subsurface description to other disciplines (e.g. to highlight sweet spots for well planning, discussing fluid flow pathways, remaining oil in place etc.) and they can be used in combination with facies proportion maps to help constrain geocellular models. It is impossible to predict precisely the presence, preservation, geometry and connectivity of shoal and other shallow water carbonate ramp bodies due to the dynamic nature of this depositional setting.

Reservoir depositional element maps are shown here for the Middle Marrat to capture the main reservoir intervals

Figure 6: Zone 60 reservoir element map

Figure 7: Zone 70 reservoir element map

Figure 8: Zone 80 reservoir element map

#### Potential Depositional Controls on Fluid Flow

The reservoir depositional element maps (RDEs) and reservoir architecture cartoons provides useful insights into potential depositional controls on fluid flow. For instance, lateral and vertical continuity of reservoir bodies are expected to be very different between the shoal dominated zone 70 and the thin shoal /thin dolomitized layers of zone 100. Other insights include element geometries and stacking patterns, and relative reservoir quality. Depositional control on reservoir quality is illustrated by the porosity-permeability cross-plots in Figure.

Figure 9: Routine core analysis (RCA) porosity-permeability cross-plots. Top left: all plug data. Top right: all plug data minus those described as fractured in the plug description. Bottom left: All plug data minus those associated with dolomitized facies interpretations. Bottom right: All plug data minus those either described as fractured or associated with dolomitized facies interpretations.

The top left figure shows all available core plug data colour-coded per facies associations, but in addition to the depositional control on porosity and permeability, this plot is likely to partly reflect fracture and diagenetic effects. On the top right figure, the plugs described as fractured in the routine core analysis reports have been removed to focus on matrix behaviour. Note that some plugs still display fracture behaviour, and this could be due to either a given plug not having a description or the description may have missed the presence of

fractures. The two top row cross-plots are repeated on the bottom row of Figure 11 with the dolomitized facies removed to remove some of the diagenetic effects. The bottom right plot reflects, as far as possible, the depositional controls on porosity and permeability. On this plot, different facies segregate relatively clearly in distinct poro-perm regions. Along the same lines, Figure 12 shows individualised porosity-permeability cross-plots for each of the facies associations (including dolomitized facies) illustrating noticeable differences in poro-perm behaviours for each facies. Figure 10: Routine core analysis (RCA) porosity-permeability cross-plots per facies association – non-fractured plugs as per plug description.

Another insight into depositional controls on fluid flow is provided by PLTs from a well Magwa well. PLTs and ILTs are key pieces of surveillance data that can be used to understand controls behind zonal contributions to flow. Fluid flow in carbonates is often affected by varying permeability, thief zone flow in which a single high-permeability zone or fracture dominates, or hybrid flow with elements of both multilayer and thief zone flow (Figure 11). In well MG-A, integrated PLT interpretation indicates that two discrete fluid flow jumps correlate with high permeability streaks. RCA data and core description show that those high permeability streaks are depositional and not diagenetic. These two examples of depositional control on fluid flow illustrate the importance of considering and capturing this type of control in reservoir models to be able to match and predict reservoir performance.

## CONCLUSIONS

- Two depositional models, i.e Ramp-barrier model and a ramp bank model have been developed, both were thought to be valid for Middle Marrat of Greater Burgan Field.
- A systematic and consistent description of facies and facies associations were done and key stratigraphic surfaces were identified.
- Reservoir depositional elements were described.
- Expected reservoir architectures across the range of reservoir intervals and ranges of reservoir permeability (based on RCA data) and quality of sweep were envisaged.
- 2D distribution of reservoir depositional elements, their stacking pattern were brought to the fore for important stratigraphic intervals.
- Depositional control on reservoir quality has been illustrated by the porosity-permeability cross-plots. Importance of PLT/ILT data in understanding zonal distribution of flow was discussed.

## REFERENCES

- Al Jadi Menayer, Pranay Kumar, Frederic Lislud, Joel Robert, Mauro Alessandrini, Christian Lefebvre, Vincent de Groen, Louise Vigier, Kalyanbrata Datta, Karam Hafez, Hans Taneja, Muktibrata Bhattacharya Deryck Bond. 2015. Integration of reservoir performance and geoscience studies in the history match of a complex carbonate reservoir – a case study from the Magwa Marrat reservoir – Kuwait. (SPE-17259). 19th Middle East Oil & Gas Show and Conference, 8-11 March, 2015, Manama, Kingdom of Bahrain
- Sharland, P. D. R. A. A. c. M., 2001. Arabian Plate Sequence Stratigraphy, GeoArabia Special Publication 2. Bahrain: s.n.
- Yousif, S., and Nouman, G., 1995. Geological model of the Jurassic section in the State of Kuwait: SPE East Oil Show, SPE 29796, p. 231-249.
- Al Moraikhi, R., Kulkarni, N., Patil, D. P., Sounderrajan, M., Verma, N. K., Quttainah, R., Al-Kandari, E., Al-Mohailan, M. (2017, November 13). Kuwait's First Successful Implementation of MPD in Deep Jurassic Reservoirs of Abdulyah Field in West Kuwait. Society of Petroleum Engineers. doi:10.2118/188649-MS
- Alsahlan, G. A., Youssef, A., Kadar, A. P., Fenton, J. P., Marshall, P. 2010. Early-Middle Jurassic Marrat formation Onshore Kuwait: A Depositional Sequence Stratigraphic Framework. GEO 2010 Middle East Geosciences Conference and Exhibition, Manama, Bahrain.
- Kadar, A. P., De Keyser, T., Neog, N., Karam, K. A. 2015. Calcareous nannofossil zonation and sequence stratigraphy of the Jurassic System, onshore Kuwait. GeoArabia, 2015, V. 20, No. 4, p.125-180. Gulf PetroLink, Bahrain.

Keywords: carbonate, Sedimentology & Stratigraphy



Figure 7: Zone 70 reservoir element map

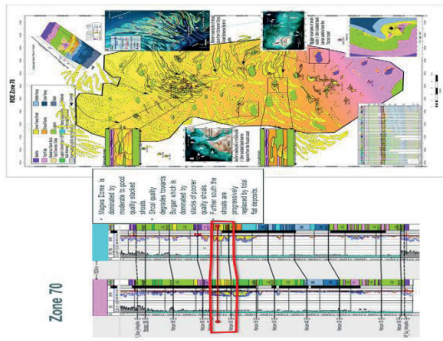


Figure 8: Zone 80 reservoir element map

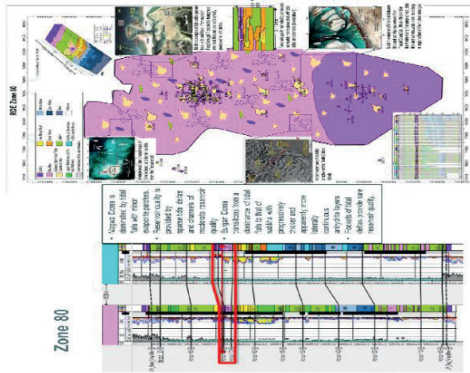


Figure 9: Routine core analysis (RCA) porosity-permeability cross-plots

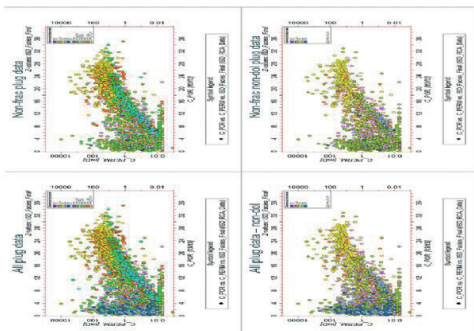
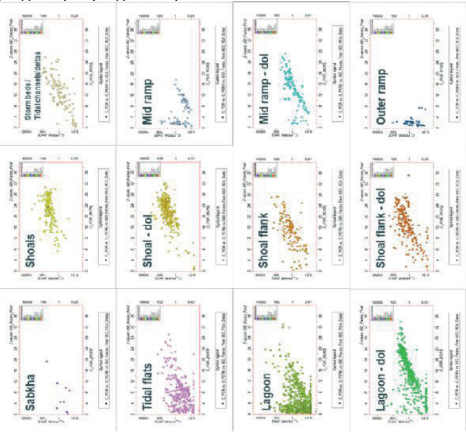


Figure 10: Routine core analysis (RCA) porosity-permeability cross-plots per facies association – non-fractured plugs as per plug description.







## **Sismik Veri Yorumlama ve Analizi**

---

---

---

# An Example of Seismic Interpretations on Listric Faults; Gulf of Gökova, Datça Fault

Yeliz Mert, Damla Doğan, Hülya Kurt

Istanbul Teknik Üniversitesi Maden Fakültesi, Jeofizik Mühendisliği, İstanbul



## SUMMARY

Listric faults are concave-upward curved normal faults where the dip angle decreases with increasing depth. Generally, it is observed that these types of normal faults merge with a low angle detachment fault at depth. Additionally, the existence of rollover anticline located on the hanging wall of the fault and the presence of antithetic and synthetic faults are commonly observed structural elements in listric faults. Multi-channel seismic reflection data that reveals the fault geometry in high resolution is widely used in the investigation of listric faults, however, there are certain aspects that need to be taken into consideration when interpreting seismic stacking or migration sections in the time domain. The most crucial of these is the velocity pull-up effect, which is a misleading consequence of the general increase in seismic velocity with depth in the subsurface. The reflections related to the fault plane in the seismic reflection sections of layers resting on a planar normal fault are moved upward due to the seismic velocity pull-up, thus forming a listric fault geometry. Therefore, by creating zero-offset synthetic seismic reflection sections, it can be investigated to what extent a normal fault can be observed as a listric fault in seismic sections.

In Western Anatolia and the Aegean Sea, where extensional tectonics dominate region, normal faults are commonly observed structural elements. One of these, the Datça Fault, which is a northward dipping listric fault extending east-west and bounding the Gulf of Gökova from the south, located in the southern Aegean Sea, is tracked up to approximately 3 seconds in time domain seismic reflection sections. In this study, the listric geometry of the fault has been comparatively investigated with synthetic seismic sections created using the ray tracing method. Additionally, structural calculations such as extension rate, extension ratio, and sedimentation rate were performed with readings from the seismic section. Accordingly, the dominant extension rate, extension factor, and sedimentation rate in the gulf have been determined as 1.26 mm/yr, 1.47, 0.45 mm/yr respectively.

## INTRODUCTION

The Gulf of Gökova, located in the Western Anatolia-Aegean Sea region, is influenced by the extensional tectonic regime (Figure 1). The active tectonics of the gulf were studied using multichannel seismic reflection data collected by the MTA Seismic-1 Vessel in 1996, and the listric Datça Fault, which delimits the gulf from the south, was identified (Kurt et al., 1999). Listric faults are convex upward normal faults where the dip decreases with depth. In this study, the multichannel

seismic reflection data collected along the EW-oriented line No. 11 in the gulf were processed conventionally, and a time migration section was constructed. Moreover, the listric nature of the interpreted Datça Fault was examined with synthetic seismic sections generated using the 2D ray tracing method, and structural calculations such as the extension rate, extension factor, and sedimentation rate in the gulf were carried out.

## MATERIALS AND METHODS

In this study, multichannel seismic reflection data collected along the approximately 21 km long, EW-oriented line No. 11 in the Gulf of Gökova were processed and interpreted (Figure 1b). The data collection parameters and an example of a shot record pertaining to the multichannel seismic reflection data collected on line No. 11 by the MTA Seismic-1 Research Vessel in the gulf in 1996, in partnership with Istanbul Technical University (ITU) and the General Directorate of Mineral Research and Exploration (MTA), are given in Figure 2.

The multichannel seismic reflection data were processed using the Echos software (V:15.5) available at the Nezihî Camtez Data Processing Laboratory of the Department of Geophysical Engineering at Istanbul Technical University (ITU), following conventional data processing steps (Figure 3). Shots were initially inspected individually to identify and remove poor-quality traces. Subsequently, the data were transferred from the seismic shot domain to the CMP (Common Mid-Point) domain and random noises were attenuated by applying a band-pass frequency filtering in the range of 12.5/25- 110/165 Hz (Figure 4). Then, to compensate for the amplitude decay with the distance of the seismic wave, amplitude gain was applied to the data. A stack section was constructed after the velocity analysis was applied to the data. A time migration section was created to enable the reflections on the stack section to be transferred to their actual locations (Figure 5a). Structural and stratigraphic interpretations are displayed in the migration section (Figure 5b). In the interpreted seismic reflection section, it can be seen that the listric character of the Datça Fault on the southern edge is followed down to a depth of 3 seconds.

In the second stage of the study, synthetic seismic sections created for different depth-velocity models using the 2D ray tracing method were examined, and the appearance of faults in planar or listric structures in time domain seismic sections were investigated. A fault that is planar in the depth section can appear planar or listric in the seismic section in the time domain. However,

due to the increase in seismic velocity with depth, the reflection level associated with a planar fault can appear curved in seismic sections due to the velocity pull-down (Figure 6). The observed listric nature of the Datça Fault in the seismic section may have occurred for similar reasons. This effect due to velocity pull-down in time domain seismic sections can only be corrected by creating a depth migration section. Indeed, a depth migration section has been created for the Datça Fault and it has been observed that this fault still exhibits a listric character (Kurt et al., 1999).

### STRUCTURAL CALCULATIONS DETERMINED FROM THE SEISMIC SECTION

Structural calculations such as extension rate, extension factor, and sedimentation rate have been made using the seismic reflection section belonging to the EW-oriented line No. 11 in the Gulf of Gökova. In the calculation of the extension rate of the Gulf of Gökova, which developed under the extensional tectonics of the Western Anatolia-Aegean Sea, the total horizontal displacements of the Datça Fault and the antithetic faults related to the fault ( $X1+X2+X3+X4+X5$ ) were used (Figure 7). These values were determined in the seismic section as 5000, 100, 350, 200, and 150 m, respectively. By relating the calculated total displacement amount to the Late Miocene-Pliocene extension age of the gulf, the extension rate of the gulf was determined to be 1.26 mm/year.

For the calculation of the extension factor, the post-extension length ( $L1=20.9$  km) of the section belonging to the seismic reflection line was first determined (Figure 8b). A synthetic section depicting how the gulf would appear in seismic reflection sections before opening was created by removing the effects of the Datça Fault and its antithetic faults (Figure 8a). Thus, by comparing the length of the gulf after extension ( $L1$ ) to its previous length ( $L0=14.2$  km), the extension factor for the gulf was found to be 1.47.

To calculate the sedimentation rates of the layers in the gulf, the depth migration section, where the horizontal and vertical scales are equal, belonging to line No. 11, is used as given in Figure 9 (Kurt et al., 1999). In the section, the layers forming the rollover anticline structure colored in yellow are assumed to be Pliocene, and the overlying layers in green are assumed to be Pleistocene (Kurt et al., 1999). The vertical thicknesses of the layers have been determined by measuring in the directions indicated by the arrows in Figure 9. The sedimentation rate for the rollover anticline was calculated in two different ways. Firstly, for the rollover anticline structure, ages were given to the layers at equal intervals from the Early Pliocene to the Late Pliocene, from 5.3 million years to 3.2 million years, and sedimentation rates were determined by dividing each layer's thickness by its age, from the deepest to the top, as 0.11, 0.14, 0.17, and 0.11 mm/year, respectively. As a second approach, dividing the entire thickness of the rollover anticline structure by the Early Pliocene age,

which is when sedimentation started, yielded 0.45 mm/year. The sedimentation rate of the overlying layers was found to be 0.42 mm/year by dividing their thickness by their age, assuming it to be 2.58 million years. The subsidence of a region can occur due to an increase in sediment thickness, tectonic activities, and the influence of isostatic events. To determine which of these factors predominates in a region, it is necessary to calculate the subsidence rate. When examining seismic line No. 11, the vertical throw of the Datça Fault necessary for the calculation of the subsidence rate is not seen in the seismic section. Therefore, it is assumed that there is only subsidence in the Gulf of Gökova due to tectonic events, and it is accepted that the sedimentation rate and the subsidence rate that could occur due to tectonic reasons are equal to each other.

### DISCUSSION AND CONCLUSIONS

Normal faults with planar geometry can appear to have a listric character in seismic sections in the time domain due to the upward curving appearance resulting from velocity pull-up. Upon examining the synthetic sections of models generated with 2D ray tracing, it is speculated that the Datça Fault, as seen in the time domain seismic migration section belonging to line No. 11, has a listric feature. Indeed, the depth migration section created by Kurt et al. (1999) supports this conclusion.

The extension rate caused by the Datça Fault in the Gulf of Gökova was determined to be 1.26 mm/year, and the extension factor was found to be 1.47. It was assumed that the only factor causing sedimentation in the region was tectonic events, and the sedimentation rate and subsidence rate were considered equal. As a result of the calculations, the sedimentation rate was found to be 0.45 mm/year for the layers in the rollover anticline structure and 0.42 mm/year for the overlying (onlap) layers. These values are in accordance with the sedimentation rates of  $0.50\pm 0.04$  to  $0.039\pm 0.003$  mm/year calculated by Uğur and Yener (2001) using cores from the Gulf of Gökova and its vicinity. While sedimentation rate calculation based on cores is the most reliable and precise method, it should not be overlooked that the time period represented by the cores corresponds to very recent times. However, the consistency of sedimentation rates from seismic data with core data supports the validity of the study.

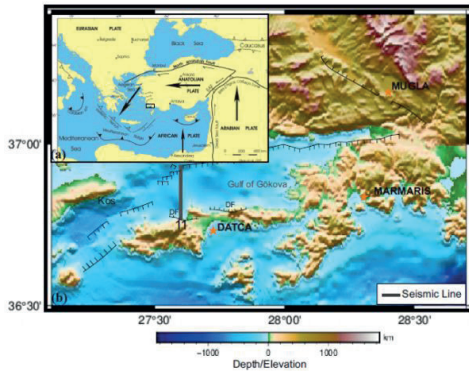
### REFERENCES

- Dikbaş, A., Akyüz, H.S., Basmenji, M. et al. Earthquake history of the Gökova fault zone by paleoseismologic trenching, SW Turkey. *Nat Hazards* (2022). <https://doi.org/10.1007/s11069-022-05284-0>
- Kurt, H., Demirbağ, E. & Kuşcu, İ., (1999). Investigation of submarine active tectonism in the Gulf of Gökova, SW Anatolia - SE Aegean Sea, by multi-channel seismic reflection data, *Tectonophysics*, 305, 477-496.
- Uğur, A., & Yener, G. (2001). Accumulation rates and sediment deposition in the Gökova Bay in Aegean Sea Turkish Coast. *Applied Radiation and Isotopes*, 55(4), 581-588.

Wessel, P., Luis, J. F., Uieda, L., Scharroo, R., Wobbe, F., Smith, W. H. F., & Tian, D. (2019). The Generic Mapping Tools version 6. *Geochemistry, Geophysics, Geosystems*, 20, 5556–5564. <https://doi.org/10.1029/2019GC008515>

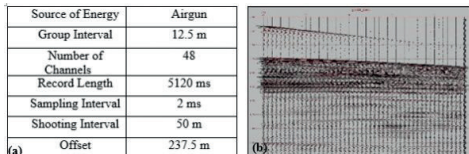
Keywords: Listric Fault, Seismic Reflection

Figure 1



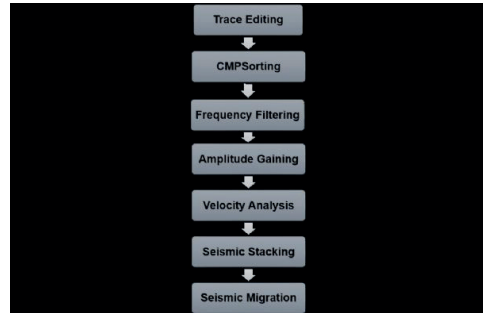
(a) Tectonic map of Turkey (Okay et al., 1999) (b) Morphology and fault map of the Gulf of Gökova and its surroundings (Morphological data from GEBCO, fault locations from Dikbas et al. (2022), seismic line from Kurt et al. (1999)). The map was created with the GMT program (Wessel and Smith, 2019). DF: Datça Fault.

Figure 2



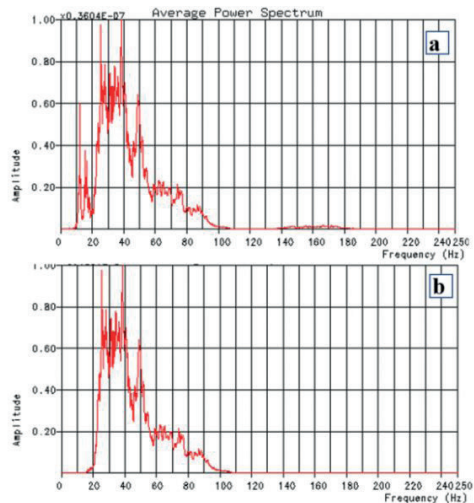
(a) Seismic data collection parameters of line 11 (b) example of a seismic shot record

Figure 3



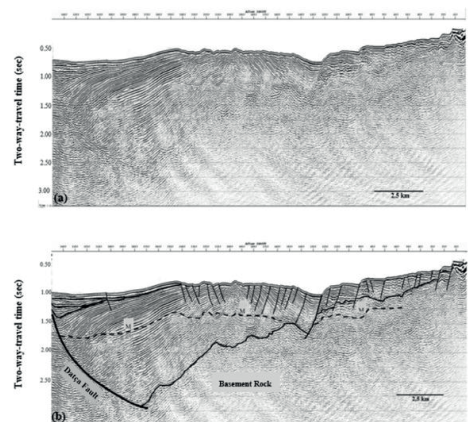
Steps followed in processing multi-channel seismic reflection

Figure 4



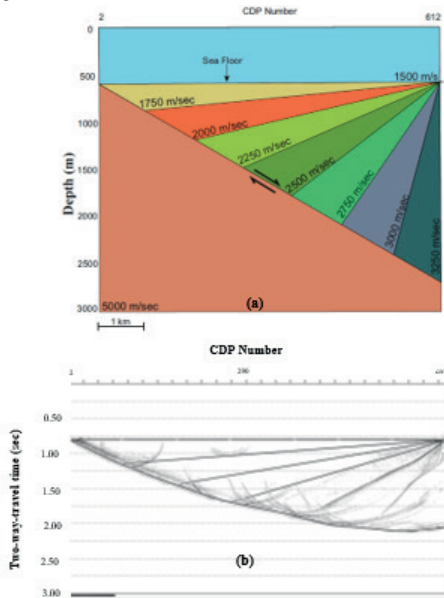
Frequency filtering process applied to seismic data. (a) Pre-filtering (b) post-filtering frequency spectrum

Figure 5



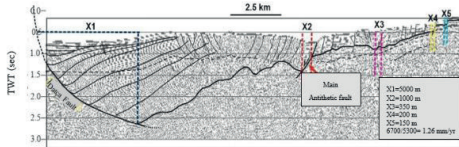
(a) Time domain seismic migration section of line 11 (b) Interpreted section. M: Multiple reflections.

Figure 6



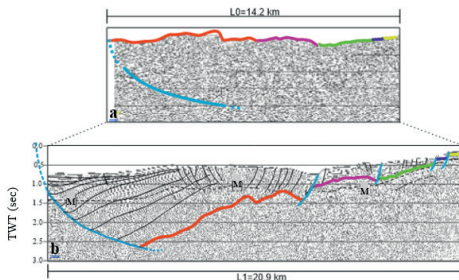
(a) Planar fault and ground model with a dip layer leaning on the fault, (b) Synthetic seismic time migration section of the planar fault model

Figure 7



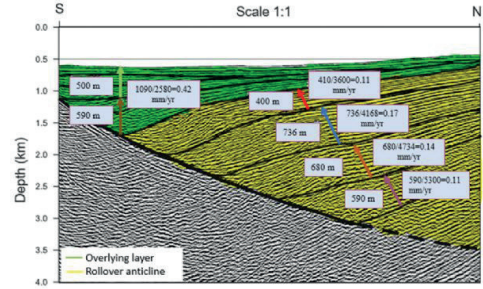
Horizontal displacements used in the calculation of the extension rate of the Gulf of Gökova

Figure 8



Calculation of the expansion coefficient of Gulf of Gökova. (a) Pre-extension seismic section of the gulf created by the retrograde method (b) post-extension seismic section, M: Multiple reflection.

Figure 9



Sedimentation rate calculations of the layers on the depth migration section of line 11 in the Gulf of Gökova (Kurt et al., 1999)

# Hesaplanmış Yansıma Katsayısı Değerleri Kullanılarak 2-B Sentetik Sismik Kesitin MATLAB Yazılımı İle Oluşturulması



**Mehmet Mert Doğu<sup>1</sup>, Altay İsa Tok<sup>1</sup>, Göktürk Mehmet Dilci<sup>2</sup>,  
Rahmi Mert Bolat<sup>2</sup>, Fatih Özdamar<sup>2</sup>**

<sup>1</sup>İstanbul Teknik Üniversitesi, Maden Fakültesi, Jeofizik Mühendisliği, İstanbul

<sup>2</sup>Türkiye Petrolleri Anonim Ortaklığı, Ankara

## ÖZET

Hidrokarbon arama amacı, jeotermal sistemlerin tespiti ve aktif tektonik çalışmalarını başta olmak üzere yer bilimlerinin pek çok alanında sismik kesitlerin yorumlanması ve yer altının karmaşık yapısının ortaya çıkarılması çok önemli bir yer tutmaktadır. Bu tarz yorumlamaları daha doğru yapmak amacıyla sentetik sismik kesitlerin oluşturulması yöntemi geçmişte pek çok araştırmacı tarafından ele alınmıştır (May & Hron, 1978; Peddy vd., 1986; Rutter vd., 1999). Bu çalışmada MATLAB yazılımı kullanılarak sentetik sismik kesitlerin kolay ve pratik bir şekilde oluşturulması ve bu yapıyı kesitlerde özellikle rezervuar seviyeleri içerisinde bulunan hidrokarbonların ne gibi yansıma görüntülerini meydana getireceği incelenmiştir. Çalışmada ilk olarak denizde bulunan hayali bir sedimanter istif çizilmiştir. Bu sedimanter istif şeyil, marn, kesif dolomit ve rezervuar dolomit araldanmasından oluşmaktadır. Bu istif içerisindeki kayaların yoğunluk değerleri ve sahip oldukları Vp (kayaç içerisinde geçen P-dalgası hızı) değerleri literatür bilgileri kullanılarak yaklaşık olarak hesaplanmıştır. Rezervuar dolomit seviyelerine farklı oranlarda porozite değerleri atanmış ve buna bağlı olarak da petrol, ıslak gaz ve su miktarları değiştirilmiştir. Bu farklı değerlere göre hazırlanan senaryolarda meydana gelebilecek 2-B (iki boyutlu) sentetik sismik kesitler oluşturulmuştur. Öncelikle sentetik sismik kesiti oluşturulmak istenen jeolojik istif AutoCad kullanılarak çizilmiştir. Çizilen bu istifte her bir tabaka sınırına belirli bir RGB (kırmızı, yeşil, mavi renkleri) değerine sahip renk yerleştirilmiştir ve her bir sınır farklı bir yansıma katsayısı değerini temsil edecek şekilde ayarlanmıştır. Ardından bu katsayılar belirlenen sinüs dalgası ile konvolüsyona sokulmuş ve görseldeki seçilen piksel kolonlarıyla uygun bir şekilde bu dalgacıklar bir bütün halinde gösterilmiştir. Nihai olarak oluşturulan 2-B sentetik sismik kesitler gerçek kesitlerin yorumlanmasında sismik kesit yorumlayan çalışan ve araştırmacılara yardım olabilecek niteliktedir. Bu kod sayesinde araştırmacılar 2-B sismik veri toplanmadan önce, eldeki mevcut jeolojik veriler ve literatür çalışmaları ışığında bir yaklaşımda bulunabilir ve sismik verinin toplanacağı güzergahı buna göre daha net bir şekilde kurgulayabilir. Bunun yanı sıra toplanmış olan verilerin yorumu yapıldığı esnada da oluşturulan sentetik sismik kesitler kullanılarak daha kapsamlı bir yorumlamaya gidilebilir.

## ABSTRACT

In many geoscience fields, such as hydrocarbon exploration, detecting geothermal systems, and studying active tectonics, interpreting seismic sections and revealing subterranean complexities is essential. To enhance the accuracy of interpretations, researchers have explored synthetic seismic section creation methods in the past (May et al., 1978; Peddy et al., 1986; Rutter et al., 1999). In this study, MATLAB software is utilized to generate synthetic seismic profiles in a straightforward and practical manner, and examines the reflection images of hydrocarbons in these artificial profiles, particularly in reservoir levels.

Initially, an imaginary sedimentary stack situated in the sea is drawn. This sedimentary stack comprises a sequence of shale, marl, clastic dolomite, and reservoir dolomite. The density and P-wave velocity values for the rocks in this stack were estimated by referencing literature. Porosity values were assigned to the reservoir dolomite levels, and the volumes of oil, wet gas, and water were adjusted accordingly. Synthetic 2-D seismic sections were then generated based on these values in the various scenarios prepared. Firstly, the geologic sequence for generating the synthetic seismic section was designed through AutoCad. Each layer boundary in this sequence was assigned a color with an individual RGB value to represent a distinct reflection coefficient. Next, the coefficients were multiplied with the intended sine wave and the resulting wavelets were exhibited as a composite, according to the designated pixel columns in the image. Finally, the 2D synthetic seismic sections created can assist seismic section interpreters and researchers in interpreting real sections. This code allows researchers to approach the task by considering existing geological data and literature studies prior to collecting 2D seismic data. As a result, they can more accurately plan the collection route of seismic data. In addition, while interpreting the collected data, synthetic seismic sections can provide a more comprehensive analysis.

## GEREÇ VE YÖNTEMLER

2 boyutlu sentetik kesit eldesi için oluşturulmuş MATLAB kodu, istif görselindeki tabaka sınırlarında bulunan renklerin RGB değerlerine göre daha önceden hazırlanan kayaç özellikleri bilgilerini taşır. Porozite, petrol oranı, ıslak gaz oranı, su oranı, yoğunluk, yığın modülü ve makaslama modülü değerleri bu kayaç özelliklerini temsil eder. Bu değerlerden yola çıkarak yansıma katsayısını oluşturan Vp (P-dalgası

hızı) ve yığın yoğunluğu değerlerini hesaplar. İstif içerisindeki kayaçların yaklaşık yansıma katsayısı değerlerinin hesaplanabilmesi için sırasıyla aşağıdaki adımlar gerçekleştirilmiştir: 1. Adım: Yığın yoğunluklarının hesaplanması (bulk modulus). Bu hesaplamayı yapabilmek için literatür verilerinden istifteki kayaçların sahip olduğu yaklaşık yoğunluk değerleri bulunmuştur (Alves vd., 2019). Buradaki yoğunluk değerlerinden yola çıkarak farklı porozite ve değişken hidrokarbon oranlarına sahip olan kayaçların yoğunlukları 1 numaralı formül vasıtasıyla bulunmuştur. Burada  $\rho_y$  değeri kayacın yığın yoğunluğunu,  $\rho_{ma}$  değeri matrisin yoğunluğunu,  $\rho_s$  değeri sıvının yani suyun yoğunluğunu,  $\Phi$  değeri ise poroziteyi temsil eder. Kayaç içerisinde hidrokarbon girdiğe formül benzer şekilde devam ettirilir.  $\rho_p = \rho_{ma}(1-\Phi) + \rho_s(\Phi)$  (1)

2. Adım: Kayaçların içerisinde geçen yaklaşık  $V_p$  hızı değerlerinin bulunması. Bu aşamada ise literatür verileri kullanılarak kayaçların sahip olduğu yığın modülü (K), makaslama modülü ( $\mu$ ) ve yığın yoğunluk ( $\rho$ ) değerleri kullanılmıştır. Bu değerler literatür bilgileri kullanılarak, yaklaşık olarak ifade edilmiştir (Cao vd., 2013). Kullanılan 2 numaralı formül aşağıdaki gibidir.  $V_p = \sqrt{((K + 4/3 \mu) / \rho)}$  (2)

3. Adım: İstifteki tabakalar arasındaki yansıma katsayısı değerlerinin hesaplanması. Bu kısımda ise 1. ve 2. adımda bulunan yoğunluk ve  $V_p$  hız değerleri kullanılarak, bu ara yüzeylerdeki yansıma katsayısı değerleri (R) hesaplanmıştır. Yansıma katsayısı değerlerinin hesaplanmasında 3 numaralı formül kullanılmıştır.  $R = (\rho_1 V_1 - \rho_2 V_2) / ((\rho_1 V_1 + \rho_2 V_2))$  (3)

Her bir tabaka sınırı için yansıma katsayıları hesaplandıktan sonra bu katsayıların hangi derinliğe denk geldiği çizilen istif görseli temel alınarak bulunur. Sismik kesit için gerekli olan görselin ortaya çıkması için yansıma katsayıları ile konvolüsyon yapılacak bir adet sinüs dalgası oluşturulup her seferinde bir dalgacığı oluşturması için katsayılar ve minimum fazlı dalga konvole edilir. Bu işlem görselin seçilen tüm piksel kolonları için tekrar edilerek çözünürlüğü ayarlanabilen bir ideal sismik kesit oluşturur. Çalışmada kullanılan kod MATLAB App Designer üzerinden kullanıcı arayüzü bir halde yazılmıştır. Program açıldığında görülen pencerenin sol tarafında görsel yükleme bölmesi yer almaktadır ve buradan sismik kesiti oluşturulacak görsel yüklenilir (Şekil 1).

İstif görseli yüklendikten sonra, Şekil 1'de görüleceği üzere görselin altında yüzdesel olarak sismik kesitin yüklenen görselin yatay piksel değerine göre çözünürlük değerinin ayarlandığı bölme bulunmaktadır. Bu bölmedeki değeri belirleyip altında bulunan "Uygula" butonu ile varsayılan ayarlardaki kayaç değerleriyle oluşturulmuş sismik kesit ekranda belirecektir. Çözünürlük optimum seviyeye getirilerek sismik kesitte daha iyi bir görüntü yakalanabilir.

Şekil 2'de pencerenin sağ bölümünde sismik kesitle birlikte kesitteki dalgaların genlik ve dalga boyu

değerlerinin güncel olarak değiştirilebildiği kaydırma butonu bulunmaktadır. Bu kaydırma butonu sayesinde dalgacığın genliği ile istenilen şekilde oynanabilir.

Şekil 3'de görselde üç butonun etkisi gözükmektedir. Görüleceği üzere Şekil 2'den farklı olarak dalga boyu ve genlik değerlerinin yanı sıra çözünürlük de artırılmıştır. Dalga boyu değeri ince tabakalarda azaltılarak dalganın ayrımlılığı artırılabilir.

Araç çubuğunda bulunan ilk eleman bize görselde belirlediğimiz bir adet piksel kolonuna ait olan ve sağlanan yansıma katsayıları değerleriyle oluşturulmuş grafiği bizlere sunar (Şekil 4). Bu değerler eğer bölgede açılan bir kuyu var ise ve burada VSP yapıldıysa değerleri eşleştirmek açısından kullanışlı bir yöntem olacaktır.

Araç çubuğunda ikinci sırada bulunan buton, Şekil 5'te görüleceği üzere kayaçların porozite, yoğunluk gibi fiziksel özelliklerinin tablo şeklinde ekranda gösterilmesini sağlar. Bu tablodaki değerler değiştirilebilir ve böylece değiştirilen değerlerin sismik kesit üzerindeki etkisi "Uygula" butonuna basılarak elde edilebilir.

Kayaçların değiştirilmiş değerleri ile oluşturulan kesit Şekil 6'daki gibi gözükmektedir. Verilen yoğunluk değeri kesitteki etkinin gözlemlenebilmesi için seçilmiştir.

## SONUÇ

Bu çalışmada kurgusal bir jeolojik istifin sadece yoğunluk, porozite, su ve hidrokarbon oranlarını değiştirilerek sentetik bir sismik kesit oluşturulmuştur. Bu sayede farklı rezervuar seviyeleri içerisinde bulunan hidrokarbonların sismik kesitte ne gibi anomalileri meydana getireceği incelenmeye çalışılmıştır. Eğer kuyu loğları gibi sondaj verileri kullanılarak bu şekilde bir model oluşturulursa gerçeğe çok daha yakın bir sentetik sismik kesitin oluşturulması öngörülmektedir. Bunun yanı sıra kodu iyileştirmek adına yapay gürültü, derinlere inildikçe sinyal gücünün azalması gibi yaklaşımlar yapılabilir. Bu tarz iyileştirmeler sonucunda oluşturulacak olan sentetik sismik kesit gerçeğe oldukça yakın bir sonuç verecektir ve bu sayede bir bölgede 2-B sentetik sismik kesit toplanmadan önce ve toplanıldıktan sonra araştırmacılara oldukça büyük katkı sağlayacaktır.

## TEŞEKKÜR

Bu çalışma 1. ve 2. yazarların Türkiye Petrolleri A. O.'nda gerçekleştirdiği yaz stajları kapsamında ortaya çıkmıştır. Çalışmanın gerçekleştirilmesinde katkısı olan tüm Akdeniz Bölge Müdürlüğü'nde görevli mühendislerle teşekkür ederiz. Çalışma esnasında bizden yardımlarını esirgemeyen arkadaşımız Yeliz Mert'e teşekkürler.

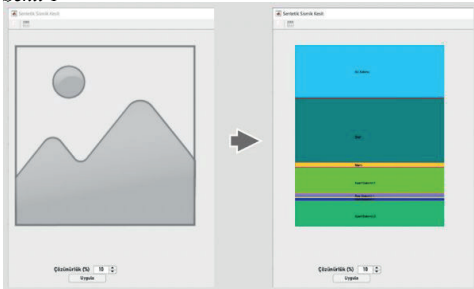


**KAYNAKÇA**

MacBeth, C., Cersosimo, G. S., Fernandez, G. A., & Rosas, F. FEASIBILITY STUDIES AND ELASTIC INVERSION APPLIED TO GEOPHYSICAL CHARACTERIZATION OF THE OFFSHORE TARANAKI BASIN, NEW ZEALAND. Cao, H., Boyd, A., & Simoes, V. D. S. (2013, August). Numerical simulation of the elastic properties of porous carbonate rocks. In 13th International Congress of the Brazilian Geophysical Society & EXPOGEF, Rio de Janeiro, Brazil, 26–29 August 2013 (pp. 1083-1088). Society of Exploration Geophysicists and Brazilian Geophysical Society. May, B. T., & Hron, F. (1978). Synthetic seismic sections of typical petroleum traps. Geophysics, 43(6), 1119-1147. Peddy, C., Brown, L. D., & Klempner, S. L. (1986). Interpreting the deep structure of rifts with synthetic seismic sections. Reflection Seismology: A Global Perspective, 13, 301-311. Rutter, E. H., Khazanehdari, J., Brodie, K. H., Blundell, D. J., & Waltham, D. A. (1999). Synthetic seismic reflection profile through the Ivrea zone–Serie dei Laghi continental crustal section, northwestern Italy. Geology, 27(1), 79-82.

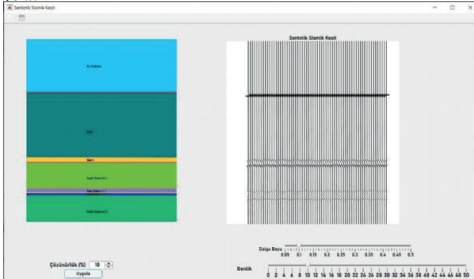
*Anahtar Kelimeler: Sentetik Sismik Kesit*

**Sekil 1**



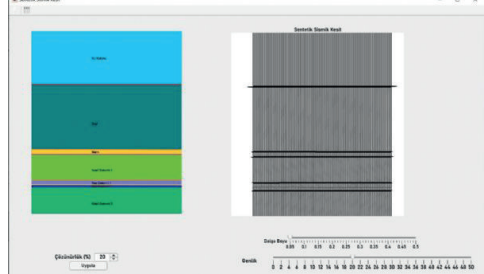
*Görsel yüklem bölgesi ve çizilen istifin bu kısımda yüklenmesi.*

**Sekil 2**



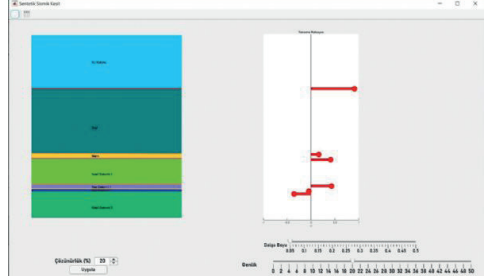
*Oluşturulan sentetik kesitin dalga boyu ve genlik değerlerinin nasıl ayarlandığının gösterilmesi.*

**Sekil 3**



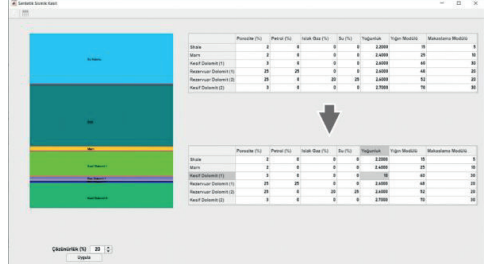
*Sinyalin sahip olduğu dalga boyu değerinin azaltılması ve genlik değerinin artırılması sonucunda sentetik sismik kesitte meydana gelen değişim.*

**Sekil 4**



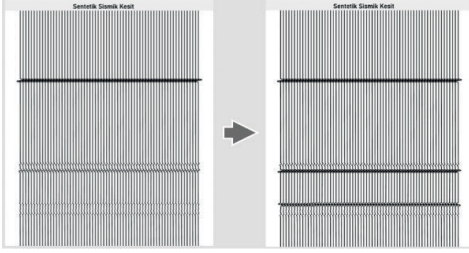
*İstif ve tabaka sınırlarına karşılık gelen yansıma katsayısı değerlerinin gösterilmesi.*

**Sekil 5**



*Kayaçların fiziksel parametrelerinin tablo halinde gösterilmesi.*

Sekil 6



Farklı porozite, yoğunluk, su oranı ve hidrokarbon oranına sahip kesitlerin karşılaştırmalı hali.

Sekil 7

```

162 - I = imread([filepath, filename]);
163
164 - a)
165 - su_soyl_Coor = R_su_soyl*double(I(:,1)) == su_soyl(1) & ...
166 - (I(:,2) == su_soyl(2) & (I(:,3) == su_soyl(3));
167 - seyl_marn_Coor = R_seyl_marn*double(I(:,1)) == seyl_marn(1) & ...
168 - (I(:,2) == seyl_marn(2) & (I(:,3) == seyl_marn(3));
169 - marn_kesifdolomit_Coor = R_marn_kesif_doloi*double(I(:,1)) == marn_kesifdolomiti(1) & ...
170 - (I(:,2) == marn_kesifdolomiti(2) & (I(:,3) == marn_kesifdolomiti(3));
171 - kesifdolomiti_rezdogolomiti_Coor = R_kesif_doloi_rez_doloi*double(I(:,1)) == kesifdolomiti_rezdogolomiti(1) & ...
172 - (I(:,2) == kesifdolomiti_rezdogolomiti(2) & (I(:,3) == kesifdolomiti_rezdogolomiti(3));
173 - rezdogolomiti_rezdogolomiti_Coor = R_rez_doloi_rez_doloi*double(I(:,1)) == rezdogolomiti_rezdogolomiti(1) & ...
174 - (I(:,2) == rezdogolomiti_rezdogolomiti(2) & (I(:,3) == rezdogolomiti_rezdogolomiti(3));
175 - rezdogolomiti_kesifdolomiti_Coor = R_rez_doloi_kesif_doloi*double(I(:,1)) == rezdogolomiti_kesifdolomiti(1) & ...
176 - (I(:,2) == rezdogolomiti_kesifdolomiti(2) & (I(:,3) == rezdogolomiti_kesifdolomiti(3));
177 -
178 - katsayi = app.KatsayiDegeriSlider.Value;
179 - matrix = katsayi*(su_soyl_Coor+ seyl_marn_Coor+ marn_kesifdolomiti_Coor+ ...
180 - kesifdolomiti_rezdogolomiti_Coor+ rezdogolomiti_rezdogolomiti_Coor+ ...
181 - rezdogolomiti_kesifdolomiti_Coor);
182
183
184 - b)
185 - k = size(I,2); % görselin yatay genişliği (piksel)
186 - spinspace = app.mpiKspisner.Value;
187 - dalga_adieti = k*spinspace/100;
188 - atlama_miktari = round(k/dalga_adieti);
189 -
190 - for i = 1:atlama_miktari:k
191 - [ud,uidx] = unique(matrix(:,i),'stable');
192 - matrix(:,i) = 0;
193 - uidx(udx == 1) = [];
194 - ud(ud == 0) = [];
195 - matrix(uidx,i) = ud;
196 -
197 - [XX,~] = find(matrix(:,i));
198 - dt2 = app.DalgaBoyuslider.Value;
199 - rt2 = 0:dt2:size(I,1);
200 - r2=zeros(1,length(rt2)); % Varyeli zamana göre genişletip açma
201 - r2(round(XX(1:length(uidx))/dt2))+[matrix(uidx,i)];
202 - y2 = conv(r2,wavelet);
203 - y2 = y2(1:length(rt2));
204 -
205 - % Ideal Seismic Section
206 -
207 - plot(app.UIAxes,rt2,y2*i*0.5,'linewidth',1,'color','k')
208 - hold(app.UIAxes,'on')
209 - app.UIAxes.View = [90 90];
210 - ax1 = app.UIAxes;
211 - ax1.XAxis.Visible = 'off';
212 - ax1.YAxis.Visible = 'off';
213 - app.UIAxes.XLim = [0,size(I,1)];
214 -
215 - end

```

a) RGB değerlerinin görselin içinden alınıp her bir kayaç için kaydedildiği kod kısmı, b) Yansıma katsayısı ve dalgacığın konvolüsyona sokulduğu kod kısmı, c) Dalgacığın oluşturulduğu kod kısmı



## Yapay Zeka ve Özdevimli Öğrenme

---

---

---

# Predicting Shear Stress in Heavy Crude Oil Using Random Forest Analysis of Magneto-Rheological Behavior



**Uğur Özveren**

Department of Chemical Engineering, Marmara University, Goztepe Campus, 34722, Kadikoy / Istanbul / Türkiye

## ABSTRACT

The prediction of shear stress in heavy oil under varying magneto-rheological conditions has become pivotal in petroleum engineering due to its direct implications on extraction and transportation efficiency. This research utilized the Random Forest (RF) algorithm, a dynamic machine learning technique, to model these shear stress dynamics. Using an extensive dataset, the data was split into training and validation subsets to meticulously evaluate the model's predictive prowess.

When trained on diverse magneto-rheological parameters, the RF model astoundingly identified the nonlinear relationships defining heavy oil's shear stress, achieving an  $R^2$  value surpassing 0.98 in testing. This remarkable achievement underscores the potential of machine learning in petroleum engineering, specifically in shear stress modeling. The insights from this research promise to greatly enhance extraction and transportation methods, offering increased efficiency and economic advantages.

## 1. INTRODUCTION

Heavy crude oil, constituting a significant portion of the world's extractable oil reservoirs, presents challenges due to its shear stress, impacting its handling and transportation [1][2][3]. Traditional methods, such as thermal enhancement, are effective in reducing viscosity but come with drawbacks like high energy costs and potential quality degradation [6][7]. Meanwhile, the addition of diluents can alter crude's chemical composition, and altering flow dynamics can be problematic in colder climates [8][9][10].

An emerging solution is magneto-rheology, which adjusts a material's viscosity when exposed to a magnetic field [11]. This technique offers a way to control heavy oil's flow properties without chemical adjustments, presenting both environmental and economic benefits [12]. However, comprehending the intricate dynamics between magnetic fields and heavy oil rheology requires robust investigative tools.

This research aims to harness machine learning, particularly the Random Forest algorithm, to predict shear stress changes in heavy oil due to magneto-rheology [13]. The algorithm's strength lies in its ability to decode complex relationships between variables such as temperature, magnetic flux density, and shear rate [14]. As the application of magneto-rheology in predicting shear stress in heavy oil remains relatively unexplored, this study introduces a groundbreaking method, potentially revolutionizing petroleum engineering's understanding of magneto-rheological

effects on heavy oil shear stress.

## 2. METHODOLOGY

### 2.1. Heavy Crude Oil

The study is anchored on a foundational dataset from Ro et al. [15] regarding extra heavy crude oil (8.5° API), comprising 1200 instances. Each instance details conditions marked by parameters like Temperature (C), Magnetic Flux Density (T), and Shear Rate (1/s), pivotal for accurate modeling of shear stress.

### 2.2. The Random Forest (RF) Algorithm

Machine learning offers a plethora of algorithms, with the Random Forest (RF) algorithm standing out due to its versatility and robustness [16]. Within the niche of heavy oil research, understanding its magneto-rheological behavior is crucial. The RF algorithm, resembling a consortium of decision trees, was employed to predict heavy oil's shear stress. By considering variables such as Temperature, Magnetic Flux Density, and Shear Rate, the RF model amasses insights from multiple decision trees, mirroring the approach of consulting multiple experts for an informed decision.

At its core, the RF model's strength derives from the bootstrap parameter. This parameter ensures each decision tree examines a unique data subset, boosting diversity and reducing overfitting risks. Parameters like `squared_error` criterion optimize the model for regression tasks by minimizing prediction discrepancies. Additionally, the `max_features` parameter stresses the significance of each feature in decision-making, while settings like `min_samples_split` and `min_samples_leaf` determine tree depth and complexity, ensuring neither oversimplification nor over-complication.

To guarantee precision and reproducibility, several hyperparameters were fine-tuned. The ensemble is bolstered by an optimal 100 trees, as denoted by the `n_estimators` value, balancing accuracy with computational speed. Furthermore, by setting the `random_state` hyperparameter to 42, the model's outcomes remain consistent across multiple runs, ensuring replicability in subsequent research efforts.

### 2.3. Statistical Performance Validation and Cross Validation

In evaluating our model's effectiveness for real-world applications, we employed several metrics, notably the RMSE, which quantified prediction accuracy, MAPE that highlighted prediction deviations in percentage terms,

and the R2 measure that indicated the predictability of variance from independent variables. Crucially, cross-validation was integrated, partitioning the dataset into multiple ‘folds’ to test different training and testing set combinations, ensuring model generalizability and reducing overfitting risks. This comprehensive evaluation approach confirmed the model’s accuracy and adaptability to diverse data scenarios.

### 3. RESULTS

#### 3.1. Interpreting Model Variables

Feature importance in the Random Forest model highlights which variables crucially influence predictions. In our research, the three examined variables—Temperature (C), Magnetic Flux Density (T), and Shear Rate (1/s)—were pivotal in predicting shear stress. Shear Rate had the most significant importance at 0.4651, followed by Temperature at 0.3828, and Magnetic Flux Density at 0.1521. Despite its lower numerical value, Magnetic Flux Density remains crucial for understanding magneto-rheological behavior in heavy crude oil. Its interaction with other variables, even if individually subtle, collectively impacts the system behavior and the model’s predictive accuracy, emphasizing the need for a comprehensive modeling approach for precise predictions.

#### 3.2. Model Accuracy

The increasing demand for accurate predictive models in oil dynamics has particularly emphasized the need to understand the magneto-rheological behavior of heavy crude oil. Accurate predictions of shear stress can significantly enhance operational efficiency. This research, supported by in-depth graphical representations and statistical analyses, highlights both the strengths of the model and areas needing improvement. Key performance metrics such as RMSE, MAPE, and the R2 value were used to gauge the model’s predictive accuracy. The training dataset revealed a promising RMSE of 56.566, a MAPE of 3.864%, and an R<sup>2</sup> value of 0.997, suggesting the model could explain 99.7% of the variability in the training data.

However, when applied to the test dataset, there was a noticeable increase in RMSE to 205.349 and a MAPE of 9.137%. The R<sup>2</sup> value for the test data was 0.958, demonstrating the model’s ability to account for 95.8% of the variability in these observations. While these results indicate the model’s substantial predictive power, the discrepancy between training and test metrics underscores the need for further optimization to improve the model’s performance on unseen data.

#### 3.3. The Effect of Temperature on Predicted Shear Stress

In the exploration of rheological properties, understanding how temperature impacts heavy crude oil’s behavior, especially under varying Magnetic Flux Density (MFD), is crucial. Temperature variations are

found to be fundamental in determining the predicted shear stress in heavy crude oil, particularly at the temperature benchmarks of 30°C, 50°C, and 70°C and a consistent shear rate of around 50.5 [1/s]. With no magnetic influence (0 T), shear stress is 549.132 Pa at 30°C and dramatically escalates to 2120.4 Pa at 50°C, an almost fourfold increase. However, raising the temperature further to 70°C results in a drop to 907.15 Pa.

Incorporating a magnetic flux density of 0.17 T reveals an intriguing pattern. The shear stress peaks at 50°C with a value of 2470.3 Pa. On the other hand, the temperatures 30°C and 70°C produce lesser shear stresses of 42.067 Pa and 817.42 Pa, respectively. Regardless of the magnetic conditions tested, the pronounced shear stress at 50°C persists, emphasizing temperature’s dominant role in the magneto-rheological dynamics of crude oil.

#### 3.4. The Effect of Magnetic Flux Density on Predicted Shear Stress

The analysis of heavy crude oil’s behavior under varying Magnetic Flux Density (MFD) is integral for optimizing extraction and transportation. Initial observations at 0T revealed that an elevation in temperature from 30°C to 70°C led to a peak shear stress of 2120.4 Pa at 50°C, only to reduce to 907.15 Pa at 70°C. As MFD was increased to 0.17T, shear stress reached 2470.3 Pa at 50°C. However, with further MFD increases to 0.35T and 0.65T, shear stress declined at 70°C, registering 723.19 Pa and 544.71 Pa respectively, indicating a non-linear relationship between MFD and shear stress.

Using this data, the study highlighted the complexities of crude oil’s rheological properties in different magnetic fields. The Random Forest method effectively predicted these patterns, emphasizing its importance in refining petroleum processes. Such insights, rooted in rigorous data analysis, are primed to direct future research and implementations in the magnetorheology of heavy crude oil.

### 4. CONCLUSIONS

The study’s exploration of magneto-rheological behaviors in heavy crude oil through the Random Forest method revealed critical non-linear relationships between variables such as Temperature, Magnetic Flux Density, and Shear Rate, and their effect on Shear Stress. Notably, temperature around 50°C emerged as a pivotal determinant of shear stress, irrespective of the magnetic context, while the impact of Magnetic Flux Density proved more intricate. Although the model showed high precision with the training data, differences in test data indicate a need for ongoing refinement. These insights, vital for the oil industry’s extraction and transportation processes, highlight the promise of machine learning in optimizing heavy crude oil operations and predicting complex behaviors. Future research in this realm stands to gain significantly from this study’s foundational methodologies and discoveries.

## REFERENCES

1. Yang, Y., et al., Economic impact of crude oil supply disruption on social welfare losses and strategic petroleum reserves. *Resources Policy*, 2022. 77: p. 102689.
2. Douglas, L.D., et al., A materials science perspective of midstream challenges in the utilization of heavy crude oil. *ACS omega*, 2022. 7(2): p. 1547-1574.
3. Yadykova, A.Y. and S.O. Ilyin, Compatibility and rheology of bio-oil blends with light and heavy crude oils. *Fuel*, 2022. 314: p. 122761.
4. Bded, A.S. and M.A. Ahmad, An overview of natural additive enhancers and their effectiveness in mitigating crude oil flow issues: Characterization and case study. *Materials Today: Proceedings*, 2023. 78: p. 18-22.
5. Lam-Maldonado, M., et al., Extra heavy crude oil viscosity and surface tension behavior using a flow enhancer and water at different temperatures conditions. *Heliyon*, 2023. 9(2).
6. Kholmurodov, T., et al., Thermochemical Upgrading of Heavy Crude Oil in Reservoir Conditions. *Processes*, 2023. 11(7): p. 2156.
7. Muñoz, J.A. and J. Ancheyta, Techno-economic analysis of heating techniques for transportation of heavy crude oils by land pipeline. *Fuel*, 2023. 331: p. 125640.
8. Rushd, S., et al., Applications of drag reducers for the pipeline transportation of heavy crude oils: A critical review and future research directions. *The Canadian Journal of Chemical Engineering*.
9. Yarmola, T., et al., Effect of Polymer Additives on the Rheological Properties of Heavy High-Viscosity Oil, in *Chemotological Aspects of Sustainable Development of Transport*. 2022, Springer. p. 19-29.
10. Martínez-Palou, R., et al., Transportation of heavy and extra-heavy crude oil by pipeline: A review. *Journal of petroleum science and engineering*, 2011. 75(3-4): p. 274-282.
11. Jiang, C., et al., Magnetic field effect on apparent viscosity reducing of different crude oils at low temperature. *Colloids and Surfaces A: Physicochemical and Engineering Aspects*, 2021. 629: p. 127372.
12. Balan, C., et al., Rheological characterization of complex fluids in electro-magnetic fields. *Journal of non-newtonian fluid mechanics*, 2008. 154(1): p. 22-30.
13. Fang, J., et al., Development of Machine Learning Algorithms for Predicting Internal Corrosion of Crude Oil and Natural Gas Pipelines. *Computers & Chemical Engineering*, 2023: p. 108358.
14. Cutler, A., D.R. Cutler, and J.R. Stevens, Random forests. *Ensemble machine learning: Methods and applications*, 2012: p. 157-175.
15. Roa, M., E. Aguilera, and R. Correa, Magneto-rheological dataset for an extra heavy crude oil (8.5° API) in the presence of a constant magnetic field. *Data in brief*, 2019. 24.
16. Sipper, M. and J.H. Moore, Conservation machine learning: a case study of random forests. *Scientific Reports*, 2021. 11(1): p. 3629.

*Keywords: Shear Stress Prediction, Random Forest Algorithm*